116

PROCEEDINGS OF THE OCEAN DRILLING PROGRAM

INITIAL REPORTS

VOLUME 126
18 April 1989–19 June 1989

NATIONAL SCIENCE FOUNDATION

JOINT OCEANOGRAPHIC INSTITUTIONS, INC.

NS1.38/2:

pages tightly bound

best copy available

DRILLING LOCATIONS

LEG	LOCATION	REP	SITES
100	Gulf of Mexico	E	625A-625C
101	Bahamas	E	626-636
102	Bermuda Rise	E	418
103	Galicia Margin	E	637-641
104	Norwegian Sea	E	642-644
105	Baffin Bay	E	645-647
106	Mid Atlantic Range	E	648-649
107	Tyrrhenian sea	E	650-656
108	Eastern Tropical Atlantic	E	657-668
109	Mid Atlantic Range	E	669-670, 395, 648
110	Northern Barbados Ridge	E	671-676
111	Costa Rica Rift	G	677-678, 504B
112	Peru Continental Margin	G	679-688
113	Weddel Sea, Antarctica	E	689-697
114	Subantarctica South Atlantic	E	698-704
115	Mascarene Plateau	G	705-716
116	Distal Bengal Fan	G	717-719
117	Oman Margin	G	720-731
118	Southwest Indian Ridge	G	732-735
119	Kerguelen Plateau Prydz Bay	E	736-746
120	Central Kerguelen Plateau	E	747-751
121	Broken Ridge & Ninetyeast Ridge	G	752-758
122	Exmouth Plateau	G	759-764
123	Argo Abyssal Plain	G	765-766
124	Celebes & Sulu Seas	G	767-771
124E	Philippine Sea	G	772-777
125	Bonin/Mariana Region	G	778-786
126	Bonin Arc-Trench System	G	787-793

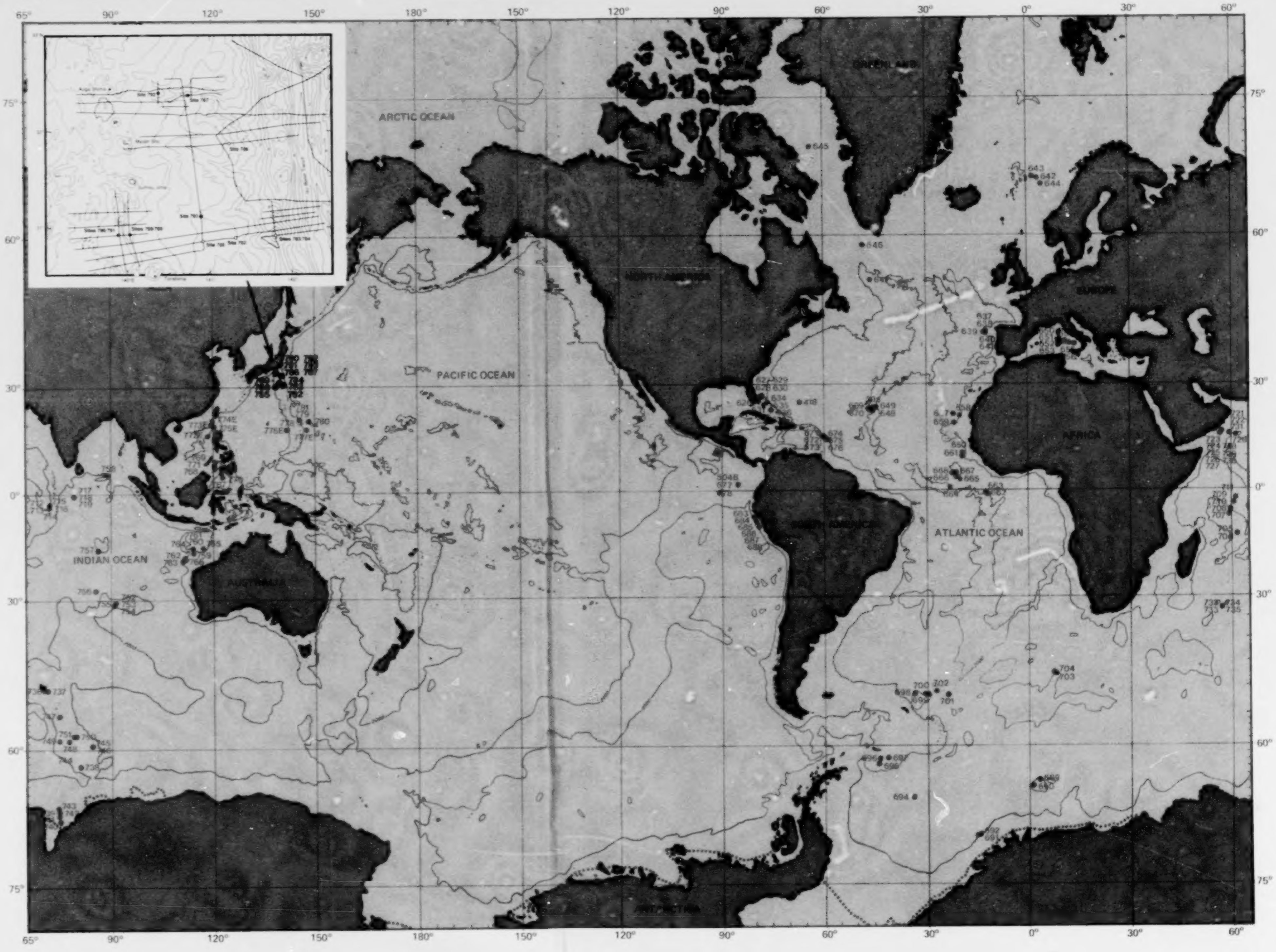
65°
90°
120°
150°
180°
150°
120°
90°
60°
30°
0°
30°
60°
75°
60°
30°
0°
30°
60°
75°
ARCTIC OCEAN
GREENLAND
NORTH AMERICA
EUROPE
PACIFIC OCEAN
AFRICA
SOUTH AMERICA
ATLANTIC OCEAN
INDIAN OCEAN
AUSTRALIA
ANTARCTICA
645
643
642
644
646
418
694
704
703
Site 762
Site 761
Site 766
Site 763
Sites 756 751
Sites 759 760
Site 764

Storage

E - East Coast Repository
G - Gulf Coast Repository

OCEAN DRILLING PROGRAM

PROCEEDINGS OF THE OCEAN DRILLING PROGRAM

VOLUME 126
INITIAL REPORTS
BONIN ARC-TRENCH SYSTEM

Covering Leg 126 of the cruises of the Drilling Vessel *JOIDES Resolution*,
Tokyo, Japan, to Tokyo, Japan, Sites 787–793,
18 April 1989–19 June 1989

Brian Taylor, Kantaro Fujioka, Thomas R. Janecek,
Jonathan Aitchison, Stanley Cisowski, Albina Colella, Patricia Ann Cooper,
Kathleen A. Dadey, Per Kristian Egeberg, John V. Firth, James B. Gill,
Yvonne Herman, Richard N. Hiscott, MaLynn Isiminger-Kelso, Kunio Kaiho,
Adam Klaus, Masato Koyama, Henriette Lapierre, Michael A. Lovell,
Kathleen Marsaglia, Akira Nishimura, Philippe A. Pezard,
Kelvin S. Rodolfo, Rex N. Taylor, Kazue Tazaki, Peter Torssander
Shipboard Scientific Party

Thomas R. Janecek
Shipboard Staff Scientist

Prepared by the
OCEAN DRILLING PROGRAM
TEXAS A&M UNIVERSITY

Eva M. Barbu and Amanda Palmer Julson
Volume Editors

in cooperation with the
NATIONAL SCIENCE FOUNDATION
and
JOINT OCEANOGRAPHIC INSTITUTIONS, INC.

This publication was prepared by the Ocean Drilling Program, Texas A&M University, as an account of work performed under the international Ocean Drilling Program, which is managed by Joint Oceanographic Institutions, Inc., under contract with the National Science Foundation. Funding for the program was provided by the following agencies at the time of this cruise:

Canada/Australia Consortium for the Ocean Drilling Program, Department of Energy, Mines and Resources (Canada) and Department of Primary Industries and Energy (Australia)

Deutsche Forschungsgemeinschaft (Federal Republic of Germany)

European Science Foundation Consortium for Ocean Drilling (Belgium, Denmark, Finland, Iceland, Italy, Greece, the Netherlands, Norway, Spain, Sweden, Switzerland, and Turkey)

Institut Français de Recherche pour l'Exploitation de la Mer (France)

National Science Foundation (United States)

Natural Environment Research Council (United Kingdom)

University of Tokyo, Ocean Research Institute (Japan)

Any opinions, findings, and conclusions or recommendations expressed in this publication are those of the author(s) and do not necessarily reflect the views of the National Science Foundation, the participating agencies, Joint Oceanographic Institutions, Inc., Texas A&M University, or Texas A&M Research Foundation.

It is recommended that reference to the whole or to part of this volume be made in one of the following forms, as appropriate:

Taylor, B., Fujioka, K., et al., 1990. *Proc. ODP, Init. Repts.*, 126: College Station, TX (Ocean Drilling Program).

Shipboard Scientific Party, 1990. Site 787. *In* Taylor, B., Fujioka, K., et al., *Proc. ODP, Init. Repts.*, 126: College Station, TX (Ocean Drilling Program), 66–96.

Effective Publication Dates of ODP *Proceedings*

According to the International Code of Zoological Nomenclature, the date of publication of a work and of a contained name or statement affecting nomenclature is the date on which the publication was mailed to subscribers, placed on sale, or when the whole edition is distributed free of charge, mailed to institutions and individuals to whom free copies are distributed. The mailing date, *not the printed date*, is the correct one.

The mailing dates of recent *Proceedings of the Ocean Drilling Program* are as follows:

Volume 123 (*Initial Reports*): May 1990
Volumes 124/124E (*Initial Reports*): May 1990
Volume 125 (*Initial Reports*) July 1990
Volume 111 (*Scientific Results*): December 1989
Volume 112 (*Scientific Results*): June 1990
Volume 113 (*Scientific Results*): July 1990

Distribution

Copies of this publication may be obtained from Publications Distribution Center, Ocean Drilling Program, 1000 Discovery Drive, College Station, Texas 77845-9547. Orders for copies will require advance payment. See current ODP publication list for price and availability of this publication.

Printed August 1990

ISSN 0884-5883
Library of Congress 87-655-674

The paper used in this publication meets the minimum requirements of American National Standard for Information Sciences—Permanence of Paper for Printed Library Materials, ANSI Z39.48–1984 ∞™

Foreword

By the National Science Foundation

The scientists of the Ocean Drilling Program (ODP) have embarked on what could prove to be one of the most important earth science initiatives of the decade—an initiative rivaling in scope and impact the exploration of the frontiers of outer space. The program explores our planet's last frontier—the Earth's structure and history as it is revealed beneath the oceans. The scope of the program's scientific goals excites the imagination, challenges the intellect, and enhances the spirit of cooperation among peoples in countries around the world.

Between 1872 and 1876, HMS *Challenger* undertook the world's first major oceanographic expedition. That expedition greatly expanded man's knowledge of the world's oceans and revolutionized our ideas about planet Earth. From 1968 to 1983, another ship named *Challenger* logged more than 375,000 miles on 96 voyages across every ocean for the Deep Sea Drilling Project (DSDP), operated by Scripps Institution of Oceanography. Among the project's many remarkable discoveries were the confirmation of seafloor spreading and the establishment of the relative youth of the seafloor, thus verifying the dynamic and changing nature of the Earth's crust.

Today, the Ocean Drilling Program, which began in 1983, brings new resources to bear on scientific ocean drilling. A new drillship is in operation—the *JOIDES Resolution*—one of the world's most modern and best equipped drillships with enhanced capability for drilling and coring in polar areas and rough weather, expanded laboratory space, facilities for more scientists, and a major drill-hole logging program. The name of the ship was derived from the international scientific partnership that directs the program—the Joint Oceanographic Institutions for Deep Earth Sampling (JOIDES)—and from the flagship of Captain Cook's second voyage to the Pacific Ocean in the late 18th century. Texas A&M University is responsible for science operations in the program, and Lamont-Doherty Geological Observatory is responsible for the logging program.

The Ocean Drilling Program truly has international participation. In 1975, the International Phase of Ocean Drilling began with member nations—the U.S.A., U.S.S.R., the Federal Republic of Germany, Japan, the United Kingdom, and France—all providing funds and scientific guidance for the project. Today, ODP partners include the U.S.A., the Canada/Australia Consortium for the Ocean Drilling Program, France, the Federal Republic of Germany, Japan, the United Kingdom, and the European Science Foundation, which represents Sweden, Finland, Norway, Iceland, Denmark, Belgium, the Netherlands, Spain, Switzerland, Italy, Greece, and Turkey. The National Science Foundation, with funds contributed by the United States and international partners, supports the scientific operations and planning for the ODP through a contract with Joint Oceanographic Institutions, Inc. (JOI).

The information gained by the program leads to a better understanding of the Earth and its dynamic processes. Drilled sediment cores and logs reveal clues to past climatic history and tie into parallel studies of paleoclimates from glacial ice cores drilled on the continents. Understanding these sediment cores will enable scientists to complete the map of major geologically active regions of the Earth, and to identify processes that lead to dynamic change such as earthquakes, volcanic eruptions, and mountain and continental growth. We are far from being able to predict such changes accurately now; but with the new tools and understanding, the accuracy of such predictions can be improved. This better understanding of the Earth's system(s) will allow us to identify regions of potential mineral and energy resource development, an issue of worldwide human interest. The Ocean Drilling Program is not in itself aimed at finding resources, but the knowledge of the Earth's processes that is gained through such a basic research program will inevitably provide pieces of information required for such resource discovery and exploitation.

The program is fully under way in its aim to further the understanding of the Earth's dynamic systems. People of our planet will benefit directly and indirectly from this research in both their daily living and work activities. This multinational endeavor will perhaps foster other cooperative efforts in science or among societies. The Ocean Drilling Program has distinguished ancestors in the original *Resolution* and *Challenger* expeditions and the Deep Sea Drilling Project. The National Science Foundation is proud to be playing a leading role in this program, and we are looking forward to significant and innovative science for many years to come.

Erich Bloch
Director
National Science Foundation

Washington, D.C.

Foreword

By Joint Oceanographic Institutions, Inc.

This volume presents results from the Ocean Drilling Program (ODP), where scientists use a specially equipped ocean drilling ship to sample and measure the properties of the submerged part of the Earth's crust. These data are then synthesized with other information to yield new insights into earth processes.

These results address the scientific goals of the program, which include providing a global description of geological and geophysical structures and materials, studying in detail areas of major geophysical activity such as mid-ocean ridges and the associated hydrothermal circulations, and studying passive and active continental margins. In addition, the ODP data support the study of sea-level and ocean-circulation changes, the effects of the Earth's orbital variations on climate, and the study of processes and mechanisms of evolution from the biological records in the cores which are recovered from drilling.

The Ocean Drilling Program is a partnership of scientists and governments. Overall scientific policy and management guidance is provided by Joint Oceanographic Institutions for Deep Earth Sampling (JOIDES), which consists of committees and panels made up of representatives of the participating institutions and other scientific and engineering experts. The JOIDES Executive Committee (EXCOM) provides general oversight; the JOIDES Planning Committee (PCOM) is the focal point for all scientific planning for the ODP and is key to the scientific success of the program.

The PCOM has a network of panels and working groups which screen drilling proposals, evaluate instrumentation and measurement techniques, and assess geophysical survey data and other safety and siting information. PCOM uses the recommendations of these panels and committees to select drilling targets, to specify the major scientific objectives of each two-month drilling segment or leg, and to provide the science operator with nominations for co-chief scientists. The science operator, Texas A&M University, in turn is responsible for planning the detailed ship's operations, actual drilling schedules, and final scientific rosters, which are developed in close cooperation with PCOM and the cognizant panels.

Many of the scientific goals can be met only with new technology. Thus the program has identified engineering goals, which include the ability to start a hole and to core on bare rock at mid-ocean ridge sites, to drill in high-temperature and corrosive regions typical of hydrothermal areas, and to core in high latitudes with minimum interference from high seas and sea ice. To meet these needs, the program operates a specially equipped drillship, the *JOIDES Resolution*, which contains laboratories and equipment that are state-of-the-art, and carries a major new logging program.

The ship, registered as SEDCO/BP 471 after her owners and her length in feet (144 meters), is 70 feet (21 meters) wide, and has a displacement of 16,595 long tons. Her derrick towers 200 feet (61 meters) above the waterline, and a computer-controlled dynamic-positioning system stabilizes the ship over a specific location while drilling in water depths up to 27,000 feet (8230 meters). The drilling system collects cores from beneath the seafloor with a derrick and drawworks that can handle 30,000 feet (9144 meters) of drill pipe. More than 12,000 square feet (1115 square meters) of space distributed throughout the ship is devoted to scientific laboratories and equipment. The ship sails with a scientific and technical crew of 50 and a ship's crew of 65.

Logging is a major part of the overall operation. The program provides a full suite of geochemical and geophysical measurements for every hole deeper than 1300 feet (400 meters). For each such hole, there are lowerings of basic oil-industry tools: nuclear, sonic, and electrical. In addition, a borehole televiewer is available for imaging the well-bore wall, a 12-channel logging tool provides accurate velocity and elastic property measurements as well as sonic waveforms for spectral analysis of energy propagation near the well bore, and a vertical seismic profiler records reflectors from below the total depth of the hole.

Texas A&M University serves as science operator for the Ocean Drilling Program. In this capacity, they operate and staff the drillship to collect cores from JOIDES-designated sites from around the world. The science operator also ensures that adequate scientific analyses are performed on the cores by maintaining the shipboard scientific laboratories and by providing logistical and technical support for shipboard scientific teams. Onshore, Texas A&M manages scientific activities after each leg, is curator for the cores, distributes samples, and coordinates the editing and publication of the scientific results. Lamont-Doherty Geological Observatory (LDGO) of Columbia University manages the program's logging operations, which include processing the data and provision of assistance to scientists in data analysis. The ODP Data Bank, a repository for geophysical data, is also managed by LDGO. Core samples from ODP and the previous Deep Sea Drilling Project are stored for future investigation at three sites: ODP Pacific and Indian Ocean cores at Texas A&M University, ODP and DSDP Atlantic and Antarctic cores at Lamont-Doherty Geological Observatory, and DSDP Pacific and Indian Ocean cores at Scripps Institution of Oceanography.

International oversight and coordination are provided by the ODP Council, a governmental consultative body of partner country representatives, chaired by the United States, which periodically reviews the general progress of the program and discusses financial plans and other management issues. Joint Oceanographic Institutions, Inc., a nonprofit consortium of U.S. oceanographic institutions, serves as the National Science Foundation's prime contractor and manages the ODP. JOI is responsible for seeing that the scientific objectives and plans are translated into scientific operations consistent with JOIDES recommendations and budgetary constraints.

Scientific achievements of the ODP already include new data on early seafloor spreading and how continents separate and their margins evolve. We have new insight into glacial cycles and the fluctuations of currents throughout geological time. Technical achievements include the first bare-rock coring, and logging data more accurate and complete than ever before. JOI is pleased to have played a facilitating role in the Ocean Drilling Program.

D. James Baker
President
Joint Oceanographic Institutions, Inc.

Washington, D.C.

OCEAN DRILLING PROGRAM

MEMBER ORGANIZATIONS OF THE JOINT OCEANOGRAPHIC INSTITUTIONS FOR DEEP EARTH SAMPLING (JOIDES):

University of California at San Diego, Scripps Institution of Oceanography

Columbia University, Lamont-Doherty Geological Observatory

University of Hawaii, Hawaii Institute of Geophysics

University of Miami, Rosenstiel School of Marine and Atmospheric Science

Oregon State University, College of Oceanography

University of Rhode Island, Graduate School of Oceanography

Texas A&M University, College of Geosciences

University of Texas at Austin, Institute for Geophysics

University of Washington, College of Ocean and Fishery Sciences

Woods Hole Oceanographic Institution

Canada/Australia Consortium for the Ocean Drilling Program, Department of Energy, Mines and Resources (Canada) and Department of Primary Industries and Energy (Australia)

European Science Foundation Consortium for Ocean Drilling (ECOD), Belgium, Denmark, Finland, Iceland, Italy, Greece, the Netherlands, Norway, Spain, Sweden, Switzerland, and Turkey

Federal Republic of Germany, Bundesanstalt für Geowissenschaften und Rohstoffe

France, Institut Français de Recherche pour l'Exploitation de la Mer

Japan, University of Tokyo, Ocean Research Institute

United Kingdom, Natural Environment Research Council

PRIME CONTRACTOR

Joint Oceanographic Institutions, Inc.
Washington, D.C.

Thomas E. Pyle
Director, Ocean Drilling Programs

OPERATING INSTITUTION

College of Geosciences
Texas A&M University
College Station, Texas

Melvin Friedman, Principal Investigator

OCEAN DRILLING PROGRAM

Philip D. Rabinowitz
Director

Louis E. Garrison
Deputy Director

Richard G. McPherson
Administrator

Audrey W. Meyer, Manager
Science Operations

Barry W. Harding, Manager
Engineering and Drilling Operations

Russell B. Merrill, Curator and Manager
Science Services

Robert E. Olivas, Manager
Technical and Logistics Support

LOGGING OPERATOR

Borehole Research Group
Lamont-Doherty Geological Observatory
Columbia University
Palisades, New York

Roger N. Anderson, Head

PARTICIPANTS ABOARD THE *JOIDES RESOLUTION* FOR LEG 126*

Brian Taylor
Co-Chief Scientist

Hawaii Institute of Geophysics
University of Hawaii
2525 Correa Road
Honolulu, Hawaii 96822

Kantaro Fujioka
Co-Chief Scientist

Ocean Research Institute
University of Tokyo
1-15-1 Minamidai Nakano-ku
Tokyo 164
Japan

Thomas R. Janecek
ODP Staff Scientist/Sedimentologist

Ocean Drilling Program
Texas A&M University
1000 Discovery Drive
College Station, Texas 77845-9547

Jonathan Aitchison
Paleontologist (radiolarians)

Department of Geology and Geophysics
University of New England
Armidale, N.S.W. 2351
Australia

Stanley Cisowski
Paleomagnetist

Department of Geological Sciences
University of California, Santa Barbara
Santa Barbara, California 93106

Albina Colella
Sedimentologist

Dipartimento Di Scienze della Terra
Universitá della Calabria
87939 Castiglione Cosentino
Scalo (CS)
Italy

Patricia Ann Cooper
Geophysicist

Hawaii Institute of Geophysics
University of Hawaii
2525 Correa Road
Honolulu, Hawaii 96822

Kathleen A. Dadey
Physical Properties Specialist

Graduate School of Oceanography
University of Rhode Island
Narragansett Bay Campus
Narragansett, Rhode Island 02882-1197

Per Kristian Egeberg
Inorganic Geochemist
Department of Geology
University of Oslo
Postboks 1047, Blindern
N-0316 Oslo 3
Norway

John V. Firth
Paleontologist (nannofossils)
Department of Geology
Florida State University
Tallahassee, Florida 32306

James B. Gill
Igneous Petrologist
Department of Earth Sciences
University of California, Santa Cruz
Santa Cruz, California 95064

Yvonne Herman
Paleontologist (foraminifers)
Department of Geology
Washington State University
Pullman, Washington 99164

Richard N. Hiscott
Sedimentologist
Earth Sciences Department
Memorial University
St. John's, Newfoundland A1B 3X5
Canada

MaLynn Isiminger-Kelso
Paleontologist (nannofossils)
Antarctic Research Facility
Florida State University
Tallahassee, Florida 32306

Kunio Kaiho
Paleontologist (foraminifers)
Institute of Geology and Paleontology
Faculty of Science
Tohoku University
Aoba, Sendai, 980
Japan

Adam Klaus
Physical Properties Specialist
Hawaii Institute of Geophysics
University of Hawaii
2525 Correa Road
Honolulu, Hawaii 96822

Masato Koyama
Paleomagnetist
Institute of Geosciences
Shizuoka University
836 Oya
Shizuoka 422
Japan

---

*Address at time of cruise.

Henriette Lapierre
Igneous Petrologist
Laboratoire de Géologie Structurale
Université d'Orléans
45067 Orléans Cedex 2
France

Michael A. Lovell
Logging Scientist
Department of Geology
University of Nottingham
University Park
Nottingham NG7 2RD
United Kingdom

Kathleen Marsaglia
Sedimentologist
Department of Geology
University of Texas at El Paso
El Paso, Texas 79968

Akira Nishimura
Sedimentologist
Marine Geology
Geological Survey of Japan
1-1-3 Higashi, Tsukuba-shi
Ibaraki 3065
Japan

Philippe A. Pezard
LDGO Logging Scientist
Borehole Research Group
Lamont-Doherty Geological Observatory
Columbia University
Palisades, New York 10964

Kelvin S. Rodolfo
Sedimentologist
Department of Geological Sciences
University of Illinois at Chicago
P.O. Box 4348
Chicago, Illinois 60680

Rex Neil Taylor
Igneous Petrologist
Geology Department
University of Southampton
Southampton SO9 5NH
United Kingdom

Kazue Tazaki
Sedimentologist
Geology Department
Shimane University
Matsue
Shimane Prefecture 690
Japan

Peter Torssander
Igneous Petrologist
Department of Geology
University of Stockholm
S-10691 Stockholm
Sweden

SEDCO OFFICIALS

Captain Anthony Ribbens
Master of the Drilling Vessel
Underseas Drilling, Inc.
707 Texas Avenue South
Suite 103D
College Station, Texas 77840-1917

Jack Tarbutton
Drilling Superintendent
Underseas Drilling, Inc.
707 Texas Avenue South
Suite 103D
College Station, Texas 77840-1917

ODP ENGINEERING AND OPERATIONS PERSONNEL

Ron Grout	Operations Superintendent
David Huey	Operations Superintendent

ODP TECHNICAL AND LOGISTICS PERSONNEL

Wendy J. Autio	Assistant Laboratory Officer
Jim Briggs	Electronics Technician
Scott Chaffey	Curatorial Representative
Valerie Clark	Chemistry Technician
Joe DeMorett	Marine Technician
David Divins	Marine Technician
Bettina Domeyer	Marine Technician
John R. Eastlund	Computer Systems Manager
Susan Erb	Marine Technician
Chris Galida	Photographer
Ted ("Gus") Gustafson	Marine Technician
Brad Julson	Laboratory Officer
Kazushi ("Kuro") Kuroki	Marine Technician
Christine Y. Mato	Marine Technician
Dwight E. Mossman	Electronics Technician
Joan Perry	Chemistry Technician
Dawn J. Wright	Yeoperson

Ocean Drilling Program Publications Staff

Publications Supervisor
William D. Rose

Chief Editor
Norman J. Stewart

Editors
Eva M. Barbu
Lona Haskins Dearmont
Sondra K. Stewart
William R. Winkler

Chief Production Editor
Jennifer Pattison Hall

Production Editors
Susan Collinsworth
Jaime A. Gracia (this volume)

Publications Coordinator
Janalisa Braziel Soltis

Assistant Publications Coordinator
Jill Mutschler-Fontenot

Hole Summary Coordinator
Laura Hammond Young

Publications Distribution Specialist
Fabiola Muñoz Byrne

Senior Photographer
John W. Beck

Photographer
Roy T. Davis

Chief Illustrator
Karen O. Benson

Illustrators
L. Michelle Curtis
Linda C. DeLeon
Garnet D. Gaither
Cindy M. Mullican

Compositor
Mary E. Betz

Production Assistants
Gudelia ("Gigi") Delgado
Lisa L. Tirey

TABLE OF CONTENTS

VOLUME 126—INITIAL REPORTS

ACKNOWLEDGMENTS 1

SECTON 1: INTRODUCTION

1. INTRODUCTION 5
B. Taylor and Shipboard Scientific Party

2. EXPLANATORY NOTES 13
Shipboard Scientific Party

3. UNDERWAY GEOPHYSICS DATA COLLECTED ON LEG 126 43
P. Cooper and Shipboard Scientific Party

4. MULTICHANNEL SEISMIC SURVEY OF THE CENTRAL IZU-BONIN ARC 51
B. Taylor, G. Moore, A. Klaus, M. Systrom, P. Cooper, and M. MacKay

SECTION 2: SITE REPORTS

5. SITE 787 63
Shipboard Scientific Party

6. SITES 788/789 97
Shipboard Scientific Party

7. SITE 790/791 127
Shipboard Scientific Party

8. SITE 792 221
Shipboard Scientific Party

9. SITE 793 315
Shipboard Scientific Party

SECTION 3: CORRELATION PAPERS

10. CORRELATION AND COMPARISON OF FOREARC SITES 407
Shipboard Scientific Party

11. CORRELATION AND COMPARISON OF BACKARC SITES 415
Shipboard Scientific Party

SECTION 4: CORES

Core description forms and core photographs for:

SITE 787 421

SITE 788 455

SITE 789 489

SITE 790 491

SITE 791 541

SITE 792 671

SITE 793 787

SECTION 5: POLICY

JOIDES ADVISORY GROUPS 997

SAMPLE-DISTRIBUTION POLICY 1001

BACK-POCKET FOLDOUT

INITIAL REPORTS: CHAPTER 4: FIGURE 3. Forearc basin multichannel seismic (MCS) data. VE = 6.7.

INITIAL REPORTS: CHAPTER 4: FIGURE 10. Sumisu Rift MCS data.

BACK-POCKET MICROFICHE

Formation microscanner images for Leg 126:

Hole 792E: depth range, 2090.0–2484.2 mbrf

Hole 793B: depth range, 3543.0–4523.0 mbrf

ACKNOWLEDGMENTS

The Ocean Drilling Program Leg 126 scientific party expresses its thanks to all who gave invaluable help to make the outcome of the drilling along the Izu-Bonin Arc a great success.

We appreciate the cooperation and professionalism of Captain Tom Ribbens, his officers, and the crew of the *JOIDES Resolution* (SEDCO/BP 471), as well as Jack Tarbutton, the drilling superintendent, and the rest of the drilling crew. Dave Huey and Ron Grout, the ODP operations superintendents, skillfully provided that vital link between the scientific goals of Leg 126 and the realities of ocean drilling. The ODP scientific technicians were thoroughly dedicated and professional in their duties.

We are indebted to the Geological Survey of Japan, the Hawaii Institute of Geophysics, and the JOIDES/ODP Site Survey Data Bank for providing us with extensive predrilling surveys of each site. The cooperation and assistance of the Japanese scientific community, the Ocean Research Institute, the University of Tokyo, and the Department of Education, Science and Culture (Monbusho) are gratefully acknowledged. We thank the JOIDES Planning Structure, especially the Western Pacific Regional Panel, for their support of Leg 126. Last of all, the support and enthusiasm of our many Japanese colleagues on shore, who saw us off to sea and greeted us on our return, will long be remembered.

SECTION 1: INTRODUCTION

Taylor, B., Fujioka, K., et al., 1990
Proceedings of the Ocean Drilling Program, Initial Reports, Vol. 126

1. INTRODUCTION[1]

Brian Taylor[2] and Shipboard Scientific Party[3]

OVERVIEW

The Izu-Bonin intraoceanic island arc is a product of the subduction of Pacific lithosphere since the Eocene. Ocean Drilling Program (ODP) Leg 126 focused on three important and poorly understood aspects of this arc system, namely:

1. the origin and evolution of the forearc, investigated by drilling a series of holes through the sediments and into the basement of the forearc basin (Sites 787 792, and 793);
2. the process and products of arc rifting, investigated by drilling holes into the center (Sites 790/791) and eastern footwall (Sites 788/789) of the Sumisu backarc rift; and
3. recycling of subducted lithosphere and evolution of the mantle, investigated indirectly from the composition of the volcanic rocks recovered from all sites.

TECTONIC SETTING AND EVOLUTION OF THE IZU-BONIN-MARIANA REGION

The present-day tectonic configuration of the Izu-Bonin-Mariana region (Fig. 1) comprises, from east to west, the trench; the forearc terrane, made up of an inner trench wall, an outer-arc high, a forearc basin, and a frontal-arc high (Fig. 2); the active Izu-Bonin and Mariana island arcs; the Izu-Bonin backarc rifts and the actively spreading Mariana backarc basin and its remnant arc, the West Mariana Ridge; the Shikoku and Parece Vela marginal basins; and the Palau-Kyushu Ridge, the westernmost remnant arc. Mesozoic Pacific oceanic lithosphere is being subducted to the west-northwest beneath the arcs at rates of 20 mm/yr in the south to 65 mm/yr in the north. The velocity at 31°N is 60 mm/yr along 288° (Seno et al., 1987).

The evolution of these arcs and backarc basins is thought to have begun in the early middle Eocene when westward subduction of Pacific lithosphere began beneath the Philippine Sea Plate (Karig, 1975). Development of the system continued throughout the early Oligocene, forming an intraoceanic volcanic arc on top of a 200-km-wide forearc composed of volcanic rocks primarily of tholeiitic and boninitic affinities (Natland and Tarney, 1981). In the Mariana area, this arc formed on or near the edge of the West Philippine Basin, whereas in the Bonin area it formed on the edge of the Amami-Oki Daito province, a series of island arcs and intervening basins of Santonian to Paleocene age. Middle Oligocene rifting split the arc, and late Oligocene to early Miocene backarc spreading in the Shikoku and Parece Vela basins isolated a remnant arc (the Kyushu-Palau Ridge) from an active Izu-Bonin-Mariana arc (Kobayashi and Nakada, 1979; Mrozowski and Hayes, 1979). The initiation of this backarc spreading event was not synchronous along the length of the Oligocene arc. Spreading began at about 31 Ma in what became the central Parece Vela Basin and propagated north and south, giving the basin its bowed-out shape. A second spreading episode began by 25 Ma in what became the northernmost Shikoku Basin and propagated south. By 23 Ma the two systems had joined at what is now approximately 25°N, and both basins shared a common spreading axis until spreading ceased at 17–15 Ma.

A repetition of this cycle of events began in the late Miocene when the southern part of the arc split again. Subsequently, 6 m.y. of spreading in the Mariana backarc basin isolated the active Mariana Arc from the West Mariana Ridge, a remnant arc, as well as increased its curvature with respect to the ridge (Karig et al., 1978; Hussong and Uyeda, 1981). Spreading in the Mariana backarc basin may now be propagating to the north, "unzipping" the Mariana Arc from the West Mariana Ridge (Stern et al., 1984). The Bonin Arc is still in the early rifting stage of backarc basin formation, undergoing extension along most of its length (Honza and Tamaki, 1985). The major zone of rifting lies immediately west of the active volcanic chain, but one volcano near 29°N is surrounded by graben (Taylor et al., 1985). Volcanism is continuing along the active and the "remnant" arcs. Volcanic centers, with bimodal basalt-rhyolite composition, also have developed in the rift basins. The basalts have major and trace element abundances that resemble the basalts of the Mariana backarc basin rather than the basalts of the adjacent Izu-Bonin island arc (Fryer et al., 1985a; Hochstaedter et al., in press).

The backarc rifts are semicontinuous along strike, segmented by structural highs and chains of submarine volcanoes extending westward from the island-arc volcanoes (Taylor et al., 1985 and in press). Similar volcanic cross-chains are located west of the Mariana volcanoes, and older chains extend westward into the Parece Vela and Shikoku basins from the West Mariana Ridge and the Izu-Bonin Arc (Hussong and Fryer, 1983; Bloomer et al., 1989).

The differences in backarc evolution between the Mariana and Izu-Bonin systems are associated with corresponding differences in their forearcs. These differences are further accentuated by the fact that seamount chains and aseismic ridges on the subducting plate have collided only with the Mariana and southernmost Izu-Bonin Arc. Compared with the Mariana forearc, the Izu-Bonin forearc has experienced little deformation since subduction began (Honza and Tamaki, 1985). It has developed a broad forearc basin, filled with volcaniclastic and hemipelagic sediments, behind an outer-arc basement high (Fig. 2). Biostratigraphic dating of the strata that lap onto this high, both submarine and subaerial (Hanazawa, 1947), indicates that this high has been a positive topographic feature since the middle Eocene. Several mature, dendritic submarine canyon systems have developed across the Izu-Bonin forearc basin and the outer-arc high by mass wasting and headward erosion. These canyons have incised as much as 1 km into the 1.5–4-km-thick sedimentary section (Taylor and Smoot, 1984).

The Mariana forearc has a broadly similar structure, but it has undergone extensive vertical uplift and subsidence resulting from seamount collision, and tensional and rotational fracturing associated with adjustments to plate subduction and to changes

---

[1] Taylor, B., Fujioka, K., et al., 1990. *Proc. ODP, Init. Repts.*, 126: College Station, TX (Ocean Drilling Program).

[2] Hawaii Institute of Geophysics, University of Hawaii at Manoa, 2525 Correa Road, Honolulu, HI 96822.

[3] Shipboard Scientific Party is as given in the list of participants preceding the contents.

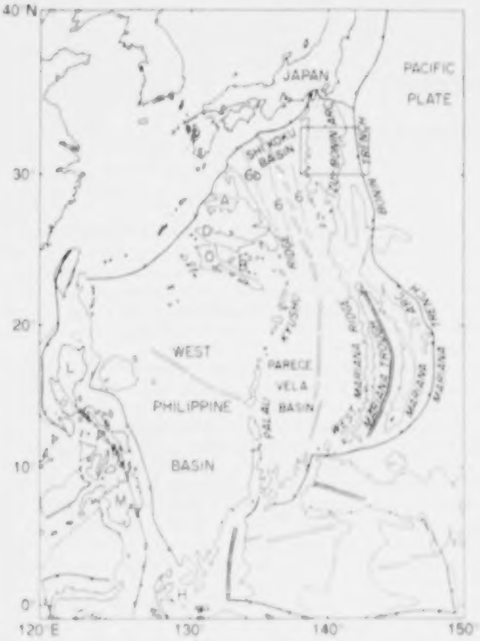

Figure 1. Active plate boundaries and relict spreading centers in the Philippine Sea region. Barbed lines locate subduction zones, medium double lines locate active spreading centers, and thin double lines locate relict spreading centers. Basins and ridges are outlined by the 4-km bathymetric contour, except for the Izu-Bonin, West Mariana, and Mariana arcs, which are outlined by the 3-km contour. Magnetic Anomalies 6 and 6B are shown by thin lines in the Shikoku Basin. A = Amami Plateau, B = Daito Basin, D = Daito Ridge, H = Halmahera, L = Luzon, M = Mindanao, and O = Oki Daito Ridge. The box shows the location of Figure 2.

in the configuration of the arc. These fractures have provided easy egress for serpentinite rising from the underlying mantle wedge. A broad zone of serpentinite seamounts, each up to 2500 m high and 30 km in diameter, 50-120 km from the trench axis, occurs along the trench-slope break (outer-arc high) of the Mariana system. These seamounts are formed by the diapiric rise and protrusion of serpentinite bodies (Bloomer, 1983; Fryer et al., 1985b; Fryer and Fryer, 1987). In the Izu-Bonin forearc, a chain of serpentinite seamounts (up to 1500 m high and 20 km in diameter) is present <50 km from the trench axis. These seamounts are spaced at intervals of 15-60 km and, together with the sediments ponded around them, form a terrace on the lower slope of the trench inner wall. Serpentinite seamounts are inferred to result from the buoyant rise of mantle hydrated by water released from crustal materials subducted beneath igneous intraoceanic forearcs. Only very minor, and probably ephemeral, accretionary complexes occur at the bases of the inner walls of the Izu-Bonin and Mariana trenches (Horine et al., 1988; Mrozowski et al., 1981).

The Izu-Bonin Arc is being subducted to the north beneath Japan. Deformation of the northern Izu-Bonin Arc is focused on the leading edge of the downgoing plate where subduction-related thrusting at the Nankai Trough is stepping seaward to the south side of Zenisu Ridge, the northernmost volcanic cross-chain of the arc (Le Pichon et al., 1987). Terranes of Izu-Bonin Arc crust have been accreted onto southern Honshu during the last 15 m.y.; the latest terrane to be accreted was the Izu Peninsula in the early Quaternary (Matsuda, 1978; Huchon and Kitazato, 1985; Taira et al., 1989).

ARC/FOREARC DEVELOPMENT: BACKGROUND TO SITES 787, 792, AND 793

With the exception of dredges from inner trench walls and large fault scarps (Bloomer and Hawkins, 1983; Bloomer and Fisher, 1987), our direct knowledge of intraoceanic forearc basement prior to ODP Legs 125 and 126 is based primarily on data from three island chains and two Deep Sea Drilling Project (DSDP) sites: the Mariana and Tonga frontal-arc islands (Guam-Saipan and 'Eua) and the Bonin Islands, which expose Eocene island-arc tholeiites and boninites (Reagan and Meijer, 1984; Ewart et al., 1977; Shiraki et al., 1980); and DSDP Leg 60 Sites 458 and 459, which sampled Eocene arc tholeiites and lower Oligocene boninites and arc tholeiites, respectively, from the Mariana outer-arc high. Prior to Leg 126, basement beneath the thickly sedimented upper-slope basin between the frontal-arc and outer-arc high had never been sampled, nor had the deep forearc basement beneath the carapace of interbedded arc pillow lavas, flows, and sills been sampled. From the available data, it appears that the present 150-230-km-wide Bonin-Mariana forearc formed, in large part, by volcanism during the initial stages of arc development in the Eocene and early Oligocene. Similar volcanism has not occurred since and cannot be studied as an active phenomenon anywhere on earth at present.

There are three main alternative hypotheses for the origin and evolution of this forearc terrane: (1) the frontal-arc and outer-arc highs could have originally been continuous and subsequently separated by forearc spreading; (2) the frontal-arc and outer-arc highs could have been built separately but nearly synchronously on former West Philippine Plate crust; or (3) the terrane could form part of a continuous Eocene arc volcanic province, possibly with overprints of later forearc volcanism. Each scenario of forearc basement development implies a different crustal structure for the forearc. The question remains: how do these different structures relate to ophiolite sheets? Many authors now ascribe a majority of ophiolites to subduction-related settings because of their chemistry and associated sediments.

Pearce et al. (1984) proposed that supra-subduction zone (SSZ) ophiolites (which have the geochemical characteristics of island arcs, but the structure of oceanic crust) formed by seafloor spreading during the initial stages of subduction prior to the development of any volcanic arc. Boninites, for which the type locality is the Bonin Islands, commonly occur in SSZ ophiolites. They appear to require hydrous partial melting at shallow depth of refractory sources that are selectively enriched in light rare earth elements and certain high-field-strength elements, as well as the typical large-ion-lithophile-element arc component (Taylor and Nesbitt, 1988). These unusual conditions and component enrichments may occur only during initial subduction or arc rifting.

However, the eruptive style and exact tectonic setting of the Eocene volcanism is unclear. Multichannel seismic (MCS) surveys of the Bonin forearc (Fig. 3) have revealed a complicated basement that is often seismically stratified and cut by dipping reflectors (see Taylor et al., this volume). These reflection characteristics imply that the Eocene volcanism may have been accompanied by stretching tectonics and/or that it was superimposed on an older-arc terrane such as the Amami Plateau (Taylor et al., 1988). Drilling in the forearc basin sampled the hitherto unstudied forearc basement to constrain some of these models for forearc evolution.

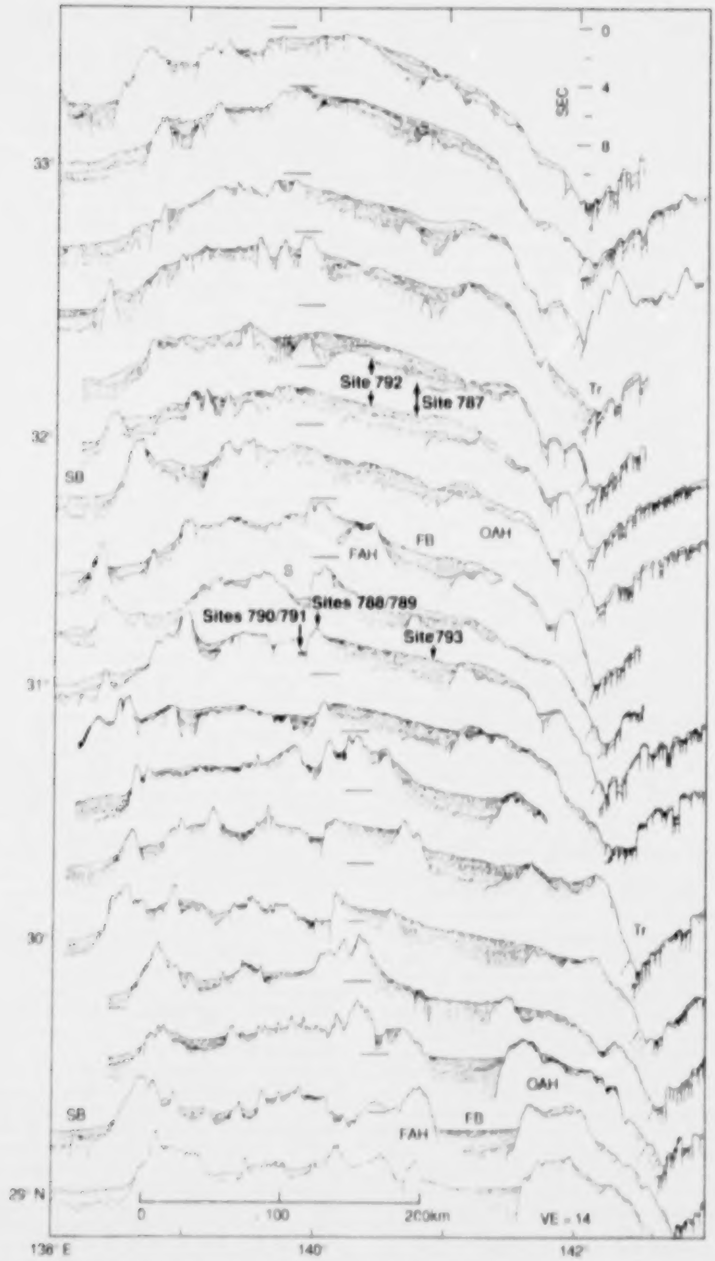
0
4
8
SEC
33°
32°
31°
30°
29° N
136° E
140°
142°
Site 792
Site 787
SB
FB
OAH
FAH
S
Sites 788/789
Sites 790/791
Site 793
Tr
Tr
OAH
SB
FAH
FB
0
100
200km
VE = 14

Figure 2. Line drawings of single-channel seismic profiles across the Izu-Bonin arc-trench system at 29°-33°N that show the location of drilled sites. Tr = trench, OAH = outer-arc high, FAH = frontal-arc high, FB = forearc basin, FAH = frontal-arc high; S = Sumisu Rift; SB = Shikoku Basin.

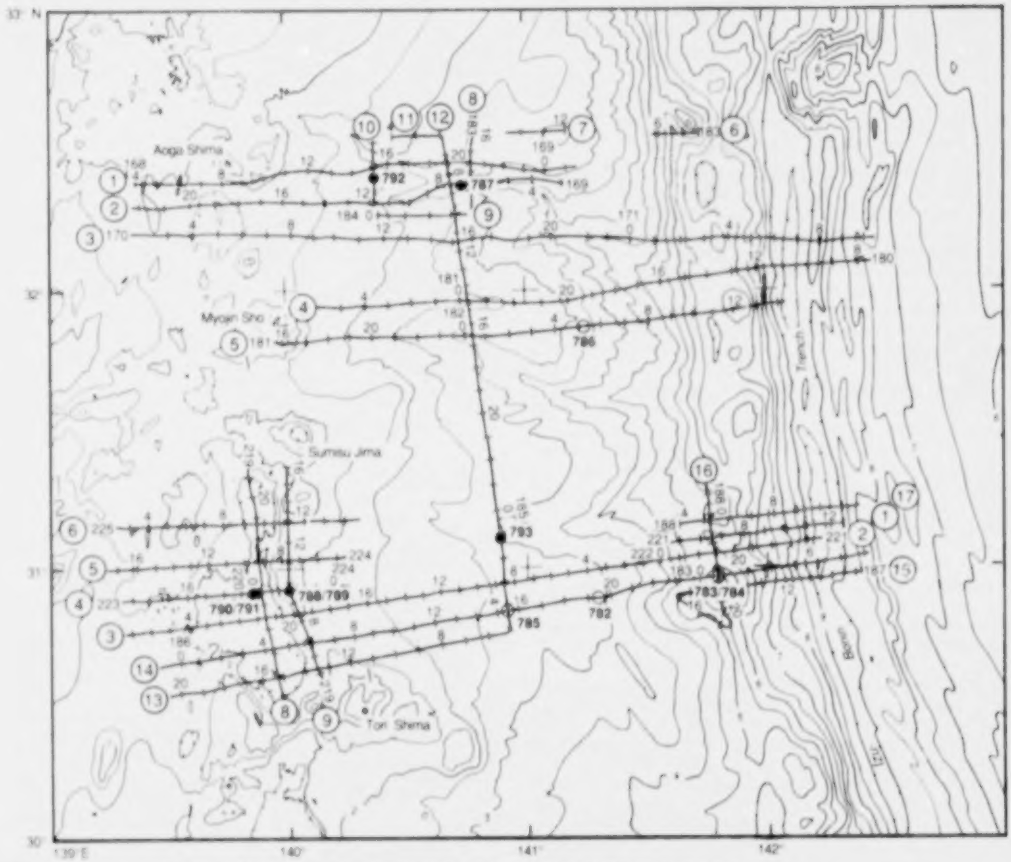

Figure 3. Locations of MCS profiles and Sites 782-786 (Leg 125) and 787-793 (Leg 126) in the Izu-Bonin region.

The presence of arc igneous rocks near the trench, together with observations of normal faulting in the forearc and interpretations of outer-arc subsidence, have been cited as evidence for large-scale removal of Mariana forearc material by tectonic erosion since the late Eocene (Hussong and Uyeda, 1981). This analysis has been questioned by Karig and Ranken (1983), who infer that the Mariana forearc has not undergone significant tectonic subsidence or erosion. Likewise, in the Bonin forearc, the presence of shallow-water Eocene fossils on the Bonin Islands, and of a well-developed submarine canyon system and lower-slope terrace elsewhere in the forearc, indicate that fairly stable conditions have prevailed since the anomalous Eocene phase of arc-basin development. This hypothesis will be tested by determining the uplift-subsidence history across the forearc by means of backstripping techniques on cored/logged holes and seismic stratigraphic analyses of interconnecting MCS profiles. Microstructures in the drill cores helped determine the intensity of faulting in space and time across the forearc terrane. Furthermore, we do not know (1) if the frontal-arc and outer-arc high developed by igneous construction or by differential uplift; (2) if the upper-slope basin between them is caused by forearc spreading or differential subsidence; and (3) if flexural loading by arc volcanoes or by coupling with the subducting plate is an important process. Determining the forearc vertical displacement field should provide some of the information on forearc flexure and basin development necessary to evaluate these hypotheses.

The forearc stratigraphy also records a history of the variations in intensity and chemistry of arc volcanism and allows the correlation of these variations with such parameters as subduction rate and backarc spreading. Karig (1975) proposed that periods of arc-volcanic maxima correlated with periods of marginal basin formation and high subduction rates. On the other hand, Scott and Kroenke (1981) hypothesized that initial periods of backarc spreading coincide with minimal arc volcanism. Contrary to both, Hussong and Uyeda (1981) inferred that arc volcanism has probably been continuous since the Eocene, but that the initiation of backarc spreading by arc rifting produced drastic subsidence of the arc volcanoes, which resulted in turn in deep-water eruptions with limited lateral transport of volcanic material. Studies of the chronology and geochemistry of tephra deposits in the forearc-basin drill cores will contribute to the evaluation of these various models. Such studies will also test whether boninitic (Beccaluva et al., 1980), alkalic (Stern et al., 1984), and/or rhyodacitic (Gill et al., 1984; Fryer et al., 1985a) volcanism characterizes periods of arc rifting.

Paleomagnetic studies of the subaerial portions of the Izu-Bonin and Mariana forearcs and from Palau have indicated clockwise rotation since the Eocene from 30° to >90° (Larson et al., 1975; Keating et al., 1983; Haston et al., 1988). These data, in conjunction with paleopoles estimated from Eocene marine magnetic anomalies in the West Philippine Basin (Louden, 1977; Shih, 1980), indicate that a general clockwise rotation characterizes the motion of the Philippine Sea Plate in the Tertiary. However, other studies have interpreted easterly declinations along the plate margin in terms of local rotations that arose from oblique subduction of the Pacific Plate (Kodama et al., 1983) or from the collisions of island arcs, rifted continental fragments, and aseismic ridges with the margin (McCabe, 1984). If the deflected declinations represent plate-wide motion, much of the clockwise rotations endemic to at least the southern parts of the Philippine Archipelago (McCabe et al., 1987) might serve as evidence for their attachment to the Philippine Sea Plate earlier in the Tertiary.

Magnetic inclination data from submerged and subaerial strata, including volcanic rocks from the Bonin Islands, also indicate significant (>20°) northward motion of the Philippine Sea Plate as well as the Philippine Islands during the Tertiary (Louden, 1977; Kinoshita, 1980; Bleil, 1981; Keating et al., 1983; Fuller et al., in press). Karig and Moore (1975) and Ogawa and Naka (1984) hypothesized that the Bonin Islands might be an exotic terrane introduced from the south by oblique motion; however, marine geophysical data indicate their structural continuity with the outer-arc high (Honza and Tamaki, 1985). However interpreted, the magnetic inclination and declination data are essential parameters for reconstructing the initial geometry of the Philippine Sea Plate and its relationship to surrounding plates, and for understanding the conditions that lead to initial subduction along the Izu-Bonin-Mariana Margin and Philippine Sea Plate evolution. The area of Leg 126 drilling is north of all previous Philippine Sea Plate paleomagnetic sampling sites and is unaffected by collision tectonics. Therefore, paleomagnetic studies of the recovered cores provide critical tests of the hypothesized plate-wide motions vs. local tectonic effects, particularly since azimuthal orientations can be obtained through the use of the formation microscanner (FMS).

RIFTING OF THE IZU-BONIN ARC: BACKGROUND TO SITES 788–791

The processes associated with the rifting and subsequent separation of continental lithosphere have been a major research focus and drilling objective for some time. In contrast, the rifting of arc lithosphere prior to backarc spreading has, until recently, received almost no attention, despite the fact that similar processes and questions are involved (e.g., the extent and nature of crustal stretching, the duration of rifting, and the interaction between vertical tectonics, rift sedimentation, and volcanism). These processes may best be observed in active rifts before the syn-rift sediments are buried by arc-volcaniclastic rocks. To date, no seaward-dipping seismic reflectors, interpreted to represent massive outpourings of volcanic material, have been recognized in backarc basins. However, SeaMARC II surveys in the Izu-Bonin region have revealed widespread syn-rift volcanism, not only on the active and "remnant" arcs but in the rift basins as well (Brown and Taylor, 1988). Most dredged samples are basalts, but andesites, dacites, and rhyolites have also been recovered. The fact that the basalts are similar to Mariana Trough basalts means that mantle little modified by a subduction component is melted even during the initial stage of backarc opening (Fryer et al., 1985a; Hochstaedster et al., in press).

The best-studied area of Izu-Bonin Arc rifting is the Sumisu Rift, located between the active arc volcanoes Sumisu Jima and Tori Shima (Fig. 3). It is a graben bounded by high-angle normal faults, in which the locus of maximum subsidence lies within an inner subgraben on its eastern side (Murakami, 1988). Faulting occurs along north-northeast-trending doglegs that form an orthorhombic fabric similar to that found in continental rifts (Brown and Taylor, 1988). The surface sediments in the rift basin include hemipelagic muds and volcaniclastic turbidites, with ash and pumice layers (Nishimura and Murakami, 1988). Whether the basement of the graben is formed of stretched, subsided arc crust, recently intruded crust, or some combination of the two, was unknown prior to Leg 126, as was the duration of rifting. The K/Ar dating of samples collected during a 1987 ALVIN program in the rift axis and on the eastern wall indicate that rift-axis volcanism began more than 0.6 Ma (Hochstaedter et al., in press). Drilling in the center and on the eastern flanks of the graben allowed us to determine if rifting began at the same time as, or subsequent to, rifting in the Mariana backarc basin (~10 Ma), if arc volcanism continued throughout its development, and when the extrusion of backarc-type basalts began.

The locus of maximum uplift and backtilting of the horst blocks that bound the basin varies back and forth along the strike between the eastern and western sides of the graben. This locus lies on the western side adjacent to the arc volcanoes and on the eastern side between them. Perhaps volcano loading suppresses the uplift. There is also some evidence of half-graben tectonics, with a master normal fault marking the edge of the dominant horst block and smaller antithetic normal faults on the other side forming the graben. However, the transfer zones linking the opposed master faults are relay zones of overlapping normal faults rather than strike-slip faults. Site survey multichannel seismic profiles have not been able to determine if the master faults are listric at depth (see Taylor et al., this volume). The uplifted footwall blocks are isolated from recent submarine volcaniclastic flow deposits and therefore were good drilling sites (1) to determine the differential vertical tectonics with respect to the graben and (2) to penetrate into the pre-rift arc basement. The nature of the frontal-arc basement between the arc volcanoes is unknown at present. Analogy with land sections such as in Japan or the Cascades would suggest that there should be numerous vents and flow fields between the large volcanic edifices. However, potential field and sidescan marine geophysical data indicate that this may not be the case in the central Izu-Bonin intraoceanic arc.

The tectonic setting and volcanic associations of the Izu-Bonin rifts are similar to those of the Hokuroku district in Japan during its ore-forming period at about 13–14 Ma (Cathles et al., 1981; Fujioka, 1983). Silica/barite/iron oxide deposits sampled with ALVIN from the rhyolite domes on the basalt ridges in the Sumisu Rift have similar trace metal abundances to the iron chert (*Tetsusekiei*) that overlies the Kuroko massive sulfide deposits (Taylor et al., in press; Urabe, in press). The chemistry of the fluids responsible for precipitating these deposits, and presumably sulfide deposits at depth, is unknown. Heat-flow measurements in the rift basin require hydrothermal circulation to explain the locally high, but widely variable, values that range from 12 to 700 mW/m^2 (Yamazaki, 1988; T. Yamazaki, pers. comm., 1988). Drilling in the Sumisu Rift was designed to enable us to investigate the metallogenic implications of arc rifting by sampling the formation fluids.

DRILLING OBJECTIVES

The Izu-Bonin and Mariana regions are the best-studied intraoceanic arc-trench systems. They are the type examples with which other older or less well-studied systems are compared. Yet fundamental questions about their evolution remain with regard to (1) arc rifting, (2) arc/forearc magmatism and structure, and (3) arc/forearc stratigraphy and vertical tectonics. To address these questions, Leg 126 drilling in the Izu-Bonin Arc had the following objectives:

1. In the arc-backarc region (Sites 788–791), we sought to determine (1) the differential uplift/subsidence history of the rift basin and adjacent arc margin; (2) the nature of volcanism and sedimentation in the rift and on the arc; (3) the duration of rifting and the nature of the rift basement; and (4) the chemistry of fluids circulating in the rift basin.

2. In the forearc region (Sites 787, 792, and 793), we sought to determine (1) the uplift/subsidence history across the forearc to provide information on forearc flexure and basin development as well as the extent of tectonic erosion; (2) the stratigraphy of the forearc with its record of sedimentation, depositional environment, and paleoceanography, as well as the variations in intensity and chemistry of arc volcanism over time; (3) the nature of the igneous basement that forms the frontal-arc high and underlies the forearc basin, to answer questions concerning the initial stages of subduction-related volcanism, the origin of boninites, and the formation of the 200-km-wide, arc-type forearc crust; and (4) the microstructural deformation and the large-scale rotation and translation of the forearc.

ACKNOWLEDGMENTS

B. Taylor acknowledges the support of the National Science Foundation. This is HIG Contribution No. 2199.

REFERENCES

Beccaluva, L., Macciotta, G., Savelli, C., Serri, G., and Zeda, O., 1980. Geochemistry and K/Ar ages of volcanics dredges in the Philippine Sea. *In* Hayes, D. E., (Ed.), *The Tectonic and Geologic Evolution of Southeast Asian Seas and Islands*. Am. Geophys. Union Monogr., 23:247–270.

Bleil, U., 1981. Paleomagnetism of Deep Sea Drilling Program Leg 60 sediments and igneous rocks from the Mariana region. *In* Hussong, D. M., Uyeda, S., et al., *Init. Repts. DSDP*, 60: Washington (U.S. Govt. Printing Office), 855–873.

Bloomer, S. H., 1983. Distribution and origin of igneous rocks from the landward slopes of the Mariana Trench. *J. Geophys. Res.*, 88:7411–7428.

Bloomer, S. H., and Fisher, R. L., 1987. Petrology and geochemistry of igneous rocks from the Tonga Trench—a non-accreting plate boundary. *J. Geol.*, 95:469–495.

Bloomer, S. H., and Hawkins, J. W., 1983. Gabbroic and ultramafic rocks from the Mariana Trench: an island arc ophiolite. *In* Hayes, D. E. (Ed.), *The Tectonic and Geologic Evolution of Southeast Asian Seas and Islands* (Pt. II). Am. Geophys. Union Monogr., 23:294–317.

Bloomer, S. H., Stern, R. J., and Smoot, N. C., 1989. Physical volcanology of the submarine Mariana and Volcano arcs. *Bull. Volcanol.*, 51:210–224.

Brown, G., and Taylor, B., 1988. Sea-floor mapping of the Sumisu Rift, Izu-Ogasawara (Bonin) Island Arc. *Bull. Geol. Surv. Jpn.*, 39(1):23–38.

Cathles, L. M., Guber, A. L., Lenagh, T. C., and Dudas, F., 1981. Failed rifts and Kuroko-type massive sulphide deposits. *Min. Geol. (Tokyo)*, 31:50–51.

Ewart, A., Brothers, R. N., and Manteen, A., 1977. An outline of the geology and geochemistry, and the possible petrogenetic evolution of the volcanic rocks of the Tonga-Kermadec-New Zealand island arc. *J. Volcanol. Geotherm. Res.*, 2(3):205–250.

Fryer, P., Ambos, E. L., and Hussong, D. M., 1985b. Origin and emplacement of Mariana forearc seamounts. *Geology*, 13:774–777.

Fryer, P., and Fryer, G. J., 1987. Origins of nonvolcanic seamounts in a forearc environment. *In* Keating, B., Fryer, P., and Batiza, R. (Eds.), *Seamounts, Islands, and Atolls*. Am. Geophys. Union Monogr., 43:61–69.

Fryer, P., Langmuir, C. H., Taylor, B., Zhang, Y., and Hussong, D. M., 1985a. Rifting of the Izu arc. III. Relationships of chemistry to tectonics. *Eos*, 66(18):421.

Fujioka, K., 1983. Where were the "Kuroko deposits" formed? Looking for the present day analogy. *Min. Geol. (Tokyo), Spec. Vol.*, 11:55–68.

Fuller, M., Haston, R., and Almasco, J., in press. Paleomagnetism of the Zambeles ophiolite, Luzon, northern Philippines. *Tectonics*.

Gill, J. B., Stork, A. L., and Whelan, P. M., 1984. Volcanism accompanying backarc basin development in the Southwest Pacific. *Tectonophysics*, 102:207–224.

Hanazawa, S., 1947. Eocene foraminifera from Hahajima. *J. Paleontol.*, 21:254–259.

Haston, R., Fuller, M., and Schmidtke, E., 1988. Paleomagnetic results from Palau, West Caroline Islands: a constraint on Philippine Sea Plate motion. *Geology*, 16:654–657.

Hochstaedter, A. G., Gill, J. B., Kusakabe, M., Newman, S., Pringle, M., Taylor, B., and Fryer, P., in press. Volcanism in the Sumisu Rift. I: the effect of distinctive volatiles on fractionation. *Earth Planet. Sci. Lett.*

Honza, E., and Tamaki, K., 1985. Bonin Arc. *In* Nairn, A.E.M., Stehli, F. G., and Uyeda, S. (Eds.), *The Ocean Basins and Margins: The Pacific Ocean* (Vol. 7): New York (Plenum Press), 459–499.

Horine, R., MacKay, M., Moore, G., and Taylor, B., 1988. Structure of the Bonin Trench landward slope. *Eos*, 69(44):1406.

Huchon, P., and Kitazato, H., 1985. Collision of the Izu block with central Japan during the Quaternary and geological evolution of the Ashigara area. *Tectonophysics*, 110:201–210.

Hussong, D., and Fryer, P., 1983. Back-arc seamounts and the SeaMARC II seafloor mapping system. *Eos*, 64(45):627–632.

Hussong, D. M., and Uyeda, S., 1981. Tectonic processes and the history of the Mariana Arc: a synthesis of the results of Deep Sea Drilling Project Leg 60. *In* Hussong, D. M., Uyeda, S., et al., *Init. Repts. DSDP*, 60: Washington (U.S. Govt. Printing Office), 909–929.

Karig, D. E., 1975. Basin genesis in the Philippine Sea. *In* Ingle, J. C., Karig, D. E., et al., *Init. Repts. DSDP*, 31: Washington (U.S. Govt. Printing Office), 857–879.

Karig, D. E., Anderson, R. N., and Bibee, L. D., 1978. Characteristics of backarc spreading in the Mariana Trough. *J. Geophys. Res.*, 83:1213–1226.

Karig, D. E., and Moore, G. F., 1975. Tectonic complexities in the Bonin Arc system. *Tectonophysics*, 27:97–118.

Karig, D. E., and Ranken, D., 1983. Marine geology of the forearc region, southern Mariana island arc. *In* Hayes, D. E. (Ed.), *The Tectonic and Geologic Evolution of Southeast Asian Seas and Islands*. Am. Geophys. Union Monogr., 23:266–280.

Keating, B., Kodama, K., and Helsley, C. E., 1983. Paleomagnetic studies of the Bonin and Mariana island arcs. *In* Shimoguru, D., and Yokoyama, I. (Eds.), *Arc Volcanism: Physics and Tectonics*: Tokyo (Terrapub).

Kinoshita, H., 1980. Paleomagnetism of sediment cores from Deep Sea Drilling Project Leg 58, Philippine Sea. *In* Klein, G. deV., Kobayashi, K., et al., *Init. Repts. DSDP*, 58: Washington (U.S. Govt. Printing Office), 765–768.

Kobayashi, K., and Nakada, M., 1979. Magnetic anomalies and tectonic evolution of the Shikoku inter-arc basin. *In* Uyeda, S., Murphy, R., and Kobayashi, K. (Eds.), *Geodynamics of the Western Pacific*: Tokyo (Japanese Sci. Soc. Press), 6:391–402.

Kodama, K., Keating, B. H., and Helsley, C. E., 1983. Paleomagnetism of the Bonin Islands and its tectonic significance. *Tectonophysics*, 95:25–42.

Larson, E. E., Reynolds, R. L., Ozima, M., Aoki, Y., Kinoshita, H., Zasshu, S., Kawai, N., Nakajima, T., Hirooka, K., Merrill, R., and Levi, S., 1975. Paleomagnetism of Miocene volcanic rocks and the curvature of the southern Mariana island arc. *Geol. Soc. Am. Bull.*, 86:346–350.

LePichon, X., Iiyama, T., Chamley, H., Charvet, J., Faure, M., Fujimoto, H., Furata, T., Ida, Y., Kagami, H., Lallement, S., Leggett, J., Murata, A., Okada, H., Rangin, C., Renard, V., Taira, A., and

Tokuyama, H., 1987. The eastern and western ends of Nankai Trough: results of Box 5 and Box 7 Kaiko survey. *Earth Planet. Sci. Lett.*, 83: 199–213.

Louden, K. E., 1977. Paleomagnetism of DSDP sediments, phase shifting of magnetic anomalies, and rotations of the West Philippine Basin. *J. Geophys. Res.*, 82:2989–3002.

Matsuda, T., 1978. Collision of the Izu-Bonin Arc with central Honshu—Cenozoic tectonics of the Fossa Magna, Japan. *J. Phys. Earth*, 26: S409–S421.

McCabe, R., 1984. Implications of paleomagnetic data on the collision related bending of island arcs. *Tectonics*, 3:409–428.

McCabe, R., Kikawa, E., Cole, J. T., Malicse, A. J., Baldauf, P. E., Yumul, J., and Almasco, J., 1987. Paleomagnetic results from Luzon and the central Philippines. *J. Geophys. Res.*, 92:555–580.

Mrozowski, C. L., and Hayes, D. E., 1979. The evolution of the Parece Vela Basin, Eastern Philippine Sea. *Earth Planet. Sci. Lett.*, 46:49–67.

Mrozowski, C. L., Hayes, D. E., and Taylor, B., 1981. Multichannel seismic reflection surveys of Leg 60 sites, Deep Sea Drilling Project. *In* Hussong, D., Uyeda, S., et al. (Eds.), *Init. Repts. DSDP*, 60: Washington (U.S. Govt. Printing Office), 57–69.

Murakami, F., 1988. Structural framework of the Sumisu Rift, Izu-Ogasawara Arc. *Bull. Geol. Surv. Jpn.*, 39(1):1–21.

Natland, J. H., and Tarney, J., 1981. Petrologic evolution of the Mariana arc and backarc basin system—a synthesis of drilling results in the South Philippine Sea. *In* Hussong, D. M., Uyeda, S., et al., *Init. Repts. DSDP*, 60: Washington (U.S. Govt. Printing Office), 877–908.

Nishimura, A., and Murakami, F., 1988. Sedimentation of the Sumisu Rift, Izu-Ogasawara Arc. *Bull. Geol. Surv. Jpn.*, 39(1):39–61.

Ogawa, Y., and Naka, J., 1984. Emplacement of ophiolitic rocks in forearc areas: examples from central Japan and Izu-Mariana-Yap island arc system. *Geol. Soc. Spec. Publ. (London)*, 13:292–304.

Pearce, J., Lippard, S., and Roberts, S., 1984. Characteristics and tectonic significance of supra-subduction zones ophiolites. *J. Geol. Soc. (London), Spec. Publ.*, 16:77–94.

Reagan, M. K., and Meijer, D., 1984. Geology and geochemistry of early sea-volcanic rocks from Guam. *Bull. Geol. Soc. Am.*, 95:701–713.

Scott, R. B., and Kroenke, L. W., 1981. Periodicity of remnant arcs and back-arc basins of the South Philippine Sea. *Oceanol. Acta*, 4:193–202.

Seno, T., Moriyama, T., Stein, S., Woods, D. F., Demets, C., Argus, D., and Gordon, R., 1987. Redetermination of the Philippine Sea Plate motion. *Eos*, 68(44):1474.

Shih, T., 1980. Marine magnetic anomalies from the western Philippine Sea: implications for the evolution of marginal basins. *In* Hayes, D. E. (Ed.), *The Tectonic and Geologic Evolution of Southeast Asian Seas and Islands*. Am. Geophys. Union Monogr., 23:49–75.

Shiraki, K., Kuroda, N., Urano, H., and Maruyama, S., 1980. Clinoenstatite in boninites from the Bonin Islands, Japan. *Nature*, 285: 31–32.

Stern, R. J., Smoot, N. C., and Rubin, M., 1984. Unzipping of the Volcano Arc, Japan. *Tectonophysics*, 102:153–174.

Taira, A., Tokuyama, H., and Soh, W., 1989. Accretion tectonics and evolution of Japan. *In* Ben-Avraham, Z. (Ed.), *Evolution of Pacific Ocean Margins*: New York (Oxford Univ. Press), 100–123.

Taylor, B., Brown, G., Fryer, P., Gill, J., Hochstaedter, A., Hotta, H., Langmuir, C., Leinen, M., Nishimura, A., and Urabe, T., in press. ALVIN-SeaBeam studies of the Sumisu Rift, Izu-Bonin Arc. *Earth Planet. Sci. Lett.*

Taylor, B., Fryer, P., Hussong, D., and Langmuir, C. H., 1985. Active volcanism in the Izu Arc and Rift: tectonic setting. *Eos*, 66(18):421.

Taylor, B., Moore, G., and McKay, M., 1988. Evidence for pre-Eocene terranes beneath the Bonin forearc. *Eos*, 66(44):1406.

Taylor, B., and Smoot, N. C., 1984. Morphology of Bonin fore-arc submarine canyons. *Geology*, 12:724–727.

Taylor, R. N., and Nesbitt, R. W., 1988. Light rare-earth enrichment of supra-subduction-zone mantle: evidence from the Troodos ophiolite, Cyprus. *Geology*, 16:448–451.

Urabe, T., and Kusakabe, M., in press. Barite-silica chimneys from the Sumisu Rift, Izu-Bonin Arc: possible analog to hematitic chert associated with Kuroko deposits. *Earth Planet. Sci. Lett.*

Yamazaki, T., 1988. Heat flow in the Sumisu Rift, Izu-Ogasawara (Bonin) Arc. *Bull. Geol. Surv. Jpn.*, 39(1):63–70.

Ms 126A-102

Taylor, B., Fujioka, K., et al., 1990
Proceedings of the Ocean Drilling Program, Initial Reports, Vol. 126

2. EXPLANATORY NOTES[1]

Shipboard Scientific Party[2]

INTRODUCTION

The standard procedures for drilling operations and preliminary shipboard analyses of the material recovered during Deep Sea Drilling Project (DSDP) and Ocean Drilling Program (ODP) drilling have been regularly amended and upgraded since drilling began in 1968. In this chapter, we have assembled information that will help the reader understand the basis for our preliminary conclusions and also help the interested investigator select samples for further analysis. This information concerns only shipboard operations and analyses described in the site reports in the *Initial Reports* volume of the Leg 126 *Proceedings of the Ocean Drilling Program*. Methods used by various investigators for shore-based analysis of Leg 126 data will be detailed in the individual scientific contributions published in the *Scientific Results* volume.

Authorship of Site Chapters

The separate sections of the site chapters were written by the following shipboard scientists (authors are listed in alphabetical order in parentheses, and no seniority is necessarily implied):

Site Summary: Fujioka, B. Taylor
Background and Objectives: B. Taylor
Seismic Stratigraphy: Cooper, Klaus, B. Taylor
Operations: Grout, Huey, Janecek
Lithostratigraphy and Accumulation Rates: Colella, Hiscott, Janecek, Marsaglia, Nishimura, Rodolfo, Tazaki
Biostratigraphy: Aitchison, Firth, Herman, Isiminger-Kelso, Kaiho
Igneous Petrology: Gill, LaPierre, R. Taylor, Torssander
Igneous Geochemistry: Gill, LaPierre, R. Taylor, Torssander
Sediment/Fluid Geochemistry: Egeberg
Paleomagnetics: Cisowski, Koyama
Physical Properties: Dadey, Klaus
Downhole Measurements: Lovell, Pezard

Following the text of each site chapter are summary core descriptions ("barrel sheets" and igneous rock visual core descriptions) and photographs of each core.

Survey Data

Survey data collected prior to Leg 126 and used in the site selection process are discussed in a separate chapter (see Taylor et al., this volume). The underway geophysics data collected aboard the *JOIDES Resolution* during Leg 126 are discussed in a separate chapter entitled "Underway Geophysics" (this volume). The underway data include bathymetry, magnetics, and seismic reflection profiles.

Drilling Characteristics

Water circulation down the hole is open; hence, cuttings were lost onto the seafloor and could not be examined. The only available information about sedimentary stratification in uncored or unrecovered intervals, other than from seismic data or wireline-logging results, is from an examination of the behavior of the drill string as observed and recorded on the drilling platform. Typically, the harder a layer, the slower and more difficult it is to penetrate. A number of other factors, however, determine the rate of penetration, so it is not always possible to relate drilling time directly to the hardness of the layers. Bit weight and revolutions per minute, recorded on the drilling recorder, influence the penetration rate.

Drilling Deformation

When cores were split, many showed signs of significant sediment disturbance, including the concave-downward appearance of originally horizontal bands, haphazard mixing of lumps of different rock types (mainly at the tops of cores), and the near-fluid state of some sediments recovered from tens to hundreds of meters below the seafloor. Core deformation probably occurred during any of several steps in which the core suffered stresses sufficient to alter its physical characteristics: cutting, retrieval (with accompanying changes in pressure and temperature), and core handling on deck.

Shipboard Scientific Procedures

Numbering of Sites, Holes, Cores, and Samples

ODP drill sites are numbered consecutively from the first site drilled by the *Glomar Challenger* in 1968. A site number refers to one or more holes drilled while the ship was positioned over one acoustic beacon. Multiple holes were drilled at a single site by pulling the drill pipe above the seafloor (out of hole), moving the ship some distance from the previous hole, and then drilling another hole.

For all ODP drill sites, a letter suffix distinguishes each hole drilled at the same site. For example, the first hole drilled was assigned the site number modified by the suffix A, the second hole took the site number and the suffix B, and so forth. Note that this procedure differs slightly from that used by DSDP (Sites 1 through 624), but it prevents ambiguity between site- and hole-number designations. It is important for sampling purposes to distinguish among the holes drilled at a site, because recovered sediments or rocks from different holes usually do not come from equivalent positions in the stratigraphic column.

The cored interval was measured in meters below seafloor (mbsf). The depth interval assigned to an individual core ranges from the depth below the seafloor that the coring operation began to the depth that the coring operation ended (Fig. 1). For example, each coring interval is generally up to 9.7 m long (the nominal capacity of a core barrel). Coring intervals may be shorter and may not necessarily be adjacent if separated by drilled intervals. In soft sediments, the drill string can be "washed ahead" with the core barrel in place without recovering sedi-

---

[1] Taylor, B., Fujioka, K., et al., 1990. *Proc. ODP, Init. Repts.*, 126: College Station, TX (Ocean Drilling Program).

[2] Shipboard Scientific Party is as given in the list of participants preceding the contents.

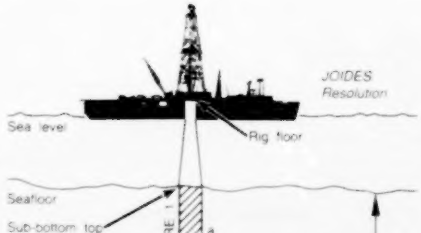

BOTTOM FELT	distance from rig floor to seafloor
TOTAL DEPTH	distance from rig floor to bottom of hole (sub-bottom bottom)
PENETRATION	distance from seafloor to bottom of hole (sub-bottom bottom)
NUMBER OF CORES	total of all cores recorded including cores with no recovery
TOTAL LENGTH OF CORED SECTION	distance from sub-bottom top to sub-bottom bottom minus drilled (but not cored) areas in between
TOTAL CORE RECOVERED	total from adding a, b, c, and d in diagram
CORE RECOVERY (%)	equals TOTAL CORE RECOVERED divided by TOTAL LENGTH OF CORED SECTION times 100

Figure 1. Diagram illustrating terms used in discussing coring operations and core recovery.

ments. This is achieved by pumping water down the pipe at high pressure to wash the sediment out of the way of the bit and up the space between the drill pipe and the wall of the hole. If thin, hard, rock layers are present, then it is possible to get "spotty" sampling of these resistant layers within the washed interval and thus to have a cored interval greater than 9.7 m. In drilling hard rock, a center bit may replace the core barrel if it is necessary to drill without core recovery.

Cores taken from a hole are numbered serially from the top of the hole downward. Core numbers and their associated cored intervals in meters below seafloor usually are unique in a given hole; however, this may not be true if an interval must be cored twice because of caving of cuttings or other hole problems. Maximum full recovery for a single core is 9.5 m of rock or sediment contained in a plastic liner (6.6-cm internal diameter) plus about 0.2 m (without a plastic liner) in the core catcher (Fig. 2). The core catcher is a device at the bottom of the core barrel that prevents the core from sliding out when the barrel is being retrieved from the hole. In certain situations (e.g., when coring gas-charged sediments that expand while being brought on deck), recovery may exceed the 9.5-m maximum.

A recovered core was divided into 1.5-m sections that were numbered serially from the top (Fig. 2). When full recovery was obtained, the sections were numbered from 1 through 7, with the last section possibly being shorter than 1.5 m (rarely, an unusually long core may require more than 7 sections). When less than full recovery was obtained, there will be as many sections as needed to accommodate the length of the core recovered; for example, 4 m of core would be divided into two 1.5-m sections and a 1-m section. If cores are fragmented (recovery less than 100%), sections are numbered serially and intervening sections are noted as void, whether shipboard scientists believe that the fragments were contiguous *in situ* or not. In rare cases, a section less than 1.5 m may be cut so that features of interest can be preserved (e.g., lithologic contacts).

By convention, material recovered from the core catcher was placed below the last section when the core was described and labeled core catcher (CC). In sedimentary cores, it was treated as a separate section. The core catcher was placed at the top of the cored interval in cases where material was only recovered in the core catcher. However, information supplied by the drillers or by other sources may allow for more precise interpretation as to the correct position of core-catcher material within an incompletely recovered cored interval.

A recovered rock (basalt, gabbro, peridotite, or serpentinite) core was also cut into 1.5-m sections and numbered serially; however, each piece of rock then was assigned a number. Fragments of a single piece were assigned a single number, and individual fragments were identified alphabetically. The core-catcher sample was placed at the bottom of the last section and treated as part of the last section rather than separately. The scientists who completed the visual core descriptions described each lithologic unit, noting core and section boundaries only as physical reference points.

When the recovered core was shorter than the cored interval, as was usually the case, the top of the core was equated with the top of the cored interval by convention so that consistency in handling the analytical data derived from the cores could be maintained. Samples removed from the cores were designated by the distance measured in centimeters from the top of the section to the top and bottom of each sample removed from that section. In curated hard-rock sections, sturdy plastic spacers were placed between pieces that did not fit together to protect them from damage in transit and in storage. Therefore, the centimeter interval noted for a hard-rock sample has no direct relationship to that sample's depth within the cored interval, but is only a physical reference to the location of the sample within the curated core.

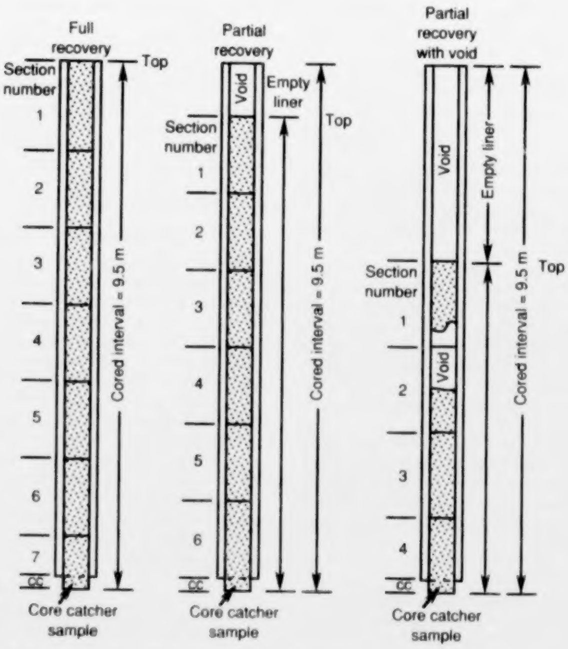

Figure 2. Diagram showing procedure for cutting and labeling core sections.

A full identification number for a sample consists of the following information: leg, site, hole, core number, core type, section number, piece number (for hard rock), and interval in centimeters measured from the top of section. For example, a sample identification of "126-787A-10R-1, 10-12 cm" would be interpreted as representing a sample removed from the interval between 10 and 12 cm below the top of Section 1, Core 10 (R designates that this core was taken with the rotary core barrel) of Hole 787A during Leg 126.

All ODP core and sample identifiers indicate core type. The following abbreviations are used: **R** = rotary core barrel (RCB); H = hydraulic piston core (HPC; also referred to as APC, or advanced hydraulic piston core); P = pressure core barrel; X = extended core barrel (XCB); B = drill-bit recovery; C = center-bit recovery; I = *in-situ* water sample; S = sidewall sample; W = wash-core recovery; and M = miscellaneous material. APC, XCB, RCB, and wash cores were cut on Leg 126.

Core Handling

Sediments

As soon as a core was retrieved on deck during Leg 126, a sample was taken from the core catcher and given to the paleontological laboratory for an initial age assessment. The core was then placed on the long horizontal rack, and gas samples were taken by piercing the core liner and withdrawing gas into a vacuum tube. Voids within the core were sought as sites for gas sampling. Some of the gas samples were stored for shore-based study, but others were analyzed immediately as part of the shipboard safety and pollution prevention program. Next, the core was marked into section lengths, each section was labeled, and the core was cut into sections. Interstitial water (IW) and organic geochemistry (OG) samples were taken. In addition, some headspace gas samples were scraped from the ends of cut sections on the catwalk and were sealed in glass vials for light-hydrocarbon analysis. Each section was then sealed at the top and bottom by gluing on color-coded plastic caps: blue to identify the top of a section and clear for the bottom. A yellow cap was placed on section ends from which a whole-round sample had been removed. The caps were usually attached to the liner by coating the end liner and the inside rim of the cap with acetone and then taping the caps to the liners.

From the deck, the cores were carried into the laboratory, where the sections were again labeled with an engraver to mark the full designation of the section more permanently. The length of the core in each section and the core-catcher sample were measured to the nearest centimeter; this information was logged into the shipboard CORELOG database program.

Next, the whole-round sections from the APC and XCB cores were run through the multisensor track (MST). This included the gamma-ray attenuation porosity evaluator (GRAPE) and *P*-wave logger (PWL) devices, which measured the bulk density, porosity, and sonic velocity, as well as an additional meter that determined the volume magnetic susceptibility. After the core was equilibrated to room temperature (approximately 3 hr), thermal conductivity measurements were performed before the cores were split.

Cores composed of rather soft material were split lengthwise into working and archive halves. The softer cores were split with a wire or saw, depending on the degree of induration. Harder cores were split with a band or diamond saw. Since cores on Leg 126 were split with wire from the bottom to top, older material could have been transported up the core on the split face of each section. One should, therefore, be aware that the very near-surface part of the split core could be contaminated.

The working half was sampled for shipboard and shore-based laboratory studies. Each extracted sample was logged into the sampling computer database program by the location and the name of the investigator receiving the sample. Records of all samples that were removed are kept by the curator at ODP. The extracted samples were sealed in plastic vials or bags and labeled. Samples were routinely taken for shipboard physical property analyses. These samples were subsequently used for calcium carbonate determinations (coulometric analyses); these data are reported in the site chapters.

The archive half was described visually. Smear slides were made from samples taken from the archive half and were supplemented by thin sections taken from the working half. Sections from the archive half that did not show evidence of drilling disturbance were run through the cryogenic magnetometer. The archive half was then photographed with black-and-white and color film, a whole core at a time. Close-up photographs (black-and-white) were taken of particular features for illustrations in the summary of each site.

Each half of the core was then put into a labeled plastic tube, sealed, and transferred to cold-storage space aboard the drilling vessel. At the end of the leg, the cores were transferred from the ship in refrigerated airfreight containers to cold storage at the Gulf Coast Repository at the Ocean Drilling Program, Texas A&M University, College Station.

Igneous and Metamorphic Rocks

Igneous and metamorphic rock cores were handled differently from sedimentary cores. Once on deck, the core catcher was placed at the bottom of the core liner, and the total core recovery was calculated by shunting the rock pieces together and taking measurements to the nearest centimeter. This information was logged into the shipboard CORELOG database program. The core was then cut into 1.5-m-long sections and transferred to the lab.

The contents of each section were transferred into 1.5-m-long sections of split core liner, where the bottom of the oriented pieces (i.e., pieces that clearly could not have rotated top to bottom about a horizontal axis in the liner) were marked with a red wax pencil. This ensured that orientation would not be lost during the splitting and labeling process. The core was split into archive and working halves, and a plastic spacer was used to separate individual pieces, and/or reconstructed groups of pieces, in the core liner. These spacers may represent a substantial interval of no recovery. Each piece was numbered sequentially from the top of each section, beginning with number 1; reconstructed groups of pieces were assigned the same number, but they were lettered consecutively. Pieces were labeled on the rounded surface, rather than on the sawn surface. If the piece was oriented, an arrow that pointed to the top of the section was added to the label.

The working half was sampled for shipboard laboratory studies. Records of all samples are kept by the curator at ODP. Minicore samples were routinely taken for physical properties and magnetic studies. Some of these samples were later subdivided for X-ray fluorescence (XRF) analysis and thin sectioning, so that as many measurements as possible were made on the same pieces of rock. At least one minicore was taken per lithologic unit when recovery permitted, generally from the freshest areas of core. Additional thin sections, X-ray diffraction (XRD) samples, and XRF samples were selected from areas of particular interest. Samples for shore-based studies were selected at a sampling party held after the drilling ended.

The archive half was described visually, then photographed with black-and-white and color film, one core at a time. Both halves of the core were shrink-wrapped in plastic to prevent rock pieces from vibrating out of sequence during transit, put into labeled plastic tubes, sealed, and transferred to cold-storage space aboard the drilling vessel. At the end of the leg, the cores were transferred from the ship in refrigerated air-freight containers to cold storage at the Gulf Coast Respository at the Ocean Drilling Program, Texas A&M University, College Station.

SEDIMENT CORE DESCRIPTION FORMS

Sediments and Sedimentary Rocks

Graphic and verbal core descriptions, smear-slide and thin-section petrographic data, sample locations, $CaCO_3$ concentrations, physical property measurements, and biostratigraphic information constitute the shipboard data summarized on the core description forms (barrel sheets) in this volume (Fig. 3). These sheets represent time-constrained field notes taken on board ship. Some ambiguities or discrepancies may be present.

The core description forms (Fig. 3), or "barrel sheets," summarize the data obtained during shipboard analysis of each sediment core, which have been recorded in detail on a section-by-section basis on visual core description forms, or VCDs. Information recorded on the VCDs is available as a searchable database through the ODP Data Librarian. The following discussion explains ODP conventions used in compiling the core descriptions and the exceptions to these procedures adopted by Leg 126 scientists.

Core Designation

Cores are designated as to leg, site, hole, core number, and core type, as previously discussed (see "Numbering of Sites, Holes, Cores, and Samples" section, this chapter). In addition, the cored interval is specified in terms of meters below sea level (mbsl) and meters below seafloor (mbsf). On the basis of drill-pipe measurements (dpm), as reported by the SEDCO coring technician and the ODP operations superintendent, depths are corrected for the height of the rig-floor, dual-elevator stool above sea level to give true water depth and the correct mbsl.

Age Data

Microfossil abundance, preservation, and zone assignment, as determined by shipboard paleontologists, appear on the core description form under the heading "Biostratigraphic Zone/Fossil Character." The geologic age determined from paleontologic and/or paleomagnetic results is shown in the "Time-Rock Unit" column. Calcareous nannofossils and planktonic foraminifers provided most age determinations. Detailed information on zonations and terms used to report abundance and preservation is presented in the "Biostratigraphy" section (this chapter).

Paleomagnetic, Physical Properties, and Chemical Data

Columns are provided on the core description form to record paleomagnetic results, physical properties values (wet-bulk density, porosity, and compressional velocity), and chemical data (% $CaCO_3$ determined by coulometric analysis). Additional information on the shipboard procedures used in collecting these types of data is found in the "Paleomagnetism," "Physical Properties," and "Inorganic Geochemistry" sections of this chapter).

Graphic Lithology Column

The lithology of the recovered material is represented on the core description forms by a single symbol or by a group of two or more symbols (see Fig. 8, this chapter) in the column titled "Graphic Lithology."

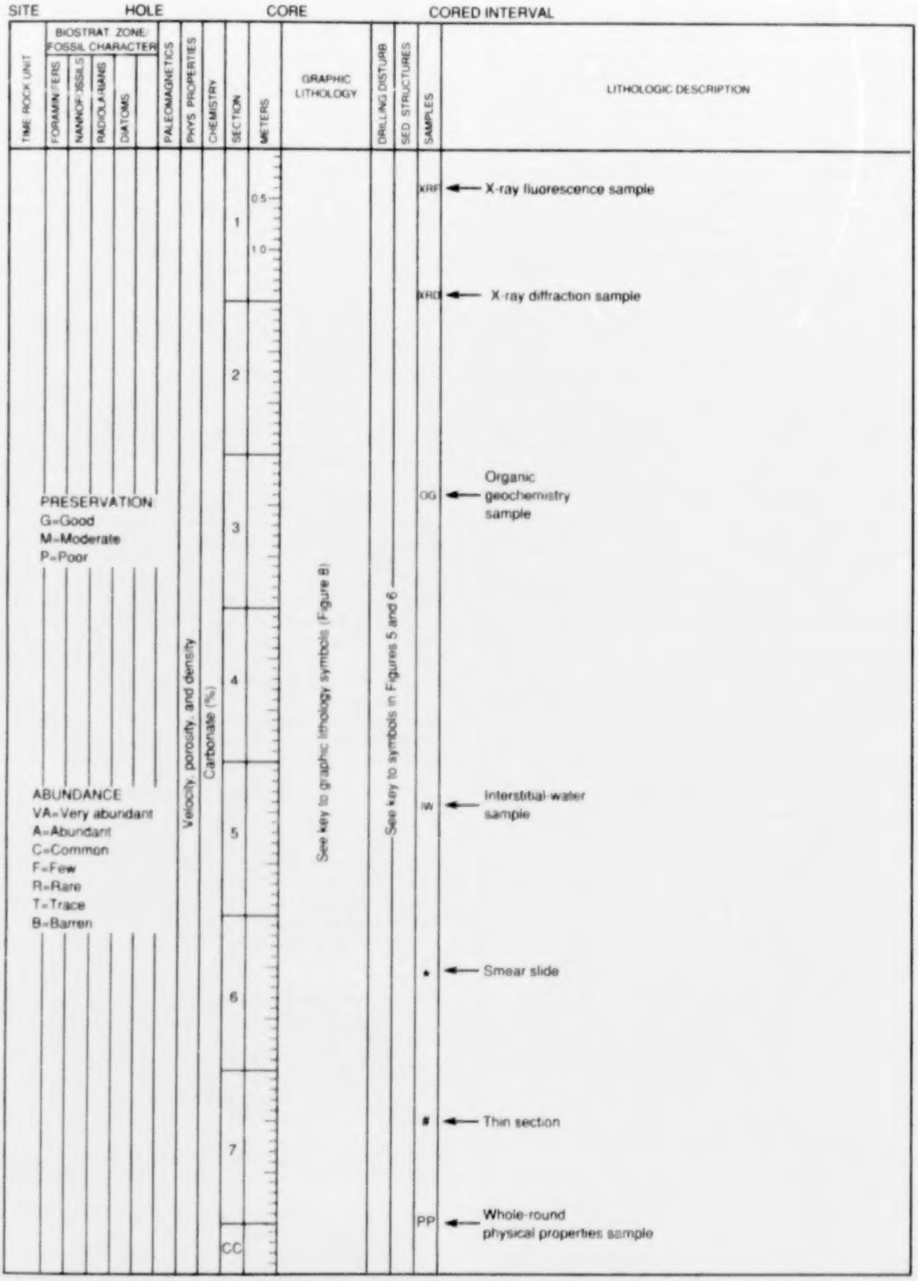
SITE
HOLE
CORE
CORED INTERVAL
TIME ROCK UNIT
BIOSTRAT. ZONE/ FOSSIL CHARACTER
FORAMINIFERS
NANNOFOSSILS
RADIOLARIANS
DIATOMS
PALEOMAGNETICS
PHYS. PROPERTIES
CHEMISTRY
SECTION
METERS
GRAPHIC LITHOLOGY
DRILLING DISTURB.
SED. STRUCTURES
SAMPLES
LITHOLOGIC DESCRIPTION
0.5
1.0
1
2
3
4
5
6
7
CC
PRESERVATION:
G=Good
M=Moderate
P=Poor
ABUNDANCE
VA=Very abundant
A=Abundant
C=Common
F=Few
R=Rare
T=Trace
B=Barren
Velocity, porosity, and density
Carbonate (%)
See key to graphic lithology symbols (Figure 8)
See key to symbols in Figures 5 and 6
XRF
X-ray fluorescence sample
XRD
X-ray diffraction sample
OG
Organic geochemistry sample
IW
Interstitial-water sample
*
Smear slide
#
Thin section
PP
Whole-round physical properties sample

Figure 3. Core description form (barrel sheet) used for sediments and sedimentary rocks.

Figure 4 illustrates the following discussion of how mixed rock types and very thin intercalated beds are drafted in the graphic columns as well as the special symbols used to describe Leg 126 cores. Where an interval is split by a solid vertical line, the sediment or sedimentary rock is an essentially homogeneous mixture of the two constituents, although each is represented by its own symbol. Examples are mixtures of biogenic and inorganic components, or mixtures of gravel and finer siliciclastic sediment. Carbonate content is not easily estimated from smear slides, and so, where chemical analyses are absent, carbonate values in the graphic column and the smear slide summary must be used only as first approximations. Where chemical analyses have been run, carbonate contents have been adjusted to conform to shipboard chemical analyses, as shown in Section 1, 30 cm, and Section 2, 10 cm, in Figure 4.

In a mixed biogenic-siliciclastic lithotype such as nannofossil-rich clay, the terrigenous constituent is noted on the right, the biogenic constituent(s) on the left side of the column, in proportions approximately equal to their respective abundances in the sediment. For example, in the uppermost interval of the core illustrated in Figure 4, the left 20% of the column has a nannofossil-ooze symbol, whereas the right 80% has a clay symbol, indicating nannofossil-rich clay or claystone composed of 20% nannofossils and 80% clay. The symbols do not indicate the quantity of primary volcanic material in the nonbiogenic fraction; this information is provided instead in the "Lithologic Description" column.

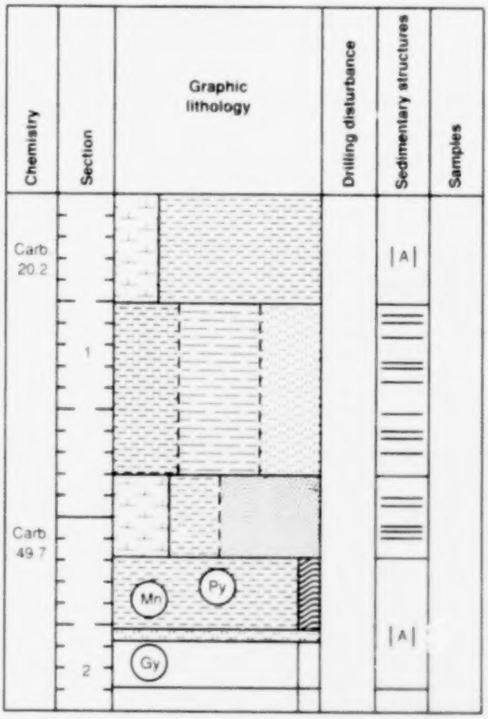

Figure 4. The graphic column and adjacent portions of the core description form (barrel sheet), illustrating Leg 126 modifications of standard ODP usage. See text for explanation.

Intervals composed of two or more sediment types that are too finely interbedded for each layer to be depicted individually show the relative abundances of the lithotypes graphically by dashed lines that vertically divide the interval into appropriate fractions. Thus, the interval in Section 1, 50–130 cm, consists of thin intercalations of clay (30%), clayey silt and silty clay (collectively 40%), and silt (30%). Some sense of the thickness of the layers is provided by the bedding lines in the "Sed. Structures" column. The numerous thin ash layers in the Pliocene-Quaternary sediments and the sedimentary rocks of Leg 126 cores are significant and required special treatment. Rather than being lumped into a vertically subdivided fraction of a core interval, the presence of these layers is noted in the "Sed. Structures" column by the letter "A."

In cases where sediment types with significant biogenic components are finely interbedded with biogenic-free lithotypes, only the lithotype with biogenic content is divided into its components by a vertical solid line. Thus, the interval from Section 1, 130 cm, to Section 2, 20 cm, consists equally of thin sand and nannofossil clay intercalations; the nannofossil clay is composed of 50% nannofossils and 50% clay, even though only 25% of the full column width is occupied by the symbol for nannofossil ooze.

Three minor, but genetically significant, mineral components encountered in Leg 126 cores were given special symbols, which appear within circles in the "Graphic Lithology" column. These were pyrite (Py), manganese oxides (Mn), and gypsum (Gy). Some of the sedimentary rocks in Leg 126 cores are hydrothermally altered. This is represented in the graphic column, as shown in the lower portions of Figure 4, by a special pattern that runs vertically along the right side of the column if the protolith is obvious, or by a pattern that occupies the full column if the original lithology could not be recognized.

Some cores recovered on Leg 126 have intercalations of sedimentary material and igneous rocks. Intervals described by igneous petrologists are indicated by the symbol "IM" (see "Hard-Rock Core Description Forms" section, this chapter).

Sediment Disturbance

The coring technique, which uses a 25-cm-diameter bit with a 6-cm-diameter core opening, results in varying degrees of mechanical disturbance of recovered core material. This is illustrated in the "Drilling Disturbance" column on the core description form (using the symbols in Fig. 5). Blank regions indicate a lack of drilling disturbance. Drilling disturbance is recognized in soft and firm sediments according to the following categories:

1. slightly deformed: bedding contacts are slightly bent;
2. moderately deformed: bedding contacts have undergone extreme bowing;
3. highly deformed: bedding is completely disturbed, sometimes showing symmetrical diapirlike or flow structures; and
4. soupy: intervals are water saturated and have lost all aspects of their original bedding.

The degree of fracturing in indurated sediments and igneous rocks is described by means of the following categories:

1. slightly fractured: core pieces are in place and contain little drilling slurry or breccia;
2. moderately fragmented: core pieces are in place or partly displaced, but original orientation is preserved or recognizable (drilling slurry may surround fragments);

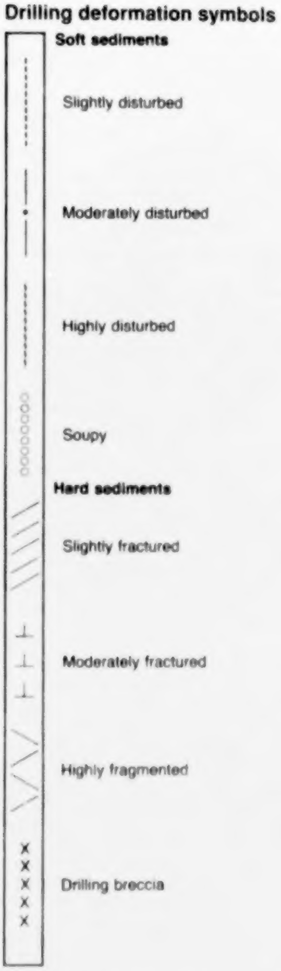
Drilling deformation symbols
Soft sediments
Slightly disturbed
Moderately disturbed
Highly disturbed
Soupy
Hard sediments
Slightly fractured
Moderately fractured
Highly fragmented
Drilling breccia

Figure 5. Drilling disturbance symbols used on Leg 126 core description forms.

3. highly fragmented: pieces are from the interval cored and are probably in the correct stratigraphic sequence (although they may not represent the entire section), but the original orientation is completely lost; and

4. drilling breccia: core pieces have lost their original orientation and stratigraphic position and may be mixed with drilling slurry.

Sedimentary Structures

The symbols used to describe the primary biogenic and physical sedimentary structures, as well as secondary structures such as microfaults, dewatering veinlets, and mineral-filled fractures, are given in Figure 6. The symbols appear in the "Sed. Structure" column of the core description form.

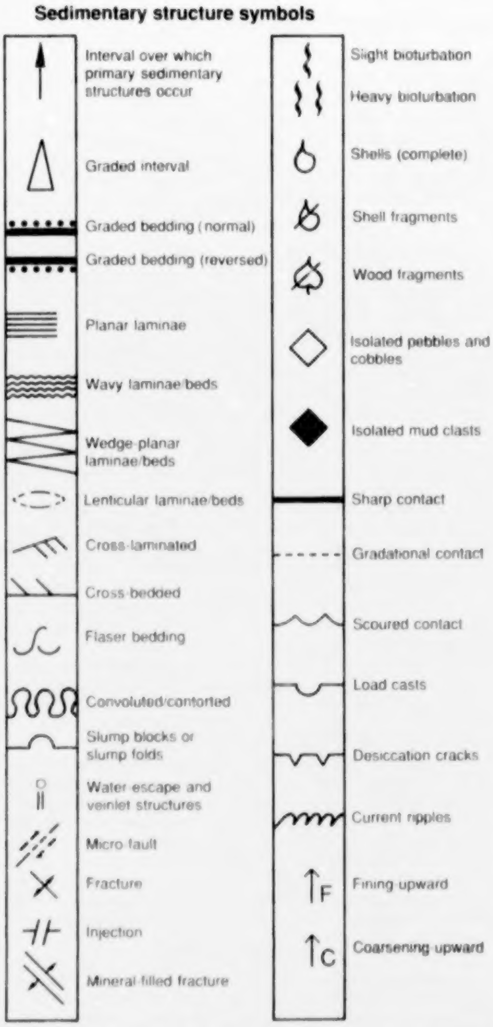
Sedimentary structure symbols
Interval over which primary sedimentary structures occur
Graded interval
Graded bedding (normal)
Graded bedding (reversed)
Planar laminae
Wavy laminae/beds
Wedge-planar laminae/beds
Lenticular laminae/beds
Cross-laminated
Cross-bedded
Flaser bedding
Convoluted/contorted
Slump blocks or slump folds
Water escape and veinlet structures
Micro fault
Fracture
Injection
Mineral-filled fracture
Slight bioturbation
Heavy bioturbation
Shells (complete)
Shell fragments
Wood fragments
Isolated pebbles and cobbles
Isolated mud clasts
Sharp contact
Gradational contact
Scoured contact
Load casts
Desiccation cracks
Current ripples
F
Fining upward
C
Coarsening upward

Figure 6. Sedimentary structure symbols for sediments and sedimentary rocks used on Leg 126 core description forms.

A common structure in the sediments from Leg 126 is a decreasing concentration upward or downward of approximately equivalent-sized particles; it occurs above and below beds of vitric ash, where the ash concentration decreases into the overlying and underlying background sediment. Termed "fining upward" or "coarsening upward" (in deference to existing definitions), or reduction of particle abundance, this structure is interpreted to be the result of animal activity redistributing ash into the sediment (Bramlette and Bradley, 1942). Gradual fining and coarsening upward are also indicated within very thick sand/sandstone or gravel/conglomerate beds that may span several cores or sections.

Color

Colors were determined by comparison with the Munsell and Geological Society of America soil-color charts (Munsell Soil Color Charts, 1975). Colors were determined immediately after the cores were split because chemical changes may occur when deep-sea sediments are exposed to the atmosphere (Moberly and Klein, 1976). Information on core colors is given in the text of the "Lithologic Description" on the core description forms and, where appropriate, in the site chapters.

Samples

The locations of samples taken from each core for shipboard analysis is indicated in the "Samples" column on the core description form. The symbol "*" indicates the location of smear slide samples. The symbols "#," "XRD," and "XRF" indicate the location of samples for shipboard thin sections, X-ray diffraction analysis, and X-ray fluorescence analysis, respectively. The symbols "IW," "OG," and "PP" designate the location of samples for whole-round interstitial water geochemistry, frozen organic geochemistry, and physical properties analyses, respectively.

Although not indicated in the "Samples" column, the positions of samples for routine physical property (porosity [%], wet-bulk density [g/cm^3], and geochemical [% $CaCO_3$]) analyses are indicated by a dot, and the analytical results are presented in the "Physical Properties" and "Chemistry" columns. Paleomagnetic results (normal and reversed polarity intervals) are indicated in the "Paleomagnetics" column.

Shipboard paleontologists generally base their age determinations on core-catcher samples, although additional samples from other parts of the core may be examined when required. An examination of such samples may lead to the recognition of zonal boundaries in the core; these are indicated in the appropriate column. All paleontological sample locations are indicated, even if they are barren.

Lithologic Description—Text

The lithologic description that appears on each core description form (barrel sheet) consists of two parts: (1) a heading that lists all the major sediment types (see "Sediment Classification" section, this chapter) observed in the core; and (2) a more detailed description of these sediments, including data on color, location in the core, significant features, etc. In cases where there are thin beds of minor lithology, a description including location information is included in the text, but the beds may be too thin (< 10 cm) to appear in the graphic lithology column.

Smear Slide Summary

A table summarizing data from smear slides and thin sections (where available) appears on each core description form. The table includes the section and interval from which the sample was taken, whether the sample represents a dominant ("D") or a minor ("M") lithology in the core, and the percentage of sand, silt, and clay, together with all identified components (total 100%). As explained in the following section, these data are used to classify and name the recovered material.

SEDIMENTARY AND PYROCLASTIC ROCK CLASSIFICATION

The sediment and pyroclastic classification scheme used during Leg 126 is descriptive in that it uses composition and texture as the only criteria to define rock types. Such genetic terms as pelagic, hemipelagic, turbidite, debris flow, ash, lapilli tephra, etc., do not appear in this classification. A primary name is based upon, and named after, a component or components that constitute 60% or more of the material. This classification scheme differs from some prior DSDP and ODP classifications in the use of compositional modifiers.

Data for classifying sedimentary and pyroclastic materials come principally from shipboard visual analyses of smear slides that use a petrographic microscope. These are qualitative optical estimates of particle characteristics (mineralogy, biogenic type, grain size, relative particle abundance, etc.) and differ from quantitative analyses of grain size, carbonate content, and mineralogy. Discrepancies between operators as well as operator inconsistencies are to be expected with these procedures.

Composition and Texture

The term "clay" is used for clay minerals and terrigenous or pyroclastic material < 4 μm in size without regard to origin. Biogenic components of silt or clay size are not described in textural terms. Thus, a sediment with 50% silt-size nannofossils and 50% terrigenous clay is called a nannofossil clay, not a nannofossil silt. The shipboard sedimentologists have chosen to use this classification (1) to maintain an internal consistency in the naming of intermediate mixtures of nonbiogenic and/or biogenic components, and (2) to provide simple descriptive modifiers that indicate the important components and their abundance in the deposits.

We have made a special effort to avoid genetic terminology in the naming of volcaniclastic sediments and pyroclastic materials. Therefore, we do not use terms otherwise employed by volcanologists, such as ash/tuff, lapilli tephra/tuff, and breccia. Instead, we use the size terms of Wentworth (1922; see Fig. 7) and then indicate composition with a modifier. The sediments may consist entirely of volcanic ejecta, but their genesis does not play a part in description and is instead discussed only in the interpretative sections of this volume.

Induration

The determination of induration is subjective. For calcareous sediments and calcareous sedimentary rocks, three classes of induration or lithification are recognized (Gealy et al., 1971): (1) soft = *ooze*, which has little strength and is readily deformed under the pressure of a finger or the broad blade of a spatula; (2) firm = chalk, which is partially lithified, readily scratched with a fingernail or the edge of a spatula; and (3) hard = well-lithified and cemented limestone or dolomite that is difficult or impossible to scratch with a fingernail.

For terrigenous sediments and pyroclastic rocks, lithified varieties are generally indicated by the addition of the suffix "-stone" to the name for soft materials. For gravels, however, the precise origin is generally unambiguous, so we use different terms for their lithified epiclastic and pyroclastic equivalents: "conglomerate" for epiclastic rocks, and "lapilli tuff" or "agglomerate" for pyroclastic rocks, depending on their grain size (lapilli = 4–64 mm diameter).

Rules for Classification

1. The principal name is determined by the component or group of components (e.g., total biogenic silica or biogenic carbonate) that constitute(s) at least 60% of the sediment or rock, except for subequal mixtures of biogenic and nonbiogenic material. The main components are as follows:

a. Nonbiogenic: If the total of a nonbiogenic component is >60%, the main name is determined by the relative proportions of sand, silt, and clay sizes when plotted on a modified Shepard (1954) classification diagram (Fig. 8). Examples of nonbiogenic principal names are *clay, silt, silty clay*, or *sand*. For nonbiogenic sediments that are composed mainly of primary volcanic particles, the modifiers "vitric" (for glassy fragments), "volcanic-lithic" (for polycrystalline volcanic grains), and "crystal"

MILLIMETERS		µm	PHI (Φ)	WENTWORTH SIZE CLASS	
			-20		
	4096		-12	Boulder (-8 to -12 Φ)	
	1024		-10		
	256		-8	Cobble (-6 to -8 Φ)	GRAVEL
	64		-6		
	16		-4	Pebble (-2 to -6 Φ)	
	4		-2		
	3.36		-1.75		
	2.83		-1.5	Granule	
	2.38		-1.25		
	2.00		-1.0		SAND
	1.68		-0.75		
	1.41		-0.5	Very coarse sand	
	1.19		-0.25		
	1.00		0.0		
	0.84		0.25		
	0.71		0.5	Coarse sand	
	0.59		0.75		
1/2	0.50	500	1.0		
	0.42	420	1.25		
	0.35	350	1.5	Medium sand	
	0.30	300	1.75		
1/4	0.25	250	2.0		
	0.210	210	2.25		
	0.177	177	2.5	Fine sand	
	0.149	149	2.75		
1/8	0.125	125	3.0		
	0.105	105	3.25		
	0.088	88	3.5	Very fine sand	
	0.074	74	3.75		
1/16	0.0625	63	4.0		
	0.053	53	4.25		MUD
	0.044	44	4.5	Coarse silt	
	0.037	37	4.75		
1/32	0.031	31	5.0		
1/64	0.0156	15.6	6.0	Medium silt	
1/128	0.0078	7.8	7.0	Fine silt	
1/256	0.0039	3.9	8.0	Very fine silt	
	0.0020	2.0	9.0		
	0.00098	0.98	10.0	Clay	
	0.00049	0.49	11.0		
	0.00024	0.24	12.0		
	0.00012	0.12	13.0		
	0.00006	0.06	14.0		

Figure 7. Grain-size categories used for classification of terrigenous sediments (after Wentworth, 1922).

(for unit crystals) may be used for clarity. These modifiers are placed immediately before the textural name; both the textural and compositional terms form the principal name.

b. Biogenic: If the total of the biogenic components is >60%, the principal name is *ooze*, or an appropriate term that denotes the sediment induration (see below).

c. Mixed sediments: In mixtures of biogenic and nonbiogenic material where neither component exceeds 60%, we have established a convention that the principal name will consist of two parts: (1) the name of the major fossil component(s), hyphenated if necessary with the least common fossil listed first, followed by (2) the textural name appropriate for the terrigenous/volcanogenic components (Fig. 8). For example, if nannofossils form 40%-60% of a sediment that contains nothing else but clay, then the name is nannofossil clay, even if nannofossils are somewhat more abundant than clay.

2. A component with an abundance of 30%-60% qualifies for major modifier status. Major modifiers are:

a. Nonbiogenic: *silty, clayey, sandy, vitric-sandy,* etc.

b. Biogenic carbonate: *nannofossil, foraminifer,* or *calcareous* (should be as specific as possible).

c. Biogenic silica: *diatom, radiolarian,* or *siliceous biogenic* (should be as specific as possible).

Note that for sediments containing from 40%-60% biogenic material, this rule is partly redundant with Rule 1c.

3. A component with an abundance of 10%-30% qualifies for minor modifier status and is hyphenated with the word *rich*. Example: nannofossil-rich clay; vitric-rich silty clay.

4. An unusual, important component that constitutes 5%-10% (e.g., bioclasts, zeolite, granules, large foraminifers) can be indicated with a minor modifier that consists of the component name hyphenated with the word *bearing*. Example: zeolite-bearing clay. This is an optional modifier.

5. The most abundant accessory component appears closest to the principal name. Major and minor modifiers are listed in order of decreasing abundance to the left of the principal name.

Example:	foraminifer-rich	nannofossil	clay
	(10%)	(30%)	(60%)

BIOSTRATIGRAPHY

General Remarks

The general correlation between the biostratigraphic zones and the magnetic polarity reversal record, the seafloor magnetic anomalies, and an absolute time scale is based on the scheme of Berggren et al. (1985). Some minor changes are discussed in the individual sections for each fossil group.

Age assignments are based mainly on core-catcher samples. Additional samples were studied when the core-catcher samples were found to be barren or restricted to narrow time intervals, or where boundaries or unconformities occur. Sample locations, preservation, and abundance for each fossil group are indicated on the barrel sheets.

Calcareous Nannofossils

The calcareous nannofossil zonations of Okada and Bukry (1980) and Sato et al. (1988) were used to identify nannofossil zones. The Pliocene/Pleistocene boundary is approximated by the first occurrence (FO) of *Gephyrocapsa oceanica* (Backman, Duncan, et al., 1988). The Oligocene/Miocene boundary is defined by the last occurrence (LO) of *Sphenolithus ciperoensis* or *Reticulofenestra bisecta* (at the top of Subzone CP19b). A list of nannofossil datums and ages, based on Berggren et al. (1985) and Backman, Duncan, et al. (1988), is given in Table 1.

Abundance and Preservation

Smear slides were prepared from all samples for the examination of calcareous nannofossils. The abundance of nannofossils was estimated as follows:

A = abundant (>10 specimens/field of view),
C = common (1-10 specimens/field of view),
F = few (1 specimen/2-10 fields of view), and
R = rare (1 specimen/>10 fields of view).

The state of preservation was estimated as:

G = good (minor or no signs of dissolution and/or overgrowth),

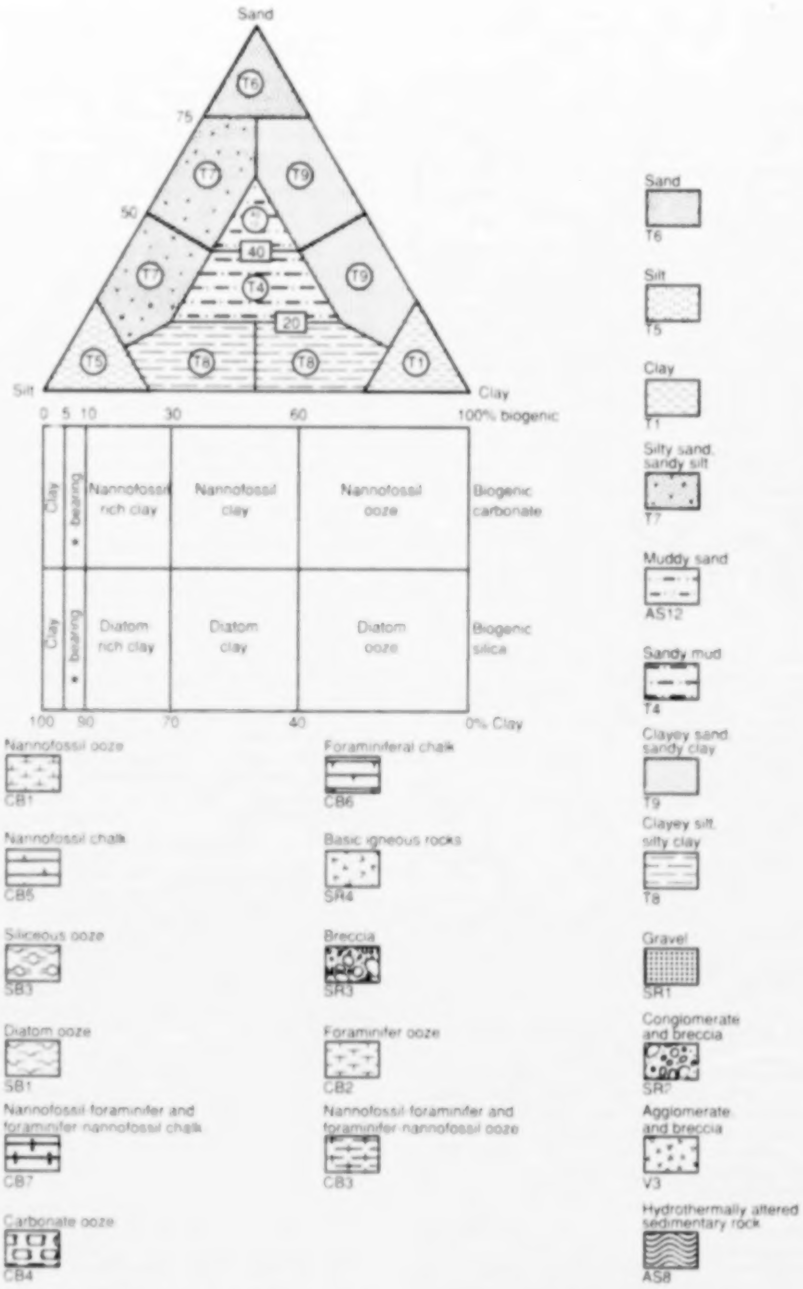
Sand
75
50
T6
T7
T9
40
T4
20
T5
T8
T1
Silt
Clay
0 5 10 30 60 100% biogenic
Clay
* bearing
Nannofossil rich clay
Nannofossil clay
Nannofossil ooze
Biogenic carbonate
Diatom rich clay
Diatom clay
Diatom ooze
Biogenic silica
100 90 70 40 0% Clay
Nannofossil ooze
CB1
Nannofossil chalk
CB5
Siliceous ooze
SB3
Diatom ooze
SB1
Nannofossil-foraminifer and foraminifer-nannofossil chalk
CB7
Carbonate ooze
CB4
Foraminiferal chalk
CB6
Basic igneous rocks
SR4
Breccia
SR3
Foraminifer ooze
CB2
Nannofossil-foraminifer and foraminifer-nannofossil ooze
CB3
Sand
T6
Silt
T5
Clay
T1
Silty sand, sandy silt
T7
Muddy sand
AS12
Sandy mud
T4
Clayey sand, sandy clay
T9
Clayey silt, silty clay
T8
Gravel
SR1
Conglomerate and breccia
SR2
Agglomerate and breccia
V3
Hydrothermally altered sedimentary rock
AS8

Figure 8. Textural classification scheme for clastic sediments and rocks; procedure for naming mixtures of biogenic and terrigenous/volcanogenic materials; and graphic symbols for lithologies, used on core description forms (barrel sheets; see Fig. 4, this chapter). The textural classification scheme is modified from Shepard (1954) by subdivision of the central triangular field into muddy sand and sandy mud. The sand-, silt-, and clay-sized fractions are defined according to the Wentworth (1922) grade scale. Asterisks indicate an unusual component, such as zeolite, that is present in amounts of 5%–10%, which give a sediment or rock the initial modifier "*-bearing," as in "zeolite-bearing siltstone."

Table 1. List of calcarous nannofossil datums and associated ages for the Eocene to Pleistocene.

Event	Species	Age (Ma)
FO	*Emiliania huxleyi*	0.275
LO	*Pseudoemiliania lacunosa*	0.460
LO	*Helicosphaera sellii*	1.37*
LO	*Calcidiscus macintyrei*	1.45*
FO	*Gephyrocapsa oceanica*	1.6*
LO	*Discoaster brouweri*	1.89*
LO	*Discoaster pentaradiatus*	2.35*
LO	*Discoaster surculus*	2.41*
LO	*Discoaster tamalis*	2.65*
LO	*Sphenolithus* spp.	3.45*
LO	*Reticulofenestra pseudoumbilica*	3.56*
FO	*Pseudoemiliania lacunosa*	3.7
LO	*Amaurolithus tricorniculatus*	3.7
FO	*Discoaster asymmetricus*	4.1
LO	*Amaurolithus primus*	4.4
FO	*Ceratolithus rugosus*	4.6*
LO	*Ceratolithus acutus*	4.6*
FO	*Ceratolithus acutus*	4.9
LO	*Triquetrorhabdulus rugosus*	4.9
LO	*Discoaster quinqueramus*	5.5
FO	*Amaurolithus primus*	6.5
FO	*Discoaster berggrenii*	8.2
FO	*Discoaster neorectus*	8.5
FO	*Discoaster loeblichii*	8.5
LO	*Discoaster hamatus*	8.9
FO	*Catinaster calyculus*	10.0
FO	*Discoaster hamatus*	10.0
FO	*Catinaster coalitus*	10.8
FO	*Discoaster kugleri*	11.5*
LO	*Sphenolithus heteromorphus*	13.2*
LO	*Helicosphaera ampliaperta*	16.2
FO	*Sphenolithus heteromorphus*	18.6*
LO	*Sphenolithus belemnos*	18.6*
FO	*Sphenolithus belemnos*	20.5*
FO	*Discoaster druggii*	23.2
LO	*Reticulofenestra bisecta*	23.7
LO	*Sphenolithus ciperoensis*	25.2
LO	*Sphenolithus distentus*	28.2
FO	*Sphenolithus ciperoensis*	30.2
LO	*Reticulofenestra umbilica*	33.8*
LO	*Coccolithus formosus*	34.9*
LO	*Discoaster saipanensis*	36.7*
LO	*Discoaster barbadiensis*	37.0*
FO	*Isthmolithus recurvus*	37.8
FO	*Chiasmolithus oamaruensis*	39.8
LO	*Chiasmolithus grandis*	40.0
LO	*Chiasmolithus solitus*	42.3
FO	*Reticulofenestra umbilica*	44.4
LO	*Nannotetrina fulgens*	45.4
LO	*Chiasmolithus gigas*	47.0
FO	*Chiasmolithus gigas*	48.8
FO	*Nannotetrina fulgens*	49.8
LO	*Discoaster lodoensis*	50.4*
FO	*Discoaster sublodoensis*	52.6
LO	*Tribrachiatus orthostylus*	53.7
FO	*Discoaster lodoensis*	55.3
LO	*Tribrachiatus contortus*	56.3
FO	*Discoaster diastypus*	56.5

Note: FO = first occurrence and LO = last occurrence. The list is based on Berggren et al. (1985) and Backman, Duncan, et al. (1988), with the latter marked by an asterisk. The FO of *Pseudoemiliania lacunosa* is based on Knuttel (1986).

M = moderate (slight to moderate dissolution and/or overgrowth), and
P = poor (severe dissolution and/or heavy overgrowth).

Planktonic Foraminifers

For correlations among the biostratigraphic zones, the magnetic reversal record, and the absolute time scale, Blow's (1969) zonal scheme was used. The correlations of planktonic foraminifer datums to magnetic polarity stratigraphy summarized by Berggren et al. (1985) were adopted in this study (Table 2).

Abundance and Preservation

For abundance estimates of planktonic foraminifer species, the following scale was used:

B = barren (no foraminifers),
R = rare (1–5 tests in the residue),
F = few (6–11 tests in the residue),
C = common (12–25 tests in the residue), and
A–VA = abundant to very abundant (>26 tests in the residue).

Preservational characteristics were divided into three categories:

Good: >90% of specimens unbroken and minor signs of dissolution or fragmentation,

Moderate: 30%–90% of specimens show dissolution effects (sugary white texture, broken chambers, preservation of only the most resistant structures), and

Poor: samples dominated by fragments and partially dissolved chambers.

Sample Preparation

Samples were disaggregated in a 30% hydrogen peroxide solution and then washed through a 63-μm sieve. For consolidated sediments, the following procedure was used: the sample was (1) covered with 30% H_2O_2 for 10–14 hr in an oven at around 40°C; (2) decanted; (3) covered with kerosene for 4–6 hr; (4) decanted; (5) covered with H_2O for several hours in an oven at 50°–100°C; (6) decanted; and (7) wet sieved through a 250-mesh screen (63 μm).

Benthic Foraminifers

The biostratigraphic determination of deep-water benthic foraminifer assemblages follows Kaiho (in press). Several large turnovers in deep-water faunas occurred during the Cenozoic: near the Paleocene/Eocene boundary (e.g., Tjalsma and Lohmann, 1983), near the middle/late Eocene boundary (e.g., Tjalsma and Lohmann, 1983), and near the middle middle Miocene (e.g., Woodruff and Douglas, 1981; Woodruff, 1985). Kaiho (in press) studied benthic foraminifers from DSDP samples of Cenozoic age from the world oceans and Paleogene samples from New Zealand and divided the Cenozoic into the following four zones in accordance with these turnovers.

Event	Species	Benthic foraminifer zone	Age
		CD4	
FO	*Cibicidoides wellerstorfi*		middle middle Miocene
		CD3	
LO	*Nuttallides truempyi*		middle/late Eocene
		CD2	
LO	*Stensioina beccariiformis*		Paleocene/Eocene
		CD1	

Paleobathymetry

Paleobathymetric determinations were estimated by benthic foraminifers following Ingle (1980), Woodruff (1985), Kaiho and Hasegawa (1986), Van Morkhoven et al. (1986), Akimoto (1989), and Yasuda (1989).

Table 2. List of planktonic foraminifer species datums, zonal boundaries, and associated ages.

Event	Species	Zonal boundary	Age (Ma)
LO	*Globigerinoides fistulosus*		1.6
FO	*Globigerina calida calida*	N23/N22	?
Pliocene/Pleistocene boundary			
FO	*Globorotalia truncatulinoides*	N22/N21	1.9
LO	*Globoquadrina altispira*		2.9
FO	*Globigerinoides fistulosus*		2.9
LO	*Sphaeroidinellopsis* spp.		3.0
FO	*Globorotalia inflata*		3.0
FO	*Globorotalia tosaensis*	N21/N19	3.1
LO	*Pulleniatina primalis*		3.5
FO	*Sphaeroidinella dehiscens*	N19/N18	5.1
FO	*Globorotalia tumida*	N18/N17	5.2
Miocene/Pliocene boundary			
FO	*Globigerinoides conglobatus*		5.3
LO	*Globoquadrina dehiscens*		5.3
FO	*Pulleniatina primalis*	N17b/N17a	5.8
FO	*Globorotalia plesiotumida*	N17/N16	8.0
FO	*Neogloboquadrina acostaensis*	N16/N15	8.6
LO	*Globorotalia siakensis*	N15/N14	10.4
FO	*Globigerina nepenthes*	N14/N13	11.3
FO	*Sphaeroidinellopsis subdehiscens*	N13/N12	11.8
FO	*Globorotalia fohsi*	N12/N11	13.5
FO	*Globorotalia praefohsi*	N11/N10	14.0
FO	*Globorotalia peripheroacuta*	N10/N9	14.6
FO	*Orbulina suturalis*	N9/N8	15.2
FO	*Praeorbulina sicanus*	N8/N7	16.3
LO	*Catapsydrax dissimilis*	N7/N6	17.6
FO	*Globigerinatella insueta*	N6/N5	17.9
LO	*Globorotalia kugleri*	N5/N4	20.1
FO	*Globorotalia kugleri*	N4/P22	23.7
Oligocene/Miocene boundary			
LO	*Paragloborotalia mendacis*		23.7
FO	*Globigerinoides primordius*		24.5
LO	*Paragloborotalia opima*	P21/P22	28.2
LO	*Streptochilus cubensis*	P21a/P21b	30.0
LO	*Globigerina ampliapertura*	P20/P21	32.8
LO	*Pseudohastigerina*	P19/P20	34.0
Eocene/Oligocene boundary			
LO	hantkeninids, *Globigerinatheka*	P17/P18	36.6
FO	*Globigerina tapuriensis*		36.6
LO	*Turborotalia cerroazulensis* group		36.7
LO	*Globigerinatheka semiinvoluta*		37.6
LO	*Acarinina*	P14/P15	40.6
LO	*Morozovella spinulosa*		41.1
FO	*Globigerinatheka semiinvoluta*		41.3
LO	*Subbotina frontosa*		42.0
LO	*Globigerinatheka beckmanni*	P13/P14	43.0
LO	*Acarinina bullbrooki*		43.0
FO	*Turborotalia pomeroli*		44.7
FO	*Globigerinatheka index*		45.0
FO	*Morozovella lehneri*	P11/P12	46.0
LO	*Morozovella aragonensis*	P11/P12	46.0
FO	*Hantkenina*	P9/P10	52.0
FO	*Morozovella aragonensis*	P7/P8	55.2
FO	*Morozovella formosa*	P6/P7	56.1
Paleocene/Eocene boundary			
LO	*Morozovella velascoensis*		57.8
LO	*Planorotalites pseudomenardii*	P4/P5	58.8
FO	*Planorotalites psuedomenardii*	P3/P4	61.0
FO	*Morozovella velascoensis*		61.7
FO	*Morozovella pusilla*	P3a/P3b	62.0
FO	*Morozovella conicotruncata*	P3a/P3b	62.0
LO	*Morozovella angulata*	P2/P3	62.3

Note: The list is based on Berggren et al. (1985).

Dissolved Oxygen in Deep Water

Predominant morphologies of benthic foraminifers found in poorly oxygenated deposits differ from those present in highly oxygenated deposits. Therefore, the morphologies of benthic foraminifer tests were used to infer relative amounts of dissolved oxygen in Cenozoic deep-sea bottom water. All the calcareous benthic foraminifers were classified into three categories: aerobic, anaerobic, and intermediate forms (Kaiho, in press). Ratios of aerobic vs. aerobic plus anaerobic forms were calculated as estimates of changes in the oxygen content of deep oceanic waters.

Abundance and Preservation

For abundance estimates of benthic foraminifers, the following scale was used:

B = barren (no foraminifers),
R = rare (< 1 specimen/10 cm^3),
F = few (1-10 specimens/10 cm^3),
C = common (10-100 specimens/10 cm^3), and
A = abundant (> 100 specimens/10 cm^3).

Preservational characteristics were divided into three categories:

Good: >90% of specimens unbroken,

Moderate: 30%-90% of specimens showing dissolution effects, and

Poor: samples dominated by fragments and partially dissolved chambers.

Sample Preparation

Samples approximately 20 cm^3 in volume were washed through a 250-mesh screen (63-μm opening) and dried. Unconsolidated sediments were soaked in water, and, when necessary, disaggregation was aided by the addition of small amounts of hydrogen peroxide. Hydrogen peroxide was also routinely added to more consolidated sediments. Kerosene was used to disaggregate highly consolidated sediments.

Radiolarians

The Cenozoic radiolarian zonation of Sanfilippo et al. (1985), derived for the tropical equatorial Pacific, was used at all sites. Sanfilippo et al. (1985) summarized the taxonomy and evolutionary lineages of all stratigraphically important radiolarian taxa commonly found in low-latitude regions of this zonation. In suggesting tentative "absolute" ages for radiolarian datum levels and zonal boundaries, the schemes of Nigrini (1985) and Barron et al. (1985), established on the basis of DSDP Leg 85 sites in the equatorial Pacific, were followed (Table 3).

The Quaternary biostratigraphic datums listed by Foreman (1981) were also used. Although much of the material obtained on Leg 85 could not be directly dated paleomagnetically, there were sufficient duplicate sites in which all major microfossil events could be identified, some of which had been correlated to the polarity time scale in nearby piston cores. Thus, the ages of Pacific radiolarian events estimated by Foreman (1981), Nigrini (1985), and Barron et al. (1985) provided a satisfactory working model.

Abundance

Qualitative assessments of the abundance (abundant, common, few, rare, trace, absent) and preservation (good, moderate, poor) of radiolarians in each slide were recorded. In assessing the relative abundances of individual taxa, the following semiquantitative criteria were used:

Abundant: $>20\%$ (of the total assemblage),
Common: $5\%-20\%$ (of the total assemblage),
Few: $1\%-5\%$ (of the total assemblage),
Rare: $0.1\%-1\%$ (of the total assemblage),
Trace: $<0.1\%$ (of the total assemblage), and
Absent: not found in an examination of the slide.

Sample Preparation

To obtain clean radiolarian concentrates for microscopic examination, the sediments were disaggregated, sieved to remove the clay-silt fraction, and acidified to eliminate the calcareous components. A 5-cm^3 sample was placed in a 400-cm^3 beaker containing 150 ml of 10% hydrogen peroxide and a small amount of calgon (to aid in disaggregating the sediment). If calcareous components were evident, they were dissolved by adding hydrochloric acid. The residue was sieved through a 63-μm sieve, and the remaining siliceous microfossils were pipetted evenly onto labeled glass slides. The accompanying water was then evaporated under a heat lamp, after which the remaining residue was mounted in a suitable medium (in this instance, Norland Optical Adhesive) and covered with a 22 × 50-mm cover slip. One slide was prepared and examined for each sample. The wet residue was retained in the event that reexamination of the material proved to be necessary.

PALEOMAGNETISM

Paleomagnetic studies performed on board *JOIDES Resolution* included measurements of remanent magnetization and magnetic susceptibility of sedimentary, igneous, and metamorphic material. The measurement of remanence was generally accompanied by alternating field (AF) or thermal demagnetization to remove secondary magnetizations.

Instruments

Two magnetometers, a Molspin spinner magnetometer and a 2-G Enterprises (Model 760R) pass-through, cryogenic, superconducting rock magnetometer, were routinely available for the measurement of remanence on board *JOIDES Resolution*. An AF demagnetizer (Model 2G600) capable of alternating fields up to 25 mT was on line with the cryogenic magnetometer. Both were controlled by a FASTCOM4 multiserial communication board in an IBM PC-AT compatible computer. To measure the archive half of the core, Leg 126 paleomagnetists used a BASIC program (126CORE) modified from the SUPERMAG program written by M. Koyama and C. Helsley during Legs 124E and 126.

The spinner magnetometer was controlled by a Digital PRO350 computer and was used only to measure individual discrete samples. In addition to these two standard sample magnetometers, a prototypic, portable, fully automatic spinner (FAS) magnetometer with a built-in AF demagnetizer (maximum field = 50 mT) and magnetic susceptibility anisotropy meter, was available for discrete sample measurement on Leg 126. This instrument was designed and built by N. Niitsuma and M. Koyama of Shizuoka University.

The superconducting quantum interference device (SQUID) sensors in the cryogenic magnetometer measure magnetization over an interval approximately 20 cm long. Each axis has a slightly different response curve. The widths of the sensor regions imply that as much as 150 cm^3 of core contributes to the sensor signals, thereby blurring sharp magnetic transitions. The large volume of core material within the sensor region permits an accurate determination of remanence for weakly magnetized samples despite the rather high background noise related to the motion of the ship. The SQUID electronics operate at the 1× scale and use the flux-counting mode for most measurements.

Remanent Magnetization Measurements

The maximum AF demagnetizing field allowed for sections from the archive half is either 15 mT or the median destructive field, whichever is lower. Discrete samples from the working half of the core were demagnetized with the Schonstedt GSD-1 AF demagnetizer and the TSD-1 thermal demagnetizer as well as the AF demagnetizer that is built into the automatic spinner magnetometer.

Sediments

Remanence measurements of sediments were performed by passing continuous archive-half core sections through the cryogenic magnetometer. Measurements of NRM before and after AF demagnetization were generally taken at 3- and 5-cm intervals. At reversal boundaries, high-density measurements at 0.5-cm intervals, at varying AF demagnetization levels, were performed. Because measurements are averaged over the broad response regions of the three sensors, deconvolution is required to recover highly detailed changes of magnetization. This work will be done during shore-based studies.

Discrete samples were taken from APC, XCB, and RCB sediment cores by pressing a standard plastic sampling box (7 cm^3) into the soft core material. The uphole direction was marked on the box. For more consolidated sediments, cubes were cut out with a spatula or minicores were cut with a drill press. Up to three discrete samples per section were taken from APC, XCB, and RCB working cores when the archive half gave a consistent paleomagnetic signal, except at certain reversal boundaries, where an even greater sampling density was employed. Azimuthal orientation of discrete samples from selected XCB and RCB core intervals was attempted by noting bedding and structural feature dip directions, when detectable, in sample coordinates. These directions were referenced to the dip directions indicated by seismic profiles or to compass-oriented bedding and fracture-dip directions, as determined by the downhole formational microscanner, so as to derive field-coordinate directions.

Igneous and Metamorphic Rocks

Drilled minicores (1-in. diameter) of the igneous portions of the cores were obtained to determine the polarity of the various "hard rock" units encountered during drilling. Archive-half sections that contained igneous rock pieces >20 cm in length were measured in the cryogenic magnetometer at 5-cm intervals.

Magnetic Stratigraphy

The magnetostratigraphic time scale of Berggren et al. (1985) was adopted for use during Leg 126.

Magnetic Susceptibility Measurements

Magnetic susceptibility measurements were routinely made on all cores employing a Bartington Instrument magnetic susceptibility meter (model M.S.1) with a M.S.1/CX 80 mm whole-core sensor loop set at 0.47 kHz. The susceptibility meter was on line with the GRAPE, and the PWL with the MST. Because the susceptibility of most core material on Leg 126 was high, all measurements were made in the low-sensitivity mode. In addition to characterizing the cored sediments, susceptibility data were used for correlation among holes and sites. The correlation of susceptibility data was performed by observing peak-to-peak spacings and general trends in the susceptibility curve.

PETROLOGY

Core Curation and Shipboard Sampling

As standard procedure, basement rocks recovered during coring were examined by petrologists to determine where the core

Table 3. List of radiolarian species datums and zones, and associated ages.

Zone	Approximate age	Top or bottom	Species
	0		
B. invaginata			
	0.17	B	*Buccinosphaera invaginata*
C. tuberosa	0.42	T	*Stylatractus universus*
	0.45	B	*Collosphaera tuberosa*
A. ypsilon	0.70	T	*Pterocorys campanula*
	0.74	T	*Anthocyrtidium nosicaae*
	0.77	B	*Pterocorys hertwigii*
	0.85	B	*Antocyrtidium euryclathrum*
	1.00	T	*Anthocyrtidium angulare*
A. angulare	1.15	B	*Lamprocyrtis nigriniae*
	1.15	T	*Lamprocyrtis neoheteroporus*
	1.50	T	*Anthocyrtidium michelinae*
	1.55	T	*Pterocanium prismatium*
P. prismatium	1.60	B	*Anthocyrtidium angulare*
	1.85	T	*Theocorythium vetulum*
	2.35	T	*Anthocyrtidium jenghisi*
	2.47	B	*Pterocorys sabae*
	2.5	B	*Theocorythium trachelium*
	2.6	T	*Stichocorys peregrina*
S. pentas	3.27	T	*Phormostichoartus fistula*
	3.35	T	*Lychnodictyum audax*
	3.53	T	*Phormostichoartus doliolum*
	3.78	B	*Amphirhopalum ypsilon*
	3.80	T	*Spongaster pentas*
	3.80	B	*Spongaster tetras*
	3.88	T	*Anthocyrtidium prolatum*
	4.3	T	*Solenosphaera omnitubus*
	4.45		*S. berminghami* → *S. pentas*
S. peregrina	4.6	B	*Pterocanium prismatium*
	5.5	T	*Acrobotrys tritubus*
	?	T	*Calocycletta caepa*
	?	T	*Siphostichartus corona*
	6.4		*S. delmontensis* → *S. peregrina*
D. penultima	6.8	B	*Solenosphaera omnitubus*
	6.9		*D. antepenultima* → *D. penultima*
	7.0	T	*Diartus hughesi*
D. antepenultima		B	*Spongaster berminghami*
		T	*Dictyocoyne ontongensis*
	7.6	B	*Acrobotrys tritubus*
		T	*Botryostrobus miralestensis*
	8.6		*D. petterssoni* → *D. hughesi*
D. petterssoni			*D. laticonus* → *D. antepenultima*
			L. neotera → *L. bacca*
		T	*Cyrtocapsella japonica*
		T	*Lithopera thornburgi*
	11.4	T	*Cyrtocapsella tetrapera*
	11.4	T	*Cyrtocapsella cornuta*
		T	*Carpocanopsis cristata*
		B	*Phormostichoartus doliolum*
		T	*Dorcadospyris alata*
		T	*Stichocorys wolffii*
		B	*Cyrtocapsella japonica*
	11.5	B	*Diartus petterssoni*
D. alata			*L. renzae* → *L. neotera*
		B	*Lithopera thornburgi*
		B	*Phormostichoartus corbula*
		T	*Dorcadospyris alata*
		T	*Calocycletta virginis*
		T	*Carpocanopsis bramlettei*
		T	*Calocycletta costata*
		T	*Didymocyrtis violina*
		T	*Didymocyrtis tubaria*
		B	*Lithopera renzae*
		T	*Docadospyris forcipata*
	15.3		*D. dentata* → *D. alata*
C. costata		T	*Eucyrtidium diaphanes*
		T	*Carpocanopsis cingulata*
		B	*Siphostichartus corona*
	16.2	T	*Didymocyrtis prismatica*
		B	*Carpocanopsis cristata*
		T	*Carpocanopsis favosa*
	16.5	T	*Lychnocanoma elongata*
	17.3	B	*Calocycletta costata*
S. wolffii	17.3	B	*Dorcadospyris dentata*
		B	*Calocycletta caepa*

Note: The list is based on Barron et al. (1985) and Nigrini (1985).

Table 3 (continued).

Zone	Approximate age	Top or bottom	Species
	18.2	B	*Stichocorys wolffii*
S. delmontensis		T	*Dorcadospyris ateuchus*
	20.3	B	*Didymocyrtis tubaria*
		B	*Didymocyrtis violina*
	21.1	B	*Stichocorys delmontensis*
	21.3	T	*Theocyrtis annosa*
C. tetrapera		B	*Carpocanopsis bramlettei*
		T	*Calocycletta serrata*
	21.5	B	*Calocycletta virginis*
	21.9		*C. pegetrum* → *C. leptetrum*
		B	*Botryostrobus miralestensis*
		B	*Carpocanopsis cingulata*
	22.1	B	*Cyrtocapsella tetrapera*
L. elongata	22.1	B	*Cyrtocapsella cornuta*
		B	*Carpocanopsis favosa*
		B	*Calocycletta serrata*
	22.6	T	*Artophormis gracilis*
	22.6	T	*Dorcadospyris papilio*
	24.1	B	*Lychnocanoma elongata*
D. ateuchus		B	*Carpocanopsis cingulata*
		B	*Dorcadospyris forcipata*
		T	*Lithocyclia angusta*
		B	*Dorcadospyris papilio*
		B	*Theocyrtis annosa*
		T	*Lithocyclia crux*
		T	*Theocyrtis tuberosa*
	33.0		*T. triceros* → *D. ateuchus*
T. tuberosa		B	*Didymocyrtis prismatica*
		B	*Lychnodictyum audax*
			A. barbadensis → *A. gracilis*
		T	*Dictyoprora mongolfieri*
		B	*Lithocyclia crux*
	36.0		*L. aristotelis* → *L. angusta*
T. bromia		T	*Calocylas turris*
		T	*Lychnocanoma bandyca*
		T	*Thyrsocyrtis bromia*
		T	*Thyrsocyrtis lochites*
		T	*Thyrsocyrtis tetracantha*
		T	*Thyrsocyrtis triacantha*
		T	*Carpocanistrum azyx*
		T	*Eusyringium fistuligerum*
		T	*Podocyrtis goetheana*
		B	*Lychnocanoma bandyca*
		T	*Podocyrtis chalara*
		B	*Calocyclas turris*
	41.0	B	*Carpocanistrum azyx*
P. goetheana		B	*Thyrsocyrtis bromia*
		B	*Thyrsocyrtis tetracantha*
		T	*Theocotylissa ficus*
		T	*Sethochytris triconiscus*
			L. ocellus → *L. aristotelis*
	42.0	B	*Podocyrtis goetheana*
P. chalara		T	*Podocyrtis trachodes*
		T	*Phormocyrtis striata striata*
		B	*Tristylospyris triceros*
	43.0		*P. mitra* → *P. chalara*
P. mitra		B	*Cryptoprora ornata*
		T	*Podocyrtis ampla*
		T	*Eusyringium lagena*
		B	*Artophormis barbadensis*
		B	*Thyrsocyrtis lochites*
		B	*Sethochytris triconiscus*
		T	*Podocyrtis fasciolata*
	45.0		*P. sinuosa* → *P. mitra*
P. ampla		B	*Podocyrtis trachodes*
			E. lagena → *E. fistuligerum*
		T	*Podocyrtis dorus*
		B	*Podocyrtis fasciolata*
		T	*Theocotyle venezuelensis*
	46.5		*P. phyxis* → *P. ampla*
T. triacantha		T	*Theocotyle nigriniae*
		T	*Theocotyle conica*
			P. diamesa → *P. phyxis*
		T	*Theocorys anaclasta*
		T	*Thyrsocyrtis hirsuta*
		T	*Thyrsocyrtis robusta*
			T. tensa → *T. triacantha*
	48.0	B	*Eusyringium lagena*

Table 3 (continued).

Zone	Approximate age	Top or bottom	Species
D. mongolfieri		B	*Podocyrtis dorus*
			T. cryptocephala → *T. conica*
		T	*Calocycloma castum*
	49.0	B	*Dictyoprora mongolfieri*
T. cryptocephala			*P. aphorma* → *P. sinuosa*
		B	*Thyrsocyrtis robusta*
		B	*Theocotyle venezuelensis*
		T	*Buryella clinata*
	50.0		*T. nigriniae* → *T. cryptocephala*
P. striata striata		T	*Podocyrtis platypus*
		T	*Lamptonium sanfilippoae*
		B	*Thyrsocyrtis rhizodon*
		B	*Podocyrtis platypus*
		B	*Podocyrtis diamesa*
		B	*Podocyrtis aphorma*
			Phormocyrtis striata exquisita → *P. striata striata*
	51.0	B	*Theocorys anaclasta*
B. clinata		T	*Theocotylissa fimbria*
		T	*Pterocodon ampla*
		T	*Bekoma bidartensis*
		T	*Buryella tetradica*
		T	*Thyrsocyrtis tarsipes*
		B	*Lithocyclia ocellus*
		B	*Thyrsocyrtis tensa*
			T. alpha → *T. ficus*
		B	*Lamptonium sanfilippoae*
		B	*Theocotyle nigriniae*
		B	*Thyrsocyrtis hirsuta*
	52.5		*P. anteclinata* → *B. clinata*
B. bidartensis		B	*Theocotylissa fimbria*
			T. auctor → *T. alpha*
		B	*Calocycloma castum*
			Lamptonium pennatum → *L. fabaeforme fabaeforme*
	55.5	B	*Bekoma bidartensis*

should be split that would best preserve unique features and/or to expose important structures. The core was split into archive and working halves using a rock saw with a diamond blade. Care was always taken to ensure that orientation was preserved during splitting and prior to labeling, usually by marking the original base of each piece with red crayon. Each piece was numbered sequentially from the top of each section on the top, uncut surface of the rock. Pieces that could be fitted together (reassembled like a jigsaw puzzle) were assigned the same number, but lettered consecutively (e.g., 1A, 1B, 1C, etc.).

Plastic spacers were placed between pieces with different numbers, but not between those with different letters and the same number. The presence of a spacer may or may not represent a substantial interval of no recovery. When the original unsplit piece was sufficiently long, such that the top and bottom could be distinguished before removal from the core liner (i.e., the piece could not have rotated top to bottom about a horizontal axis in the liner during drilling), an arrow was added to the label pointing to the top of the section. Because pieces were free to turn about a vertical axis during drilling, azimuthal orientation was not possible.

After the core was split, the working half was sampled for shipboard physical properties, magnetics, XRF, XRD, and thin-section studies. These samples were often of minicores and, when appropriate, were stored in seawater prior to measurement. When recovery permitted, samples were taken from each lithologic unit. The archive half was described on the visual core description (VCD) form, which is used for such nondestructive physical properties measurements as magnetic susceptibility, and was photographed before storage.

Visual Core Descriptions

Igneous VCD forms were used in the description of the igneous rock cores (Fig. 9). In Figure 9, the left column is a graphic representation of the archive half. A horizontal line across the entire width of the column denotes a plastic spacer glued between rock pieces inside the liner. Oriented pieces are indicated on the form by an upward-pointing arrow to the right of the piece. Shipboard samples and studies are indicated on the VCD in the column headed "shipboard studies," using the following notations: XRD = X-ray diffraction analysis, XRF = X-ray fluorescence analysis, TSB = petrographic thin section, and PP = physical properties analysis.

Because igneous and metamorphic rocks were classified mainly on the basis of macroscopic mineralogy and texture, shipboard petrologists followed a checklist of features that ensured consistent and complete descriptions. To this end, VCDs were entered directly into a computerized database (HARVI). The describer is prompted by the HARVI program with a set of questions pertaining to petrologic features that must all be diagnosed and entered in the database. The descriptions on the VCD forms will, to a certain extent, reflect the rigidity of the HARVI program. It is relevant, therefore, to discuss the organization of the database briefly. Fine-grained rocks were entered into a data set called HARVI-F, and coarse-grained rocks were entered into the data set HARVI-C. Each record was checked by the database program for consistency, and a hard copy was printed in a format that resembles the final barrel sheets. The "clean-copy" print-out was directly pasted onto a copy of the barrel sheet for subsequent curatorial record keeping.

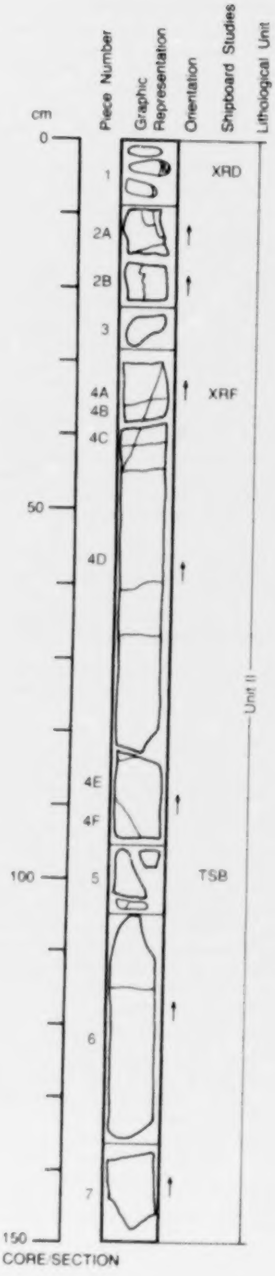
cm
Piece Number
Graphic Representation
Orientation
Shipboard Studies
Lithological Unit
0
50
100
150
1
2A
2B
3
4A
4B
4C
4D
4E
4F
5
6
7
XRD
XRF
TSB
Unit II
CORE/SECTION

126-793B-1R-1

UNIT II: DIABASE

Pieces 1-7

CONTACTS: Upper baked; lower chilled
PHENOCRYSTS: In glomeroporphyritic clots and at lower chilled margin
Olivine - 5-7%; 1-3 mm; subhedral; altered to smectite
Clinopyroxene - 2-15%; 2-6 mm; euhedral; twinned; with exsolution lamellae
Orthopyroxene - 1%; 1-2 mm; sometimes rounded
GROUNDMASS: Plagioclase (41%, 0.1-0.5 mm); clinopyroxene (18%, 0.1-0.5 mm); orthopyroxene (<1%, 0.1 mm); opaque (4%, 0.05-0.5 mm); glass (26%); vesicles (8%)
VESICLES: 8%; 0.1 mm; equant; random
Miaroles: In bands and inclusions
COLOR: Gray
STRUCTURE: Sill
ALTERATION: Smectite
VEINS/FRACTURES: 1%; 5-10 mm; subhorizontal; roughly at 10 cm spacing

Figure 9. Sample visual core description (VCD) form used for metamorphic and igneous rocks.

When describing sequences of fine- to coarse-grained rocks, the core was subdivided into lithologic units according to the criteria of changes in petrographic types, mineral abundances, and rock-clast types. For each lithologic unit, section, and rock type, the following information was recorded as appropriate using the HARVI system:

A.1. Leg, site, hole, core number and type, and section.

A.2. Unit number (consecutive downhole), position in the section, number of pieces of the same lithologic type being described, the name of the describer, and rock name.

A.3. Color of the rock according to the Munsell chart (recorded when the rock piece was dry) as well as the presence of layering and deformation and the character of each.

A.4. The number of mineral phases and their distribution within the unit. For each mineral phase, abundance, average size in millimeters, shape, the degree of alteration, and any additional comments were given.

A.5. Groundmass texture: glassy, microcrystalline, fine-grained (< 1 mm), medium-grained (1-5 mm), or coarse-grained (> 5 mm). Relative grain size changes within the unit (e.g., coarsening from Pieces 1 to 5) were also noted.

A.6. Presence of alteration and characteristics, including structures imposed during the formation of secondary minerals, type of alteration and abundance, and abundance of secondary minerals.

A.7. Vesicles: percentage abundance, distribution, size, shape, and fillings and their relationships (including proportion of vesicles that were filled by alteration minerals).

A.8. Structure: massive flow, pillow lava, thin flow, breccia, hyaloclastite, etc., and comments.

A.9. Alteration: fresh (<2%), slight (2%-10%), moderate (10%-40%), high (40%-80%), very high (80%-95%), or complete (95%-100%). The type, form, and distribution of the alteration were also given.

A.10. Veins/Fractures: percent present, width, orientation, fillings, and relationships. The relationship of the veins and fractures to the alteration was also noted.

A.11. Comments: appropriate notes on the continuity of the unit within the core and the interrelationship of units.

Basalts are termed aphyric, sparsely phyric, moderately phyric, or highly phyric, depending upon the proportion of phenocrysts visible with the hand lens or binocular microscope (approximately 10X). Basalts were called aphyric if phenocrysts clearly amounted to <1% of the rock, sparsely phyric if they ranged from 1% to 2%, moderately phyric if 2%-10%, and highly phyric if phenocrysts amounted to >10% of the rock. Basalts were further classified by phenocryst type (e.g., a moderately plagioclase-olivine phyric basalt contains 2%-10% phenocrysts, mostly plagioclase, with subordinate olivine).

During Leg 126, the following volcanic rock names were used for the initial core descriptions. ***Basalts*** have any combination of olivine, augite, and plagioclase phenocrysts. ***Andesites*** differ in that they have essential orthopyroxene and plagioclase phenocrysts plus or minus augite and olivine. ***Dacites*** and ***rhyolites*** were not distinguished from each other petrographically. They differ from andesites either by containing essential quartz or by lacking orthopyroxene. ***Boninites*** lack plagioclase and have more orthopyroxene than clinopyroxene or olivine.

More specific nomenclature was determined from chemical analyses. For consistency, we used the MgO-SiO_2 fields adopted during Leg 125. However, we did name some fields differently (Fig. 10) to avoid using "picrite" for pyroxene-rich basalts and "boninite" for plagioclase-rich rocks. Broadly speaking, the "high-Mg series" corresponds to the "low-Ca boninitic series" of Crawford et al. (1989), and our "low-Mg series" corresponds to the island-arc tholeiitic series of Jakes and Gill (1970). (However, the low-Mg series can be calcalkaline, low- to high-K, and low- or high-Al in detail.) Because of the delay that occurred between the initial core descriptions and the later chemical analyses, there are discrepancies between the lithostratigraphic and geochemical sections of this report. The geochemical classification is preferred.

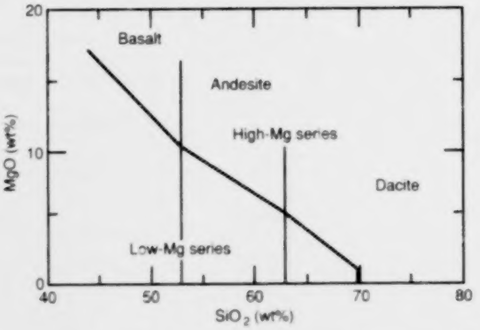

Figure 10. Nomenclature used to describe volcanic rocks recovered during Leg 126.

Serpentinized rocks were classified on the basis of the original phase proportions present in the protolith, using the IUGS classification system for ultramafic rocks. For example, "serpentinized dunite" is a rock with >90% modal olivine originally present that has some specified proportion of serpentinization.

Synoptic versions of the Leg 126 igneous/metamorphic VCD forms are published with this volume and are available on microfilm at all three ODP repositories.

Thin-Section Descriptions

Thin-section billets of basement rocks were examined to (1) confirm the identity of petrographic groups in the cores; (2) understand the textures and interrelationships of the mineral phases better; (3) help define unit boundaries indicated by hand-specimen core descriptions; and (4) define the secondary alteration mineralogy. Percentages of individual mineral phases were estimated and were reported in the detailed thin-section description sheets (available on microform at the repositories). The terminology for thin-section description was used in the same manner as in the macroscopic descriptions. In cases where discrepancies arose between hand-specimen and thin-section analyses over the composition and abundance of mineral phases, the thin-section descriptions were used in preference.

X-Ray Diffraction Analyses

A Philips ADP 3520 X-ray diffractometer was used for the XRD analyses of the mineral phases. Instrument conditions in normal use were as follows: CuK-alpha radiation with a Ni filter, 40 kV, 35 mA, Goniometer scan from 2° to 70° 2θ, step size = 0.02°, with a count time = 1 s per step.

Samples normally were ground with the Spex 8000 Mixer Mill or, when the sample was very small, an agate mortar and pestle. The material was then pressed into the sample holders, or smeared on glass plates and placed in the sample holders, for analysis.

Diffractograms were interpreted with the help of a computerized search and match routine using Joint Committee on Powder Diffraction Standards (JCPDS) powder files.

X-Ray Fluorescence Analysis

Prior to analysis, samples were normally crushed in the Spex 8510 Shatterbox with a tungsten carbide barrel. This produced some tantalum and massive tungsten contamination of the sample. If post-cruise studies for these elements, or instrumental neutron activation analyses were envisaged with the shipboard XRF powders (as on Leg 125), samples were crushed with an agate-lined barrel.

A fully automated wavelength-dispersive ARL8420 XRF (3 kW) system equipped with a Rh target X-ray tube was used to determine the major oxide and trace element abundances of whole-rock samples. Analyses of the major oxides were carried out on lithium borate glass disks doped with lanthanum as a "heavy absorber" (Norrish and Hutton, 1969). The disks were prepared from 500 mg of rock powder, ignited for 2 hr at about 1030°C, mixed with 6.0 g of dry flux consisting of 80% lithium tetraborate and 20% La_2O_3. This mixture was then melted at 1150°C in a Pt-Au crucible for about 10 min and poured into a Pt-Au mold using a Claisse Fluxer. The 12:1 flux-to-sample ratio, and the use of the lanthanum absorber, made matrix effects insignificant over the normal range of igneous rock compositions. Hence, the following linear relationship between X-ray intensity and concentration holds:

$$Ci = (Ii \times mi) - bi,$$

where

Ci = the concentration of oxide i (wt%);
Ii = the net peak X-ray intensity of oxide i;
mi = the slope of the calibration curve for oxide i (wt%/cps); and
bi = apparent background concentration for oxide i (wt%).

The slope, *mi*, was calculated from a calibration curve derived from the measurement of well-analyzed reference rocks (BHVO-1, G-2, AGV-1, PCC-1, JGB-1, JP-1, BR, DR-N, UB-N). The background, *bi*, was determined on blanks or was derived by regression analysis from the calibration curves.

Systematic errors resulting from short- or long-term fluctuations in X-ray tube intensity were corrected by normalizing the measured intensities of the samples to those of a standard that was always run together with a set of six samples. To reduce shipboard weighing errors, two glass disks were prepared for each sample. Accurate weighing was difficult on board the moving platform of the *JOIDES Resolution* and was performed with particular care, therefore, since weighing errors can be a major source of imprecision in the final analysis. Loss-on-ignition (LOI) values were determined by drying the sample at 110°C for 8 hr and then weighing them before and after ignition at 1030°C.

Trace element determinations used pressed-powder pellets prepared by pressing (with 7 tons of pressure) a mixture of 5.0 g of dry rock powder (dried at 110°C for >2 hr) and 30 drops of polyvinylalcohol binder into an aluminum cap. A modified Compton scattering technique based on the intensity of the Rh Compton peak was used for matrix absorption corrections (Reynolds, 1967).

An outline of the computation methods is given below.

1. Input X-ray intensities: Dead-time corrected X-ray intensities were read into the program from an ARL result file.

2. Make drift corrections: All peak and background intensities were corrected for machine drift by using a one-point correction of the form:

$$Di = Si/Mi, \text{ and}$$
$$Idi = Ii \times Di,$$

where

Di = the drift factor for element i, generally 1.00 ± 0.01;
Si = the peak intensity for element i, measured on a synthetic standard ("POOP") at the time of calibration;
Mi = the measured peak intensity for element i, measured on "POOP" at any time after the calibration;
Ii = the uncorrected peak or background intensity, element i; and
Idi = the drift corrected peak or background intensity, element i.

3. Subtract backgrounds. Peak intensities were corrected for nonlinear backgrounds by measuring a peak to average background ratio (***BFi***). This was determined for each element, on synthetic and natural blank standards, at the time of calibration.

$$BFi = PKi/AVBgi.$$

Thus, when measuring unknowns, the true or modified background (***MBgi***) was calculated by multiplying the average measured background for element i (***AVBgi***) by the ***BFi***. This new modified background value was then subtracted from the peak intensity (***PKi***) to arrive at the net peak intensity (***NETPKi***) for element i.

$$MBgi = AVBgi \times BFi, \text{ and}$$
$$NETPKi = PKi - MBgi.$$

4. Remove spectral interferences. During calibration, interferences were measured on synthetic pellets containing pure quartz and the interfering element. A ratio of the interference intensity to the net peak of the interfering element was calculated and assumed constant with respect to concentration. When measuring an unknown, the net interference (***INTFERi,j***) was calculated and removed by

$$INTFERi,j = NETPKi \times IRi,j \text{ and}$$
$$CNETPKj = NETPKj - INTFERi,j,$$

where

$INTFERi,j$ = the net interference intensity of element i on element j and
$CNETPKj$ = the net intensity of element j with the interference element i removed.

In the case of mutually interfering elements, an iterative approach to this same calculation was used until all the elements involved converge on their respective corrected values.

5. Measure mass absorption coefficients. To correct for matrix differences between samples, three separate mass absorption coefficients were determined following a modification of the Compton scattering technique of Reynolds (1967). Measured intensities from the rhodium K-series Compton, FeKa, and TiKa lines were compared with the calculated absorption coefficients of Rb (ARb), Cr (ACr), and V (AV), respectively. From this comparison, three equations can be written to describe the relationship between each coefficient and its respective line. The three equations derived from the Leg 126 calibration were as follows:

$$ARb = 104/[(Rhcps \times 0.0698) + 57.79],$$
$$ACr = ARb/[(\text{Fecps} \times 1.044 \times 10^{-6}) + 0.081], \text{ and}$$
$$AV = ACr/[(\text{Ticps} \times 6.140 \times 10^{-6}) + 0.778).$$

By using this method, unknowns were measured and corrected for matrix differences without calculating the absorption coefficients for each sample.

6. Calculate concentrations. Once all the spectral and matrix corrections have been calculated, the equation to calculate elemental concentrations reduces to:

$$Ci = (CNETPKi \times Ai)/Ki,$$

where

Ci = the concentration of element i in parts per million;
$CNETPKi$ = corrected net peak intensity, element i;
Ai = mass absorption coefficient for element i; and
Ki = calibration factor (ppm/cps) for element i.

The value Ki is analogous to the calibration curve slope (mi) for major elements; it was determined in the same manner on natural rock (AGV-1, UB-N, G-2, BHVO-1, RGM-1, DRN) and synthetic (compressed, spiked quartz powders) standards.

Details of the analytical conditions for each element determined are given in Table 4. Tables 5-7 summarize information about the precision and accuracy of XRF analyses during Leg 126. Given the results presented in these tables, the major element data are precise to within 0.5%-2.5% and are considered accurate to ± 1% for Si, Ti, Fe, Ca, and K, and to ± 3%-5% for Al, Mn, Na, and P. Periodic summations to 101-102 wt% occurred but were irreproducible and attributed to weighing errors or gremlins. The trace element data are considered accurate to ± 2%-3% or 1 ppm, whichever is greater, for Rb, Sr, Y, and Zr, and to ± 5%-10% or 1 ppm for the others, except for Ba and Ce. Precision also was within 3% for Ni, Cr, and V at concentrations >100 ppm.

The range of trace element concentrations over which these claims hold true encompasses those encountered during Leg 126—from basalts with 10% MgO to rhyolites with 75% SiO_2—with the following exceptions: Zr may be systematically 5 ppm too low, although agreement for BIR was excellent; Rb may be 0.5 ppm too low; Cr may be up to 5 ppm too low below 25 ppm; Ce contents are thought to be accurate to ± 15 ppm so that concentrations between 0 and 25 ppm are indistinguishable, which applies to most Leg 126 results; and Ba is accurate to within 10% at concentrations >250 ppm, but most Leg 126 results were <100 ppm where Ba was essentially uncalibrated. Moreover, BIR, with a nominal 6 ppm Ba concentration, gave results ranging from −10 to +35 ppm. Nonetheless, average concentrations for seafloor Sumisu Rift basalts agree with those measured at UCSC and L-DGO to within 5 ppm at ranges from 10 to 15 ppm. Consequently, Ce and Ba contents less than 20 and 30 ppm, respectively, indicate that these concentrations are indeed below those levels, but these values are too imprecise for us to be confident of more than that.

SEDIMENT/FLUID GEOCHEMISTRY AND ELECTRICAL RESISTIVITY

Fluid Geochemistry

Hydrocarbon Gases

As required by safety considerations, the concentrations of the hydrocarbons methane (C_1), ethane (C_2), and propane (C_3) were monitored in the sediment cores at intervals of about 10 m. The hydrocarbon gases were extracted from the bulk sediment by means of a headspace-sampling technique. A 5-cm^3 plug of sediment was taken as soon as the core arrived on deck, using a No. 4 cork borer. This sample was placed immediately in a glass vial sealed with a septum and metal crimp and heated to 70°C. The gas driven off was drawn into a syringe and injected into a Hach-Carle AGC Series 100 model 211 gas chromatograph equipped with a thermal conductivity detector. Where high concentrations of propane were suspected, a second sample was taken by the same method and analyzed for C_1 through C_6 hy-

Table 4. X-ray fluorescence analytical conditions, Leg 126.

Element	Line	Crystal	Detector	Collimator	Peak angle (degrees)	Background offset (degrees)	Total count time (s) peak	background
SiO_2	Kα	PET(002)	FPC	Coarse	109.25	0	40	0
TiO_2	Kα	LIF(200)	FPC	Fine	86.14	0	40	0
Al_2O_3	Kα	PET(002)	FPC	Coarse	145.27	0	100	0
[a]Fe_2O_3	Kα	LiF(200)	FPC	Fine	57.52	0	40	0
MnO	Kα	LiF(200)	KrSC	Fine	62.98	0	40	0
MgO	Kα	TLAP	FPC	Coarse	44.87	± 0.80	200	200
CaO	Kα	LiF(200)	FPC	Coarse	113.16	0	40	0
Na_2P	Kα	TLAP	FPC	Coarse	54.71	− 1.20	200	200
K_2O	Kα	LiF(200)	FPC	Fine	136.65	0	40	0
P_2O_5	Kα	Ge(111)	FPC	Coarse	140.94	0	100	0
Rh	K-C	LiF(200)	Scint	Fine	18.59	0	100	0
Nb	Kα	LiF(200)	Scint	Fine	21.37	± 0.35	200	200
Zr	Kα	LiF(200)	Scint	Fine	22.53	± 0.35	100	100
Y	Kα	LiF(200)	Scint	Fine	23.78	± 0.40	100	100
Sr	Kα	LiF(200)	Scint	Fine	25.13	± 0.40	100	100
Rb	Kα	LiF(200)	Scint	Fine	26.60	± 0.60	100	100
Zn	Kα	LiF(200)	Scint	Fine	41.79	± 0.40	60	60
Cu	Kα	LiF(200)	Scint	Fine	45.02	± 0.40	60	60
Ni	Kα	LiF(200)	Scint	Coarse	48.67	± 0.60	60	60
Cr	Kα	LiF(200)	FPC	Fine	69.35	± 0.50	60	60
Fe	Kα	LiF(220)	FPC	Fine	85.37	− 0.40 + 0.70	40	40
V	Kα	LiF(220)	FPC	Fine	122.84	− 0.50	60	60
TiO_2	Kα	LiF(200)	FPC	Fine	86.14	± 0.50	40	40
[b]Ce	Lα	LiF(220)	FPC	Coarse	137.92	± 1.50	100	100
[b]Ba	Lβ	LiF(220)	FPC	Coarse	128.53	± 1.50	100	100

Note: All elements were analyzed under vacuum on goniometer 1 at generator settings of 60 kV and 50 mA. FPC = flow proportional counter using P_{10} gas; KrSC = sealed krypton gas counter; and Scint = NaI scintillation counter.

[a] Total Fe as Fe_2O_3.

[b] Calibrated but not analyzed on basalts.

drocarbons using a Hewlett-Packard 5980A Natural Gas Analyzer, a gas chromatograph equipped with Poropak-Q, molecular-sieve, and silicone-oil-coated columns, and a flame ionization detector. After the headspace gas had been analyzed, the actual volume of the sediment sample was measured to the nearest 0.5 cm^3 by the displacement method using water. Details of this method and the complete configuration of both gas chromatographs are given in the Explanatory Notes for Leg 112 (Suess, von Huene, et al., 1988).

Interstitial Water

On Leg 126, interstitial water was obtained by squeezing and by *in-situ* extraction using the Barnes pore-water sampler. We squeezed 10-cm-long, whole-round sections of cores that were cut from the core as soon as it arrived on deck by slicing the plastic core liner and capping both ends. Following the electrical resistivity measurements, the core was removed from the core liner, scraped with a stainless-steel spatula to remove the outer, contaminated layer, and placed in a stainless-steel squeezer (Manheim and Sayles, 1974). The squeezer was placed in a Carver hydraulic press and squeezed at pressures of up to 40,000 psi. Interstitial water was collected directly into a 50-mL plastic syringe, from which the various aliquots for analysis were ejected through an on-line 0.45-μm polysulfone filter mounted in a Gelman "acrodisc" disposable filter holder. Squeezed interstitial waters are designated here as "IW" samples.

The *in-situ* pore-water sampler is the new version designed by Dr. R. Barnes and first used on Leg 110 (Barnes, 1988). This tool collects interstitial water while making simultaneous measurements of sediment temperature and pore pressure. It is lowered on the sand line to the end of the drill string, where it is locked into an assembly just above the bit. To keep the hole free of fill during the descent of the sampler, the hole is flushed with drilling fluid with the bit just off bottom. After the sampler is latched into place, the bit is lowered into the bottom with the sampling probe projecting about 20 cm through the bit. A timer-operated valve opens and interstitial water is drawn under negative pressure through two 40-μm stainless-steel filters and one 1-μm polyester filter into the sampler. There it passes through a stainless-steel entry tube of 12 mL volume into two sample coils arranged in series and separated by an open ball valve, and then into a steel overflow cylinder of 1200 mL volume that also contains the sample coils and valving. The length of time required to fill the Barnes sampler varies with the permeability of the sediment, but typically is about 15 min. Interstitial water samples collected with the Barnes tool are designated here as "BW". On removal from the stainless-steel coil, they are filtered at 0.45 μm as for the squeezed samples.

Drilling Mud Filtrate

To evaluate the extent of contamination by drilling mud filtrate, samples of drilling mud were taken when new batches were prepared. The drilling mud filtrate was separated by centrifugation, filtered and treated similar to interstitial water samples. Drilling mud filtrate is designated here as "MW".

Sample Analysis

The waters were analyzed immediately on recovery for pH, alkalinity by potentiometric titration, salinity by refractive index, and, when an odor was detected, hydrogen sulfide by colorimetry using methylene blue. Aliquots were acidified to a pH of about 2 by adding concentrated HCl, refrigerated, and analyzed within a few days for sodium, strontium, lithium, potassium, iron, and manganese by atomic absorption spectrophotometry. When required, ionization suppressors were added to samples, blanks, and standards. All samples were diluted to within the linear range of the instrument. Calcium and magnesium were determined by titration as described by Gieskes and Peretsman (1986). A separate aliquot was taken for the determination of chloride, silicon, sulfate, and ammonium. The concentration of chloride was determined by means of argentiometric titration; sulfate by ion chromatography; and silicon and ammonium by colorimetry. All shipboard anion analyses were carried out using standard ODP techniques as detailed by Gieskes and Peretsman (1986) and described briefly in the Explanatory Notes for Leg 112 (Suess, von Huene, et al., 1988). IAPSO standard seawater was used as the primary standard for the determination of chlorinity, calcium, magnesium, and sulfate and as a secondary standard for lithium, potassium, strontium, and sodium.

Electrical Resistivity

The electrical resistivity and formation factor of the sediments was measured by means of a four-electrode configuration (Wenner configuration) similar to the one used by Manheim and Waterman (1974). The electrodes were made of 2-mm-diameter stainless-steel rods. Specially designed equipment allows the electrodes to be inserted into the short end of the whole-round sections in exactly (fraction of a millimeter) the same position relative to the core liner. A 20-kHz square-wave current was applied to the outer electrodes and the difference in potential between the two inner electrodes was measured. The size of the current (typically 50 mAmps) was measured over a resistor in the outer circuit. The temperature of the sediment was measured with a thermocouple. For an infinite and homogeneous medium the resistivity was given by the equation,

$$R = 2 \times \pi \times a \times \Delta V/I,$$

where

R = the specific resistivity,
a = the distance between the electrodes,
ΔV = the difference in potential between the inner electrodes, and
I = the current (Jakosky, 1940).

However, because of edge effects and the large diameter of the electrodes relative to the distance between them (13 mm), the "$2 \times \pi \times a$" term in the equation had to be replaced by a cell constant. The cell constant was determined by measuring the resistivity of a 35‰ NaCl solution held in a container made from a core liner and of the same length as the whole rounds on which the electrical resistivity was measured. Determination of the formation factor involved the following steps:

1. Correction of the measured apparent resistivity of the reference fluid to 25°C by means of the temperature calibration curve (Fig. 11).
2. Determination of the cell constant as the ratio between the theoretical resistivity of the reference fluid at 25°C (0.195 ohm-m) to the temperature-corrected theoretical resistivity of the reference fluid from Step 1.
3. Determination of the resistivity of the sediment at the measuring temperature by means of the cell constant and the measured current and voltage.
4. Correction of the sediment resistivity to 25°C by means of the temperature calibration curve (Fig. 11).
5. Making the assumption that the resistivity of the pore water of a given salinity (estimated from the chloride concentration) has the same resistivity as pure sodium chloride solution, and using the calibration curve (Fig. 12) to estimate the pore-water resistivity at 25°C.
6. The formation factor is the ratio between the output from Step 4 to 5.

Table 5. Consensus values and Leg 126 values (in wt%) obtained for major and trace element standards during initial calibration of shipboard X-ray fluorescence.

Element	BIR-1 anhydrous	JN-2 anhydrous	JB-3 anhydrous	All 92-29-1 anhydrous	BHVO anhydrous	BEN anhydrous	BR anhydrous	UBN anhydrous	JA-1 anhydrous	DRN anhydrous	STM-1 anhydrous
SiO_2 [1]	48.04*	53.4*	51.16*	49.39*	49.69*	39.58*	39.43*	44.93*	64.75*	54.03*	60.63*
[2]	47.96	53.44	51.45	49.48	50.15	39.87	39.87	45.06	64.4	54.13	59.94
TiO_2	0.96*	1.19	1.45*	1.75*	2.7*	2.7*	2.7	0.13	0.88	1.08*	0.153
	0.97	1.16	1.43	1.74	2.74	2.71	2.7	0.12	0.96	1.1	0.14
Al_2O_3	15.53	14.73*	16.93*	15.49*	13.6*	10.43*	10.49*	3.3	15.14*	17.84*	18.82*
	15.57	14.94	17.47	15.51	13.65	10.24	10.23	3.17	15.37	18.09	18.74
Fe_2O_3	11.34*	14.39*	11.91*	10.85*	12.3*	13.3*	13.31*	9.5	7.02*	9.82*	5.3*
	11.44	14.35	11.92	10.96	12.49	13.23	13.17	9.5	6.92	9.89	5.31
MnO	0.18*	0.2	0.16	0.18*	0.17*	0.21*	0.21*	0.14	0.154*	0.21*	0.22*
	0.18	0.23	0.18	0.18	0.18	0.21	0.21	0.15	0.158	0.23	0.23
MgO	9.71*	4.68*	5.21*	7.52*	7.26*	13.62*	13.71*	40.12	1.63*	4.45*	0.092
	9.4	4.8	5.25	6.94	6.82	14.08	14.15	39.86	1.93	4.63	0.17
CaO	13.34*	9.93*	9.88*	11.16*	11.39*	14.37*	14.23*	1.37	5.78*	7.16*	1.12*
	13.52	9.95	9.92	11.1	11.52	14.56	14.29	1.39	5.7	7.17	1.13
NaO_2	1.82*	2.04*	2.83*	3.07*	2.29*	3.3*	3.11*	0.11	3.9*	3.02*	9.07*
	1.81	2.03	2.72	2.87	2.14	3.21	3.15	0.19	3.85	3.14	9.21
K_2O	0.03	0.43*	0.8*	0.17*	0.52*	1.44*	1.45*	0.02	0.83*	1.73*	4.38*
	0.023	0.424	0.786	0.161	0.52	1.48	1.44	0.02	0.777	1.76	4.35
P_2O_5	0.021	0.1*	0.29*	0.16*	0.28*	1.09*	1.08*	0.05	0.16	0.22	0.16
	0.0266	0.103	0.291	0.171	0.27	1.05	1.05		0.16	0.22	0.14
H_2O+	0.09	0.31	0.2		−0.69	2.24	.48	10.84	0.8		
H_2O−	0.08	0.07	0.03			0.5		1.26	0.26		
CO_2				0.23		0.74		0.39			
LOI	0.17	0.38	0.23	0.23	−0.69	3.48	2.48	12.49	1.06	0	0
Total [1]	100.8	100.71	100.39	99.51	100.89	98.56	97.24	87.18	99.18	99.56	99.95
[2]	100.73	101.05	101.19	98.88	101.17	97.16	97.78	86.97	99.27	100.36	99.36

Element	BIR-1	JB-2	JB-3	BHVO	BEN	BR	JA-1	DRN	GH	STM-1	Mica Mg	RGM-1	Mica Fe	G2	AGV-1
Nb [1]	2.3	0.8*	2.3	19*	173	100*	1.7	6*	83*	270*	120*	9*	270*	12*	15*
[2]	0.4	0.8	1.7	17.5	109	103.8	1.8	7.5	95	268.5	128.4	9.8	281.4	12.2	13.6
Zr	18	52*	100*	180*	265*	250*	87*	125*	150*	130*0	20	245*	80*	300*	231*
	16	46.4	96.1	170	271.2	269.6	85.4	125	153	1337	11.7	243	76.5	319.5	229.7
Y	16*	26*	28*	26.5*	30*	30*	31.4*	29*	70*	46*	—	22.4	25	10*	19*
	16.7	25.1	28.1	27.9	29.7	2	31.8	28.3	88.8	51.5	—	25.7	34.9	9.6	19.5
Sr	107*	178*	395*	420*	1370*	1320*	266*	400*	10	700*	2.5	106*	5	480*	656*
	107	172.2	410.9	386	1355	1330.7	262	395.7	9	726.9	27.2	108.7	5.6	500	645.9
Rb	2.2	6.2	13	9.1*	47*	47*	11.8	70*	390*	120*	1300*	152*	2200*	170*	67*
	0.5	5.6	14.2	8.4	46	47	10.5	73.1	411.6	120.4	1326	159.8	2057	178.9	65.6
Zn	70	110*	106*	113*	120*	65*	90.6*	145	85	230	—	36	—	90*	89
	54.7	108.5	90.5	100	100	[156.3]	85.6	[264]	46.8	[295.3]	—	[17.9]	—	83.88	127.2
Cu	125*	230*	197*	140*	72*	72*	41.7*	50*	14	4*	4	11*	4	11	59
	120.4	191	191	133.4	77.6	75.3	43.2	47	2.8	4	6.6	11.8	10.7	11.6	57.5
Ni	166*	14.2	38.8	120*	267*	260*	1.8	16*	5*	2.1	110	6	35	5*	16*
	157.3	13.3	38.8	115.3	274	265	2.7	15.8	5.3	4.7	125.6	7	40.8	5.3	15.3
Cr	373*	27.4*	60.4*	300*	360*	380*	7.3	42	6	2.6	100*	4	90*	8	10
	397	26.3	55.34	292.5	385	345.3	—	28.7	—	—	99.6	10.4	87.7	3.8	1
V	312*	578*	383*	320*	235*	240*	105*	225*	5	2	—	13	135*	35*	125*
	321.9	623	373	328.3	272	242.6	110.4	216	—	5.2	—	9.7	152.8	30.6	115.8
Ce	1.6	6.5	20.5	38*	152*	140	13	44	70	260*	—	49	—	160*	71
	—	5.1	—	39.2	145.2	144.5	6	28	53.2	271.5	—	52	—	188.6	50.1
Ba	6	208	251*	135*	1025*	1050*	307*	385	850	560*	—	800*	—	1880*	1208*
	—	251	242.6	129.8	1080	1161	295	398	—	596	—	818.4	—	1877	1102

Note: The consensus values are largely from Govindaraju (1984), revised in some cases to conform to experience in other XRF labs (Stork et al., 1987). The major element results from these sources were recalculated to an anhydrous basis by multiplying published values by 1.0 plus the sum of (H_2O^+ + H_2O^- + CO_2) given at the base of each column. The Leg 126 entries are those obtained during calibration for ignited powders. The trace and major element calibration curves were based on the standards that have an asterisk for that element. [1] = consensus values and [2] = Leg 126 values. Entries in brackets are analytically uncertain.

The uncertainty introduced by making the assumption that the pore-water resistivity was the same as for a NaCl solution of the same salinity was small when the disturbance of the sediments caused by inserting the electrodes and by drilling and retrieval is considered.

Sediment Geochemistry

Sediments were analyzed on board ship for inorganic carbon and for total nitrogen, carbon, and sulfur. The organic carbon content of the sediments was calculated by difference. Inorganic carbon and total nitrogen, carbon and sulfur were determined on all sediment samples taken for physical properties measurements and on the squeezed sections. All samples were freeze dried prior to analysis.

Total inorganic carbon was determined using a Coulometrics 5011 Coulometer equipped with a System 140 carbonate carbon analyzer. Depending on the carbonate content, 15-70 mg of ground and weighed sediment was reacted in a 2N HCl solution. The liberated CO_2 was titrated in a monoethanolamine solution with a colorimetric indicator, while monitoring the change in light transmittance with a photo-detection cell.

Total nitrogen, carbon, and sulfur were determined with a N/C/S analyzer (Model NA 1500) from Carlo Erba Instruments. Bulk samples were combusted at 1000°C in an oxygen atmo-

Table 5 (continued).

NBS 688 anhydrous	GH anhydrous	Mica Mg anhydrous	JDF2 anhydrous	RGM-1 anhydrous	K1919 anhydrous	JGB-1 anhydrous	Mica Fe anhydrous	G2 anhydrous	AGV-1 anhydrous	JP-1 anhydrous
48.01*	76.42*	39.32*	50.33*	73.42*	49.73*	44*	35.65*	69.31*	59.96	43.74
48.43	76.28	39.08	49.9	73.41	49.25	43.76	35.13	69.06	59.84	43.31
1.16*	0.08	1.67*	1.95	0.28	2.83	1.64*	2.6*	0.48*	1.07*	0.01
1.16	0.08	1.68	1.88	0.28	2.83	1.6	2.56	0.5	1.06	0.02
17.22*	12.6	15.61*	13.68*	13.8*	13.75*	17.89*	20.21*	15.47*	17.29	0.64*
17.53	12.83	15.38	13.48	13.96	13.62	17.69	19.63	15.51	17.37	0.649
10.27*	1.35*	9.71*	13.41*	1.89	12.21*	15.35*	26.38*	2.68*	6.86*	8.61*
10.34	1.15	9.7	13.37	1.76	12.1	15.21	26.33	2.41	6.8	8.68
0.17*	0.05	0.27*	0.22*	0.04	0.18	0.17	0.36*	0.03	0.1*	0.12
0.17	0.05	0.27	0.22	0.03	0.17	0.17	0.36	0.03	0.1	0.12
8.33*	0.03	20.94	6.56*	0.29	6.83*	7.93*	4.71*	0.75	1.53	46.14
8.34	0.13	19.02	6.48	0.37	6.33	7.56	4.83	0.9	1.9	46.5
12.07*	0.7*	0.08	10.68*	1.2*	11.32*	12.13*	0.45	1.97*	4.97*	0.58*
12.62	0.69	0.01	10.75	1.2	11.25	12.09	0.38	1.92	4.92	0.57
2.13*	3.88*	0.123	2.74	4.16*	2.35*	1.25	0.31	4.06*	4.35*	0.022
2.1	4.04	0.18	2.86	4.24	2.28	1.36	0.19	4.09	4.39	0.03
0.19*	4.8*	10.27*	0.19	4.34*	0.53*	0.26	9.07*	4.48*	2.94*	0.003
0.19	4.81	10.4	0.23	4.35	0.53	0.23	9.21	4.48	2.96	0.005
0.13	0.01*	0.01	0.24*	0.05*	0.28*	0.05*	0.47	0.13*	0.51*	
0.1	0.01		0.21	0.05	0.26	0.05	0.39	0.13	0.48	
	0.46	2.09		0.38		1.23	2.91	0.5	0.78	2.68
	0.14	0.31				0.04	0.43			0.4
0.05	0.3	0.15					0.19	0.08	0.02	
0.05	0.9	2.55	0	0.38	0	1.27	3.53	0.58	0.8	3.08
99.63	99.02	95.45	100	99.09	100.01	99.4	96.88	99	99.78	96.79
100.93	99.17	93.17	99.38	99.27	98.62	98.45	95.48	98.45	99.02	96.80

sphere with the addition of vanadium pentoxide, converting organic and inorganic carbon to CO_2 and sulfur to SO_2. These gases, along with nitrogen, were then separated by gas chromatography and measured with a thermal conductivity detector.

PHYSICAL PROPERTIES

Physical property measurements made on cores recovered during Leg 126 included MST logging (GRAPE, magnetic susceptibility, and compressional sonic velocity measurements), thermal conductivity, undrained vane shear strength, Hamilton Frame compressional velocity, electrical resistivity, index properties, and carbonate analyses. Downhole temperatures were measured at one site. Representative samples of the core or section were taken in areas of least disturbance. Sample selection and spacing depended on the rate of core recovery, the type of measurement (see below), as well as the thickness and homogeneity of the recovered sequences.

The testing methods employed during Leg 126 are discussed in the order in which they were performed on each core. The MST logging and soft-sediment thermal conductivity determinations were performed on whole cores. Other measurements were conducted on discrete samples taken from the split cores.

Gamma-Ray Attenuation Porosity Evaluator

The gamma-ray attenuation porosity evaluator (GRAPE) makes continuous measurements of wet-bulk density on whole cores by comparing the attenuation of gamma rays through the cores with attenuation through an aluminum standard (Boyce, 1976). Individual core sections were placed horizontally on the MST and moved on a conveyor belt through the GRAPE sensors. The attenuation of the gamma rays passing through the liner and core was measured every 2.5 cm, and bulk density was calculated from the attenuation values. The GRAPE data were filtered to remove values that resulted from gas, gaps, or end-cap effects before averaging over 0.2-m intervals. All bulk density data are reported in units of g/cm³.

P-Wave Logger

The *P*-wave logger (PWL), which also operates on the MST, produces a 500-kHz compressional wave pulse at a repetition rate of 1 kHz. Both signal and receiving transducers are aligned perpendicular to the core axis. A pair of displacement transducers monitor the separation between the compressional wave transducers, allowing variations in the outside liner diameter without degrading the accuracy of the velocities. Measurements were taken at 2.5-cm intervals.

Water was applied to the core liner to improve acoustic contact between the transducers and the liner. As with the GRAPE, generally only APC and the first few XCB cores were measured. The deeper XCB cores and all RCB cores have annular voids between the core and the liner which caused loss of transmission of compressional waves. The PWL data were filtered to remove data that resulted from gas, gaps, or end-cap effects. Weak returns with signal strengths below a threshold value of 200 also were removed. All velocity data are reported in units of km/s.

Thermal Conductivity

Whole-round cores were allowed to equilibrate to room temperature for at least 3 hr, until drift rates were reduced to less than 0.1 mV/min prior to running thermal conductivity measurements. The thermal conductivity techniques used are described by Von Herzen and Maxwell (1959) and Vacquier (1985). All thermal conductivity data are reported in units of W/m · K.

Soft-Sediment Thermal Conductivity

Needle probes connected to a Thermcon-85 unit were inserted into the sediment through holes drilled into the core liner and the thermal drift was monitored. An additional probe was inserted into a reference material. Once the temperature (estimated from voltage) stabilized, the probes were heated and the coefficient of thermal conductivity was calculated as a function of the change in probe resistance. When the sediment became

Table 6. Elemental wt% obtained during multiple analyses of major element standard AII-92-19-1 run throughout Leg 126.

Result file →	Run 1	Run 2	Run 3	Run 4	Run 5	Run 6	Run 7	Run 8	Run 9	Run 10	Run 11	Run 12	Run 13	Run 14	Run 15
SiO_2	49.73	49.41	49.7	49.41	49.51	49.65	49.62	49.6	49.78	49.36	49.37	49.5	49.15	49.52	49.37
TiO_2	1.74	1.73	1.74	1.73	1.73	1.74	1.73	1.74	1.73	1.74	1.73	1.74	1.72	1.74	1.74
Al_2O_3	15.46	15.47	15.47	15.43	15.5	15.59	15.41	15.5	15.68	15.38	15.41	15.46	15.42	15.56	15.5
Fe_2O_3	10.89	10.91	10.86	10.76	10.87	10.9	10.87	10.9	10.91	10.85	10.77	10.92	10.77	10.84	10.83
MnO	0.15	0.15	0.15	0.15	0.15	0.15	0.15	0.15	0.15	0.14	0.15	0.15	0.15	0.15	0.14
MgO	7.14	6.96	7.5	7.08	7.12	7.08	7.08	6.97	6.93	7.17	6.6	6.95	6.83	6.91	7.22
CaO	11.06	11.06	11.1	11.04	11.09	11.11	11.11	11.06	11.1	11.06	11.09	11.08	10.97	11.1	11.11
NaO_2	3.02	3.04	3.07	3.03	2.98	2.99	2.88	2.77	2.65	2.78	2.75	2.81	2.78	2.85	2.94
K_2O	0.17	0.17	0.17	0.17	0.17	0.17	0.16	0.16	0.16	0.16	0.16	0.16	0.17	0.17	0.16
P_2O_5	0.16	0.16	0.16	0.16	0.17	0.16	0.17	0.16	0.15	0.15	0.15	0.15	0.15	0.16	0.15
Total	99.52	99.06	99.92	98.96	99.29	99.54	99.18	99.01	99.24	98.79	98.18	98.92	98.11	99.03	99.18

Note: SD = standard deviation and Real dev. = real deviation.

too stiff to allow easy insertion of the probe, holes were drilled into the core material prior to insertion. An attempt was made to insert the probes at locations along each core section that appeared to be the least disturbed. However, an annulus of disturbed sediment and drill fluid was often present along the inside of the liner, preventing visual identification of disturbance and resulting in possible erroneous values.

Hard-Rock Thermal Conductivity

Thermal conductivity measurements on well-lithified sediments and rocks were conducted on split cores using the half-space technique with a needle probe partially embedded in a slab of insulating material. The surface of a sample of split core was polished with 240-, then 600-grit sandpaper, and placed on top of the slab. Dow Corning 3 silicone was used to improve the thermal contact between the slab and the sample. The sample and the slab were immersed in a saltwater bath. After reaching thermal equilibrium, the probe was heated and measurements of resistance changes in the probe were made over a 6-min interval. Thermal conductivity was determined from the most linear portion of the resulting temperature vs. log-time plot.

Undrained Shear Strength

Undrained shear strength was determined by means of a Wykeham-Farrance motorized vane shear apparatus equipped with a four-bladed vane that has a diameter of 1.28 cm and a length of 1.28 cm. The vane was inserted into the split-core section perpendicular to the core axis, to a point where the top of the blade was covered by between 2 and 4 mm of sediment. The vane was then rotated at a rate of 89°/min until the sediment failed. The undrained shear strength was calculated from the peak torque (stress) obtained at failure. Shear strength testing was suspended at the point where significant disturbance occurred or where the material became too stiff for the vane to penetrate without severe cracking. No shear strength measurements were done on rotary-drilled cores. All shear strengths are reported in units of kPa.

Hamilton Frame Compressional Wave Velocity

Compressional-wave velocity measurements were taken on discrete samples that were sufficiently competent to provide adequate signal strength. Velocities were calculated from the determination of the travel time of a 500-kHz compressional wave through a measured thickness of sample, using a Hamilton Frame Velocimeter and Tektronix DC 5010 counter/timer system. Samples of soft sediment were taken with a special parallel-sided sampling tool. A double-bladed diamond saw was used in more lithified sediments. Basement rock samples were obtained using either a double-bladed diamond saw or a 2.5-cm-diameter rock corer. Sample thicknesses (distance) were measured directly with calipers.

Zero traveltimes for the velocity transducers were estimated by linear regressions of the traveltime vs. distance for a series of aluminum and lucite standards. Filtered seawater was used to improve the acoustic contact between the sample and the transducers. Velocities were not recorded when insufficient or extremely variable signals were obtained.

Electrical Resistivity/Formation Factor

The electrical resistivity of soft sediments was measured perpendicular and parallel to the core axis with a Wenner electrode array composed of two current and two potential electrodes. Alternating current with a voltage of 200 kHz was applied to the sediment and the resulting resistances were measured with a Wayne-Kerr Precision Component Analyzer. Formation factors were calculated as:

formation factor = sediment resistivity/pore-fluid resistivity.

Pore-water resistivity was measured with the same electrode array in a seawater-filled core liner; care was taken to simulate the same configuration as used for the sediment measurements.

Index Properties

Index properties, wet- and dry-bulk density, porosity, water content, and grain density were determined on samples of sediment and rock (Lambe and Whitman, 1969). Where possible, samples for index property analyses were taken adjacent to compressional wave velocity and/or vane shear strength measurements. Samples were weighed using two calibrated Scientech 202 electronic balances. An average of 200 sample weighings compensated for ship motion. Samples were freeze dried for at least 18 hr (Site 787) or oven dried at 105°C for 24 hr (Sites 788–793). Wet and dry volumes were measured with a Quantochrome helium penta-pycnometer.

Porosities and water contents are reported as percentages; water contents are on a dry-weight basis (Lambe and Whitman, 1969). Wet- and dry-bulk densities and grain density are reported as g/cm^3. All values were corrected for the salt content of the pore fluid, assuming seawater salinity of 35‰.

Calcium Carbonate

Calcium carbonate was calculated from weight percent inorganic carbon, assuming that all inorganic carbon is in the form of $CaCO_3$. Inorganic carbon was determined on index property samples with a Coulometrics Carbon Dioxide Coulometer.

Table 6 (continued).

Run 16	Run 17	Element	Average	SD	Real dev. (%)
49.38	49.25	SiO_2	49.49	0.18	0.36
1.74	1.73	TiO_2	1.73	0.01	0.41
15.45	15.48	Al_2O_3	15.48	0.09	0.56
10.79	10.81	Fe_2O_3	10.85	0.06	0.52
0.15	0.15	MnO	0.15	0	2.83
6.84	7.01	MgO	7.02	0.18	2.49
11.02	10.96	CaO	11.07	0.05	0.49
2.82	2.86	NaO_2	2.89	0.08	2.75
0.17	0.16	K_2O_5	0.17	0	2.92
0.15	0.15	P_2O_5	0.16	0	2.69
98.5	98.56	Avg. total	99.00	0.40	

Freeze-dried samples were dissolved in 2.0 N HCl, and inorganic carbon was estimated from the amount of CO_2 evolved (see Backman, Duncan, et al., 1988).

Heat Flow

Downhole-temperature measurements were successfully completed at Site 792. The Uyeda probe, a ½-in.-diameter thermistor probe, was attached to the end of the coring shoe and extended beyond the shoe into undisturbed sediment. The electrical resistance in the sediment was recorded for approximately 20 min during each deployment at 1-min intervals. During this time, the temperature probe was effectively decoupled from ship motion by means of a heave compensator. Electrical resistance data was then converted into temperatures when the probe arrived back on deck. Reported temperatures are extrapolated to *in-situ* equilibrium values.

DOWNHOLE MEASUREMENTS

Measurement Descriptions

Downhole measurements determine the physical and chemical properties of formations adjacent to the borehole. Interpretation of these continuous, *in-situ* measurements can yield a stratigraphic, lithologic, structural, geophysical, and geochemical characterization of the site. After coring is completed, a combination of sensors are lowered downhole on a 7-conductor cable, and each of several measuring devices continuously monitored properties of the adjacent formation. Of the dozens of different combinations commonly used in the petroleum industry, four combinations of Schlumberger sensors were used on Leg 126: (1) the geophysical combination, (2) the geochemical combination, (3) the formation microscanner (FMS), and (4) a vertical seismic profile (VSP). Each combination was not necessarily deployed in each hole; reference should be made to individual site chapters for details.

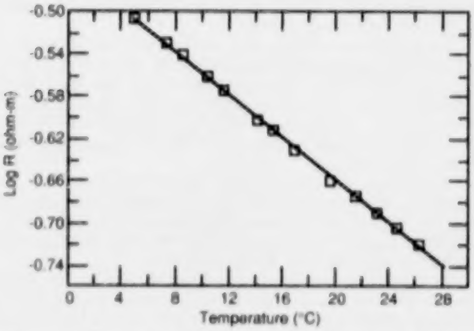

Figure 11. Temperature calibration curve used for the correction of measured apparent electrical resistivity of a reference fluid and of sediment resistivity.

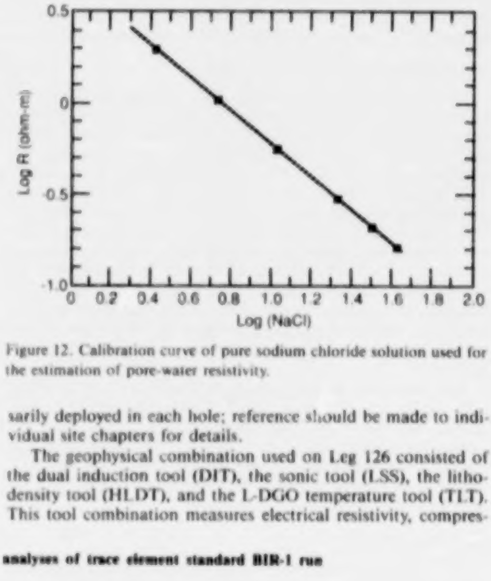

Figure 12. Calibration curve of pure sodium chloride solution used for the estimation of pore-water resistivity.

The geophysical combination used on Leg 126 consisted of the dual induction tool (DIT), the sonic tool (LSS), the lithodensity tool (HLDT), and the L-DGO temperature tool (TLT). This tool combination measures electrical resistivity, compres-

Table 7. Elemental wt% obtained during multiple analyses of trace element standard BIR-1 run throughout Leg 126.

Result file →	Run 1	Run 2	Run 3	Run 4	Run 5	Run 6	Run 7	Run 8	Average	SD
Nb	0.8	0.7	0.9	0.5	1	0.7	0.8	0.4	0.7	0.20
Zr	15.9	16.4	15.3	16.1	15.2	15.3	15	15.8	15.6	0.49
Y	16.5	17	16.6	16.5	16.2	16.8	17.3	16.4	16.7	0.35
Sr	106.5	107.5	105.9	106.1	106.6	106.9	108.1	106.3	106.7	0.74
Rb	0	0	0	0.6	0.1	−0.06	0	0.1	0.1	0.21
Zn	55.9	88.4	92.5	90.5	91.4	91	89.3	88.9	86.0	12.23
Cu	125.4	96.6	96.7	96.6	99.1	95.8	98.4	99.3	101.0	9.95
Ni	154.7	156.4	156.1	156.4	156.9	155.6	157.3	156.4	156.2	0.80
Cr	391.7	—	388.9	402.2	395.5	398.6	391	403.6	395.9	5.73
V	336.4	—	310.1	326.2	328.7	327.1	315.8	336	325.8	9.77
TiO_2	0.94	—	0.94	0.95	0.94	0.93	0.95	0.94	0.9	0.01
Ce	—	—	—	—	—	−5	5.9	0	0.3	5.46
Ba	23.1	—	—	11	22.4	34.8	0	0	15.1	13.88

Note: SD = standard deviation.

sional wave velocity, formation density, and the spectral content of naturally occurring radiation.

The geochemical combination consists of a natural gamma-ray spectrometry tool (NGT), an aluminum clay tool (ACT), an induced gamma-ray spectrometry tool (GST), and the L-DGO temperature tool (TLT). This tool combination measures the *relative* concentrations of 11 elements, including silicon, calcium, iron, sulfur, manganese, hydrogen, chlorine, potassium, thorium, and uranium.

The FMS is a microresistivity imaging device that was deployed for the first time in the Ocean Drilling Program during Leg 126. It allows for the visual characterization of the borehole wall from measurements related to the formation's electrical resistivity in the vicinity of the borehole wall.

Vertical seismic profiles were conducted in two of the holes drilled. The VSPs can provide much information on the seismic nature of reflective interfaces penetrated by the borehole, as well as provide predictive information on the nature of, and depth to, interfaces below the total depth of the borehole.

Measurement Devices

A brief description of *in-situ* sensors used during Leg 126 is given below. A more detailed description of the physical principles of these sensors and their applications is provided in Schlumberger (1972), Hearst and Nelson (1984), and Ellis (1987).

Electrical Resistivity

The dual induction instrument (DIT) provides three different measurements of electrical resistivity, each one with a different radial depth of investigation. Two induction devices ("deep" and "medium" resistivity) send high-frequency alternating currents through transmitter coils, creating magnetic fields that induce secondary (Foucault) currents in the formation. These ground-loop currents produce new inductive signals that are proportional to the conductivity of the formation. The signals are recorded by a series of receiving coils, and the measured conductivities are converted to resistivities. A third device, the "spherically" focused resistivity (SFR), measures the current necessary to maintain a constant voltage drop across a fixed interval. The vertical resolution is on the order of 2 m for the two induction devices and about 1 m for the spherically focused resistivity.

To a first-order approximation, resistivity responds to the inverse square root of porosity (Archie, 1942). In addition, water salinity, clay content, and temperature are important factors controlling the electrical resistivity of rocks. Other factors that may influence the resistivity of a rock include the concentration of hydrous and metallic minerals, the presence of vesicles, and the geometry of interconnected pore spaces.

Sonic Velocity

The digital sonic measurement (LSS) uses two acoustic transmitters and two receivers to measure the time required for sound waves to travel along the borehole wall over source-receiver distances of 2.4, 3.0, and 3.6 m. The raw data are expressed as the time required for a sound wave to travel through 0.31 m of formation; these traveltimes are then converted to sonic velocities. First arrivals for the individual source-receiver paths are used to calculate the velocities of the different waves traveling in the formation (compressional, shear, etc.). Only compressional wave velocity is determined on board the ship, but the full sonic waveforms are recorded for postcruise processing to determine shear wave and Stoneley wave velocities. The vertical resolution of the tool is 0.61 m. Compressional wave velocity is primarily controlled by porosity and lithification; decreases in porosity and increases in lithification generally cause velocity to increase.

Temperature

The L-DGO temperature tool is a self-contained tool that can be attached to any of the sensor combinations. Data from two thermistors and a pressure transducer are collected every 0.5-5.0 s and stored within the tool. Once the *in-situ* measurement is completed the data are transferred to a shipboard computer for analysis. The fast-response thermistor, though low in accuracy, is able to detect sudden, very small temperature excursions caused by fluid flow from the formation. The slow-response thermistor has a high accuracy and can be used to estimate the temperature gradient. Data are recorded as a function of time, with conversion to depth being based on the pressure transducer (or preferably, on simultaneous recording by Schlumberger of both depth and time).

Lithodensity Measurement

The lithodensity tool (HLDT) uses a Ce^{137} gamma-ray source to measure the resulting flux at fixed distances from the source. Under normal operating conditions, attenuation of gamma rays is chiefly caused by Compton scattering (Ellis, 1987). Formation density is extrapolated from this energy flux by assuming that the atomic weight of most rock-forming elements is approximately twice the atomic number. A photoelectric effect factor (PEF) is also provided. Photoelectric absorption occurs in the energy window below 150 Kev and depends on the energy of the incident gamma ray, the atomic cross section, and the nature of the atom. This measurement is almost independent of porosity and can therefore be used directly as a matrix lithology indicator. The radioactive source and detector array are placed in a tool that is pressed against the borehole wall by a spring-loaded caliper arm. Excessive roughness of the borehole wall allows drilling fluid between the skid and the formation. Consequently, the density measurement will give rise to false low values. Approximate corrections can be applied using caliper data. The vertical resolution of the measurement is about 0.30 m.

Gamma-Ray Spectrometry Measurement

This induced gamma-ray device (GST) consists of a pulsed source of 14 Mev neutrons and a gamma-ray scintillation detector. A surface computer performs spectral analysis of gamma-ray counts resulting from the interactions of neutrons emitted by the source with atomic nuclei in the formation. Characteristic sets of gamma rays from six elements dominate the spectrum: Ca, Si, Fe, Cl, H, and S. As their sum is always unity, they do not reflect the actual elemental composition. Consequently, ratios of these elements are used in interpreting the lithology and porosity of the formation and the salinity of the formation fluid.

Aluminum Clay Measurement

Aluminum abundance as measured by the aluminum clay tool (ACT) is determined by neutron-induced (Californium chemical source), gamma-ray spectrometry. The contribution to the gamma-ray spectrum by natural radiation is removed by placing NaI gamma-ray detectors above and below the neutron source; the one above measures the natural radiation before activation, and the one below, the induced radiation after activation. It is then possible to subtract the naturally occurring component from the total measured after activation. Calibration to elemental weight per cent (wt%) is performed by taking irradiated core samples of known volume and density and measuring their gamma-ray output while placed in a jig attached to the logging tool.

Natural Gamma-Ray Measurement

The natural gamma-ray measurement (NGT) measures the natural radioactivity of the formation. Most gamma rays are emitted by the radioactive isotope K^{40} and by the radioactive elements of the U and Th series. The gamma radiation originating in the formation close to the borehole wall is measured by a scintillation detector mounted inside the sonde. The analysis is achieved by subdividing the entire incident gamma-ray spectrum into five discrete energy windows. The total counts recorded in each window, for a specified depth in the well, are processed at the surface to give elemental abundances of K, U, and Th.

Radioactive elements tend to be most abundant in clay minerals, and consequently the gamma-ray curve is commonly used to estimate the clay or shale content. There are rock matrixes, however, for which the radioactivity ranges from moderate to extremely high values, as a result of the presence of volcanic ash, potassic feldspar, or other radioactive minerals.

Borehole Inclination Measurement

The general purpose inclination tool (GPIT) contains a three-component accelerometer and a three-component magnetometer. The device is used to measure the orientation of the downhole sensors within the borehole, and the orientation (or deviation) of the borehole itself, as well as to compensate for instrument accelerations in the axis of the borehole during data acquisition. It is included as a part of the FMS.

Formation Microscanner

The formation microscanner (Fig. 13) produces high-resolution borehole images from electrical conductivity measurements (Ekstrom et al., 1986; Pezard and Luthi, 1988). Its application in the context of the oil industry since 1986 has been precluded in the Ocean Drilling Program because of diameter constraints imposed by the internal diameter (4.125 in.) of the drill pipe. A modified sensor was consequently developed by Schlumberger for ODP and first deployed during Leg 126. The FMS has a vertical resolution of approximately 1 cm, but a detection threshold for conductive features on the order of microns. With this fine-scale detection ability (raw data points are recorded every 2.5 mm), it allows for the detailed study of subsurface structures. This compares with typical conventional downhole measurements that are averaged over 150 mm; the sampling rate of the FMS is consequently 60 times larger than most other logging devices. The FMS has four orthogonal pads that are pressed against the borehole wall. In the original version developed by Schlumberger, two adjacent pads each carry an array of 27 closely spaced electrodes, from which two electrical images are derived. The electrode currents probe the conductivity of the rock to a depth of a few centimeters into the borehole wall, thus responding to such variations in physical and chemical properties of the rock as porosity or surface conduction when clay minerals are present. The series of conductivity traces are displayed side by side, then coded into an image where black represents the most conductive values and white, the most resistive ones. The new ODP sensor was designed in such a way that four images (of 16 traces each), instead of 2, are recorded simultaneously (Fig. 14). In addition, the resolution of the images is improved because of the smaller size of the electrode array. Once the data have been acquired in the borehole, the images are processed on a devoted workstation to allow for on-site comparison with the cores.

Possible applications of the FMS-derived images include the orientation of cores, the mapping of fractures, foliations, sedimentary features, and the direct analysis of depositional environments (with information on transport direction, structure of the pore space, nature of contacts, and depositional sequences).

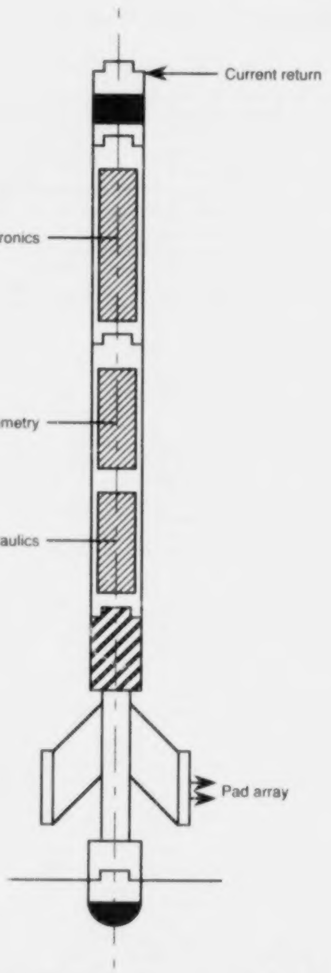

Figure 13. Sketch of the formation microscanner (FMS). Four images are recorded from four pad arrays of 16 electrodes each. The 4 antipodal arrays are located on separate pads that open up in the borehole just as an umbrella would.

Vertical Seismic Profiles

The technical specifications and experimental procedure for the vertical seismic profiles (VSP) are described in great detail by Phillips (Shipboard Scientific Party, 1988). During Leg 126 the sound source used was the *JOIDES Resolution*'s large-volume (400 in.), high-pressure (2000 psi/106 bar) water gun (SSI P400 Model 02). This choice was made on the basis of providing the best possible results from a single experiment within the time constraints of the program.

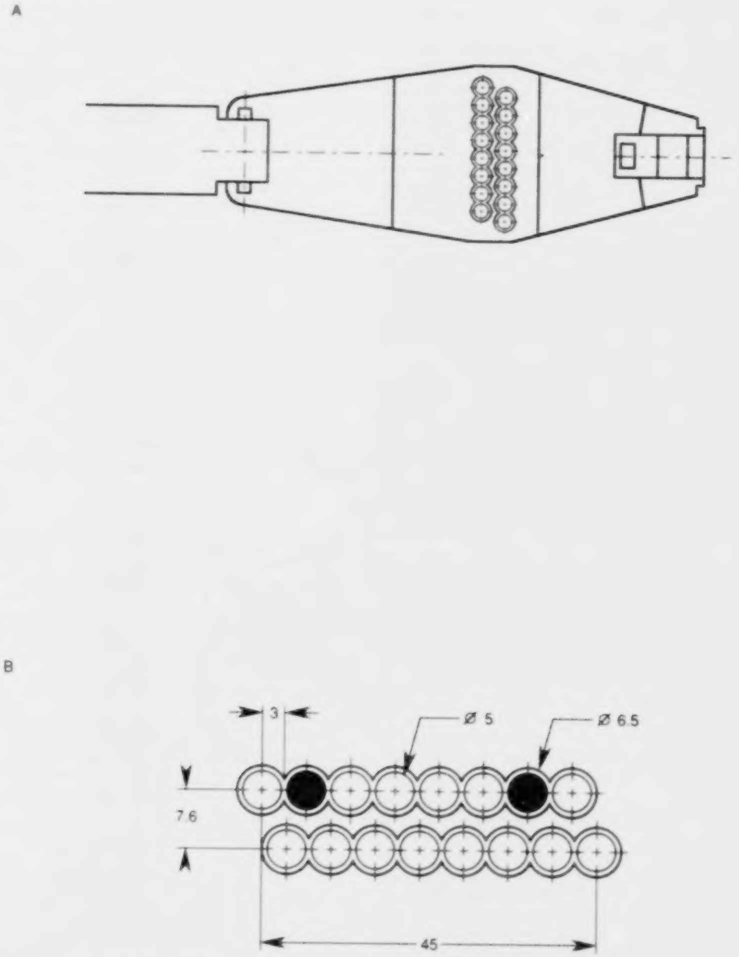

Figure 14. **A**. Sketch of an FMS pad with a 16-electrode array. **B**. Geometry of the FMS array. Dimensions are in millimeters.

Data Quality

Downhole data quality may be seriously degraded in excessively large sections of the borehole or by rapid changes in the hole diameter. Electrical resistivity and velocity measurements are least sensitive to such borehole effects. The nuclear measurements (of density, neutron porosity, and both natural and induced spectral gamma rays) are most seriously impaired because of the large attenuation by the borehole fluid. Corrections can be applied to the original data to reduce the effects of these conditions.

Different logs may have small depth mismatches, caused by either cable stretch or ship heave during recording. Small errors in depth matching can impair the results in zones of rapidly varying lithology. To minimize such errors, a hydraulic heave compensator adjusts for ship motion in real time. Downhole data cannot be precisely matched with core data in zones where core recovery is low because of the inherently ambiguous placement of the recovered section within the interval cored.

Data Analysis

Throughout the acquisition of downhole measurements, incoming data are observed in real time on a monitor oscilloscope and simultaneously recorded on digital tape. After the completion of a set of downhole measurements, tapes are reformatted to allow interpretation using shipboard software; an interactive log-interpretation software package with a versatile array of manipulative and plotting options is available for this purpose. The precise nature of the interpretation procedure varies for each site. Although initial appraisal of the downhole data is carried out on board ship, further analyses and interpretation are undertaken after the end of the leg.

Reprocessing of Downhole Data

Raw count rates for six elements (Ca, Si, Fe, S, Cl, and H) are obtained in real time by the Schlumberger data acquisition software. In the past, these count rates have commonly exhibited some inversion interference from chlorine; this is manifest as a strong but spurious correlation between chlorine and calcium, and weaker correlations with other elements. This interference, which is attributable to the dominance of the induced gamma-ray spectrum by chlorine, has until now been unavoidable in ODP holes because the minimum pipe diameter is too small to permit the use of a boron sleeve for chlorine count suppression (see Harvey and Lovell, in press). On Leg 126, however, a modification to the tool allowed the inclusion of a slimmer boron sleeve.

The data is reprocessed after the cruise using proprietary Schlumberger software. The gamma-ray spectrum at each depth is inverted for titanium, gadolinium, and potassium in addition to the six elements listed above. Though gadolinium is present in concentrations of only a few parts per million, its neutron-capture cross section is so large that gadolinium can account for 10%-30% of the total gamma-ray spectrum. Inclusion of these additional elements improves the quality of the overall inversion, particularly the accuracy of calculated calcium abundance, by converting sources of unaccounted variance to signals. The potassium concentrations determined, however, are less accurate than those from the NGT, and the hydrogen concentrations similarly are less accurate than those from the neutron tool (CNT).

Aluminum concentrations from the ACT require correction for variations in cable speed. Changes in speed affect the time lag between neutron irradiation of the formation and recording of the induced gamma-ray spectrum because the number of induced gamma rays decreases rapidly with time. Post-cruise correction for this effect is possible with techniques used in land holes; this correction may be less reliable in ODP holes where ship heave affects the measurement in spite of mechanical compensation devices.

After geophysical and geochemical downhole measurement combinations have been completed, it is possible to reprocess the geochemical downhole data further. The relative abundances of Ca, Si, Fe, Ti, Al, K, S, Th, U, and Gd are used to calculate a log of predicted photoelectric effect. The difference between this calculated curve and the actual photoelectric curve may be attributed to the only two major elements not directly measured, Mg and Na. Major elements are converted from volume percent to weight percent using downhole data curves of total porosity and density. Major elements are expressed in terms of oxide weight percent, based on the assumption that oxygen is 50% of the total dry weight.

If GST data are available, but not enough log types are run to permit complete solution for oxide weight percentage, one further processing step is made. Omitting chlorine and hydrogen, the yields of the other GST-derived elements (Ca, Si, Fe, Ti, S, K, and Gd) are summed, and each is expressed as a fraction of this total yield. This procedure corrects for porosity and count-rate variations. Although the absolute abundance of each element is not determined, downhole variations in relative abundance are indicated.

Downhole sonic data obtained in real time are not based on full-waveform analyses but on a threshold-measuring technique that attempts to detect the compressional wave arrival by first-break criteria. Occasionally, this technique fails, and either the threshold is exceeded by noise, or the amplitude of the first compressional arrival is smaller than the threshold. The latter of these effects is known as cycle skipping and creates spurious spikes on the sonic log. Such problems may often be eliminated by reprocessing the data.

In-Situ Stress Measurements

The FMS was used during Leg 126 to determine principal horizontal stress directions from elongation caused by stress-induced borehole breakouts. In an isotropic, linearly elastic rock subject to differential stresses, breakouts form along the borehole wall as a result of compressive stress concentrations exceeding the strength of the rock. Under these conditions, the breakout orientation will develop in the direction of the least principal horizontal stress. It has been demonstrated in different areas that stress orientations deduced from breakouts are consistent with other independent indicators (Bell and Gough, 1979; Zoback et al., 1988). See individual site chapters for detailed explanations of FMS operations.

REFERENCES

Akimoto, K., 1989. Recent foraminifera from Enshunada. *In* Takayanagi, Y., and Ishizaki, K. (Eds.), *Collected Papers on Foraminifera from the Japanese Islands:* Sendai (Toko Press), 93-104 (in Japanese).

Archie, G. E., 1942. The electrical resistivity log as an aid in determining some reservoir characteristics. *J. Petrol. Tech.*, 5:1-8.

Backman, J., Duncan, R. A., et al., 1988. *Proc. ODP, Init. Repts.*, 115: College Station, TX (Ocean Drilling Program).

Barnes, R. O., 1988. ODP *in-situ* fluid sampling and measurement: a new wireline tool. *In* Mascle, A., Moore, J. C., et al., *Proc. ODP, Init. Repts.*, 110: College Station, TX (Ocean Drilling Program), 55-63.

Barron, J. A., Nigrini, C. A., Pujos, A., Saito, T., Theyer, F., Thomas, E., and Weinreich, N., 1985. Synthesis of biostratigraphy, central equatorial Pacific, Deep Sea Drilling Project Leg 85: refinement of Oligocene to Quaternary biochronology. *In* Mayer, L., Theyer, F., et al., *Init. Repts. DSDP,* 85: Washington (U.S. Govt. Printing Office), 905-934.

Bell, J. S., and Gough, D. I., 1979. Northeast-southwest compressive stress in Alberta: evidence from oil wells. *Earth Planet. Sci. Lett.*, 45:475-482.

Berggren, W. A., Kent, D. V., Flynn, J. J., and Van Couvering, J. A., 1985. Cenozoic geochronology. *Geol. Soc. Am. Bull.*, 96:1407-1418.

Blow, W. H., 1969. Late middle Eocene to Recent planktonic foraminiferal biostratigraphy. *In* Renz, H. H., and Brönnimann, P. (Eds.), *Proceedings of the First International Conference on Planktonic Microfossils:* Leiden (E. J. Brill), 1:199-422.

Boyce, R. E., 1976. Sound velocity-density parameters of sediment and rock from DSDP drill sites 315-318 on the Line islands chain, Manihiki Plateau, and Tuamoto Ridge in the Pacific Ocean. *In* Schlanger, S. O., Jackson, E. D., et al., *Init. Repts. DSDP,* 33: Washington (U.S. Govt. Printing Office), 695-728.

Bramlette, M. N., and Bradley, W. H., 1942. Geology and biology of North Atlantic deep-sea cores between Newfoundland and Ireland. Pt. 1, Lithology and geologic interpretations. *Geol. Surv. Prof. Pap. (U.S.),* 196A:1-55.

Crawford, A. J., Falloon, T. J., and Green, D. H., 1989. Classification, petrogenesis and tectonic setting of boninites. *In* Crawford, A. J. (Ed.), *Boninites:* London (Unwin Hyman), 2-49.

Ekstrom, M. P., Dahan, C. A., Chen, M.-Y., Lloyd, P. M., and Rossi, D. J., 1986. Formation imaging with microelectrical scanning arrays. *Trans. SPWLA Annu. Logging Symp.*, 27th, Pap. No. BB.

Ellis, D. V., 1987. *Well Logging for Earth Scientists:* Amsterdam (Elsevier).

Foreman, H. P., 1981. Radiolaria. *In* Emiliani, C. (Ed.), *The Sea* (Vol. 7): *The Oceanic Lithosphere:* New York (Wiley-Interscience), 1121-1144.

Gealy, E. L., Winterer, E. L., and Moberly, R. M., Jr., 1971. Methods, conventions, and general observations. *In* Winterer, E. L., Riedel, W. R., et al., *Init. Repts. DSDP,* 7, Pt. 1: Washington (U.S. Govt. Printing Office), 9-26.

Gieskes, J. M., and Peretsman, G., 1986. Water chemistry procedures aboard *JOIDES Resolution*—some comments. *ODP Tech. Note,* No. 5.

Govindaraju, K. (Ed.), 1984. *Geostand. Newsl.*, Spec. Issue, No. 8.

Harvey, P. K., and Lovell, M. A., in press. Basaltic lithostratigraphy of DSDP Hole 504B. *Nucl. Geophys.*

Hearst, J. R., and Nelson, P. H., 1984. *Well Logging for Physical Properties:* New York (McGraw-Hill).

Ingle, J. C., 1980. Cenozoic paleobathymetry and depositional history of selected sequences within the southern California continental borderland. *Cushman Found. Foraminiferal Res., Spec. Publ.*, 19:163–195.

Jakes, P., and Gill, J., 1970. Rare earth elements and the island arc tholeiitic series. *Earth Planet. Sci. Lett.*, 9:17–28.

Jakosky, J. J., 1940. *Exploration Geophysics:* Los Angeles (Times-Mirror Press).

Kaiho, K., in press. Morphotype changes of deep-sea benthic foraminifera during the Cenozoic Era and their paleoenvironmental implications. *Kaseki* (Fossils) (in Japanese with English abstract).

Kaiho, K., and Hasegawa, S., 1986. Bathymetric distribution of benthic foraminifera in bottom sediments off Onahama, Fukushima Prefecture, northeast Japan. *In* Matoba, Y., and Kato, M. (Eds.), *Studies on Benthic Foraminifera:* Akita (Akita Univ.), 43–52 (in Japanese).

Knuttel, S., 1986. Calcareous nannofossil biostratigraphy of the central East Pacific Rise, Deep Sea Drilling Project Leg 92: evidence for downslope transport of sediments. *In* Leinen, M., Rea, D. K., et al., *Init. Repts. DSDP,* 92: Washington (U.S. Govt. Printing Office), 255–290.

Lambe, T., and Whitman, R., 1969. *Soil Mechanics:* New York (Wiley).

Manheim, F. T., and Sayles, F. L., 1974. Composition and origin of interstitial waters of marine sediments based on deep sea drill cores. *In* Goldberg, E. D. (Ed.), *The Sea* (Vol. 5): *Marine Chemistry:* New York (Wiley-Interscience), 527–568.

Manheim, F. T., and Waterman, L. S., 1974. Diffusimetry (diffusion constant estimation) on sediment cores by resistivity probe. *In* von der Borch, C. C., Slater, J. G., et al., *Init. Repts. DSDP,* 22: Washington (U.S. Govt. Printing Office), 663–670.

Moberly, R., and Klein, G. deV., 1976. Ephemeral color in deep-sea cores. *J. Sediment. Petrol.*, 46:216–225.

Munsell Soil Color Charts, 1975. Baltimore (Munsell Color).

Nigrini, C. A., 1985. Radiolarian biostratigraphy in the central equatorial Pacific, Deep Sea Drilling Project Leg 85. *In* Mayer, L., Theyer, F., et al., *Init. Repts. DSDP,* 85: Washington (U.S. Govt. Printing Office), 511–551.

Norrish, K., and Hutton, J. T., 1969. An accurate X-ray spectrographic method for the analysis of a wide range of geological samples. *Geochim. Cosmochim. Acta,* 33:431–453.

Okada, H., and Bukry, D., 1980. Supplementary modification and introduction of code numbers to the low-latitude coccolith biostratigraphic zonation. *Mar. Micropaleontol.*, 5(3):321–325.

Pezard, P. A., and Luthi, S. M., 1988. Borehole electrical images in the basement of the Cajon Pass Scientific Drillhole, California; fracture identification and tectonic implications. *Geophys. Res. Lett.*, 15: 1017–1020.

Reynolds, R. C., 1967. Estimations of mass absorption coefficients by Compton scattering: improvements and extensions of the method. *Am. Mineral.*, 48:1133–1143.

Sanfilippo, A., Westberg-Smith, M. J., and Reidel, W. R., 1985. Cenozoic radiolarian. *In* Bolli, H. M., Saunders, J. B., and Perch-Nielson, K. (Eds.), *Plankton Stratigraphy:* Cambridge (Cambridge Univ. Press), 631–712.

Sato, T., Takayama, T., Kato, M., Kudo, T., and Kameo, K., 1988. Calcareous microfossil biostratigraphy of the uppermost Cenozoic formations distributed in the coast of the Japan Sea—Part 4: Conclusion. *J. Japan. Assoc. Petrol. Tech.*, 53(6):13–29.

Schlumberger Ltd., 1972. *Log Interpretation* (Vol. 1).

Shepard, F. P., 1954. Nomenclature based on sand-silt-clay ratios. *J. Sediment. Petrol.*, 24:151–158.

Shipboard Scientific Party, 1988. Site 504B. *In* Becker, K., Sakai, H., et al., *Proc. ODP, Init. Repts.*, 111: College Station, TX (Ocean Drilling Program), 124–152.

Stork, A. L., Smith, D. K., and Gill, J. B., 1987. Evaluation of geochemical reference standards by X-ray fluorescence analysis. *Geostand. Newsl.*, 11:107–113.

Suess, E., von Huene, R., et al., 1988. *Proc. ODP, Init. Repts.*, 112: College Station, TX (Ocean Drilling Program), 25–44.

Tjalsma, R. C., and Lohmann, G. P., 1983. Paleocene-Eocene bathyal and abyssal benthic foraminifera from the Atlantic Ocean. *Micropaleontol., Spec. Publ.*, 4:1–90.

Vacquier, V., 1985. The measurement of thermal conductivity of solids with a transient linear heat source on the plane surface of a poorly conducting body. *Earth Planet. Sci. Lett.*, 74:275–279.

Van Morkhoven, F.P.C.M., Berggren, W. A., and Edwards, A. S., 1986. Cenozoic cosmopolitan deep-water benthic foraminifera. *Bull. Cent. Rech. Explor.-Prod. Elf-Aquitaine*, Mem. No. 11.

Von Herzen, R. P., and Maxwell, A. E., 1959. The measurement of thermal conductivity of deep-sea sediments by a needle-probe method. *J. Geophys. Res.*, 64:1557–1563.

Wentworth, C. K., 1922. A scale of grade and class terms of clastic sediments. *J. Geol.*, 30:377–390.

Woodruff, F., 1985. Changes in Miocene deep-sea benthic foraminiferal distribution in the Pacific Ocean: relationship to paleoceanography. *Mem. Geol. Soc. Am.*, 163:131–175.

Woodruff, F., and Douglas, R. G., 1981. Response of deep-sea benthic foraminifera to Miocene paleoclimatic events, DSDP Site 289. *Mar. Micropaleontol.*, 6:617–632.

Yasuda, H., 1989. Benthic foraminifera and sedimentary facies of the lower slope basin off Shikoku, Japan. *In* Takayanagi, Y., and Ishizaki, K. (Eds.), *Collected Papers on Foraminifera from the Japanese Islands:* Sendai (Toko Press), 83–92.

Zoback, M. D., Zoback, M. L., Mount, V. S., Suppe, J., Eaton, J. P., Healy, J. H., Oppenheimer, D., Reasenberg, P., Jones, L., Raleigh, C. B., Wong, I. G., Scotti, O., and Wentworth, C., 1988. New evidence on the state of stress of the San Andreas Fault. *Science,* 238: 1105–1111.

Ms 126A-103

Taylor, B., Fujioka, K., et al., 1990
Proceedings of the Ocean Drilling Program, Initial Reports, Vol. 126

3. UNDERWAY GEOPHYSICS DATA COLLECTED ON LEG 126[1]

Patricia A. Cooper[2] and Shipboard Scientific Party[3]

INTRODUCTION

Ocean Drilling Program (ODP) Leg 126 drilled seven sites (787–793) in the Izu-Bonin region. The *JOIDES Resolution* was underway for 4 of the 57 days at sea, traveling approximately 103 nmi between the port of Tokyo and the first site (787); the ship departed Tokyo, Japan, on 22 April 1989 to begin Leg 126, and it arrived at the eastern edge of the Izu-Bonin forearc on 23 April 1989.

The first site, in the axis of Aoga Shima Canyon (proposed site BON-5C; ODP Site 787), was occupied from 24 to 26 April 1989. Drilling commenced at the next site (proposed site BON-2; ODP Sites 788 and 789), located on top of a horst on the eastern flank of the Sumisu Rift, on 28 April. Sites 790 and 791 (proposed site BON-1) within the rift graben were occupied between 29 April and 13 May 1989. Site 788 was reoccupied on 14 May and drilling was completed by 16 May. Site 792 (proposed site BON-4), which was occupied from 16 to 26 May 1989, is located within the Izu-Bonin forearc basin. Drilling at Site 793 (proposed site BON-6D) commenced 26 May.

The *JOIDES Resolution* departed from the Izu-Bonin forearc on 18 June 1989 and completed Leg 126 at Tokyo, Japan, on 19 June 1989. The track line of the cruise is shown in Figure 1. This plot was generated from global positioning system (GPS) transit satellite and Loran-C positions, course- and speed-changing data, and on- and off-site information compiled from the bridge log, the underway geophysical log, and the HIGHRES (shipboard seismic data acquisition and processing software) tape headers. The final site locations are an average of positions collected while on site.

NAVIGATION

It was not possible to carry out all site approach surveys during GPS windows; therefore, the information used to reconstruct the ship's track around each drill site is combined Loran-C and GPS data. The GPS data are preferable to Loran-C and dead-reckoning positions because of the continually updated, higher quality data available during a GPS "window." This "window" is a period of up to 12 hr each day when positioning data from three or more GPS satellites can be received. Navigation data were recorded in the Underway Geophysics Lab (UGL) by a Magnavox 1107 GPS Transit Satellite Receiver.

The GPS fixes were printed to hard copy at a user-specified rate; Loran-C fixes were logged from the UGL repeater. The sampling density depended on the nature of the survey; it was generally one fix per 15–30 min in the initial part of the survey, increasing to one fix per 1 min when approaching the site. The ship's track was assumed to proceed from point to point unless otherwise indicated from course-change information listed in the HIGHRES headers. The density of points illustrated is less than the actual amount of data collected, but it is sufficient to ensure an accurate reconstruction of the ship's track.

DATA ACQUISITION

Shipboard geophysical instrumentation included two precision echo sounders (3.5 and 12.5 kHz), a magnetometer, seismic reflection profilers, and satellite navigation systems. The instruments were maintained and operated by ODP marine technicians, in cooperation with the scientific party and the officers and crew of SEDCO-FOREX, Inc. Table 1 summarizes the amounts and types of geophysical data collected. Bathymetry, seismic reflection profiles, and magnetic data were continuously recorded along the transits. Bathymetric data were obtained from 3.5- and 12.5-kHz (Raytheon line-scan recorder system) echo sounders. The 3.5- and 12.5-kHz data are not presented here because of the volume of data involved; the data are available upon request from the ODP Database Librarian.

The seismic sources used on board the *JOIDES Resolution* during Leg 126 were two synchronized 80-in.^{3} Seismic System, Inc., water guns operating at approximately 1800 psi. One 100-m-long Teledyne streamer containing 60 active sections, combined to produce a single signal, was deployed from the fantail and towed about 500 m behind the vessel at a depth of 10 m.

Five seismic lines were recorded during Leg 126, covering approximately 30 nmi (Table 1); copies are available from the ODP Database Librarian. Single-channel seismic data were displayed in real-time analog format on two Raytheon line-scan dry-paper recorders, using only streamers, an amplifier, and band-pass filters. Seismic data were also recorded with a Masscomp 561 computer (Table 2), which functions as the central unit to record, process, and display the data. Data were processed and displayed in real time on a 15-in.-wide Printronix high-resolution graphic printer (160 dots/in.) according to the parameters listed in Table 3. Raw data were recorded on magnetic tapes by means of a SEG-Y format and a density of 1600 bits/in. Seismic lines recorded with the Masscomp were reprocessed on board, using SIOSEIS software. The reprocessed data were displayed on a 22-in.-wide Versatec plotter (200 dots/in.).

MAGNETIC DATA AND BATHYMETRY

A Geometrics 801 proton precession magnetometer, towed approximately 300 m astern, was used during transits and site surveys. Total-intensity, magnetic-field data were recorded in analog format on a strip chart recorder, in digital format via the HIGHRES headers (one reading per shot), and manually every 5 min in the underway geophysics log. The magnetic field values were reduced to anomaly values by subtracting the 1985 International Geophysical Reference Field. Figure 2 shows bathymetry, magnetic anomaly, course, and speed data, plotted in profile as functions of time and distances.

SINGLE-CHANNEL SEISMIC REFLECTION PROFILES

A map view of the bathymetry of the Izu-Bonin region traversed on Leg 126 is shown together with the ship's track in Figure 1. The single-channel seismic reflection profiles with their

---

[1] Taylor, B., Fujioka, K., et al., 1990. *Proc. ODP, Init. Repts.*, 126: College Station, TX (Ocean Drilling Program).

[2] Hawaii Institute of Geophysics, University of Hawaii at Manoa, 2525 Correa Road, Honolulu, HI 96822.

[3] Shipboard Scientific Party is as given in the list of participants preceding the contents.

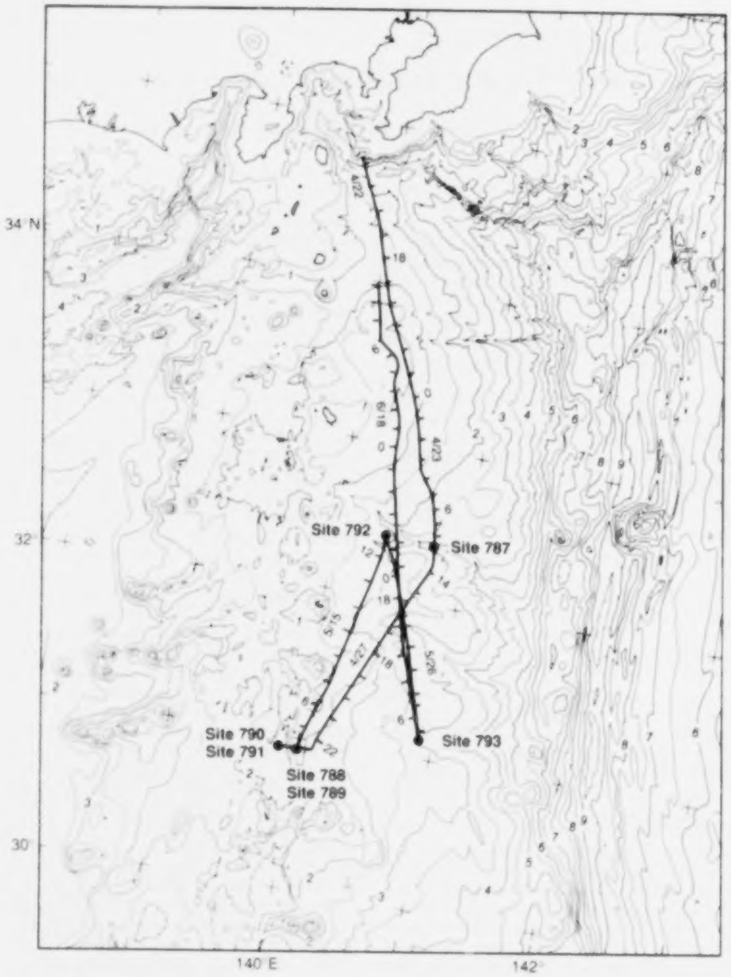

Figure 1. Leg 126 track line on a bathymetric map contoured at 500 m by B. Taylor.

corresponding track segments are shown in Figures 3 through 10. Bad traces were blanked. The traces were band-pass filtered (25-65 Hz); a three-trace, equally weighted, running-slant mix and automatic gain control were applied to all traces. For Lines 2 through 4, the signal was muted to seafloor; signal losses caused by water-gun malfunctions made the seafloor somewhat difficult to distinguish in parts of Line 1. The seismic lines are summarized below.

Seismic Line 1 was collected en route to Site 787 along the track segment shown in Figure 3. The processed digital seismic profile is shown in Figure 4 (from Julian Day 113/0723 UTC, shotpoint 4147, to Julian Day 113/1155 UTC, shotpoint 5281). Basement depth is highly variable, from 4.8 s beneath the canyon walls to approximately 6.0 s at Site 787.

Seismic Line 2 was collected en route to Site 788 along the track segment shown in Figure 5. The processed digital seismic profile is shown in Figure 6 (from Julian Day 117/2237 UTC, shotpoint 5815, to Julian Day 118/0030 UTC, shotpoint 6317). The profile shows a stratified sequence, cut by normal faults, on the footwall uplift forming the eastern flank of the Sumisu Rift.

No single-channel seismic data were collected en route to Site 789.

Seismic Line 3 was collected en route to Site 790 along the track segment shown in Figure 7. The processed digital seismic profile is shown in Figure 8 (from Julian Day 119/0450 UTC, shotpoint 6375, to Julian Day 119/0700 UTC, shotpoint 7017). This section shows a half graben filled with syn-rift sedimentary sequence. To the west, the base of the syn-rift sequence cannot

Table 1. Geophysical data coverage.

Port: Tokyo	to Site 787	to Site 788	to Site 790	to Site 792	to Site 793
Line number	Line 1	Line 2	Line 3	Line 4	Line 5
Navigation and bathymetric data:					
Start time	JD 112/1600	JD 117/1200	JD 119/0445	JD 136/0356	JD 145/2209
End time	JD 113/1200	JD 118/0030	JD 119/0703	JD 136/1556	JD 146/0728
Shotpoint intervals	3588–5401	5442–6368	6370–7047	7182–8553	8648–8988
Distance (nmi)	68.0	51.0	5.4	46.6	40.2
Total: 211.2 nmi					
Magnetic data:					
Shotpoint intervals	3590–5298	5448–6333	6373–7018	7195–8553	8648–8696
Distance (nmi)	67.0	50.0	5.0	45.9	39.0
Total: 206.9 nmi					
Seismic reflection data:					
Shotpoint intervals	4147–5401	5821–6367	6395–7030	7490–8527	None
Distance (nmi)	12.4	4.3	5.0	7.8	
Total: 29.5 nmi					

Table 2. Seismic data, real-time recording parameters.

	Line 1	Line 2	Line 3	Line 4
Start at	32°30.970′N, 140°45.010′E	30°55.271′N, 140°06.452′E	30°54.910′N, 140°00.810′E	32°18.748′N, 140°22.940′E
End at	32°22.580′N, 140°39.700′E	30°55.298′N, 140°00.327′E	30°54.890′N, 139°51.080′E	32°24.040′N, 140°22.779′E
Source				
(water/air guns, size)	two 80-in.^{3} water guns 1800 psi	two 80-in.^{3} water guns 1800 psi	two 80-in.^{3} water guns 1800 psi	two 80-in.^{3} water guns 1800 psi
Streamer				
(port or starboard)	Port	Port	Port	Port
Analog 1:				
Low cut (Hz)	150	150	150	145
High cut (Hz)	40	40	40	40
Gain: amp (db)	80	80	80	80
Analog 2:				
Low cut (Hz)	100	100	100	100
High cut (Hz)	30	30	30	30
Gain: amp (db)	80	80	80	80

Table 3. Seismic data processing parameters.

	Line 1	Line 2	Line 3	Line 4
Data window (ms):				
From	3000	1000	1000	1000
To	7750	5750	5750	5750
AGC:				
Response time (ms)	3000	1000	1000	1000
Gain (%)	20	20	20	20
Zero-phase band-pass filter:				
High cut (Hz)	150	150	150	150
Taper width	24	24	24	24
Low cut (Hz)	30	30	30	30
Taper width	24	24	24	24

be readily discerned, but it appears to "step up" via a series of antithetic normal faults that extend into basement. The syn-rift sediments are cut by numerous synthetic and antithetic normal growth faults, some of which extend from the basement to the surface. To the east, the graben is bounded by a large normal fault zone with bathymetric relief of more than 1000 m.

No single-channel seismic data were collected en route to Site 791.

No single-channel seismic data were collected en route to the reoccupation of Site 788.

Seismic Line 4 was collected en route to Site 792 along the track segment shown in Figure 9. The processed digital seismic profile is shown in Figure 10 (from Julian Day 136/1215 UTC, shotpoint 7490, to Julian Day 136/1553 UTC, shotpoint 8526). Basement depth is highly variable, approximately 3.2 s at Site 792.

No single-channel seismic data were collected en route to Site 793.

No single-channel seismic data were collected en route to Tokyo, Japan, after leaving Site 793.

Ms 126A-104

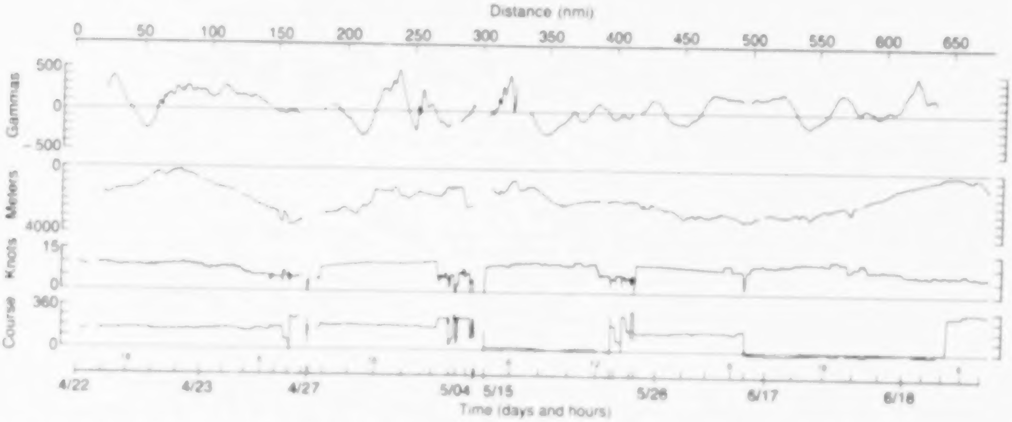

Figure 2. Magnetic anomaly, bathymetry, speed, and course data, plotted as functions of linear distance and nonlinear time.

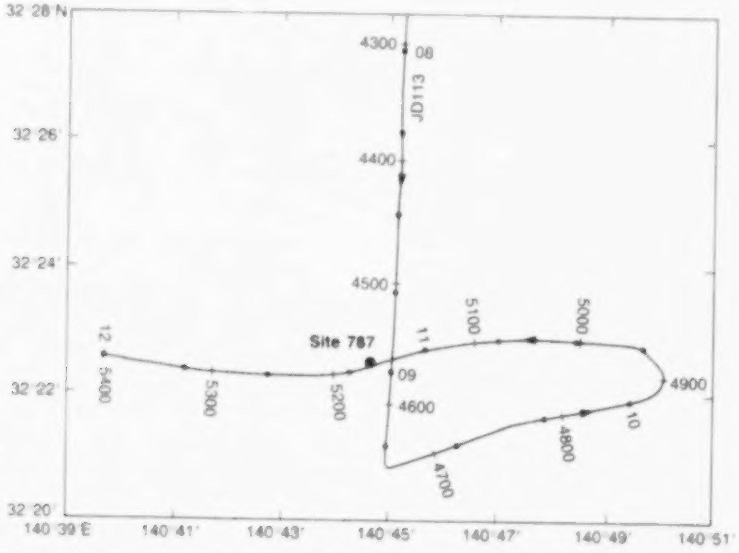
32°28'N
32°26'
32°24'
32°22'
32°20'
140°39'E
140°41'
140°43'
140°45'
140°47'
140°49'
140°51'
4300
08
JD113
4400
4500
5100
5000
Site 787
11
12
09
5400
5300
5200
4600
4900
10
4800
4700

Figure 3. Ship track for single-channel seismic Line 1 (from south of Tokyo, Japan, to Site 787).

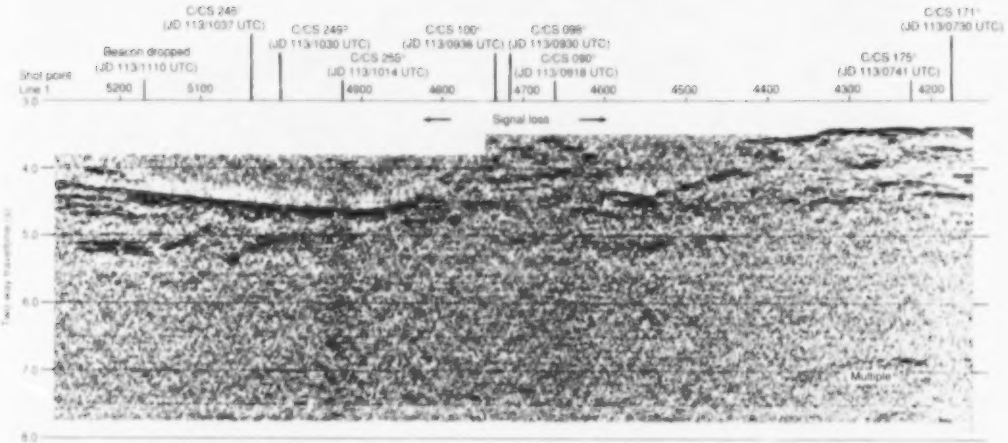

Figure 4. Processed single-channel seismic reflection from Line 1. Track line is shown in Figure 3.

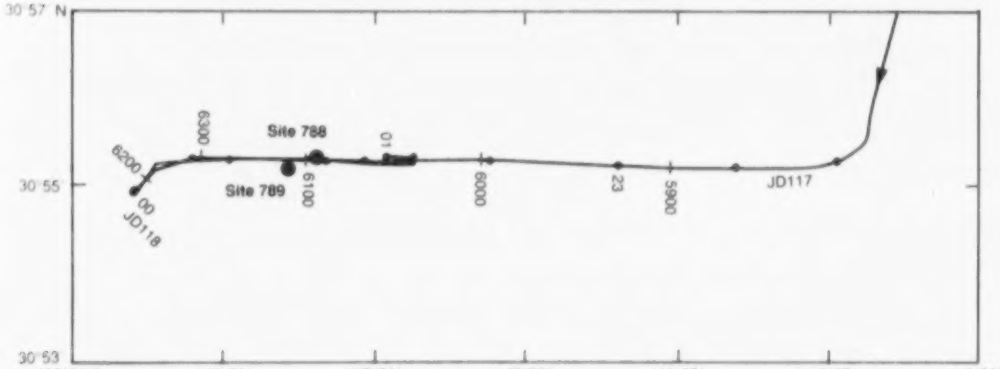
30°57' N
30°55'
30°53'
139°57' E
139°59'
140°01'
140°03'
140°05'
140°07'
140°09'
6300
6200
00
JD118
Site 788
Site 789
6100
01
6000
23
5900
JD117

Figure 5. Ship track for single-channel seismic Line 2 (from Site 787 to Site 788).

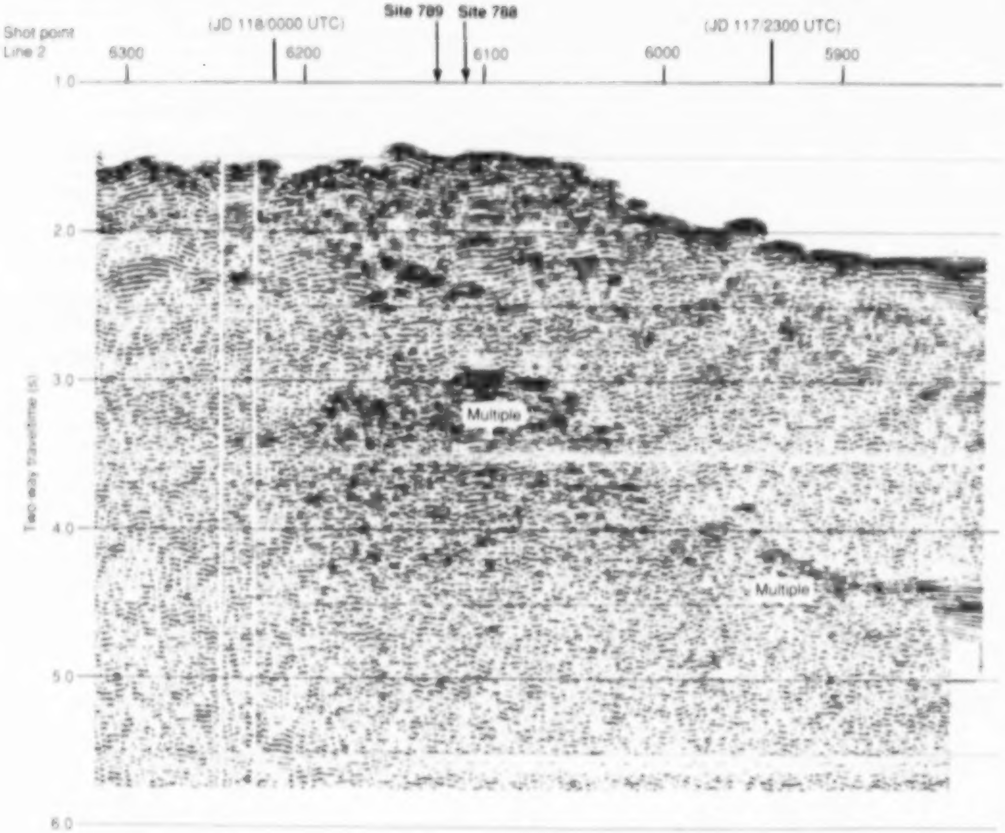

Figure 6. Processed single-channel seismic reflection from Line 2. Track line is shown in Figure 5.

30°57' N
30°55'
30°53'
139°48' E
139°50'
139°52'
139°54'
139°56'
139°58'
140°00'
140°02'
Site 790
Site 791
6900
7000
07
6800
06
6700
6600
6500
6400
05
JD119

Figure 7. Ship track for single-channel seismic Line 3 (from Site 789 to Site 790).

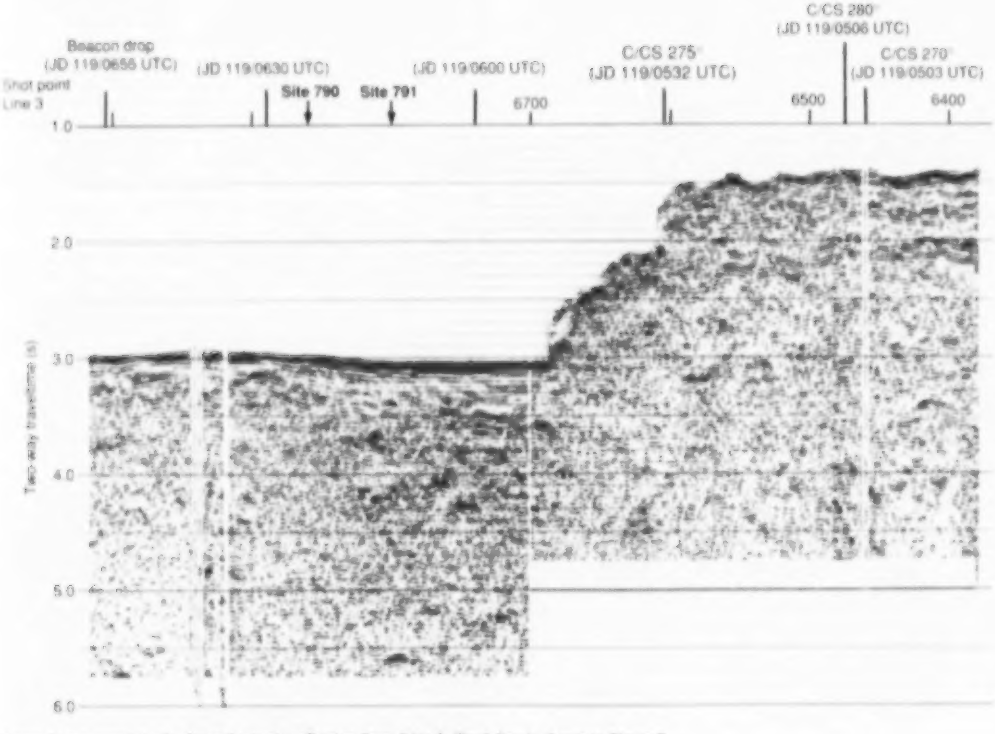

Figure 8. Processed single-channel seismic reflection from Line 3. Track line is shown in Figure 7.

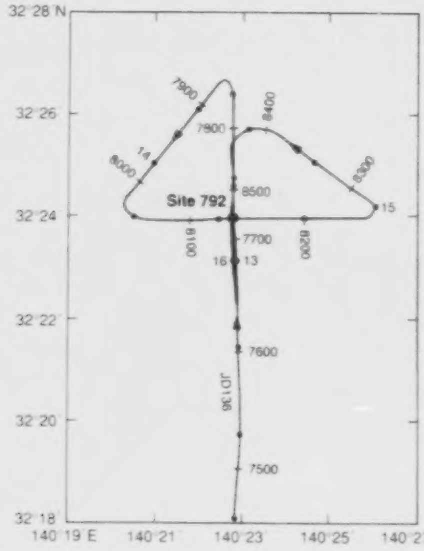
32°28'N
32°26'
32°24'
32°22'
32°20'
32°18'
140°19'E
140°21'
140°23'
140°25'
140°27'
Site 792
7900
8000
14
7800
8400
8300
8500
15
7700
8100
8200
16
13
7600
JD136
7500

Figure 9. Ship track for single-channel seismic Line 4 (from Site 788 to Site 792).

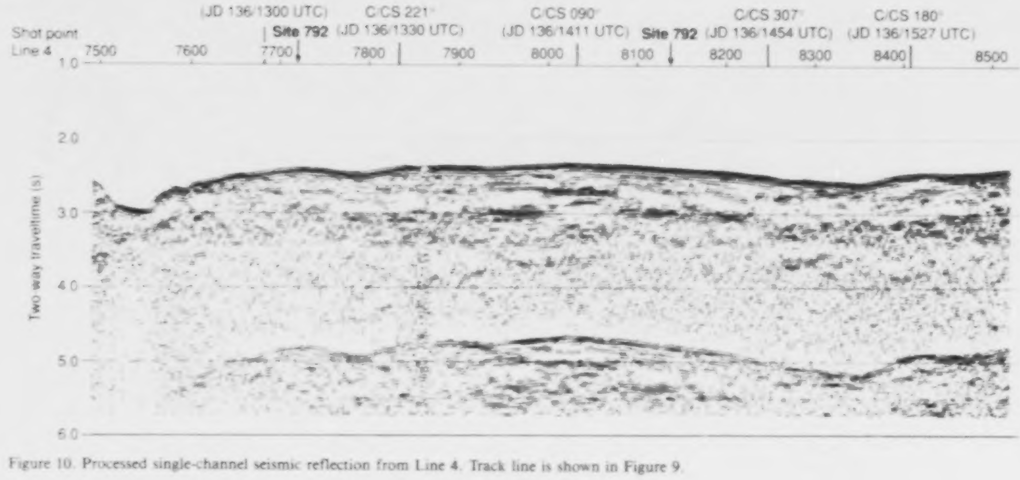

Figure 10. Processed single-channel seismic reflection from Line 4. Track line is shown in Figure 9.

Taylor, B., Fujioka, K., et al., 1990
Proceedings of the Ocean Drilling Program, Initial Reports, Vol. 126

4. MULTICHANNEL SEISMIC SURVEY OF THE CENTRAL IZU-BONIN ARC[1]

Brian Taylor, Gregory Moore, Adam Klaus, Martha Systrom,
Patricia Cooper, and Mary MacKay[2]

INTRODUCTION

Multichannel seismic (MCS) data were collected in the central Izu-Bonin island arc in preparation for Legs 125 and 126 of the Ocean Drilling Program, and as part of our continuing research into the evolution of intraoceanic arc-trench systems (Fig. 1). Our seismic investigation focused on the processes of arc, forearc, and backarc formation, tectonics, and sedimentation. In the forearc basin, the MCS data provide insights into the nature and mode of basin formation, lithospheric flexure that results from arc volcano loading, and forearc sedimentation processes and evolution. Major issues addressed by the MCS survey in the arc/backarc region include the nature and style of arc volcanism and backarc rift-basin sedimentation, faulting, and volcanism.

For an overview of the tectonic evolution of the Izu-Bonin Arc, see the "Introduction" chapter (this volume). In this paper we present the processed MCS data from our surveys of the Sumisu Rift (Profiles 3–6, 8, 9, 13, and 14) and the arc to outer-arc high portion of the forearc (Profiles 1–5 and 8–14; Fig. 2). Interpretations of the trench-slope MCS data appear in Horine et al. (in press). Papers presenting our interpretation of the backarc rift and forearc basin MCS data are in preparation. Detailed correlations of the MCS data and the Leg 126 drilling results are presented in the "Seismic Stratigraphy" sections of each site chapter in this volume.

DATA ACQUISITION AND PROCESSING

We collected over 3000 km of 96-channel seismic data from the Izu-Bonin Arc during two cruises of the *Fred Moore* (FM 3505, 17 June to 7 July 1987; FM 3507, 4–16 August 1987; see Fig. 2). The seismic source consisted of a tuned array of six Bolt air guns (total = 1065 $in.^3$) and a single large air gun (2000 $in.^3$), which resulted in sources that ranged from 1065 to 3065 $in.^3$. Shot intervals ranged from 16 to 67 m (average ~35 m) depending on ship speed and shot repetition rate. The streamer was configured into 96 groups consisting of 40 hydrophones each. Groups were separated by 33.3 m with a near offset (channel 96) of 170 m and a far offset (channel 1) of 3337 m. Loran C and the global positioning system (GPS) provided navigation data. The 2-ms-sampled seismic data were band-pass filtered at 5 Hz (24 dB/octave) to 100 Hz (54 dB/octave) and recorded on a GUS 4200 system in demultiplexed SEGD format using an integer floating point gain.

We processed the data at the University of Tulsa on a VAX 11/750 equipped with a Phoenix processing system (Seismograph Service Corporation). The processing sequence began by resampling the data to 4 ms and removing noisy traces and bad shots. Next, the source-receiver geometry was defined from the navigation and the data were sorted into 16.7-m common midpoints. After velocity analysis, normal moveout (NMO), and muting of severe NMO stretch, the data were stacked (~ 48 fold). The data were then deconvolved (200 ms operator, with 3% white noise added), time-varying band-pass filtered, migrated using finite difference migration, band-pass filtered at 6-10-50-60 Hz, gained using 500-ms automatic gain control, muted to water bottom, and plotted.

FOREARC BASEMENT

Figures 3 (in back pocket) and 4–6 show our migrated MCS profiles from the volcanic arc to the outer-arc high. The acoustic basement surface is strongly reflective on the outer-arc high, but it becomes less so beneath the forearc basin where the velocity contrast with the deep basin sediments is less. Basement cannot be followed west to the volcanic front, primarily because of the water-bottom multiple reflection. The basement is seismically stratified, with strong reflectors that dip both east and west beneath the outer-arc high. The high is presumed to be formed of Eocene boninites and island-arc tholeiites, similar to those cropping out on the Bonin Islands along strike to the south. The basement surface has significant relief, commonly 500–1000 m, but more than 2000 m in places. The outer-arc basement high is bounded on the west by a series of west-dipping buried escarpments that are probably normal faults. Further west, basement blocks form numerous ridges with intervening troughs beneath the forearc sedimentary basin. Several of the troughs appear to be half grabens (e.g., Profile 14, 1300–1600Z near 5 s; see Fig. 3, in back pocket). The strong east-dipping reflector within the basement at 1600–1700Z on Profile 14 (Fig. 3, in back pocket) may be from a crustal detachment surface. Profile 2/3 crossed the northern flank of a large buried seamount at 0500–0600Z (Fig. 3, in back pocket). Frontal-arc basement highs, spaced about 100 km apart, are present east of Aoga Shima, Sumisu Jima, and Tori Shima. Our survey crossed only the smallest of these highs (Profile 10, Fig. 4), which are reflected by shallow bathymetry (Fig. 2). Where dredged further south (25°–30°N) by the Geological Survey of Japan, these highs yield upper Eocene volcaniclastics (M. Yuasa, pers. comm., 1987). These highs were probably formed by late Eocene and early Oligocene arc volcanoes.

FOREARC SEDIMENTS

The forearc sedimentary section can be subdivided into three major seismic-stratigraphic units. The first caps (and is restricted to) the outer-arc high basement. It is a thin, finely layered, often-eroded unit of presumed (hemi-) pelagic sediments. It is best seen on Profile 5 east of 0245Z (Fig. 3, in back pocket). Further east, the inner-trench slope is nearly devoid of sediments (e.g., Profile 14 of Fig. 3, in back pocket), except where ponded around the serpentinite seamounts at 5–6 km water depth (Fig. 2). The second unit forms the bulk of the forearc basin sedimentary fill. It is characterized by strong, continuous, subparallel reflectors, typical of turbidites, which lap onto the basement highs (e.g., 0700–0900Z on Profile 2; see Fig. 3, in back pocket). In areas of

---

[1] Taylor, B., Fujioka, K., et al., 1990. *Proc. ODP, Init. Repts.*, 126: College Station, TX (Ocean Drilling Program).

[2] All at Hawaii Institute of Geophysics, University of Hawaii at Manoa, 2525 Correa Road, Honolulu, HI 96822.

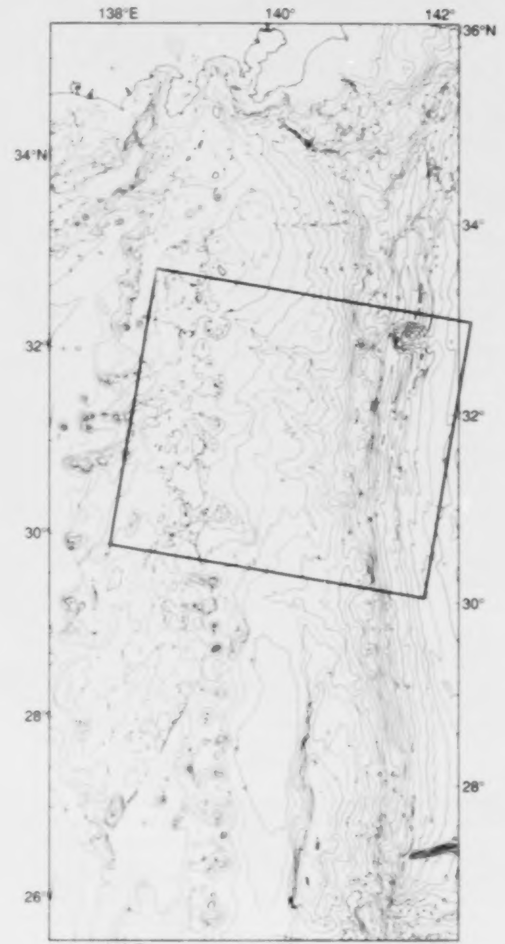

Figure 1. Bathymetry of the Izu-Bonin Arc at 500-m contour intervals showing the area (boxed) of our MCS survey and Figure 2.

deep basement depressions such as the previously discussed example, there is a lower subunit that is separated from the main upper unit by an angular unconformity. The MCS data show that normal faulting is pervasive throughout the entire unit. The third unit unconformably overlies the two lower units; in the center of the basin it is less faulted than the underlying unit and is characterized by discontinuous reflectors of varying amplitude, with migrating sediment packages indicative of channel cut and fill. This presumed hemipelagic unit is itself cut by major submarine channels and canyons (Figs. 3 [in back pocket] and 4). The least-eroded section is seen on Profile 4 (Fig. 3, in back pocket), which traverses an intercanyon high (Fig. 2). The unit thickens to the west toward the arc volcanoes. The reflectors increase in continuity and amplitude, presumably as a result of the coarsening volcaniclastic facies. Loading by the arc volcanoes appears to have flexed the forearc lithosphere, creating a proximal moat (filled with the volcaniclastic sediments) and an arch (onto which the sediments lap). This is particularly evident on the three northern profiles (Profiles 1–3, Fig. 3, in back pocket), but it can also be seen on Profile 13 (Fig. 6). The sedimentary sections in the moat and on the arch are cut by normal faults.

SUMISU RIFT

Figure 7 shows the detailed location, and Figures 8 and 9 show variable-area plots of our migrated MCS profiles across the Sumisu Rift and its margins. Figure 10 (in back pocket) shows wiggle-trace plots of the same data as Figure 8, but at less vertical exaggeration (VE = 2.1). The seismic stratification of the pre-rift margins and "basement" of the 30–40-km-wide rift is highly variable as a result of significant syn-rift normal faulting and volcanism. The presumed arc-proximal, volcaniclastic, pre-rift section is often difficult to distinguish from the poorly stratified early syn-rift sediments because of this overprinting tectonism. Only the late syn-rift stage, strong, subparallel reflectors are easily correlated throughout the basin. These presumed volcaniclastic turbidites are offset by active normal faults. Fault offsets and reflector dips increase with depth, indicating syndepositional faulting.

The rift-basin development and sedimentation is fault controlled. Most of the intra-rift and rift-margin volcanism is also fault localized. Sumisu Rift is bounded on the east by a major fault zone (see Profiles 14 and 3–6, Figs. 8 and 10 [in back pocket]). To the east of this master fault zone, the arc margin has been uplifted, exposing pre-rift arc volcaniclastics. The lack of footwall uplift on Profile 6 may be the result of loading by the nearby arc volcano. In the south, on Profile 13, the master fault zone and rift-flank uplift is on the west side of the rift (Figs. 8 and 10 [in back pocket]). The transfer zone between the two opposing master fault systems is located at and south of Profile 14. It is a relay zone of distributed normal faulting rather than an oblique slip zone (see Profile 8, Fig. 8). Away from the master fault zones the pre-rift section gradually rises up and out of the basin, as seen on Profiles 13, 14, and 3. Further north, two antithetic fault zones have downdropped the western margin, producing a more symmetric rift profile (see Profiles 4–6, Fig. 8). On all of the east-west profiles, there is an inner-rift graben of maximum subsidence on the eastern side of the rift. This inner rift has been intruded by an en echelon volcanic ridge (Fig. 4) that was crossed on Profiles 5 and 8 (Figs. 8 and 9).

ACKNOWLEDGMENTS

This work was supported by NSF grants OCE86-14687 to B. Taylor and OCE-8700826 and OCE-8996141 to G. Moore. The authors would like to thank the officers, crew, and technicians of the *Fred Moore* as well as E. W. Behrems, R. Horine, Y. Nakamura, Y. Nogi, and Y. Okamura for their help in acquiring the seismic data at sea. This is HIG Contribution No. 2200.

REFERENCES

Horine, R. L., Moore, G. F., and Taylor, B., in press. Structure of the Outer Izu-Bonin Forearc from reflection seismic profiling and gravity modeling. *In* Fryer, P., Pearce, J., Stokking, L. B., et al., *Proc. ODP Init. Repts.*, 125: College Station, TX (Ocean Drilling Program).

Ms 126A-105

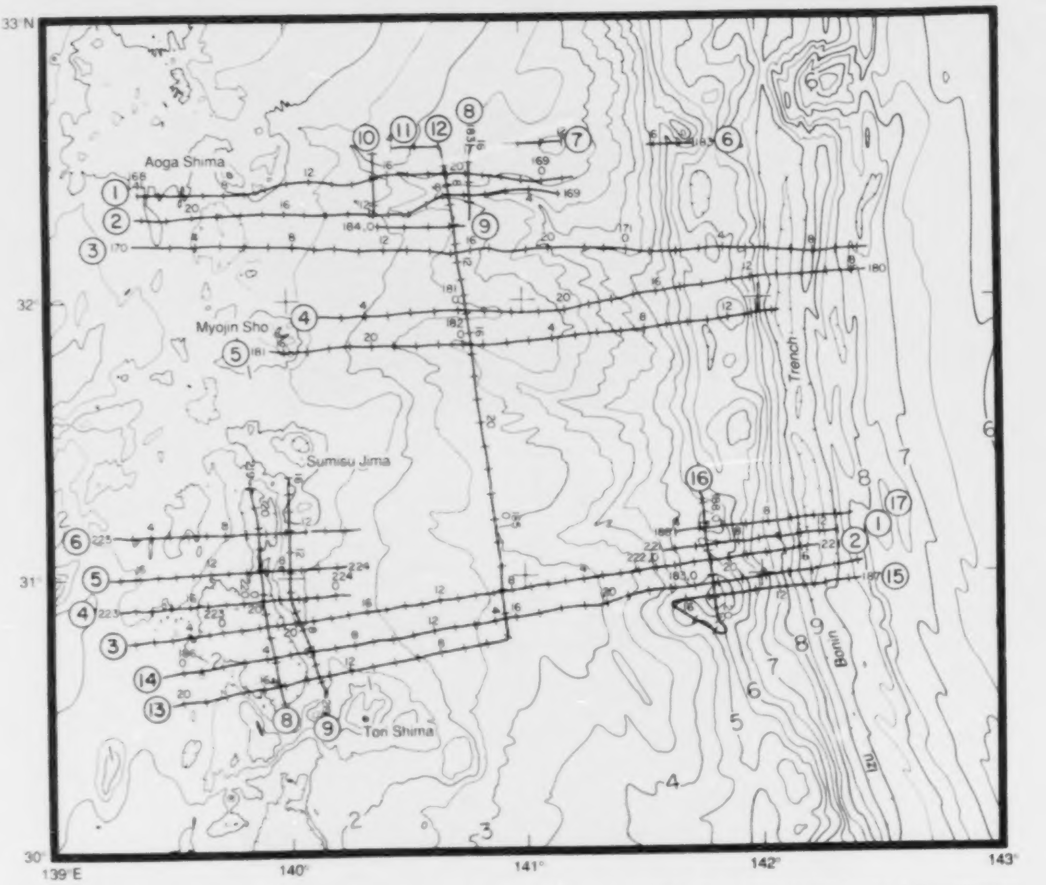
33°N
32°
31°
30°
139°E
140°
141°
142°
143°
Aoga Shima
Myojin Sho
Sumisu Jima
Tori Shima
Izu
Bonin
Trench

Figure 2. Track chart of the 1987 *Fred Moore* cruises 3505 and 3507 showing the location of MCS Profiles 1–17 (cruise 3505) and 1–6, 8, and 9 (cruise 3507). Tick marks every hour are annotated every 4 hr along track. The Julian Day is annotated at the beginning of every new track segment and at the beginning of each day. The contour interval is 0.5 km.

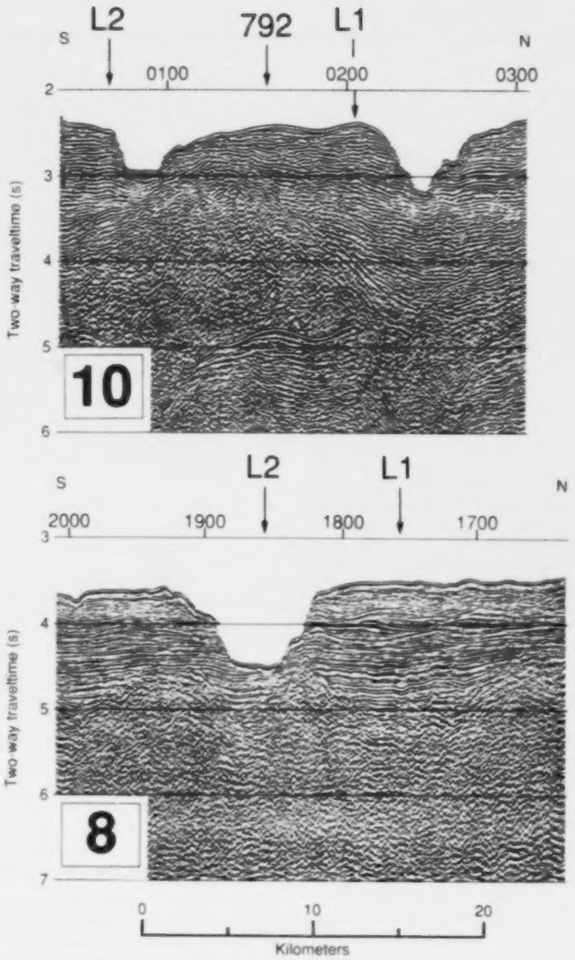

Figure 4. MCS Profiles 8 and 10 across Aoga Shima Canyon. VE = 6.7. See Figure 2 for location.

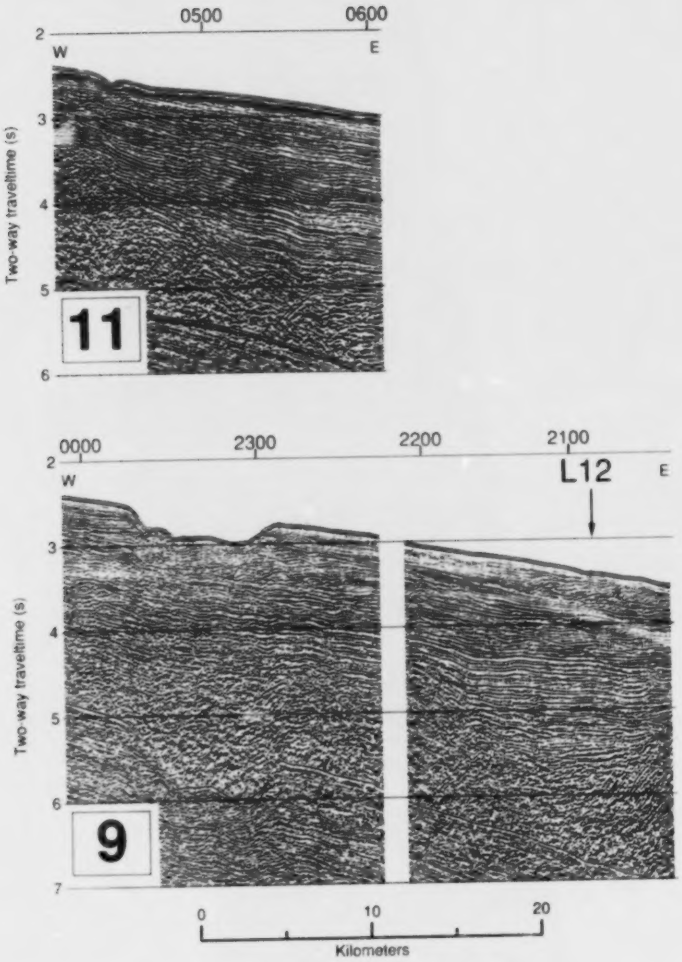

Figure 5. MCS Profiles 9 and 11. VE = 6.7. See Figure 2 for location.

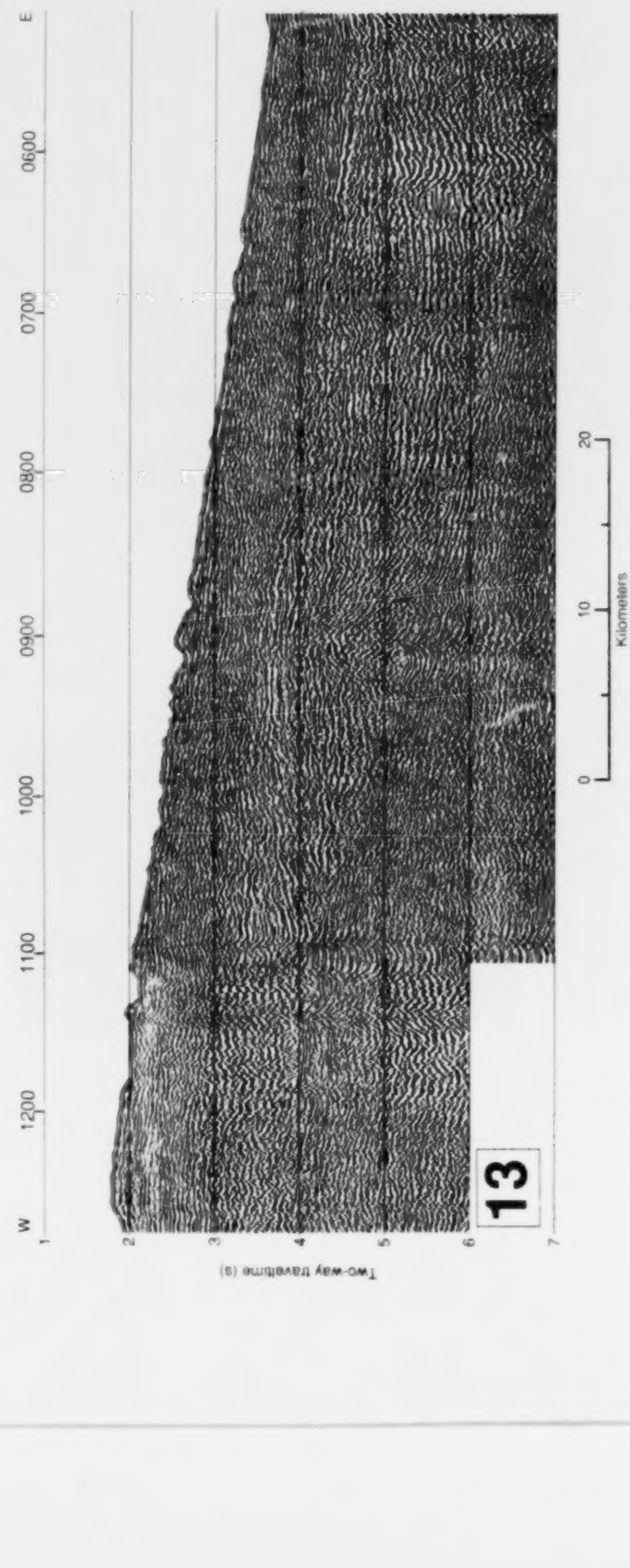

Figure 6. MCS Profile 13 across the inner forearc. VE = 6.7. See Figure 2 for location.

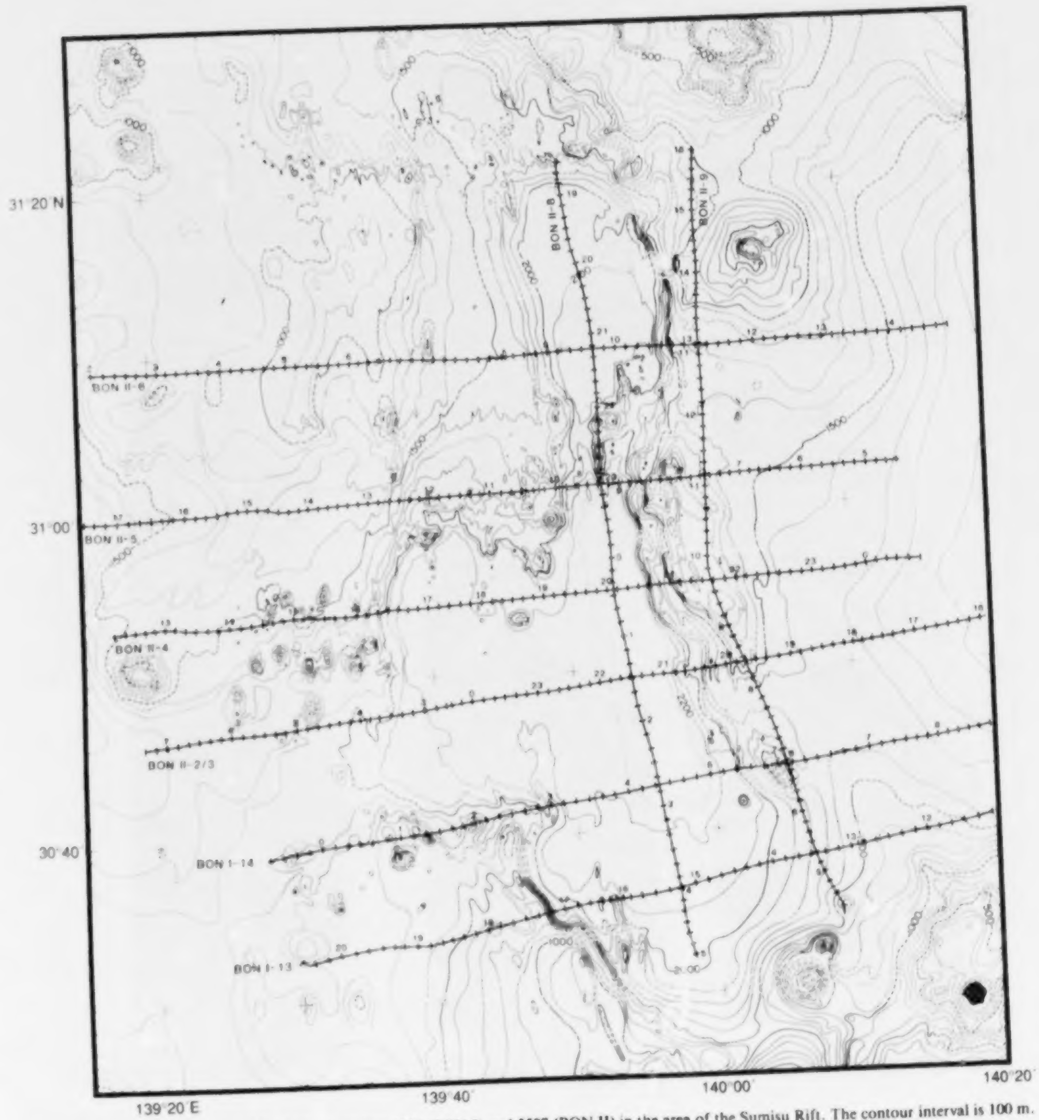
31°20'N
31°00'
30°40'
139°20'E
139°40'
140°00'
140°20'
BON II-8
BON II-9
BON II-6
BON II-5
BON II-4
BON II-2/3
BON I-14
BON I-13
500
1000
2000

Figure 7. Detailed track chart of *Fred Moore* cruises 3505 (BON I) and 3507 (BON II) in the area of the Sumisu Rift. The contour interval is 100 m.

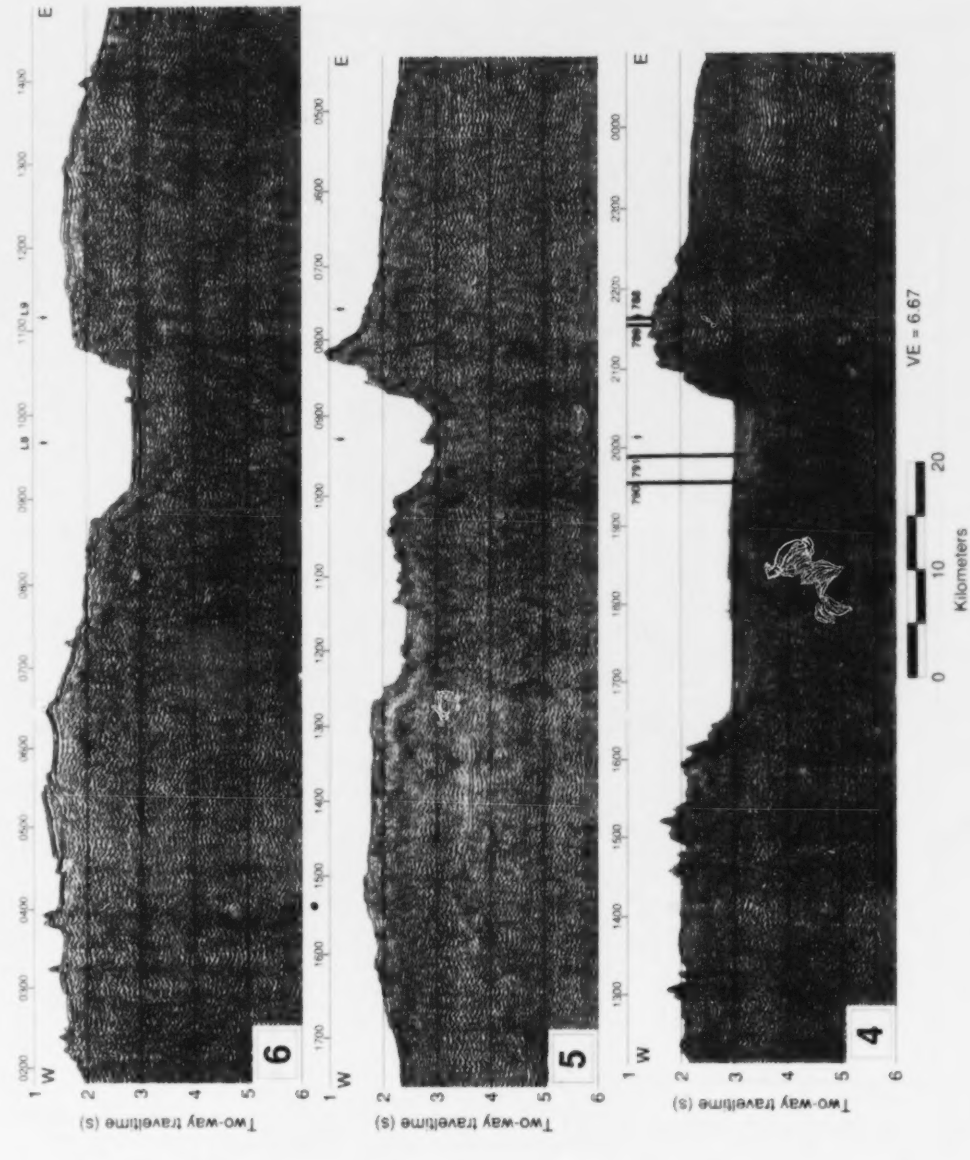
6
5
4
W
E
Two-way traveltime (s)
L8
L9
790
791
788
VE = 6.67
0
10
20
Kilometers

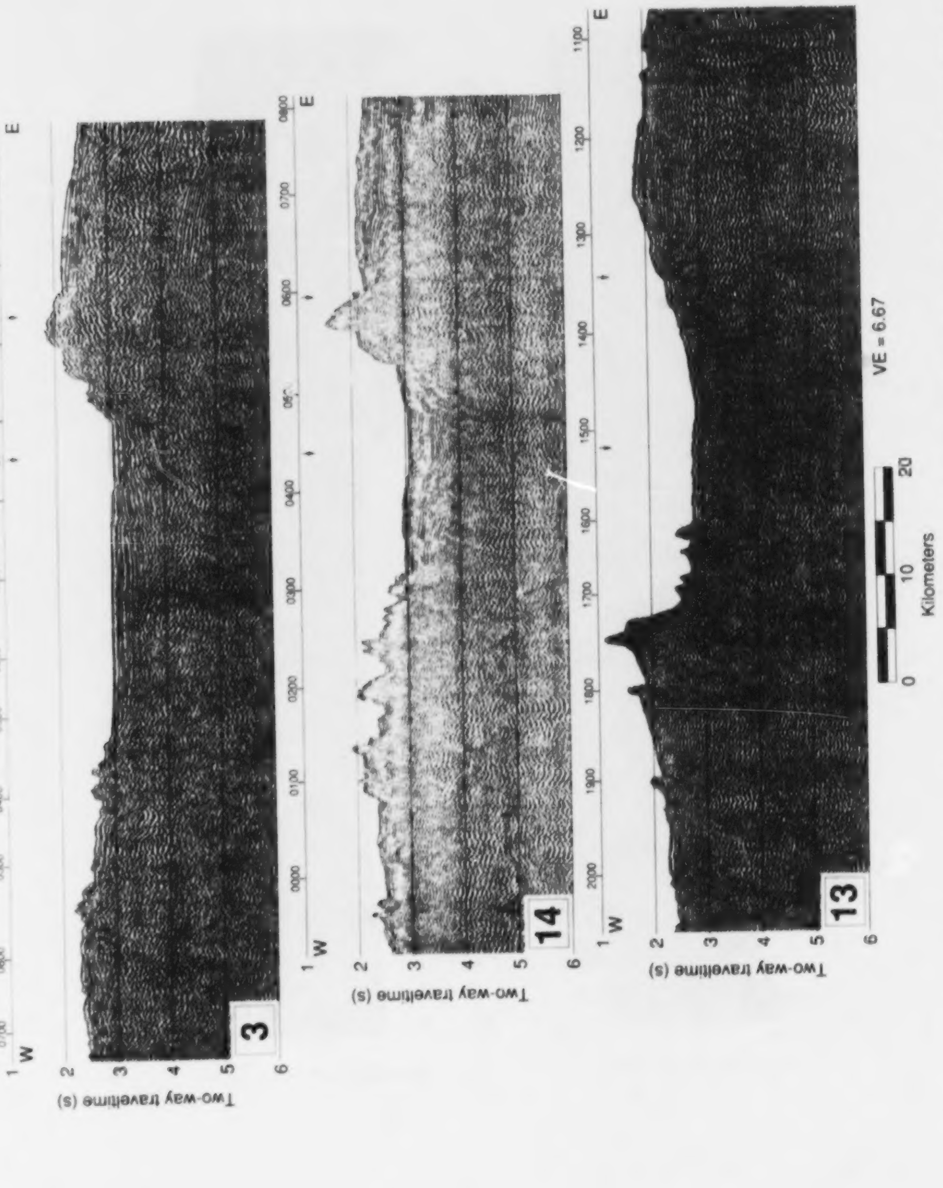

Figure 8. MCS Profiles 3–6, 13, and 14 across the Sumisu Rift and its margins. See Figure 7 for location. The profiles are aligned with respect to the crossing Profile 8.

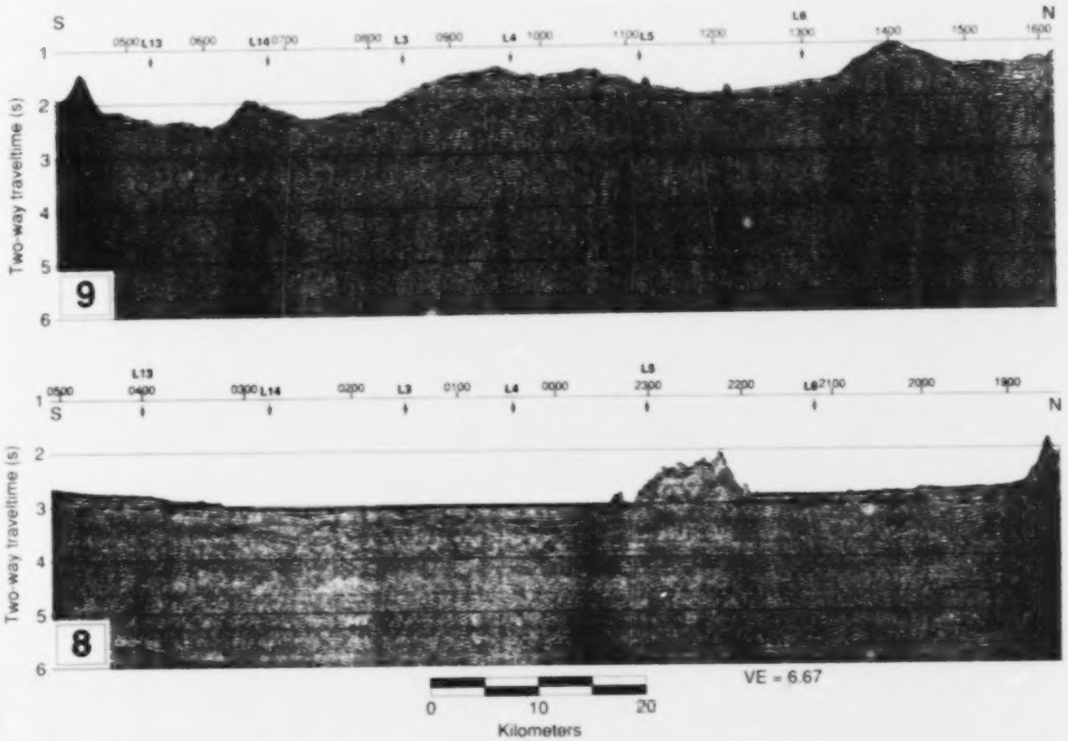

Figure 9. MCS Profiles 8 (along the axis) and 9 (along the arc margin) of the Sumisu Rift. See Figure 7 for location.

SECTION 2: SITE REPORTS

Taylor, B., Fujioka, K., et al., 1990
Proceedings of the Ocean Drilling Program, Initial Reports, Vol. 126

5. SITE 787[1]

Shipboard Scientific Party[2]

HOLE 787A

Date occupied: 23 April 1989

Date departed: 24 April 1989

Time on hole: 18 hr, 45 min

Position: 32°22.50′N, 140°44.64′E

Bottom felt (rig floor; m, drill pipe measurement): 3265.0

Distance between rig floor and sea level (m): 10.50

Water depth (drill pipe measurement from sea level, m): 3254.5

Total depth (rig floor; m): 3299.50

Penetration (m): 34.50

Number of wash cores (including cores with no recovery): 1

Total length of washed section (m): 34.50

Total core recovered (m): 6.00

Core recovery (%): 17

Oldest sediment cored:
Depth (mbsf): 34.50
Nature: scoriaceous and pumiceous sand and gravel
Age: late Miocene

HOLE 787B

Date occupied: 24 April 1989

Date departed: 27 April 1989

Time on hole: 2 days, 21 hr

Position: 32°22.50′N, 140°44.64′E

Bottom felt (rig floor; m, drill pipe measurement): 3269.4

Distance between rig floor and sea level (m): 10.50

Water depth (drill pipe measurement from sea level, m): 3258.9

Total depth (rig floor; m): 3589.5

Penetration (m): 320.10

Number of cores (including cores with no recovery): 34

Total length of cored section (m): 320.10

Total core recovered (m): 159.89

Core recovery (%): 50

Oldest sediment cored:
Depth (mbsf): 320.10
Nature: nannofossil-rich silty claystone and nannofossil claystone
Age: late Oligocene
Measured velocity (km/s): 2.25

Principal results: Site 787 is located on the eastern edge of the Izu-Bonin forearc sedimentary basin, about 95 km east of the arc volcano Aoga Shima and 135 km west of the axis of the Izu-Bonin Trench. It is located in the axis of Aoga Shima Canyon; the canyon has incised and removed up to 1 km of the sedimentary section. The principal objectives of this site were to determine:

1. the stratigraphy of the forearc basin, which would help us understand temporal variations in sedimentation, depositional environment, and paleoceanography, and the history of intensity and chemistry of arc volcanism;
2. the uplift and subsidence history across the forearc, which would provide information on forearc flexure and basin development, as well as on the extent of any vertical tectonic activity that may have taken place following the formation of the forearc terrane; and
3. the post-Eocene microstructural deformation and large-scale rotation and translation of the forearc terrane.

The site was selected on the basis of multichannel seismic records and a short shipboard seismic survey, and lies on *Fred Moore* 3505, Line 2, at 0710Z. Site 787 was occupied from 1110Z on 24 April to 0300Z on 27 April 1989.

Hole 787A was spudded for rotary core barrel (RCB) operations at 0400Z on 24 April 1989. We washed 34.5 m below sea floor (mbsf) and recovered 6 m during the jet-in test. We continued RCB operations at Hole 787B, which cored 320.1 mbsf and recovered 50.0% (recovery was 7[illegible]% from 127 to 282 mbsf). This hole penetrated the first strong seismic reflector before the pipe became stuck (probably a result of hole collapse) and eventually had to be severed with explosives 10 m below the mud line. Operations in Hole 787B ended at 0300Z on 27 April.

We defined four lithostratigraphic units at Site 787:

1. Unit I (0-21.4 mbsf): Quaternary sandy gravel, gravelly sand, gravel, and silty sand, all scoriaceous and pumiceous.
2. Unit II (21.4-40.3 mbsf): lower Pliocene and upper Miocene interbedded nannofossil ooze, nannofossil-rich silty clay, and nannofossil-rich clay.
3. Unit III (40.3-118.9 mbsf): upper Oligocene nannofossil-rich claystone, vitric silty claystone, claystone, and nannofossil chalk, with a lower 2.6-m-thick welded crystal-lithic lapilli tuff.
4. Subunit IVA (118.9-281.7 mbsf): upper Oligocene graded, sharp-based beds of sandstone, siltstone, and silty sandstone interbedded with bioturbated vitric silty claystone, nannofossil-rich silty claystone, and nannofossil-rich claystone; Subunit IVB (281.7-320.1 mbsf): upper Oligocene granule-rich and pebble-rich sandstone, silty claystone, silty sandstone, nannofossil chalk, and pebble conglomerate.

We dated Units I and II by means of nannofossil, foraminifer, and radiolarian biostratigraphy. Units III and IV are well dated by nannofossil biochronology and magnetostratigraphy (Chrons 6CN-9R). Sedimentation rates in the upper Oligocene range from 120 m/m.y. (at 29 Ma) to 33 m/m.y. (at 24 Ma).

Units I and II are unconsolidated, whereas Units III and IV are lithified. All sediments consist of mixtures of volcanogenic and biogenic (mainly nannofossil) materials that were deposited in water depths below 2000 m and above the carbonate compensation depth (CCD). Smectite is the dominant clay mineral in Units III and IV.

The volcaniclastic sands and gravels of Unit I represent Quaternary canyon fill. Unconformities form the upper and lower boundaries of Unit II, as well as internal separations within the unit. Unit II records intermittent hemipelagic deposition during canyon erosion. The lithification of the Oligocene section requires significant former overburden; we infer that canyon formation did not remove this overburden until the (probably late) Miocene or Pliocene.

---

[1] Taylor, B., Fujioka, K., et al., 1990. *Proc. ODP, Init. Repts.*, 126: College Station, TX (Ocean Drilling Program).

[2] Shipboard Scientific Party is as given in the list of participants preceding the contents.

The clastic component in Unit III results from distal turbidite deposition and volcanic ashfall, as well as one andesitic submarine pyroclastic flow. Subunit IVA represents basin-plain volcaniclastic turbidite deposits interbedded with fine-grained hemipelagic sediments. The biogenic component of the hemipelagic sediments decreases upward. Subunit IVB is probably a channel deposit, although the seismic data show evidence that this higher velocity coarse material is regionally distributed. All bedding is horizontal, except near a syndepositional slump unit at 189-195 mbsf that is 75% overturned. The upper Oligocene section is strongly burrowed. Extensional microfaults, conjugate fracture sets, low-angle shear planes, clastic injections, and dewatering veinlets all indicate extensional deformation.

Physical property measurements indicate that (1) carbonate content reaches a maximum in Unit III and varies inversely with clastic dilution from 0%-65%; (2) average bulk densities increase downward from 1700 to 2200 g/cm^3; (3) sonic velocities average 1.8 km/s in Unit III and 2.2 km/s in Unit IV, with the exception of some thin coarse layers in these units that have velocities from 2.7 to 3.5 km/s; and (4) magnetic susceptibility is at a maximum in Units I and IV and at a minimum in Unit III. Magnetic inclination data cluster around ±40°, which indicates 8° of northward motion since the late Oligocene.

Analyses of sediment and fluid geochemistry indicate that the interstitial waters are of marine origin and are modified by low-temperature alteration of volcanogenic material in the sediments. Reversal of K, Ca, and Mg concentration trends below 275 mbsf may be interpreted as the result of seawater circulation in a deeper layer. Uniformly high concentrations of sulfate, along with hydrocarbon gas levels below detection limits, are evidence of very low bacterial activity. The concentration of sedimentary organic carbon varies from 0% to 0.54%.

The principal results of this site are (1) characterization of late Oligocene hemipelagic and turbidite deposition in this deep-water forearc basin; (2) documentation of arc volcanism associated with moderate to high sedimentation rates in the late Oligocene, and extrapolation of average rates greater than 500 m/m.y. back to the presumed mid-Oligocene base of the forearc sediments (see "Site 792" and "Site 793" chapters, this volume); (3) paleomagnetic evidence that this site was translated about 8° to the north during the Neogene; (4) microstructural evidence of extensional deformation; (5) constraints on the time of major submarine canyon formation in this area to the (probably late) Miocene-Pliocene; and (6) pore-water indications of a possible seawater aquifer within the basin.

BACKGROUND AND OBJECTIVES

Site 787 is located at 32°22.50′ N, 140°44.64′ E, at 3259 mbsl (meters below sea level) on the eastern edge of the Izu-Bonin forearc sedimentary basin, about 95 km east of the arc volcano Aoga Shima ("Blue Island") and 135 km west of the axis of the Izu-Bonin Trench (Fig. 1). It is located in the axis of Aoga Shima Canyon (Fig. 2); the canyon has incised and removed up to 1000 m of the sedimentary section. Beneath the site, forearc-basin turbidites (>3 km total thickness) lap onto the western edge of the outer-arc basement high of presumed middle Eocene age (Fig. 3).

This first site of Leg 126 continued the drilling transect of the Izu-Bonin forearc region that was begun on Leg 125. The purpose of this program was to study the history of the Izu-Bonin forearc and to compare results of drilling in the Izu-Bonin forearc region with that accomplished in the Mariana forearc region by Deep Sea Drilling Project (DSDP) Leg 60 (Hussong, Uyeda, et al., 1982). By drilling in the forearc we sought to determine the following:

1. The stratigraphy of the forearc, and thus the temporal variations in sedimentation, depositional environment and paleoceanography, and the history of the intensity and chemistry of arc volcanism.
2. The uplift and subsidence history across the forearc, which would provide information on forearc flexure and basin development, as well as on the extent of any tectonic erosion.
3. The nature of the forearc igneous basement, which would resolve uncertainties concerning the nature of volcanism in the initial stages of subduction, the origin of boninites, and the formation of the 200-km-wide arc-type forearc crust.
4. The post-Eocene microstructural deformation and large-scale rotation and translation of the forearc terrane.

The first of these objectives was addressed partly through detailed studies of sediments retrieved at Site 787. The type of sedimentation and style of deposition in the forearc basin was expected to change with time as (1) the provenance changed from combined arc and outer-arc high to solely arc-derived, (2) the basin filled, (3) the volume and eruptive style of arc products varied, and (4) the development of submarine canyons eroded and redistributed sedimentary material. Geostrophic currents (e.g., the paleo-Kuroshio) and changes in global sea level may also have affected the pattern of sedimentation; these effects may be deciphered from the stratigraphic record.

The forearc sediments also contain a temporal record of the variations in the intensity and composition of arc volcanism. Studies of the chronology and geochemistry of tephra deposits at this site tested various conflicting models concerning the complex relationships between tectonic and volcanic phenomena in island arcs, such as changes in subduction rate, periodicity in backarc rifting and spreading, pulses of arc volcanism, and variations in arc geochemistry (see "Introduction" chapter, this volume, for elaboration).

The second objective was investigated through a combination of paleontological estimates of paleobathymetry, backstripping of the sedimentation history using the physical property and logging data, and seismic-stratigraphic analyses of interconnecting multichannel seismic (MCS) profiles. Determining the forearc vertical-displacement history provided some of the information necessary to decide whether (1) comparatively stable conditions have prevailed since the mid-Tertiary, as suggested by the well-developed submarine canyon system and lower-slope terrace of serpentinite seamounts; (2) the frontal arc and outer-arc high resulted from igneous construction or from differential uplift; (3) the upper-slope basin between them was formed by forearc spreading or differential subsidence; and (4) flexural loading of the forearc (either by arc volcanoes or by coupling with the subducting plate) is an important process.

The >80-m-thick Pleistocene pumice bed encountered at Site 785 limited penetration of the forearc-basin sedimentary section during Leg 125 (Fryer, Pearce, Stokking, et al., in press). Therefore, on Leg 126, we located Site 787 on the edge of the sedimentary basin (rather than at the initially proposed location on the edge of the outer-arc high) so that we could recover a sedimentary section representative of forearc-basin deposition. The site was drilled in a canyon axis so as to avoid a thick Pliocene-Pleistocene volcaniclastic sequence. However, the third objective of our forearc drilling (i.e., determining the nature of igneous basement) could not be addressed at this site because basement lies deeper than 2000 mbsf.

The fourth objective of the site, the study of microstructures and plate rotations, was addressed through a study of the structural and paleomagnetic properties of the cored materials. Microstructures in the drill cores indicate the intensity of faulting in space and time across the forearc terrane and define the syndepositional structures. Measurements of the paleomagnetic properties of subaerial portions of the Izu-Bonin and Mariana forearcs have shown at least 20° of northward drift, and from 30° to >90° of clockwise rotation since the Eocene (see "Introduction" chapter, this volume, for more details). Studies of the paleomagnetism of the cores constrained the numerous different models for the nature and timing of these motions, and their relationship to the overall structural evolution of the forearc.

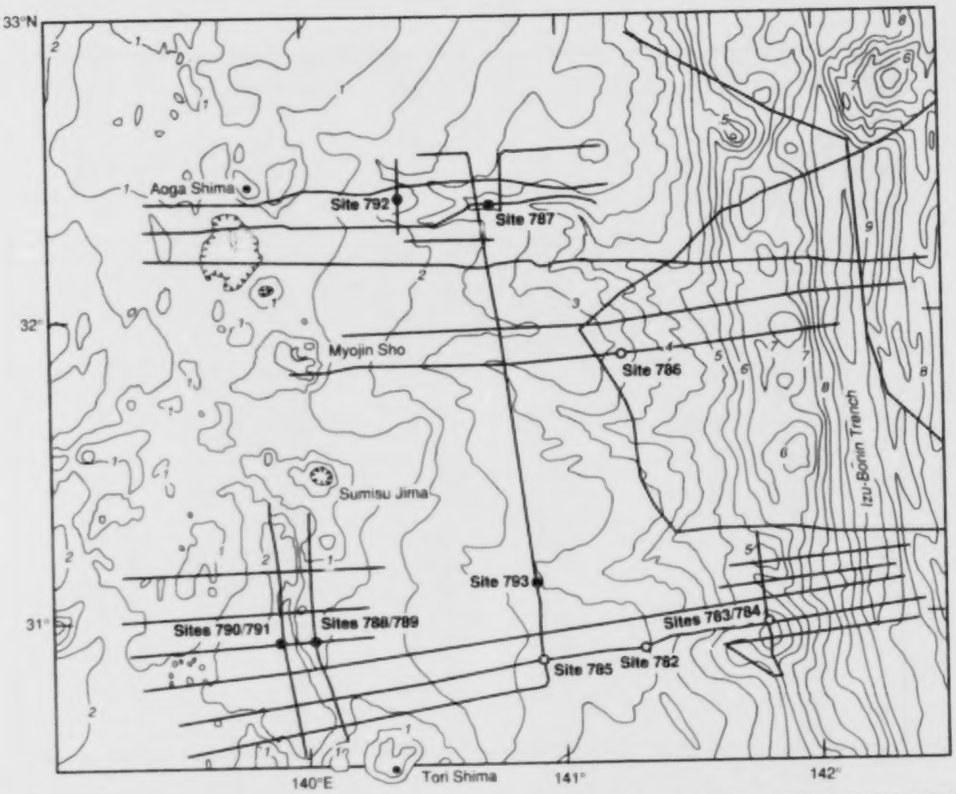

Figure 1. Bathymetric map of the Izu-Bonin arc-trench system between 30.5°N and 33°N. The locations of sites drilled on ODP Legs 125 (open circles) and 126 (solid circles) are shown on the map as are the locations of site survey multichannel seismic lines. Contour interval = 500 m (numbers on contour lines indicate depth in km).

SEISMIC STRATIGRAPHY

Correlation of site-survey MCS reflection data with recovered core material (Fig. 4) was accomplished by using the physical property velocity determinations, averaged over each lithologic unit (see "Physical Properties" section, this chapter), to convert sub-bottom depths (mbsf) into two-way traveltimes. The location chosen for Site 787 lies on *Fred Moore* 3505, Line 2, at 0710Z. The unconformity-bound Units I and II cannot be seismically characterized because they occur within the seismic bubble pulse. Low-amplitude, parallel, downlapping reflectors characterize Unit III and Subunit IVA. However, the automatic gain control (500-ms window) has lowered their amplitude with respect to the rest of the section as a result of the surrounding high-amplitude events associated with the seafloor and the coarse sand and gravel of Subunit IVB. Therefore, the entire seismic section at Site 787, from the bubble pulse to 5.36 s, is characterized by parallel, continuous, medium- to high-amplitude reflectors typical of basin-fill turbidites, with two extra-high-amplitude reflectors associated with the top and bottom of Subunit IVB. These reflectors lap onto a westward-dipping, high-amplitude sequence (5.36–5.77 s) that in turn laps onto the seismically chaotic acoustic basement.

OPERATIONS

Tokyo to Site 787

JOIDES Resolution departed Tokyo at 1700 hr (all times given in UTC) on 22 April 1989, and steamed toward Site 787 (proposed Site BON-5C). The first site was selected on the basis of our need to occupy the deepest-water site first; the new television (TV) coaxial cable had to be paid out to maximum depth and allowed to detorque prior to its first use in conjunction with the drill pipe. We selected proposed Site BON-5C and the ship proceeded directly to that site. The availability of either a global positioning satellite (GPS) window or adequate Loran navigation coverage would determine whether or not we performed the pre-site survey and dropped the beacon prior to the cable detorquing exercise. As it turned out, GPS was unavailable but the Loran fixes appeared to be accurate, so we conducted the pre-site survey in a normal fashion (see "Underway Geophysics" chapter, this volume). One north-south pass was made over the site, followed by an east-west pass during which the beacon was dropped. One beacon, poised over the side and ready for release on command, broke free without weights and drifted away. A backup beacon was readied in just 6 min and released as the ship was about to leave the acceptable drop zone.

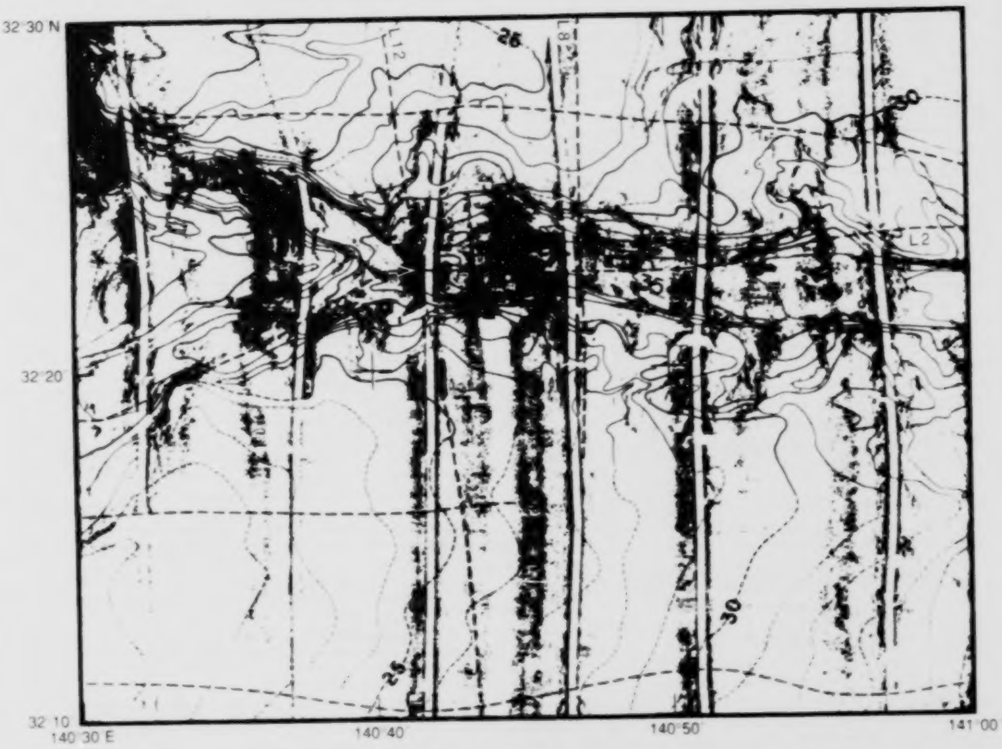

Figure 2. SeaMARC II sidescan and bathymetry (contour interval = 100 m) of Aoga Shima Canyon (Klaus and Taylor, in press). The locations of MCS site-survey tracks and of Site 787 (open circle) are also shown. The segment of MCS Line 2 shown in Figure 3 is delineated by arrows.

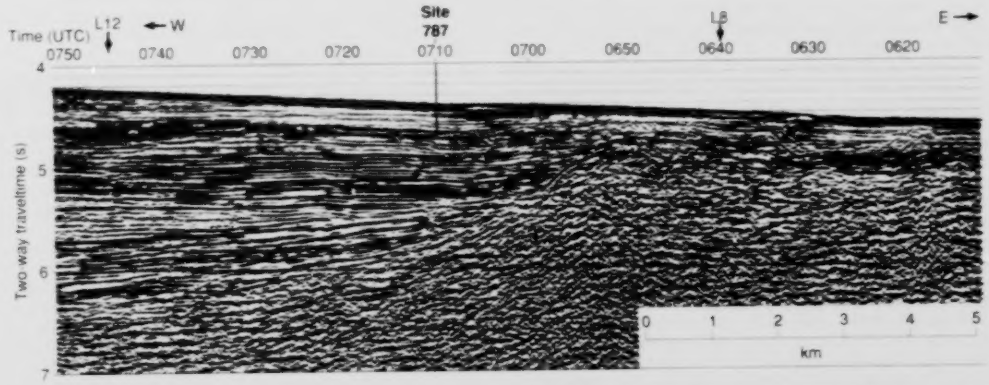

Figure 3. MCS Line 2 (Taylor et al., this volume) across the Izu-Bonin forearc sedimentary basin and outer-arc high. This profile was shot along the axis of Aoga Shima Canyon (see Fig. 2 for location). Site 787 is located on the eastern edge of the basin, where the deeper sedimentary section laps onto the outer-arc high.

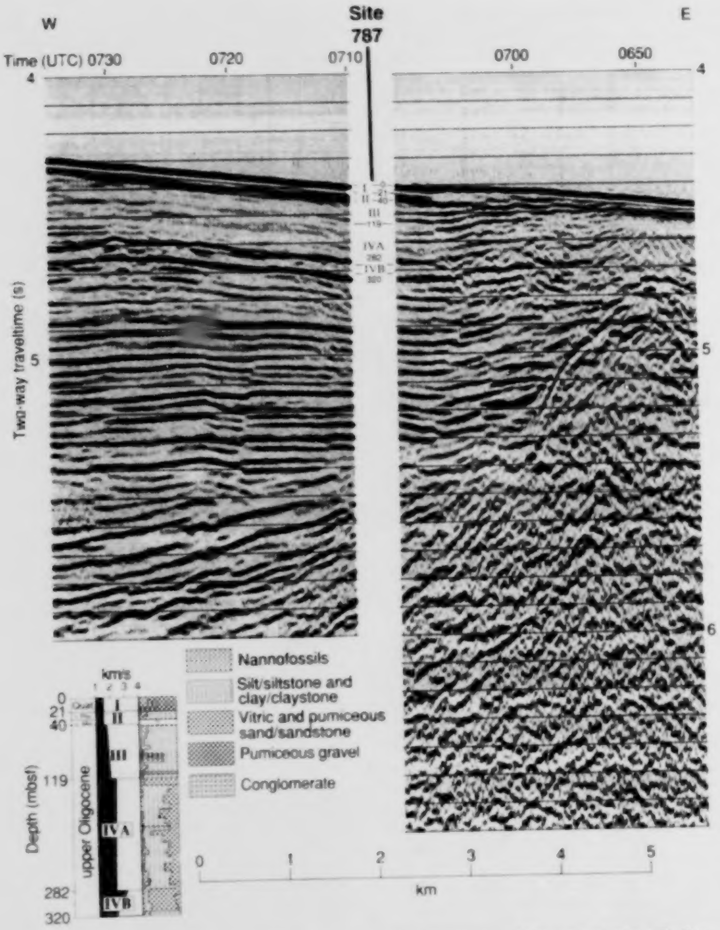

Figure 4. Correlation of Site 787 lithostratigraphy with site-survey multichannel seismic reflection data. Lithologic units are identified on the seismic section, unit boundaries are given in mbsf, and the lithologic column (see "Lithostratigraphy and Accumulation Rates," this chapter) is presented in the lower left corner. The location of the *Fred Moore* seismic line is shown in Figure 2. The seismic section has been stacked (48-fold), deconvolved, migrated, and filtered 10-60 Hz. Vertical exaggeration is about 4X.

Site 787

The second beacon was deployed at 1110 hr on 23 April, initiating Site 787. The seismic survey line was continued for 5 nmi before the gear was pulled. As the ship returned over the beacon and the thrusters were lowered, heavy seas dislodged several large portions of a reentry-cone assembly that were loose on the main deck. These steel brackets moved across the deck and landed partly on an exposed section of the TV coaxial cable that had been strung out in preparation for the detorquing run. The damage to the cable made its watertightness suspect, so the detorquing exercise was postponed.

Hole 787A

The potential target depth for the site was as deep as 1400 mbsf, which was expected to require more than one bit. One of the possible scenarios for operations at the site was the emplacement of a full reentry cone and installation of casing. Accordingly, Hole 787A was to be a jet-in test to determine the depth for jetting in 16-in. casing with a full-size reentry cone.

The anticipated seafloor conditions suggested lithified sediments at or near the surface, and interbedded volcaniclastic materials and claystones below. The RCB was deemed best for the type of formation expected, and a standard nine-drill-collar bottom-hole assembly (BHA) with a hydraulic bit release (HBR) was assembled and run to the seafloor. The precision depth recorder (PDR) indicated a firm reflector at the seafloor in 3272.0 m of water.

The seafloor proved to be more suitable for jetting than anticipated. The hole was spudded at 0400 hr on 24 April, and the bit was successfully jetted in to a presumed sub-bottom depth of 34.5 mbsf, on the basis of apparent mud-line contact at 3254.5 mbsl. At that point, firmer material was encountered. The bit was pulled clear of the seafloor at 0555 hr, and we retrieved the core barrel used for the jet-in test. Unexpectedly, 6.00 m of pumiceous and scoriaceous gravel had been trapped in the core barrel. Scientific interest in the material was high, so the core was designated a wash core and the jet-in hole became Hole 787A.

Hole 787B

The ship was offset 20 m northeast, and Hole 787B was spudded at 0747 hr. Coring with the RCB in the unconsolidated sand and gravel at the seafloor was unexpectedly successful. The first three cores each recovered an average of 3.74 m of material, with circulation, pipe rotation, and weight on the bit all at a minimum (Table 1). The following five RCB cores were from an interval of apparently firm but loose sand or gravel in which recovery was almost impossible. Only the more consolidated nannofossil-rich claystones were recovered. Despite this ominous start, the conditions for rotary coring improved dramatically at that point, and the next 22 cores (126-787B-9R to -30R) were very good in terms of the percentage and quality of core recovered. The formation contained just enough claystone and clay-bearing sedimentary material to stabilize the hole and, evidently, "make its own mud," thus preventing loose material near the surface from causing fill or pipe-sticking problems. We recovered several well-preserved rock/claystone contacts, which indicated unusually favorable conditions not typically encountered during RCB coring of interbedded lithologies.

Table 1. Coring summary, Site 787.

Core no.	Date (April 1989)	Time (UTC)	Depth (mbsf)	Cored (m)	Recovered (m)	Recovery (%)
126-787A-						
1W	24	0710	0.0	34.5	6.00	17
Coring totals				0.0	0.00	
Washing totals				34.5	6.00	
Combined totals				34.5	6.00	
126-787B-						
1R	24	0830	0.0-2.3	2.3	2.32	101.0
2R	24	1025	2.3-11.9	9.6	5.29	55.1
3R	24	1145	11.9-21.4	9.5	3.61	38.0
4R	24	1300	21.4-30.9	9.5	0.46	4.8
5R	24	1420	30.9-40.3	9.4	0.39	4.2
6R	24	1525	40.3-49.8	9.5	2.20	23.1
7R	24	1700	49.8-59.3	9.5	1.80	18.9
8R	24	1800	59.3-69.0	9.7	0.57	5.9
9R	24	1900	69.0-78.7	9.7	3.48	35.9
10R	24	2020	78.7-88.4	9.7	3.86	39.8
11R	24	2145	88.4-98.1	9.7	3.38	34.8
12R	24	2335	98.1-107.8	9.7	2.49	25.7
13R	25	0135	107.8-117.5	9.7	3.78	38.9
14R	25	0400	117.5-127.2	9.7	4.22	43.5
15R	25	0555	127.2-136.8	9.6	6.76	70.4
16R	25	0730	136.8-146.5	9.7	6.43	66.3
17R	25	0900	146.5-156.2	9.7	7.46	76.9
18R	25	1040	156.2-165.8	9.6	4.27	44.5
19R	25	1215	165.8-175.5	9.7	9.46	97.5
20R	25	1340	175.5-185.1	9.6	5.82	60.6
21R	25	1500	185.1-194.8	9.7	9.82	101.0
22R	25	1620	194.8-204.4	9.6	0.98	10.2
23R	25	1745	204.4-214.1	9.7	7.69	79.3
24R	25	1855	214.1-223.7	9.6	9.78	102.0
25R	25	2010	223.7-233.4	9.7	8.22	84.7
26R	25	2130	233.4-243.0	9.6	7.68	80.0
27R	25	2240	243.0-252.7	9.7	5.32	54.8
28R	25	2350	252.7-262.4	9.7	8.01	82.6
29R	26	0100	262.4-272.0	9.6	7.62	79.4
30R	26	0215	272.0-281.7	9.7	7.68	79.2
31R	26	0340	281.7-291.3	9.6	1.87	19.5
32R	26	0500	291.3-300.8	9.5	2.60	27.3
33R	26	0645	300.8-310.5	9.7	2.68	27.6
34R	26	0815	310.5-320.1	9.6	1.89	19.7
Coring totals				320.1	159.89	50.0

The good drilling conditions ended abruptly after encountering an interval of unconsolidated coarse sandstone at 282 mbsf. The hole was deepened to 320.1 mbsf, with recovery averaging 2.2 m/core over the last four cores. The low recovery rate suggested a highly unstable zone, but hole conditions were quasi-stable until the sinker bars stabbed into the top-drive swivel to retrieve Core 126-787B-34R. At that point, severe backflow indicated the probability of hole collapse. After the sinker bars were in place and the wireline blowout preventer could be closed, we found the bit to be plugged. The core barrel was stuck briefly at the bit, suggesting flow-in of loose material around the core barrel at the bit. By the time we retrieved the core barrel to the deck, the pipe was firmly stuck. Although we regained circulation, we could not work the pipe free. After 3½ hr of continuous overpulls, we decided to sever the pipe and abandon the hole.

The first 31-pellet high-energy engineering (HEE) severing charge was fired in the 5½-in. transition joints at the top of the BHA, but the charge was a partial failure and the pipe did not come free. We fired the second charge 10 m below the mud line, as the first charge could have failed because it had been applied below the free point of the drill string. The second shot was successful, and the pipe came free with minimum pull. The pipe was then pulled, and the severed joint reached the deck at 0300 on 27 April.

LITHOSTRATIGRAPHY AND ACCUMULATION RATES

We recognized four lithologic units at Site 787 (Table 2, Fig. 5). The upper two units are unconsolidated, whereas the lower two are lithified. The contacts between Units I, II, and III were not recovered. All sediments at this site consist of mixtures of volcanogenic and biogenic materials (mainly nannofossils). Bedding in the entire section is essentially horizontal, except immediately above a slide unit in Core 126-787B-21R. Minor deformation and dewatering features include subvertical veinlets, extensional microfaults, low-angle shear planes, and clastic injections.

Figure 5 also shows downhole distribution of carbonate minerals (mainly nannofossil tests) and trends in magnetic susceptibility. In many cases, peaks in magnetic susceptibility correspond to concentrations of magnetic minerals and mafic volcanic glass, particularly in fine-grained sediments that contain bioturbation-disseminated ash.

Unit I

Interval: Cores 126-787B-1R through -3R
Age: Quaternary
Depth: 0-21.4 mbsf

Unit I (0-21.4 mbsf) consists mainly of sandy gravel (49%), gravelly sand (28%), gravel (11%), and silty sand (9%), all scoriaceous and pumiceous; recovery averaged 52%. We interpret the complete lack of primary structures and the occurrence of coarsest material in the lower part of each core to be the result of drilling disturbance.

Table 2. Lithostratigraphic units, Hole 787B.

Unit	Lithology	Sedimentary structures	Interval (mbsf)	Age	Occurrence
I	Pumiceous and scoriaceous sandy gravel, gravelly sand, gravel, and silty sand.	Cores all show upward fining owing to drilling disturbance. No primary structures noted. Maximum clast size is 3 cm.	0–21.4	Quaternary	126-787B-1R to -3R
II	Interbedded nannofossil ooze, nannofossil-rich silty clay, and nannofossil-rich clay.	None observed (poor recovery).	21.4–40.3	early Pliocene to late Miocene	126-787B-4R and 126-787B-5R
III	Nannofossil-rich claystone, vitric silty and sandy claystone, claystone, and nannofossil chalk. Cores 126-787B-12R and -13R contain a welded crystal-lithic lapilli tuff.	Sediment contains disseminated ash and is bioturbated; burrows include *Zoophycos*, *Planolites*, and *Chondrites*. Common dewatering veinlets, clastic dikes, and microfaults.	40.3–118.9	late Oligocene	126-787B-6R to -14R-1, 135 cm
IVA	Graded, sharp-based, parallel- to ripple-laminated beds of sandstone, siltstone, and silty sandstone interbedded with bioturbated vitric silty claystone, nannofossil-rich silty claystone, and nannofossil-rich claystone. Carbonate content increases downhole.	Fine-grained sediments contain local concentrations of sand-sized ash and are bioturbated; burrows include: *Zoophycos*, *Planolites*, and *Chondrites*. Silty sandstone beds have sharp bases, are graded, and show internal structures of the Bouma sequence (generally the parallel-laminated and rippled divisions). Injections and extensional microfaults characterize this subunit. Core 126-787B-21R contains two overturned intervals and slide folds.	118.9–281.7	late Oligocene	126-787B-14R-1, 135 cm, to -30R
IVB	Granule-rich and pebble-rich sandstone, silty claystone, silty sandstone, nannofossil chalk, and pebble conglomerate.	No primary structures in the sandstone; burrows and microfaults in the finer sediment.	281.7–320.1	late Oligocene	126-787B-31R to -34R

Maximum clast size in Unit I is approximately 3 cm. The major clast types are pumice (white, gray, rarely red) and black scoria (Fig. 6). Other grains include plagioclase, quartz, and minor bioclasts (benthic foraminifers, gastropods, and bryozoans).

Unit II

Interval: Cores 126-787B-4R and -5R
Age: early Pliocene to late Miocene
Depth: 21.4–40.3 mbsf

Unit II was sampled in only two, short, core sections (total recovery = 85 cm) and consists of lithic-vitric-rich nannofossil ooze (58%), nannofossil-rich volcanic-lithic silty clay (35%), and nannofossil-rich clay (7%). Total recovery was 4.5% of the cored interval. This material contains no primary structures other than bedding.

Unit III

Interval: Core 126-787B-6R through Section 126-787B-14R-1 at 135 cm
Age: late Oligocene
Depth: 40.3–118.9 mbsf

Unit III is dominated (60%) by nannofossil-bearing sediment types: nannofossil-rich claystone (38%), nannofossil chalk (19%), nannofossil vitric silty claystone (3%), and nannofossil claystone (1%). Noncalcareous sediments and rocks make up the remaining 40% of the unit: predominantly vitric silty and sandy claystone (18%), claystone (10%), and a 2.6-m-thick crystal-lithic lapilli tuff (13%). Some laminated claystones and minor graded bedding are present; however, most of the sediment in this unit is bioturbated. Trace fossils include *Zoophycos*, *Planolites*, and *Chondrites* (Figs. 7 and 8). Sand-size volcanic ash is commonly scattered throughout the burrowed sediment (Figs. 5 and 9). Total recovery was 29% of the cored interval.

Unit III, unlike the overlying Units I and II, is lithified and has been deformed by extension. Evidence of this deformation includes rotated (kinked), subvertical, mineral-filled veinlets with braided and anastomosing geometries (Figs. 7 and 8), low-angle shear planes or zones (Fig. 7), and numerous microfaults (Fig. 10). The mineral-filled veinlets are identical to those described from the Middle America Trench slope by Ogawa and Miyata (1985) and from the Japan Trench by Arthur et al. (1980) and Lundberg and Leggett (1986); they are particularly common in Cores 126-787B-7R through -10R. The low-angle shear zones generally are planar bands of homogeneous claystone, a few millimeters thick, which offset primary structures. These zones are very subtle, and many may not have been recognized in dark-colored sections. The extensional stress field also may have helped promote the injection of clastic dikes, which are common in this unit (Fig. 11).

Near the base of Unit III, there is a 2.6-m-thick andesitic crystal-lithic lapilli tuff with welded texture (Fig. 12). The base of this unit is chilled and contains vesicles (Fig. 13); the top is overlain sharply by nannofossil-rich vitric silty claystone. Clasts consist of gray andesite, and clots of plagioclase and pyroxene crystals. In thin section (Sample 126-787B-13R-1, 27–30 cm), the welded lapilli tuff is formed mainly of andesitic clasts (2–4 mm in size) and crystal fragments (1 mm in size). The andesitic clasts are generally moderately porphyritic, with zoned plagioclase and clinopyroxene phenocrysts in a glassy groundmass. Locally, the feldspar microlites within these clasts are aligned.

The glassy groundmass found in Unit III is partly hydrated to brown palagonite, which contains a few feldspar microlites formed during devitrification; vesicles (<0.5 mm) are abundant and filled with zeolites and palagonite. A few clasts are formed of glomeroporphyritic plagioclase with small clinopyroxenes. The crystal fragments consist of complete or broken plagioclase and clinopyroxene. The plagioclase crystals show oscillatory zoning. Some of the clinopyroxene crystals are corroded and exhibit orthopyroxene lamellae inclusions that suggest a fairly slow cooling rate. The groundmass consists predominantly of clear, amorphous, volcanic glass or possibly amorphous silica and minor brown devitrified glass.

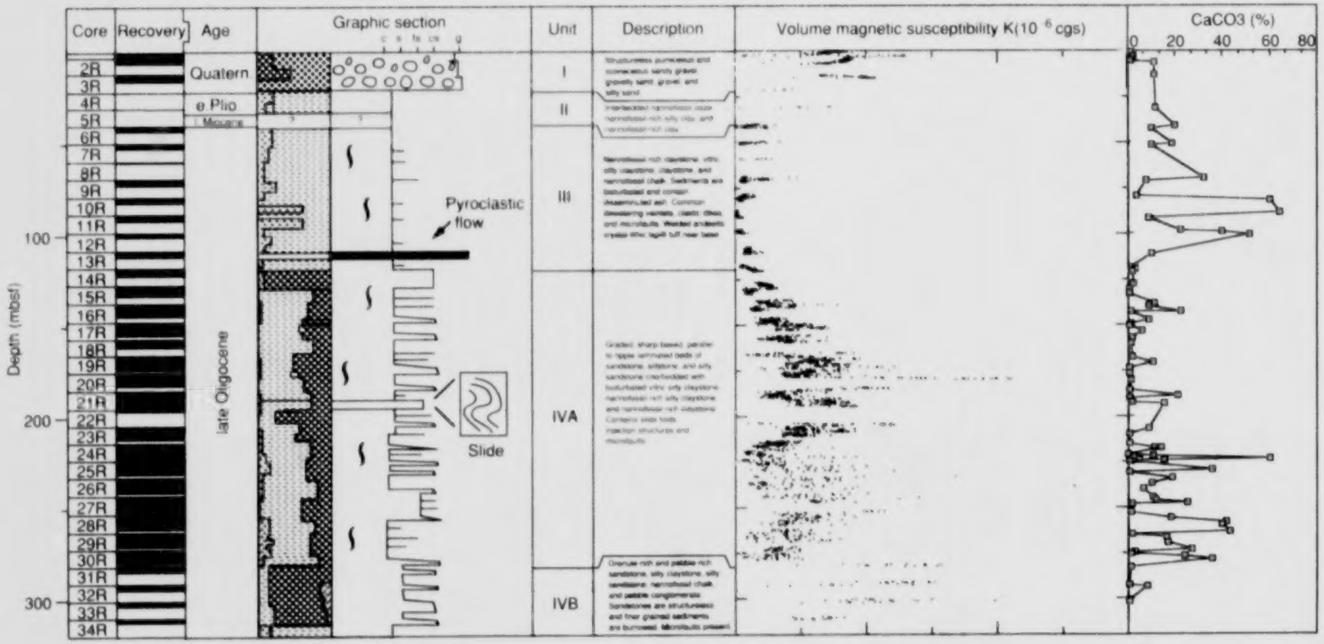

Figure 5. Lithostratigraphic summary for Site 787, including a graphic display of core recovery and the downhole distributions of carbonate minerals and magnetic susceptibility. The carbonate curve is primarily a function of nannofossil distribution throughout the section, whereas the magnetic susceptibility data reflect the distribution of coarse mafic volcanic lithic rocks and crystals. The proportions of sediment types at Hole 787B are shown in the lithology column (see Fig. 4 for key to patterns). The format is more generalized than in the core descriptions (which appear at the back of this volume), reflecting the percent of lithologic groups observed in the cored intervals (e.g., silt + clay, sand, gravel, carbonate), and does not show mixed biogenic/siliciclastic sediments. The graphic column is a simplified sedimentological log that displays relative grain size on the horizontal axis (c = clay/claystone, s = silt, fs = fine sand, cs = coarse sand and g = gravel/conglomerate). On this column, sedimentary structures (see Fig. 6, "Explanatory Notes" chapter, this volume) and bedding within the cored units are schematically displayed.

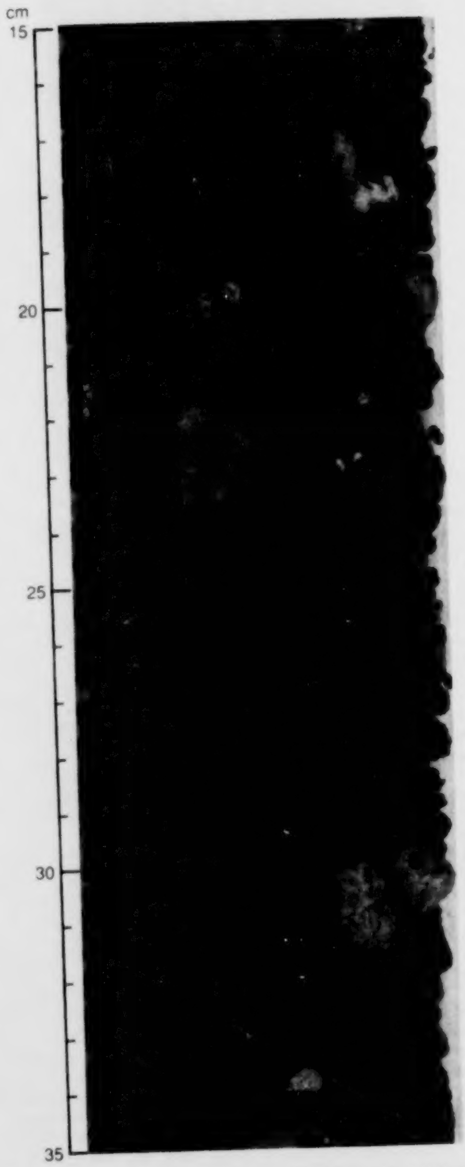

Figure 6. Dark, scoriaceous gravel of Unit I, with interspersed light gray pumice pebbles. Interval shown is 126-787B-1R-2, 15–35 cm.

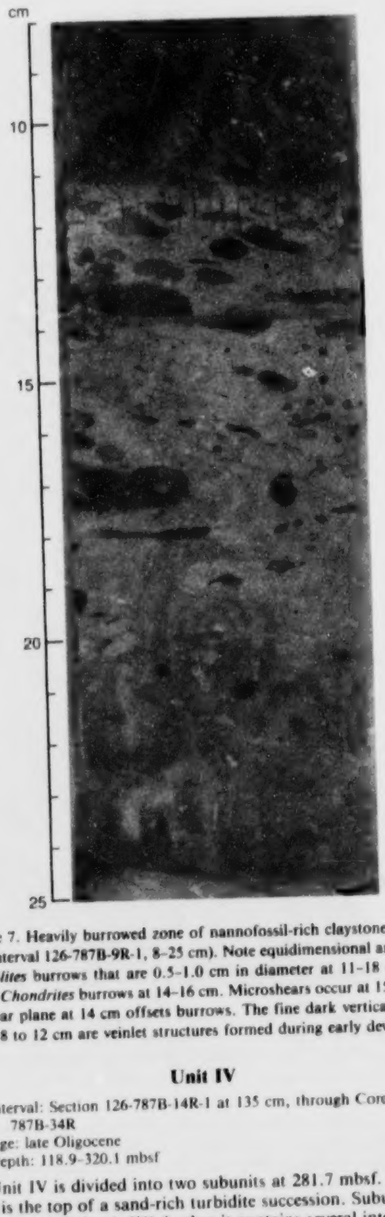

Figure 7. Heavily burrowed zone of nannofossil-rich claystone in Unit III (Interval 126-787B-9R-1, 8–25 cm). Note equidimensional and ovoid *Planolites* burrows that are 0.5–1.0 cm in diameter at 11–18 cm, and small *Chondrites* burrows at 14–16 cm. Microshears occur at 15–18 cm. A shear plane at 14 cm offsets burrows. The fine dark vertical streaks from 8 to 12 cm are veinlet structures formed during early dewatering.

Unit IV

Interval: Section 126-787B-14R-1 at 135 cm, through Core 126-787B-34R
Age: late Oligocene
Depth: 118.9–320.1 mbsf

Unit IV is divided into two subunits at 281.7 mbsf. Subunit IVA is the top of a sand-rich turbidite succession. Subunit IVB differs from Subunit IVA in that it contains several intervals of granule-rich coarse sandstone and pebbly sandstone. Recovery was 71% for Subunit IVA, and 24% for Subunit IVB. As in Unit III, all finer grained intervals are burrowed and contain variable amounts of disseminated sand- to silt-size volcanic ash

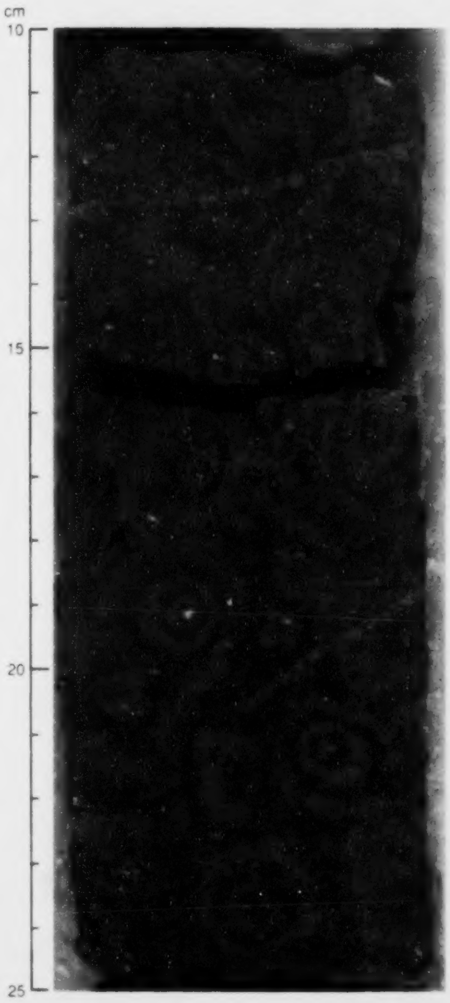

Figure 8. Indistinctly mottled claystone is crosscut by two simple *Zoophycos* burrows (12-13 and 19-20 cm). The upper burrow is deformed by closely spaced, wavy, vertical veinlet structures that extend across the interval from 11 to 17 cm. Interval shown is 126-787B-10R-1, 10-25 cm.

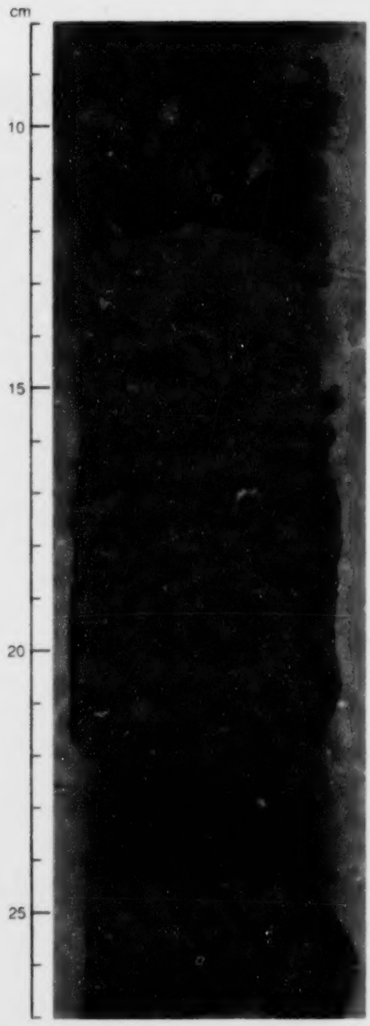

Figure 9. Black sand-size ash disseminated throughout a bioturbated nannofossil-rich claystone. Interval shown is 126-787B-8R-1, 8-27 cm.

(Figs. 5 and 14). Volcanic ash is also commonly concentrated in discrete beds of brownish black, lithic-crystal-vitric siltstone and fine-grained sandstone (Fig. 15).

Subunit IVA is characterized by the intercalation of two sediment types. The first consists of dark-colored, thin- to thick-bedded, sharp-based, graded, vitric sandstones (23% of the total material recovered), vitric silty sandstone (15%), and vitric siltstone (6%) beds. The second sediment type consists of strongly burrowed claystones (11%), vitric silty claystones to clayey siltstones (7%), and nannofossil-bearing sediments (36%). The burrows extend downward into the upper part of the graded silty sandstone and siltstone beds (Fig. 16), creating mixed nannofossil-bearing sediments: nannofossil-rich vitric silty claystone (19%), nannofossil-rich claystone (12%), nannofossil-rich siltstone (3%), and nannofossil claystone (2%). The quantity of biogenic carbonate (i.e., nannofossils) in the finer grained lithologies increases downward in Subunit IVA, and beds of nannofossil-rich claystone and nannofossil-rich silty claystone, etc., become common below Core 126-787B-22R (Fig. 5).

Internal structures in the graded silty sandstone and siltstone beds include parallel lamination, ripple lamination, rare convo-

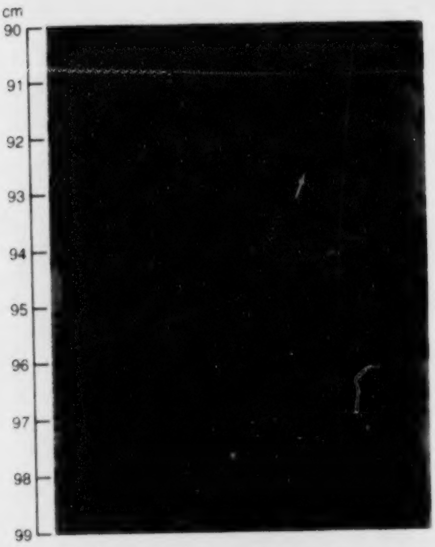

Figure 10. Microfractures with an apparent dip of 45° cutting bioturbated vitric-rich nannofossil chalk. Note 1.5-cm-diameter pumice pebble at 92 cm (indicated by arrow). Interval shown is 126-787B-7R-1, 90-99 cm.

lute lamination, and silt-mud laminae at the top. The sequences of structures are identical to those described for turbidites by Bouma (1962). Bases of the beds are almost always sharp, and in some cases have basal scour marks. Trace fossils include *Planolites*, *Zoophycos*, and *Chondrites*.

The sandstone percentage and the relative thickness of sandstone beds are greatest near the top of Subunit IVA. Below Core 126-787B-15R, graded silty sandstone and siltstone beds are thin, and burrowed claystone and nannofossil-rich claystone units are thick; some cores contain very little sand. In Cores 126-787B-19R and -20R, sandstone beds are comparatively thick (1-2 m maximum). In general, sandstone/siltstone bed thicknesses and the sandstone/shale ratio vary between cores, suggesting cyclicity in these parameters on a scale of tens of meters.

Core 126-787B-21R contains a deformed interval from Section 126-787B-21R-3 at 110 cm, to -21R-7 at 70 cm (thickness = 5.6 m). Approximately 75% of the sediment in this interval is overturned, and two horizons of sandy mudstone and clayey siltstone are plastically folded (Fig. 17). The deformed interval is accompanied by extensional microfaults (Fig. 18) and sandstone injections (Fig. 19). The overturned bedding is confirmed by a reversal in magnetic polarity in this interval (see "Paleomagnetics" section, this chapter). Immediately above this zone, the beds show as much as 20° of apparent dip, but they are horizontal well above and below the overturned sequence.

Smear-slide data show that the silty sandstones and siltstones are formed almost entirely of volcanic grains. The vitric/lithic/crystal ratios are variable. The vitric component consists of dark brown to clear glass shards and pumice fragments. Crystals are mainly plagioclase, with less abundant pyroxene and rare epidote. Volcanic lithic fragments are mainly microlitic in texture. Many beds are rich in black sand in their basal parts, particularly in the lower part of the subunit, and in smear slides we observed this material to consist of dark glass and lithic grains.

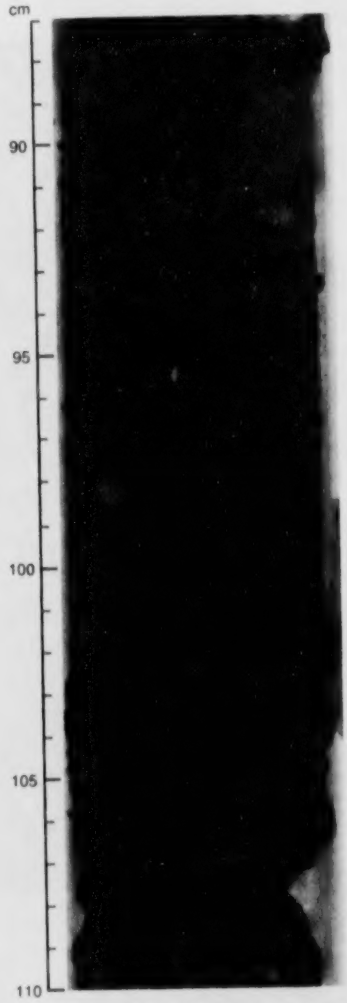

Figure 11. V-shaped, subvertical clastic dike crosscutting silty claystone. The dike consists of brecciated silty claystone clasts within a poorly sorted matrix. Interval shown is 126-787B-14R-1, 87-110 cm.

Subunit IVA contains structural features that indicate brittle deformation under extension has taken place, predominantly microfaults that locally have conjugate fracture sets (Fig. 20). Healed fractures are visible in some cores.

Subunit IVB consists of granule-rich and pebbly sandstone (46%), silty claystone (20%), silty sandstone (14%), nannofossil chalk (11%), and pebble conglomerate (9%). The coarse sandstone and minor conglomerate are structureless and contain scattered large-pebble- and cobble-size claystone clasts that have

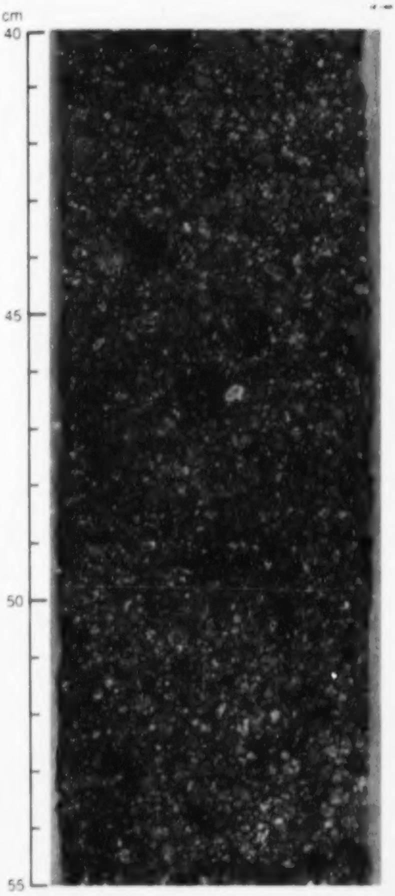

Figure 12. Welded lapilli tuff near the base of Unit III. Interval shown is 126-787B-13R-1, 40-55 cm.

the same composition and approximate age as the interbedded sediment, as determined from nannofossil dates. Pebbles, granules, and sand grains are composed of mafic and felsic volcanic lithic rocks, pumice, quartz, feldspar, and rare red pumice. Microfaults are present in the fine-grained units. Recovery in this subunit was relatively low, probably because the weakly cemented coarse sandstone tended to crumble; therefore, the percentage of fine-grained lithologies may be significantly lower than that calculated from recovered intervals.

X-Ray Diffraction Analysis

X-ray diffraction (XRD) results for Units I, III, and IV in Hole 787B are shown in Table 3. In Unit I, the clay fraction contains chlorite, smectite, mica, and kaolinite. Calcite, quartz, and siderite are also present in this unit.

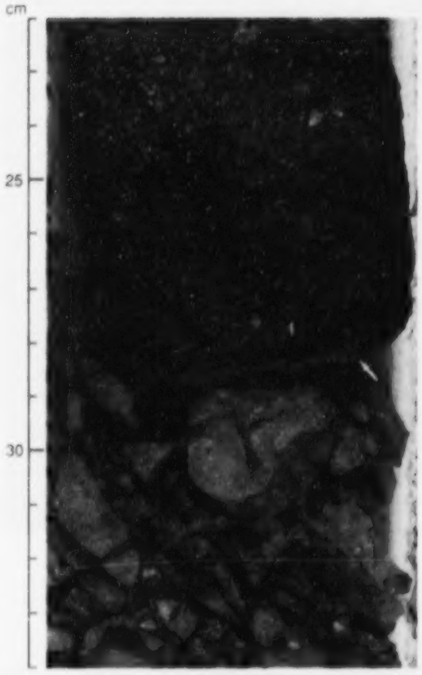

Figure 13. Vesicular base of lapilli tuff unit (indicated by arrow) shown in Figure 12. Interval shown is 126-787B-13R-3, 22-34 cm.

Vitric silty claystone and vitric siltstone of Unit III contain traces of 1.4-nm clays in bulk samples, along with large amounts of feldspar, quartz, and calcite. Maghemite and halite (from pore water) are accessory minerals.

The silty claystone, clayey siltstone, and fine-grained sandstone in Subunit IVA are rich in smectite, with traces of mica (1.0 nm) and chlorite (Fig. 21A). Feldspar, calcite, quartz, and zeolite are also present. Clinoptilolite in clayey siltstone (Sample 126-787B-24R-1, 143 cm) is well crystallized (Fig. 21B). Clinoptilolite is a low-temperature alteration product commonly found in siliceous deep-sea sediments buried 100 m or more below the sediment/water interface (Kastner, 1979). A broad background in the XRD records indicates the presence of amorphous materials.

A nannofossil silty claystone in Subunit IVB contains a large amount of smectite with a trace of mica. Feldspar, quartz, and calcite are also present.

Sediment Accumulation Rates

Sedimentation rates for Site 787 were established from calcareous nannofossil ages and paleomagnetic data (Table 4), which were used to construct the age-depth curve shown in Figure 22. Sedimentation rates in the late Oligocene are 120 m/m.y. at the base of the hole (< 30.3-27.74 Ma) and 26 m/m.y. in the interval between 27.01 and 24.21 Ma.

Most of the Miocene section was not recovered. Only a short interval of Zone CN8 appears to be present in Core 126-787B-5R. Similarly, only a short section of Pliocene sediment (3.5-4.6 Ma) was recovered; this interval has a sedimentation rate of 9.2 m/m.y. One nannofossil datum was present in the Pleisto-

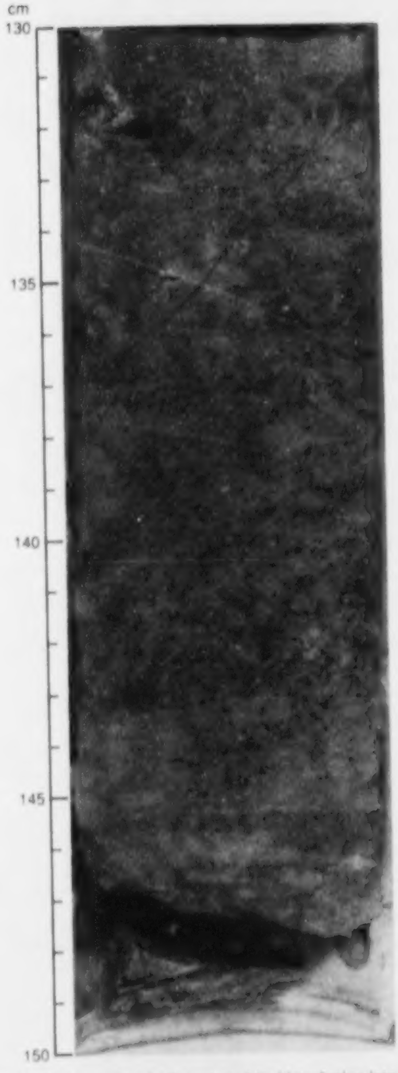

Figure 14. Black, sandy ash disseminated by bioturbation into nannofossil chalk. Interval shown is 126-787B-30R-1, 130-150 cm.

cene (first occurrence, or FO, of *Emiliana huxleyi*), giving an estimated sedimentation rate of 67.2 m/m.y. for the Quaternary. However, this rate may be suspect because we may not have recovered the surface (i.e., zero age) sediments.

Interpretation

Unit I

The sandy gravels and sands that characterize this unit appear to form a veneer of coarse, volcaniclastic, unconsolidated

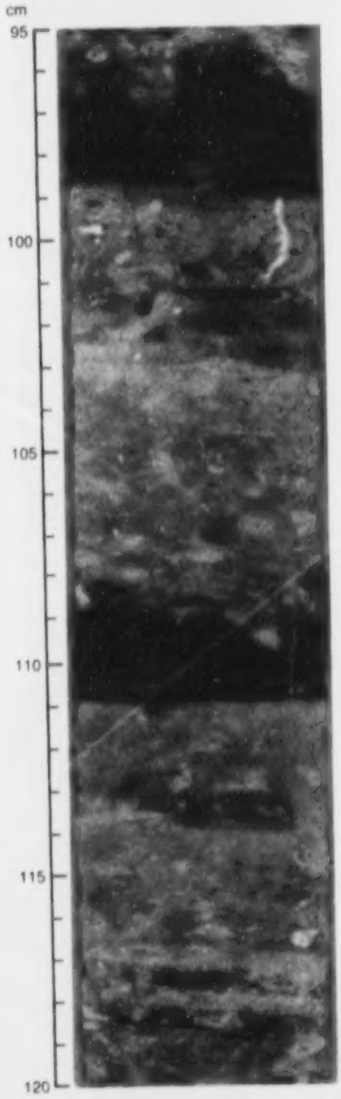

Figure 15. Black, lithic-crystal-vitric siltstone/fine sandstone beds (94-98.5 and 107-110.5 cm) with tops disrupted by bioturbation. The interval from 117 to 120 cm is probably a thin ash that has been almost completely disrupted by burrowers. Interval shown is 126-787B-25R-2, 95-120 cm.

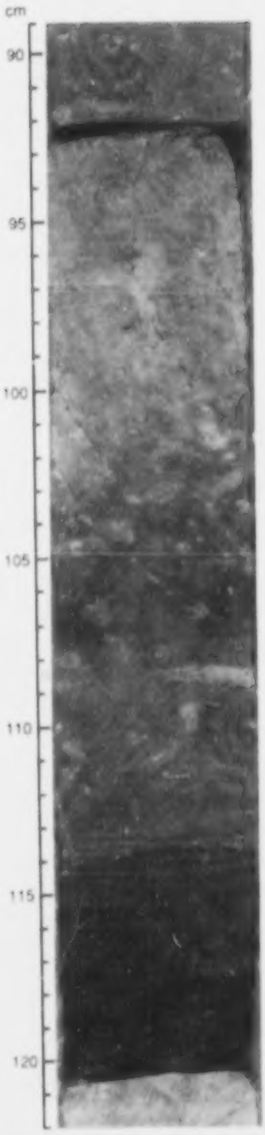
cm
90
95
100
105
110
115
120

Figure 16. Graded silty sandstone to siltstone with wavy laminations, overlain by light-colored, bioturbated nannofossil-rich claystone, with burrows extending downward into the top of the clastic unit. Interval shown is 126-787B-29R-4, 89–122 cm.

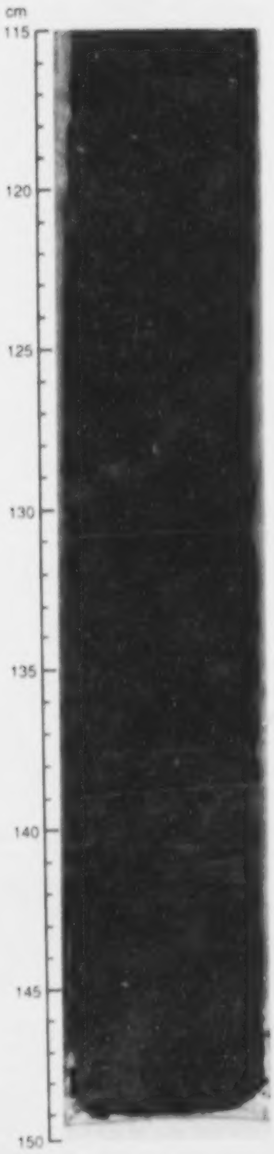
cm
115
120
125
130
135
140
145
150

Figure 17. Plastically folded sandy mudstone and clayey siltstone in overturned section. Interval shown is 126-787B-21R-5, 115–150 cm.

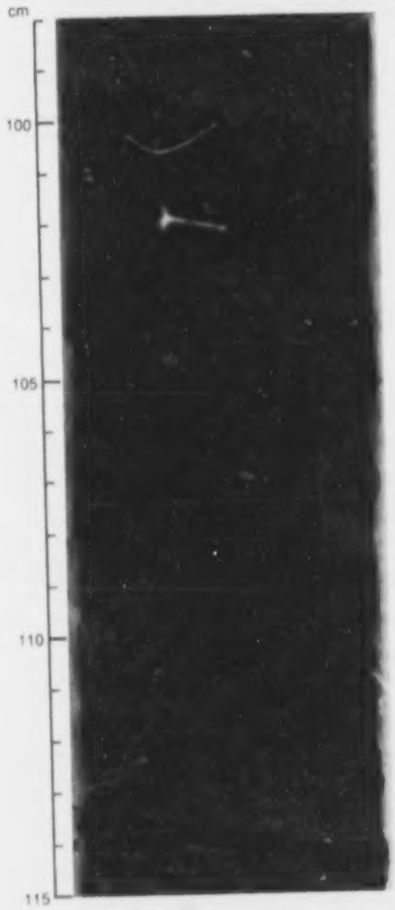

Figure 18. Extensional microfaults (apparent dips 45°-60°) crosscutting very fine-grained sandstones and siltstones with apparent normal offset of 1-2 cm. Interval shown is 126-787B-21R-6, 98-115 cm.

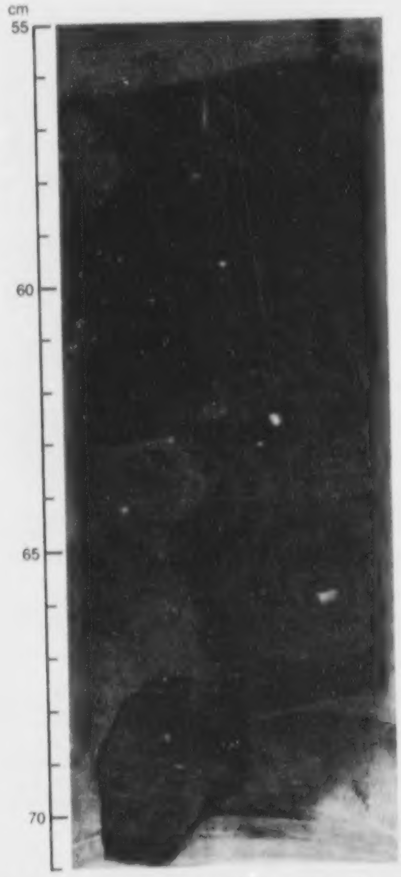

Figure 19. Sandstone injection into finely laminated silty claystone. The left-most, rotated, silty claystone piece at 67-70 cm was surrounded by sandstone (which occurs in the core catcher of Core 126-787B-21R) and was therefore detached from the wall of the sandstone dike. Interval shown is 126-787B-21R-7, 55-71 cm.

material on the southern marginal terrace of Aoga Shima Canyon (see Figs. 3 and 4). Biostratigraphic data indicate an age of late Quaternary (<0.275 Ma) for Unit I, suggesting that sand and gravel are not being transported in Aogo Shima Canyon.

The texture of the material in Unit I and its location on the floor of a submarine canyon suggest transport by sediment gravity flows, perhaps high-concentration turbidity currents that were characterized by intense clast interactions (dispersive pressure) (Pickering et al., 1989).

Unit II

Recovery of this unit was very limited (4.5%). We interpret these nannofossil oozes and nannofossil-rich silty clays as pelagic or hemipelagic deposits. The vitric silt grains indicate fallout from volcanic eruptions along the volcanic arc.

There is a marked difference in texture between Units I and II, and a sharp change in consolidation from Unit II to III, the latter being lithified. These contrasts, together with the biostratigraphic data (see "Biostratigraphy" section, this chapter), suggest that the upper and lower boundaries of Unit II are unconformities. The erosional surface between the rocks of Unit III and the soft sediments of Unit II may be part of the basal surface of a Miocene or Pliocene paleocanyon that cut into upper Oligocene rocks (Unit III).

Unit III

The fine-grained, strongly burrowed rocks of Unit III are predominantly hemipelagic sediments deposited in a distal, deep-water setting. The main sources of Unit III detritus were nannofossils that settled from the sea surface, infrequent fine-grained

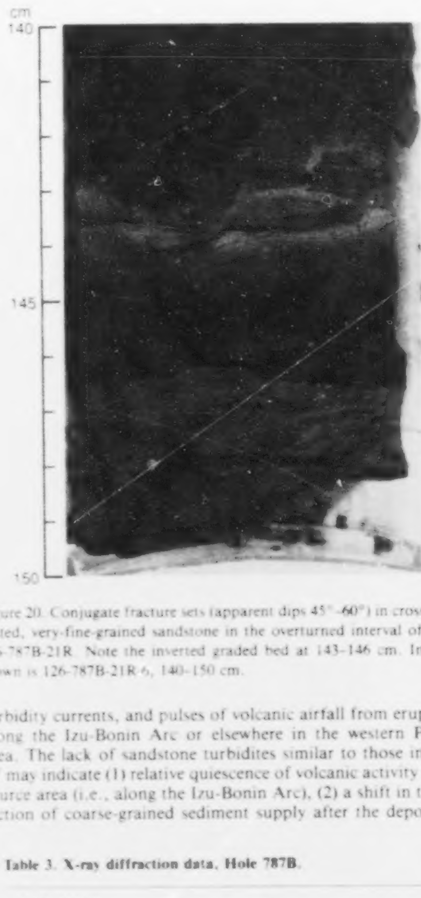

Figure 20. Conjugate fracture sets (apparent dips 45°-60°) in cross-laminated, very-fine-grained sandstone in the overturned interval of Core 126-787B-21R. Note the inverted graded bed at 143-146 cm. Interval shown is 126-787B-21R-6, 140-150 cm.

turbidity currents, and pulses of volcanic airfall from eruptions along the Izu-Bonin Arc or elsewhere in the western Pacific area. The lack of sandstone turbidites similar to those in Unit IV may indicate (1) relative quiescence of volcanic activity in the source area (i.e., along the Izu-Bonin Arc), (2) a shift in the direction of coarse-grained sediment supply after the deposition of Unit IV, or (3) relative tectonic uplift of this area, with contemporaneous turbidity currents moving primarily along the deeper forearc-basin axis. The pyroclastic flow deposit near the base of Unit III and the presence of some disseminated ash within Unit III indicate some local (as well as regional) volcanicity at this time. The occurrence of turbidite sandstones of this age at Site 792, about 40 km to the west (see "Correlation and Comparison of Forearc Sites," this volume), supports the second hypothesis.

The deformation fabrics in Unit III all formed in an extensional stress field. Movement on the microfaults is consistently extensional. The subvertical, kinked, veinlet structures are identical to those that Ogawa and Miyata (1985) interpreted to be extensional fracture cleavages formed in rapidly consolidating (wet) sediments. Clastic injections are also compatible with an extensional regime: early fractures were opened by extension and filled with poorly sorted, liquefied sediment.

Unit IV

We interpret the graded silty sandstone and siltstone beds in Subunit IVA, which show incomplete Bouma sequences (Bouma, 1962), as volcaniclastic turbidites. The interbedded massive and bioturbated finer grained sediments, including nannofossil-rich silty claystones and nannofossil-rich claystones, are primarily hemipelagic deposits. The bed thicknesses, sandstone/shale ratios, and sedimentary structures are typical of basin-plain turbidite settings (e.g., Ricci Lucchi and Valmori, 1980). Sedimentation rates were about 120 m/m.y. (Fig. 22), which is relatively low compared with rates for submarine fans and tectonically active basins of the California Borderland (Stow et al., 1985).

The slide unit in Core 126-787B-21R indicates a favorable combination of high water content in the sediment, probable seismic activity, and possibly bottom slopes of a few degrees in this part of the forearc basin. The paleoslope direction cannot be determined from the cores. After lithification, the sedimentary succession was fractured under extension, which accounts for the observed microfaults.

Subunit IVB contains significant thicknesses of structureless, volcaniclastic granule-rich and pebbly sandstone, interbedded with thin-bedded, fine-grained sandstones and siltstones that we interpreted as turbidites. Similar massive pebbly sand-

Table 3. X-ray diffraction data, Hole 787B.

Core, section interval (cm)	Unit	Color	Texture	Clay minerals (1.4-0.7 nm)	Minerals
126-787B-					
1R-CC, 4-6	I	10YR 6/6	Very coarse sand with yellowish clay	Bulk of clay parts chlorite + smectite < mica + kaolinite	Calcite > quartz > siderite Siderite is $FeCO_3$
7R-1, 65	III	5Y 4/1	Dark gray vitric nannofossil-rich silty claystone	Bulk 1.4-nm traces	Feldspar > maghemite Quartz, calcite
10R-2, 94	III	5Y 7/2	Vitric siltstone (ash)	Bulk 1.4-nm clays	Calcite > quartz > halite
19R-5, 134	IVA	5GY 4/1	Silty claystone	Fine 1.482-nm abundant smectites Medium 1.499-nm common smectites Coarse 1.243-nm, trace	Feldspar, zeolite, amorphous materials
24R-1, 15	IVA	5G 2/1	Burrowed clayey siltstone with scattered sand grains	Bulk 1.482-nm abundant 1.0-nm traces 0.7-nm chlorite, traces	Feldspar, trace calcite Trace quartz
24R-1, 143		5G 2/1	Burrowed clayey siltstone with pods of fine sand (ash?)	Bulk 1.4-nm traces 1.0-nm traces 0.7-nm chlorite, traces	Calcite, clinoptilolite, feldspar
25R-4, 112-113	IVA	5Y 2.5/1	Very dark gray very fine sandstone to siltstone	Bulk 1.43-nm abundant 0.7-nm chlorite, trace	Calcite, mordenite, or stilbite, Feldspar
33R-2, 104-107	IVB	N5	Nannofossil silty claystone	Bulk 1.497-nm abundant 0.999-nm mica, trace	Feldspar > quartz > calcite 0.8458-nm, trace

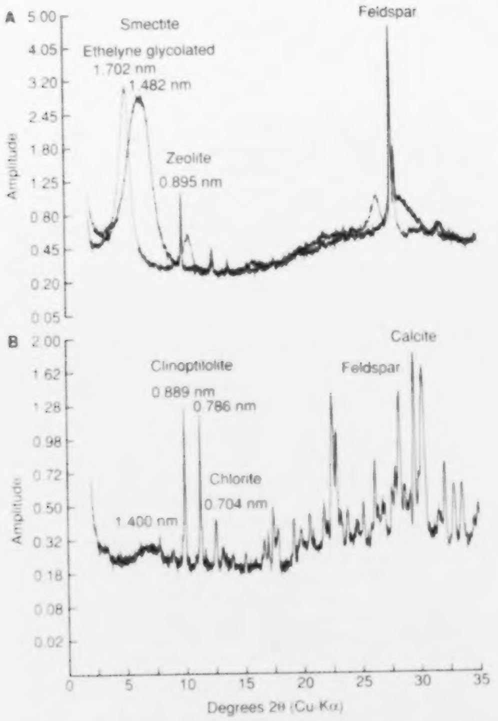

Figure 21. X-ray diffraction analyses. **A.** Sample 126-787B-19R-5, 134 cm, showing a large amount of smectite with feldspar and zeolite. The 1.482 nm peak was shifted to 1.702 nm by ethylene glycol treatment. **B.** Sample 126-787B-24R-1, 143 cm, showing large amounts of clinoptilolite, feldspar, and calcite with a small amount of chlorite (0.704 nm) and a trace of 1.4-nm minerals.

stones, which include large intraclasts of silty claystone, are typically present in channelized units in well-documented ancient successions (Nilsen and Abbott, 1981).

BIOSTRATIGRAPHY

Calcareous Nannofossils

Hole 787A

Sample 126-787A-1W-CC contains *Discoaster berggrenii*, *D. bollii*, *D. loeblichii*, and *D. calcaris*. Ordinarily, the ranges of these species do not overlap but occur in adjacent zones (Zones CN7, CN8, and CN9) in the upper Miocene. However, this sample was from a core catcher at the bottom of a washed hole, and the species could easily have been mixed together as a result of drilling.

Hole 787B

Samples 126-787B-1R-CC through 126-787B-3R-CC contain *Gephyrocapsa oceanica* and *Emiliania huxleyi*, and fall within Zone CN15 (late Quaternary). This interval contains a moderate amount of reworked Pliocene and Miocene species, such as *Re-*

Table 4. Chronostratigraphic data, Hole 787B.

Biostratigraphic event[1]		Core, section, interval (cm) (126-787B-)	Depth (mbsf)	Age (Ma)
Calcareous nannofossils				
Emiliania huxleyi	FO	3R-CC	15.51-21.47	<0.275
R. psuedoumbilica	LO	4R-1, 7-8	15.51-21.47	3.5
C. rugosus	FO	5R, 10-11	31.00-40.30	4.6
R. bisecta	LO	6R, 82-88	31.29-41.10	ca. 23.7
S. distensus	LO	27R-CC	250.7-252.7	28.2
S. ciperoensis	FO	34R-CC	320.1	<30.3
Paleomagnetic events				
Base of third normal in Anomaly 6c		7R, 130	51.1-58.8	24.21
Top of second normal in Anomaly 8		14R/15R-2	121.7-131.5	27.01
Base of second normal in Anomaly 8		19R-4, 50	170.8-171.04	27.74
Top of first normal in Anomaly 9		25R-4, 110	229.3-230.78	28.15
Base of first normal in Anomaly 9		31R/32R	283.5-298.2	28.74
Biostratigraphic zones				
Nannofossil Zone CN8		5R-CC	30.9-40.3	8.2-8.9

[1] FO = first occurrence, LO = last occurrence.

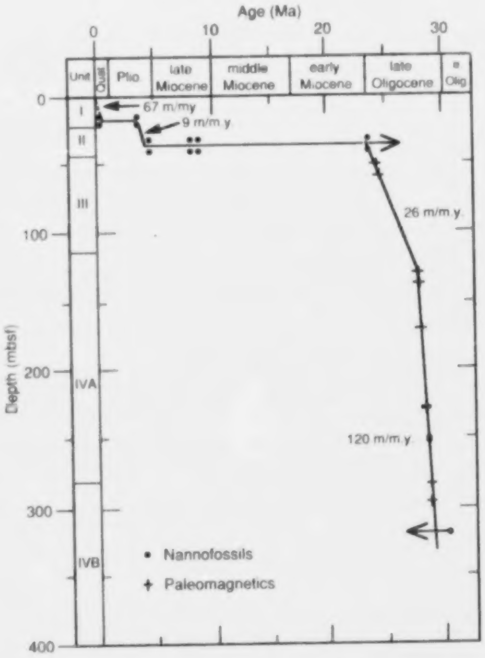

Figure 22. Age-depth plot of paleomagnetic and nannofossil data for Hole 787B. Upper and lower depth limits are given for each biostratigraphic and paleomagnetic datum. See Table 4 for details.

ticulofenestra pseudoumbilica, *Discoaster brouweri*, *D. variabilis*, *D. pentaradiatus*, *D. berggrenii*, and *Calcidiscus macintyrei*.

Samples 126-787B-4R-1, 7–8 cm, -4R-2, 4–5 cm, -4R-CC, and -5R-1, 10–11 cm, contain *Reticulofenestra pseudoumbilica*, *Sphenolithus abies*, *Discoaster variabilis*, *D. surculus*, *D. brouweri*, *Pseudoemiliania lacunosa*, and *Ceratolithus rugosus*, which would place them in the lower Pliocene Zones CN10C–CN11. These samples also contain moderate amounts of reworked Miocene species, such as *Discoaster berggrenii*, *D. quinqueramus*, *D. loeblichii*, *D. deflandrei*, and *Minylitha convallis*.

Sample 126-787B-5R-CC contains *Minylitha convallis*, *Discoaster neohamatus*, and *D. bergeni*, and is constrained to upper Miocene Zone CN8. Other species present are *Discoaster brouweri*, *D. prepentaradiatus*, *D. icarus*, *D. pentaradiatus*, *D. variabilis*, *Reticulofenestra pseudoumbilica*, *Coccolithus pelagicus*, *Calcidiscus leptoporus*, and *Sphenolithus moriformis*.

Samples 126-787B-6R-1, 87–88 cm, through -34R-CC are located between the last occurrence (LO) of *Reticulofenestra bisecta*, marking the Oligocene/Miocene boundary, and the first occurrence (FO) of *Sphenolithus ciperoensis*, which marks the base of upper Oligocene Zone CP19. The LO of *Sphenolithus distentus*, which marks the boundary between Subzones CP19A and CP19B, occurs in Sample 126-787B-27R-CC. The Oligocene sediments in Hole 787B contain a low-diversity assemblage with moderate preservation throughout most of the section, with scattered samples exhibiting higher diversity. Typical species in this interval include *Discoaster deflandrei*, *D. calculosus*, *D. adamanteus*, *Coccolithus pelagicus*, *Reticulofenestra bisecta*, *Cyclicargolithus floridanus*/*C. abisectus*, and *Sphenolithus moriformis*.

The abundance of discoasters in the upper Miocene and upper Oligocene sections of Holes 787A and 787B suggest warm-water conditions during the corresponding time intervals.

Planktonic Foraminifers

Hole 787B

Cores 126-787B-1R, -2R, and -3R are assigned to Zone N22 of early Pleistocene age, given the presence of rare *Globorotalia truncatulinoides* and *G. menardii* (sinistral), and the absence of *Globigerinoides ruber* (pink), *G. calida calida*, and *Pulleniatina finalis*.

Sample 126-787B-4R-CC contains rare specimens of *Globorotalia tosaensis* and *Sphaeroidinella dehiscens*, placing it in Pliocene Zones N19–N21.

The Pleistocene and Pliocene assemblages are dominated by *Globorotalia inflata* and *Globigerinoides* spp.

Sample 126-787B-5R-CC contains rare specimens of *Globorotalia plesiotumida*, *G. merotumida*, *Globigerina* cf. *falconensis*, and *G. drury*, placing this sample in the upper Miocene Zones N16–N18.

A single specimen of *Catapsydrax dissimilis* (upper Oligocene to lower Miocene range) was present in Sample 126-787B-19R-CC.

The planktonic foraminiferal assemblages do not show dissolution effects under the reflected-light microscope at about 100X magnification. The fair to good preservation of foraminifer shells is probably the result of rapid clastic sedimentation rates.

Paleoceanography

The planktonic foraminifer assemblages in Quaternary Samples 126-787B-1R-CC and -2R-CC are represented by warm-water taxa such as *Globigerinoides sacculifer*, *G. ruber*, *G. quadrilobatus*, *G. conglobatus*, *Pulleniatina obliquiloculata*, and *Globorotalia menardii*, as well as by cooler water species including *Globigerina bulloides*, *G. pachyderma* (dextral), *Globigerinita glutinata*, and *Globigerina quinqueloba*. These two intervals are preceded in Sample 126-787B-3R-CC by colder water faunas dominated by *Globorotalia truncatulinoides* and *Globorotalia inflata*, with less abundant *G. bulloides* and dextral *G. pachyderma*. Warm-water taxa occur in lower abundances in this sample.

The paleotemperatures indicated by the upper Pliocene faunas (Core 126-787B-4R) were probably somewhat higher than those that prevailed during the deposition of sediments in Core 126-787B-3R. We make this interpretation given the dominance of the *Globorotalia menardii* group, globigerinoids, and *Sphaeroidinelopsis* spp., as well as the lower abundances of globigerinids. As several representative species in this core are extinct, our interpretation is tentative, pending confirmation by $\delta^{18}O$ measurements. Sample 126-787B-5R-CC contains cold and warm surface and subsurface morphotypes. Water paleotemperatures were slightly higher for this sample than for the late Pliocene. Our basis for this assumption, to be confirmed by oxygen-isotope measurements, is the predominance of menardiform globorotalids, globigerinoids, and *Sphaerodinelopsis* spp., as well as the lower abundances of globigerinids.

Benthic Foraminifers

Samples 126-787B-1R-CC through -5R-CC contain *Cibicidoides wellerstorfi* and are correlative with the cosmopolitan benthic foraminiferal Zone CD4 (Kaiho, in press), which corresponds to the post-middle middle Miocene turnover event. This fauna is characterized by deep-oceanic taxa such as *C. wellerstorfi*, *Oridorsalis umbonatus*, *Melonis barleeanus*, *Hoeglundina elegans*, *Pleurostomella* spp., *Pullenia bulloides*, *Uvigerina* spp., *Pyrgo* sp., and *Epistominella exigua*. The presence of these taxa indicates depositional water depths of 2000–4000 m and normal oxygen conditions in the surface sediments. Sample 126-787B-3R-CC contains the inner neritic species *Elphidium crispum*, which was probably transported from shallower depths.

Benthic foraminifers from Samples 126-787B-8R-1, 32–34 cm through -27R-CC are rare, moderately preserved, and include *Cibicidoides* sp., *Oridorsalis umbonatus*, *Pullenia bulloides*, *Stilostomella* spp., *Pleurostomella* spp., and *Chrysalogonium* sp. The presence of these calcareous species and rare planktonic foraminifers indicates depositional water depths of 3000–4000 m. The absence of *C. wellerstorfii* and *Nuttallides truempyi* in these samples allows assignment to Zone CD3, which corresponds to the interval between the LO of *N. truempyi* (near the middle/upper Eocene contact) and the FO of *C. wellerstorfi* (middle middle Miocene).

Radiolarians

Quaternary sediments from Site 787 contain abundant radiolarians. With the exception of rare, poorly preserved specimens in Core 126-787B-13R, identifiable radiolarians are absent below Core 126-787B-5R, although we commonly observed infilled and highly corroded radiolarian ghosts.

An abundant and well-preserved radiolarian assemblage was recovered from Samples 126-787B-1R-CC through -3R-CC. This assemblage contains *Lamprocyclas maritalis*, *Anthocyrtidium angulare*, *Axoprunum angelinum*, *Theocorythium trachelium*, and *Eucyrtidium calvertense* and is typical of the lower Pleistocene *Anthocyrtidium angulare* Zone.

Sample 126-787B-5R-CC contains a radiolarian assemblage that is diluted by volcanogenic debris. This assemblage includes *Diartus hughesi*, which indicates the upper Miocene *Didymocyrtis antepenultima* Zone.

A single identifiable specimen *Lithocyclia angusta* was recovered from Sample 126-787B-13R-CC. The specimen is poorly preserved but permits tentative assignment to the upper Oligocene *Dorcadospyris ateuchus* Zone.

Summary

Biostratigraphy

A summary of the biostratigraphic results for Site 787 is presented in Figure 23.

We washed Hole 787A down to 34.5 mbsf and recovered one core-catcher sample, which contained the upper Miocene calcareous nannofossils *Discoaster bollii, D. loeblichii, D. calcaris*, and *D. berggrenii*.

The presence of the calcareous nannofossil *Emiliania huxleyi* in Cores 126-787B-1R, -2R, and -3R indicates a late Quaternary age for this interval. Some reworking is evidenced by the presence of early Pleistocene or older calcareous nannofossils, planktonic foraminifers, and radiolarians. This interval corresponds to Unit I (see "Lithostratigraphy and Accumulation Rates," this chapter).

The interval from Samples 126-787B-4R-1, 7–8 cm, to -5R-1, 10–11 cm, contains a calcareous nannofossil assemblage indicative of the lower Pliocene (Zones CN10C–CN11). The planktonic foraminifers in Sample 126-787B-4R-CC are indicative of the lower to upper Pliocene (Zones N19–N21). Therefore, this interval is assigned an early Pliocene age.

Sample 126-787B-5R-CC is assigned a late Miocene age on the basis of calcareous nannofossils, planktonic foraminifers, and radiolarians. A hiatus probably separates this sample from the overlying Pliocene sediments, but because of poor core recovery in Core 126-787B-5R we cannot estimate the extent of this hiatus. The Miocene and Pliocene sediments correspond to Unit II (see "Lithostratigraphy and Accumulation Rates," this chapter).

Interval 126-787B-6R-1, 87–88 cm, through -34R-CC is assigned a late Oligocene age, primarily on the basis of calcareous nannofossils. The low-diversity assemblage contains *Reticulofenestra bisecta, Discoaster deflandrei, D. calculosus, Cyclicargolithus floridanus/C. abisectus, Sphenolithus ciperoensis*, and *S. distentus*. Single specimens of the planktonic foraminifer *Catapsydrax dissimilis* in Sample 126-787B-19R-CC and the radiolarian *Lithocyclia angusta* in Sample 126-787B-13R-CC also corroborate the late Oligocene age assignment for this interval. This interval corresponds to Unit III and Subunits IVA and IVB (see "Lithostratigraphy and Accumulation Rates," this chapter) and is separated from the overlying Miocene sediments by a hiatus of at least 14.8 m.y.

Paleoenvironments

Planktonic foraminiferal evidence suggests that surface-water temperatures were warm in the Pliocene and Quaternary, except for a cooler interval in Core 126-787B-3R (Quaternary), when the colder water species *Globorotalia truncatulinoides* and *G. inflata* dominated the fauna. The dominance of the *Globorotalia menardii* group, globigerinoids, and *Sphaeroidinelopsis* spp. suggest warm-water conditions in the late Miocene. An abundance of discoasters in the Miocene and Oligocene intervals also indicates warm-water conditions during these times.

The calcareous benthic foraminiferal fauna indicates deep-oceanic conditions (lower bathyal to upper abyssal depths; >2000

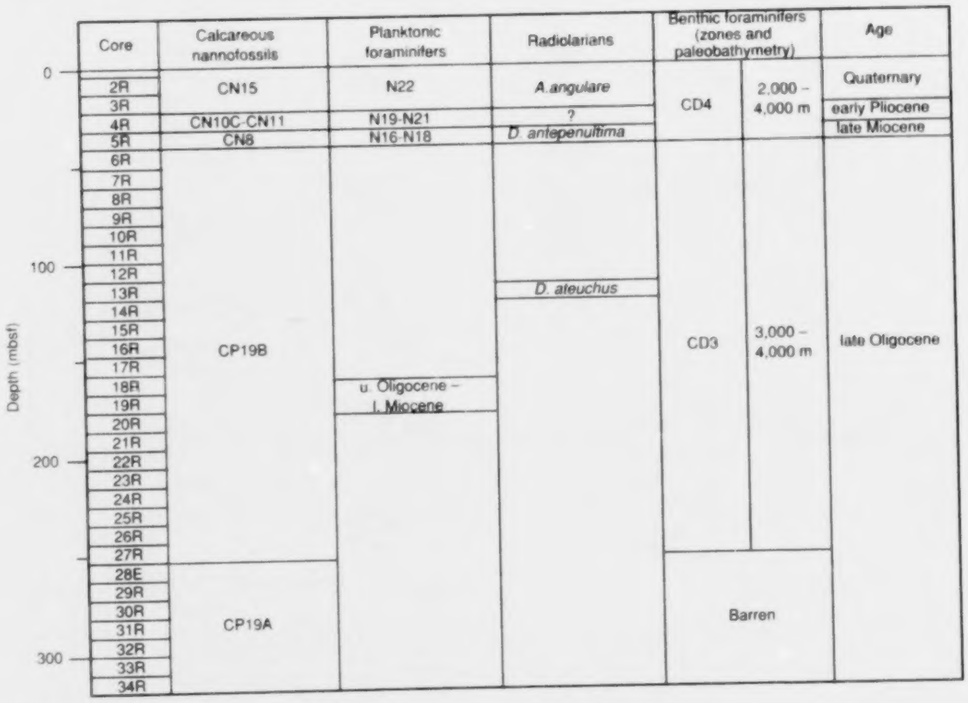

Figure 23. Summary of the biostratigraphic and paleobathymetric results for Hole 787B.

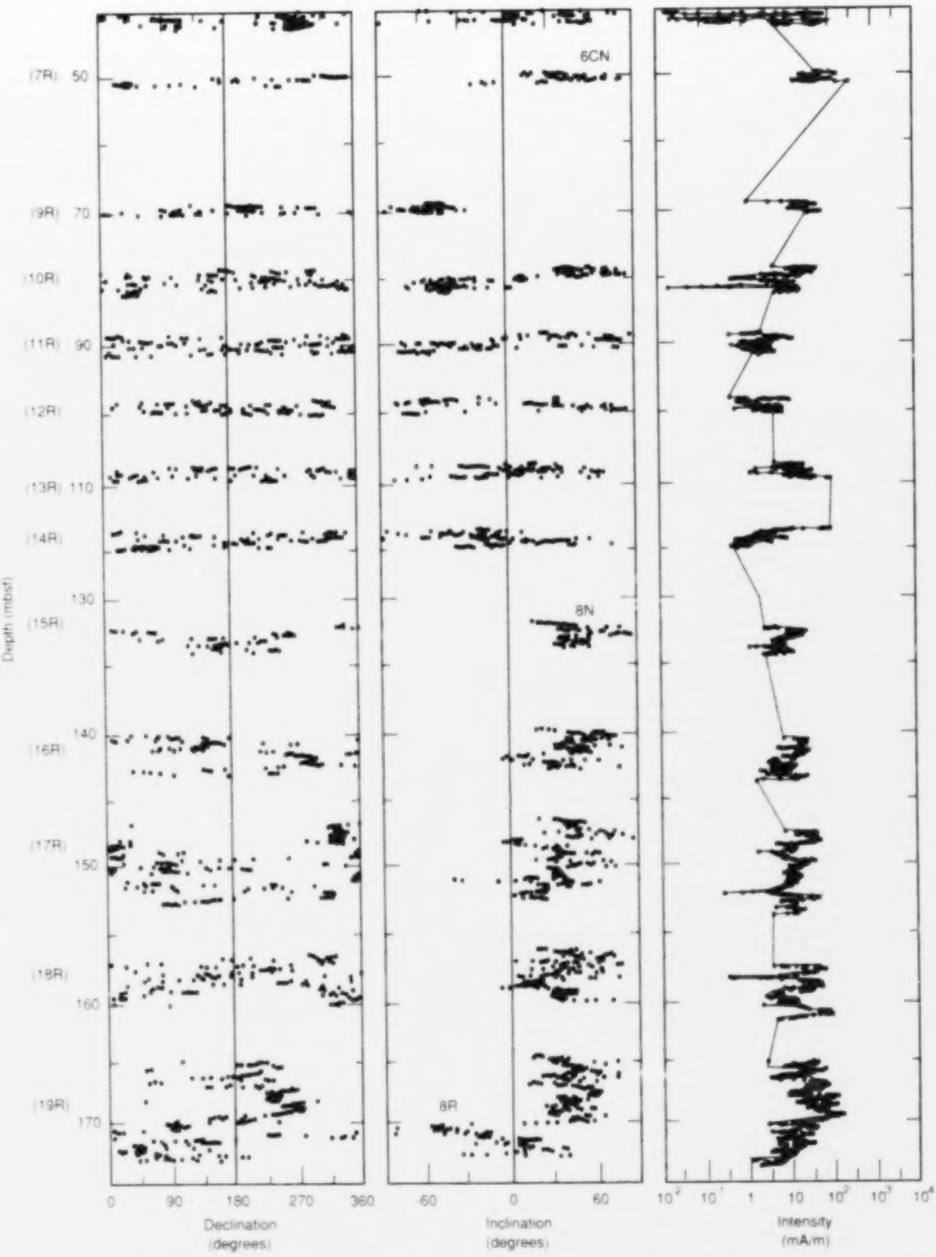

Figure 24. Paleomagnetic results vs. depth (mbsf) for Hole 787B. All data are obtained after optimum AF demagnetization. Core numbers are indicated in parentheses. Probable beginnings of polarity chrons are indicated with inclination data.

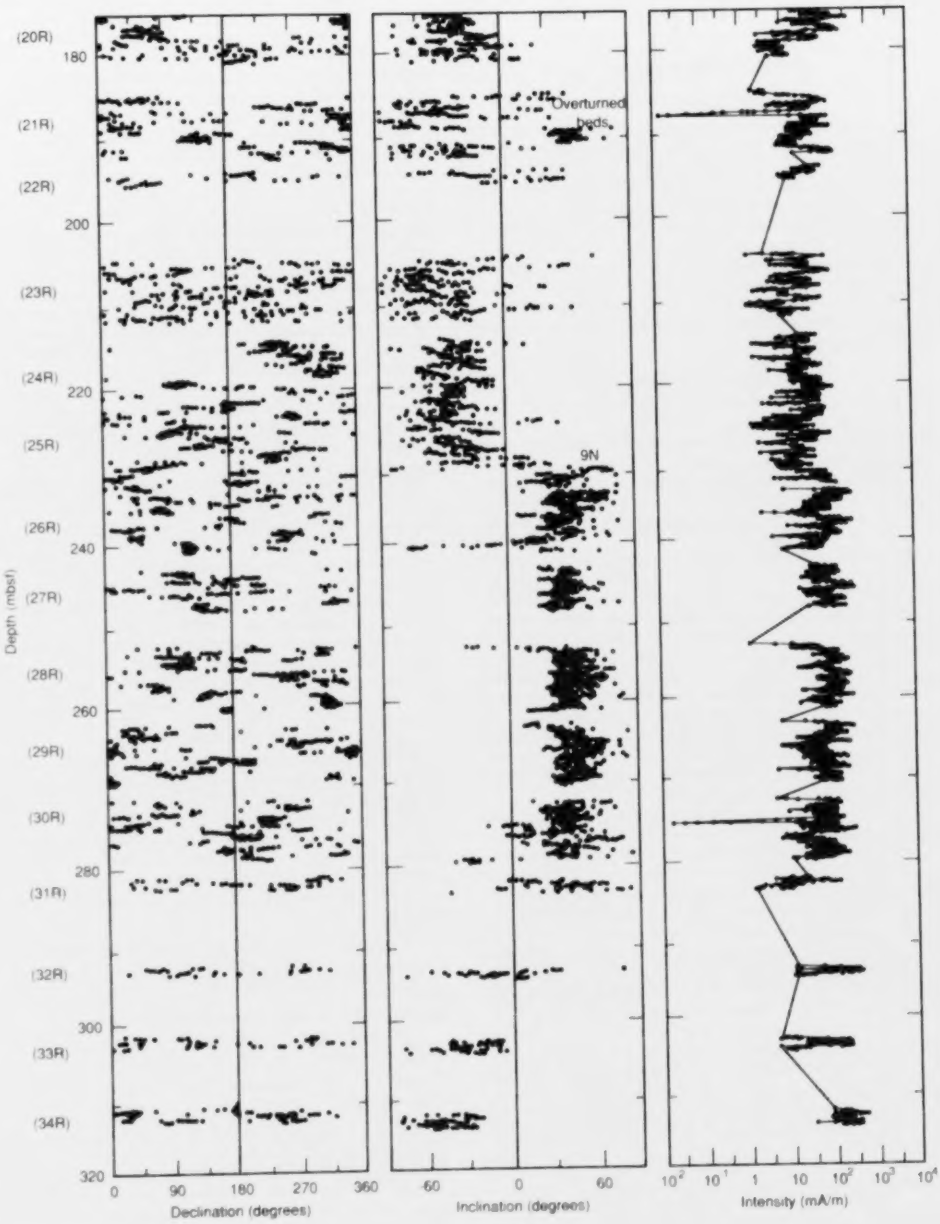

Figure 24 (continued).

m and above the CCD) during most of the depositional interval at Site 787. In Samples 126-787B-3R-CC and -5R-CC, the inner neritic species *Elphidium crispum* indicates downslope transport from shallow waters.

PALEOMAGNETISM

Introduction

To establish the magnetostratigraphy and detect possible latitudinal movement of Site 787, we measured the remanent magnetization of the cores. We measured most archive halves with the 2G-Enterprises pass-through cryogenic magnetometer. Several discrete samples were also measured using the Molspin magnetometer and the Fully Automatic Spinner (FAS) magnetometer (see "Explanatory Notes" chapter, this volume). Archive halves were subjected to alternating field (AF) demagnetization using the three-axial-coil system attached to the cryogenic magnetometer. Discrete samples were stepwise demagnetized using a Schonstedt AF Demagnetizer or the AF demagnetizer attached to the FAS magnetometer.

Magnetostratigraphy

Hole 787B

The natural remanent magnetization (NRM) of most archive halves from Hole 787B was measured at 3-cm intervals. Magnetic directions and intensity after the highest AF demagnetization step are shown in Figure 24. Declinations are arbitrary because all cores were drilled with an unoriented rotary core barrel.

A primary component of remanent magnetization generally appears to be preserved in the cores. The NRM intensities decreased by 10%-50% after 15-mT AF demagnetization for almost all claystone and siltstone samples. The weaker, coarse-grained sandstone samples are much less resistant to AF demagnetization; therefore, to preserve some magnetic signal in the archive halves, we used lower maximum alternating fields (2-8 mT). The NRMs of the sandstones were commonly overprinted with a present-field normal component of magnetization that masked the polarity of the primary remanence; the claystones were less commonly overprinted. In general, AF demagnetization was effective in removing this "soft" component to reveal the underlying primary polarity (Fig. 25).

The first three cores from this hole were coarse grained and highly disturbed, so we did not measure their remanence. After AF demagnetization, we could discern several short and long magnetic-polarity intervals for some of the core segments measured (Fig. 24). We divided the magnetostratigraphy of the site into four parts, accordingly: (1) the upper part (Sections 126-787B-4R-1 to -14R-3) was characterized by incomplete recovery and has several short normal/reversed intervals; (2) the upper-middle part (Sections 126-787B-15R-1 to -19R-4) is a long, normal-polarity interval; (3) the lower-middle part (Section 126-787B-19R-4 to -25R-4) is dominated by reversed polarity (note that the onset of a short, normal-polarity interval at Sample 126-787B-21R-5, 115 cm [189.5 mbsf; Fig. 24], correlates with an overturned slump unit [see "Lithostratigraphy and Accumulation Rates," this chapter, Fig. 17]); and (4) the lower part (Sections 126-787B-25R-4 to -34R-2) is characterized by a long, normal-polarity interval with a zone of reversed polarity at the bottom of the hole.

We carried out additional NRM measurements and stepwise AF demagnetizations on selected discrete samples collected from the working halves to examine the stability of remanent magnetization (Table 5). Many of these samples have a dominant, primary component of NRM that one can discern after removal of a "soft" secondary component (Fig. 26). These results confirm the validity of the polarity sequence obtained from our measurement of the archive halves. The magnetization associated with the bioturbated claystones appears to be consistent in both direction and intensity with that of the finely laminated intervals, indicating that the remanent magnetization was acquired after deposition and bioturbation.

According to the biostratigraphic ages of the cores (see "Biostratigraphy," this chapter), the age of the upper part of Hole 787B ranges from late Oligocene to Pliocene, whereas the age of the other three parts is late Oligocene (nannofossil Zone NP24 or NP25). The normal-polarity interval associated with the top of Unit III (Core 126-787B-7R, ~50 mbsf) may represent the bottom part of normal-polarity Chron 6C (Fig. 27). If this is true, then the many short normal- and reversed-polarity intervals recorded in the underlying cores would be the result of hiatuses in sedimentation and/or the rapid magnetic reversal rate in the mid-late Oligocene. Because paleontological datums are absent within the upper upper Oligocene (see "Biostratigraphy," this chapter), a firm polarity chron assignment within this zone is not possible. For the lower three parts of the hole, we correlate the long N-R-N-R polarity interval sequence with Chrons 8N, 8R, 9N, and the short reversed zone within 9N (Fig. 27), on the basis of the nannofossil biochronology (see "Biostratigraphy," this chapter).

In general, magnetization is assumed to have been acquired sequentially in an upward direction. The correlation between the sharp polarity reversal and the beginning of the slump unit in Section 126-787B-21R-3 (centered at 190 mbsf; Fig. 24) indicates that magnetization was acquired before the slumping event. However, in Section 126-787B-26R-5 (~240 mbsf), a short interval of reversed polarity (55-110 cm) occurs in the upper half of the long-normal-polarity Chron 9N. This reversed interval correlates precisely with an unusual zone of diffuse bedding laminations (Fig. 28), suggesting a restricted zone of remagnetization associated with diagenesis, and having remanence acquired after the polarity of the magnetic field had reversed.

Paleolatitude

The mean inclination values shown in Figure 24 are approximately 40°, although in Core 126-787B-28R, zones of low scatter have inclinations of ~32° (Fig. 29). These data indicate that Site 787 was situated at a latitude of 17°N in middle Oligocene time, which is 15° lower than the present latitude for this site. This implies that the Site 787 locale has been shifted from an area of lower latitude by plate motion, as may be the case for the West Philippine Basin (Louden, 1977) and the Daito Ridge (Kinoshita, 1980).

SEDIMENT/FLUID GEOCHEMISTRY

Nine 10-cm-long, whole-round samples were obtained from Hole 787B for electrical resistivity measurements, pore-water squeezing, and sediment and fluid analyses.

The headspace hydrocarbon analyses did not show any gases above background level and thus are not reported.

Sediment Resistivity

The formation factors calculated from the resistivity measurements vary between 4.8 and 28.6 (Table 6), and the vertical distribution exhibits a pronounced maximum at 130.3 mbsf (Section 126-787B-15R-2; Fig. 30). This section consists of a strongly lithified silty sandstone. In general, formation factors in claystones and mudstones vary between 8 and 20. It is possible that the maximum reading has been affected by the measurement

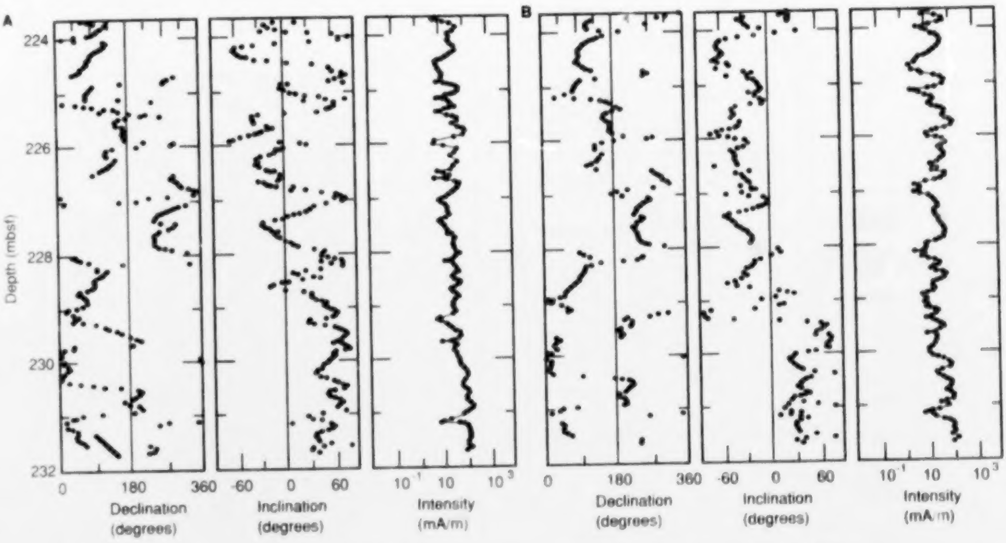

Figure 25. Paleomagnetic results for Core 126-787B-25R. **A.** Before AF demagnetization to 15 mT. **B.** After demagnetization.

Table 5. **Remanence properties of discrete samples, Hole 787B.**

Core, section, interval (cm)	Optimum AF (mT)	Inc (deg)	J_o ($\times 10^{-3}$ mA/M)	J_{AF} ($\times 10^{-3}$ mA/M)	Lithology
126-787B-					
4R-1, 22	100	+45	59.4	8.67	Clay
5R-1, 22	30	+43	128.0	7.72	Clay
7R-1, 11	45	+38	128.0	41.4	Claystone
7R-2, 3	25	+49	42.0	26.6	Clay
13R-1, 36	50	−35	72.6	12.4	Agglomerate
13R-1, 104	50	−32	57.5	14.4	Agglomerate
13R-3, 87	30	+42	119.0	23.5	Claystone
14R-2, 37	30	+48	3.75	0.44	Sandstone
14R-3, 43	10	+50	7.86	3.70	Sandstone
15R-2, 22	15	+44	5.98	1.45	Sandstone
15R-4, 39	30	+44	27.0	13.3	Claystone
16R-4, 61	15	+42	11.6	12.4	Siltstone

procedure, which involves drilling holes for the electrodes. Although the exact magnitude of the maximum may be dubious, its presence is supported by neighboring data.

Sediment Geochemistry

Sediments from Site 787 were analyzed on board ship for inorganic carbon and total carbon and nitrogen (see "Explanatory Notes," this volume), and these data are presented in Table 7. The carbonate analyses are reported in the physical property section. The concentration of organic carbon in Hole 787B is generally <0.5%. There is an overall decrease of organic carbon from the top to the bottom of the hole. The concentration of total nitrogen varies between 0.06% and less than the detection limit.

Fluid Geochemistry

Because we drilled Hole 787B with the RCB, we paid special attention to possible contamination of the pore water by drilling-mud filtrate. Starting with Core 126-787B-4R, drilling mud was used during the drilling of alternate cores. The analytical results presented in Table 8 show that the drilling-mud filtrate has a chloride concentration about 1/20 of the pore waters. Thus, the comparatively low concentrations of sodium and chloride in the sample from Section 126-787B-12R-1 probably reflect some mixing with drilling-mud filtrate.

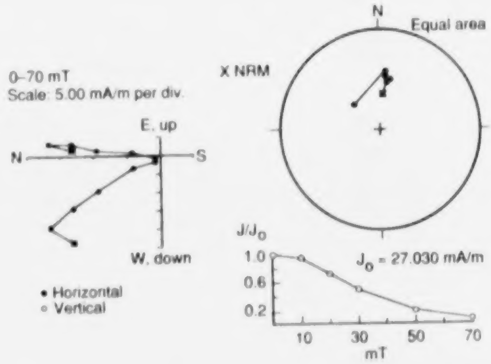

Figure 26. Example of change of NRM direction, intensity, and orthogonal components of magnetization with AF demagnetization, Sample 126-787B-15R-4, 39 cm.

Qualitatively, the distribution of dissolved constituents in the upper 140 m of the sediment is typical of most deep-sea sediments and includes decreasing potassium and magnesium concentrations (Fig. 31) and increasing concentrations of calcium and strontium. These changes are related to reactions involving

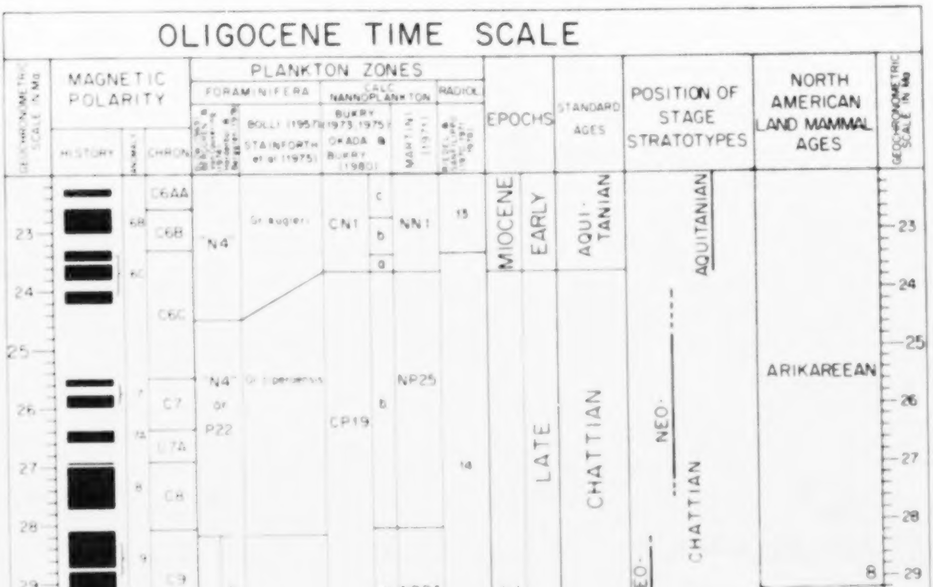

Figure 27. Oligocene time scale (from Berggren et al., 1985).

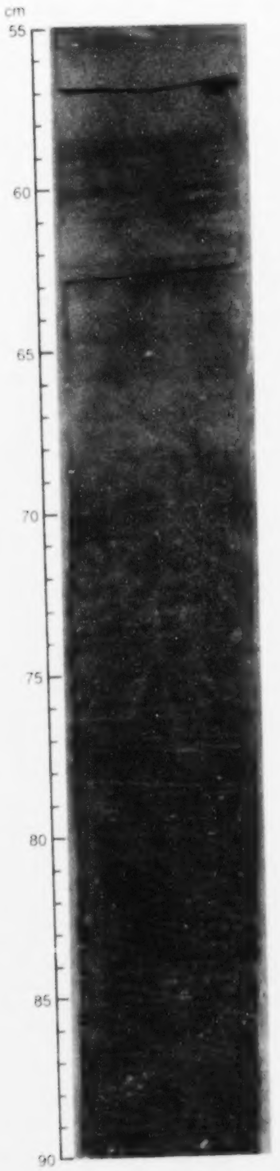

Figure 28. Transition from normal to diffuse bedding laminations, Interval 126-787B-26R-5, 55-90 cm. The laminations correlate to a zone of anomalous magnetic polarity in Section 126-787B-26R-5.

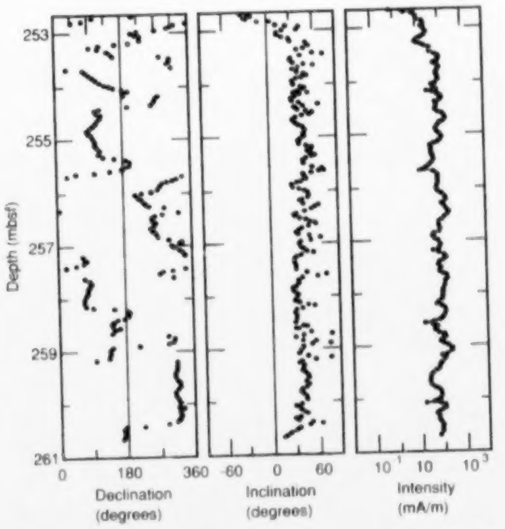

Figure 29. Paleomagnetic results, after AF demagnetization to 15 mT, for Core 126-787B-28R.

Table 6. Sediment resistivity, measurement temperature, pore-water resistivity at 25°C, and formation factor of sediments from Hole 787B.

Core, section, interval (cm)	Depth (mbsf)	K_c (m)	R_s (ohm-m)	t (°C)	R_{pw} (ohm-m)	F
123-787B						
9R-2, 65-75	71.20	0.1007	1.33	13.5	0.198	4.8
12R-1, 3-13	98.18	0.0946	1.49	14.9	0.204	5.0
15R-2, 146-156	130.21	0.0908	8.23	14.9	0.198	28.6
18R-1, 80-90	157.05	0.1031	4.59	11.9	0.192	17.7
21R-2, 140-150	187.95	0.1050	2.65	11.4	0.195	10.2
24R-2, 140-150	217.05	0.0959	2.81	13.1	0.189	10.7
27R-2, 42-52	244.97	0.0976	1.78	16.6	0.193	6.1
30R-2, 140-150	274.95	0.0956	1.49	17.9	0.190	5.0
33R-1, 58-60	301.43	0.0952	2.42	13.6	0.194	7.8

Note: K_c = cell constant; R_s = sediment resistivity at measurement temperature (t); R_{pw} = pore water resistivity at 25°C; F = formation factor.

the alteration of volcanogenic material in the sediments as well as alteration reactions in the oceanic crust (e.g., Gieskes, 1983). Quantitatively, however, the changes are much more pronounced than usually observed. This is caused by the combined effect of abundant volcanogenic material, high formation factors, and rather high rates of sedimentation. The latter two factors render diffusive communication with the overlying seawater less efficient, thus allowing steeper concentration gradients to be maintained. The pronounced minimum of dissolved silica between 130 and 157 mbsf (Cores 126-787B-15R through -18R) indicates that silica is removed rapidly from the pore water in this region.

In contrast, below 140 mbsf the distribution of dissolved constituents is unusual. In deep-sea sediments the magnitude of the slopes of the various concentration profiles discussed above may vary vertically. However, except for sites with high bacterial activity, the slopes rarely change sign. At Site 787 the concentration profiles of potassium, magnesium, calcium, strontium, and

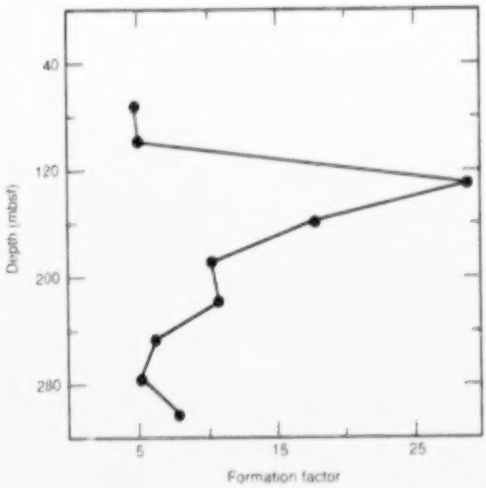

Figure 30. Formation factor of sediments from Hole 787B. The data are given in Table 6.

Table 7. Concentration of carbon and total nitrogen in sediments from Hole 787B.

Core, section, interval (cm)	Depth (mbsf)	Total carb (%)	Inorg carb (%)	Org carb (%)	Total N (%)
126-787B-					
1R-1, 88.0-90.0	0.88	0.15	0.13	0.02	LD
2R-1, 80.0-82.0	3.10	0.33	0.28	0.05	0.01
2R-2, 120.0-122.0	5.00	0.15	0.15	LD	LD
2R-3, 47.0-49.0	5.77	1.84	1.30	0.54	0.06
3R-1, 56.0-58.0	12.46	1.44	1.35	0.09	0.01
3R-3, 29.0-31.0	15.19	0.20	0.17	0.03	LD
5R-1, 13.0-15.0	31.03	1.66	1.43	0.23	0.02
6R-1, 52.0-53.0	40.82	2.42	2.21	0.21	0.03
6R-2, 61.0-62.0	42.41	1.38	1.21	0.17	0.04
7R-1, 84.0-85.0	50.64	2.44	2.26	0.18	0.03
7R-2, 9.0-11.0	51.39	1.37	1.17	0.20	0.02
9R-1, 56.0-57.0	69.56	3.08	3.07	LD	0.03
9R-2, 34.0-35.0	70.84	1.28	0.92	0.36	0.03
9R-2, 65.0-75.0	71.15	4.28	4.09	0.19	0.03
9R-2, 65.0-75.0	71.15	4.52	4.15	0.37	0.03
9R-3, 33.0-34.0	71.58	0.99	0.86	0.13	0.04
10R-1, 64.0-66.0	79.34	0.57	0.34	0.23	0.04
11R-1, 27.0-29.0	88.67	7.96	7.73	0.23	0.03
11R-CC, 5.0-7.0	91.68	1.38	1.05	0.33	0.03
11R-CC, 5.0-7.0	91.68	1.20	1.05	0.15	0.04
12R-1, 3.0-13.0	98.13	4.35	4.14	0.21	0.05
12R-1, 3.0-13.0	98.13	4.91	4.75	0.16	0.02
12R-1, 88.0-90.0	98.98	2.78	2.66	0.12	0.03
12R-2, 63.0-65.0	100.23	6.31	6.19	0.12	0.01
14R-2, 12.0-14.0	119.12	0.32	0.34	0.00	LD
14R-3, 52.0-54.0	120.73	0.28	0.18	0.10	0.01
15R-1, 43.0-44.0	127.63	0.56	0.30	0.26	0.01
15R-2, 140.0-150.0	130.03	0.13	0.09	0.04	LD
18R-1, 80.0-90.0	157.00	0.15	0.12	0.03	LD
20R-1, 133.0-135.0	176.83	0.10	0.08	0.02	LD
20R-2, 32.0-34.0	180.32	0.19	0.13	0.06	0.01
21R-2, 140.0-150.0	188.00	2.69	2.49	0.20	0.01
24R-2, 140.0-150.0	217.00	1.69	1.68	0.01	0.01
27R-2, 42.0-52.0	244.92	1.48	1.43	0.05	0.01
30R-2, 140.0-150.0	274.90	0.47	0.37	0.10	LD
33R-1, 58.0-68.0	301.38	0.11	0.07	0.04	LD

Note: LD = less than detection limit.

sodium (Fig. 31) are reversed towards the bottom of the hole. DSDP Site 453, drilled in a sediment pond on the west side of the Mariana Trough, is one of the few Ocean Drilling Program (ODP)/DSDP sites showing this type of distribution pattern. Gieskes and Johnson (1982) reported concentration profiles of calcium, magnesium, strontium, potassium, lithium, and silica similar to the results obtained at Site 787. Their interpretation was that the pore water in the lower part of the sediment column is affected by the circulation of seawater through brecciated igneous and metamorphic rocks at the depth of maximum penetration. None of the explanations for the breccias suggested by the Leg 60 Shipboard Scientific Party (e.g., talus pile, avalanche deposits, drilling in a fault plane) could explain their character (Hussong, Uyeda, et al., 1982).

Because of insufficient penetration at Site 787, only a small portion of the lower part of the concentration profiles could be established. Therefore, the idea that the pore-water concentration profiles are shaped by circulating seawater will remain a vague hypothesis. On the basis of a rough extrapolation of the concentration profiles, the "aquifer" could be situated about 40-60 m below our maximum penetration of 320.1 mbsf. A less attractive interpretation of the concentration profiles involves progressive contamination of the pore water with the surface seawater with which we cleaned the bit. We took great care in choosing the part of the core to be squeezed, and only continuous, 10-cm-long, whole-round sections were sampled. The whole rounds were examined and the outer parts scraped off before squeezing. Unfortunately, there are no shipboard analyses that can be used to assess this question. Onshore analyses for one of the isotopes produced by nuclear testing (e.g., ^{3}H, ^{90}Sr) or in nuclear reactors (e.g., ^{85}Kr) are needed.

Concentrations of sulfate and ammonia do not vary much, indicating that the bacterial activity in these low-organic-carbon sediments is minimal. This is further substantiated by the low levels of dissolved iron and manganese (Table 8). Evidently, the sub-bottom redox conditions are not sufficiently low enough to mobilize iron or manganese, except in the shallower intervals. The downhole decrease in alkalinity is probably caused by the precipitation of calcium carbonate in response to an increase in calcium from the alteration of volcanogenic material.

PHYSICAL PROPERTIES

Introduction

The techniques employed to acquire the physical property data at Site 787 are described in the "Explanatory Notes" chapter (this volume). Rotary drilling at this site resulted in significant disturbance to the unlithified sediment in Cores 126-787B-1R through -5R. Below Core 126-787B-5R, the recovered samples consisted of lithified or semilithified sediment (see "Lithostratigraphy and Accumulation Rates," this chapter). Consequently, no vane shear strength measurements were performed. Gamma-ray attenuation porosity evaluation (GRAPE) bulk-density measurements were run on most of the cores, but because the core sections did not completely fill the liners, the results are considered inaccurate (see the following discussion of index properties for more details).

Physical property measurements conducted on Hole 787B sediments include thermal conductivity, sonic (*P*-wave) velocity on discrete samples, wet-bulk density, porosity, water content, and grain density. Hole 787A, which consists of a single wash core, was not tested. Obviously spurious data are not recorded on the figures. However, all index property data are included in Table 9; anomalous data points are noted.

Index Properties

The results of all index property tests on Hole 787B sediments are presented in Table 9. Plots of the index property val-

Table 8. Composition of pore water from Site 787 sediments and of drilling-mud filtrate used during the drilling of Hole 787B.

Core, section, interval (cm)	Depth (mbsf)	pH	Alk. (mM)	Sal. (g/kg)	Cl^- (mM)	SO_4^{2-} (mM)	Na^+ (mM)	Mg^{2+} (mM)	Ca^{2+} (mM)	K (mM)	Li (μM)	Sr (μM)	Fe (μM)	Mn (μM)	SiO_2 (μM)	NH_4^+ (μM)
126-787B-																
9R-2, 65-75	71.20	7.43	1.52	36.0	561	28.4	476	44.5	23.4	7.1	18.4	124	LD	51	843	100
12R-1, 3-13	98.18	7.16	1.09	35.0	542	27.6	444	37.9	35.3	3.9	16.9	151	12	95	559	69
15R-2, 146-156	130.21	ND	ND	ND	562	23.9	476	7.2	57.8	3.0	7.7	172	ND	ND	68	56
19R-1, 80-90	157.05	8.07	0.99	36.5	582	27.8	476	4.3	72.5	2.1	7.7	188	LD	9	94	60
21R-2, 140-150	187.95	8.54	0.62	37.5	572	25.5	465	1.3	79.0	1.9	9.2	180	LD	7	354	76
24R-2, 140-150	217.05	7.04	ND	38.0	580	26.3	467	3.5	79.8	2.0	7.7	170	LD	9	581	55
27R-2, 42-52	244.97	8.67	0.76	37.5	578	27.2	464	1.8	76.1	2.2	7.7	178	LD	9	485	47
30R-2, 140-150	274.95	8.55	0.37	38.0	586	29.7	480	2.6	76.6	2.7	7.7	195	LD	5	528	31
33R-1, 58-68	301.43	ND	ND	ND	575	30.7	488	15.5	55.1	4.2	12.3	163	LD	24	516	68
Drilling mud filtrate		9.90	3.77	ND	25	5.0	90	2.9	0.3	1.4	15.8	2	LD	LD	132	11

Note: LD = less than detection; ND = not determined.

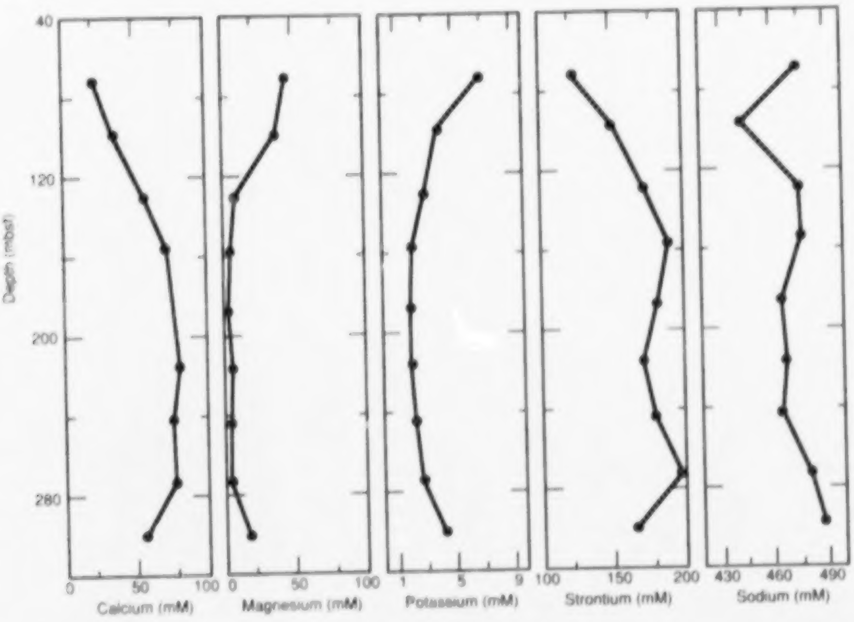

Figure 31. Composition of sediment pore waters, Hole 787B.

ues vs. sub-bottom depth in Hole 787B are presented in Figure 32.

The persistence of relatively high porosity values in deeper parts of the hole (e.g., as much as 60% at 280 mbsf, within the Oligocene sandstone unit) is surprising. Porosity values estimated from hand specimens and thin sections (see "Lithostratigraphy and Accumulation Rates," this chapter) of the recovered material are extremely low. Furthermore, applying Archie's Law (Archie, 1942), we calculated porosity values of approximately 20% and 30% for Samples 126-787B-13R-1, 56-58 cm, and -20R-1, 81-83 cm, respectively, from resistivity measurements. Index property measurements of these samples indicate porosities of 47% and 50%, respectively (Table 10).

There are several possible causes for these different porosity values. Archie's Law, which is empirically derived, may not be appropriate for these samples. However, sampling with a water-cooled rock saw and/or uncertainties in the reliability of wet volumes determined by the penta-pycnometer (Becker, Sakai, et al., 1988) also may bias the data (Table 11). In addition, porosity calculations using weights and dry volumes (Becker, Sakai, et al., 1988) are generally within 7% of the values obtained using the wet volumes. On the other hand, the porosity results obtained in Hole 787B are comparable to those previously reported for sediments from similar depositional/tectonic environments cored during ODP Leg 125 (Fryer, Pearce, Stokking, et al., in press) and DSDP Leg 60 (Hussong, Uyeda, et al., 1982).

Other explanations for the high porosity values include the presence of highly angular, porous volcaniclastic particles and an abundance of smectite minerals (see "Lithostratigraphy and

Table 9. Physical property data collected at Hole 787B.

Core, section, interval (cm)	Depth (mbsf)	Velocity (m/s)	Wet-bulk density (g/cm^3)	Grain density (g/cm^3)	Porosity (%)	Water content (%)	CaCO$_3$ (%)	Thermal conductivity (W/m·K)
126-787B-								
1R-1, 34-35	0.34							^{a}0.357
1R-1, 88-90	0.88		^{a}2.11	^{a}2.54	^{a}37.8	^{a}22.5	1.1	
2R-1, 43-45	2.73	4462						
2R-1, 80-82	3.10		^{a}1.80	^{a}2.67	^{a}53.8	^{a}40.6	2.3	
2R-2, 120-122	5.00		^{a}1.99	^{a}2.52	^{a}44.5	^{a}29	1.2	
2R-3, 47-49	5.77		^{a}1.62	^{a}2.53	^{a}72.1	^{a}83.9	10.8	
3R-1, 54-55	12.44							0.770
3R-1, 56-57	12.46		^{a}1.7	^{a}2.65	^{a}65.6	^{a}65.6	11.2	
3R-3, 28-29	15.18		^{a}1.99	^{a}1.85	^{a}84.5	^{a}77.3		
5R-1, 14-15	31.04		1.91	2.76	60.4	47.8	11.9	
6R-1, 52-54	40.42	1676	1.77	2.79	70.2	68.4	20.0	
6R-1, 102-103	41.32							^{a}0.246
6R-2, 59-61	42.39	1667	1.72	2.71	70.4	72.0	10.1	^{a}0.067
7R-1, 84-86	50.64	1765	1.74	2.82	60.1	54.7	18.8	
7R-1, 93-94	50.73							^{a}0.728
7R-2, 9-11	51.39	1592	1.78	2.67	58.4	50.5	9.7	
8R-1, 24-26	59.53	1986	1.67	2.83	69.3	73.9		
8R-1, 37-38	59.67							^{a}1.094
9R-1, 44-45	69.44							0.697
9R-1, 55-57	69.55	1680	^{a}1.66	^{a}2.79	^{a}68.2	^{a}72.5	12.2	
9R-2, 35-37	70.85	1708	1.80	2.87	63.6	56.5	7.7	
9R-3, 33-35	71.58	1836	1.93	2.77	67.3	55.7		
9R-3, 38-39	70.88							0.774
10R-1, 55-56	79.25							1.007
10R-1, 64-66	79.34	1825	1.68	2.77	65.5	66.8	3.3	
10R-2, 94-96	81.14	1841	1.87	2.82	56.3	44.6	60.0	
10R-3, 20-21	80.40							1.271
11R-1, 27-29	88.67	1486	1.92	2.67	51.7	38.2	64.4	
11R-1, 107-108	89.47							1.247
11R-2, 70-71	90.60							1.205
11R-CC, 5-7	91.60	1775	1.60	2.61	64.0	64.8	8.7	
12R-1, 3-13	98.13		2.04	2.86	52.5	35.9	22.2	
12R-1, 88-90	98.98	1671	1.94	2.74	53.4	39.4	39.6	
12R-1, 111-112	98.21							^{a}1.532
12R-2, 48-49	100.08							1.234
12R-2, 63-65	100.23	1845	2.02	2.57	60.4	44.1	51.6	
13R-1, 56-58	108.36	3093	2.20	2.74	46.9	27.9		
13R-1, 64-68	108.44	3013	2.14	2.73	41.2	24.6		
13R-1, 94-96	108.74	3057	2.23	2.76	43.6	25.0		
13R-1, 111-113	108.91	3047	2.21	2.72	44.5	26.0		
13R-1, 123-136	109.03							1.190
13R-3, 115-117	111.25	1786	2.00	2.57	65.7	65.6	10.1	
13R-3, 119-120	111.99							1.003
14R-1, 115-117	118.65	2206	1.60	2.30	61.4	59.9	1.3	
14R-2, 12-14	119.12	2610	1.96	2.49	46.5	32.2	2.8	
14R-3, 52-54	120.73	2872	2.05	2.60	44.2	28.4	1.5	
15R-1, 72-74	127.92	2773	2.05	2.54	46.5	30.3	2.5	
15R-3, 29-31	130.44	2773	2.17	2.71	45.5	27.4	0.8	
15R-4, 89-90	220.70							0.970
15R-4, 92-94	132.57	2206	1.72	2.54	65.9	64.6	0.8	
16R-1, 138-140	138.18	1980	1.83	2.64	60.7	51.4	11.3	
16R-2, 90-91	139.20							1.081
16R-2, 125-127	139.55	1942	1.89	2.71	58.8	46.7	8.7	
16R-3, 72-73	140.52							0.929
16R-4, 103-105	142.33	1980	1.82	2.58	58.8	49.4	21.9	
16R-CC, 17-19	142.97	2210	1.92	2.55	58.7	45.7	0.9	
17R-1, 75-77	147.25	1945	^{a}1.92	^{a}3.01	^{a}36.0	^{a}23.7	8.6	
17R-1, 80-81	147.31							1.102
17R-2, 123-125	149.23	2220	1.98	2.74	60.8	45.9	1.0	
17R-3, 66-68	150.16	2340	2.08	2.97	61.7	43.7	0.7	
17R-5, 20-21	152.70							^{a}1.140
17R-5, 74-76	153.24	1960	1.85	2.47	53.5	42.2	6.1	
18R-1, 46-48	156.66	2055	1.96	2.51	46.3	32.3	1.8	
18R-1, 80-90	157.00		2.07	2.52	43.1	27.0		
18R-2, 10-11	157.80							^{a}1.190
18R-3, 118-120	159.78	1924	1.90	2.62	54.1	41.3	1.0	
19R-2, 38-40	167.68	2186	1.99	2.78	61.7	46.5	1.8	
19R-4, 46-48	170.76	1952	2.08	3.01	55.8	38.3	10.5	
19R-6, 52-54	173.82	2235	2.11	2.83	54.6	36.0	0.7	
20R-1, 81-83	176.31	2433	2.13	2.81	52.2	33.5	0.7	
20R-1, 133-135	176.83	2516	2.07	2.71	48.1	31.2	0.8	
20R-2, 7-9	177.07	2628	2.07	2.74	49.9	32.7		
20R-2, 57-60	177.57	2257	1.94	2.70	59.3	45.8		
20R-4, 32-34	180.32	2168	2.10	2.77	45.8	28.7	1.1	
21R-1, 52-54	185.62	2498	2.23	2.94	41.8	23.7	0.7	

Table 9 (continued).

Core, section, interval (cm)	Depth (mbsf)	Velocity (m/s)	Wet-bulk density (g/cm^3)	Grain density (g/cm^3)	Porosity (%)	Water content (%)	CaCO$_3$ (%)	Thermal conductivity (W/m·K)
126-787B-								
21R-2, 140-150	188.00		2.12	2.55	49.4	31.3		
21R-3, 65-67	188.75	2033	2.05	2.80	50.8	34.1	20.7	
21R-4, 35-37	189.95	2251	2.05	2.75	50.4	33.6	0.7	
21R-5, 100-102	192.10	2212	2.03	2.83	51.6	35.2	1.7	
21R-6, 93-95	193.53	1964	1.97	2.75	51.8	36.9	15.0	
22R-1, 75-77	195.55	2490	2.21	2.75	39.2	22.3		
23R-2, 52-54	206.42	2237	1.96	2.67	51.0	36.4	8.9	
23R-4, 63-65	209.53	2565	2.31	2.88	36.7	19.4	0.7	
23R-5, 77-79	211.17	3130	2.40	2.81	37.2	18.9	1.7	
24R-1, 110-112	215.20	2442	2.11	2.70	46.8	29.5	0.8	
24R-2, 140-150	217.00		1.84	2.44	57.0	46.7	11.0	
24R-3, 29-31	217.39	2095	2.07	2.68	53.9	36.5	14.0	
24R-4, 77-79	219.37	2266	1.95	2.49	48.2	33.9		
24R-5, 97-99	221.07	2161	1.76	2.42	55.9	48.2	0.2	
24R-6, 25-27	221.85	2355	1.84	2.51	58.5	48.4	10.4	
24R-7, 58-60	223.08	2537	2.14	2.90	50.5	31.9	60.0	
25R-1, 53-55	224.23	2139	1.74	2.49	61.5	56.8	15.3	
25R-1, 67-69	224.37	2043	1.74	2.49	61.5	57.0	4.8	
25R-1, 84-86	224.54	2034	1.74	2.37	57.0	50.4	0.9	
25R-1, 95-97	224.65	2069	1.79	2.32	58.0	49.8	0.3	
25R-1, 117-119	224.87	2113	1.79	*2.99	*38.6	*28.4	0.5	
25R-4, 117-119	229.37	2252	2.08	2.66	47.2	30.3	35.8	
25R-6, 4-6	231.24	2531	2.27	2.79	51.6	30.4	0.8	
26R-1, 82-84	234.22	2173	2.06	2.73	46.1	29.8	18.7	
26R-3, 86-88	237.26	2130	1.74	2.73	66.8	64.5		
26R-4, 145-147	239.35	2292					1.4	
26R-5, 47-49	239.87	2304	1.75	2.63	63.2	58.8	6.2	
27R-1, 122-124	244.22	2075	2.02	2.84	52.4	36.2	10.7	
27R-2, 42-52	244.92		2.01	2.83	51.0	35.1		
27R-2, 122-124	245.72	2432	1.97	2.75	59.0	44.8	11.9	
27R-4, 81-83	247.58	1987	1.87	2.80	59.7	48.6	25.1	
27R-CC, 11-13	248.24	3483	2.22	2.92	45.1	26.2	1.8	
28R-1, 45-47	253.15	2695	2.15	2.91	47.2	28.9	1.2	
28R-2, 146-148	255.66	2243	1.93	2.82	58.3	44.8	18.2	
28R-4, 93-95	258.13	2416	*2.33	*2.76	*35.3	*18.4	41.3	
28R-5, 122-124	259.77	2039	1.96	2.85	60.0	45.5	39.7	
29R-1, 95-97	263.35	2336	*2.28	*2.82	*35.4	*18.9	43.3	
29R-2, 70-72	264.60	1991	1.82	2.67	59.1	49.7	1.7	
29R-3, 69-71	266.09	2140	1.89	2.81	60.9	49.4	16.4	
29R-4, 43-45	267.33	1856	1.73	2.59	62.3	58.2		
29R-5, 107-109	269.47	2166	1.86	2.85	61.0	50.4	17.2	
30R-1, 104-106	273.04	2069	1.79	2.85	65.3	59.5	26.8	
30R-2, 140-150	274.90		1.79	2.57	59.9	52.2	3.1	
30R-3, 60-62	275.60	1991	1.94	2.57	58.9	45.1	0.9	
30R-4, 55-57	277.05	1993	1.88	2.78	58.4	46.8	23.7	
30R-5, 75-77	278.75	2090	1.87	2.83	63.1	52.7	35.7	
31R-1, 112-114	282.82	2899	2.28	2.94	41.8	23.2	26.8	
32R-1, 122-124	292.52	2850	2.31	2.89	44.4	24.5	0.9	
32R-2, 81-83	293.61	2660	2.07	2.72	51.9	34.5	8.2	
33R-1, 58-68	301.38		2.29	2.94	38.2	20.5	0.6	
33R-2, 61-63	302.09	2690	2.13	2.84	47.3	29.5	0.6	
34R-1, 50-52	311.00	2246	2.00	2.95	55.1	39.2		

* Indicates a value that is obviously spurious and has not been plotted in Figures 33, 34, 36, or 37.

Accumulation Rates," this chapter). Angular particles will result in a less densely packed, higher porosity sediment; smectite is associated with high porosity and water content because of its small size, high specific surface area, and propensity for adsorption of water (e.g., see discussion by Mitchell, 1976). Nevertheless, we recommend that the index property data be considered primarily as trends, rather than as absolute values.

GRAPE wet-bulk density measurements were conducted on Cores 126-787B-3R through -13R. However, rotary drilling caused reduction of core diameters, resulting in gaps between the core and liner. Because the GRAPE technique requires that the sediment completely fill the liners (Boyce, 1976), the GRAPE measurements are probably incorrect. A comparison of GRAPE and gravimetric bulk-density values for the depth interval between Sections 126-787B-9R-1 and -9R-3 (Fig. 33) supports this hypothesis. All GRAPE data fall below the gravimetrically determined values.

Porosity and water content values decrease downhole and are overprinted by significant small-scale variability. Much of the variability of the index properties, particularly in Subunit IVA, may be attributed to the existence of turbidite beds. Because our sampling scheme included representative samples from all turbidite lithologies, the high variability in the properties is not surprising. A detailed investigation of one turbidite sequence showed that physical properties change dramatically over short depth intervals within a single turbidite bed (Fig. 34).

An exception to the trend of decreasing porosity and water content with depth is found in Unit I, where these parameters actually increase with depth (Fig. 32). Sediments in this unit consist primarily of unlithified sand and are strongly disturbed

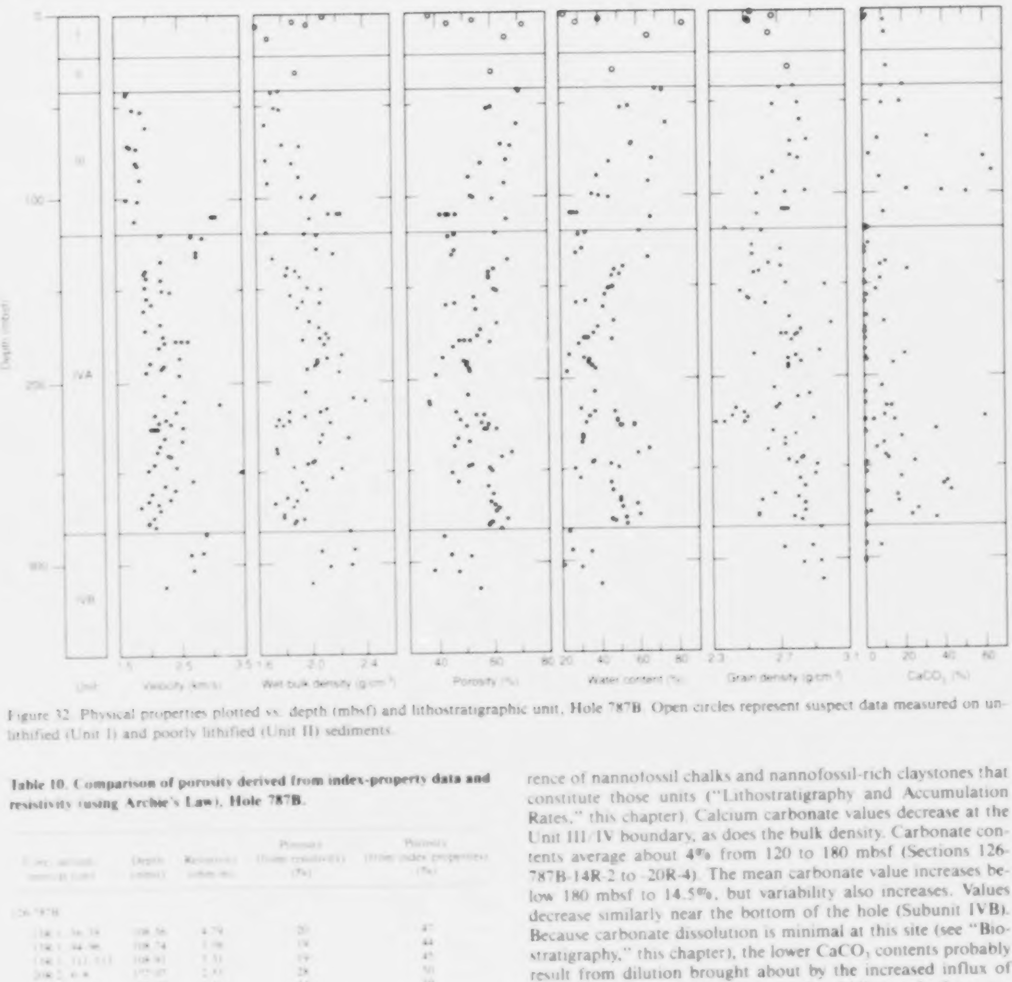

Figure 32. Physical properties plotted vs. depth (mbsf) and lithostratigraphic unit, Hole 787B. Open circles represent suspect data measured on unlithified (Unit I) and poorly lithified (Unit II) sediments.

Table 10. Comparison of porosity derived from index-property data and resistivity (using Archie's Law), Hole 787B.

Core, section, interval (cm)	Depth (mbsf)	Resistivity (ohm-m)	Porosity (from resistivity) (%)	Porosity (from index properties) (%)
126-787B				
13R-1, 36-38	108.56	4.79	20	47
13R-1, 54-56	108.74	5.06	19	44
13R-1, 71-73	108.91	5.31	19	45
20R-2, 6-8	177.07	2.83	28	50
20R-2, 57-59	177.57	1.66	34	59
20R-3, 81-83	178.31	1.74	34	52

by drilling. The anomalous increases in porosity and water content are probably the result of sample contamination by drilling fluid.

Contacts between the four lithologic units are clearly visible in the index property data. Distinct changes in porosity, bulk density, and water content are observed at these depths (Fig. 32). In addition, porosity and bulk-density data display slightly different trends within the different units. The lapilli tuff reported at the base of Unit III (see "Lithostratigraphy and Accumulation Rates," this chapter) is delineated in the index property values by low porosities and high bulk-density values.

Calcium carbonate content is relatively high in the upper three lithologic units (Fig. 32), with a maximum of 65% at 89 mbsf (Section 126-787B-11R-1); it is consistent with the occurrence of nannofossil chalks and nannofossil-rich claystones that constitute those units ("Lithostratigraphy and Accumulation Rates," this chapter). Calcium carbonate values decrease at the Unit III/IV boundary, as does the bulk density. Carbonate contents average about 4% from 120 to 180 mbsf (Sections 126-787B-14R-2 to -20R-4). The mean carbonate value increases below 180 mbsf to 14.5%, but variability also increases. Values decrease similarly near the bottom of the hole (Subunit IVB). Because carbonate dissolution is minimal at this site (see "Biostratigraphy," this chapter), the lower CaCO₃ contents probably result from dilution brought about by the increased influx of volcaniclastic material in the form of turbidites and other gravity-controlled sedimentary flows. The influence of turbidites on CaCO₃ content is shown in Figure 34. Within this single turbidite bed, low CaCO₃ contents are observed in the coarse lower parts and higher CaCO₃ contents in the upper hemipelagic division. Variations in carbonate content also are influenced by our sampling scheme, which included single samples from numerous different turbidite layers (see discussion above and Fig. 34).

We observed a positive relationship between grain density and bulk density, and an inverse correlation between wet-bulk density and porosity at this site. These relationships have been observed elsewhere in Pacific sediments (e.g., Wilkens and Handyside, 1983). However, bulk-density values from Hole 787B tend to be greater than expected, compared to calculated relationships for constant grain density (Wilkens and Handyside, 1983). Again, the possibility of inaccurate porosity values may explain some of this discrepancy.

Table 11. Calibration measurements for the penta-pycnometer, Hole 787B.

Run no.	Volume (cm^3)
1	16.3205
2	16.3227
3	16.3352
4	16.3242
5	16.3337
6	16.3456
7	16.3538
8	16.3534
9	16.3410
10	16.3694
11	16.3524
12	16.3359
13	16.3540
14	16.3518
15	16.3504
16	16.3457
17	16.3303
18	16.3469
19	16.3446
20	16.3401
21	16.3395
22	16.3382
23	16.3470
24	16.3440
25	16.3491

Note: standard known volume = 16.38 cm^3, mean value = 16.3428; standard deviation = ±0.0112.

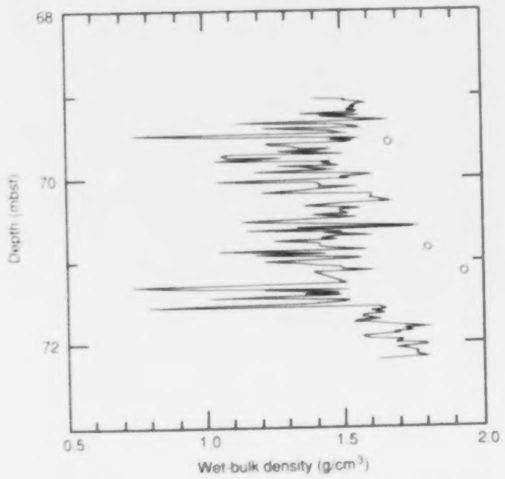

Figure 33. Plot of wet-bulk density determined gravimetrically (open circles) and by GRAPE (solid line) for Core 126-787B-9R.

Sonic Velocity

Sonic velocity measurements were performed on discrete samples from Site 787 cores (Tables 9 and 12; Figs. 32, 34, and 35). Because of the reduced core diameters that were a result of the rotary drilling, multisensor track (MST) sonic velocities were not measured. Coarse, unconsolidated sediments at the top of the hole also prevented Hamilton Frame velocity analyses on Cores 126-787B-1R through -4R. We observed a general increase in sonic velocity with depth. Unit III is characterized by relative uniform velocities ranging from 1.67 to 3.1 km/s. Above the lapilli tuff in Unit III, velocities average 1.71 km/s. Velocities from four samples within the lapilli tuff are 3.0–3.1 km/s, whereas below this tuff, velocities drop to 1.79 km/s within a fine-grained sedimentary unit.

At the top of Subunit IVA, velocities range from 2.21 to 2.87 km/s within a coarse, consolidated sand unit. Velocities within Subunit IVA range from 1.92 to 3.50 km/s and average 2.26 km/s. This unit is characterized by high-frequency fluctuations in velocity that may be attributed to the abundance of turbidite beds and other sedimentary structures indicative of downslope processes. As we usually performed the velocity measurements on one sample per section, we took representative samples from various levels within turbidite beds from section to section, but not within a single turbidite. This may explain the high-frequency scatter observed in the data shown in Figure 32. To illustrate this point, the results of a detailed study of a single turbidite sequence from Core 126-787B-25R-1 are shown in Figure 34. In this core, the physical property measurements exhibit significant changes, including a velocity variation of over 100 m/s. This study exemplifies the problem of sampling only once per section in areas of rapidly changing, thinly bedded lithologies. Subunit IVB, a pebbly sandstone, is characterized by velocities that range from 2.25 to 2.90 km/s and average 2.67 km/s.

Thermal Conductivity

All thermal conductivity results are presented in Table 9. Only values that fall within acceptable temperature drift rates ($< 0.04°C/min$) and curve fit parameters (< 0.015) are shown in Figure 36. Thermal conductivity measurements range from 0.697 to 1.271 W/m · K. Values measured above 75 mbsf are distinctly lower (average = ~0.75 W/m · K) than those below (average = ~1.11 W/m · K). Higher thermal conductivity values below 75 mbsf correlate with increased wet-bulk density and decreased porosity.

REFERENCES

Archie, G., 1942. The electrical resistivity log as an aid in determining some reservoir characteristics. *AIME Trans.*, 146:54.

Arthur, M. A., Carson, B., and von Huene, R., 1980. Initial tectonic deformation of hemipelagic sediment at the leading edge of the Japan convergent margin. *In* Langseth, M., Okada, H., et al., *Init. Repts. DSDP*, 56, 57, Pt. 1: Washington (U.S. Govt. Printing Office), 569–613.

Becker, K., Sakai, H., et al., 1988. *Proc. ODP, Init. Repts.*, 111: College Station, TX (Ocean Drilling Program).

Berggren, W. A., Kent, D. V., Flynn, J. J., and Van Couvering, J. A., 1985. Cenozoic geochronology. *Geol. Soc. Am. Bull.*, 96:1407–1418.

Bouma, A. H., 1962. *Sedimentology of Some Flysch Deposits:* Amsterdam (Elsevier).

Boyce, R., 1976. Definitions and laboratory techniques of compressional sound velocity parameters and wet-water content, wet-bulk density, and porosity parameters by gravimetric and gamma-ray attenuation techniques. *In* Schlanger, S., Jackson, E., et al., *Init. Repts. DSDP*, 33: Washington (U.S. Govt. Printing Office), 695–728.

Fryer, P., Langmuir, C. H., Taylor, B., Zhang, Y., and Hussong, D. M., 1985. Rifting of the Izu Arc, III. Relationship of chemistry to tectonics. *Eos*, 66(18):421.

Fryer, P., Pearce, J., Stokking, L. B., et al., in press. *Proc. ODP, Init. Repts.*, 125: College Station, TX (Ocean Drilling Program).

Gieskes, J. M., 1983. The chemistry of interstitial waters of deep-sea sediments: interpretation of deep sea drilling data. *In* Riley, J. P., and Chester, R. (Eds.), *Chemical Oceanography* (Vol. 8): London (Academic Press), 221–269.

Gieskes, J. M., and Johnson, J., 1982. Interstitial water studies, Deep Sea Drilling Project Leg 60. *In* Hussong, D. M., Uyeda, S., et al., *Init. Repts. DSDP*, 60: Washington (U.S. Govt. Printing Office), 749–754.

Hussong, D. M., and Uyeda, S., 1982. Tectonic processes and the history of the Mariana Arc: a synthesis of the results of Deep Sea Drilling Project Leg 60. *In* Hussong, D. M., Uyeda, S., et al., *Init. Repts. DSDP*, 60: Washington (U.S. Govt. Printing Office), 909–929.

Hussong, D., Uyeda, S., et al., 1982. *Init. Repts. DSDP*, 60: Washington (U.S. Govt. Printing Office).

Kaiho, K., in press. Morphotype changes of deep-sea benthic foraminifera during the Cenozoic Era and their paleoenvironmental implications. *Kaseki* (Fossils).

Kastner, M., 1979. Zeolites. *Reviews in Mineralogy*, 6:111-122.

Kinoshita, H., 1980. Paleomagnetism of sediment cores from Deep Sea Drilling Project Leg 58, Philippine Sea. *In* Klein, G. deV., Kobayashi, K., et al., *Init. Repts. DSDP*, 58: Washington (U.S. Govt. Printing Office), 765–768.

Klaus, A., and Taylor, B., in press. Submarine canyon development in the Izu-Bonin forearc: a SeaMARC II survey of Aoga Shima canyon. *GSA Bull.*

Louden, K. E., 1977. Paleomagnetism of DSDP sediments, phase shifting of magnetic anomalies, and rotations of the West Philippine Basin. *J. Geophys. Res.*, 82:2989–3002.

Lundberg, N., and Leggett, J. K., 1986. Structural features in cores from the slope landward of the Japan Trench, Deep Sea Drilling Project Leg 87B. *In* Kagami, H., Karig, D. E., Coulbourn, W. T., et al., *Init. Repts. DSDP*, 87: Washington (U.S. Govt. Printing Office), 807–842.

Mitchell, J., 1976. *Fundamentals of Soil Behavior*: New York (Wiley and Sons).

Nilsen, T. H., and Abbott, P. L., 1981. Paleogeography and sedimentology of Upper Cretaceous turbidites, San Diego, California. *AAPG Bull.*, 5:1256-1284.

Ogawa, Y., and Miyata, Y., 1985. Vein structure and its deformation history in the sedimentary rocks of the Middle America Trench slope off Guatemala, Deep Sea Drilling Project Leg 84. *In* von Huene, R., Aubouin, J., et al., *Init. Repts. DSDP*, 84: Washington (U.S. Govt. Printing Office), 811–829.

Okada, H., and Bukry, D., 1980. Supplementary modification and introduction of code numbers to the low-latitude coccolith biostratigraphic zonation. *Mar. Micropaleontol.*, 5:321–325.

Pickering, K. T., Hiscott, R. N., and Hein, F. J., 1989. *Deep Marine Environments: Clastic Sedimentation and Tectonics*: London (Unwin Hyman).

Ricci Lucchi, F., and Valmori, E., 1980. Basin-wide turbidites in a Miocene, over-supplied deep-sea plain: a geometrical analysis. *Sedimentology*, 27:241–270.

Stow, D. A. V., Howell, D. G., and Nelson, C. H., 1985. Sedimentary, tectonic, and sea-level controls. *In* Bouma, A. H., Normark, W. R., and Barnes, N. E. (Eds.), *Submarine Fans and Related Turbidite Systems*: Berlin-Heidelberg-New York (Springer-Verlag), 15–22.

Wilkens, R., and Handyside, T., 1983. Physical properties of equatorial Pacific sediments. *In* Mayer, L., Theyer, F., et al., *Init. Repts. DSDP*, 85: Washington (U.S. Govt. Printing Office), 839–847.

Ms 126A-106

NOTE: All core description forms ("barrel sheets") and core photographs have been printed on coated paper and bound as Section 3, near the back of the book, beginning on page 421.

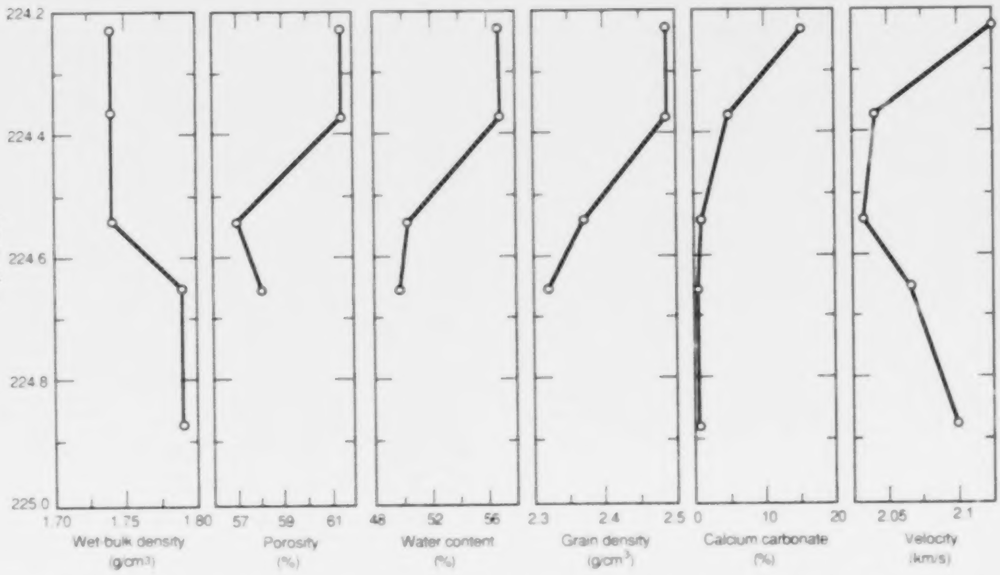

Figure 34. Physical properties plotted vs. depth for five samples from a single turbidite bed within Subunit IVA, including (from bottom to top): the lower coarse part of the basal parallel-laminated sand division, the upper fine part of the basal parallel-laminated sand division, the cross-laminated T_c division, the finely-laminated T_d division, and a bioturbated hemipelagic unit.

Table 12. Results of Hamilton Frame calibration using lucite and aluminum standards of varying length.

	Thickness (mm)	Traveltime (µs)
Cores 126-787B-1R to -20R		
Lucite	10.00	4.69
	20.10	8.46
	40.10	15.97
	50.19	19.68
	65.70	25.55
$t = 0.941 + 0.347x$ for $x = 0$, $t = 0.941$ µs		
Aluminum	20.00	4.10
	30.00	5.62
	40.00	7.16
	50.00	8.70
$t = 1.026 + 0.153x$ for $x = 0$, $t = 1.026$ µs; Average delay time = 0.984 µs		
Cores 126-787B-21R to -34R		
Lucite	9.70	4.66
	19.75	8.39
	39.75	15.90
	49.90	19.66
	65.55	25.51
$t = 1.033 + 0.374x$ for $x = 0$, $t = 1.033$ µs		
Aluminum	19.90	4.03
	29.90	5.52
	40.00	7.07
	50.00	8.60
$t = 0.993 + 0.152x$ for $x = 0$, $t = 0.993$ µs; Average delay time = 1.013 µs		

Note: data are plotted in Figure 35.

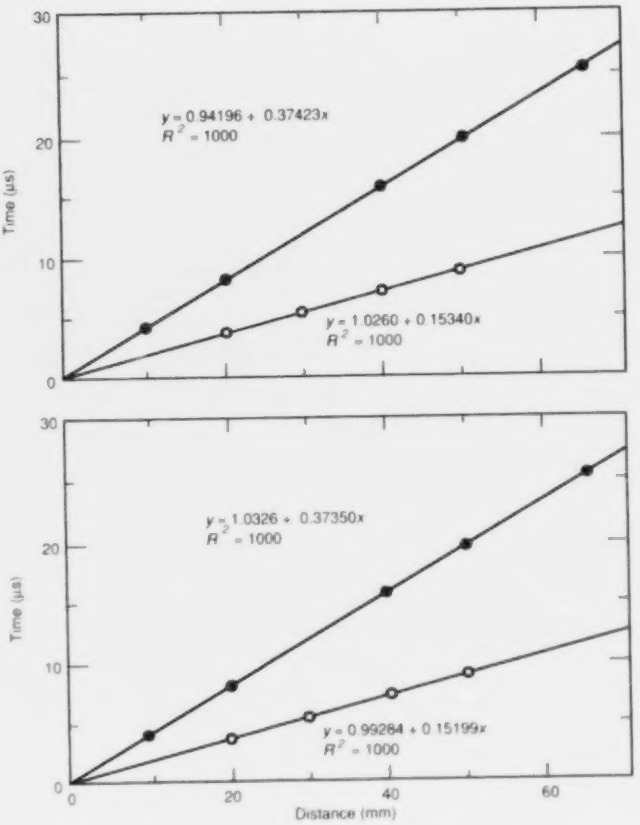

Figure 35. Plots of Hamilton Frame velocimeter calibrations showing the results from lucite (solid circles) and aluminum (open circles) standards. **A.** Cores 126-787B-1R through -20R. **B.** Cores 126-787B-21R through -34R.

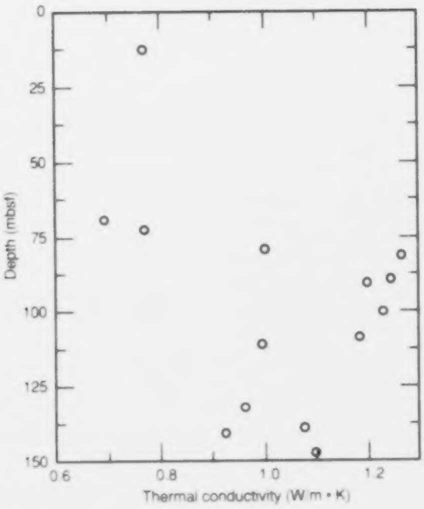

Figure 36. Thermal conductivity vs. depth, Hole 787B.

Taylor, B., Fujioka, K., et al., 1990
Proceedings of the Ocean Drilling Program, Initial Reports, Vol. 126

6. SITES 788/789[1]

Shipboard Scientific Party[2]

HOLE 788A

Date occupied: 28 April 1989

Date departed: 28 April 1989

Time on hole: 12 hr, 45 min

Position: 30°55.35′N, 140°00.27′E

Bottom felt (rig floor; m, drill-pipe measurement): 1111.0

Distance between rig floor and sea level (m): 10.50

Water depth (drill-pipe measurement from sea level, m): 1100.5

Total depth (rig floor; m): 1156.30

Penetration (m): 45.30

Number of cores (including cores with no recovery): 5

Total length of cored section (m): 45.30

Total core recovered (m): 1.24

Core recovery (%): 3

Oldest sediment cored:
Depth (mbsf): 45.30
Nature: pumiceous pebbly vitric sand and vitric sand
Age: Quaternary

HOLE 788B

Date occupied: 28 April 1989

Date departed: 28 April 1989

Time on hole: 5 hr

Position: 30°55.38′N, 140°00.17′E

Bottom felt (rig floor; m, drill-pipe measurement): 1113.0

Distance between rig floor and sea level (m): 10.50

Water depth (drill-pipe measurement from sea level, m): 1102.5

Total depth (rig floor; m): 1148.60

Penetration (m): 35.60

Number of cores (including cores with no recovery): 4

Total length of cored section (m): 35.60

Total core recovered (m): 0.00

Core recovery (%): 0

Oldest sediment cored:
Depth (mbsf): 35.60
Nature: no recovery

HOLE 788C

Date occupied: 13 May 1989

Date departed: 14 May 1989

Time on hole: 1 day, 2 hr

Position: 30°55.36′N, 140°00.21′E

Bottom felt (rig floor; m, drill-pipe measurement): 1113.0

Distance between rig floor and sea level (m): 10.50

Water depth (drill-pipe measurement from sea level, m): 1102.5

Total depth (rig floor; m): 1375.50

Penetration (m): 262.50

Number of cores (including cores with no recovery): 28

Total length of cored section (m): 258.50

Total core recovered (m): 146.15

Core recovery (%): 56

Oldest sediment cored:
Depth (mbsf): 262.50
Nature: nannofossil clast
Age: Pliocene
Measured velocity (km/s): 2.42

HOLE 788D

Date occupied: 14 May 1989

Date departed: 16 May 1989

Time on hole: 1 day, 9 hr, 15 min

Position: 30°55.37′N, 140°00.22′E

Bottom felt (rig floor; m, drill-pipe measurement): 1113.0

Distance between rig floor and sea level (m): 10.50

Water depth (drill-pipe measurement from sea level, m): 1102.5

Total depth (rig floor; m): 1487.00

Penetration (m): 374.00

Number of cores (including cores with no recovery): 16

Total length of cored section (m): 154.40

Total core recovered (m): 12.28

Core recovery (%): 8

Oldest sediment cored:
Depth (mbsf): 374.00
Nature: vitric siltstone and vitric sandstone
Age: early Pliocene
Measured velocity (km/s): 2.61

HOLE 789A

Date occupied: 29 April 1989

Date departed: 29 April 1989

Time on hole: 8 hr, 45 min

Position: 30°55.24′N, 139°59.84′E

Bottom felt (rig floor; m, drill-pipe measurement): 1128.5

Distance between rig floor and sea level (m): 10.50

Water depth (drill-pipe measurement from sea level, m): 1118.0

Total depth (rig floor; m): 1182.60

---

[1] Taylor, B., Fujioka, K., et al., 1990. *Proc. ODP, Init. Repts.*, 126: College Station, TX (Ocean Drilling Program).

[2] Shipboard Scientific Party is as given in the list of participants preceding the contents.

Penetration (m): 54.10

Number of cores (including cores with no recovery): 6

Total length of cored section (m): 54.10

Total core recovered (m): 0.10

Core recovery (%): 0.2

Oldest sediment cored:
Depth (mbsf): 54.10
Nature: pumice
Age: Pliocene-Quaternary

Principal results: Sites 788 and 789 are located on the eastern margin of the Sumisu Rift between the active Izu-Bonin arc volcanoes Sumisu Jima (58 km north) and Tori Shima (55 km south-southeast). The sites are just over 0.5 km apart and are situated on the summit of the rift-flank footwall uplift, which is cut by high-angle normal faults dipping away on both sides from Site 788. The principal objectives of these sites were to determine (1) the vertical-motion history of the rift margin; (2) the time of initial rifting; and (3) the nature and history of volcanism and sedimentation between the major arc volcanoes. Site selection was made on the basis of multichannel seismic (MCS) records and a short shipboard seismic survey; the sites chosen lie on *Fred Moore* 3507, Line 4, at 2138Z (Site 788) and at 2133Z (Site 789). Sites 788 and 789 were occupied from 0030 hr (all times given in UTC), 28 April, to 0400 hr, 29 April; Site 788 was reoccupied from 1620 hr, 13 May, to 0330 hr, 16 May 1989.

Hole 788A was spudded at 0755 hr on 28 April 1989, rotary coring 45.3 m with 1.24 m of recovery. After offsetting 100 m northwest, four RCB cores were taken in Hole 788B, penetrating 35.6 m with zero recovery. The hole began to cave in and so was abandoned at 1820 hr on 28 April. Hole 789A was spudded at 2005 hr on 28 April, rotary coring 54.1 m with only 0.1-m recovery. Further coring was deferred until after drilling Sites 790 and 791. Hole 788C was spudded at 2144 hr on 13 May, and APC cored from 4 to 248.2 m below seafloor (mbsf) with 60% recovery. The hole was continued with extended core barrel (XCB) coring to 262.5 mbsf with 1% recovery before the pipe became stuck. After we freed the pipe, the string was tripped. Hole 788D was spudded with RCB coring at 0035 hr on 15 May and drilled with a center bit to 219.6 mbsf. Coring continued to 374 mbsf with 8% recovery. Because we had met our primary scientific objectives, we ended coring in the hole so that we would not jeopardize another bottom-hole assembly (BHA).

Two lithologic units were defined at Site 788:

1. Unit I (0-249 mbsf) is upper Quaternary and Pliocene sandy, granule and pebble, pumiceous gravel locally interbedded with vitric sands and rare vitric silts. There is a transition to the basal 20 m, which is a subunit (IB) lithified to conglomerate.
2. Unit II was divided into two subunits: Subunit IIA (249-277.6 mbsf) is Pliocene, interbedded nannofossil-rich claystone and vitric sandstone, silty claystone, and siltstone, moderately burrowed; and Subunit IIB (277.6-374 mbsf) is lower Pliocene, interbedded pumiceous conglomerate and vitric sandstone, siltstone, and silty claystone.

At Site 789, 0.1 m of Pliocene-Quaternary pumice was recovered from the surficial core.

Units I and II were dated by means of nannofossils, foraminifers, and paleomagnetics. There is an unconformity at about 30 mbsf between pumice less than 275 Ka and pumice 2.35-3.56 Ma. Pliocene sedimentation rates are >140 but <240 m/m.y. in Unit I and average 140 m/m.y. in Unit II, varying between as low as 40 m/m.y. in Subunit IIA and up to 280 m/m.y. in Subunit IIB. Benthic foraminifers indicate a depositional water depth of 1500-3000 m for Subunit IIA sediments.

The sediments are dominantly arc-derived volcaniclastic rocks, mostly pumiceous gravel and conglomerate. No igneous rocks were recovered. The silt/clay component and all biogenic materials were virtually absent in the coarse clastic rocks (carbonate is <0.5% in Unit I), probably as a result of winnowing. Carbonate-rich sections such as in Subunit IIA and middle Subunit IIB reflect slower deposition during volcanic minima lasting up to 300 k.y. Upward-coarsening intervals in Unit I represent four large eruptions, or four periods during which volcanism built up to climaxes, three in the Pliocene and one in the late Quaternary. The pumice is mainly rhyolitic, although the lower two cycles have more diverse clast types, including high-silica andesite.

Bedding is horizontal in Unit I to subhorizontal in Unit II. A zone of 30°-60° normal faulting occurs near 297 mbsf. Lithification was caused by compaction and pressure-welding in Subunits IB and IIA, plus carbonate and local zeolite cementation in Subunit IIB. The degree of compaction suggests that the overburden was formerly greater than at present.

Physical property measurements indicate that (1) average bulk density values increase from 1.5 g/cm^3 in Unit I to 2.0 g/cm^3 in Unit II; (2) porosity values range from 50%-90% (average 73%) in Unit I to 45%-70% (average 60%) in Unit II; and (3) sonic velocity data average 1.6 km/s in Unit I, 2.7 km/s (ranging from 2.4 to 3.3 km/s) in Subunit IIA, and 2.8 km/s (ranging from 2.0 to 3.4 km/s) in Subunit IIB.

The principal results of these sites are (1) the arc-margin footwall of Sumisu Rift has been uplifted between 200 and 1700 m; (2) the footwall uplift, and therefore the initiation of rifting, occurred since 2.35-3.56 Ma; (3) present-day and pre-rift volcanism and sedimentation along the volcanic front is dominated by rhyolitic pumice eruptions; and, (4) unlike other arcs such as Japan and the Cascades, there is no evidence at this site of igneous vents or lava flows between the large frontal-arc volcanoes during the last 5 m.y.

BACKGROUND AND OBJECTIVES

Site 788 is located at 30°55.36′N, 140°00.21′E, at 1102 m below sea level (mbsl), and Site 789 is located at 30°55.24′N, 139°59.84′E, at 1118 mbsl. Both sites are on the eastern margin of the Sumisu Rift between the active Izu-Bonin arc volcanoes Sumisu Jima (58 km north) and Tori Shima (55 km south-southeast; Figs. 1 and 2). The submarine arc caldera South Sumisu is 35-40 km to the north. The sites are just over 0.5 km apart and are located on the summit of the rift-flank footwall uplift (Figs. 2-4). The section is cut by active normal faults dipping ~45° away from Site 788 (Fig. 4). By drilling in the arc margin of the rift, we sought to determine (1) the vertical-motion history of the rift margin, (2) the time of initial rifting, and (3) the nature and history of volcanism and sedimentation between the major arc volcanoes.

The first of these objectives was addressed through a combination of paleontological estimates of paleobathymetry, backstripping the sedimentation history using the physical property and logging data, and seismic stratigraphic analyses of the interconnecting MCS profiles. The second objective was obtained by dating the unconformity resulting from the uplift of the rifted arc margin, assuming that the footwall uplift is a flexural and isostatic response to the unloading of the hanging wall block (Weissel and Karner, 1989). To meet the third objective required recovery, dating, and characterization of the upper part of the more than 1.5-km-thick margin section. The frequency, chemistry, and eruptive style of the pre-rift volcanism was ascertained from studies of the volcaniclastic sediments encountered.

Although the nature of the frontal-arc material between the arc volcanoes was unknown, analogy with such land sections as those in Japan or the Cascades suggested that there should be numerous vents and flow fields between the large volcanic edifices. Samples collected during an ALVIN dive indicate that the lower eastern rift wall consists of interbedded volcaniclastic rocks, pumice, and basalt (Taylor et al., in press). However, potential-field and sidescan marine geophysical data suggest a paucity of volcanic centers between the large edifices in the central Izu-Bonin intraoceanic arc.

SEISMIC STRATIGRAPHY

Correlation of MCS site survey data with recovered core material (Fig. 5) was accomplished by using physical properties velocity data, averaged over each lithologic unit (see "Physical

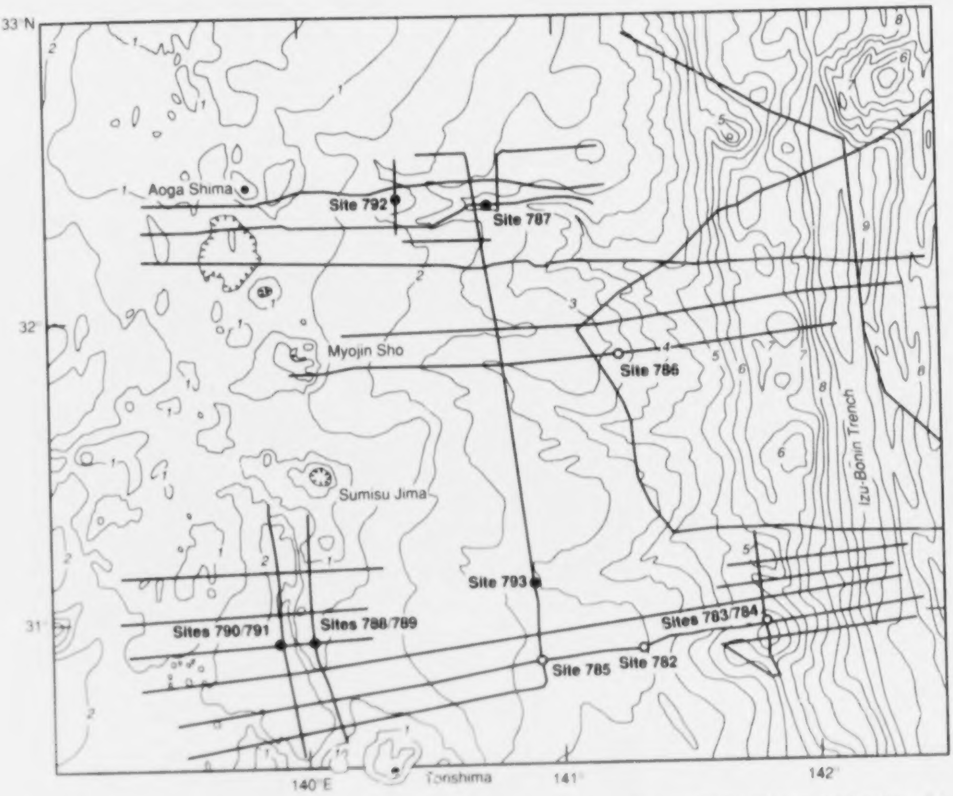

Figure 1. Bathymetric map, at 0.5-km contour intervals, of the Izu Bonin arc-trench system between 30.5°N and 33°N. The locations of sites drilled on ODP Legs 125 (open circles) and 126 (filled circles) are shown on the map, as are the locations of MCS site survey lines.

Properties" section, this chapter), to convert depths (mbsf) into two-way traveltimes. The entire seismic section is characterized by relatively continuous reflectors observed down to multiple and is cut by active normal faults dipping away on either side of Site 788. Site 789, drilled to 54.1 mbsf, did not even pass through the seismic bubble pulse. At Site 788, Unit I is characterized by horizontal, slightly discontinuous, low-amplitude reflectors. The Unit I/II boundary correlates with a high-amplitude reflector (at 1.77 s). The large impedance contrast caused by the change from conglomerate (Subunit IB) to nannofossil claystones (Unit II) is responsible for generating this high-amplitude event. This reflector can be traced locally throughout this rift-flank uplift.

Unit I appears to be conformably deposited on this reflector at Site 788, but appears to be disconformable beneath Site 789. Unit II is characterized by discontinuous, low-amplitude reflections. Below the bottom of Site 788, a series of high-amplitude, well-layered reflectors are observed down to the water-bottom multiple reflection. It is inferred from the character of these reflectors that they represent sedimentary strata and that acoustic basement is not observed in the >1000 m of seismically imaged section.

OPERATIONS

Site 787 to Site 788

Before departing from Site 787, the televiewer (TV) umbilical cable detorquing procedure was conducted. A dead weight was attached to the TV cable and lowered to 3000 mbsl. As we slowly reeled in the cable, the ship drifted away from a point directly over the weight and the cable became angled in such a way that it dragged against the edge of the moonpool, resulting in eight lost strands over an interval of 2635–2850 m of paid-out cable. The remainder of the cable was recovered without further incident, and it was checked and found to have proper electrical continuity. Although the cable looked bad and spooled poorly, it was serviceable for the remainder of the leg.

The ship departed the site at 1200 hr on 27 April 1989 and arrived at Site 788 (proposed Site BON-2) with a routine beacon drop at 0030 hr on 28 April.

Site 788

The beacon was dropped near what appeared to be a fault, so the ship was offset 100 m from the beacon location along bearing 060° to place the hole as far as possible from the sus-

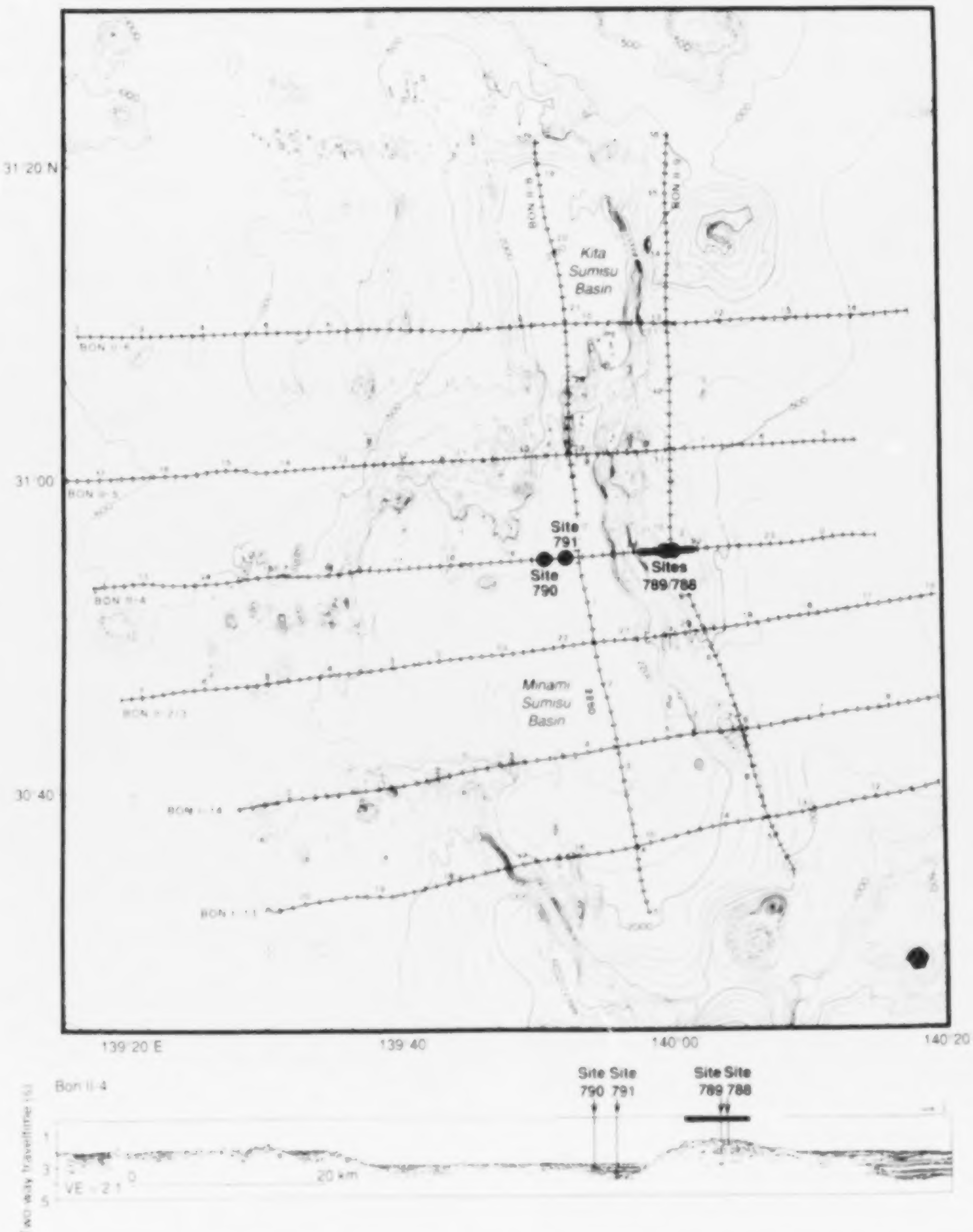
31°20'N
31°00'
30°40'
139°20'E
139°40'
140°00'
140°20'
Kita Sumisu Basin
Minami Sumisu Basin
Site 791
Site 790
Sites 789/788
BON II-6
BON II-5
BON II-4
BON II-2/3
BON II-8
BON II-9
BON I-14
BON I-11
500
2000
Bon II-4
Site 790
Site 791
Site 789
Site 788
Two-way traveltime (s)
1
3
5
VE = 2:1
0
20 km

Figure 2. Bathymetric map (100-m contour intervals) of Sumisu Rift and surrounding area showing the location of MCS site survey tracks and of Sites 788–791. A line drawing of MCS Line BON II-4 (*Fred Moore* 35-07) is shown at the bottom of the figure. The segment of this line shown in Figure 4 is indicated by the solid bars in the upper and lower parts of the figure.

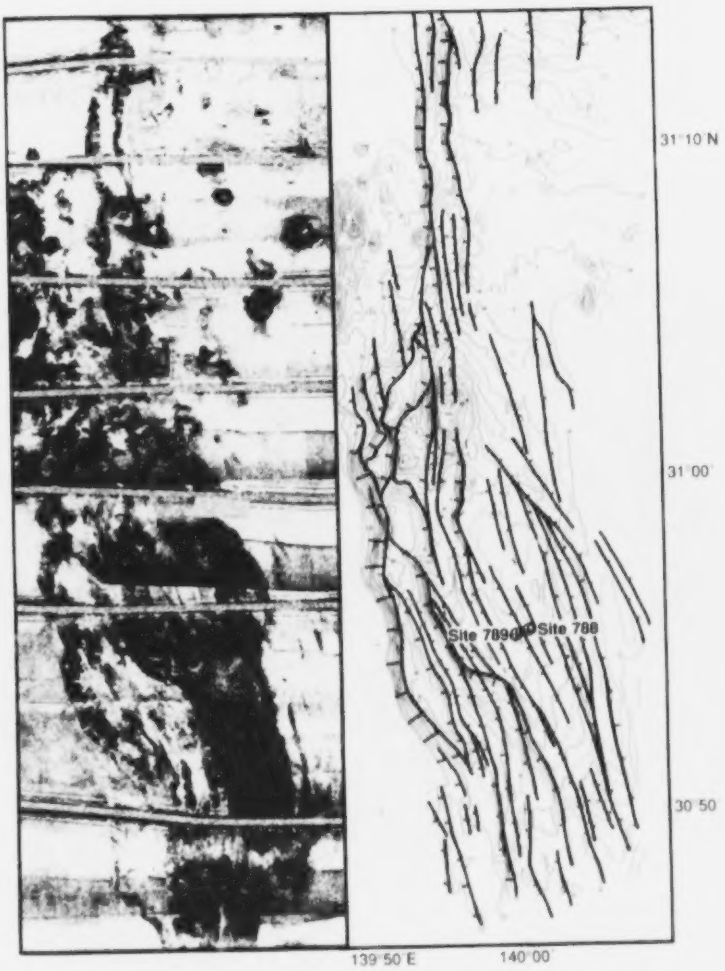

Figure 3. SeaMARC II sidescan image (left) and SeaBeam bathymetry (right) of the eastern margin of the Sumisu Rift showing the anastomosing and relay pattern of normal faults (from Taylor et al., in press) and the location of Sites 788 and 789.

pected fault. The precision depth recorder (PDR) water depth was 1112 mbsl.

Hole 788A

A new RCB BHA was put together and lowered slowly until contact with a very firm mud line was felt 1111 m below rig floor at 0755 hr. No penetration was possible without slight drill-pipe rotation, so a jet-in test was voided. The material near the surface of the formation behaved like loose sand, and this suspicion was strengthened by the fact that four of the first five core barrels were empty (Table 1). After recovering only 1.24 m of loose, pebbly sand in the upper 45 m of penetration, the hole was declared undrillable. The hole was abandoned, and the pipe cleared the seafloor at 1315 hr on 28 April 1989.

Hole 788B

The ship was moved to a new location 100 m due north of the beacon to try another spud, in the hope of finding at least some sediment or cohesive material. The results were again disappointing. Virtually identical circumstances prevailed, and four cores were taken without any recovery. After penetrating 35.6 m, the hole began to exhibit signs of caving in, and some overpull was necessary to free the pipe. The hole was abandoned at 1820 hr on 28 April.

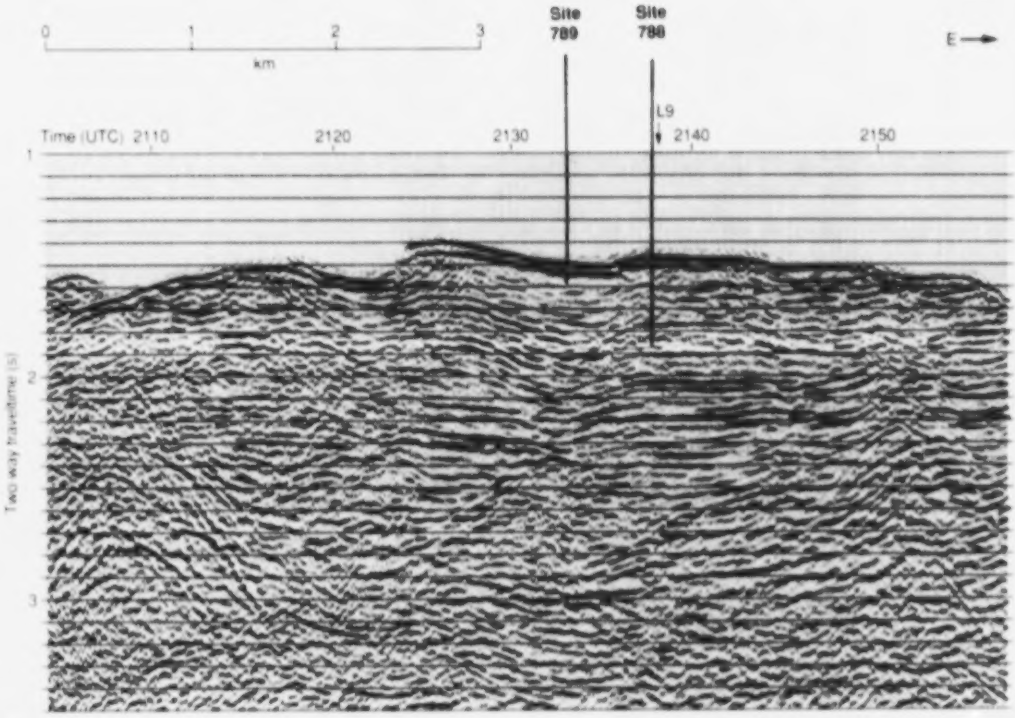

Figure 4. Latitudinal MCS profile BON II-4 (Taylor et al., this volume) across the eastern footwall uplift of the Sumisu Rift at 30°55′N (see Fig. 2 for location). Sites 788 and 789 are located on the summit of the uplift where the MCS data indicate a stratigraphic thickness greater than 1.5 km. The section is cut by active normal faults that dip at ~45° away from the central block into which Site 788 was drilled.

Site 789

Hole 789A

The ship was offset to a location of a shallow sediment pond where conditions at the seafloor might allow for some sediment recovery and better hole stability. The move was beyond beacon range, so a separate beacon was dropped and a new site designated. The hole was spudded 1128.5 m below rig floor at 2005 hr on 28 April. Six RCB cores were taken with only traces of recovery. After experiencing a 50,000-lb overpull to lift the pipe at a sub-bottom depth of only 54.1 m, the hole was declared undrillable and abandoned. The string was pulled and the bit was on deck at 0400 hr, 29 April.

Return to Site 788

The original attempts to core at Site 788 had been with the RCB coring system. Recovery, after four to five cores in very loose sand and gravel, had been essentially nil and the site was declared uncorable since it was thought that the APC also would fare poorly in the incompressible vitric material. Surprising success in piston coring in similar material at Sites 790 and 791 demonstrated that the APC was a viable coring approach after all. Armed with this new knowledge, the vessel returned in dynamic positioning mode to the still-active beacon at Site 788.

Hole 788C

A six-collar XCB BHA was assembled with a 10½-in., five-cone bit, and the pipe was run to the seafloor. The hole was spudded with the first shot being taken from a point 4 m below the mud line to avoid any chance of repeating the buckled core-barrel problem experienced at Hole 791A. The piston-coring results were successful and continued until Core 126-788C-26H at a depth of 248.2 mbsf, where APC refusal was defined by the lack of penetration in apparently firm, granular material. The XCB coring system was then applied for two core attempts, but problems ensued. During the piston-coring sequence, sand or cuttings had infiltrated the BHA and plugged off the five $^{14}/_{32}$-in. bit nozzles.

Because of the obstruction, the flow to the bit was channeled entirely into the cutting-shoe flow path on the XCB core barrel. Core 126-788C-27X was declared a misrun when the cutting-shoe inner-flow sleeve collapsed completely because of high nozzle pressures and blocked the throat of the core barrel. Core 126-788C-28X was attempted at very low flow rates in an at-

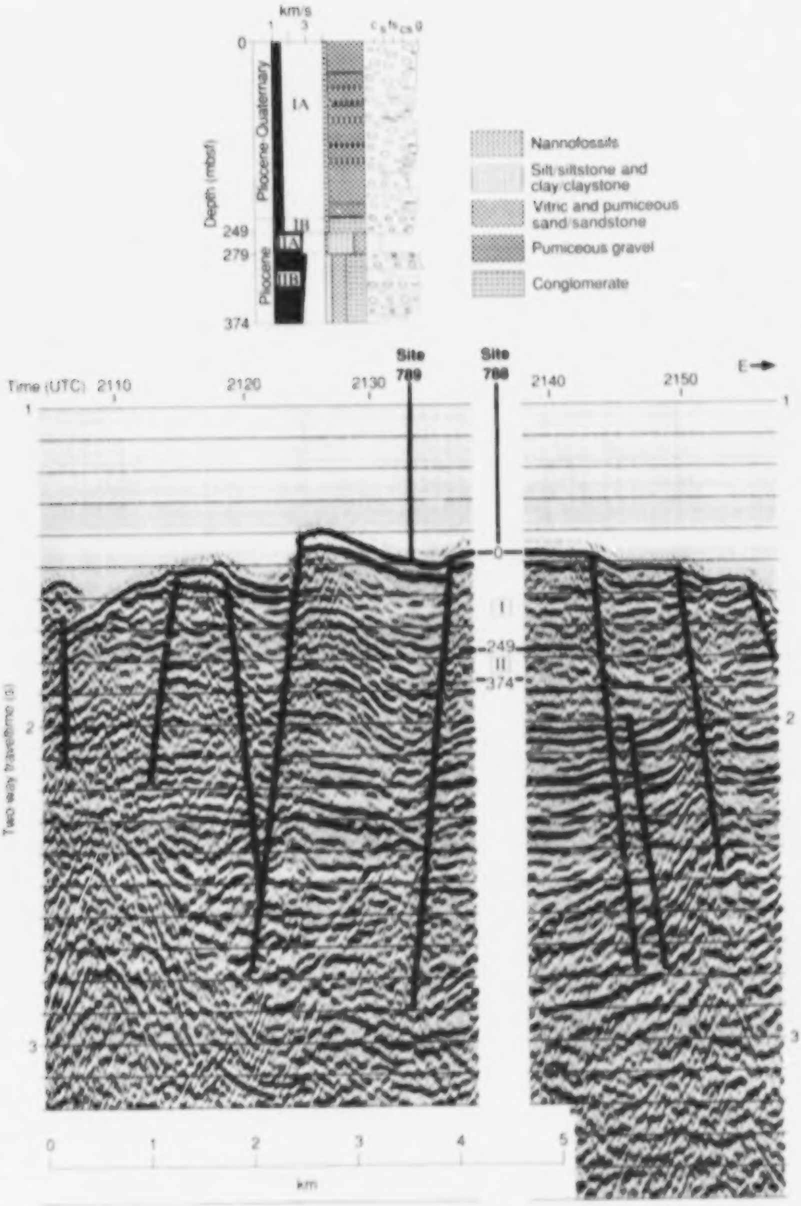

Figure 5. Correlation of Site 788 lithostratigraphy with MCS site survey data. Lithologic units are identified on the seismic section, unit boundaries are given in meters below seafloor (mbsf), and the lithologic column (see "Lithostratigraphy and Accumulation Rates" section, this chapter) is presented above the seismic section. The location of the *Fred Moore* seismic line is shown in Figure 2. The seismic profile has been stacked (48 fold), deconvolved, migrated, and filtered from 10 to 60 Hz. The vertical exaggeration is ~4×.

Table 1. Coring summary, Sites 788 and 789.

Core no.	Date (1989)	Time (UTC)	Depth (mbsf)	Cored (m)	Recovered (m)	Recovery (%)
Hole 788A:						
1R	Apr 28	0845	0-7.0	7.0	0	0
2R	Apr 28	0945	7.0-16.6	9.6	0	0
3R	Apr 28	1030	16.6-26.2	9.6	0.01	0.1
4R	Apr 28	1115	26.2-35.8	9.6	1.23	12.8
5R	Apr 28	1225	35.8-45.3	9.5	0	0
Coring totals				45.3	1.24	2.7
Hole 788B:						
1R	Apr 28	1455	0-7.0	7.0	0	0
2R	Apr 28	1600	7.0-16.5	9.5	0	0
3R	Apr 28	1640	16.5-26.0	9.5	0	0
4R	Apr 28	1715	26.0-35.6	9.6	0	0
Coring totals				35.6	0	0
Hole 788C:						
1H	May 13	2110	4.0-13.3	9.3	5.17	55.6
2H	May 13	2150	13.3-20.2	6.9	0.98	14.2
3H	May 13	2240	20.2-29.7	9.5	9.34	98.3
4H	May 13	2330	29.7-39.2	9.5	5.48	57.7
5H	May 14	0000	39.2-48.7	9.5	8.89	93.6
6H	May 14	0025	48.7-58.2	9.5	9.08	95.6
7H	May 14	0050	58.2-67.7	9.5	3.65	38.4
8H	May 14	0125	67.7-77.2	9.5	3.52	37.0
9H	May 14	0150	77.2-86.7	9.5	9.35	98.4
10H	May 14	0210	86.7-96.2	9.5	8.99	94.6
11H	May 14	0235	96.2-105.7	9.5	6.40	67.4
12H	May 14	0300	105.7-115.2	9.5	9.15	96.3
13H	May 14	0335	115.2-124.7	9.5	9.18	96.6
14H	May 14	0425	124.7-134.2	9.5	8.92	93.9
15H	May 14	0455	134.2-143.7	9.5	6.21	65.4
16H	May 14	0525	143.7-153.2	9.5	3.07	32.3
17H	May 14	0600	153.2-162.7	9.5	9.00	94.7
18H	May 14	0650	162.7-172.2	9.5	4.63	48.7
19H	May 14	0720	172.2-181.7	9.5	8.78	92.4
20H	May 14	0750	181.7-191.2	9.5	3.56	37.5
21H	May 14	0820	191.2-200.7	9.5	2.30	24.2
22H	May 14	0845	200.7-210.2	9.5	1.41	14.8
23H	May 14	0915	210.2-219.7	9.5	5.12	53.9
24H	May 14	0940	219.7-229.2	9.5	5.17	54.4
25H	May 14	1010	229.2-238.7	9.5	0.16	1.7
26H	May 14	1035	238.7-248.2	9.5	0.28	3.0
27X	May 14	1200	248.2-257.9	9.7	0.00	0.0
28X	May 14	1245	257.9-262.5	4.6	0.18	3.9
Coring totals				258.5	146.15	56.5
Drilled interval = 4.0 m						
Total penetration and recovery				262.5	146.15	56.5
Hole 788D:						
1R	May 15	0930	219.6-229.2	9.6	0.79	8.2
2R	May 15	1000	229.2-238.9	9.7	0.19	2.0
3R	May 15	1055	238.9-248.5	9.6	0.20	2.1
4R	May 15	1205	248.5-258.2	9.7	1.15	11.8
5R	May 15	1315	258.2-267.9	9.7	1.90	19.6
6R	May 15	1410	267.9-277.5	9.6	0.75	7.8
7R	May 15	1505	277.5-287.2	9.7	2.03	20.9
8R	May 15	1605	287.2-296.9	9.7	0.69	7.1
9R	May 15	1715	296.9-306.5	9.6	1.32	13.7
10R	May 15	1815	306.5-316.0	9.5	0.37	3.9
11R	May 15	1900	316.0-325.6	9.6	0.77	8.0
12R	May 15	1950	325.6-335.3	9.7	0.43	4.4
13R	May 15	2040	335.3-345.0	9.7	0.25	2.6
14R	May 15	2140	345.0-354.7	9.7	0.14	1.4
15R	May 15	2230	354.7-364.3	9.6	0.58	6.0
16R	May 15	2340	364.3-374.0	9.7	0.72	7.4
Coring totals				154.4	12.20	7.9
Drilled interval = 219.6 m						
Total penetration and recovery				374.0	12.20	7.9
Hole 789A:						
1R	Apr 28	2100	0-8.5	8.5	0.10	1.2
2R	Apr 28	2200	8.5-18.0	9.5	0	0
3R	Apr 28	2245	18.0-27.5	9.5	0	0
4R	Apr 28	2330	27.5-37.1	9.6	0	0
5R	Apr 29	0000	37.1-46.6	9.5	0	0
6R	Apr 29	0045	46.6-54.1	7.5	0	0
Coring totals				54.1	0.10	0.2

tempt to reduce the nozzle back pressure. The combination of low flow levels and the unstable formation caused the hole to collapse in the vicinity of the BHA and the pipe became stuck. Repeated overpulls of 260,000 lb freed the string after about 30 min. With the bit nozzles plugged and the hole deteriorating, the only choice was to pull out of the hole. The bit was on deck at 1815 hr on 14 May 1989, ending Hole 788C.

Hole 788D

In the final XCB core of Hole 788C (cut short by the hole collapse and stuck pipe), a sample of material representing a significant change in lithology was recovered. This, plus the possibility of still more lithology alternations nearby, dictated that the scientific goals of the hole were not quite accomplished. Thus, an RCB BHA was made up and run back to the seafloor. Hole 788D was spudded at 0035 hr on 15 May and drilled with a center bit to 219.6 mbsf. We took 16 RCB cores and then ended the hole at 374 mbsf. Recovery was poor but adequate enough to satisfy the first-order scientific objectives. The hole was abandoned and the bit was on deck after the pipe trip at 0330 hr on 16 May 1989.

LITHOSTRATIGRAPHY AND ACCUMULATION RATES

Introduction

Sites 788 and 789 are located atop the east flank of the Sumisu Rift graben. Site 789, 0.5 km southwest of Site 788, was cored with the RCB coring system. Penetration was 54.1 m, and only 0.1 m of pumiceous gravel was recovered (Section 126-789A-1R-CC) and received by the paleontology laboratory before the hole and the site were abandoned. This discussion is based principally upon the more successful results of APC and XCB coring of Hole 788C, and RCB coring of Hole 788D. Recovery was reasonably good in Hole 788C. The top of Hole 788D overlapped the basal portion of the 788C column, but recovery from Hole 788D was poor.

The stratigraphic succession at Site 788 consists of two lithologic units (Table 2 and Fig. 6), both of which are overwhelmingly dominated by volcanogenic components, much of it gravel and conglomerate. No igneous basement rock was recovered. Biogenic materials are virtually absent in the upper unit, and in the lower unit they are fairly abundant within only one interval. The contact between Units I and II was not recovered in Hole 788C but was recovered at 249 mbsf in Hole 788D. Table 3 summarizes the recovery of sediments and sedimentary rocks for Units I and II in Holes 788A, 788C, 788D, and 789A.

Description of Units

Unit I

Intervals: Core 126-788A-4H, Cores 126-788C-1H through -26H, and Cores 126-788D-1R through -4R at 55 cm
Age: Pliocene to Quaternary
Depth: 0-249 mbsf

Sediments and sedimentary rocks assigned to Unit I were recovered from Holes 788A, 788C, and 788D. Hole 788A recovered only a single core-catcher sample. Hole 788D cored the basal 26 m of Unit I and recovered the contact with Unit II. Only Hole 788C cored the entire unit; it provides the principal basis for the lithologic description that follows.

Unit I consists primarily of light olive gray (5Y 6/2), olive black (5Y 2/1), and grayish black (N2), pumiceous granule and pebble gravel (Fig. 7) that, over a transitional interval from 172 to 230 mbsf (Section 126-788C-18H-CC to Core 126-788C-25H), progressively lithified to a conglomerate of essentially identical composition with that of the gravel that immediately overlies it.

Table 2. Summary of sediment types and sedimentary structures at Site 788.

Subunit	Lithology	Sedimentary structures	Interval (mbsf)	Age	Occurrence
IA	Pumiceous sandy granule and pebble gravel locally interbedded with vitric sands and rare vitric silts. Mean sand:granule:pebble ratio is 24:30:45. Maximum clast size is 130 mm. Oxidized coatings on clasts in Cores 126-788C-1H to -7H. Mn-oxide coatings on clasts in Cores 126-788C-5H to -8H. Transition to conglomerate in Cores 126-788C-19H through -24H.	Gravel predominantly structureless; local normal grading may be drilling artifact. Rare grading of vitric sand to vitric silt within interbeds.	0–229.2	Quaternary to Pliocene	126-788A-4R, 126-788C-1H to -24H 126-788D-1R
(Transitional)					
IB	Pumiceous sandy pebble-granule conglomerate. Mean sand:granule:pebble ratio is 15:32:52. Maximum clast size is 45 cm.	Structureless.	229.2–249	Pliocene	126-788C-25H to -26H 126-788D-2R to -4R, 55 cm
IIA	Interbedded nannofossil-rich claystone, vitric sandstone, vitric silty claystone, and vitric siltstone.	Vitric sandstones grade upward into vitric clayey siltstone and vitric silty claystone. Moderate burrowing; *Chondrites* common. Parallel lamination present.	249–278.6	Pliocene	126-788C-28X 126-788D-4R, 55 cm, to -7R, 8 cm
IIB	Interbedded pumiceous conglomerate, vitric sandstone, vitric siltstone, and vitric silty claystone. Toward the base, sandstone, siltstone, and claystone are carbonate bearing or carbonate rich. Faulting and fracturing in Cores 126-788D-8R through -10R.	Parallel lamination, wavy lamination, and locally intense bioturbation.	278.6–374	Pliocene	126-788D-7R, 8 cm, to -16R

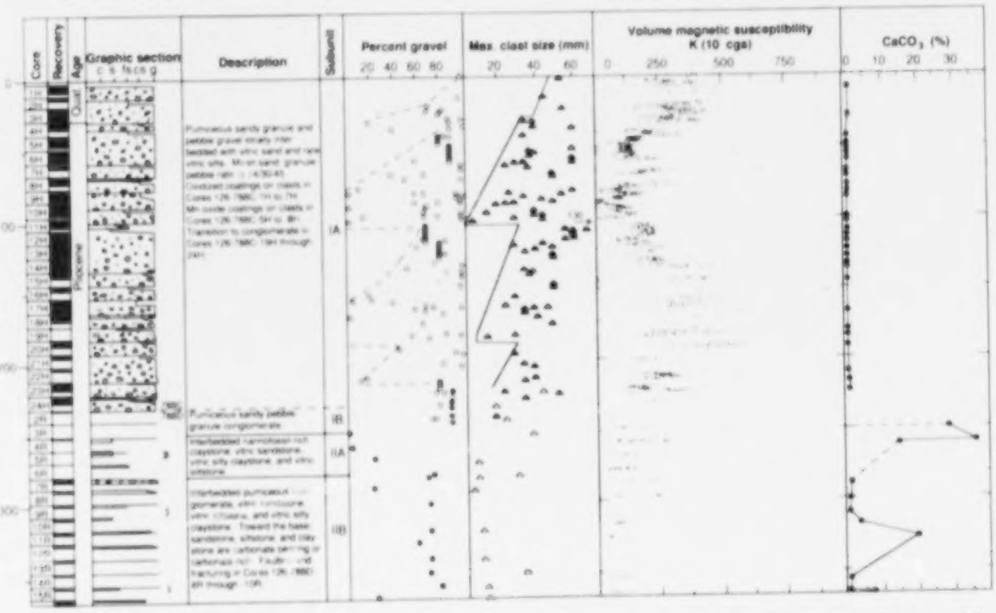

Figure 6. Lithostratigraphic summary diagram for Site 788, including a graphic display of core recovery, percent gravel, maximum clast size, and the downhole distributions of carbonate content and magnetic susceptibility. The carbonate curve is primarily a function of the distribution of nannofossil tests throughout the section, whereas the magnetic susceptibility data reflect the distribution of coarse mafic volcanic lithic rocks and crystals. The proportions of sediment types at Holes 788C and 788D are shown in the "Graphic section" column; the format is more generalized than in the core descriptions in that it reflects the percent of groups of lithotypes observed within any cored section (i.e., silt and clay, sand, gravel, carbonate), and does not show mixed biogenic/siliciclastic lithotypes. The graphic column is a simplified sedimentological log displaying relative grain size on the horizontal axis (c = clay/claystone, s = silt/siltstone, fs = fine-grained sand/sandstone, cs = coarse-grained sand/sandstone, and g = gravel/conglomerate); on this column, bedding within the core units is schematically displayed. Burrowed intervals are indicated to the right (see Fig. 6, "Explanatory Notes" chapter, this volume, for key to sedimentary structure symbols). The "Percent gravel" and "Maximum clast size" columns delineate four upward-coarsening cycles within Unit I, indicated by dashed and solid lines, respectively.

Table 3. Sediment recovery data for Units I and II at Site 788 and 789.

Subunit	Hole	Interval (core-core)	Depth (mbsf)	Cored (m)	Recovery (m)	Recovery (%)
IA	788A	1R	0			
		4R	45.3	45.3	1.24	3
	788B	1R	0			
		4R	35.6	35.6	0	0
	788C	1H	0			
		24H	229.2	229.2	[a]138.5	[a]60
	788D	1R	219.6			
		1R	229.2	9.6	0.79	8
	789A	1R	0			
		6R	54.1	54.1	0.10	0.2
IB	788C	25H	229.2			
		27H	249.0	19.8	0.63	3
	788D	2R	229.2			
		4R	249.0	19.8	0.94	5
IIA	788C	27X	249.0			
		28X	262.5	13.5	0.2	1.5
	788D	4R	249.0			
		7R	277.6	28.6	3.4	12
IIB	788D	7R	277.6			
		16R	374.0	96.4	7.2	7

Note: The Subunit IA/IB boundary is at the top of Core 126-788C-25H (229.2 mbsf) and the top of Core 126-788D-2R (229.2 mbsf). The Subunit IIA/IIB boundary is in Section 126-788D-7R-1 at 8 cm (277.58 mbsf, reported here as 277.6 mbsf).

[a] These figures are inflated by cave-in and flow-in at the tops and bottoms of cores, especially of vitric sand. The ODP coring summary reported a recovery of 8.78 m for Core 126-788C-19H, which contained large voids and actually contained only 1.94 m, the number used here.

This change in induration is the basis for dividing the unit into two subunits. The gravels and conglomerates of Unit I contain very little silt and clay and, consequently, very few microfossils.

Pumiceous, sandy, granule and pebble gravel constitutes 86% of Subunit IA. The sand/granule/pebble ratios in individual cores range from about 5/5/90 to 90/10/0; the mean ratio for the subunit is 24/30/45. The pumice is predominantly olive gray (5Y 4/1) to light olive gray (5Y 5/2) in color; however, from 0 to 58.2 mbsf (Cores 126-788C-1H through -6H), some pumice is oxidized to various shades of yellow, orange, and brown (10YR 6/8, 5/8, 7/4, 5/4; 5Y 7/2, 6/2). From 39.2 to 61.9 mbsf (Core 126-788C-5H to Section 126-788C-7H-CC), some of the pumice pebbles have thin (< 1 mm) surface coatings of olive black (5Y 2/1), brownish black (5YR 2/1), and grayish black (N2) manganese oxides (Fig. 8), some of which occur as microspherules (Fig. 9).

The dominant clast lithology in all of Unit I is pumice. Rhyolite pumice clasts are mostly aphyric, but some contain microlites (< 0.1 mm) of plagioclase and quench phases of clinopyroxene. With the exception of the interval from 48.8 to 97.0 mbsf (Cores 126-788C-6H, 14 cm, to 126-788C-11H-1, 58 cm), Unit I also contains clasts of glassy, commonly scoriaceous andesite in typical abundances of < 1%. These lithic clasts are significantly smaller than the associated pumice pebbles, ranging in intermediate diameters from 3 to 10 mm. Chemical data from the analysis of a clast of this andesite scoria are presented elsewhere (see "Igneous Geochemistry" section, this chapter). In smear slides, small amounts (< 2% total) of plagioclase, clinopyroxene, orthopyroxene, and oxide fragments are present in addition to the dominant glass shards. In the top of Core 126-788C-9H (78 mbsf), there are two clasts up to 6 cm in diameter of olive gray (5Y 3/2), vitric silty claystone, much more lithified than the sediments in this interval. Below about 135 mbsf (Core 126-788C-15H), clasts of mottled-green pumiceous breccia (Fig. 10) are also present.

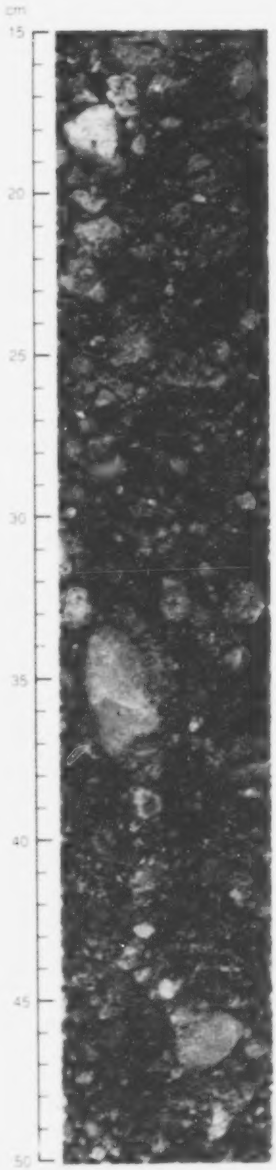

Figure 7. Pumiceous gravel in Subunit IA. The dominant color of the pumice is grayish black (N2); some clasts are yellowish brown (10YR 5/4). There are mixed basaltic and felsic clasts (Interval 126-788C-4H-3, 15-50 cm).

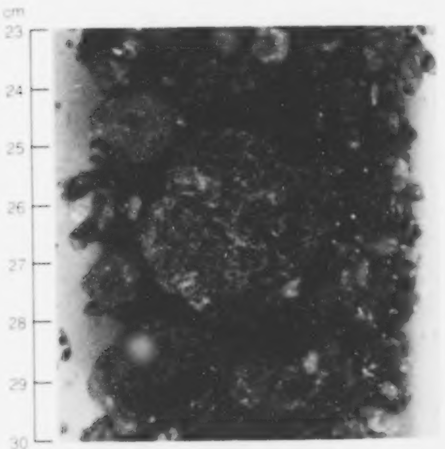

Figure 8. Pumice pebble with a black surface coating of manganese oxide (MnO_2). The diameter of the pebble is 3.5 cm (Interval 126-788C-5H-1, 23-30 cm).

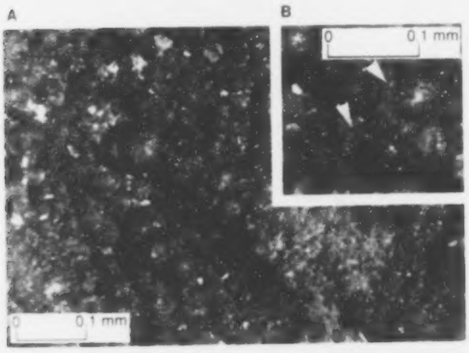

Figure 9. Microspherules of manganese oxide (todorokite) on the surface of a pumice pebble (Sample 126-788C-7H-CC, 20 cm). **A.** General view of the microspherules. Bar scales are 0.1 mm. **B.** Enlargement of an area just to the left of this inset, showing radial crystal habit of the todorokite where a microspherule has been broken open. Bar scales are 0.1 mm.

The rest of Subunit IA is mainly structureless, silicic, vitric sand, much of which is present in disturbed intervals (cave-ins and flow-ins) at the tops and bottoms of cores; therefore, the relative abundance of this lithology (14%) within Subunit IA is overestimated in recovery figures (see Table 3). Minor, undisturbed sand beds within the cores (Fig. 11) are only 6-58 cm thick; two of these grade upward into 4- and 77-cm-thick intervals of vitric silt, the only appearances of this lithotype in the subunit. Beginning at 172 mbsf (Section 126-788C-18H-CC and Core 126-788C-19H), drilling biscuits of the semilithified gravel and conglomerate increase irregularly in abundance downhole (Fig. 12), with a corresponding decrease in the proportions of original unconsolidated gravel (or lithified material disaggregated by drilling). No cement was recognized, and induration is most likely a result of compaction.

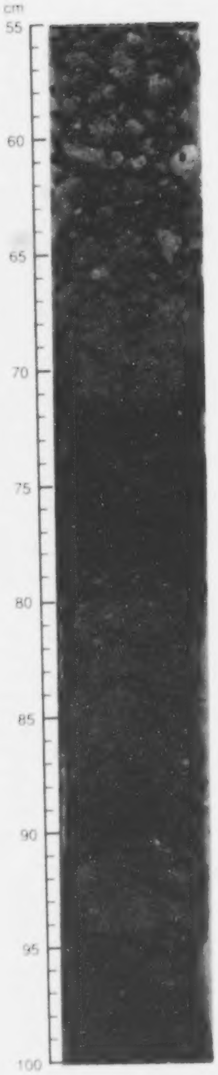

Figure 10. A light olive gray (5Y 6/1), fine vitric sand bed (64-70 cm) and a locally pebbly, dark gray (N4) vitric sand bed (70-79 cm) intercalated with well-sorted, pebbly granule gravel (Interval 126-788C-8H-2, 55-100 cm). Both sand beds are interpreted as ash layers.

The downhole trend in lithification is accompanied by a pronounced decrease in recovery to only 4% in Core 126-788C-

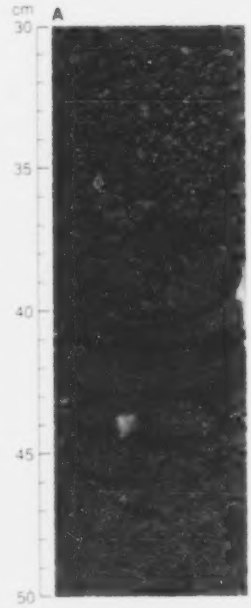

Figure 11. Transitional facies from granule gravel to granule conglomerate. **A.** In this example, the lithified fragments are "drilling biscuits" (40–44 cm) produced by coring. Above and below the lithified fragments, respectively, is granule gravel (sand 30%, granules 60%, pebbles 10%) and pumiceous medium sand (Interval 126-788C-20H-2, 30–50 cm). **B.** Lithified "biscuits" of pumiceous pebble conglomerate, surrounded by pumiceous gravel (sand 30%, granules 40%, pebbles 30%; Interval 126-788C-22H-1, 27–45 cm).

25H, where the lithified clasts are as thick as 7 cm in diameter and more abundant than unconsolidated or disaggregated material, and so the contact with Subunit IB was placed here, at 229.2 mbsf (Fig. 13). Apart from its lithification, the conglomerate of Subunit IB is compositionally and texturally similar to the gravel of the lower part of Subunit IA, sand/granule/pebble ratios ranging from 10/30/60 to 60/30/10 in individual sections and averaging 15/33/52 for the subunit.

Core 126-788C-26H recovered only 0.28 m of rock, after which XCB coring began. Core 126-788C-27X recovered no material, so the contact of Units I and II, which may have occurred either in Core 126-788C-26H or -27X, was missed in Hole 788C. Core 126-788C-28X recovered a totally different lithology and was placed in Unit II (Fig. 13).

Unit II

Intervals: Core 126-788C-28X and Cores 126-788D-4R at 55 cm through -16R
Age: Pliocene
Depth: 249–374 mbsf

The first recovery of Unit II in Hole 788C (Core 126-788C-28X), 9 m below the contact recovered in Hole 788D, is a nannofossil-rich claystone that also shows a fraction of a percent of foraminifers on the split-core surface (Fig. 13). In Hole 788D, nannofossil-rich claystone occurs beneath drilling biscuits of

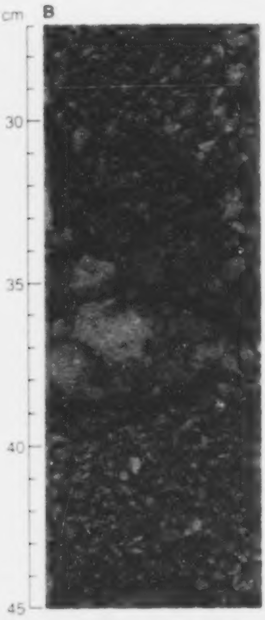

Figure 11 (continued).

Unit I conglomerate in Section 126-788D-4R-1. The uppermost claystone is 0.52 m below the top of this core, which is 248.5 mbsf, and so the contact between Units I and II is placed at 249 mbsf (Fig. 13).

The five sediment types delineated in Table 2 are based upon poor (8%) recovery. To qualify and organize these sparse data, Figure 14 presents the recovered thicknesses of each lithology and their depths of occurrence in the hole as a basis for lithostratigraphic reconstruction. The columns of sediment types are arranged by coarseness, which increases from left to right. Pumice conglomerate and vitric sandstone are the most abundant sediment types in Unit II (29% and 27% of total thickness recovered, respectively), followed by nannofossil-rich claystone (21%), vitric silty claystone (12%), and vitric siltstone (11%). Nannofossil-rich claystone is restricted to the upper portion of the unit, where no pumice conglomerates were recovered. These distributions are genetically significant and are the basis for dividing the unit into two subunits, IIA and IIB, at the base of the lowest nannofossil claystone, 277.6 mbsf (Section 126-788D-7R-1 at 8 cm).

Figure 14 provides some sense of how thinly intercalated the various lithotypes in Subunit IIA are. Nannofossil-rich claystone layers from 8 to 54 cm thick constitute 62% of the subunit. These rocks are slightly to heavily bioturbated (Fig. 15). Trace fossils include *Chondrites*. Carbonate contents average 18%; one sample (126-788D-4R-1, 107–109 cm) was calcareous enough (36.14%) to be termed a nannofossil claystone. Foraminifer and nannofossil tests are clearly visible but are poorly preserved. Much of the interstitial carbonate is micrite. Small amounts of glauconite contribute to the grayish green (5GY 6/1) and dark greenish gray (10Y 5/1, 4/1) colors of these rocks.

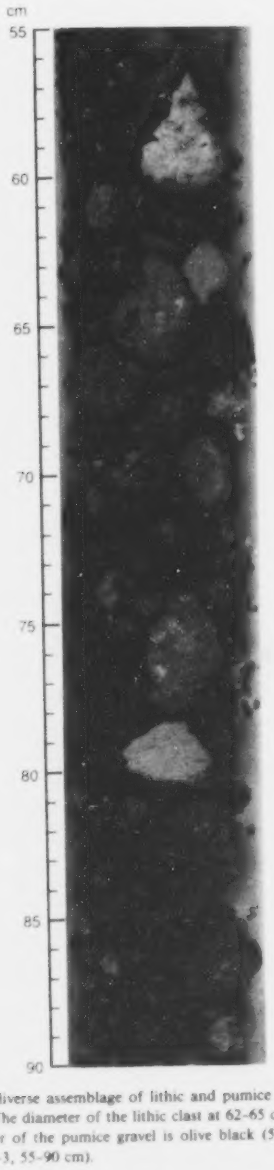

Figure 12. A diverse assemblage of lithic and pumice clasts in pumiceous gravel. The diameter of the lithic clast at 62–65 cm is 4 cm. The dominant color of the pumice gravel is olive black (5Y 2/1; Interval 126-788C-15H-3, 55–90 cm).

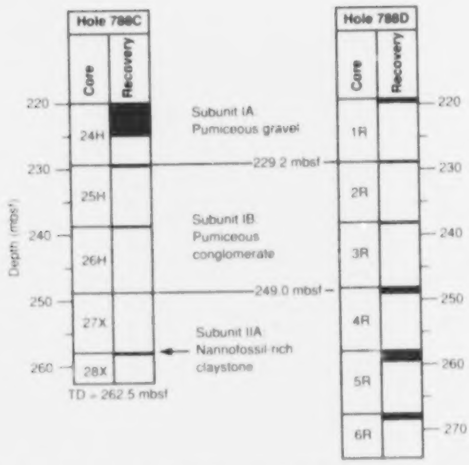

Figure 13. The basis for establishing the Subunit IA/IB and Unit I/II contacts at Site 788.

The nannofossil-rich claystone is interbedded with black (N1), very fine- to medium-grained vitric sandstone layers, 1–40 cm thick, that constitute 18% of Subunit IIA. Brown volcanic glass is the principal constituent of the sandstones. The thicker beds are planar laminated, and graded beds are succeeded by very dark greenish gray (10Y 3/1), clayey vitric siltstone, which comprises 8% of the subunit. The remaining 12% of the subunit consists of dark greenish gray (10Y 5/2) and greenish black (5GY 2/1), bioturbated mixtures of interbedded vitric sandstones and nannofossil claystones.

Subunit IIB is composed of pumiceous conglomerate (44%), vitric sandstone (30%), vitric siltstone (12%), and vitric silty claystone (9%). The conglomerate is grayish black (N2) and brownish black (5YR 2/1; Fig. 16). It is more poorly sorted than the gravel and conglomerate of Unit I and contains more sand (20%–40% vs. an average of 15%). Typical granule and pebble contents are 60%–80%, and maximum clast sizes are about 10 mm. Clasts are colored light olive gray (5Y 6/2), olive black (5Y 2/1), and grayish black (N2).

The vitric sandstone is grayish black (N2), medium to very fine grained, and is present in layers 5–36 cm thick (Fig. 17). Planar lamination is common, and one bed displays wavy laminations at its base. Vitric siltstone layers are 4–37 cm thick, grayish black (N2), and planar laminated, or they are light olive gray (5Y 6/2) or medium dark gray (N4) and either structureless or bioturbated (Fig. 18). Vitric silty claystone occurs as two laminated layers: one dark gray (5GY 4/1) and 60 cm thick (Core 126-788D-9R), the other greenish black (5G 2/1) and only 5 cm thick (Core 126-788D-13R, 0–5 cm).

Although Subunit IIB is generally characterized by the coarseness of its material and the scarcity of carbonate, it tends to become more calcareous in its middle portions and toward the bottom of the hole (Fig. 6). The enrichment in carbonate affects all lithotypes; conglomerate in Core 126-788D-12R, where nannofossils and foraminifers are part of the matrix, and vitric siltstone and silty claystone in Cores 126-788D-15R and -16R.

The rocks of Subunit IIB have been deformed by faulting (288–297 mbsf). In Section 126-788D-8R-CC, hanging-wall vitric sandstone has been juxtaposed against pebble-granule conglomerate along a healed, 7-mm-wide, siltstone-filled microfault zone that dips at 60° (Fig. 19). Another healed microfault dipping at 30° is located at the top of Core 126-788D-9R; here, granule conglomerate is the hanging-wall lithology, resting on vitric silty claystone with laminae that dip at 5° in the same direction as the fault. A total of six subvertical microfractures occur lower in the same core and in the next (Core 126-788D-10R),

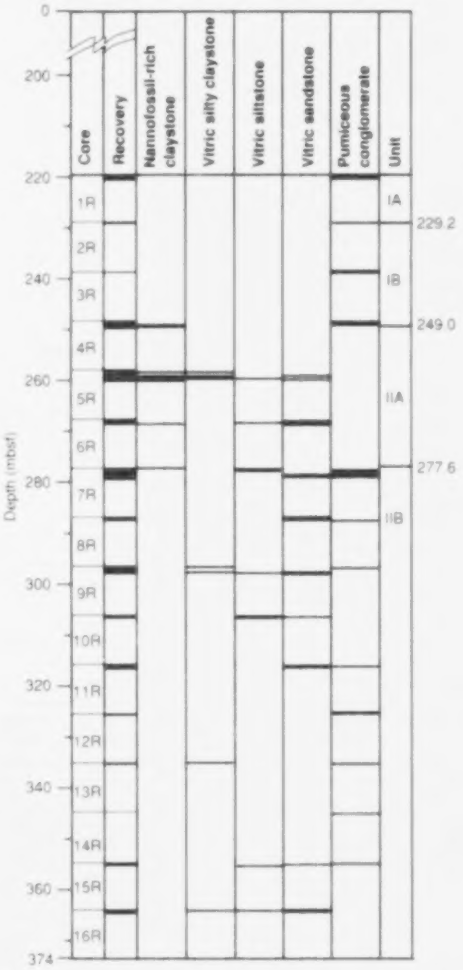

Figure 14. The lithotypes of Hole 788D, and the bases for defining the Unit I/II and Subunit IIA/IIB boundaries.

below which no additional evidence of tectonic deformation was seen.

Lithification and Diagenesis

Because lithification and diagenetically influenced parameters, such as nannofossil content, have been used to define subunit boundaries, these processes warrant further discussion. Petrographic examination of thin sections from Subunits IA (IA to IIB transition; Sample 126-788D-1R-1, 25 cm), IIA (Sample 126-788D-6R-1, 41 cm), and IIB (Samples 126-788D-9R-1, 89 cm; 126-788D-11R-1, 12 cm; and 126-788D-12R-1, 11 cm) show a downhole variation in lithification processes. Compaction and pressure welding are prevalent at the base of Subunit IA and in

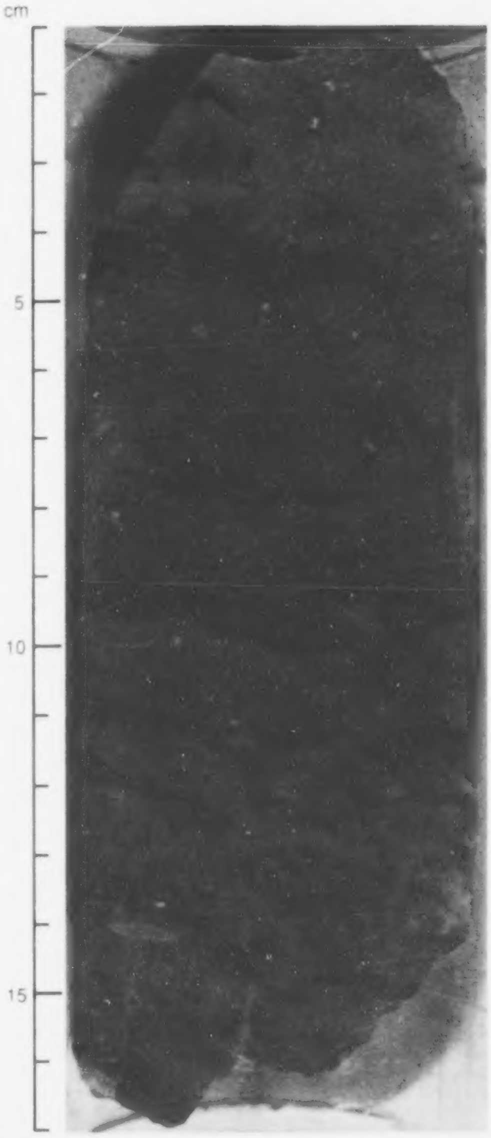

Figure 15. Strongly burrowed nannofossil claystone of Unit IIA with scattered white foraminifers (Interval 126-788C-28X-CC, 0-17 cm).

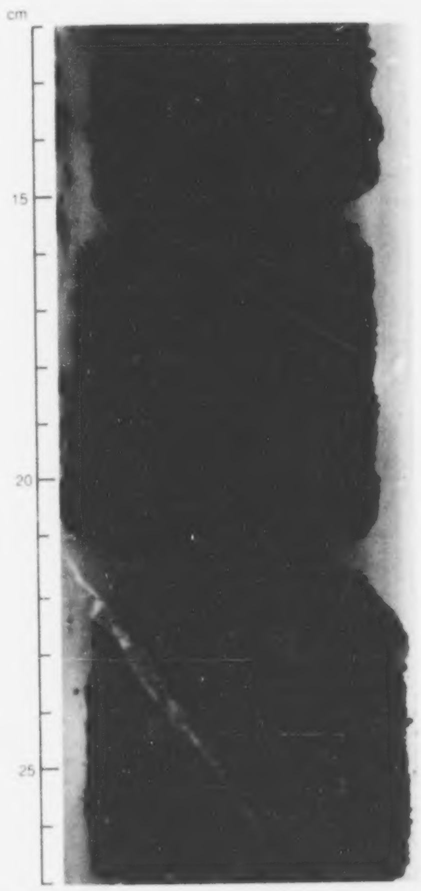

Figure 16. Black (N2), pebble-granule conglomerate characteristic of Subunit IIB (sand 30%, granules 40%, pebbles 30%; Interval 126-788D-7R-2, 12–27 cm).

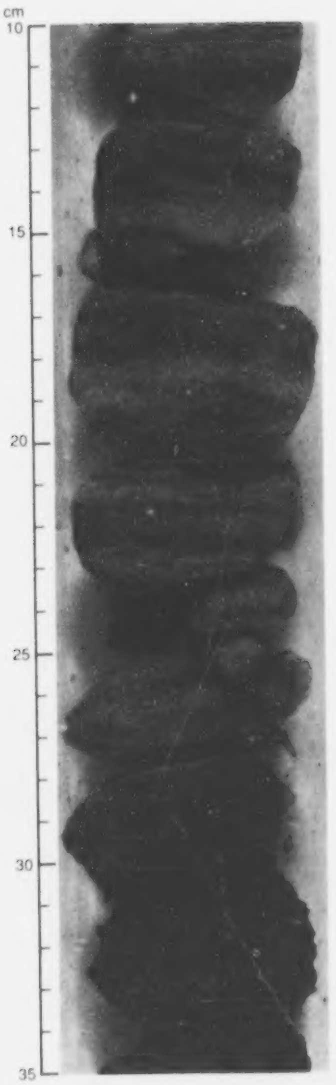

Figure 17. Pumiceous medium-grained sandstone (above 28 cm) and vitric sandy granule-pebble conglomerate (below 28 cm; Interval 126-788D-11R-1, 10–35 cm).

Subunit IIA, whereas compactional textures are accompanied by cementation in Subunit IIB. Smear-slide description of Sample 126-788C-21H-1, 2 cm, indicates that recrystallization of clay-mineral matrix material may also be an important binding agent in these sediments.

The uppermost occurrence of carbonate cement (high-Mg calcite; see XRD data) in Subunit IIB coincides with a shift in the preservation of calcareous fauna: Subunit IIA is nannofossil-rich, in direct contrast with Subunit IIB, which is relatively devoid of nannofossils but is locally enriched in foraminifers. Carbonate cements in Subunit IIB samples exhibit needle to microspar morphologies and also form needle overgrowths on foraminifer tests. Only one sample showed two-phase cementation: initial precipitation of carbonate needles, followed by precipitation of microcrystalline, low-birefringent zeolite. The paragenetic sequence is documented by the inclusion of carbonate crystals within the later zeolite phase. This local zeolite cementation could be related to glass hydration reactions within adjacent sediments.

Constituent grains of different morphologies and mineralogy have responded to compaction in different ways during induration. Where compactional processes have resulted in induration,

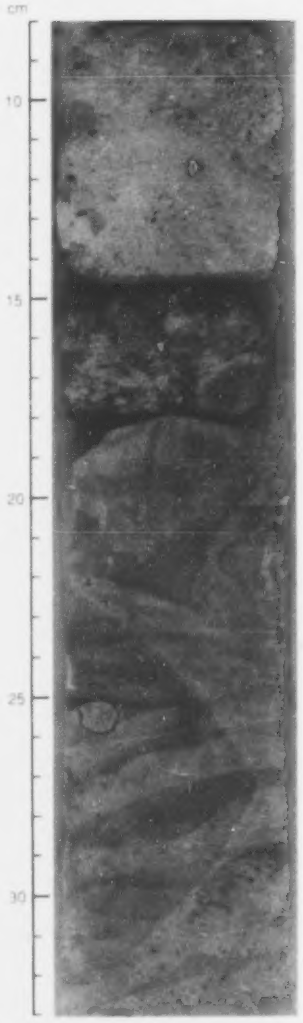

Figure 18. Strongly burrowed vitric siltstone in Subunit IIB. *Zoophycos* is the predominant trace fossil from 23-33 cm (Interval 126-788D-16R-1, 8-33 cm).

grain contacts are straight and interpenetrating, and deformed grains are common. Microporous pumice fragments, the most common grain type within Site 788 sandstones, are less competent than interspersed or interlaminated, altered microlitic to holocrystalline intermediate glass fragments. The glass fragments are embedded therefore into (interpenetrated) pumice grains or deform pumice grains at pressure-welded grain contacts. This pressure welding, caused by simple compactional processes within a pumiceous sequence, mimics high-temperature welding effects.

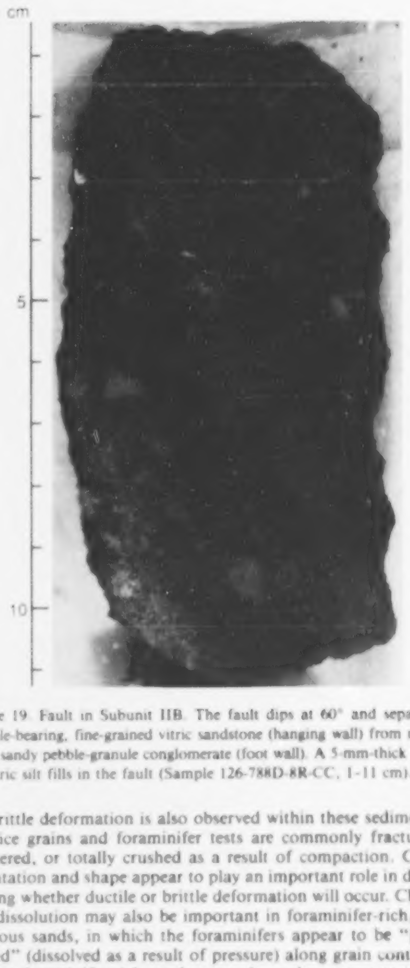

Figure 19. Fault in Subunit IIB. The fault dips at 60° and separates granule-bearing, fine-grained vitric sandstone (hanging wall) from mafic vitric sandy pebble-granule conglomerate (foot wall). A 5-mm-thick band of vitric silt fills in the fault (Sample 126-788D-8R-CC, 1-11 cm).

Brittle deformation is also observed within these sediments. Pumice grains and foraminifer tests are commonly fractured, shattered, or totally crushed as a result of compaction. Grain orientation and shape appear to play an important role in determining whether ductile or brittle deformation will occur. Chemical dissolution may also be important in foraminifer-rich, pumiceous sands, in which the foraminifers appear to be "pressolved" (dissolved as a result of pressure) along grain contacts. Within foraminifer-rich sandstones, the carbonate cements are localized around crushed foraminifers; thus, liberated carbonate may have been locally reprecipitated as microcrystalline cement.

X-Ray Diffraction Analysis

X-ray diffraction (XRD) results are summarized in Table 4. In Unit I, handpicked black microspherules (Fig. 9) on the surface of a pebble of pumice (Sample 126-788C-7H-CC, 20 cm) display a very strong peak at 0.95 nm, reflecting abundant todorokite $(Ca,K,Na)_{0.21}(Mn^{2+},Mg^{2+},Mn^{4+})_{6.40}O_{12} \cdot 3.6H_2O$ as well as large amounts of amorphous glass (Fig. 20). The black, manganiferous material coats the surface of pumice pebbles and granules from 38 to 78 mbsf (Cores 126-788C-4H to -9H). Buserite is not present in the microspherules. The todorokite is stable and did not change to birnessite after 15 days of air drying.

In the top of Subunit IIA, micrite-rich claystone contains glauconite, in association with smectite, calcite, and feldspar

Table 4. X-ray diffraction data from Site 788.

Core, section, interval (cm)	Depth (mbsf)	Unit	Color	Texture	Clay minerals 1.4-nm	Clay minerals 1.0-nm Mica	0.7-nm Chlorite	Minerals	1.0-1.1 nm 0.44 nm Palagonite	Amorphous materials
126-788C-										
7H-CC, 20	61.7	I	5YR2/1	Mn spherule	—	—	—	Todorokite >>> halite	—	Abundant
8H-3, 10	70.8	I	5Y4/1	Granular sand	—	—	—	Feldspar, halite	Common	Abundant
13H-1, 50	115.7	I	5GY3/2	Welded tuff	1.41-nm chlorite	Present	Abundant	Quartz, feldspar > halite	Present	Abundant
28X-CC, 15	257.9	II	5GY6/1	Micrite-rich claystone	1.76-nm mica-smectite interstratified	0.45-nm glauconite	Trace	Calcite > feldspar > quartz, halite	Common	Abundant
126-788D-										
1R-1, 50	220.1	II	5GY4/1	Conglomerate	Present	Present	Present	Feldspar >>> quartz, halite	Present	Common
6R-1, 20	268.1	II	5G4/1	Siltstone	1.76-nm smectite	Trace	Abundant	Feldspar >>> quartz > halite	—	Common
6R-1, 30	268.2	II	N1	Mafic vitric sandstone	1.76-nm smectite	—	—	Feldspar >>> halite	Common	Abundant
6R-1, 50	268.5	II	5Y2/1	Mafic vitric sandstone	Present	—	—	Feldspar	Present	Abundant
6R-1, 70	268.6	II	10Y4/1	Claystone	Present	—	Trace	Feldspar >>> calcite	Present	Abundant
11R-1, 13	316.1	II	5Y5/4	Pumiceous sandstone	Present	—	Trace	Calcite (Mg-rich) > feldspar > halite	Trace	Abundant

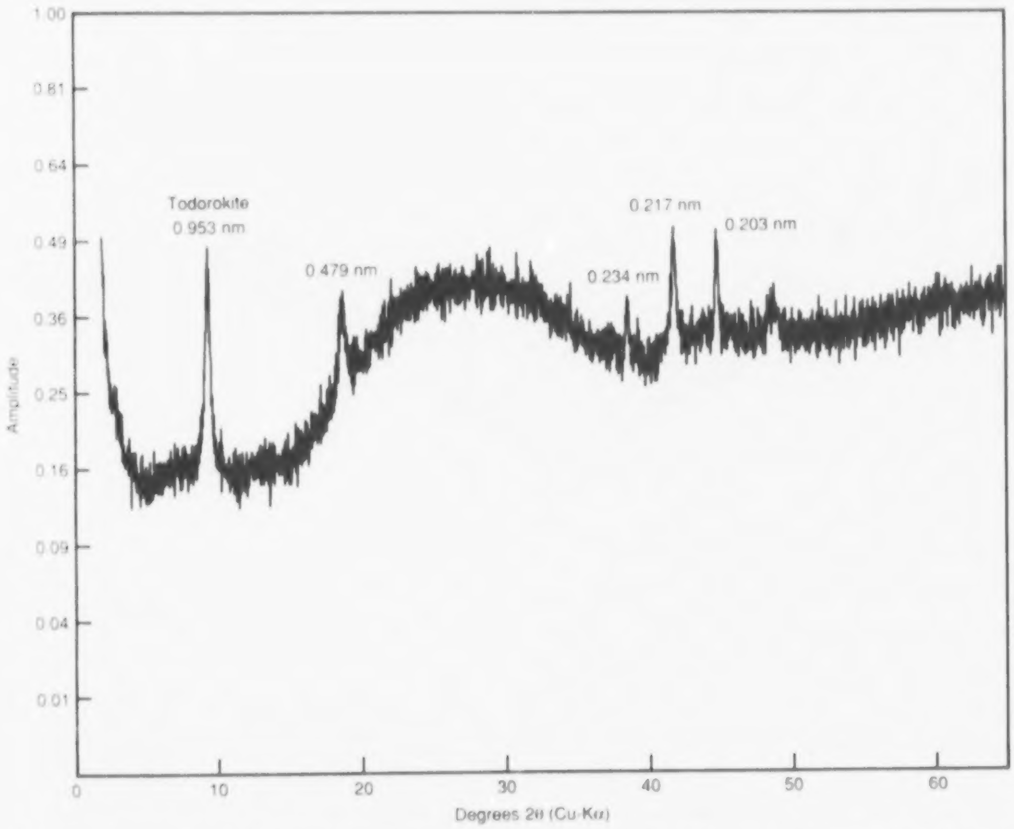

Figure 20. XRD pattern for handpicked spherules of manganese oxide, indicating the characteristic peak of todorokite (Sample 126-788C-7H-CC, 20 cm).

(Fig. 21). The sediment contains foraminifers and interstratified mica-smectite clay minerals. Glauconite is commonly confused with celadonite, an iron-rich, dioctahedral mica with almost the same chemical composition as glauconite. The Site 788 material shows a distinctive glauconite <060> reflection at a *d*-spacing of 0.151-0.152 nm that is larger than the analogous *d*-spacing of celadonite at 0.150 nm. This distinction of glauconite from celadonite is important, because celadonite is an alteration product or hydrothermal mineral associated with volcanic rocks. In contrast, glauconite indicates *in-situ* sediment alteration under reducing conditions with fairly slow sedimentation rates (Berner, 1981; Odin and Matter, 1981).

Green to black vitric siltstone and sandstone beds in Units I and II contain large amounts of amorphous material, principally volcanic glass. The glass, which is green to brown in color, is partially altered to smectite, chlorite, and palagonite. Feldspar is abundant in the vitric siltstones and sandstones, whereas mica group minerals and quartz are very rare.

A sample of pumiceous medium-grained sandstone (Sample 126-788D-11R-1, 1-13 cm) has a peak at 0.300 nm, suggesting the presence of Mg-calcite rather than calcite; calcite has its characteristic <104> peak at 0.3035 nm.

Sediment Accumulation Rates

Sedimentation rates for Site 788 were determined from calcareous nannofossils datums, nannofossil biozones, and paleomagnetic events (Table 5), which were used to construct the age-depth curves shown in Figures 22 and 23. Sedimentation rates were not determined for Site 789 because of the lack of recovery at this site.

Sedimentation rates for Unit II at Site 788 average 124 m/m.y. over the interval from 4.77 to 3.88 Ma (Fig. 22). However, Figure 23 (an expanded version of the lower sedimentary section of Site 788) shows that sedimentation rates during this interval are quite variable, ranging from 39 m/m.y. to as much as 282 m/m.y. The lowest rates occur at the top of Subunit IIA, the nannofossil-rich claystone interval, and coincide with other lithologic indicators (see "Interpretation" section that follows) of reduced sediment accumulation at this time.

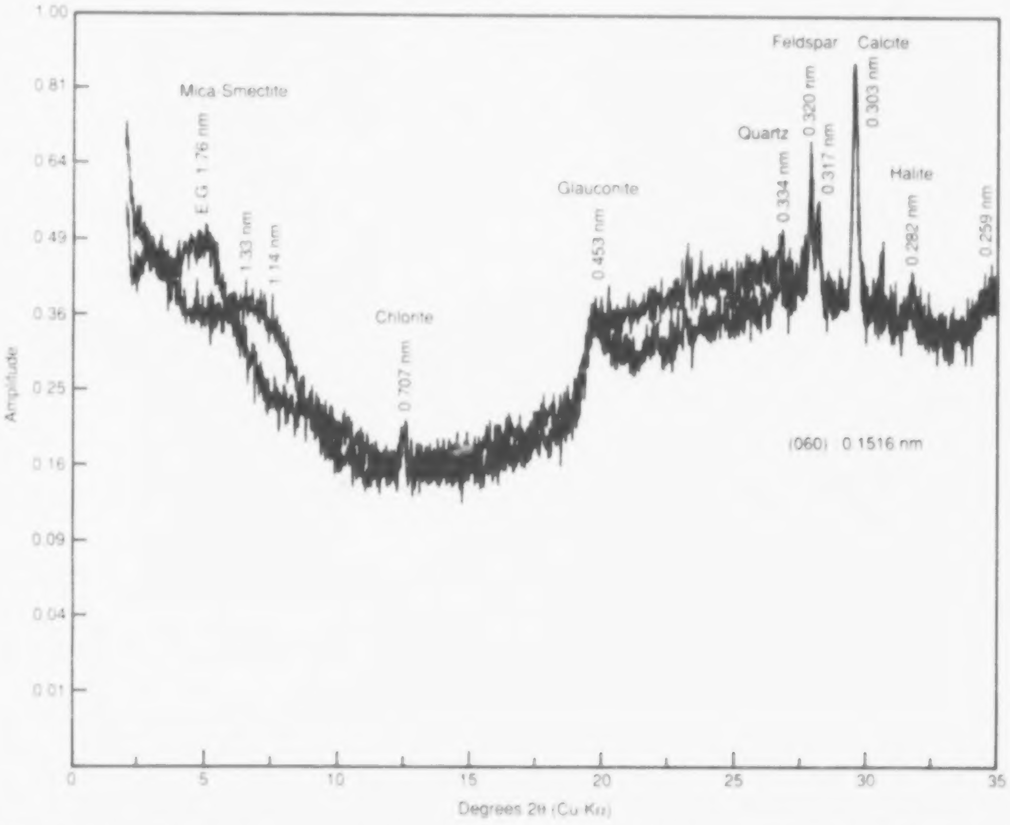

Figure 21. XRD pattern for micrite-rich claystone (Sample 126-788C-28X-CC, 15 cm) showing glauconite with mica-smectite interlayers, quartz, feldspar, and calcite.

Table 5. Chronostratigraphic events at Site 788 and associated depth intervals used to construct the age-depth curves shown in Figures 22 and 23.

Chronostratigraphic event	Core, section, interval (cm)	Depth (mbsf)	Age (Ma)
Biostratigraphy:			
FO *E. huxleyi*	788A-4R-CC	27.43–35.80	<0.275
LO *D. pentaradiatus*	788C-4H-1, 0–1	29.70–33.73	>2.350
Presence *Geophrocapsa* sp.	788C-19H-CC	180.98–181.78	<3.560
Paleomagnetics:			
Gilbert R to N	788D-4R, 85	249.35–257.90	3.88
N to R	788D-4R/5R	249.65–266.00	3.97
R to N	788D-5R, 15	258.35–266.15	4.10
N to R	788D-9R	297.00–306.50	4.24
R to N	788D-10R/11R	306.87–324.83	4.40
N to R	788D-11R, 55	316.55–325.38	4.47
R to N	788D-11R/12R	316.77–334.87	4.57
N to R	788D-15R/16R	355.28–373.28	4.77

Note: A slash ("/") between core numbers indicates that the polarity reversal occurred between the two cores listed. The two values for each depth datum represent the possible depth range a sample may have if less than 100% recovery occurred within a core. R = reversed polarity sequence and N = normal polarity sequence.

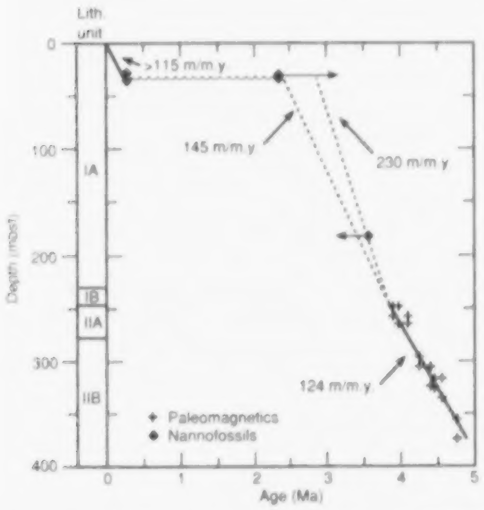

Figure 22. Age-depth curve for Site 788. See text and Table 5 for details of the chronostratigraphic horizons. Two points at any given event (age) indicate the possible depth range over which the event may have occurred.

Sedimentation rates in Unit I, the pumiceous sandy granule and pebble gravels, are constrained by nannofossil datums and biozones to vary between 145 to 230 m/m.y. for the interval between 30 and 250 mbsf (>2.35 Ma but <3.56 Ma). A hiatus, over 2.0 m.y. in duration, is present in the upper Pliocene to upper Quaternary sequence (2.35-0.275 Ma). Upper Quaternary (<0.275 Ma) sedimentation rates are no less than 115 m/m.y. and may be equivalent to rates in the pumiceous gravel below the hiatus.

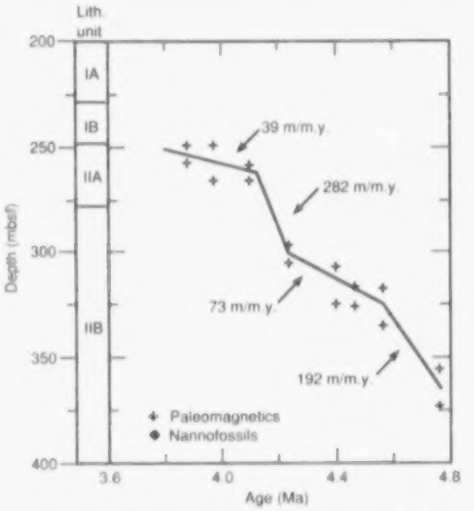

Figure 23. Age-depth curve for Site 788 for the interval from 250 to 370 mbsf. See Table 5 for details of chronostratigraphic horizons. Two points at any given event (age) indicate the possible depth range over which the event may have occurred.

Interpretation

Any attempt to reconstruct the history of Site 788 (Table 6) must be qualified by the poor recovery from Hole 788D. However, these rocks are a varied suite of lithotypes from which paleoenvironmental information of tectonic as well as sedimentologic significance may be extracted, with the caveat that the proportions of the recovered rock types, particularly that of easily disaggregated pumice conglomerate, probably do not accurately reflect the true proportions.

We begin with the environments and events recorded by the sedimentary rocks recovered from the bottom of Hole 788D (Subunit IIB). Initially high sedimentation rates (Fig. 23) accompanied nearby volcanism at 4.8-4.6 Ma. The carbonate contents of 4.6-4.2-Ma rocks, in the form of foraminifers and nannofossils, suggest that they were deposited during a fairly quiescent stage of volcanism. Otherwise, they would have been diluted by volcaniclastic debris. The relative abundance of foraminifers with respect to nannofossils may indicate that the site was already a bathymetric high subjected to winnowing by bottom currents this early in its history.

The pumiceous conglomerate in the upper portion of Subunit IIB was produced by active rhyolitic volcanism and was deposited on Site 788 some time between 4.2 and 4.1 Ma (Figs. 22 and 23). The presence of pressure welding and brittle compactional effects in the rocks of this subunit suggest that a significantly greater thickness of pumice may have been deposited, subjecting the rocks to high overburden pressures. If this is so, the overlying rock column must have been subsequently truncated by erosion, because the thickness of the present column is insufficient to create such effects. Sufficient overlying rock and

Table 6. Summary of geological events as deduced from the sedimentary data in Holes 788C and 788D.

Sedimentary event	Time period (Ma)	Environmental setting
1. Accumulation of pelagic carbonate and detrital component of basal Subunit IIB	4.8–4.2	Nearby volcanism, then volcanic quiescence; site bathymetrically high?
2. Accumulation of Subunit IIB pumiceous conglomerate	4.2–4.1	Massive silicic eruptions
3. Accumulation of Subunit IIA nannofossil-rich clays and associated rock types; glauconite diagenesis/authigenesis	4.1–3.8	Possibly volcanic fall-distal volcanism; possible that [illegible] site was a bathymetric high, but with less relief and at greater water depth than during Subunit IA time
4. Accumulation of major part of Unit I pumiceous conglomerates and gravels	3.8–2.55 or later	Massive silicic eruptions; deposition of the first three cycles of pumice (from 249 up to 29.7 mbsf); the first two of these record andesitic-rhyolitic events or eruptive periods
5. Erosional truncation (tectonically triggered?) of Unit I pumice deposits	Sometime during 2.55–0.27?	Site bathymetrically high
6. Accumulation of Subunit I manganese oxides		
7. Deposition of uppermost Unit I pumice layer (35.1–0 mbsf) on the manganiferous interval	Post-0.27?	Massive silicic eruption(s)
8. Oxidation and reworking of surface pumice; remobilization of manganese oxides	Post-uppermost pumice deposition to Present	Site bathymetrically high

overburden pressure may not have accumulated until the time that Subunit IA was deposited.

The restriction of carbonate cementation to the interval immediately below the Subunit IIA/IIB boundary could be explained in three ways:

1. Fault- or unconformity-related juxtaposition of young, incipiently compacted sediments on more deeply buried, cemented sediments. This fault or unconformity would have to be situated between Cores 126-788D-6R (compacted only) and -9R (cemented and compacted), and would best correspond to the faulting observed in the interval from 288 to 297 mbsf (Sections 126-788D-8H-CC and 126-788D-9H-1).
2. A change in depositional environment (e.g., shallowing) between Subunits IA and IIB. This could best be verified by foraminiferal paleoenvironmental analyses.
3. Burial-related recrystallization and dissolution of nannofossil tests and associated pressolving of foraminiferal tests with reprecipitation in the form of needle and microspar cements in porous sandstones.

There is evidence to support the first and third of these hypotheses.

Another period of quiescence and slow deposition from 4.1 to 3.8 Ma is recorded by the lack of pumiceous conglomerates and the dominance of nannofossil-rich claystones in the rocks of Subunit IIA. Regional, distal volcanic activity, as recorded by the presence of thin vitric sandstones in the subunit, may have continued during this period but at a reduced scale. The glauconite in the nannofossil-rich claystones indicates that the claystones accumulated slowly and resided at the surface long enough for the glauconite to form authigenetically or from the diagenesis of other clay minerals.

In the modern marine environment, the typical site for glauconite accumulation is a submarine high, under conditions of either slow deposition or nondeposition, and nonoxidizing microenvironments (Odin and Matter, 1981) such as the tests of foraminifers. Berner (1981) has characterized the depositional environment of glauconite as one in which organic matter and sulfides are scarce or absent, and all oxygen has already been consumed by aerobic bacteria. If Site 788 was a bathymetric high during the time Unit II was deposited, the presence of significant amounts of fine material in the calcareous portions of the unit may signify that local relief was significantly less than at present. The site may also have experienced weaker bottom currents and other winnowing agents during Unit II deposition than it did during Unit I deposition because it was at greater depths.

After this period of slow deposition, explosive silicic volcanism was renewed at about 3.8 Ma, producing the first pumiceous gravels of Unit I. Upward-coarsening trends in the deposits indicate four major episodes of pumice eruption in late Pliocene to Quaternary time, or four extended periods over which silicic volcanism built up to climaxes. Each deposit is 30–50 m thick. These are roughly as thick as the individual Quaternary pumice layers at Site 791 and substantially thicker than those at Site 790. Being on the rift-basin floor, Sites 790 and 791 would be expected to accumulate thicker deposits than such high-standing localities as Sites 788 and 789. The Unit I pumice deposits of Pliocene age at Site 788 were either produced by individual events of greater magnitude than those recorded in the Quaternary deposits of Sites 790 and 791, or they were deposited during extended cycles of eruption. The top of the third upward-coarsening trend (29.7 mbsf; Interval 126-788-C-4H-1, 0–1 cm) is marked by an unconformity. The last of these accumulations is Quaternary in age, and thus is separated in time from the first three (see discussion below).

If the site stood above the surrounding submarine terrain during the accumulation of the Unit I pumice conglomerate and gravel, there are two plausible mechanisms that would have brought pumice clasts to the site and deposited them there as blankets. The pumice could have arrived more or less directly as air fall, or, alternatively, it may have rafted (or floated in the water column) to the site. That Subunit IA gravels are variably rounded, but very well-rounded pumice clasts in some intervals implies that they were subjected to extensive abrasion, perhaps from wave activity before or during their journey to the seafloor. This rounding supports the rafting transport mechanism rather than the direct air-fall one.

The occurrence of todorokite at depths of 39.2–61.9 mbsf is noteworthy. It addresses the question of whether hydrothermal activity has been significant at Site 788, and it bears upon the problem of locating a Pliocene hiatus at the site. Marine manganese oxides may be deposited (1) hydrothermally; (2) as a result of the slow oxidation of Mn^{2+} to Mn^{4+} during diagenesis, or (3) as hydrogenous precipitates from Mn-enriched seawater at the ocean floor. If manganese is derived from hydrothermal leaching of basalts in the basement, then the temperature range for this leaching would be in the 200°–500°C range.

Todorokite of Holocene hydrothermal origin has been found and studied in the Bonin region, in the vicinity of Nishinoshima Island, approximately 400 km south of Site 788. It is especially widespread on Kaikata Seamount. Usui et al. (1987) reported that the hydrothermal todorokite takes three forms, each characterized by its thickness and stability. Deposits thicker than 5 cm have stable, heat-resistant interiors, although their external portions may be unstable when heated at 110°C, as are deposits 1-5 cm thick, becoming transformed to birnessite. Deposits several millimeters to a centimeter thick are even less stable, becoming birnessite when air dried at room temperatures for 1 hr.

The todorokite in Subunit IA, although no more than a millimeter thick, remained unchanged after 15 days at room temperature, and probably has a different origin than the hydrothermal todorokites from the Nishinoshima area. A diagenetic or hydrogenous origin, on the other hand, would produce stable manganese minerals. The restriction of the manganese oxides to a relatively thin, near-surface interval far above the igneous basement is difficult to account for by hydrothermal origin *in situ*. Furthermore, the geochemistry of pore waters from Hole 788C (see "Sediment/Fluid Geochemistry" section, this chapter) is not very different from that of normal seawater. The manganese contents of these interstitial waters are only 30 ppm at depths of 135-215 mbsf, increase to 60 ppm at 60 mbsf, the lowest (and most abundant) occurrence of manganese, and then diminish to 50 ppm at 10 mbsf. It appears that the manganese in the pore waters is being remobilized out of the deposits. There is no other geochemical evidence for hydrothermal alteration of the sediment column or of its water content.

The manganese oxides occur close to an unconformity at approximately 30 mbsf (see "Biostratigraphy" section, this chapter). Nannofossil data established a Quaternary (< 0.275 Ma) age for Section 126-788A-4R-CC at a depth between 27.5 and 35.8 mbsf. In Hole 788C, however, nannofossil data indicate a Pliocene age (≥ 2.35 Ma) at 29.7-33.7 mbsf (Sample 126-788C-4H-1, 0-1 cm, Table 5). These biostratigraphic data require that an unconformity exists at some depth between 27.5 and 33.7 mbsf. This is the cored interval of Cores 126-788C-3H to -4H. If the manganese in the depth range from 39.2 to 61.9 mbsf has a hydrogenous origin, it may mark a period of virtual nondeposition some time during the 2-m.y. hiatus. It remains to be demonstrated, however, that manganese could have precipitated on the pumice at some depth beneath, instead of directly on, the seafloor.

An explanation for the unconformity is that it was caused by rift-related Pliocene-Quaternary tectonism. As a result of tectonically triggered movements, a thick cap of gravel and other sediments that may have accumulated during all or part of the 2 m.y. of hiatus could have been removed by mass movements. This would account for the missing column of sediment necessary to provide the pressure to compact the conglomerates of Subunits IB and IIB. The compactional history of this sequence of sediments could be of great importance in estimating relative uplift rates during rifting in the Sumisu region. With the present limited data base, it is not possible to determine the amount of Pliocene-Pleistocene overburden that may have been removed by erosion during flank uplift.

The uppermost 30 m of pumiceous gravel atop the manganese at Hole 788C could have been deposited at any time after 2.35 Ma. Assuming that it correlates with the sequences of Hole 788A, it is 0.275 Ma in age or younger. Marked as the uppermost upward-coarsening sequence in Figure 6, this layer differs from the rest of the subunit in two ways. Many of its pumice pebbles are oxidized, and, although the entire subunit is depleted in fines, this uppermost layer is exceptionally so (Fig. 6). These features suggest that these surface deposits have resided for an extended period of time at the present seafloor atop this high-standing site, where the sediment is subjected to winnowing by currents and the slow oxidation of volcanic glass.

BIOSTRATIGRAPHY

Site 788

Calcareous Nannofossils

Hole 788A

Samples 126-788A-1R-CC, 126-788A-4R-1, 0-1 cm, and 126-788A-4R-CC contain *Emiliania huxleyi*, which falls within Zone CN15. Other species present in these samples are *Helicosphaera carteri*, *Gephyrocapsa* spp., *Pontosphaera* spp., *Reticulofenestra* sp., *Oolithotus antillarum*, and reworked specimens of *Pseudoemiliania lacunosa*.

Sample 126-788A-3R-CC is barren of calcareous nannofossils. Sample 126-788A-5R-CC contains only the species *P. lacunosa*, which has a range from the middle Pliocene to the Pleistocene (Zones CN11b-CN14a).

Hole 788B

No samples were taken or analyzed from this hole.

Hole 788C

Samples 126-788C-4H-1, 0-1 cm, 126-788C-4H-4, 30 cm, 126-788C-28X-1, 0-1 cm, and 126-788C-28X-CC contain species *Discoaster pentaradiatus*, *Discoaster brouweri*, and *Calcidiscus macintyrei* and do not contain *Discoaster surculus*, *Discoaster tamalis*, or *Reticulofenestra pseudoumbilica*, which suggests assignment to upper Pliocene Zone CN12c. Other species present in these samples are *Gephyrocapsa* spp., *Calcidiscus leptoporus*, *Coccolithus pelagicus*, *Helicosphaera sellii*, *Syracosphaera* sp., and small *Reticulofenestra* sp.

Samples 126-788C-4H-CC and 126-788C-19H-CC contain only rare specimens of *Gephyrocapsa* sp. The presence of *Gephyrocapsa* sp. in Sample 126-788C-28X-CC indicates that the bottom of this hole is no older than the middle Pliocene (Perch-Nielsen, 1985).

Preservation in these samples is generally poor to moderate because of dissolution of the calcareous nannofossils. This suggests that the absence of index species older than CN12c could be a result of dissolution. If so, the oldest constraint for the hole would then be based upon the first occurrence (FO) of *Discoaster pentaradiatus* in middle Miocene Zone CN7a (Perch-Nielsen, 1985).

All other samples taken from this hole are barren of calcareous nannofossils.

Hole 788D

Samples 126-788D-4R-CC, 126-788D-10R-1, 37 cm, 126-788D-12R-1, 28 cm, Core 126-788D-14R, and Sample 126-788D-16R-1, 12 cm, contain *Calcidiscus macintyrei*, which indicates an age range from the early Miocene to the early Pleistocene (Zones CN3-CN14a).

Sample 126-788D-5R-1, 10 cm, contains *C. macintyrei* and *Discoaster* sp. Therefore, it is no younger than the late Pliocene based on the last occurrence (LO) of the genus *Discoaster*, and no older than the early Miocene (Zone CN3) based on the FO of *C. macintyrei*. *Reticulofenestra* sp., *Gephyrocapsa* sp., and *C. leptoporus* are present in Samples 126-788D-6R-CC; 126-788D-11R-1, 18 cm; 126-788D-11R-CC; 126-788D-12R-CC; 126-788D-13R-1, 5 cm; and 126-788D-15R-1, 55 cm. All other samples analyzed from this hole are barren of calcareous nannofossils.

Planktonic Foraminifers

Hole 788C

Sample 126-788C-28X-CC, 5–6 cm, contains dextral *Globorotalia menardii*, dextral *Globorotalia tumida*, *G. crassaformis* s.l., *G. margaritae*, *G. scitula*, *Globigerinoides sacculifer*, *G. obliquus*, *G. bollii*, *Globoquadrina altispira*, *G. humerosa*, *G. venezuelana*, *Globigerina praedigitata*, and dextral *G. pachyderma*. The presence of *G. margaritae* and other assemblage species limits the age to Zones N18–N19 (Bolli et al., 1985).

Sample 126-788C-28X-CC, 13–14 cm, contains most species present in Sample 126-788C-28X-CC, 5–6 cm, plus *Globigerina ruber*, which makes its appearance in the middle of Zone N18 (Bolli et al., 1985). This sample is assigned to the middle of Zones N18–N19 according to the zonation of Berggren et al. (1985).

Sample 126-788C-28X-CC, 14–18 cm, contains, in addition to the species present in the previous sample, *Globorotalia merotumida-plesiotumida*, which ranges from the top of Zone N17 to lower Zone N19 (Bolli et al., 1985). This sample is assigned to middle Zone N18 to lower Zone N19.

Hole 788D

Sample 126-788D-4R-CC contains dextral *Globorotalia tumida*, dextral *G. menardii*, *Globigerinoides ruber*, *Globoquadrina altispira*, *G. humerosa*, *Orbulina universa*, and *Globigerina quinqueloba* placing this sample in the middle of Zones N18–N19 (Bolli et al., 1985).

Rare specimens of *Globorotalia margaritae*, in addition to *Globigerinoides conglobatus*, *G. humerosa*, *G. altispira*, *G. dutertrei*, dextral *Globigerina pachyderma*, and *Globorotalia crassaformis* s.l., were observed in Sample 126-788D-6R-CC, placing it in Zones N18–N19 (Bolli et al., 1985).

Samples 126-788D-15R-1, 38–40 cm, and 126-788D-16R-1, 37–39 cm, contain planktonic foraminifer shell fragments, which could not be identified at 100× magnification. The shells may belong to *Globoquadrina* sp., *Turborotalia* sp., *Globigerina* sp., and a menardiform-tumidaform species. They will be reexamined under the scanning electron microscope (SEM) during shore-based analyses for species identification.

Benthic Foraminifers

The benthic foraminifer fauna from Samples 126-788C-28X-CC, 5–6 cm, 126-788C-28X-CC, 13–14 cm, 126-788C-28X-CC, 14–18 cm, 126-788D-4R-CC, and 126-788D-6R-CC is characterized by an abundance of small, unornamented *Stilostomella* spp. Other common species are *Chilostomella* sp., *Pyrgo murrhina*, *Uvigerina hispida*, *Cassidulinoides* sp., *Pleurostomella* sp., and *Cibicidoides* sp. This fauna indicates a depositional water depth of 1500–3000 m (Ingle, 1980; Woodruff, 1985; Van Morkhoven et al., 1986; Yasuda, 1989). Abundant occurrences of anaerobic fauna (Bernhard, 1986) composed of small unornamented *Stilostomella* spp., *Chilostomella* sp., *Pleurostomella* sp., and a few occurrences of aerobic fauna from three samples from 126-788C-28X-CC indicate low- to medium-dissolved oxygen content. The fauna from the other samples have a higher ratio of aerobic fauna than the fauna from Sample 126-788C-28X-CC and show medium oxygen content.

Radiolarians

All samples analyzed from Holes 788A, 788B, 788C, and 788D were found to be barren of radiolarians.

Site 789

Hole 789A

Sample 126-789-1R-CC contains the calcareous nannofossil *Pseudoemiliania lacunosa*, which constrains the age of this sample from the early Pliocene to the Pleistocene (Zones CN11–CN14a of Okada and Bukry, 1980). Other nannofossil species present are small *Reticulofenestra* sp., *Calcidiscus leptoporus*, and *Helicosphaera carteri*.

No planktonic foraminifers, benthic foraminifers, or radiolarians were found at this site.

Summary

Calcareous nannofossils recovered from Hole 788A suggest a Quaternary age. Calcareous nannofossils suggest a middle to late Pliocene age for samples in Hole 788C. Planktonic foraminifers indicate an early to middle Pliocene age for Samples 126-788C-28X-CC, 5–6 cm, and 126-788C-28X-CC, 14–18 cm.

Most samples in Hole 788D were barren of calcareous nannofossils and planktonic foraminifers. Samples that did contain nannofossils show the effects of strong dissolution. However, planktonic foraminifers in Samples 126-788D-4R-CC and 126-788D-6R-CC restrict their age to the early Pliocene.

Benthic foraminifers indicate a depositional water depth between 1500 and 3000 m for Holes 788C and 788D. Most assemblages from these holes indicate a low to medium dissolved oxygen content.

PALEOMAGNETICS

Introduction

Magnetic measurements for Site 788 were confined to the cores with the finer-grained or more consolidated lithologies, because previous polarity assignments on coarse-grained, unconsolidated material drilled with the APC proved difficult because of the remanence acquired during drilling. Archive halves of all cores judged suitable for paleomagnetic study by this criteria, excluding cores composed of fragments too small to insure vertical orientation, were measured on the cryogenic magnetometer system.

In addition, a small number of discrete samples were demagnetized and measured on the fully automatic spinner (FAS) magnetometer (see "Explanatory Notes" chapter, this volume). These samples were taken from intervals of specific interest or where continuous core measurements were ambiguous. Alternating field (AF) demagnetizations at higher alternating fields in these cases provided a more confident picture of the characteristic polarity.

Magnetostratigraphy

Holes 788A and 788B

No magnetic results were obtained from these holes because of low core recovery.

Hole 788C

Based on lithology and degree of consolidation, only Core 126-788C-28X (257.9-262.5 mbsf) was judged suitable for polarity assignment The core exhibited a normal polarity after AF demagnetization to 8 mT. The lower to middle Pliocene fossil assemblage of this core (see "Biostratigraphy" section, this chapter) suggests that this normal polarity represents either the Gauss (indicated by the nannofossil assemblage) or Gilbert normal (indicated by the foraminiferal assemblage) polarity chron (Table 7).

Hole 788D

Cores 126-788D-4R through -16R (except Core 126-788D-14R, which has small fragments that may have rotated vertically) were all judged suitable for paleomagnetic measuring. Figure 24 summarizes the polarity designations, and Figure 25 shows the directional and intensity stability of several of the discrete samples measured from this hole. The increase in remanence intensity with AF demagnetization at 25 mT for Sample 126-788D-10R-1,

Table 7. Depth ranges for Gilbert and Gauss normal polarity chron datums.

Absolute age (Ma)		Depth range (mbsf)
Gilbert	Gauss	
3.88	2.47	249.35-257.90
3.97	—	249.65-258.2
4.10	—	258.35-266.15
4.24	2.92	297.0-298.32
4.40	2.99	306.87-316.0
4.47	3.08	316.55-325.38
4.57	3.18	316.77-325.6
4.77	3.40	355.28-364.3

30 cm, is characteristic of removal of the present-field normal overprint from a reversely magnetized sample.

The polarity sequence in Figure 24 may be correlated with either the Gilbert (#4) or Gauss (#3) normal polarity chrons. The compressed N-R polarity interval at the top of the section in the Gilbert correlation (Fig. 24A) would agree with the low sedimentation rate postulated for Cores 126-788D-4R and -5R, based on the presence of claystone and glauconite (see "Lithostratigraphy and Accumulation Rates" section, this chapter). The correlation with the older Gilbert normal chron requires that the reversely magnetized tuff bed (as measured in the continuous pass-through and the discrete sampling modes), which occurs in the upper 10 cm of Section 126-788D-5R-1, be representative of a full reverse polarity zone. The planktonic foraminifer assemblages of various cores from this hole have been associated with Zone N19 (see "Biostratigraphy" section, this chapter) and is consistent with the correlation to the Gilbert polarity chron.

Hole 789A

No magnetic results were obtained from this hole because of the limited recovery (0.10 m).

IGNEOUS GEOCHEMISTRY

Although the Pliocene-Pleistocene lavas hoped for at Site 788 did not materialize, there are white and black vitreous pumices in Subunit IA (see "Lithostratigraphy and Accumulation Rates" section, this chapter). Bulk chemical analyses of two of these, one rhyolitic, the other andesitic, are given in Table 8, together with seven analyses of Pleistocene rhyolite pumices from Sites 790, 791, and 792. For comparison, analyses are given for Quaternary acid andesite from the Izu-Bonin Arc (Tori Shima;

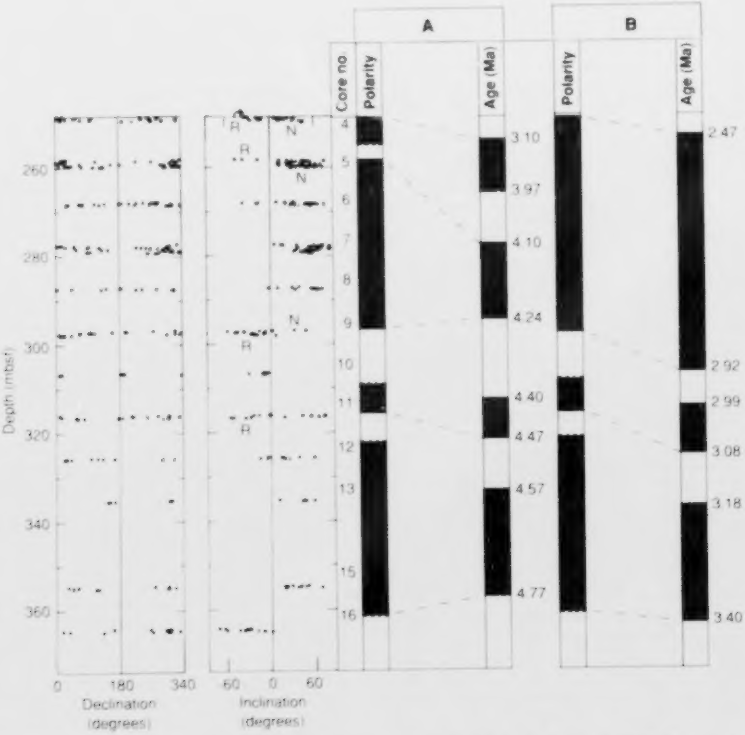

Figure 24. Declination, inclination, and polarity sequence vs. depth (mbsf) for Cores 126-788D-4R through -16R after demagnetization. Rough edges on boundaries indicate polarity transitions that occur between core sections. Datums and polarity sequence at the far right of each section are for the (**A**) Gilbert (#4) and (**B**) Gauss (#3) normal polarity chrons (Berggren et al., 1985).

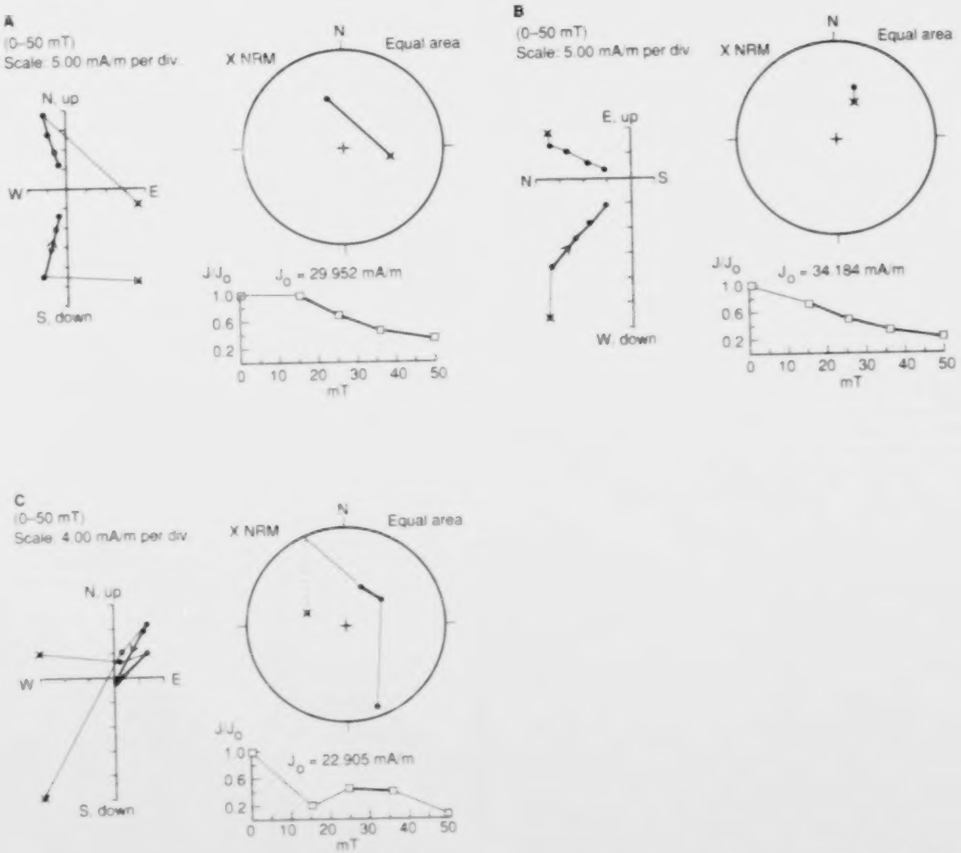

Figure 25. Orthogonal components, field-vector directions, and remanence intensities, as a function of AF demagnetization, for three discrete samples taken from Hole 788D. The heavy lines indicate segments of the AF demagnetization sequence characterized by high directional stability. Negative inclination paths (upper hemisphere) are indicated by a dashed line on the field-vector plots. **A.** Sample 126-788D-5R-1, 15 cm. **B.** Sample 126-788D-10R-1, 30 cm. **C.** Sample 126-788D-15R-1, 38 cm.

Y. Zhang, pers. comm., 1989), for 250-Ka rhyolite lava from a dome atop the en echelon pillow ridges in the Sumisu Rift (Hochstaedter et al., in press), and for dredged rhyolite pumice from the Minami Sumisu submarine caldera (Daisan Sumisu knoll) and another site east of it on the arc (Ikeda and Yuasu, 1989). All pumices were scrubbed, treated several times with ultrasound in deionized water, dried, and handpicked to ensure freshness.

The andesite is similar to the most-differentiated sample from Tori Shima with respect to Si, Mg, and Na. However, it has fractionated more plagioclase, resulting in almost 50% greater iron enrichment (higher Fe, Ti, and V) and lower Al and Ca. Relative to SiO_2, its K, Rb, and Y are about 20%–30% higher than at Tori Shima, whereas its Ba is that much lower in concentration. If confirmed by post-cruise work, this difference in incompatible elements may indicate progressive enrichment of the Izu-Bonin arc in subduction-related incompatible elements during the Pliocene-Quaternary. The Eocene lavas of the outer arc high and the basement lavas at Site 792 are known to have even lower concentrations (see Fryer, Pearce, Stokking, et al., 1990, "Igneous Geochemistry" sections, Sites 781 and 782 chapters). Thus, progressive enrichment in subduction-related incompatible elements through time may characterize the entire Cenozoic history of the arc.

All analyzed Quaternary rhyolite pumices from Sites 788, 790, 791, and 792 are from arc rather than backarc volcanoes. That is, all have lower concentrations of Rb, Zr, Nb, Ce, and Y relative to SiO_2 than do rift rhyolites. In part, this is because the pumices are less differentiated (i.e., they have higher Ti, Fe, Mg, Ca, and P). However, they also have arc-like ratios of incompatible trace elements that the backarc rhyolites lack (e.g., Ba/Zr ~2 rather than 0.5. (REE patterns also should differ, but concentrations even in the rhyolites are too low for shipboard Ce analyses to be sufficiently reliable.)

Indeed, the pumices are extremely depleted in incompatible elements for rhyolitic rocks (e.g., 0.6%–1.0% K_2O and 80–100

Table 8. Shipboard X-ray fluorescence analyses of pumices from Sites 788, 790, 791, and 792.

Site Section, interval (cm) Unit Rock type Chemical type	791A 1H-3, 0-150 Pumice I Pumice B	790B 7H, 0-40 Pumice II Pumice A	790B 10H, 80-150 Pumice III Pumice A	791A 22H-2, 26-28 Pumice III Pumice A	788C 5H-1, 0-150 Pumice IV Pumice B	791B 9R-CC, 2-3 Lith I Pumice B	788C 12H-[illegible], 10-13 Lith IA Pumice A	792B 1H-3, 30-31 Lith I Pumice A	788C 14H-CC, 5-15 Lith IA Scoria	789 Tori Shima Andesite	1888-4 Sumisu Rift Rhyolite	D865-2 Minami Sumisu Pumice A/B	D866-1 Arc Pumice B
SiO_2	71.45	70.76	72.55	69.56	73.38	73.08	72.4	69.9	60.86	61.05	72.71	70.65	73.22
TiO_2	0.41	0.56	0.6	0.62	0.48	0.4	0.52	0.62	0.93	0.90	0.30	0.49	0.32
Al_2O_3	13.42	13.66	13.35	13.96	13.16	13.36	13.06	13.9	14.98	15.01	14.65	14.57	13.28
Fe_2O_3*	3.79	4.22	3.84	4.8	3.74	3.55	3.62	4.91	[illegible]	7.74	2.81	3.68	2.23
MnO	0.11	0.14	0.15	0.14	0.12	0.13	0.12	0.16	0.18	0.16	0.10	0.14	0.09
MgO	0.8	1.02	0.70	1.1	0.86	0.84	1.16	[illegible]	3.6	3.97	0.28	0.9	0.42
CaO	2.27	3.80	3.56	4.07	3.12	2.98	3.15	4.09	6.51	7.72	1.93	3.61	2.65
Na_2O	5.42	5.17	4.3	4.44	4.18	4.97	4.5	4.40	3.16	3.00	5.93	4.06	5.96
K_2O	1.29	0.75	0.65	0.77	0.87	0.91	1.02	0.76	0.62	0.48	1.03	0.91	1.22
P_2O_5	0.08	0.13	0.1	0.14	0.09	0.07	0.1	0.14	0.11	0.09	0.05	0.11	0.06
LOI	2.11	1.8	2.96	4.25	3.72	0.38	3.80	3.63	1.84		1.64	0.76	5.02
Sum	99.06	100.26	99.9	99.59	99.98	100.29	99.6	99.90	100.0	99.86	99.78	99.12	99.41
(ppm)													
Rb		9.7	8.6	7.8		9.9	10.5		8		23		
Sr		172	169	176		162	166		100	101	132		
Ba		162	155	161		162	116		73	110	150		
Zr		86	83	80		92	112		60	56	291		
Nb		2.7	3.7	3.1		1.1	1.8		1.5		4.5		
Cu		25	28	18		11	15			7.8	39		
Y		44	45	44		47	46		12	23	69		
Ni		0	0	0		1	0		8	12	5		
Cr		0	0	0		0	0			45	1		
V		12	28	34			17		236	186	6		
Zn		116	125	124		112	96		152				
Ce		8	9	5		6	8		40	77			

Note: The stratigraphic unit is either one of the pumice units from within Unit I of Sites 790/791 or a lithologic unit from the site (see "Lithostratigraphy and Accumulation Rates" section, this chapter). The chemical type (A or B) refers to the extent of differentiation (see text). Columns 11–14 are surface samples from the arc and backarc, for comparison (see text for references). LOI = loss on ignition.

ppm Zr at 70%–73% SiO_2) and similar to those described as abundant "quartz keratophyres" in ancient arc terranes (e.g., Brouxel et al., 1987). These very low concentrations, together with the apparent bimodality of volcanism (basaltic andesite plus rhyolite), suggest an anatectic origin for the rhyolites. However, thorough evaluations of similar young bimodal suites in arcs (e.g., Stork and Gill, in press) and backarcs (e.g., Hochstaedter et al., in press) usually show no differences in isotope or trace element ratios between rhyolites and coeval mafic rocks, leaving the nature of their genetic link ambiguous.

There is a range of differentiation among the rhyolites. Based on shipboard study, they are roughly divided into two categories, as shown in Tables 8 and 9, with Type B being more differentiated than Type A. Unfortunately, most Type B pumice clasts are <5 mm in diameter so that shipboard sampling gave insufficient mass for trace element analysis by XRF. All pumice clasts that we encountered were too small for thin sections to be made from the analyzed samples. The six thin sections that have been made of Pliocene-Pleistocene pumices indicate no variation in the phenocryst assemblage of plagioclase-clinopyroxene-orthopyroxene-oxide. However, the differences in chemical composition between Types A and B are similar in magnitude to those among the voluminous 7-Ma, low-K rhyolites in Fiji, which also presage-backarc basin initiation and have differences in phenocryst assemblages (Stork and Gill, in press).

Table 9. Summary of differences between rhyolite types A vs. B.

Oxide	Type A	Type B
SiO_2	69–73	73–74
TiO_2	0.5–0.6	0.4–0.5
Fe_2O_3	3.8–5.0	3.6–3.8
MgO	1.0–1.2	0.8–0.9
CaO	3.5–4.1	2.3–3.1
Na_2O	4.3–4.5	5.0–5.5
K_2O	0.6–0.8	0.9–1.3
P_2O_5	0.10–0.14	0.07–0.09
Zr (ppm)	80–90	>90
Y	44–46	>46

Rhyolite geochemistry and mineralogy may have stratigraphic utility. Except for the rhyolite from Site 792 for which a precise age is unknown, the samples are listed in apparent stratigraphic sequence in Table 8. The first five are from the pumice units that punctuate Unit I of Sites 790 and 791 at roughly 60-Ka intervals (see "Lithostratigraphy and Accumulation Rates" sections, "Sites 790/791" chapter, this volume), whereas the sixth underlies them. The two samples from pumice Unit III belong to chemical Type A. The few differences between them (in Si, Fe, and Mg) make the sample from Site 790 atypical of Type A (i.e., more differentiated). This pumice was pure white, whereas some of the Unit III pumices from Site 791 were visibly mixed, with gray lenses mixed into a white host. Thus, although there are differences among the pumices that are broadly correlative between sites, the occurrence of mingled magma eruptions may damp out the stratigraphically useful geochemical contrasts. The Pliocene pumice from Site 788 differs from the others in some of the same ways the Pliocene andesite differs from the Quaternary andesites (e.g., it has lower concentrations of Ba despite higher Rb).

The two oldest Quaternary pumices are the most differentiated (Type B), whereas pumice Units II and III are more mafic (Type A). Were these from one caldera, it might indicate eruption of increasingly mafic rhyolite from the arc as the new episode of explosive volcanism developed in the late Quaternary. This temporal sequence is common in rhyolitic calderas. The sequence also occurs in low-K arc rhyolite volcanoes, (e.g., Usu, though over much smaller volumes and shorter time scales).

The most recent pumice reverses the "trend," becoming more differentiated again. It is similar in composition to one pumice dredged from the Minami Sumisu submarine caldera (Daisan Sumisu knoll), but pumices from that caldera, and from the arc generally, are diverse and have been studied only in reconnaissance fashion (Table 8). Nonetheless, the volcanic component in the upper Neogene stratigraphic section at all sites of Leg 126 is dominated by rhyolitic pumice. Their stratigraphic variations and origin will be difficult to decipher but are pivotal to understanding the history of Izu-Bonin arc volcanism. In turn, this history is relevant to most ancient arcs in which "quartz keratophyres" play a comparably prominent role.

SEDIMENT/FLUID GEOCHEMISTRY

Seven 10-cm long, whole-round samples from Hole 788C were obtained for electrical resistivity measurements, pore-water squeezing, and sediment and fluid analyses.

Sediment Resistivity

Because of the coarse-grained nature of the sediments, the resistivity measurements could not be conducted.

Sediment Geochemistry

Sediments from Site 788 were analyzed on board ship for inorganic carbon, total carbon, nitrogen, and sulfur (see "Explanatory Notes" chapter, this volume). Analytical results are presented in Table 10. The concentration of organic carbon is unusually low throughout the cored interval, varying from less than the detection limit (about 0.01%) to 0.23%. Nitrogen could not be detected in any of the samples. The concentration of sulfur is uniformly low, with an average of about 0.05%.

Fluid Geochemistry

The headspace hydrocarbon analyses did not show any gases above the background level and thus are not reported.

Sodium, strontium, and iron could not be analyzed because of a shortage of acetylene. The composition of the interstitial water is unusually uniform and only shows a slight enrichment of calcium and a depletion of magnesium relative to seawater of similar chlorinity. As one would expect in organic-poor sediments like this, there is no indication of bacterial sulfate reduction. This is further substantiated by the low concentrations of ammonium. However, the elevated manganese and dissolved silicon concentrations (Table 11) clearly distinguish the pore waters from seawater. Thus, despite the coarse-grained nature of the squeezed sediments, the pore waters do not appear to have been appreciably contaminated by seawater. The high concentrations of dissolved manganese show that the subsurface redox conditions are sufficiently low to stabilize Mn(II). Thus, at present, the manganese overgrowths observed in Unit I (see "Lithostratigraphy and Accumulation Rates" section, this chapter) are being remobilized.

Despite the abundance of volcanogenic material, there are no strong signs of low-temperature alteration reactions. This may be related to the coarseness of the sediments, resulting in a small, reactive surface area/water ratio and effective exchange with the overlying seawater.

PHYSICAL PROPERTIES

Introduction

Multisensor track (MST) logging, index property, and velocity measurements were made on cores from Holes 788C and 788D. MST logging was suspended following Core 126-788D-9R, and only MST logging measurements were made in Hole 788A. No physical property measurements were made on sediments from Hole 788B or Site 789. The primary lithology of the upper unconsolidated material (Subunit IA) consists of coarse, pumice-rich sediment (see "Lithostratigraphy and Accumulation Rates" section, this chapter) and is particularly susceptible to disturbance. Therefore, no vane shear strength analyses were made and even the index property data should be viewed with caution. The unconsolidated, friable nature of this material made Hamilton Frame velocity measurements impractical and only one measurement was made. No thermal conductivity measurements were made on cores from Sites 788 or 789.

Index Properties

Unit I consists of structureless, pumiceous sandy gravel and is highly disturbed by drilling. Although the most obvious anomalous values are not included in the figures and interpretations, all the data from the pebbly and gravelly intervals are suspect. Nevertheless, it is possible to recognize certain trends in the index property data. More confidence may be placed in data obtained from Unit II, which is finer grained and more consolidated (see "Lithostratigraphy and Accumulation Rates" section, this chapter).

Grain density values display the least downhole variability of the index properties (Table 12 and Fig. 26) and exhibit a slight increase downhole. Grain density values in Unit I range from 2.3 to 2.8 g/cm³ and average 2.56 g/cm³. The range in Unit II is from 2.4 to 2.79 g/cm³, but the average is slightly higher (2.63 g/cm³). As expected, fewer anomalous values exist in Unit II (Table 12). Unlike the previous three sites (787, 790, and 791), only a weak correlation between grain density values and carbonate contents was observed. A slight increase in mean grain density values from Unit I to Unit II is probably related to the higher average $CaCO_3$ content (in Unit II), but it may also correlate to an increase in heavy minerals, such as olivine and hornblende.

Only five data points remain after filtering and averaging the GRAPE bulk-density measurements made on a single core sec-

Table 10. Concentration of organic carbon, total nitrogen, and sulfur in samples from Holes 788C and 788D.

Core, section, interval (cm)	Depth (mbsf)	Inorg C (%)	$CaCO_3$ (%)	Tot C (%)	Org C (%)	Tot N (%)	Tot S (%)
126-788C-							
1H-3, 140-150	8.4	0.06	0.5	0.02	LD	LD	LD
3H-5, 140-150	27.6	0.05	0.42	0.02	LD	LD	0.03
5H-4, 19-21	43.89	0.01	0.08	0.02	0.01	LD	0.04
5H-6, 32-34	47.02	0.02	0.17	0.02	LD	LD	0.09
6H-3, 55-57	52.25	0.01	0.08	0.01	LD	LD	0.08
6H-5, 24-26	54.94	0.02	0.17	0.01	LD	LD	0.07
7H-1, 35-37	58.55	0.01	0.08	0.03	0.02	LD	0.08
7H-1, 140-150	59.6	0.04	0.33	0.03	LD	LD	0.08
7H-2, 23-25	59.93	0.01	0.08	0.01	LD	LD	0.05
8H-1, 81-83	68.51	0.01	0.08	0.01	LD	LD	0.07
8H-2, 90-92	70.1	0.01	0.08	ND	ND	ND	ND
9H-1, 25-27	77.45	0.01	0.08	ND	ND	ND	ND
9H-3, 39-41	80.59	0.02	0.17	ND	ND	ND	ND
9H-3, 140-150	81.6	0.04	0.33	ND	ND	ND	ND
9H-5, 63-65	83.83	0.01	0.08	0.01	LD	LD	0.11
11H-3, 82-85	100.02	0.01	0.08	0.03	0.02	LD	0.09
11H-4, 132-134	102.02	0.01	0.08	ND	ND	ND	ND
11H-5, 11-13	102.31	0.02	0.17	ND	ND	ND	ND
12H-3, 59-61	109.29	0.01	0.08	ND	ND	ND	ND
12H-6, 34-36	113.54	0.01	0.08	0.01	LD	LD	0.05
13H-3, 71-73	118.91	0.02	0.17	0.03	0.01	LD	0.09
13H-5, 69-71	121.89	0.02	0.17	0.03	0.01	LD	0.05
13H-6, 0-10	122.7	0.05	0.42	0.01	LD	LD	0.03
14H-4, 48-50	129.68	0.01	0.08	0.02	0.01	LD	0.07
14H-5, 90-93	131.6	0.01	0.08	0.01	LD	LD	0.05
15H-1, 46-48	134.66	0.02	0.17	0.03	0.01	LD	0.07
16H-1, 89-90	144.59	0.02	0.17	0.04	0.02	LD	0.09
16H-3, 140-150	145.1	0.02	0.17	0.01	LD	LD	0.02
18H-2, 89-90	165.09	0.01	0.08	0.03	0.02	LD	0.07
19H-6, 67-68	180.37	0.02	0.17	0.01	LD	LD	0.04
20H-2, 63-64	183.83	0.01	0.08	0.03	0.02	LD	0.07
21H-1, 17-18	191.37	0.02	0.17	0.04	0.02	LD	0.1
23H-1, 62-64	210.82	0.01	0.08	0.04	0.03	LD	0.08
23H-3, 140-150	214.6	0.02	0.17	0.01	LD	LD	0.02
24H-2, 108-110	222.28	0.02	0.17	ND	ND	ND	ND
126-788D-							
4R-1, 107-109	249.57	3.49	29.07	3.56	0.07	LD	LD
5R-1, 7-8	258.27	4.34	36.15	4.57	0.23	LD	0.07
5R-1, 146-147	259.66	1.75	14.58	1.86	0.11	LD	0.03
8R-1, 14-16	287.34	0.09	0.75	0.1	0.01	LD	0.03
9R-1, 31-33	297.21	0.02	0.17	0.04	0.02	LD	0.04
9R-1, 91-93	297.81	0.14	1.17	0.16	0.02	LD	0.02
10R-1, 21-23	306.71	0.14	1.17	ND	ND	ND	ND
11R-1, 21-23	316.21	0.47	3.92	0.52	0.05	LD	0.04
12R-1, 31-33	325.91	2.39	19.91	2.55	0.16	LD	LD
13R-1, 3-5	335.33	0.07	0.58	ND	ND	ND	ND
15R-1, 42-44	355.12	0.09	0.75	0.1	0.01	LD	0.04
16R-1, 36-38	364.66	0.02	0.17	0.04	0.02	LD	0.04
16R-1, 60-62	364.9	0.99	8.25	1.04	0.05	LD	0.03

Note: LD = less than the detection limit and ND = not determined.

Table 11. Composition of pore water for samples from Site 788.

Core, section, interval (cm)	Depth (mbsf)	pH	Alk (meq/l)	Sal. (g/kg)	Cl^- (mM)	SO_4^{2-} (mM)	Mg^{2+} (mM)	Ca^{2+} (mM)	K (mM)	Li (μm)	Mn (μm)	SiO_2 (μm)	NH_4 (μm)
126-788C-													
1H-3, 140-150	8.45	7.27	2.31	35.5	557	28.3	51.9	11.2	11.3	26.3	53	497	18
3H-5, 140-150	27.65	7.44	2.36	35.5	554	29.7	51.8	11.2	11.0	22.3	58	459	23
7H-1, 140-150	59.65	7.49	2.38	35.0	552	28.9	51.9	11.1	11.3	24.3	60	440	LD
9H-3, 140-150	81.65	7.51	2.48	35.0	557	28.8	52.2	11.5	11.2	24.3	48	518	LD
13H-6, 0-5	122.75	8.03	2.53	35.0	556	29.6	52.1	11.4	10.9	21.6	39	585	LD
16H-1, 140-150	145.15	8.09	2.59	35.0	556	27.9	52.6	11.5	11.0	23.0	30	537	LD
23H-3, 140-150	214.65	7.97	2.50	35.5	556	28.3	52.5	11.4	11.3	23.7	29	495	LD

Note: LD = less than the detection limit.

tion in Hole 788A (126-788A-4R-1). These data agree well with those obtained at similar depths in Hole 788C. A comparison of GRAPE density measurements in Hole 788D with gravimetrically derived values (Fig. 27) further illustrates the previously reported problems associated with GRAPE data from rotary-drilled sections. The two data sets are nearly mirror images of each other. This, along with other data from Sites 787, 790, and 791 (see "Physical Properties" sections, Sites 787 and 790/791 chapters), is enough evidence to suspend any further acquisition of GRAPE data on rotary-drilled sections. Consequently, only GRAPE density data from Hole 788C (i.e., Unit I) are discussed here.

GRAPE and gravimetric bulk densities in Hole 788C (Unit I) correlate reasonably well despite the high degree of disturbance and poor sample quality within this unit (Fig. 27). However, several gravimetric values fall significantly below the curve of GRAPE density. Introduction of additional water into these core sections during the splitting process may contribute to these low bulk density values.

Variability in both types of density measurements is noted at scales of approximately 10-30 m. Preliminary comparisons with the lithostratigraphy (see "Lithostratigraphy and Accumulation Rates" section, this chapter) suggest that the higher bulk density values are associated with vitric sand and silt layers. Furthermore, these sediments may contain large amounts of dense, mafic minerals.

Gravimetrically determined wet-bulk density values generally exhibit a significant degree of scatter. However, the Unit I/II boundary is well defined on the basis of a sharp increase in bulk density from an average of 1.48 g/cm^3 in Unit I to an average of 1.96 g/cm^3 in Unit II. Despite the poor quality and scatter of the data in Unit I, this change is distinct and obvious. The primary cause of this density increase is thought to be the transition from unconsolidated to lithified material (see "Lithostratigraphy and Accumulation Rates" section, this chapter). Unfortunately, because of very low recovery in Subunit IB, no physical property samples were obtained in this unit. Therefore, the boundary between these two consolidation states is not well defined.

Sharp changes are also observed in the porosity and water content data. Unit I is characterized by fairly constant to slightly increasing downhole trends with mean values of 72.8% (porosity) and 105% (water content). The wide range of values in both parameters (50.8%-89.1% and 32.2%-178%, in porosity and water content, respectively) is probably the result of drilling disturbance. Porosity values in Unit II are much lower, averaging 60%; water contents average 52%. A fair amount of scatter in the values persists. This scatter most likely results from sampling different lithologies, specifically vitric sand and siltstones vs. nannofossil-rich claystones.

Calcium Carbonate

Calcium carbonate contents in the upper 249 m (Unit I) never exceed 0.5%, and most values are <0.2% (Fig. 26). An increase to values as high as 36% occurs in Unit II. Two distinct layers with high carbonate contents, centered at 258 and 326 mbsf, consist of nannofossil-rich claystones (see "Lithostratigraphy and Accumulation Rates" section, this chapter). The remainder of Unit II is composed of sediment with carbonate contents comparable to those in Unit I.

Sonic Velocity

Hamilton Frame velocity measurements are shown in Figure 26 and are compared with MST *P*-wave logger results in Figure 28. Within Unit I, the coarse, unconsolidated, pumiceous nature of the majority of the sediments (see "Lithostratigraphy and Accumulation Rates" section, this chapter) allowed only one Hamilton Frame velocity measurement on a vitric silt unit. The resulting velocity of 1.60 km/s is in close agreement with MST velocity measurements at this depth (Fig. 28). MST velocity values within Unit I average 1.58 km/s and range from 1.56 to 1.62 km/s. These velocity data should be viewed with caution because of coring disturbances in these unconsolidated sediments.

Velocity measurements in Unit II are significantly higher than in Unit I. Hamilton Frame velocity values in Unit IIA average 2.68 km/s and range from 2.37 to 3.29 km/s (Table 12 and Fig. 26). This distinct increase in velocity, as well as in index property data, between Units I and II indicates a significant difference in the degree of consolidation between these units.

Within Subunit IIB, velocity data averaged 2.79 km/s and ranged from 2.00 to 3.46 km/s. These faster velocities are probably a result of increased consolidation caused by increased overburden, as well as the greater amount of coarse sediments (see "Lithostratigraphy and Accumulation Rates" section, this chapter).

REFERENCES

Berggren, W. A., Kent, D. V, Flynn, J. J., and Van Couvering, J. A., 1985. Cenozoic geochronology. *Geol. Soc. Am. Bull.*, 96:1407-1418.

Berner, R. A., 1981. A new geochemical classification of sedimentary environments. *J. Sediment. Petrol.*, 51:359-365.

Bernhard, J. M., 1986. Characteristic assemblages and morphologies of benthic foraminifera from anoxic, organic-rich deposits: Jurassic through Holocene. *J. Foram. Res.*, 16:207-215.

Bolli, H. M., Saunders, J. B., and Perch-Nielsen, K. (Eds.), 1985. *Plankton Stratigraphy*: Cambridge (Cambridge Univ. Press).

Brouxel, M., Lapierre, H., Michard, A., and Albarede, F., 1987. The deep layers of a Paleozoic arc: geochemistry of the Copley-Balaklala series, northern California. *Earth Planet. Sci. Lett.*, 86:386-400.

Fryer, P., Pearce, J. A., Stokking, L., et al., 1990. *Proc. ODP, Init. Repts.*, 125: College Station, TX (Ocean Drilling Program).

Hochstaedter, A. G., Gill, J. B., Newman, S., Pringle, M., Taylor, B., and Fryer, P., in press. Volcanism in the Sumisu Rift I: The effect of distinctive volatiles on fractionation. *Earth Planet. Sci. Lett.*

Ikeda, Y., and Yuasu, M., 1989. Volcanism in Nascent back-arc basins behind the Shichito Ridge and adjacent areas in the Izu-Ogasawara arc, Northwest Pacific: evidence for mixing between E-type MORB and island arc magmas and the initiation of backarc rifting. *Contrib. Mineral. Petrol.*, 101:377-393.

Ingle, J. C., Jr., 1980. Cenozoic paleobathymetry and depositional history of selected sequences within the southern California continental borderland. *Spec. Publ. Cushman Found. Foraminiferal Res.*, 19: 163-195.

Odin, G. S., and Matter, A., 1981. Die glauconarium origine. *Sedimentology*, 28:611-643.

Okada, H., and Bukry, D. 1980. Supplementary modification and introduction of code numbers to the "Low-latitude coccolith biostratigraphic zonation" (Bukry, 1973; 1975). *Mar. Micropaleontol.*, 5: 321-325.

Perch-Nielsen, K., 1985. Cenozoic calcareous nannofossils. *In* Bolli, H. M., Saunders, J. B., and Perch-Nielsen, K. (Eds.), *Plankton Stratigraphy*: Cambridge (Cambridge Univ. Press), 427-554.

Stork, A. L., and Gill, J. B., in press. Low-K rhyolites and high-Mg andesites accompany the early stages of backarc basin formation in the southwest Pacific. *J. Geol.*

Taylor, B., Brown, G., Fryer, P., Gill, J., Hochstaedter, A., Hotta, H., Langmuir, C., Leinen, M., Nishimura, A., and Urabe, T., in press. ALVIN-SeaBeam studies of the Sumisu Rift, Izu-Bonin Arc. *Earth Planet. Sci. Lett.*

Usui et al., 1987. Local variability of manganese nodules facies on small abyssal hills of the Central Pacific Basin. *Mar. Geol.*, 74:237-276.

Van Morkhoven, F.P.C.M., Berggren, W. A., and Edwards, A. S., 1986. Cenozoic cosmopolitan deep-water benthic foraminifera. *Bull. Cent. Rech. Explor.-Prod. Elf-Aquitaine, Mem.*, No. 11.

Weissel, J. K., and Karner, G. D., 1989. Flexural uplift of rift flanks due to tectonic denudation of the lithosphere during extension. *J. Geophys. Res.*, 94:13913-13950.

Woodruff, F., 1985. Changes in Miocene deep-sea benthic foraminiferal distribution in the Pacific Ocean: relationship to paleoceanography. *In* Kennett, J. P. (Ed.), *The Miocene Ocean: Paleoceanography and Biogeography*. Mem. Geol. Soc. Am., 163:131-175.

Yasuda, H., 1989. Benthic foraminifers and sedimentary facies of the lower slope basin off Shikoku, Japan. *In* Takayanagi, Y., and Ishizaki, K. (Eds), *Collected Papers on Foraminifera from the Japanese Islands*: Sendai (Toko Press), 83-92.

Ms 126A-107

NOTE: All core description forms ("barrel sheets") and core photographs have been printed on coated paper and bound as Section 3, near the back of the book, beginning on page 421.

Table 12. Physical property data of samples from Holes 788C and 788D.

Core, section, interval (cm)	Depth (mbsf)	Wet-bulk density (g/cm³)	Dry-bulk density (g/cm³)	Porosity (%)	Water content (%)	Grain density (g/cm³)	Void ratio	Carbonate content (%)	Velocity (km/s)
126-788C-									
1H-3, 75-76	7.75	1.57	0.94	64	71	2.42	1.77	0.5	
3H-3, 87-88	24.07	1.52	0.85	68	84	2.46	2.12	0.4	
4H-2, 113-115	32.33	1.50	0.85	66	82	2.22	1.92		
4H-4, 40-41	34.60	1.42*	0.63*	79*	135*	2.52*	3.85*		
5H-4, 20-21	43.90	1.71	1.15	57	52	2.39	1.31	0.1	
5H-6, 32-34	47.02	1.32	0.51	82	175	2.42	4.60	0.2	
6H-3, 57-59	52.27	1.39	0.67	73	116	2.56	2.69	0.1	
6H-5, 26-28	54.96	1.33	0.71	63	93	3.34	1.68	0.2	
7H-1, 36-38	58.56	1.35	0.54	82	163	2.51	4.42	0.1	
7H-1, 140-150	59.60							0.3	
7H-2, 24-26	59.94	1.16	0.49	68	148	1.89	2.10	0.1	
8H-1, 81-83	68.51	1.48	0.61	88	157	1.93	7.49	0.1	
8H-2, 91-93	70.11	1.64	0.99	65	69	2.65	1.87	0.1	
9H-1, 26-28	77.46	1.59	0.95	65	72	2.52	1.85	0.1	
9H-3, 40-41	80.60	1.40	0.62	79	138	2.31	3.76	0.2	
9H-3, 140-150	81.60								
9H-5, 63-66	83.83	1.37	0.58	80	150	2.59	4.10	0.1	
11H-3, 82-84	100.01	1.50*	0.80*	71*	95*	2.54*	2.49*	0.1	1.6
11H-4, 132-133	102.02	1.99*	1.11*	89*	85*	2.51*	8.16*	0.1	
11H-5, 11-12	102.31	1.63*	0.97*	66*	71*	2.56*	1.94*	0.2	
12H-3, 60-63	109.30	1.38	0.80	78	139	2.59	3.58	0.1	
12H-6, 35-37	113.55	1.54	0.68	68	82	2.47	2.12	0.1	
13H-3, 70-72	118.90	1.52	0.81	71	91	2.50	2.39	0.2	
13H-5, 70-72	121.90	1.58	1.00	64	71	2.45	1.79	0.2	
13H-6, 0-10	122.70							0.4	
14H-4, 48-50	129.68	1.43	0.66	78	125	2.80	3.44	0.1	
14H-5, 92-94	131.62	1.62	0.89	65	69	2.54	1.84	0.1	
15H-1, 46-48	134.66							0.2	
16H-1, 90-92	144.60	1.42*	0.41*	81*	140*	2.69*	4.26*	0.2	
16H-1, 140-150	145.10							0.2	
17H-4, 112-114	158.82	1.57	0.91	77	102	2.54	3.35		
18H-2, 90-92	165.10	1.52	0.95	76	106	2.72	3.19	0.1	
19H-6, 67-69	180.37	2.13	1.65	51	32	2.80	1.03	0.2	
20H-2, 63-65	183.83	1.59	0.87	71	85	2.55	2.45	0.1	
21H-1, 16-18	191.36	1.61	0.63	72	84	2.75	2.57	0.2	
23H-1, 62-64	210.82	1.39	0.77	82	152	2.69	4.61	0.1	
24H-2, 106-108	222.26	1.35	0.52	84	178	2.72	5.30	0.2	
126-788D-									
1R-1, 9-11	219.69	1.68	0.7	80	94	2.47	3.90		
4R-1, 109-111	249.59	2.12	1.32	95	85	2.27	18.46	29.1	2.58
5R-1, 7-8	258.27							36.2	
5R-1, 143-145	259.63	2.11	1.52	47	30	2.40	0.88	14.6	3.29
5R-2, 16-19	259.86	1.95	1.4	55	40	2.72	1.22		2.76
6R-1, 35-37	268.26	1.86	1.31	58	46	2.60	1.35		2.37
7R-1, 92-94	278.42	1.88	1.33	49	37	2.52	0.97		2.94
7R-2, 32-34	279.32	1.92	1.38	51	38	2.59	1.05		2.39
8R-1, 0-2	287.20	1.68	1.25	64	64	2.27	1.76		
8R-1, 1-2	287.21	1.68		64	64	2.49	1.79		
8R-1, 14-16	287.34	2.03	1.77	62	46	2.73	1.65	0.8	2.51
9R-1, 31-33	297.21							0.2	
9R-1, 89-91	297.79	2.19	1.44	48	29	2.72	0.91	1.2	3.06
10R-1, 21-23	306.71	2.47	1.26	45	23	2.69	0.83	1.2	3.46
11R-1, 20-22	316.20	1.76	1.66	73	73	2.72	2.64	3.9	2.04
12R-1, 30-33	325.90	1.91	1.21	64	53	2.79	1.81	19.9	2.64
13R-1, 5-6	335.35	1.84	1.2	59	49	2.57	1.46	0.6	2.65
14R-1, 12-14	345.12	2.00	1.83	55	39	2.43	1.20		
15R-1, 42-46	355.12	1.97	1.27	52	37	2.75	1.06	0.8	2.80
16R-1, 36-38	364.66	1.80		61	53	2.62	1.55	0.2	2.61
16R-1, 58-60	364.88	2.21	1.95	51	31	2.75	1.02	8.3	2.88

Note: Asterisks (*) mark measurements from finer grained, more consolidated beds that are considered more accurate values than those from the coarse, pumiceous sediments in the upper 230 mbsf. Other data are suspect.

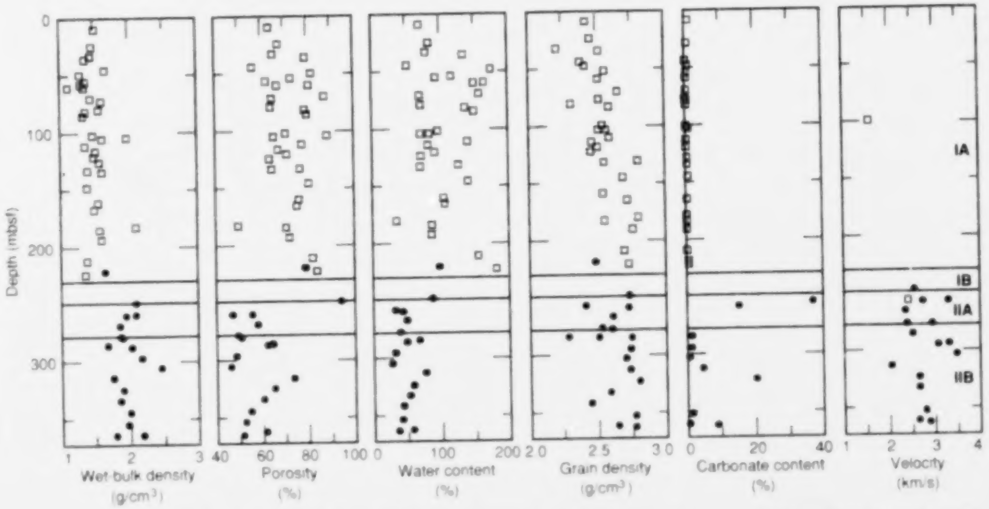

Figure 26. Physical property data from Site 788, Holes 788C (open squares) and 788D (solid circles). Locations of lithostratigraphic unit boundaries are indicated.

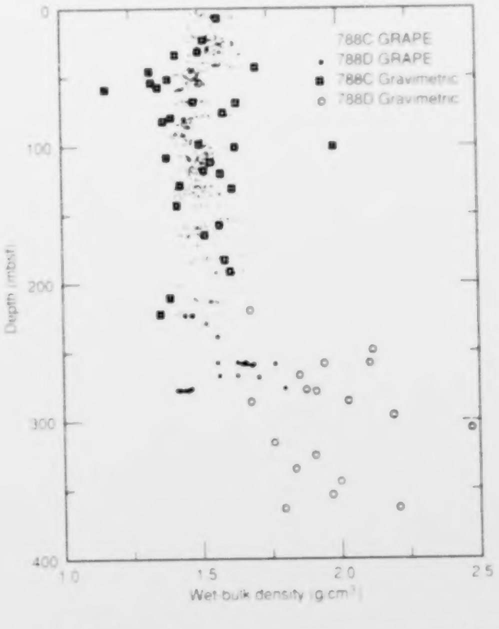

Figure 27. GRAPE and gravimetric wet-bulk density values from Holes 788C and 788D.

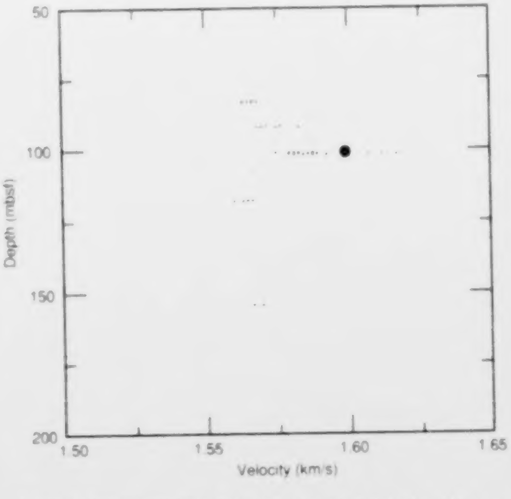

Figure 28. Comparison of Hamilton Frame (solid circle) and multisensor track *P*-wave logger (small points) analyses on sediments from Hole 788C.

Taylor, B., Fujioka, K., et al., 1990
Proceedings of the Ocean Drilling Program, Initial Reports, Vol. 126

7. SITES 790/791[1]

Shipboard Scientific Party[2]

HOLE 790A

Date occupied: 29 April 1989

Date departed: 29 April 1989

Time on hole: 14 hr, 30 min

Position: 30°54.95′N, 139°50.66′E

Bottom felt (rig floor; m, drill-pipe measurement): 2232.7

Distance between rig floor and sea level (m): 10.50

Water depth (drill-pipe measurement from sea level, m): 2222.2

Total depth (rig floor; m): 2270.10

Penetration (m): 37.40

Number of cores (including cores with no recovery): 4

Total length of cored section (m): 37.40

Total core recovered (m): 35.71

Core recovery (%): 95.5

Oldest sediment cored:
Depth (mbsf): 37.40
Nature: vitric sand
Age: Quaternary
Measured velocity (km/s): 1.59

HOLE 790B

Date occupied: 29 April 1989

Date departed: 1 May 1989

Time on hole: 1 day, 5 hr, 45 min

Position: 30°45.96′N, 139°50.66′E

Bottom felt (rig floor; m, drill-pipe measurement): 2234.0

Distance between rig floor and sea level (m): 10.50

Water depth (drill-pipe measurement from sea level, m): 2223.5

Total depth (rig floor; m): 2372.90

Penetration (m): 138.90

Number of cores (including cores with no recovery): 15

Total length of cored section (m): 138.90

Total core recovered (m): 88.71

Core recovery (%): 63.7

Oldest sediment cored:
Depth (mbsf): 138.90
Nature: vitric sand and silt
Age: Quaternary
Measured velocity (km/s): 1.57

HOLE 790C

Date occupied: 1 May 1989

Date departed: 3 May 1989

Time on hole: 2 days, 19 hr

Position: 30°54.95′N, 139°50.69′E

Bottom felt (rig floor; m, drill-pipe measurement): 2234.0

Distance between rig floor and sea level (m): 10.50

Water depth (drill-pipe measurement from sea level, m): 2223.5

Total depth (rig floor; m): 2621.10

Penetration (m): 387.10

Number of cores (including cores with no recovery): 33

Total length of cored section (m): 302.10

Total core recovered (m): 127.32

Core recovery (%): 42.1

Oldest sediment cored:
Depth (mbsf): 387.10
Nature: nannofossil-rich silty clay, nannofossil-rich sandy mud (Core 126-790C-20X) and sandy silt (Core 126-790C-33X)
Age: Quaternary
Measured velocity (km/s): 1.56 (Core 126-790C-20X)

HOLE 791A

Date occupied: 4 May 1989

Date departed: 6 May 1989

Time on hole: 2 days, 6 hr

Position: 30°54.96′N, 139°52.20′E

Bottom felt (rig floor; m, drill-pipe measurement): 2279.0

Distance between rig floor and sea level (m): 10.50

Water depth (drill-pipe measurement from sea level, m): 2268.5

Total depth (rig floor; m): 2736.00

Penetration (m): 457.00

Number of cores (including cores with no recovery): 49

Total length of cored section (m): 457.00

Total core recovered (m): 179.86

Core recovery (%): 39.4

Oldest sediment cored:
Depth (mbsf): 428.40
Nature: crystal-vitric silty sand and sandy siltstone
Age: Quaternary
Measured velocity (km/s): 1.56

HOLE 791B

Date occupied: 6 May 1989

Date departed: 13 May 1989

Time on hole: 7 days, 6 hr

---

[1] Taylor, B., Fujioka, K., et al., 1990. *Proc. ODP, Init. Repts.*, 126: College Station, TX (Ocean Drilling Program).

[2] Shipboard Scientific Party is as given in the list of participants preceding the contents.

Position: 30°54.98′N, 139°52.19′E

Bottom felt (rig floor; m, drill-pipe measurement): 2279.0

Distance between rig floor and sea level (m): 10.50

Water depth (drill-pipe measurement from sea level, m): 2268.5

Total depth (rig floor; m): 3424.00

Penetration (m): 1145.00

Number of cores (including cores with no recovery): 79

Total length of cored section (m): 915.00

Total core recovered (m): 114.39

Core recovery (%): 15.48

Oldest sediment cored:
Depth (mbsf): 983.70
Nature: nannofossil-foraminifer claystone (Core 126-791B-47R) and crystal-vitric silt and sandy mud (Core 126-791B-62R)
Age: Quaternary
Measured velocity (km/s): 1.56 (Core 126-791B-39X)

Hard rock:
Depth (mbsf): 829.60
Nature: basalt breccia, basalt mousse, diabase
Measured velocity (km/s): 4.26–4.48

Principal results: Sites 790 and 791 are located near the center of Sumisu Rift, a backarc graben west of the Izu-Bonin island-arc volcanoes Sumisu Jima and Tori Shima. The sites are 2.4 km apart and are situated on the western side of the eastern inner-rift half-graben. The syn-rift sediments dip to the east with regional basal dips of 15° and are cut by 45°–60°, dominantly west-dipping, normal faults.

The principal objectives of this site were to determine (1) the vertical-motion history of the rift basin, (2) the nature of volcanism and sedimentation in the rift, (3) the duration of rifting and the nature of the rift basement, and (4) the chemistry of fluids circulating in the sediments. Site selection was determined from multichannel seismic (MCS) records and a short shipboard seismic survey; the sites chosen lie on *Fred Moore* 35-07, Line 4, at 1933Z (Site 790) and at 1953Z (Site 791). Sites 790 and 791 were occupied from 0656 hr (all times UTC), 29 April, to 1345 hr, 13 May 1989.

Hole 790A was spudded with the advanced hydraulic piston corer (APC) at 1400 hr on 29 April 1989, coring 35.7 m with 96% recovery. Potential entanglement with fishing line required a pipe round trip. Hole 790B recored the mud line and continued with an APC to 100.3 m below seafloor (mbsf) with 88% recovery before switching to the extended core barrel (XCB) for a further 38.6 m with 2% recovery. A top-drive electrical short ended the hole. Hole 790C overlapped the poorly recovered basal section of 790B, recovering 98% of the interval from 85 to 155.2 mbsf with the APC and continued with the XCB to 271.1 mbsf with 50% recovery. Recovery with the XCB in the basal 116 m of Hole 790C to 387.1 m total depth (TD) was 0.5%. Operations in Hole 790C ended at 2210 hr on 3 May after the lockable flapper valve jammed open and short trips showed repeated hole filling that made logging unsafe.

Hole 791A was spudded with an APC at 0730 hr on 4 May, coring 207.9 m with 83% recovery. The hole was continued with an XCB to 457 mbsf with 3% recovery. Hole 791B was spot cored and washed down to 416.3 mbsf and was then cored with the rotary core barrel (RCB) to 1145 mbsf. Recovery between 457 and 834 mbsf was 23% and in the basement below was 9%. Extensive hole conditioning in preparation for logging was ended when the pipe stuck at 825 mbsf. After geochemical logging through the pipe of the sedimentary section, the pipe was severed at 46 mbsf with the third explosive charge.

Three lithologic units were defined at Sites 790 and 791:

1. Unit I, deposited in the last 0.2 m.y., is vitric silt and sand, pumiceous gravel, and vitric silty clay at Site 790, 0–165 mbsf, and is pumiceous gravel and sand, vitric silt, pumiceous pebbly sand, and nannofossil-rich silty clay at Site 791, 0–428 mbsf.
2. Unit II, deposited between 0.2 and 1.1 Ma, is burrowed nannofossil clay, nannofossil-rich clay, silty clay, and clayey silt at Site 790, 165–271 mbsf, and is nannofossil claystone, sandy mudstone, and vitric silt at Site 791, 428–834 mbsf.
3. Unit III is scoriaceous basalt at Site 790, 269–387 mbsf, and, in order of first occurrence downsection, is composed of basalt breccia, basalt, diabase, basaltic "mousse," and mafic to felsic tuff and lapilli tuff at Site 791, 834–1145 mbsf. A vitric siltstone occurs at 329 mbsf in Site 790, and a coarse sandy silt occurs at 975 mbsf in Site 791. Both sedimentary layers are Pleistocene.

Units I and II are well dated using nannofossils, foraminifers, radiolarians, and paleomagnetics. Eight chronostratigraphic datums at each site show that sedimentation rates increased exponentially from 80 and 300 m/m.y. at 1 Ma to 1000 and 2250 m/m.y. in the last 100 k.y. at Sites 790 and 791, respectively. The rapid sedimentation provides high-resolution records of bioevolution and magnetic reversals. Applying the average sedimentation rates for the period 0.46–0.83 Ma to the Brunhes/Matuyama polarity transition indicates that the decrease of dipole intensity is limited to about 600 yr and that the reversal in inclination occurred in perhaps as little as 100 yr. However, it is possible that we recovered only one of several reversals in the polarity transition zone.

Bimodal mafic-felsic volcanism is recorded throughout the sedimentary history of the basin, although the relative proportions of each component change. Explosive arc volcanism, possibly from Sumisu and/or South Sumisu calderas, provided thick deposits of felsic pumiceous sand and gravel four times during the deposition of Unit I at approximately 60-k.y. intervals. One geochemical analysis indicates that the mafic scoria and ash probably derived from intra-rift basaltic eruptions. Thin ash beds and scattered clasts of basaltic scoria and felsic pumice, with the mafic components dominant, are present throughout Unit II and increase in proportion downhole.

Carbonate contents are <3% in the coarse clastic rocks of Unit I, up to 20% in the finer interbeds, and 20%–40% in Unit II. Because of the high sedimentation rates in Unit II at Site 791, the burial of organic carbon led to reducing conditions in the sediment and precipitation of iron sulfides. Concentrations of sedimentary organic carbon vary from below detection in the coarse clastic rocks to as much as 1.2%. Fluid geochemistry studies indicate that fluids other than seawater are not circulating through the sediments.

The differential subsidence between the two sites is matched by the clastic and the biogenic sedimentation, with rates for Unit II at Site 791 almost four times those at Site 790. This, and the lack of coeval material on at least the eastern rift flank, requires that a large proportion of the pyroclastic and pelagic materials were (re)deposited by submarine mass flows. Benthic foraminifers are consistent with deposition in 2-km water depths during the Brunhes Chron and at somewhat greater depths during earlier time intervals.

Bedding at Site 790 is near horizontal, but at Site 791 the dip gradually increases to 15°–20° by 600 mbsf and then abruptly increases to 35°–45° by 760 mbsf down to basement. The MCS data indicate that the dips are easterly above 650 mbsf, and magnetic declinations, after tilt corrections, indicate that the dips remain easterly above basement. Near basement, Hole 791B may have crossed into the footwall of an intra-rift fault, thereby missing a few hundred meters (about 0.1 m.y.) of the early syn-rift sediments. The dips of the basement rocks vary from 40° at the top to 5°–40° in some of the basal fault slices.

The sparsely phyric basaltic volcanic rocks at Sites 790 and 791 are highly vesicular, despite their eruption in deep water, probably because of their high pre-eruption water contents. One more-differentiated lava contains clinopyroxene in addition to the olivine and plagioclase typical of the more mafic lavas that it overlies. The diabase intrusions range from relatively olivine rich and as mafic as any of the basalts, to Fe-Ti-rich and more differentiated than any of the basalts. The 135-m-thick basaltic "mousse" consists primarily of highly expanded basaltic glass, with vesicular "clasts" in an even more vesicular glassy matrix of the same composition. It is interpreted as the product of a large-volume, deep-submarine eruption of gas-rich basalt.

The rift basement basalts may be distinguished from Izu-Bonin Arc basalts by lower Ba (<30 ppm) and higher TiO_2 (>0.95%) contents with respect to MgO, Zr, and V. They are inferred to be of syn-rift origin, but are more similar to rift-wall rocks dated at 1.0–1.4 Ma and to seamounts in the outer rift than to the 250-ka pillow ridges of the inner rift, which implies a temporal evolution of rift volcanism toward compositions more depleted in high-field-strength elements.

The basalts at Hole 791B have lower concentrations of Ba and Rb than do those at Hole 790C and the younger rocks of the inner rift. These concentrations are as low as those in Mid-Ocean Ridge basalts (MORB) and in the most mature backarc basins.

The tuff and lapilli tuffs at the base of Hole 791B show strong flattening of pumice shards and the development of a eutaxitic texture. They are interpreted as a sequence of hot pyroclastic flows from a proximal eruption site. They are dominantly andesitic, with one basal basaltic unit. Their most immobile elements have strong island-arc characteristics (Ti/Zr = 195 and Zr/Y = 1.5), implying that the tuffs cap an arc basement of unknown age. However, alteration effects make this conclusion preliminary. Alteration increases down the basement section from fresh to zeolite or lower greenschist facies in the basal 41 m, which penetrated a fault zone evidenced by slickensides, fault gouge, massive gypsum, and minor pyrite.

Physical properties measurements of the sediments indicate that (1) average bulk density values increase downhole from 1.55 to 1.8 g/cm^3 at Site 790 and to 1.9 g/cm^3 at Site 791; (2) average porosity values decrease from 70% to 60% at Site 790 and to 55% at Site 791; (3) sonic velocity data range from 1.53 to 1.61 km/s in Unit I, in Unit II to 1.52–1.55 km/s at Site 790 (a small velocity inversion), and to 1.61–1.84 km/s at Site 791; and (4) average thermal conductivity measurements increase downhole from 0.9 to 1.1 and 1.2 W/m · K at Sites 790 and 791, respectively.

The range of basement physical properties data at Site 791 includes (1) bulk density, 2.2–3.0 g/cm^3; (2) porosity, 8%–44%; (3) sonic velocity, 2.6–5.2 km/s, and (4) thermal conductivity, 1.0–1.2 W/m · K. The lower velocity and density and the higher porosity values are from the basaltic "mousse." The lowest porosity values are from the basal lapilli tuffs, and the highest velocity value is from a gypsum vein.

Geochemical logging at Site 791 identified isolated natural gamma-ray peaks with some of the silty clay beds. These high values are mostly caused by thorium. Long sections in Unit I with uniformly low gamma-ray values are associated with unrecovered pumiceous sand and gravel.

The principal results of this site are as follows:

1. Rifting began, and rift basement depths exceeded 2 km, prior to 1.1 Ma.
2. Basement was formed by early rift basaltic lavas and intrusives, as well as by arc pyroclastic rocks metamorphosed to zeolite or lower greenschist facies.
3. A large-volume, deep-submarine eruption of water-rich basalt produced basaltic "mousse," a highly expanded basaltic glass, with vesicular "clasts" in an even more vesicular glassy matrix of the same composition.
4. Extremely rapid, differential, and accelerating subsidence and sedimentation occurred in the inner-rift half-graben in the last 1.1 m.y.
5. Intra-rift basaltic eruptions and rhyolitic arc eruptions were common 1.1–0.2 Ma, but explosive arc volcanic activity dramatically increased about 0.2 Ma.
6. A large proportion of the pyroclastic and pelagic materials were (re)deposited by submarine mass flows.
7. Fluids other than seawater are not circulating locally through the sediments.
8. The decrease of dipole intensity and the reversal in inclination associated with the Brunhes/Matuyama polarity transition is limited to about 600 yr and occurred in perhaps as little as 100 yr, respectively.

BACKGROUND AND OBJECTIVES

Site 790 is located at 30°54.96′N, 139°50.66′E, at 2223 m below sea level (mbsl), and Site 791 is located at 30°54.97′N, 139°52.20′E, at 2268 mbsl. Each site is near the center of Sumisu Rift, a backarc graben west of the active Izu-Bonin Arc volcanoes Sumisu Jima and Tori Shima (Figs. 1 and 2). The sites are 2.4 km apart and are located on the western side of the eastern inner-rift half-graben (Figs. 2–5). The syn-rift sediments dip to the east with regional basal dips up to 15° and are cut by 45°–60°, dominantly west-dipping, normal faults (Fig. 5).

The pre-rift "basement" is not well imaged by the MCS profiles, probably because of the structural complexity. By drilling in the rift, we sought to determine the following: (1) the vertical-motion history of the rift basin, (2) the nature of volcanism and sedimentation in the rift, (3) the duration of rifting and the nature of the rift basement, and (4) the chemistry of fluids circulating in the sediments.

The first of these objectives was addressed through a combination of paleontological estimates of paleobathymetry, backstripping the sedimentation history using the physical properties and logging data, and seismic stratigraphic analyses of the interconnecting MCS profiles. To meet the second and third objectives required recovery, dating, and characterization of the syn-rift section. The surface sediments in the rift basin include hemipelagic muds and volcaniclastic turbidites, with ash and pumice layers (Nishimura and Murakami, 1988). However, the rates and styles of deposition of the up to 1.5-km-thick rift-basin sediment fill and the duration of rifting were unknown prior to drilling.

The frequency, chemistry, and eruptive style of the syn-rift arc margin and the rift basin volcanism was ascertained from studies of the volcaniclastic sediments. The basement petrology determined whether the rift is floored by stretched, subsided arc crust, recently intruded crust, or some combination of the two. Finally, the fourth objective, which is concerned with the chemistry of the fluids that heat-flow and mineralization studies indicate are circulating in the basin, was investigated by examining the chemistry of pore fluids squeezed from the cores and hydrothermal alteration products.

SEISMIC STRATIGRAPHY

Correlation of site-survey MCS data with recovered core material (Fig. 6) was accomplished by using physical properties velocity data, averaged over each lithologic unit (see "Physical Properties" section, this chapter), to convert depths (mbsf) into two-way traveltimes. Sites 790 and 791 were drilled in the eastern inner-rift graben of Sumisu Rift, bounded to the east by a west-dipping master fault zone. Normal faulting, synthetic to the master fault, has created a series of east-dipping tilted fault blocks within the rift basin. These fault blocks are also cut by minor antithetic faulting. Both fault sets extend to the seafloor, indicating that they are currently active.

The pattern of faulting is responsible for concentrating basin subsidence adjacent to the eastern margin of the rift and for thinning the sedimentary section toward the west. Synthetic faulting has created sedimentary reflectors that exhibit increasing dip with depth, indicating that subsidence is syn-depositional. Continuous tilting of the fault blocks has resulted in progressive onlap and, in some cases, erosional truncation by younger sedimentary strata.

Unit I (see "Lithostratigraphy and Accumulation Rates" section, this chapter) is characterized by a series of rather continuous, high-amplitude reflections that can be traced between the two sites. Several strong reflectors within Unit I, which are correlatable throughout the south Sumisu Rift basin, document that subsidence is greatest in the eastern inner-rift graben. The upper portion of Unit I at Site 791 (seafloor to 3.22 s, 0–167 mbsf) returns discontinuous low-amplitude reflections that possibly are a result of the greater amount of coarse debris-flow material accumulating in this topographic low. The base of these discontinuous low-amplitude reflections corresponds to the base of pumice bed II (see "Lithostratigraphy and Accumulation Rates" section, this chapter).

The Unit I/II boundary occurs at 3.17 s at Site 790 and 3.56 s at Site 791. At Site 791, this boundary is near high-amplitude reflection events; however, at Site 790, onlap has juxta-

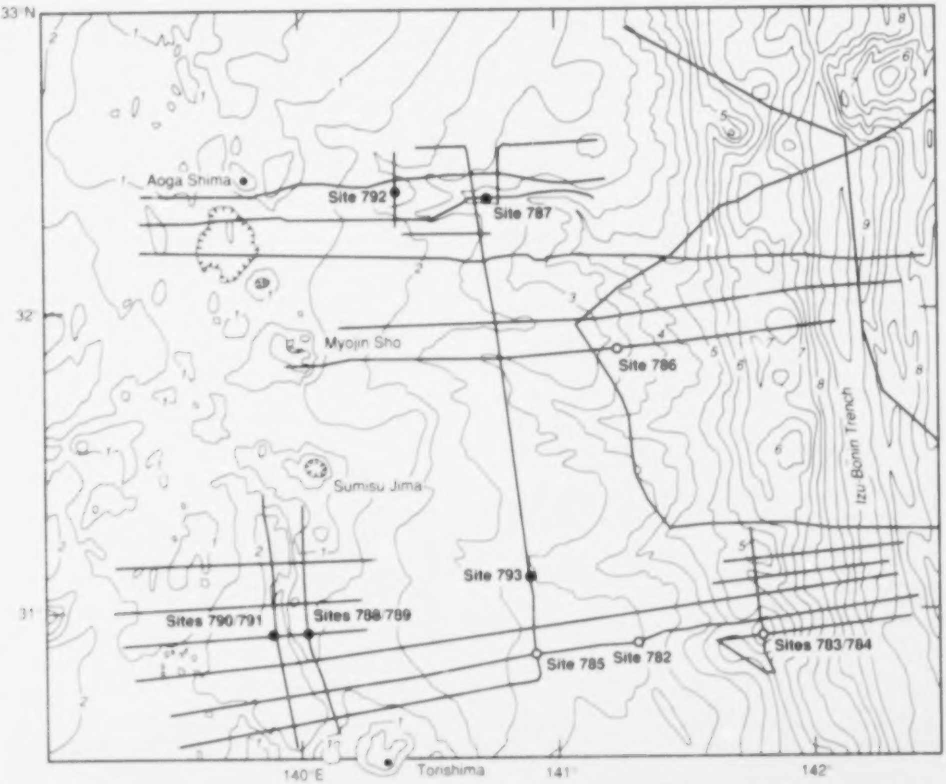

Figure 1. Bathymetric map at 0.5-km-contour interval of the Izu-Bonin arc-trench system between 30.5° and 33°N. The locations of sites drilled on Legs 125 (open circles) and 126 (filled circles) are shown on the map as are the locations of MCS site survey lines.

posed strata with less impedance contrast. Unit II is characterized at each site by an absence of any strong or continuous reflectors. This is probably a result of low-impedance contrasts within this unit (see "Physical Properties" section, this chapter) combined with structural disruption by pervasive rift faulting. Correlation of this unit throughout the rift basin is difficult because of the lack of strong continuous reflectors, complex faulting, and local deposition in small, fault-block-bounded depocenters. A strong reflection event between 3.25 and 3.30 s at Site 790 does not appear to correlate with a distinct lithologic or physical property change and may be an out-of-plane reflection.

Two-way traveltimes for lithostratigraphic, biostratigraphic, and paleomagnetic horizons observed at Sites 790 and 791 were calculated using physical properties velocity data (Table 1). These horizons include the base of the coarse pumice unit above Key Bed #7, Key Bed #7, lithologic unit boundaries I/II and II/III (see "Lithostratigraphy and Accumulation Rates" section, this chapter), the first occurrence (FO) of *Emiliania huxleyi* at 275 ka and the last occurrence (LO) of *Pseudoemiliania lacunosa* at 460 ka (see "Biostratigraphy" section, this chapter), and the Brunhes/Matuyama boundary (730 ka; see "Paleomagnetics" section, this chapter). These horizons and the correlation of major seismic reflectors are shown in Figure 7. This figure demonstrates the dramatic thickening of the sedimentary section from Site 790 east to Site 791 as a result of rift-basin faulting and differential subsidence. This structural evolution has created reflectors that onlap older tilted horizons and sometimes cause erosional truncation by younger horizons.

The pattern of recent sediment accumulation in this area of actively subsiding and rotating fault blocks is a modern analogue for the deposition of deeper seismic reflectors. The transparent, surficial layer observed in the high-resolution seismic record (3.5 kHz; Fig. 8) at Site 791 thins considerably, and may onlap, toward Site 790. Thicker and coarser recovered core material at Site 791 and seismically observed stratigraphic onlap supports this interpretation of structurally controlled sedimentation.

Correlation of these horizons to the east of Site 791 shows that sedimentation rates there are even higher than those observed at Site 791. Reflector correlation, although complicated by tilting, faulting, and onlap, is possible down to the horizon corresponding to the FO of *E. huxleyi* (Horizon H; Fig. 7). However, below this horizon, seismic correlation between Sites 790 and 791 is not possible. The difficulty in correlating the three lowermost horizons (L, B, and II, Fig. 7) probably results from a combination of (1) complex faulting that progressively

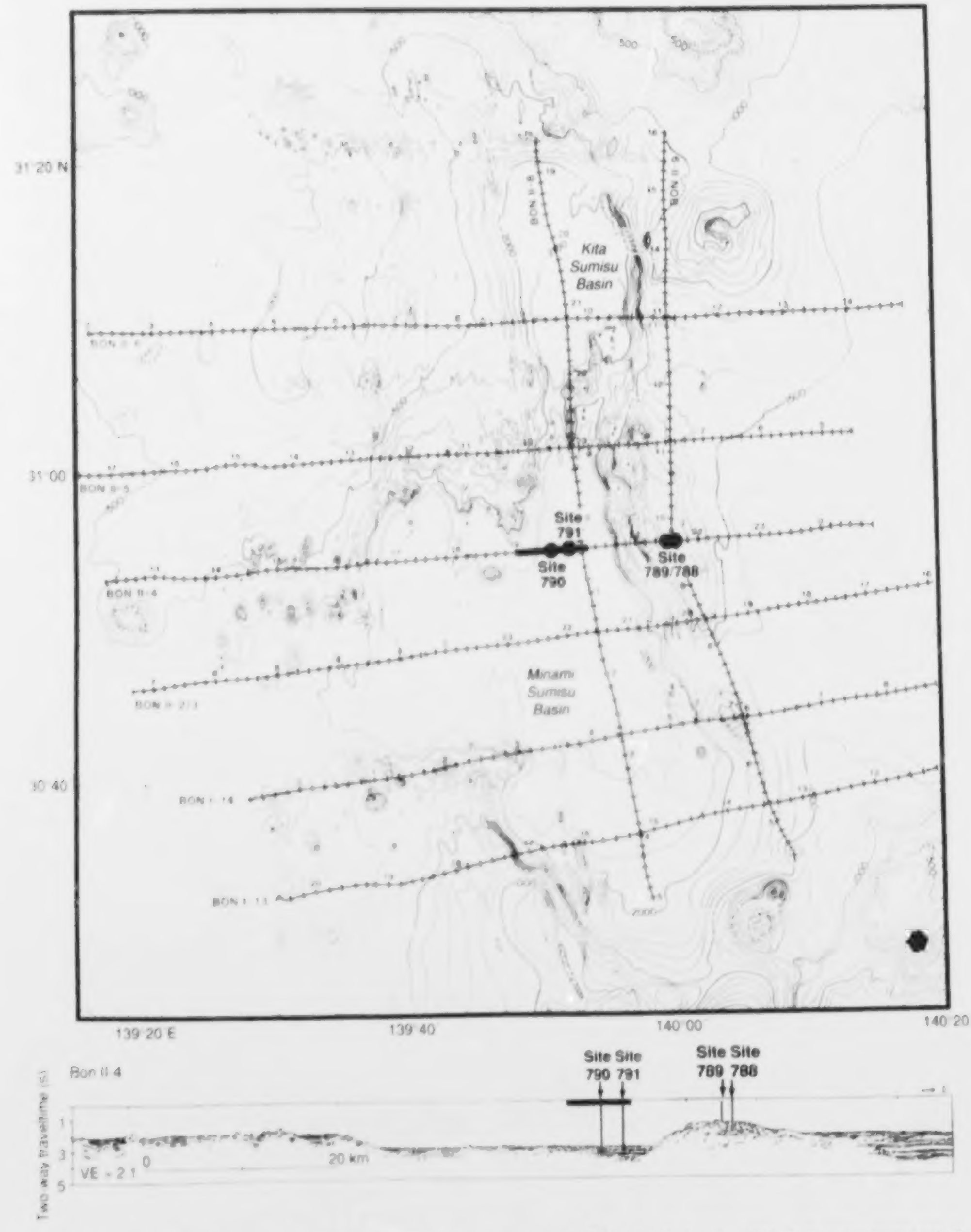
31°20'N
31°00'
30°40'
139°20'E
139°40'
140°00'
140°20'
Kita Sumisu Basin
Minami Sumisu Basin
Site 791
Site 790
Site 789/788
BON II-6
BON II-5
BON II-4
BON II-2/3
BON I-14
BON I-13
BON II-8
BON II-9
500
1000
2000
Bon II 4
Site 790
Site 791
Site 789
Site 788
Two-way traveltime (s)
1
3
5
0
20 km
VE = 2:1

Figure 2. Bathymetric map (100-m-contour interval) of Sumisu Rift and surrounding area showing the location of MCS site survey tracks and of Sites 788–791. A line drawing of MCS line BON II-4 (*Fred Moore* 35-07) is shown at the bottom of the figure. The segment of this line shown in Figure 6 is indicated by the solid bars in the upper and lower parts of the figure.

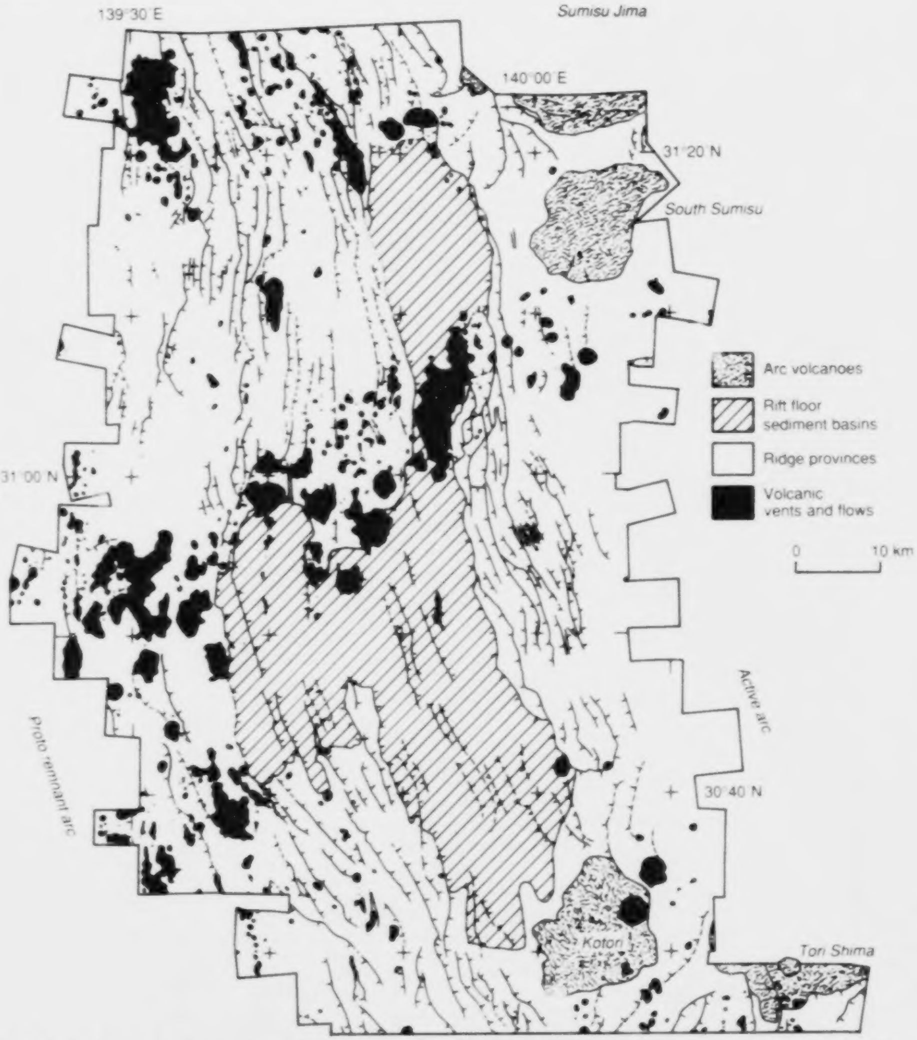
139°30'E
Sumisu Jima
140°00'E
31°20'N
South Sumisu
Arc volcanoes
Rift floor sediment basins
Ridge provinces
Volcanic vents and flows
0
10 km
31°00'N
Active arc
30°40'N
Proto remnant arc
Kotori
Tori Shima

Figure 3. Simplified geological interpretation of the Sumisu Rift SeaMARC II sidescan data (Taylor et al., 1988a, 1988b) showing the main faults, volcanic fields, sedimentary basins, and adjacent arc volcanoes (from Taylor et al., in press).

offsets deeper horizons to a greater degree, (2) pre-rift and early syn-rift volcanism that overprints and obscures the sedimentary horizons, and (3) high-amplitude, possibly out-of-plane seismic reflections.

The Unit II/III boundary occurs at 3.32 s at Site 790 and 4.05 s at Site 791. At Site 791, this boundary correlates very well with a high-amplitude reflection that is a result of the large impedance contrast across this boundary (see "Physical Properties" section, this chapter). This high-amplitude reflection is interpreted to be a fault surface with Unit II claystones in fault contact with Unit III basaltic lavas. At Site 790, the Unit II/III boundary does not correspond to a similar high-amplitude reflection. Furthermore, correlations of seismic "basement" documented by drilling at Site 791 to any similar reflector at Site 790 indicates that acoustic basement at Site 790 may occur as deep as 3.5–3.6 s. This implies that acoustic basement may be more than 200 m below the basalt scoria at the bottom of Site 790. Furthermore, at Site 790, the basalt scoria is characterized by transparent to low-amplitude discontinuous reflections that are different from the acoustic basement observed at Site 791. Acoustic basement throughout the rift basin is characterized by discontinuous, chaotic reflections.

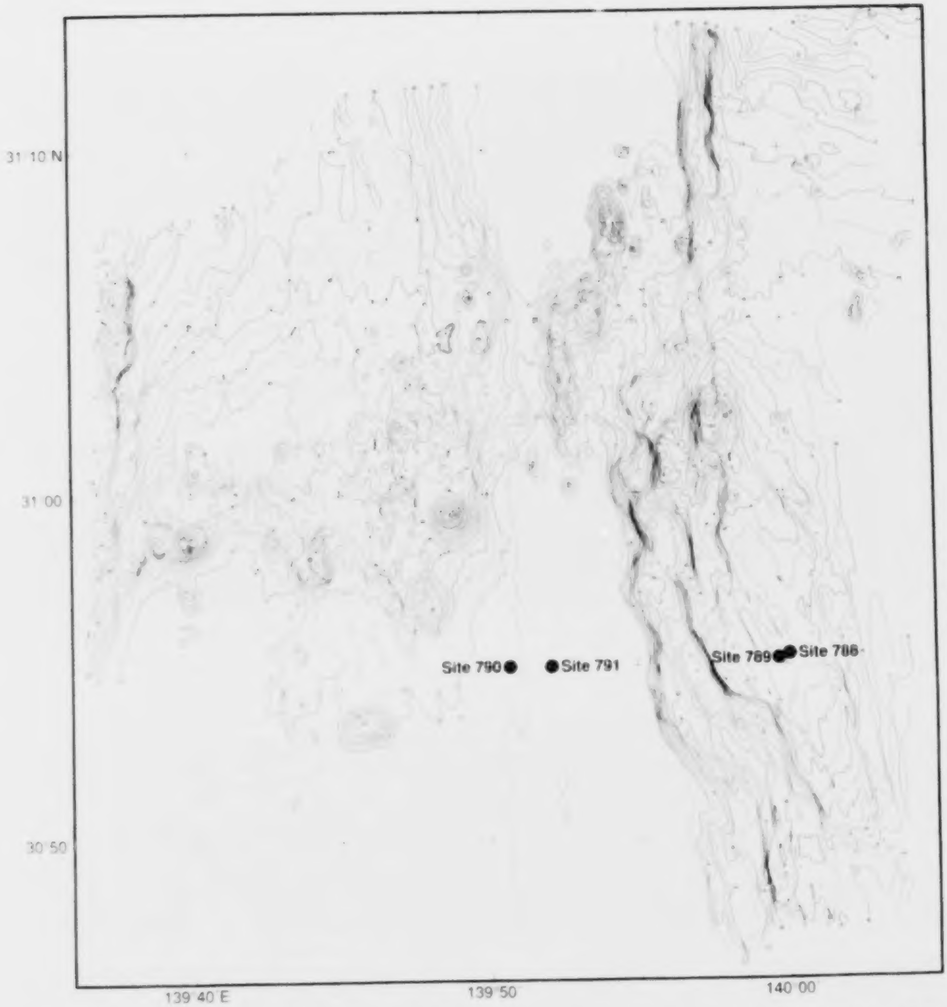

Figure 4. SeaBeam bathymetric map (50-m-contour interval) of the central Sumisu Rift showing the location of Sites 788–791 (after Taylor et al., in press a).

OPERATIONS

Site 790 (BON-1A)

The vessel made the transit from Site 789 to Site 790 in 3 hr and dropped a beacon at 0656 hr (all times UTC) on 29 April 1989.

Hole 790A

Because the seafloor sediments were assumed to be soft enough for piston coring, an APC/XCB bottom-hole assembly (BHA) was made up and run to the seafloor. It included a lockable float valve (to allow logging through the bit, if desired) and a nonmagnetic drill collar (to allow magnetic orientation of the piston cores). The mud-line APC core was taken at 1425 hr on 29 April 1989. Four APC cores were recovered (Table 2). While Core 126-790A-4H was being retrieved, a lighted buoy and several smaller floats from nearby fishing vessels were observed floating in the water on both sides of the ship. If the floats were attached to nets or long fishing lines, they were close enough to represent a hazard to the dynamic-positioning thrusters. As a precautionary measure, the thrusters were shut down and retracted. Because station-keeping ability could not be guaranteed, the drill string was pulled clear of the seafloor until the fishing-float problem could be solved. The bit cleared the seafloor at

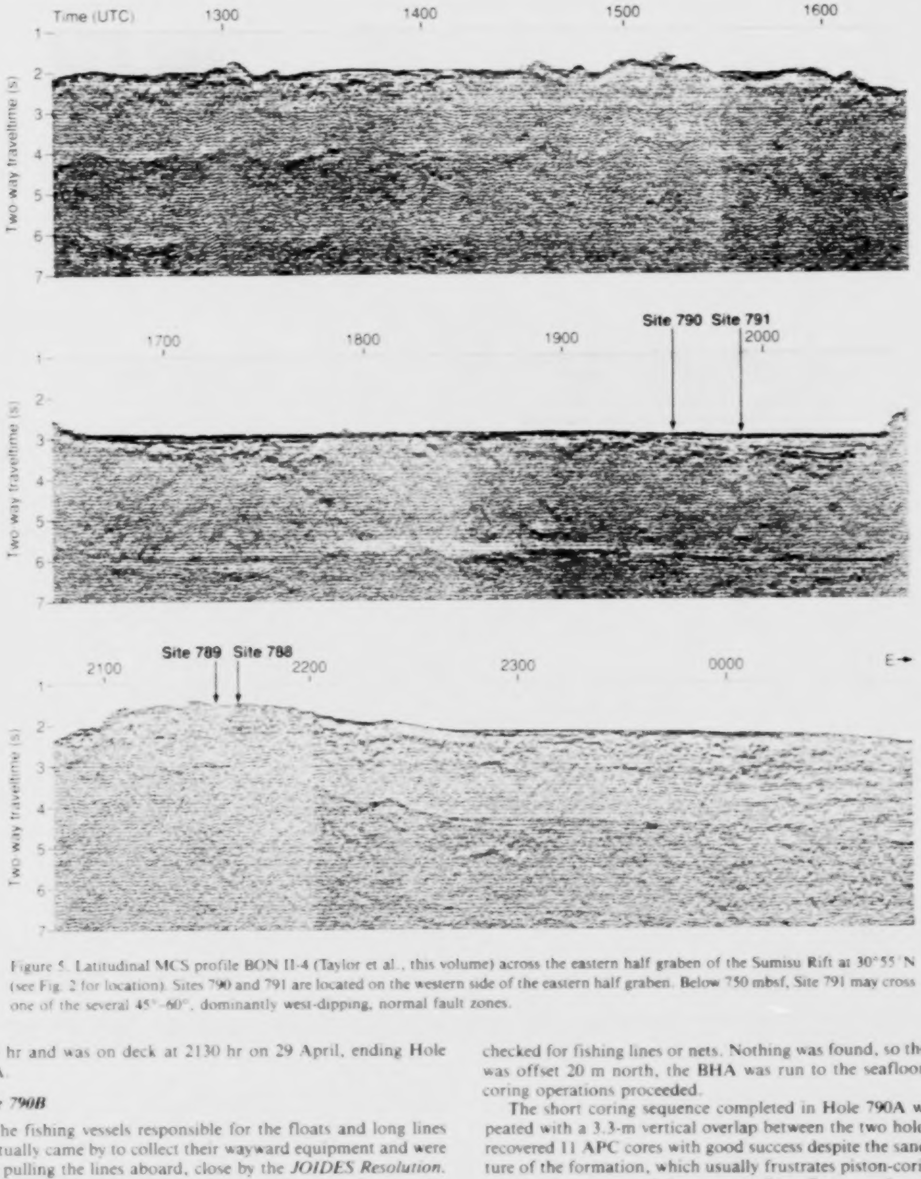

Figure 5. Latitudinal MCS profile BON II-4 (Taylor et al., this volume) across the eastern half graben of the Sumisu Rift at 30°55′N (see Fig. 2 for location). Sites 790 and 791 are located on the western side of the eastern half graben. Below 750 mbsf, Site 791 may cross one of the several 45°–60°, dominantly west-dipping, normal fault zones.

1655 hr and was on deck at 2130 hr on 29 April, ending Hole 790A.

Hole 790B

The fishing vessels responsible for the floats and long lines eventually came by to collect their wayward equipment and were seen pulling the lines aboard, close by the *JOIDES Resolution*. While pulling in their lines, they apparently snagged one under the drillship in the vicinity of the drill pipe. They seemed to cut that line, and then they departed, leaving the potential problem of lines fouled around the drill string. The thrusters could not be lowered safely because we could not see the lines in the water in the darkness. Without positive station-keeping ability, drilling could not proceed, so the drill bit was pulled to the deck and checked for fishing lines or nets. Nothing was found, so the ship was offset 20 m north, the BHA was run to the seafloor, and coring operations proceeded.

The short coring sequence completed in Hole 790A was repeated with a 3.3-m vertical overlap between the two holes. We recovered 11 APC cores with good success despite the sandy nature of the formation, which usually frustrates piston-coring attempts. An unsuccessful pore-water/heat-flow sample run was attempted after Core 126-790B-5H was cut.

Following Core 126-790B-11H, a 55,000-lb overpull in a sticky clay interval dictated a change to the XCB coring system. The switch was apparently too soon, however, because the next four XCB cores netted a total of only 0.8 m of loose, sandy material. Before more coring could be accomplished, a serious ground

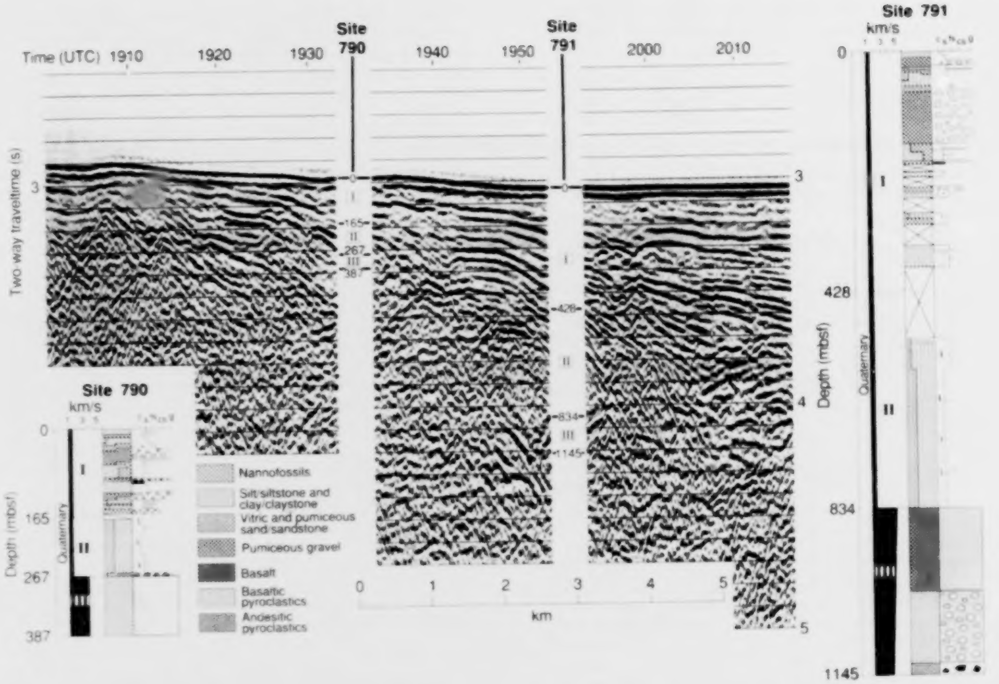

Figure 6. Correlation of Sites 790/791 lithostratigraphy with MCS seismic data. Lithologic units are identified on the seismic section, unit boundaries are given in meters below seafloor (mbsf), and lithologic columns (see "Lithostratigraphy and Accumulation Rates" section, this volume) are presented. The location of the *Fred Moore* seismic line is shown in Figure 2. The seismic profile has been stacked (48 fold), deconvolved, migrated, and filtered 10-60 Hz. The vertical exaggeration is ~4×; c = clay, s = silt, fs = fine sand, cs = coarse sand, and g = gravel/conglomerate.

fault in the top-drive power cables was discovered. Because the problem appeared to be one that would require many hours to fix, we ended drilling in Hole 790A and pulled the bit above the seafloor at 0315 hr on 1 May 1989.

Hole 790C

After 20.5 hr, the shorted-out umbilical lines to the top drive were repaired and coring operations were continued. Hole 790C was spudded at 1610 hr on 1 May, and the bit was washed without coring to 85 mbsf where piston coring resumed. This time the overpull through the sticky zone from 90 to 100 mbsf was tolerable (< 30 Kpsi), and we extended APC coring to Core 126-790C-8H at 155.2 mbsf. During most of this sequence, the APC did not achieve full stroke in the sand/silt-dominated sediment and the high recovery rate observed was probably because of flow-in.

We changed to XCB coring at Core 126-790C-9X and proceeded with fine results through Core 126-790C-20X at 271 mbsf. At that point, a new lithologic unit was encountered that resisted all recovery attempts with XCB-coring methods. The traces of material trapped in the recesses of the core catchers indicated that the missing sediment was very loose sand or gravel. The lack of recovery continued to frustrate all efforts until Core 126-790C-31X at 367 mbsf.

While running in with the sand line to retrieve Core 126-790C-31X, the bit plugged. The core barrel was also found to be stuck, undoubtedly by sand packed around the cutting shoe and bit throat. To remedy the stuck core barrel situation, the drill string was pulled until the bit was out of the gravel/sand zone at 261 mbsf. At that point, circulation was again achieved and an extensive mud treatment was pumped through the system to stabilize the hole and wash away the material jamming the core barrel.

The pipe was washed back to total depth through 44 m of fill that had collected when the hole partially caved in, and XCB coring resumed. Three more cores were cut, but with negligible recovery, in a formation consisting of pebbly gravels. At each connection and when attempting to insert the sinker-bar assembly, severe backflow was observed. The implication was that the hole annulus was heavily laden with sand and/or cuttings. Because backflow did not decrease when the core barrels were out of the string, it was assumed that the float valve was jammed open and therefore unable to prevent the ingress of sand. Temporary bit plugs were experienced after each backflow. We ended Hole 790C at 387.1 mbsf when the backflow was deemed to be too great a hazard to personnel and downhole equipment.

Before pulling the pipe completely out of the hole, the possibility of logging the lower unrecovered interval was evaluated by doing a short pipe trip up 100 m and back down. The short trip took less than 1 hr, but the hole was already filled with more than 30 m of sand. The possibility of getting a logging tool into the unstable zone was considered remote, and we abandoned

Table 1. Depth (mbsf) and two-way traveltimes for stratigraphic horizons observed at Sites 790 and 791.

Horizon	Site 790	Site 791
Base of pumice bed II (P)	54.65 mbsf 0.070 s	167 mbsf 0.214 s
Key Bed #7 (K)	87.85 mbsf 0.112 s	205 mbsf 0.262 s
I/II Boundary (I)	165 mbsf 0.210 s	428 mbsf 0.543 s
FO *Emiliania huxleyi* (H) (275 ka)	187 mbsf 0.239 s	518 mbsf 0.654 s
LO *Pseudoemiliania huxleyi* (L) (460 ka)	219 mbsf 0.280 s	659 mbsf 0.828 s
Brunhes/Matuyama (B) (730 ka)	244 mbsf 0.313 s	750 mbsf 0.933 s
II/III Boundary (II)	271 mbsf 0.350 s	834 mbsf 1.024 s
Total depth	387 mbsf 0.410 s	1145 mbsf 1.188 s

Notes: The stratigraphic boundaries include lithologic unit boundaries I/II and II/III (see "Lithostratigraphy and Accumulation Rates" section, this chapter), the Brunhes/Matuyama boundary, the first occurrence of *E. huxleyi* (see "Biostratigraphy" section, this chapter), Key Bed #7, and the base of pumice bed II (see "Lithostratigraphy and Accumulation Rates" section, this chapter). Letters and numbers in parentheses identify horizons shown in Figure 7. Two-way traveltimes are given in seconds below seafloor and are derived from physical properties velocities (see "Physical Properties" section, this chapter). FO = first occurrence and LO = last occurrence.

logging plans. The pipe was pulled out of the hole, and the bit reached the deck at 2215 hr, 3 May 1989.

Site 790 to 791

Although we had planned to run the drill string back to the bottom at Site 790 for coring Hole 790D with the RCB system, a change of heart occurred when geophysical interpretation determined that the site had been located too far from the sediment structure originally targeted. Thus, the site was abandoned and the vessel made a very short transit to a position 1.5'E of Site 790. The move was beyond beacon offset range, so a new beacon was dropped at 0138 hr on 4 May 1989 and Site 791 (proposed Site BON-1A) was begun.

Hole 791A

An APC/XCB BHA was put together and run to the seafloor. It included the nonmagnetic drill collar to enable oriented piston coring. A prototype set of Hydrolex mechanical jars were also included, and an extra stand of drill collars was added above the jars for hammer weight if needed. The mud-line coring attempt with the APC encountered unexpectedly firm material at the surface, and the core barrel was not able to extend to its full length. Since the roller cone bit and drill string were hanging some 5 m above the seafloor, the column-loaded piston corer barrel was unsupported and it subsequently buckled. The bent barrel could not at first be pulled back into the drill string. The stuck barrel was dislodged after a few minutes of hammering with the sand-line link jars. On deck, it was found that the lower 15-ft core-barrel section had broken off from the upper section. The upper barrel was bent beyond reuse, and the cutting shoe, core catchers, and the core itself were lost.

Rather than risk another buckled core barrel with a mud-line shot, the next core was taken at the normal location for the second core in the sequence with the BHA buried 4.5 m. The results were good, and piston coring continued for a total of 23 cores to a depth of 207.9 mbsf. The formation penetrated in the APC sequence was dominated by sand and pebbly gravel. The coring results were unusual for APC performance in sands, with recovery averaging 82% and over half of the shots registering full stroke of the core barrel. The recovery figures in the cases of partial stroke were clearly augmented by flow-in. Poor penetration finally dictated APC refusal and the change was made to the XCB.

Recovery in the XCB sequence (Cores 126-791A-24X through -49X) was poor, as the material continued to be dominated by vitric silts and sands that were virtually impossible to coax into the core barrel. No combination of drilling parameters or core-barrel mechanical adjustments could be found to improve the results. Of the 26 XCB cores recovered, 17 contained less than 1 cm of material. Penetration rates were naturally very quick, and an enforced cautious pace in advancing the drill string did not improve the core recovery. It probably helped, however, in keeping the unstable material from collapsing around the drill string. Liberal gel mud sweeps were used after each second core in an attempt to hold off erosion of the walls in the hole.

The hole was abruptly ended when the rope socket on top of the sinker-barrel assembly backed off, leaving the sinker bars and core barrel in the pipe. An attempt was made to wireline fish for the sinker bars using a jury-rigged taper tap, but the tap broke off after engaging the fish. The drill string was pulled, and the core-barrel wash was removed on deck. Hole 791A ended when the bit reached the deck at 0745 hr on 6 May 1989.

Hole 791B

With the basement objective and firmer lithology expected to appear only a little deeper than the total depth of Hole 791A, the RCB was chosen for Hole 791B. A 12-drill-collar BHA was assembled, including the Hydrolex jars. The hole was spudded at 1640 hr on 6 May and drilled with a center bit to 173 mbsf. Some tight-hole conditions were experienced at that point that required 45 min of remedial hole conditioning. Center-bit drilling continued to 230 mbsf where the first spot core was attempted but with no recovery. The pipe was washed down to 250 mbsf where it became stuck while making a connection. The new jars were used to hammer the BHA free. The wash interval ended at 416 mbsf, where routine RCB coring commenced.

Cores 126-791B-4R to -8R were overlaps of the base of the XCB coring interval at Hole 791A. Recovery was virtually zero over this zone, but it picked up slightly as the hole deepened and some clay layers were encountered. While attempting to retrieve Core 126-791B-19R, the sinker-bar assembly came apart at the 3-lug quick release (Q/R). The Q/R was successfully fished with another wireline run, and coring continued without further difficulties.

Fairly normal RCB coring conditions and results prevailed through Core 126-791B-46R as a series of interbedded units of claystones and silts were recovered. At 834 mbsf, a hard interval was detected by the driller, and basalt breccia was recovered in the core barrel (Core 126-791B-47R). Core recovery dropped off dramatically as a zone of gravel and pumice material was penetrated. Hole stability in this zone was significantly poorer than in the clays above, but it was not enough to prohibit advancing the drill string. As at Hole 791A, liberal usage of gel mud was applied throughout the coring of the hole.

At about 1100 mbsf, the formation turned to hard rock, and the rapid penetration rates fell off to a range of 2-5 m/hr. The

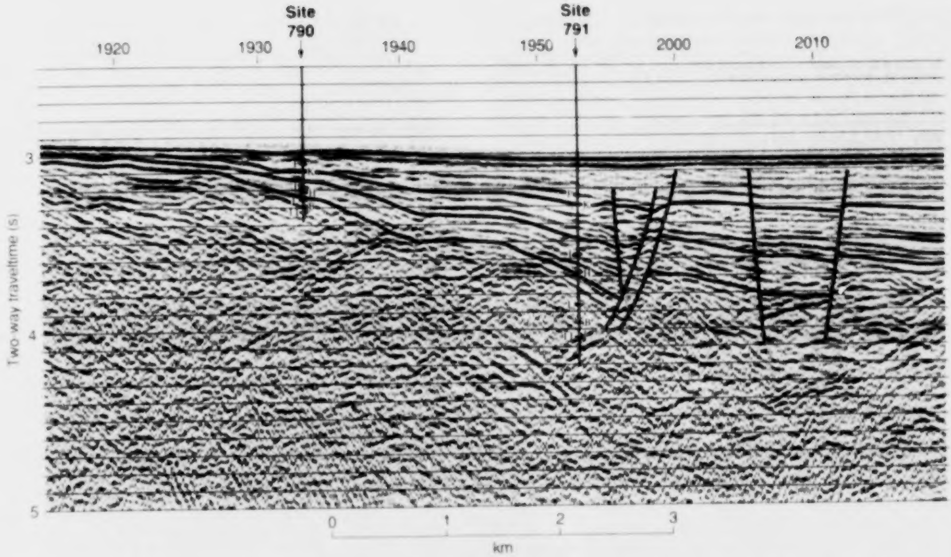

Figure 7. Detailed seismic correlation of specific stratigraphic horizons identified at Sites 790 and 791. Horizons identified on the seismic section are (P) the base of the coarse pumice unit above Key Bed #7, (K) Key Bed #7, (I) Unit I/II boundary, (H) the FO of ***Emiliania huxleyi*** (275 ka), (L) the LO of ***Pseudoemiliania lacunosa*** (460 ka), (B) Brunhes/Matuyama boundary (730 ka), and (II) Unit II/III boundary. Solid lines represent general seismic stratigraphic correlation and principal faults. Note the distinct difference in seismic character at and below the Unit II/III boundary between the two drill sites. The difficulty in correlating the three lowermost horizons (L, B, and II) results from a combination of (1) complex faulting that progressively offsets deeper horizons to a greater degree, (2) pre-rift and early syn-rift volcanism that overprints and obscures the sedimentary horizons, and (3) possible out-of-plane seismic reflections. The location of this seismic line is shown in Figure 2. The vertical exaggeration is ~2×.

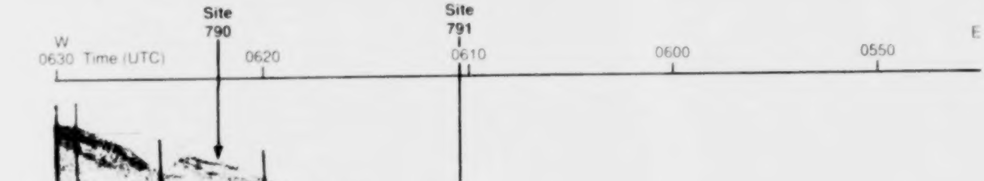

Figure 8. High-resolution seismic record (3.5 kHz) illustrating the pattern of recent sediment accumulation in this area of actively subsiding and rotating fault blocks. Note the thicker transparent ash layer observed at Site 791 that thins considerably toward Site 790.

Table 2. Coring summary for Sites 790 and 791.

Core no.	Date (1989)	Time (UTC)	Depth (mbsf)	Cored (m)	Recovered (m)	Recovery (%)
126-790A-						
1H	Apr 29	1425	0-8.8	8.8	8.81	100.0
2H	Apr 29	1510	8.8-18.3	9.5	9.65	101.0
3H	Apr 29	1600	18.3-27.8	9.5	9.60	101.0
4H	Apr 29	1645	27.8-37.4	9.6	7.65	79.7
Coring totals				37.4	35.71	95.5
126-790B-						
1H	Apr 30	0230	0-4.5	4.5	4.44	98.2
2H	Apr 30	0325	4.5-14.0	9.5	8.82	92.8
3H	Apr 30	0405	14.0-23.5	9.5	9.40	98.9
4H	Apr 30	0510	23.5-33.0	9.5	9.35	98.4
5H	Apr 30	0600	33.0-42.5	9.5	8.58	90.3
6H	Apr 30	1000	42.5-52.0	9.5	5.84	61.5
7H	Apr 30	1050	52.0-61.6	9.6	9.23	96.1
8H	Apr 30	1140	61.6-71.3	9.7	9.66	99.6
9H	Apr 30	1225	71.3-81.0	9.7	4.18	43.1
10H	Apr 30	1340	81.0-90.7	9.7	9.25	95.3
11H	Apr 30	1445	90.7-100.3	9.6	9.16	91.6
12X	Apr 30	1550	100.3-110.0	9.7	0	0
13X	Apr 30	1640	110.0-119.6	9.6	0	0
14X	Apr 30	1730	119.6-129.3	9.7	0	0
15X	Apr 30	1845	129.3-138.9	9.6	0.80	8.3
Coring totals				138.9	88.71	63.9
126-790C-						
1H	May 1	1910	85.0-94.5	9.5	9.53	100.0
2H	May 1	1955	94.5-104.2	9.7	10.01	103.2
3H	May 1	2040	104.2-113.9	9.7	9.84	101.0
4H	May 1	2120	113.9-123.5	9.6	8.79	91.5
5H	May 1	2215	123.5-133.2	9.7	9.00	92.8
6H	May 1	2300	133.2-142.7	9.5	9.68	102.0
7H	May 1	2345	142.7-145.7	3.0	2.54	84.6
8H	May 2	0035	145.7-155.2	9.5	9.39	98.8
9X	May 2	0140	155.2-164.9	9.7	0	0
10X	May 2	0230	164.9-174.6	9.7	1.71	17.6
11X	May 2	0310	174.6-184.2	9.6	7.05	73.4
12X	May 2	0400	184.2-193.9	9.7	1.77	18.2
13X	May 2	0445	193.9-203.6	9.7	4.89	50.4
14X	May 2	0530	203.6-213.2	9.6	3.74	38.9
15X	May 2	0615	213.2-222.8	9.6	0.38	4.0
16X	May 2	0700	222.8-232.4	9.6	8.12	84.6
17X	May 2	0800	232.4-242.1	9.7	9.79	101.0
18X	May 2	0845	242.1-251.7	9.6	6.44	67.1
19X	May 2	0940	251.7-261.4	9.7	8.47	87.3
20X	May 2	1040	261.4-271.1	9.7	5.32	54.8
21X	May 2	1130	271.1-280.6	9.5	0.09	1.0
22X	May 2	1245	280.6-290.2	9.6	0	0
23X	May 2	1425	290.2-299.9	9.7	0.06	0.6
24X	May 2	1630	299.9-309.5	9.6	0.26	2.7
25X	May 2	1800	309.5-319.2	9.7	0	0
26X	May 2	1920	319.2-328.8	9.6	0	0
27X	May 2	2100	328.8-338.5	9.7	0.26	2.7
28X	May 2	2240	338.5-348.1	9.6	0	0
29X	May 3	0035	348.1-353.0	4.9	0.01	0.2
30X	May 3	0355	353.0-358.1	5.1	0	0
31X	May 3	0820	358.1-367.7	9.6	0	0
32X	May 3	1215	367.7-377.4	9.7	0.03	0.3
33X	May 3	1440	377.4-387.1	9.7	0.15	1.5
Coring totals				302.1	127.32	42.1
126-791A-						
1H	May 4	0820	0-4.5	4.5	0	0
2H	May 4	0910	4.5-14.0	9.5	9.76	103.0
3H	May 4	1000	14.0-23.5	9.5	4.63	48.7
4H	May 4	1040	23.5-33.0	9.5	7.27	76.5
5H	May 4	1145	33.0-42.5	9.5	9.15	96.3
6H	May 4	1225	42.5-52.0	9.5	2.83	29.8
7H	May 4	1300	52.0-61.6	9.6	6.84	71.2
8H	May 4	1350	61.6-71.3	9.7	9.76	100.0
9H	May 4	1440	71.3-81.0	9.7	9.36	96.5
10H	May 4	1520	81.0-90.7	9.7	8.88	91.5
11H	May 4	1600	90.7-100.4	9.7	8.84	91.1
12H	May 4	1640	100.4-110.1	9.7	9.16	94.4
13H	May 4	1715	110.1-119.8	9.7	9.01	92.9
14H	May 4	1805	119.8-129.5	9.7	8.80	90.7
15H	May 4	1845	129.5-139.2	9.7	8.88	91.5

Table 2 (continued).

Core no.	Date (1989)	Time (UTC)	Depth (mbsf)	Cored (m)	Recovered (m)	Recovery (%)
126-791A- (Cont.)						
16H	May 4	1925	139.2-148.8	9.6	9.35	97.4
17H	May 4	2010	148.8-158.5	9.7	8.65	89.2
18H	May 4	2055	158.5-168.1	9.6	9.38	97.7
19H	May 4	2330	168.1-177.7	9.6	9.69	101.0
20H	May 5	0000	177.7-187.4	9.7	8.87	91.4
21H	May 5	0035	187.4-196.9	9.5	1.65	17.3
22H	May 5	0110	196.9-206.4	9.5	9.46	99.6
23H	May 5	0145	206.4-207.9	1.5	2.02	134.0
24X	May 5	0240	207.9-217.1	9.2	0	0
25X	May 5	0345	217.1-226.7	9.6	0.92	9.6
26X	May 5	0430	226.7-236.4	9.7	0	0
27X	May 5	0525	236.4-246.0	9.6	0	0
28X	May 5	0615	246.0-255.6	9.6	1.29	13.4
29X	May 5	0745	255.6-265.3	9.7	0	0
30X	May 5	0840	265.3-274.9	9.6	0.33	3.4
31X	May 5	0915	274.9-284.6	9.7	0.03	0.3
32X	May 5	1000	284.6-294.3	9.7	0.02	0.2
33X	May 5	1052	294.3-304.0	9.7	1.24	12.8
34X	May 5	1140	304.0-313.6	9.6	0.98	10.2
35X	May 5	1230	313.6-323.3	9.7	0.03	0.3
36X	May 5	1310	323.3-332.9	9.6	0.01	0.1
37X	May 5	1350	332.9-342.6	9.7	0	0
38X	May 5	1425	342.6-352.3	9.7	0.01	0.1
39X	May 5	1525	352.3-362.0	9.7	1.18	12.1
40X	May 5	1620	362.0-371.7	9.7	0.54	5.6
41X	May 5	1705	371.7-381.4	9.7	0.07	0.7
42X	May 5	1750	381.4-391.0	9.6	0.67	7.0
43X	May 5	1830	391.0-399.8	8.8	0	0
44X	May 5	1910	399.8-409.1	9.3	0	0
45X	May 5	1955	409.1-418.8	9.7	0	0
46X	May 5	2050	418.8-428.4	9.6	0.30	3.1
47X	May 5	2130	428.4-437.7	9.3	0	0
48X	May 5	2215	437.7-447.3	9.6	0	0
49X	May 6	0745	447.3-457.0	9.7	0	0
Coring totals				457.0	179.86	39.4
126-791B-						
1R	May 7	0100	230.0-239.5	9.5	0	0
2W	May 7	0450	239.5-339.7	100.2	0.01	Wash core
3W	May 7	0802	339.7-416.3	76.6	0.10	Wash core
4R	May 7	0900	416.3-425.7	9.4	0	0
5R	May 7	1015	425.7-435.0	9.3	0.01	0.1
6R	May 7	1100	435.0-444.7	9.7	0	0
7R	May 7	1200	444.7-454.3	9.6	0	0
8R	May 7	0835	454.3-463.6	9.3	0	0
9R	May 7	1325	463.6-473.3	9.7	0.24	2.5
10R	May 7	1405	473.3-482.9	9.6	1.02	10.6
11R	May 7	1500	482.9-492.6	9.7	0.18	1.9
12R	May 7	1550	492.6-502.1	9.5	0	0
13R	May 7	1635	502.1-511.8	9.7	2.76	28.4
14R	May 7	1715	511.8-521.5	9.7	0	0
15R	May 7	1800	521.5-531.2	9.7	0.24	2.5
16R	May 7	1850	531.2-540.9	9.7	0.49	5.1
17R	May 7	2000	540.9-550.6	9.7	0.14	1.4
18R	May 7	2045	550.6-560.3	9.7	0.61	6.3
19R	May 7	2245	560.3-569.7	9.4	0	0
20R	May 7	2340	569.7-579.3	9.6	0.38	4.0
21R	May 8	0015	579.3-589.0	9.7	0.15	1.5
22R	May 8	0100	589.0-598.7	9.7	0.91	9.4
23R	May 8	0140	598.7-608.4	9.7	5.38	55.4
24R	May 8	0220	608.4-618.1	9.7	1.23	12.7
25R	May 8	0300	618.1-627.7	9.6	3.02	31.4
26R	May 8	0345	627.7-637.0	9.3	0.99	10.6
27R	May 8	0430	637.0-646.6	9.6	0.89	9.3
28R	May 8	0515	646.6-656.3	9.7	5.85	60.3
29R	May 8	0600	656.3-666.0	9.7	0.24	2.5
30R	May 8	0645	666.0-675.6	9.6	5.94	61.9
31R	May 8	0730	675.6-685.3	9.7	4.93	50.8
32R	May 8	0810	685.3-695.0	9.7	1.51	15.5
33R	May 8	0850	695.0-704.6	9.6	0.32	3.3
34R	May 8	0945	704.6-714.3	9.7	6.51	67.1
35R	May 8	1025	714.3-723.6	9.3	1.25	13.4
36R	May 8	1110	723.6-733.2	9.6	6.40	66.6
37R	May 8	1155	733.2-742.8	9.6	2.62	27.3
38R	May 8	1235	742.8-752.4	9.6	5.25	54.7
39R	May 8	1320	752.4-762.1	9.7	3.09	31.8
40R	May 8	1400	762.1-771.7	9.6	3.74	38.9
41R	May 8	1445	771.7-781.3	9.6	4.40	45.8
42R	May 8	1530	781.3-791.0	9.7	4.49	46.3

Table 2 (continued).

Core no.	Date (1989)	Time (UTC)	Depth (mbsf)	Cored (m)	Recovered (m)	Recovery (%)
126-791B- (Cont.)						
43R	May 8	1605	791.0-800.7	9.7	1.60	16.5
44R	May 8	1655	800.7-810.3	9.6	2.76	28.7
45R	May 8	1745	810.3-820.0	9.7	3.35	34.5
46R	May 8	1835	820.0-829.6	9.6	2.84	29.6
47R	May 8	1945	829.6-839.2	9.6	1.21	12.6
48R	May 8	2120	839.2-848.9	9.7	0.25	2.6
49R	May 8	2240	848.9-858.6	9.7	0.22	2.
50R	May 9	0005	858.6-868.3	9.7	0.17	1.8
51R	May 9	0125	868.3-878.0	9.7	0.17	8
52R	May 9	0315	878.0-887.6	9.6	0.30	3.1
53R	May 9	0440	887.6-897.3	9.7	0.27	2.8
54R	May 9	0605	897.3-906.6	9.3	0.02	0.2
55R	May 9	0730	906.6-916.3	9.7	0.04	0.4
56R	May 9	0920	916.3-925.9	9.6	0.34	3.5
57R	May 9	1100	925.9-935.5	9.6	1.02	10.6
58R	May 9	1225	935.5-945.2	9.7	0.06	0.6
59R	May 9	1335	945.2-954.8	9.6	0.64	6.7
60R	May 9	1525	954.8-964.5	9.7	0.25	2.6
61R	May 9	1740	964.5-974.1	9.6	0.17	1.8
62R	May 9	1920	974.1-983.7	9.6	1.07	11.1
63R	May 9	2115	983.7-993.0	9.3	0.98	10.5
64R	May 9	2245	993.0-1002.7	9.7	1.48	15.2
65R	May 10	0015	1002.7-1012.4	9.7	0.89	9.2
66R	May 10	0150	1012.4-1022.1	9.7	1.52	15.7
67R	May 10	0335	1022.1-1031.8	9.7	3.05	31.4
68R	May 10	0615	1031.8-1041.5	9.7	0.43	4.4
69R	May 10	0805	1041.5-1051.1	9.6	0.30	3.1
70R	May 10	1000	1051.1-1060.8	9.7	0.58	6.0
71R	May 10	1215	1060.8-1070.4	9.6	0.34	3.5
72R	May 10	1425	1070.4-1080.0	9.6	2.93	30.5
73R	May 10	1640	1080.0-1089.7	9.7	2.70	27.8
74R	May 10	1805	1089.7-1099.3	9.6	0.16	1.7
75R	May 10	2000	1099.3-1109.0	9.7	0.56	5.8
76R	May 11	0000	1109.0-1118.6	9.6	2.06	21.4
77R	May 11	0445	1118.6-1128.3	9.7	2.60	26.8
78R	May 11	0800	1128.3-1137.6	9.3	0.77	8.3
79R	May 11	1235	1137.6-1145.0	7.4	1.00	13.5
Coring totals				738.2	114.28	15.5
Washing totals				176.8	0.11	
Drilled interval = 230.0						
Combined totals				1145.0	114.39	

coring operation was continued to 1145.0 mbsf, at which point the scientific objectives were deemed satisfied. The final core was cut short by 2 m when a sudden increase in torque with the bit on the bottom indicated possible bit failure.

The hole was displaced several times with both sweep mud and seawater before beginning a wiper trip to the logging depth (121 mbsf) and back to total depth. Greater-than-normal care was taken during the wiper trip in an attempt to prepare a potentially unstable formation for open-hole logging runs. The top drive was engaged to ream a tight hole from 165 to 336 mbsf. The bit was lowered without rotation through a 548-m interval of open hole without encountering any bridges or detectable obstructions. At 261 m above the former total depth (884 mbsf), a solid bridge was found and just above a probable gauge-sized pinch spot immediately overlying the basal zone. After the top drive was picked up, the pipe was found to be stuck and the annulus packed off, apparently around the lower drill collars. The Hydrolex jars again were used to free the pipe by applying up to 60,000-lb jars. With the pipe again free to move, the bit was pulled up to 826 mbsf to regain circulation. The hole was swept with high-viscosity mud, and the process of drilling out the fill/bridge began.

Before the redrilling process could proceed, the annulus was again apparently packed off as stand-pipe pressure increased dramatically. Neither rotation nor circulation was lost, but the pipe was only free to move vertically about 4 m before becoming stuck in either the up or down direction. With free rotation of the bit, it was not possible to apply left-hand torque to cock the Hydrolex jars. It could not even be determined if the upper stuck point was above or below the jars. Within the hour, rotation and the limited amount of vertical movement were both lost as the hole apparently began to slough ever faster. After 3 hr of pulling and attempting to rotate the pipe without any success, it became evident that the pipe would not come free.

The geochemical log was run through the stuck drill pipe before severing the pipe. The geochemical tools (NGT/ACT/GST/TEMP) were rigged and run into the pipe until they encountered an "obstruction" in the pipe apparently 203 m above the bit. (Later log analysis and inventory of the pipe in the rackers revealed that a 203-m pipe tally error had occurred during the downgoing portion of the wiper trip [one layer of the 5½-in. pipe racker had been missed]. The "obstruction" in the pipe was actually the bit itself.) As the logging tools would not go any deeper, the logging run commenced. Data were acquired solely on the uphole run of the combination tool, at a speed of 450 ft/hr (137 m/hr), starting at a depth of 811.67 mbsf.

After logging, one more attempt was made to free the stuck pipe by picking up the top drive and circulating while attempting to rotate, pull free, and activate the drilling jars. All our efforts were fruitless and the severing charges were rigged. In the hope of saving the experimental, and much needed, Hydrolex jars, the first severing shot was intended to be fired in the drill collars just below the jars. The severing charges, of course, were stopped by the mysterious "obstruction" since the pipe tally error still had not been discovered. The 84-pellet high energy engineering (HEE) severing charge was triggered at the "obstruction" point, but it did not fire because of a flooded firing assembly.

A second severing charge was rigged, run to the "obstruction" point, and fired. The pipe was still found to be stuck after the severing charge was removed. It was assumed that the shot had been fired near the top of the BHA (rather than near the bit as it actually was), so the depth for the next severing attempt was chosen to be near the seafloor to guarantee that the pipe would be freed on the next attempt. The charge was run in the pipe and detonated at a point 46 mbsf and the pipe was freed. The remains of the drill string were recovered with the severed stub arriving on deck at 1345 hr on 13 May.

LITHOSTRATIGRAPHY AND ACCUMULATION RATES

Sites 790 and 791 are located west of the Izu-Bonin Arc in the eastern half-graben of the Sumisu Rift. The sites are 2.4 km apart (Figs. 6–7). Site 791 was drilled on the western edge of the flat basin floor of the eastern half-graben, whereas Site 790 is situated on a slight rise and structural high to the west of the flat basin floor. The sedimentary section at Site 791 is about three times thicker than the time-equivalent section at Site 790. Nevertheless, lithotypes and generalized stratigraphy at the two sites are similar. The successions at Sites 790 and 791 are first described separately and then are interpreted in a common section.

Site 790

Three APC/XCB holes were drilled at Site 790. Cores from these holes were correlated by means of sets of key beds, and a 377.6-m-thick composite section was constructed (Figs. 9 and 10). The stratigraphic succession (Table 3) consists of three lithologic units composed predominantly of volcanogenic materials; the upper two are sedimentary, whereas the basal unit is igneous. The sedimentary units also contain variable quantities of biogenic materials, mainly nannofossils. The contact between Units I and II was not recovered, but it is placed at 165 mbsf; the contact between Units II and III was recovered at 266.6

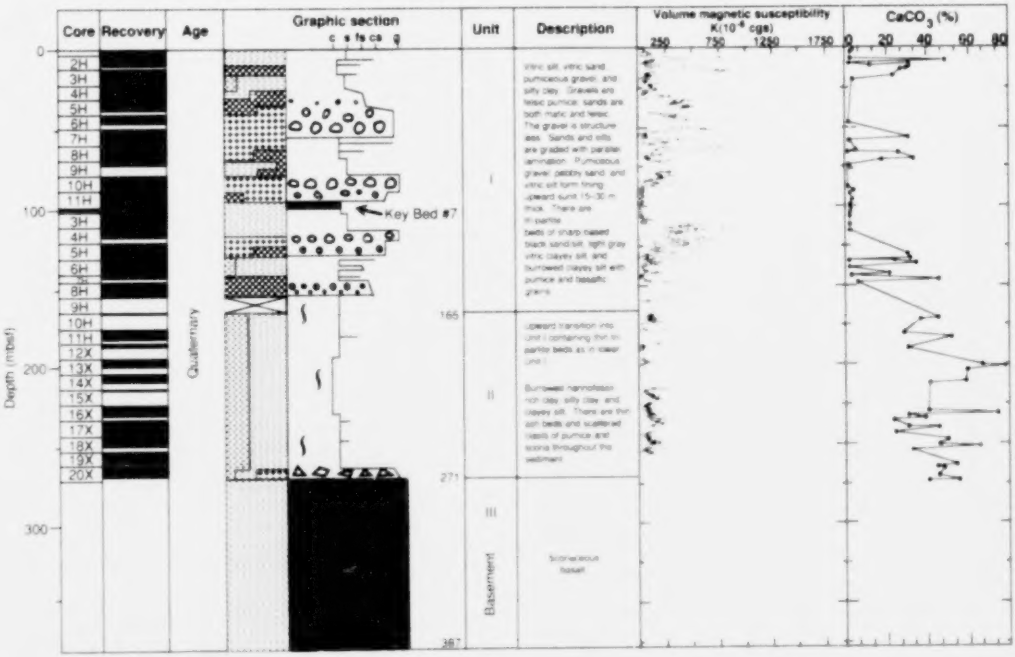

Figure 9. Composite stratigraphic section for Site 790 showing unit boundaries and downhole variations in magnetic susceptibility and total carbonate. The carbonate curve is primarily a function of the distribution of nannofossil tests throughout the section, whereas the magnetic susceptibility data reflect the distribution of coarse mafic volcanic lithics and crystals. The proportions of sediment types in Holes 790B and 790C have been combined and are shown in the Lithology column (see Fig. 6 for key); the format is more generalized than in core descriptions in that it reflects the percentages of groups of sediment types observed within any cored section (i.e., silt + clay, sand, gravel, carbonate), and does not show mixed biogenic/siliclastic lithotypes. The graphic column is a simplified sedimentologic log displaying relative grain size on the horizontal axis (c = clay/claystone, st = silt/siltstone, ss = sand/sandstone, and g = gravel/conglomerate); on this column, sedimentary structures (Fig. 6, "Explanatory Notes" chapter, this volume) and bedding within the cored units are schematically displayed.

mbsf. Although the lithology for Unit III is shown in Figure 9, this material is described in a later section (see "Igneous Petrology" section, this chapter). The recovery for Unit I varied in the three holes, ranging from as low as 64% to as high as 95% between the top and bottom parts of the unit (Table 4). Some of the "apparent" high recoveries in Unit I are artificial, caused by cave-in or flow-in (see "Description" sections that follow). Recovery was 54% for Unit II but extremely low (1%) in Unit III (Table 4).

Sediment types and sedimentary structures (Units I and II) are summarized in Table 3. Also shown in Figure 9 are plots of the downhole distribution of carbonate content and magnetic susceptibility. Peaks in magnetic susceptibility correlate with relative concentrations of ferromagnetic or paramagnetic minerals (e.g., magnetite, ilmenite, pyrrhotite, and hematite), either as solitary phases or as minute inclusions in basaltic glass. Units I and II contain numerous ash layers (a total of 135 were catalogued in Hole 790C) that vary in thickness from millimeters to meters (Table 5). Sediments of Unit II tend to have carbonate contents of 20%-40%, whereas sediments of Unit I generally contain less than 20% carbonate. High values of magnetic susceptibility are generally restricted to Unit I.

Bedding is horizontal in all cores, and there is no evidence for either syn-sedimentary or tectonic deformation.

Unit I

Intervals: Cores 126-790A-1H through -4H, Cores 126-790B-1H through -15X, and Cores 126-790C-1H through -9X
Age: Quaternary
Depth: 0-165 mbsf

Sediments assigned to Unit I were recovered from all three holes at this site, but the unit was completely penetrated only in Hole 790C. Sets of key beds showing identical composition, sedimentary structures, thickness, and mutual stratigraphic separation are recognizable in each hole. Six key beds allow detailed correlation of sections and intervals in Hole 790A with Hole 790B (Fig. 11), which demonstrates that a continuous section was recovered at Site 790 down to a depth of 41.58 mbsf. A similar correlation can be made between Holes 790B and 790C (Figs. 12 and 13); the main key bed for this correlation is "Key Bed #7." The percentages of sediment types indicated below are determined for a composite section on the basis of the above correlations.

There are large-scale alternations in Unit I of (1) pumiceous gravel, pebbly sand, and vitric silt in intervals 15-30 m thick; and (2) 10- to 15-m-thick intervals of clayey silts interbedded with thin- to thick-bedded (3-100 cm) sand and silty sand. The basal contact of Unit I is placed just below the lowest interval of

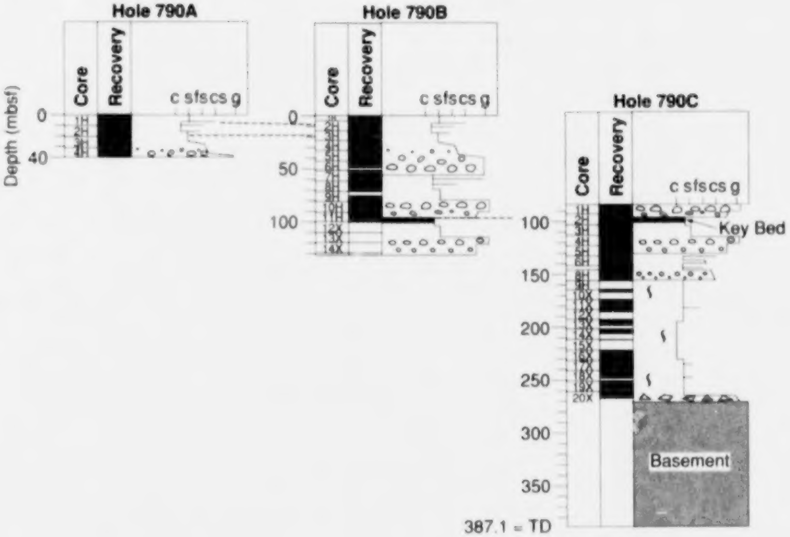

Figure 10. Detailed correlation between stratigraphic sections recovered at Holes 790A, 790B, and 790C. Stratigraphic columns constructed as in Figure 9.

Table 3. Summary of lithology and sedimentary structures of units at Site 790.

Unit	Lithology	Sedimentary structures	Interval (mbsf)	Age	Occurrence
I	Vitric silt, vitric sand, pumiceous gravel, clayey silt, and silty clay. Gravels are felsic; sands are mafic and felsic. Triplet beds of black sand/silt, light gray vitric clayey silt, and burrowed clayey silt with pumice and basaltic grains.	Structureless gravel, graded sands and silts with parallel lamination. Pumiceous gravel, pebbly sand, and vitric silt units are 15–30 m thick and fine upward. Sharp-based black silts/sands and burrows in hemipelagic intervals.	0–165	Quaternary	126-790A-1H to -4H 126-790B-1H to -15X 126-790C-1H to -9X
II	Nannofossil clay, nannofossil-rich clay, silty clay, and clayey silt. Thin ash beds. Scattered pumice and scoria clasts. Triplet beds from 165 to 184 mbsf as in Unit I.	Burrow mottling.	165–266.6	Quaternary	126-790C-10X to 20X-CC, 34 cm
III	Scoriaceous basalt.		266.6–387	Quaternary	126-790C-20X-CC, 34 cm, to -33X

Table 4. Calculated recovery for units at Site 790.

Unit	Hole	Interval (core-core)	Depth (mbsf)	Cored (m)	Recovery (m)	Recovery (%)
I	790A	1H–4H*	0–37.4	37.4	35.7	95
	790B	1H–15H*	0–138.9	138.9	88.71	64
	790C	1H–9X	0–165.0	80.0	68.38	86
II	790C	10X–20X	165.0–266.6	106.1	57.68	54
III	790C	20X–33X	266.6–387.1	120.5	1.00	1

Note: Asterisk (*) indicates that the lower contact of Unit I was not penetrated.

pumiceous gravel and pebbly sand. Gravel- to silt-size sediments throughout Unit I are composed almost exclusively of volcanogenic glass, pumice, minor crystals, and rare microcrystalline lithic fragments. For brevity, therefore, the modifier "vitric" will generally be omitted from lithologic names in this site chapter, except where emphasis is desired. Glass is predominantly transparent and colorless in the pumiceous units and brown to colorless in the thinner interbedded sandy and silty beds.

Unit I consists of 40% silt, 35% sand, 15% gravel, and 10% silty clay. The gravel, and much of the sand and silt, is present in thick to very thick beds (maximum apparent bed thickness about 15 m) that are commonly structureless or, less commonly, normally graded. Gravel-size clasts are angular to subrounded. The gravel is poorly sorted, with abundant sand- to silt-size matrix (Fig. 14). The coarsest gravels tend to occur at the tops or

Table 5. Volcanic ash layers at Site 790.

Core, section, interval (cm)	Thickness (cm)	Description and remarks
126-790B-		
1H-1, 14 (top)- 2H-2-140 (base)	726	Thick pumice layer I
2H-2, 145-150 2H-3, 0-5	5/3/2	Very dark gray (5Y3/1)/brownish black (5YR2/1)/grayish black (N2); silt/silt/very fine sand
2H-3, 7-11	4	Brownish black (5YR2/1); silt
2H-3, 17-20	3	Brownish black (5YR2/1); silt
2H-3, 39-46	7	Grayish black (N2)/brownish black (5YR2/1); silt
2H-3, 148-150 2H-4, 0-18	20	Grayish black (N2); silt (laminated at lowest 5 cm)
2H-4, 61-74	13	Light olive gray (5Y6/1); silt
2H-4, 127-150 2H-5, 0-138	76/85	Light olive gray (5Y4/1); silt/very fine sand-medium sand (grading)
2H-6, 42-77	35	Brownish black (5YR2/1); silt
3H-1, 27-56	29	Grayish black (N2); silt
3H-1, 70-150 3H-2, 0-29	44/65	Grayish black (N2); silt/fine-medium sand (laminated)
3H-2, 58-150 3H-3, 0-137	152/77	Olive gray (5Y5/2)/olive gray (5Y4/2)/dark olive gray (5Y3/2); silt/silt-medium sand (graded)
3H-4, 29 (top)- 7H-3-7 (base)	3628	Thick pumice layer II
7H-3, 27-31	4	Brownish black (5YR2/1); silt
7H-3, 63-66	3	Olive black (5Y2/1); silt
7H-3, 85-93	3/3/2	Olive gray (5Y4/1)/olive gray (5Y4/2)/olive gray (5Y4/1); silt/silt/silt
7H-3, 115-150 7H-4, 0-150 7H-5, 0-150 7H-6, 0-130	50/55/230/ 45/35/50	Gray (5Y5/1)/olive gray (5Y4/1)/(5Y4/1)/olive gray (5Y4/2)/(5Y4/2)/(5Y4/2); silt/silt/very fine sand/very fine sand/fine sand/medium sand with dark olive gray (5Y3/2) laminations
7H-6, 143-147	4	Reddish gray (10R6/1); silt
8H-1, 0-150 8H-2, 0-90	+ 90/25/11/ 1/23/70/17/3	Light gray (5Y7/1)/gray (5Y5/1)/(5Y5/1)/olive gray (5Y4/1)/(5Y5/1)/(5Y4/1)/dark olive gray (5Y3/2)/olive black (5Y2/1); pumice granule (maximum diameter = 3.5 cm)/mixture of pumice pebble and silt/silt/silt/silt/silt/very fine sand/fine sand
8H-2, 106-150 8H-3, 0-85	39/1/40/9/ 32/8	Brownish black (5YR2/1)/grayish black (N2)/olive black (5Y2/1)/(N2)/(N2)/dark olive gray (5Y3/2); silt/very fine sand/silt with grayish black, very fine sand thin layers/very fine sand/fine sand/very fine sand
8H-3, 143-148	5	Dark olive gray (5Y3/2); very fine sand
8H-4, 0-38	35/3	Olive black (5Y2/1); silt/fine sand (laminated)
8H-4, 48-62	10/2/2	Olive black (5Y2/1)/grayish black (N2)/olive black (5Y2/1); silt/very fine sand/silt
8H-4, 115-150 8H-5, 0-9	26/18	Olive black (5Y2/1)/grayish black (N2); silt with very fine sand laminated/very fine-fine sand (graded)
8H-5, 38-131	11/41/41	Brownish black (5YR2/1)/olive black (5Y2/1)/grayish black (N2); fine sand with pumice medium sand laminated/silt with grayish black (N2) very fine sand thin layers/very fine-medium sand (graded)
8H-6, 14-17	3	Dark olive gray (5Y3/2); silt
8H-6, 33-35	2	Dark olive gray (5Y3/2); silt
8H-6, 54-63	9	Gray (5Y5/1); silt
8H-6, 74-92	3/2/7/2/2	Olive black (5Y2/1)/grayish black (N2)/olive black (5Y2/1)/grayish black (N2)/olive black (5Y2/1); silt/very fine sand/silt/very fine sand/silt/
8H-7, 43 (top)- 10H-5, -15 (base)	1622	Thick pumice layer III
10H-5, 22-24	2	Brownish black (5YR2/1); silt
10H-5, 32-150 10H-6, 0-146	5/5/83/2/ 23//8/1/4/ 5/6/44/34/ 14/2/8/20	Olive gray (5Y4/1)/dark greenish gray (5GY4/1)/(5Y4/1)/very dark gray (5Y3/1)/(5Y4/1)/(5Y4/1)/olive gray (5Y4/2)/(5Y4/1)/(5Y4/2)/(5Y4/1)/(5Y4/2)/dark olive gray (5Y3/2)/(5Y3/2)/gray (5Y5/1)/olive black (5Y2/1)/(5Y3/2); silty clay/silty clay/silt/silt/silt/very fine sand/silty very fine sand/silt/very fine sand/silt/coarse silt/very fine sand/fine sand/fine sand/medium sand
126-790C-		
1H-4, 70-72	2	Olive gray (5Y4/1); very fine sand
1H-4, 115 (top)- 5H-3, -43 (base)	3628	Thick pumice layer IV
5H-3, 55-59	4	Olive (5Y5/4); fine sand
5H-3, 67-70	3	Olive (5Y5/4); fine sand
5H-3, 87	< 1	Dusky green (5G3/2); silt
5H-3, 91-111	20	Grayish black (N2); clayey silt-fine sand (graded)
5H-3, 111-150	39/60	Grayish black (N2)/dark gray (N3); silt/coarse sand (graded)

Table 5 (continued).

Core, section, interval (cm)	Thickness (cm)	Description and remarks
126-790C- (Cont.)		
5H-4, 0-60		
5H-4, 96-136	26/14	Dark gray (N3)/black (N1); clayey silt/medium sand
5H-5, 6-15	9	Dark gray (N3); silt
5H-5, 20-35	15	Dark gray (N3); clayey silt/very fine sand
5H-5, 43-95	49/3	Dark gray (N3)/grayish black (N2); clayey silt/medium sand
5H-6, 6-21	15	Medium dark gray (N4); silt–very fine sand (graded)
5H-6, 62-72	10	Medium dark gray (N4); silt–very fine sand (graded)
5H-6, 82	<1	Dusky green (5G3/2); silt
5H-6, 85	<	Dusky green (5G2/1); silt
5H-6, 120-150	2/28	Medium light gray (N6)/olive gray (5Y4/1); silt/silt
6H-1, 0-150	150/31	Olive gray (5Y4/1)/olive gray (5Y4/1); fine–medium sand/
6H-2, 0-31		Pumiceous medium–coarse sand (graded) (laminated)
6H-2, 47-65	18	Light olive gray (5Y6/1); fine sand (graded)
6H-2, 80-144	57/7	Light olive gray (5Y6/1)/dark gray (N3); silty clay/medium sand
6H-3, 34-135	29/73	Light olive gray (5Y6/1)/medium gray (N5); silt/medium sand (graded) (pumice maximum diameter = 1 mm)
6H-4, 5-51	5/25/16	Light olive gray (5Y6/1)/light olive gray (5Y6/1)/dark gray (N3); fine sand/silty clay/medium sand
6H-4, 60-81	11/10	Light olive gray (5Y6/1)/dark gray (N3); silty clay with scattered pumice/fine sand with an erosive base
6H-4, 99-140	2/23/16	Olive gray (5Y4/1)/olive gray (5Y4/1)/dark gray (N3); silty very fine sand/silty clay/medium sand
6H-5, 7-77	52/18	Light olive gray (5Y6/1)/dark gray (N3); clayey silt/fine sand (laminated)
6H-5, 96-118	14/8	Light olive gray (5Y6/1)/dark gray (N3); clayey silt/fine sand (laminated)
6H-5, 141-150	29/17	Light olive gray (5Y6/1)/dark gray (N3); clayey silt/silty
6H-6, 0-37		Very fine sand
6H-6, 41-47	6	Light olive gray (5Y6/1); very fine sand
6H-6, 73-142	11/53/5	Light olive gray (5Y6/1)/light olive gray (5Y6/1)/dark gray (N3); silty clay/silty fine sand/fine sand
7H-1, 0 (top)- 8H-CC, -18 (base)	1250	Thick pumice layer V
11X-1, 25	<1	Silt
11X-2, 10-16	6	Very light gray (N8); clayey silt–very fine sand (graded)
11X-2, 45-50	5	(10Y6/2); silt (graded)
11X-3, 17-30	12/1	Olive gray (5Y5/2)/very light gray (N8); clayey silt–very fine sand (graded)/clayey silt
11X-3, 109-110	1	Very light gray (N8); silt
11X-4, 32-47	10/5	Olive gray (5Y5/2)/dark gray (N3); clayey silt/coarse sand
11X-4, 70-72	2	Medium light gray (N6); very fine sand
11X-4, 110-120	10	Dark gray (N3); silt (graded)
11X-4, 139-150	15/4/3/3	Olive gray (5Y5/2)/olive gray (5Y5/2)/light gray (N7)/
11X-5, 0-14		Medium dark gray (N4); silt/medium sand/silt/very fine sand with an erosive base
12X-1, 5-14	9	Olive gray (5Y4/1); silt
12X-1, 20-23	3	Olive gray (5Y4/1); silt
12X-1, 26-28	2	Olive gray (5Y4/1); silt
12X-1, 35-37	2	Olive gray (5Y4/1); silt
12X-1, 40-42	2	Olive gray (5Y4/1); silt
12X-1, 45-69	5/4/6/4/5	Olive gray (5Y4/2)/olive gray (5Y4/1)/olive gray (5Y4/2)/olive black (5Y2/1)/olive black (5Y2/1); silt/silt/medium sand with pumice coarse sand/fine sand/silt
12X-1, 71-76	5	Olive black (5Y2/1); fine sand
12X-1, 130-140	43	Light olive gray (5Y4/1); silt
12X-CC, 0-33		
13X-1, 18-44	7/5/4	Gray (5Y5/1)/olive gray (5Y4/1)/olive black (5Y2/1); clayey silt/silt/fine sand
13X-1, 50-52	2	Olive gray (5Y4/2); silt
13X-1, 66-68	2	Olive black (5Y2/1); silt
13X-1, 71-72	1	Olive black (5Y2/1); silt
13X-1, 79	<1	Olive black (5Y2/1); silt
13X-1, 81	<1	Olive black (5Y2/1); silt
13X-2, 15-55	31/9	Gray (5Y5/1)/gray (5Y5/1); clayey silt/silt
13X-3, 71-75	4	Gray (5Y5/1); silt
14X-1, 0-7	+7	Gray (5Y5/1); silt
14X-1, 87-88	1	Light brownish gray (5YR6/1); clayey silt
14X-2, 136-147	6/5	Very dark gray (N2)/olive gray (5Y4/1); fine sand/scoria granule (maximum diameter = 1 cm)
15X-1, 7-8	1	Olive black (5Y2/1); silty very fine sand
15X-1, 12-17	10	Olive black (5Y2/1); medium sand
15X-CC, 0-5		
15X-CC, 10-22	12	Olive black (5Y2/1); medium sand
16X-1, 0-28	7/3/16/2	Gray (5Y5/1)/very dark gray (5Y3/1)/gray (5Y5/1)/very dark gray (5Y3/1); silt/silt/silt/very fine sand

Table 5 (continued).

Core, section, interval (cm)	Thickness (cm)	Description and remarks
126-790C- (Cont.)		
16X-1, 99-104	5	Olive gray (5Y4/1); silt
16X-1, 108	< 1	Olive gray (5Y4/1); silt (5 mm thick)
16X-2, 8-12	4	Olive gray (5Y5/2); silt
16X-2, 35-38	3	Gray (5Y5/1); silt
16X-4, 63-67	1/3	Dark olive gray (5Y3/2)/olive gray (5Y4/1); silt
16X-5, 52-66	14	Very dark gray (5Y3/1); medium sand
16X-5, 118-120	2	Light olive gray (5Y6/1); silt
16X-6, 17-20	3	Olive gray (5Y4/2); silt
16X-CC, 0-4	4	Dark olive gray (5Y3/2); silt
16X-CC, 18-20	1/1	Gray (5Y5/1)/dark olive gray (5Y3/2); silt
17X-1, 130-145	15	Olive gray (5Y4/1); silt-sandy silt (graded)
17X-7, 27-32	2/2/1	Very dark gray (5Y3/1)/olive gray (5Y4/2)/olive black (5Y2/1); silt/silt/medium sand
17X-CC, 34-35	1	Light olive gray (5Y6/1); silt
18X-1, 145	< 1	Silt
18X-3, 135-136	1	Silt
18X-4, 58-60	2	Very light gray (N8); silt
18X-4, 100	< 1	Very light gray (N8); silt
18X-4, 123-124	1	Very light gray (N8); silt
19X-1, 46-53	7	Olive gray (5Y4/2); silt
19X-1, 65-68	3	Olive gray (5Y4/2); silt
19X-1, 94-96	2	Gray (5Y5/1); silt
19X-2, 98-106	8	Gray (5Y5/1); silt
19X-3, 52-60	8	Olive gray (5Y4/2); clayey silt
19X-3, 81-85	4	Olive gray (5Y4/2); clayey silt
19X-4, 92-150 19X-5, 0-3	36/14/11	Dark gray (N3)/grayish black (N2)/olive black (5Y2/1); Pebble-granule gravel with sandy silt matrix/very coarse sand-granule/granule with medium sand matrix
19X-5, 57-59	2	Olive gray (5Y4/2); silt
19X-6, 13-14	1	Medium light gray (N6); silt
19X-6, 20	1	Medium light gray (N6); silt pocket
19X-6, 39-45	4/2	Olive gray (5Y5/2)/light olive gray (5Y6/1); silt
20X-2, 63-150 20X-3, 0-130	217	Pumice gravel scattered in sandy mud (maximum diameter = 4 cm)
20X-CC, 28-50	6/16	Light olive gray (5Y6/1)/grayish black (N2); sand/scoria (maximum diameter = 2 cm)

Note: 126-790B-10H-6, 140 cm, is correlative to 126-790C-1H-4, 57 cm.

bases of cores; excluding the uppermost coarse material, several cores are graded from coarser gravel at the base to finer gravel, pebbly sand, sand, or silt at the top. Some of this grading may be an artifact of drilling. A detailed correlation of Holes 790A and 790B (Fig. 11) indicates that some pebbly sand and gravel intervals may not be primary features of the sedimentary succession. For example, the pebbly sand bed in Sections 126-790A-1H-3 to 126-790A-1H-6 is unlike the sediment found in Cores 126-790B-1H and -2H at the same sub-bottom depth, and key-bed correlation indicates that the pebbly sand bed overlaps with sediment in Section 126-790A-2H-1. This overlap can only be explained by flow-in of the pebbly sand.

In downhole plots, thick vitric silt units are clearly marked by very low magnetic susceptibility values (Fig. 9) forming distinct intervals that can be correlated between Holes 790A and 790B, and that can also be traced to Site 791 (Fig. 15).

Crude parallel stratification in a few of the gravel and pebbly sand units, defined by concentrations of brown-black glass (Fig. 16), implies little drilling deformation in these intervals. Elsewhere, the unconsolidated nature of the gravels in cores makes it difficult to discriminate unequivocally between *in-situ* sediment, and cave-in or flow-in material.

In Hole 790B (Fig. 10), the intervals 6-20.5, 55-70, and 87-100 mbsf consist predominantly of two distinct sequences. The first is sharp-based, thin- to thick-graded beds (Fig. 17), consisting of a lower sand or silt division, overlain by beds of silty clay that contain scattered sand- and granule-size grains of pumice. The second sequence is characterized by millimeter- to centimeter-thick layers of white or dusky green ash (Fig. 18). The sands and silts appear black (N2) because of a predominance of brown glass, scoria, and dark mineral grains, as indicated by smear slide analysis. Where the sands have not been liquefied by drilling, they commonly show parallel lamination, in some cases above a basal division that is graded but otherwise massive. Some of these sand beds contain intraclasts of soft silty clay similar to the interbedded sediments.

Below 127 mbsf, there are distinctive tripartite units (triplets) (Fig. 19), each beginning with a sharp or erosional base. The lowest division of a triplet is a thin black sand or silt layer that is poorly graded or ungraded and may be plane-parallel laminated (Fig. 20) or burrowed (Fig. 21). The black sand/silt is overlain with a sharp contact by a subtly graded, gray, structureless vitric clayey silt. This second division is succeeded over a thin transition by an uppermost division of strongly burrowed and color mottled, greenish gray, nannofossil-rich clayey silt with scattered sand- to pebble-size clasts of pumice and scoria (Figs. 22 and 23). The nannofossil-rich clayey silt also contains widely spaced, white to dark green, silty to sandy ash layers, generally less than 5 cm thick (Fig. 24). Tripartite beds of this type are also found in the uppermost part of underlying Unit II (above 184 mbsf).

The composition of the pumiceous gravels and sands in Unit I is predominantly felsic, given the pale color of the pumice (clear in smear slides and thin sections), although 10%-20% of the sand-size grains consist of black basaltic fragments. Rare grains of olivine were also identified in the smear slides, although these may have been in beds partially mixed by drilling disturbance.

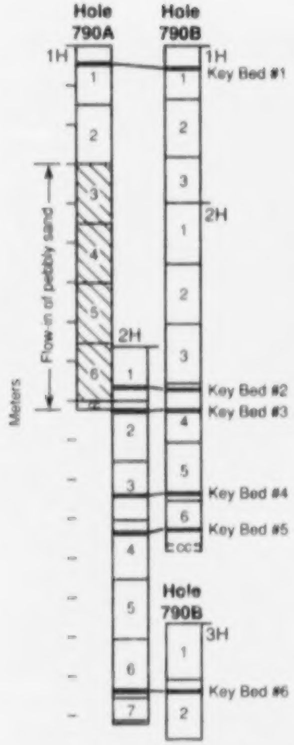
Hole 790A
Hole 790B
1H
1H
Key Bed #1
2H
Flow-in of pebbly sand
Meters
2H
Key Bed #2
Key Bed #3
Key Bed #4
Key Bed #5
CC
Hole 790B
3H
Key Bed #6
1
2
3
4
5
6
7

Figure 11. Correlation of sections in Cores 126-790A-1H to -2H with sections in Cores 126-790B-1H to -3H, based on positions of the bases of six key beds recognized in both holes. The apparent overlap between Cores 126-790A-1H and -2H is the result of flow-in of pebbly sand that is present at 4.5–6.0 mbsf in Core 126-790B-1H. Note scale in meters.

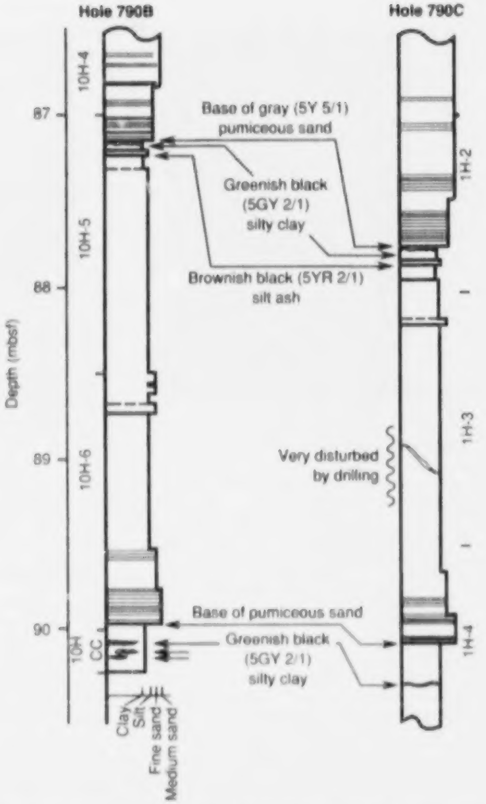
Hole 790B
Hole 790C
Depth (mbsf)
87
88
89
90
10H-4
10H-5
10H-6
10H CC
1H-2
1H-3
1H-4
Base of gray (5Y 5/1) pumiceous sand
Greenish black (5GY 2/1) silty clay
Brownish black (5YR 2/1) silt ash
Very disturbed by drilling
Base of pumiceous sand
Greenish black (5GY 2/1) silty clay
Clay
Silt
Fine sand
Medium sand

Figure 12. Graphic representation of the key elements in Sections 126-790B-10H-4 to -7 and Sections 126-790C-1H-2 to -4 that allow correlation between Holes 790B and 790C. Photographs of Key Bed #7, consisting of greenish black silty clay, are shown in Figure 13.

The black sands in the thinner-bedded intervals consist of dark brown glass, clinopyroxene, orthopyroxene, plagioclase, volcanic lithic grains, and rare olivine and epidote. A grain was tentatively identified as pumpellyite in Sample 126-790C-5H-4, 112 cm.

Unit II

Intervals: Core 126-790C-10X through Section 126-790C-20X-CC at 34 cm
Age: Quaternary
Depth: 165–266.6 mbsf

Unit II is entirely restricted to Hole 790C. The top of Unit II was not recovered, and its contact with Unit I is placed between Cores 126-790C-9X and -10X at 165 mbsf (Fig. 9), based upon the presence of massive sandy beds, magnetic susceptibility data, carbonate content, and comparison with the logging results for Site 791. The basal contact of Unit II with the igneous rocks of Unit III (see "Igneous Petrology" section, this chapter) was recovered in Core 126-790C-20X.

Unit II consists of 67% nannofossil clay and nannofossil-rich clay, 21% silty clay and clayey silt, 8% clay, 2% silt (vitric ash), and 1% each of sand and gravel. The nannofossil clays are concentrated in the interval 193.9–210 mbsf (Fig. 9). Nannofossil clays and nannofossil-rich clays are generally structureless except for widely spaced, very thin (< 5 cm), medium-grained sand to silt beds of dark grayish green to white ash (Fig. 25).

From 184 mbsf to the top of Unit II at 165 mbsf, there are thin tripartite beds of black vitric sand/silt, light gray vitric silt, and burrowed nannofossil clayey silt like those found in the lower part of Unit I. These reflect an upward transition from the nannofossil clay and related sediment types of the lower part of Unit II to the coarser volcaniclastic section of Unit I.

Below 230 mbsf, grain size increases to clayey silt, and the sediment becomes greener in color. Burrowing is strong and marked by dark greenish gray (5G 4/1) mottles. Thin silty or sandy ash bands of the same color are common. The abundance and size of scattered felsic pumice and basaltic clasts increases downcore; the lower 3 m of Unit II, immediately above the igneous rocks of Unit III, contains pumice clasts with maximum diameters of 5 cm (Fig. 26). In this basal interval, color mottling

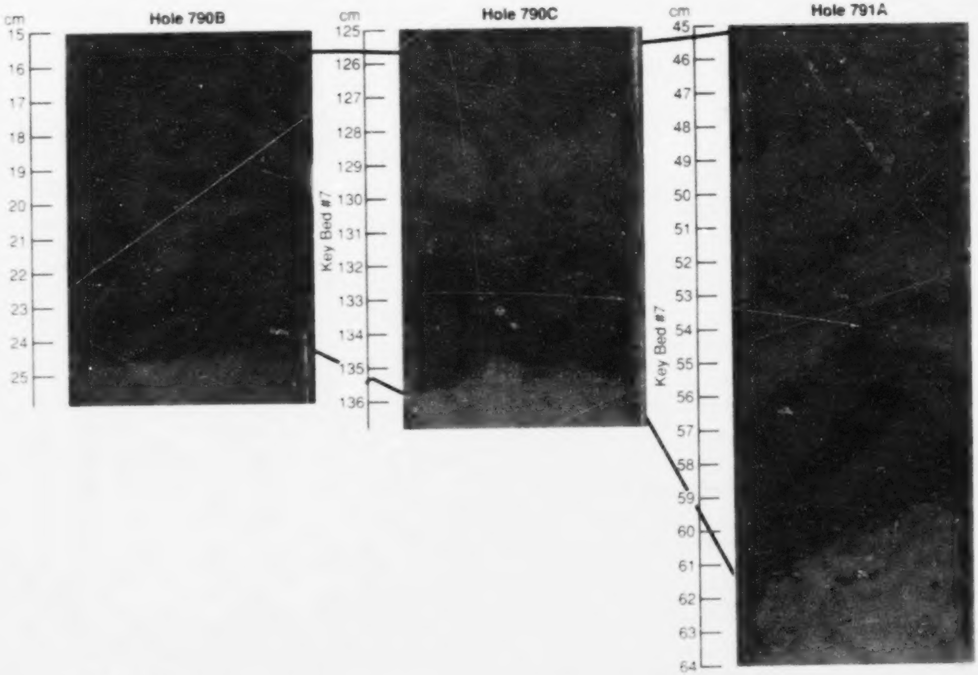

Figure 13. Key Bed #7, a greenish black silty clay bed, at Hole 790B (Interval 126-790B-10H-5, 15-25 cm, 87.25 mbsf), Hole 790C (Interval 126-790C-1H-2, 125-136 cm, 87.85 mbsf), and Hole 791A (Interval 126-791A-22H-6, 44-60 cm, 205.0 mbsf).

increases dramatically, and both sediment and pumice clasts contain secondary coloration in shades of grayish green (5GY 6/1, 10GY 5/2) and grayish yellow green (5GY 7/2).

Site 791

Two holes were drilled at Site 791. The recovery in these holes does not overlap, so the description below is made on the basis of a single column (Fig. 27) that comes from Holes 791A (0-419.1 mbsf) and 791B (463.3-1138.6 mbsf). Recovery of the sedimentary section in Hole 791B with the RCB was low (20%); recovery of sediments at Hole 791A with the XCB was even lower (3%). In contrast, APC recovery in the upper part of Hole 791A was very high (83%). The generally low recovery rates below 208 mbsf decrease the reliability of our description of the sedimentary succession in this interval.

The succession at Site 791 is divided into three lithologic units (Fig. 27). The upper two units are sedimentary and the lower one is igneous. Although part of the lithology for Unit III is shown in Figure 27, this material, including a 22-cm interval of silt and sandy silt in Core 126-791B-62R (igneous Unit 9), is described in a later section (see "Igneous Petrology" section, this chapter). Several lines of evidence (see "Correlation" section that follows) indicate that Unit I at this site is correlative both in time and in sedimentary facies with Unit I at Site 790, although it is much thicker.

In the interval of good recovery at Site 791 (Cores 126-791A-2H to -22H), Unit I consists mainly of very thick beds (up to 65 m thick) of pumiceous gravel with clasts up to 7.5 cm long, and thinner beds of sand, pumiceous pebbly sand, and vitric silt. Thin interbeds of clay, silty clay, and black vitric sand/silt like those in Unit I at Site 790 are present in this section but are much less common. The lower part of Unit I, characterized by very low recovery, consists mainly of vitric silt/siltstone and nannofossil-rich silty clay/claystone.

The top of Unit II is placed at a depth of 428.4 mbsf, based partly on seismic stratigraphic results (see "Seismic Stratigraphy" section, this chapter). Below this depth, most sediments are sufficiently lithified to be called "-stones," although some unlithified vitric silt beds are present even near the base of Unit II.

Unit II consists mainly of burrowed nannofossil-rich claystone and nannofossil claystone, both with scattered sand-size basaltic grains. Bedding dips increase gradually to 15°-20° at a depth of 600 mbsf. Dip then increases more rapidly and reaches values of 45° by a depth of 760-770 mbsf. Below this latter depth, the quantity of disseminated mafic grains, including dark glass and heavy minerals, increases markedly. The change in dip and variation in mafic content may be the result of faulting in the section.

Sediment types and sedimentary structures (Units I and II) are summarized in Table 6. Plots of the downhole distribution of total carbonate and magnetic susceptibility are shown in Figure 27. As at Site 790, peaks in magnetic susceptibility correlate with relative concentrations of ferromagnetic or paramagnetic minerals (e.g., magnetite, ilmenite, pyrrhotite, and hematite), either as solitary phases or as minute inclusions in basaltic glass.

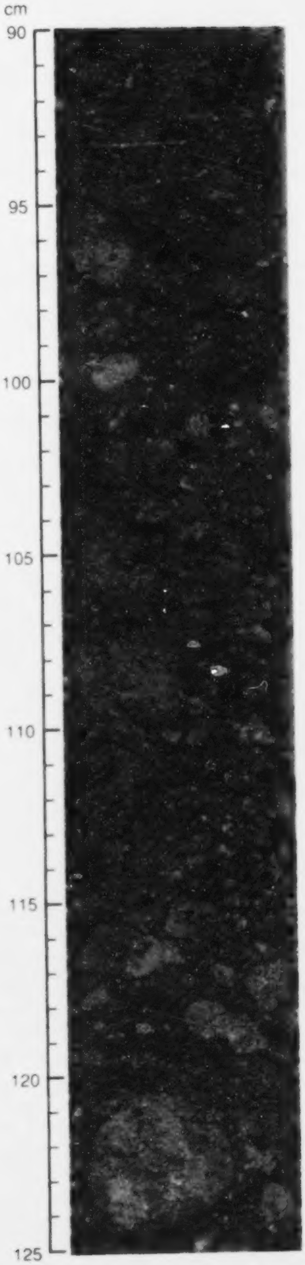

Figure 14. Poorly sorted pumiceous gravel of Unit I (Interval 126-790B-5H-4, 90–125 cm).

Unit I

Interval: Cores 126-791A-1H through -46X and Cores 126-791B-1R through -5R-2, 120 cm
Age: Quaternary
Depth: 0–428.4 mbsf

All sediment recovered in Hole 791A is assigned to Unit I. Cores 126-791B-1R through -5R also penetrated sediments of Unit I, but there was no recovery. Unit I consists of 44% pumiceous gravel; 30% pumiceous and vitric sand, granule sand, and pebbly sand; 14% vitric silt; 7% silty clay and clayey silt; 1.5% nannofossil-rich clay and nannofossil-rich silty clay; and 2% clay. The pumiceous gravel, pebbly sand, granule sand, and sand beds are similar in composition and texture to facies in Unit I at Site 790. Notable differences between these gravels and those of Site 790 are that they form a higher percentage of the succession at Site 791, are thicker (Figs. 9 and 27), and are generally coarser (Fig. 28) with clasts up to 7.5 cm in diameter. In some cores, the gravel has partly flowed within the core barrel, so that the true thickness of some units cannot be determined.

Sand and pebbly sand generally occur in structureless, very thick beds that are light in color from the pumice content (Fig. 29). In many cases, this material is strongly disturbed by drilling (flow-in). Intraclasts of vitric silt up to 7 cm in diameter are present locally (Fig. 30). Rarely, the vitric sand in Unit I is black (Fig. 31); smear slide analysis shows the sand consists of abundant brown glass and mafic minerals. This black sand occurs as the basal part of graded sand to silty clay couplets that characterize the thinner bedded intervals of Unit I. The sand lies with an erosional or sharp contact on burrowed silty clay, is in many cases plane-parallel laminated, and grades upward into silt and burrowed silty clay. Black sand also appears in widely spaced, crude laminae in the very thick pumiceous sand beds.

The vitric silt component is commonly very light colored and can form structureless beds up to 20 m thick (Fig. 27) or millimeter-thick beds within silty clay units. Very thin beds of dark silt (ash) also occur locally. One such bed, in Core 126-791A-22H-6, 55-60 cm (205.0 mbsf), has also been identified in Holes 790B (87.25 mbsf) and 790C (87.85 mbsf; Key Bed #7, Fig. 13).

Light-colored vitric silt, pumiceous and vitric sand, nannofossil-rich clay/claystone, and nannofossil-rich silty clay/claystone characterize the interval of poor recovery in Unit I below 206 mbsf. The biogenic-rich sediment types also contain variable amounts of siliceous microfossils (mainly diatoms and sponge spicules). These sediment types are similar to those present in the lower part of Unit I at Site 790. The contact between Units I and II at Site 791 is placed below the lowest recovered bed of pumiceous sand at 428.4 mbsf. The tripartite beds present in the lower part of Unit I and the upper part of Unit II at Site 790 were not recovered at Site 791. However, their presence in this interval is implied by peaks in the total gamma-ray logs (see "Downhole Measurements" section, this chapter) from 330 to 485 mbsf. These peaks may mark burrowed, nannofossil-rich clayey silts that form one division of the tripartite beds.

Unit II

Interval: Cores 126-791A-47X to -48X and Core 126-791B-5R-2, 120 cm to Section 126-791B-47R-1 at 44 cm
Age: Quaternary
Depth: 428.4–834 mbsf

The first recovery of sediment in Unit II is in Section 126-791B-9R-CC. Recovery in Unit II was low (25%, 34% below 599 mbsf). The sediments consist of 27% carbonate claystone, 22% carbonate-rich claystone, 28% carbonate-rich silty claystone, and 15% carbonate silty claystone, plus very minor amounts of unlithified, light-colored, carbonate-rich vitric silt and vitric silt (3%), carbonate-rich sandy mudstone (2%), silty

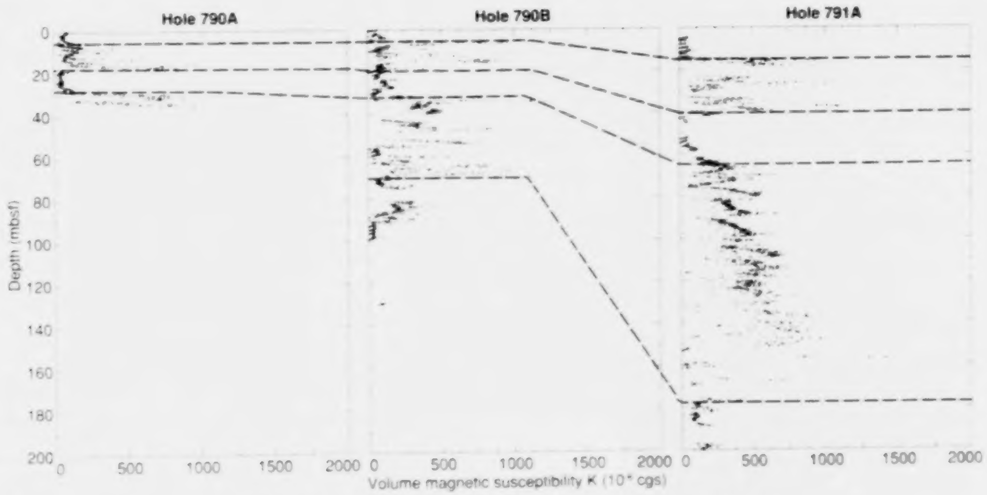

Figure 15. Plots of magnetic susceptibility for Holes 790A, 790B, and 790C. Dashed lines mark correlative sections.

claystone (1%), and chalk (1%). The carbonate component is primarily nannofossils, but some sediments contain 10%-20% foraminifers. Biogenic silica is present in all samples in minor amounts, mainly as diatoms, radiolarians, and sponge spicules. In some cores, scattered, white, elliptical masses, about 1 mm across, consist of clusters of sponge spicules, probably biologically pelletized.

The sediments of Unit II are generally burrowed by *Chondrites*, *Zoophycos*, and *Scolites* (Fig. 32). From 580 to 770 mbsf, secondary pyrite is common in burrows; other minor pyrite persists to the bottom of Unit II. Most burrowed sediments contain disseminated, black, sand-size basaltic rock fragments and scattered pumice clasts up to about 1.5 cm in diameter. The basaltic fragments are locally concentrated into dark disseminated bands, very thin beds, or burrows. Isolated basaltic clasts are as large as 2 cm. The abundance of basaltic fragments increases downward from a depth of about 695 mbsf toward the basalts of underlying Unit III; below 780 mbsf, the mean size of the basaltic clasts increases to a maximum of about 1-2 mm.

An important minor lithology in Unit II below 570 mbsf is very light to medium gray (N8-N6), locally parallel-laminated vitric silt beds, generally 1-10 cm thick (Fig. 33). The apparent original contacts of these soft beds were generally lost during drilling (Fig. 34). The bed thicknesses, therefore, are significantly reduced. In some cases, the soft vitric silt beds were squeezed to fill the core liner completely (the core diameter of lithified sediments is considerably less; Fig. 35).

At a depth of about 600 mbsf, bedding in Unit II dips at angles of 15°-20°. By 760 mbsf, dips are about 45° (Figs. 33 and 34). Two faults are present in the lower 15 m of Unit II (819-834 mbsf), just above the basalt contact (Fig. 36).

X-ray Diffraction Analysis

Site 790

The X-ray diffraction (XRD) results for Site 790 are summarized in Table 7. In Unit I, glass grains have fresh surfaces with only traces of clay alteration products. The XRD analyses of vitric silt and sand from Unit I show very high, broad backgrounds, reflecting abundant, amorphous volcanic glass. Smectite and chlorite are present in this material. Mica group minerals are present in small amounts in all vitric units. Light olive gray (5Y 6/1) to greenish gray (5GY 6/1) ash beds contain abundant calcite, reflecting the high contents of microfossils. Feldspars and quartz are present in all the sediments analyzed; clay minerals are present only in trace amounts (Fig. 37).

Diaspore (AlO[OH]) is common in Unit I, indicating the circulation of hydrothermal fluids with temperatures of 300°-400°C, a result not consistent with sediment pore-water geochemistry (see "Sediment/Fluid Geochemistry" section, this chapter). Handpicked, medium yellowish green (10GY 6/4) glass grains and dark yellowish green (10GY 4/4) ash beds show a strong, but unidentified, peak at 0.203 nm (Fig. 38) probably caused by a mineral containing reduced, divalent iron (Fe^{2+}).

A moderate, reddish brown (10R 4/6) pumice clast (Fig. 23; Sample 126-790C-5H-6 at 22 cm) contains quartz, feldspar, cristobalite, calcite, smectite, chlorite, the 0.203-nm unknown mineral, and amorphous volcanic glass. The presence of cristobalite indicates hydrothermal conditions and temperatures of 200°-300°C. Clasts of this color are exceedingly rare and are probably material incorporated from locally distinct rocks in the vicinity of the volcanic vent as accidental inclusions during eruptions.

In Unit I, dark greenish gray mottles in light olive gray sandy ash (Sample 126-790C-5H-6 at 6 cm) contain calcite, feldspar, quartz, pyrolusite ($Mn0_2$), pyrite (FeS_2), and the 0.203-nm unknown mineral. The characteristic peaks of pyrolusite and pyrite overlap, but they can be distinguished by high intensities at 0.314 (pyrolusite) and 0.163 nm (pyrite).

In Unit II, gritty, light olive gray nannofossil sandy mud (Samples 126-790C-20X-2, 80 cm, and 126-790C-20X-3, 46 cm and 90 cm) contains abundant calcite, feldspar, quartz, the unknown 0.203-nm mineral, and a trace of 1.4-nm clay minerals. Other clay minerals, such as mica group minerals, are very rare.

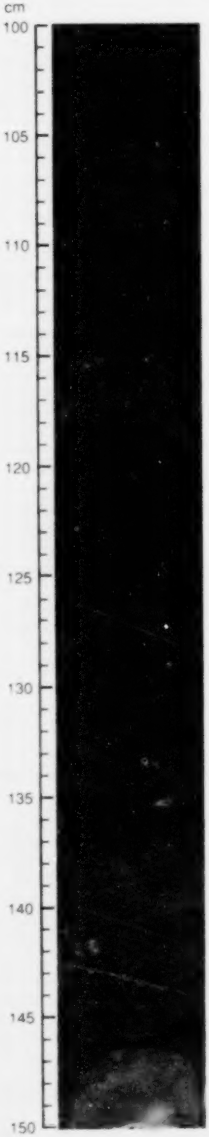
cm
100
105
110
115
120
125
130
135
140
145
150

Figure 16. Basal, parallel-laminated part of a sharp-based, graded, pumiceous sand bed that is 120 cm thick (Interval 126-790B-10H-6, 100–150 cm). The pumice pebbles at 115 cm may mark a surface of amalgamation in the bed.

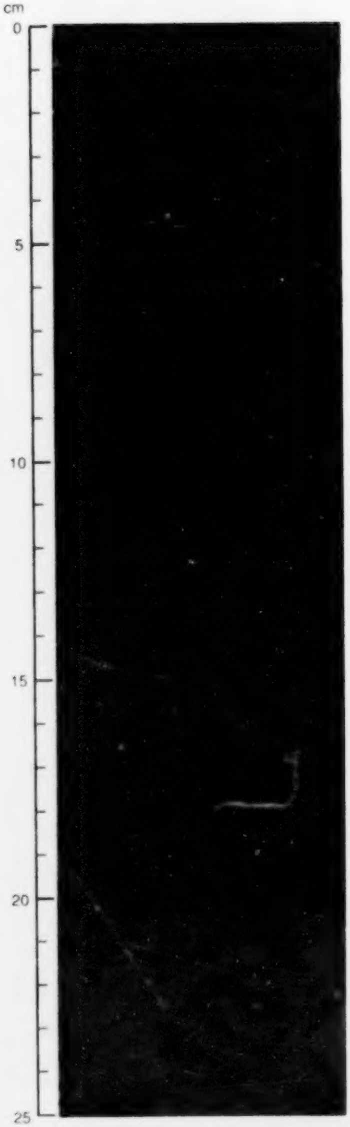
cm
0
5
10
15
20
25

Figure 17. Thin, sharp-based, graded beds of silt to silty clay (Interval 126-790B-2H-3, 0–25 cm). The silty clay in this example is burrowed and contains scattered sand-size grains of pumice.

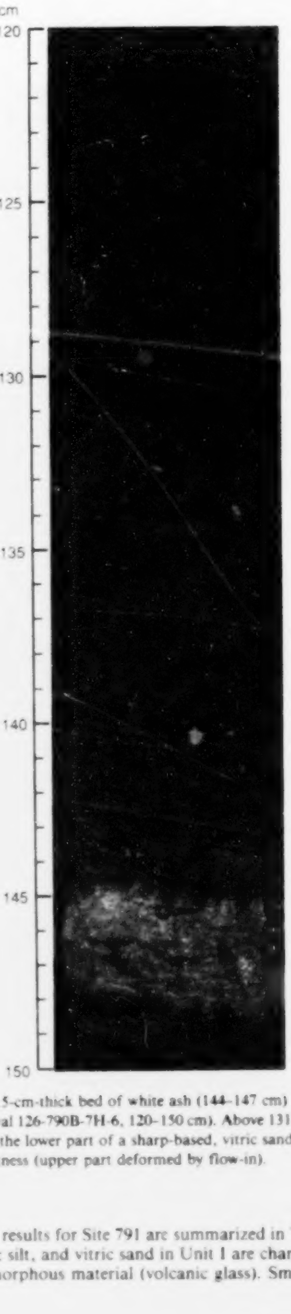

Figure 18. A 2.5-cm-thick bed of white ash (144–147 cm) within a silty clay bed (Interval 126-790B-7H-6, 120–150 cm). Above 131 cm, the photograph shows the lower part of a sharp-based, vitric sand bed of indeterminate thickness (upper part deformed by flow-in).

Site 791

The XRD results for Site 791 are summarized in Table 8. Vitric clay, vitric silt, and vitric sand in Unit I are characterized by abundant amorphous material (volcanic glass). Small amounts of smectite, chlorite, and mica group minerals are present in samples from Cores 126-791A-18H and -19H, whereas clay minerals are present in only trace amounts in Core 126-791A-20H. A trace of diaspore is present in all samples.

Samples from Core 126-791A-18H contain calcite and quartz as major mineral species; feldspar and an unknown mineral with a *d*-spacing of 0.209 nm are also present. The 0.209-nm peak corresponds to minerals containing Fe and/or Ni (e.g, FeS minerals troilite and mackinawite, both characteristic of reduced sediments; Berner, 1964). Abundances are so low, however, that additional peaks that discriminate between the various possible minerals in this group cannot be discerned. Also, poor crystallinity of the iron monosulfides may contribute to difficulties in identifying secondary peaks. Substitutions of small amounts of Mn, Zr, Ti, Co, and Si in the lattice of the unknown mineral would subtly affect its *d*-spacing. Identification of this mineral, as well as the mineral with the 0.2030-nm peak at Site 790, can only be achieved with chemical data using SEM-EDX and TEM-electron diffraction patterns.

In Unit II, calcite is abundant in sediments that contain nannofossils (e.g., Cores 126-791B-9R, -21R, and -22R). All cores contain large amounts of amorphous volcanic glass. Mica group minerals, chlorite, and quartz are major minerals, whereas feldspar and cristobalite are minor minerals in nannofossil-rich claystones.

In Section 126-791B-22R-1, thin lens-shaped masses of black (5G 2/1), vitric clayey silt contain abundant amorphous glass and pyrite and only traces of clay minerals, calcite, feldspar, and cristobalite. The pyrite and abundant glass indicate high sedimentation rates (see "Sediment Accumulation Rates" section that follows) associated with reducing conditions.

Pyrite crystals are scattered in the nannofossil-rich silty claystone in the Interval 126-791B-25R-2, 18–46 cm. Handpicked pyrite yields the characteristic peaks of pyrite (FeS_2) as well as peaks attributed to troilite (FeS), traces of calcite, quartz, and the 1.4-nm clay minerals (Fig. 39).

Foraminifer-nannofossil claystone just above the basalts of Unit III (Section 126-791B-47R-1) contains calcite and alunite ($KAl_3[SO_4]_2[OH]_6$). Alunite has characteristic peaks at 0.301, 0.190, and 0.175 nm, which indicates low-temperature hydrothermal alteration.

Sediment Accumulation Rates

Sedimentation rates for Sites 790 and 791 were determined from calcareous nannofossil and radiolarian datums and from paleomagnetic events (Table 9), which were used to construct the age-depth curve shown in Figure 40. Data from Hole 790C were used to construct the curve for Site 790. At Site 791 all the datums (except the ash-bed correlation) come from Hole 791B. A distinctive correlatable ash bed was found at Holes 790C and 791A (Fig. 13). The age of the ash bed in Hole 790C (0.091 Ma) was determined by dividing the sub-bottom depth (87 m) of the bed by the linear sedimentation rate for the interval (958 m/m.y.). This age was then used to constrain the age-depth curve even further for the top of Site 791.

Sedimentation rates at each site exhibit an exponential increase over the recovered interval. At Site 791, sedimentation rates increase from 344 m/m.y. at the base of Unit II (approximately 1 Ma) to over 2200 m/m.y. at the top Unit I. At Site 790, sedimentation rates increase from 90 m/m.y. around 1 Ma to ~1000 m/m.y. at present. Prior to the LO of *Pseudoemiliania lacunosa* (0.275 Ma), sedimentation rates at Site 791 were approximately four times those found at Site 790. Between 0.275 and 0.10 Ma, linear sedimentation rates at Site 791 were greater by a factor of 3, although this ratio declined to 2:1 over the past 0.10 Ma.

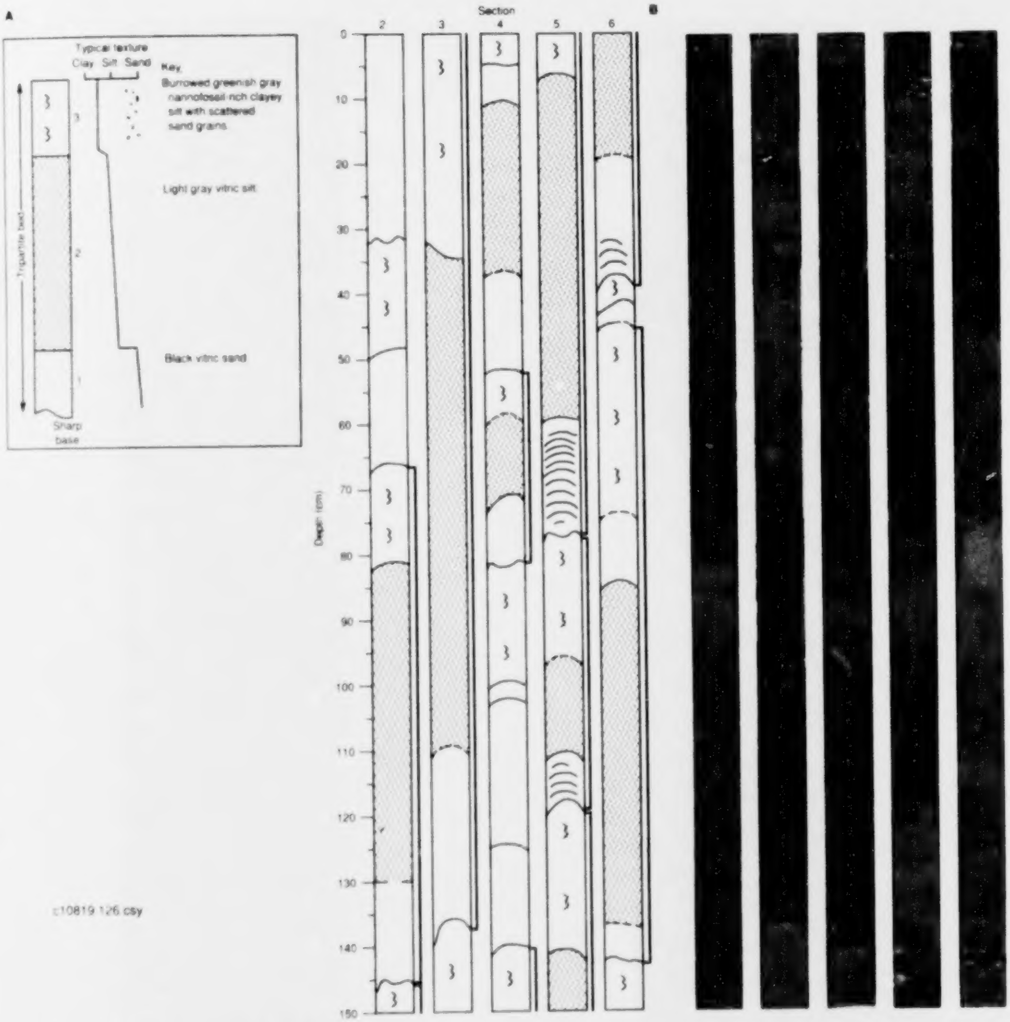
A
Typical texture
Clay Silt Sand
Key
Burrowed greenish gray nannofossil-rich clayey silt with scattered sand grains
Light gray vitric silt
Black vitric sand
Tripartite bed
3
2
1
Sharp base
c10819 126 csy
Section
2
3
4
5
6
Depth (cm)
0
10
20
30
40
50
60
70
80
90
100
110
120
130
140
150
B

Figure 19. A. Positions and internal lithology of seven tripartite beds in Core 126-790C-6H. Note that the middle division of vitric silt (fine stipple) is generally considerably thicker than the lower division of black vitric sand (coarse stipple). Burrowed nannofossil-rich silty clays contain scattered sand- and granule-size pumice grains. **B.** Corresponding core photograph of the tripartite beds.

Correlation of Sites 790 and 791

Sites 790 and 791 are located on the western margin and in the central part of the eastern half-graben of the Sumisu Rift, respectively (Figs. 2–5). The recovery at both sites of the contact between the sedimentary sequence and the underlying basaltic rocks demonstrates that the sedimentary section at Site 791 is about three times thicker than the section at Site 790. The biostratigraphic and paleomagnetic data used to construct the age-depth curves at Sites 790 and 791 (Fig. 40 and Table 9) indicate that the successions at the two sites are essentially time equivalent.

Lithostratigraphic correlation between Sites 790 and 791 is made on the basis of the following characteristics: (1) lithology and sedimentary facies (Fig. 41); (2) identification of Key Bed #7 (volcanic ash) at both sites (Fig. 13); (3) bulk magnetic susceptibility (Fig. 15); (4) carbonate contents (Fig. 42); and (5) a correlatable seismic horizon. Correlation between the two sites

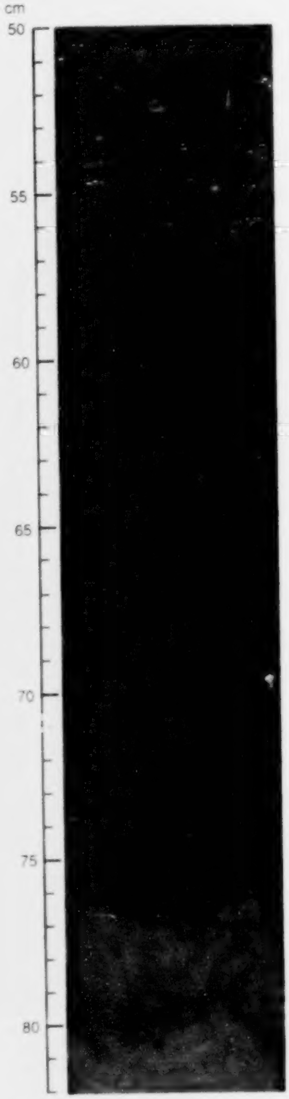

Figure 20. Parallel-laminated lower division of the tripartite bed illustrated in Figure 19 (Interval 126-790C-6H-5, 50–82 cm). The curvature of the laminae is a result of coring disturbance.

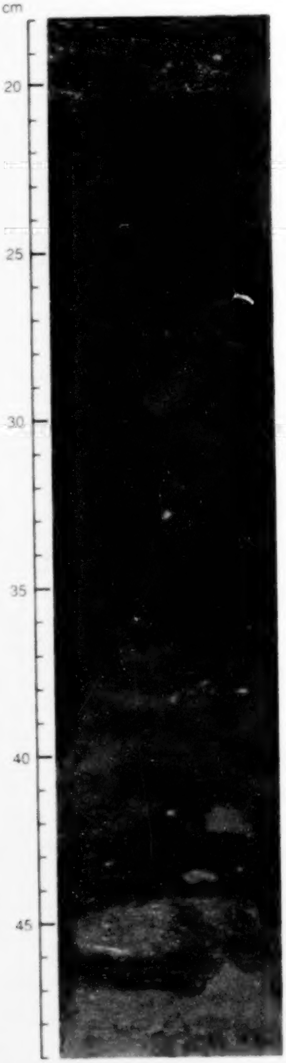

Figure 21. Cylindrical burrows in black vitric sand divisions of tripartite beds illustrated in Figure 19 (Interval 126-790C-6H-6, 18–49 cm). Burrows in the sand are filled with nannofossil-rich silty clay (29–31 cm, 42 cm), whereas burrows in the nannofossil-rich silty clay are filled with sand (45–47 cm).

is well constrained above Key Bed #7, based mainly on the marked differences in magnetic susceptibility between thick units of felsic vitric silt (volume magnetic susceptibility $< 125 \times 10^{-6}$) and thin- to thick-bedded intervals containing magnetic minerals and mafic grains of basaltic composition. These latter intervals include black vitric sand/silt beds and pumiceous gravels and pebbly sands (e.g., Site 791, 60–150 mbsf) that contain scattered scoria grains.

At Sites 790 and 791, there is a sharp lithologic contrast between Units I and II, with Unit I containing thick intervals of pumiceous gravel and pumiceous sand. The contact between the two units is reasonably well defined at Site 790, although the

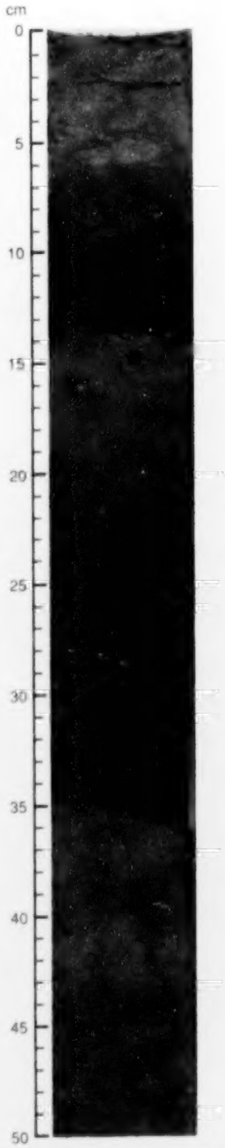

Figure 22. Scattered sand-size volcanic fragments in burrowed nannofossil-rich silty clay (14–20 cm) that forms the upper division of a tripartite bed from 14 to 35 cm (Interval 126-790C-5H-5, 0–50 cm). The basal division of vitric sand is saturated with water in this photograph as a result of coring-induced liquefaction.

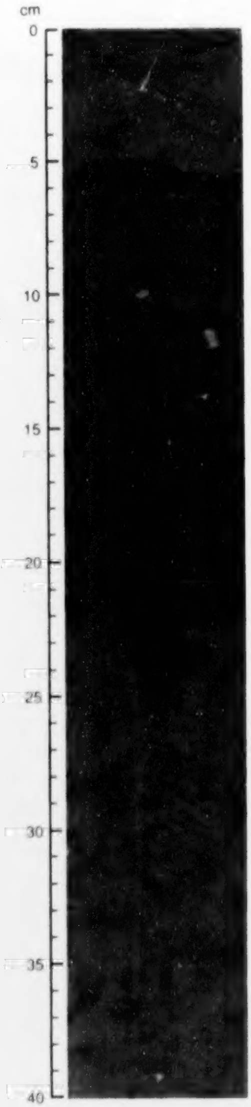

Figure 23. Scattered volcanic fragments (sand to pebble sizes) in burrowed nannofossil-rich silty clay (Interval 126-790C-5H-6, 0–40 cm). The 2-cm pebble is in the lowermost lithology, not in the overlying dark gray vitric silt.

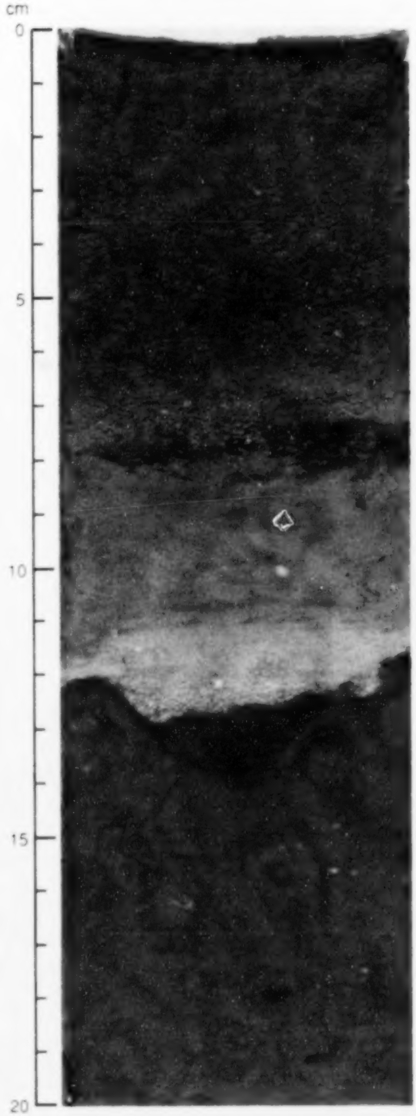

Figure 24. Photograph of a scour, filled partially by a light olive gray, 1-cm-thick vitric sand lens, and blanketed by a light gray, very fine, vitric sand (ash) bed (Interval 126-790C-11X-5, 0–20 cm).

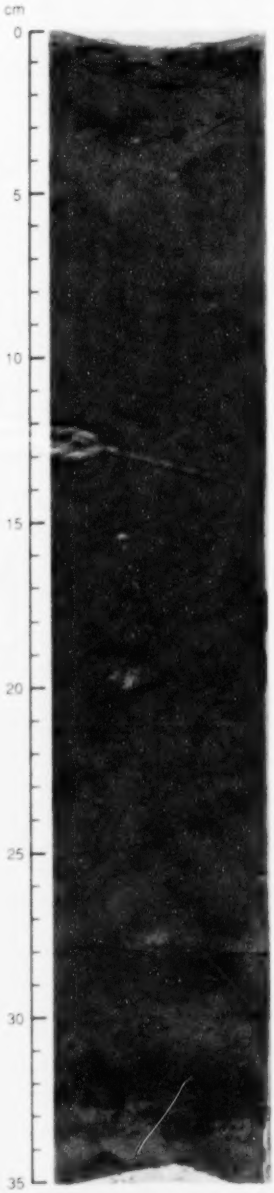

Figure 25. Dark grayish green (31–33 cm) and light gray (28 cm) ash beds in nannofossil-rich clay of Unit II (Interval 126-790C-17X-CC, 0–35 cm).

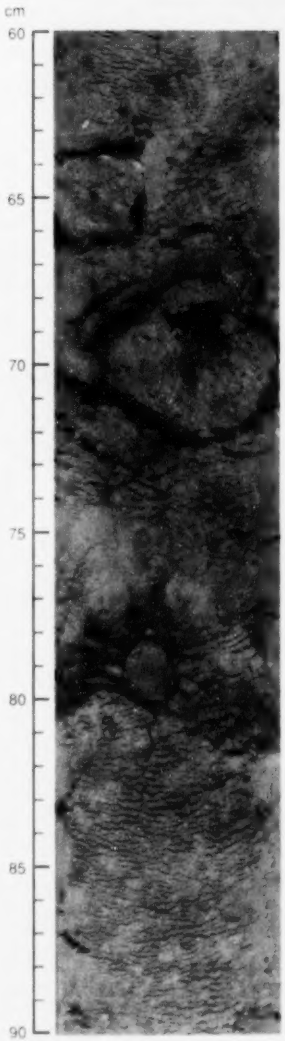

Figure 26. Dispersed, large pumice pebbles (64–66, 68–71, and 78–80 cm) near the base of Unit II (Interval 126-790C-20X-2, 60–90 cm).

contact itself was not recovered in the cores. At Site 791, however, very poor recovery does not allow a confident assessment of the position of the contact, given only the lithology. Therefore, we used three criteria to estimate the true depth of the contact between Units I and II at Site 791: (1) the age correlation as determined from the age-depth curves (Fig. 40); (2) a comparison of downhole trends in carbonate content at the two sites; and (3) seismic stratigraphic correlations (see "Seismic Stratigraphy" section, this chapter).

Poor recovery near the contact between Units I and II at Site 790 permits the contact to be placed anywhere in the interval from 155 to 165 mbsf. On the basis of the age-depth curves, the contact at Site 790 (155–165 mbsf) has the same age (about 0.2 Ma) as sediment at a depth of 415–430 mbsf at Site 791. To minimize the apparent difference in age between the base of Unit I at the two sites, the base at Site 790 is assigned its maximum possible depth of 165 mbsf, and the base at Site 791 is assigned to the bottom of Core 126-791A-46X.

At Site 790, Unit II has carbonate contents of 20%–40%, whereas Unit I has <20% carbonate (Fig. 42). The carbonate curve for Site 791 shows the same trend, with the upward transition from high to low carbonate values occurring at about 375–500 mbsf. This depth is consistent with the independent estimate of the position of the contact between Units I and II at 428.4 mbsf, but it is not sufficiently well defined in the carbonate curves to allow a more accurate definition of the contact (see "Physical Properties" section, this chapter, for further discussion of these data).

Interpretation

The sedimentary succession recovered at Sites 790 and 791 shows stratigraphic variation caused by changes in the amount, texture, and composition of volcaniclastic materials, and the amount of biogenic (pelagic) input to the backarc basin. Sites 790 and 791 have undergone differential subsidence, resulting in a thickening of the basin fill toward the eastern margin of the half-graben and the volcanic arc. The gravel material that characterizes the pumice units in Unit I at both sites also increases in grain size from west to east.

The volcanogenic components in the sediments are bimodal in composition, consisting of felsic pumice and dark grains of mafic glass, ferromagnesian minerals, and lithic fragments. This bimodal signature is present throughout the sedimentary history of the basin, although the relative amounts of the two end members has changed with time. In particular, the proportion of felsic material increased dramatically during the last 0.2 Ma (Fig. 40), whereas more mafic components are dominant in Unit II at both sites.

Some of the mafic volcanic material may have been produced within the backarc basin at volcanic centers like those that are found today along the transverse volcanic ridge to the north, or in the vicinity of Shadow Mountain to the south (Hochstaedter et al., in press). The felsic pumice, in contrast, was probably produced by explosive eruptions of submarine/subaerial volcanoes of the Izu-Bonin Arc to the east, like the Minami Sumisu and Sumisu calderas (see "Igneous Petrology" section, this chapter).

The sedimentary sequence at Sites 790 and 791 coarsens upward from the nannofossil-rich and nannofossil claystones of Unit II to the pumiceous gravels and sands of Unit I. This coarsening upward is not produced by a decrease in water depth or an encroachment of source areas but is the result, instead, of increased volcanic activity and the tectonic development of basin-margin and intrabasinal relief. Benthic foraminifers indicate that the entire sedimentary sequence was deposited in a bathyal setting ranging in depth from 1500 to >2000 m (see "Biostratigraphy" section, this chapter).

Limited paleontological data from a thin sedimentary unit within the basaltic section indicate that there is no significant time gap between the eruption of the underlying basalts and the deposition of the lowest sediments of Unit II. The sediments of Unit II, summarized in Figures 9 and 27, are predominantly fine grained and burrowed and contain 20%–40% biogenic carbonate. They were deposited in a low-energy environment where burrowers were able to rework the sediment continuously and

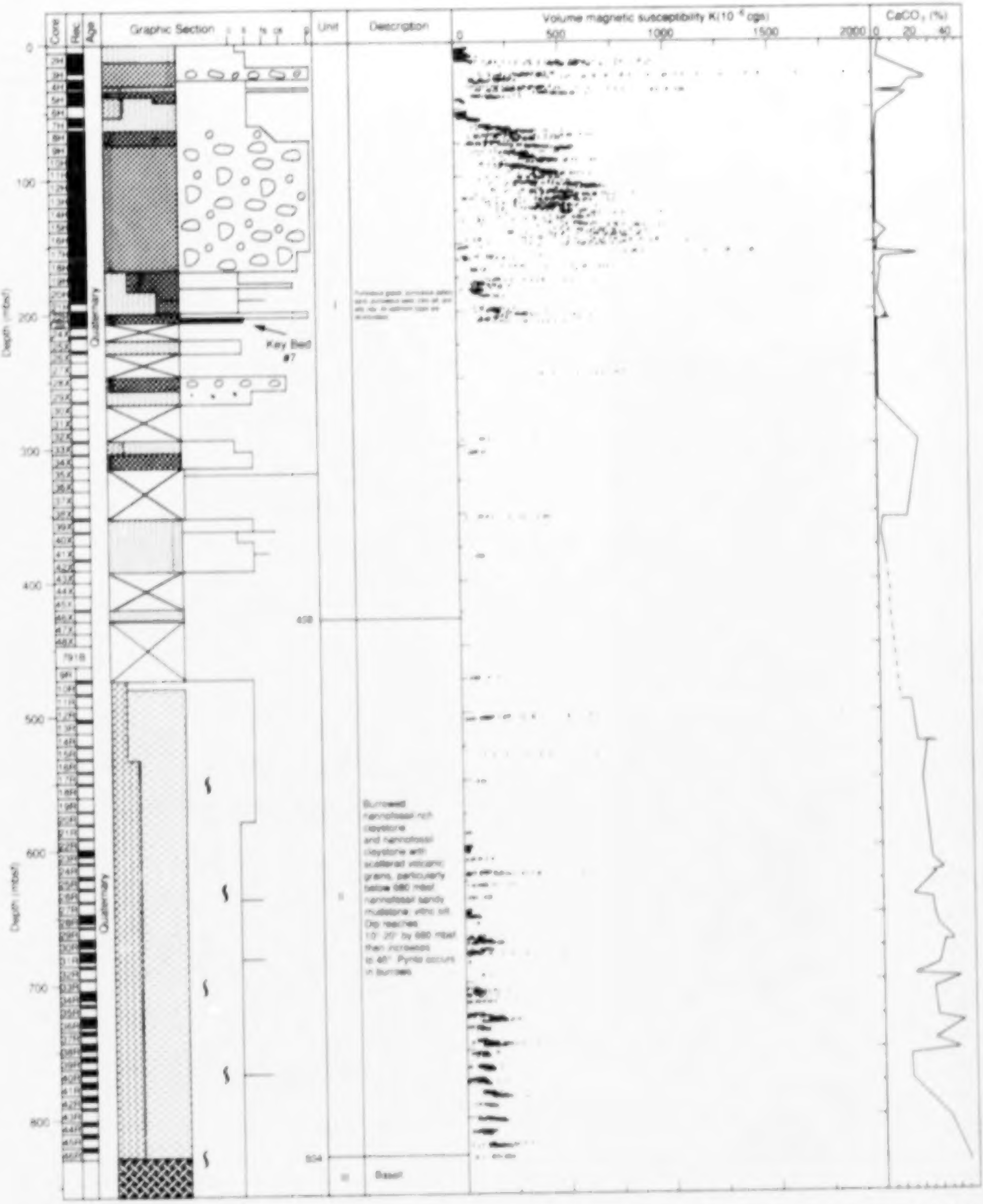

Figure 27. Composite stratigraphic succession for Site 791 showing unit boundaries and downhole variations in magnetic susceptibility and total carbonate. See Figures 6 and 9 for key to graphic lithology.

Table 6. Summary of lithology and sedimentary structures of units at Site 791.

Unit	Lithology	Sedimentary structures	Interval (mbsf)	Age	Occurrence
I	Pumiceous gravel, pumiceous pebbly sand and sand, vitric silt with minor clay, silty clay, and nannofossil-rich silty clay.	Generally structureless.	0–428.4	Quaternary	126-791A-1H to -46X 126-791B-1R to -5R-2, 120 cm
II	Nannofossil-rich claystone and nannofossil claystone with scattered volcanic grains, particularly below 680 mbsf; nannofossil sandy mudstone; vitric silt. Dip reaches 10°–20° by 600 mbsf, then increases to 45° by 760 m. Pyrite occurs in burrows.	Burrows of *Chondrites* and *Zoophycos* (1-cm burrows). Vitric silt beds may be parallel laminated.	428.4–834	Quaternary	126-791B-5R-2, 120 cm to -47R-1, 44 cm
III	Basalt, diabase, basaltic mousse, felsic ash to lapilli tuff, and rare dark vitric silt.		834–1145	Quaternary	126-791B-47R-1, 44 cm, to 126-791B-79R

destroy any primary physical structures. Nevertheless, depositional rates were high, about 90 (Site 790) to 345 m/m.y. (Site 791). At Site 791, burial of organic carbon at high sedimentation rates led to reducing conditions in the sediment and the precipitation of iron sulfides (troilite and pyrite) in burrows and as disseminations.

The high sedimentation rates demand a constant supply of fine-grained material to the basin and enhanced delivery of this material to areas with the highest subsidence rates. This material includes volcanogenic ash and clays as well as nannofossils. Because Unit II in the Sumisu Rift is not evenly draped across the basin, its deposition must have involved an interplay of processes that include settling from the overlying water column, supply from dilute density currents, and redistribution by weak bottom currents.

To provide a proper evaluation of the depositional processes for the fine-grained sediments of Unit II requires the determination of the mass budget of fine volcanogenic and biogenic carbonate materials within the basin and around the basin margins. It is known from dredging and seismic profiling that basement highs east of Sites 790 and 791 are covered only by a thin, discontinuous blanket of Holocene pelagic sediments and pumiceous clastic rocks. Also, Pleistocene to Pliocene sediments recovered from Site 788 (see "Lithostratigraphy and Accumulation Rates" section, "Site 788" chapter, this volume) are represented mainly by winnowed pumiceous gravel and conglomerates. At or near the seafloor, this gravel, unlike the pumiceous gravel at Sites 790 and 791, contains no mud matrix or nannofossils; some pumice clasts are coated by black manganese oxides, and others are oxidized.

We interpreted the features at Site 788 to be the result of winnowing by bottom currents that swept clays and microfossils away from the highs and into the adjacent basins. Fine clay and nannofossil particles are easily resuspended and may, in fact, never be deposited under strong bottom currents (Nowell and Hollister, 1985). Similar hydrodynamic conditions probably persisted throughout the Quaternary, carrying clay particles and nannofossils from bathymetric highs into the Sumisu Rift. Suspended fines from the highs around the rift may have traveled down into the basin as plumes of suspended material along density interfaces in the water column or as dilute lutite flows (McCave, 1972). These flows and plumes could then have fed a nepheloid layer above the basin floor from which clay and fine-silt particles settled to the seafloor. Because of severe bioturbation, we do not see evidence for density current deposits in Unit II; it is essential, however, that the depositional mechanism of these sediments involved control by bathymetry of the rift basin.

The foregoing discussion assumes that the recovered sediments at Site 791, where Unit II is thicker, are representative. This may not be true, because there are several examples in remnant cores of vitric silt beds that have been almost completely lost during drilling (Figs. 33 and 34). Preliminary interpretation of the total gamma-ray log for Site 791 is not inconsistent with the presence of about 20% vitric silt beds in the unrecovered intervals (see "Downhole Measurements" section, this chapter). If these vitric silt beds are much thinner at Site 790, then the degree to which the fine-grained, burrowed, carbonate-rich facies must thicken to the east may be less than assumed above. However, there must be significant eastward thickening of all sediments to account for the 400% increase in the thickness of Unit II from Sites 790 to 791.

An important characteristic of the nannofossil-rich and nannofossil claystones of Unit II at Site 791 is the presence of scattered basaltic sand grains that decrease in abundance away from the contact with the basalts. These mafic-rich intervals are also characterized by high smectite contents, implying that submarine, and possibly even subaerial, weathering and erosion of basaltic outcrops was prevalent during the earliest phase of rift sedimentation. These basaltic materials may have been transported from submarine volcanoes east and north of Sites 790 and 791. Alternatively, the basaltic grains in the lower part of Unit II may have been derived from the erosion of basalt from intrabasinal highs and from hyaloclastite-forming eruptions on the irregular floor of the embryonic rift.

Despite the relative abundance of the mafic component directly above basement, clear (felsic) glass shards are still present, indicating that bimodal volcanism prevailed in this region throughout the sedimentary history of the site. Light-colored, thin beds of felsic fine ash that occur throughout Unit II were probably derived from distant volcanic eruptions around the western Pacific rim.

The contact between syn-rift basalts and the sediments of Unit II was recovered at Site 790, but not at Site 791. Even at Site 791, however, the lowest-recovered sediments came from less than 10 m above the volcanic rocks. At neither site is there evidence for hydrothermal alteration (such as from the recrystallization of microfossils). The alunite present at Site 791 may be detrital.

The basaltic basement rocks that underlie the eastern half-graben near Sites 790 and 791 can account for some of the basaltic detritus in the lower part of Unit II, but similar detritus in younger sediments must have come from different volcanic centers. A possible source for basaltic detritus in the upper part of the basin fill is the basaltic fissure ridges north of the Minami Sumisu Basin (see "Igneous Petrology" section, this chapter).

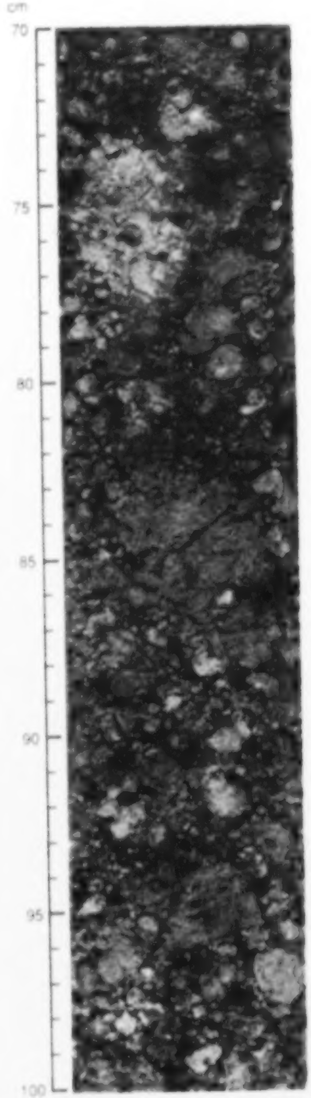

Figure 28. Structureless, poorly sorted, pumiceous gravel from the upper part of Unit I (Interval 126-791A-13H-4, 70–100 cm).

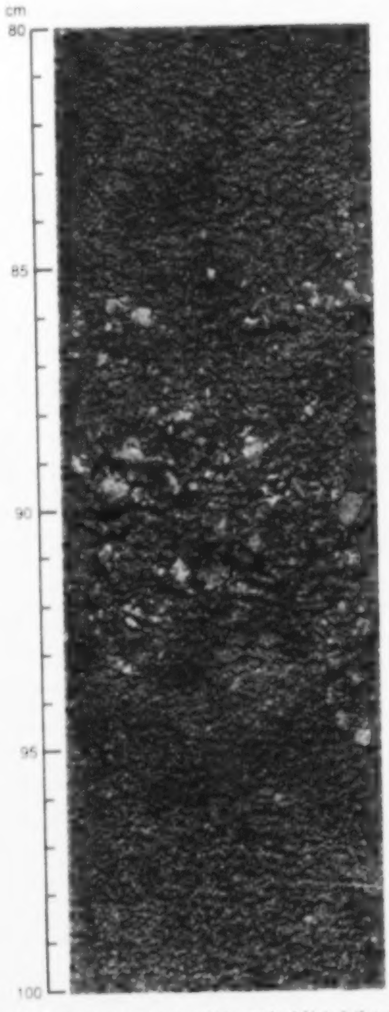

Figure 29. Pumiceous sand and pebbly sand of Unit I (Interval 126-791A-8H-5, 80–100 cm).

The upper part of Unit II contains decimeter-scale, tripartite beds of sharp-based, black sand/silt, thick vitric silt, and burrowed nannofossil-rich clayey silt that are interpreted as pyroclastic deposits because of their thick cap of glass shards (vitric silt). This facies, which typifies the transition between Units I and II, records the initial phase of the paroxysmic volcanic activity that characterizes Unit I.

Unit I is characterized by a sequence of thick, coarse, silicic volcanogenic materials. Possible mechanisms to transport the volcanic ash and coarser ejecta include (1) air fall; (2) the rafting of floating pumice until it is water saturated; (3) an entire spectrum of mass movements (both hot and cold), including submarine slumps, debris flows, and turbidity currents; and (4) hyaloclastite-induced submarine density flows. The first three mechanisms would be predominantly associated with felsic eruptions in the nearby arc volcanoes, whereas the last process may be one of the agencies responsible for the mafic ash layers. The dramatic lateral thinning of the pumiceous gravels from Sites 791 to 790, the mounded reflectors that characterize these gravels in high-resolution air-gun records of the Geological Survey

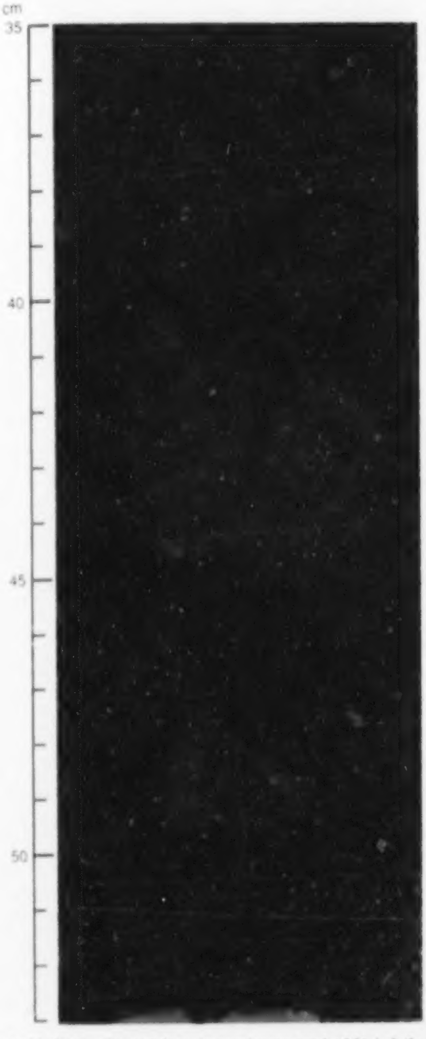

Figure 30. Vitric silt intraclasts in pumiceous sand of Unit I (Interval 126-791A-19H-7, 35–53 cm). Because this is an APC core, the intraclasts cannot be drilling biscuits.

of Japan, the presence of intraclasts of vitric silt, and the lack of coeval pumiceous gravels on the basin slopes, all favor resedimentation by debris flow for final emplacement of the gravels. The pumiceous gravel probably was initially deposited as blankets on the basin floor as well as metastably perched on adjacent basin slopes. Shortly after each was laid down, gravitational failure or seismic shaking remobilized the gravels on the basin slopes into debris flows that moved onto the basin floor, preferentially filling in the deeper parts of the half-graben.

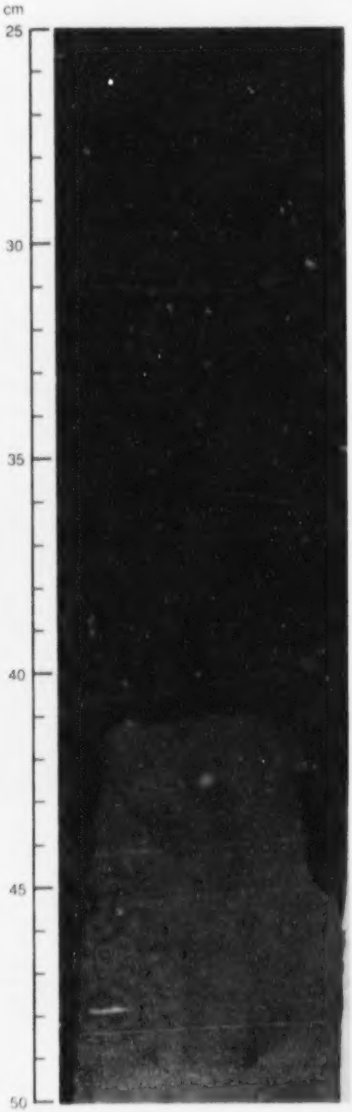

Figure 31. Sharp base of a faintly laminated black sand bed that is about 20 cm thick (Interval 126-791A-5H-3, 25–50 cm).

Explosive volcanism provided large thicknesses of pumiceous gravel five times during the deposition of Unit I. Figure 43 summarizes an attempt to date these occurrences. It assumes that the layers of strongly burrowed silty clay and clayey silt with variable amounts of biogenic carbonate were contributed to the

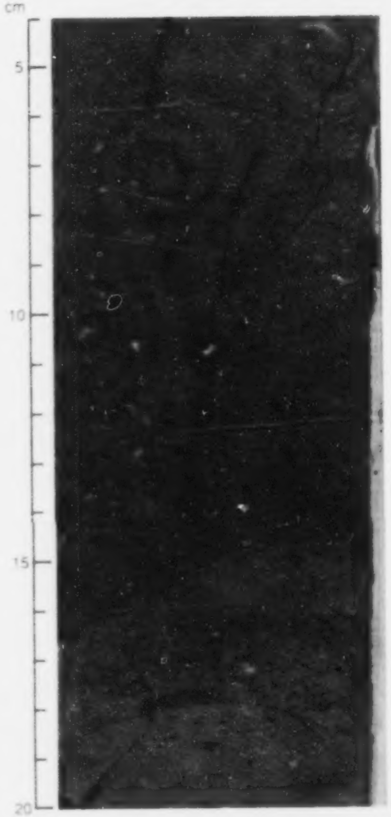

Figure 32. *Chondrites* (11–19 cm), *Zoophycos* (5–10 cm), and unidentified cylindrical burrows in Unit II (Interval 126-791B-13R-2, 4–20 cm).

basin at a fairly constant rate. Specifically, the 21.33 m of muddy sediment deposited in Unit I at Site 790 since the FO of the *Emiliania huxleyi* datum (275,000 yr ago) accumulated at a rate of about 77.5 mm/1000 yr. Applying this uniform rate, and treating each massive influx of pumice as an essentially instantaneous event, yields dates for the explosive eruptions of 194, 128, 122, 59, and 2 ka.

BIOSTRATIGRAPHY

Calcareous Nannofossils

Hole 790A

Samples 126-790A-1H-1, 0–1 cm, through 126-790A-4H-CC contain *Emiliania huxleyi* and are placed within Zone CN15. Rare reworked specimens of *Calcidiscus macintyrei* and *Pseudoemiliania lacunosa* are present in Cores 126-790A-1H, -2H, and -4H. Other species present include *Umbilicosphaera sibogae*, *Helicosphaera carteri*, *Rhabdosphaera clavigera*, and *Gephyrocapsa oceanica*.

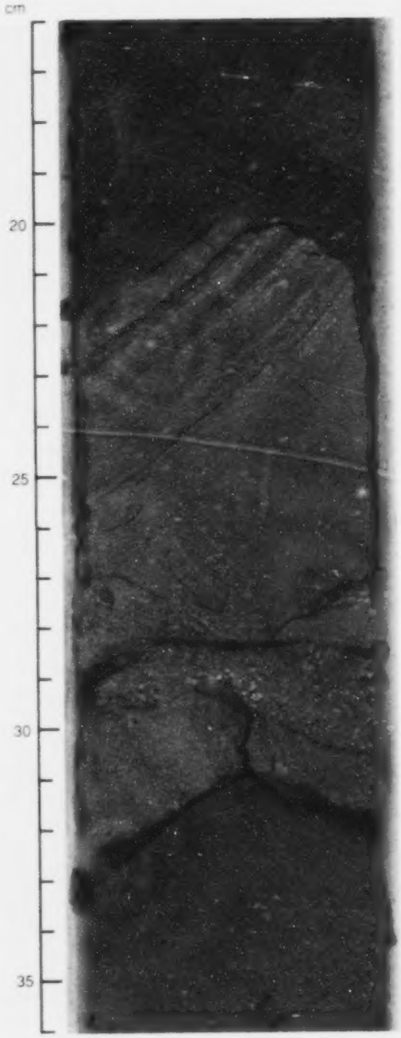

Figure 33. Dipping bed of predominantly vitric silt (20–30 cm), with 1–2-mm pumice grains at the base (Interval 126-791B-42R-1, 16–36 cm). The base is in a different drilling biscuit than the top of the bed, and its apparent dip is horizontal. The vitric silt is soft, and the top of the bed has been truncated during drilling.

Hole 790B

Samples 126-790B-1H-1, 3 cm, through 126-790B-15X-CC contain *E. huxleyi* and are placed within Zone CN15. Rare reworked specimens of *P. lacunosa* and *C. macintyrei* are present in most samples. One reworked specimen of the upper Miocene *Discoaster quinqueramus* was found in Sample 126-790B-15X-CC.

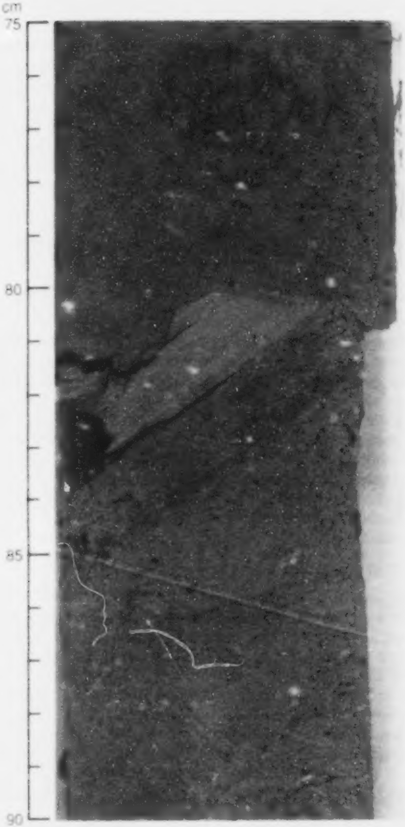

Figure 34. Remnant of a dipping bed of vitric silt (81–83 cm) that has been almost completely destroyed by drilling (Interval 126-791B-44R-2, 75–90 cm).

Hole 790C

Samples 126-790C-1H-CC through 126-790C-11X-CC contain *E. huxleyi* and are placed within Zone CN15. Samples 126-790C-12X-1, 120–121 cm, through 126-790C-15X-CC are located below the FO of *E. huxleyi* and above the LO of *P. lacunosa* and are assigned to Zone CN14b. Samples 126-790C-16X-1, 40–41 cm, through 126-790C-20X-CC contain *P. lacunosa* and *G. oceanica* and are assigned to Zone CN14a. Sample 126-790C-19X-1, 40–41 cm, contains the highest occurrence of common *Reticulofenestra* sp. A that marks the datum of Takayama and Sato (1987) and Sato et al. (1988) (about 0.83 Ma). *Reticulofenestra* sp. A commonly are present throughout Cores 126-790C-19X and -20X.

Samples 126-790C-21X-CC, 126-790C-23X-CC, 126-790C-32X-CC, and 126-790C-33X-CC consist of fragments of volcanic rocks (scoria) that had small particles of sediment stuck to them. These sediment particles contain *P. lacunosa*, *Gephyrocapsa* spp., *Calcidiscus* sp., and *Coccolithus pelagicus*, which would indicate assignment to Zone CN14a. However, these assemblages may be downhole contaminants.

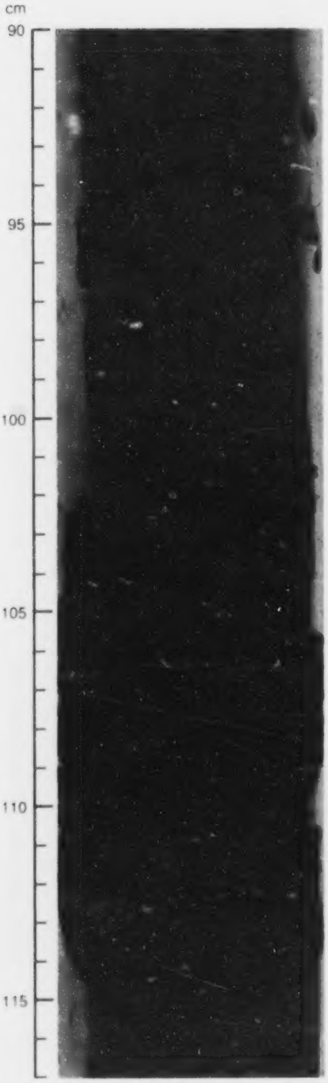

Figure 35. Squeezed and expanded bed of unlithified vitric silt (106–113 cm) sandwiched between hard, lithified sediments that form the bulk of Unit II (Interval 126-791B-25R-1, 90–117 cm).

Hole 791A

All core-catcher samples contain *E. huxleyi*, and are assigned to Zone CN15. Other species present in these samples include

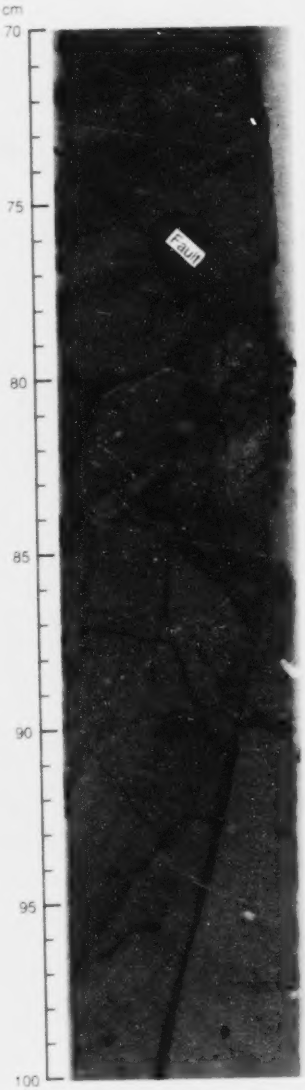

Figure 36. Fault with a dip of about 45°, left to right (73–78 cm), near the base of Unit II (Interval 126-791B-46R-1, 70–100 cm). Note the high concentration of sand-size basaltic rock fragments above 75 cm.

Umbilicosphaera sibogae, Coccolithus pelagicus, Gephyrocapsa spp., *Ceratolithus cristatus, Rhabdosphaera clavigera, Helicosphaera* spp., and *Thoracosphaera* sp.

Hole 791B

Samples 126-791B-5R-CC through 126-791B-11R-CC contain *E. huxleyi* and are assigned to Zone CN15. Samples 126-791B-13R-CC through 126-791B-28R-CC contain neither *E. huxleyi* nor *P. lacunosa*, but do contain *G. oceanica*, indicating placement in Subzone CN14b. Samples 126-791B-29R-CC through 126-791B-49R-CC contain *P. lacunosa* and *G. oceanica* and are placed within Subzone CN14a. The LO of common *Reticulofenestra* sp. A in Sample 126-791B-41R-CC indicates an age of about 0.83 Ma at this level (Takayama and Sato, 1987; Sato et al., 1988). Other species present throughout Hole 791B are *Calcidiscus leptoporus, R. clavigera, U. sibogae, Helicosphaera carteri, Scapholithus fossilis, Pontosphaera* spp., *Thoracosphaera* sp., and *Syracosphaera* spp.

Samples 126-791B-56R-1 (Pieces 1, 2, and 6), 126-791B-75R-CC, and 126-791B-78R-CC are barren of calcareous nannofossils.

Planktonic Foraminifers

Hole 790A

Samples 126-790A-1H, 1–2 cm, 2–4 cm, and 7–9 cm, contain *Globigerina calida, Globorotalia tumida* (sinistral), *Globorotalia truncatulinoides* (dextral), and *Globorotalia menardii* (sinistral), in addition to about 30 long-ranging, warm-water taxa, placing these samples in the upper Pleistocene Zone N23 (Blow, 1969). Samples 126-790A-1H-CC and 126-790A-2H-CC contain colder water faunas than the three topmost samples; dominant taxa include *Globigerina pachyderma* (dextral), *Globigerina hermanae* (dextral), *Globigerina cryophila, Globigerina quinqueloba, Globigerina bulloides, Globigerinita uvula*, and *Globorotalia scitula*.

Hole 790B

Samples 126-790B-3H-CC and 126-790B-7H, 98–102 cm, contain *Pulleniatina obliquiloculata* and other warm-water taxa, in addition to cool-water and eurythermal species such as *G. bulloides, G. quinqueloba, G. uvula, G. truncatulinoides, Globorotalia inflata, Globigerinoides gomitulus, Globoquadrina dutertrei-pachyderma* (dextral), *Globorotalia falconensis, Globorotalia crassaformis, Orbulina universa, Globigerinella aequilateralis*, and others, indicating that the sediments were deposited during interglacial periods. Samples 126-790B-10H-CC and 126-790B-11H-CC contain interglacial faunas, and the presence of *G. calida* and *Globigerina digitata* places these samples in upper Pleistocene Zone N23.

Hole 790C

Sample 126-790C-9H-CC contains only two juvenile specimens of warm-water species (*Globigerinoides ruber* s.s. white and *Globigerinoides trilobus sacculifer*) in an ash fall. Sedimentation rates were very high during the deposition of this ash bed and more than 99% of the fraction >63 μm is composed of volcanic ash. Sample 126-790C-13X-3, 104–106 cm, contains high percentages of cool-water dextral *G. pachyderma, G. quinqueloba, G. bulloides*, and *Globigerinita glutinata* as well as low percentages of warm-water *G. menardii, G. tumida*, and *P. obliquiloculata*. In Sample 126-790C-14X-CC, warm-water taxa (*Globigerinoides trilobus, Globigerinoides conglobatus, G. tumida*, and *P. obliquiloculata*) dominate the faunal assemblage. Samples 126-790C-15X-CC, 126-790C-18X-CC, and 126-790C-19X-CC contain transitional faunal assemblages (e.g., *G. gomitulus, G. dutertrei*, etc.). Sample 126-790C-20X, 36–41 cm, contains an interglacial warm-water fauna that is dominated by *Sphaeroidinella dehiscens, P. obliquiloculata, G. ruber, G. trilobus, G. conglobatus, G. sacculifer, G. tumida, G. menardii*, and others.

Hole 791A

Sample 126-791A-4H-3, 60–62 cm, contains cool- and warm-water species (e.g., *G. quinqueloba, Globigerina glutinata, Globigerina scitula, G. sacculifer, G. conglobatus, S. dehiscens*, etc.);

Table 7. X-ray diffraction data from Site 790.

Core, section, interval (cm)	Unit	Color	Sample description	Clay minerals			Minerals	Amorphous materials
				1.3 ~ 1.4 nm	1.0 nm	0.7 nm		
126-790A-								
1H-1, 1	I	10YR3/3	Green grains in clayey vitric silt	Trace	Trace		0.203 nm > Feldspar-diaspore	Abundant
3H-3, 90	I	5Y6/1	Vitric silt	Present		Present	0.209 nm > halite > diaspore, calcite, 0.203 nm > feldspar	Abundant
4H-1, 140	I	N5	Green grains in vitric medium to coarse sand	Trace		Trace	0.203 nm > diaspore	Abundant
126-790B-								
1H-1, 5	I	5YR3/4	Clayey vitric silt	Trace (chlorite)	Present	Present	Calcite > quartz > halite > 0.203 nm > feldspar, diaspore	Abundant
10H-5, 14	I	5Y5/1	Very fine sand (ash)	Trace	Trace	Trace	Halite > calcite > diaspore, 0.203 nm > feldspar, quartz	Abundant
10H-5, 20	I	5GY2/1	Silty clay	Trace	Trace	Trace	Halite, calcite > diaspore, 0.203 nm > feldspar, quartz	Abundant
10H-5, 24	I	5YR2/1	Silt (ash)	Present (smectite)	Trace	Trace	Halite > 0.203 nm, calcite > feldspar, quartz	Abundant
126-790C-								
2H-2, 150	I	5Y6/1	Vitric silt (ash)	1.65 nm (smectite) 1.41 nm (chlorite)	Trace	Present	Halite > 0.203 nm > calcite, quartz, feldspar, > diaspore	Abundant
5H-6, 22	I	5Y5/3	Reddish pumice in vitric clayey silt	Present		Present	Quartz, feldspar, cristobalite > calcite > 0.203 nm	Abundant
5H-6, 6	I	5Y5/3	Vitric silt (ash)	Trace			Pyrolusite, pyrite, 0.203 nm > calcite, feldspar > quartz	Abundant
11X-5, 10	II	5Y5/2	Very fine sand	Trace			Halite > calcite > 0.203 nm, feldspar > quartz, diaspore	Abundant
20X-2, 80	II	5G4/1	Pumice gravel-bearing nannofossil mud	Trace			Calcite > feldspar, quartz, halite, 0.203 nm	Abundant
20X-3, 46	II	5GY7/2	Pumice gravel-bearing nannofossil mud	Trace			Calcite > feldspar, quartz, halite, 0.203 nm	Abundant
20X-3, 90	II	5GY6/1	Pumice gravel-bearing nannofossil mud	Trace			Calcite >> feldspar, quartz, halite, 0.203 nm	Abundant

the presence of *G. calida* and *G. digitata* places this sample in Zone N23. Sample 126-791A-5H-3, 52-54 cm, contains specimens of *Globorotalia tumida flexuosa*. Cool-water elements dominate the assemblage in Sample 126-791A-16H-2, 95-97 cm. The presence of *G. calida* places this sample in Zone N23. Sample 126-791A-31X-CC contains cool- and warm-water faunas, including *G. truncatulinoides* (dextral), *G. pachyderma, G. falconensis, G. tumida, G. menardii, G. ruber, P. obliquiloculata,* and *G. trilobus*.

Hole 791B

Sample 126-791B-24R-CC contains cool-water foraminifers such as dextral *G. pachyderma*, dextral *G. hermanae, G. bulloides*, and *G. falconensis*. Cool foraminiferal elements including dextral *G. pachyderma*, dextral *G. hermanae*, dextral *G. cryophila, G. bulloides*, and *G. glutinata* are present in Samples 126-791B-30R-CC and 126-791B-32R-CC. Sample 126-791B-37R-CC (just above the Brunhes/Matuyama boundary; see "Paleomagnetics" section, this chapter) contains a transitional fauna and is dominated by *G. glutinata, G. aequilateralis, G. dutertrei*, dextral *G. pachyderma, G. scitula*, and *G. gomitulus*. Sample 126-791B-38R-CC, immediately below the Brunhes/Matuyama boundary, contains a predominantly warm-water foraminiferal fauna (e.g., *G. trilobus, G. ruber, S. dehiscens, P. obliquiloculata*, and *G. tumida*). Sample 126-791B-39R-CC is characterized by high percentages of cool-water taxa (dextral *G. pachyderma* complex, *G. bulloides, G. glutinata, G. crassaformis*, and *G. uvula*) deposited during a period henceforth termed the Matuyama *G. pachyderma* acme Zone 1. The estimated age of this event is about 780 ka, based on the paleomagnetic stratigraphy of Hole 791B. Sample 126-791B-45R-CC, deposited during the Jaramillo Event about 920 ka, contains warm-water species (e.g. *G. menardii, G. tumida, G. sacculifer, G. trilobus, S. dehiscens, P. obliquiloculata*, and *G. ruber*). Sample 126-791B-46R-CC contains mostly cool-water taxa characterized by the dominance of the *G. pachyderma* dextral complex and accompanied by *G. quinqueloba, G. glutinata*, and *G. falconensis*. The fauna was deposited during a period henceforth termed the Matuyama *G. pachyderma* acme Zone 2. The estimated age of this event is about 1 Ma, based on the paleomagnetic stratigraphy of Hole 791B and extrapolated sedimentation rates below the base of the Jaramillo event in Hole 791B. Sample 126-791B-47R-1, 41-43 cm, at the contact with the underlying basalt, contains both cool- and warm-water species such as dextral *G. pachyderma, G. falconensis, G. gomitulus, G. ruber, G. crassaformis, G. tumida, G. menardii, S. dehiscens, P. obliquiloculata*, and *G. ruber*. This sample is placed in lower Pleistocene Zone N22.

Benthic Foraminifers

Quaternary strata at Sites 790 and 791 may be subdivided biostratigraphically into six biozones based on benthic foraminifers (Fig. 44). Water mass depths are estimated mainly on the

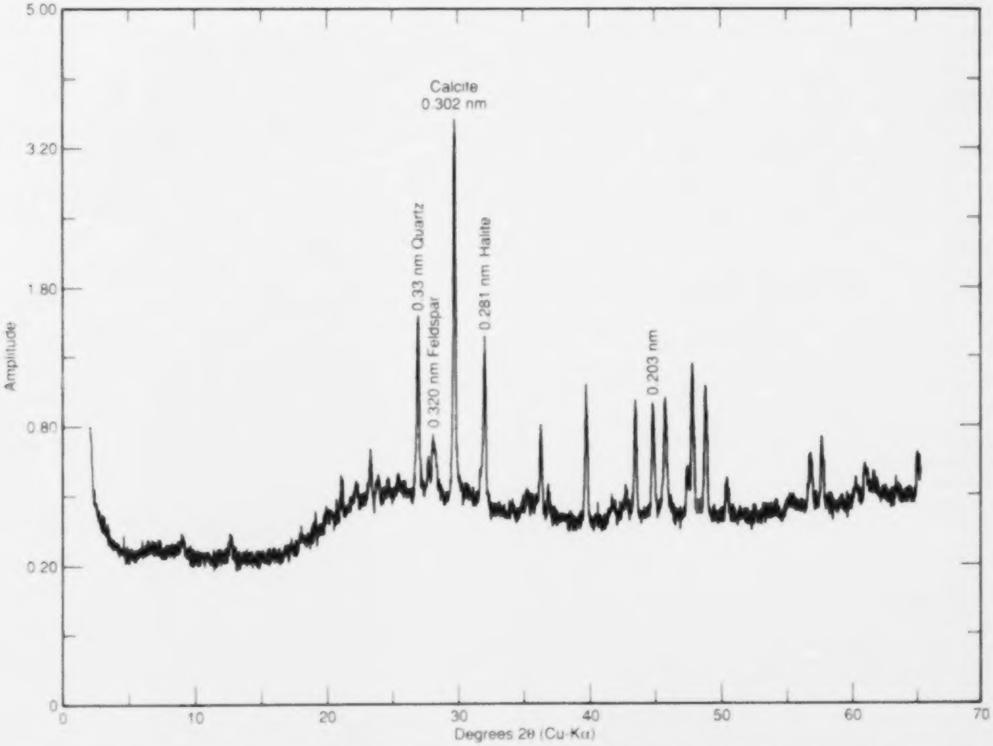

Figure 37. X-ray diffraction chart of brown vitric clayey silt (Sample 126-790B-1H-1, 5 cm) showing high calcite abundance, with quartz, feldspar, halite (from pore water), diaspore, and small amounts of clay minerals.

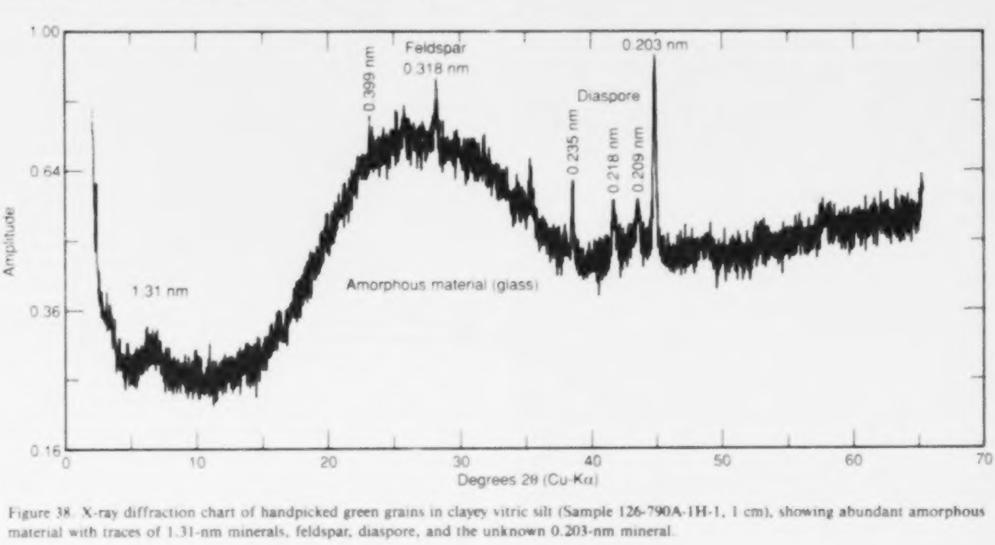

Figure 38. X-ray diffraction chart of handpicked green grains in clayey vitric silt (Sample 126-790A-1H-1, 1 cm), showing abundant amorphous material with traces of 1.31-nm minerals, feldspar, diaspore, and the unknown 0.203-nm mineral.

Table 8. X-ray diffraction data from Site 791.

Core, section, interval (cm)	Unit	Color	Sample description	Clay minerals			Minerals	Amorphous material
				1.4 nm	1.0-nm Mica	0.7-nm Chlorite		
126-791A-								
18-1, 40	I	N4	Silty clay	1.66 nm (smectite) 1.40 nm (chlorite) Present	— Common	— Present	Calcite > quartz > 0.209-nm > feldspar > diaspore	Abundant
18-2, 100	I	5Y4/1	Clayey silt	Present	—	Present	Calcite > quartz > feldspar, 0.209 nm > diaspore	Abundant
19-7, 43	I	5Y5/2	Gravel-rich sand	Present	Trace	Present	Halite > quartz, feldspar, calcite > diaspore	Abundant
20H-2, 92	I	5Y6/1	Graded fine sand	Trace	—	—	Halite > quartz, feldspar, calcite > diaspore	Abundant
126-791B-								
9R-CC, 20	II	5Y2/1	Nannofossil-rich silty claystone	1.43 nm (chlorite)	Common	Common	Calcite > quartz > feldspar	Abundant
21R-CC, 8	II	5Y4/2	Claystone	1.40 nm (chlorite)	Common	Common	Calcite > quartz > feldspar	Abundant
22R-1, 10	II	5Y4/1	Claystone	Trace	Common	Common	Calcite > quartz > feldspar cristobalite	Abundant
22R-1, 30	II	5G4/1	Claystone	1.77 nm (smectite) 1.44 nm (chlorite)	Common	Common	Calcite > quartz > feldspar	Abundant
22R-1, 51	II	5G4/1	Claystone	1.71 nm (smectite) 1.43 nm (chlorite)	Common	Common	Quartz > calcite > feldspar, cristobalite	Abundant
22R-1, 53	II	5G2/1	Vitric clayey silt	Trace	Trace	Present	Pyrite > quartz > calcite, cristobalite > feldspar	Abundant
22R-1, 58	II	5G4/1	Vitric clayey silt	Trace	—	Present	Quartz > calcite > feldspar, cristobalite	Abundant
22R-1, 60	II	5G2/1	Vitric clayey silt	Trace	—	Present	Quartz > calcite, feldspar	Abundant
22R-1, 70	II	5G4/1	Vitric clayey silt	1.65 nm (smectite) 1.40 nm (chlorite)	Common	Common	Calcite > quartz >> feldspar, cristobalite	Abundant
25R-2, 18	II	5Y3/2	Pyrite grains	Trace	—	—	Pyrite >> troilite > calcite, quartz	Abundant
25R-2, 46	II	5Y3/2	Pyrite grains	—	—	—	Pyrite >>> calcite > quartz	Abundant
42R-3, 70	II	5Y6/1	Nannofossil silty claystone	Trace	Trace	—	Calcite >>> quartz, feldspar	Abundant
47R-1, 43	II	5GY6/1	Nannofossil-foraminifer claystone	Trace	—	Trace	Calcite >>> alunite, quartz, feldspar > cristobalite	Abundant

basis of benthic foraminiferal data from Shizuoka and Shikoku, southwest Japan (Akimoto, 1989; Yasuda, 1989).

These six biozones are as follows:

1. *Pleurostomella* spp.-*Stilostomella* spp. assemblage zone

Definition: This assemblage zone is marked by the joint occurrence of *Pleurostomella* spp. and *Stilostomella* spp.

Characteristic species: *Uvigerina hispidocostata, Oridorsalis umbonatus, Cibicidoides wellerstorfi, Stilostomella* spp., *Melonis barleeanus, Melonis pompilioides, Pullenia bulloides,* and *Pleurostomella* spp.

Samples: 126-790C-20X-CC through 126-790C-18X-CC, and 126-791B-47R-1, 41-43 cm, through 126-791B-37R-CC

Depositional water depth: 2000-3500 mbsl

Dissolved oxygen: high

Environment: deep open ocean, or basin with open-ocean access

2. *Bulimina aculeata* assemblage zone

Definition: This zone corresponds to an interval from the LO of *Pleurostomella* spp. to the base of the acme zone of *Uvigerina proboscidea.*

Characteristic species: *U. hispidocostata, Bulimina aculeata, O. umbonatus,* and *M. barleeanus*

Samples: 126-790C-17X-CC and 126-791B-36R-CC

Original water-mass depth (this depth may be the depth of a sill surrounding the basin): 1600-2300 mbsl

Dissolved oxygen: medium to high

Event: slight shallowing or closing of the basin started

3. *Uvigerina proboscidea* acme zone

Definition: This zone corresponds to the acme zone of *Uvigerina proboscidea.*

Characteristic species: *Hoeglundina elegans, U. proboscidea, Bulimina striata, B. aculeata, M. barleeanus, M. pompilioides, P. bulloides, Sphaeroidina bulloides,* and *O. umbonatus*

Samples: 126-790C-15X-CC through 126-790C-13X-3, 104-106 cm, and 126-791B-35R-CC through 126-791B-25R-CC

Original water-mass depth (this depth may be the depth of a sill surrounding the basin): 1000-1800 mbsl

Dissolved oxygen: low-medium to partly low. Low oxygen in Samples 126-790C-14X-2, 61-63 cm, 126-790C-13X-CC, 126-791B-29R-CC, and 126-791B-28R-CC because of the occurrence of *Globobulimina pacifica* and low ratios of aerobic forms

Event: closing of the basin probably occurred and dissolved oxygen decreased in this basin. A shallower fauna entered into this basin and faunal change occurred

4. *Bulimina striata-Bulimina aculeata* assemblage zone

Definition: This zone represents a body of strata characterized by the joint occurrence of *B. striata* and *B. aculeata*

Characteristic species: *U. hispidocostata, H. elegans, B. aculeata, B. striata, O. umbonatus, M. barleeanus,* and *M. pompilioides*

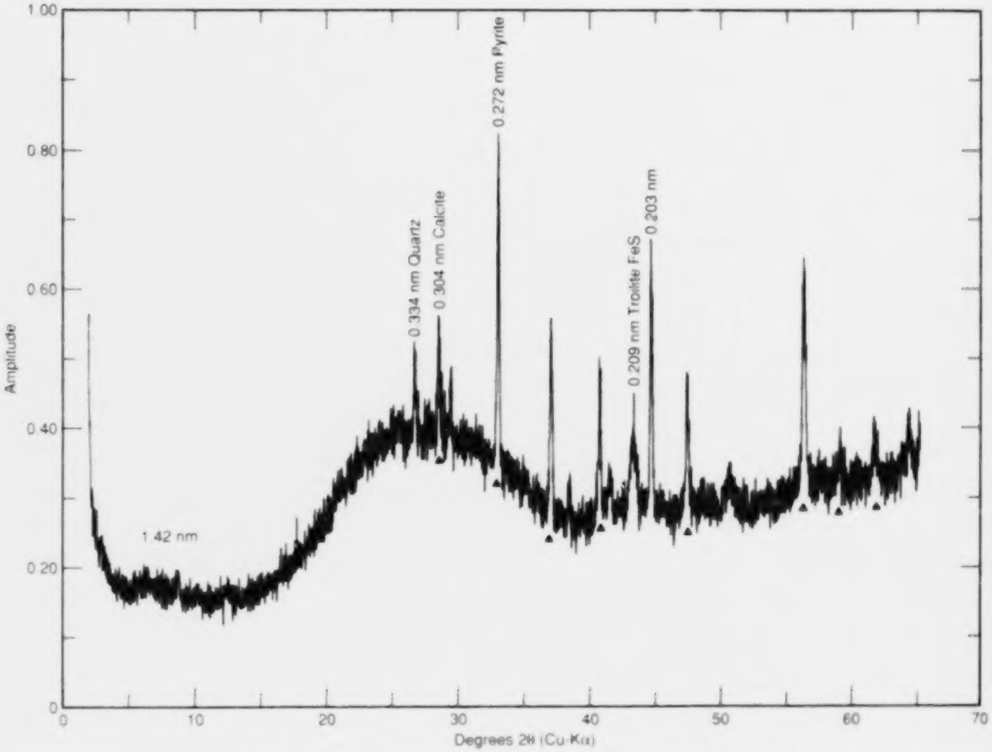

Figure 39. X-ray diffraction analysis of handpicked pyrite grains from Sample 126-791B-25R-2, 18 cm (nannofossil-rich silty claystone) showing pyrite (filled triangle) and troilite with traces of quartz, calcite, and 1.42-nm clay minerals.

Samples: 126-790C-12X-CC through 126-790B-10H-CC, and 126-791B-24R-CC through 126-791A-38X-CC

Original water-mass depth: 1000–1800 mbsl

Dissolved oxygen: medium

Event: closed environment still continued but dissolved oxygen increased

5. *Bulimina aculeata-Uvigerina hispidocostata* assemblage zone

Definition: The present zone represents a body of strata characterized by the joint occurrence of *B. aculeata* and *U. hispidocostata.*

Characteristic species: *U. hispidocostata, M. barleeanus, O. umbonatus, B. aculeata, P. bulloides, Pyrgo murrhina,* and *Tosaia hanzawai*

Samples: 126-790B-8H-6, 29–31 cm, through 126-790B-7H-CC, and 126-791A-33X-1, 6–8 cm, through 126-791A-16H-6, 58–60 cm

Original water-mass depth: 1600–2300 mbsl

Dissolved oxygen: medium

Event: sill depth probably deepened. Thick volcanic ash was deposited above the present zone and faunal change occurred.

6. *Chilostomella oolina-Uvigerina hispidocostata* assemblage zone

Definition: The zonal base is defined by a rapid increase in the abundance of *Chilostomella oolina.*

Characteristic species: *Chilostomella oolina, U. hispidocostata, M. barleeanus,* and *Globobulimina pacifica*

Samples: 126-790B-3H-1, 0–2 cm, through 126-790A-1H-1, 7–9 cm, 126-791A-5H-3, 52–54 cm, and 126-791A-4H-3, 60–62 cm

Original water-mass depth: 1600–2300 mbsl

Dissolved oxygen: low-medium to partly low. Low oxygen in Samples 126-790A-2H-3, 98–100 cm, 126-790A-2H-1, 129–131 cm, 126-791A-5H-3, 52–54 cm, and 126-791A-4H-3, 60–62 cm, because of occurrences of *C. oolina* and *G. pacifica* and the low ratios of aerobic forms.

Event: anaerobic fauna increased

A deep, open-ocean benthic foraminiferal fauna (>2000 mbsl) was distributed in this area between 1.0 and 0.7 Ma. The appearance of the low-to-medium-oxygen shallower fauna (1000–2000 mbsl) between 0.7 to 0.5 Ma implies that a closing of the basin may have started at this time, while dissolved oxygen decreased. After a part of the deep, open ocean fauna became extinct, a shallower fauna entered into the basin and the low-to-medium-oxygen fauna survived. The slight change of the fauna at 0.4 Ma indicates that dissolved oxygen increased slightly. The minor change to a deeper fauna at 0.2 to 0.1 may imply a slight

Table 9. Biostratigraphic, paleomagnetic, and other correlatable horizons used to construct the age-depth curve in Figure 40.

Chronostratigraphic event	Core, section, interval (cm)	Depth (mbsf)	Age (Ma)
Nannofossils:			
	Hole 790C		
FO *E. huxleyi*	11X-CC to 12X-CC	181.6-193.9	0.275
LO *A. angelinum*	14X-CC to 15X-CC	207.3-222.8	0.410
LO *P. lacunosa*	15X-CC to 19X-1, 40	213.6-224.6	0.460
Reticulofenestra sp. A	18X-CC to 19X-1, 40	248.5-253.3	0.830
	Hole 791B		
FO *E. huxleyi*	13R-CC to 15R-CC	504.9-531.0	0.275
LO *A. angelinum*	23R-CC to 24R-CC	604.1-618.1	0.410
LO *P. lacunosa*	28R-CC to 29R-CC	652.5-666.0	0.460
Reticulofenestra sp. A	41R-3 to 41R-CC	774.7-781.3	0.830
Paleomagnetics:			
	Hole 790C		
Blake	Between 2H-6 and 2H-7	103.5	0.108
Brunhes/Matuyama	Between 17X-CC and 18X-1	241.7-245.3	0.730
Top of Jaramillo	Between 19X-3 and 19X-4	256.2-257.4	0.910
Bottom of Jaramillo	Between 19X-6 and 20X-1	260.0-265.9	0.980
	Hole 791B		
Brunhes/Matuyama	38R-4, 40	747.8-752.2	0.730
Top of Jaramillo	Between 43R-CC and 44R-1	792.6-807.5	0.910
Bottom of Jaramillo	46R-1, 80	820.8-827.6	0.980
Other:			
Ash bed 126-790C-1H-2, 132-135 126-790B-10H-5, 22-24	22H-6, 55-60	205.0	0.091

Note: See text for discussion of ash-bed correlation.

deepening of the sill water depth. After a thick pile of volcanic ash was deposited at about 0.06 Ma, a low-oxygen fauna occupied the basin.

Radiolarians

Well-preserved radiolarians are present in many samples and indicate a late Pliocene to Recent age for the sediments cored at Sites 790/791. The abundance of radiolarians is variable, and they are often diluted by volcanic ash. Preservation is generally good. A diverse radiolarian assemblage that includes *Didymocyrtis tetrathalamus*, *Lamprocyclas maritalis maritalis*, *Theocorythium trachelium dianae*, *Stylochlamydium asteriscus*, *Botryostrobus aurita/australis* group, *Porodiscus* sp., *Amphirhopalum ypsilon*, *Eucyrtidium* spp., *Tetrapyle octacantha*, and *Spongaster tetras* are found in samples throughout all of the holes drilled at Sites 790/791. The common occurrence of *T. trachelium dianae* indicates a late Pliocene age, at the oldest.

Specimens of *Druppatractus acquilonius* are present in Sample 126-790C-12X-CC and in samples below this level. This species is also observed at Site 791 in and below Sample 126-791B-17R-CC. The occurrence of *D. acquilonius* indicates an age greater than 0.3 Ma (Foreman, 1981) for samples deeper than 184.2 mbsf at Site 790 and more than 540.9 mbsf at Site 791. Specimens of *Axoprunum angelinum* are present in Sample 126-790C-15X-CC. This species is first observed downhole at Site 791 in Sample 126-791B-24R-CC. The LO of *A. angelinum* was dated at 0.41 Ma (Foreman, 1981), and its presence indicates an age greater than this for samples below 213.2 mbsf at Site 790 and below 608.4 mbsf at Site 791. More precise dating using radiolarians was not possible as published upper Quaternary zonations are based on the occurrence of rare equatorial forms (Sanfilippo et al., 1985), which were not observed at Sites 790 and 791.

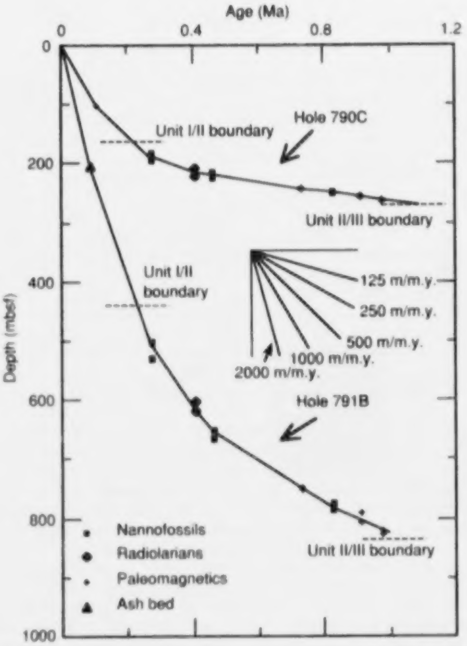

Figure 40. Age-depth curves for Sites 790 and 791. See text and Table 9 for details of the chronostratigraphic horizons. Two points at any given event (age) indicate the possible depth range for the event.

Summary

A summary of biostratigraphic and benthic foraminifer results for Sites 790 and 791 is presented in Figures 44, 45, and 46. Hole 790C ends at about 1.1 Ma, whereas the bottom sediments of Hole 791B are estimated to have an age of 1 Ma on the basis of the extrapolated sedimentation rates (Fig. 40).

Calcareous nannofossils are generally common to abundant in the samples studied. Three nannofossil datums are identified: the FO of *Emiliania huxleyi* (0.275 Ma), the LO of *Pseudoemiliania lacunosa* (0.46 Ma), and the LO of the acme of *Reticulofenestra* sp. A (0.83 Ma).

The abundance of planktonic foraminifers in the Pleistocene and Holocene sediments ranges from rare to very abundant, and their preservation ranges from poor to excellent. Based on preliminary data, three planktonic foraminiferal datum levels are recognized. In an upward sequence these are (1) the Matuyama *Globigerina pachyderma* acme II zone, about 1 Ma, marking the first major late Neogene global cold event; (2) the Matuyama *G. pachyderma* acme I zone, deposited about 780 ka; and (3) the *Globigerina calida-Globigerina digitata* Zone (Blow, 1969; N23) ranging between the Holocene and the base of the Brunhes Epoch (Blow, 1969; Berggren et al., 1985). Confirmation of these correlations must await additional faunal data as well as stable isotope analyses and absolute age determination.

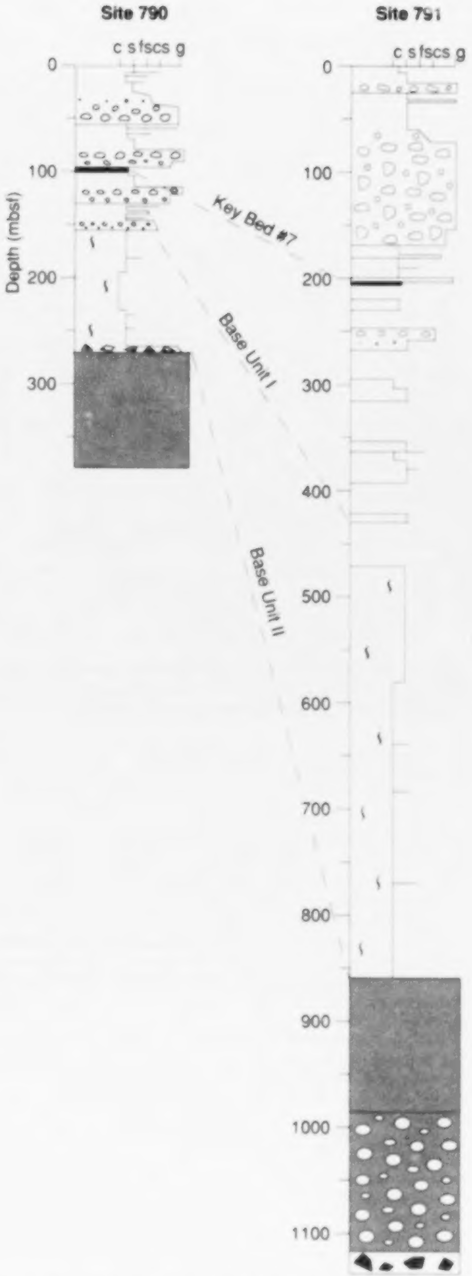
Site 790
Site 791
c s fscs g
c s fscs g
Depth (mbsf)
0
100
200
300
400
500
600
700
800
900
1000
1100
Key Bed #7
Base Unit I
Base Unit II

Figure 41. Detailed correlation between stratigraphic summary sections for Sites 790 (Fig. 9) and 791 (Fig. 27).

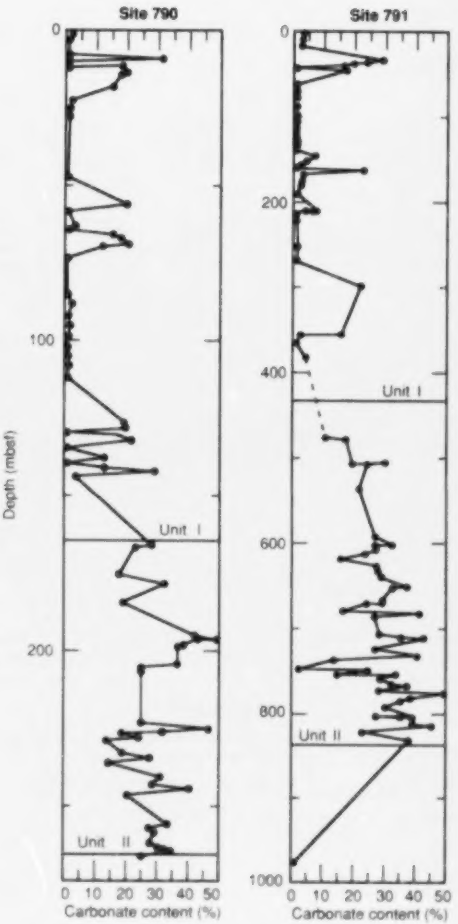

Figure 42. Downhole plots of carbonate content for Sites 790 and 791. Note that the depth scale is different in each plot.

Radiolarians are generally common to abundant in the examined samples except when diluted by volcanic ash. Preservation is typically moderate to good. Two radiolarian datums are recognized: the last appearance of ***Druppatractus acquilonius*** at 300 ka and the last appearance of ***Axoprunum angelinum*** at 410 ka (Foreman, 1981). Diatoms and silicoflagellates are also common in many samples.

The benthic foraminifer fauna indicates that a deep ocean (>2000 m) or a basin with open-ocean access existed between 1.0 and 0.7 Ma. The appearance of a low-to-medium-oxygen shallower fauna (1000–2000 mbsl) between 0.7 and 0.5 Ma implies that the basin may have started closing at this time and is continuing to close at present.

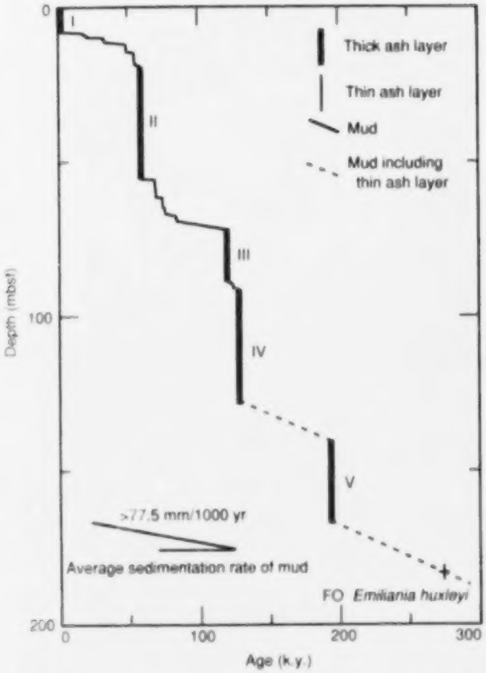

Figure 43. Plot of age vs. depth for Unit I sediments recovered at Holes 790B and 790C, illustrating the periodicity of explosive pumice eruptions as recorded by five thick pumiceous beds (I–V). Eruption and deposition of pumice is treated as an instantaneous event.

PALEOMAGNETICS

Introduction

Paleomagnetic measurements were carried out on all archive halves of cores from Sites 790 and 791 that were not composed only of unconsolidated gravel or coarse sand or were not highly disturbed by drilling, or where the segments of recovered sample were long enough not to have rotated vertically during drilling. For cores that contained igneous rocks, only longer segments were measured after transfer to separate fiberglass boats, to eliminate the signals from short segments that may have rotated vertically. Alternating field (AF) demagnetization levels were adjusted according to the expected magnetic hardness of the various sampled sediment types, as coarser-grained intervals generally were less resistant to AF demagnetization.

In addition to the pass-through core measurements on the cryogenic magnetometer, a large number of discrete samples were measured with the fully automatic spinner (FAS) magnetometer (see "Explanatory Notes" chapter, this volume). The discrete samples were taken at specific zones of interest as well as at regular intervals to serve as a backup and check of the continuous core measurements. The use of AF values >15 mT was often essential in determining the true polarity of the primary remanence, and the stable "end point" direction of magnetization that characterizes the field direction at the time of primary remanence acquisition.

Magnetostratigraphy

Holes 790A and 790B

Magnetostratigraphic determinations on cores from these two holes were severely hampered by large ambient fields (up to thousands of gammas) in the region of the AF demagnetization coils within the cryogenic magnetometer shield assembly. We realized that an apparent polarity reversal in Core 126-790A-4H, and the large number of apparent polarity reversals in the first 11 cores of Hole 790B were inconsistent with the late Pleistocene nannofossil assemblages present throughout this interval (see "Biostratigraphy" section, this chapter).

We then noted that the reversed zones of magnetization generally corresponded to the coarse-grained (i.e., magnetically "soft") sediment types, and that the negative inclinations had appeared only after AF demagnetizations of the cores. Subsequently, a number of discrete samples from the apparent reversed intervals were measured and demagnetized on the spinner magnetometers and the Schonstedt sample demagnetizer, and they retained their positive inclinations throughout the demagnetization process.

Measurement of the ambient field in the region of the cryogenic system's AF coils with the Applied Physics Systems APS 520 fluxgate magnetometer revealed that the strong ambient field was directed upcore. Therefore, reversed inclinations in the coarse sediment types most likely resulted from the acquisition of an anhysteretic remanent magnetization (ARM). From this point on, the mu-metal shielding that surrounds the cryogenic measuring system was periodically demagnetized with degaussing coils already built into the shielding. With repetitive degaussing the field level in the AF coil region was reduced to < 100 gammas; however, frequent monitoring of the field indicated that fields of > 1000 gammas could build up in a period of several hours.

The cause of the instabilities in the mu-metal shielding is currently unknown. It may have been the result of metal degradation from heat generated by the AF coils, or from exposure to cold helium during instrument filling. The consistent magnetostratigraphic results obtained for Hole 787B indicated that a substantial ambient field was not present during measurement and demagnetization at that location. This may have been a fortuitous circumstance, as the shielding was not disassembled or in any other way disturbed between drilling at Site 787 and at the following sites.

Hole 790C

The first 17 cores from this hole were magnetized mostly in a normal sense, even after AF demagnetization. A short reversed-polarity interval revealed after AF demagnetization in Section 126-790C-2H-7 (~104 mbsf) may represent the Blake Event (~0.108 Ma), which has been recorded in sediments from Japan and the Pacific, including the Marianas region (C. Helsley, pers. comm., 1989). Another short reversed-polarity interval was recorded in Section 126-790C-13X-4 (198.5 mbsf), possibly corresponding to the Biwa II excursion, which has been recorded in deposits from Lake Biwa, Japan, dating to 0.295 Ma (Tarling, 1983).

The first major reversed-polarity zone occurred at the very bottom of Sections 126-790C-17X-7 and 126-790C-17X-CC (241.8 mbsf) and continued into Core 126-790C-19X (Fig. 47). Although the continuous core measurements did not reveal a consistent polarity for Sections 126-790C-19X-1 and 126-790C-19X-3 even after AF demagnetization to 15 mT, measurements on discrete samples indicated that a reversed polarity characterizes these sections (Table 10).

The measurement of Section 126-790C-19X-4 (~256–258 mbsf) was hampered by the extreme variation of remanence in-

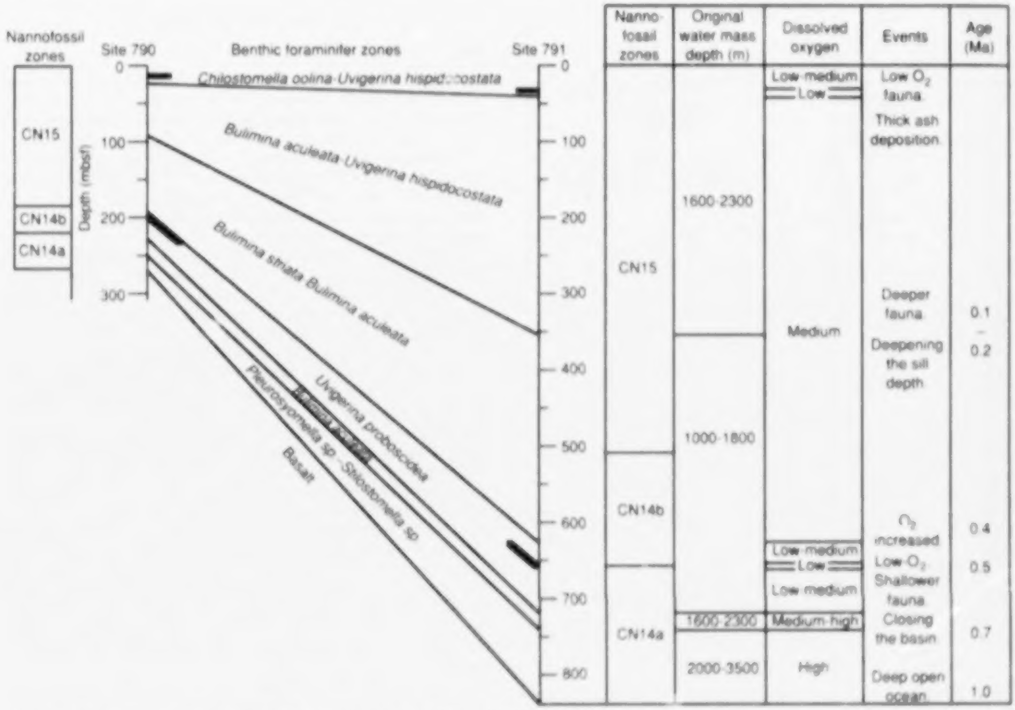
Nannofossil zones
CN15
CN14b
CN14a
Site 790
Depth (mbsf)
0
100
200
300
Benthic foraminifer zones
Site 791
Chilostomella oolina-Uvigerina hispidocostata
Bulimina aculeata-Uvigerina hispidocostata
Bulimina striata-Bulimina aculeata
Uvigerina proboscidea
Pleurosyomella sp.-Stilostomella sp.
Basalt
400
500
600
700
800
Nanno-fossil zones
Original water mass depth (m)
Dissolved oxygen
Events
Age (Ma)
Low-medium
Low
Low O_2 fauna
Thick ash deposition
1600-2300
Medium
Deeper fauna
0.1
0.2
Deepening the sill depth
1000-1800
O_2 increased
0.4
Low-medium
Low
Low O_2
0.5
Low-medium
Shallower fauna
1600-2300
Medium-high
Closing the basin
0.7
2000-3500
High
Deep open ocean
1.0

Figure 44. Quaternary benthic foraminiferal biozones at Sites 790 and 791.

tensity in the section, with the signal from the bottom of the section (pumiceous gravel) exceeding the range of the cryogenic magnetometer. However, measurements on a discrete clay sample (126-790C-19X-4, 52 cm) from above the gravel bed (Table 10) confirmed that this section marked a return to normal polarity. Positive inclinations also characterized Sections 126-790C-19X-5 and 126-790C-19X-6, whereas reversed inclinations returned at the bottom of Core 126-790C-19X (261.4 mbsf; Fig. 47).

Although the bottom sections of Core 126-790C-20X (beginning at about 263.5 mbsf) exhibited predominantly positive inclinations when measured on the cryogenic pass-through system (Fig. 47), higher AF demagnetizations of discrete samples taken from this same pumiceous interval revealed an underlying reversed primary magnetization (Table 10).

Because the paleontology indicated only Quaternary faunal assemblages in the above cores (see "Biostratigraphy" section, this chapter), we identified the polarity transition recorded at the bottom of Core 126-790C-17X as the Brunhes/Matuyama boundary (0.73 Ma), and the subsequent short normal-polarity zone at 256.2-261.4 mbsf as the Jaramillo interval (0.91-0.98 Ma). The base of the sedimentary section in this hole corresponds to an age of ~1.1 Ma, based on extrapolation of the age-depth curve (see Fig. 40 in "Lithostratigraphy and Accumulation Rates" section, this chapter).

Holes 791A and 791B

Magnetostratigraphic results from Hole 791A were inconsistent, apparently because of the unconsolidated and soupy nature of the sediments. Although the more consolidated sections generally indicated normal polarities, as expected for upper Quaternary sediments, many of the less-coherent sections displayed a highly inclined reversed magnetization before and after AF demagnetization. The almost vertical nature of their remanence implies that it was acquired during drilling, probably in the field associated with the drill string.

Fortunately, the magnetic signal associated with the cores from Hole 791B, which began recovery just below the bottom depth of Hole 791A, seemed more representative of the predrilling remanence signal in the sediments. This probably resulted from the more lithified nature of these deeper strata. Cores 126-791B-10R through -38R were consistently magnetized in a normal sense. A sharp transition to reversed polarity, revealed only after AF demagnetization, took place near the bottom of Section 126-791B-38R-4 (747.8 mbsf; Fig. 48B), and the reversed polarities continued from this point until the top of Core 126-791B-44R, where another normal polarity zone began at 800.7 mbsf. The normal polarities persisted over this and the following core and ended at the base of Section 126-791B-46R-1 (820.9 mbsf; Fig. 48C).

The next sedimentary and igneous cores that were measured were reversely magnetized for the most part or trended toward reversed polarity with AF demagnetization (e.g., Core 126-791B-47R at ~830 mbsf). Cores 126-791B-72R, -73R, -75R, and -76R (from ~1070 to ~1110 mbsf) consisted of basaltic "mousse" (see "Igneous Petrology" section, this chapter) and displayed indeterminate polarities. Subsequent measurements on discrete samples taken from the "mousse" indicate wide variations in in-

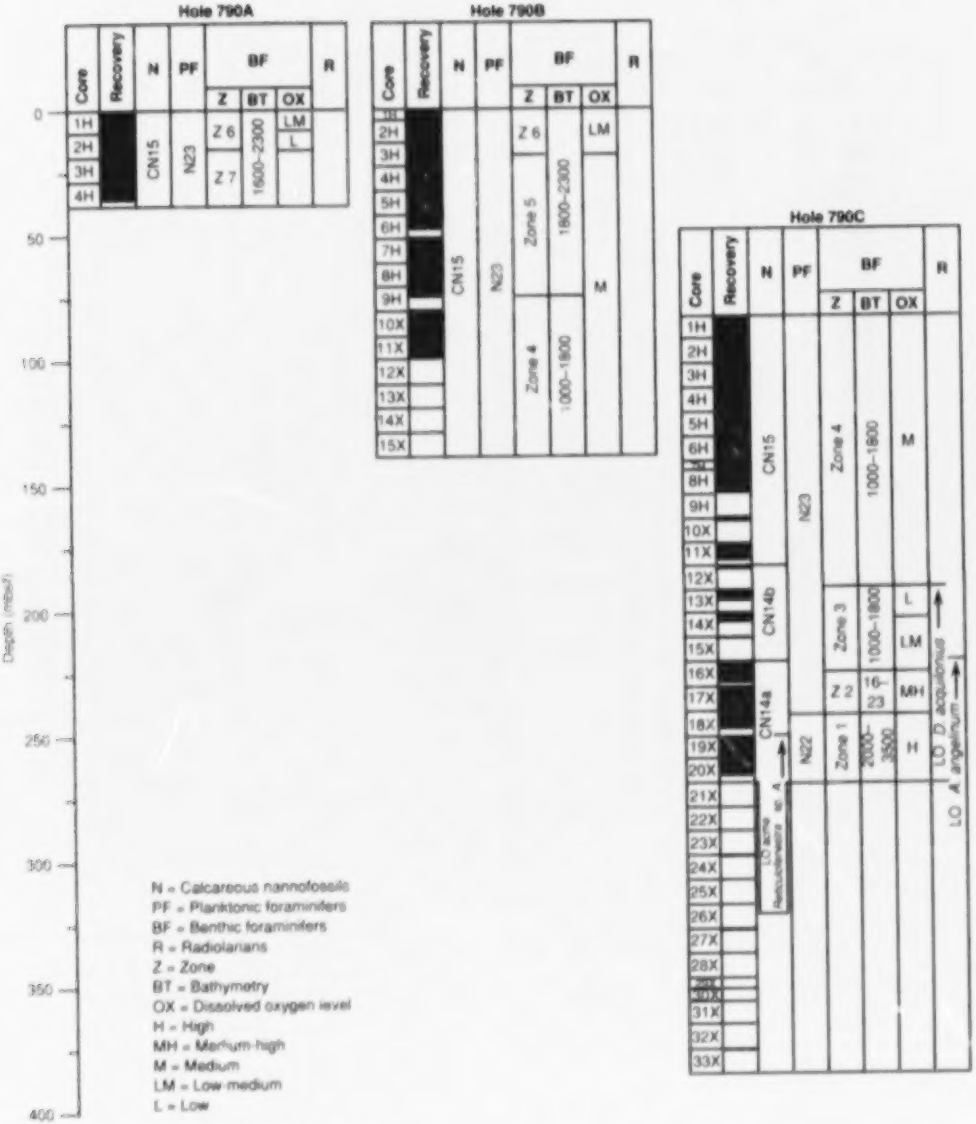

Figure 45. Biostratigraphic summary chart for Site 790.

clination, implying that separate cooling units of the mousse moved with respect to each other after welding.

The next two cores also had indeterminate polarities and contained tuff, basalt, and diabase intruded by gypsum veins (see "Igneous Petrology" section, this chapter). However, the final core obtained from the hole (Core 126-791B-79X; 1137.6-1145 mbsf), which consisted of lapilli tuff and diabase, could again be characterized as reversely magnetized (Fig. 48D).

As with Hole 790C, the restriction of the fossil assemblages in the sedimentary portions of this hole to the Quaternary allows us to label with confidence the transition in Core 126-791B-38R as the Brunhes/Matuyama boundary, with the following short normal-polarity interval corresponding to the Jaramillo zone. By extrapolation of the age-depth curve (see Fig. 40 in "Lithostratigraphy and Accumulation Rates" section, this chapter), the initiation of sediment accumulation began at 1

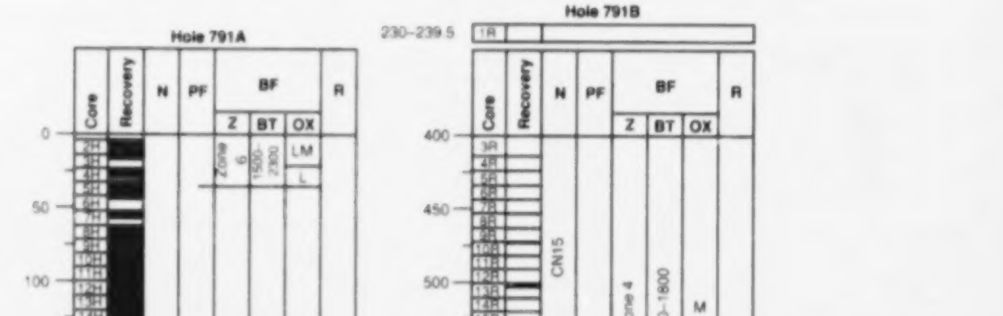

Figure 46. Biostratigraphic summary chart for Site 791.

Ma, implying that the sediment recovered from the bottom of Hole 790C was ~0.1 Ma older than that recovered above the igneous units in Hole 791B.

The higher sedimentation rate at Site 791 compared with Site 790 is illustrated by the length of the normal polarity zone identified as the Jaramillo and the overlying reversed (Matuyama) zone, which in Hole 791B occupies more than seven cores, compared with only two cores in Hole 790C (Fig. 49). This indicates a sedimentation rate increase by almost a factor of 4 (344 vs. 90 m/Ma) between the bottom portions of Hole 791B and 790C (see Fig. 40 in "Lithostratigraphy and Accumulation Rates" section, this chapter).

Brunhes/Matuyama Reversal Record

In Holes 790C and 791B, sedimentary sections containing the Brunhes/Matuyama polarity transition were recovered from nannofossil-rich clayey silt and claystone, respectively. Despite the high sedimentation rates for Hole 791B, the observed change from negative to positive inclination is very sharp, occurring over an interval of only a few centimeters. A pronounced decrease in remanence intensity that accompanies the reversal spans only about 20 cm (Fig. 50).

If the average sedimentation rate is applied to these intervals, then the change from positive to negative inclination occurred in perhaps as little as 100 yr, with the pronounced demise of dipole intensity limited to ~600 yr. However, the ~35% recovery rate in Hole 791B for the interval between the Brunhes/Matuyama reversal and the bottom of the Jaramillo zone could mean that the actual sedimentation rate across the reversal was up to one third lower than the average rate, or ~100 m/Ma, if the unrecovered portions of these cores consisted entirely of rapidly deposited pumice and volcanic ash. However, in Hole 790C, ~75% recovery was achieved in the same stratigraphic interval with only minor recovery of rapidly deposited pumiceous gravel (see "Lithostratigraphy and Accumulation Rates" section, this chapter).

Continuous pass-through measurements on the archive core halves that record the reversal were supplemented by extensive sampling across the reversal as well as in the sections of core immediately beneath the boundary. Although the ~100% recov-

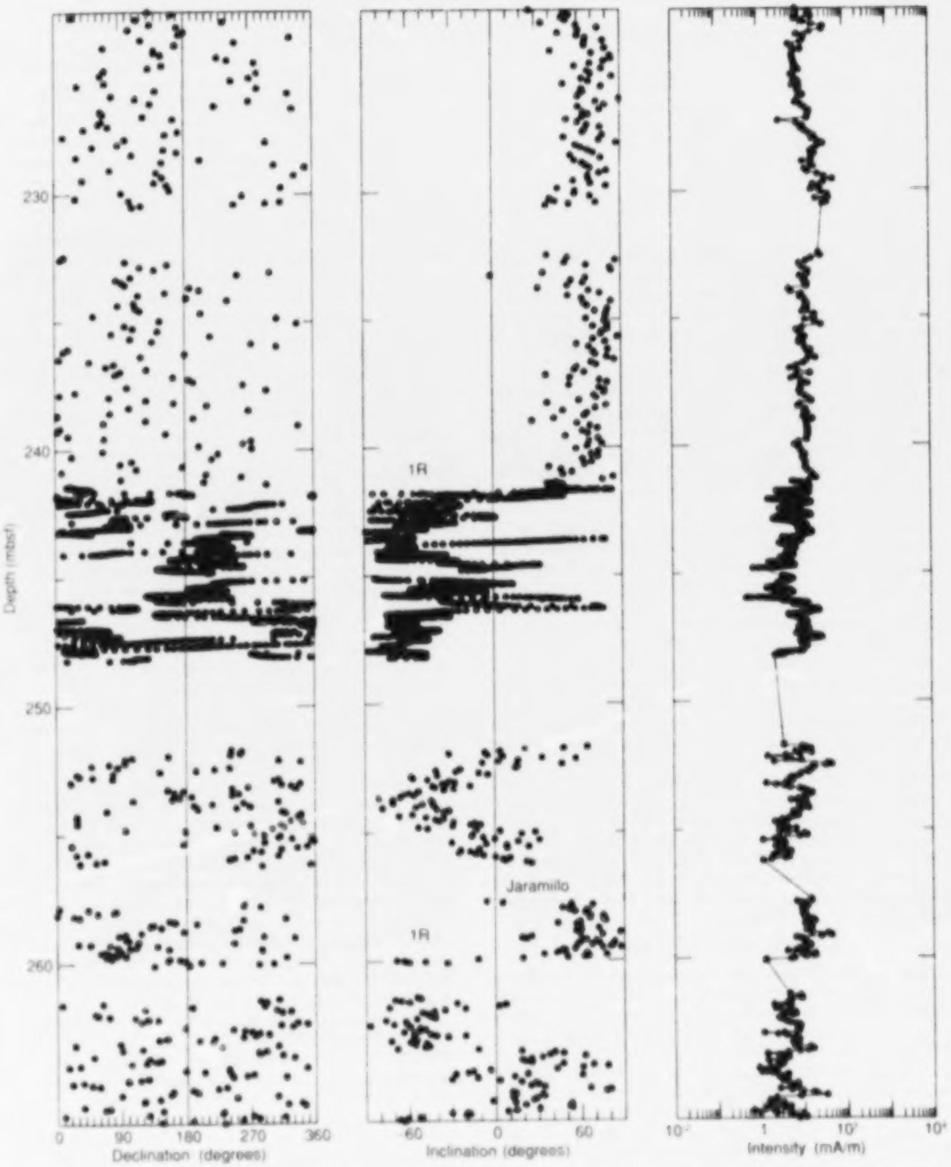

Figure 47. Paleomagnetic results vs. depth (mbsf) for Cores 126-790C-16X through -20X, after maximum AF demagnetization. Identifications of polarity chrons are indicated above inclination polarity changes.

Table 10. Remanence properties, before and after 35-mT AF demagnetization, of selected discrete samples from Hole 790C.

Core, section, interval (cm)	NRM $(\times 10^{-3}$ mA/m)	Inclination (degrees)	AF(35 mT) $(\times 10^{-3}$ mA/m)	Inclination (degrees)
126-790C-				
19X-1, 12	4.8	−31	4.4	−32
19X-1, 64	4.5	−16	3.4	−34
19X-1, 104	18.3	−67	16.4	−73
19X-3, 25	14.1	−37	4.2	−48
19X-3, 83	3.3	+19	0.4	−57
19X-4, 52	5.9	+83	1.5	+60
20X-3, 75	3.7	+44	1.7	−36
20X-3, 133	5.0	+24	0.8	−6

ery in Core 126-790C-17X indicates a near-continuous record of the magnetic field before and after the reversal, 55% recovery in Core 126-791B-38R leaves open the possibility of a significant hiatus in the magnetic record before and/or after the transition. However, in this case, recovery in the immediate vicinity of the reversal seems to be complete, with no severe drilling disturbance, except for horizontal rotation of drilling biscuits (Fig. 51).

In general, AF demagnetization of discrete samples taken near the reversal boundary revealed a high degree of directional stability after the removal of a soft normal component of magnetization at the lowest demagnetization step (Fig. 52). This indicates that an accurate representation of the behavior of the magnetic field can be obtained from these sediments around the time of the polarity transition.

Although the cores from these holes were not oriented by azimuth, the high dips (20°–45°) of the vitric silt beds near the reversal plane in Hole 791B, combined with the easterly dip directions apparent from the seismic profiles at shallower depths (see Fig. 7 in "Seismic Stratigraphy" section, this chapter), allowed for estimates of true declinations for discrete samples taken near to highly dipping laminations (Fig. 51B). Figure 53 shows the migration of the field vector derived in this manner for the polarity transition recorded in Core 126-791B-38R-4. These data indicate a far-sided pole path for the reversal.

For both holes, the core catcher is present just below the sections that include the polarity transition. The core catchers for each hole record a brief reverse-normal-reverse polarity event preceding the final reverse to normal transition (Fig. 50). Given the average sedimentation rate, the complete sequence of reversals appears to have taken place over a >1,000-yr period. Okada and Niitsuma (1989), in an examination of rapidly deposited sediments on the Boso Peninsula, Japan, which also record the Brunhes/Matuyama boundary, have found evidence for rapid, multiple reversals of inclination associated with a longer-term polarity transition.

IGNEOUS PETROLOGY

Highly vesicular, sparsely phyric volcanic rocks were drilled at the base of two sites in the Sumisu Rift. At Site 790, these rocks lay 256.9–387 mbsf below sediment estimated to be 1.1 Ma in age (see "Lithostratigraphy and Accumulation Rates" section, this chapter). Only 1.03 m of scoriaceous basalt was recovered, all in core catchers (Fig. 54). At Site 791, the volcanic rocks are similar in composition to those at Site 790 but were found much deeper (834–1145 mbsf). Altogether, 27.83 m (8.9% recovery) of basalt lava, basalt "mousse" (see below), diabase, and felsic crystal-lithic tuffs were recovered below sediments also estimated to be 1.1 Ma in age (Fig. 55).

Alteration increases downsection from fresh to zeolite or lower greenschist facies. Below about 1110 mbsf all rocks have been sheared, hydrothermally altered, and metamorphed. Consequently, it is unclear if the metamorphism is a result of greater burial or hydrothermal alteration. The transition in metamorphic grade is gradual and begins within basalt units interpreted as syn-rift in origin rather than as arc basement, based on their petrography and chemical composition. The ubiquitous and extensive vesiculation of these basalts, despite an inferred deep-water site of eruption (see "Biostratigraphy" section, this chapter), is attributed to high, pre-eruption water contents. The origin of the volcaniclastic felsic rocks at the base of the hole is rendered ambiguous by their alteration, but they are more similar in texture and some immobile trace elements to rocks from the arc than from the rift. Whether they were deposited on the arc before rifting or within the basin during rifting is not constrained by petrology.

At Site 791, the volcanic rocks lie immediately beneath lithologic Unit II (Section 126-791B-62R-1, 18 cm). No contact was recovered, but the overlying sediments are nonvolcanogenic (see "Lithostratigraphy and Accumulation Rates" section, this chapter). The underlying rocks were divided on the basis of macroscopic texture and mineralogy into 29 units: 7 basalt flows, 2 basalt breccias, 3 units of enigmatic frothy basalt that we called "basaltic mousse" in a fit of gastronomic deprivation, 7 diabase intrusives, 7 units of intermediate to felsic ash to lapilli tuffs, 1 unit of interlava sediment, and 2 units of fault gouge (Fig. 55). Chemical analyses show that the basalt flows are of two types (see "Igneous Geochemistry" section, this chapter), the more differentiated (Unit 2) above the more mafic (Units 3, 5, and 7). The three basaltic mousse units (Units 11, 12, and 14) constitute the thickest deposit encountered, spanning 135 m (from 980 mbsf in Core 126-791B-62R to 1115 mbsf in Section 126-791B-76R-2), and may represent one lava type and perhaps one eruption event. The diabase intrusions are variable in mineralogy and composition, ranging from olivine-rich and as mafic as any basalt at this site (Units 15 and 23) to Fe-Ti-oxide-rich and more differentiated than any basalt at this site (Units 4 and 29).

The ash and lapilli tuffs at the base of Hole 791B (Units 16, 18–22, and 28) are interpreted as a sequence of hot pyroclastic flows. With the exception of Units 16 and 22, all of the tuffs exhibit strong flattening of pumice shards and development of eutaxitic texture. Even the coarsest lapilli tuffs, with lava clasts up to 30 mm, contain pronounced fiamme. The pyroclastic sequence as a whole contains clasts of andesite, which, combined with the evidence of coarse-grained lapilli tuffs and hot eruptions, indicates that it was produced in close proximity to the volcanic source. In light of the apparent propinquity of hot ash flows to calderas, it could be concluded that the felsic sequence is a manifestation of arc volcanism. Hence, the sequence may represent pre-rift arc-basement to the Sumisu Rift system. However, the effects of alteration on texture, mineralogy, and bulk composition, render this conclusion speculative. Unit 20, a crystal-lithic ash tuff, also shows the development of a weak metamorphic fabric. This runs at an angle of approximately 45° to the eutaxitic fabric and can only be recognized as an alignment of chlorite fibers in cross-polarized light.

The age range of the basement rocks is unknown, but all cores are reversely magnetized except for the gypsum-filled veins, which are normally magnetized (see "Paleomagnetism" section, this chapter). The similarity of all basaltic rocks to each other, and to basalts from the rift wall dated from 1.1 to 1.4 Ma (Hochstaedter et al., in press), implies emplacement in a short time interval prior to 1.1 Ma at both sites. The underlying tuffs could be older-arc basement, but present information is inconclusive.

The characteristics of the individual units are discussed below. The basement lithostratigraphy of Sites 790 and 791 is illustrated in Figures 54 and 55, respectively.

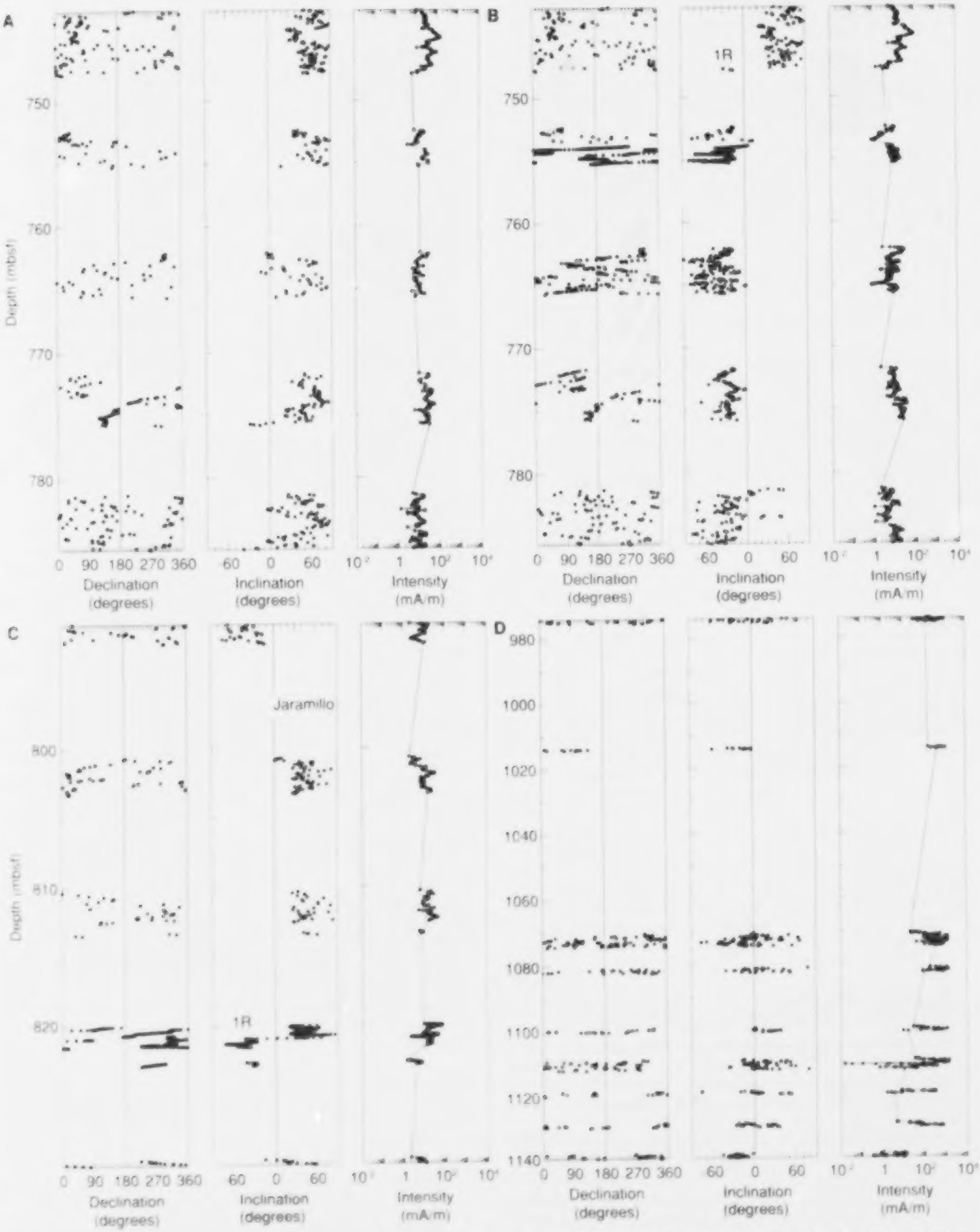

Figure 48. Paleomagnetic results vs. depth (mbsf) for Hole 791B. **A** and **B**. Cores 126-791B-38R to -42R before and after AF demagnetization. **C**. Cores 126-791B-43R to -47R after AF demagnetization. **D**. Cores 126-791B-62R to -79R after AF demagnetization.

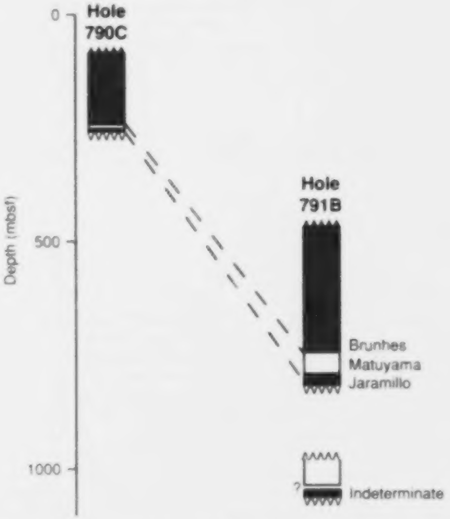

Figure 49. Polarity zones vs. depth (mbsf) for Holes 790C and 791B. Note increased thickness of polarity zones in Hole 791B.

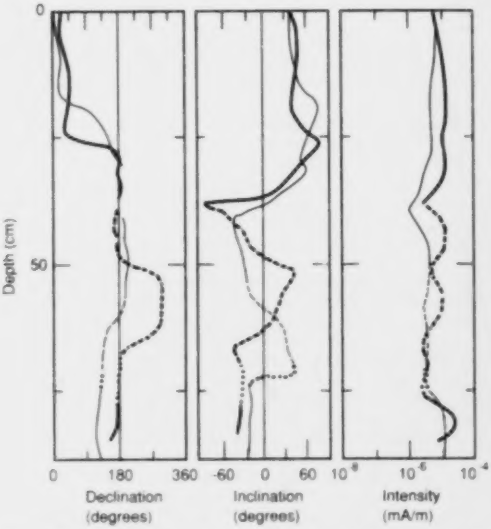

Figure 50. Paleomagnetic results for archive half of cores from Holes 790C and 791B, which include the Brunhes/Matuyama polarity transition. Thick line = Core 126-790C-17X-7 and core catcher. Thin line = Core 126-791B-38R-4 and core catcher. Declination segments were adjusted to eliminate rotations between core segments. Dashed lines indicate core-catcher data. Dotted lines are interpolations to the underlying core.

Site 790

Unit 1

Description: basalt
Intervals: Cores 126-790C-18X through -28X

The pieces and gravel are highly vesicular (20%-50%), nearly aphyric, basalt scorias. They contain microphenocrysts of olivine and plagioclase in an intersertal groundmass. Typical modal proportions, morphology, and sizes of the phenocrysts are 1% euhedral, 0.1-0.2-mm-diameter olivine and 5% euhedral, 0.1-0.3-mm-diameter plagioclase. One comparatively dense piece (126-790C-21X-CC, Piece 2) is an exception as clinopyroxene is present as both phenocrysts (1% euhedral, 0.1 mm diameter) and in the groundmass. The groundmass in all the samples consists of plagioclase laths in partially devitrified glass. The vesicles are round and range from 0.2 to 0.3 mm in size. Yellow translucent crystals occur on the vesicle walls and exposed surfaces.

Site 791

Unit 1

Description: basalt breccia
Interval: Section 126-791B-47R-1 at 45-150 cm

Vesicular olivine-plagioclase-clinopyroxene basalt clasts, 0.5-2.0 cm in diameter, lie in a matrix of glass shards, olivine and plagioclase crystals, and smaller basaltic fragments. In the 1.03 m recovered from Unit 1, a distinct visual difference is apparent between the upper 40 cm and the lower 75 cm. In thin section, the upper part has a glassy matrix, which is isotropic, but difficult to confirm as being either a mass of fine shards or a continuous "liquid" matrix. If the matrix is continuous, the style of this flow may be similar to that of the basaltic mousse described below in Unit 11, the key physical difference being the lack of microvesiculation in Unit 1.

The lower part is composed of fragmental vitric material. It is layered with bands of dark clast-rich material and concentrations of pale glass shards. This lower section may be a hyaloclastite, a vitric debris flow, or a hot pyroclastic flow.

The entire unit contains olivine, plagioclase, and clinopyroxene as phenocrysts in the clasts and as crystals in the matrix (Table 11). This three-phase assemblage is similar to the underlying Unit 2 basalt.

Unit 2

Description: glomeroporphyritic basalt
Intervals: Cores 126-791B-48R through -53R

Unit 2 is a vesicular olivine-plagioclase-clinopyroxene basalt with fresh phenocrysts that are characteristically in large glomeroporphyritic clots. The presence of clinopyroxene contrasts with its absence from the next lower basalt, which is more mafic, thus reflecting the more differentiated character of Unit 2. The vesicles are up to 3 mm in diameter. They have thin, blue smectite linings at the top of the unit but become increasingly filled with smectite and calcite toward the base. Exotic pebbles are present only at the top of cores and may have fallen from higher units rather than represent interbedded material. One is a silt-rich foraminiferal nannofossil chalk at the top of Core 126-791B-49R; another is a greenish (10GY) lapilli tuff at the top of Core 126-791B-52R. A total of 1.38 m was recovered from 58 m of cored interval.

Unit 3

Description: vesicular, sparsely phyric, olivine-plagioclase basalt
Intervals: Cores 126-791B-54R through -56R

Glomeroporphyritic clots are present but are less common than in Unit 2. Clinopyroxene phenocrysts are absent. Vesicle abundance, size, and filling are similar to Unit 2. We recovered

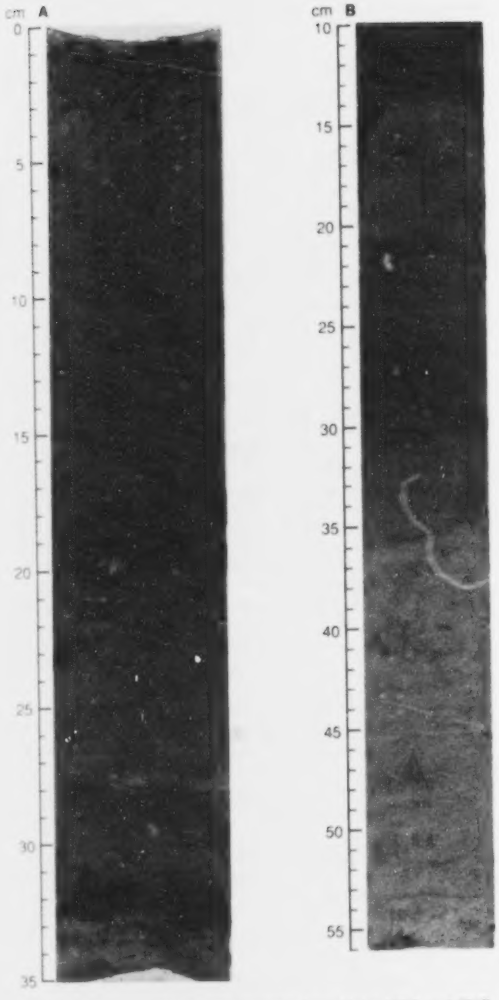

Figure 51. Photographs of core intervals from Holes 790C and 791B, which include the Brunhes/Matuyama polarity transition. **A.** Interval 126-790C-17X-CC (0-35 cm). **B.** Interval 126-791B-38R-4, 10-56 cm.

1 piece from each of Cores 126-791B-54R and -55R and 11 pieces from Core 126-791B-56R, for a total of 0.30 m.

Unit 4

Description: diabase
Intervals: Sample 126-791B-56R-1, Pieces 8 and 10, to 126-791B-57R-1 at 22 cm

Unit 4 is a fine-grained, mostly holocrystalline dike or sill (no contacts recovered) of differentiated basaltic material containing plagioclase, clinopyroxene, olivine, and magnetite. There is devitrified glass and microvesicles, even in this more intrusive rock. Only 0.30 m of core was recovered.

Unit 5

Description: vesicular, sparsely phyric, olivine-plagioclase basalt
Intervals: Sample 126-791B-57R-1 at 22 cm to 126-791B-58R-1, Piece 1

This unit is similar to Unit 3 and may be the lower portion of a single flow unit cut by the diabase. Alteration is more evident in the middle of Core 126-791B-57R, where brownish halos surround a spherical grey interior. However, the two areas are almost indistinguishable in thin section. A total of 0.85 m of core was recovered.

Unit 6

Description: basalt
Intervals: Sample 126-791B-58R-1, Piece 2, to 126-791B-60R-1, Piece 1

Unit 6 is a vesicular, sparsely phyric, olivine-plagioclase basalt similar to Units 3 and 5. A glassy margin, possibly a chilled contact, separates it from Unit 5. In comparison with Unit 5, Unit 6 is less vesicular (10% vs. 25%); however, the phenocryst content and texture are similar, so it may be only a different lava flow of the same magma type. In Sample 126-791B-50R-1 (Piece 8), the basalt invades a xenolith of basalt breccia similar to Unit 2, but is not chilled against it. A total of 0.74 m of core was recovered.

Unit 7

Description: basalt
Interval: Samples 126-791B-60R-1, Pieces 2 through 13

Unit 7 is a vesicular, sparsely phyric, olivine-plagioclase basalt similar to Units 3, 5, and 6. It is distinguished from the latter by being more vesicular, but its similarity in mineralogy and composition indicate that it, too, belongs to the same magma type, if not the same flow. A total of 0.15 m of core was recovered. Altogether, 2.0 m of this basalt type was recovered from 59 m of cored interval, interrupted by one diabase intrusion. Thus, potentially, a similar thickness (≤ 60 m) of more mafic basalt (Units 3, 5, 6, and 7) underlies a less mafic basalt (Unit 2).

Unit 8

Description: diabase
Intervals: Core 126-791B-61R

Unit 8 is a fine-grained, equigranular, plagioclase-clinopyroxene-olivine rock. Its flow-aligned plagioclase laths, glass, and microvesicularity indicate a shallow level of emplacement. A similar pebble occurs at the top of Core 126-791B-62R.

Unit 9

Description: sediment
Interval: Section 126-791B-62R-1 at 0-28 cm

A bedded sand-clay-gravel/sand sequence of volcanic clasts is interpreted to be air-fall deposit. The lowest lapilli may be accretionary, but identification is inconclusive (see "Lithostratigraphy and Accumulation Rates" section, this chapter).

Unit 10

Description: basalt
Interval: Sample 126-791B-62R-1, Piece 1

Unit 10 consists of one clast of vesicular basalt with only plagioclase phenocrysts, often in clots. Because it lies below the sediment and no similar material was recovered higher in the core, it is considered a separate lava.

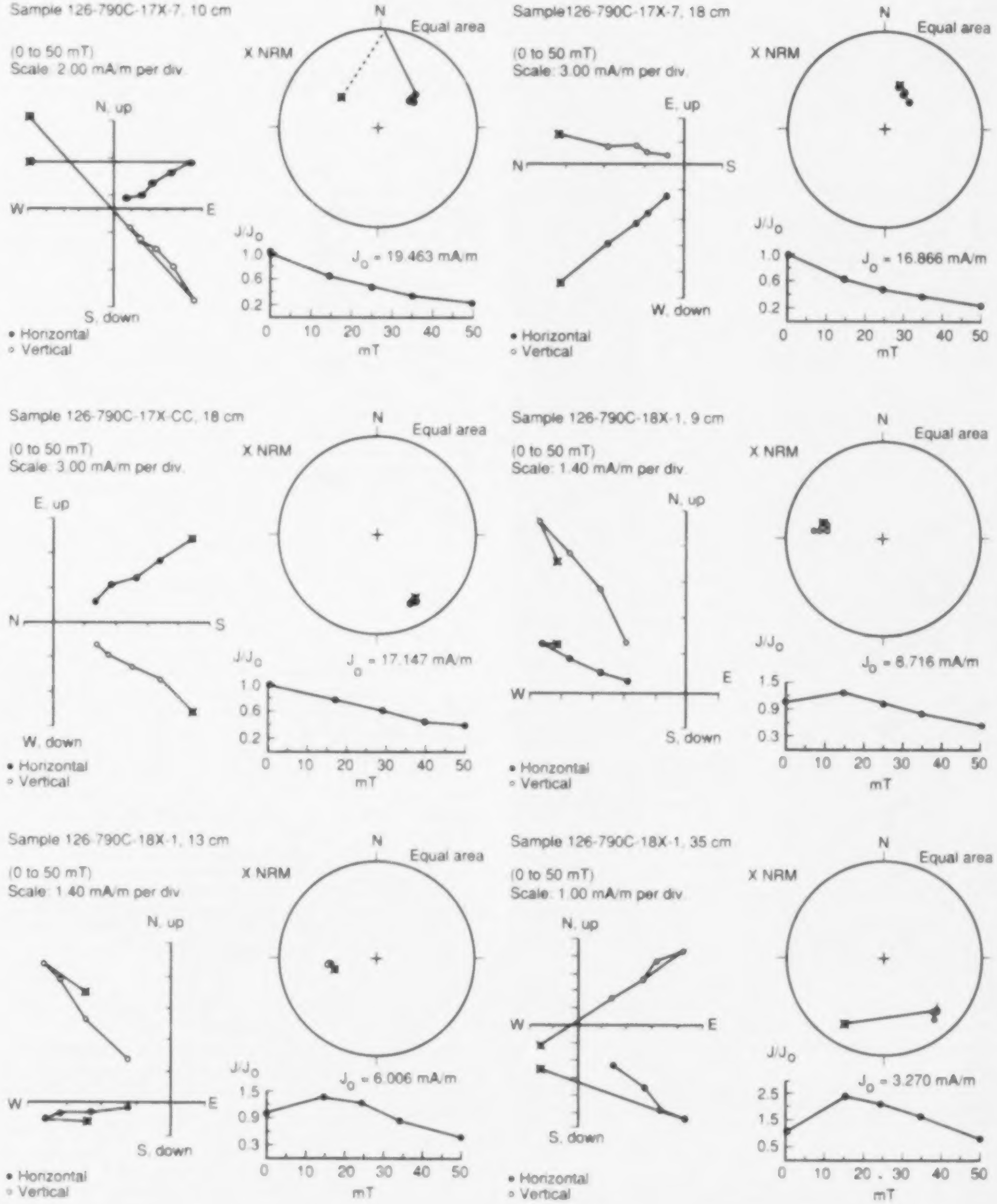

Figure 52. Orthogonal component field vector directions, and remanence intensities, as a function of AF demagnetization, for discrete samples taken across the Brunhes/Matuyama boundary interval (from ~65 cm below to ~35 cm above the inclination reversal horizon) in Hole 790C.

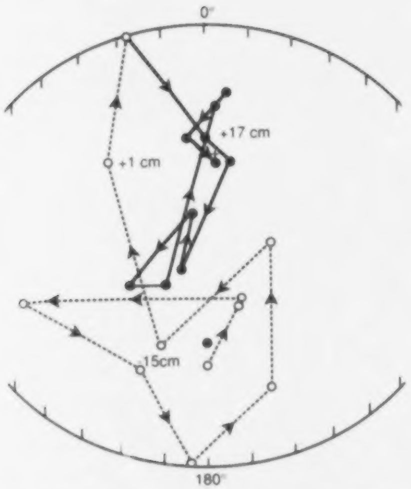

Figure 53. Field-vector directions (after AF demagnetization to 35 mT) as a function of distance below (−) and above (+) the Brunhes/Matuyama reversal plane recovered in Core 126-791B-38R-4. Upper hemisphere (negative inclination) paths are plotted as dashed lines. Azimuthal directions were determined from the directions of dipping laminations. (•) and (+) represent the present normal (reversed) dipole field direction for this latitude. All field vectors are corrected for bedding dips. Samples from the core catcher were not included in this plot.

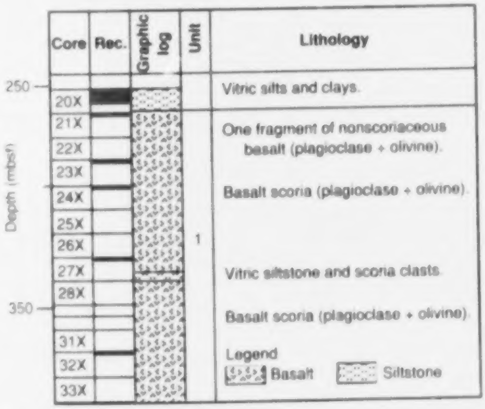
Core
Rec.
Graphic log
Unit
Lithology
250
350
Depth (mbsf)
20X
21X
22X
23X
24X
25X
26X
27X
28X
31X
32X
33X
1
Vitric silts and clays.
One fragment of nonscoriaceous basalt (plagioclase + olivine).
Basalt scoria (plagioclase + olivine).
Vitric siltstone and scoria clasts.
Basalt scoria (plagioclase + olivine).
Legend
Basalt
Siltstone

Figure 54. Lithostratigraphy of Hole 790C basement.

Unit 11

Description: basalt mousse
Samples 126-791B-62R-1, Pieces 2 through 11, through Core 126-791B-74R

This 135-m-thick unit is enigmatic and exotic. Macroscopically, it looks like a breccia of vesicular grey basalt clasts in a greenish matrix. However, in detail, "clasts" and "matrix" are very similar, and both consist primarily of highly expanded basaltic glass. Thus, the texture is like that of a mousse. The unit is interpreted as the product of a large-volume, deep-submarine eruption of gas-rich basalt. Its youth and very rapid burial have preserved it from collapse.

Most "clasts" are sparsely olivine-plagioclase phyric. The olivines contain spinel inclusions. Both minerals are euhedral and fresh near the top of the section. The plagioclases are optically zoned. The two minerals commonly form glomeroporphyritic clots that are set in a microvesicular groundmass of devitrified glass. The total vesicle content in the "clasts" is about 30%–40%, so that the glass usually consists of vesicle walls <0.5 mm thick. The measured porosity is also 35%–45% (see "Physical Properties" section, this chapter).

The vesicles are round and open at the top of the section, and some have thin linings of blue smectite. In some "clasts," the rim is less vesicular than the interior, as in a pillow (e.g., Sample 126-791B-73R-2, Piece 1B). However, the "clast" margins are not dense glass but are like scoria margins, that is, highly angular and irregular because of burst vesicles. Near the base of the section, plagioclase-clinopyroxene clasts appear infrequently. The clinopyroxene is subhedral; olivine is absent. Why clinopyroxene is present, or olivine is absent, in some clasts or at some depths but not at others is not yet clear.

All of the above description applies equally to the mousse "matrix" as well. The only difference is that the glass in the matrix is fresher. Throughout Unit 11 the matrix glass is fresh and isotropic, lending a greenish hue to hand specimens. This is especially evident around the glomeroporphyritic clots, where microvesiculation is absent. Again, the vesicles near the top of the section are empty except for occasional thin smectite linings (Figs. 56 and 57). The matrix glass vesicle walls may be thicker adjacent to "clasts," and vesicle walls as thin as 0.1 mm are often "clast" margins. These are the only characteristics that indicate a difference in strength between the components, perhaps as a result of the cooling history prior to their intermingling.

Both clasts and matrix become more altered with depth, resulting in smectite forming along cracks in olivine, and vesicles filling with thicker smectite, calcite, or zeolite(?). Plagioclase minerals remain fresh throughout. The glass becomes more devitrified, but it always is fresher in the matrix than in the clasts, preserving a color contrast in hand specimens.

Unit 12

Description: basalt mousse
Intervals: Samples 126-791B-74R-1, Piece 2, through 126-791B-75R-1, Piece 10

These pieces are similar to an uncommon clast type found near the base of Unit 11. They contain only plagioclase phenocrysts, usually in clots. Clinopyroxene is visible in the groundmass, whereas it is small or absent in most of Unit 11. Most pieces are partially rimmed by thin, greenish, microvesicular "mousse matrix." This, plus the similarity in bulk composition to Unit 11 (see "Igneous Geochemistry" section, this chapter) and the resumption of two-component mousse in Unit 14, may mean that Units 11, 12, and 14 are one flow unit. However, it is unclear whether the magma type is homogeneous. Unit 12 is the most different of the three units.

Unit 13

Description: fault gouge
Intervals: Sample 126-791B-75R-1, Piece 12

Unit 13 is a smectite-feldspar-rich clay.

Unit 14

Description: basalt mousse
Intervals: Samples 126-791B-75R-1, Piece 13, through 126-791B-76R-2, Piece 7

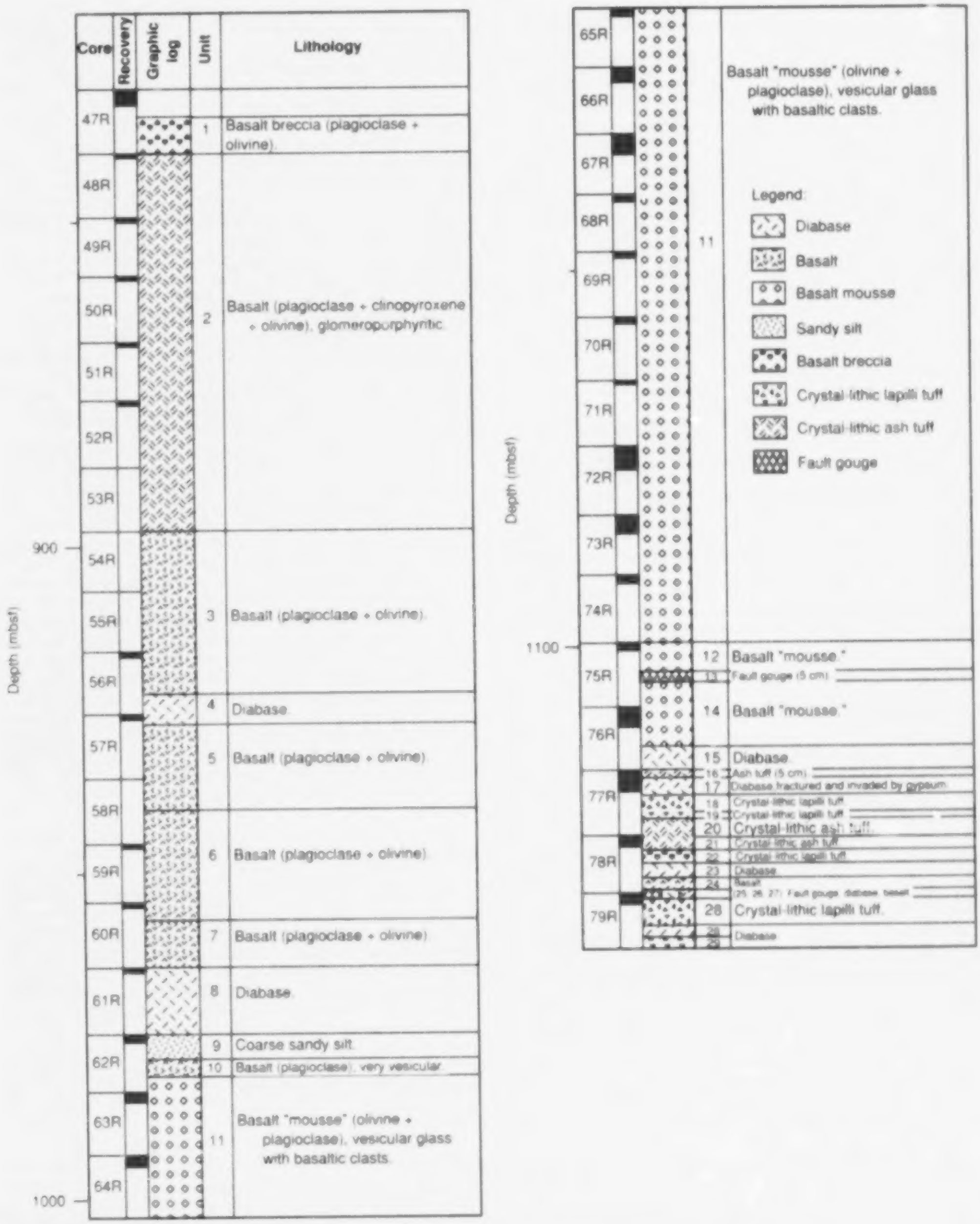
Core
Recovery
Graphic log
Unit
Lithology
Depth (mbsf)
900
1000
1100
47R
48R
49R
50R
51R
52R
53R
54R
55R
56R
57R
58R
59R
60R
61R
62R
63R
64R
65R
66R
67R
68R
69R
70R
71R
72R
73R
74R
75R
76R
77R
78R
79R
1 Basalt breccia (plagioclase + olivine).
2 Basalt (plagioclase + clinopyroxene + olivine), glomeroporphyritic.
3 Basalt (plagioclase + olivine).
4 Diabase.
5 Basalt (plagioclase + olivine).
6 Basalt (plagioclase + olivine).
7 Basalt (plagioclase + olivine).
8 Diabase.
9 Coarse sandy silt.
10 Basalt (plagioclase), very vesicular.
11 Basalt "mousse" (olivine + plagioclase), vesicular glass with basaltic clasts.
Basalt "mousse" (olivine + plagioclase), vesicular glass with basaltic clasts.
11
12 Basalt "mousse."
13 Fault gouge (5 cm)
14 Basalt "mousse."
15 Diabase.
16 Ash tuff (5 cm)
17 Diabase fractured and invaded by gypsum.
18 Crystal-lithic lapilli tuff.
19 Crystal-lithic lapilli tuff.
20 Crystal-lithic ash tuff.
21 Crystal-lithic ash tuff.
22 Crystal-lithic lapilli tuff.
23 Diabase.
24 Basalt
(25, 26, 27) Fault gouge, diabase, basalt
28 Crystal-lithic lapilli tuff.
29 Diabase
Legend:
Diabase
Basalt
Basalt mousse
Sandy silt
Basalt breccia
Crystal-lithic lapilli tuff
Crystal-lithic ash tuff
Fault gouge

Figure 55. Lithostratigraphy of Hole 791B basement.

Table 11. Summary of phenocryst percentages observed in shipboard thin sections.

Core, section, piece no.	Rock type	Olivine	Plagioclase	Cpx	Others	Alteration
47R, 3	Breccia	1	3	0		
47R, 10	Breccia	2	2	5	Cr-sp	
47R, 17		2	3	0		
48R, 9	Glom basalt	2	4	2		
53R, 5	Glom basalt	1	3	2		
55R, 1	Basalt	3	5	0	sp	
56R, 2	Basalt	2	5	0	sp	
56R, 13	Diabase	3	60	15		
57R, 4	Basalt	5	10	0	sp	
59R, 5	Basalt	3	3	0	sp	
60R, 13	Basalt	1	3	0	sp	
61R, 1	Diabase	0	12	3		
62R, 1B	Plag basalt	0	5	0		
62R, 5B	Mousse C and M	2	5	0	sp	fresh gl and ol
63R, 13B	C and M	2	4	0		devit and fresh gl ves filled smec excell M/C
64R-1, 13	C	0	2	0.5		devit xline gms
64R-2, 1	C and M	1	5	0	sp	gl alt ves more filled
65R, 17	C and M	3	5	0		ol alt
67R-1, 5	C and M	2	4	0	sp	
67R-2, 9	C and M	2	4	0		ol alt, gl fresg ves open
68R, 9	C	0.5	2	0		
70R, 10	C and M	0	2	0		C gl alt M gl fresh ves filled smec
72R-1, 18	C and M	2	4	0		M gl devit ves filled zeol
72R-3, 2A	C and M	2	4	0		M gl devit ves filled zeol
73R-3, 10	C	1	6	0		
75R, 10	C	1	10	0		ol alt calcite
76R-1, 12	C and M(?)	4	4	0		ol pseudo gl alt ves filled
76R-2, 6B	C and M(?)	4	10	1		ol pseudo gl alt ves filled
76R-3, 4A	Diabase	2	40	30		
77R-1, 1	Tuff		?			
77R-1, 7	Diabase	2	60	10		
77R-2, 2A	Tuff	0	3	1	qtz, ox	
77R-2, 6A	Tuff	0	8	0	qtz, ox	
77R-3, 1A	Tuff	0	5	1		
78R, 2	Tuff	0	15	0	ox	
78R, 3B	Diabase	5	60	5		
78R, 8	Basalt	2	2	0		
78R, 10A	Diabase	5	60	10		
78R, 12A	Basalt	0	65	1		
79R, 3	Tuff	0	30	0		
79R, 6	Tuff	0	40	0		
79R, 7	Diabase	7	65	5		

Note: Cr-sp = chromium spinel, sp = spinel, alt = alteration/altered, gl = glass, ol = olivine, devit = devitrified, ves = vesicles, smec = smectite, zeol = zeolite, cpx = clinopyroxene, qtz = quartz, C = clast, M = matrix, xline = crystalline, gms = groundmass, Glom = glomeroporphyritic, pseudo = pseudomorphs, and ox = oxides.

This unit is a more altered version of Unit 11. Compared with Unit 11, the vesicles in the "clasts" are less abundant but larger. The glomeroporphyritic clots are larger (to centimeter scale) and have cumulate textures. The margins between clast and matrix are more convoluted. Olivine is largely pseudomorphed by chlorite, vesicles are largely filled with smectite and calcite, and the glass is more devitrified and iron stained. Plagioclase remains fresh.

Unit 15

Description: diabase
Intervals: Sample 126-791B-76R-2, Piece 8, through Section 126-791B-76R-3

This intrusive rock has 40% euhedral plagioclase <0.5 mm in size, 30% euhedral clinopyroxene as large as 1 mm in size, and around 30% glass and oxides. The glass and 2% euhedral olivine (0.5 mm in size) are altered to smectite. A total of 0.76 m of core was recovered.

Unit 16

Description: crystal-lithic tuff
Interval: Sample 126-791B-77R-1, Piece 1

This unwelded pyroclastic rock could be a drop-in as it is the first piece in the core. However, because nothing like it occurs higher in the sequence, it is treated as a new unit, the first of a fundamentally different kind that constitutes the base of the core. The contact with the mousse was not recovered. The piece contains 5% partially sericitized plagioclase and 10% lithic lava fragments replaced by various assemblages, including calcite and hematite. Of the original vitric shards, 85% are altered to chlorite. The rock may represent an air-fall deposit because there is no evidence for crushing of the pumice shards. A total of 0.03 m of core was recovered.

Unit 17

Description: diabase
Interval: Samples 126-791B-77R-2, Pieces 3 through 8

The diabase is fine grained with a subophitic and intersertal texture and is very similar to the diabase in Unit 15. The phenocrysts in this rock are as large as 1 mm in size and predominantly plagioclase (60%). All of the glass (30%) and olivine (2%) are altered to chlorite. Gypsum veins cut the pieces. A total of 0.80 m of core was recovered.

Unit 18

Description: gypsum-mineralized fracture breccia in lapilli tuff
Interval: Samples 126-791B-77R-2, Pieces 1A through 1E

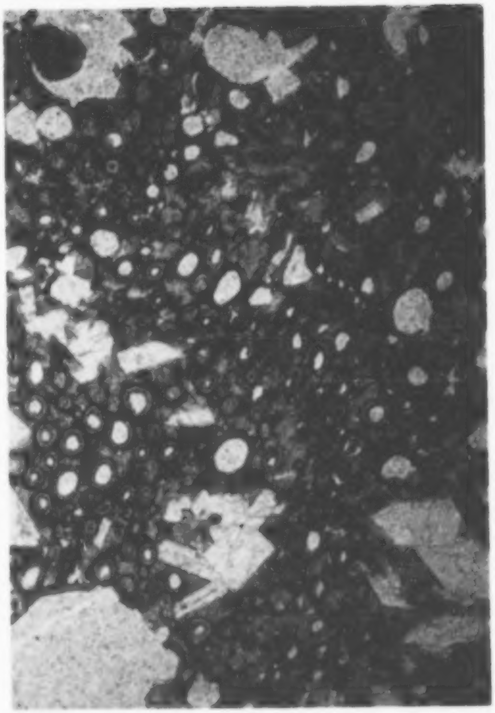

Figure 56. Basalt mousse (Unit 11). Microvesicular basalt glass with glomeroporphyritic clots of plagioclase and olivine. Vesicle walls are lined with smectite (95 × magnification, plane-polarized light, Sample 126-791B-62R-1, Piece 13).

This rock consists of large fracture blocks (0.5–4.0 cm in size) randomly aligned. The clasts are crystal-lithic lapilli tuff and welded, lithic-vitric lapilli tuff. The fractures in the rock are filled with gypsum. The breccia is caused by fault plane movement followed by fracturing and infilling of fluid-precipitated gypsum. A sharp basal contact with the unbrecciated Unit 19 is present.

Unit 19

Description: crystal-lithic lapilli tuff
Interval: Samples 126-791B-77R-2, Pieces 1E through 4

The rock is a eutaxitic, welded, well-sorted tuff (Fig. 58). It consists of 50% vitric fragments that are present mainly as compressed flattened pumice with fiamme, 40% lithic fragments, and 10% crystals (quartz, calcite, and magnetite). The vitric rocks are completely altered to chlorite. The rock shows two fabrics: an igneous eutaxitic one with flattened pumice, and a metamorphic overprint with chlorite aligned 45° to the igneous one. A total of 0.45 m of core was recovered.

Unit 20

Description: crystal-lithic tuff
Interval: Samples 126-791B-77R-2, Pieces 5–6, through Samples 126-791B-77R-3, Pieces 1–2

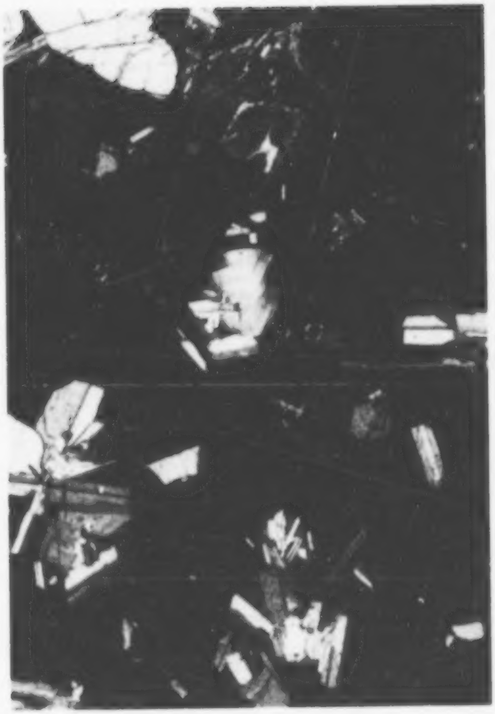

Figure 57. Basalt mousse (Unit 11). Glomeroporphyritic texture with clots of plagioclase and olivine. Birefringent haloes mark the smectite-lined microvesicles (95 × magnification, cross-polarized light, Sample 791B-62R-1, Piece 13).

This welded tuff has the same compositional characteristics as Unit 19, but a much finer grain size (< 2 mm), and hence is a new flow unit. This rock consists of 70% compressed and flattened pumice altered to chlorite. Minor amounts of calcite are also present (Fig. 59). The metamorphic fabric resulting from chlorite alignment is more pronounced in this unit. A total of 0.45 m of core was recovered.

Unit 21

Description: crystal-lithic tuff
Interval: Sample 126-791B-77R-3, Pieces 3–4

The difference between Units 20 and 21 is that the Unit 21 pumices are not flattened as in Unit 20. A total of 0.15 m of core was recovered.

Unit 22

Description: lithic lapilli tuff
Sample 126-791B-77R-3, Piece 6, through Sample 126-791B-78R-1, Piece 2

This is a poorly sorted, unwelded rock. Altered andesitic lava constitutes the lithic fragments. The clinopyroxenes are replaced by epidote. A total of 0.10 m of core was recovered.

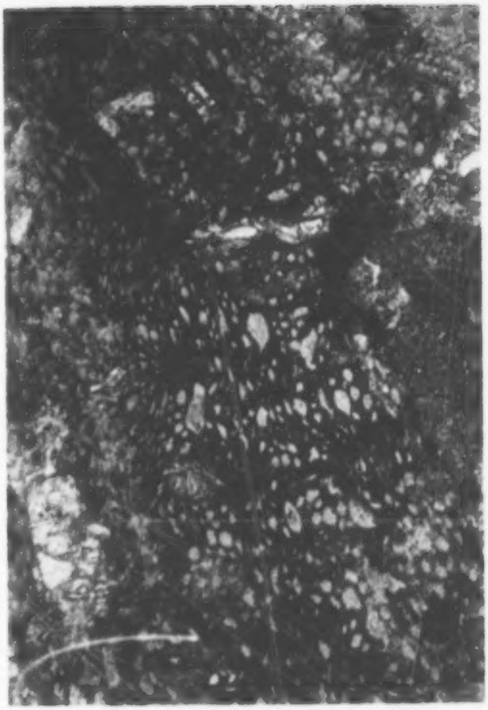

Figure 58. Crystal lithic lapilli tuff (Unit 19). Semiflattened scoriaceous pumice shards, in a matrix of vitric, lithic, and crystal fragments (95× magnification, plane-polarized light, Sample 126-791B-77R-2, Piece 2).

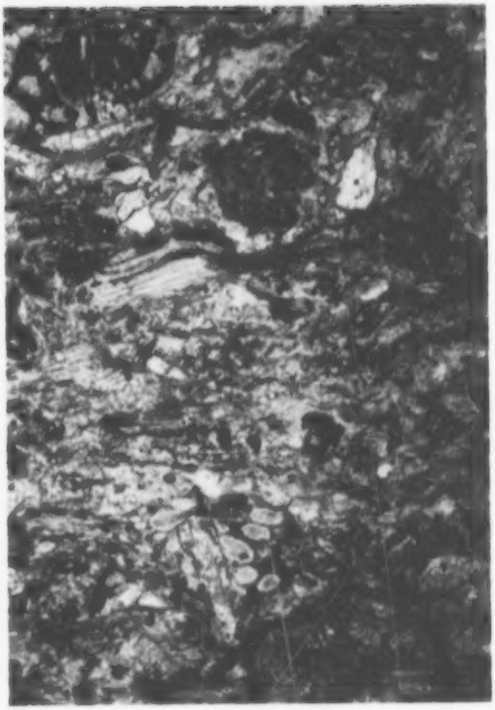

Figure 59. Crystal-lithic tuff (Unit 20). Flattened, elongate pumice shards compacted around crystal and lithic fragments in a eutaxitic texture (95× magnification, plane-polarized light, Sample 126-791B-77R-2, Piece 6A).

Unit 23

Description: diabase
Interval: Sample 126-791B-78R-1, Piece 3

This diabase has an intersertal, subophitic texture similar to that of the other diabases. The only difference is that this rock has slightly more olivine (5%), the crystals are smaller, and it contains gypsum. A total of 0.09 m of core was recovered.

Unit 24

Description: basalt
Interval: Samples 126-791B-78R-1, Pieces 4 through 8

This basalt is plagioclase phyric with an intersertal, vesicular texture. It is highly altered and composed of plagioclase and chlorite. It contains rounded vesicles filled with radially grown chlorite. The vesicles contain tiny laths of plagioclase in a glassy matrix, which could imply that the vesicles are filled with differentiated melt. A total of 0.4 m of core was recovered.

Unit 25

Description: felsic clast and fault gouge
Interval: Sample 126-791B-78R-1, Piece 9

A silicic rock, mineralized with pyrite and containing an epidote vein, was recovered in the same interval as green fault gouge. Pyrite also is disseminated in the rock, which consists of plagioclase and some chlorite in a fine-grained groundmass. The XRD patterns from the fault gouge showed the presence of chlorites and quartz. A total of 0.04 m of core was recovered.

Unit 26

Description: diabase
Interval: Samples 126-791B-78R-1, Pieces 10 to 11, through Sample 126-791B-79R-1, Piece 1

This diabase unit has essentially the same characteristics as Unit 23. It is mineralized in fractures with pyrite, calcite, and gypsum. The alignment of plagioclase laths may be the result of shearing. A total of 0.14 m of core was recovered.

Unit 27

Description: basalt
Interval: Sample 126-791B-78R-1, Piece 12

This rock has a porphyritic texture with partly altered plagioclase phenocrysts and epidote resembling clinopyroxene pseudomorphs. Plagioclase is the dominant phenocryst (65%), with 1% clinopyroxene. The secondary mineralogy consists of smectite, chlorite, and quartz. A total of 0.09 m of core was recovered.

Unit 28

Description: welded crystal-lithic tuff
Interval: Sample 126-791B-79R-1, Pieces 2 through 6 and Piece 11

This deposit has variable composition and variable vesicularity of the lithic fragments and pumice, implying a difference in competence. Part of the plagioclase and all of the crushed pumice and glass shards are altered to smectite and chlorite. A total 0.80 m of core was recovered.

Unit 29

Description: diabase
Interval: Samples 126-791B-79R-1, Pieces 7 through 10

This diabase has a mineralogy similar to that of the other diabases, but it is more extensively altered. All of the clinopyroxene is altered to chlorite and parts of the plagioclase are altered to sericite. This unit is mineralized with secondary calcite, pyrite, and gypsum as in Unit 26. A total of 0.20 m of core was recovered.

X-ray Diffraction Results

The XRD results are summarized in Table 12. In Units 1-11, samples from vesicle walls have very high, broad backgrounds that reflect abundant amorphous glass as well as large amounts of smectite. This blue clay alteration product coats vesicle interiors. Greenish, elongated crystals in vesicles are calcite with traces of 1.4-nm minerals (chlorite or smectite) and feldspar also present.

The matrix of the basalt mousse in Unit 11 (Sample 126-791B-65R-1, Piece 13) contains abundant smectite together with feldspar, augite, glass, and halite. The smectite is an alteration product of the glass and seawater. The white, vein-filling material in Cores 126-791B-76R to -79R was confirmed as gypsum ($CaSO_4 \cdot 2H_2O$) with characteristic peaks at 0.76, 0.43, 0.38, and 0.306 nm (Fig. 60). The tuff of Unit 20 in Sample 126-791B-77R-3 (Piece 1) contains calcite, quartz, and chlorite, together with lesser amounts of mica group minerals, feldspar, and glass, but no smectite (Fig. 61).

Two types of fault gouge are present. The one within the basalt mousse (Unit 13, Sample 126-791B-75R-1, Piece 12) contains smectite and feldspar (Fig. 62). In contrast, the gouge associated with a felsic clast within the lapilli tuff section is rich in chlorites and quartz. The different mineral suites show that the rock being faulted affects the gouge mineralogy.

IGNEOUS GEOCHEMISTRY

We analyzed 4 samples from Site 790 and 20 from Site 791 by X-ray fluorescence (XRF) for major elements; all except 2 were also analyzed for 12 trace elements (Table 13). One basalt scoria from Hole 790A and one rhyolite pumice from Hole 791B were from Unit I. The rest were from Unit III, the basement (see "Lithostratigraphy and Accumulation Rates" section, this chapter).

The basement rocks of Units 1-15 are predominantly basaltic. Their high TiO_2 with respect to MgO, low Ba contents (< 30 ppm), and Ti/V ratios closer to 20 than 10, distinguish them from basalts and andesites of the Izu-Bonin Arc (Fig. 63). Consequently, the younger basement volcanism is inferred to be syn-rift in origin.

In detail, the basement basalts are more similar to those from the rift wall, dated at 1.1-1.4 Ma, and from seamounts in the outer rift, than to basalts from the 250-ka en echelon pillow ridges of the inner rift (Hochstaedter et al., in press). That is, the basement volcanics have 17% vs. 16% Al_2O_3, 1.0% vs. 0.85% TiO_2, 11% vs. 12% CaO, 2.5% vs. 2.0% Na_2O, 0.2% vs. 0.1% P_2O_5, and 60-70 vs. 40-50 ppm Zr at 7%-8% MgO. These contrasts indicate percent fusion increases with time. The higher Ca/Al_2O_3 ratios in younger basalts implies that clinopyroxene has remained a residual phase, as it also is during MORB genesis. This contrasts with the more extensive melting and refractory harzburgite beneath the arc.

The basement basalts also have higher Fe with respect to Mg, implying higher pressure fusion (e.g., Klein and Langmuir, 1987). Taken together, these intra-rift comparisons indicate that the crust has thinned, allowing the mantle to rise closer to the surface and, therefore, melt more extensively during the last million years, at least beneath the en echelon ridges. One observation inconsistent with this idea is that the basement basalts apparently become saturated in clinopyroxene at a later stage of differentiation (between 7% and 6% MgO) than do the younger rift basalts, making them more similar to MORB and implying lower-pressure conditions of fractionation.

The basement basalts at Site 791 have lower concentrations of Ba, Rb, and perhaps Ce than do those at Site 790 or the younger rocks of the inner rift. Indeed, Ba and Rb concentrations in Site 791 basalts are as low as in MORB. Previously, such low concentrations have been found only in the basalts of well-evolved backarc basins such as the Lau and West Philippine Basins (Hawkins and Melchior, 1985; Mattey et al., 1981). In the Sumisu Rift, such differences occurred at approximately the same time, only 1 km apart, early in the basin history. The more depleted variant erupted in deeper water.

At Hole 791B, the volcanic rock stratigraphic units can be subdivided into four types. The most mafic is sparsely olivine-plagioclase phyric and has about 8% MgO, 100 ppm Ni, and 250-300 ppm Cr. This also characterizes the least-differentiated lavas from the major en echelon pillow ridges of the inner rift between the North and South Sumisu basins (Hochstaedter et al., in press). It applies to petrologic Units 3, 5, 6, and probably

Table 12. X-ray diffraction analysis of Site 791 rocks.

Core, section, piece no.	Unit	Sample description	Clay minerals: 1.4 nm	Clay minerals: 1.0-nm Mica	Clay minerals: 0.7-nm Chlorite	Minerals	Amorphous materials
126-791B-							
47R-1, 4	1	Basalt breccia	1.73 nm (smectite)	—	—	Feldspar	Abundant
53R-1, 7	2	Hand-picked green grains in a vesicle of basalt	Trace	—	—	Calcite > feldspar	Abundant
65R-1, 13	11	Hand-picked coating materials in vesicles of basalt breccia	1.68 nm (smectite)	—	—	Feldspar	Abundant
65R-1, 13	11	Matrix of basalt breccia	1.60 nm (smectite)	—	—	Feldspar > halite > augite	Abundant
75R-1, 12	13	Fault gouge	1.65 nm (smectite)	—	Trace	Feldspar >>> quartz	Abundant
76R-1, 12	14	White part of vein in basaltic mousse	—	—	—	Gypsum	—
76R-2, 10A	15	White parts in diabase	—	—	—	Gypsum	—
791B-77R-3, 1	20	Welded coarse-ash tuff	1.456 nm (chlorite)	Present	Common	Calcite > quartz >> feldspar	Present
791B-78R-1, 5	25	Fault gouge	1.42 nm (chlorite)	Present	Common	Quartz >>> feldspar	Present

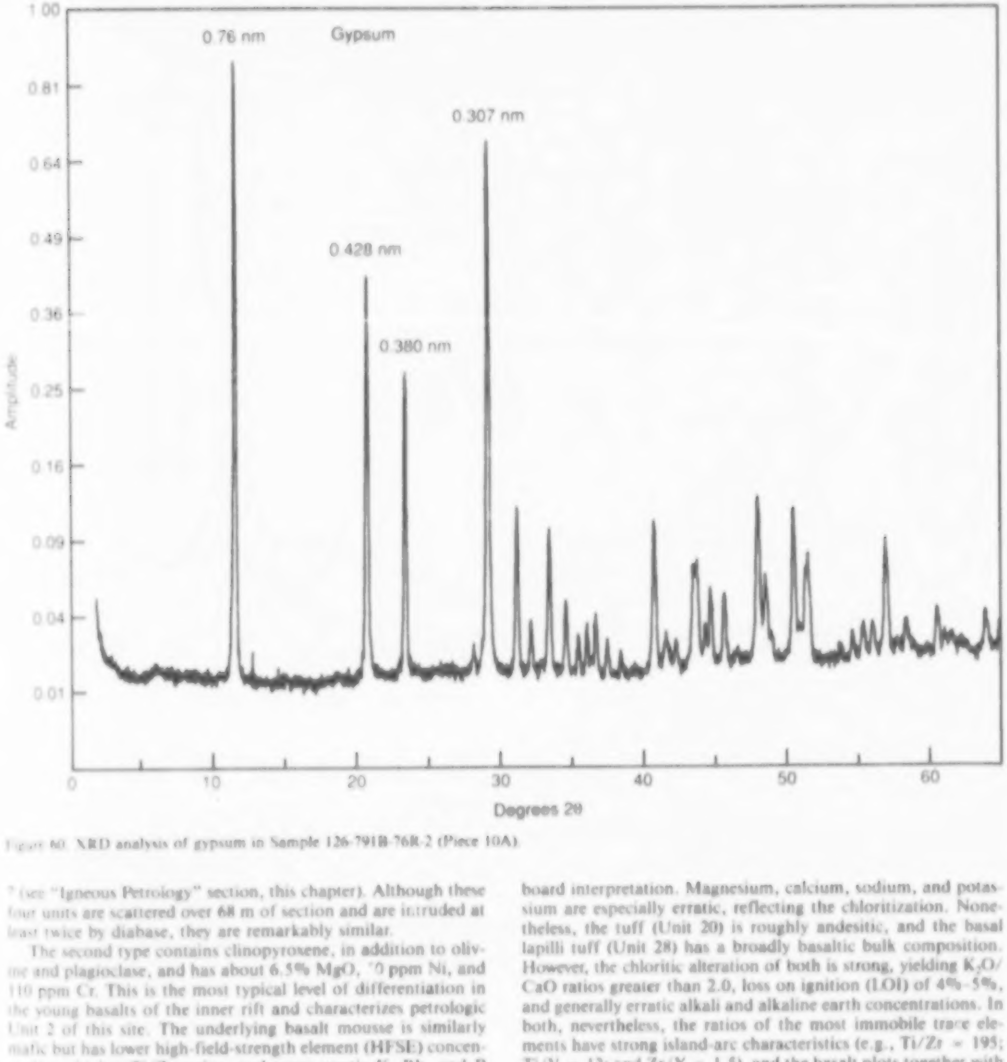

Figure 60. XRD analysis of gypsum in Sample 126-791B-76R-2 (Piece 10A).

7 (see "Igneous Petrology" section, this chapter). Although these four units are scattered over 68 m of section and are intruded at least twice by diabase, they are remarkably similar.

The second type contains clinopyroxene, in addition to olivine and plagioclase, and has about 6.5% MgO, 70 ppm Ni, and 110 ppm Cr. This is the most typical level of differentiation in the young basalts of the inner rift and characterizes petrologic Unit 2 of this site. The underlying basalt mousse is similarly mafic but has lower high-field-strength element (HFSE) concentrations, higher Ti/Zr ratios, and more erratic K, Rb, and P concentrations. This type may also characterize Units 24 and 27, which are interspersed with the tuffs near the base of the hole, but alteration makes assignment of those basalts ambiguous.

Diabases constitute the third rock type. They range in composition from being as mafic as type I (Unit 15), to being similar to type II (Unit 8), to being more differentiated than type II (Units 4 and 29). The TiO_2 contents increase regularly in that order from 1.1% to 1.9%, although Zr remains oddly constant at about 60-70 ppm.

Finally, the tuffs and lapilli tuffs at the base of the section in Units 16-22 and 28 appear broadly intermediate to felsic in nature, but they are too fine grained and altered for clear shipboard interpretation. Magnesium, calcium, sodium, and potassium are especially erratic, reflecting the chloritization. Nonetheless, the tuff (Unit 20) is roughly andesitic, and the basal lapilli tuff (Unit 28) has a broadly basaltic bulk composition. However, the chloritic alteration of both is strong, yielding K_2O/CaO ratios greater than 2.0, loss on ignition (LOI) of 4%-5%, and generally erratic alkali and alkaline earth concentrations. In both, nevertheless, the ratios of the most immobile trace elements have strong island-arc characteristics (e.g., Ti/Zr = 195; Ti/V = 12; and Zr/Y = 1.5), and the basalt plots together with data from the modern Bonin Arc in the Ba-Zr and Ti-V diagrams of Figure 63. Thus, the eutaxitic textures, which imply proximity to the eruption site, and the preliminary bulk geochemistry suggest that Units 16-28 are an arc basement of unknown age. However, Units 24 and 27 are intercalated yet similar in composition and mineralogy to the overlying syn-rift basalts. Consequently, the provenance of the tuffs remains ambiguous.

SEDIMENT/FLUID GEOCHEMISTRY

Eleven 10-cm long, whole-round samples from Holes 790A, 790B, and 790C and 15 whole-round samples from Holes 791A

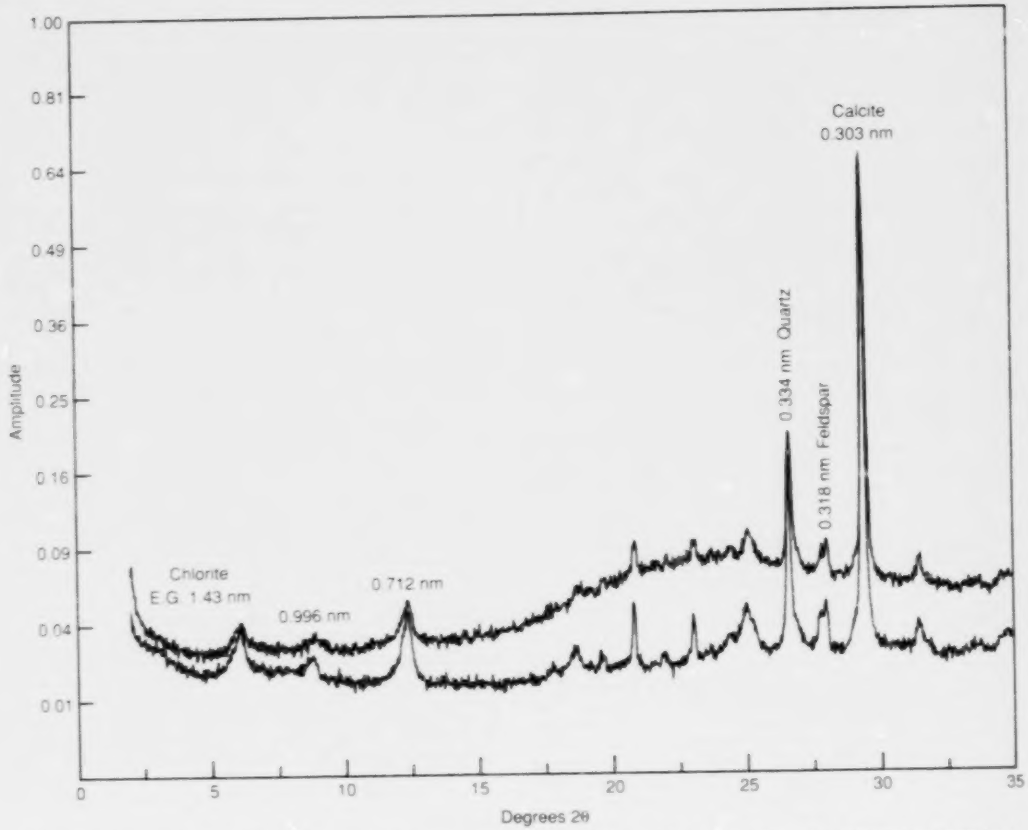

Figure 61. XRD analysis of ash tuff showing chlorite, mica group minerals, quartz, feldspar, calcite, and amorphous glass in Sample 126-791B-77R-3 (Piece 1) before (bottom) and after glycolation (EG).

and 791B were obtained for electrical resistivity measurements, pore-water squeezing, and sediment and fluid analyses.

Sediment Resistivity

The formation factors calculated from the resistivity measurements vary between 2.0 and 7.5 (Table 14). The sample from Core 126-790B-6H consists of coarse sand, and the high formation factor (5.5) is caused by water draining away from the electrodes during measuring. At Site 791, the same phenomenon precluded recording of meaningful data on Cores 126-791A-9H, -12H and -15H. There is a tendency for slightly higher formation factors in the lower parts of the holes, consistent with the more compacted nature of these sediments (Fig. 64). The magnitude of the formation factors is the same as determined by other investigations on similar sediments at the same stage of compaction (e.g., Manheim and Waterman, 1974).

Sediment Geochemistry

Sediments from Sites 790 and 791 were analyzed on board ship for inorganic carbon, total carbon, nitrogen, and sulfur (see "Explanatory Notes" chapter, this volume). Sulfur was not determined quantitatively because vanadium pentoxide was not added to the samples for capacity reasons. Analytical results are presented in Table 15. The distribution pattern of organic carbon at the two sites shows the same features, with low values in the upper part of the holes and a broad maximum in the lower half (Fig. 65).

Despite a three-fold difference in the rate of sediment accumulation, the concentration of organic carbon at the two sites is not very different. The concentration of organic carbon is positively correlated with sedimentary carbonate. This probably relates to the fact that sections with high concentrations of sedimentary carbonate (mainly nannofossils) represent periods with high planktonic productivity and/or reduced input of clastic material. However, for samples with high concentrations of carbonate, the correlation may be enhanced by the method used for determining the concentration of organic carbon, which involves subtracting inorganic carbon and total carbon (see "Explanatory Notes" chapter, this volume).

The concentration of total nitrogen varies from less than the detection limit to 0.2%. Although most of the nitrogen is organically bound, there is no significant correlation between or-

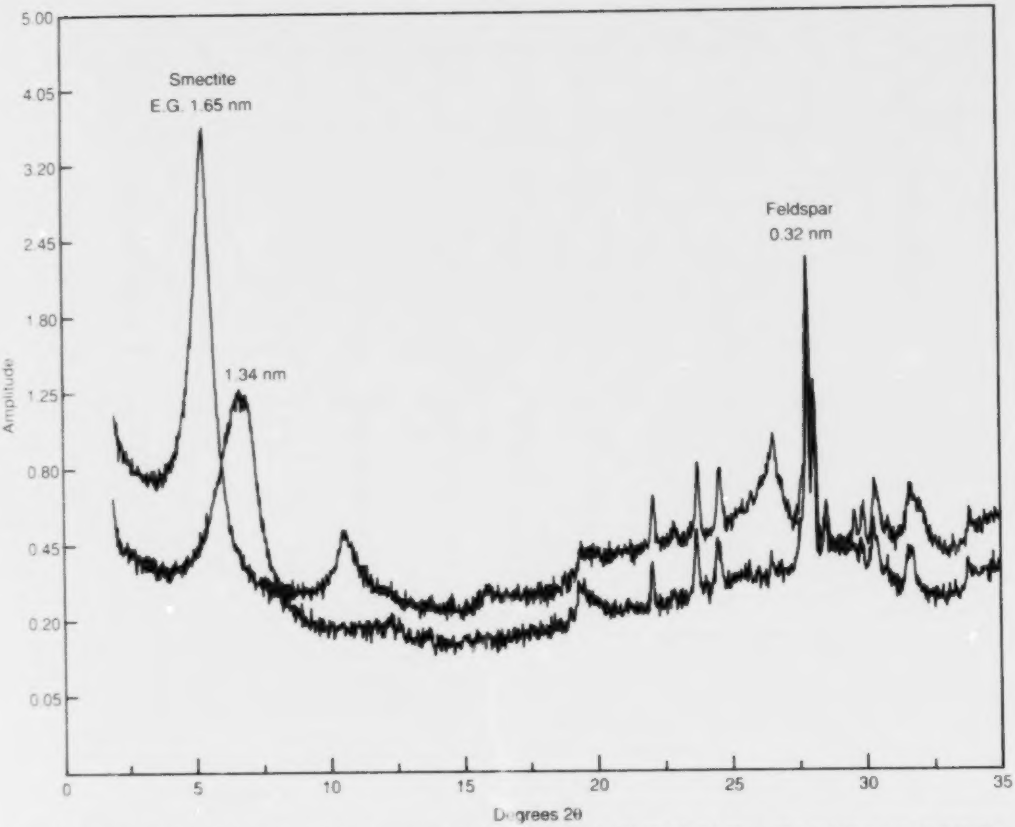

Figure 62. XRD analysis of fault gouge showing abundant smectite and feldspar in Sample 126-791B-75R-1 (Piece 12). The 1.34-nm peak is shifted to 1.65 by glycolation. (EG)

ganic carbon and sedimentary nitrogen. Except for Core 126-790A-2H, sulfur could only be detected between 88 (Core 126-790C-1H) and 247 mbsf (Core 126-790C-18X) at Site 790. The fact that sulfur is more abundant in the part of the hole where sulfate reduction is taking place (see discussion that follows) attests to its biogenic origin.

Fluid Geochemistry

The headspace hydrocarbon analyses did not show any gases above background level and are not reported. Special attention was paid to possible contamination of the pore water by drilling-mud filtrate because of the extensive use of mud while drilling Holes 790A, 790B, 790C, 791A, and 791B. The composition of the mud filtrate is given in Table 16. Uniform chloride concentrations at typical seawater levels (Table 16) indicate that none of the samples were measurably contaminated by drilling-mud filtrate.

Concentrations of sodium, magnesium, and strontium in pore waters recovered from Holes 790A, 790B, and 790C deviate little from concentrations in seawater of similar chlorinity. Concentrations of potassium decrease to about 50% of its seawater level at 100 mbsf (Core 126-790C-2H) and increase to normal seawater concentrations at 254 mbsf (Core 126-790C-18X; Table 16). A similar trend is observed at Site 791.

At Site 790, the concentration of lithium exhibits a pronounced subsurface maximum of 63 μM at 100 mbsf (Core 126-790C-2H; Fig. 66), whereas at Site 791 the highest lithium concentration is recorded at 37 mbsf (Core 126-791A-5H). Very few sources of lithium other than high-temperature alteration of volcanic material have been identified. However, Gieskes (1983) proposed that lithium can be enriched in pore waters during dissolution and recrystallization of biogenic silica.

At Site 790, alkalinity remains at about 4 mM down to 131 mbsf (Core 126-790C-5H) and then increases to about 9.3 mM in Cores 126-790C-13X through -16X (197–227 mbsf), below which it decreases to 6.0 mM at 255 mbsf (Core 126-790C-2X; Fig. 66). The concentration profile of calcium mirrors the alkalinity profile (Fig. 66) and shows calcium concentrations only slightly higher than in seawater in Cores 126-790C-2H and -5H. The alkalinity maximum and calcium minimum coincide with the minimum in the sulfate concentration profile between 197 and 227 mbsf. Evidently, the concentration of calcium is af-

Table 13. Shipboard X-ray fluorescence analyses of rocks from Sites 790 and 791.

Hole, core	790A-4H	790C-21X	790C-24X	790C-24X	791B-9R	791B-48R	791B-53R	791B-55R	791B-56R	791B-57R	791B-59R
Section, interval (cm)	2, 57-59	CC, 3-8	CC, 8-10	15-72	CC, 2-3	1, 46-49	1, 10-12	1, 2-5	1, 69-71	1, 31-34	1, 41-44
Piece number	—	2	2A	2B	—	9	4	1	13	4	5
Depth (mbsf)	32.1	275	305	305	472	845	890	910	922	930	950
Petrologic unit	1	1	1	1	1	2	2	3	4	5	6
Lithology[a]	basalt	basalt	basalt	basalt	pumice	basalt	basalt	basalt	diabase	basalt	basalt
Major elements:											
SiO_2	49	51.43	48.71	49.61	73.08	49.22	50.08	49.2	48.81	48.55	48.91
TiO_2	1.07	1.35	0.97	0.97	0.4	1.2	1.24	1.06	1.74	1.78	1
Al_2O_3	16.4	16.89	17.57	17.21	13.36	16.84	17.36	17.33	15.12	16.78	17.46
Fe_2O_3	11.21	10.9	9.64	10.62	3.55	11.27	10.35	11.1	14.63	10.59	10.7
MnO	0.16	0.16	0.13	0.15	0.13	0.13	0.15	0.14	0.17	0.14	0.13
MgO	8.1	4.69	7.8	8.49	0.84	6.81	5.85	8.03	5.65	6.45	8.53
CaO	10.87	10.14	11.63	10.44	2.98	10.71	10.77	10.9	9.63	12.35	10.54
Na_2O	2.44	3.23	2.44	2.49	4.97	2.85	2.93	2.53	2.93	2.67	2.68
K_2O	0.37	0.54	0.4	0.56	0.91	0.26	0.28	0.31	0.2	0.41	0.2
P_2O_5	0.19	0.25	0.27	0.14	0.07	0.23	0.24	0.17	0.27	0.17	0.16
LOI	0	0.24	0.21	0.49	0.38	0.56	0.15	0.35	0.24	2.14	1.39
Total	99.81	99.58	99.56	100.68	100.29	99.52	99.25	100.77	99.15	99.18	100.31
Trace elements:											
P	828.59	1090.25	1177.47	610.54	305.27	1003.03	1046.64	741.37	1177.47	741.37	697.76
Zr	61.4	90.5			92.1	75.8	79	69.8	67.9	68.5	61.1
Y	21.2	29			47	26.1	26.5	23.1	26.4	22.1	20.7
Rb	4.9	7.9			9.9	2.4	3.1	3.6	0.3	7.3	2.6
Sr	222	287			162	243	260	237	258	356	266
Ba	42	38			162	8	13	20	24		11
V	291	663				336	356	320	516	279	300
Nb	3.4	2.1			1.3	2.1	1.6	1.8	1.5	1.2	1.2
Ni	102	12			1	45	51	98	8	115	124
Cr	920	21				106	118	278		266	261
Zn	68	120			112	114	116	101	131	95	91
Cu	67	35			4	48	46	47	50	48	35
Ce	26	10			11		5	1		3	
Mg#	61.4	48.64	64.04	63.76	34.25	57.08	55.44	61.42	45.95	57.27	63.7

Note: Major elements in wt%, trace elements in ppm.

[a] Msse = mousse, c = clast, m = matrix, lap = lapilli.

fected by precipitation of calcium carbonate in response to the increase in alkalinity resulting from bacterial sulfate reduction. Further evidence for bacterial activity in this interval is provided by the ammonium profile exhibiting a pronounced maximum between 197 and 227 mbsf (Fig. 67).

The ammonium profile also shows that the pore water from the coarse sand in Core 126-790B-6H probably has been severely mixed with seawater. At Site 791, the low concentrations of ammonium in Cores 126-791A-5H, -9H, and -12H probably reflect the same phenomenon.

There are several interpretations of the minimums in the sulfate profile at 197 (Core 126-790C-13X) and 651 mbsf (Core 126-791B-28R): (1) contamination of deeper samples by surface seawater used during drilling, (2) subsurface flow of seawater, and (3) nonsteady-state sulfate reduction. Contamination cannot be entirely excluded. However, at Site 790 the whole rounds taken for squeezing were thoroughly examined, and all of them consisted of continuous, undisturbed, coherent sediments.

Given the distribution of sedimentary sulfur and organic carbon, and the young age of these sediments, the nonsteady-state interpretation is preferred. Circulation of seawater in the basement is also a possibility, but in this case, a less likely interpretation. At Site 791, the quality of the cores was low, and some contamination of the deeper samples by seawater may have occurred. However, it is interesting to note that the sulfate minimum at Site 791 is present at about the same age as at Site 790 (0.32 Ma).

High calcium and low magnesium concentrations in the pore waters recovered from Cores 126-791A-2H and -5H are the only direct indications of ongoing low-temperature alteration of volcanogenic material at these two sites, despite the abundance of pyroclastic material. It is speculated that this is related to the very high sedimentation rates, which give the reactions too little time to impose their signal on the pore-water composition.

PHYSICAL PROPERTIES

Introduction

Multisensor track (GRAPE and *P*-wave) logging, thermal conductivity, index property, and Hamilton Frame (HF) sonic velocity measurements were completed on sediments from all three holes at Site 790 (see "Explanatory Notes" chapter, this volume). In addition, vane shear strength was measured on sections of Holes 790B and 790C that appeared the least disturbed. Velocity measurements were completed on one igneous sample recovered from the base of Hole 790C.

The full suite of physical property measurements were attempted on cores recovered from Hole 791A. However, because of the nature of the material, many intervals of poor recovery, and extensive drilling disturbance, sample spacing is variable. See the individual sections below for details. Multisensor track (MST) logging, thermal conductivity, index property, and velocity measurements were performed on cores throughout the sedimentary section at Hole 791B. Within the igneous section at Hole 791B, velocity and index property analyses were obtained on discrete samples; four igneous samples were measured for thermal conductivity. Because of disturbance resulting from rotary drilling, no vane shear strength analyses were made on any of the material recovered in Hole 791B. In addition, *P*-wave logging and GRAPE measurements were suspended at the base of the sedimentary section.

Samples of hard rock used for physical property analyses were removed from the cores at different time intervals. Some

Table 13 (continued).

791B-61R	791B-62R	791B-64R	791B-67R	791B-72R	791B-73R	791B-75R	791B-77R	791B-77R	791B-78R	791B-78R	791B-79R	791B-79R
1, 1-4	1, 88-92	1, 8-81	1, 61-63	3, 14-17	3, 112-115	1, 57-59	1, 92-95	2, 128-130	1, 79-82	1, 113-115	1, 17-20	1, 94-97
1	5B	13	5	2A	10	10	7	5B	8	12A	3	7
967	982	1001	1025	1077	1088	1103	1121	1125	1133	1137	1139	1143
8	11	11	11	11	11	12	17	20	24	27	28	29
diabase	mousse-c	mousse-c	mousse-m + c	mousse-c + m	mousse-c	mousse-c	diabase	lap-tuff	basalt	basalt	lap-tuff	diabase
50.14	48.59	48.94	49.76	50.21	49.61	49.68	48.51	60.66	52.62	51.59	51.04	49.09
1.17	0.96	0.99	1.06	0.92	1.01	0.98	1.09	0.96	1	1.05	0.68	1.59
17.69	16.99	16.89	17.58	16.56	16.59	17.11	18.6	15.66	17.09	17.98	18.78	16.9
10.45	10.67	12.16	12.02	10.94	10.79	10.13	11.69	8.92	10.12	10.48	11.16	14.96
0.13	0.15	0.16	0.18	0.17	0.12	0.11	0.2	0.12	0.09	0.14	0.21	0.22
5.97	8.25	9.17	8.72	10.83	7.95	8.94	7.82	7.22	9.58	8.71	8.98	5.43
11.66	12.11	10.02	8.43	4.78	10.17	10.74	10.05	1.64	6.6	7.59	1.67	5.9
2.63	2.28	2.12	2.41	4.52	2.9	2.41	2.6	1.76	3.02	2.82	3.96	5.15
0.3	0.15	0.3	0.54	1.15	0.52	0.15	0.15	3.26	0.47	0.22	3.41	0.73
0.18	0.48	0.07	0.07	0.1	0.23	0.19	0.15	0.24	0.23	0.21	0.06	0.16
0.64	1.49	1.56	6.32	6.4	2.1	1.95	1.5	4.48	2.94	2.45	4.32	3.34
100.32	100.63	100.82	100.75	100.18	99.89	100.44	100.86	100.44	100.82	100.79	99.95	100.13
784.98	2093.28	305.27	305.27	436.1	1003.03	829.[illegible]	654.15	1046.64	1003.03	915.81	261.66	697.76
71.7	46.8	45.7	46.3	40.1	47.5	43.9	56.1	84.3	62.4	63.9	20.9	59.6
25	29.1	16.2	15.9	16.7	26.2	18.7	20.1	45.5	20.3	16.4	13.8	20.9
5.3	2	3.1	4.8	5.5	1.4	1.1	0.9	71.3	3.3	1.4	26.3	9.7
242	260	183	172	227	275	203	220	59	256	286	292	358
5	1	25		25	22		3	147	43	37	209	33
455	353	321	355	165	387	361	123	306	327	352	419	
1.9	0.9	0.7	1.1	0.7	1.2	1.2	1.1	1.6	2	2.3	0.4	1.1
55	43	56	52	55	40	53	97	5	58	51	22	0
167	186	164	181	165	167	180	226	1	166	160	26	6
103	106	102	95	88	99	99	92	164	98	95	100	111
51	55	58	54	47	52	49	50	12	48	62	27	18
6	11		7		12	11	7		1	4		3
55.7	62.99	62.4	61.49	68.54	61.86	66.01	59.55	64.05	67.57	64.66	63.91	44.41

were taken and measured immediately after the cores were split; others were taken after all pieces had their surface dried for labeling (approximately 2-3 hr after core splitting). The largest group of samples were taken 2-4 days after the cores had been retrieved.

Even in these relatively short time periods, a significant loss of pore fluid may have occurred (e.g., Hay, Sibuet, et al., 1984) and permanent alteration of the rock resulted, induced by changes in the hydration and crystallographic states of the minerals. Attempts to resaturate these samples in seawater did, indeed, increase the amount of water in the rock, but the resulting material properties may have little relation to those of the *in-situ* rock. Consequently, those samples measured directly after splitting are the most reliable indicators of the original state and properties of the rock.

Site 790

Index Properties

Trends in wet-bulk density and grain density roughly parallel each other throughout the entire sedimentary section. Throughout lithologic Unit I (see "Lithostratigraphy and Accumulation Rates" section, this chapter), both properties are characterized by high variability and no real systematic downhole trends. Values in Unit II increase fairly regularly from approximately 160 to 250 mbsf, at which point both parameters again become highly variable (Fig. 68 and Table 17).

Gravimetrically determined wet-bulk densities range from approximately 1.4 to 2.0 g/cm^3, averaging 1.61 g/cm^3 in Unit I and 1.69 g/cm^3 in Unit II. This downhole increase is primarily the result of increased consolidation from the weight of overburden. However, a distinct change at the Unit I/II boundary (Fig. 68) implies that higher calcium carbonate contents within Unit II are also influencing the wet-bulk densities, probably through their effect on grain densities (see below).

GRAPE wet-bulk density values correlate very well in the overlapping intervals between Holes 790A and 790B and between Holes 790B and 790C (Fig. 69). Slight offsets may be attributed to small variations in the cored interval (see "Lithostratigraphy and Accumulation Rates" section, this chapter) and/or coring disturbance.

In general, agreement between GRAPE and gravimetrically determined wet-bulk density values is good throughout Holes 790A, 790B, and 790C. With the exception of the upper 20 m of Hole 790B, gravimetric bulk density measurements fall within 0.1 g/cm^3 of the GRAPE values (Fig. 69). Gravimetric bulk density values in the upper 20 m of Hole 790B display significantly greater scatter than either those in Hole 790A or GRAPE-generated values. These discrete samples are from thin layers with extreme bulk density values, such as vitric sand and silt beds. When the GRAPE data are averaged (over 20-cm intervals), much of the scatter in the data is minimized.

The downhole increase in wet-bulk density is mirrored by decreases in water content and porosity. Porosity data range from 50% to over 80%, and average 68% and 66% in Units I and II, respectively. Water contents generally fall between approximately 30% and 110% and average 79% and 68% in Units I and II, respectively (Table 17 and Fig. 68). Variability in water content and porosity decreases near the lithologic boundary, similar to the trend in wet-bulk density and grain density.

Grain density values in the upper unit range from 2.1 to ~3.0 g/cm^3, with a mean of 2.57 g/cm^3. Intervals of high grain density in Unit I correspond to beds with high calcium carbonate contents (11-28 and 55-70 mbsf; Fig. 68; see discussion that follows). Grain density values in Unit II display less variability, averaging 2.66 g/cm^3. This increase in grain density from Units I to II is related to higher calcium carbonate contents below 130-150 mbsf.

The magnitude and trends of the gravimetrically determined index properties agree well in the depth overlaps between the

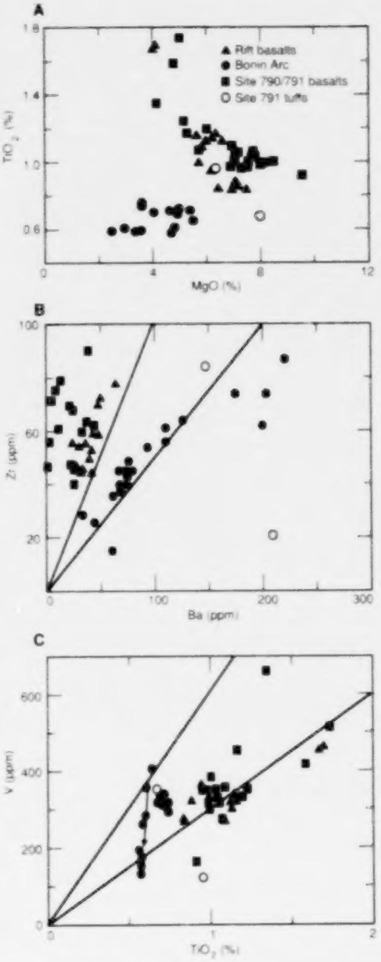

Figure 63. **A.** TiO_2 vs. MgO. The rift basalts are representatives of the 0.6–0.05 Ma basalts dredged and sampled by ALVIN (Hochstaedter et al., in press; Fryer et al., in press). The Bonin Arc samples are basalt to andesites from Tori Shima, Sumisu Jima, and Oshima (Y. Zhang, pers. comm., 1989; Wood et al., 1980). The two Site 791 tuffs are from Units 20 and 28. Note the slightly higher TiO_2 content of the younger "rift" vs. older Site 790/791 basalts. **B.** Ba vs. Zr. Symbols and data as above. Lines of constant Ba/Zr ratios of 1 and 2 are shown for reference. Arc lavas generally have Ba/Zr >1; MORB and oceanic-island basalt (OIB) ratios are about 0.15 and 0.8, respectively. The Site 790/791 shipboard Ba data are tentative, but unquestionably <50 ppm, indicating Ba/Zr ratios intermediate between MORB and the arc, but overlapping OIB. **C.** TiO_2 vs. V. Symbols and data as above. Lines of constant Ti/V ratios of 10 and 20 are shown for reference. Arc lavas generally have Ti/V of 10–20 vs. 20–25 in MORB and >30 in OIB. The arrow shows the differentiation path of Tori Shima lavas, implying a low Ti/V parent and early magnetite fractionation.

Table 14. Sediment resistivity, measurement temperature, and pore-water resistivity at 25°C and formation factor of sediments from Sites 790 and 791.

Core, section, interval (cm)	Depth (mbsf)	R_s (ohm-m)	Temperature (°C)	R_{pw} (ohm-m)	F
126-790A-					
2H-3, 140–150	13.25	0.675	10.0	0.200	2.4
3H-5, 140–150	25.75	0.704	10.9	0.200	2.5
126-790B-					
6H-3, 140–150	46.95	1.445	13.1	0.200	5.5
8H-5, 140–150	69.05	0.709	13.7	0.198	2.7
9H-2, 140–150	74.25	0.657	13.6	0.198	2.5
126-790C-					
2H-4, 140–150	100.45	0.530	11.9	0.196	2.0
5H-5, 140–150	130.95	0.761	14.9	0.198	3.0
10X-1, 101–111	165.96	0.717	14.3	0.197	2.8
13X-2, 140–150	196.85	0.662	15.3	0.196	2.7
16X-3, 140–150	227.25	0.791	15.3	0.197	3.2
18X-2, 140–150	254.65	0.695	18.7	0.198	3.0
126-791A-					
2H-5, 140–150	11.95	0.619	11.1	0.196	2.3
5H-3, 140–150	37.45	0.856	13.8	0.193	3.4
18H-6, 90–100	166.95	0.886	13.3	0.195	3.5
22H-6, 140–150	205.85	0.902	14.2	0.194	3.6
126-791B-					
10R-1, 86–96	474.21	1.253	14.5	0.199	5.0
13R-1, 140–150	503.55	0.964	14.9	0.196	4.2
23R-3, 115–125	602.9	0.790	14.6	0.198	5.0
28R-3, 140–150	651.05	1.049	16.1	0.198	4.3
34R-3, 140–150	709.05	1.246	16.4	0.199	5.1
39R-1, 140–150	753.85	0.872	14	0.198	3.4
42R-2, 0–10	782.85	0.951	15.6	0.198	3.9
45R-2, 140–150	813.2	1.864	15.8	0.199	7.5

Note: R_s = sediment resistivity, R_{pw} = pore-water resistivity, and F = formation factor.

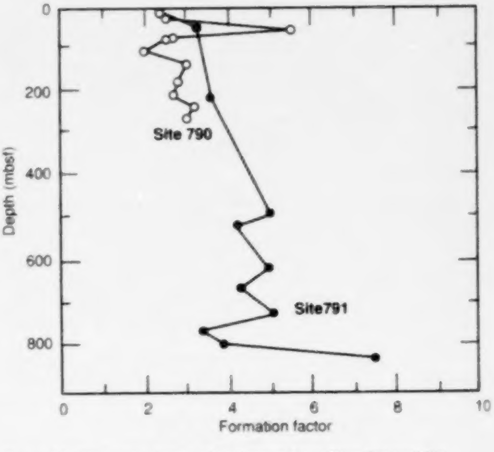

Figure 64. Formation factor of sediments from Sites 790 and 791.

Table 15. Concentration of organic carbon and total nitrogen and sulfur in sediments from Sites 790 and 791.

Core, section, interval (cm)	Depth (mbsf)	Inorg. carbon (%)	$CaCO_3$ (%)	Total carbon (%)	Org. carbon (%)	Tot N (%)	Tot S (%)
126-790A-1H-1, 52–54	0.52	0.22	1.8	0.40	0.18	0.09	
126-790B-1H-1, 62–65	0.62	0.29	2.4	0.50	0.21	0.08	
126-790A-1H-2, 87–89	2.38	0.18	1.5	0.33	0.15		
126-790B-1H-2, 106–109	2.58	0.13	1.1	0.26	0.13		
126-790B-1H-3, 22–25	3.23	0.13	1.1	0.28	0.15	0.08	
126-790A-1H-3, 23–25	3.23	0.15	1.2	0.32	0.17		
126-790B-2H-2, 53–56	6.55	0.16	1.3	0.32	0.16	0.06	
126-790A-1H-6, 25–27	7.76	0.15	1.2	0.28	0.13		
126-790B-2H-3, 113–116	8.65	3.71	30.9	4.97	1.26	0.17	
126-790A-2H-1, 84–85	9.64	0.07	0.6	0.17	0.10	0.01	0.04
126-790B-2H-4, 88–91	9.90	1.95	16.2	2.82	0.87	0.13	
126-790A-2H-2, 71–73	11.02	2.35	19.6	3.11	0.76	0.06	
126-790B-2H-5, 61–64	11.13	0.11	0.9	0.20	0.09		
126-790B-2H-6, 36–39	12.37	2.38	19.8	3.29	0.91	0.13	
126-790A-2H-3, 122–123	13.02	2.22	18.5	3.00	0.78	0.09	
126-790A-2H-3, 140–150	13.25	2.04	17.0	2.87	0.83	0.13	
126-790A-2H-6, 132–133	17.62	1.77	14.7	2.45	0.68	0.11	
126-790A-3H-2, 102–104	20.83	0.23	1.9	0.43	0.20	0.08	
126-790A-3H-4, 40–42	23.21	0.18	1.5	0.34	0.16	0.07	
126-790A-3H-5, 140–150	25.75	0.16	1.3	0.30	0.14	0.06	
126-790A-3H-6, 57–59	26.38	0.14	1.2	0.29	0.15		
126-790B-6H-3, 140–150	46.95	0.05	0.4	0.11	0.06		
126-790B-7H-3, 72–76	55.74	2.32	19.3	3.08	0.76	0.13	
126-790B-7H-4, 62–65	57.14	0.10	0.8	0.30	0.20		
126-790B-7H-5, 24–27	58.26	0.05	0.4	0.18	0.13		
126-790B-8H-1, 134–135	62.94	0.34	2.8	0.59	0.25	0.09	
126-790B-8H-2, 132–134	64.33	0.05	0.4	0.16	0.11	0.05	
126-790B-8H-3, 130–132	65.91	1.83	15.2	2.42	0.59	0.11	
126-790B-8H-4, 10–12	66.21	2.07	17.2	2.63	0.56	0.10	
126-790B-8H-5, 140–150	69.05	2.52	21.0	3.22	0.70	0.13	
126-790B-8H-6, 47–49	69.58	1.37	11.4	1.99	0.62	0.12	
126-790B-9H-1, 124–126	72.55	0.07	0.6	0.17	0.10	0.07	
126-790B-9H-2, 140–150	74.25	0.20	1.7	0.15	-0.05	0.06	
126-790B-9H-3, 13–15	74.44	0.05	0.4	0.14	0.09	0.05	
126-790B-10H-4, 57–60	86.09	0.05	0.4	0.12	0.07		
126-790B-10H-5, 81–84	87.83	0.26	2.2	0.42	0.16	0.07	
126-790C-1H-3, 34–36	88.32	0.27	2.2	0.40	0.13	0.08	0.14
126-790B-10H-6, 96–99	89.48	0.10	0.8	0.20	0.10	0.05	
126-790B-11H-1, 114–117	91.86	0.13	1.1	0.24	0.11	0.05	
126-790B-11H-2, 89–92	93.11	0.18	1.5	0.34	0.16	0.08	
126-790C-1H-6, 107–109	93.58	0.17	1.4	0.27	0.10	0.06	0.11
126-790B-11H-4, 114–117	96.36	0.16	1.3	0.31	0.15	0.07	
126-790C-2H-2, 106–109	97.08	0.08	0.7	0.15	0.07	0.06	0.08
126-790B-11H-6, 15–18	98.37	0.15	1.2	0.25	0.10	0.07	
126-790C-2H-5, 0–5	100.53	0.08	0.7	0.16	0.08		
126-790C-2H-6, 79–82	102.81	0.07	0.6	0.23	0.16	0.07	
126-790C-3H-3, 62–65	107.84	0.08	0.7	0.21	0.13		
126-790C-3H-6, 38–41	112.10	0.06	0.5	0.28	0.22		0.17
126-790C-5H-3, 81–84	127.33	2.26	18.8	2.76	0.50	0.11	0.08
126-790B-15X-1, 10–13	129.42	2.38	19.8	2.80	0.42	0.09	
126-790B-15X-1, 45–47	129.76	0.07	0.6	0.18	0.11		
126-790C-5H-5, 59–61	130.10	0.04	0.3	0.13	0.09	0.07	0.40
126-790C-5H-5, 140–150	130.95	1.86	15.5	2.23	0.37		
126-790C-5H-6, 91–94	131.93	2.58	21.5	3.18	0.60	0.11	
126-790C-6H-1, 126–129	134.47	0.05	0.4	0.13	0.08	0.13	
126-790C-6H-2, 91–93	135.62	0.09	0.7	0.19	0.10		
126-790C-6H-4, 88–92	138.60	1.57	13.1	1.88	0.31	0.09	0.14
126-790C-6H-5, 62–65	139.84	0.08	0.7	0.13	0.05	0.03	0.09
126-790C-6H-6, 67–69	141.38	1.66	13.8	2.07	0.41	0.10	
126-790C-6H-7, 22–25	142.44	3.42	28.5	4.03	0.61	0.12	0.11
126-790C-7H-2, 25–28	144.47	0.36	3.0	0.55	0.19		
126-790C-10X-1, 101–111	165.96	3.38	28.2	4.28	0.90	0.12	
126-790C-10X-2, 36–39	166.78	2.71	22.6	3.38	0.67	0.14	
126-790C-11X-1, 103–106	175.65	2.06	17.2	2.57	0.51	0.11	
126-790C-11X-3, 52–54	178.13	3.87	32.2	4.48	0.61	0.13	0.12
126-790C-11X-5, 42–45	181.04	2.96	24.7	4.09	1.13	0.20	0.24
126-790C-12X-1, 43–45	184.64	2.22	18.5	2.82	0.60	0.15	0.14
126-790C-12X-2, 6–8	185.77	4.76	39.7	5.19	0.43	0.12	0.12
126-790C-13X-1, 115–116	195.06	5.07	42.2	5.60	0.53	0.11	
126-790C-13X-2, 99–100	196.39	5.88	49.0	6.45	0.57	0.14	
126-790C-13X-2, 140–150	196.85	5.16	43.0	5.70	0.54	0.08	
126-790C-13X-3, 100–101	197.91	4.60	38.3	5.40	0.80	0.14	0.10
126-790C-13X-4, 14–16	198.55	4.38	36.5	5.18	0.80	0.15	0.14
126-790C-14X-1, 127–128	204.88	4.38	36.5	5.20	0.82	0.14	
126-790C-14X-2, 125–126	206.36	2.93	24.4	3.73	0.80	0.17	0.13

Table 15 (continued).

Core, section, interval (cm)	Depth (mbsf)	Inorg. carbon (%)	$CaCO_3$ (%)	Total carbon (%)	Org. carbon (%)	Tot N (%)	Tot S (%)
126-790C-14X-3, 35-36	206.96	3.02	25.2	3.68	0.66	0.15	
126-790C-16X-1, 90-91	223.71	2.93	24.4	3.54	0.61	0.16	
126-790C-16X-2, 104-105	225.35	5.63	46.9	6.43	0.80	0.19	
126-790C-16X-3, 68-69	226.49	3.77	31.4	4.56	0.79	0.15	
126-790C-16X-3, 140-150	227.25	2.16	18.0	2.58	0.42	0.09	
126-790C-16X-4, 109-110	228.40	2.87	23.9	3.46	0.59	0.13	
126-790C-16X-5, 91-92	229.72	1.62	13.5	2.18	0.56	0.12	0.17
126-790C-17X-1, 101-103	233.42	2.22	18.5	2.63	0.41	0.12	
126-790C-17X-2, 74-77	234.66	3.31	27.6	4.15	0.84	0.14	
126-790C-17X-3, 111-113	236.52	1.69	14.1	2.09	0.40	0.75	0.16
126-790C-17X-4, 14-16	237.05	1.79	14.9	2.42	0.63	0.10	0.15
126-790C-17X-6, 105-108	240.97	3.73	31.1	4.26	0.53	0.12	0.19
126-790C-18X-2, 35-38	243.97	3.35	27.9	3.86	0.51	0.12	
126-790C-18X-2, 140-150	245.05	4.91	40.9	5.35	0.44	0.08	
126-790C-18X-4, 82-85	247.44	2.37	19.7	2.69	0.32	0.07	0.16
126-790C-19X-2, 44-47	253.66	6.97	58.1	6.59		0.09	
126-790C-19X-3, 115-118	255.87	4.02	33.5	4.56	0.54	0.11	
126-790C-19X-4, 124-127	257.46	3.26	27.2	3.75	0.49	0.10	
126-790C-19X-5, 72-73	258.43	3.52	29.3	3.94	0.42	0.08	
126-790C-20X-1, 112-114	262.53	3.29	27.4	3.72	0.43	0.09	
126-790C-20X-2, 57-59	263.48	3.58	29.8	3.90	0.32	0.08	
126-790C-20X-3, 38-41	264.78	4.09	34.1	4.07		0.07	
126-790C-20X-3, 38-41	264.80	3.84	32.0	4.07	0.23	0.07	
126-790C-20X-4, 12-15	266.04	3.02	25.2	3.32	0.30	0.07	
126-791A-2H-1, 81-84	5.31	0.33	2.7	0.54	0.21		
126-791A-2H-2, 92-95	6.92	0.23	1.9	0.39	0.16		
126-791A-2H-5, 140-150	11.90	0.23	1.9	0.42	0.19		
126-791A-2H-6, 48-51	12.48	0.21	1.7	0.36	0.15		
126-791A-4H-3, 96-97	27.46	3.37	28.1	4.46	1.09	0.16	0.10
126-791A-4H-4, 119-120	29.19	2.92	24.3	3.98	1.06	0.15	0.13
126-791A-4H-5, 55-56	30.05	2.33	19.4	3.32	0.99	0.13	0.08
126-791A-5H-2, 120-121	35.70	1.91	15.9	2.76	0.85	0.14	
126-791A-5H-3, 56-57	36.56	1.80	15.0	2.18	0.38	0.10	
126-791A-5H-3, 140-150	37.40	0.12	1.0	0.24	0.12	0.05	0.07
126-791A-5H-4, 23-24	37.73	0.11	0.9	0.24	0.13	0.07	0.20
126-791A-5H-5, 73-74	39.73	2.05	17.1	2.74	0.69	0.11	0.11
126-791A-7H-3, 62-65	55.62	0.14	1.2	0.30	0.16	0.07	
126-791A-7H-4, 134-137	57.84	0.14	1.2	0.30	0.16	0.07	
126-791A-8H-4, 70-72	66.80	0.07	0.6	0.16	0.09		0.08
126-791A-9H-6, 140-150	80.20	0.07	0.6	0.15	0.08		
126-791A-12H-5, 140-150	107.80	0.04	0.3	0.15	0.11		
126-791A-15H-6, 25-35	137.25	0.04	0.3	0.11	0.07	0.04	0.08
126-791A-16H-2, 74-76	141.44	0.82	6.8	1.17	0.35	0.09	
126-791A-16H-5, 60-63	145.80	0.44	3.7	0.63	0.19	0.07	0.13
126-791A-17H-1, 81-83	149.61	0.09	0.7	0.20	0.11	0.06	
126-791A-17H-3, 86-88	152.66	0.14	1.2	0.21	0.07	0.04	0.08
126-791A-17H-6, 79-81	157.09	0.04	0.3	0.11	0.07		0.09
126-791A-18H-1, 46-49	158.96	2.75	22.9	3.26	0.51	0.14	
126-791A-18H-2, 102-104	161.02	0.41	3.4	0.61	0.20	0.07	
126-791A-18H-6, 90-100	166.90	0.20	1.7	0.27	0.07		
126-791A-19H-1, 107-109	169.17	0.36	3.0	0.59	0.23	0.09	
126-791A-19H-6, 123-125	176.83	0.22	1.8	0.43	0.21	0.07	
126-791A-20H-2, 110-112	180.30	0.19	1.6	0.39	0.20	0.10	
126-791A-20H-6, 76-79	185.96	0.07	0.6	0.22	0.15	0.07	
126-791A-22H-6, 140-150	205.80	0.40	3.3	0.54	0.14	0.08	0.10
126-791A-22H-7, 16-19	206.06	0.90	7.5	1.27	0.37	0.11	
126-791A-23H-2, 72-75	207.76	0.04	0.3	0.10	0.06		0.08
126-791A-25X-CC, 15-217	0.18	0.12	0.5	0.06	0.50		
126-791A-28X-1, 68-70	246.68	0.09	0.7	0.25	0.16	0.04	
126-791A-28X-CC, 25-247	0.17	0.12	0.4	0.05	0.40		
126-791A-30X-CC, 15-265	0.12	0.03	0.7	0.09	0.70		
126-791A-33X-1, 16-18	294.46	2.62	21.8	3.20	0.58	0.11	
126-791A-39X-1, 12-13	352.42	1.88	15.7	2.74	0.86	0.13	
126-791A-39X-1, 42-45	352.72	0.22	1.8	0.43	0.21	0.09	
126-791A-40X-1, 2-3	362.02	0.13	1.1	0.26	0.13		
126-791A-42X-1, 10-11	381.50	0.45	3.7	0.71	0.26	0.09	
126-791B-10R-1, 34-35	473.64	1.24	10.3	1.80	0.56	0.06	0.07
126-791B-10R-1, 86-96	474.16	1.98	16.5	2.40	0.42	0.04	
126-791B-13R-1, 46-50	502.56	2.29	19.1	2.79	0.50	0.06	0.17
126-791B-13R-1, 140-150	503.50	3.59	29.9	4.14	0.55	0.05	0.06
126-791B-13R-2, 44-47	504.04	2.91	24.2	3.40	0.49	0.04	0.11
126-791B-16R-1, 23-25	531.43	2.58	21.5	3.23	0.65	0.05	0.14
126-791B-18R-1, 4-7	550.64	0.56	4.7	0.68	0.12	0.02	0.21
126-791B-22R-1, 69-71	589.69	3.14	26.2	4.12	0.98	0.08	0.05
126-791B-23R-1, 77-79	599.47	3.90	32.5	4.92	1.02	0.09	0.14
126-791B-23R-2, 84-86	601.04	3.18	26.5	4.18	1.00	0.10	0.21
126-791B-23R-3, 115-125	602.85	3.32	27.7	4.37	1.05	0.03	
126-791B-23R-CC, 2-4	603.91	3.26	27.2	4.05	0.79	0.08	0.43

Table 15 (continued).

Core, section, interval (cm)	Depth (mbsf)	Inorg. carbon (%)	$CaCO_3$ (%)	Total carbon (%)	Org. carbon (%)	Tot N (%)	Tot S (%)
126-791B-24R-1, 54-56	608.94	2.81	23.4	3.43	0.62	0.06	0.02
126-791B-25R-1, 25-27	618.35	1.86	15.5	2.40	0.54	0.07	0.13
126-791B-25R-2, 13-15	619.73	3.22	26.8	3.86	0.64	0.07	0.78
126-791B-26R-1, 4-6	627.74	3.27	27.2	3.81	0.54	0.04	0.03
126-791B-27R-1, 37-39	637.37	3.46	28.8	4.23	0.77	0.07	0.03
126-791B-28R-1, 120-121	647.80	4.46	37.2	5.25	0.79	0.08	0.07
126-791B-28R-3, 81-83	650.41	4.53	37.7	5.32	0.79	0.08	0.02
126-791B-28R-3, 140-150	651.00	3.86	32.2	4.74	0.88	0.07	0.10
126-791B-30R-1, 146-147	667.46	3.51	29.2	4.11	0.60	0.05	
126-791B-30R-3, 107-108	670.07	2.85	23.7	3.45	0.60	0.06	0.04
126-791B-31R-1, 83-84	676.43	1.98	16.5	2.48	0.50	0.06	0.05
126-791B-31R-3, 70-71	679.30	4.93	41.1	5.45	0.52	0.05	0.03
126-791B-32R-1, 30-32	685.60	3.17	26.4	3.75	0.58	0.05	0.08
126-791B-34R-1, 116-118	705.76	3.38	28.2	4.05	0.67	0.06	0.07
126-791B-34R-3, 37-39	707.97	5.12	42.6	5.79	0.67	0.06	
126-791B-34R-3, 140-150	709.00	4.21	35.1	4.91	0.70	0.05	0.22
126-791B-34R-4, 68-70	709.78	5.17	43.1	5.70	0.53	0.05	
126-791B-36R-1, 28-30	723.88	3.18	26.5	3.84	0.66	0.07	0.02
126-791B-36R-4, 134-136	729.44	4.86	40.5	5.31	0.45	0.04	
126-791B-37R-2, 66-67	735.36	1.62	13.5	2.06	0.44	0.04	0.03
126-791B-38R-2, 8-10	744.38	4.01	33.4	4.49	0.48		0.06
126-791B-38R-4, 15-18	747.45	2.46	20.5	2.56	0.10		0.04
126-791B-39R-1, 9-11	752.49	4.03	33.6	4.51	0.48		0.04
126-791B-39R-1, 140-150	753.80	1.72	14.3	1.86	0.14	0.02	0.05
126-791B-39R-2, 108-109	754.98	3.42	28.5	3.82	0.40	0.04	
126-791B-40R-1, 9-11	762.19	3.78	31.5	4.12	0.34	0.04	0.04
126-791B-40R-3, 50-52	765.60	4.53	37.7	4.98	0.45	0.05	
126-791B-41R-1, 17-19	771.87	3.41	28.4	3.88	0.47	0.05	
126-791B-41R-3, 72-74	775.42	6.03	50.2	6.47	0.44	0.05	
126-791B-42R-1, 36-38	781.66	4.59	38.2	5.03	0.44	0.04	
126-791B-42R-2, 0-10	782.80	4.24	35.3	4.76	0.52		
126-791B-43R-1, 9-11	791.09	3.64	30.3	4.14	0.50	0.07	
126-791B-44R-1, 40-41	801.10	4.66	38.8	5.17	0.51	0.04	
126-791B-44R-1, 98-99	801.68	4.22	35.2	4.53	0.31	0.03	
126-791B-44R-2, 97-98	803.17	3.25	27.1	3.62	0.37	0.04	
126-791B-45R-2, 96-99	812.76	4.74	39.5	5.18	0.44	0.04	
126-791B-45R-2, 140-150	813.20	5.46	45.5	5.95	0.49		
126-791B-46R-1, 43-45	820.43	2.70	22.5	3.07	0.37	0.04	
126-791B-46R-2, 15-18	821.65	4.88	40.7	5.31	0.43	0.04	

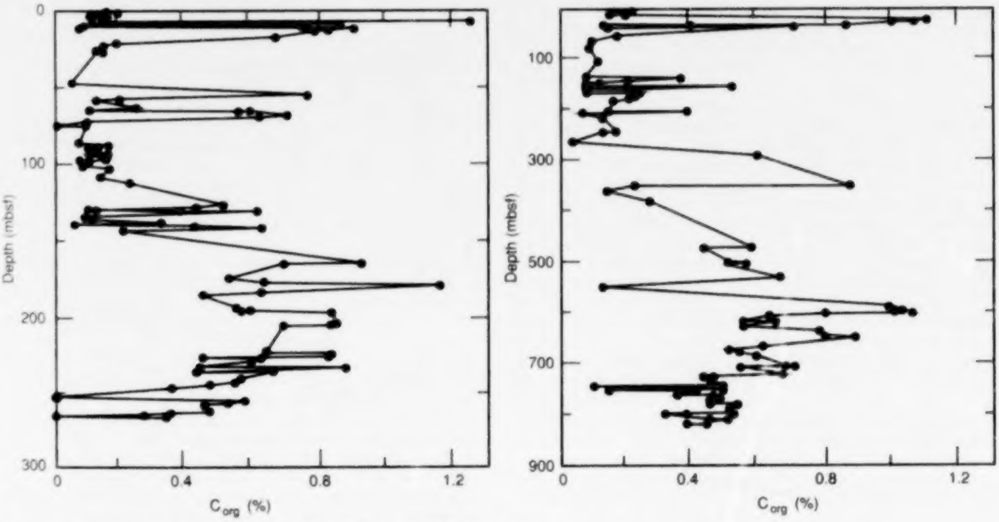

Figure 65. Concentrations of organic carbon, Sites 790 (left) and 791 (right).

Table 16. Composition of pore water and drilling mud filtrate at Sites 790 and 791.

Core, section, interval (cm)	Depth (mbsf)	pH	Alk. (mM)	Sal. (g/kg)	Cl^- (mM)	SO_4^{2-} (mM)	Na (mM)	Mg^{2+} (mM)	Ca^{2+} (mM)	K (mM)	Li (μM)	Sr (μM)	Fe (μM)	Mn (μM)	SiO_2 (μM)	NH_4 (μM)
126-790A																
2H-3, 140-150	13.25	7.66	4.46	35.5	554	27.9	474	53.5	9.7	10.2	25.1	90	9	39	677	271
3H-5, 140-150	25.75	7.62	3.94	35.0	553	27.4	470	53.1	10.2	9.3	25.1	90	7	28	477	197
126-790B																
6H-3, 140-150	46.95	7.93	2.70	35.0	555	27.8	478	53.0	10.8	9.2	23.3	89	7	13	239	56
8H-5, 140-150	69.05	7.64	4.79	35.0	560	27.6	475	52.2	9.6	8.0	35.9	97	12	25	823	695
9H-2, 140-150	74.25	7.56	4.90	35.5	561	27.2	485	52.6	10.3	6.5	39.4	98	7	22	500	733
126-790C																
2H-4, 140-150	100.45	7.69	3.99	36.5	563	26.8	483	53.8	11.7	5.4	62.8	100	13	19	392	572
5H-5, 140-150	130.95	7.62	3.40	35.5	567	25.3	478	51.9	11.0	6.7	50.2	98	12	24	718	894
10X-1, 101-111	165.96	7.45	5.68	35.5	563	21.2	472	52.3	9.5	7.1	48.4	105	6	10	956	1234
13X-2, 140-150	196.85	7.36	9.29	35.0	560	15.1	472	52.0	5.6	8.1	30.5	111	11	9	962	1468
16X-3, 140-150	227.25	7.39	9.40	35.0	560	18.2	473	51.9	5.7	8.7	30.5	103	11	10	942	1425
18X-2, 140-150	254.65	7.4	5.99	35.0	560	22.9	478	50.0	7.5	9.9	30.2	98	16	7	1003	752
126-791A																
2H-5, 140-150	11.95	7.47	4.11	36.0	569	28.5	487	45.8	19.2	6.8	80.7	105	88	74	284	281
5H-3, 140-150	37.45	7.56	3.01	36.0	576	27.5	493	44.3	19.7	7.3	93.5	103	35	40	576	331
9H-6, 140-150	80.25	7.86	3.19	36.0	563	28.1	478	52.8	12.0	9.5	40.4	95	LD	27	269	175
12H-5, 140-150	107.85	7.77	3.54	35.5	558	28.8	473	52.1	12.3	8.8	42.2	95	LD	34	338	271
15H-6, 25-35	137.30	7.82	3.72	36.0	565	26.6	478	52.8	10.9	8.3	45.9	95	4	21	263	266
18H-6, 90-100	166.95	7.77	4.66	36.5	570	26.9	484	53.0	10.8	6.6	55.0	95	LD	14	506	440
22H-6, 140-150	205.85	7.53	4.55	36.0	571	26.5	486	52.7	10.8	6.6	64.2	95	1	22	487	415
126-791B																
10R-1, 86-96	474.21	7.53	3.76	36.0	557	27.6	484	48.7	15.7	5.8	60.5	99	2	26	717	536
13R-1, 140-150	503.55	7.48	2.39	36.0	566	26.8	483	49.5	16.1	5.6	51.4	96	3	36	850	417
23R-3, 115-125	602.90	7.33	4.58	36.0	561	25.5	481	49.5	15.7	5.7	53.2	107	LD	33	1001	811
28R-3, 140-150	651.05	7.34	3.98	35.5	562	24.2	491	47.9	14.2	6.3	58.7	121	2	12	1049	1110
34R-3, 140-150	709.05	7.39	3.77	36.0	558	25.9	469	49.6	13.1	9.6	36.7	103	2	23	947	310
39R-1, 140-150	753.85	7.45	4.10	36.0	561	26.2	481	50.4	13.0	9.7	40.4	109	13	12	856	398
42R-2, 0-10	782.85	7.32	3.33	36.5	562	26.1	480	50.3	13.2	10.2	40.4	107	3	16	999	196
45R-2, 140-150	813.20	7.48	2.32	36.5	558	26.7	483	49.6	12.5	10.6	27.5	99	1	12	682	47
Drilling mud filtrate		9.01	0.87		267	14.3	251	5.4	6.0	4.0	23.8	93	LD	LD	16	LD
Surface seawater		8.05	2.67		563	28.6	475	53.3	10.7	10.0	31.2	29	LD	LD	2	LD

Note: LD = less than the detection limit.

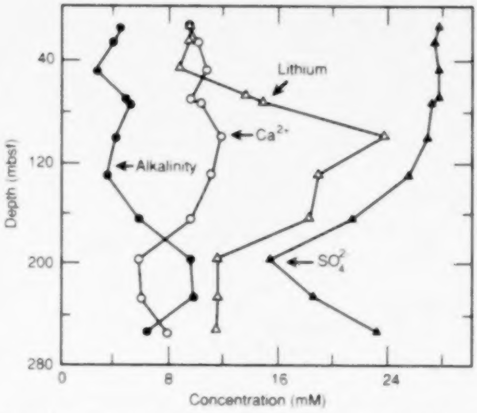

Figure 66. Composition of sedimentary pore water from Site 790.

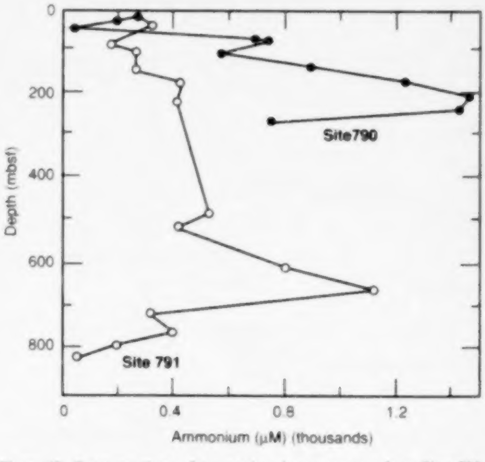

Figure 67. Concentrations of ammonium in pore waters from Sites 790 and 791.

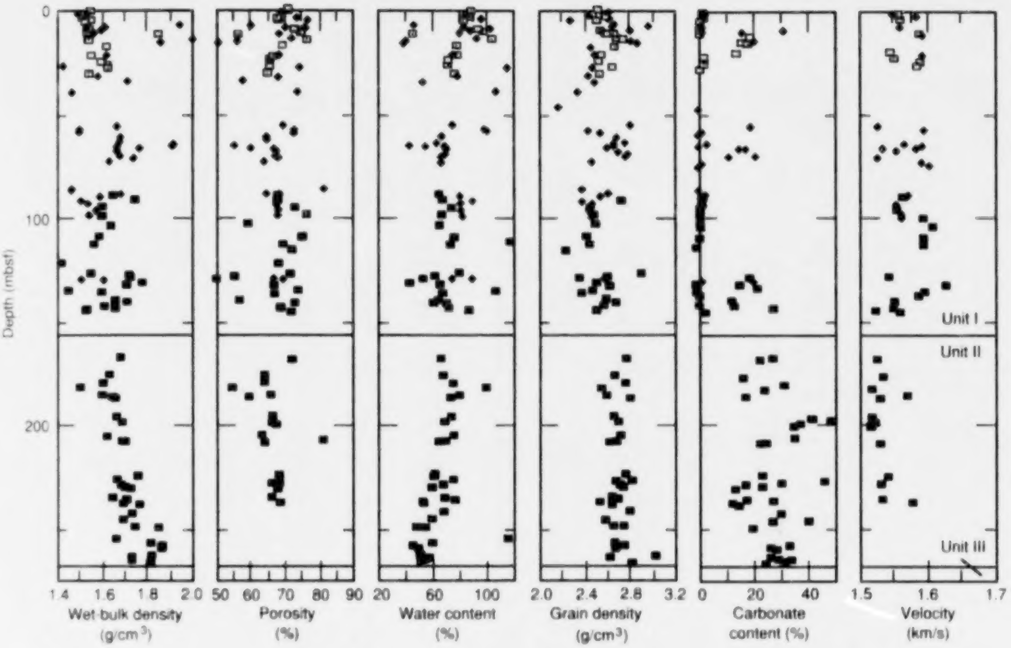

Figure 68. Downhole plots of index properties, carbonate content, and velocity for Holes 790A (open squares with dots), 790B (diamonds), and 790C (closed squares). Horizontal lines indicate Unit I, II, and III boundaries.

three holes. Particularly good correlation is observed in the grain density values. It is likely that grain density is the parameter least changed by drilling disturbance.

Calcium Carbonate

The upper 140 m of Unit I at Site 790 is characterized by low calcium carbonate contents, generally <2-3 wt% (Fig. 68). These low values are usually associated with thick beds of silt- to gravel-size volcanogenic material rich in pumice (see "Lithostratigraphy and Accumulation Rates" section, this chapter). Thinner layers, 5-10 m thick, in which $CaCO_3$ contents reach 30%, are also present within this unit. Dilution of pelagic carbonate sedimentation by thick, sporadic, geologically instantaneous volcanogenic sediment input is the probable cause of these variations.

At the transition to Unit II, average carbonate contents increase to approximately 30%. The magnitude of the carbonate content fluctuations increases in Unit II, ranging from a low of 13.5% to a high of 49%.

Vane Shear Strength

Vane shear strength measurements in Holes 790B and 790C range from <5 to 110 kPa; values in the sediments above 240 mbsf never exceed 65 kPa (Fig. 70). Trends in the shear strength measurements between 80 and 240 mbsf correlate well with those in water content. A fairly consistent inverse trend between the two parameters is observed (Tables 17 and 18). Much of the variation in shear strength, water content, and other index properties may be attributed to lithologic and mineralogical variations such as grain size, carbonate content, degree of consolidation, and changes in the clay mineral assemblages (see "Lithostratigraphy and Accumulation Rates" section, this chapter). However, the effects of coring disturbance and other artifacts attributed to the sampling procedure cannot be disregarded (e.g., Becker, Sakai, et al., 1988, "Sites 677 and 678" chapter).

Sonic Velocity

Sonic velocity measurements were performed on discrete samples from Site 790 (Holes 790A, 790B, and 790C) with the HF method (Table 17 and Fig. 68). In addition, all cores from Holes 790A and 790B and Cores 126-790C-1H through -20X were passed through the MST and sonic velocity measurements were obtained (Fig. 71). The MST *P*-wave data, obtained at 2.5-cm intervals, were filtered to remove low signal strengths and then averaged over 10-cm intervals to reduce the number of data points to a manageable size. A comparison of HF and MST velocity measurements shows good correlation of these data for the upper parts of the APC holes (Figs. 71 and 72). The MST values obtained deeper in the section are faster than those given by the HF method. Because variable contact with the core liner from XCB coring (reduced core diameters) should result in a lower MST velocity, the cause of these higher MST velocity values is problematic.

Drilling three separate holes at Site 790 provided means for an independent check on velocity measurements in the overlapping regions of Holes 790A and 790B and Holes 790B and 790C. Velocity measurements at the same depth below seafloor in different holes produced almost identical values, indicating that (1) similar sediments were present and (2) there is a high degree of precision in these measurements between holes and be-

Table 17. Physical properties (index, velocity, and carbonate) data for Site 790.

Core, section, interval (cm)	Depth (mbsf)	Wet-bulk density (g/cm³)	Dry-bulk density (g/cm³)	Porosity (%)	Water content (%)	Grain density (g/cm³)	Void ratio	Velocity (km/s)	Carbonate (%)
126-790A-									
1H-1, 52–54	0.52	1.54	0.84	71	88.9	2.52	2.43	1.56	1.8
1H-2, 92–94	2.42	1.52	0.84	69	87.3	2.61	2.25	1.57	1.5
1H-3, 23–25	3.23	1.54	0.86	69	83.9	2.54	2.19	[a]1.89	1.2
1H-6, 25–27	7.75	1.54	0.82	73	94.4	2.35	2.73		1.2
2H-1, 82–84	9.62	1.55	0.81	75	97.7	2.61	2.98	1.59	0.6
2H-2, 70–72	11.00	1.85	1.30	56	45.1	2.67	1.28		19.6
2H-3, 123–125	13.03	1.54	0.78	76	103.9	2.73	3.24	[a]1.50	18.5
2H-3, 140–150	13.20								17.0
2H-6, 134–136	17.64	1.62	0.94	69	77.5	2.67	2.24	1.55	14.7
3H-2, 102–104	20.82	1.56	0.90	67	78.2	2.53	2.02	1.55	1.9
3H-4, 39–41	23.19	1.60	0.95	66	72.9	2.53	1.92	1.59	1.5
3H-5, 140–150	25.70								1.3
3H-6, 56–58	26.36	1.63	0.97	66	71.1	2.63	1.94		1.2
4H-1, 140–142	29.20	1.55		66	76.7	2.53	1.90		
126-790B-									
1H-1, 62–65	0.62	1.53	0.74	68	84	2.60	2.15	1.55	2
1H-2, 106–109	2.56	1.49	0.81	69	89	2.45	2.19	1.59	1
1H-3, 23–25	3.23	1.52	0.80	73	96	2.63	2.70		1
2H-1, 51–53	5.01	[a]1.4	[a]0.64	[a]76.6	[a]127.6	[a]2.27	[a]3.27		
2H-2, 53–55	6.53	[a]1.94	[a]1.35	[a]59.3	[a]45.5	[a]2.97	[a]1.46	1.56	1
2H-3, 112–115	8.62	1.53	0.78	75	103	2.65	3.07	1.51	31
2H-4, 89–92	9.89	1.59	0.87	73	88	2.79	2.65	1.51	16
2H-5, 61–64	11.11	1.56	0.89	68	81	2.60	2.15	1.59	1
2H-6, 36–39	12.36	1.54	0.83	72	92	2.66	2.55	1.51	20
3H-1, 39–41	14.39	2.00	1.45	56	40	2.80	1.27		
3H-1, 139–140	15.39	1.85	1.26	50	39	2.86	1.01		
3H-3, 76–78	17.76	[a]1.44	0.77	[a]67	[a]92	2.46	2.06		
3H-5, 121–123	21.21	1.62	0.95	68	1	2.49	2.09	1.59	
4H-3, 75–77	27.25	[a]1.43	[a]0.69	[a]74	[a]113	2.47	[a]2.88		
4H-6, 101–103	32.01	[a]1.58	[a]0.91	[a]67	[a]77	2.43	[a]2.09		
5H-1, 108–110	34.08	[a]1.71	[a]1.15	[a]56	[a]51	2.49	[a]1.32		
5H-4, 88–90	38.38	[a]1.46	[a]0.73	[a]73	[a]106	2.34	[a]2.73		
6H-1, 61–62	43.11	[a]1.38	[a]0.58	[a]80	[a]147	[a]2.15	[a]4.09		
6H-3, 140–150	46.90								0
7H-3, 74–76	55.74	1.66	0.98	69	74	2.80	2.21	1.53	19
7H-4, 62–64	57.12	1.50	0.78	73	98	2.41	2.65	1.60	1
7H-5, 25–27	58.25	1.49	0.77	73	99	2.53	2.65		0
7H-CC, 9–11	61.09	1.68	1.06	65	65	2.67	1.83		
8H-1, 134–135	62.94	1.68	1.04	65	65	2.74	1.83	1.57	3
8H-2, 132–134	64.42	1.92	1.38	55	42	2.64	1.22	1.59	0
8H-3, 123–134	65.92	1.67	1.02	66	68	2.61	1.92	1.54	15
8H-4, 9–11	66.19	1.76	1.17	60	53	2.65	1.48	1.59	17
8H-4, 94–96	67.04	1.67	1.01	67	69	2.67	2.00	1.55	
8H-5, 140–150									21
8H-6, 42–44	69.52	1.68	1.02	66	68	2.78	1.98	1.52	11
8H-6, 110–112	70.20	1.74	1.07	68	67	2.74	2.11	1.53	
9H-1, 124–126	72.54	1.53	1.00	64	66	2.45	1.75	1.59	1
9H-3, 13–16	74.43								0
10H-4, 58–60	86.08	[a]1.46	[a]0.66	[a]81	[a]131	2.35	[a]4.30		0
10H-5, 81–83	87.81	1.68	1.05	64	64	2.61	1.78	1.57	2
10H-6, 96–98	89.46	1.59	0.92	69	79	2.54	2.19		1
11H-1, 114–116	91.84	[a]1.51	[a]0.82	[a]68	[a]87	2.37	[a]2.18		1
11H-2, 90–93	93.10	1.53	0.88	67	80	2.46	1.99	1.58	2
11H-4, 112–115	96.32	1.57	0.90	68	80	2.43	2.11	1.56	1
11H-6, 16–19	98.36	1.54	0.87	68	82	2.46	2.11	1.57	1
15X-1, 12–15	129.40	1.60	0.94	67	75	2.58	2.02		20
15X-1, 46–48	129.76	1.51	0.83	69	88	2.56	2.25		1
126-790C-									
1H-3, 34–36	88.34	1.65	1.02	64	66	2.61	1.79	1.57	2.2
1H-4, 63–65	90.13	1.75	1.07	69	67	2.71	2.18		
1H-6, 107–109	93.57	1.60	0.95	66	74	2.45	1.98	1.56	1.4
2H-2, 107–109	97.07	1.60	0.98	64	68	2.48	1.74	1.59	0.7
2H-5, 0–5	100.50								0.7
2H-6, 80–82	102.80	1.64	1.01	63	65	2.51	1.72	1.61	0.6
3H-3, 62–65	107.82	1.59	0.93	67	76	2.42	2.04	1.60	0.7
3H-6, 39–41	112.09	1.57	0.92	66	75	2.45	1.90	1.60	0.5
4H-1, 60–62	114.50	[a]1.32	[a]0.60	[a]72	[a]127	[a]2.23	[a]2.57		
4H-5, 71–73	120.61	[a]1.43	[a]0.67	[a]75	[a]118	[a]1.71	[a]3.11		
5H-2, 38–40	125.38	1.56	0.89	68	80	2.91	2.10		
5H-3, 81–83	127.31	1.72	1.08	65	63	2.61	1.84	1.55	18.8

Table 17 (continued).

Core, section, interval (cm)	Depth (mbsf)	Wet-bulk density (g/cm^3)	Dry-bulk density (g/cm^3)	Porosity (%)	Water content (%)	Grain density (g/cm^3)	Void ratio	Velocity (km/s)	Carbonate (%)
126-790C- (Cont.)									
5H-4, 35-38	128.35	[a]1.75	[a]1.15	[a]59	[a]53	[a]2.35	[a]1.47	[a]1.49	
5H-5, 59-61	130.09	1.79	1.26	54	44	2.50	1.16	1.63	0.3
5H-5, 104-150	130.90								15.5
5H-6, 91-94	131.91	1.71	1.05	66	66	2.62	1.96		21.5
6H-1, 125-127	134.45	1.46	0.73	74	108	2.47	2.84	1.60	0.4
6H-2, 91-94	135.61	1.60	0.99	63	68	2.39	1.72	1.59	0.7
6H-4, 88-91	138.58	1.66	1.03	64	65	2.59	1.76	1.56	13.1
6H-5, 63-66	139.83	1.71	1.08	64	62	2.67	1.75	1.50	0.7
6H-6, 67-70	141.37	1.61	0.95	66	73	2.57	1.94	1.56	13.8
6H-7, 22-25	142.42	[a]1.67	[a]0.99	[a]67.7	[a]71		[a]2.10	1.53	28.5
7H-2, 25-27	143.94	1.53	0.84	70	88	2.50	2.30	1.56	3.0
10X-1, 101-111	165.91								
10X-2, 36-39	166.37	1.69	1.05	65	66	2.78	1.89	1.53	28.2
11X-1, 103-106	175.63	1.64	1.01	64	67	2.67	1.81	1.54	22.6
11X-3, 51-55	178.11	1.62	0.95	68	76	2.78	2.14	1.52	17.2
11X-5, 42-45	181.02	1.51	0.79	74	99	2.55	2.78	1.52	32.2
12X-1, 43-47	184.63	1.60	0.92	70	80	2.61	2.27	1.57	24.7
12X-CC, 6-9	185.66	1.65	0.98	68	73	2.82	2.15	1.53	18.5
13X-1, 116-118	195.06	1.68	0.99	70	74	2.66	2.32	1.52	42.2
13X-2, 99-100	196.39	[a]1.24	[a]1.01	[a]23.8	[a]24.4	[a]2.68			49.0
13X-2, 140-150	196.60								43.0
13X-3, 97-99	197.87	1.69	1.02	68	71	2.69	2.17	1.53	38.3
13X-4, 14-16	198.54	[a]1.86	[a]1.00	[a]65	[a]68	[a]2.69		1.52	36.5
14X-1, 126-128	204.86	1.63	0.95	69	76	2.72	2.17	1.52	36.5
14X-2, 122-124	206.32	[illegible]	1.02	69	71	2.65	2.18	1.52	24.4
14X-3, 32-34	206.92	1.69	1.04	66	66	2.68	1.91	1.53	25.2
16X-1, 91-93	223.71	1.76	1.12	66	62	2.76	1.90	1.54	24.4
16X-2, 104-106	225.34	1.68	0.98	71	76	2.82	2.41	1.52	46.9
16X-3, 67-71	226.49	1.69	1.08	64	63	2.71	1.78	1.53	31.4
16X-3, 140-150	227.20		1.05						18.0
16X-4, 99-101	228.29	1.71		67	68	2.71	2.07	1.53	23.9
16X-5, 91-93	229.71	1.74	1.11	64	61	2.75	1.79		13.5
17X-1, 101-103	233.41	1.65	0.99	67	71	2.67	2.02	1.54	18.5
17X-2, 74-77	234.64	1.71	0.93	72	76	2.70	2.60	1.52	27.6
17X-3, 111-113	236.51	1.70	1.12	59	54	2.52	1.41	1.58	14.1
17X-4, 13-16	237.03	1.77	1.17	61	54	2.64	1.55		14.9
17X-6, 105-108	240.95	1.74	1.06	69	68	2.79	2.18		31.1
18X-2, 35-38	243.95	1.70	1.08	63	61	2.47	1.67		27.9
18X-2, 140-150	245.00								40.9
18X-4, 82-85	247.42	1.86	1.26	61	50	2.75	1.54		19.7
18X-4, 126-129	247.86	1.75	1.14	62	57	2.66	1.63		
19X-2, 43-46	253.63	[a]1.67	[a]0.80	[a]87	[a]116	[a]2.22	[a]6.92		
19X-3, 115-118	255.85	1.82	1.16	67	60	2.66	2.02		33.5
19X-4, 124-127	257.44	1.87	1.27	58	46	2.75	1.37		27.2
19X-5, 72-73	258.42	1.87	[a]1.21	61	50	2.68	1.54		29.3
20X-1, 111-115	262.51	[a]1.82	1.13	[a]60	[a]52	[a]3.04	1.55		27.4
20X-2, 57-60	263.47	1.73	[a]1.10	61	56	2.63	1.56		29.8
20X-3, 38-41	264.78	[a]1.74	1.22	[a]59	[a]54	[a]3.03	[a]1.49		33.0
20X-4, 12-15	266.02	1.82	1.30	61	52	2.81	1.57		25.2
33X-CC, 9-11	378.30							4.26	

[a] Results are of uncertain quality.

tween the two techniques (HF and MST; Fig. 72). The HF velocity data at this site exhibit minimal variation, with a total range of 1.51-1.63 km/s in the entire recovered section.

A general increase in velocity is observed from the seafloor down to about 155 mbsf (Unit I). Velocity measurements in this unit average 1.57 km/s (HF). A good correlation is observed between the velocity data obtained by both methods, although there is a wider range of scatter in the MST velocity data. A small (~40 m/s), but distinct, velocity inversion occurs between Units I and II (Figs. 68 and 71).

Within Unit II, velocity data average 1.54 km/s, are relatively uniform, and show a slight increase downhole to 266.7 mbsf. The HF and MST methods within Unit II show similar trends, but the MST measurements are consistently higher. This offset may result from the effect of XCB coring methods used over this interval, which can result in a lack of sediment contact with the core liner. A scoriaceous basalt (Unit III) lies beneath Unit II. Because of the low recovery, only one velocity measurement was performed, yielding a velocity of 4.26 km/s (Section 126-790C-33X-CC; 378.30 mbsf).

Thermal Conductivity

Thermal conductivity values of sediments from Holes 790A and 790B (Fig. 73 and Table 19) generally increase downhole. Values in Unit I (especially in the upper 50 m) are variable, averaging 0.902 W/m · K and ranging up to 1.06 W/m · K. This variability may be related to lithologic changes, with higher values in carbonate-rich sediments and lower values in carbonate-poor sands and gravels. Within Unit II, values tend to increase downhole and exhibit less overall variability than in Unit I. Ther-

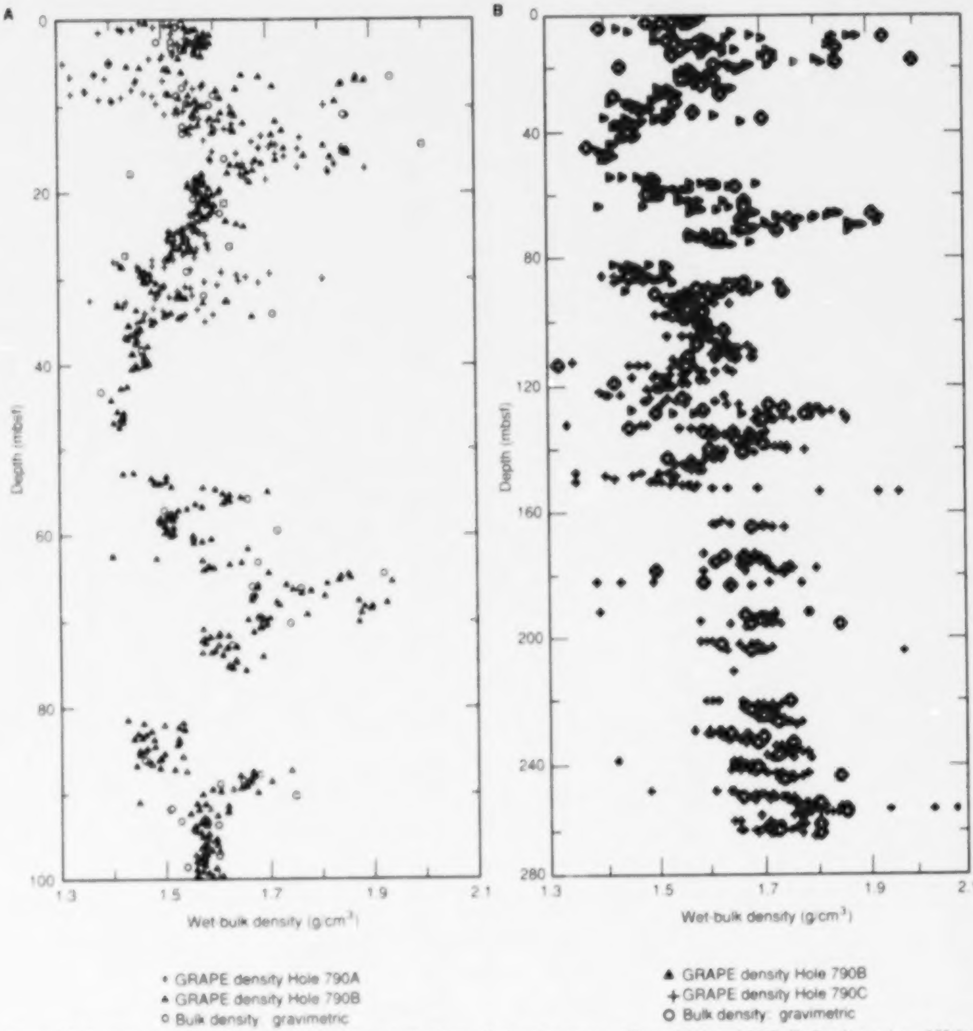

Figure 69. Comparison of gravimetric and GRAPE wet-bulk density. **A.** Overlap region of Holes 790A and 790B. **B.** Overlap region of Holes 790B and 790C.

mal conductivity values in this unit are higher than in Unit I and average 1.069 W/m · K (with a range of 0.983 – 1.183 W/m · K).

Thermal conductivity measurements are made before cores are split, not allowing assessment of coring disturbance prior to making the measurements. Because lower thermal conductivity values may result from coring disturbance (e.g., an increase in water content), we suspect that the higher values are more representative of *in-situ* conditions. Because of the low recovery, no thermal conductivity measurements were conducted on Unit III rocks.

Site 791

Index Properties

As at Site 790, wet-bulk density and grain density at Site 791 increase with depth. Mean values in Unit I are 1.64 and 2.52 g/cm³ (Fig. 74), respectively. Unit II wet-bulk and grain density

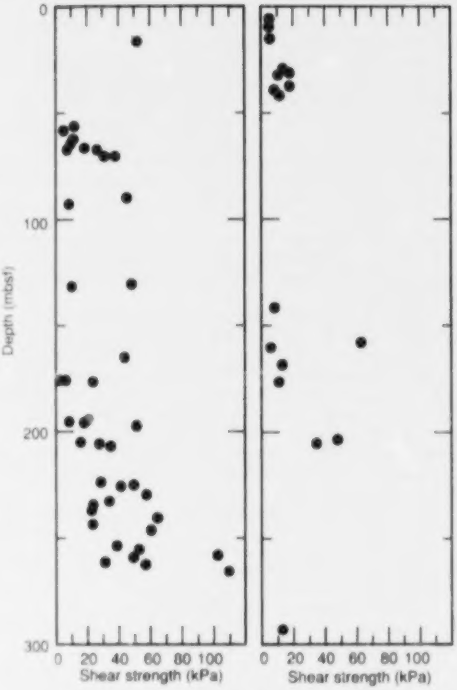

Figure 70. Plots of shear strength vs. depth, Sites 790 (left) and 791 (right).

averages are 1.86 and 2.7 g/cm^3, respectively. Concurrent decreases in porosity (averages of 65.9% in Unit I and 59.1% in Unit II) and water content (averages of 73.6% in Unit I and 48.8% in Unit II) are also noted (Table 20 and Fig. 74). With the exception of grain density, the majority of these downhole changes can be attributed to increased consolidation with depth.

Because the first eight cores in Hole 791B had essentially no recovery, no samples were taken for index properties. Therefore, a gap of about 80 m occurs in the data and no information on the overlap in the cored intervals exists. However, trends observed in Hole 791A appear to continue, at least in a general way, in Hole 791B.

Variations in wet-bulk density and grain density, especially within Hole 791A (Unit I), may be related to the sporadic input of pumice-rich material derived from volcanic eruptions (see "Lithostratigraphy and Accumulation Rates" section, this chapter). Porosity and water content trends are similar in shape, but inverse to the bulk-density trends. However, the majority of index properties measured within these pumice-rich layers are suspect. The coarse, unconsolidated nature of this material makes it especially prone to coring disturbance. Therefore, most measured properties may not be representative of the *in-situ* state of the sediment. The parameter that is expected to most resemble the *in-situ* value is grain density. Grain density variations display a strong similarity to those of $CaCO_3$. This is the case even below 450 mbsf where both properties are highly variable (Fig. 74).

Table 18. Shear strength data from Site 790.

Core, section, interval (cm)	Depth (mbsf)	Shear strength (kPa)
126-790B-		
3H-2, 40	15.9	52.2
7H-3, 72	55.7	12.2
7H-5, 27	58.3	5.0
8H-1, 132	62.9	11.1
8H-2, 135	64.5	9.7
8H-3, 136	66.0	18.3
8H-4, 7	66.2	8.2
8H-4, 92	67.0	27.1
8H-6, 42	69.5	30.7
8H-6, 113	70.2	38.1
11H-2, 129	93.5	8.9
126-790C-		
1H-4, 63	90.1	48.7
5H-5, 106	130.6	10.5
5H-6, 58	131.6	43.4
10X-2, 30	166.3	2.3
11X-2, 12	176.2	6.1
11X-2, 28	176.4	23.3
11X-2, 115	177.3	19.8
13X-1, 121	195.1	8.4
13X-2, 90	196.3	18.2
13X-2, 103	196.4	50.8
13X-3, 96	197.9	15.9
14X-1, 125	204.9	28.0
14X-2, 121	206.3	34.7
14X-3, 31	206.9	28.4
16X-1, 87	223.7	49.2
16X-2, 101	225.3	41.0
16X-3, 66	226.5	56.9
16X-5, 95	229.8	34.0
17X-1, 98	233.4	22.9
17X-2, 77	234.7	22.2
17X-3, 114	236.5	64.4
17X-6, 108	241.0	23.6
18X-2, 32	243.9	60.6
18X-4, 80	247.4	39.2
19X-2, 39	253.6	52.7
19X-3, 121	255.9	102.6
19X-5, 121	258.9	49.4
19X-6, 70	259.9	30.9
20X-1, 103	262.4	57.0
20X-2, 50	263.4	109.4

Index property variability is damped within Unit II (Hole 791B). Except for anomalous points that result from coring disturbance and measurement errors, the range of values in the sediments of these four index properties is much less below 450 mbsf (wet-bulk density: 1.64–2.0 g/cm^3; grain density: 2.56–2.89 g/cm^3; porosity: 30%–75%; water content: 21%–75%; Table 20). The unfortunate coincidence of the change in lithologic unit and the change of coring technique makes unequivocal interpretation impossible. However, a comparison with Site 790, which was not rotary cored, but which does display similar index property trends over these stratigraphic intervals, indicates that much of the decrease in variability between Units I and II is real. The difference in the rate of change in the index properties in Unit II of Site 791 compared with Site 790 (approximately 3×10^{-4} g/cm^3/m at Site 791 vs. 1.7×10^{-3} g/cm^3/m at Site 790 for wet-bulk density) may be related to greater depth higher overburden stresses, and a more advanced state of consolidation in Unit II at Site 791.

The correlation between GRAPE and gravimetrically determined wet-bulk densities in Hole 791A is excellent (Fig. 75). Even in the XCB drilled holes below 200 mbsf, where recovery

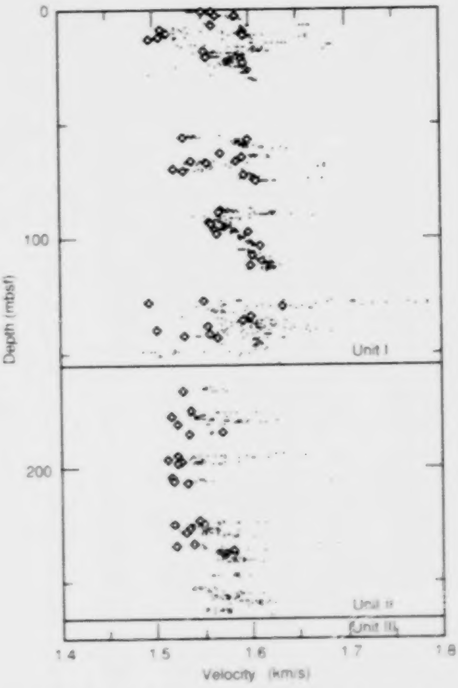

Figure 71. Comparison of sonic velocity determined by Hamilton Frame (diamonds) and multisensor track (small dots) methods for Site 790. Horizontal lines indicate lithologic unit boundaries.

was low and coring disturbance increased, values from the two data sets match extremely well. In contrast, the situation in rotary-drilled Hole 791B is the opposite. Virtually all the gravimetrically derived bulk densities are greater than those determined by the GRAPE, as expected from rotary-drilled sections. The GRAPE volume calculations assume that the core fills the liner. The real core diameter is less than this because of drilling effects. Consequently, the core volume is overestimated and the density underestimated.

An analogous situation was noted in the rotary-drilled section at Site 787 (see "Physical Properties" section, "Site 787" chapter, this volume). However, the dissimilarity between the trends in the two types of measurements is unexpected. Although the GRAPE data is characterized by a high degree of scatter, not even well-defined trends seen in the gravimetric bulk density are observed in the GRAPE data (e.g., compare the densities between 650 and 770 mbsf in Fig. 75). The probable cause of this discrepancy is from variations in the way that the two measurements are made; specifically, differences in the true and GRAPE-estimated volumes of the cores.

A sharp, but not unexpected, change in all measured physical properties occurs at the transition from sediment to igneous rocks (Fig. 74). In general, bulk and grain density values increase, and porosity and water content values decrease. However, these properties are by no means constant within the hard-rock section. Some variability may be attributed to measurement errors related to differences in the sampling times (see "Explanatory Notes" chapter, this volume), but most appears to be related to the inherent properties of the rocks (see "Igneous Petrology" section, this chapter).

After filtering out anomalous data points that are obviously erroneous, some clear-cut trends emerge. The basaltic "mousse," a mixture of vesicular glass matrix and basaltic clasts, is characterized by lower wet-bulk density values and higher porosity values and water contents than the other igneous units. Porosity values as high as 44% were measured in this unit, with a mean value of approximately 36%. Porosity data in the other igneous units in Hole 791B rarely exceed 25% (Table 21). The properties of the clast vs. matrix material in the "mousse" indicate that the porosity and water content of the clasts is lower and the bulk density higher than those of the matrix glass. Samples composed of a mixture of both tend to exhibit intermediate values (Table 21).

Variations in porosity and density values between the various units are linked closely with the mineralogy and chemistry of the different rocks. This is supported by the high grain density of the diabase in Sample 126-791B-57R-1, 7 cm (926 mbsf). The high iron content of this unit (see "Igneous Geochemistry" section, this chapter) is probably the cause of this extreme value (the highest measured). In contrast, the sample with the lowest grain density is that of Sample 126-791B-76R-2, 108 cm (within the diabase, Unit 15), which contained a large amount of low-density gypsum in veins.

In general, the diabase units display low porosity values, ranging from 13.7% in Unit 4 to 17.2% in Unit 17. Again, this variation in properties appears to be tied to chemical and mineralogical changes, not to such variations in compaction as those common in the sedimentary section.

The lowest measured porosity values are found in the deepest recovered unit, a lapilli tuff. Three samples, taken within 50 cm of each other, exhibit an average porosity of 8.5%. These samples are from an upward-fining sequence. A slight positive correlation between porosity and grain size is observed.

Generally, agreement between the visual petrographic estimate of vesicle pore space and the gravimetrically determined porosity data is good (see "Igneous Petrology" section, this chapter). The greatest discrepancies between the two determinations is found in the denser, low-porosity units, such as the diabase units. Although the gravimetric and visual porosity trends are the same, the gravimetrically determined absolute values are often significantly greater in these samples.

Grain density values range from a low of 2.6 g/cm³ to a high of 3.03 g/cm³ in the igneous section. Values exhibit a high degree of scatter throughout the hard-rock sequence and may be related to variations in composition.

Calcium Carbonate

The basic trend of low calcium carbonate content in Unit I and increased values in Unit II noted at Site 790 was also observed at Site 791 (Fig. 74). Average $CaCO_3$ contents and small-scale variability increase significantly at the Unit I/II boundary. A more pronounced trend is indicated in Unit I at Site 791. Calcium carbonate values at the base of the sedimentary section at Site 791 are somewhat higher than those at Site 790.

Vane Shear Strength

Unfortunately, poor recovery and drilling disturbance resulted in only a small number of vane shear strength measurements, most of which fall below 15 kPa. Increased values at 36 mbsf and isolated peaks below 150 mbsf are probably related to an increase in grain size (Fig. 70 and Table 22).

Sonic Velocity

Sonic velocity measurements were performed on discrete samples from Holes 791A and 791B with the HF method (Table 20 and Fig. 74). In addition, Cores 126-791A-1H through -42X and

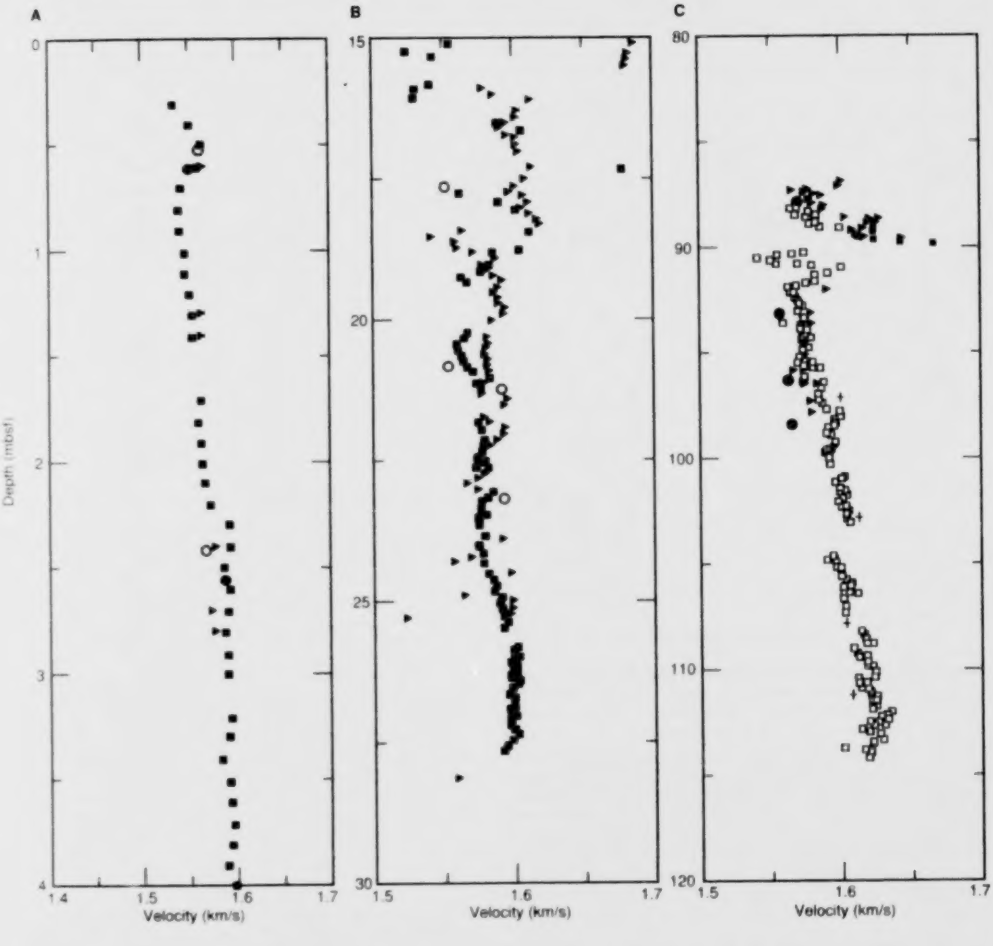

Figure 72. Detailed comparison of sonic velocity measurements between overlapping holes and methods of measurement. **A.** and **B.** Overlap of Holes 790A and 790B. Note that the vertical scales for each graph are different. **C.** Overlap of Holes 790B and 790C.

126-791B-1R through -46R were passed through the MST, and sonic velocity measurements were obtained with the sonic wave (*P*-wave) logger (Fig. 76).

Velocity values in Unit I (0–425 mbsf) range from 1.53 to 1.61 km/s and average 1.58 km/s. Several distinct velocity lows are observed between 27–37 and 158–168 mbsf and are seen in the HF and MST data (see Fig. 76). Both methods show similar values and trends in this unit.

Unit II is characterized by average sonic velocity values of 1.70 km/s with a range from 1.61 to 1.84 km/s. A distinct increase in velocity with depth was observed, with the highest sediment velocity measurements (~1.8 km/s) just above basement. This increase is mainly a result of increased induration.

In Unit III, velocity data range from 2.60 to 5.22 km/s and average 3.80 km/s. Unit III is characterized by two relative highs (~830-900 and >1100 mbsf). This wide variation in velocity

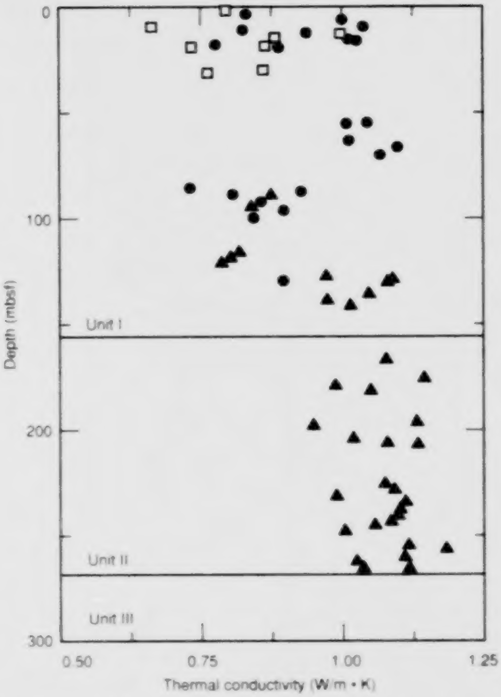

Figure 73. Plot of thermal conductivity, Site 790. Horizontal lines indicate lithologic unit boundaries. Open square = Hole 790A; closed circle = Hole 790B; closed triangle = Hole 790C.

(similar to that observed in the index properties) is probably caused by the variability of igneous rocks in Unit III (see "Igneous Petrology" section, this chapter; a summary of igneous rock types and physical property measurements is given in Table 21). The large velocity and density contrast is responsible for the strong reflection observed between 4.0 and 4.2 s on seismic Line BON II-4 (see "Site Survey" chapter, this volume, and "Seismic Stratigraphy" section, this chapter). The fastest velocity measured was 5.22 km/s in a gypsum vein within a diabase unit.

Thermal Conductivity

Thermal conductivity measurements were performed on as many undisturbed cores as possible from the sedimentary column, as well as on four igneous rock samples (with the half-space method) from below 830 mbsf (Fig. 77 and Table 23). Thermal conductivity values show a distinct increase with depth to the basement, at which point the values drop off slightly. Thermal conductivity data show distinct correlations with index property data. Within Unit I, thermal conductivity data average 0.913 W/m · K. Unit II exhibits higher conductivity values, with an average of 1.193 W/m · K. Unit III is characterized by slightly lower values that average 1.133 W/m · K.

DOWNHOLE MEASUREMENTS

At Hole 791B, the drill pipe became stuck during hole-conditioning procedures in preparation for downhole measurements.

Table 19. Thermal conductivity data from Site 790.

Core, section, interval (cm)	Depth (mbsf)	Thermal conductivity (W/m · K)
126-790A-		
1H-1, 28-29	0.28	0.817
1H-2, 15-16	1.65	0.793
1H-3, 57-58	3.57	[a]2.017
1H-5, 101-102	7.01	[a]2.317
2H-1, 51-52	9.31	[a]0.660
2H-3, 99-100	12.79	0.994
2H-5, 43-44	15.23	0.877
2H-7, 19-20	17.99	0.857
3H-1, 82-83	19.12	[a]0.730
3H-5, 63-64	24.93	0.881
3H-7, 53-54	27.83	1.041
4H-2, 72-73	30.02	0.855
4H-3, 33-34	31.13	0.758
126-790B-		
1H-1, 27-28	0.27	0.8212
1H-3, 11-12	3.11	0.8291
2H-2, 40-41	6.40	0.9972
2H-4, 43-44	9.43	1.0331
2H-5, 24-25	10.74	0.8216
2H-6, 50-51	12.50	0.9362
3H-1, 105-106	15.05	1.0086
3H-2, 41-42	15.91	1.0212
3H-3, 81-82	17.81	0.7763
3H-4, 20-21	18.70	0.8854
7H-2, 119-120	54.69	1.0397
7H-3, 48-49	55.48	1.0039
8H-2, 96-97	64.06	1.008
8H-4, 74-75	65.84	1.097
8H-6, 80-81	69.90	1.065
10H-4, 65-66	86.15	[a]0.7268
10H-5, 82-83	87.82	0.9232
10H-6, 49-50	88.99	0.8022
11H-2, 44-45	92.64	0.8528
11H-4, 87-88	96.07	0.8919
11H-6, 72-73	98.92	0.8382
15X-1, 53-54	129.83	0.8924
126-790C-		
1H-3, 46-47	88.46	0.8695
1H-5, 67-68	91.67	[a]1.45652
1H-7, 27-28	94.27	0.8395
4H-2, 53-54	115.93	0.8119
4H-4, 30-31	118.70	0.8003
4H-6, 41-42	121.81	0.7839
5H-3, 64-65	127.14	0.9686
5H-4, 81-82	128.81	1.0798
5H-6, 75-76	131.75	1.075
6H-2, 34-35	135.04	1.0456
6H-4, 83-84	138.53	0.9691
6H-6, 62-63	141.32	1.0105
10X-2, 25-26	166.26	1.0738
11X-1, 53-54	175.13	1.139
11X-3, 66-67	178.26	0.9824
11X-5, 56-57	181.16	1.0438
13X-2, 77-78	196.17	1.1263
13X-3, 72-73	197.62	0.945
14X-1, 80-81	204.80	1.0157
14X-2, 81-82	205.91	1.0727
14X-3, 28-29	206.88	1.1311
16X-2, 46-47	224.76	1.0692
16X-4, 73-74	228.03	1.0876
16X-6, 16-17	230.46	0.9833
17X-2, 39-40	234.29	1.1076
17X-4, 76-77	237.66	1.1009
17X-6, 83-84	240.73	1.0944
18X-1, 77-78	242.87	1.0821
18X-2, 73-74	244.33	1.0514
18X-4, 101-102	247.61	0.9982
19X-2, 63-64	253.83	1.1138
19X-4, 63-64	256.83	1.1806
19X-6, 56-57	259.76	1.1036
20X-1, 130-131	262.70	1.0221
20X-3, 42-43	264.82	1.1142
20X-4, 27-28	266.17	1.0258

[a] Results are of uncertain quality.

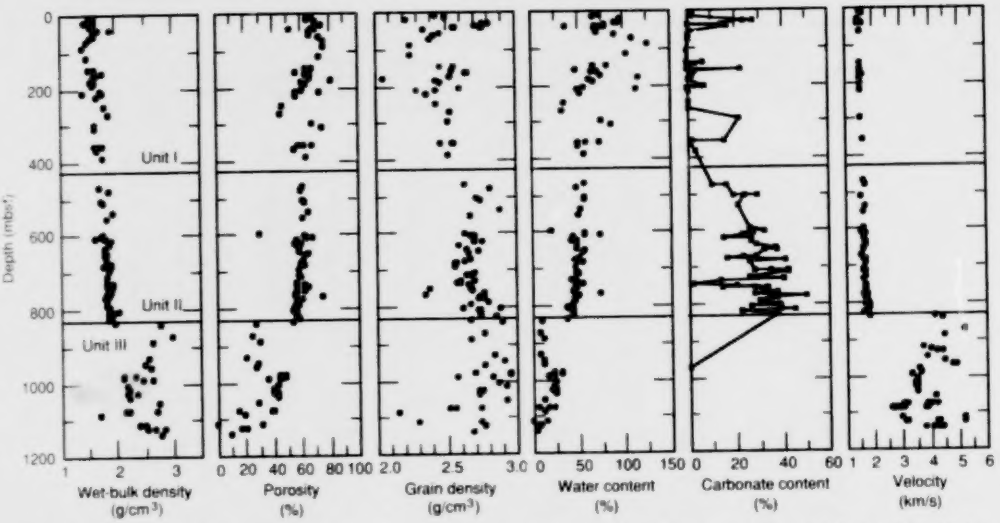

Figure 74. Downhole plots of index properties, carbonate content, and velocity for Site 791. Horizontal lines indicate lithologic unit boundaries.

This resulted in a decision to reduce the program to the deployment of the geochemical combination, the only one with the capability of recording measurements through the drill pipe. This series of measurements provides quantitative assessments of the natural gamma radiation (specifically K, Th, and U) emanating from the formation, together with the relative proportions of the elements Si, Ca, Fe, S, H, Cl, and Al (determined from neutron capture and activation). A detailed description of the geochemical measurements is given in the "Explanatory Notes" chapter (this volume). Further processing onshore may enable the extraction of two additional elements (Ti and Gd).

The base of the drill string was located at a depth of 830 mbsf (i.e., 315 m above the total depth of the hole). This depth coincides with the depth to the top of basement. Data was acquired solely on the uphole run of the combination, at a speed of approximately 450 ft/hr (137 m/hr) starting at a depth of 811.67 mbsf.

Data Quality

The geochemical combination is designed for use in open-hole conditions. When run inside the drill pipe, the quality of the data pertaining to the formations is inevitably degraded in comparison with data obtained in an open hole. The natural gamma-ray measurements suffer from attenuation in the pipe through Compton Scattering, whereas the measurement of the remaining elements is affected by the pipe in terms of the outward passage of neutrons from the tool to the formation as well as the return of the generated gamma rays to the detector from the formation through the drill pipe. The natural gamma-ray measurement technique uses five windows in the spectrometric determination of the contributions of Th, U, and K. Of the measured energy spectrum, the lower energy gamma rays are preferentially attenuated in passing through the wall of the drill pipe and, consequently, the measured spectrum is unfairly weighted toward the higher energies. This has a pronounced effect on the quality of the acquired data, since only 10% of the spectrum (in terms of counting rates) is derived from this higher energy region (Schlumberger, 1983).

In addition to the inevitable decrease in signal-to-noise ratio, the drill pipe itself provided additional input in terms of the chemical signals observed; this was expected particularly for iron and the other elements that compose the drill pipe. These effects were not constant throughout the hole but varied with the thickness of the pipe, the pipe collars, the BHA, and other special components. Because there were no additional measurements made in the borehole other than the geochemical analyses, there is no quantitative determination of borehole size or physical state.

Given the conditions encountered in terms of hole instability and the presence of the drill pipe, the quality of the acquired data was surprisingly good. Careful analysis of the relative variations of individual elemental yields allowed us to identify large- and small-scale sedimentary features that correlate well with the sediments recovered from Holes 790B, 790C, 791A, and 791B. It was also possible to identify sections of the hole that were most affected by the presence of the drill string.

All of the signals received (Figs. 78 and 79) showed responses that were strongly modified with respect to those expected in open-hole conditions. With the exception of the Fe (and possibly S) responses, which were positively increased by the drill-string effect, the remaining signals were all heavily attenuated. The relative values for the elements determined from the neutron bombardment of the formation (Si, Fe, S, Ca, H, Cl, and Al) appeared to be the most severely affected and did not show much variation with depth. No corrections for this attenuation were applied to the data, and no processing of the responses to remove the effects of variations in the contribution of pipe and pipe collars was attempted. Depth shifting was not necessary for this single downhole-measurements experiment.

Geochemical Variations with Depth

Hydrogen and Chlorine

Hydrogen and chlorine values (Fig. 78) provided estimates of the total amount of seawater in the formation as well as between the detector and the formation. Consequently, high values may

Table 20. Physical properties (index, velocity, and carbonate) data for Site 791.

Core, section, interval (cm)	Depth (mbsf)	Wet-bulk density (g/cm³)	Dry-bulk density (g/cm³)	Porosity (%)	Water content (%)	Grain density (g/cm³)	Void ratio	Carbonate content (%)	Velocity (km/s)
126-791A-									
2H-1, 82-85	5.32	1.63	0.96	68	75	2.50	2.11	2.7	1.60
2H-2, 92-95	6.92	1.59	0.95	65	72	2.43	1.87	1.9	1.59
2H-5, 140-150	11.90							1.9	
2H-6, 49-52	12.49	1.64	1.01	65	67	2.50	1.83	1.7	1.61
3H-2, 73-74	16.23	[a]1.47	[a]0.76	[a]71	[a]98	[a]2.23	[a]2.45		
4H-3, 101-102	27.51	1.58	0.84	75	95	2.78	3.03	28.1	[a]1.52
4H-4, 120-122	29.20	1.62	0.88	75	90	2.81	3.00	24.3	[a]1.52
4H-5, 56-58	30.06	1.62	0.92	71	81	2.72	2.41	19.4	1.53
5H-2, 120-122	35.70	1.64	0.93	71	80	2.57	2.46	15.9	1.53
5H-3, 59-61	36.59	1.65	0.96	69	75	2.58	2.24	15.0	1.53
5H-3, 140-150	37.40							1.0	1.61
5H-4, 28-30	37.78	1.93	1.41	53	39	2.76	1.12	0.9	
5H-5, 71-73	39.71	1.69	1.02	68	70	2.78	2.11	17.1	1.55
6H-2, 77-78	44.77	1.65	0.99	66	70	2.35	1.95		
7H-3, 62-63	55.62	1.64	0.98	67	71	2.46	2.00	1.2	
7H-4, 135-136	57.85	1.58	0.86	73	90	2.42	2.72	1.2	1.60
8H-4, 72-73	66.82	[a]1.49	0.73	[a]75	[a]109	[a]2.40	[a]3.12	0.6	
9H-6, 140-150	80.20							0.6	
10H-3, 79-80	84.79	[a]1.41	0.65	[a]77	[a]126.4	[a]2.26	[a]3.35		
12H-5, 140-150	107.80							0.3	
13H-2, 68-70	112.28	[a]1.49	[a]0.75	[a]73	[a]103	[a]2.26	[a]2.83		
15H-6, 25-35	137.25							0.3	
16H-2, 74-76	141.44	1.62	0.99	63	67	2.56	1.73	6.8	1.58
16H-4, 63-65	144.33	[a]1.54	[a]0.86	[a]68	[a]83	[a]2.46	[a]2.14		
16H-5, 60-63	145.80							3.7	
17H-1, 81-83	149.61							0.7	
17H-3, 86-88	152.66							1.2	
17H-6, 80-82	157.10	[a]1.77	[a]1.20	[a]56	[a]48	[a]2.55	[a]1.30	0.3	
18H-1, 48-50	158.98	1.67	1.03	64	65	2.65	1.80	22.9	1.55
18H-2, 103-107	161.03	1.63	0.97	66	72	2.66	1.96	3.4	1.57
18H-6, 99-100	166.90							1.7	
19H-1, 108-110	169.18	1.60	0.93	67	76	2.53	2.06	3.0	1.54
19H-6, 123-126	176.83	[a]1.57	[a]0.75	[a]82	[a]115	[a]2.05	[a]4.63	1.8	1.61
20H-2, 110-112	180.30	1.62	1.01	62	64	2.43	1.62	1.6	1.59
20H-6, 78-80	185.98	1.61	0.98	64	69	2.46	1.77	0.6	1.59
22H-6, 71-73	205.11	1.73	1.12	61	57	2.60	1.57	6.1	1.59
22H-6, 140-150	205.80							3.3	
22H-7, 16-18	206.06	1.76	1.20	57	50	2.44	1.34	7.5	
23H-2, 73-75	207.77	[a]1.42	[a]0.68	[a]74	[a]114	[a]2.30	[a]2.86	0.3	
25X-CC, 13-16	217.84	1.68	1.12	56	52	2.36	1.29	0.5	
28X-1, 68-70	246.68							0.7	1.56
28X-CC, 21-23	247.16	1.82	1.35	48	37	2.43	0.91	0.4	
30X-CC, 12-14	265.42	1.88	1.43	46	34	2.54	0.86	0.7	
33X-1, 17-19	294.47	1.62	0.95	68	75	2.52	2.10	21.8	1.56
34X-1, 5-8	304.05	[a]1.65	[a]0.53	[a]74	[a]85	[a]4.28	[a]2.91		
39X-1, 12-15	352.42	1.64	1.19	68	73	2.57	2.08	15.7	
39X-1, 42-45	352.72	1.76	1.09	59	52	2.55	1.42	1.8	1.61
39X-CC, 11-12	353.40	1.70	0.97	62	60	2.47	1.66		
40X-1, 2-3	362.02	[a]1.66	[a]1.11	[a]55	[a]51	[a]1.48	[a]1.23	1.1	
42X-1, 10-11	381.50	1.77	1.14	63	58	2.52	1.73	3.7	
126-791B-									
9R-CC, 19-21	463.79	1.72	1.12	61	57	2.63	1.56	10.3	1.61
10R-1, 34-36	473.64	1.87	1.28	60	49	2.81	1.48	16.5	1.71
13R-1, 46-48	502.56	1.75	1.14	61	56	2.72	1.58	19.1	3.14
13R-1, 140	503.50							29.9	
13R-2, 46-48	504.06	1.77	1.14	63	58	2.75	1.71	24.2	1.58
16R-1, 23-24	531.43	1.94	1.30	65	52	2.89	1.84	21.5	1.72
18R-1, 5-7	550.65	1.83	1.17	61	51	2.67	1.54		1.64
22R-1, 69-71	589.69	[a]1.76	[a]1.46	[a]30	[a]21	[a]3.37	[a]0.44	26.2	1.63
23R-1, 75-77	599.45	1.75	1.13	63	58	2.63	1.67	32.5	1.64
23R-2, 82-84	601.02	1.64	0.97	67	73	2.70	2.07	26.5	1.61
23R-3, 115-125	602.85							27.7	
23R-CC, 3-6	603.92	1.81	1.18	64	56	2.68	1.74	27.2	1.60
24R-1, 57-59	608.97	1.91	1.34	57	44	2.70	1.33	23.4	1.69
25R-1, 27-29	618.37	1.87	1.33	55	43	2.71	1.23	15.5	1.67
25R-2, 14-17	619.74	1.88	1.34	60	49	2.76	1.50	26.8	1.67
26R-1, 6-9	627.76	1.81	1.24	58	49	2.59	1.38	27.2	1.69
27R-1, 35-37	637.35	1.81	1.24	58	48	2.65	1.36	28.8	1.71
28R-1, 129-131	647.89	1.84	1.20	65	57	2.73	1.85	37.2	1.65
28R-3, 81-83	650.41	1.82	1.20	63	54	2.66	1.67	37.7	1.63
28R-3, 140-150	651.00							32.2	
30R-1, 145-148	667.45	1.85	1.24	61	51	2.68	1.59	29.2	1.59

Table 20 (continued).

Core, section, interval (cm)	Depth (mbsf)	Wet-bulk density (g/cm^3)	Dry-bulk density (g/cm^3)	Porosity (%)	Water content (%)	Grain density (g/cm^3)	Void ratio	Carbonate content (%)	Velocity (km/s)
126-791B- (Cont.)									
30R-3, 104–108	670.06	1.91	1.32	60	47	2.64	1.49	23.7	
31R-1, 81–83	676.41	1.91	1.30	62	50	2.56	1.62	16.5	1.69
31R-3, 67–69	679.27	1.79	1.17	63	56	2.58	1.67	41.1	1.67
32R-1, 28–30	685.58	1.88	1.30	58	46	2.56	1.39	26.4	1.72
34R-1, 116–118	705.76	1.85	1.28	59	48	2.71	1.41	28.2	1.64
34R-3, 37–39	707.97	1.86	1.27	60	49	2.65	1.49	42.6	1.64
34R-3, 140–150	709.00							35.1	
34R-4, 68–69	709.78	1.85	1.26	60	50	2.68	1.53	43.1	1.67
36R-1, 27–29	723.87	1.95	1.39	57	42	2.70	1.30	26.5	1.72
36R-3, 134–136	727.94	1.83	1.26	58	47	2.61	1.35		
36R-4, 86–88	728.96	1.95	1.33	63	50	2.58	1.71		
36R-4, 134–136	729.44	1.83		58	47	2.61	1.35	40.5	1.65
37R-2, 8–10	734.78	1.92		62	49	2.68	1.64		
37R-2, 65–67	735.35	1.91	1.26	65	54	2.66	1.88	13.5	
38R-2, 8–10	744.38	1.92	1.31	62	49	2.68	1.64	33.4	1.70
38R-4, 16–18	747.46	1.88	1.31	58	46	2.38	1.35	20.5	
39R-1, 10–12	752.50	1.84	1.28	57	46	2.69	1.32	33.6	1.70
39R-1, 140–150	753.80							14.3	
39R-2, 107–109	754.97	1.88	1.32	56	44	2.77	1.27	28.5	1.72
40R-1, 10–13	762.20	[a]1.80	[a]0.82	[a]74	[a]73	[a]2.35	[a]2.92	31.5	1.73
40R-3, 50–53	765.60	1.85	1.25	61	50	2.74	1.53	37.7	1.73
41R-1, 17–20	771.87	1.83	1.28	56	46	2.73	1.29	28.4	1.66
41R-3, 71–74	775.41	1.86	1.28	58	47	2.78	1.40	50.2	1.76
42R-1, 35–38	781.65	1.85	1.27	58	47	2.80	1.37	38.2	1.74
42R-2, 0–10	782.80							35.3	
43R-1, 9–11	791.09	1.87	1.32	56	44	2.68	1.26	30.3	1.75
44R-1, 38–41	801.08	1.90	1.36	55	42	2.62	1.20	38.8	1.74
44R-1, 98–100	801.68	2.04	1.49	56	39	2.89	1.25	35.2	1.84
44R-2, 96–99	803.16	1.89		57	44	2.74	1.30	27.1	1.79
44R-2, 97–99	803.17	1.96	1.41	56	41	2.73	1.25	39.5	
45R-2, 17–19	811.97	1.89		57	45	2.86	1.32	39.5	
45R-2, 96–99	812.76	1.89	1.33	57	44	2.74	1.30	22.5	1.84
45R-2, 140–150	813.20							45.5	
46R-1, 43–45	820.43	1.92	1.35	58	44	2.75	1.36		1.66
46R-2, 17–19	821.67	1.89	1.33	57	45	2.86	1.32		1.77
47R-1, 41–42	830.01	1.99	1.45	54	39	2.68	1.18	37.99	1.87
47R-1, 88–90	[b]830.48					2.94			4.20
48R-1, 31–33	[b]839.51	2.78		28	11	2.90	0.38		4.45
51R-1, 5–9	[b]868.35	[a]3.01		[a]25	[a]9	[a]2.78	[a]0.34		5.19
53R-1, 15–23	[b]887.75	2.67		30	13	[a]2.68	0.44		4.53
56R-1, 25–31	916.55								3.71
56R-1, 4–6	921.30								4.04
57R-1, 6–8	925.96								4.22
57R-1, 7–8	925.97	2.80		14		3.03			4.26
57R-1, 55–64	926.45	2.59	2.39	21	9	2.84	0.26		4.46
59R-1, 36–38	945.56	2.51	2.21	30	14	2.92	0.42		3.90
60R-1, 16–19	[b]954.96	2.63		27	12	2.78	0.37		4.50
61R-1, 43–45	[b]964.93	3.19		15		2.83			4.81
62R-1, 5–7	974.15	2.13	1.65	49	31	2.96	0.97	0.71	
62R-1, 97–99	975.07	2.34	1.90	44	24	2.71	0.79		3.57
63R-1, 49–51	984.19	2.48	2.05	44	22	[a]2.65	0.78		3.65
63R-1, 76–79	[b]984.46	2.67		36	16	2.83	0.57		3.67
64R-1, 37–44	[b]993.37					[a]2.70			3.33
65R-1, 55–56	1003.25	2.21	1.84	43	25	2.87	0.75		3.56
66R-1, 65–67	[b]1013.05	2.22	1.81	41	23	2.93	0.69		3.49
66R-2, 46–48	[b]1014.24					[a]2.56			3.52
67R-1, 62–64	1022.72								3.52
67R-1, 90–91	1023.00	2.19	1.76	43	25	2.73	0.76		3.46
67R-2, 26–28	1023.86	2.20	1.79	42	24	2.76	0.71		3.45
67R-3, 24–26	[b]1025.34	2.37		40	21	2.73	0.68		3.46
68R-1, 49	1032.29	2.23	1.83	43	24	2.73	0.74		
68R-2, 60–65	1038.80								3.52
70R-1, 0–4	[b]1051.1	2.76		29	12	2.93	0.41		4.14
72R-1, 120–126	[b]1071.6	2.23		15	7	2.74	0.17		3.07
72R-2, 116–118	[b]1073.06	2.13		35		2.75			3.19
72R-2, 117–119	1073.07								3.87
72R-2, 135–140	[b]1073.25	2.73		39	17	[a]2.57	[a]0.64		4.21
72R-3, 35–37	1073.75	2.23	2.12	23		2.50			4.05
73R-2, 20–24	[b]1081.3					2.79			2.93
73R-2, 77–79	1081.87								2.69
73R-2, 77–79	1081.87								3.89
73R-2, 87–89	1081.97	2.00		42		2.75			2.71
73R-2, 87–89	1081.97								2.60
73R-2, 87–89	1081.97								2.69
73R-3, 18–21	[b]1082.7	2.09		37		2.72			3.02
73R-3, 18–21	[b]1082.7								2.76

Table 20 (continued).

Core, section, interval (cm)	Depth (mbsf)	Wet-bulk density (g/cm³)	Dry-bulk density (g/cm³)	Porosity (%)	Water content (%)	Grain density (g/cm³)	Void ratio	Carbonate content (%)	Velocity (km/s)
126-791B- (Cont.)									
73R-3, 72-74	1083.24	[a]1.69		[a]19.2	[a]13	[a]2.15	[a]0.24		3.82
76R-1, 117-120	[b]1110.17					2.75			2.96
76R-2, 37-38	1110.87	2.41	2.10	32	16	2.75	0.47		2.94
76R-2, 106-109	[b]1111.56	[a]2.52				[a]2.29			5.22
77R-1, 58-64	[b]1119.18	[a]2.85		[a]16.3	[a]6	[a]2.77	0.19		4.35
77R-1, 85-89	1119.45	2.68	2.51	17	7	2.78	0.21		4.21
77R-2, 43-45	1120.04								5.21
77R-2, 93-95	[b]1120.54					2.71			3.16
77R-2, 131-134	1120.92	2.54	2.33	21	10	3.21	0.27		3.09
79R-1, 19-21	[b]1137.79	[a]2.79		[a]9	[a]4	[a]2.69	[a]0.10		4.31
79R-1, 21-24	[b]1137.81	2.64		8		2.79			4.11
79R-1, 21-24	[b]1137.81								4.12
79R-1, 40-42	[b]1138.00	2.59	8.00			2.74			4.12
79R-1, 41-42	[b]1138.00								3.81
79R-1, 72-74	[b]1138.32	2.61	9.00			2.76			4.41
79R-1, 73-76	[b]1138.32								4.45

[a] Results are of uncertain quality.

[b] Samples that were not measured immediately after cores were split.

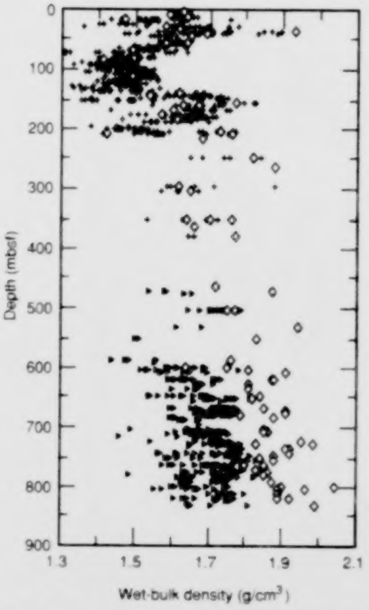

Figure 75. Comparison of gravimetric and GRAPE wet-bulk density data for Holes 791A and 791B. Open diamond = gravimetric bulk density; closed triangle = Hole 791B GRAPE density.

indicate either high porosities or the possibility of large hole conditions existing outside the pipe. Several distinct intervals are present (Fig. 78):

1. 0–42 mbsf: very high values; variable H and Cl values indicate bad hole conditions with a seawater pool developed around the pipe as a result of erosion of sediments through drill-string action (Fig. 78, 0–150 mbsf).

2. 42–182 mbsf: high values; fairly constant H and Cl values over this depth interval indicate either a higher *in-situ* porosity compared with the zone below (Fig. 78, 0–300 mbsf) or an oversized hole.

3. 182–560 mbsf: constant values; low values of H and Cl indicate that the best hole conditions were encountered within this hole.

4. 560–710 mbsf: variable values; H and Cl values imply variable lithology.

The high values correspond to zones of low Si and Fe, but high Th, U, and K (Fig. 78).

Natural Gamma-Ray Components

The total gamma-ray signal exhibits detailed variation downhole. Although the signal strength was particularly low throughout the section and was particularly affected by the pipe, the variations appeared to be lithologically related. The quantitative nature of the individual spectrometric determinations is, however, questionable because of the bias resulting from the differential attenuation of gamma rays at different energy levels. All three elements (Th, U, and K) contributed to the natural gamma-ray signal.

Silicon, Iron, Calcium, Sulfur, and Aluminum

All five of these elements showed little gross variation over the logged section (Fig. 78). There were variations evident, however, in the Fe, Si, Al, and S traces, which appeared to correlate with the main features of the hole described below. Calcium, however, did not show any substantial variation downhole; this is in contrast to the substantial variation exhibited by laboratory measurements of calcium carbonate on individual samples. With the exception of Fe and S (which increased because of contributions from the drill pipe), the measured signal strengths are very low when compared with the levels obtained in an open hole.

Stratigraphic Observations from Downhole Geochemical Data

Major Features

Three clearly separate units or zones were identifiable from the downhole data, selected on the basis of comparable geochemical signatures.

Table 21. Synthesis of physical property data from igneous rock samples from Hole 791B.

Core, section, interval (cm)	Depth (mbsf)	Wet-bulk density (g/cm³)	Porosity (%)	Grain density (g/cm³)	Velocity (km/s)	Rock type and unit	Comments
126-791B-							
47R-1, 89	830.49	—	—	2.94	4.20	Basalt breccia, Unit 1	Days; no salt correction
48R-1, 32	839.52	2.78	27.8	2.90	4.45	Vesicular basalt, Unit 2	Days
51R-1, 7	868.35	[a]3.01	[a]25.4	[a]2.78	5.19	Vesicular basalt, unit 2	Days; numerous large vesicles
53R-1, 20	887.80	[a]2.67	[1]30.4	[a]2.68	4.53	Vesicular basalt, Unit 2	Days
57R-1, 7	925.97	2.80	13.7	3.03	4.26	Diabase, Unit 4; high Fe content	Days; no salt correction
57R-1, 55	926.45	2.59	20.7	2.84	4.46	Basalt, Unit 5	Minutes
59R-1, 37	945.57	2.51	29.6	2.92	3.90	Basalt, Unit 6	Minutes
60R-1, 18	954.98	2.63	27.1	2.78	4.50	Basalt, Unit 7	Days
61R-1, 44	964.94	[a]3.19	[1]14.5	[1]2.83	4.90	Diabase, Unit 8	Days; no salt correction
62R-1, 98	975.08	2.34	44.1	2.71	3.57	Basaltic "mousse," Unit 11	Hours
63R-1, 50	984.20	2.48	43.9	2.65	3.65	Basaltic "mousse," Unit 11	Hours; mixture
63R-1, 78	984.48	2.67	36.3	2.83	3.67	Basaltic "mousse," Unit 11	Days; clast with large vesicles
64R-1, 40	993.40	—	—	2.70	3.33	Basaltic "mousse," Unit 11	Days; mixture; no salt correction
65R-1, 55	1003.25	2.21	42.9	2.87	3.56	Basaltic "mousse," Unit 11	Minutes; mixture
66R-1, 66	1013.05	2.22	40.7	2.93	3.49	Basaltic "mousse," Unit 11	Minutes; mixture
66R-2, 47	1014.24	—	—	[a]2.56	3.52	Basaltic "mousse," Unit 11	Days; matrix; no salt correction
67R-1, 90	1023.00	2.19	43.2	2.73	3.46	Basaltic "mousse," Unit 11	Minutes; mixture
67R-2, 27	1023.87	2.20	41.6	2.76	3.45	Basaltic "mousse," Unit 11	Minutes; mixture
67R-3, 25	1025.35	2.37	40.4	2.73	3.46	Basaltic "mousse," Unit 11	Days; mixture
68R-1, 50	1032.30	2.23	42.6	2.73		Basaltic "mousse," Unit 11	Minutes; mixture
70R-1, 2	1051.12	2.76	29.2	2.93	4.14	Basaltic "mousse," Unit 11	Days; clast ("dense")
72R-1, 124	1071.64	2.23	14.7	2.74	3.07	Basaltic "mousse," Unit 11	Days; matrix
72R-2, 117	1073.00	2.13	35.5	2.75	3.19	Basaltic "mousse," Unit 11	Days; mixture; no salt correction
72R-2, 138	1073.28	[a]2.73	[a]38.9	[a]2.57	4.21	Basaltic "mousse," Unit 11	Days; clast
72R-3, 37	1073.77	2.23	23.1	2.60	4.05	Basaltic "mousse," Unit 11	Hours; matrix; no salt correction
73R-2, 22	1081.32	—	—	2.79	2.93	Basaltic "mousse," Unit 11	Days; mostly matrix; no salt correction
73R-2, 89	1081.98	2.00	42.4	2.75	2.60	Basaltic "mousse," Unit 11	
73R-3, 20	1082.70	2.09	36.7	2.72	2.76	Basaltic "mousse," Unit 11	Days; mixture; no salt correction
73R-3, 73	1083.23	[a]1.69	[1]19.2	[a]2.15	3.82	Basaltic "mousse," Unit 11	Hours; clast
76R-1, 119	1110.19	—	—	2.75	2.96	Basaltic "mousse," Unit 14	Days; no salt correction; "not mousse"
76R-2, 37	1110.87	2.41	31.9	2.75	2.94	Basaltic "mousse," Unit 14	Hours; clast
76R-2, 108	1111.58	[a]2.52	—	[1]2.29	5.22	Diabase, Unit 15	Days; diabase with gypsum veins
77R-1, 60	1119.18	[a]2.85	[a]16.3	[a]2.77	4.35	Diabase, Unit 17	Days; sheared, slickensided
77R-1, 87	1119.47	2.68	17.2	2.78	4.21	Diabase, Unit 17	Minutes
77R-2, 94	1120.54	—	—	2.71	3.16	Lapilli tuff, Unit 19	Days; coarse grained
77R-2, 132	1120.92	2.54	21.4	[a]3.21	3.09	Ash tuff, Unit 20	Minutes
79R-1, 20	1137.80	[a]2.79	[a]9.2	[a]2.69	4.31	Lapilli tuff, Unit 28	Days; coarse grained
79R-1, 23	1137.83	2.64	8.3	2.79	4.11	Lapilli tuff, Unit 28	Days; no salt correction
79R-1, 41	1138.01	2.59	8.5	2.74	4.12	Lapilli tuff, Unit 28	Days; no salt correction
79R-1, 73	1138.33	2.61	8.6	2.76	4.41	Lapilli tuff, Unit 28	Days; no salt correction

Notes: Days, hours and minutes refer to the approximate amount of time between splitting and sampling. The term "mixture" in the basaltic "mousse" unit refers to a sample composed of both matrix and clast material. "No salt correction" = values have not been corrected for 35 ppt salt content in the pore fluid.

[a] Denotes suspicious values.

Table 22. Shear strength data from Site 791.

Core, section, interval (cm)	Depth (mbsf)	Shear strength (kPa)
126-791A-		
2H-1, 95	5.45	5.4
2H-2, 94	6.94	5.1
2H-6, 41	12.41	4.7
4H-3, 96	27.46	13.9
4H-4, 122	29.22	12
4H-5, 58	30.08	17.6
5H-2, 116	35.66	17.9
5H-3, 54	36.54	18.2
5H-4, 27	37.77	8.2
5H-5, 69	39.69	11.2
16H-2, 70	141.4	8.6
18H-1, 44	158.94	62
18H-2, 109	161.09	5.8
19H-1, 104	169.14	12.4
19H-6, 120	176.8	10.7
22H-6, 72	205.12	47.3
22H-7, 16	206.06	33.8
33X-1, 16	294.46	12.8

Unit A starts at the mud line, is approximately 42 m thick, and is contained within the depth limits of lithologic Unit I (see "Lithostratigraphy and Accumulation Rates" section, this chapter). It is characterized by very low values of Th, U, K, Fe, Si, and Al; these elements increase with depth over the interval observed (Fig. 79, 0–150 mbsf). Some of the observations may be explained by the large hole size below the mud line, where sediment eroded by the action of the drill string formed a seawater pool in the immediate vicinity of the pipe. This observation was supported by higher than average values of H and Cl over this interval (Fig. 78, 0–150 mbsf).

This section of hole, however, contains two compatible sets of observations that support the separation of this unit from the one below. First, this zone is one of high magnetic susceptibility (see "Lithostratigraphy and Accumulation Rates" section, this chapter, Fig. 9). Second, the recovered material from Holes 790B and 791A, for comparable depths (after correcting for variations in sedimentation rates), is described as a pumiceous sandy gravel; shipboard measurements of porosity for recovered cores are on the order of 60%–80%.

Unit B is also contained within lithologic Unit I. It starts at approximately 42 mbsf and is 140 m thick. It is characterized by low values of Th, U, K, Fe, Si, and Al (Fig. 79, 0–150 mbsf).

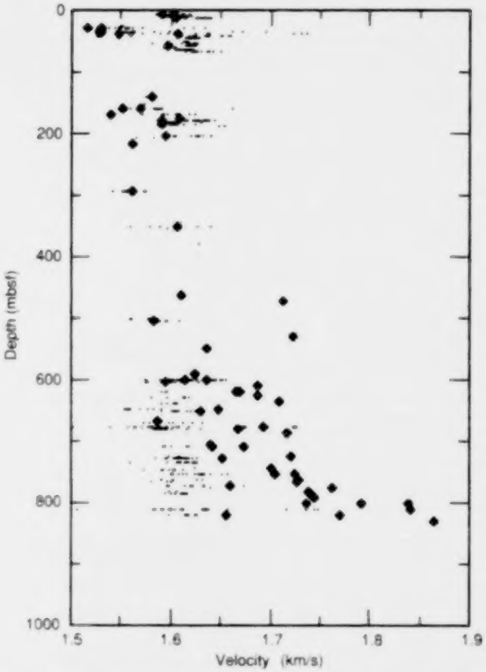

Figure 76. Comparison of sonic velocity determined by Hamilton Frame and multisensor track methods for Site 791. Dots = multisensor track; closed diamond = Hamilton Frame.

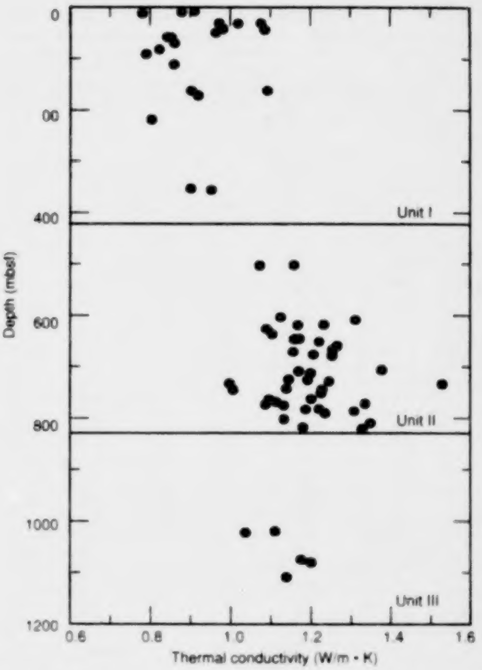

Figure 77. Plot of thermal conductivity, Site 791. Horizontal lines indicate lithologic unit boundaries.

The overall decrease in most of the elements studied might be a result of the increase in hole size. However, this section corresponds to a zone of steadily increasing magnetic susceptibility (see "Lithostratigraphy and Accumulation Rates" section, this chapter), reflected by a gradual increase in Fe content. Descriptions of recovered core material indicate that this interval is predominantly pumiceous sandy gravel and pebbly sand.

Unit C starts at 182 mbsf. It is characterized by a constant value of Al and a gradual increase in Th, Si, and K with depth (Fig. 79, 0-300 mbsf). The base of the unit is indistinct, however, within the terms of the present analysis. Consequently, it extends over parts of lithologic Units I and II. Toward the base of this unit, a narrow zone from 585 to 600 mbsf is characterized by high Th and U and low Fe, Al, and Si values. It may be possible to subdivide the unit by placing a boundary at either 471 or 534 mbsf on the basis of the trends described above (Fig. 79, 150-650 mbsf).

High Gamma Ray Horizons

Throughout the borehole we observed a series of narrow zones with high readings of natural gamma rays (Fig. 79). For example, the base of Unit A is defined by three of these horizons at 33, 38, and 43 mbsf (Fig. 79, 0-150 mbsf), which correlate with clay beds associated with black sand/silt beds recovered in Holes 790B (Core 126-790B-3H) and 791A (Core 126-791A-5H). The occurrence of these high natural gamma log features increases with depth.

Presence of Pyrite

Sulfur values increase toward the base of the analyzed section and correlate well with observations of pyrite in recovered cores. Between 585 and 685 mbsf, the Fe and S responses are effectively parallel. Unfortunately, further detailed analysis of this trend is hampered, at present, by the use of sulfur in the drill-string composition.

Nongeological Observations

At 645 mbsf (Figs. 78 and 79, 650-800 mbsf), a noticeable increase in iron results from the increased thickness in the wall of the drill string just above the BHA, where a 60-m-long section of 5½-in.-diameter drill pipe is present. At 710 mbsf, a massive increase in measured iron and a decrease in total natural gamma rays occur. This continues to the bottom 115 m of the logged portion of the hole, which is the length of the BHA.

Conclusions

This report is a preliminary assessment of the downhole geochemical data obtained in Hole 791B during Leg 126. The data are of good quality, given the difficult conditions encountered in the hole. Initial appraisals indicate that (1) it is possible to identify three major zones or units within the section studied, which may be either lithologically or hole-condition related; (2) high Fe concentrations are found in zones exhibiting high magnetic susceptibility values; (3) high gamma-ray values are found where clay beds are associated with black sands; (4) in lithologic

Unit I, low gamma-ray values are associated with unrecovered pumice gravels; and (5) the presence of pyrite in the lower part of the section is shown by a positive correlation between S and Fe.

Further detailed analysis can only be accomplished after the data have been evaluated for the effects of both attenuation and modification caused by the presence of the drill string.

REFERENCES

Akimoto, K., 1989. Recent foraminifera from Enshunada. *In* Takayanagi, Y., and Ishizaki, K. (Eds.), *Collected Papers on Foraminifera from the Japanese Islands:* Sendai (Toko Press), 93–104.

Becker, K., Sakai, H., et al., 1988. *Proc. ODP, Init. Repts.*, 111: College Station, TX (Ocean Drilling Program).

Berggren, W. A., Kent, D. V., Flynn, J. J., and Van Couvering, J. A., 1985. Cenozoic geochronology. *Geol. Soc. Am. Bull.*, 96:1407–1418.

Berner, R. A., 1964. Iron sulfides formed from aqueous solution at low temperatures and atmospheric pressure. *J. Geol.*, 72:293–306.

Blow, W. H., 1969. Late middle Eocene to Recent planktonic foraminiferal biostratigraphy. *In* Renz, H. H., and Brönniman, P. (Eds.), *Proceedings of the First International Conference on Planktonic Microfossils:* Leiden (E. J. Brill), 1:199–422.

Ericson, D. B., and Wollin, G., 1968. Pleistocene climates and chronology in deep-sea sediments. *Science*, 162:1227–1234.

Foreman, H. P., 1981. Radiolaria. *In* Emiliani, C. (Ed.), *The Sea* (Vol. 7): *The Oceanic Lithosphere:* New York (Wiley-Interscience), 1121–1144.

Fryer, P., Taylor, B., Langmuir, C., and Hochstaedter, A. G., in press. Petrology and geochemistry of lavas from the Sumisu and Torishima backarc rifts. *Earth Planet. Sci. Lett.*

Gieskes, J. M., 1983. The chemistry of interstitial waters of deep sea sediments: interpretation of deep sea drilling data. *In* Riley, J. P., and Chester, R. (Eds.), *Chemical Oceanography* (Vol. 8): London (Academic Press), 221–269.

Hawkins, J. W., and Melchior, J. T., 1985. Petrology of Mariana Trough and Lau Basin basalts. *J. Geophys. Res.*, 90:11,431–11,468.

Hay, W. W., Sibuet, J.-C., et al., 1984. *Init. Repts. DSDP,* 75, Pts. 1 and 2: Washington (U.S. Govt. Printing Office).

Hochstaedter, A. G., and Gill, J. B., in press. Petrology and geochemistry of lavas from the Sumisu Rift: an incipient back-arc basin. *Earth Planet. Sci. Lett.*

Klein, E. M., and Langmuir, C. H., 1987. Global correlations of ocean ridge chemistry with axial depth and crustal thickness. *J. Geophys. Res.*, 92:8089–8115.

Manheim, F. T., and Waterman, L. S., 1974. Diffusimetry (diffusion constant estimation) on sediment cores by resistivity probe. *In* von der Borch, C. C., Sclater, J. G., et al., *Init. Repts. DSDP,* 22: Washington (U.S. Govt. Printing Office), 663–670.

Mattey, D. P., Marsh, N. G., and Tarney, J., 1981. The geochemistry, mineralogy, and petrology of basalts from the West Philippine and Parece Vela basins and from the Palau-Kyushu and West Mariana ridges, Deep Sea Drilling Program Leg 59. *In* Kroenke, L., Scott, R. B., et al., *Init. Repts. DSDP,* 59: Washington (U.S. Govt. Printing Office), 753–796.

McCave, I. N., 1972. Transport and escape of fine-grained sediment from shelf areas. *In* Swift, D.J.P, Duane, D. B., and Pilkey, O. H. (Eds.), *Shelf Sediment Transport: Process and Pattern:* Stroudsburg, PA (Dowden, Hutchinson and Ross), 225–248.

Niitsuma, N., 1982. Paleomagnetic results, Middle America Trench off Mexico, Deep Sea Drilling Project Leg 66. *In* Watkins, J. S., Moore, J. C., et al., *Init. Repts. DSDP,* 66: Washington (U.S. Govt. Printing Office), 737–770.

Nishimura, A., and Murakami, F., 1988. Sedimentation of the Sumisu Rift, Izu-Ogasawara Arc. *Bull. Geol. Surv. Jpn.*, 39:39–61.

Nowell, A.R.M., and Hollister, C. D. (Eds.), 1985. Deep ocean sediment transport—preliminary results of the High Energy Benthic Boundary Layer Experiments. *Mar. Geol.*, Spec. Issue, No. 66.

Okada, H., and Bukry, D., 1980. Supplementary modification and introduction of code numbers to the "Low-latitude coccolith biostratigraphic zonation" (Bukry, 1973; 1975). *Mar. Micropaleontol.*, 5: 321–325.

Sanfilippo, A., Westberg-Smith, M. J., and Reidel, W. R., 1985. Cenozoic radiolaria. *In* Bolli, H. M., Saunders, J. B., and Perch-Nielson, K. (Eds.), *Plankton Stratigraphy:* Cambridge (Cambridge Univ. Press), 631–712.

Sato, T., Takayama, T., Kato, M., Kudo, T., and Kameo, K., 1988. Calcareous microfossil biostratigraphy of the uppermost Cenozoic formations distributed in the Coast of the Japan Sea—Part 4: Conclusion. *J. Jpn. Assoc. Petrol. Tech.*, 53:13–29.

Schlumberger, 1983. *Natural Gamma Ray Spectrometry: Essentials of NGS Interpretation:* Houston (Schlumberger).

Takayama, T., and Sato, T., 1987. Coccolith biostratigraphy of the North Atlantic Ocean, Deep Sea Drilling Project Leg 94. *In* Ruddiman, W. F., Kidd, R. B., Thomas, E., et al., *Init. Repts. DSDP,* 94, Pt. 2: Washington (U.S. Govt. Printing Office), 651–702.

Tarling, D. H., 1983. *Palaeomagnetism, Principles and Applications in Geology, Geophysics and Archaeology:* London (Chapman and Hall).

Taylor, B., Brown, G., Fryer, P., Gill, J., Hochstaedter, A., Hotta, H., Langmuir, C., Leinen, M., Nishimura, A., and Urabe, T., in press. ALVIN-SeaBeam studies of the Sumisu Rift, Izu-Bonin Arc. *Earth Planet. Sci. Lett.*

Taylor, B., Brown, G., Hussong, D., and Fryer, P., 1988a. SeaMARC II sidescan acoustic imagery, Sumisu and Torishima rifts, Izu-Ogasawara Island Arc, 1:200,000. *Mar. Geol. Map Ser.*, Tsukuba (Geol. Surv. Jpn.), No. 31.

————, 1988b. SeaMARC II bathymetry, Sumisu and Torishima rifts, Izu-Ogasawara Island Arc, 1:200,000. *Mar. Geol. Map Ser.*, Tsukuba (Geol. Surv. Jpn.), No. 31.

Wood, D. A., Joron, J.-L., Marsh, N. G., Tarney, J., and Treuil, M., 1980. Major- and trace-element variations in basalts from the North Philippine Sea drilled during Deep Sea Drilling Program Leg 58: a comparative study of back-arc-basin basalts with lava series from Japan and mid-ocean ridges. *In* Klein, G. deV., Kobayashi, K., et al., *Init. Repts. DSDP,* 58: Washington (U.S. Govt. Printing Office), 873–894.

Yasuda, H., 1989. Benthic foraminifers and sedimentary facies of the lower slope basin off Shikoku, Japan. *In* Takayanagi, Y., and Ishizaki, K. (Eds.), *Collected Papers on Foraminifera from the Japanese Islands:* Sendai (Toko Press), 83–92.

Ms 126A-108

NOTE: All core description forms ("barrel sheets") and core photographs have been printed on coated paper and bound as Section 3, near the back of the book, beginning on page 421.

Table 23. Thermal conductivity data from Site 791.

Core, section, interval (cm)	Depth (mbsf)	Thermal conductivity (W/m · K)
126-791A-		
2H-1, 52	5.02	0.907
2H-3, 95	8.45	0.777
2H-4, 66	9.66	0.874
4H-3, 56	27.06	0.970
4H-4, 122	29.22	1.072
4H-5, 49	29.99	1.013
5H-3, 96	36.96	0.974
5H-4, 19	37.69	1.075
5H-6, 106	41.56	0.958
7H-4, 16	56.66	0.848
7H-5, 14	58.14	0.837
8H-3, 30	64.90	0.856
8H-4, 17	66.27	[a]1.950
9H-6, 34	79.14	0.815
10H-6, 37	88.87	0.787
11H-4, 87	96.07	[a]0.158
11H-6, 68	98.88	0.125
12H-6, 50	108.40	0.854
18H-1, 52	159.02	1.089
18H-2, 82	160.82	0.899
19H-1, 73	168.83	0.914
25X-1, 17	217.27	0.803
39X-1, 35	352.65	0.899
39X-1, 82	353.12	0.953
126-791B-		
10R-1, 28	473.58	[a]1.190
13R-1, 83	502.93	1.156
13R-2, 48	504.08	1.071
16R-1, 18	531.38	[a]1.1724
23R-1, 82	599.52	[a]1.204
23R-3, 51	602.21	1.123
23R-4, 52	603.72	[a]0.805
24R-1, 36	608.76	1.303
25R-1, 117	619.27	1.164
25R-2, 47	620.07	1.229
26R-1, 8	627.78	1.086
27R-1, 44	637.44	1.101
28R-1, 33	646.93	1.160
28R-3, 24	649.84	1.154

Table 23 (continued).

Core, section, interval (cm)	Depth (mbsf)	Thermal conductivity (W/m · K)
126-791B- (Cont.)		
28R-4, 49	651.59	1.217
30R-1, 70	666.70	1.255
30R-2, 79	668.29	1.245
30R-3, 102	670.02	1.156
31R-1, 118	676.78	1.201
31R-3, 63	679.23	0.285
31R-4, 24	680.34	1.249
34R-1, 90	705.50	1.373
34R-3, 80	708.40	1.170
34R-5, 24	710.84	1.197
36R-1, 110	724.70	1.192
36R-2, 91	726.01	1.142
36R-3, 118	727.78	1.245
37R-1, 70	733.90	1.000
37R-2, 26	734.96	1.524
38R-1, 99	743.79	1.141
38R-3, 55	746.35	1.011
39R-1, 42	752.82	1.222
39R-2, 88	754.78	1.215
38R-4, 98	767.28	1.112
40R-1, 25	762.35	1.198
40R-2, 83	764.43	1.095
40R-3, 40	765.50	1.114
41R-1, 35	772.05	1.329
41R-2, 127	774.47	1.134
41R-3, 70	775.40	1.086
42R-1, 62	781.92	1.188
42R-2, 50	783.30	1.215
42R-3, 59	784.89	1.304
43R-1, 28	791.28	1.234
44R-1, 87	801.57	1.136
45R-2, 76	812.56	1.344
46R-1, 90	820.90	1.178
46R-2, 35	821.85	[a]2.2924
46R-CC, 18	822.80	1.323
67R-1, 40	1022.5	1.114
67R-2, 115	1024.8	1.042
72R-2, 85	1075.8	1.1731
73R-3, 32	1083.3	1.2007
76R-1, 128	1110.3	1.1365

[a] Results are of uncertain quality.

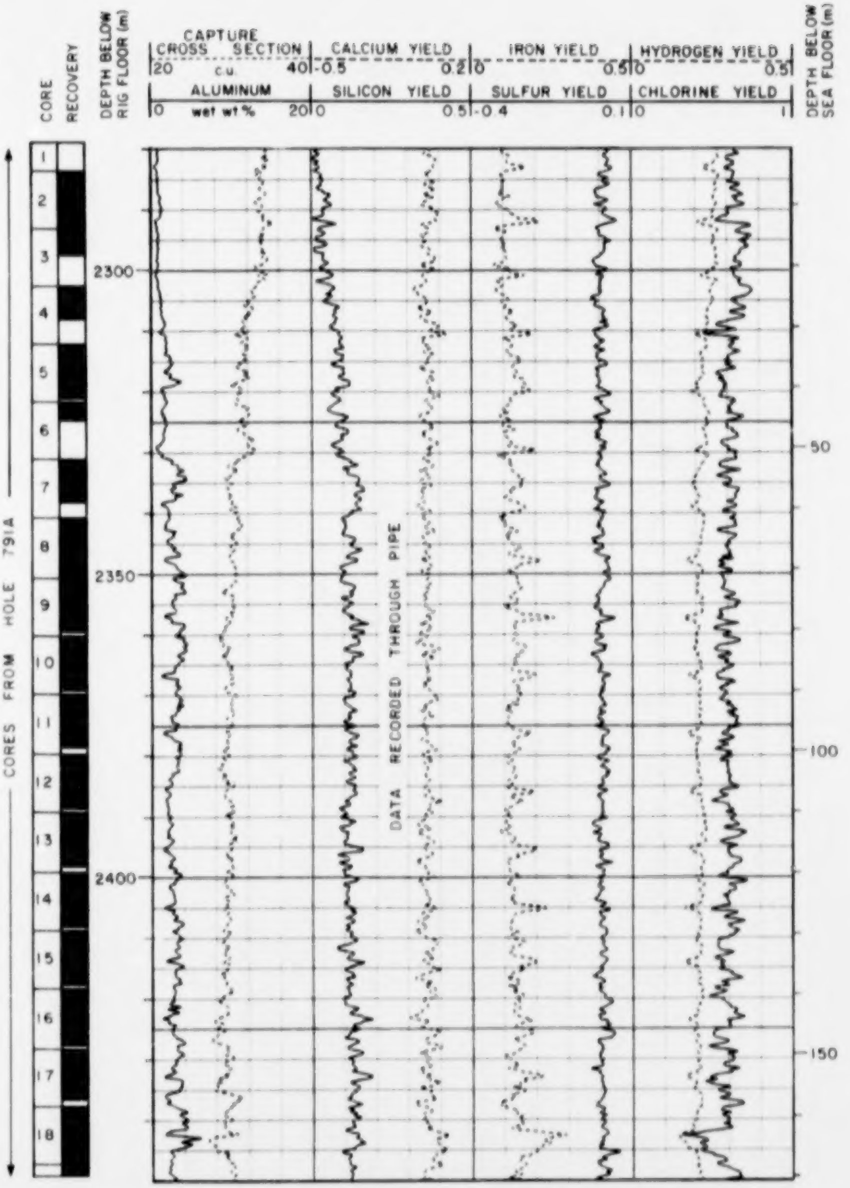

Figure 78. Summary log for hydrogen and chlorine (far right) obtained with the aluminum clay tool (ACT) for the interval from 0 to 830 mbsf. Also shown are the plots for aluminum, calcium, silicon, iron, and sulfur.

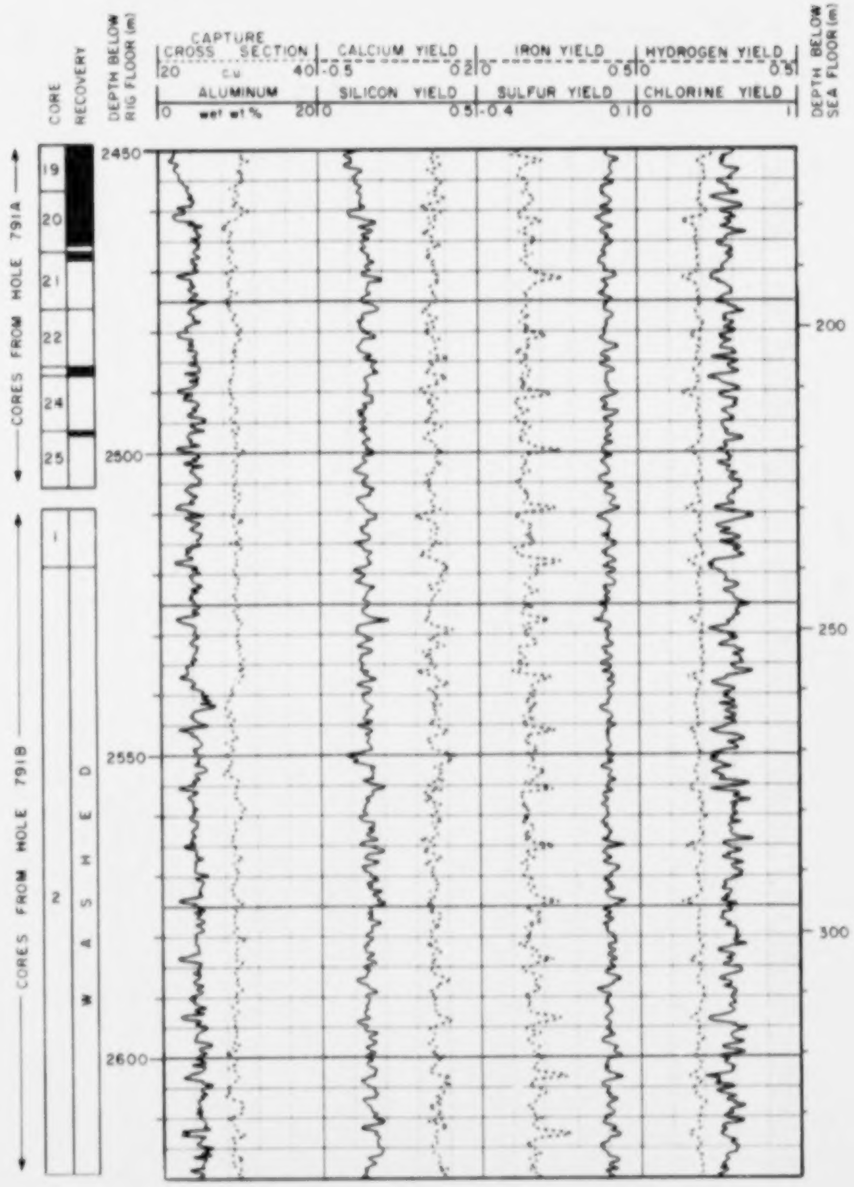

Figure 78 (continued).

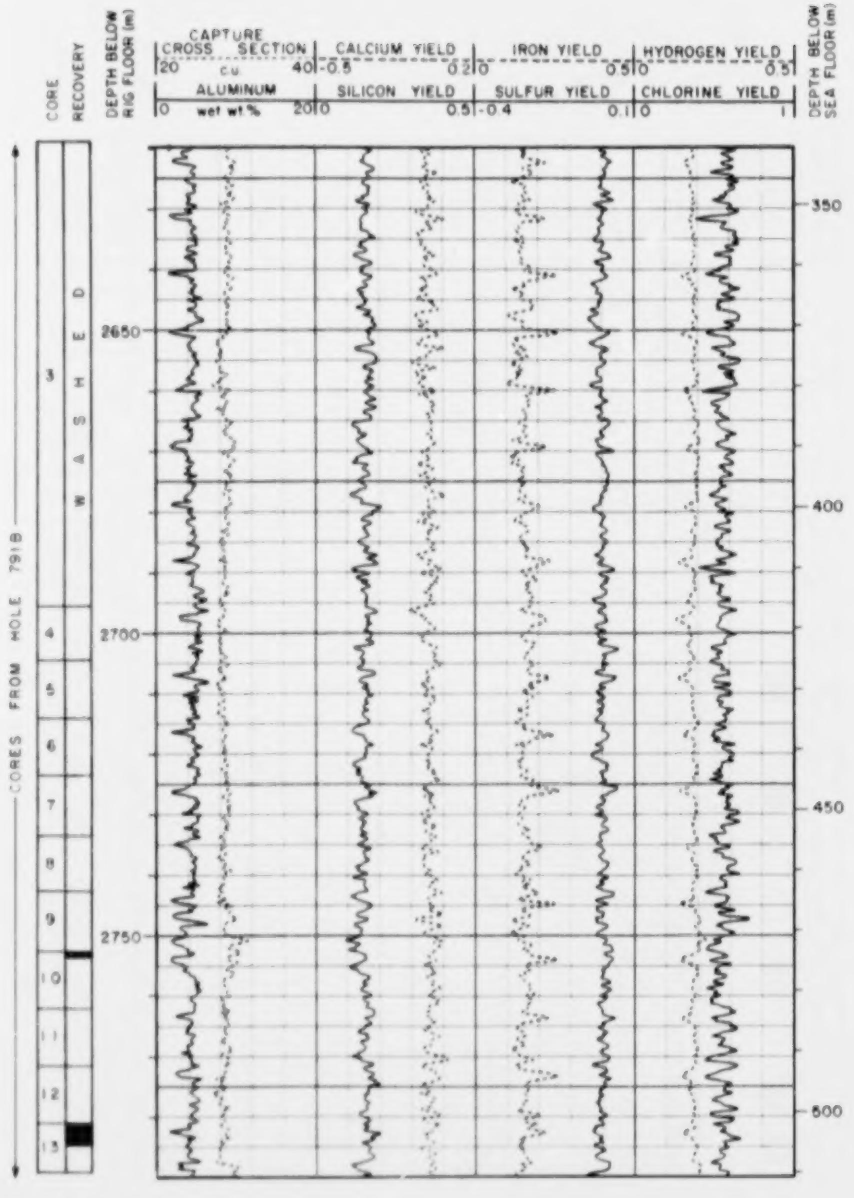

Figure 78 (continued).

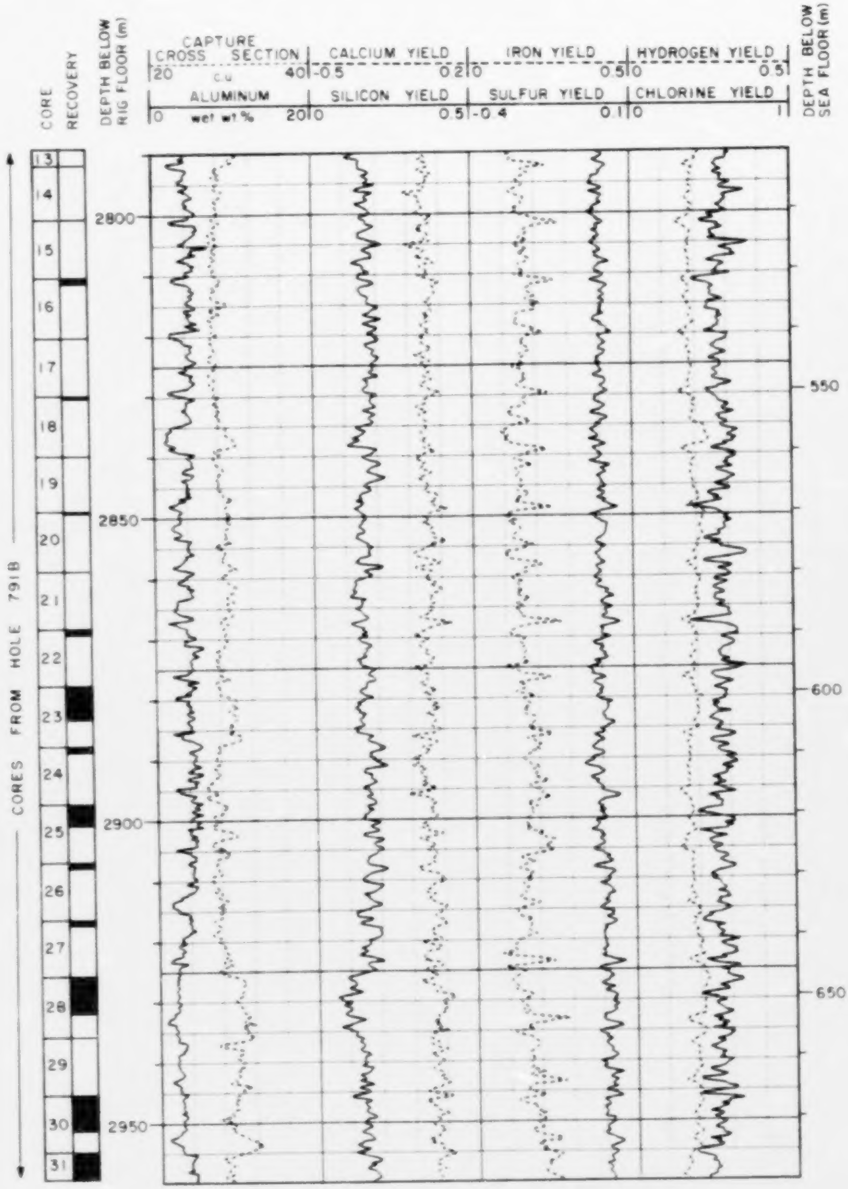

Figure 78 (continued).

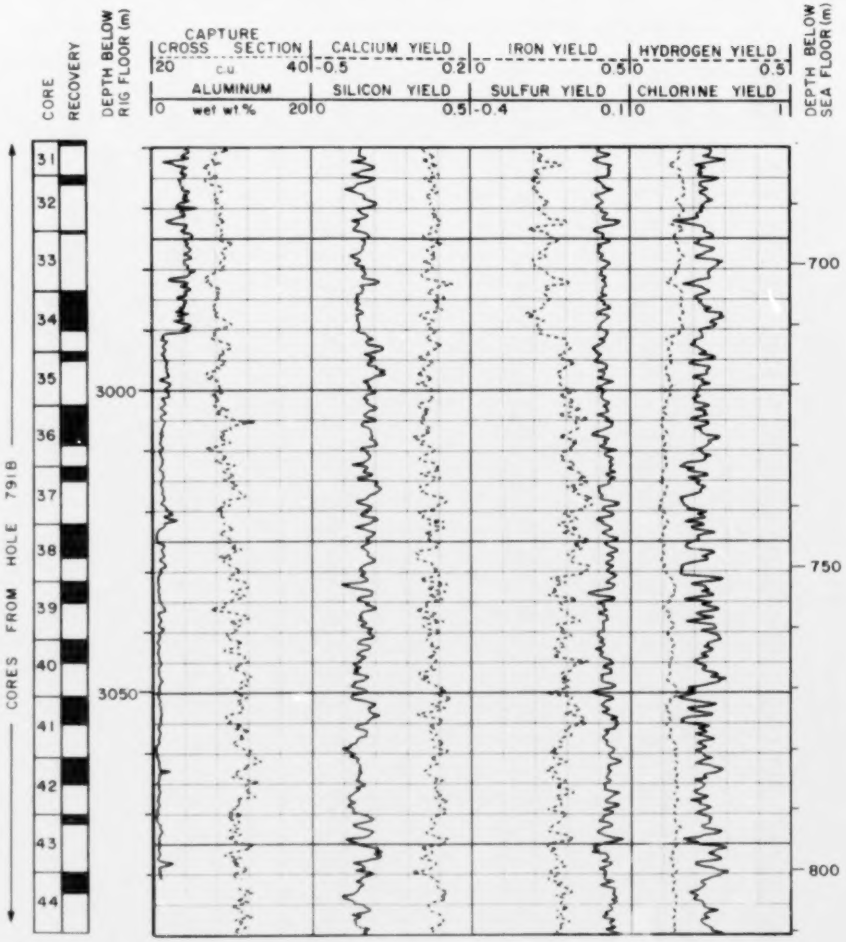

Figure 78 (continued).

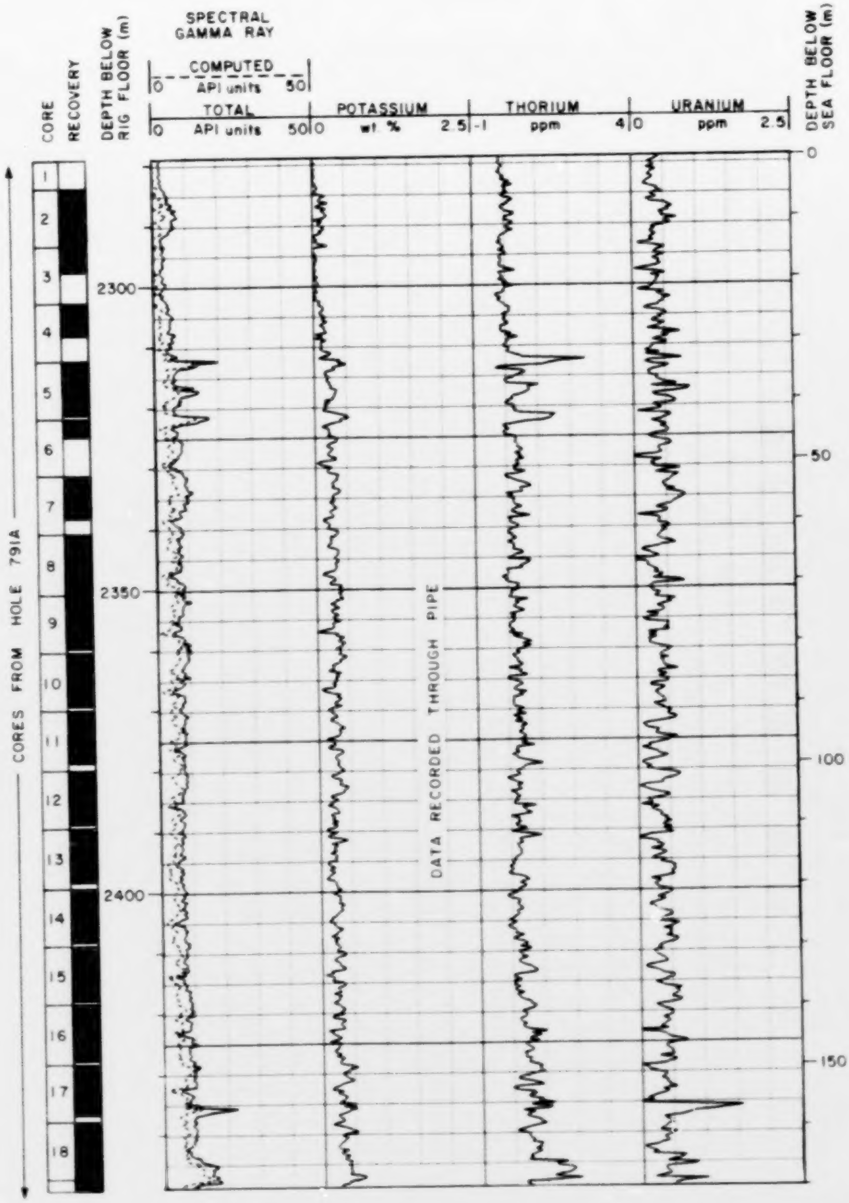

Figure 79. Summary log for potassium, thorium, and uranium obtained with the natural gamma-ray tool (NGT) for the interval from 0 to 830 mbsf. Also shown is the plot for spectral gamma-ray measurements.

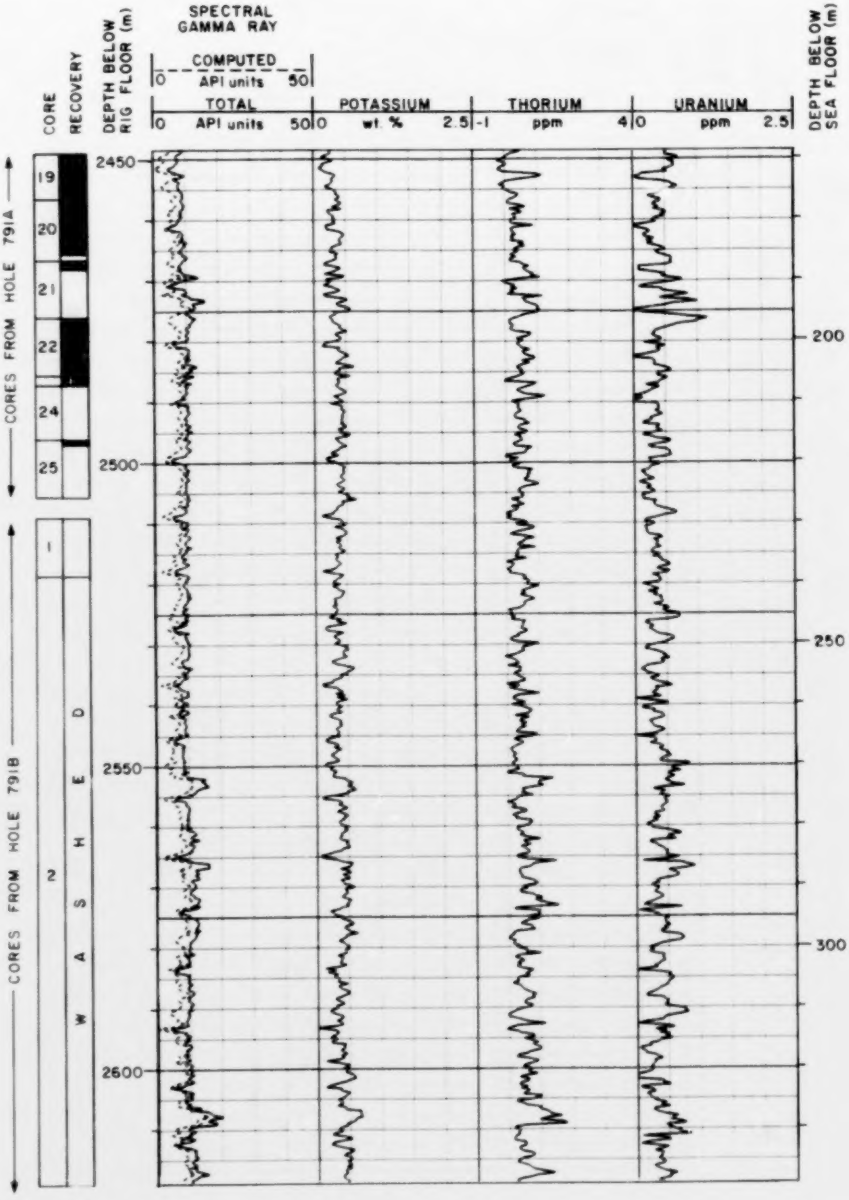

Figure 79 (continued).

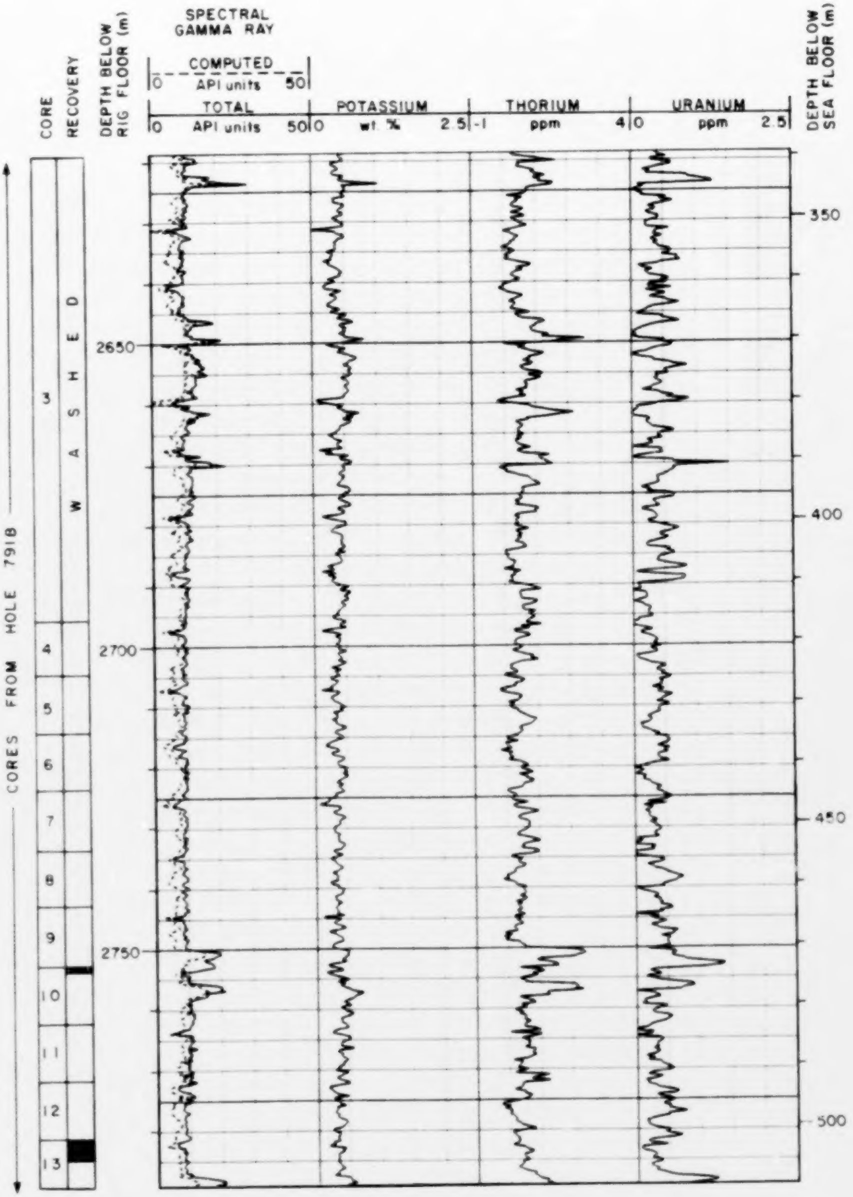

Figure 79 (continued).

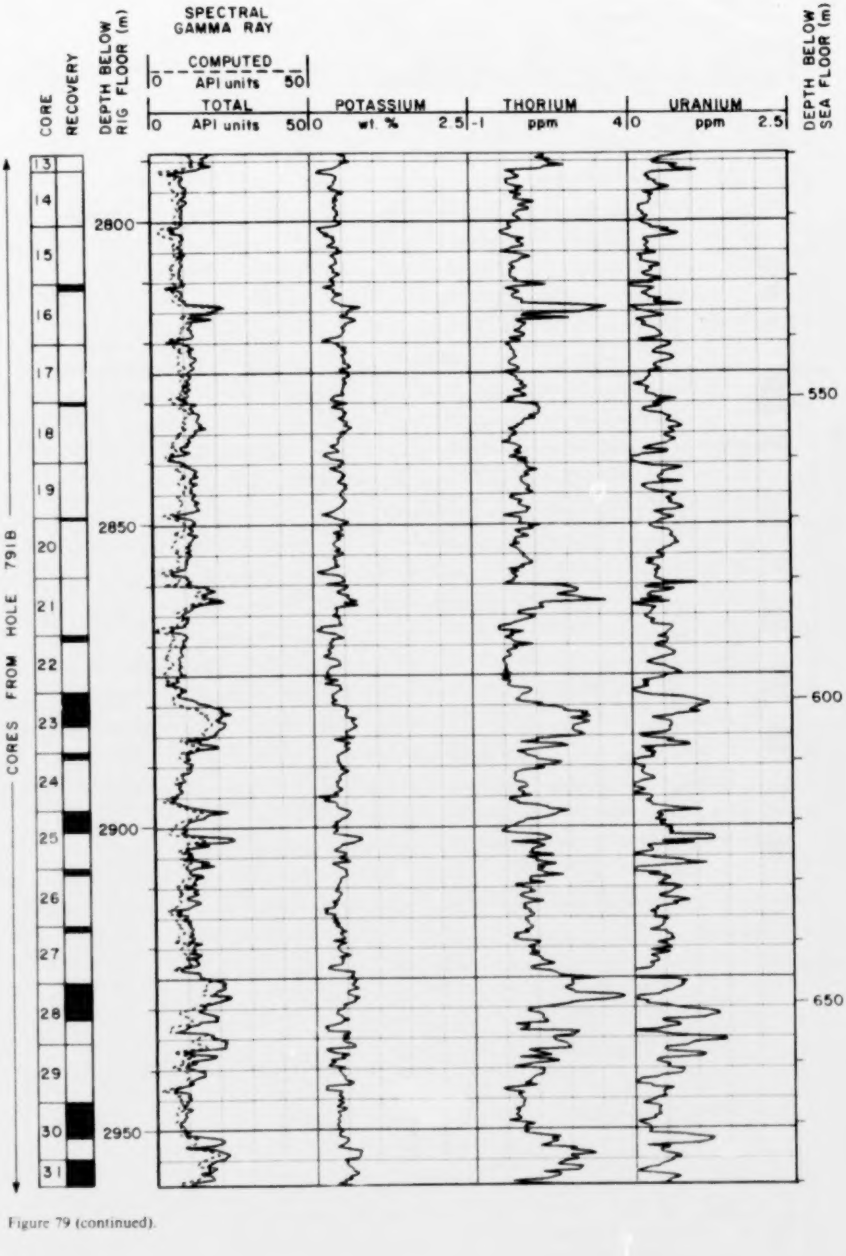

Figure 79 (continued).

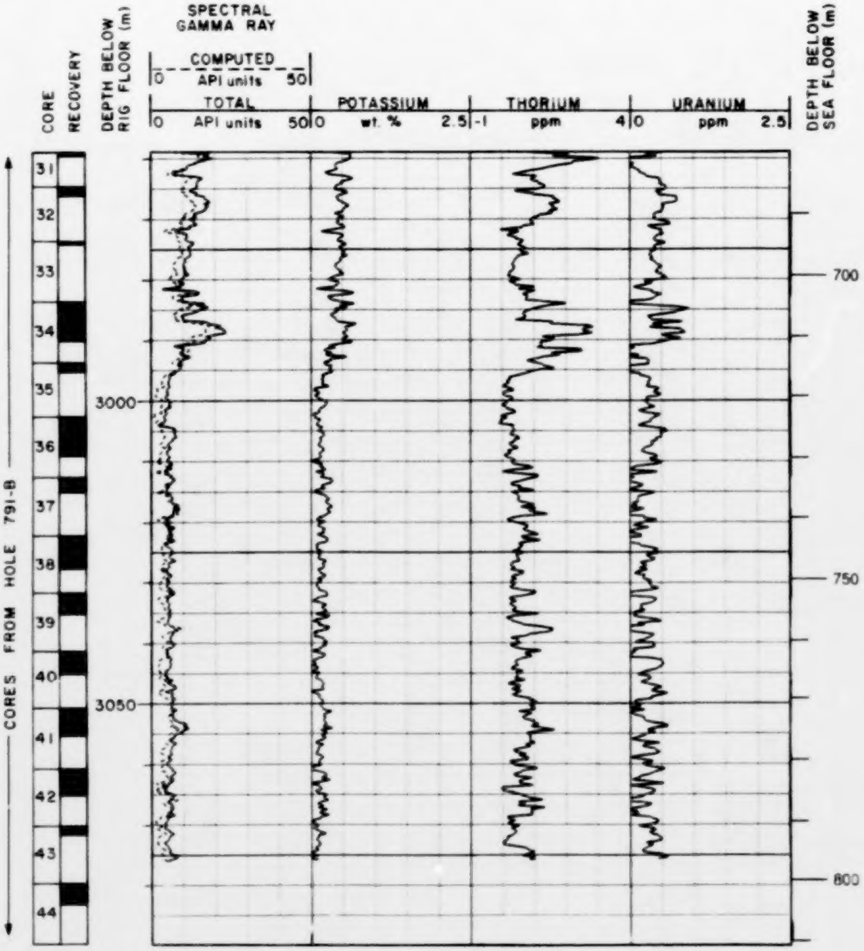

Figure 79 (continued).

Taylor, B., Fujioka, K., et al., 1990
Proceedings of the Ocean Drilling Program, Initial Reports, Vol. 126

8. SITE 792[1]

Shipboard Scientific Party[2]

HOLE 792A

Date occupied: 16 May 1989

Date departed: 17 May 1989

Time on hole: 15 hr, 49 min

Position: 30°23.97′N, 140°22.81′E

Bottom felt (rig floor; m, drill pipe measurement): 1797.8

Distance between rig floor and sea level (m): 10.50

Water depth (drill pipe measurement from sea level, m): 1787.3

Total depth (rig floor, m): 1892.8

Penetration (m): 95.00

Number of cores (including cores with no recovery): 10

Total length of cored section (m): 95.00

Total core recovered (m): 72.09

Core recovery (%): 75.9

Oldest sediment cored:
  Depth (mbsf): 95.00
  Nature: vitric sand and foraminifer-nannofossil vitric silty clay
  Age: Pleistocene
  Measured velocity (km/s): 1.59

HOLE 792B

Date occupied: 17 May 1989

Date departed: 17 May 1989

Time on hole: 14 hr, 45 min

Position: 32°23.96′N, 140°22.81′E

Bottom felt (rig floor; m, drill pipe measurement): 1798.2

Distance between rig floor and sea level (m): 10.50

Water depth (drill pipe measurement from sea level, m): 1787.7

Total depth (rig floor, m): 1944.6

Penetration (m): 146.4

Number of cores (including cores with no recovery): 11

Total length of cored section (m): 100.70

Total core recovered (m): 43.59

Core recovery (%): 43.3

Oldest sediment cored:
  Depth (mbsf): 146.40
  Nature: biogenic, silica-rich, lithic-vitric silty clay and nannofossil-rich vitric silty clay
  Age: late Pliocene
  Measured velocity (km/s): 1.59

HOLE 792C

Date occupied: 17 May 1989

Date departed: 18 May 1989

Time on hole: 9 hr, 35 min

Position: 32°23.94′N, 140°22.78′E

Bottom felt (rig floor; m, drill pipe measurement): 1798.2

Distance between rig floor and sea level (m): 10.50

Water depth (drill pipe measurement from sea level, m): 1787.7

Total depth (rig floor, m): 1944.6

Penetration (m): 146.4

Number of cores (including cores with no recovery): 1

Total length of cored section (m): 9.60

Total core recovered (m): 0.59

Core recovery (%): 6.1

Oldest sediment cored:
  Depth (mbsf): 146.40
  Nature: nannofossil-rich vitric silty clay
  Age: late Pliocene

HOLE 792D

Date occupied: 18 May 1989

Date departed: 18 May 1989

Time on hole: 6 hr, 50 min

Position: 32°23.93′N, 140°22.80′E

Bottom felt (rig floor; m, drill pipe measurement): 1798.2

Distance between rig floor and sea level (m): 10.50

Water depth (drill pipe measurement from sea level, m): 1787.7

Total depth (rig floor, m): 1944.6

Penetration (m): 146.4

Number of cores (including cores with no recovery): 1

Total length of cored section (m): 9.60

Total core recovered (m): 0.84

Core recovery (%): 8.8

Oldest sediment cored:
  Depth (mbsf): 146.4
  Nature: nannofossil-rich vitric silty clay
  Age: late Pliocene

HOLE 792E

Date occupied: 19 May 1989

Date departed: 26 May 1989

Time on hole: 7 days, 6 hr, 5 min

Position: 32°23.96′N, 140°22.79′E

Bottom felt (rig floor; m, drill pipe measurement): 1798.2

---

[1] Taylor, B., Fujioka, K., et al., 1990. *Proc. ODP, Init. Repts.*, 126: College Station, TX (Ocean Drilling Program).

[2] Shipboard Scientific Party is as given in the list of participants preceding the contents.

Distance between rig floor and sea level (m): 10.50

Water depth (drill pipe measurement from sea level, m): 1787.7

Total depth (rig floor, m): 2684.1

Penetration (m): 885.9

Number of cores (including cores with no recovery): 78

Total length of cored section (m): 750.30

Total core recovered (m): 361.89

Core recovery (%): 48.2

Oldest sediment cored:
Depth (mbsf): 800.20
Nature: hydrothermally altered volcanic pebble-granule conglomerate and other volcaniclastic rocks of uncertain grain size
Age: late Oligocene
Measured velocity (km/s): 2.01

Basement:
Depth (mbsf): 804.00
Nature: porphyritic andesite
Measured velocity (km/s): 4.59

Principal results: Site 792 is located on the western half of the Izu-Bonin forearc sedimentary basin, about 60 km east of the arc volcano Aoga Shima and 170 km west of the axis of the Izu-Bonin Trench. It is upslope of a fork in the Aoga Shima Canyon where the forearc sediments lap onto the edge of a basement high. The principal objectives of this site were to determine (1) the stratigraphy of the forearc basin, and hence the temporal variations in sedimentation, depositional environment, and paleoceanography, and the history of the intensity and chemistry of the arc volcanism; (2) the uplift and subsidence history across the forearc; (3) the nature of the igneous basement and the formation of the 200-km-wide forearc crust; and (4) the microstructural deformation and large-scale rotation and translation of the forearc terrane since the Eocene. We selected the site on the basis of multichannel seismic records and a short shipboard seismic survey; the location chosen lies on *Fred Moore* 3505, Line 10, at 0134Z. Site 792 was occupied from 1636 hr (UTC) on 16 May, to 2140 hr on 25 May 1989.

Hole 792A was spudded for advanced piston corer (APC) operations at 2130Z on 17 May 1989. We cored 95 m at a recovery rate of 76% before an overpull resulted in a severed piston rod, thus ending operations at the hole. Hole 792B re-cored the mud line, washed to 50 m below sea floor (mbsf), and continued with the APC to 69.2 mbsf; at this point we switched to the extended core barrel (XCB) and cored to 146.4 mbsf, with overall recovery of 43%. Holes 792B–D all ended operations in the interval from 137 to 146 mbsf, owing to separation of the XCB cutting shoe in each case. We spudded Hole 792E with a rotary core barrel (RCB) at 0207Z on 19 May, washed to 135.6 mbsf, and then cored to 885.9 mbsf; recovery was 52% in the sediments above 804 mbsf, and 16% in the underlying basement. As we pulled the pipe from the hole to prepare for logging it became stuck, the bit resting at 286 mbsf. After attempts to save the bottom-hole assembly (BHA) proved fruitless, we ran a full suite of standard geophysical and geochemical logs above 878 mbsf. The first use of formation microscanner (FMS) logging in the Ocean Drilling Program (ODP) was successfully completed, and a vertical seismic profile (VSP) was also collected. Finally, we severed the pipe with explosives at 134 mbsf.

We defined six lithostratigraphic units at Site 792:

1. Unit I (0–183.7 mbsf): upper Pliocene to Holocene nannofossil-rich, vitric silty clay and clayey silt, interbedded with vitric silts and sands and minor pumiceous and scoriaceous gravels.
2. Unit II (183.7–357.4 mbsf): middle and upper Miocene sandy mudstone, muddy sandstone, and silty claystone (all with nannofossil-rich intervals), and vitric sand- and siltstone.
3. Unit III (357.4–429.3 mbsf): lower Miocene to upper Oligocene intensely bioturbated, nannofossil-rich claystone and nannofossil chalk, and rare crystal-vitric silt- and sandstone.
4. Unit IV (429.3–783.4 mbsf): upper Oligocene vitric sandstone and sandy conglomerate with claystone intraclasts, with minor silty claystone and claystone that contain nannofossil-rich intervals.
5. Unit V (783.4–804 mbsf): altered volcanic sandstone with claystone intraclasts.
6. Unit VI (804–885.9 mbsf): porphyritic andesite with minor basaltic andesite and dacite.

Units I–IV were dated by means of nannofossils, foraminifers, and paleomagnetics, with the addition of radiolarians for Units I–II. Four lacunae occur, at 1–2.2, 3.5–6, 8–9, and 13–19 Ma. The second and fourth lacunae correspond to the basal boundaries of the first two units. Average sedimentation rates in the intervals between these lacunae are (in order of increasing age) 90 and 122 m/m.y. (Unit I), and 43 and 23 m./m.y. (Unit II), respectively. Sedimentation rates for Unit III are 14 and 4 m/m.y., respectively, for intervals above and below a normal fault that cuts out strata from 23 to 24 Ma. Sedimentation rates for Unit IV (27–29 Ma) were about 300 m/m.y. and greater prior to 28 Ma, but slowed to 40 m/m.y. thereafter. Benthic foraminifers indicate that depositional water depths shallowed from 3.5–4.5 km in the late Oligocene to <2.3 km since the middle Pleistocene, which is evidence for 1–2 km of basement uplift since 29 Ma.

The >200 ash layers in Unit I are evidence of ongoing explosive volcanism since the late Pliocene. Unit II records hemipelagic and turbidite deposition of biogenic and volcanic components, mixed by burrowers. Unit III marks a period of slow bathyal deposition without significant volcanic input. Unit IV consists of thick- to thin-bedded turbidites and debris-flow deposits, and fine-grained hemipelagic sediments. The volcanogenic detritus includes the products of concurrent volcanism and erosion of older volcanic terranes. Bedding is subhorizontal, with maximum dips <5°–10°. Extensional microfaults, conjugate high-angle fractures, slickensided horizontal shears, clastic injections, and dewatering veinlets in Units III and IV are all evidence of postdepositional extensional deformation. Zeolites and gypsum fill many of the veins and fractures. Correlation to multichannel seismic data suggests that we drilled through a major unconformity somewhere between 690 and 730 mbsf at this site. Although there is no lithologic change in this interval, physical property and logging data suggest a significant boundary at 715 mbsf. The age of Unit IV strata from 715 to 770 mbsf is constrained by biostratigraphic results to <34 Ma. This implies that the >1-km-thick forearc basin section, which laps onto the unconformity below the level reached at Site 792, was deposited in the middle Oligocene (29–34 Ma). The age of the (hydrothermally) altered Unit V and of the igneous basement is middle Oligocene or older. Radiometric dating of the igneous rocks will be attempted during shore-based investigations.

The basement lavas are massive flows with intercalated hyaloclastite and breccia layers. They are dominantly porphyritic, plagioclase-orthopyroxene-clinopyroxene andesites, with high aluminum, early oxide-mineral precipitation and concomitant iron depletion. They are less enriched in low-field-strength elements such as K, Rb, Sr, and Ba than are most arc lavas. Ratios between the high-field-strength elements (e.g., Zr/Y = ~1.9) are consistent with a depleted mantle source. The presence of quartz xenocrysts, along with other geochemical evidence, may indicate that magmas from two distinct sources were mixed during a high-level fractionation process to produce the andesites.

The most extensively altered pore water of seawater origin ever sampled by the Deep Sea Drilling Project (DSDP) or ODP (except for Site 793) is located from 500 to 700 mbsf, with characteristic concentrations of sulfate = 15, magnesium = 0–4, calcium = 155, and silica = 0.1–0.4 (all in mM). The maximum calcium concentration (170 mM) at 600 mbsf is the highest ever recorded, except at Site 793 and in evaporite settings. This unique geochemistry is not a basement alteration effect but is the result of low-temperature alteration of the volcanogenic sediments. It is reflected in the marked downward increase (below 350 mbsf) in smectite and zeolite at the expense of the volcanic glass in Units III and IV. This alteration releases Ca and consumes Mg, Si, and Na. Below 500 mbsf, the pore waters are saturated with respect to gypsum, which by precipitation lowers the sulfate concentration. The concentration of organic carbon decreases exponentially from a near-surface high of 0.76% to <0.15% in Unit II and below.

Magnetic inclinations on cores younger than 15 Ma show no latitudinal shift, but some northward motion is required for cores older than 25 Ma. The inclination and declination records of the Brunhes-Matuyama reversal show a double transition during a period of decreased field intensity lasting about 3000 yr. This polarity transition period is about five times longer than at Site 791, but this may be an averaging affect caused by the threefold decrease in sedimentation rate (120 m/m.y.).

Physical property measurements indicate that (1) average bulk density values increase downward from 1.7 to 1.9 g/cm^3 in Unit I, then decrease from 2.1–1.9 g/cm^3 in Unit II to 1.85 g/cm^3 in Unit III; (2) average porosity values decrease from 65% at the top of Unit I to 55% at its base, then increase through Unit II to 65% at the base of Unit III; (3) sonic velocity data average 1.59, 1.85, and 1.87 km/s in Units I–III respectively; and (4) carbonate values range from 1%–36% at the top to 3%–21% at the base of Unit I, from 0%–4% at the top to 3%–22% at the base of Unit II, and are commonly 20%–67% in Unit III. The physical property measurements of Unit IV vary downward in concert with the lithologic changes. We defined four subunits of Unit IV, which broadly correspond to alternating finer (first and third) and coarser (second and fourth) material, subdivided at 514, 590, and 715 mbsf. In order of increasing depth, the average values in the four subunits (and Units V and VI) are (1) bulk density: 1.87, 2.16, 2.09, 2.28, 2.02, and 2.64 g/cm^3; (2) porosity: 58%, 44%, 50%, 42%, 50%, and 17%; and (3) sonic velocity: 2.3, 2.7, 2.2, 2.6, 2.2, and 4.3 km/s. Carbonate contents are 1%–10% (and rarely as high as 25%) in the upper subunit, and are typically <1%–2% below, except for thin nannofossil-rich layers with values of 10%–20%. Thermal conductivities increase downward, averaging 1.01, 1.02, 1.05, and 1.61 W/m · K in Units I–III and VI. Three excellent Uyeda-probe temperature measurements down to 110 mbsf, together with the bottom-water temperature, define a linear geothermal gradient of 55°C/km. The heat flow is 56 mW/m^2.

Although the downhole measurement logs are excellent, they mostly require shore-based analysis before final interpretation. The *in-situ* geophysical measurements show physical properties similar to the laboratory measurements. All of the lithostratigraphic and physical property unit boundaries can be recognized in the logs. The FMS clearly imaged features such as ash layers <1 cm thick. The temperature and caliper records identify permeable zones at 400–430 mbsf and at the top and bottom of Unit V, which are most likely fault zones. The borehole is slightly elongated in a direction 020° throughout the sedimentary section, but is circular in basement.

The principal results of this site are:

1. the characterization of varying rates of volcanogenic input to the forearc (extremely rapid prior to 27 Ma, minimal between 27 and 13 Ma, and from moderate to increasingly fast between 13 Ma and the present);
2. the documentation of ongoing explosive volcanism since the late Pliocene;
3. the correlation between coring results and seismic stratigraphy by means of VSP and logging, indicating sedimentary filling of the basin between the frontal arc and outer-arc highs in the middle Oligocene;
4. the first recovery of igneous basement beneath such an intraoceanic forearc basin and initial description of its unusual trace-element chemistry, characterized by weak enrichment in low-field-strength elements and depletion in high-field-strength elements (the latter indicates derivation from a refractory mantle source);
5. benthic foraminiferal evidence of 1–2 km of basement uplift since 29 Ma;
6. microstructural evidence of extensional deformation;
7. pore-water indications of low-temperature alteration of the volcanogenic sediments, producing fluids extremely enriched in calcium and depleted in magnesium, silica, and sulfate;
8. paleomagnetic evidence that the Brunhes-Matuyama reversal involved a double polarity transition during a period of decreased field intensity lasting 3000 yr or less; and
9. measurement of heat flow at 56 mW/m^2.

BACKGROUND AND OBJECTIVES

Site 792 (proposed Site BON-4) is located at 32°23.96′N, 140°22.80′E, and 1787 m below sea level (mbsl) in the western half of the Izu-Bonin forearc sedimentary basin, about 60 km east of the arc volcano Aoga Shima ("Blue Island") and 170 km west of the axis of the Izu-Bonin Trench (Fig. 1). It is located between two forks of Aoga Shima Canyon (Fig. 2). Beneath the site, the normally >3-km-thick section of forearc-basin turbidites laps onto the edge of a basement high (Fig. 3).

By drilling at this site we sought to determine the following:

1. The stratigraphy of the forearc, and hence the temporal variations in sedimentation, depositional environment, and paleoceanography, and the history of the intensity and chemistry of arc volcanism.
2. The uplift/subsidence history across the forearc to provide information on forearc flexure and basin development.
3. The nature of the forearc igneous basement, to resolve problems concerning the nature of volcanism in the initial stages of subduction and the formation of the 200-km-wide forearc crust, including the possibility of later forearc volcanism.
4. The microstructural deformation and the large-scale rotation and translation of the forearc terrane since the Eocene.

The first of these objectives was addressed partly through detailed studies of sediments retrieved at Site 792. The type of sedimentation and style of deposition in the forearc basin was expected to change with time as the proximity to arc volcanoes changed, as the volume and eruptive style of arc products varied, as the basin filled, and as the development of submarine canyons eroded and redistributed sedimentary material. Geostrophic currents, such as the paleo-Kuroshio, and changes in global sea level may also affect the pattern of sedimentation, and their effects may be deciphered from the stratigraphic record.

These sediments also contain a temporal record of the variations in the intensity and composition of arc volcanism. Studies of the chronology and nature of tephras at this site tested various conflicting models concerning the complex relationships between tectonic and volcanic phenomena in island arcs (e.g., changes in subduction rate, periodicity in backarc rifting and spreading, pulses of arc volcanism, and variations in arc geochemistry; see "Introduction" chapter, this volume, for elaboration).

The second objective was investigated through a combination of paleontological estimates of paleobathymetry, backstripping of the sedimentation history using the physical property and logging data, and seismic stratigraphic analyses of interconnecting multichannel seismic (MCS) profiles. Determining the forearc vertical-displacement history should provide some of the information necessary to decide if (1) fairly stable conditions have prevailed since the mid-Tertiary, as suggested by the well-developed submarine canyon system and lower-slope terrace of serpentinite seamounts; (2) the frontal-arc and outer-arc high resulted from igneous construction or from differential uplift; (3) the intervening forearc basin was formed by spreading or by differential subsidence; and (4) flexural loading of the forearc (by arc volcanoes or by coupling with the subducting plate) is an important process.

The third objective was investigated through studies of the basement rocks retrieved at this site. Basement beneath the thickly sedimented upper-slope basin (between the frontal-arc and outer-arc highs) had never been sampled in this or any other intraoceanic arc-trench system. From the available data, it appears that the present 150–230-km-wide Bonin-Mariana forearc formed, in large part, by volcanism during the initial stages of arc development in the Eocene and early Oligocene (see "Introduction" chapter, this volume, for elaboration). Similar volcanism has not occurred since and cannot be studied as an active phenomenon anywhere on earth at present. Studies of the basement rocks permitted evaluation of the three main alternative

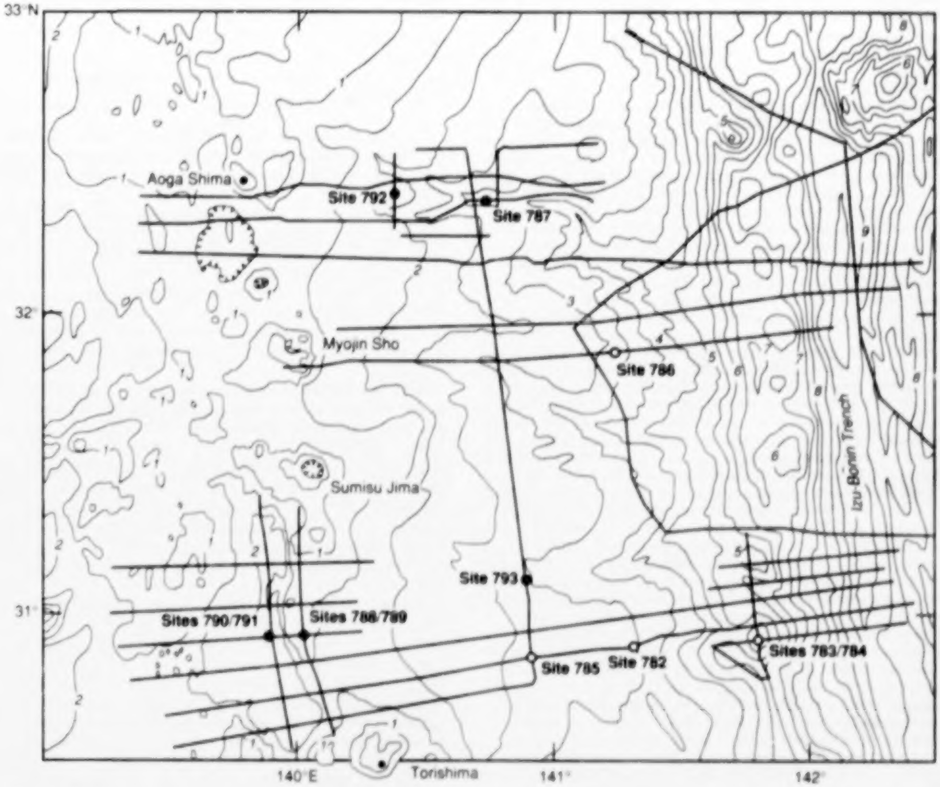

Figure 1. Bathymetric map (0.5-km contour interval) of the Izu-Bonin arc-trench system between 30.5° and 33°N. The locations of sites drilled on ODP Legs 125 (open circles) and 126 (filled circles) are shown on the map, as are the locations of site survey multichannel seismic lines.

hypotheses for the origin and evolution of this forearc terrane, namely: (1) the frontal arc and outer-arc highs could have originally been continuous and subsequently separated by forearc spreading; (2) the frontal-arc and outer-arc highs could have been built separately but nearly synchronously on former West Philippine plate crust; or (3) the terrane could form part of a continuous Eocene arc volcanic province, possibly with overprints of later forearc volcanism. Each scenario of forearc basement development implies a different crustal structure for the forearc.

The fourth objective of the site, the study of microstructures and plate rotations, was addressed through a study of FMS images and of the structural and paleomagnetic properties of the cored materials. Microstructures in the cores and on the FMS images of the borehole wall helped us to determine the intensity of faulting in space and time across the forearc terrane, as well as to define the syndepositional structures. Measurements of the paleomagnetic properties of subaerial portions of the Izu-Bonin and Mariana forearcs have shown at least 20° of northward drift and from 30° to >90° of clockwise rotation since the Eocene (see "Introduction" chapter, this volume, for more details). Studies of the paleomagnetism of the cores constrained the numerous different models for the nature and timing of these motions, and their relationship to the overall structural evolution of the forearc. The FMS data helped orient the rotary cores so that declinations, and hence rotations, could be determined.

SEISMIC STRATIGRAPHY

The correlation of site-survey multichannel seismic (MCS) reflection data to recovered core material (Fig. 4) was accomplished by using physical property velocity data, averaged over each lithologic unit (see "Physical Properties," this chapter), to convert depths (mbsf) into two-way traveltimes. The site chosen lies on *Fred Moore* 3505, line 10, at 0134Z. The reflector sequence can be divided into five seismic units:

1. Seismic Unit 1 (2.4–2.72 s) consists of numerous subparallel, divergent (lenticular near Site 792), high-amplitude reflectors, and corresponds to lithologic Unit I and the upper portion

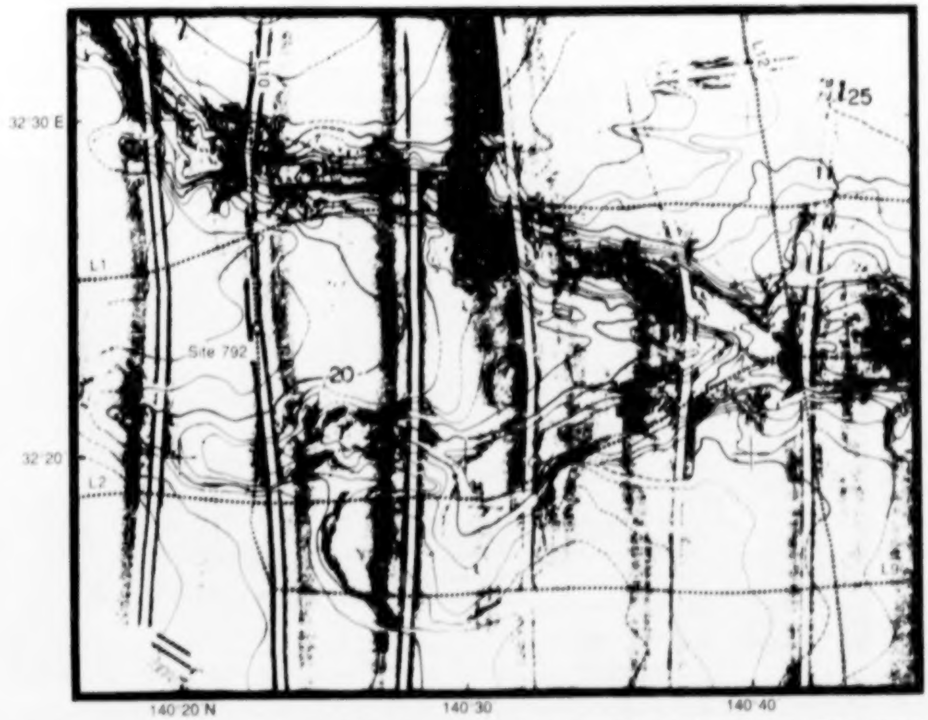

Figure 2. SeaMARC II sidescan and bathymetry (100-m contours) of Aoga Shima canyon (Klaus and Taylor, in press.). The locations of MCS site survey tracks and Site 792 (open circle) are also shown.

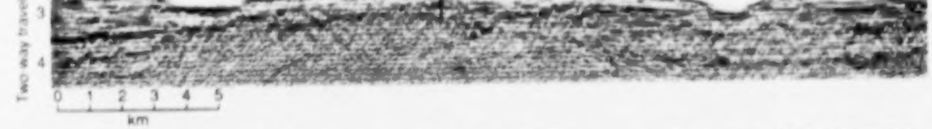

Figure 3. MCS profile 10 (Taylor et al., this volume) across the Izu-Bonin forearc sedimentary basin, crossing both forks of Aoga Shima canyon (see Fig. 2 for location). Site 792 is in the western half of the forearc basin, located where the deeper sedimentary section laps onto a basement high.

of Unit II. The lenticular reflector package may be interpreted as either channel deposits or as a bottom-current-induced depositional feature.

2. Seismic Unit 2 (2.72–2.88 s) consists of parallel, continuous, undulating, low-amplitude reflectors, and corresponds to the lower portion of lithologic Unit II and Unit III.

3. Seismic Unit 3 (2.88–3.12 s) is characterized by northward divergent, high-amplitude reflectors, offset by normal faults. It corresponds to the turbiditic lithologic Unit IV.

4. Seismic Unit 4 (3.12–3.2 s) laps off the basement in the vicinity of Site 792 and is present only as a thin horizon above basement. Subparallel to discontinuous, medium-amplitude reflectors characterize this unit farther east. The onlap of reflectors onto seismic Unit 4 indicates that a major unconformity is present near 715 mbsf at Site 792.

5. Acoustic basement (>3.2 s) at this site on the western margin of the forearc basin is characterized by chaotic, discontinuous reflectors of low to medium amplitude.

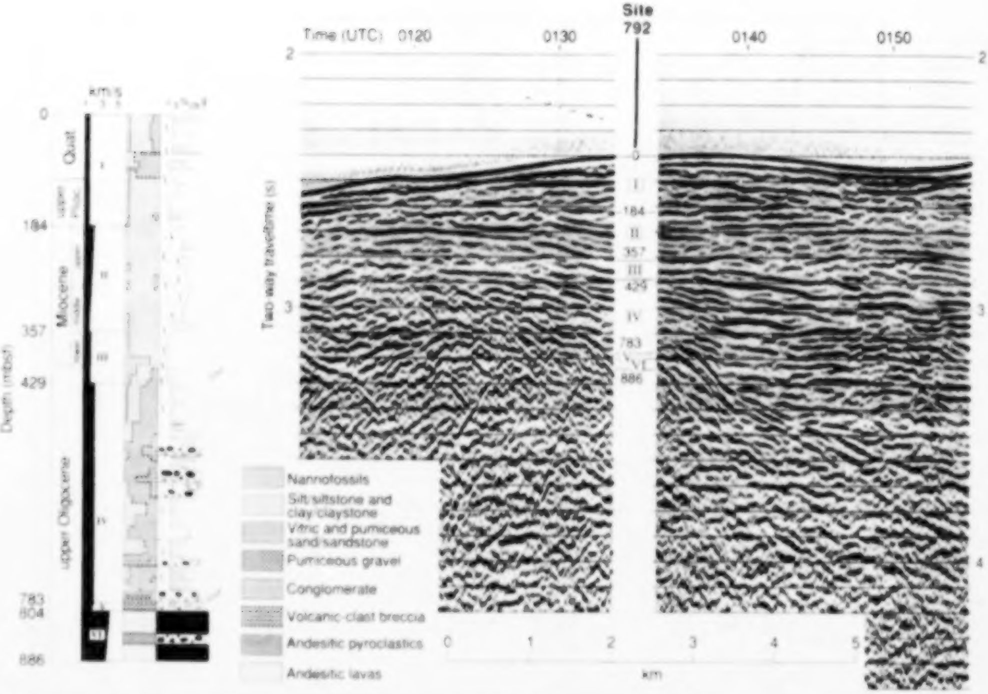

Figure 4. Correlation of Site 792 lithostratigraphy with site-survey multichannel seismic reflection data. The lithologic column for this site (see "Lithostratigraphy and Accumulation Rates" section, this chapter) appears on the left-hand side of the figure (c = clay, fs = fine sand, cs = coarse sand, and g = gravel). The location of the *Fred Moore* seismic line (MCS profile 10) is shown in Figure 2; lithologic units are identified on the seismic section, and unit boundaries are given in mbsf. The seismic section has been stacked (48-fold), deconvolved, migrated, and filtered 10-60 Hz. Vertical exaggeration is about 4×.

OPERATIONS

Site 788 to Site 792

JOIDES Resolution departed from Site 788 at full speed for Site 792 at 0330 hr (all times given in UTC) on 16 May 1989 and arrived in the vicinity of the new site at 1215 hr the same day. After a 4.5 hr survey, the first beacon was deployed at 1636 hr. Within 30 min, this beacon exhibited erratic pulse-time behavior, and a second unit had to be launched.

Site 792A

Hole 792A

A standard six-collar APC/XCB BHA with a nonmagnetic drill collar was lowered to just above the mud line, and the first APC core was shot at 2130 hr on 16 May. Although the retrieved core was 9.7 m in length, it was used to establish mud-line depth at 1797.8 mbsl. After the fifth piston core was cut, a Uyeda heat-flow experiment was conducted, and piston coring resumed. Another heat flow experiment was conducted after Core 126-792A-10H was cut. Recovery for the first 10 APC cores averaged 76% (Table 1).

The eleventh piston core was shot at 95.1 mbsf, but the core barrel resisted all efforts to extract it from the formation until an overpull of 170,000 lb was applied. The piston rod severed at the rod connection and the inner core barrel, and 5 m of piston rod remained in the hole. The remnants of the APC prevented any further coring efforts, so the BHA was short-tripped above the mud line. The BHA cleared the mud line, officially ending Hole 792A operations at 0825 hr on 17 May.

Hole 792B

The ship was offset 20 m farther south of the beacon, and Hole 792B was spudded at 0925 hr on 17 May. The mud-line core established the seafloor at 1798.2 mbsl. The drill string was then washed to 50 mbsf, where a second piston core was shot, followed by another heat-flow experiment. The third and last piston core was shot at 59.6 mbsf. The APC core barrel was retracted, and XCB coring was initiated at 78.8 mbsf. Cores 126-792B-4X through -10X averaged <28% recovery. When Core 126-792B-11X was tripped to the surface, we discovered that the cutting shoe had broken off near the 1/4-in. radius immediately behind the cutting structure.

Because the fractured shoe in the hole could have destroyed the rotary cones if coring had been continued, we ended operations at the hole and pulled out the BHA. The BHA cleared the seafloor at 2310 hr, thus ending Hole 792B and commencing Hole 792C.

Table 1. **Coring summary, Site 792.**

Core no.	Date (May 1989)	Time (UTC)	Depth (mbsf)	Cored (m)	Recovery (m)	Recovery (%)
126-792A-						
1H	16	2145	0.0-9.7	9.7	9.72	100.0
2H	16	2225	9.7-19.1	9.4	5.74	61.0
3H	16	2300	19.1-28.4	9.3	9.75	105.0
4H	16	2325	28.4-37.8	9.4	9.79	104.0
5H	17	0010	37.8-47.2	9.4	8.72	92.7
6H	17	0155	47.2-56.6	9.4	7.49	79.7
7H	17	0225	56.6-66.0	9.4	7.46	79.3
8H	17	0335	66.0-75.6	9.6	3.46	36.0
9H	17	0415	75.6-85.3	9.7	4.54	46.8
10H	17	0450	85.3-95.0	9.7	5.42	55.9
Coring totals				95.0	72.09	75.9
126-792B-						
1H	17	0935	0.0-4.3	4.3	4.28	99.5
2H	17	1205	50.0-59.6	9.6	8.60	89.6
3H	17	1425	59.6-69.2	9.6	10.05	104.7
4X	17	1545	69.2-78.8	9.6	4.76	49.6
5X	17	1640	78.8-88.5	9.7	0.38	3.9
6X	17	1720	88.5-98.2	9.7	0.15	1.5
7X	17	1810	98.2-107.9	9.7	0.37	3.8
8X	17	1900	107.9-117.5	9.6	6.22	64.8
9X	17	1955	117.5-127.1	9.6	2.08	21.6
10X	17	2100	127.1-136.8	9.7	4.66	48.0
11X	17	2210	136.8-146.4	9.6	2.04	21.2
Coring totals				100.7	43.59	43.3
126-792C-						
1X	18	0745	136.8-146.4	9.6	0.59	6.1
Coring totals				9.6	0.59	6.1
126-792D-						
1X	18	1355	136.0-145.6	9.6	0.84	8.8
Coring totals				9.6	0.84	8.8
126-792E-						
1R	19	0540	135.6-145.2	9.6	1.04	10.8
2R	19	0630	145.2-154.8	9.6	0.48	5.0
3R	19	0710	154.8-164.5	9.7	2.84	29.3
4R	19	0755	164.5-174.1	9.6	3.25	33.8
5R	19	0830	174.1-183.7	9.6	0.93	9.7
6R	19	0915	183.7-193.4	9.7	1.43	14.7
7R	19	0950	193.4-203.1	9.7	0.40	4.1
8R	19	1025	203.1-212.6	9.5	0.30	3.2
9R	19	1055	212.6-222.2	9.6	5.54	57.7
10R	19	1130	222.2-231.9	9.7	5.28	54.4
11R	19	1205	231.9-241.5	9.6	2.65	27.6
12R	19	1240	241.5-251.2	9.7	4.34	44.7
13R	19	1315	251.2-260.9	9.7	1.85	19.1
14R	19	1345	260.9-270.5	9.6	0.24	2.5
15R	19	1420	270.5-280.2	9.7	3.49	36.0
16R	19	1455	280.2-289.9	9.7	2.66	27.4
17R	19	1530	289.9-299.5	9.6	5.30	55.2
18R	19	1600	299.5-309.0	9.5	5.95	62.6
19R	19	1635	309.0-318.6	9.6	3.91	40.7
20R	19	1710	318.6-328.3	9.7	3.88	40.0
21R	19	1740	328.3-337.9	9.6	2.22	23.1
22R	19	1810	337.9-347.6	9.7	4.71	48.5
23R	19	1845	347.6-357.3	9.7	2.07	21.3
24R	19	1925	357.3-367.0	9.7	1.30	13.4
25R	19	2005	367.0-376.6	9.6	1.74	18.1
26R	19	2045	376.6-386.3	9.7	1.28	13.2
27R	19	2130	386.3-396.0	9.7	5.32	54.8
28R	19	2225	396.0-405.6	9.6	3.03	31.5
29R	19	2310	405.6-415.2	9.6	3.03	31.5
30R	20	0030	415.2-424.9	9.7	8.29	85.4
31R	20	0125	424.9-434.6	9.7	4.41	45.4
32R	20	0240	434.6-444.2	9.6	4.84	50.4
33R	20	0355	444.2-453.9	9.7	4.13	42.6
34R	20	0520	453.9-463.5	9.6	5.12	53.3
126-792E- (Cont.)						
35R	20	0655	463.5-473.2	9.7	2.68	27.6
36R	20	0800	473.2-482.8	9.6	6.93	72.2
37R	20	0910	482.8-492.5	9.7	9.82	101.0
38R	20	1020	492.5-502.2	9.7	9.02	93.0
39R	20	1125	502.2-511.9	9.7	6.98	71.9
40R	20	1225	511.9-521.6	9.7	8.80	90.7
41R	20	1330	521.6-531.2	9.6	6.80	70.8
42R	20	1435	531.2-540.6	9.4	9.39	99.9
43R	20	1555	540.6-550.3	9.7	9.71	100.0
44R	20	1725	550.3-560.0	9.7	6.59	67.9
45R	20	1840	560.0-569.7	9.7	5.70	58.7
46R	20	2010	569.7-579.4	9.7	9.75	100.0
47R	20	2150	579.4-588.6	9.2	4.66	50.6
48R	20	2300	588.6-597.8	9.2	9.60	104.0
49R	21	0130	597.8-607.4	9.6	9.72	101.0
50R	21	0230	607.4-617.1	9.7	9.61	99.1
51R	21	0340	617.1-626.8	9.7	4.86	50.1
52R	21	0440	626.8-636.4	9.6	7.97	83.0
53R	21	0600	636.4-646.1	9.7	0.00	0.0
54R	21	0725	646.1-655.7	9.6	8.33	86.8
55R	21	0835	655.7-665.4	9.7	3.57	36.8
56R	21	0945	665.4-675.1	9.7	8.77	90.4
57R	21	1055	675.1-684.8	9.7	8.95	92.2
58R	21	1200	684.8-694.4	9.6	5.20	54.1
59R	21	1500	694.4-704.0	9.6	8.21	85.5
60R	21	1610	704.0-713.6	9.6	9.83	102.0
61R	21	1720	713.6-722.9	9.3	5.98	64.3
62R	21	1830	722.9-732.5	9.6	9.88	103.0
63R	21	1940	732.5-742.2	9.7	4.73	48.7
64R	21	2140	742.2-751.8	9.6	3.55	37.0
65R	21	0005	751.8-761.5	9.7	2.27	23.4
66R	22	0110	761.5-771.2	9.7	7.77	80.1
67R	22	0255	771.2-780.9	9.7	4.92	50.7
68R	22	0435	780.9-790.6	9.7	2.69	27.7
69R	22	0610	790.6-800.2	9.6	7.68	80.0
70R	22	0830	800.2-809.9	9.7	0.19	2.0
71R	22	1135	809.9-819.5	9.6	3.05	31.8
72R	22	1435	819.5-829.2	9.7	1.45	14.9
73R	22	1700	829.2-838.8	9.6	2.31	24.0
74R	22	1900	838.8-848.2	9.4	2.15	22.9
75R	22	2110	848.2-857.7	9.5	1.57	16.5
76R	22	2245	857.7-867.1	9.4	1.24	13.2
77R	23	0110	867.1-876.6	9.5	0.40	4.2
78R	23	0445	876.6-885.9	9.3	1.36	14.6
Coring totals				750.3	361.89	48.2

Hole 792C

The vessel was offset an additional 20 m farther south of the beacon. The bottom of the drill string "felt" the seafloor at 1798.2 mbsl and was washed down to 137 mbsf, where another XCB attempt was made. The cutting shoe failed again, in the same manner as at Hole 792B. At this point, we decided that the two cutting shoe failures may have been caused by a defect in the fabrication of the entire lot of cutting shoes. A diamond-impregnated, three-bladed cutting shoe was selected for the next attempt. The drill string was short-tripped above the seafloor. The BHA cleared the seafloor at 0845 hr on 18 May, thus ending Hole 792C and initiating Hole 792D.

Hole 792D

The center bit was run down to the drill bit, and the drill string was lowered to the mud line at 1798.2 mbsl. We washed the drill string down to 136 mbsf and made another attempt to cut the core. After coring for 52 min, the driller noticed that penetration had stopped. We retrieved the core barrel and found that the cutting shoe had separated in the same manner as in the other two incidents.

The drill string was pulled out of the hole, and the BHA cleared the mud line at 1535 hr on 18 May.

Hole 792E

Hole 792E was spudded with a standard nine-collar RCB BHA and drilled to 135.6 mbsf, at which depth normal rotary coring was initiated. No problems were encountered at the level where the three XCB cutting shoes had previously fractured. We cut 78 cores to a depth of 885.9 mbsf during the next 83 hr.

After cutting Core 126-792E-78R, a multishot survey was conducted from the bottom (885.9 mbsf) up to 60 mbsf at 100-m increments. This survey took about 30 min, during which time there was no circulation or drill-pipe rotation. The survey indicated that the hole never exceeded 2.5° from vertical.

After retrieving the survey and just before removing the sinker bars, the formation started to flow into the bit and the hole began to slough in, trapping the BHA. From 0425 to 0940 hr on 23 May a successful (albeit temporary) effort was conducted to save the BHA and the hole. After mud treatment and some minor hole reaming, we decided that luck had been pushed long enough and it was time to withdraw to the logging depth.

The bit was lifted just off bottom and released at 1110 hr. The drill string stuck at 286 mbsf, at which point overpulls of 230,000 lb proved futile in moving the pipe farther up the hole. We then decided to start the downhole measurement program.

With the uncertainty of downhole conditions a prime consideration, the first log was a reduced geophysical combination (DIT/LSS/NGT-TEMP) without the density tool (HLDT). The tool was run in the hole at 2245 hr on 23 May to a depth of 877.1 mbsf, and returned at 0345 hr on 24 May. The results of this log were excellent and provided a good match with the shipboard physical property data.

The formation microscanner (FMS-NGT-TEMP) was rigged up for its maiden voyage with ODP. The tool was deployed at 0445 hr on 24 May and was successfully used to log the hole from 285 to 878.6 mbsf. All conductivity curves were visibly active and promised to yield first-class images. Both calipers showed that the borehole was cylindrical to slightly elliptical, with a typical diameter of 10 in. throughout the hole, except between 370 and 400 mbsf, where the radius exceeded 15 in.

In spite of the rough going while trying to retrieve the drill string, the hole was in excellent shape, and the absence of fill suggested that the zone that sloughed in on the pipe was essentially sealed off by the BHA.

The FMS was rigged down at 0845 hr, and the geochemical (GST-ACT-NGT-TEMP) logging suite was prepared. Between 0945 and 1830 hr on 24 May, the GST logged the borehole including through the pipe up to the mud line, with excellent results.

Completing the standard suite of logs was a rerun of the geophysical combination with the density tool (HLDT-LSS-NGT-TEMP), which also completed a successful excursion of the hole between 2000 on 24 May and 0200 hr on 25 May, although the short-spacing density sensor failed downhole. The final log at this site was a vertical seismic profile (VSP), which obtained a high-grade log. Apparently, the firm anchoring of the drill pipe in the sediment caused the ambient noise level of the log to be extremely low.

After the logging program was completed, the top drive was put up and a final attempt was made to free the stuck pipe. When this proved unsuccessful, we decided to sever the pipe. A 31-pellet severing charge was run in the hole and fired.

The pipe was tripped to the surface, and the string cleared the mud line at 1945 hr and the rotary table at 2140 hr on 25 May, ending Site 792E. An unsuccessful attempt was made to recall the commandable beacon. Finally, the thrusters and hydrophones were pulled and the *JOIDES Resolution* made way at full speed to Site 793 at 2230 hr on 25 May.

LITHOSTRATIGRAPHY AND ACCUMULATION RATES

We drilled five holes at Site 792. The upper part of the sedimentary sequence was cored primarily in Holes 792A and 792B; the middle and lower portions were penetrated by Hole 792E. We recognized six lithologic units at this site (Table 2 and Fig. 5). A composite section incorporates data from Hole 792A for the interval from 0 to 98.2 mbsf, from Hole 792B for the interval from 98.2 to 135.6 mbsf, and from Hole 792E for the rest of the section (see Fig. 30, "Biostratigraphy" section, this chapter). The upper five units are composed of volcanogenic and biogenic sediments and sedimentary rocks, and the lowest unit is igneous rock. Contacts between adjacent units were recovered, with the exception of the Unit I/II and Unit III/IV contacts.

Although defined by lithologic changes, two contacts between lithologic units at Site 792 roughly coincide with unconformities suggested by biostratigraphic data. The Unit I/II boundary is marked by a hiatus between upper Pliocene and upper Miocene sedimentary rocks, and the Unit II/III boundary is also characterized by a hiatus between upper and lower Miocene sedimentary rocks. The Unit IV/V boundary is marked by a fault.

Biostratigraphic data suggest that three more hiatuses occur within Units I, II, and III. The oldest discontinuity coincides with a fault between the upper Oligocene and the lower Miocene in Unit III, in Core 126-792E-29R, and the middle discontinuity corresponds to a color change in the middle part of Unit II in Section 126-792E-15R-1 at 20 cm.

Unit I

Intervals: Cores 126-792A-1H through -10H, Cores 126-792B-1H through -11H, Core 126-792C-1X, Core 126-792D-1X, and Cores 126-792E-1X through -5R
Age: Holocene to late Pliocene
Depth: 0-183.7 mbsf

Unit I extends from the sediment/water interface to 183.7 mbsf, where there is a change from unconsolidated deposits, mainly nannofossil-rich fine-grained sediments, to lithified sedimentary rocks, mainly sandy mudstone and muddy sandstone. This contact was not recovered and is placed at the top of Core 126-792E-6R.

Unit I consists predominantly (62%) of dark gray (5GY 4/1) and olive gray (5Y 4/1), nannofossil-rich clayey silt and nannofossil-rich silty clay, which is composed of nannofossils, volcanic glass, and clay. Calcium carbonate contents in the highly bioturbated nannofossil-rich deposits range from 10% to 30%. Minor sediment types include foraminifer-rich silty clay (5%), nannofossil-rich vitric silt (2%), and clay (1%).

Interbedded with the nannofossil-rich muddy sediments are beds of vitric sand (19%), vitric silt (8%), and scoriaceous and pumiceous gravel (3%). These beds, which compose 30% of the core, are generally < 20 cm thick, but locally exceed 100 cm in thickness (Table 3). Several layers show planar lamination and normal grading, but scoured bases are rare. The sediments are variably mafic and dark colored (dark gray, N3, 5Y 4/1; black, 5Y 3/1; brownish black, 5YR 2/1), or felsic and light colored (light gray, N6; gray, 5Y 6/1) (Figs. 6 and 7); however, the total thickness of mafic sand is almost twice that of felsic sand. Mafic vitric sand and silt are mainly composed of brown and opaque glass with variable amounts of orthopyroxene, clinopyroxene, and plagioclase crystals, whereas the felsic sediments consist of translucent bubble wall and pumice-type glass shards with only minor crystals. Many intervals are mixtures of mafic

Table 2. Lithologic units, Site 792.

Unit	Lithology	Sedimentary structures	Interval (mbsf)	Age	Occurrence
I	Nannofossil-rich vitric silty clay and nannofossil-rich clayey silt, interbedded with vitric silts, vitric sands, and pumiceous and scoriaceous gravels. Locally rich in foraminifers and/or biogenic silica.	Vitric silt and sand layers show plane-parallel lamination, graded bedding, and burrowed tops.	0–183.7	Quaternary to late Pliocene	126-792A-1H through -10H, 126-792B-1H through -11H, 126-792C-1X, 126-792D-1X, 126-792E-1R through -5R
II	Sandy mudstone, muddy sandstone, silty claystone, vitric sandstone, and vitric siltstone, all with nannofossil-rich intervals. Nannofosil content increases irregularly with depth. Local granule- and pebble-rich intervals.	Vitric siltstone beds show plane-parallel lamination and sharp bases. Finer lithologies are strongly burrowed. Trace fossils include *Zoophycos* and *Chondrites*.	183.7–357.4	late Miocene to middle Miocene	126-792E-6R to -24R-1, 10 cm
III	Nannofossil-rich claystone, nannofossil claystone and nannofossil chalk. Rare crystal-vitric siltstone and crystal-vitric sandstone.	Some intervals show dewatering fractures and sandstone dikes. Fault zone at 407 mbsf.	357.4–429.3	early Miocene to late Oligocene	126-792E-24R-1, 10 cm through -31R
IV	Vitric sandstone, volcanic and intraclastic sandy conglomerate, with minor silty claystone, nannofossil-rich silty claystone, nannofossil-rich claystone and claystone.	Vitric sands show plane-parallel lamination, cross-lamination, scoured bases, load casts, and frame structures. Claystone cobble intraclasts are associated with scours and may be reversely graded. Microfaults, fractures, and clastic dikes occur locally. *Zoophycos* and *Chondrites* burrows are present.	429.3–783.4	late Oligocene to early Oligocene	126-792E-32R through -68R-2, 100 cm
V	Altered volcanic sandstone with claystone intraclasts.	Mottled and brecciated, possibly in association with hydrothermal alteration.	783.4–804	?	126-792E-68R-2, 100 cm through -70R-CC
VI	Plagioclase-orthopyroxene-clinopyroxene andesite.		804–885.9	?	126-792E-70R-CC to -78R

and felsic vitric material. Scoriaceous and pumiceous pebble to granule gravel beds, from 6 to 180 cm in thickness, occur mainly in the upper part of Unit I (Cores 126-792A-1H through -10H).

Sediments of Unit I are unconsolidated, except for a thin bed of dark gray (5Y 4/1) vitric siltstone in Interval 126-792E-5R-1, 25–32 cm, and lack tectonic deformation.

Unit II

Interval: Cores 126-792E-6R through Section 126-792E-24R-1 at 10 cm
Age: late to middle Miocene
Depth: 183.7–357.4 mbsf

The uppermost recovered sediment of Unit II is a poorly sorted sandy mudstone containing granules and pebbles (Fig. 8). The lower boundary of Unit II is the lithologic change from nannofossil-rich sandy mudstone/muddy sandstone to finer grained sediment types, which have much higher nannofossil contents and are assigned to Unit III. This boundary occurs in Section 126-792E-24R-1 at 10 cm, at the base of a black, fine-grained sandstone layer.

Unit II consists mainly of olive black (5Y 2/1) to dark gray (5Y 4/1, 5GY 4/1) vitric sandy mudstone (37%), vitric muddy sandstone (30%), and silty claystone (15%), all of which have nannofossil-rich intervals and minor sandstone (10%), siltstone (5%), and claystone (3%). Disseminated sand and silt grains are predominantly brown scoria, clear volcanic glass shards, and volcanic rock fragments. Bioclasts include nannofossils, foraminifers, radiolarians, and sponge spicules. Granules scattered throughout the muddy sandstone include rhyolitic pumice in Cores 126-792E-9R to -15R, and basaltic scoria in Cores 126-792E-12R to -20R. Below Core 126-792E-22R, granules of scoria are absent, and the sequence is composed mainly of very dark gray to dark gray (5Y 3/1 to 5Y 4/1), nannofossil-rich vitric silty claystone and vitric silty claystone.

The muddy sandstone and sandy mudstone layers are burrowed, and trace fossils include *Zoophycos* (Fig. 9). These poorly sorted, bioturbated units are lithified primarily by recrystallization of matrix minerals, predominantly clay minerals and carbonate. In better sorted ash layers, thin birefringent rims of hydrated glass and/or clay minerals bind the sediments. Calcium carbonate contents of the muddy sediments generally increase downhole, from 5%–15% to 10%–20% (Fig. 5), whereas the color of the sedimentary rocks abruptly changes from olive black (5Y 2/1) to dark gray (N3) in Section 126-792E-15R-1 at 20 cm. Very dark green (5GY 2/1), glauconite-bearing, fine-grained sandstone (see X-ray diffraction [XRD] analysis that follows) is present just below this boundary.

The vitric sandstone and siltstone layers of Unit II, mostly dark colored (N2, 5Y 2/1), are 1–10 cm thick (Figs. 10 and 11). Rare, light-colored (5R 2/1, N7), siltstone beds are limited to the upper part of the unit. A pumiceous granule-to-pebble conglomerate bed is present in Interval 126-792E-9R-3, 96–103 cm.

No tectonic deformation was observed in Unit II. Unconsolidated vitric siltstone and vitric sandstone beds rarely occur in the upper part of the unit (above Core 126-792E-11R).

Unit III

Interval: Section 126-792E-24R-1 at 10 cm through Core 126-792E-31R
Age: early Miocene to late Oligocene
Depth: 357.4–429.3 mbsf

The upper boundary of Unit III is placed at the top of a dark gray (5Y 4/1) layer of nannofossil claystone that underlies the lowest black sandstone bed of Unit II. The lower boundary of

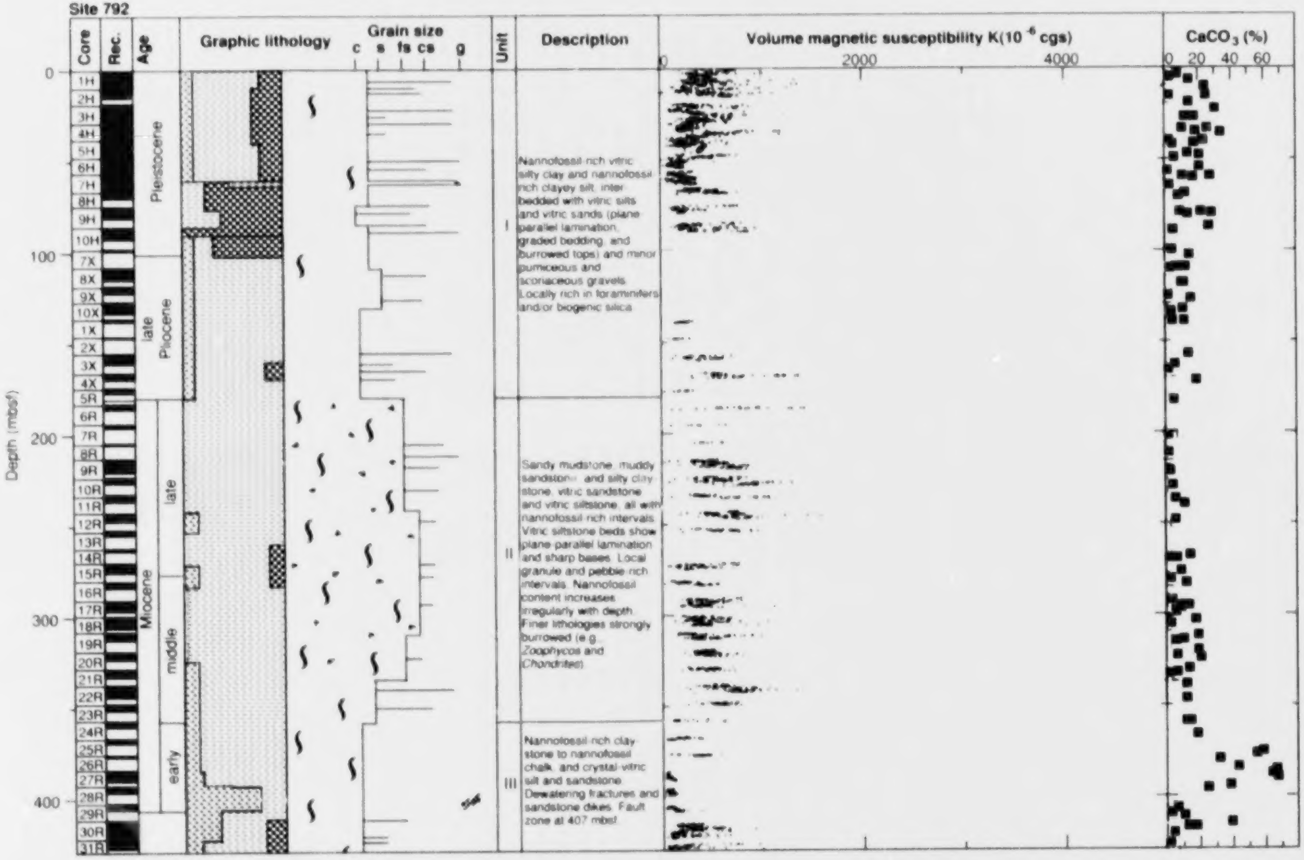
Site 792
Core
Rec.
Age
Graphic lithology
Grain size
c s fs cs g
Unit
Description
Volume magnetic susceptibility K(10⁻⁶ cgs)
CaCO₃ (%)
Depth (mbsf)
0
100
200
300
400
0
2000
4000
0 20 40 60
1H
2H
3H
4H
5H
6H
7H
8H
9H
10H
7X
8X
9X
10X
1X
2X
3X
4X
5R
6R
7R
8R
9R
10R
11R
12R
13R
14R
15R
16R
17R
18R
19R
20R
21R
22R
23R
24R
25R
26R
27R
28R
29R
30R
31R
Pleistocene
late Pliocene
Miocene
late
middle
early
I
II
III
Nannofossil-rich vitric silty clay and nannofossil-rich clayey silt, interbedded with vitric silts and vitric sands (plane parallel lamination, graded bedding, and burrowed tops) and minor pumiceous and scoriaceous gravels. Locally rich in foraminifers and/or biogenic silica
Sandy mudstone, muddy sandstone, and silty claystone, vitric sandstone and vitric siltstone, all with nannofossil-rich intervals. Vitric siltstone beds show plane-parallel lamination and sharp bases. Local granule and pebble-rich intervals. Nannofossil content increases irregularly with depth. Finer lithologies strongly burrowed (e.g., Zoophycos and Chondrites)
Nannofossil-rich claystone to nannofossil chalk, and crystal-vitric silt and sandstone. Dewatering fractures and sandstone dikes. Fault zone at 407 mbsf

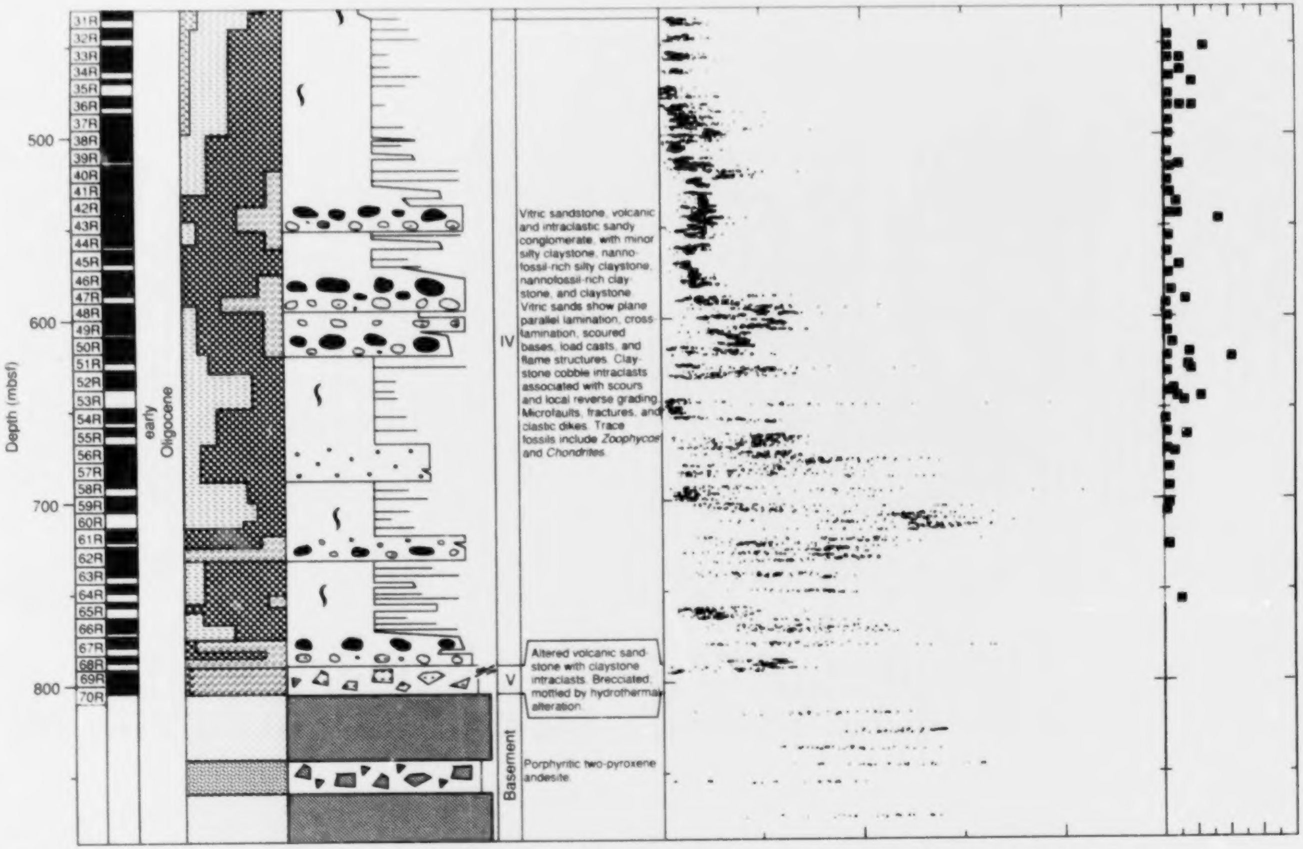

Figure 5. Composite stratigraphic section for Site 792 showing unit boundaries and downhole variations in magnetic susceptibility and total carbonate. (See Fig. 4 for legend.)

Table 3. Ash layers, Site 792.

Core, section, interval (cm)	Thickness (cm)	Description and remarks
126-792A-		
1H-1, 0-19	19	Fine scoria (dispersed in silty clay)
1H-1, 34-42	3/5	Light brownish gray (5YR6)/very light gray (N8); silt-clay/sand
1H-1, 57-58	1	Coarse sand-granule scoria
1H-1, 63-64	1	Coarse sand-granule scoria
1H-1, 67-69	1	Coarse sand-granule scoria
1H-1, 80-82	2	Black; fine sand
1H-1, 124-130	6	Brownish black (5YR2/1); fine scoria lapilli (maximum diameter = 4 mm)
1H-2, 30-34	4	Medimum light gray (N6); coarse sand (pumice and lithic)
1H-2, 51-79	9/12/7	Light gray (N7)/dark gray (N3); silt-clay/fine sand/coarse sand-granule
1H-2, 120-124	4	Dark gray (N3); fine sand
1H-2, 125-132	7	White; fine ash (dispersed)
1H-2, 139-140	1	Brownish black (5YR2/1); scoria; very coarse sand (maximum diameter = 1 mm)
1H-3, 4-5	1	Scoria; coarse sand
1H-3, 24-25	1	Olive gray (5Y4/1); medium sand
1H-3, 73-80	4/3	Brownish gray (5YR4/1); silt/coarse sand (pumice and scoria)
1H-3, 126-145	19	Light gray (N7) (purple); clay-fine sand (grading)
1H-4, 144-146	2	Olive black (5Y2/1); silt
1H-5, 15-16	1	Medium light gray (N6); silt
1H-5, 28-32	2/2	Black/black; medium sand/scoria (maximum diameter = 2 mm)
1H-5, 32-38	4/2	Medium light gray (N6)/white; clay/silt-clay
1H-5, 47-52	3/2	Black/black; fine sand/scoria (maximum diameter = 2 mm)
1H-5, 60-62	2	Dark gray (N3); scoria (maximum diameter = 1 mm)
1H-5, 80-83	2/1	Medium light gray (N6)/gray; silt/coarse sand
1H-5, 98-99	1	Dark gray (N3); scoria; coarse sand (dispersed)
1H-6, 44-55	11	Dark gray (N3); fine coarse sand (graded)
1H-6, 81-110	29	Dark gray (N3); fine coarse sand with granules (graded)
1H-6, 118-122	4	Medium light gray (N6); fine sand
1H-6, 122-124	2	Black; fine sand
1H-6, 131-132	1	Black; fine medium sand
1H-6, 144-147	1/2	Grayish green (10GY5/2)/medium light gray (N6); silt-clay
1H-7, 37-39	2	White; fine ash (dispersed)
2H-1, +0-90	+60/14/16	Medium dark gray (N4)/grayish black (N2); silt/fine sand
2H-1, 100-105	5	Grayish black (N2); fine sand
2H-1, 140-150	18/22	Medium dark gray (N4)/light olive gray (5Y6/1); pumiceous very coarse
2H-2, 10-30		Sand (pumice maximum diameter = 2 cm)/medium sand
2H-2, 64-74	8/2	Light olive gray (5Y6/1)/grayish black (N2); coarse tuff (pumice and granules)/scoria; coarse sand
2H-2, 82-94	7/3/2	Light gray (5Y6/1)/olive gray (5Y4/1)/brownish gray (5YR4/1) (purple); clay/sand/silt
2H-2, 133-150 2H-3, 0-8	12/13	Light olive gray (5Y6/1); pumiceous lapilli (pumice maximum diameter = 2 cm, lithic maximum diameter = 5 mm)/pumiceous sandy lapilli (pumice maximum diameter = 1 cm)
2H-3, 40-46	6	Dark gray (N3); silt-medium sand (graded)
2H-3, 59-64	5	Light gray; clay
2H-3, 90-98	8	Dark gray (N3); silt-fine sand (graded)
2H-4, 27-113 2H-CC 0-12+	98+	Fine sand-pumiceous gravel (pumice maximum diameter = 1 cm, two kinds of pumice, white porous and gray dense)
3H-1, 27-39	12	Gray; pumice lapilli tuff (pumice maximum diameter = 2 cm)
3H-1, 50-52	2	Medium gray (N5); lithic tuff, silt-very fine sand (graded)
3H-1, 69-70	1	Lithic tuff coarse sand
3H-1, 80-94	10/4	Medium light gray (N6)/medium gray (N5); silt-very fine sand/pumice coarse sand, crystal (plagioclase) rich (diameter = 1 mm)
3H-1, 108-113	5	Medium gray (N5); tuff, medium very fine sand
3H-1, 122-127	4/1	Medium light gray (N6)/medium gray (N5); silt/very fine sand
3H-2, 3-6	1/2	Grayish green (5G5/2)/light gray (N7); silt
3H-2, 25-27	2	Grayish black (N2); silt
3H-2, 81-84	3	Medium light gray (N6); silt
3H-2, 97-117	20	Olive gray (5Y4/1); clayey silt
3H-2, 147-148	1	White; fine tuff
3H-3, 55-57	7	Medium dark gray (N4); silt-very fine sand
3H-3, 65-73	8	Gray; pumice lapilli (pumice maximum diameter = 2 cm)
3H-3, 102-115	12/1	White; silt/pumiceous coarse sand (lithic tuff)
3H-4, 2-6	4	Grayish black (N2); fine sand
3H-4, 17-22	5	Dark gray (N3); silt
3H-4, 77-78	1	Black; very fine sand (dispersed)
3H-4, 99-104	4/1	Dark gray (N3); very fine sand/scoria, very coarse sand (maximum diameter = 2 mm)
3H-4, 141-147	6	Medium dark gray (N4); silt-medium sand (grading)
3H-5, 15-19	2/2	Olive gray (5Y4/1)/dark gray (N3); very fine sand/very coarse sand; lithic tuff (lithic maximum diameter = 1 mm)
3H-5, 54-57	2/1	Dark gray (N3); silt/scoria; coarse sand (maximum diameter = 1 mm)

Table 3 (continued).

Core, section, interval (cm)	Thickness (cm)	Description and remarks
126-792A- (Cont.)		
3H-5, 67-76	9	Grayish black (N2); very coarse silt
3H-5, 78-79	1	Medium light gray (N6); silt
3H-5, 110-114	4	White; fine tuff pocket
3H-6, 29-32	3	Light olive gray (5Y6/1); silt
3H-6, 47	<1	Pumice tuff (maximum diameter = 1 mm)
3H-6, 58-60	2	Grayish black (N2); scoria; coarse sand (maximum diameter = 2 mm)
3H-6, 82-88	3/3	Light gray (N7)/very light gray (N8); silt
3H-6, 100-115	15	Medium dark gray (N4); silt medium sand
3H-7, 16-17	1	Olive gray (5Y4/1); silt
3H-7, 42-45	17	Light gray (N7); silt
3H-CC, 0-14		
4H-1, 10-16	6	Dark gray (N3); silt/very fine sand
4H-1, 115-120	5	Dark gray (N3); silt
4H-2, 8-15	4/3	Olive gray (5Y4/1)/grayish black (N2); silt/fine sand
4H-2, 19-23	3/1	Grayish black (N2); silt/coarse sand
4H-2, 33-46	13	Light olive gray (5Y6/1); silty/coarse-medium sand
4H-2, 50-53	3	Grayish black (N2); very coarse sand with granules (maximun diameter = 4 mm)
4H-2, 73-80	7	Dark gray (N3); silt-very fine sand (graded)
4H-2, 101	<1	Dark gray (N3); lithic tuff (5 mm thick)
4H-2, 123-131	8	Dark gray (N3); silt
4H-3, 10-15	5	Black; coarse sand (burrowed)
4H-3, 30-33	3	Olive gray (5Y4/1); pumice pebble (maximum diameter = 5 mm)
4H-3, 50-52	2	Dark gray (N3); silt
4H-3, 79	<1	Dark gray (N3); silt
4H-3, 100-104	4	Dark gray (N3); silt-fine sand (graded)
4H-3, 128-129	1	Grayish black (N2); medium sand
4H-4, 6-7	1	Light olive gray (5Y6/1); fine sand
4H-4, 31-32	1	Gray; fine tuff
4H-4, 35	<1	White; fine tuff (dispersed)
4H-4, 39	<1	Dark gray (N3); fine tuff (5 mm thick)
4H-4, 48-50	2	Light olive gray (5Y6/1); fine sand
4H-4, 90-91	1	Dark gray (N3); fine sand
4H-4, 94-103	8/1	Light olive gray (5Y6/1); silt/medium sand
4H-5, 10-17	7	Grayish black (N2); scoria; coarse sand
4H-5, 28-30	2	Grayish black (N2); scoria; coarse sand
4H-5, 38-43	5	Grayish black (N2); scoria; granule
4H-5, 49-64	13/2	Dark gray (N3); silt/medium sand
4H-5, 81	<1	Grayish black (N2); scoria; coarse sand (5 mm thick)
4H-5, 102-105	3	Grayish black (N2); scoria; coarse sand (maximum diameter = 2 mm)
4H-5, 108-110	2	Grayish black (N2); scoria
4H-6, 0-2	2	Grayish black (N2); scoria; coarse sand
4H-6, 12-15	3	Light olive gray (5Y6/1); silt
4H-6, 35-36	1	Grayish black (N2); fine sand-silt
4H-6, 48-50	2	Dark gray (N3); silt with scoria (maximum diameter = 1 mm)
4H-6, 68-69	1	Dark gray (N3); medium sand
4H-6, 86-87	1	Dark gray (N3); silt
4H-6, 107-108	1	Dark gray (N3); silt
4H-6, 126-128	2	Dark gray (N3); silt
4H-6, 146-150	4	Dark gray (N3); silt
4H-7, 12-13	1	Light olive gray (5Y6/1) (reddish), silt
4H-CC 12-17	5	Dark gray (N3); silt
5H-1, +0-3	+3	Light olive gray (5Y6/1); silt
5H-1, 18-20	2	Olive gray (5Y4/1); silt
5H-1, 38-43	4/<1	Light olive gray (5Y6/1)/olive gray (5Y4/1); silt/very fine sand (5 mm thick)
5H-1, 69-72	3	Black (5Y2/1)/light olive gray (5Y4/1); silt/medium sand with pumice (5 mm thick)
5H-1, 118-119	1	Very dark gray (5Y3/1); very fine sand
5H-1, 140-142	2	Olive gray (5Y4/1); silt/very fine sand (5 mm thick)
5H-2, 20-22	2	Olive gray (5Y4/1); pumice; very coarse sand
5H-2, 31-33	2	Olive gray (5Y4/1); silt
5H-2, 40-44	4	Light olive gray (5Y6/1); silt
5H-2, 51-55	4	Very dark gray (5Y3/1); medium sand with scoria (maximum diameter = 1 cm)
5H-2, 65-68	3	Olive gray (5Y4/1); silt
5H-2, 80-89	4/5	Olive gray (5Y4/1); silt/pumice; fine sand (maximum diameter = 3 mm)
5H-2, 129-130	1	Olive gray (5Y4/2); silt
5H-2, 140-143	3	Grayish black (N2); silt
5H-3, 8-19	10/1	Olive gray (5Y4/1); silt/very fine sand
5H-3, 30	<1	Black; silt (5 mm thick, dispersed)
5H-3, 54-61	3/1/3	Light olive gray (5Y6/1)/olive gray (5Y4/1)/light olive gray (5Y6/1); silt/fine silt with a 5-mm-thick very fine sand basal part

Table 3 (continued).

Core, section, interval (cm)	Thickness (cm)	Description and remarks
126-792A- (Cont.)		
5H-3, 75-76	1	Light olive gray (5Y6/1); fine tuff
5H-3, 103-108	5	Black, fine tuff (dispersed)
5H-3, 114-150	11/79	Light gray (5Y4/1)/light (5Y4/1); silt/clayey silt
5H-4, 0-54		
6H-1, 14-70	56	Olive gray (5Y4/1); pumiceous pebbly sand
6H-1, 96	<1	Black; silt (dispersed)
6H-1, 124-125	1	Grayish black (N2); silt
6H-2, 8-26	7/6/5	Light olive gray (5Y6/1)/light gray (N7)/olive gray (5Y4/1); silt/silt/pumiceous very fine sand
6H-2, 27-28	1	Olive gray (5Y4/2); very fine sand
6H-2, 38-45	5/2	Light olive gray (5Y6/1)/dark olive gray (5Y3/2); silt/medium sand
6H-2, 92-101	6/3	Olive gray (5Y4/1); silt/very fine sand (laminated)
6H-3, 4-10	6	Light olive gray (5Y6/1); silt
6H-3, 34-36	10/2	Grayish black (N2); fine sand/very fine sand (laminated)
6H-3, 58-68	10	Brownish black (5YR2/1); silt with scoria scatterd basal part (maximum diameter = 5 mm)
6H-3, 114-136	5/17	Dark olive gray (5Y3/2); grayish black (N2) silt/silt-fine sand (grading)
6H-4, 3-10	1/6	Olive gray (5YR4/1)/olive gray (5Y4/2); silt/clayey silt
6H-4, 21-24	3	Light olive gray (5Y6/1); silt pocket
6H-4, 34-85	4/47	Dark olive gray (5Y3/2); grayish black (N2); silt/medium fine sand
6H-4, 93-104	10/1	Light olive gray (5Y6/1)/olive gray (5Y4/1); silt/very fine sand
6H-4, 114-120	6	Light olive gray (5Y6/1); silt
6H-4, 140-150	17	Dark olive gray (5Y3/2)/olive black (5Y2/1); clayey silt
6H-5, 0-7		silt
6H-5, 14-135	113/5/17+	Grayish black (N2); fine sand with pumice/medium coarse sand/silt
6H-CC, 0-14+	14	Medium sand
7H-1, +0-1	+1	Olive black (5Y2/1); very fine sand
7H-1, 12-13	1	Olive gray (5Y4/1); very fine sand
7H-1, 21-29	8	Light olive gray (5Y6/1); silt
7H-1, 40-57	3/6/3/5	Greenish gray (5GY6/1)/olive black (5Y2/1)/light olive gray (5Y6/1)/olive gray (5Y4/1); silt/very fine sand/silt/sandy silt
7H-1, 103-131	28	Grayish black (N2); alternation of fine sand and very fine sand
7H-2, 19-21	2	Light olive gray (5Y6/1); silt pocket
7H-2, 41-52	11	Light olive gray (5Y6/1); silt
7H-2, 112-114	2	Grayish black (N2); very fine sand pocket
7H-2, 119-121	2	Grayish black (N2); very fine sand
7H-3, 12-14	2	Brownish black (5YR2/1); very fine sand
7H-3, 27-32	5	Olive gray (5YR4/1); very fine sand
7H-3, 38-39	1	Light olive gray (5Y6/1); silt
7H-3, 46-48	2	Grayish black (N2); scoria sand pocket
7H-3, 57-67	3/5/2	Dark reddish brown (5YR2/1)/dark reddish brown (5YR2/1); very fine sand/sandy mud with scattered pumice (maximum diameter = 5 mm)/very fine sand
7H-3, 81-86	3/2	Dark reddish brown (5YR2/1)/grayish black (N2); silt/fine sand (laminated)
7H-3, 98-114	72	Light olive gray (5Y6/1); silt
7H-4, 0-56		
7H-4, 87-92	1/1/3	Brownish black (5YR2/1); silt/fine sand (pumice and foraminifers included)/very fine sand with thin (2 mm) scoria base
7H-4, 101-106	3/2	Brownish black (5YR2/1)/grayish black (N2); silt/very fine sand
7H-4, 143-145	6/146/30+	Dark reddish brown (5YR3/2)/grayish black (N2); clayey
7H-5, 0-150		Silt/fine sand with gravel (maximum diameter = 10 mm)/scoria pebble
7H-6, 0-16		
7H-CC, 0-14+		
8H-1, +0-6	+6	Grayish black (N2); scoria; medium sand
8H-1, 33-42	9	Grayish black (N2); very fine sand
8H-1, 48-55	7	Grayish black (N2); scoria; coarse sand
8H-1, 75-77	2	Grayish black (N2); medium sand
8H-1, 85-86	1	Grayish black (N2); medium sand
8H-1, 131-137	6/47	Dark olive gray (5Y3/2)/olive black (5Y2/1); clayey silt
8H-2, 0-47		Very fine sand (medium sand pumice included)
8H-2, 66-83	2/12/3	Dark reddish brown (5YR2/1)/olive black (5Y2/1)/grayish black (N2); silt/very fine sand/sandy silt
8H-2, 93-135	4/38	Brownish black (5YR2/1)/olive black (5Y2/1); silt/fine-medium sand (graded) (pumice and foraminifers included)
8H-2, 135-148	13	Scoria pebble (maximum diameter = 7 mm) scattered in dark olive gray sandy mud)
8H-2, 148-150	2	Grayish black (N2); medium sand
8H-3, 10-12	2	Pumice; granule
8H-3, 19-21	2	Pumice; granule
8H-3, 25	<1	Pumice; granule, seam
8H-3, 30	<1	Pumice; granule, seam

Table 3 (continued).

Core, section, interval (cm)	Thickness (cm)	Description and remarks
126-792A- (Cont.)		
8H-3, 39-43 8H-CC, 0-16+	9/11+	Light olive gray (5Y6/1)/olive black (5Y2/1); sandy silt medium sand
9H-1, +0-50	+50	Olive black (5Y2/1); scoria; pebble-granule gravel
9H-1, 60	<1	Medium sand (pumice) seam
9H-1, 60-78	18	Olive gray (5Y4/2); silt
9H-2, 29-65	36	Olive black (5Y2/1); fine sand-very fine sand (graded)
9H-2, 84-99	15	Olive black (5Y2/1); very fine sand
9H-2, 113-150	3/37	Olive black (5Y2/1); silt
9H-3, 0-3		Olive black (5Y2/1); medium sand (laminated)
9H-3, 37-54	17	Light olive gray (5Y6/1); silt
9H-3, 54-87 9H-4, 4-64	93	Olive gray (5Y4/1); very fine sand
9H-CC, 7	1	Light olive gray (5Y6/1); silt pocket
10H-1, +0-7	+7	Grayish black (N2); scoria granule
10H-1, 16-18	2	Grayish black (N2); scoria granule
10H-1, 36-100	64	Olive gray (5Y4/1); pumiceous granule-coarse sand (pumice pebble concentrated at 65-68, 72-73, and 85-87 cm)
10H-1, 132-148	16	Olive gray (5Y5/2); pumiceous medium sand (laminated)
10H-2, 6-8	2	Olive gray (5Y4/1); silt
10H-2, 29-31 10H-3, 4-8	2/4	Grayish black (N2); scoria medium sand/scoria granule
10H-3, 18-34	12/4	Light olive gray (5Y6/1); silt/fine sand
10H-3, 39-44	5	Light olive gray (5Y6/1); silt
10H-3, 78	<1	Medium dark gray (N4); very fine sand
10H-3, 93	<1	Medium gray (N5); silty clay
10H-3, 95	<1	Grayish black (N2); silt
10H-3, 118-124	6	Olive black (5YR2/1); scoria granules
10H-3, 129-132	3	Olive black (5YR2/1); fine sand
10H-3, 144-145	1	Medium dark gray (N4); silt
10H-4, 0-5	5	Grayish black (N2); very fine sand
10H-4, 24-84	16/44	Olive gray (5Y4/2)/olive black (5Y2/1); pumiceous medium sand/pumiceous medium sand (scoria concentrated)
10H-4, 101-150 10H-5, 0-40 10H-CC, 0-20+	109+	Olive black (5Y2/1); pumiceous medium sand (pumice maximum diameter = 6 mm, laminated in the upper part)

Unit III is defined by a change in lithologic character from finer grained rocks with high calcium carbonate contents to interbedded coarser vitric sandstone, clayey siltstone (generally with 0%-20% calcium carbonate), and sandy conglomerate. This contact was not recovered and is placed just below Core 126-792E-31R (see "Downhole Measurements" section, this chapter).

The high calcium carbonate contents (15%-60%) of Unit III rocks are mainly attributed to calcareous nannofossils. The principal sediment types are nannofossil-rich claystone (42%), nannofossil claystone (22%), and nannofossil chalk (14%); the minor sediment types include claystone (10%), vitric sandstone (7%), vitric siltstone (5%), and breccia (1%). Calcium carbonate contents are reflected in the color of the rocks: nannofossil chalk is white (5Y 8/1) to light gray (5Y 7/1); nannofossil clay is yellowish gray (5Y 7/2); and nannofossil-rich claystone is dark gray (5Y 4/1). The nonbiogenic component is primarily clay, with low contents of volcanic glass compared with those of fine-grained sediments in other units. Bioturbation is intense. The minor sediment types that make up the remaining 22% of the core are very thin to thin beds of olive black (5Y 2/1), greenish black (5G 2/1), and brownish black (5YR 2/1) vitric clayey siltstone, very fine-grained vitric sandstone, and vitric siltstone. Constituent grains include brown to opaque glass and feldspars. These minor sediment types rarely show planar lamination.

Dewatering veinlets occur in Unit III (Fig. 12) in Cores 126-792E-26R, -30R, and -31R, and some intervals of nannofossil chalk and nannofossil clay are highly fractured into subvertical wavy fragments along the veinlet surfaces. A fault zone in the lower part of Section 126-792E-29R-1 consists of a 30-cm-thick fault gouge characterized by highly fractured, grayish green (5GY 5/1) claystone with slickensides and lens-shaped pieces of greenish black (5GY 2/1), very fine-grained sandstone. This fault zone is clearly identified in downhole logs (see "Downhole Measurements" section, this chapter).

Unit IV

Interval: Cores 126-792E-32R through Section 126-792E-68R-2 at 100 cm
Age: late to early Oligocene
Depth: 429.3-783.4 mbsf

The lower boundary of Unit IV is a fault between sandstone and the highly altered volcanic conglomerate and sandstone of Unit V. Unit IV is composed mainly of vitric sandstone (58%) and a sandy pebble-granule conglomerate (10%). The rest of the unit is silty claystone (9%), nannofossil-rich silty claystone (6%), nannofossil-rich claystone (5%), claystone (4%), and intermediate sediment types (siltstone, 4%; nannofossil claystone, clayey siltstone, sandy mudstone, and sandy siltstone, all 1% each).

In the upper part of this unit (Cores 126-792E-32R through -40R), graded beds of vitric sandstone and vitric siltstone are interbedded with muddy intervals (Fig. 13). Parallel- and ripple-laminated beds of siltstone and very fine- to fine-grained sandstone, from one to several centimeters in thickness, predominate in Cores 126-792E-34R, -36R, -37R, and -38R. Massive sandstones beds, 60-280 cm thick, occur in Cores 126-792E-32R, -33R, -38R, and -39R.

The conglomerate is confined to the middle and lower parts of the unit; it is absent in Cores 126-792E-52R through -59R (Fig. 5). The upper conglomerates contain clasts of andesite to dacite and pumice fragments (Fig. 14). Claystone intraclasts that

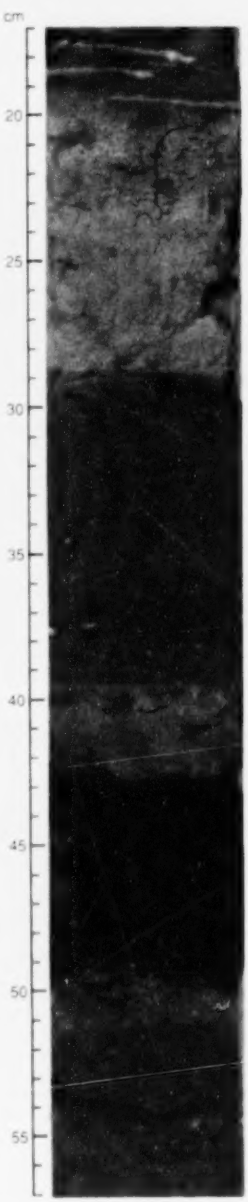

Figure 6. Interbedded light and dark colored ash, composed of vitric sand and silt and nannofossil-rich vitric clayey silt, in Unit I (Interval 126-792A-7H-1, 17-57 cm). The color of the ash layers varies from gray (5Y 6/1) in the 21-29 cm and 40-43 cm intervals, to brownish black (5YR 2/1) at 43-49 cm.

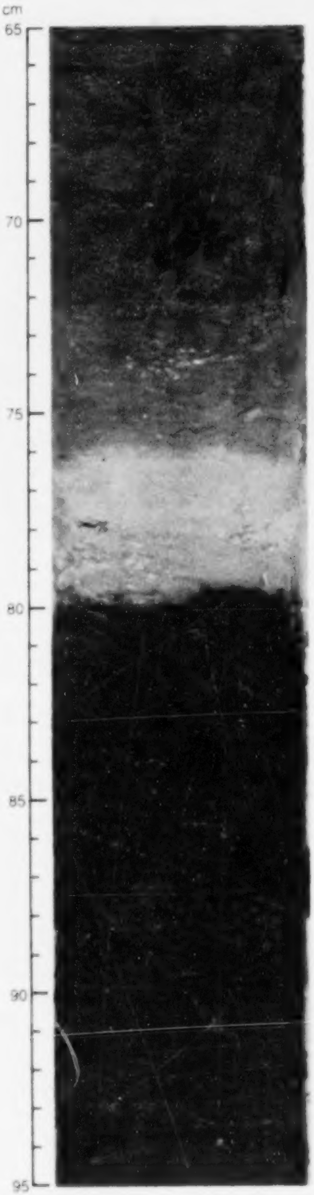

Figure 7. Interbedded light and dark ash layers of Unit I (Interval 126-792B-10X-1, 65-95 cm). The 72-75 and 75-79 cm intervals are adjacent light olive gray (5Y 6/2) and light gray (5Y 7/1) vitric silt; 79-84 cm is the host lithology (nannofossil-rich vitric silty mud); 84-89 is olive gray (5Y 4/2) pumiceous granule gravel; 89-93 cm is very dark gray (5Y 3/1) vitric silt, laminated in the basal 1 cm.

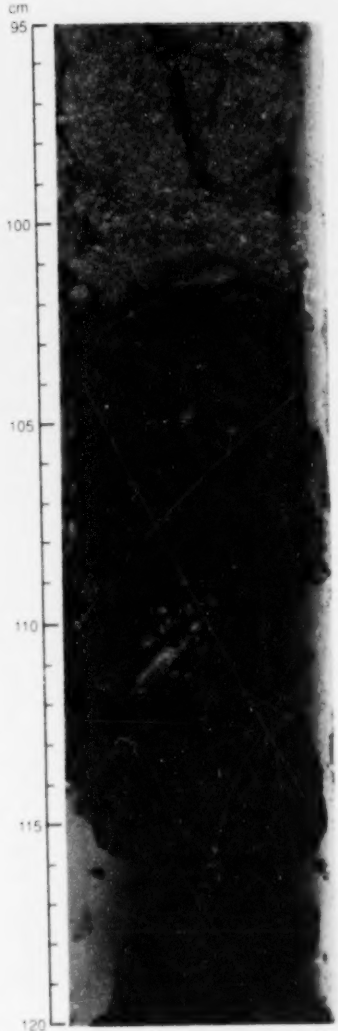

Figure 8. Lithified, poorly-sorted sandy mudstone containing granules 3 mm in diameter at the top of Unit II (Interval 126-792E-6R-1, 95-120 cm).

cm
7
8
9
10
11
12
13
14
15
16

Figure 9. Intensely bioturbated nannofossil-rich vitric silty claystone in Unit II (Interval 126-792E-21R-2, 7-16 cm). The horizontal feature at 13 cm is a *Zoophycos* burrow.

exceed the diameter of the core (maximum dimension about 8 cm) are present locally (Figs. 15 and 16). Intraclast sediment types resemble those of underlying units. Conglomerates below Core 126-792E-59R are greenish black (5GY 2/1, 5G 2/1) and also contain large claystone, siltstone, and sandstone intraclasts that exceed 7 cm in diameter. This lower conglomerate interval is mainly composed of thick sandstone and conglomerate beds, generally from tens of centimeters to 100 cm thick, with a maximum bed thickness of about 300 cm. In some cases, conglomerate grades upward into sandstone (Fig. 17). The grain size of the sandstone beds varies from very coarse to very fine. The thicker sandstone beds are generally massive, except for normal grading; they rarely have laminated tops. Thin- to medium-thickness beds are graded and contain a variety of sedimentary structures, including planar and cross lamination, flute casts, and flame structures (Figs. 18 and 19). Reddish brown epiclastic volcanic lithic grains occur in the thick, medium- to coarse-grained sandstones of the lower part of this unit.

Sandstones and siltstones in this unit are dominated by either felsic or mafic glass. Mixed felsic and mafic intervals are not common, and crystal contents are variable but generally low. Diagenetic products within these beds include fibroradiating zeolite cements, incipient clay-rim cements, and glass hydration rims.

The fine-grained sediments are strongly bioturbated (Fig. 20). Trace fossils include *Zoophycos* and *Chondrites*. Calcium carbonate contents are highly variable, ranging from <5% to 40%. A concentration of plant debris is present in burrowed siltstone in Section 126-792E-52R-5 (Fig. 21).

Unit IV shows moderate tectonic disturbance. Microfaults that are present in Cores 126-792E-45R, -50R, -59R and -67R rarely have slickensides, although horizontal microfaults in Section 126-792E-59R-5 show slickensides. Mineral-filled fractures (calcite and zeolite) are present in Cores 126-792E-37R through -40R, and Core 126-792E-66R, fractures in Core 126-792E-54R, subvertical fractures in Cores 126-792E-60R and -65R, and sandstone dikes (Fig. 22) in Cores 126-792E-32R, -35R, -39R, -41R, and -62R. The lowest conglomerate bed in Unit IV (Core 126-792E-67R) shows a variety of colors that are attributed to alteration (Figs. 23 and 24).

Unit V

Interval: Sections 126-792E-68R-2 at 100 cm through -70R-CC
Age: unknown
Depth: 783.4-804 mbsf

The top of Unit V is a fault. The lower contact separates the altered volcanic conglomerate of this unit from the underlying andesite lava of Unit VII (see "Igneous Petrology" section, this chapter). The lower contact occurs in Section 126-792E-70R-CC at 12 cm.

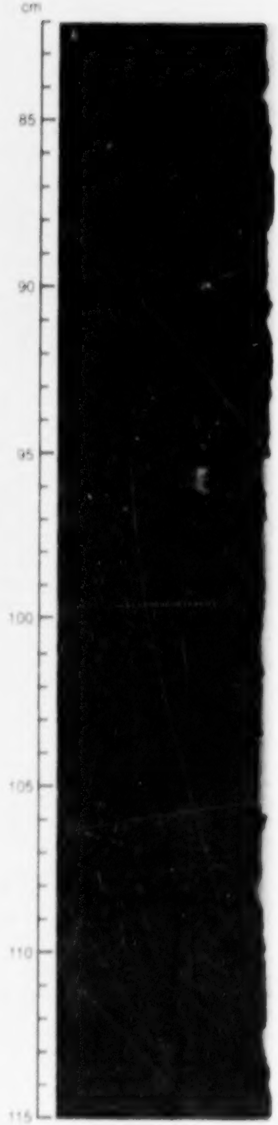

Figure 10. Dark ash beds in Unit II (Interval 126-792E-10R-2, 82-115 cm). The interval from 83-85 cm is a grayish black (N2) layer of angular to subangular, 2-4 mm granules; 85-91 cm and 102-108 cm are greenish black (5GY 2/1), laminated vitric silty claystone; 91-102 cm and 108-110 cm are intercalations of slightly bioturbated sandy siltstone.

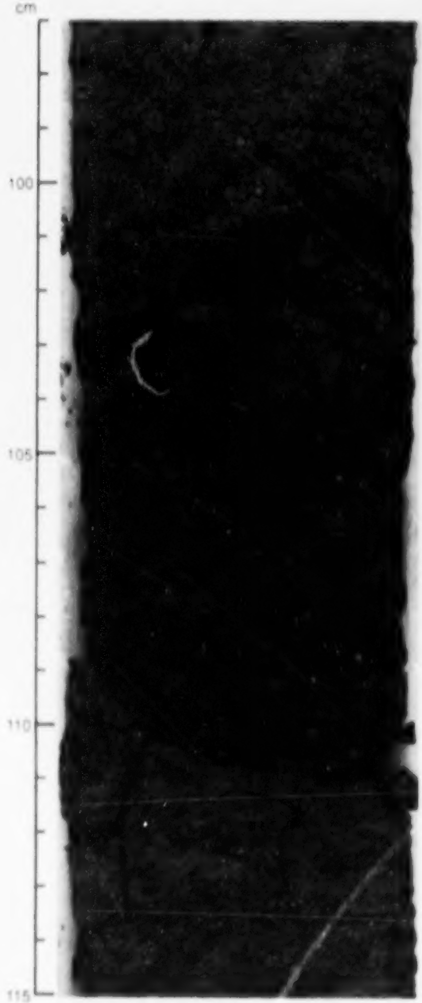

Figure 11. Grayish black (N2) ash bed of normally graded vitric sandstone to siltstone (105-111 cm), in nannofossil-rich sandy mudstone of Unit II (Interval 126-792E-18R-2, 97-115 cm).

Unit V is composed of very dark green (7.5GY 3/2) and dark grayish blue (5BG 5/1), altered volcanic pebble-granule conglomerate and sandstone. We could not determine grain sizes either visually or under the binocular microscope because of severe alteration. Greenish black (5G 2.5/1), silicified claystone and siltstone (probably clasts in the altered sandstone) and a brecciated mixture of altered volcaniclastic rock and claystone in the lower part of this unit suggest that the protolith of this material was a sedimentary rock of similar lithology to the sandstone and conglomerate in the lower part of Unit IV. Petro-

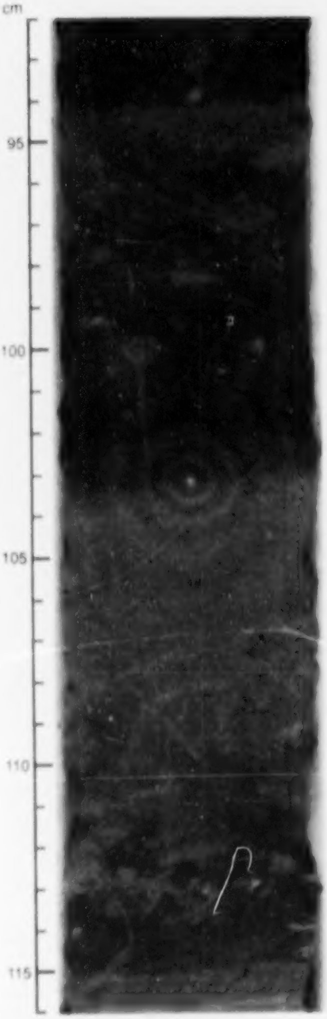

Figure 12. Intensely bioturbated nannofossil-rich claystone, medium dark gray (N4) vitric siltstone and sandstone, and grayish green (5GY 6/1) claystone of Unit III (Interval 126-792E-31R-1, 92–116 cm). Note wavy, subvertical dewatering structures (103–110 cm).

graphic examination of the unit shows it to be composed of highly altered pumiceous material, including pressure-flattened sand-size grains that are commonly wrapped around more competent crystal fragments. A pebble of highly altered andesite with a peculiar reddish color, and lumps of black manganese oxides are present within the fault that separates this unit from Unit IV (Fig. 25).

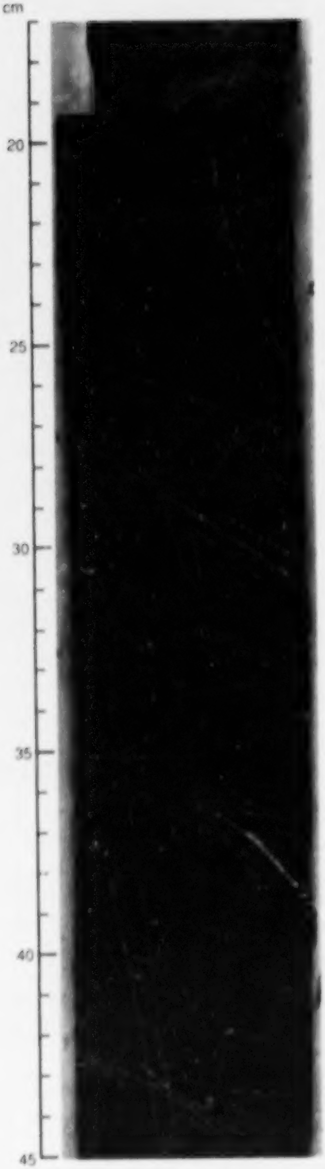

Figure 13. An interval consisting of five graded beds of very-fine-grained sandstone with parallel or cross lamination; Unit IV (Interval 126-792E-38R-1, 17–45 cm). Only the tops of these units are burrowed.

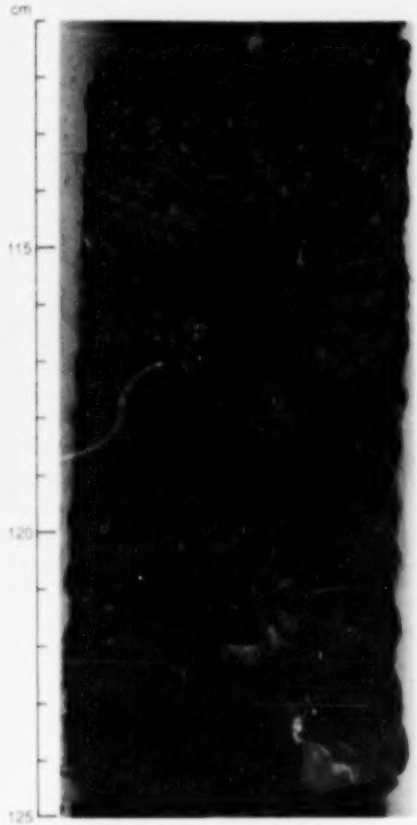

Figure 14. Pumiceous conglomerate and underlying very fine sandstone of Unit IV (Interval 126-792E-40R-2, 111-125 cm). Note the healed subvertical fracture at 114-124 cm.

Unit VI

Interval: Section 126-792E-70R-CC through -78R
Age: unknown
Depth: 804-885.9 mbsf

This unit consists of plagioclase-(± quartz)-orthopyroxene-clinopyroxene andesite lava, hyaloclastite, and breccia, with minor basaltic andesite and dacite (see "Igneous Petrology" section, this chapter).

X-Ray Diffraction Analysis

The results of XRD analyses of 44 samples from Site 792 are summarized in Table 4 and Figure 26, which present semiquantitative measurements derived from the characteristic main peaks of clay and other minerals. The quantities of calcite, reflecting the amount of microfossils in nannofossil-rich vitric silty clay, claystone, or chalk, increase irregularly with depth to 600 mbsf. The XRD calcite data are much the same as calcium carbonate values obtained from chemical analysis and display the same trends. Calcite is rare below 600 mbsf. Quartz is ubiquitous, but

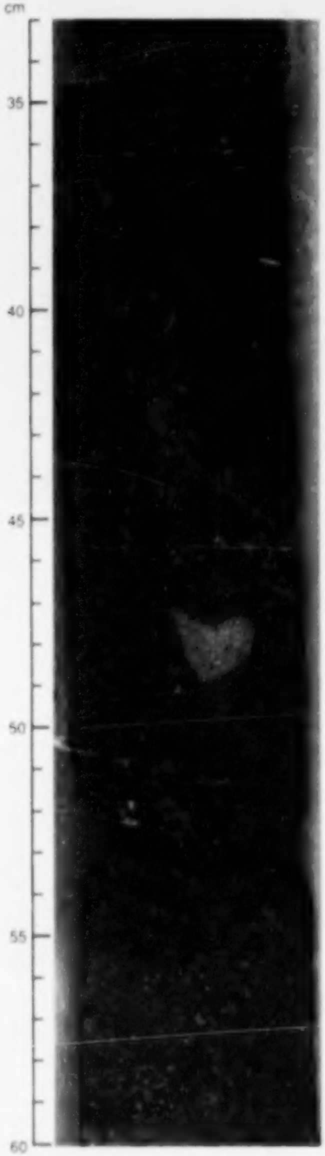

Figure 15. Matrix-supported polymictic conglomerate of Unit IV (Interval 126-792E-46R-7, 33-60 cm), with black (N1) intrabasinal clasts of claystone at 33-41 cm.

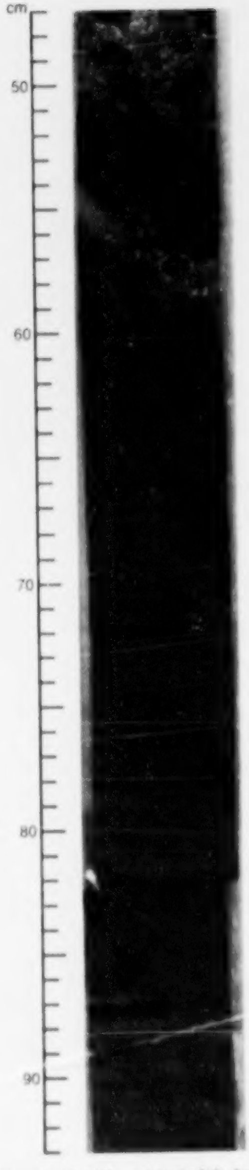

Figure 16. A sequence in Unit IV consisting of (1) the lower portion of a debris-flow deposit that has its base at 58–71 cm, (2) a plastically deformed, fine-grained sandstone (58–78 cm); (3) a medium-grained sandstone (78–82 cm); and (4) the fine-grained top and laminated portion of a graded turbidite (78–93 cm) in Unit IV (Interval 126-792E-48R-1, 47–93 cm).

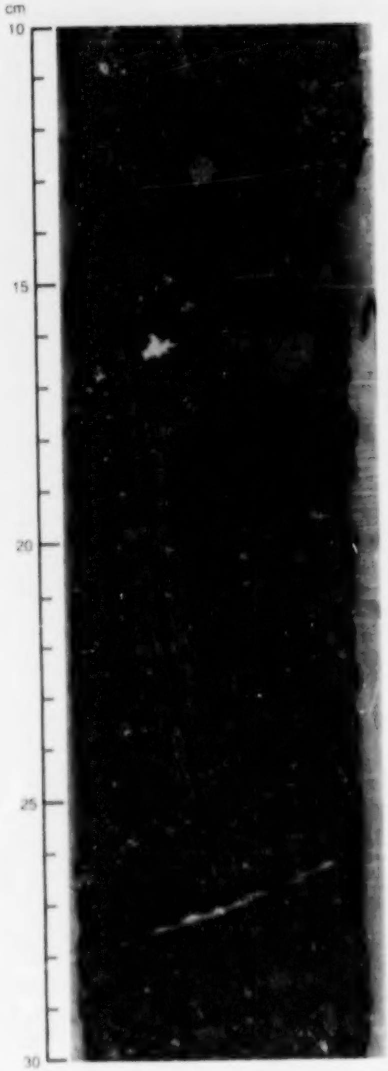

Figure 17. Volcanic granular and pebbly coarse sandstone of Unit IV (Interval 126-792E-43R-1, 10–30 cm). This is the upper part of an interval that has conglomerate at its base.

it is especially abundant in Units I and II and decreases with depth from Unit III to Unit IV. Chlorite is very rare at Site 792.

The quantity of amorphous materials, principally volcanic glass (estimated from the broad enhancement at 0.33 nm), decreases with depth, accompanied by increases in the clay mineral and zeolite contents.

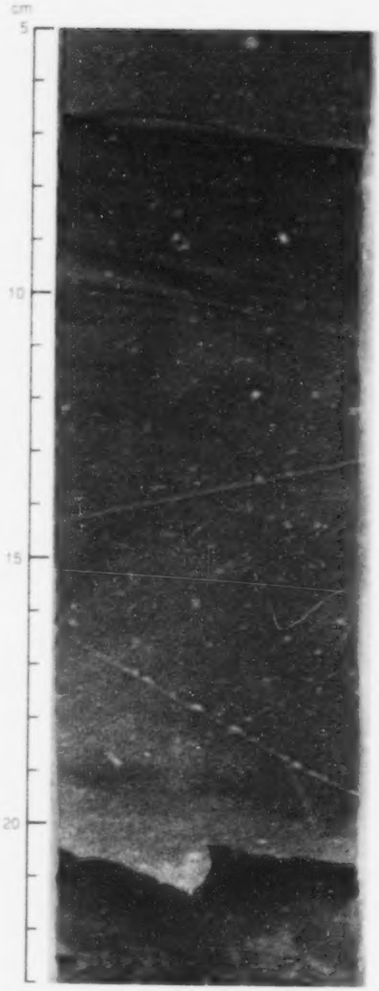

Figure 18. Turbidite bed of medium to fine-grained sandstone in Unit IV (Interval 126-792E-48R-4, 5–23 cm). The top of the turbidite (7–11 cm) is cross laminated. The bed rests with a load cast on burrowed claystone.

Smectite is present in varying amounts in all the samples and increases in abundance below 350 mbsf. The glass in Units II through IV is green to brown in color and is commonly altered to smectite and palagonite. Glauconite or palagonite is present in a green, fine-grained sandstone at 270 mbsf (Section 126-792E-15R-1 at 21 cm), at a sharply defined hiatus in Unit II.

Zeolites are absent in Units I and II, but they are present in Units III–V (below 350 mbsf). The phillipsite, analcime, wairakite, heulandite-clinoptilolite, and stilbite species of the zeolite group, characterizing the earliest stages of the zeolite facies, intermediate between diagenesis and metamorphism (Coombs et al., 1959), were classified according to their characteristic peaks.

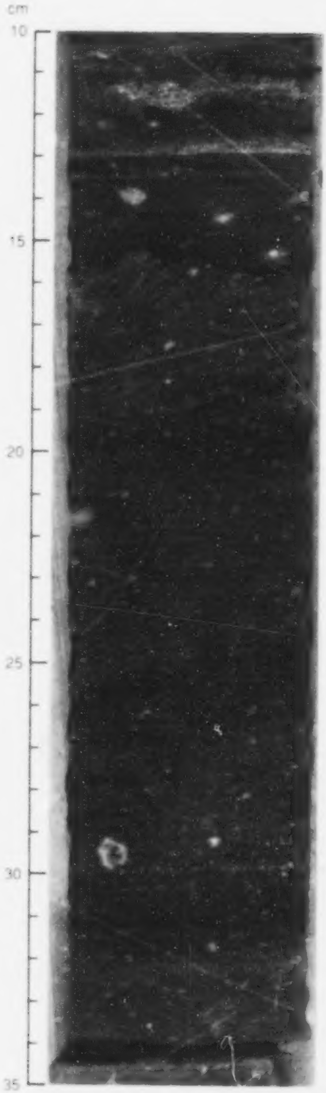

Figure 19. Laminated medium- to fine-grained sandstone turbidite (cross laminated at the top), grading into clayey siltstone, Unit IV (Interval 126-792E-56R-4, 10–35 cm).

Below 400 mbsf, the zeolite minerals change downhole from phillipsite and analcime to wairakite, accompanying the increase in smectite. Heulandite-clinoptilolite and stilbite replace analcime, phillipsite, and wairakite below 670 mbsf.

In Units IV and V, minor mineral components such as gypsum, diaspore, and cristobalite are present, and numerous white to green-colored veins in Unit IV are filled with zeolite and gyp-

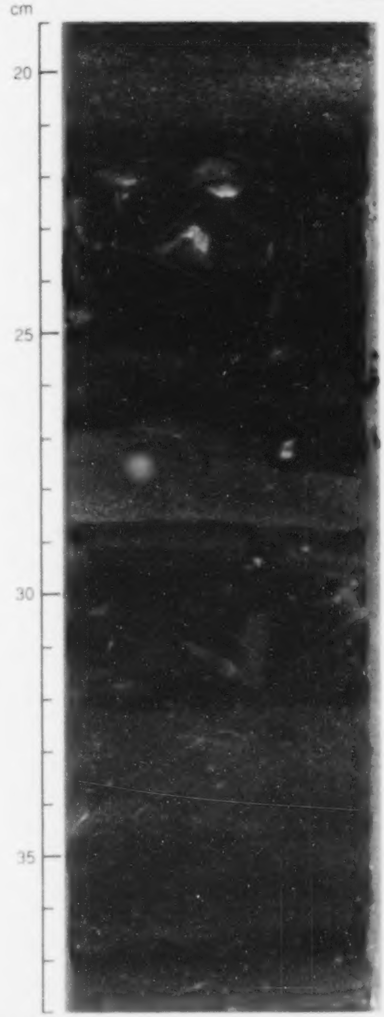

Figure 20. Bioturbated silty claystone overlying fine sandstone; Unit IV (Interval 126-792E-48R-3, 19–38 cm).

sum. A granule conglomerate layer in the middle portion of Unit IV (Section 126-792E-51R-4 at 21 cm) contains a pale reddish volcanic clast. Abundant smectite and diaspore in this clast suggests high-temperature (260°-290°C) alteration.

Sediment Accumulation Rates

We established sedimentation rates for Site 792 by using calcareous nannofossil datums and paleomagnetic reversal data (Tables 5 and 6) to construct the age-depth curves shown in Figures 27–29. The sedimentary section at Site 792 is marked by four lacunae: 1–2.2 Ma, 3.5–6 Ma, 8–9 Ma, and 13–19 Ma. The second and fourth lacunae correspond to the basal boundaries of the first two lithologic units.

Sedimentation rates in the late Oligocene (29–28 Ma) are 300 m/m.y, but they decrease almost an order of magnitude to 40 m/m.y. during the interval from 28 to 27 Ma. This sharp break occurs toward the top of Unit IV. In Unit III, sedimentation rates below and above a short normal fault that cuts out strata deposited 23–24 Ma are 4 m/m.y. and 14 m/m.y., respectively. Sedimentation rates for the Miocene section (23.7–5.0 Ma) range from 14 m/m.y. for the lower Miocene (Unit III) to values of 23 to 43 m/m.y. for the upper Miocene (Unit II).

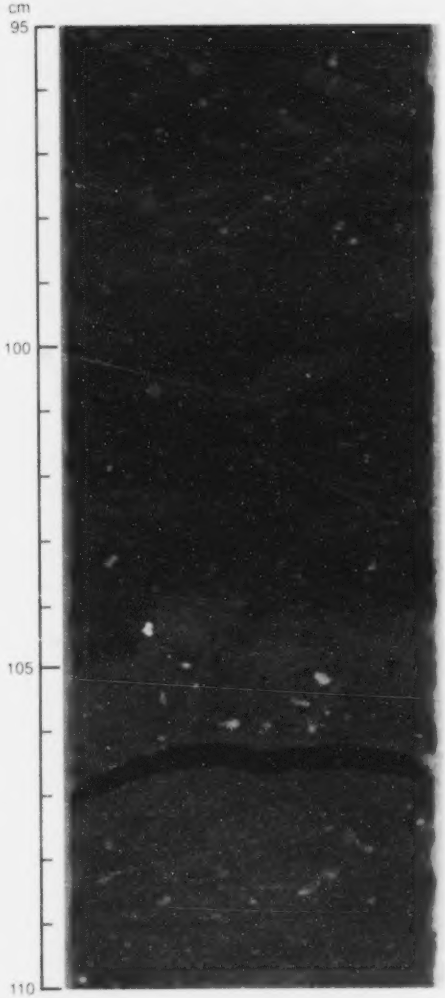

Figure 21. Concentration of carbonaceous plant debris (101–105 cm) in burrowed claystone of Unit IV (Interval 126-792E-52R-5, 95–110 cm).

A large increase in the sedimentation rate is apparent in the Pliocene and Quaternary sedimentary sections (Unit I). Following the early Pliocene lacuna at 6–3.56 Ma, sedimentation rates

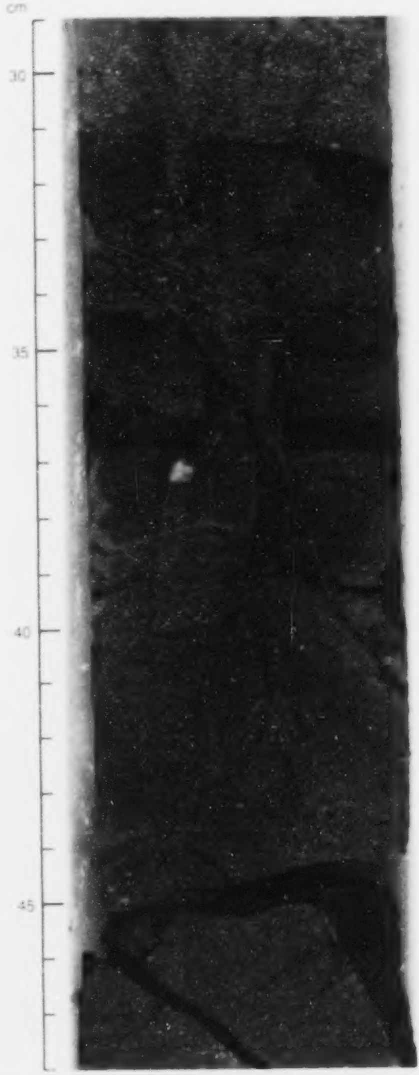

Figure 22. Subvertical sandstone dike, 5 mm wide, invading medium- to fine-grained sandstone of Unit IV (Interval 126-792E-32R-2, 29–48 cm).

increased from 40 m/m.y. to >120 m/m.y. for the late Pliocene. Similarly, sedimentation rates for the Quaternary remained high, ranging from 80 to 120 m/m.y.

Interpretation

Unit I

The nannofossil-rich clayey silt and nannofossil-rich silty clay of Unit I are interpreted as hemipelagic deposits that accumulated in water depths of 1.5–3 km (see "Biostratigraphy" section, this chapter) east of the Izu-Bonin Arc. The >200 volcanic ash layers and the pumiceous and scoriaceous gravel that are interbedded with the fine-grained sediments were mostly derived from volcanoes of the Izu-Bonin Arc, either as primary airfall or, in some cases, as resedimented ash that was transported to the site by turbidity currents (Table 3). The abundance of volcanic ash layers indicates continuous explosive volcanic activity in the arc throughout the late Pliocene and Pleistocene. The wide range of grain size, bed thickness, and composition of the ash and associated volcanogenic turbidites suggest large variations of eruption styles and composition of magma for the Izu-Bonin volcanoes during this period. Some caution is required, however, because contrasts in grain size and bed thickness may also reflect multiple source volcanoes at different distances from the site.

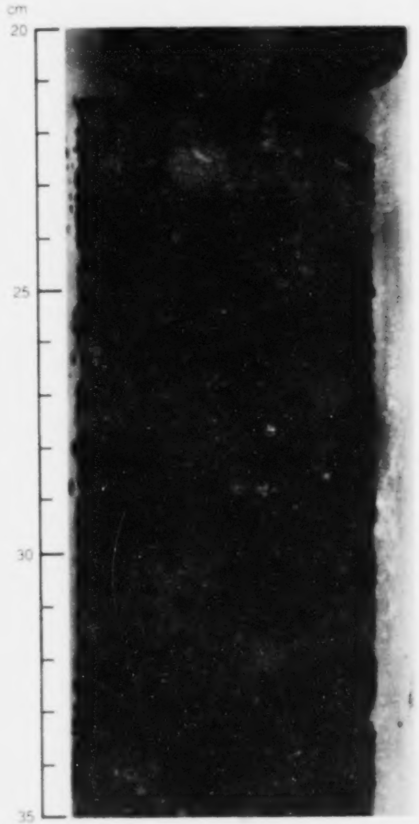

Figure 23. Polymictic, pebble conglomerate to fine-grained-sand conglomerate near the base of Unit IV (Interval 126-792E-67R-1, 20–35 cm). The mottled matrix is a result of variable hydrothermal alteration and cementation.

Unit II

Muddy sandstones and sandy mudstones that characterize Unit II were probably produced by bioturbative mixing of hemi-

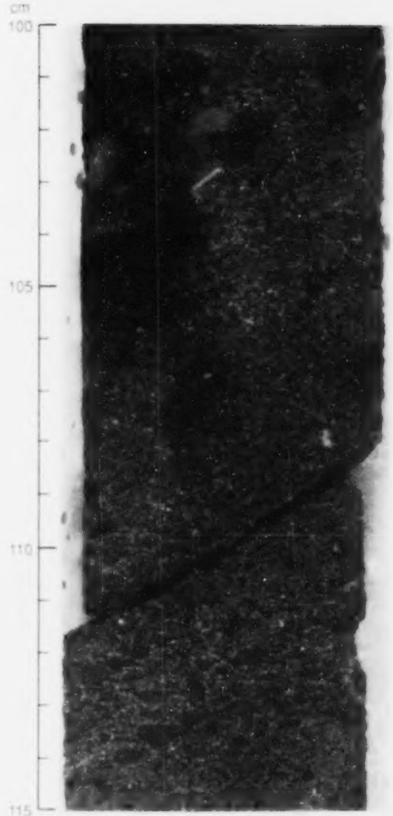

Figure 24. Polymictic granule conglomerate with a fine-grained sand matrix, near base of Unit IV (lower in the same section of Fig. 22; Interval 126-792E-67R-1, 100–115 cm). Pebbles are light red (10R 6/6), red (10R 4/6), very dusky red purple (5RP 2/2), light greenish gray (5G 8/1), greenish black (5G 2/1), medium light gray (N6), and gray (5YR 6/1); the more unusual shades are the result of hydrothermal alteration. Healed microshears displace and smear out some pebble horizons above and below the break at 108–111 cm, which is also a healed microshear fractured by drilling.

pelagic mud with thin beds of sand-size scoria grains and silt-size volcanic glass. This interpretation requires the coarser volcanic material to have been supplied at a slow rate, or as very thin beds, so that burrowers could rework and disperse the material into surrounding muds. The sedimentation rate of this unit suggests a large flux of volcanogenic material, even though instantaneous rates must have been slow.

Contrasts in ash abundance and composition from the base to the top of Unit II suggest temporal changes in volcanic supply to the site; ash is more scarce in the lower part of the unit, and lighter colored felsic ash is found only in the upper part of the unit.

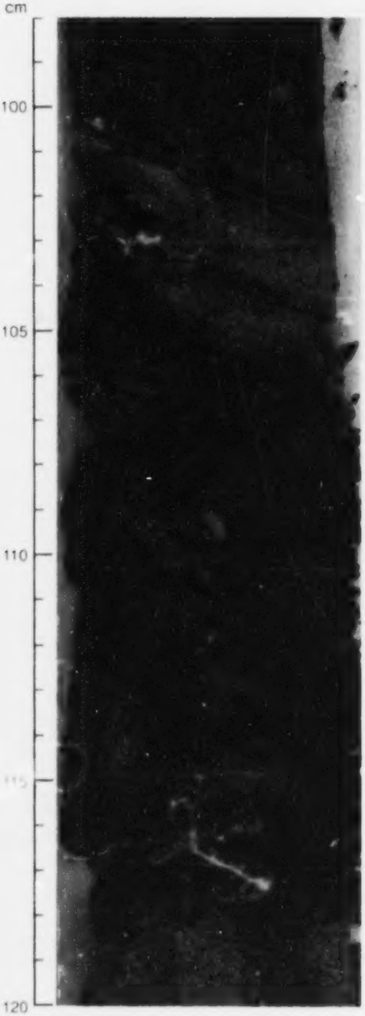

Figure 25. The fault-zone contact between Units V and IV (Interval 126-792E-68R-2, 98–120 cm). It includes a red (2.5YR 5/6) clast of altered andesite at 110 cm, and three black (N1) igneous clasts at 106–110 cm. The interval 110–116 cm is altered sandstone, mottled dark greenish gray (5G 4/1) and reddish yellow (7.5YR 6/6). Below the fault (116–120 cm) is vitric silty claystone and vitric sandy mudstone of Unit V, hydrothermally altered to mottled, very dark green (7.5 GY 3/2) and dark grayish blue (5BG 5/1) colors.

Table 4. Results of X-ray diffraction (XRD) analyses, Site 792.

Core, section, interval (cm)	Depth (mbsf)	Unit	Color	Texture	Clay minerals			Minerals	Amorphous materials
					1.4 nm	1.0 nm	0.7 nm		
126-792A-									
1H-1, 33	0.3	I	5GY 6/1	Vitric silt	Common	—	Present	Quartz, feldspar	Abundant
1H-3, 100	4	I	5Y 4/1	Nannofossil silty clay	Common	Present	Present	Calcite, quartz, feldspar	Abundant
1H-3, 140	4.4	I	N7	Sand, silt	Present	—	Trace	Quartz, feldspar	Abundant
1H-6, 145	9	I	10GY 5/2	Vitric silt	Trace	—	—	Quartz, feldspar	Abundant
2H-4, 100	15.2	I	N2	Sand	Trace	—	—	Calcite, quartz, feldspar	Abundant
3H-3, 100	23.1	I	5GY 4/1	Sand	Trace	—	—	Quartz, feldspar	Abundant
4H-3, 25	31.7	I	5Y 5/2	Nannofossil clayey silt	Trace	Trace	Present	Calcite, quartz, feldspar	Abundant
5H-3, 103	41.8	I	5Y 4/1	Vitric silt	Present	—	Present	Quartz, feldspar, cristobalite	Abundant
126-792B-									
1H-1, 47	0.5	I	10GY 5/2	Vitric silt	Common	Trace	Present	Calcite, quartz, feldspar	Common
7H-2, 112	62.2	I	N2	Sand	Common	—	—	Quartz, feldspar	Abundant
7H-3, 83	63.4	I	N8	Vitric silt	Trace	—	Trace	Calcite, quartz, feldspar	Abundant
7H-6, 40	67.5	I	5YR 4/1	Vitric sand	Trace	—	—	Calcite, quartz, feldspar	Abundant
8X-2, 74	110.1	I	N2	Foraminifer-rich vitric silt	Abundant	—	Common	Calcite, quartz, feldspar	Common
126-792D-									
1X-CC, 10	136	I	5Y 3/2	Silty clay	Present	—	—	Feldspar	Abundant
126-792E-									
14R-CC, 10	261	II	5GY 4/1	Silty sandstone	Trace	—	—	Calcite, quartz, feldspar	Common
15R-1, 23	270.7	II	5GY 2/1	Sandstone	Trace	—	—	Calcite, quartz, feldspar	Common
15R-2, 6	272.2	II	5GY 6/1	Silty sandstone	Trace	—	—	Calcite, quartz, feldspar, palagonite, glauconite	Common
16R-1, 7	280.3	II	5Y 4/1	Nannofossil sandstone	—	—	—	Calcite, quartz, feldspar, palagonite, glauconite	Common
17R-2, 14	291.5	II	5R 6/2	Pale red ash bed	—	—	—	Calcite, quartz, feldspar, palagonite, glauconite	Abundant
17R-4, 22	295.6	II	5Y 6/1	Vitric clayey silt	—	—	—	Quartz, feldspar	Common
17R-4, 29	295.7	II	5BG 3/2	Vitric clayey silt	Abundant	Trace	Trace	Feldspar, calcite, palagonite	Common
18R-2, 145	302.5	II	5YR 4/1	Tan ash	Present	—	—	Quartz, feldspar, glauconite	Common
19R-1, 123	310.2	II	5Y 2/1	Clayey siltstone	Present	—	Present	Quartz, feldspar, glauconite	Common
20R-4, 25	323.4	II	5Y 2/1	Vitric silty claystone	Present	—	Trace	Calcite, quartz, feldspar, glauconite	Common
21R-2, 16	330	II	N2	Vitric claystone	Present	—	—	Calcite, quartz, feldspar, glauconite	Common
29R-CC, 5	405.6	III	5GY 2/1	Vitric siltstone	Abundant	—	Present	Calcite, quartz, glauconite, zeolite	Common
32R-2, 130	437.4	IV	5GY 4/1	Silty claystone	Present	—	Present	Calcite, quartz, feldspar, palagonite, glauconite, zeolite	Common
32R-3, 75	438.4	IV	5G 3/2	Claystone	Abundant	Present	Present	Calcite, feldspar, palagonite, glauconite	Common
34R-1, 130	455.2	IV	5GY 4/1	Siltstone	Abundant	—	Present	Feldspar, palagonite, glauconite, zeolite	Present
35R-1, 78	464.3	IV	N3	Vein in sandstone	Abundant	—	Abundant	Calcite, feldspar, glauconite, zeolite	Present
35R-1, 77	464.3	IV	N3	Sandstone	Abundant	—	Present	Calcite, feldspar, glauconite, zeolite	Present
37R-3, 48	492.3	IV	5GY 8/1	Vein in sandstone	Present	—	Common	Calcite, feldspar, zeolite	Present
38R-2, 71	504.4	IV	N3	Vein in vitric silty claystone	Trace	—	—	Gypsum, zeolite	
38R-3, 103	506.2	IV	N2	Vein in sand	Trace	—	Present	Calcite, feldspar, zeolite	
43R-1, 117	561.4	IV	5GY 2/1	Vein in vitric sandstone	Trace	—	—	Gypsum	
44R-5, 97	576.7	IV	5GY 2/1	Pebbly sandstone	Abundant	—	Common	Feldspar, zeolite	
46R-4, 42	593.5	IV	N3	Very fine turbidites sand/shale	Abundant	—	—	Feldspar, palagonite, glauconite, celadonite	Common
47R-3, 93	601.7	IV	5G 5/2	Graded very fine sand to claystone	Abundant	—	—	Quartz, feldspar, palagonite, glauconite, celadonite	Common
49R-4, 21	621.8	IV	5G 6/2	Pale red rock	Abundant	—	—	Quartz, feldspar, palagonite, diaspore, celadonite	
56R-4, 110	671	IV	5G 5/2	Sandstone	Abundant	—	—	Feldspar, amphiboles, cristobalite, palagonite, zeolite	Present
56R-6, 110	674	IV	5G 5/2	Fine sandstone	Abundant	—	Trace	Feldspar, glauconite, zeolite	Present
58R-3, 126	689.1	IV	5GY 4/1	Silty claystone	Present	—	Trace	Zeolite	Present
69R-3, 102	794.6	V	5G 3/2	Altered sandstone	Abundant	—	Present	Feldspar, glauconite, cristobalite	Present
69R-3, 105	794.7	V	5G 5/1	Altered sandstone	Abundant	—	Present	Feldspar, glauconite, tridymite	Present

Unit III

The nannofossil chalk marks a period of slow deposition at 2–4 km water depth (see "Biostratigraphy" section, this chapter) without significant volcanic input; ash layers and terrigenous sandstone/siltstone beds are very rare. The lesser epiclastic input relative to that of the underlying Unit IV may be the result of tectonic subsidence of the source area and a significant rise in global sea level from the mid-Oligocene into the Miocene (Haq et al., 1988).

The FMS data (see "Downhole Measurements" section, this chapter) indicate that the bedding dip abruptly increases to 30° in the uppermost 1 m of Unit III, just below the bounding unconformity. This local steepening of bedding may be caused by slumping or may indicate rotation of bedding within a fault zone.

Unit IV

This unit consists mainly of sandstone, sandy conglomerate, and silty claystone. The range of bed thicknesses and grain sizes are like those found in the middle and outer parts of submarine fans, or in oversupplied basin plains (e.g., Ricci Lucchi and Valmori, 1980). Seismic data (see "Seismic Stratigraphy" section, this chapter), calibrated by the sedimentary deposits recovered at Sites 787, 792, and 793, indicate that the upper Oligocene fill of the forearc basin is a rapidly deposited turbidite blanket that onlaps both the eastern and western margins of the basin. In such an oversupplied basin, individual morphological elements like submarine fans probably cannot be distinguished (Pickering, 1982).

Structural features in Unit IV include subvertical veinlets and numerous microfaults. Similar features occur in Unit III and in the Eocene and Oligocene sections at Sites 787 and 793 (see "Site 787" and "Site 793" chapters, this volume). The veinlets are identical to those described from the Middle America Trench slope by Ogawa and Miyata (1985) and from the Japan Trench by Arthur et al. (1980) and Lundberg and Leggett (1986), and are interpreted as extensional fracture cleavages formed in rapidly consolidating (wet) sediments. The microfaults in Units III and IV also formed in an extensional regime. An extensional stress field may have also facilitated injection of the clastic dikes that are common in this unit.

The conglomerate beds of Unit IV represent a spectrum of deposits, from those in which grading is absent and bed tops are sharp, to those that are normally graded. Beds of both types contain outsized, floating intraclasts as large as 7 cm in diameter. Some beds also contain scattered large pebbles of andesite, dacite, and porphyritic rocks from the Izu-Bonin Arc. The

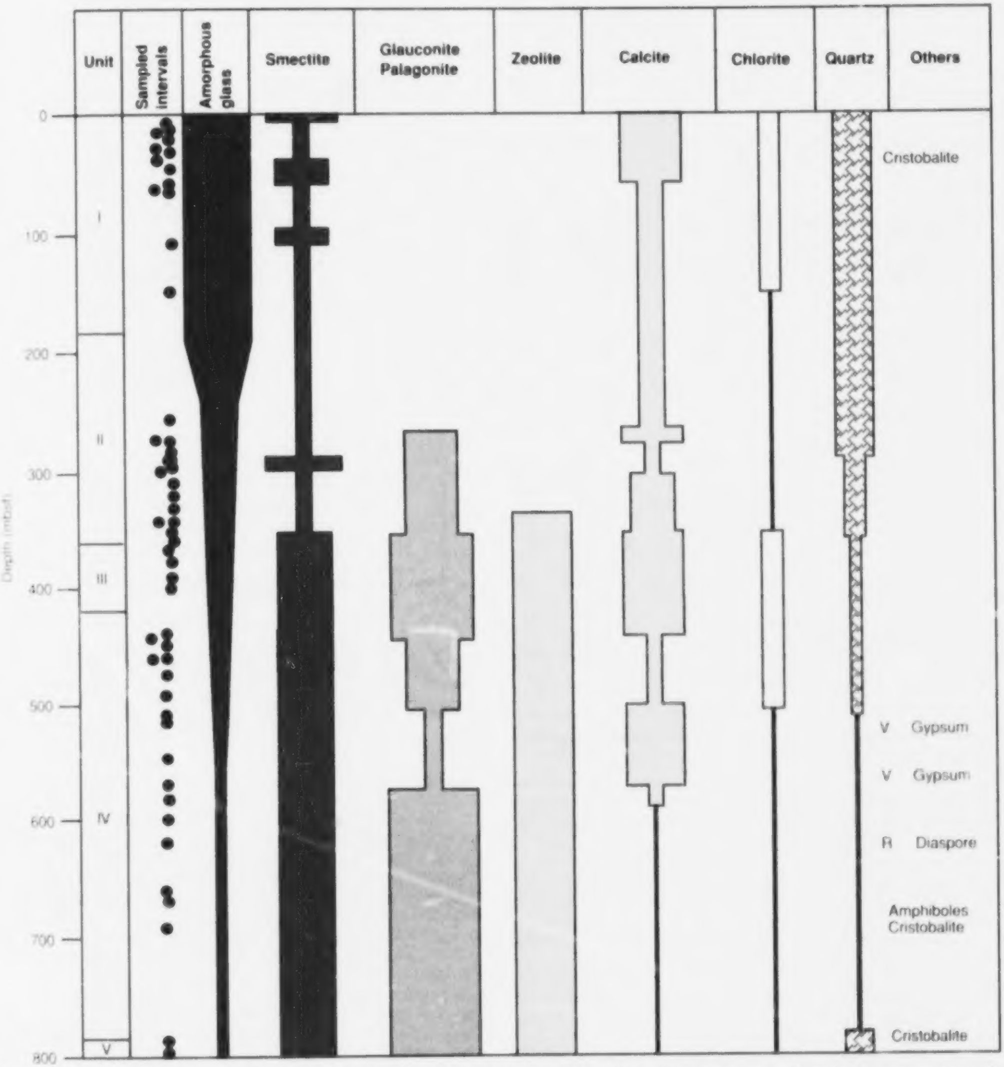

Figure 26. Summary diagram of X-ray diffraction data from Site 792 in which the relative widths of bars represent semiquantitative measurements of clay and other mineral abundances (filled circles = sampled intervals; V = vein or microfault; R = pale reddish volcanic clast).

structureless conglomerates with sharp tops and floating clasts are interpreted as debris-flow deposits. The graded beds of conglomerate are like the normally graded conglomerates of Walker (1975) and are interpreted as turbidites deposited from high-concentration flows. Thick pebbly sandstone beds and thin- to medium-bedded, graded sandstone beds with planar lamination, cross lamination, and flame structures are also turbidites.

There is no evidence that the conglomerates at this site were deposited in channels, although similar sediments in some ancient successions do reside in shallow channels or large scours. Conglomerates of this type are known from the inner to middle parts of ancient submarine fans, within and beyond fan channels, and from coarse-grained slope aprons (Nelson and Maldonado, 1988).

The composition of sand and gravel clasts indicates that part of the volcanogenic detritus is not the product of syndepositional volcanism, but instead was derived by the erosion of volcanoes along the nearby arc. In particular, pebble types include

Table 5. Biostratigraphic datums used to construct the age-depth curves for Site 792.

Chronostratigraphic event	Core, section, interval (cm)	Depth (mbsf)	Age (ma)
Hole 792A			
FO *E. huxleyi*	2H-CC to 3H-CC	15.55–28.40	0.275
LO *P. lacunosa*	4H-3, 40–41 to 4H-CC	31.80–37.60	0.460
LO acme *R.* Sp. A	8H-CC to 9H-1, 64–65	69.46–81.41	0.830
Hole 792B			
FO *E. huxleyi*	1H-CC to 2H-CC	4.26–59.60	0.275
LO acme *R.* Sp. A	4X-CC to 5X-CC	73.96–88.50	0.830
LO *D. brouweri*	6X-CC to 7X-CC	88.65–107.90	1.890
LO *D. pentaradiatus*	7X-CC to 8X-1, 33–34	98.57–111.62	2.350
LO *D. surculus*	8X-1, 36–37 to 8X-CC	108.26–117.50	2.410
LO *D. tamalis*	11X-1, 25 to 11X-CC	137.05–146.40	2.650
Hole 792C			
LO *D. tamalis* to LO *R. pseudoumbilica*	1X-CC	137.39–146.40	2.65 3.56
Hole 792D			
LO *D. tamalis* to LO *R. pseudoumbilica*	1X-CC	136.84–145.60	2.65 3.56
Hole 792E			
LO *R. pseudoumbilica*	5R-CC to 6R-1, 39–40	175.03–192.37	3.56
FO *P. lacunosa*	6R-1, 39–40 to 6R-CC	185.13–193.40	3.70
LO *D. quinqueramus*	6R-1, 39–40 to 6R-CC	185.13–193.40	5.30
FO *D. berggrenii*	15R-1, 11–12, to 15R-2, 39–40	270.16–278.6	8.20
LO *D. hamatus*	15R-1, 11–12 to 15R-39–40	270.16–278.6	8.90
FO *C. calyculus*	15R-CC to 16R-1, 40–41	273.99–287.64	10.0
FO *D. hamatus*	16R-CC to 17R-1, 40–41	282.56–294.61	10.0
FO *C. coalitus*	17R-2, 41–42 to 17R-3, 37–38	291.80–297.56	10.8
FO *D. kugleri*	20R-CC to 21R-1, 40–41	322.48–336.09	11.5
LO *S. heteromorphus*	23R-CC to 24R-1, 46–47	349.67–366.10	13.2
LO *S. belemnos*	23R-CC to 24R-1, 46–47	349.67–366.10	18.6
FO *S. belemnos*	24R-CC to 25R-1, 40–41	358.66–375.27	20.5
FO *D. druggii*	28R-CC to 29R-1, 108–109	399.03–413.26	23.2
LO *R. bisecta*	28R-CC to 29R-1, 108–109	399.03–413.26	23.7
LO *S. distentus*	36R-CC to 37R-CC	480.13–492.50	28.2

Note: Data are plotted in Figures 27, 28, and 29.

Table 6. Paleomagnetic reversal events used to construct the age-depth curves for Site 792.

Chronostratigraphic event	Interval	Depth (mbsf)	Age (Ma)
Hole 792A			
Brunhes/Matuyama	7H-1, 140	58.0–59.9	0.73
Top of Jaramillo	9H-3, 140	80.0–85.2	0.91
Base of Jaramillo	10H-1, 130	86.8–91.1	0.98
Hole 792B			
Brunhes/Matuyama	3H, 40	60.1	0.73
Top of Jaramillo	4X/5X	74.0–88.1	0.91
Top of Anomaly 2A	9X/10X	119.6–132.1	2.47
Hole 792E			
Base of Anomaly 2A	5R/6R	175.0–192.7	3.40
Top of normal between Anomalies 3A and 4	8R-1, 30	203.4–212.4	6.37
Top of Anomaly 4	9R-3, 20	215.4–219.8	6.70
Base of 1st normal in Anomaly 4	9R-3, 100	216.6–220.6	6.78
Base of 2nd normal in Anomaly 4	12R/13R	245.8–258.45	7.28
Top of Anomaly 5	15R-1, 59	271.0–277.2	8.92
Top of 2nd normal in Anomaly 5A	21R/22R	330.53–342.89	11.69
Top of 1st normal in Anomaly 8	31R-3, 140	418.45–419.86	26.86
Top of 1st normal in Anomaly 9	35R/36R	466.2–475.9	28.15
Base of 1st normal in Anomaly 9	51R/52R	621.96–628.43	28.74
Top of 2nd normal in Anomaly 9	55R-2, 50	657.7–664.33	28.80

Note: Data are plotted in Figures 27, 28, and 29.

andesite, dacite, and some porphyritic rocks; sandstones contain abundant reddish brown, epiclastic, sand-size scoria grains and local concentrations of plant debris. The pumice clasts present in the upper conglomerates suggest some contemporaneous volcanic activity in the region.

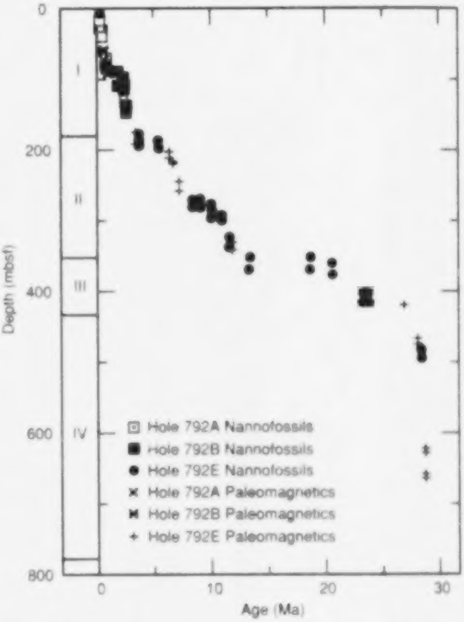

Figure 27. Age-depth plot for Site 792, constructed from the biostratigraphic datums and paleomagnetic reversal events listed in Tables 5 and 6. Lithologic unit boundaries are plotted on the right-hand side of the graph. Two data points at any one age represent possible depth range of datum or event.

Unit V

This unit is composed of severely altered volcanic pebble-granule conglomerate and sandstone. Although grain boundaries are not visible with a binocular microscope, "ghosts" of flattened pumiceous grains are visible petrographically. This alteration may be hydrothermal; the fluids responsible for it probably moved along the fault planes that bound Unit V (see "Downhole Measurements" section, this chapter). Manganese oxides that occur just below the upper fault have a hydrothermal origin. Slight alteration is also present above this fault in the lowest sandstones of Unit IV and may be the result of movement of hydrothermal fluids along the faults. The suggestion of hydrothermal circulation appears to be at odds with temperature measurements at the base of the sedimentary section that are consistently less than 30°C (see "Downhole Measurements" section, this chapter). Higher fluid temperatures may have been short lived, however, and possibly were restricted to the Oligocene or Miocene.

BIOSTRATIGRAPHY

Calcareous Nannofossils

Hole 792A

Samples 126-792A-1H-CC and -2H-CC contain *Emiliania huxleyi* and are placed within Zone CN15. The following species are also present in these samples: *Gephyrocapsa oceanica,*

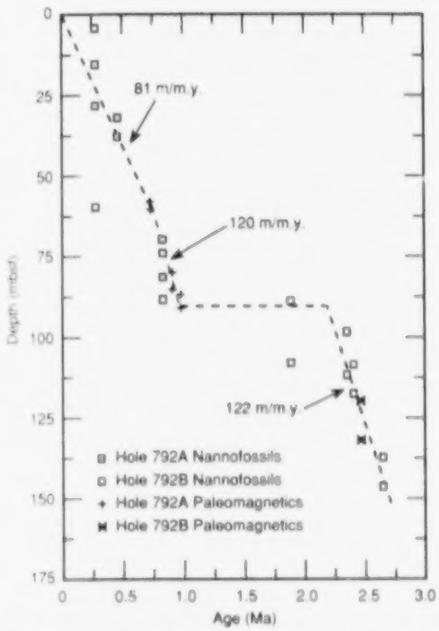

Figure 28. Expanded age-depth plot of the Pliocene-Pleistocene section, Site 792 (shown in Fig. 27), constructed from the biostratigraphic datums and paleomagnetic reversal events listed in Tables 5 and 6. Two data points at any one age represent possible depth range of datum or event. Average sedimentation rates are shown in m/m.y.

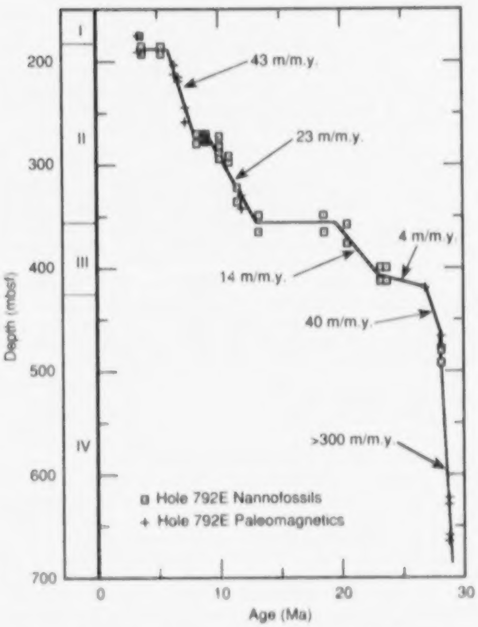

Figure 29. Expanded age-depth plot of the Miocene and Oligocene section, Site 792 (shown in Fig. 27), constructed from the biostratigraphic datums and paleomagnetic reversal events listed in Tables 5 and 6. Lithologic unit boundaries are plotted on the right-hand side of the graph. Two data points at any one age represent possible depth range of datum or event. Average sedimentation rates are shown in m/m.y.

Helicosphaera carteri, *Umbilicosphaera irregularis*, *Rhabdosphaera clavigera*, and *Coccolithus pelagicus*. Reworked *Sphenolithus* sp. was found in Sample 126-792A-1H-CC.

E. huxleyi and *Pseudoemiliania lacunosa* are not present in Samples 126-792A-3H-CC, -4H-1, 40–41 cm, and -4H-3, 40–41 cm, which are placed within Zone CN14b. Other species present include *Syracosphaera* sp., *Pontosphaera japonica*, *Calcidiscus leptoporus*, *G. oceanica*, and *H. carteri*.

P. lacunosa is present in Samples 126-792A-4H-CC through -10H-CC, which are assigned to Zone CN14a. Sample 126-792A-9H-1, 64–65 cm, contains the last occurrence (LO) of the acme of *Reticulofenestra sp. A.*, which marks the 0.83 Ma datum proposed by Takayama and Sato (1987). Other species found in these samples are *G. oceanica*, small *Gephyrocapsa* sp., *Scapholithus fossilis*, *C. pelagicus*, *C. leptoporus*, *Thoracosphaera* sp., and *Helicosphaera* spp.

Hole 792B

Emiliania huxleyi is present in Sample 126-792B-1H-CC, which indicates that the sample falls within Zone CN15. Other species present in the sample are *C. leptoporus*, *G. oceanica*, *Ceratolithus cristatus*, *H. carteri*, and *Oolithotus antillarum*.

Samples 126-792B-2H-CC through -6X-CC contain *P. lacunosa* and are assigned to Zone CN14a (of Okada and Bukry, 1980). We found the *Reticulofenestra* sp. A datum (0.83 Ma) in Sample 126-792B-5X-CC. Other calcareous nannofossils in these samples are *G. oceanica*, *P. japonica*, *R. clavigera*, *C. leptoporus*, and *Umbilicosphaera sibogae*. Sample 126-792B-6X-CC does not contain *Helicosphaera sellii* or *Calcidiscus macintyrei*, which suggests that this sample is younger than the LOs of both of these species (1.37 and 1.45 Ma, respectively).

We found *Discoaster brouweri* in Sample 126-792B-7X-CC, but not *Discoaster pentaradiatus*, which indicates a late Pliocene age and assignment to Zone CN12d. A hiatus or period of reduced sedimentation rate occurs within Core 126-792B-7X, between Samples 126-792B-6X-CC (Zone CN14a, <1.37 Ma) and -7X-CC (Zone CN12d, >1.89 Ma). Samples 126-792B-8X-1, 33–34 cm, and -8X-1, 36–37 cm, contain *D. pentaradiatus* and do not contain *Discoaster surculus*, which indicates Zone CN12c. Samples 126-792B-8X-CC, -9X-CC, -10X-1, 42–43 cm, and -11X-1, 25 cm, contain *D. surculus* and do not contain *Discoaster tamalis*, which indicates Zone CN12b. Sample 126-792B-11X-CC contains *D. tamalis*, but it does not contain *Reticulofenestra pseudoumbilica*, which constrains this sample to Zone CN12a. Other species present in these samples include *P. japonica*, *Helicosphaera sellii*, *Calcidiscus macintyrei*, *Coccolithus streckerii*, *Syracosphaera pulchra*, *D. brouweri*, and *Helicosphaera* spp.

Hole 792C

D. surculus is present in Sample 126-792C-1X-CC but *R. pseudoumbilica* is absent, which suggests a range in age from Zones CN12a to CN12b. Other species found in this sample are *D. brouweri*, *D. pentaradiatus*, *C. pelagicus*, *H. sellii*, *Thoracosphaera* sp., *P. lacunosa*, and *C. leptoporus*.

Hole 792D

Sample 126-792D-1X-CC contains *D. surculus* and does not contain *R. pseudoumbilica;* it falls within Zones CN12a to CN12b. Other calcareous nannofossils found in the sample are *D. pentaradiatus, Ceratolithus rugosus, P. lacunosa, C. pelagicus, Syracosphaera* spp., and *Discoaster asymmetricus.*

Hole 792E

D. brouweri, D. pentaradiatus, D. surculus, and *D. asymmetricus* are present in Samples 126-792E-1R-CC through -5R-CC, but *R. pseudoumbilica* is absent, which indicates Zones CN12a to CN12b. Sample 126-792E-6R-1, 39–40 cm, contains the aforementioned species plus common *R. pseudoumbilica* and is assigned to Zone CN11b. These Pliocene samples also contain common *P. lacunosa, C. leptoporus,* and *C. macintyrei.*

Samples 126-792E-6R-CC through -15R-1, 11–12 cm, contain *Discoaster quinqueramus* and *Discoaster berggrenii;* they are assigned to the upper Miocene Zone CN9. Also present within this interval are *Discoaster pansus, Sphenolithus abies,* and *Minylitha convallis.*

Zone CN7b is indicated by *Discoaster hamatus* and *Catinaster calyculus* being present in Samples 126-792E-15R-2, 39–40 cm, through -15R-CC. Zone CN8, defined as the interval between the LO of *D. hamatus* and the first occurrence (FO) of *D. berggrenii,* is either missing or is restricted to the interval between Samples 126-792E-15R-1, 11–12 cm, and -15R-2, 39–40 cm, which suggests the presence of a hiatus.

Samples 126-792E-16R-1, 40–41 cm, through -16R-CC contain *D. hamatus* but do not contain *C. calyculus;* they are assigned to the middle Miocene Zone CN7a. Samples 126-792E-17R-1, 40–41 cm, and -17R-2, 41–42 cm, contain *Catinaster coalitus* but do not contain *D. hamatus,* and are assigned to Zone CN6. Samples 126-792E-17R-3, 37–38 cm, through -20R-CC are located below the FO of *C. coalitus* and above the FO of *Discoaster kugleri,* and are assigned to Zone CN5b. Samples 126-792E-21R-1, 40–41 cm, through -23R-CC occur below the FO of *D. kugleri* and do not contain *Sphenolithus heteromorphus,* but they do contain *Cyclicargolithus floridanus* and *C. macintyrei* and thus are assigned to Zone CN5a. The middle Miocene assemblages also contain common *R. pseudoumbilica* and *C. pelagicus.*

We found *Sphenolithus belemnos* and *C. floridanus* in Samples 126-792E-24R-1, 46–47 cm, and -24R-CC but did not find *C. macintyrei,* and thus assign those samples to lower Miocene Zone CN2. The lack of an interval containing *S. heteromorphus* indicates that Zones CN3 and CN4 are missing in this hole. Samples 126-792E-25R-1, 40–41 cm, through -28R-CC are located below the FO of *S. belemnos* and above the FO of *Discoaster druggii,* and are assigned to Zone CN1c. The lower Miocene interval also contains rare to few *Reticulofenestra bisecta,* and common *C. floridanus* and *Discoaster deflandrei.*

The LO of consistently occurring, few to common *R. bisecta* in Sample 126-792E-29R-1, 106–109 cm, in the absence of any exclusively Miocene species, suggests that the top of Oligocene Zone CP19b occurs in this sample. Therefore, Subzones CN1a and CN1b do not occur in this section, indicating the presence of a short hiatus between Samples 126-792E-28R-CC and -29R-1, 106–109 cm. Samples 126-792E-29R-1, 106–109 cm, through -36R-CC contain *R. bisecta* and rare *Sphenolithus ciperoensis,* but no *Sphenolithus distentus;* they are assigned to Zone CP19b. Samples 126-792E-37R-CC through -57R-CC contain *S. distentus* and *S. ciperoensis,* and are assigned to Zone CP19a. Samples 126-792E-62R-CC, -63R-CC, and -66R-2, 99–101 cm, contain *Sphenolithus predistentus* and *S. distentus,* but they do not contain *S. ciperoensis.* We thus assigned these samples to lower Oligocene Zones CP17–CP18. *Sphenolithus distentus* and *S. ciperoensis* have rare and sporadic occurrences in this section; therefore, the boundaries between Zones CP17-18, CP19a, and CP19b are tentative. The Oligocene assemblages in Hole 792E are characterized by common *R. bisecta, C. floridanus,* and *D. deflandrei.*

Planktonic Foraminifers

Hole 792A

The faunas in Samples 126-792A-1H-CC, -2H-2, 57–62 cm, -3H-CC, -5H-CC, and 126-792A-6H-CC are dominated by *Globorotalia inflata,* dextral *Globorotalia truncatulinoides, Globigerinoides ruber* complex, *Globigerinoides sacculifer,* and dextral *Globigerina pachyderma.* Co-occurring species are the sinistral *Globorotalia menardii-tumida* complex, *Globigerinoides trilobus, Globigerinoides conglobatus, Globigerina bulloides, Globorotalia scitula, Globorotalia menardii flexuosa, Pulleniatina obliquiloculata,* and *Globigerinita glutinata.* The presence of *Globigerina digitata,* pink *G. ruber,* and *G. menardii flexuosa* places this sample in Zone N23 (Bielak and Briskin, 1978). Pink *G. ruber* indicates that the sample was deposited before 123 Ka (the LO of *G. ruber,* pink).

The dominant species in Sample 126-792A-7H-1, 59–61 cm, is *G. inflata;* co-occurring species include the *G. ruber* complex, *G. trilobus, P. obliquiloculata, Globorotalia crassaformi,* dextral *G.* pachyderma, dextral *G. truncatulinoides,* and sinistral *G. tumida.* The presence of *Globigerina calida* places this sample in the Brunhes Epoch (Zone N23, Blow, 1969). Sample 126-792A-8H-1, 93–97 cm, contains *G. inflata, G. sacculifer,* the *G. ruber* complex, dextral *G. truncatulinoides, G. crassaformis, G. scitula,* sinistral *G. menardii,* sinistral *G. tumida,* and dextral *G. pachyderma.* This sample is assigned to Zone N22 (Blow, 1969). Samples 126-792A-9H-CC and -10H-CC contain *G. inflata, G. truncatulinoides, Globorotalia tosaensis-truncatulinoides, Globorotalia tosaensis,* the *G. sacculifer* complex, sinistral *G. menardii, Sphaeroidinella dehiscens,* and the *G. ruber* complex, and are assigned to Zone N22 (Blow, 1969).

Hole 792B

Sample 126-792B-5X-CC is characterized by abundant *G. inflata, G. gomitulus, P. obliquiloculata,* and *G. crassaformis;* co-occurring taxa include *G. truncatulinoides-tosaensis* and *G. tosaensis.* The dominance of the sinistral *G. menardii-tumida* complex and the presence of *G. truncatulinoides* places this sample in Zone N23 (Blow, 1969; Bielak and Briskin, 1978). Sample 126-792B-7X-CC does not contain zonal markers.

Hole 792D

Sample 126-792D-1X-CC contains rare specimens of *G. tosaensis* and abundant to common representatives of the *G. ruber* complex, *G. conglobatus* and dextral *G. pachyderma.* The dominance of sinistrally coiled specimens in the *G. menardii-tumida* complex places this sample in Zone N22. However, the absence of *G. truncatulinoides* (the Pleistocene and Holocene zonal index species), generally present in low percentages, as well as the absence of such late Pliocene zonal markers as *Globigerinoides fistulosus,* make the zonal assignment of this sample tentative.

Hole 792E

Sample 126-792E-1R-CC contains about 50% sinistrally coiled *G. menardii-tumida.* Bielak and Briskin (1978) noticed a similar short-term change in the coiling direction of this species at about 1.65 Ma in a Pacific deep-sea core. Using the revised time scale of Berggren et al. (1985), we place this sample in the latest Pliocene (Zone N21). Samples 126-792E-2R-1, 13–15 cm, and -2R-CC are characterized by the predominance of sinistral *G. me-*

nardii-tumida and rare specimens of *G. tosaensis*, in addition to *Globigerinoides tenellus*, *Globoquadrina humerosa*, *G. trilobus*, *G. sacculifer*, *G. ruber*, *G. gomitulus*, *S. dehiscens*, etc., which places these samples near the top of Zone N21 in the *T. tosaensis* Subzone (Bielak and Briskin, 1978). The compositions of the foraminiferal faunas in Samples 126-792E-3R-1, 64-69 cm, and -5R-CC resemble that of the previous sample, placing them near the top of Zone N21. Sample 126-792E-6R-1, 58-60 cm, is located below an unconformity (Fig. 30). Representative taxa include *Globorotalia merotumida*, *Globigerinoides obliquus*, *Sphaeroidinellopsis sphaeroides*, and predominantly dextrally coiled *G. tumida-menardii*, placing this sample in upper Miocene Zone N17 (Bolli et al., 1985).

Samples 126-792E-7R-CC through -11R-CC are barren or contain only rare foraminiferal shell fragments unidentifiable at 100X magnification. Sample 126-792E-12R-CC contains rare foraminifers. The presence of *Globigerina nepenthes* tentatively places this sample in Zone N17. Samples 126-792E-13R-1, 30-32 cm, through -15R-1, 115-117 cm, are barren or contain rare foraminiferal fragments unidentifiable at 100X magnification. Samples 126-792E-15R-CC through -17R-CC contain *S. sphaeroides* and *G. nepenthes*, and are placed in Zone N17 (Bolli et al., 1985). Samples 126-792E-16R-CC and -17R-CC are characterized by *G. menardii* A, *Globoquadrina venezuelana*, *S. sphaeroides*, and *G. obliquus* and are assigned to Zone N17 (Bolli et al., 1985). Samples 126-792E-18R-CC through -20R-CC are barren or contain unidentifiable foraminiferal shell fragments.

An unconformity exists between Samples 126-792E-17R-CC and -23R-1, 59-60 cm, which contains specimens of *Globorotalia praemenardii*, *Globorotalia fohsi peripheronda*, *Globorotalia scitula*, *Globigerina bulloides*, and *Orbulina suturalis*, and is placed in middle Miocene Zones N8-N9 (Bolli et al., 1985; Fig. 30). Another unconformity is detected between the previous sample and Sample 126-792E-24R-CC; the latter contains specimens of *Catapsydrax stainforthi* and *Globorotalia continuosa*, and is assigned to early Miocene Zone N6 (Bolli et al., 1985). *Catapsydrax dissimilis* and *G. trilobus* were observed in Sample 126-792E-26R-CC, placing it in Zones N5-N6 (Bolli et al., 1985). Sample 126-792E-28R-1, 62-63 cm, contains *C. dissimilis*, *Globorotalia siakensis*, *Globigerina praebulloides*, and *Globigerina brevispira*; this sample is assigned to Zone N5 (Bolli et al., 1985).

The foraminiferal fauna in Sample 126-792E-28R-CC indicates an unconformity between this and the previous sample; the presence of *C. dissimilis*, *Globigerina quinqueloba*, *Globorotalia obesa*, *G. siakensis*, *Globorotalia kugleri*, and *Globorotalia opima nana* places this sample in the upper Oligocene Zone P22/N3 (Bolli et al., 1985). Sample 126-792E-29R-CC contains *G. opima nana* and *C. dissimilis*, placing this sample in Zones P18/19-P22/N3 (Bolli et al., 1985). Samples 126-792E-30R-CC through -37R-CC are barren or contain unidentifiable foraminiferal shell fragments. Sample 126-792E-40R-3, 62-64 cm, which contains *G. opima nana* and *G. venezuelana*, is placed in Zone P22/N3 (Bolli et al., 1985). Samples 126-792E-40R-CC through -57R-1, 97-99 cm, are barren or contain unidentifiable foraminiferal shell fragments. Sample 126-792E-57R-CC contains specimens of *G. venezuelana*, *G. opima nana* and *C. dissimilis*; this sample is assigned to Zones P18/19-P22/N3 (Bolli et al., 1985).

The preservation and abundance of species ranges from excellent to poor and very abundant to absent, respectively.

Benthic Foraminifers

We subdivided the Tertiary strata at Site 792 into twelve zonules on the basis of benthic foraminifer assemblages (Fig. 30). Our estimations of depositional water depths are mainly in comparison with (1) Holocene and Quaternary benthic foraminifer data from Holes 792B (1798 mbsl), 790A (2222 mbsl), 790B (2223 mbsl), 791A (2268 mbsl), 793A (2975 mbsl), and 787B (3254 mbsl; see "Biostratigraphy" sections in appropriate site chapters, this volume); (2) offshore data from Shizuoka and Shikoku, Japan (Akimoto, 1989; Yasuda, 1989) for the Pliocene and Pleistocene strata; and (3) Cenozoic benthic foraminifer data (Ingle, 1980; Woodruff, 1985; van Morkhoven et al., 1986) for the Miocene and Oligocene strata. We determined the age of each zonule on the basis of the calcareous nannofossil, radiolarian, and planktonic foraminifer zonations in this report. Dissolved oxygen contents were estimated from the ratios of aerobic to anaerobic forms of benthic foraminifers (Bernhard, 1986; Kaiho, in press).

Rhabdammina sp. Assemblage-Zonule

Characteristic species: agglutinated foraminifers such as *Rhabdammina* sp., *Rhizammina* sp., *Reophax* sp., *Thalmannamina* sp., *Subreophax* sp, and *Haplophragmoides* sp.; barren of calcareous foraminifers

Abundance: few
Samples: 126-792E-64R-1, 131-134 cm, -64R-1, 17-18 cm, and -63R-CC
Age: early Oligocene
Depositional water depth: Between 3.5 and 4.5 km
Dissolved oxygen: ?

Barren Zonule

Samples: 126-792E-62R-CC through -59R-CC
Age: early Oligocene

Stilostomella spp.-*Oridorsalis umbonatus* Assemblage-Zonule

Characteristic species: *Stilostomella* spp., *Oridorsalis umbonatus*, and *Pleurostomella* spp.

Abundance: few
Samples: 126-792E-57R-CC and -57R-1, 97-99 cm
Age: late Oligocene
Depositional water depth: between 2 and 4 km
Dissolved oxygen: high

Barren Zonule

Samples: 126-792E-56R-3, 25-27 cm, through -37R-CC
Age: late Oligocene

Rhabdammina sp.-*Stilostomella* spp. Assemblage-Zonule

Characteristic species: *Rhabdammina* sp., *Stilostomella* spp., and *Nodosaria longiscata*

Abundance: few
Samples: 126-792E-36R-CC through -30R-CC
Age: late Oligocene
Depositional water depth: between 2 and 4 km
Dissolved oxygen: ?

Oridorsalis umbonatus-*Pleurostomella* spp. Assemblage-Zonule

Characteristic species: *Oridorsalis umbonatus*, *Pleurostomella* spp., *Stilostomella* spp., and *Cibicidoides* spp.

Abundance: few
Samples: 126-792E-28R-CC through -24R-1, 61-63 cm
Age: early Miocene
Depositional water depth: between 2 and 4 km
Dissolved oxygen: high

Cibicidoides renzi-*Cibicidoides wellerstorfi* Assemblage-Zonule

Characteristic species: *Cibicidoides renzi*, *Cibicidoides wellerstorfi*, *Oridorsalis umbonatus*, *Pleurostomella* spp., and *Stilostomella* spp.

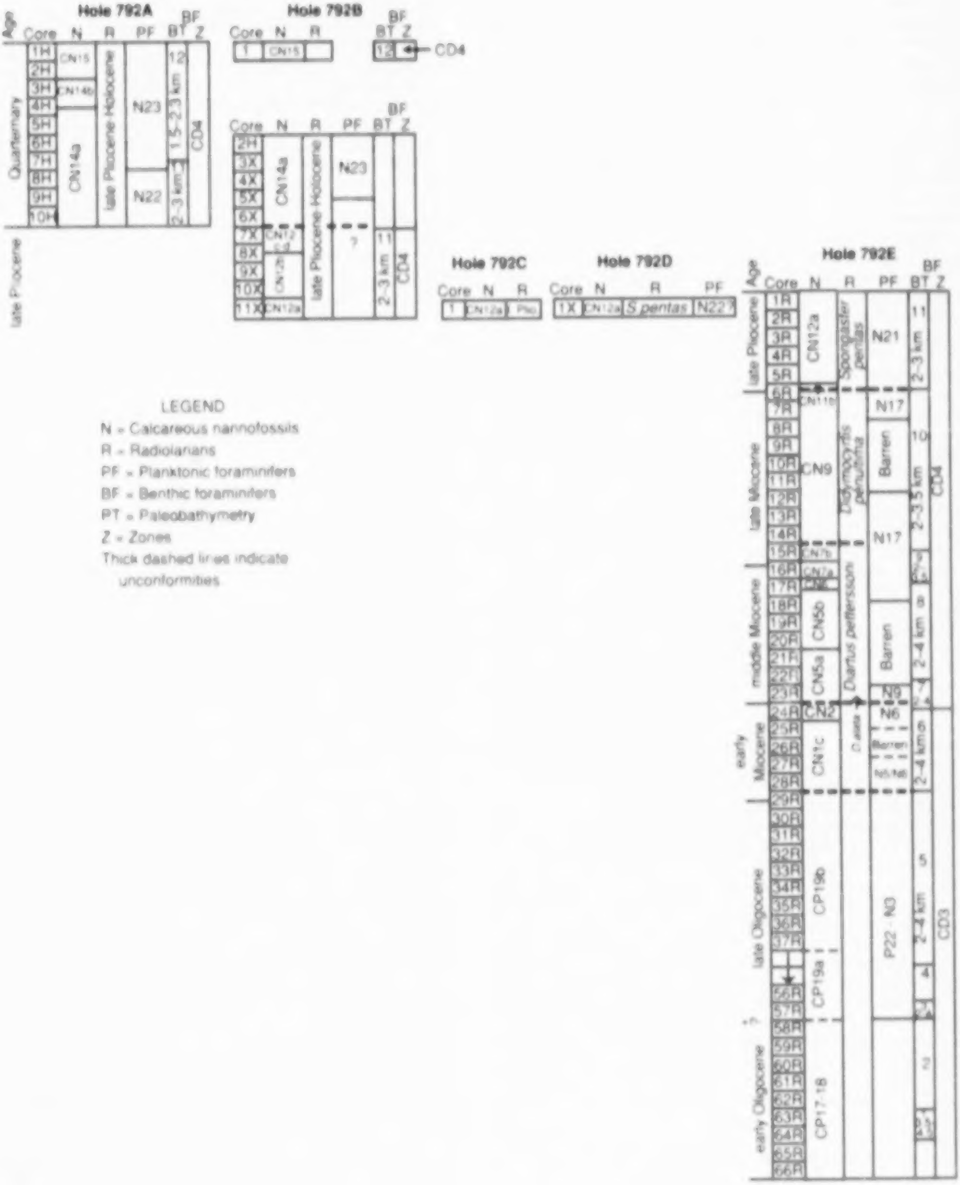
Hole 792A
Hole 792B
Hole 792C
Hole 792D
Hole 792E
Age
Core
N
R
PF
BF
BT
Z
Quaternary
late Pliocene
late Miocene
middle Miocene
early Miocene
late Oligocene
early Oligocene
CN15
CN14b
CN14a
CN12a
CN11b
CN9
CN7b
CN7a
CN6
CN5b
CN5a
CN2
CN1c
CP19b
CP19a
CP17-18
late Pliocene-Holocene
Spongaster pentas
S. pentas
Didymocyrtis penultima
Diartus petterssoni
N23
N22
N22?
N21
N17
N9
N6
N5/N6
P22 - N3
Barren
1.5-2.3 km
2-3 km
2-3.5 km
2-4 km
CD4
CD3
LEGEND
N = Calcareous nannofossils
R = Radiolarians
PF = Planktonic foraminifers
BF = Benthic foraminifers
PT = Paleobathymetry
Z = Zones
Thick dashed lines indicate unconformities

Figure 30. Summary of the biostratigraphic and paleobathymetric results for Site 792. See text for discussion of individual microfossil zones.

Abundance: few to common

Samples: 126-792E-23R-1, 59–61 cm, and -22R-CC

Age: middle Miocene

Depositional water depth: between 2 and 3.7 km

Dissolved oxygen: high

Cibicidoides spp.-*Epistominella* sp. Assemblage-Zonule

Characteristic species: *Cibicidoides* spp. and *Epistominella* sp.

Abundance: rare

Samples: 126-792E-22R-3, 60–65 cm, through -17R-3, 60–63 cm

Age: middle Miocene

Depositional water depth: between 2 and 3.5 km

Dissolved oxygen: high

Uvigerina sp. Assemblage-Zonule

Characteristic species: *Uvigerina* sp., *Cibicidoides* spp., *Sphaeroidina bulloides*, *Oridorsalis umbonatus*, *Gyroidinoides* sp., *Bulimina rostrata*, *Pleurostomella* spp., *Cibicidoides wellerstorfi*, *Melonis barleeanus*, and *Lenticulina* sp.

Abundance: common

Samples: 126-792E-16R-CC and -15R-CC

Age: middle Miocene

Depositional water depth: between 2 and 3.5 km

Dissolved oxygen: high

Stilostomella spp.-*Cibicidoides wellerstorfi* Assemblage-Zonule

Characteristic species: *Stilostomella* spp., *Cibicidoides* spp. and *Cibicidoides wellerstorfi*

Abundance: few

Samples: 126-792E-15R-1, 115–117 cm, through -7R-CC

Age: late Miocene

Depositional water depth: between 2 and 3.5 km

Dissolved oxygen: high

Stilostomella spp.-*Pleurostomella* spp. Assemblage-Zonule

Characteristic species: *Stilostomella* spp., *Oridorsalis umbonatus*, *Cibicidoides wellerstorfi*, *Pleurostomella* spp., *Sigmoilopsis schlumbergeri*, *Pullenia bulloides*, *Uvigerina hispidocostata*, *Uvigerina probosidea*, *Lenticulina* spp., *Amphicoryna* sp. (lower part of this zonule), and *Bolivinita* sp. (middle part of this zonule)

Abundance: abundant

Samples: 126-792E-6R-1, 58–60 cm, through -8H-1, 93–97 cm

Age: Pliocene to Pleistocene

Depositional water depth: between 2 and 3 km

Dissolved oxygen: high

Bulimina aculeata Assemblage-Zonule

Characteristic species: *Melonis barleeanus*, *Pullenia bulloides*, *Bulimina aculeata*, *Uvigerina hispidocostata*, *Oridorsalis umbonatus*, *Sphaeroidina bulloides*, *Chilostomella oolina*, *Cibicidoides wellerstorfi*, *Uvigerina hispida*, and *Globobulimina pacifica*

Abundance: abundant

Samples: 126-792A-7H-1, 59–61 cm, through -1H-CC.

Age: Quaternary

Depositional water depth: between 1.5 and 2.3 km

Dissolved oxygen: high

Remarks: The depositional age of the base of this assemblage-zonule is approximately 0.7 Ma, as determined from magnetic datums. This faunal change also occurred at the same time in Sites 790 and 791.

Samples 126-792A-1H-CC through -23R-1, 59–61 cm, contain *Cibicidoides wellerstorfi* and are correlative with the cosmopolitan benthic foraminiferal Zone CD4 (Kaiho, in press), corresponding to the post-middle middle Miocene turnover event. Samples 126-792E-24R-1, 61–63 cm, through -64R-1, 131–134 cm, are correlative with Zone CD3 given the absence of *C. wellerstorfi* and *Nuttallides truempyi*. Benthic foraminifer faunas in all the zonules below the *Bulimina aculeata* Zonule that contain *Pleurostomella* and *Stillostomella* and lack shallower fauna (e.g., *Bulimina aculeata*) indicate a deep-ocean basin environment (see Woodruff, 1985, table 5). However, the fauna in the uppermost zonule, which contains *Bulimina aculeata*, suggests a marginal ocean environment on the basis of previous studies (e.g., Kaiho and Hasegawa, 1986; Akimoto, 1989; Yasuda, 1989).

Radiolarians

Radiolarians are common to abundant and generally well preserved in Miocene to Quaternary sections of holes drilled at Site 792.

Hole 792A

Moderately diverse, well-preserved faunas are present in Samples 126-792A-1H-CC, -3H-CC, -4H-CC, -5H-CC and -9H-CC, and indicate a Quaternary age. The faunas typically include *Didymocyrtis tetrathalamus*, *Lamprocyclas maritalis*, *Botryostrobus aurita/australis* group, *Amphirhopalum ypsilon*, *Didymocyrtis tetrathalamus*, and *Spongaster tetras*. The occurrence of *Druppatractus acquilonius* in Sample 126-792A-5H-CC and *Axoprunum angelinum* in Sample 126-792A-9H-CC provides minimum age constraints of 0.3 and 0.41 Ma, respectively, for samples at and below these levels (Foreman, 1981).

Hole 792B

Moderately diverse, well-preserved radiolarian faunas are present in core-catcher samples from all cores of Hole 792B except for Samples 126-792B-4X-CC, -8X-CC, and -10X-CC. The occurrence of faunas including *Tetrapyle octacantha*, *Didymocyrtis tetrathalamus*, and *Spongaster tetras* suggest a late Pliocene to Holocene age.

Hole 792C

Upper Pliocene to Holocene radiolarians are common and well-preserved in Sample 126-792C-1X-CC and include the *Botryostrobus aurita/australis* group, *Lamprocyclas maritalis*, and *Acrosphaera spinosa*.

Hole 792D

Sample 126-792D-1X-CC contains abundant well-preserved radiolarians. The co-occurrence of *Spongaster tetras* and *Spongaster pentas* in this sample suggests assignment to the upper part of the upper Pliocene *Spongaster pentas* Zone of Sanfilippo et al. (1985).

Hole 792E

Well-preserved, lower Miocene to upper Pliocene radiolarians are common in the upper half of Hole 792E. All samples from below the level of Sample 126-792E-28R-2, 20–21 cm, are devoid of identifiable radiolarians. However, extremely poorly preserved, infilled radiolarians occur in Sample 126-792E-30R-CC and were also observed rarely below this sample.

Samples 126-792E-1R-1, 2–3 cm, through -5R-1, 19–20 cm, contain an assemblage that includes *Druppatractus acquilonius*, *Axoprunum angelinum*, *Amphirhopalum ypsilon*, *Spongaster tetras*, *Spongaster pentas*, *Pterocanium prismatium*, and *Stichocorys peregrina*. The presence of *Amphirhopalum ypsilon* and *Spongaster tetras* in these samples indicates ages less than

3.78 and 3.8 Ma, respectively (Backman, Duncan, et al., 1988). The morphotypic top of *Stichocorys peregrina*, which indicates an age greater than 2.6 Ma (Sanfilippo et al., 1985), and the presence of this species along with *Didymocyrtis avita* in Sample 126-792E-2R-1, 5–6 cm, suggests assignment to the *Spongaster pentas* Zone of late Pliocene age (Sanfilippo et al., 1985). No radiolarians were recovered between Samples 126-792E-5R-1, 19–20 cm, and -9R-1, 21–22 cm.

Sample 126-792E-9R-1, 21–22 cm, contains *Stichocorys delmontensis*, and is therefore no younger than the late Miocene (6.4 Ma; Backman, Duncan, et al. 1988). This sample is tentatively assigned to the *Didymocyrtis penultima* Zone of Sanfilippo et al. (1985).

An upper middle Miocene fauna is present in Samples 126-792E-15R-CC through -22R-CC, which includes *Stichocorys delmontensis*, *Cyrtocapsella japonica*, and *Didymocyrtis laticonus*. The presence of *Didymocyrtis laticonus* suggests assignment to the upper middle Miocene *Diartus petterssoni* Zone of Sanfilippo et al. (1985). *Stichocorys wolffii* is present in and below Sample 126-792E-18R-CC. The LO of this species in the latest middle Miocene was at 11.6 Ma (Nigrini, 1985).

Both *Stichocorys wolffii* and *Cyrtocapsella japonica* occur in Sample 126-792E-23R-CC. *Didymocyrtis laticonus* is absent, which suggests assignment to the lower middle Miocene *Dorcadospyris alata* Zone of Sanfilippo et al. (1985). Samples 126-792E-24R-CC through -27R-CC are barren of radiolarians.

One identifiable species, *Cyrtocapsella japonica*, is present in Sample 126-792E-28R-2, 20–21 cm, which allows the assignment of a Miocene age. This species is known to occur in the *Cyrtocapsella tetrapera* through *Diartus petterssoni* Zones (Nigrini and Lombari, 1984). No identifiable radiolarians were recovered from below Samples 126-792E-28R-2, 20–21 cm.

Summary

We recognize a sedimentary sequence from lower Oligocene through Quaternary on the basis of calcareous nannofossils, foraminifers, and radiolarians. The age of the sediment above the basement is late early Oligocene, as determined from calcareous nannofossils.

The following four hiatuses were recognized (Table 7):

1. from 5.6 Ma through 3.6 Ma (upper Miocene–upper Pliocene), CN10–CN11a and N18–N20 absent, 2.0 m.y. duration, between Samples 126-792E-6R-1, 58–60 cm, and -6R-1, 39–40 cm;
2. from 8.9 Ma through 7.0 Ma (within the upper Miocene), CN8 and *D. antepenultima* Zone absent, 1.9 m.y. duration, between Samples 126-792E-15R-2, 39–40 cm, and -15R-1, 11–12 cm;
3. from 18.6 Ma through 13.2 Ma (lower Miocene–middle Miocene), CN3–CN4 and N7–N9 absent, 5.4 m.y. duration, between Samples 126-792E-24-1, 46–47 cm, and -23R-CC; and
4. from 24.5 Ma through 21.8 Ma, (upper Oligocene–lower Miocene), CN1a, CN1b, and N4 absent, 2.7 m.y. duration, between Samples 126-792E-28R-1, 62–63 cm, and -29R-1, 106–109 cm.

Table 7. Age and duration of hiatuses, Site 792.

Age of hiatus (Ma)	Minimum duration (m.y.)	Biozones absent
late Miocene–late Pliocene (5.6–3.6)	2.0	CN10–CN11a, N18–N20
late Miocene (8.9–7.0)	1.9	CN8, *D. antepenultima*
early Miocene–middle Miocene (18.6–13.2)	5.4	CN3–CN4, N7–N9
late Oligocene–early Miocene (24.5–21.8)	2.7	CN1a–b, N4

Although we recognized the absence of CN13 and the lower part of CN14a (0.5 m.y. duration), we are uncertain if the absence of these biozones are due to actual hiatuses or the result of low core recovery.

Benthic foraminifer faunal changes show shallowing water depths from 3.5–4.5 km, in the late early Oligocene, to 1.5–2.3 km today. This estimate means that 1–2 km of total basement uplift has occurred since about 30 Ma in the Bonin inner fore arc. The lower trench slope in the Mariana outer forearc, in contrast, has been subsiding since the Eocene (Hussong and Uyeda, 1982).

PALEOMAGNETICS

Introduction

Paleomagnetic measurements were made on the cores recovered from Site 792 to determine magnetostratigraphic ages, to estimate paleolatitude, and to observe the detailed behavior of the geomagnetic field during polarity transitions. Measurements were carried out by means of the 2G cryogenic magnetometer and the fully automatic spinner (FAS) magnetometer (see "Explanatory Notes" chapter, this volume).

Almost all archive halves (except for those highly disturbed by drilling or that consisted of gravels) were measured and demagnetized with the cryogenic magnetometer system. We made our measurements at 5- or 10-cm intervals, except in those sections that contained a polarity transition zone, for which we chose a 0.5-cm interval. The peak alternating field (AF) demagnetization level varied from 2 to 15 mT, according to the magnetic stability of each core section. During measurement, the intensity of the remnant magnetic field around the AF demagnetizing coil in the cryogenic system was periodically monitored. If the field exceeded 500 nT, the inner shield was degaussed to suppress the ambient field.

In addition to the archive half measurements, we measured a number of discrete samples to obtain a more detailed picture of the magnetic properties and to check the reliability of results from archive halves. Discrete samples were measured and stepwise demagnetized with the FAS magnetometer and the AF demagnetizer incorporated into it. Stepwise AF demagnetizations enabled us to discriminate the stable component of remanent magnetization on an orthogonal component vector endpoint plot (Zijderveld diagram). These diagrams show that most discrete samples from this site have stable directions of remanence, and also confirm the reliability of results from archive halves (Fig. 31).

Magnetostratigraphy

Hole 792A

The downhole plot of paleomagnetic direction and polarity in Hole 792A, after AF demagnetization, and the correlation of this data with the standard polarity time scale (Berggren et al., 1985) is shown in Figure 32. All cores were drilled with the APC, and the lower six cores (Cores 126-792A-5H through -10H) were oriented azimuthally with the multishot tool. The natural remanent magnetization (NRM) intensities ranged from 2 (clay) to 700 mA/m (scoria layer).

We recognized two major magnetic polarity intervals in Hole 792A (Fig. 32). The upper one, which ranges from the top of Core 126-792A-1H (0 mbsf) to the top of Section 126-792A-7H-2 (about 58.5 mbsf), is dominated by normal polarity. The lower interval, which ranges from the top of Core 126-792A-7H to the bottom of Core 126-792A-10H (95.0 mbsf), is dominated by re-

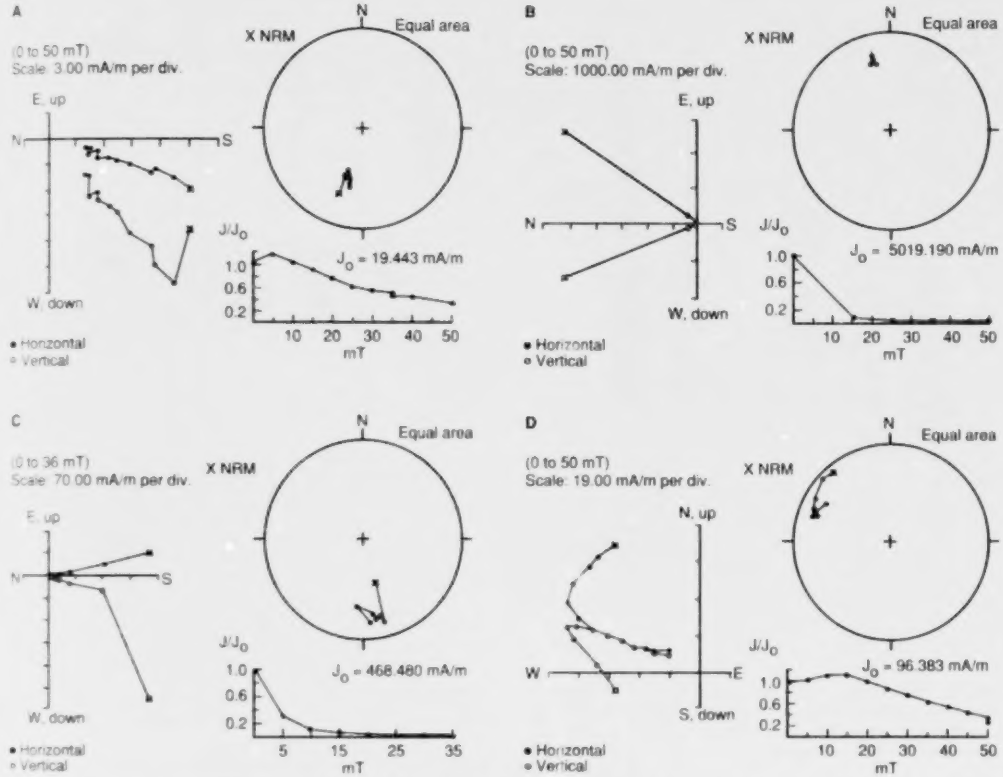

Figure 31. Examples of orthogonal component diagrams, changes of remanence vector direction, and total intensity during stepwise AF demagnetization for discrete samples from Site 792. **A.** Sample 126-792B-2H-1, 57 cm. **B.** Sample 126-792E-15R-1, 35 cm. **C.** Sample 126-792E-59R-2, 61 cm. **D.** Sample 126-792E-52R-5, 64 cm.

versed polarity. On the basis of the biostratigraphic data (see "Biostratigraphy" section, this chapter), we correlated the upper and lower intervals with the Brunhes normal and the Matuyama reversed polarity chrons, respectively. The lower interval also includes several short normal polarity intervals. We correlated the interval from the bottom of Core 126-792A-9H (~80 mbsf) to the middle part of Core 126-792A-10H (88 mbsf) to the Jaramillo normal polarity subchron on the basis of the biostratigraphic data.

Azimuthally corrected declination data were available from Core 126-792A-5H through -10H (37.8–95.0 mbsf). In Cores 126-792A-6H, -7H, -8H, and -10H, the declinations show reasonable directions, nearly aligned with north and south in the normal and the reversed polarity intervals, respectively. However, the declinations from Cores 126-792A-6H and -9H are significantly deflected, particularly from 37.8 to 47.2 mbsf, where the declination varies over 90° and approximates a sine curve. Such deflections may be caused by twisting of the core in the core liner during drilling or handling on the catwalk.

Hole 792B

The downhole plot of paleomagnetic direction and polarity in Hole 792B, after AF demagnetization, and the correlation of this data with the standard polarity time scale is shown in Figure 33. The upper three cores (Cores 126-792B-1H through -3H, 0–69.2 mbsf) were drilled with the APC and two cores (Cores 126-792B-2H and -3H, 50.0–69.2 mbsf) were oriented azimuthally. Most NRM intensity values ranged from 2 (clay) to 200 mA/m (ash layer).

Three magnetic polarity intervals were recognized in Hole 792B (Fig. 33). The upper interval, which ranges from the top of Core 126-792B-1H to the top of Core 126-792B-3H (0–60 mbsf), is dominated by normal polarity, although the directions from Cores 126-792B-2H and -3H are scattered owing to the coarse lithology (Fig. 34). The middle interval, which ranges from the top of Core 126-792B-3H to the bottom of -9X (~59–~120 mbsf), is dominated by reversed polarity. The lower interval of normal polarity ranges from the top of Core 126-792B-10X (127.1 mbsf) to the bottom of the hole (Core 126-792B-11X). Several short, normal polarity intervals exist in Cores 126-792B-3H and -4X (59.6–78.8 mbsf, Fig. 34). Although some intervals appear to be a result of scatter in coarse materials, others (in the finer sediment types) are probably true reversal zones.

On the basis of the biostratigraphic data (see "Biostratigraphy" section, this chapter), we can correlate the upper, middle, and lower intervals with the Brunhes normal, Matuyama re-

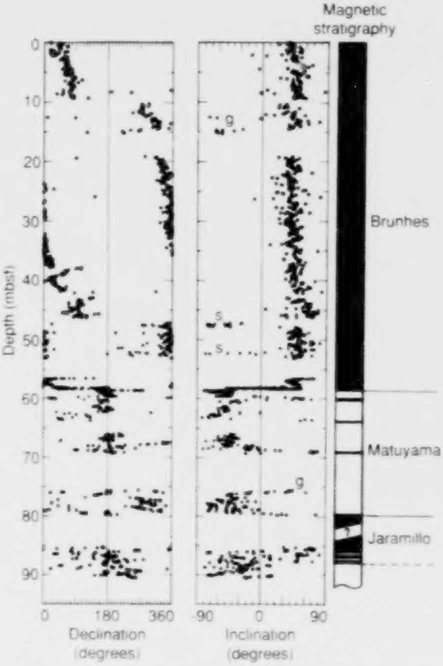

Figure 32. Paleomagnetic data vs. depth (mbsf) for Hole 792A, and correlation with the standard polarity time scale (Berggren et al., 1985). Directional deflections are the result of coarse sediments (g = gravels, s = coarse sandstones) in some intervals.

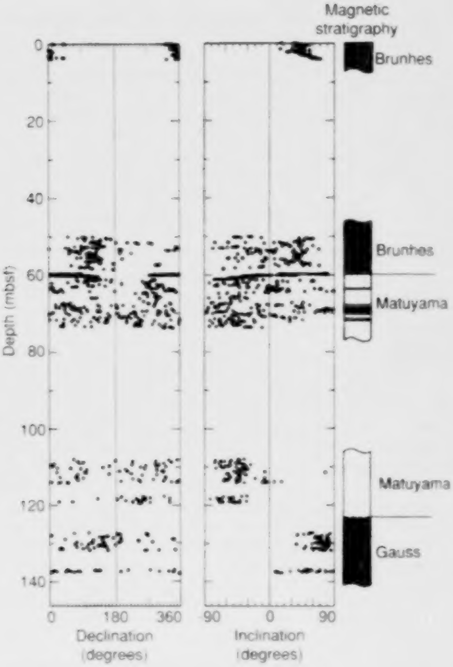

Figure 33. Paleomagnetic data vs. depth (mbsf) for Hole 792B, and correlation with the standard polarity time scale (Berggren et al., 1985).

versed, and Gauss normal polarity chrons, respectively. Although normal polarity intervals do exist between 60 and 75 mbsf in the upper Matuyama Chron, the Jaramillo normal polarity subchron seems to have been missed in this hole, as the biostratigraphic datum of 0.83 Ma was not recovered between Sections 126-792B-4X-CC and -5X-CC (~74–~79 mbsf).

Holes 792C and 792D

Only one core-catcher sample was measured in each hole (Sections 126-792C-1X-CC and -1X-CC, Fig. 35). Section 126-792C-1X-CC is normally magnetized, except for the lower 10 cm, which has reversed polarity. Section 126-792D-1X-CC is normally magnetized. We correlated both sections to the Gauss normal polarity chron on the basis of the biostratigraphic data (see "Biostratigraphy" section, this chapter).

Hole 792E

The downhole plot of paleomagnetic direction and polarity in Hole 792E, after AF demagnetization, and correlation of this data to the standard polarity time scale is shown in Figure 36. All cores were drilled with the RCB, and thus the declinations are arbitrary. The NRM intensities ranged from 0.3 (clay) to 700 mA/m (conglomerate) in sedimentary rocks, and from 10 to 1000 mA/m in volcanic rocks.

In Hole 792E, NRM directions indicate that several sections between Cores 126-792E-41R and -78R have been significantly remagnetized. This is apparent from the concentration of NRM declination values around the 0° or 360° "core north" direction, and by the systematically increasing inclination with depth within these cores (Fig. 37; e.g., Cores 126-792E-48R, 589–598 mbsf, and -50R, 607–617 mbsf). Although the remagnetization features were at least partially removed by AF demagnetization in these particular cores, in other cores they still exist after demagnetization (e.g., Core 126-792E-44R, 550–560 mbsf). The directions of discrete samples taken from these remagnetized intervals are generally concordant with the archive half results, and so the working halves also seem to be remagnetized. Because of this remagnetization problem, we chose to consider only the data from the less contaminated cores. Figure 36 shows the magnetostratigraphic results after the contaminated cores are filtered out.

The many normal and reversed polarity intervals recognized in Hole 792E have been correlated with the standard polarity time scale (Fig. 36) on the basis of biostratigraphic data (see "Biostratigraphy" section, this chapter). These data indicate four hiatuses or unconformity horizons (Fig. 36) in this hole. The polarity intervals found in Hole 792E can be correlated with the Gauss and Gilbert polarity chrons (Chrons 3 and 4, 135.6–193 mbsf), Chron 6 to 8 (193–272 mbsf), Chron 11 (or C5) to Chron C5AN (272–357 mbsf), the C6 Chrons (357–405 mbsf), and the C7 Chrons to Chron 9N (405–780 mbsf). The interval that includes Chron C9 is by far the longest, which reflects the high sedimentation rates associated with the increased abundance of turbidites toward the bottom of the hole (see "Lithostratigraphy and Accumulation Rates" section, this chapter). Although normal and reversed polarities were found in the lowest

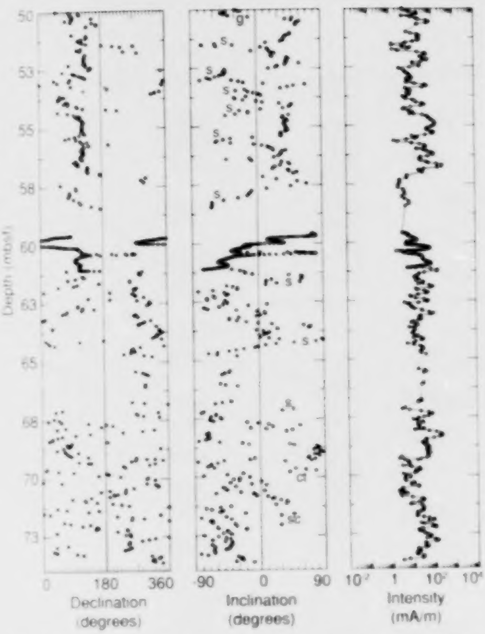

Figure 34. Paleomagnetic data vs. depth (50–74 mbsf) for Hole 792B. Directional deflections are the result of coarse sediments (g = gravels, s = coarse sandstones, ct = coarse tuffs, sc = scorias) in some intervals.

volcanic sequence, a magnetostratigraphic age assignment has not been made because of the lack of biostratigraphic data.

Figure 38 shows the magnetostratigraphic correlation of Site 792 with Site 787. Chrons C8N and C9Na exist in both sites, allowing for a precise correlation between their top and bottom horizons. Although the interval of Chron C9Na (~140 m) is longer at Site 792 than at Site 787 (~60 m), the interval of Chron C8 (N + R) at Site 792 (~55 m) is shorter than at Site 787 (105 m). This indicates a sharp decrease in the sedimentation rate above ~500 mbsf at Site 792, which is near the top of a thick turbidite sequence in the upper part of Unit IV (see "Lithostratigraphy and Accumulation Rates" section, this chapter). At Site 787, the intervals that include Chrons C8 and C9 are also dominated by thick turbidites, but there is no major lithologic change near the chron boundary (see "Lithostratigraphy and Accumulation Rates" section, "Site 787" chapter).

Paleolatitude

Figure 39 shows the relationship between the age and the mean inclinations for each core. The data from the cores that display severe remagnetization, as discussed above, or from cores composed primarily of coarse sediment types (i.e., conglomerate, lapilli tuff, and volcanic breccia), were deleted from the figure. The inclinations of cores younger than 13 Ma are concordant with the axial geocentric dipole at the latitude of Site 792, whereas the inclinations for cores older than 20 Ma are generally shallower than the present mean inclination. Thus, we conclude that Site 792, along with Site 787, occupied a lower latitude in late Oligocene time. Future shore-based analyses of the data and the measurement of additional discrete samples should refine this result.

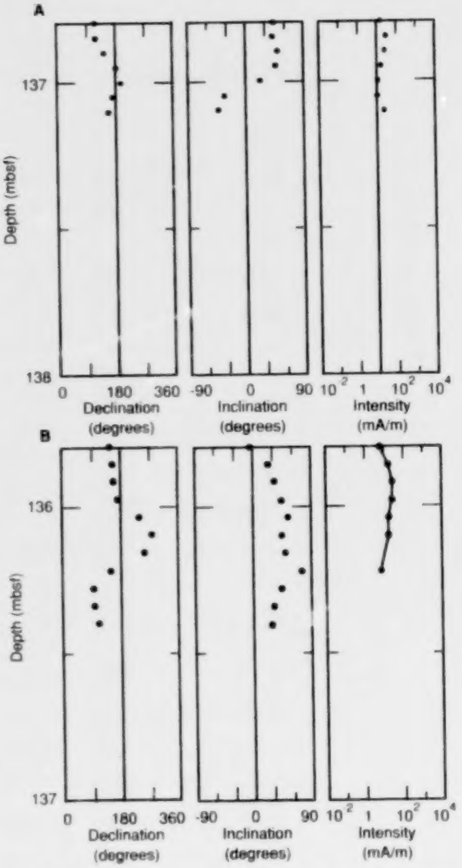

Figure 35. Paleomagnetic data vs. depth (mbsf). A. Hole 792C. B. Hole 792D.

The generally lower inclinations associated with the reversed (negative inclination) cores are a result of the incomplete removal of the present-field normal component, which will steepen the inclination vector for the normal cores, but will have the opposite effect on the reversed cores. Rotation of the drilling biscuits, which commonly is a result of rotary drilling into lithified sediments, will have the effect of randomizing the horizontal components of the remanence vector, which would steepen the apparent inclinations of both normal and reversed cores.

Brunhes/Matuyama Reversal Record in Holes 792A and 792B

We carried out detailed measurements on the intervals (Cores 126-792A-7H and 126-792B-3H) that included the Brunhes/Matuyama transition zone (Figure 40). Both piston cores were azimuthally oriented by the multishot tool. The transition curves

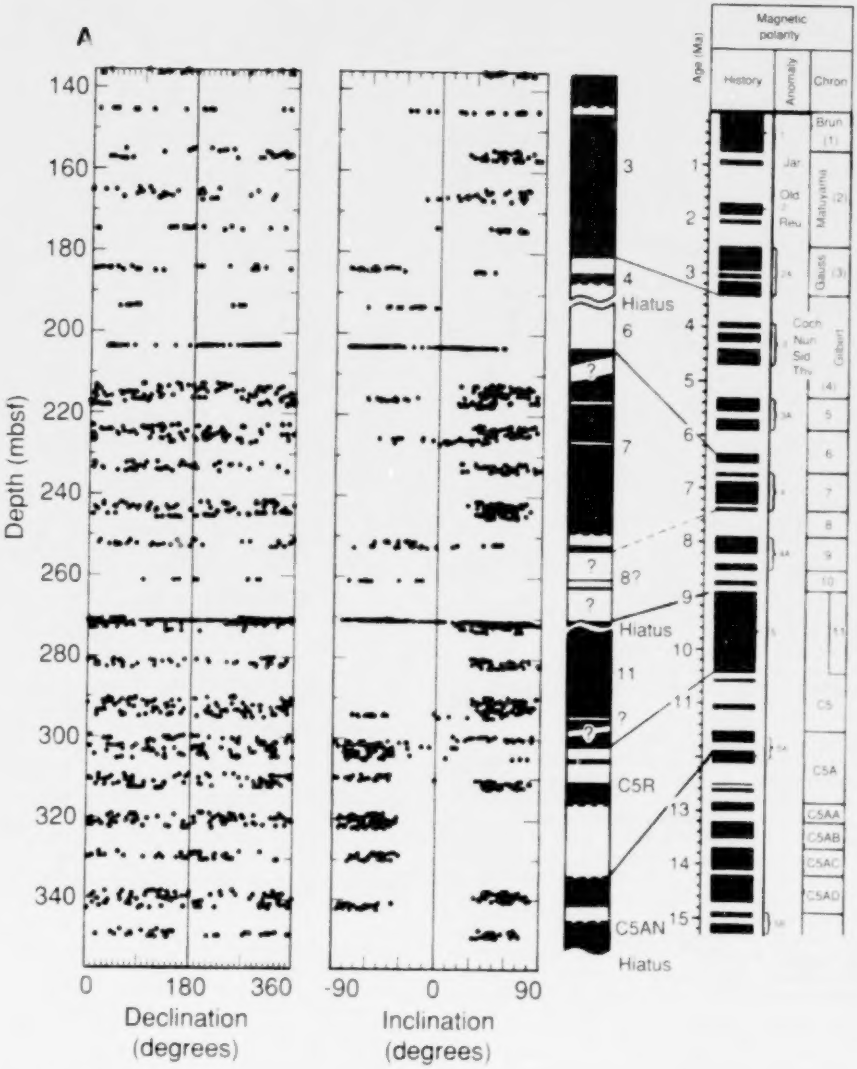

Figure 36. Paleomagnetic data vs. depth (mbsf) for Hole 792E, and correlation with the standard polarity time scale (Berggren et al., 1985). Numbers beside polarity column show chron number; hiatuses (estimated from biostratigraphic data) are indicated. **A.** Cores 126-792E-1R through -23R. **B.** Cores 126-792E-24R through -52R. **C.** Cores 126-792E-54R through -78R. Directional deflections are the result of coarse sediments (cg = conglomerates, lt = lapilli tuffs, s = sandstones) and/or alteration (= a) in some intervals.

of inclination and declination show multiple transitions in Hole 792A and possibly in 792B. Of these, the short reversed polarity interval "A" in Hole 792A and the short normal polarity interval "J" in Hole 792B are likely to be false, because they correspond to intervals disturbed by drilling.

The lithology of the transition zone is laminated clay in Hole 792A, and clay with a sandy burrow and a scoria layer in Hole 792B. The reversed intervals also correspond to an apparent decrease in remanence intensity in Hole 792A. The rapid transitions of polarity and the more extended decrease of intensity

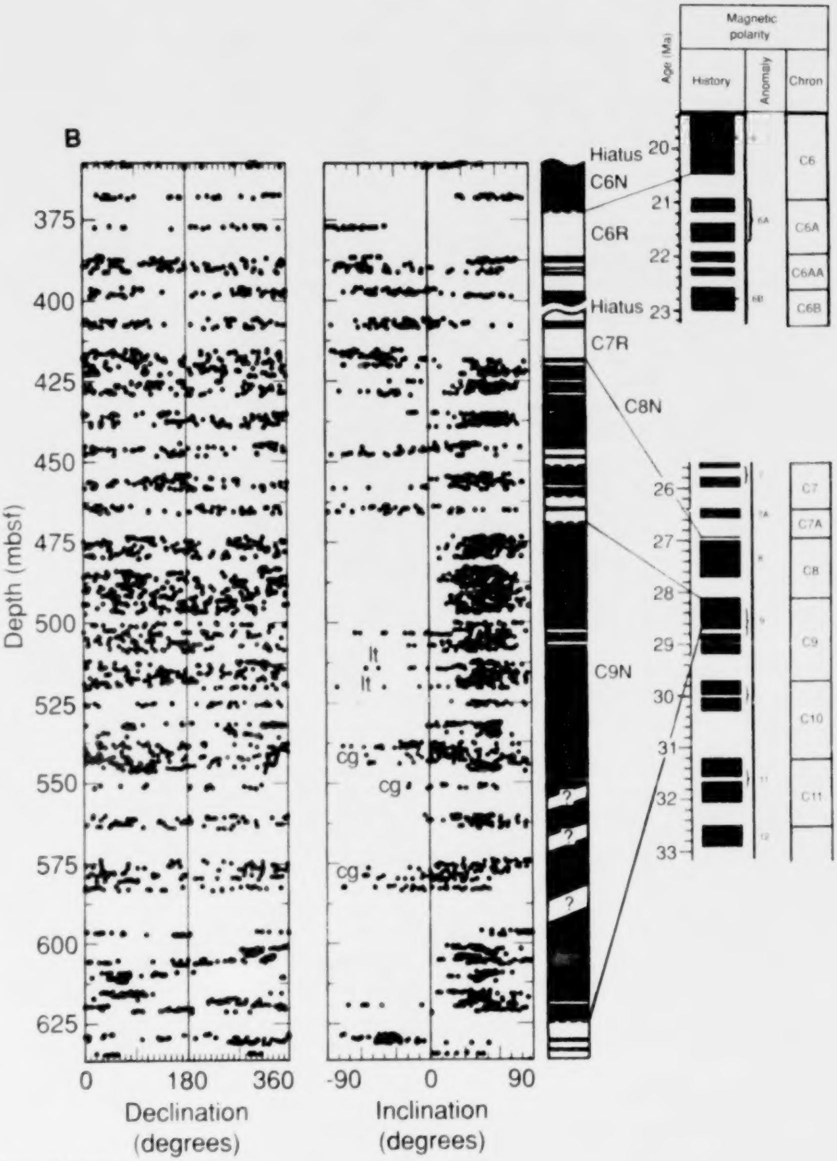

Figure 36 (continued).

were also detected at the Brunhes/Matuyama boundary in Holes 790C and 791B (see "Paleomagnetics" section, "Site 790/791" chapter, this volume). Detailed features of the reversal zone, such as double transitions and intensity decreases, are not apparent in Core 126-792B-3H, probably owing to the greater disturbance in that core.

The length of the transition zone in Hole 792A is about 40 cm, which corresponds to about 4000 yr on the basis of the average sedimentation rate for that portion of the core (see "Lithostratigraphy and Accumulation Rates" section, this chapter, and Fig. 28). Thus, the polarity transition time scale appears to be considerably longer than that for Holes 790C and 791B.

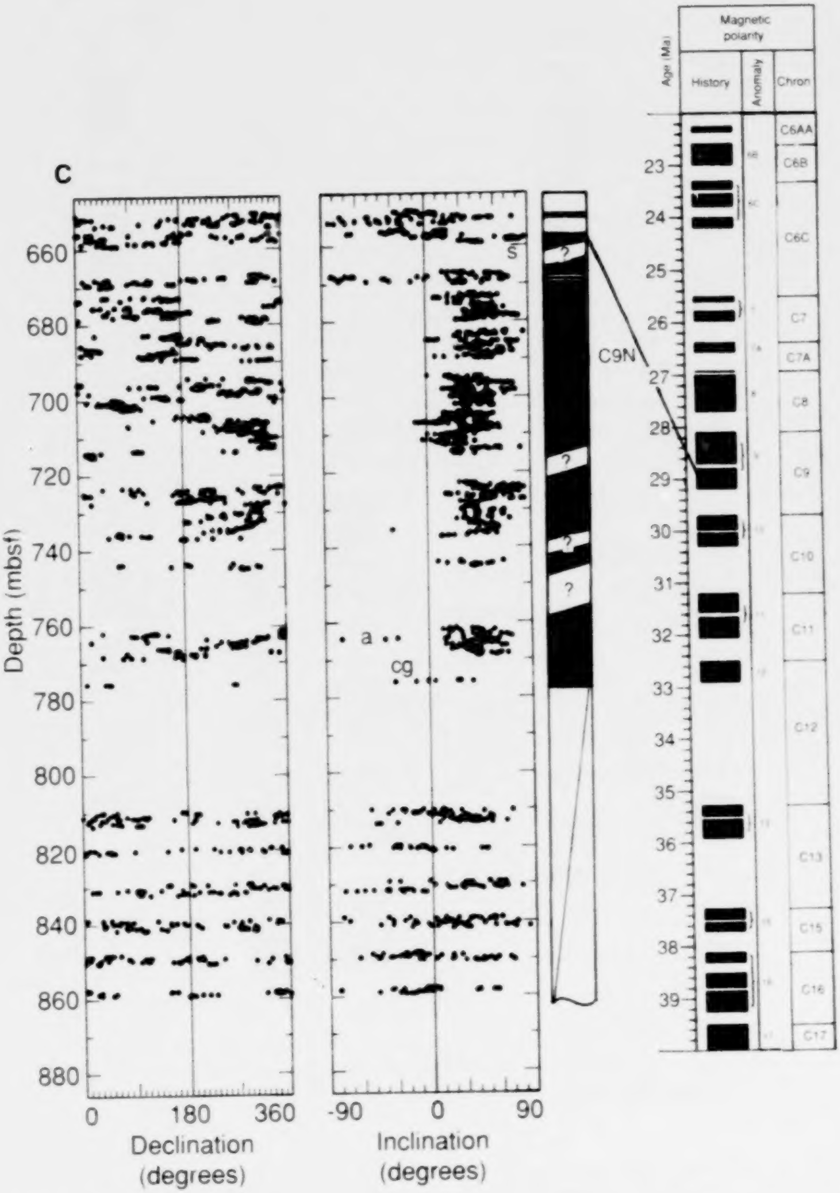

Figure 36 (continued).

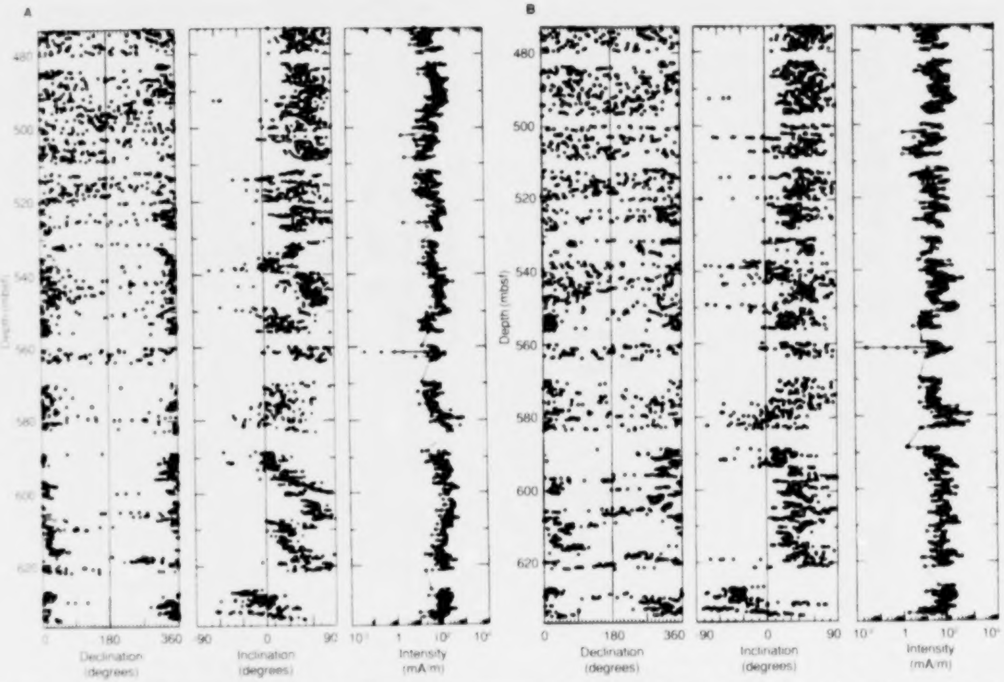

Figure 37. Comparison between the downhole plots before and after demagnetization of Cores 126-792E-36R to -52R. **A.** Before demagnetization (i.e., NRM). **B.** After AF demagnitization (AFD).

However, this may be an averaging effect caused by either the lower resolution that results from a threefold decrease in sedimentation rate (~100 m/m.y.) in Hole 792A as compared with Hole 791B (300 m/m.y.), or the ~20 cm sensing region for the Z-axis sensor of the cryogenic magnetometer. Within the transition zone in Hole 792A, each of the three "true" inclination reversals (e.g., the top and bottom of intervals C and D; Fig. 40) occur over <10 cm, which, as in Holes 790C and 791B, suggests a time scale of only hundreds of years.

Problems with Measurements

The magnetic field intensity around the AF demagnetizing coil in the cryogenic magnetometer often increased above 1000 nT during measurements on cores from this site, as it did during measurements on materials from Sites 790/791. After the transit to Site 792, the field intensity grew up to 5000 nT, which is about 10% of the total geomagnetic field intensity. The direction of the field varied over time. The correlation of the record of this change with the ship's orientation data obtained from the dynamic positioning (DP) room revealed that the magnetic field intensity in the cryogenic's shield varied with the ship's rotation. Apparently, the change of the ambient field in the laboratory magnetized the inner shield, probably owing to the poor shielding ability of the outer shield. The cause of this phenomenon is still unknown.

The remagnetization in Hole 792E cores (i.e., the clustering of declinations around the core north direction in archive and working halves) shows that the remagnetization was superimposed after the core barrels were lifted on deck and before the cores were split into working and archive halves rather than during drilling. This is because the orientation of RCB core barrels in a drill pipe is arbitrary. Thus, the remagnetization must have occurred in a location where the cores reside in the same orientation (e.g., in the core rack, in the GRAPE assembly, or around the super saw). The intensity of the magnetic field at the core rack in the core-cutting room was measured at >0.13 mT, larger than the ambient geomagnetic field by a factor of 3. This high field apparently results from the presence of a magnetized beam within the adjoining wall, and may be one reason for the anomalous inclination and declination trends. Remagnetization may also have occurred when the cores were split, because the ambient field within the super saw assembly was found to be horizontal, or parallel to the N-S direction in the cores.

IGNEOUS PETROLOGY

The first basement rocks ever drilled from beneath the forearc sedimentary basin of the Izu-Bonin arc-trench system were recovered at Site 792. At a depth of about 804 mbsf in Hole 792E, the drill-string penetration rate increased from 3.4 to over 8.6 m/hr, marking the transition from hydrothermally altered volcanogenic sediment to fairly unaltered volcanic rock. A further 82 m of penetration was achieved in basement, resulting in a total hole depth of 885.9 mbsf. We also found other igneous rocks as clasts in the Oligocene to Quaternary conglomerates and gravels of the sedimentary sequence.

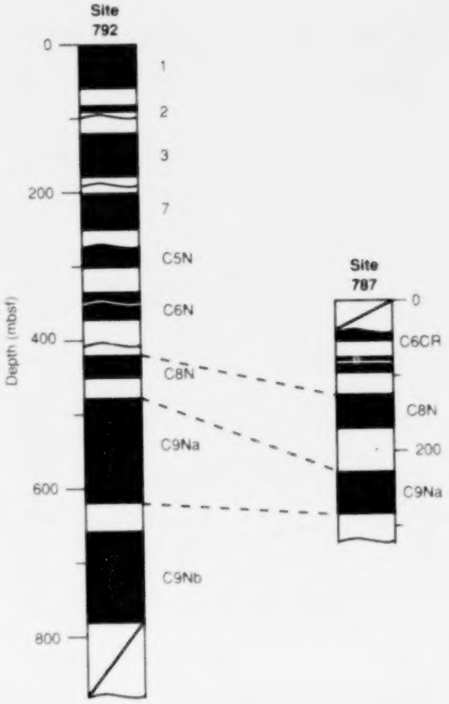

Figure 38. Magnetostratigraphic correlation of the results from Site 792 with those from Site 787. Numbers beside columns are chron numbers from in the standard polarity time scale (Berggren et al., 1985).

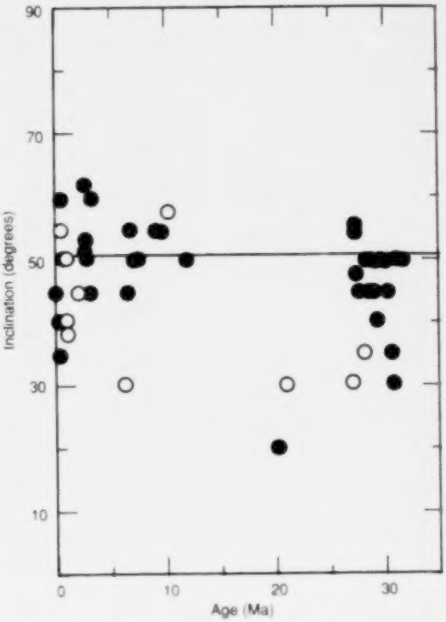

Figure 39. Plot of mean inclination of remanent magnetization from continuous core measurements vs. age (solid circle = positive inclinations, open circle = negative inclinations). Horizontal line shows the inclination value of axial geocentric dipole field at the present latitude of Site 792.

Basement Petrology

The dominant volcanic lithology recovered in the basal section of Hole 792E was highly porphyritic, two-pyroxene andesite, the only variant being thin layers of volcaniclastic and hyaloclastic material. On the basis of homogeneous crystallinity, long-core fragments, and the lack of any features indicative of pillow structure, the andesite was considered to be part of a sequence of massive lava flows.

Mineralogically, there is little variation in the porphyritic andesite. Plagioclase is the dominant phenocryst, forming 25%-35% of the mode, with clinopyroxenes and orthopyroxenes together usually <15%. An opaque mineral is present in all rocks as both a groundmass and phenocryst phase. In the uppermost part of Unit 1 (see below), very rare skeletal olivine pseudomorphs were recognized, now replaced by smectite and an opaque mineral. In the lower 70% of the section, from the top of Core 126-792E-73R to the base of the hole, subhedral to rounded quartz grains are present in almost all of the thin sections examined (Fig. 41). The rounded nature of most of these grains indicates dissolution at crystal apices and, therefore, disequilibrium with the original host liquid. However, only a few of the crystals show any signs of embayment. In addition to this possible xenocrystal material, evidence for lithic inclusion is found throughout the sequence. Lithic inclusions take the form of rounded clasts of diabase, quartz-bearing volcanics, and intersertal andesites. Representative modal analyses of the basement rocks from Hole 792E are given in Table 8.

The groundmass texture of the lava is generally intersertal or vitric-microphyric, although at most levels in the sequence, original glass is not well preserved. Remnants of vitric material are found as pale-brown isotropic interstices in the upper 10 m of the lava and in some fragments within the interlayered hyaloclastites.

Orthopyroxene is the only member of the mineral assemblage that has been significantly affected by posteruptive alteration processes. With the exception of the uppermost 10 m of lava, orthopyroxene is totally pseudomorphed by smectite. The XRD analyses of this pseudomorph material indicate that cristobalite is also present. Some pyroxene grains in the basement and in the overlying sedimentary sequence show all the characteristics of orthopyroxene (form, cleavage, pleochroism, and birefringence), are fresh, have extinction angles ranging from 0° to 10°, and occasionally have multiple twinning. These pyroxenes may represent a late-stage form or resistant compositional variant of the dominant, altered orthopyroxenes. Alteration is most visible in the interflow hyaloclastites. Most of the original glass is now smectite, which gives these layers a green-gray tinge. Another indication of the low-temperature hydrothermal alteration is the fracturing found scattered through the basement section. The fractures are filled with a mixture of celadonite, palagonite, cristobalite, and smectite.

The age of the basement lavas is uncertain owing to the absence of intercalated fossil-bearing sedimentary horizons and

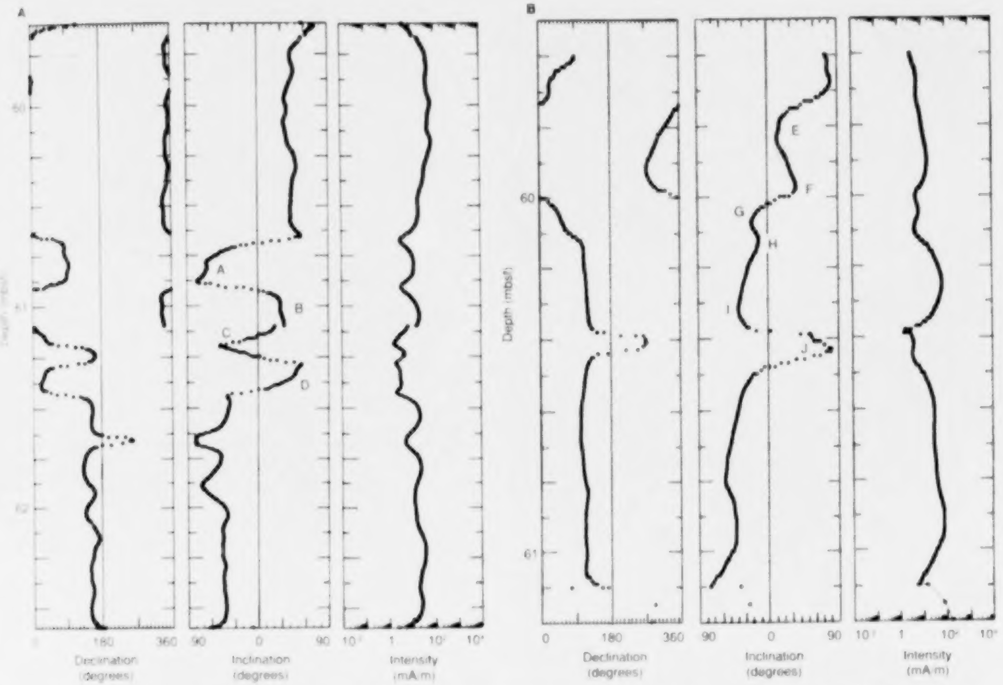

Figure 40. Azimuthally oriented paleomagnetic data vs. depth (mbsf) for the Brunhes-Matuyama polarity transition zone. Possible short polarity intervals in the transition zone are marked A–J; A and J correspond to highly disturbed zones, and probably do not represent true polarity changes. **A.** Hole 792A. **B.** Hole 792B.

barren sediments in the section immediately above basement. We obtained fossil ages that range from early to late Oligocene from the sediments of lithologic Unit IV (see "Biostratigraphy" section, this chapter). Paleomagnetic data indicate that five reversals are present in the Site 792 basement section. Such a narrow spacing of reversals within 82 m of section suggests that the lavas were erupted in a period of rapid reversals (such as the late Eocene) or that the magnetic polarity has been disrupted by hydrothermal activity.

Lava Stratigraphy

We divided the volcanic sequence into five units. This includes three levels of andesitic lava flows with intercalated hyaloclastite bands, and two major hyaloclastite-volcanic breccia horizons (Fig. 42).

Unit 1: Porphyritic Andesite Flow

Interval: Samples 126-792E-70R-1, Piece 1, through -74R-1, Piece 3
Description: pale gray-lilac porphyritic andesite lava (see Table 8 for modal analysis of lava)

This andesite unit is typical of the extrusive rocks recovered in the basement sequence. It contains about 30% euhedral fresh plagioclase, 0.5–3 mm in diameter, with < 10% total pyroxenes. The feldspars show oscillatory zoning (Fig. 43) and abundant two-phase fluid inclusions that were entrained during crystal growth. The clinopyroxenes are easily recognized as bottle-green, euhedral crystals up to 5 mm in length and are always fresh in thin section. However, the orthopyroxenes are dominantly pseudomorphed by smectite and appear as dark laths in hand specimens.

The upper section of Unit 1 (Cores 126-792E-70R and -71R) contains the only examples of fresh orthopyroxene phenocrysts. This material is present as the central portions of large crystals, and is surrounded and crosscut by smectite alteration. In some cases these orthopyroxenes are rimmed by fresh clinopyroxene (Fig. 44), which indicates a change in magma composition or crystallization pressure. The upper section of this unit (Section 126-792E-71R-1) contains rare pseudomorphs of skeletal olivine that were recognized in hand specimens and in one thin section. Toward the base of the unit, quartz first appears as a xenocrystal phase.

Xenoliths are common in the Unit 1 andesites, as well as in Units 3 and 5. All are rounded and < 3 cm in diameter. In Unit 1, they consist of coarser grained variants of the andesite, notably orthopyroxene diabase, and intersertal andesite (Fig. 45).

Within Unit 1 are two layers of hyaloclastite material (Fig. 42). The uppermost band is 4 cm thick and probably represents an interflow volcanic-glass spall layer. Other similar horizons were found throughout the volcanic sequence, although it is not

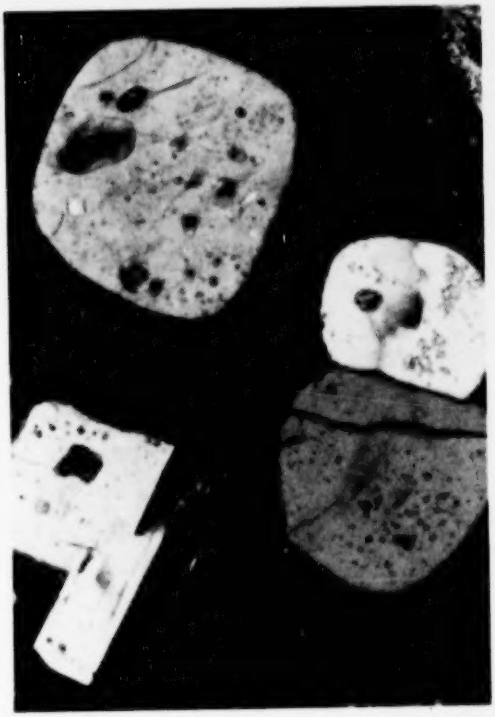

Figure 41. Rounded to subhedral quartz grains in a devitrified glassy matrix. Interval 126-792E-74R-1, 84–85 cm, Unit 2. Cross-polarized light, 95 ×.

clear with the limited thin sections available if all examples are genuine fragmental deposits or simply glassy sections of flows that are more susceptible to hydrothermal alteration.

Unit 2: Andesitic Hyaloclastite Breccia

Interval: Samples 126-792E-74R-1, Piece 4 through -74R-1, Piece 9

This unit is similar to the hyaloclastite bands seen in Unit 1, but it is represented by only 110 cm of recovered material. It differs from Unit 1 in that it has 1–4 cm clasts of dense lava sparsely distributed in a matrix of glass shards and xenocryst fragments. The mineral assemblage is similar to the andesite lavas in the lower part of Unit 1. In addition to the quartz crystals, there are clasts of dacitic lava that contain euhedral phenocrysts of quartz (Fig. 46). The majority of the clasts present in the unit and, in particular, the larger clasts are porphyritic andesite similar to the adjacent lavas. The core appears to have numerous dark porphyritic clasts in the crystal-bearing matrix, but on close inspection we found many of these "clasts" to be less-altered sectors of the matrix.

At the base of the unit we observed a contact with the underlying andesite flow. A 3-mm-layer, rich in a fragmented opaque mineral, is present above the contact (see modal analysis B in Table 8, and Fig. 47). We extracted samples from this layer and analyzed them by XRD. Figure 48 presents part of the XRD patterns of the ore-bearing layer and a normal andesite. These data suggest that the opaque mineral present at the base of Unit 2 is ilmenite, as indicated by the characteristic peak at 0.28 nm, which is notably much less intense in the analysis of normal andesite. The accumulation of ilmenite at the base of Unit 2 indicates that a gravity-settling mechanism may have operated during its formation. Hence, the unit was probably generated as a glassy debris flow in a submarine environment.

Table 8. Modal mineralogy of basement rocks, Hole 792E.

Core, section, interval (cm)	Depth (mbsf)	Plag	Opx	Cpx	Qtz	Opaques
126-792E-						
71R-CC, 10[a]	812.9	36.5	5.0	3.5	—	1.7
74R-1, 146[b]	840.3	23.1	0.1	6.3	—	8.9
74R-1, 146[c]	840.3	30.7	5.9	1.8	—	2.4
76R-1, 61[d]	858.3	35.5	6.5	1.2	1.5	1.2
78R-1, 134[e]	877.9	32.8	6.5	4.4	1.3	1.3

Note: all analyses performed by point counting (>400 counts per section). Reported values are percentages, with groundmass the residual percentage (including microphenocrysts of plagioclase, pyroxene, and opaques).

[a] Porphyritic andesite, Unit 1.

[b] Basal 1.4-cm-thick layer of hyaloclastite breccia, Unit 2 (upper half of thin section).

[c] Top of porphyritic andesite flow, Unit 3, in contact with Unit 2 (lower half of thin section).

[d] Porphyritic quartz-bearing andesite, Unit 5.

[e] Porphyritic quartz-bearing andesite, Unit 5.

Unit 3: Porphyritic Andesite Flows

Interval: Samples 126-792E-74R-1, Piece 10, through -75R-2, Piece 9

This unit is similar to Unit 1 in phenocryst abundance and proportion. Quartz xenocrysts are present in the andesitic assemblage of Unit 3, as they were near the base of Unit 1. Two <10-cm layers of altered pale green hyaloclastite material are present in the unit and probably represent massive flow boundaries. Sample 126-792E-75R-1 (Piece 3), from directly above the lower hyaloclastite band, is a darker, apparently fresher lava. However, in thin section, the melanocratic nature can be assigned to the devitrification of glass.

Unit 4: Volcanic Breccia

Interval: Samples 126-792E-76R-1, Piece 1 through -76R-1, Piece 3

We recovered only 40 cm of this lithology. It consists of rounded, pebble-size clasts of lava in an altered, green hyaloclastic matrix. This matrix is similar to that in Unit 2, but the Unit 4 matrix contains a greater proportion and diversity of lava clasts. We found three clasts in the three pieces recovered: (1) a silicified, celadonite-stained andesitic lava; (2) a porphyritic andesite similar to the adjacent flows; and (3) a metabasaltic rock with no original mineralogy preserved. The latter clast contains abundant prehnite, chlorite, and clay minerals, which have replaced the groundmass and phenocryst assemblage. The only relics of igneous texture are minor lathlike chlorite-clay patches rimmed by smectite, which could be pseudomorphs after orthopyroxene. In hand specimens, the basaltic pebble appears to contain pseudomorphs after a pyroxene, now a mixture of hematite and a white clay mineral.

This volcanic breccia is likely to be associated with a submarine debris flow that entrained glassy debris, crystal fragments, and lava pebbles. The presence of a prehnite-grade basaltic clast suggests that an area of low-grade metamorphic basement was exposed and then entrained during the eruption of the frontal-arc andesites.

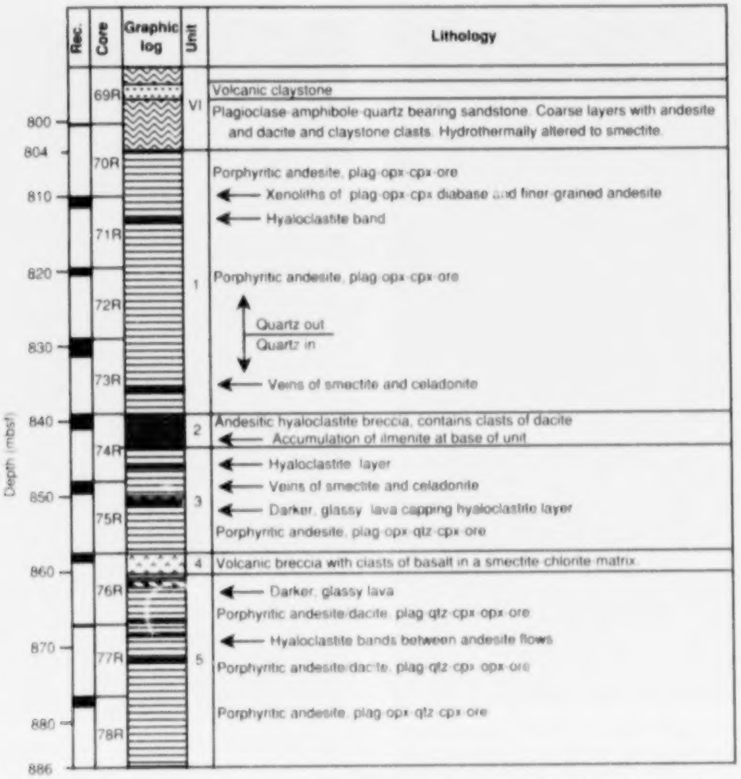
Rec.
Core
Graphic log
Unit
Lithology
Depth (mbsf)
800
804
810
820
830
840
850
860
870
880
886
69R
70R
71R
72R
73R
74R
75R
76R
77R
78R
VI
1
2
3
4
5
Volcanic claystone
Plagioclase-amphibole-quartz bearing sandstone. Coarse layers with andesite and dacite and claystone clasts. Hydrothermally altered to smectite.
Porphyritic andesite, plag-opx-cpx-ore
Xenoliths of plag-opx-cpx diabase and finer-grained andesite
Hyaloclastite band
Porphyritic andesite, plag-opx-cpx-ore
Quartz out
Quartz in
Veins of smectite and celadonite
Andesitic hyaloclastite breccia, contains clasts of dacite
Accumulation of ilmenite at base of unit
Hyaloclastite layer
Veins of smectite and celadonite
Darker, glassy lava capping hyaloclastite layer
Porphyritic andesite, plag-opx-qtz-cpx-ore
Volcanic breccia with clasts of basalt in a smectite-chlorite matrix
Darker, glassy lava
Porphyritic andesite/dacite, plag-qtz-cpx-opx-ore
Hyaloclastite bands between andesite flows
Porphyritic andesite/dacite, plag-qtz-cpx-opx-ore
Porphyritic andesite, plag-opx-qtz-cpx-ore

Figure 42. Stratigraphic summary of basement rock sequence at Hole 792E, Cores 126-792E-69R through -78R. Recovery within each core is proportionally expanded to fill the total core penetration.

Unit 5: Porphyritic Andesite Flows

Interval: Samples 126-792E-76R-1, Piece 4, through -78R-2, Piece 2

At the top of this unit, a contact with a 35° dip was observed between the volcanic breccia of Unit 4 and the uppermost andesite flow of Unit 5. The flow top beneath the contact has a pale, 5-mm chill zone underlain by 10 cm of andesite that contains 5-mm-diameter irregular pipe vesicles; notably, this is the only vesiculation observed in the Hole 792E basement section. Unit 5 is similar to Unit 3 in that it contains quartz, interflow hyaloclastic bands, and a darker, glassy interval amidst the porphyritic andesite flows (see Fig. 42).

IGNEOUS GEOCHEMISTRY

The 82-m basement penetration in Hole 792E revealed a sequence of andesitic massive flows with intercalated hyaloclastite bands. We analyzed 11 basement samples and 2 samples of lava clasts from the overlying sedimentary sequence with X-ray fluorescence spectrometry (XRF) for both major and trace elements. The SiO_2 content within the 11 basement samples ranged from 53.3 to 74 wt%, corresponding to a suite of compositional rock types between basaltic andesite and rhyolite (Table 9). However, a classification of individual samples on the basis of silica alone may be erroneous, owing to the presence of quartz xenocrysts (see "Igneous Petrology" section, this chapter) and alteration (see below). Analyses of clasts from the sedimentary section are probably affected by alteration since the Al_2O_3, K_2O, and loss on ignition results are anomalously high. However, Sample 126-792E-47R-1, 15-20 cm ("Pebble A" in Table 9), shows similar characteristics to the basement lavas of Site 792. This also is true for concentrations and ratios of most trace elements in Pebble A, especially Zr, Y, Rb, Sr, Nb, and V.

Major Element Geochemistry

Low-temperature alteration has affected the Hole 792E basement rocks and must be considered in the interpretation of both major and trace elements. With the exception of Sample 126-792E-78R-1 (Piece 15) and the two silicified samples outlined below, K_2O percentages remain remarkably consistent within the sequence. Two "dacite" samples from Section 126-792E-76R-1 (Table 9) have partially silicified groundmasses; this appears to have had the effect of diluting the concentrations of most elements. However, the dacites do not merely reflect secondary addition of silica to andesite. For example, if the Zr concentration of Sample 126-792E-76R-1 (Piece 4) is increased to the same level as the average andesite from Unit 1, and if silica is proportionally decreased, the SiO_2 level is only reduced from 73.3 to 68.5 wt%, whereas the Unit 1 andesites have around 57 wt% SiO_2. However, this serves to demonstrate that

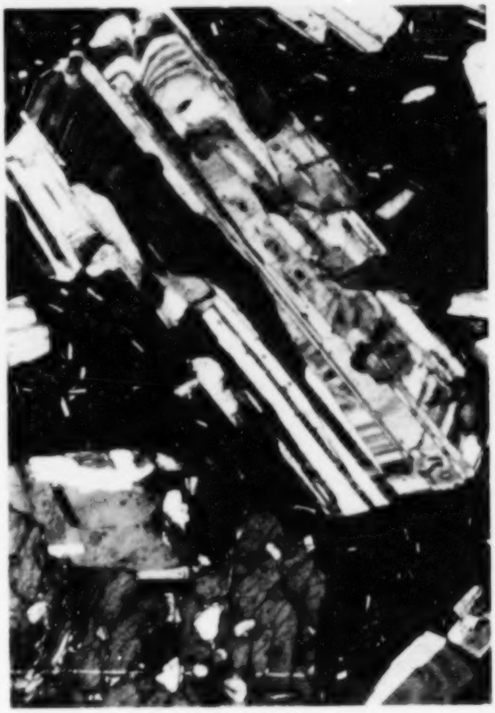

Figure 43. Typical texture of the porphyritic andesite. Oscillatory zoned plagioclase and euhedral clinopyroxene in a microphyric groundmass of feldspar and glass. Section 126-792E-71R-CC, Unit 1. Cross-polarized light, 95 ×.

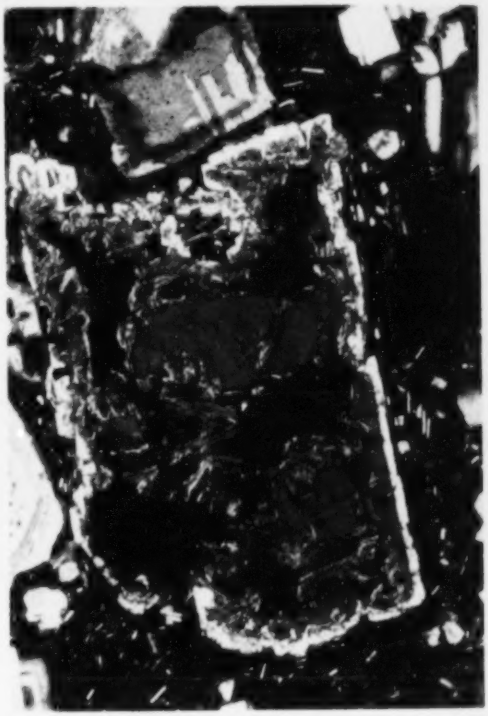

Figure 44. Orthopyroxene phenocryst partially altered to smectite, and plucked during sectioning. This crystal is rimmed by clinopyroxene (pale), and set in a microphyric groundmass. Section 126-792E-71R-CC, Unit 1. Cross-polarized light, 95 ×.

the original composition lies between the average of Unit 1 andesites and the measured composition. This also may be true for all elements except Fe and V, which are too low.

In addition to the dacites, the geochemistry of most of the basement section from Hole 792E may be affected by hydrothermal alteration. Although this hypothesis must await further laboratory-based analyses, mobile elements (e.g., Rb, K, and Sr) show internally consistent values and variations, comparable to suitable fractionation schemes. The compositional range of incompatible, immobile trace elements (e.g., Ti and Zr) is narrow and presumably reflects fractionation processes. However, the Y and P variation within the sequence is not consistent with simple crystal fractionation. Further studies of the mobility of these elements in this system is required to determine whether they might have been mobilized by alteration.

Major element variation diagrams show well-defined trends with limited scatter. For example, there is a positive correlation between total iron and MgO (Fig. 49), which suggests the removal of an iron-oxide phase at an early stage of fractionation and is characteristic of a calc-alkaline suite. This association is examined further in Figure 50, which compares the Site 792 lavas with selected rock suites on an alkali-iron-magnesium (AFM) plot. The trend indicates a calc-alkaline affinity, with a typical lack of iron enrichment and an associated increase in alkali elements. However, concentrations of K_2O and Na_2O in most of the andesites are remarkably low and increase by only a small amount as compared to normal calc-alkaline extrusives. The calc-alkaline trend of these samples is confirmed on the FeO^*/MgO-SiO_2 plot (Fig. 51), which also serves to compare the Site 792 basement with the Oligocene tholeiitic lavas drilled in the remnant arc at DSDP Site 448.

Trace Element Geochemistry

Of the 12 trace elements analyzed on the shipboard XRF, only Ce and Ba data are considered unreliable because these concentrations are close to their detection limits. The concentrations of high-field-strength (HFS) elements (Ti, Zr, Y, Nb, and P) in the samples from Site 792 basement lavas are all low relative to normal mid-ocean ridge basalts (MORB) with the same level of SiO_2 or MgO. In addition, ratios between the HFS elements are consistent with a depleted mantle source (e.g., $Zr/Y \leq 2$) that typifies oceanic island-arc systems. The low Ti/Zr and Ti/Y ratios are unlikely to be source characteristics because of the unquantified amount and type of iron-oxide removal during crystallization processes.

The Site 792 basement lavas are low in Rb, Sr, and (as far as analytical methods will allow) Ba, relative to regional arc andesites (Table 10), concordant with the low K_2O values described above. These low-field-strength (LFS) elements normally are en-

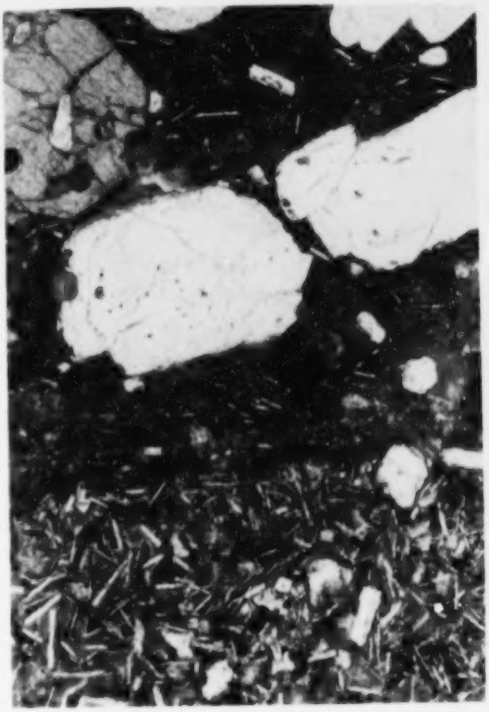

Figure 45. Intersertal textured andesite xenolith within porphyritic andesite. Sample 126-792E-71R-3, 33-34 cm, Unit 1. Plane polarized light, 95×.

riched in supra-subduction-zone magmas and especially in calc-alkaline lavas. Thus, it is surprising that the basement lavas of Hole 792E, with such marked calc-alkaline characteristics, are comparatively unenriched in LFS elements.

The basaltic andesite flows in Units 3 and 5 (see Table 9), and the andesites and dacitic lavas from the rest of the sequence, have distinctly different Zr/Y ratios (averages of 7.3 and 1.9, respectively). In light of the major element variations between the evolved and more primitive end members of the sequence, such a difference in Zr/Y is difficult to explain by variations in the degree of partial melting or crystal fractionation. Assuming that the HFS elements are comparatively unaffected by alteration, a more likely explanation is that magmas from two distinct sources were involved.

As a whole, the Site 792 basement lavas have most of the characteristics of a calc-alkaline suite: they are porphyritic, two-pyroxene andesitic lavas, with high aluminum, early oxide mineral precipitation, and concomitant iron depletion. However, they are unusual because of their low LFS element concentrations. In Table 10, an average analysis of the four Unit 1 samples is compared with three examples of Oligocene-Miocene arc volcanic rocks from the western Pacific arc system, and with an average calc-alkaline lava from Japan. None of these lavas provide a suitable analogue for the Hole 792E basement lavas.

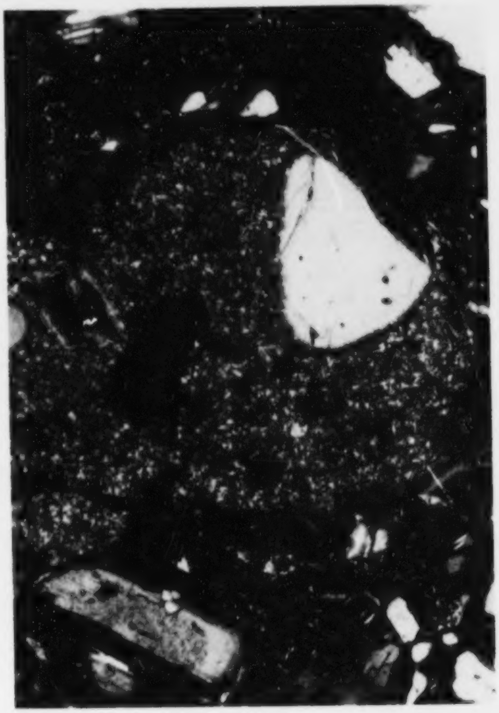

Figure 46. Dacitic clast in Unit 2 hyaloclastite. This clast contains a quartz phenocryst and a pseudomorph after a mafic phase, set in a devitrified and silicified glass. Sample 126-792E-74R-1, 84-85 cm. Cross-polarized light, 95×.

SEDIMENT/FLUID GEOCHEMISTRY

We obtained 26 whole-round samples (each 10 cm long) from Holes 792A, 792B, and 792E for electrical resistivity measurements, squeezing of pore water, and sediment and fluid analyses.

Sediment Resistivity

Electrical resistivity could only be measured on 17 of the whole-round samples because of the geometry of the cores. The results are presented in Table 11. The formation factor calculated from the resistivity measurements remains fairly stable from 3.1 to 341 mbsf (Core 126-792E-22R). Near 400 mbsf, the formation factor increases abruptly to a maximum of 15.8 at 620 mbsf (Core 126-792E-51R), then decreases to 7.2 by 796 mbsf (Core 126-792E-69R; see Fig. 52 and Table 11). The formation factors in the upper 350 m are typical for poorly compacted sediments, whereas the maximum readings are similar to those measured in claystones and siltstones. There is a positive correlation between the formation factor and the sonic velocity data (see "Physical Properties" section, this chapter), indicating that some of the decrease in the formation factor below 620 mbsf (Core 126-792E-51R) is the result of changes in the physi-

Figure 47. Accumulation layer at the base of Unit 2. Broken ilmenite grains in a groundmass of glass shards and fragmented phenocrysts. Contact is observed with underlying andesite flow (Unit 3), which contains only sparse opaque mineral. Sample 126-792E-74R-1, 145–148 cm. Plane polarized light, 95 ×.

cal properties of the rock. However, much of the apparent decrease probably is caused by the abundance of smectites. Because of the large ion-exchange capacity of the smectites, their presence can significantly contribute to the electric conductivity of the rock (Atlan et al., 1968).

Sediment Geochemistry

Sediments from Site 792 were analyzed on board ship for inorganic carbon, total carbon, nitrogen, and sulfur (see "Explanatory Notes" chapter, this volume). Analytical results are presented in Table 12. The concentration of organic carbon decreased exponentially from a level of about 0.6%–0.8% in the upper 60 mbsf to about 0.05% below 185 mbsf (Core 126-792E-6R; Fig. 53). This change corresponds to the boundary between lithologic Units I and II (see "Lithostratigraphy and Accumulation Rates" section, this chapter). Thus, the distribution of organic carbon probably is lithologically controlled, and decomposition plays a minor role. The concentration of total sedimentary sulfur varied from less than the detection limit to 0.55%, with the highest concentrations in the interval from 4 to 26 mbsf (Cores 126-792A-1H to -3H), which corresponds to the interval where the pore waters are depleted in sulfate on account of bacterial consumption (see below).

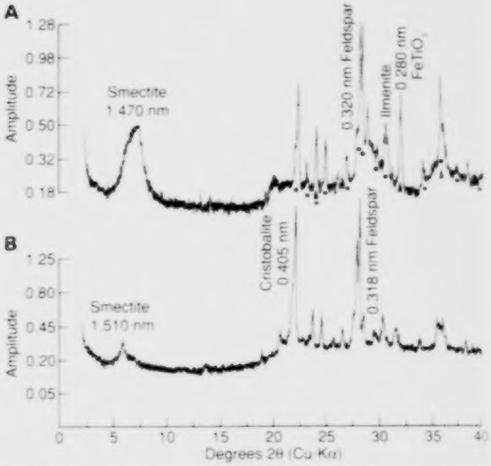

Figure 48. X-ray diffraction patterns, Site 792. **A.** Sample 126-792E-74R-1, 146 cm, taken from the accumulation layer at the base of Unit 2. Arrows mark ilmenite d-spacings, filled circles mark feldspar d-spacings. **B.** 126-792E-75R-1, 18 cm, taken from a sample of porphyritic andesite in Unit 3.

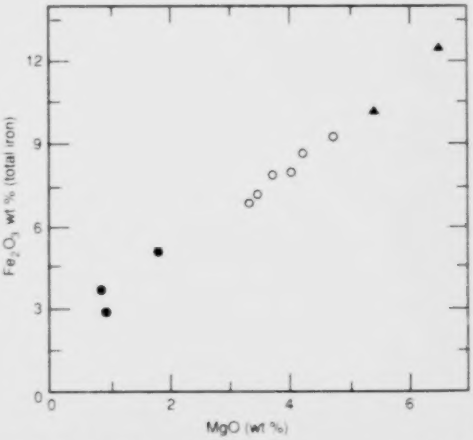

Figure 49. Fe_2O_3–MgO variation for Site 792 basement lavas listed in Table 9. Total iron is represented as Fe_2O_3. Open circles = andesite; closed circles = dacite; closed triangles = basalt-andesite.

Fluid Geochemistry

The headspace hydrocarbon analyses did not show any gases above background level and thus are not reported.

Because of a shortage of acetylene, calcium and magnesium are the only cations that we could analyze. To clean the hole, drilling mud was pumped between alternate cores. The composition of the drilling mud filtrate is presented in Table 13. On the

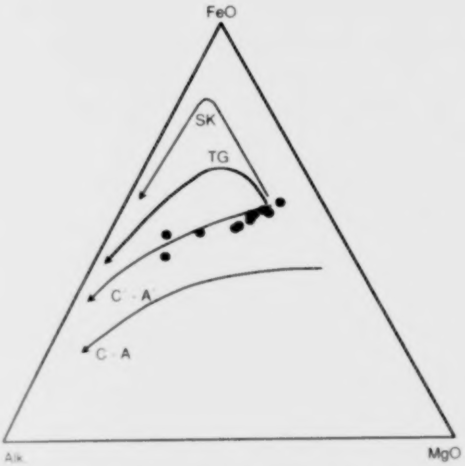

Figure 50. $Na_2O + K_2O$-FeO^*-MgO (AFM) triangular diagram for Site 792 basement lavas and selected lava suites (SK = Skaergaard fractionation trend; TG = Thingmuli fractionation trend). C-A and C'-A' represent typical calc-alkaline fractionation trends, and constrain the calc-alkaline lavas of New Zealand, the Cascades, and Aleutians (After Ringwood, 1974).

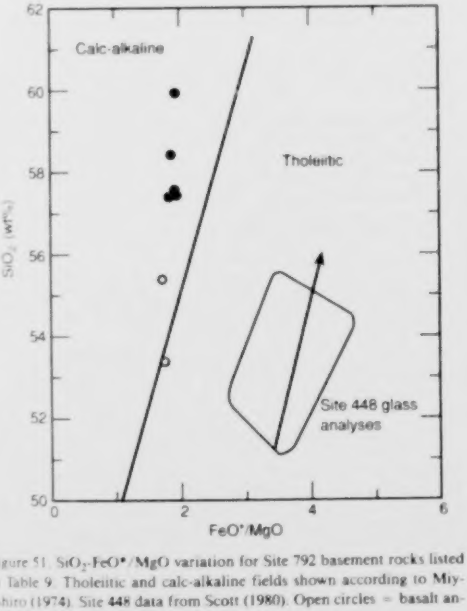

Figure 51. SiO_2-FeO^*/MgO variation for Site 792 basement rocks listed in Table 9. Tholeiitic and calc-alkaline fields shown according to Miyashiro (1974). Site 448 data from Scott (1980). Open circles = basalt andesites; closed circles = andesites.

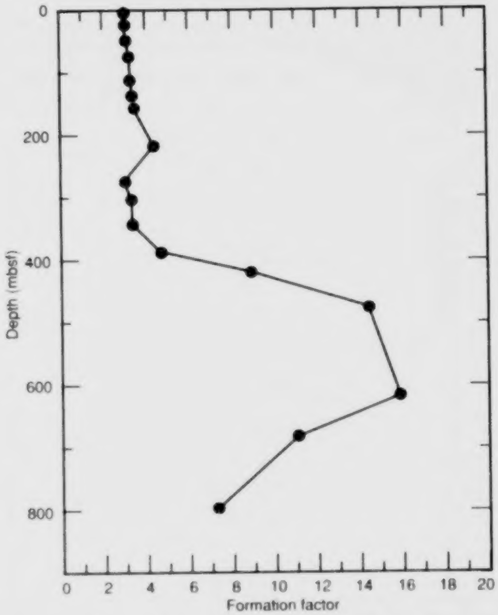

Figure 52. Formation factor of sediments from Holes 792A, 792B, and 792E.

basis of chloride analyses, we estimated that no sample contained >3% drilling-mud filtrate. The concentrations of calcium and magnesium (Fig. 54) are strongly affected by low-temperature alteration of volcanogenic material. Down to about 400 mbsf, the distribution of calcium and magnesium is typical for sediments that overlie basaltic basement, with an almost linear relationship between magnesium and calcium, and a $\delta Ca/\delta Mg$ ratio of about −1.5 (e.g., McDuff, 1981). However, the continuous increase in calcium below 450 mbsf is unusual, and the pore water between 500 and 700 mbsf is the most extensively altered pore water of seawater origin ever sampled by the DSDP/ODP programs (except for pore waters sampled from Site 793). Calcium concentrations reach 170 mM at 600 mbsf (Core 126-792E-48R), which is higher than ever recorded (except at Site 793 and in evaporitic settings). Note that the reaction zone giving rise to these highly altered pore waters is not situated in the basement, but instead lies within the interval between 500 and 700 mbsf. Although some of the samples may have been contaminated by surface seawater, none of the samples below 500 mbsf contains >10% seawater and most contain <5%, if any (as determined from the magnesium data). Thus, we have no doubt that the calcium maximum is real and defines the location of the reaction zone.

There are several possible interpretations for the deep calcium maximum. It may correspond to a zone with a particularly high concentration of reactive volcanogenic components. However, unless the reactions were triggered recently, diffusion would have eliminated the downward gradient by now. It is difficult to envisage any such triggering mechanism in the middle of a sediment column. The action of a process that removes calcium in the lower part of the section seems to us a more plausible interpretation. Although we could not confirm this by shipboard

Table 9. Major and trace element data from XRF analysis of basement rocks and two volcanic pebbles from Hole 792E.

Core, section, interval (cm) (126-792E)	47R-1, 15-20	67R-4, 6-10	71R-1, 9-13	71R-3, 34-38	72R-1, 111-115	73R-1, 15-18	74R-2, 53-57	75R-1, 50-55
Piece #	—	—	2	2a	10	2	5	3
Depth (mbsf)	—	—	810.5	818.2	825.5	829.5	845	850.5
Unit	IV	V	1	1	1	1	3	3
Lithology	Pebble A	Pebble B	Andesite	Andesite	Andesite	Andesite	Andesite	Basalt-andesite
SiO_2	50.14	52.13	57.48	57.55	57.48	57.39	59.91	53.26
TiO_2	0.80	0.68	0.54	0.56	0.55	0.56	0.54	0.53
Al_2O_3	20.94	21.35	18.92	18.20	19.04	17.93	17.50	17.66
Fe_2O_3	6.76	8.95	6.90	8.65	7.84	9.26	7.17	12.37
MnO	0.40	0.24	0.15	0.14	0.08	0.10	0.05	0.16
MgO	5.56	5.24	3.28	4.17	3.68	4.68	3.41	6.47
CaO	10.17	6.44	9.67	9.06	9.50	8.99	8.21	7.85
Na_2O	3.41	2.59	2.31	2.21	2.18	1.98	2.57	1.80
K_2O	1.23	2.08	0.23	0.15	0.13	0.14	0.20	0.12
P_2O_5	1.07	0.31	0.11	0.05	0.13	0.04	0.04	0.02
LOI	7.04	3.67	1.01	0.81	1.05	1.10	1.44	2.23
Total	100.48	100.01	99.59	100.74	100.61	101.07	99.60	100.24
Ti	4796	4077	3237	3357	3297	3357	3237	3177
P	4666	1352	480	218	567	174	174	87
Zr	41	80	40	40	42	41	39	44
Y	22	29	20	20	28	22	18	6
Rb	2.0	10.8	1.4	1.4	1.2	1.3	2.4	1.6
Sr	174	212	176	176	188	175	166	155
Ba	20	175	31	31	16	12	28	33
V	256	150	258	258	260	244	242	186
Nb	0.7	1.1	0.9	0.9	1.3	1.1	0.6	0.5
Ni	10	5	9	9	9	9	6	5
Cr	13	8	12	12	11	12	0	0
Zn	93	77	86	86	82	93	79	134
Cu	26	30	34	34	28	27	39	18
Ce	2	6	N	N	3	N	7	N
Mg#	64.42	56.31	51.13	51.48	50.81	52.66	51.14	53.51

Note: major and minor element contents in wt%, trace element contents in ppm; N = no data.

analysis, the concentration of sodium probably increases downward from the calcium maximum to maintain the charge balance. These concentration trends are opposite to what is observed during seawater/basalt interactions and actually shift the composition of the pore waters toward seawater composition. Thus, the possibility that the downward decrease in calcium below 600 mbsf (Core 126-792B-48R) is caused by recent lateral movement of seawater in the lower part of the sediment section should be considered. Although of more recent origin, the circulating seawater must have been in the sediments for a sufficiently long time to have its magnesium removed by water/rock interactions. Unit IV consists of mottled and brecciated, highly altered, volcanic sandstone with claystone interclasts (see "Lithostratigraphy and Accumulation Rates" section, this chapter). The high porosity of this unit (average 38%, see "Physical Properties" section, this chapter) and the low formation factor (Table 11) indicate that this unit is the most permeable interval below 400 mbsf. The extensive alteration of this unit is in itself an indication of a high cumulative water/rock ratio.

The calcium gradient between 300 and 500 mbsf is much steeper than would be established by simple diffusion in a homogeneous, porous media. This is caused by the rapidly changing diffusive properties of the rocks in this region (as revealed by the formation factor; Fig. 52). Most probably, the growth of authigenic smectite at the expense of volcanic glass constitutes the major sink for magnesium. Calcium is probably derived from this reaction and from the alteration of plagioclase. Shipboard (semiquantitative) XRD analyses show that at about 400 mbsf there is a pronounced increase in the abundance of smectites, and that the zeolite facies changes downhole from phillipsite and analcime to wairakite. Heulandite, clinoptilolite, and stilbite are present at 670 mbsf (see "Lithostratigraphy and Accumulation Rates" section, this chapter). Charge balance calculations show that the pore waters are severely depleted in sodium, although we could not confirm this by shipboard analyses. The most likely sink for sodium is the formation of zeolites (see "Lithostratigraphy and Accumulation Rates" section, this chapter).

Sulfate concentration profiles in marine sediments usually have a steep gradient close to the seafloor. However, except for a subsurface sulfate minimum at 26.55 mbsf (Core 126-792A-3H), the sulfate concentration remains close to seawater values down to 303 mbsf (Core 126-792E-18R), and then decreases to a level between 15 and 17 mM (Fig. 54). The peak in the ammonium profile at 26.55 mbsf (Core 126-792A-3H; Fig. 54) suggests that the subsurface sulfate minimum is the result of bacterial activity. Below this maximum, the concentration of ammonium decreases toward the bottom of the hole, indicating that the low-sulfate concentrations below about 500 mbsf are not related to bacterial activity.

Saturation index estimates (determined on the basis of thermodynamic data from National Bureau of Standards) demonstrate that below about 500 mbsf, pore waters are saturated with respect to gypsum (Fig. 54). Evidently, the sulfate concentrations are controlled by the precipitation of gypsum in response to the release of calcium by the low-temperature alteration of volcanogenic material. Thus, the fracture-filling gypsum observed below 500 mbsf (see "Lithostratigraphy and Accumulation Rates" section, this chapter) is not necessarily linked to a previous hydrothermal event, but may be precipitating at the present time. The data presented in Figure 54 show that the reactions taking place in the alteration zone consume silica faster than it can be supplied by diffusion from above. The considerable variations in the dissolved silica concentration in this region indicate that the reaction zone may consist of subzones characterized by different reactions or reaction rates.

Table 9 (continued).

76R-1, 43-46	76R-1, 60-64	76R-1, 85-87	78R-1, 80-85	78R-1, 131-136
4	6	7	9	15
860.1	861	862.2	880.2	883
5	5	5	5	5
Dacite	Basalt-andesite	Dacite	Andesite	Dacite
73.24	55.28	74.04	58.41	64.87
0.41	0.56	0.40	0.51	0.49
14.03	19.32	14.43	18.74	17.77
2.92	10.04	3.72	7.94	5.08
0.02	0.14	0.02	0.07	0.03
0.87	5.36	0.79	3.96	1.75
6.13	8.31	6.23	8.88	8.35
2.23	2.04	2.31	2.30	2.45
0.24	0.14	0.22	0.14	0.37
0.06	0.02	0.04	0.04	0.17
1.28	3.10	1.49	1.62	0.69
100.15	101.21	102.20	100.99	101.33
2458	3357	2398	3057	2938
262	87	174	174	741
35	49	36	44	42
15	7	22	10	31
2.7	2.1	3.1	1.2	3.9
134	166	138	170	162
42	2	211	6	43
153	247	125	260	233
1.4	0.7	1.0	0.7	1.2
0	7	4	5	4
0	2	2	8	4
41	98	78	80	55
26	17	31	28	18
2	N	1	N	9
39.61	54.02	31.85	52.33	43.12

Table 10. Representative analyses of Oligocene and Miocene basalts and andesites from Philippine Sea arc systems.

	Average Unit I andesite Hole 792E[a]	Palau-Kyushu Ridge Hole 448A[b]	Palau-Kyushu Ridge Site 1397[c]	West Mariana Ridge Hole 451[b]	Average Japan calc-alkaline[b]
SiO_2	57.94	50.00	54.20	49.90	53.80
TiO_2	0.56	1.11	1.15	0.71	0.95
Al_2O_3	18.67	15.30	19.00	18.20	17.79
FeO*	7.40	11.09	9.90	8.71	8.80
MnO	0.12	0.19	0.22	0.25	0.19
MgO	3.99	4.54	2.50	5.75	5.87
CaO	9.38	9.73	8.50	10.88	8.79
Na_2O	2.19	3.55	3.50	2.44	2.76
K_2O	0.16	1.38	0.45	0.73	0.62
P_2O_5	0.08	0.14		0.14	
Total	100.50	98.74	99.42	97.71	99.57
Ni	9	16	40	8	
Cr	12	25	260	31	
Rb	1	13		9	14
Sr	179	171	270	478	550
Zr	41	71		45	40
Y	23	31		19	15

Note: Major elements oxides reported in wt%, trace elements in ppm.

[a] Average of four analyses.

[b] Data from Mattey et al. (1980).

[c] Data from IGCP "Ophiolites" project (1977).

Table 11. Sediment resistivity (R_s), measurement temperature, pore-water resistivity (R_{pw}) at 25°C, and formation factor of sediments from Holes 792A, 792B, and 792E.

Core, section, interval (cm)	Depth (mbsf)	Cell constant (m)	R_s (ohm-m)	Temp. (°C)	R_{pw} (ohm-m)	F
126-792A-						
1H-5, 140-150	7.45	0.1002	0.855	11.9	0.201	3.1
3H-5, 140-150	26.55	0.1016	0.826	12.5	0.199	3.1
6H-2, 140-150	50.15	0.0997	0.952	12.6	0.198	3.1
9H-1, 89-97	76.54	0.1009	0.872	14.4	0.198	3.4
126-792B-						
8X-3, 140-150	112.35	0.1008	0.857	14.0	0.198	3.3
11X-1, 75-85	137.60	0.0996	0.866	14.2	0.199	3.4
126-792E-						
3R-2, 60-70	156.95	0.1024	0.945	11.8	0.199	3.5
9R-4, 40-50	217.55	0.1023	1.072	15.7	0.198	4.4
15R-2, 115-125	273.20	0.0978	0.697	18.8	0.199	3.0
18R-3, 115-125	303.70	0.1002	0.760	18.3	0.199	3.3
22R-2, 140-150	340.85	0.0975	0.802	16.1	0.198	3.3
27R-1, 27-37	386.62	0.0998	1.111	17.7	0.198	4.7
30R-5, 11-21	421.36	0.0998	2.185	16.6	0.201	8.9
36R-4, 67-77	478.42	0.1012	3.571	15.4	0.198	14.4
51R-2, 140-150	620.05	0.0962	3.723	16.2	0.192	15.8
57R-5, 140-150	682.55	0.1024	2.624	16.9	0.197	11.0
69R-4, 136-146	796.51	0.1007	1.814	15.6	0.202	7.2

PHYSICAL PROPERTIES

Introduction

Multi-sensor track (MST) logging, thermal conductivity, vane shear strength, electrical resistivity, Hamilton Frame (HF) compressional sonic velocity, index properties, and $CaCO_3$ content measurements were made on relatively undisturbed sections of APC and XCB cores from Holes 792A and 792B. We took only one sample for carbonate analysis from Hole 792C, and two samples from the 84 cm of sediment recovered from Hole 792D.

Thermal conductivity, HF sonic velocity, index property, and carbonate analyses were performed on rotary-drilled sections

Table 12. Concentration of carbonate, organic carbon, total nitrogen, and total sulfur in Site 792 sediments.

Core, section, interval (cm)	Depth (mbsf)	Inorg. carbon (%)	$CaCO_3$ (%)	Total carbon (%)	Org. carbon (%)	Total N (%)	Total S (%)
126-792B-1H-1, 6-7	0.06	1.32	11.0	1.90	0.58	0.05	0.11
126-792A-1H-1, 70-73	0.70	1.20	10.0	1.56	0.36	0.02	0.09
126-792B-1H-1, 113-117	1.13	1.31	10.9				
126-792B-1H-2, 47-48	1.97	2.45	20.4				
126-792B-1H-2, 47-48	1.97	2.45	20.4	3.09	0.64	0.05	0.04
126-792A-1H-2, 64-65	2.14	0.07	0.6	0.09	0.02	LD	0.2
126-792A-1H-2, 96-99	2.46	1.32	11.0	1.69	0.37	0.03	0.13
126-792B-1H-2, 102-105	2.52	1.39	11.6				
126-792B-1H-3, 50-53	3.50	1.61	13.4				
126-792B-1H-3, 95-96	3.95	1.90	15.8	2.66	0.76	0.05	0.26
126-792B-1H-3, 95-96	3.95	1.90	15.8				
126-792A-1H-3, 99-102	3.99	1.48	12.3	1.88	0.40	0.03	0.19
126-792A-1H-4, 108-111	5.58	0.95	7.9	1.33	0.38	0.02	0.11
126-792A-1H-5, 140-150	7.40	0.50	4.2	0.67	0.17	LD	0.16
126-792A-1H-6, 113-116	8.63	0.21	1.7	0.26	0.05	LD	0.08
126-792A-1H-7, 24-27	9.24	1.92	16.0	2.22	0.30	0.02	0.05
126-792A-2H-1, 129-131	10.99	3.22	26.8	3.66	0.44	0.03	0.03
126-792A-2H-2, 102-105	12.22	1.82	15.2	2.26	0.44	0.03	0.15
126-792A-2H-3, 120-122	13.90	0.59	4.9	0.72	0.13	0.01	0.14
126-792A-2H-4, 39-41	14.59	0.08	0.7	0.08	LD	LD	0.22
126-792A-3H-2, 56-59	21.16	2.10	17.5	2.49	0.39	0.03	0.55
126-792A-3H-3, 78-81	22.88	3.98	33.2	4.27	0.29	0.02	0.05
126-792A-3H-4, 122-125	24.82	1.51	12.6	1.89	0.38	0.03	0.14
126-792A-3H-5, 91-94	26.01	2.14	17.8	2.60	0.46	0.03	0.13
126-792A-3H-5, 140-150	26.50	2.08	17.3	2.43	0.35	0.03	0.09
126-792A-3H-7, 22-25	28.32	2.27	18.9	2.60	0.33	0.03	0.04
126-792A-4H-1, 99-102	29.39	1.85	15.4	2.17	0.32	0.03	0.06
126-792A-4H-2, 118-121	31.08	2.54	21.2	2.74	0.20	0.02	0.03
126-792A-4H-3, 64-67	32.04	3.29	27.4	3.59	0.30	0.02	0.05
126-792A-4H-4, 116-119	34.06	4.33	36.1	4.87	0.54	0.04	0.05
126-792A-4H-5, 89-92	35.29	3.33	27.7	3.69	0.36	0.03	0.15
126-792A-4H-7, 40-43	37.80	1.23	10.2	1.48	0.25	0.02	0.08
126-792A-5H-1, 101-104	38.81	3.00	25.0				
126-792A-5H-2, 34-37	39.64	0.59	4.9	0.63	0.04	LD	0.09
126-792A-5H-3, 93-95	41.73	2.26	18.8				
126-792A-5H-4, 129-131	43.59	2.30	19.2				
126-792A-5H-6, 62-65	45.92	2.39	19.9				
126-792A-6H-1, 117-119	48.37	2.24	18.7				
126-792A-6H-2, 67-69	49.37	0.94	7.8				
126-792A-6H-2, 140-150	50.10	1.67	13.9	1.97	0.30	0.03	0.06
126-792A-6H-3, 26-27	50.46	2.11	17.6				
126-792B-2H-1, 110-113	51.10	2.87	23.9	3.33	0.46	0.02	0.02
126-792B-2H-2, 64-67	52.14	1.45	12.1				
126-792A-6H-4, 118-119	52.88	2.56	21.3				
126-792B-2H-4, 70-73	55.20	2.03	16.9				
126-792B-2H-5, 63-66	56.63	2.46	20.5	3.00	0.54	0.03	0.05
126-792A-7H-1, 95-96	57.55	0.62	5.2	0.86	0.24	0.01	0.05
126-792A-7H-2, 91-94	59.01	3.56	29.7				
126-792B-3H-1, 12-15	59.72	2.01	16.7				
126-792A-7H-3, 74-75	60.34	1.30	10.8				
126-792B-3H-3, 83-86	63.43	0.08	0.7	0.08	0.00	LD	0.07
126-792A-8H-1, 68-70	66.68	1.11	9.2				
126-792B-3H-6, 40-43	67.50	0.03	0.2				
126-792A-8H-2, 92-94	68.29	0.60	5.0	0.68	0.08	0.01	0.06
126-792B-3H-7, 39-42	68.99	2.06	17.2	2.36	0.30	0.02	0.18
126-792A-8H-3, 35-38	69.22	0.65	5.4				
126-792B-4X-1, 24-27	69.44	1.77	14.7				
126-792B-4X-2, 130-133	72.00	0.17	1.4	0.18	0.01	LD	0.18
126-792B-4X-3, 110-113	73.30	1.06	8.8				
126-792A-9H-1, 71-74	76.31	1.42	11.8				
126-792A-9H-1, 87-97	76.47	2.01	16.7	2.28	0.27	0.02	0.06
126-792A-9H-2, 100-103	77.82	3.55	29.6				
126-792A-9H-3, 17-20	78.49	2.95	24.6				
126-792A-9H-4, 20-23	79.39	2.06	17.2	2.34	0.28	0.01	0.05
126-792A-10H-1, 112-115	86.42	3.48	29.0				
126-792A-10H-3, 108-110	88.19	3.67	30.6				
126-792A-10H-4, 95-98	89.56	1.02	8.5				
126-792B-7X-CC, 26-29	98.46	0.74	6.2	0.96	0.22	0.03	0.16
126-792B-8X-1, 38-41	108.28	1.92	16.0				
126-792B-8X-2, 38-41	109.78	0.71	5.9	0.99	0.28	0.03	0.13
126-792B-8X-3, 92-95	111.82	1.81	15.1				
126-792B-8X-3, 140-150	112.30	1.31	10.9	1.55	0.24	0.02	0.14
126-792B-8X-4, 53-56	112.93	1.08	9.0				
126-792B-9X-1, 113-116	118.63	1.56	13.0				
126-792B-9X-2, 20-23	119.20	1.24	10.3				
126-792B-10X-1, 95-98	128.05	0.50	4.2	0.73	0.23	0.03	0.19
126-792B-10X-2, 141-144	130.01	0.69	5.7				

Table 12 (continued).

Core, section, interval (cm)	Depth (mbsf)	Inorg. carbon (%)	$CaCO_3$ (%)	Total carbon (%)	Org. carbon (%)	Total N (%)	Total S (%)
126-792B-10X-3, 69-72	130.79	2.18	18.2	2.47	0.29	0.04	0.08
126-792E-1R-1, 36-38	135.96	1.55	12.9	1.81	0.26	0.02	0.09
126-792D-1X-1, 37-38	136.37	0.94	7.8	1.12	0.18	0.02	0.07
126-792C-1X-CC, 13-14	136.93	0.72	6.0				
126-792B-11X-1, 24-26	137.04	0.88	7.3				
126-792B-11X-1, 54-55	137.34	1.19	9.9				
126-792B-11X-1, 75-85	137.55	1.66	13.8	1.97	0.31	0.02	0.03
126-792B-11X-2, 35-37	138.00	0.62	5.2				
126-792B-11X-CC, 25-27	138.78	0.68	5.7				
126-792E-3R-1, 109-111	155.89	1.74	14.5				
126-792E-3R-2, 60-70	156.90	1.85	15.4	2.13	0.28	0.03	0.1
126-792E-3R-3, 26-29	157.26	1.83	15.2				
126-792E-4R-1, 84-87	165.34	1.11	9.3	1.33	0.22	0.02	0.14
126-792E-4R-2, 107-109	167.07	0.40	3.3				
126-792E-5R-1, 65-66	174.75	2.50	20.8	2.76	0.26	0.03	0.03
126-792E-6R-1, 13-14	183.83	0.87	7.3				
126-792E-6R-1, 120-121	184.90	0.04	0.3	0.04	0.00	0.01	LD
126-792E-8R-1, 13-15	203.23	0.42	3.5				
126-792E-9R-1, 17-19	212.77	0.19	1.6	0.23	0.04	0.01	0.04
126-792E-9R-2, 24-26	214.34	0.24	2.0				
126-792E-9R-3, 74-76	216.34	0.07	0.6				
126-792E-9R-4, 40-50	217.50	0.30	2.5	0.37	0.07	0.01	0.03
126-792E-9R-5, 31-35	217.91	0.24	2.0				
126-792E-10R-1, 48-50	222.68	0.11	0.9				
126-792E-10R-3, 6-8	225.26	0.06	0.5	0.06	0.00	0.01	0.46
126-792E-10R-3, 124-127	226.44	0.38	3.2				
126-792E-11R-1, 94-96	232.84	0.69	5.8				
126-792E-11R-2, 3-5	233.43	0.92	7.7	0.95	0.03	0.02	0.06
126-792E-11R-2, 64-66	234.04	0.08	0.7				
126-792E-12R-1, 116-119	242.66	1.43	11.9				
126-792E-12R-3, 20-22	244.70	0.97	8.1	1.04	0.07	0.01	0.15
126-792E-13R-1, 11-12	251.31	0.89	7.4				
126-792E-15R-1, 71-72	271.21	1.02	8.5				
126-792E-15R-1, 79-80	271.29	1.74	14.5	1.86	0.12	0.02	0.07
126-792E-15R-1, 99-101	271.49	0.78	6.5				
126-792E-15R-2, 16-18	272.16	1.76	14.7				
126-792E-15R-2, 115-125	273.15	0.31	2.6	0.31	0.00	0.01	0.04
126-792E-16R-1, 26-28	280.46	1.18	9.8				
126-792E-16R-2, 7-9	281.77	0.30	2.5				
126-792E-17R-1, 14-16	290.04	0.41	3.4				
126-792E-17R-1, 42-43	290.32	1.71	14.2	1.86	0.15	0.01	0.03
126-792E-17R-2, 140-142	292.80	0.05	0.4	0.06	0.01	0.01	0.05
126-792E-17R-3, 139-141	294.29	0.31	2.6				
126-792E-17R-4, 42-44	294.82	1.76	14.7				
126-792E-18R-1, 15-17	299.65	0.81	6.8				
126-792E-18R-2, 104-106	302.04	0.17	1.4				
126-792E-18R-2, 137-138	302.37	1.48	12.3				
126-792E-18R-3, 107-109	303.57	1.13	9.4				
126-792E-18R-3, 115-125	303.65	0.85	7.1	0.95	0.10	0.01	0.02
126-792E-18R-4, 124-126	305.24	2.00	16.7				
126-792E-19R-1, 47-48	309.47	0.09	0.8				
126-792E-19R-2, 21-23	310.71	0.60	5.0	0.66	0.06	0.02	0.03
126-792E-19R-3, 48-50	312.48	2.49	20.7				
126-792E-20R-1, 34-36	318.94	2.64	22.0				
126-792E-20R-2, 124-126	321.34	1.45	12.1				
126-792E-20R-3, 19-21	321.79	1.04	8.7	1.13	0.09	0.02	0.1
126-792E-21R-1, 13-15	328.43	2.61	21.7				
126-792E-21R-2, 49-51	330.29	0.96	8.0				
126-792E-22R-1, 79-81	338.69	0.77	6.4				
126-792E-22R-2, 5-7	339.45	1.87	15.6				
126-792E-22R-2, 140-150	340.80	0.87	7.3	0.96	0.09	0.01	0.02
126-792E-22R-3, 52-54	341.42	0.35	2.9				
126-792E-23R-1, 74-75	348.34	1.67	13.9				
126-792E-24R-1, 26-27	357.56	1.62	13.5				
126-792E-25R-1, 111-112	368.11	1.68	14.0				
126-792E-25R-1, 129-131	368.29	1.90	15.8				
126-792E-26R-1, 10-12	376.70	2.58	21.5				
126-792E-26R-1, 69-70	377.29	2.31	19.2				
126-792E-27R-1, 27-37	386.57	6.88	57.3				
126-792E-27R-2, 43-44	387.35	7.16	59.6				
126-792E-27R-4, 87-88	390.79	3.98	33.2				
126-792E-28R-1, 35-36	396.35	7.75	64.6	7.84	0.09	0.03	0.04
126-792E-28R-1, 69-71	396.69	5.53	46.1				
126-792E-28R-2, 42-43	397.92	8.12	67.6	8.19	0.07	0.02	LD
126-792E-29R-1, 99-100	406.59	4.71	39.2				
126-792E-29R-2, 5-6	407.15	3.03	25.2	3.05	0.02	0.02	0.07
126-792E-29R-2, 23-24	407.33	0.22	1.8				
126-792E-30R-1, 107-108	416.27	0.06	0.5				

Table 12 (continued).

Core, section, interval (cm)	Depth (mbsf)	Inorg. carbon (%)	$CaCO_3$ (%)	Total carbon (%)	Org. carbon (%)	Total N (%)	Total S (%)
126-792E-30R-3, 85-86	419.05	1.12	9.3	1.11	0.00	0.01	0.11
126-792E-30R-5, 10-12	421.30	0.50	4.2				
126-792E-30R-5, 11-21	421.31	0.10	0.8	0.07	0.02	0.02	0.08
126-792E-30R-7, 37-39	423.28	1.33	11.1				
126-792E-31R-1, 54-55	425.44	5.12	42.7				
126-792E-31R-1, 127-128	426.17	4.93	41.1	4.90	0.00	0.03	0.06
126-792E-31R-2, 22-23	426.62	0.11	0.9				
126-792E-31R-2, 48-49	426.88	0.05	0.4				
126-792E-31R-3, 97-98	428.87	2.47	20.6	2.38	0.00	0.02	0.06
126-792E-31R-3, 118-119	429.08	1.67	13.9				
126-792E-32R-1, 38-40	434.98	0.69	5.8				
126-792E-32R-3, 100-101	438.60	0.59	4.9				
126-792E-33R-1, 90-92	445.10	0.09	0.8				
126-792E-33R-2, 95-105	446.65	0.17	1.4	0.19	0.02	0.01	0.19
126-792E-33R-3, 60-62	447.60	0.48	4.0				
126-792E-34R-1, 67-69	454.57	3.00	25.0	3.06	0.06	0.02	0.11
126-792E-34R-2, 104-106	456.44	1.05	8.8				
126-792E-34R-3, 78-80	457.68	1.16	9.7				
126-792E-35R-1, 105-107	464.55	0.12	1.0	0.12	0.00	0.01	0.06
126-792E-35R-2, 47-49	465.47	1.00	8.3				
126-792E-36R-1, 73-75	473.93	0.82	6.8				
126-792E-36R-2, 139-141	476.09	0.62	5.2	0.67	0.05	0.01	0.04
126-792E-36R-3, 129-131	477.49	1.75	14.6				
126-792E-36R-4, 67-77	478.37	0.23	1.9	0.24	0.01	0.01	0.02
126-792E-36R-5, 92-94	479.39	0.75	6.3				
126-792E-37R-1, 73-74	483.53	2.26	18.8	2.32	0.06	0.02	0.06
126-792E-37R-1, 132-134	484.12	0.95	7.9				
126-792E-37R-3, 52-55	486.32	1.67	13.9				
126-792E-37R-5, 126-128	490.06	0.65	5.4				
126-792E-37R-7, 16-18	491.96	0.13	1.1	0.20	0.07	0.01	0.03
126-792E-38R-1, 41-43	492.91	0.16	1.3				
126-792E-38R-3, 118-120	496.68	0.04	0.3	0.05	0.01	0.01	0.09
126-792E-38R-5, 30-32	498.80	0.09	0.8				
126-792E-38R-6, 6-8	501.00	0.05	0.40	3.3			
126-792E-39R-1, 128-130	503.48	0.33	2.8	0.41	0.08	0.01	0.03
126-792E-39R-2, 115-125	504.85	0.18	1.5	0.21	0.03	0.01	0.02
126-792E-39R-3, 36-38	505.56	0.34	2.8				
126-792E-39R-5, 60-62	508.80	0.07	0.6	0.08	0.01	LD	0.03
126-792E-40R-1, 103-105	512.93	0.28	2.3				
126-792E-40R-3, 15-17	515.05	0.07	0.6				
126-792E-40R-5, 107-109	518.97	0.06	0.5				
126-792E-40R-6, 75-77	520.15	1.29	10.7				
126-792E-41R-1, 20-22	521.80	0.07	0.6				
126-792E-41R-1, 118-119	522.78	0.07	0.6	0.08	0.01	0.01	0.03
126-792E-41R-2, 56-58	523.66	0.31	2.6				
126-792E-41R-3, 82-84	525.42	0.07	0.6				
126-792E-41R-5, 99-101	528.32	0.07	0.6				
126-792E-42R-3, 118-119	535.38	0.07	0.6				
126-792E-42R-4, 140-150	537.10	0.07	0.6	0.07	0.00	0.01	0.02
126-792E-42R-5, 121-122	538.41	0.10	0.8				
126-792E-43R-1, 76-78	541.36	0.07	0.6	0.07	0.00	0.01	0.02
126-792E-43R-3, 56-58	543.97	1.17	9.8				
126-792E-43R-3, 110-111	544.51	0.85	7.1				
126-792E-43R-5, 82-84	547.25	0.11	0.9				
126-792E-43R-5, 100-101	547.43	3.91	32.6				
126-792E-43R-7, 30-32	549.63	0.06	0.5				
126-792E-44R-1, 60-61	550.90	0.07	0.6				
126-792E-44R-3, 53-54	553.84	0.08	0.7				
126-792E-44R-5, 34-35	556.65	0.08	0.7				
126-792E-45R-1, 64-65	560.64	0.10	0.8	0.08	0.00	0.01	0.05
126-792E-45R-2, 0-10	561.45	0.08	0.7	0.12	0.04	0.01	LD
126-792E-45R-3, 4-5	562.96	0.19	1.6				
126-792E-45R-4, 132-133	565.55	0.10	0.8				
126-792E-46R-1, 78-79	570.48	0.10	0.8				
126-792E-46R-3, 122-124	573.65	0.08	0.7				
126-792E-46R-5, 119-121	576.55	1.03	8.6				
126-792E-46R-7, 31-33	578.56	1.29	10.7				
126-792E-47R-1, 114-116	580.54	0.13	1.1				
126-792E-47R-3, 47-49	582.48	0.09	0.7				
126-792E-48R-1, 35-37	588.95	0.10	0.8	0.12	0.02	0.01	0.02
126-792E-48R-3, 37-39	591.27	0.22	1.8				
126-792E-48R-3, 52-53	591.42	0.64	5.3				
126-792E-48R-5, 63-65	594.21	0.05	0.4	0.08	0.03	0.01	0.02
126-792E-48R-6, 83-84	595.88	1.70	14.2				
126-792E-48R-7, 140-150	597.55	0.05	0.4	0.06	0.01	0.01	0.02
126-792E-48R-8, 19-21	597.84	0.07	0.6				
126-792E-49R-3, 63-65	601.43	0.47	3.9				
126-792E-49R-5, 112-114	604.77	0.50	4.2				

Table 12 (continued).

Core, section, interval (cm)	Depth (mbsf)	Inorg. carbon (%)	$CaCO_3$ (%)	Total carbon (%)	Org. carbon (%)	Total N (%)	Total S (%)
126-792E-50R-1, 23-25	607.63	0.15	1.3				
126-792E-50R-3, 7-9	610.47	0.07	0.6				
126-792E-50R-5, 16-18	613.57	0.10	0.8				
126-792E-50R-7, 11-13	616.52	0.29	2.4				
126-792E-51R-1, 32-34	617.42	0.73	6.1				
126-792E-51R-2, 106-108	619.66	0.31	2.6				
126-792E-51R-2, 140-150	620.00	0.19	1.6	0.24	0.05	0.01	0.08
126-792E-51R-3, 14-16	620.24	0.75	6.3	0.81	0.06	0.01	0.22
126-792E-52R-1, 38-40	627.18	1.92	16.0				
126-792E-52R-1, 100-102	627.80	5.10	42.5				
126-792E-52R-2, 29-31	628.59	0.11	0.9				
126-792E-52R-3, 22-24	630.02	0.07	0.6				
126-792E-52R-4, 49-51	631.79	1.77	14.7				
126-792E-52R-5, 50-52	633.30	0.10	0.8				
126-792E-52R-6, 8-10	634.38	0.09	0.7				
126-792E-54R-1, 136-137	647.46	0.08	0.7				
126-792E-54R-2, 49-50	648.09	0.76	6.3				
126-792E-54R-3, 11-12	649.21	0.17	1.4				
126-792E-54R-3, 140-150	650.50	1.07	8.9	1.12	0.05	0.01	0.05
126-792E-54R-5, 83-84	652.93	1.64	13.7				
126-792E-54R-6, 8-9	653.68	2.79	23.2				
126-792E-55R-1, 53-55	656.23	1.45	12.1				
126-792E-55R-2, 99-101	658.19	0.10	0.8				
126-792E-56R-2, 77-79	667.67	0.27	2.2				
126-792E-56R-4, 16-18	670.06	0.08	0.7				
126-792E-56R-6, 136-138	673.98	0.05	0.4				
126-792E-57R-1, 98-100	676.08	1.56	13.0				
126-792E-57R-3, 3-5	678.13	0.06	0.5				
126-792E-57R-5, 85-87	681.95	0.03	0.2				
126-792E-57R-5, 140-150	682.50	0.04	0.3	0.04	0.00	0.01	LD
126-792E-57R-6, 49-51	683.09	0.81	6.7				
126-792E-58R-1, 70-72	685.50	0.06	0.5				
126-792E-58R-2, 92-94	687.22	0.28	2.3				
126-792E-58R-CC, 20-22	689.90	0.05	0.4				
126-792E-59R-1, 65-67	695.05	0.44	3.7				
126-792E-59R-2, 49-51	696.39	0.05	0.4				
126-792E-59R-3, 101-103	698.28	0.13	1.1				
126-792E-59R-4, 72-74	699.21	0.08	0.7				
126-792E-59R-5, 47-49	700.40	0.73	6.1				
126-792E-60R-1, 121-123	705.21	0.08	0.7				
126-792E-60R-2, 71-72	706.21	0.05	0.4				
126-792E-60R-3, 16-17	707.16	0.05	0.4				
126-792E-60R-4, 140-141	709.90	0.04	0.3				
126-792E-60R-6, 27-28	711.77	0.04	0.3				
126-792E-60R-6, 140-150	712.90	0.05	0.4	0.05	0.00	0.01	0.02
126-792E-61R-2, 119-121	716.29	0.04	0.3				
126-792E-61R-3, 130-132	717.90	0.05	0.4				
126-792E-61R-4, 88-90	718.98	0.07	0.6				
126-792E-62R-1, 4-5	722.94	0.15	1.2				
126-792E-62R-2, 95-96	724.53	0.10	0.8				
126-792E-62R-4, 37-38	726.54	0.13	1.1				
126-792E-62R-7, 69-70	730.80	0.07	0.6				
126-792E-62R-8, 6-7	731.67	0.21	1.7				
126-792E-63R-1, 109-111	733.59	0.06	0.5				
126-792E-63R-3, 5-7	735.41	0.32	2.7				
126-792E-63R-3, 138-150	736.74	0.35	2.9	0.35	0.00	0.01	0.02
126-792E-64R-1, 14-15	742.34	0.27	2.2				
126-792E-64R-2, 51-53	744.16	0.05	0.4				
126-792E-65R-1, 12-14	751.92	0.07	0.6				
126-792E-65R-2, 13-14	753.36	0.06	0.5				
126-792E-66R-1, 52-54	762.02	1.17	9.7				
126-792E-66R-3, 144-146	765.94	0.08	0.7				
126-792E-66R-5, 139-149	768.91	0.14	1.2	0.15	0.01	0.01	0.03
126-792E-66R-6, 10-12	769.11	0.13	1.1				
126-792E-67R-1, 74-76	771.94	0.05	0.4				
126-792E-67R-2, 110-112	773.80	0.11	0.9				
126-792E-67R-3, 23-25	774.43	0.08	0.7				
126-792E-68R-1, 50-52	781.40	1.93	16.1				
126-792E-68R-2, 82-84	782.96	0.06	0.5				
126-792E-68R-2, 124-126	783.38	0.03	0.2				
126-792E-69R-3, 107-108	794.67	0.06	0.5				
126-792E-69R-4, 136-146	796.28	0.04	0.3	0.04	0.00	0.01	0.03

Note: Samples are listed according to depth (mbsf); LD = less than detection limit.

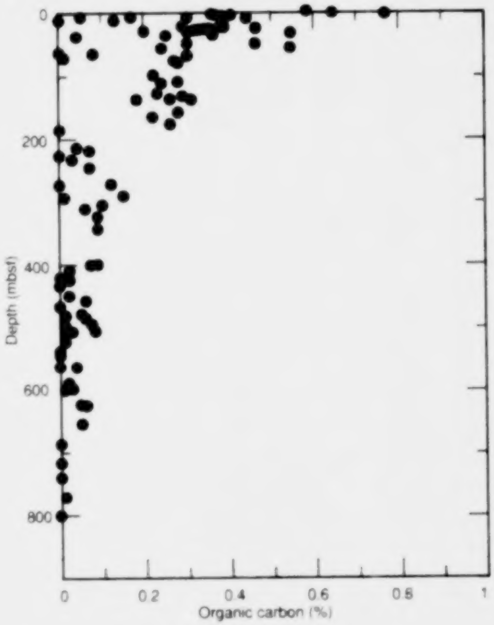

Figure 53. Organic carbon, Site 792.

from Hole 792E. We obtained MST logging from Cores 126-792E-1R through -31R, but we report only the sonic data for Hole 792E (see "Physical Properties" sections in previous site chapters, this volume, for details). Vane shear strength measurements were discontinued after five cores because of drilling disturbance. Thermal conductivity was suspended at Core 126-792E-32R, below which the material became too lithified for the needle-probe method.

We conducted HF velocity, index property, and thermal conductivity analyses on igneous rock samples. All igneous samples for physical property analyses were taken from core sections within minutes of splitting to minimize the effects of dessication. Thermal conductivity was measured on six samples with the half-space method.

Four downhole temperature measurements were attempted by means of a Uyeda temperature probe at Site 792, two in Hole 792A and two in Hole 792C. Of these, three were successful (at depths of 47.2, 67, and 110 mbsf). The fourth measurement (at 95 mbsf) produced an anomalous temperature-vs.-time plot and was not included in further analyses. Bottom-water temperature was used as a fourth data point to constrain the geothermal gradient.

Index Properties

Index property measurements overlap at two depth intervals in Holes 792A and 792B: 0–4.3 mbsf and 50–73 mbsf (Figs. 55 and 56; Table 14). Trends agree reasonably well with absolute values, although values in Hole 792A exhibit greater variability. Depth overlap between Hole 792B and Holes 792C, 792D, and 792E is minimal. The physical property measurements and lithologic units are displayed in Figure 55, and relationships among the parameters are discussed below.

Table 13. Pore-water composition, Site 792.

Core, section, interval (cm)	Depth (mbsf)	pH	Alk (mM)	Sal (g/kg)	Cl (mM)	SO_4^{2-} (mM)	Mg^{2+} (mM)	Ca^{2+} (mM)	SiO_2 (μM)	NH_4^+ (μM)
126-792A-										
1H-5, 140-150	7.45	7.74	3.18	35.5	550	28.4	52.2	9.4	521	192
3H-5, 140-150	26.55	7.80	4.27	35.5	556	25.5	52.5	7.9	629	536
6H-2, 140-150	50.15	7.80	3.33	35.5	561	26.3	53.0	9.2	595	453
9H-1, 89-97	76.54	7.82	2.66	35.5	562	26.9	52.0	10.2	650	296
126-792B-										
8X-3, 140-150	112.35	7.60	3.09	35.5	561	27.6	51.8	11.0	710	250
11X-1, 75-85	137.60	7.69	2.64	36.0	560	27.1	50.6	15.1	794	199
126-792E-										
3R-2, 60-70	156.95	7.52	2.15	35.5	557	27.2	50.2	16.5	805	187
9R-4, 40-50	217.55	7.69	0.23	36.0	560	27.8	46.0	23.5	765	212
15R-2, 115-125	273.20	7.93	1.62	36.0	559	28.5	46.6	23.0	875	161
18R-3, 115-125	303.70	7.58	2.34	36.0	559	28.2	46.4	23.9	938	165
22R-2, 140-150	340.85	7.53	1.43	36.0	559	27.2	43.6	28.8	979	147
27R-1, 27-37	386.62	7.34	1.37	36.0	560	26.6	40.0	36.9	924	118
30R-5, 11-21	421.36	7.79	1.20	36.0	551	25.5	31.2	53.7	157	92
33R-2, 95-105	446.70	ND	ND	ND	559	23.2	22.2	71.5	135	106
36R-4, 67-77	478.42	7.94	0.12	36.5	560	19.7	12.0	98.5	118	133
39R-2, 115-125	504.90	ND	ND	ND	562	16.7	4.2	130.6	118	105
42R-4, 140-150	537.15	ND	ND	ND	578	15.2	2.6	159.0	375	114
45R-2, 0-10	561.55	ND	ND	ND	579	15.6	4.6	156.1	123	108
48R-7, 140-150	599.05	8.48	0.35	39.0	579	15.3	0.4	169.3	262	44
51R-2, 140-150	620.05	ND	ND	ND	577	15.1	3.2	153.1	343	58
54R-3, 140-150	650.55	ND	ND	ND	560	15.2	2.4	153.1	123	60
57R-5, 140-150	682.55	8.11	0.47	38.0	563	16.3	1.4	143.1	447	80
60R-6, 140-150	712.95	ND	ND	ND	568	18.8	3.2	135.6	282	82
63R-3, 138-150	736.94	ND	ND	ND	567	17.3	0.3	143.8	203	113
66R-5, 139-150	768.95	ND	ND	ND	569	16.8	5.4	121.7	146	55
69R-4, 136-146	796.51	ND	ND	ND	549	16.2	4.3	114.2	508	72
Drilling mud filtrate		9.69	0.80	ND	215	12.0	2.7	7.0	19	58

Note: ND = not determined.

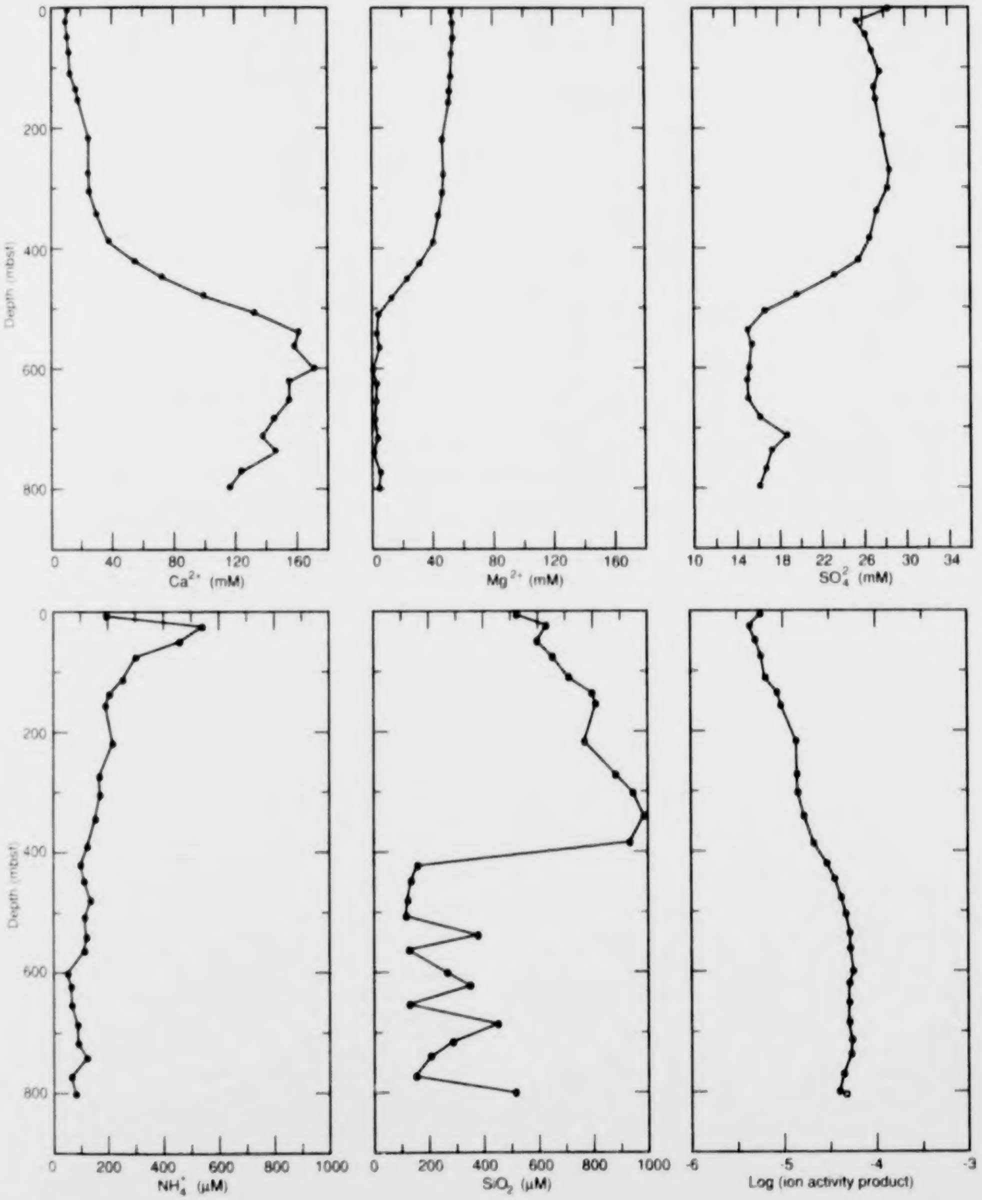

Figure 54. Composition of pore waters, Site 792.

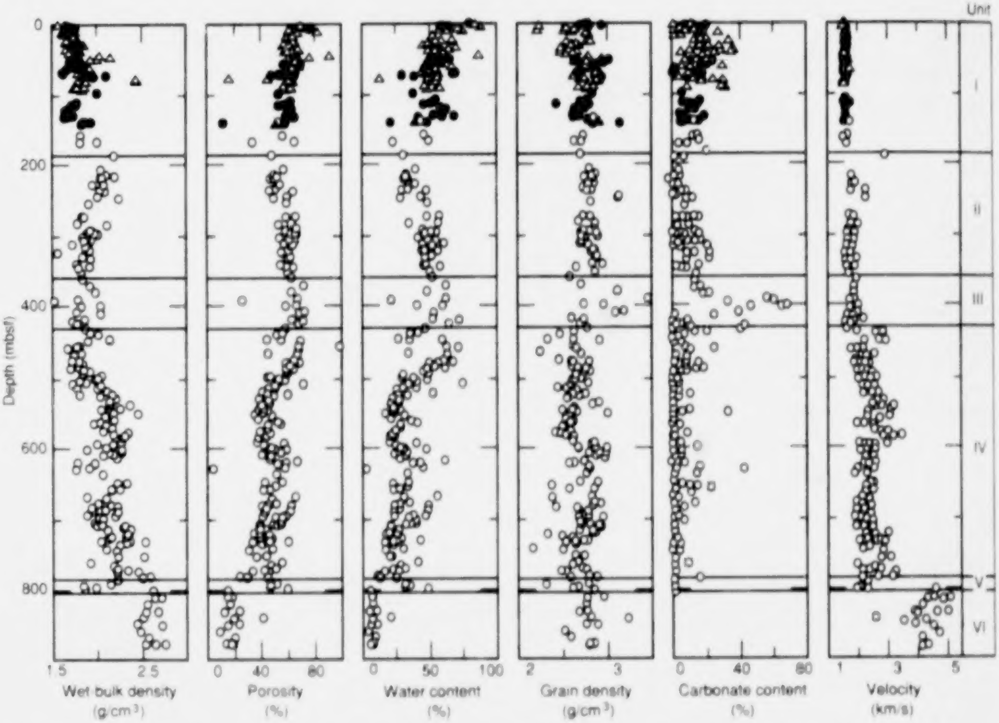

Figure 55. Downhole plots of index properties, carbonate content, and velocity for Holes 792A (open triangles), 792B (closed circles), and 792E (open circles). Horizontal lines indicate lithologic units.

In Unit I, average porosity, water content, and wet-bulk density values are 62.5%, 56.4%, and 1.8 g/cm^3, respectively. Porosity and water content values decrease downward, whereas wet-bulk density increases. Values of porosity and water content increase from Unit II (averages of 58.1% and 45%, respectively) to Unit III (averages of 66% and 58.5%, respectively). We observed a steady decrease in porosity and water content in the top 100 m of Unit IV, from average values of 61% and 52% to 43% and 24%, respectively (Fig. 55). Average porosity and water content values for the remainder of Unit IV (542-783.4 mbsf) are 46% and 29%, respectively. Wet-bulk density data mirror the trends in porosity and water content data. Wet-bulk density values in Units II and III are similar (means of 1.95 g/cm^3 and 1.86 g/cm^3, respectively). Wet-bulk density increases from about 2.0 g/cm^3 at the top of Unit IV to 2.23 g/cm^3 at approximately 535 mbsf, and then remains constant (but variable) to the base of Unit IV (averaging 2.16 g/cm^3 from 542 to 783.4 mbsf).

Smaller scale fluctuations in porosity, water content, and wet-bulk density values within the lithologic units are probably related to compositional and grain-size variations. In general, coarser grained intervals are associated with lower porosity and water content values and higher wet-bulk density values. In the upper two lithologic units, index property data correlate with variations in clay mineralogy. All four zones of high porosity above 350 mbsf (Fig. 55) correspond to smectite-rich intervals (see "Lithostratigraphy and Accumulation Rates" section, this chapter). Smectite minerals have high water-adsorption capacities and are thus associated with high water contents and porosities (e.g., Mitchell, 1976).

Increases in porosity and water content below Unit II may be related to increased concentrations of high-porosity zeolites in the unit. Intervals of high porosity observed in Unit IV (410 and 630 mbsf) may also be associated with increased glauconite and palagonite concentrations (see "Lithostratigraphy and Accumulation Rates" section, this chapter). Furthermore, the sharp change in porosity, water content, and wet-bulk density observed at approximately 540 mbsf is most likely related to the increase in grain size at this depth (see "Lithostratigraphy and Accumulation Rates" section, this chapter).

The GRAPE wet-bulk density measurements from Holes 792A and 792B and the gravimetric values from the same depth intervals are shown in Figure 56. Agreement between the two types of measurements is good. Three intervals of low wet-bulk density are observed in the GRAPE data (at approximately 12 and 87 mbsf in Hole 792A and at 50 mbsf in Hole 792B) but not in the gravimetric measurements. These intervals are associated with drilling disturbance. Although the gravimetric samples were chosen from areas that appeared the least disturbed, the GRAPE measures continuously and thus does not discriminate disturbed and undisturbed regions of the core.

Grain density values are highly variable. The data fall into three distinct depth zones (Figs. 55 and 56). From 0 to 350 mbsf

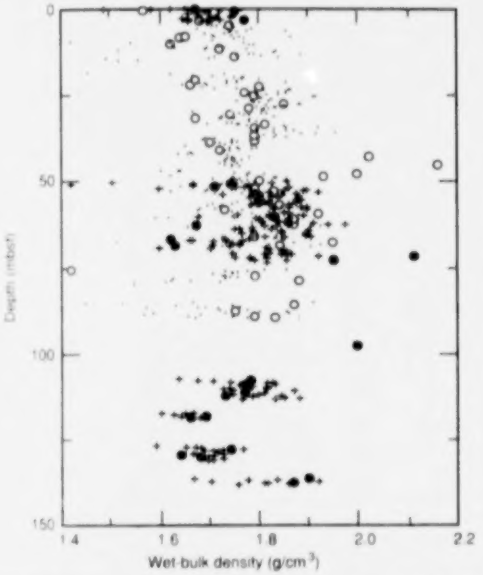

Figure 56. Comparison of gravimetric and GRAPE wet-bulk density, Holes 792A and 792B. Small closed circles = Hole 792A GRAPE; crosses = Hole 792B GRAPE; open circles = Hole 792A gravimetric; closed large circles = Hole 792B gravimetric.

(Units I and II), grain density data average 2.76 g/cm^3 and have a relatively narrow range of values from 2.52 to 3.01 g/cm^3. Within Unit III (from approximately 350 to 430 mbsf), grain density displays variable but high values (the range of values is 2.58-3.46 g/cm^3; the average is 2.87 g/cm^3). Some of this increase in grain density values can be attributed to the increased carbonate content of this unit. However, of the 13 data points within this unit, nine exceed the average carbonate density of 2.71 g/cm^3. These high values are associated with increased concentrations of opaque, heavy minerals in this unit.

In the sediments below 410 mbsf, grain density variability increases, with values ranging from 2.31 to 3.0 g/cm^3 (Figs. 55 and 56; Table 14). The mean (2.66 g/cm^3) is lower than that in the upper 350 m. Grain density increases from the base of the sediment toward the basement, but rarely attains values as high as those observed in Unit III, which ranges from 2.51 to 3.22 g/cm^3, and averages 2.79 g/cm^3 in Unit VI.

Porosity and water contents in Unit V increase relative to values at the base of Unit IV (averages of 51% and 37%, respectively), whereas wet-bulk density decreases to an average of 1.97 g/cm^3. These changes probably are caused by low-temperature hydrothermal alteration in this unit (see "Lithostratigraphy and Accumulation Rates" section, this chapter). Porosity and water content values decrease sharply near the Unit V/Unit VI contact and average 18.7% and 8.1%, respectively, within Unit VI. One sample, at 839.6 mbsf, has a porosity of 42% and a water content of 21%. The wet-bulk density and HF velocity (see below) are correspondingly low. This sample is from a zone of andesitic hyaloclastite breccia (see "Igneous Petrology" section, this chapter).

Calcium Carbonate

Calcium carbonate contents generally exhibit trends consistent with the lithologic unit boundaries (Fig. 55; see "Lithostratigraphy and Accumulation Rates" section, this chapter). Carbonate values in Unit I are quite variable (with a range of 0.6%-36.1% and an average of 13.8%) and represent samples of interbedded nannofossil-rich and nannofossil-poor beds (see "Lithostratigraphy and Accumulation Rates" section, this chapter). Carbonate values in Unit II correlate with irregularly increasing nannofossil contents with depth (see "Lithostratigraphy and Accumulation Rates" section, this chapter). Carbonate contents range from 0.3% at 184.9 mbsf to 22% near the base of Unit II. However, the average is relatively low (7.5%). This downward trend in carbonate content within Unit II continues through Unit III, where values range from 13.5% to a maximum of 67% at 398 mbsf (the average $CaCO_3$ content in Unit III is 25%). Unit IV is characterized by generally low $CaCO_3$ contents; the average is 4.0%. Isolated high carbonate peaks represent samples from microfossil-rich pelagic intervals. Two $CaCO_3$ analyses from Unit V average 0.4%.

Vane Shear Strength

Vane shear strength measurements in Holes 792A and 792B overlap in the depth intervals from 0 to 3.5 mbsf and 51 to 73 mbsf (Fig. 57; Table 15). Correlation between the two holes is good in the upper zone and below 55 mbsf. Data from Hole 792B between 51 and 55 mbsf are significantly lower than values in Hole 792A at these depths, and probably are the result of greater drilling disturbance in Hole 792B. Shear strength values are highly variable, even when one ignores anomalously low values in which disturbance is suspected. We noted three intervals displaying different strength characteristics. Shear strength values in the upper 13 m are low, exceeding 20 kPa in only two samples. The section between 13 and 78 mbsf has the highest shear strengths measured at this site, with an average of 30.8 kPa and values as high as 46.6 kPa. Below 78 mbsf, shear strength decreases, averaging 16.9 kPa and reaching values as low as those observed in the upper 13 m. Most of these low shear strength values in the deeper interval are from cores drilled by XCB or RCB operations; therefore, they are expected to display low shear strengths as a result of drilling disturbance. However, the zone of lower strengths actually starts within the APC-cored interval in Hole 792A. We noted no obvious change in porosity or wet-bulk density trends at this depth, so the origin of the low shear strengths remains unknown.

Sonic Velocity

We performed sonic velocity measurements on discrete samples from Holes 792A, 792B, and 792E with the Hamilton Frame velocimeter (Table 14; Fig. 55). In addition, we passed Cores 126-792A-1H through -10H and 126-792E-1R through -31R through the multi-sensor track (MST) and obtained sonic velocity measurements from the sonic wave (*P*-wave) logger (Fig. 58).

Velocity values average 1.59 km/s (with a range of 1.55-1.67 km/s) within Unit I (0-183.7 mbsf), 1.85 km/s (with a range of 1.65-2.28 km/s) in Unit II (183.7-357.4 mbsf), and 1.87 km/s (with a range of 1.76-2.05 km/s) in Unit III (Figs. 55 and 58). Two samples, near 240-250 mbsf, with velocity values exceeding 2.20 km/s, are from coarser grained lithologies (Figs. 55 and 58).

We observed a 1.0-km/s increase in velocity across the Unit III/Unit IV contact. This velocity contrast is the result of a high-velocity zone (average = 2.77 km/s; 429-450 mbsf) in the

Table 14. Physical property (index-property, velocity, and carbonate) data, Site 792.

Core, section, interval (cm)	Depth (mbsf)	Wet-bulk density (g/cm^3)	Dry-bulk density (g/cm^3)	Porosity (%)	Water content (%)	Grain density (g/cm^3)	Void ratio	Carbonate content (%)	Velocity (km/s)
126-792A-									
1H-1, 70-73	0.70	1.57	0.87	71	86	2.78	2.42	10.0	1.55
1H-2, 60-64	2.14							0.6	
1H-2, 97-99	2.47	1.71^a	0.94	77^a	87^a	2.23^a	3.32^a	11.0	1.55
1H-3, 99-101	3.99	1.68	1.01	68	71	2.56	2.11	12.3	1.56
1H-4, 108-111	5.58	1.74	1.13	62	57	2.66	1.62	7.9	1.61
1H-5, 140-150	7.40							4.2	
1H-6, 113-115	8.63	1.65	1.03	62	63	2.51	1.64	1.8	1.56
1H-7, 24-28	9.24	1.64^a	0.83	82^a	105^a	2.22^a	4.67^a	16.0	1.56
2H-1, 128-131	10.98	1.62	0.95	67	74	2.59	2.05	26.8	1.60
2H-2, 102-105	12.22	1.72	1.08	65	63	2.75	1.84	15.2	1.59
2H-3, 120-122	13.90							4.9	1.59
2H-4, 39-42	14.59	1.75	1.16	60	54	2.78	1.49	0.7	
3H-2, 57-59	21.17	1.67	1.07	65	67	2.80	1.89	17.5	1.53
3H-3, 78-81	22.88	1.66	1.02	65	66	2.56	1.83	33.2	1.54
3H-3, 119-123	23.29	1.80	1.19	62	55	2.77	1.64		
3H-4, 122-125	24.82	1.77	1.14	64	59	2.58	1.76	12.6	1.62
3H-5, 91-94	26.01	1.79	1.22	57	49	2.63	1.34	17.8	1.61
3H-5, 140-150	26.50							17.3	
3H-7, 22-25	28.32	1.85	1.29	56	45	2.61	1.29	18.9	1.59
4H-1, 99-102	29.39	1.78	1.17	61	53	2.68	1.58	15.4	1.56
4H-2, 118-121	31.08	1.74	1.13	62	57	2.60	1.61	21.2	1.56
4H-3, 64-67	32.04	1.67	1.01	67	70	2.59	2.05	27.4	1.55
4H-4, 116-119	34.06	1.81	1.23	59	50	2.48	1.41	36.1	1.56
4H-5, 88-91	35.28	1.79	1.11	68	64	2.63	2.15	27.7	1.57
4H-7, 31-34	37.71	1.79	1.18	61	54	2.66	1.59		1.57
4H-7, 40-43	37.80							10.3	
5H-1, 101-105	38.81	1.79	1.18	61	54	2.62	1.56	25.0	1.57
5H-2, 35-38	39.65	1.70	1.09	62	60	2.48	1.66	4.9	1.60
5H-3, 92-96	41.72	1.72	1.10	63	60	2.55	1.71	18.8	1.57
5H-4, 129-132	43.59	2.02^a	1.12	91^a	86^a	2.62^a	10.55^a	19.2	1.57
5H-6, 62-65	45.92	2.16^a	1.40	76^a	56^a	2.78^a	3.23^a	19.9	1.58
6H-1, 107-109	48.27	2.00	1.34	67	52	2.65	1.99		1.62
6H-1, 117-119	48.37							18.7	
6H-2, 67-69	49.37	1.93	1.25	69	57	2.94	2.18	7.8	1.59
6H-2, 140-150	50.10							13.9	
6H-3, 26-28	50.46	1.80	1.18	63	56	2.66	1.71	17.6	1.58
6H-4, 118-119	52.88							21.3	
6H-4, 126-128	52.96	1.79	1.16	63	57	2.66	1.74		1.59
6H-5, 17-19	53.37	1.83	1.24	59	50	2.74	1.45		
7H-1, 94-96	57.54	1.88	1.23	63	53	2.75	1.67	5.2	1.59
7H-2, 91-94	59.01	1.73	1.06	68	67	2.87	2.07	29.7	1.55
7H-3, 74-75	60.34	1.92	1.30	62	50	2.74	1.65	10.8	
7H-4, 114-117	61.91	1.87	1.27	60	49	2.77	1.50		1.58
7H-5, 90-92	63.17	1.87	1.26	62	51	2.71	1.61		
8H-1, 68-70	66.68	1.79	1.17	63	56	2.88	1.68	9.3	1.58
8H-2, 92-93	68.29	1.95	1.37	59	44	2.90	1.41	5.0	1.63
8H-3, 35-37	69.22	1.84		58	48	2.64	1.40	5.4	
9H-1, 72-74	76.32	1.42	0.97	46	49	2.74	0.83	11.8	1.61
9H-1, 87-97	76.47							16.7	
9H-2, 75-77	77.57	2.44^a	2.10	83^a	54^a	2.88^a	5.09^a		
9H-2, 100-103	77.82							29.6	1.58
9H-3, 15-21	78.50	1.79	1.18	61	54	2.69	1.56	24.6	1.59
9H-4, 20-23	79.39	1.88	1.26	63	52	2.88	1.71	17.2	1.59
10H-1, 112-114	86.42	1.87	1.30	58	46	2.65	1.37	29.0	
10H-3, 104-107	88.15	1.75	1.14	62	57	2.68	1.63	30.6	
10H-4, 94-97	89.55	1.79	1.17	63	56	2.78	1.70	8.5	
10H-5, 20-22	90.31	1.83	1.25	58	48	2.78	1.39		
126-792B-									
1H-1, 6-7	0.06							11.0	
1H-1, 113-115	1.13	1.75	1.11	65	61	2.93	1.85	10.9	1.56
1H-2, 47-48	1.97							20.4	
1H-2, 102-105	2.52	1.71	1.06	65	65	2.70	1.89	11.6	1.56
1H-3, 49-51	3.49	1.77	1.14	64	58	2.79	1.74	13.4	1.57
1H-3, 95-96	3.95							15.8	
2H-1, 110-113	51.10	1.78	1.07	68	66	3.01	2.09	23.9	1.57
2H-2, 63-66	52.13	1.71	1.12	60	56	2.67	1.52	12.1	1.62
2H-3, 29-30	53.29	1.79	1.17	63	56	2.97	1.68		
2H-4, 70-73	55.20	1.80	1.19	62	54	2.75	1.62	16.9	1.56
2H-5, 62-66	56.62	1.80	1.23	58	49	2.88	1.37	20.5	1.61
3H-1, 12-15	59.72							16.7	
3H-1, 112-115	60.72	1.83	1.27	57	47	2.81	1.33		1.62
3H-3, 81-84	63.41	1.67	1.09	58	56	2.69	1.40	0.7	
3H-6, 39-42	67.49	1.62	0.98	65	69	2.69	1.83	0.3	1.62

Table 14 (continued).

Core, section, interval (cm)	Depth (mbsf)	Wet-bulk density (g/cm³)	Dry-bulk density (g/cm³)	Porosity (%)	Water content (%)	Grain density (g/cm³)	Void ratio	Carbonate content (%)	Velocity (km/s)
126-792B- (Cont.)									
3H-7, 39-42	68.99	1.73		68	67	3.00		17.2	1.57
4X-1, 24-27	69.44	1.63	0.99	64	66	2.64	1.80	14.7	
4X-2, 130-132	72.00	2.11	1.64	47	30	2.88	0.89	1.4	
4X-3, 110-114	73.30	1.95	1.42	54	39	2.93	1.16	8.8	1.67
7X-CC, 28-33	98.48	2.00	1.46	54	38	2.83	1.17	6.2	
8X-1, 37-44	108.27	1.78	1.19	60	53	2.78	1.52	16.0	1.59
8X-2, 37-40	109.77	1.77	1.18	60	53	2.70	1.47	5.9	1.60
8X-3, 92-95	111.82	1.77	1.19	59	51	2.80	1.42	15.1	1.60
8X-3, 140-150	112.30							10.9	
8X-4, 53-56	112.93	1.73	1.21	53	46	2.43	1.13	9.0	1.67
9X-1, 113-116	118.63	1.69	1.09	61	58	2.64	1.51	13.0	1.60
9X-2, 20-23	119.20	1.66	1.04	63	63	2.76	1.68	10.3	1.61
10X-1, 95-96	128.05	1.74	1.15	59	54	2.62	1.45	4.2	
10X-2, 141-144	130.01	1.64	0.99	65	69	2.62	1.86	5.8	1.59
10X-3, 70-72	130.80	1.68	1.07	62	60	2.69	1.60	18.2	
11X-1, 25-28	137.05	1.90	1.35	56	43	2.79	1.25	7.3	1.62
11X-1, 54-55	137.34							9.9	
11X-1, 75-85	137.55							13.8	
11X-2, 35-38	138.00	1.87	1.28	59	48	3.14	1.46	5.2	1.59
11X-CC, 25-26	138.78	0.7ᵃ	0.58	12.2ᵃ	21.8ᵃ	2.86ᵃ	0.14ᵃ	5.7	
126-792C-									
1X-CC, 13-14	136.93							6	
126-792D-									
1X-1, 37-38	136.37							7.83	
1X-1, 72-74	136.52	1.89	1.37	53	40	2.91	1.11		
126-792E-									
1R-1, 38-40	135.98	1.86	1.31	55	44	2.85	1.23	12.9	1.67
3R-1, 109-111	155.89	1.82	1.27	56	46	2.73	1.28	14.5	1.61
3R-2, 60-70	156.9							15.4	1.58
3R-3, 26-29	157.26							15.2	
4R-1, 66-67	165.16	2.00	1.36	65	49	2.63	1.82		
4R-1, 84-87	165.34							9.3	
4R-2, 106-107	167.06	1.81	1.48	33	23	2.71	0.50	3.3	1.65
5R-1, 65-66	174.75							20.8	
6R-1, 13-14	183.83							7.3	
6R-1, 120-122	184.90	2.20	1.70	51	31	2.70	1.02	0.3	2.89
8R-1, 13-15	203.23	2.04	1.48	57	40	2.80	1.31	3.5	
9R-1, 19-21	212.79	2.11	1.61	50	32	2.87	1.01	1.6	
9R-2, 25-27	214.35	2.20	1.68	52	32	2.82	1.08	2.0	1.83
9R-3, 74-76	216.34	2.06	1.56	50	33	2.83	1.01	0.6	
9R-4, 40-50	217.5							2.5	
9R-5, 31-34	217.91	2.05ᵃ	1.58	47ᵃ	31ᵃ	2.74ᵃ	0.91ᵃ	2.0ᵃ	
10R-1, 48-50	222.68							0.9	1.82
10R-3, 6-8	225.26	1.96	1.43	54	40	2.79	1.19	0.5	1.80
10R-3, 124-126	226.44	2.08ᵃ	1.57	52ᵃ	35ᵃ	2.86ᵃ	1.11ᵃ	3.17ᵃ	
11R-1, 94-96	232.84	2.07	1.57	51	34	2.74	1.04	5.8	1.80
11R-2, 2-4	233.42	2.03ᵃ	1.39	64ᵃ	48ᵃ	2.82ᵃ	1.81ᵃ	7.7ᵃ	
11R-2, 64-66	234.04	2.10	1.64	47	30	2.77	0.89	0.7	2.28
12R-1, 116-119	242.66	2.01	1.42	60	44	3.13	1.49	11.9	
12R-3, 19-21	244.69	2.26	1.76	50	29	3.12	0.99	8.1	2.24
13R-1, 11-13	251.31	1.91	1.32	60	47	2.82	1.47	7.4	
15R-1, 71-72	271.21							8.5	
15R-1, 79-81	271.29							14.5	
15R-1, 99-102	271.49	1.87	1.28	59	48	2.81	1.46	6.5	1.80
15R-2, 16-18	272.16	1.85	1.20	66	57	2.73	1.91	14.7	1.77
15R-2, 115-125	273.15							2.6	
16R-1, 27-29	280.47	1.79	1.17	63	56	2.68	1.69	9.8	1.77
16R-2, 8-11	281.78	2.12	1.59	54	35	2.87	1.15	2.5	2.01
17R-1, 15-17	290.05	1.95	1.36	59	45	2.86	1.46	3.4	1.82
17R-1, 42-43	290.32							14.2	
17R-2, 141-143	292.81	1.96		65	51	2.81	1.86	0.4	1.82
17R-3, 139-141	294.29	2.01	1.39	63	47	2.71	1.68	2.6	1.91
17R-4, 43-45	294.83	1.89	1.24	66	55	2.88	1.91	14.7	1.70
18R-1, 15-17	299.65	1.85	1.22	63	54	2.89	1.72	6.8	1.74
18R-2, 102-106	302.02	1.89	1.36	54	41	2.71	1.17	1.4	1.74
18R-2, 137-138	302.37							12.3	
18R-3, 107-109	303.57	1.93	1.32	62	49	2.74	1.60	9.4	1.75
18R-3, 115-125	303.65							7.1	
18R-4, 124-126	305.24	1.87	1.23	65	55	2.71	1.82	16.7	1.73
19R-1, 10-12	309.10	1.73	1.10	64	60	2.69	1.75		1.69
19R-1, 47-49	309.47							0.8	

Table 14 (continued).

Core, section, interval (cm)	Depth (mbsf)	Wet-bulk density (g/cm³)	Dry-bulk density (g/cm³)	Porosity (%)	Water content (%)	Grain density (g/cm³)	Void ratio	Carbonate content (%)	Velocity (km/s)
126-792E- (Cont.)									
19R-2, 21-24	310.71	1.91	1.34	58	45	2.75	1.38	5.0	1.77
19R-3, 41-51	312.41	1.88	1.26	62	52	2.79	1.66	20.7	1.71
20R-1, 36-38	318.96	1.92	1.34	59	46	2.85	1.46	22.0	1.73
20R-2, 123-126	321.33	1.57[a]	1.02	55	57	2.82	1.24	12.1	1.73
20R-3, 19-21	321.79	1.89	1.33	57	45	2.84	1.32	8.7	1.76
21R-1, 15-17	328.45	1.85	1.24	62	52	2.89	1.63	21.7	1.74
21R-2, 50-53	330.30	1.93	1.33	60	47	2.88	1.50	8.0	1.93
22R-1, 79-81	338.69	1.78	1.23	56	47	2.83	1.26	6.4	1.79
22R-2, 5-7	339.45	1.92	1.33	59	46	2.94	1.44	15.6	1.69
22R-2, 140-150	340.8							7.3	
22R-3, 52-54	341.42							2.9	
22R-3, 74-77	341.64	1.80	1.16	64	58	2.65	1.80		1.87
23R-1, 74-77	348.34	1.82	1.23	60	51	2.86	1.48	13.9	1.74
24R-1, 25-27	357.55	1.85	1.24	62	52	2.58	1.64	13.5	1.95
25R-1, 108-111	368.08	1.92	1.21	72	63	2.70	2.57	14.0	1.91
25R-1, 129-131	368.29							15.8	
26R-1, 10-12	376.7							21.5	
26R-1, 68-70	377.28	1.98	1.36	63	48	3.11	1.68	19.2	1.86
27R-1, 27-37	386.57							57.3	
27R-2, 42-44	387.34	1.80	1.13	68	62	3.46	2.08	59.6	1.80
27R-4, 88-90	390.80	1.50[a]	1.24	26[a]	22[a]	3.80[a]	0.35[a]	33.2	1.83
28R-1, 35-36	396.35								
28R-1, 69-70	396.69	1.82	1.16	67	60	2.74	2.01	64.6	2.05
28R-2, 41-43	397.91	2.04	1.46	59	42	2.95	1.41	67.6	1.79
29R-1, 97-100	406.57	1.78	1.07	72	71	3.19	2.55	39.2	1.96
29R-2, 5-7	407.15							25.2	
29R-2, 21-23	407.31	2.04	1.35	69	53	3.09	2.22	1.8	1.76
30R-1, 108-110	416.28	1.87	1.24	63	53	2.60	1.71	0.5	2.20
30R-3, 84-86	419.04	1.73	1.03	71	72	2.73	2.42	9.3	1.80
30R-5, 10-12	421.3	1.73		72	75	2.79		4.2	
30R-5, 11-21	421.31							0.8	1.78
30R-7, 37-39	423.28	1.79	1.12	68	64	2.69	2.16	11.1	1.69
31R-1, 54-55	425.44							42.7	1.67
31R-1, 127-128	426.17							41.1	
31R-2, 22-23	426.62							0.9	
31R-2, 48-49	426.88							0.4	
31R-3, 96-98	428.86	1.88	1.31	58	46	2.78	1.39	20.6	1.99
31R-3, 118-119	429.08							13.9	
32R-1, 35-37	434.95	1.93	1.38	55	41	2.62	1.22	5.8	2.60
32R-3, 98-101	438.58	2.02	1.50	52	36	2.47	1.08	4.9	2.81
33R-1, 15-17	444.35	2.14	1.59	55	36	2.62	1.22		2.80
33R-1, 89-90	445.09	2.15	1.71	44	27	2.33	0.79	0.8	2.87
33R-2, 95-105	446.65							1.4	
33R-3, 58-60	447.58	1.90	1.22	69	59	2.91	2.24	4.0	2.24
34R-1, 67-69	454.57	1.78[a]	0.81	99[a]	131[a]	1.83[a]	73[a]	25.0	1.82
34R-2, 102-104	456.42	1.80	1.13	68	63	2.61	2.10	8.8	2.15
34R-3, 79-81	457.69	1.68	1.01	68	71	2.64	2.14	9.7	2.05
35R-1, 107-110	464.57	1.83	1.38	45[a]	33[a]	2.24[a]	0.82	1.0	2.52
35R-2, 48-50	465.49	1.75	1.09	67	64	2.71	1.99	8.3	2.22
36R-1, 75-77	473.95	1.73	1.10	64	61	2.46	1.76	6.8	2.14
36R-2, 139-141	476.09	1.81	1.23	59	50	2.61	1.41	5.2	2.33
36R-3, 129-132	477.49	1.73	1.06	69	68	2.79	2.18	14.6	1.95
36R-4, 67-77	478.37							1.9	
36R-5, 91-93	479.38	1.85	1.21	65	56	2.59	1.86	6.3	2.17
37R-1, 73-74	483.53							18.8	
37R-1, 131-135	484.11	1.80	1.19	62	54	2.60	1.60	7.9	2.12
37R-3, 54-57	486.34	1.71	1.08	64	62	2.67	1.75	13.9	2.03
37R-5, 16-18	488.96	1.86	1.28	59	48	2.76	1.45		
37R-5, 128-130	490.08	1.92	1.34	59	46	2.80	1.43	5.4	2.23
37R-7, 16-18	491.96							1.1	2.33
38R-1, 43-45	492.93	1.84	1.25	59	49	2.74	1.46	1.3	2.47
38R-3, 119-121	496.69	2.04	1.57	47	31	2.64	0.89	0.3	2.63
38R-5, 30-33	498.80	2.01	1.56	45	30	2.64	0.82	0.8	2.60
38R-CC, 6-8	501.25	1.99	1.46	53	38	2.70	1.14	0.4	2.37
39R-1, 128-130	503.48	1.81	1.24	58	48	2.63	1.36	2.8	2.18
39R-2, 115-125	504.85							1.5	
39R-3, 36-38	505.56	1.88	1.35	53	41	2.60	1.13	2.8	2.21
39R-5, 63-66	508.83	2.03	1.53	50	34	2.59	1.00	0.6	2.47
40R-1, 103-106	512.93	1.79	1.29	51	41	2.55	1.03	2.3	2.36
40R-3, 15-17	515.05	2.00	1.55	45	30	2.43	0.83	0.6	2.51
40R-5, 107-110	518.97	2.11	1.70	42	26	2.66	0.73	0.5	2.67
40R-6, 75-77	520.15							10.7	
41R-, 20-22	521.80	2.17	1.73	44	27	2.76	0.79	0.6	2.48
41R-1, 118-119	522.78							0.6	
41R-2, 56-59	523.66	1.81	1.30	60	52	2.61	1.52	2.6	2.23
41R-3, 82-85	525.42	2.03	1.53	50	34	2.69	0.99	0.6	2.32

Table 14 (continued).

Core, section, interval (cm)	Depth (mbsf)	Wet-bulk density (g/cm^3)	Dry-bulk density (g/cm^3)	Porosity (%)	Water content (%)	Grain density (g/cm^3)	Void ratio	Carbonate content (%)	Velocity (km/s)
126-792E- (Cont.)									
41R-5, 100-102	528.33	2.20	1.82	39	22	2.56	0.63	0.6	2.79
42R-1, 52-54	531.72	2.15	1.70	45	27	2.55	0.82		2.63
42R-3, 116-118	535.36	2.14	1.69	46	28	2.89	0.85	0.6	2.52
42R-4, 140-150	537.1							0.6	
42R-5, 119-120	538.39	2.38	1.98	41	21	2.83	0.68	0.8	2.75
43R-1, 77-79	541.37	2.27	1.86	42	23	2.62	0.71	0.6	2.78
43R-3, 56-58	543.97	2.04	1.66	39	24	2.50	0.63	9.8	3.10
43R-3, 110-111	544.51							7.1	
43R-5, 82-84	547.25	2.07	1.62	45	29	2.60	0.83	0.9	2.32
43R-5, 100-101	547.43							32.6	
43R-7, 30-33	549.63	2.19	1.78	41	24	2.65	0.70	0.5	3.11
44R-1, 60-62	550.90	2.46	2.11	35	17	3.00	0.54	0.6	3.09
44R-3, 52-55	553.83	2.09	1.61	49	31	2.57	0.94	0.7	2.26
44R-5, 34-36	556.65	2.19	1.82	38	22	2.53	0.62	0.7	2.73
45R-1, 65-67	560.65	2.03	1.50	53	37	2.61	1.14	0.8	2.22
45R-2, 0-10	561.45							0.7	
45R-3, 1-3	562.93	1.97	1.43	55	40	2.58	1.21	1.6	2.04
45R-4, 133-135	565.56	2.10	1.65	46	29	2.57	0.83	0.8	2.52
46R-1, 73-75	570.43	2.17	1.72	45	27	2.50	0.82	0.8	2.60
46R-3, 122-124	573.65	2.07	1.68	40	24	2.59	0.65	0.7	2.76
46R-5, 119-120	576.55	2.35	1.90	46	25	2.42	0.84	8.6	3.00
46R-7, 31-35	578.56	2.19	1.79	40	23	2.48	0.68		3.55
47R-1, 114-116	580.54	2.31	1.88	44	24	2.52	0.77	1.1	2.91
47R-3, 48-50	582.49	2.29	1.91	38	21	2.62	0.62	0.8	3.15
48R-1, 35-37	588.95	2.27	1.90	38	21	2.61	0.61	0.8	3.03
48R-3, 38-40	591.28	2.01	1.45	57	41	2.84	1.32	1.8	2.11
48R-3, 52-53	591.42							5.3	
48R-5, 63-65	594.21	2.18	1.77	42	25	2.83	0.73	0.4	2.52
48R-6, 83-84	595.88							14.2	2.33
48R-7, 140-150	597.55							0.4	2.40
48R-8, 19-21	577.84	2.10		47	30	2.67	0.89	0.6	2.32
49R-1, 120-121	599.00	2.17	1.71	46	28	2.86	0.86		2.32
49R-2, 37-41	599.67	2.28	1.77	51	30	2.67	1.05		2.55
49R-3, 63-66	601.43	1.89	1.31	58	46	2.99	1.40	3.9	2.15
49R-5, 111-114	604.76	2.13	1.67	46	28	2.89	0.84	4.2	2.34
49R-6, 37-39	605.52	2.27	1.73	55	33	2.98	1.22		2.33
50R-1, 23-26	607.63	2.18	1.78	40	23	2.79	0.67	1.3	2.48
50R-3, 8-10	610.48	2.07	1.60	48	31	2.87	0.91	0.6	2.25
50R-5, 16-18	613.57	2.22	1.76	46	27	2.97	0.86	0.8	2.35
50R-7, 11-13	616.52							2.4	2.37
51R-1, 33-35	617.43	1.79	1.14	66	61	2.73	1.96	6.1	2.26
51R-2, 106-109	619.66	2.00	1.48	52	37	2.57	1.10	2.6	2.55
51R-2, 140-150	620							1.6	
51R-3, 14-17	620.24	1.98	1.41	58	43	2.62	1.41	6.3	2.42
52R-1, 38-40	627.18	1.91	1.33	58	45	2.79	1.37	16.0	2.08
52R-1, 100-102	627.8							42.5	
52R-2, 31-34	628.61	1.78[a]	1.73	5[a]	3[a]	2.80[a]	0.05[a]	0.9	1.98
52R-3, 22-24	630.02							0.6	2.53
52R-4, 49-51	631.79							14.7	2.06
52R-5, 50-52	633.3							0.8	1.94
52R-6, 8-10	634.38	2.07	1.56	51	34	2.77	1.03	0.7	2.30
54R-1, 136-137	647.46	2.23	1.69	55	34	2.69	1.23	0.7	2.40
54R-2, 49-51	648.09							6.3	
54R-3, 11-12	649.21	2.33	1.91	43	23	2.89	0.74	1.4	2.51
54R-3, 140-150	650.5							8.9	
54R-5, 83-84	652.93	2.10	1.59	51	33	2.38	1.05	13.7	2.31
54R-6, 8-9	653.68							23.2	
55R-1, 53-55	656.23	2.17	1.72	46	28	2.57	0.85	12.1	2.37
55R-2, 99-101	658.19	2.25	1.84	41	23	2.85	0.71	0.8	2.46
56R-2, 78-80	667.68	1.89	1.25	65	55	2.82	1.89	2.2	2.16
56R-4, 16-18	670.06	2.11	1.64	48	30	2.38	0.93	0.7	2.36
56R-6, 136-138	673.98							0.4	2.00
57R-1, 96-99	679.06	2.00	1.49	51	36	2.87	1.06	13.0	2.15
57R-3, 4-6	678.14	2.16	1.71	46	28	2.92	0.83	0.5	2.42
57R-5, 84-87	681.94	2.22	1.81	41	23	2.83	0.70	0.2	2.38
57R-5, 140-150	682.5							0.3	
57R-6, 50-52	683.10	1.94	1.32	63	49	2.41	1.67	6.7	2.07
58R-1, 69-71	685.49	2.10	1.67	44	27	2.66	0.78	0.5	2.30
58R-2, 93-95	687.23	1.95	1.34	62	48	2.67	1.62	2.3	2.22
58R-CC, 19-21	689.89	2.23	1.82	42	24	2.78	0.72	0.4	2.41
59R-1, 68-68	695.05	1.89	1.31	59	47	2.78	1.41	3.7	1.96
59R-2, 46-48	696.36	2.20	1.79	41	24	2.76	0.69	0.4	2.41
59R-3, 101-103	689.28	2.03	1.48	55	39	2.67	1.24		2.25
59R-4, 73-75	699.22	2.07	1.57	51	34	2.94	1.06	0.7	2.30
59R-5, 47-50	700.40	2.03	1.49	56	39	2.77	1.25	6.1	2.07
60R-1, 121-123	705.21	1.98	1.44	55	40	2.69	1.21	0.7	2.02

Table 14 (continued).

Core, section, interval (cm)	Depth (mbsf)	Wet-bulk density (g/cm^3)	Dry-bulk density (g/cm^3)	Porosity (%)	Water content (%)	Grain density (g/cm^3)	Void ratio	Carbonate content (%)	Velocity (km/s)
126-792E- (Cont.)									
60R-2, 70-73	706.20	2.06	1.58	49	32	2.70	0.95	0.4	2.20
60R-3, 16-19	707.16	2.01	1.50	52	36	2.80	1.06	0.4	2.03
60R-4, 140-143	709.90	2.32	1.94	38	21	2.90	0.62	0.3	2.50
60R-6, 28-30	711.78	2.29	1.91	38	21	2.92	0.62	0.3	2.54
60R-6, 140-150	712.9							0.4	
61R-1, 143-145	715.03	2.12	1.70	43	26	2.68	0.76		2.34
61R-2, 119-121	716.29	2.37	1.99	39	20	2.83	0.63	0.3	2.52
61R-3, 130-133	717.90	2.35	1.97	38	20	2.86	0.62	0.4	2.61
61R-4, 87-89	718.97	2.33	1.99	34	18	2.83	0.52	0.6	3.02
62R-1, 3-5	722.93	2.32	1.86	46	26	2.54	0.85	1.2	2.29
62R-2, 94-96	724.52	2.17	1.78	39	23	2.49	0.64	0.8	2.61
62R-4, 36-39	726.53	2.13	1.68	46	29	2.61	0.86	1.1	2.35
62R-6, 114-116	729.83	2.36	1.90	46	25	2.78	0.86		2.62
62R-7, 69-71	730.80	2.54	2.10	45	22	2.73	0.81	0.6	2.77
62R-8, 6-8	731.67	2.05	1.46	60	43	2.63	1.49	1.7	2.09
63R-1, 109-111	733.59	2.32	1.99	33	17	2.53	0.50	0.5	2.86
63R-3, 5-7	735.41	2.25	1.85	41	23	2.64	0.68	2.7	2.43
63R-3, 138-150	736.74							2.9	
64R-1, 15-17	742.35	2.10	1.62	48	31	2.15	0.92	2.2	2.17
64R-2, 51-53	744.16	2.22	1.92	31	17	2.50	0.45	0.4	2.85
65R-1, 11-13	751.91	2.23	1.87	36	20	2.63	0.57	0.6	3.07
65R-2, 16-18	753.39	2.52	2.08	44	22	2.73	0.78	0.5	2.80
66R-1, 52-54	762.02	1.92	1.38	55	41	2.67	1.21	9.7	1.96
66R-3, 144-146	765.94	2.19	1.60	47	28	2.60	0.90	0.7	2.56
66R-5, 139-149	768.91							1.2	
66R-6, 10-12	769.11	2.23	1.72	51	31	2.72	1.05	1.1	2.41
67R-1, 75-77	771.95	2.33	1.91	42	23	2.76	0.73	0.4	2.74
67R-2, 111-113	773.81	2.46	2.13	34	16	2.53	0.51	0.9	3.26
67R-3, 23-25	774.43	2.22	1.78	45	26	2.49	0.81	0.7	2.22
68R-1, 51-53	781.41	2.59	2.35	25	11	2.79	0.33	16.1	3.25
68R-2, 83-85	782.97	2.51	2.23	29	13	2.88	0.41	0.5	2.68
68R-2, 124-126	783.38	2.23	1.79	44	25	2.58	0.78	0.2	2.18
69R-1, 19-21	790.79	2.15	1.65	51	32	2.79	1.03		2.34
69R-2, 90-92	793.00	1.85	1.38	47	35	2.31	0.88		2.16
69R-3, 107-108	794.67							0.5	
69R-4, 24-26	795.16	1.99	1.53	46	31	2.67	0.86		2.37
69R-4, 136-146	796.28		1.28					0.3	
69R-5, 89-91	797.27	1.87		60	49	2.61	1.52		2.01
70R-CC, 2-5	800.22	2.62	2.48	15	6	2.85	0.18		4.59
71R-1, 52-54	810.42	2.65	2.50	15	6	2.77	0.18		4.50
71R-2, 22-24	811.55	2.71	2.53	18	7	2.94	0.22		4.39
71R-2, 83-85	812.16		2.66						5.09
71R-3, 5-7	812.88	11.10^a	2.61	4^a	3^a	0.12^a			4.88
73R-1, 68-70	820.18	2.56	2.39	17	7	2.75	0.20		4.17
73R-1, 49-51	829.69		2.67						5.03
73R-1, 123-125	830.43	2.68	2.56	12	5	2.68	0.14		4.66
73R-2, 99-101	831.64	2.54	2.30	24	11	2.77	0.31		3.94
73R-2, 141-143	832.06								3.91
74R-1, 77-78	839.57	2.51	2.09	42	21	2.81	0.71		2.62
74R-2, 28-30	840.51	3.23	3.03	20	7	3.22	0.25		4.29
74R-2, 46-48	840.69		2.21						3.58
75R-1, 71-73	848.91	2.45	2.22	23	11	2.75	0.31		3.94
75R-2, 35-37	850.05	2.72	2.58	15	6	2.88	0.18		4.47
76R-1, 96-98	858.66	2.48	2.39	9	4	2.51	0.10		4.75
77R-1, 44-46	867.54	2.57	2.37	20	9	2.58	0.25		4.16
78R-1, 22-24	876.82	2.76	2.61	15	6	2.80	0.17		4.30
78R-1, 37-39	876.97	2.53	2.37	17	7	2.77	0.20		4.12
78R-1, 61-63	877.21	2.64	2.46	18	8	2.84	0.22		4.22

[a] Data of uncertain quality.

uppermost part of Unit IV. Below this high-velocity layer, velocity data increase downward from an average of 2.15 km/s at 450-480 mbsf to 2.77 km/s at 540–590 mbsf. At 590 mbsf, we observed a velocity decrease of 0.5 km/s. From 590-708 mbsf, velocity values show little variation and average 2.28 km/s. Between 708 mbsf and the bottom of Unit IV (783 mbsf), variability increases and velocity values increase slightly (average = 2.58 km/s).

A distinct decrease (~0.5 km/s) in velocity is observed across the Unit IV/Unit V contact. The few velocity measurements made within Unit V average 2.22 km/s (with a range from 2.01 to 2.37 km/s). These lower velocities may be the result of the alteration that we observed in these sediments (see "Lithostratigraphy and Accumulation Rates" section, this chapter).

The contact of the sedimentary section with igneous basement (Unit VI; composed of andesite) at 804 mbsf is marked by a 2.58-km/s increase (from 2.01-4.59 km/s) in velocity. Velocity data in basement rocks average 4.26 km/s (range = 2.62-5.09 km/s). Velocity values decrease downward in the basement rocks, probably the result of an increase in alteration.

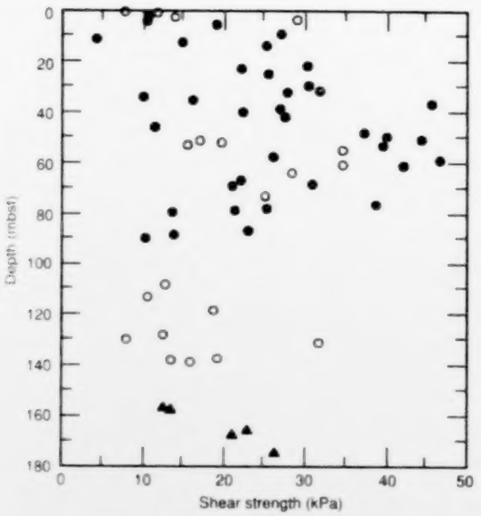

Figure 57. Plots of shear strength vs. depth for Holes 792A (closed circles), 792B (open circles), and 792E (triangles).

A comparison of MST *P*-wave and Hamilton Frame velocity data reveals a close agreement within depths drilled by the APC (Hole 792A; Fig. 58. In rotary-drilled Hole 792E, there is a large difference between MST and HF velocity measurements. This is attributed to a large annulus of air between the core and the core liner that resulted from rotary coring. This evidence, coupled with the results from previous holes (see "Physical Properties" section, "Site 787" and "Site 790/791" chapters, this volume) suggests that MST *P*-wave logging should not be attempted on rotary cores.

Thermal Conductivity

Thermal conductivity measurements were performed on as many undisturbed cores as possible from the sedimentary column, by means of the needle-probe method (Fig. 59; Table 16). In addition, thermal conductivity measurements were made on two well-lithified sedimentary samples and four igneous rock samples by means of the half-space method (Fig. 59, Table 16).

Thermal conductivity values within Units I, II, III, and IV are highly variable. However, we observed a slight increase in thermal conductivity with depth. Thermal conductivity values increase from 1.000 to 1.050 between Units I and IV, and average 1.010, 1.018, 1.047, and 1.052 W/m · K in Units I, II, III, and IV, respectively.

The two well-lithified sedimentary rocks from the lower parts of Unit IV (Sample 126-792E-67R-1, 60 cm; 771.80 mbsf) and Unit V (Sample 126-792E-69R, CC, 10 cm; 798.20 mbsf) yielded thermal conductivity values of 1.172 and 1.038 W/m · K, respectively.

Thermal conductivity data within the andesitic "basement" (Unit VI; see "Lithostratigraphy and Accumulation Rates" section, this chapter) increase sharply. Average values for this unit are 1.610 W/m · K (with a range of 1.456–1.838 W/m · K).

Heat Flow

Plots of temperature vs. time for the three successful downhole temperature runs are shown in Figure 60. These three mea-

Table 15. Shear strength data, Site 792.

Core, section, interval (cm)	Depth (mbsf)	Shear strength (kPa)
126-792A-		
1H-2, 100	2.50	10.7
1H-3, 110	4.10	10.4
1H-4, 94	5.44	19.0
1H-7, 20	9.20	26.8
2H-1, 114	10.84	4.2
2H-2, 107	12.27	14.7
2H-3, 114	13.84	25.3
3H-2, 70	21.30	30.2
3H-3, 82	22.92	22.1
3H-4, 116	24.76	25.4
4H-1, 105	29.45	30.4
4H-2, 115	31.05	31.7
4H-3, 55	31.95	27.8
4H-4, 123	34.13	10.0
4H-5, 94	35.34	16.1
4H-6, 45	36.35	45.6
5H-1, 100	38.80	26.8
5H-2, 42	39.72	22.2
5H-3, 97	41.77	27.4
5H-6, 49	45.79	11.4
6H-1, 106	48.26	37.2
6H-2, 71	49.41	39.9
6H-3, 29	50.49	44.3
6H-4, 129	52.99	39.6
7H-1, 92	57.52	26.1
7H-2, 89	58.99	46.6
7H-3, 75	60.35	42.0
7H-4, 92	61.69	42.0
8H-1, 65	66.65	21.9
8H-2, 95	68.32	30.8
8H-3, 34	69.21	21.0
9H-1, 74	76.34	38.7
9H-2, 104	77.86	25.2
9H-3, 17	78.49	21.2
9H-4, 24	79.43	13.5
10H-1, 115	86.45	22.9
10H-3, 109	88.20	13.8
10H-4, 96	89.57	10.3
126-792B-		
1H-1, 37	0.37	7.7
1H-1, 118	1.18	11.7
1H-2, 105	2.55	14.0
1H-3, 53	3.53	28.9
2H-1, 109	51.09	16.8[a]
2H-2, 63	52.13	19.6[a]
2H-3, 29	53.29	15.4[a]
2H-4, 73	55.23	34.5
3H-1, 125	60.85	34.5
3H-3, 131	63.91	28.4
4H-3, 112	73.32	25.0
8H-1, 44	108.34	12.8
8H-4, 64	113.04	10.7
9H-1, 110	118.60	18.7
10H-1, 99	128.09	12.4
10H-2, 139	129.99	7.9
10H-3, 75	130.85	31.7
11H-1, 23	137.03	19.1
11H-2, 32	137.91	13.5
11H-CC, 25	138.78	15.9
126-792E-		
3R-1, 115	155.95	12.4
3R-3, 25	157.25	13.5
4R-1, 66	165.16	22.9
4R-2, 106	167.06	21.0
5R-1, 64	174.74	26.3

[a] Data of uncertain quality.

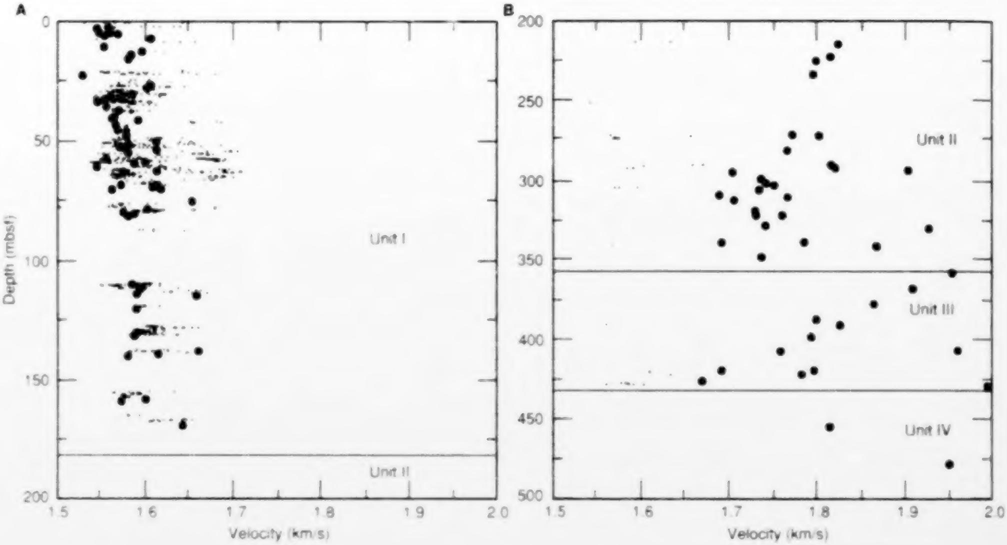

Figure 58. Comparison of sonic velocity determined by Hamilton Frame (large closed circles) and multi-sensor track (small dots) methods for Site 792. Horizontal lines indicate lithologic units. Note good correlation between methods in APC cores and poor correlation in RCB cores (shown at different vertical scales). **A.** APC cores. **B.** RCB cores.

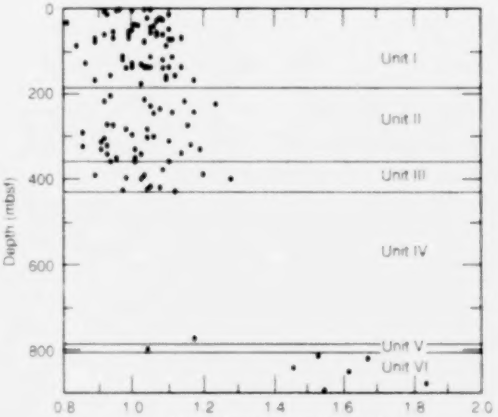

Figure 59. Plot of thermal conductivity vs. depth from Site 792. Horizontal lines indicate lithologic unit boundaries.

surements produced excellent data (Table 17) from which we made preliminary estimates of *in-situ* temperatures by extrapolation of the temperature-vs.-time data through the use of theoretical decay equations (Table 17; shipboard computer system software developed by K. Becker, unpubl. data). The linearity of the resulting geothermal gradient (0.054°C/m; Fig. 61) suggests that no convection is occurring through this deposit. Therefore, heat flow may be calculated as

$$Q = k\, dT/dz, \tag{1}$$

where Q = the calculated heat flow,
k = the average thermal conductivity, and
dT/dz = the geothermal gradient.

If we use an average thermal conductivity (not corrected to *in-situ* values) of 1.012 W/m · K for the upper 110 mbsf, an average heat flow of 0.0546 W/m^2 (1.3 heat flow units, or HFU) is determined. Predicted heat-flow values, determined on the basis of half-space models of purely conductive flow (Davis and Lister, 1977; Parsons and Sclater, 1977) and various estimates for the age of basement, range as high as 2.19 HFU (assuming a minimum basement age of 30 Ma) to as low as 1.6 HFU (assuming a 50-Ma basement age).

DOWNHOLE MEASUREMENTS

At Hole 792E, the drill pipe became stuck at a depth of 287.0 mbsf as we attempted to pull out of the hole to the proposed logging depth of 120.0 mbsf. Thus, we decided to deploy a reduced combination of geophysical sensors in the open-hole section. The density tool was excluded to eliminate the risk of leaving a radioactive source in the hole if the tool became stuck. The first run consisted of resistivity, velocity, natural gamma, and temperature sensors. In total, we conducted a series of five experiments in Hole 792E. The second run consisted of the formation microscanner (FMS), natural gamma ray, and temperature sensors. The geochemical, natural gamma ray, and temperature sensors were deployed during the third run, whereas the density, natural gamma ray, and temperature sensors were com-

Table 16. Thermal conductivity data, Site 792.

Core, section, interval (cm)	Depth (mbsf)	Thermal conductivity (W/m · K)
792B-1H-1, 111	1.11	1.047
792A-1H-1, 119	1.19	0.958
792B-1H-2, 95	2.45	1.028
792B-1H-3, 75	3.75	0.950
792A-1H-3, 98	3.98	0.999
792A-1H-5, 104	7.04	0.913
792A-2H-3, 61	13.31	0.926
792A-2H-3, 128	13.98	1.098
792A-2H-6, 86	18.66	0.668
792A-3H-2, 45	21.05	1.074
792A-3H-3, 33	22.43	1.044
792A-3H-5, 51	25.61	1.083
792A-4H-1, 70	29.10	1.070
792A-4H-3, 69	32.09	0.813
792A-4H-6, 60	36.50	1.005
792A-5H-1, 59	38.39	1.012
792A-5H-3, 89	41.69	1.060
792A-5H-5, 25	44.05	1.049
792A-6H-1, 81	48.01	1.102
792A-6H-3, 66	50.86	0.993
792B-2H-3, 73	53.73	0.939
792B-2H-4, 73	55.23	0.986
792B-2H-5, 73	56.73	1.065
792A-7H-1, 18	56.78	1.052
792A-7H-2, 78	58.88	0.984
792A-7H-3, 55	60.15	0.918
792B-3H-1, 107	60.67	1.083
792B-3H-3, 60	63.20	1.068
792A-8H-1, 103	67.03	1.138
792A-8H-2, 102	68.39	0.892
792B-3H-7, 48	69.08	0.989
792A-8H-3, 36	69.23	0.942
792B-4X-1, 77	69.97	1.141
792B-4X-2, 123	71.93	1.099
792B-4X-3, 17	72.37	1.112
792A-9H-1, 70	76.30	1.028
792A-9H-2, 105	77.87	1.028
792A-9H-3, 34	78.66	0.893
792A-10H-1, 53	85.83	0.838
792A-10H-1, 120	86.50	1.090
792A-10H-2, 28	87.08	0.622[a]
792B-8X-2, 99	110.39	0.971
792B-8X-3, 88	111.78	1.049
792B-8X-4, 73	113.13	1.112
792B-9X-1, 102	118.52	1.082
792B-9X-2, 18	119.18	0.970
792B-10X-1, 117	128.27	0.992
792B-10X-2, 33	128.93	0.862
792B-10X-3, 94	131.04	1.026
792E-1R-1, 19	135.79	1.137
792E-1R-1, 34	135.94	1.031
792D-1X-1, 43	136.43	1.104
792B-11X-1, 10	136.90	0.993
792C-1X-CC, 14	136.94	1.049
792C-1X-CC, 32	137.12	1.043
792B-11X-2, 28	137.93	0.974
792B-11X-CC, 12	138.65	1.087
792E-3R-1, 75	155.55	0.932
792E-3R-2, 44	156.74	1.121
792E-3R-3, 33	157.33	1.092
792E-4R-1, 12	164.62	1.095
792E-4R-2, 108	167.08	1.173
792E-4R-CC, 5	167.55	0.893
792E-5R-1, 61	174.71	1.024
792E-8R-1, 24	203.34	0.932
792E-9R-1, 84	213.44	1.034
792E-9R-3, 109	216.69	0.918
792E-9R-5, 33	217.93	1.150
792E-10R-2, 48	224.18	1.232
792E-10R-4, 44	227.14	1.046
792E-11R-1, 55	232.45	1.117[a]
792E-11R-1, 126	233.16	1.073
792E-11R-2, 54	233.94	0.7891[a]
792E-12R-1, 115	242.65	1.114
792E-12R-2, 67	243.67	1.175
792E-12R-3, 103	245.53	1.058
792E-13R-1, 44	251.64	1.039[a]
792E-13R-2, 24	252.94	0.673[a]
792E-15R-1, 104	271.54	0.923
792E-15R-2, 27	272.27	1.151
792E-15R-3, 20	273.70	0.943
792E-16R-1, 72	280.92	1.040
792E-16R-2, 33	282.03	0.978
792E-17R-1, 9	289.99	0.946[a]
792E-17R-2, 8	291.48	0.851
792E-17R-3, 100	293.90	0.993
792E-18R-1, 23	299.73	1.062
792E-18R-2, 13	301.13	1.038
792E-18R-4, 34	304.34	0.916
792E-19R-1, 100	310.00	1.103
792E-19R-2, 76	311.26	0.905
792E-19R-3, 22	312.22	0.896[a]
792E-20R-1, 21	318.81	1.164
792E-20R-2, 23	320.33	0.929
792E-20R-3, 46	322.06	0.850
792E-21R-1, 47	328.77	1.193
792E-21R-1, 117	329.47	1.006
792E-21R-2, 21	330.01	0.905
792E-22R-1, 15	338.05	1.138
792E-22R-2, 40	339.80	1.026
792E-22R-3, 20	341.10	0.924
792E-23R-1, 68	348.28	0.953
792E-23R-2, 21	349.31	1.004
792E-24R-1, 27	357.57	1.099
792E-24R-1, 57	357.87	0.929
792E-24R-1, 96	358.26	1.006
792E-25R-1, 87	367.87	0.951[a]
792E-26R-1, 108	377.68	1.087
792E-27R-2, 66	387.58	1.201
792E-27R-3, 105	389.47	1.032
792E-27R-4, 68	390.60	0.891
792E-28R-1, 16	396.16	0.976
792E-28R-2, 54	398.04	1.279
792E-28R-2, 115	398.65	1.024
792E-30R-2, 70	417.40	1.049
792E-30R-3, 64	418.84	1.078
792E-30R-6, 73	422.14	1.037
792E-31R-1, 96	425.86	0.971
792E-31R-2, 35	426.75	1.124
792E-31R-3, 124	429.14	1.129[a]
792E-67R-1, 60	771.8	1.172
792E-69R-CC, 10	798.2	1.038
792E-71R-3, 68	813.58	1.531
792E-72R-1, 14	819.64	1.673
792E-73R-2, 28	893.98	1.546
792E-74R-2, 61	840.91	1.456
792E-75R-2, 53	850.23	1.617
792E-78R-1, 114	877.74	1.838

[a] Data of uncertain quality.

bined for the fourth run. The velocity sensor was added to this fourth combination to obtain a second velocity profile in an attempt to reduce the noise level encountered during the first run. The last run consisted of a vertical seismic profile (VSP) experiment. The wireline heave compensator was used for downhole measurements in Hole 792E, but it failed at the beginning of the third run. A summary of the operational timing is provided in Table 18.

Prior to releasing the drill bit, we displaced the borehole fluid with KCl mud. With the exception of a short section located at the top of the open hole (297.0–317.0 mbsf), and two fault zones (407.5–430.0 and 779.0–804.0 mbsf), the borehole was generally cylindrical to slightly elliptical, with a diameter constrained to < 11.0 in. The deviation of the borehole axis

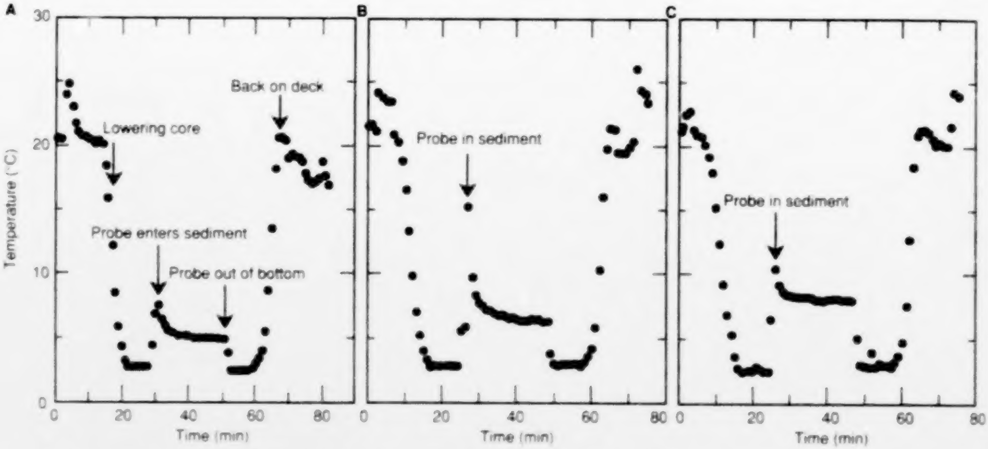

Figure 60. Plots of temperature versus time for the three Uyeda temperature probe runs. **A.** Hole 792A (47.2 mbsf). **B.** Hole 792C (67.0 mbsf). **C.** Hole 792C (110.0 mbsf).

Table 17. *In-situ* temperatures from Uyeda temperature probe runs, Site 792.

Depth (mbsf)	*In-situ* temperature (°C)
0	2.02
47.2	4.5
67	5.6
110	7.92

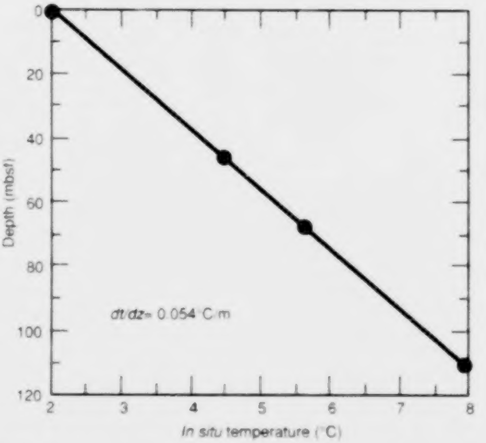

Figure 61. *In-situ* temperature vs. depth, Site 792.

Table 18. Summary of downhole measurement operations, Site 792.

Date	Time[a] (UTC)	Operation	Run no.	Sensors[b]
May 23, 1989	2115	Rig-Up		
	2245	RIH tool #1	Run 1	DIL-LSS-NGT-TLT
May 24, 1989	0345	POOH tool #1		(1500 ft/hr)
	0445	RIH tool #2	Run 2	FMS-NGT-TLT
	0845	POOH tool #2		(1400 ft/hr)
	0945	RIH tool #3	Run 3	GST-ACT-NGT-TLT
	1830	POOH tool #3		(600 ft/hr)
	2000	RIH tool #4	Run 4	HLDT-LSS-NGT-TLT
May 25, 1989	0200	POOH tool #4		(1000 ft/hr)
	0330	Set-up for VSP		
	0600	RIH tool #5	Run 5	WST
	1400	POOH tool #5		(64 stations in 4.5 hr)
	1415	Rig-down		

[a] Times reported are those at which each sensor combination was run into the hole (RIH) and pulled out of the hole (POOH).

[b] Logging speed is given in parentheses.

from vertical is on the order of 3.0° (N235E), between 292.0 and 878.0 mbsf. Because of the early lithification of this sediment column, the borehole conditions were ideal for downhole experiments and, consequently, the data recorded in Hole 792E are of excellent quality. The sampling distance for FMS data is the smallest of any presently available downhole sensor (25.2 mm), whereas a VSP station was recorded every 9.45 m, and temperature data were acquired every 0.5 s. All of the other records presented in this report were sampled with a 0.152 m digitization interval. A detailed description of each of the sensors and measurement principles is provided in the "Explanatory Notes" chapter (this volume).

Run 1 (Resistivity-Sonic-Natural Gamma-Temperature)

The first run in Hole 792E consisted of a combination of two induction resistivity sensors (with deep and shallow radii of investigation for the deep-phasor induction measurement [IDPH] and the medium-phasor induction measurement [IMPH], respectively), a spherically focused resistivity sensor (SFLU), the long-spacing sonic sensor (LSS), a spectral natural-gamma sensor (NGT), and the Lamont-Doherty Geological Observatory temperature tool (TLT). These last two sensors were included in each of the first four runs and are discussed separately at the end of this section. The NGT was included in each combination for the purpose of depth correlation. The TLT was included to record a temperature profile from seafloor to total depth for each of the four successive runs. Such consecutive profiles allowed us to evaluate the decay of the thermal anomaly introduced by drilling and extrapolate these measurements to obtain an estimate of the temperature at equilibrium for each depth level.

The resistivity data are of excellent quality, recording such features as a series of upward-fining sequences that we observed in the core from 545.0 to 580.0 mbsf (Cores 126-792E-43R through -46R; Fig. 62, 540-580 mbsf). The steplike decrease in resistivity at 587.0 mbsf occurs at the base of a thick conglomeratic bed (Core 126-792E-47R), and is also the location of a sharp increase in (1) smectite concentration observed in XRD analysis, and (2) magnetic susceptibility measured on cores (see "Lithostratigraphy and Accumulation Rates" section, this chapter). The transition from sediment to basement rock is characterized by an order of magnitude increase in resistivity at 804.5 mbsf. Within basement, we observed a series of units with near-constant resistivity values and thicknesses (about 4.1 m). These units have varying mean resistivity values, with low values that correspond to altered and/or brecciated zones observed in the core.

The main characteristic of the sonic data during acquisition was the high noise level, which interfered with the signal from the formation. This noise was primarily a result of the absence of adequate centralization of the sonic tool used aboard the *JOIDES Resolution;* it is a consequence of the small diameter of the drill pipe, which does not allow for the use of centralizers. This lack of centralization resulted in asymmetrical arrivals at the level of the receivers and in "road noise" caused by occasional direct contact between the tool and the formation. The final velocity profile (Fig. 62) was consequently computed by choosing three of the four measured transit times (LTT1, LTT2, LTT3, LTT4; Shipboard Scientific Party [Leg 105], 1987). The sonic sensor was run in the hole during Run 4 at a slower velocity (900 ft/hr instead of 1500 ft/hr) to reduce "road noise". The number of noise-related cycle-skipping events was reduced in the basement section where they were the most numerous in the earlier run.

Run 2 (FMS Images–Natural Gamma–Temperature)

The second run provided the first opportunity to record FMS images during ODP operations. The log was originally recorded from the bottom of the hole up to the drill pipe but, unfortunately, about 200 m of images from the lower part of the hole were overwritten during backup copying after the ship departed Site 792. Four continuous images (from 650.0 to 280.0 mbsf), each covering about 10% of the internal surface of the borehole, will subsequently be produced for analysis. Primary shipboard image analysis of a small interval (347.0-409.0 mbsf) shows the data to be of excellent quality. The FMS picked up features < 1 cm in thickness (e.g., dark ash layers in Core 126-792E-28R; Fig. 63). We also observed a change in dip azimuth and direction at the contact between Units II and III. The average dip is 10° (N070E) in the 10.0 m located above the contact, and changes abruptly to about 30° (N250E) for a 1-m-long interval. Below this level, we observed no significant dip.

We recorded measurements pertaining to hole shape and direction (including two orthogonal measurements of drillhole diameter) from 292.0 mbsf to the bottom of the hole. The average hole diameter is approximately 10.5 in., and its shape is predominantly cylindrical to slightly elliptical. Below the fault zone located at 780.0 mbsf, the ellipticity has no preferred orientation but tends to align in a N20E-N200E direction over the rest of the sedimentary column (Fig. 64). This constrains the maximum horizontal stress direction in the sediments of Hole 792E to be approximately parallel to the relative velocity vector between the Pacific and Philippines plates in the Bonins island arc region (N110E-N290E).

Run 3 (Geochemical Combination–Natural Gamma–Temperature)

The geochemical data recorded during the third run into the drill hole are of excellent quality (Figs. 65 and 66). The data were recorded over the entire length of the drill hole, in the open hole for the lower part of the section, and in the pipe for the upper 287.0 m. Some correlations between several of the analyzed elements in the sedimentary section are shown in Figures 67 and 68, and are generally valid for the basement section as well. They show that Al, Si, Fe, and possibly S are positively correlated with the physical property data (resistivity, velocity, and density), whereas H is negatively correlated. In basement rocks, the low resistivity/velocity/density/Al/Fe/Si, high-H sections are those in which the most intense alteration was observed. The Ca curve is a mirror image of the Si curve in the sediments, and the highest Ca values in this hole are recorded in the middle section of Unit III, as observed in the laboratory core data (see "Sediment/Fluid Geochemistry" section, this chapter). The upper boundary of the Ca-rich zone is also the location of a seismic reflector identified by the VSP experiment (see Run 5, below).

Run 4 (Density–Sonic–Natural Gamma–Temperature)

The short-spacing density detector failed while going into the hole. Therefore, we present only the long-spacing density measurement (LSRH) data (Fig. 62). Because of the small size of the drill hole, however, the data are of good quality and agree with wet-bulk density core measurements. The log was run at 900 ft/hr, which yielded an improved sonic log in comparison with Run 1 (recorded at a speed of 1500 ft/hr). In combination with the velocity data, the wet-bulk density measurements permitted the computation of an impedance profile used as input to a synthetic seismogram shown in Figure 69.

Natural Gamma Spectrometry

In each of the first four runs, natural gamma data were recorded. The four records are of good quality, with a generally low uranium concentration throughout the analyzed section. In the upper part of the sediments (Units II and III), and in the basement rocks (Unit VI), the main source for natural gamma radiation is thorium. Within Units IV and V (430.0-804.5 mbsf), however, natural gamma rays are mostly generated by potassium. In this sedimentary interval, the potassium is inversely related to resistivity, velocity, density (Figs. 62 and 66), and, in some cases, grain size (430.0-500.0 and 555.0-585.0 mbsf). Throughout most of the hole, uranium and potassium are negatively correlated. Thorium and uranium are negatively correlated in the upper part of the basement section (Unit VI, 804.5-842.0 mbsf) and positively correlated in the lower section (842.0-875.0 mbsf).

Temperature Measurements

Out of the four temperature runs, only the first and last ones (Fig. 70) are presented here. The temperature data were recorded upon entering and exiting the hole, starting from a point approximately 100 m above seafloor. The temperature measured at the seafloor during the first run was 2.02°C. Upon entering the hole, the average fluid temperature inside the pipe was approximately 7.0°C. The entrance into the open hole is outlined by a

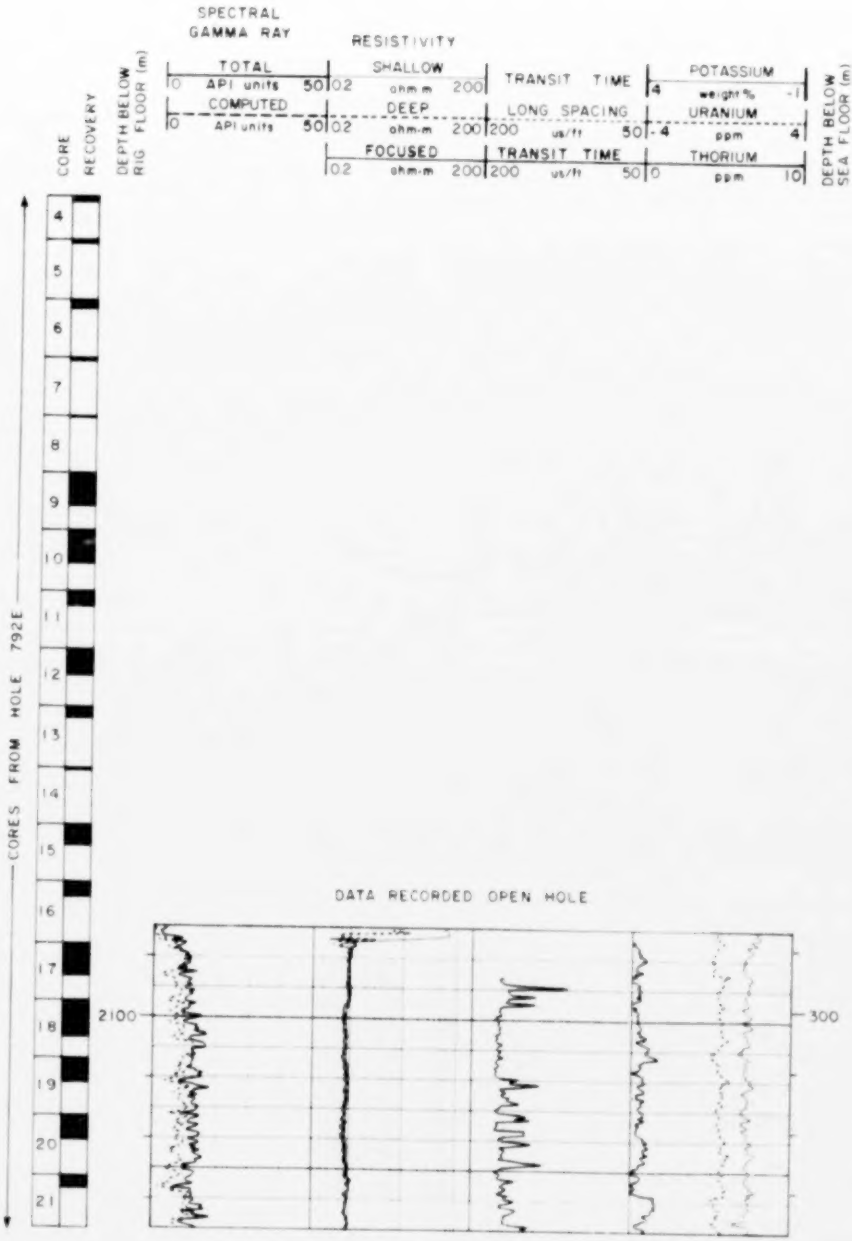

Figure 62. Summary logging figure, DIT, Hole 793E.

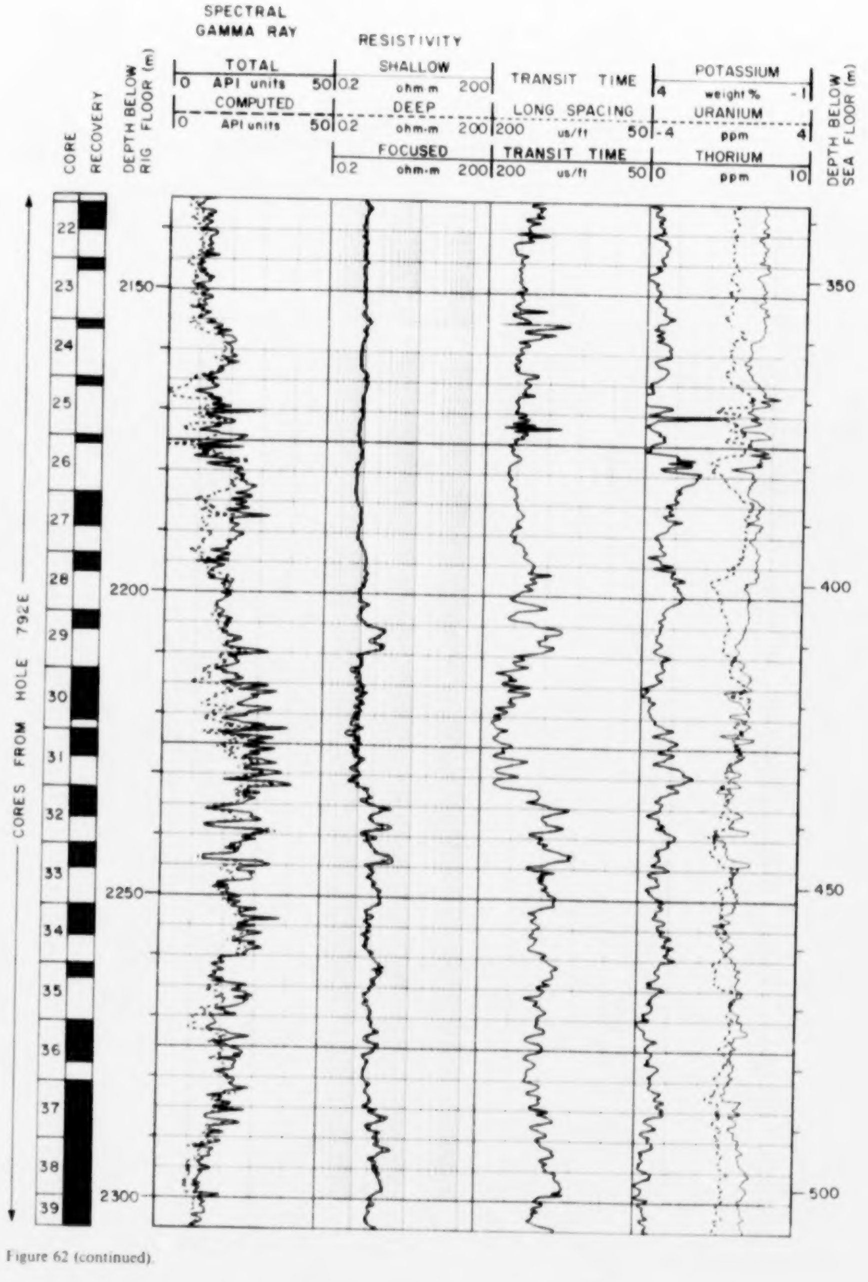

Figure 62 (continued).

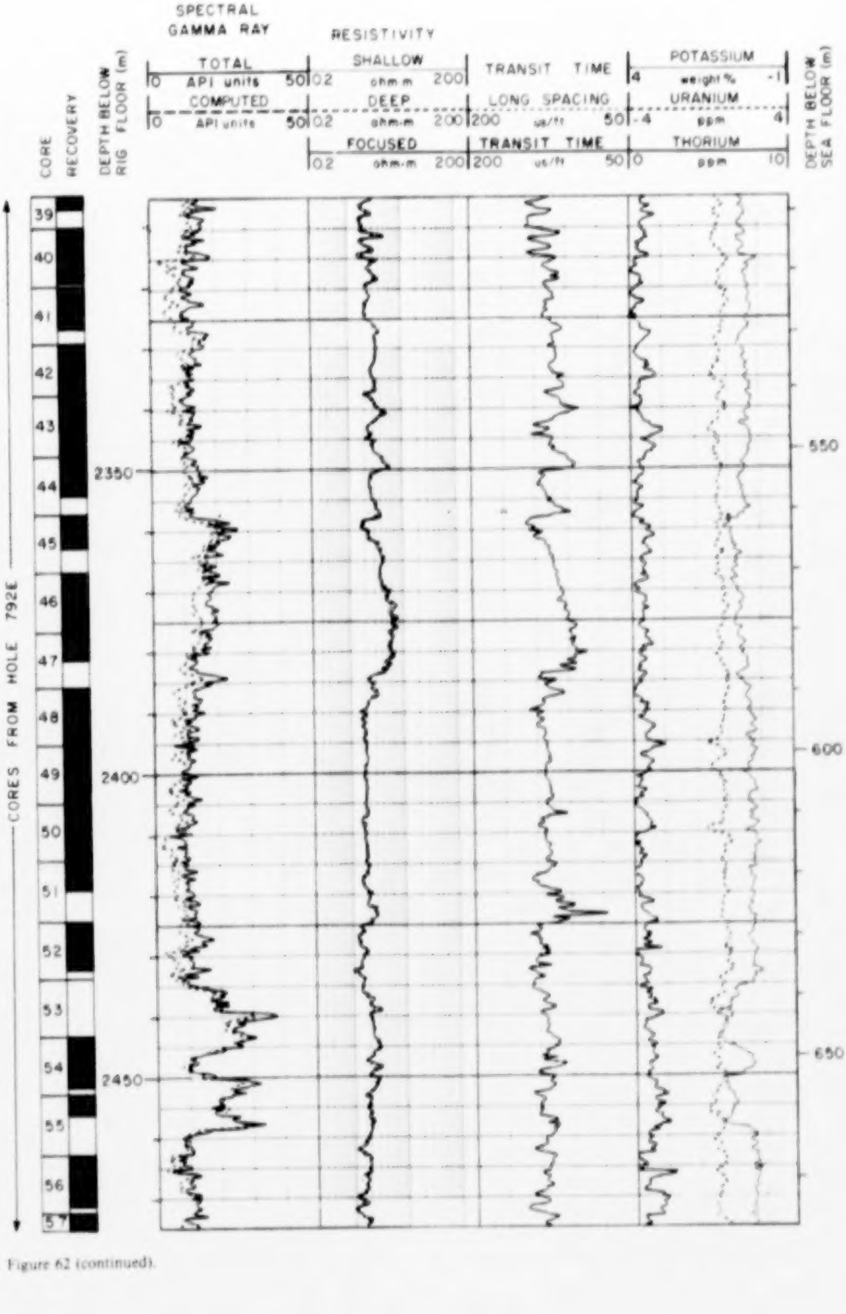

Figure 62 (continued).

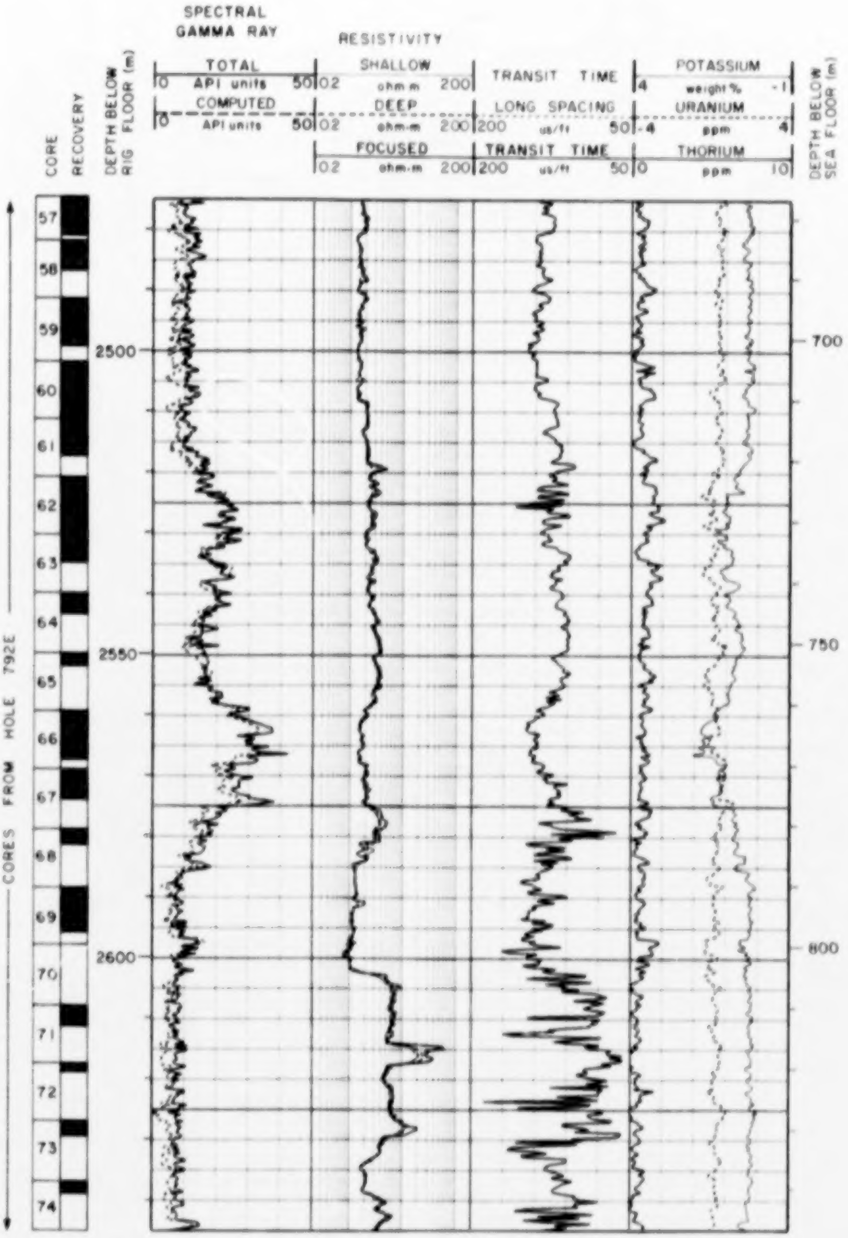

Figure 62 (continued).

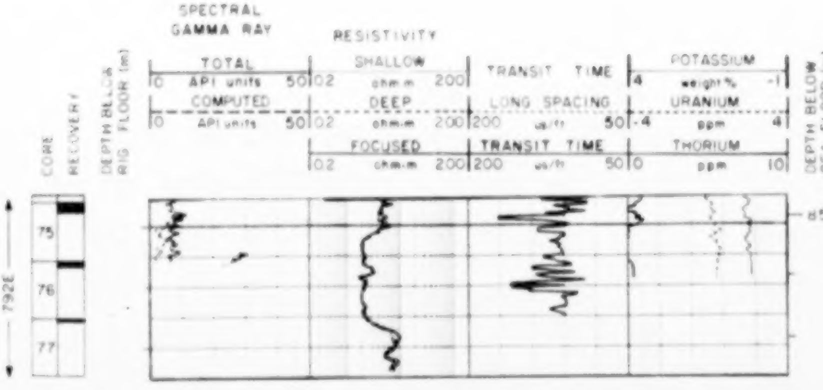

Figure 62 (continued).

sharp temperature increase. From this depth (285.0 mbsf) to the top of the basement (804.5 mbsf), the temperature profile is generally linear. A definitive statement on the nature of the heat transfer at this site must await shore-based analysis of the data-set. We observed a linear gradient of steeper slope in basement rocks.

We observed a total of seven departures from these linear gradients in the sedimentary section, two of which represent positive temperature anomalies. We discuss these below with respect to the fourth temperature run. The profile recorded upon exiting the hole generally has less character than the one obtained upon entering the hole. This probably is caused by physical displacement and the mixing of borehole fluid by the downhole sensors. Seawater is injected into permeable zones during drilling and it flows back into the drill hole after pumping stops; thus, it is in unstable equilibrium with the denser mud placed into the drill hole prior to downhole measurements. The passage of the tool disrupts this equilibrium, and the lighter seawater is displaced upward. This mechanically generated "advective" process results in a smoothed temperature profile and an overall temperature increase of more than 2.0°C. As a consequence, warm fluid from the open-hole section was displaced into the lower section of the drill pipe (as shown by the upward smearing of the temperature anomaly located just below the drill pipe, or the upward increase in chlorine concentration detected by the geochemical measurements).

A similar flow of water from the formation into the drill hole is visible on the log recorded during the fourth run. A steeper gradient during Run 4 indicates the progressive return to thermal equilibrium over the 21 hr that separated these two runs. Only five departures from the linear gradients are visible in the fourth temperature profile. Below the drill pipe, a positive anomaly emphasizes inflow from a permeable zone within Unit 2, with water warmer than borehole fluid. At 350.0 mbsf, the anomaly turns negative, still showing inflow from a permeable zone, but with a fluid colder than borehole fluid in this case. This crossover point indicates the nearby crossing of geothermal and drilling-temperature profiles (Serra, 1984). Above the crossover point, the drilling fluid temperature is warmer than the formation temperature, and below it is colder. Below the crossover point, the temperature profile meets the linear gradient over a short interval within Unit III, and then indicates a permeable zone from which a fault zone was described (407.5–430.0 mbsf) in the cores and from geophysical logs (Figs. 62 and 66).

The amplitudes of these three anomalies are reduced between Run 1 and Run 4, indicating a slow return to equilibrium over this time interval. A fourth, small-amplitude, positive anomaly is evident in both profiles (500.0–600.0 mbsf). It remains similar between Runs 1 and 4 and may be related to a variation in thermal conductivity. The two small negative anomalies detected in the first profile, at approximately 650.0 and 700.0 mbsf, are not visible in the fourth run. The last anomaly, represented as a doublet in the first profile, is also present in the fourth, although attenuated. This doublet corresponds to two permeable zones that have larger than normal hole diameters (Fig. 66), and which may be faults bounding Unit V. Evidence for faulting was noticed in the cores (see "Lithostratigraphy and Accumulation Rates" section, this volume).

Run 5 (Vertical Seismic Profile)

The primary objectives of the vertical seismic experiment conducted in Hole 792E were to enhance velocity analysis, to identify and locate the primary reflectors, to correlate the lithostratigraphy with identified reflectors, and to tie the surface multichannel seismics to well logs for regional scale correlations.

Data Acquisition

The sound source used for the Hole 792E VSP experiment was the large-volume (400 $in.^3$, or 16.0 L), high-pressure (2000 psi, or 140 bar) water gun (SSI H400) aboard the *JOIDES Resolution*. The gun was suspended 15 mbsl from a buoy tethered from the drill ship's aft port crane boom, about 24 m abeam. The downhole seismic signals were received by a Schlumberger Well Seismic Tool (WST) single vertical component seismometer. The seismometer has four, series-connected, 10-Hz (F_o) geophones (Geospace Model HS-1) mounted at its base. All downhole equipment functioned flawlessly. The water-gun acoustic signals were also detected by a separate, calibrated hydrophone suspended directly from the crane boom, 3 m below the water gun. This hydrophone configuration provided a stable, zero-time reference relative to the seafloor, allowing real-time summing of the seismic records observed for the several shots fired at each seismometer clamping level. During the operation period, weather conditions were optimal and a total of 64 clamping levels were occupied, amounting to 4.5 hr of recording time.

The WST was lowered to the bottom of the hole (Level 1, 868.0 mbsf) and clamped to the well bore. The cable was then

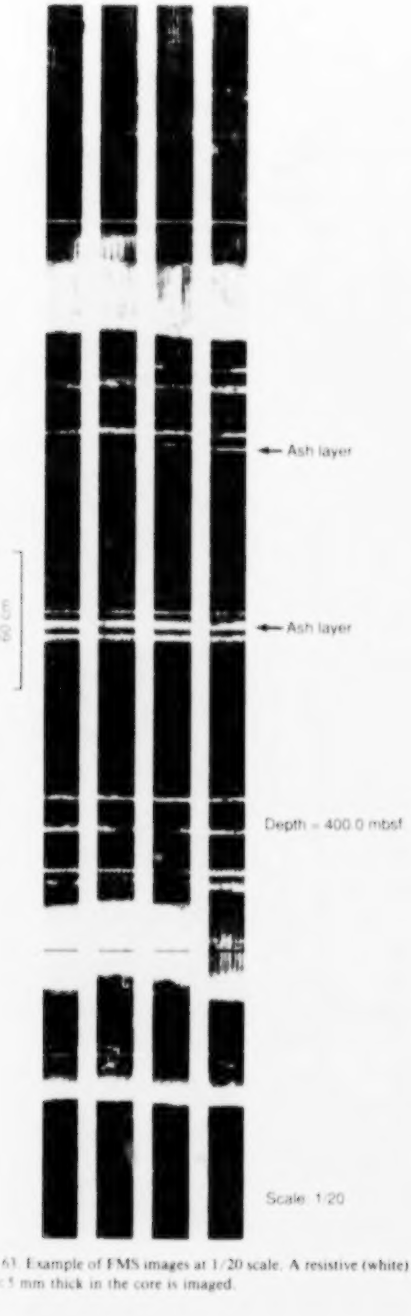

Figure 63. Example of FMS images at 1/20 scale. A resistive (white) ash layer <5 mm thick in the core is imaged.

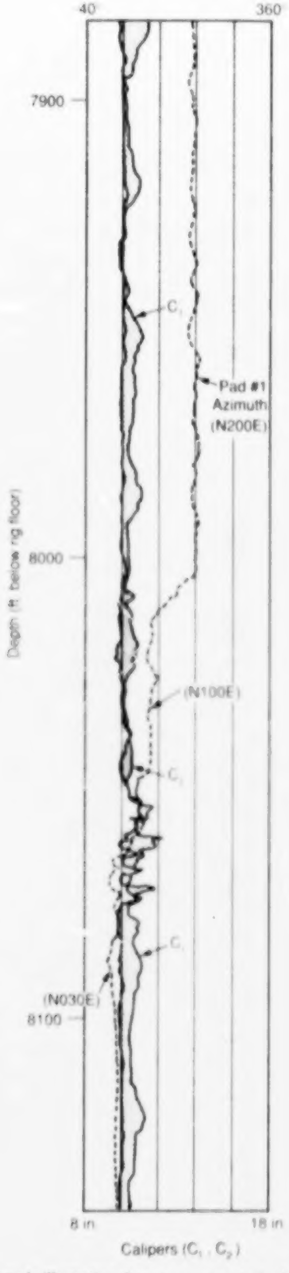

Figure 64. Example illustrating the very constant hole elongation direction as observed with FMS calipers in the sedimentary section. The tool rotated 90° at 8010.0 and 8050.0 ft below rig floor. The largest hole dimension remains oriented close to the north-south axis.

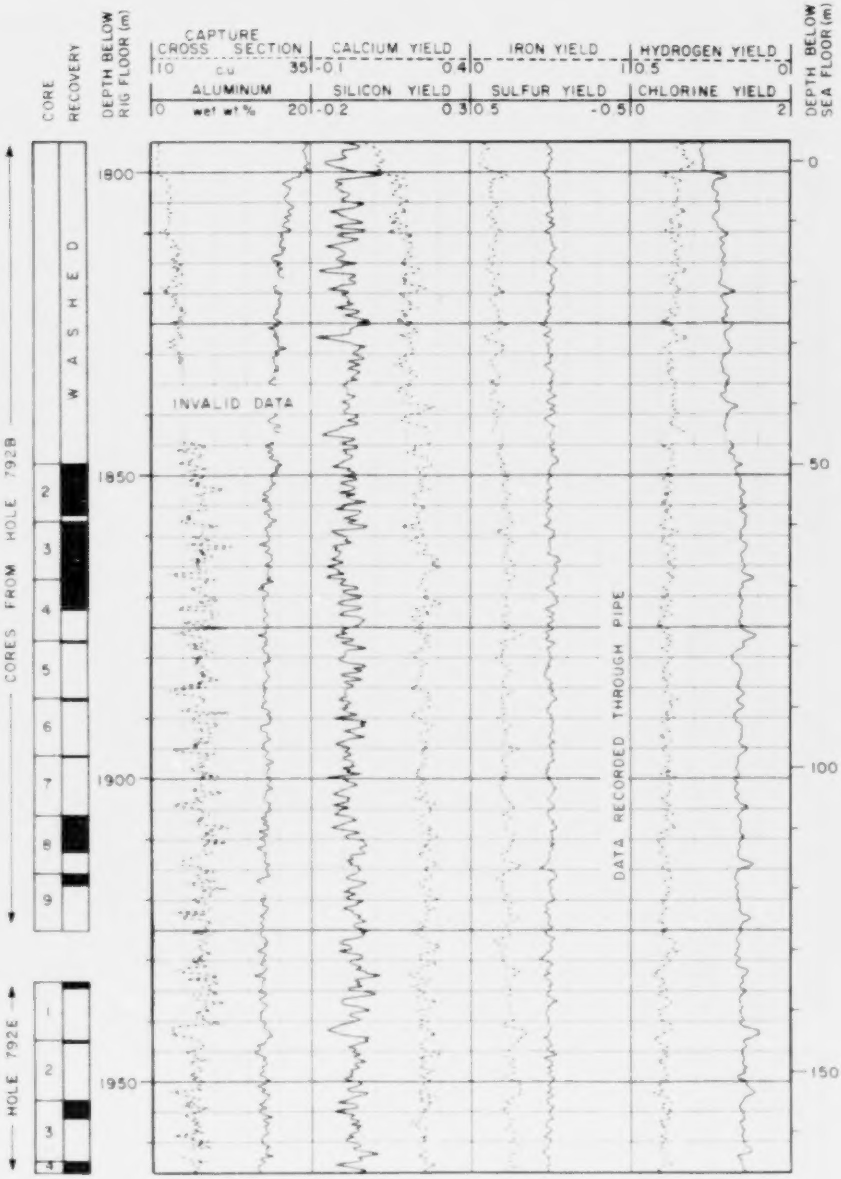

Figure 65. Summary logging figure, ACT, Hole 792E.

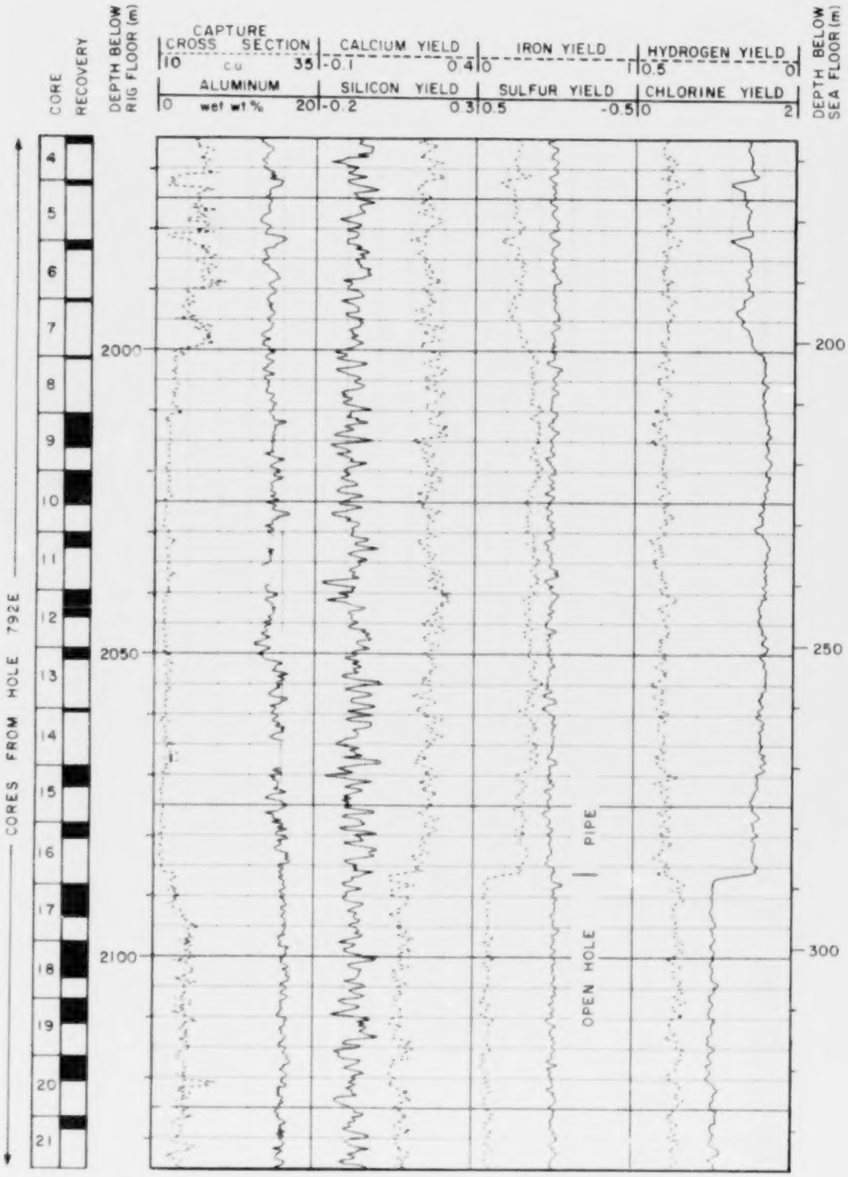

Figure 65 (continued).

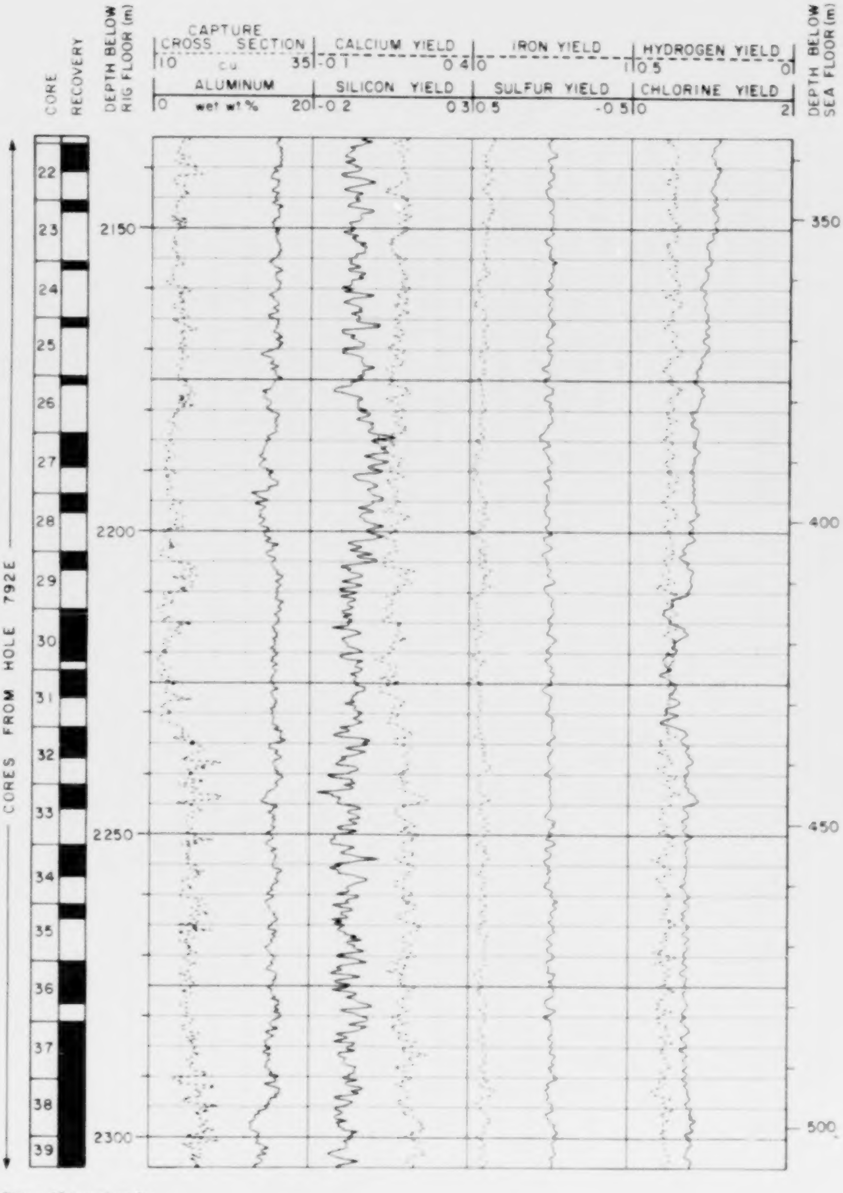

Figure 65 (continued).

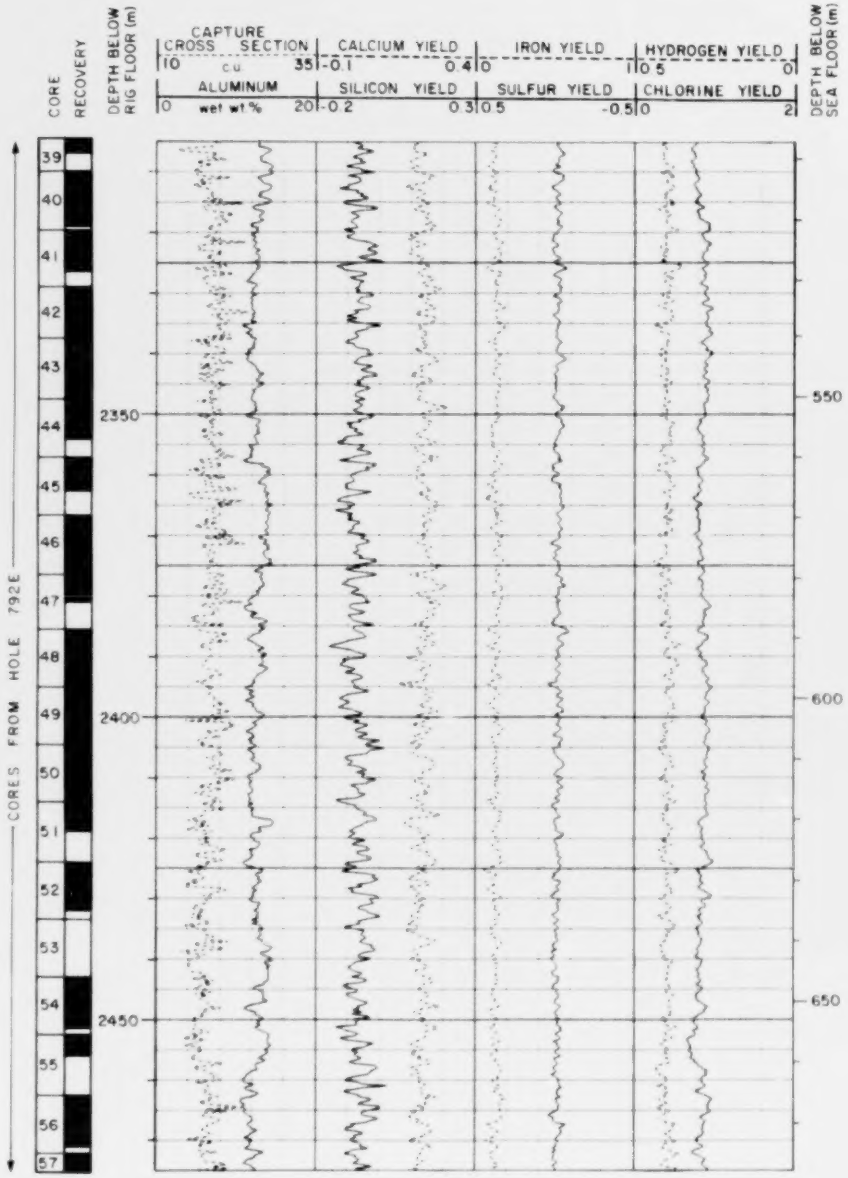

Figure 65 (continued).

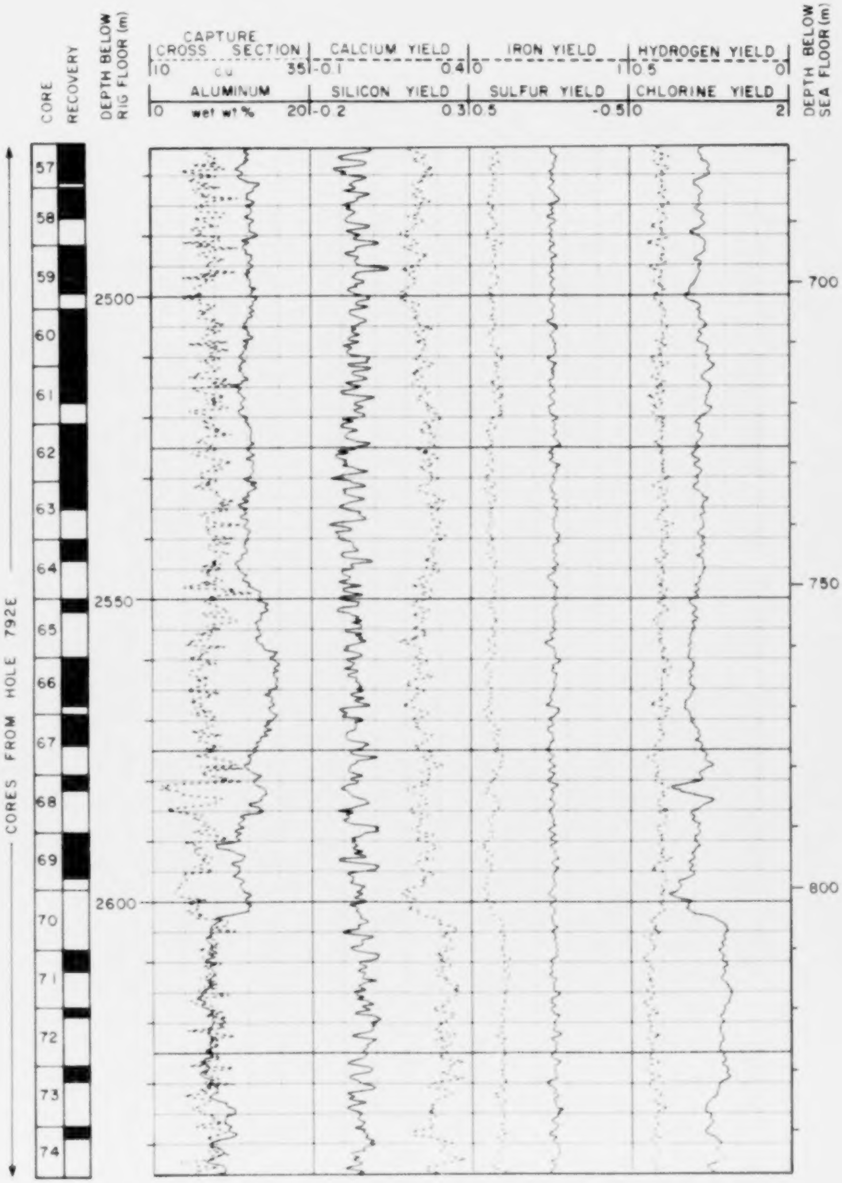

Figure 65 (continued).

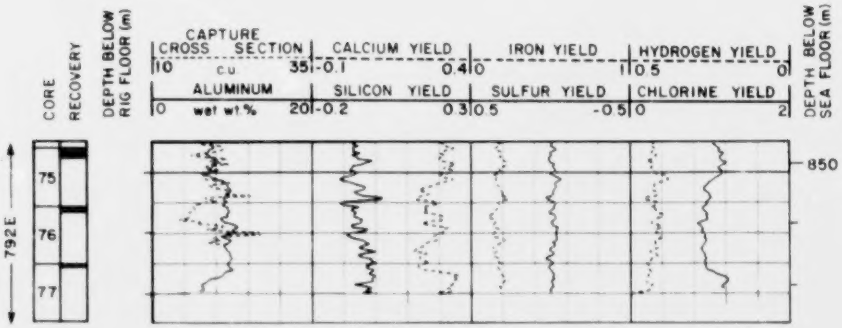

Figure 65 (continued).

slacked 2 m, and a single shot was fired to test for noise or poor coupling to the borehole wall. The seismogram waveforms recorded for each shot were displayed in quasi-real time after the shot on a TEKTRONIX graphics terminal. After we ascertained that the seismometer was properly clamped to the well bore, additional shots were taken as deemed necessary by the operators and stacked for real-time display. Each waveform was visually inspected and either accepted for stacking or rejected. The resultant normalized stacked trace was then displayed and inspected before moving on to the next clamping level. A satisfactory signal-to-noise ratio was obtained using an average of five stacked shots per clamping level, with a maximum of seven. Following the shooting/inspection/stacking sequence, the WST seismometer package was raised 9.45 m (30 ft) and the shooting/inspection/stacking sequence was repeated at 9.45-m (30 ft) intervals to the last clamping level at 301.0 mbsf. A total of 409 shots were used. Because the drill pipe was firmly stuck in the hole, no further efforts were taken to reduce downhole seismic noise aside from adjusting the ship's heading to minimize roll and slacking the cable after clamping. The logging winch wireline heave compensator was not used, as it had failed during Run 3.

Water-gun-generated signals received by the WST borehole seismometer were preamplified downhole, transmitted up the logging cable, and digitally recorded along the hydrophone signals by the PDP-11 minicomputer and A/D converter of the Schlumberger CSU logging data acquisition system. Timing information was logged with millisecond accuracy. First-break transit traveltimes were calculated to 0.1 ms from the stacked shots at each clamping level. The data sampling rate was 1.00 ms with a record length of 3.00 s. The record delay (blanking time) ranged from 1.45 s at the maximum observation depth (868.0 mbsf) to 1.25 s at the shallowest depth (301.0 mbsf). An attempt to continue sampling inside the drill pipe was aborted because of unacceptable noise levels.

Data Processing

Shipboard seismic processing of the VSP data used the same PDP-11-based Schlumberger CSU computer used for data acquisition. The CSU system's Seismic Quick Look (SQL) software performed the primary data editing and the preliminary processing tasks immediately following the experiment. These processing steps are summarized as follows:

1. The addition or elimination of shot records from real-time, field-summed, stack trace at each clamping level. "Good" data records were re-summed to obtain a final stacked trace for each depth position.
2. Application of a static shift correction for recording delay (blanking) time and combining the final stacked traces into a composite depth vs. one-way traveltime section.
3. Application of a static shift correction equal to the first-break time of the direct wave for each stacked depth trace, to align the reflection wavetrain pattern along constant arrival times and to combine the stacked traces into a composite depth vs. two-way traveltime section.
4. Calculation of the velocity-depth profile from time differences in the direct-wave, first-break transit times for the sequential depth intervals.
5. Preliminary wavefield separation into upgoing (reflection) and downgoing (direct) waves using spatial velocity filtering (specifically, narrow-reject f-k filtering).
6. Performance of preliminary source deconvolution. A wavelet-shaping operator is derived from the downgoing waveforms of the deepest four stacked traces (1, 2, 3, and 4) and is applied to the upgoing energy.

Results

The signal-to-noise ratio was good throughout the experiment. Borehole diameter was fairly uniform except in the region of Levels 47, 48, and 49 (see Fig. 71, stacks 47–49). High-frequency tool resonance, seen in the upper level traces, increased as the tool neared the base of the drill pipe.

Figure 71 shows the one-way traveltime, stacked-trace, composite depth section for all the raw VSP data obtained at Hole 792E over the depth interval from 868.0 to 301.0 mbsf. The bottom of the drill pipe was at 287.0 mbsf, which prevented shallower seismometer clamping. The depth section includes 64 observations made in the uncased open hole. The data are unfiltered; a spreading-loss-type, 1.5-power exponential time gain factor was applied to display the weaker, deeper reflections. Each trace amplitude scale is normalized. The downgoing direct waves are the strong first arrivals with traveltime increasing with depth (Fig. 71). Note that no water-bottom multiple arrivals were seen on the section because the one-way traveltime through the water column is 1200 ms. The three-way traveltime (3600 ms) for a VSP-type, water-bottom multiple is well beyond the record length displayed. The upgoing, reflected waves are the late, weak (but coherent) events, with traveltime increasing as depth decreases. The divergence of the downgoing and upgoing wavetrains results from the decreasing range to the sound source for the direct waves and the increasing range from the reflecting interface as the seismometer is raised. The reflected wavetrains intersect the direct wave's first break arrival at the depth of the interface causing the reflection; in practice, if the direct wave is

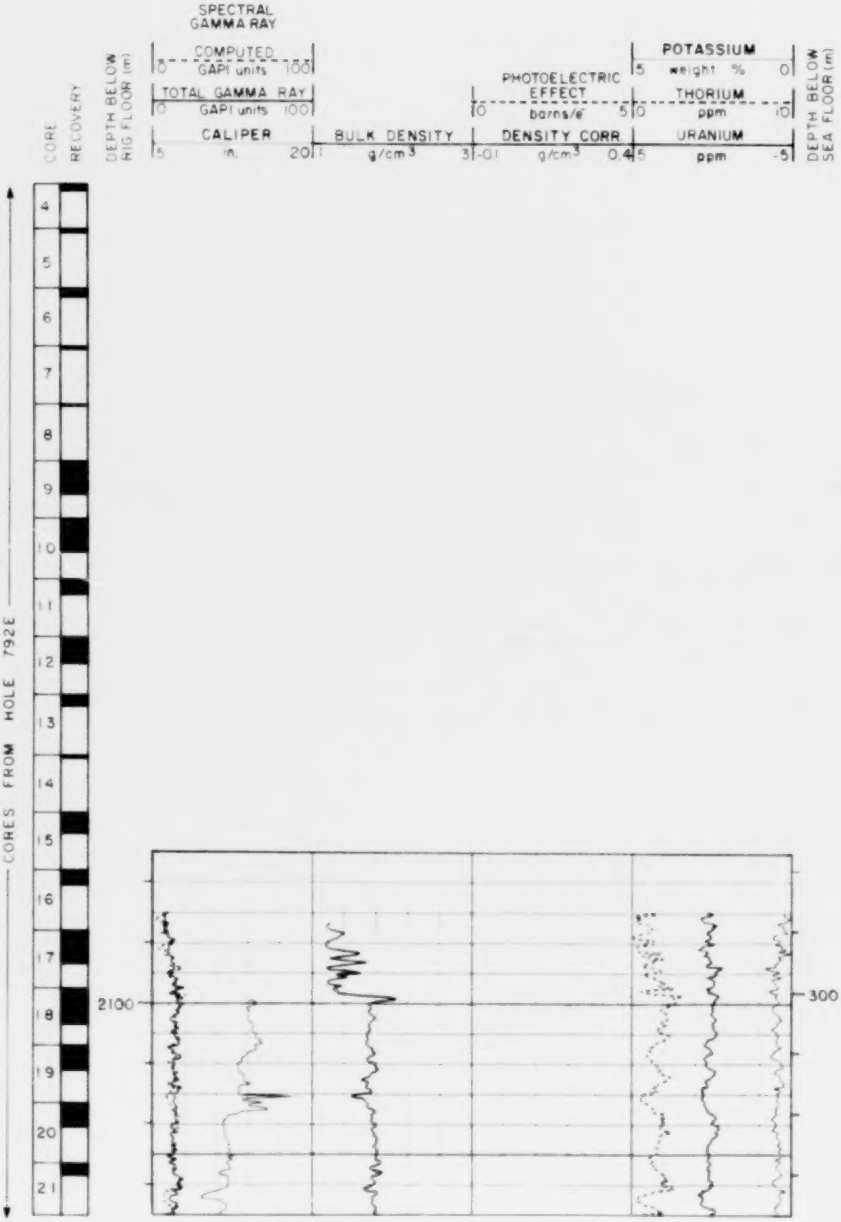

Figure 66. Summary logging figure, LDT, Hole 792E.

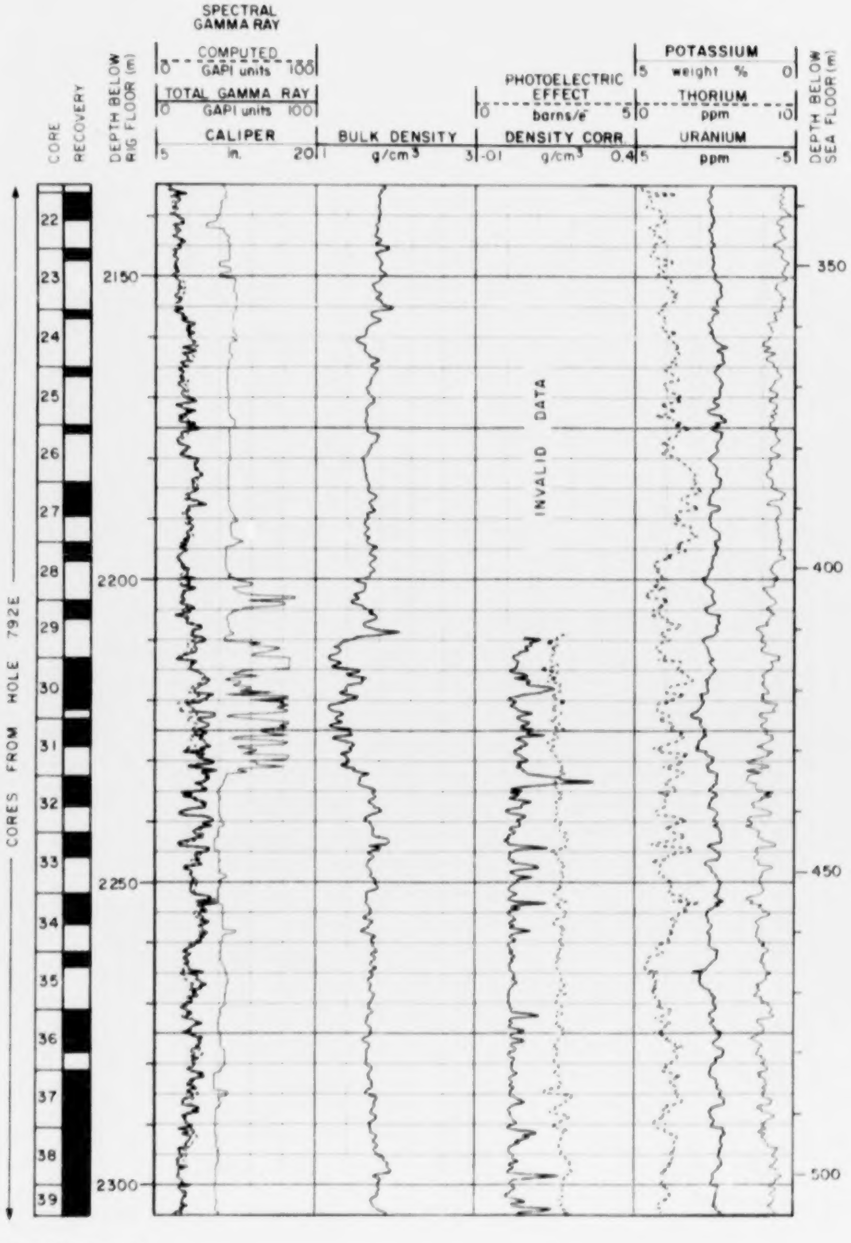

Figure 66 (continued).

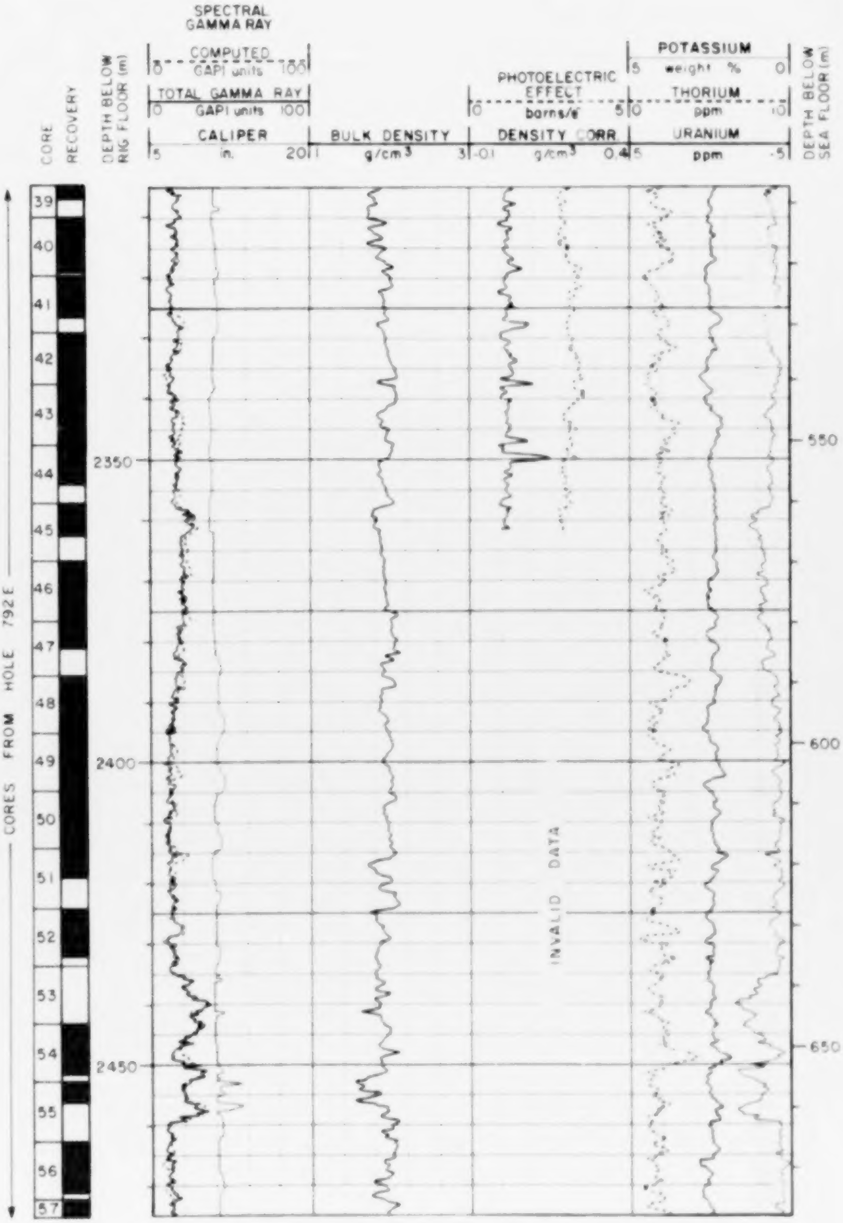

Figure 66 (continued).

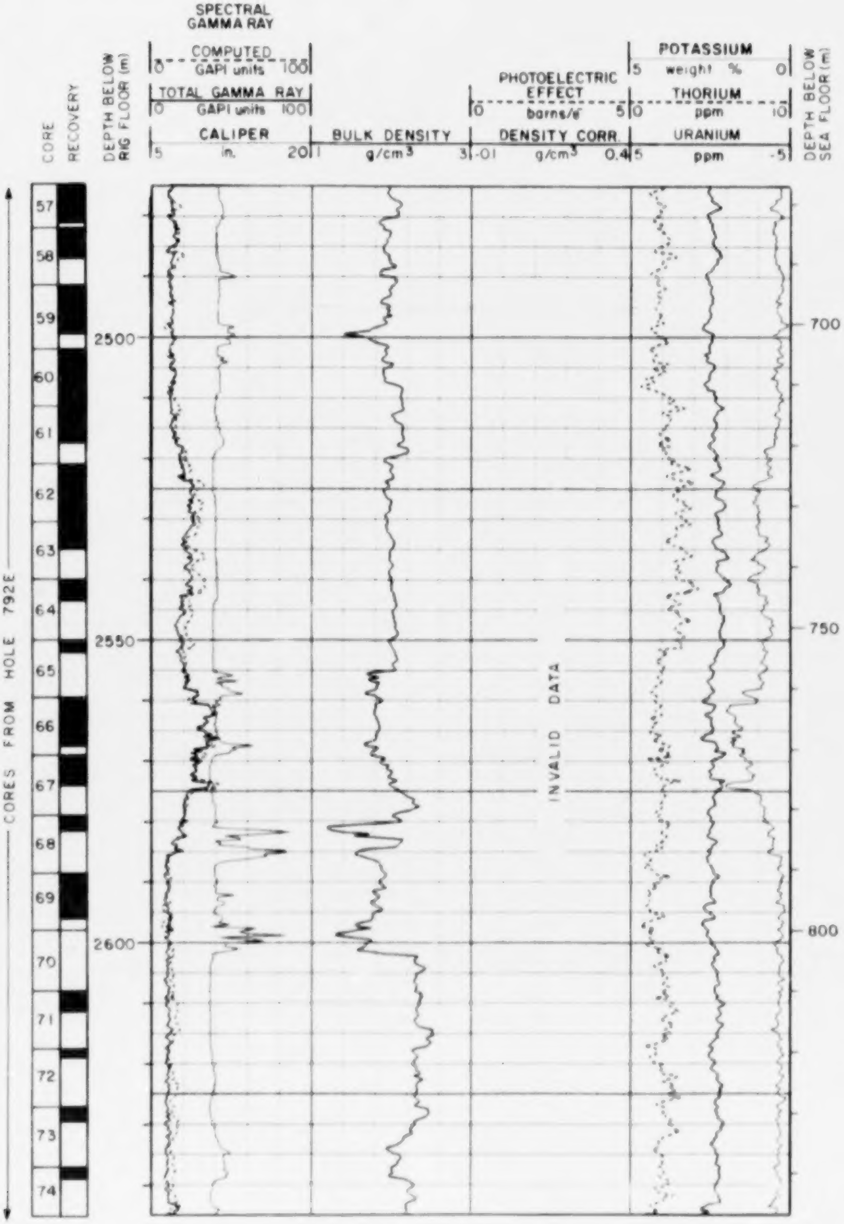

Figure 66 (continued).

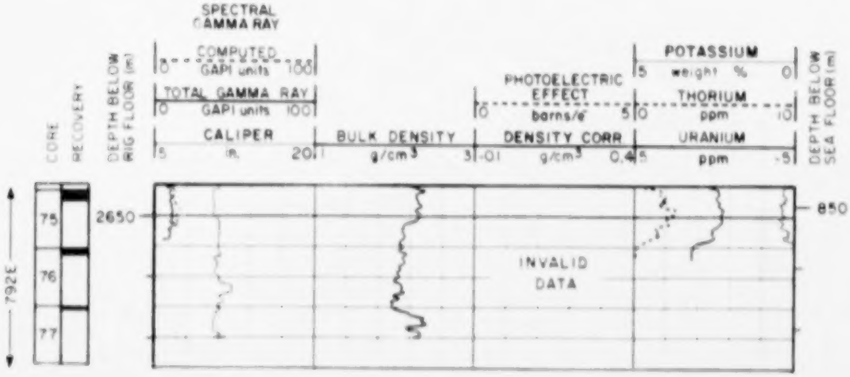

Figure 66 (continued).

of a complex nature, it is sometimes difficult to define that intersection. Numerous reflection events are evident in this essentially raw data display, demonstrating the overall good signal-to-noise ratio.

A preliminary determination of the interval velocity-depth structure was made by dividing the interval distance between sequential clamping levels by the difference in their direct-wave, first-break, arrival traveltimes. The results of this simple calculation are shown in Figure 72 together with the one-way traveltimes over the same depth range. Figure 73 illustrates the excellent correlation between VSP interval velocity data averaged over the designated lithostratigraphic intervals with velocity data obtained by physical properties measurements and downhole measurements.

The traces were time-shifted by an amount equal to the direct wave's first break arrival. A spatial velocity filter was then applied to the resulting partial two-way traveltime section to separate the upward propagating reflected wavetrains from the downward propagating wavetrains. The data were not corrected for the minor deviation of the borehole from vertical. Figure 74 is a display of the upgoing reflected wavetrains; prominent reflectors have been identified and, whenever possible, related to lithologic units or subunits. Reflectors defining major unit boundaries (Units III through VI) are identified on this figure and also on the multichannel data (Fig. 74). At this point in the analysis, the precision to which depths can be determined in this data is ± 1 depth level. The curvature of the deepest reflections is caused by the dip of basement beds and is analogous to the curvature often observed in CDP gathers that results from the normal moveout effect.

Preliminary Stratigraphic Results from Downhole Measurements

The downhole measurements are analyzed here with respect to the stratigraphic column defined from the cores. Because the total recovery in this hole was only 48.23%, such an analysis is necessary to define unit thicknesses and boundaries with precision, and to check if any major lithologic event was skipped as a result of partial recovery. The location of unit boundaries is discussed here in terms of variations of *in-situ* physical properties and in the context of VSP results. As a summary, the average value for *in-situ* measurements of resistivity, velocity, and density for each sedimentary unit are reported in Table 19. A comparison of laboratory and *in-situ* velocity data is given in Table 20.

The geochemical combination is the only sensor that recorded data through pipe within Unit I. The contact between Unit I and Unit II (183.7 mbsf, from core data) cannot be detected at present from the geochemical logging dataset. The open-hole data start within Unit II (~ 287.0 mbsf). Unit II is characterized by near-constant resistivity (about 0.9 Ω · m) and wet-bulk density (1.76 g/cm³; Fig. 62; Table 19). Temperature records indicate that this section is permeable.

A lacuna (a 5-m.y. gap in the middle Miocene record, at 357.4 mbsf; see "Lithostratigraphy and Accumulation Rates" section, this chapter) defines the contact between Unit II and Unit III. The wet-bulk density decreases below this depth to an average value of 1.67 g/cm³, and the resistivity is more variable than in Unit II. We found a reflector within Unit III at 386.0 mbsf (Reflector T; Fig. 74), where the calcium concentration increases abruptly in the core and in the downhole geochemical record.

The next boundary in the hole is the top of a fault zone cored at 407.1 mbsf, and defined by large caliper values (Fig. 66), a seismic reflector in the VSP data (Reflector S; Fig. 75), and an anomaly in the temperature profiles (Fig. 70). With reference to the caliper and *in-situ* physical property data, this fault zone extends to approximately 430.0 mbsf, the lower contact of Unit III (Table 19). The entire fault zone is seen as permeable in the temperature records. In the upper part of Unit IV (from 430.0 to approximately 515.0 mbsf), the physical property profiles have a bimodal character, with high resistivity/velocity/wet-bulk density, low natural gamma-ray values, alternating with beds of opposite characteristics. The main source of natural gamma rays is potassium, and the low resistivity/high natural gamma values appear where we found high smectite concentrations in Core 126-792E-40R.

At about 515.0 mbsf, the overall character of physical property measurements changes, marked by an increase in average wet-bulk density, velocity, and resistivity. The profiles lose their high-frequency character below 560 mbsf as a result of the appearance of thicker, often conglomeratic units. This boundary is Reflector N in the VSP experiment (Fig. 74). In the lower part of Unit IV, the next reflector is found at about 590.0 mbsf (Fig. 74), close to the location of a sharp (1) decrease of resistivity, (2) increase in smectite content (see "Lithostratigraphy and Accumulation Rates" section, this chapter), (3) increase in magnetic susceptibility (see "Lithostratigraphy and Accumulation Rates" section, this chapter), and (4) variation in pore-water Ca^{2+} and Mg^{2+} concentrations (see "Sediment/Fluid Geochemistry" sec-

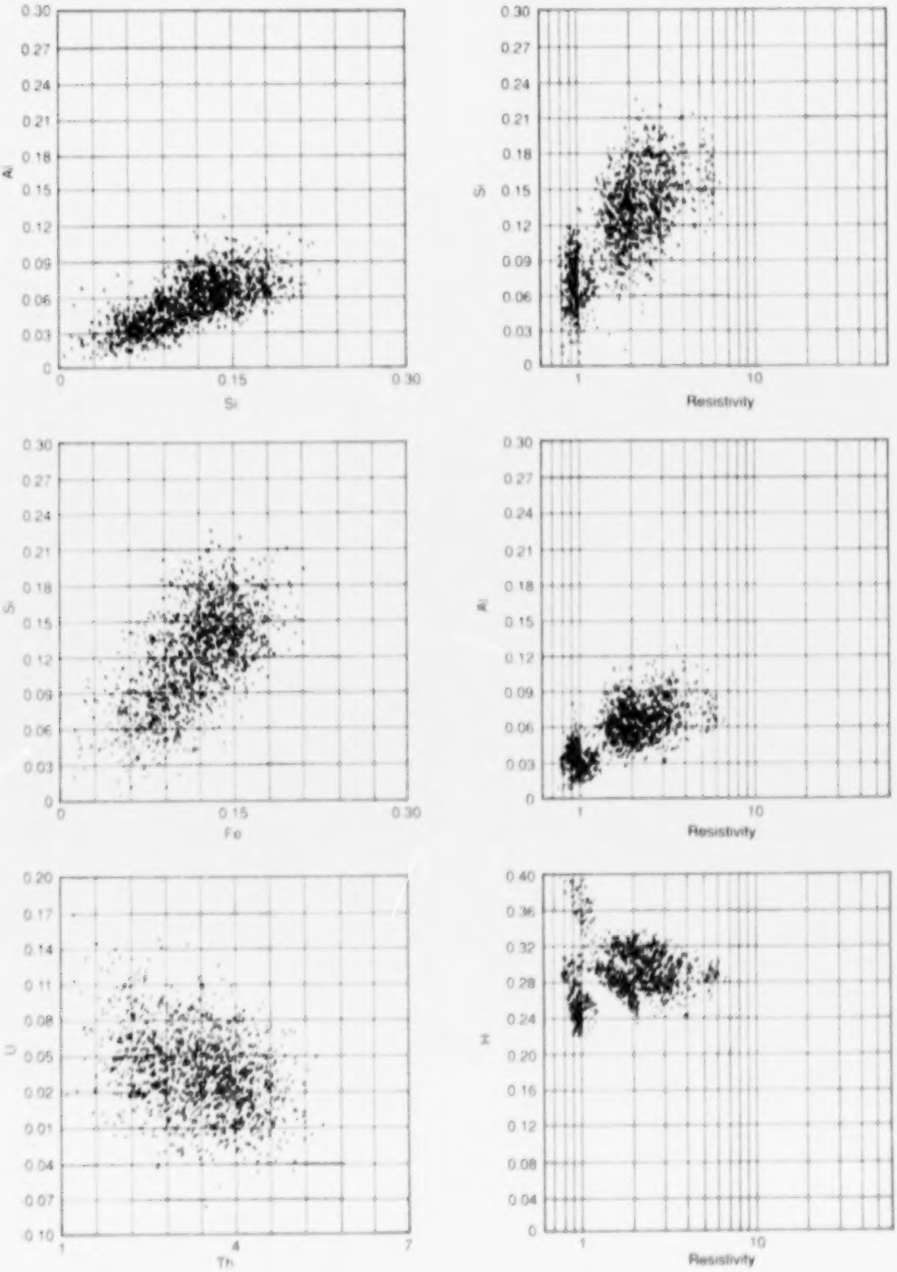

Figure 67. Crossplots of *in-situ* geochemical measurements in the sediments, Site 792.

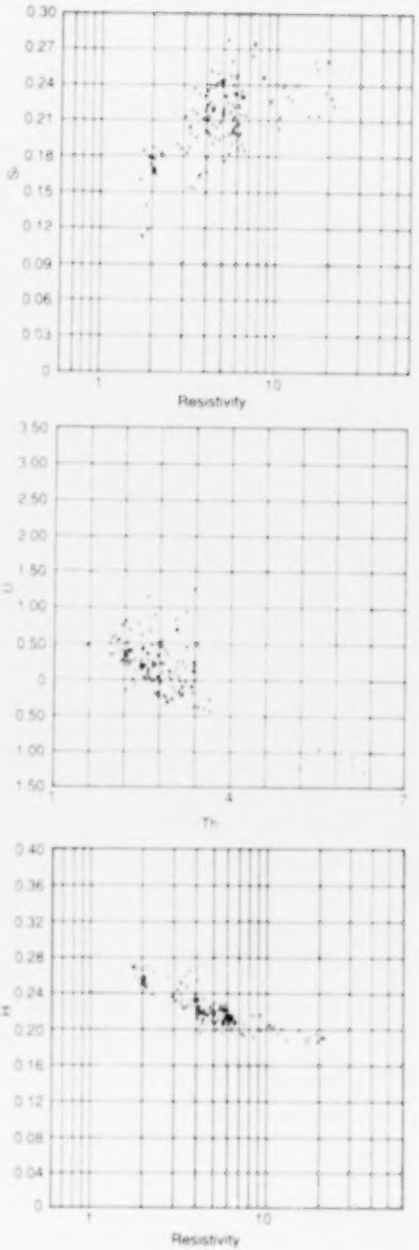

Figure 68. Crossplots of *in-situ* geochemical measurements in the basement, Site 792.

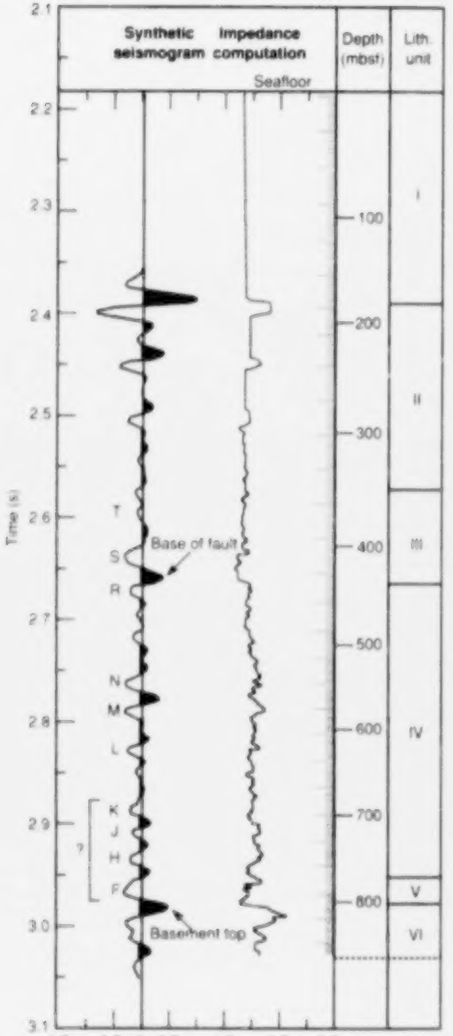

Figure 69. Synthetic seismogram and impedance log for Site 792, computed from velocity and bulk density *in-situ* measurements, then convolved with a 30-Hz Ricker wavelet.

tion, this chapter). Except for a high-resistivity region associated with coarser units (717.0–758.0 mbsf), the *in-situ* physical properties remain constant to the base of Unit IV, at 780.0 mbsf.

The highly altered rocks of Unit V are characterized by low physical property values (Table 19), bounded by two permeable faults (Fig. 74), and outlined by the VSP with Reflectors F and G (Fig. 74). The top of the basement is, therefore, the site of a

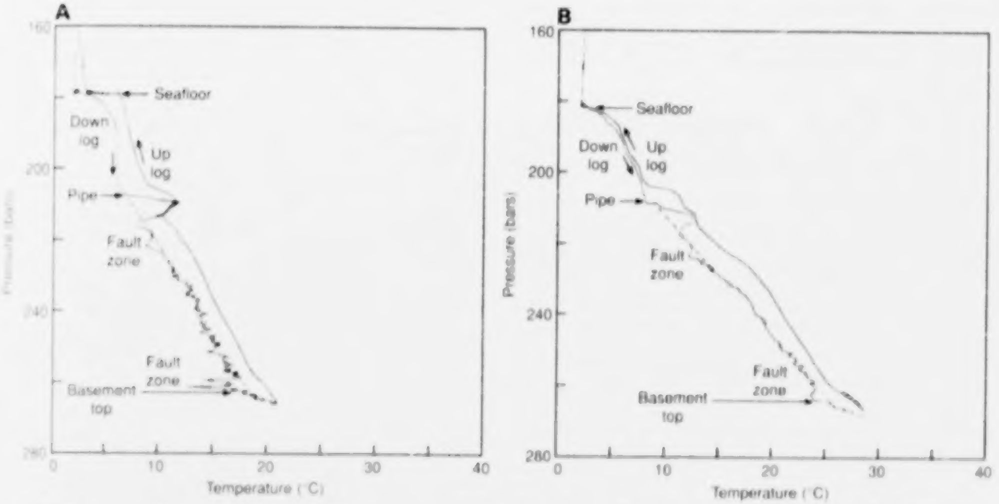

Figure 70. Temperature data (in °C) plotted against lithostatic pressure (in bars), Hole 792E. **A.** Data recorded during the first run. **B.** Data recorded during the second run (24 hr after the first run).

sharp increase in physical properties (Table 19) and of a decrease in natural gamma radiation.

Conclusions

A complete set of downhole measurements has succeeded, within the limits of shipboard analysis capabilities, in identifying the major structural and lithologic events within sediments and basement rocks. One of the most interesting results is the hole elongation seen in the sedimentary section, which shows compression aligned with the relative velocity vector between the Pacific and Philippine plates. In the basement, the FMS caliper was not able to detect any borehole breakouts, which does not rule out the possibility of a small stress anisotropy in the horizontal plane. The FMS imaged features < 1 cm in thickness. We measured a geothermal gradient of 3.0°C/100 m, 30 hr after the end of the drilling operation. Further processing of geochemical, temperature, FMS, and VSP data in combination with calibrations obtained from laboratory measurements should bring more insight into the geological processes active in the inner forearc basin over the last 30 m.y.

REFERENCES

Akimoto, K., 1989. Recent foraminifera from Enshunada. *In* Takayanagi, Y., and Ishizaki, K. (Eds.), *Collected Papers on Foraminifera from the Japanese Islands:* Sendai (Toko Press), 93–104.

Arthur, M. A., Carson, B., and von Huene, R., 1980. Initial tectonic deformation of hemipelagic sediment at the leading edge of the Japan convergent margin. *In* Langseth, M., Okada, H., et al., *Init. Repts. DSDP,* 56, 57 (Pt. 1): Washington (U.S. Govt. Printing Office), 569–614.

Atlan, Y., Bardon, C., Minssieux, L., Quint, M., and Delvaux, P., 1968. Conductivite en milieu poreux argileux. Interpretation des diagraphies. Troisieme colloque de l'association de recherche sur les techniques de forage et de production. *Pau. Comm.*, No. 31.

Backman, J., Duncan, R. A., et al., 1988. *Proc. ODP, Init. Repts.*, 115: College Station, TX (Ocean Drilling Program).

Berggren, W. A., Kent, D. V., Flynn, J. J., and Van Couvering, J. A., 1985. Cenozoic geochronology. *Geol. Soc. Am. Bull.*, 96:1407–1418.

Bernhard, J. M., 1986. Characteristic assemblages and morphologies of benthic foraminifera from anoxic, organic-rich deposits: Jurassic through Holocene. *J. Foram. Res.*, 16:207–215.

Bielak, L. E., and Briskin, M., 1978. Pleistocene biostratigraphy, chronostratigraphy and paleocirculation of the southeast Pacific central water core RC 11-220. *Mar. Micropaleontol.*, 3:51–94.

Blow, W. H., 1969. Late middle Eocene to Recent planktonic foraminiferal biostratigraphy. *In* Renz, H. H., and Brönniman, P. (Eds.), *Proc. 1st Internat. Conf. Planktonic Microfossils*, 1:199–422.

Bolli, H. M., Saunders, J. B., and Perch-Nielsen, K. (Eds.), 1985. *Plankton Stratigraphy:* Cambridge (Cambridge Univ. Press).

Coombs, D. S., Ellis, A. J., Fyfe, W. S., and Taylor, A. M., 1959. The zeolite facies, with comments on the interpretation of hydrothermal syntheses. *Geochim. Cosmochim. Acta*, 17:53–107.

Davis, E. E., and Lister, C.R.B., 1977. Heat flow measured over the Juan de Fuca Ridge: evidence for widespread hydrothermal circulation in a highly heat transportive crust. *J. Geophys. Res.*, 82:4845–4860.

Foreman, H. P., 1981. Radiolaria. *In* Emiliani, C. (Ed.), *The Sea* (Vol. 7): New York (Wiley), 1121–1144.

Haq, B. U., Hardenbol, J., and Vail, P. R., 1987. Chronology of fluctuating sea levels since the Triassic. *Science*, 235:1156–1167.

Hussong, D. M., and Uyeda, S., 1981. Tectonic processes and the history of the Mariana arc: a synthesis of the results of Deep Sea Drilling Project Leg 60. *In* Hussong, D. M., Uyeda, S., et al., *Init. Repts. DSDP,* 60: Washington (U.S. Govt. Printing Office), 909–929.

Ingle, J. C., Jr., 1980. Cenozoic paleobathymetry and depositional history of selected sequences within the southern California continental borderland. *Spec. Publ. Cushman Found. Foraminiferal Res.*, 19:163–195.

Kaiho, K., in press. Morphotype changes of deep-sea benthic foraminifera during the Cenozoic Era and their paleoenvironmental implications. *Kaseki* (Fossils).

Kaiho, K., and Hasegawa, S., 1986. Bathymetric distribution of benthic foraminifera in bottom sediments off Onahama, Fukushima Prefecture, northeast Japan. *In* Matoba, Y., and Kato, M. (Eds.), *Studies on Cenozoic Benthic Foraminifera in Japan:* Akita University, 43–52.

Klaus, A., and Taylor, B., in press. Submarine canyon development in the Izu-Bonin forearc: a SeaMARC II and seismic survey of Aoga Shima Canyon. *Mar. Geophys. Res.*

Lundberg, N., and Leggett, J. K., 1986. Structural features in cores from the slope landward of the Japan Trench, Deep Sea Drilling Project Leg 87B. *In* Kagami, H., Karig, D. E., Coulbourn, W. C., et al., *Init. Repts. DSDP,* 87: Washington (U.S. Govt. Printing Office), 809–826.

Mattey, D. P., Marsh, N. G., and Tarney, J., 1980. The geochemistry, mineralogy, and petrology of basalts from the West Philippine and Parece Vela basins and from the Palau-Kyushu and West Mariana ridges, Deep Sea Drilling Project Leg 59. *In* Kroenke, L., Scott, R., et al., *Init. Repts. DSDP,* 59: Washington (U.S. Govt. Printing Office), 753–796.

McDuff, R. E., 1981. Major cation gradients in DSDP interstitial waters: the role of diffusive exchange between seawater and the upper oceanic crust. *Geochim. Cosmochim. Acta,* 45:1705–1713.

Mitchell, J., 1976. *Fundamentals of Soil Behavior:* New York (Wiley).

Miyashiro, A., 1974. Volcanic rock series in island arcs and active continental margins. *Am. J. Sci.,* 274:321–355.

Nelson, C. H., and Maldonado, A., 1988. Factors controlling depositional patterns of Ebro turbidite systems, Mediterranean Sea. *AAPG Bull.,* 72:698–716.

Nigrini, C. A., 1985. Radiolarian biostratigraphy in the central equatorial Pacific, Deep Sea Drilling Project Leg 85. *In* Mayer, L., Theyer, F., et al., *Init. Repts. DSDP,* 85: Washington (U.S. Govt. Printing Office), 511–551.

Nigrini, C., and Lombari, G., 1984. *A Guide to Miocene Radiolaria.* Spec. Publ. Cushman Found. Foraminiferal Res., No. 22.

Ogawa, Y., and Miyata, Y., 1985. Vein structure and its deformation history in the sedimentary rocks of the Middle America Trench slope off Guatemala, Deep Sea Drilling Project Leg 84. *In* von Huene, R., Aubouin, J., et al., *Init. Repts. DSDP,* 84: Washigton (U.S. Govt. Printing Office), 811–829.

Parsons, B., and Sclater, J. G., 1977. An analysis of the variation of oceanic bathymetry and heat flow with age. *J. Geophys. Res.,* 82:803–827.

Pickering, K. T., 1982. The shape of deep-sea siliciclastic systems—a discussion. *Geo-Mar. Lett.,* 2:41–46.

Ricci Lucchi, F., and Valmori, E., 1980. Basin-wide turbidites in a Miocene, over-supplied deep-sea plain: a geometrical analysis. *Sedimentology,* 27:248–270.

Ringwood, A. E., 1974. The petrological evolution of island arc systems. *J. Geol. Soc. London,* 130:183–204.

Sanfilippo, A., Westberg-Smith, M. J., and Riedel, W. R., 1985. Cenozoic radiolarian. *In* Bolli, H. M., Saunders, J. B., and Perch-Nielson, K. (Eds.), *Plankton Stratigraphy:* Cambridge (Cambridge Univ. Press), 631–712.

Scott, R. B., 1980. Petrology and geochemistry of arc tholeiites on the Palau-Kyushu Ridge, Site 448, Deep Sea Drilling Project Leg 59. *In* Kroenke, L., Scott, R., et al., *Init. Repts. DSDP,* 59: Washington (U.S. Govt. Printing Office), 753–796.

Serra, O., 1984. *Fundamentals of Well Log Interpretation* (Vol. 1): *The Acquistion of Logging Data:* Amsterdam (Elsevier).

Shipboard Scientific Party, 1987. Site 645. *In* Srivastava, S. P., Arthur, M., et al., *Proc. ODP, Init. Repts.,* 105: College Station, TX (Ocean Drilling Program), 61–418.

Takayama, T., and Sato, T., 1987. Coccolith biostratigraphy of the North Atlantic Ocean, Deep Sea Drilling Project Leg 94. *In* Ruddiman, W. F., Kidd, R. B., Thomas, E., et al., *Init. Repts. DSDP,* 94 (Pt. 2): Washington (U.S. Govt. Printing Office), 651–702.

Van Morkhoven, F.P.C.M., Berggren, W. A., and Edwards, A. S., 1986. Cenozoic cosmopolitan deep-water benthic foraminifera. *Bull. Cent. Rech. Explor.-Prod. Elf-Aquitaine,* No. 11.

Walker, R. G., 1975. Upper Cretaceous resedimented conglomerates at Wheeler Gorge: description and field guide. *J. Sediment. Petrol.,* 45:105–112.

Woodruff, F., 1985. Changes in Miocene deep-sea benthic foraminiferal distribution in the Pacific Ocean: relationship to paleoceanography. *In* Kennett, J. P. (Ed.), *The Miocene Ocean: Paleoceanography and Biogeography:* Geol. Soc. Am. Mem., 163:131–175.

Yasuda, H., 1989. Benthic foraminifera and sedimentary facies of the lower slope basin off Shikoku, Japan. *In* Takayanagi, Y. and Ishizaki, K. (Eds.), *Collected Papers on Foraminifera from the Japanese Islands:* Sendai (Toko Press), 83–92.

Ms 126A-109

NOTE: All core description forms ("barrel sheets") and core photographs have been printed on coated paper and bound as Section 3, near the back of the book, beginning on page 421.

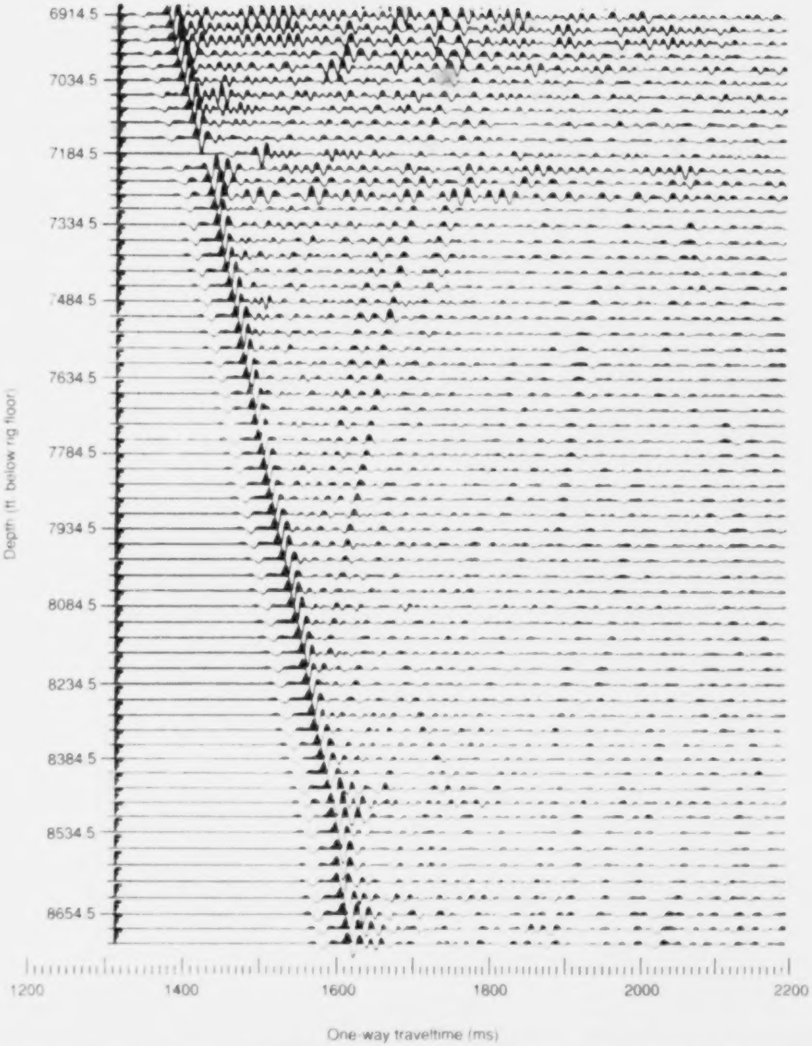

Figure 71. One-way traveltime plot of unprocessed, stacked traces, Hole 792E. Vertical scale is depth (in ft below rig floor) at which the stacked trace was obtained. The horizontal scale is one-way traveltime (in ms).

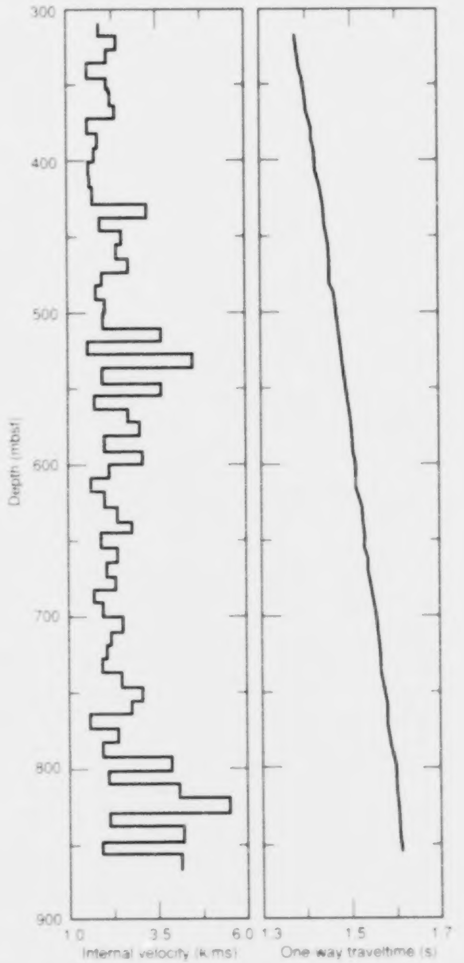

Figure 72. Raw (unsmoothed) interval velocity and one-way traveltime vs. depth, Hole 792E.

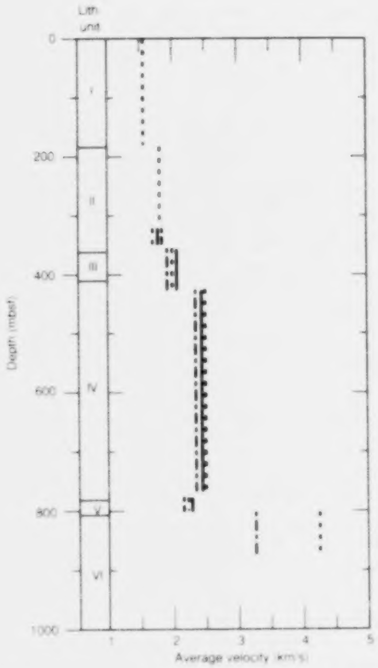

Figure 73. Comparison of VSP (solid line), laboratory (dashed line), and *in-situ* (dot-and-dashed line) velocity measurements for Hole 792E. Lithologic units are shown for reference.

Table 19. Average resistivity, interval velocity, and bulk density computed for lithologic units, Site 792.

Unit/subunit	Depth (mbsf)	Resistivity[a] (Ω · m)	Interval velocity[b] (km/s)	Bulk density[c] (g/cm^3)
IIB	287.0–357.4	0.91	1.82	1.76
III	357.4–430.0	1.02	1.83	1.53
IV	430.0–783.4	2.40	2.39	1.88
V	783.4–804.0	1.21	2.21	1.79
VI (upper basement)	804.0–831.5	8.59	3.39	2.35
VI (lower basement)	831.5–878.0	3.38	2.54	2.15

Note: Values are reported from *in-situ* measurements.

[a] From deep-induction measurement (IDPH).

[b] Compressional velocity (V_p).

[c] LSRH.

Table 20. Average compressional velocity data, Site 792.

Unit/subunit	Depth (mbsf)	VSP velocity (km/s)	Laboratory velocity (km/s)	*In-situ* velocity (km/s)
I	000.0–183.7	—	1.59	—
IIA	183.7–317.0	—	1.85	—
IIB	317.0–357.4	1.80	1.76	1.82
III	357.4–430.0	2.00	1.89	1.83
IV	430.0–783.4	2.44	2.47	2.39
V	783.4–804.0	2.23	2.22	2.21
VI (upper basement)	804.0–886.0	—	4.26	3.39

Note: Data obtained from VSP transit times, laboratory measurements, and *in-situ* measurements.

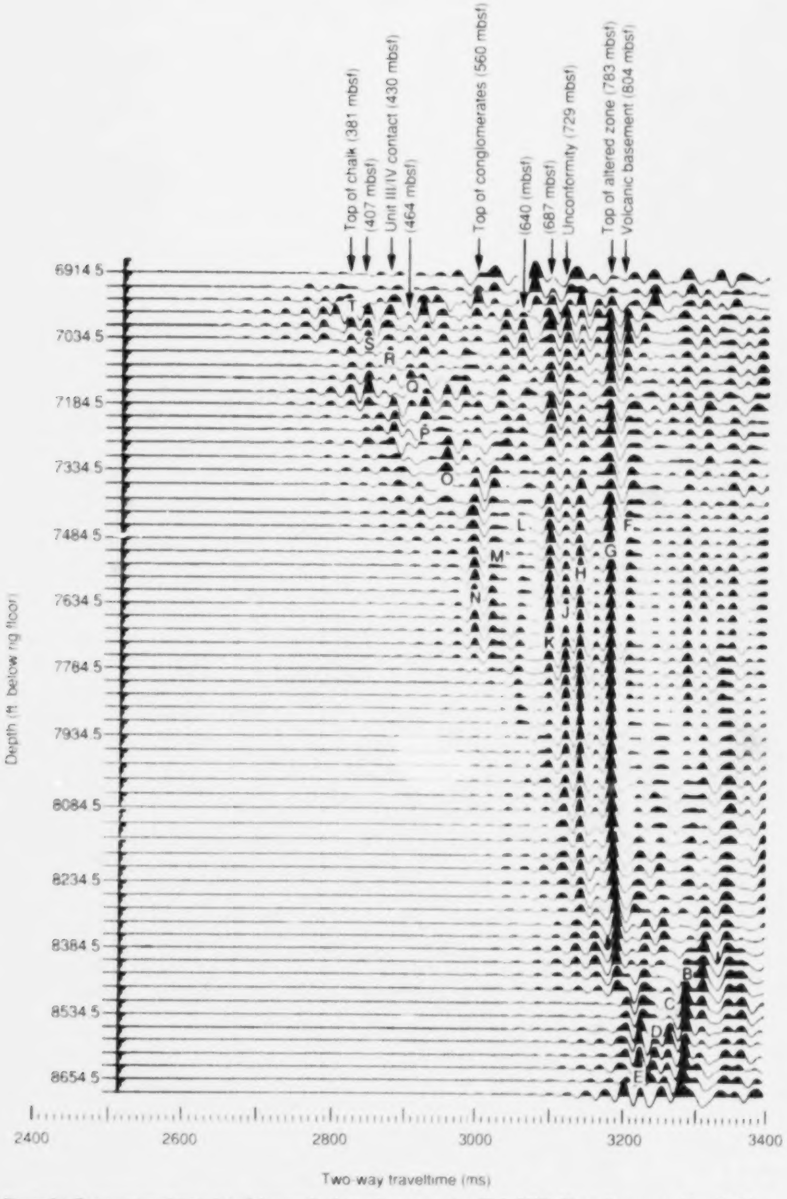

Figure 74. Two-way traveltime plot of deconvolved upgoing wavetrains, Hole 792E. The reflectors are identified by letter (for correlation with synthetic seismogram, Fig. 69, and MCS, Fig. 75) and by corresponding lithological unit (or depth) wherever possible.

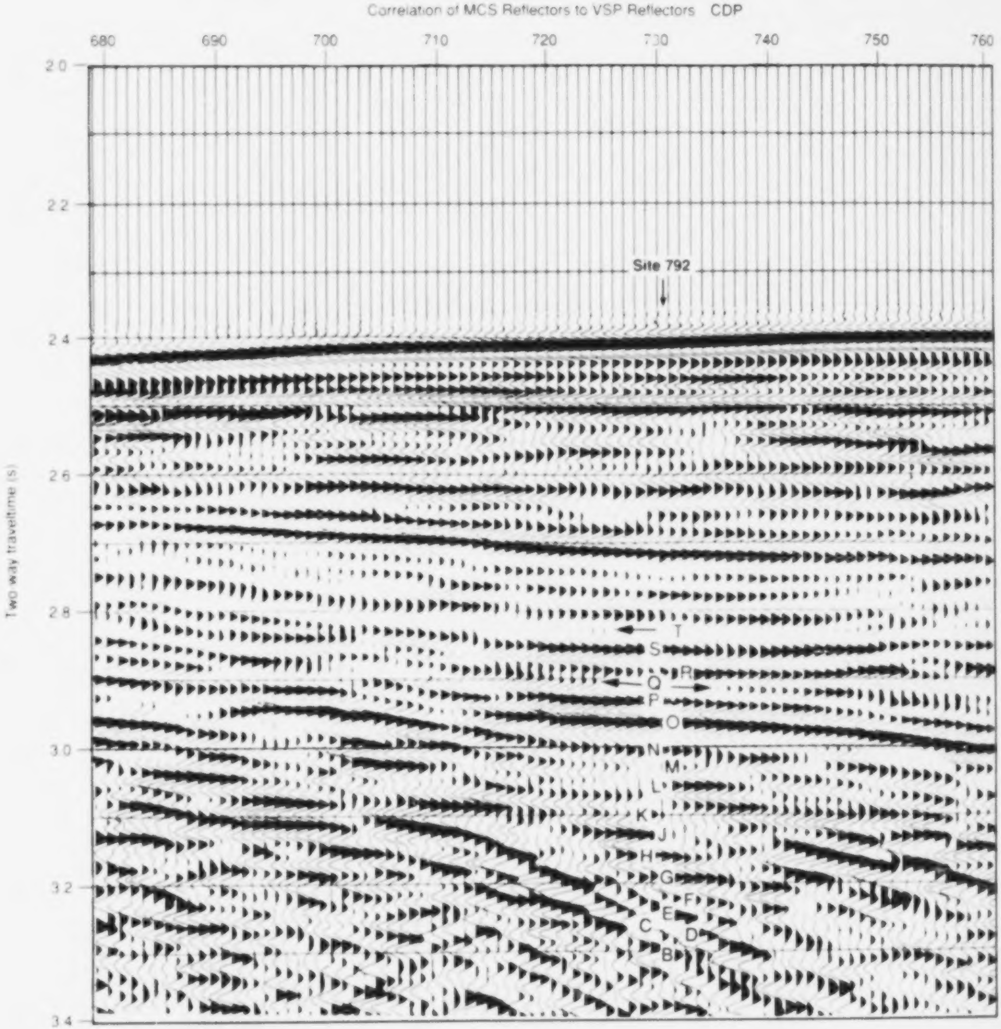

Figure 75. Correlation of MCS and VSP reflectors, Site 792. See text for discussion.

Taylor, B., Fujioka, K., et al., 1990
Proceedings of the Ocean Drilling Program, Initial Reports, Vol. 126

9. SITE 793[1]

Shipboard Scientific Party[2]

HOLE 793A

Date occupied: 26 May 1989

Date departed: 27 May 1989

Time on hole: 21 hr, 20 min

Position: 31°06.35′N, 140°53.26′E

Bottom felt (rig floor; m, drill pipe measurement): 2975.3

Distance between rig floor and sea level (m): 10.50

Water depth (drill pipe measurement from sea level, m): 2964.8

Total depth (rig floor; m): 3075.0

Penetration (m): 99.70

Number of cores (including cores with no recovery): 11

Total length of cored section (m): 99.70

Total core recovered (m): 78.96

Core recovery (%): 79.2

Oldest sediment cored:
Depth (mbsf): 99.70
Nature: vitric sand and vitric silt
Age: Pliocene Pleistocene
Measured velocity (km/s): 1.64

HOLE 793B

Date occupied: 27 May 1989

Date departed: 17 June 1989

Time on hole: 21 days, 5 hr, 20 min

Position: 31°06.33′N, 140°53.27′E

Bottom felt (rig floor; m, drill pipe measurement): 2975.3

Distance between rig floor and sea level (m): 10.50

Water depth (drill pipe measurement from sea level, m): 2964.8

Total depth (rig floor; m): 4657.3

Penetration (m): 1682.0

Number of cores (including cores with no recovery): 114

Total length of cored section (m): 1095.50

Total core recovered (m): 697.94

Core recovery (%): 63.7

Oldest sediment cored:
Depth (mbsf): 1403.9
Nature: volcanic breccia and microbreccia
Age: early Oligocene (Core 126-793B-81R)
Measured velocity (km/s): 2.55

Basement:
Depth (mbsf): 1403.90
Nature: volcanic to hyaloclastite breccia
Measured velocity (km/s): 3.1

Comments: Deepest hole reaching basement in Deep Sea Drilling Project (DSDP) or Ocean Drilling Program (ODP) history (longest occupation of any ODP or DSDP hole on a single leg).

Principal results: Site 793 is located in the center of the Izu-Bonin forearc sedimentary basin, about 75 km east of the volcanic front between the islands of Sumisu Jima and Tori Shima, and 125 km west of the axis of the Izu-Bonin Trench. It is located in an interchannel area on the southern side of the broad Sumisu Jima Canyon. The principal objectives of this site were to determine (1) the stratigraphy of the forearc basin and, hence, both the temporal variations in sedimentation, depositional environment, and paleoceanography, and the history of the intensity and chemistry of the arc volcanism; (2) the uplift and subsidence history across the forearc; (3) the nature of the igneous basement and the formation of the 200-km-wide forearc crust; and (4) the microstructural deformation and the large-scale rotation and translation of the forearc terrane since the Eocene. We selected the site on the basis of multichannel seismic records; the site chosen lies on *Fred Moore* 3505, Line 12, at 0109:30Z. Site 793 was occupied from 0745 hr (UTC, or Universal Time Coordinate), 26 May, to 1230 hr, 17 June 1989.

We spudded Hole 793A with the advanced hydraulic piston corer (APC) at 1745 hr on 26 May 1989 and cored 99.7 m with 79% recovery until an overpull and resulting severed piston rod ended operations at the hole. A reentry cone was spudded into the sediment at 0930 hr on 28 May, and Hole 793B was begun by drilling a 14-$^{3}/_{4}$-in. hole to 586.5 mbsf, which was then lined with 46 joints (562.66 m) of 11-$^{3}/_{4}$-in. casing. We obtained special permission not to core this section so that we could meet the deep stratigraphic and basement objectives in the time available. We took 114 rotary core barrel (RCB) cores during the next 12 days, with a pipe trip and subsequent reentry after Core 126-793B-87R (1422.9 mbsf) to change the drill bit. At 0320 hr on 14 June, Hole 793B reached a total penetration of 1682 mbsf, with 74% recovery in the sediments above 1403.9 mbsf and 33% recovery in the basement below.

Following a pipe trip to release the bit and add a casing landing tool, a full suite of geophysical and geochemical logs, including the formation microscanner (FMS) and vertical seismic profiling (VSP), was planned. Several bridges were encountered, which required clearing with the pipe, so the hole was logged in stages. The density tool failed. The other physical property and temperature tools logged the intervals 1565.6–1034, 947.8–775.9, and 708.2–586.5 mbsf. The FMS was run from 1539 to 1034 mbsf and from 764.1 to 586.5 mbsf. The geochemistry combination was used in the open hole from 1531 to 1034 mbsf, and through the pipe from 917 to 586.5 mbsf. Poor clamping, a result of formation conditions, limited an attempted VSP to only a few good recording levels.

We defined seven lithostratigraphic units at Site 793:

Unit I (0–98.9 mbsf): Quaternary pumiceous gravel, sandy gravel, and vitric sand; nannofossil clay, clayey silt, and silty clay; and nannofossil-rich clayey silt and clay, with rare vitric sand and silt.

Unit II (586.5–591 mbsf): olivine-clinopyroxene diabase.

Unit III (591–735.7 mbsf): lower to middle Miocene nannofossil-rich silty claystone, silty claystone, nannofossil-rich and nannofossil claystone, vitric siltstone and sandstone, clayey siltstone, and nannofossil-rich clayey siltstone.

Unit IV (735.7–759 mbsf): lower Miocene claystone, nannofossil and nannofossil-rich claystone, and vitric siltstone.

---

[1] Taylor, B., Fujioka, K., et al., 1990. *Proc. ODP, Init. Repts.*, 126: College Station, TX (Ocean Drilling Program).

[2] Shipboard Scientific Party is as given in the list of participants preceding the contents.

Unit V (759-1373.1 mbsf): lower to upper Oligocene vitric sandstone, pumiceous sandstone, granule- to fine-pebble conglomerate, siltstone, clayey siltstone, and silty claystone.

Unit VI (1373.1-1403.9 mbsf): upper-lower Oligocene(?) very poorly sorted volcanic breccia with sandy matrix, and mixed fresh to altered clasts of mainly plagioclase-rich andesite.

Unit VII (1403.9-1678.4 mbsf): upper-lower Oligocene(?) breccias and massive to pillowed flows of porphyritic and aphyric clinopyroxene-orthopyroxene basaltic andesites and andesites. Note that this unit is subdivided into 17 igneous rock units in the "Igneous Petrology" section (this chapter).

We dated Units I and III-V by means of nannofossils, radiolarians (Units I and III), foraminifers, and paleomagnetics; Units VI-VII were dated by paleomagnetics. Sedimentation rates in Units V and VI are 250 m/m.y. (31-29 Ma) and in the upper part of Unit V are 80 m/m.y. (29-27 Ma). Unit IV was deposited very slowly (~7 m/m.y.) with a probable lacuna at 18-21 Ma. Sedimentation rates are 70 m/m.y. in Unit III, 40 m/m.y. in the uncored interval, and 105 m/m.y. in Unit I (< 0.83 Ma). Benthic foraminifers indicate that depositional water depths shallowed from 4-5 km in the late-early Oligocene to 2-4 km at present.

Unit VI represents a debris or talus apron, eroded from local basement topography. Several of the clasts are geochemically similar to the basement calcalkaline andesites at Site 792. Unit V, >600 m thick, records the rapid filling of the forearc basin by turbiditic sandstones, conglomeratic debris flows, and finer interbeds. These sediments were produced by concurrent volcanism as well as by erosion of surrounding highs. Hemipelagic Unit IV was deposited in oxygenated bottom waters during a time of regional volcanic quiescence. Unit III represents an alternation of fine-grained turbidites fed by renewed arc volcanism and hemipelagic sediments. Unit II is a high-Mg series tholeiitic diabase, intruded in the middle Miocene or younger. Unit I records the continuation in the late Pleistocene of the infilling, begun in the early Pliocene, of a broad canyon that was probably incised during the latest Miocene. The increased pumiceous input to the upper part of Unit I records a late Quaternary increase in explosive arc volcanism.

Units III-VI contain numerous normal microfaults and locally abundant subvertical dewatering veinlets, indicative of an extensional regime throughout the basin history. The minimum horizontal compressive stress direction determined from hole ellipticity is N65°E. Paleomagnetic inclination data from the sediments and lavas show that the forearc has been translated about 15° north since 30 Ma.

Volcanism without epiclastic sedimentation accompanied the initial mid-Oligocene forearc basin subsidence, as the formerly contiguous Eocene frontal- and outer-arc highs were separated. This separation probably resulted from rifting rather than spreading at a well-defined axis, given the scale of the basin (40-70 km wide) and multichannel seismic data that imply the presence of half grabens and low-angle detachments in the basement. Most of the Site 793 basement lavas and breccias belong to a high-Mg series of basaltic andesites and andesites that have boninitic affinities. The aphyric lavas and clasts belong to a low-Mg series that has tholeiitic affinities. Both series have < 5% vesicles. They are less enriched in Ti, P, Y, Zr, and Ba than most arc lavas. Their high-field-strength element ratios indicate a depleted mantle source.

The pore waters below 787 mbsf broke the record of the previous site for the most extensively altered pore water of seawater origin ever sampled by the DSDP/ODP. Characteristic concentrations include sulfate = 12-16, magnesium = ~0, calcium = 290-300, and silica = 0.14-0.23 (all in mM). Unlike values at Site 792, even the concentration of chloride has been shifted relative to seawater, to stable levels of around 715 mM below 1000 mbsf. These highly altered interstitial Ca-Cl-type waters result from the low-temperature alteration of volcanogenic sedimentary components into smectites, zeolites, and gypsum, in a virtually closed system, as indicated by the high formation factors.

Physical property measurements indicate that

1. the sedimentary section is characterized by generally decreasing porosity, from an average of 68% in Unit I to 31% in Unit VI;
2. wet-bulk density increases concurrently from a mean of 1.68 g/cm^3 (Unit I) to 2.53 g/cm^3 (Unit VI);
3. superimposed on these general trends are cyclic fluctuations, similar to those observed at Site 792;
4. carbonate contents average 25%, 10%, and 21% in Units I, III, and IV, respectively, and values are consistently low throughout Units V and VI, generally <4%;
5. sonic velocity data in Units I, II, and IV display relatively low values with little variability, averaging 1.6, 2.0, and 2.0 km/s, respectively;
6. the diabase intrusion (Unit II) is characterized by extremes in all the physical properties, with averages of 10.4% (porosity), 2.76 g/cm^3 (bulk density), and 5.04 km/s (velocity); and
7. the sediment/basement contact is not well defined by the physical property data (or *in-situ* measurements) because of the gradual transition through the breccias.

However, the volcanic breccia and lava flows within the basement are clearly different with regard to their physical properties. Deeper layers, containing a greater abundance of flow units, are characterized by generally lower porosity values (average of 23.3%) and higher bulk density (2.62 g/cm^3) and velocity values (3.84 km/s), compared with values in breccia units (averages of 28%, 2.5 g/cm^3, and 3.4 km/s, respectively).

The principal results of this site, which made the deepest penetration reaching basement in the history of the DSDP/ODP, are

1. documentation of the absence of pre-mid-Oligocene sediments in the forearc basin depocenter;
2. benthic foraminiferal evidence that depositional water depths shallowed from 4-5 km in the mid-Oligocene to 2-4 km at present;
3. interpretation that the forearc basin formed by mid-Oligocene rifting that separated the formerly contiguous Eocene frontal- and outer-arc highs;
4. recovery of the igneous basement beneath the center of the forearc basin, which includes high-Mg series basaltic andesites and andesites with boninitic affinities as well as a low-Mg series with tholeiitic affinities;
5. confirmation of varying volcanogenic input to the forearc, including volcanic quiescence during the early Miocene and a dramatic increase in volcanic activity in the late Quaternary;
6. documentation of a Neogene intrusion 70 km in front of the "volcanic front";
7. microstructural evidence of an extensional regime throughout the forearc basin history;
8. paleomagnetic evidence that the forearc has been translated about 15° northward since 30 Ma;
9. pore-water indications of low-temperature alteration of the volcanogenic sediments, producing Ca-Cl-type waters; and
10. establishment of a deep, open, reentry site for future investigators.

BACKGROUND AND OBJECTIVES

Site 793 is located at 31°06.33'N, 140°53.27'E, at 2965 m below sea level (mbsl) in the center of the Izu-Bonin forearc sedimentary basin, about 75 km east of the volcanic front between the islands of Sumisu Jima and Tori Shima, and 125 km west of the axis of the Izu-Bonin Trench (Fig. 1). It is located on the southern side of the broad Sumisu Jima Canyon (Fig. 2).

By drilling at this site we sought to determine the following:

1. the stratigraphy of the forearc and, hence, both the temporal variations in sedimentation, depositional environment, and paleoceanography, and the history of the intensity and chemistry of arc volcanism;
2. the uplift/subsidence history across the forearc to obtain information on forearc flexure and basin development;
3. the nature of the forearc igneous basement to answer questions concerning the nature of volcanism in the initial stages of subduction and the formation of the 200-km-wide forearc crust, including the possibility of later forearc volcanism; and
4. the microstructural deformation and the large-scale rotation and translation of the forearc terrane since the Eocene.

The first of these objectives was addressed partly through detailed studies of sediments retrieved at Site 793. The type of sed-

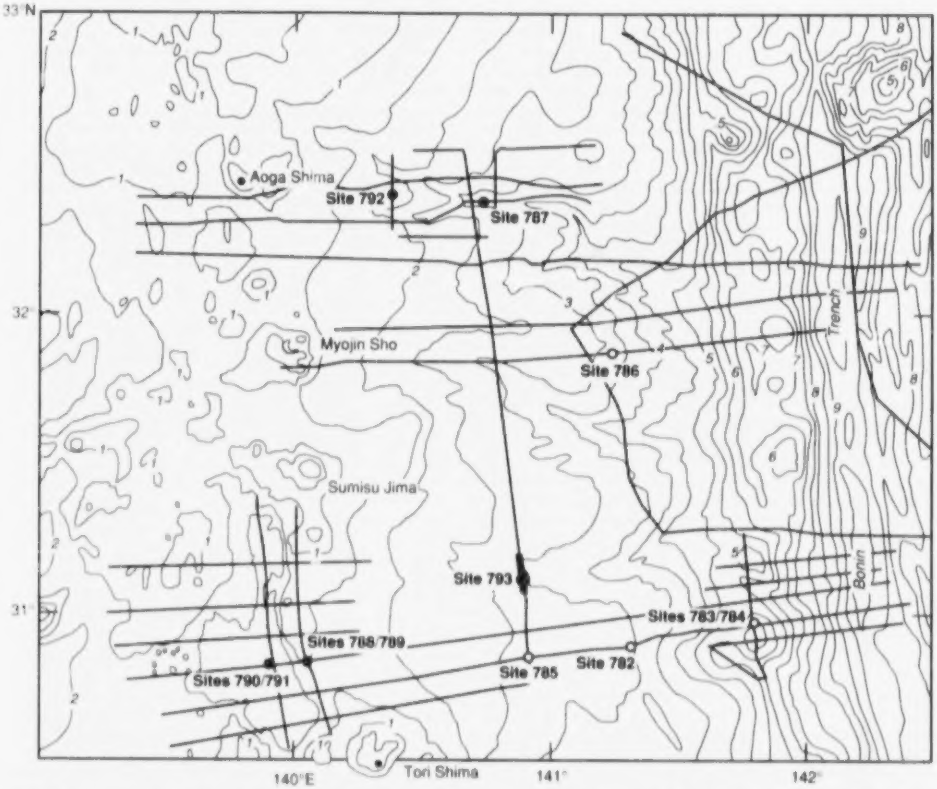
33°N
32°
31°
140°E
141°
142°
Aoga Shima
Site 792
Site 787
Myojin Sho
Site 786
Sumisu Jima
Site 793
Sites 783/784
Sites 788/789
Sites 790/791
Site 785
Site 782
Tori Shima
Trench
Bonin

Figure 1. Bathymetric map (500-m-contour interval) of the Izu-Bonin arc-trench system between 30.5° and 33°N. The locations of sites drilled on ODP Legs 125 (open circles) and 126 (filled circles) are shown on the map, as are the locations of site survey multichannel seismic (MCS) lines. The segment of MCS Line 12 (shown in Fig. 2) is delineated by the thicker line segment.

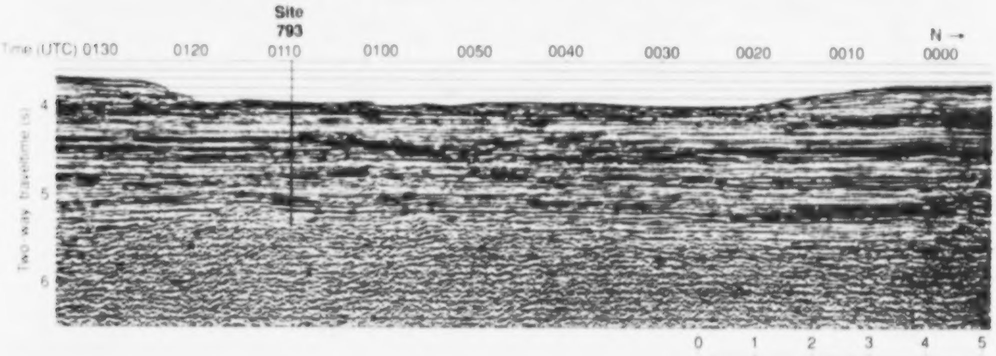

Figure 2. MCS profile 12 (Systrom, Taylor, et al., in prep.) along the Izu-Bonin forearc sedimentary basin, crossing Sumisu Jima Canyon (see Fig. 1 for location).

imentation and style of deposition in the forearc basin was expected to change with time as the proximity to arc volcanoes changed, as the volume and eruptive style of arc products varied, as the basin filled, and as the development of submarine canyons eroded and redistributed sedimentary material. Geostrophic currents, such as the paleo-Kuroshio, and changes in global sea level also may have affected the pattern of sedimentation and their effects may be deciphered from the stratigraphic record.

These sediments also contain a temporal record of the variations in the intensity and composition of arc volcanism. Studies of the chronology and nature of tephras at this site will test various conflicting models concerning the complex relationships between tectonic and volcanic phenomena in island arcs, such as changes in subduction rate, periodicity in backarc rifting and spreading, pulses of arc volcanism, and variations in arc geochemistry (see "Introduction" chapter, this volume, for elaboration).

The second objective was investigated through a combination of paleontological estimates of paleobathymetry, backstripping of the sedimentation history using the physical property and logging data, and seismic stratigraphic analyses of interconnecting multichannel seismic (MCS) profiles. Determination of the forearc vertical displacement history provided some of the information necessary to decide (1) whether fairly stable conditions have prevailed since the mid-Tertiary, as suggested by the well-developed submarine canyon system and lower-slope terrace of serpentinite seamounts; (2) whether the frontal- and outer-arc high resulted from igneous construction or from differential uplift; (3) whether the upper-slope basin between them is caused by forearc spreading or differential subsidence; and (4) whether flexural loading of the forearc by arc volcanoes or by coupling with the subducting plate is an important process.

The third objective was investigated by studies of the basement rocks retrieved at this site. Basement beneath the thickly sedimented upper-slope basin between the frontal- and outer-arc highs had never been sampled in this or any other intraoceanic arc-trench system. From the available data, it appears that the present 150–230-km-wide Bonin-Mariana forearc formed, in large part, by volcanism during the initial stages of arc development in the Eocene and early Oligocene, (see "Introduction" chapter, this volume, for elaboration). Similar volcanism has not occurred since and cannot be studied as an active phenomenon anywhere on Earth at present. Studies of the basement rocks permitted evaluation of the three main alternative hypotheses for the origin and evolution of this forearc terrane, namely: (1) the frontal- and outer-arc highs could have originally been continuous and subsequently separated by forearc spreading; (2) the frontal- and outer-arc highs could have been built separately but nearly synchronously on former West Philippine Plate crust; or (3) the terrane could form part of a continuous Eocene arc volcanic province, possibly with overprints of later forearc volcanism. Each scenario of forearc basement development implies a different crustal structure for the forearc.

The fourth objective of the site, the study of microstructures and plate rotations, was addressed through a study of FMS images as well as the structural and paleomagnetic properties of the cored materials. Microstructures in the drill cores and on the FMS images of the drill-hole wall helped us to determine the intensity of faulting in space and time across the forearc terrane and to define the syndepositional structures. Measurements of the paleomagnetic properties of subaerial portions of the Izu-Bonin and Mariana forearcs have shown at least 20° of northward drift and from 30° to >90° of clockwise rotation since the Eocene (see "Introduction" chapter, this volume, for more details). Studies of the paleomagnetism of the cores constrained the numerous different models for the nature and timing of these motions, and their relationship to the overall structural evolution of the forearc. The FMS data helped orient the rotary cores so that declinations, and hence rotations, could be determined.

Given the previous drilling in the Izu-Bonin forearc on this leg and on Leg 125, the remaining primary objectives were to recover the mid-Oligocene and older stratigraphy and basement of the forearc basin. To meet these objectives required a deep penetrating reentry hole, but the estimated site time was 3 days more than that available. To save this time, a request was made and approved to drill without coring the interval below APC refusal to 600 mbsf.

SEISMIC STRATIGRAPHY

Site 793 lies on *Fred Moore* 3505, Line 12, at 0109:30Z. We correlated the MCS reflection data with recovered core material (Fig. 3) by using velocity data obtained from physical properties measurements, averaged over each lithologic unit (see "Physical Properties" section, this chapter), to convert depths (mbsf) into two-way traveltimes. For the uncored interval between 99.7 and 586.5 mbsf, we used stacked velocity values derived from the reflection data to make the conversion. Physical properties and stacking velocities are in close agreement for the cored intervals at this site.

Two of the active channels within the broad submarine valley can be seen at 0053–0100Z and 0116–0121Z on Line 12 (Fig. 3). Site 793 is located in the interchannel area. Unit I recovered Quaternary material filling a paleo-canyon, the base of which can be seen at 4.46 s and 0053Z in Figure 3. Because of the canyon fill and the uncored interval between 99.7 and 586.5 mbsf, the uppermost seismic stratigraphic units adjacent to the site were not sampled. These include a unit of discontinuous, high-amplitude reflectors down to 4.1 s, which overlies a unit of subparallel, weak reflectors down to 4.36 s. Unit II, a diabase sill, corresponds to the strong reflector at 4.62 s that is at the base of an uncored interval of subparallel, continuous, mainly strong reflectors, typical of turbidites. Lower amplitude, less continuous reflectors between 4.63 and 4.79 s correlate with Units III and IV. Unit V is seismically expressed as a series of subparallel reflectors, laterally varying in amplitude, that are offset by several normal faults. High-amplitude reflectors at 5.03 to 5.18 s correlate with the coarse sediments in the lower half of this unit. There is a gradual transition in physical properties data from the basal sediments, including the volcanic-clast breccia of Unit VI, to the andesitic basement (see "Physical Properties" section, this chapter). Acoustic basement (>5.25 s) is characterized by chaotic and discontinuous reflectors underlying the stratified sedimentary sequences.

OPERATIONS

Site 792 to Site 793 (BON 6D)

The transit from Sites 792 to 793 (proposed Site BON 6D) took 8.6 hr to traverse 82 nmi at an average speed of 9.5 kt. At 0715 hr (all times in UTC) on 26 May 1989, the first of two beacons was dropped. As the bottom-hole assembly (BHA) for the first hole was being made up, the first beacon died and the backup beacon had to be deployed at 0813 hr.

The drilling program for this site called for coring 1700 mbsf into mid-Oligocene forearc sediments. To complete operations within the remaining 22 days, some changes in scientific objectives were needed, and a plan of action was established that included blind drilling, spot coring, and the setting of a reentry cone with 11-3/4-in. casing. A summary of drilling operations at this site is presented in Table 1.

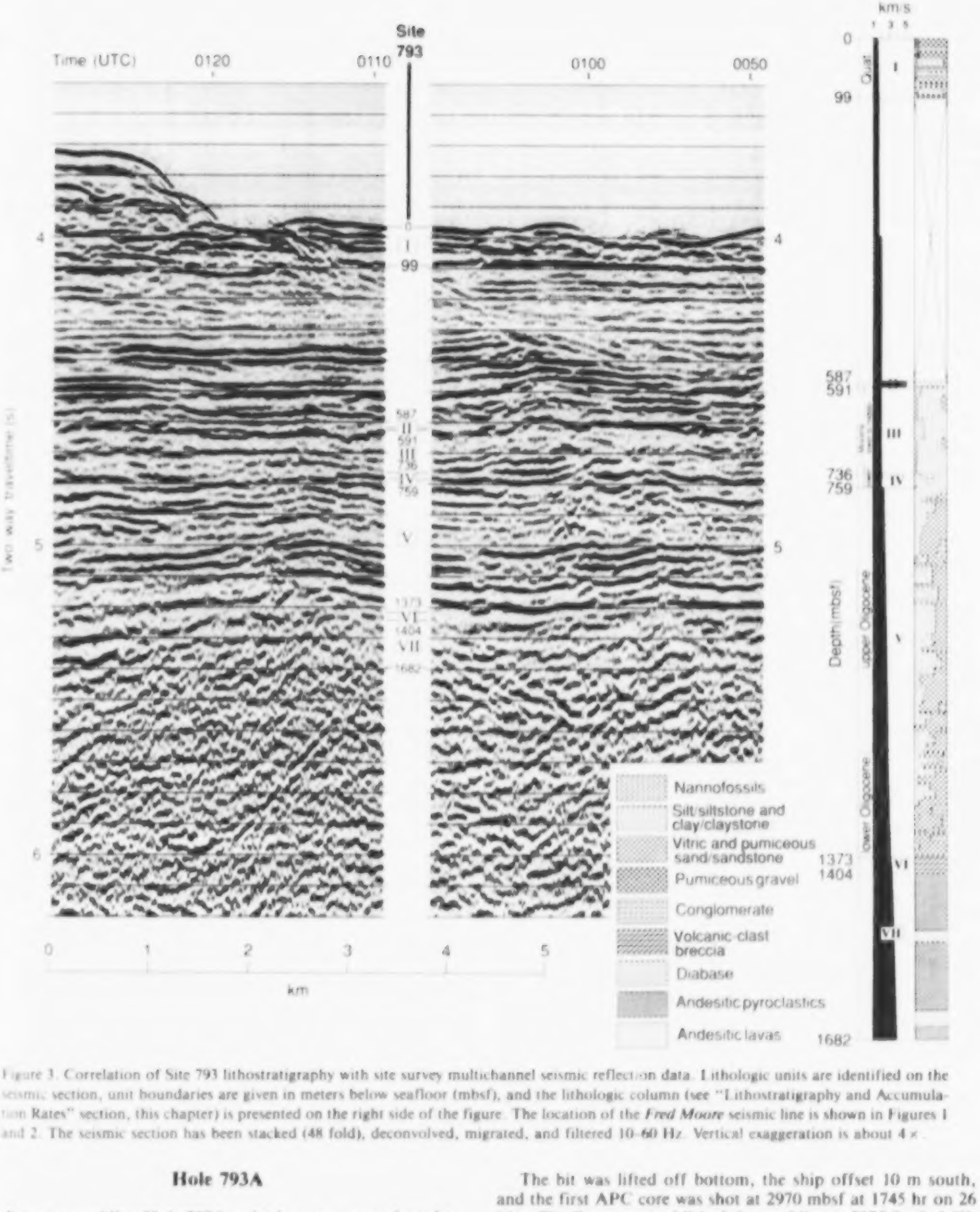

Figure 3. Correlation of Site 793 lithostratigraphy with site survey multichannel seismic reflection data. Lithologic units are identified on the seismic section, unit boundaries are given in meters below seafloor (mbsf), and the lithologic column (see "Lithostratigraphy and Accumulation Rates" section, this chapter) is presented on the right side of the figure. The location of the *Fred Moore* seismic line is shown in Figures 1 and 2. The seismic section has been stacked (48 fold), deconvolved, migrated, and filtered 10–60 Hz. Vertical exaggeration is about 4 ×.

Hole 793A

Prior to spudding Hole 793A, a jet-in test was conducted to examine the capabilities of the sediment to support a reentry cone and to determine what length to make the 16-in. casing shoe. At 1735 hr on 26 May, the jet-in test concluded with a final penetration of 22 m.

The bit was lifted off bottom, the ship offset 10 m south, and the first APC core was shot at 2970 mbsf at 1745 hr on 26 May. The first core established the mud line at 2975.3 mbsf. We routinely obtained Cores 126-793A-2H through -10H encountering overpulls as much as 60,000 lb. Orientation of the cores commenced with Core 126-793B-6H. The percentage recovery of the first 11 cores was 79%.

Table 1. Coring summary, Site 793.

Core no.	Date (1989)	Time (UTC)	Interval (mbsf)	Cored (m)	Recovered (m)	Recovery (%)
126-793A-						
1H	May 26	1845	0.0-4.2	4.2	4.21	100.0
2H	26	1935	4.2-13.5	9.3	7.08	76.1
3H	26	2010	13.5-23.0	9.5	9.35	98.4
4H	26	2055	23.0-32.5	9.5	9.56	100.0
5H	26	2130	32.5-42.0	9.5	9.76	103.0
6H	26	2220	42.0-51.6	9.6	8.82	91.9
7H	26	2310	51.6-61.2	9.6	6.42	66.9
8H	26	2355	61.2-70.9	9.7	7.19	74.1
9H	27	0040	70.9-80.5	9.6	7.78	81.0
10H	27	0130	80.5-90.1	9.6	1.99	20.7
11H	27	0215	90.1-99.7	9.6	8.80	91.6
Coring totals				99.7	78.96	79.2
126-793B-						
1R	June 2	0250	586.5-594.7	8.2	3.79	46.2
2R	2	0415	594.7-604.3	9.6	0.47	4.9
3R	2	0525	604.3-614.0	9.7	4.97	51.2
4R	2	0630	614.0-623.6	9.6	5.88	61.2
5R	2	0730	623.6-633.3	9.7	6.63	68.3
6R	2	0830	633.3-642.8	9.5	3.41	35.9
7R	2	0935	642.8-652.4	9.6	0.63	6.6
8R	2	1030	652.4-662.1	9.7	2.00	20.6
9R	2	1155	662.1-671.8	9.7	3.91	40.3
10R	2	1300	671.8-681.4	9.6	4.25	44.3
11R	2	1405	681.4-691.1	9.7	8.07	83.2
12R	2	1500	691.1-700.8	9.7	2.20	22.7
13R	2	1600	700.8-710.4	9.6	5.56	57.9
14R	2	1645	710.4-720.1	9.7	2.07	21.3
15R	2	1740	720.1-729.7	9.6	5.58	58.1
16R	2	1910	729.7-739.1	9.4	8.89	94.6
17R	2	2120	739.1-748.8	9.7	8.25	85.0
18R	2	2250	748.8-758.4	9.6	9.83	102.0
19R	3	0020	758.4-768.0	9.6	5.05	52.6
20R	3	0150	768.0-777.7	9.7	9.84	101.0
21R	3	0310	777.7-787.3	9.6	8.97	93.4
22R	3	0435	787.3-797.0	9.7	4.63	47.7
23R	3	0620	797.0-806.7	9.7	6.53	67.3
24R	3	0810	806.7-816.4	9.7	8.87	91.4
25R	3	0945	816.4-825.7	9.3	9.03	97.1
26R	3	1150	825.7-835.4	9.7	9.88	102.0
27R	3	1330	835.4-845.1	9.7	9.31	96.0
28R	3	1510	845.1-854.7	9.6	9.91	103.0
29R	3	1650	854.7-864.4	9.7	7.22	74.4
30R	3	1835	864.4-874.0	9.6	8.50	88.5
31R	3	2025	874.0-883.7	9.7	9.14	94.2
32R	3	2235	883.7-893.3	9.6	6.45	67.2
33R	4	0020	893.3-903.0	9.7	9.83	101.0
34R	4	0200	903.0-912.6	9.6	8.28	86.2
35R	4	0335	912.6-922.3	9.7	9.35	96.4
36R	4	0520	922.3-932.0	9.7	8.09	83.4
37R	4	0705	932.0-941.6	9.6	9.89	103.0
38R	4	0905	941.6-951.3	9.7	7.44	76.7
39R	4	1115	951.3-961.0	9.7	0.69	7.1
40R	4	1310	961.0-970.6	9.6	10.01	104.3
41R	4	1505	970.6-980.3	9.7	9.57	98.6
42R	4	1710	980.3-989.7	9.4	7.11	75.6
43R	4	1905	989.7-999.4	9.7	8.61	88.7
44R	4	2115	999.4-1009.1	9.7	9.95	102.0
45R	4	2240	1009.1-1018.7	9.6	1.30	13.5
46R	5	0025	1018.7-1028.0	9.3	10.49	112.8
47R	5	0200	1028.0-1037.6	9.6	6.62	68.9
48R	5	0345	1037.6-1047.3	9.7	8.58	88.4
49R	5	0545	1047.3-1057.0	9.7	4.11	42.4
50R	5	0745	1057.0-1066.7	9.7	8.92	91.9
51R	5	1035	1066.7-1076.4	9.7	9.76	100.0
52R	5	1345	1076.4-1086.1	9.7	6.11	63.0
53R	5	1540	1086.1-1095.7	9.6	5.63	58.6
54R	5	1735	1095.7-1105.4	9.7	5.91	60.9
55R	5	1950	1105.4-1115.0	9.6	3.96	41.2
56R	5	2150	1115.0-1124.7	9.7	7.22	74.4
57R	5	2340	1124.7-1134.0	9.3	4.20	45.1
58R	6	0225	1134.0-1143.6	9.6	9.79	102.0
59R	6	0625	1143.6-1153.2	9.6	9.92	103.0
60R	6	0840	1153.2-1162.9	9.7	9.62	99.2
61R	6	0930	1162.9-1172.6	9.7	4.18	43.1
62R	6	1040	1172.6-1182.2	9.6	4.80	50.0
63R	6	1235	1182.2-1191.9	9.7	5.23	53.9
64R	6	1500	1191.9-1201.5	9.6	9.82	102.0
65R	6	1710	1201.5-1211.1	9.6	9.38	97.7
66R	6	1915	1211.1-1220.8	9.7	9.29	95.8

Table 1 (Continued).

Core no.	Date (1989)	Time (UTC)	Interval (mbsf)	Cored (m)	Recovered (m)	Recovery (%)
126-793B- (cont.)						
67R	6	2110	1220.8-1230.5	9.7	9.27	95.5
68R	6	2300	1230.5-1240.2	9.7	8.69	89.6
69R	7	0110	1240.2-1249.8	9.6	9.58	99.8
70R	7	0330	1249.8-1259.4	9.6	9.85	102.0
71R	7	0600	1259.4-1268.7	9.3	9.30	100.0
72R	7	0825	1268.7-1278.4	9.7	9.71	100.0
73R	7	1045	1278.4-1288.0	9.6	6.35	66.1
74R	7	1450	1288.0-1297.7	9.7	9.36	96.5
75R	7	1735	1297.7-1307.3	9.6	9.56	99.6
76R	7	2050	1307.3-1317.0	9.7	9.51	98.0
77R	8	0040	1317.0-1326.7	9.7	8.71	89.8
78R	8	0335	1326.7-1336.4	9.7	9.78	101.0
79R	8	0615	1336.4-1346.0	9.6	7.65	79.7
80R	8	0945	1346.0-1355.7	9.7	8.78	90.5
81R	8	1155	1355.7-1365.3	9.6	8.31	86.5
82R	8	1450	1365.3-1374.9	9.6	9.54	99.4
83R	8	1745	1374.9-1384.5	9.6	2.51	26.1
84R	8	2035	1384.5-1394.2	9.7	3.02	31.1
85R	9	0040	1394.2-1403.9	9.7	3.35	34.5
86R	9	0450	1403.9-1413.6	9.7	2.78	28.6
87R	9	0900	1413.6-1422.9	9.3	5.02	54.0
88R	9	1115	1422.9-1431.4	8.5	2.15	25.3
89R	10	1520	1431.4-1441.1	9.7	4.88	50.3
90R	10	1840	1441.1-1450.4	9.3	0.05	0.5
91R	10	2155	1450.4-1460.1	9.7	0.00	0.0
92R	11	0520	1460.1-1469.7	9.6	4.09	42.6
93R	11	0910	1469.7-1479.4	9.7	3.01	31.0
94R	11	1320	1479.4-1489.0	9.6	2.59	27.0
95R	11	1635	1489.0-1498.7	9.7	3.08	31.7
96R	11	1855	1498.7-1508.3	9.6	1.41	14.7
97R	11	2205	1508.3-1518.0	9.7	1.08	11.1
98R	12	0050	1518.0-1527.6	9.6	5.74	59.8
99R	12	0325	1527.6-1537.3	9.7	1.90	19.6
100R	12	0630	1537.3-1546.9	9.6	2.06	21.4
101R	12	0920	1546.9-1556.6	9.7	1.31	13.5
102R	12	1245	1556.6-1566.3	9.7	2.14	22.0
103R	12	1530	1566.3-1575.9	9.6	3.45	35.9
104R	12	1820	1575.9-1585.5	9.6	5.30	55.2
105R	12	2120	1585.5-1595.2	9.7	4.42	45.5
106R	13	0010	1595.2-1604.8	9.6	1.69	17.6
107R	13	0350	1604.8-1614.4	9.6	5.52	57.5
108R	13	0645	1614.4-1624.1	9.7	3.55	36.6
109R	13	1005	1624.1-1633.8	9.7	3.71	38.2
110R	13	1230	1633.8-1643.4	9.6	5.88	61.2
111R	13	1535	1643.4-1653.1	9.7	2.49	25.7
112R	13	1900	1653.1-1662.7	9.6	2.54	26.4
113R	13	2225	1662.7-1672.4	9.7	4.09	42.1
114R	13	0320	1672.4-1682.0	9.6	6.02	62.7
Coring totals				1095.5	697.94	63.7

After Core 125-793A-12H was shot, the core barrel became firmly imbedded in the sediment and required 120,000-lb overpull to be extracted. The excessive overpull was too much for the piston rod connection and it sheared, leaving part of the piston rod and the core barrel in the hole. Having completed the scientific objectives of this hole, the drill pipe was tripped to the surface and broke the plane of the rotary table at 0435 hr on 27 May, thereby officially ending Hole 793A.

Hole 793B

As soon as the advanced-hydraulic-piston-core/extended-core-barrel (APC/XCB) bottom-hole assembly (BHA) was laid down, work began on configuring the reentry cone running assembly. The cone was skidded over the center of the moonpool, a commandable beacon permanently attached to the upper lip of the cone, and the 16-in. casing shoe spaced out. The BHA was lowered through the rotary table and latched to the reentry cone. The reentry cone and BHA were lowered through the moonpool doors at 0300 hr on 28 May.

There were two short stops on the way to the seafloor to reduce the buoyancy of the drill pipe, and at 0933 hr the casing shoe was spudded in at the mud line. The jet-in procedure was finished and the reentry cone released by 1130 hr.

The drilling phase of this hole began at 1130 hr on 28 May and continued until 0745 hr on 29 May, when a total depth of 596.5 mbsf was attained. The hole was stopped short of the original target depth of 600 mbsf when a formation change at 575 mbsf indicated harder material that would be suitable for anchoring the bottom of the casing string. The hole was then swept twice and displaced with potassium chloride-treated mud. The top drive was racked, and at 1415 hr we began to pull the drillstring out of the hole.

The bit cleared the seafloor at 1610 hr and was on deck at 2200 hr. The casing running tools were made up and 46 joints (562.66 m) of 11-3/4-in. casing were run to the bottom. When the end of the casing reached a depth corresponding to 9 m above the reentry cone, we conducted a 2-hr television (TV) search for the cone starting at 1800 hr on 30 May. At 2015 hr, the casing string was stabbed into the reentry cone.

The casing string encountered resistance almost immediately upon entering the 16-in. casing hanger. After pumping mud and repositioning the vessel, the casing started to feed into the hole. The casing was worked while maintaining circulation to advance down the bore slowly. At 0425 hr on 31 May, the casing hanger was successfully landed in the reentry cone. The casing was then secured in place with a cement slurry, after which the pipe began its trip to the surface at 1145 hr.

First Reentry

A 6-collar RCB BHA was made up without a bit release because the only mechanical bit release (MBR) on board had sustained numerous cracks in the box connection during Leg 125 and was considered a total loss. The BHA was run in the hole to 2961.5 mbsl with the vibration-isolated television (VIT) system. At 0630 hr on 1 June, a TV search for the reentry cone commenced and found its target within 10 min. Reentry of the cone with the RCB occurred at 0650 hr.

At 1115 hr, the tedious process of drilling out the cement plug began; after cleaning up the rat hole, RCB coring commenced at 2330 hr on June 1, at a depth of 3561.8 mbsl (586.5 mbsf). The first core taken in Hole 793B took 115 min to cut 8.2 m, which corresponds to a rate of penetration of 4 m/hr. We discovered that the casing had been anchored in a diabase sill. This zone virtually ended with Core 126-793B-1R.

The remaining cores for the day took a more "reasonable" time (on the order of 40 m/hr) to penetrate the sediment. By the end of the first day, 114.3 m had been cored with 40% recovery.

By the end of the June 3, the material had compacted, the rate of penetration (ROP) slowed to a more stable level, and recovery improved to 79%. We continued RCB coring into upper Oligocene vitric sandstone and claystone. Hole surveys conducted at 1000, 1105, and 1201.5 mbsf found the hole angle at 1° or less.

On the morning of 8 June, one of the two heave compensator hoses ruptured. There were no spares on board, so coring continued with one hose and with limited performance potential on the heave compensator. Fortunately, the seas remained fairly calm for the rest of the leg. The penetration rate slowly but relentlessly continued to decrease with depth so that by the end of June 8, the ROP had dropped to 10 m/hr.

As the morning of 9 June approached, the ROP had slowed to 1.5 m/hr. Although there were no visible signs of bit distress such as erratic torque and undergauged core diameter, the high number of rotating hours (74 hr), the hardness of bottom, the light BHA (only six drill collars), and nearly 5 days remaining on site dictated that a bit change would be a prudent course of action. The progress up to that time had been 836.4 m cored with 73.4% recovery (613.9 m).

Starting at 0930 hr on 9 June, the drill bit began to be pulled to the surface. The drill bit broke the plane of the rotary table at 1830 hr on 9 June. Examination of the bit showed it to be in fair condition with about 25 inserts missing.

Second Reentry

A nine-collar BHA was rapidly made up and the new bit was run in the hole to 2170 mbsl at 2330 hr. The cone was reentered at 0210 hr on 10 June, and the drillstring was run to the bottom.

Cores 126-793B-88R through -90R (1442.3-1450.4 mbsf) recovered lower Oligocene volcanic breccia. While pumping down the core barrel for Core 126-793B-90R, an increase in pump pressure was observed. This was ascribed initially to a plugged jet, and Core 126-793B-90R was cut and retrieved. Recovery for this core was 5 cm of breccia.

The core barrel for Core 126-793B-91R was then pumped down with the slightly higher pressure still in evidence. When this core was retrieved with no recovery, it was assumed that the problem of the abnormally higher pressure was caused by an obstruction in the core throat or a partially jammed flapper, not a clogged jet orifice. A core barrel with a "deplugger" was pumped down and the pump pressure monitored for a drop to normal operating pressure. A couple of taps with the wireline jars were needed to unseat the deplugger, which was then tripped to the surface. There was no drop in pressure.

We dropped a center bit in hopes that this would clear the obstruction. Still the pressure remained high. The center bit was tripped out and the deplugger run in for a second time, this time with success. The pressure dropped, the deplugger was withdrawn, and a standard core barrel was run in the hole.

Normal coring operations resumed at 0145 hr on 11 June with Core 126-793B-92R, which yielded 4 m of volcanic breccia. The average rate of penetration for the day was 4 m/hr. Surveys were run at Cores 126-793B-96R and -106R, which found the hole at 1.75° and 2.0° from vertical, respectively.

Early in the morning of 14 June, Hole 793B reached total depth at 1682 mbsf and became the deepest hole ever cored into basement during DSDP or ODP operations. The drill string was pulled out of the hole, and the bit reached the rotary table at 1300 hr on 14 June.

Third Reentry

The logging BHA was assembled and run into the hole in the late hours of 14 June. The bit reentered the cone at 2214 hr. The first log attempted was a geophysical combination (DIL/LSS/NGT/TEMP). Several bridges were encountered, which required clearing with the pipe, so the hole was logged in stages. The density tool failed. Other physical properties and temperature tools logged the intervals 1565.6-2034, 947.8-775.9, and 708.2-586.5 mbsf. The FMS was run from 1539 to 1034 mbsf and from 764.1 to 586.5 mbsf. The geochemistry combination was used in the open hole from 1531 to 1034 mbsf, and through the pipe from 917 to 586.5 mbsf. Poor clamping, a result of formation conditions, limited an attempted VSP to only a few good recording levels. Logging was completed in Hole 793B at 0415 hr on 17 June.

Site 793 to Tokyo

JOIDES Resolution was underway for Tokyo by 2130 hr on 17 June. Leg 126 ended officially when the first anchor was dropped in Tokyo harbor at 0700 hr on 19 June 1989.

LITHOSTRATIGRAPHY AND ACCUMULATION RATES

Site 793 is located in the central part of the forearc basin of the Izu-Bonin Arc. The drill site is near the southern side of the east-west-trending Sumisu Jima Canyon, which heads east of the arc volcanoes, passes through structural lows at the outer-arc high, and ends at a mid-slope terrace on the inner wall of the Izu-Bonin Trench (Taylor and Smoot, 1984). Near the drill site, Sumisu Jima Canyon is a broad, flat-floored depression that contains three active, leveed, thalweg channels; it does not, therefore, possess the features of a true submarine canyon, such as a V-shaped profile and steep walls with rock outcrops (Shepard, 1963); instead, in the following discussion, we refer to this feature as a submarine valley. Site 793 is located in an interchannel setting between the southern two leveed channels. Seismic data (Fig. 2) indicate an older (probably Pliocene) erosional surface of similar width beneath the modern submarine valley; to the north, the paleo-valley fill is up to 400 m thick.

We drilled Hole 793A to a depth of 99.7 mbsf and recovered part of the Quaternary section that infills the paleo-valley. We then set a reentry cone and casing and recommenced coring at 586.5 mbsf, so that we bypassed the lower part of the paleo-valley fill, including its erosional contact with underlying sediments, and a considerable thickness of probable Pliocene and possibly upper Miocene deposits. The successions recovered in Holes 793A and 793B are separated by a long uncored interval, and so the sediments in these two holes are described and interpreted separately. The characteristics and depths of all units recognized at Site 793 are summarized in Table 2, and in Figures 4 and 5.

Hole 793A

The recovery in Hole 793A was 79%. The predominant sediment types recovered are pumiceous gravel, pumiceous pebbly sand, pumiceous sand, black vitric sand and silt, nannofossil clay, nannofossil clayey silt, and nannofossil-rich clayey silt. The pumiceous gravel is concentrated in the upper 32.5 m (Cores 126-793A-1H through -3H). The carbonate content of the fine-grained sediments (Fig. 4) is higher than in any other Pleistocene section drilled during Leg 126, with values as high as 60%.

We recognized only one lithologic unit in Hole 793A. Contrasts in the abundance of pumiceous gravel are sufficient to justify division of the succession into two subunits, with the base of Subunit IA placed at 32.5 mbsf (Fig. 4).

Unit I

Interval: Cores 126-793A-1H through -11H
Age: Quaternary
Depth: 0–98.9 mbsf

Subunit IA

Subunit IA (0–32.5 mbsf; Cores 126-793A-1H through -4H) consists of 71% pumiceous gravel and sandy gravel, 15% nan-

Table 2. Lithostratigraphic units, Site 793.

Unit/ subunit	Lithology	Sedimentary structures	Interval (mbsf)	Age	Occurrence
IA	Intermediate to felsic, pumiceous gravel and sandy gravel, nannofossil clay, nannofossil clayey silt, nannofossil-rich clayey silt, and nannofossil-rich clay. Rare vitric sand and vitric silt.	Gravel, structureless, poorly sorted, maximum clast size = 5 cm. Fine-grained sediments are burrowed and contain scattered granules and pebbles of pumice.	0–32.5	Quaternary	126-793A-1H through -4H
IB	Pumiceous and vitric sand, nannofossil-rich clayey silt, nannofossil-rich clay, nannofossil silty clay, vitric silt, and pumiceous gravel.	Sand and gravel beds, graded, parallel laminated to locally ripple laminated; maximum pebble size = 5 cm. Fine-grained sediments are burrowed and contain scattered pumice granules and pebbles. Includes a very thick, gravel-matrix debris-flow deposit with cobbles and boulders of fine-grained sediments.	32.5–98.9	Quaternary	126-793A-5H through -11H
II	Olivine-clinopyroxene diabase sill		586.5–591.0	post-middle Miocene	126-793B-1R
III	Nannofossil-rich silty claystone, silty claystone, nannofossil-rich claystone, nannofossil claystone, vitric siltstone, vitric sandstone, clayey siltstone, and nannofossil-rich clayey siltstone.	Graded beds, lower division parallel- to ripple-laminated vitric sandstone/siltstone; middle division parallel-laminated silty claystone/clayey claystone; fine-grained burrowed top, rich in nannofossils, contains scattered grains of mafic glass or felsic pumice. Dip is 3°–4°. Sub-vertical veinlets and normal microfaults.	591.0–735.7	early to middle Miocene	126-793B-2R through -16R-4, 0 cm
IV	Claystone, nannofossil claystone, nannofossil-rich claystone, and vitric siltstone. Maximum $CaCO_3$ is 60%. Uppermost rocks are pale red and contain todorokite (MnO_2) and gypsum. Carbonate content is negligible near base. Scattered large benthic foraminifers.	Top of unit strongly burrowed and contains abundant dewatering veinlets and slickensided microfaults. The base contains few burrows and is fissile. Dip is 8°–10°.	735.7–759.0	early Miocene	126-793B-16R-5, 0 cm, through -19R-1, 60 cm
V	Vitric sandstone, pumiceous sandstone, granule to fine-pebble conglomerate, siltstone, clayey siltstone, and silty claystone.	Graded sandstone beds with Bouma sequences and erosional bases. Thick to very thick sandstones, pebbly sandstones, and conglomerates contain fluid-escape pillars, dish structures, decimeter-scale intraclasts, large reworked benthic foraminifers, fragments of calcareous red algae, and pumice. Fine-grained lithologies are parallel-laminated upper divisions of turbidites. Some ungraded conglomerates and pebbly sandstones. Dip is <10°. Fractures, microfaults, and gypsum-filled veins occur. Entire unit fines upward.	759.0–1373.1	early to late Oligocene	126-793B-19R-1, 60 cm, through -82R-6, 78 cm
VI	Very poorly sorted volcanic breccia with sandy matrix, and mixed fresh to altered clasts of plagioclase-rich andesite.	Chaotic	1373.1–1403.9	early(?) Oligocene	126-793B-82R-6, 78 cm, through -85R
VII	Breccias and massive to pillowed lava flows of porphyritic and aphyric clinopyroxene-orthopyroxene basic andesite.	Local clast-supported breccia with zeolite cements and internal sediments in cavities.	1403.9–1678.4	early(?) Oligocene	126-793B-86R to -114R

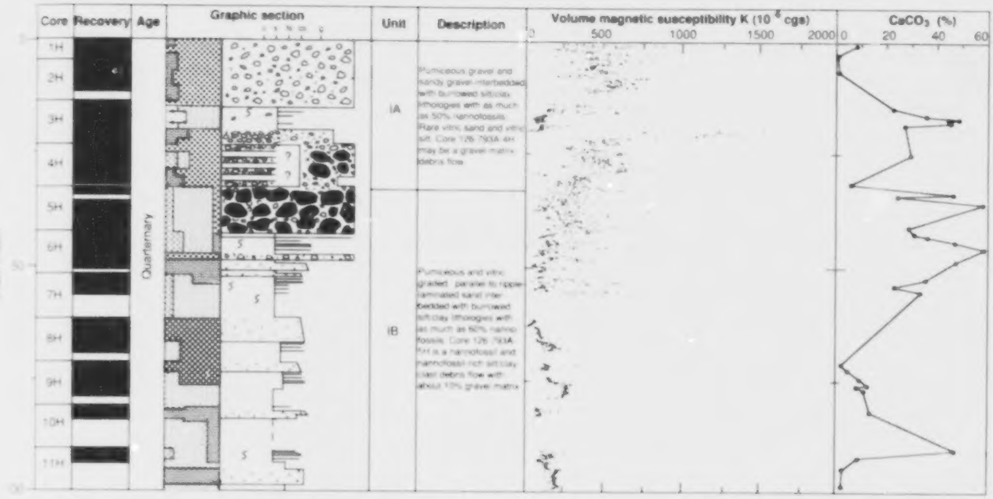

Figure 4. Lithostratigraphic summary for Hole 793A, including a graphic display of core recovery and the downhole distributions of carbonate minerals and magnetic susceptibility. The carbonate curve is primarily a function of the distribution of nannofossils throughout the section, whereas the magnetic susceptibility data reflect the distribution of coarse mafic volcanic lithics and crystals or their dilution by carbonate. The proportions of rock types are shown in the lithology column (see Fig. 3 for legend); the format is more generalized than in core descriptions in that it reflects the percent of groups of rock types observed within a given cored section (i.e., carbonate, gravel, sand, and silt plus clay), and does not show mixed biogenic/siliciclastic lithologies. The graphic column is a simplified sedimentological log displaying relative grain size on the horizontal axis (c = clay, s = silt, fs = fine-grained sand, cs = coarse-grained sand, and g = gravel); on this column, sedimentary structures (see Fig. 4, "Explanatory Notes" chapter, this volume) and bedding within the cored units are schematically displayed; in addition, clast types are illustrated as follows: black ovals = sedimentary intraclasts; unfilled, sharp-edged shapes = volcanic pebbles and cobbles; and dark, sharp-edged shapes = angular fragments of andesite. We cannot determine whether disturbance in Core 126-793A-4H is a result of drilling or presence of a debris flow with gravel matrix.

nofossil clay and nannofossil clayey silt, 10% nannofossil-rich clay and nannofossil-rich clayey silt, and <1% each of vitric sand, vitric silt, and vitric silty sand. The upper 6 cm of Core 126-793A-1H is a sample of the surface sediment just below the mud line and consists of grayish brown (10YR 5/2) nannofossil-rich vitric clayey silt and nannofossil-rich vitric silty clay.

The pumiceous gravel is generally structureless and poorly sorted (Fig. 6). Maximum clast diameter is about 5 cm. Pumice composition is variable, including rhyolite and andesite. The pumice is highly vesicular (Fig. 7).

The fine-grained sediment types differ from one another in color, nannofossil content, and in the relative proportions of silt and clay. They are generally burrowed and contain scattered granules and pebbles of pumice as large as 3 cm in diameter (Fig. 8). In Core 126-793A-4H, nannofossil clay is very disturbed and consists of masses of this material surrounded by pumiceous gravel. The original relationship of the gravel to the fine-grained sediments is not clear, but local apparent stratigraphic continuity suggests that the pumice layers may have formed thin (<5-cm-thick) beds in the fine-grained sequence (Fig. 9). Conversely, the mixture of fine-grained sediment types and pumice gravel may be analogous to features in Core 126-793A-5H (see the following discussion) that are not believed to reflect drilling disturbance.

There are a few, thin, graded beds of light gray to black vitric sand in Subunit IA (Fig. 10). These may have erosional bases and are parallel laminated.

Subunit IB

Subunit IB (32.5-98.9 mbsf; Cores 126-793A-5H through -11H) consists of 39% pumiceous and vitric sand, 21% nannofossil-rich clay and nannofossil-rich clayey silt, 16% nannofossil clay and nannofossil silty clay, 11% vitric silt, 6% pumiceous gravel, and 4% nannofossil-rich silt. The fine-grained sediment types are generally bioturbated and may contain isolated clasts of pumice as large as 2-3 cm in diameter.

A significant proportion of the pumiceous gravel occurs as matrix around stiff fragments of fine-grained sediments in Core 126-793A-5H (see whole-core photograph in Section 3, this volume). Individual fragments are up to 30 cm thick. The arrangement of sediment types in this core does not appear to be a result of drilling disturbance because long intervals of fine-grained lithologies are tilted, we recorded a full stroke of the APC, recovery was 100%, and no apparent suction and flow-in occurred.

Sections 126-793A-6H-4 and -6H-5 contain an undisturbed bed of sandy pumiceous gravel 140 cm thick. Maximum clast size is 5 cm at the top of this bed. This gravel bed contains crude horizontal stratification (Fig. 11) and appears to be amalgamated, with a sharp grain-size break in Section 126-793A-6H-4 at 139 cm. Immediately above this contact, the upper gravel layer is normally graded, although it has a sharp top.

The beds of pumiceous and vitric sand are variable in thickness and composition, with the two end members being thick horizons of black fine sand in Core 126-793A-8H, and thin to

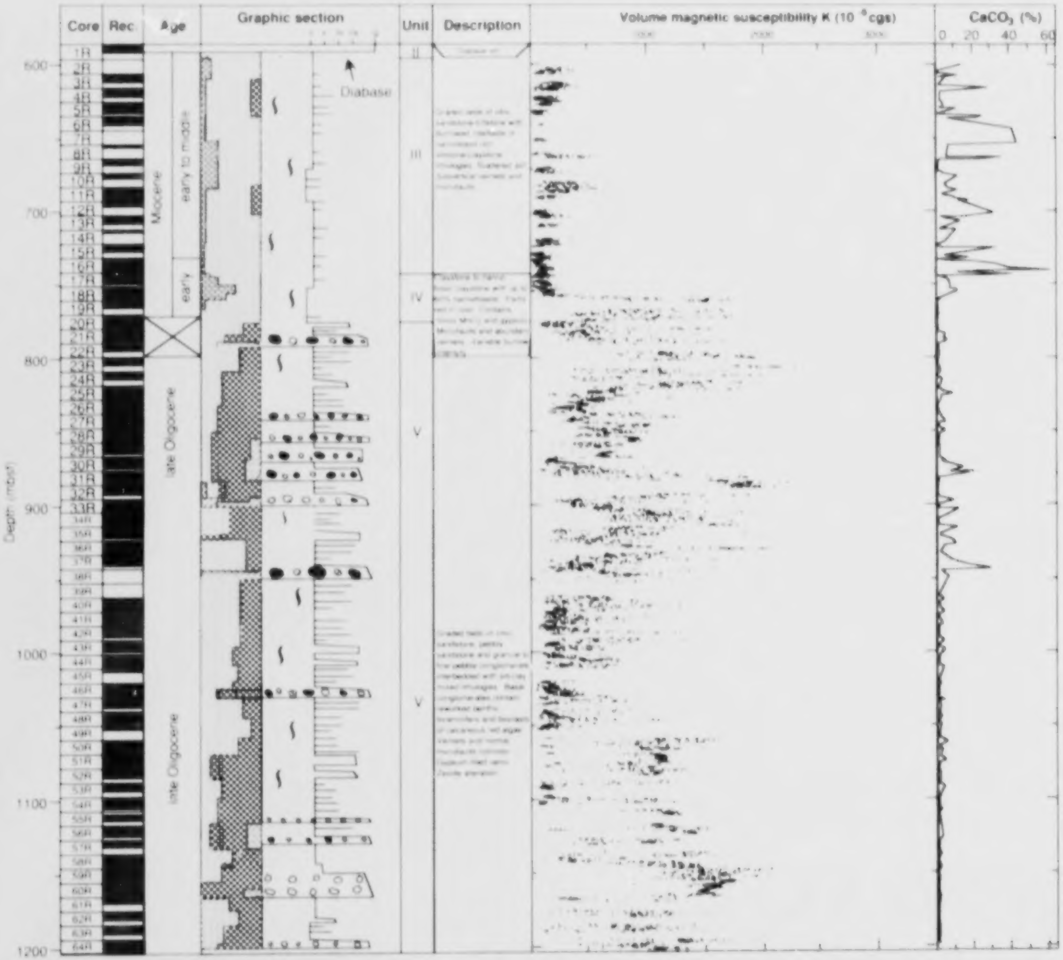

Figure 5. Lithostratigraphic summary for Hole 793B, to the base of Unit VI, including a graphic display of core recovery and the downhole distributions of carbonate minerals and magnetic susceptibility. Symbols are th same as in Figure 4 except that c = claystone, s = siltstone, fs = finegrained sandstone, cs = coarse-grained sandstone, and g = conglomerate.

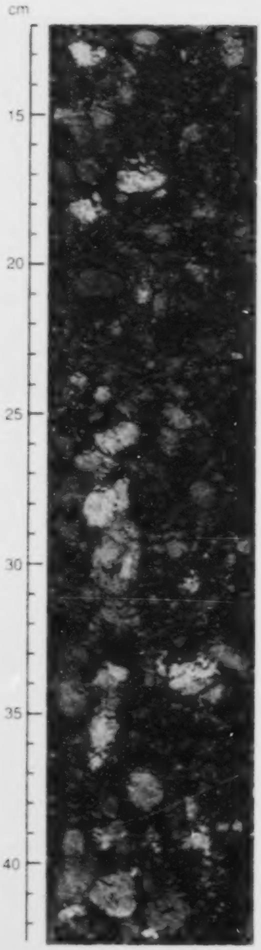

Figure 6. Poorly sorted pumiceous sandy gravel of Unit IA (Interval 126-793A-2H-5, 12-42 cm).

very thin beds of black or white sand throughout (Fig. 12). Thin to medium beds tend to have sharp bases, normal grading (Fig. 13), parallel lamination (Fig. 14), and local cross lamination (Fig. 15). Parallel laminae are defined by grain size fluctuations and by compositional variation (Fig. 16). The tops of the thinner sand beds grade upward into vitric silt. In two cases, this upper silt division is enriched in dusky green (5G 3/2) celadonite (Fig. 15).

The beds of vitric silt tend to be < 10 cm thick, dark gray to black, and graded. Some beds contain delicate parallel lamination (Fig. 17). One thin bed of graded vitric silt is overlain by an inversely graded mixture of nannofossil silty clay and sand- to pebble-size pumice clasts (Fig. 18).

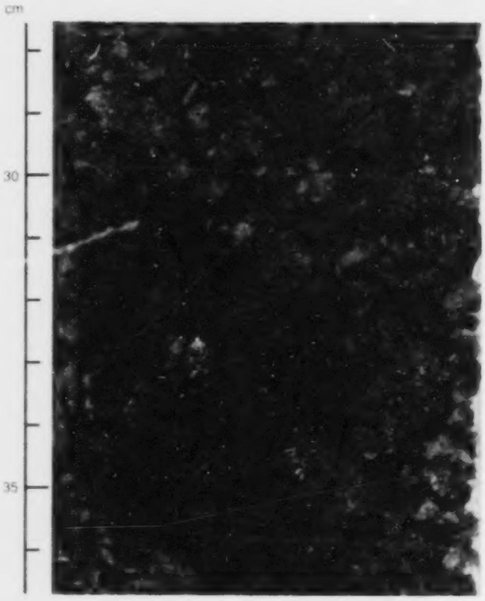

Figure 7. Vesicular pumice clasts in Subunit IA (Interval 126-793A-4H-1, 28-36 cm).

Interpretation of Hole 793A

The pumiceous gravels of Subunit IA are structureless and probably represent the accumulation of waterlogged ejecta from silicic to intermediate caldera eruptions along the nearby Izu-Bonin Arc. Many of the minor vitric sand beds in this subunit contain scour marks and sedimentary structures like those of turbidites (Bouma, 1962), although the turbidity currents in this case may have been generated directly by submarine or subaerial volcanic eruptions feeding large amounts of sandy ash to the water column and to submarine slopes around the arc volcanoes. The burrowed fine-grained sediments in Subunit IA, containing variable amounts of biogenic carbonate as great as 50%, represent quiescent periods between eruptive phases. At these times, the seafloor received pelagic carbonate via settling from the sea surface as well as arc-derived siliciclastic material that was transported by weak bottom currents and/or by surface or mid-water plumes.

Some of the pumiceous gravel in the upper part of Subunit IB may represent primary ejecta that settled to form thin layers in an otherwise fine-grained succession. The disturbed mixture of these materials in Core 126-793A-5H, however, probably represents older deposits that were remobilized into a debris flow, which was probably triggered by a sediment failure along the margin of the paleo-valley (Fig. 2). The failure involved somewhat compacted nannofossil clay, nannofossil silty clay, nannofossil-rich clayey silt, and interbeds of fairly cohesionless pumiceous gravel. The high percentage of fine-grained clasts would have impeded the upward escape of pore fluids, creating elevated pore-fluid pressures in the flow. These elevated pore-fluid pressures account for mobility of the flow in spite of little clay-size matrix (Pierson, 1981).

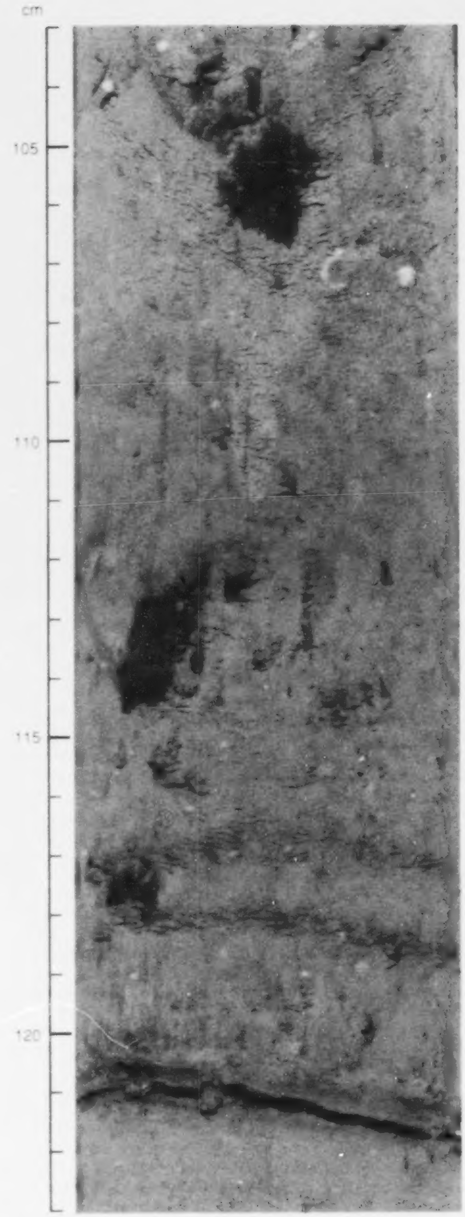

Figure 8. Fine pebbles of dark gray pumice at 104, 105–106, 113–114, and 117–118 cm, partially smeared during the core-splitting process. The surrounding sediment is nannofossil-rich silty clay (Interval 126-793A-3H-2, 103–123 cm).

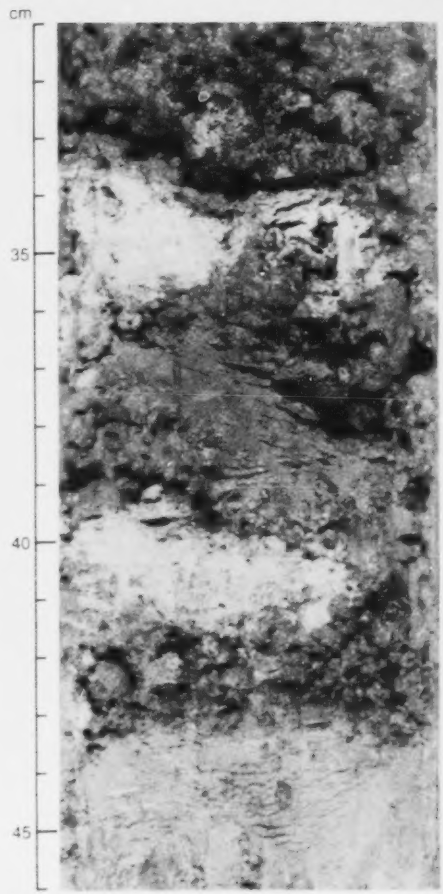

Figure 9. Disturbed nannofossil clay (white), nannofossil-rich clay (gray) and interstitial pumiceous gravel (Interval 126-793A-4H-3, 31–46 cm). The interval from 41 to 44 cm suggests that the pumiceous gravel forms thin interbeds in the fine-grained sediments but this sediment may have been disturbed before coring.

Some graded beds with homogeneous and distinctive composition (e.g., Fig. 12) probably represent primary accumulations of volcanic ash. Most of the pumiceous and vitric sand beds, however, contain tractional structures like those characteristic of turbidite facies. Mixed compositions in some sand beds (e.g., Fig. 16) require some degree of mixing of different source materials before final deposition, a typical feature of resedimented deposits. The thick vitric sand beds in Cores 126-793A-8H through -11H were probably emplaced by high-concentration turbidity currents, although the extent of drilling disturbance prevents recognition of diagnostic primary structures. Such high-concentration flows would have been maintained by turbulence, elevated pore pressures, and grain interaction (dispersive pressure).

Some of the vitric silt beds are probably fine-grained turbidites, and others likely consist of primary ejecta from subma-

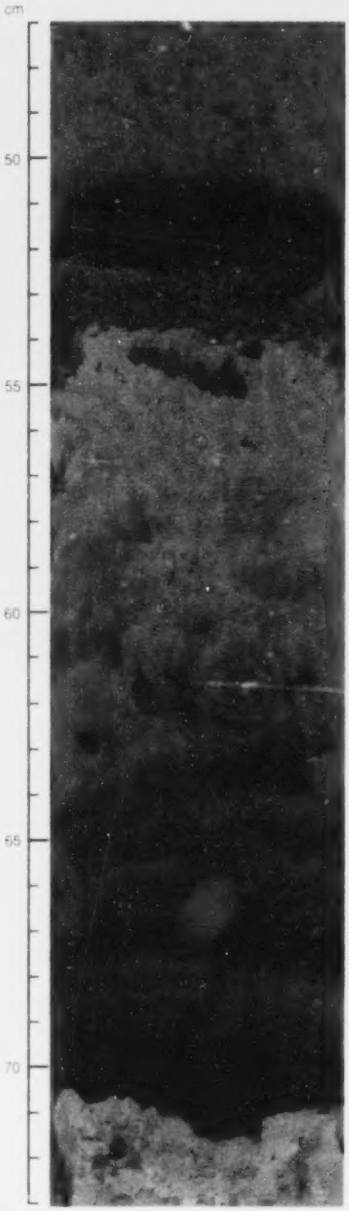

Figure 10. Graded beds of parallel-laminated, fine-grained, black vitric sand, overlain gradationally by burrowed nannofossil-rich silty clay (Interval 126-793A-3H-2, 47–73 cm). The lower sand bed has an erosional base.

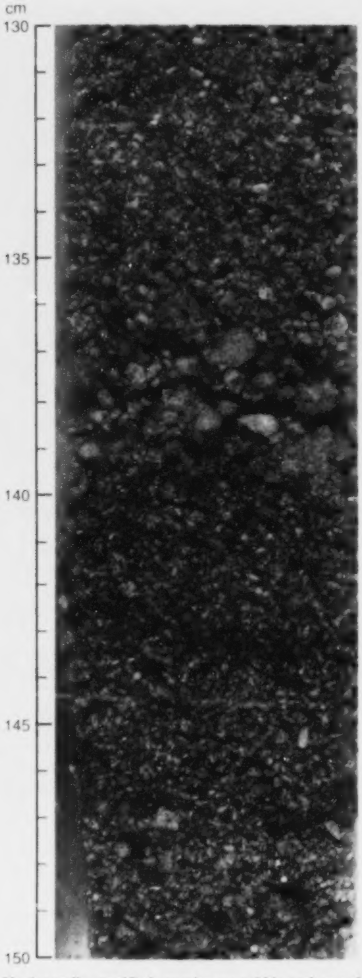

Figure 11. Horizontally stratified, pumiceous pebble and granule gravel in Subunit IB (Interval 126-793A-6H-4, 130–150 cm).

rine or subaerial eruptions. One striking example of a primary volcanic deposit is shown in Figure 18, in which a thin, graded, vitric silt bed is immediately overlain by an inversely graded accumulation of pumice sand and pebbles. A plausible scenario for deposition of these volcaniclastic materials begins with a volcanic eruption, producing high-density black sand and silt grains, probably andesitic glass, and low-density pumice ash. The black sand and silt settled rapidly to form a graded bed. Next, the pumice ash was progressively saturated by water, the smallest grains becoming waterlogged and settling first, followed by increasingly coarser grains.

Biogenic carbonate content in the fine-grained sediments of Subunit IB is commonly 30%–60%, corresponding to times of

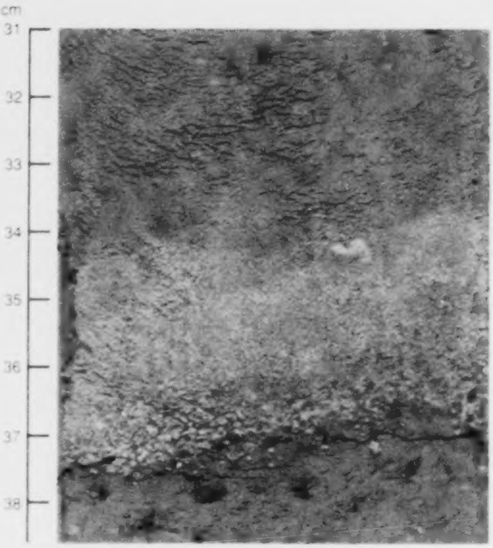

Figure 12. White, graded, pumiceous ash bed, interbedded with nannofossil-rich clayey silt (Interval 126-793A-7H-3, 31–38 cm).

slow supplies of volcanogenic materials, either by direct air fall or as a result of resedimentation.

All sediments of Unit I were deposited in an erosional valley that extended into the forearc basin from the landward slope of the trench. The erosional surface has been onlapped and smoothed by the accumulation of carbonate-rich, fine-grained sediments ("hemipelagites"), air-fall/suspension deposits of pumice, thin ash beds, and thinly bedded sand/silt turbidites. Most of the succession in Unit I was deposited between two active, leveed channels on the floor of the valley; the predominance of fine-grained sediments may reflect this interchannel setting. The only facies that reflects deposition in a major submarine valley is the chaotic debris flow in Core 126-793A-5H.

Hole 793B

Hole 793B was cored from a depth of 586.5 mbsf. Units II–VI are described below. Igneous Unit II and the basement Unit VII are described and discussed in detail in the "Igneous Geochemistry" section (this chapter). The other units are sedimentary.

Unit II

Interval: Core 126-793B-1R
Age: younger than middle Miocene
Depth: 586.5–591.0 mbsf

Unit II, consisting of olivine-clinopyroxene diabase, is described in detail in the "Igneous Petrology" section (this chapter). The base of Unit II was determined from drilling records. The top includes 10 cm of epidote-carbonate-rich silicified sediment that is the baked upper contact of the diabase.

Unit III

Interval: Core 126-793B-2R through Section 126-793B-16R-4
Age: early to middle Miocene
Depth: 591.0–735.7 mbsf

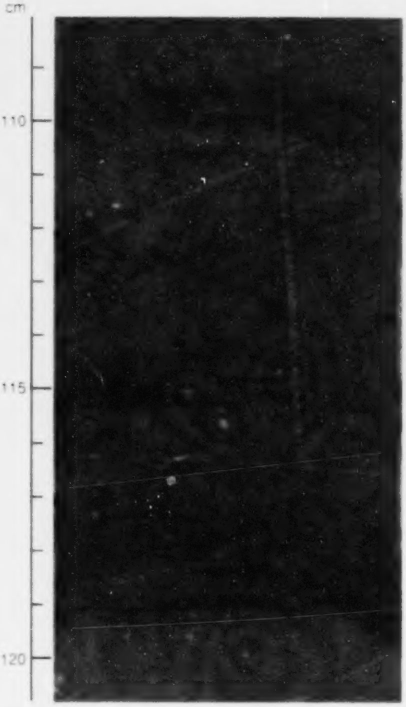

Figure 13. Sharp-based, parallel-laminated, graded beds of vitric sand in Subunit IB (Interval 126-793A-7H-2, 109–120 cm).

The contact of Unit III with the diabase sill was not recovered. The lower contact of Unit III is placed at a sharp change in lithology and color at the top of burrowed nannofossil claystones of Unit IV. The color change is striking, with the drab gray colors of Unit III being replaced downward by light reddish brown (5YR 6/4) sediment at the top of Unit IV. Recovery in Unit III was 43%.

Unit III consists of 24% nannofossil-rich silty claystone, 24% silty claystone, 13% nannofossil-rich claystone, 8% nannofossil claystone, 8% vitric siltstone, 7% vitric sandstone, 4% clayey siltstone, 4% nannofossil-rich clayey siltstone, 3% sandy siltstone, and 2% sandy mudstone. Much of the section consists of graded beds with a lower division of parallel- to ripple-laminated vitric siltstone or vitric sandstone, a middle division of parallel-laminated clayey siltstone to silty claystone, and a cap of strongly burrowed, fine-grained sedimentary rock containing variable amounts of nannofossils (Fig. 19). Carbonate contents in some of the burrowed facies are as high as 40% (Fig. 5). The burrowed rock locally contains disseminated sand-size grains of mafic volcanic glass and/or felsic pumice (Fig. 20). Isolated pebbles of pumice also occur in the burrowed, fine-grained sedimentary rock.

Interval 126-793B-3R-1, 73–107 cm, consists of a bed of very poorly sorted, pebbly, very coarse-grained muddy sandstone, containing large tilted intraclasts of nannofossil-rich clayey siltstone and a cobble of vesicular, intersertal, clinopyroxene-plagioclase basalt 7 cm in diameter (Fig. 21). Chemical analysis of

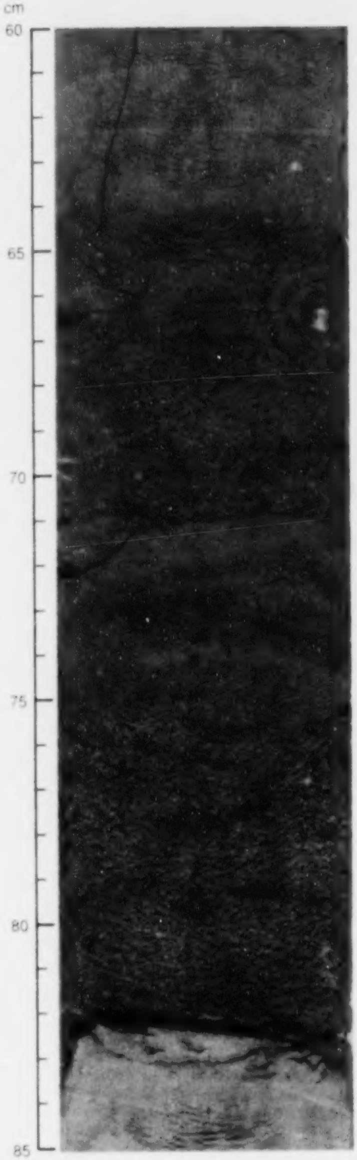

Figure 14. Two beds of parallel-laminated, medium- to fine-grained, pumiceous sand in Subunit IB (Interval 126-793A-6H-2, 60-85 cm). The bases of the beds are at 71 and 82 cm.

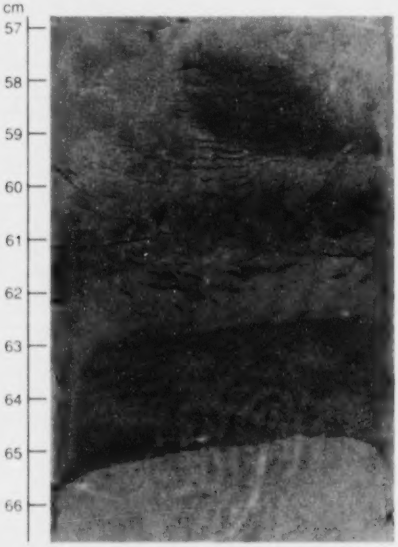

Figure 15. Sharp-based, cross-laminated, graded bed of vitric sand (63-65 cm), overlain by a band of celadonite-rich sediment (60-61 cm). The underlying and overlying sediment is nannofossil clayey silt (Interval 126-793A-7H-2, 57-66 cm).

the basalt is presented in Table 2 (see "Igneous Geochemistry" section, this chapter).

The beds in Unit III dip at 3°-4°. Between 610 and 660 mbsf, there are several occurrences of subvertical veinlets (Fig. 22) like those described from Sites 787 and 792 (see site chapters, this volume), from the Middle America Trench slope by Ogawa and Miyata (1985) and from the Japan Trench by Arthur et al. (1980) and Lundberg and Leggett (1986). Below a depth of 625 mbsf, steeply dipping microfaults and fractures are present (Fig. 23).

Unit IV

Interval: Sections 126-793B-16R-5 through -19R-1 at 60 cm
Age: early Miocene
Depth: 735.7-759.0 mbsf

Recovery of Unit IV was 92%. The most significant lithologic difference between Unit IV and the surrounding sedimentary rocks is the uniformly fine grain size of the material. The unit consists of 47% claystone, 43% nannofossil claystone, 5% nannofossil-rich claystone, 3% vitric siltstone, and 1% each of vitric sandstone and silty claystone. Maximum contents of calcium carbonate (60%) occur in Section 126-793B-17R-1. From the top to the base of Core 126-793B-17R, the color changes downward from light reddish brown (5YR 6/4), through pale red and weak red (10R 6/4, 10R 5/4), through pale yellowish brown (10YR 6/2), to light olive gray (5Y 5/2). Core 126-793B-18R contains intervals with the following colors: light olive gray (5Y 5/2), pale yellowish brown (10YR 6/2), dark gray (5GY 4/1), grayish green (10GY 5/2), olive gray (5Y 3/2), and reddish brown (5YR 4/4). The lower contact of Unit IV, in Section 126-793B-19R-1 at 60 cm, is a rapid downward change from pale yellowish brown (10YR 6/2), slightly burrowed, fissile claystone to

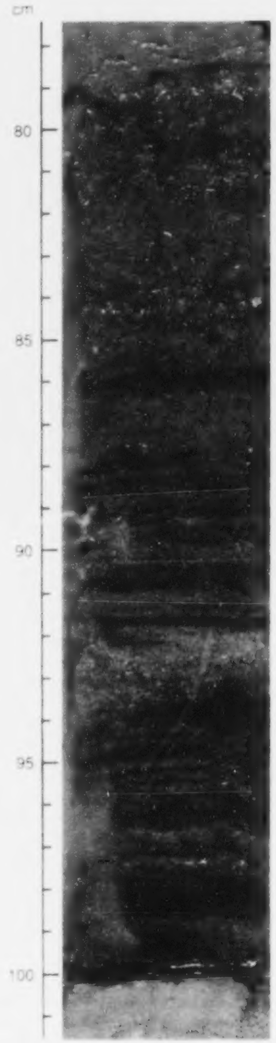

Figure 16. Parallel-laminated sand bed with dark laminae composed of mafic glass and light laminae composed of felsic pumice (Interval 126-793A-7H-1, 78-101 cm). The granules at the top of the bed are low-density pumice clasts. The core is partially obscured by water in the liner.

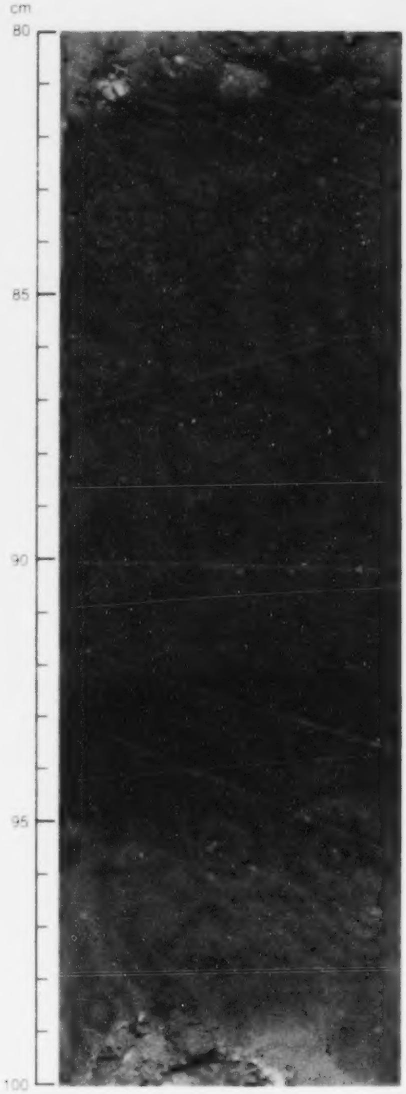

Figure 17. Two probable ash beds that grade from coarse to fine vitric silt. The upper bed (82–87 cm) has delicate parallel laminae in its upper part (Interval 126-793A-5H-4, 80–100 cm).

the typical, slightly calcareous, grayish green (5GY 5/1), strongly burrowed silty claystone of Unit V. This lithologic change is most easily explained by a modification of the surface current pattern and consequent reduction in nannofossil production. A less likely alternative explanation is a change in bottom-water chemistry, causing dissolution of calcareous nannofossils. The 88 cm of silty claystone and claystone between the highest sandstone bed and the contact are much more like the fine-grained rocks of Unit V than the mudrocks of Unit IV.

The main primary structure in these sedimentary rocks is variable degrees of bioturbation. The intensity of burrowing varies directly with the carbonate content, so that the noncalcareous claystones near the base of the unit generally lack bur-

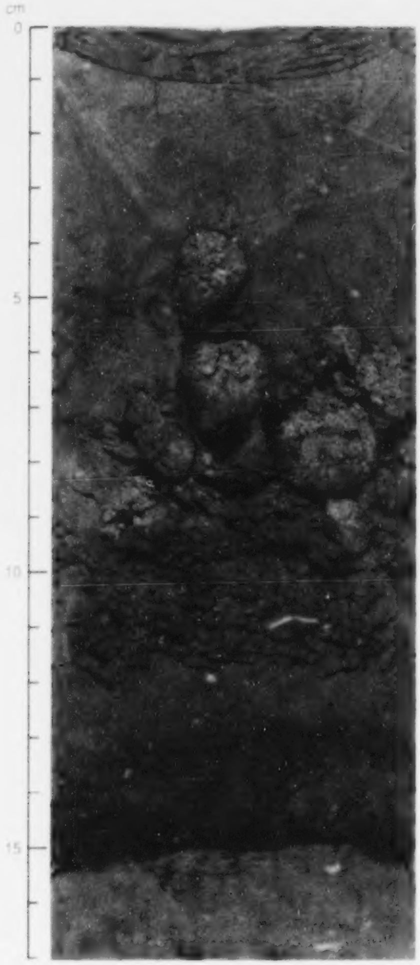

Figure 18. Graded bed of vitric silty ash, overlain by an inversely graded layer of sand- to pebble-sized pumice clasts (Interval 126-793A-6H-2, 0-17 cm). See text for discussion.

rows. These claystones contain only a few very thin (1-3 cm) interbeds of parallel- to ripple-laminated vitric siltstone. Scattered benthic foraminifers are visible in the core.

Unit IV is characterized by a suite of mineralogical and structural features. Sample 126-793B-17R-1, 85 cm, contains a 2 × 4 cm nodule of gypsum. Just below this (Interval 126-793B-17R-2, 10-70 cm), there are black smears and poorly developed dendrites of todorokite (manganese oxide). Much of the rock is cut by subvertical, wavy, dewatering veinlets along which the core is strongly fractured (Fig. 24). There are several, irregular, slickensided microfaults that dip at about 45°-60°. From Section 126-793B-18R-6 to the base of the unit, the claystone is fis-

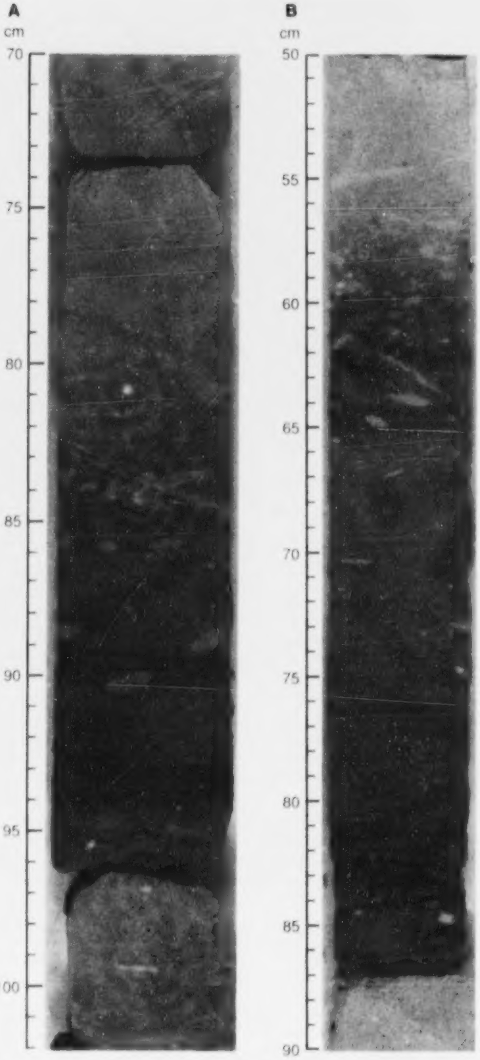

Figure 19. Two examples of graded beds of vitric siltstone, overlain first by parallel-laminated clayey siltstone and silty claystone and then by strongly burrowed nannofossil silty claystone or nannofossil claystone. **A.** A bed with a basal division of cross lamination, overlain by parallel-laminated siltstone cut by a few deep burrows; trace fossils include flattened ***Planolites***, ***Zoophycos***, and ***Chondrites*** (Interval 126-793B-4R-4, 70-102 cm). **B.** A bed with a basal division of parallel lamination, partly modified by soft-sediment deformation, overlain by finely laminated clayey siltstone, and then by nannofossil claystone (Interval 126-793B-6R-2, 50-90 cm).

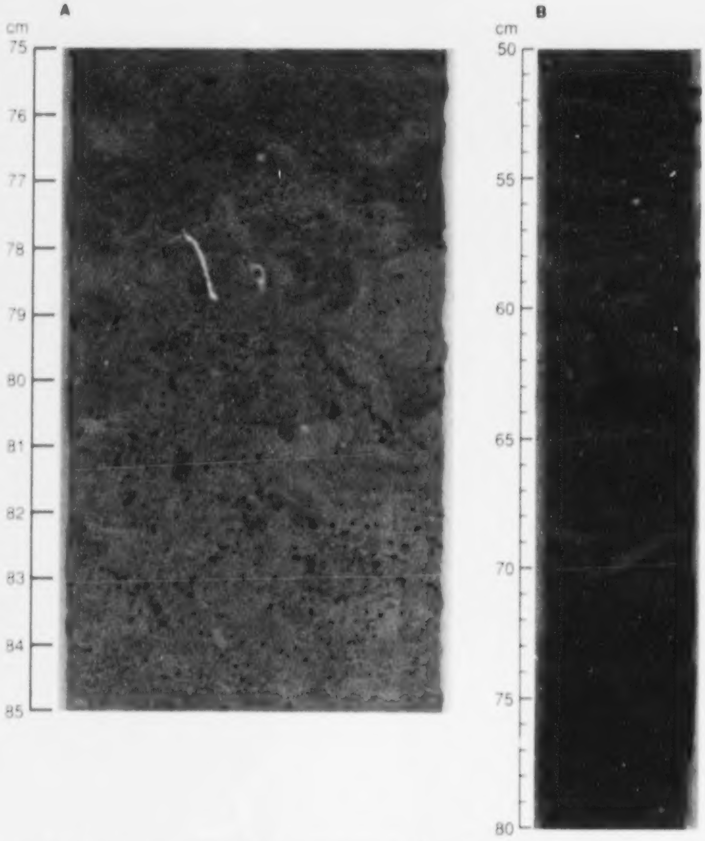

Figure 20. **A.** Sandy mudstone formed by biogenic mixing of fine-grained sediment and mafic ash. (Interval 126-793B-15R-2, 75–85 cm). **B.** Interbedded very thin, graded, parallel- and cross-laminated beds of black vitric siltstone and very fine sandstone, and burrowed silty claystone. From 49–58 cm, the burrowed material contains abundant, dispersed, black sand (Interval 126-793B-11R-1, 50–80 cm).

sile, with a well-developed, bedding-parallel parting. Bedding dips at 8°–10° in this unit.

Unit V

Interval: Sections 126-793B-19R-1 at 60 cm through -82R-6 at 78 cm
Age: early to late Oligocene
Depth: 759.0–1373.1 mbsf

The sharp lithologic change from Unit IV to Unit V is described above. This contact may mark a hiatus. The base of Unit V is a fault that separates the graded sandstone beds of this unit from the volcanic breccia of Unit VI. Recovery of Unit V was 83%.

Unit V is characterized by thin to very thick graded beds of vitric sandstone (Fig. 25) and, in some intervals, pumiceous sandstone (Fig. 26); together, these constitute 50% of the unit. The bases of these beds are sharp, and basal scour marks (e.g., flutes) are present on a few beds (Fig. 27). Fine-grained, carbonate-poor rocks, typically with <5% calcium carbonate, collectively constitute 42% of the unit (claystone, 3%; silty claystone and clayey siltstone, 22%; siltstone, 17%); whereas nannofossil-rich, fine-grained rocks containing about 20% calcium carbonate constitute only 1.5%. Much of the fine-grained sedimentary rock is either the upper, parallel-laminated to slightly burrowed parts of graded sandstone beds, or consists of graded beds of clayey siltstone to silty claystone that are parallel to ripple laminated. Some fine-grained facies in Unit V contain features attributed to wet-sediment deformation of water-rich sediments (Fig. 28). A fine-grained sandstone bed in Interval 126-793B-59R-3, 74–146 cm, contains a small quantity of plant debris.

The sandstones, siltstones, and finer grained sedimentary rocks of Unit V are associated in some parts of the section with thick to very thick beds of pebbly sandstone or granule to fine-pebble conglomerate, some apparently as thick as 5–10 m. The conglomerates constitute 8% of Unit V. The coarsest and thickest beds are concentrated in the lower part of the unit (Figs. 5 and 29). Higher in the section, thick and very thick sandstone

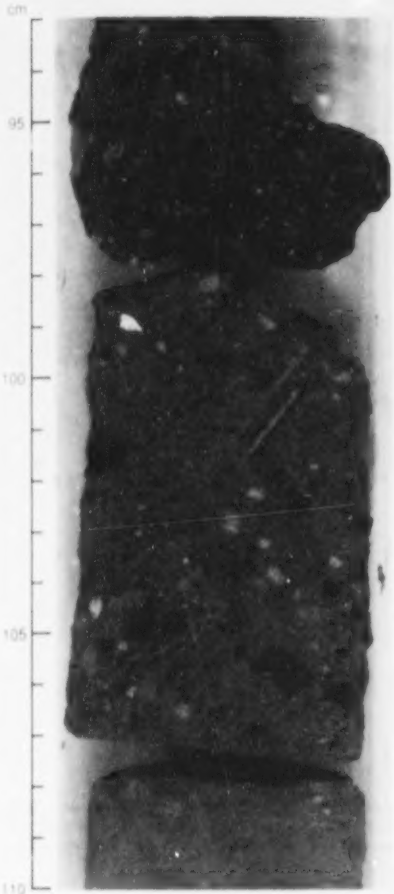

Figure 21. The lower part of a sharp-based, very poorly sorted bed of very coarse-grained gravel-rich muddy sandstone (98–107 cm). Above the sediment shown in this photograph (73–93 cm), the bed contains large, tilted intraclasts of nannofossil-rich clayey siltstone that are a minimum of 15 cm across. A cobble-sized clast of basalt, 7 cm across, is shown in the upper part of the photograph (93–98 cm; Interval 126-793B-3R-1, 93–110 cm).

beds appear to be randomly distributed and are absent in the uppermost part of the unit. This distribution defines an overall upward-fining trend throughout Unit V.

Examples of five of the very thick beds are sketched in Figure 30. Examples A, B, and C are characterized by very poor sorting, poorly developed clast fabric and grading (the latter, if present, is restricted to the top of the bed in divisions of parallel or ripple lamination), and concentrations of cobble- to boulder-size intraclasts well above the base of the bed. Example C contains fluid-escape pillars in its upper part (Fig. 31A); Examples D and E contain intraclasts that are tens of centimeters in diameter, but these tend to be confined to the lower part of the bed.

cm
17
18
19
20
21
22
23
24
25
26

Figure 22. S-shaped, subvertical, locally bifurcated dewatering veinlets in silty claystone of Unit III (Interval 126-793B-12R-1, 17–26 cm).

Thick divisions of parallel- and ripple-laminated sandstone form the upper parts of these beds, and step-wise normal grading is well developed. Some beds are inversely graded at the base (Fig. 32).

Some of the intraclasts in the conglomerates are composed of more than one lithology. These clasts were probably partly consolidated before incorporation into the flows; otherwise, they would have been quickly disaggregated by shear during transport.

The very thick sandstone beds in Unit V are also poorly organized and lack tractional structures except at the top of the bed. A 6-m-thick sandstone bed in Core 126-793B-51R contains dish structures in its lower part (Fig. 31B) and broad fluid-escape pillars and injections of sandstone near its top.

Volcanic clasts in the conglomerates of Unit V are mainly clinopyroxene-orthopyroxene-plagioclase andesite + opaques ± quartz. There are minor clasts of hornblende-augite dacite; intersertal, quenched basalt; brick-red rhyolite with quartz phenocrysts, orthopyroxene and magnetite; white and red pumice; and basaltic scoria.

Smear-slide estimates of Unit V sandstone and siltstone compositions were hampered by intense diagenetic alteration of constituent grains and an abundance of authigenic cements. The vitric and crystal components of these rocks have been altered (possibly by dissolution-precipitation reactions) to clay minerals and zeolites that are often indistinguishable from pore-filling cements; thus, smear-slide descriptions are an unsatisfactory way to recognize original framework detrital modes. Additional problems are related to sandstone induration, which required that sediment be forcefully scraped to make the smear slide, breaking up grains and artificially increasing the amount of silt- to clay-size material. Often silt-size, clay-mineral vesicle fillings could be seen in smear slides, implying that vesicular altered glass had been crushed during sample preparation. Thin sections were prepared to help resolve these problems.

We examined 14 sandstone thin sections. This sample set spans the entire Unit V, from the top (Sample 126-793B-20R-4, 96 cm; 773.5 mbsf) to the base (Sample 126-793B-82R-CC, 11

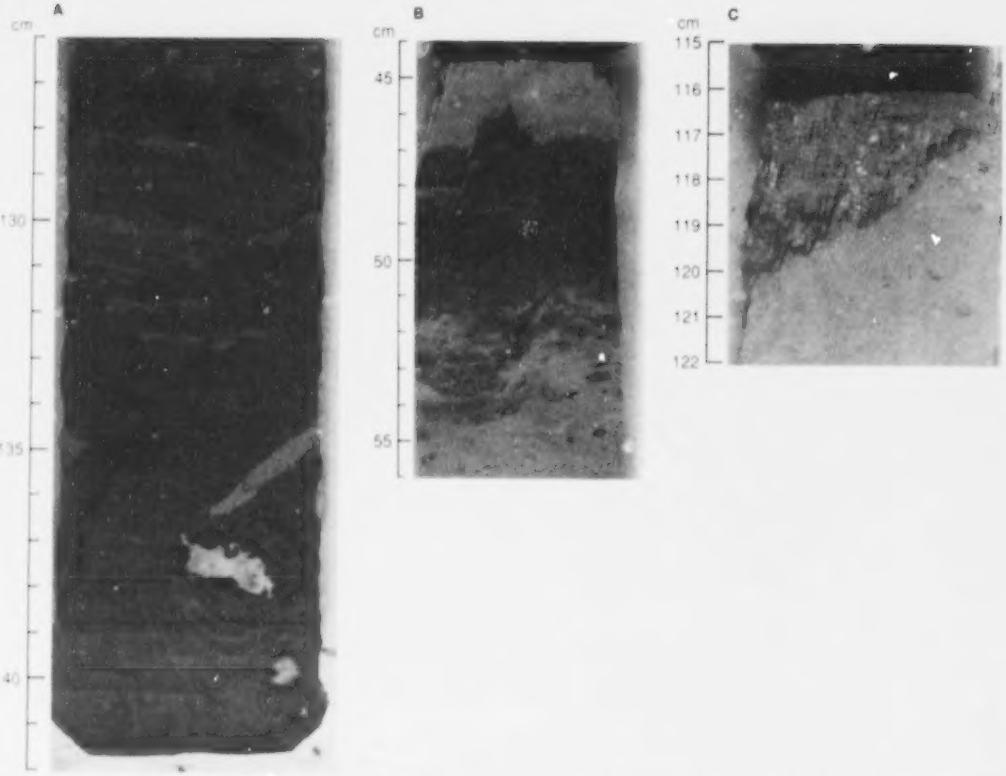

Figure 23. Normal microfaults in Unit III. **A.** Steeply dipping, curved fault with a few millimeters of displacement in parallel-laminated silty claystone (Interval 126-793B-5R-4, 126–142 cm). **B.** Steeply dipping, conjugate faults with displacements of about 1 cm in nannofossil-rich silty claystone (light gray), and burrowed sandy mudstone (Interval 126-793B-14R-1, 44–56 cm). **C.** Slickensides on a fault surface that cuts across nannofossil-rich claystone (Interval 126-793B-8R-1, 115–122 cm).

cm; 1375.3 mbsf). Visual estimates of grain and cement percentages show no distinct trends with depth. The sandstones are generally rich in vitric components, with less abundant crystals and lithic grains; hence, they are best described as crystal-vitric or lithic-crystal-vitric sandstones. Mean estimates of the proportion of the various framework grain types is as follows: 71% volcanic glass, 15% plagioclase feldspar, 4% lithics, and 9% heavy minerals. Included in the volcanic glass category are vitric grains exhibiting a wide range of vesicularity (nonvesicular to pumiceous) and containing variable percentages of plagioclase microlites and phenocrysts. The majority of the vitric material, except for opaque, dark brown to black glass, appears to be altered to zeolites and/or green to brownish green clay minerals. The major crystal component, plagioclase feldspar, is moderately to completely replaced by zeolites throughout the unit. Accessory minerals are predominantly pyroxene and opaques with rare hornblende. Rock fragments include (1) holocrystalline, polymineralic, hypabyssal volcanic or intrusive grains consisting of plagioclase in various combinations with hornblende, opaques, and clinopyroxene; and (2) metavolcanic grains altered by hydrothermal or low-grade metamorphic processes. Microfossils/bioclasts include planktonic foraminifers, reworked benthic foraminifers, fragments of calcareous red algae, bryozoans, and very rare coral. The reworked bioclastic debris is predominantly in the lower part of the unit, mainly in Cores 126-793B-74R through -80R.

Interparticle porosity appears to be minor because two major phases of cementation permeate sandstones within Unit V. The first type is a green to greenish brown, clay-mineral rim to pore-fill cementation, which is followed by stage(s) of zeolite rim to pore-fill cementation. Zeolite crystals are fibroradiating to lath-shaped to blocky. These cements are ubiquitous throughout Unit V except for the lowermost sample studied (Sample 126-793B-82R-CC, 11 cm). Whole-rock X-ray diffraction (XRD) results indicate the presence of a wide range of authigenic minerals: heulandite, clinoptilolite, analcime, phillipsite, mixed-layer mica-smectite, pyrophyllite, and chabazite (Table 3).

A common diagenetic feature noted during visual core description of sandstones was "snowflake" alteration, consisting of closely spaced, 1–2-mm-scale, delicate, white, lacelike spots. A thin-section of this material displays localized centers of low-birefringent, fibroradiating zeolite (heulandite or chabazite) as

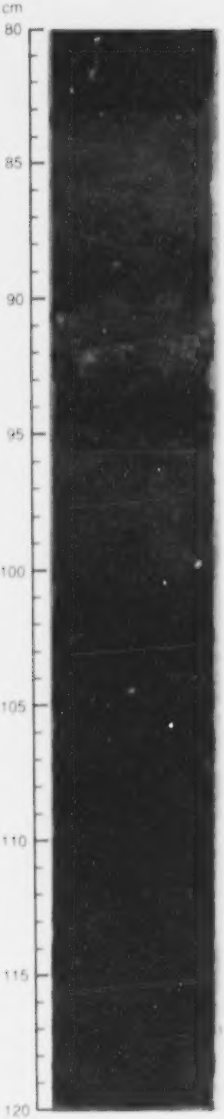

Figure 24. Strongly burrowed nannofossil claystone of Unit IV, cut by abundant subvertical dewatering veinlets (Interval 126-793B-16R-5, 80–120 cm). In places, the core is fractured along the length of the veinlets.

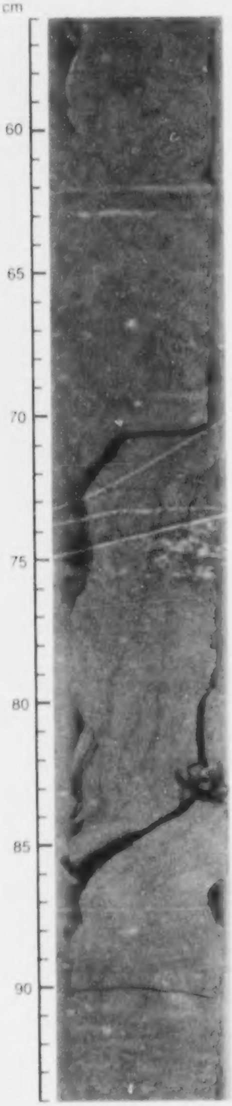

Figure 25. Very thin to medium graded beds of fine-grained vitric sandstone, separated by burrowed horizons of clayey siltstone, in the upper part of Unit V (Interval 126-793B-19R-3, 56–94 cm).

both grain alteration and cement (Sample 126-793B-60R-3, 128 cm).

Where cementation/alteration is minor, smear-slide estimates are similar to thin-section percentages. For example, smear-slide Sample 126-793B-21R-1, 80 cm, had the following framework composition: 10% feldspar, 3% lithics, 82% vitric grains, and 5% accessory minerals. A thin section from an adjacent interval (Sample 126-793B-21R-1, 83 cm) contains 11% feldspar, a trace of lithics, 84% vitric grains, and 5% accessory minerals (same operator).

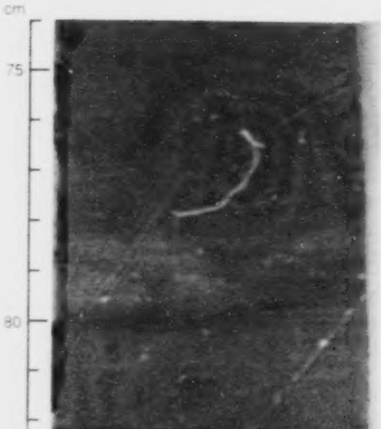

Figure 26. Sharp-based, graded, parallel-laminated bed of pumiceous medium-grained sandstone. There is a thin ripple-laminated division at 82-83 cm, beneath the upper parallel-laminated division of very fine-grained sandstone. The base of this bed is irregular as a result of erosion, possibly modified by loading. The underlying lithology is vitric siltstone (Interval 126-793B-20R-7, 74-93 cm).

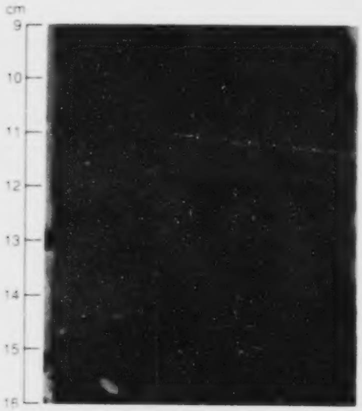

Figure 27. Example of a nose of a flute cast on the base of a graded, fine-grained sandstone bed (Interval 126-793B-47R-3, 9-16 cm). Note the accumulation of coarse and very coarse sand grains in the former zone of flow separation at the upstream end of the flute cast. Ripple laminations in the sandstone bed confirm that flow was from right to left.

Unit V is just over 600 m thick, and parts of this section are characterized by distinctive bedding styles or grain compositions. Rather than describing all parts of the unit in detail, two examples of the facies associations that occur in this unit are highlighted (Fig. 29).

The first of these associations (Fig. 29A) is characterized by an alternation of very thin- to medium-bedded, graded sandstone with thick to very thick beds of pebbly sandstone or granule to fine-pebble conglomerate. The conglomeratic beds contain intraclasts of silty claystone as large as 70 cm across, some of which are internally folded (Fig. 33).

An interval from ~ 900 to 1020 mbsf, partly shown in Figure 29A, is characterized by large quantities of pumice in sandstone beds (Fig. 34). This partly overlaps with an interval of anomalously low sediment bulk density from 950 to 1050 mbsf (see "Physical Properties" section, this chapter). Alteration of much of the pumice to celadonite (see the following discussion of XRD analysis) results in a dusky blue-green (5BG 3/2) color for this rock. The pumice tends to occur well above the base of the beds, as concentrated bands in parallel-laminated sandstone. In many beds, the increase in pumice size and abundance away from the base of the bed produces inverse grading. Low-density pumice granules and fine pebbles appear to have been transported by flows that also carried more sand-size dense crystals and glass grains. Laminae rich in pumice may have formed as a result of subtle changes in flow velocity and concentration.

The second facies association that we use as an example of Unit V is typified by very thick beds of pebbly sandstone and volcanic-lithic conglomerate (Fig. 29B). The thickest beds with no evidence for internal amalgamation are 10-15 m thick (e.g., Fig. 30A). These conglomerates and pebbly sandstones, as in the overlying section to a depth of about 1180 mbsf, contain scattered, resedimented benthic foraminifers up to ~5 mm in diameter (Fig. 35). Beds in Cores 126-793B-72R through -80R also contain pebble-size bioclasts, up to 2 cm in diameter, of calcareous red algae and coral-bearing limestone (Fig. 36).

Bedding in Unit V dips at a maximum of about 10°. Structural features include steeply dipping fractures, mineral-filled fractures and faults, and microfaults (Fig. 37), as well as more significant faults that juxtapose different rock types (Fig. 38). Most faults dip at about 45°-60°, and many have slickensided surfaces. Gypsum is the most common mineral along fault planes and in veins or fractures (Fig. 39).

The lower part of Unit V contains steeply dipping (about 60°) or cross-cutting (Fig. 40), light-colored, 1-3-mm-thick bands or zones in sandstone beds that appear to differ from the surrounding rock only in clay content. The dip of these features is

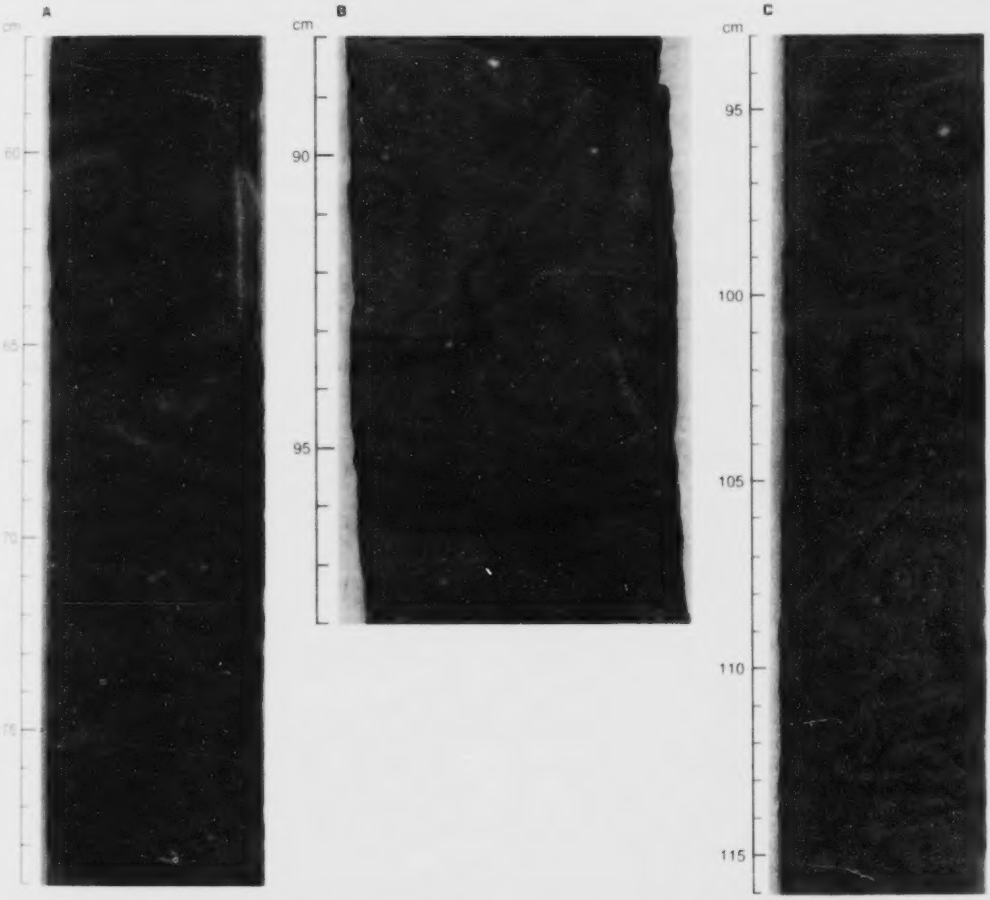

Figure 28. Examples of wet-sediment deformation in Unit V. **A.** The upper, predominantly ripple-laminated division of a bed that grades from coarse-grained to very fine-grained sandstone. The base of the bed is at 107 cm in this section. There is a liquefied, partly homogenized zone from 69 to 74 cm, and synsedimentary faults and clastic injections from 60 to 67 cm (Interval 126-793B-40R-3, 57-79 cm). **B.** Plastically folded parallel laminae and oversteepened cross laminae in a graded siltstone bed with base at 96 cm (Interval 126-793B-42R-1, 88-98 cm). **C.** Plastically folded fine-grained sandstone and siltstone interbeds (Interval 126-793B-72R-3, 93–116).

similar to the dip of associated microfaults in the fine-grained sediments.

Unit VI

Interval: Section 126-793B-82R-6 at 78 cm through Core 126-793B-85R
Age: early(?) Oligocene
Depth: 1373.1–1403.9 mbsf

The top of Unit VI is a fault of unknown displacement. The base is also a sheared fault zone (see "Downhole Measurements" section, this chapter), but it is defined as well by the shipboard petrologists as the place where volcanic clasts that are identical in composition to lava flows in the basement form essentially 100% of the coarser material in the rock. The composition of these flows is clinopyroxene-orthopyroxene-plagioclase andesite, with pyroxene more abundant than plagioclase (see thorough discussion of the definition of this contact in the "Igneous Geochemistry" section, this chapter). Recovery was 34%. The only lithology in this unit is grayish green (5G 5/2), very poorly sorted volcanic breccia and microbreccia. Most clasts are angular (Fig. 41), although some are subangular to subrounded. In Section 126-793B-83R-1, this material has a matrix of zeolitic claystone that forms about 10% of the rock. Below this level, there is little claystone matrix between sand- and granule-size volcanic grains and crystals.

Clasts, up to 30 cm in diameter, are fragments (with chilled margins) of vesicular, clinopyroxene-orthopyroxene-plagioclase

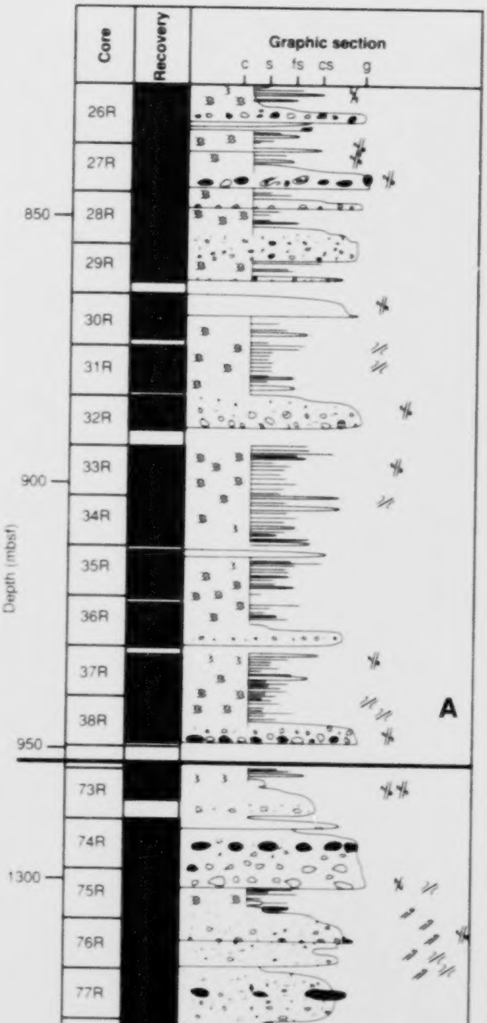

Figure 29. Examples of facies associations in Unit V. See text for discussion. The width of the column varies with grain size. Symbols are the same as those used on barrel sheets and explained in the caption to Figure 5. **A** and **B** indicate separate examples.

andesite + opaques ± quartz. Plagioclase is more abundant than pyroxene. The chemistry of these clasts is similar to the chemistry of the basement at Site 792 (see "Igneous Geochemistry" section, "Site 792" chapter), but different from the chemistry of the immediately underlying basement (see Table 3 and "Igneous Petrology" section, this chapter). Smectite occurs in the vesicles of these clasts. In Cores 126-793B-84R and -85R, there are also clasts of andesitic tuff and clinopyroxene-phyric basaltic andesite. Some other clasts resemble hyaloclastites.

X-Ray Diffraction Analysis

The results from XRD analysis of 97 samples from Units I through VI are summarized in Table 3. The main processes that these data record are replacement of volcanic glass by clay minerals and zeolites, alteration of feldspar, and cementation in coarse-grained sediments. Presentation of mineralogical data for Unit V is divided into six parts, each corresponding to a particular depth, because of the great thickness of this unit, and because diagenetic alteration varies considerably from the top to the bottom of the unit.

Unit I

The XRD data confirm that the nannofossil-rich silty clays of Unit I contain abundant calcite. Vitric silts and sands contain little calcite. Quartz, feldspar, smectite, and chlorite are common in all samples. Chlorite reflects the high Mg concentration of interstitial water (see "Sediment/Fluid Geochemistry" section, this chapter). Mica-group minerals are present in silts and clayey silts. Pyrolusite (MnO_2) and maghemite (γ-Fe_2O_3) occur in a black vitric silt (ash) bed (Sample 126-793A-5H-6, 70 cm). Volcanic glass is partially altered to palagonite and smectite. Most glass, however, is still amorphous, producing a high background around 0.33 nm; this glass is clear and colorless in smear slides. Pyrite (FeS_2) is present in nannofossil-rich silty clay near the base of the unit (Sample 126-793A-11H-1, 36 cm).

Unit III

The XRD analyses show abundant calcite in the fine-grained, burrowed sediment types of Unit III. Calcite abundance decreases below 705 mbsf, a feature also shown by bulk calcium carbonate analysis (Fig. 5). Quartz, feldspar, and smectite are common in all samples, whereas mica-group minerals and chlorite are rare or present in only trace amounts. This latter feature distinguishes these sedimentary rocks from the sediments of Unit I. In detail, the minor chlorite decreases rapidly from the top of Unit III, reflecting a sharp decline in the concentration of Mg in interstitial waters from 600 to 800 mbsf (see "Sediment/Fluid Geochemistry" section, this chapter).

Unit IV

The XRD data show a sharp increase in the proportions of calcite, chlorite, quartz, Ca-feldspar, and smectite at the top of Unit IV, coincident with a sharp increase in Ca concentration and a sharp decrease in Mg concentration in the interstitial waters (see "Sediment/Fluid Geochemistry" section, this chapter). The lithology here is nannofossil claystone. Gypsum and todorokite (manganese oxide) are also present in the upper part of Unit IV.

The distinctive clay-mineral assemblage of Unit IV may reflect intense alteration of fine-grained volcanic components in the sediments, leading to uptake of Mg and release of Ca.

Unit V

Sediments in the depth interval from 780 to 870 mbsf are characterized by relatively high abundances of smectite, in association with analcime, gypsum, ankerite, and smectite-mica

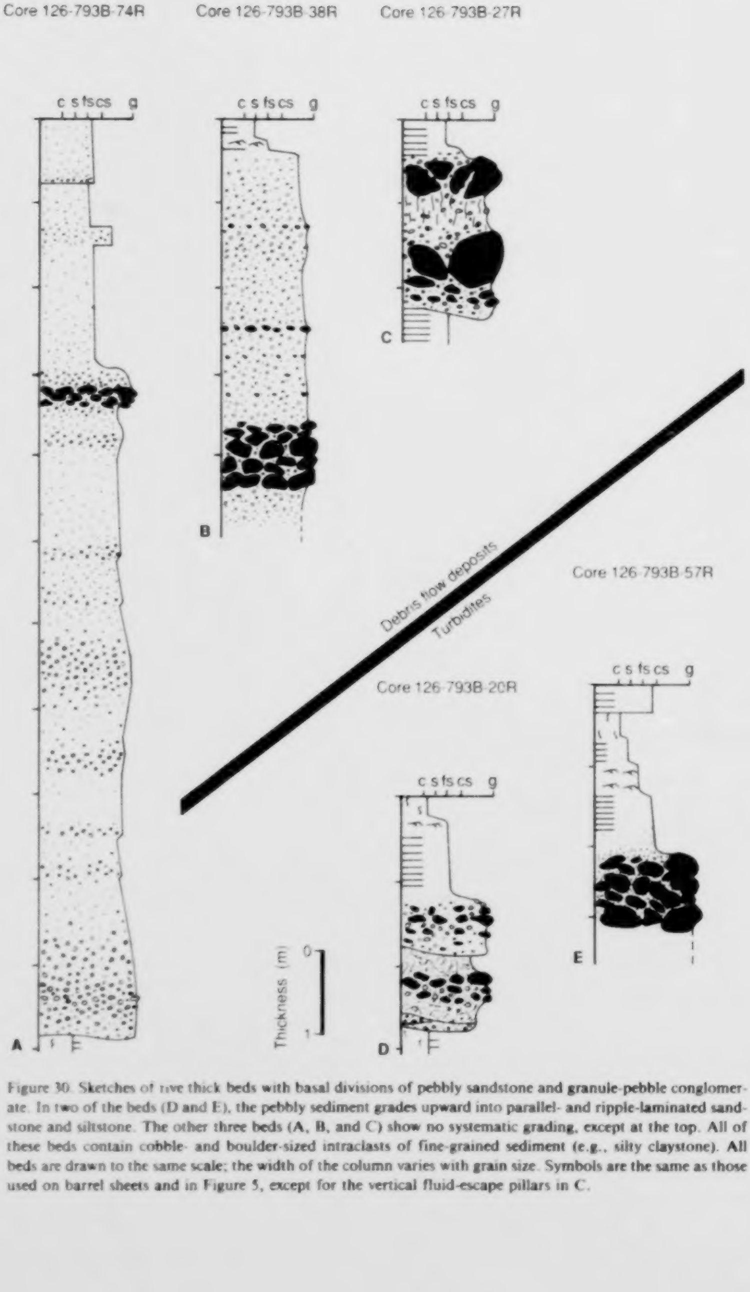
Core 126-793B-74R
Core 126-793B-38R
Core 126-793B-27R
Core 126-793B-57R
Core 126-793B-20R
c s fs cs g
A
B
C
D
E
Debris flow deposits
Turbidites
Thickness (m)
0
1

Figure 30. Sketches of five thick beds with basal divisions of pebbly sandstone and granule-pebble conglomerate. In two of the beds (D and E), the pebbly sediment grades upward into parallel- and ripple-laminated sandstone and siltstone. The other three beds (A, B, and C) show no systematic grading, except at the top. All of these beds contain cobble- and boulder-sized intraclasts of fine-grained sediment (e.g., silty claystone). All beds are drawn to the same scale; the width of the column varies with grain size. Symbols are the same as those used on barrel sheets and in Figure 5, except for the vertical fluid-escape pillars in C.

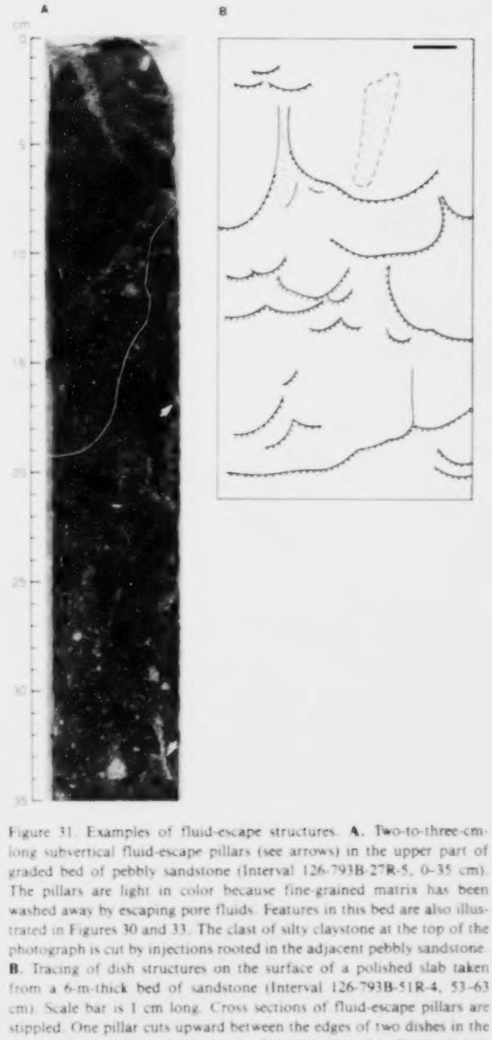

Figure 31. Examples of fluid-escape structures. **A.** Two-to-three-cm-long subvertical fluid-escape pillars (see arrows) in the upper part of graded bed of pebbly sandstone (Interval 126-793B-27R-5, 0–35 cm). The pillars are light in color because fine-grained matrix has been washed away by escaping pore fluids. Features in this bed are also illustrated in Figures 30 and 33. The clast of silty claystone at the top of the photograph is cut by injections rooted in the adjacent pebbly sandstone. **B.** Tracing of dish structures on the surface of a polished slab taken from a 6-m-thick bed of sandstone (Interval 126-793B-51R-4, 53–63 cm). Scale bar is 1 cm long. Cross sections of fluid-escape pillars are stippled. One pillar cuts upward between the edges of two dishes in the upper left-hand part of the sketch. The unpatterned sediment is medium-grained sandstone.

mixed-layer clays. The Na and Mg required for formation of analcime and smectite were derived from modified seawater that constitutes the pore water. From 800 to 870 mbsf, analcime and smectite are associated with albite.

Relative to overlying sediments, there is an increase in the interval from 870 to 895 mbsf in the amounts of chlorite, quartz, smectite, and smectite-mica mixed-layer clays. The zeolite phase changes from analcime to heulandite. Pyrophyllite and Ca-feldspar are also present. The smectite shows a ⟨060⟩ reflection at 0.153–0.154 ηm, indicating that this is a trioctahedral smectite, rich in Mg and Ca. Sample 126-793B-30R-5, 45 cm, contains a small amount of phillipsite in association with smectite. Phillipsite is a common submarine alteration product of volcanic glass.

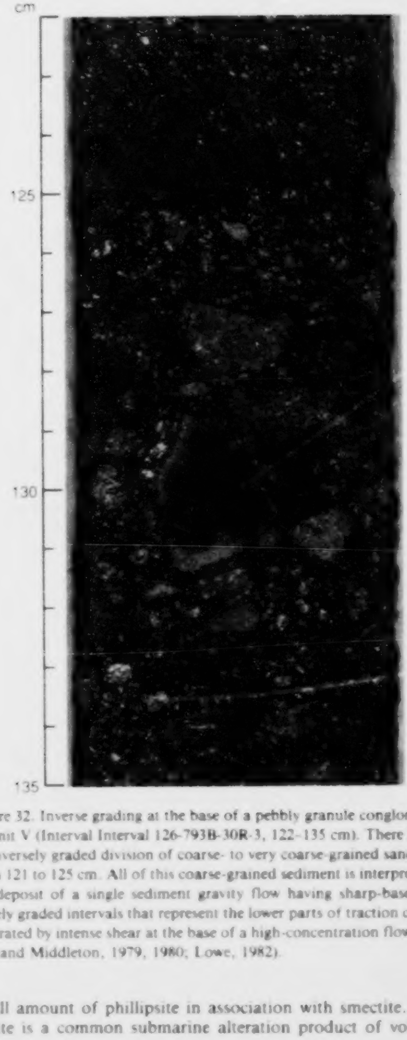

Figure 32. Inverse grading at the base of a pebbly granule conglomerate in Unit V (Interval Interval 126-793B-30R-3, 122–135 cm). There is also an inversely graded division of coarse- to very coarse-grained sandstone from 121 to 125 cm. All of this coarse-grained sediment is interpreted as the deposit of a single sediment gravity flow having sharp-based, inversely graded intervals that represent the lower parts of traction carpets generated by intense shear at the base of a high-concentration flow (Hiscott and Middleton, 1979, 1980; Lowe, 1982).

The interval from 920 to 1060 mbsf is characterized by a lack of chlorite, perhaps because of severe depletion of Mg in pore waters at this depth (see "Sediment/Fluid Geochemistry" section, this chapter). The main minerals in the sedimentary rocks are smectite, calcite, quartz, Na-feldspar, and heulandite. Analcime is not present. A mineral-filled vein in this interval (Sample 126-793B-44R-3, 16 cm) consists of heulandite-clinoptilolite.

Very fine-grained sandstones in the part of the section from 1130 to 1150 mbsf contain abundant smectite, local celadonite, chabazite ($Ca[Al_2Si_4]O_{12} \cdot 6H_2O$), and Ca-feldspar. Chlorite, calcite, and quartz are rare. The smectite has a ⟨060⟩ reflection at 0.15388 nm (Sample 126-793B-58R-5, 20 cm) and is, therefore, a trioctahedral, Mg- and Ca-rich variety. This is consistent

Table 3. X-ray diffraction data for Holes 793A and 793B.

Core, section, interval (cm)	Depth (mbsf)	Unit	Color	Texture	Clay minerals			Mineral
					1.4 nm	1.0 nm	0.7 nm	
126-793A-								
[illegible]	1.5	I	2.5Y 6/2	Pumiceous gravel	Trace	—	—	Calcite, quartz, feldspar
[illegible]	16.2	I	5G 5/2	Silt	Present	Present	Present	Calcite, quartz, feldspar
[illegible]	18.3	I	5G 2/1	Silt	Present	—	Present	Calcite, quartz, feldspar
[illegible]	26.9	I	5Y 6/1	Nannofossil clay	Present	Trace	Present	Calcite, quartz, feldspar
[illegible]	33.4	I	5Y 6/1	Nannofossil-rich silty clay	Present	Present	Present	Calcite, quartz, feldspar
[illegible]	40.7	I	5G 2/1	Vitric silt	Present	—	Trace	Calcite, quartz, feldspar, pyrolusite, maghemite
[illegible]	42.7	I	5Y 6/1	Nannofossil-rich silty clay	Present	Present	Present	Calcite, quartz, feldspar
[illegible]	53.7	I	5G 3/2	Silt	Present	—	Present	Calcite, quartz, feldspar, palagonite, glauconite
[illegible]	61.7	I	N1	Vitric very fine-grained sand	Trace	—	—	Calcite, feldspar
[illegible]	74.0	I	5Y 2/1	Vitric silt	Present	Present	Present	Calcite, quartz, feldspar
[illegible]	90.5	I	5GY 2/1	Nannofossil-rich silty clay	Present	—	Trace	Calcite, quartz, feldspar, pyrite
126-793B-								
[illegible]	594.4	III	5GY 6/1	Claystone	Present	Trace	Trace	Calcite, quartz, feldspar
[illegible]	594.8	III	5GY 6/1	Pebble	Present	Trace	Trace	Calcite, quartz, feldspar
[illegible]	595.1	III	5GY 6/1	Nannofossil claystone	Present	—	Trace	Calcite, quartz, feldspar
[illegible]	604.4	III	N4	Very fine-grained sandstone	Present	—	—	Quartz, feldspar, palagonite
[illegible]	604.7	III	5GY 4/1	Silty claystone	Present	—	—	Calcite, quartz, feldspar
[illegible]	605.8	III	5GY 4/1	Very fine-grained sandstone	Present	Trace	—	Calcite, quartz, feldspar
[illegible]	606.2	III	5GY 4/1	Siltstone	Present	—	—	Calcite, quartz, feldspar, hematite, magnetite
[illegible]	606.8	III	5GY 4/1	Coarse-grained sandstone	Present	—	—	Calcite, quartz, feldspar, palagonite
[illegible]	607.8	III	5GY 4/1	Siltstone	Present	—	—	Calcite, quartz, feldspar
[illegible]	608.9	III	5GY 4/1	Siltstone	Present	—	—	Calcite, quartz, feldspar
[illegible]	614.5	III	5GY 4/1	Vitric silty claystone	Present	—	Trace	Calcite, quartz, feldspar
[illegible]	616.3	III	5GY 4/1	Vitric sandstone	Present	Trace	—	Calcite, quartz, feldspar
[illegible]	618.3	III	5GY 6/1	Vitric silty claystone	Present	—	—	Calcite, quartz, feldspar
[illegible]	619.0	III	5GY 4/1	Vitric silty claystone	Present	Present	Present	Calcite, quartz, feldspar, glauconite
[illegible]	633.7	III	N7	Silty sandstone	Trace	—	—	Calcite, quartz, feldspar
[illegible]	633.8	III	5G 3/1	Siltstone	Present	—	Trace	Quartz, feldspar
[illegible]	635.3	III	N6	Siltstone	Trace	—	—	Quartz, feldspar
[illegible]	635.5	III	5G 3/1	Siltstone	Present	—	Present	Calcite, quartz, feldspar
[illegible]	635.6	III	5Y 4/1	Siltstone	Present	—	—	Calcite, quartz, feldspar
[illegible]	645.0	III	5Y 4/1	Siltstone	Present	—	—	Calcite, quartz, feldspar
[illegible]	655.3	III	5Y 3/1	Siltstone	Trace	—	—	Calcite, quartz, feldspar
[illegible]	683.7	III	5Y 2/1	Claystone	Present	—	—	Calcite, quartz, feldspar, glauconite
[illegible]	710.5	III	5GY 5/1	Nannofossil-rich silty claystone	Present	—	—	Calcite, quartz, feldspar, glauconite
[illegible]	722.6	III	5GY 4/1	Sandy claystone	Present	—	Present	Calcite, quartz, feldspar
[illegible]	733.1	III	5YR 4/1	Vitric siltstone	Present	—	—	Calcite, quartz, feldspar
[illegible]	736.2	IV	5YR 6/1	Nannofossil-rich claystone	Abundant	Present	Present	Calcite, quartz, feldspar, glauconite
[illegible]	740.0	IV		Gypsum nodule	Common	—	—	Gypsum
[illegible]	740.8	IV	10R 6/4	Nannofossil claystone	Abundant	Present	Present	Calcite, quartz, feldspar, palagonite
[illegible]	741.2	IV	10R 6/4	Black manganese blotches	Present	—	—	Calcite, quartz, feldspar, todorokite
[illegible]	746.1	IV	5Y 5/2	Claystone	Abundant	Present	Present	Calcite, quartz, feldspar, palagonite
[illegible]	755.8	IV	10Y 6/2	Vitric claystone	Abundant	Present	Common	Calcite, quartz, feldspar, palagonite
[illegible]	774.9	V	5GY 6/1	Clayey siltstone clasts	Common	Present	—	Quartz, feldspar, palagonite heulandite-clinoptilolite
[illegible]	785.6	V	5G 2/1	Crystal-vitric nannofossil sandstone	Abundant	—	Present	Calcite, quartz, heulandite-clinoptilolite
[illegible]	789.6	V	5GY 2/1	Crystal-vitric siltstone	Abundant	—	Present	Calcite, quartz, feldspar, heulandite-clinoptilolite, smectite-mica mixed
[illegible]	797.1	V	5G 6/1	Very fine-grained sandstone	Trace	—	—	Gypsum, analcime
[illegible]	797.4	V	5G 6/1	Very fine-grained sandstone vein	Present	—	—	Gypsum
[illegible]	821.1	V	5YR 2/1	Very fine-grained sandstone	Common	—	—	Analcime
[illegible]	838.1	V	5GY 4/1	Fine-grained sandstone vein	Trace	Present	—	Gypsum, feldspar
[illegible]	839.7	V	5GY 4/1	Clayey siltstone	Abundant	Trace	Common	Calcite, quartz, feldspar, analcime
[illegible]	859.8	V	5GY 4/1	Fine-grained sandstone	Abundant	—	Trace	Feldspar, analcime
[illegible]	870.9	V	5GY 4/1	Very fine-grained siltstone	Abundant	—	Common	Quartz, feldspar, heulandite-clinoptilolite, analcime, phillipsite
[illegible]	881.1	V	5GY 4/1	Very fine-grained sandstone	Abundant	—	Present	Calcite
[illegible]	881.7	V	5G 2/1	Very fine-grained sandstone	Abundant	Trace	Common	Quartz, feldspar, smectite-mica mixed
[illegible]	891.2	V	N3	Vitric fine-grained sandstone	Abundant	—	Present	Calcite, quartz, feldspar, pyrophyllite, analcime heulandite, heulandite-clinoptilolite
[illegible]	902.0	V	5BG 3/2	Pumiceous sandstone	Common	—	—	Calcite, quartz, heulandite
[illegible]	911.8	V	N7	Fine-grained sandstone	Abundant	—	Trace	Calcite, feldspar, heulandite, analcime, heulandite-clinoptilolite
[illegible]	915.0	V	5G 2/1	Crystal-vitric fine-grained sandstone	Common	—	—	Calcite, feldspar, heulandite, analcime, heulandite-clinoptilolite
[illegible]	971.9	V	5G 6/1	Silty claystone	Common	—	—	Calcite, feldspar, heulandite
[illegible]	992.2	V	5B 5/1	Siltstone	Abundant	—	—	Calcite, quartz, feldspar, heulandite
[illegible]	1002.6	V	5GY 2/1	Silty claystone	Trace	—	—	Calcite, quartz, feldspar, heulandite-clinoptilolite
[illegible]	1021.2	V	5G 3/1	Vitric siltstone	Common	—	—	Calcite, quartz, feldspar, heulandite
[illegible]	1039.4	V	5GY 2/1	Clayey siltstone	Abundant	—	—	Calcite, quartz, feldspar, heulandite
[illegible]	1052.0	V	5GY 2/1	Fine-grained sandstone	Common	—	—	Calcite, quartz, feldspar, heulandite
[illegible]	1061.6	V	5YR 2/1	Very fine-grained sandstone	Common	—	—	Calcite, feldspar, heulandite, analcime, heulandite-clinoptilolite
[illegible]	1089.6	V	5Y 4/1	Very fine-grained sandstone	Abundant	—	—	Calcite, feldspar, heulandite-clinoptilolite
[illegible]	1099.3	V	5Y 2/1	Clayey sandstone	Abundant	—	—	Calcite, quartz, feldspar, heulandite-clinoptilolite
[illegible]	1109.4	V	N2	Very fine-grained crystal-vitric sandstone	Abundant	—	—	Calcite, quartz, feldspar, heulandite, heulandite-clinoptilolite
[illegible]	1119.0	V	5BG 5/2	Very fine-grained sandstone	Abundant	—	—	Calcite, quartz, feldspar, heulandite
[illegible]	1128.6	V	5Y 2/1	Silty claystone vein	Abundant	—	—	Calcite, quartz, feldspar, heulandite, heulandite-clinoptilolite, analcime
[illegible]	1136.5	V	5BG 4/6	Sandstone	—	Common (celadonite)	—	Dolomite, analcime
[illegible]	1140.2	V	5GY 4/1	Very fine-grained sandstone	Abundant	Trace	—	Quartz, feldspar, analcime, chabazite
[illegible]	1152.8	V	5YR 2/1	Very fine-grained sandstone	Abundant	—	—	Quartz, feldspar, analcime, heulandite, chabazite
[illegible]	1154.3	V	N2	Crystal-vitric sandstone	Abundant	—	—	Feldspar, analcime, heulandite, chabazite
[illegible]	1173.2	V	5GY 2/1	Siltstone	Abundant	—	—	Quartz, feldspar, heulandite
[illegible]	1201.0	V	5GY 2/1	Medium-grained sandstone	Abundant	—	—	Calcite, feldspar, analcime, heulandite
[illegible]	1205.6	V	5G 2/1	Conglomerate	Abundant	—	—	Calcite, feldspar, analcime, heulandite-clinoptilolite
[illegible]	1211.9	V	5G 1/2	Very fine-grained sandstone	Abundant	—	—	Quartz, feldspar, analcime, heulandite-clinoptilolite
[illegible]	1229.1	V	5GY 2/1	Siltstone	Abundant	Present	—	Calcite, quartz, feldspar, analcime, heulandite-clinoptilolite
[illegible]	1232.6	V	5GY 2/1	Sandy siltstone	Abundant	Trace	Present	Quartz, feldspar, analcime
[illegible]	1240.5	V	5GY 4/1	Medium-grained crystal-vitric sandstone	Abundant	—	—	Calcite, quartz, feldspar, heulandite, heulandite-clinoptilolite
[illegible]	1253.4	V	N1	Very fine-grained sandstone with slickensides	Abundant	—	—	Heulandite
[illegible]	1275.3	V	5G 5/2	Very fine-grained sandstone	Abundant	—	—	Calcite, dolomite, quartz, feldspar, heulandite-clinoptilolite
[illegible]	1281.7	V	5G 4/1	Siltstone	Abundant	—	—	Dolomite, quartz, feldspar, heulandite
[illegible]	1288.2	V	5G 2/1	Silty claystone	Abundant	—	—	Calcite, feldspar, heulandite-clinoptilolite
[illegible]	1309.3	V	5GY 2/1	Conglomerate	Abundant	—	—	Calcite, dolomite, quartz, feldspar, heulandite-clinoptilolite
[illegible]	1312.3	V	5GY 2/1	Pebbly sandstone	Common	Present	—	Quartz, feldspar, heulandite, heulandite-clinoptilolite
[illegible]	1317.3	V	5GY 2/1	Fine-grained sandstone	Abundant	—	—	Calcite, dolomite, quartz, feldspar, heulandite, heulandite-clinoptilolite
[illegible]	1328.7	V	5G 2/1	Volcanic sandy granule conglomerate	Abundant	—	—	Feldspar, analcime, heulandite-clinoptilolite
[illegible]	1333.8	V	5GY 4/1	Fine-grained crystal-vitric sandstone	Abundant	Trace	—	Calcite, quartz, feldspar, heulandite-clinoptilolite, analcime
[illegible]	1347.0	V	5GY 2/1	Granule-rich coarse-grained sandstone	Abundant	—	—	Calcite, feldspar, heulandite-clinoptilolite, analcime
[illegible]	1361.2	V	2YR 2/1	Siltstone	Common	Trace	—	Quartz, feldspar, heulandite-clinoptilolite, palagonite
[illegible]	1368.5	V	5G 2/1	Granule-rich medium-grained sandstone	Abundant	—	—	Quartz, feldspar, heulandite-clinoptilolite, palagonite
[illegible]	1373.6	V/VI	5GY 2/1	Fault shear zone	Present	Present	—	Feldspar, palagonite
[illegible]	1379.6	VI	5G 5/2	Microbreccia	Present	—	—	Quartz, feldspar, analcime, palagonite
[illegible]	1384.7	VI	5G 5/2	Volcanic breccia	Present	Trace	Present	Analcime
[illegible]	1394.8	VI	5G 5/2	Volcanic breccia	Abundant	—	Present	Feldspar

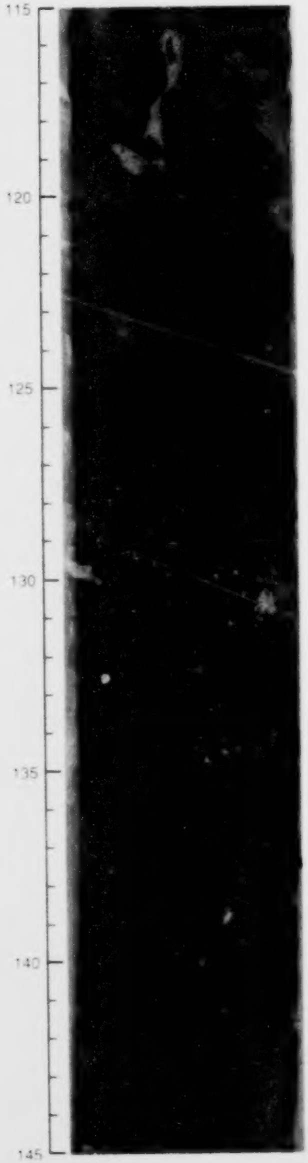

Figure 33. The lower part of a deformed sedimentary clast, at least 70 cm across, that occurs 35 cm above the base of a 2.3-m-thick graded bed of pebbly sandstone (Interval 126-793B-27R-5, 115-145 cm). The sedimentary structures and grain size of this bed are shown in Figure 30.

with the fact that interstitial waters are almost saturated with respect to Ca at this depth (see "Sediment/Fluid Geochemistry" section, this chapter).

Cobalt-blue celadonite is present in a sandstone bed (Sample 126-793B-58R-2, 96 cm) in this interval, associated with dolomite and analcime. Both celadonite and trioctahedral (magnesian) smectite suggest low-temperature, nonoxidative alteration of volcanic glass.

Siltstone to conglomerate beds in the interval from 1200 to 1230 mbsf contain abundant smectite, analcime, and heulandite-clinoptilolite. Chlorite, quartz, and feldspar are rare. Calcite concentration is elevated in beds containing tests and broken tests of benthic foraminifers.

In the interval from 1250 to 1373 mbsf, a slickensided fault surface at 1253 mbsf (Sample 126-793B-70R-3, 63 cm) contains a high concentration of heulandite and smectite. Dolomite is present from 1275 to 1320 mbsf. Analcime is present below 1330 mbsf in fine-grained crystal-vitric sandstone and coarse-grained sandstone, in association with abundant smectite. The surface of the fault that separates Units V and VI (1373 mbsf) contains abundant palagonite with a small amount of smectite-mica mixed-layer clay.

Unit VI

The volcanic breccia at the base of the sedimentary succession contains significantly more feldspar than the overlying section, in association with smectite and palagonite. The feldspar is albite.

Sediment Accumulation Rates

Sedimentation rates for Site 793 were established from calcareous nannofossil datums and paleomagnetic reversals (Table 4), which were used to construct the age-depth curve shown in Figure 42. The interval between 98.9 and 586.5 mbsf was drilled without taking any cores; thus, age-depth information for the sedimentary section between those depths is not available.

Sedimentation rates in Unit V (late early to early late Oligocene; 30.33-29.21 Ma) are >250 m/m.y., similar in magnitude to rates in equivalent sedimentary sections of early late Oligocene age at Sites 787 and 792 (see "Lithostratigraphy and Accumulation Rates" section, "Site 787" and "Site 792" chapters, this volume). Toward the top of Unit V (29.21-26.86 Ma), sedimentation rates decline to about 80 m/m.y. The high rates throughout Unit V reflect the influx of volcaniclastic material to the forearc basin at this time.

The early Miocene sediments were deposited very slowly (~7 m/m.y.). These low sedimentation rates occur in Unit IV and the lower part of Unit III, which are characterized by nannofossil claystones and nannofossil-rich claystones that slowly accumulated in the absence of significant volcanic input. These low sedimentation rates may also reflect a stratigraphic discontinuity at or near the Unit III/IV contact. Sedimentation rates rise sharply to 70 m/m.y. in the middle Miocene (Unit III) and average 40 m/m.y. in the uncored interval.

Pleistocene sedimentation rates (Unit I) are over 100 m/m.y., similar to rates seen at Sites 792 (see "Lithostratigraphy and Accumulation Rates" section, "Site 792" chapter, this volume) for the same time interval. This rate reflects renewed volcaniclastic input to the forearc basin.

Interpretation of Sedimentary Units in Hole 793B

Unit III

The sharp-based, graded beds in this unit are typical fine-grained turbidites, except that their parallel- to ripple-laminated

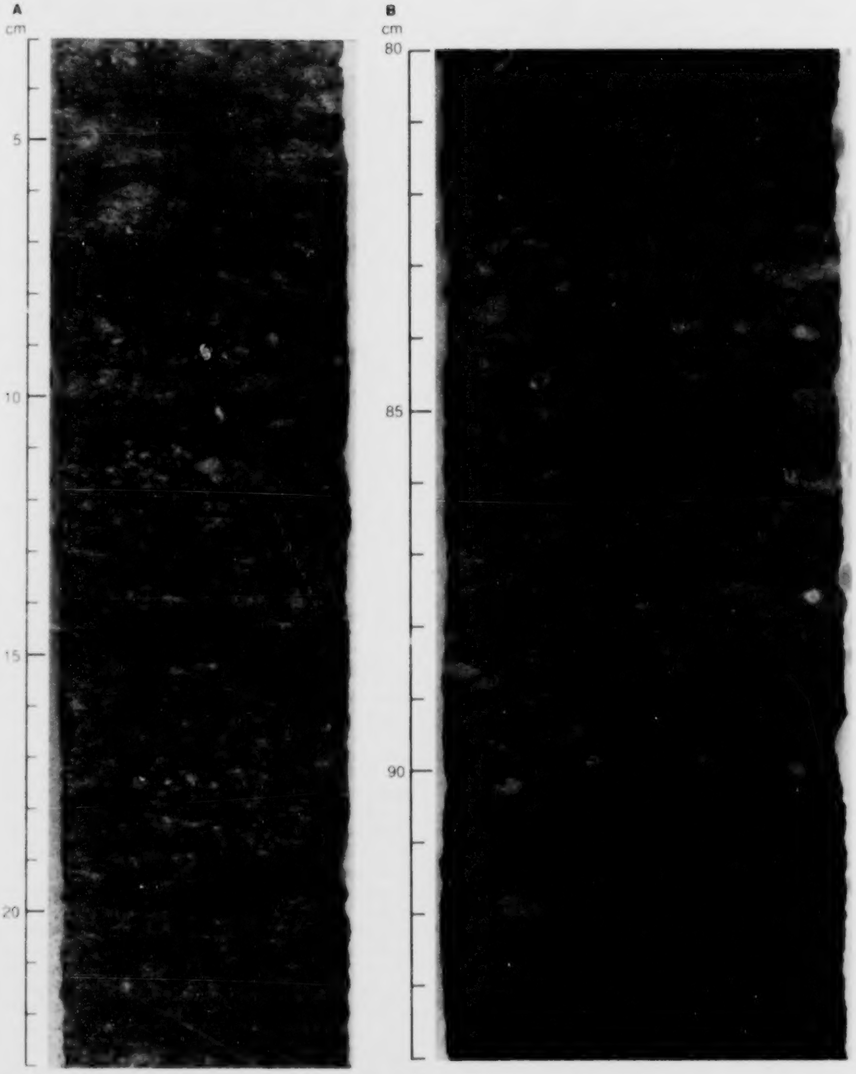

Figure 34. Examples of pumiceous, granule-rich, and pebbly sandstones in Unit V. **A.** Part of a parallel-laminated sandstone bed with light-colored, low-density pumice grains concentrated in bands within the finer grained sandstone. There are dark-colored clasts of pumice, altered to clay minerals, concentrated in bands at 14–15 and 19–20 cm (Interval 126-793B-37R-4, 3-23 cm). **B.** A high concentration of pumice granules and pebbles in a matrix of fine-grained sandstone (Interval 126-793B-43R-5, 80–94 cm).

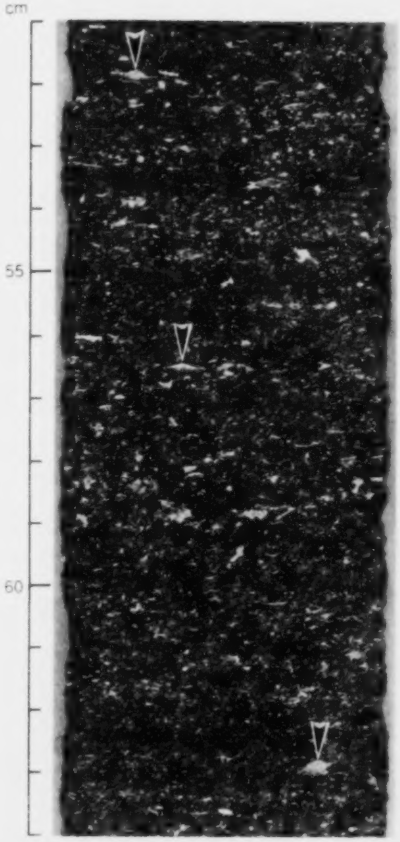

Figure 35. Medium-grained, parallel-laminated sandstone rich in tests of *Discocyclina* and other larger benthic foraminifers (Interval 126-793B-63R-3, 51–64 cm). The foraminifers (at 52, 56, and 63 cm; see arrows) have a discoid shape.

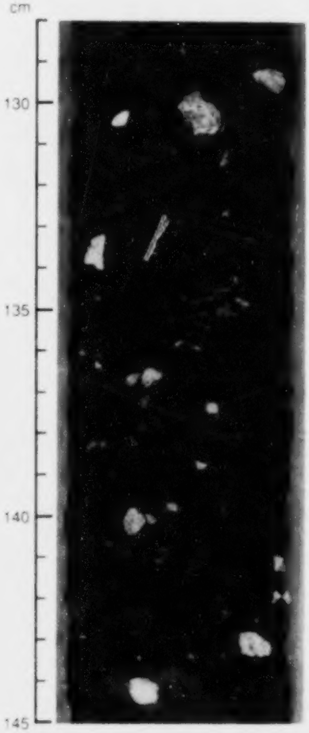

Figure 36. Volcanic-lithic conglomerate with large white bioclasts of calcareous red algae (Interval 126-793B-75R-2, 128–145 cm).

siltstone and silty claystone divisions (T_d division of Bouma, 1962) are several times thicker than the basal sandstone/siltstone division. Some of these fine-grained turbidites are on the order of 50 cm thick. Given the lack of thick-bedded, coarse-grained beds in Unit III, and sheetlike geometry of the basin fill on seismic profiles, we interpret the depositional setting to have been a rather featureless basin plain over which dilute, unconfined turbidity currents spread out to form sheetlike deposits. The interbedded facies are strongly burrowed siltstone-claystone sediment types with high contents of biogenic carbonate and scattered sand- to granule-size grains of mafic volcanic glass and felsic pumice. These are interpreted as hemipelagic deposits produced by the settling of biogenic and volcanogenic fractions, as well as mixing by burrowers. In some cases, the fallout of volcanic ash formed very thin layers of coarse silt to granules. The grain size and total volume of volcanic ejecta in this unit is much less than in Unit I, suggesting limited activity of the nearby arc volcanoes at this time. As at Sites 787 and 792 (see "Site 787" and "Site 792" chapters, this volume), the volcanogenic input to the basin was compositionally bimodal.

The 35-cm-thick bed of muddy sandstone, with large intraclasts and basalt cobbles, is interpreted as a thin debris-flow deposit. This is the only such bed in Unit III and probably represents an unusual event like a seismically triggered failure on the margin of the forearc basin. Only a thin feather-edge of what was probably a thicker flow reached this part of the basin.

As at Sites 787 and 792, subvertical veinlets are the expression of a fracture cleavage that formed during early dewatering of unlithified, wet, muddy sediments (Ogawa and Miyata, 1985). The extensional regime inferred from these veinlets is consistent with numerous extensional microfaults noted in cores from Unit III.

Unit IV

Unit IV consists entirely of variable mixtures of biogenic carbonate, both nannofossils and foraminifers, and siliciclastic claystone, except for rare, thin, graded siltstone beds (turbidites). We interpret these rocks as hemipelagic deposits that accumulated in a low-energy environment. The clay fraction was probably advected from the vicinity of the volcanic front by storm waves and fairly weak marine currents; there is no evidence for bottom-current reworking. Slow depositional rates, and an almost complete absence of direct volcanogenic input, indicate

cm
44
45
46
47
48
49
50
51
52
53
54

Figure 37. Steeply dipping, curved, anastomosing microfaults, with the total displacement of 8 mm partitioned between two of the faults from 48 to 53 cm (Interval 126-793B-54R-2, 44–54 cm).

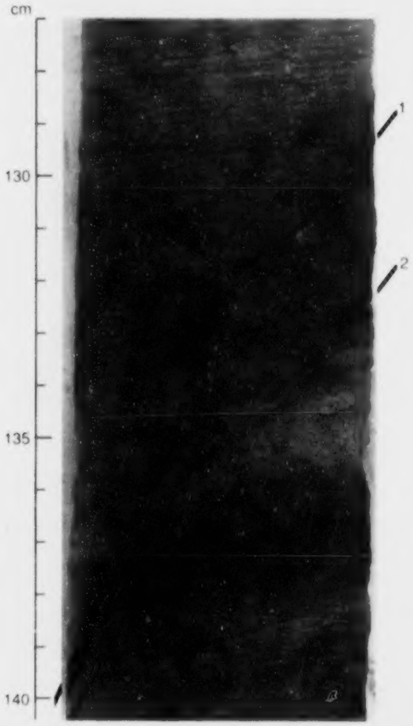

Figure 38. Complex set of braided faults, with different lithologies on the opposite sides of fault plane 2. The sediments above and below this fault are, respectively, very fine-grained and fine-grained pumiceous sandstone. Fault surfaces 1 and 2 merge below 135 cm (Interval 126-793B-54R-4, 127–140 cm).

that the Izu-Bonin Arc was largely inactive during this part of the early Miocene. This suggestion is corroborated by results from Site 792 (see "Lithostratigraphy and Accumulation Rates" section, "Site 792" chapter, this volume), where lower Miocene nannofossil chalk marks a period of very slow deposition without significant volcanic input. As at Site 792, the lower epiclastic input in Unit IV of Site 793, relative to that of the underlying Unit V, may partly be a response to the significant rise in global sea level from the mid-Oligocene into the Miocene (Haq et al., 1987).

The upper part of Unit IV is characterized by strongly burrowed, red-colored (oxidized) sedimentary rock, diagenetic manganese oxide (todorokite), and biogenic carbonate contents of about 40%–60%. We interpret these features to be the product of a very slow delivery of siliciclastic detritus. Oxygenated bottom waters were in contact with the surface sediment long enough to oxidize the organic fraction and any iron-rich minerals completely.

In the rocks of the lower part of Unit IV, the color is drabber, burrow density is drastically reduced, and carbonate content is low. Fissility, a product of recrystallization of clay minerals parallel to the bedding, is probably better developed in the claystone in this part of the section because of a primary, undisturbed alignment of phyllosilicate grains in the unburrowed sediments. On the basis of the lack of bioturbation, we interpret this part of the unit to have been deposited beneath poorly oxygenated bottom waters. The changes in lithology and burrow intensity from the top to the base of Unit IV may either reflect higher rates of accumulation in the older strata or temporal differences in the character of bottom waters. Benthic foraminifers are rare in the lower part of Unit IV, and no samples were processed from the fissile interval to aid in our assessment of the bottom-water character. Organic carbon content in this sedimentary rock is low, about 0.2% (see "Sediment/Fluid Geochemistry" section, this chapter).

A striking feature of Unit IV is the abundance of dewatering veinlets. Veinlets are also present in Unit III, but they are absent from the upper part of the more sandy Unit V. The claystones of Unit IV are impermeable, and it is possible that the large quantities of pore water that must have been expelled from the more permeable Unit V generated and maintained a dense network of veinlets to accommodate the high flow volumes. The veinlets contain a greater proportion of zeolite precipitates than at other Leg 126 sites, consistent with greater net transport of pore fluids through the veinlet network. The kinked geometry of the veinlets is attributed to compaction, perhaps with a component of directed shear, after the early phase of dewatering.

The gypsum nodule in Unit IV reflects the Ca-rich, pore-water chemistry of this site (see "Sediment/Fluid Geochemistry" section, this chapter).

Unit V

All sediments in Unit V were deposited by sediment gravity flows, ranging in character from debris flows to turbidity currents of both high and low concentration, that diluted the pe-

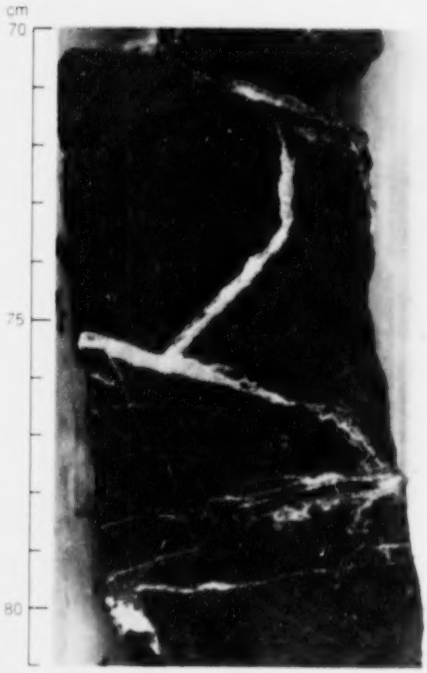

Figure 39. Gypsum-filled fractures in very fine-grained sandstone of Unit V (Interval 126-793B-27R-3, 70–81 cm).

lagic input to this part of the section to insignificant levels. The debris-flow deposits are structureless and are characterized by poorly developed fabric and grading. Large silty claystone intraclasts are commonly present well above the base of the bed (Fig. 30). Gravel-size material in some of these beds consists only of such intraclasts, whereas in other beds there is a polymictic assemblage of volcanic pebbles, including clasts of andesite flows. In the lower part of Unit V, the conglomeratic beds also contain large benthic foraminifers, bioclasts of calcareous red algae, bryozoans, rare coral, and lithified algal micrite clasts.

Many of the pebble-size volcanic clasts were derived by subaerial or coastal/nearshore erosion of arc volcanoes. The bioclastic debris was derived from shallow-marine areas around the same volcanoes. These larger clasts were mixed, in shallow water or during resedimentation, with finer grained erosional products, and with primary volcanic ejecta (vitric sand) on the seafloor around the volcanic edifices.

The graded sandstones and pebbly sandstones of Unit V were deposited by turbidity currents during a period of rapid sediment supply that diluted pelagic and primary pyroclastic input to the forearc basin. Much of the detritus in these beds, however, may have been produced along the arc by nonexplosive volcanic activity, with the abundant primary material being contributed directly, or quickly resedimented, into the forearc basin. The necessity to derive a large fraction of the coarser siliciclastic material from active volcanoes is a consequence of the great volumetric difference between the sedimentary fill of the forearc basin, and the probable area of emergent arc volcanoes that could have acted as sources for epiclastic material.

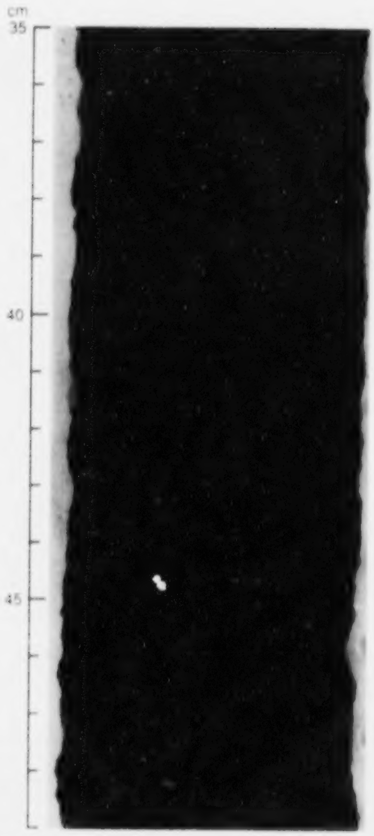

Figure 40. Orthogonal sets of light-colored bands or zones in fine-grained sandstone. There is no sharp fracture in the middle of these zones. Examination of a thin section indicates that the lighter areas contain more clay minerals than the darker areas. The set that dips from right to left has the same orientation as microfaults at this general depth in Unit V (Interval 126-793B-77R-1, 35–49 cm).

In part of Unit V, there is direct evidence for contemporaneous, explosive, and acidic volcanic activity. In the interval from 900 to 1020 mbsf (28.3–29.5 Ma; Fig. 32), most sandstone beds contain abundant pumice clasts that were probably transported into the basin as a part of the load of the turbidity currents. There is no evidence for the direct accumulation of pumice by air fall to the sea surface and settling. For other parts of Unit V, there are apparently no macroscopic criteria to distinguish resedimented volcanogenic material from detritus supplied directly by submarine eruptions, followed by flow as a density current into the basin.

There is no evidence that the conglomerates in the lower part of Unit V were deposited in channels, although similar sediments in ancient successions commonly reside in shallow channels or large scours. Conglomerates of this type are known from the inner to middle parts of ancient submarine fans, both within

cm
130
135
140
145
150

Figure 41. Angular cobbles of porphyritic lava in a matrix of sandstone of the same composition. Much of the field of view consists of clasts (Interval 126-793B-83R-1, 130-150 cm).

and beyond fan channels, and from coarse-grained slope aprons (Nelson and Maldonado, 1988). Conglomeratic beds higher in the section (825-900 mbsf; Figs. 5 and 29A) are interbedded with thin- to medium-bedded turbidites and seem to represent unique, high-volume events rather than channel-fill deposits. Some of these events were debris flows that may have been generated by catastrophic failure of parts of the coarse-grained

Table 4. Calcareous nannofossil datums and paleomagnetic reversal events used to construct the Site 793 age-depth curve.

Chronostratigraphic event	Core	Depth (mbsf)	Age (Ma)
Nannofossils:			
	Hole 793A		
FO *E. huxleyi*	2H-CC	11.28-23.0	0.275
LO *P. lacunosa*	5H-1, 141 cm	32.56-33.91	0.460
younger than LO acme of *Reticulofenestra* sp. A	11H-CC	98.9-99.7	< 0.830
	Hole 793B		
FO *S. heteromorphus*	14R-CC	706.36-720.10	17.2-18.6
FO *D. druggi*	18R-4, 23-25 cm	753.55-758.40	23.2
LO *S. ciperoensis*	23R-CC	791.93-806.7	25.2
LO *S. distensus*	30R-CC	861.92-874.0	28.2
FO *S. ciperoensis*	57R-CC	1128.9-1143.4	30.2
Paleomagnetics:			
	Hole 793A		
Brunhes/Matuyama	9H-3 to 9H-4	75.4-77.2	0.73
Top of Jaramillo	9H/10H	78.68-90.9	0.91
	Hole 793B		
Base of second normal in Anomaly 5B	1R/2R	590.29-603.83	15.27
Base of third normal in Anomaly 5C	9R, 20 cm	662.3-668.09	16.22
Base of second normal in Anomaly 6A	16R-5, 130 cm	737.0-737.5	21.71
Top of first normal in Anomaly 6AA	17R-2, 70 cm	741.3-742.7	21.90
Top of first normal in Anomaly 8	20R-6, 110 cm	776.6	26.86
Base of second normal in Anomaly 8	25R-5, 20 cm	824.1-824.4	27.74
Top of first normal in Anomaly 9	31R-3, 110 cm	878.1-878.7	28.15
Base of second normal in Anomaly 9	40R-5, 90 cm	967.9	29.21
Top of first normal in Anomaly 10	53R/54R	1091.73-1099.5	29.73
Top of second normal in Anomaly 10	63R-1, 30 cm	1182.5-1187.0	30.09
Top of second normal in Anomaly 10	70R-4, 120 cm	1255.5	30.33

Note: Site 793 age-depth plot appears in Figure 42; FO = first occurrence; LO = last occurrence.

apron surrounding the arc volcanoes, perhaps associated with tectonic rejuvenation of the flanks of the basin. The global sea level was fairly low at this time (Haq et al., 1987), which may have also aided the delivery of coarser grained material to the basin (Mutti, 1985). Within error limits for biostratigraphic and paleomagnetic datums, this upper conglomeratic interval (28 ± 0.5 Ma; Fig. 42) is broadly contemporaneous with conglomerates at the base of the sedimentary section at Site 792 (see "Lithostratigraphy and Accumulation Rates" section, "Site 792" chapter, this volume).

The overall upward fining in Unit V from the basal conglomerates and pebbly sandstones to the uppermost thin- to medium-bedded turbidites is probably controlled by tectonic evolution of the forearc basin. The basin was apparently formed by rifting of a wide Eocene arc terrane, with the western and eastern flanks now exposed at the frontal- and outer-arc highs, respectively (see "Principal Results" section, this chapter). Uplift of the flanks of this rift, deepening of the basin, steepening of bottom slopes, increased seismic activity, and perhaps augmented volcanicity would have all contributed to the coarse-grained and very thickly bedded interval at the base of the unit. The upward fining above the conglomeratic interval may have been produced

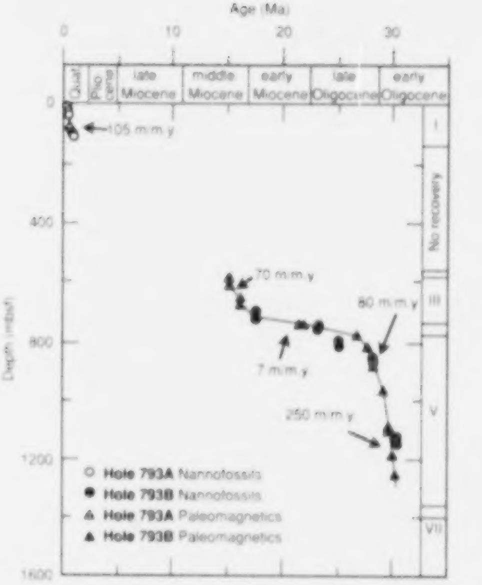

Figure 42. Age-depth curve for Site 793 constructed from data in Table 4. Lithologic unit boundaries are located along the right-hand side of the figure.

by a combination of effects: (1) a decreasing rate of extension; (2) a decline in the elevation and extent of the source area; and (3) a decrease in seafloor gradients along the basin-margin slopes caused by the infilling of the basin.

Unit VI

The lack of organization, very poor sorting, and clast angularity of the volcanic breccias of Unit VI suggest a very local source area. The features of the sediment are like those of rockfall or talus deposits, although there is sufficient mud matrix in the upper part of the unit to have permitted downslope transport by debris flow. We interpret this material to be a debris or talus apron along the flanks of a volcanic edifice or intrabasinal fault scarp. Petrologic differences between the clasts in Unit VI and the basement (see "Igneous Petrology" section, this chapter) indicate that this volcanic breccia was derived from a separate volcano or flow field.

History of Volcanic Activity

The lower to upper Oligocene turbidite succession contains little direct air fall of pumice or other ejecta except for a pumice-rich interval from 900 to 1020 mbsf. Nevertheless, it is difficult to account for the enormous volume of sediment deposited in the forearc basin, at rates of about 80–250 m/m.y., without invoking contemporaneous production of large quantities of volcanogenic material. Continuous volcanic activity, combined with relentless subaerial and coastal erosion, maintained a constant flux of detritus to the steep flanks of the arc volcanoes. From this position, the materials were periodically carried out onto the forearc basin plain.

There is a general upward fining toward the top of Unit V (759–825 mbsf), signaling a decline in the rate of production and input of volcanic products, perhaps caused in part by drowning of the source area as a result of a significant rise in global sea level from the mid-Oligocene into the Miocene (Haq et al., 1987). The presence of only a few percent of volcanic ash in Unit IV (present as vitric siltstone and vitric sandstone) combined with slow rate of deposition (7–13 m/m.y.) point to a period of volcanic quiescence in the early Miocene.

Unit III contains significant quantities of volcanic ejecta, both as disseminated grains in burrowed sediments, and as primary or resedimented volcanic glass of sand and silt size. The rate of input of volcanogenic material is less than in Unit V, but much more than in Unit IV. After an early Miocene hiatus, therefore, volcanic activity resumed at a moderate level from the late early Miocene into the middle Miocene.

Unit I is separated from Unit III by about 500 m for which no sedimentary record was recovered. We cannot comment, therefore, about trends in volcanic activity between the middle Miocene and the Quaternary. In the Quaternary (Unit I), there are large amounts of volcanogenic gravel, sand, and silt, all indicating important input from volcanoes of the Izu-Bonin Arc. Subunit IA, in particular, consists mainly of pumiceous gravel and sandy gravel produced by large caldera eruptions along the arc. Pumice from the same phase of intense volcanic activity was recovered at several other Leg 126 sites, particularly in the backarc.

BIOSTRATIGRAPHY

Calcareous Nannofossils

Hole 793A

We placed Samples 126-793A-1H-CC and -2H-CC, which contain *Emiliania huxleyi*, in Zone CN15. Samples 126-793A-3H-4, 0 cm, -3H-CC, and -4H-CC contain neither *E. huxleyi* nor *Pseudoemiliania lacunosa* and thus belong in Zone CN14b. We assigned Samples 126-793A-5H-1, 141 cm, through -11H-CC, which contain *P. lacunosa* and *Gephyrocapsa oceanica*, to Zone CN14a. Sample 126-793A-11H-CC does not contain the acme of *Reticulofenestra* sp. A, which implies that this sample is younger than that datum (0.83 Ma; Takayama and Sato, 1987). Other species recovered from Hole 793A include *G. oceanica*, *Calcidiscus leptoporus*, *Umbilicosphaera sibogae*, and *Coccolithus pelagicus*.

Hole 793B

Core 126-793B-1R was drilled through a diabase sill and is barren of calcareous nannofossils. We placed the interval from Sample 126-793B-2R-CC through -10R-CC in Zone CN4, given that *Sphenolithus heteromorphus* and *Calcidiscus macintyrei* are present. Samples 126-793B-11R-5, 85–87 cm, through -14R-CC occur below the first occurrence (FO) of *C. macintyrei* and above the FO of *S. heteromorphus*, and were assigned to Zone CN3. Other species present in these two zones are *Cyclicargolithus floridanus*, *Discoaster deflandrei*, and *Coccolithus pelagicus*. *Sphenolithus belemnos* occurs with *S. heteromorphus* in Sample 126-793B-14R-1, 42–44 cm, which is evidence that this sample is near the base of Zones CN3–CN4.

Samples 126-793B-15R-3, 1–2 cm, through -18R-4, 23–25 cm, do not contain *S. heteromorphus* or *S. belemnos*, and lie above the FO of *Discoaster druggii* in Sample 126-793B-18R-4, 23–25 cm. Therefore, we assigned this interval to Zone CN1c. The absence of *S. belemnos* in this section implies that Zone CN2 is missing and that a hiatus occurs between Samples 126-793B-14R-CC and -15R-3, 1–2 cm. Other species present in Zone CN1c are *C. floridanus*, *D. deflandrei*, and *Reticulofenestra bisecta*. *R. bisecta* may be reworked in this interval.

Samples 126-793B-18R-CC through -20R-CC are barren. Samples 126-793B-21R-CC and below contain typical Oligocene assemblages, including *R. bisecta*, *C. floridanus* and *D. deflan-*

drei; in the absence of exclusively Miocene species, we consider these assemblages to be of Oligocene age. Because of the rare and sporadic occurrences of the index species *Sphenolithus ciperoensis* and *Sphenolithus distentus* in the Oligocene interval, the zonal boundaries are tentative. We placed Samples 126-793B-21R-CC through -30R-CC, which lie above the last occurrence (LO) of *S. distentus*, in Zone CP19b. The LO of *S. ciperoensis* is in Sample 126-793B-23R-CC. We assigned Samples 126-793B-31R-CC through -54R-CC to Zone CP19a, given the co-occurrence of *S. ciperoensis* and *S. distentus*. Samples 126-793B-55R-CC and -56R-CC are barren. The interval from Samples 126-793B-57R-3, 82-83 cm, through -81R-1, 86 cm, contains sporadic occurrences of *R. bisecta*, *C. floridanus*, *D. deflandrei*, *S. distentus*, and *Sphenolithus predistentus* and does not contain *S. ciperoensis*. Therefore, we tentatively placed this interval in Zones CP17-CP18. The occurrence of one questionable specimen of *Reticulofenestra umbilica* in Sample 126-793B-81R-1, 86 cm, may be a result of reworking. All samples examined below Sample 126-793B-81R-1, 86 cm, are barren of calcareous nannofossils.

Planktonic Foraminifers

Hole 793A

Minute juvenile planktonic foraminifers and specimens of *Globigerina quinqueloba* are present in Samples 126-793A-1H-1, 0-2 cm, and -1H-1, 2-5 cm, which consist predominantly of volcanic ash. Zonal markers were not observed in these samples. Sample 126-793A-1H-1, 6-8 cm, is similar to the previous samples, but several additional adult planktonic foraminifers are present, including *Globorotalia inflata*, *Globigerinoides ruber*, *Globigerinoides trilobus*, dextral and sinistral *Globigerina pachyderma*, *Globigerinoides tenellus*, *Globigerinita glutinata*, and *Orbulina universa*. Zonal markers are not present in this sample. *Globorotalia truncatulinoides* is abundant in Sample 126-793A-3H-4, 0 cm, in addition to the species present in the samples above. Rare specimens of *Globorotalia tosaensis* are also present in this core. The overlap of these two species ranges between 0.2 and 1.8 Ma in the subtropical Northwest Pacific (Keller, 1979). Other Pleistocene species present in Sample 126-793A-3H-4, 0 cm, are sinistral *Globorotalia menardii*, sinistral *Globorotalia tumida*, and *Globigerina calida*, placing this sample in Zone N23 (sensu Blow, 1969).

Samples 126A-793A-5H-3, 2-4 cm, and -5H-CC contain *G. inflata*, *G. tosaensis*, *Globigerina hexagona*, and other long-ranging taxa. The absence of *G. truncatulinoides* assigns these samples to the zonal range of *G. tosaensis* (>0.2 Ma and <2 Ma; Keller, 1979). Sample 126-793A-7H-3, 60-65 cm, contains *G. inflata* and *G. tosaensis-truncatulinoides*. The absence of *G. truncatulinoides* s.s. places this sample in the zonal range of *G. tosaensis* (Keller, 1979). Sample 126-793A-7H-CC consists mainly of volcanic ash. Zonal markers were not observed in this sample. Sample 126-793A-9H-CC contains *G. tosaensis*, *Globorotalia crassaformis hessi*, and a primitive form of *G. tumida*; we assigned this core to the zonal range of *G. crassaformis hessi* (Keller, 1979; Fig. 43). Samples 126-793A-10H-2, 102-104 cm, and -11H-CC contain mainly volcanic ash. Planktonic foraminifers are similar to those found in Sample 126-793A-9H-CC. We placed these samples in the zonal range of *Globorotalia crassaformis hessi*.

The abundance and preservation of foraminifers ranges from very abundant to rare and good to moderate, respectively.

Hole 793B

Samples 126-793B-2R-1, 36-38 cm, -2R-1, 64-65 cm, and -2R-CC, are dominated by *Globoquadrina venezuelana*, *Globoquadrina dehiscens*, *Globigerinoides immaturus*, *Globorotalia scitula*, *Sphaeroidinellopsis disjuncta*, *Globorotalia peripheronda*, and *Catapsydrax parvula*. They were placed in Zone N10. Samples 126-793B-8R-1, 60-62 cm, and -8R-CC contain *Globigerina continuosa* and *Globigerina drury*, in addition to the species mentioned above, and were assigned to Zone N10.

Globoquadrina venezuelana, *G. dehiscens*, *G. scitula*, *Globorotalia praescitula*, and *S. disjuncta* are present in Samples 123-793B-9R-2, 64-65 cm, and -9R-3, 61-62 cm. The overlap of *G. scitula* with *G. praescitula* places this sample in Zone N9 (Bolli et al., 1985). One specimen of *Globorotalia foshi lobata* was found in Sample 126-793B-9R-1, 60-65 cm. The stratigraphic range of this species spans the N11/12 boundary (Berggren et al., 1985), and its presence in this sample remains anomalous.

Samples 126-793B-12R-2, 46-49 cm, and -12R-2-CC, contain *S. disjuncta*, *Globigerina continuosa*, *Globoquadrina altispira*, *Catapsydrax parvula*, and others, and were assigned to Zone N9.

Sample 126-793B-16R-CC contains a few broken, flattened, and deformed specimens, tentatively identified as *Catpsydrax* sp., a minute globorotalid, and two specimens of *Chiloguembelina cubensis*, the range of which is late Eocene-mid-Oligocene. This sample may contain reworked faunas.

Minute benthonic calcareous and planktonic foraminifers, including juvenile specimens of *Catapsydrax* sp., are present in Sample 126-793-17R-4, 59-60 cm. These sediments may have been redeposited by a turbidity current. We cound not assign an age to this sample. Sample 126-793B-31R-2, 93-95 cm, contains specimens of *C. cubensis*, *Globigerina praebulloides*, and *Globigerina* sp. cf. *G. venezuelana*, and was tentatively placed in Zone "N4" (sensu Berggren et al., 1985). Sample 126-793B-52R-2, 33-35 cm, contains a recrystallized specimen of *Globigerina ampliapertura* and one specimen of *Globoquadrina pseudovenezuelana*. The ranges of both these species is late Eocene to early Oligocene. This sample is tentatively assigned to Zones "N4"/P21 (Berggren et al., 1985). Sample 126-793B-74R-1, 5-7 cm, contains one large broken globigerinid that we could not identify at the species level.

The abundance and preservation of specimens ranges from barren to abundant and from poor to good, respectively.

Benthic Foraminifers

Tertiary strata at Site 793 may be subdivided biostratigraphically into seven zonules on the basis of benthic foraminifers (Fig. 43). We estimated depositional water depths mainly on the basis of a comparison of (1) Holocene and Quaternary benthic foraminifer data from Holes 792B (1798 mbsl), 790A (2222 mbsl), 790B (2223 mbsl), 791A (2268 mbsl), 793A (2975 mbsl), and 787B (3254 mbsl) (see "Biostratigraphy" sections in other site chapters, this volume); (2) Pleistocene strata from offshore Shizuoka and Shikoku, Japan (Akimoto, 1989; Yasuda, 1989); and (3) Cenozoic benthic foraminifer data (Ingle, 1980; Woodruff, 1985; van Morkhoven et al., 1986) for the Miocene and Oligocene strata. We determined the age of each zonule on the basis of calcareous nannofossil zonations in this chapter.

The seven assemblage-zonules are as follows:

1. *Rhabdammina* spp.-*Thalmannammina*? sp. Assemblage Zonule

Characteristic species: deep-water agglutinated foraminifers such as *Rhabdammina* spp., *Thalmannammina*? sp., and *Haplophragmoides* sp. from mudstones and reworked larger inner neritic benthic foraminifers from coarse sandstone

Abundance: few agglutinated foraminifers; larger foraminifers are rare in Cores 126-793B-72R through -67R and common in Cores 126-793B-66R through -64R

Samples: 126-793B-67R-1, 2-4 cm, -73R-CC, and -74R-1, 5-7 cm, from mudstones

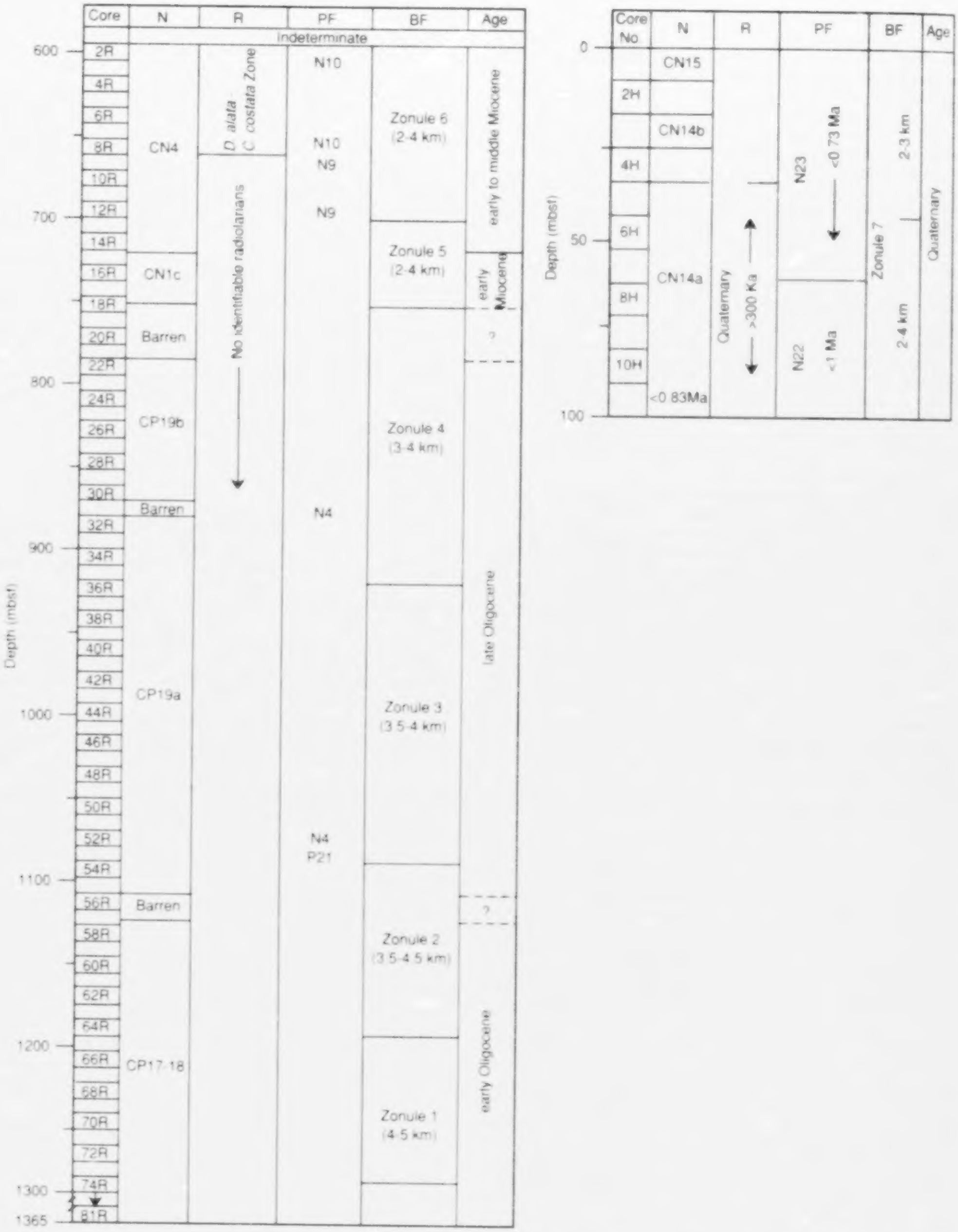

Figure 43. Biostratigraphic results from Site 793. N = calcareous nannofossils, R = radiolarians, PF = planktonic foraminifers, BF = benthic foraminifers.

Age: late early Oligocene

Depositional water depth: between 4 and 5 km

Remarks: This zonule is characterized by primitive agglutinated foraminifers and the absence of calcareous foraminifers. These benthic foraminifers show depositional water depths below the CCD. Larger foraminifers from sandstones may be reworked from an inner neritic zone to abyssal depths.

2. *Rhizammina* sp.-*Marginulina*? sp. Assemblage Zonule

Characteristic species: *Rhizammina* sp., *Marginulina*? sp., *Rhabdammina* sp., *Thalmannammina*? sp., *Haplophragmoides* sp., and *Nodosaria* sp. A

Abundance: few

Samples: from 126-793B-53R-CC through -61R-CC

Age: late early-early late Oligocene

Depositional water depth: between 3.5 and 4.5 km

Remarks: This assemblage zonule is composed of primitive agglutinated foraminifers and primitive calcareous foraminifers. This assemblage indicates depositional water depths near the carbonate compensation depth (CCD).

3. *Stilostomella* sp.-*Nodosaria* sp. A Assemblage Zonule

Characteristic species: *Rhizammina* sp., *Stilostomella* sp., *Nodosaria* sp. A., *Glomospira gordialis, Reophanus oviculus, Rhabdammina* sp., *Labrospira* sp., *Trochammina* sp. and *Pleurostomella* spp.

Abundance: few

Samples: 126-793B-36R-2, 108-111 cm, through -52R-2, 33-35 cm

Age: early late Oligocene

Depositional water depth: between 3.5 and 4 km

Remarks: This assemblage, which consists of primitive agglutinated foraminifers and primitive calcareous foraminifers plus *Stilostomella* sp. and *Pleurostomella* sp., shows depositional water depths above the CCD.

4. *Rhabdammina* spp.-*Oridorsalis umbonatus* Assemblage Zonule

Characteristic species: *Rhabdammina* spp., *Rhizammina* sp., *Stilostomella* spp., *Thalmannammina*? sp., *Gyroidinoides* sp., *Oridorsalis umbonatus, Pullenia* spp., *Reophax* spp., and *Glomospira gordialis*

Abundance: few; common in Samples 126-793B-35R-CC and 35R-3, 109-111 cm

Samples: 126-793B-18R-3, 102-104 cm, through -35R-CC

Age: late Oligocene

Depositional water depth: between 3 and 4 km

Remarks: The zonule is marked by the occurrence of primitive agglutinated foraminifers, *Stilostomella* spp., plus deep-sea trochospiral and planispiral calcareous forms such as *Oridorsalis umbonatus, Gyroidinoides* sp., and *Pullenia* spp.

5. *Cibicidoides* spp.-*Rhizammina* sp. Assemblage Zonule

Characteristic species: *Stilostomella* spp., *Cibicidoides* spp., *Globocassidulina subglobosa, Rhizammina* sp., *Oridorsalis umbonatus, Pullenia bulloides, Gyroidinoides* sp., *Pullenia* spp., *Pleurostomella* spp., *Anomalinoides* spp., *Rhabdammina* sp., *Bulimina grata*, and *Eggerella* sp.

Abundance: abundant in Samples 126-793B-17R-4, 59-60 cm, and -16R-CC; few in Samples 126-793B-16R-1, 70-72 cm, and -12R-CC

Samples: 126-793B-12R-CC through -17R-4, 59-60 cm

Age: early Miocene

Depositional water depth: between 2 and 4 km

Remarks: This zonule is characterized by the fauna from the subjacent zonule and the dominance of calcareous foraminifers such as *Pullenia bulloides, Cibicidoides* spp., *Anomalinoides* spp., and *Globocassidulina subglobosa*. Complex agglutinated foraminifers such as *Vulvulina* sp. and *Eggerella* sp. have their FO in this zonule.

6. *Stilostomella* spp.-*Pullenia bulloides* Assemblage Zonule

Characteristic species: *Stilostomella* spp., *Oridorsalis umbonatus, Pullenia bulloides, Globocassidulina subglobosa, Gyroidinoides* spp., *Anomalinoides* spp., *Cibicidoides* spp., *Pullenia* spp., and *Chrysalogonium* sp.

Abundance: common below Sample 126-793B-8R-1, 60-62 cm; few above Sample 126-793B-7R-CC.

Samples: 126-793B-2R-1, 36-38 cm, through -12R-2, 46-49 cm

Age: late early-early middle Miocene

Depositional water depth: between 2 and 4 km.

Remarks: This zonule is characterized by the fauna from the subjacent zonule without primitive agglutinated foraminifers genera such as *Rhizammina, Rhabdammina*, and *Bathysiphon*.

7. *Pullenia bulloides*-*Melonis barleeanus* Assemblage Zonule

Characteristic species: *Pullenia bulloides, Melonis barleeanus, Epistominella exigua, Melonis pompilioides, Oridorsalis umbonatus, Cibicidoides wellerstorfi, Sphaeroidina bulloides, Pyrgo murrhina, Tosaia hanzawai*, and *Uvigerina proboscidea*.

Abundance: abundant

Samples: 126-793A-3H-4, 0-2 cm, through -11H-CC

Age: Pleistocene

Depositional water depth: between 2 and 4 km below Sample 126-793A-7H-3, 60-65 cm; between 2 and 3 km above Sample 126-793A-5H-CC, as determined by presence of *Uvigerina proboscidea*, etc.

Radiolarians

Hole 793A

We examined all core-catcher samples from this hole. Quaternary radiolarians are present in all samples except 126-793A-2H-CC and -8H-CC. The occurrence of *Druppatractus aquilonius* in and below Sample 126-793A-3H, 0 cm, indicates an age >300 Ka for samples at and below this level (Foreman, 1981).

Hole 793B

Rare, moderately preserved radiolarians are present in Sample 126-793B-2R-CC and Samples 126-793B-4R-CC through -8R-CC. The presence of *Cyrtocapsella tetrapera* and *Stichocorys wolffii* in these samples suggests assignment to the late early to early middle Miocene *Calocycletta costata* or *Didymocyrtis alata* zones. No identifiable faunas were found in, or below, Sample 126-793B-9R-CC. Radiolarians are present in many samples, but they are typically infilled and have suffered extreme dissolution.

Summary

Radiolarians, calcareous nannofossils, and planktonic foraminifers indicate a Quaternary age for all cores from Hole 793A (Fig. 43). A maximum age of no greater than 0.83 Ma is indicated from nannofossil data. Calcareous nannofossils, radiolarians, and planktonic foraminifers indicate an early middle to late early Miocene age range for samples down to the level of Sample 126-793B-14R-CC in Hole 793B. A possible hiatus occurs between Samples 126-793B-14R-CC and -15R-3, 1-2 cm, below which early Miocene (Zone CN1c) nannofossils occur. The hiatus is equivalent to nannofossil Zone CN2 (approximately 1.9 m.y. duration).

We could not determine an age for the interval between Samples 126-793B-18R-CC and -20R-CC. Biostratigraphic data are insufficient to determine whether or not there is a hiatus at this level. Below Sample 126-793B-21R-CC nannofossils and rare planktonic foraminifers indicate late Oligocene (Zone CP19b) through late early Oligocene ages (Zones CP17-18). Reworked upper Eocene planktonic foraminifers may indicate the age of the source area for detrital sediments.

Benthic foraminifer faunal changes show shallowing water depths from 4–5 km in the early Oligocene to 2–3 km at present. As the present water depth is 3 km, this estimate means that 1–2 km shallowing of the sea floor, and 0.3–0.7 km of total basement uplift has occurred since about 32 Ma.

PALEOMAGNETICS

Introduction

We made magnetic measurements on the archive halves of all but the first two cores (coarse gravels) from Hole 793A and on all sediment cores from Hole 793B. Below Core 126-793B-82R, we measured only selected core sections or cores containing possible lava flows because many of the lower cores consisted of coarse volcanic breccia. We also carried out stepwise alternating field (AF) demagnetizations on selected discrete samples (in the form of 7 cm^3 cubes from Hole 793A and 10-cm^3 minicores) from Hole 793B, employing the fully automatic spinner (FAS) (see "Explanatory Notes" chapter, this volume). In some cases, we used the Schonstedt AF demagnetizer in conjunction with the FAS instrument to extend discrete sample demagnetization beyond 50 mT. The results from discrete sample analysis (Fig. 44) show that a stable magnetization component is dominant in most of the cores and confirm the reliability of the results from archive halves.

Although core sections were not stored in the core rack in the core cutting room, natural remanent magnetization (NRM) declinations below Core 126-793B-24R nevertheless exhibited a strong tendency to cluster at 0° or 360°, whereas in some cases the inclinations systematically became more positive with increasing depth within the core (see "Paleomagnetics" section, "Site 792" chapter, this volume). This was a particular problem for cores from the lower parts of the hole (Fig. 45). During sawing, the cores were deliberately rotated 180° from their normal orientation several times. However, this did not consistently alter the direction of declination clustering. In most cases, AF demagnetization to 15 mT was effective in removing much of this remanence contamination; but, in some instances (e.g., Cores 126-793B-76R through -82R, 1305–1375 mbsf), it had little effect. Only ~30% of the discrete samples from cores with archive half declinations clustered at 0° or 360° exhibited similar biased declinations. The remaining discrete samples had NRM declinations significantly different from their archive halves. This suggests that the precautions taken in storing the cores may have been of some benefit. However, an additional (and as yet unidentified) source of magnetic contamination remains.

Magnetostratigraphy

Hole 793A

Figure 46 shows the declination and inclination data for the archive halves of the cores from Hole 793A. We have filtered highly scattered data from cores severely disturbed by drilling, or consisting of coarse-grained material, out of this plot for the sake of clarity. The < 1-Ma paleontologic age determination for all cores from Hole 793A (see "Biostratigraphy" section, this chapter) allows us to label the normal-to-reverse polarity change in Core 126-793A-9H-3 (75.4 mbsf) as the Brunhes-Matuyama reversal. The short normal polarity interval in Core 126-793A-10H (beginning at ~81 mbsf) is tentatively identified as the Jaramillo Polarity Zone. A short reversed zone of magnetization in Core 126-793A-6R-1 (42.4–43.0 mbsf), the existence of which was confirmed by discrete sample AF demagnetization, may correspond to a reversed polarity event at ~0.5 Ma reported in rapidly deposited glacial loess deposits in eastern Europe (Champion et al., 1988).

Hole 793B

Figure 47 summarizes the magnetostratigraphy of the cores from Hole 793B. Below Core 126-793B-25R, core sections composed of coarse-grained sediment types (i.e., sandstones and clastic debris flows) displayed high (~50°) inclinations and normal polarities after AF demagnetization, even for intervals where the finer grained sediment types displayed reversed polarities. Because this probably represents a recently acquired viscous magnetization, we have filtered these core sections out of the composite figure. In addition, we have also deleted cores displaying persistent clustering of declinations at 0° and 360°, or those from which discrete samples exhibited intermediate or contradictory polarities after high AF demagnetization.

Because paleontologic evidence indicates a late early to middle Miocene age for the first 14 cores of Hole 793B (see "Biostratigraphy" section, this chapter), we tentatively assigned the long reversed interval represented by Cores 126-793B-2R through -8R (595–660 mbsf) as reversed Chron C5B (Berggren et al., 1985), with the normal sill in Core 126-793B-1R probably representing the normal part of the same chron. Thus, the following sequences of mostly normal-polarity (660–690 mbsf) and mostly reversed-polarity cores (690–718 mbsf) would correspond to Chron C5C, normal and reversed, respectively. A depositional hiatus or unconformity near the top of Core 126-793B-15R is directly followed by a sequence of tightly spaced, multiple reversed- and normal-polarity zones (720–750 mbsf), probably representing the C6 reversed through C6A or C6B polarity chrons (Fig. 47A). This is consistent with the 20.5–23.2 Ma paleontological age assignment for this interval (see "Biostratigraphy" section, this chapter).

Low sedimentation rates, as indicated by a paucity of volcanic input and a barren interval (see "Lithostratigraphy and Accumulation Rates" section, this chapter) may account for the apparent compressed section represent[illegible], Cores 126-793B-19R and -20R, as the succeeding cores [illegible] characterized by a late Oligocene paleontologic assemblage (see "Biostratigraphy" section, this chapter).

The long normal and reversed polarity zones distributed over Cores 126-793B-21R through -85R (the last sedimentary core before basement) can be correlated with Chrons C8 through C10 in Figure 47 (B–D), which represent a time period of ~4 m.y. The mixed polarities in the sedimentary cores below 1320 mbsf almost certainly reflect incomplete removal of the present-field normal component of magnetization in the coarser grained rock types, rather than field reversals. The underlying volcanic breccia and flows are predominantly of normal polarity, but with an apparent reversed flow (recognized only after discrete sample analysis) in Core 126-793B-104R. This sequence likely represents the C11 normal polarity chron (assuming that no major hiatus or unconformity exists between the sediment and basement), with the reversed flow at ~1580 mbsf corresponding to the short reversed polarity zone at 31.6 Ma (Fig. 47D).

We correlate the reddish, carbonate-rich claystone in Cores 126-793B-16R and -17R, centered at ~740 mbsf (see "Lithostratigraphy and Accumulation Rates" section, this chapter) with a similar carbonate zone occurring in Core 126-792E-27R, as both encompass a short zone of reversed polarity (Chron C6A?). Unlike the multiple polarity zones that characterize the basement rocks at Site 792, the extrusive units at the base of Site 793 appear to represent a simpler normal-reverse-normal polarity sequence.

Table 5 summarizes the datums derived from the best determined polarity chron boundaries in the preceding discussion.

Paleolatitude

Despite scatter in the data, and a distinct variation between inclinations associated with normally and reversely magnetized

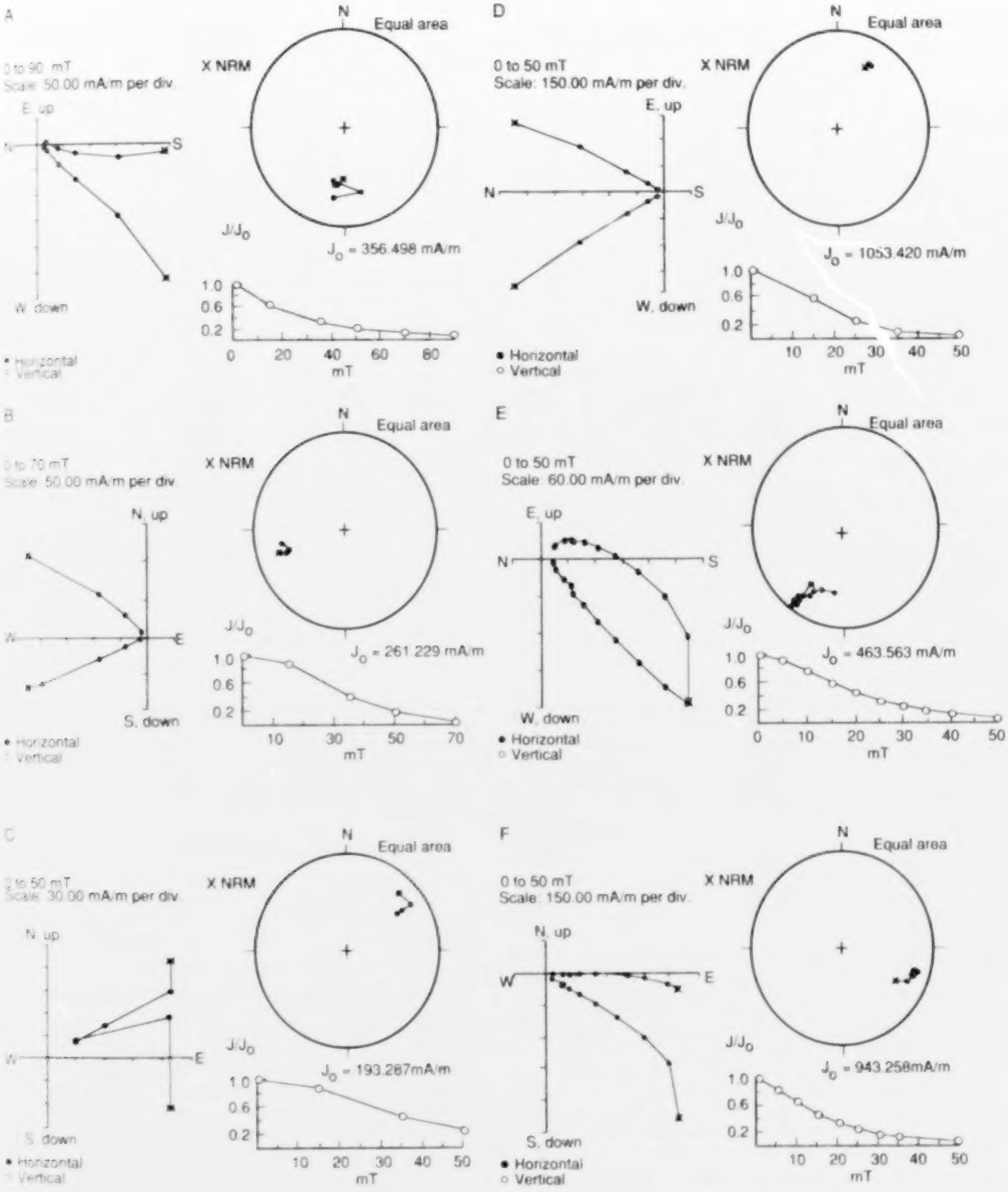

Figure 44. Examples of orthogonal directions, changes of remanence vector direction, and total intensity during stepwise AF demagnetization for discrete sedimentary and igneous rock samples. Numerical values of remanence intensity and inclination for these samples are given in Table 5. **A.** Sample 126-793B-35R-3, 102 cm. **B.** Sample 126-793B-71R-2, 135 cm. **C.** Sample 126-793B-74R-1-15 cm. **D.** Sample 126-793B-92R-3, 11 cm. **E.** Sample 126-793B-104R-1, 118 cm. **F.** Sample 126-793B-110R-2, 68 cm.

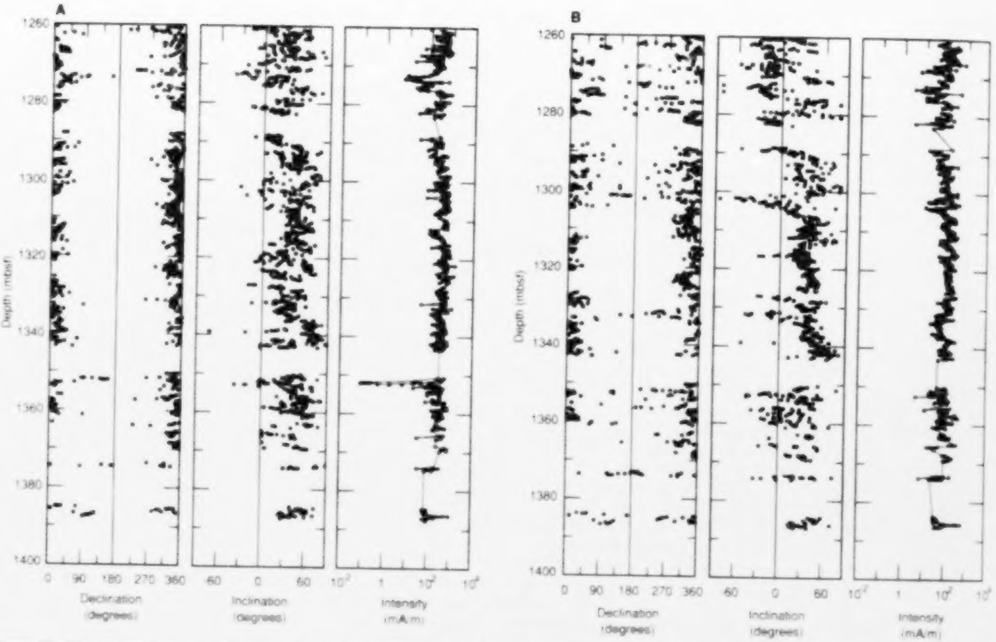

Figure 45. Comparison between paleomagnetic results for Cores 126-793B-71R to -84R. **A.** Before AF demagnetization. **B.** After AF demagnetization.

core intervals, the mean inclinations of the various archive halves and discrete samples suggest a progressive decrease from ~40° in the middle Miocene (represented by the top of Hole 793B) to near 30° for the middle Oligocene sediments (directly above basement) (Fig. 48). Inclination data from cores that exhibit low directional scatter near the bottom of Hole 793B, including both sedimentary and igneous rock types (archive halves, Fig. 49; discrete samples, Table 6) support the idea that this site was situated at a significantly lower latitude in mid-Oligocene time. This result is consistent with DSDP results from the West Philippine Basin (as summarized in fig. 3 of Seno and Maruyama, 1984), which also suggests ~15° of northward translation since the middle Oligocene.

The directional inconsistency between the data of normal and reversed polarities in the Oligocene (Fig. 48) probably results from incomplete removal of the secondary viscous remanence caused by the present geomagnetic field. Although the maximum field intensity of AF demagnetization of archive halves is limited by ODP policy, this inconsistency may be eliminated by further shore-based demagnetization and measurement of additional discrete samples. Paleomagnetic evidence for or against progressive azimuthal rotation of this site should also be forthcoming, following shore-based paleomagnetic measurement of discrete samples and processing of FMS data.

Reversal Studies

The use of the multishot tool in Hole 793A enabled us to recover an azimuth-corrected reversal record of the Brunhes-Matuyama polarity transition (Fig. 50). Unfortunately, the sediment immediately above and below the reversal interval was watery and highly disturbed by the drilling process. Therefore, the discrete samples taken across this zone did not produce a usable detailed record of the geomagnetic field behavior during the time of the reversal. However, as at the previous sites, the inclination data suggest two rapid polarity reversals, although part of the second inclination reversal is missing between Sections 126-793A-9H-3 and -9H-4 (75.4 mbsf).

IGNEOUS PETROLOGY

This section describes the three main occurrences of igneous rocks in Hole 793B: (1) a diabase that intrudes middle Miocene sedimentary rocks, (2) volcanic clasts throughout the sedimentary sequence, and (3) the basement lava flows and breccias.

Olivine Diabase Intrusion

A total of 3.65 m of an olivine-diabase (lithologic Unit II) was penetrated in the first rotary core (126-793B-1R) of Hole 793B (586.5 mbsf). The approximate thickness of the diabase inferred from the drilling log is 4.5 m (90% recovery; Fig. 51). The diabase is directly overlain by 15 cm of epidote-carbonate-rich silicified sediments (Core 126-793B-1R; Fig. 52) that contain small bubbles and 5-mm pieces of diabase. The epidote and bubbles in the sediment are evidence for baking by the intrusion. The underlying sediments are middle Miocene in age, yielding a maximum age for the intrusion. The basal contact with the sediments was not recovered, but petrographic features of the lowest diabase indicate that its lower chilled margin was recovered. The diabase is of normal polarity, whereas the underlying sediments are reversed (see "Paleomagnetism" section, this chapter). The measured sonic velocity values of the intrusion are in the range of 5.00–5.14 km/s, whereas in the underly-

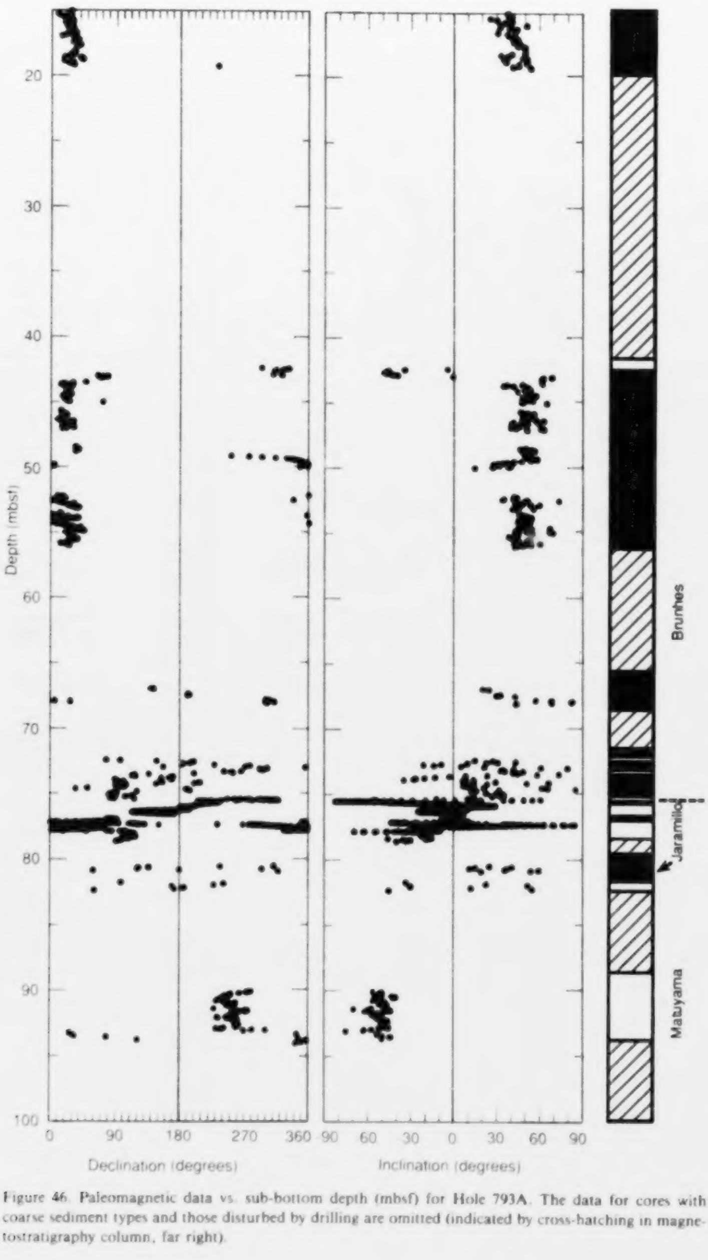

Figure 46. Paleomagnetic data vs. sub-bottom depth (mbsf) for Hole 793A. The data for cores with coarse sediment types and those disturbed by drilling are omitted (indicated by cross-hatching in magnetostratigraphy column, far right).

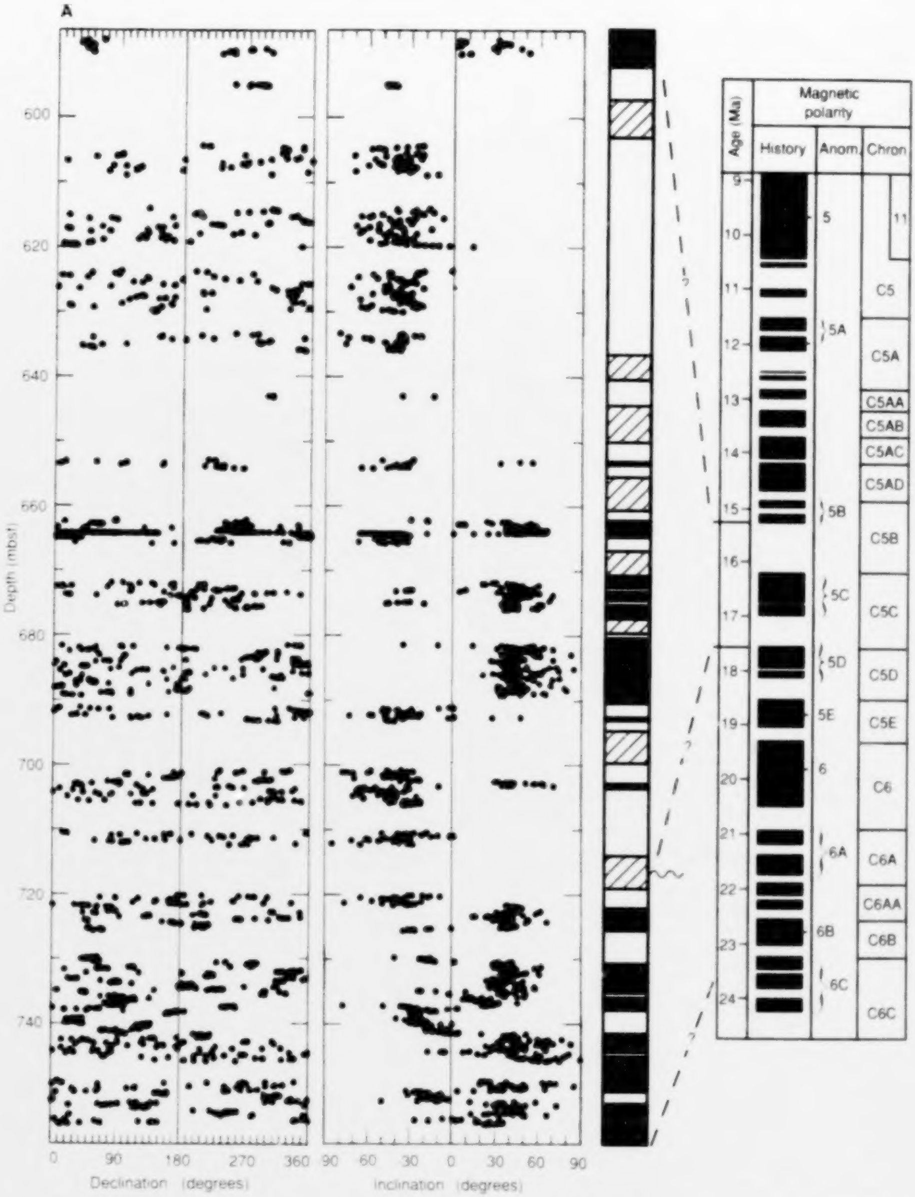

Figure 47. **A.** Paleomagnetic data vs. sub-bottom (mbsf) for Cores 126-793B-1R through -18R and correlation with the standard polarity time scale (Berggren et al., 1985). Cores with coarse sediment types and those disturbed by drilling are omitted (indicated by cross-hatching in magnetostratigraphy column, far right). Wavy lines beside the polarity column indicates hiatus/unconformity horizons estimated from biostratigraphic data (see "Biostratigraphy" section, this chapter). **B.** Data from Cores 126-793B-19R through -39R. **C.** Data from Cores 126-793B-40R through -61R. **D.** Data from Cores 126-793B-62R through -85R.

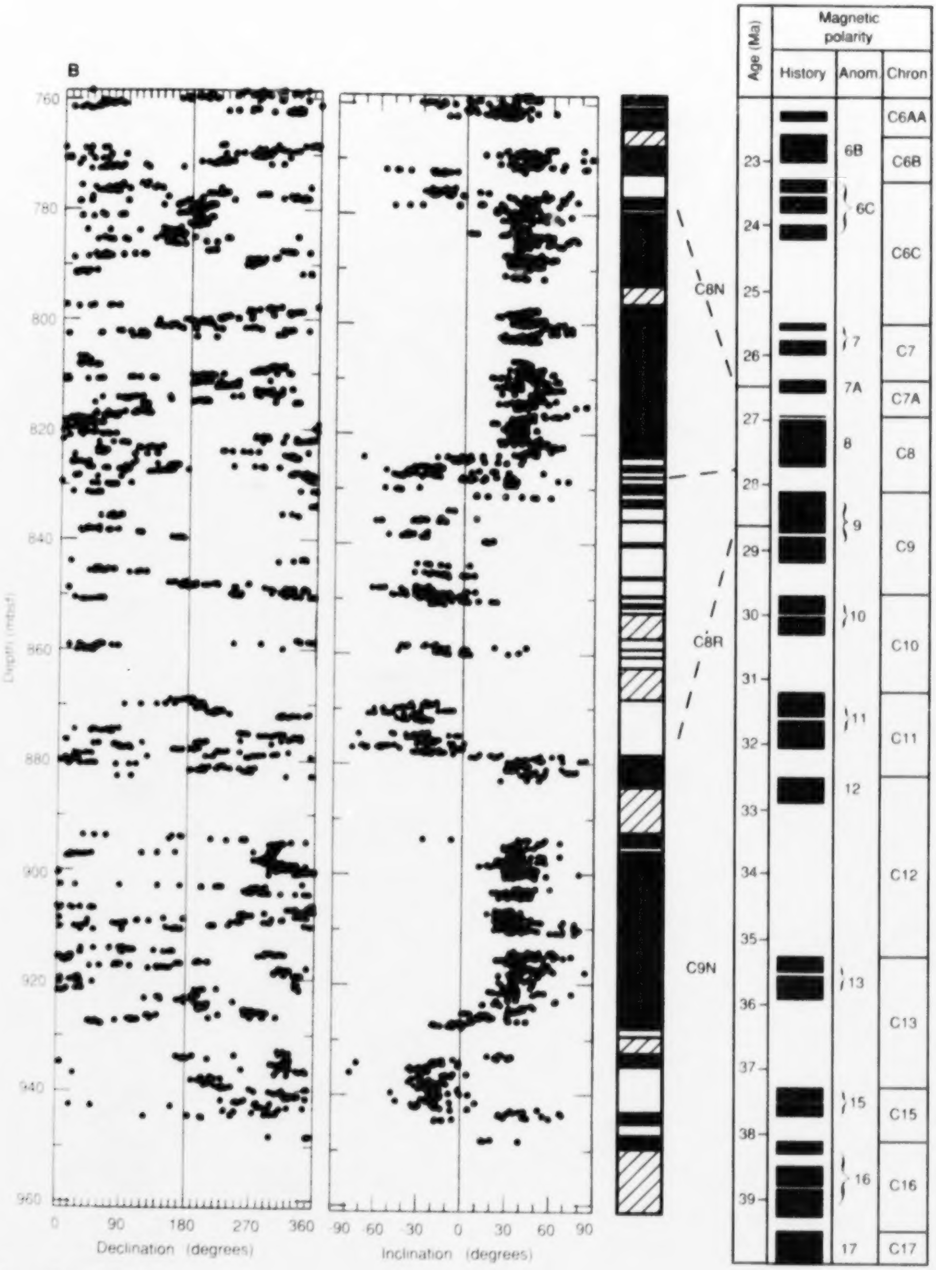

Figure 47 (continued).

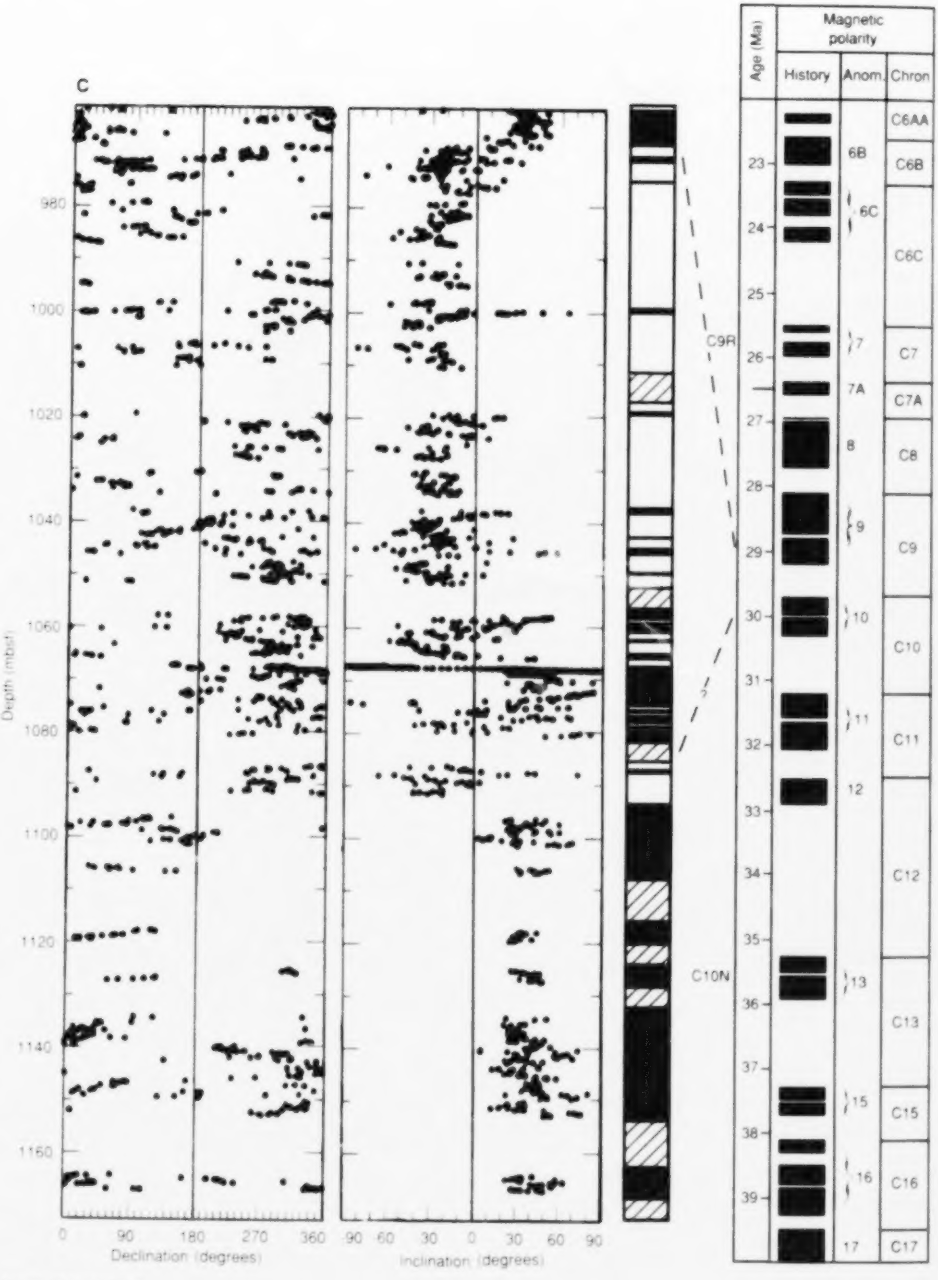

Figure 47 (continued).

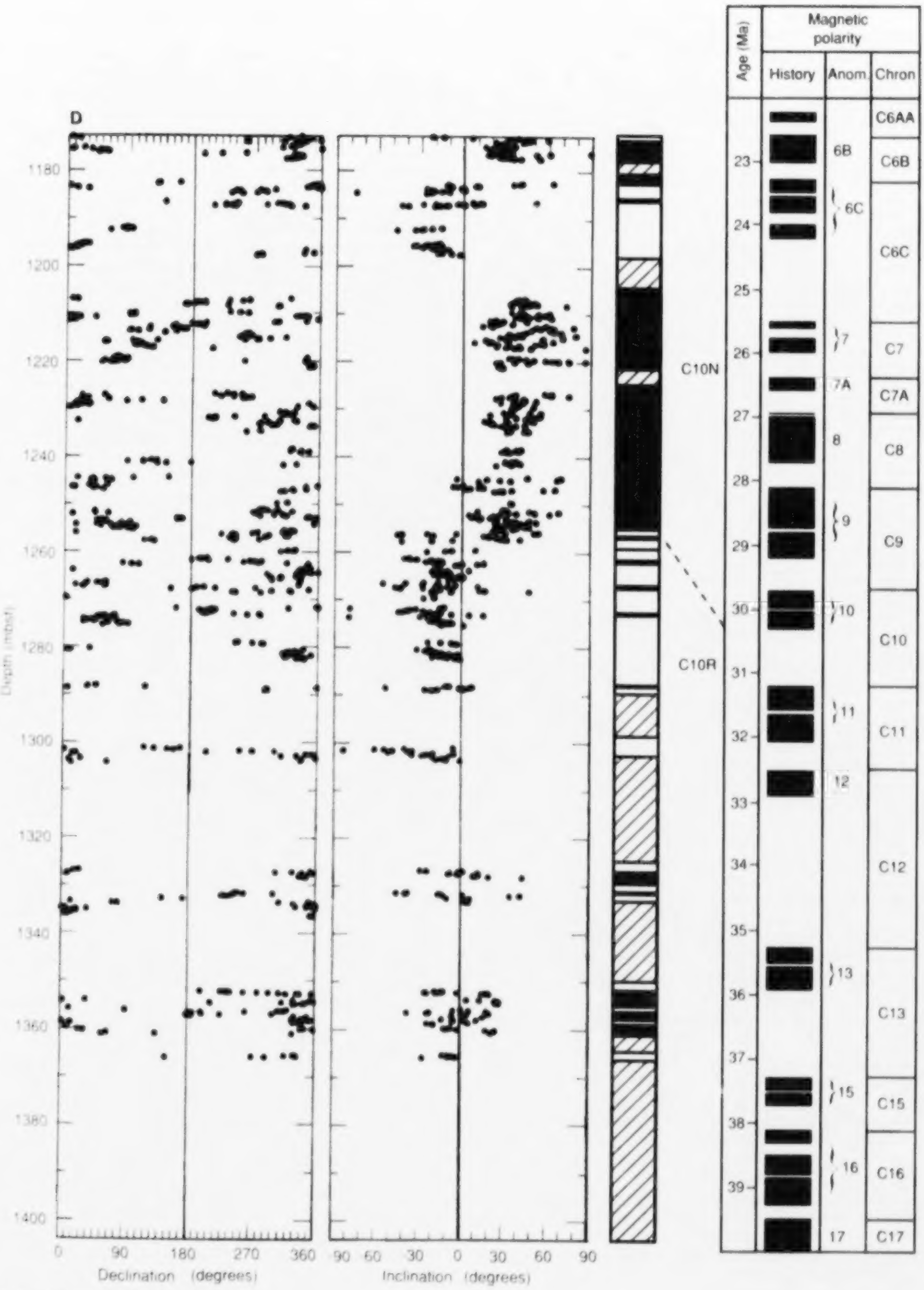

Figure 47 (continued).

Table 5. Datums derived from the polarity chron boundaries judged as most reliable in Site 793.

Age (Ma)	Chron	Depth (mbsf)
0.73	1-2	75.4-77.2
0.91	Jaramillo	80.5-88.1
15.27	C5B	594.7-603.8
16.22	C5C	662.3-668.1
21.71	C6A	737.0-737.5
21.90	C6AA	741.3-742.7
26.86	C8	776.6
27.74	C8	824.1-824.4
28.15	C9	878.1-878.7
29.21	C9	967.9
29.73	C10	1095.7-1099.9
30.09	C10	1102.8-1107.3
30.33	C10	1255.5

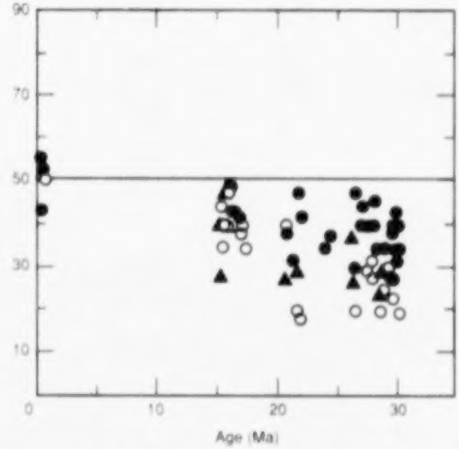

Figure 48. Mean inclinations for archive halves and discrete samples (mean value per core) vs. age for Site 793. Solid and open circles represent normal and reversed intervals, respectively. Triangles represent discrete samples. Horizontal line shows the inclination value of the axial geocentric dipole field for the present latitude of this site.

ing sediments they are much lower, 2.03 km/s; (see "Physical Properties" section, this chapter).

The differences in density and porosity between the intrusion and the underlying sediments are also striking (porosity = 9%-12% vs. 64% in the underlying sediments; density = 2.7 g/cm^3 vs. 1.78 g/cm^3 in the underlying sediments; see "Physical Properties" section, this chapter). The intrusion is too thin to be resolved by MCS profiles, so its lateral extent is unknown. The difference in magnetic polarity between the diabase and the underlying sediments, the contrast of the textures between the upper and lower margins of the unit, and the presence of a thermal contact with the overlying sediments provide evidence that this unit is intrusive. However, on the basis of the textural and structural evidence from the intrusive, we cannot conclude whether it is a concordant or discordant feature.

Petrographic Description

Minerals in the groundmass of the olivine-diabase are fresh, in contrast with the interstitial glass and olivine phenocrysts, which are altered to smectites. The top (Sections 126-793B-1R-1 through -1R-2, 60 cm) of the intrusion is fine grained with few glomeroporphyritic clots, whereas the middle to lower part (Interval 126-793B-1R-2, 60 cm, to -1R-3) has large (5-10 mm) subspherical dark inclusions and larger, more abundant, crystal clots (Fig. 53). The base of the unit is characterized by the presence of large olivine, clinopyroxene, orthopyroxene, and pseudomorphosed olivine phenocrysts in a fine-grained glassy groundmass, implying accumulation at a chilled margin (Fig. 54).

Subparallel, subhorizontal, dark-colored glassy bands (3-10 mm thick) are present at about 10-cm intervals in the intrusion. They are formed, like the subspherical inclusions, of a more vesiculated and finer grained material. These glassy bands or inclusions include quenched clinopyroxene and plagioclase crystals, abundant opaque minerals (up to 10%), and vesicles. The dark color is caused by the presence of smectites that fill the vesicles and replace the glass. These bands and inclusions probably represent more differentiated melts, squeezed during cooling into thermal contraction cracks of the intrusion by a filter-press process. The inclusions sometimes are tadpole shaped, tapering downward, with vesicles at the top. This particular example may have formed from more hydrous magma than mid-ocean ridge basalt (MORB).

Three thin sections from the upper, middle, and lower parts of the sill are representative of the recovered material and show the textural differences within this diabase (Fig. 54). The upper part consists of subhedral olivine phenocrysts altered to smectites in an intersertal to intergranular groundmass of subhedral zoned plagioclase laths, subhedral clinopyroxene, subhedral orthopyroxene, and opaque minerals. Point counting on thin section Sample 126-793B-1R-1, 102-104 cm, produced the following modal proportions: olivine pseudomorphs, 2.9%; plagioclase, 41%; clinopyroxene, 18.3%; orthopyroxene, <0.5%; opaque mineral, 4.2%; and glass, 33.8%.

The central part of the intrusion differs in that it has a greater abundance of olivine-clinopyroxene-orthopyroxene glomeroporphyritic aggregates in an intersertal groundmass containing clinopyroxene-plagioclase-opaque mineral. These clots are formed of olivine pseudomorphs of partly fresh orthopyroxene and fresh clinopyroxene. Also, the fine-grained inclusions are more abundant in this part of the intrusion (Fig. 51).

Finally, at the base of the unit is a 3-cm-thick vitrophyric layer with olivine-clinopyroxene-orthopyroxene glomeroporphyritic aggregates and isolated plagioclase phenocrysts, which represents the chilled margin. Subhedral olivine (~10% of the thin section), altered to smectites and calcite, is present either as isolated corroded phenocrysts (2 mm) or clustered with pyroxenes. In the aggregates, euhedrally zoned clinopyroxene crystals (up to 6 mm) exhibit multiple-style twinning and exsolution lamellae, and the orthopyroxenes are rounded crystals (3 mm) that are often surrounded by clinopyroxene. Tiny plagioclase laths (0.1 mm) are sometimes included in the orthopyroxene. Glass, altered to smectite, is caught in the glomeroporphyritic aggregates. These glomeroporphyritic aggregates (40% of the basal chilled margin) indicate accumulation. Finally, the cryptocrystalline groundmass (60%) includes abundant, small, quenched plagioclase and clinopyroxene microphenocrysts and crystallites. Rounded vesicles, 0.1 mm in diameter, are filled with smectites.

The crystallization sequence within the sill is inferred to be olivine, followed by orthopyroxene + clinopyroxene, followed by plagioclase, followed by the opaque mineral. The lack of the opaque mineral in the chilled margin and its abundance in the dark-colored inclusions and bands indicate that this is a late

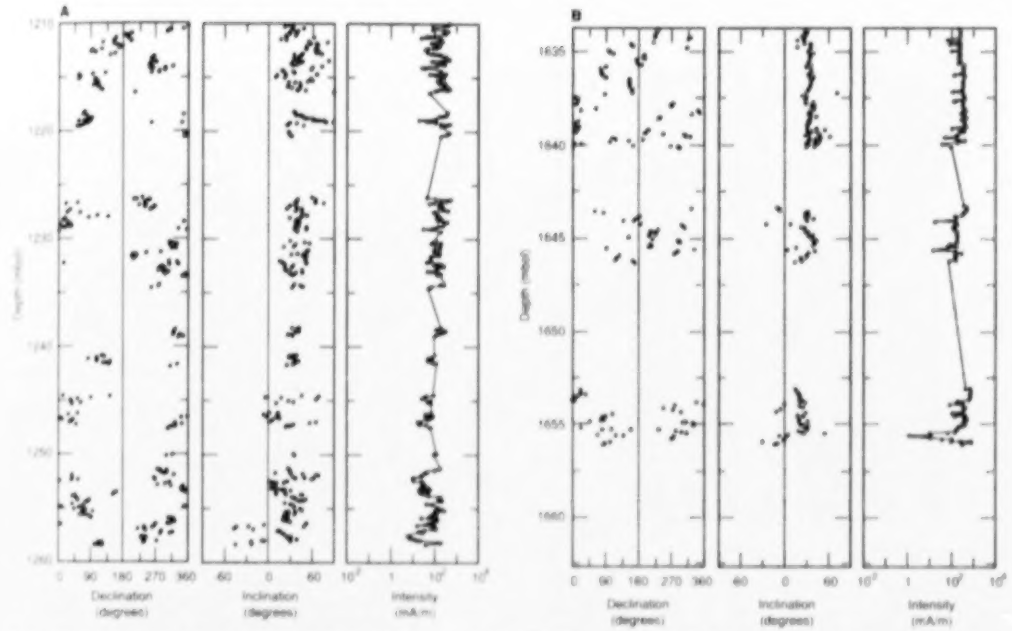

Figure 69. Paleomagnetic data vs. sub-bottom depth (mbsf). **A.** Cores 126-793B-66R through -70R. **B.** Cores 126-793B-110R through -112R.

Table 6. **Results from paleomagnetic analysis of discrete samples, Site 793.**

Core, section, interval (cm)	J(0)	Inc (0) (degrees)	Optimum AF (mT)	J(AF)	Inc (AF) (degrees)
126-793B					
Sediments					
33R-1, 102	356	+47.0	90	15.6	+30.0
71R-2, 136	261	−24.1	35	109	−31.0
74R-1, 15	191	+20.0	50	45	−33.0
Igneous rocks					
92R-1, 11	1050	+30.6	25	259	+28.2
104R-1, 110	464	+29.8	50	42	−31.5
110R-2, 68	943	+46.7	35	93	+31.2

Note: Abbreviations are as follows: J(0) = intensity of natural remanent magnetization (NRM); Inc (0) = inclination of NRM; Optimum AF = optimum field intensity of AF demagnetization; J(AF) = remanence intensity after optimum AF demagnetization; Inc (AF) = inclination after optimum AF demagnetization. Demagnetization characteristics of these samples are plotted in Figure 44.

crystallizing phase and, hence, that the diabase has a tholeiitic differentiation trend. The absence of plagioclase phenocrysts in glomeroporphyritic clots, despite its presence as phenocrysts in the chilled margin as well as its abundance in the groundmass, is striking and indicates hydrous conditions.

Volcanic Clasts in Units III, V, and VI

One basaltic pebble (Sample 126-793B-3R-1, 92–98 cm) was recovered in the lower to middle Miocene section (lithologic Unit III), which consists of siltstones and claystones (see "Lithostratigraphy and Accumulation Rates" section, this chapter). This basalt displays porphyritic intersertal texture with clinopyroxene and plagioclase phenocrysts often in glomeroporphyritic clots, within a groundmass of trachytic plagioclase laths.

Lithologic Unit V, a 600-m-thick lower to mid-Oligocene section, consists of granule- to fine-pebble conglomerate, vitric and/or pumiceous sandstones, siltstones, and claystones. The volcanic clasts consist of plagioclase-clinopyroxene-orthopyroxene andesite, hornblende-clinopyroxene dacite, intersertal basalt, and pumice. Plagioclase-clinopyroxene-orthopyroxene andesite (Sample 126-793B-32R-3, 125–128 cm, and Samples 126-793-56R-3, 75–76 cm, and -56R-3, 85–86 cm) is the most common type. This andesite has a porphyritic and/or fluidal texture with abundant phenocrysts of plagioclase (up to 30%) and fresh clinopyroxene and orthopyroxene. Plagioclase and orthopyroxene are generally replaced by zeolite and smectites. Opaque minerals are included in the pyroxene phenocrysts and thus represent an early crystallization phase. The groundmass is often very altered, but the glass of some clasts (e.g., Sample 126-793B-56R-2, 75–76 cm) is surprisingly fresh. Uncommon hornblende-clinopyroxene-bearing crystal tuff is present in Sample 126-793B-37R-1, 68–69 cm. It contains perfectly fresh, green hornblende, clinopyroxene, and oscillatory-zoned plagioclase. The rare intersertal basalt clasts in Sample 126-793B-56R-2, 85–86 cm, show quenched clinopyroxene and plagioclase microlites in a highly vesicular groundmass.

Unit VI (lower[?] Oligocene) is a poorly sorted volcaniclastic breccia and microbreccia with a sandy matrix. Most clasts are angular. Porphyritic andesite with abundant plagioclase phenocrysts (20%–35%) represents the predominant type of clast (Samples 126-793B-83R-1, 120–121 cm, -84R-2, 39–40 cm, and -85R-2, 39–40 cm; Table 7). Clinopyroxene is always well pre-

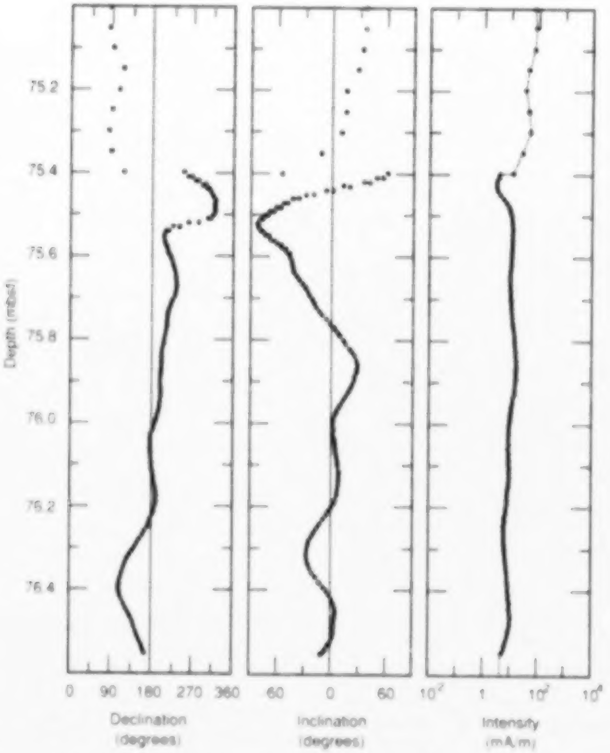

Figure 50. Downhole plot of azimuthally corrected declination, inclination, and intensity of remanent magnetization for the part of Core 126-793A-8H (archive half) that includes the Brunhes-Matuyama polarity transition.

served and forms glomeroporphyritic aggregates with orthopyroxene pseudomorphs. Plagioclase and orthopyroxene may be altered to smectites and zeolites (Sample 126-793B-84R-2, 39-40 cm; Table 7). Opaque minerals are included in these pyroxene phenocrysts, indicating their early crystallization. Sparse rounded quartz microphenocrysts may be present (e.g., Sample 126-793B-84R-2, 39-40 cm). The vesicles are lined by smectites and filled with zeolites. Where the phenocrysts display fluidal texture, the vesicles are flattened and lobate (Samples 126-793B-85R-1, 8-10 cm, and -85R-2, 39-40 cm).

Rare clinopyroxene phyric basic andesite with a few plagioclase phenocrysts (Sample 126-793B-84R-1, 16-18 cm) and intersertal basalt with quenched clinopyroxene and plagioclase microlites (Sample 126-793B-85R-1, 8-10 cm) are the two other types of clasts in this polymictic breccia. The former is similar to clasts in basement breccias.

The most common volcanic clast present in the conglomeratic volcaniclastic beds of Unit V as well as in the breccias of Unit VI is a plagioclase-clinopyroxene-orthopyroxene andesite that displays many similarities to the andesites recovered in the basement of Site 792 (i.e., abundance of plagioclase, presence of orthopyroxene and clinopyroxene that includes opaque minerals, and occasional occurrence of quartz) (see "Igneous Petrology" section, "Site 792" chapter, this volume).

The Basement

At Hole 793B, basement was reached at 1404 mbsf, and a further 278 m of penetration was achieved, reaching a total depth of 1682 mbsf. The rate of recovery for basement rocks was 33%. A lithostratigraphic column for Hole 793B basement is shown in Figure 55. We defined the upper contact of the basement with the overlying breccia (Unit VI, Core 126-793B-85R and above) on the basis of the lithology and diversity of the volcanic clasts, the type of the matrix, and the presence of a sheared zone in Core 126-793B-86R. The most common volcanic clast found in Unit VI is plagioclase-rich andesite with two pyroxenes, an early crystallizing opaque mineral, and minor quartz. In contrast, the andesitic clasts in the uppermost volcanic breccia of the basement (Unit 1, Core 126-793B-86R through Section 126-793B-92R-1) never have >10% plagioclase phenocrysts, and opaque minerals are absent (see the following discussion and Table 7). The Unit VI volcaniclastic breccia contains up to 40% sand-size matrix. In contrast, the matrix of the Unit 1 volcanic breccia is hyaloclastitic with a zeolitic cement.

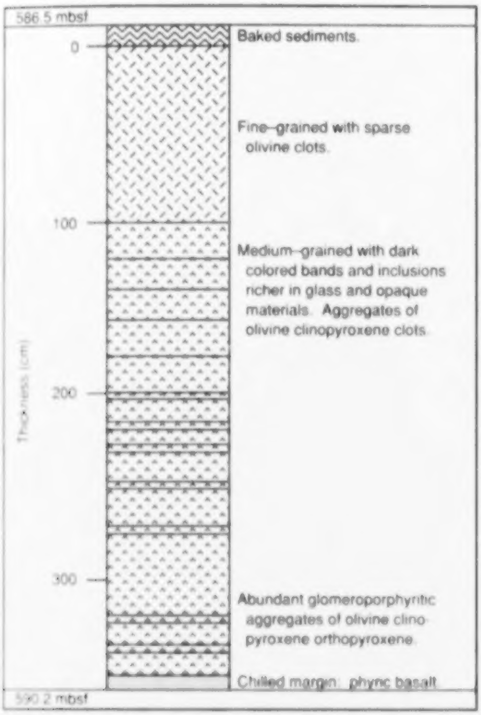
586.5 mbsf
0
100
200
300
Thickness (cm)
Baked sediments.
Fine-grained with sparse olivine clots.
Medium-grained with dark colored bands and inclusions richer in glass and opaque materials. Aggregates of olivine clinopyroxene clots.
Abundant glomeroporphyritic aggregates of olivine clinopyroxene orthopyroxene.
Chilled margin: phyric basalt
590.2 mbsf

Figure 51. Schematic diagram of the diabase sill showing the textural differences between the upper, middle, and lower sections and the distribution of the dark-colored bands and inclusions.

The top of the Unit 1 volcanic breccia is sheared, which could suggest a fault contact between the forearc sediments and the basement. Basement-like clasts are reworked in Unit VI breccias, but clasts similar to those of Unit VI are absent from the basement.

Pillowed and massive lava flows in the basement contain one reversal of magnetic polarity (see "Paleomagnetism" section, this chapter). The pillowed lava in Units 2 and 14 (Cores 126-793B-92R and -110R through -112R) are normally magnetized, whereas the massive flow in Unit 10 (Core 126-793B-104R) is reversed. The latter may represent the short reversal at about 31.6 Ma in the middle of Chron C11. Thus, the basement at Site 793 may have formed within as little as 0.1-0.9 m.y.

The basement consists of the following units:

Unit 1

Description: heterolithic andesitic breccia
Interval: 126-793B-86R to -92R-1 at 140 cm
Depth: 1404-1461 mbsf

This breccia is formed of 60% clasts, which range in size from 1 to 10 cm, in a hyaloclastitic matrix. The clasts have chilled margins on some surfaces and some are preshaped. They are interpreted as pillow fragments. They include clinopyroxene-rich porphyritic andesite or plagioclase-rich porphyritic andesite, and sparsely phyric andesite lithologic suites. The porphyritic clinopyroxene-rich andesite (Samples 126-793B-86R-2, 29-30 cm, -87R-4, 21-22 cm, -89R-2, 3-4 cm, and -89R-3, 111-113 cm; Table 7) displays porphyritic texture with an intersertal groundmass and includes large, abundant clinopyroxene and orthopyroxene phenocrysts (15%-23%) and variable amounts of smaller plagioclase crystals (5%-10%). The two pyroxenes are often clustered in glomeroporphyritic aggregates in which the orthopyroxene is frequently mantled by the clinopyroxene.

The porphyritic plagioclase-rich andesite (Sample 126-793B-86R-1, 117-119 cm; Table 7) differs mainly in having fewer pyroxene phenocrysts. The sparsely phyric andesite (Sample 126-793B-88R-1, 69-70 cm; Table 7) has a few (< 10%) plagioclase, orthopyroxene, and clinopyroxene phenocrysts in a trachytic groundmass that includes late-crystallizing opaque minerals. In all clasts, the vesicles (< 5%) are rounded or flattened and filled with smectites and/or zeolites, and the orthopyroxene is partly replaced by smectites. The hyaloclastitic matrix is formed of glass shards and clinopyroxene-orthopyroxene crystals. The cement is a mixture of heulandite-clinoptilolite containing small sheets of native copper.

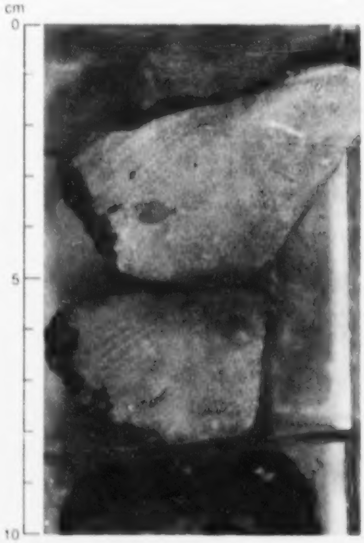

Figure 52. Photograph of the upper contact of the diabase sill with the baked sediments (Interval 126-793B-1R-1, 0-10.0 cm).

Unit 2

Description: pyroxene-rich andesite pillow lava and an interlayer of monolithic breccia
Interval: 126-793B-92R-1 at 140 cm, through 93R-1 at 120 cm
Depth: 1461-1471 mbsf

The top of this unit was first regarded as representing the sediment/basement contact because of the occurrence of pillowed lavas. Beneath these, the hyaloclastitic breccia includes 1-6-cm pillow fragments in a matrix rich in glass shards and pyroxene crystals. More pillow lavas are present in Section 126-

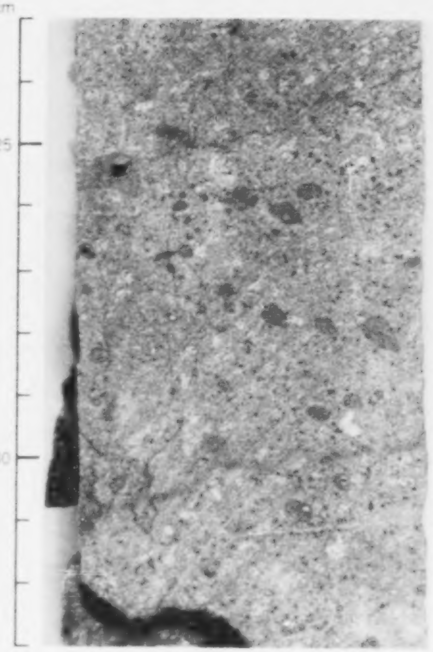

Figure 53. The glassy inclusions in the diabase with their rounded, empty, or smectite-filled vesicles are distinguished from the rest of the diabase sill by their black color and finer grain size. In contrast, the glomeroporphyritic clots are light colored and coarse grained (Interval 126-793B-1R-3, 23-33 cm).

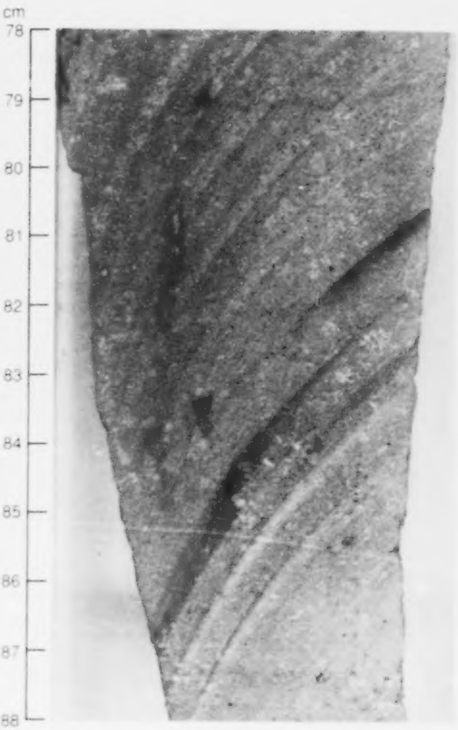

Figure 54. Photograph of the basal chilled margin of the diabase intrusion characterized by its larger and abundant glomeroporphyritic aggregates and its fine-grained groundmass. Just above the chilled margin, inclusions are sometimes tadpole-shaped, tapering downward with vesicles at the top (Interval 126-793B-1R-3, 78-88 cm).

793B-93R-1. The pillows and pillow fragments are formed of highly porphyritic andesite (Sample 126-793B-93R-1, 84-85 cm; Table 7) with orthopyroxene (up to 15%) and clinopyroxene (up to 10%) phenocrysts and rare plagioclase-lath phenocrysts (1%).

Unit 3

Description: monolithic sparsely phyric andesite breccia
Interval: 126-793B-93R-1 at 120 cm, through -96R-1 at 33 cm
Depth: 1471-1499 mbsf

The andesitic pillow fragments (0.5-10 cm) are included in a hyaloclastitic matrix formed of altered glass shards and pyroxene crystals cemented by zeolites and smectites. Sparsely phyric clasts predominate over coarsely porphyritic ones. The sparsely phyric andesite (Sample 126-793B-93R-2, 27-28 cm; Table 7) has an abundant felty groundmass that contains ~2% small, disseminated orthopyroxene and clinopyroxene phenocrysts.

Unit 4

Description: pyroxene-rich andesite pillow lava
Interval: 126-793B-96R-1, 33 cm, to -96R-CC
Depth: 1471-1499 mbsf

This unit is formed of porphyritic pyroxene-rich andesite pillow lava (Sample 126-793B-96R, 81-83 cm; Table 7) similar to the clinopyroxene-rich andesitic clasts present in Unit 1: predominant orthopyroxene phenocrysts (~12%), and clinopyroxene (~5%) approximately equal to plagioclase (~ 3%). The pillows show radial fractures. A thin breccia horizon formed of sparsely phyric and porphyritic andesitic pillow fragments is present between the pillows. The sparsely phyric andesitic fragments are similar to those of Unit 3.

Unit 5

Description: pyroxene-rich andesitic massive lava
Interval: Core 126-793B-97R
Depth: 1508-1518 mbsf

This andesite (Sample 126-793B-97R-1, 123-124 cm; Table 7) displays an intersertal trachytic groundmass with abundant (15%) orthopyroxene and clinopyroxene phenocrysts.

Unit 6

Description: monolithic, sparsely phyric andesite breccia
Interval: 126-793B-98R-1 through -99R-1 at 38 cm
Depth: 1518-1528 mbsf

This breccia is very similar to that of Unit 3 in containing mostly aphyric clasts (0.2-10 cm in diameter) in a hyaloclastitic matrix. The chilled fragments are characterized by elongate open-pipe vesicles that imply degassing processes. Their groundmass is

Table 7. Original percent of phenocrysts in thin sections of the basement at Site 793 as estimated without point counting.

Core, section, interval (cm)	Unit	Plagioclase (%)	Cpx (%)	Opx (%)	Olivine (%)	Opaques (%)	
Core 793B							
[illegible]R-1, 2-4	II	41	18	0	3	4	
[illegible]R-2, 115-116	II	37	20	1	7	5	
[illegible]R-3, 86-89	II	5	15	5	10	0	
[illegible]R-1, 95-96	III	5	3	0	0	0	
[illegible]R-3, 129-131	V	30	10	1	0	0	
[illegible]R-3, 125-128	V	10	2	1	0	0	
[illegible]R-2, 75-76	V	5-15	5	0-2	0	0	
[illegible]R-?, 80-82	VI	30	10	6	0	1	
[illegible]R-1, 120-121	VI	20	10	3	0	1	
[illegible]R-1, 76-78	VI	0	7	0	0	1	
[illegible]R-2, 39-40	VI	30	10	5	0	1	+ Qtz
[illegible]R-1, 8-10	VI	5	5	3	0	0	
[illegible]R-2, 39-40	VI	35	10	8	0	1	
[illegible]R-1, 117-119	1	10	6	2	0	0	
[illegible]R-2, 29-30	1	5	20	3	0	0	
[illegible]R-4, 21-22	1	10	20	10	0	0	
[illegible]R-1, 69-70	1	6	3	?	0	0	
[illegible]R-2, 3-4	1	1	15	5?	0	0	
[illegible]R-3, 111-113	1	1	15	10	0	0	
[illegible]R-1, 84-85	2	1	10	15	0	0	
[illegible]R-2, 27-28	3	2	1	1	0	0	
[illegible]R-1, 81-83	4	3	5	15	0	0	
[illegible]R-1, 123-124	5	0	7	8	0	0	
99R-1, 54-55	7	< 1	5	4	1	0	
100R-1, 28-29	9	0.2	[illegible]	0.3	0	0	
104R-2, 48-49	10	8	8	1.5	0	0	
105R-1, 126-127	11	10	4	6	0	0	
107R-1, 17-18	12	7	5	1	0	0	
110R-1, 4-5	13	0	9	7	4	< 1 Cr-Sp	
[illegible]R-1, 63-64	14	0	7	10	0	0	
[illegible]R-1, 136-137	16	3	0	0	0	0	

Note: Cpx = clinopyroxene; Opx = orthopyroxene; Qtz = quartz; Cr-Sp = chromium-spinel.

crossed by smectitic veinlets. Open cracks, filled with zeolites, crosscut the fragments and the matrix. Toward the base, in contact with the underlying porphyritic pillows, this breccia includes porphyritic and sparsely phyric andesitic clasts.

Unit 7

Description: boninitic pillow lava
Interval: 126-793B-99R-1, 38-150 cm
Depth: 1528-1529 mbsf

The pillows (Sample 126-793B-99R-1, 54-55 cm; Table 7) have rounded olivine (1%, 1 mm in size), euhedral clinopyroxene, and orthopyroxene phenocrysts. The chromium-spinels are included in the olivine. The groundmass contains up to 50% plagioclase laths and aligned vesicles (5%) partly filled with smectites and zeolites. This flow represents one of the two most mafic units of the basement.

Unit 8

Description: heterolithic andesitic breccia
Interval: 126-793B-99R-2 through -100R-1 at 132 cm
Depth: 1529-1539 mbsf

This breccia differs from the other heterolithic layers because differences are present between the top and base of the unit. The upper portion contains only small (< 3 cm) porphyritic and sparsely aphyric clasts enclosed in a matrix mainly formed of nonvesicular glassy shards and isolated pyroxene crystals. In contrast, the base includes larger clasts (up to 10 cm) and isolated aphyric pillows, and the zeolitic cement is more developed and forms larger crystals. The margins of the isolated pillows are chilled against the surrounding breccia. In thin section (Sample 126-793B-100R-1, 28-29 cm; Table 7), this pillow is characterized by a trachytic groundmass in which small amounts of clinopyroxene, orthopyroxene, and plagioclase euhedral microphenocrysts (0.1-0.3 mm) are present. The cores of the spherical vesicles are filled with smectites, whereas zeolites are in the rims and walls.

Unit 9

Description: monolithic sparsely-phyric andesite breccia
Interval: 126-793B-100R-1 at 132 cm, through -103R-CC
Depth: 1539-1576 mbsf

Compared to the later, sparsely phyric breccias (Units 3 and 4), this horizon differs in having a downward increase in the size and abundance of clasts.

Unit 10

Description: plagioclase-rich andesitic massive lava
Interval: Core 126-793B-104R
Depth: 1576-1586 mbsf

The top and base of the flow are clearly chilled against the overlying and underlying breccias. This andesite (Sample 126-793B-104R-2, 48-49 cm, through -104R-CC, 0-30 cm) differs from those above in that it contains equal proportions of plagioclase and clinopyroxene phenocrysts (~8%) and little orthopyroxene (< 1.5%).

Unit 11

Description: monolithic plagioclase-rich andesitic breccia
Interval: 126-793B-105R-1 through -107R-1 at 53 cm
Depth: 1586-1615 mbsf

These porphyritic andesitic pillows (Sample 126-793B-105R-1, 126-127 cm; Table 7) and pillow fragments are very similar to the plagioclase-rich andesite of Unit 10. At the base of the unit, the chilled pillow rims in contact with the hyaloclastitic breccia are marked by abundant (30%) flattened vesicles filled with zeolites and smectites, and by the presence of vertical and radial fractures filled with vesicles.

Unit 12

Description: monolithic plagioclase-rich andesitic breccia in a tuffaceous matrix
Interval: 126-793B-107R-1 at 53 cm, through -109R-3 at 108 cm
Depth: 1615-1628 mbsf

The upper section of this unit is formed of large chilled clasts (~20 cm) similar to those in Unit 11, whereas the middle and lower sections contain smaller clasts (2-0.5 cm), decreasing in size downward. The tuffaceous matrix is a crystal tuff with entire or broken plagioclase and clinopyroxene crystals, and altered glass shards in a smectitic cement. The chilled andesitic fragments (Sample 126-793B-107R-1, 17-18 cm; Table 7) are very similar to the andesitic massive flow of Unit 11 in that phenocrysts of plagioclase outnumber those of clinopyroxene, in an intersertal to microphyric groundmass that includes late-crystallizing opaque minerals.

Unit 13

Description: boninitic massive lava, "orange spot lava"
Interval: 126-793B-110R-1 through -110R-5 at 74 cm
Depth: 1628-1650 mbsf

This flow (Sample 126-793B-110R-1, 4-5 cm; Table 7) best displays boninitic features, such as lack of plagioclase phenocrysts, presence of rounded olivine pseudomorphs, Cr-spinels in the olivine pseudomorphs and groundmass, and orthopyroxene rimmed by clinopyroxene. Moreover, there is an equal abundance of clinopyroxene and orthopyroxene phenocrysts. The groundmass includes abundant subhedral plagioclase laths and quenched clinopyroxene and orthopyroxene microphenocrysts (~0.02 mm). The interstitial glass is probably replaced by zeolites. The orange spots represent cumulate glomeroporphyritic aggregates of aligned, rounded, euhedral pseudomorphs after olivine, mantled by the two pyroxenes and associated with Cr-spinels and native copper. Olivine is replaced by calcite and

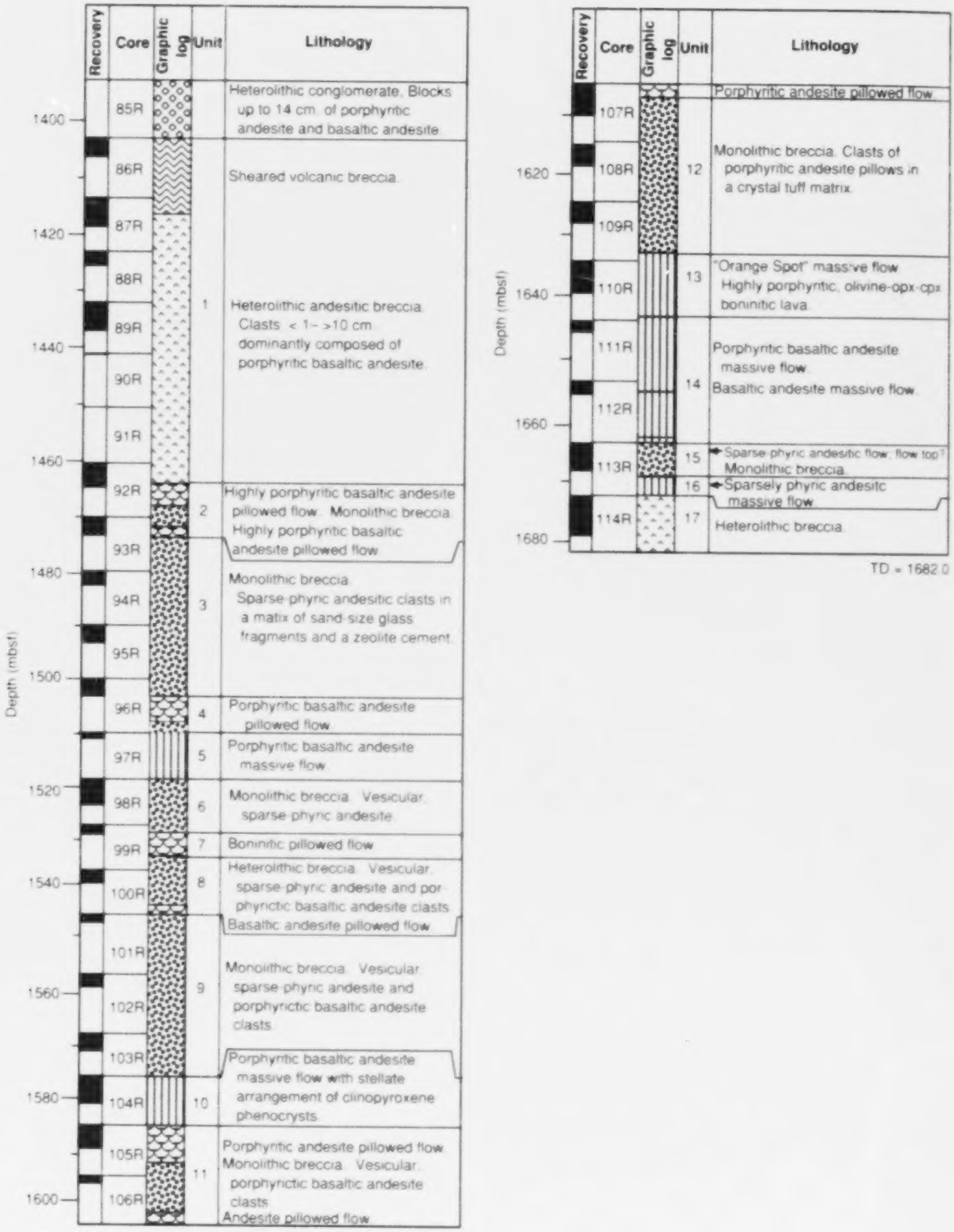
Recovery
Core
Graphic log
Unit
Lithology
Depth (mbsf)
1400
1420
1440
1460
1480
1500
1520
1540
1560
1580
1600
85R
86R
87R
88R
89R
90R
91R
92R
93R
94R
95R
96R
97R
98R
99R
100R
101R
102R
103R
104R
105R
106R
Heterolithic conglomerate. Blocks up to 14 cm. of porphyritic andesite and basaltic andesite.
Sheared volcanic breccia.
1
Heterolithic andesitic breccia. Clasts < 1– >10 cm. dominantly composed of porphyritic basaltic andesite.
2
Highly porphyritic basaltic andesite pillowed flow. Monolithic breccia. Highly porphyritic basaltic andesite pillowed flow.
3
Monolithic breccia. Sparse-phyric andesitic clasts in a matrix of sand-size glass fragments and a zeolite cement.
4
Porphyritic basaltic andesite pillowed flow.
5
Porphyritic basaltic andesite massive flow.
6
Monolithic breccia. Vesicular, sparse-phyric andesite.
7
Boninitic pillowed flow.
8
Heterolithic breccia. Vesicular, sparse-phyric andesite and porphyrictic basaltic andesite clasts.
Basaltic andesite pillowed flow.
9
Monolithic breccia. Vesicular, sparse-phyric andesite and porphyrictic basaltic andesite clasts.
Porphyritic basaltic andesite massive flow with stellate arrangement of clinopyroxene phenocrysts.
10
11
Porphyritic andesite pillowed flow.
Monolithic breccia. Vesicular, porphyrictic basaltic andesite clasts.
Andesite pillowed flow.
1620
1640
1660
1680
107R
108R
109R
110R
111R
112R
113R
114R
Porphyritic andesite pillowed flow.
12
Monolithic breccia. Clasts of porphyritic andesite pillows in a crystal tuff matrix.
13
"Orange Spot" massive flow. Highly porphyritic, olivine-opx-cpx boninitic lava.
14
Porphyritic basaltic andesite massive flow.
Basaltic andesite massive flow.
15
Sparse-phyric andesitic flow; flow top?
Monolithic breccia.
16
Sparsely phyric andesitc massive flow.
17
Heterolithic breccia.
TD = 1682.0

Figure 55. Lithostratigraphic column of the basement at Site 793.

smectites. Smectites are also present along fractures in orthopyroxenes.

Unit 14

Description: pyroxene-rich andesite massive lava
Interval: 126-793B-110R-5, 74 cm, through -112R-2 at 150 cm
Depth: 1650-1656 mbsf

The porphyritic andesite (Sample 126-793B-112R-1, 63-64 cm; Table 7) is characterized by clinopyroxene and orthopyroxene phenocrysts in an intersertal trachytic groundmass. Smectites replace glass and fill fractures. The vesicles are filled by zeolites and smectites.

Unit 15

Description: monolithic pyroxene-rich andesitic breccia
Interval: 126-793B-113R-1 through -113R-3 at 118 cm
Depth: 1656-1660 mbsf

The chilled andesitic clasts (1-10 cm) are set in a hyaloclastitic matrix formed of 1-10-mm glass shards and pyroxene crystals in a smectitic cement. The porphyritic andesite is similar to that of Unit 1.

Unit 16

Description: high-silica, sparsely phyric andesite massive lava
Interval: 126-793B-113R-3 at 118 cm, through -113R-4 at 35 cm
Depth: 1660-1661 mbsf

This aphyric andesite (Sample 126-793B-113R-3, 136-137 cm; Table 7) is characterized by uncommon clinopyroxene microphenocrysts, an abundant trachytic intersertal groundmass, and late-crystallizing magnetite.

Unit 17

Description: heterolithic plagioclase-rich andesitic breccia
Interval: Core 126-793B-114R
Depth: 1661-1682 mbsf

Most clasts in this heterolithic breccia are 1-10 cm in size, but we also recovered some 40-cm-diameter isolated pillows. The clasts contain less plagioclase than pyroxene, but clasts in the bottom of this unit are more typical of Units 10, 11, and 15 (i.e., with plagioclase < orthopyroxene < clinopyroxene).

Conclusions

The basement of Hole 793B is predominantly formed of andesitic massive or pillowed lavas, interbedded with monolithic and/or heterolithic hyaloclastitic breccias. Four main lithologic types can be distinguished using the following criteria: (1) porphyritic or aphyric, (2) olivine and Cr-spinels present, (3) relative abundance of plagioclase vs. pyroxenes, and (4) relative proportions of the two pyroxenes.

The first type consists of olivine and Cr-spinel-bearing basaltic andesite and is located in Units 7 and 13 (Samples 126-793B-99R-1, 54-55 cm and -110R-1, 4-5 cm). It is the most mafic lithology in the basement and displays some features in common with boninites. Plagioclase is present only as laths in the groundmass, which also includes two pyroxenes as microphenocrysts. Orthopyroxene phenocrysts are rimmed by clinopyroxene.

The porphyritic clinopyroxene-rich andesite in Units 2, 4, 5, and 14 (Samples 126-793B-86R-2, 29-30 cm; -89R-2, 3-4 cm; -89R-3, 111-112 cm; -93R-1, 81-85 cm; -96R-1, 81-83 cm; -97R-1, 123-124 cm; and -112R-1, 63-64 cm) is apparently the most common rock type in the basement and is present in breccias and as lavas. It contains a large amount of clinopyroxene and orthopyroxene phenocrysts (up to 30%). Clinopyroxene predominates over orthopyroxene, and plagioclase phenocrysts are very few (0%-3%).

The porphyritic plagioclase-rich andesite in Units 10 and 12 (Samples 126-793B-93R-2, 28-28 cm; -104R-2, 48-49 cm; -105R-1, 126-127 cm; and -105R-1, 17-18 cm) is present as pillow fragments in heterolithic and monolithic breccias, as well as massive and pillowed. It is characterized by an intersertal and felty groundmass and an equal proportion of plagioclase (2%-10%) and pyroxenes (5%-10%).

The last type is aphyric to sparsely phyric andesite and is present in Units 6, 9, and 16 (Samples 126-793B-100R-1, 28-29 cm and -113R-1, 136-137 cm; Table 7). It is present as pillow fragments and as massive flows. It is characterized by an intersertal trachytic groundmass (40% plagioclase laths), a few plagioclase, orthopyroxene, and clinopyroxene microphenocrysts (< 0.3 mm), and a late-crystallizing opaque mineral (magnetite?). It represents the most-differentiated rock type of the andesitic suite in the Hole 793B basement.

Overall, the basement of Hole 793B consists of an andesitic suite that ranges from olivine-Cr-spinel basaltic andesite (Mg rich) to more evolved siliceous andesite (Mg poor). All rock types have <2% vesicles, which are present in lavas and in hyaloclastitic breccia clasts. In all of the rock types, the plagioclase and pyroxene phenocrysts are euhedral and largely unzoned. The orthopyroxenes are nonpleochroic and are the most highly altered (to smectite) mineral. The cements vary in smectite/zeolite ratio, and native copper is prominent in Units 1 and 10-13.

IGNEOUS GEOCHEMISTRY

This section deals with the geochemistry of the three main occurrences of igneous rocks in Hole 793B: (1) an olivine diabase that intrudes middle Miocene sedimentary rocks, (2) volcanic clasts throughout the sedimentary sequence, and (3) the basement lava flows and breccias.

Olivine Diabase Intrusion

Hole 793B encountered an *in-situ* igneous unit at 586.5 mbsf. This unit appears to be a single diabase intrusion, 4.5 m thick (90% recovery), which is bound above and below by sediments. The age of the underlying sediments is late early to early middle Miocene (~14-17 Ma; see "Biostratigraphy" section, this chapter). The mineralogy of the diabase consists of olivine phenocrysts in a groundmass dominated by plagioclase, clinopyroxene, and opaque minerals. In the lowermost parts of the unit, including the chilled margin, clinopyroxene and orthopyroxene phenocrysts occur (see "Igneous Petrology" section, this chapter).

Three samples were analyzed by wavelength spectrometer X-ray fluorescence (XRF) for major and trace element abundances (Table 8). The samples come from the upper, middle, and lower sections of the intrusion.

The main geochemical features of this olivine diabase are its high concentrations of SiO_2 (~53.2%) and MgO (~9%; Table 8) and its low concentrations of Al_2O_3 (~15%), Na_2O (<1.7%), and K_2O (<0.28%). The high SiO_2 levels explain the presence of orthopyroxene phenocrysts. With a Mg number ranging between 64.8 and 67.9, this diabase intrusion is more mafic than any diabase drilled at Site 791 (see "Igneous Petrology" section, "Sites 790/791" chapter, this volume). The Fe_2O_3 values decrease slightly, whereas Cr and Ni contents, and to a lesser extent MgO, increase from the top to the base of the sill. This indicates a more differentiated upper section and more mafic middle and lower parts (the latter is a result of the presence of olivine-clinopyroxene-orthopyroxene glomeroporphyritic aggregates; see "Igneous Petrology" section, this chapter). This differentiation trend is probably related to the accumulation of the olivine and pyroxenes toward the base of the intrusion. The Fe

Table 8. Shipboard XRF analyses of rocks from Hole 793B.

Hole, core	126-793A-1H	126-793A-1H	126-793A-1H	126-793B-3R	126-793B-83R	126-793B-84R	126-793B-85R	126-793B-86R
Section, interval (cm)	1, 27-32	2, 59-62	3, 60-64	1, 95-98	1, 115-118	2, 35-40	2, 39-54	2, 26-30
Piece number	4A	5A	1D					
Depth (mbsf)	586.5	586.5						1409
Unit	II	II	II	III (sediments)	VI (sediments)	VI (sediments)	VI (sediments)	1 (basement)
Lithology	diabase	diabase	diabase	basalt				
SiO_2	53.25	52.36	52.28	52.81	55.55	51.46	53.2	55
TiO_2	0.59	0.55	0.54	0.66	0.45	0.45	0.47	0.33
Al_2O_3	15.14	14.59	14.33	17.07	17.96	19.52	20.01	15.94
Fe_2O_3	10.2	9.68	9.61	10.42	8.46	8.42	8.23	7.62
MnO	0.14	0.14	0.14	0.16	0.14	0.28	0.12	0.13
MgO	8.55	8.97	9.24	5.27	3.93	4.91	5.76	7.43
CaO	10.83	10.89	10.9	11.7	3.11	7.82	9.78	10.77
Na_2O	1.68	1.67	1.71	1.91	6.11	5.1	2.11	1.52
K_2	0.28	0.28	0.23	0.3	4.05	1.46	0.29	1.14
P_2O_5	0.03	0.03	0.03	0.04	0.09	0.36	0.03	0
LOI	0.96	1.32	1.13	0.33	12.23	6.95	2.5	2.23
Total	100.68	99.14	99	100.36	99.85	99.78	100.02	100.18
Zr	30	29.8	30.2		59.9	50.8	55.8	39.7
Y	16.6	15.6	15.5		33.9	53.7	13.8	9.6
Rb	2	2.6	2.9		31.5	13.8	1	10.1
Sr	115.5	111.2	110.4		89.5	107.9	180.3	124.5
Ba	44.1	23.6	39.9		173.5	246.5	20.7	—
V	295.2	269.6	285.7		223.7	203.7	261.4	201.9
Nb	0.7	0.5	0.9		1.1	1.2	1.1	1.1
Ni	88.9	104	109		31	29.8	29.7	50.4
Cr	266	344.1			87.2	40.1	51	377.9
Zn	91.1	92.4	85.2		104.7	107.4	103.2	87.2
Cu	73.6	97.7	75.2		33.5	53.7	119	16.8
Ce	7.4	2.3	0		12	5.1	—	—
Ti/Zr	118	110.7	107.2		45.07	53.14	50.53	52.89
Zr/Y	1.8	1.91	1.94		1.07	0.94	4.04	4.13
Ti/V	11.99	12.24	11.34		12.06	13.25	10.78	10.41

Note: Major elements are measured in wt% oxide, and trace elements are measured in parts per million (ppm); LOI = loss on ignition.

Table 8 (Continued).

Hole, core	126-793B-87R	126-793B-88R	126-793B-89R	126-793B-92R	126-793B-93R	126-793B-93R	126-793B-96R	126-793B-97R
Section, interval (cm)	4, 22-25	1, 65-68	2, 0-4	3, 25-28	1, 85-87	2, 27-29	1, 81-83	1, 124-127
Piece number								
Depth (mbsf)	1419.6	1424.4	1432.4	1468.7	1471.2	1475.4	1507.1	1516
Unit	1 (basement)	1 (basement)	1 (basement)	2 (basement)	2 (basement)	3 (basement)	4 (basement)	5 (basement)
Lithology								
SiO_2	54.89	54.73	55.65	54.58	52.89	53.71	53.48	53.28
TiO_2	0.32	0.35	0.26	0.28	0.28	0.37	0.29	0.28
Al_2O_3	15.14	18.85	13.74	13.97	13.08	17.9	14.46	13.78
Fe_2O_3	7.66	8	9.24	8.63	9.27	8.7	8.98	9.1
MnO	0.14	0.11	0.13	0.13	0.16	0.14	0.16	0.18
MgO	8.25	4.8	8.73	8.46	12.51	6.34	10.37	11.93
CaO	10.68	10.47	9.39	10.48	10.35	10.53	10.57	10.02
Na_2O	1.48	1.88	1.36	1.92	1.24	1.72	1.9	1.56
K_2	0.65	0.92	1.08	0.89	0.24	0.47	0.36	0.19
P_2O_5	0.01	0.03	0	0.32	0	0	0.01	0
LOI	2.42	2.66	2.19	1.4	1.56	1.84	1.68	2.14
Total	99.22	100.17	99.54	99.6	100.06	99.89	100.57	100.32
Zr	38.9	40.7	25.3	27.3	25.9	34.6	27.2	26
Y	8.9	15.5	18.5	19.6	8.8	9.8	10	7.8
Rb	3.7	13.5	18.5	15.9	3.2	3.9	6.4	1.4
Sr	123.1	154.7	145.1	161.7	141.5	184	149.3	141.3
Ba	—	12.4	—	18.2	15.1	13.1	21.6	8.6
V	204.8	204.5	193.6	224.2	225.5	260.3	235.8	196.6
Nb	0.6	0.6	0	0.6	0.5	0.5	0.6	0.3
Ni	56	38.4	102	110	172.5	55.2	140.2	124.7
Cr	335.5	133.4	627.9	437.3	589.6	144.1	599.9	513.1
Zn	86.8	95.3	87.3	79.3	83	88.4	100.7	82.2
Cu	65.7	26	16.4	16.1	18.2	75.5	19.4	24
Ce	3.3	—	3.2	—	—	—	—	—
Ti/Zr	53.98	57.49	68.77	65.93	71.8	65.02	66.17	69.23
Zr/Y	4.37	2.62	1.36	1.39	2.94	3.53	2.72	3.3
Ti/V	10.25	11.44	8.98	8.02	8.24	8.64	7.93	9.15

Table 8 (Continued).

Hole, core	126-793B-99R	126-793B-100R	126-793B-104R	126-793B-105R	126-793B-107R	126-793B-110R	126-793B-112R	126-793B-113R
Section, interval (cm)	1, 54-55	1, 28-30	2, 49-54	1, 127-131	1, 17-20	1, 1-3	1, 59-63	3, 137-141
Piece number								
Depth (mbsf)	1527.6	1537.58						
Unit	7 (basement)	9 (basement)	10 (basement)	11 (basement)	12 (basement)	13 (basement)	14 (basement)	16 (basement)
Lithology								
SiO_2	53.04	53.42	53.54	57	53.93	54.11	55.45	59.75
TiO_2	0.28	0.34	0.31	0.28	0.32	0.26	0.29	0.31
Al_2O_3	13.86	18.05	14.56	13.07	16.58	12.7	14.75	16.36
Fe_2O_3	9.75	9.13	9.37	9.26	9.43	9.06	8.11	7.58
MnO	0.14	0.11	0.15	0.15	0.12	0.13	0.11	0.07
MgO	9.33	5.68	7.91	8.53	7.08	10.14	7.04	3.76
CaO	11.07	10.28	11.93	10.43	10.38	9.9	9.44	8.26
Na_2O	1.64	2.11	2.09	1.82	2.24	2.23	2.7	2.74
K_2O	0.78	0.7	0.53	0.44	0.48	0.66	1.16	1.66
P_2O_5	0.02	0	0.05	0.01	0	0.02	0.6	0.05
LOI	2	1.61	1.06	2.57	6.14	1.17	2.03	1.17
Total	99.9	99.84	100.45	100.99	100.05	99.2	99.64	100.51
Zr	23.3	32.4	31.6	28.8	34.2	24	29.5	33.5
Y	8.9	9.8	15.2	9.6	8.5	12.4	18.3	20.3
Rb	18.2	10.9	8.4	3.8	8.7	11.1	25.4	32.9
Sr	134.6	191	174.5	127	180.1	143.3	182.5	189.1
Ba	13.1	15.5	19.7	17.3	17.3	21.6	32.9	19.2
V	243.4	246	251.2	251.5	242.2	214.9	209.8	227
Nb	0.4	0.8	0.7	0.4	0.5	0.7	0.9	1
Ni	120.5	45.7	47.45	36.6	34.7	126.4	81.9	23.2
Cr	700	88.5	294.6	249.2	174.1	706.2	249.6	24.6
Zn	93.9	107.8	97.6	82.7	107.9	81.3	78.4	64.9
Cu	15.3	19.4	17.8	72	168.7	102.4	19.2	37.8
Ce	—	—	—	—	—	—	—	8.4
Ti/Zr	72.1	64.81	66.45	66.6	61.4	67.5	63.05	59.1
Zr/Y	2.61	3.3	2.07	3	4.02	1.93	1.61	1.65
Ti/V	6.9	8.5	8.35	7.63	8.67	6.69	8.86	8.72

enrichment in the upper part may be a result of the extraction of clinopyroxene and orthopyroxene, whereas Fe in the base may have been diluted by pyroxene. Thus, the analysis of the upper part of the sill is more representative of the diabase magma, whereas the analysis of the middle and lower parts shows the increasing effects of crystal accumulation. The low values of aluminum and total alkalis indicate that this diabase displays tholeiitic affinities, using the criteria of Kuno (1960).

The trace element geochemistry of the olivine diabase is characterized by the depletion in high-field-strength elements (e.g., TiO_2, P, Zr, Y, and Nb) relative to N-MORB (Table 8), which appears to be a constant feature of this arc-forearc system. Indeed, the basaltic andesites and andesites that form the basement in Hole 792E (see "Igneous Petrology" section, Site 792 chapter, this volume), as well as the Tori Shima basalts (Zhang et al., in press), display a depletion in high-field-strength elements similar to that in the diabase. However, the diabase also has low concentrations of Rb (2-3 ppm), Ba (~36 ppm), and Sr (~110 ppm) compared with most island-arc suites, including the Marianas (Stern and Ito, 1983).

Volcanic Pebbles in Unit VI

Unit VI is a poorly sorted volcaniclastic breccia with a sandy matrix. Porphyritic andesite with abundant plagioclase phenocrysts is the most common clast type. We analyzed three samples by XRF for major and trace elements to compare their geochemistry with the basement rocks of Sites 793 and 792. The high K_2O (4.50 wt%) and loss on ignition (or LOI, 12.23%; Table 8) contents of one of the analyzed samples show the high degree of alteration of some of these andesitic clasts. Nevertheless, the clasts display many similarities with the basement calc-alkaline andesites at Site 792 (i.e., they are Fe-poor and Ti-rich, their Al_2O_3 contents are high, and they are depleted in high-field-strength elements).

The Basement

The 278 m of basement in Hole 793B revealed a sequence of andesitic pillowed and massive lavas intercalated with monolithic and heterolithic breccias with hyaloclastitic and tuffaceous matrices. The lavas and clasts belong to both the high-Mg and low-Mg series (Fig. 56). Four main lithologic types were recognized, and are listed from the more mafic to the more acidic (see "Igneous Petrology" section, this chapter):

1. olivine and Cr-spinel-bearing basalt andesite, which displays some features in common with boninites;
2. clinopyroxene-rich andesite, which contains a fairly large amount of clinopyroxene and orthopyroxene phenocrysts;
3. plagioclase-rich andesite, which is characterized by a more equal proportion of plagioclase and pyroxenes; and
4. aphyric to sparsely phyric andesite, which differs from the other types by the lack of large phenocrysts, an abundant intersertal trachytic groundmass, and late-crystallizing opaque minerals.

To examine the magmatic affinities of the basement andesites, their fractionation history, and their geochemical analogies, 17 samples were analyzed by XRF for major and trace elements (see "Explanatory Notes" chapter, this volume).

Within the 17 basement samples, the SiO_2 content ranged from 53 to 60 wt%, corresponding to a range from basaltic to acidic andesites (Table 8). The K_2O contents are generally low, mostly 0.4-1.2 wt%, indicating unaltered compositions. The TiO_2 contents range from 0.26 to 0.37 wt% and are lower than in the andesites of the basement rocks at Site 792 and of most island arcs. In contrast, Fe_2O_3 contents are similar in all andesite types at Site 793 (7.56-9.75 wt%), but are higher than in the andesitic basement of Site 792 (Table 8). The difference between

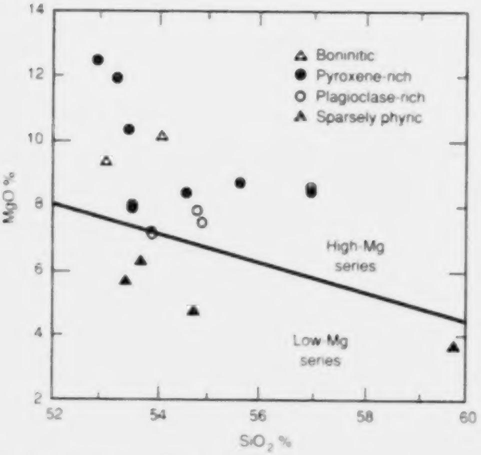

Figure 56. MgO wt% vs. SiO_2 wt% diagram. The boundary between the high-Mg and low-Mg series is discussed in the "Explanatory Notes" chapter (this volume) and is the same as for Leg 125.

the Fe-rich but Ti-poor andesites in the Site 793 basement rocks, and the Fe-poor but Ti-rich andesites in the Site 792 basement rocks, illustrates the tholeiitic affinity of the Site 793 andesitic suite vs. the calc-alkaline affinity of the Site 792 andesites. This contrast is also shown in the occurrence of opaque minerals, which are only present in the groundmass of the more differentiated andesites at Site 793, but which are included in the plagioclase and pyroxene phenocrysts of Site 792 basement andesites (see "Igneous Petrology" section, this chapter).

Another striking feature of the Site 793 basement suite is the relationship between MgO, Cr, and Ni contents. Chrome and nickel (and to a lesser extent, MgO) concentrations differ between the main petrographic types of andesite. The olivine-Cr-spinel-bearing basaltic andesites have the highest Cr (~700 ppm) and Ni (172.5-126.4 ppm) contents, whereas MgO contents are in the range of the clinopyroxene-rich andesite (9.33-10.14 wt%). The clinopyroxene-rich andesite shows a wider range of Cr (~249-628 ppm) and Ni (~50-140 ppm) contents, and the MgO contents of some samples (12.51%) are even higher than those of the olivine-Cr-spinel basaltic andesites. Even the plagioclase-rich andesites have rather high Cr (130-144 ppm), Ni (~38-55 ppm), and MgO (~8 wt%) contents compared with island-arc tholeiites. Only the sparsely to aphyric andesites display low Cr (< 100 ppm), Ni (< 50 ppm), and MgO (~3.78-5.68 wt%) contents. Thus, the first three types belong to a high-Mg series whereas the last type belongs to the more conventional low-Mg series (Fig. 56).

The Hole 793B andesites show the customary negative correlation between Al_2O_3 and MgO and can be subdivided into two groups on the basis of their Al_2O_3 contents. The olivine-Cr-spinel basaltic andesites and the clinopyroxene-rich andesites with MgO contents >7 wt% are Al_2O_3-poor (13-16 wt%). In contrast, the plagioclase-rich andesites and the sparsely phyric to aphyric andesites, with MgO ranging between 8 and 4 wt%, are Al_2O_3 rich (16-18 wt%).

In the MgO wt% vs. SiO_2 wt% diagram (Fig. 56), the Hole 793B andesitic suite fails to show a good negative correlation, implying that none of these rocks are linked by closed-system differentiation. In contrast, there is a very good positive correlation between TiO_2 and Al_2O_3 (Fig. 57), which indicates that these andesites are derived either from a similar mantle source through differing degrees of partial melting or from variably depleted sources.

Of the 17 trace elements analyzed, only Ce and (in some cases) Ba are considered unreliable, because their concentrations were close to the detection limits of the shipboard XRF.

The Site 793 andesites, compared with N-MORB, are enriched in the low-field-strength elements such as Rb, Sr, and Ba, features that are common to island-arc volcanic rocks. However, compared with many island-arc suites, including the Marianas, the Hole 793B basement andesites are depleted in Ba and Sr.

The Site 793 basement andesites also show rather low contents of high-field-strength elements (Fig. 58), especially Nb, which is always < 1 ppm. However, they differ by a factor of 2 in Y contents in all four types of andesite; Y contents are either 8-10 ppm or 14-20 ppm (Table 8). Most Site 793 andesites have a Zr/Y ratio ranging between 1 and 5 (see Fig. 59), with the exception of some clinopyroxene-rich porphyritic andesites and the aphyric siliceous andesites that have Zr/Y ratios < 1. The differences in the Y contents, like those in the Ti and Al contents of the Site 793 andesites, imply either variations in the degree of partial melting or differences in source compositions. The Cr vs. Y diagram (Fig. 60) shows that the andesites form three different groups on the basis of their Y contents. Within each group, the trend displayed by the andesites is consistent with crystal fractionation. Multiple lithologic suites constitute each group, with the most mafic members being boninitic, and the most differentiated being sparsely phyric.

Compared with the basement andesites of Site 792 that have the same ranges of SiO_2 and MgO values, those at Site 793 have lower Ti, P, and Zr contents. Andesites at both sites show two-fold ranges in Y contents in otherwise similar rock types.

Finally, the basement volcanic rocks at Site 793 are exclusively andesitic, whereas the Eocene basement rocks of the outer-arc high at Site 786 are more diversified, being made up of basalts, dacites, and rhyolites, as well as andesites. The andesites of Site 793 are mostly high-Mg andesites, whereas the

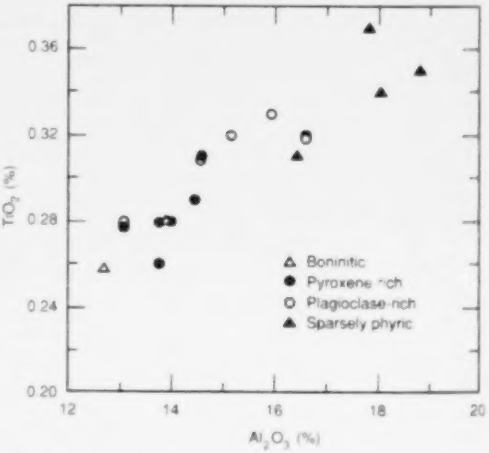

Figure 57. TiO_2 wt% vs. Al_2O_3 wt% diagram. There is a very good correlation between TiO_2 and Al_2O_3 in the basement andesites in Hole 793B.

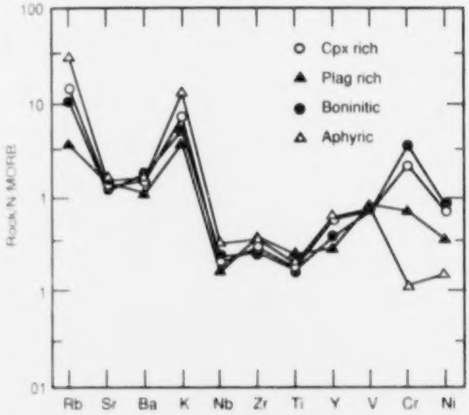

Figure 58. The four andesitic types are shown normalized to N-MORB. These patterns show a relative enrichment in the large-ion lithophile elements and depletion in the high-field-strength elements.

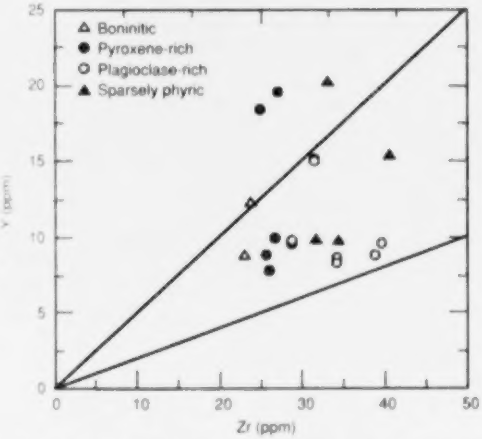

Figure 59. Y (ppm) vs. Zr (ppm) diagram showing the two-fold ranges in Y contents in the basement andesites in Hole 793B.

volcanic rocks of Site 786 are predominantly members of the low-Mg series. Finally, for the same range of SiO_2 contents, the basement volcanic rocks at Site 786 have lower TiO_2 contents and are more depleted in all the high-field-strength elements and Y. Thus, the temporal evolution noted above applies to the entire Cenozoic history of the Izu-Bonin Arc.

SEDIMENT/FLUID GEOCHEMISTRY

We obtained twelve 10-cm, six 25-cm, and thirteen 30-cm-long, whole-round samples from Holes 793A and 793B for electrical resistivity measurements, squeezing of pore water, and fluid and sediment analyses. Seven of the whole rounds did not yield any water.

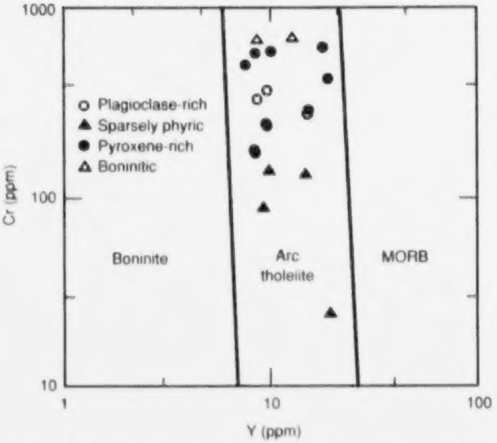

Figure 60. Y (ppm) vs. Cr (ppm). The boundaries between boninite, arc tholeiite, and MORB are those used during Leg 125 (J. Pearce, pers. comm.; see "Igneous Geochemistry" section, "Site 781" chapter [Fryer, Pearce, et al., 1990]) and are arbitrary. The failure to discriminate between the high-Mg and low-Mg series at Site 793 is unimportant, but the slope of the boundaries parallels typical crystal fractionation trends.

The deepest pore-water sample previously recovered by ODP was obtained from 1143.7 mbsf at Site 645. Here, we report data from samples down to 1258.95 mbsf.

Sediment Resistivity

Electric resistivity could only be measured on 20 of the whole rounds because of the geometry of some of the cores. For the samples below 1022 mbsf, resistivity was measured on slices cut from the whole rounds, and the electrode lengths were adjusted for each sample. The slices were cut < 10 min after the core arrived on deck, holes for the electrodes were drilled, and the slices were submerged in 35 g/kg NaCl solution for 48 hr prior to measurement. The results are presented in Table 9.

The formation factors calculated from the resistivity measurements are fairly stable, at about 2.5, to a depth of 77 mbsf (Core 126-793A-9H). In Unit III of Hole 793B (Cores 126-793B-2R to -16R), the formation factors scatter about a mean value of 5.7 and then increase abruptly through Unit IV (Cores 126-793B-16R to -19R) to an average level of 22 in Unit V (Cores 126-793B-19R to -82R; Fig. 61). Much of the variation observed in Unit V can be attributed to varying particle size. In Units I and III, the magnitude of the formation factors is the same as determined by other investigators for similar sediments at the same stage of compaction (e.g., Manheim and Waterman, 1974). However, the formation factors measured in Unit V are exceptionally high for the given porosity (see "Physical Properties" section, this chapter).

The measured rock resistivities compare favorably with resistivity measurements performed with other electrode configurations aboard the ship and thus seem to be real and characteristic of vitric sand and siltstones. We are not aware of other published data on the resistivity of similar rock types.

Fluid Geochemistry

The headspace hydrocarbon analyses did not show any gases above background level and thus are not reported.

Table 9. Sediment resistivity (R_s), measurement temperature, pore-water resistivity (R_{pw}) at 25°C and formation factor (F) of sediments from Holes 793A and 793B.

Core, section, interval (cm)	Depth (mbsf)	Cell constant (m)	R_s (ohm-m)	Temp. (°C)	R_{pw} (ohm-m)	F
126-793A-						
3H-3, 140-150	17.95	0.0914	0.649	11.6	0.200	2.4
6H-1, 140-150	43.45	0.1040	0.721	12.7	0.198	2.7
9H-4, 140-150	76.85	0.0997	0.827	12.6	0.198	2.5
126-793B-						
3R-1, 130-140	608.65	0.1037	1.499	16.5	0.198	6.2
6R-3, 0-10	636.35	0.0989	1.133	18.2	0.198	4.8
9R-2, 132-142	664.97	0.0910	1.249	17.3	0.196	5.3
5R-3, 117-127	724.32	0.1018	1.611	15.3	0.197	6.5
8R-3, 115-125	753.00	0.0952	2.296	15.1	0.196	9.3
21R-6, 133-143	786.58	0.0994	2.456	17.4	0.190	10.8
33R-6, 0-25	900.93	0.1001	4.371	17.8	0.167	22.1
36R-3, 113-138	926.56	0.1003	4.593	15.6	0.168	21.9
40R-5, 96-121	968.09	0.0935	3.496	18.4	0.165	18.1
43R-5, 120-150	997.05	0.0991	5.206	16.4	0.162	26.3
46R-3, 116-141	1022.99	0.0937	4.213	22.3	0.159	24.9
58R-4, 76-106	1139.41	0.0540[a]	5.932	24.4	0.195[b]	30.1
61R-3, 56-86	1166.61	0.0505[a]	2.737	23.3	0.195[b]	13.5
64R-6, 117-147	1200.75	0.0921[a]	5.990	16.6	0.195[b]	24.9
70R-7, 0-30	1225.45	0.0565[a]	4.227	23.0	0.195[b]	20.5
73R-4, 120-150	1284.25	0.0565[a]	5.663	23.0	0.195[b]	27.6
80R-5, 0-30	1352.15	0.0587[a]	4.619	24.2	0.195[b]	22.8

[a] Rocks were saturated with 35 g/kg NaCl solution prior to measurements.
[b] Lengths of electrodes were adjusted to fit individual samples.

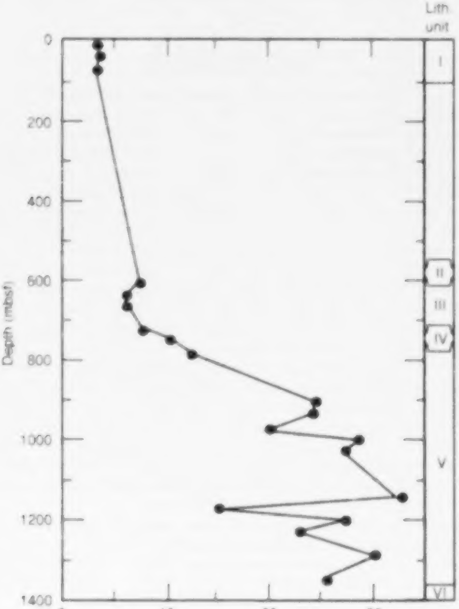

Figure 61. Formation factor, Holes 793A and 793B.

Because of a shortage of acetylene, the only cations that we could analyze were calcium and magnesium. To clean the hole, drilling mud was pumped between every second core. The drilling mud was the same as used at Site 792, and the composition of the drilling-mud filtrate is given in Table 10. There is no indication that any of the samples have been contaminated by drilling-mud filtrate. The distribution of calcium and magnesium (Fig. 62) follows the common evolution for marine sediments of decreasing magnesium and increasing calcium concentrations down to about 725 mbsf (Core 126-793B-15R). However, the continuous increase of calcium further down the hole is very unusual, and the pore waters below 786 mbsf (Core 126-793B-21R) are the most highly altered pore waters of marine origin ever recovered by DSDP/ODP, including the pore waters recovered at Site 792.

At Site 792, the highest calcium concentration was 169 mM at 600 mbsf (Core 126-792E-48R). At Site 793, we reached this level at 786 mbsf (Core 126-793B-21R), below which the calcium concentration continued to increase until it reached a stable level of about 300 mM at a depth of 1139 mbsf (Core 126-793B-58R). The pore waters below 850 mbsf are so highly altered that an isolated sample would have been difficult to recognize as altered seawater. Subsurface waters of similar composition are present in a few deep sedimentary basins and are classified as Ca-Cl-type waters, the origin of which has been disputed. The concentration of magnesium drops to about zero at 786 mbsf (Core 126-793B-21R). The sporadic occurrence of magnesium concentrations greater than the detection limit (about 0.2 mM) below this depth is probably a result of the precision of the methods. However, because of the limited sample volumes, other analyses were given priority above replicate magnesium analyses.

The data presented in Figure 62 show that even the concentration of chloride has been shifted relative to seawater. The concentration of chloride remains near seawater level through Unit III (Section 126-793B-15R-3) and then increases to a stable level of about 715 mM below 1023 mbsf (Core 126-793B-46R). Several processes leading to enhanced chloride concentrations in pore waters have been recognized. These are the dissolution of evaporites, gas hydrate formation, shale membrane filtration, and the uptake of water by authigenic mineral phases. Because of the absence of evaporites and the low concentration of organic carbon (Table 11), the first two of these may be excluded.

It has been observed that when shales become sufficiently compacted they may act as semipermeable membranes, which are more permeable to water than to ions (e.g., Kharaka and Berry, 1973). However, the efficiency of this process is dependent on the state of compaction, and none of the claystones at Site 793 have sufficiently low porosities to act as semipermeable membranes. Furthermore, if the elevated chloride concentrations were caused by shale-membrane filtration, one would expect to observe a corresponding chloride minimum on the low-pressure side (Unit III).

On the basis of this background, we concluded that the high chloride concentrations are caused during the uptake of water by the formation of authigenic mineral phases (smectites, gypsum, and zeolites). To our knowledge, this is the most extensive uptake of water ever reported for deep-sea sediments. This raises the question of the location of the reactions responsible for the dramatic changes in pore-water composition. The composition of pore waters is a dynamic equilibrium determined by the relative rates of reactions and processes (diffusion and advection) that remove or add a given component. At Site 792, the highly altered pore waters were attributed to low-temperature alteration of volcanogenic material. Because of the much higher formation factors at Site 793 (slower diffusion), the even more highly altered pore waters presumably could have been formed by the same reactions as at Site 792. The much slower diffusion

Table 10. Composition of pore water at Site 793.

Core, section,	Depth (mbsf)	pH	Alk (meq/l)	S (g/kg)	Cl^- (mM)	SO_4^{-2} (mM)	Mg^{+2} (mM)	Ca^{+2} (mM)	SiO_2 (μM)	NH_4 (μM)
126-793A-										
1H-2, 140-150	2.95	7.78	2.71	35.5	554	29.5	53.5	10.7	250	LD
3H-3, 140-150	17.95	7.74	2.71	36.0	555	29.5	52.8	10.4	589	11
6H-1, 140-150	43.45	7.77	3.32	36.5	561	28.2	52.8	9.5	623	282
9H-4, 140-150	76.85	7.85	3.36	ND	561	29.1	52.9	9.8	478	378
126-793B-										
3R-3, 130-140	608.65	7.69	2.07	35.0	560	29.1	51.4	19.2	725	LD
6R-3, 0-10	636.35	7.40	1.57	36.0	560	28.0	46.8	24.7	890	106
9R-2, 132-142	664.97	7.52	1.19	37.0	568	29.3	41.6	41.2	764	LD
12R-1, 100-110	692.15	7.65	1.40	37.5	566	29.0	37.4	52.3	905	104
15R-3, 117-127	724.32	7.64	0.88	37.5	569	29.5	25.4	80.2	914	58
18R-3, 115-125	753.00	7.63	0.62	38.5	588	22.5	14.8	108.6	158	33
21R-6, 133-143	786.58	ND	ND	ND	586	17.3	0.2	171.5	226	21
27R-7, 33-58	844.85	8.41	0.66	45.0	643	14.2	LD	213.2	172	LD
30R-4, 110-135	870.13	8.81	0.64	46.5	662	13.8	LD	237.3	143	LD
33R-6, 0-25	900.93	9.01	0.48	47.5	677	13.0	LD	255.2	196	LD
36R-3, 113-138	926.56	ND	ND	ND	671	11.9	LD	265.1	196	LD
40R-5, 96-121	968.09	ND	ND	ND	685	14.8	LD	276.3	196	ND
43R-5, 120-150	997.05	8.83	0.69	50.0	700	16.3	2.7	285.1	216	LD
46R-3, 116-141	1022.99	ND	ND	ND	715	16.6	LD	307.5	298	ND
58R-4, 76-106	1139.41	ND	ND	ND	710	15.7	LD	292.2	167	ND
61R-3, 56-86	1166.61	ND	ND	ND	724	14.4	1.1	298.7	197	LD
67R-4, 0-30	1225.45	ND	ND	ND	717	14.6	LD	293.9	138	ND
70R-7, 0-30	1258.95	ND	ND	ND	722	15.3	0.4	296.8	196	ND
Drilling mud filtrate		9.69	0.80	ND	215	12.0	2.7	7.0	19	58

Note: ND = not determined; LD = less than the detection limit.

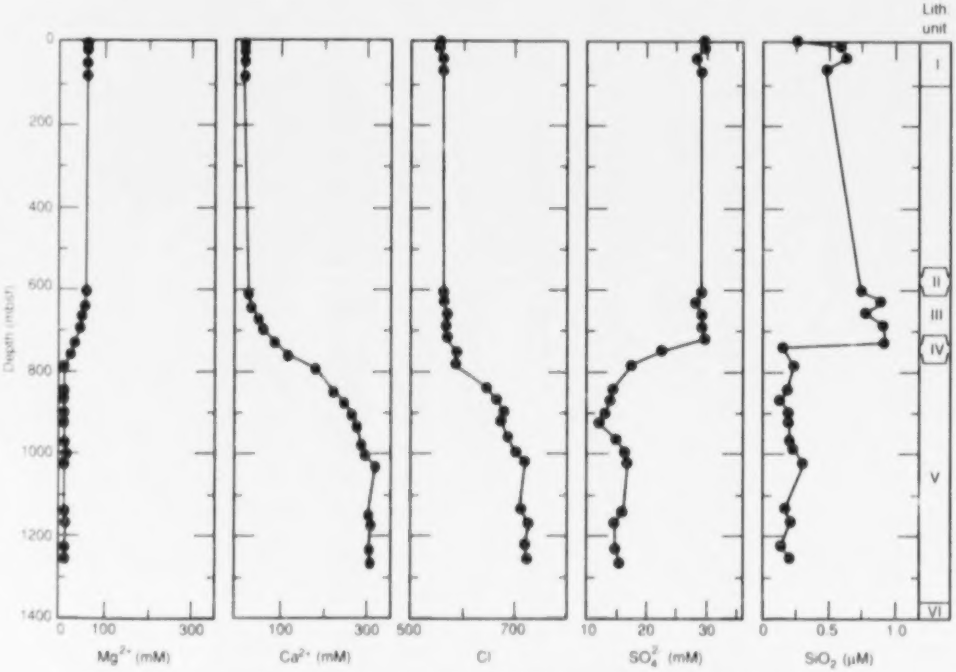

Figure 62. Pore-water characteristics, Holes 793A and 793B. Unit boundaries are shown at far right-hand side.

Table 11. Concentration of inorganic carbon, carbonate, total carbon, organic carbon, total nitrogen, and total sulfur in sediments from Site 793.

Core, section, interval (cm)	Depth (mbsf)	Inorg. C (%)	$CaCO_3$ (%)	Total C (%)	Org. C (%)	Total N (%)	Total S (%)
126-793A-							
1H-1, 68-70	0.68	0.97	8.1				
1H-2, 140-150	2.90	0.08	0.7	0.08	LD	LD	0.03
2H-2, 70-72	6.40	0.12	1				
3H-1, 115-118	14.65	2.71	22.6				
3H-2, 125-128	16.25	4.31	35.9				
3H-3, 46-47	16.96	5.88	49	6.16	0.28	0.03	0.02
3H-3, 83-86	17.33	5.39	44.9				
3H-3, 140-150	17.90	5.46	45.5	5.72	0.26	0.02	0.05
3H-4, 61-64	18.61	3.27	27.2				
4H-2, 40-42	24.90	3.56	29.7				
4H-6, 92-94	31.42	0.69	5.8	0.73	0.04	0.01	0.04
5H-1, 142-145	33.92	5.62	46.8				
5H-3, 21-25	34.32	2.95	24.6				
5H-4, 41-44	36.02	7.07	58.9				
5H-7, 118-120	41.29	3.45	28.7	3.83	0.38	0.05	0.06
6H-1, 77-79	42.77	3.72	31				
6H-1, 140-150	43.40	4.37	36.4	4.67	0.3	0.03	LD
6H-2, 114-116	44.64	5.69	47.4	5.91	0.22	0.03	LD
6H-3, 103-105	46.03	7.13	59.4				
6H-5, 64-66	48.64	5.75	47.9	6.08	0.33	0.04	0.01
7H-1, 119-121	52.79	4.31	35.9				
7H-2, 122-124	54.32	2.72	22.7				
7H-3, 93-95	55.53	4.05	33.7				
9H-1, 92-93	71.82	0.25	2.1	0.25	LD	0.01	0.01
9H-2, 76-79	73.16	0.56	4.7				
9H-3, 103-105	74.93	1.16	9.7	1.32	0.16	0.02	0.014
9H-4, 101-104	76.41	1.53	12.7				
9H-4, 140-150	76.80	0.97	8.1	1.11	0.14	0.02	0.1
9H-5, 75-78	77.65	1.34	11.2	1.49	0.15	0.02	0.1
10H-2, 136-137	82.27	1.66	13.8	1.7	0.04	0.02	0.07
11H-1, 81-82	90.91	5.72	47.7				
11H-2, 91-92	92.51	1.09	9.1				
11H-4, 34-37	94.94	0.33	2.8	0.33	LD	0.01	0.14
11H-7, 52-54	98.61	0.29	2.4				
126-793B-							
2R-1, 33-35	595.03	3.68	30.7	3.79	0.11	0.03	0.09
3R-1, 53-55	604.83	0.02	0.2				
3R-2, 19-21	605.79	0.04	0.3	0.07	0.03	0.01	0.1
3R-3, 5-7	607.09	1.34	11.2				
3R-3, 130-140	608.34	0.12	1	0.12	LD	LD	0.05
3R-4, 31-33	608.75	0.56	4.7				
4R-1, 62-64	614.62	0.14	1.2	0.17	0.03	0.01	0.05
4R-2, 9-11	615.59	3.26	27.2				
4R-3, 108-110	617.75	0.32	2.7				
4R-4, 70-72	618.90	0.24	2				
5R-1, 72-74	624.32	0.22	1.8				
5R-2, 118-120	626.18	0.39	3.3	0.43	0.04	0.01	0.09
5R-3, 128-130	627.63	0.44	3.7				
5R-4, 112-114	628.84	0.17	1.4				
5R-5, 44-46	629.57	1.28	10.7				
6R-1, 49-51	633.79	0.04	0.3	0.1	0.06	0.02	0.11
6R-2, 30-33	635.02	2.96	24.7	3.23	0.27	0.03	0.02
6R-3, 0-10	636.01	2.36	19.7	2.52	0.16	0.02	0.04
6R-CC, 3-5	636.54	0.69	5.8				
7R-1, 23-25	643.03	4.84	40.3	4.98	0.14	0.02	0.02
8R-1, 103-106	653.43	5.14	42.8				
8R-2, 17-18	653.98	0.75	6.3	0.8	0.05	0.01	0.03
9R-1, 29-31	662.39	0.63	5.3				
9R-1, 110-111	663.20	4.10	34.2	4.24	0.14	0.02	LD
9R-2, 45-46	664.01	2.47	20.6				
9R-2, 132-142	664.88	0.19	1.6	0.18	LD	LD	0.02
9R-3, 23-24	665.21	0.11	0.9				
10R-1, 40-42	672.20	0.07	0.6				
10R-1, 105-106	672.85	0.26	2.2	0.29	0.03	0.01	0.03
10R-2, 36-38	673.66	0.42	3.5				
10R-3, 109-111	675.86	1.34	11.2				
11R-1, 47-48	681.87	0.53	4.4				
11R-2, 86-87	683.65	0.69	5.8				
11R-3, 131-132	685.51	1.29	10.8				
11R-5, 134-135	688.38	0.34	2.8				
11R-6, 68-69	689.11	0.92	7.7				
12R-1, 33-35	691.43	1.19	9.9				

Table 11 (Continued).

Core, section, interval (cm)	Depth (mbsf)	Inorg. C (%)	CaCO$_3$ (%)	Total C (%)	Org. C (%)	Total N (%)	Total S (%)
126-793B-							
12R-1, 100-110	692.10	2.04	17	2.11	0.07	0.01	0.03
12R-2, 87-89	693.07	1.39	11.6				
13R-1, 43-45	701.23	3.68	30.7				
13R-2, 80-82	703.04	1.69	14.1				
13R-3, 33-34	704.01	0.22	1.8				
13R-4, 92-93	706.08	1.52	12.7				
14R-1, 120-121	711.60	0.17	1.4				
14R-2, 28-30	712.11	1.20	10				
15R-1, 45-47	720.55	0.55	4.6				
15R-2, 111-113	722.71	0.04	0.3				
15R-3, 75-77	723.67	0.04	0.3				
15R-3, 117-127	724.09	0.27	2.3	0.27	ID	ID	0.05
15R-4, 107-109	725.26	3.72	31				
16R-1, 29-31	729.99	0.47	3.9				
16R-2, 8-10	731.29	2.03	16.9	2.09	0.06	0.02	0.01
16R-3, 30-32	732.95	0.02	0.2				
16R-4, 21-23	734.28	2.68	22.3				
16R-5, 69-72	736.30	3.87	32.2				
16R-6, 107-109	738.18	4.66	38.8				
17R-1, 44-46	739.54	7.32	61	7.29	ID	0.02	0.06
17R-2, 41-43	740.36	4.73	39.4				
17R-3, 75-77	742.06	1.34	11.2				
17R-4, 75-77	743.50	4.81	40.1				
17R-5, 55-57	744.80	0.07	0.6	0.11	0.04	ID	ID
17R-6, 30-32	746.02	0.54	4.5				
17R-6, 92-93	746.64	0.74	6.2				
18R-1, 84-86	749.64	0.87	7.3				
18R-3, 38-40	752.18	0.87	7.3				
18R-3, 115-125	752.95	1.13	9.4				
18R-4, 22-24	753.52	1.29	10.8	1.31	0.02	ID	ID
19R-1, 123-125	759.63	0.08	0.7				
19R-2, 11-13	759.77	0.20	1.7				
19R-3, 54-56	761.63	0.04	0.3	0.08	0.04	ID	ID
19R-4, 81-83	763.36	0.04	0.3				
20R-1, 53-55	768.53	0.08	0.7				
20R-2, 120-122	770.63	0.11	0.9				
20R-3, 30-32	771.07	0.03	0.3	0.08	0.05	ID	ID
20R-4, 55-57	772.72	0.03	0.3				
20R-5, 123-125	774.85	0.03	0.3				
20R-7, 20-22	776.76	0.04	0.3				
21R-1, 77-78	778.47	0.03	0.3	0.06	0.03	ID	ID
21R-3, 94-96	781.64	0.07	0.6				
21R-5, 19-21	783.89	0.52	4.3				
21R-6, 133-143	786.53	0.41	3.4	0.45	0.04	ID	ID
22R-1, 81-82	788.11	0.66	5.5				
22R-3, 31-32	790.55	0.06	0.5				
23R-1, 58-60	797.58	0.15	1.3				
23R-3, 65-67	800.52	0.06	0.5	0.06	ID	ID	ID
23R-5, 40-41	803.13	0.05	0.4				
24R-2, 67-69	808.87	0.21	1.8				
24R-4, 7-9	811.16	0.03	0.3				
24R-4, 141-151	812.50	0.03	0.3	0.03	ID	ID	ID
24R-6, 55-57	814.67	0.29	2.4				
25R-1, 121-122	817.61	0.24	2				
25R-3, 29-30	819.58	0.08	0.7				
25R-5, 81-82	823.10	0.37	3.1	0.4	0.03	ID	ID
25R-6, 105-106	824.84	1.00	8.3				
26R-1, 45-47	826.15	0.27	2.3				
26R-3, 76-78	829.33	0.17	1.4				
26R-4, 18-20	830.25	0.13	1.1				
26R-5, 17-20	831.74	0.05	0.4	0.09	0.04	ID	ID
27R-2, 3-5	836.93	0.08	0.7				
27R-4, 21-23	839.91	0.23	1.9				
27R-6, 110-112	843.65	0.50	4.2				
27R-7, 33-58	844.38	0.21	1.8	0.23	0.02	ID	ID
28R-2, 85-87	846.62	0.05	0.4				
28R-4, 38-40	849.14	0.48	4				
28R-6, 100-102	852.63	0.06	0.5	0.08	0.02	ID	ID
28R-8, 37-39	854.81	0.12	1				
29R-1, 52-54	855.22	0.09	0.8				
29R-3, 22-24	857.58	0.06	0.5	0.1	0.04	ID	ID
29R-5, 90-92	860.90	0.13	1.1				
30R-1, 39-41	864.79	0.14	1.2				
30R-3, 56-58	867.96	0.14	1.2				
30R-4, 110-135	870.00	0.53	4.4	0.53	ID	ID	ID
30R-5, 40-42	870.65	0.30	2.5				
31R-1, 96-98	874.96	1.62	13.5				

Table 11 (Continued).

Core, section, interval (cm)	Depth (mbsf)	Inorg. C (%)	CaCO$_3$ (%)	Total C (%)	Org. C (%)	Total N (%)	Total S (%)
126-793B-							
31R-3, 62-63	877.27	0.83	6.9	0.86	0.03	LD	LD
31R-4, 14-16	877.99	2.37	19.7				
31R-6, 69-71	881.39	0.06	0.5	0.07	0.01	LD	LD
32R-1, 48-50	884.18	0.06	0.5	0.07	0.01	LD	LD
32R-3, 70-72	887.11	0.04	0.3				
32R-4, 128-130	889.19	0.05	0.4				
33R-1, 85-86	894.15	0.04	0.3				
33R-3, 87-89	897.02	1.03	8.6				
33R-5, 57-58	899.31	0.05	0.4				
33R-6, 0-25	900.09	0.08	0.7	0.08	LD	LD	LD
33R-7, 60-61	902.19	0.09	0.8				
34R-1, 31-32	903.31	1.35	11.3				
34R-3, 58-59	906.50	0.57	4.8				
34R-5, 88-89	909.16	0.03	0.3	0.04	0.01	LD	LD
34R-7, 27-28	911.06	0.05	0.4				
35R-1, 75-76	913.35	0.06	0.5				
35R-3, 53-54	916.01	1.26	10.5	1.37	0.11	LD	LD
35R-5, 125-126	919.51	0.19	1.6				
35R-6, 57-58	920.33	0.18	1.5				
36R-1, 115-117	923.45	0.94	7.8				
36R-3, 115-130	926.33	1.17	9.8	1.23	0.06	LD	LD
36R-5, 85-86	928.62	0.43	3.6				
37R-1, 33-34	932.33	0.17	1.4				
37R-5, 69-70	938.30	0.88	7.3	0.97	0.09	LD	LD
37R-7, 73-74	940.96	1.90	15.8				
38R-1, 138-140	942.98	3.47	28.9				
38R-3, 64-66	945.11	0.24	2.0	0.28	0.04	LD	LD
38R-5, 143-145	948.37	0.67	5.6				
40R-2, 54-56	961.81	0.07	0.6				
40R-4, 106-108	965.14	0.39	3.3				
40R-5, 98-121	966.25	0.09	0.8	0.13	0.04	LD	LD
40R-6, 133-135	967.83	0.12	1				
40R-8, 109-111	970.40	0.14	1.2				
41R-2, 45-46	972.53	0.42	3.5				
41R-4, 59-61	975.32	0.05	0.4				
41R-6, 97-99	978.42	0.18	1.5				
42R-1, 43-45	980.73	0.32	2.7				
42R-3, 22-24	983.37	0.06	0.5				
43R-1, 17-19	989.87	0.08	0.7				
43R-3, 59-61	992.83	0.39	3.3				
43R-5, 68-70	995.62	0.09	0.8				
43R-5, 120-150	996.14	0.06	0.5				
43R-7, 5-7	997.87	0.41	3.4				
44R-1, 60-62	1000.00	0.42	3.5				
44R-3, 49-51	1002.77	0.15	1.3				
44R-5, 7-9	1005.21	0.10	0.8				
44R-7, 24-26	1008.27	0.09	0.8				
45R-1, 45-47	1009.55	0.13	1.1				
45R-1, 100-102	1010.10	0.37	3.1				
46R-1, 27-28	1018.97	0.08	0.7				
46R-3, 19-20	1020.83	0.14	1.2				
46R-3, 116-141	1021.80	0.18	1.5				
46R-5, 43-44	1024.00	0.08	0.7				
47R-1, 61-62	1028.61	0.06	0.5				
47R-3, 80-81	1031.34	0.06	0.5				
47R-4, 78-79	1032.82	0.44	3.7				
47R-5, 12-13	1033.52	0.11	0.9				
48R-1, 82-84	1038.42	0.18	1.5				
48R-3, 54-56	1041.14	0.07	0.6				
48R-5, 31-33	1043.91	0.23	1.9				
48R-6, 57-59	1045.46	0.06	0.5				
49R-1, 88-89	1048.18	0.13	1.1				
49R-2, 108-109	1049.88	0.19	1.6				
49R-3, 45-75	1050.52	0.18	1.5				
50R-1, 78-80	1057.78	0.06	0.5				
50R-3, 57-59	1060.57	0.57	4.8				
50R-5, 121-123	1064.13	0.18	1.5				
50R-6, 127-129	1065.69	0.05	0.4				
51R-2, 14-16	1067.28	0.27	2.3				
51R-4, 64-66	1070.78	0.13	1.1				
51R-6, 93-95	1073.92	0.51	4.3				
51R-8, 5-7	1075.83	0.18	1.5				
52R-1, 75-77	1077.15	0.07	0.6				
52R-1, 108-138	1077.38	0.06	0.5				
52R-3, 67-69	1079.95	0.05	0.4				
52R-5, 40-42	1082.07	0.15	1.3				
53R-1, 39-41	1086.49	0.13	1.1				

Table 11 (Continued).

Core, section, interval (cm)	Depth (mbsf)	Inorg. C (%)	$CaCO_3$ (%)	Total C (%)	Org. C (%)	Total N (%)	Total S (%)
126-793B-							
53R-3, 69-71	1089.66	0.07	0.6				
53R-CC, 8-10	1091.67	0.41	3.4				
54R-2, 35-37	1096.43	0.17	1.4				
54R-4, 32-34	1099.22	0.07	0.6				
55R-2, 0-30	1105.56	0.06	0.5				
55R-2, 134-136	1106.90	0.24	2				
55R-4, 103-105	1109.20	0.05	0.4				
56R-3, 70-74	1118.70	0.18	1.5				
57R-1, 48-50	1125.18	0.27	2.3				
57R-3, 15-17	1127.85	0.06	0.5				
58R-1, 37-39	1134.37	0.05	0.4				
58R-3, 94-96	1137.64	0.16	1.3				
58R-4, 76-106	1138.96	0.11	0.9				
58R-5, 122-124	1140.58	0.04	0.3				
58R-7, 87-89	1143.20	0.05	0.4				
59R-1, 45-46	1144.05	0.04	0.3				
59R-3, 75-77	1147.09	0.18	1.5				
59R-3, 132-133	1147.66	0.03	0.3	0.19	0.16	LD	LD
59R-5, 72-74	1149.89	0.04	0.3				
59R-7, 136-138	1153.26	0.04	0.3				
60R-1, 102-103	1154.22	0.06	0.5				
60R-3, 60-62	1156.80	0.05	0.4				
60R-5, 83-84	1159.84	0.03	0.3				
60R-7, 29-31	1161.90	0.05	0.4				
61R-1, 22-24	1163.12	0.04	0.3				
61R-3, 40-42	1166.05	0.10	0.8				
61R-3, 56-86	1166.21	0.09	0.8				
62R-1, 46-47	1173.06	0.05	0.4				
62R-2, 108-110	1174.89	0.05	0.4				
62R-4, 64-66	1177.14	0.04	0.3				
63R-1, 74-76	1182.94	0.05	0.4				
63R-4, 67-69	1187.34	0.06	0.5				
64R-1, 46-48	1192.36	0.06	0.5				
64R-3, 81-83	1195.33	0.05	0.4				
64R-5, 122-124	1198.56	0.07	0.6				
64R-6, 117-147	1200.01	0.13	1.1				
64R-7, 99-101	1201.30	0.74	6.2				
65R-1, 80-82	1202.30	0.03	0.2				
65R-5, 30-32	1207.64	0.04	0.3				
65R-6, 74-76	1209.58	0.23	1.9				
65R-7, 35-37	1210.69	0.04	0.3				
66R-1, 65-67	1211.75	0.03	0.2				
66R-3, 81-83	1214.81	0.03	0.2				
66R-4, 34-36	1215.84	0.04	0.3				
66R-4, 117-118	1216.67	0.21	1.8				
66R-6, 140-142	1219.69	0.37	3.1				
67R-1, 97-99	1221.77	0.05	0.4				
67R-3, 69-71	1224.35	0.20	1.7				
67R-4, 0-30	1225.11	0.04	0.3				
67R-5, 121-123	1227.82	0.05	0.4				
68R-1, 115-117	1231.65	0.26	2.2				
68R-3, 38-40	1233.78	0.11	0.9				
68R-4, 91-93	1235.67	0.10	0.8				
68R-6, 26-28	1237.95	0.10	0.8				
69R-1, 72-74	1240.92	0.60	5				
69R-3, 73-75	1243.85	0.07	0.6				
69R-5, 47-49	1246.38	0.77	6.4				
69R-7, 12-14	1248.99	0.06	0.5				
70R-1, 92-96	1250.72	0.26	2.2				
70R-3, 74-76	1253.49	0.14	1.2				
70R-5, 62-64	1255.93	0.35	2.9				
70R-7, 0-30	1258.31	0.11	0.9				
70R-7, 45-47	1258.76	0.13	1.1				
71R-1, 88-90	1260.28	0.27	2.2				
71R-7, 83-85	1268.11	0.12	1				
72R-1, 58-60	1269.28	0.32	2.7				
72R-3, 79-81	1272.49	0.09	0.7				
72R-5, 81-83	1275.51	0.33	2.7				
72R-7, 12-14	1277.54	0.06	0.5				
73R-1, 102-104	1279.42	0.14	1.2				
73R-3, 38-40	1281.54	0.08	0.7				
73R-4, 120-150	1283.71	0.37	3.1				
73R-5, 56-58	1284.57	0.31	2.6				
74R-5, 64-66	1294.17	0.32	2.7				
74R-7, 81-83	1296.83	0.59	4.9				
75R-1, 75-77	1298.45	0.45	3.7				
75R-5, 71-73	1304.34	0.65	5.4				

Table 11 (Continued).

Core, section, interval (cm)	Depth (mbsf)	Inorg. C (%)	$CaCO_3$ (%)	Total C (%)	Org. C (%)	Total N (%)	Total S (%)
126-793B-							
75R-7, 6-8	1306.69	0.13	1.1				
76R-1, 71-73	1308.01	0.08	0.7				
76R-5, 104-134	1314.25	0.06	0.5				
77R-1, 63-65	1317.63	0.11	0.9				
77R-3, 120-122	1321.13	0.57	4.7				
77R-5, 101-103	1323.88	0.09	0.7				
78R-1, 64-66	1327.34	0.21	1.7				
78R-3, 64-66	1330.31	0.09	0.7				
78R-5, 56-58	1332.68	0.26	2.2				
78R-7, 123-125	1336.11	0.24	2				
79R-1, 63-64	1337.03	0.24	2				
79R-5, 43-44	1342.15	0.54	4.5				
79R-6, 60-61	1343.77	0.22	1.8				
80R-1, 95-97	1346.95	0.21	1.7				
80R-3, 86-88	1349.86	0.24	2				
80R-5, 0-30	1351.63	0.10	0.8				
80R-5, 73-74	1352.36	0.81	6.7				
80R-7, 4-6	1354.49	0.55	4.6				
82R-1, 73-75	1366.03	0.05	0.4				
82R-3, 70-71	1368.80	0.05	0.4				
82R-5, 96-97	1371.78	0.04	0.3				
82R-7, 49-51	1374.18	0.03	0.2				
83R-1, 96-98	1375.86	0.06	0.5				
83R-2, 28-30	1376.68	0.05	0.4				
84R-1, 22-24	1384.72	0.03	0.2				
84R-2, 98-100	1386.98	0.04	0.3				
85R-1, 25-27	1394.15	0.04	0.3				
87R-3, 45-75	1416.91	0.05	0.4				
88R-1, 79-81	1423.69	0.07	0.6				
88R-2, 23-25	1424.55	0.07	0.6				
89R-1, 34-36	1431.74	0.07	0.6				
89R-3, 48-50	1434.80	0.05	0.4				

Note: LD = less than detection limit.

of dissolved constituents would sustain steeper concentration gradients and more prominent extremes. However, the possibility that the highly altered composition of the pore waters in Unit V is a result of reactions occurring in Unit VI must be considered.

At present, there are two lines of observations contradicting this hypothesis:

1. The concentration of magnesium drops to zero at the top of Unit V, which shows that reactions are taking place at the same rate that magnesium is diffusing from above.
2. None of the dissolved constituents show prominent gradients in the lower half of Unit V, indicating that exchange with the underlying unit is limited.

Most probably, any previous hydrothermal pore-water signal has now been overprinted by the prominent low-temperature alteration reactions and the growth of authigenic smectite at the expense of volcanic glass, which constitutes the major sink for magnesium. Calcium is probably derived from this reaction and from the alteration of plagioclase. Shipboard, semiquantitative XRD analyses show that smectites, gypsum, and zeolites are abundant constituents of Unit V and VI sediments (see "Lithostratigraphy and Accumulation Rates" section, this chapter). Although this cannot be confirmed by shipboard analyses, charge-balance calculations show that the pore waters are severely depleted in sodium. The most likely sink for sodium is the formation of zeolites.

The low alkalinities in Units IV and V (Table 10) are a result of the precipitation of carbonate in response to the release of calcium. The reason that alkalinities are not even lower is probably the formation of $CaHCO_3$ ion pairs, although this can only be confirmed by more detailed speciation studies. Note that the precipitation of this amount of carbonate would result in <0.01% calcite. Thus, this hypothesis does not conflict with the very low concentrations of sedimentary carbonate (Table 11).

Sulfate concentration profiles in marine sediments usually have a steep gradient close to the seafloor. At Site 793, the concentration of sulfate remains close to seawater levels down to 724 mbsf (Core 126-793B-15R) and then decreases to a minimum of 11.9 mM at 927 mbsf (Core 126-793B-36R; Fig. 62). As at Site 792, the concentration of sulfate appears to be controlled by the precipitation of gypsum, although saturation-state calculations show an apparent supersaturation with respect to this mineral below about 800 mbsf. This supersaturation probably is an artifact resulting from the use of constant-activity coefficients for calcium and sulfate similar to the activity constants in seawater. In these pore waters, the coefficients presumably are considerably smaller than in seawater as a result of the formation of $CaSO_4$ ion pairs.

The low concentrations of ammonia in Unit V substantiate the hypothesis that the removal of sulfate is a result of mineral precipitation rather than of bacterial consumption.

The concentration of dissolved silica increases from about 500 μM in Unit I to about 900 μM in Unit III, then decreases abruptly to about 200 μM in Units IV and V (Fig. 62). The steep gradient between Unit III and IV is another indication of high reaction rates.

Sediment Geochemistry

Sediments from Site 793 were analyzed on board ship for inorganic carbon, total carbon, nitrogen, and sulfur (see "Explanatory Notes" chapter, this volume). Analytical results are presented in Table 11. The concentration of organic carbon is very low, ranging from less than the detection limit to 0.38%, with an average of 0.07%. The concentration of total sedimentary sulfur varies from less than the detection limit to 0.14%.

PHYSICAL PROPERTIES

Introduction

Physical property measurements completed on APC cores in Hole 793A included multisensor track (MST) logging, thermal conductivity, vane shear strength, Hamilton Frame (HF) compressional sonic velocity, index properties, and carbonate analyses. Rotary-drilled cores from Hole 793B were measured for HF velocity, index properties, and calcium carbonate. Details of procedures are included in the "Explanatory Notes" chapter (this volume). As nearly 500 m of unrecovered section separates Holes 793A and 793B, and because significant differences in lithification exist between the sediments in the two holes, we will discuss the properties of each separately.

Index Properties

Hole 793A

Porosity and water content values decrease slightly with depth in Unit I, and correlate inversely with wet-bulk density (Table 12, Fig. 63). We did not observe any obvious changes at the Subunit IA/IB contact, but general downward trends are reflected in the average values of these index properties for the two subunits: porosity, 70.1% and 66.2%; water content, 79.4% and 66.4%; and wet-bulk density, 1.65 and 1.71 g/cm^3 in Subunits IA and IB, respectively. We note a tenuous correlation between porosity, water content, and carbonate content. High carbonate contents in this unit are associated with higher percentages of clay-size material and, therefore, higher porosities. The GRAPE and gravimetric wet-bulk density data from Hole 793A are shown in Figure 64. Similar density values are obtained by both methods. Higher variability in the GRAPE measurements, and intervals of noticeably lower GRAPE density values (e.g., between 40 and 50 mbsf), probably result from coring disturbance, which is generally avoided in gravimetric sampling.

Grain density values in Unit I are fairly high; the majority of values fall above 2.7 g/cm^3. In addition, grain density values correlate well with carbonate contents. One exception is the interval between 60 and 85 mbsf in which grain density is high, but carbonate contents are lower than average (Table 12). Grain density values increase slightly from Subunit IA (average 2.70 g/cm^3) to IB (average 2.77 g/cm^3).

Hole 793B

Unit II, a diabase sill, is characterized by very low porosity and high wet-bulk density values. Porosity and water content values from the diabases are the lowest measured at this site (averages of 10.4% and 4.0%, respectively), whereas wet-bulk density averages 2.76 g/cm^3 and grain density averages 2.79 g/cm^3.

With the exception of Unit II, correlation between the lithologic units and the index property measurements is marginal. Although fairly sharp changes in index properties were observed at several unit boundaries (e.g., Unit III/IV and Unit IV/V boundaries; see Fig. 63), similar changes were noted at numerous other depths within the section. Particularly interesting is the lack of a significant variation in the index property values from the base of the sediments into basement rock, probably the result of the gradual transition from the sediments to igneous breccias (see "Lithostratigraphy and Accumulation Rates" and "Igneous Petrology" sections, this chapter).

We recognized some general trends. Units III and IV have high porosity (means of 60.3% and 46.5%) and water content (means of 50.9% and 32%) values. A sharp change in these parameters is observed at the Unit III/IV boundary (e.g., porosity decreases from approximately 60% to 40%). Trends reverse within Unit IV and values comparable to those in Unit III are reached toward the base of Unit IV. Mean values of porosity and water content in lithologic Units VI and VII are lower: 31% and 27% (porosity) and 15% and 12% (water content), respectively. Fluctuations similar to those observed in Hole 792E are superimposed on these gross trends. Values of porosity and water content decrease from a maximum of 64% and 60%, respectively, at 600 mbsf, to a minimum of 25% and 10% at 900 mbsf, then increase to 40% and 30% at approximately 1000 mbsf. Another decrease occurs over the interval from 1000 to 1120 mbsf, below which values of both parameters remain essentially unchanged to a depth of 1280 mbsf. A fairly sharp decrease in porosity and water content follows. Minima at 1320 mbsf represent the lowest porosity and water content values in the hole, with the exception of the diabase of Unit II. This depth interval coincides with the occurrence of abundant opaque minerals.

No other obvious correlation between the lithology (in particular, grain size or mineralogy) is observed in this hole (see "Lithostratigraphy and Accumulation Rates" section, this chapter). Porosity and water content values increase to a depth of 1350 mbsf, then remain fairly stable to about 1480 mbsf, at which point both increase sharply. The volcanic breccia and lava flow units within the basement rocks are clearly differentiated by the index property measurements (Table 12). Samples from the flow units are characterized by generally low porosity and water content values, and high wet-bulk density values, compared with those in the breccia.

Wet-bulk density trends in Hole 793B mirror those observed in porosity and water content. Bulk density values increase from about 1.7 g/cm^3 at the top of the sediment (means of 1.86 and 2.05 g/cm^3 in Units III and IV, respectively) to 2.2 g/cm^3 at approximately 900 mbsf. The trend then reverses and values decrease sharply to a depth of 1000 mbsf, followed by a steady increase in wet-bulk density to the Unit VII boundary; the mean value in Unit VI is 2.5 g/cm^3. Values in basement rocks are quite stable, averaging 2.54 g/cm^3.

Grain density values display a high degree of variability throughout the sedimentary section in both Holes 793A and 793B. Values average 2.71 g/cm^3 within Unit III and 2.62 g/cm^3 in Unit IV. Average grain density values in Units V, VI, and VII are 2.57, 2.66, and 2.79 g/cm^3, respectively. In general, high values correspond to intervals of high carbonate content (Fig. 63). Grain density values above 2.8 g/cm^3 are probably associated with concentrations of heavy minerals.

Carbonate Content

Ranges and averages of carbonate contents in Units III (0.2%–43%; average 10%) and IV (1.0%–61%; mean 21%) are similar to those in the upper 100 mbsf (Unit I; Hole 793A). Much of the variability in carbonate is a result of the presence of nannofossil-rich layers. Except for a zone between 867 and 956 mbsf in which values reach 30%, carbonate contents are generally <4% in Units V and VI (averages are 2.0% and 0.4%, respectively). Lithologic Unit IV, which has the highest average carbonate content, has been interpreted as a pelagic unit deposited during a period of volcanic quiescence (see "Lithostratigraphy and Accumulation Rates" section, this chapter). This implies that much of the variation in $CaCO_3$ content is the result of dilution by volcanogenic input.

Vane Shear Strength

Hole 793A

Only 16 successful vane shear strength measurements were acquired in Hole 793A because of the short APC section. These values are shown in Table 13 and are plotted in Figure 65. Sev-

Table 12. **Physical property (index properties, velocity, and calcium carbonate content) data from Holes 793A and 793B.**

Core, section, interval (cm)	Depth (mbsf)	Wet-bulk density (g/cm³)	Dry-bulk density (g/cm³)	Porosity (%)	Water content (%)	Grain density (g/cm³)	Void ratio	Carbonate content (%)	Velocity (km/s)
126-793A-									
1H-1, 69-71	0.69	1.59	0.88	72	86	2.81	2.55	8.1	
1H-2, 140-150	2.9							0.7	
2H-2, 67-71	6.39	1.10[a]	0.90	20[a]	23[a]	2.31[a]	0.25[a]	1.0	
3H-1, 114-116	14.64	1.67	0.98	70	75	2.71	2.31	22.6	1.52
3H-2, 125-128	16.25	1.73	1.04	71	72	2.89	2.39	35.9	1.53
3H-3, 46-47	16.96							49.0	
3H-3, 82-84	17.32	1.60	0.92	68	78	2.68	2.14	44.9	1.52
3H-3, 140	150							45.5	
3H-4, 61-64	18.61	1.67	0.97	70	76	2.79	2.37	27.2	
3H-5, 105-107	20.55	1.60[a]	0.73	88[a]	130[a]	1.62[a]	7.51[a]		
4H-2, 40-42	24.90	1.65	0.98	68	72	2.65	2.10	29.7	1.54
4H-4, 115-117	28.65	1.72	1.19	54	48	2.41	1.19		1.53
4H-6, 92-94	31.42							5.7	
5H-1, 142-145	33.92	1.57	0.87	71	87	2.81	2.50	46.8	1.53
5H-3, 21-25	34.32	1.81	1.22	59	51	2.66	1.46	24.6	1.58
5H-4, 41-45	36.02	1.71	1.03	68	69	2.75	2.16	58.9	1.53
5H-7, 118-121	41.29	1.75	1.12	64	60	2.83	1.77	28.7	1.55
6H-1, 76-79	42.76	1.73	1.03	70	71	3.24	2.35	31.0	1.52
6H-1, 140-150	43.4							36.4	
6H-2, 114-116	44.64	1.73	1.08	66	64	2.72	1.91	47.4	1.55
6H-3, 103-105	46.03	1.72	1.00	73	76	3.01	2.68	59.4	1.52
6H-5, 63-65	48.63	1.70	1.02	69	71	2.86	2.26	47.9	1.53
7H-1, 119-121	52.79	1.65	0.99	67	71	2.76	2.00	35.9	1.55
7H-2, 121-124	54.31	1.64	0.94	71	79	2.70	2.42	22.7	1.52
7H-3, 92-95	55.52	1.68	1.04	65	66	2.68	1.89	33.7	1.54
8H-1, 42-45	61.62	1.68	1.04	65	65	2.85	1.83		
8H-5, 140-141	68.08	1.73	1.20	53	46	2.82	1.12		
9H-1, 92-93	71.82	1.79	1.17	63	56	2.76	1.70	2.1	
9H-2, 76-78	73.16	1.91	1.26	66	54	2.87	1.90	4.7	1.58
9H-3, 107-110	74.97	1.74	1.05	70	71	2.82	2.37	9.7	1.58
9H-4, 103-107	76.43	1.79	1.16	64	58	2.82	1.78	12.7	1.61
9H-4, 140-150	76.8							8.1	
9H-5, 75-78	77.65	1.78	1.15	64	58	2.61	1.74	11.2	1.56
10H-1, 38-40	80.86	1.58	0.88	71	85	2.74	2.43		
10H-2, 135-138	82.26	1.78	1.14	64	59	2.86	1.81	13.8	
11H-1, 81-83	90.91							47.6	1.58
11H-1, 135-138	91.45	1.72	1.00	73	77	2.79	2.69		
11H-2, 90-92	92.50	1.63	0.98	65	70	2.49	1.88	9.1	1.61
11H-4, 34-37	94.94	1.62	0.99	64	67	2.44	1.76	2.7	1.65
11H-7, 52-53	98.61	1.64	1.02	63	64	2.56	1.68	2.4	1.65
126-793B-									
1R-1, 19-20	586.69	2.75	2.66	9	3	2.75[a]	0.10		5.14
1R-1, 66-68	587.16	2.88	2.77	12	4	2.93	0.13		4.66
1R-1, 123-125	587.73	3.13	3.00	13	4	3.13	0.15		5.06
1R-1, 101-103	589.01	3.07	2.94	13	5	3.21	0.15		4.66
1R-2, 113-115	589.13	2.76	2.66	10	4	2.79	0.11		5.00
1R-2, 18-20	589.53	3.27	3.17	10	3	3.14	0.12		4.63
1R-3, 70-73	590.05	2.77	2.65	12	5	2.82	0.14		4.99
2R-1, 32-34	595.02	1.63	0.94	70	78	2.63	2.29	30.7	1.86
3R-1, 54-57	604.84	1.69	1.08	61	59	2.65	1.57	0.2	2.10
3R-2, 20-22	605.80	1.97	1.43	55	40	2.70	1.20	0.3	1.97
3R-3, 6-8	607.10	1.78	1.13	66	61	2.68	1.91	11.2	1.94
3R-3, 130-140	608.34							1.0	
3R-4, 32-34	608.76	1.78	1.12	67	62	2.72	2.02	4.7	2.04
4R-1, 64-66	614.64	1.81	1.15	67	60	2.76	1.99	1.2	2.28
4R-2, 11-13	615.61	1.78	1.19	61	53	2.73	1.53	27.2	1.93
4R-2, 102-104	616.52	1.89	1.22	67	58	2.42	2.07		2.08
4R-3, 109-111	617.76	1.88	1.28	60	49	2.47	1.50	2.7	1.94
4R-4, 71-73	618.91	1.71	1.13	58	54	2.47	1.39	2.0	1.83
5R-1, 75-77	624.35	1.68	1.03	66	67	2.71	1.96	1.8	1.86
5R-2, 20-22	625.20	1.70	1.10	60	57	2.49	1.52		1.91
5R-2, 118-120	626.18							3.3	
5R-3, 129-131	627.64	1.84	1.24	60	51	2.57	1.51	3.7	2.01
5R-4, 111-113	628.83	1.77[a]	1.33	45[a]	35[a]	3.34[a]	0.82[a]	1.4	1.91
5R-5, 44-46	629.57	1.74	1.16	59	53	2.47	1.45	10.7	1.91
6R-1, 51-53	633.81	1.69	1.05	65	65	2.71	1.83	0.3	1.85
6R-2, 30-33	635.02	1.79	1.18	62	55	2.73	1.62	24.7	1.90
6R-3, 0-10	636.01							19.7	
6R-CC, 3-5	636.54	1.67	1.10	57	54	2.27	1.34	5.8	1.89
7R-1, 24-26	643.04	1.92	1.34	59	46	2.82	1.46	40.3	2.00
8R-1, 103-105	653.43	1.87	1.28	61	49	2.97	1.53	42.8	1.93
8R-2, 18-20	653.99	2.04	1.41	64	48	2.48	1.79	6.3	1.92

Table 12 (Continued).

Core, section, interval (cm)	Depth (mbsf)	Wet-bulk density (g/cm³)	Dry-bulk density (g/cm³)	Porosity (%)	Water content (%)	Grain density (g/cm³)	Void ratio	Carbonate content (%)	Velocity (km/s)
126-793B-									
9R-1, 29-30	662.39	1.90	1.24	66	56	2.66	1.97	5.3	1.92
9R-1, 110-112	663.20	2.01	1.38	64	48	2.89	1.76	34.2	1.97
9R-2, 44-46	664.00	1.93	1.29	65	52	3.08	1.85	20.6	2.06
9R-2, 132-142	664.88							1.6	
9R-3, 22-24	665.20	2.03	1.53	59	43	3.10	1.44	0.9	2.09
10R-1, 41-43	672.21	1.81	1.21	61	53	2.80	1.56	0.6	2.07
10R-1, 105-107	672.85	1.88	1.23	65	56	2.93	1.89	2.2	1.97
10R-2, 35-37	673.65	1.86	1.22	64	55	2.74	1.80	3.5	1.96
10R-2, 110-112	674.40	1.83	1.20	64	56	2.58	1.80		2.02
10R-3, 107-109	675.84	2.05	1.33	72	57	3.02	2.61	11.2	2.01
10R-3, 110-112	675.87	1.91	1.35	57	44	2.69	1.32		2.12
11R-1, 47-49	681.87	1.74	1.20	55	48	2.57	1.21	4.4	2.14
11R-2, 84-86	683.63	2.17	1.67	50	31	2.86	1.01	5.8	2.18
11R-3, 131-133	685.51	2.16	1.48	69	48	3.16	2.19	10.8	2.09
11R-4, 90-92	686.49	2.11	1.50	61	42	3.10	1.58		2.08
11R-5, 134-136	688.38	1.72	1.13	60	55	2.34[a]	1.50	2.8	1.92
11R-6, 68-70	689.11	1.95	1.37	58	44	2.98	1.38	7.7	2.19
12R-1, 33-35	691.43	1.79	1.18	62	54	2.66	1.60	9.9	2.07
12R-1, 100-110	692.10							17.0	
12R-2, 86-88	693.06	1.82	1.26	57	47	2.52	1.33	11.6	2.02
13R-1, 43-45	701.23	1.85	1.22	64	55	2.66	1.76	30.7	1.95
13R-2, 80-82	703.04	1.86	1.23	64	54	2.70	1.78	14.1	1.98
13R-3, 33-35	704.01	1.85	1.23	62	53	2.69	1.66	1.8	1.85
13R-4, 92-94	706.08	1.75	1.15	61	55	2.45	1.54	12.7	2.18
14R-1, 118-121	711.58	1.83		56	46	2.67	1.27	1.4	2.00
14R-2, 29-31	712.12	1.77	1.17	61	55	2.66	1.56	10.0	2.07
15R-1, 44-46	720.54	1.75	1.20	56	49	2.54	1.29	4.6	2.03
15R-2, 110-112	722.70	1.75	1.14	61	56	2.43	1.57	0.3	1.99
15R-3, 75-77	723.67	1.81	1.21	61	52	2.45	1.54	0.3	2.08
15R-3, 117-127	724.09							2.3	
15R-4, 106-108	725.25	1.97	1.42	56	41	2.87	1.27	31.0	2.09
16R-1, 29-31	729.99	1.80	1.22	59	50	2.69	1.41	3.9	2.00
16R-2, 7-10	731.28	1.81	1.25	57	47	2.56	1.31	16.9	2.05
16R-3, 30-32	732.95							0.2	
16R-3, 37-40	733.02	1.93	1.46	48	34	2.57	0.94		2.33
16R-4, 22-24	734.29	2.02	1.48	54	38	2.78	1.18	22.3	1.88
16R-5, 69-71	736.30	2.12	1.71	41	25	2.67	0.71	32.2	1.96
16R-6, 106-109	738.17	2.18	1.79	39	22	2.60	0.63	38.8	2.02
17R-1, 43-46	739.53	2.24	1.90	34	19	2.71	0.52	61.0	2.14
17R-2, 41-43	740.36	2.17	1.77	40	23	2.78	0.66	39.4	1.99
17R-3, 75-77	742.06	2.09	1.63	47	30	2.75	0.87	11.2	1.93
17R-4, 74-76	743.49	2.20	1.80	41	23	2.52	0.68	40.1	2.08
17R-5, 54-57	744.79	2.00	1.54	47	[illegible]	2.65	0.89	0.6	1.94
17R-6, 31-33	746.03	1.92	1.38	54	41	2.41	1.18	4.5	2.03
17R-6, 92-93	746.64							6.2	
18R-1, 85-87	749.65	2.12	1.64	49	31	2.59	0.97	7.3	1.92
19R-3, 39-41	752.19	1.78	1.25	53	45	2.49	1.15	7.3	1.97
18R-3, 115-125	752.95							9.4	
18R-4, 22-25	753.52	1.77	1.11	66	63	2.61	1.98	10.8	1.98
19R-1, 122-124	759.62	2.02	1.50	53	37	2.54	1.12	0.7	1.79
19R-2, 11-14	759.77	1.89	1.37	52	40	2.46	1.10	1.7	1.81
19R-3, 54-57	761.63	2.11	1.78	34	20	2.47	0.51	0.3	3.27
19R-4, 80-82	763.35	2.22	1.90	33	18	2.58	0.48	0.3	3.31
20R-1, 54-56	768.54	2.21	1.81	41	23	2.76	0.68	0.7	2.85
20R-2, 119-122	770.62	2.06	1.63	44	28	2.66	0.77	0.9	2.32
20R-3, 29-31	771.06	2.14	1.70	44	27	2.73	0.79	0.3	2.08
20R-4, 56-58	772.73	2.28	1.94	34	18	2.77	0.52	0.3	2.94
20R-5, 123-125	774.85	2.19	1.82	38	21	2.78	0.60	0.3	2.96
20R-7, 20-22	776.76	2.10	1.69	42	26	2.65	0.71	0.3	2.01
21R-1, 77-79	778.47	2.01	1.53	48	33	2.60	0.93	0.3	2.18
21R-2, 130-132	780.50	2.12	1.64	48	30	2.76	0.93		2.13
21R-3, 93-96	781.63	2.24	1.89	36	19	2.70	0.55	0.6	2.74
21R-4, 135-137	783.55	2.15	1.63	52	33	2.73	1.10		2.02
21R-5, 19-21	783.89	1.92		62	50	2.74	1.64	4.3	2.34
21R-6, 99-101	786.19	2.13	1.55	58	39	2.76	1.38		2.25
21R-6, 133-153	786.53							3.4	
22R-1, 81-83	788.11	2.09	1.64	46	29	2.68	0.84	5.5	2.16
22R-3, 32-34	790.56	2.20	1.87	34	19	2.34[a]	0.51	0.5	2.99
23R-1, 59-61	797.59	2.14	1.77	37	22	2.66	0.59	1.3	3.11
23R-3, 65-67	800.52	2.08	1.66	42	26	2.65	0.73	0.5	2.60
23R-5, 39-41	803.12	2.23	1.79	44	26	2.68	0.80	0.4	2.79
24R-2, 66-68	808.86	2.17	1.63	55	35	2.74	1.20	1.8	2.24
24R-4, 8-10	811.17	2.39	2.10	29	14	2.62	0.41	0.3	3.27
24R-4, 141-151	812.50							0.3	
24R-6, 54-56	814.66	1.96	1.38	58	44	2.92	1.38	2.4	2.05

Table 12 (Continued).

Core, section, interval (cm)	Depth (mbsf)	Wet-bulk density (g/cm^3)	Dry-bulk density (g/cm^3)	Porosity (%)	Water content (%)	Grain density (g/cm^3)	Void ratio	Carbonate content (%)	Velocity (km/s)
126-793B-									
25R-1, 121–123	817.61	2.00	1.57	43	29	2.64	0.76	2.0	2.30
25R-3, 29–31	819.58	2.15	1.69	47	29	2.64	0.88	0.7	2.55
25R-5, 80–82	823.09	2.06	1.60	47	30	2.60	0.88	3.1	2.32
25R-6, 105–106	824.84	2.22		54	33	3.02		8.3	2.14
26R-1, 45–47	826.15	1.98	1.46	53	38	2.55	1.13	2.3	2.18
26R-2, 61–63	827.67	1.94	1.56	39	26	2.45	0.64		2.73
26R-3, 75–77	829.32	2.11	1.74	38	23	2.51	0.61	1.4	2.79
26R-4, 18–20	830.25	2.21	1.73	48	29	2.50	0.92	1.1	2.74
26R-5, 3–5	831.60	2.27	1.88	40	22	6.32^{a}	0.66		3.00
26R-5, 17–20	831.74							0.4	
26R-6, 63–65	833.70	2.19	1.81	38	22	2.58	0.62		2.96
26R-6, 139–141	834.46	2.22	1.82	40	23	2.30^{a}	0.66		3.07
27R-2, 3–5	836.93	2.20	1.85	36	20	2.66	0.57	0.7	3.22
27R-4, 22–24	839.92	2.04	1.60	45	29	2.56	0.81	1.9	2.56
27R-6, 109–111	843.64	2.40	1.82	59	34	2.62	1.44	4.2	2.26
27R-7, 33–58	844.38							1.8	
28R-2, 85–88	846.62	2.05	1.68	38	23	2.50	0.61	0.4	2.74
28R-4, 38–40	849.14	1.97	1.47	50	35	2.65	1.00	4.0	2.27
28R-6, 99–101	852.62	1.93	1.50	44	30	2.32^{a}	0.78	0.5	2.58
28R-8, 37–39	854.81	2.15	1.77	38	22	2.55	0.62	1.0	2.76
29R-1, 52–55	855.22	2.22	1.88	34	19	2.58	0.52	0.8	3.02
29R-3, 22–24	857.58	2.21	1.88	33	18	2.53	0.49	0.5	3.16
29R-5, 90–92	860.90	1.94	1.45	50	36	2.48	1.01	1.1	2.34
30R-1, 38–41	864.78	2.24	1.90	35	19	2.64	0.53	1.2	3.18
30R-3, 55–58	867.95	2.16	1.81	36	20	2.62	0.55	1.2	3.19
30R-4, 110–135	870.00							4.4	
30R-5, 40–42	870.65	1.94	1.38	57	43	2.96	1.32	2.5	2.28
31R-1, 95–97	874.95	2.13	1.72	42	25	2.86	0.72	13.5	2.43
31R-2, 128–131	879.56	1.92	1.44	48	35	2.48	0.93		2.53
31R-3, 10–12	879.75	1.86	1.37	50	38	2.56	0.98		2.43
31R-3, 25–28	876.90	1.97	1.46	51	36	2.45	1.04		2.49
31R-3, 62–63	877.27							6.9	
31R-4, 14–16	877.99	2.09	1.72	38	23	2.88	0.61	19.7	2.45
31R-6, 68–70	881.38	2.21	1.89	32	18	2.68	0.48	0.5	2.76
32R-1, 48–51	884.18	2.25	1.94	32	17	2.74	0.47	0.5	2.92
32R-3, 70–73	887.11	2.29	2.03	27	14	2.61	0.37	0.3	3.35
32R-4, 127–130	889.18	2.43	2.20	23	11	2.62	0.30	0.4	3.76
33R-1, 85–87	894.15	2.21	1.97	25	13	2.42	0.33	0.3	3.32
33R-3, 87–89	897.02	2.05	1.62	43	28	2.69	0.76	8.6	2.42
33R-5, 57–60	899.31	2.23	1.90	34	18	2.62	0.51	0.4	2.89
33R-6, 0–25	900.09							0.7	
33R-7, 60–63	902.19	2.01	1.62	39	25	2.43	0.63	0.8	2.73
34R-1, 31–33	903.31	2.28	1.86	42	23	2.80	0.71	11.3	2.39
34R-3, 57–59	906.49	2.28	1.95	33	18	2.68	0.50	4.8	2.75
34R-5, 87–89	909.15	2.44	2.23	21	10	2.58	0.26	0.3	3.59
34R-7, 25–27	911.04	2.27	1.91	37	20	2.56	0.59	0.4	2.95
35R-1, 75–77	913.35	2.28	1.99	30	16	2.53	0.43	0.5	3.19
35R-3, 55–57	916.03	2.26	1.92	35	19	2.60	0.53	10.5	2.87
35R-5, 125–127	919.51	2.11	1.67	45	28	2.39	0.82	1.6	2.62
35R-6, 57–59	920.33	2.29	1.85	44	25	2.70	0.79	1.5	2.54
36R-1, 66–68	922.96	2.25	1.78	48	28	2.80	0.91		2.29
36R-1, 116–118	923.46	2.10	1.64	46	29	2.68	0.86	7.8	
36R-3, 94–96	926.14	2.20	1.77	44	26	2.64	0.78		2.38
36R-3, 113–138	926.33							9.8	
36R-4, 12–14	926.70	2.32	1.90	43	23	2.71	0.75		
36R-5, 84–86	928.61	2.29	2.01	28	14	2.62	0.39	3.6	3.02
36R-6, 96–99	930.18	2.39	2.04	35	18	2.64	0.54		
37R-1, 32–34	932.32	2.15	1.81	35	20	2.60	0.53	1.4	2.77
37R-3, 58–61	935.54	2.23	1.90	34	19	2.64	0.51		2.85
37R-5, 69–71	938.30	2.12	1.70	42	26	2.51	0.74	7.3	2.49
37R-7, 73–75	940.96	2.25	1.83	43	24	2.70	0.74	15.8	2.47
38R-1, 138–140	942.98	2.32	2.01	32	16	2.62	0.46	28.9	2.82
38R-3, 64–66	945.15	2.23	1.80	44	25	0.82^{a}	0.78	2.0	2.87
38R-5, 143–145	948.37	2.06	1.55	52	35	2.58	1.07	5.6	2.34
39R-1, 14–16	951.44	2.18	1.82	37	21	2.65	0.58		2.60
40R-2, 54–60	961.81	2.01	1.64	38	24	2.36^{a}	0.61	0.6	2.75
40R-4, 106–108	965.14	1.95	1.54	41	28	2.33^{a}	0.70	3.3	2.74
40R-5, 96–121	966.25							0.8	
40R-6, 133–135	967.83	2.30	1.95	34	18	2.64	0.53	1.0	2.92
40R-8, 109–111	970.48	2.02	1.61	42	27	2.21^{a}	0.72	1.2	2.62
41R-2, 45–47	972.53	1.97	1.55	43	29	2.40	0.74	3.5	2.58
41R-4, 59–62	975.32	2.07	1.68	40	25	2.56	0.67	0.4	2.75
41R-6, 97–99	978.42	2.00	1.55	45	30	2.42	0.82	1.5	2.56
42R-1, 43–46	980.73	1.89	1.45	45	32	2.08^{a}	0.81	2.7	2.61
42R-2, 4–6	981.77								2.60

Table 12 (Continued).

Core, section, interval (cm)	Depth (mbsf)	Wet-bulk density (g/cm^3)	Dry-bulk density (g/cm^3)	Porosity (%)	Water content (%)	Grain density (g/cm^3)	Void ratio	Carbonate content (%)	Velocity (km/s)
126-793B-									
42R-3, 23-25	983.38	2.00	1.60	40	26	2.33^{a}	0.66	0.5	2.77
42R-4, 59-61	985.14	2.09	1.64	46	29	2.71	0.84		2.60
42R-4, 133-135	985.88	2.12	1.63	49	31	2.51	0.96		2.48
42R-5, 76-78	986.71	2.02	1.60	42	27	2.29^{a}	0.74		2.69
43R-1, 17-19	989.87	1.97	1.57	40	27	2.48	0.68	0.7	2.69
43R-3, 59-61	992.83	1.86	1.46	41	29	2.51	0.70	3.3	2.67
43R-5, 68-71	995.62	2.03	1.62	42	27	2.51	0.71	0.8	2.61
43R-5, 120-150	996.14							0.5	
43R-7, 4-7	997.86	2.02	1.60	42	27	2.45	0.73	3.4	2.56
44R-1, 60-62	1000.00	1.89	1.42	48	35	2.40	0.91	3.5	2.59
44R-3, 48-51	1002.76	2.02	1.58	44	29	2.54	0.78	1.3	2.67
44R-5, 7-9	1005.21	2.06	1.66	40	25	2.51	0.68	0.8	2.83
44R-7, 26-29	1008.29	1.98	1.57	41	27	2.46	0.70	0.8	3.04
45R-1, 45-47	1009.55	2.10	1.73	37	22	2.61	0.60	1.1	2.83
45R-1, 100-103	1010.10	1.90	1.48	42	30	2.37	0.73	3.1	2.61
46R-1, 26-29	1018.96	2.10	1.77	33	20	2.54	0.50	0.7	2.99
46R-2, 90-92	1020.04	2.00	1.55	46	31	2.49	0.84		2.00
46R-3, 21-23	1020.85	1.98	1.53	46	31	2.42	0.83	1.2	2.64
46R-3, 116-141	1021.80							1.5	
46R-4, 80-82	1022.85	1.88	1.47	41	29	2.41	0.71		1.98
46R-5, 42-44	1023.99	1.95	1.46	50	36	2.54	1.01	0.7	2.46
46R-6, 86-88	1025.93	2.04	1.57	47	31	2.59	0.89		2.03
46R-7, 119-121	1027.76	2.08	1.66	43	27	2.56	0.75		2.95
47R-1, 61-62	1028.61	2.01	1.65	36	23	2.46	0.56	0.5	3.19
47R-3, 80-81	1031.34	2.05	1.55	51	34	2.62	1.04	0.5	2.89
47R-4, 78-80	1032.82	1.97	1.46	51	36	2.45	1.05	3.7	2.28
47R-5, 12-14	1033.52	2.11	1.69	43	26	2.57	0.75	0.9	2.69
48R-1, 81-83	1038.41	1.96	1.53	44	30	2.40	0.78	1.5	2.63
48R-3, 54-56	1041.14							0.6	2.64
48R-5, 31-33	1043.91	1.98	1.54	44	30	2.38^{a}	0.79	1.9	2.61
48R-6, 58-60	1045.47	2.35	1.98	38	20	2.84	0.61	0.5	2.89
49R-1, 87-89	1048.17	2.11	1.74	38	23	2.57	0.61	1.1	2.95
49R-2, 107-109	1049.87	1.98	1.54	45	30	2.33^{a}	0.82	1.6	2.58
49R-3, 45-75	1050.52							1.5	
49R-4, 27-29	1051.09	1.62^{a}	1.15^{a}	48^{a}	44^{a}	1.88^{a}	0.93^{a}		2.56
50R-1, 80-82	1057.80	2.27	1.90	38	21	2.90	0.61	0.5	2.80
50R-3, 56-58	1060.56	2.09	1.58	51	33	2.73	1.03	4.8	2.37
50R-5, 120-122	1064.12	2.35	1.95	40	21	2.68	0.66	1.5	2.76
50R-6, 126-128	1065.68	2.38	2.11	28	14	2.63	0.38	0.4	3.20
51R-2, 14-16	1067.28	1.81^{a}	1.18	64^{a}	57^{a}	2.41^{a}	1.81^{a}	2.3	2.29
51R-2, 78-80	1067.92	2.39	2.00	40	20	2.99	0.65		2.22
51R-4, 64-66	1070.78	2.36	2.10	26	13	2.51	0.36	1.1	3.58
51R-5, 61-63	1072.25	2.38	2.10	29	14	2.55	0.40		2.60
51R-6, 93-95	1073.92	2.19	1.75	45	27	2.51	0.83	4.3	3.14
51R-7, 72-74	1075.06	2.25	1.91	34	18	2.64	0.52		2.26
51R-8, 6-8	1075.84	1.98	1.56	42	28	2.38	0.73	1.5	2.63
52R-1, 76-78	1077.16	2.28	2.00	29	15	2.39	0.40	0.6	3.52
52R-1, 108-138	1077.48							0.5	
52R-3, 66-68	1079.94	2.31	2.04	28	14	2.49	0.38	0.4	3.57
52R-5, 40-42	1082.07	2.56^{a}	2.01	56^{a}	29^{a}	2.29^{a}	1.29^{a}	1.3	3.73
53R-1, 39-42	1086.49	2.31	1.94	38	20	2.91	0.60	1.1	2.78
53R-3, 69-72	1089.66	2.10	1.67	44	27	2.70	0.78	0.6	2.53
53R-CC, 10-12	1091.69	2.06	1.55	52	35	2.54	1.06	3.4	2.43
54R-2, 36-38	1096.44	2.00	1.55	45	30	2.33^{a}	0.83	1.4	2.67
54R-4, 31-33	1099.21	2.23	1.89	34	19	2.85	0.51	0.6	2.79
55R-2, 0-30	1105.56							0.5	
55R-2, 134-137	1106.90	2.17	1.77	40	23	2.62	0.66	2.0	1.85
55R-4, 104-107	1109.21	2.33	2.04	30	15	2.58	0.42	0.4	2.18
56R-1, 46-48	1115.46	2.36	2.11	25	12	2.64	0.34		2.44
56R-2, 47-50	1116.97	2.30	2.06	25	12	2.62	0.33		2.43
56R-3, 50-53	1118.50	1.92	1.50	43	30	2.26^{a}	0.75		1.99
56R-3, 70-74	1118.70							1.5	
56R-3, 86-89	1118.86	1.90	1.49	41	28	2.30^{a}	0.70		2.02
56R-4, 1-4	1119.51	2.23	1.86	37	21	2.71	0.59		2.00
56R-5, 60-62	1121.34	2.44	2.18	26	12	2.65	0.34		2.34
57R-1, 48-50	1125.18	2.01	1.88	13	7	2.93	0.15	2.3	1.93
57R-3, 14-17	1127.84	2.26	1.92	34	18	2.69	0.52	0.5	1.99
58R-1, 37-39	1134.37	2.26	1.97	30	16	2.64	0.42	0.4	2.20
58R-3, 94-97	1137.64	2.02	1.58	45	29	2.47	0.81	1.3	1.86
58R-4, 76-106	1138.96							0.9	
58R-5, 122-124	1140.58	2.21	1.89	32	17	2.60	0.46	0.3	2.13
58R-7, 87-89	1143.20	2.35	2.11	25	12	2.58	0.34	0.4	2.43
59R-1, 44-47	1144.04	2.31	2.08	24	12	2.52	0.31	0.3	2.46
59R-3, 74-77	1147.08	2.31	2.05	26	13	2.60	0.35	1.5	2.29
59R-3, 132-133	1147.66							0.3	

Table 12 (Continued).

Core, section, interval (cm)	Depth (mbsf)	Wet-bulk density (g/cm^3)	Dry-bulk density (g/cm^3)	Porosity (%)	Water content (%)	Grain density (g/cm^3)	Void ratio	Carbonate content (%)	Velocity (km/s)
126-793B-									
59R-5, 72–75	1149.89	2.35	2.10	26	13	2.49	0.34	0.3	2.46
59R-7, 107–109	1152.97	2.37	2.10	27	14	2.58	0.38		
59R-7, 136–138	1153.27							0.3	2.37
60R-1, 102–104	1154.22	2.41	2.16	25	12	2.67	0.33	0.5	3.30
60R-3, 60–62	1156.80	2.31	2.03	28	14	2.43	0.40	0.4	2.98
60R-5, 82–84	1159.83	2.66	2.41	25	11	2.85	0.34	0.3	3.29
60R-7, 29–31	1161.90	2.53	2.31	22	10	2.92	0.28	0.4	3.54
61R-1, 22–24	1163.12	2.33[a]	1.68	66[a]	41[a]	2.22[a]	1.90	0.3	2.97
61R-1, 55–57	1163.45	2.62	2.42	20	9	2.73	0.25		3.65
61R-2, 69–71	1164.93	2.02	1.60	43	27	2.33[a]	0.74		2.69
61R-3, 41–43	1166.06	2.11	1.74	37	22	2.44	0.59	0.8	2.86
61R-4, 28–30	1166.79	2.40	2.07	34	17	2.83	0.52		2.79
62R-1, 45–47	1173.05	2.08	1.66	43	27	2.44	0.77	0.4	2.55
62R-2, 108–110	1174.89	2.24	1.91	34	18	2.55	0.51	0.4	2.78
62R-4, 64–66	1177.14	2.34	2.01	33	17	2.64	0.48	0.3	2.73
63R-1, 74–76	1182.94	2.22	1.84	39	22	2.70	0.65	0.4	2.41
63R-3, 33–35	1185.53	2.42	2.18	24	11	2.61	0.32		3.43
63R-4, 69–71	1187.36	2.26	1.86	40	22	2.63	0.68	0.5	2.64
64R-1, 46–48	1192.36	2.25	1.90	36	19	2.64	0.55	0.5	2.54
64R-3, 81–83	1195.33	2.20	1.81	40	23	2.61	0.66	0.4	2.44
64R-5, 122–124	1198.56	2.32	2.01	31	16	2.53	0.45	0.6	3.04
64R-6, 117–147	1200.01							1.1	
64R-7, 97–99	1201.28	2.58	2.33	25	11	2.68	0.34	6.2	3.44
65R-1, 78–81	1202.28	2.44	2.22	22	10	2.65	0.28		3.48
65R-3, 47–50	1204.89	2.50	2.32	18	8	2.66	0.23		4.23
65R-5, 31–33	1207.65	2.14	1.84	30	17	2.57	0.43		2.68
65R-6, 74–76	1209.58							1.9	
65R-7, 34–37	1210.68	2.12	1.71	42	25	2.44	0.72	0.3	2.51
66R-1, 65–68	1211.75	2.33	2.10	24	12	2.38	0.31	0.2	3.13
66R-3, 81–84	1214.81	2.23	1.92	32	17	2.53	0.46	0.2	2.99
66R-4, 33–36	1215.83	2.22	1.90	33	18	2.53	0.49	0.1	3.08
66R-4, 117–118	1216.67							1.1	
66R-5, 3–6	1216.88	1.75[a]	1.39	36[a]	26[a]	1.86[a]	0.55[a]		3.03
66R-6, 140–142	1219.69	2.03	1.67	36	23	2.33	0.57	3.[illegible]	2.94
67R-1, 97–99	1221.77	2.30	2.01	29	15	2.69	0.41	0.4	2.96
67R-3, 69–71	1224.35	2.46	2.18	29	14	2.84	0.40	1.7	3.14
67R-5, 121–123	1227.82	2.04	1.66	39	24	2.49	0.63	0.4	2.65
67R-6, 59–62	1228.56	2.26	2.07	19	10	2.75	0.24		
68R-1, 115–118	1231.65	2.21	1.83	38	22	2.69	0.62	2.2	2.58
68R-3, 38–40	1233.78	2.49	2.22	27	13	2.68	0.37	0.9	3.29
68R-4, 91–93	1235.67	2.09	1.66	43	27	2.36	0.76	0.1	2.70
68R-5, 26–28	1236.45	2.50	2.23	27	12	2.68	0.37		
68R-6, 26–28	1237.95							0.8	3.13
69R-1, 73–75	1240.93	2.04	1.66	38	24	2.42	0.62	5.0	2.71
69R-3, 73–75	1243.85	2.33	2.08	26	13	2.63	0.35	0.6	3.14
69R-5, 47–49	1246.38	2.04	1.64	40	25	2.39	0.67	6.4	2.69
69R-7, 12–14	1248.99	2.41	2.16	26	12	2.67	0.35	0.5	3.29
70R-1, 93–95	1250.73	2.40	2.14	26	12	2.68	0.35	2.2	3.28
70R-3, 74–76	1253.49	2.36	2.12	24	11	2.58	0.31	1.2	3.30
70R-5, 62–64	1255.93	2.33	1.95	39	20	2.71	0.63	2.9	2.60
70R-7, 0–30	1258.31							0.9	
70R-7, 45–47	1258.76	2.28	1.96	33	17	2.58	0.49	1.1	3.01
71R-1, 94–96	1260.34	2.37	2.10	27	13	2.64	0.37	2.2	3.23
71R-3, 12–14	1262.19	2.27	1.85	43	24	2.74	0.75		2.64
71R-4, 77–79	1264.02	2.02	1.65	37	23	2.36	0.59		2.97
71R-5, 83–85	1265.35								2.95
71R-7, 82–84	1268.10	2.33	2.04	30	15	2.39	0.43	1.0	3.06
72R-1, 60–62	1269.30	2.28	1.93	36	19	2.70	0.55	2.7	2.68
72R-3, 79–81	1272.49	2.02	1.58	44	29	2.36	0.80	0.7	2.70
72R-5, 80–82	1275.50	1.88[a]	1.49	39[a]	27[a]	2.13[a]	0.64[a]	2.7	2.84
72R-7, 12–14	1277.54	2.61	2.37	24	10	2.73	0.32	0.5	3.57
73R-1, 102–104	1279.42	2.29	1.95	35	18	2.63	0.53	1.2	2.91
73R-3, 37–39	1281.53	1.96[a]	1.58	39[a]	25[a]	2.25[a]	0.63[a]	0.7	3.05
73R-4, 120–150	1283.71							3.1	
73R-5, 56–58	1284.57	2.45	2.17	29	14	2.72	0.40	2.6	3.49
74R-1, 24–28	1288.24	2.34	2.06	28	14	2.57	0.40		3.35
74R-3, 118–121	1292.01	2.32	2.09	23	12	2.38	0.30		3.47
74R-5, 63–66	1294.16	2.47	2.19	28	13	2.60	0.39	2.7	3.26
74R-7, 81–84	1296.83	2.67	2.38	29	12	2.66	0.40	4.9	3.36
75R-1, 75–78	1298.45	2.44	2.16	28	13	2.70	0.38	3.7	3.45
75R-2, 86–89	1300.06	2.38	2.12	26	13	2.64	0.35		3.46
75R-5, 71–73	1304.34	2.41	2.10	31	15	2.70	0.46	5.4	2.84
75R-7, 6–9	1306.69	2.35	2.14	21	10	2.42	0.27	1.1	3.73
76R-1, 70–73	1308.00	2.39	2.18	20	10	2.47	0.26	0.7	3.70
76R-2, 44–47	1309.23	2.38	2.22	16	8	2.40	0.19		4.13

Table 12 (Continued).

Core, section, interval (cm)	Depth (mbsf)	Wet-bulk density (g/cm³)	Dry-bulk density (g/cm³)	Porosity (%)	Water content (%)	Grain density (g/cm³)	Void ratio	Carbonate content (%)	Velocity (km/s)
126-793B-									
76R-3, 71-74	1311.01	2.38	2.20	19	9	2.48	0.23		4.03
76R-5, 6-9	1313.27	2.38	2.20	19	9	2.42	0.23		4.04
76R-5, 104-134	1314.25							0.5	
77R-1, 62-65	1317.62	2.42	2.29	13	6	2.39	0.15	0.9	4.32
77R-3, 120-123	1321.13	2.45	2.28	18	8	2.50	0.21	4.7	3.83
77R-5, 101-104	1323.88	2.41	2.30	11	5	2.54	0.13	0.7	4.40
78R-1, 64-66	1327.34	2.19	1.86	33	18	2.62	0.49	1.7	2.71
78R-3, 64-66	1330.31	2.59	2.46	13	6	2.61	0.15	0.7	4.29
78R-5, 56-59	1332.68	2.39	2.16	24	11	2.60	0.31	2.2	3.13
78R-7, 124-126	1336.12	2.34	2.06	28	14	2.59	0.39	2.0	3.13
79R-1, 63-65	1337.03	2.45	2.24	22	10	2.56	0.28	2.0	3.87
79R-3, 84-85	1339.78	2.35	2.08	27	13	2.52	0.36		3.57
79R-5, 43-44	1342.15	2.17	1.79	39	22	2.58	0.63	4.5	2.45
79R-6, 60-61	1343.77	2.38	2.28	10	4	2.56	0.11	1.8	3.88
80R-1, 95-97	1346.95	2.30	2.09	21	11	2.43	0.27	1.7	3.46
80R-3, 86-88	1349.86	2.20	1.90	31	17	2.40	0.45	2.0	3.25
80R-5, 0-30	1351.63							0.8	
80R-5, 72-74	1352.35	2.35	2.06	30	15	2.63	0.42	6.7	2.80
80R-7, 4-6	1354.49	2.36	2.05	32	16	2.68	0.48		2.84
81R-2, 126-128	1358.39	2.45	2.09	36	18	2.77	0.57		2.91
81R-3, 40-43	1359.03	2.27	1.92	36	19	2.62	0.55		2.87
81R-5, 43-46	1361.74	2.42	2.10	33	16	2.68	0.49		2.99
81R-5, 127-129	1362.58	2.32	2.01	32	17	2.59	0.47		2.94
81R-6, 37-39	1363.12	2.30	1.92	39	21	2.46	0.63		2.88
81R-6, 69-71	1363.44	2.27	1.95	33	18	2.67	0.49		2.88
82R-1, 75-77	1366.05	2.33	2.04	30	15	2.60	0.42		2.93
82R-3, 70-72	1368.80	2.30	2.06	24	12	2.69	0.32		3.12
82R-5, 85-87	1371.67	2.37	2.12	25	12	2.58	0.34		3.14
82R-6, 61-63	1372.93	2.21	2.02	20	10	2.50	0.25		3.60
82R-7, 49-51	1374.18	2.40	2.14	26	13	2.58	0.35		3.43
82R-CC, 20-22	1374.77	2.31	2.07	24	12	2.52	0.32		3.21
83R-1, 47-49	1375.37	2.89	2.40	51	22	2.49	1.02		2.70
83R-1, 48-50	1375.38	2.37	2.04	33	17	2.78	0.50		
83R-1, 98-100	1375.88	2.25	1.82	43	24	2.76	0.76		2.78
83R-2, 27-29	1376.67	2.45	2.16	29	14	2.33[a]	0.41		2.89
83R-2, 39-41	1376.79	2.51	2.24	27	12	2.53	0.37		2.91
84R-1, 21-23	1384.71	2.32	2.03	29	15	2.66	0.41		3.03
84R-2, 98-100	1386.98	2.48	2.25	23	11	2.58	0.30		3.11
85R-1, 24-27	1394.44	2.46	2.22	24	11	2.61	0.32		3.26
85R-1, 63-65	1394.93								3.53
85R-2, 34-36	1396.04								3.35
85R-2, 125-128	1396.95	2.55	2.27	29	13	2.78	0.40		2.96
86R-1, 29-32	1404.19	2.25	1.93	33	18	2.58	0.49		3.10
86R-2, 8-10	1405.48	2.61	2.42	19	8	2.78	0.23		4.30
87R-1, 84-87	1414.44	2.41	2.14	30	15	2.74	0.44		3.06
87R-2, 107-110	1416.16	2.42	2.13	29	14	2.73	0.41		3.30
87R-4, 82-84	1418.03	2.75	2.59	17	7	2.83	0.21		4.47
88R-1, 78-81	1423.68	2.43	2.14	30	14	2.79	0.42		3.27
88R-1, 121-124	1424.11								3.31
88R-2, 21-23	1424.53	2.42	2.11	31	15	2.73	0.45		3.18
89R-1, 34-36	1431.74	2.40	2.09	32	16	2.60	0.46		3.05
89R-3, 48-50	1434.80	2.43	2.12	31	15	2.67	0.45		3.08
89R-4, 25-27	1436.04	2.58	2.36	23	10	2.79	0.29		3.82
92R-1, 46-48	1460.56	2.57	2.33	25	11	2.95	0.33		3.75
92R-2, 137-139	1462.97	2.80	2.62	18	7	3.09	0.23		4.09
92R-3, 6-8	1463.13	2.84		18	7	3.02	0.23		4.04
93R-1, 137-140	1471.07	2.40		32	16	2.81	0.48		4.04
93R-2, 95-98	1472.15	2.63		24	10	3.13	0.31		3.57
94R-1, 54-57	1479.94	2.30		29	15	2.62	0.42		3.83
94R-2, 82-85	1481.54	2.56		19	8	2.62	0.23		3.47
95R-1, 78-80	1489.78	2.31		36	19	2.69	0.56		3.05
95R-1, 138-140	1490.38	2.40		32	16	2.64	0.47		3.10
95R-2, 64-66	1491.10	2.49		29	14	2.81	0.41		3.04
96R-1, 35-37	1499.05	2.52		53	28	2.57	1.14		3.32
96R-CC, 13-15	1500.06	2.21		38	22	2.67	0.62		3.15
97R-1, 89-93	1509.19	2.61		23	10	2.90	0.29		3.74
98R-1, 87-89	1518.87	2.37		31	16	2.55	0.46		3.41
98R-2, 67-69	1520.02	2.45		28	13	2.64	0.39		3.85
98R-2, 143-146	1520.78	2.37		27	13	2.61	0.36		3.41
98R-3, 73-75	1521.55	2.66		62	31	2.51	1.63		3.76
98R-4, 10-13	1522.33	2.34		26	13	2.55	0.35		3.51
98R-4, 44-46	1522.67	2.57		23	10	2.66	0.30		3.85
99R-1, 13-16	1527.73	2.44		25	12	2.57	0.34		3.96
99R-1, 88-91	1528.48	2.67		24	10	2.98	0.32		3.83
100R-1, 7-10	1537.37	2.49		24	11	2.50	0.32		3.61

Table 12 (Continued).

Core, section, interval (cm)	Depth (mbsf)	Wet-bulk density (g/cm³)	Dry-bulk density (g/cm³)	Porosity (%)	Water content (%)	Grain density (g/cm³)	Void ratio	Carbonate content (%)	Velocity (km/s)
126-793B-									
100R-CC, 12-16	1539.24	2.57		27	12	2.90	0.37		3.62
101R-1, 44-48	1547.34	2.33		30	15	2.50	0.43		3.35
102R-1, 79-84	1551.39	2.55		25	11	2.88	0.33		3.37
102R-2, 27-30	1558.25	2.42		29	14	2.63	0.40		3.55
102R-CC, 6-9	1558.47	2.44		29	14	2.60	0.41		3.59
103R-1, 26-28	1566.56	2.36		35	18	2.57	0.54		3.50
103R-2, 43-45	1568.12	2.35		30	15	2.58	0.42		3.24
103R-3, 37-39	1569.46	2.37		66	40	3.68*	1.93		3.94
104R-1, 47-50	1576.37	2.67		25	11	2.93	0.34		3.45
104R-2, 26-28	1577.66	2.57		27	12	3.04	0.37		3.62
104R-3, 41-43	1579.21	3.40		29	9	3.64	0.40		3.32
104R-4, 35-37	1580.45	2.53		27	12	2.95	0.37		3.28
105R-1, 87-89	1586.37	2.68		17	7	2.78	0.21		4.30
105R-1, 123-125	1586.73	2.76		22	9	2.66	0.27		3.80
105R-3, 82-83	1589.15	2.67		28	12	3.00	0.39		3.39
105R-3, 115-117	1589.48	2.67		19	8	2.75	0.23		4.00
106R-1, 69-71	1595.89	2.71		20	8	2.86	0.25		4.24
106R-2, 24-26	1596.92	2.65		26	11	2.71	0.35		3.86
107R-1, 59-62	1605.39	2.54		27	12	2.77	0.37		3.52
107R-2, 38-40	1606.68	2.39		26	12	2.65	0.35		3.58
107R-3, 100-102	1608.64	2.45		29	14	2.56	0.41		3.56
107R-4, 128-132	1610.42	2.72		19	8	2.99	0.24		3.74
108R-1, 121-124	1615.61	2.48		28	13	2.69	0.38		3.90
108R-2, 115-117	1616.97	2.61		22	10	2.96	0.29		4.04
109R-1, 113-116	1625.23	2.45		28	13	2.60	0.38		3.55
109R-2, 144-147	1626.93	2.79		20	8	2.88	0.24		3.88
110R-1, 56-58	1634.36	2.64		24	10	2.90	0.32		3.73
110R-2, 39-41	1635.56	2.69		20	8	2.97	0.25		3.93
110R-4, 43-45	1638.23	2.71		21	9	2.96	0.26		3.81
111R-1, 23-25	1643.63	2.56		23	10	2.89	0.30		3.76
111R-2, 99-101	1645.89	2.92		19	7	2.94	0.24		3.97
112R-1, 25-27	1653.35	2.68		22	9	2.94	0.28		3.91
112R-2, 85-87	1655.45	2.63		23	10	2.90	0.31		3.81
113R-1, 100-102	1663.70	2.45		28	14	2.76	0.40		3.53
113R-4, 18-21	1667.21	2.90		13	5	2.77	0.15		4.57
114R-1, 40-42	1672.80	2.43		29	14	2.80	0.41		3.55
114R-4, 87-89	1677.57	2.43		29	14	2.76	0.40		3.66

* Data of uncertain quality.

eral trends were noted despite the wide sample spacing and paucity of data. The most obvious aspect of the shear strength curve is the peak at 40 mbsf, which is defined by four data points, and includes a maximum of 109 kPa. These high strength values do not correlate with either porosity or water content values, which are variable and display no consistent trends over this interval. The high strengths may be associated with intervals of interbedded nannofossil silty clays and nannofossil-rich silty clays.

A similar lithology (see "Lithostratigraphy and Accumulation Rates" section, this chapter) is reported at 90 mbsf where a secondary strength peak is located. Low shear strength values between 70 and 80 mbsf are associated with low $CaCO_3$ percentages. However, the primary cause of the low strengths between 70 and 80 mbsf is probably drilling disturbance (see "Lithostratigraphy and Accumulation Rates" section, this chapter).

Hole 793B

No vane shear strength measurements were made in Hole 793B because of the lithified state of the sediments.

Sonic Velocity

Hole 793A

Sonic velocity measurements were performed on discrete samples from Hole 793A using the HF method (Table 12, Fig. 66). In addition, all cores from Hole 793A were passed through the MST to obtain *P*-wave velocity data (Fig. 66). Although HF and MST methods exhibit the same general trends, the MST velocity values are higher. From the seafloor to 60 mbsf, HF velocity data remain fairly constant (~1.53-1.55 km/s; average = 1.54 km/s) and show little (if any) change across the Subunit IA/IB boundary. We observed a distinct downward increase (from 1.58 to 1.65 km/s; average = 1.60 km/s) from 70 mbsf to the bottom of Hole 793A.

Hole 793B

Sonic velocity measurements were performed on discrete samples from Holes 793B using the HF method (Fig. 63, Table 12). The first rocks recovered in Hole 793B, the Unit II diabase (Core 126-793B-1R; 586.5-591.0 mbsf), have the highest velocity values of the entire cored section at this site, averaging 4.88 km/s (range = 4.63-5.14 km/s).

The Unit II/III boundary is characterized by a decrease in velocity of more than 2.5 km/s. Velocity data exhibit the least variability (range = 1.85-2.33 km/s; average = 2.01 km/s) in Unit III (Cores 126-793B-2R through Section -16R-5; 591.0-735.7 mbsf), and do not show any significant downward trends. Velocity values across the Unit III/IV boundary and within Unit IV are fairly constant. The average velocity in Unit IV is 2.18 km/s, with little overall variation (range = 1.92-2.14 km/s).

At the Unit IV/V boundary (759.0 mbsf), velocity values increase by an average of 0.5 km/s. In contrast to Unit IV, Unit V

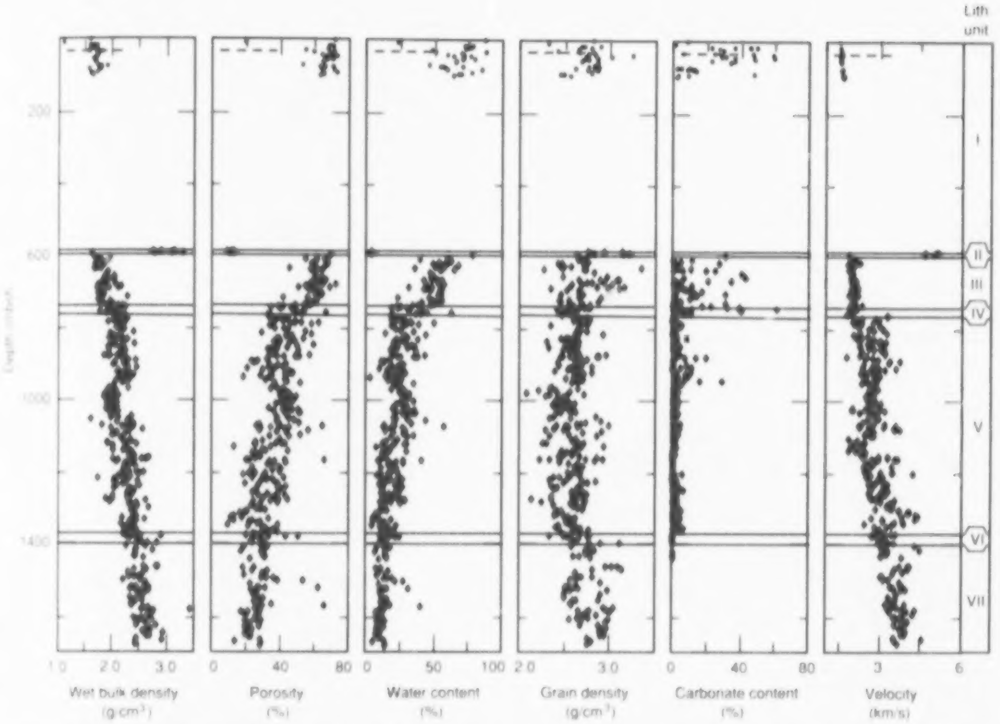

Figure 63. Physical properties, Holes 793A (circles) and 793B (diamonds). Horizontal solid lines indicate lithologic units. The dashed line indicates the Subunit IA/IB contact.

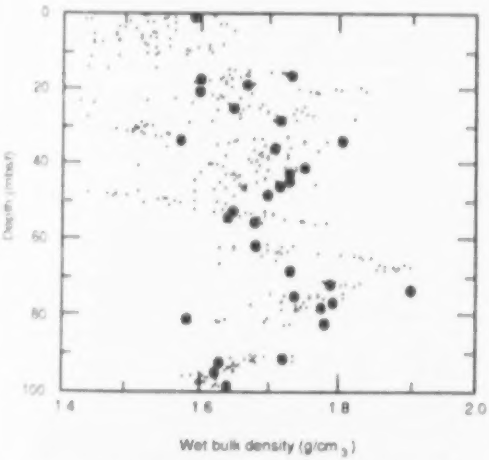

Figure 64. Comparison of gravimetric (large dots) and GRAPE wet-bulk density (small dots) for Hole 793A.

Table 13. Shear strength data from Site 793.

Core, section, interval (cm)	Depth (mbsf)	Shear strength (kPa)
126-793A-		
3H-1, 119	14.69	40.6
3H-2, 129	16.29	38.0
3H-3, 82	17.32	48.3
3H-4, 64	18.64	53.2
5H-4, 128	36.89	79.0
5H-7, 112	41.23	109.1
6H-1, 83	42.83	75.3
6H-3, 119	46.19	63.9
7H-1, 125	52.85	40.8
7H-2, 120	54.30	42.9
7H-3, 98	55.58	51.3
9H-3, 110	75.00	27.3
9H-5, 79	77.69	17.0
10H-2, 139	82.30	40.1
11H-1, 80	90.90	70.9
11H-2, 90	92.50	12.1

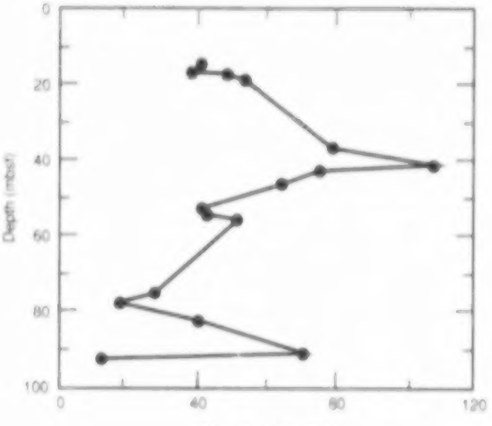

Figure 65. Plot of shear strength vs. depth for Hole 793A.

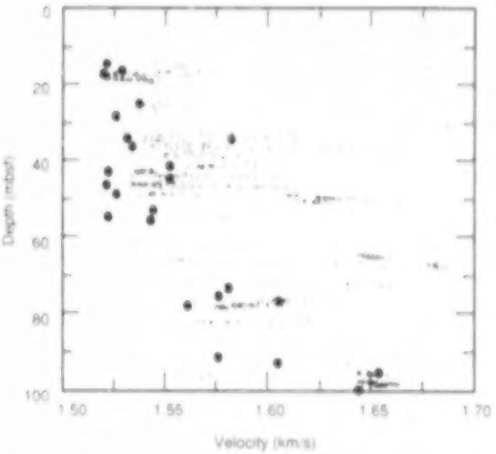

Figure 66. Comparison of sonic velocity determined by Hamilton Frame (HF; large circles) and multisensor track (MST; small dots) methods for Hole 793A.

is characterized by (1) rapidly fluctuating velocity values (total range >2.0 km/s); (2) a downward increase in velocity; (3) a distinct velocity minimum (1107–1150 mbsf); and (4) an average velocity of 2.81 km/s. We observed fluctuations of over 1.0 km/s between samples, which are related to the rapidly changing sediment types present in this unit (turbidites, debris flows; see "Lithostratigraphy and Accumulation Rates" section, this chapter). The downward velocity increase in this unit is illustrated by comparing the average velocity values in the upper part of Unit V (~759–1107 mbsf), which are 2.67 km/s, and those in the lower part of this unit (~1150–1373), which are 3.14 km/s. In the middle part of Unit V, a velocity minimum (average = 2.17 km/s) exists at 1107–1150 mbsf. This minimum has a velocity difference of 0.5 km/s with the overlying sediments and >1.0 km/s with those below.

Velocity values generally increase from 1200 to 1700 mbsf, but no significant increase marks the Unit VI/VII boundary, where we encountered igneous rocks. Within the igneous section, velocity data increase downward and are quite variable. The wide range of values (3.05–4.57 km/s) is likely related to alteration, changes in the relative proportion of clasts vs. matrix in the hyaloclastites, and the presence of interlayered high-velocity andesite flows and pillows. The uppermost part of the unit (1403–1440 mbsf) has an average velocity of 3.41 km/s, whereas the average is 3.84 km/s in the lowermost part (1560–1682 mbsf). Velocity values within Unit VI show no significant difference from the lower part of Unit V. Velocity values in this unit average 3.10 km/s (range = 2.78–3.55 km/s).

Thermal Conductivity

Hole 792A

Thermal conductivity measurements of samples from Hole 793A are shown in Figure 67 (Table 14). Subunit IA thermal conductivity values increase downward from 0.944 to 1.103 W/m · K (average = 1.007 W/m · K). Thermal conductivity values in Subunit IB decrease downward from 1.197 to ~0.900 (average 1.038 W/m · K).

Hole 792B

No thermal conductivity measurements were made on Hole 793B.

DOWNHOLE MEASUREMENTS

The drill pipe was pulled out of the hole on 14 June 1989, and the bit was removed in preparation for downhole measurements. The hole was reentered on 15 June, and the first downhole sensor was rigged up. Because the density tool failed to operate correctly at the surface, a reduced combination of geophysical sensors was deployed. Consequently, the first run consisted of resistivity, velocity, natural gamma, and temperature sensors. The assembly ran into an obstruction at 727.0 mbsf, and the short section located between that depth and the casing shoe (568.0 mbsf) was

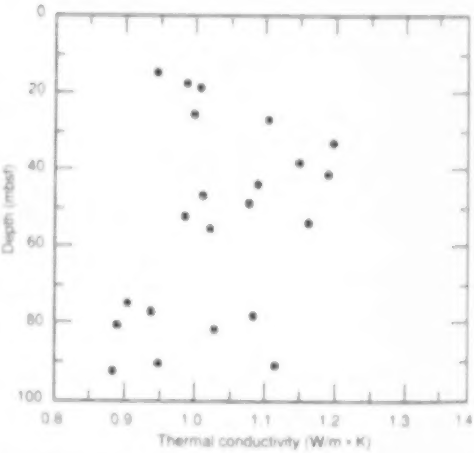

Figure 67. Plot of thermal conductivity vs. depth from Site 793.

Table 14. Thermal conductivity data from Site 793.

Core, section, interval (cm)	Depth (mbsf)	Thermal conductivity (W/m · K)
126-793A-		
1H-1, 12	0.12	0.738[a]
1H-3, 60	3.60	0.694[a]
3H-1, 119	14.69	0.964
3H-3, 107	17.57	0.986
3H-4, 55	18.55	1.006
4H-2, 92	25.42	0.997
4H-3, 108	27.08	1.103
5H-1, 36	32.86	1.197
5H-5, 82	37.93	1.148
5H-7, 108	41.17	1.191
6H-2, 41	43.91	1.088
6H-4, 12	46.62	1.009
6H-5, 55	48.55	1.075
7H-1, 67	52.27	0.983
7H-2, 75	53.85	1.161
7H-3, 71	55.31	1.019
9H-3, 44	74.34	0.902
9H-5, 24	77.14	0.937
9H-5, 104	77.94	1.001
10H-1, 22	80.72	0.887
10H-2, 84	81.75	1.027
11H-1, 29	90.39	0.945
11H-1, 78	90.88	1.114
11H-2, 35	91.95	0.881

[a] Data of uncertain quality.

logged. The drill pipe was lowered to clear the borehole, and the bit was set below the obstruction at 774.0 mbsf. The same combination of sensors encountered a second bridge at 965.0 mbsf. After logging this 191.0-m-long interval, the previous operation was repeated and the pipe set below the bridge at 1034.0 mbsf. The third run of the geophysical assembly was more successful, as the tool stopped at 1580 mbsf, allowing us to record data over a 546.0-m-long interval. Because this third interval was the longest open section of the borehole in which data could be recorded, we decided to keep the pipe at the depth of 1034.0 mbsf and to proceed with the rest of the measurements.

The second logging assembly consisted of the FMS, natural gamma, and temperature sensors. A depth of only 1539.0 mbsf was reached because the hole began filling up with debris as a result of clearing the two first bridges.

The geochemical (GLT), natural gamma (NGT), and temperature sensors were deployed as the third combination. The interval from 1532.0 to 1034.0 mbsf was logged in the open hole, and data were recorded through the drill pipe up to the casing shoe (568.0 mbsf). At this point we decided to run a reduced vertical seismic profile (VSP) because of time constraints. Poor clamping of the downhole sensor in the hole precluded the recording of good data, reducing the final dataset to only a few good shots at five discrete levels. The last run in Hole 793B consisted of the FMS, natural gamma, and temperature sensors deployed in the upper part of the open hole, from 762.0 mbsf to the casing shoe (568.0 mbsf), after pulling the drill pipe into the casing.

In the upper interval logged with the FMS (762.0–768.0 mbsf), the borehole was often measured to be larger than 15.5 in. in diameter. In the lower interval, the hole is generally cylindrical to slightly elliptical, with an average diameter of 12.0 in. Near the sediment/basement contact, the hole is caved and larger than 15.5 in. The deviation of the borehole axis from vertical is approximately 2.0°. The borehole conditions were favorable to downhole experiments because of the lithified nature of the sediments. As a consequence, the data recorded in Hole 793B are of excellent quality. The sampling distance of 2.52 mm for FMS data is the smallest of any presently available downhole sensor. Besides VSP checkshots, all the other records presented in this report have been sampled with a 0.152-m digitization interval. A detailed description of each of the sensors and measurement principles is provided in the "Explanatory Notes" chapter, this volume. Summary log figures appear as Figures 68 and 69. A summary of downhole measurements operations appears in Table 15.

Runs 1, 2, and 3

The first three runs (resistivity, sonic, natural gamma, and temperature) in Hole 793B consisted of a combination of two induction resistivity sensors (with deep and shallow radii of investigation for the deep-phasor induction measurement [IDPH] and the medium-phasor induction measurement [IMPH], respectively), a spherically focussed resistivity sensor (SFL), the long-spacing sonic sensor (LSS), a spectral natural gamma sensor (NGT), and the Lamont-Doherty Geological Observatory temperature tool (TLT). These last two sensors were included in each of the logging runs (the NGT for the purpose of depth correlation) and are discussed separately at the end of this section.

The SFL calibration sequence was found to be in error for Runs 1 and 2. Prior to Run 3, the cartridge of the resistivity sonde was changed and the problem disappeared. As a consequence, the SFL profiles provided for Runs 1 and 2 were normalized to the induction logs and should not be considered quantitative. They were kept because of the better vertical resolution of the SFL over the induction measurements. The resistivity data are otherwise of excellent quality, outlining, for example, numerous upward-fining sequences. The transition from sediments to basement is characterized at 1408.0 mbsf by the lowest resistivity value recorded in the lower part of the basement; this may correlate with a fault.

The main characteristic of the sonic data during acquisition was the high noise level that interfered with the signal from the formation. This noise is primarily the result of the absence of adequate centralization of the sonic tool, a consequence of the small diameter of the drill pipe, which does not allow for the use of centralizers. This lack of centralization resulted in asymmetrical arrivals at the receivers and "road-noise" caused by occasional direct contact between the tool and the formation. The final velocity profile was computed choosing mostly three of the four measured transit times (LTT1, LTT2, LTT3, and LTT4; see discussion of Site 645, Shipboard Scientific Party, 1987, for further details).

Runs 4 and 7

Runs 4 and 7 collected FMS images and natural gamma-ray and temperature data. The four continuous FMS images, which spanned the intervals 1539.0 to 1034.0 mbsf and 762.0 to 568 mbsf each covered about 10% of the internal surface of the borehole; the images will be produced after shore-based analysis. Shipboard image analysis showed the data to be of excellent quality. Features < 1 cm in thickness are evident in the FMS results, and numerous turbidite sequences are visible.

The measurements pertaining to hole shape and direction (including two orthogonal measurements of drill hole diameter) were recorded over the same intervals. In basement, below the fault zone located at 1408.0 mbsf, the ellipticity of the drillhole tends to align in a N065°E direction. This constrains the maximum horizontal stress direction in the basement of Hole 793B to N155°E, significantly different from that observed in Hole 792E (N110°E).

Run 5

The geochemical data recorded during the fifth run (geochemical combination, natural gamma, and temperature) are of

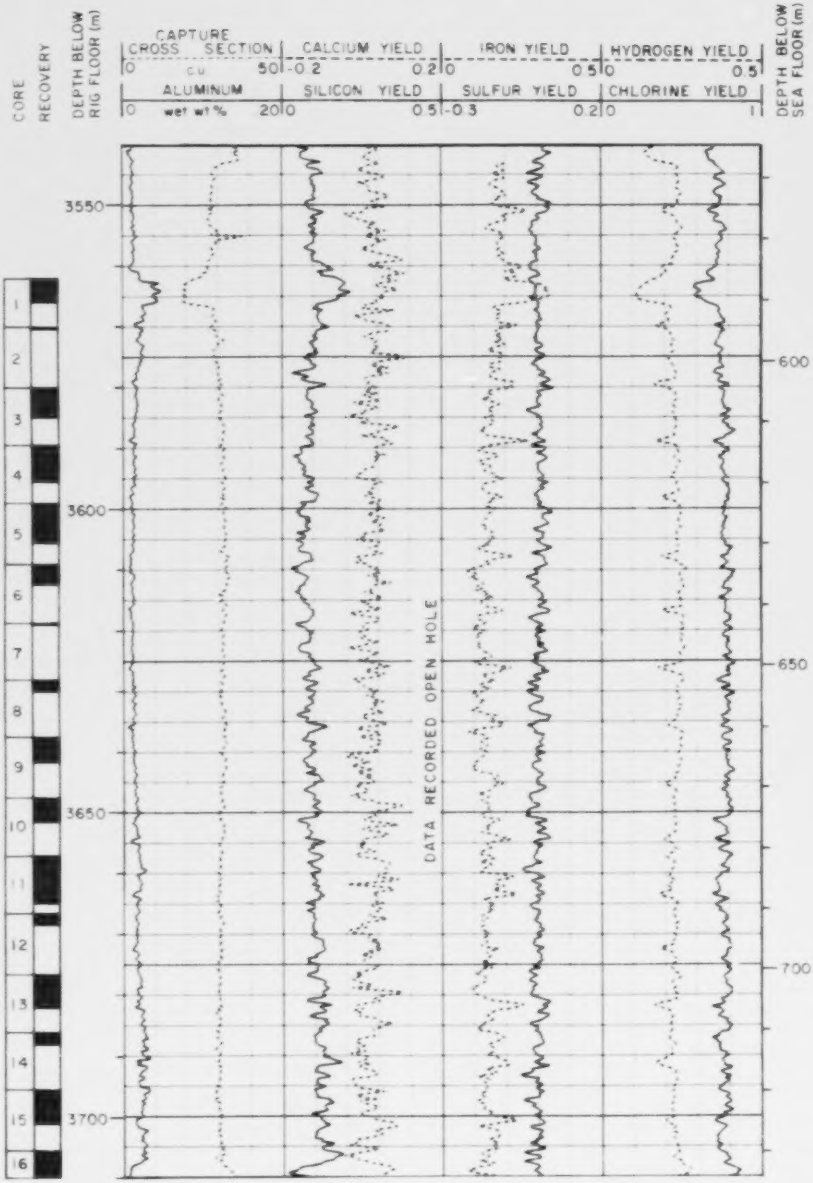

Figure 68. Summary log figure, ACT, Hole 793B.

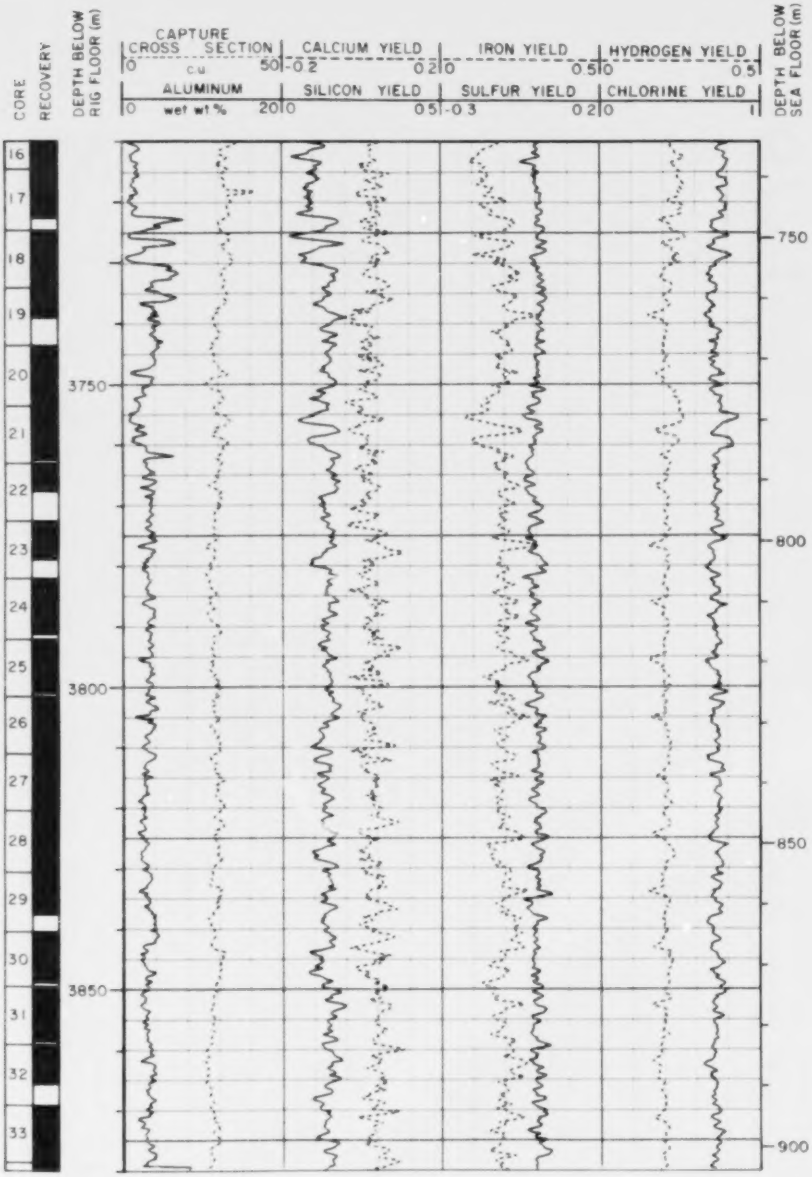

Figure 68 (continued).

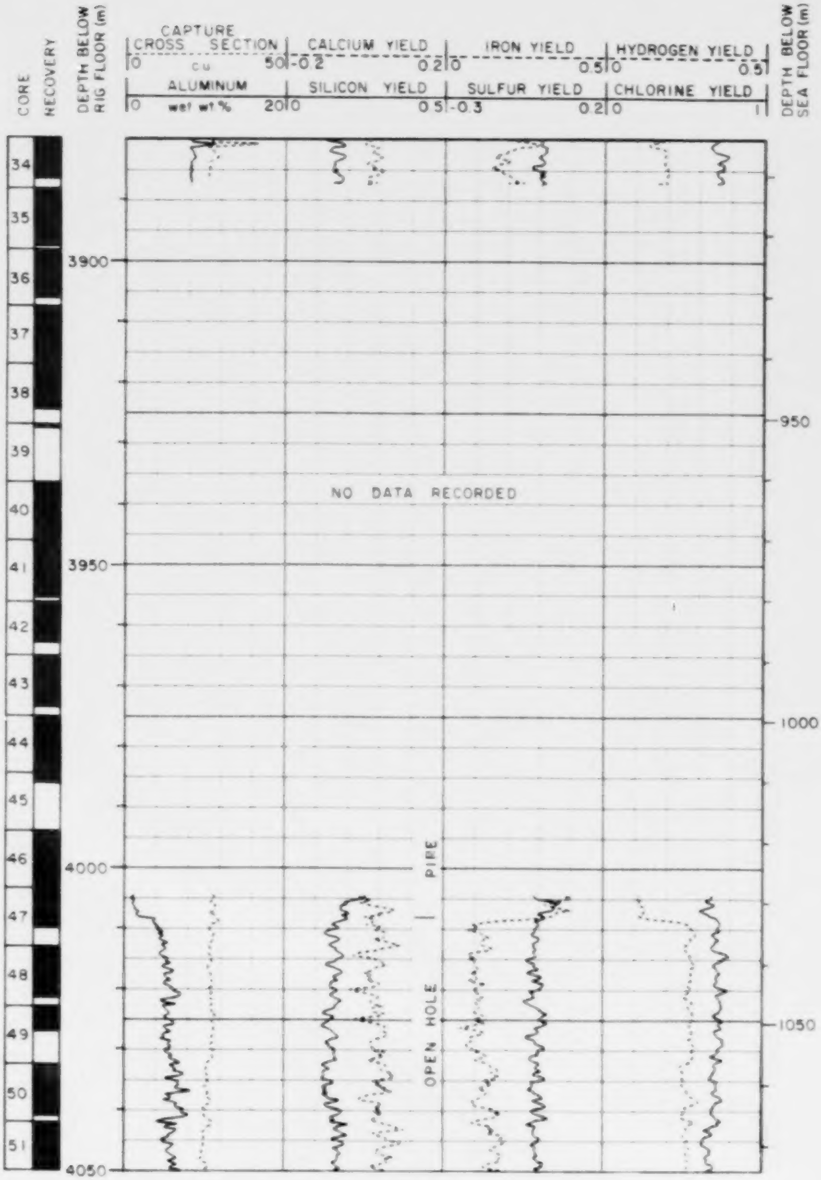

Figure 68 (continued).

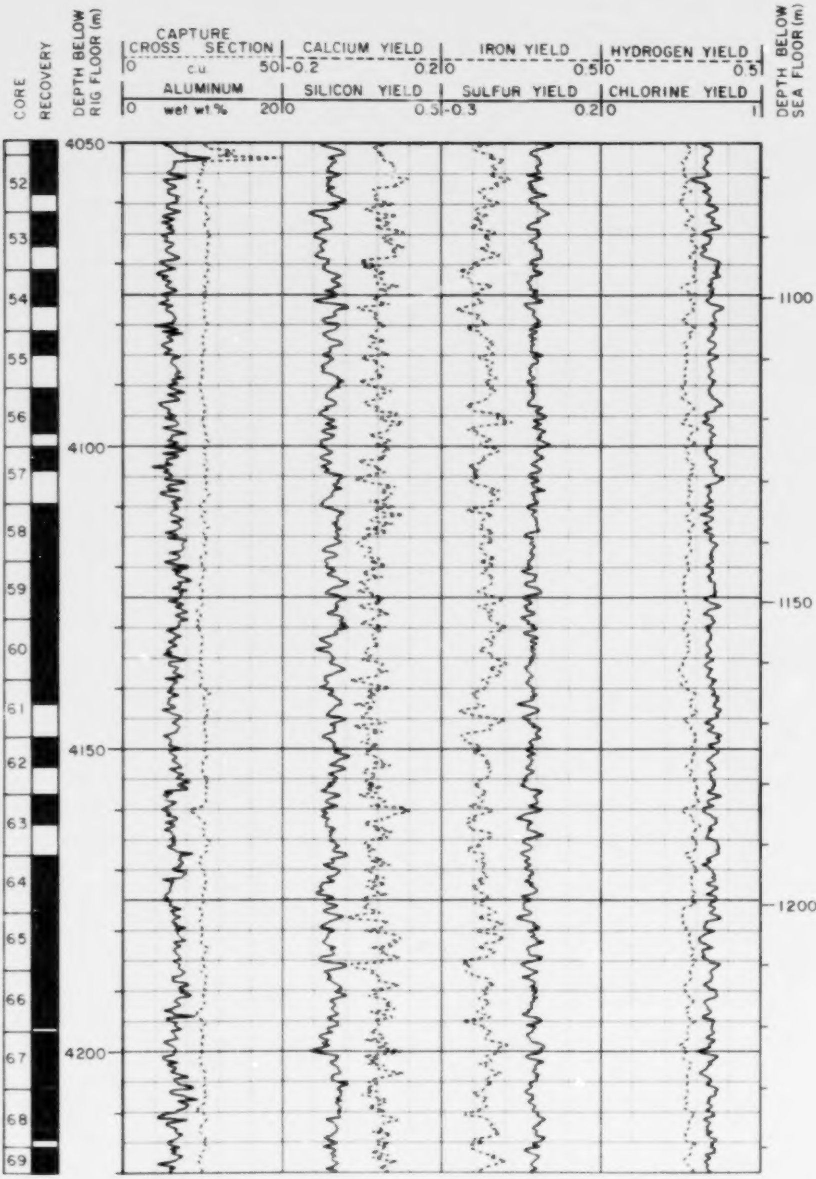

Figure 68 (continued).

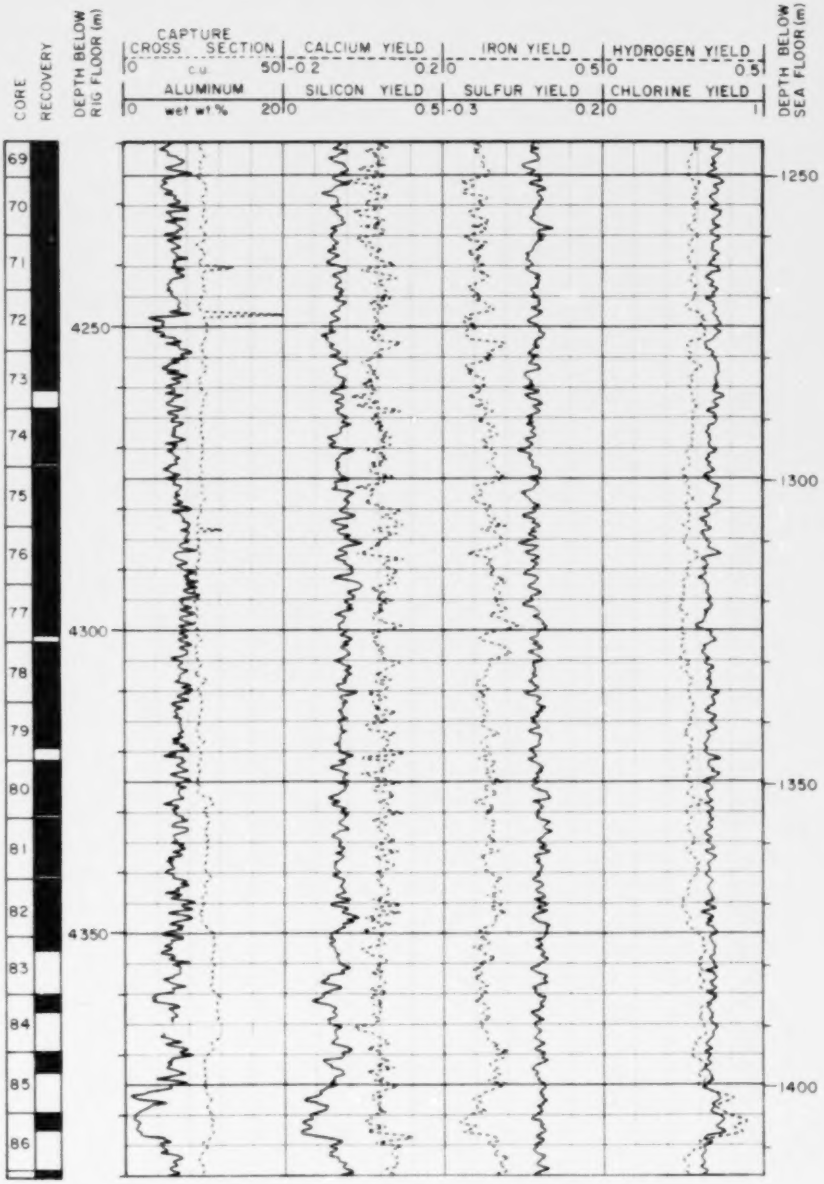

Figure 68 (continued).

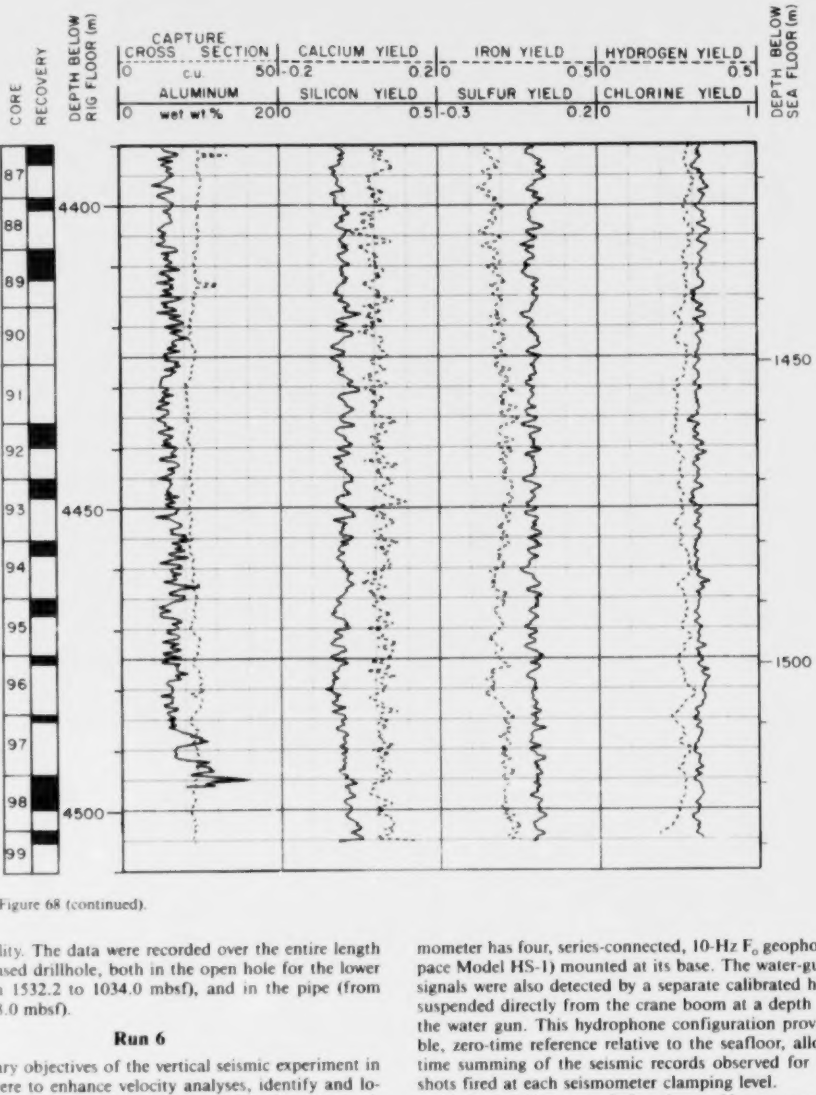

Figure 68 (continued).

excellent quality. The data were recorded over the entire length of the non-cased drillhole, both in the open hole for the lower section (from 1532.2 to 1034.0 mbsf), and in the pipe (from 1034.0 to 568.0 mbsf).

Run 6

The primary objectives of the vertical seismic experiment in Hole 793B were to enhance velocity analyses, identify and locate primary reflectors, correlate the lithostratigraphy with identified reflectors, and tie the surface multichannel seismics to well logs for regional-scale correlations. The data acquisition began near the bottom of the hole (1530 mbsf, 4505 mbsl).

Data Acquisition

The sound source used for the Hole 793B VSP experiment was the *JOIDES Resolution*'s large-volume (400 in.^{3}/16.0 L), high-pressure (2000 psi/140 bar) water gun (SSI H400). The gun was suspended 15 mbsl from a buoy, tethered from the drillship's aft port crane boom about 24 m abeam. The downhole seismic signals were received by a Schlumberger Well Seismic Tool (WST) single vertical component seismometer. The seismometer has four, series-connected, 10-Hz F_0 geophones (Geospace Model HS-1) mounted at its base. The water-gun acoustic signals were also detected by a separate calibrated hydrophone suspended directly from the crane boom at a depth 3 m below the water gun. This hydrophone configuration provided a stable, zero-time reference relative to the seafloor, allowing real-time summing of the seismic records observed for the several shots fired at each seismometer clamping level.

Unfortunately, repeated clamping problems were encountered because the tool slid downhole when the cable was slacked to allow for good coupling to the borehole wall. Only five acceptable shots were recorded at an average depth of 1300 mbsf. They may eventually provide reliable transit-time data to calibrate surface multichannel data. Transit time may also be recovered from six other noisy shots recorded at approximately the same depth.

Water-gun-generated signals received by the WST borehole seismometer are preamplified downhole, transmitted up the logging cable, and digitally recorded along the hydrophone signals by the PDP-11 minicomputer and A/D converter of the Schlumberger CSU logging data acquisition system. Timing information was logged with millisecond accuracy. First-break transit

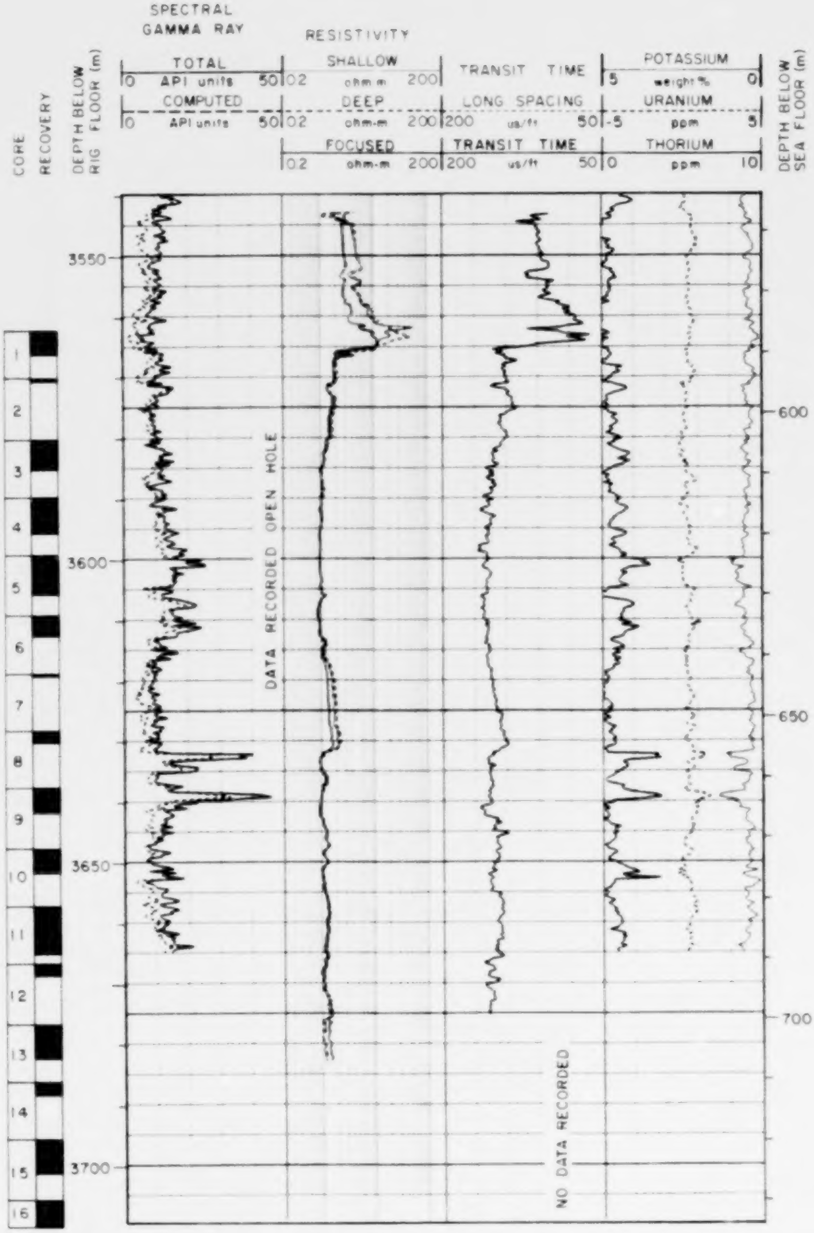

Figure 69. Summary log figure, DIT, Hole 793B.

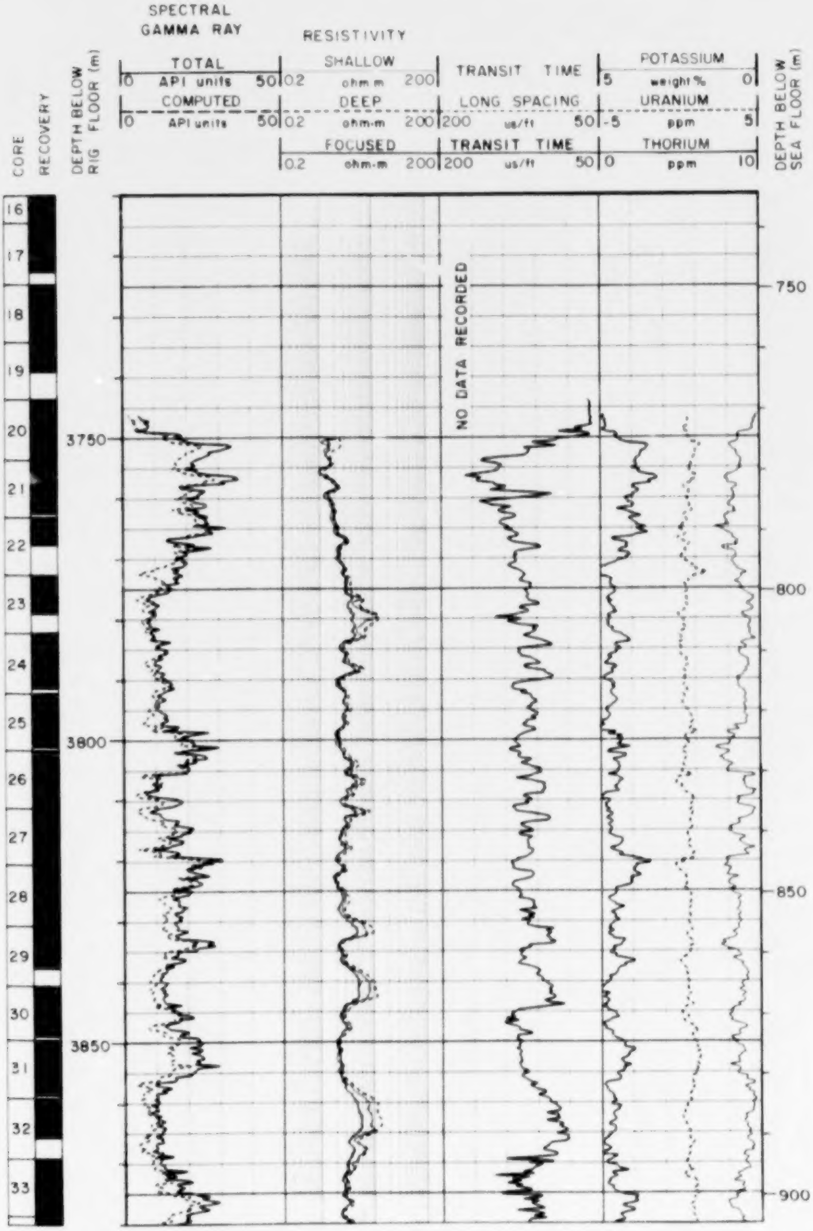

Figure 69 (continued).

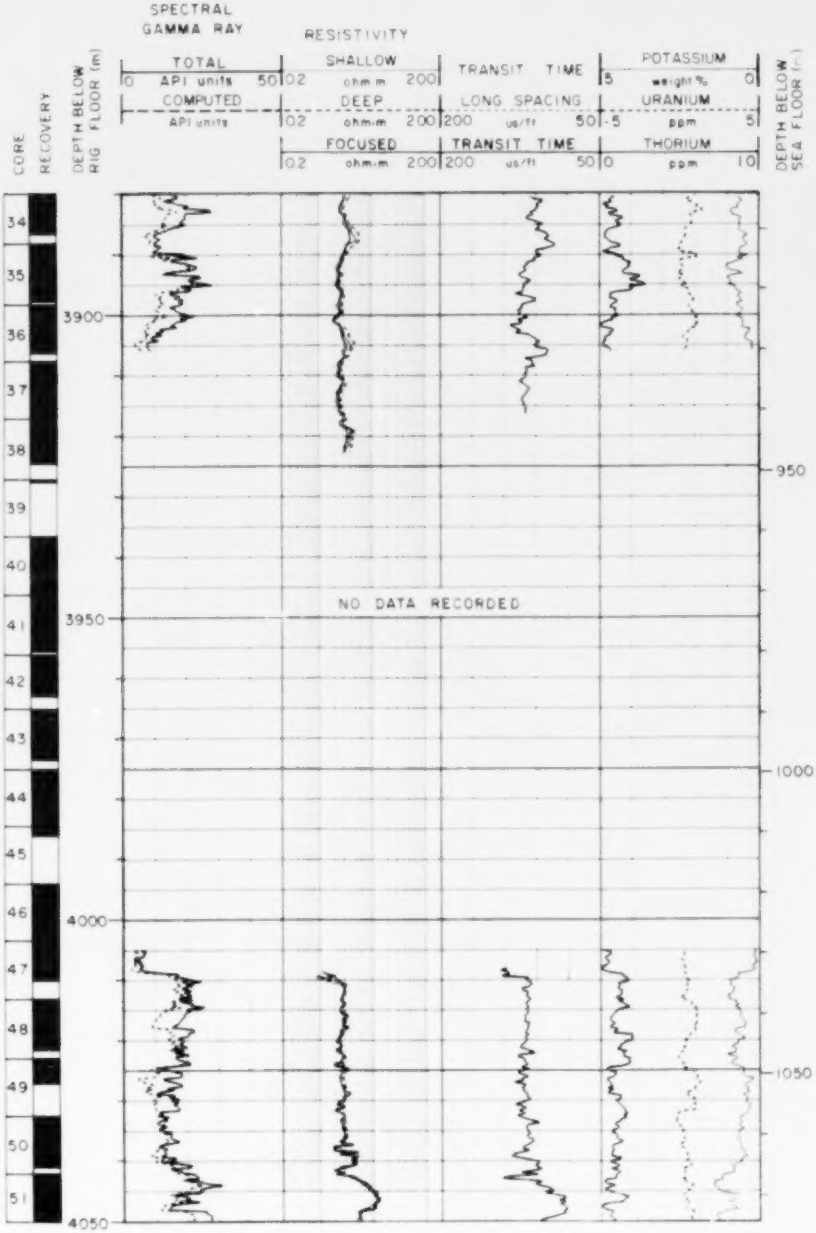

Figure 69 (continued).

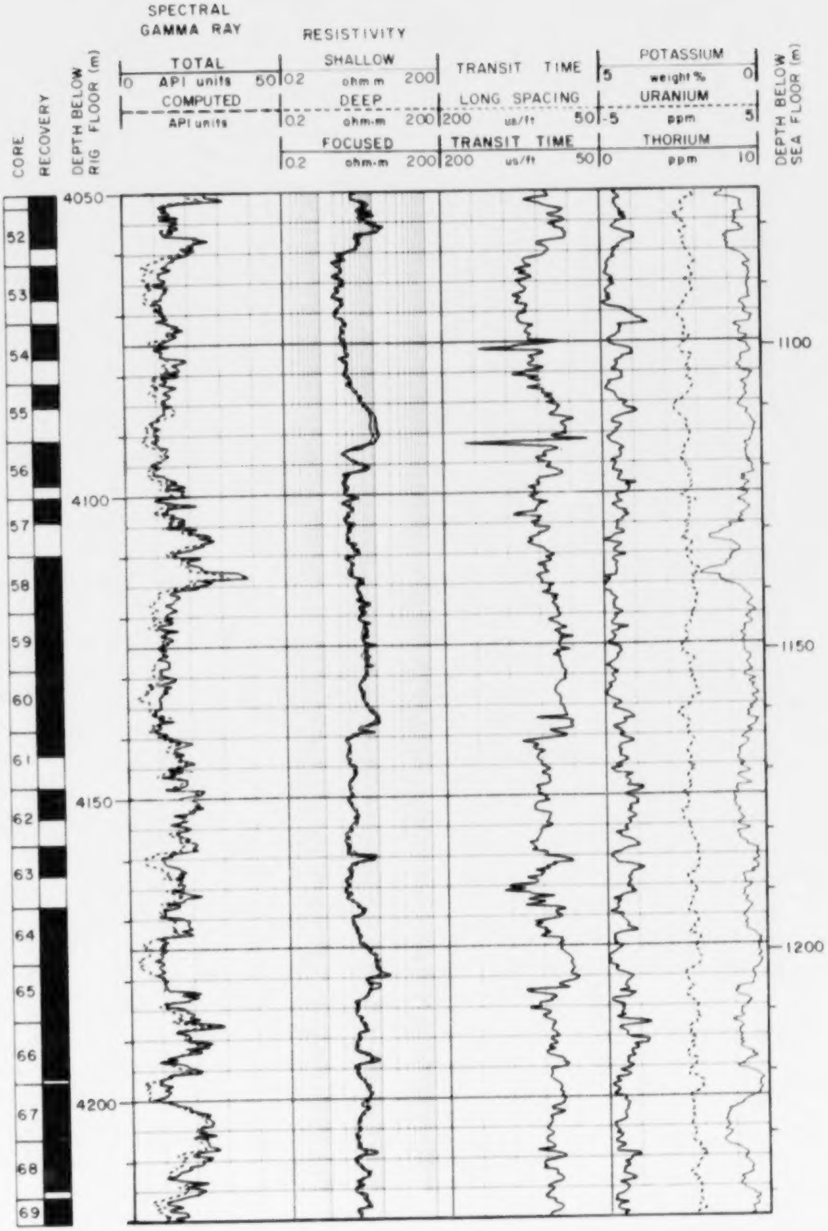

Figure 69 (continued).

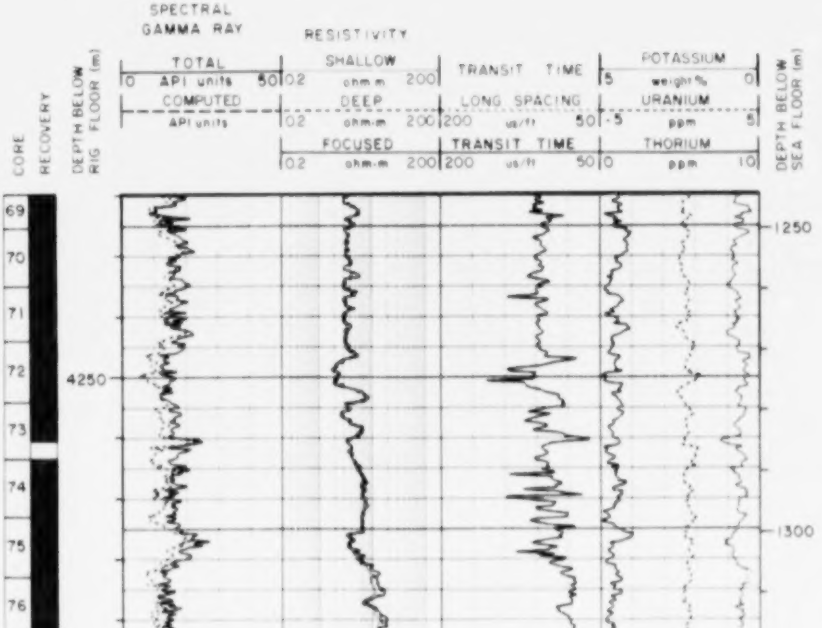

Figure 69 (continued).

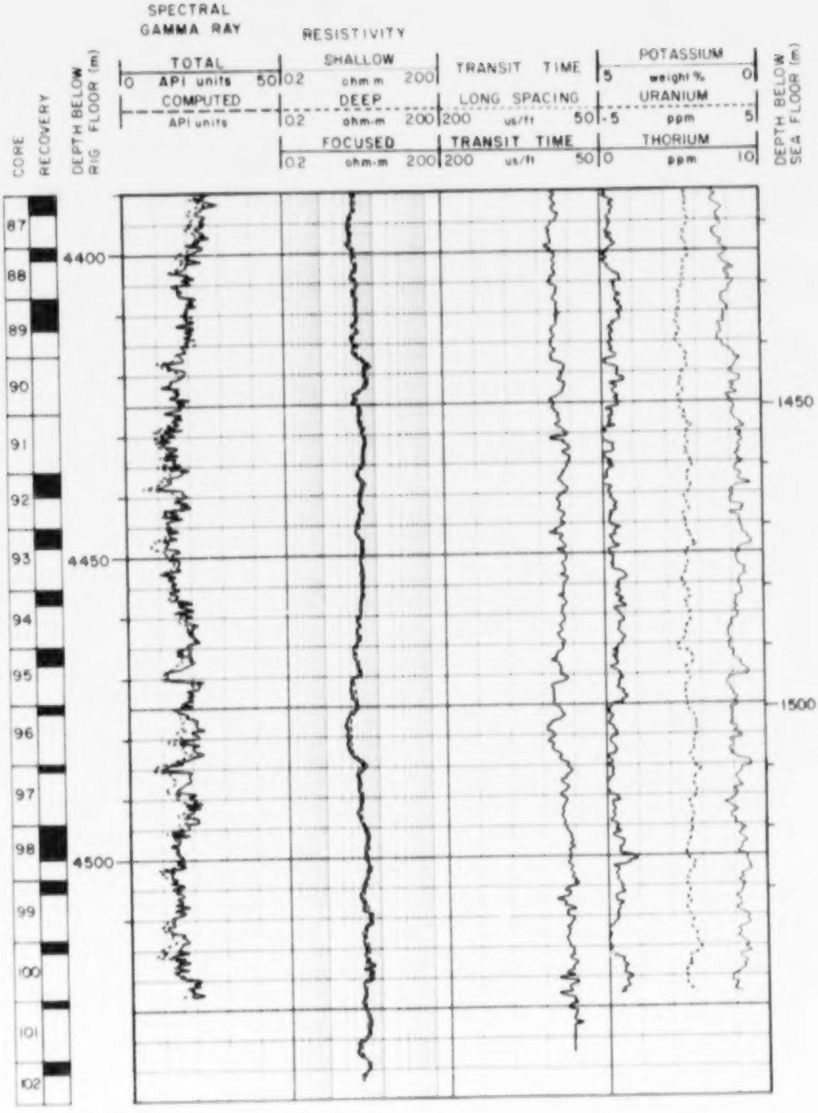

Figure 69 (continued).

traveltimes were calculated to 0.1 ms from the stacked shots at each clamping level.

Preliminary Stratigraphic Results from Downhole Measurements

The downhole measurements are analyzed here with respect to the stratigraphic column defined from cores. Because of the discontinuous nature of this dataset, we infer only limited results with respect to the stratigraphy.

As no data were recorded inside the 11-3/4-in. casing (from the seafloor to the casing shoe, located at 568.0 mbsf), Unit I is not represented by downhole measurements. Velocity and resistivity were measured in Units II (a diabase sill located from 586.0 to 591.0 mbsf) and III during Run 1. The FMS images re-

Table 15. Summary of downhole measurement operations, Site 793.

Date	Time (UTC)	Operation
June 15, 1989	0730	Rig-Up. Attempting DIL-LDT-LSS-NGT-TEMP HLDT failed with SS at surface—IMPH not working.
	1115	RIH with DIL-LSS-NGT-TEMP—Second DIL used.
	1315	Hit bridge at 12,090 ft. Log up to shoe at 11,624 ft. Good data.
	1600	Out of the hole with DIL (Run 1). Rig down to break through bridge with pipe.
	2000	Rig up DIL-LSS-NGT-TEMP.
	2215	Hit bridge at 12,886 ft. Log up to pipe at 12,301 ft. Good data.
June 16, 1989	0130	Out of the hole with DIL (Run 2). Rig down to break through bridge with pipe.
	0515	Rig up DIL-LSS-NGT-TEMP.
	0730	Hit bridge at 14,896 ft. Log up to pipe at 13,153 ft. (about 120 m off bottom). Good data. 77% of open hole covered.
	1015	Out of the hole with DIL (Run 3).
	1100	RIH with FMS-NGT-TEMP.
	1300	Hit bottom at 14,810 ft. Log up to pipe at 13,153 ft. Good data.
	1500	Out of the hole with FMS.
	1630	RIH with GST-ACT-NGT-TEMP.
	1900	Hit bottom at 14,785 ft. Log up to pipe at 13,153 ft. Good data.
	2200	Skip BHA. Logging through pipe from 12,770 ft. to casing shoe (11,624 ft.).
June 17, 1989	0100	Out of the hole with GLT.
	0130	RIH with WST.
Plan for the end of logging:		
	0300	Start recording about twelve levels from the bottom of the hole, and for a maximum of 90 min.
	0600	Out of the hole with WST. Rig down and trip pipe above casing shoe.
	0800	RIH with FMS-NGT-TEMP to log the upper part of the hole.
	1300	Rig down. Start pulling pipe out of the hole.
	2300	Sailing to Tokyo.

corded during the last run in the hole span approximately the same interval. Although Unit IV is not represented by downhole mesurements, Unit V is largely sampled. The base of Unit V (1374.5 mbsf) is the site of a large natural gamma peak, apparently the result of local potassium enrichment. The drill hole is generally oval in shape in Unit VI and caved at its base in what appears to be a faulted sediment/basement contact (from 1405.5 to 1408.2 mbsf). Basement (Unit VII) is characterized by uniform physical properties and generally featureless, mottled FMS images.

REFERENCES

Akimoto, K., 1989. Recent foraminifera from Enshunada. *In* Takayanagi, Y., and Ishizaki, K. (Eds.), *Collected Papers on Foraminifera from the Japanese Islands*: Sendai (Toko Press), 93-104.

Arthur, M. A., Carson, B., and von Huene, R. 1980. Initial tectonic deformation of hemipelagic sediment at the leading edge of the Japan convergent margin. *In* Langseth, M., Okada, H., et al., *Init. Repts. DSDP*, 56, 57, Pt. 1: Washington (U.S. Govt. Printing Office), 569-614.

Berggren, W. A., Kent, D. V., Flynn, J. J., and Van Couvering, J. A., 1985. Cenozoic geochronology. *Geol. Soc. Am. Bull.*, 96:1407-1418.

Blow, W. H., 1969. Late middle Eocene to Recent planktonic foraminiferal biostratigraphy. *In* Renz, H. H., and Bronniman, P. (Eds.), *Proc. 1st Intern. Conf. Planktonic Microfossils*: Leiden (E. J. Brill), 199-422.

Bolli, H. M., Saunders, J. B., and Perch-Nielsen, K. (Eds.), 1985. *Plankton Stratigraphy*: Cambridge (Cambridge Univ. Press).

Bouma, A. H., 1962. *Sedimentology of Some Flysch Deposits*: Amsterdam (Elsevier).

Champion, D. E., Lanphere, M. A., and Kuntz, M. A., 1988. Evidence for a new geomagnetic reversal from lava flows in Idaho: discussion of short polarity reversals in the Brunhes and late Matuyama polarity chrons. *J. Geophys. Res.*, 93:11,667-11,680.

Foreman, H. P., 1981. Radiolaria. *In* Emiliani, C. (Ed.), *The Sea* (Vol. 7): *The Oceanic Lithosphere*: New York (Wiley), 1121-1144.

Fryer, P., Pearce, J., et al., in press. *Proc. ODP, Init. Repts.*, 125: College Station, TX (Ocean Drilling Program).

Haq, B. U., Hardenbol, J., and Vail, P. R., 1987. Chronology of fluctuating sea levels since the Triassic. *Science*, 235:1156-1167.

Hiscott, R. N., and Middleton, G. V., 1979. Depositional mechanics of thick-bedded sandstones at the base of a submarine slope, Tourelle Formation (Lower Ordovician), Quebec, Canada. *In* Doyle, L. J., and Pilkey, O. H. (Eds.), *Geology of Continental Slopes*. Soc. Econ. Paleontol. Mineral. Spec. Publ., 27:307-326.

———, 1980. Fabric of coarse deep-water sandstones, Tourelle Formation, Quebec, Canada. *J. Sediment. Petrol.*, 50:703-722.

Ingle, J. C., Jr., 1980. Cenozoic paleobathymetry and depositional history of selected sequences within the southern California continental borderland. *Spec. Publ. Cushman Found. Foraminiferal Res.*, 19:163-195.

Keller, G., 1979. Early Pliocene to Pleistocene planktonic foraminiferal datum levels in the North Pacific: DSDP Sites 173, 310, 296. *Mar. Micropaleontol.*, 4:281-294.

Kharaka, Y. K., and Berry, F. A. W., 1973. Simultaneous flow of water and solutes through geological membranes. *Geochim. Cosmochim. Acta*, 37:2577-2603.

Kuno, H., 1960. High-alumina basalt. *J. Petrol.*, 1:121-145.

Lowe, D. R., 1982. Sediment gravity flows: II. Depositional models with special reference to the deposits of high-density turbidity currents. *J. Sediment. Petrol.*, 52:279-297.

Lundberg, N., and Leggett, J. K., 1986. Structural features in cores from the slope landward of the Japan Trench, Deep Sea Drilling Project Leg 87B. *In* Kagami, H., Karig, D. E., Coulbourn, W. C., et al., *Init. Repts. DSDP*, 87: Washington (U.S. Govt. Printing Office), 809-826.

Manheim, F. T., and Waterman, L. S., 1974. Diffusimetry (diffusion constant estimation) on sediment cores by resistivity probe. *In* von der Borch, C. C., Sclater, J. G., et al., *Init. Repts. DSDP*, 22: Washington (U.S. Govt. Printing Office), 663-670.

Mutti, E., 1985. Turbidite systems and their relations to depositional sequences. *In* Zuffa, G. G. (Ed.), *Provenance of Arenites*: Dordrecht (D. Reidel), 65-93.

Nelson, C. H., and Maldonado, A., 1988. Factors controlling depositional patterns of the Ebro turbidite systems, Mediterranean Sea. *AAPG Bull.*, 72:698–716.

Ogawa, Y., and Miyata, Y., 1985. Vein structure and its deformation history in the sedimentary rocks of the Middle America Trench slope off Guatemala, Deep Sea Drilling Project Leg 84. *In* von Huene, R., Aubouin, J., et al., *Init. Repts. DSDP,* 84: Washington (U.S. Govt. Printing Office), 811–829.

Pierson, T. C., 1981. Dominant particle support mechanisms in debris flows at Mt. Thomas, New Zealand, and implications for flow mobility. *Sedimentology,* 28:49–60.

Seno, T., and Maruyama, S., 1984. Paleogeographic reconstruction and origin of the Philippine Sea. *Tectonophysics,* 102:53–84.

Shepard, F. P., 1963. Submarine canyons. *In* Hill, M. N. (Ed.), *The Sea* (Vol. 3): Huntington, NY (Krieger), 480–506.

Shipboard Scientific Party, 1987. Site 645. *In* Srivastava, S. P., Arthur, M., et al., *Proc. ODP, Init. Repts.*, 105: College Station, TX (Ocean Drilling Program), 61–418.

Stern, R. J., and Ito, E., 1983. Trace element and isotopic constraints on the source of magmas in active volcano and Mariana island arcs. *J. Volc. Geothermal. Res.*, 18:461–482.

Takayama, T., and Sato, T., 1987. Coccolith biostratigraphy of the North Atlantic Ocean, Deep Sea Drilling Project Leg 94. *In* Ruddiman, W. F., Kidd, R. B., Thomas, E., et al., *Init. Repts. DSDP,* 94, Pt. 2: Washington (U.S. Govt. Printing Office), 651–702.

Taylor, B., and Smoot, N. C., 1984. Morphology of Bonin fore-arc submarine canyons. *Geology,* 12:24–727.

Van Morkhoven, F.P.C.M., Berggren, W. A., and Edwards, A. S., 1986. Cenozoic cosmopolitan deep-water benthic foraminifera. *Bull. Cent. Rech. Explor.-Prod. Elf-Aquitaine,* No. 11.

Woodruff, F., 1985. Changes in Miocene deep-sea benthic foraminiferal distribution in the Pacific Ocean: relationship to paleoceanography. *In* Kennett, J. P. (Ed.), *The Miocene Ocean: Paleoceanography and Biogeography.* Mem. Geol. Soc. Am., 163:131–175.

Yasuda, H., 1989. Benthic foraminifera and sedimentary facies of the lower slope basin off Shikoku, Japan. *In* Takayanagi, Y., and Ishizaki, K. (Eds.), *Collected Papers on Foraminifera from the Japanese Islands:* Sendai (Toko Press), 83–92.

Zhang, Y., Langmuir, C. H., and Taylor, B., in press. Petrogenesis of Tori-shima and Sumisu-jima volcanoes of the Izu-Bonin arc. *Earth Planet. Sci. Lett.*

Ms 126A-110

NOTE: All core description forms ("barrel sheets") and core photographs have been printed on coated paper and bound as Section 3, near the back of the book, beginning on page 421.

SECTION 3: CORRELATION PAPERS

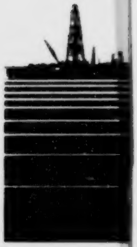

Taylor, B., Fujioka, K., et al., 1990
Proceedings of the Ocean Drilling Program, Initial Reports, Vol. 126

10. CORRELATION AND COMPARISON OF FOREARC SITES[1]

Shipboard Scientific Party[2]

INTRODUCTION

Three sites were drilled in the forearc basin of the Izu-Bonin Arc (Figs. 1 and 2). A lithologic and graphic summary of each site is presented in Figure 3. This chapter provides general comments as a framework for a comparison of the sites; the reader is directed to the respective site chapters for details (see "Site 787," "Site 792," and "Site 793" chapters, this volume).

BASEMENT AND BASAL SEDIMENTS

The forearc basement was cored at Sites 792 and 793. At Site 792, plagioclase-orthopyroxene-clinopyroxene andesites with minor basaltic andesite and dacite form massive flows with intercalated hyaloclastite and breccia layers. At Site 793, the breccias and massive to pillowed flows are mostly clinopyroxene-orthopyroxene basaltic andesites and andesites that belong to a high-Mg series with boninitic affinities. Minor aphyric lavas and clasts belong to a low-Mg series with tholeiitic affinities.

Basement at Sites 792 and 793 is overlain by brecciated rock. At Site 792, the brecciation appears to be the result of postdepositional hydrothermal alteration of volcanogenic sandstones. At Site 793, the breccia (about 30 m thick) is composed mainly of angular clasts of plagioclase-orthopyroxene-clinopyroxene andesite of a different composition from the underlying basement. Nevertheless, the poor organization of the breccia suggests local derivation from a submarine volcano or intrabasinal fault scarp.

The sedimentary rocks overlying the basement at Site 793 date from about 31 Ma, based on extrapolation of age-depth plots to the top of the basement (Fig. 4). The basal sedimentary strata at Site 792 are probably of similar age. They are biostratigraphically dated as younger than 34 Ma, but sedimentation rates cannot be extrapolated to basement because a major unconformity was crossed near 715 mbsf (about 29 Ma).

OLIGOCENE TURBIDITES (31–27 Ma)

Sedimentary rocks that overlie the basal breccia and that are older than 27 Ma constitute a thick Oligocene turbidite succession deposited at undecompacted rates of 80–300 m/m.y. (Figs. 4 and 5). The coarsest Oligocene deposits were recovered from the 28–29-Ma section (all sites) and the pre-30-Ma succession (Site 793 only). Very thick beds of pebbly sandstone and pebble conglomerate with large floating intraclasts and volcanic cobbles were recovered at Sites 792 and 793. Some of these coarse-grained deposits are interpreted as submarine debris-flow deposits.

All three forearc sites have a relatively complete record of sedimentation from 27–29 Ma, but only Site 793 has a good record of sedimentation from 29–31 Ma (Figs. 5 and 6). The older sediments were not reached at Site 787, and they lap out against a thin basal section above a basement high at Site 792. Depocenters to the north of Site 792 and to the west of Site 787 have sedimentary sections more than 100% thicker than at Site 793. Contemporaneous rates of deposition varied between the sites, so that Site 792 has the thickest 28–29-Ma record, whereas Sites 787 and 793 have thicker 27–28-Ma records. This probably reflects space-time variations in subsidence rates as well as spatial shifts in the positions of feeder channels supplying detritus from the Izu-Bonin Arc to the west, and from the outer-arc high that forms the eastern margin of the basin (Fig. 2). Site 792 is closest to the Izu-Bonin Arc, which may account for the significantly thicker 28–29-Ma record there.

UPPER OLIGOCENE–LOWER MIOCENE STRATA (27–18 Ma)

Sedimentation rates dramatically decreased during the latest Oligocene (23.7–27 Ma) to 4–9 m/m.y. at Sites 792 and 793 and to 20–24 m/m.y. at Site 787. The deposits are generally fine grained and burrowed, with minor distal turbidites. At Sites 787 and 792, the claystones and siltstones locally contain 10%–30% nannofossils. This calcareous component is absent at Site 793, possibly because local paleoceanographic variations caused reduced surface productivity and/or increased bottom-water dissolution.

Canyon cutting at Site 787 left no early Miocene sedimentary section. At Sites 792 and 793, claystones and nannofossil claystones that contain up to 60% nannofossils accumulated at undecompacted rates of 10–13 m/m.y. between 21–23.7 Ma. The overlying, often nannofossil-rich, silty claystones and clayey siltstones accumulated at 5–9 m/m.y. between 18–21 Ma. The carbonate-rich, very fine-grained, condensed sections at Sites 792 and 793 indicate a widespread low flux of volcanogenic detritus to the forearc basin during the early Miocene. In general, the only significant terrigenous component in the sediments is clay.

UPPERMOST LOWER MIOCENE–UPPER MIOCENE STRATA (18–5 Ma)

The middle and late Miocene record either is punctuated by unconformities (Sites 787 and 792) or was bypassed to reach deeper objectives (Site 793). At least two phases of submarine valley cutting at Site 787 left essentially no Miocene record, except for one core-catcher sample of unknown lithology.

Uppermost lower Miocene and lower middle Miocene (18–15 Ma) strata are only present at Site 793 (Figs. 4 and 6). The vitric siltstones and sandstones and the clayey siltstones with nannofossil-rich intervals record a renewal of arc volcanism beginning at 17–18 Ma. Sedimentation rates varied between 40 and 70 m/m.y. (Fig. 4).

Sediments of late middle Miocene and late Miocene age were only recovered at Site 792 (Fig. 4), as the equivalent section at Site 793 was not cored and Site 787 was drilled in Aoga Shima Canyon to bypass this section. The sediments consist mainly of strongly burrowed sandy mudstone and muddy sandstone with nannofossil-rich intervals, deposited at undecompacted rates of 20–50 m/m.y. The disseminated sand and silt grains are mainly brown scoria, clear volcanic glass shards, and volcanic rock fragments.

---

[1] Taylor, B., Fujioka, K., et al., 1990. *Proc. ODP, Init. Repts.*, 126: College Station, TX (Ocean Drilling Program).

[2] Shipboard Scientific Party is as given in the list of participants preceding the contents.

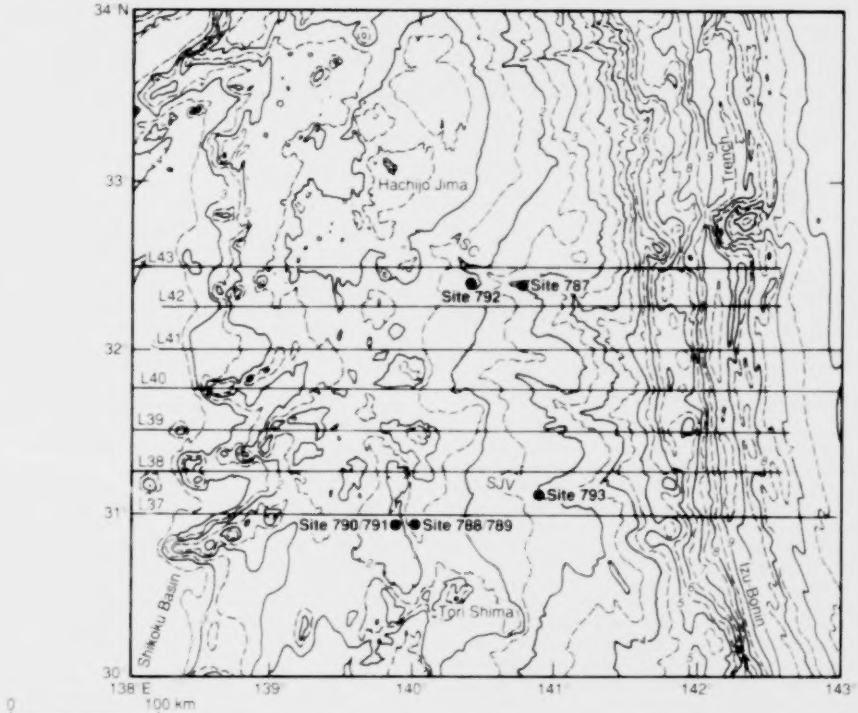

Figure 1. Bathymetric map of the Izu-Bonin Arc between the Shikoku Basin and Izu-Bonin Trench. Leg 126 sites and seismic profiles shown in Figure 2 are indicated; all but Lines 41 and 42 (L41 and L42) end just west of the map boundary in the Shikoku Basin. Bathymetric contour interval is 500 m. Note the positions of Sites 787 and 793 in Aoga Shima Canyon (ASC) and Sumisu Jima Valley (SJV), respectively.

PLIOCENE AND QUATERNARY STRATA (5–0 Ma)

The Quaternary and Pliocene sections at the three sites vary in their depositional environment, but all reflect a large volcanogenic input. At Sites 787 and 793, sediments of this age were deposited in deep-sea canyons cut into the forearc basin deposits; they consist (in whole or in part) of mixtures of pumiceous and scoriaceous sand and gravel. Drilling at Site 792 recovered a Quaternary and Pliocene fine-grained sedimentary section of predominantly nannofossil-rich, clayey silt and silty clay, punctuated by graded beds of vitric silt, vitric sand, and minor scoriaceous and pumiceous gravel that are interpreted as primary or resedimented volcanic ash.

STRUCTURAL FEATURES

All sedimentary rocks in the forearc basin that are older than 15 Ma contain a range of extensional features: (1) normal faults and microfaults; (2) steeply dipping fractures that may contain minerals like gypsum or injected sediment; and (3) subvertical, locally kinked dewatering veinlets like those described from the Middle America Trench slope by Ogawa and Miyata (1985) and from the Japan Trench by Arthur et al. (1980) and Lundberg and Leggett (1986). These latter structures are inferred to be the expression of a spaced cleavage that formed during early dewatering of unlithified, wet, muddy sediments (Ogawa and Miyata, 1985).

The Izu-Bonin forearc basin did not form until the mid-Oligocene. It is bounded to the east by Eocene volcanic rocks, which crop out on the Bonin Islands and were drilled at 31°–32°N (Fryer, Pearce, Stokking, et al., 1989). Basement to the west of the basin is also Eocene in age, as determined from the ages of rocks dredged from the frontal-arc high (M. Yuasa, pers. comm.) and the remnant arc (Kyushu-Palau Ridge; Shiki et al., 1985). Eocene margins to the Oligocene forearc basin suggest that the basin originated as an intra-arc rift (see "Site 793" chapter, this volume). Rifting can also explain the extensional structures that characterize the Oligocene section. Extensional microfaulting in the forearc continued into the Miocene, during the time of backarc spreading in the Shikoku Basin (25–15 Ma). Multichannel seismic profiles indicate that the center of the forearc basin is little faulted after 15 Ma, but that in the inner part of the forearc basin even the Pliocene-Pleistocene section is cut by normal faults (Taylor et al., this volume).

REFERENCES

Arthur, M. A., Carson, B., and von Huene, R., 1980. Initial tectonic deformation of hemipelagic sediment at the leading edge of the Japan convergent margin. *In* Langseth, M., Okada, H., et al., *Init. Repts.*

DSDP, 56, 57, Pt. 1: Washington (U.S. Govt. Printing Office), 569–613.

Fryer, P., Pearce, J., Stokking, L. B., et al., 1990. *Proc. ODP, Init. Repts.,* 125: College Station, TX (Ocean Drilling Program).

Honza, E., and Tamaki, K. 1985. The Bonin Arc. *In* Nairn, A.E.M., Stehli, F. G., and Uyeda, S. (Eds.), *The Ocean Basins and Margins,* (Vol. 7A): New York (Plenum), 459–502.

Lundberg, N., and Leggett, J. K., 1986. Structural features in cores from the slope landward of the Japan Trench, Deep Sea Drilling Project Leg 87B. *In* Kagami, H., Karig, D. E., et al., *Init. Repts. DSDP,* 87: Washington (U.S. Govt. Printing Office), 809–826.

Ogawa, Y., and Miyata, Y., 1985. Vein structure and its deformation history in the sedimentary rocks of the Middle America Trench slope off Guatemala, Deep Sea Drilling Project Leg 84. *In* von Huene, R., Aubouin, J., et al., *Init. Repts. DSDP,* 84: Washington (U.S. Govt. Printing Office), 811–829.

Shiki, T., Mizuno, A., and Kobayashi, K., 1985. Data listing of the bottom materials dredged and cored from the Northern Philippine Sea. *In* Shiki, T. (Ed.), *Geology of the Northern Philippine Sea:* (Tokai Univ. Press), 23–41.

Ms 126A-111

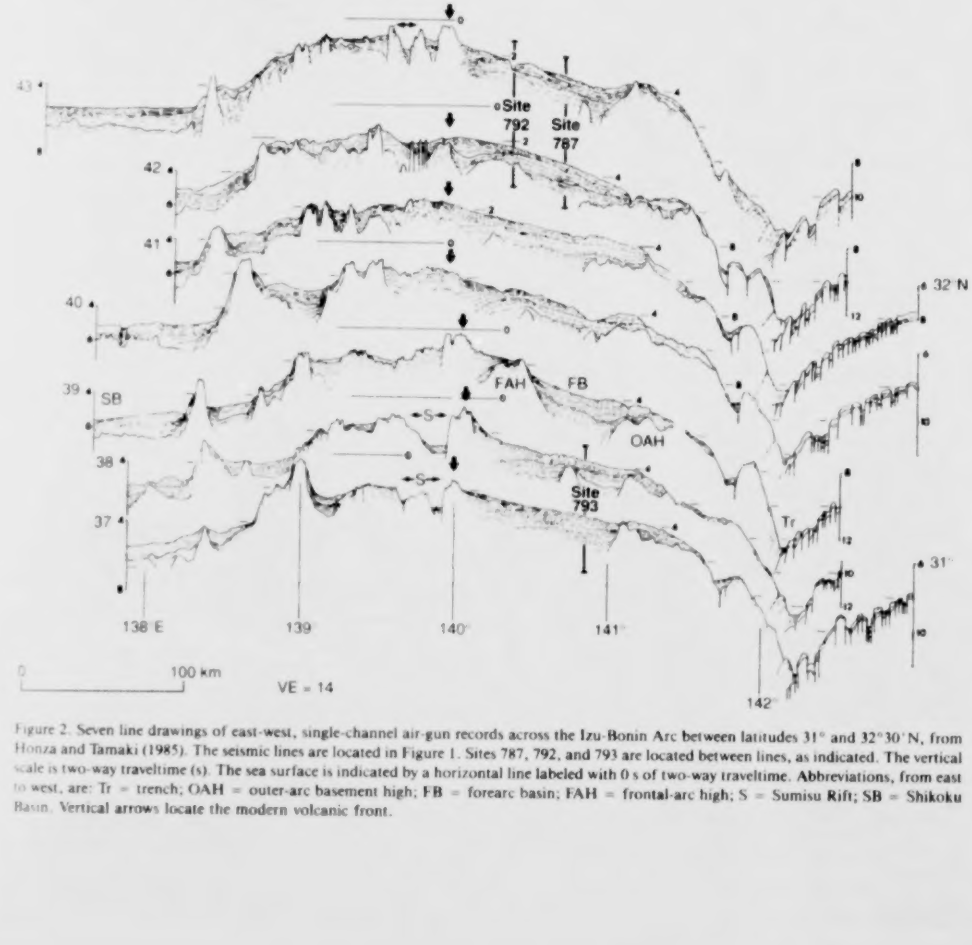

Figure 2. Seven line drawings of east-west, single-channel air-gun records across the Izu-Bonin Arc between latitudes 31° and 32°30′N, from Honza and Tamaki (1985). The seismic lines are located in Figure 1. Sites 787, 792, and 793 are located between lines, as indicated. The vertical scale is two-way traveltime (s). The sea surface is indicated by a horizontal line labeled with 0 s of two-way traveltime. Abbreviations, from east to west, are: Tr = trench; OAH = outer-arc basement high; FB = forearc basin; FAH = frontal-arc high; S = Sumisu Rift; SB = Shikoku Basin. Vertical arrows locate the modern volcanic front.

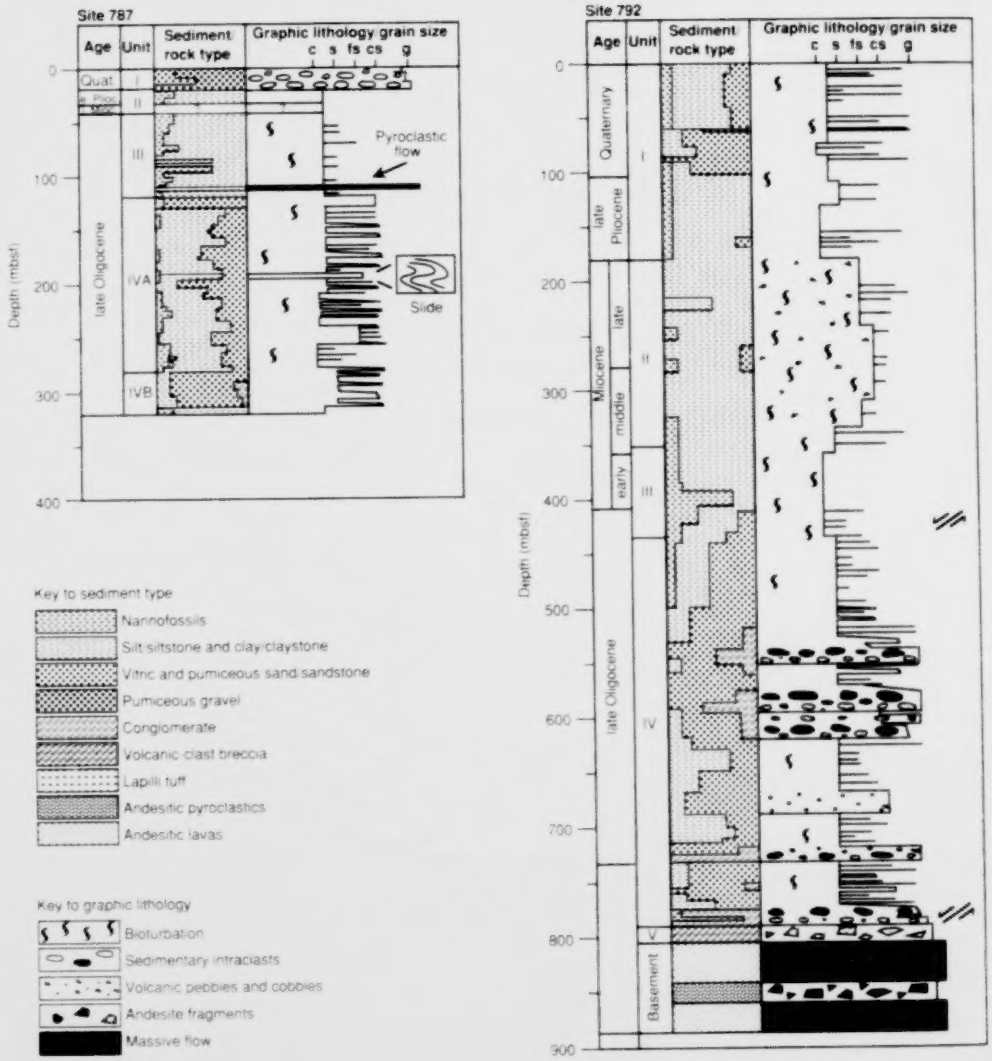
Site 787
Age
Unit
Sediment/rock type
Graphic lithology/grain size
c s fs cs g
Quat
e. Plioc.
Mioc.
late Oligocene
I
II
III
IVA
IVB
Pyroclastic flow
Slide
Depth (mbsf)
0
100
200
300
400
Site 792
Quaternary
late Pliocene
Miocene
late
middle
early
late Oligocene
Basement
V
500
600
700
800
900
Key to sediment type
Nannofossils
Silt/siltstone and clay/claystone
Vitric and pumiceous sand/sandstone
Pumiceous gravel
Conglomerate
Volcanic clast breccia
Lapilli tuff
Andesitic pyroclastics
Andesitic lavas
Key to graphic lithology
Bioturbation
Sedimentary intraclasts
Volcanic pebbles and cobbles
Andesite fragments
Massive flow

Figure 3. Summary columns for forearc sites, showing depth (mbsf), age, lithologic units, sediment/rock type, and graphic lithology/grain size (c = clay/claystone, s = silt/siltstone, fs = fine-grained sand/sandstone, cs = coarse-grained sand/sandstone, and g = gravel/conglomerate).

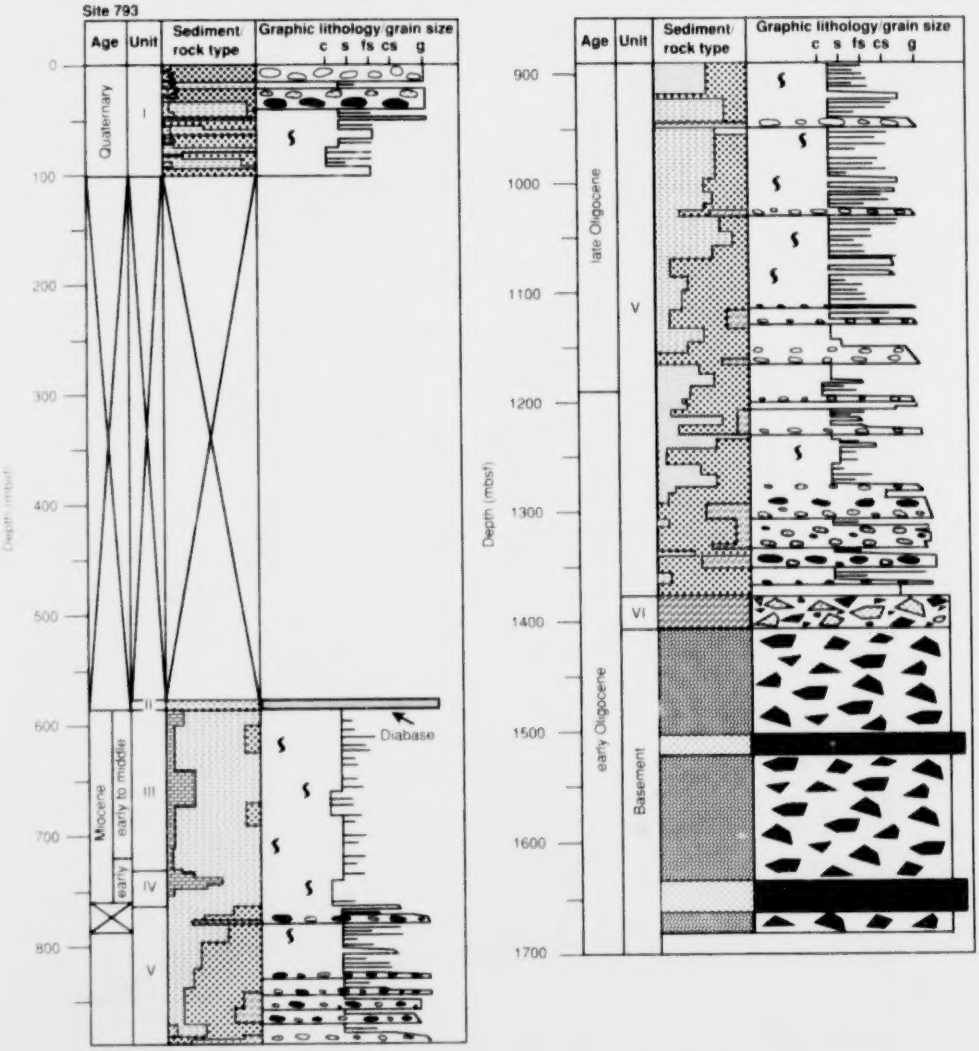
Site 793
Age
Unit
Sediment/ rock type
Graphic lithology/grain size
c s fs cs g
Depth (mbsf)
0
100
200
300
400
500
600
700
800
Quaternary
I
II
Diabase
Miocene
early to middle
early
III
IV
V
900
1000
1100
1200
1300
1400
1500
1600
1700
late Oligocene
early Oligocene
VI
Basement

Figure 3 (continued).

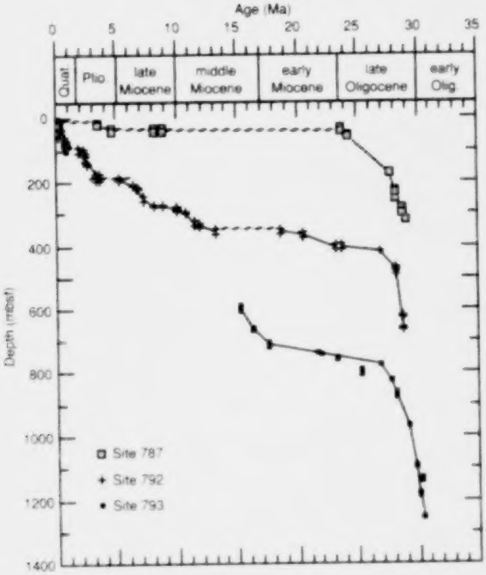

Figure 4. Age-depth plots for forearc sites, with inferred unconformities indicated by wavy lines. Raw data are tabulated in each of the site chapters.

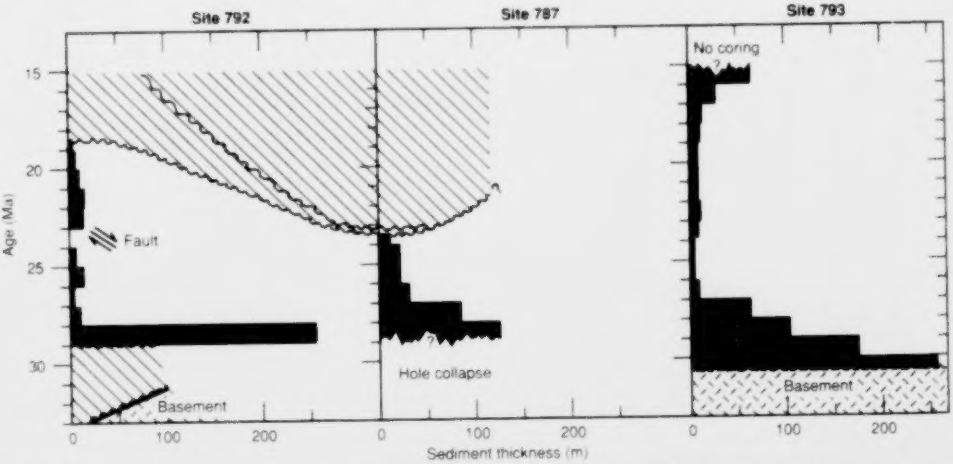

Figure 5. Histograms of undecompacted sediment thickness in each 1-m.y. interval before 15 Ma, determined from age-depth curves (Fig. 4). Hiatuses are indicated by hatched areas.

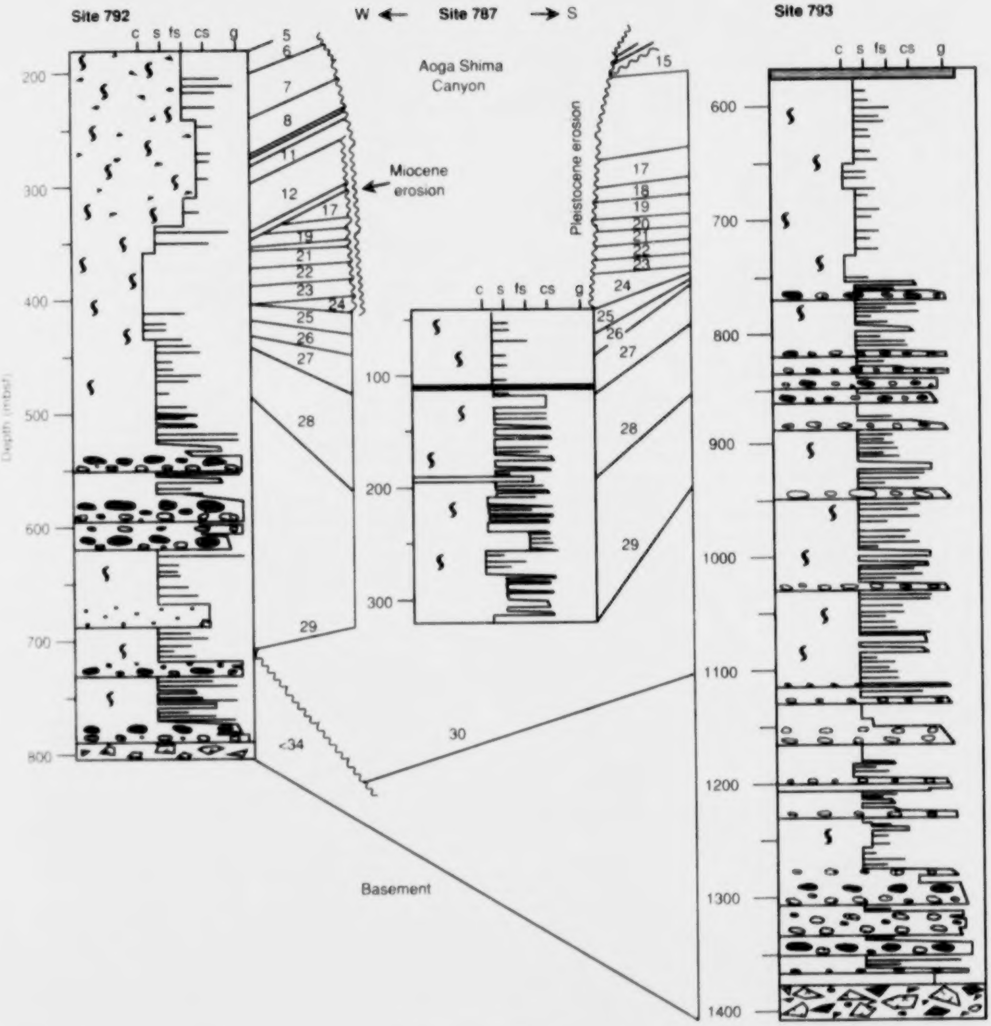
Site 792
c s fs cs g
Depth (mbsf)
200
300
400
500
600
700
800
5
6
7
8
11
12
17
19
21
22
23
24
25
26
27
28
29
<34
W
Site 787
S
Aoga Shima Canyon
Miocene erosion
Pleistocene erosion
15
17
18
19
20
21
22
23
24
25
26
27
28
29
100
200
300
30
Basement
Site 793
600
700
800
900
1000
1100
1200
1300
1400

Figure 6. Time lines (at 1-m.y. intervals) joining horizons of equal age at Sites 787, 792, and 793. Ages are determined from age-depth curves (Fig. 4). The arrangement in the figure allows easy comparison of adjacent sites (Sites 787 and 792 and Sites 787 and 793) located in the central part of the forearc basin (Fig. 2). The legend is the same as in Figure 3.

Taylor, B., Fujioka, K., et al., 1990
Proceedings of the Ocean Drilling Program, Initial Reports, Vol. 126

11. CORRELATION AND COMPARISON OF BACKARC SITES[1]

Shipboard Scientific Party[2]

INTRODUCTION

This chapter provides a comparative, generalized, spatial, and geochronological context for the four sites that were drilled in and on the margin of the Sumisu Rift in the Izu-Bonin Arc. In the corresponding chapter on the forearc sites, Figures 1 and 2 show how the forearc and backarc sites are spatially related; the backarc sites alone are shown in Figure 1 of this chapter. Sites 788 and 789 are located on the eastern rift flank footwall uplift in water 1100 m deep. Sites 790 and 791 were drilled in water about twice as deep (2223 and 2271 m, respectively) into the flat floor of the rift basin. Site 790, 15 km west of Site 788, is situated on the western side of the eastern half-graben of the rift on the margin of an intrabasinal high; Site 791 was drilled 2.4 km east of Site 790. Each backarc site is more fully described in its own site chapter in this volume. A lithologic and graphic summary for the backarc sites is presented in Figure 2.

The sedimentary record of the eastern margin of the rift was recovered at Site 788, from Holes 788C and 788D. Recovery of the lower part of the section was poor (Hole 788D, Subunits IIA and IIB), and so the earlier lithostratigraphic record from the margin is fragmentary and must be interpreted with caution. However, recovery of the younger sediments from Hole 788C was good. In contrast, the sedimentary successions of the rift basin have been reconstructed from three holes at Site 790 (Holes 790A, 790B, and 790C) and two holes at Site 791 (Holes 791A and 791B), at which recovery and stratigraphic overlap were reasonably good.

There is little stratigraphic overlap between the strata encountered on the rift flank uplift and in the rift basin. The sedimentary succession of the margin is older and, except for the uppermost ~30 m, entirely predates the rifting. The 30-m surface capping of the uplift as well as the total fill of the rift basin postdate the initiation of rifting. Massive igneous rock was cored only at Site 791 in the basin. On the rift flank uplift, we did not see basement in the seismic reflection records; therefore, the igneous rock must lie far below the greatest depth reached by the drill. Scoriaceous basalts recovered from the basal interval drilled at Site 790 are probably fragmental syn-rift volcanic rocks.

PLIOCENE-QUATERNARY SEDIMENTARY SUCCESSION OF THE RIFT FLANK MARGIN

The oldest rocks recovered from the backarc region are from the base of Hole 788D (Subunit IIB, 278.6–374 mbsf), paleomagnetically dated at 4.77 to about 4.2 Ma (early Pliocene). These rocks are mainly volcaniclastic: interbedded pumiceous conglomerate, vitric sandstone, vitric siltstone, and vitric silty claystone. They are generally low in carbonate content, but are somewhat more calcareous from the middle part of the subunit downward. Sedimentation rates varied during the deposition of this subunit from 192 to 73 m/m.y., then to 282 m/m.y. (Fig. 3). Minor faults, presumably of normal displacement associated with rifting, cut these rocks at 288–297 mbsf.

From 249 to 278.6 mbsf (Site 788, Subunit IIA), the rocks, paleomagnetically dated at about 4.2–3.8 Ma, are also dominated by volcaniclastic components, but they do contain significant epiclastic and pelagic components. They are interbedded nannofossil-rich claystone, vitric sandstone, vitric silty claystone, and vitric siltstone; conglomerate is notably absent. Sedimentation rates were low, measured at 39 m/m.y. in the upper portion of the subunit (Site 788, Subunit IIA; see Fig. 3).

Unit I of Site 788 overlies Unit II at 249 mbsf. Unit I has an estimated basal age of 3.66 Ma and is composed of sandy, granule, and pebble pumiceous gravel that contains little interstitial mud, locally interbedded with vitric sand and rare vitric silt. The basal 19 m (Subunit IB) is transitionally lithified to conglomerate. The unit is composed of four coarsening-upward intervals, each 30–50 m thick. The uppermost, 30-m-thick interval is biostratigraphically separated from the others by an unconformity. Below the hiatus, the age of these pumiceous gravel beds is somewhere between 2.85 and 2.36 Ma, depending upon the actual sedimentation rate, which could be as high as 230 m/m.y. or as low as 145 m/m.y. (Fig. 3).

The gravel layer immediately above the hiatus was biostratigraphically dated at 0.275 Ma; it accumulated at rates in excess of 115 m/m.y. The age of the top of this uppermost interval is not known, but discolored pumice clasts, and a lack of interstitial mud that is exceptional even for Unit I, indicate that the surface deposits have resided for some time at the seafloor where they were subjected to oxidation and winnowing. It is only this 30-m surficial interval on the rift flank uplift that correlates stratigraphically with the (upper) sediments at the basin sites.

PLEISTOCENE IGNEOUS ROCK OF THE RIFT BASIN SITES

At Site 790, 116 m of igneous rock was drilled from 271 to 387 mbsf. Recovery was poor (0.9%), totaling only 1 m of scoriaceous basalt fragments, all from core catchers. The quality of seismic reflections indicates that this interval is not massive igneous rock. At Site 791, igneous rock was cored from 834 to 1145 mbsf. Recovery from this 311-m interval was 27.83 m, or 8.9%, and consisted of a lithologically complex suite of rocks. The downhole sequence consisted of basalt breccia, basalt, a diabase intrusion, basaltic "mousse," and mafic to felsic tuff and lapilli tuff. The basalts recovered at both sites are highly vesicular and sparsely phyric, typically with olivine and plagioclase phenocrysts, although one lava at Site 791 also contains clinopyroxene.

The basalt "mousse" at Site 791 consists of clasts of highly vesicular basalt glass in a matrix of even more vesicular glass of the same composition. Inconclusive igneous-petrological evidence has led to the speculation that the tuffs at the bottom of Hole 791B may represent pre-rift sediments. The diabase intrusions at Site 791 range from olivine to clinopyroxene rich. Some volcaniclastic sedimentary material of Pleistocene age occurs in the igneous rocks of Sites 790 and 791. At Site 790, sedimentary particles admixed with basaltic scoria contain nannofossils that indicate an age of 0.83–1.6 Ma (Zone CN14a), but this material

---

[1] Taylor, B., Fujioka, K., et al., 1990. *Proc. ODP, Init. Repts.*, 126: College Station, TX (Ocean Drilling Program).

[2] Shipboard Scientific Party is as given in the list of participants preceding the contents.

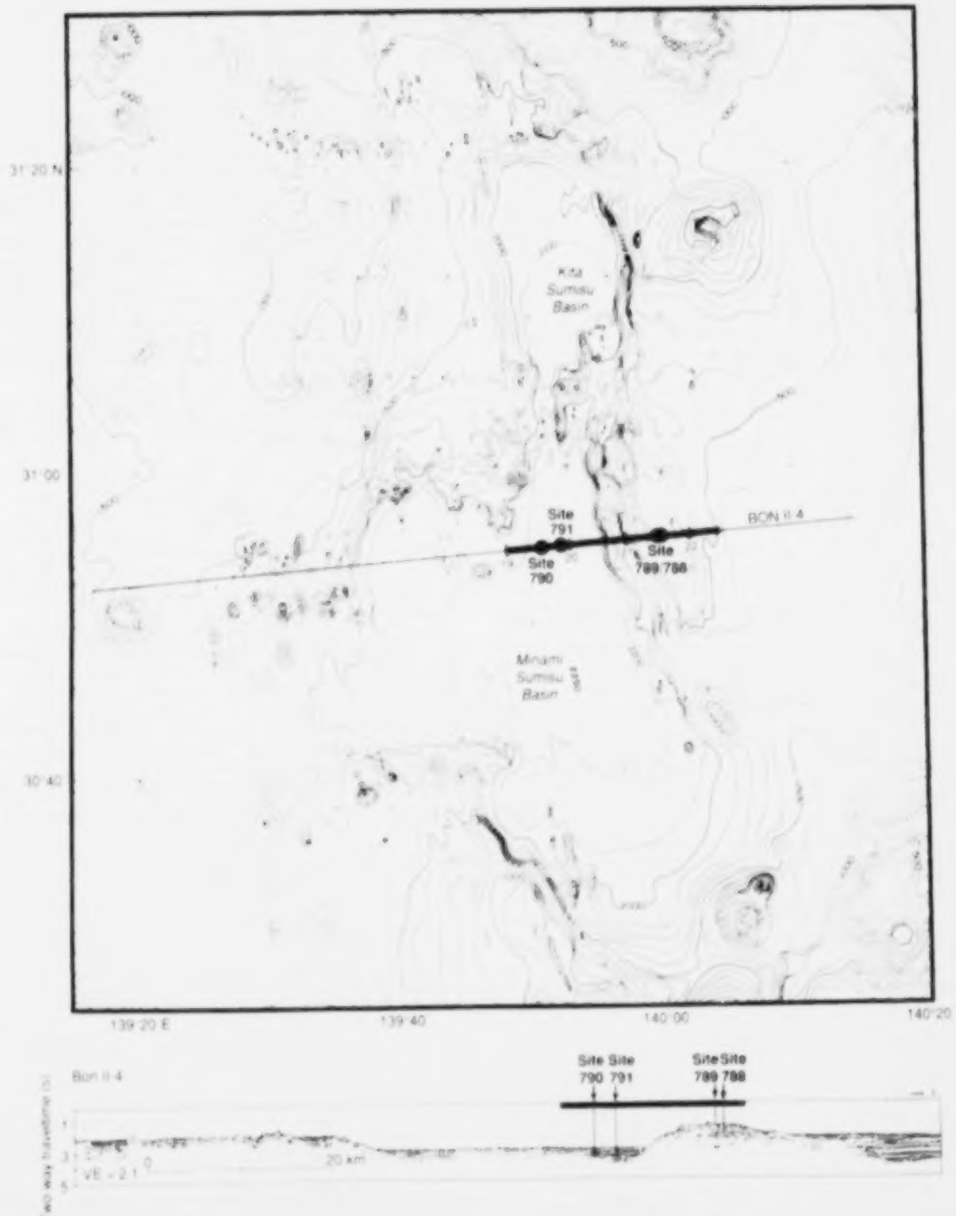
31°20'N
31°00'
30°40'
139°20'E
139°40'
140°00'
140°20'
Kita Sumisu Basin
Minami Sumisu Basin
Site 791
Site 790
Site 789 788
BON II-4
Bon II-4
Site 790
Site 791
Site 789
Site 788
Two way traveltime (s)
1
3
5
0
20 km
VE = 2:1

Figure 1. Bathymetry (100-m contour interval) of Sumisu Rift (modified from Taylor et al., 1988), showing the location of multichannel seismic (MCS) Line BON II-4 and the backarc sites. A line drawing of the seismic reflection profile is shown at the bottom of figure. The solid bar above the profile indicates the segment of Line BON II-4 that is depicted in Figure 2.

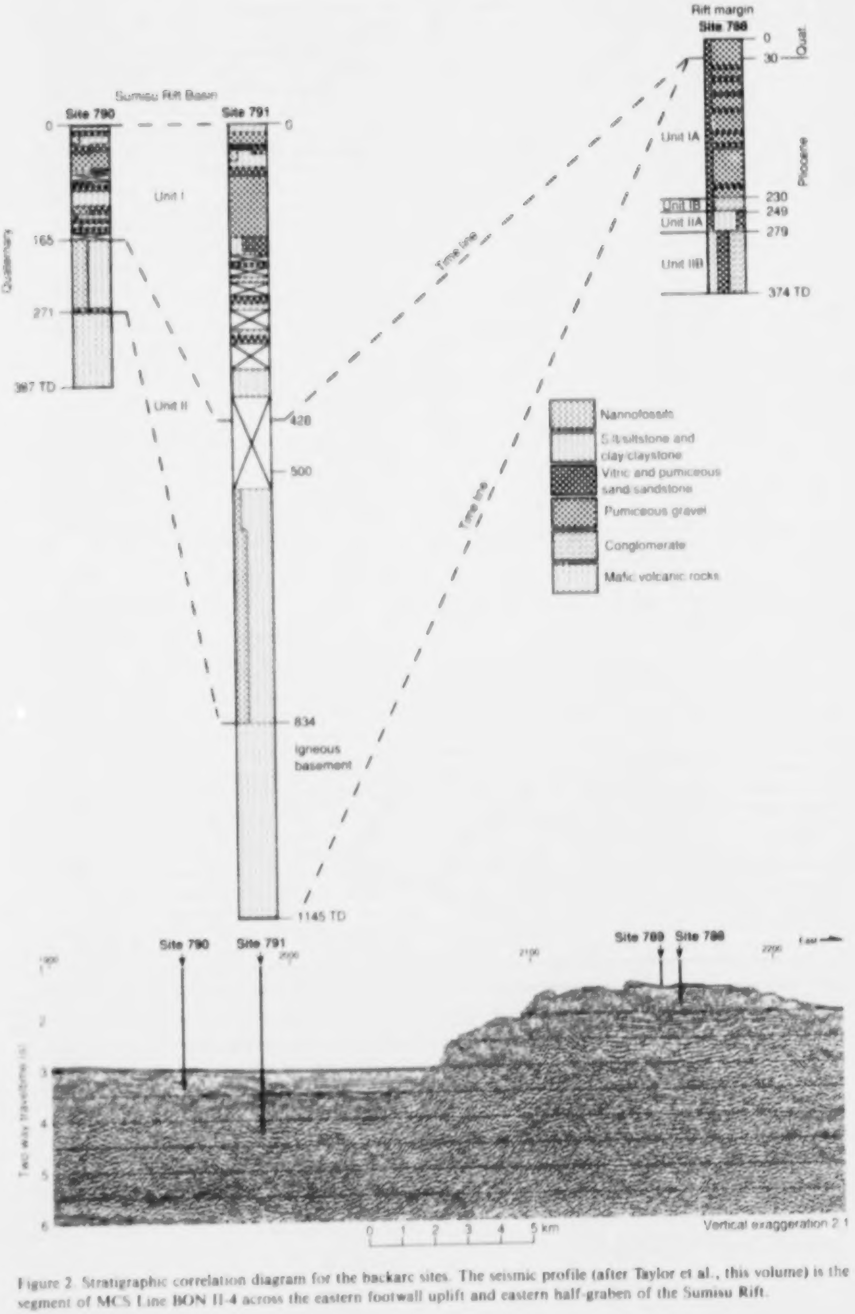
Rift margin
Site 788
0
30
Quat.
Unit IA
Pliocene
Unit IB
230
249
Unit IIA
279
Unit IIB
374 TD
Sumisu Rift Basin
Site 790
Site 791
0
165
271
387 TD
Quaternary
Unit I
Unit II
428
500
834
Igneous basement
1145 TD
Time line
Time line
Nannofossils
Silt/siltstone and clay/claystone
Vitric and pumiceous sand/sandstone
Pumiceous gravel
Conglomerate
Mafic volcanic rocks
Site 790
Site 791
Site 789
Site 788
1900
2000
2100
2200
East
Two way traveltime (s)
2
3
4
5
6
0 1 2 3 4 5 km
Vertical exaggeration 2:1

Figure 2. Stratigraphic correlation diagram for the backarc sites. The seismic profile (after Taylor et al., this volume) is the segment of MCS Line BON II-4 across the eastern footwall uplift and eastern half-graben of the Sumisu Rift.

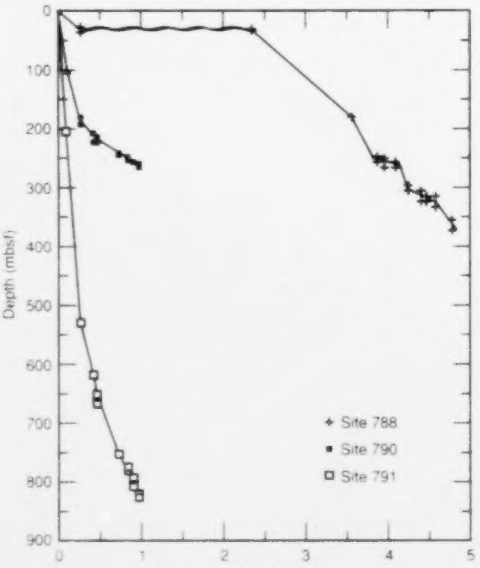

Figure 3. Age-depth plots for the backarc sites. The wavy line on the Site 788 curve is an unconformity.

may be downhole contamination. At Site 791, a 22-cm-thick interval of crystal-vitric silt and sandy mud occurs at 974 mbsf.

QUATERNARY SEDIMENTARY RIFT BASIN FILL

The sedimentary section at Site 791 is about three times thicker than the section at Site 790. The biostratigraphic and paleomagnetic data used to construct the age-depth curves (Fig. 3) indicate that the successions at the two sites are essentially time equivalent. The greater overburden pressures of the thicker column at Site 791 have compacted and lithified its basal sediments, whereas the sedimentary accumulation at Site 790 [illegible] entirely unlithified. Sedimentation rates at the base of Unit II were 90 and 344 m/m.y. at Sites 790 and 791, respectively; they increased to ~1000 and 2200 m/m.y. from 0.1 Ma to the present.

Lithostratigraphic correlation between Sites 790 and 791 is based on the following characteristics: (1) lithology and sedimentary facies (Fig. 41 in "Sites 790/791" chapter, this volume); (2) identification of Key Bed #7 (volcanic ash) at both sites (Fig. 13 in "Sites 790/791" chapter); (3) bulk magnetic susceptibility (Fig. 15 in "Sites 790/791" chapter); (4) carbonate contents (Fig. 42 in "Sites 790/791" chapter); and (5) seismic reflection records (see "Seismic Stratigraphy" section, "Sites 790/791" chapter). Correlation between the two sites is well constrained above Key Bed #7, based mainly on the marked differences in magnetic susceptibility between thick units of felsic vitric silt (volume magnetic susceptibility $< 125 \times 10^{-6}$), and thin- to thick-bedded intervals containing magnetic minerals and mafic grains of basaltic composition. These latter intervals include black vitric sand/silt beds and pumiceous gravels and pebbly sands (e.g., Site 791, 60–150 mbsf) that contain scattered scoria grains.

At Sites 790 and 791, there is a sharp lithologic contrast between Units I and II. Unit II, deposited between 1.1 and 0.2 Ma, is burrowed nannofossil-rich clay, silty clay, and clayey silt, collectively 106 m thick at Site 790 (271–165 mbsf), and the lithified equivalents of these sediment types at Site 791, where the unit is 406 m thick (834–428 mbsf). The bedding in Unit II is subhorizontal in the sediments of Site 790, but at Site 791 the dip gradually decreases upward from 45° at 760 mbsf to only 15°–20° at about 600 mbsf. Unit I consists mainly of thick intervals of vitric silt. The contact between the two units is constrained to within 10 m at Site 790 (1.55–1.65 mbsf), although the contact itself was not recovered in cores. At Site 791, however, very poor recovery does not allow a confident assessment of the position of the contact based only on lithology. We therefore used four criteria to estimate the true depth of the contact between Units I and II at Site 791: (1) the lowest recovered bed of pumiceous sand, (2) a correlatable seismic horizon (see Fig. 6 in "Seismic Stratigraphy" section, "Sites 790/791" chapter, this volume), (3) the age correlation based on age-depth curves (Fig. 3), and (4) a comparison of downhole trends in carbonate content at the two sites.

At Site 790, Unit II has carbonate contents of 20%–40%, whereas Unit I has less than 20% carbonate (Fig. 42 in "Sites 790/791" chapter). The carbonate curve for Site 791 shows the same trend, with the upward transition from high to low carbonate values occurring at about 375–500 mbsf. This depth is consistent with the independent estimate of the position of the contact between Units I and II at 428 mbsf, but it is not sufficiently defined in the carbonate curves to allow a more accurate definition of the contact.

INTERPRETATION

In brief, the results from the backarc sites document the following: rifting began no earlier than 3.56 (and probably 2.35–2.85) Ma and no later than 1.1 Ma. The region in pre-rift time underwent a period of relative volcanic quiescence that began prior to 4.77 Ma and lasted to 4.2 Ma, terminated by a series of massive silicic eruptions that lasted until 4.1 Ma. The period from 4.1 to about 3.9 or 3.8 Ma was characterized by another volcanic lull in the region, although distal volcanism provided thin ashfalls to Site 788. This lull was terminated by silicic eruptions that left at least three massive deposits of pumiceous gravels on what is now the rift flank uplift, and ended at a poorly constrained time that could have been as early as 2.85 Ma or, more likely, as late or even later than 2.35 Ma.

Uplift of the rift flank sites, probably associated with the initiation of rifting, occurred some time after ~2.8 Ma, causing erosional truncation of the sedimentary succession there. At the rift basin sites, rift initiation and emplacement of the igneous rocks occurred before 1.1 Ma; it was likely closer to this time than to 2.35 Ma. As rifting continued, there was first a period of relative volcanic quiescence, during which time the hemipelagic Unit II sediments of basin-floor Sites 790 and 791 accumulated. No contemporaneous sedimentary record is preserved on the rift flank. At about 0.2 Ma, renewed, episodic, explosive silicic volcanism resulted in the deposition of the Unit I pumiceous layers at the basin-floor sites and the uppermost 30 m of Site 788 on the rift flank uplift.

REFERENCE

Taylor, B., Brown, G., Hussong, D., and Fryer, P., 1988. SeaMARC II bathymetry, Sumisu and Torishima rifts, Izu-Ogasawara Arc, 1:200,000. *Mar. Geol. Map Ser.*, Tsukuba (Geol. Surv. Jpn.), No. 31.

Ms 126A-112

SECTION 4: CORES

SITE 787 HOLE A CORE 1W CORED INTERVAL 0-24.5 mbsf

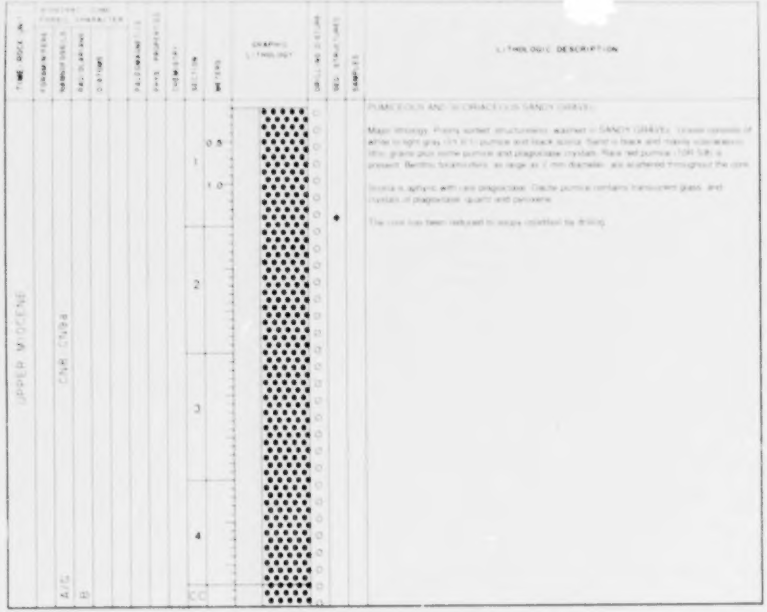

TIME-ROCK UNIT	FORAMINIFERS	NANNOFOSSILS	RADIOLARIANS	DIATOMS	PALEOMAGNETICS	PHYS. PROPERTIES	CHEMISTRY	SECTION	METERS	GRAPHIC LITHOLOGY	DRILLING DISTURB.	SED. STRUCTURES	SAMPLES	LITHOLOGIC DESCRIPTION
UPPER MIOCENE		CN8-CN9a A/G	B					1 2 3 4 CC	0.5 1.0					PUMICEOUS AND SCORIACEOUS SANDY GRAVEL Major lithology: Poorly sorted, structureless, washed in SANDY GRAVEL. Gravel consists of white to light gray (5Y 8/1) pumice and black scoria. Sand is black and mainly volcaniclastic lithic grains plus some pumice and plagioclase crystals. Rare red pumice (10R 5/6) is present. Benthic foraminifers, as large as 2 mm diameter, are scattered throughout the core. Scoria is aphyric with rare plagioclase. Dacite pumice contains translucent glass, and crystals of plagioclase, quartz and pyroxene. The core has been reduced to soupy (clotted) by drilling.

Information on Core Description Forms, for ALL sites, represents field notes taken aboard ship. Some of this information has been refined in accord with post-cruise findings, but production schedules prohibit definitive correlation of these forms with subsequent findings. Thus, the reader should be alerted to the occasional ambiguity or discrepancy.

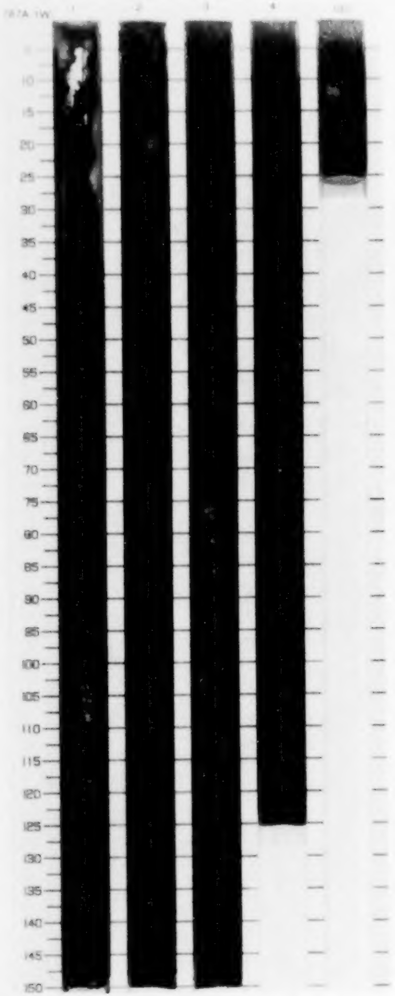

SITE 787 HOLE B CORE 1R CORED INTERVAL 0.0-2.3 mbsf

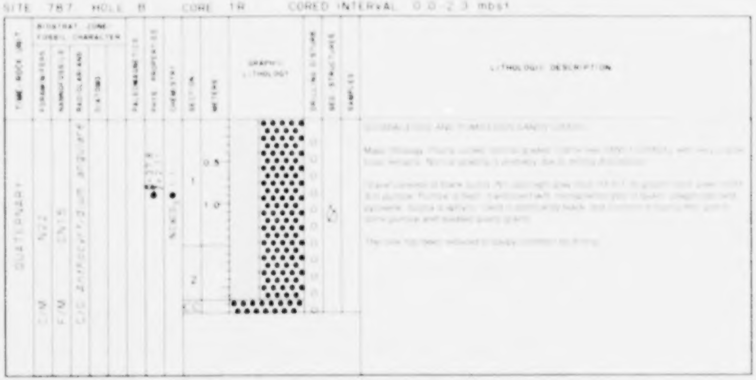
TIME-ROCK UNIT
BIOSTRAT. ZONE/ FOSSIL CHARACTER
FORAMINIFERS
NANNOFOSSILS
RADIOLARIANS
DIATOMS
PALEOMAGNETICS
PHYS. PROPERTIES
CHEMISTRY
SECTION
METERS
GRAPHIC LITHOLOGY
DRILLING DISTURB.
SED. STRUCTURES
SAMPLES
QUATERNARY
N22
CN15
Anthocyrtidium angulare
C/M
F/M
C/G
0.5
1.0
1
2
CC

LITHOLOGIC DESCRIPTION

SCORIACEOUS AND PUMICEOUS SANDY GRAVEL

Major lithology: [illegible]

[illegible]

[illegible]

SITE 787 HOLE B CORE 2R CORED INTERVAL 2.3-11.9 mbsf

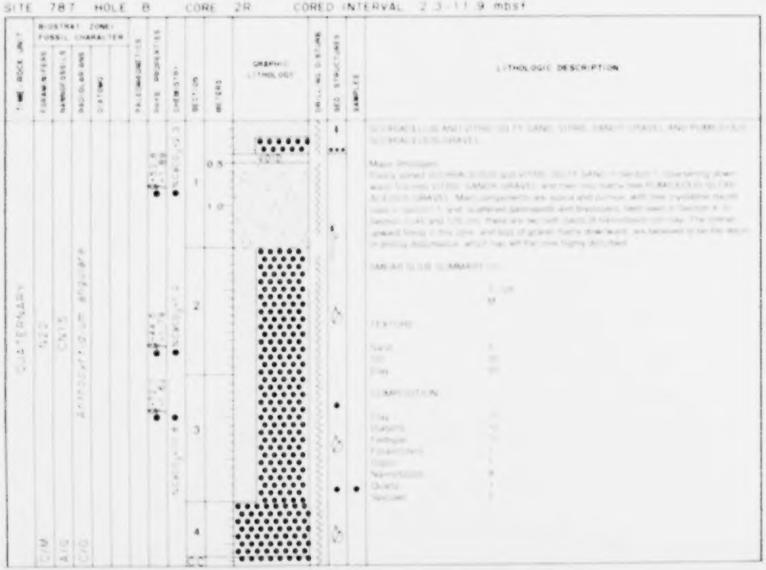
TIME-ROCK UNIT
BIOSTRAT. ZONE/ FOSSIL CHARACTER
FORAMINIFERS
NANNOFOSSILS
RADIOLARIANS
DIATOMS
PALEOMAGNETICS
PHYS. PROPERTIES
CHEMISTRY
SECTION
METERS
GRAPHIC LITHOLOGY
DRILLING DISTURB.
SED. STRUCTURES
SAMPLES
QUATERNARY
N22
CN15
Anthocyrtidium angulare
C/M
A/G
C/G
0.5
1.0
1
2
3
4
CC

LITHOLOGIC DESCRIPTION

SCORIACEOUS AND VITRIC SILTY SAND, VITRIC SANDY GRAVEL AND PUMICEOUS SCORIACEOUS GRAVEL

Major lithologies:
[illegible]

SMEAR SLIDE SUMMARY (%):

1, 125
M

TEXTURE:

Sand
Silt
Clay

COMPOSITION:

Clay
Diatoms
Feldspar
Foraminifers
Glass
Nannofossils 8
Quartz
Volcanic

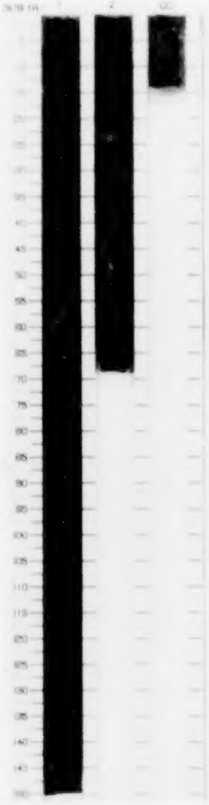
787B-1R
1
2
CC
0
5
10
15
20
25
30
35
40
45
50
55
60
65
70
75
80
85
90
95
100
105
110
115
120
125
130
135
140
145
150

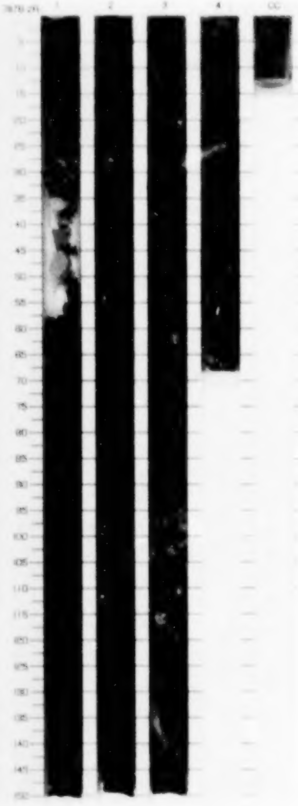
787B-2R
1
2
3
4
CC

SITE 787 HOLE B CORE 3R CORED INTERVAL 17.9-27.4 mbsf

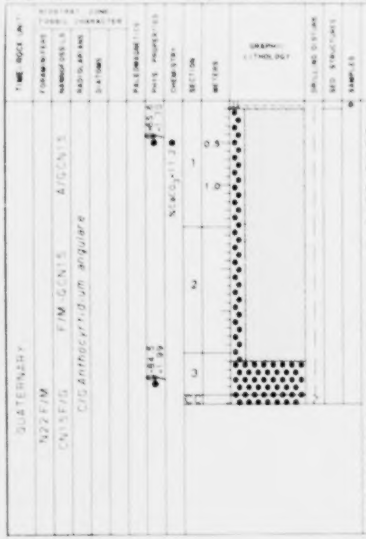
TIME-ROCK UNIT
BIOSTRAT. ZONE/ FOSSIL CHARACTER
FORAMINIFERS
NANNOFOSSILS
RADIOLARIANS
DIATOMS
PALEOMAGNETICS
PHYS. PROPERTIES
CHEMISTRY
SECTION
METERS
GRAPHIC LITHOLOGY
DRILLING DISTURB.
SED. STRUCTURES
SAMPLES
QUATERNARY
N22 F/M
CN15F/G
F/M-CGN15
A/GCN15
C/G Anthocyrtidium angulare
NCaCO3=11.3
1
2
3
CC
0.5
1.0

LITHOLOGIC DESCRIPTION

VITRIC SAND

Major lithology: Poorly sorted dark gray to black (N3 to N2) medium- to coarse VITRIC SAND with white pumice gravel (1-3 cm diameter), foraminiferal tests, and shell fragments. The sand is principally scoria and pumice fragments. Grayish black (N2) pumice granules and pebbles occur in Section 3, 12-50 cm, and in the core catcher.

Minor lithology: The top 12 cm of Section 1 is grayish black (N2) homogeneous NANNOFOSSIL-RICH CLAY with an isolated pumice clast.

The core is moderately disturbed by drilling.

SMEAR SLIDE SUMMARY (%):

	1, 4
	D
TEXTURE:	
Sand	[illegible]
Silt	4
Clay	[illegible]
COMPOSITION:	
Accessory minerals	Tr
Clay	78
Diatoms	[illegible]
Feldspar	Tr
Foraminifers	4
Glass	[illegible]
Micrite	Tr
Nannofossils	[illegible]
Radiolarians	Tr
Rock fragment	[illegible]
Silicoflagellates	[illegible]
Spicules	[illegible]

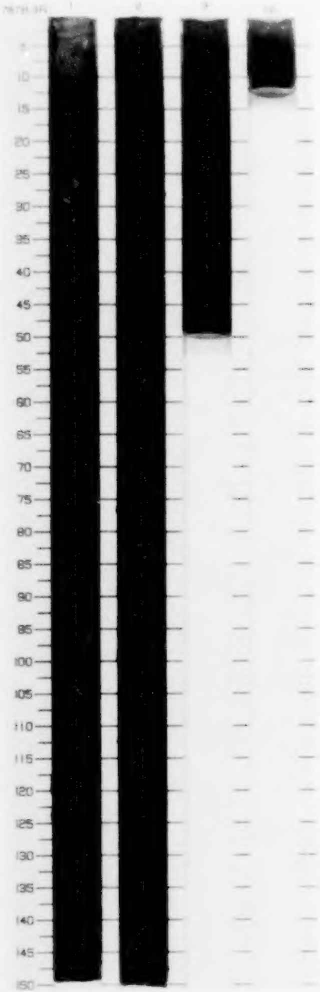
787B-3R
1
2
3
CC
5
10
15
20
25
30
35
40
45
50
55
60
65
70
75
80
85
90
95
100
105
110
115
120
125
130
135
140
145
150

SITE 787 HOLE B CORE 4R CORED INTERVAL 21.4-30.9 mbsf

TIME-ROCK UNIT	FORAMINIFERS	NANNOFOSSILS	RADIOLARIANS	DIATOMS		PALEOMAGNETICS	PHYS. PROPERTIES	CHEMISTRY	SECTION	METERS	GRAPHIC LITHOLOGY	DRILLING DISTURB.	SED. STRUCTURES	SAMPLES	LITHOLOGIC DESCRIPTION
LOWER PLIOCENE	N18-N19/M	CN10c-CN11	B			N			1 CC					●●●	[illegible] NANNOFOSSIL OOZE AND NANNOFOSSIL [illegible] CLAY Major lithology: [illegible] Minor lithology: [illegible] The core is moderately disturbed by drilling. SMEAR SLIDE SUMMARY (%): TEXTURE: Sand Silt Clay COMPOSITION: Accessory minerals [illegible] Clay [illegible] Feldspar Foraminifers Glass Mica Nannofossils Radiolarians Rock fragments [illegible] Sponge spicules

787B-4R
1
CC
5
10
15
20
25
30
35
40
45
50
55
60
65
70
75
80
85
90
95
100
105
110
115
120
125
130
135
140
145
150

SITE 787 HOLE B CORE 5R CORED INTERVAL 30.8-40.1 mbsf

TIME-ROCK UNIT	FORAMINIFERS	NANNOFOSSILS	RADIOLARIANS	DIATOMS		PALEOMAGNETICS	PHYS. PROPERTIES	CHEMISTRY	SECTION	METERS	GRAPHIC LITHOLOGY	DRILLING DISTURB.	SED. STRUCTURES	SAMPLES	LITHOLOGIC DESCRIPTION
LOWER PLIOCENE UPPER MIOCENE	N18/N19 R/M	CN11b or older A/G CN9 A/G	*Didymocyrtis antepenultima* R/G			N	● [illegible]	● [illegible]	1					●●●	NANNOFOSSIL-RICH VOLCANIC LITHIC SILTY CLAY

NANNOFOSSIL-RICH VOLCANIC LITHIC SILTY CLAY

Major lithology: Most of the core [illegible] is very dark grayish brown [illegible] NANNOFOSSIL-RICH VOLCANIC LITHIC SILTY CLAY.

Minor lithology: The lowermost 1 cm of the core is dark gray [illegible] CLAY.

The core is slightly disturbed by drilling.

SMEAR SLIDE SUMMARY (%):

	[illegible]	[illegible]	[illegible]
	M	D	D
TEXTURE:			
Sand	[illegible]	[illegible]	[illegible]
Silt	[illegible]	[illegible]	[illegible]
Clay	[illegible]	[illegible]	[illegible]
COMPOSITION:			
Accessory minerals	[illegible]	[illegible]	[illegible]
Clay	[illegible]	[illegible]	[illegible]
Diatoms	[illegible]	[illegible]	[illegible]
Feldspar	[illegible]	[illegible]	[illegible]
Foraminifers	[illegible]	[illegible]	[illegible]
Glass	[illegible]	[illegible]	[illegible]
Nannofossils	[illegible]	[illegible]	[illegible]
Pellets	[illegible]	[illegible]	[illegible]
Radiolarians	[illegible]	[illegible]	[illegible]
Rock fragments	[illegible]	[illegible]	[illegible]
Silicoflagellates	[illegible]	[illegible]	[illegible]
Spicules	[illegible]	[illegible]	[illegible]

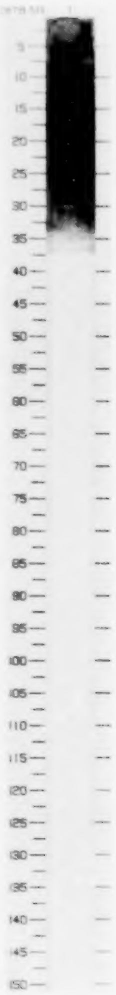

SITE 787 HOLE B CORE 6R CORED INTERVAL 40.3-49.8 mbsf

TIME-ROCK UNIT	FORAMINIFERS	NANNOFOSSILS	RADIOLARIANS	DIATOMS	PALEOMAGNETICS	SECTION	METERS
UPPER OLIGOCENE	F/B	C/G CP19b C/M CP19b A/G CP19b	B		N	1	0.5
							1.0
						2	

LITHOLOGIC DESCRIPTION

NANNOFOSSIL CLAYSTONE, NANNOFOSSIL-RICH CLAYSTONE, AND CLAYSTONE

Major lithology: Variegated shades of greenish gray [illegible] NANNOFOSSIL CLAYSTONE and NANNOFOSSIL-RICH CLAYSTONE, in which most of the carbonate is [illegible]. The core is [illegible] in Section 1, [illegible] Section 1, [illegible] to Section 2, [illegible]

Minor lithology: [illegible] CLAYSTONE [illegible] in Section 1, [illegible] of Section 2, [illegible]

The core is [illegible]

SMEAR SLIDE SUMMARY (%):

TEXTURE:

Sand
Silt
Clay

COMPOSITION:

Accessory minerals
Clay
Feldspar
Foraminifers
Glass
Micrite
Nannofossils
Radiolarians
Rock fragments
Spicules

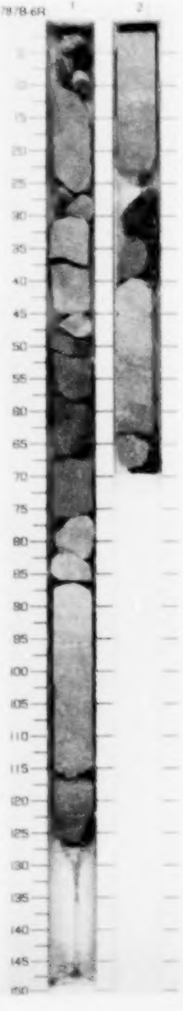
787B-6R
1
2
5
10
15
20
25
30
35
40
45
50
55
60
65
70
75
80
85
90
95
100
105
110
115
120
125
130
135
140
145
150

SITE 787 HOLE B CORE 7R CORED INTERVAL 49.8-59.3 mbsf

TIME-ROCK UNIT	FORAMINIFERS	NANNOFOSSILS	RADIOLARIANS	DIATOMS	PALEOMAGNETICS	PHYS. PROPERTIES	CHEMISTRY	SECTION	METERS	GRAPHIC LITHOLOGY	DRILLING DISTURB.	SED. STRUCTURES	SAMPLES
UPPER OLIGOCENE	B	C/M C/G CP19b	B		N R?			1 2 CC	0.5 1.0				

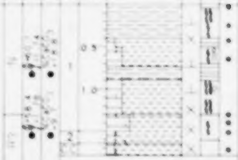

LITHOLOGIC DESCRIPTION

NANNOFOSSIL-RICH CLAYSTONE AND VITRIC SILTY CLAYSTONE

Major lithology: Lightly to moderately bioturbated, dark gray (5Y 4/1) NANNOFOSSIL-RICH CLAYSTONE is the dominant lithology of the core from Section 1, 50 cm to CC. Brownish black (5YR 2/1) VITRIC SILTY CLAYSTONE occurs in Section 1, 0-50 and 74-88 cm.

Minor lithology: Gray (5Y 5/1) NANNOFOSSIL-RICH CLAYSTONE occurs in the core catcher.

Drilling has highly fractured the core, and portions are drilling breccia.

SMEAR SLIDE SUMMARY (%):

	1, 3 D	1, 25 D	1, 40 D	1, 65 M	1, 130 D	1, 140 D	2, 1 D
TEXTURE:							
Sand	65	2	20	5	95	5	Tr
Silt	30	28	30	25	3	30	20
Clay	5	70	50	65	2	65	80
COMPOSITION:							
Accessory minerals	—	—	—	2	—	—	—
Amphibole	—	—	—	—	—	—	—
Clay	5	55	50	55	5	65	70
Feldspar	1	5	5	5	5	—	5
Glass	60	20	40	20	45	25	15
Mica	—	—	—	—	—	—	—
Micrite	1	5	—	—	—	—	—
Nannofossils	1	5	10	20	2	10	10
Pyroxene	—	—	—	—	3	—	—
Quartz	3	1	—	—	—	2	—
Rock fragment	30	5	—	—	40	—	—

SMEAR SLIDE SUMMARY (%):

	CC, 7 D
TEXTURE:	
Sand	—
Silt	5
Clay	95
COMPOSITION:	
Accessory minerals	1
Clay	80
Feldspar	1
Quartz	1
Nannofossils	10
Rock fragment	5
Spicules	5

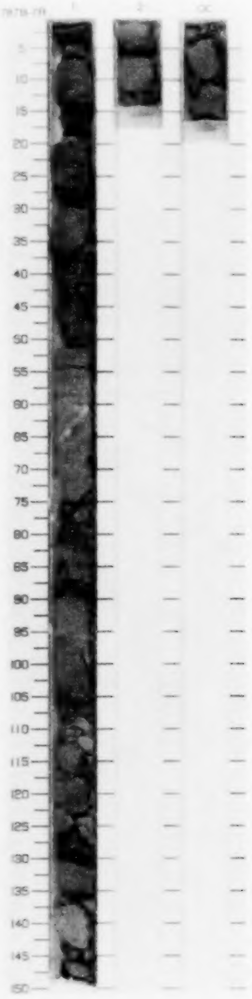

SITE 787 HOLE B CORE 8R CORED INTERVAL 59.3-69.0 mbsf

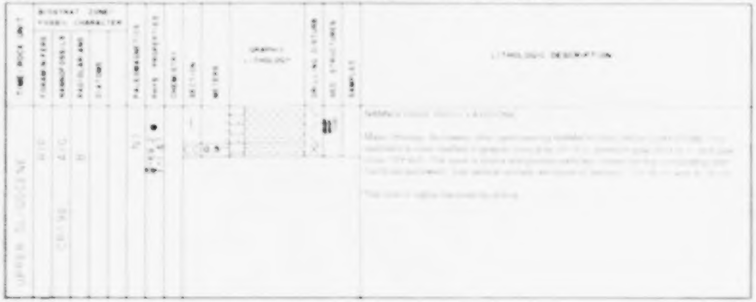
TIME-ROCK UNIT
BIOSTRAT. ZONE/FOSSIL CHARACTER
FORAMINIFERS
NANNOFOSSILS
RADIOLARIANS
DIATOMS
PALEOMAGNETICS
PHYS. PROPERTIES
CHEMISTRY
SECTION
METERS
GRAPHIC LITHOLOGY
DRILLING DISTURB.
SED. STRUCTURES
SAMPLES
UPPER OLIGOCENE
1
0.5

LITHOLOGIC DESCRIPTION

[illegible]

[illegible]

The core is highly disturbed by drilling.

SITE 787 HOLE B CORE 9R CORED INTERVAL 69.0-78.7 mbsf

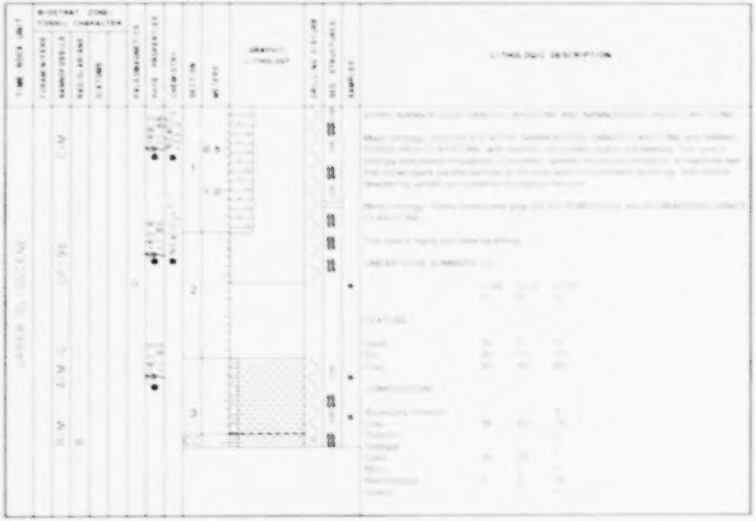
TIME-ROCK UNIT
BIOSTRAT. ZONE/FOSSIL CHARACTER
FORAMINIFERS
NANNOFOSSILS
RADIOLARIANS
DIATOMS
PALEOMAGNETICS
PHYS. PROPERTIES
CHEMISTRY
SECTION
METERS
GRAPHIC LITHOLOGY
DRILLING DISTURB.
SED. STRUCTURES
SAMPLES
UPPER OLIGOCENE
1
2
3
0.5
1.0

LITHOLOGIC DESCRIPTION

[illegible]

[illegible]

[illegible]

The core is highly disturbed by drilling.

SMEAR SLIDE SUMMARY (%):

TEXTURE:

Sand
Silt
Clay

COMPOSITION:

[illegible]

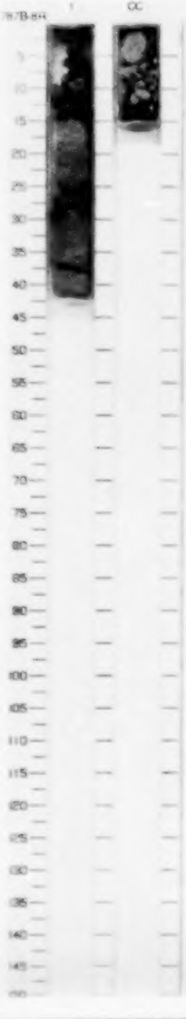
787B-8R
1
CC
5
10
15
20
25
30
35
40
45
50
55
60
65
70
75
80
85
90
95
100
105
110
115
120
125
130
135
140
145
150

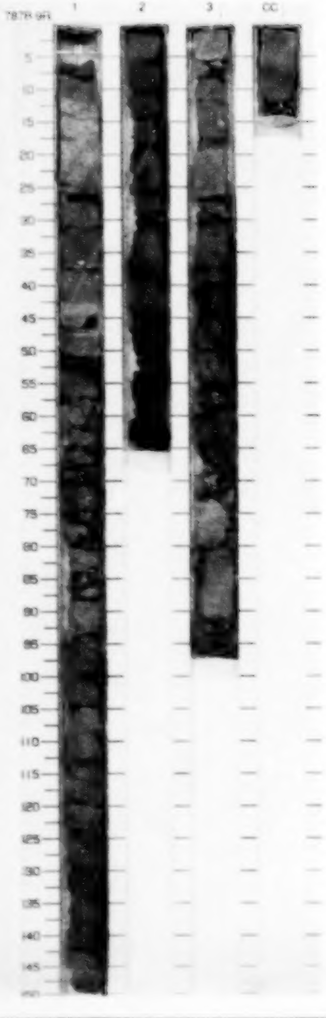
787B-9R
1
2
3
CC
5
10
15
20
25
30
35
40
45
50
55
60
65
70
75
80
85
90
95
100
105
110
115
120
125
130
135
140
145
150

SITE 787 HOLE B CORE 10R CORED INTERVAL 78.7-88.4 mbsf

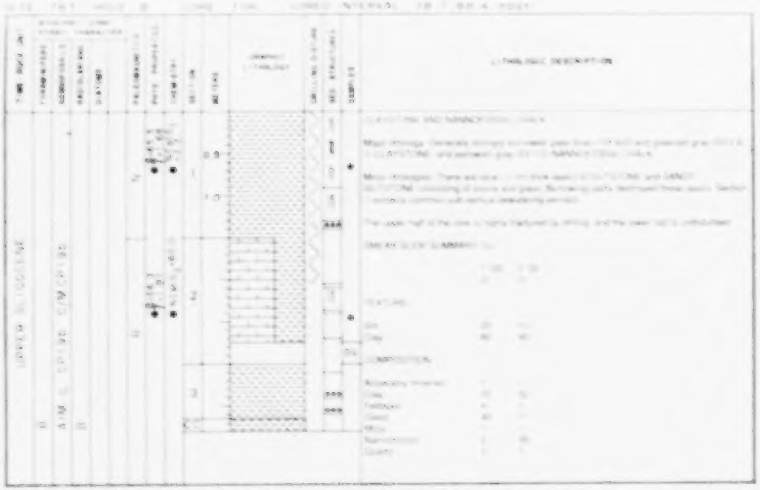
TIME ROCK UNIT
BIOSTRAT. ZONE/FOSSIL CHARACTER
FORAMINIFERS
NANNOFOSSILS
RADIOLARIANS
DIATOMS
PALEOMAGNETICS
PHYS. PROPERTIES
CHEMISTRY
SECTION
METERS
GRAPHIC LITHOLOGY
DRILLING DISTURB.
SED. STRUCTURES
SAMPLES
UPPER OLIGOCENE
A/M C CP19B C/M CP19B
0.5
1.0
1
2
3

LITHOLOGIC DESCRIPTION

CLAYSTONE AND NANNOFOSSIL CHALK

Major lithology: Generally strongly burrowed [illegible] CLAYSTONE, and [illegible] NANNOFOSSIL CHALK.

Minor lithologies: There are [illegible] SILTSTONE and SANDY SILTSTONE consisting of [illegible] and glass. Burrowing [illegible] these layers. Section [illegible] contains common sub-vertical dewatering veinlets.

The upper half of the core is highly fractured by drilling, and the lower half is undisturbed.

SMEAR SLIDE SUMMARY (%):

TEXTURE:

COMPOSITION:

SITE 787 HOLE B CORE 11R CORED INTERVAL 88.4-98.1 mbsf

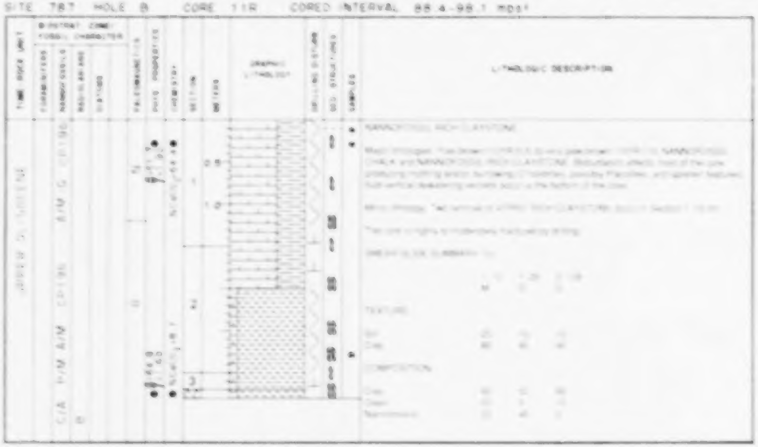
TIME ROCK UNIT
BIOSTRAT. ZONE/FOSSIL CHARACTER
FORAMINIFERS
NANNOFOSSILS
RADIOLARIANS
DIATOMS
PALEOMAGNETICS
PHYS. PROPERTIES
CHEMISTRY
SECTION
METERS
GRAPHIC LITHOLOGY
DRILLING DISTURB.
SED. STRUCTURES
SAMPLES
UPPER OLIGOCENE
C/A R/M A/M CP19B A/M C CP19B
0.5
1.0
1
2
3

LITHOLOGIC DESCRIPTION

NANNOFOSSIL RICH CLAYSTONE

Major lithologies: [illegible] NANNOFOSSIL CHALK and NANNOFOSSIL RICH CLAYSTONE. Bioturbation [illegible] of the core [illegible] burrowing [illegible] vertical dewatering veinlets occur in the bottom of the core.

Minor lithology: [illegible] RICH CLAYSTONE occur in Section [illegible]

The core is slightly to moderately fractured by drilling.

SMEAR SLIDE SUMMARY (%):

TEXTURE:

COMPOSITION:

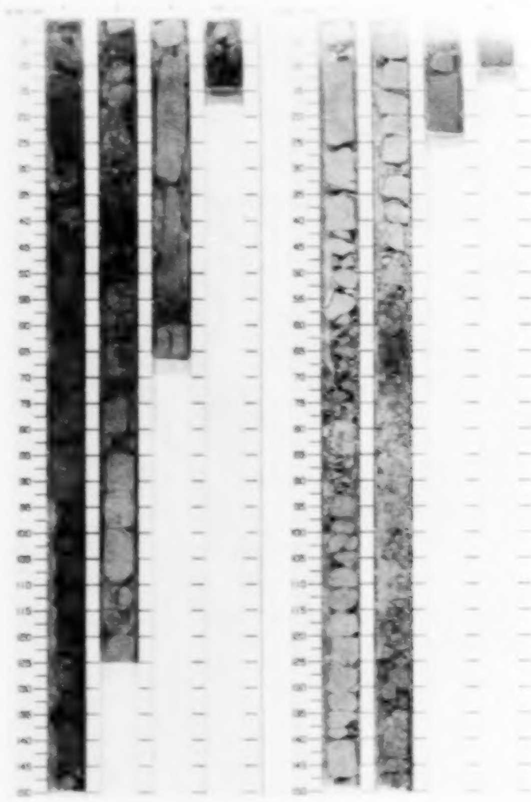

SITE 787 HOLE B CORE [illegible] CORED INTERVAL [illegible]

LITHOLOGIC DESCRIPTION

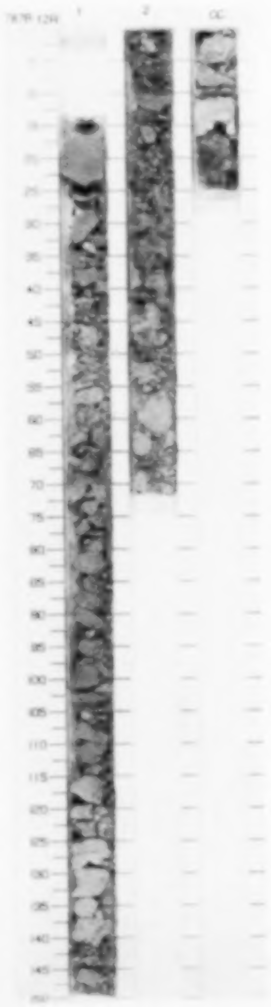
TOP (CM)
1
2
CC
25
30
35
40
45
50
55
60
65
70
75
80
85
90
95
100
105
110
115
120
125
130
135
140
145
150

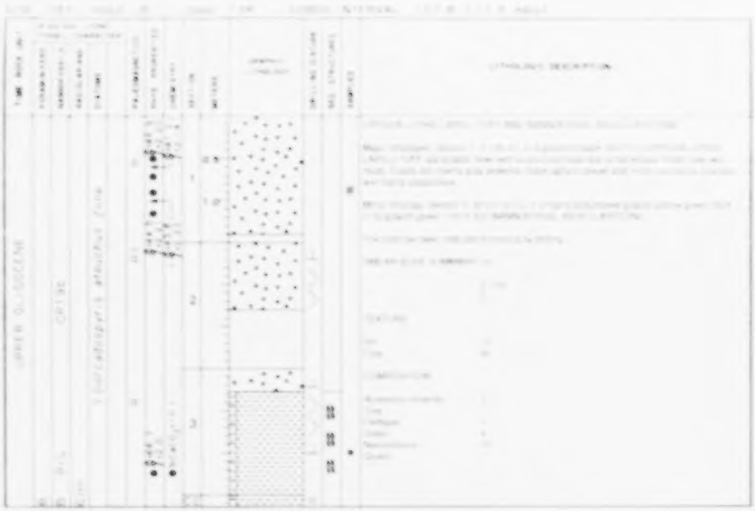
LITHOLOGIC DESCRIPTION
UPPER OLIGOCENE

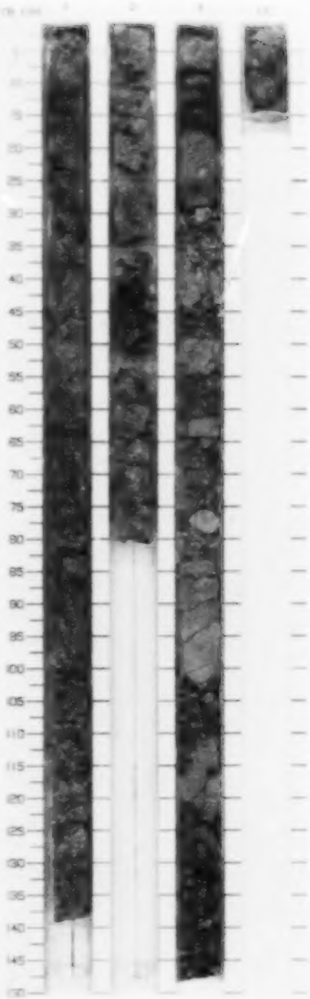
1
2
3
CC

SITE 787 HOLE B CORE 14R CORED INTERVAL 117.5-127.2 mbsf

BIOSTRAT. ZONE/ FOSSIL CHARACTER	GRAPHIC LITHOLOGY	LITHOLOGIC DESCRIPTION
[illegible]	[illegible]	[illegible]

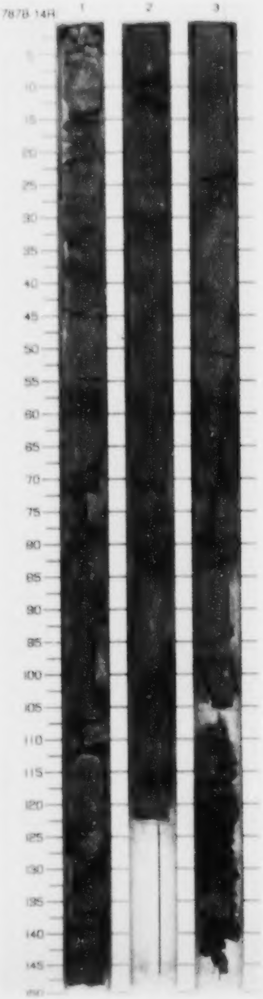
787B 14R
1
2
3
5
10
15
20
25
30
35
40
45
50
55
60
65
70
75
80
85
90
95
100
105
110
115
120
125
130
135
140
145
150

SITE 787 HOLE B CORE 15R CORED INTERVAL 127.2-136.8 mbsf

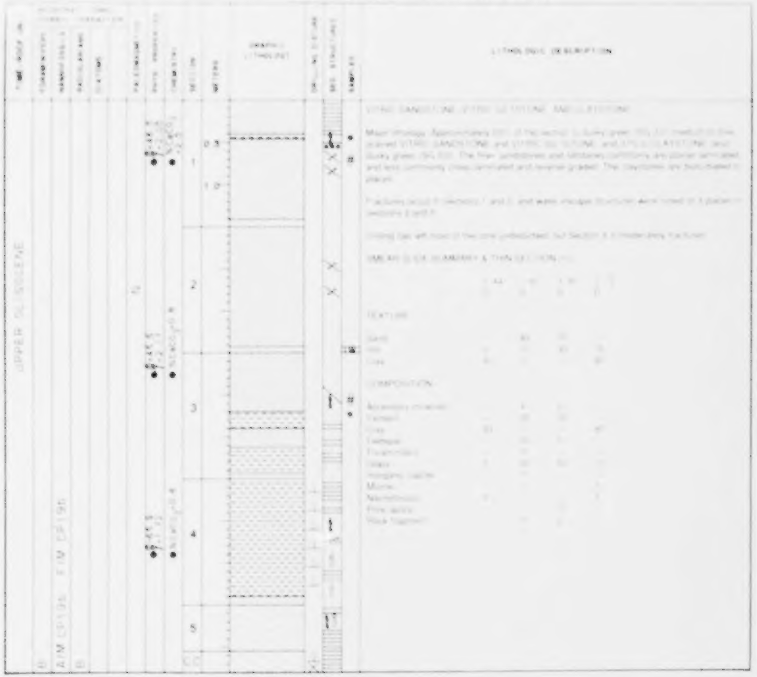
TIME-ROCK UNIT
BIOSTRAT. ZONE / FOSSIL CHARACTER
FORAMINIFERS
NANNOFOSSILS
RADIOLARIANS
DIATOMS
PALEOMAGNETICS
PHYS. PROPERTIES
CHEMISTRY
SECTION
METERS
GRAPHIC LITHOLOGY
DRILLING DISTURB.
SED. STRUCTURES
SAMPLES
UPPER OLIGOCENE
A/M CP19b F/M CP19b
B
B
0.5
1
1.0
2
3
4
5
CC

LITHOLOGIC DESCRIPTION

VITRIC SANDSTONE, VITRIC SILTSTONE, AND CLAYSTONE

Major lithology: Approximately [illegible] of the section is dusky green ([illegible]) medium to fine-grained VITRIC SANDSTONE and VITRIC SILTSTONE, and [illegible] CLAYSTONE (also dusky green ([illegible])). The finer sandstones and siltstones commonly are planar laminated and less commonly cross-laminated and reverse graded. The claystones are bioturbated in places.

Fractures (about [illegible]) in Sections 1 and 2, and water escape structures were noted in [illegible] places in Sections 3 and 4.

Drilling has left most of the core undisturbed, but Section 3 is moderately fractured.

SMEAR SLIDE SUMMARY & THIN SECTION (%):

	[illegible]	[illegible]	[illegible]	[illegible]
TEXTURE:				
Sand	—	[illegible]	[illegible]	—
Silt	[illegible]	[illegible]	[illegible]	[illegible]
Clay	[illegible]	[illegible]	—	[illegible]
COMPOSITION:				
Accessory minerals	—	[illegible]	[illegible]	—
Cement	—	[illegible]	[illegible]	—
Clay	[illegible]	—	—	[illegible]
Feldspar	—	[illegible]	[illegible]	—
Foraminifers	—	[illegible]	—	—
Glass	[illegible]	[illegible]	[illegible]	[illegible]
Inorganic calcite	—	[illegible]	—	—
Micrite	—	—	—	[illegible]
Nannofossils	[illegible]	—	—	[illegible]
Pore space	—	—	[illegible]	—
Rock fragments	—	[illegible]	[illegible]	—

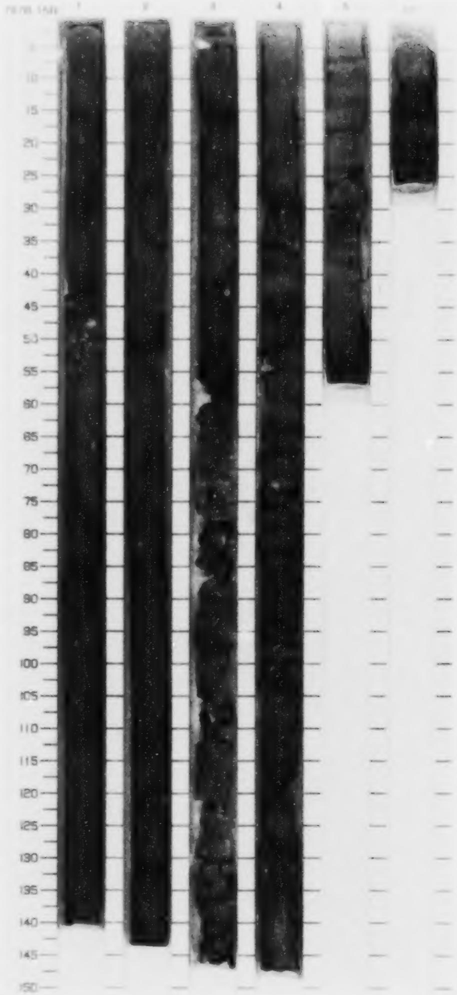
78/787B-15R
1
2
3
4
5
CC
0
10
15
20
25
30
35
40
45
50
55
60
65
70
75
80
85
90
95
100
105
110
115
120
125
130
135
140
145
150

SITE 787 HOLE B CORE 16R CORED INTERVAL 136.8-146.5 mbsl

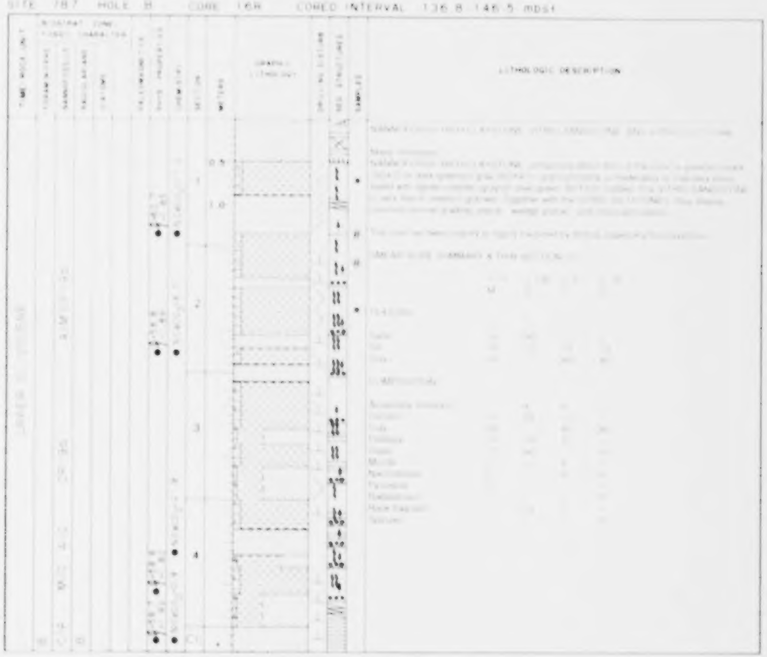
TIME-ROCK UNIT
BIOSTRAT. ZONE/FOSSIL CHARACTER
FORAMINIFERS
NANNOFOSSILS
RADIOLARIANS
DIATOMS
PALEOMAGNETICS
PHYS. PROPERTIES
CHEMISTRY
SECTION
METERS
GRAPHIC LITHOLOGY
DRILLING DISTURB.
SED. STRUCTURES
SAMPLES
0.5
1.0
1
2
3
4
CC

LITHOLOGIC DESCRIPTION

[illegible]

Major lithology:

[illegible]

[illegible]

SMEAR SLIDE SUMMARY (%): [illegible]

TEXTURE:

Sand
Silt
Clay

COMPOSITION:

Accessory minerals
[illegible]
Clay
[illegible]
Glass
Micrite
Nannofossils
[illegible]
Radiolarians
Rock fragments
Spicules

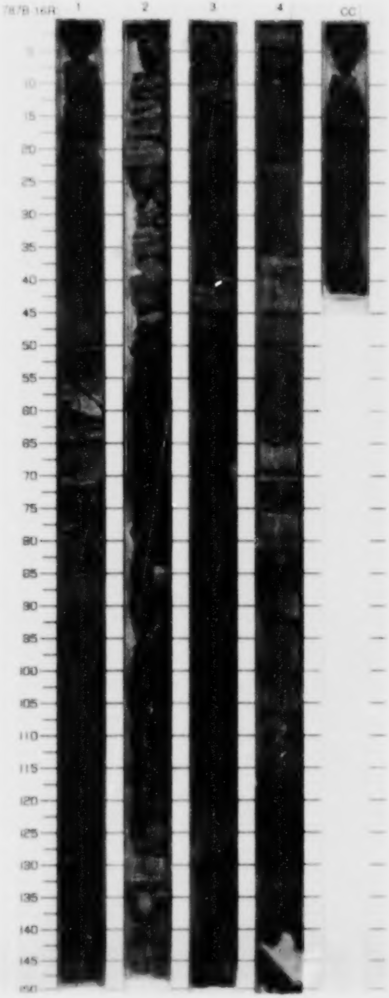
787B-16R
1
2
3
4
CC
5
10
15
20
25
30
35
40
45
50
55
60
65
70
75
80
85
90
95
100
105
110
115
120
125
130
135
140
145
150

SITE 787 HOLE B CORE [illegible] CORED INTERVAL [illegible]

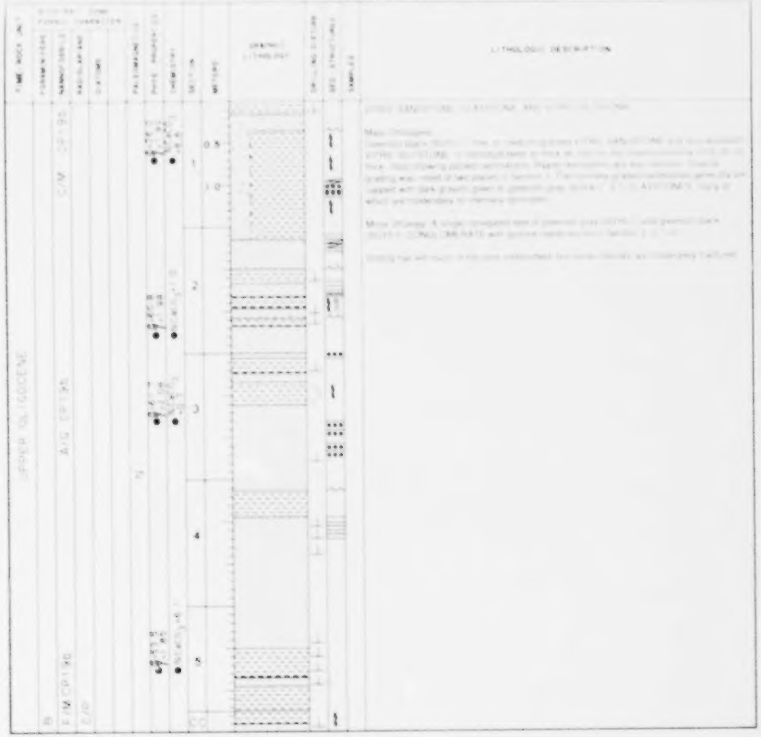
TIME-ROCK UNIT
BIOSTRAT. ZONE / FOSSIL CHARACTER
FORAMINIFERS
NANNOFOSSILS
RADIOLARIANS
DIATOMS
PALEOMAGNETICS
PHYS. PROPERTIES
CHEMISTRY
SECTION
METERS
GRAPHIC LITHOLOGY
DRILLING DISTURB.
SED. STRUCTURES
SAMPLES
UPPER OLIGOCENE
B
F/M CP19b
A/G CP19b
C/M CP19b
C/P
N
1
2
3
4
5
CC
0.5
1.0

LITHOLOGIC DESCRIPTION

[illegible] SANDSTONE, [illegible], AND [illegible]

Major lithologies: [illegible]

Minor lithology: A single [illegible] CONGLOMERATE [illegible]

[illegible]

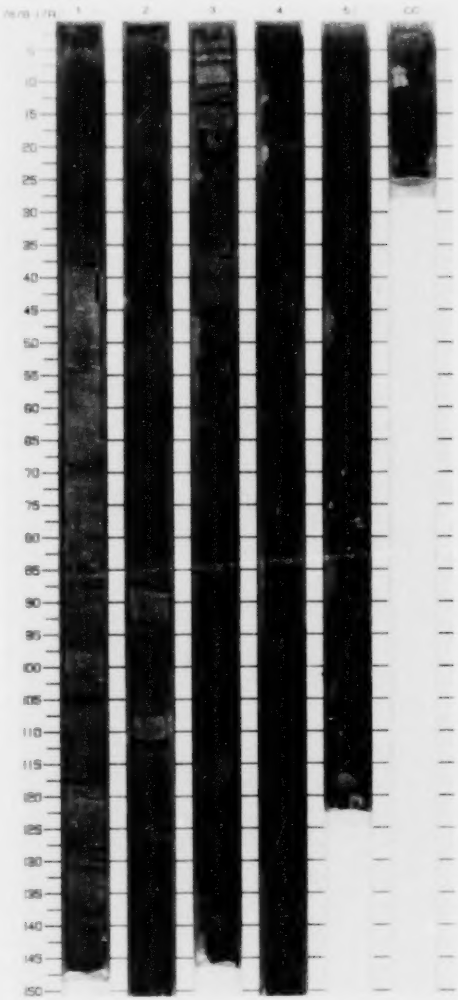
787B-17R
1
2
3
4
5
CC
5
10
15
20
25
30
35
40
45
50
55
60
65
70
75
80
85
90
95
100
105
110
115
120
125
130
135
140
145
150

SITE 787 HOLE B CORE 18R CORED INTERVAL 156.2-165.8 mbsf

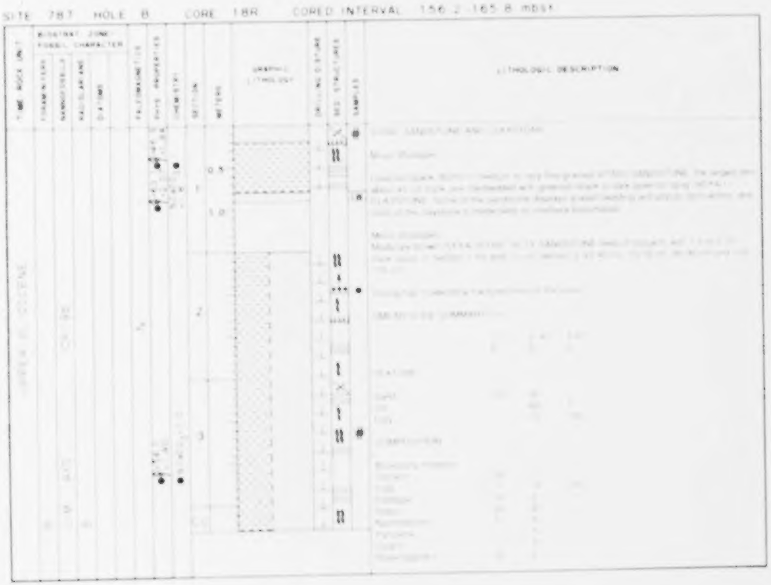
TIME-ROCK UNIT
BIOSTRAT. ZONE/ FOSSIL CHARACTER
FORAMINIFERS
NANNOFOSSILS
RADIOLARIANS
DIATOMS
PALEOMAGNETICS
PHYS. PROPERTIES
CHEMISTRY
SECTION
METERS
GRAPHIC LITHOLOGY
DRILLING DISTURB.
SED. STRUCTURES
SAMPLES
0.5
1.0
1
2
3

LITHOLOGIC DESCRIPTION

[illegible]

[illegible]

SMEAR SLIDE SUMMARY (%):

TEXTURE:

Sand

Silt

Clay

COMPOSITION:

[illegible]

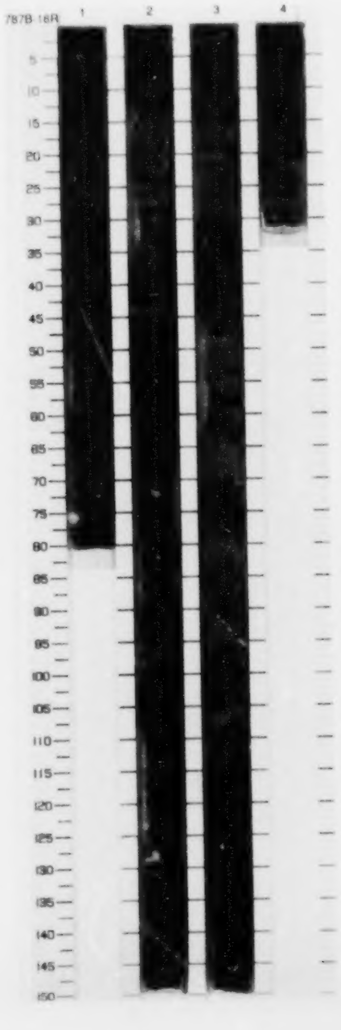
787B-18R
1
2
3
4
5
10
15
20
25
30
35
40
45
50
55
60
65
70
75
80
85
90
95
100
105
110
115
120
125
130
135
140
145
150

SITE 787 HOLE B CORE 19R CORED INTERVAL 165.8-175.5 mbsf

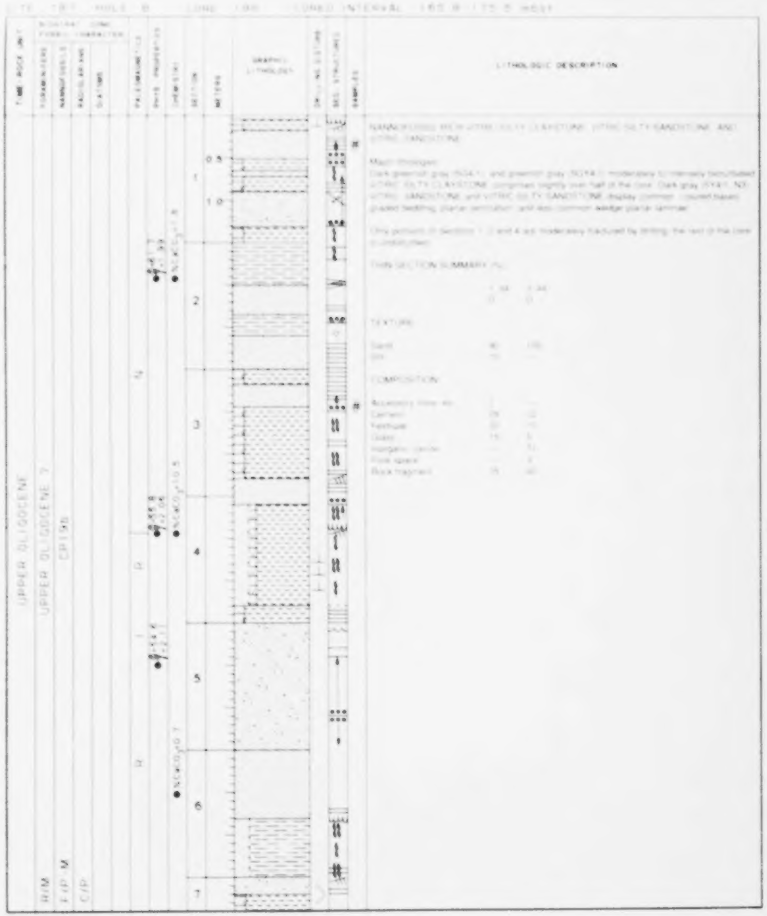
TIME-ROCK UNIT
BIOSTRAT. ZONE/FOSSIL CHARACTER
FORAMINIFERS
NANNOFOSSILS
RADIOLARIANS
DIATOMS
PALEOMAGNETICS
PHYS. PROPERTIES
CHEMISTRY
SECTION
METERS
GRAPHIC LITHOLOGY
DRILLING DISTURB.
SED. STRUCTURES
SAMPLES
UPPER OLIGOCENE
UPPER OLIGOCENE ?
CP19b
R/M
F/P M
C/P
N
R
I
R
0.5
1.0
1
2
3
4
5
6
7

LITHOLOGIC DESCRIPTION

NANNOFOSSIL-RICH VITRIC SILTY CLAYSTONE, VITRIC SILTY SANDSTONE, AND VITRIC SANDSTONE

Major lithologies:

Dark greenish gray (5G4/1) and greenish gray (5GY4/1) moderately to intensely bioturbated VITRIC SILTY CLAYSTONE comprises slightly over half of the core. Dark gray (5Y4/1, N3) VITRIC SANDSTONE and VITRIC SILTY SANDSTONE display common, scoured-based, graded bedding, planar lamination, and also common wedge planar laminae.

Only portions of Sections 1, 3 and 4 are moderately fractured by drilling; the rest of the core is undisturbed.

THIN SECTION SUMMARY (%):

	1, 60	3, 34
	D	D
TEXTURE:		
Sand	90	100
Silt	10	—
COMPOSITION:		
Accessory minerals	1	—
Cement	25	12
Feldspar	20	15
Glass	15	5
Inorganic calcite	—	11
Pore space	—	8
Rock fragment	35	40

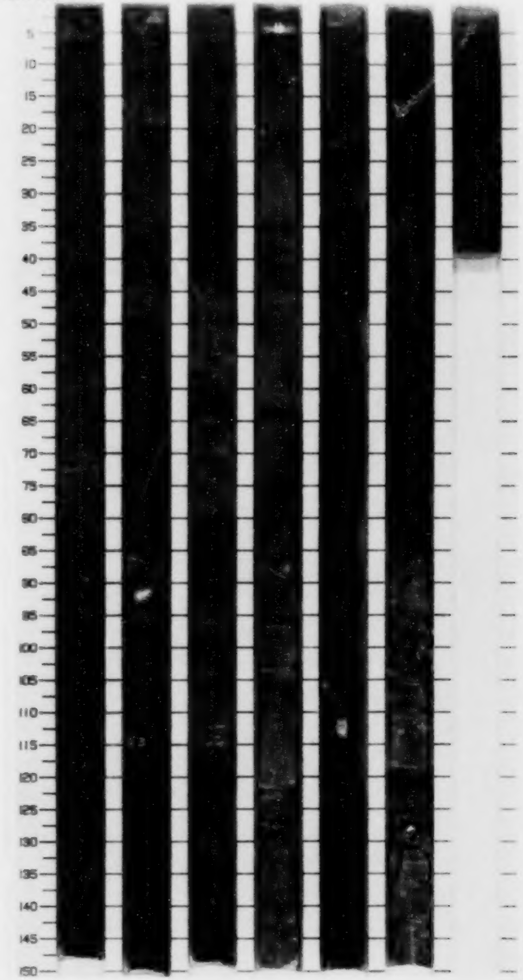
787B 19R
1
2
3
4
5
6
7
5
10
15
20
25
30
35
40
45
50
55
60
65
70
75
80
85
90
95
100
105
110
115
120
125
130
135
140
145
150

SITE 787 HOLE B CORE 20R CORED INTERVAL 175.5-185.1 mbsf

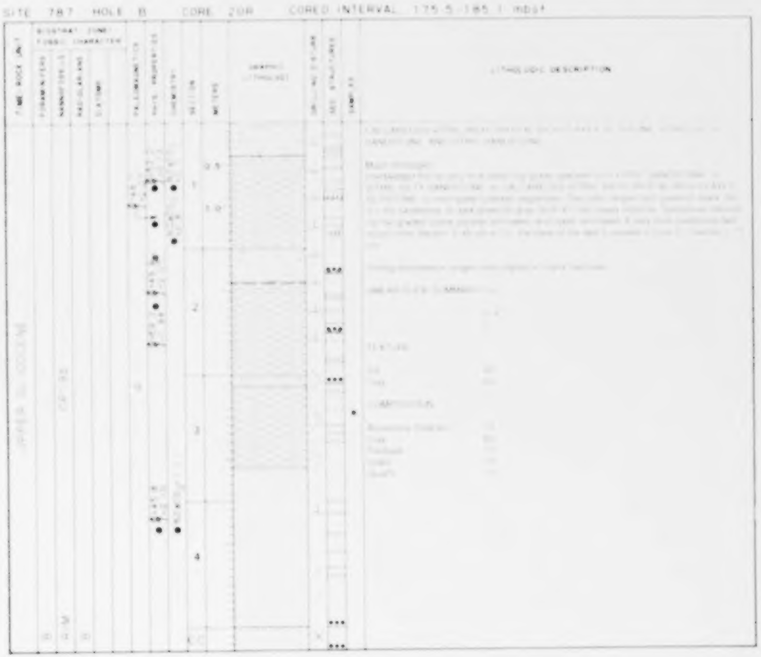
TIME-ROCK UNIT
BIOSTRAT. ZONE/ FOSSIL CHARACTER
FORAMINIFERS
NANNOFOSSILS
RADIOLARIANS
DIATOMS
PALEOMAGNETICS
PHYS. PROPERTIES
CHEMISTRY
SECTION
METERS
GRAPHIC LITHOLOGY
DRILLING DISTURB.
SED. STRUCTURES
SAMPLES
0.5
1.0
1
2
3
4
CC

LITHOLOGIC DESCRIPTION

[illegible]

Major lithologies:

[illegible]

SMEAR SLIDE SUMMARY (%):

TEXTURE:

Silt

Clay

COMPOSITION:

Accessory minerals

Clay

Feldspar

Glass

Quartz

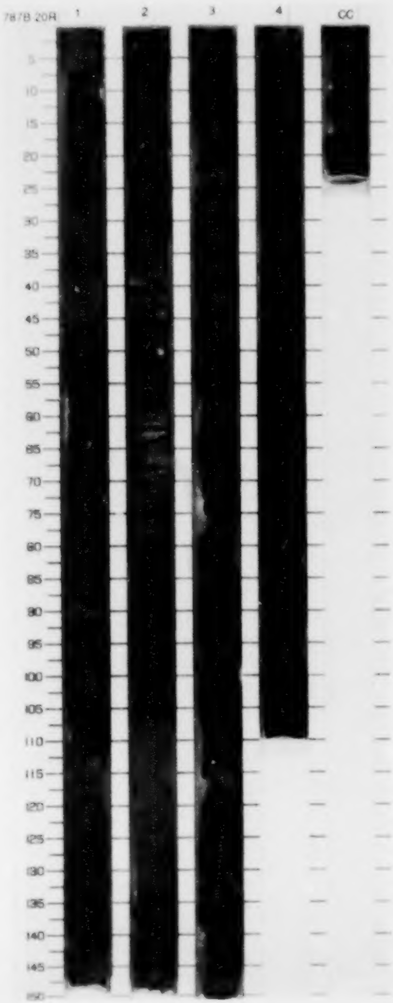
787B 20R
1
2
3
4
CC
5
10
15
20
25
30
35
40
45
50
55
60
65
70
75
80
85
90
95
100
105
110
115
120
125
130
135
140
145
150

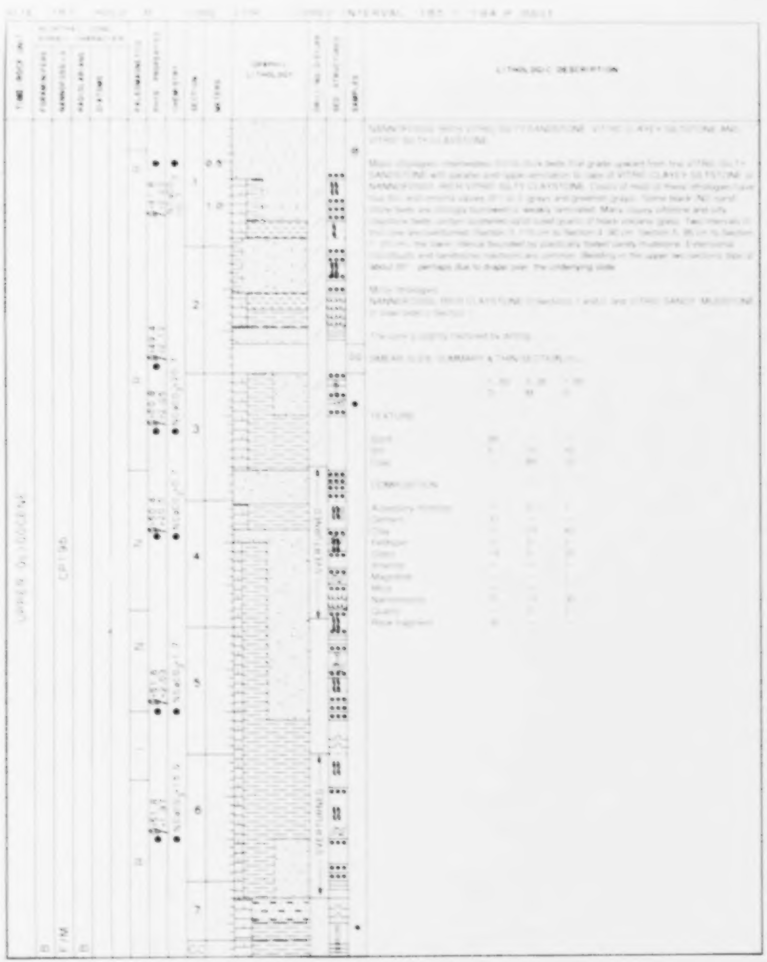
GRAPHIC LITHOLOGY
LITHOLOGIC DESCRIPTION
UPPER OLIGOCENE
1
2
3
4
5
6
7
CC

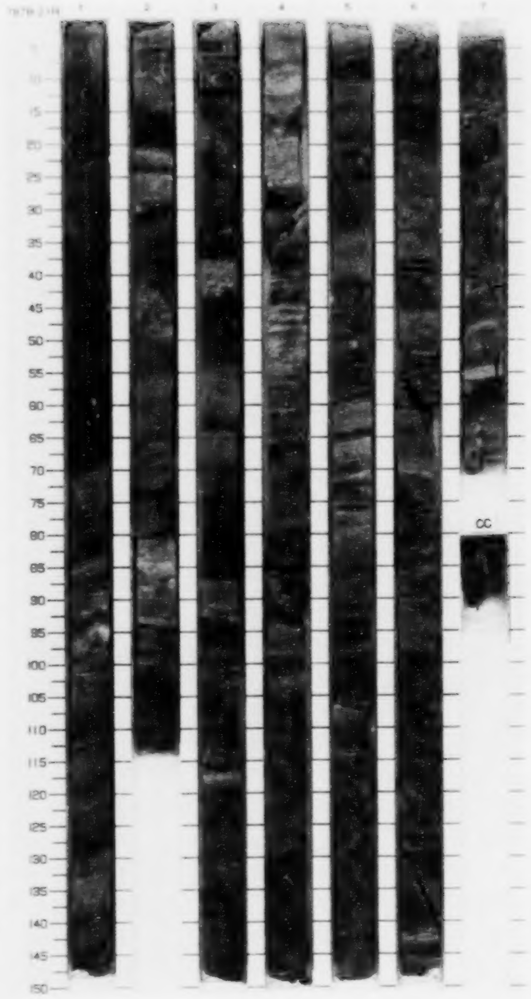
787B-21R
1
2
3
4
5
6
7
CC
5
10
15
20
25
30
35
40
45
50
55
60
65
70
75
80
85
90
95
100
105
110
115
120
125
130
135
140
145
150

SITE 787 HOLE B CORE 22R CORED INTERVAL 194.8-204.4 mbsf

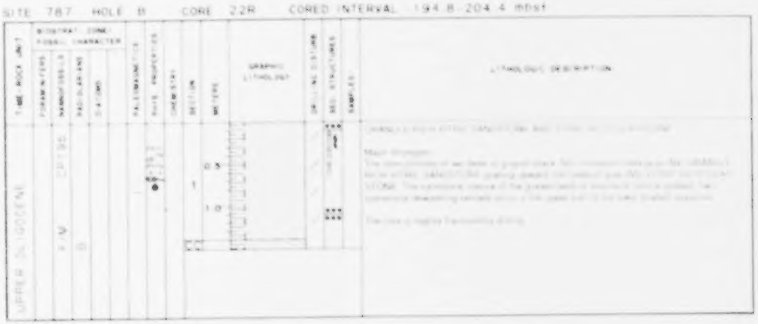
TIME-ROCK UNIT
BIOSTRAT. ZONE/ FOSSIL CHARACTER
FORAMINIFERS
NANNOFOSSILS
RADIOLARIANS
DIATOMS
PALEOMAGNETICS
PHYS. PROPERTIES
CHEMISTRY
SECTION
METERS
GRAPHIC LITHOLOGY
DRILLING DISTURB.
SED. STRUCTURES
SAMPLES
LITHOLOGIC DESCRIPTION
UPPER OLIGOCENE
CP19b
F/M
B
1
0.5
1.0
CC

[illegible]

Major lithologies:
[illegible]

[illegible]

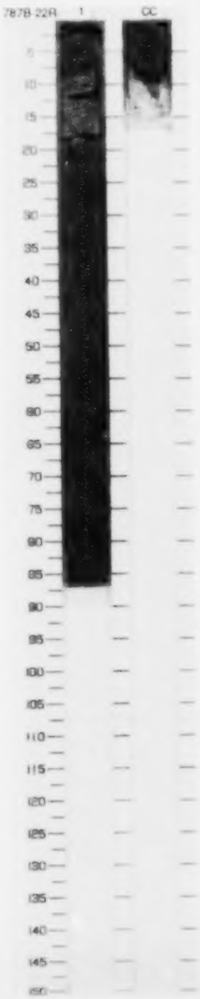
787B-22R
1
CC
5
10
15
20
25
30
35
40
45
50
55
60
65
70
75
80
85
90
95
100
105
110
115
120
125
130
135
140
145
150

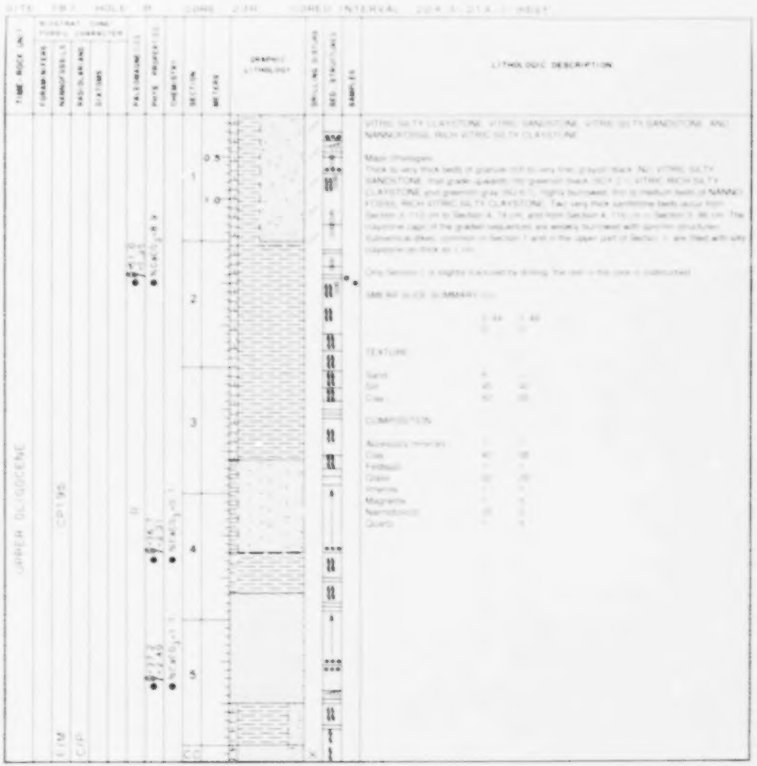
TIME-ROCK UNIT
BIOSTRAT. ZONE/FOSSIL CHARACTER
FORAMINIFERS
NANNOFOSSILS
RADIOLARIANS
DIATOMS
PALEOMAGNETICS
PHYS. PROPERTIES
CHEMISTRY
SECTION
METERS
GRAPHIC LITHOLOGY
DRILLING DISTURB.
SED. STRUCTURES
SAMPLES
UPPER OLIGOCENE
CP19b
C/M
C/P
0.5
1.0
1
2
3
4
5
CC

SITE 787 HOLE B CORE 23R CORED INTERVAL [illegible]

LITHOLOGIC DESCRIPTION

VITRIC SILTY CLAYSTONE, VITRIC SANDSTONE, VITRIC SILTY SANDSTONE, AND NANNOFOSSIL-RICH VITRIC SILTY CLAYSTONE

Major lithologies:
Thick to very thick beds of granule-rich to very fine, grayish black (N2) VITRIC SILTY SANDSTONE that grade upwards into greenish black (5GY 2/1) VITRIC-RICH SILTY CLAYSTONE and greenish gray (5G 6/1), highly burrowed, thin to medium beds of NANNOFOSSIL-RICH VITRIC SILTY CLAYSTONE. Two very thick sandstone beds occur from Section 3, 115 cm to Section 4, 74 cm, and from Section 4, 110 cm to Section 5, 96 cm. The claystone caps of the graded sequences are weakly burrowed with Zoophycos structures. Subvertical dikes, common in Section 1 and in the upper part of Section 3, are filled with silty claystone as thick as 1 cm.

Only Section 1 is slightly fractured by drilling; the rest of the core is undisturbed.

SMEAR SLIDE SUMMARY (%):

	2, 44	2, 48
	D	D
TEXTURE:		
Sand	5	—
Silt	45	40
Clay	50	60
COMPOSITION:		
Accessory minerals	[illegible]	[illegible]
Clay	40	58
Feldspar	[illegible]	[illegible]
Glass	30	20
[illegible]	[illegible]	[illegible]
Magnetite	[illegible]	[illegible]
Nannofossils	[illegible]	[illegible]
Quartz	[illegible]	[illegible]

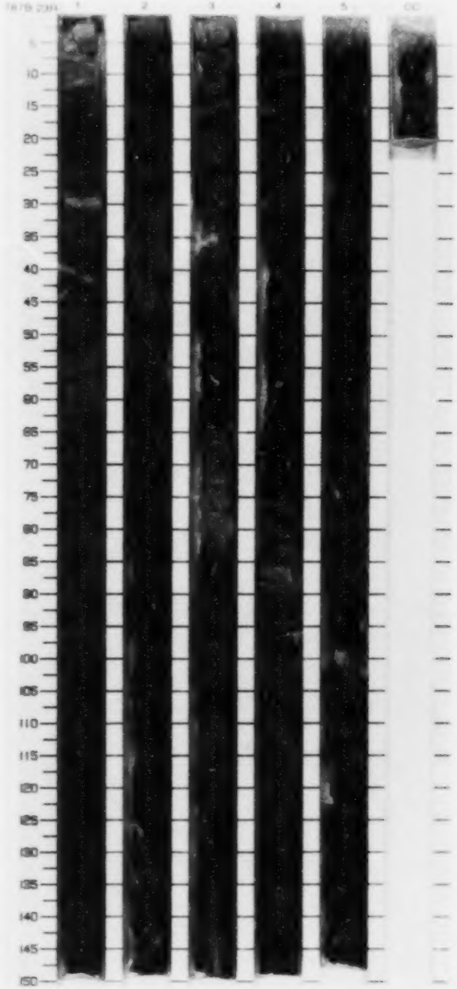
787B-23R
1
2
3
4
5
CC
5
10
15
20
25
30
35
40
45
50
55
60
65
70
75
80
85
90
95
100
105
110
115
120
125
130
135
140
145
150

SITE 787 HOLE B CORE 24R CORED INTERVAL 214.1-223.7 mbsf

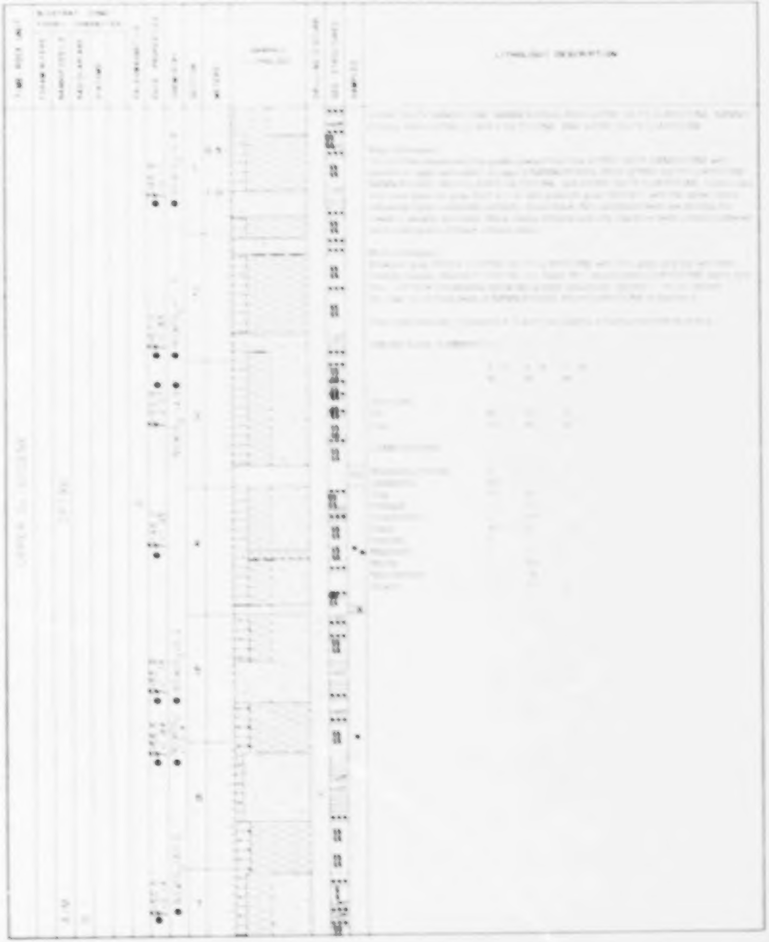
LITHOLOGIC DESCRIPTION

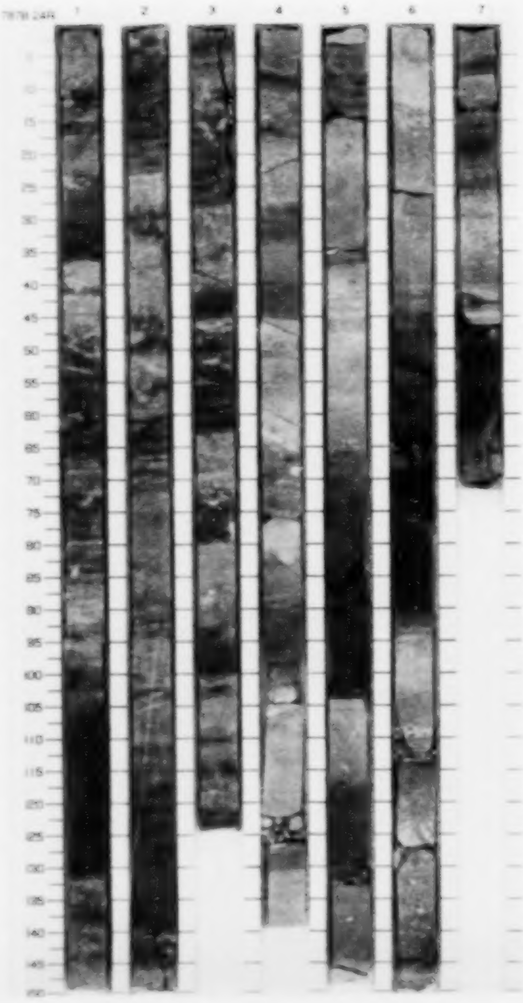
787B-24R
1
2
3
4
5
6
7
5
10
15
20
25
30
35
40
45
50
55
60
65
70
75
80
85
90
95
100
105
110
115
120
125
130
135
140
145
150

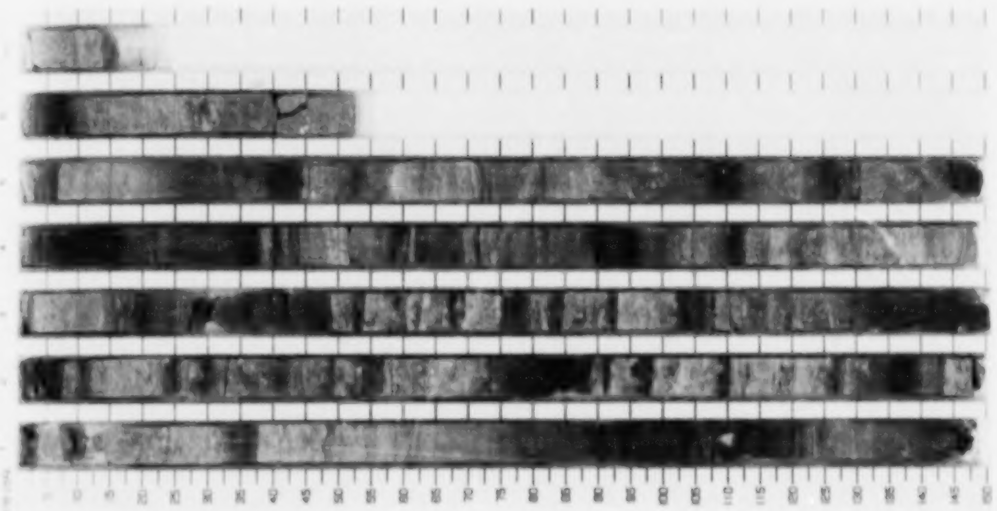

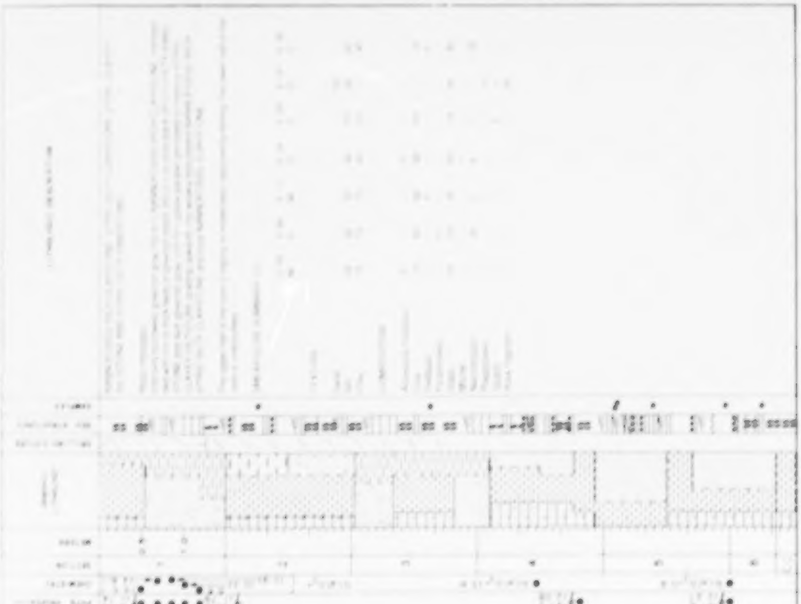

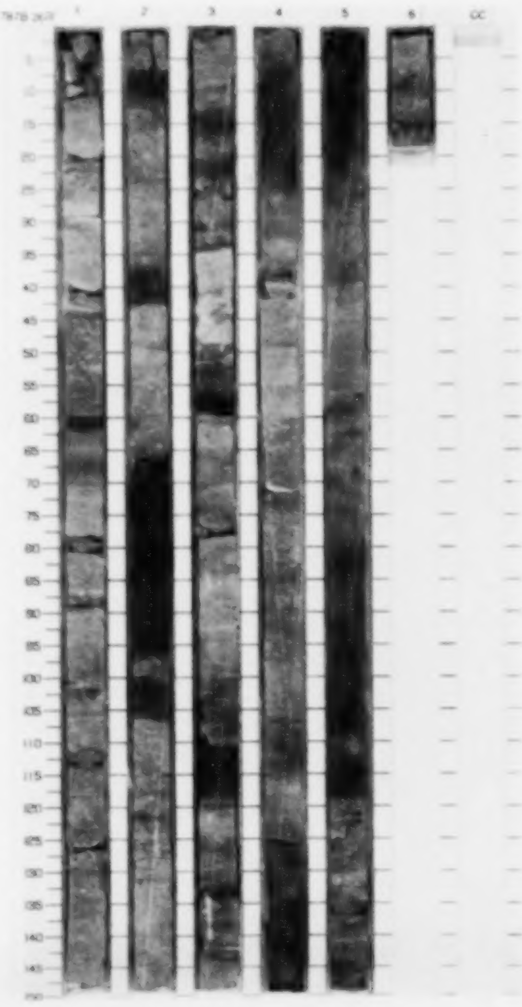
787B 26X
1
2
3
4
5
6
CC
5
10
15
20
25
30
35
40
45
50
55
60
65
70
75
80
85
90
95
100
105
110
115
120
125
130
135
140
145
150

SITE 787 HOLE B CORE 26X CORED INTERVAL 233.4-243.0 mbsf

LITHOLOGIC DESCRIPTION

[illegible]

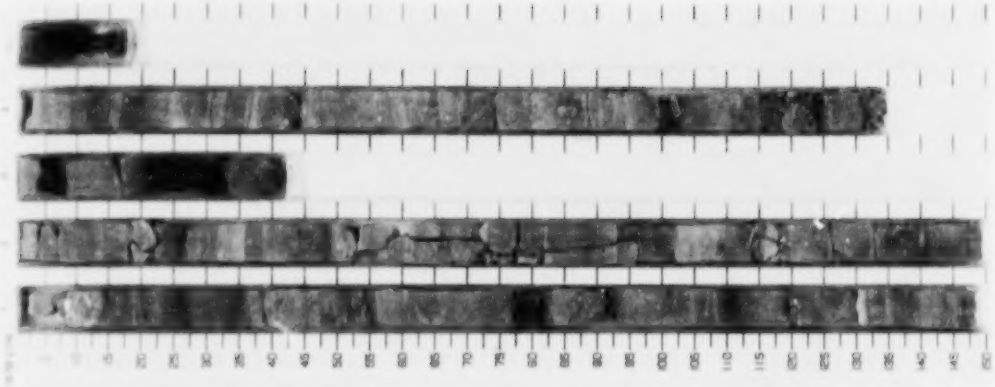
0
5
10
15
20
25
30
35
40
45
50
55
60
65
70
75
80
85
90
95
100
105
110
115
120
125
130
135
140
145
150

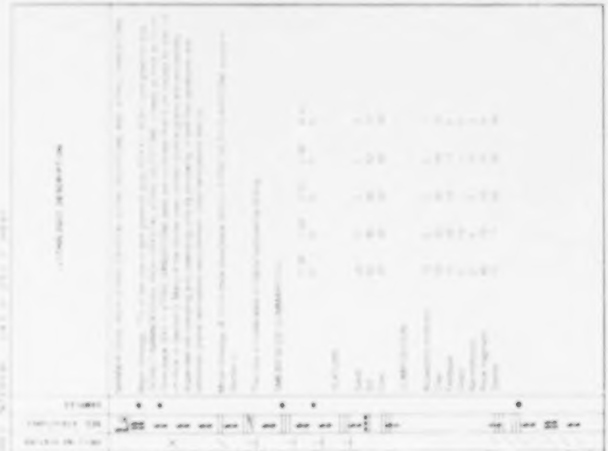
GRAPHIC LITHOLOGY
LITHOLOGIC DESCRIPTION
1
2
3
4
SMEAR SLIDE SUMMARY (%):
TEXTURE:
Sand
Silt
Clay
COMPOSITION:
Accessory minerals
Clay
Feldspar
Glass
Nannofossils
Rock fragments
Quartz

SITE 787 HOLE B CORE 28R CORED INTERVAL 252.7-262.4 mbsf

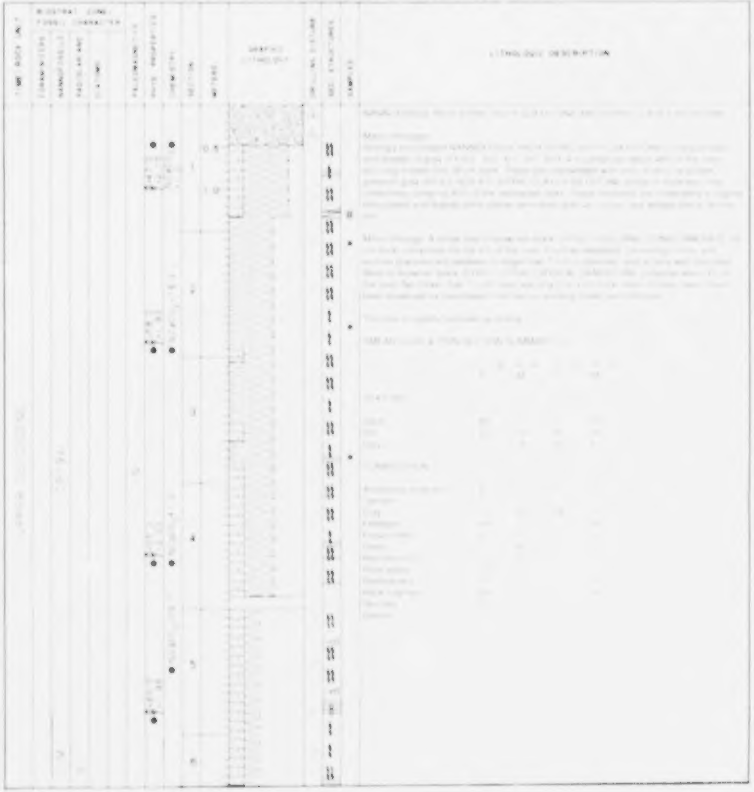
TIME-ROCK UNIT
BIOSTRAT. ZONE/FOSSIL CHARACTER
FORAMINIFERS
NANNOFOSSILS
RADIOLARIANS
DIATOMS
PALEOMAGNETICS
PHYS. PROPERTIES
CHEMISTRY
SECTION
METERS
GRAPHIC LITHOLOGY
DRILLING DISTURB.
SED. STRUCTURES
SAMPLES
LITHOLOGIC DESCRIPTION
0.5
1.0
1
2
3
4
5
6

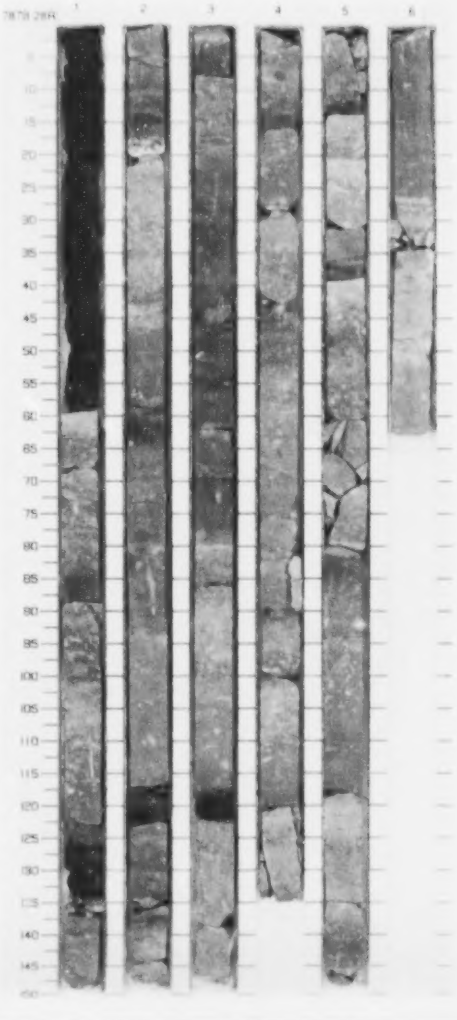
787B 28R
1
2
3
4
5
6
5
10
15
20
25
30
35
40
45
50
55
60
65
70
75
80
85
90
95
100
105
110
115
120
125
130
135
140
145
150

SITE 787 HOLE B CORE 29R CORED INTERVAL 262.4-272.0 mbsf

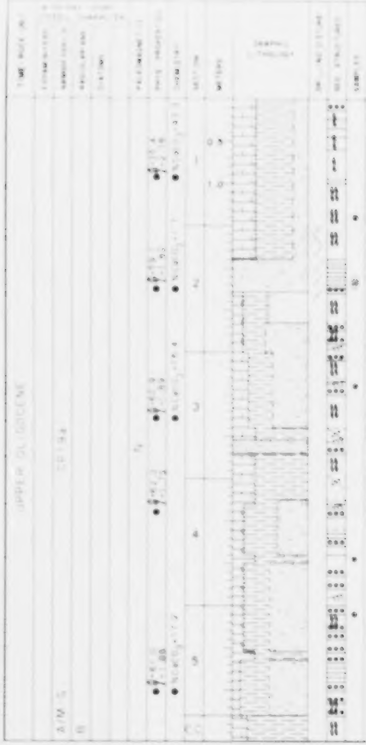
TIME-ROCK UNIT
BIOSTRAT. ZONE/FOSSIL CHARACTER
FORAMINIFERS
NANNOFOSSILS
RADIOLARIANS
DIATOMS
PALEOMAGNETICS
PHYS. PROPERTIES
CHEMISTRY
SECTION
METERS
GRAPHIC LITHOLOGY
DRILLING DISTURB.
SED. STRUCTURES
SAMPLES
UPPER OLIGOCENE
A/M G
B
N
0.5
1.0
1
2
3
4
5
CC

LITHOLOGIC DESCRIPTION

VITRIC-LITHIC SILTY SANDSTONE, NANNOFOSSIL VITRIC SILTY CLAYSTONE, AND NANNOFOSSIL-RICH VITRIC SILTY CLAYSTONE

Major lithologies:
Interbedded graded, laminated and cross-laminated greenish black (5GY 2.5/1) VITRIC-LITHIC SILTY SANDSTONES and burrowed intervals of light greenish gray (5GY 8/1) NANNOFOSSIL CHALK, and greenish gray (5G 5/1) NANNOFOSSIL VITRIC SILTY CLAYSTONE and NANNOFOSSIL-RICH VITRIC SILTY CLAYSTONE that commonly contain dispersed sand-sized volcanic grit. There are healed fractures in the lower part of Section 3 and the upper part of Section 4.

The core is undisturbed by drilling except for Section 2, which is slightly to highly fractured by drilling.

SMEAR SLIDE & THIN SECTION SUMMARY (%):

	1, 24	2, 142	3, 42	4, 30	5, [illegible]
	[illegible]	[illegible]	M	[illegible]	M
TEXTURE:					
Sand	[illegible]	[illegible]	[illegible]	[illegible]	[illegible]
Silt	[illegible]	[illegible]	[illegible]	[illegible]	[illegible]
Clay	[illegible]	[illegible]	[illegible]	[illegible]	[illegible]
COMPOSITION:					
Accessory minerals	[illegible]	[illegible]	[illegible]	[illegible]	[illegible]
Clay	[illegible]	[illegible]	[illegible]	[illegible]	[illegible]
Feldspar	[illegible]	[illegible]	[illegible]	[illegible]	[illegible]
Foraminifers	[illegible]	[illegible]	[illegible]	[illegible]	[illegible]
Glass	[illegible]	[illegible]	[illegible]	[illegible]	[illegible]
Nannofossils	[illegible]	[illegible]	[illegible]	[illegible]	[illegible]
Pore space	[illegible]	[illegible]	[illegible]	[illegible]	[illegible]
Radiolarians	[illegible]	[illegible]	[illegible]	[illegible]	[illegible]
Rock fragment	[illegible]	[illegible]	[illegible]	[illegible]	[illegible]
Zeolite	[illegible]	[illegible]	[illegible]	[illegible]	[illegible]

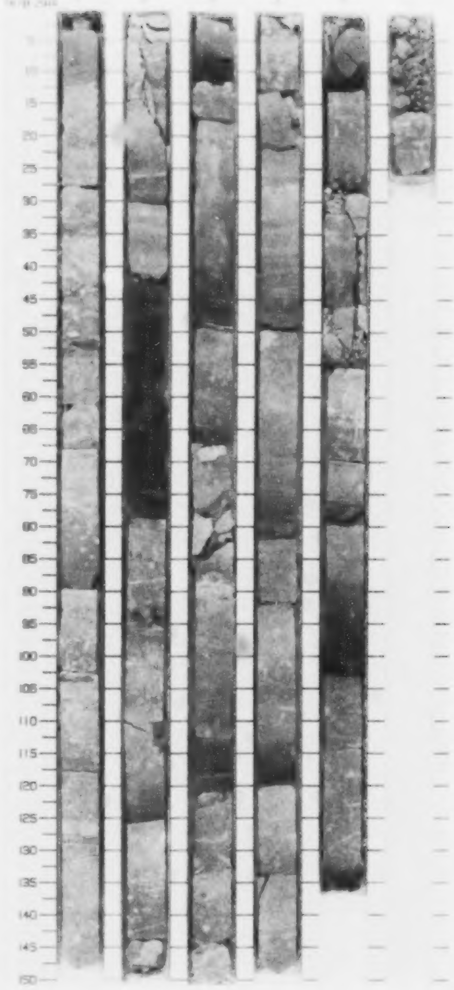
787B-29R
1
2
3
4
5
6
0
5
10
15
20
25
30
35
40
45
50
55
60
65
70
75
80
85
90
95
100
105
110
115
120
125
130
135
140
145
150

SITE 787 HOLE B CORE 30R CORED INTERVAL 272.0-281.7 mbsf

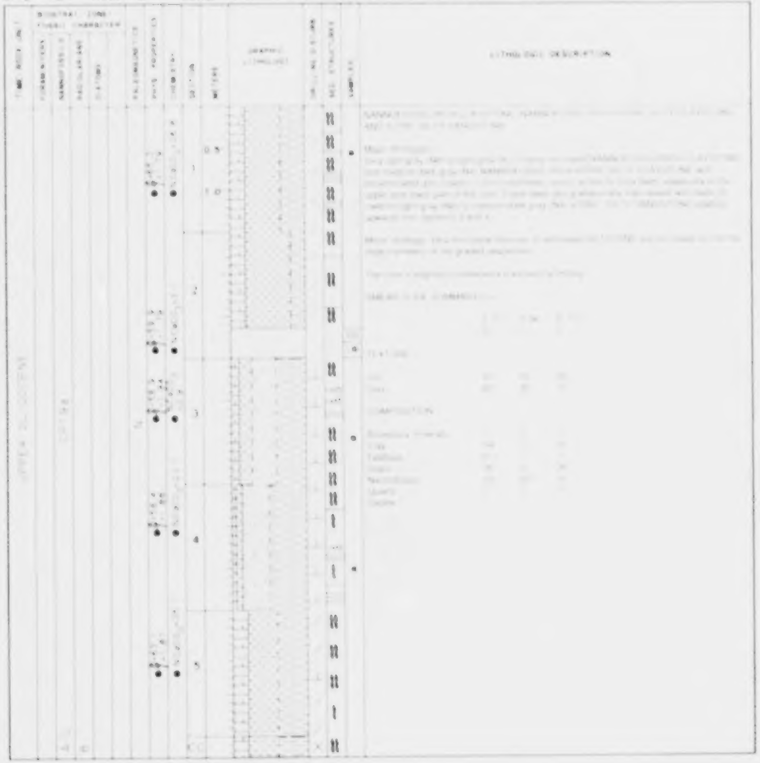
TIME-ROCK UNIT
BIOSTRAT. ZONE/FOSSIL CHARACTER
FORAMINIFERS
NANNOFOSSILS
RADIOLARIANS
DIATOMS
PALEOMAGNETICS
PHYS. PROPERTIES
CHEMISTRY
SECTION
METERS
GRAPHIC LITHOLOGY
DRILLING DISTURB.
SED. STRUCTURES
SAMPLES
LITHOLOGIC DESCRIPTION
0.5
1.0
1
2
3
4
5
CC

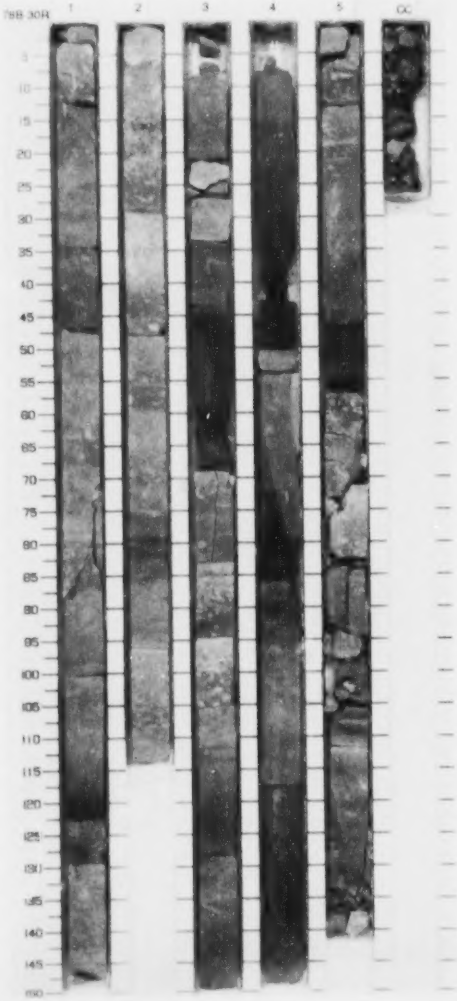
788 30R
1
2
3
4
5
CC
5
10
15
20
25
30
35
40
45
50
55
60
65
70
75
80
85
90
95
100
105
110
115
120
125
130
135
140
145
150

SITE 787 HOLE B CORE [illegible] CORED INTERVAL [illegible]

TIME-ROCK UNIT	FORAMINIFERS	NANNOFOSSILS	RADIOLARIANS	DIATOMS	PALEOMAGNETICS	PHYS. PROPERTIES	CHEMISTRY	SECTION	METERS	GRAPHIC LITHOLOGY	DRILLING DISTURB.	SED. STRUCTURES	SAMPLES	LITHOLOGIC DESCRIPTION
[illegible]		[illegible]	[illegible]		[illegible]	● [illegible]	● [illegible]	1	0.5 1.0		× × × × ×	●	▨	[illegible]
								2						

THIN SECTION SUMMARY [illegible]

TEXTURE:

[illegible]

COMPOSITION:

[illegible]

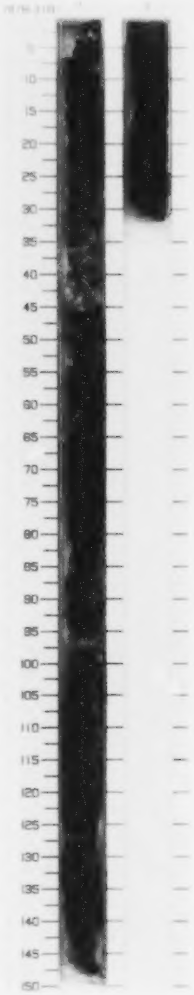

[illegible]
1
2
0
5
10
15
20
25
30
35
40
45
50
55
60
65
70
75
80
85
90
95
100
105
110
115
120
125
130
135
140
145
150

SITE 787 HOLE B CORE 32R CORED INTERVAL 291.3-300.8 mbsf

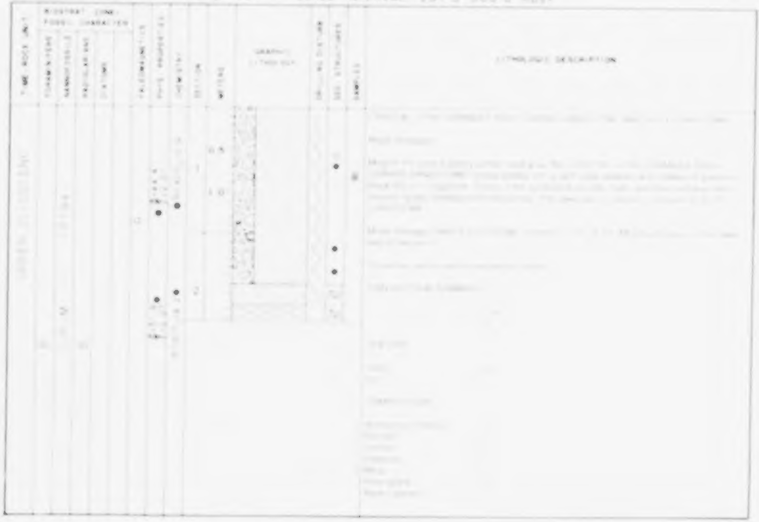
TIME-ROCK UNIT
BIOSTRAT. ZONE/FOSSIL CHARACTER
FORAMINIFERS
NANNOFOSSILS
RADIOLARIANS
DIATOMS
PALEOMAGNETICS
PHYS. PROPERTIES
CHEMISTRY
SECTION
METERS
0.5
1.0
GRAPHIC LITHOLOGY
DRILLING DISTURB.
SED. STRUCTURES
SAMPLES
LITHOLOGIC DESCRIPTION

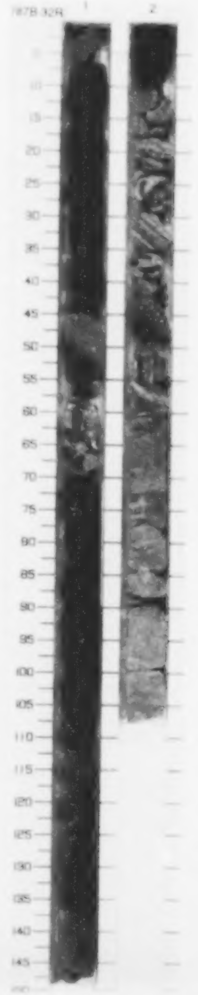
787B-32R
1
2
5
10
15
20
25
30
35
40
45
50
55
60
65
70
75
80
85
90
95
100
105
110
115
120
125
130
135
140
145
150

SITE 787 HOLE B CORE [illegible] CORED INTERVAL [illegible]

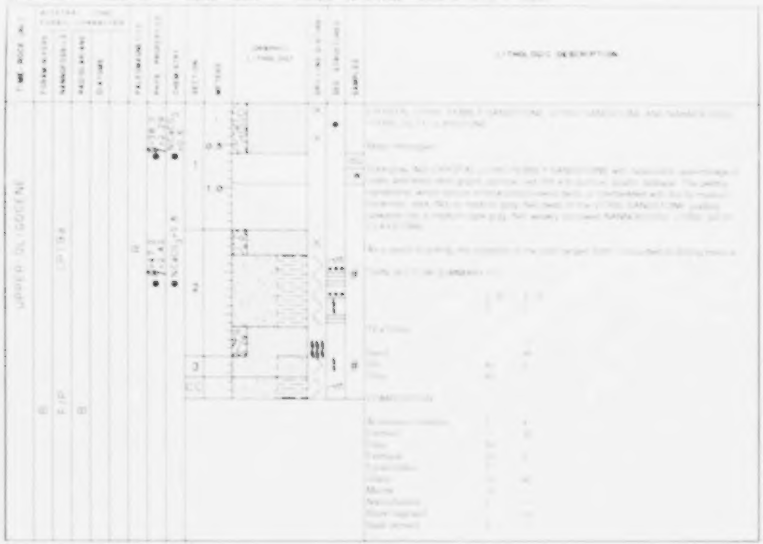
TIME-ROCK UNIT
BIOSTRAT. ZONE/FOSSIL CHARACTER
FORAMINIFERS
NANNOFOSSILS
RADIOLARIANS
DIATOMS
PALEOMAGNETICS
PHYS. PROPERTIES
CHEMISTRY
SECTION
METERS
GRAPHIC LITHOLOGY
DRILLING DISTURB.
SED. STRUCTURES
SAMPLES
UPPER OLIGOCENE
B
F/P
B
0.5
1.0
1
2
3
CC

LITHOLOGIC DESCRIPTION

[illegible]

TEXTURE:

Sand
Silt
Clay

COMPOSITION:

Accessory minerals
Clay
Glass
Micrite
Nannofossils

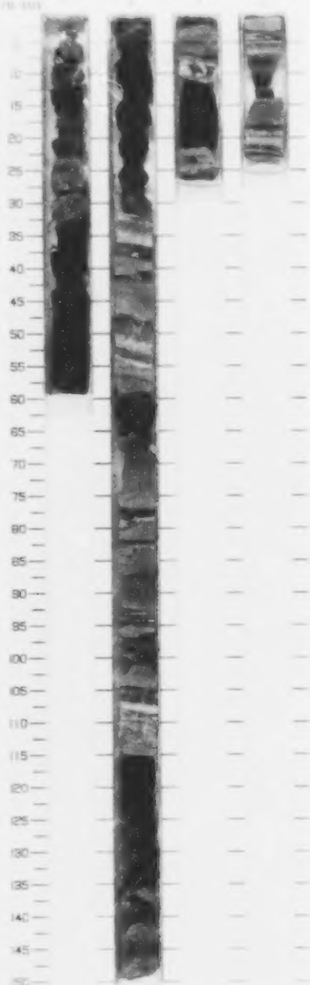
1
2
3
4
5
10
15
20
25
30
35
40
45
50
55
60
65
70
75
80
85
90
95
100
105
110
115
120
125
130
135
140
145
150

SITE 787 HOLE B CORE 34R CORED INTERVAL 310.5-320.1 mbsf

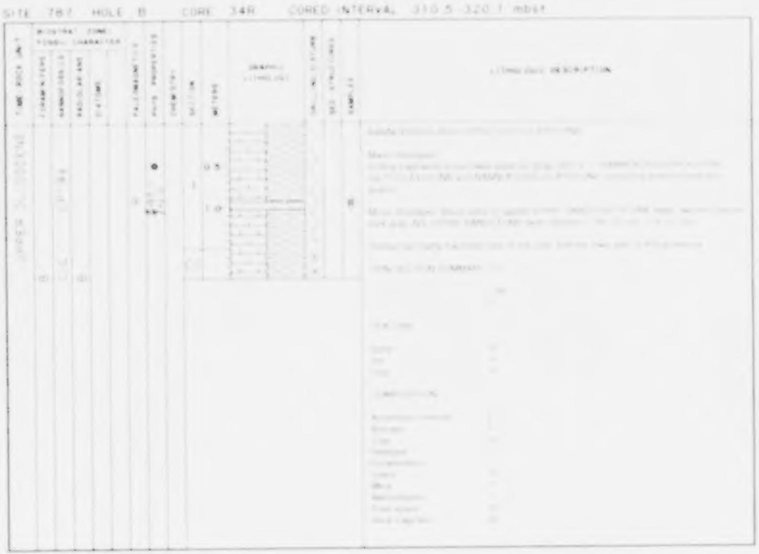
TIME-ROCK UNIT
BIOSTRAT. ZONE/FOSSIL CHARACTER
FORAMINIFERS
NANNOFOSSILS
RADIOLARIANS
DIATOMS
PALEOMAGNETICS
PHYS. PROPERTIES
CHEMISTRY
SECTION
METERS
GRAPHIC LITHOLOGY
DRILLING DISTURB.
SED. STRUCTURES
SAMPLES
0.5
1.0
LITHOLOGIC DESCRIPTION

[illegible]

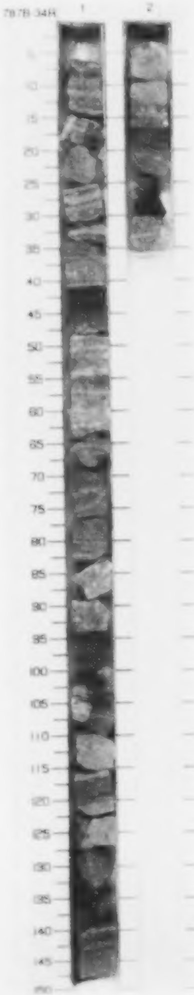
787B-34R
1
2
5
10
15
20
25
30
35
40
45
50
55
60
65
70
75
80
85
90
95
100
105
110
115
120
125
130
135
140
145
150

```
[illegible]87B-2R-01 (44-45 cm)                 OBSERVER: GIL        WHERE SAMPLED: Top of core (Pliocene-Pleistocene)

ROCK NAME: Andesite

GRAIN SIZE: Fine

TEXTURE: Intersertal

-------------------------------------------------------------------------------------------------------------------

PRIMARY        PERCENT PERCENT  SIZE        COMPO-
MINERALOGY     PRESENT ORIGINAL (mm)        SITION              MORPHOLOGY              COMMENTS

PHENOCRYSTS
PLAGIOCLASE     10      10      0.5                             Euhedral
CLINOPYROXENE   3       3       0.5                             Euhedral
ORTHOPYROXENE   1       1       0.5                             Euhedral
MAGNETITE       Tr      N/A     0.1                             Anhedral

GROUNDMASS
[illegible]     N/A     N/A     N/A                             N/A
-------------------------------------------------------------------------------------------------------------------
VESICLES/                       SIZE
CAVITIES       PERCENT LOCATION (mm)                FILLING                          SHAPE
VESICLES        15              0.1                 Zeolite                          Circular
-------------------------------------------------------------------------------------------------------------------
COMMENTS: Vesicular 2 pyroxene andesite with glomeroporphyritic clots. Contains an inclusion of less phyric
          non-vesicular plagioclase and augite and magnetite andesite; sample is 2 cm clast. No piece # given.

[illegible]87B-3R-01 (31-32 cm)                 OBSERVER: GIL        WHERE SAMPLED: Base gravel section

ROCK NAME: Dacite

GRAIN SIZE: Fine

TEXTURE: Glassy

-------------------------------------------------------------------------------------------------------------------

PRIMARY        PERCENT PERCENT  SIZE        COMPO-
MINERALOGY     PRESENT ORIGINAL (mm)        SITION              MORPHOLOGY              COMMENTS

PHENOCRYSTS
PLAGIOCLASE     15      15      2-3         Andesine 40-45      Anhedral                Zoned and corroded.
CLINOPYROXENE   2       2       1                               Euhedral                In clots with plagioclase.
MAGNETITE       Tr      N/A     0.1                             Anhedral                Fresh.

GROUNDMASS
GLASS           N/A     N/A     N/A                             N/A                     Seems to be devitrified glass but
                                                                                        peculiar.
-------------------------------------------------------------------------------------------------------------------
VESICLES/                       SIZE
CAVITIES       PERCENT LOCATION (mm)                FILLING                          SHAPE
VESICLES        3
-------------------------------------------------------------------------------------------------------------------
COMMENTS: No piece # given.

[illegible]87B-10R-01 (17-19 cm)                OBSERVER: LTP        WHERE SAMPLED: Tuff

ROCK NAME: Welded andesitic lapilli

GRAIN SIZE:

TEXTURE: Vitroclastic

-------------------------------------------------------------------------------------------------------------------

PRIMARY        PERCENT PERCENT  SIZE        COMPO-
MINERALOGY     PRESENT ORIGINAL (mm)        SITION              MORPHOLOGY              COMMENTS

PHENOCRYSTS
PLAGIOCLASE     [illegible] N/A 0.1-1                           Subhedral to            Rock predominantly formed of andesitic
                                                                euhedral                vitric clasts and plagioclase-pyroxene
                                                                                        crystals.
CLINOPYROXENE   2       N/A     0.1-0.5                         Subhedral to
                                                                euhedral

GROUNDMASS
GLASS           N/A     N/A     N/A                             N/A                     Partly devitrified.
-------------------------------------------------------------------------------------------------------------------
VESICLES/                       SIZE
CAVITIES       PERCENT LOCATION (mm)                FILLING                          SHAPE
VESICLES        1
-------------------------------------------------------------------------------------------------------------------
COMMENTS: No piece # given.
```

126 788A 1R NO RECOVERY

126 788A 2R NO RECOVERY

126 788A 3R NO RECOVERY

SITE 788 HOLE A CORE 4R CORED INTERVAL 26.2-35.8 mbsf

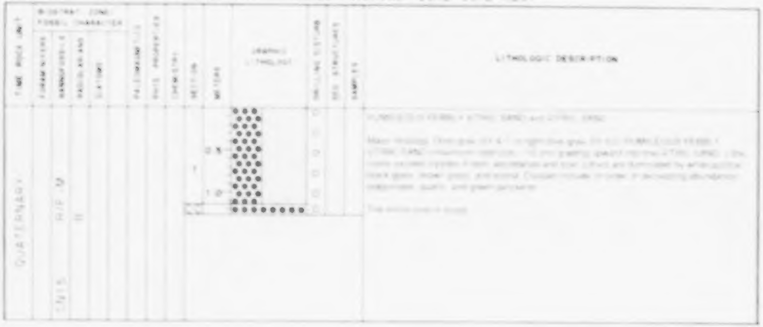
TIME ROCK UNIT
BIOSTRAT. ZONE/ FOSSIL CHARACTER
FORAMINIFERS
NANNOFOSSILS
RADIOLARIANS
DIATOMS
PALEOMAGNETICS
PHYS. PROPERTIES
CHEMISTRY
SECTION
METERS
GRAPHIC LITHOLOGY
DRILLING DISTURB.
SED. STRUCTURES
SAMPLES
LITHOLOGIC DESCRIPTION
QUATERNARY
NN 19
B
0.5
1
1.0
CC

PUMICEOUS PEBBLY VITRIC SAND and VITRIC SAND

Major lithology: Olive gray (5Y 4/1) to light olive gray [illegible] PUMICEOUS PEBBLY VITRIC SAND [illegible] VITRIC SAND [illegible]

[illegible]

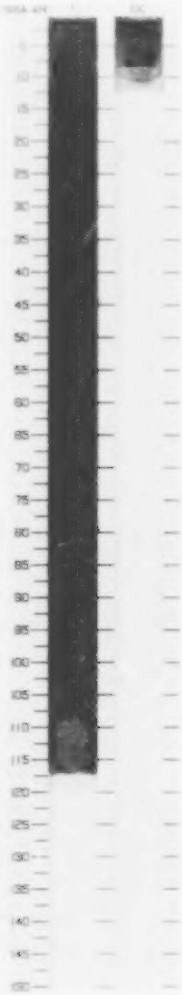
788A 4R
1
CC
5
10
15
20
25
30
35
40
45
50
55
60
65
70
75
80
85
90
95
100
105
110
115
120
125
130
135
140
145
150

126 788A 5R NO RECOVERY

126 788B 1R NO RECOVERY

126 788B 2R NO RECOVERY

126 788B 3R NO RECOVERY

126 788B 4R NO RECOVERY

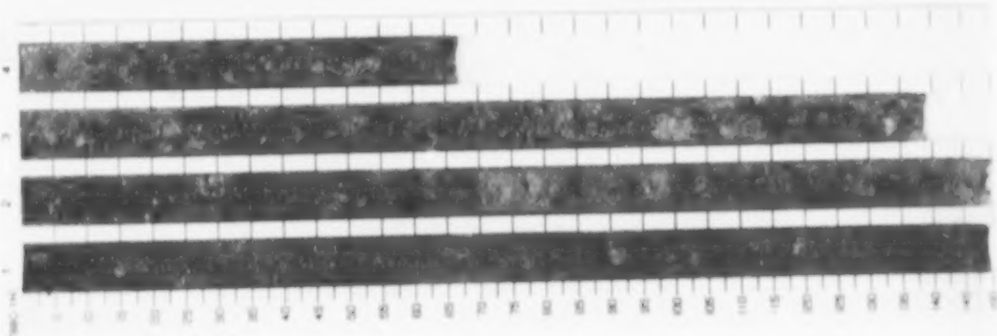
CORE 1H
1
2
3
4
cm

SITE 788 HOLE C CORE 1H CORED INTERVAL
BIOSTRAT. ZONE/ FOSSIL CHARACTER
GRAPHIC LITHOLOGY
LITHOLOGIC DESCRIPTION
QUATERNARY

GRAPHIC LITHOLOGY
LITHOLOGIC DESCRIPTION

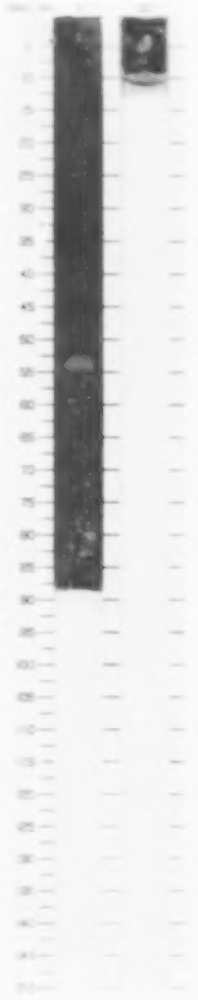
5
10
15
20
25
30
35
40
45
50
55
60
65
70
75
80
85
90
95
100
105
110
115
120
125
130
135
140
145
150

SITE 788 HOLE C CORE 3H CORED INTERVAL 20.2-29.7 mbsf

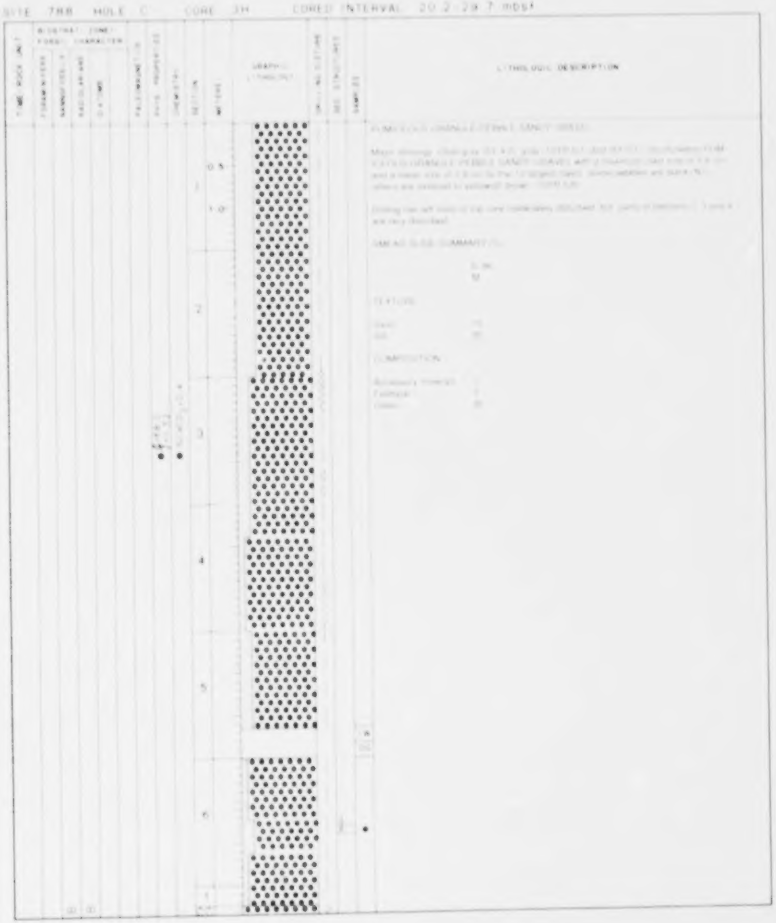
TIME-ROCK UNIT
BIOSTRAT. ZONE/FOSSIL CHARACTER
FORAMINIFERS
NANNOFOSSILS
RADIOLARIANS
DIATOMS
PALEOMAGNETICS
PHYS. PROPERTIES
CHEMISTRY
SECTION
METERS
GRAPHIC LITHOLOGY
DRILLING DISTURB.
SED. STRUCTURES
SAMPLES
0.5
1.0
1
2
3
4
5
6
7
CC

LITHOLOGIC DESCRIPTION

PUMICEOUS GRANULE-PEBBLE SANDY GRAVEL

Major lithology: [illegible] ... PUMICEOUS GRANULE-PEBBLE SANDY GRAVEL with [illegible] and a mean size of [illegible] ... [illegible] yellowish brown [illegible]

Drilling has left much of the core [illegible] ... [illegible] are very disturbed.

SMEAR SLIDE SUMMARY (%):

3, 96
M

TEXTURE:

Sand
Silt

COMPOSITION:

Accessory minerals
Feldspar
Glass

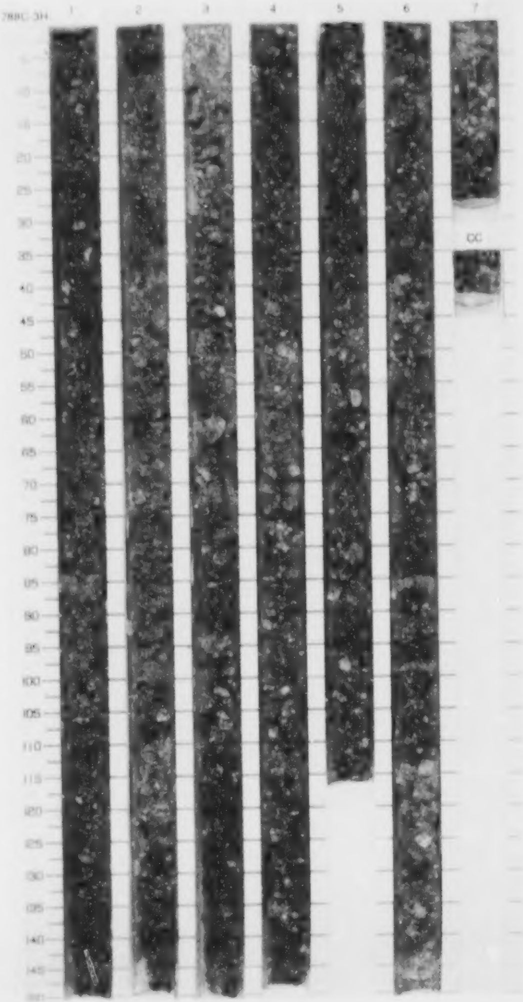
788C-3H
1
2
3
4
5
6
7
CC
5
10
15
20
25
30
35
40
45
50
55
60
65
70
75
80
85
90
95
100
105
110
115
120
125
130
135
140
145
150

SITE 788 HOLE C CORE 4R CORED INTERVAL 29.7-39.2 mbsf

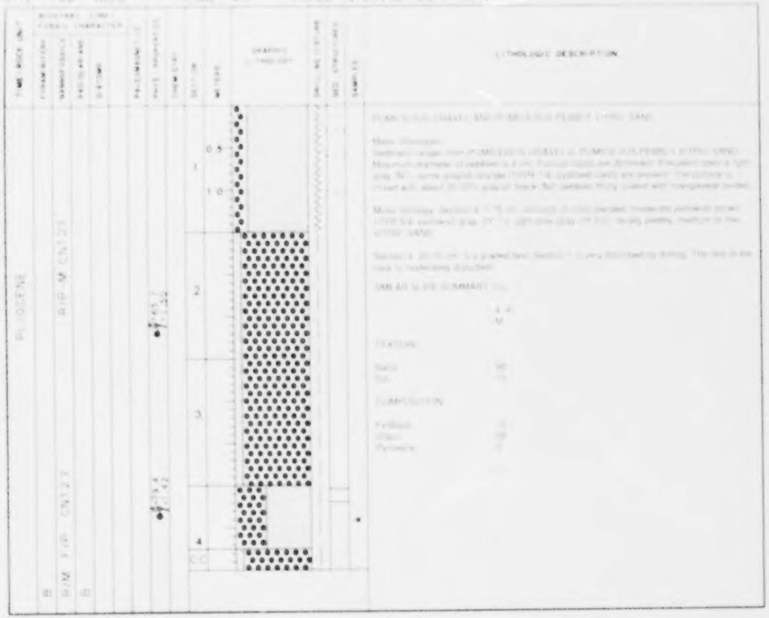
TIME-ROCK UNIT
BIOSTRAT. ZONE/FOSSIL CHARACTER
FORAMINIFERS
NANNOFOSSILS
RADIOLARIANS
DIATOMS
PALEOMAGNETICS
PHYS. PROPERTIES
CHEMISTRY
SECTION
METERS
GRAPHIC LITHOLOGY
DRILLING DISTURB.
SED. STRUCTURES
SAMPLES
PLIOCENE
B
R/M F/P CN12?
R/P-M CN12?
B
0.5
1.0
1
2
3
4
CC

LITHOLOGIC DESCRIPTION

PUMICEOUS GRAVEL AND PUMICEOUS PEBBLY VITRIC SAND

Major lithologies:
Sediment ranges from PUMICEOUS GRAVEL to PUMICEOUS PEBBLY VITRIC SAND. Maximum diameter of pebbles is 4 cm. Pumice clasts are dominant; [illegible] light gray (N7); some grayish orange (10YR 7/4) [illegible] are present. The pumice is mixed with about 20-30% [illegible] black [illegible] pebbles [illegible] with manganese [illegible].

Minor lithology: Section 4, 7-75 cm, consists of [illegible] bedded moderate yellowish brown (10YR 5/4) [illegible] gray (5Y 7/2) [illegible] gray (5Y 6/1) [illegible] pebbly [illegible] VITRIC SAND.

Section 4, 20-75 cm, is a graded bed. Section 1 is very disturbed by drilling. The rest of the core is moderately disturbed.

SMEAR SLIDE SUMMARY (%):

	4, 41
	M
TEXTURE:	
Sand	90
Silt	10
COMPOSITION:	
Feldspar	[illegible]
Glass	[illegible]
Pyroxene	[illegible]

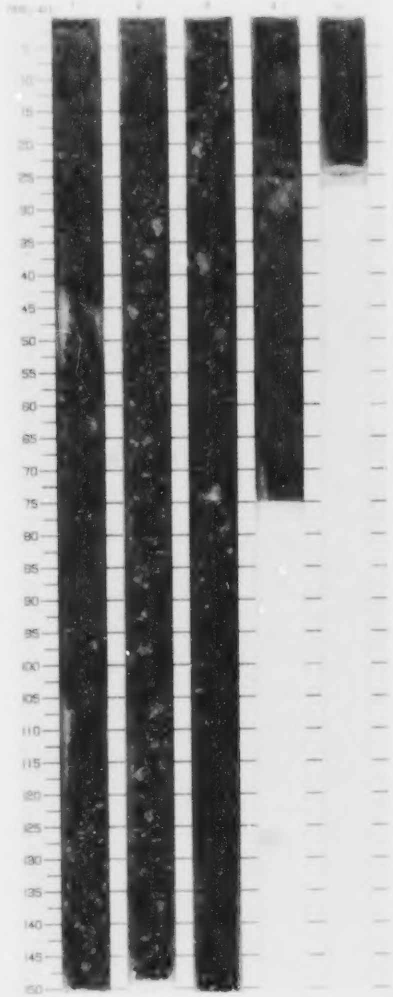
788C-4R
1
2
3
4
5
0
5
10
15
20
25
30
35
40
45
50
55
60
65
70
75
80
85
90
95
100
105
110
115
120
125
130
135
140
145
150

SITE 788 HOLE C CORE 5H CORED INTERVAL 39.2-48.7 mbsf

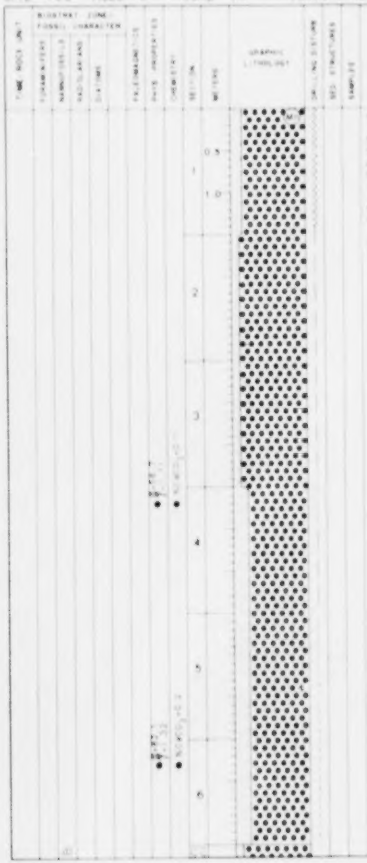
BIOSTRAT. ZONE/FOSSIL CHARACTER
GRAPHIC LITHOLOGY
0.5
1.0
1
2
3
4
5
6

LITHOLOGIC DESCRIPTION

PUMICEOUS SANDY GRAVEL

Major lithology: Light olive gray (5Y 6/2) poorly sorted, structureless PUMICEOUS SANDY GRAVEL. Maximum pebble size is 3.5 cm; mean size of the largest 10 pebbles is 2.5 cm. Some clasts have been oxidized to pale olive (10Y 6/2), grayish black (N2) and dusky yellow (5Y 6/4) colors; others have grayish black (N2) with thin coats of manganese oxides.

Minor lithology: Section 4, [illegible] consists of very thin beds of fine light olive gray (5Y 6/2) [illegible].

Section 1 is very disturbed by drilling. Sections 2 and 3 are moderately disturbed, and the rest of the core is only slightly disturbed.

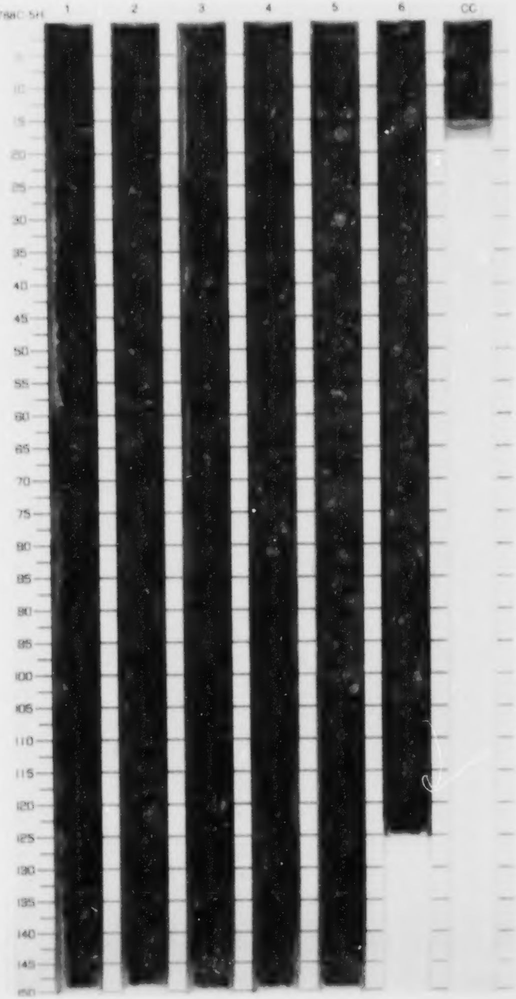
788C 5H
1
2
3
4
5
6
CC
5
10
15
20
25
30
35
40
45
50
55
60
65
70
75
80
85
90
95
100
105
110
115
120
125
130
135
140
145
150

SITE 788 HOLE C CORE 6H CORED INTERVAL 48.7-58.2 mbsf

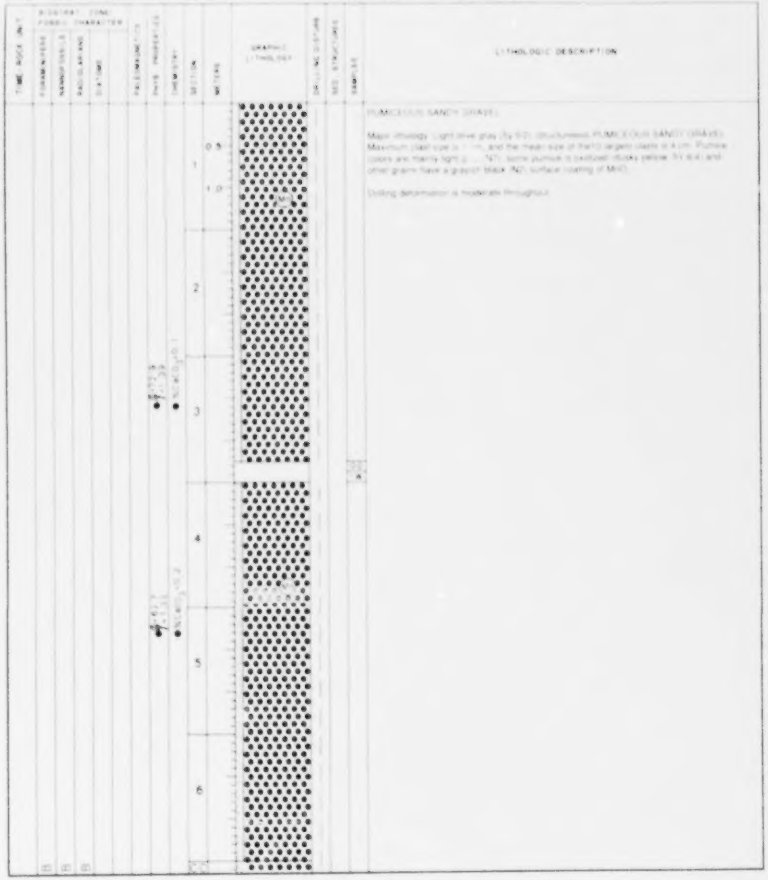
TIME-ROCK UNIT
BIOSTRAT. ZONE/FOSSIL CHARACTER
FORAMINIFERS
NANNOFOSSILS
RADIOLARIANS
DIATOMS
PALEOMAGNETICS
PHYS. PROPERTIES
CHEMISTRY
SECTION
METERS
GRAPHIC LITHOLOGY
DRILLING DISTURB.
SED. STRUCTURES
SAMPLES
LITHOLOGIC DESCRIPTION
0.5
1.0
1
2
3
4
5
6
●%CaCO3=0.1
●%CaCO3=0.2

PUMICEOUS SANDY GRAVEL

Major lithology: Light olive gray (5Y 6/2) structureless PUMICEOUS SANDY GRAVEL. Maximum clast size is [illegible], and the mean size of the 10 largest clasts is 4 cm. Pumice colors are mainly light g[illegible] (N7); some pumice is oxidized (dusky yellow, 5Y 6/4) and other grains have a grayish black (N2) surface coating of MnO.

Drilling deformation is moderate throughout.

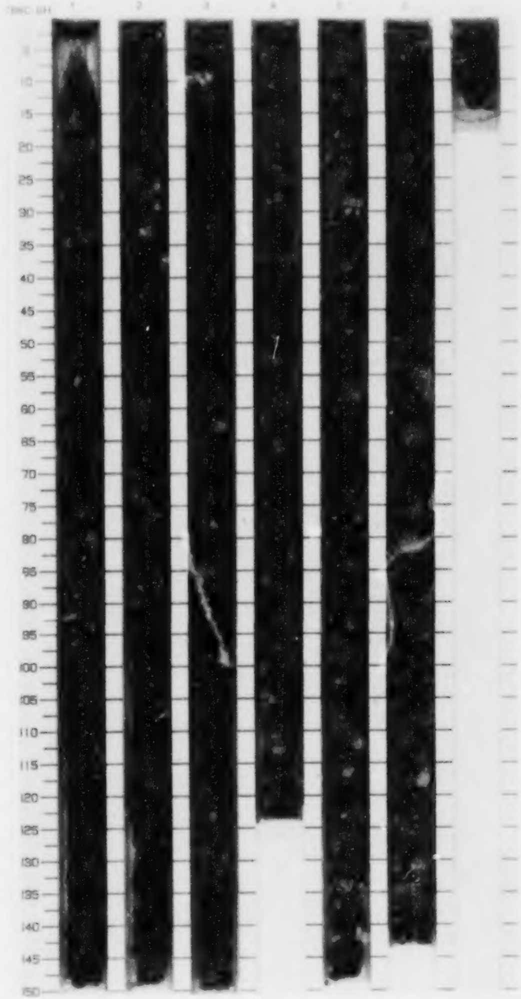
CM
1
2
3
4
5
6
5
10
15
20
25
30
35
40
45
50
55
60
65
70
75
80
85
90
95
100
105
110
115
120
125
130
135
140
145
150

SITE 788 HOLE C CORE 7H CORED INTERVAL 58.2-67.7 mbsf

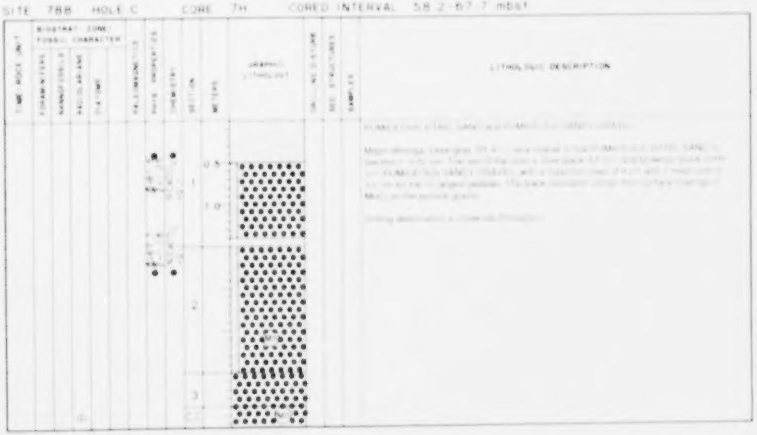
TIME-ROCK UNIT
BIOSTRAT. ZONE/ FOSSIL CHARACTER
FORAMINIFERS
NANNOFOSSILS
RADIOLARIANS
DIATOMS
PALEOMAGNETICS
PHYS. PROPERTIES
CHEMISTRY
SECTION
METERS
GRAPHIC LITHOLOGY
DRILLING DISTURB.
SED. STRUCTURES
SAMPLES
LITHOLOGIC DESCRIPTION
0.5
1.0
1
2
3
CC

SITE 788 HOLE C CORE 8H CORED INTERVAL 67.7-77.2 mbsf

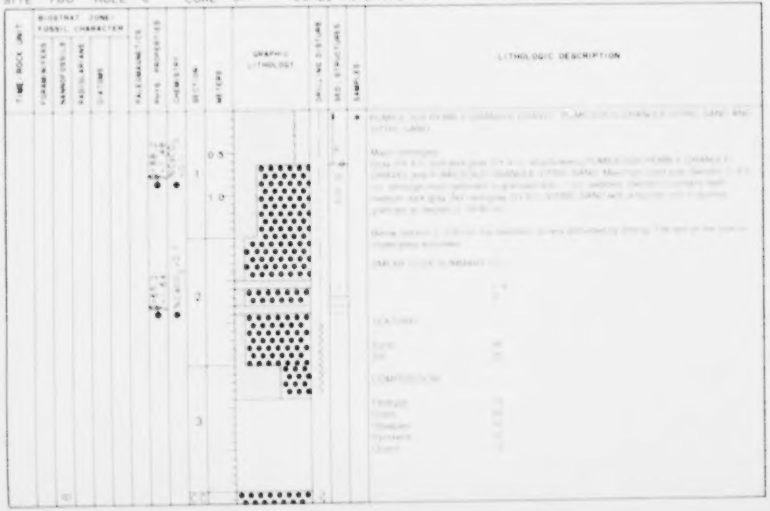
TIME-ROCK UNIT
BIOSTRAT. ZONE/ FOSSIL CHARACTER
FORAMINIFERS
NANNOFOSSILS
RADIOLARIANS
DIATOMS
PALEOMAGNETICS
PHYS. PROPERTIES
CHEMISTRY
SECTION
METERS
GRAPHIC LITHOLOGY
DRILLING DISTURB.
SED. STRUCTURES
SAMPLES
LITHOLOGIC DESCRIPTION
0.5
1.0
1
2
3
CC

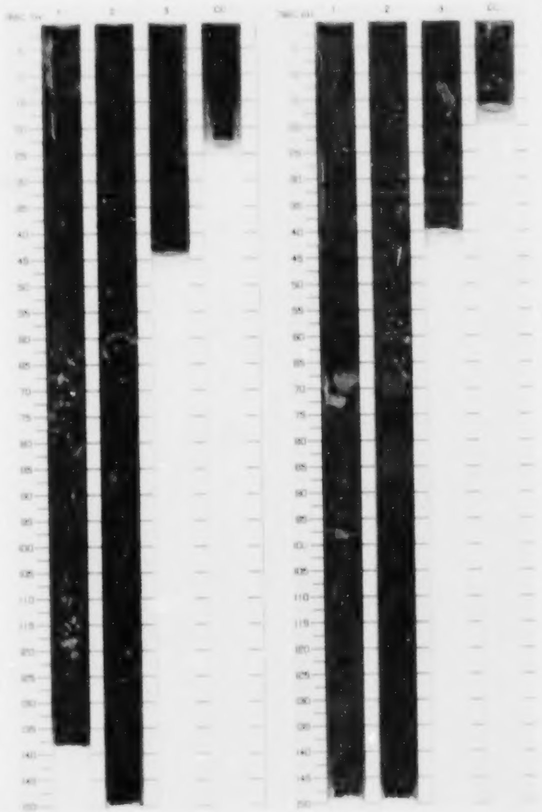
1
2
3
CC
1
2
3
CC

SITE 788 HOLE C CORE 9H CORED INTERVAL 77.2-86.7 mbsf

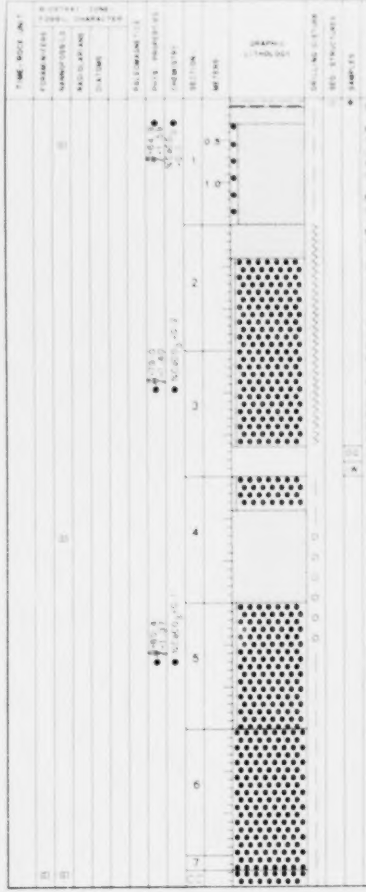
TIME-ROCK UNIT
BIOSTRAT. ZONE/FOSSIL CHARACTER
FORAMINIFERS
NANNOFOSSILS
RADIOLARIANS
DIATOMS
PALEOMAGNETICS
PHYS. PROPERTIES
CHEMISTRY
SECTION
METERS
GRAPHIC LITHOLOGY
DRILLING DISTURB.
SED. STRUCTURES
SAMPLES
0.5
1.0
1
2
3
4
5
6
7
CC
IW
*

LITHOLOGIC DESCRIPTION

PUMICEOUS SANDY GRAVEL, PUMICEOUS PEBBLY SAND AND VITRIC SAND

Major lithologies:
This core consists of an alternation of the following lithologies: PUMICEOUS SANDY GRAVEL, PUMICEOUS PEBBLY SAND and VITRIC SAND. Colors are light olive gray (5Y 6/2), dark gray (5Y 4/1) and brownish black (5YR 2/1). Maximum clast size is 4.5 cm and the mean size of the 10 largest clasts is 4 cm.

Minor lithology: Section 1, 0-13 cm, contains two 4-cm diameter clasts of consolidated olive gray (5Y 5/2), laminated CLAYEY VITRIC SILTSTONE.

Most sediment from the top of Section 1 to Section 5, 50 cm, is strongly disturbed to soupy. The rest of the core is moderately disturbed by drilling.

SMEAR SLIDE SUMMARY (%):

	1, 4
	M
TEXTURE:	
Silt	60
Clay	40
COMPOSITION:	
Clay	35
Feldspar	5
Glass	60
Quartz	1

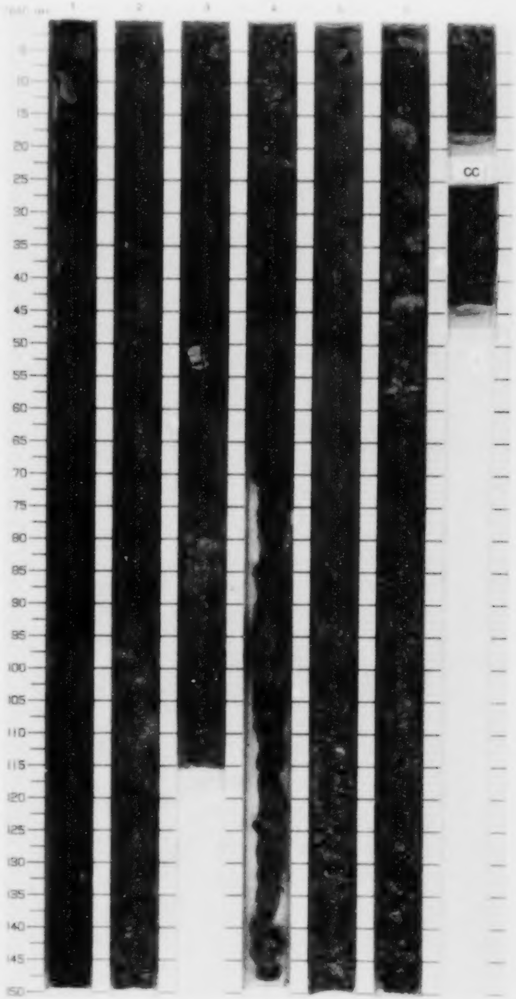
CM
1
2
3
4
5
6
CC
0
5
10
15
20
25
30
35
40
45
50
55
60
65
70
75
80
85
90
95
100
105
110
115
120
125
130
135
140
145
150

SITE 788 HOLE C CORE 10H CORED INTERVAL 86.7-96.2 mbsf

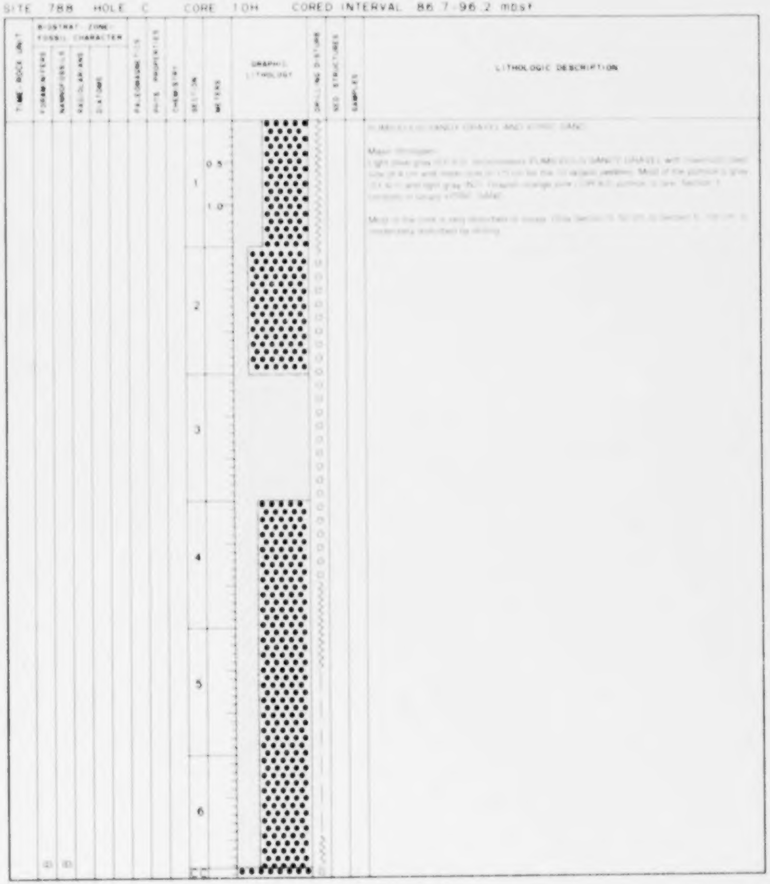
TIME-ROCK UNIT
BIOSTRAT. ZONE/FOSSIL CHARACTER
FORAMINIFERS
NANNOFOSSILS
RADIOLARIANS
DIATOMS
PALEOMAGNETICS
PHYS. PROPERTIES
CHEMISTRY
SECTION
METERS
GRAPHIC LITHOLOGY
DRILLING DISTURB.
SED. STRUCTURES
SAMPLES
LITHOLOGIC DESCRIPTION
0.5
1.0
1
2
3
4
5
6
CC

PUMICEOUS SANDY GRAVEL AND VITRIC SAND

Major lithologies:
Light olive gray (5Y 6/1), unconsolidated PUMICEOUS SANDY GRAVEL with maximum clast size of 4 cm and mean size of 1.5 cm for the 10 largest pebbles. Most of the pumice is gray (5Y 6/1) and light gray (N7). Grayish orange pink (10R 8/2) pumice is rare. Section 1 consists of largely VITRIC SAND.

Most of the core is very disturbed or soupy. [illegible] moderately disturbed by drilling.

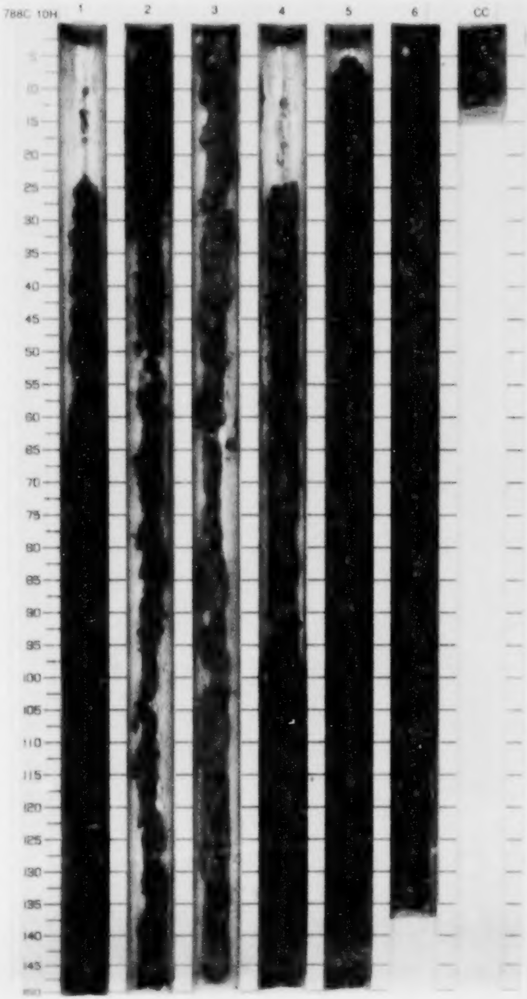
788C 10H
1
2
3
4
5
6
CC
5
10
15
20
25
30
35
40
45
50
55
60
65
70
75
80
85
90
95
100
105
110
115
120
125
130
135
140
145
150

SITE 788 HOLE C CORE 11H CORED INTERVAL 98.2-105.7 mbsf

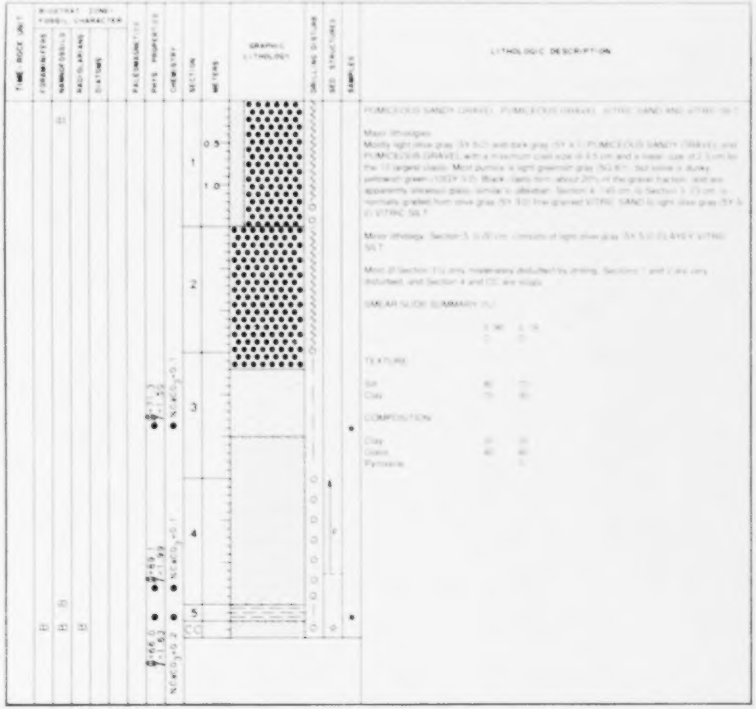
TIME-ROCK UNIT
BIOSTRAT. ZONE/FOSSIL CHARACTER
FORAMINIFERS
NANNOFOSSILS
RADIOLARIANS
DIATOMS
PALEOMAGNETICS
PHYS. PROPERTIES
CHEMISTRY
SECTION
METERS
GRAPHIC LITHOLOGY
DRILLING DISTURB.
SED. STRUCTURES
SAMPLES
B
B
B
B
B
ϕ=71.3
γ=1.55
ϕ=69.1
γ=1.59
ϕ=66.0
γ=1.62
%CaCO3=0.1
%CaCO3=0.1
%CaCO3=0.2
1
2
3
4
5
CC
0.5
1.0

LITHOLOGIC DESCRIPTION

PUMICEOUS SANDY GRAVEL, PUMICEOUS GRAVEL, VITRIC SAND AND VITRIC SILT

Major lithologies:
Mostly light olive gray (5Y 6/2) and dark gray (5Y 4/1) PUMICEOUS SANDY GRAVEL and PUMICEOUS GRAVEL, with a maximum clast size of 4.5 cm and a mean size of 2.5 cm for the 10 largest clasts. Most pumice is light greenish gray (5G 8/1), but some is dusky yellowish green (10GY 3/2). Black clasts form about 20% of the gravel fraction, and are apparently obsidian glass, similar to obsidian. Section 4, 140 cm, to Section 5, 23 cm, is normally graded from olive gray (5Y 3/2) fine-grained VITRIC SAND to light olive gray (5Y 5/2) VITRIC SILT.

Minor lithology: Section 5, 0-20 cm, consists of light olive gray (5Y 5/2) CLAYEY VITRIC SILT.

Most of Section 3 is only moderately disturbed by drilling. Sections 1 and 2 are very disturbed, and Section 4 and CC are soupy.

SMEAR SLIDE SUMMARY (%):

	3, 90	5, 19
	D	M
TEXTURE:		
Silt	80	70
Clay	20	30
COMPOSITION:		
Clay	20	20
Glass	80	80
Pyroxene	—	Tr

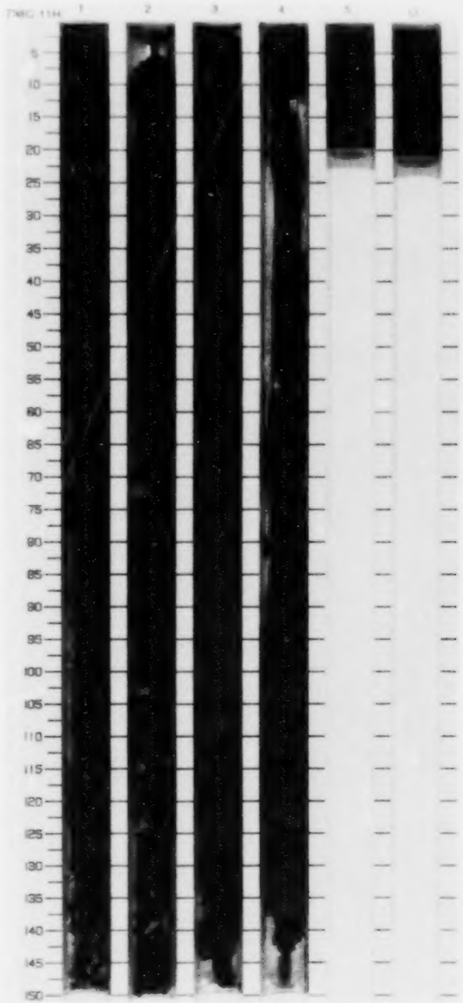
788C 11H
1
2
3
4
5
CC
5
10
15
20
25
30
35
40
45
50
55
60
65
70
75
80
85
90
95
100
105
110
115
120
125
130
135
140
145
150

SITE 788 HOLE C CORE 12H CORED INTERVAL 105.7-115.2 mbsf

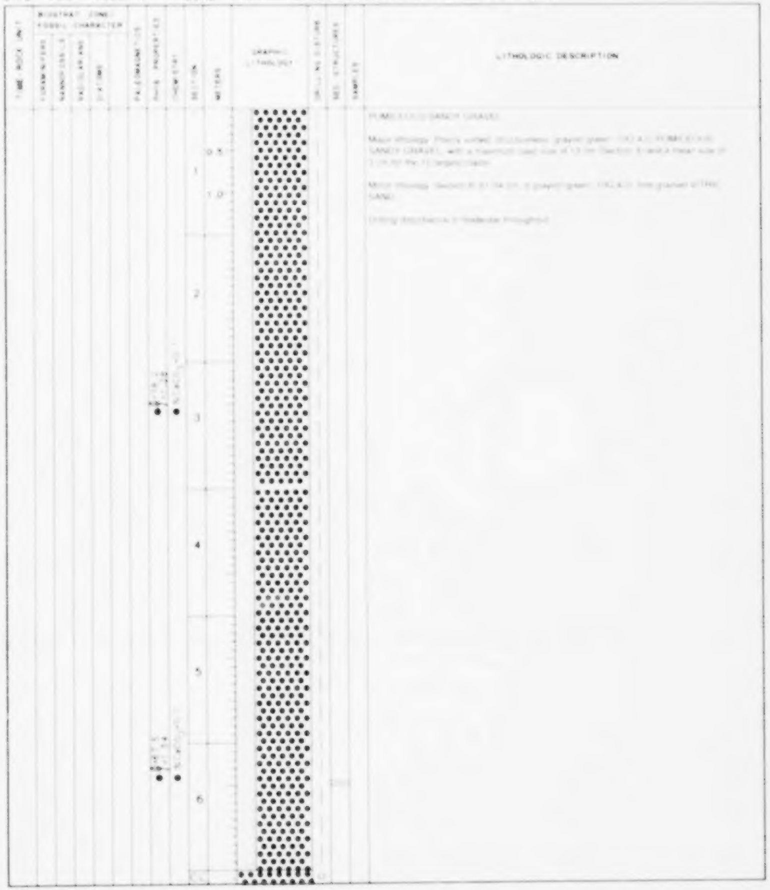

LITHOLOGIC DESCRIPTION

PUMICEOUS SANDY GRAVEL

Major lithology: Poorly sorted, structureless, grayish green (10G 4/2) PUMICEOUS SANDY GRAVEL, with a maximum clast size of 13 cm (Section 3) and a mean size of 3 cm for the 10 largest clasts.

Minor lithology: Section 6, 0–34 cm, is grayish green (10G 4/2) fine-grained VITRIC SAND.

Drilling disturbance is moderate throughout.

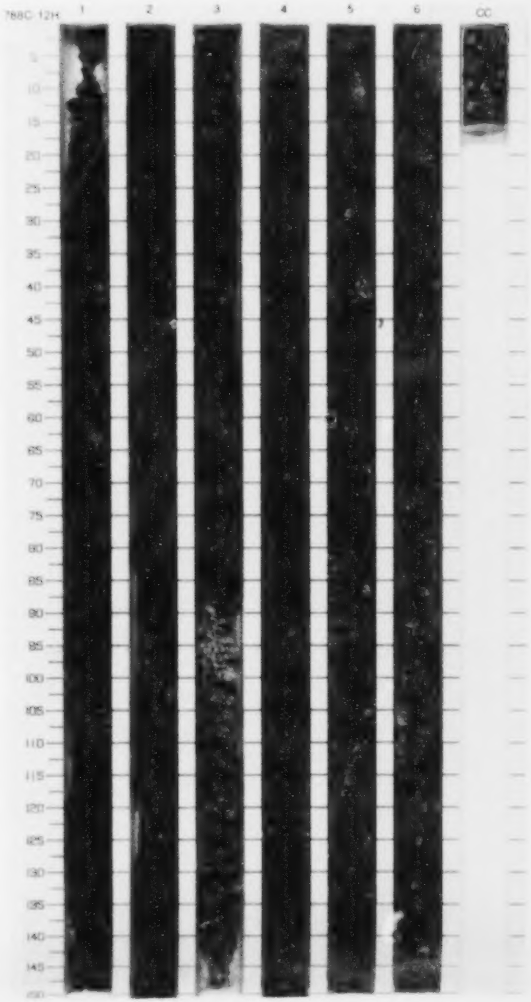
788C-12H
1
2
3
4
5
6
CC
5
10
15
20
25
30
35
40
45
50
55
60
65
70
75
80
85
90
95
100
105
110
115
120
125
130
135
140
145
150

SITE 788 HOLE C CORE 13H CORED INTERVAL 115.2-124.7 mbsf

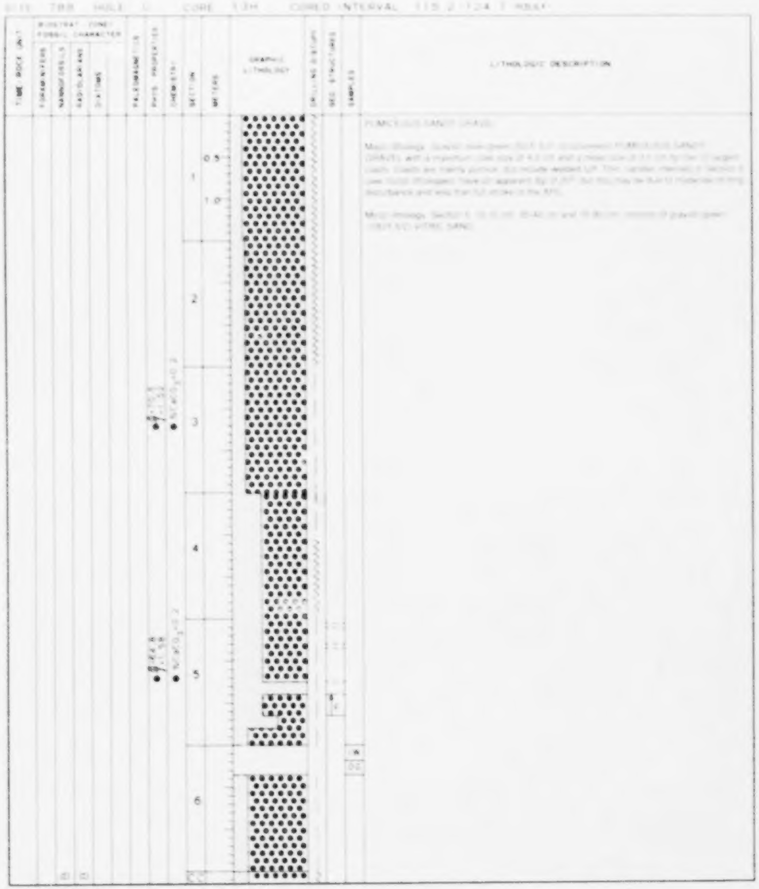
TIME-ROCK UNIT
BIOSTRAT. ZONE/ FOSSIL CHARACTER
FORAMINIFERS
NANNOFOSSILS
RADIOLARIANS
DIATOMS
PALEOMAGNETICS
PHYS. PROPERTIES
CHEMISTRY
SECTION
METERS
GRAPHIC LITHOLOGY
DRILLING DISTURB.
SED. STRUCTURES
SAMPLES
0.5
1
1.0
2
3
4
5
6

LITHOLOGIC DESCRIPTION

PUMICEOUS SANDY GRAVEL

Major lithology: [illegible] PUMICEOUS SANDY GRAVEL, with a maximum clast size of [illegible] and a mean size of [illegible] for the 10 largest clasts. Clasts are mainly pumice, [illegible]

Minor lithology: Section 5, [illegible] VITRIC SAND.

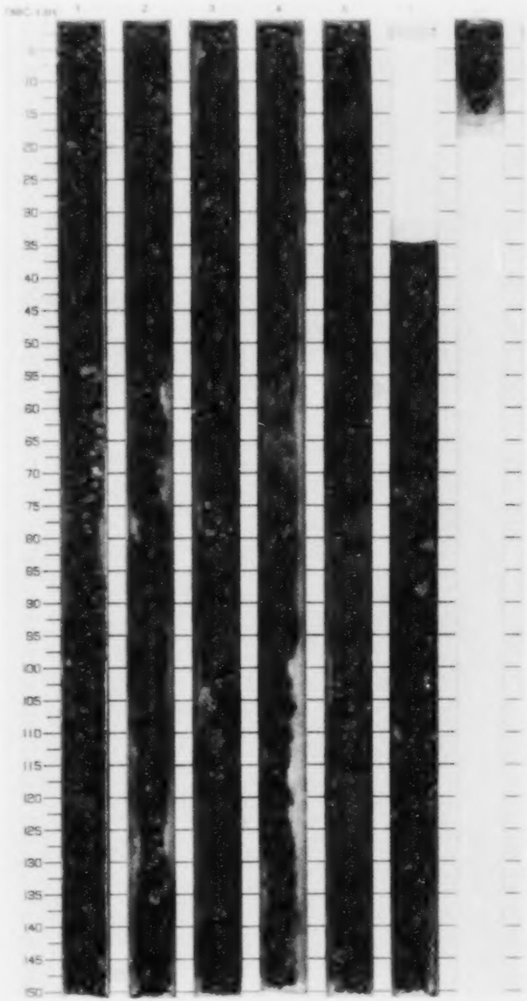
(MC-13H)
1
2
3
4
5
6
7
0
10
15
20
25
30
35
40
45
50
55
60
65
70
75
80
85
90
95
100
105
110
115
120
125
130
135
140
145
150

SITE 788 HOLE C CORE 14H CORED INTERVAL 124.7-134.2 mbsf

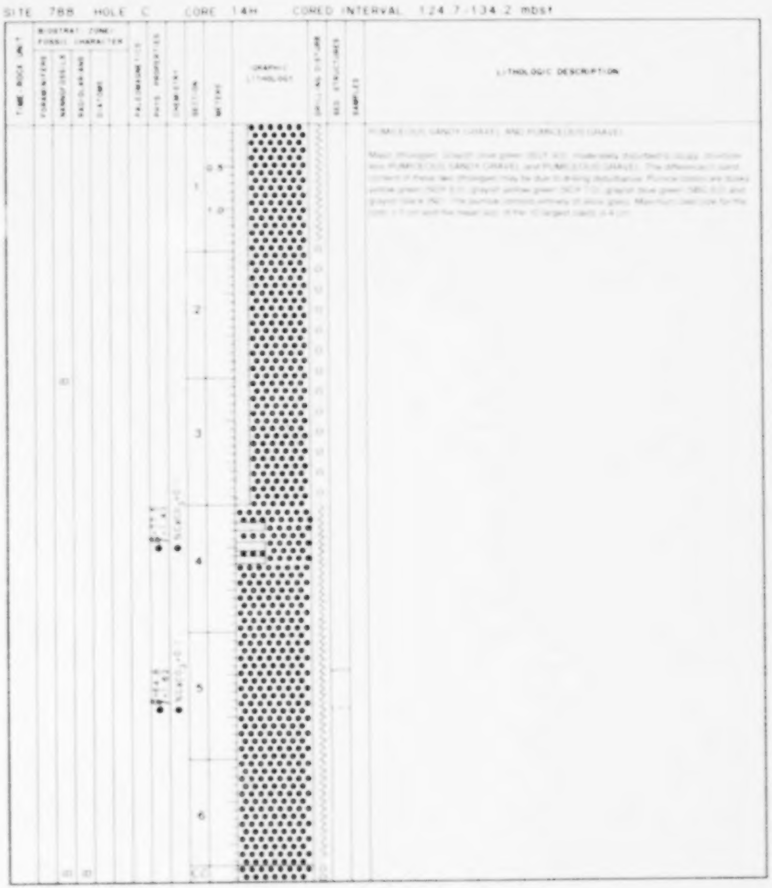
TIME-ROCK UNIT
BIOSTRAT. ZONE/ FOSSIL CHARACTER
FORAMINIFERS
NANNOFOSSILS
RADIOLARIANS
DIATOMS
PALEOMAGNETICS
PHYS. PROPERTIES
CHEMISTRY
SECTION
METERS
GRAPHIC LITHOLOGY
DRILLING DISTURB.
SED. STRUCTURES
SAMPLES
0.5
1.0
1
2
3
4
5
6
CC

LITHOLOGIC DESCRIPTION

PUMICEOUS SANDY GRAVEL AND PUMICEOUS GRAVEL

Major lithologies: Grayish blue green ([illegible]), moderately disturbed to soupy, structureless PUMICEOUS SANDY GRAVEL and PUMICEOUS GRAVEL. The difference in sand content of these two lithologies may be due to drilling disturbance. Pumice clasts are dusky yellow green ([illegible]), grayish yellow green ([illegible]), grayish blue green ([illegible]) and grayish black (N2). The pumice consists entirely of silicic glass. Maximum clast size for the core: [illegible] cm and the mean size of the 10 largest clasts is 4 cm.

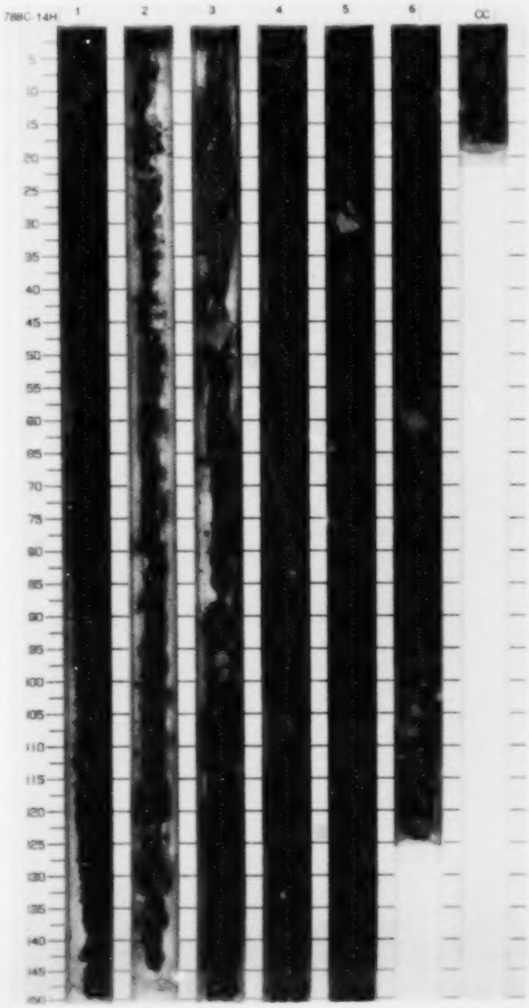
788C-14H
1
2
3
4
5
6
CC
5
10
15
20
25
30
35
40
45
50
55
60
65
70
75
80
85
90
95
100
105
110
115
120
125
130
135
140
145
150

SITE 788 HOLE C CORE 15H CORED INTERVAL 134.2-143.7 mbsf

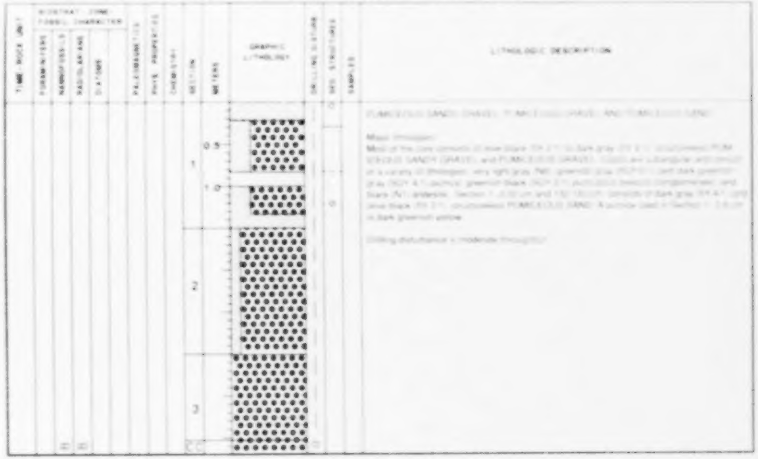
TIME-ROCK UNIT
BIOSTRAT. ZONE/ FOSSIL CHARACTER
FORAMINIFERS
NANNOFOSSILS
RADIOLARIANS
DIATOMS
PALEOMAGNETICS
PHYS. PROPERTIES
CHEMISTRY
SECTION
METERS
GRAPHIC LITHOLOGY
DRILLING DISTURB.
SED. STRUCTURES
SAMPLES
LITHOLOGIC DESCRIPTION
0.5
1.0
1
2
3
CC

PUMICEOUS SANDY GRAVEL, PUMICEOUS GRAVEL, AND PUMICEOUS SAND

Major lithologies:
Most of the core consists of olive black (5Y 2/1) to dark gray (5Y 4/1) structureless PUMICEOUS SANDY GRAVEL and PUMICEOUS GRAVEL. Clasts are subangular and consist of a variety of lithologies: very light gray (N8) greenish gray (5GY 6/1) and dark greenish gray (5GY 4/1) pumice; greenish black (5GY 2/1) pumiceous breccia conglomerate; and black (N1) andesite. Section 1, [illegible] cm and [illegible] cm, consists of dark gray (5Y 4/1) to olive black (5Y 2/1), structureless PUMICEOUS SAND. A pumice clast in Section 1, [illegible] cm is dark greenish yellow.

Drilling disturbance is moderate throughout.

SITE 788 HOLE C CORE 16H CORED INTERVAL 143.7-153.2 mbsf

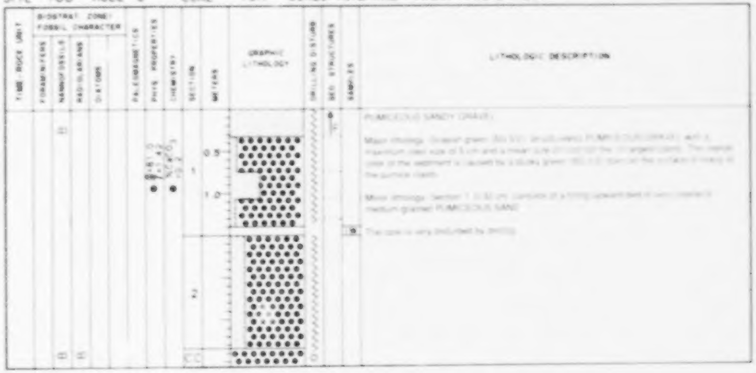
TIME-ROCK UNIT
BIOSTRAT. ZONE/ FOSSIL CHARACTER
FORAMINIFERS
NANNOFOSSILS
RADIOLARIANS
DIATOMS
PALEOMAGNETICS
PHYS. PROPERTIES
CHEMISTRY
SECTION
METERS
GRAPHIC LITHOLOGY
DRILLING DISTURB.
SED. STRUCTURES
SAMPLES
LITHOLOGIC DESCRIPTION
0.5
1.0
1
2
CC

PUMICEOUS SANDY GRAVEL

Major lithology: Grayish green (5G 5/2) structureless PUMICEOUS GRAVEL with a maximum clast size of 5 cm and a mean size of [illegible] for the 10 largest clasts. The overall color of the sediment is caused by a dusky green (5G 3/2) stain on the surface of many of the pumice clasts.

Minor lithology: Section 1, [illegible] cm, consists of a fining-upward bed of very coarse to medium-grained PUMICEOUS SAND.

The core is very disturbed by drilling.

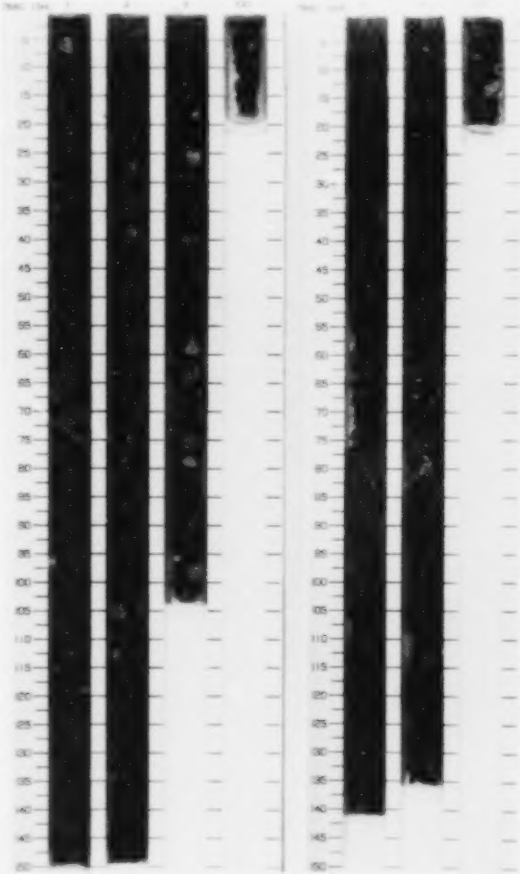
1
2
3
CC
0
5
10
15
20
25
30
35
40
45
50
55
60
65
70
75
80
85
90
95
100
105
110
115
120
125
130
135
140
145
150

SITE 788 HOLE C CORE 17H CORED INTERVAL 153.2-163.7 mbsf

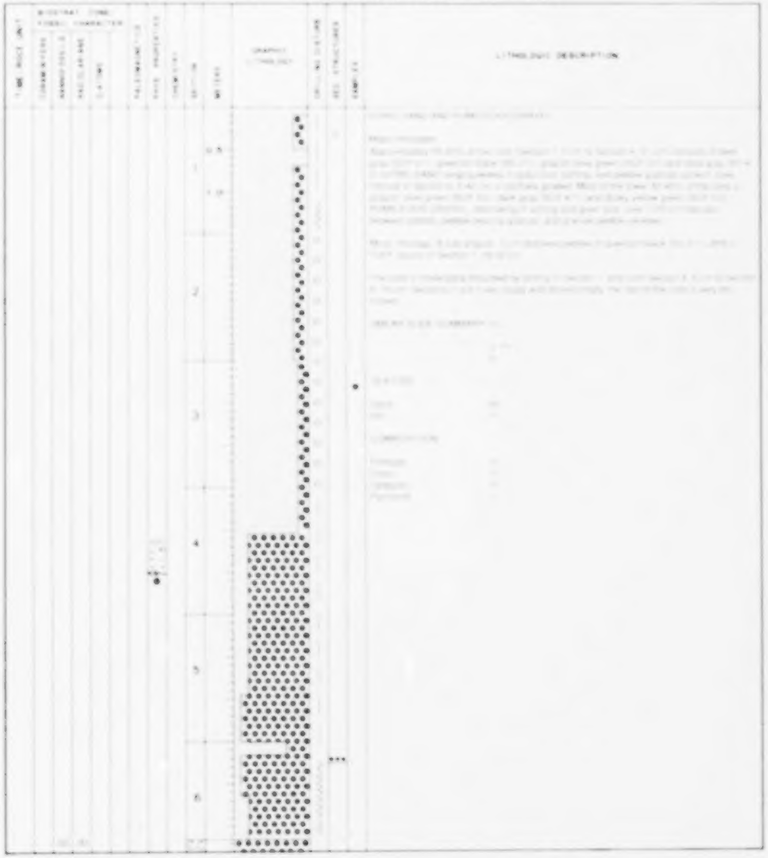
LITHOLOGIC DESCRIPTION
GRAPHIC LITHOLOGY
SECTION
METERS
1
2
3
4
5
6
CC

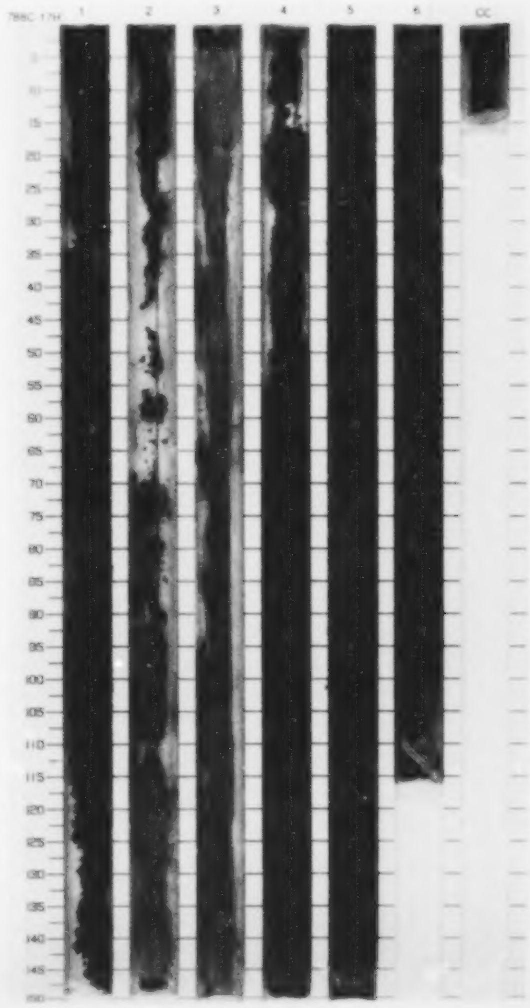
788C-17H
1
2
3
4
5
6
CC
0
5
10
15
20
25
30
35
40
45
50
55
60
65
70
75
80
85
90
95
100
105
110
115
120
125
130
135
140
145
150

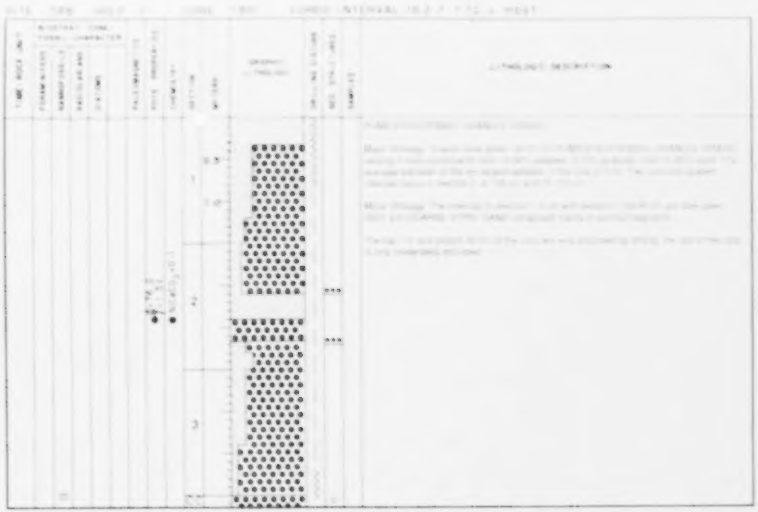
LITHOLOGIC DESCRIPTION
GRAPHIC LITHOLOGY
BIOSTRAT. ZONE/ FOSSIL CHARACTER
0.5
1.0
1
2
3
CC

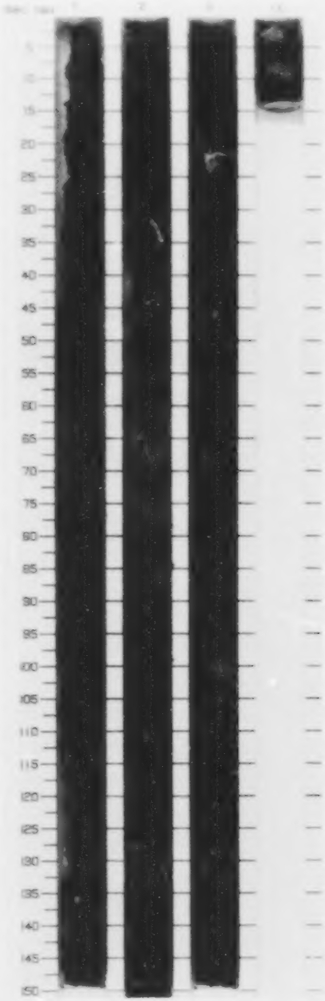
1
2
3
CC
5
10
15
20
25
30
35
40
45
50
55
60
65
70
75
80
85
90
95
100
105
110
115
120
125
130
135
140
145
150

SITE 788 HOLE C CORE 19H CORED INTERVAL 172.2-181.7 mbsf

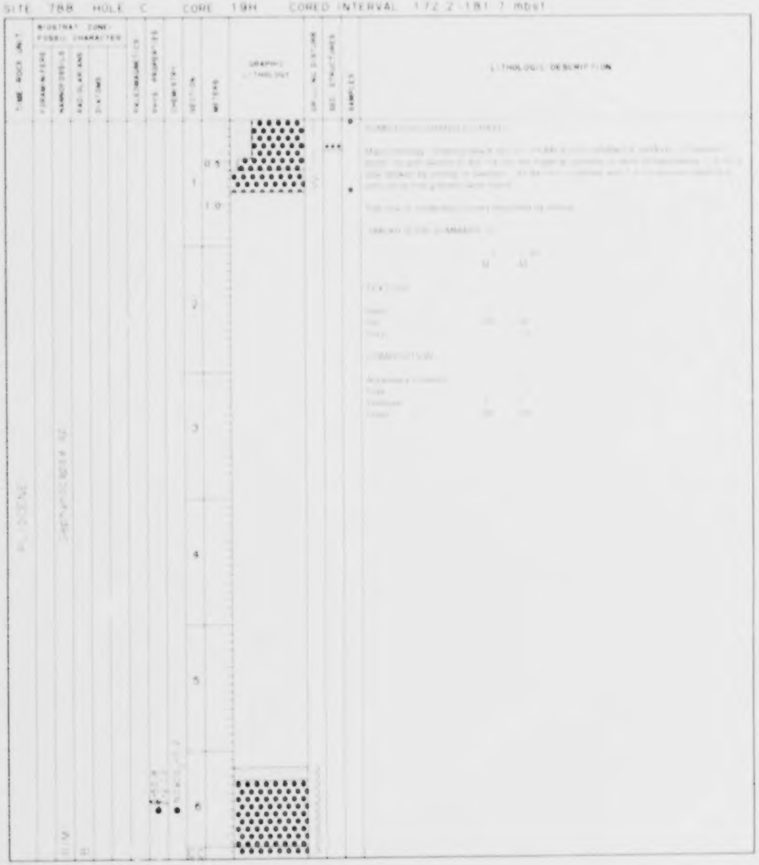
TIME-ROCK UNIT
BIOSTRAT. ZONE/ FOSSIL CHARACTER
FORAMINIFERS
NANNOFOSSILS
RADIOLARIANS
DIATOMS
PALEOMAGNETICS
PHYS. PROPERTIES
CHEMISTRY
SECTION
METERS
GRAPHIC LITHOLOGY
DRILLING DISTURB.
SED. STRUCTURES
SAMPLES
PLIOCENE
0.5
1.0
1
2
3
4
5
6
CC

LITHOLOGIC DESCRIPTION

[illegible]

[illegible]

[illegible]

SMEAR SLIDE SUMMARY (%):

TEXTURE:

Sand

Silt

Clay

COMPOSITION:

Accessory minerals

[illegible]

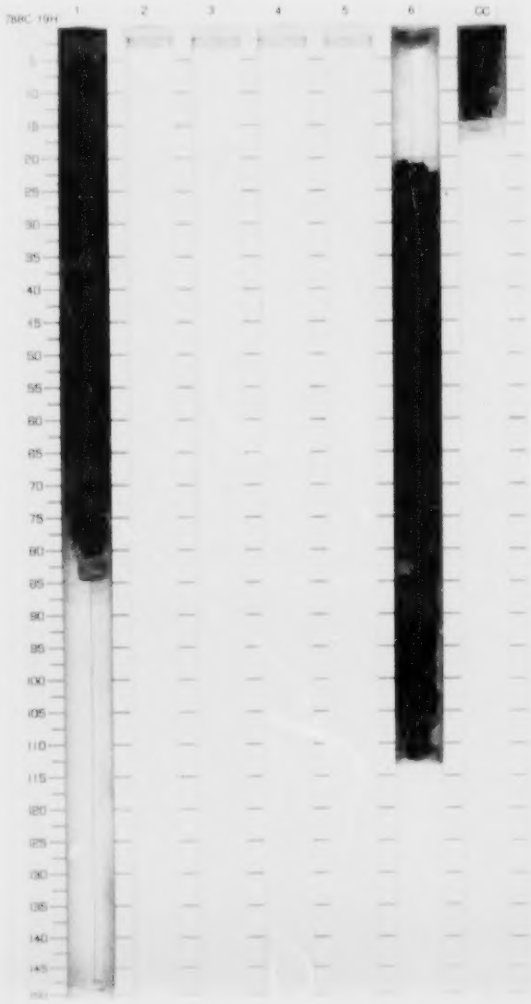
788C-19H
1
2
3
4
5
6
CC
5
10
15
20
25
30
35
40
45
50
55
60
65
70
75
80
85
90
95
100
105
110
115
120
125
130
135
140
145
150

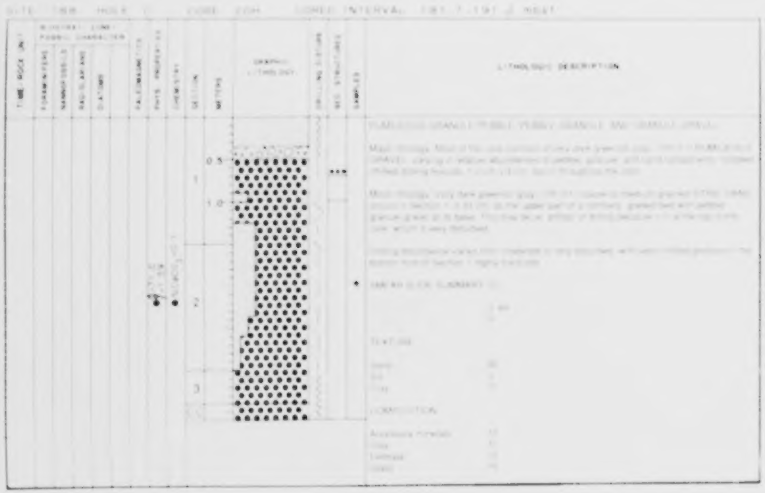

LITHOLOGIC DESCRIPTION

[illegible]

SMEAR SLIDE SUMMARY (%):

TEXTURE:

Sand
Silt
Clay

COMPOSITION:

Accessory minerals
Clay
Feldspar
Glass

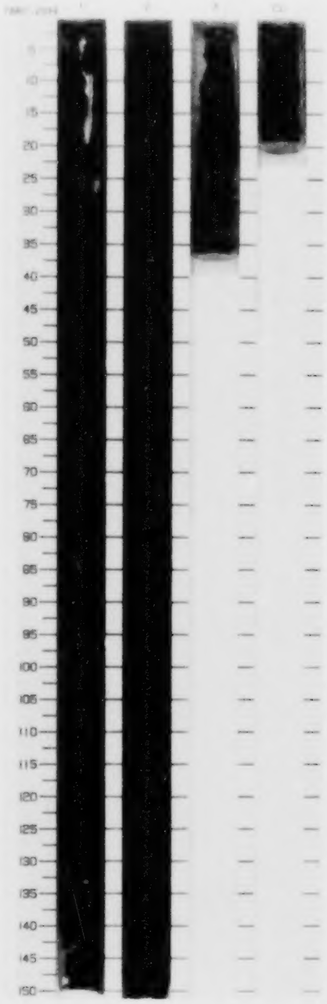
1
2
3
CC
5
10
15
20
25
30
35
40
45
50
55
60
65
70
75
80
85
90
95
100
105
110
115
120
125
130
135
140
145
150

SITE 788 HOLE C CORE 21H CORED INTERVAL 191.2-200.7 mbsf

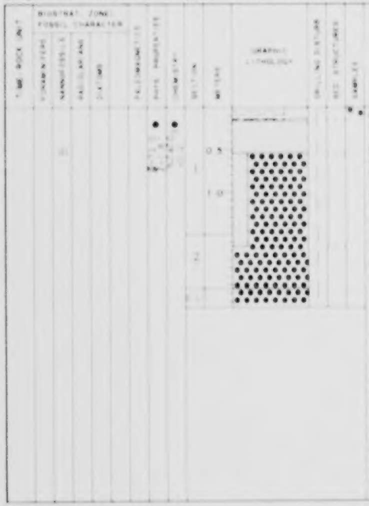

LITHOLOGIC DESCRIPTION

PUMICEOUS SANDY GRANULE GRAVEL AND PUMICEOUS GRANULE PEBBLE GRAVEL

Major lithologies: The bottom 80% of the core consists of very dark gray (5Y 3/1) PUMICEOUS GRANULE PEBBLE GRAVEL that grades upward into PUMICEOUS SANDY GRANULE GRAVEL and into the minor lithologies.

Minor lithologies:
The major lithologies continue grading upward into [illegible] cm of dark gray (5Y 4/1) very coarse to very fine grained VITRIC SAND and [illegible] cm of dark gray (5Y 4/1) CRYSTAL LITHIC VITRIC SILT. The top [illegible] cm of the core consists of two lithified very dark gray (5Y 3/1) CRYSTAL VITRIC SANDSTONE pebbles [illegible] cm in diameter.

Drilling disturbance is moderate.

SMEAR SLIDE SUMMARY (%):

	[illegible]	[illegible]
	M	M
TEXTURE:		
Sand	[illegible]	[illegible]
Silt	[illegible]	[illegible]
Clay	[illegible]	[illegible]
COMPOSITION:		
Accessory minerals	15	[illegible]
Clay	[illegible]	[illegible]
Feldspar	[illegible]	[illegible]
Glass	[illegible]	[illegible]
Rock fragments	[illegible]	

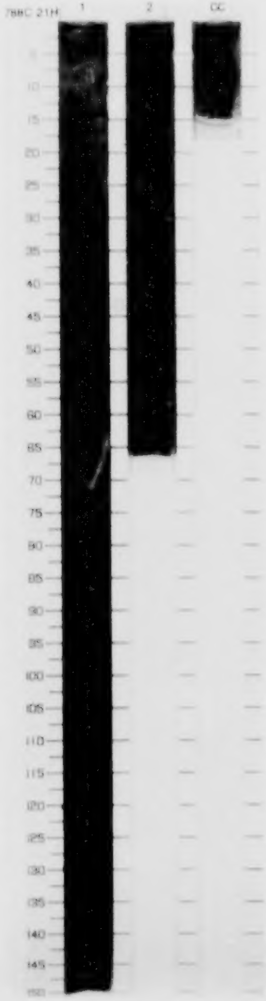
788C 21H
1
2
CC
5
10
15
20
25
30
35
40
45
50
55
60
65
70
75
80
85
90
95
100
105
110
115
120
125
130
135
140
145
150

SITE 788 HOLE C CORE 22H CORED INTERVAL 200.7-210.2 mbsf

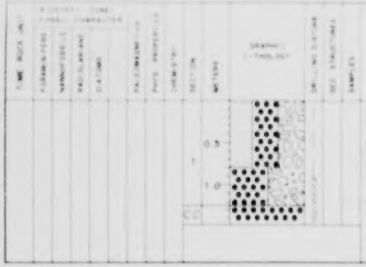
TIME-ROCK UNIT
BIOSTRAT. ZONE/FOSSIL CHARACTER
FORAMINIFERS
NANNOFOSSILS
RADIOLARIANS
DIATOMS
PALEOMAGNETICS
PHYS. PROPERTIES
CHEMISTRY
SECTION
METERS
GRAPHIC LITHOLOGY
DRILLING DISTURB.
SED. STRUCTURES
SAMPLES
1
0.5
1.0
CC

LITHOLOGIC DESCRIPTION

PUMICEOUS PEBBLE-GRANULE GRAVEL AND PUMICEOUS PEBBLE-GRANULE CONGLOMERATE

Major lithologies: Dark greenish gray (10Y 4/1) PUMICEOUS PEBBLE-GRANULE GRAVEL, partially lithified into PUMICEOUS PEBBLE-GRANULE CONGLOMERATE of the same color. Both lithologies consist of about 30% gray (5Y 6/1) pumice pebbles, 40% pumice granules, and 30% sand dominated by black volcanic lithic fragments.

Minor lithology: In Section 1, 0-30 cm, the underlying major lithology grades upwards into unconsolidated, fine-grained, dark gray (5GY 4/1) VITRIC SAND.

A larger percentage of the core may have been lithified, but has been disaggregated by drilling: moderate to very disturbed.

SITE 788 HOLE C CORE 23H CORED INTERVAL 210.2-219.7 mbsf

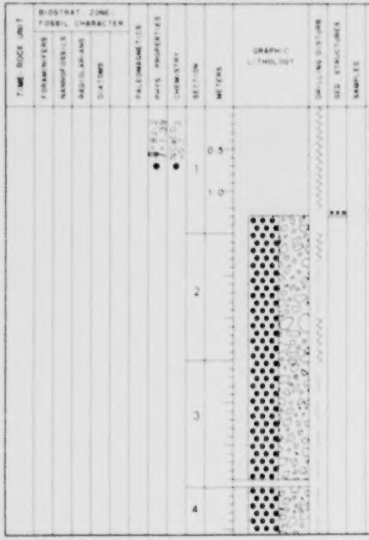
TIME-ROCK UNIT
BIOSTRAT. ZONE/FOSSIL CHARACTER
FORAMINIFERS
NANNOFOSSILS
RADIOLARIANS
DIATOMS
PALEOMAGNETICS
PHYS. PROPERTIES
CHEMISTRY
SECTION
METERS
GRAPHIC LITHOLOGY
DRILLING DISTURB.
SED. STRUCTURES
SAMPLES
1
2
3
4
0.5
1.0

LITHOLOGIC DESCRIPTION

CRYSTAL-VITRIC SAND, PUMICEOUS SANDY PEBBLE-GRANULE GRAVEL, AND PUMICEOUS SANDY PEBBLE-GRANULE CONGLOMERATE

Major lithologies:
The upper 25% of the core (Section 1, 0-130 cm) is dark gray (5GY 4/1) fine-grained CRYSTAL-VITRIC SAND. The rest of the core consists of dark greenish gray (10Y 4/1) PUMICEOUS SANDY PEBBLE-GRANULE GRAVEL and its consolidated equivalent, PUMICEOUS SANDY PEBBLE-GRANULE CONGLOMERATE. The largest lithified pieces are 4.5 x 5 cm, have pumice clasts about 1 cm in diameter, and fine- to coarse-grained sand and granules for matrix.

The relative proportions of the two major lithologies is uncertain, because the whole core has been moderately to very disturbed by drilling.

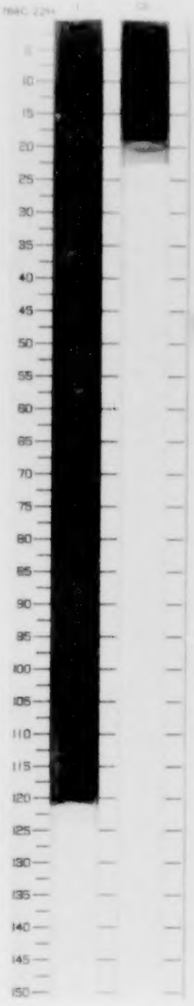
788C-22H
1
CC
5
10
15
20
25
30
35
40
45
50
55
60
65
70
75
80
85
90
95
100
105
110
115
120
125
130
135
140
145
150

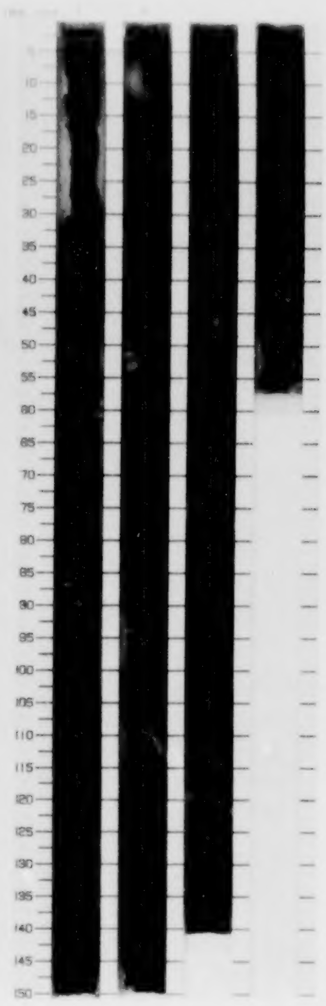
5
10
15
20
25
30
35
40
45
50
55
60
65
70
75
80
85
90
95
100
105
110
115
120
125
130
135
140
145
150

SITE 788 HOLE C CORE 24H CORED INTERVAL 219.7-229.2 mbsf

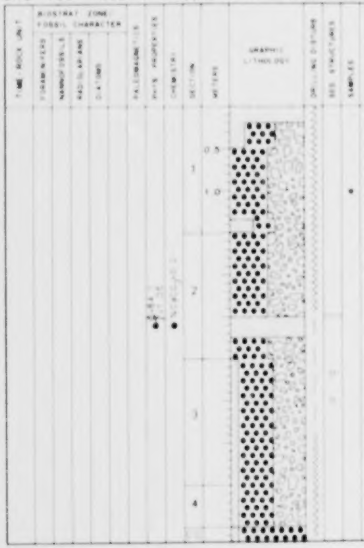
TIME-ROCK UNIT
BIOSTRAT. ZONE/FOSSIL CHARACTER
FORAMINIFERS
NANNOFOSSILS
RADIOLARIANS
DIATOMS
PALEOMAGNETICS
PHYS. PROPERTIES
CHEMISTRY
SECTION
METERS
GRAPHIC LITHOLOGY
DRILLING DISTURB.
SED. STRUCTURES
SAMPLES
0.5
1.0
1
2
3
4

LITHOLOGIC DESCRIPTION

PUMICEOUS GRANULE-PEBBLE GRAVEL AND PUMICEOUS GRANULE-PEBBLE CONGLOMERATE

Major lithology: Grayish green (10Y 5/2) and very dark greenish gray (10Y 3/1) PUMICEOUS GRANULE-PEBBLE GRAVEL and PUMICEOUS GRANULE-PEBBLE CONGLOMERATE in [illegible] proportions, uncertain because the core is [illegible] disturbed by drilling. Typical texture is [illegible] pebbles, [illegible] granules, and [illegible] coarse sand. Maximum pumice clast size is [illegible] cm. Pebble colors are [illegible] green [illegible] gray (10Y 6/1), dark greenish gray (10Y 4/1), and very dark greenish gray (10Y 3/1).

Minor lithology: The top [illegible] cm of the core is very dark greenish gray (10Y 3/1), fine- to coarse-grained LITHIC PUMICE SAND [illegible] grades upward from the underlying gravel.

Section 1, [illegible] cm, to Section 2, [illegible] cm, is completely disturbed by drilling. The rest of the core is very disturbed.

SMEAR SLIDE SUMMARY (%):

TEXTURE:

Sand [illegible]
Silt [illegible]

COMPOSITION:

Accessory minerals [illegible]
Feldspar [illegible]
Glass [illegible]

SITE 788 HOLE C CORE 25H CORED INTERVAL 229.2-238.7 mbsf

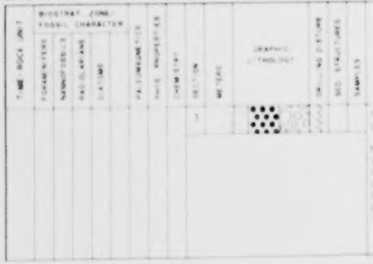
TIME-ROCK UNIT
BIOSTRAT. ZONE/FOSSIL CHARACTER
FORAMINIFERS
NANNOFOSSILS
RADIOLARIANS
DIATOMS
PALEOMAGNETICS
PHYS. PROPERTIES
CHEMISTRY
SECTION
METERS
GRAPHIC LITHOLOGY
DRILLING DISTURB.
SED. STRUCTURES
SAMPLES
1

LITHOLOGIC DESCRIPTION

PUMICEOUS PEBBLE-GRANULE GRAVEL AND PUMICEOUS PEBBLE-GRANULE CONGLOMERATE

Major lithology:
Very dark greenish gray (10Y 3/1) PUMICEOUS PEBBLE-GRANULE GRAVEL and PUMICEOUS PEBBLE-GRANULE CONGLOMERATE in approximately equal proportions. Most of the gravel is probably disaggregated conglomerate, as the core is very disturbed by drilling. The material consists of [illegible] pebbles, [illegible] granules, and [illegible] sand. Maximum pumice clast size is about 2.5 cm, and pebble colors are olive [illegible] and grayish green [illegible].

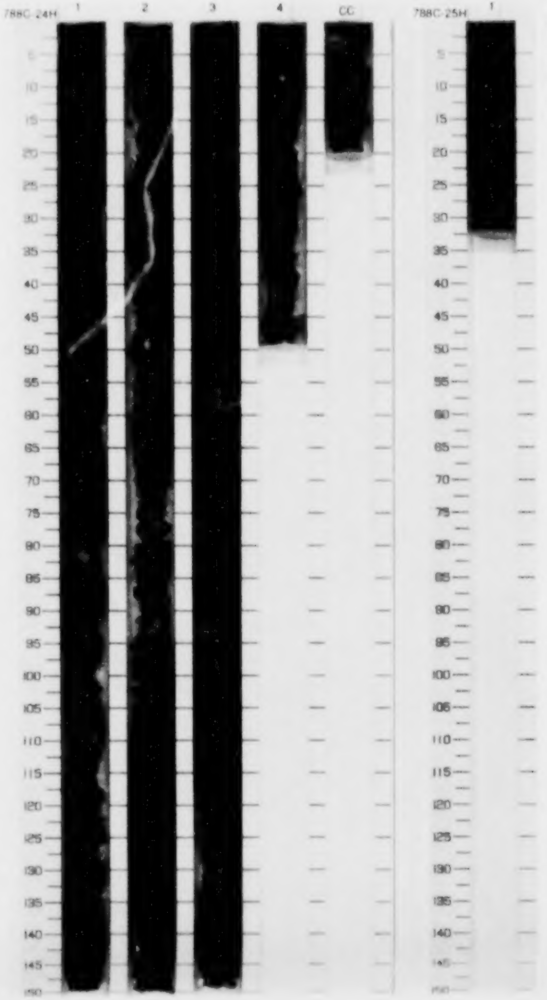
788C-24H
1
2
3
4
CC
788C-25H
1
5
10
15
20
25
30
35
40
45
50
55
60
65
70
75
80
85
90
95
100
105
110
115
120
125
130
135
140
145
150

SITE 788 HOLE C CORE 26X CORED INTERVAL 238.7-248.2 mbsf

TIME-ROCK UNIT	FORAMINIFERS	NANNOFOSSILS	RADIOLARIANS	DIATOMS	PALEOMAGNETICS	PHYS. PROPERTIES	CHEMISTRY	SECTION	METERS	GRAPHIC LITHOLOGY	DRILLING DISTURB.	SED. STRUCTURES	SAMPLES
		B						1					

LITHOLOGIC DESCRIPTION

PUMICEOUS GRANULE-PEBBLE CONGLOMERATE AND PUMICEOUS GRANULE-PEBBLE GRAVEL

Major lithologies:
Very dark greenish gray (10Y 3/1) PUMICEOUS GRANULE-PEBBLE CONGLOMERATE and its unconsolidated or disaggregated equivalent, PUMICEOUS GRANULE-PEBBLE GRAVEL. Textural composition is: pebbles 60%, granules 30%, sand 10%.

Minor lithology: The top 4 cm of the core is dark greenish gray (10Y 4/1) medium-grained VITRIC SAND composed of pumice grains.

126 788C 27X NO RECOVERY

SITE 788 HOLE C CORE 28X CORED INTERVAL 257.9-262.5 mbsf

TIME-ROCK UNIT	FORAMINIFERS	NANNOFOSSILS	RADIOLARIANS	DIATOMS	PALEOMAGNETICS	PHYS. PROPERTIES	CHEMISTRY	SECTION	METERS	GRAPHIC LITHOLOGY	DRILLING DISTURB.	SED. STRUCTURES	SAMPLES
PLIOCENE	N19 - N18 F/C	CN12? F/C	B		N			CC					

LITHOLOGIC DESCRIPTION

NANNOFOSSIL CLAYSTONE

Major lithology: Grayish green (5G 4/2) NANNOFOSSIL CLAYSTONE, slightly to heavily burrowed. The burrows are [illegible] mm wide, [illegible]

Minor lithology: The bottom [illegible] cm of the core is grayish green (5G [illegible]) [illegible] CLAYSTONE.

The core is moderately fractured by drilling.

SMEAR SLIDE SUMMARY (%):

	CC, 4	CC, [illegible]
	M	D
TEXTURE:		
Sand	5	5
Silt	20	15
Clay	75	80
COMPOSITION:		
Accessory minerals	20	[illegible]
Cement	—	[illegible]
Clay	—	[illegible]
Feldspar	[illegible]	[illegible]
Foraminifers	[illegible]	[illegible]
Glass	[illegible]	—
Micrite	[illegible]	[illegible]
Nannofossils	[illegible]	[illegible]
Opaques	2	—
Zeolite	—	[illegible]

788C 26X 1
788C 28X CC
5
10
15
20
25
30
35
40
45
50
55
60
65
70
75
80
85
90
95
100
105
110
115
120
125
130
135
140
145
150

SITE 788 HOLE D CORE 1R CORED INTERVAL 219.6-229.2 mbsf

TIME-ROCK UNIT	FORAMINIFERS	NANNOFOSSILS	RADIOLARIANS	DIATOMS	PALEOMAGNETICS	PHYS. PROPERTIES	CHEMISTRY	SECTION	METERS	GRAPHIC LITHOLOGY	DRILLING DISTURB.	SED. STRUCTURES	SAMPLES	LITHOLOGIC DESCRIPTION
						●	●	1	0.5 1.0		× × ×			PUMICEOUS CONGLOMERATE Major lithology: Dark gray [illegible] PUMICEOUS CONGLOMERATE. Pumice clasts range from [illegible] yellow green [illegible] to dusky green [illegible]. Maximum clast diameter [illegible] cm.
								2			×			
								3			×			

SITE 788 HOLE D CORE 2R CORED INTERVAL 229.2-238.9 mbsf

TIME-ROCK UNIT	FORAMINIFERS	NANNOFOSSILS	RADIOLARIANS	DIATOMS	PALEOMAGNETICS	PHYS. PROPERTIES	CHEMISTRY	SECTION	METERS	GRAPHIC LITHOLOGY	DRILLING DISTURB.	SED. STRUCTURES	SAMPLES	LITHOLOGIC DESCRIPTION
								1			×			PUMICEOUS CONGLOMERATE Major lithology: Dark gray [illegible] PUMICEOUS CONGLOMERATE. Pumice clasts range from [illegible] yellow green [illegible] to dusky green [illegible]. Maximum clast diameter [illegible] cm.

SITE 788 HOLE D CORE 3R CORED INTERVAL 238.9-248.5 mbsf

TIME-ROCK UNIT	FORAMINIFERS	NANNOFOSSILS	RADIOLARIANS	DIATOMS	PALEOMAGNETICS	PHYS. PROPERTIES	CHEMISTRY	SECTION	METERS	GRAPHIC LITHOLOGY	DRILLING DISTURB.	SED. STRUCTURES	SAMPLES	LITHOLOGIC DESCRIPTION
								1			×			PUMICEOUS CONGLOMERATE Major lithology: Dark gray [illegible] PUMICEOUS CONGLOMERATE. Pumice clasts range from [illegible] yellow green [illegible] to dusky green [illegible]. Maximum clast diameter [illegible] cm.

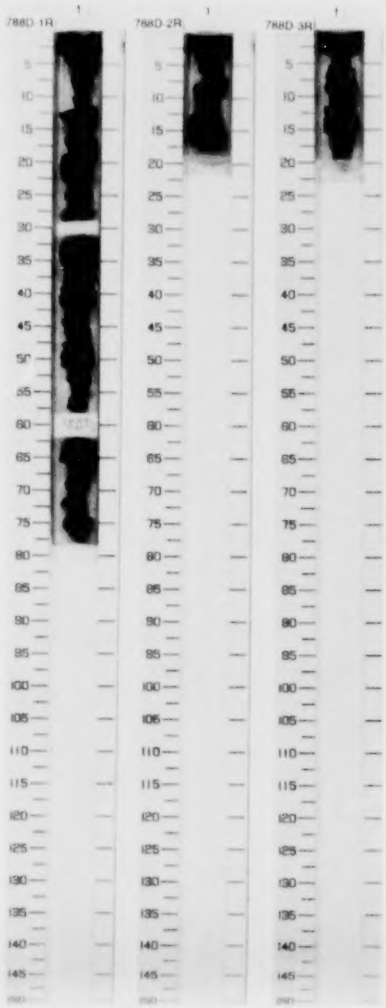

SITE 788 HOLE D CORE 4R CORED INTERVAL 248.5-258.8 mbsf

TIME-ROCK UNIT	BIOSTRAT. ZONE / FOSSIL CHARACTER: FORAMINIFERS	NANNOFOSSILS	RADIOLARIANS	DIATOMS	PALEOMAGNETICS	PHYS. PROPERTIES	CHEMISTRY	SECTION	METERS	GRAPHIC LITHOLOGY	DRILLING DISTURB.	SED. STRUCTURES	SAMPLES	LITHOLOGIC DESCRIPTION
PLIOCENE	N18 - N19 C	CN3 - CN14a F/P	B		R N	[illegible]	● %CaCO$_3$=[illegible]	1	0.5 1.0	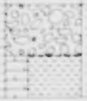	× × × × ×		●	PUMICEOUS CONGLOMERATE AND NANNOFOSSIL-RICH CLAYSTONE Major lithologies: The top 50% of the core is [illegible] black (5GY 2/1) PUMICEOUS CONGLOMERATE. Pumice clasts are up to 1 cm in diameter and grayish green (5G 5/2), gray (5Y 6/1), and pale olive (10Y 6/2) in color. The matrix is grayish black (N2) in color. The lower half of the core is grayish green (5GY 5/1) NANNOFOSSIL-RICH CLAYSTONE with scattered, clearly visible foraminifer tests, and slight burrowing. The entire core is drilling breccia. One piece at 18 cm shows a contact between the major lithologies. SMEAR SLIDE SUMMARY (%): 1, 80 D TEXTURE: Silt 10 Clay 90 COMPOSITION: Accessory minerals [illegible] Clay [illegible] Feldspar [illegible] Glass [illegible] Micrite [illegible] Nannofossils [illegible] Opaques [illegible]

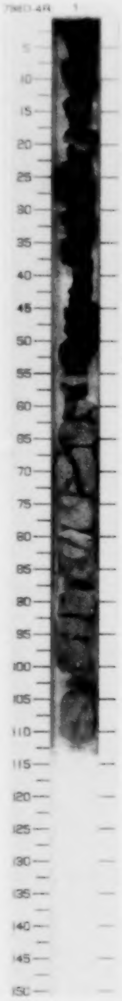

SITE 788 HOLE D CORE 5R CORED INTERVAL 258.2–267.9 mbsf

TIME-ROCK UNIT	FORAMINIFERS	NANNOFOSSILS	RADIOLARIANS	DIATOMS	PALEOMAGNETICS	PHYS. PROPERTIES	CHEMISTRY	SECTION	METERS	GRAPHIC LITHOLOGY	DRILLING DISTURB.	SED. STRUCTURES	SAMPLES
PLIOCENE	[illegible]	[illegible]	[illegible]		[illegible]	● ●	● ●	1 2	0.5 1.0				● ● ● ●

LITHOLOGIC DESCRIPTION

NANNOFOSSIL-RICH CLAYSTONE

Major lithology: Dark greenish gray [illegible], heavily burrowed NANNOFOSSIL-RICH CLAYSTONE [illegible] [illegible] of the core. [illegible] burrows are recognized. Several burrows [illegible] are lined with [illegible]. [illegible] pumice clasts [illegible] in Section 1, [illegible] pumice pebble at the top probably caved in and is not stratigraphically intact.

Minor lithologies:
In Section 1, [illegible] is a layer of black (N1), very fine-grained VITRIC SANDSTONE [illegible]. Section 1, [illegible] cm are laminated intervals of the same VITRIC SANDSTONE. [illegible] of these intervals grade upward into [illegible] VITRIC CLAYEY SILTSTONE and VITRIC SILTY CLAYSTONE.

A fracture occurs in Section 1, [illegible] cm. The entire core is moderately fractured by drilling.

SMEAR SLIDE SUMMARY (%):

	1, 6	1, 24	1, 96	1, 110
	D	D	M	M
TEXTURE:				
Sand	5	—	90	—
Silt	15	45	10	25
Clay	80	55	—	75
COMPOSITION:				
Accessory minerals	[illegible]	[illegible]	[illegible]	[illegible]
Clay	[illegible]	[illegible]	[illegible]	[illegible]
Feldspar	[illegible]	[illegible]	[illegible]	[illegible]
Foraminifers	[illegible]	[illegible]	[illegible]	[illegible]
Glass	[illegible]	[illegible]	98	[illegible]
Mica	[illegible]	[illegible]	[illegible]	[illegible]
Nannofossils	[illegible]			
Opaques	[illegible]	[illegible]		
Zeolite	[illegible]			

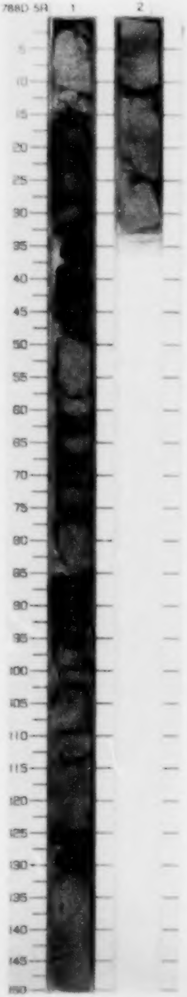

SITE 788 HOLE D CORE 6R CORED INTERVAL 267.8-277.5 mbsf

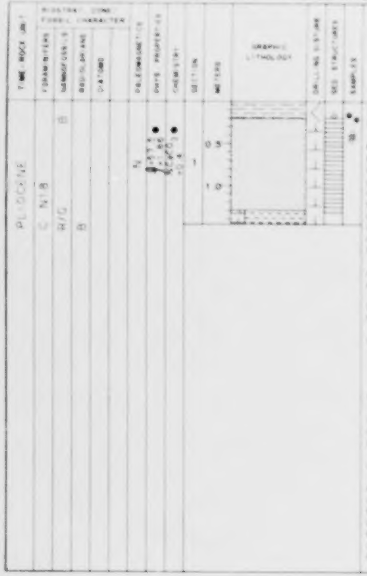
TIME-ROCK UNIT
BIOSTRAT. ZONE/ FOSSIL CHARACTER
FORAMINIFERS
NANNOFOSSILS
RADIOLARIANS
DIATOMS
PALEOMAGNETICS
PHYS. PROPERTIES
CHEMISTRY
SECTION
METERS
GRAPHIC LITHOLOGY
DRILLING DISTURB.
SED. STRUCTURES
SAMPLES
PLIOCENE
C N18
B
R/G
B
N
1
0.5
1.0

LITHOLOGIC DESCRIPTION

VITRIC SANDSTONE, VITRIC SILTY CLAYSTONE, AND NANNOFOSSIL-RICH CLAYSTONE

Major lithologies:
Black (N1), very fine-grained to medium-grained, laminated VITRIC SANDSTONE constitutes 55% of the core in a single bed from 26-[illegible] cm. The bed is laminated and normally graded, from medium grained at the base, to fine grained in the middle, to very fine grained in the upper third. Except for the lowest [illegible] cm of the bed [illegible], the middle and lower thirds are pumiceous granule and pebble bearing. The sandstone grades upward into dark greenish gray (10Y 3/2, 5GY 4/1) VITRIC SILTY CLAYSTONE (26% of the core) that contains an isolated 1-cm diameter pumice clast. The lowermost [illegible] cm (19%) of the core is dark greenish gray (10Y 4/1) NANNOFOSSIL-RICH CLAYSTONE containing large, well-tested foraminifers.

An oxidized light gray (N7) pumice pebble at the top [illegible]

Drilling disturbance: The top 10 cm is highly fractured; the rest of the core is moderately fractured.

SMEAR SLIDE & THIN SECTION SUMMARY (%):

	1, 16	1, 20	1, 41
	M	M	T
TEXTURE:			
Sand	—	—	95
Silt	25	25	5
Clay	75	75	—
COMPOSITION:			
Accessory minerals	Tr	Tr	—
Clay	75	75	—
Feldspar	Tr	Tr	—
Glass	25	25	70
Pore space	—	—	25
Quartz	—	Tr	—
Rock fragments	Tr	Tr	5

SITE 788 HOLE D CORE 7R CORED INTERVAL 277.5-287.2 mbsf

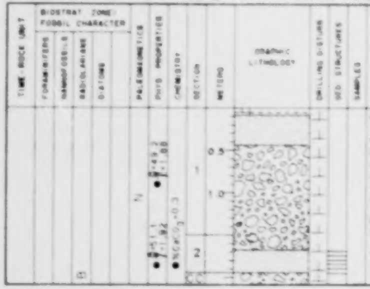
TIME-ROCK UNIT
BIOSTRAT. ZONE/ FOSSIL CHARACTER
FORAMINIFERS
NANNOFOSSILS
RADIOLARIANS
DIATOMS
PALEOMAGNETICS
PHYS. PROPERTIES
CHEMISTRY
SECTION
METERS
GRAPHIC LITHOLOGY
DRILLING DISTURB.
SED. STRUCTURES
SAMPLES
B
N
φ=49.2 γ=1.88
φ=51.1 γ=1.82
%CaCO3=0.3
1
2
CC
0.5
1.0

LITHOLOGIC DESCRIPTION

PUMICEOUS CONGLOMERATE AND VITRIC SANDSTONE

Major lithologies:
Grayish black (N2) PUMICEOUS CONGLOMERATE comprises 62% of the core. It consists of 20-30% sand, 40-60% granules, and 10-40% pebbles, which are round to subangular and as large as 32 mm in diameter. Grayish black (N2), poorly sorted, coarse to fine-grained VITRIC SAND comprises 37% of the core. It displays some planar laminations in Section 2 and contains scattered pumice clasts 3 mm in diameter.

Minor lithology: The topmost 8% of the core is dark greenish gray (10Y 4/1) NANNOFOSSIL-RICH CLAYSTONE containing scattered white, sand-sized foraminifers.

The whole core is moderately fractured by drilling.

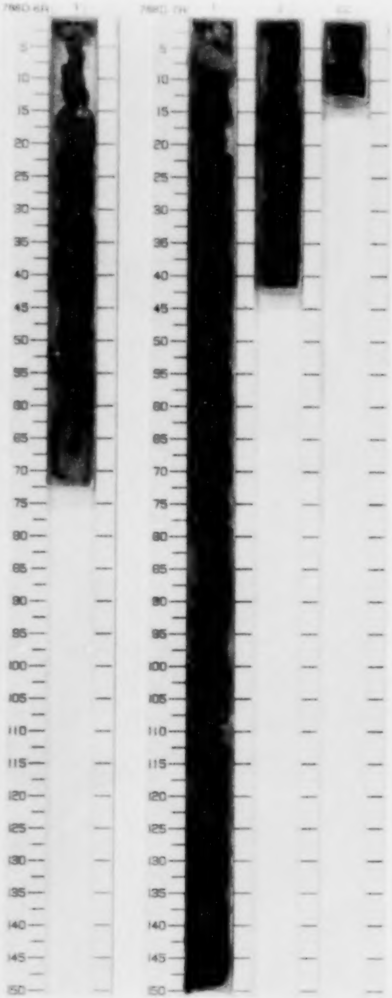
788D-6R
1
788D-7R
1
2
CC
5
10
15
20
25
30
35
40
45
50
55
60
65
70
75
80
85
90
95
100
105
110
115
120
125
130
135
140
145
150

SITE 788 HOLE D CORE 8R CORED INTERVAL 287.2-296.9 mbsf

TIME-ROCK UNIT	BIOSTRAT. ZONE/ FOSSIL CHARACTER: FORAMINIFERS	NANNOFOSSILS	RADIOLARIANS	DIATOMS	PALEOMAGNETICS	PHYS. PROPERTIES	CHEMISTRY	SECTION	METERS	GRAPHIC LITHOLOGY	DRILLING DISTURB.	SED. STRUCTURES	SAMPLES	LITHOLOGIC DESCRIPTION
					[illegible]	●	●	1					●	[illegible]

788D 8R
1
CC
5
10
15
20
25
30
35
40
45
50
55
60
65
70
75
80
85
90
95
100
105
110
115
120
125
130
135
140
145
150

[illegible] CORED INTERVAL [illegible]

TIME-ROCK UNIT	BIOSTRAT. ZONE/FOSSIL CHARACTER				PALEOMAGNETICS	PHYS. PROPERTIES	CHEMISTRY	SECTION	METERS	GRAPHIC LITHOLOGY	DRILLING DISTURB.	SED. STRUCTURES	SAMPLES	LITHOLOGIC DESCRIPTION
	FORAMINIFERS	NANNOFOSSILS	RADIOLARIANS	DIATOMS										

LITHOLOGIC DESCRIPTION

[illegible]

Major lithology: [illegible]

Minor lithologies: [illegible] PEBBLE GRANULE CONGLOMERATE [illegible]

[illegible]

The core is moderately fractured by drilling throughout.

SMEAR SLIDE & THIN-SECTION SUMMARY (%):

	[illegible]	[illegible]	[illegible]
TEXTURE:			
Sand	—	—	[illegible]
Silt	[illegible]	[illegible]	[illegible]
Clay	[illegible]	[illegible]	—
COMPOSITION:			
Accessory minerals	—	[illegible]	[illegible]
Cement	—	—	[illegible]
Clay	[illegible]	[illegible]	—
Feldspar	[illegible]	[illegible]	[illegible]
Foraminifers	—	—	[illegible]
Glass	[illegible]	[illegible]	[illegible]
Glauconite		[illegible]	—
Opaques		[illegible]	—
Plant debris			[illegible]
Rock fragment		[illegible]	[illegible]
Zeolite		[illegible]	—

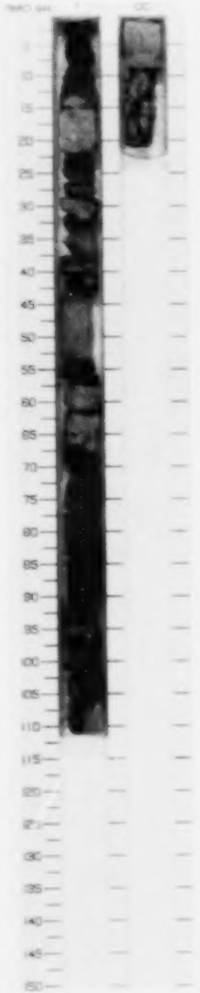
CM
1
CC
5
10
15
20
25
30
35
40
45
50
55
60
65
70
75
80
85
90
95
100
105
110
115
120
125
130
135
140
145
150

SITE 788 HOLE D CORE 10R CORED INTERVAL 306.5-316.0 mbsf

TIME-ROCK UNIT	FORAMINIFERS	NANNOFOSSILS	RADIOLARIANS	DIATOMS	PALEOMAGNETICS	PHYS. PROPERTIES	CHEMISTRY	SECTION	METERS	GRAPHIC LITHOLOGY	DRILLING DISTURB.	SED. STRUCTURES	SAMPLES	LITHOLOGIC DESCRIPTION
LOWER MIOCENE - PLEISTOCENE		CN2 - CN14				●	●	1					●	[illegible]

SITE 788 HOLE D CORE 11R CORED INTERVAL 316.0-325.6 mbsf

TIME-ROCK UNIT	FORAMINIFERS	NANNOFOSSILS	RADIOLARIANS	DIATOMS	PALEOMAGNETICS	PHYS. PROPERTIES	CHEMISTRY	SECTION	METERS	GRAPHIC LITHOLOGY	DRILLING DISTURB.	SED. STRUCTURES	SAMPLES	LITHOLOGIC DESCRIPTION
	B/M					●	●	1						[illegible]

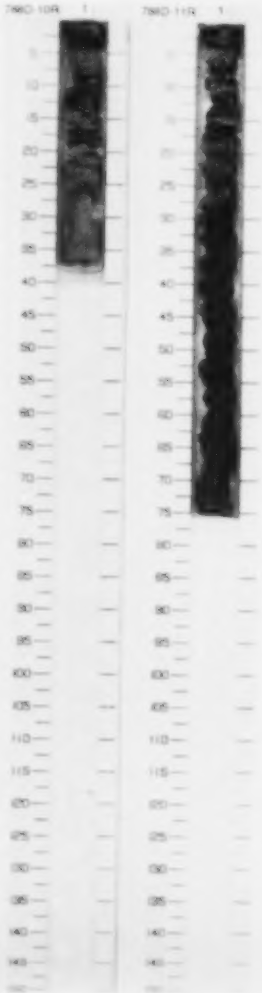
788D-10R 1
788D-11R 1
5
10
15
20
25
30
35
40
45
50
55
60
65
70
75
80
85
90
95
100
105
110
115
120
125
130
135
140
145
150

SITE 788 HOLE D CORE 12R CORED INTERVAL 325.6-335.3 mbsf

TIME-ROCK UNIT	FORAMINIFERS	NANNOFOSSILS	RADIOLARIANS	DIATOMS	PALEOMAGNETICS	PHYS. PROPERTIES	CHEMISTRY	SECTION	METERS	GRAPHIC LITHOLOGY	DRILLING DISTURB.	SED. STRUCTURES	SAMPLES
LOWER MIOCENE - PLEISTOCENE		C/M CN2 - CN14A	B		?	●	●	1					●

LITHOLOGIC DESCRIPTION

[illegible] CONGLOMERATE

Major lithology: [illegible]

Minor lithology: [illegible]

The core is moderately fractured by drilling.

SMEAR SLIDE & THIN SECTION SUMMARY (%):

	1, [illegible] D	1, [illegible] [illegible]
TEXTURE:		
Sand	[illegible]	[illegible]
Silt	[illegible]	[illegible]
Clay	[illegible]	[illegible]
COMPOSITION:		
Accessory minerals	[illegible]	
Cement	[illegible]	
Clay	[illegible]	[illegible]
Feldspar	[illegible]	[illegible]
Foraminifers	[illegible]	[illegible]
Glass	[illegible]	[illegible]
Micrite	[illegible]	[illegible]
Nannofossils	[illegible]	[illegible]
Rock fragment	[illegible]	[illegible]

SITE 788 HOLE D CORE 13R CORED INTERVAL 335.3-345.0 mbsf

TIME-ROCK UNIT	FORAMINIFERS	NANNOFOSSILS	RADIOLARIANS	DIATOMS	PALEOMAGNETICS	PHYS. PROPERTIES	CHEMISTRY	SECTION	METERS	GRAPHIC LITHOLOGY	DRILLING DISTURB.	SED. STRUCTURES	SAMPLES
		B/P			?	●	●	1					●

LITHOLOGIC DESCRIPTION

PUMICEOUS PEBBLE GRANULE CONGLOMERATE AND [illegible] SILTY CLAYSTONE

Major lithology: The bottom 80% of the core consists of black (N2) PUMICEOUS PEBBLE GRANULE CONGLOMERATE composed of [illegible] pebbles, [illegible] granules, and [illegible] fine grained sand. The uppermost 20% of the core is [illegible] VITRIC SILTY CLAYSTONE.

The core is moderately fractured by drilling.

SMEAR SLIDE SUMMARY (%):

	1, [illegible] M
TEXTURE:	
Sand	[illegible]
Silt	[illegible]
Clay	[illegible]
COMPOSITION:	
Calcite	[illegible]
Clay	[illegible]
Glass	[illegible]
Micrite	[illegible]

788D-12R 1
788D-13R 1
5
10
15
20
25
30
35
40
45
50
55
60
65
70
75
80
85
90
95
100
105
110
115
120
125
130
135
140
145
150

SITE 788 HOLE D CORE 14R CORED INTERVAL 345.0-354.7 mbsf

TIME-ROCK UNIT	FORAMINIFERS	NANNOFOSSILS	RADIOLARIANS	DIATOMS		PALEOMAGNETICS	PHYS. PROPERTIES	CHEMISTRY	SECTION	METERS	GRAPHIC LITHOLOGY	DRILLING DISTURB.	SED. STRUCTURES	SAMPLES	LITHOLOGIC DESCRIPTION
LOWER MIOCENE - PLEISTOCENE		CN1 - CN14a					●	●	1						[illegible] Major lithology: [illegible] [illegible]

788D 14R 1
10
15
20
25
30
35
40
45
50
55
60
65
70
75
80
85
90
95
100
105
110
115
120
125
130
135
140
145
150

[illegible] INTERVAL 354.7-364.3 [illegible]

TIME-ROCK UNIT	FORAMINIFERS	NANNOFOSSILS	RADIOLARIANS	DIATOMS	PALEOMAGNETICS	PHYS. PROPERTIES	CHEMISTRY	SECTION	METERS	GRAPHIC LITHOLOGY	DRILLING DISTURB.	SED. STRUCTURES	SAMPLES	LITHOLOGIC DESCRIPTION
MIOCENE - LOWER PLIOCENE		R/M	B		N	●	●	1						[illegible]

SMEAR SLIDE SUMMARY (%):

	M	M	M	M	M
TEXTURE:					
Sand	[illegible]	[illegible]	[illegible]		
Silt	[illegible]	[illegible]	[illegible]	[illegible]	[illegible]
Clay	[illegible]	[illegible]	[illegible]	[illegible]	[illegible]
COMPOSITION:					
Accessory minerals	[illegible]		[illegible]	[illegible]	[illegible]
Clay	[illegible]			[illegible]	[illegible]
Feldspar	[illegible]		[illegible]	[illegible]	
[illegible]	[illegible]		[illegible]		
Glass	[illegible]	[illegible]	[illegible]	[illegible]	[illegible]
Micrite		[illegible]	[illegible]	[illegible]	[illegible]
Nannofossils	[illegible]	[illegible]	[illegible]	[illegible]	[illegible]
Opaques			[illegible]		[illegible]
Rock fragments					[illegible]
[illegible]					

SITE 788 HOLE D CORE 16R CORED INTERVAL 364.3-374.0 mbsf

TIME-ROCK UNIT	BIOSTRAT. ZONE/ FOSSIL CHARACTER: FORAMINIFERS	NANNOFOSSILS	RADIOLARIANS	DIATOMS	PALEOMAGNETICS	PHYS. PROPERTIES	CHEMISTRY	SECTION	METERS	GRAPHIC LITHOLOGY	DRILLING DISTURB.	SED. STRUCTURES	SAMPLES	LITHOLOGIC DESCRIPTION
LOWER MIOCENE – PLEISTOCENE	B M. MIOCENE-PLIOCENE	CN3 – CN14a A/M				● ●	● ● %CaCO3						● ●	VITRIC SILTSTONE AND VITRIC SANDSTONE

VITRIC SILTSTONE AND VITRIC SANDSTONE

Major lithology: Most of the core is VITRIC SANDSTONE. [illegible]

Minor lithologies: [illegible] VITRIC SILTSTONE. [illegible] CLAYEY VITRIC SILTSTONE. [illegible] VITRIC SILTY CLAYSTONE with pumice [illegible].

The core is moderately fractured [illegible].

SMEAR SLIDE SUMMARY (%):

M

TEXTURE:

Sand

Silt

Clay

COMPOSITION:

Clay

Feldspar

Glauconite

Glass

Micrite

Nannofossils

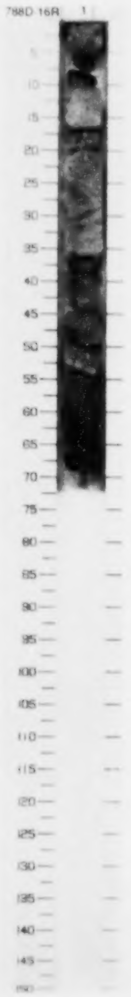

788D 16R 1
5
10
15
20
25
30
35
40
45
50
55
60
65
70
75
80
85
90
95
100
105
110
115
120
125
130
135
140
145
150

SITE 789 HOLE A CORE 1G CORED INTERVAL 0.0-8.5 mbsf

TIME-ROCK UNIT	BIOSTRAT. ZONE/ FOSSIL CHARACTER					PALEOMAGNETICS	PHYS. PROPERTIES	CHEMISTRY	SECTION	METERS	GRAPHIC LITHOLOGY	DRILLING DISTURB.	SED. STRUCTURES	SAMPLES	LITHOLOGIC DESCRIPTION
	FORAMINIFERS	NANNOFOSSILS	RADIOLARIANS	DIATOMS											
															All recovery went to Paleontology and Igneous Petrology Laboratories

126 789A 1R NO RECOVERY

126 789A 2R NO RECOVERY

126 789A 3R NO RECOVERY

126 789A 4R NO RECOVERY

126 789A 5R NO RECOVERY

126 789A 6R NO RECOVERY

SITE 790 HOLE A CORE 1H CORED INTERVAL 0.0-8.8 mbsf

TIME-ROCK UNIT	FORAMINIFERS	NANNOFOSSILS	RADIOLARIANS	DIATOMS	PALEOMAGNETICS	PHYS. PROPERTIES	CHEMISTRY	SECTION	METERS	GRAPHIC LITHOLOGY	DRILLING DISTURB.	SED. STRUCTURES	SAMPLES
QUATERNARY	N23	CN15	UPPER PLIOCENE–RECENT C/G R/G A/G R/G			[illegible]	[illegible]	1 2 3 4 5 6 CC	0.5 1.0				

LITHOLOGIC DESCRIPTION

CLAYEY VITRIC SILT, VITRIC SILT, PUMICEOUS SAND AND PUMICEOUS GRAVEL

Major lithologies:
The uppermost 95 cm (11%) of the core is a CLAYEY VITRIC SILT, with a 5-cm dark brown (10YR 3/3) top rich in amorphous iron oxide aggregates. The rest of the core is dark gray and gray (5Y 4/1, 5Y 5/1). This unit grades downward into a gray (5Y 5/1) and dark gray (5Y 4/1) VITRIC SILT 2.1 m thick (25% of the core), which is succeeded by 4.1 m (53%) of core of dark gray, gray, and light olive gray (5Y 4/1, 5/1, 5/2), coarse, very poorly sorted, gravelly PUMICEOUS SAND and PUMICEOUS GRAVEL that is, in large part, very badly disturbed by drilling.

Minor lithology: Two 1-2-cm thick layers of VITRIC SILT occur near the top of Section 3.

SMEAR SLIDE SUMMARY (%):

	1, 2 D	1, 30 M	1, 50 D	1, 85 D	2, 27 M	2, 90 D	3, 129 D
TEXTURE:							
Sand	5	10	5	—	5	10	20
Silt	50	60	70	90	75	90	80
Clay	45	30	25	10	20	—	Tr
COMPOSITION:							
Accessory minerals	—	Tr	—	—	—	—	—
Clay	30	30	25	10	10	—	Tr
Diatoms	Tr	Tr	1	1	—	—	—
Feldspar	Tr	Tr	1	Tr	5	2	1
Foraminifers	2	1	1	—	Tr	—	—
Glass	65	68	69	89	64	97	98
Lithic fragments	—	—	—	—	—	1	1
Micrite	—	Tr	—	—	—	—	Tr
Oxide	3	1	—	—	20	—	—
Spicules	—	Tr	Tr	—	—	—	—

SMEAR SLIDE SUMMARY (%):

	3, 70 D	3, 118 D	4, 80 D	6, [illegible] D
TEXTURE:				
Sand	60	90	80	95
Silt	40	10	20	5
COMPOSITION:				
Bioclast	—	—	—	1
Feldspar	3	5	—	20
Foraminifers	5	2	25	1
Glass	90	93	68	70
Lithic fragments	1	—	2	2
Micrite	1	—	—	—
Nannofossils	—	—	—	Tr
Opaques	1	—	2	2
Pyroxene	Tr	—	—	1

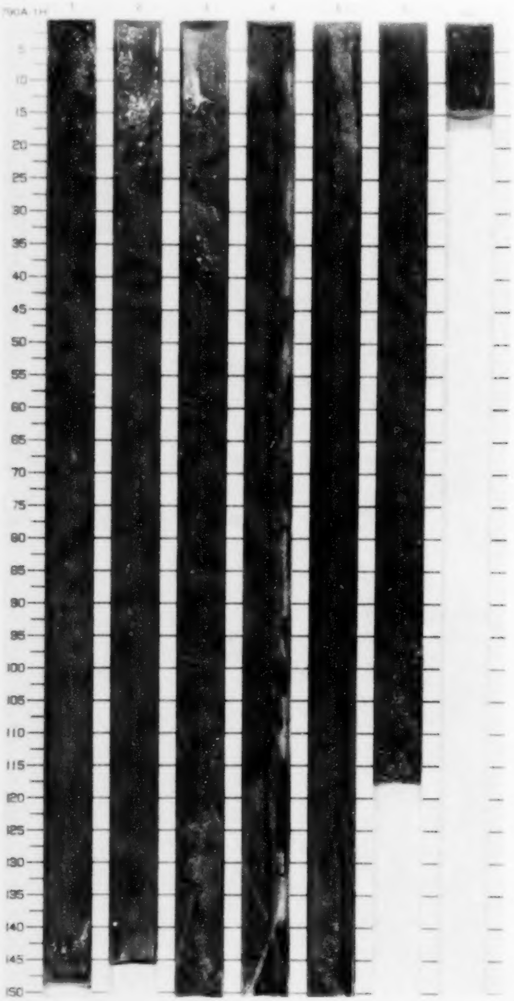

SITE 790 HOLE A CORE 2H CORED INTERVAL 8.8-18.3 mbsf

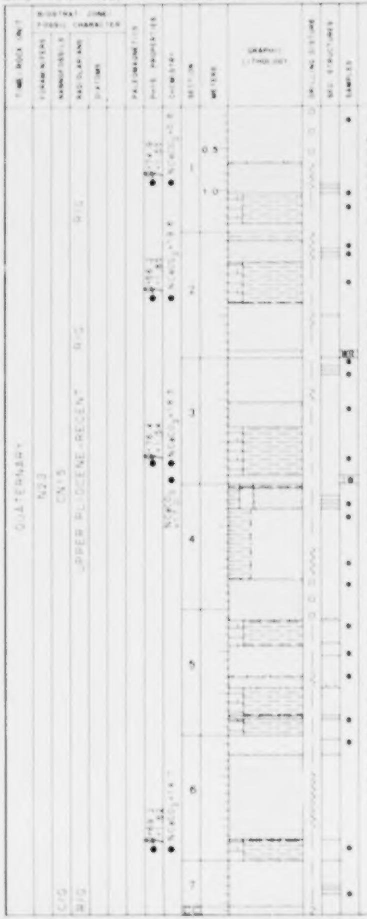

LITHOLOGIC DESCRIPTION

VITRIC SILT, NANNOFOSSIL-RICH SILTY CLAY, AND VITRIC SAND

Major lithologies:
Dark gray (5Y 4/1, 4/2) VITRIC SILT beds, 25 to 120 cm thick, that comprise 42% of the core, interbedded with olive gray (5Y 4/2) NANNOFOSSIL-RICH SILTY CLAY beds, 25-80 cm thick (36% of recovery), and five layers of black (N2, 5YR 2/1) VITRIC SAND that together constitute 24% of the core. Some of the sandy and silty intervals are graded, and several are planar laminated.

SMEAR SLIDE SUMMARY (%):

	1, 78 D	1, 102 D	1, 120 D	2, [illegible] D	2, 37 D	2, 80 D	2, 114 D
TEXTURE:							
Sand	1	25	3	10	80	15	—
Silt	59	65	31	90	20	35	95
Clay	40	10	66	—	—	50	5
COMPOSITION:							
Accessory minerals	—	—	—	—	—	—	1
Clay	33	5	61	—	—	48	5
Diatoms	15	—	10	Tr	—	10	Tr
Feldspar	—	15	—	5	1	2	—
Foraminifers	3	—	2	Tr	2	3	—
Glass	5	50	2	93	93	5	92
Micrite	—	—	—	—	Tr	—	—
Nannofossils	40	20	20	1	Tr	30	2
Opaques	—	—	—	—	1	—	—
Oxide	2	5	2	—	—	1	—
Pyroxene	—	5	—	—	1	—	—
Radiolarians	—	—	Tr	—	Tr	1	Tr
Silicoflagellates	Tr	—	—	—	Tr	Tr	—
Spicules	2	—	3	—	1	Tr	Tr

SMEAR SLIDE SUMMARY (%):

	3, 4 D	3, 70 D	3, 80 D	3, 120 D	4, 24 D	4, 40 D	4, 95 D
TEXTURE:							
Sand	90	5	88	2	70	5	70
Silt	10	95	12	28	10	30	20
Clay	—	—	Tr	70	20	65	10
COMPOSITION:							
Accessory minerals	—	—	2	—	5	—	—
Clay	—	—	—	67	10	63	10
Diatoms	—	—	—	Tr	—	10	—
Feldspar	5	5	5	1	15	Tr	5
Foraminifers	Tr	—	Tr	3	—	1	—
Glass	95	95	90	5	60	5	67
Lithic fragments	—	—	3	—	10	—	15
Nannofossils	—	—	Tr	15	Tr	20	1
Radiolarians	—	—	—	2	—	1	—
Silicoflagellates	—	—	—	5	—	—	—
Spicules	—	—	—	1	—	Tr	—

cont.

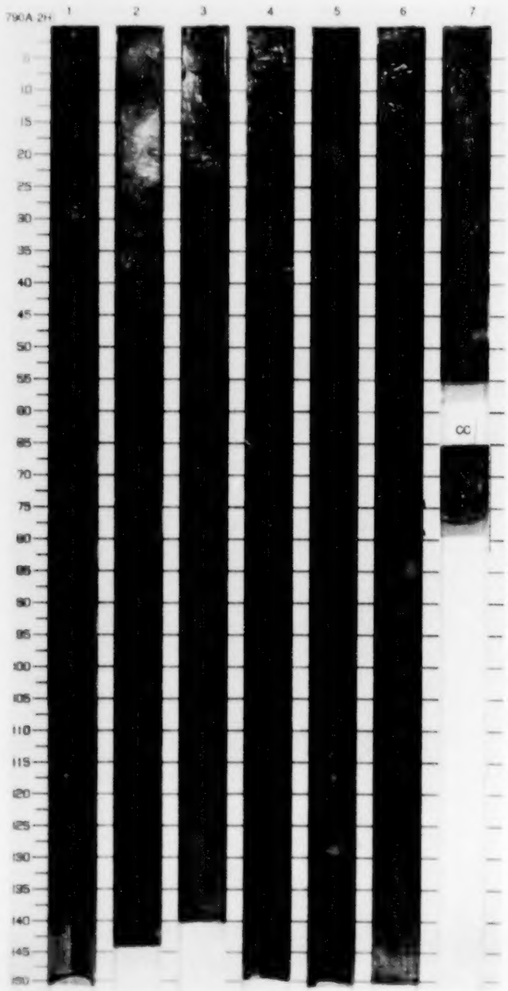

SITE 790 HOLE A CORE 2H CORED INTERVAL 8.8-18.3 mbsf

TIME-ROCK UNIT	BIOSTRAT. ZONE/FOSSIL CHARACTER: FORAMINIFERS	NANNOFOSSILS	RADIOLARIANS	DIATOMS	PALEOMAGNETICS	PHYS. PROPERTIES	CHEMISTRY	SECTION	METERS	GRAPHIC LITHOLOGY	DRILLING DISTURB.	SED. STRUCTURES	SAMPLES	LITHOLOGIC DESCRIPTION
														[illegible]

SMEAR SLIDE SUMMARY (%):

	4, 100 D	5, 20 D	5, 52 D	5, 80 D	6, 110 D	[illegible] D	[illegible] D
TEXTURE:							
Sand	70	3	40	50	75	55	10
Silt	25	47	55	45	15	35	60
Clay	5	50	5	5	10	10	30
COMPOSITION:							
Accessory minerals	—	—	1	1	5	2	—
Clay	—	46	5	5	10	10	30
Diatoms	—	15	5	—	5	Tr	10
Feldspar	15	2	3	7	5	15	—
Foraminifers	Tr	—	—	—	—	—	2
Glass	72	10	55	20	50	54	35
Lithic fragments	10	—	25	67	20	15	—
Nannofossils	Tr	25	1	—	5	1	15
Oxide	—	2	—	—	—	—	—
Pyroxene	3	—	—	—	—	—	—
Quartz	—	—	—	—	—	5	—
Radiolarians	—	Tr	—	—	Tr	—	—
Silicoflagellates	—	Tr	—	—	—	—	—
Spicules	—	Tr	—	—	—	—	—

SMEAR SLIDE SUMMARY (%):

	7, 40 D
TEXTURE:	
Sand	20
Silt	75
Clay	5
COMPOSITION:	
Accessory minerals	1
Clay	5
Diatoms	10
Feldspar	2
Foraminifers	Tr
Glass	80
Nannofossils	2

SITE 790 HOLE A CORE 3H CORED INTERVAL 18.3-27.8 mbsf

TIME-ROCK UNIT: QUATERNARY

BIOSTRAT. ZONE / FOSSIL CHARACTER: FORAMINIFERS N23; NANNOFOSSILS CN15, C/G; RADIOLARIANS B/G; DIATOMS

SECTION: 1, 2, 3, 4, 5, 6, 7, CC

LITHOLOGIC DESCRIPTION

VITRIC SILT

Major lithology: Gray [illegible] VITRIC SILT consisting of [illegible] glass, with a few percent of siliceous microfossils (diatoms, radiolarians, sponge spicules) and silicoflagellates. The core is almost structureless except for small graded intervals in Sections [illegible] and a few scattered [illegible] bedded pieces.

Minor lithology: Gray [illegible] fine VITRIC SAND layers, [illegible] thick, [illegible]

SMEAR SLIDE SUMMARY (%):

TEXTURE:

Sand

Silt

COMPOSITION:

Diatoms

Glass

Radiolarians

Silicoflagellates

Spicules

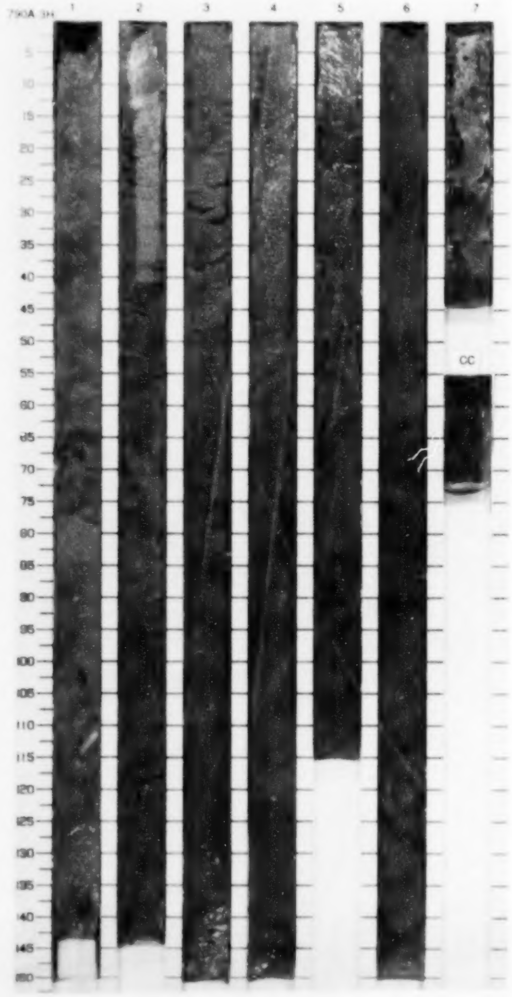
790A 3H
1
2
3
4
5
6
7
CC
5
10
15
20
25
30
35
40
45
50
55
60
65
70
75
80
85
90
95
100
105
110
115
120
125
130
135
140
145
150

SITE 790 HOLE A CORE 4H CORED INTERVAL 27.8-37.6 mbsf

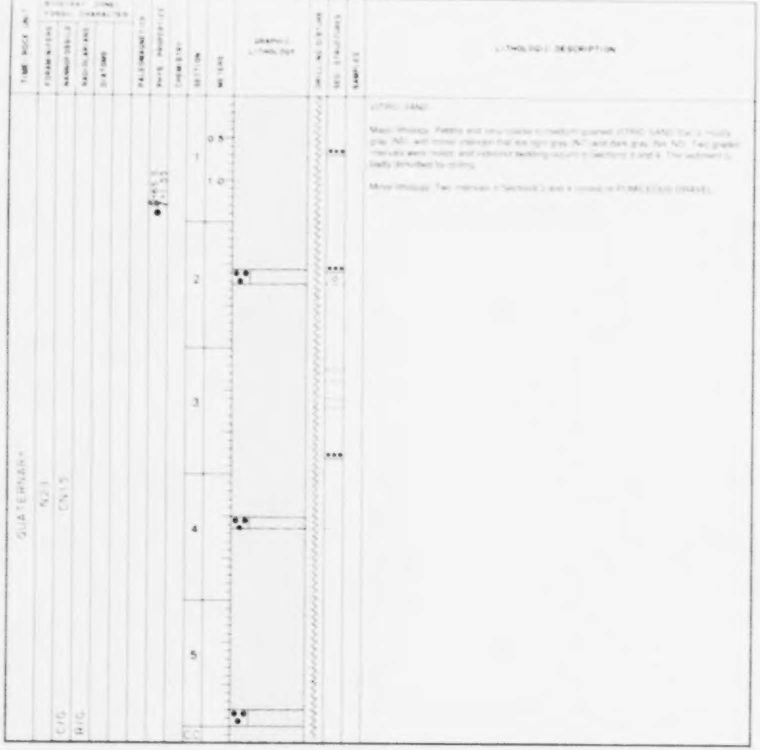
TIME-ROCK UNIT
BIOSTRAT. ZONE/ FOSSIL CHARACTER
FORAMINIFERS
NANNOFOSSILS
RADIOLARIANS
DIATOMS
PALEOMAGNETICS
PHYS. PROPERTIES
CHEMISTRY
SECTION
METERS
GRAPHIC LITHOLOGY
DRILLING DISTURB.
SED. STRUCTURES
SAMPLES
LITHOLOGIC DESCRIPTION
QUATERNARY
N23
CN15
C/G
B/G
1
2
3
4
5
CC
0.5
1.0

VITRIC SAND

Major lithology: Pebbly and very coarse to medium-grained VITRIC SAND that is mostly gray (N6), with minor intervals that are light gray (N7) and dark gray (N4, N3). Two graded intervals were noted, and indistinct bedding occurs in Sections 3 and 4. The sediment is badly disturbed by coring.

Minor lithology: Two intervals in Sections 2 and 4 consist of PUMICEOUS GRAVEL.

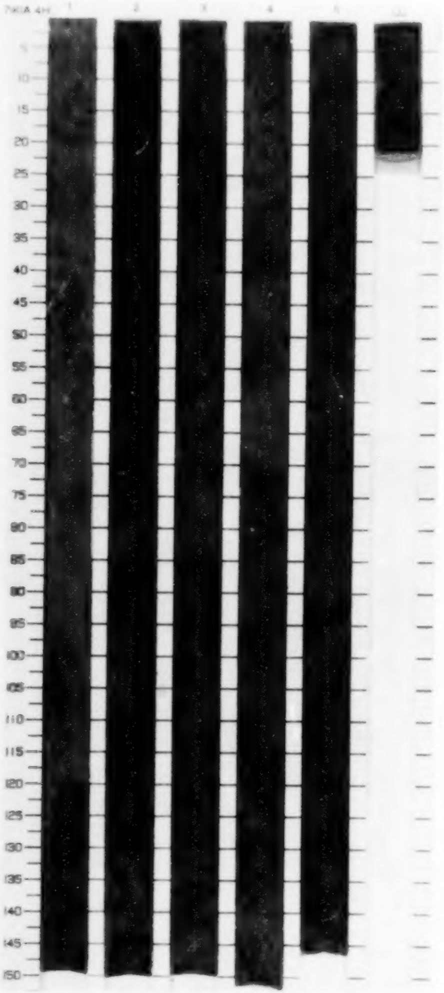
790A 4H
1
2
3
4
5
CC
5
10
15
20
25
30
35
40
45
50
55
60
65
70
75
80
85
90
95
100
105
110
115
120
125
130
135
140
145
150

SITE 790 HOLE B CORE 1H CORED INTERVAL 0.0-4.5 mbsf

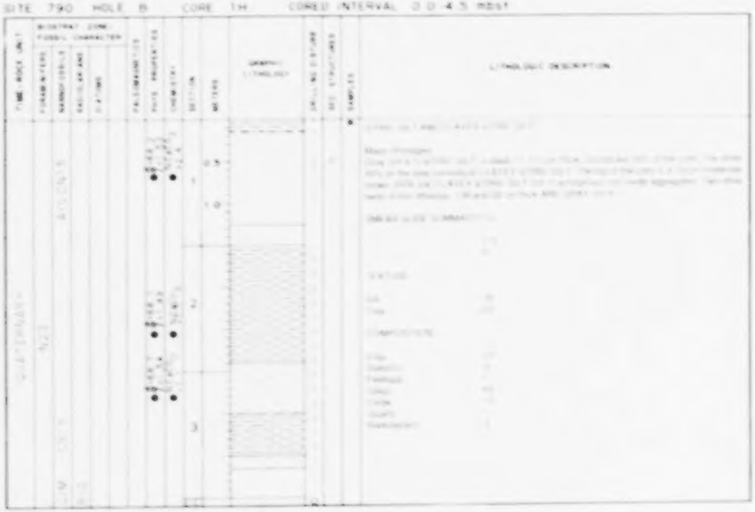
TIME-ROCK UNIT
BIOSTRAT. ZONE/FOSSIL CHARACTER
FORAMINIFERS
NANNOFOSSILS
RADIOLARIANS
DIATOMS
PALEOMAGNETICS
PHYS. PROPERTIES
CHEMISTRY
SECTION
METERS
GRAPHIC LITHOLOGY
DRILLING DISTURB.
SED. STRUCTURES
SAMPLES
LITHOLOGIC DESCRIPTION
0.5
1.0
1
2
3

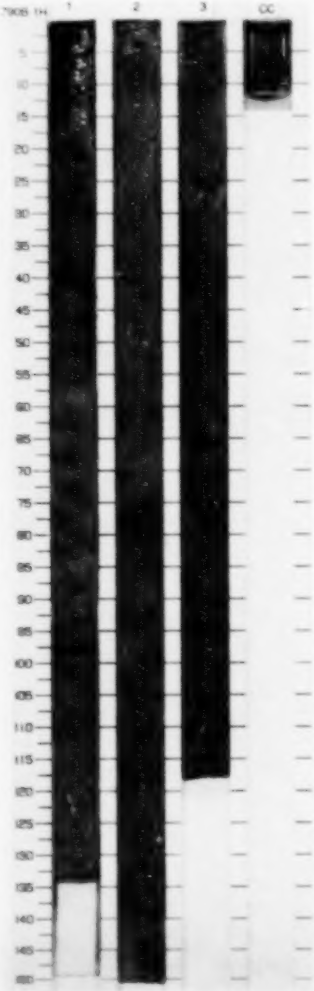
790B 1H
1
2
3
CC
5
10
15
20
25
30
35
40
45
50
55
60
65
70
75
80
85
90
95
100
105
110
115
120
125
130
135
140
145
150

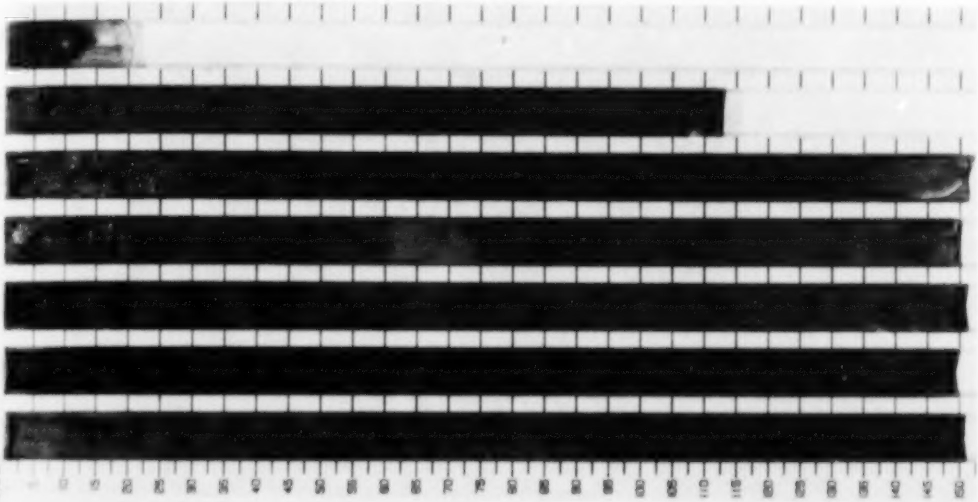

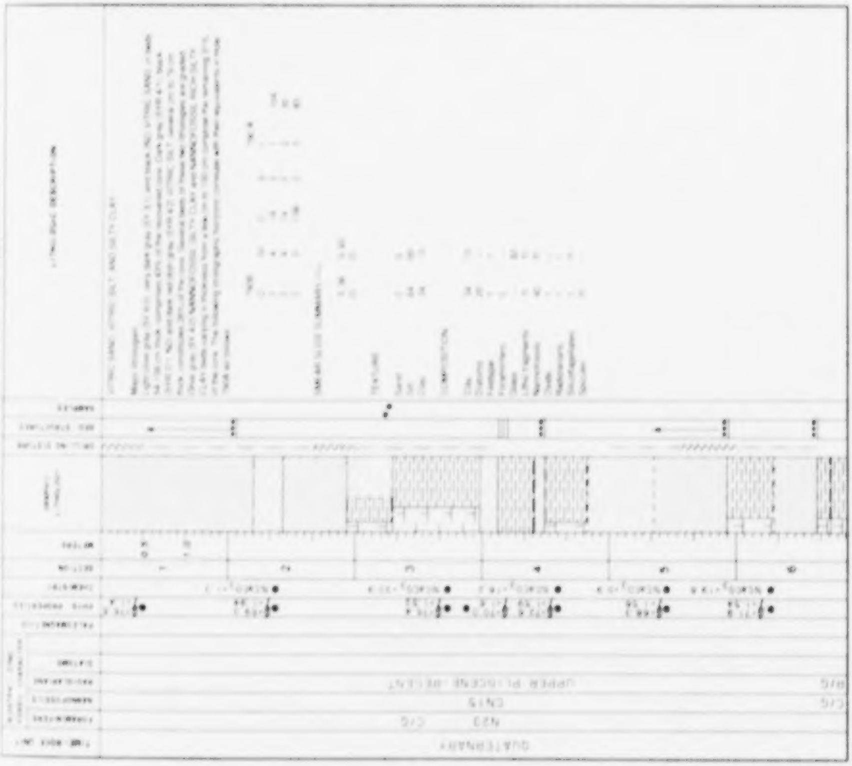
QUATERNARY
N23
C/G
CN15
C/G
UPPER PLIOCENE-RECENT
B/G
LITHOLOGIC DESCRIPTION

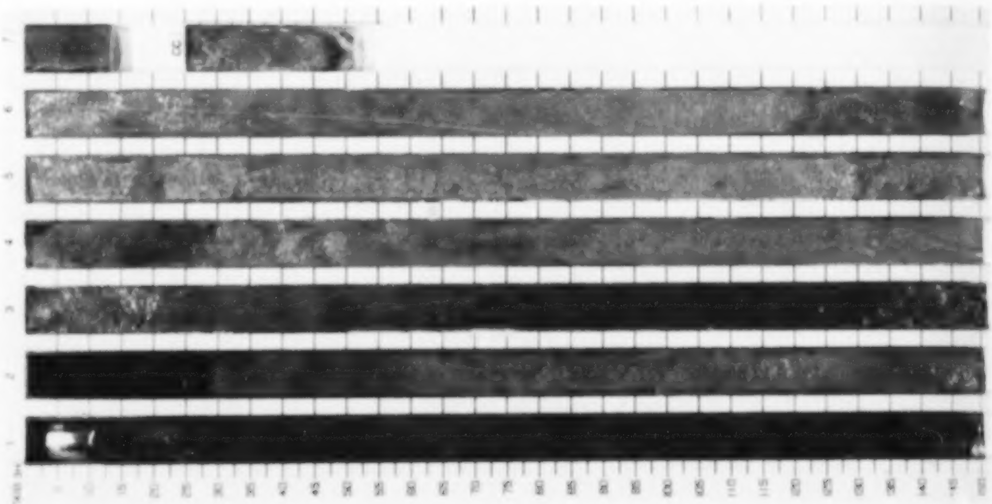
790B-3H
1
2
3
4
5
6
7
CC

SITE 790 HOLE B CORE 3H CORED INTERVAL 14.0-23.5 mbsf

LITHOLOGIC DESCRIPTION
QUATERNARY

SITE 790 HOLE B CORE 4H CORED INTERVAL 23.5-33.0 mbsf

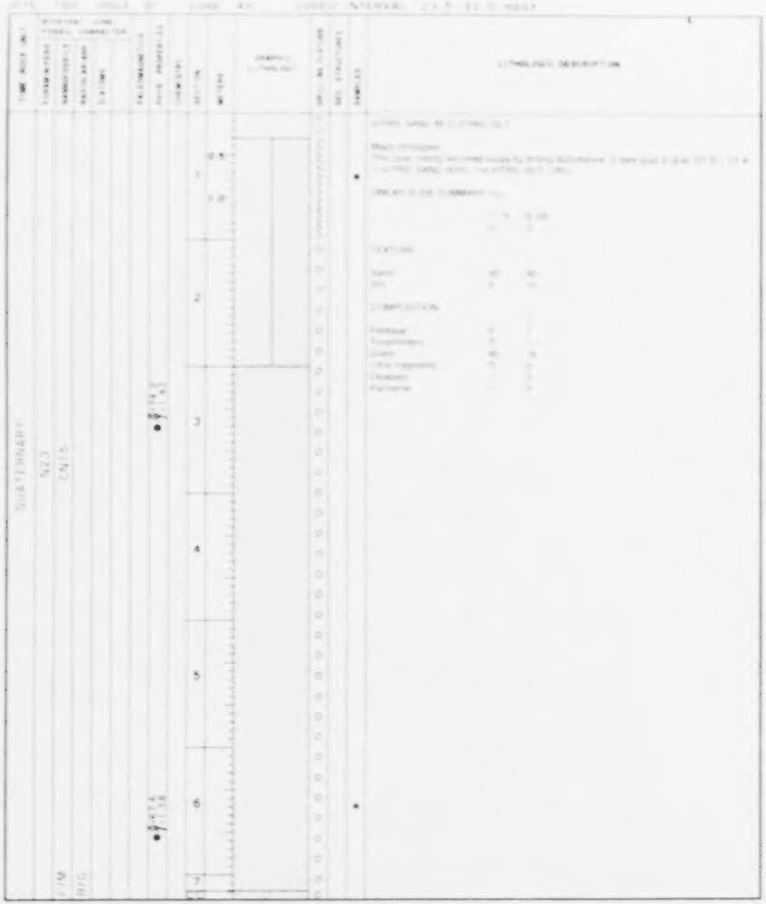
TIME-ROCK UNIT
BIOSTRAT. ZONE/ FOSSIL CHARACTER
FORAMINIFERS
NANNOFOSSILS
RADIOLARIANS
DIATOMS
PALEOMAGNETICS
PHYS. PROPERTIES
CHEMISTRY
SECTION
METERS
GRAPHIC LITHOLOGY
DRILLING DISTURB.
SED. STRUCTURES
SAMPLES
QUATERNARY
N23
CN15
F/M
M/G
1
2
3
4
5
6
7
0.5
1.0

LITHOLOGIC DESCRIPTION

VITRIC SAND to CLAYEY VITRIC SILT

Major lithologies:
[illegible]

SMEAR SLIDE SUMMARY (%):

TEXTURE:

Sand
Silt

COMPOSITION:

Feldspar
[illegible]
Glass
[illegible]
Opaques
Pyroxene

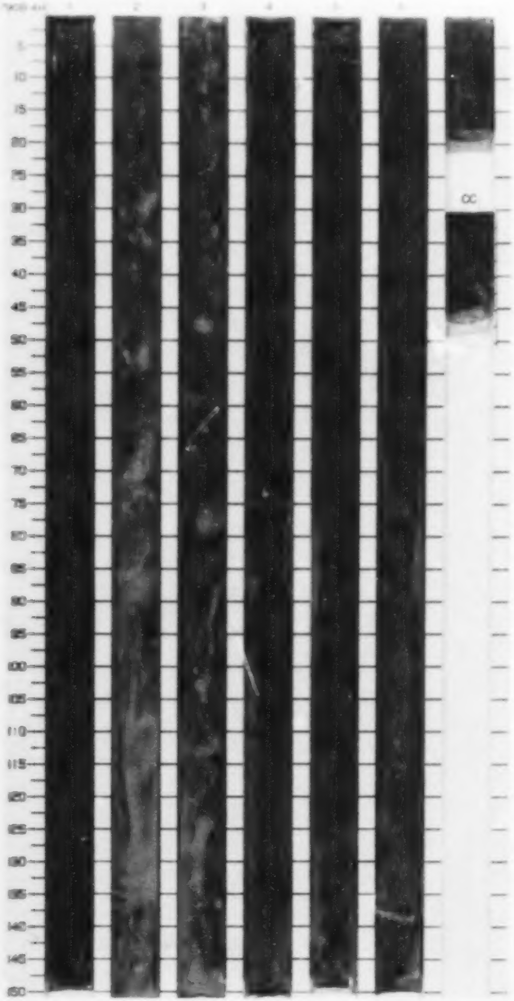
790B-4H
1
2
3
4
5
6
7
CC
5
10
15
20
25
30
35
40
45
50
55
60
65
70
75
80
85
90
95
100
105
110
115
120
125
130
135
140
145
150

SITE 790 HOLE B CORE 5H CORED INTERVAL 33.0-42.5 mbsf

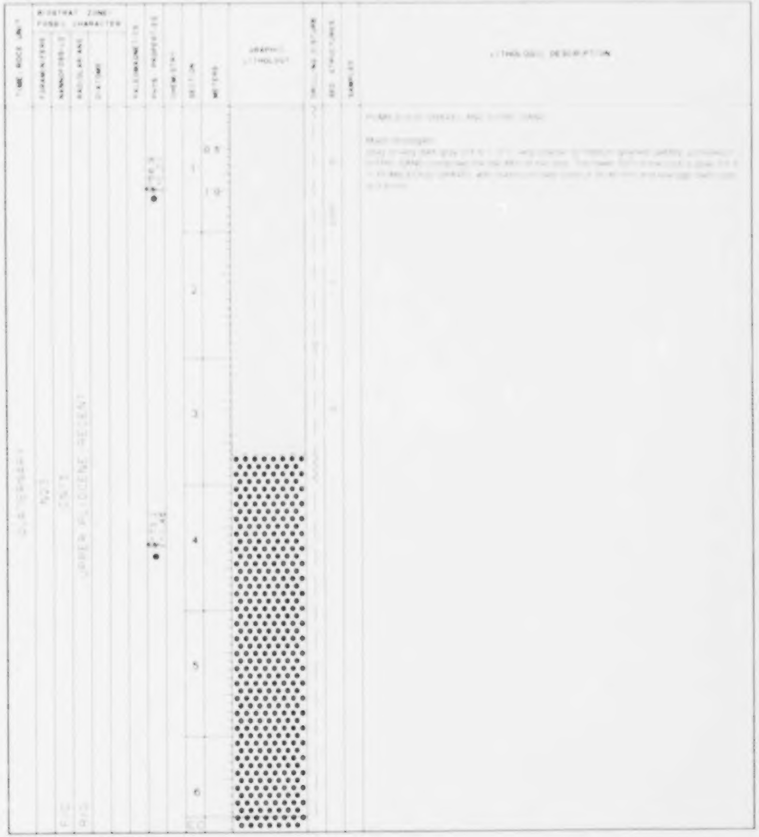
TIME-ROCK UNIT
BIOSTRAT. ZONE/ FOSSIL CHARACTER
FORAMINIFERS
NANNOFOSSILS
RADIOLARIANS
DIATOMS
PALEOMAGNETICS
PHYS. PROPERTIES
CHEMISTRY
SECTION
METERS
GRAPHIC LITHOLOGY
DRILLING DISTURB.
SED. STRUCTURES
SAMPLES
LITHOLOGIC DESCRIPTION
QUATERNARY
N22
UPPER PLIOCENE-RECENT
0.5
1.0
1
2
3
4
5
6
CC

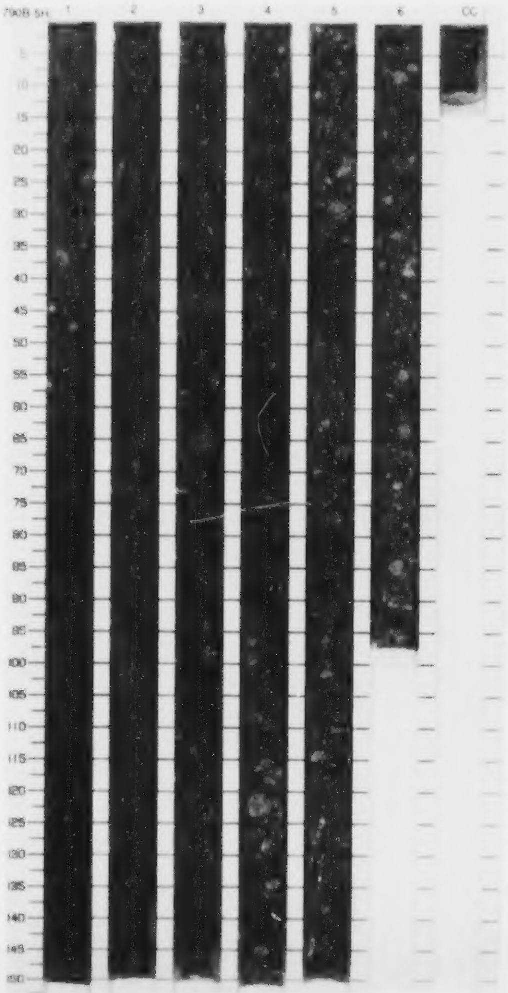
790B 5H
1
2
3
4
5
6
CC
5
10
15
20
25
30
35
40
45
50
55
60
65
70
75
80
85
90
95
100
105
110
115
120
125
130
135
140
145
150

SITE 790 HOLE B CORE 6H CORED INTERVAL 42.5-52.0 mbsf

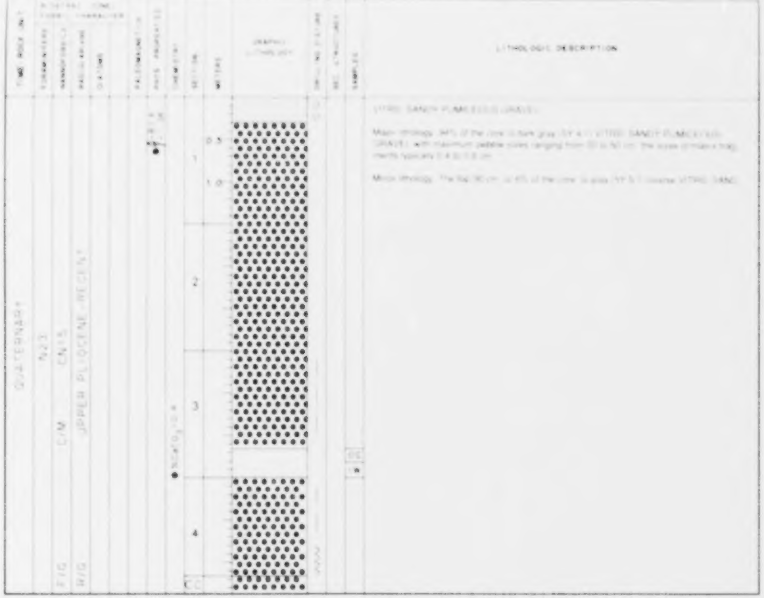
TIME-ROCK UNIT
BIOSTRAT. ZONE/FOSSIL CHARACTER
FORAMINIFERS
NANNOFOSSILS
RADIOLARIANS
DIATOMS
PALEOMAGNETICS
PHYS. PROPERTIES
CHEMISTRY
SECTION
METERS
GRAPHIC LITHOLOGY
DRILLING DISTURB.
SED. STRUCTURES
SAMPLES
QUATERNARY
N23
C/M CN15
UPPER PLIOCENE-RECENT
F/G
R/G
1
2
3
4
CC
0.5
1.0
IW
OG

LITHOLOGIC DESCRIPTION

VITRIC SANDY PUMICEOUS GRAVEL

Major lithology: 94% of the core is dark gray (5Y 4/1) VITRIC SANDY PUMICEOUS GRAVEL with maximum pebble sizes ranging from 30 to 50 cm; the sizes of matrix fragments typically 0.4 to 0.8 cm.

Minor lithology: The last 90 cm (or 6% of the core) is gray (5Y 5/1) coarse VITRIC SAND.

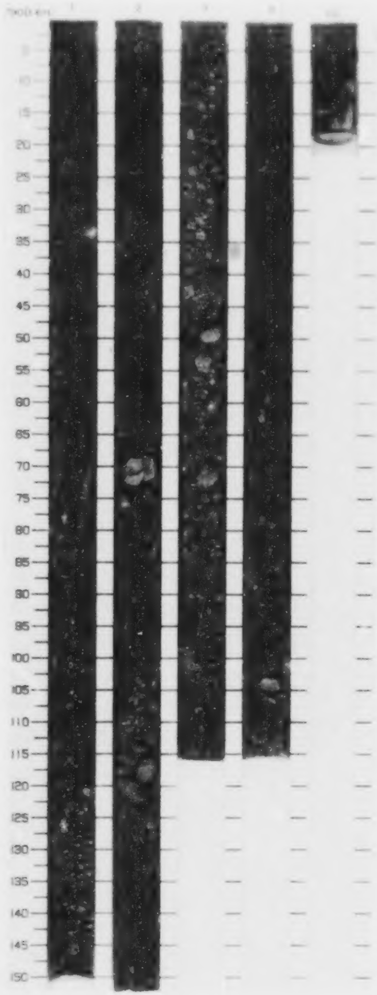
790B-6H
1
2
3
4
CC
0
5
10
15
20
25
30
35
40
45
50
55
60
65
70
75
80
85
90
95
100
105
110
115
120
125
130
135
140
145
150

SITE 790 HOLE B CORE 7H CORED INTERVAL 52.0-61.6 mbsf

TIME-ROCK UNIT	FORAMINIFERS	NANNOFOSSILS	RADIOLARIANS	DIATOMS	PALEOMAGNETICS	PHYS. PROPERTIES	CHEMISTRY	SECTION	METERS	GRAPHIC LITHOLOGY	DRILLING DISTURB.	SED. STRUCTURES	SAMPLES	LITHOLOGIC DESCRIPTION
QUATERNARY	N22	CN15	UPPER PLIOCENE - RECENT					1 2 3 4 5 6 CC	0.5 1.0					
	A/G	C/G												

LITHOLOGIC DESCRIPTION

[illegible]

Major lithologies:

[illegible]

Minor lithologies:

[illegible]

SMEAR SLIDE SUMMARY (%):

TEXTURE:

Sand
Silt
Clay

COMPOSITION:

[illegible]

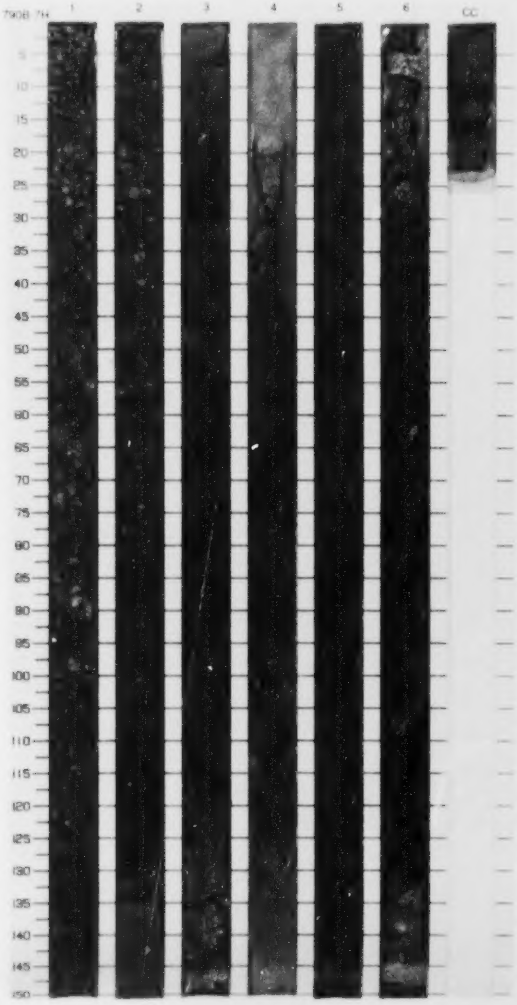
790B 7H
1
2
3
4
5
6
CC
5
10
15
20
25
30
35
40
45
50
55
60
65
70
75
80
85
90
95
100
105
110
115
120
125
130
135
140
145
150

SITE 790 HOLE B CORE [illegible] CORED INTERVAL [illegible]-71.3 mbsf

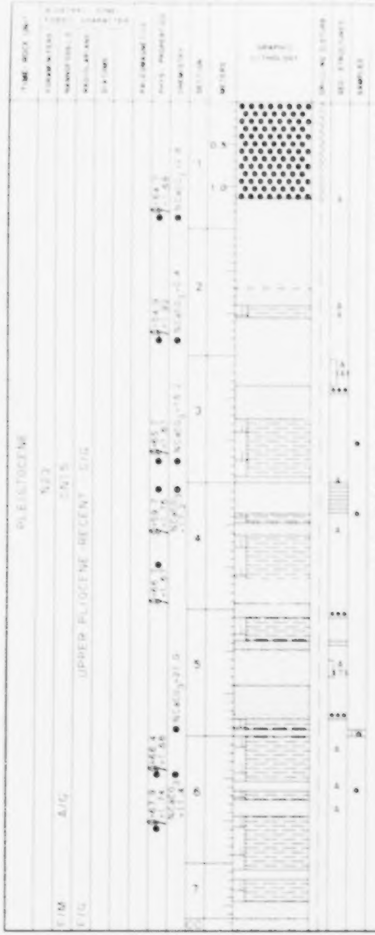
TIME-ROCK UNIT
BIOSTRAT. ZONE / FOSSIL CHARACTER
FORAMINIFERS
NANNOFOSSILS
RADIOLARIANS
DIATOMS
PALEOMAGNETICS
PHYS. PROPERTIES
CHEMISTRY
SECTION
METERS
GRAPHIC LITHOLOGY
DRILLING DISTURB.
SED. STRUCTURES
SAMPLES
PLEISTOCENE
N22
CN15
UPPER PLIOCENE-RECENT
A/G
F/M
F/G
0.5
1.0
1
2
3
4
5
6
7
CC

LITHOLOGIC DESCRIPTION

VITRIC SILT AND NANNOFOSSIL-RICH SILTY CLAY

Major lithologies:
VITRIC SILT in varying shades of gray to black (5Y 5/1, 4/1, 3/1, 2/2; 5YR 2/1; N2), in beds [illegible] cm thick, makes up 41% of the core. Most ([illegible]%) of the remaining core consists of olive gray (5Y 4/2) NANNOFOSSIL-RICH SILTY CLAY beds 5–50 cm thick; some containing dispersed vitric (ash) grains.

Minor lithologies:
A light gray (5Y 7/1) granule-pebble VITRIC PUMICEOUS GRAVEL with maximum clast sizes of 3.5 cm comprises the top 13% of the core. Black (5Y 2.5/1; N2) VITRIC SAND beds from a few millimeters to 40 cm thick constitute 11% of the recovered core. Graded bedding and lamination occur in places in the sandy and silty intervals.

SMEAR SLIDE SUMMARY (%):

	[illegible]	[illegible]	[illegible]
	D	D	D
TEXTURE:			
Sand	—	[illegible]	[illegible]
Silt	[illegible]	[illegible]	[illegible]
Clay	[illegible]	—	—
COMPOSITION:			
Clay	[illegible]	—	—
Diatoms	[illegible]	—	—
Feldspar	[illegible]	[illegible]	[illegible]
Foraminifers	[illegible]	—	—
Glass	[illegible]	[illegible]	[illegible]
Lithic Fragments	[illegible]	[illegible]	[illegible]
Mica	—	—	[illegible]
Nannofossils	[illegible]	—	[illegible]
Opaques	[illegible]	—	—
Pyroxene	—	[illegible]	[illegible]
Radiolarians	[illegible]	—	—
Silicoflagellates	[illegible]	—	—
Spicules	[illegible]	—	—

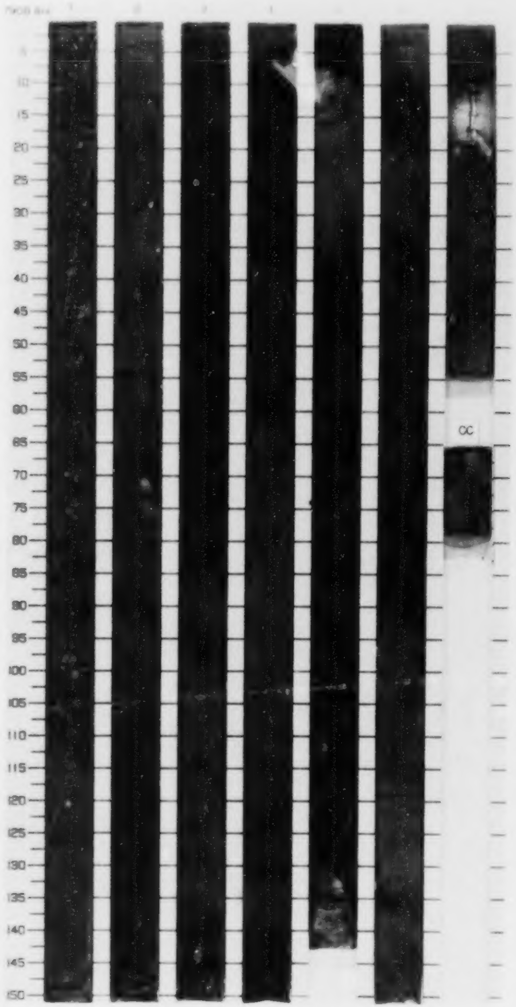
CM
1
2
3
4
5
6
7
CC
5
10
15
20
25
30
35
40
45
50
55
60
65
70
75
80
85
90
95
100
105
110
115
120
125
130
135
140
145
150

SITE 790 HOLE B CORE 9H CORED INTERVAL 71.3-81.0 mbsf

TIME-ROCK UNIT	FORAMINIFERS	NANNOFOSSILS	RADIOLARIANS	DIATOMS	PALEOMAGNETICS	PHYS. PROPERTIES	CHEMISTRY	SECTION	METERS	GRAPHIC LITHOLOGY	DRILLING DISTURB.	SED. STRUCTURES	SAMPLES	LITHOLOGIC DESCRIPTION
QUATERNARY	N23	CN15 F/P	R/G			[illegible]	● NC&CO₃=0.8 ● NC&CO₃=0.4	1 2 3 CC	0.5 1.0				● IW ● ●	VITRIC SILT AND VITRIC SAND Major lithologies: [illegible] SMEAR SLIDE SUMMARY (%): TEXTURE: Sand Silt COMPOSITION: Feldspar Glass Lithic fragments Pyroxene

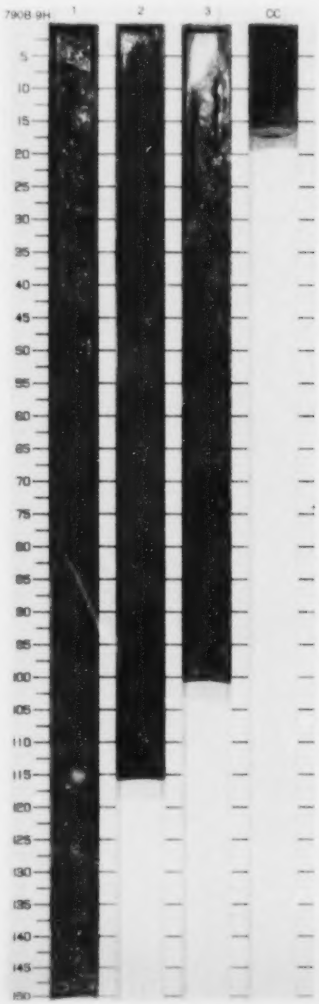
790B-9H
1
2
3
CC
5
10
15
20
25
30
35
40
45
50
55
60
65
70
75
80
85
90
95
100
105
110
115
120
125
130
135
140
145
150

SITE 790 HOLE B CORE 10H CORED INTERVAL 81.0-90.7 mbsf

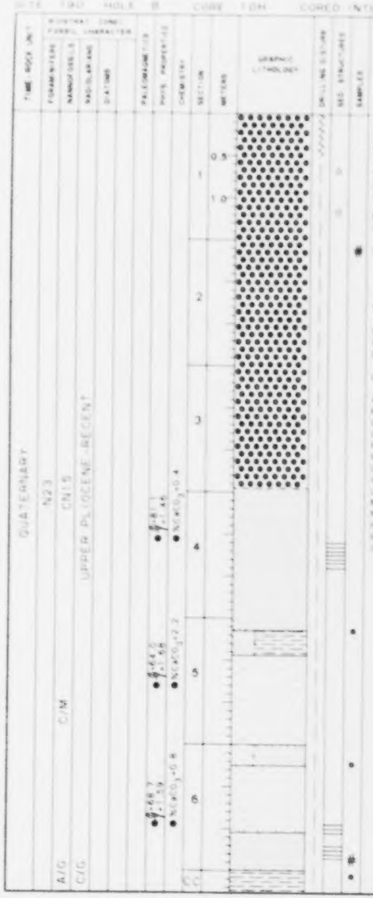
TIME-ROCK UNIT
BIOSTRAT. ZONE/ FOSSIL CHARACTER
FORAMINIFERS
NANNOFOSSILS
RADIOLARIANS
DIATOMS
PALEOMAGNETICS
PHYS. PROPERTIES
CHEMISTRY
SECTION
METERS
GRAPHIC LITHOLOGY
DRILLING DISTURB.
SED. STRUCTURES
SAMPLES
QUATERNARY
N23
CN15
C/M
A/G
UPPER PLIOCENE-RECENT
C/G
φ=61.1 γ=1.46
%CaCO3=0.4
φ=64.0 γ=1.66
%CaCO3=2.2
φ=68.7 γ=1.59
%CaCO3=0.8
1
2
3
4
5
6
CC
0.5
1.0

LITHOLOGIC DESCRIPTION

VITRIC PUMICEOUS GRAVEL, VITRIC SAND AND VITRIC SILT

Major lithologies:
The top 445 cm (50%) of the core is light olive gray, olive gray, gray, and black (5Y 6/2, 5Y 4/2, 5/2) granule and pebble VITRIC PUMICEOUS GRAVEL. Gray, olive gray and black (5Y 5/1, 4/1, 5/2) VITRIC SAND beds comprise 27% of the core, and dark gray (5Y 4/1) VITRIC SILT beds 15% of the core.

Minor lithology: Dark olive gray (5Y 3/2) SILTY CLAY, 5% of the core, occurs in thin beds near the top of Section 5.

SMEAR SLIDE SUMMARY & THIN SECTIONS (%):

	2, 100 D	5, 14 D	6, 20 D	6, 130 D	CC, 8 M
TEXTURE:					
Sand	100	90	100	95	1
Silt	—	10	—	5	77
Clay	—	—	—	—	22
COMPOSITION:					
Accessory minerals	—	—	—	2	—
Biotite	—	Tr	—	—	—
Clay	—	—	—	—	22
Diatoms	—	Tr	—	—	1
Feldspar	2	8	10	5	Tr
Foraminifers	—	—	—	Tr	1
Glass	95	90	88	88	63
[illegible]	—	—	—	1	—
Lithic fragments	—	Tr	—	—	—
Micrite	—	—	—	—	1
Nannofossils	—	—	—	—	12
Pyroxene	—	Tr	2	—	Tr
Rock fragment	3	—	—	3	—
Spicules	—	—	—	—	Tr

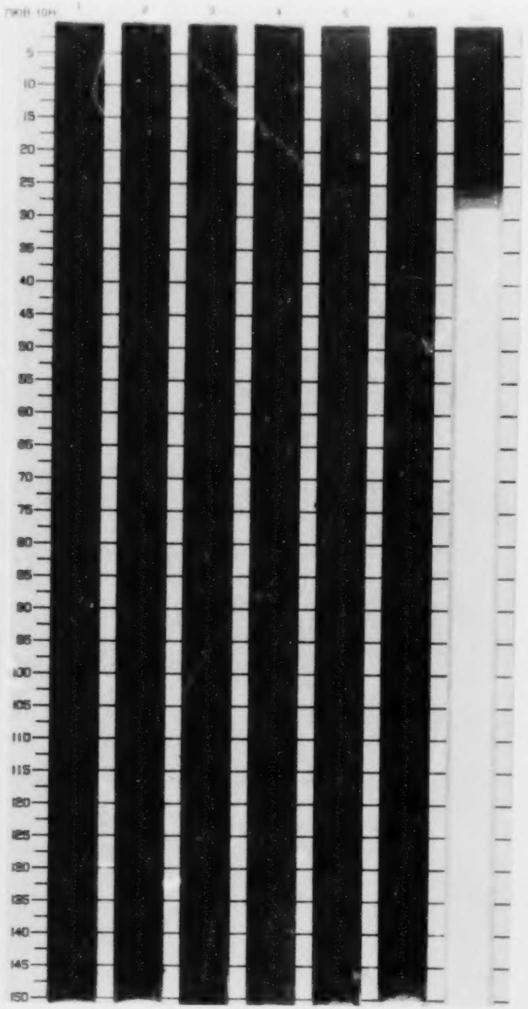
790B-10H
1
2
3
4
5
6
CC
5
10
15
20
25
30
35
40
45
50
55
60
65
70
75
80
85
90
95
100
105
110
115
120
125
130
135
140
145
150

SITE 790 HOLE B CORE 11H CORED INTERVAL 90.7-100.3 mbsf

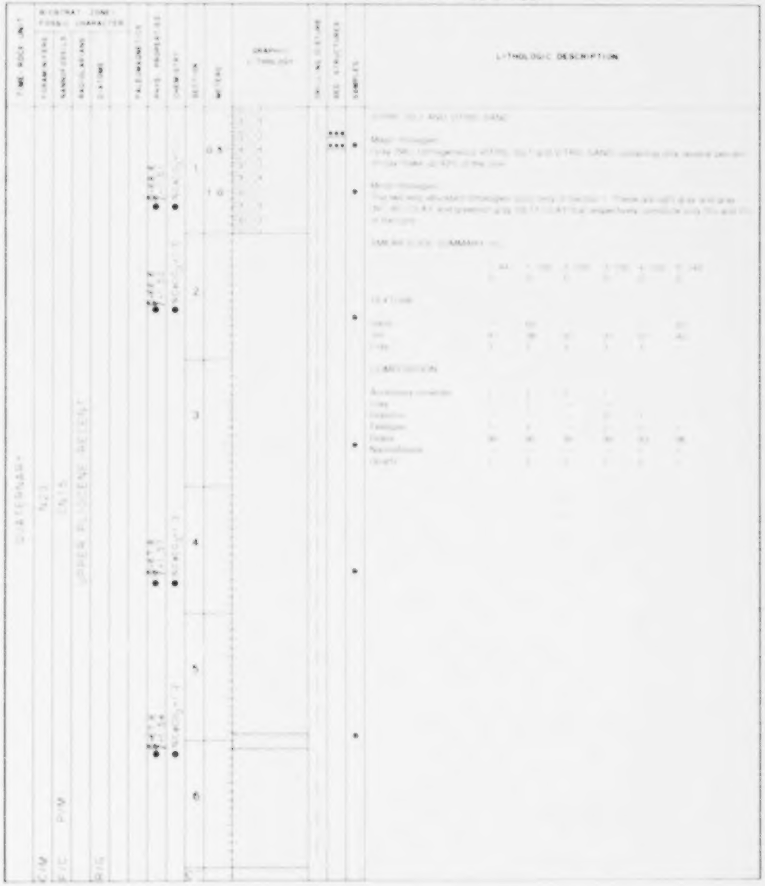
TIME-ROCK UNIT
BIOSTRAT. ZONE/FOSSIL CHARACTER
FORAMINIFERS
NANNOFOSSILS
RADIOLARIANS
DIATOMS
PALEOMAGNETICS
PHYS. PROPERTIES
CHEMISTRY
SECTION
METERS
GRAPHIC LITHOLOGY
DRILLING DISTURB.
SED. STRUCTURES
SAMPLES
QUATERNARY
N23
CN15
UPPER PLIOCENE–RECENT
C/M
F/C
P/M
B/G
1
2
3
4
5
6
0.5
1.0

LITHOLOGIC DESCRIPTION

VITRIC SILT AND VITRIC SAND

Major lithologies:

[illegible]

Minor lithologies:

[illegible]

SMEAR SLIDE SUMMARY (%):

	1, 41	1, 100	2, 100	3, 100	4, 100	5, 140
	D	D	D	D	D	D
TEXTURE:						
Sand	[illegible]	[illegible]	[illegible]	[illegible]	[illegible]	[illegible]
Silt	[illegible]	[illegible]	[illegible]	[illegible]	[illegible]	[illegible]
Clay	[illegible]	[illegible]	[illegible]	[illegible]	[illegible]	[illegible]
COMPOSITION:						
Accessory minerals	[illegible]	[illegible]	[illegible]	[illegible]	[illegible]	[illegible]
Clay	[illegible]	[illegible]	[illegible]	[illegible]	[illegible]	[illegible]
Dolomite	[illegible]	[illegible]	[illegible]	[illegible]	[illegible]	[illegible]
Feldspar	[illegible]	[illegible]	[illegible]	[illegible]	[illegible]	[illegible]
Glass	[illegible]	[illegible]	[illegible]	[illegible]	[illegible]	[illegible]
Nannofossils	[illegible]	[illegible]	[illegible]	[illegible]	[illegible]	[illegible]
Quartz	[illegible]	[illegible]	[illegible]	[illegible]	[illegible]	[illegible]

126 790B 12X NO RECOVERY

126 790B 13X NO RECOVERY

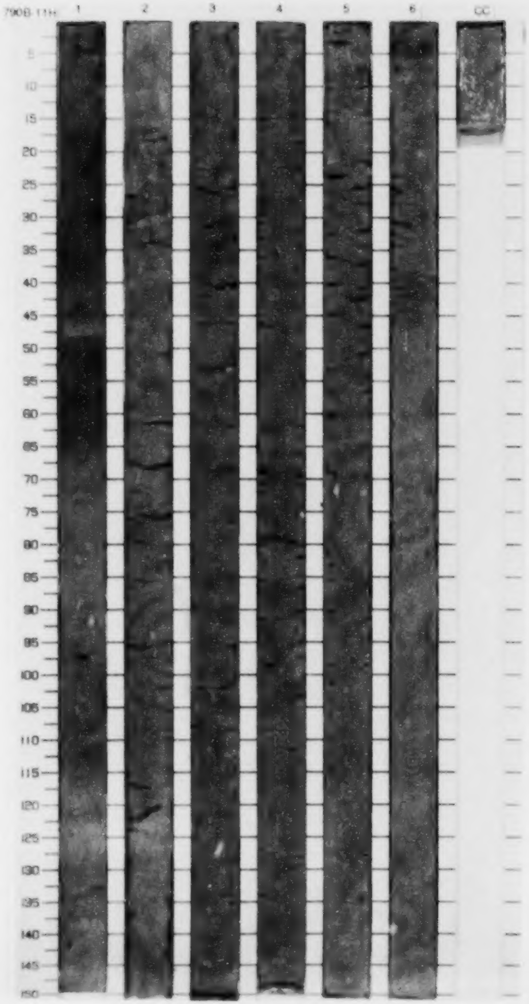
790B 11H
1
2
3
4
5
6
CC
5
10
15
20
25
30
35
40
45
50
55
60
65
70
75
80
85
90
95
100
105
110
115
120
125
130
135
140
145
150

126 790B 14X NO RECOVERY

SITE 790 HOLE B CORE 15X CORED INTERVAL 129.3-138.9 mbsf

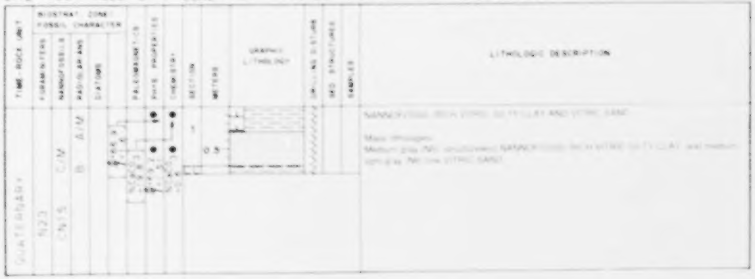

TIME-ROCK UNIT	FORAMINIFERS	NANNOFOSSILS	RADIOLARIANS	DIATOMS	PALEOMAGNETICS	PHYS. PROPERTIES	CHEMISTRY	SECTION	METERS	GRAPHIC LITHOLOGY	DRILLING DISTURB.	SED. STRUCTURES	SAMPLES	LITHOLOGIC DESCRIPTION
QUATERNARY	N23	CN15 C/M	B A/M			● ●	● ●	1	0.5					NANNOFOSSIL-RICH VITRIC SILTY CLAY AND VITRIC SAND Major lithologies: Medium gray (N5), structureless NANNOFOSSIL-RICH VITRIC SILTY CLAY and medium light gray (N6) fine VITRIC SAND.

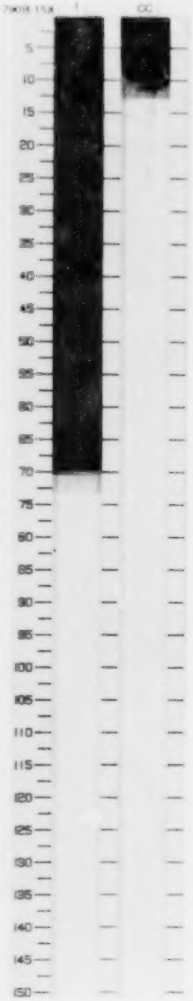
790B 15X
1
CC
5
10
15
20
25
30
35
40
45
50
55
60
65
70
75
80
85
90
95
100
105
110
115
120
125
130
135
140
145
150

SITE 790 HOLE C CORE 1H CORED INTERVAL 85.0-94.5 mbsf

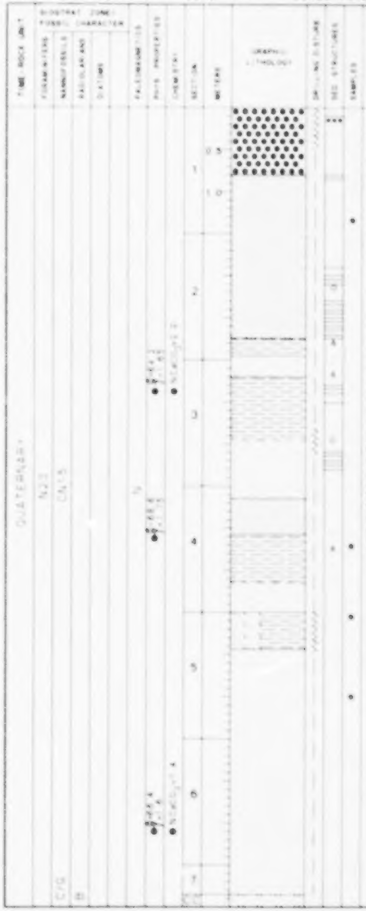

LITHOLOGIC DESCRIPTION

VITRIC SILT, VITRIC SAND AND SILTY CLAY

Major lithologies:

Dark gray [illegible] VITRIC [illegible] interbedded with the other lithologies in the upper part of the core, and comprising the basal [illegible] of the core [illegible] of the recovery. Dark gray [illegible] and black [illegible] VITRIC SAND [illegible] in the [illegible] and dark gray [illegible] SILTY CLAY [illegible] recovery.

Minor lithology: The uppermost [illegible] of recovery [illegible] VITRIC PUMICEOUS GRAVEL with maximum [illegible] Planar laminations [illegible] some of the sands and silts [illegible] places.

SMEAR SLIDE SUMMARY (%):

	[illegible]	[illegible]	[illegible]	[illegible]
TEXTURE:				
Sand	50	90	90	5
Silt	45	5	10	90
Clay	5	[illegible]		5
COMPOSITION:				
Clay	5	[illegible]		3
Diatoms	[illegible]	[illegible]		
Feldspar	8	[illegible]		
Foraminifers	[illegible]	[illegible]		
Glass	54	90	100	97
Lithic fragments	[illegible]			
Micrite	[illegible]			
Nannofossils	[illegible]	[illegible]	[illegible]	[illegible]
Pyrite	[illegible]			
Pyroxene	[illegible]			
Radiolarians	[illegible]	[illegible]		

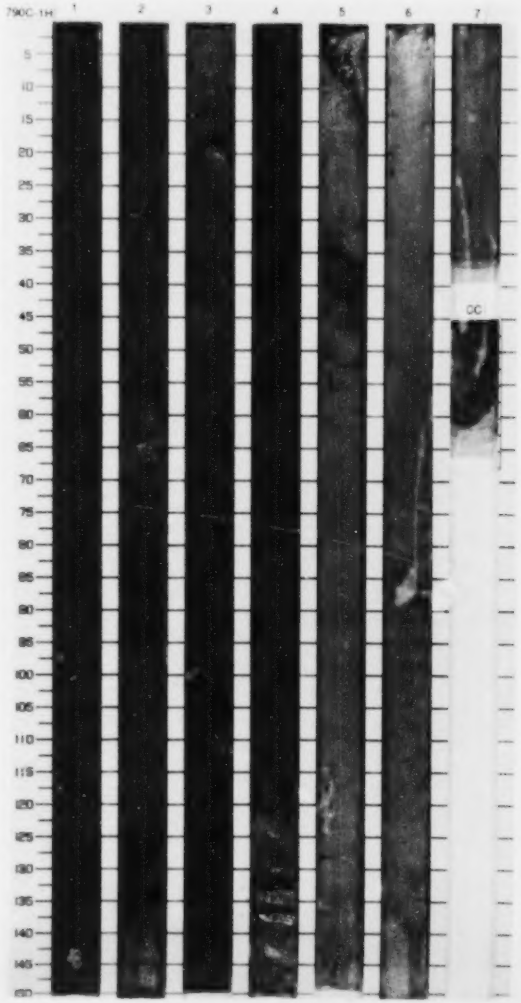
790C-1H
1
2
3
4
5
6
7
CC
5
10
15
20
25
30
35
40
45
50
55
60
65
70
75
80
85
90
95
100
105
110
115
120
125
130
135
140
145
150

SITE 790 HOLE C CORE 1H CORED INTERVAL 104.2-113.9 mbsl

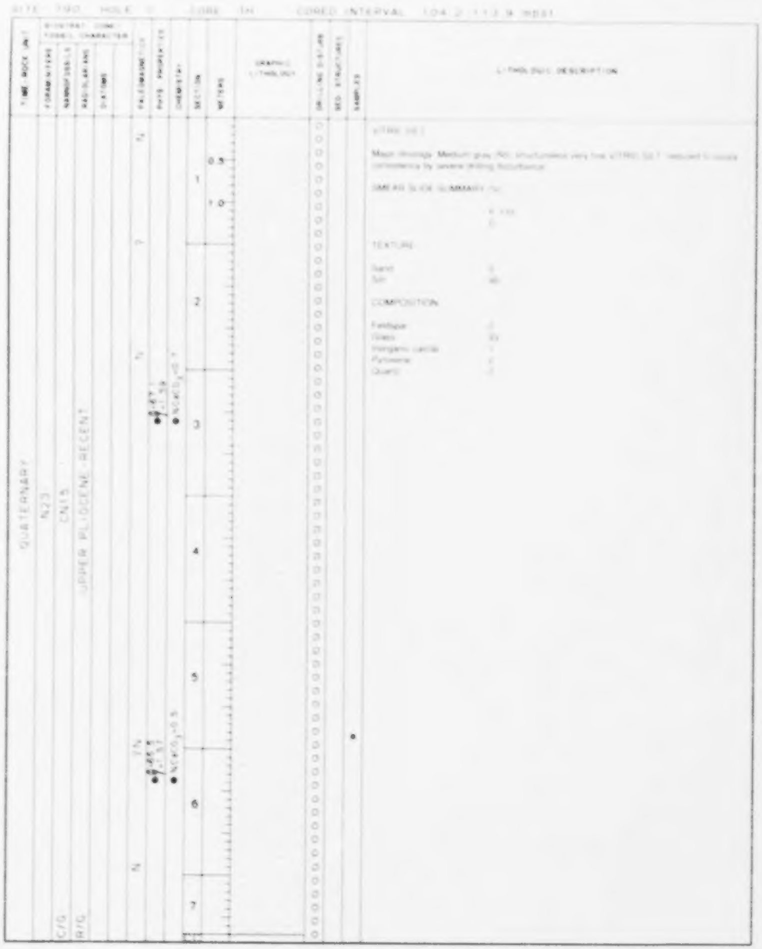
TIME-ROCK UNIT
BIOSTRAT. ZONE/FOSSIL CHARACTER
FORAMINIFERS
NANNOFOSSILS
RADIOLARIANS
DIATOMS
PALEOMAGNETICS
PHYS. PROPERTIES
CHEMISTRY
SECTION
METERS
GRAPHIC LITHOLOGY
DRILLING DISTURB.
SED. STRUCTURES
SAMPLES
QUATERNARY
N23
CN15
UPPER PLIOCENE-RECENT
C/G
R/G
N
?
N
?N
N
●NCaCO3=0.7
●NCaCO3=0.5
1
2
3
4
5
6
7
0.5
1.0

LITHOLOGIC DESCRIPTION

VITRIC SILT

Major lithology: Medium gray (N5) structureless very fine VITRIC SILT reduced to soupy consistency by severe drilling disturbance.

SMEAR SLIDE SUMMARY (%):

	6, 130
	D
TEXTURE:	
Sand	5
Silt	95
COMPOSITION:	
Feldspar	2
Glass	93
Inorganic calcite	1
Pyroxene	2
Quartz	2

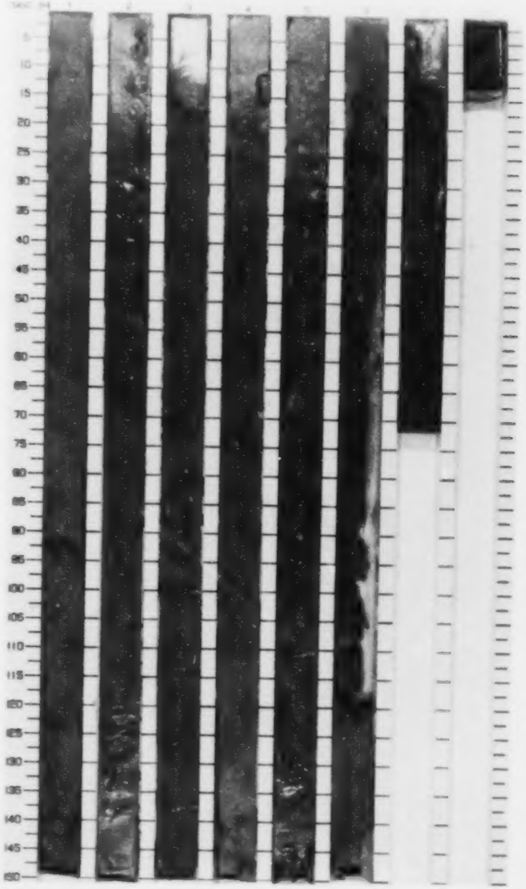
CM
1
2
3
4
5
6
7
8
5
10
15
20
25
30
35
40
45
50
55
60
65
70
75
80
85
90
95
100
105
110
115
120
125
130
135
140
145
150

SITE 790 HOLE C CORE 2H CORED INTERVAL 94.5-104.2 mbsf

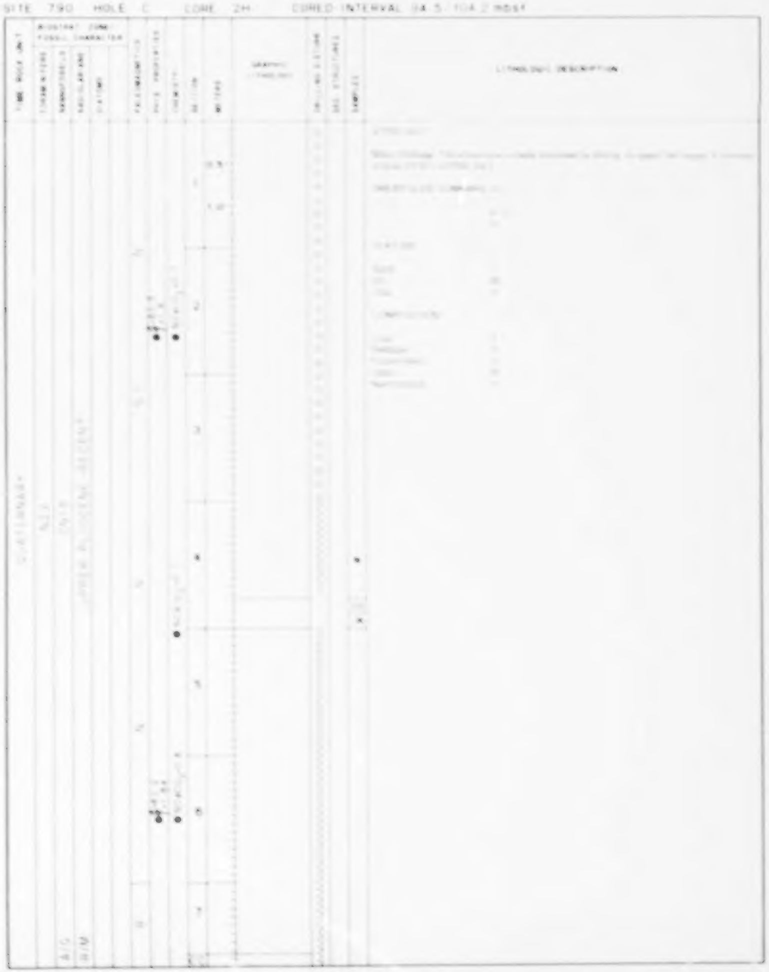

TIME-ROCK UNIT
BIOSTRAT. ZONE/ FOSSIL CHARACTER
FORAMINIFERS
NANNOFOSSILS
RADIOLARIANS
DIATOMS
PALEOMAGNETICS
PHYS. PROPERTIES
CHEMISTRY
SECTION
METERS
GRAPHIC LITHOLOGY
DRILLING DISTURB.
SED. STRUCTURES
SAMPLES
QUATERNARY
N22
CN15
UPPER PLIOCENE-RECENT
A/G
R/M
1
2
3
4
5
6
7
CC

LITHOLOGIC DESCRIPTION

[illegible]

SMEAR SLIDE SUMMARY (%):

TEXTURE:

Sand

Silt

Clay

COMPOSITION:

[illegible]

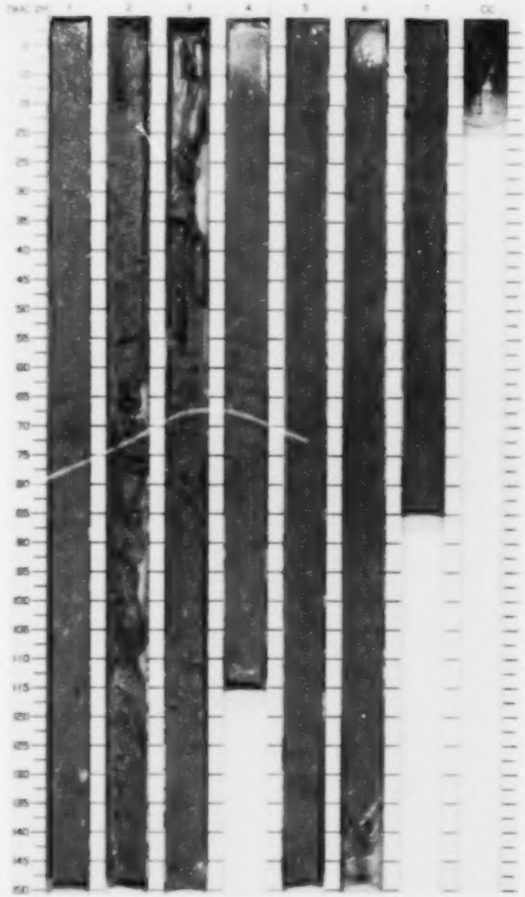

790C-2H
1
2
3
4
5
6
7
CC
0
5
10
15
20
25
30
35
40
45
50
55
60
65
70
75
80
85
90
95
100
105
110
115
120
125
130
135
140
145
150

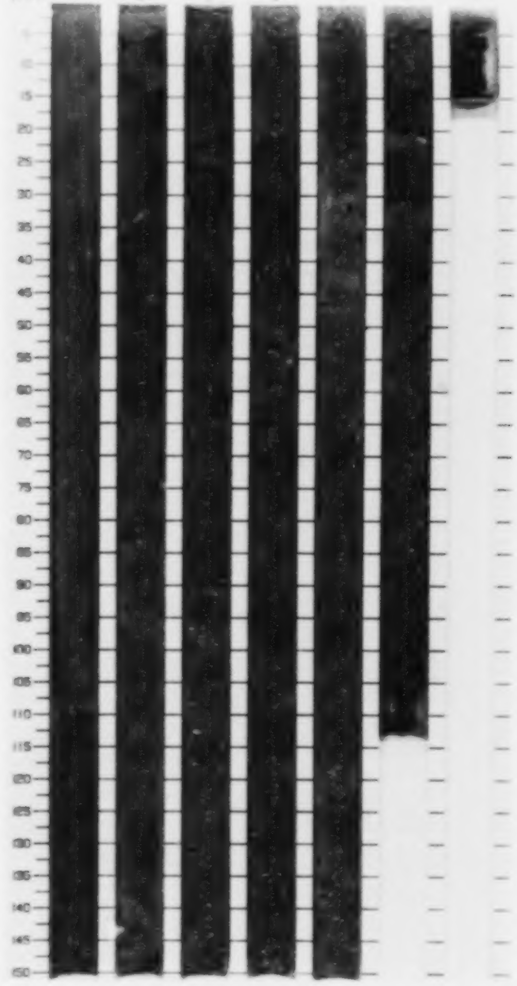
CM
0
5
10
15
20
25
30
35
40
45
50
55
60
65
70
75
80
85
90
95
100
105
110
115
120
125
130
135
140
145
150

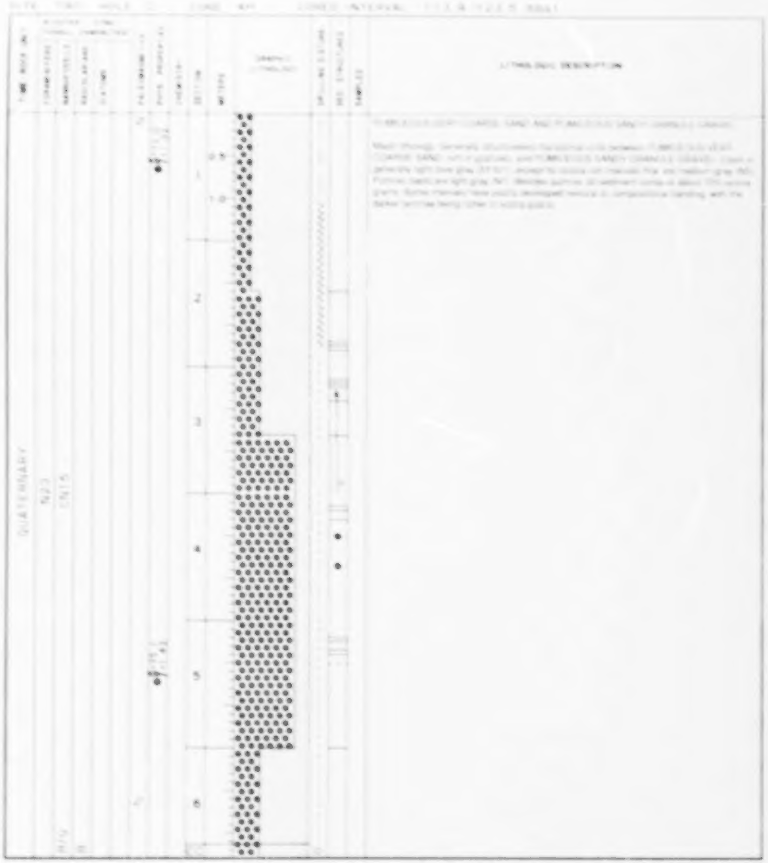
TIME-ROCK UNIT
BIOSTRAT. ZONE/FOSSIL CHARACTER
FORAMINIFERS
NANNOFOSSILS
RADIOLARIANS
DIATOMS
PALEOMAGNETICS
PHYS. PROPERTIES
CHEMISTRY
SECTION
METERS
GRAPHIC LITHOLOGY
DRILLING DISTURB.
SED. STRUCTURES
SAMPLES
QUATERNARY
N23
CN15
0.5
1
1.0
2
3
4
5
6

LITHOLOGIC DESCRIPTION

PUMICEOUS VERY COARSE SAND AND PUMICEOUS SANDY GRANULE GRAVEL

[illegible] through. Generally structureless horizontal units between PUMICEOUS VERY COARSE SAND [illegible] and PUMICEOUS SANDY GRANULE GRAVEL. Clasts generally light olive gray (5Y 6/1) [illegible] medium gray (N5). Pumice clasts are light gray (N7). Besides pumice, [illegible] sediment consists of about [illegible] volcanic grains. Some intervals have poorly developed normal to compositional banding, with the darker laminae being richer in volcanic grains.

SITE 790 HOLE C CORE 5H CORED INTERVAL 123.5-133.2 mbsf

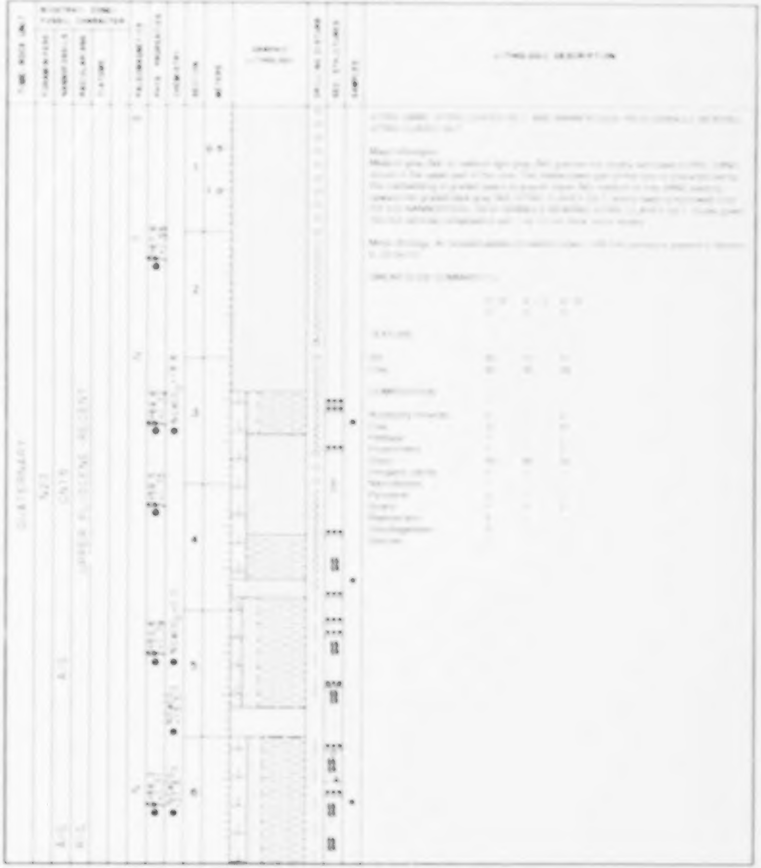
BIOSTRAT. ZONE/
FOSSIL CHARACTER
GRAPHIC
LITHOLOGY
LITHOLOGIC DESCRIPTION
QUATERNARY
N22
CN15
1
2
3
4
5
6

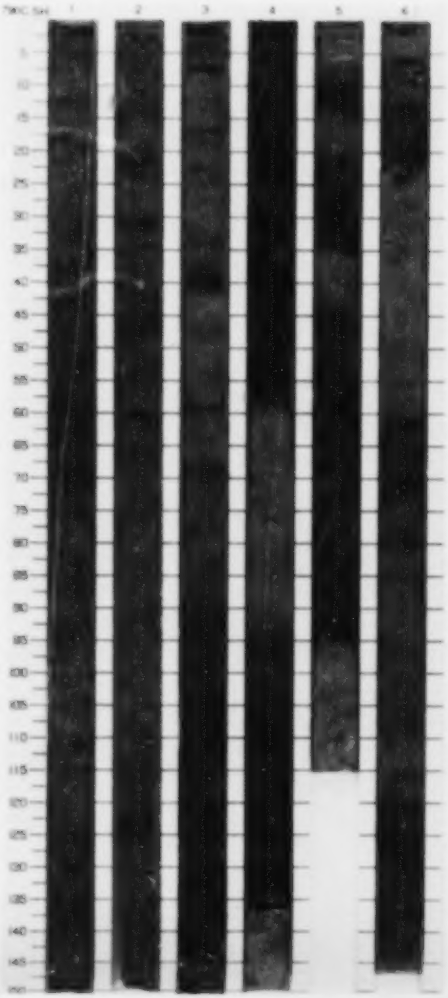
790C-5H
1
2
3
4
5
6
0
5
10
15
20
25
30
35
40
45
50
55
60
65
70
75
80
85
90
95
100
105
110
115
120
125
130
135
140
145
150

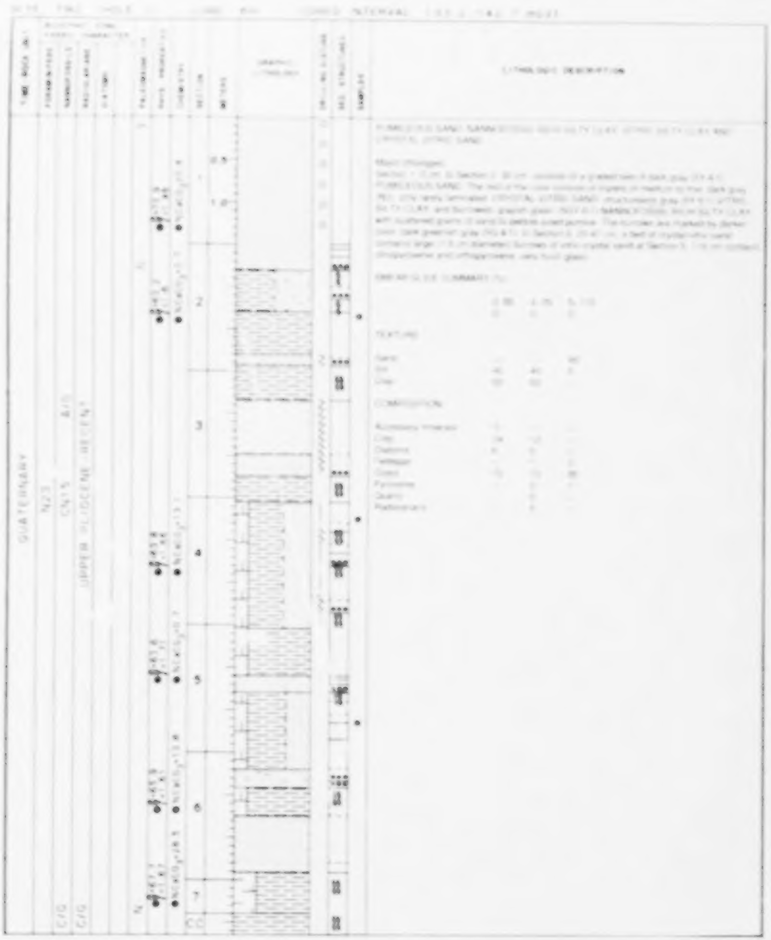
TIME ROCK UNIT
BIOSTRAT. ZONE / FOSSIL CHARACTER
FORAMINIFERS
NANNOFOSSILS
RADIOLARIANS
DIATOMS
PALEOMAGNETICS
PHYS. PROPERTIES
CHEMISTRY
SECTION
METERS
GRAPHIC LITHOLOGY
DRILLING DISTURB.
SED. STRUCTURES
SAMPLES
QUATERNARY
N23
CN15
A/G
UPPER PLIOCENE - RECENT
C/G
C/G
N
1
2
3
4
5
6
7
CC
0.5
1.0

LITHOLOGIC DESCRIPTION

PUMICEOUS SAND, NANNOFOSSIL-RICH SILTY CLAY, VITRIC SILTY CLAY, AND CRYSTAL VITRIC SAND

Major lithologies:

[illegible]

SMEAR SLIDE SUMMARY (%):

	2, 80	2, 75	5, 110
	D	D	D
TEXTURE:			
Sand	—	—	90
Silt	40	40	5
Clay	60	60	—
COMPOSITION:			
Accessory minerals	[illegible]	—	—
Clay	24	12	—
Diatoms	5	5	—
Feldspar	—	—	[illegible]
Glass	[illegible]	[illegible]	85
Pyroxene	—	[illegible]	[illegible]
Quartz	—	[illegible]	—
Radiolarians	—	[illegible]	—

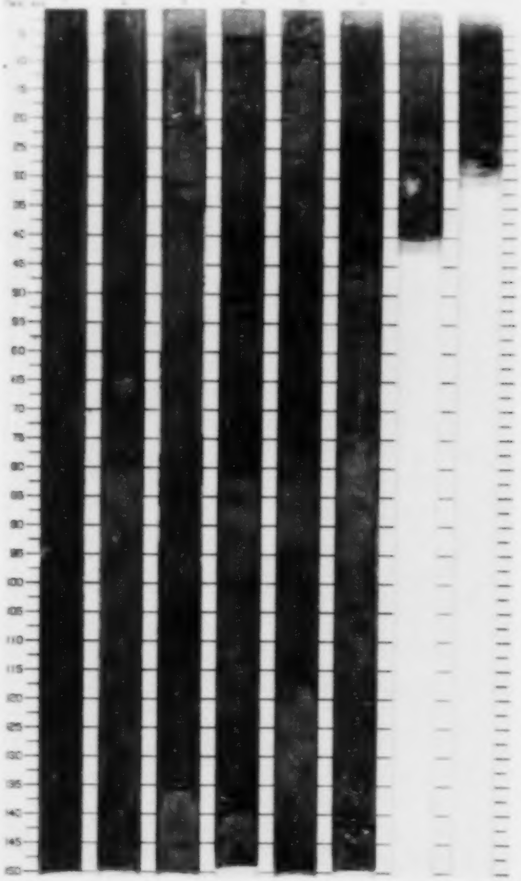
CM
1
2
3
4
5
6
7
CC
0
5
10
15
20
25
30
35
40
45
50
55
60
65
70
75
80
85
90
95
100
105
110
115
120
125
130
135
140
145
150

SITE 790 HOLE C CORE 7H CORED INTERVAL 142.7-145.7 mbsf

TIME-ROCK UNIT	BIOSTRAT. ZONE/FOSSIL CHARACTER: FORAMINIFERS	NANNOFOSSILS	RADIOLARIANS	DIATOMS	PALEOMAGNETICS	PHYS. PROPERTIES	CHEMISTRY	SECTION	METERS	GRAPHIC LITHOLOGY	DRILLING DISTURB.	SED. STRUCTURES	SAMPLES	LITHOLOGIC DESCRIPTION
[illegible]	[illegible]	[illegible]	[illegible]			●	●	1 2	0.5 1.0					[illegible]

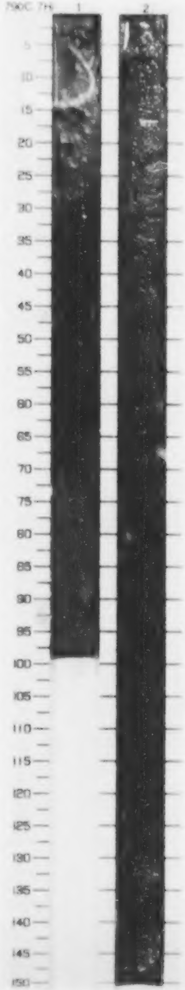
790C 7H
1
2
5
10
15
20
25
30
35
40
45
50
55
60
65
70
75
80
85
90
95
100
105
110
115
120
125
130
135
140
145
150

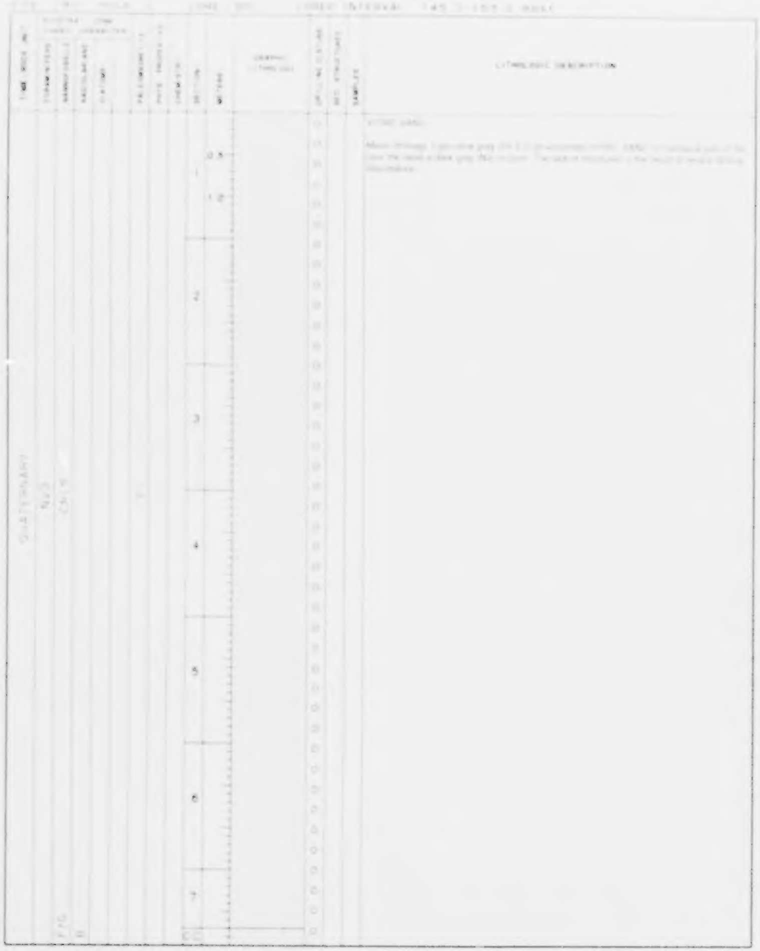
CORED INTERVAL 145.3-155.3 mbsf
TIME-ROCK UNIT
BIOSTRAT. ZONE/FOSSIL CHARACTER
FORAMINIFERS
NANNOFOSSILS
RADIOLARIANS
DIATOMS
PALEOMAGNETICS
PHYS. PROPERTIES
CHEMISTRY
SECTION
METERS
GRAPHIC LITHOLOGY
DRILLING DISTURB.
SED. STRUCTURES
SAMPLES
LITHOLOGIC DESCRIPTION
VITRIC SAND
QUATERNARY
N22
CN14
0.5
1.0
1
2
3
4
5
6
7
CC

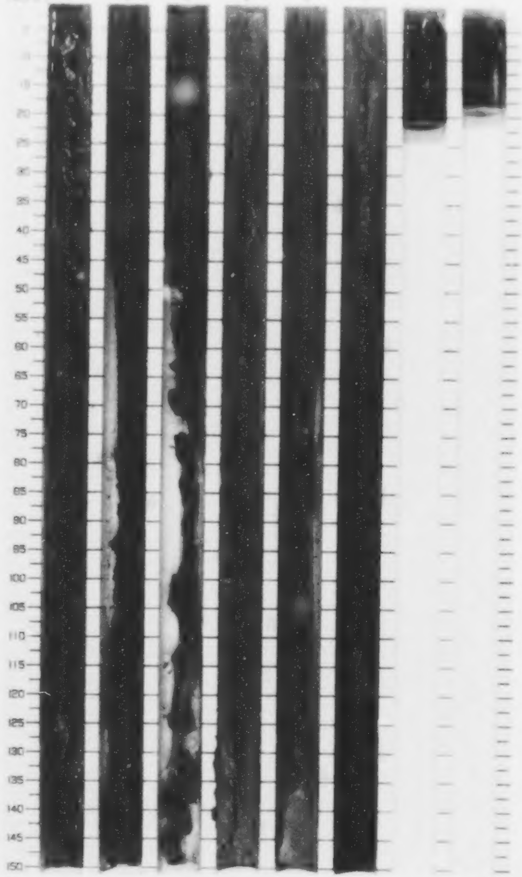
0
5
10
15
20
25
30
35
40
45
50
55
60
65
70
75
80
85
90
95
100
105
110
115
120
125
130
135
140
145
150

126 790C 9X NO RECOVERY

SITE 790 HOLE C CORE 10X CORED INTERVAL 164.9-174.6 mbsf

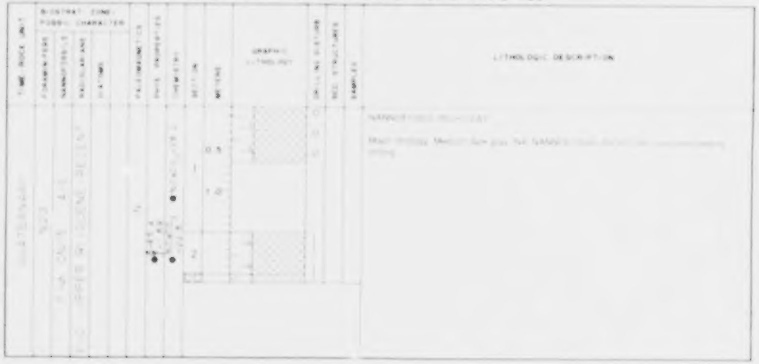
TIME-ROCK UNIT
BIOSTRAT. ZONE/FOSSIL CHARACTER
FORAMINIFERS
NANNOFOSSILS
RADIOLARIANS
DIATOMS
PALEOMAGNETICS
PHYS. PROPERTIES
CHEMISTRY
SECTION
METERS
GRAPHIC LITHOLOGY
DRILLING DISTURB.
SED. STRUCTURES
SAMPLES
LITHOLOGIC DESCRIPTION
0.5
1
1.0
2

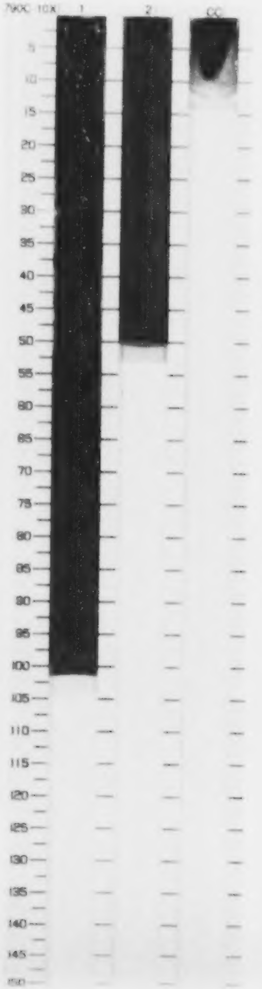
790C 10X
1
2
CC
5
10
15
20
25
30
35
40
45
50
55
60
65
70
75
80
85
90
95
100
105
110
115
120
125
130
135
140
145
150

SITE 790 HOLE [illegible] CORE 17X CORED INTERVAL 174.0-184.2 mbsf

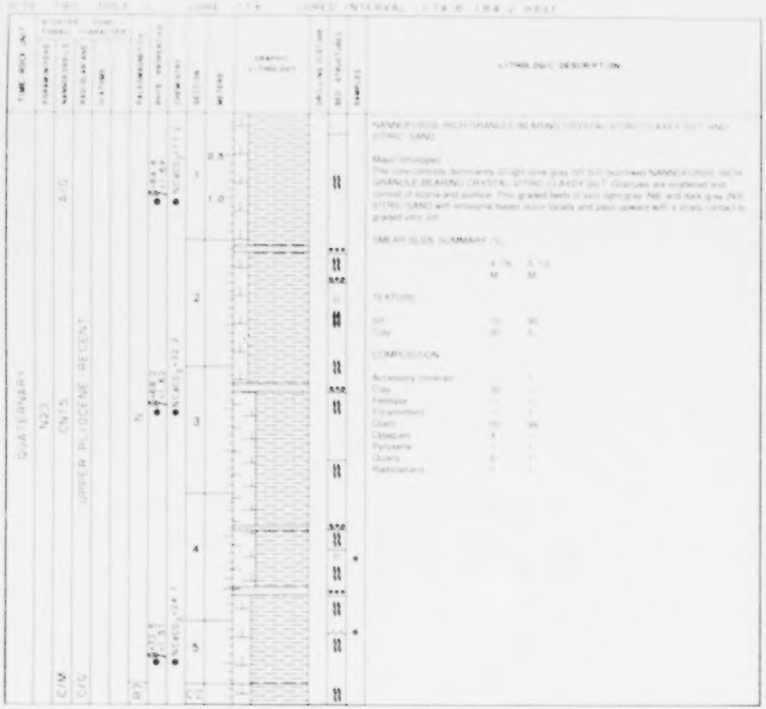
TIME-ROCK UNIT
BIOSTRAT. ZONE/ FOSSIL CHARACTER
FORAMINIFERS
NANNOFOSSILS
RADIOLARIANS
DIATOMS
PALEOMAGNETICS
PHYS. PROPERTIES
CHEMISTRY
SECTION
METERS
GRAPHIC LITHOLOGY
DRILLING DISTURB.
SED. STRUCTURES
SAMPLES
QUATERNARY
N23
CN15
A/G
C/M
UPPER PLIOCENE-RECENT
C/G
N
RY
1
2
3
4
5
CC
0.5
1.0

LITHOLOGIC DESCRIPTION

NANNOFOSSIL-RICH GRANULE-BEARING CRYSTAL-VITRIC CLAYEY SILT AND VITRIC SAND

Major lithologies:
The core consists dominantly of light olive gray (5Y 5/2) burrowed NANNOFOSSIL-RICH GRANULE-BEARING CRYSTAL-VITRIC CLAYEY SILT. Granules are scattered and consist of scoria and pumice. Thin graded beds of very light gray (N8) and dark gray (N3) VITRIC SAND with erosional bases occur locally and pass upward with a sharp contact to graded vitric silt.

SMEAR SLIDE SUMMARY (%):

	4, 79 M	5, 13 M
TEXTURE:		
Silt	70	95
Clay	30	5
COMPOSITION:		
Accessory minerals	—	1
Clay	30	—
Feldspar	—	[illegible]
Foraminifers	—	1
Glass	[illegible]	94
Opaques	3	—
Pyroxene	—	[illegible]
Quartz	[illegible]	[illegible]
Radiolarians	—	[illegible]

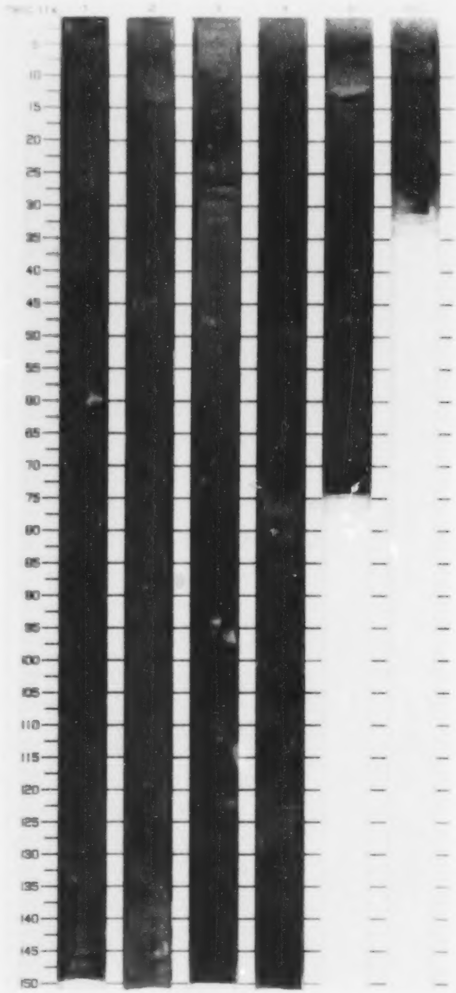
1
2
3
4
5
CC
5
10
15
20
25
30
35
40
45
50
55
60
65
70
75
80
85
90
95
100
105
110
115
120
125
130
135
140
145
150

SITE 790 HOLE C CORE 12X CORED INTERVAL 184.2-193.9 mbsf

TIME-ROCK UNIT	BIOSTRAT. ZONE/FOSSIL CHARACTER: FORAMINIFERS	NANNOFOSSILS	RADIOLARIANS	DIATOMS	PALEOMAGNETICS	PHYS. PROPERTIES	CHEMISTRY	SECTION	METERS	GRAPHIC LITHOLOGY	DRILLING DISTURB.	SED. STRUCTURES	SAMPLES	LITHOLOGIC DESCRIPTION
QUATERNARY	N23	CN14b	UPPER PLIOCENE-RECENT			● ●	●	1 CC	0.5 1.0				● ●	[illegible]

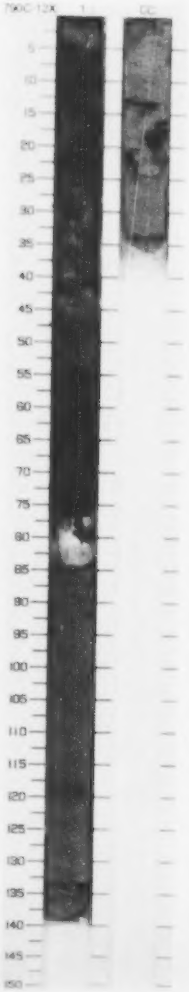
790C-12X
1
CC
5
10
15
20
25
30
35
40
45
50
55
60
65
70
75
80
85
90
95
100
105
110
115
120
125
130
135
140
145
150

SITE 790 HOLE C CORE 13X CORED INTERVAL 193.9-203.6 mbsf

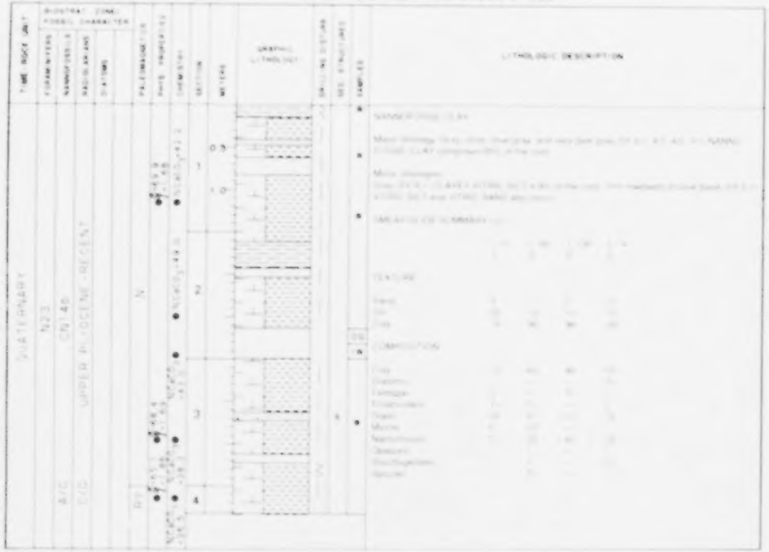
TIME-ROCK UNIT
BIOSTRAT. ZONE/ FOSSIL CHARACTER
FORAMINIFERS
NANNOFOSSILS
RADIOLARIANS
DIATOMS
PALEOMAGNETICS
PHYS. PROPERTIES
CHEMISTRY
SECTION
METERS
GRAPHIC LITHOLOGY
DRILLING DISTURB.
SED. STRUCTURES
SAMPLES
LITHOLOGIC DESCRIPTION
QUATERNARY
N23
CN14b
UPPER PLIOCENE-RECENT
A/G
C/G
N
R?
1
2
3
4
0.5
1.0
OG
NANNOFOSSIL CLAY
Major lithology
Minor lithologies
SMEAR SLIDE SUMMARY (%):
TEXTURE:
Sand
Silt
Clay
COMPOSITION:
Clay
Diatoms
Feldspar
Foraminifers
Glass
Micrite
Nannofossils
Opaques
Rock fragments
Spicules

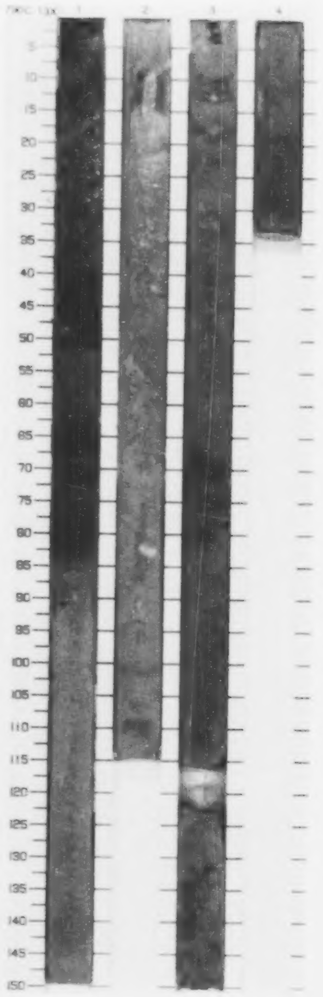
790C-13X
1
2
3
4
5
10
15
20
25
30
35
40
45
50
55
60
65
70
75
80
85
90
95
100
105
110
115
120
125
130
135
140
145
150

SITE 790 HOLE C CORE 14X CORED INTERVAL 203.6-213.2 mbsf

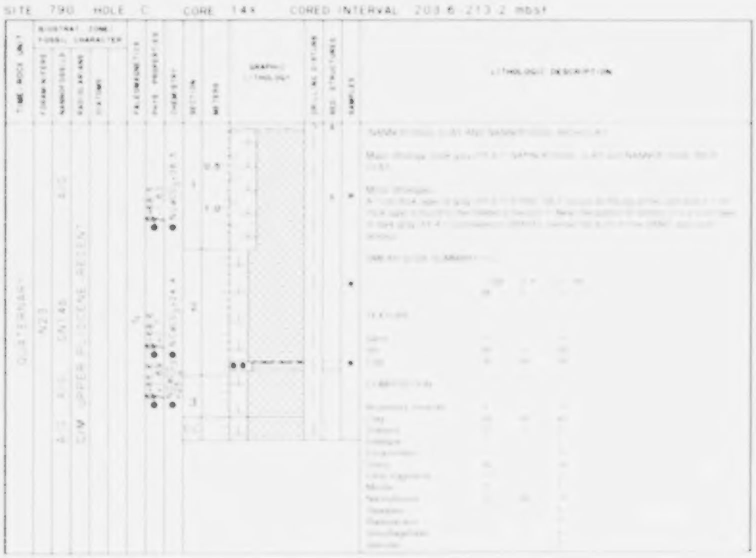
TIME-ROCK UNIT
BIOSTRAT. ZONE/FOSSIL CHARACTER
FORAMINIFERS
NANNOFOSSILS
RADIOLARIANS
DIATOMS
PALEOMAGNETICS
PHYS. PROPERTIES
CHEMISTRY
SECTION
METERS
GRAPHIC LITHOLOGY
DRILLING DISTURB.
SED. STRUCTURES
SAMPLES
QUATERNARY
N23
A/G
CN14b
A/G
C/M UPPER PLIOCENE-RECENT
1
2
3
CC
0.5
1.0

LITHOLOGIC DESCRIPTION

[illegible]

Major lithology: [illegible]

Minor lithologies: [illegible]

SMEAR SLIDE SUMMARY (%):

TEXTURE:

Sand

Silt

Clay

COMPOSITION:

[illegible]

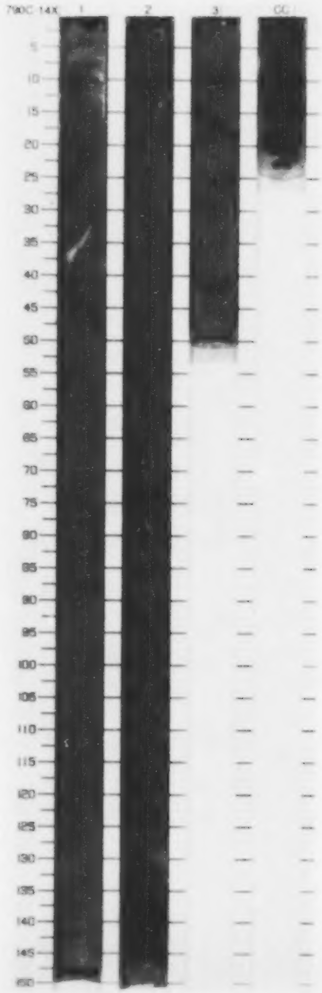
790C-14X
1
2
3
CC
5
10
15
20
25
30
35
40
45
50
55
60
65
70
75
80
85
90
95
100
105
110
115
120
125
130
135
140
145
150

SITE 790 HOLE C CORE 15X CORED INTERVAL 213.2-222.8 mbsf

TIME-ROCK UNIT	FORAMINIFERS	NANNOFOSSILS	RADIOLARIANS	DIATOMS	PALEOMAGNETICS	PHYS. PROPERTIES	CHEMISTRY	SECTION	METERS	GRAPHIC LITHOLOGY	DRILLING DISTURB.	SED. STRUCTURES	SAMPLES
QUATERNARY	N23	CN14b A/G	UPPER PLIOCENE - PLEISTOCENE C/M		B?			1 CC					● ●

LITHOLOGIC DESCRIPTION

SILTY SAND AND NANNOFOSSIL CLAY

Major lithologies:
The 36 cm of recovered sediment consists of 23 cm [illegible] of olive black [illegible] SILTY SAND interbedded with [illegible] of dark gray [illegible] NANNOFOSSIL CLAY.

SMEAR SLIDE SUMMARY (%):

	1, 8 D	CC, 3 D
TEXTURE:		
Sand	—	40
Silt	10	50
Clay	90	10
COMPOSITION:		
Accessory minerals	2	15
Clay	40	15
Diatoms	1	—
Feldspar	3	10
Foraminifers	—	4
Glass	10	50
Mica	2	1
Nannofossils	40	10
Radiolarians	—	2
Silicoflagellates	2	

790C-15X
1
CC
5
10
15
20
25
30
35
40
45
50
55
60
65
70
75
80
85
90
95
100
105
110
115
120
125
130
135
140
145
150

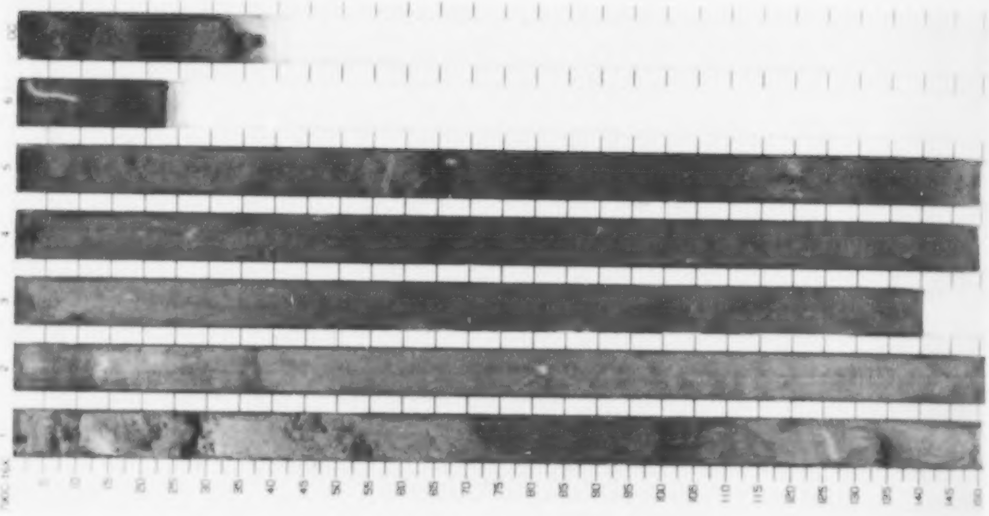
790C-16X
1
2
3
4
5
6
CC

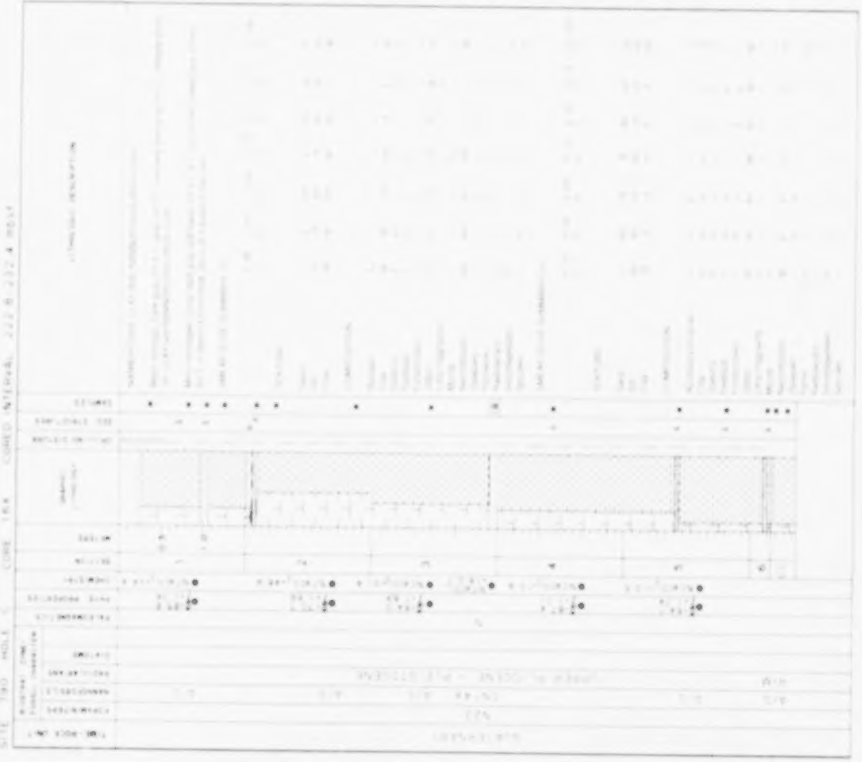
SITE 790 HOLE C CORE 16X CORED INTERVAL 222.8-232.4 mbsf
LITHOLOGIC DESCRIPTION

SITE 790 HOLE [illegible] CORE [illegible] CORED INTERVAL [illegible]

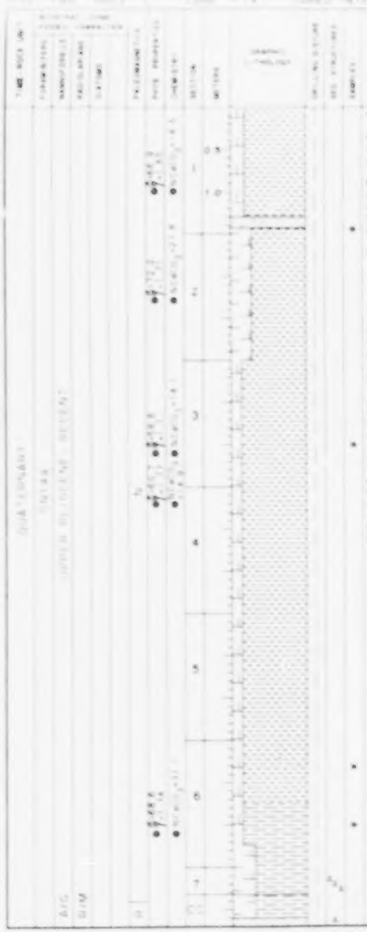
TIME-ROCK UNIT
BIOSTRAT. ZONE/FOSSIL CHARACTER
FORAMINIFERS
NANNOFOSSILS
RADIOLARIANS
DIATOMS
PALEOMAGNETICS
PHYS. PROPERTIES
CHEMISTRY
SECTION
METERS
GRAPHIC LITHOLOGY
DRILLING DISTURB.
SED. STRUCTURES
SAMPLES
QUATERNARY
CN14a
UPPER PLIOCENE - RECENT
A/G
B/M
0.5
1.0
1
2
3
4
5
6
7
CC

LITHOLOGIC DESCRIPTION

NANNOFOSSIL-RICH VITRIC CLAY AND NANNOFOSSIL VITRIC CLAY

Major lithologies:
Gray (5Y 5/1) and olive gray (5Y 4/2) NANNOFOSSIL-RICH VITRIC CLAY (5Y 4/2) occurs from Section 1, 0-130 cm and from Section 2, 145 cm to Section 6, 75 cm.

Minor lithologies:
Dark gray (5Y 4/1) NANNOFOSSIL VITRIC CLAYEY SILT occurs from Section 6, 75 cm to the base of the core catcher. Dark gray (5Y 4/1) VITRIC SANDY SILT occurs in Section 1, 130-145 cm. Three 1-2 cm beds of olive black (5Y 2/1), olive gray (5Y 4/2), and very dark gray (5Y 3/1) VITRIC SANDY SILT occur at the base of Section 7.

SMEAR SLIDE SUMMARY (%):

	1, 144 D	2, 100 D	6, 37 M	6, 150 D
TEXTURE:				
Sand	20	5	5	10
Silt	58	60	50	35
Clay	22	35	45	55
COMPOSITION:				
Accessory minerals	3	—	—	2
Clay	20	35	40	52
Diatoms	—	5	Tr	—
Feldspar	3	Tr	Tr	—
Foraminifers	Tr	2	—	Tr
Glass	60	28	50	15
Lithic fragments	Tr	—	—	—
Micrite	2	2	2	2
Nannofossils	2	25	Tr	20
Opaques	5	2	1	—
Radiolarians	—	—	Tr	5
Silicoflagellates	—	Tr	—	—
Spicules	—	2	Tr	—

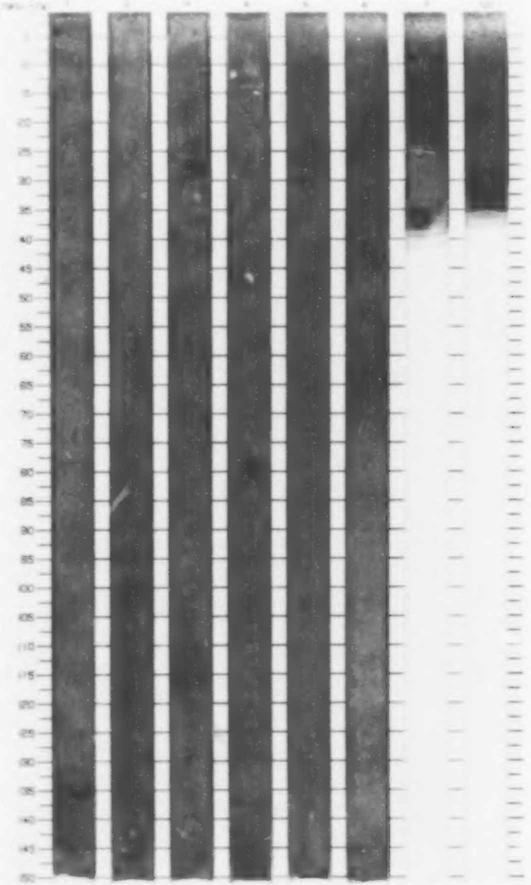
CM
1
2
3
4
5
6
7
CC
0
5
10
15
20
25
30
35
40
45
50
55
60
65
70
75
80
85
90
95
100
105
110
115
120
125
130
135
140
145
150

SITE 790 HOLE C CORE 18X CORED INTERVAL 242.1-251.7 mbsf

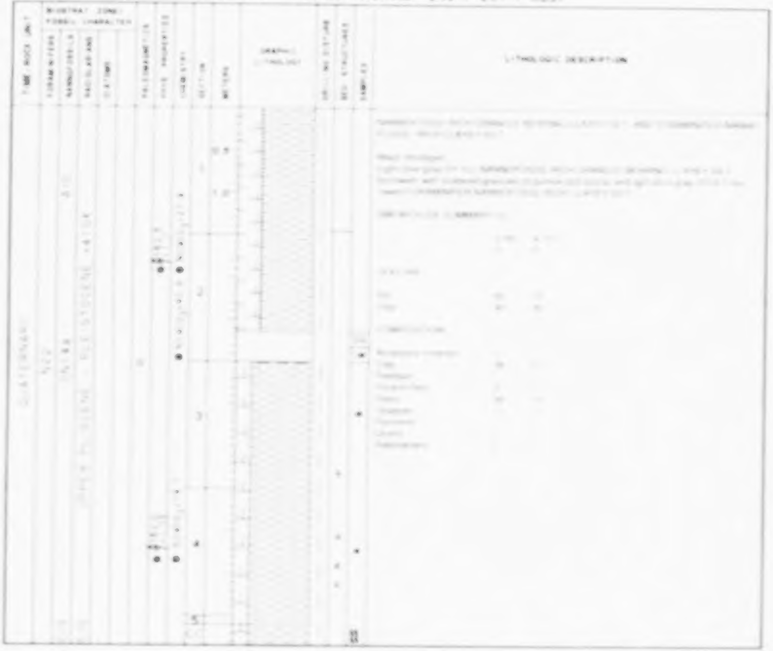
LITHOLOGIC DESCRIPTION
GRAPHIC LITHOLOGY
BIOSTRAT. ZONE/ FOSSIL CHARACTER
QUATERNARY

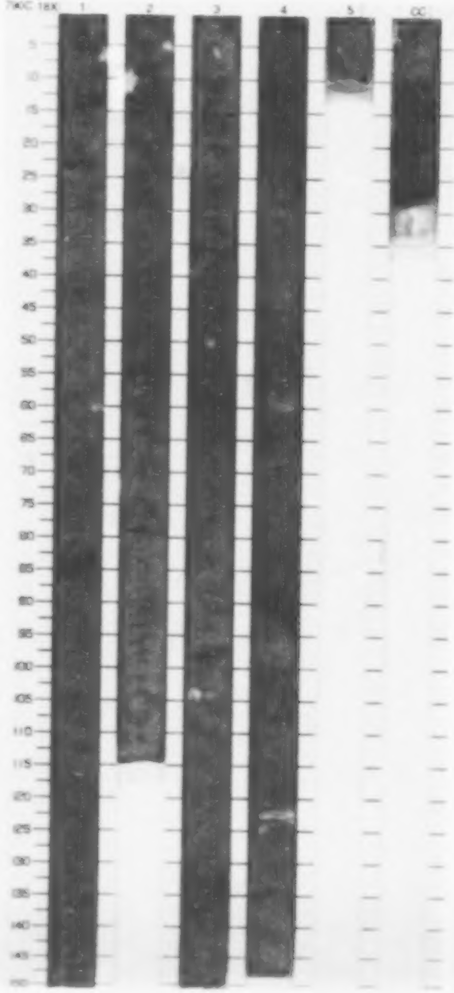
790C 18X
1
2
3
4
5
CC
5
10
15
20
25
30
35
40
45
50
55
60
65
70
75
80
85
90
95
100
105
110
115
120
125
130
135
140
145
150

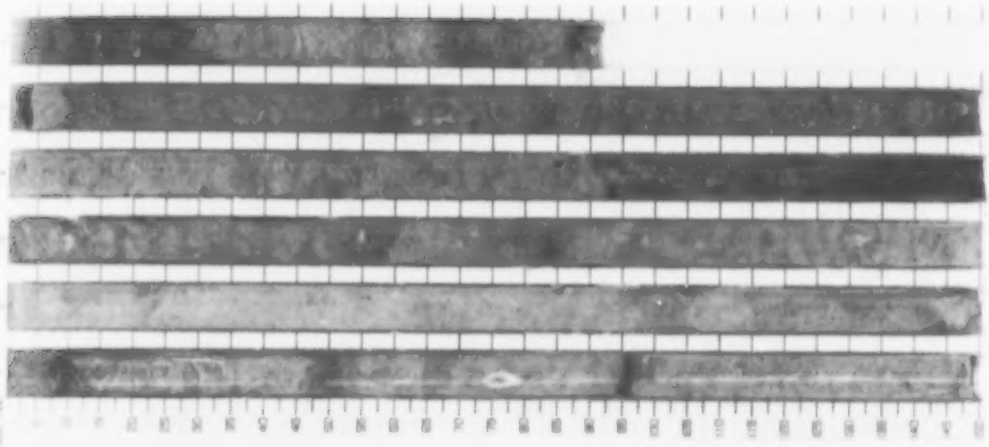

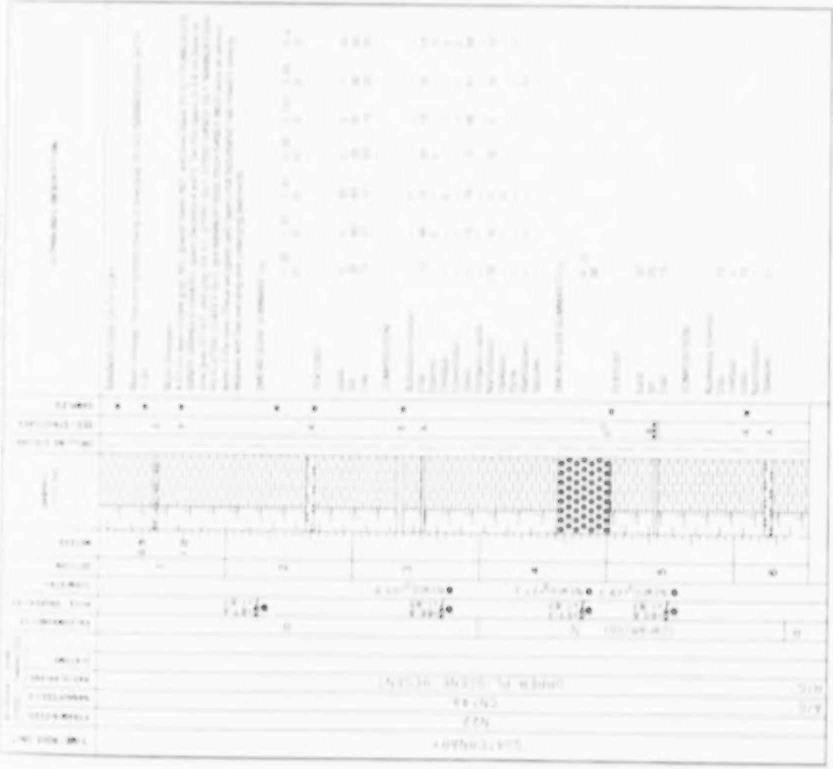

SITE 790 HOLE C CORE 20X CORED INTERVAL 261.4-271.1 mbsf

LITHOLOGIC DESCRIPTION

[illegible]

Major lithologies:

[illegible]

Minor lithologies:

[illegible]

SMEAR SLIDE SUMMARY (%):

TEXTURE:

Sand
Silt
Clay

COMPOSITION:

Accessory minerals
Epidote
Feldspar
Foraminifers
Glass
Mica
Nannofossils
Opaques
Quartz
Radiolarians

SITE 790 HOLE C CORE 21X CORED INTERVAL 271.1-280.6 mbsf

LITHOLOGIC DESCRIPTION

All recovery went to the Paleontology and Igneous Petrology Laboratories.

126 790C 22X NO RECOVERY

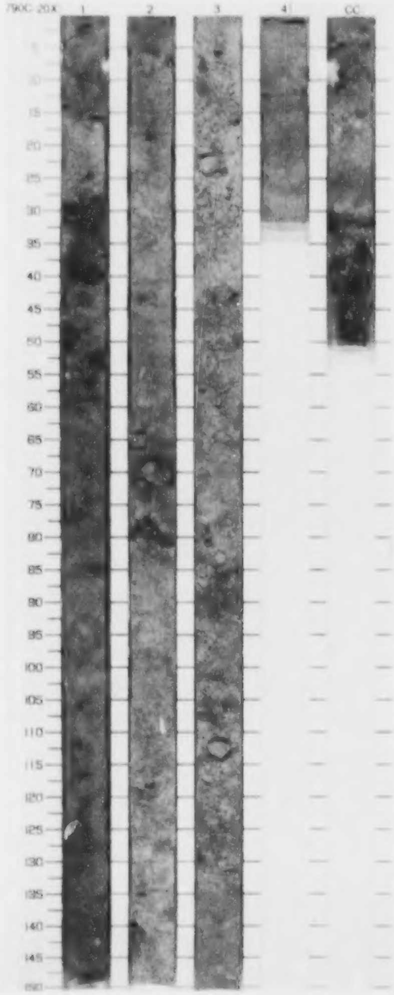
790C-20X
1
2
3
4
CC
5
10
15
20
25
30
35
40
45
50
55
60
65
70
75
80
85
90
95
100
105
110
115
120
125
130
135
140
145
150

SITE 790 HOLE C CORE 23X CORED INTERVAL 290.2-299.9 mbsf

TIME-ROCK UNIT	BIOSTRAT. ZONE/ FOSSIL CHARACTER					PALEOMAGNETICS	PHYS. PROPERTIES	CHEMISTRY	SECTION	METERS	GRAPHIC LITHOLOGY	DRILLING DISTURB.	SED. STRUCTURES	SAMPLES	LITHOLOGIC DESCRIPTION
	FORAMINIFERS	NANNOFOSSILS	RADIOLARIANS	DIATOMS											
QUATERNARY		R/P CN14a?							1	0.5 1.0					All recovery went to the Paleontology and Igneous Laboratory.

SITE 790 HOLE C CORE 24X CORED INTERVAL 299.9-309.5 mbsf

TIME-ROCK UNIT	BIOSTRAT. ZONE/ FOSSIL CHARACTER					PALEOMAGNETICS	PHYS. PROPERTIES	CHEMISTRY	SECTION	METERS	GRAPHIC LITHOLOGY	DRILLING DISTURB.	SED. STRUCTURES	SAMPLES	LITHOLOGIC DESCRIPTION
	FORAMINIFERS	NANNOFOSSILS	RADIOLARIANS	DIATOMS											
		▨													All recovery went to the Paleontology and Igneous Petrology Laboratories.

SITE 790 HOLE C CORE 25X CORED INTERVAL 309.5-319.2 mbsf

TIME-ROCK UNIT	BIOSTRAT. ZONE/ FOSSIL CHARACTER					PALEOMAGNETICS	PHYS. PROPERTIES	CHEMISTRY	SECTION	METERS	GRAPHIC LITHOLOGY	DRILLING DISTURB.	SED. STRUCTURES	SAMPLES	LITHOLOGIC DESCRIPTION
	FORAMINIFERS	NANNOFOSSILS	RADIOLARIANS	DIATOMS											
															All recovery went to the Igneous Petrology Laboratory.

126 790C 26X NO RECOVERY

SITE 790 HOLE C CORE 27X CORED INTERVAL 328.2-338.5 mbsf

TIME-ROCK UNIT	BIOSTRAT. ZONE/ FOSSIL CHARACTER					PALEOMAGNETICS	PHYS. PROPERTIES	CHEMISTRY	SECTION	METERS	GRAPHIC LITHOLOGY	DRILLING DISTURB.	SED. STRUCTURES	SAMPLES	LITHOLOGIC DESCRIPTION
	FORAMINIFERS	NANNOFOSSILS	RADIOLARIANS	DIATOMS											
	▨	▨	▨												All recovery went to the Paleontology and Igneous Petrology Laboratories.

126 790C 28X NO RECOVERY

126 790C 29X NO RECOVERY

126 790C 30X NC RECOVERY

126 790C 31X NO RECOVERY

SITE 790 HOLE C CORE 32X CORED INTERVAL 367.7-377.4 mbsf

TIME-ROCK UNIT
BIOSTRAT. ZONE/FOSSIL CHARACTER
FORAMINIFERS
NANNOFOSSILS
RADIOLARIANS
DIATOMS
PALEOMAGNETICS
PHYS. PROPERTIES
CHEMISTRY
SECTION
METERS
GRAPHIC LITHOLOGY
DRILLING DISTURB.
SED. STRUCTURES
SAMPLES
LITHOLOGIC DESCRIPTION
QUATERNARY
B
R/M PLIOCENE - PLEISTOCENE
B
1
2
0.5
1.0

All recovery went to the Paleontology and Igneous Petrology Laboratories.

SITE 790 HOLE C CORE 33X CORED INTERVAL 377.4-387.1 mbsf

TIME-ROCK UNIT
BIOSTRAT. ZONE/FOSSIL CHARACTER
FORAMINIFERS
NANNOFOSSILS
RADIOLARIANS
DIATOMS
PALEOMAGNETICS
PHYS. PROPERTIES
CHEMISTRY
SECTION
METERS
GRAPHIC LITHOLOGY
DRILLING DISTURB.
SED. STRUCTURES
SAMPLES
LITHOLOGIC DESCRIPTION
QUATERNARY
B
R/C CN 14a
B
1
0.5
1.0

All recovery went to the Paleontology and Igneous Petrology Laboratories.

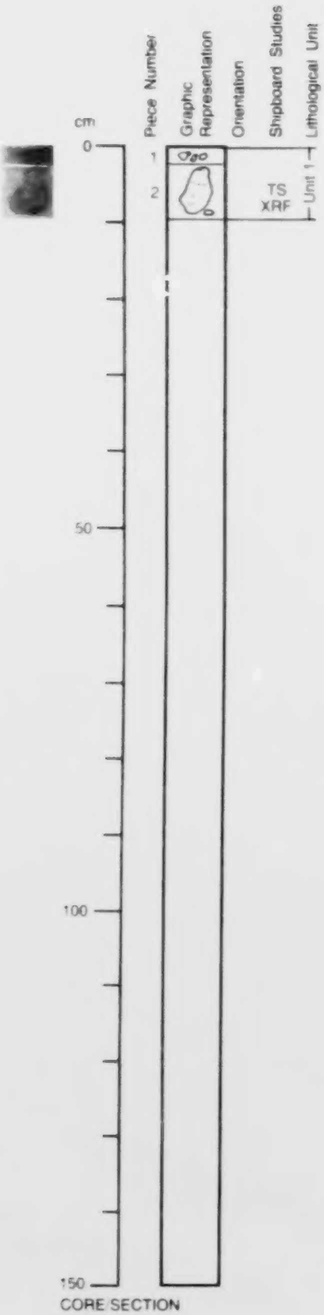
cm
Piece Number
Graphic Representation
Orientation
Shipboard Studies
Lithological Unit
0
1
2
TS
XRF
Unit 1
50
100
150
CORE/SECTION

126-790C-21X-CC

UNIT 1: BASALT

Pieces 1-2

CONTACTS: None
PHENOCRYSTS:
Olivine - 1%, 0.1-0.2 mm, euhedral, fresh
Plagioclase - 5%, 0.1 mm, euhedral, fresh
Cr-Spinel - <0.01%, <0.01 mm, euhedral, in olivine
GROUNDMASS: Dark brown glass, translucent in smear slide
VESICLES: 45%, 0.5-4 mm, round, even
COLOR: Pale green-brown to very dark gray
STRUCTURE: None
ALTERATION: Glass to smectite in vesicles
VEINS/FRACTURES: None

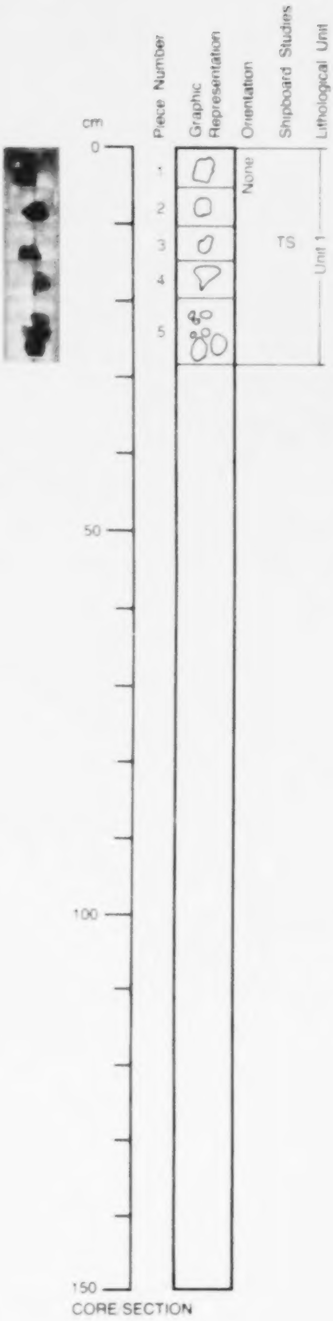
cm
Piece Number
Graphic Representation
Orientation
Shipboard Studies
Lithological Unit
0
1
2
3
4
5
None
TS
Unit 1
50
100
150
CORE SECTION

126-790C-23X-CC

UNIT 1: BASALT

Pieces 1-5

CONTACTS: None
PHENOCRYSTS:
  Olivine - 1%, 0.1-0.2 mm, euhedral, fresh
  Plagioclase - 5%, 0.1 mm, euhedral, fresh
  Cr Spinel - <0.01%, <0.01 mm, euhedral, in olivine
GROUNDMASS: Dark brown glass, translucent in smear slide
VESICLES: 45%, 0.5-4 mm, round, even
COLOR: Pale green brown to very dark gray
STRUCTURE: None
ALTERATION: Glass to smectite in vesicles
VEINS/FRACTURES: None

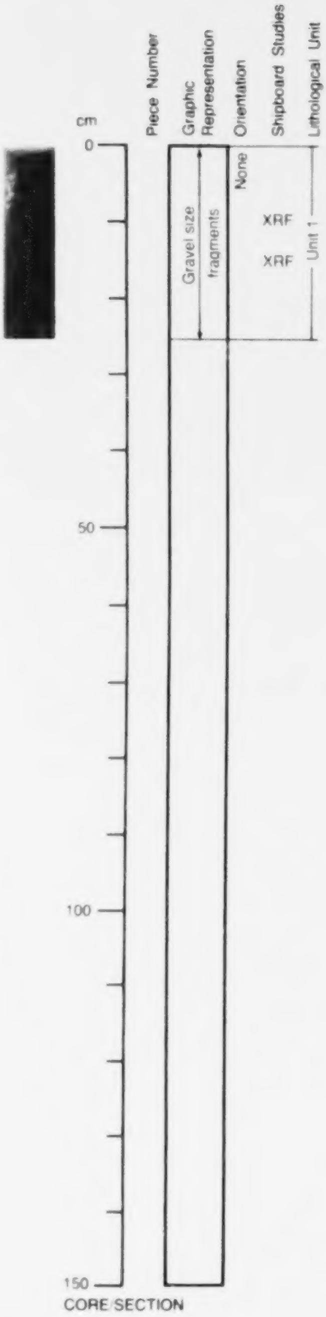
cm
Piece Number
Graphic Representation
Orientation
Shipboard Studies
Lithological Unit
0
50
100
150
Gravel size fragments
None
XRF
XRF
Unit 1
CORE/SECTION

126-790C-24X-CC

UNIT 1: BASALT

CONTACTS: None
PHENOCRYSTS:
- Olivine - 1%; 0.1-0.2 mm; euhedral, fresh
- Plagioclase - 5%; 0.1 mm; euhedral, fresh
- Cr-Spinel - <0.01%; <0.01 mm; euhedral, in olivine

GROUNDMASS: Dark brown glass, translucent in smear slide
VESICLES: 45%; 0.5-4 mm; round; even
COLOR: Pale green-brown to very dark gray
STRUCTURE: None
ALTERATION: Glass to smectite in vesicles
VEINS/FRACTURES: None

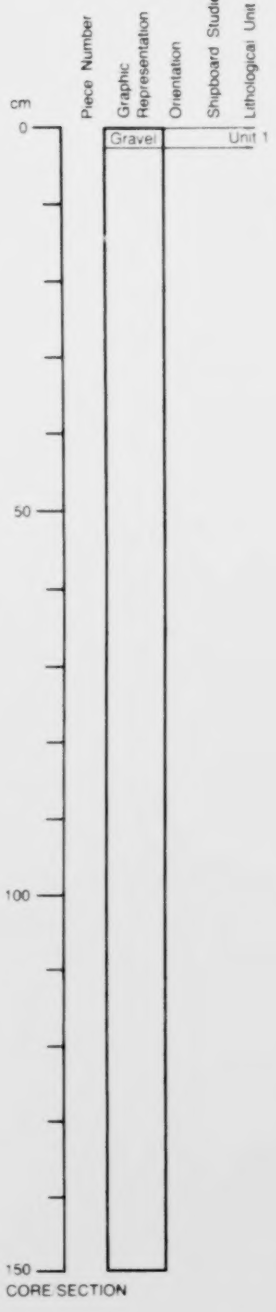
cm
Piece Number
Graphic Representation
Orientation
Shipboard Studies
Lithological Unit
0
Gravel
Unit 1
50
100
150
CORE/SECTION

126-790C-25X-CC

UNIT 1: BASALT

CONTACTS: None
PHENOCRYSTS:
- Olivine - 1%, 0.1-0.2 mm, euhedral, fresh.
- Plagioclase - 5%, 0.1 mm, euhedral, fresh.
- Cr-Spinel - <0.01%, <0.01 mm, euhedral, in olivine.

GROUNDMASS: Dark brown glass, translucent in smear slide.
VESICLES: 45%, 0.5-4 mm, round, even.
COLOR: Pale green-brown to very dark gray.
STRUCTURE: None.
ALTERATION: Glass to smectite in vesicles.
VEINS/FRACTURES: None.

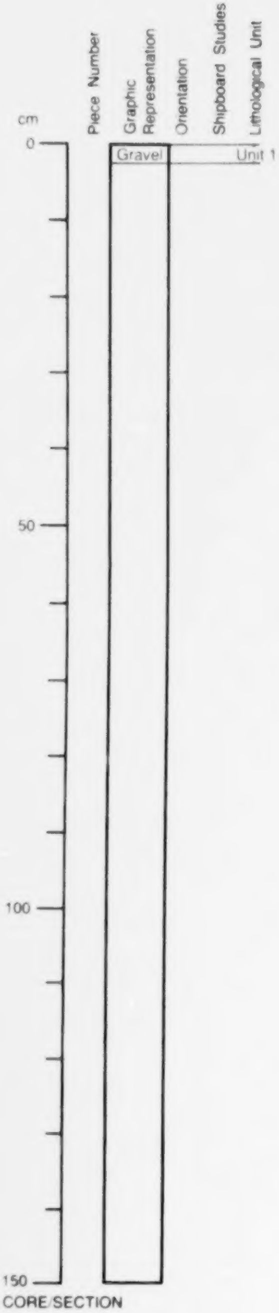
cm
Piece Number
Graphic Representation
Orientation
Shipboard Studies
Lithological Unit
0
Gravel
Unit 1
50
100
150
CORE/SECTION

126-790C-26X-CC

UNIT 1: BASALT

CONTACTS: None
PHENOCRYSTS:
- Olivine - 1%, 0.1-0.2 mm, euhedral, fresh.
- Plagioclase - 5%, 0.1 mm, euhedral, fresh.
- Cr-Spinel - <0.01%; <0.01 mm, euhedral, in olivine.

GROUNDMASS: Dark brown glass, translucent in smear slide.
VESICLES: 45%, 0.5-4 mm, round, even.
COLOR: Pale green-brown to very dark gray.
STRUCTURE: None.
ALTERATION: Glass to smectite in vesicles.
VEINS/FRACTURES: None.

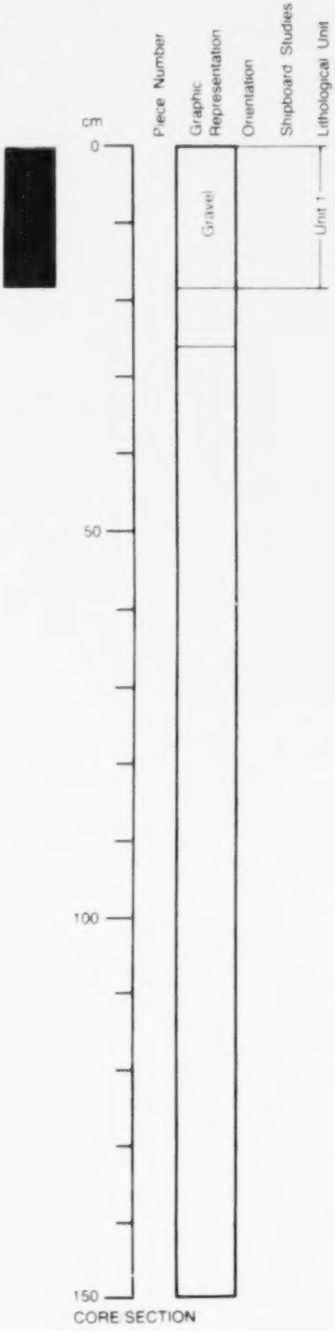
cm
Piece Number
Graphic Representation
Orientation
Shipboard Studies
Lithological Unit
0
50
100
150
Gravel
Unit 1
CORE/SECTION

126-790C-27X-CC

UNIT 1: BASALT

CONTACTS: None.
PHENOCRYSTS:
Olivine - 1%, 0.1-0.2 mm, euhedral, fresh.
Plagioclase - 5%, 0.1 mm, euhedral, fresh.
Cr-Spinel - <0.01%, <0.01 mm, euhedral, in olivine.
GROUNDMASS: Dark brown glass, translucent in smear slide.
VESICLES: 45%, 0.5-4 mm, round, even.
COLOR: Pale green-brown to very dark gray.
STRUCTURE: None.
ALTERATION: Glass to smectite in vesicles.
VEINS/FRACTURES: None.

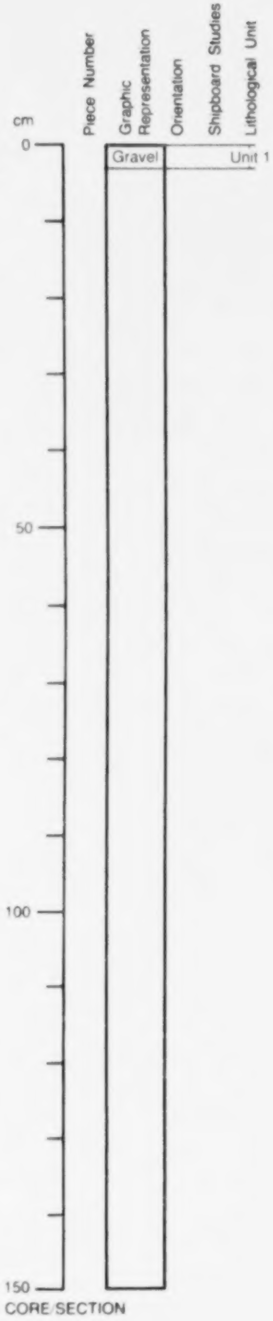
cm
Piece Number
Graphic Representation
Orientation
Shipboard Studies
Lithological Unit
0
50
100
150
Gravel
Unit 1
CORE/SECTION

126-790C-29X-CC

UNIT 1: BASALT

PHENOCRYSTS:
Olivine - 1%; 0.1-0.2; euhedral, fresh.
Plagioclase - 5%; 0.1; euhedral, fresh.
CR-Spinel - <0.01%; <0.01; euhedral, in olivine.
GROUNDMASS: Dark brown glass, translucent in smear slide.
VESICLES: 45%, 0.5-4 mm, round, even, none.
Miaroles: None.
COLOR: Pale green-brown to very dark gray.
ALTERATION: Glass to smectite in vesicules.

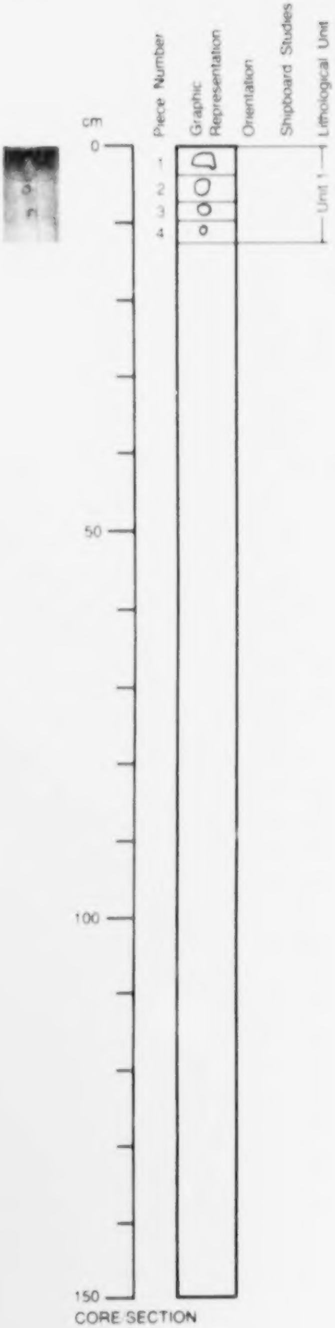
cm
Piece Number
Graphic Representation
Orientation
Shipboard Studies
Lithological Unit
0
50
100
150
1
2
3
4
Unit 1
CORE/SECTION

126-790C-32X-CC

UNIT 1: BASALT

Pieces 1-4

CONTACTS: None
PHENOCRYSTS:
Olivine - 1%; 0.1-0.2 mm; euhedral; fresh.
Plagioclase - 5%; 0.1 mm; euhedral; fresh.
Cr-Spinel - <0.01%; <0.01 mm; euhedral; in olivine.
GROUNDMASS: Dark brown glass; translucent in smear slide.
VESICLES: 45%; 0.5-4 mm; round; even.
COLOR: Pale green-brown to very dark gray.
STRUCTURE: None.
ALTERATION: Glass to smectite in vesicles.
VEINS/FRACTURES: None.

126-790C-33X-CC

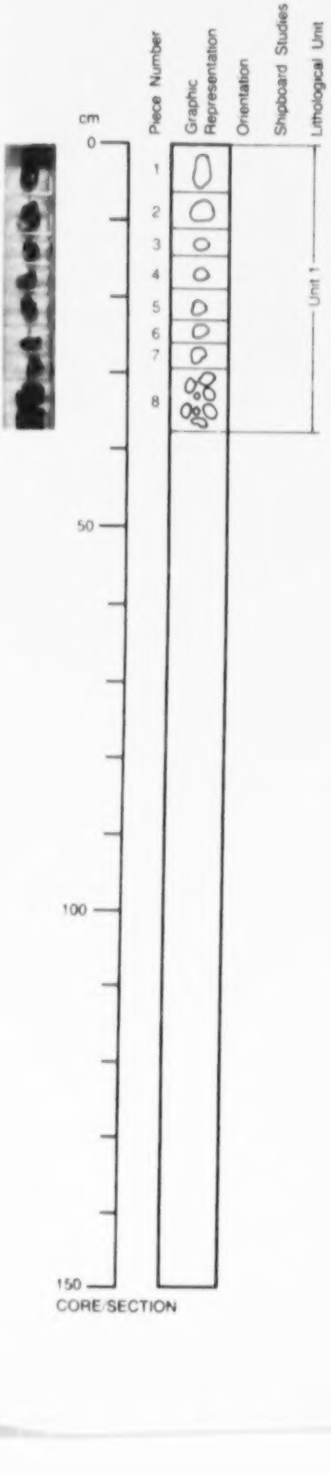
cm
0
50
100
150
Piece Number
Graphic Representation
Orientation
Shipboard Studies
Lithological Unit
1
2
3
4
5
6
7
8
Unit 1
CORE/SECTION

UNIT 1: BASALT

Pieces 1-8

CONTACTS: None
PHENOCRYSTS:
  Olivine - 1%, 0.1-0.2 mm, euhedral, fresh
  Plagioclase - 5%, 0.1 mm, euhedral, fresh
  Cr-Spinel - <0.01%, <0.01 mm, euhedral, in olivine
GROUNDMASS: Dark brown glass, translucent in smear slide
VESICLES: 45%, 0.5-4 mm, round, even
COLOR: Pale green-brown to very dark gray
STRUCTURE: None
ALTERATION: Glass to smectite in vesicles
VEINS/FRACTURES: None

```
[illegible]                                  OBSERVER: [illegible]     WHERE SAMPLED: [illegible]

ROCK NAME: Basalt

GRAIN SIZE: Fine

TEXTURE: Vesicular
------------------------------------------------------------------------------------------------

PRIMARY            PERCENT PERCENT   SIZE      COMPO-
MINERALOGY         PRESENT ORIGINAL  (mm)      SITION          MORPHOLOGY          COMMENTS

PHENOCRYSTS
Olivine            [illegible]                                 Euhedral            Fresh.
Plagioclase        [illegible]                                 Subhedral           Fresh.

GROUNDMASS
Devitrified        N.A.    N.A.      N.A.                      N.A.
glass
------------------------------------------------------------------------------------------------
VESICLES/                            SIZE
CAVITIES           PERCENT LOCATION  (mm)            FILLING                       SHAPE
Vesicles           [illegible]                       Empty                         Round
------------------------------------------------------------------------------------------------
COMMENTS: [illegible]

[illegible]                                  OBSERVER: [illegible]     WHERE SAMPLED: [illegible]

ROCK NAME: [illegible]

GRAIN SIZE:

TEXTURE:
------------------------------------------------------------------------------------------------

PRIMARY            PERCENT PERCENT   SIZE      COMPO-
MINERALOGY         PRESENT ORIGINAL  (mm)      SITION          MORPHOLOGY          COMMENTS

PHENOCRYSTS
Olivine            [illegible]                                 N.A.                [illegible]
Plagioclase        [illegible]                                 N.A.                Fresh.

GROUNDMASS
Devitrified        N.A.    N.A.      N.A.                      N.A.                [illegible]
glass                                                                              [illegible]
------------------------------------------------------------------------------------------------
VESICLES/                            SIZE
CAVITIES           PERCENT LOCATION  (mm)            FILLING                       SHAPE
Vesicles           [illegible]                       Empty                         Round
------------------------------------------------------------------------------------------------
COMMENTS: [illegible]
```

126-790C-21X-CC (Piece 2,)   OBSERVER: GIL   WHERE SAMPLED:

ROCK NAME: Basalt

GRAIN SIZE: Fine

TEXTURE: Vesicular

PRIMARY MINERALOGY	PERCENT PRESENT	PERCENT ORIGINAL	SIZE (mm)	COMPO-SITION	MORPHOLOGY	COMMENTS
PHENOCRYSTS						
Olivine	4	4	0.3-1.0		Equant	One 0.6 mm long. Includes spinel.
Plagioclase	20	20	0.1-0.7		Euhedral	
Clinopyroxene	1	1	N/A		Equant	Olivine vs clinopyroxene difficult.
GROUNDMASS						
Glass	N/A	N/A	N/A		N/A	Devitrifying.

VESICLES/ CAVITIES	PERCENT	LOCATION	SIZE (mm)	FILLING	SHAPE	COMMENTS
Vesicles	27		0.2-0.3	Open	Elongate, some yellow crystals.	Elongate, large elongate/ associated with veinlets of finer-grained material which parallel plagioclase alignment; more vesicular than rest.
Vesicles	10		0.2-1.0	Open		

COMMENTS: Also elongate patches of finer-grained vitrophyric material enclosed within above lava. Same assemblage, but finer grained (plagioclase<0.2 mm). Probably inclusion of chill material during eruption. No top or bottom interval given.

126-790C-[illegible] (Piece 7,)   OBSERVER: GIL   WHERE SAMPLED:

ROCK NAME: Basalt Scoria

GRAIN SIZE: Fine

TEXTURE: Vesicular

PRIMARY MINERALOGY	PERCENT PRESENT	PERCENT ORIGINAL	SIZE (mm)	COMPO-SITION	MORPHOLOGY	COMMENTS
PHENOCRYSTS						
Olivine	1	1	0.1-0.2		Acicular	Fo?, zoned, plucked. Some clots. Includes spinel.
Plagioclase	5	5	0.1-0.3		Euhedral	Fresh. Some clots.
GROUNDMASS						
Glass	N/A	N/A	N/A		N/A	Devitrified.

VESICLES/ CAVITIES	PERCENT	LOCATION	SIZE (mm)	FILLING	SHAPE	COMMENTS
Vesicles	40		0.2	Little	Round	Some yellow crystals on walls.

COMMENTS: 2 cm diameter clast; looks more altered in hand specimen than thin section. No top or bottom intervals given.

126 791A 1H NO RECOVERY

SITE 791 HOLE A CORE 2H CORED INTERVAL 4.5-14.0 mbsf

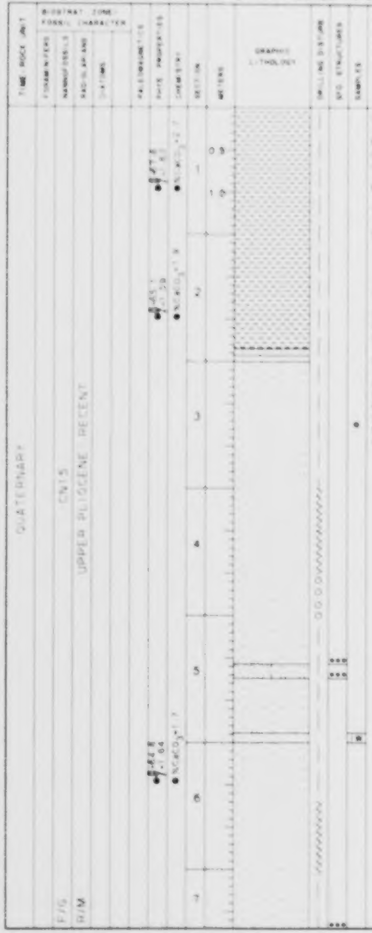
TIME-ROCK UNIT
BIOSTRAT. ZONE/FOSSIL CHARACTER
FORAMINIFERS
NANNOFOSSILS
RADIOLARIANS
DIATOMS
PALEOMAGNETICS
PHYS. PROPERTIES
CHEMISTRY
SECTION
METERS
GRAPHIC LITHOLOGY
DRILLING DISTURB.
SED. STRUCTURES
SAMPLES
QUATERNARY
CN15
UPPER PLIOCENE-RECENT
F/G
R/M
0.5
1.0
1
2
3
4
5
6
7
1.64
%CaCO₃=1.7

LITHOLOGIC DESCRIPTION

CLAY AND VITRIC SILT

Major lithologies:
Light olive gray (5Y 6/2) CLAY and VITRIC SILT respectively comprise [illegible] and [illegible] of the core.

Minor lithology: A 2 cm thick FINE VITRIC SAND layer in Section 5 grades upward into silt.

This core is structureless for the most part, having moderately to very disturbed by drilling.

SMEAR SLIDE SUMMARY (%):

	4, 78
	D
TEXTURE:	
Sand	15
Silt	75
Clay	10
COMPOSITION:	
Diatoms	5
Feldspar	1
Foraminifers	2
Glass	[illegible]
Nannofossils	3
Quartz	1

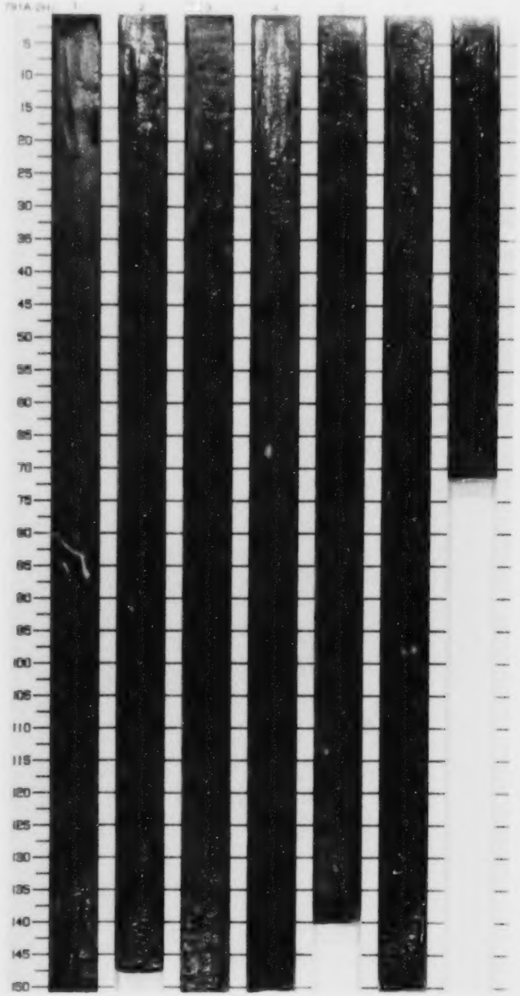
791A-2H
1
2
3
4
5
6
7
5
10
15
20
25
30
35
40
45
50
55
60
65
70
75
80
85
90
95
100
105
110
115
120
125
130
135
140
145
150

SITE 791 HOLE A CORE 3H CORED INTERVAL 14.0-23.5 mbsf

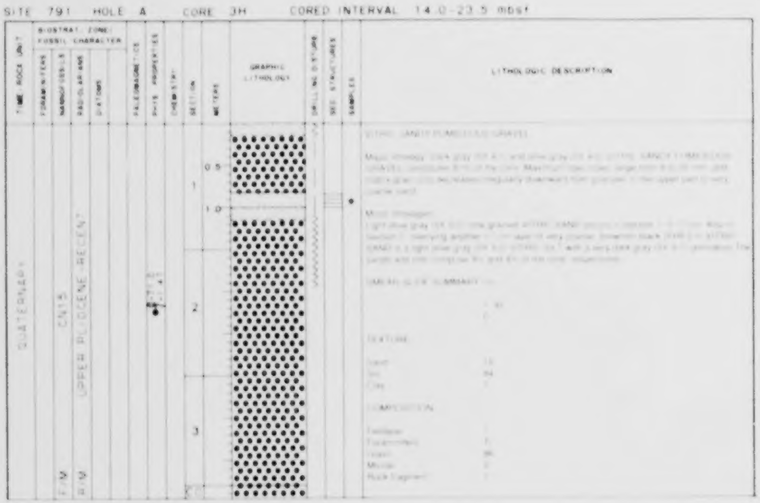
TIME-ROCK UNIT
BIOSTRAT. ZONE/FOSSIL CHARACTER
FORAMINIFERS
NANNOFOSSILS
RADIOLARIANS
DIATOMS
PALEOMAGNETICS
PHYS. PROPERTIES
CHEMISTRY
SECTION
METERS
GRAPHIC LITHOLOGY
DRILLING DISTURB.
SED. STRUCTURES
SAMPLES
LITHOLOGIC DESCRIPTION
QUATERNARY
F/M
CN15
R/M
UPPER PLIOCENE-RECENT
0.5
1.0
1
2
3
CC

VITRIC SANDY PUMICEOUS GRAVEL

Major lithology: [illegible]

Minor lithologies: [illegible]

SMEAR SLIDE SUMMARY (%):

1, 40
D

TEXTURE:

Sand 15
Silt 84
Clay 1

COMPOSITION:

Feldspar [illegible]
Foraminifers [illegible]
Glass 96
Micrite [illegible]
Rock fragment [illegible]

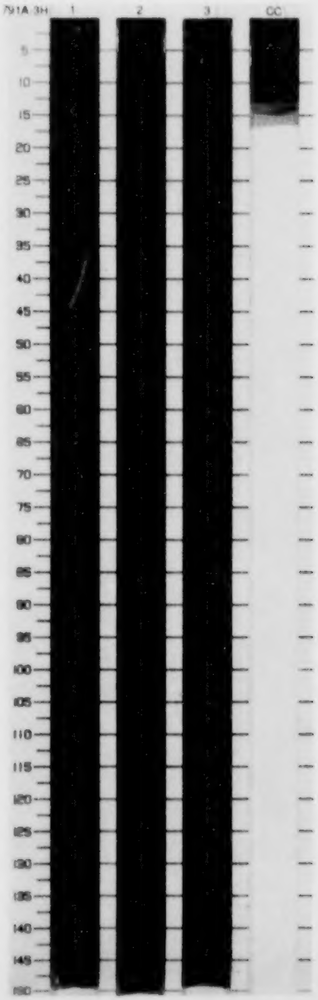
791A-3H
1
2
3
CC
5
10
15
20
25
30
35
40
45
50
55
60
65
70
75
80
85
90
95
100
105
110
115
120
125
130
135
140
145
150

SITE 791 HOLE A CORE 4H CORED INTERVAL 23.5-33.0 mbsf

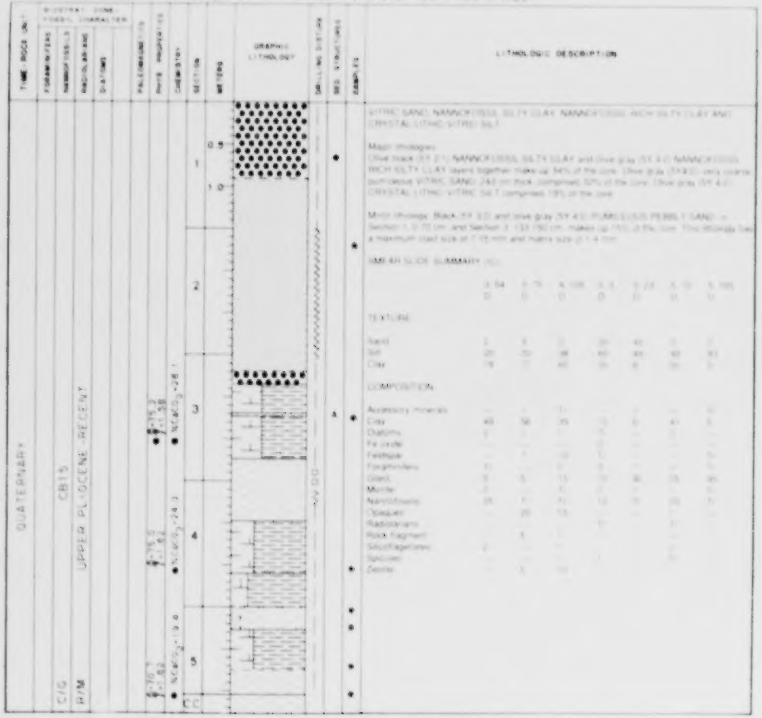
TIME-ROCK UNIT
BIOSTRAT. ZONE/FOSSIL CHARACTER
FORAMINIFERS
NANNOFOSSILS
RADIOLARIANS
DIATOMS
PALEOMAGNETICS
PHYS. PROPERTIES
CHEMISTRY
SECTION
METERS
GRAPHIC LITHOLOGY
DRILLING DISTURB.
SED. STRUCTURES
SAMPLES
QUATERNARY
CB15
C/G
UPPER PLIOCENE-RECENT
R/M
φ=75.2
γ=1.58
φ=75.5
γ=1.62
φ=70.7
γ=1.62
%CaCO3=28.1
%CaCO3=24.3
%CaCO3=19.4
1
2
3
4
5
CC
0.5
1.0
OO

LITHOLOGIC DESCRIPTION

VITRIC SAND, NANNOFOSSIL SILTY CLAY, NANNOFOSSIL-RICH SILTY CLAY AND CRYSTAL-LITHIC VITRIC SILT

Major lithologies:
Olive black (5Y 2/1) NANNOFOSSIL SILTY CLAY and olive gray (5Y 4/2) NANNOFOSSIL-RICH SILTY CLAY layers together make up 54% of the core. Olive gray (5Y 4/2) very coarse pumiceous VITRIC SAND, 243 cm thick, comprises 10% of the core. Olive gray (5Y 4/2) CRYSTAL-LITHIC VITRIC SILT comprises 19% of the core.

Minor lithology: Black (5Y 2/2) and olive gray (5Y 4/2) PUMICEOUS PEBBLY SAND in Section 1, 0-70 cm, and Section 3, 133-150 cm, makes up 15% of the core. This lithology has a maximum clast size of 7-15 mm and matrix size 0.1-4 mm.

SMEAR SLIDE SUMMARY (%):

	3, 54	3, 79	4, 108	5, 5	5, 23	5, 70	5, 105
	D	D	D	D	D	M	M
TEXTURE:							
Sand	2	5	2	20	45	5	7
Silt	20	25	38	60	49	62	83
Clay	78	70	60	20	6	33	10
COMPOSITION:							
Accessory minerals	—	1	Tr	—	2	—	10
Clay	40	56	25	15	6	41	6
Diatoms	1	2	2	Tr	—	2	—
Fe oxide	—	—	—	2	—	—	—
Feldspar	—	7	10	5	—	—	5
Foraminifers	Tr	—	2	3	—	—	5
Glass	8	5	15	50	80	15	65
Mica	2	—	Tr	2	2	—	5
Nannofossils	35	5	20	10	10	35	5
Opaques	—	20	15	—	—	1	—
Radiolarians	—	—	—	Tr		Tr	
Rock fragment	—	5	2	—		—	
Silicoflagellates	2	—	—			2	
Spicules	—	—	—	1		Tr	
Zeolite	—	5	10				

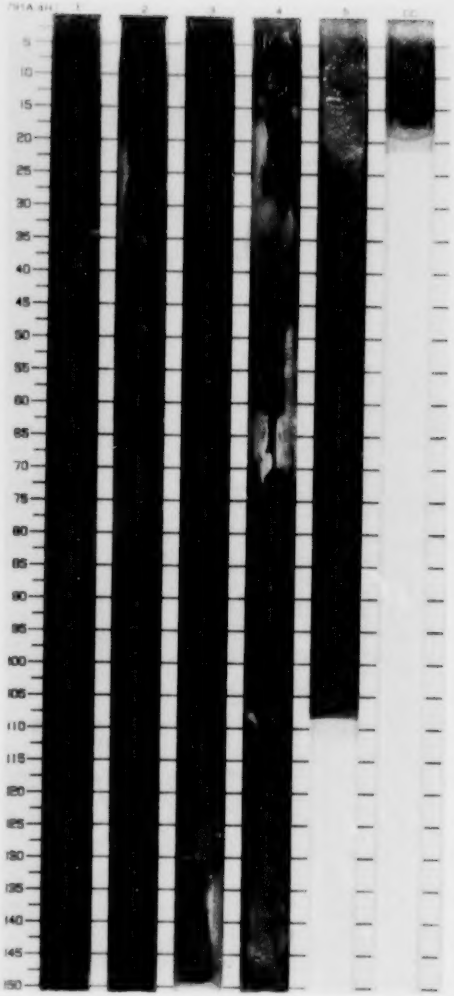
791A-4H
1
2
3
4
5
CC
5
10
15
20
25
30
35
40
45
50
55
60
65
70
75
80
85
90
95
100
105
110
115
120
125
130
135
140
145
150

SITE 791 HOLE A CORE 5H CORED INTERVAL 33.0-42.5 mbsf

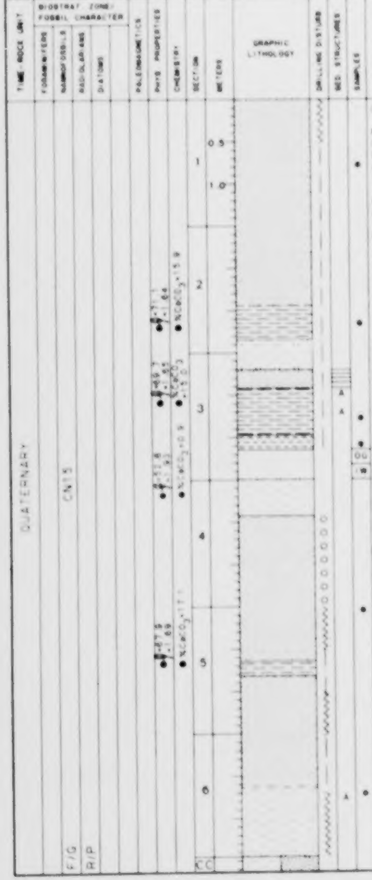
TIME-ROCK UNIT
BIOSTRAT. ZONE/ FOSSIL CHARACTER
FORAMINIFERS
NANNOFOSSILS
RADIOLARIANS
DIATOMS
PALEOMAGNETICS
PHYS. PROPERTIES
CHEMISTRY
SECTION
METERS
GRAPHIC LITHOLOGY
DRILLING DISTURB.
SED. STRUCTURES
SAMPLES
QUATERNARY
CN15
F/G
R/P
φ=71.1 γ=1.64
φ=69.7 γ=1.65
φ=52.8 γ=1.93
φ=67.8 γ=1.69
%CaCO₃=15.9
%CaCO₃=13.0
%CaCO₃=0.9
%CaCO₃=17.1
1
2
3
4
5
6
CC
0.5
1.0
OG

LITHOLOGIC DESCRIPTION

CRYSTAL VITRIC SAND AND VITRIC-CRYSTAL SAND

Major lithologies:
Olive black (5Y 2/1) CRYSTAL VITRIC SAND occurs in the uppermost 244 cm of the core. Grayish black (N2) VITRIC-CRYSTAL SAND forms a 171-cm-thick layer in Sections 4 and 5, a 134-cm layer in Sections 5 and 6, and two thin (10 and 21 cm) layers in Sections 2 and 3. This unit comprises 74% of the core.

Minor lithologies:
Olive gray (5Y 4/2) CLAYEY VITRIC SILT in Section 2, 84-134 cm. Olive gray (5Y 4/2) VITRIC SILT in Section 2, 144 cm, to Section 3, 41 cm; Section 4, 0-42 cm; and Section 6, 86-145 cm. A 19-cm layer of black (N2) CLAY occurs in Section 3, 96-115 cm.

SMEAR SLIDE SUMMARY (%):

	1, 78 D	2, 117 D	3, 78 D	3, 106 D	5, 5 D	6, 71 D
TEXTURE:						
Sand	95	7	90	—	85	2
Silt	2	63	10	5	15	98
Clay	3	30	—	95	—	—
COMPOSITION:						
Accessory minerals	15	—	10	—	5	Tr
Clay	2	55	—	80	—	—
Diatoms	—	2	—	—	—	—
Epidote	—	—	Tr	—	—	—
Feldspar	15	—	10	Tr	5	Tr
Foraminifers	Tr	3	—	—	Tr	Tr
Glass	68	30	75	2	87	100
Micrite	—	2	—	—	—	—
Nannofossils	Tr	5	—	—	—	Tr
Opaques	—	1	3	5	3	—
Rock fragment	—	—	2	—	—	—
Silicoflagellates	—	2	—	—	—	—
Zeolite	—	—	—	10	—	—

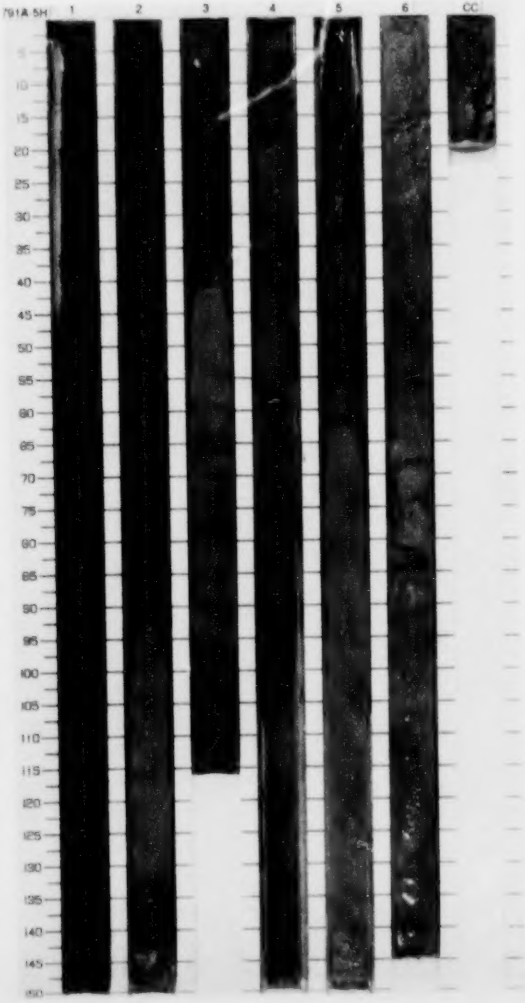
791A-5H
1
2
3
4
5
6
CC
5
10
15
20
25
30
35
40
45
50
55
60
65
70
75
80
85
90
95
100
105
110
115
120
125
130
135
140
145
150

SITE 791 HOLE A CORE 6H CORED INTERVAL 42.5-52.0 mbsf

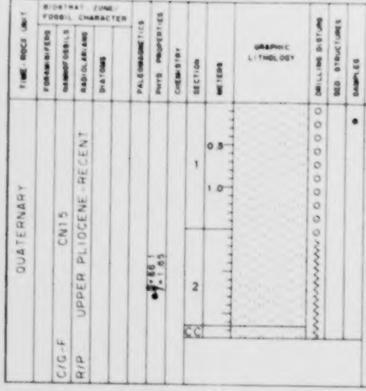
TIME-ROCK UNIT
BIOSTRAT. ZONE/ FOSSIL CHARACTER
FORAMINIFERS
NANNOFOSSILS
RADIOLARIANS
DIATOMS
PALEOMAGNETICS
PHYS. PROPERTIES
CHEMISTRY
SECTION
METERS
GRAPHIC LITHOLOGY
DRILLING DISTURB.
SED. STRUCTURES
SAMPLES
QUATERNARY
C/G-F
CN15
R/P
UPPER PLIOCENE-RECENT
φ-66.1
γ-1.65
1
2
CC
0.5
1.0

LITHOLOGIC DESCRIPTION

VITRIC SILT

Major lithology: The entire core is light olive gray (5Y 5/2) VITRIC SILT, homogenized by drilling and in very disturbed and soupy condition.

SMEAR SLIDE SUMMARY (%):

	1, 20
	D
TEXTURE:	
Silt	100
COMPOSITION:	
Feldspar	2
Glass	97
Micrite	1
Nannofossils	Tr

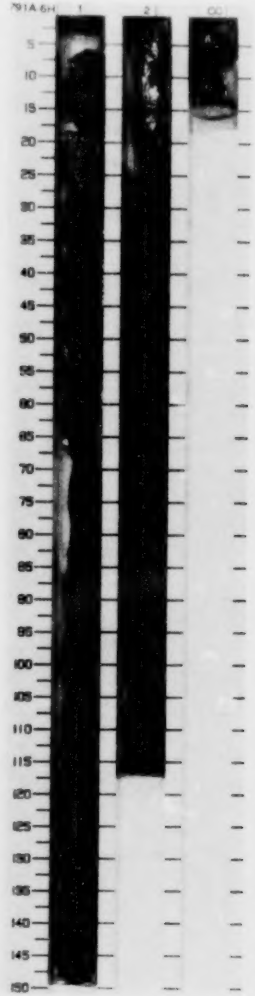
791A-6H
1
2
CC
5
10
15
20
25
30
35
40
45
50
55
60
65
70
75
80
85
90
95
100
105
110
115
120
125
130
135
140
145
150

SITE 791 HOLE A CORE 7H CORED INTERVAL 52.0-61.6 mbsf

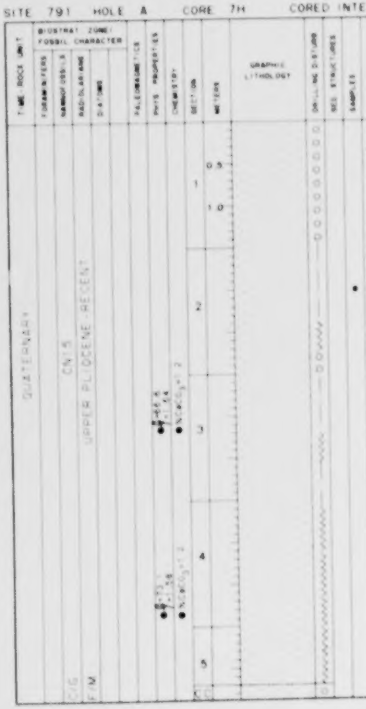
TIME-ROCK UNIT
BIOSTRAT. ZONE/ FOSSIL CHARACTER
FORAMINIFERS
NANNOFOSSILS
RADIOLARIANS
DIATOMS
PALEOMAGNETICS
PHYS. PROPERTIES
CHEMISTRY
SECTION
METERS
GRAPHIC LITHOLOGY
DRILLING DISTURB.
SED. STRUCTURES
SAMPLES
QUATERNARY
CN15
UPPER PLIOCENE-RECENT
C/G
F/M
φ=66.4
γ=1.44
%CaCO3=1.2
φ=73.1
γ=1.38
%CaCO3=1.2
1
2
3
4
5
CC
0.5
1.0

LITHOLOGIC DESCRIPTION

VITRIC SILT

Major lithology: The entire core is light olive gray (5Y 6/2) vitric silt. Homogenized by drilling and is moderately disturbed to soupy [illegible]

SMEAR SLIDE SUMMARY (%):

2, 40
D

TEXTURE:

Silt 100
Clay Tr

COMPOSITION:

Accessory minerals Tr
Feldspar 5
Foraminifers Tr
Glass 95
Nannofossils Tr

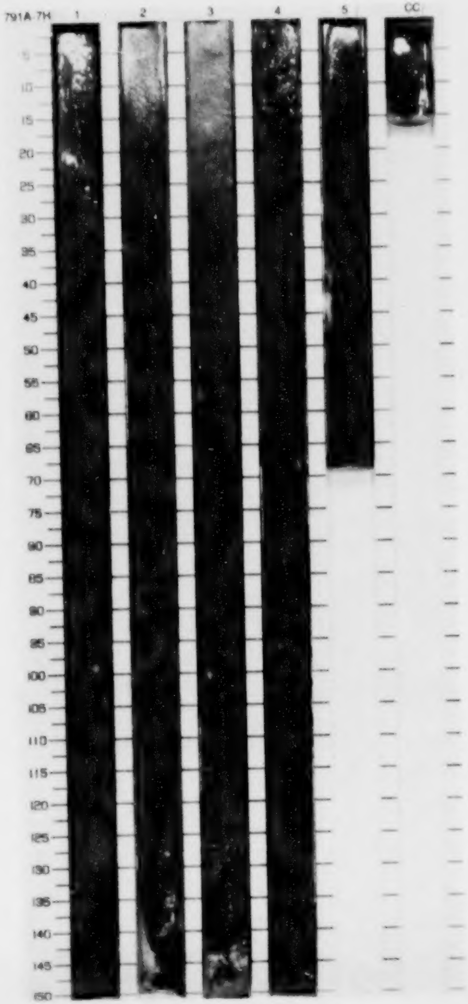
791A-7H
1
2
3
4
5
CC
5
10
15
20
25
30
35
40
45
50
55
60
65
70
75
80
85
90
95
100
105
110
115
120
125
130
135
140
145
150

SITE 791 HOLE A CORE 8H CORED INTERVAL 61.6-71.3 mbsf

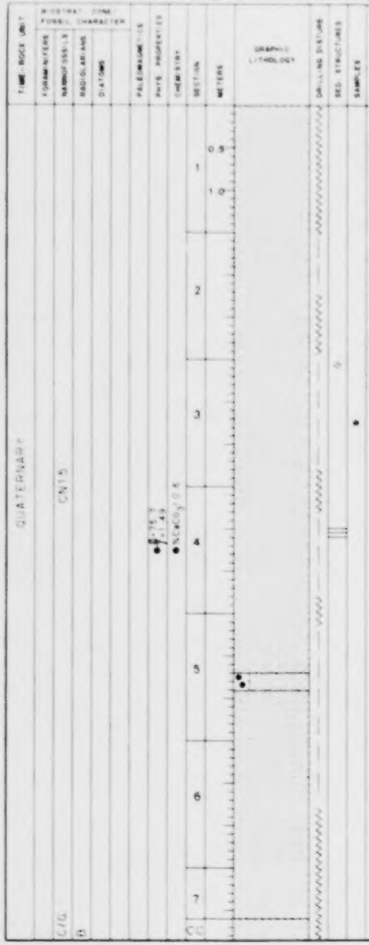
TIME-ROCK UNIT
BIOSTRAT. ZONE/ FOSSIL CHARACTER
FORAMINIFERS
NANNOFOSSILS
RADIOLARIANS
DIATOMS
PALEOMAGNETICS
PHYS. PROPERTIES
CHEMISTRY
SECTION
METERS
GRAPHIC LITHOLOGY
DRILLING DISTURB.
SED. STRUCTURES
SAMPLES
QUATERNARY
CN15
C/G
B
%CaCO$_3$=0.4
1
2
3
4
5
6
7
CC
0.5
1.0

LITHOLOGIC DESCRIPTION

CRYSTAL VITRIC SAND

Major lithology: The entire core consists of very disturbed to soupy, dark gray (5Y 4/1), fine to medium CRYSTAL VITRIC SAND, somewhat coarser from Section 4, 130 cm downwards. An 8-mm pumice clast is located at the top of Section 3, and thin intervals containing concentrations of pumice pebbles/granules occur in Section 5. Minor laminated zones of finer material occur in Sections 2 and 4.

SMEAR SLIDE SUMMARY (%):

	3, 75
	D
TEXTURE:	
Sand	95
Silt	5
COMPOSITION:	
Accessory minerals	15
Feldspar	15
Foraminifers	Tr
Glass	70
Nannofossils	Tr

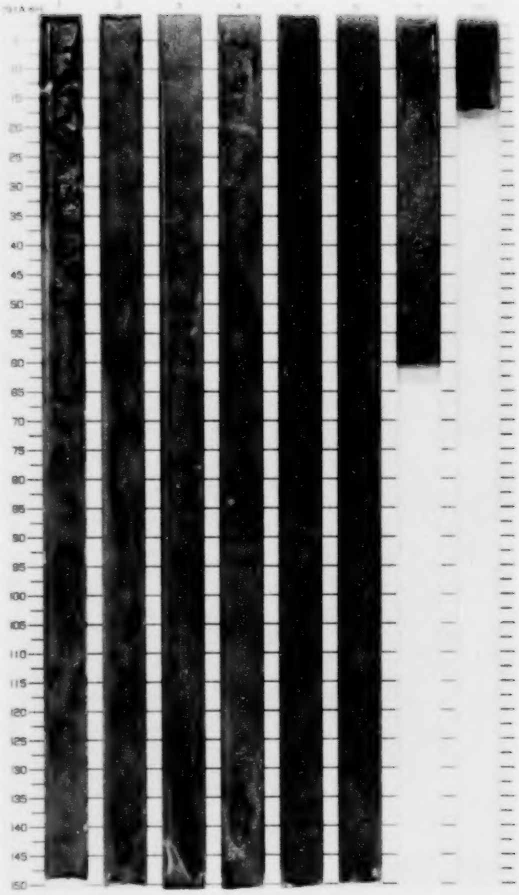
791A-8H
1
2
3
4
5
6
7
CC
5
10
15
20
25
30
35
40
45
50
55
60
65
70
75
80
85
90
95
100
105
110
115
120
125
130
135
140
145
150

SITE 791 HOLE A CORE 9H CORED INTERVAL 71.3-81.0 mbsf

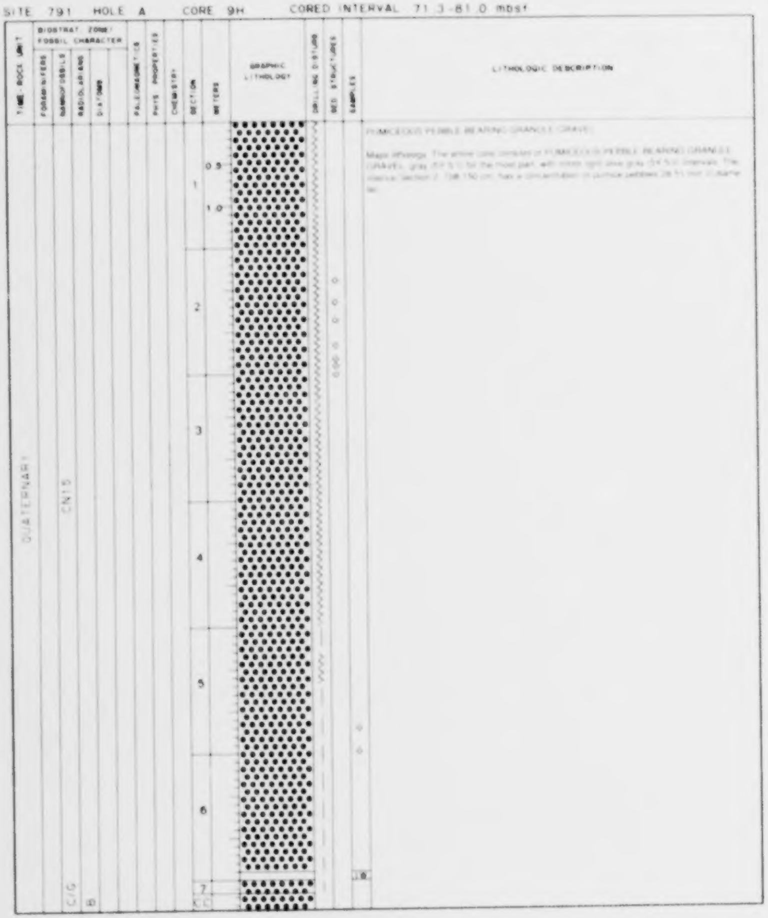
TIME-ROCK UNIT
BIOSTRAT. ZONE/ FOSSIL CHARACTER
FORAMINIFERS
NANNOFOSSILS
RADIOLARIANS
DIATOMS
PALEOMAGNETICS
PHYS. PROPERTIES
CHEMISTRY
SECTION
METERS
GRAPHIC LITHOLOGY
DRILLING DISTURB.
SED. STRUCTURES
SAMPLES
LITHOLOGIC DESCRIPTION
QUATERNARY
CN15
C/G
B
0.5
1.0
1
2
3
4
5
6
7
CC
IW

PUMICEOUS PEBBLE BEARING GRANULE GRAVEL

Major lithology: The entire core consists of PUMICEOUS PEBBLE BEARING GRANULE GRAVEL, gray (5Y 5/1) for the most part, with minor light olive gray (5Y 5/2) intervals. The interval Section 2, 108-150 cm, has a concentration of pumice pebbles (8-11 mm in diameter).

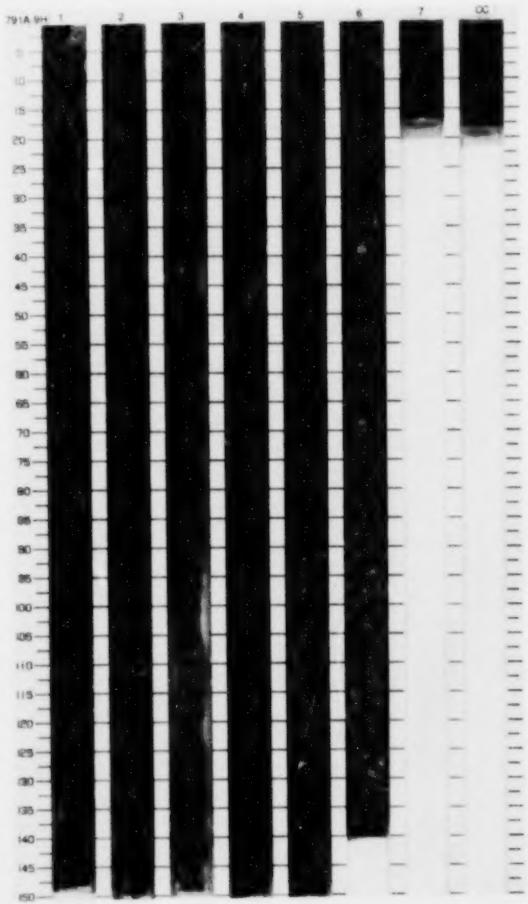
791A-9H
1
2
3
4
5
6
7
CC
5
10
15
20
25
30
35
40
45
50
55
60
65
70
75
80
85
90
95
100
105
110
115
120
125
130
135
140
145
150

SITE 791 HOLE A CORE 10H CORED INTERVAL 81.0-90.7 mbsf

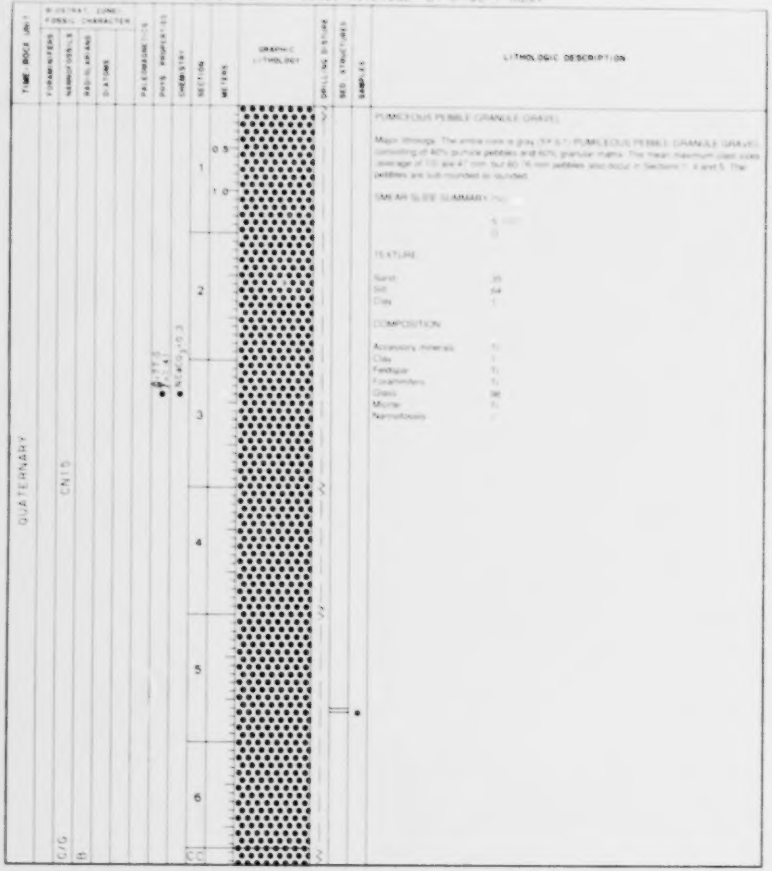
TIME-ROCK UNIT
BIOSTRAT. ZONE/ FOSSIL CHARACTER
FORAMINIFERS
NANNOFOSSILS
RADIOLARIANS
DIATOMS
PALEOMAGNETICS
PHYS. PROPERTIES
CHEMISTRY
SECTION
METERS
GRAPHIC LITHOLOGY
DRILLING DISTURB.
SED. STRUCTURES
SAMPLES
LITHOLOGIC DESCRIPTION
QUATERNARY
CN15
C/G
B
%CaCO3=0.3
0.5
1.0
1
2
3
4
5
6
CC

PUMICEOUS PEBBLE GRANULE GRAVEL

Major lithology: The entire core is gray (5Y 5/1) PUMICEOUS PEBBLE GRANULE GRAVEL consisting of 40% pumice pebbles and 60% granular matrix. The mean maximum clast sizes (average of 10) are 47 mm, but 60-76 mm pebbles also occur in Sections 1, 4 and 5. The pebbles are sub-rounded to rounded.

SMEAR SLIDE SUMMARY (%):

	5, 107
	D
TEXTURE:	
Sand	35
Silt	64
Clay	1
COMPOSITION:	
Accessory minerals	Tr
Clay	1
Feldspar	Tr
Foraminifers	Tr
Glass	98
Micrite	Tr
Nannofossils	1

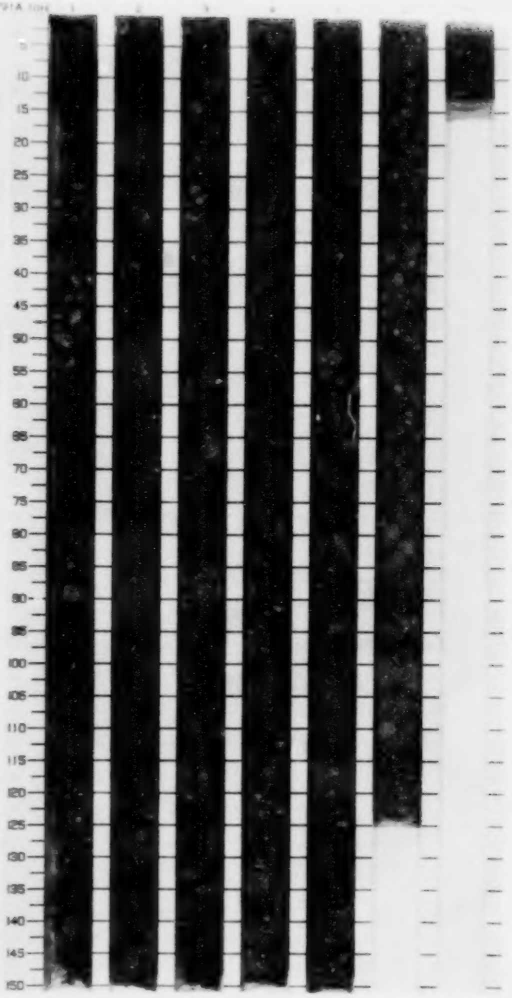
791A 10H
1
2
3
4
5
6
7
5
10
15
20
25
30
35
40
45
50
55
60
65
70
75
80
85
90
95
100
105
110
115
120
125
130
135
140
145
150

SITE 791 HOLE A CORE 11H CORED INTERVAL 90.7-100.4 mbsf

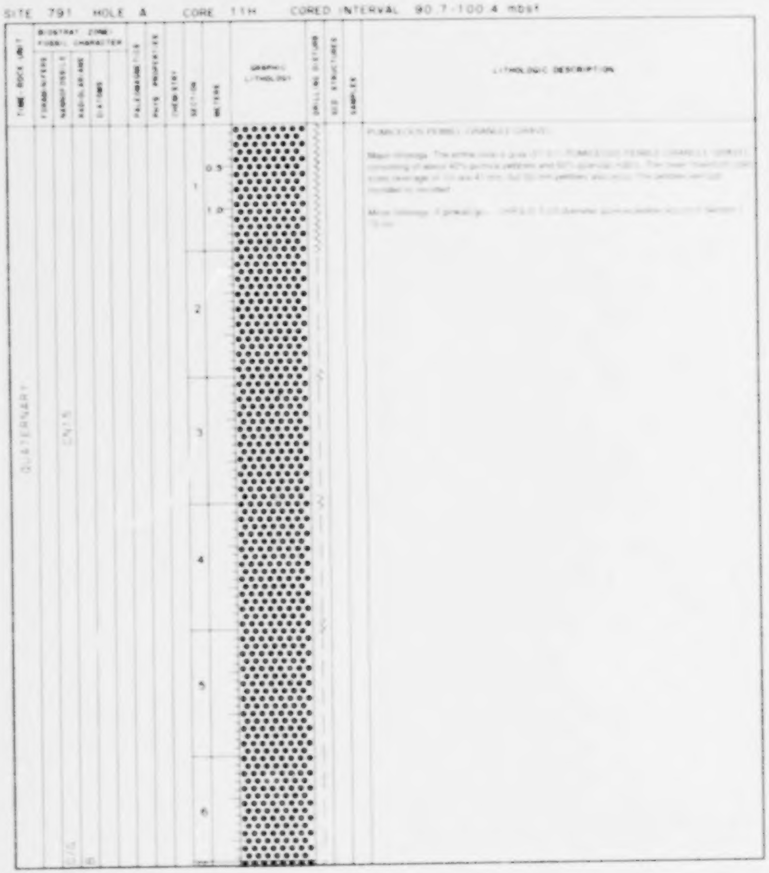
TIME-ROCK UNIT
BIOSTRAT. ZONE/ FOSSIL CHARACTER
FORAMINIFERS
NANNOFOSSILS
RADIOLARIANS
DIATOMS
PALEOMAGNETICS
PHYS. PROPERTIES
CHEMISTRY
SECTION
METERS
GRAPHIC LITHOLOGY
DRILLING DISTURB.
SED. STRUCTURES
SAMPLES
QUATERNARY
CN15
0.5
1.0
1
2
3
4
5
6

LITHOLOGIC DESCRIPTION

PUMICEOUS PEBBLE (GRANULE) GRAVEL

Major lithology: The entire core is gray [illegible] PUMICEOUS PEBBLE (GRANULE) GRAVEL, consisting of about 40% pumice pebbles and 60% [illegible]. The [illegible] sizes average of [illegible] and 4 mm, but [illegible] pebbles also occur. The pebbles are [illegible] rounded to rounded.

Minor lithology: A greenish gray [illegible] diameter pumice pebble occurs in Section 1, [illegible] cm.

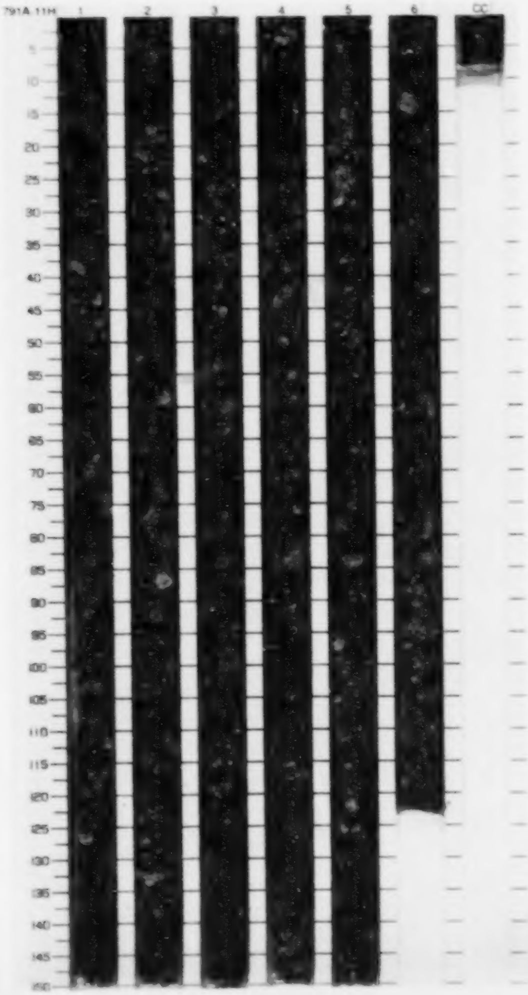
791A-11H
1
2
3
4
5
6
CC
5
10
15
20
25
30
35
40
45
50
55
60
65
70
75
80
85
90
95
100
105
110
115
120
125
130
135
140
145
150

SITE 791 HOLE A CORE 12H CORED INTERVAL 100.4-110.1 mbsf

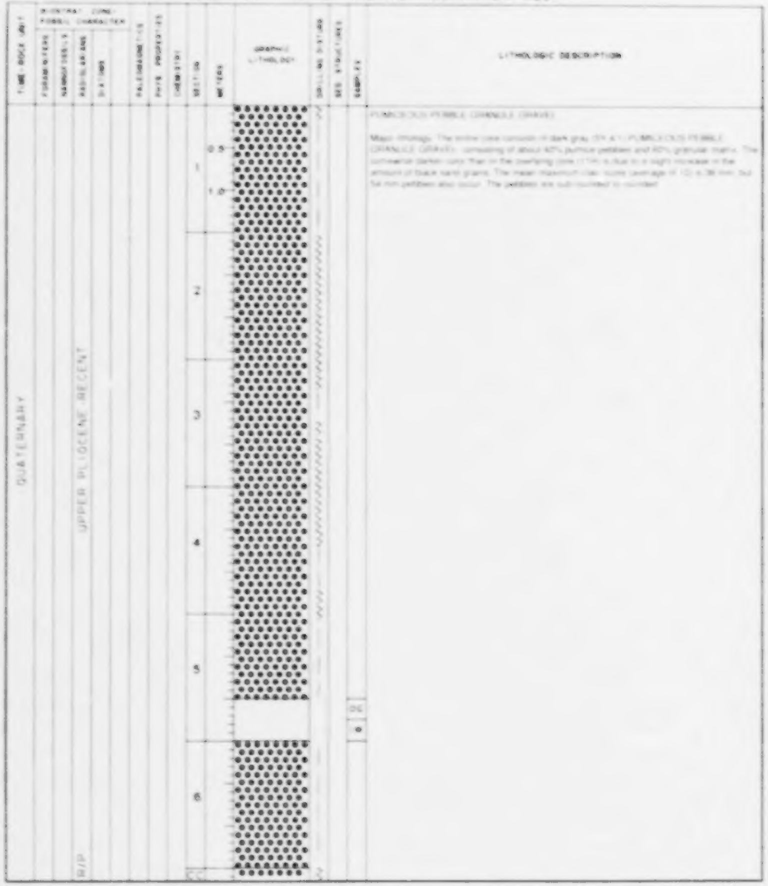
TIME-ROCK UNIT
BIOSTRAT. ZONE/FOSSIL CHARACTER
FORAMINIFERS
NANNOFOSSILS
RADIOLARIANS
DIATOMS
PALEOMAGNETICS
PHYS. PROPERTIES
CHEMISTRY
SECTION
METERS
GRAPHIC LITHOLOGY
DRILLING DISTURB.
SED. STRUCTURES
SAMPLES
LITHOLOGIC DESCRIPTION
QUATERNARY
UPPER PLIOCENE-RECENT
B/P
0.5
1.0
1
2
3
4
5
6
CC
OG
♦

PUMICEOUS PEBBLE GRANULE GRAVEL

Major lithology: The entire core consists of dark gray (5Y 4/1) PUMICEOUS PEBBLE GRANULE GRAVEL, consisting of about 40% pumice pebbles and 60% granular matrix. The somewhat darker color than in the overlying core (11H) is due to a slight increase in the amount of black sand grains. The mean maximum clast sizes (average of 10) is 38 mm, but 54 mm pebbles also occur. The pebbles are sub-rounded to rounded.

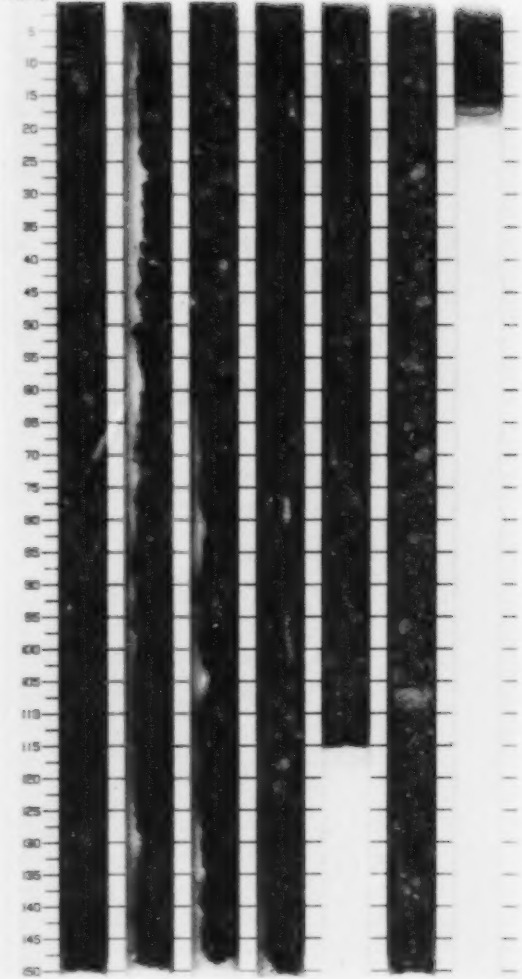
791A 12H
1
2
3
4
5
6
7
5
10
15
20
25
30
35
40
45
50
55
60
65
70
75
80
85
90
95
100
105
110
115
120
125
130
135
140
145
150

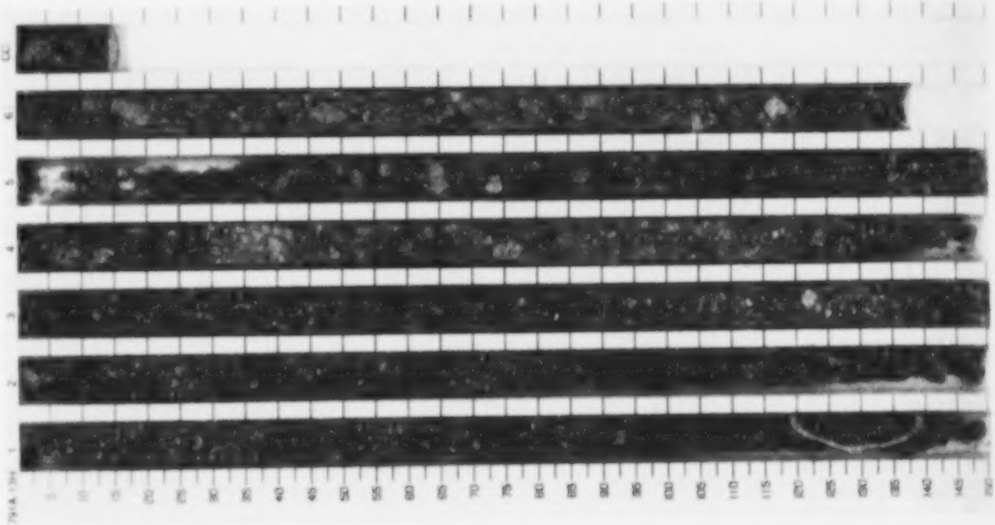
CC
6
5
4
3
2
1
791A 13H
5
10
15
20
25
30
35
40
45
50
55
60
65
70
75
80
85
90
95
100
105
110
115
120
125
130
135
140
145
150

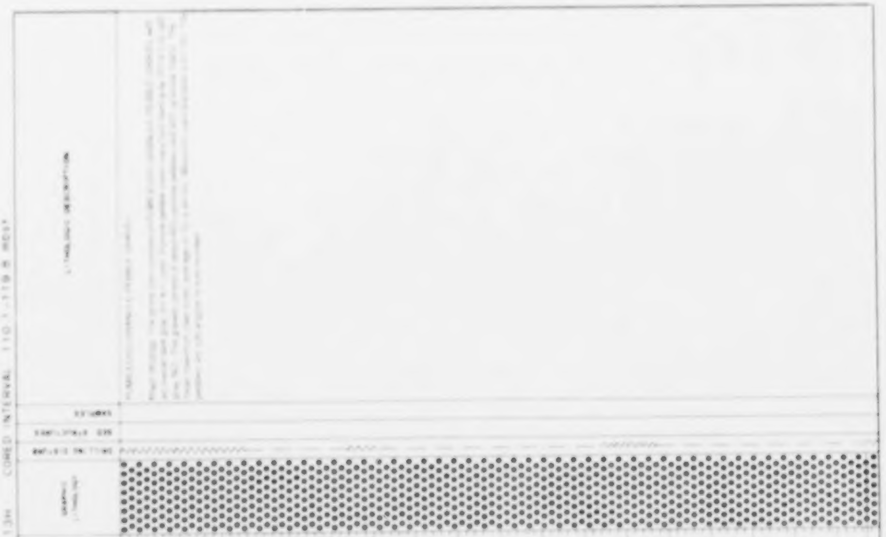
SITE 791 HOLE A CORE 13H CORED INTERVAL 1110.1-1119.6 mbsf
TIME-ROCK UNIT
BIOSTRAT. ZONE/FOSSIL CHARACTER
FORAMINIFERS
NANNOFOSSILS
RADIOLARIANS
DIATOMS
PALEOMAGNETICS
PHYS. PROPERTIES
CHEMISTRY
SECTION
METERS
GRAPHIC LITHOLOGY
DRILLING DISTURB.
SED. STRUCTURES
SAMPLES
LITHOLOGIC DESCRIPTION
QUATERNARY
CN15
A/G
1
2
3
4
5
6
CC

SITE 791 HOLE A CORE 14H CORED INTERVAL 119.8-129.5 mbsf

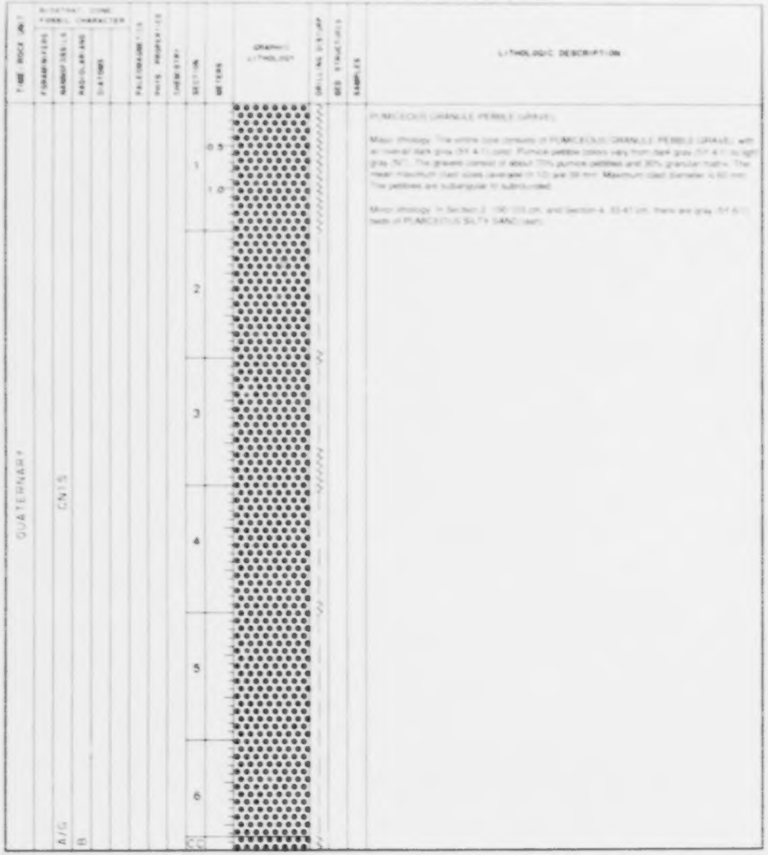
TIME-ROCK UNIT
BIOSTRAT. ZONE/FOSSIL CHARACTER
FORAMINIFERS
NANNOFOSSILS
RADIOLARIANS
DIATOMS
PALEOMAGNETICS
PHYS. PROPERTIES
CHEMISTRY
SECTION
METERS
GRAPHIC LITHOLOGY
DRILLING DISTURB.
SED. STRUCTURES
SAMPLES
LITHOLOGIC DESCRIPTION
QUATERNARY
CN15
A/G
B
0.5
1.0
1
2
3
4
5
6
CC

PUMICEOUS GRANULE PEBBLE GRAVEL

Major lithology: The entire core consists of PUMICEOUS GRANULE PEBBLE GRAVEL with an overall dark gray (5Y 4/1) color. Pumice pebble colors vary from dark gray (5Y 4/1) to light gray (N7). The gravels consist of about 70% pumice pebbles and 30% granular matrix. The mean maximum clast sizes (average of 10) are 39 mm. Maximum clast diameter is 60 mm. The pebbles are subangular to subrounded.

Minor lithology: In Section 2, 100-103 cm, and Section 4, 33-41 cm, there are gray (5Y 6/1) beds of PUMICEOUS SILTY SAND (ash).

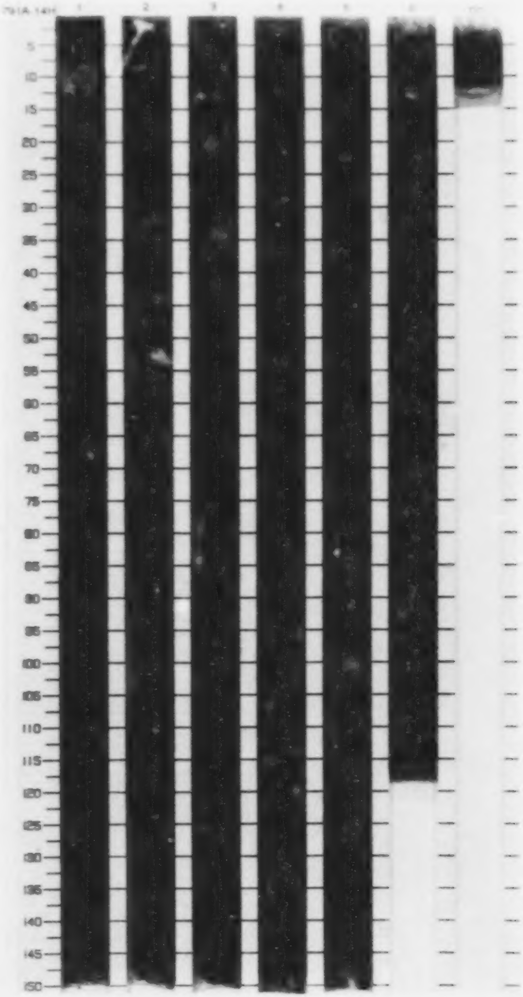
791A-14H
1
2
3
4
5
6
CC
5
10
15
20
25
30
35
40
45
50
55
60
65
70
75
80
85
90
95
100
105
110
115
120
125
130
135
140
145
150

SITE 791 HOLE A CORE 15H CORED INTERVAL 129.5-139.2 mbsf

TIME-ROCK UNIT	BIOSTRAT. ZONE/ FOSSIL CHARACTER: FORAMINIFERS	NANNOFOSSILS	RADIOLARIANS	DIATOMS	PALEOMAGNETICS	PHYS. PROPERTIES	CHEMISTRY	SECTION	METERS	GRAPHIC LITHOLOGY	DRILLING DISTURB.	SED. STRUCTURES	SAMPLES	LITHOLOGIC DESCRIPTION
QUATERNARY		CN15						1	0.5 1.0					[illegible] PUMICEOUS GRAVEL, SAND, AND PEBBLY SAND Major lithologies: The sediment consists of both poorly sorted, dark gray (5Y 4/1) PUMICEOUS GRAVEL, and horizons of SAND and PEBBLY SAND of similar color and composition. Pumice colors are very light gray (N8), light gray (N7), and gray (5Y 6/1). The sediment contains about 10% scoria granules and coarse sand. Maximum pumice clast size is 5 cm, and the average diameter of the 10 largest pebbles is 1 cm. The core may be severely mixed by drilling.
								2						
								3						
								4						
								5					OG IW	
								6						
		A/G	R/P					CC						

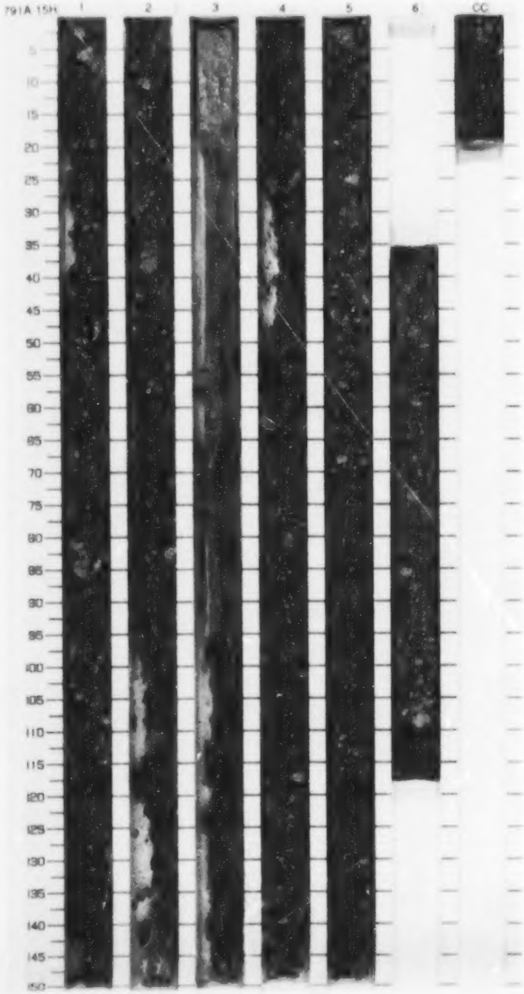

791A 15H
1
2
3
4
5
6
CC
5
10
15
20
25
30
35
40
45
50
55
60
65
70
75
80
85
90
95
100
105
110
115
120
125
130
135
140
145
150

SITE 791 HOLE A CORE 16H CORED INTERVAL 139.2-148.8 mbsf

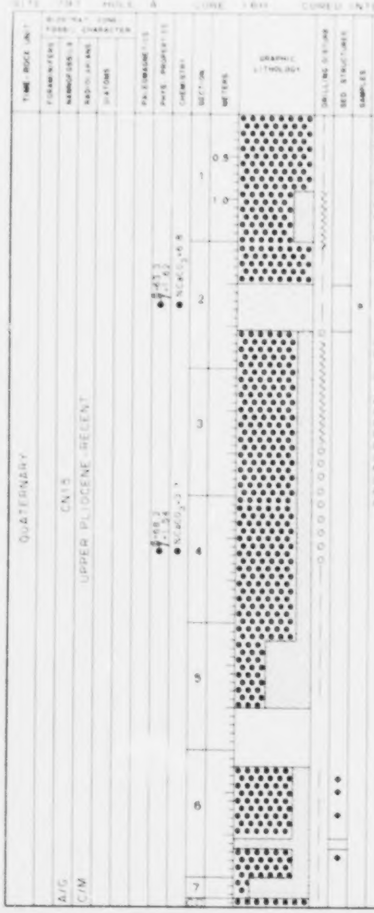
TIME-ROCK UNIT
BIOSTRAT. ZONE/FOSSIL CHARACTER
FORAMINIFERS
NANNOFOSSILS
RADIOLARIANS
DIATOMS
PALEOMAGNETICS
PHYS. PROPERTIES
CHEMISTRY
SECTION
METERS
GRAPHIC LITHOLOGY
DRILLING DISTURB.
SED. STRUCTURES
SAMPLES
QUATERNARY
CN15
UPPER PLIOCENE-RECENT
A/G
C/M
φ=63.3
γ=1.62
%CaCO3=6.8
φ=68.2
γ=1.54
%CaCO3=3.1
1
2
3
4
5
6
7
0.5
1.0

LITHOLOGIC DESCRIPTION

PUMICEOUS GRAVEL, PUMICEOUS SANDY GRAVEL, PEBBLY SAND, AND SAND

Major lithologies:
Poorly sorted, dark gray (5Y 4/1) PUMICEOUS GRAVEL, PUMICEOUS SANDY GRAVEL, and horizons of SAND and PEBBLY SAND of similar color and composition. The sediment contains about 10% scoria granules and coarse sand. Maximum pumice clast size is 3 cm, and the average diameter of the 10 largest clasts is 2 cm. The sediment in Section 6, 60-140 cm, contains large (cm diameter), angular, soft clasts of clayey silt, perhaps disrupted by drilling.

Minor lithology: Section 2, 50-100 cm, consists of a bed of VITRIC SILT.

SMEAR SLIDE SUMMARY (%):

	2, 75
	D
TEXTURE:	
Silt	60
Clay	40
COMPOSITION:	
Accessory minerals	[illegible]
Clay	30
Diatoms	[illegible]
Feldspar	[illegible]
Foraminifers	[illegible]
Glass	60
Nannofossils	[illegible]
Opaques	[illegible]
Radiolarians	[illegible]
Rock fragments	[illegible]

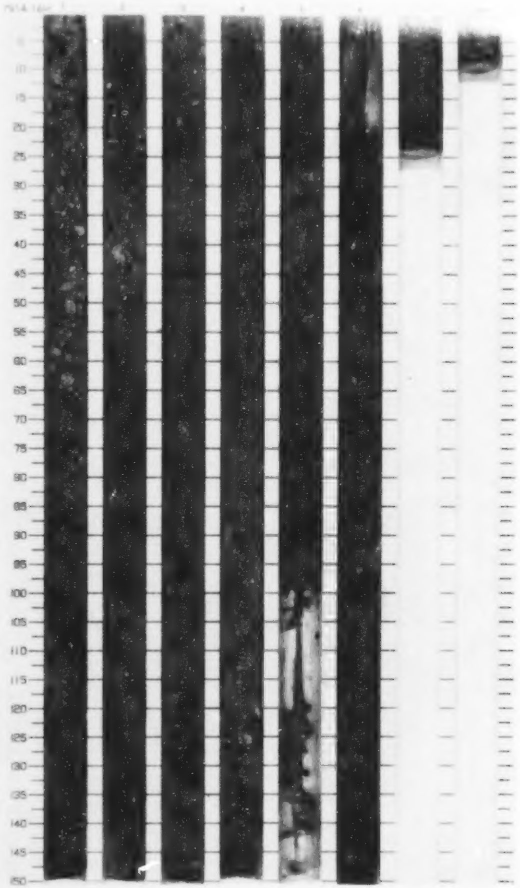
791A-16H
1
2
3
4
5
6
7
CC
0
10
15
20
25
30
35
40
45
50
55
60
65
70
75
80
85
90
95
100
105
110
115
120
125
130
135
140
145
150

SITE 791 HOLE A CORE 17H CORED INTERVAL 148.8-158.5 mbsf

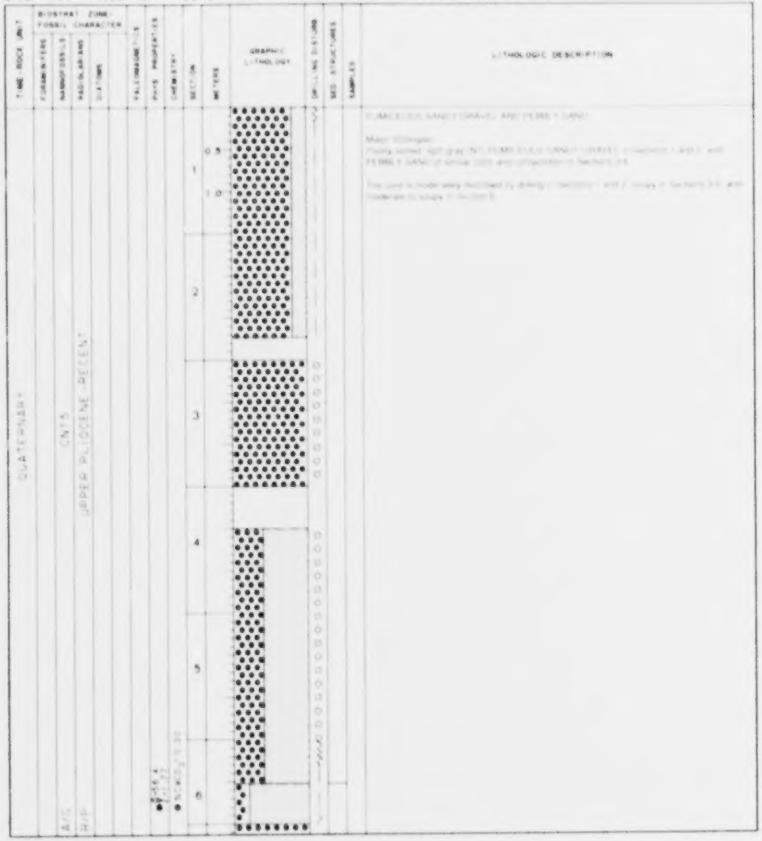
TIME-ROCK UNIT
BIOSTRAT. ZONE/ FOSSIL CHARACTER
FORAMINIFERS
NANNOFOSSILS
RADIOLARIANS
DIATOMS
PALEOMAGNETICS
PHYS. PROPERTIES
CHEMISTRY
SECTION
METERS
GRAPHIC LITHOLOGY
DRILLING DISTURB.
SED. STRUCTURES
SAMPLES
QUATERNARY
CN15
A/C
UPPER PLIOCENE-RECENT
R/P
0.5
1.0
1
2
3
4
5
6

LITHOLOGIC DESCRIPTION

PUMICEOUS SANDY GRAVEL AND PEBBLY SAND

Major lithologies:
Poorly sorted, light gray (N7) PUMICEOUS SANDY GRAVEL in Sections 1 and 2, and PEBBLY SAND of similar color and composition in Sections 3-6.

The core is moderately disturbed by drilling in Sections 1 and 2, soupy in Sections 3-5, and moderate to soupy in Section 6.

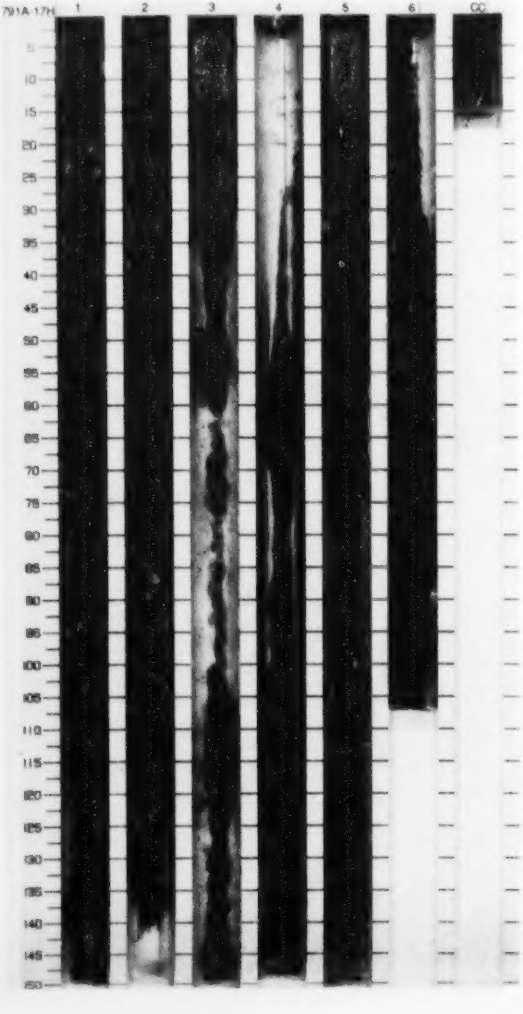
791A-17H
1
2
3
4
5
6
CC
5
10
15
20
25
30
35
40
45
50
55
60
65
70
75
80
85
90
95
100
105
110
115
120
125
130
135
140
145
150

SITE 791 HOLE A CORE 18H CORED INTERVAL 158.5-168.1 mbsf

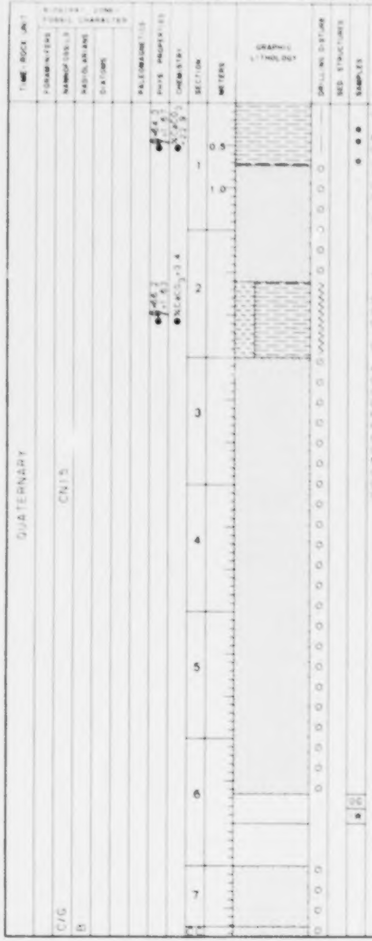
TIME-ROCK UNIT
BIOSTRAT. ZONE/ FOSSIL CHARACTER
FORAMINIFERS
NANNOFOSSILS
RADIOLARIANS
DIATOMS
PALEOMAGNETICS
PHYS. PROPERTIES
CHEMISTRY
SECTION
METERS
GRAPHIC LITHOLOGY
DRILLING DISTURB.
SED. STRUCTURES
SAMPLES
QUATERNARY
CN15
C/G
B
0.5
1.0
1
2
3
4
5
6
7
CC
OG

LITHOLOGIC DESCRIPTION

VITRIC SAND AND VITRIC SILTY CLAY

Major lithologies:
Olive gray (5Y 4/1) medium to granule-rich to pebbly SAND grading downward into dark gray (N3) coarse sand. Medium to thick graded beds of medium dark gray (N4) to olive gray (5Y 5/1) VITRIC SILTY CLAY are slightly mottled. Drilling has moderately disturbed the upper 75 cm of the core; the rest of it is very disturbed to soupy. The sand is structureless, and may be mainly flow-in material.

SMEAR SLIDE SUMMARY (%):

	1, 30 M	1, 41 D	1, 68 D
TEXTURE:			
Sand	75	—	—
Silt	25	40	30
Clay	—	60	70
COMPOSITION:			
Accessory minerals	1	—	—
Chlorite	—	1	1
Clay	19	60	42
Diatoms	2	2	1
Fe-oxide	—	—	1
Feldspar	1	1	1
Foraminifers	1	1	1
Glass	75	30	30
Nannofossils	—	—	20
Opaques	1	1	—
Quartz	—	—	1
Spicules	—	—	1

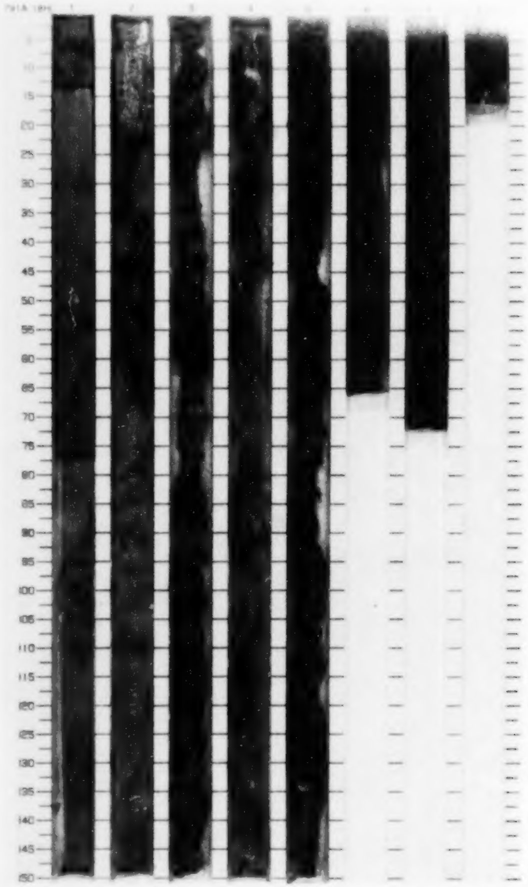
791A 18H
1
2
3
4
5
6
7
CC
0
5
10
15
20
25
30
35
40
45
50
55
60
65
70
75
80
85
90
95
100
105
110
115
120
125
130
135
140
145
150

SITE 791 HOLE A CORE 19H CORED INTERVAL 168.1-177.7 mbsf

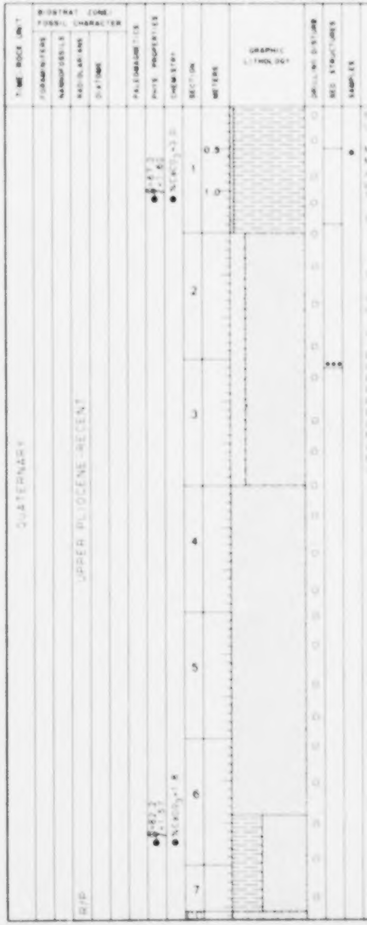

LITHOLOGIC DESCRIPTION

PUMICEOUS SAND, PUMICEOUS GRANULE-RICH SAND, VITRIC SILT AND VITRIC CLAYEY SILT

Major lithologies:

Medium dark gray (N4) to light olive gray (5Y 6/2) fine to very coarse PUMICEOUS SAND and PUMICEOUS GRANULE-RICH SAND with a minor percentage of scoria. In the upper part of the core sand grades into olive gray (5Y 6/2) VITRIC SILT and VITRIC CLAYEY SILT. The sediment is highly disturbed flow-in material.

SMEAR SLIDE SUMMARY (%):

	1, 35
	D
TEXTURE:	
Silt	[illegible]
Clay	[illegible]
COMPOSITION:	
Chlorite	[illegible]
Clay	[illegible]
Diatoms	[illegible]
Fe oxide	[illegible]
Feldspar	[illegible]
Foraminifers	[illegible]
Glass	[illegible]
Nannofossils	[illegible]
Opaques	[illegible]
Pyroxene	[illegible]
Quartz	[illegible]

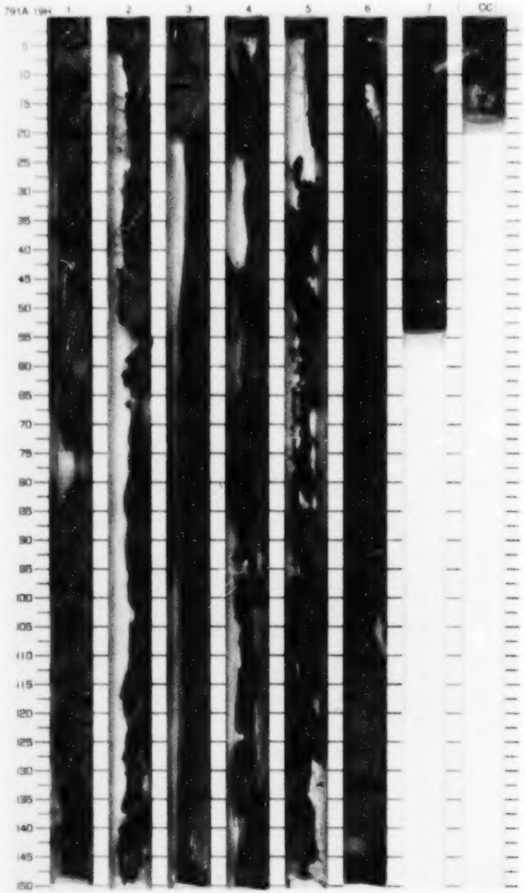
791A 19H
1
2
3
4
5
6
7
CC
5
10
15
20
25
30
35
40
45
50
55
60
65
70
75
80
85
90
95
100
105
110
115
120
125
130
135
140
145
150

SITE 791 HOLE A CORE 20H CORED INTERVAL 177.7-187.4 mbsf

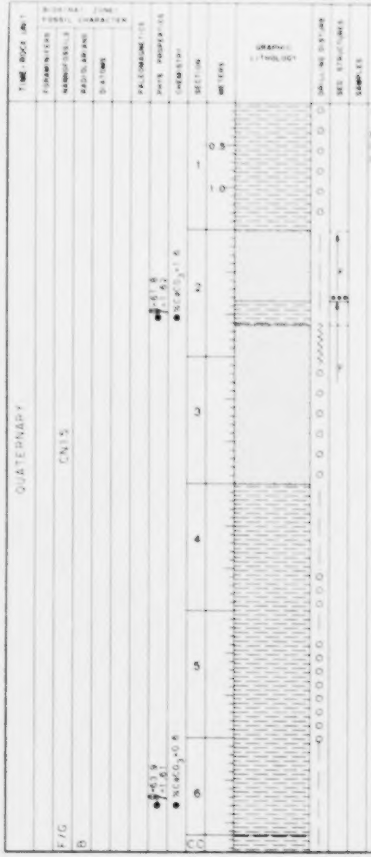
TIME-ROCK UNIT
BIOSTRAT. ZONE/ FOSSIL CHARACTER
FORAMINIFERS
NANNOFOSSILS
RADIOLARIANS
DIATOMS
PALEOMAGNETICS
PHYS. PROPERTIES
CHEMISTRY
SECTION
METERS
GRAPHIC LITHOLOGY
DRILLING DISTURB.
SED. STRUCTURES
SAMPLES
QUATERNARY
CN15
F/G
B
φ=61.8
γ=1.62
%CaCO₃=1.6
φ=63.9
γ=1.61
%CaCO₃=0.8
1
2
3
4
5
6
CC
0.5
1.0

LITHOLOGIC DESCRIPTION

VITRIC CLAYEY SILT AND PUMICEOUS SAND

Major lithologies:
Dark gray (5Y 4/1) structureless VITRIC CLAYEY SILT, interbedded with two thick beds of graded PUMICEOUS SAND. This core is strongly deformed by drilling.

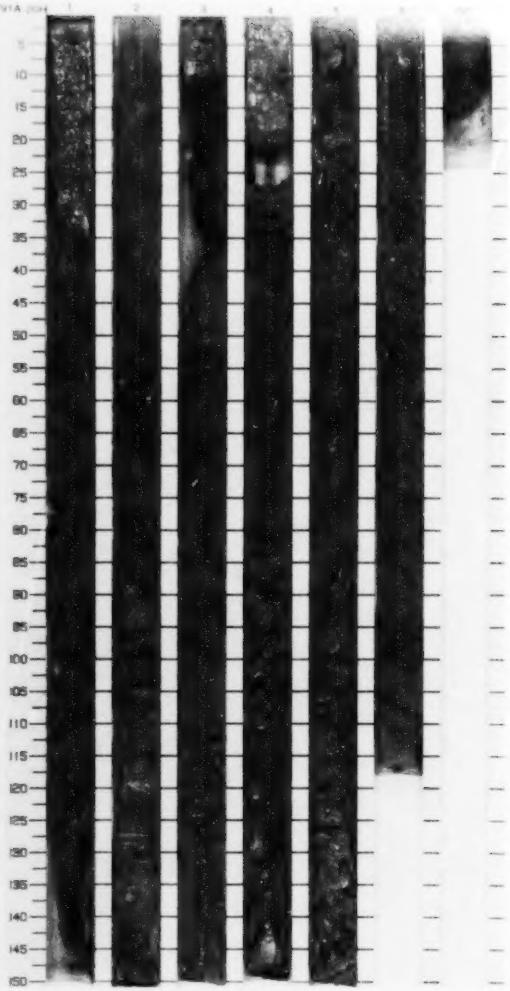
791A 20H
1
2
3
4
5
6
CC
5
10
15
20
25
30
35
40
45
50
55
60
65
70
75
80
85
90
95
100
105
110
115
120
125
130
135
140
145
150

SITE 791 HOLE A CORE 21H CORED INTERVAL 187.4-196.9 mbsf

TIME-ROCK UNIT	BIOSTRAT. ZONE/ FOSSIL CHARACTER: FORAMINIFERS	NANNOFOSSILS	RADIOLARIANS	DIATOMS	PALEOMAGNETICS	PHYS. PROPERTIES	CHEMISTRY	SECTION	METERS	GRAPHIC LITHOLOGY	DRILLING DISTURB.	SED. STRUCTURES	SAMPLES	LITHOLOGIC DESCRIPTION
QUATERNARY		CN15 F/G	UPPER PLIOCENE-RECENT R/P					1 CC	0.5 1.0		○ ○ ○ ○ ○ ○ ○ ○ ○ ○			VITRIC SAND Major lithology: Dark gray (5Y 4/1) fine VITRIC SAND, strongly deformed by drilling. Minor lithology: Dark gray (5Y 4/1) VITRIC SILT present only in the core catcher.

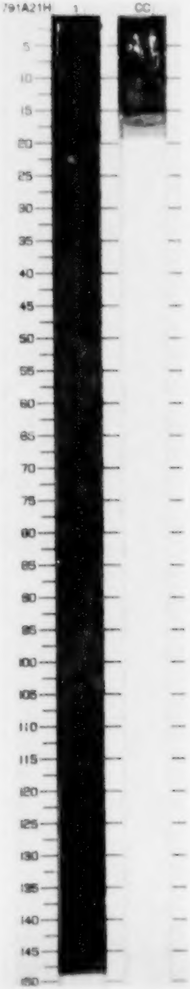
791A21H
1
CC
5
10
15
20
25
30
35
40
45
50
55
60
65
70
75
80
85
90
95
100
105
110
115
120
125
130
135
140
145
150

SITE 791 HOLE A CORE 22H CORED INTERVAL 196.9-206.4 mbsf

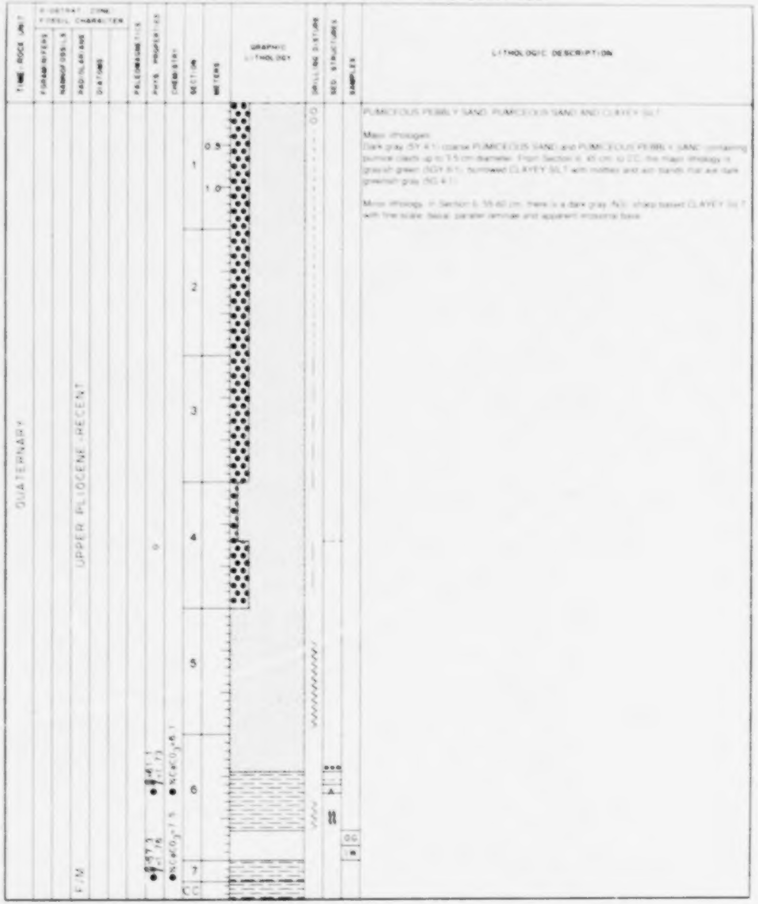
TIME-ROCK UNIT
BIOSTRAT. ZONE/FOSSIL CHARACTER
FORAMINIFERS
NANNOFOSSILS
RADIOLARIANS
DIATOMS
PALEOMAGNETICS
PHYS. PROPERTIES
CHEMISTRY
SECTION
METERS
GRAPHIC LITHOLOGY
DRILLING DISTURB.
SED. STRUCTURES
SAMPLES
LITHOLOGIC DESCRIPTION
QUATERNARY
UPPER PLIOCENE-RECENT
F/M
0.5
1.0
1
2
3
4
5
6
7
CC
φ=41.1
γ=1.73
%CaCO₃=6.1
φ=47.2
γ=1.76
%CaCO₃=7.5
OG
IW

PUMICEOUS PEBBLY SAND, PUMICEOUS SAND AND CLAYEY SILT

Major lithologies:
Dark gray (5Y 4/1) coarse PUMICEOUS SAND and PUMICEOUS PEBBLY SAND containing pumice clasts up to 1.5 cm diameter. From Section 6, 45 cm, to CC, the major lithology is grayish green (5GY 5/1), burrowed CLAYEY SILT with mottles and ash bands that are dark greenish gray (5G 4/1).

Minor lithology: In Section 6, 55-60 cm, there is a dark gray (N3), sharp based CLAYEY SILT with fine scale, basal, parallel laminae and apparent erosional base.

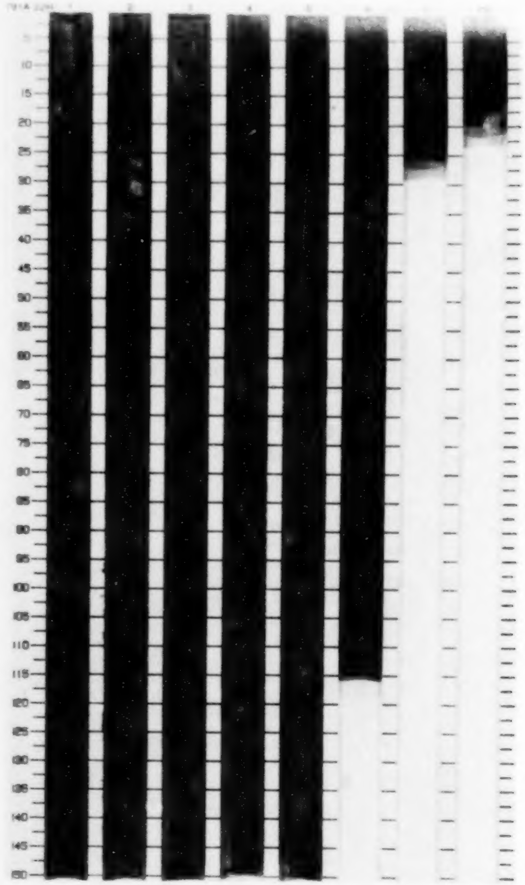
791A-22H
1
2
3
4
5
6
7
CC
5
10
15
20
25
30
35
40
45
50
55
60
65
70
75
80
85
90
95
100
105
110
115
120
125
130
135
140
145
150

SITE 791 HOLE A CORE 23H CORED INTERVAL 206.4-207.9 mbsf

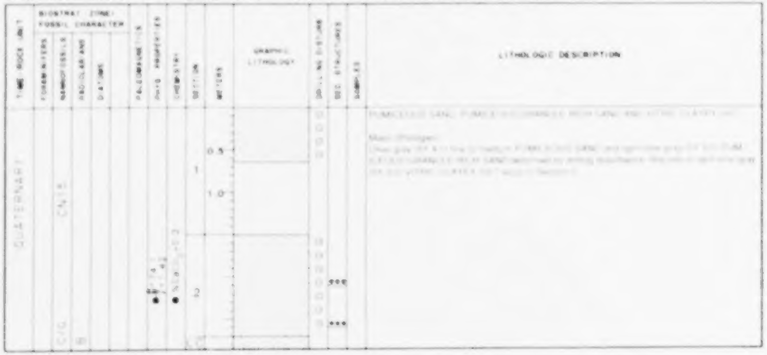
TIME-ROCK UNIT
BIOSTRAT. ZONE/ FOSSIL CHARACTER
FORAMINIFERS
NANNOFOSSILS
RADIOLARIANS
DIATOMS
PALEOMAGNETICS
PHYS. PROPERTIES
CHEMISTRY
SECTION
METERS
GRAPHIC LITHOLOGY
DRILLING DISTURB.
SED. STRUCTURES
SAMPLES
LITHOLOGIC DESCRIPTION
QUATERNARY
CN15
C/G
B
0.5
1
1.0
2
CC
Major lithologies:

126 791A 24X NO RECOVERY

SITE 791 HOLE A CORE 25X CORED INTERVAL 217.1-226.7 mbsf

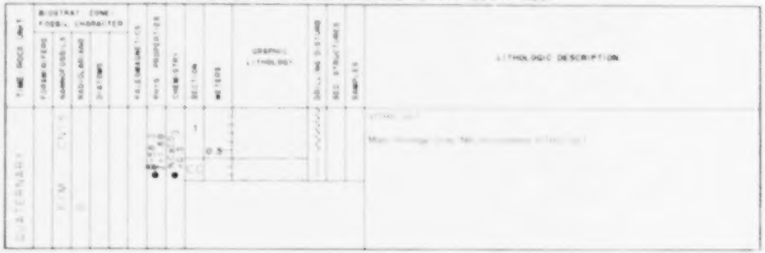
TIME-ROCK UNIT
BIOSTRAT. ZONE/ FOSSIL CHARACTER
FORAMINIFERS
NANNOFOSSILS
RADIOLARIANS
DIATOMS
PALEOMAGNETICS
PHYS. PROPERTIES
CHEMISTRY
SECTION
METERS
GRAPHIC LITHOLOGY
DRILLING DISTURB.
SED. STRUCTURES
SAMPLES
LITHOLOGIC DESCRIPTION
QUATERNARY
CN15
F/M
B
1
0.5
CC

126 791A 26X NO RECOVERY

126 791A 27X NO RECOVERY

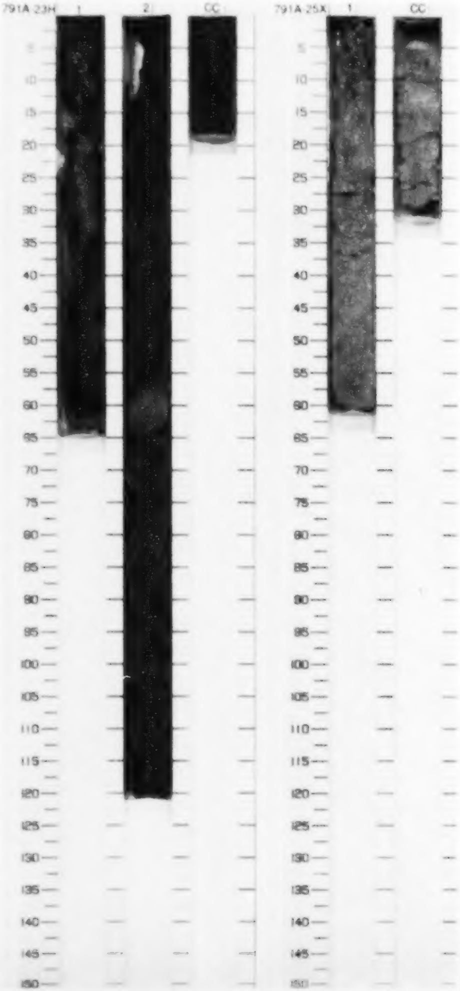
791A 23H
1
2
CC
791A 25X
1
CC
5
10
15
20
25
30
35
40
45
50
55
60
65
70
75
80
85
90
95
100
105
110
115
120
125
130
135
140
145
150

SITE 791 HOLE A CORE 28X CORED INTERVAL 246.0-255.6 mbsf

TIME-ROCK UNIT	BIOSTRAT. ZONE/ FOSSIL CHARACTER				PALEOMAGNETICS	PHYS. PROPERTIES	CHEMISTRY	SECTION	METERS	GRAPHIC LITHOLOGY	DRILLING DISTURB.	SED. STRUCTURES	SAMPLES	LITHOLOGIC DESCRIPTION
	FORAMINIFERS	NANNOFOSSILS	RADIOLARIANS	DIATOMS										
QUATERNARY		CN15 F/M	B			● Φ=47.6 γ=1.82	● %CaCO$_3$=0.4	1 CC	0.5 1.0					PUMICEOUS SAND AND VITRIC SILT Major lithologies: Light gray (N7) to medium light gray (N6) PUMICEOUS SAND with [illegible] and medium light gray (N6) VITRIC SILT. The sediment is structureless because of flow-in.

126 791A 29X NO RECOVERY

SITE 791 HOLE A CORE 30X CORED INTERVAL 265.3-274.9 mbsf

TIME-ROCK UNIT	BIOSTRAT. ZONE/ FOSSIL CHARACTER				PALEOMAGNETICS	PHYS. PROPERTIES	CHEMISTRY	SECTION	METERS	GRAPHIC LITHOLOGY	DRILLING DISTURB.	SED. STRUCTURES	SAMPLES	LITHOLOGIC DESCRIPTION
	FORAMINIFERS	NANNOFOSSILS	RADIOLARIANS	DIATOMS										
QUATERNARY		R/M CN15	B			● Φ=46.3 γ=1.88	● %CaCO$_3$=0.7	CC						VITRIC SAND AND VITRIC SILT Major lithology: Medium light gray (N6) crudely laminated, fine to coarse VITRIC SAND a VITRIC SILT.

126 791A 31X NO RECOVERY

126 791A 32X NO RECOVERY

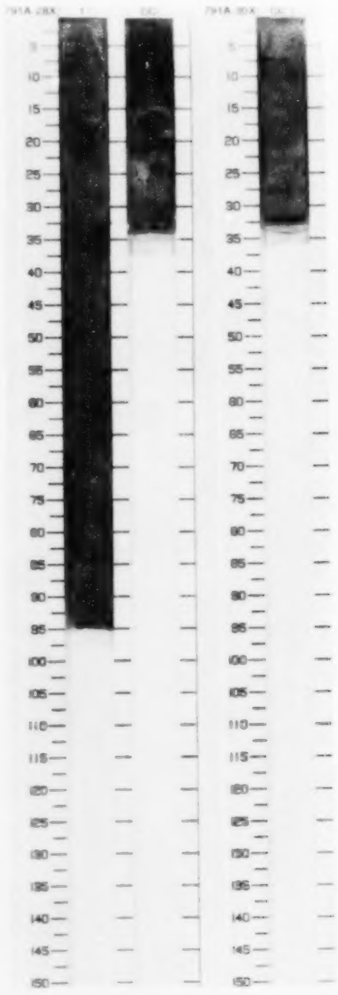

SITE 791 HOLE A CORE 33X CORED INTERVAL 296.3-304.0 mbsf

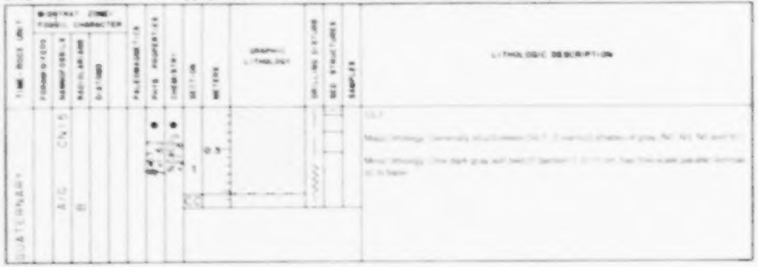
TIME-ROCK UNIT
BIOSTRAT. ZONE/ FOSSIL CHARACTER
FORAMINIFERS
NANNOFOSSILS
RADIOLARIANS
DIATOMS
PALEOMAGNETICS
PHYS. PROPERTIES
CHEMISTRY
SECTION
METERS
GRAPHIC LITHOLOGY
DRILLING DISTURB.
SED. STRUCTURES
SAMPLES
LITHOLOGIC DESCRIPTION
QUATERNARY
A/G
CN15
B
1
0.5
CC

SILT

Major lithology: Generally structureless SILT in various shades of gray (N4, N5, N6 and N7).

Minor lithology: One dark gray ash bed(?) Section 1, [illegible] cm, has fine-scale parallel laminae at its base.

SITE 791 HOLE A CORE 34X CORED INTERVAL 304.0-313.6 mbsf

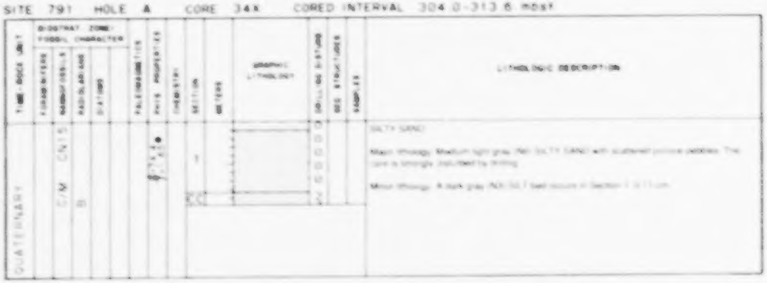
TIME-ROCK UNIT
BIOSTRAT. ZONE/ FOSSIL CHARACTER
FORAMINIFERS
NANNOFOSSILS
RADIOLARIANS
DIATOMS
PALEOMAGNETICS
PHYS. PROPERTIES
CHEMISTRY
SECTION
METERS
GRAPHIC LITHOLOGY
DRILLING DISTURB.
SED. STRUCTURES
SAMPLES
LITHOLOGIC DESCRIPTION
QUATERNARY
C/M
CN15
B
1
CC

SILTY SAND

Major lithology: Medium light gray (N6) SILTY SAND with scattered pumice pebbles. The core is strongly disturbed by drilling.

Minor lithology: A dark gray (N3) SILT bed occurs in Section 1, [illegible] cm.

SITE 791 HOLE A CORE 35X CORED INTERVAL 313.6-323.3 mbsf

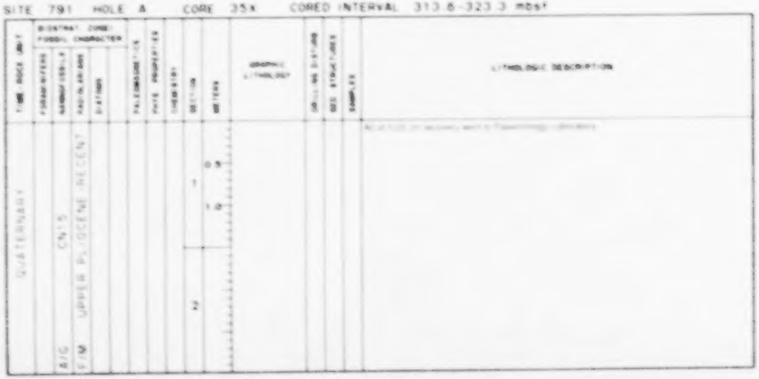
TIME-ROCK UNIT
BIOSTRAT. ZONE/ FOSSIL CHARACTER
FORAMINIFERS
NANNOFOSSILS
RADIOLARIANS
DIATOMS
PALEOMAGNETICS
PHYS. PROPERTIES
CHEMISTRY
SECTION
METERS
GRAPHIC LITHOLOGY
DRILLING DISTURB.
SED. STRUCTURES
SAMPLES
LITHOLOGIC DESCRIPTION
QUATERNARY
A/G
F/M
CN15
UPPER PLIOCENE-RECENT
1
2
0.5
1.0

ALL CORE (in recovery) went to Paleontology Laboratory.

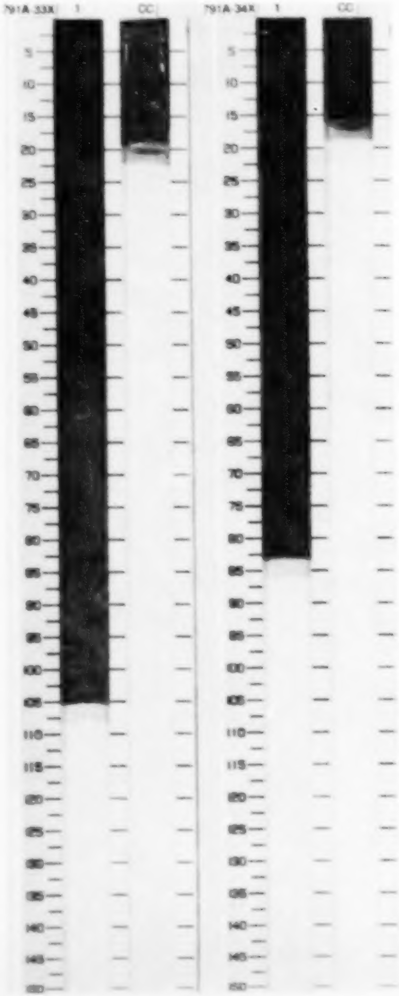
791A-33X
1
CC
791A-34X
1
CC
5
10
15
20
25
30
35
40
45
50
55
60
65
70
75
80
85
90
95
100
105
110
115
120
125
130
135
140
145
150

SITE 791 HOLE A CORE 36X CORED INTERVAL 323.3-332.9 mbsf

TIME-ROCK UNIT
BIOSTRAT. ZONE/ FOSSIL CHARACTER
FORAMINIFERS
NANNOFOSSILS
RADIOLARIANS
DIATOMS
PALEOMAGNETICS
PHYS. PROPERTIES
CHEMISTRY
SECTION
METERS
GRAPHIC LITHOLOGY
DRILLING DISTURB.
SED. STRUCTURES
SAMPLES
LITHOLOGIC DESCRIPTION
QUATERNARY
R/M CN15
1
2
0.5
1.0

All [illegible] cm recovery went to Paleontology Laboratory.

126 791A 37X NO RECOVERY

SITE 791 HOLE A CORE 38X CORED INTERVAL 342.6-352.3 mbsf

TIME-ROCK UNIT
BIOSTRAT. ZONE/ FOSSIL CHARACTER
FORAMINIFERS
NANNOFOSSILS
RADIOLARIANS
DIATOMS
PALEOMAGNETICS
PHYS. PROPERTIES
CHEMISTRY
SECTION
METERS
GRAPHIC LITHOLOGY
DRILLING DISTURB.
SED. STRUCTURES
SAMPLES
LITHOLOGIC DESCRIPTION
QUATERNARY
A/G CN15
C/M UPPER PLIOCENE-RECENT
1
2
0.5
1.0

All [illegible] cm recovery went to Paleontology Laboratory.

SITE 791 HOLE A CORE 39X CORED INTERVAL 352.3-362.0 mbsf

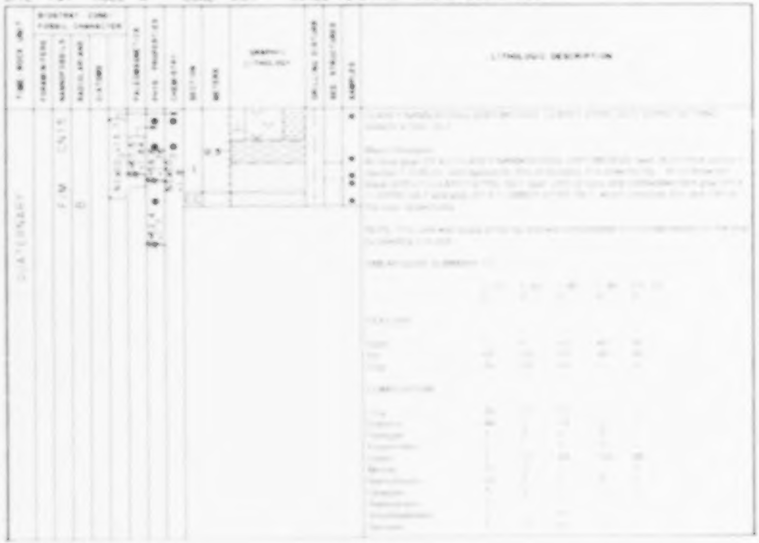
TIME-ROCK UNIT
BIOSTRAT. ZONE/FOSSIL CHARACTER
FORAMINIFERS
NANNOFOSSILS
RADIOLARIANS
DIATOMS
PALEOMAGNETICS
PHYS. PROPERTIES
CHEMISTRY
SECTION
METERS
GRAPHIC LITHOLOGY
DRILLING DISTURB.
SED. STRUCTURES
SAMPLES
QUATERNARY
F/M
CN15
1
CC

LITHOLOGIC DESCRIPTION

[illegible]

SMEAR SLIDE SUMMARY (%):

TEXTURE:

COMPOSITION:

791A-39X
1
CC
5
10
15
20
25
30
35
40
45
50
55
60
65
70
75
80
85
90
95
100
105
110
115
120
125
130
135
140
145
150

SITE 791 HOLE A CORE 40X CORED INTERVAL 362.0-371.7 mbsf

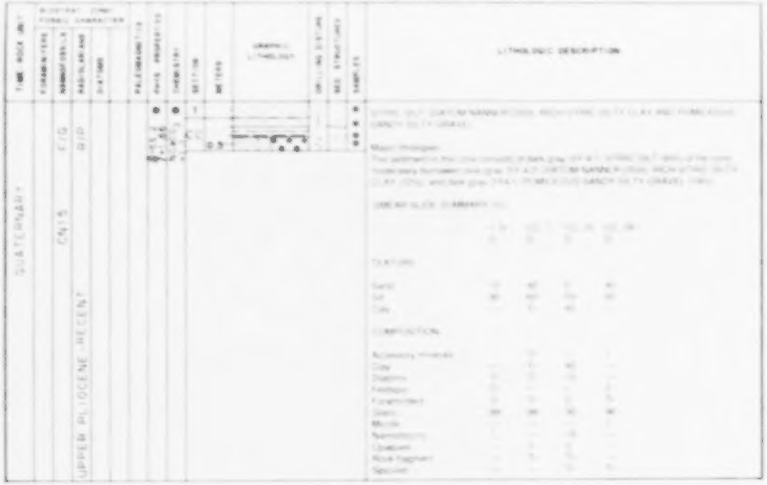
TIME-ROCK UNIT
BIOSTRAT. ZONE/ FOSSIL CHARACTER
FORAMINIFERS
NANNOFOSSILS
RADIOLARIANS
DIATOMS
PALEOMAGNETICS
PHYS. PROPERTIES
CHEMISTRY
SECTION
METERS
GRAPHIC LITHOLOGY
DRILLING DISTURB.
SED. STRUCTURES
SAMPLES
LITHOLOGIC DESCRIPTION
QUATERNARY
CN15
UPPER PLIOCENE-RECENT
F/G
R/P
1
CC
0.5

VITRIC SILT, DIATOM NANNOFOSSIL-RICH VITRIC SILTY CLAY AND PUMICEOUS SANDY SILTY GRAVEL

Major lithologies:
The sediment in this core consists of dark gray (5Y 4/1) VITRIC SILT ([illegible] of the core), moderately burrowed olive gray (5Y 4/2) DIATOM NANNOFOSSIL-RICH VITRIC SILTY CLAY ([illegible]), and dark gray (5Y 4/1) PUMICEOUS SANDY SILTY GRAVEL ([illegible]).

SMEAR SLIDE SUMMARY (%):

	[illegible]	[illegible]	[illegible]	[illegible]
TEXTURE:				
Sand	[illegible]	[illegible]	[illegible]	[illegible]
Silt	[illegible]	[illegible]	[illegible]	[illegible]
Clay	[illegible]	[illegible]	[illegible]	[illegible]
COMPOSITION:				
Accessory minerals	[illegible]	[illegible]	[illegible]	[illegible]
Clay	[illegible]	[illegible]	[illegible]	[illegible]
Diatoms	[illegible]	[illegible]	[illegible]	[illegible]
Feldspar	[illegible]	[illegible]	[illegible]	[illegible]
Foraminifers	[illegible]	[illegible]	[illegible]	[illegible]
Glass	[illegible]	[illegible]	[illegible]	[illegible]
Micrite	[illegible]	[illegible]	[illegible]	[illegible]
Nannofossils	[illegible]	[illegible]	[illegible]	[illegible]
Opaques	[illegible]	[illegible]	[illegible]	[illegible]
Rock fragment	[illegible]	[illegible]	[illegible]	[illegible]
Spicules	[illegible]	[illegible]	[illegible]	[illegible]

SITE 791 HOLE A CORE 41X CORED INTERVAL 371.7-381.4 mbsf

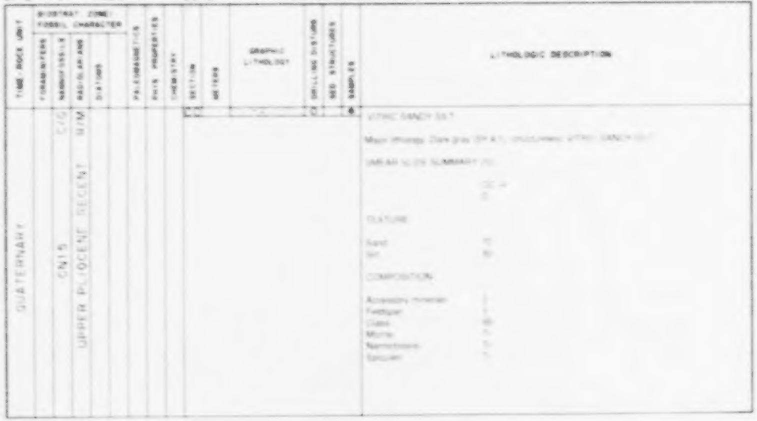
TIME-ROCK UNIT
BIOSTRAT. ZONE/ FOSSIL CHARACTER
FORAMINIFERS
NANNOFOSSILS
RADIOLARIANS
DIATOMS
PALEOMAGNETICS
PHYS. PROPERTIES
CHEMISTRY
SECTION
METERS
GRAPHIC LITHOLOGY
DRILLING DISTURB.
SED. STRUCTURES
SAMPLES
LITHOLOGIC DESCRIPTION
QUATERNARY
CN15
UPPER PLIOCENE-RECENT
C/G
R/M
CC

VITRIC SANDY SILT

Major lithology: Dark gray (5Y 4/1), structureless VITRIC SANDY SILT.

SMEAR SLIDE SUMMARY (%):

	CC, 4 D
TEXTURE:	
Sand	[illegible]
Silt	[illegible]
COMPOSITION:	
Accessory minerals	[illegible]
Feldspar	[illegible]
Glass	[illegible]
Micrite	[illegible]
Nannofossils	[illegible]
Spicules	[illegible]

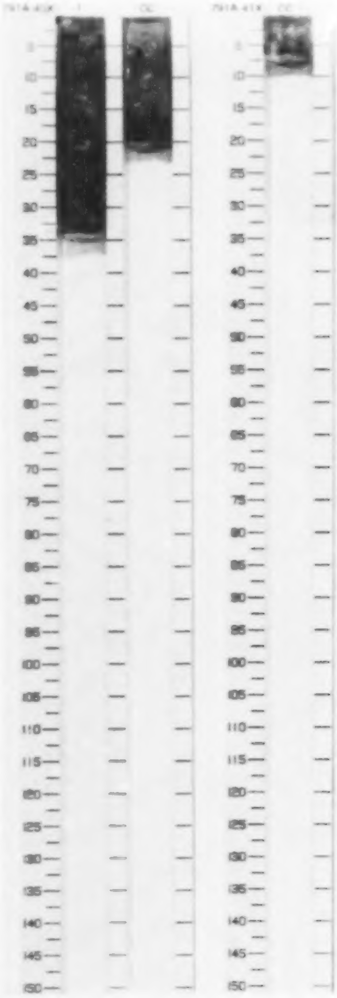
791A-40X 1
CC
791A-41X CC
0
5
10
15
20
25
30
35
40
45
50
55
60
65
70
75
80
85
90
95
100
105
110
115
120
125
130
135
140
145
150

SITE 791 HOLE A CORE 42X CORED INTERVAL 381.4-391.0 mbsf

TIME-ROCK UNIT	BIOSTRAT. ZONE/ FOSSIL CHARACTER: FORAMINIFERS	NANNOFOSSILS	RADIOLARIANS	DIATOMS		PALEOMAGNETICS	PHYS. PROPERTIES	CHEMISTRY	SECTION	METERS	GRAPHIC LITHOLOGY	DRILLING DISTURB.	SED. STRUCTURES	SAMPLES	LITHOLOGIC DESCRIPTION
QUATERNARY		A/G CN15	B				●	●	1 CC					▪ ▲	NANNOFOSSIL-RICH CLAYEY SILT Major lithology: Gray (5Y 5/1) structureless NANNOFOSSIL-RICH CLAYEY SILT. Minor lithology: Section 1, 2-4 cm: [illegible] dark gray (5Y 4/1) NANNOFOSSIL-RICH CLAY. SMEAR SLIDE SUMMARY (%): TEXTURE: Sand Silt Clay COMPOSITION: Accessory minerals Clay Feldspar Foraminifers Glass Mica Nannofossils Opaques Shell fragments Spicules

791A 42X
1
CC
5
10
15
20
25
30
35
40
45
50
55
60
65
70
75
80
85
90
95
100
105
110
115
120
125
130
135
140
145
150

126 791A 43X NO RECOVERY

126 791A 44X NO RECOVERY

126 791A 45X NO RECOVERY

SITE 791 HOLE A CORE 48X CORED INTERVAL 418.8-428.4 mbsf

TIME-ROCK UNIT	BIOSTRAT. ZONE/FOSSIL CHARACTER: FORAMINIFERS	NANNOFOSSILS	RADIOLARIANS	DIATOMS		PALEOMAGNETICS	PHYS. PROPERTIES	CHEMISTRY	SECTION	METERS	GRAPHIC LITHOLOGY	DRILLING DISTURB.	SED. STRUCTURES	SAMPLES	LITHOLOGIC DESCRIPTION
QUATERNARY		CN15 C/G	UPPER PLIOCENE-RECENT R/P						CC			✗		●	CRYSTAL VITRIC SILTY SAND AND SANDY SILTSTONE Major lithologies: Severe drilling disturbance has reduced CC, 0-19 cm, to a soupy mixture of dark gray (5Y 4/1) CRYSTAL VITRIC SILTY SAND in which angular rock fragments are imbedded; identical fragments that are not imbedded in unconsolidated sediment constitute the bottom 13 cm of the core-catcher sample. These fragments are highly indurated, conchoidally fractured, grayish black (N2) and black (5Y 2.5/1) SANDY SILTSTONES, some with fine laminations <1 mm in thickness. SMEAR SLIDE SUMMARY (%): CC, 8 D TEXTURE: Sand 80 Silt 20 COMPOSITION: Feldspar 10 Foraminifers 5 Glass 75 Nannofossils Tr

126 791A 47X NO RECOVERY

126 791A 48X NO RECOVERY

126 791B 1R NO RECOVERY

126 791B 2W WASH CORE

126 791B 3W WASH CORE

126 791B 4R NO RECOVERY

126 791B 5R NO RECOVERY

126 791B 6R NO RECOVERY

126 791B 7R NO RECOVERY

126 791B 8R NO RECOVERY

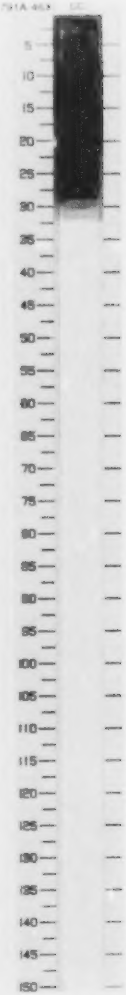

SITE 791 HOLE B CORE 9R CORED INTERVAL 463.6-473.3 mbsf

TIME-ROCK UNIT	BIOSTRAT. ZONE/ FOSSIL CHARACTER: FORAMINIFERS	NANNOFOSSILS	RADIOLARIANS	DIATOMS		PALEOMAGNETICS	PHYS. PROPERTIES	CHEMISTRY	SECTION	METERS	GRAPHIC LITHOLOGY	DRILLING DISTURB.	SED. STRUCTURES	SAMPLES	LITHOLOGIC DESCRIPTION
QUATERNARY		A/G CN15	R/M UPPER PLIOCENE-RECENT				●	●	CC					●	NANNOFOSSIL-RICH SILTY CLAYSTONE

Major lithology: Greenish gray [illegible] bioturbated NANNOFOSSIL-RICH SILTY CLAYSTONE.

SMEAR SLIDE SUMMARY (%):

CC, [illegible]
D

TEXTURE:

Sand [illegible]
Silt [illegible]
Clay [illegible]

COMPOSITION:

Accessory minerals [illegible]
Clay [illegible]
Dolomite [illegible]
Feldspar [illegible]
Foraminifers [illegible]
Glass [illegible]
Nannofossils [illegible]
Opaques [illegible]
Radiolarians [illegible]
[illegible] [illegible]
[illegible] [illegible]

791B-9R, CC

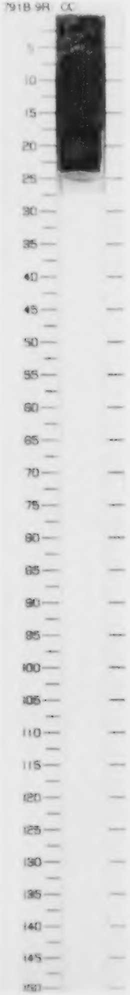
5
10
15
20
25
30
35
40
45
50
55
60
65
70
75
80
85
90
95
100
105
110
115
120
125
130
135
140
145
150

SITE 791 HOLE B CORE 10R CORED INTERVAL 473.3-482.9 mbsf

TIME-ROCK UNIT	FORAMINIFERS	NANNOFOSSILS	RADIOLARIANS	DIATOMS	PALEOMAGNETICS	PHYS. PROPERTIES	CHEMISTRY	SECTION	METERS	GRAPHIC LITHOLOGY	DRILLING DISTURB.	SED. STRUCTURES	SAMPLES
QUATERNARY		CN15 A/G	UPPER PLIOCENE-RECENT C/M		N	●	●	1	0.5 1.0				● ● ● IW

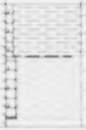

LITHOLOGIC DESCRIPTION

SILTY CLAYSTONE AND NANNOFOSSIL-RICH VITRIC SILTY CLAYSTONE

Major lithologies:
Olive gray (5Y 4/2) SILTY CLAYSTONE, containing foraminifers, and NANNOFOSSIL-RICH VITRIC SILTY CLAYSTONE of the same color.

Minor lithology: A CRYSTAL VITRIC CLAYEY SILTSTONE (ash bed) occurs in Section 1, [illegible] cm.

SMEAR SLIDE SUMMARY (%):

	1, 19 M	1, 30 D	1, 40 D
TEXTURE:			
Sand	5	—	—
Silt	[illegible]	[illegible]	40
Clay	50	[illegible]	60
COMPOSITION:			
Accessory minerals	[illegible]	—	[illegible]
Clay	[illegible]	[illegible]	[illegible]
Diatoms	Tr	Tr	Tr
Feldspar	[illegible]	[illegible]	[illegible]
Foraminifers	—	Tr	—
Glass	[illegible]	[illegible]	[illegible]
Lithic fragments	Tr	—	—
Micrite	[illegible]	4	[illegible]
Nannofossils	[illegible]	[illegible]	25
Opaques	[illegible]	[illegible]	[illegible]
Silicoflagellates	[illegible]	[illegible]	[illegible]
Spicules	Tr	—	[illegible]

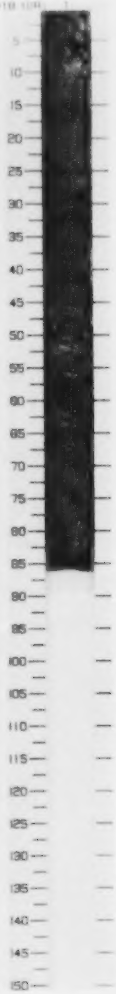

SITE 791 HOLE B CORE 11R CORED INTERVAL 482.9-492.6 mbsf

TIME-ROCK UNIT	BIOSTRAT. ZONE/ FOSSIL CHARACTER: FORAMINIFERS	NANNOFOSSILS	RADIOLARIANS	DIATOMS	PALEOMAGNETICS	PHYS. PROPERTIES	CHEMISTRY	SECTION	METERS	GRAPHIC LITHOLOGY	DRILLING DISTURB.	SED. STRUCTURES	SAMPLES	LITHOLOGIC DESCRIPTION
QUATERNARY		CN15 F/G	B		N			CC					●	CRYSTAL VITRIC SAND Major lithology: Dark gray (5Y 4/1), structureless fine CRYSTAL VITRIC SAND (sand consisting of transparent white pumice clasts, olive (5Y 5/4) glass, and dark rock fragments). Minor lithology: A VITRIC SAND, identical in appearance to the above material but lacking significant crystals, occurs in CC, 0-4 cm. SMEAR SLIDE SUMMARY (%): CC, 10 D TEXTURE: Sand 75 Silt 20 Clay 5 COMPOSITION: Accessory minerals 1 Bioclast 1 Clay 11 Feldspar [illegible] Foraminifers [illegible] Glass 87 Micrite [illegible] Nannofossils [illegible]

126 791B 12R NO RECOVERY

791B-11R CC
5
10
15
20
25
30
35
40
45
50
55
60
65
70
75
80
85
90
95
100
105
110
115
120
125
130
135
140
145
150

SITE 791 HOLE B CORE 13R CORED INTERVAL 502.1-511.8 mbsf

TIME-ROCK UNIT	BIOSTRAT. ZONE/ FOSSIL CHARACTER				PALEOMAGNETICS	PHYS. PROPERTIES	CHEMISTRY	SECTION	METERS	GRAPHIC LITHOLOGY	DRILLING DISTURB.	SED. STRUCTURES	SAMPLES
	FORAMINIFERS	NANNOFOSSILS	RADIOLARIANS	DIATOMS									
QUATERNARY		A/G CN14b	C/M UPPER PLIOCENE-RECENT			[illegible]	[illegible]	1 2 CC	0.5 1.0				● ● ● ● ●

LITHOLOGIC DESCRIPTION

NANNOFOSSIL-RICH CLAYSTONE AND NANNOFOSSIL-RICH SILTY CLAYSTONE

Major lithologies:
Most of the core consists of olive gray (5Y 4/2) locally burrowed (Zoophycos, Chondrites) NANNOFOSSIL-RICH CLAYSTONE and NANNOFOSSIL-RICH SILTY CLAYSTONE.

Minor lithologies:
In Section 1, 17-19 cm, there is a bed of GRANULE GRAVEL with silty claystone clasts and pumice clasts. In Section 2, 50-53 cm and 55-60 cm, there are two thin beds of VITRIC SILT (ash). From Section 2, 110 cm to CC, the sediment consists of parallel laminated DIATOM CLAYSTONE.

SMEAR SLIDE SUMMARY (%):

	1, 46 D	1, 135 D	2, 11 D	2, 53 M	CC, 9 D
TEXTURE					
Sand	3	—	2	Tr	—
Silt	37	45	38	100	58
Clay	60	55	60	Tr	42
COMPOSITION					
Accessory minerals	—	Tr	1	Tr	—
Clay	18	55	51	—	—
Diatoms	Tr	—	—	Tr	58
Feldspar	2	1	1	Tr	—
Foraminifers	1	1	5	Tr	1
Glass	13	5	1	97	41
Lithic fragments	—	Tr	—	Tr	—
Micrite	3	1	3	Tr	—
Nannofossils	25	35	25	1	2
Opaques	—	—	10	Tr	2
Radiolarians	—	Tr	—	—	—
Silicoflagellates	Tr	—	2	—	—
Spicules	Tr	Tr	—	—	—

126 791B 14R NO RECOVERY

SITE 791 HOLE B CORE 15R CORED INTERVAL 521.5-531.2 mbsf

TIME-ROCK UNIT	BIOSTRAT. ZONE/ FOSSIL CHARACTER				PALEOMAGNETICS	PHYS. PROPERTIES	CHEMISTRY	SECTION	METERS	GRAPHIC LITHOLOGY	DRILLING DISTURB.	SED. STRUCTURES	SAMPLES
	FORAMINIFERS	NANNOFOSSILS	RADIOLARIANS	DIATOMS									
QUATERNARY		A/G CN14b	B		N			1 CC			O		

LITHOLOGIC DESCRIPTION

SAND

Major lithology: Dark gray (5Y 4/1) and black (5Y 3/2) medium to coarse SAND, consisting of pumice clasts and black rock fragments.

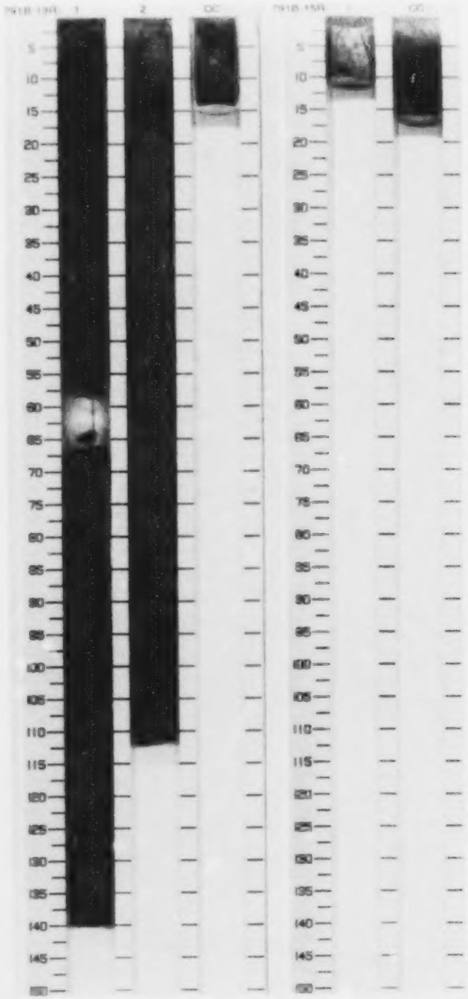

SITE 791 HOLE B CORE 16R CORED INTERVAL 531.2-540.9 mbsf

TIME-ROCK UNIT	BIOSTRAT. ZONE/ FOSSIL CHARACTER: FORAMINIFERS	NANNOFOSSILS	RADIOLARIANS	DIATOMS		PALEOMAGNETICS	PHYS. PROPERTIES	CHEMISTRY	SECTION	METERS	GRAPHIC LITHOLOGY	DRILLING DISTURB.	SED. STRUCTURES	SAMPLES
QUATERNARY		CN14b C/M	UPPER PLIOCENE-RECENT R/M			N	●	●	1 CC					● ●

LITHOLOGIC DESCRIPTION

NANNOFOSSIL-RICH CLAYSTONE AND NANNOFOSSIL-RICH VITRIC CLAYEY SILTSTONE

Major lithologies:
Locally burrowed (Zoophycos), olive gray (5Y 4/2) and brownish black (5YR 2/1) NANNOFOSSIL-RICH CLAYSTONE and NANNOFOSSIL-RICH VITRIC CLAYEY SILTSTONE.

SMEAR SLIDE SUMMARY (%):

	1, 20	CC, 4
	D	D
TEXTURE:		
Sand	—	10
Silt	40	50
Clay	60	40
COMPOSITION:		
Accessory minerals	—	Tr
Clay	50	40
Diatoms	—	Tr
Feldspar	5	Tr
Foraminifers	2	Tr
Glass	3	30
Mica	—	Tr
Nannofossils	40	10
Opaques	Tr	—
Quartz	—	15
Silicoflagellates	Tr	—
Zeolite	—	5

791B-16R
1
CC
5
10
15
20
25
30
35
40
45
50
55
60
65
70
75
80
85
90
95
100
105
110
115
120
125
130
135
140
145
150

SITE 791 HOLE B CORE 17R CORED INTERVAL 540.9-550.6 mbsf

TIME-ROCK UNIT	FORAMINIFERS	NANNOFOSSILS	RADIOLARIANS	DIATOMS	PALEOMAGNETICS	PHYS. PROPERTIES	CHEMISTRY	SECTION	METERS	GRAPHIC LITHOLOGY	DRILLING DISTURB.	SED. STRUCTURES	SAMPLES
QUATERNARY		C/M CN14b	R/M UPPER PLIOCENE-Recent					CC					●●

LITHOLOGIC DESCRIPTION

VITRIC CLAYEY SILT AND VITRIC SILT

Major lithologies:
This CC contains structureless dark gray (5Y 4/1) VITRIC CLAYEY SILT (0-15 cm) and gray (5Y 5/1) parallel laminated VITRIC SILT, 9-12 cm.

SMEAR SLIDE SUMMARY (%):

	CC, 1 D	CC, 15 D
TEXTURE:		
Sand	5	2
Silt	75	88
Clay	20	10
COMPOSITION:		
Accessory minerals	Tr	—
Clay	30	10
Feldspar	2	3
Foraminifers	—	Tr
Glass	63	80
Lithic fragments	Tr	—
Mica	—	Tr
Nannofossils	5	2
Opaques	2	Tr

SITE 791 HOLE B CORE 18R CORED INTERVAL 550.6-560.3 mbsf

TIME-ROCK UNIT	FORAMINIFERS	NANNOFOSSILS	RADIOLARIANS	DIATOMS	PALEOMAGNETICS	PHYS. PROPERTIES	CHEMISTRY	SECTION	METERS	GRAPHIC LITHOLOGY	DRILLING DISTURB.	SED. STRUCTURES	SAMPLES
QUATERNARY		A/G CN14b	R/P UPPER PLIOCENE-RECENT		N	● [illegible]		1					●

LITHOLOGIC DESCRIPTION

VITRIC CLAYEY SILT

Major lithology: Gray (5Y 5/1) structureless VITRIC CLAYEY SILT.

SMEAR SLIDE SUMMARY (%):

	1, 80 D
TEXTURE:	
Sand	5
Silt	75
Clay	20
COMPOSITION:	
Accessory minerals	Tr
Clay	20
Feldspar	3
Foraminifers	Tr
Glass	70
Glauconite	Tr
Nannofossils	5
Opaques	Tr

126 791B 19R NO RECOVERY

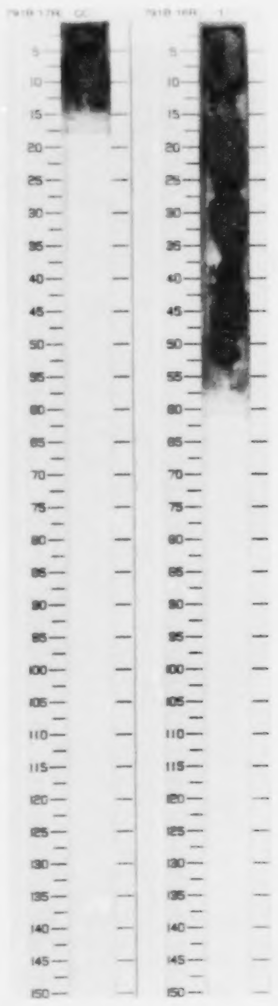

SITE 791 HOLE B CORE 20R CORED INTERVAL 569.7-579.3 mbsf

TIME-ROCK UNIT	BIOSTRAT. ZONE/FOSSIL CHARACTER: FORAMINIFERS	NANNOFOSSILS	RADIOLARIANS	DIATOMS	PALEOMAGNETICS	PHYS. PROPERTIES	CHEMISTRY	SECTION	METERS	GRAPHIC LITHOLOGY	DRILLING DISTURB.	SED. STRUCTURES	SAMPLES	LITHOLOGIC DESCRIPTION
QUATERNARY		A/G CN14a	C/M UPPER PLIOCENE-RECENT					1 CC					● ●	VITRIC SILT AND DIATOM NANNOFOSSIL CLAYSTONE

Major lithologies:

Brownish gray [illegible] VITRIC SILT with [illegible] DIATOM NANNOFOSSIL CLAYSTONE

SMEAR SLIDE SUMMARY (%):

TEXTURE:

Sand
Silt
Clay

COMPOSITION:

Clay
Diatoms
Feldspar
Foraminifers
Glass
Micrite
Nannofossils
Opaques
Radiolarians
Silicoflagellates
Sponge spicules

SITE 791 HOLE B CORE 21R CORED INTERVAL 579.3-589.0 mbsf

TIME-ROCK UNIT	BIOSTRAT. ZONE/FOSSIL CHARACTER: FORAMINIFERS	NANNOFOSSILS	RADIOLARIANS	DIATOMS	PALEOMAGNETICS	PHYS. PROPERTIES	CHEMISTRY	SECTION	METERS	GRAPHIC LITHOLOGY	DRILLING DISTURB.	SED. STRUCTURES	SAMPLES	LITHOLOGIC DESCRIPTION
QUATERNARY		A/G CN14a	C/M UPPER PLIOCENE-RECENT					CC					●	NANNOFOSSIL DIATOM RICH CLAYSTONE

Major lithology: Olive gray [illegible] NANNOFOSSIL DIATOM RICH CLAYSTONE

SMEAR SLIDE SUMMARY (%):

TEXTURE:

Silt
Clay

COMPOSITION:

Clay
Quartz
Feldspar
Ferromagnesian
Glass
Nannofossils
Pyrite
Radiolarians
Sponge spicules
Zeolite

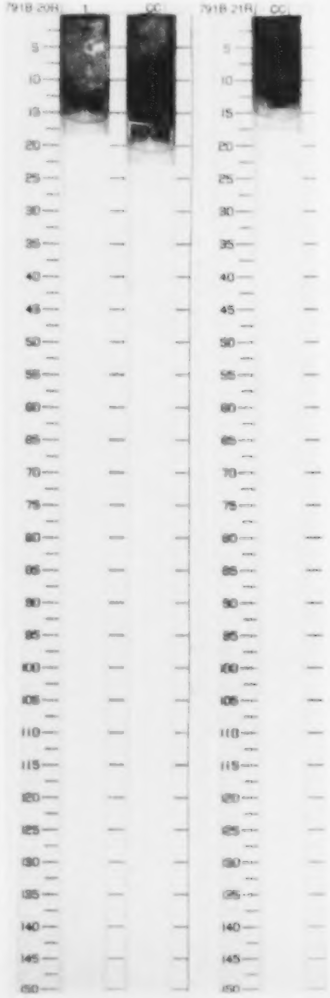

SITE 791 HOLE B CORE 22R CORED INTERVAL 589.0-598.7 mbsf

TIME-ROCK UNIT	FORAMINIFERS	NANNOFOSSILS	RADIOLARIANS	DIATOMS		PALEOMAGNETICS	PHYS. PROPERTIES	CHEMISTRY	SECTION	METERS	GRAPHIC LITHOLOGY	DRILLING DISTURB.	SED. STRUCTURES	SAMPLES	LITHOLOGIC DESCRIPTION
QUATERNARY		CN14b A/G	UPPER PLIOCENE-RECENT C/M			N	● [illegible]	● [illegible]	1	0.5				● ●	DIATOM NANNOFOSSIL CLAYSTONE Major lithology: Dark greenish gray (5G 4/1) microfaulted DIATOM NANNOFOSSIL CLAYSTONE, with sponge spicules and diatoms. Minor lithology: Two beds, Section 1, 30-32 cm and 58-60 cm, of greenish black (5G 2/1) NANNOFOSSIL-RICH VITRIC CLAYEY SILT.

SMEAR SLIDE SUMMARY (%):

	1, 30	1, 52
	D	M
TEXTURE:		
Sand	—	5
Silt	15	25
Clay	85	70
COMPOSITION:		
Accessory minerals	2	1
Clay	80	10
Diatoms	10	2
Feldspar	5	2
Foraminifers	10	1
Glass	—	20
Lithic fragments	—	1
Nannofossils	30	41
Opaques	2	10
Quartz	1	8
Spicules	5	1

791B-22R 1

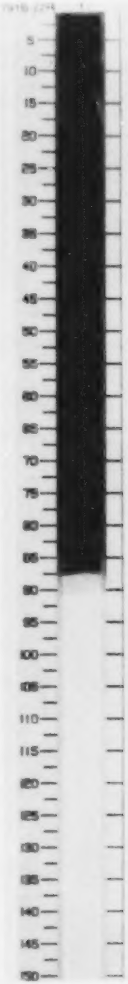

SITE 791 HOLE B CORE 23R CORED INTERVAL 598.7-608.4 mbsf

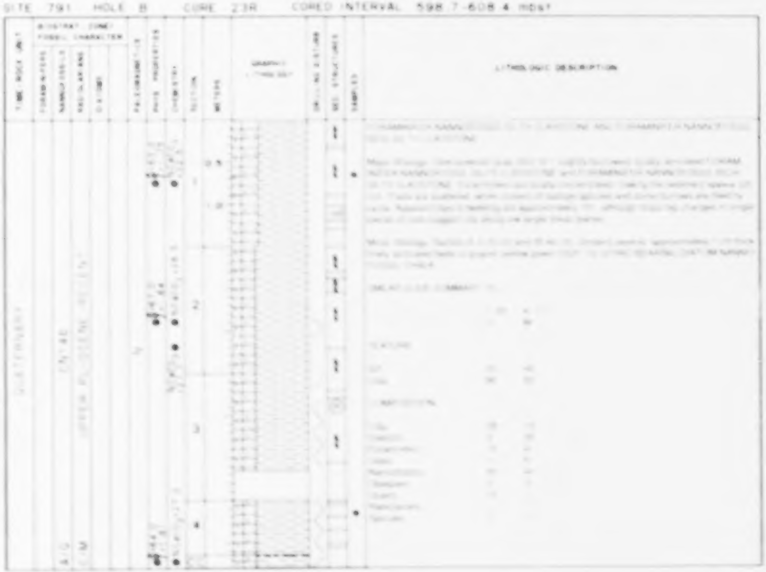
TIME-ROCK UNIT
BIOSTRAT. ZONE/ FOSSIL CHARACTER
FORAMINIFERS
NANNOFOSSILS
RADIOLARIANS
DIATOMS
PALEOMAGNETICS
PHYS. PROPERTIES
CHEMISTRY
SECTION
METERS
GRAPHIC LITHOLOGY
DRILLING DISTURB.
SED. STRUCTURES
SAMPLES
QUATERNARY
CN14a
upper Pleistocene
A/G
C/M
1
2
3
4
0.5
1.0

LITHOLOGIC DESCRIPTION

FORAMINIFER NANNOFOSSIL [illegible] SILTY CLAYSTONE AND FORAMINIFER NANNOFOSSIL [illegible] SILTY CLAYSTONE

Major lithology: [illegible]

Minor lithology: [illegible]

SMEAR SLIDE SUMMARY (%):

TEXTURE:

Silt

Clay

COMPOSITION:

Clay

[illegible]

Foraminifers

Glass

Nannofossils

[illegible]

Quartz

Radiolarians

Sponge spicules

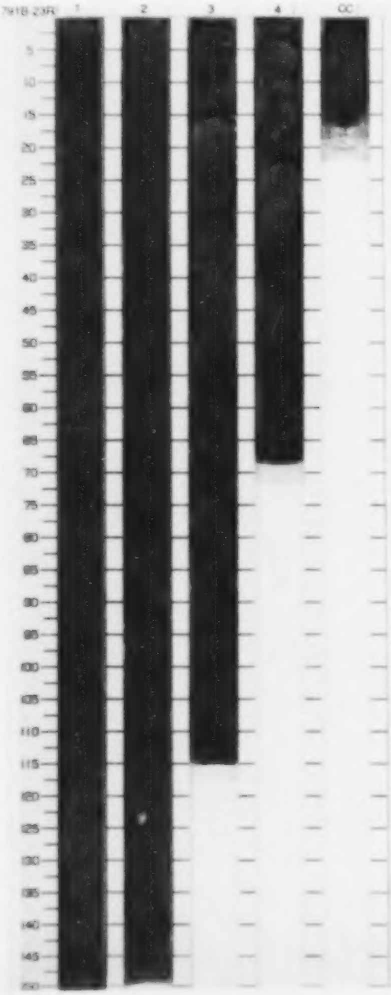
791B-23R
1
2
3
4
CC
5
10
15
20
25
30
35
40
45
50
55
60
65
70
75
80
85
90
95
100
105
110
115
120
125
130
135
140
145
150

SITE 791 HOLE B CORE [illegible] CORED INTERVAL [illegible]

TIME-ROCK UNIT	FORAMINIFERS	NANNOFOSSILS	RADIOLARIANS	DIATOMS	PALEOMAGNETICS	PHYS. PROPERTIES	CHEMISTRY	SECTION	METERS	GRAPHIC LITHOLOGY	DRILLING DISTURB.	SED. STRUCTURES	SAMPLES	LITHOLOGIC DESCRIPTION
QUATERNARY		CN14b	UPPER PLIOCENE - MIDDLE PLEISTOCENE [illegible]					1	0.5 1.0				● ●	[illegible]

Major lithologies:

[illegible]

SMEAR SLIDE SUMMARY (%):

TEXTURE:

Sand
Silt
Clay

COMPOSITION:

Accessory minerals
Clay
[illegible]
Feldspar
Foraminifers
Glass
Inorganic calcite
Nannofossils
[illegible]
Quartz
[illegible]
[illegible]

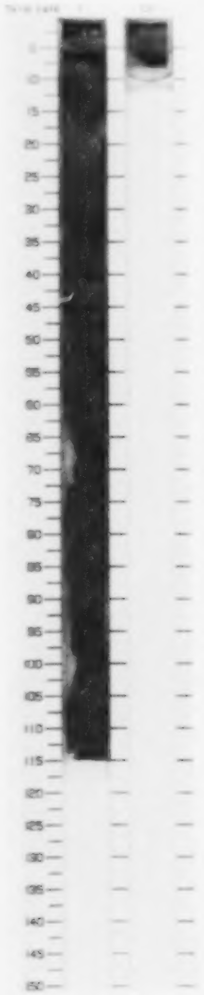

0
10
15
20
25
30
35
40
45
50
55
60
65
70
75
80
85
90
95
100
105
110
115
120
125
130
135
140
145
150

SITE 791 HOLE B CORE 25R CORED INTERVAL 618.1-627.7 mbsf

TIME-ROCK UNIT
BIOSTRAT. ZONE/ FOSSIL CHARACTER
FORAMINIFERS
NANNOFOSSILS
RADIOLARIANS
DIATOMS
PALEOMAGNETICS
PHYS. PROPERTIES
CHEMISTRY
SECTION
METERS
GRAPHIC LITHOLOGY
DRILLING DISTURB.
SED. STRUCTURES
SAMPLES
LITHOLOGIC DESCRIPTION
QUATERNARY
CN14a
UPPER PLEISTOCENE (N22)
1
2
0.5
1.0

SITE 791 HOLE B CORE 26R CORED INTERVAL 627.7-637.0 mbsf

TIME-ROCK UNIT
BIOSTRAT. ZONE/ FOSSIL CHARACTER
FORAMINIFERS
NANNOFOSSILS
RADIOLARIANS
DIATOMS
PALEOMAGNETICS
PHYS. PROPERTIES
CHEMISTRY
SECTION
METERS
GRAPHIC LITHOLOGY
DRILLING DISTURB.
SED. STRUCTURES
SAMPLES
LITHOLOGIC DESCRIPTION
QUATERNARY
CN14a
UPPER PLEISTOCENE
1
0.5

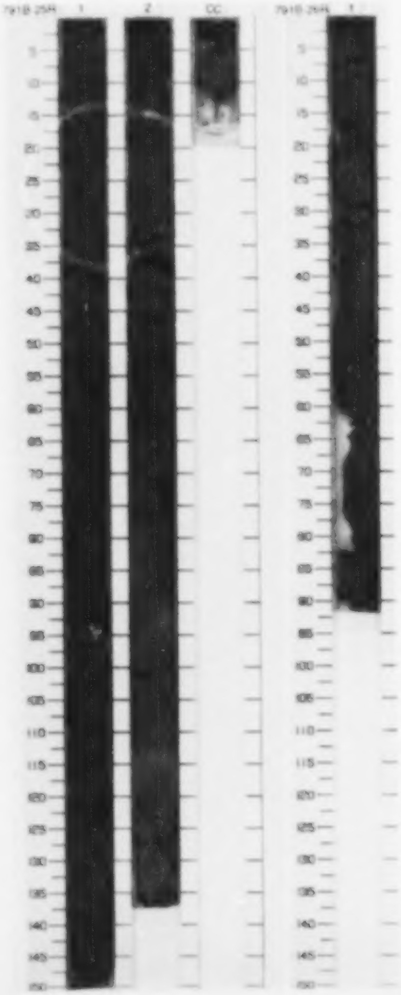
791B-25R 1
2
CC
791B-26R 1

SITE 791 HOLE B CORE [illegible] CORED INTERVAL [illegible]

TIME-ROCK UNIT	FORAMINIFERS	NANNOFOSSILS	RADIOLARIANS	DIATOMS	PALEOMAGNETICS	PHYS. PROPERTIES	CHEMISTRY	SECTION	METERS	GRAPHIC LITHOLOGY	DRILLING DISTURB.	SED. STRUCTURES	SAMPLES	LITHOLOGIC DESCRIPTION
QUATERNARY		CN14b A/G	UPPER PLIOCENE–RECENT B/M			●	●	1					●	NANNOFOSSIL-RICH CLAYSTONE Major lithologies: [illegible] NANNOFOSSIL-RICH CLAYSTONE [illegible] [illegible] NANNOFOSSIL [illegible] SMEAR SLIDE SUMMARY (%): TEXTURE: Sand [illegible] Silt [illegible] Clay [illegible] COMPOSITION: Feldspar [illegible] Rock fragments [illegible] Glass [illegible] Inorganic calcite [illegible] Nannofossils [illegible] Diatoms [illegible] Quartz [illegible] Radiolarians [illegible]

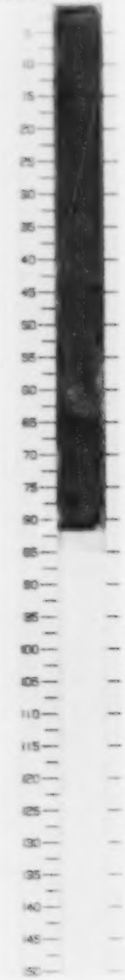

SITE 791 HOLE B CORE 28R CORED INTERVAL 646.6-656.3 mbsf

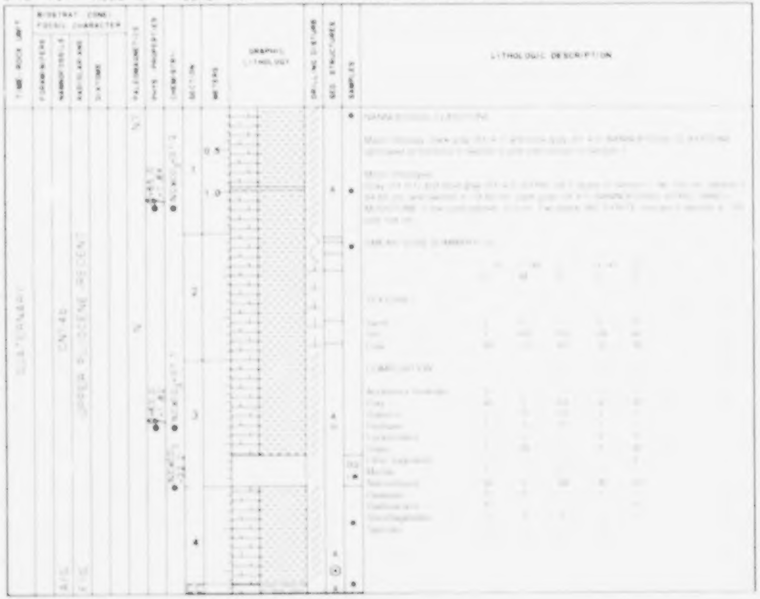
TIME-ROCK UNIT
BIOSTRAT. ZONE/FOSSIL CHARACTER
FORAMINIFERS
NANNOFOSSILS
RADIOLARIANS
DIATOMS
PALEOMAGNETICS
PHYS. PROPERTIES
CHEMISTRY
SECTION
METERS
GRAPHIC LITHOLOGY
DRILLING DISTURB.
SED. STRUCTURES
SAMPLES
LITHOLOGIC DESCRIPTION
QUATERNARY
CN14b
UPPER PLIOCENE-RECENT
N
0.5
1.0
1
2
3
4
CC

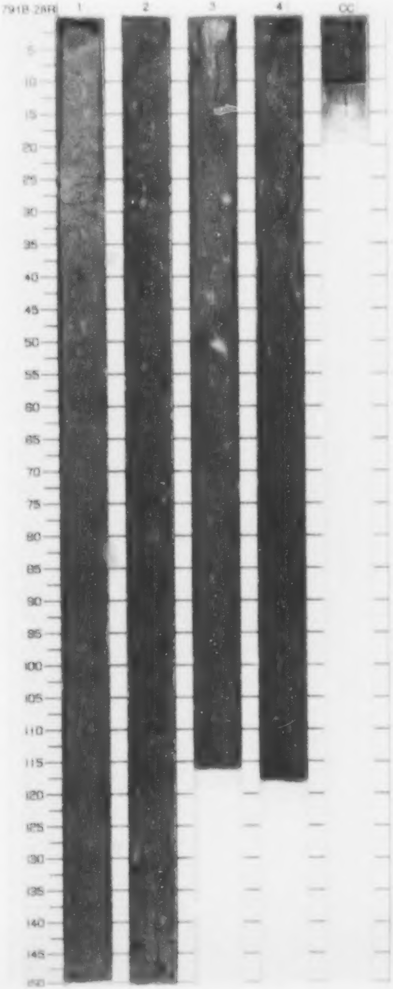
791B-28R
1
2
3
4
CC
5
10
15
20
25
30
35
40
45
50
55
60
65
70
75
80
85
90
95
100
105
110
115
120
125
130
135
140
145
150

SITE 791 HOLE B CORE 29R CORED INTERVAL 656.2-666.0 mbsf

TIME-ROCK UNIT	FORAMINIFERS	NANNOFOSSILS	RADIOLARIANS	DIATOMS		PALEOMAGNETICS	PHYS. PROPERTIES	CHEMISTRY	SECTION	METERS	GRAPHIC LITHOLOGY	DRILLING DISTURB.	SED. STRUCTURES	SAMPLES	LITHOLOGIC DESCRIPTION
QUATERNARY		A/G CN14b	R/M UPPER PLIOCENE-RECENT						CC			/		●	NANNOFOSSIL CLAYSTONE

NANNOFOSSIL CLAYSTONE

Major lithology: Olive gray (5Y 4/2) NANNOFOSSIL CLAYSTONE; the top [illegible] is drilling breccia, the remaining [illegible] slightly bioturbated.

Minor lithology: Black (N 2) PUMICE [illegible]

SMEAR SLIDE SUMMARY (%):

CC, [illegible]
D

TEXTURE:

Sand [illegible]
Silt 30
Clay [illegible]

COMPOSITION:

Clay [illegible]
Volcanic glass [illegible]
Feldspar [illegible]
Quartz [illegible]
Nannofossils [illegible]
Opaques [illegible]
Radiolarians [illegible]

791B-29R-1

5
10
15
20
25
30
35
40
45
50
55
60
65
70
75
80
85
90
95
100
105
110
115
120
125
130
135
140
145
150

SITE 791 HOLE B CORE 30R CORED INTERVAL 666.6-675.6 mbsf

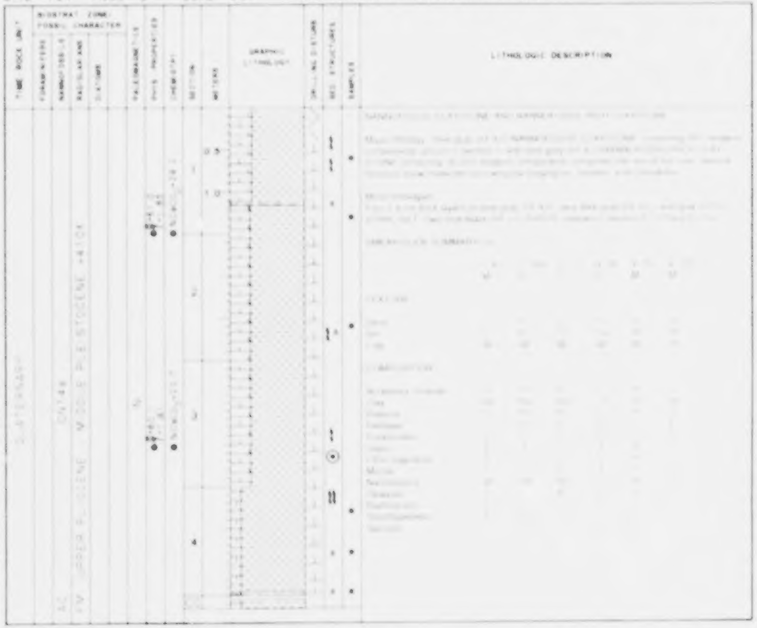
TIME-ROCK UNIT
BIOSTRAT. ZONE/ FOSSIL CHARACTER
FORAMINIFERS
NANNOFOSSILS
RADIOLARIANS
DIATOMS
PALEOMAGNETICS
PHYS. PROPERTIES
CHEMISTRY
SECTION
METERS
GRAPHIC LITHOLOGY
DRILLING DISTURB.
SED. STRUCTURES
SAMPLES
LITHOLOGIC DESCRIPTION
AC CN14a
RV UPPER PLIOCENE - MIDDLE PLEISTOCENE
0.5
1.0
1
2
3
4
Major lithology:
Minor lithology:
SMEAR SLIDE SUMMARY (%):
TEXTURE:
Sand
Silt
Clay
COMPOSITION:
Clay

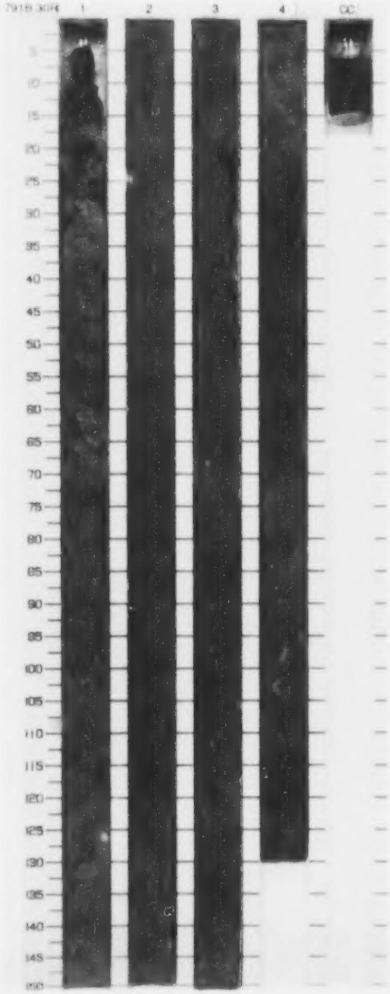
791B-30R
1
2
3
4
CC
5
10
15
20
25
30
35
40
45
50
55
60
65
70
75
80
85
90
95
100
105
110
115
120
125
130
135
140
145
150

SITE 791 HOLE B CORE 31R CORED INTERVAL 675.6-685.3 mbsf

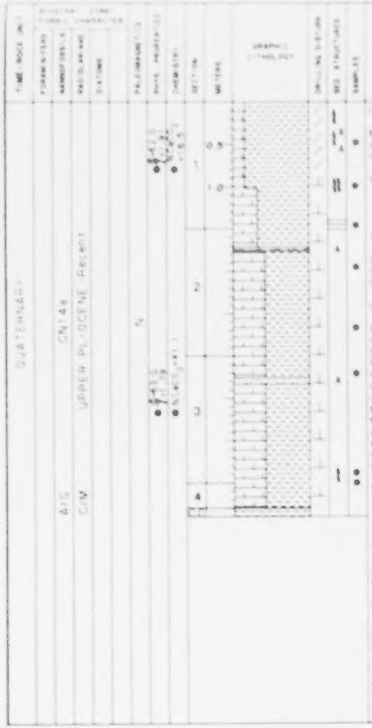
TIME-ROCK UNIT
BIOSTRAT. ZONE/FOSSIL CHARACTER
FORAMINIFERS
NANNOFOSSILS
RADIOLARIANS
DIATOMS
PALEOMAGNETICS
PHYS. PROPERTIES
CHEMISTRY
SECTION
METERS
GRAPHIC LITHOLOGY
DRILLING DISTURB.
SED. STRUCTURES
SAMPLES
QUATERNARY
CN14a
A/G
UPPER PLIOCENE-Recent
C/M
N
1
2
3
4
CC
0.5
1.0

LITHOLOGIC DESCRIPTION

CLAYSTONE and NANNOFOSSIL CLAYSTONE

Major lithology: CLAYSTONE and NANNOFOSSIL CLAYSTONE, olive gray (5Y 4/2) occurs in Section 1, 0-80 cm. Nannofossil and other biogenic contents increase down the core, with colors changing to gray (5Y 5/1 and 5Y 6/1) in Sections 3, 4 and 5.

SMEAR SLIDE SUMMARY (%):

	1, 40 D	1, 47 D	1, 100 D	2, 50 D	2, 125 M	3, 29 M	3, 104 D
TEXTURE:							
Sand	2	—	1	—	5	1	2
Silt	15	20	10	6	70	14	7
Clay	83	80	89	94	25	85	91
COMPOSITION:							
Accessory minerals	—	Tr	—	—	—	—	—
Clay	83	73	63	24	15	73	28
Diatoms	Tr	Tr	Tr	—	—	—	1
Feldspar	5	2	3	—	1	1	1
Foraminifers	—	1	1	3	Tr	Tr	1
Glass	10	10	8	—	75	10	6
Lithic fragments	—	—	Tr	—	—	Tr	—
Micrite	Tr	3	2	1	10	Tr	—
Nannofossils	Tr	1	24	70	1	13	60
Opaques	2	2	—	Tr	2	2	—
Radiolarians	—	—	Tr	1	Tr	—	—
Silicoflagellates	—	8	1	2	—	1	1
Spicules	—	Tr	1	1	Tr	—	—

SMEAR SLIDE SUMMARY (%):

	3, 148 D
TEXTURE:	
Silt	5
Clay	95
COMPOSITION:	
Accessory minerals	Tr
Clay	30
Diatoms	1
Foraminifers	1
Quartz	1
Nannofossils	65
Radiolarians	Tr
Silicoflagellates	1

791B-31R

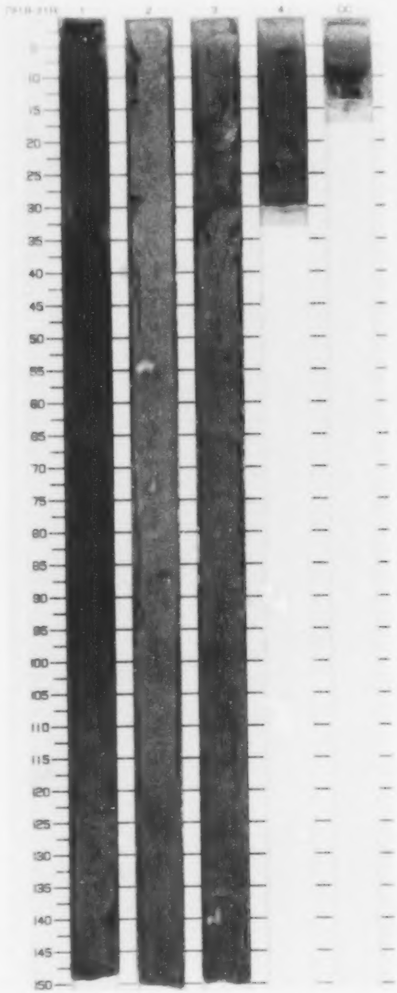
1
2
3
4
CC
0
5
10
15
20
25
30
35
40
45
50
55
60
65
70
75
80
85
90
95
100
105
110
115
120
125
130
135
140
145
150

SITE 791 HOLE B CORE 32R CORED INTERVAL 685.3-695.0 mbsf

TIME-ROCK UNIT	FORAMINIFERS	NANNOFOSSILS	RADIOLARIANS	DIATOMS	PALEOMAGNETICS	PHYS. PROPERTIES	CHEMISTRY	SECTION	METERS	GRAPHIC LITHOLOGY	DRILLING DISTURB.	SED. STRUCTURES	SAMPLES	LITHOLOGIC DESCRIPTION
QUATERNARY		A/G	R/P			●	●	1	0.5 1.0				● ●● ●	NANNOFOSSIL [illegible] Major lithologies: [illegible] SMEAR SLIDE SUMMARY (%): TEXTURE: Sand, Silt, Clay COMPOSITION: [illegible]

SITE 791 HOLE B CORE 33R CORED INTERVAL 695.0-704.8 mbsf

TIME-ROCK UNIT	FORAMINIFERS	NANNOFOSSILS	RADIOLARIANS	DIATOMS	PALEOMAGNETICS	PHYS. PROPERTIES	CHEMISTRY	SECTION	METERS	GRAPHIC LITHOLOGY	DRILLING DISTURB.	SED. STRUCTURES	SAMPLES	LITHOLOGIC DESCRIPTION
QUATERNARY		CN14a A/G	UPPER PLIOCENE-RECENT R/P		B			1					●	NANNOFOSSIL CLAY Major lithology: [illegible] NANNOFOSSIL CLAY [illegible] SMEAR SLIDE SUMMARY (%): TEXTURE: Silt, Clay COMPOSITION: Accessory minerals, Clay, Feldspar, Foraminifers, Glass, Micrite, Nannofossils, Opaques, Plant fragments

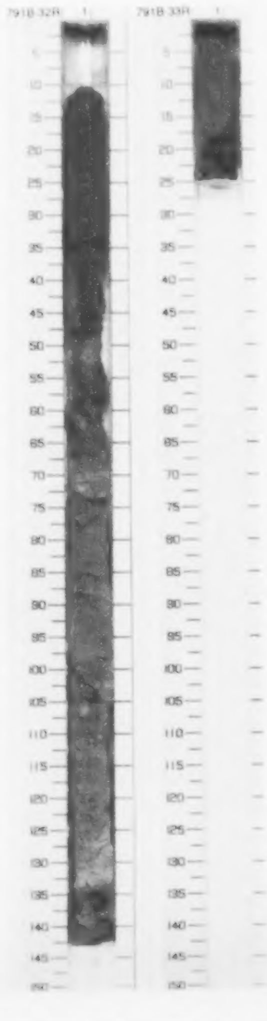
791B-32R 1
791B-33R 1
5
10
15
20
25
30
35
40
45
50
55
60
65
70
75
80
85
90
95
100
105
110
115
120
125
130
135
140
145
150

SITE 791 HOLE B CORE 14R CORED INTERVAL 704.6-714.0 mbsf

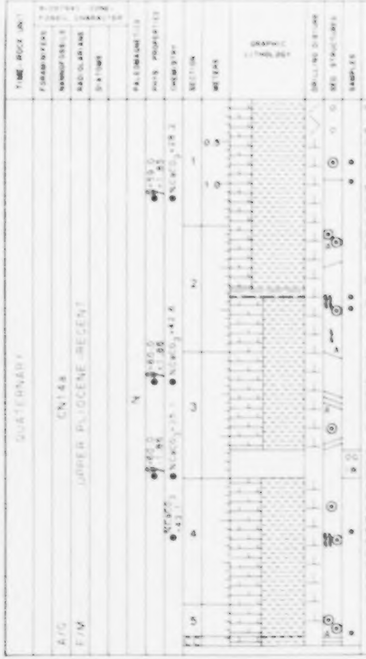
TIME-ROCK UNIT
BIOSTRAT. ZONE/FOSSIL CHARACTER
FORAMINIFERS
NANNOFOSSILS
RADIOLARIANS
DIATOMS
PALEOMAGNETICS
PHYS. PROPERTIES
CHEMISTRY
SECTION
METERS
GRAPHIC LITHOLOGY
DRILLING DISTURB.
SED. STRUCTURES
SAMPLES
QUATERNARY
CN14a
UPPER PLIOCENE-RECENT
A/G
F/M
N
1
2
3
4
5
0.5
1.0

LITHOLOGIC DESCRIPTION

NANNOFOSSIL-RICH CLAY AND NANNOFOSSIL CLAY

Major lithologies:

Olive gray (5Y 4/2) NANNOFOSSIL-RICH CLAY [illegible]. Most of the core is gray (5Y 5/1) NANNOFOSSIL CLAY, moderately to strongly bioturbated by [illegible] at several intervals.

Minor lithologies:

Olive gray (5Y 4/2) VITRIC SILT and CLAYEY VITRIC SILT [illegible] Section 3, [illegible] and in Section 4, [illegible] in diameter [illegible] Section 1 at 74 cm, [illegible] Section 4, [illegible] and Section 5, [illegible] BASALT pebbles [illegible] in diameter [illegible]

Bedding planes in Sections [illegible] and 4 display apparent dips of [illegible]

SMEAR SLIDE SUMMARY (%):

TEXTURE:

Sand
Silt
Clay

COMPOSITION:

Accessory minerals
Clay
Dolomite
Feldspar
Foraminifers
Glass
Mica
Micrite
Nannofossils
Opaques
Radiolarians
Rock fragments
Silicoflagellates
Spicules

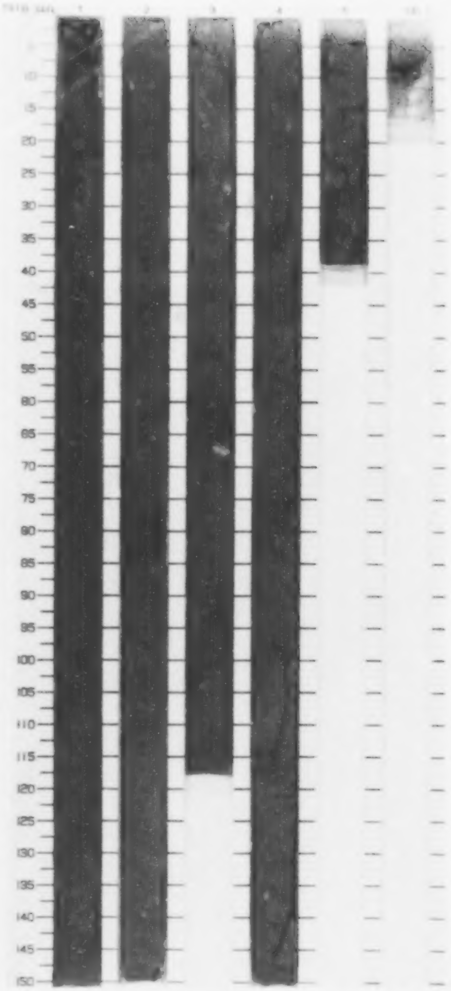
1
2
3
4
5
CC
0
5
10
15
20
25
30
35
40
45
50
55
60
65
70
75
80
85
90
95
100
105
110
115
120
125
130
135
140
145
150

SITE 791 HOLE B CORE 35R CORED INTERVAL 714.3-723.6 mbsf

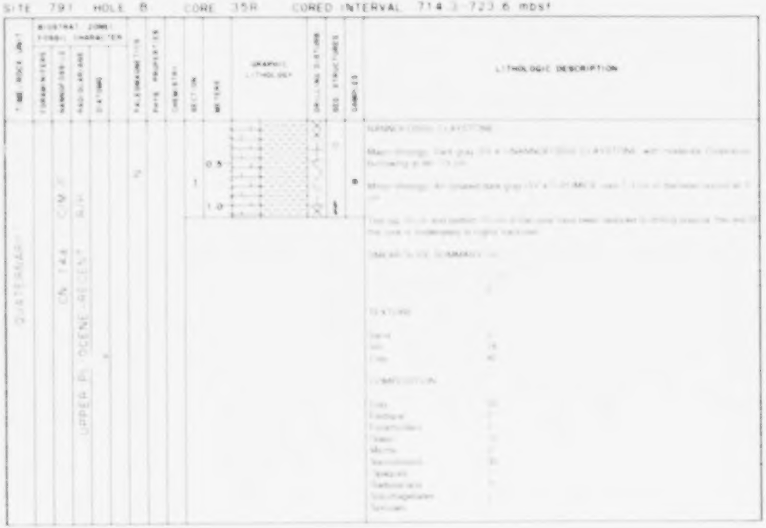

TIME-ROCK UNIT	FORAMINIFERS	NANNOFOSSILS	RADIOLARIANS	DIATOMS	PALEOMAGNETICS	PHYS. PROPERTIES	CHEMISTRY	SECTION	METERS	GRAPHIC LITHOLOGY	DRILLING DISTURB.	SED. STRUCTURES	SAMPLES	LITHOLOGIC DESCRIPTION
QUATERNARY		CN 14a CM 9	UPPER PLIOCENE-RECENT R/M		N			1	0.5 1.0				●	NANNOFOSSIL CLAYSTONE

NANNOFOSSIL CLAYSTONE

Major lithology: Dark gray (5Y 4/1) NANNOFOSSIL CLAYSTONE, with moderate Chondrites burrowing at 80-115 cm.

Minor lithology: An [illegible] dark gray (5Y 4/1) PUMICE [illegible] 1 cm in diameter [illegible] at 5 cm.

The top [illegible] and bottom [illegible] of the core have been disturbed by drilling process. The rest of the core is moderately to highly fractured.

SMEAR SLIDE SUMMARY (%):

TEXTURE:

Sand	[illegible]
Silt	15
Clay	85

COMPOSITION:

Clay	[illegible]
Feldspar	[illegible]
Foraminifers	[illegible]
Glass	[illegible]
Micrite	[illegible]
Nannofossils	[illegible]
Opaques	[illegible]
Radiolarians	[illegible]
Silicoflagellates	[illegible]
Spicules	[illegible]

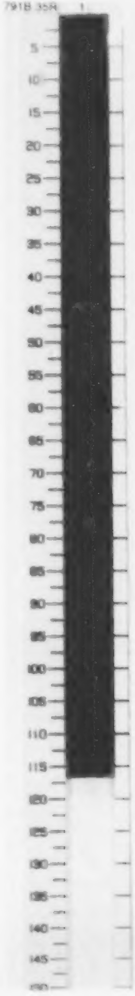
791B 35R 1
5
10
15
20
25
30
35
40
45
50
55
60
65
70
75
80
85
90
95
100
105
110
115
120
125
130
135
140
145
150

SITE 791 HOLE B CORE 3R CORED INTERVAL 7[illegible] m

TIME-ROCK UNIT	FORAMINIFERS	NANNOFOSSILS	RADIOLARIANS	DIATOMS	PALEOMAGNETICS	PHYS. PROPERTIES	CHEMISTRY	SECTION	METERS	GRAPHIC LITHOLOGY	DRILLING DISTURB.	SED. STRUCTURES	SAMPLES	LITHOLOGIC DESCRIPTION
QUATERNARY		A/G CN14a	F/M UPPER PLIOCENE–RECENT		N	[illegible]	[illegible]	1 2 3 4 5 CC	0.5 1.0				●	NANNOFOSSIL CLAY and NANNOFOSSIL-RICH CLAY

Major lithologies:
Olive (5Y 4/[illegible]) NANNOFOSSIL CLAY, except in Section [illegible], which is olive gray (5Y [illegible]) NANNOFOSSIL-RICH CLAY. [illegible]

Minor lithology: [illegible] PUMICE [illegible] Section [illegible] and Section [illegible]

The interval in Section [illegible] cm is [illegible] composed of NANNOFOSSIL CLAY and PUMICE fragments. The rest of the core has been moderately to highly fractured.

SMEAR SLIDE SUMMARY (%):

	1, [illegible]	1, [illegible]	2, [illegible]	3, [illegible]	4, [illegible]	4, [illegible]	4, [illegible]
	D	D	D	D	D	M	D
TEXTURE:							
Sand	—	—	—	[illegible]	[illegible]	[illegible]	[illegible]
Silt	[illegible]	[illegible]	[illegible]	[illegible]	[illegible]	[illegible]	[illegible]
Clay	[illegible]	[illegible]	[illegible]	[illegible]	[illegible]	[illegible]	[illegible]
COMPOSITION:							
Accessory minerals	—	—	—	—	—	[illegible]	[illegible]
Clay	[illegible]	[illegible]	[illegible]	[illegible]	[illegible]	[illegible]	[illegible]
Dolomite	[illegible]	[illegible]	[illegible]	[illegible]	[illegible]	[illegible]	[illegible]
Feldspar	[illegible]	[illegible]	[illegible]	[illegible]	[illegible]	[illegible]	[illegible]
Foraminifers	[illegible]	[illegible]	[illegible]	[illegible]	[illegible]	[illegible]	[illegible]
Glass	[illegible]	[illegible]	[illegible]	[illegible]	[illegible]	[illegible]	[illegible]
Micrite	[illegible]	[illegible]	[illegible]	[illegible]	[illegible]	[illegible]	[illegible]
Nannofossils	[illegible]	[illegible]	[illegible]	[illegible]	[illegible]	[illegible]	[illegible]
Opaques	[illegible]	[illegible]	[illegible]	[illegible]	[illegible]	[illegible]	[illegible]
Radiolarians	[illegible]	[illegible]	[illegible]	[illegible]	[illegible]	[illegible]	[illegible]
Rock fragment	[illegible]	[illegible]	[illegible]	[illegible]	[illegible]	[illegible]	[illegible]
Silicoflagellates	[illegible]	[illegible]	[illegible]	[illegible]	[illegible]	[illegible]	[illegible]
Sponge spicules	[illegible]	[illegible]	[illegible]	[illegible]	[illegible]	[illegible]	[illegible]

SMEAR SLIDE SUMMARY (%):

	5, [illegible]
	D
TEXTURE:	
Sand	[illegible]
Silt	[illegible]
Clay	[illegible]
COMPOSITION:	
Clay	[illegible]
Feldspar	[illegible]
Foraminifers	[illegible]
Glass	[illegible]
Nannofossils	[illegible]
Opaques	[illegible]

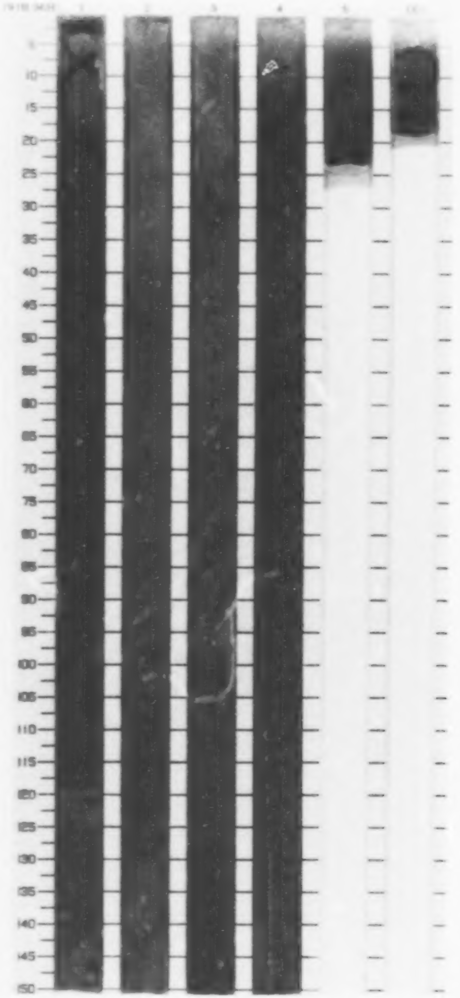

SITE 791 HOLE B CORE 37R CORED INTERVAL 733.6-742.8 mbsf

TIME-ROCK UNIT	BIOSTRAT. ZONE/FOSSIL CHARACTER: FORAMINIFERS	NANNOFOSSILS	RADIOLARIANS	DIATOMS	PALEOMAGNETICS	PHYS. PROPERTIES	CHEMISTRY	SECTION	METERS	GRAPHIC LITHOLOGY	DRILLING DISTURB.	SED. STRUCTURES	SAMPLES	LITHOLOGIC DESCRIPTION
QUATERNARY		A/C CN14a	C/C UPPER PLIOCENE-RECENT			[illegible]	[illegible]	1 2 CC	0.5 1.0				● ●	[illegible]

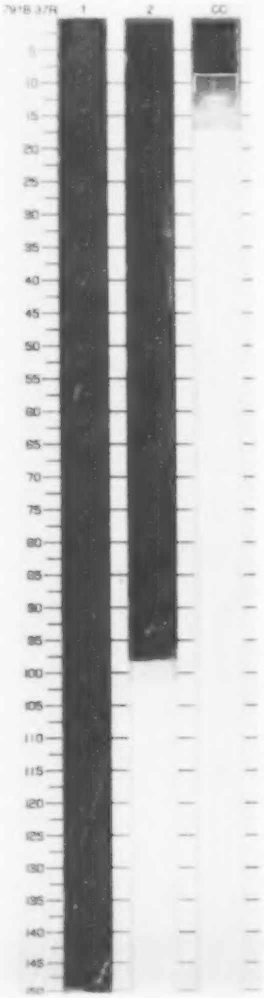

791B 37R
1
2
CC
5
10
15
20
25
30
35
40
45
50
55
60
65
70
75
80
85
90
95
100
105
110
115
120
125
130
135
140
145
150

SITE 791 HOLE B CORE [illegible] CORED INTERVAL [illegible] mbsf

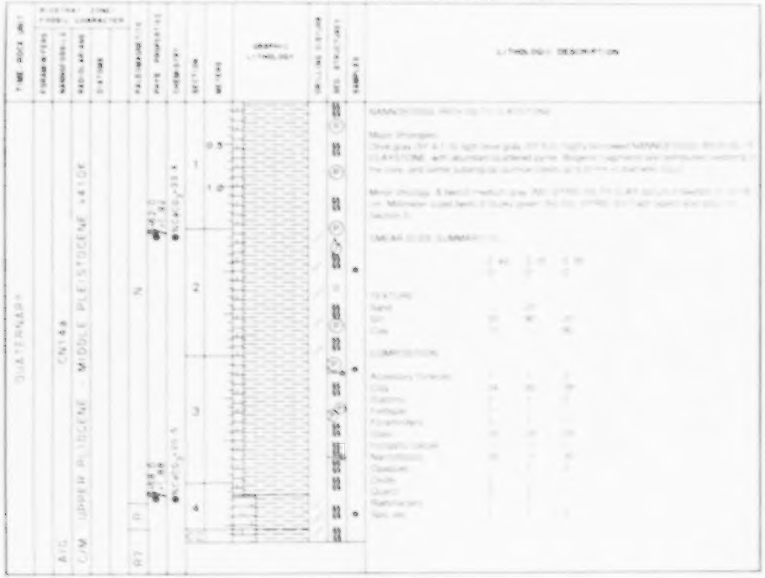
TIME-ROCK UNIT
BIOSTRAT. ZONE/ FOSSIL CHARACTER
FORAMINIFERS
NANNOFOSSILS
RADIOLARIANS
DIATOMS
PALEOMAGNETICS
PHYS. PROPERTIES
CHEMISTRY
SECTION
METERS
GRAPHIC LITHOLOGY
DRILLING DISTURB.
SED. STRUCTURES
SAMPLES
LITHOLOGIC DESCRIPTION
QUATERNARY
A/G
CN14a
C/M UPPER PLIOCENE - MIDDLE PLEISTOCENE
N
R?
1
2
3
4
CC
0.5
1.0

NANNOFOSSIL-RICH SILTY CLAYSTONE

Major lithologies:

Olive gray (5Y 4/2) to light olive gray (5Y [illegible]) slightly bioturbated NANNOFOSSIL-RICH SILTY CLAYSTONE, with abundant scattered pyrite. [illegible]

Minor lithology: [illegible] medium gray [illegible] SILTY CLAY [illegible] cm. Millimeter-sized [illegible] Section 3.

SMEAR SLIDE SUMMARY (%):

	[illegible]	[illegible]	[illegible]
TEXTURE:			
Sand	[illegible]	[illegible]	[illegible]
Silt	[illegible]	[illegible]	[illegible]
Clay	[illegible]	[illegible]	[illegible]
COMPOSITION:			
Accessory minerals	[illegible]	[illegible]	[illegible]
Clay	[illegible]	[illegible]	[illegible]
Diatoms	[illegible]	[illegible]	[illegible]
Feldspar	[illegible]	[illegible]	[illegible]
Foraminifers	[illegible]	[illegible]	[illegible]
Glass	[illegible]	[illegible]	[illegible]
Inorganic calcite	[illegible]	[illegible]	[illegible]
Nannofossils	[illegible]	[illegible]	[illegible]
Opaques	[illegible]	[illegible]	[illegible]
Oxide	[illegible]	[illegible]	[illegible]
Quartz	[illegible]	[illegible]	[illegible]
Radiolarians	[illegible]	[illegible]	[illegible]
Volcanic	[illegible]	[illegible]	[illegible]

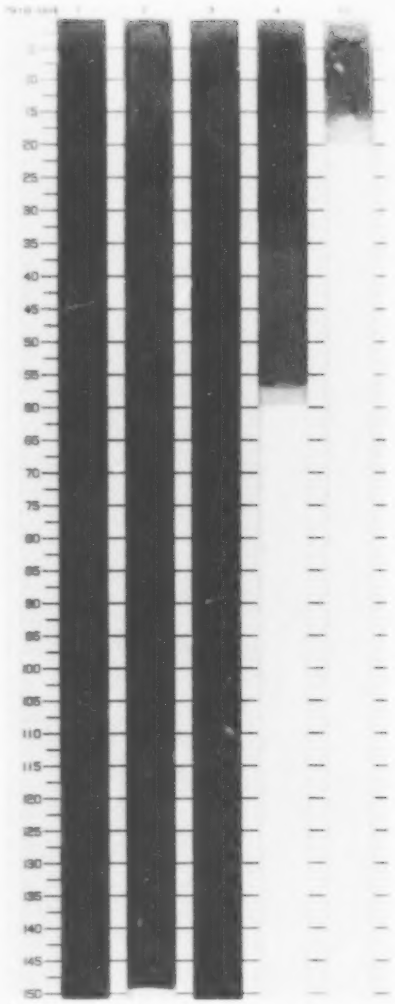
1
2
3
4
CC
5
10
15
20
25
30
35
40
45
50
55
60
65
70
75
80
85
90
95
100
105
110
115
120
125
130
135
140
145
150

SITE 791 HOLE B CORE 39R CORED INTERVAL 752.4-762.1 mbsf

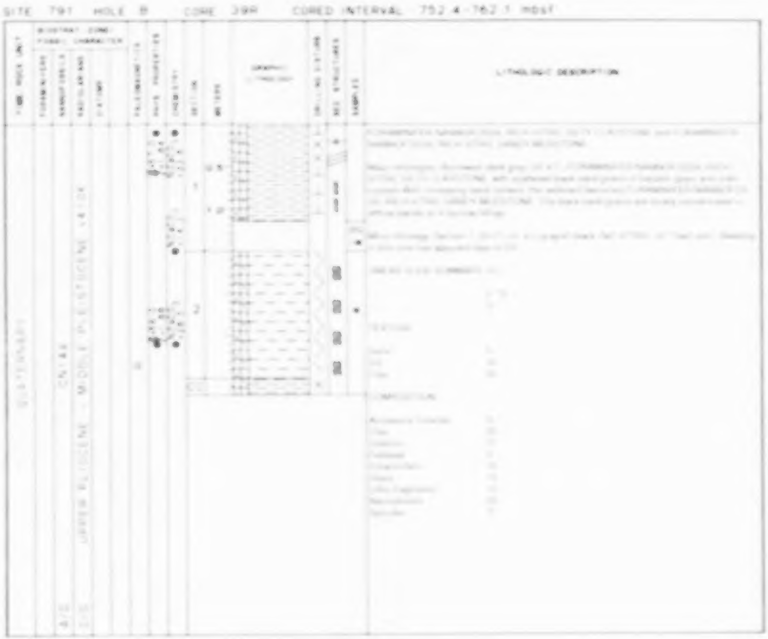
TIME-ROCK UNIT
BIOSTRAT. ZONE/FOSSIL CHARACTER
FORAMINIFERS
NANNOFOSSILS
RADIOLARIANS
DIATOMS
PALEOMAGNETICS
PHYS. PROPERTIES
CHEMISTRY
SECTION
METERS
GRAPHIC LITHOLOGY
DRILLING DISTURB.
SED. STRUCTURES
SAMPLES
QUATERNARY
CN14a
UPPER PLIOCENE - MIDDLE PLEISTOCENE
A/G
C/G
1
2
CC
0.5
1.0

LITHOLOGIC DESCRIPTION

[illegible]

SMEAR SLIDE SUMMARY (%):

TEXTURE:

Sand [illegible]
Silt [illegible]
Clay [illegible]

COMPOSITION:

Accessory minerals [illegible]
Clay [illegible]
[illegible]
Feldspar [illegible]
Foraminifers [illegible]
Glass [illegible]
Lithic fragments [illegible]
Nannofossils [illegible]
Spicules [illegible]

791B-39R 1 2 CC

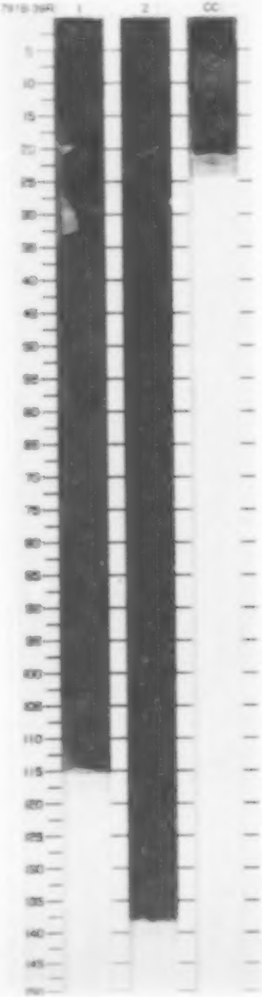
5
10
15
20
25
30
35
40
45
50
55
60
65
70
75
80
85
90
95
100
105
110
115
120
125
130
135
140
145
150

SITE 791 HOLE B CORE [illegible] CORED INTERVAL [illegible] mbsf

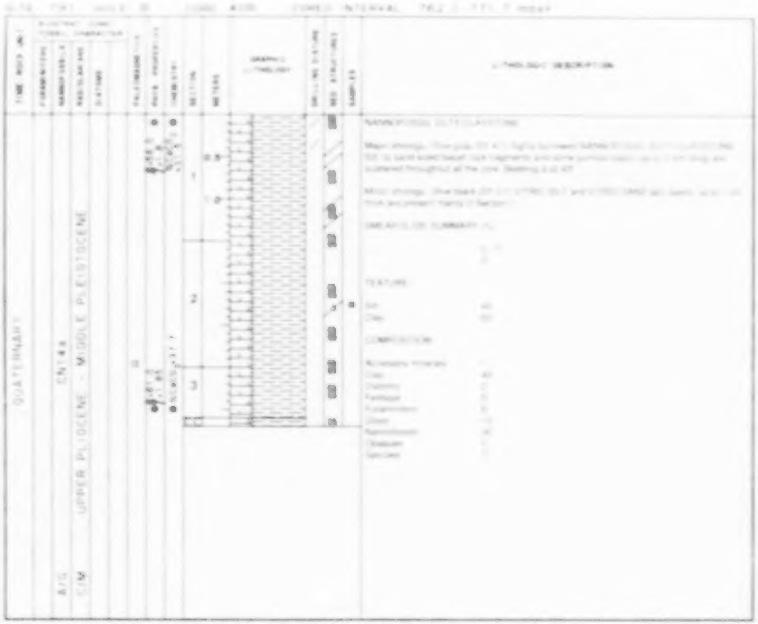
TIME-ROCK UNIT
BIOSTRAT. ZONE / FOSSIL CHARACTER
FORAMINIFERS
NANNOFOSSILS
RADIOLARIANS
DIATOMS
PALEOMAGNETICS
PHYS. PROPERTIES
CHEMISTRY
SECTION
METERS
GRAPHIC LITHOLOGY
DRILLING DISTURB.
SED. STRUCTURES
SAMPLES
QUATERNARY
A/G CN14a
C/M UPPER PLIOCENE - MIDDLE PLEISTOCENE
1
2
3
0.5
1.0

LITHOLOGIC DESCRIPTION

NANNOFOSSIL SILTY CLAYSTONE

Major lithology: Olive gray (5Y 4/1) highly burrowed NANNOFOSSIL SILTY CLAYSTONE. Silt- to sand-sized basalt rock fragments and some pumice clasts [illegible] are scattered throughout all the core. Bedding [illegible]

Minor lithology: Olive black [illegible] VITRIC SILT and VITRIC SAND [illegible] thick are present mainly in Section 1.

SMEAR SLIDE SUMMARY (%):

TEXTURE:

Silt	40
Clay	60

COMPOSITION:

Accessory minerals	[illegible]
Clay	40
Dolomite	[illegible]
Feldspar	[illegible]
Foraminifers	[illegible]
Glass	[illegible]
Nannofossils	[illegible]
Opaques	[illegible]
Spicules	[illegible]

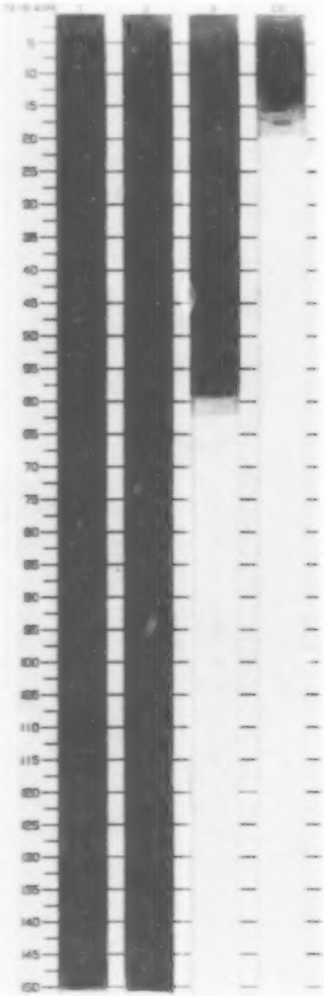
1
2
3
CC
5
10
15
20
25
30
35
40
45
50
55
60
65
70
75
80
85
90
95
100
105
110
115
120
125
130
135
140
145
150

SITE 791 HOLE B CORE 41R CORED INTERVAL 771.7-781.3 mbsf

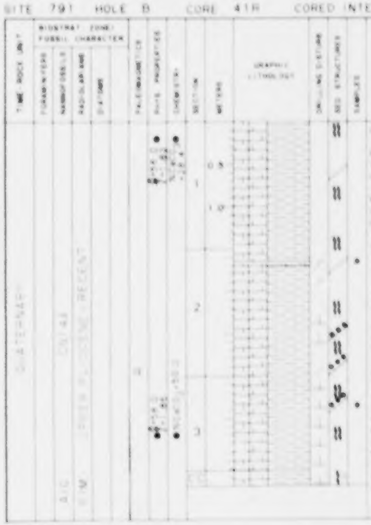
TIME-ROCK UNIT
BIOSTRAT. ZONE/ FOSSIL CHARACTER
FORAMINIFERS
NANNOFOSSILS
RADIOLARIANS
DIATOMS
PALEOMAGNETICS
PHYS. PROPERTIES
CHEMISTRY
SECTION
METERS
GRAPHIC LITHOLOGY
DRILLING DISTURB.
SED. STRUCTURES
SAMPLES
QUATERNARY
A/G CN 14
R/M UPPER PLIOCENE - RECENT
0.5
1.0
1
2
3
CC

LITHOLOGIC DESCRIPTION

FORAMINIFER NANNOFOSSIL VITRIC SILTY CLAYSTONE

Major lithologies: Olive gray (5Y 4/1), highly fractured FORAMINIFER NANNOFOSSIL VITRIC SILTY CLAYSTONE with abundant scattered angular fragments of basalt rock as large as 4 cm in diameter.

Minor lithology: A 5-cm-thick bed of light olive gray (5Y 6/2) nannofossil-bearing VITRIC SILT occurs in Section 2, 5-10 cm. A few very thin beds of olive black (5Y 2/1) SAND containing fragments of basalt rock fragments are present. Bedding planes have apparent dips of 40°.

SMEAR SLIDE SUMMARY (%):

	2, [illegible]	3, [illegible]
	M	M
TEXTURE:		
Sand	—	[illegible]
Silt	[illegible]	[illegible]
Clay	[illegible]	
COMPOSITION:		
Accessory minerals	[illegible]	[illegible]
Diatoms	[illegible]	[illegible]
Feldspar	[illegible]	[illegible]
Foraminifers	[illegible]	[illegible]
Glass	[illegible]	[illegible]
Nannofossils	[illegible]	[illegible]
Opaque		[illegible]
Radiolarians		[illegible]
Sponge spicules		[illegible]

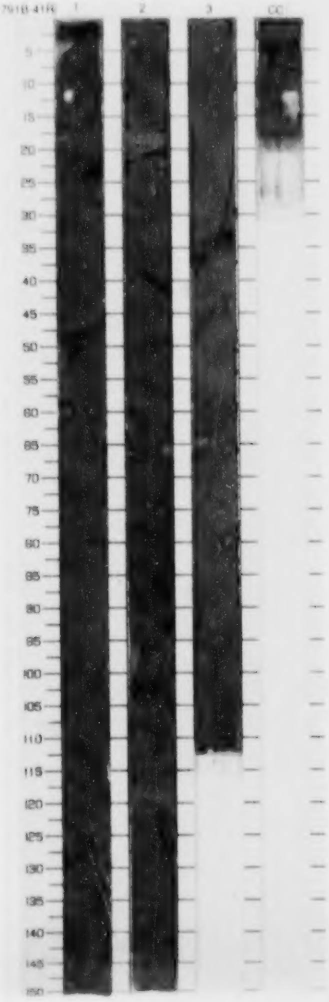
791B-41R
1
2
3
CC
5
10
15
20
25
30
35
40
45
50
55
60
65
70
75
80
85
90
95
100
105
110
115
120
125
130
135
140
145
150

SITE 791 HOLE B CORE 42R CORED INTERVAL 781.3-791.0 mbsf

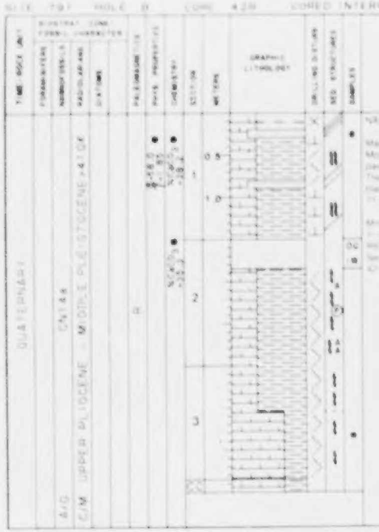
TIME-ROCK UNIT
BIOSTRAT. ZONE/ FOSSIL CHARACTER
FORAMINIFERS
NANNOFOSSILS
RADIOLARIANS
DIATOMS
PALEOMAGNETICS
PHYS. PROPERTIES
CHEMISTRY
SECTION
METERS
GRAPHIC LITHOLOGY
DRILLING DISTURB.
SED. STRUCTURES
SAMPLES
QUATERNARY
A/G CN14a
C/M UPPER PLIOCENE - MIDDLE PLEISTOCENE >41GK
R
1
2
3
0.5
1.0
CC

LITHOLOGIC DESCRIPTION

NANNOFOSSIL SILTY CLAYSTONE AND NANNOFOSSIL CHALK

Major lithologies:
Most of this core consists of dark gray (5Y 4/1) NANNOFOSSIL SILTY CLAYSTONE, passing gradationally downward in Section 3 into gray (5Y 5/1) NANNOFOSSIL CHALK. These sediments are bioturbated, and contain scattered grains and local concentrations of black basaltic sand (dark glass and mafic minerals). Highest concentrations are in Section 1, 71-76 cm and Section 3, 17-18 cm and 41-58 cm. Some burrows are filled with pyrite.

Minor lithologies:
Thin beds of light gray (N7) and medium gray (N5) VITRIC SILT and NANNOFOSSIL-RICH VITRIC SILT occur in Section 1, [illegible] cm, [illegible] cm, Section 2, [illegible] cm, and Section 3, [illegible] cm. The bed in Section 1, [illegible] cm, is parallel laminated. Bedding dips at [illegible]. Much of the core [illegible] of drilling biscuits.

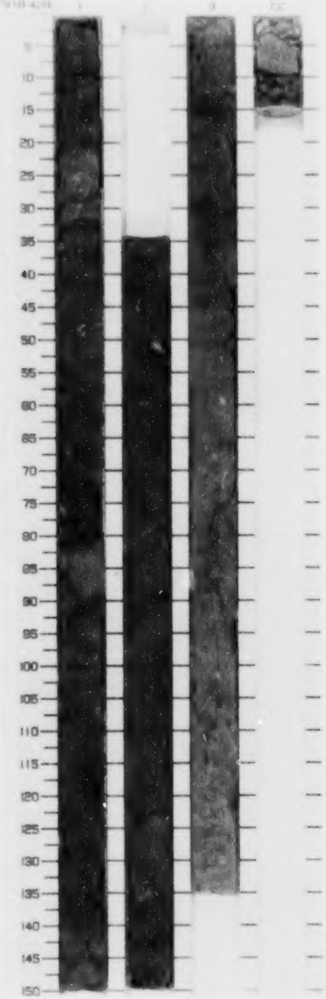
791B-42R
1
2
3
CC
5
10
15
20
25
30
35
40
45
50
55
60
65
70
75
80
85
90
95
100
105
110
115
120
125
130
135
140
145
150

SITE 791 HOLE B CORE 43R CORED INTERVAL 791.0-800.7 mbsf

TIME-ROCK UNIT	FORAMINIFERS	NANNOFOSSILS	RADIOLARIANS	DIATOMS	PALEOMAGNETICS	PHYS. PROPERTIES	CHEMISTRY	SECTION	METERS	GRAPHIC LITHOLOGY	DRILLING DISTURB.	SED. STRUCTURES	SAMPLES
QUATERNARY		CN14a A/G	UPPER PLIOCENE-RECENT R/M			●	●	1 CC	0.5 1.0		⊥	⊙	● ●●

LITHOLOGIC DESCRIPTION

NANNOFOSSIL-RICH CLAYSTONE

Major lithology: From 0-134 cm, the core consists of light olive gray (5Y 5/2) NANNOFOSSIL-RICH CLAYSTONE.

Minor lithology: From 134-145 cm, the core is gray (5Y 5/1) NANNOFOSSIL-RICH CLAYEY VITRIC SILT. Black (5Y 2/2) PYRITE nodules 0.22-0.3 cm in diameter occur in Section 1, 73 and 122 cm. Two dark gray (5GY 4/1) laminae, 3 mm thick, show apparent dips of 4°.

The core has been moderately fractured by drilling.

SMEAR SLIDE SUMMARY (%):

	1, 50 M	1, 140 D	CC, 11 D
TEXTURE:			
Sand	Tr	1	1
Silt	6	30	28
Clay	95	69	65
COMPOSITION:			
Clay	75	40	58
Feldspar	1	1	—
Foraminifers	—	2	1
Glass	6	25	10
Mica	1	1	—
Nannofossils	20	30	30
Opaques	1	—	—
Silicoflagellates	Tr	—	—
Spicules	Tr	1	Tr

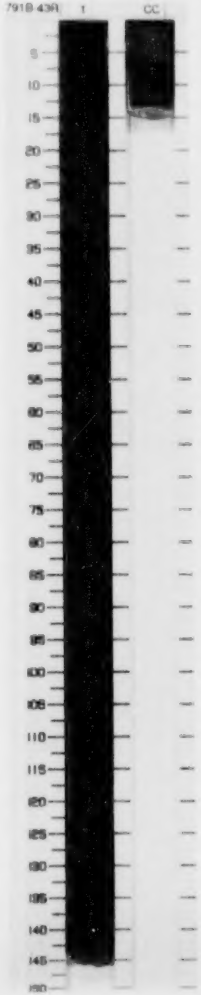

SITE 791 HOLE B CORE 44R CORED INTERVAL 800.7-810.3 mbsf

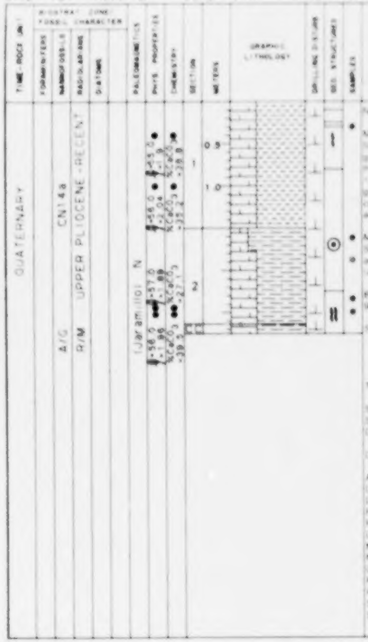
TIME-ROCK UNIT
BIOSTRAT. ZONE/ FOSSIL CHARACTER
FORAMINIFERS
NANNOFOSSILS
RADIOLARIANS
DIATOMS
PALEOMAGNETICS
PHYS. PROPERTIES
CHEMISTRY
SECTION
METERS
GRAPHIC LITHOLOGY
DRILLING DISTURB.
SED. STRUCTURES
SAMPLES
QUATERNARY
A/G
CN14a
R/M
UPPER PLIOCENE - RECENT
(Jaramillo) N
1
2
CC
0.5
1.0

LITHOLOGIC DESCRIPTION

NANNOFOSSIL CLAYSTONE AND NANNOFOSSIL SILTY CLAYSTONE

Major lithologies:
Section 1 is gray (5Y 5/1) NANNOFOSSIL CLAYSTONE. Black granules and fine to medium grained sand grains of brown glass and much fewer lithic fragments are scattered throughout this section, with greater concentrations at 10-26, 41-50, 74-78, 83-92, 95-101, 129-131, and 134-136 cm. The interval from Section 2, 29-114 cm to the bottom of the core catcher is dark gray (5Y 4/1) NANNOFOSSIL SILTY CLAYSTONE. It has some Scolithus burrowing and contains disseminated black sand grains with greater concentrations in Section 2, 31-35, 38, and 78 cm.

Minor lithologies:
Section 2, 0-29 cm is gray (5Y 5/1) NANNOFOSSIL-RICH VITRIC SILTY CLAYSTONE with a 0.3 cm-diameter black (5Y 3/2) PYRITE nodule at 23 cm. Gray (5Y 6/1, 5/1) VITRIC SILT (ash) beds occur in Section 1, 96-98 cm, and Section 2, 8-39 and 82-83 cm.

Bedding planes in Section 1 show apparent dips of 40° at 25-30 cm, 20° at 83-90 cm, 35° at 96-105 cm, and 20° at 110-120 cm. In Section 2, 80-87 cm, the apparent dip is 35°.

SMEAR SLIDE SUMMARY (%):

	1, 30 D	2, 11 D	2, 38 M	2, 82 M	2, 99 D
TEXTURE:					
Sand	1	5	15	25	5
Silt	9	30	35	65	15
Clay	90	65	50	10	80
COMPOSITION:					
Accessory minerals	Tr	Tr	1	—	Tr
Clay	60	46	40	10	47
Diatoms	—	Tr	—	Tr	—
Feldspar	1	Tr	1	2	1
Foraminifers	2	2	2	Tr	1
Glass	5	30	45	83	20
Micrite	1	1	Tr	—	1
Nannofossils	30	20	10	2	30
Opaques	—	—	1	2	Tr
Radiolarians	—	—	—	1	—
Rock fragment	—	—	Tr	—	—
Silicoflagellates	—	1	—	—	—
Spicules	1	—	—	—	—

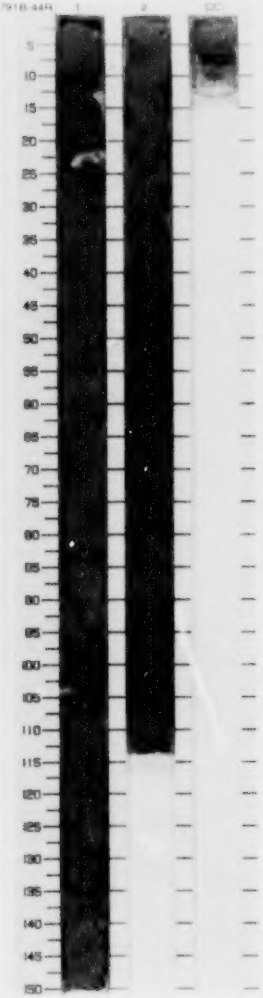
791B-44R
1
2
CC
5
10
15
20
25
30
35
40
45
50
55
60
65
70
75
80
85
90
95
100
105
110
115
120
125
130
135
140
145
150

SITE 791 HOLE B CORE 45R CORED INTERVAL 810.3-820.0 mbsf

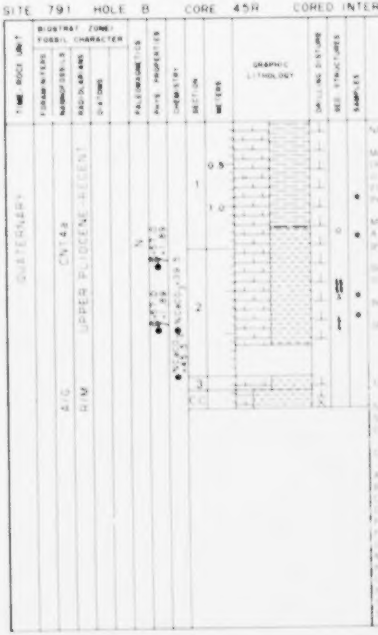
TIME-ROCK UNIT
BIOSTRAT. ZONE/ FOSSIL CHARACTER
FORAMINIFERS
NANNOFOSSILS
RADIOLARIANS
DIATOMS
PALEOMAGNETICS
PHYS. PROPERTIES
CHEMISTRY
SECTION
METERS
GRAPHIC LITHOLOGY
DRILLING DISTURB.
SED. STRUCTURES
SAMPLES
QUATERNARY
CN14a
A/G
UPPER PLIOCENE-RECENT
R/M
N
0.5
1.0
1
2
3
CC

LITHOLOGIC DESCRIPTION

NANNOFOSSIL SILTY CLAYSTONE AND NANNOFOSSIL CLAYSTONE

Major lithologies:
Olive gray (5Y 4/2) and light olive gray (5Y 6/2) NANNOFOSSIL SILTY CLAYSTONE occurs in Section 1, 0–104 cm, with scattered black fine to medium sand grains concentrated at 14–21 cm and 30–31 cm. From Section 1, 104 cm to Section 3, 18 cm and in the Core Catcher, the core is light olive gray (5Y 6/2) and olive gray (5Y 4/2) NANNOFOSSIL CLAYSTONE.

Minor lithologies:
A black (5Y 2/2) layer of VITRIC SILTY SAND occurs in Section 2, 56–57 cm. An isolated light gray (5Y 7/1) PUMICE clast, 1.5 cm in diameter, is located in Section 1, 13 cm.

Slight to moderate burrowing by *Teichichnus* and *Chondrites* occurs in Section 1, 11–18 cm, and in Section 2, 42–46 cm, 52–56 cm, and 81–86 cm.

Bedding planes in Section 1, 125–150 cm display apparent dips of 15°.

SMEAR SLIDE SUMMARY (%):

	1, 80	1, 117	2, 50	2, 80
	D	D	M	D
TEXTURE:				
Sand	[illegible]	[illegible]	60	10
Silt	18	[illegible]	30	[illegible]
Clay	80	89	10	85
COMPOSITION:				
Accessory minerals	[illegible]	[illegible]	[illegible]	[illegible]
Biotite	[illegible]	[illegible]	[illegible]	[illegible]
Clay	60	80	10	83
Diatoms	[illegible]	[illegible]	[illegible]	[illegible]
Feldspar	[illegible]	[illegible]	[illegible]	[illegible]
Foraminifers	4	[illegible]	[illegible]	[illegible]
Glass	10	[illegible]	78	[illegible]
Micrite	[illegible]	4	[illegible]	5
Nannofossils	20	10	5	10
Opaques	[illegible]	[illegible]	[illegible]	[illegible]
Rock fragments	[illegible]	[illegible]	[illegible]	[illegible]
Silicoflagellates	[illegible]	[illegible]	[illegible]	[illegible]
Spicules	[illegible]	[illegible]	[illegible]	[illegible]

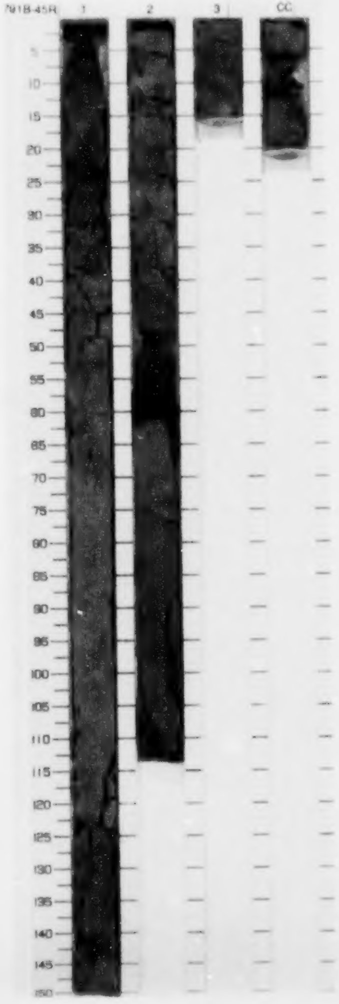
791B-45R
1
2
3
CC
5
10
15
20
25
30
35
40
45
50
55
60
65
70
75
80
85
90
95
100
105
110
115
120
125
130
135
140
145
150

SITE 791 HOLE B CORE 46R CORED INTERVAL 820.0-829.6 mbsf

TIME-ROCK UNIT	FORAMINIFERS	NANNOFOSSILS	RADIOLARIANS	DIATOMS	PALEOMAGNETICS	PHYS. PROPERTIES	CHEMISTRY	SECTION	METERS	GRAPHIC LITHOLOGY	DRILLING DISTURB.	SED. STRUCTURES	SAMPLES
QUATERNARY	A/G	CN14a	R/P		N (Jaramillo) R	●	●	1 2 CC	0.5 1.0				●

LITHOLOGIC DESCRIPTION

NANNOFOSSIL RICH CLAYSTONE AND NANNOFOSSIL RICH VITRIC SILTY CLAYSTONE

Major lithologies:
Section 1, 4-143 cm and the interval from Section 2, 94 cm to the base of the core catcher is olive gray (5Y 4/2) NANNOFOSSIL RICH CLAYSTONE. The interval from Section 1, 143 cm to Section 2, 94 cm is light olive gray (5Y 5/2) NANNOFOSSIL RICH VITRIC SILTY CLAYSTONE, with slight burrowing by Chondrites in Section 2, 78-82 cm.

Minor lithologies:
An olive gray (5Y 4/2) layer of VITRIC SILT occurs in Section 1, 0-4 cm. Thin layers of gray (5Y 5/1) CLAYEY VITRIC SILT occur in Section 1, 13-17 cm and 106-110 cm, and in Section 2, 14-15 and 94-95 cm. An isolated black (5Y 3/2) SCORIA clast 1.1 cm in diameter is in Section 1, 90 cm. Two isolated light gray (5Y 7/1) PUMICE clasts 2.2 and 3.7 cm in diameter are found in Section 2, 90-95 cm.

Two microfaults, dipping 45°, are situated in Section 1, 72-81 cm and 99-100 cm, the upper one cutting bedding planes with an apparent dip of 10°. Apparent dips below the lower microfault (Section 1, 105-150 cm) are 20°.

SMEAR SLIDE SUMMARY (%):

	1, 14	1, 49	2, 13	2, 50	CC, 15
	M	D	M	D	D
TEXTURE:					
Sand	5	3	2	15	0
Silt	73	12	83	18	15
Clay	22	85	15	72	80
COMPOSITION:					
Accessory minerals	2	Tr	Tr	Tr	Tr
Clay	20	75	15	58	59
Diatoms	—	Tr	—	—	—
Feldspar	1	1	2	2	1
Foraminifers	Tr	2	1	5	8
Glass	72	10	80	20	13
Micrite	Tr	1	Tr	5	—
Nannofossils	2	15	Tr	10	20
Opaques	—	—	1	—	—
Rock fragment	Tr	—	Tr	—	—
Silicoflagellates	—	Tr	—	—	—
Spicules	—	Tr	—	Tr	—

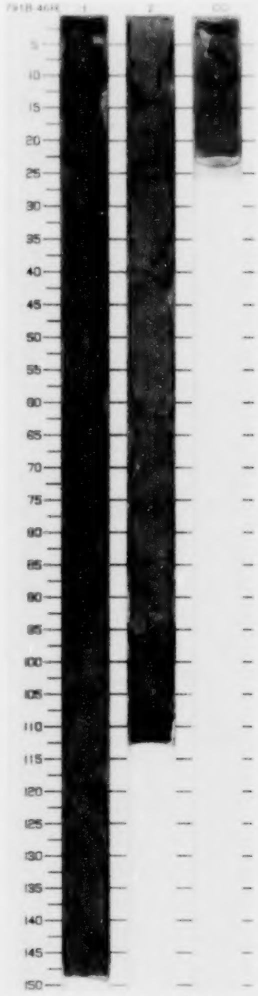

SITE 791 HOLE B CORE 47R CORED INTERVAL 829.6-839.2 mbsf

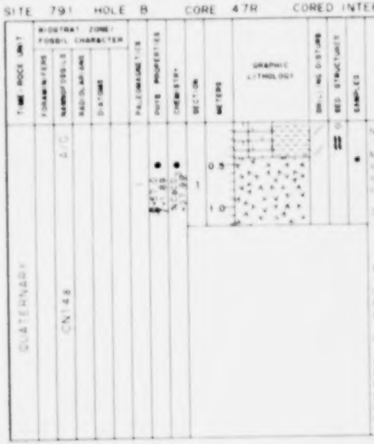
TIME-ROCK UNIT
BIOSTRAT. ZONE/ FOSSIL CHARACTER
FORAMINIFERS
NANNOFOSSILS
RADIOLARIANS
DIATOMS
PALEOMAGNETICS
PHYS. PROPERTIES
CHEMISTRY
SECTION
METERS
GRAPHIC LITHOLOGY
DRILLING DISTURB.
SED. STRUCTURES
SAMPLES
QUATERNARY
A/G
CN14B
1
0.5
1.0

LITHOLOGIC DESCRIPTION

NANNOFOSSIL FORAMINIFER CLAYSTONE

Major lithology: Grayish green (5GY 6/1) NANNOFOSSIL FORAMINIFER CLAYSTONE with local intervals of intense burrowing, isolated pumice granules at 0-4 cm and 17-38 cm, and sand-sized basalt fragments. A shear surface with an apparent dip of about 40° is at 20-25 cm. Igneous rocks occupy the rest of the core.

SMEAR SLIDE SUMMARY (%):

	1, 43
	D
TEXTURE:	
Sand	25
Silt	35
Clay	40
COMPOSITION:	
Accessory minerals	1
Clay	30
Feldspar	2
Foraminifers	40
Glass	5
Nannofossils	15

791B-47R 1

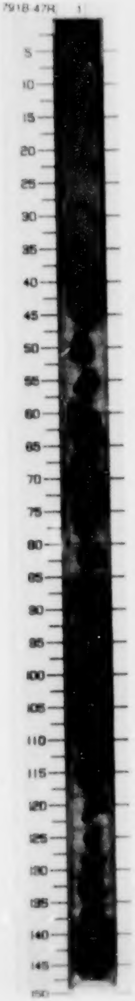
5
10
15
20
25
30
35
40
45
50
55
60
65
70
75
80
85
90
95
100
105
110
115
120
125
130
135
140
145
150

SITE 791 HOLE B CORE 62R CORED INTERVAL 974.1-983.7 mbsf

TIME-ROCK UNIT	BIOSTRAT. ZONE/ FOSSIL CHARACTER: FORAMINIFERS	NANNOFOSSILS	RADIOLARIANS	DIATOMS		PALEOMAGNETICS	PHYS. PROPERTIES	CHEMISTRY	SECTION	METERS	GRAPHIC LITHOLOGY	DRILLING DISTURB.	SED. STRUCTURES	SAMPLES
QUATERNARY		CN14a F/M				R	● φ=49.8 γ=2.13	● %CaCO$_3$ =0.71	1					● ●

LITHOLOGIC DESCRIPTION

CRYSTAL VITRIC SILT AND SANDY MUD

Major lithologies:
The top 12 cm of the core is brownish black (5YR 2/1) CRYSTAL VITRIC SILT. In a smear slide the material consists principally of opaque glass, feldspar, pyroxene, and olivine grains. From 12-22 cm the material is dark gray (5Y 4/1) SANDY MUD, consisting of opaque glass, clay-sized zeolites (?), and accessory minerals.

These sediments are homogeneous and firm but unconsolidated, and rest on basalt, which constitutes the remainder of the core.

SMEAR SLIDE SUMMARY (%):

	1, 1 D	1, 21 D
TEXTURE:		
Sand	10	40
Silt	85	30
Clay	5	30
COMPOSITION:		
Accessory minerals	10	15
Clay	—	30
Feldspar	25	15
Glass	65	40
Spar cement	Tr	—

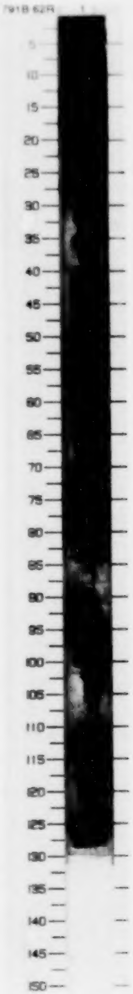

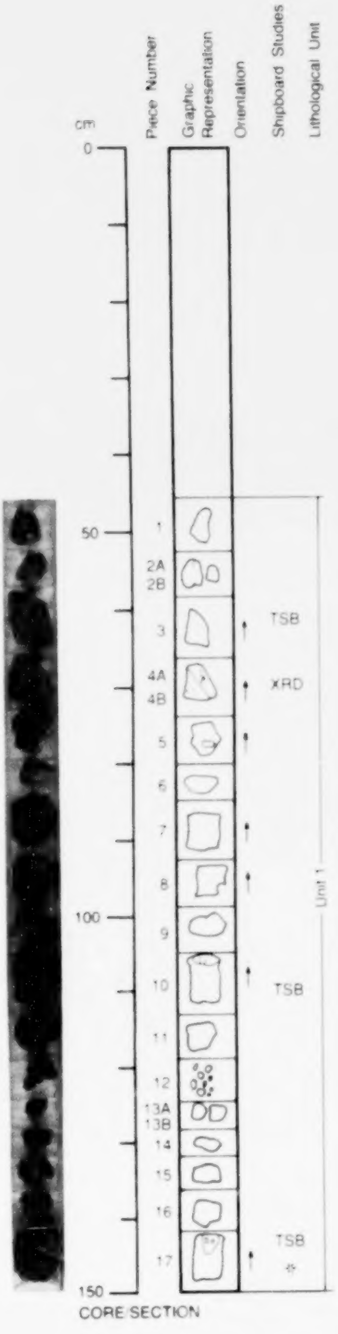
cm
Piece Number
Graphic Representation
Orientation
Shipboard Studies
Lithological Unit
0
50
100
150
1
2A
2B
3
4A
4B
5
6
7
8
9
10
11
12
13A
13B
14
15
16
17
TSB
XRD
TSB
TSB
Unit 1
CORE SECTION

126-791B-47R-1

UNIT 1: BASALT BRECCIA

Pieces 1-17

CONTACTS: None
PHENOCRYSTS:
Olivine - 1-2%, 0.2-0.5 mm, fresh, euhedral
Plagioclase - 3%, 0.5-2.0 mm, fresh, euhedral
GROUNDMASS: Intersertal
VESICLES: 30%, 0.3-2.0, round, random, some smectite linings
COLOR: Dark gray, N4
STRUCTURE: None
ALTERATION: Slight
VEINS/FRACTURES: None
ADDITIONAL COMMENTS: The clasts (0.5-2.0 cm) described above occur in a crystal-lithic nonvesicular glass matrix of the same mineralogy.

126-791B-48R-1

UNIT 2: GLOMEROPORPHYRITIC BASALT

Pieces 1-10

CONTACTS: None.
PHENOCRYSTS: Often in glomeroporphyritic clots.
    Plagioclase - 3-4%; 1-3 mm; fresh, euhedral.
    Olivine - 1-2%; 0.1-0.5 mm; fresh, euhedral.
    Clinopyroxene - 1-3%; 1.5-3.0 mm; fresh, euhedral.
GROUNDMASS: Intersertal.
VESICLES: 20%; 0.5 mm; round; random; smectite linings.
COLOR: Dark gray, N4.
STRUCTURE: None.
ALTERATION: Slight.
VEINS/FRACTURES: None.

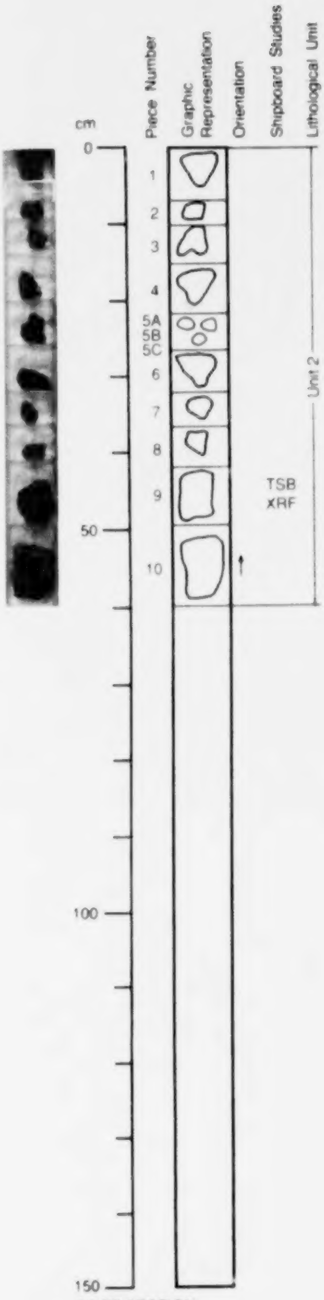
cm
Piece Number
Graphic Representation
Orientation
Shipboard Studies
Lithological Unit
0
50
100
150
1
2
3
4
5A
5B
5C
6
7
8
9
10
TSB
XRF
Unit 2
CORE/SECTION

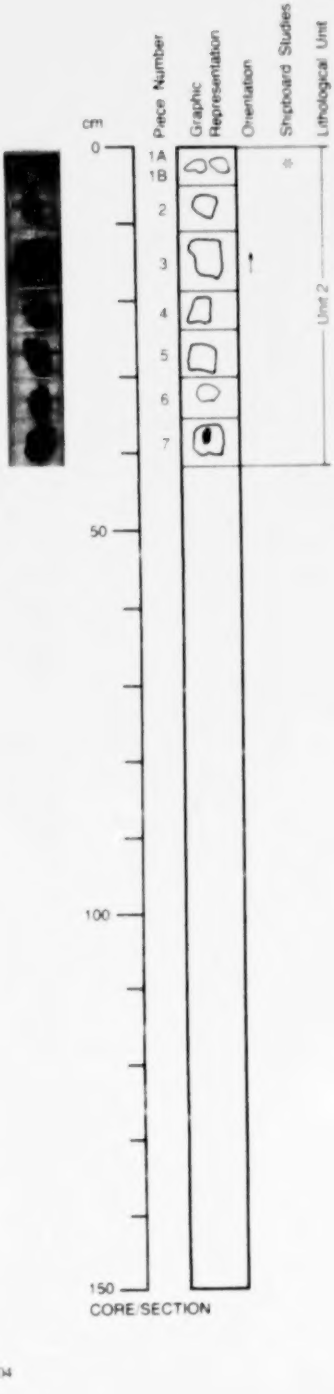
cm
Piece Number
Graphic Representation
Orientation
Shipboard Studies
Lithological Unit
0
1A
1B
2
3
4
5
6
7
Unit 2
50
100
150
CORE/SECTION

126-791B-49R-1

UNIT 2: GLOMEROPORPHYRITIC BASALT

Pieces 1-7

CONTACTS: None
PHENOCRYSTS: Often in glomeroporphyritic clots
Plagioclase - 3-4%, 1-3 mm, fresh, euhedral
Olivine - 1-2%, 0.1-0.5 mm, fresh, euhedral
Clinopyroxene - 1-3%, 1.5-3.0 mm, fresh, euhedral
GROUNDMASS: Intersertal
VESICLES: 20%, 0.5 mm, round, random, smectite linings
COLOR: Dark gray, N4
STRUCTURE: None
ALTERATION: Slight
VEINS/FRACTURES: None

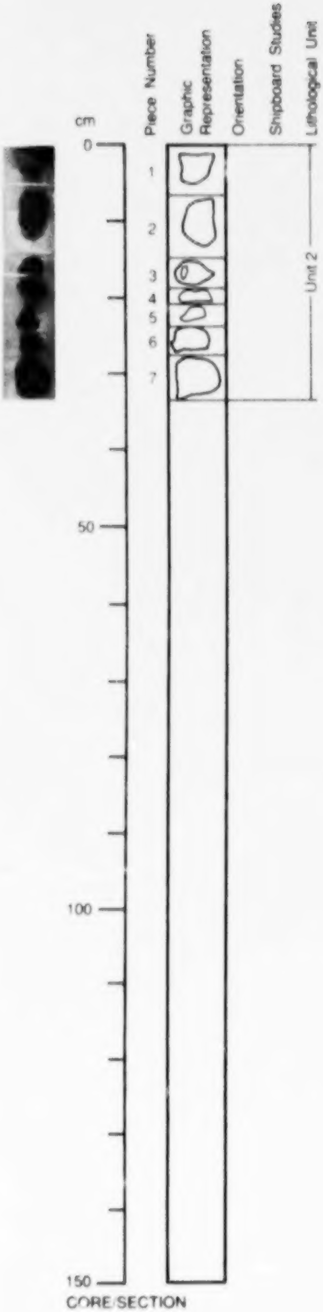
cm
Piece Number
Graphic Representation
Orientation
Shipboard Studies
Lithological Unit
0
1
2
3
4
5
6
7
Unit 2
50
100
150
CORE/SECTION

126-791B-50R-1

UNIT 2: GLOMEROPORPHYRITIC BASALT

Pieces 1-7

CONTACTS: None
PHENOCRYSTS: Often in glomeroporphyritic clots
Plagioclase - 3-4%, 1-3 mm, fresh, euhedral
Olivine - 1-2%, 0.1-0.5 mm, fresh, euhedral
Clinopyroxene - 1-3%, 1.5-3.0 mm, fresh, euhedral
GROUNDMASS: Intersertal
VESICLES: 20%, 0.5 mm, round, random, smectite linings
COLOR: Dark gray, N4
STRUCTURE: None
ALTERATION: Slight
VEINS/FRACTURES: None

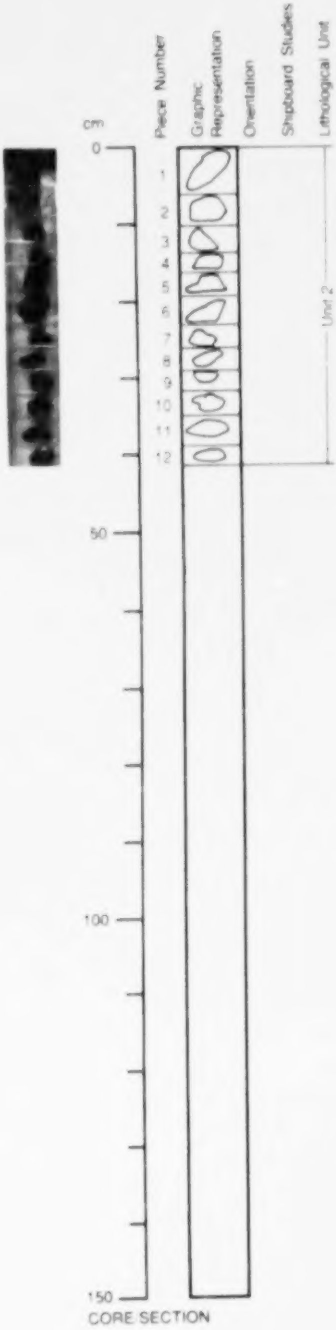
cm
Piece Number
Graphic Representation
Orientation
Shipboard Studies
Lithological Unit
0
1
2
3
4
5
6
7
8
9
10
11
12
Unit 2
50
100
150
CORE SECTION

126-791B-51R-1

UNIT 2: GLOMEROPORPHYRITIC BASALT

Pieces 1-12

CONTACTS: None
PHENOCRYSTS: Often in glomeroporphyritic clots.
Plagioclase - 3-4%, 1-3 mm, fresh, euhedral.
Olivine - 1-2%, 0.1-0.5 mm, fresh, euhedral.
Clinopyroxene - 1-3%, 1.5-3.0 mm, fresh, euhedral.
GROUNDMASS: Intersertal.
VESICLES: 20%, 0.5 mm, round, random, smectite linings.
COLOR: Dark gray N4.
STRUCTURE: None.
ALTERATION: Slight.
VEINS/FRACTURES: None.

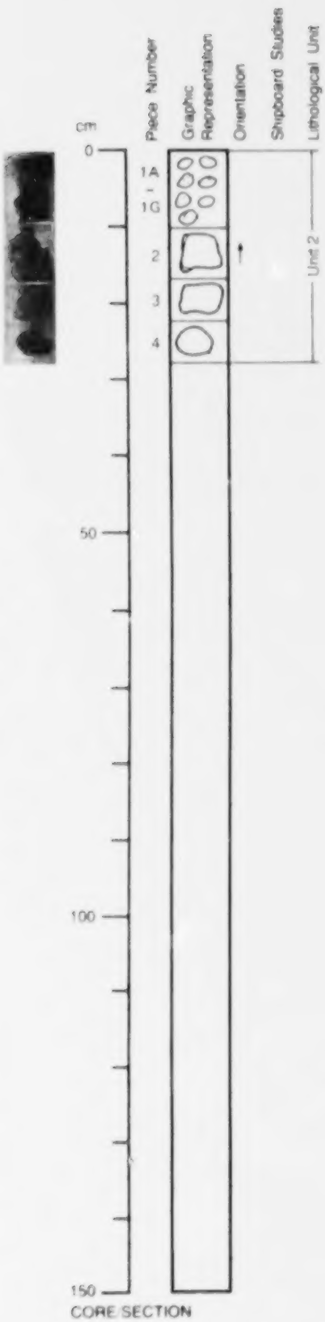
cm
Piece Number
Graphic Representation
Orientation
Shipboard Studies
Lithological Unit
0
1A
-
1G
2
3
4
Unit 2
50
100
150
CORE/SECTION

126-791B-52R-CC

UNIT 2: GLOMEROPORPHYRITIC BASALT

Pieces 1-4

CONTACTS: None
PHENOCRYSTS: Often in glomeroporphyritic clots
Plagioclase - 3-4%, 1-3 mm, fresh, euhedral
Olivine - 1-2%, 0.1-0.5 mm, fresh, euhedral
Clinopyroxene - 1-3%, 1.5-3.0 mm, fresh, euhedral
GROUNDMASS: Intersertal
VESICLES: 20%, 0.5 mm, round, random, smectite linings
COLOR: Dark gray N4
STRUCTURE: None
ALTERATION: Slight
VEINS/FRACTURES: None

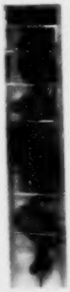

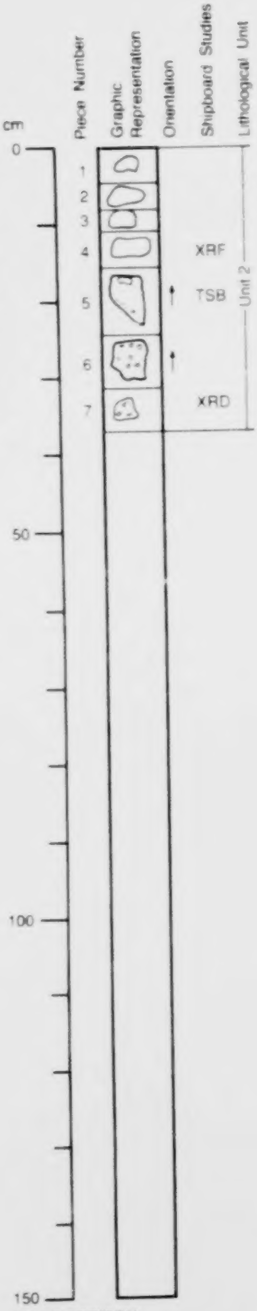
cm
Piece Number
Graphic Representation
Orientation
Shipboard Studies
Lithological Unit
0
1
2
3
4
XRF
5
TSB
Unit 2
6
7
XRD
50
100
150
CORE/SECTION

126-791B-53R-1

UNIT 2: GLOMEROPORPHYRITIC BASALT

Pieces 1-7

CONTACTS: None
PHENOCRYSTS: Often in glomeroporphyritic clots
    Plagioclase - 3-4%, 1-3 mm, fresh, euhedral
    Olivine - 1-2%, 0.1-0.5 mm, fresh, euhedral
    Clinopyroxene - 1-3%, 1.5-3.0 mm, fresh, euhedral
GROUNDMASS: Intersertal
VESICLES: 20%, 0.5 mm, round, random, smectite linings
COLOR: Dark gray, N4
STRUCTURE: None
ALTERATION: Slight
VEINS/FRACTURES: None

126-791B-54R-1

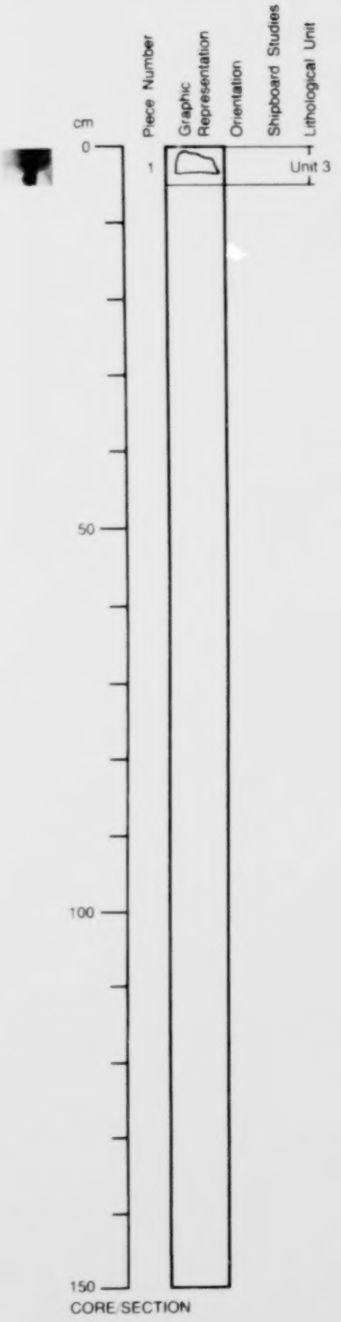
cm
Piece Number
Graphic Representation
Orientation
Shipboard Studies
Lithological Unit
0
50
100
150
1
Unit 3
CORE/SECTION

UNIT 3: BASALT

Piece 1

CONTACTS: None.
PHENOCRYSTS: Some glomeroporphyritic clots.
Plagioclase - 5%; 0.2-0.5 mm, fresh, euhedral.
Olivine - 1-3%, 0.2-1.5 mm, euhedral.
GROUNDMASS: Intersertal, microvesicular, devitrified glass.
VESICLES: 20%, 1-2 mm, round, random, smectite, calcite fillings.
COLOR: Dark gray, N4.
STRUCTURE: None.
ALTERATION: Slight.
VEINS/FRACTURES: None.

126-791B-55R-1

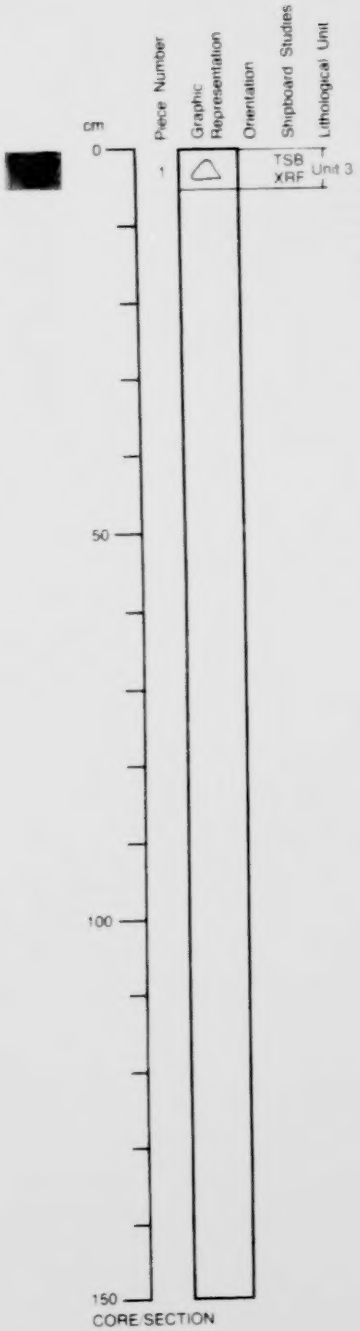
cm
Piece Number
Graphic Representation
Orientation
Shipboard Studies
Lithological Unit
0
1
TSB
XRF
Unit 3
50
100
150
CORE/SECTION

UNIT 3: BASALT

Piece 1

CONTACTS: None
PHENOCRYSTS: Some glomeroporphyritic clots.
    Plagioclase - 5%, 0.2-0.5 mm, fresh, euhedral
    Olivine - 1-3%, 0.2-1.5 mm, euhedral
GROUNDMASS: intersertal, microvesicular, devitrified glass.
VESICLES: 20%, 1-2 mm, round, random, smectite, calcite fillings.
COLOR: Dark gray, N4
STRUCTURE: None
ALTERATION: Slight
VEINS/FRACTURES: None

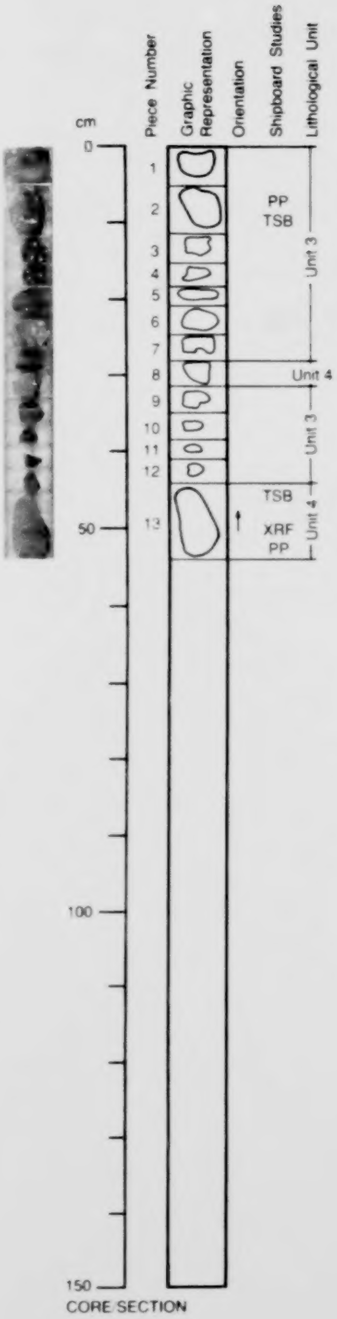
cm
Piece Number
Graphic Representation
Orientation
Shipboard Studies
Lithological Unit
0
50
100
150
1
2
3
4
5
6
7
8
9
10
11
12
13
PP
TSB
Unit 3
Unit 4
Unit 3
TSB
XRF
PP
Unit 4
CORE/SECTION

126-791B-56R-1

UNIT 3: BASALT

Pieces 1-7 and 9-12

CONTACTS: None
PHENOCRYSTS: Some glomeroporphyritic clots.
Plagioclase - 5%, 0.2-0.5 mm; fresh, euhedral.
Olivine - 1-3%, 0.2-1.5 mm; euhedral.
GROUNDMASS: Intersertal, microvesicular, devitrified glass.
VESICLES: 20%, 1-2 mm; round; random; smectite, calcite fillings.
COLOR: Dark gray, N4
STRUCTURE: None
ALTERATION: Slight.
VEINS/FRACTURES: None

UNIT 4: DIABASE

Pieces 8 and 13

CONTACTS: None
PHENOCRYSTS:
Plagioclase - 60%, 0.2 mm; fresh.
Clinopyroxene - 15%, 0.05 mm.
Olivine - 2-3%, 0.05 mm.
Magnetite - 3%, 0.05 mm.
GROUNDMASS: Devitrified glass.
VESICLES: 5%, 0.2 mm; circular; random; smectite linings.
COLOR: Gray
STRUCTURE: None
ALTERATION: Slight.
VEINS/FRACTURES: None

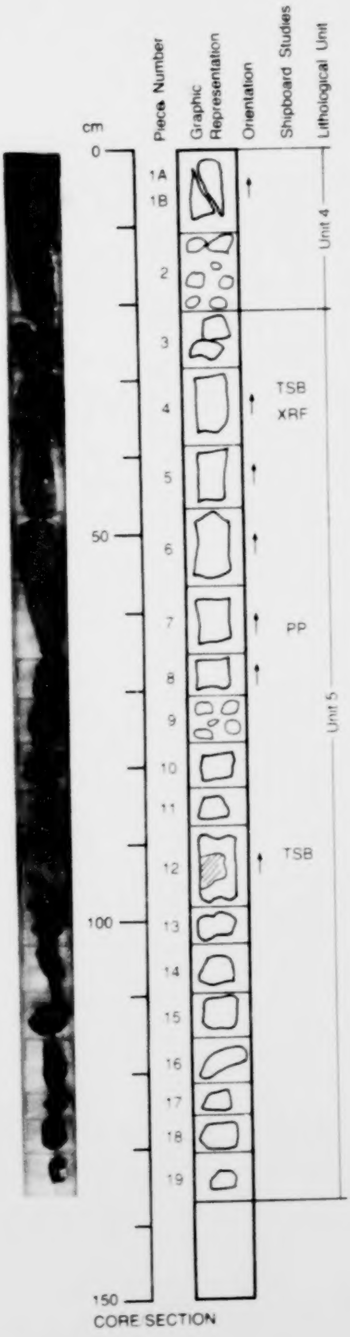
cm
Piece Number
Graphic Representation
Orientation
Shipboard Studies
Lithological Unit
0
50
100
150
1A
1B
2
3
4
5
6
7
8
9
10
11
12
13
14
15
16
17
18
19
TSB
XRF
PP
TSB
Unit 4
Unit 5
CORE/SECTION

126-791B-57R-1

UNIT 4: DIABASE

Pieces 1-2

CONTACTS: None
PHENOCRYSTS:
- Plagioclase - 60%, 0.2 mm, fresh
- Clinopyroxene - 15%, 0.05 mm
- Olivine - 2-3%, 0.05 mm
- Magnetite - 3%, 0.05 mm

GROUNDMASS: Devitrified glass
VESICLES: 5%, 0.2 mm, circular, random, smectite linings.
COLOR: Gray
STRUCTURE: None
ALTERATION: Slight
VEINS/FRACTURES: None

UNIT 5: BASALT

Pieces 3-19

CONTACTS: None
PHENOCRYSTS:
- Plagioclase - 5-10%, 0.2-0.5 mm, fresh, euhedral
- Olivine - 2-5%, 1-2 mm, euhedral, partly altered

GROUNDMASS: Intergranular, microvesicular
VESICLES: 25%, 0.2-1.5 mm, circular, random; ranges from open with blue smectite linings, to filled with calcite or zeolite
COLOR: Dark gray, N4
STRUCTURE: None
ALTERATION: Alteration halos surround fresher cores.
VEINS/FRACTURES: None

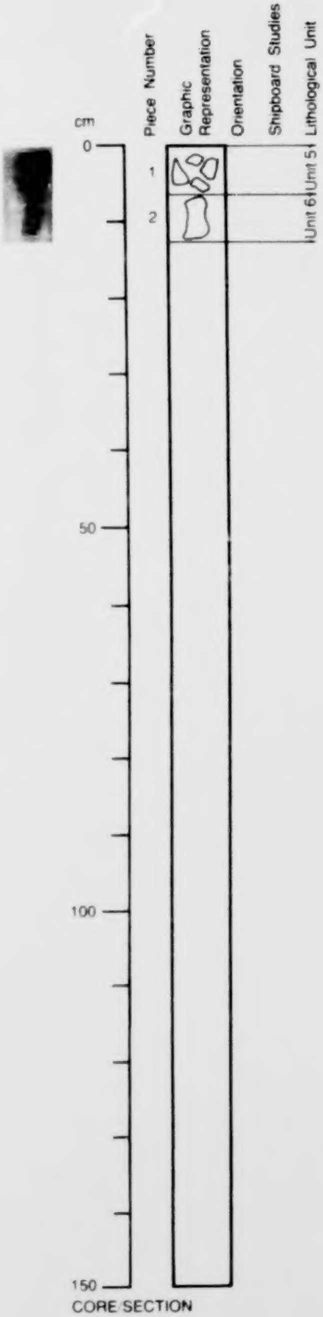
cm
Piece Number
Graphic Representation
Orientation
Shipboard Studies
Lithological Unit
0
1
2
Unit 5
Unit 6
50
100
150
CORE/SECTION

126-791B-58R-1

UNIT 5: BASALT

Piece 1

CONTACTS: None.
PHENOCRYSTS:
Plagioclase - 5-10%, 0.2-0.5 mm, fresh, euhedral.
Olivine - 2-5%, 1-2 mm, euhedral, partly altered.
GROUNDMASS: Intergranular, microvesicular.
VESICLES: 25%, 0.2-1.5 mm, circular, random, ranges from open with blue smectite linings, to filled with calcite or zeolite.
COLOR: Dark gray, N4.
STRUCTURE: None.
ALTERATION: Alteration halos surround fresher cores.
VEINS/FRACTURES: None.

UNIT 6: BASALT

Piece 2

CONTACTS: Glass at top.
PHENOCRYSTS:
Olivine - 1-2%, 0.3-1.0 mm, partly altered, euhedral.
Plagioclase - 1-3%, 0.3-1.0 mm, fresh, euhedral.
GROUNDMASS: Intersertal, microvesicular.
VESICLES: 10%, 0.2-1.0 mm, circular, random, smectite linings.
COLOR: Dark gray, N4.
STRUCTURE: None.
ALTERATION: None.
VEINS/FRACTURES: None.

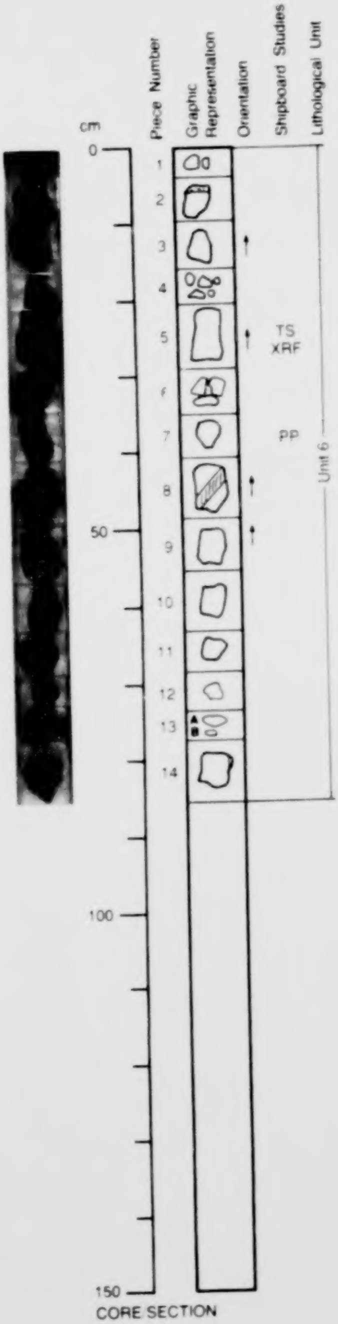
cm
Piece Number
Graphic Representation
Orientation
Shipboard Studies
Lithological Unit
0
50
100
150
1
2
3
4
5
6
7
8
9
10
11
12
13
A
B
14
TS
XRF
PP
Unit 6
CORE SECTION

126-791B-59R-1

UNIT 6: BASALT

Pieces 1-14

CONTACTS: Glass at top
PHENOCRYSTS:
Olivine - 1-2%; 0.3-1.0 mm; partly altered, euhedral.
Plagioclase - 1-3%; 0.3-1.0 mm; fresh, euhedral.
GROUNDMASS: Intersertal, microvesicular.
VESICLES: 10%; 0.2-1.0 mm; circular; random; smectite linings.
COLOR: Dark gray, N4.
STRUCTURE: None.
ALTERATION: None.
VEINS/FRACTURES: None.

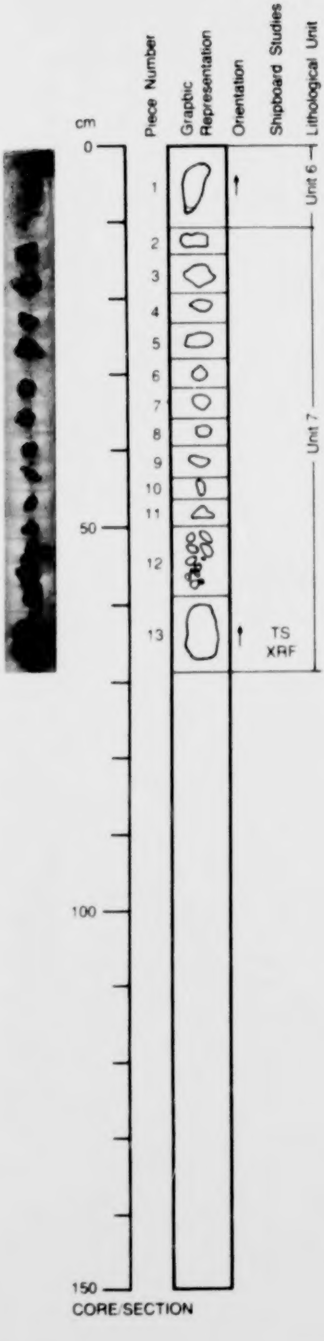
cm
Piece Number
Graphic Representation
Orientation
Shipboard Studies
Lithological Unit
0
50
100
150
1
2
3
4
5
6
7
8
9
10
11
12
13
Unit 6
Unit 7
TS
XRF
CORE/SECTION

126-791B-60R-1

UNIT 6: BASALT

Piece 1

CONTACTS: Glass at top.
PHENOCRYSTS:
Olivine - 1-2%; 0.3-1.0 mm; partly altered, euhedral.
Plagioclase - 1-3%; 0.3-1.0 mm; fresh, euhedral.
GROUNDMASS: Intersertal, microvesicular.
VESICLES: 10%; 0.2-1.0 mm; circular; random; smectite linings.
COLOR: Dark gray, N4.
STRUCTURE: None.
ALTERATION: None.
VEINS/FRACTURES: None.

UNIT 7: BASALT

Pieces 2-13

CONTACTS: None.
PHENOCRYSTS:
Olivine - 1-3%; 0.5-2.0 mm; fresh, euhedral.
Plagioclase - 1-2%; 0.5-2.0 mm; fresh, euhedral.
GROUNDMASS: Intersertal, devitrified glass.
VESICLES: 20%; 1-3 mm; circular; random; smectite linings.
COLOR: Medium gray, N5.
STRUCTURE: None.
ALTERATION: None.
VEINS/FRACTURES: None.

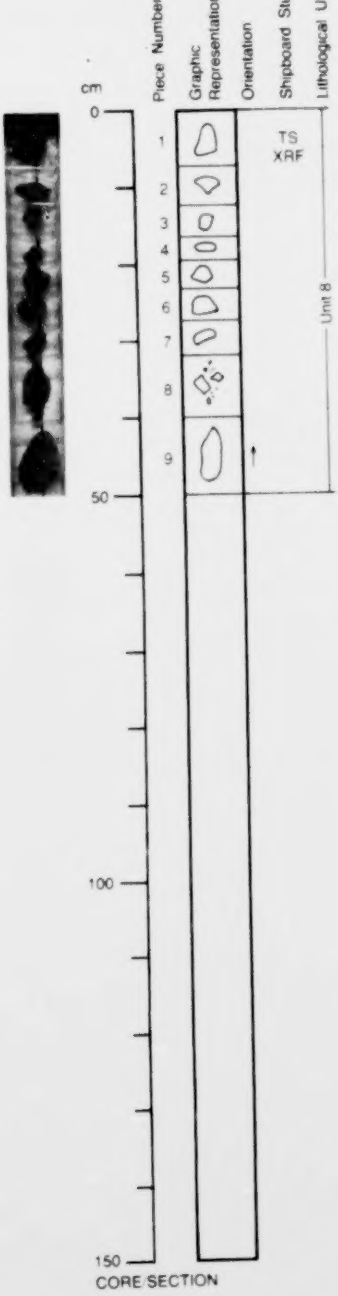
cm
Piece Number
Graphic Representation
Orientation
Shipboard Studies
Lithological Unit
0
1
2
3
4
5
6
7
8
9
TS
XRF
Unit 8
50
100
150
CORE/SECTION

126-791B-61R-1

UNIT 8: DIABASE

Pieces 1-9

CONTACTS: None
PHENOCRYSTS:
Plagioclase - 2%, 1-2 mm, fresh
GROUNDMASS: Flow aligned plagioclase, clinopyroxene, microvesicular glass
VESICLES: <1 mm
COLOR: Medium gray, N5
STRUCTURE: None
ALTERATION: Slight
VEINS/FRACTURES Chlorite vein in one piece

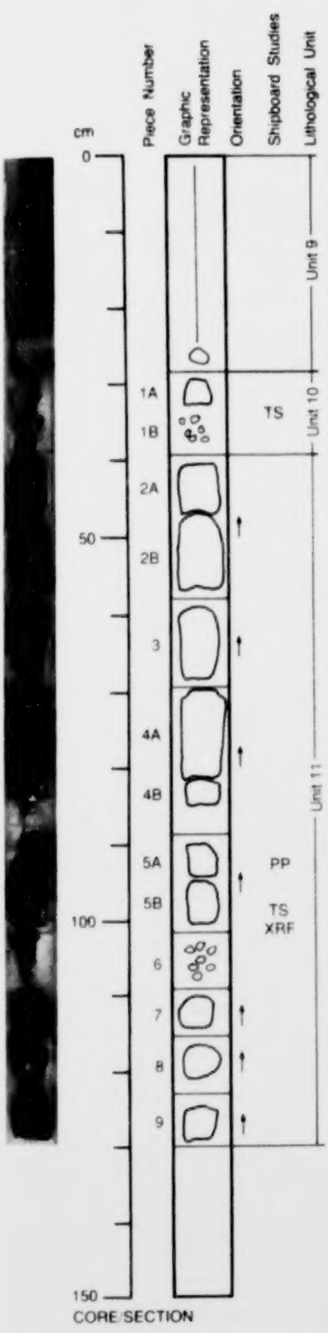
cm
Piece Number
Graphic Representation
Orientation
Shipboard Studies
Lithological Unit
0
50
100
150
1A
1B
2A
2B
3
4A
4B
5A
5B
6
7
8
9
TS
PP
TS
XRF
Unit 9
Unit 10
Unit 11
CORE/SECTION

126-791B-62R-1

UNIT 9: SEDIMENT: CRYSTAL VITRIC SILT (0-10 CM); CRYSTAL VITRIC SANDY CLAY (10-22 CM)

See sedimentary visual core description.

UNIT 10: BASALT

Piece 1

CONTACTS: None.
PHENOCRYSTS: Often in clots.
Plagioclase - 2-5%; 0.2-1.0 mm; euhedral, fresh.
GROUNDMASS: Intersertal, microvesicular with quench pyroxenes.
VESICLES: 10-30%; 0.2-1.0 mm; circular; random; smectite linings.
COLOR: Dark gray, N4.
STRUCTURE: None.
ALTERATION: Slight.
VEINS/FRACTURES: None.

UNIT 11: BASALT MOUSSE

Pieces 1-9

CONTACTS: None.
PHENOCRYSTS:
Olivine - 2%; <1 mm; euhedral, equant, fresh.
Plagioclase - <=5%; <1 mm; euhedral, elongate, fresh.
GROUNDMASS: Microvesicular, devitrified glass.
VESICLES: 50%; <0.2 mm; round; random; smectite lining plus occasional zeolite.
COLOR: Gray, N5.
STRUCTURE: None.
ALTERATION: Slight.
VEINS/FRACTURES: None.
ADDITIONAL COMMENTS: Above description applies to the most common type of "clast" in a matrix which is very similar in composition. The matrix also has <1 mm olivine and plagioclase crystals, often in clots, within a vesicular glass (30%, 0.1-0.5 mm) which is less devitrified than the clasts, and less vesicular around crystal clots.

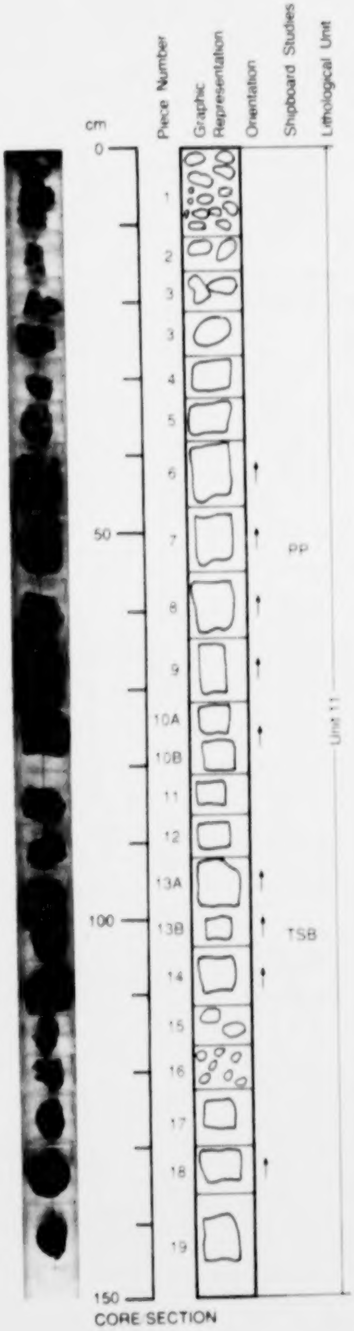
cm
Piece Number
Graphic Representation
Orientation
Shipboard Studies
Lithological Unit
0
50
100
150
1
2
3
3
4
5
6
7
8
9
10A
10B
11
12
13A
13B
14
15
16
17
18
19
PP
TSB
Unit 11
CORE SECTION

126-791B-63R-1

UNIT 11: BASALT MOUSSE

Pieces 1-19

CONTACTS: None
PHENOCRYSTS:
Olivine - 2%, <1 mm, euhedral, equant, fresh.
Plagioclase - <=5%, <1 mm, euhedral, elongate, fresh.
GROUNDMASS: Microvesicular, devitrified glass.
VESICLES: 50%, <0.2 mm, round, random, smectite lining plus occasional zeolite.
COLOR: Gray, N5.
STRUCTURE: None
ALTERATION: Slight
VEINS/FRACTURES: None
ADDITIONAL COMMENTS: Above description applies to the most common type of "clast" in a matrix which is very similar in composition. The matrix also has <1 mm olivine and plagioclase crystals, often in clots, within a vesicular glass (30%, 0.1-0.5 mm) which is less devitrified than the clasts, and less vesicular around crystal clots.

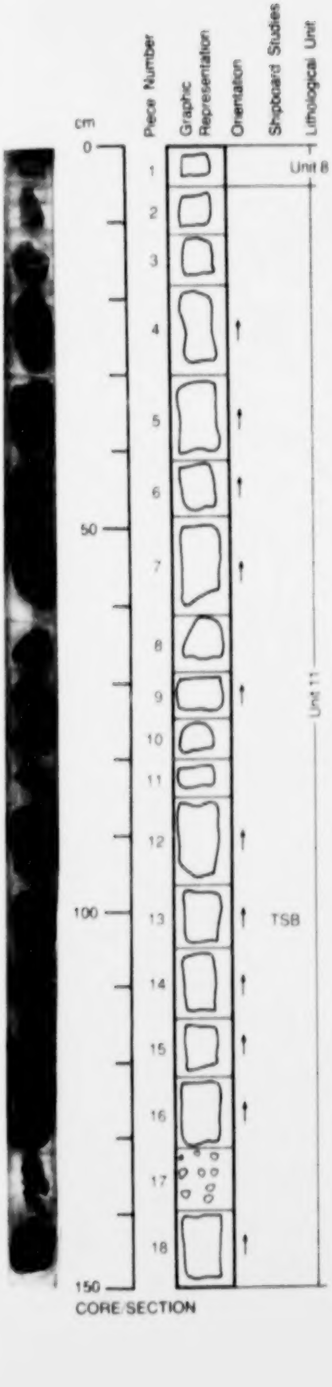
cm
Piece Number
Graphic Representation
Orientation
Shipboard Studies
Lithological Unit
0
50
100
150
1
2
3
4
5
6
7
8
9
10
11
12
13
14
15
16
17
18
Unit 8
Unit 11
TSB
CORE/SECTION

126-791B-64R-1

UNIT 8: DIABASE

Piece 1

CONTACTS: None
PHENOCRYSTS:
Plagioclase : 2%, 1-2 mm, fresh
GROUNDMASS: Flow aligned plagioclase, clinopyroxene, microvesicular glass
VESICLES: <1 mm
COLOR: Medium gray, N5
STRUCTURE: None
ALTERATION: Slight
VEINS/FRACTURES: Chlorite vein in one piece

UNIT 11: BASALT MOUSSE

Pieces 2-18

CONTACTS: None
PHENOCRYSTS:
Olivine : 2%, <1 mm, euhedral, equant, fresh
Plagioclase : <=5%, <1 mm, euhedral, elongate, fresh
GROUNDMASS: Microvesicular, devitrified glass
VESICLES: 50%, <0.2 mm, round, random, smectite lining plus occasional zeolite
COLOR: Gray, N5
STRUCTURE: None
ALTERATION: Slight
VEINS/FRACTURES: None
ADDITIONAL COMMENTS: Above description applies to the most common type of "clast" in a matrix which is very similar in composition. The matrix also has <1 mm olivine and plagioclase crystals, often in clots within a vesicular glass (30%, 0.1-0.5 mm) which is less devitried than the clasts, and less vesicular around crystal clots.

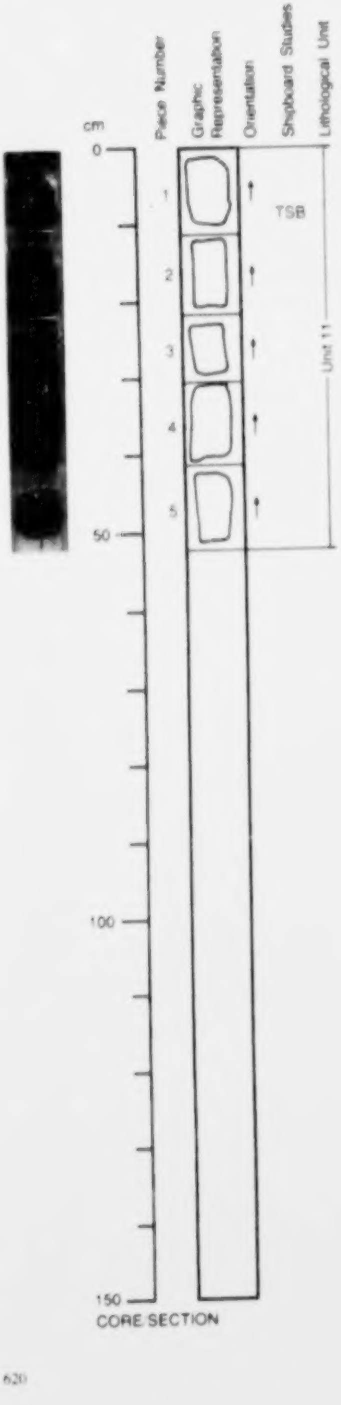
cm
0
50
100
150
Piece Number
Graphic Representation
Orientation
Shipboard Studies
Lithological Unit
1
2
3
4
5
TSB
Unit 11
CORE/SECTION

126-791B-64R-2

UNIT 11: BASALT MOUSSE

Pieces 1-5

CONTACTS: None
PHENOCRYSTS:
Olivine - 2%, <1 mm, euhedral, equant, fresh
Plagioclase - <=5%, <1 mm, euhedral, elongate, fresh
GROUNDMASS: Microvesicular, devitrified glass
VESICLES: 50%, <0.2 mm, round, random, smectite lining plus occasional zeolite
COLOR: Gray, N5
STRUCTURE: None
ALTERATION: Slight
VEINS/FRACTURES: None
ADDITIONAL COMMENTS: Above description applies to the most common type of "clast" in a matrix which is very similar in composition. The matrix also has <1 mm olivine and plagioclase crystals, often in clots, within a vesicular glass (30%, 0.1-0.5 mm) which is less devitrified than the clasts, and less vesicular around crystal clots.

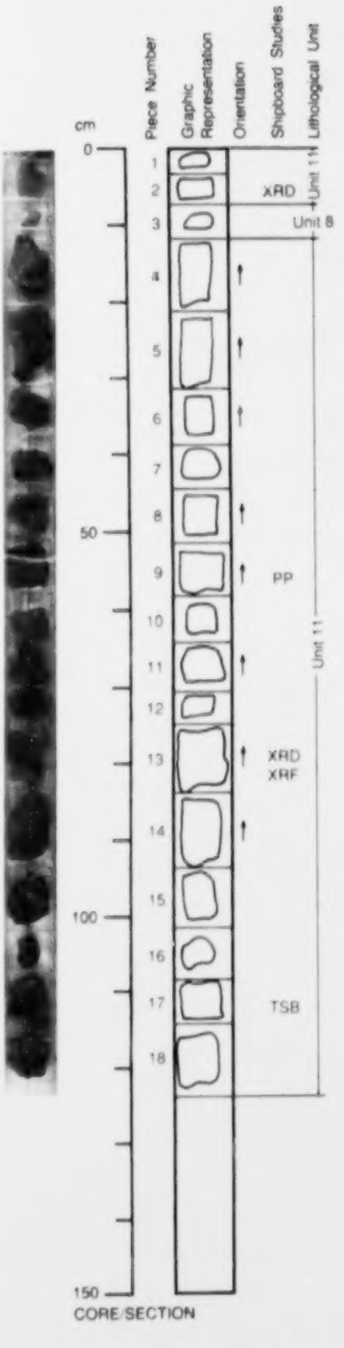
cm
Piece Number
Graphic Representation
Orientation
Shipboard Studies
Lithological Unit
0
50
100
150
1
2
3
4
5
6
7
8
9
10
11
12
13
14
15
16
17
18
XRD
PP
XRD
XRF
TSB
Unit 11
Unit 8
Unit 11
CORE/SECTION

126-791B-65R-1

UNIT 11: BASALT MOUSSE

Pieces 1-2 and 4-18

CONTACTS: None
PHENOCRYSTS:
Olivine - 2%; <1 mm; euhedral, equant, fresh.
Plagioclase - <=5%; <1 mm; euhedral, elongate, fresh.
GROUNDMASS: Microvesicular, devitrified glass.
VESICLES: 50%; <0.2 mm; round; random; smectite lining plus occasional zeolite.
COLOR: Gray, N5.
STRUCTURE: None.
ALTERATION: Slight.
VEINS/FRACTURES: None.
ADDITIONAL COMMENTS: Above description applies to the most common type of "clast" in a matrix which is very similar in composition. The matrix also has <1 mm olivine and plagioclase crystals, often in clots, within a vesicular glass (30%, 0.1-0.5 mm) which is less devitrified than the clasts, and less vesicular around crystal clots.

UNIT 8: DIABASE

Piece 3

CONTACTS: None.
PHENOCRYSTS:
Plagioclase - 2%; 1-2 mm, fresh.
GROUNDMASS: Flow-aligned plagioclase, clinopyroxene, microvesicular glass.
VESICLES: <1 mm.
COLOR: Medium gray, N5.
STRUCTURE: None.
ALTERATION: Slight.
VEINS/FRACTURES: Chlorite vein in one piece.

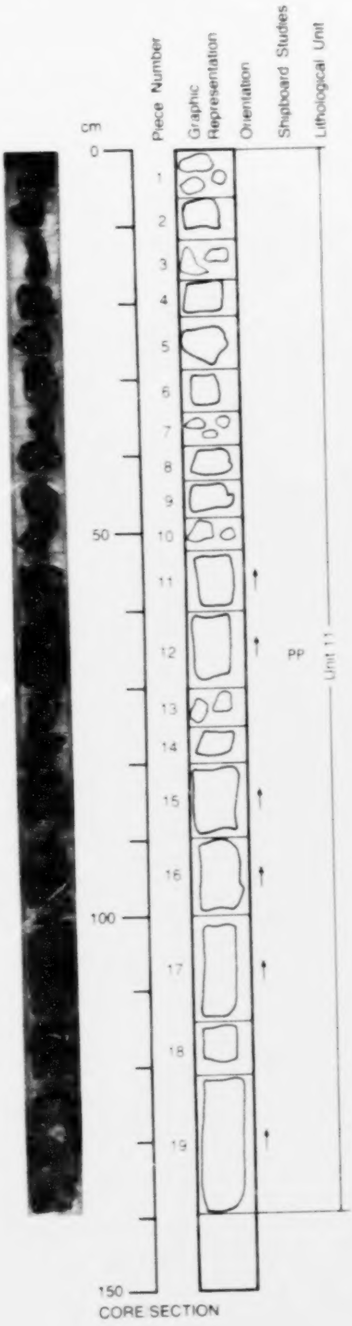
cm
Piece Number
Graphic Representation
Orientation
Shipboard Studies
Lithological Unit
0
50
100
150
1
2
3
4
5
6
7
8
9
10
11
12
13
14
15
16
17
18
19
PP
Unit 11
CORE SECTION

126-791B-66R-1

UNIT 11: BASALT MOUSSE

Pieces 1-19

CONTACTS: None
PHENOCRYSTS:
Olivine - 2%, <1 mm, euhedral, equant, fresh.
Plagioclase - <=5%, <1 mm, euhedral, elongate, fresh.
GROUNDMASS: Microvesicular, devitrified glass.
VESICLES: 50%, <0.2 mm, round, random, smectite lining plus occasional zeolite.
COLOR: Gray, N5.
STRUCTURE: None.
ALTERATION: Slight.
VEINS/FRACTURES: None.
ADDITIONAL COMMENTS: Above description applies to the most common type of "clast" in a matrix which is very similar in composition. The matrix also has <1 mm olivine and plagioclase crystals, often in clots, within a vesicular glass (30%, 0.1-0.5 mm) which is less devitried than the clasts, and less vesicular around crystal clots.

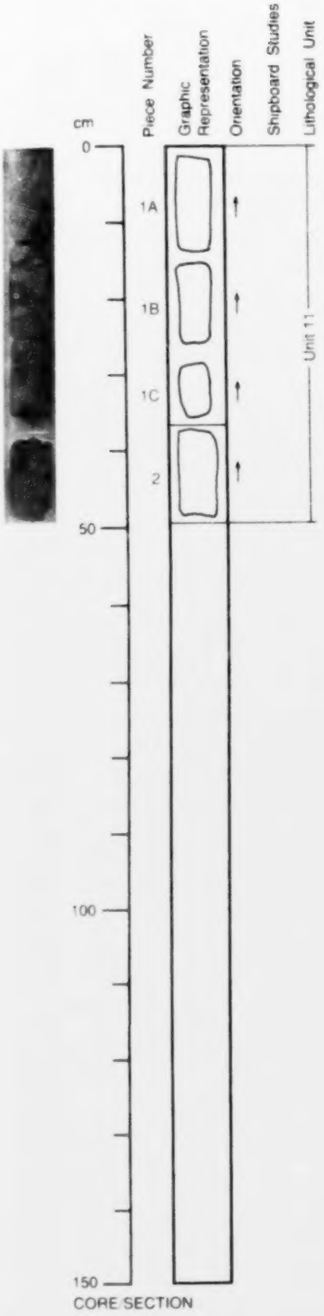
cm
Piece Number
Graphic Representation
Orientation
Shipboard Studies
Lithological Unit
0
1A
1B
1C
2
50
100
150
Unit 11
CORE/SECTION

126-791B-66R-2

UNIT 11: BASALT MOUSSE

Pieces 1-2

CONTACTS: None
PHENOCRYSTS:
  Olivine - 2%, <1 mm, euhedral, equant, fresh
  Plagioclase - <=5%, <1 mm, euhedral, elongate, fresh
GROUNDMASS: Microvesicular, devitrified glass
VESICLES: 50%, <0.2 mm, round, random, smectite lining plus occasional zeolite
COLOR: Gray, N5
STRUCTURE: None
ALTERATION: Slight
VEINS/FRACTURES: None
ADDITIONAL COMMENTS: Above description applies to the most common type of "clast" in a matrix which is very similar in composition. The matrix also has <1 mm olivine and plagioclase crystals, often in clots, within a vesicular glass (30%, 0.1-0.5 mm) which is less devitrified than the clasts, and less vesicular around crystal clots.

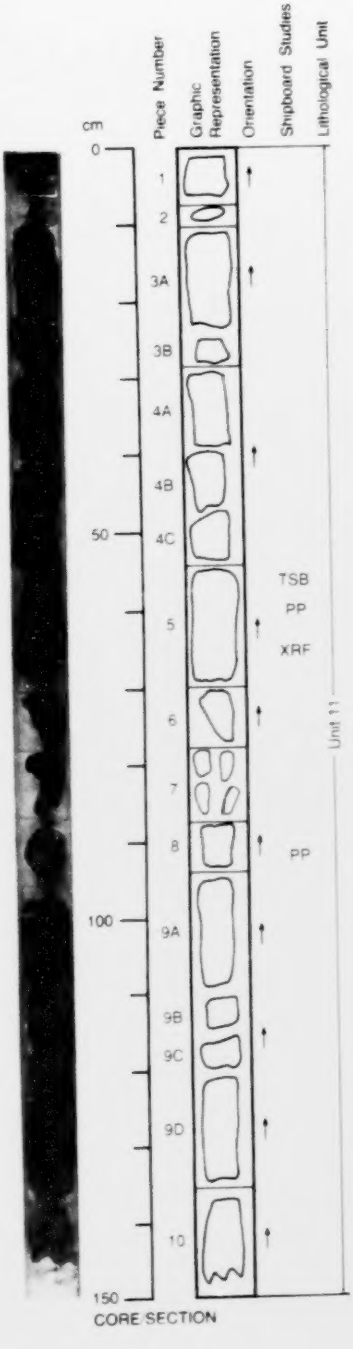
cm
Piece Number
Graphic Representation
Orientation
Shipboard Studies
Lithological Unit
0
50
100
150
1
2
3A
3B
4A
4B
4C
5
6
7
8
9A
9B
9C
9D
10
TSB
PP
XRF
PP
Unit 11
CORE/SECTION

126-791B-67R-1

UNIT 11: BASALT MOUSSE

Pieces 1-10

CONTACTS: None
PHENOCRYSTS:
Olivine - 2%, <1 mm, euhedral, equant, fresh
Plagioclase - <=5%, <1 mm, euhedral, elongate, fresh
GROUNDMASS: Microvesicular, devitrified glass
VESICLES: 50%, <0.2 mm, round, random, smectite lining plus occasional zeolite
COLOR: Gray, N5
STRUCTURE: None
ALTERATION: Slight
VEINS/FRACTURES: None
ADDITIONAL COMMENTS: Above description applies to the most common type of "clast" in a matrix which is very similar in composition. The matrix also has <1 mm olivine and plagioclase crystals, often in clots, within a vesicular glass (30%, 0.1-0.5 mm) which is less devitrified than the clasts, and less vesicular around crystal clots.

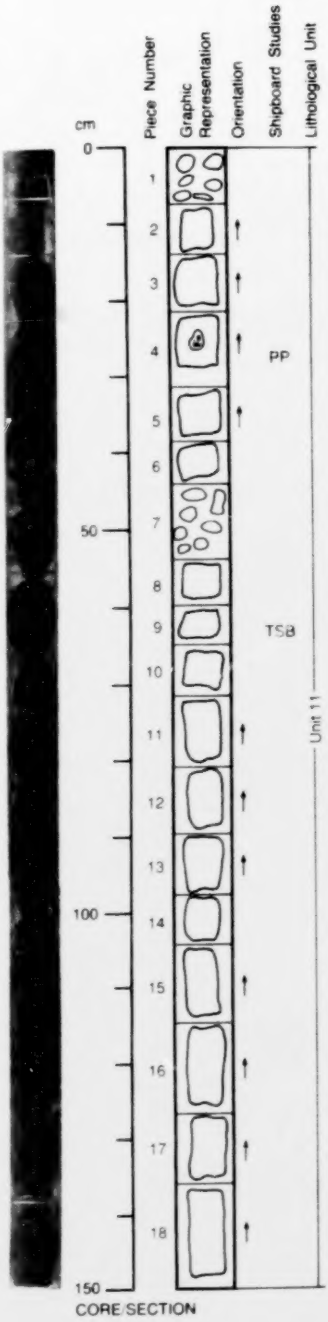
cm
Piece Number
Graphic Representation
Orientation
Shipboard Studies
Lithological Unit
0
50
100
150
1
2
3
4
5
6
7
8
9
10
11
12
13
14
15
16
17
18
PP
TSB
Unit 11
CORE/SECTION

126-791B-67R-2

UNIT 11: BASALT MOUSSE

Pieces 1-18

CONTACTS: None.
PHENOCRYSTS:
Olivine - 2%; <1 mm; euhedral, equant, fresh.
Plagioclase - <=5%; <1 mm; euhedral, elongate, fresh.
GROUNDMASS: Microvesicular, devitrified glass.
VESICLES: 50%; <0.2 mm; round; random; smectite lining plus occasional zeolite.
COLOR: Gray, N5.
STRUCTURE: None.
ALTERATION: Slight.
VEINS/FRACTURES: None.
ADDITIONAL COMMENTS: Above description applies to the most common type of "clast" in a matrix which is very similar in composition. The matrix also has <1 mm olivine and plagioclase crystals, often in clots, within a vesicular glass (30%, 0.1-0.5 mm) which is less devitried than the clasts, and less vesicular around crystal clots.

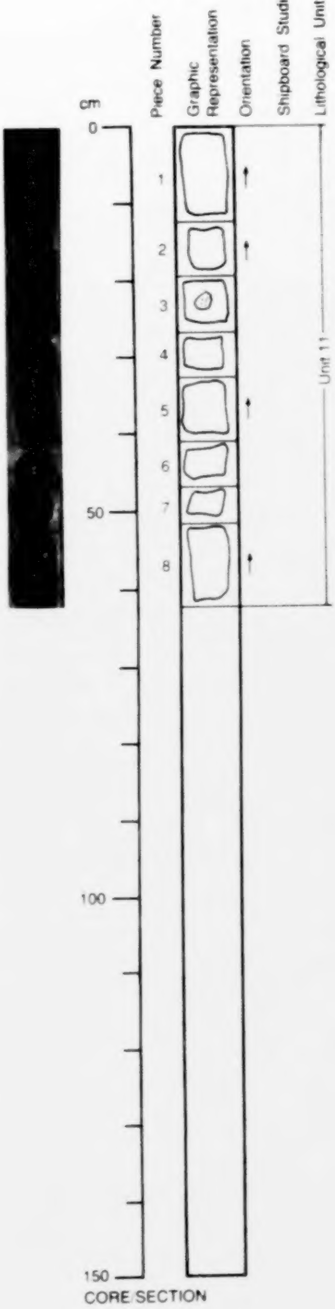
cm
Piece Number
Graphic Representation
Orientation
Shipboard Studies
Lithological Unit
0
50
100
150
1
2
3
4
5
6
7
8
Unit 11
CORE/SECTION

126-791B-67R-3

UNIT 11: BASALT MOUSSE

Pieces 1-8

CONTACTS: None.
PHENOCRYSTS:
Olivine - 2%, <1 mm, euhedral, equant, fresh.
Plagioclase - <=5%, <1 mm, euhedral, elongate, fresh.
GROUNDMASS: Microvesicular, devitrified glass.
VESICLES: 50%, <0.2 mm, round, random, smectite lining plus occasional zeolite.
COLOR: Gray, N5.
STRUCTURE: None.
ALTERATION: Slight.
VEINS/FRACTURES: None.
ADDITIONAL COMMENTS: Above description applies to the most common type of "clast" in a matrix which is very similar in composition. The matrix also has <1 mm olivine and plagioclase crystals, often in clots, within a vesicular glass (30%, 0.1-0.5 mm) which is less devitried than the clasts, and less vesicular around crystal clots.

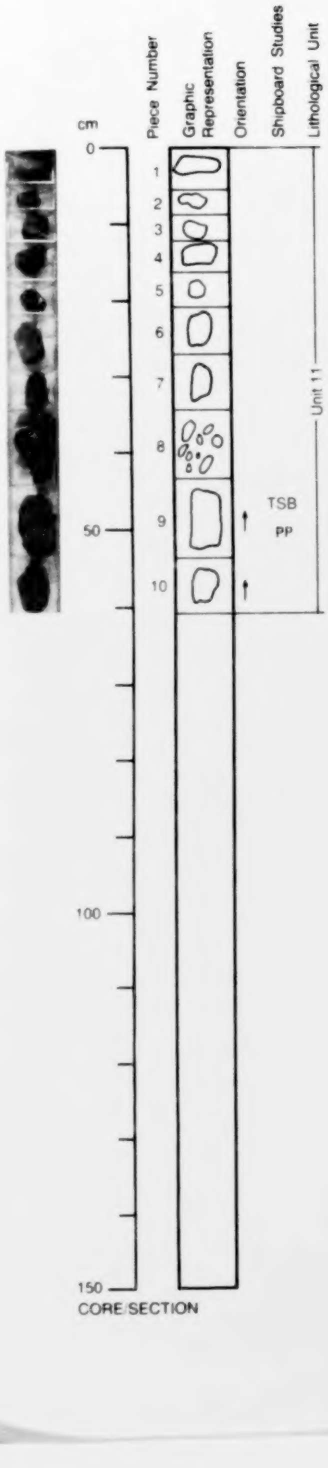
cm
Piece Number
Graphic Representation
Orientation
Shipboard Studies
Lithological Unit
0
50
100
150
1
2
3
4
5
6
7
8
9
10
TSB
PP
Unit 11
CORE/SECTION

126-791B-68R-1

UNIT 11: BASALT MOUSSE

Pieces 1-10

CONTACTS: None.
PHENOCRYSTS:
Olivine - 2%; <1 mm; euhedral, equant, fresh.
Plagioclase - <=5%; <1 mm; euhedral, elongate, fresh.
GROUNDMASS: Microvesicular, devitrified glass.
VESICLES: 50%; <0.2 mm; round; random; smectite lining plus occasional zeolite.
COLOR: Gray, N5.
STRUCTURE: None.
ALTERATION: Slight.
VEINS/FRACTURES: None.
ADDITIONAL COMMENTS: Above description applies to the most common type of "clast" in a matrix which is very similar in composition. The matrix also has <1 mm olivine and plagioclase crystals, often in clots, within a vesicular glass (30%, 0.1-0.5 mm) which is less devitried than the clasts, and less vesicular around crystal clots.

126-791B-69R-1

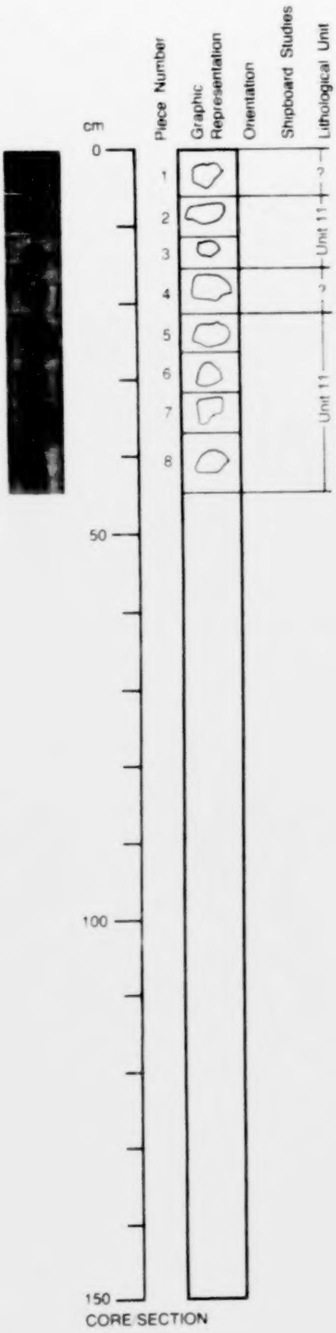
cm
Piece Number
Graphic Representation
Orientation
Shipboard Studies
Lithological Unit
0
50
100
150
1
2
3
4
5
6
7
8
?
Unit 11
?
Unit 11
CORE SECTION

UNIT 11: BASALT MOUSSE

Pieces 1-8

CONTACTS: None
PHENOCRYSTS:
Olivine - 2%, <1 mm, euhedral, equant, fresh
Plagioclase - <=5%, <1 mm, euhedral, elongate, fresh
GROUNDMASS: Microvesicular, devitrified glass
VESICLES: 50%, <0.2 mm, round, random, smectite lining plus occasional zeolite
COLOR: Gray, N5
STRUCTURE: None
ALTERATION: Slight
VEINS/FRACTURES: None
ADDITIONAL COMMENTS: Above description applies to the most common type of "clast" in a matrix which is very similar in composition. The matrix also has <1 mm olivine and plagioclase crystals, often in clots, within a vesicular glass (30%, 0.1-0.5 mm) which is less devitried than the clasts, and less vesicular around crystal clots.

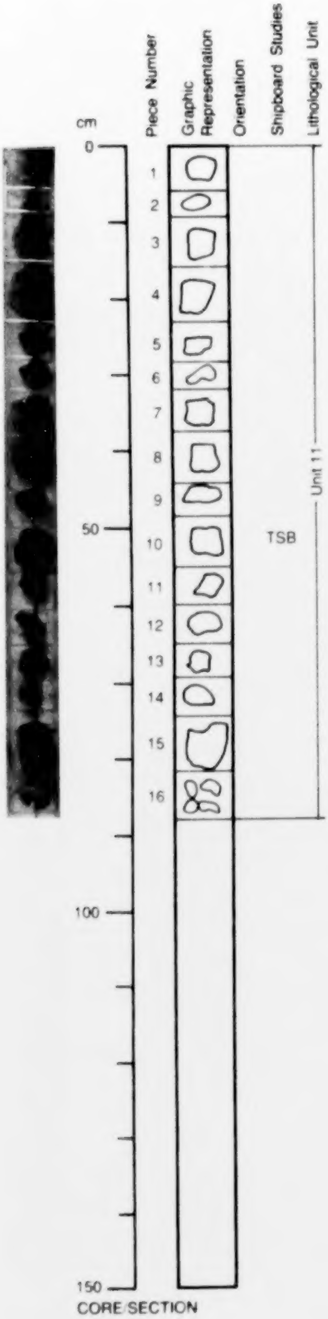
cm
Piece Number
Graphic Representation
Orientation
Shipboard Studies
Lithological Unit
0
50
100
150
1
2
3
4
5
6
7
8
9
10
11
12
13
14
15
16
TSB
Unit 11
CORE/SECTION

126-791B-70R-1

UNIT 11: BASALT MOUSSE

Pieces 1-16

CONTACTS: None.
PHENOCRYSTS:
Olivine - 2%; <1 mm; euhedral, equant, fresh.
Plagioclase - <=5%; <1 mm; euhedral, elongate, fresh.
GROUNDMASS: Microvesicular, devitrified glass.
VESICLES: 50%; <0.2 mm; round; random; smectite lining plus occasional zeolite.
COLOR: Gray, N5.
STRUCTURE: None.
ALTERATION: Slight.
VEINS/FRACTURES: None.
ADDITIONAL COMMENTS: Above description applies to the most common type of "clast" in a matrix which is very similar in composition. The matrix also has <1 mm olivine and plagioclase crystals, often in clots, within a vesicular glass (30%, 0.1-0.5 mm) which is less devitried than the clasts, and less vesicular around crystal clots.

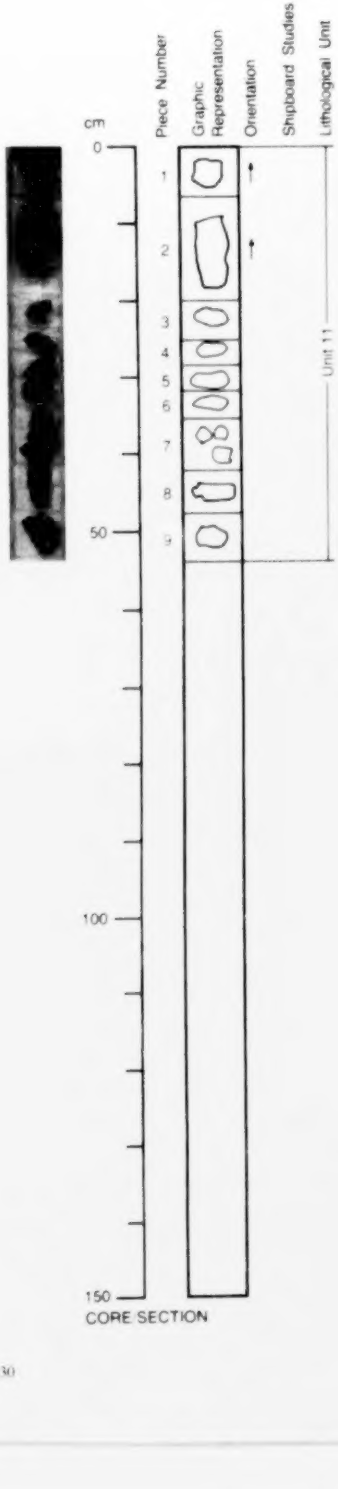
cm
Piece Number
Graphic Representation
Orientation
Shipboard Studies
Lithological Unit
0
50
100
150
1
2
3
4
5
6
7
8
9
Unit 11
CORE/SECTION

126-791B-71R-1

UNIT 11: BASALT MOUSSE

Pieces 1-9

CONTACTS: None
PHENOCRYSTS:
Olivine - 2%, <1 mm, euhedral, equant, fresh
Plagioclase - <=5%, <1 mm, euhedral, elongate, fresh
GROUNDMASS: Microvesicular, devitrified glass
VESICLES: 50%, <0.2 mm, round, random, smectite lining plus occasional zeolite
COLOR: Gray, N5
STRUCTURE: None
ALTERATION: Slight
VEINS/FRACTURES: None
ADDITIONAL COMMENTS: Above description applies to the most common type of "clast" in a matrix which is very similar in composition. The matrix also has <1 mm olivine and plagioclase crystals, often in clots, within a vesicular glass (30%, 0.1-0.5 mm) which is less devitrified than the clasts, and less vesicular around crystal clots.

126-791B-72R-1

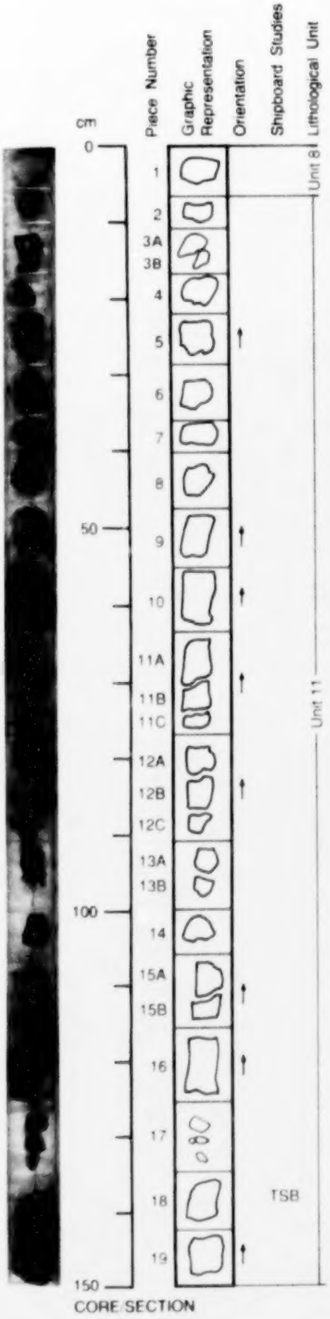
cm
Piece Number
Graphic Representation
Orientation
Shipboard Studies
Lithological Unit
0
50
100
150
1
2
3A
3B
4
5
6
7
8
9
10
11A
11B
11C
12A
12B
12C
13A
13B
14
15A
15B
16
17
18
19
Unit 8
Unit 11
TSB
CORE/SECTION

UNIT 8: DIABASE

Piece 1

CONTACTS: None.
PHENOCRYSTS:
Plagioclase - 2%, 1-2 mm, fresh.
GROUNDMASS: Flow-aligned plagioclase, clinopyroxene, microvesicular glass.
VESICLES: <1 mm.
COLOR: Medium gray, N5.
STRUCTURE: None.
ALTERATION: Slight.
VEINS/FRACTURES: Chlorite vein in one piece.

UNIT 11: BASALT

Pieces 2-19

CONTACTS: None.
PHENOCRYSTS: Olivine altering to smectite in cracks.
Olivine - 2%, <1 mm, euhedral, equant.
Plagioclase - <5%, <1 mm, euhedral, elongate, fresh.
GROUNDMASS: Microvesicular, more devitrified than higher in Unit 11.
VESICLES: 50%, <0.2 mm, round, random, increasing smectite and zeolite.
COLOR: Gray, N5.
STRUCTURE: None.
ALTERATION: As noted above.
VEINS/FRACTURES: None.
ADDITIONAL COMMENTS: Above description applies to the most common type of "clast" in a matrix which is very similar in composition. The matrix also has <1 mm olivine and plagioclase crystals, often in clots, within vesicular (30%, 0.1-0.5 mm) glass which is less devitrified than the clasts, and less vesicular around crystal clots.

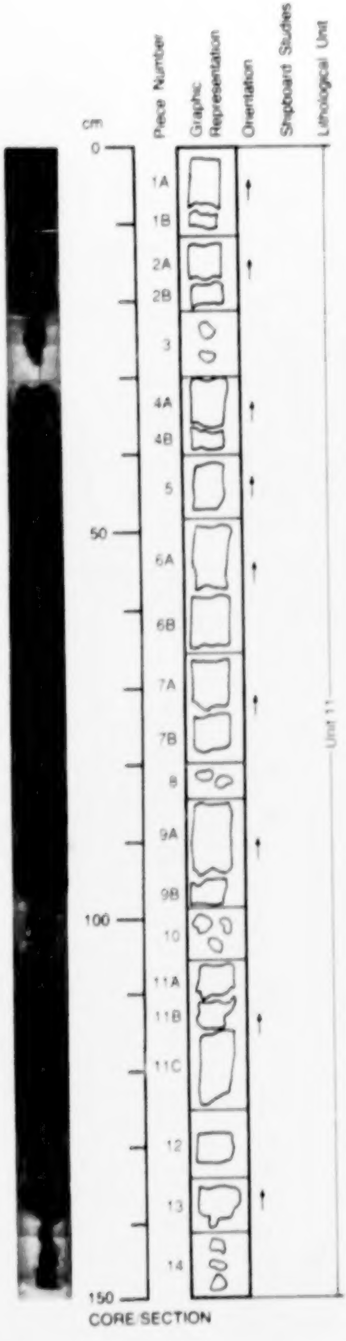
cm
Piece Number
Graphic Representation
Orientation
Shipboard Studies
Lithological Unit
0
50
100
150
1A
1B
2A
2B
3
4A
4B
5
6A
6B
7A
7B
8
9A
9B
10
11A
11B
11C
12
13
14
Unit 11
CORE/SECTION

126-791B-72R-2

UNIT 11: BASALT MOUSSE

Pieces 1-14

CONTACTS: None
PHENOCRYSTS: Olivine altering to smectite in cracks.
Olivine - 2%; <1 mm; euhedral; equant.
Plagioclase - <5%; <1 mm; euhedral; elongate; fresh.
GROUNDMASS: Microvesicular, more devitrified than higher in Unit 11.
VESICLES: 50%; <0.2 mm; round; random; increasing smectite and zeolite.
COLOR: Gray, N5.
STRUCTURE: None.
ALTERATION: As noted above.
VEINS/FRACTURES: None.
ADDITIONAL COMMENTS: Above description applies to the most common type of "clast" in a matrix which is very similar in composition. The matrix also has <1 mm olivine and plagioclase crystals, often in clots, within vesicular (30%, 0.1-0.5 mm) glass which is less devitrified than the clasts, and less vesicular around crystal clots.

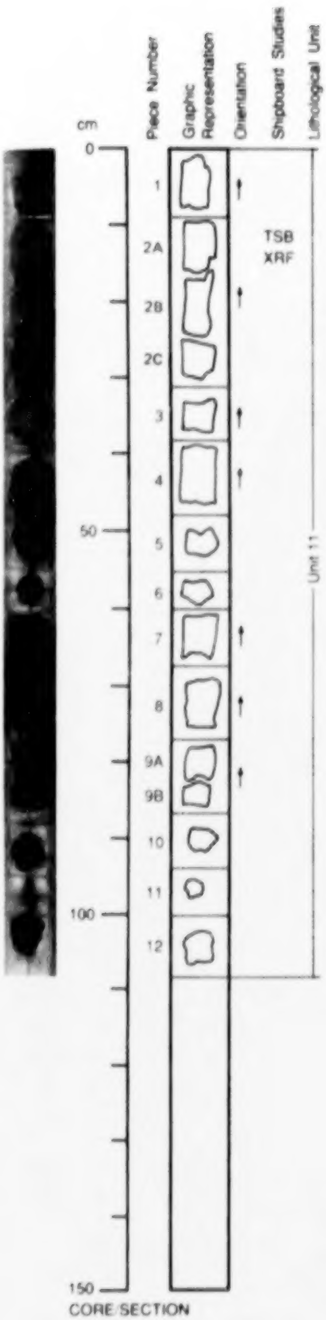
cm
Piece Number
Graphic Representation
Orientation
Shipboard Studies
Lithological Unit
0
50
100
150
1
2A
2B
2C
3
4
5
6
7
8
9A
9B
10
11
12
TSB
XRF
Unit 11
CORE/SECTION

126-791B-72R-3

UNIT 11: BASALT MOUSSE

Pieces 1-12

CONTACTS: None
PHENOCRYSTS: Olivine altering to smectite in cracks
    Olivine - 2%, <1 mm, euhedral, equant
    Plagioclase - <5%, <1 mm, euhedral, elongate, fresh
GROUNDMASS: Microvesicular, more devitrified than higher in Unit 11
VESICLES: 50%, <0.2 mm, round, random, increasing smectite and zeolite
COLOR: Gray, N5
STRUCTURE: None
ALTERATION: As noted above
VEINS/FRACTURES: None
ADDITIONAL COMMENTS: Above description applies to the most common type of "clast" in a matrix which is very similar in composition. The matrix also has <1 mm olivine and plagioclase crystals, often in clots, within vesicular (30%, 0.1-0.5 mm) glass which is less devitrified than the clasts, and less vesicular around crystal clots.

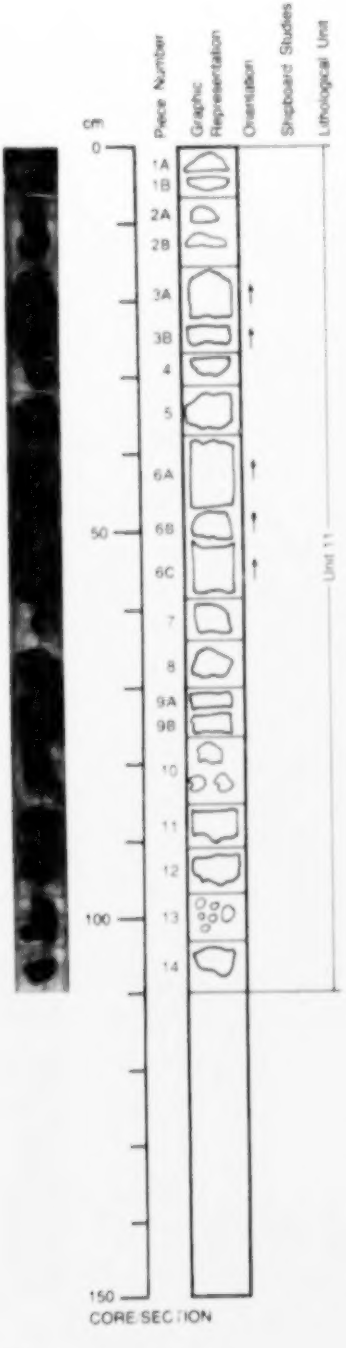
cm
Piece Number
Graphic Representation
Orientation
Shipboard Studies
Lithological Unit
0
1A
1B
2A
2B
3A
3B
4
5
6A
6B
6C
7
8
9A
9B
10
11
12
13
14
50
100
150
Unit 11
CORE/SECTION

126-791B-73R-1

UNIT 11: BASALT MOUSSE

Pieces 1-14

CONTACTS: None.
PHENOCRYSTS: Olivine altering to smectite in cracks.
  Olivine - 2%; <1 mm; euhedral; equant.
  Plagioclase - <5%; <1 mm; euhedral; elongate; fresh.
GROUNDMASS: Microvesicular; more devitrified than higher in Unit 11.
VESICLES: 50%; <0.2 mm; round; random; increasing smectite and zeolite.
COLOR: Gray, N5.
STRUCTURE: None.
ALTERATION: As noted above.
VEINS/FRACTURES: None.
ADDITIONAL COMMENTS: Above description applies to the most common type of "clast" in a matrix which is very similar in composition. The matrix also has <1 mm olivine and plagioclase crystals, often in clots, within vesicular (30%, 0.1-0.5 mm) glass which is less devitrified than the clasts, and less vesicular around crystal clots.

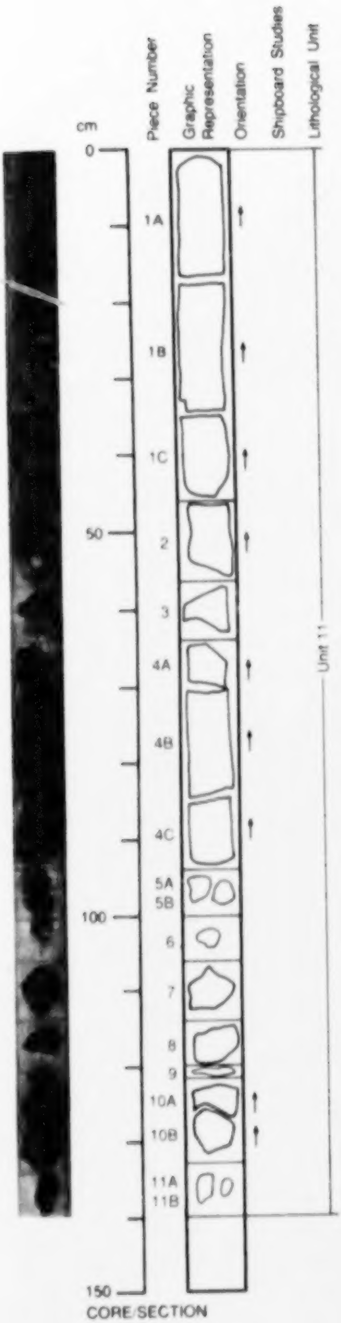
cm
Piece Number
Graphic Representation
Orientation
Shipboard Studies
Lithological Unit
0
50
100
150
1A
1B
1C
2
3
4A
4B
4C
5A
5B
6
7
8
9
10A
10B
11A
11B
Unit 11
CORE/SECTION

126-791B-73R-2

UNIT 11: BASALT MOUSSE

Pieces 1-11

CONTACTS: None
PHENOCRYSTS: Olivine altering to smectite in cracks.
    Olivine - 2%; <1 mm; euhedral, equant.
    Plagioclase - <5%; <1 mm; euhedral, elongate, fresh.
GROUNDMASS: Microvesicular, more devitrified than higher in Unit 11.
VESICLES: 50%; <0.2 mm; round; random; increasing smectite and zeolite.
COLOR: Gray, N5.
STRUCTURE: None.
ALTERATION: As noted above.
VEINS/FRACTURES: None.
ADDITIONAL COMMENTS: Above description applies to the most common type of "clast" in a matrix which is very similar in composition. The matrix also has <1 mm olivine and plagioclase crystals, often in clots, within vesicular (30%, 0.1-0.5 mm) glass which is less devitrified than the clasts, and less vesicular around crystal clots.

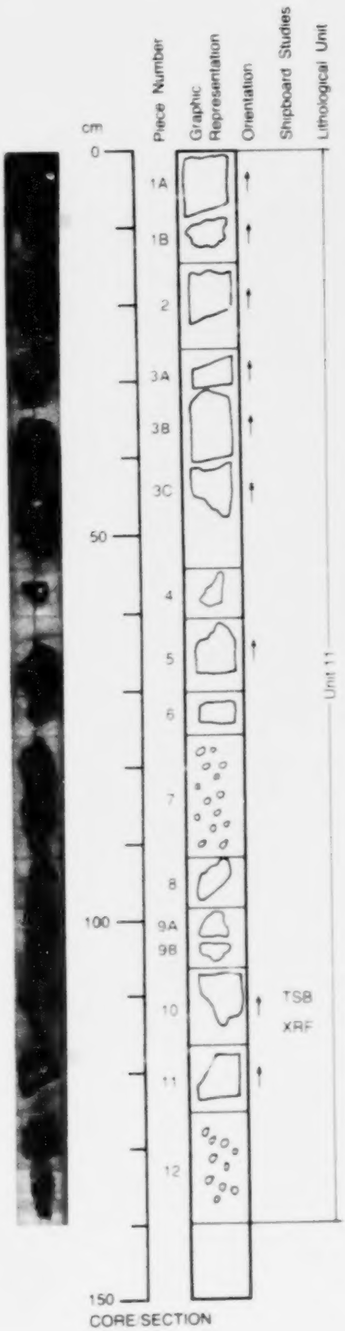
cm
Piece Number
Graphic Representation
Orientation
Shipboard Studies
Lithological Unit
0
50
100
150
1A
1B
2
3A
3B
3C
4
5
6
7
8
9A
9B
10
11
12
TSB
XRF
Unit 11
CORE/SECTION

126-791B-73R-3

UNIT 11: BASALT MOUSSE

Pieces 1-12

CONTACTS: None.
PHENOCRYSTS: Olivine altering to smectite in cracks.
Olivine - 2%, <1 mm, euhedral, equant.
Plagioclase - <5%, <1 mm, euhedral, elongate, fresh.
GROUNDMASS: Microvesicular, more devitrified than higher in Unit 11.
VESICLES: 50%, <0.2 mm, round, random, increasing smectite and zeolite.
COLOR: Gray, N5.
STRUCTURE: None.
ALTERATION: As noted above.
VEINS/FRACTURES: None.
ADDITIONAL COMMENTS: Above description applies to the most common type of "clast" in a matrix which is very similar in composition. The matrix also has <1 mm olivine and plagioclase crystals, often in clots, within vesicular (30%, 0.1-0.5 mm) glass which is less devitrified than the clasts, and less vesicular around crystal clots.

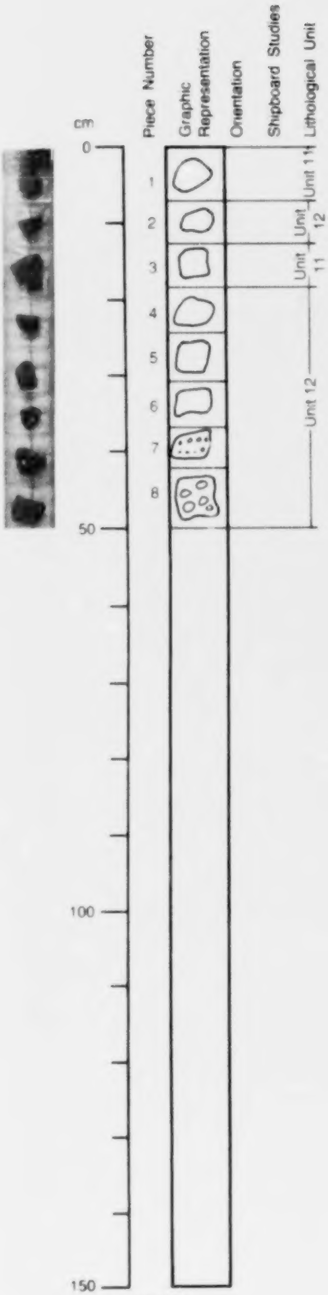
cm
Piece Number
Graphic Representation
Orientation
Shipboard Studies
Lithological Unit
0
50
100
150
1
2
3
4
5
6
7
8
Unit 11
Unit 12
Unit 11
Unit 12
CORE/SECTION

126-791B-74R-1

UNIT 11: BASALT MOUSSE

Pieces 1, 3

CONTACTS: None
PHENOCRYSTS: Olivine altering to smectite in cracks.
Olivine - 2%, <1 mm, euhedral, equant.
Plagioclase - <5%, <1 mm, euhedral, elongate, fresh.
GROUNDMASS: Microvesicular, more devitrified than higher in Unit 11.
VESICLES: 50%, <0.2 mm, round, random, increasing smectite and zeolite.
COLOR: Gray, N5.
STRUCTURE: None.
ALTERATION: As noted above.
VEINS/FRACTURES: None.
ADDITIONAL COMMENTS: Above description applies to the most common type of "clast" in a matrix which is very similar in composition. The matrix also has <1 mm olivine and plagioclase crystals, often in clots, within vesicular (30%, 0.1-0.5 mm) glass which is less devitrified than the clasts, and less vesicular around crystal clots.

UNIT 12: BASALT CLASTS

Pieces 2 and 4-8

CONTACTS: None.
PHENOCRYSTS:
Plagioclase - 10%, <1.5 mm, euhedral, elongate, fresh.
GROUNDMASS: Intersertal, clinopyroxene + plagioclase + devitrified glass, microvesicular.
VESICLES: 10%, <1 mm, round, random, smectite, zeolite fillings.
COLOR: Gray, N5.
STRUCTURE: None.
ALTERATION: As above.
VEINS/FRACTURES: None.
ADDITIONAL COMMENTS: Mostly clasts with thin, partial coatings of greenish matrix such as the Unit 11 mousse.

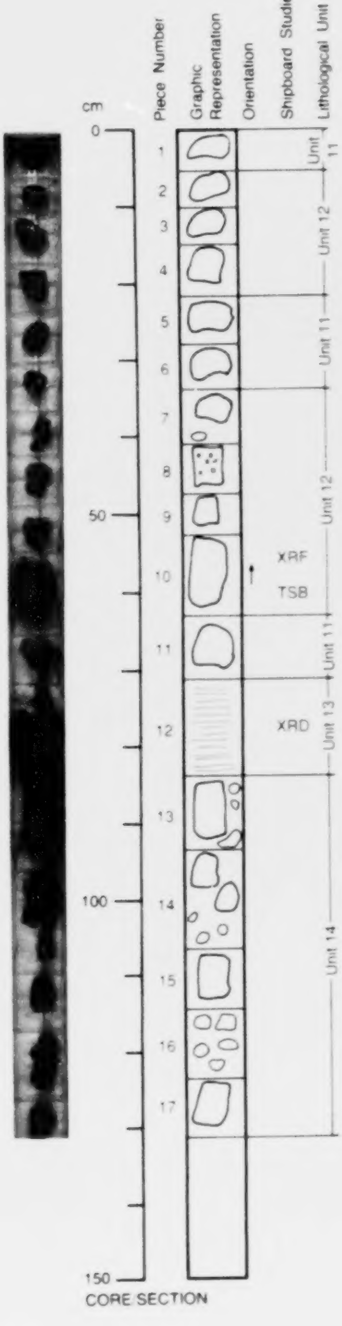
cm
Piece Number
Graphic Representation
Orientation
Shipboard Studies
Lithological Unit
0
50
100
150
1
2
3
4
5
6
7
8
9
10
11
12
13
14
15
16
17
Unit 11
Unit 12
Unit 11
Unit 12
Unit 11
Unit 13
Unit 14
XRF
TSB
XRD
CORE SECTION

126-791B-75R-1

UNIT 11: BASALT MOUSSE

Pieces 1, 5, 6, 11

CONTACTS: None
PHENOCRYSTS: Olivine altering to smectite in cracks
Olivine: 2%, <1 mm, euhedral, equant
Plagioclase: <5%, <1 mm, euhedral, elongate, fresh
GROUNDMASS: Microvesicular, more devitrified than higher in Unit 11
VESICLES: 50%, <0.2 mm; round, random; increasing smectite and zeolite
COLOR: Gray, N5
STRUCTURE: None
ALTERATION: As noted above
VEINS/FRACTURES: None
ADDITIONAL COMMENTS: Above description applies to the most common type of "clast" in a matrix which is very similar in composition. The matrix also has <1 mm olivine and plagioclase crystals, often in clots, within vesicular (30%, 0.1-0.5 mm) glass which is less devitrified than the clasts, and less vesicular around crystal clots.

UNIT 12: BASALT CLASTS

Pieces 2-4 and 7-10

CONTACTS: None
PHENOCRYSTS:
GROUNDMASS: Intersertal, clinopyroxene + plagioclase + devitrified glass, microvesicular
VESICLES: 10%, <1 mm, round, random, smectite, zeolite fillings
COLOR: Gray, N5
STRUCTURE: None
ALTERATION: As above
VEINS/FRACTURES: None
ADDITIONAL COMMENTS: Mostly clasts with thin, partial coatings of greenish matrix such as the Unit 11 mousse.

UNIT 14: BASALT MOUSSE

Pieces 13-17

CONTACTS: None
PHENOCRYSTS:
Olivine: 1.5%, <5 mm, pseudomorphed by smectite and iron oxide
Plagioclase: 1.5%, <5 mm, fresh
GROUNDMASS: Microvesicular, devitrified iron-stained glass (60%)
VESICLES: 10%, <0.2 mm, round, random, smectite, zeolite fillings
COLOR: Green-gray
STRUCTURE: None
ALTERATION: More than in Unit 11
VEINS/FRACTURES: None
ADDITIONAL COMMENTS: Above description applies to "clasts" in a matrix which is very similar in composition. The matrix also has <5 mm altered olivine and fresh plagioclase crystals, often in clots, within vesicular (30%, <0.1 mm, slightly flattened) glass.

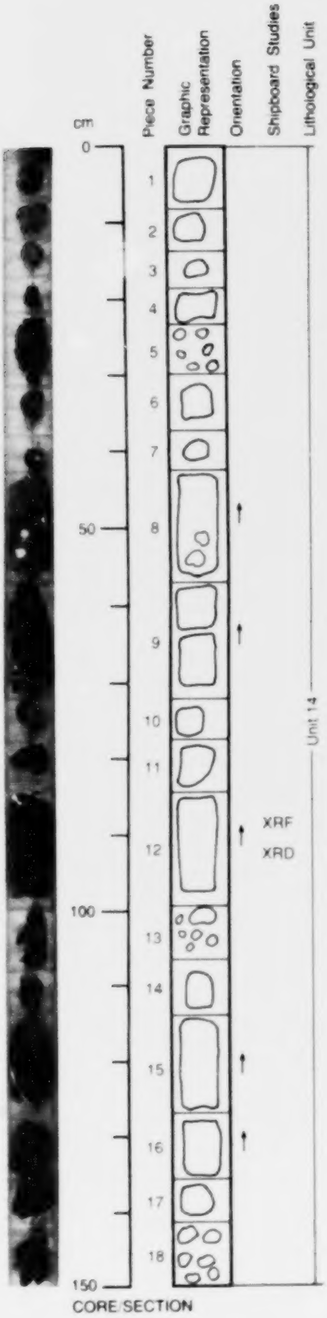
cm
Piece Number
Graphic Representation
Orientation
Shipboard Studies
Lithological Unit
0
50
100
150
1
2
3
4
5
6
7
8
9
10
11
12
13
14
15
16
17
18
XRF
XRD
Unit 14
CORE/SECTION

126-791B-76R-1

UNIT 14: BASALT MOUSSE

Pieces 1-18

CONTACTS: None
PHENOCRYSTS:
  Olivine - 1-5%, <5 mm, pseudomorphed by smectite and iron oxide
  Plagioclase - 1-5%, <5 mm, fresh
GROUNDMASS: Microvesicular, devitrified iron-stained glass (60%)
VESICLES: 10%, <0.2 mm, round, random, smectite, zeolite fillings
COLOR: Green-gray
STRUCTURE: None
ALTERATION: More than in Unit 11
VEINS/FRACTURES: None
ADDITIONAL COMMENTS: Above description applies to "clasts" in a matrix which is very similar in composition. The matrix also has <5 mm altered olivine and fresh plagioclase crystals, often in clots, within vesicular (30%, <0.1 mm, slightly flattened) glass.

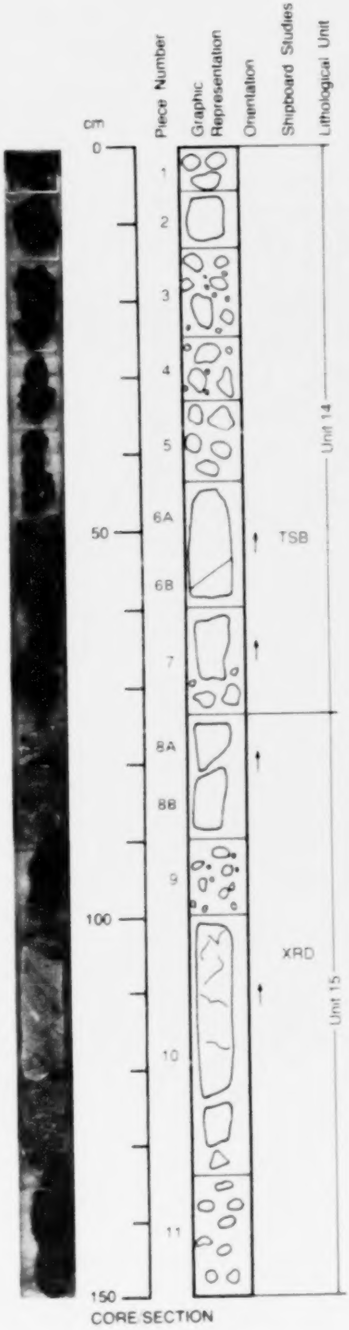
cm
Piece Number
Graphic Representation
Orientation
Shipboard Studies
Lithological Unit
0
50
100
150
1
2
3
4
5
6A
6B
7
8A
8B
9
10
11
TSB
XRD
Unit 14
Unit 15
CORE SECTION

126-791B-76R-2

UNIT 14: BASALT MOUSSE

Pieces 1-7

CONTACTS: None
PHENOCRYSTS:
Olivine - 1-5%, <5 mm, pseudomorphed by smectite and iron-oxide
Plagioclase - 1-5%, <5 mm, fresh
GROUNDMASS: Microvesicular, devitrified iron stained glass (60%)
VESICLES: 10%, <0.2 mm, round, random, smectite, zeolite fillings
COLOR: Green-gray
STRUCTURE: None
ALTERATION: More than in Unit 11
VEINS/FRACTURES: None
ADDITIONAL COMMENTS: Above description applies to "clasts" in a matrix which is very similar in composition. The matrix also has <5 mm altered olivine and fresh plagioclase crystals, often in clots, within vesicular (30%, <0.1 mm, slightly flattened) glass.

UNIT 15: DIABASE

Pieces 8-11

PHENOCRYSTS:
Plagioclase - 40%, <0.5 mm
Olivine - 2%, 0.5 mm, altered to smectite, oxide
Clinopyroxene - 30%, <0.1 mm
FeTi oxide - 30%, 0.1 mm
GROUNDMASS: Devitrified glass
VESICLES: None
COLOR: Gray
ALTERATION: As above
VEINS/FRACTURES: 0.25%, 0.5 - 2 cm, subvertical gypsum veins in Pieces 8 and 10

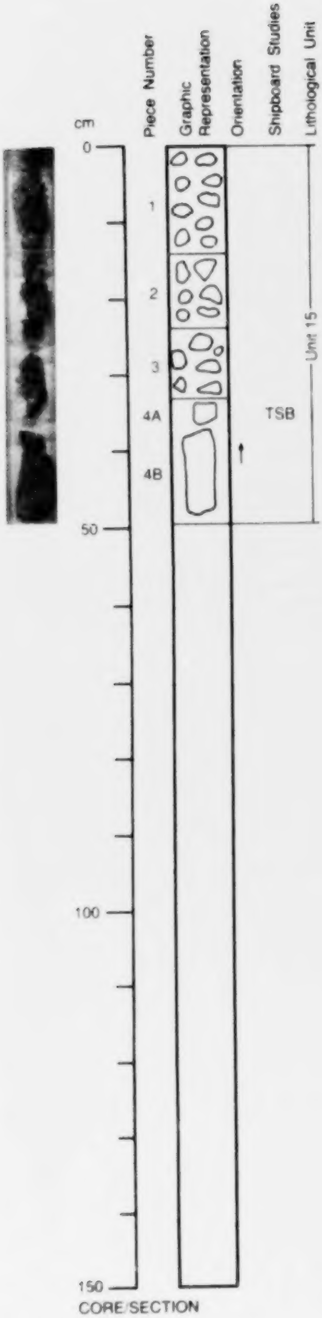
cm
Piece Number
Graphic Representation
Orientation
Shipboard Studies
Lithological Unit
0
1
2
3
4A
4B
TSB
Unit 15
50
100
150
CORE/SECTION

126-791B-76R-3

UNIT 15: DIABASE

Pieces 1-4

CONTACTS: None
PHENOCRYSTS:
- Plagioclase - 40%; <0.5 mm
- Clinopyroxene - 30%; <1.0 mm
- FeTi oxide - 30%; 0.1 mm
- Olivine - 2%; 0.5 mm; altered to smectite, oxide

GROUNDMASS: Devitrified glass
VESICLES: None
COLOR: Gray
STRUCTURE: None

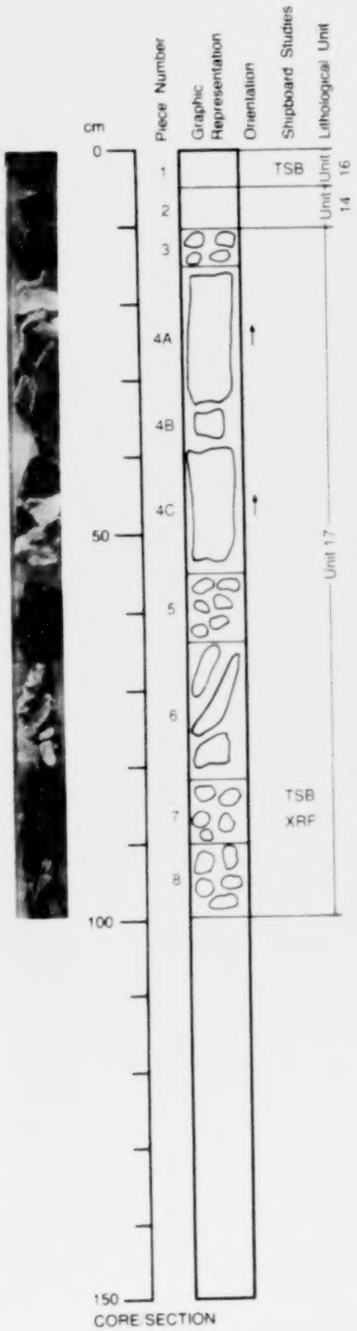
cm
0
50
100
150
Piece Number
Graphic Representation
Orientation
Shipboard Studies
Lithological Unit
1
2
3
4A
4B
4C
5
6
7
8
TSB
TSB
XRF
Unit 16
Unit 14
Unit 17
CORE SECTION

126-791B-77R-1

UNIT 16: CRYSTAL-LITHIC ASH TUFF

Piece 1

CONTACTS: None
PHENOCRYSTS:
Plagioclase - 5%, 0.1-0.2 mm, some sericitization
GROUNDMASS: Fine-grained
VESICLES: None
COLOR: Overall mottled dark greenish gray
STRUCTURE: None
ALTERATION: Chlorite, hematite, calcite
VEINS/FRACTURES: None
ADDITIONAL COMMENTS: Unwelded, undeformed pumice and lithic (10%, 0.2-0.5 mm) fragments.

UNIT 14: BASALT MOUSSE

Piece 2

CONTACTS: None
PHENOCRYSTS:
Olivine - 1-5%, <5 mm, pseudomorphed by smectite and iron-oxide
Plagioclase - 1-5%, <5 mm, fresh
GROUNDMASS: Microvesicular, devitrified iron-stained glass (60%)
VESICLES: 10%, <0.2 mm, round, random, smectite, zeolite fillings
COLOR: Green gray
STRUCTURE: None
ALTERATION: More than in Unit 11
VEINS/FRACTURES: None
ADDITIONAL COMMENTS: Above description applies to "clasts" in a matrix which is very similar in composition. The matrix also has <5 mm altered olivine and fresh plagioclase crystals, often in clots, within vesicular (30%, <0.1 mm, slightly flattened) glass.

UNIT 17: DIABASE

Pieces 3-8

CONTACTS: None
PHENOCRYSTS:
Plagioclase - 60%, 0.2-1.0 mm, subhedral
Clinopyroxene - 10%, 0.5-1.0 mm, anhedral
Olivine - 2%, <0.5 mm, altered to smectite, chlorite
GROUNDMASS: None
VESICLES: None
COLOR: Olive black
STRUCTURE: Slickensides in Piece 5
ALTERATION: Glass altered to chlorite and smectite
VEINS/FRACTURES: None

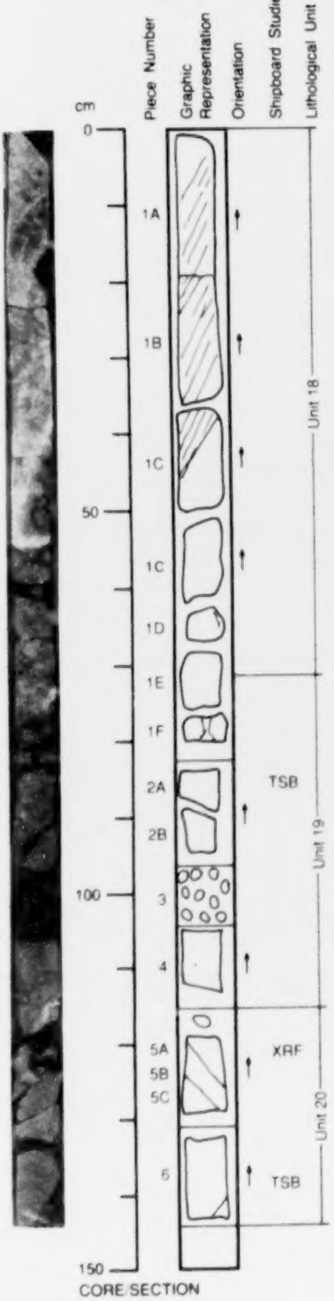
cm
Piece Number
Graphic Representation
Orientation
Shipboard Studies
Lithological Unit
0
50
100
150
1A
1B
1C
1C
1D
1E
1F
2A
2B
3
4
5A
5B
5C
6
TSB
XRF
TSB
Unit 18
Unit 19
Unit 20
CORE/SECTION

126-791B-77R-2

UNIT 18: GYPSUM-MINERALIZED FRACTURE BRECCIA IN LAPILLI TUFF

Pieces 1A-1E

CONTACTS: Sharp, depositional with Unit 19
PHENOCRYSTS: None
GROUNDMASS: Fine-grained.
VESICLES: None
COLOR: Purple, gray, green clasts
STRUCTURE: Complex
ALTERATION: Extensive
VEINS/FRACTURES: 3 sets of fracture-filling events, at about 45 degrees to core axis; gypsum in veins
ADDITIONAL COMMENTS: Breccia clasts (1-4 cm) are crystal-lithic and welded lithic-vitric lapilli tuffs.

UNIT 19: CRYSTAL-LITHIC LAPILLI TUFF

Pieces 1E-4

CONTACTS: Separated from Unit 18 by pale fine ash, 3 mm thick
PHENOCRYSTS: None
GROUNDMASS: Fine-grained
VESICLES: None
COLOR: Green and gray
STRUCTURE: Crudely layered, fining upward
ALTERATION: 50% chlorite, smectite, calcite
VEINS/FRACTURES: Possible cleavage fabric at high angle to bedding
ADDITIONAL COMMENTS: Welded tuff with eutaxitic textures. Clasts: 50% vitric fragments of flattened pumice, 40% equant lithic (andesite-dacite?) clasts, 5% Fe-Ti oxides, 3% calcite after mafic minerals(?), 2% recrystallized quartz. Clasts are 2-10 mm and well-sorted.

UNIT 20: CRYSTAL-LITHIC ASH TUFF

Pieces 5-6

CONTACTS: None
PHENOCRYSTS: None
GROUNDMASS: Fine
VESICLES: None
COLOR: Pale green, 10G 8/2
STRUCTURE: Bedded
ALTERATION: Chlorite, calcite, quartz
VEINS/FRACTURES: Incipient cleavage in chlorite at 45 degrees to bedding
ADDITIONAL COMMENTS: Fining upward bedding. Welded eutaxitic textures. 70-80% pumice/glass shards altered to 6:1 chlorite-calcite assemblage. Lithics and crystals 10-20% each.

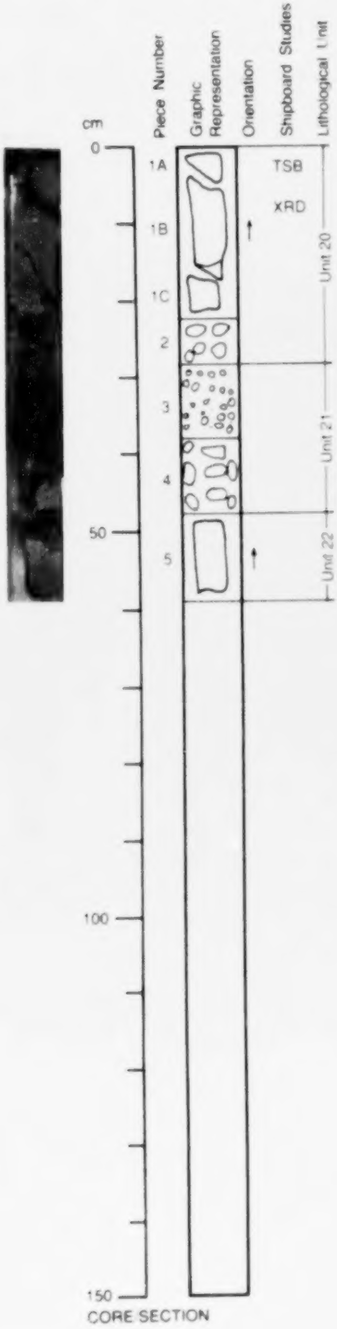
cm
Piece Number
Graphic Representation
Orientation
Shipboard Studies
Lithological Unit
0
50
100
150
1A
1B
1C
2
3
4
5
TSB
XRD
Unit 20
Unit 21
Unit 22
CORE SECTION

126-791B-77R-3

UNIT 20: CRYSTAL-LITHIC ASH TUFF

Pieces 1-2

CONTACTS: None
PHENOCRYSTS: None
GROUNDMASS: Fine
VESICLES: None
COLOR: Pale green, 10G 8/2
STRUCTURE: Bedded
ALTERATION: Chlorite, calcite, quartz
VEINS/FRACTURES: Incipient cleavage in chlorite at 45 degrees to bedding
ADDITIONAL COMMENTS: Fining upward bedding. Welded eutaxitic textures. 70-80% pumice/glass shards altered to 6:1 chlorite: calcite assemblage. Lithics and crystals, 10-20% each.

UNIT 21: CRYSTAL-LITHIC ASH TUFF

Pieces 3-4

CONTACTS: Gradational
PHENOCRYSTS: None
GROUNDMASS: Fine
VESICLES: None
COLOR: Mottled greenish grey; darker green than Unit 20
STRUCTURE: Bedded
ALTERATION: Chlorite, epidote
VEINS/FRACTURES: None
ADDITIONAL COMMENTS: Pumice not as flattened as in Unit 20.

UNIT 22: LITHIC LAPILLI TUFF

Piece 5

CONTACTS: None
PHENOCRYSTS: Plagioclase and clinopyroxene microphenocrysts in lithics
GROUNDMASS: Fine
VESICLES: None
COLOR: Pale green
STRUCTURE: None
ALTERATION: Chlorite after glass, epidote after clinopyroxene
VEINS/FRACTURES: None
ADDITIONAL COMMENTS: Unwelded, poorly sorted. Lithic lava fragments (50%). Fine chlorite after glass (50%).

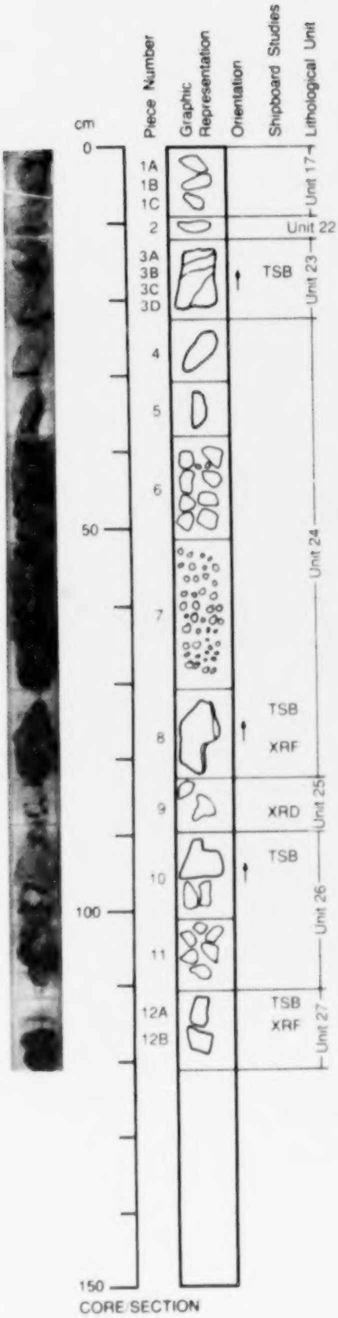
cm
Piece Number
Graphic Representation
Orientation
Shipboard Studies
Lithological Unit
0
50
100
150
1A
1B
1C
2
3A
3B
3C
3D
4
5
6
7
8
9
10
11
12A
12B
TSB
TSB
XRF
XRD
TSB
TSB
XRF
Unit 17
Unit 22
Unit 23
Unit 24
Unit 25
Unit 26
Unit 27
CORE/SECTION

126-791B-78R-1

UNIT 17: DIABASE

Piece 1

CONTACTS: None
PHENOCRYSTS:
Plagioclase - 60%; 0.2-1.0 mm; subhedral
Clinopyroxene - 10%; 0.5-1.0 mm; anhedral
Olivine - 2%; <0.5 mm; altered to smectite, chlorite
GROUNDMASS: None
VESICLES: None
COLOR: Olive black
STRUCTURE: Slickensides in Piece 5
ALTERATION: Glass altered to chlorite and smectite
VEINS/FRACTURES: None

UNIT 22: LITHIC LAPILLI TUFF

Piece 2

CONTACTS: None
PHENOCRYSTS: Plagioclase and clinopyroxene microphenocrysts in lithics
GROUNDMASS: Fine
VESICLES: None
COLOR: Pale green
STRUCTURE: None
ALTERATION: Chlorite after glass, epidote after clinopyroxene
VEINS/FRACTURES: None
ADDITIONAL COMMENTS: Unwelded, poorly sorted. Lithic lava fragments (50%) Fine chlorite after glass (50%)

UNIT 23: DIABASE

Piece 3

CONTACTS: None
PHENOCRYSTS:
Plagioclase - 60%; <0.1-0.3 mm, sericitized
Clinopyroxene - 5%; <0.3-1.0 mm, subhedral, partly chlorite
Olivine - 5%; <0.5 mm, chlorite
GROUNDMASS: Intersertal, fine grained
VESICLES: None
COLOR: Dark greenish grey, 5G 4/1
STRUCTURE: None
ALTERATION: Chlorite
VEINS/FRACTURES: 5%, random, gypsum-filled

UNIT 24: BASALT

Pieces 4-8

CONTACTS: None
PHENOCRYSTS:
Olivine - 2-3%, <0.5 mm, altered to chlorite
Plagioclase - 2%; 0.3-0.7 mm, euhedral
GROUNDMASS: 50% plagioclase + 50% chlorite after glass, intersertal microvesicular
VESICLES: Radial chlorite fillings
COLOR: Dark greenish gray, 5G 4/1
STRUCTURE: None
ALTERATION: As above
VEINS/FRACTURES: Gypsum veins in Pieces 4 and 8
ADDITIONAL COMMENTS: Rounded microvesicular glassy clasts with plagioclase laths are present, perhaps as xenoliths

126-791B-78R-1 (continued)

UNIT 25: FELSIC CLAST + FAULT GOUGE

Piece 9

CONTACTS: None
PHENOCRYSTS:
- Plagioclase - 5-10%, <0.5 mm
- Chlorite - 2%, <0.5 mm

GROUNDMASS: Fine grained
VESICLES: None
COLOR: Medium gray, N5
STRUCTURE: None
ALTERATION: Chlorite, epidote
VEINS/FRACTURES: Disseminated pyrite in mm veins.
ADDITIONAL COMMENTS: Above applies to 3 cm clast present with fault gouge in interval 9. Gouge contains chlorite and quartz.

UNIT 26: DIABASE

Pieces 10 and 11

CONTACTS: None
PHENOCRYSTS:
- Plagioclase - 60%, 0.2-1.0 mm
- Clinopyroxene - 10%, 0.5 mm
- Olivine - 5%, 0.5 mm, altered to chlorite

GROUNDMASS: Intersertal glass altered to chlorite (30%)
VESICLES: None
COLOR: Dark greenish gray, 5GY 4/1
STRUCTURE: None
ALTERATION: Disseminated pyrite and gypsum
VEINS/FRACTURES: Weak alignment of plagioclase may be due to shearing.

UNIT 27: BASALT

Piece 12

CONTACTS: None
PHENOCRYSTS:
- Plagioclase - 65%, <5 mm, altered to clay, chlorite
- Clinopyroxene - 1%, <5 mm, altered to epidote

GROUNDMASS: Microcrystalline, altered to chlorite, clay, quartz
VESICLES: 20%, 1-2 mm, round, random, zeolite fillings
COLOR: Medium blue gray, 5B 5/1
STRUCTURE: None
ALTERATION: As above
VEINS/FRACTURES: None
ADDITIONAL COMMENTS: Too altered to identify

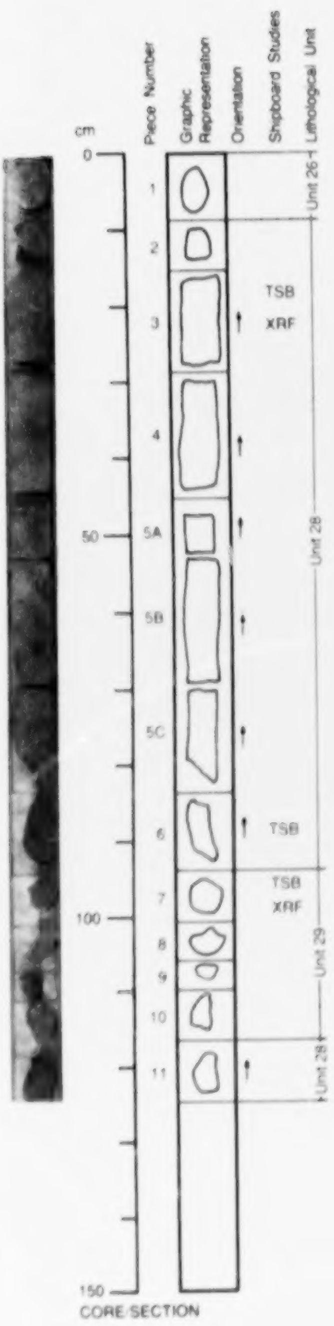
cm
Piece Number
Graphic Representation
Orientation
Shipboard Studies
Lithological Unit
0
50
100
150
1
2
3
4
5A
5B
5C
6
7
8
9
10
11
TSB
XRF
TSB
TSB
XRF
Unit 26
Unit 28
Unit 29
Unit 28
CORE/SECTION

126-791B-79R-1

UNIT 26: DIABASE

Piece 1

CONTACTS: None
PHENOCRYSTS:
  Plagioclase - 60%; 0.2-1.0 mm
  Clinopyroxene - 10%; 0.5 mm
  Olivine - 5%; 0.5 mm; altered to chlorite
GROUNDMASS: Intersertal glass altered to chlorite (30%)
VESICLES: None
COLOR: Dark greenish gray, 5GY 4/1
STRUCTURE: None
ALTERATION: Disseminated pyrite and gypsum
VEINS/FRACTURES: Weak alignment of plagioclase may be due to shearing

UNIT 28: CRYSTAL-LITHIC TUFF

Pieces 2-6, and 11

CONTACTS: None
PHENOCRYSTS: Plagioclase in clasts
GROUNDMASS: Fine grained in clasts
VESICLES: Elongate vesicles in clasts
COLOR: Medium bluish gray, 5B 5/1
STRUCTURE: Overall fining upwards
ALTERATION: Shards altered to smectite, chlorite
VEINS/FRACTURES: None
ADDITIONAL COMMENTS: Eutaxitic, well sorted tuff consisting up 1-2 mm plagioclase (partly altered to chlorite) 40%, 1-4 mm heterolithologic lithic fragments (basalt rhyolite? indeterminate) 20%, crushed pumice (altered to smectite chlorite) 40%

UNIT 29: DIABASE

Pieces 7-10

CONTACTS: None
PHENOCRYSTS:
  Plagioclase - 10%; 0.2-0.5 mm; euhedral subhedral, altered to sericite
  Clinopyroxene - 3%; 0.2-0.3 mm; euhedral, altered to chlorite
  Olivine - 3%; 0.2-0.5 mm; euhedral, altered to chlorite
GROUNDMASS: Plagioclase laths in fine grained altered glass
VESICLES: None
COLOR: Medium blue gray, 5B 5/1
STRUCTURE: None
ALTERATION: Highly altered as above
VEINS/FRACTURES: Gypsum, pyrite, calcite in veins

[illegible] (Piece 3, 57-60 cm) OBSERVER: LIP WHERE SAMPLED: Unit 1

ROCK NAME: Basaltic breccia/olivine basalt

GRAIN SIZE: Fine

TEXTURE: Medium porphyritic

PRIMARY MINERALOGY	PERCENT PRESENT	PERCENT ORIGINAL	SIZE (mm)	COMPOSITION	MORPHOLOGY	COMMENTS
PHENOCRYSTS						
Olivine	[illegible]	1	0.8		Euhedral	Partly altered to smectites.
Plagioclase	3	3	[illegible]		Euhedral	
GROUNDMASS						
Feldspars	1	1	[illegible]		Euhedral	Abundant glassy groundmass.
Glass	74	N/A	N/A		N/A	

VESICLES/CAVITIES	PERCENT	LOCATION	SIZE (mm)	FILLING	SHAPE
Fractures	10			Smectites	

COMMENTS: The matrix of the breccia is partly transformed glass. It contains centimetric clasts of olivine (?) little phyric basalts. Sometimes the groundmass is unaltered fresh glass. Not vesicular. [illegible] Unit 1.

[illegible] OBSERVER: ARK WHERE SAMPLED: Unit 1

ROCK NAME: Basalt breccia

GRAIN SIZE: [illegible]

TEXTURE: Fragmented glass + basalt clasts

PRIMARY MINERALOGY	PERCENT PRESENT	PERCENT ORIGINAL	SIZE (mm)	COMPOSITION	MORPHOLOGY	COMMENTS
PHENOCRYSTS						
Olivine	1	1	[illegible]		Euhedral	Chromium-spinel inclusions.
Plagioclase	[illegible]	[illegible]	N/A		Euhedral	Large 2.2 mm fluid inclusions and strong zoning.
Clinopyroxene	[illegible]	[illegible]	N/A		Euhedral	
GROUNDMASS						
Plagioclase	10	10	[illegible]		Euhedral	
Glass	85	85	N/A		N/A	

VESICLES/CAVITIES	PERCENT	LOCATION	SIZE (mm)	FILLING	SHAPE
[illegible]	[illegible]				

COMMENTS: Clastic glass breccia. Two main clast types: dark, altered, aphyric basalt, and a pale green [illegible] basalt, which forms most of the matrix of the breccia.

[illegible] (Piece 17,141-145 cm) OBSERVER: LTF WHERE SAMPLED: Unit 1

ROCK NAME: Basaltic breccia/olivine basalt

GRAIN SIZE: Fine

TEXTURE: Pyroclastic/porphyritic

PRIMARY MINERALOGY	PERCENT PRESENT	PERCENT ORIGINAL	SIZE (mm)	COMPO-SITION	MORPHOLOGY	COMMENTS
PHENOCRYSTS						
Olivine	2	N/A	</=0.5		Euhedral	Basaltic clasts.
Plagioclase	3	N/A	</=2		Euhedral	
GROUNDMASS						
Olivine	1	N/A	</=0.1		Euhedral	Basaltic clast.
Plagioclase	1	N/A	</=0.6		Euhedral	Flow altered basaltic clast; Glassy groundmass partly altered.

VESICLES/CAVITIES	PERCENT	LOCATION	SIZE (mm)	FILLING	SHAPE
Vesicles	<25		0.3-3	Smectite + glass	Circular

COMMENTS: This basaltic breccia is mainly free of olivine-phyric basalt clasts. The matrix of breccia includes olivine and plagioclase fragments as well as basaltic fragments with very fresh glass and not vesicular. Unit 1.

[illegible] (Piece 9,43-46 cm) OBSERVER: LTF WHERE SAMPLED: Unit 2

ROCK NAME: Olivine-clinopyroxene-plagioclase phyric basalt

GRAIN SIZE: Fine

TEXTURE: Porphyritic

PRIMARY MINERALOGY	PERCENT PRESENT	PERCENT ORIGINAL	SIZE (mm)	COMPO-SITION	MORPHOLOGY	COMMENTS
PHENOCRYSTS						
Olivine	2	2	[illegible]		Euhedral	Fresh.
Plagioclase	4	4	[illegible]		Subeuhedral	Often clustered sometimes with clinopyroxene.
Clinopyroxene	3	3	[illegible]		Euhedral	
GROUNDMASS						
Plagioclase	[illegible]	[illegible]	[illegible]		N/A	Flow aligned.
Olivine	<1	N/A	[illegible]		N/A	
Clinopyroxene	2	N/A	[illegible]		N/A	
Altered glass	N/A	N/A	N/A		N/A	

VESICLES/CAVITIES	PERCENT	LOCATION	SIZE (mm)	FILLING	SHAPE
Vesicles	<25		[illegible]	Smectites, zeolites	

COMMENTS: Glomeroporphyritic clots abundant.

126-791B-12R-1, (Piece 1,19-21 cm) OBSERVER: LTP WHERE SAMPLED:

ROCK NAME: Olivine-clinopyroxene-plagioclase phyric basalt

GRAIN SIZE: Fine.

TEXTURE: Intersertal and porphyritic.

PRIMARY MINERALOGY	PERCENT PRESENT	PERCENT ORIGINAL	SIZE (mm)	COMPO-SITION	MORPHOLOGY	COMMENTS
PHENOCRYSTS						
Olivine	<1	1	0.3		Euhedral	Partly altered to smectites + calcite.
Plagioclase	1	1	1-1.5		Euhedral	Crystals often cluster.
Clinopyroxene	1.5	1.5	~0.3		Euhedral	Plagioclase inclusions.
GROUNDMASS						
Feldspar	[illegible]	N/A	[illegible]		N/A	Flow aligned.
Clinopyroxene	[illegible]	N/A	[illegible]		N/A	Partly devitrified glass.

SECONDARY MINERALOGY	PERCENT	REPLACING/ FILLING	COMMENTS
Clays			Filling up vesicles.

VESICLES/ CAVITIES	PERCENT	LOCATION	SIZE (mm)	FILLING	SHAPE
Vesicles	N/A		0.5-2.5	Smectites + glass	

COMMENTS: Glomeroporphyritic [illegible]

126-791B-79R-1, (Piece 1,3-5 cm) OBSERVER: TPB WHERE SAMPLED:

ROCK NAME: Moderately plagioclase-olivine-phyric basalt

GRAIN SIZE: Fine.

TEXTURE: Vesicular intersertal

PRIMARY MINERALOGY	PERCENT PRESENT	PERCENT ORIGINAL	SIZE (mm)	COMPO-SITION	MORPHOLOGY	COMMENTS
PHENOCRYSTS						
Olivine	1	1	0.2-1.0		Euhedral	Fresh, partly embayed. Includes spinel.
Plagioclase	5	5	0.2-1.5		Euhedral	Fresh.
GROUNDMASS						
Olivine	N/A	N/A	<0.2		N/A	
Plagioclase	N/A	N/A	<0.2		N/A	
Glass	N/A	N/A	N/A		Devitrifying.	

VESICLES/ CAVITIES	PERCENT	LOCATION	SIZE (mm)	FILLING	SHAPE
Vesicles	20	Even	0.2-1.0		Round

COMMENTS: Unit 1.

[illegible] (Piece 2, 5-11 cm) OBSERVER: REX WHERE SAMPLED:

ROCK NAME: Moderately plagioclase olivine phyric basalt

GRAIN SIZE: Fine

TEXTURE: Porphyritic, intersertal

PRIMARY MINERALOGY	PERCENT PRESENT	PERCENT ORIGINAL	SIZE (mm)	COMPO-SITION	MORPHOLOGY	COMMENTS
PHENOCRYSTS						
Olivine	1-2	2	0.5-1		Euhedral	Altered along fractures (smectite occasionally glomeroporphyritic clusters).
Spinel	N/A	N/A	<0.05		N/A	Included in olivine.
GROUNDMASS						
Plagioclase	40	40	0.1		Laths	
Glass	57	N/A	N/A		N/A	Altered.

SECONDARY MINERALOGY	PERCENT	REPLACING/ FILLING	COMMENTS
Clay	5	Olivine	Smectite replacing olivine.
Calcite	<1	Vesicles	Calcite replacing olivine along small veins and vesicles.

VESICLES/ CAVITIES	PERCENT	LOCATION	SIZE (mm)	FILLING	SHAPE
Vesicles	20	Ubiquitous	1-2	Calcite	Elongate-spherical

COMMENTS: Unit 1.

[illegible] (Piece 13, 45-48 cm) OBSERVER: TUR WHERE SAMPLED:

ROCK NAME: Highly plagioclase-clinopyroxene-olivine diabase

GRAIN SIZE: Fine

TEXTURE: Intersertal

PRIMARY MINERALOGY	PERCENT PRESENT	PERCENT ORIGINAL	SIZE (mm)	COMPO-SITION	MORPHOLOGY	COMMENTS
PHENOCRYSTS						
Olivine	2-3	2-3	0.05		Euhedral	Fresh.
Plagioclase	40	40	0.2		Euhedral	Laths fresh.
Clinopyroxene	15	15	0.05		Euhedral	Fresh.
Magnetite	3	3	0.05		Euhedral	
GROUNDMASS						
Glass	N/A	15	N/A		N/A	Altered to clay; smectite.

SECONDARY MINERALOGY	PERCENT	REPLACING/ FILLING	COMMENTS
Clay	15	Glass	

VESICLES/ CAVITIES	PERCENT	LOCATION	SIZE (mm)	FILLING	SHAPE	COMMENTS
Vesicles	7	Even	0.2		Round	Vesicles partly filled with smectite

COMMENTS: Unit 6.

126-791B-[illegible] (Piece 4,) OBSERVER: LTP WHERE SAMPLED:

ROCK NAME: Intersertal olivine plagioclase basalt

GRAIN SIZE: Fine

TEXTURE: Intersertal-[illegible] sparsely porphyritic

PRIMARY MINERALOGY	PERCENT PRESENT	PERCENT ORIGINAL	SIZE (mm)	COMPO-SITION	MORPHOLOGY	COMMENTS
PHENOCRYSTS						
Olivine	5	5	1-1.5		Euhedral	Fresh, beginning to be altered along fractures. Includes spinel.
Plagioclase	11	11	[illegible]		Euhedral	
GROUNDMASS						
Plagioclase	N/A	N/A	[illegible]		N/A	Partly devitrifying.
Clinopyroxene	N/A	N/A	[illegible]		N/A	

VESICLES/CAVITIES	PERCENT	LOCATION	SIZE (mm)	FILLING	SHAPE
Vesicles	[illegible]	Even	[illegible]	Calcite, smectite, zeolite	Round

COMMENTS: No top or bottom interval given. Unit [illegible].

126-791B-[illegible] (Piece 12,) OBSERVER: LTP WHERE SAMPLED:

ROCK NAME: Olivine-clinopyroxene-intersertal basalt

GRAIN SIZE: Fine

TEXTURE: Intersertal/medium porphyritic

PRIMARY MINERALOGY	PERCENT PRESENT	PERCENT ORIGINAL	SIZE (mm)	COMPO-SITION	MORPHOLOGY	COMMENTS
PHENOCRYSTS						
Olivine	1-2	[illegible]	1-2		Euhedral	Clustered and partly altered to calcite, smectite and iddingsite.
Spinel	[illegible]	[illegible]	[illegible]		N/A	In inclusions in olivine.
GROUNDMASS						
Clinopyroxene	[illegible]	[illegible]	[illegible]		Sub-euhedral	
Plagioclase	[illegible]	[illegible]	[illegible]		N/A	Very little glass and completely transformed.

VESICLES/CAVITIES	PERCENT	LOCATION	SIZE (mm)	FILLING	SHAPE	COMMENTS
Vesicles	[illegible]		[illegible]			Calcite, smectite.

COMMENTS: Different from the previous one more coarse grained, tending to a [illegible] texture. Unit [illegible]. Altered area. [illegible] in hand specimen but no difference apparent in thin section. No top or bottom interval given.

[illegible]-6R-1 (Piece 5, 46-47 cm) OBSERVER: TOR WHERE SAMPLED: Unit 6

ROCK NAME: Moderately plagioclase-olivine-phyric basalt

GRAIN SIZE: Fine

TEXTURE: Vesicular, intersertal

PRIMARY MINERALOGY	PERCENT PRESENT	PERCENT ORIGINAL	SIZE (mm)	COMPO-SITION	MORPHOLOGY	COMMENTS
PHENOCRYSTS						
Olivine	[illegible]	3	0.3-1		Euhedral	Embayed, replaced by calcite. Includes spinel.
Plagioclase	1	1	0.3-2.?		Euhedral	
GROUNDMASS						
Plagioclase	N/A	N/A	N/A		Laths	
Glass	N/A	N/A	N/A		N/A	Devitrified.

SECONDARY MINERALOGY	PERCENT	REPLACING/ FILLING	COMMENTS
Clay	3	Glass	
Carbonate	3	Olivine, vein	Fills vein throughout.

VESICLES/ CAVITIES	PERCENT	LOCATION	SIZE (mm)	FILLING	SHAPE	COMMENTS
Vesicles	15	Scattered	0.2-1		Irregular	Smectite on the vesicle walls.

COMMENTS: Unit 6.

[illegible] (Piece 13,?) OBSERVER: LTP WHERE SAMPLED:

ROCK NAME: Olivine-plagioclase-phyric basalt

GRAIN SIZE: Fine grained.

TEXTURE: Microporphyritic, intersertal

PRIMARY MINERALOGY	PERCENT PRESENT	PERCENT ORIGINAL	SIZE (mm)	COMPO-SITION	MORPHOLOGY	COMMENTS
PHENOCRYSTS						
Olivine	2	1	N/A		Euhedral	Corroded olivine, sometimes clustered.
Plagioclase	[illegible]	0.5-1	N/A		Euhedral	
Chrome spinel	N/A	N/A	N/A		N/A	Inclusion in olivine.
GROUNDMASS						
Glass	N/A	<0.1	N/A		N/A	Altered brown glass.
Plagioclase	N/A	.1-.3	N/A		N/A	

VESICLES/ CAVITIES	PERCENT	LOCATION	SIZE (mm)	FILLING	SHAPE	COMMENTS
Vesicles	20		1-3			Smectites.

COMMENTS: No top or bottom interval given. Unit 7.

126-791B-[illegible] (Piece [illegible], [illegible] cm)   OBSERVER: [illegible]   WHERE SAMPLED: [illegible]

ROCK NAME: Moderately plagioclase-olivine-phyric basalt.

GRAIN SIZE: Fine.

TEXTURE: Vesicular; intersertal.

PRIMARY MINERALOGY	PERCENT PRESENT	PERCENT ORIGINAL	SIZE (mm)	COMPOSITION	MORPHOLOGY	COMMENTS
PHENOCRYSTS:						
Olivine	<1	N/A	[illegible]		Euhedral	Embayed, some skeletal.
Plagioclase	<1	N/A	[illegible]		Euhedral	
GROUNDMASS:						
Olivine	N/A	N/A	[illegible]		N/A	
Plagioclase	N/A	N/A	N/A		N/A	Needles.
Glass	N/A	N/A	N/A		N/A	Devitrified.

VESICLES/ CAVITIES	PERCENT	LOCATION	SIZE (mm)	FILLING	SHAPE
Vesicles	[illegible]	Scattered	[illegible]		Irregular

126-791B-[illegible] (Piece [illegible])   OBSERVER: [illegible]   WHERE SAMPLED: [illegible]

ROCK NAME: Plagioclase phyric basalt.

GRAIN SIZE: Fine.

TEXTURE: Vitrophyric; intersertal.

PRIMARY MINERALOGY	PERCENT PRESENT	PERCENT ORIGINAL	SIZE (mm)	COMPOSITION	MORPHOLOGY	COMMENTS
PHENOCRYSTS:						
Plagioclase	[illegible]	N/A	[illegible]		Euhedral	Clustered in glomeroporphyritic clots.
GROUNDMASS:						
Plagioclase	[illegible]	N/A	[illegible]		N/A	
Clinopyroxene	N/A	N/A	[illegible]		N/A	Quenched crystals are plumose.
Glass	N/A	N/A	N/A		N/A	Highly vesicular.

VESICLES/ CAVITIES	PERCENT	LOCATION	SIZE (mm)	FILLING	SHAPE	COMMENTS
Vesicles	[illegible]		[illegible]	Smectites, zeolite	Rounded	Sometimes joining.

COMMENTS: Quenched clinopyroxene crystals. Only [illegible] top or bottom interval given.

[illegible] (Piece 18, 95-100 cm) OBSERVER: TOR WHERE SAMPLED:

ROCK NAME: Breccia unit II - matrix

GRAIN SIZE: Fine

TEXTURE: Vesicular, intersertal, porphyritic

PRIMARY MINERALOGY	PERCENT PRESENT	PERCENT ORIGINAL	SIZE (mm)	COMPO-SITION	MORPHOLOGY	COMMENTS
PHENOCRYSTS Olivine	N/A	N/A	N/A		Euhedral	Perfectly fresh as clots; includes spinel.
Plagioclase	N/A	N/A	N/A		Euhedral	Perfectly fresh as clots.
GROUNDMASS Glass	N/A	N/A	N/A		N/A	Devitrified. Glass held together by clots.
Plagioclase	N/A	N/A	N/A		N/A	Needles.

SECONDARY MINERALOGY	PERCENT	REPLACING/ FILLING	COMMENTS
Clays	1	Vesicles	

VESICLES/ CAVITIES	PERCENT	LOCATION	SIZE (mm)	FILLING	SHAPE	COMMENTS
Vesicles	10	Random	0.1-0.5			Vesicles w/ smectite lining; vesicle walls.

COMMENTS: Phenocrysts are light beige and isotropic. The glass looks "bubbly" and fresh. Contact: embayed but sharp edges of clasts poke into matrix, even vesicle walls of clasts can be edges (i.e., vesicle chilled before inclusion in matrix).

[illegible] (Piece 5B, 95-100 cm) OBSERVER: TOR WHERE SAMPLED:

ROCK NAME: Breccia unit III clasts

GRAIN SIZE: Fine

TEXTURE: Vesicular, intersertal, porphyritic

PRIMARY MINERALOGY	PERCENT PRESENT	PERCENT ORIGINAL	SIZE (mm)	COMPO-SITION	MORPHOLOGY	COMMENTS
PHENOCRYSTS Olivine	1	1	0.5-1		Euhedral	Partly altered to smectite; clasts. Includes spinel.
Plagioclase	1	1	0.5-1		Euhedral	Fresh clasts.
GROUNDMASS Plagioclase	N/A	N/A	N/A		N/A	Needles.
Glass	N/A	N/A	N/A		N/A	Devitrified.

SECONDARY MINERALOGY	PERCENT	REPLACING/ FILLING	COMMENTS
Clays	3	Vesicles and olivine	

VESICLES/ CAVITIES	PERCENT	LOCATION	SIZE (mm)	FILLING	SHAPE	COMMENTS
Vesicles	20	Even	0.1-0.2			Rimmed with smectite and yellow minerals.

COMMENTS: Unit III breccia.

126-791B-43R-1 (Piece 15B, 132-134 cm)   OBSERVER: LTF   WHERE SAMPLED: Unit 11

ROCK NAME: Basaltic breccia

GRAIN SIZE:

TEXTURE: Porphyritic, intersertal

PRIMARY MINERALOGY	PERCENT PRESENT	PERCENT ORIGINAL	SIZE (mm)	COMPO-SITION	MORPHOLOGY	COMMENTS
PHENOCRYSTS						
Olivine	2	2	0.7		Subhedral	Pseudomorphs of olivine and smectites.
Plagioclase	8	8	1.5		Euhedral	Clustered in glomero-porphyritic aggregates.
GROUNDMASS						
Feldspar	N/A	N/A	0.11		N/A	Some are microphenocrysts, others are devitrifying microlites.
Groundmass	40	N/A	N/A		N/A	Highly vesicular glass now replaced by brown opaque material.

SECONDARY MINERALOGY	PERCENT	REPLACING/ FILLING	COMMENTS
Clays		Smectites	Filling vesicles

VESICLES/ CAVITIES	PERCENT	LOCATION	SIZE (mm)	FILLING	SHAPE	COMMENTS
Vesicles	10		0.01-2.0		Elongated	Filled with smectite and hematite.

COMMENTS: Clasts: smaller clasts identical to the big one. Matrix: contains clots of fresh/perfectly fresh olivine and plagioclase. Some of these clots are in a very fresh glass or were very small fragments of both minerals. Highly vesicular glass, very fresh.

126-791B-44R-1 (1-2 cm)   OBSERVER: LTF   WHERE SAMPLED:

ROCK NAME: Plagioclase phyric basalt

GRAIN SIZE: Fine

TEXTURE: Porphyritic

PRIMARY MINERALOGY	PERCENT PRESENT	PERCENT ORIGINAL	SIZE (mm)	COMPO-SITION	MORPHOLOGY	COMMENTS
PHENOCRYSTS						
Plagioclase	.2	N/A	0.2-1		Euhedral	Clustered with clinopyroxene.
Clinopyroxene	0.1	N/A	0.8		Subhedral	
GROUNDMASS						
Plagioclase	.2	N/A	0.1		N/A	Devitrified brown glass.
Clinopyroxene	0.1	N/A	N/A		N/A	Vesicles filled with smectites.

VESICLES/ CAVITIES	PERCENT	LOCATION	SIZE (mm)	FILLING	SHAPE	COMMENTS
Vesicles	N/A		0-0.02			Smectites.

COMMENTS: No piece # given (Rubble).

[illegible] [illegible]-14R-02 (Piece 1, 8-9 cm) OBSERVER: TOR WHERE SAMPLED: Unit 11

ROCK NAME: Basalt mousse-only clasts

GRAIN SIZE: Fine

TEXTURE: Vesicular, intersertal, porphyritic

PRIMARY MINERALOGY	PERCENT PRESENT	PERCENT ORIGINAL	SIZE (mm)	COMPO-SITION	MORPHOLOGY	COMMENTS
PHENOCRYSTS						
Olivine	0	1(+1)	0.2-1		Euhedral	Altered to smectite.
Plagioclase	1	5	0.2-1		Euhedral	Clots are glomeroporphyritic.
GROUNDMASS						
Glass	N/A	N/A	N/A		N/A	Devitrified, completely altered.
Plagioclase	N/A	N/A	N/A		Laths	
Clinopyroxene	N/A	N/A	N/A		Subeuhedral	Microphenocryst composition unknown.

SECONDARY MINERALOGY	PERCENT	REPLACING/ FILLING	COMMENTS
Clays	1	Olivine	

VESICLES/ CAVITIES	PERCENT	LOCATION	SIZE (mm)	FILLING	SHAPE	COMMENTS
Vesicles	40	Random	0.3-1		Round	Clasts.

COMMENTS: Matrix: small piece on thin section with one 0.3 mm euhedral olivine. Olivine and and glass are fresh. Vesicles 0/<0.01 mm are filled with smectites (not completely). Clasts: small fragments of basalt (as altered as the clasts). One clast contains clinopyroxene in the groundmass (intergranular).

[illegible]-14R-02 (Piece 17, 109-111 cm) OBSERVER: TOR WHERE SAMPLED: Unit 11

ROCK NAME: Basalt mousse

GRAIN SIZE: Fine

TEXTURE: Porphyritic/flow aligned

PRIMARY MINERALOGY	PERCENT PRESENT	PERCENT ORIGINAL	SIZE (mm)	COMPO-SITION	MORPHOLOGY	COMMENTS
PHENOCRYSTS						
Olivine	1	1	0.2-1		Euhedral	Altered to smectite, chlorite clasts.
Plagioclase	5	5	0.2-1		Euhedral	Glomeroporphyritic.
Clinopyroxene	N/A	N/A	0.5		Euhedral	Intergranular texture with plagioclase. Plagioclase olivine or clinopyroxene form glomeroporphyritic aggregates.
GROUNDMASS						
Glass, plagioclase, clinopyroxene	N/A	N/A	N/A		Laths	Clasts 1,-2 no clinopyroxene.

VESICLES/ CAVITIES	PERCENT	LOCATION	SIZE (mm)	FILLING	SHAPE	COMMENTS
Vesicles	10	Random	0.1-0.2		Round	Matrix

COMMENTS: 2 types of clasts. Clast 1 vesicular (very different from the previous ones). Clast 2: 30% vesicles. Contains altered olivine and fresh plagioclase. Matrix: glassy "bubbly", with 1% euhedral fresh olivine (0.5 mm) and 5% glomeroporphyritic plagioclase (fragments of plagioclase and olivine).

126-791B-[illegible] (Piece [illegible] cm) OBSERVER: [illegible] WHERE SAMPLED: Unit II

ROCK NAME: Basaltic breccia.

GRAIN SIZE: Fine.

TEXTURE: Porphyritic.

PRIMARY MINERALOGY	PERCENT PRESENT	PERCENT ORIGINAL	SIZE (mm)	COMPO-SITION	MORPHOLOGY	COMMENTS
PHENOCRYSTS						
Olivine	2	N/A	[illegible]		Euhedral	
Plagioclase	4	N/A	[illegible]		Euhedral	Clustered (glomeroporphyritic).
Spinel + Chromium	N/A	N/A	N/A		Euhedral	Inclusion in olivine (few).
GROUNDMASS						
Few feldspar	2	N/A	[illegible]		N/A	Highly vesicular glass.
Few olivine	N/A	N/A	[illegible]		N/A	

SECONDARY MINERALOGY	PERCENT	REPLACING/FILLING	COMMENTS
Clays		Smectites	Filling up the vesicles/replacing altered glass.

VESICLES/CAVITIES	PERCENT	LOCATION	SIZE (mm)	FILLING	SHAPE
Vesicles	[illegible]		[illegible]		

COMMENTS: Unit II "basaltic mousse". Clastic [illegible] basalt with altered glass (now smectite) and vesicles filled with smectites. Very fresh medium porphyritic basalt with very fresh glass. Crystal fragments: olivine and plagioclase. Matrix: highly vesicular glass.

126-791B-[illegible] (Piece [illegible] cm) OBSERVER: [illegible] WHERE SAMPLED: Unit II

ROCK NAME: Basaltic breccia mousse.

GRAIN SIZE: Fine.

TEXTURE: Porphyritic, vesicular.

PRIMARY MINERALOGY	PERCENT PRESENT	PERCENT ORIGINAL	SIZE (mm)	COMPO-SITION	MORPHOLOGY	COMMENTS
PHENOCRYSTS						
Olivine	[illegible]	2	[illegible]		Euhedral	Pseudomorphs in calcite and smectites.
Plagioclase	4	N/A	[illegible]		Subeuhedral	Clustered in glomeroporphyritic aggregates sometimes with olivine.
GROUNDMASS						
Plagioclase + clinopyroxene	N/A	[illegible]	[illegible]		N/A	Intergranular texture.
Plagioclase	N/A	[illegible]	N/A		N/A	Microlites and microphenocrysts.
Devitrified glass	N/A	[illegible]	N/A		N/A	Brown opaque material.

SECONDARY MINERALOGY	PERCENT	REPLACING/FILLING	COMMENTS
Clays		Smectites and [illegible]	

VESICLES/CAVITIES	PERCENT	LOCATION	SIZE (mm)	FILLING	SHAPE	COMMENTS
Vesicles	[illegible]		[illegible]	Smectites	Rounded	Smectites jointed

COMMENTS: Clast: olivine-plagioclase phyric basalt. Matrix: glass highly vesicular including fresh olivine and plagioclase [illegible], glass is fresh. Vesicles are fresh and lined by smectites.

[illegible] (Piece 8,1?? cm)   OBSERVER: LTP   WHERE SAMPLED: Unit 11

ROCK NAME: Olivine (only clast)-plagioclase (phyric) basalt

GRAIN SIZE: Fine

TEXTURE: Porphyritic

PRIMARY MINERALOGY	PERCENT PRESENT	PERCENT ORIGINAL	SIZE (mm)	COMPOSITION	MORPHOLOGY	COMMENTS
PHENOCRYSTS						
Olivine	0.5	N/A	0.5		Euhedral	Altered sometimes.
Plagioclase	2	N/A	0.1-0.5		Subeuhedral	Clustered in ± glomeroporphyritic aggregates.
GROUNDMASS						
Glass	N/A	N/A	N/A		N/A	Few microlites. Abundant vesicular glassy groundmass. Glass partly transformed in brown secondary products.

VESICLES/CAVITIES	PERCENT	LOCATION	SIZE (mm)	FILLING	SHAPE
Vesicles	50		1-3		Round, elongated.

COMMENTS: Top of section intervals given.

[illegible] (Piece 13,51-54 cm)   OBSERVER: LTP   WHERE SAMPLED: Unit 11

ROCK NAME: Basaltic breccia "Scoria"

GRAIN SIZE: Fine

TEXTURE: Highly vesicular porphyritic

PRIMARY MINERALOGY	PERCENT PRESENT	PERCENT ORIGINAL	SIZE (mm)	COMPOSITION	MORPHOLOGY	COMMENTS
PHENOCRYSTS						
Plagioclase	3	3	0.5		Euhedral	Clustered in glomeroporphyritic aggregates.
GROUNDMASS						
Plagioclase	N/A	N/A	N/A		N/A	Microlites (devitrification).
[illegible]	95	95	N/A		N/A	Now completely altered.

SECONDARY MINERALOGY	PERCENT	REPLACING/FILLING	COMMENTS
Clay			Filling up vesicles.

VESICLES/CAVITIES	PERCENT	LOCATION	SIZE (mm)	FILLING	SHAPE
Vesicles	40		0.01-0.3		Circular; sometimes pointed.

COMMENTS: Few clasts. Highly vesicular basalt. Abundant matrix: fresh olivine (one or two crystals); fresh plagioclase abundant, fresh glass. Flattened, elongated vesicles filled with smectites. Feldspars are broken crystals.

[illegible] (Piece 1A,117-124 cm) OBSERVER: [illegible] WHERE SAMPLED:

ROCK NAME: Basaltic breccia, Unit 11

GRAIN SIZE:

TEXTURE: Highly vesicular/porphyritic

PRIMARY MINERALOGY	PERCENT PRESENT	PERCENT ORIGINAL	SIZE (mm)	COMPO-SITION	MORPHOLOGY	COMMENTS
PHENOCRYSTS						
Olivine	3	2	up to 1		Euhedral	Pseudomorph smectite.
Plagioclase	<1	1	1-5		N/A	Fractures are filled with zeolites.
GROUNDMASS						
Plagioclase	N/A	N/A	N/A		N/A	In microlites, devitrification.
Glass	N/A	97	N/A		N/A	Altered, highly vesicular.

SECONDARY MINERALOGY	PERCENT	REPLACING/FILLING	COMMENTS
Clays			Vesicles are lined by smectites and filled with zeolites.

VESICLES/CAVITIES	PERCENT	LOCATION	SIZE (mm)	FILLING	SHAPE	COMMENTS
Vesicles	40		up to mm	Smectites + zeolites		[illegible]

COMMENTS: Clasts: Olivine presents bigger crystals. Plagioclase partly replaced by zeolite. Matrix: glass, altered olivine, fresh plagioclase laths, highly vesicular glass. Small flattened vesicles filled with smectites.

[illegible] (Piece 1A,[illegible] cm) OBSERVER: [illegible] WHERE SAMPLED:

ROCK NAME: Basaltic breccia

GRAIN SIZE: Fine

TEXTURE: Porphyritic

PRIMARY MINERALOGY	PERCENT PRESENT	PERCENT ORIGINAL	SIZE (mm)	COMPO-SITION	MORPHOLOGY	COMMENTS
PHENOCRYSTS						
Olivine	<1	<1	[illegible]		N/A	Altered.
Plagioclase	<1	N/A	[illegible]		Euhedral	
GROUNDMASS						
Plagioclase	N/A	N/A	N/A		N/A	Only microlites(no abundant groundmass; devitrified glass (brown)).

SECONDARY MINERALOGY	PERCENT	REPLACING/FILLING	COMMENTS
Zeolites			Filling of the vesicles.

VESICLES/CAVITIES	PERCENT	LOCATION	SIZE (mm)	FILLING	SHAPE
Vesicles	N/A		[illegible]	Zeolites, smectites	Round

COMMENTS: Unit 11. Clasts: a big clast of olivine (altered) and plagioclase medium phyric basalt. There is isolated plagioclase phenocrysts (entire and broken). Matrix: little matrix: glass with vesicles and zeolites (glass partly devitrified, yellow color).

```
[illegible] -[illegible]R-[illegible] (Piece [illegible], 111-113 cm)     OBSERVER: LYP       WHERE SAMPLED:

ROCK NAME: Olivine-plagioclase basalt

GRAIN SIZE:

TEXTURE: [illegible]

------------------------------------------------------------------------------------------

[illegible]       PERCENT PERCENT  SIZE      COMPO-
[illegible]       PRESENT ORIGINAL (mm)      SITION          MORPHOLOGY            COMMENTS

[illegible]
[illegible]        0       2      <1-1                       Euhedral              Altered.
[illegible]        6       6      <1-1.5                     Subeuhedral

[illegible]
[illegible]        N/A     [illegible]  <1-0.7               N/A                   Glass; partly devitrified. [illegible]

[illegible]                 REPLACING/
[illegible]       PERCENT   FILLING                                                COMMENTS
[illegible]                 Filling vesicles/replacing olivine
[illegible]                 Filling
------------------------------------------------------------------------------------------
[illegible]                        SIZE
[illegible]       PERCENT LOCATION (mm)            FILLING                     SHAPE
[illegible]       [illegible]        up to [illegible]                                     Rounded
                                                                               and
                                                                               [illegible]
------------------------------------------------------------------------------------------
COMMENTS: Unit [illegible]: Clast only.

[illegible] (Piece [illegible], [illegible] cm)        OBSERVER: LYP        WHERE SAMPLED: Unit [illegible]

ROCK NAME: [illegible] basalt

GRAIN SIZE: Fine

TEXTURE: Intersertal porphyritic

------------------------------------------------------------------------------------------

[illegible]       PERCENT PERCENT  SIZE      COMPO-
[illegible]       PRESENT ORIGINAL (mm)      SITION          MORPHOLOGY            COMMENTS

[illegible]
[illegible]       [illegible]  [illegible]  [illegible]      Euhedral              Altered to calcite.
[illegible]       [illegible]  [illegible]  [illegible]      Euhedral              Clustered.

[illegible]
Plagioclase       [illegible]  [illegible]  [illegible]      Euhedral
Clinopyroxene     [illegible]  [illegible]  [illegible]      Subeuhedral
[illegible]       4[illegible] 4[illegible] N/A              N/A
[illegible]

[illegible]                 REPLACING/
[illegible]       PERCENT   FILLING                                                COMMENTS
[illegible]
[illegible]                                              Olivine replaced by calcite.
------------------------------------------------------------------------------------------
[illegible]                        SIZE
[illegible]       PERCENT LOCATION (mm)            FILLING                     SHAPE
[illegible]       [illegible]      [illegible]     Zeolites, smectites
------------------------------------------------------------------------------------------
```

126-791B-76R-01 (Piece 12,93-94 cm) OBSERVER: LTP WHERE SAMPLED: Unit 14

ROCK NAME: Basaltic breccia

GRAIN SIZE:

TEXTURE: Porphyritic

PRIMARY MINERALOGY	PERCENT PRESENT	PERCENT ORIGINAL	SIZE (mm)	COMPO-SITION	MORPHOLOGY	COMMENTS
PHENOCRYSTS						
Olivine	0	-3-5	</=1-0.5		Euhedral	Pseudomorphs of iddingsite, smectites, chlorite and iron.
Plagioclase	-4	-4	0.5		Euhedral	Beginning to alter.
GROUNDMASS						
Feldspars	N/A	0.01	N/A		N/A	
Groundmass	60	N/A	N/A		N/A	Glass completely transformed into smectites + iron stained (hematite?).

SECONDARY MINERALOGY	PERCENT	REPLACING/ FILLING	COMMENTS
Clays		Smectites	
Zeolites		filling vesicles	

VESICLES/ CAVITIES	PERCENT	LOCATION	SIZE (mm)	FILLING	SHAPE	COMMENTS
Vesicles	30		</=3		Rounded	Jointed vesicles forming a sort of net.

COMMENTS: Clast and matrix: very similar to core 126-76R-02, piece 6B. Altered olivine clast is plagioclase phyric basalt. Olivine clusters showing "cumulate" process. Matrix: highly vesicular matrix with olivine and plagioclase clots. The vesicles are a little flattened and filled with smectites. Glass is completely devitrified. Vesicle size-0.1 and 0.5 mm.

126-791B-76R-02 (Piece 6B,54-55 cm) OBSERVER: LTP WHERE SAMPLED: Unit 14

ROCK NAME: Olivine basalt breccia

GRAIN SIZE: Fine to medium

TEXTURE: Porphyritic

PRIMARY MINERALOGY	PERCENT PRESENT	PERCENT ORIGINAL	SIZE (mm)	COMPO-SITION	MORPHOLOGY	COMMENTS
PHENOCRYSTS						
Olivine	0	4	</=2		Euhedral	Altered (iron and smectites/clustered glomeroporphyritic).
Plagioclase	10	10	</=1		Subeuhedral	
Clinopyroxene	1	1	N/A		N/A	Sometimes with olivine.
GROUNDMASS						
Feldspars	2	2	0.01		N/A	Devitrified glass (40%).
Glass	10	83	N/A		N/A	

SECONDARY MINERALOGY	PERCENT	REPLACING/ FILLING	COMMENTS
Clays	12	Filling vesicles	
Carbonate		Filling vesicles	
Chlorite	60	Replacing olivine and glass	
Hematite	5	Replacing olivine	

VESICLES/ CAVITIES	PERCENT	LOCATION	SIZE (mm)	FILLING	SHAPE
Vesicles	10	In glass	</=0.1	Chlorite	Rounded

COMMENTS: Unit 14. Clasts: (centimeter size) olivine, plagioclase, highly porphyritic basalt. Olivine and plagioclase clots. Crystals: olivine and plagioclase. Matrix: highly vesicular glass (this glass is now beginning to devitrify).

12 91B-76R-03 (Piece 4A,36-37 cm) OBSERVER: LTP WHERE SAMPLED:

ROCK NAME: Diabase

GRAIN SIZE:

TEXTURE:

PRIMARY MINERALOGY	PERCENT PRESENT	PERCENT ORIGINAL	SIZE (mm)	COMPO-SITION	MORPHOLOGY	COMMENTS
PHENOCRYSTS						
Olivine	0	~2	0.5		Euhedral	Altered to smectites.
Plagioclase	40	40	</=0.5		Euhedral	
Clinopyroxene	30	30	</=1		Subeuhedral	
GROUNDMASS						
Oxides	N/A	30	N/A		N/A	
Altered glass	N/A	30	N/A		N/A	

VESICLES/ CAVITIES	PERCENT	LOCATION	SIZE (mm)	FILLING	SHAPE
Vesicles	0				

COMMENTS: Rather altered in spite of the preserved clinopyroxene. Unit 15.

126-791B-77R-01 (Piece 1,7-9 cm) OBSERVER: REX WHERE SAMPLED: (drop-in) unit 16

ROCK NAME: Crystal-lithic ash tuff

GRAIN SIZE: Ash (<2 mm)

TEXTURE: Unwelded, vitroclastic

PRIMARY MINERALOGY	PERCENT PRESENT	PERCENT ORIGINAL	SIZE (mm)	COMPO-SITION	MORPHOLOGY	COMMENTS
PHENOCRYSTS						
Plagioclase	4.5	5	0.1-0.2		Euhedral	Some sericitization.
Lithic lava-fragment	10	10	0.5-2		N/A	Various alteration to hematite, calcite and chlorite.
GROUNDMASS						
Vitric shards	0	85	N/A		N/A	Complete alteration to chlorite.

SECONDARY MINERALOGY	PERCENT	REPLACING/ FILLING	COMMENTS
Chlorite	85	Replacing	Replacing shards of pumice/volcanic glass.
Sericite	0.5	Replacing	Replacing plagioclase.

VESICLES/ CAVITIES	PERCENT	LOCATION	SIZE (mm)	FILLING	SHAPE
Vesicles	0				

COMMENTS: Unwelded pyroclastic rock. Could be fall-deposit. No evidence for crushing of pumice shards. Lithic fragments replaced by various assemblages, including hematite-calcite.

126-791B-77R-01 (Piece 7,88-92 cm) OBSERVER: REX WHERE SAMPLED: Unit 17

ROCK NAME: Diabase

GRAIN SIZE: 0.5-1 mm

TEXTURE: Subophitic and intersertal

PRIMARY MINERALOGY	PERCENT PRESENT	PERCENT ORIGINAL	SIZE (mm)	COMPO-SITION	MORPHOLOGY	COMMENTS
PHENOCRYSTS						
Olivine	0	2	0.2		Subhedral	Chlorite and smectite.
Plagioclase	60	60	0.2-1		Subhedral	Some sericite?
Clinopyroxene	10	10	0.5-1		Anhedral	Some smectite?
GROUNDMASS						
Glass/ microcrystalline	0	28	N/A		N/A	Replaced by chlorite smectite.

SECONDARY MINERALOGY	PERCENT	REPLACING/ FILLING	COMMENTS
Clays	2	Replacing	Smectite in olivine and some matrix.
Chlorite	28	Replacing	Mostly replaces groundmass, also olivine.

VESICLES/ CAVITIES	PERCENT	LOCATION	SIZE (mm)	FILLING	SHAPE
Vesicles	0				

COMMENTS: Mixture of original subophitic and intersertal domains.

126-791B-77R-02 (Piece 2A,87-90 cm) OBSERVER: REX WHERE SAMPLED: Unit 19

ROCK NAME: Crystal-lithic lapilli tuff

GRAIN SIZE: >2 mm

TEXTURE: Eutaxitic welded tuff

PRIMARY MINERALOGY	PERCENT PRESENT	PERCENT ORIGINAL	SIZE (mm)	COMPO-SITION	MORPHOLOGY	COMMENTS
PHENOCRYSTS						
Lithic (lava) clasts	40	40	1-7		N/A	
Plagioclase	1	3	0.3		N/A	
Clinopyroxene	0	1	0.1		N/A	Calcite + sericite.
Quartz	2	2	0.01		N/A	Recrystallized granular clusters.
Magnetite / ilmenite	5	5	0.5		Euhedral	
GROUNDMASS						
Vitric shards-pumice	0	50	N/A		N/A	Difficult to judge proportion.

SECONDARY MINERALOGY	PERCENT	REPLACING/ FILLING	COMMENTS
Clays	5		Smectite.
Carbonate	20		
Chlorite	27		Replacing vitric clasts.

VESICLES/ CAVITIES	PERCENT	LOCATION	SIZE (mm)	FILLING	SHAPE
Vesicles	0				

COMMENTS: May have a minor meta-fabric as well as the eutaxitic development.

```
126-791B-77R-02 (Piece 6A,138-141 cm)      OBSERVER: REX          WHERE SAMPLED: Unit 20

ROCK NAME: Coarse crystal-lithic ash tuff

GRAIN SIZE: 0.2-2 mm

TEXTURE: Eutaxitic

--------------------------------------------------------------------------------------------------------------------------

PRIMARY          PERCENT PERCENT  SIZE         COMPO-
MINERALOGY       PRESENT ORIGINAL (mm)         SITION               MORPHOLOGY                  COMMENTS

 PHENOCRYSTS
Ilmenite          1       1       0.3                              N/A
Plagioclase       8       N/A     0.5                              N/A
Quartz            1       1       0.2                              N/A                   Granular clumps.
Lithic-(lava)     20      20      0.2-2                            N/A
clasts

 GROUNDMASS
Pumice-glass      0       70      0.1-2                            Elongate
shards

SECONDARY                 REPLACING/
MINERALOGY       PERCENT    FILLING                                                      COMMENTS
Clays             10      Replacing                                 Smectite replaces glass and minerals.
Carbonate         10      Replacing                                 Calcite replaces plagioclase.
Chlorite          50      Replacing                                 Replaces shards.
--------------------------------------------------------------------------------------------------------------------------
VESICLES/                           SIZE
CAVITIES         PERCENT  LOCATION  (mm)                  FILLING                              SHAPE
Vesicles          0
--------------------------------------------------------------------------------------------------------------------------

126-791B-77R-03 (Piece 1A,3-5 cm)          OBSERVER: REX          WHERE SAMPLED: Unit 20

ROCK NAME: Welded, graded ash tuff

GRAIN SIZE:

TEXTURE: Welded, eutaxitic

--------------------------------------------------------------------------------------------------------------------------

PRIMARY          PERCENT PERCENT  SIZE         COMPO-
MINERALOGY       PRESENT ORIGINAL (mm)         SITION               MORPHOLOGY                  COMMENTS

 PHENOCRYSTS
Plagioclase       5       5       0.2-0.5                          Euhedral
Clinopyroxene     1       1       0.2                              Subhedral
Lithic (lava)     8       8       0.5                              Irregular             Internally altered to hematite, chlorite
fragments                                                                                 calcite.

 GROUNDMASS
Shard matrix      0       86      0.5                              Irregular             Glassy

SECONDARY                 REPLACING/
MINERALOGY       PERCENT    FILLING                                                      COMMENTS
Carbonate                                                           Some calcite as veins and maybe some plagioclase.
Chlorite          86      Replacing                                 Glassy pumice shards.
--------------------------------------------------------------------------------------------------------------------------
VESICLES/                           SIZE
CAVITIES         PERCENT  LOCATION  (mm)                  FILLING                              SHAPE
Vesicles          0
--------------------------------------------------------------------------------------------------------------------------
COMMENTS: This ash has two fabrics: (1) a relict igneous eutaxitic texture, flattened pumice fragments easily picked-out
          in PPL. (2) a metamorphic fabric-shown in XPL by chlorite lineation at ~45 degrees to eutaxitic development,
          much fainter than fabric 1.
```

```
126-791B-78R-01 (Piece 2,9-12 cm)          OBSERVER: REX         WHERE SAMPLED: Unit 22

ROCK NAME: Lithic lapilli tuff

GRAIN SIZE: 0.5-1.5 mm

TEXTURE: Unwelded pyroclastic?

-----------------------------------------------------------------------------------------------------------------

PRIMARY          PERCENT PERCENT  SIZE        COMPO-
MINERALOGY       PRESENT ORIGINAL (mm)        SITION                MORPHOLOGY                  COMMENTS

 PHENOCRYSTS
Plagioclase       15      15      0.2                               Subhedral
Ilmenite          1       1       0.1                               Euhedral
Lithic (lava      50      50      15-5                              N/A                Altered andesitic lava with epidote
clast)                                                                                 replacing clinopyroxene.

 GROUNDMASS
Ash matrix        0       36      N/A                               N/A                Very fine glassy ash matrix.

SECONDARY                      REPLACING/
MINERALOGY       PERCENT       FILLING                                                 COMMENTS
Clays             1                                                   Smectite after plagioclase or clinopyroxene?
Carbonate         3        Filling                                    Veins cutting matrix.
Chlorite          30
-----------------------------------------------------------------------------------------------------------------
VESICLES/                          SIZE
CAVITIES         PERCENT  LOCATION  (mm)                  FILLING                        SHAPE
Vesicles          0
-----------------------------------------------------------------------------------------------------------------
COMMENTS: Unwelded, poorly sorted deposit. Could be base-surge layer? Lava clasts have plagioclase phenocrysts. Also
          clinopyroxene-plagioclase phyric variety.

126-791B-78R-01 (Piece 3,16-19 cm)          OBSERVER: TOR         WHERE SAMPLED: Unit 23

ROCK NAME: Olivine-plagioclase-clinopyroxene phyric diabase

GRAIN SIZE: Fine

TEXTURE: Intersertal, subophitic

-----------------------------------------------------------------------------------------------------------------

PRIMARY          PERCENT PERCENT  SIZE        COMPO-
MINERALOGY       PRESENT ORIGINAL (mm)        SITION                MORPHOLOGY                  COMMENTS

 PHENOCRYSTS
Olivine           0       5       <0.5                              Euhedral           Altered to chlorite, smectite.
Plagioclase       60      60      0.1-0.3                           Euhedral
Clinopyroxene     4       5       0.3-1                             Subhedral          Altered to chlorite, sericite.

 GROUNDMASS
Glass             0       30      N/A                               N/A                Altered to chlorite, smectite.

SECONDARY                      REPLACING/
MINERALOGY       PERCENT       FILLING                                                 COMMENTS
Chlorite          36      Glass, olivine                              Together with smectite replacing glass and olivine.
Sericite                                                              Fractures filled with sericite?
-----------------------------------------------------------------------------------------------------------------
VESICLES/                          SIZE
CAVITIES         PERCENT  LOCATION  (mm)                  FILLING                        SHAPE
Vesicles          0
-----------------------------------------------------------------------------------------------------------------
```

12 -791B-78R-01 (Piece 8,79-82 cm) OBSERVER: TOR WHERE SAMPLED: Unit 24

ROCK NAME: Moderately plagioclase phyric basalt

GRAIN SIZE: Fine

TEXTURE: Intersertal-vesicular

PRIMARY MINERALOGY	PERCENT PRESENT	PERCENT ORIGINAL	SIZE (mm)	COMPO-SITION	MORPHOLOGY	COMMENTS
PHENOCRYSTS						
Olivine	0	2-3	0.3-0.7		Euhedral	Altered to chlorite.
Plagioclase	2	2	0.3-0.7		Euhedral	
GROUNDMASS						
Plagioclase	48	N/A	<0.2		Laths	
Glass	0	48	N/A		N/A	Altered to chlorite.

SECONDARY MINERALOGY	PERCENT	REPLACING/ FILLING	COMMENTS
Chlorite	50	Glass and olivine	

VESICLES/ CAVITIES	PERCENT	LOCATION	SIZE (mm)	FILLING	SHAPE	COMMENTS
Vesicles	N/A	Clasts	0.1-0.5	Chlorite	Round	Clasts nearly completely altered to chlorite. The vesicles are interconnected to each other with radially grown chlorite.

COMMENTS: The tiny plagioclase laths in the clasts could indicate a clast origin as xenolithic in the basalt magma. PHENOCRYSTS: rounded clasts with vesicles filled with chlorite. GROUNDMASS: clasts - glassy matrix with tiny plagioclase laths.

126-791B-78R-01 (Piece 10A,94-96 cm) OBSERVER: TOR WHERE SAMPLED: Unit 26

ROCK NAME: Plagioclase-olivine-clinopyroxene phyric diabase

GRAIN SIZE: Fine

TEXTURE: Subophitic-intersertal

PRIMARY MINERALOGY	PERCENT PRESENT	PERCENT ORIGINAL	SIZE (mm)	COMPO-SITION	MORPHOLOGY	COMMENTS
PHENOCRYSTS						
Olivine	0	5	N/A		Euhedral	Altered to chlorite, smectite.
Plagioclase	60	60	N/A		Euhedral	
Clinopyroxene	10	10	N/A		Euhedral	
GROUNDMASS						
Glass	0	25	N/A		N/A	Altered to chlorite, smectite.

SECONDARY MINERALOGY	PERCENT	REPLACING/ FILLING	COMMENTS
Carbonate			Vein fracture in thin section.
Chlorite	30	Olivine and glass	Together with smectite.

VESICLES/ CAVITIES	PERCENT	LOCATION	SIZE (mm)	FILLING	SHAPE
Vesicles	0				

COMMENTS: Weak alignment of plagioclase laths due to shearing.

126-791B-78R-01 (Piece 12A,112-114 cm) OBSERVER: REX WHERE SAMPLED: Unit 27

ROCK NAME: Basalt-andesite

GRAIN SIZE: One phenocryst of 2 mm

TEXTURE: Microcrystalline-porphyritic

PRIMARY MINERALOGY	PERCENT PRESENT	PERCENT ORIGINAL	SIZE (mm)	COMPO-SITION	MORPHOLOGY	COMMENTS
PHENOCRYSTS						
Plagioclase	65	75	N/A		N/A	
Clinopyroxene	0	1	N/A		N/A	
GROUNDMASS						
Altered glass?	0	24	N/A		N/A	

SECONDARY MINERALOGY	PERCENT	REPLACING/ FILLING	COMMENTS
Clays	5	Replacing	Matrix.
Chlorite	24	Replacing	Matrix.
Epidote	1	Replacing	Clinopyroxene.
Quartz	5		

VESICLES/ CAVITIES	PERCENT	LOCATION	SIZE (mm)	FILLING	SHAPE	COMMENTS
Vesicles	20	Here and there!	1-2	Zeolite?	Round	Thin section too this.

COMMENTS: Section at 20 microns.

126-791B-79R-01 (Piece 3,17-20 cm) OBSERVER: REX WHERE SAMPLED: Unit 28

ROCK NAME: Lithic-crystal tuff

GRAIN SIZE: 1-4 mm

TEXTURE: Eutaxitic, well sorted

PRIMARY MINERALOGY	PERCENT PRESENT	PERCENT ORIGINAL	SIZE (mm)	COMPO-SITION	MORPHOLOGY	COMMENTS
PHENOCRYSTS						
Plagioclase	30	40	1-2		N/A	
Lithic(lava) clasts	5	5	1-4		N/A	Variable range in composition and competence (scoria-pumice).
GROUNDMASS						
Crushed pumice shard	0	40	N/A		N/A	

SECONDARY MINERALOGY	PERCENT	REPLACING/ FILLING	COMMENTS
Clays	15	Replacing	Smectite replacing feldspar and matrix.
Carbonate	5	Filling	Filling fractures.
Chlorite	45	Replacing	Replacing glass/pumice shards.

VESICLES/ CAVITIES	PERCENT	LOCATION	SIZE (mm)	FILLING	SHAPE
Vesicles	0				

COMMENTS: Variation in the vesicularity of the pumice-scoria fragments, hence difference in the degree of competence and variable amount of crushing/welding.

126-791B-79R-01 (Piece 6,85-87 cm) OBSERVER: TOR WHERE SAMPLED: Unit 28 bottom

ROCK NAME: Welded lithic crystal tuff

GRAIN SIZE: 1-2 mm

TEXTURE: Eutaxitic

PRIMARY MINERALOGY	PERCENT PRESENT	PERCENT ORIGINAL	SIZE (mm)	COMPO-SITION	MORPHOLOGY	COMMENTS
PHENOCRYSTS						
Plagioclase	30	40	-1		N/A	
Lithics	10	10	1-2		N/A	
GROUNDMASS						
Crushed pumice shard	0	50	N/A		N/A	

SECONDARY MINERALOGY	PERCENT	REPLACING/ FILLING	COMMENTS
Clays	30		Smectite replacing glass and pumice shards.
Carbonate			Calcite filling fracture.
Chlorite	30		Replacing glass and pumice shards.

VESICLES/ CAVITIES	PERCENT	LOCATION	SIZE (mm)	FILLING	SHAPE	COMMENTS
Vesicles	N/A	in glass	N/A	Chlorite	Flat	Small compacted vesicles in crushed glass shards.

126-791B-79R-01 (Piece 7,94-97 cm) OBSERVER: TOR WHERE SAMPLED: Unit 29

ROCK NAME: Altered olivine-plagioclase-clinopyroxene phyric diabase

GRAIN SIZE: Fine

TEXTURE: Intersertal

PRIMARY MINERALOGY	PERCENT PRESENT	PERCENT ORIGINAL	SIZE (mm)	COMPO-SITION	MORPHOLOGY	COMMENTS
PHENOCRYSTS						
Olivine	0	N/A	0.3-0.5		Euhedral	Altered to chlorite, smectite, calcite.
Plagioclase	5	5	0.3-0.5		Euhedral	
Clinopyroxene	5	5	0.3-0.5		Euhedral	
Magnetite	3	3	N/A		N/A	
GROUNDMASS						
Glass	0	N/A	N/A		N/A	Altered to chlorite, smectite.
Plagioclase	60	60	N/A		Laths	

SECONDARY MINERALOGY	PERCENT	REPLACING/ FILLING	COMMENTS
Clays			Replacing olivine and glass (together with chlorite).
Carbonate	Trace		
Zeolite	Trace		
Chlorite	27		Replacing glass and olivine.
Gypsum		Vein	

VESICLES/ CAVITIES	PERCENT	LOCATION	SIZE (mm)	FILLING	SHAPE
Vesicles	0				

SITE 792 HOLE A CORE 1H CORED INTERVAL 0.0-9.7 mbsf

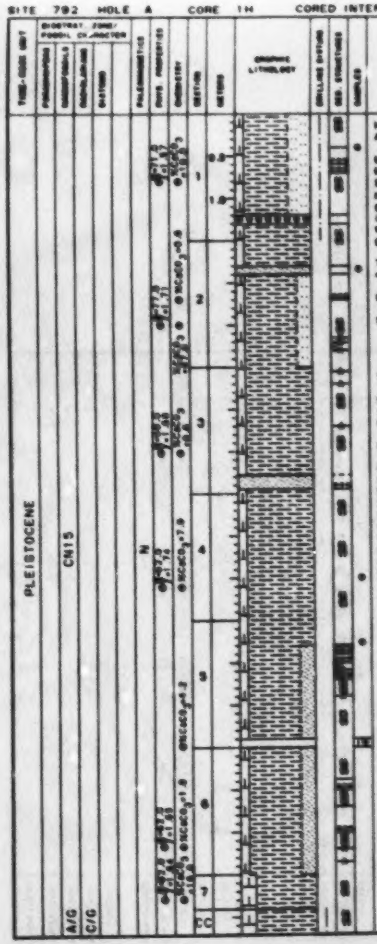
TIME-ROCK UNIT
BIOSTRAT. ZONE/ FOSSIL CHARACTER
FORAMINIFERS
NANNOFOSSILS
RADIOLARIANS
DIATOMS
PALEOMAGNETICS
PHYS. PROPERTIES
CHEMISTRY
SECTION
METERS
GRAPHIC LITHOLOGY
DRILLING DISTURB.
SED. STRUCTURES
SAMPLES
PLEISTOCENE
CN15
A/G
C/G
N
1
2
3
4
5
6
7
CC
0.5
1.0

LITHOLOGIC DESCRIPTION

NANNOFOSSIL-RICH SILTY CLAY, NANNOFOSSIL-RICH CLAYEY SILT, VITRIC SILT AND SAND

Major lithologies:
Most of the core is medium dark gray (N4) and dark gray (5GY 4/1), burrowed NANNOFOSSIL-RICH SILTY CLAY and NANNOFOSSIL-RICH CLAYEY SILT, with scattered sand-to pebble-sized pumice clasts. The remaining 20% of the core consists of graded beds, generally <10 cm thick, of dark gray (N3) or medium light gray (N6) VITRIC SILT and SAND (ash). The ash beds have sharp, locally scoured bases, do not show lamination, and their tops are partly mixed with overlying sediment by burrows. A few of these beds contain granules and pebbles of pumice at their base.

The dark gray sands consist of basaltic lithic fragments, plagioclase, and ferromagnesian minerals.

Only Section 1 is moderately disturbed by drilling. The rest of the core is undisturbed.

SMEAR SLIDE SUMMARY (%):

	1, 40 M	2, 32 M	4, 100 D	5, 20 M
TEXTURE:				
Sand	—	80	15	—
Silt	80	20	40	80
Clay	20	—	45	20
COMPOSITION:				
Chlorite	—	—	—	2
Clay	5	—	44	2
Diatoms	—	—	1	16
Feldspar	—	40	5	—
Foraminifers	—	10	5	—
Glass	90	30	3	80
Nannofossils	—	Tr	30	—
Opaques	—	—	5	—
Pyroxene	5	20	5	—
Radiolarians	—	—	Tr	—
Silicoflagellates	—	—	1	—
Spicules	—	—	1	—

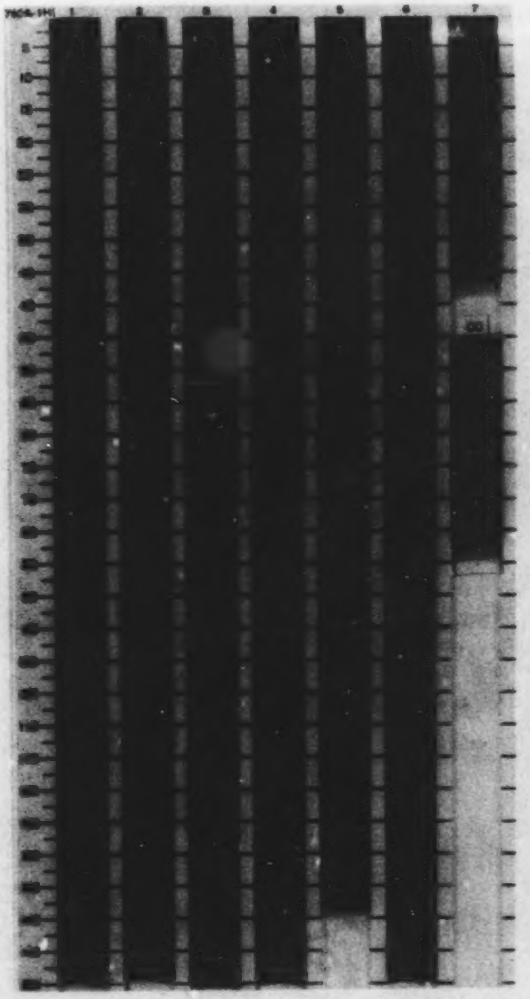

SITE 792 HOLE A CORE 2H CORED INTERVAL 9.7-19.1 mbsf

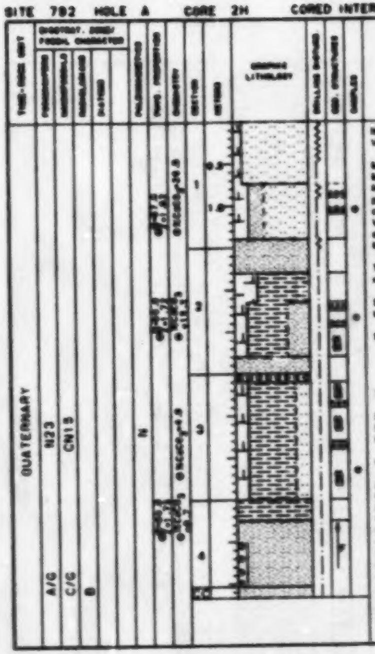
TIME-ROCK UNIT
BIOSTRAT. ZONE/FOSSIL CHARACTER
FORAMINIFERS
NANNOFOSSILS
RADIOLARIANS
DIATOMS
PALEOMAGNETICS
PHYS. PROPERTIES
CHEMISTRY
SECTION
METERS
GRAPHIC LITHOLOGY
DRILLING DISTURB.
SED. STRUCTURES
SAMPLES
QUATERNARY
N23
CN15
A/G
C/G
B
N
1
2
3
4
CC
0.5
1.0

LITHOLOGIC DESCRIPTION

NANNOFOSSIL-RICH SILTY CLAY, NANNOFOSSIL-RICH CLAYEY SILT, SILTY CLAY, VITRIC SILT AND SAND

Major lithologies:
Most of the core is dark gray (5GY 4/1), burrowed NANNOFOSSIL-RICH SILTY CLAY, NANNOFOSSIL-RICH CLAYEY SILT and SILTY CLAY, with scattered sand to pebble-sized pumice clasts, and medium dark gray (N4) VITRIC SILT. The remaining 20% of the core consists of graded beds, generally <10 cm thick, of dark gray (N3) or medium light gray (N6) VITRIC SILT and SAND (ash). The ash beds have sharp, locally scoured bases, do not show lamination, and their tops are partly mixed with overlying sediment by burrowers. A few of these beds contain granules and pebbles of pumice at their base.

The black sands consist of basaltic lithic fragments, plagioclase, and ferromagnesian minerals.

Section 1, 0-50 cm, is very disturbed by drilling. The rest of the core is moderately disturbed.

SMEAR SLIDE SUMMARY (%)

	1, 105 M	2, 80 M	3, 115 D
TEXTURE			
Sand	80	—	5
Silt	20	80	40
Clay	—	20	55
COMPOSITION			
Accessory minerals	—	Tr	—
Clay	—	—	30
Diatoms	—	—	1
Feldspar	15	10	20
Foraminifers	10	Tr	1
Glass	60	90	—
Lithic fragments	5	—	10
Nannofossils	—	—	20
Opaques	—	—	5
Pyroxene	10	—	3
Radiolarians	—	—	Tr
Silicoflagellates	—	—	Tr
Sponge spicules	—	—	Tr

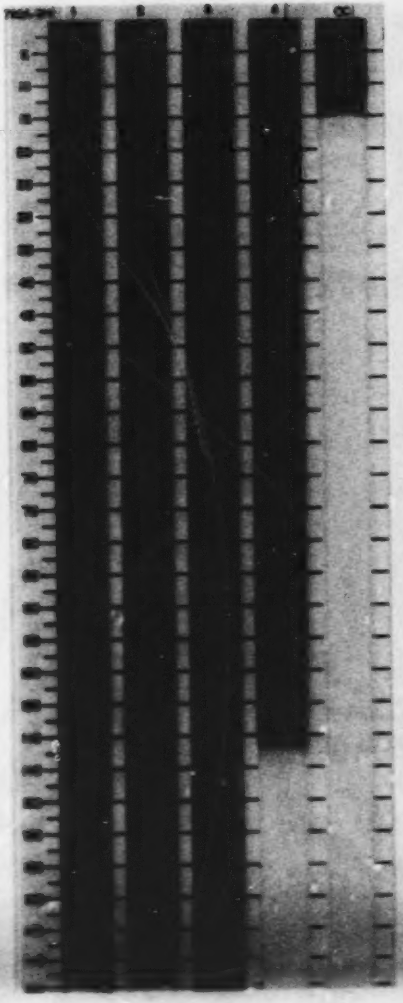
792A-2H
1
2
3
4
CC

SITE 792 HOLE A CORE 3H CORED INTERVAL 19.1-28.4 mbsf

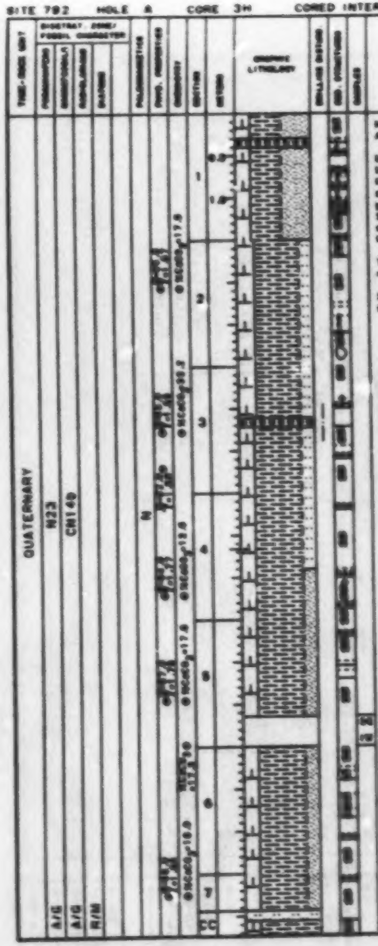

LITHOLOGIC DESCRIPTION

NANNOFOSSIL-RICH SILTY CLAY, NANNOFOSSIL-RICH CLAYEY SILT, VITRIC SILT AND VITRIC SAND

Major lithologies:
Most of the core is dark gray (5GY 4/1), burrowed NANNOFOSSIL-RICH SILTY CLAY and NANNOFOSSIL-RICH CLAYEY SILT, and SILTY CLAY, with scattered sand-to pebble-sized pumice clasts and medium dark gray (N4). The remaining 20% of the core consists of graded beds, generally <10 cm thick, of dark gray (N3) or medium light gray (N6) VITRIC SILT and VITRIC SAND (ash). The ash beds have sharp, locally scoured bases, do not show lamination, and their tops are partly mixed with overlying sediment by burrowers. A few of these beds contain granules and pebbles of pumice at their base.

The black sands consist of basaltic lithic fragments, plagioclase, and ferromagnesian minerals.

Section 1, 0-50 cm, is very disturbed by drilling. The rest of the core is moderately disturbed.

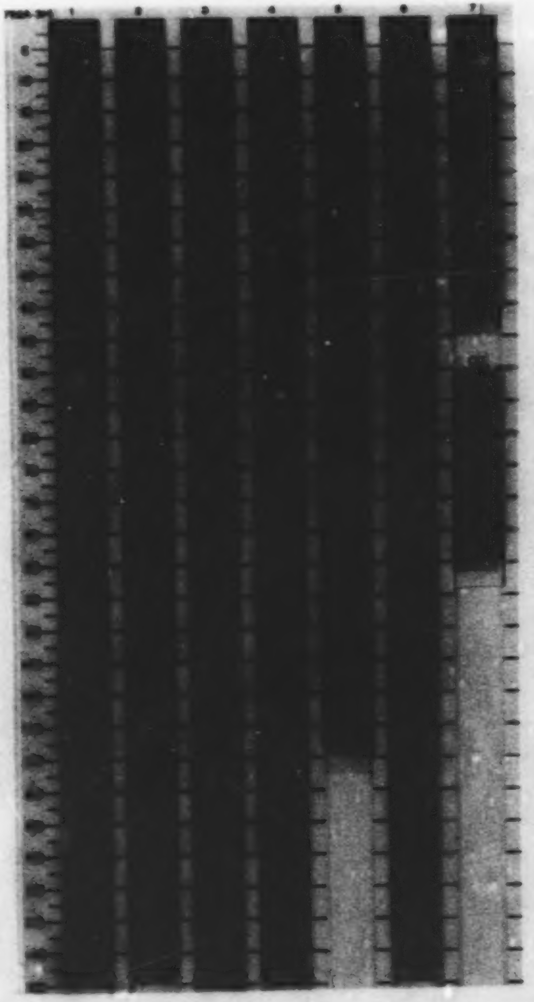

SITE 792 HOLE A CORE 4H CORED INTERVAL 28.4-37.8 mbsf

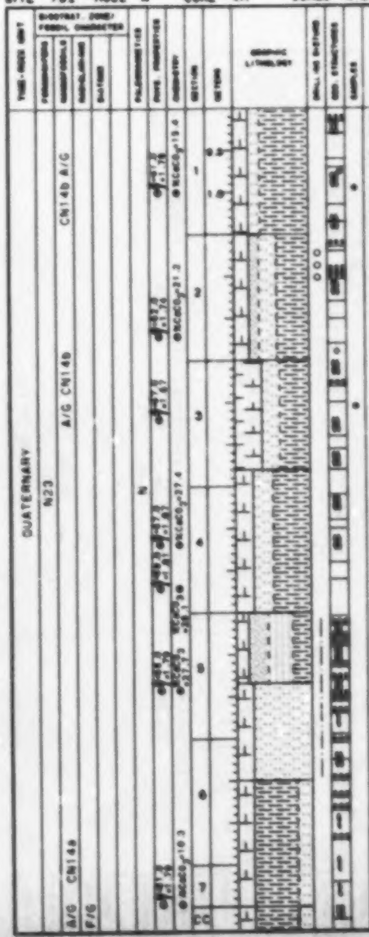

LITHOLOGIC DESCRIPTION

NANNOFOSSIL-RICH CLAYEY SILT, NANNOFOSSIL-RICH SILTY CLAY, VITRIC SILT AND CLAYEY SAND

Major lithologies:
Most of the core consists of burrowed olive gray (5Y 4/1) NANNOFOSSIL-RICH CLAYEY SILT, and light olive gray (5Y 5/2) NANNOFOSSIL-RICH SILTY CLAY with scattered sand- to granule and pebble-sized pumiceous clasts. VITRIC SILT is intercalated as thin beds of light olive gray (5Y 6/1), and thick beds of olive gray (5Y 4/1) sediment. The SAND is dark gray (N3) to grayish black (N2) in color, and forms sharp-based thin to medium beds, with a lower graded division, followed locally by a plane-parallel laminated division. Locally, these divisions grade upward into an olive gray (5Y 4/1) division of CLAYEY SAND. Some of the sand beds contain granules at the base.

Minor lithologies: Dark greenish gray (5G 4/1), very thin ash layers of VITRIC SILT are present.

A few of the beds of vitric silt are soupy. Section 5, 0 cm, to Section 6, 50 cm, is moderately disturbed by drilling.

SMEAR SLIDE SUMMARY (%):

	1, 80 D	3, 55 D
TEXTURE:		
Silt	30	35
Clay	70	65
COMPOSITION:		
Clay	40	40
Diatoms	1	1
Feldspar	1	1
Foraminifers	2	1
Glass	30	25
Inorganic calcite	—	1
Nannofossils	20	20
Opaques	1	1
Oxide	—	1
Pyroxene	—	1
Quartz	1	1
Radiolarians	1	—
Spicules	1	2

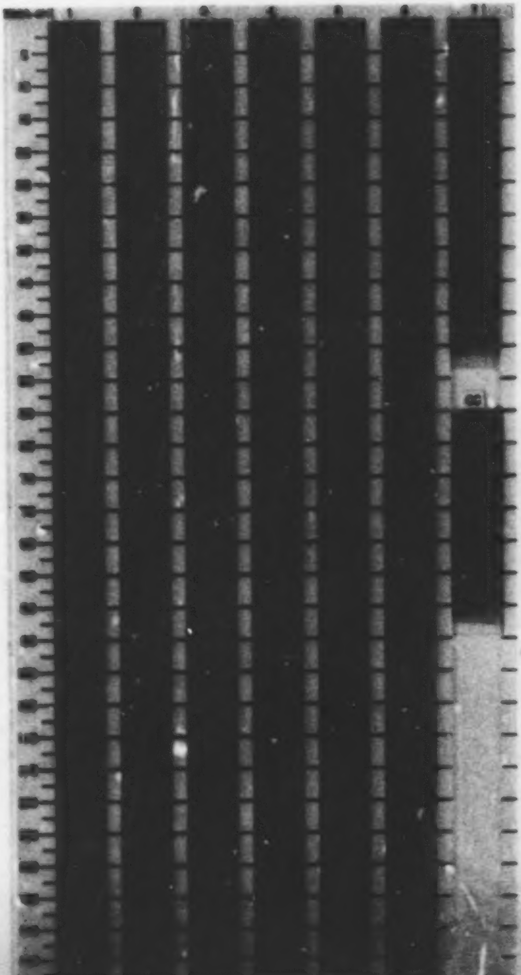

SITE 792 HOLE A CORE 5H CORED INTERVAL 37.8-47.2 mbsf

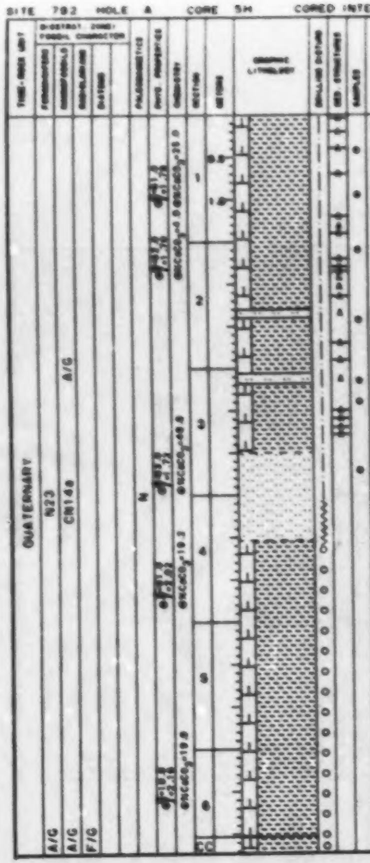
TIME-ROCK UNIT
BIOSTRAT. ZONE/FOSSIL CHARACTER
FORAMINIFERS
NANNOFOSSILS
RADIOLARIANS
DIATOMS
PALEOMAGNETICS
PHYS. PROPERTIES
CHEMISTRY
SECTION
METERS
GRAPHIC LITHOLOGY
DRILLING DISTURB.
SED. STRUCTURES
SAMPLES
QUATERNARY
N23
CN14a
A/G
A/G
A/G
F/G
N
CaCO3=19.8
CaCO3=19.2
CaCO3=48.8
CaCO3=25.0
1
2
3
4
5
6
CC
0.5
1.0

LITHOLOGIC DESCRIPTION

NANNOFOSSIL-RICH CLAY AND NANNOFOSSIL-RICH VITRIC SILTY CLAY

Major lithologies:
Olive gray (5Y 4/2) NANNOFOSSIL-RICH CLAY and NANNOFOSSIL-RICH VITRIC SILTY CLAY together comprise 78% of the core. They are slightly to heavily burrowed, and contain isolated pumice and scoria clasts.

Minor lithologies:
Dark gray (5Y 4/1) VITRIC SILT in a disturbed (flow-in) unit 105 cm thick (Section 3) comprises 12% of the core. Gray (5Y 5/1) and dark gray (5Y 5/1, 5Y 4/1) VITRIC SAND, VITRIC SILTY SAND and VITRIC SILT (ash), in layers 1-11 cm thick, together constitute 11% of the core.

The upper half of the core is moderately disturbed by drilling, and the rest is slightly.

SMEAR SLIDE SUMMARY (%):

	1, 42 M	1, 95 D	2, 13 D	2, 140 M	3, 16 M	3, 40 D	3, 121 M
TEXTURE:							
Sand	85	2	10	15	5	Tr	40
Silt	15	18	30	60	95	25	30
Clay	—	80	60	25	—	75	30
COMPOSITION:							
Accessory minerals	—	Tr	1	2	—	—	—
Clay	2	46	40	25	—	67	30
Diatoms	Tr	1	2	—	—	1	Tr
Feldspar	1	3	2	5	3	1	3
Foraminifers	Tr	2	2	—	1	2	Tr
Glass	95	6	20	35	93	15	60
Lithic fragments	Tr	3	Tr	25	Tr	—	Tr
Mica	—	—	—	—	—	1	—
Nannofossils	2	35	30	—	2	10	3
Opaques	—	2	—	—	—	1	1
Quartz	—	—	—	15	—	—	—
Pyroxene	Tr	—	—	—	1	—	3
Radiolarians	—	Tr	Tr	—	—	—	—
Silicoflagellates	—	1	2	—	—	1	Tr
Sponge spicules	—	1	1	—	Tr	1	Tr

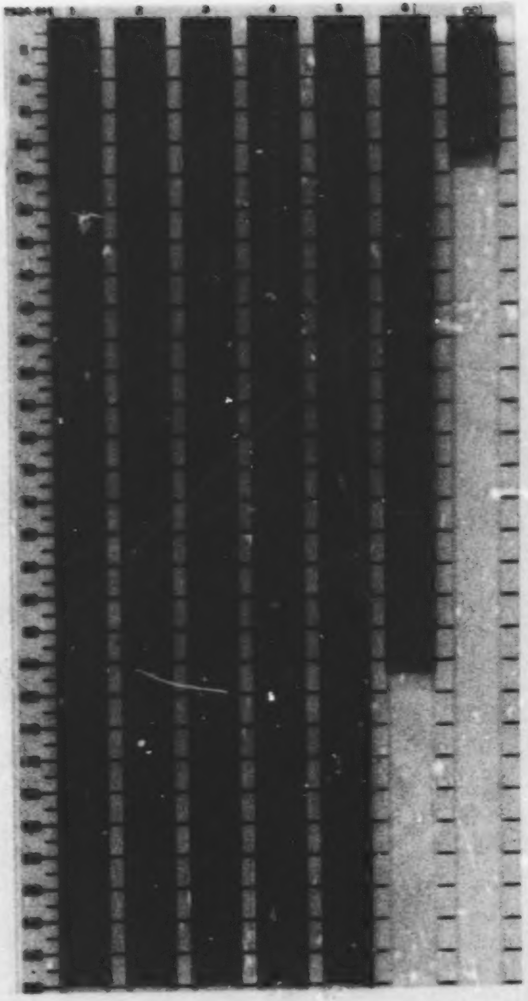

SITE 792 HOLE A CORE 6H CORED INTERVAL 47.2-56.8 mbsf

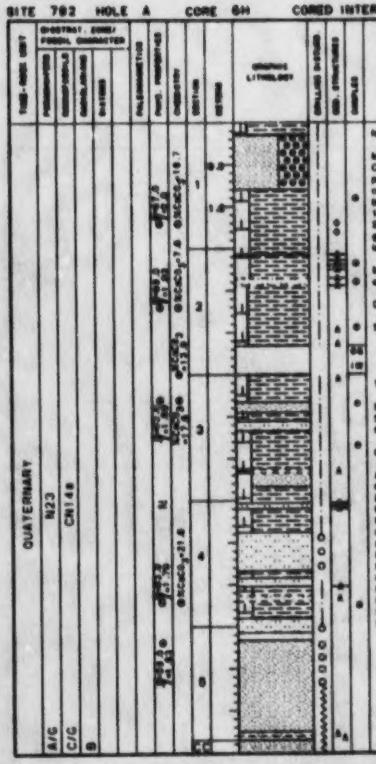
TIME-ROCK UNIT
BIOSTRAT. ZONE/ FOSSIL CHARACTER
FORAMINIFERS
NANNOFOSSILS
RADIOLARIANS
DIATOMS
PALEOMAGNETICS
PHYS. PROPERTIES
CHEMISTRY
SECTION
METERS
GRAPHIC LITHOLOGY
DRILLING DISTURB.
SED. STRUCTURES
SAMPLES
QUATERNARY
N23
CN14a
A/G
C/G
B
%CaCO3=18.7
%CaCO3=7.6
%CaCO3=17.8
%CaCO3=21.6
1
2
3
4
5
CC
0.5
1.0

LITHOLOGIC DESCRIPTION

NANNOFOSSIL-RICH VITRIC SILTY CLAY AND VITRIC SAND

Major lithologies:
Olive gray (5Y 4/2) and black (5Y 3/2) NANNOFOSSIL-RICH VITRIC SILTY CLAY comprises 40% of the core. Some intervals are slightly burrowed, and Section 2, 6-12 and 20-35 cm are heavily burrowed. Most of the rest of the core (30%) is dark gray (5Y 4/1), brownish black (5YR 2/1), black (5Y 3/2) and grayish black (N2) VITRIC SAND, typically in layers 1-14 cm thick. Thicker beds occur in Section 1, 14-70 cm, and as thick flow-in layers in Sections 4, 5 and CC. The unit in Section 1 contains 5-30% pumice pebbles and 20-35% granules; the other sands are medium to very fine-grained. Some of the thicker layers are laminated, others are graded, or both.

Minor lithology: Nine, gray (5Y 6/1) and light gray (N7) VITRIC SILT layers, 5-12 cm thick, occur throughout and constitute 5% of the core.

Drilling disturbance is moderate to soupy.

SMEAR SLIDE SUMMARY (%)

	1, 90 D	2, 18 M	2, 40 M	2, 94 M	3, 30 M	3, 84 D	4, 125 D
TEXTURE							
Sand	Tr	85	40	90	95	5	—
Silt	30	15	60	10	5	45	20
Clay	70	—	—	—	—	50	80
COMPOSITION							
Accessory minerals	1	1	—	—	—	1	1
Clay	60	—	—	—	—	50	50
Diatoms	Tr	Tr	—	—	Tr	3	3
Feldspar	2	8	2	2	10	1	1
Foraminifers	5	1	—	Tr	1	4	4
Glass	10	90	97	95	85	15	10
Lithic fragments	1	Tr	1	Tr	2	1	—
Micrite	2	—	—	—	—	2	1
Nannofossils	10	Tr	Tr	Tr	Tr	15	20
Opaques	1	—	Tr	1	—	—	1
Pyroxene	—	—	—	1	2	—	—
Radiolarians	—	—	—	—	—	2	Tr
Silicoflagellates	Tr	—	—	—	Tr	5	—
Spicules	2	—	—	—	—	1	1

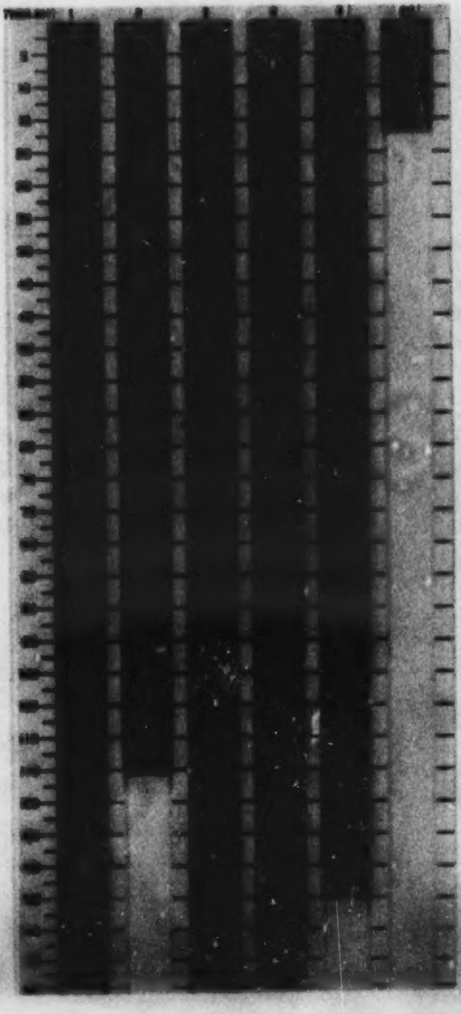

SITE 792 HOLE A CORE 7H CORED INTERVAL 56.6-66.0 mbsf

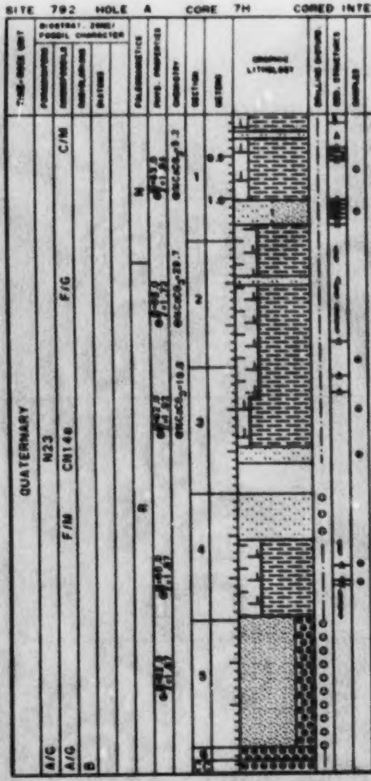
TIME-ROCK UNIT
BIOSTRAT. ZONE/ FOSSIL CHARACTER
FORAMINIFERS
NANNOFOSSILS
RADIOLARIANS
DIATOMS
PALEOMAGNETICS
PHYS. PROPERTIES
CHEMISTRY
SECTION
METERS
GRAPHIC LITHOLOGY
DRILLING DISTURB.
SED. STRUCTURES
SAMPLES
QUATERNARY
N23
A/G
C/M
F/G
CN14b
F/M
A/G
B
N
R
●CaCO₃=9.2
●CaCO₃=29.7
●CaCO₃=19.8
1
2
3
4
5
CC
0.5
1.0

LITHOLOGIC DESCRIPTION

NANNOFOSSIL-RICH CLAY and NANNOFOSSIL-RICH VITRIC SILTY CLAY

Major lithologies:

Olive gray (5Y 4/2) NANNOFOSSIL-RICH CLAY and NANNOFOSSIL-RICH VITRIC SILTY CLAY comprise 50% of the core. Slight bioturbation occurs at the top of the core, Section 2, and the top of Section 3.

Minor lithologies:

Dark gray (5Y 4/1), olive gray (5Y 4/2) and gray (5Y 5/1) VITRIC SILT layers varying in thickness from 1-10 cm, together with a single 55-cm interval in Section 4, constitute 10% of the core. Another 5% of the core is olive black (5Y 2/1) VITRIC SAND, in layers 2-11 cm thick. Section 5 is an olive black (5Y 2/1) sandy mixture of SCORIA GRAVEL and fine-grained VITRIC SAND. Grayish black (N2) SCORIACEOUS PEBBLE GRAVELS in Section 6 and the core catcher represent 4% of the core.

Drilling disturbance varies from moderate to slight.

SMEAR SLIDE SUMMARY (%):

	1, 87 D	1, 115 M	2, 141 D	3, 80 D	3, 100 M	4, 83 D	4, 105 M
TEXTURE:							
Sand	20	70	1	20	10	85	75
Silt	20	20	6	30	85	5	10
Clay	60	10	93	40	5	10	20
COMPOSITION:							
Accessory minerals	Tr	Tr	—	Tr	Tr	—	1
Clay	50	10	61	20	5	6	18
Diatoms	1	—	1	Tr	—	—	—
Feldspar	1	2	1	2	1	8	3
Foraminifers	1	Tr	1	25	—	1	15
Glass	30	83	8	25	94	80	55
Lithic fragments	1	5	1	Tr	—	Tr	Tr
Mica	2	Tr	—	—	Tr	—	1
Nannofossils	12	Tr	25	15	—	Tr	5
Opaques	1	—	2	5	—	—	1
Pyroxene	—	—	—	—	—	2	—
Radiolarians	—	—	Tr	—	—	—	—
Silicoflagellates	1	—	2	1	—	—	1
Sponge spicules	—	Tr	1	2	—	—	—

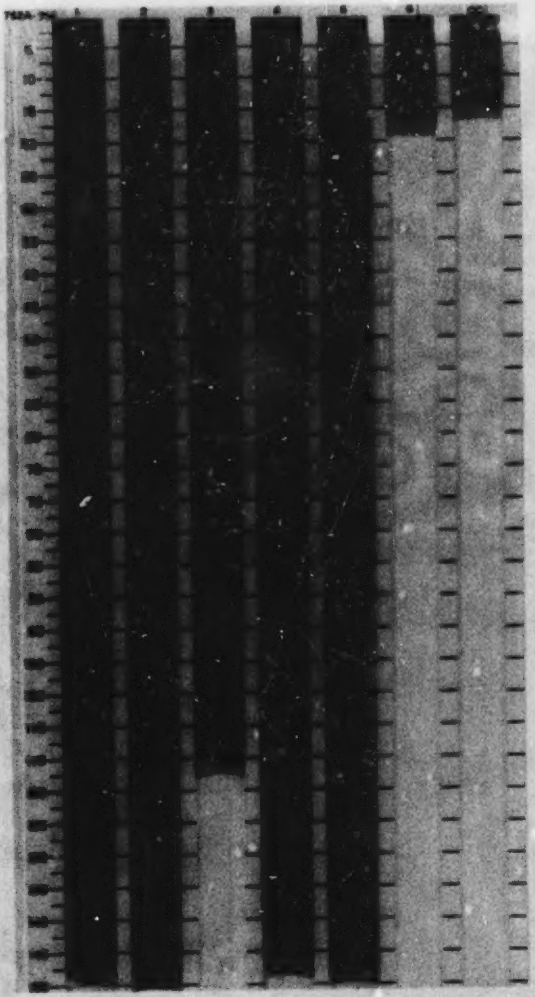
792A-7H
1
2
3
4
5
6
CC

SITE 792 HOLE A CORE 8H CORED INTERVAL 68.0-75.6 mbsf

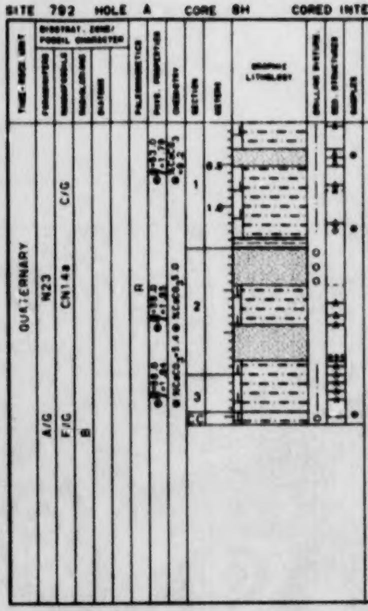
TIME-ROCK UNIT
BIOSTRAT. ZONE/ FOSSIL CHARACTER
FORAMINIFERS
NANNOFOSSILS
RADIOLARIANS
DIATOMS
PALEOMAGNETICS
PHYS. PROPERTIES
CHEMISTRY
SECTION
METERS
GRAPHIC LITHOLOGY
DRILLING DISTURB.
SED. STRUCTURES
SAMPLES
QUATERNARY
N23
A/G
CN14a
C/G
F/G
B
R
1
2
3
CC
0.5
1.0

LITHOLOGIC DESCRIPTION

NANNOFOSSIL RICH VITRIC SANDY MUD, VITRIC SANDY MUD AND VITRIC SAND

Major lithologies:
Olive gray (5Y 4/2) and black (5Y 2/2) NANNOFOSSIL RICH VITRIC SANDY MUD and VITRIC SANDY MUD comprise 56% of the core. Slight burrowing occurs only in Section 1, 26-32 cm and 98-104 cm. Grayish black (N2) VITRIC SAND occurs as ash layers, 1-9 cm thick, and in Section 2, 97-135 cm, where it is a normally graded, medium- to fine-grained bed that contains scattered pumice grains and foraminifers.

Minor lithology: Black (5Y 2/2) CLAYEY VITRIC SILT, comprising 6% of the core, occurs as a separate ash bed at the bottom of Section 1, and as caps, 1-5 cm thick, over sand layers.

Drilling disturbance is mostly moderate, but the top of Section 2 is soupy.

SMEAR SLIDE SUMMARY (%):

	1, 30 M	1, 128 D	CC, 3 M
TEXTURE:			
Sand	75	40	40
Silt	15	35	50
Clay	10	25	5
COMPOSITION:			
Accessory minerals	—	2	—
Clay	10	25	5
Diatoms	—	1	—
Feldspar	5	5	2
Foraminifers	2	10	—
Glass	74	40	87
Glauconite	—	Tr	—
Lithic fragments	5	Tr	5
Micrite	—	1	—
Nannofossils	2	15	Tr
Pyroxene	2	—	1
Radiolarians	—	Tr	—
Silicoflagellates	Tr	1	—
Spicules	—	Tr	—

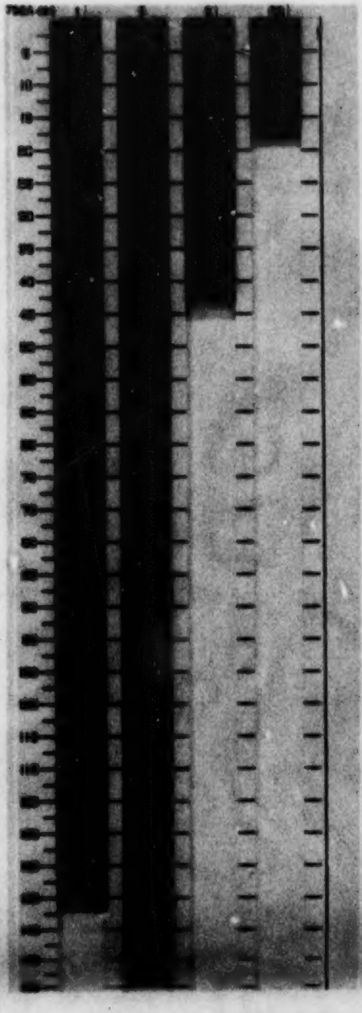
792A-8H
1
2
3
CC

SITE 792 HOLE A CORE 9H CORED INTERVAL 75.6-85.3 mbsf

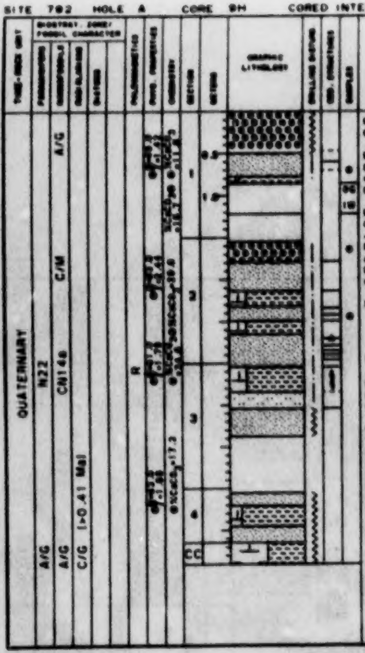
TIME-ROCK UNIT
BIOSTRAT. ZONE/ FOSSIL CHARACTER
FORAMINIFERS
NANNOFOSSILS
RADIOLARIANS
DIATOMS
PALEOMAGNETICS
PHYS. PROPERTIES
CHEMISTRY
SECTION
METERS
GRAPHIC LITHOLOGY
DRILLING DISTURB.
SED. STRUCTURES
SAMPLES
QUATERNARY
N22
A/G
CN14a
A/G
C/M
A/G
C/G (>0.41 Ma)
R
1
2
3
4
CC
0.5
1.0
OG
IW

LITHOLOGIC DESCRIPTION

NANNOFOSSIL-RICH CLAY, VITRIC SAND AND PUMICEOUS PEBBLE-GRANULE GRAVEL

Major lithologies:
Light olive gray (5Y 6/2) NANNOFOSSIL-RICH CLAY, in intervals 9-24 cm thick, comprises 42% of the core. It is structureless except for slight burrowing in Section 3. Another 42% of the core is composed of olive black (5Y 2/1) and dark gray (5Y 4/1) VITRIC SAND.

Minor lithologies:
Olive gray (5Y 4/2), gray (5Y 6/1) and very minor olive black (5Y 2/1) VITRIC SILT units, <10 cm thick, comprise 12% of the core. The top 50 cm of Section 1 is olive black (5Y 2/1) PUMICEOUS PEBBLE-GRANULE GRAVEL. Its thickness, and that of the sand in Section 4 and the core catcher, probably are exaggerated because the top (Section 1, 0-50 cm) and bottom (Section 3, 54 cm to cc) of the core is very disturbed by drilling. Disturbance is moderate in the rest of the core.

SMEAR SLIDE SUMMARY (%):

	1, 67 M	2, 16 D	2, 94 D
TEXTURE:			
Sand	5	5	20
Silt	75	15	50
Clay	20	80	30
COMPOSITION:			
Accessory minerals	—	Tr	—
Clay	25	45	30
Diatoms	—	1	Tr
Feldspar	1	1	2
Foraminifers	Tr	5	2
Glass	70	7	40
Lithic fragments	Tr	Tr	Tr
Micrite	1	3	2
Nannofossils	3	35	15
Opaques	—	—	1
Pyroxene	—	—	2
Radiolarians	—	Tr	—
Silicoflagellates	Tr	1	Tr
Spicules	Tr	2	Tr

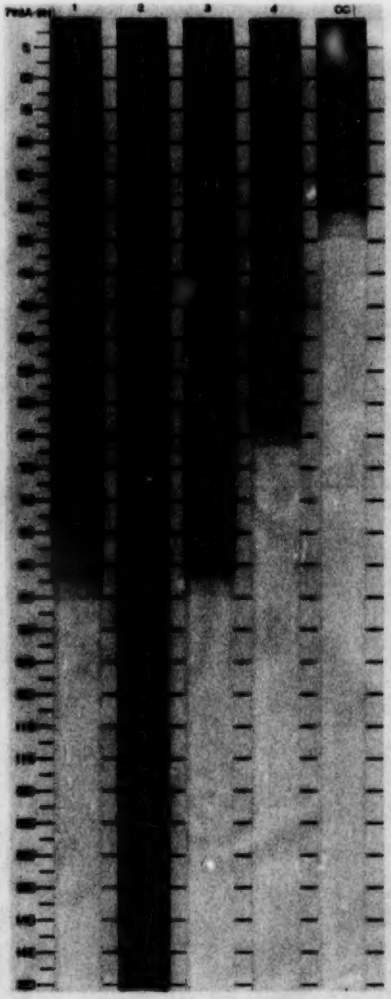
792A-9H
1
2
3
4
CC

SITE 792 HOLE A CORE 10H CORED INTERVAL 85.3-95.0 mbsf

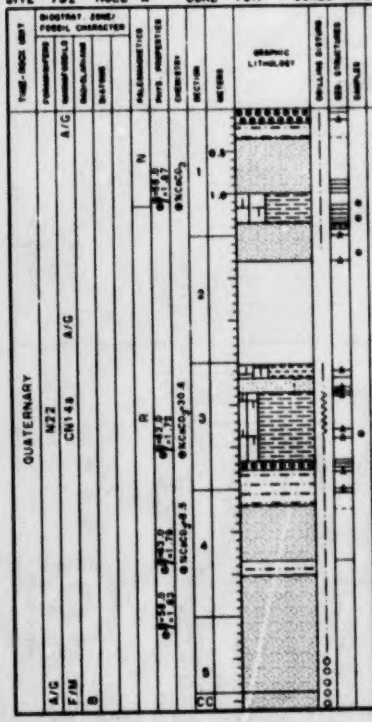
TIME-ROCK UNIT
BIOSTRAT. ZONE/FOSSIL CHARACTER
FORAMINIFERS
NANNOFOSSILS
RADIOLARIANS
DIATOMS
PALEOMAGNETICS
PHYS. PROPERTIES
CHEMISTRY
SECTION
METERS
GRAPHIC LITHOLOGY
DRILLING DISTURB.
SED. STRUCTURES
SAMPLES
QUATERNARY
N22
CN14a
A/G
A/G
A/G
A/G
F/M
B
N
R
CaCO3
CaCO3=30.4
CaCO3=8.5
1
2
3
4
5
CC
0.5
1.0

LITHOLOGIC DESCRIPTION

VITRIC SAND AND FORAMINIFER-NANNOFOSSIL VITRIC SILTY CLAY

Major lithologies: Gray (5Y 6/1), light olive gray (5Y 5/2) dark gray (5Y 4/1), and olive black (5Y 2/1) VITRIC SAND, in intervals 16-60 cm thick, comprises 51% of the core. Medium-grained, laminated intervals occur in Section 1, 132-150 cm, and in Section 4, 100-107 and 130-137 cm. A fine-grained unit in Section 3, 25-33 cm, is normally graded.

Most of the rest of the core (34%) is light olive gray (5Y 5/2) and dark gray (5Y 4/1) FORAMINIFER-NANNOFOSSIL VITRIC SILTY CLAY, with slight burrowing only in Section 1, 108-114 cm.

Minor lithologies:
Olive gray (5Y 4/2) and dark gray (5Y 4/1) VITRIC SANDY MUD (8% of the core) occurs in Sections 1 and 4, in layers 5-18 cm thick. Thin VITRIC SILT layers, dark gray (5Y 4/1) in Section 2, 6-8 cm, and gray (5Y 6/1) in Section 3, 39-44 cm, are probably ash.

Most of the core is only moderately disturbed by drilling, but Section 3, 34-85 cm is very disturbed, and Section 5 and the core catcher are soupy.

SMEAR SLIDE SUMMARY (%):

	1, 113	1, 130	2, 16	3, 86
	M	M	D	D
TEXTURE:				
Sand	10	10	15	15
Silt	10	20	25	35
Clay	80	70	60	50
COMPOSITION:				
Accessory minerals	Tr	1	Tr	—
Clay	38	22	43	36
Diatoms	1	—	1	—
Feldspar	2	2	5	2
Foraminifers	20	40	10	1
Glass	13	10	20	50
Glauconite	—	—	Tr	—
Lithic fragments	Tr	Tr	—	—
Micrite	2	5	3	2
Nannofossils	20	10	15	7
Opaques	—	Tr	—	1
Pellets	—	—	Tr	—
Pyroxene	—	—	—	2
Radiolarians	—	—	1	—
Silicoflagellates	3	—	2	—
Sponge spicules	1	1	Tr	—

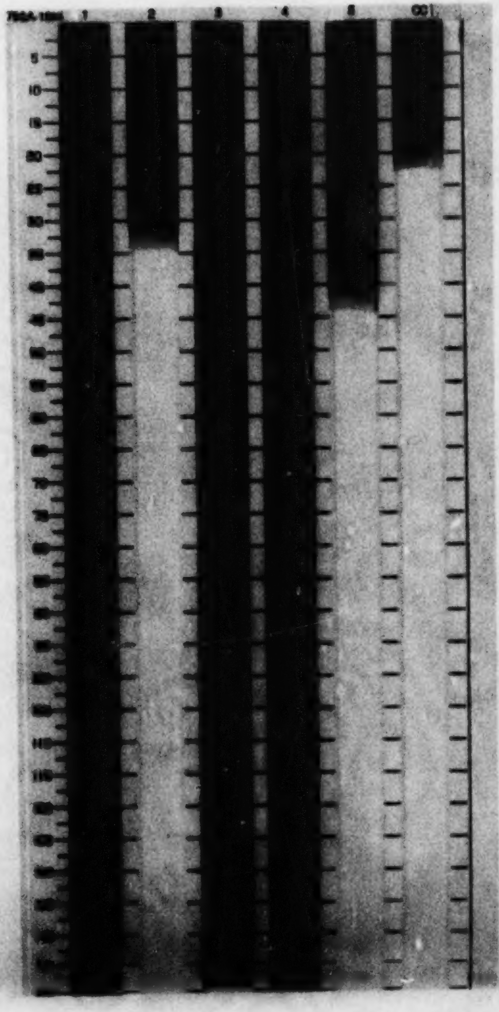
792A-10H
1
2
3
4
5
CC
5
10
15
20
25
30
35
40
45
50
55
60
65
70
75
80
85
90
95
100
105
110
115
120
125
130
135
140
145
150

SITE 792 HOLE B CORE 1H CORED INTERVAL 0.0-4.3 mbsf

TIME-ROCK UNIT	FORAMINIFERS	NANNOFOSSILS	RADIOLARIANS	DIATOMS	PALEOMAGNETICS	PHYS. PROPERTIES	CHEMISTRY	SECTION	METERS	GRAPHIC LITHOLOGY	DRILLING DISTURB.	SED. STRUCTURES	SAMPLES
QUATERNARY		CN15 C/G	C/G		N			1 2 3 CC	0.5 1.0				● ● ●

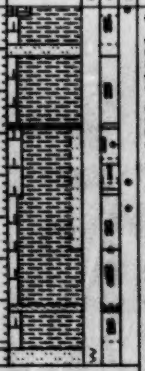

LITHOLOGIC DESCRIPTION

NANNOFOSSIL-RICH CLAYEY SILT and VITRIC SILT

Major lithologies:
Most of the core consists of dark gray (5Y 4/1), burrowed, NANNOFOSSIL-RICH CLAYEY SILT with scattered sand-sized volcanic ash grains and in Section 3, 29-32 cm, a 3-cm diameter pumice clast. The remaining 10-15% of the core is mainly medium light gray (N6) and light gray (N7), sharp-based, locally parallel laminated beds of VITRIC SILT (ash).

Minor lithologies:
Section 1, 0-8 cm, represents the surface sediment in this area, and consists of dark grayish brown (2.5Y 4/2), FORAMINIFER-NANNOFOSSIL-RICH CLAYEY SILT. Section 3, 61-67 cm, is an olive black (5Y 2/1) GRANULE-RICH SAND with abundant granules of pumice.

The core is essentially undisturbed by drilling.

SMEAR SLIDE SUMMARY (%):

	1, 2 M	2, 50 M	2, 80 D
TEXTURE:			
Silt	70	70	60
Clay	30	30	40
COMPOSITION:			
Clay	20	22	40
Diatoms	2	1	1
Feldspar	2	4	10
Foraminifers	2	—	5
Glass	60	70	20
Inorganic calcite	—	—	1
Lithic fragments	—	—	3
Nannofossils	10	1	10
Opaques	1	1	2
Quartz	1	—	—
Pyroxene	—	—	1
Radiolarians	1	—	1
Silicoflagellates	—	—	Tr
Spicules	1	—	2

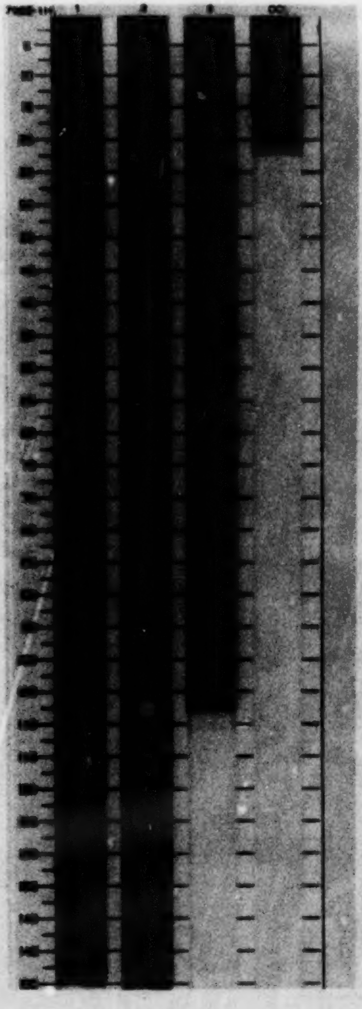

SITE 792 HOLE B CORE 2H CORED INTERVAL 50.0-59.6 mbsf

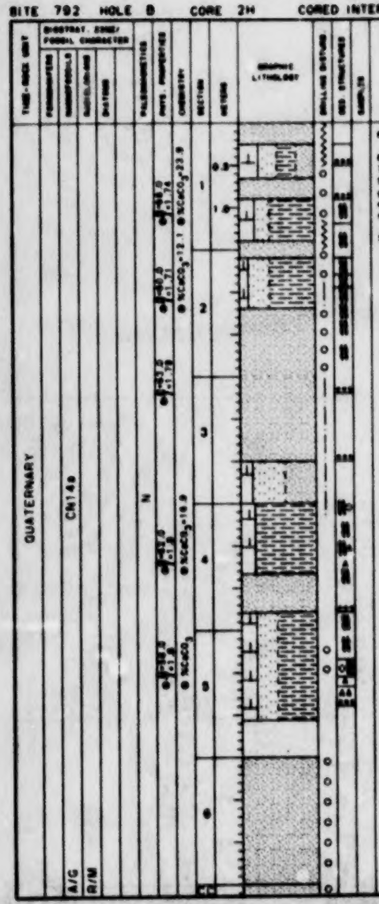
TIME-ROCK UNIT
BIOSTRAT. ZONE/ FOSSIL CHARACTER
FORAMINIFERS
NANNOFOSSILS
RADIOLARIANS
DIATOMS
PALEOMAGNETICS
PHYS. PROPERTIES
CHEMISTRY
SECTION
METERS
GRAPHIC LITHOLOGY
DRILLING DISTURB.
SED. STRUCTURES
SAMPLES
QUATERNARY
CN14a
A/G
R/M
N
%CaCO3=23.9
%CaCO3=12.1
%CaCO3=18.9
%CaCO3
0.5
1.0
1
2
3
4
5
6
CC

LITHOLOGIC DESCRIPTION

NANNOFOSSIL-RICH SILTY CLAY, VITRIC SILT AND VITRIC SAND

Major lithologies:
The background lithology in this core is dark gray (5Y 4/1), burrowed NANNOFOSSIL SILTY CLAY. This is interbedded with very thin to thick beds of grayish black (N2) to light gray (N7) VITRIC SILT and VITRIC SAND (ash beds), which are generally structureless except for local grading. All of Section 6 and the core catcher consists of dark gray (N3), medium- to coarse-grained VITRIC SAND.

Sections 1-3 are moderately disturbed to soupy. Section 6 is soupy.

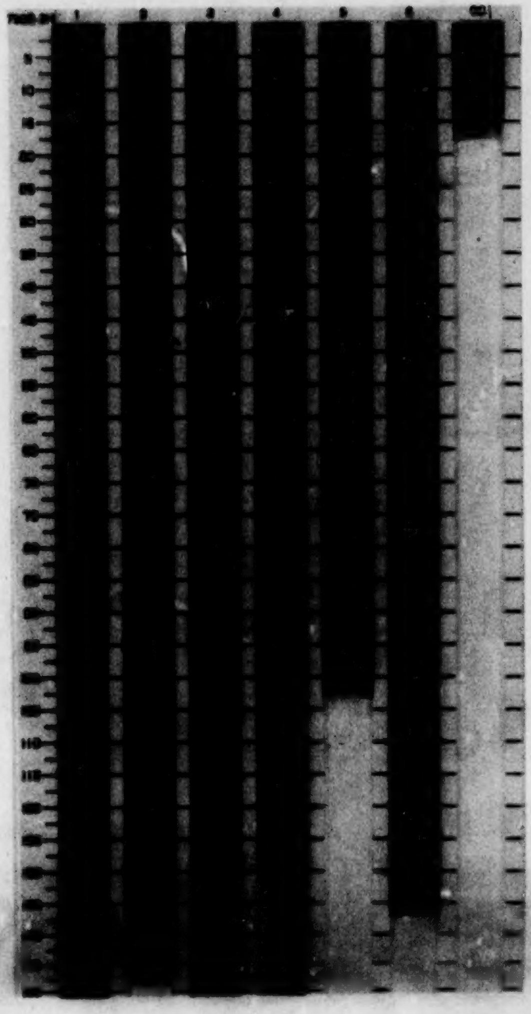

SITE 792 HOLE B CORE 3H CORED INTERVAL 59.6-69.2 mbsf

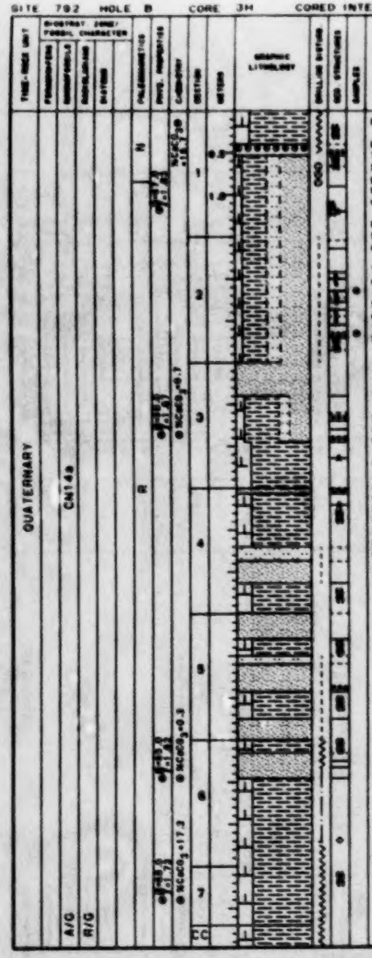
TIME-ROCK UNIT
BIOSTRAT. ZONE/ FOSSIL CHARACTER
FORAMINIFERS
NANNOFOSSILS
RADIOLARIANS
DIATOMS
PALEOMAGNETICS
PHYS. PROPERTIES
CHEMISTRY
SECTION
METERS
GRAPHIC LITHOLOGY
DRILLING DISTURB.
SED. STRUCTURES
SAMPLES
QUATERNARY
CN14a
A/G
R/G
N
R
%CaCO3=0.7
%CaCO3=0.3
%CaCO3=17.3
1
2
3
4
5
6
7
CC
0.5
1.0
OG

LITHOLOGIC DESCRIPTION

NANNOFOSSIL-RICH CLAYEY SILT, VITRIC SILT AND VITRIC SAND

Major lithologies:
This core consists of an intimate interbedding of burrowed, dark gray (5Y 4/1), NANNOFOSSIL-RICH CLAYEY SILT, and generally very thin to medium beds of black (N1) to very light gray (N8) VITRIC SILT and VITRIC SAND. Many normally graded sequences consist of a tri-partite bed of vitric silt/sand, overlain by very fine, structureless vitric silt, overlain by nannofossil-rich clayey silt.

Minor lithologies:
Section 1, 40-55 cm, consists of a bed of scoriaceous gravel with pebbles up to 1 cm in diameter. There is a 4.5-cm diameter clast of scoria near the base of Section 6.

The complexity of the interbedded lithologies in this core can be appreciated best from whole-core photographs.

Section 1, 0-40 cm, and Section 6, 18 cm to the base of the core, have been strongly disturbed by flow-in. Other parts of the core are only slightly disturbed.

SMEAR SLIDE SUMMARY (%)

	2, 65 D	2, 116 D
TEXTURE:		
Sand	—	80
Silt	20	20
Clay	80	—
COMPOSITION:		
Accessory minerals	1	Tr
Clay	80	—
Feldspar	2	2
Foraminifers	2	Tr
Glass	—	98
Nannofossils	14	—
Opaques	1	—

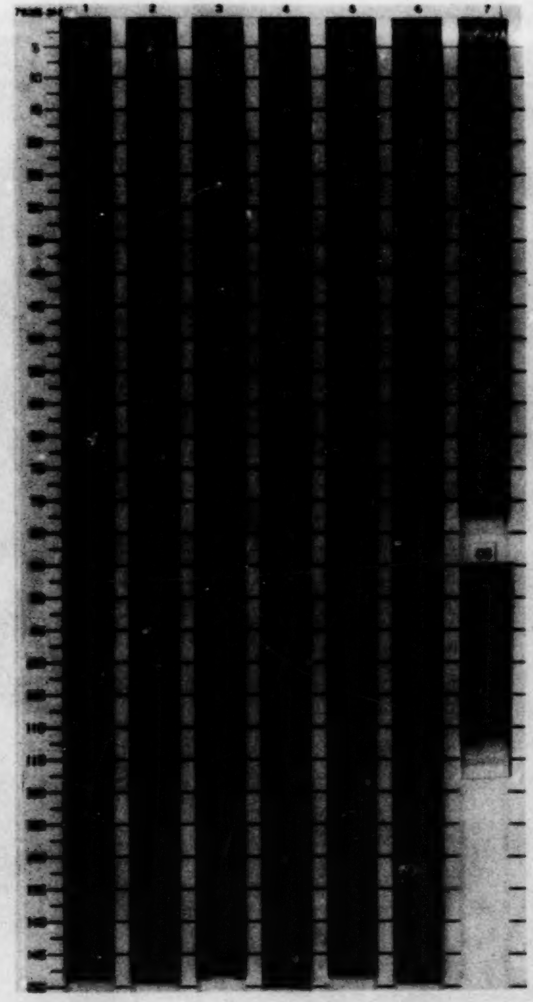

SITE 792 HOLE B CORE 4X CORED INTERVAL 69.2-78.8 mbsf

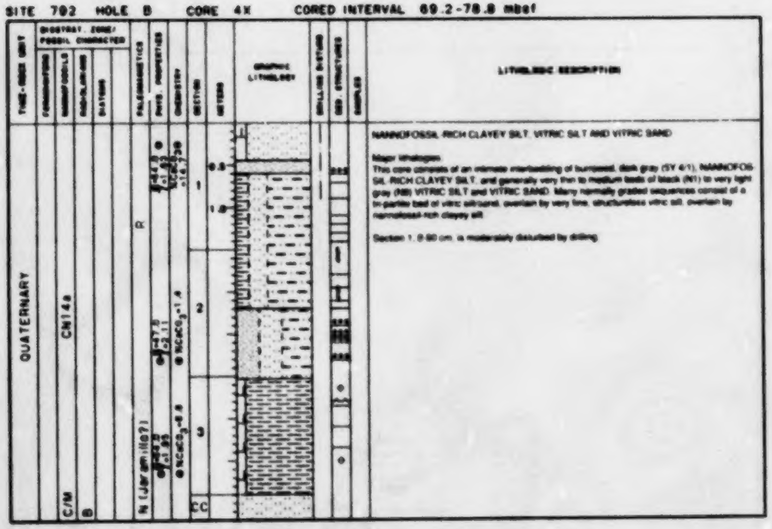
TIME-ROCK UNIT
BIOSTRAT. ZONE/ FOSSIL CHARACTER
FORAMINIFERS
NANNOFOSSILS
RADIOLARIANS
DIATOMS
PALEOMAGNETICS
PHYS. PROPERTIES
CHEMISTRY
SECTION
METERS
GRAPHIC LITHOLOGY
DRILLING DISTURB.
SED. STRUCTURES
SAMPLES
QUATERNARY
C/M
CN14a
B
R
N (Jaramillo?)
●%CaCO3=1.4
●%CaCO3=8.8
1
2
3
CC
0.5
1.0

LITHOLOGIC DESCRIPTION

NANNOFOSSIL-RICH CLAYEY SILT, VITRIC SILT AND VITRIC SAND

Major lithologies:
This core consists of an intimate interbedding of burrowed, dark gray (5Y 4/1), NANNOFOSSIL-RICH CLAYEY SILT, and generally very thin to medium beds of black (N1) to very light gray (N8) VITRIC SILT and VITRIC SAND. Many normally graded sequences consist of a tri-partite bed of vitric silt/sand, overlain by very fine, structureless vitric silt, overlain by nannofossil-rich clayey silt.

Section 1, 0-90 cm, is moderately disturbed by drilling.

SITE 792 HOLE B CORE 5X CORED INTERVAL 78.8-88.5 mbsf

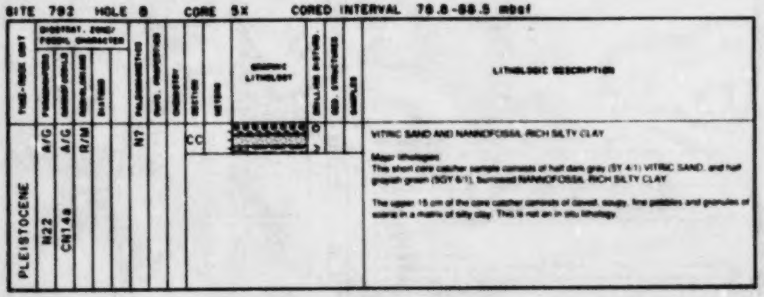
TIME-ROCK UNIT
BIOSTRAT. ZONE/ FOSSIL CHARACTER
FORAMINIFERS
NANNOFOSSILS
RADIOLARIANS
DIATOMS
PALEOMAGNETICS
PHYS. PROPERTIES
CHEMISTRY
SECTION
METERS
GRAPHIC LITHOLOGY
DRILLING DISTURB.
SED. STRUCTURES
SAMPLES
PLEISTOCENE
A/G
N22
A/G
CN14a
R/M
N?
CC

LITHOLOGIC DESCRIPTION

VITRIC SAND AND NANNOFOSSIL-RICH SILTY CLAY

Major lithologies:
This short core catcher sample consists of half dark gray (5Y 4/1) VITRIC SAND, and half grayish green (5GY 6/1), burrowed NANNOFOSSIL-RICH SILTY CLAY.

The upper 15 cm of the core catcher consists of caved, soupy, fine pebbles and granules of scoria in a matrix of silty clay. This is not an in situ lithology.

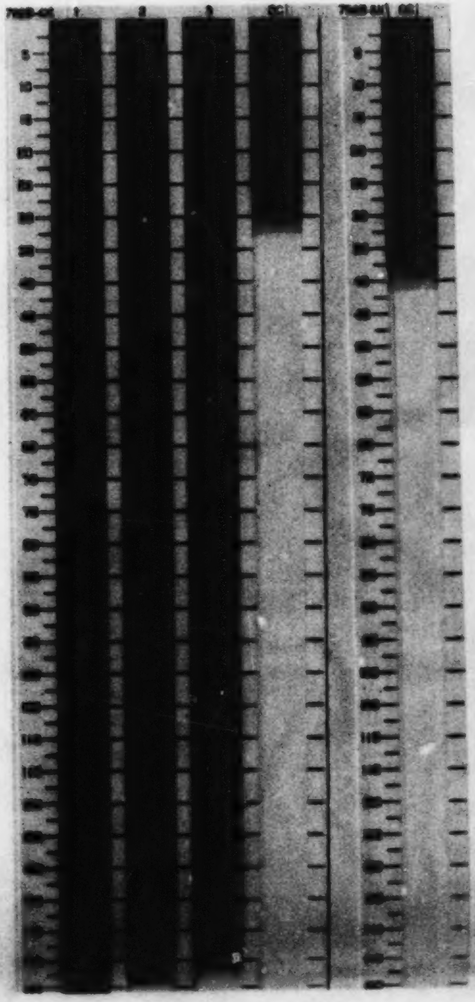
792B-4X
1
2
3
CC
792B-5X
CC

SITE 792 HOLE B CORE 6X CORED INTERVAL 88.5-98.2 mbsf

TIME-ROCK UNIT	BIOSTRAT. ZONE/ FOSSIL CHARACTER				PALEOMAGNETICS	PHYS. PROPERTIES	CHEMISTRY	SECTION	METERS	GRAPHIC LITHOLOGY	DRILLING DISTURB.	SED. STRUCTURES	SAMPLES	LITHOLOGIC DESCRIPTION
	FORAMINIFERS	NANNOFOSSILS	RADIOLARIANS	DIATOMS										
PLEISTOCENE		CN14a A/G	R/P					CC			O			SCORIACEOUS GRAVEL Major lithology: The only material in this short core catcher sample is a soupy, dark gray (N3) SCORIACEOUS GRAVEL. This is probably 100% cavings, and should not be considered as in situ sediment.

SITE 792 HOLE B CORE 7X CORED INTERVAL 98.2-107.9 mbsf

TIME-ROCK UNIT	BIOSTRAT. ZONE/ FOSSIL CHARACTER				PALEOMAGNETICS	PHYS. PROPERTIES	CHEMISTRY	SECTION	METERS	GRAPHIC LITHOLOGY	DRILLING DISTURB.	SED. STRUCTURES	SAMPLES	LITHOLOGIC DESCRIPTION
	FORAMINIFERS	NANNOFOSSILS	RADIOLARIANS	DIATOMS										
UPPER PLIOCENE	? C/G	CN12a A/G	R/P			[illegible]	[illegible]	CC						CLAYEY SILT Major lithology: This short core catcher sample consists of dark gray (5GY 4/1), strongly disturbed CLAYEY SILT.

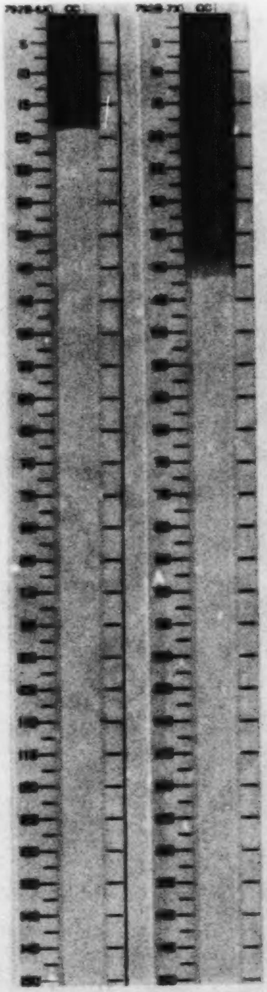

SITE 792 HOLE B CORE 8X CORED INTERVAL 107.9-117.5 mbsf

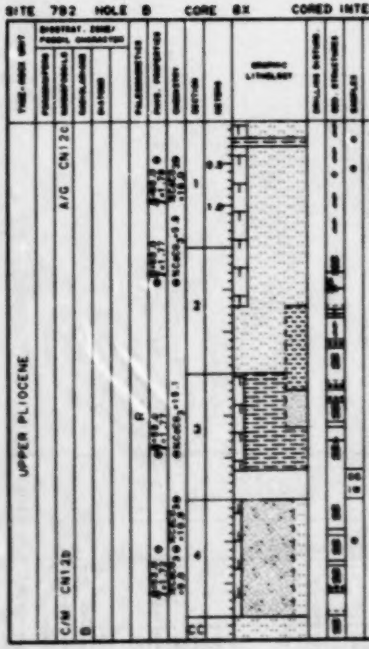
TIME-ROCK UNIT
BIOSTRAT. ZONE/ FOSSIL CHARACTER
FORAMINIFERS
NANNOFOSSILS
RADIOLARIANS
DIATOMS
PALEOMAGNETICS
PHYS. PROPERTIES
CHEMISTRY
SECTION
METERS
GRAPHIC LITHOLOGY
DRILLING DISTURB.
SED. STRUCTURES
SAMPLES
UPPER PLIOCENE
A/G CN12c
C/M CN12b
B
R
1
2
3
4
CC
0.5
1.0

LITHOLOGIC DESCRIPTION

FORAMINIFER-RICH VITRIC SILT, VITRIC SILTY CLAY, VITRIC SILT, VITRIC SAND, VITRIC SILTY SAND AND VITRIC SANDY SILT

Major lithologies:

The bulk of this core consists of one of the following bioturbated lithologies: dark gray (5Y 4/1) FORAMINIFER-RICH VITRIC SILT, dark gray (5Y 4/1) VITRIC SILT, or dark gray (5Y 4/1) to dark gray (5GY 4/1) VITRIC SILTY SAND to VITRIC SANDY SILT. The remainder of the core consists of grayish black (N2) to light gray (N7) thin to medium beds of VITRIC SILTY CLAY, VITRIC SILT and VITRIC SAND (ash beds).

The core is essentially undisturbed by drilling.

SMEAR SLIDE SUMMARY (%):

	1, 22 M	1, 58 D	4, 90 D
TEXTURE:			
Sand	—	10	60
Silt	40	80	30
Clay	60	10	10
COMPOSITION:			
Clay	30	—	10
Diatoms	Tr	—	—
Feldspar	10	12	10
Foraminifers	—	20	10
Glass	60	60	70
Nannofossils	Tr	5	—
Pyroxene	—	3	Tr
Spicules	—	Tr	—

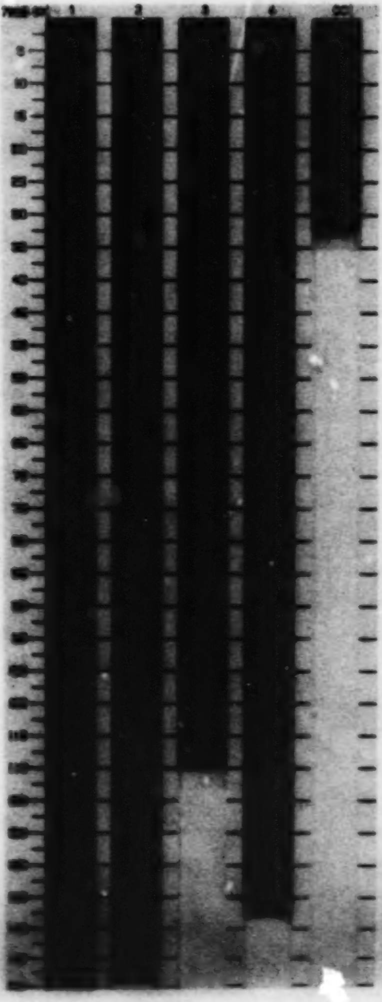
792B-8X
1
2
3
4
CC

SITE 792 HOLE B CORE 9X CORED INTERVAL 117.5-127.1 mbsf

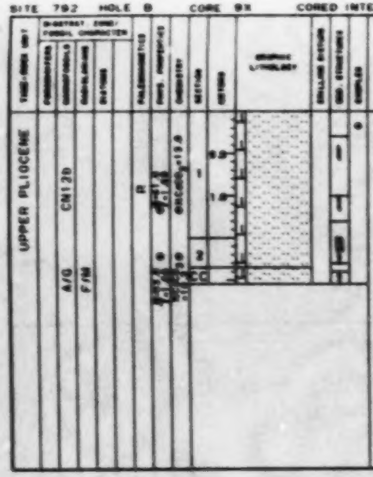

LITHOLOGIC DESCRIPTION

NANNOFOSSIL-RICH VITRIC SILT

Major lithology: The core is almost entirely dark gray (5Y 4/1), slightly burrowed NANNOFOSSIL-RICH VITRIC SILT, interbedded with widely separated beds, generally <2 cm thick, of light gray (N7) VITRIC SILT (ash).

The core is essentially undisturbed by drilling.

SMEAR SLIDE SUMMARY (%):

	1, 20
	D
TEXTURE:	
Silt	20
Clay	80
COMPOSITION:	
Clay	62
Diatoms	1
Feldspar	2
Foraminifers	1
Glass	20
Inorganic calcite	1
Nannofossils	10
Opaques	1
Pyroxene	1
Spicules	1

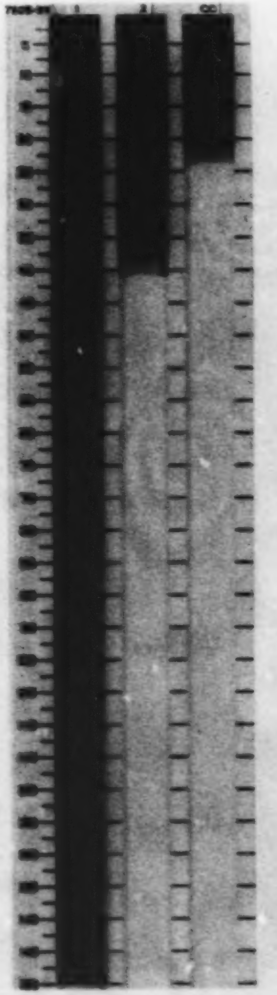

SITE 792 HOLE B CORE 10X CORED INTERVAL 127.1-136.8 mbsf

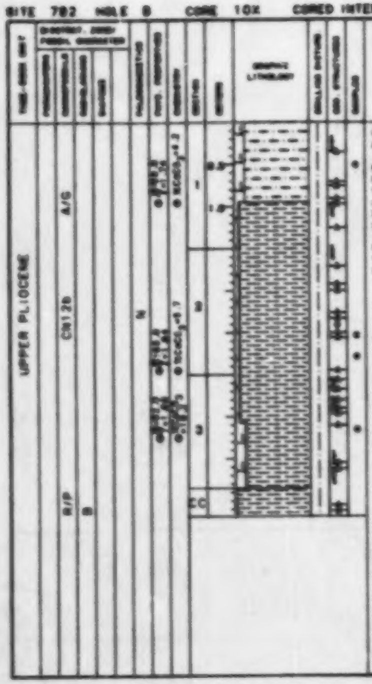
TIME-ROCK UNIT
BIOSTRAT. ZONE/FOSSIL CHARACTER
FORAMINIFERS
NANNOFOSSILS
RADIOLARIANS
DIATOMS
PALEOMAGNETICS
PHYS. PROPERTIES
CHEMISTRY
SECTION
METERS
GRAPHIC LITHOLOGY
DRILLING DISTURB.
SED. STRUCTURES
SAMPLES
UPPER PLIOCENE
A/G
CN12b
B/P
B
N
● %CaCO3=4.2
● %CaCO3=6.7
1
2
3
CC
0.5
1.0

LITHOLOGIC DESCRIPTION

VITRIC CLAYEY SILT, VITRIC SILTY CLAY, NANNOFOSSIL RICH VITRIC SILTY CLAY AND NANNOFOSSIL RICH VITRIC SANDY MUD

Major lithologies:
More than half (51%) of the core consists of olive gray (5Y 4/2) VITRIC CLAYEY SILT, VITRIC SILTY CLAY and NANNOFOSSIL RICH VITRIC SILTY CLAY. Two closely associated lithologies with the same color are VITRIC SILTY CLAY (18% of the core) and in Section 1, 0-72 cm, NANNOFOSSIL RICH VITRIC SANDY MUD (17% of the core). These sediments are slightly burrowed.

Minor lithologies:
Very dark gray (5Y 3/1), dark gray (5Y 4/1), olive gray (5Y5/2) light olive gray (5Y 6/2), and light gray (5Y 7/1) VITRIC SILT and VITRIC SAND occur throughout the core as ash layers 1-7 cm thick. Several of the thicker ones are planar laminated.

The entire core has been moderately disturbed by drilling.

SMEAR SLIDE SUMMARY (%):

	1, 50 D	2, 102 M	2, 139 D	3, 67 D
TEXTURE:				
Sand	35	3	10	20
Silt	30	77	65	35
Clay	35	20	25	45
COMPOSITION:				
Accessory minerals	Tr	Tr	2	—
Barite	—	—	Tr	Tr
Clay	25	20	20	41
Dolomite	Tr	—	1	1
Feldspar	1	2	2	—
Foraminifers	1	—	Tr	1
Glass	55	60	68	40
Glauconite	—	—	—	Tr
Lithic fragments	1	1	—	—
Micrite	2	—	2	5
Nannofossils	10	Tr	3	10
Opaques	3	15	—	Tr
Radiolarians	—	—	1	Tr
Silicoflagellates	—	—	—	1
Spicules	2	—	1	1

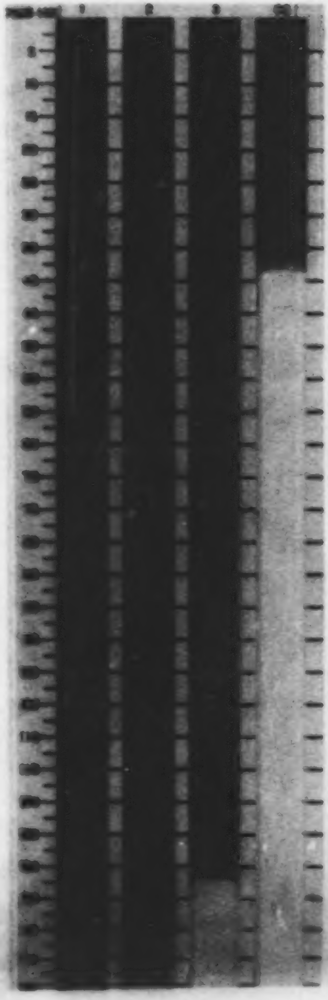

SITE 792 HOLE B CORE 11X CORED INTERVAL 130.8-140.4 mbsf

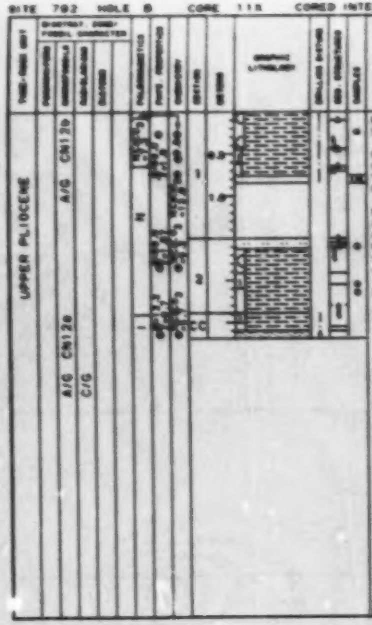

LITHOLOGIC DESCRIPTION

BIOGENIC SILICA-RICH LITHIC VITRIC SILTY CLAY AND NANNOFOSSIL-RICH VITRIC SILTY CLAY

Major lithologies:
51% of the core is composed of olive gray (5Y 3/2) BIOGENIC SILICA-RICH LITHIC VITRIC SILTY CLAY that is slightly bioturbated in places. Dark gray (5Y 4/1), structureless NANNOFOSSIL-RICH VITRIC SILTY CLAY comprises another 28% of the core.

Minor lithologies:
Light and dark-colored VITRIC SILT and VITRIC SAND ash layers 1-6 cm thick, in approximately equal abundances, together comprise 21% of the core. The dark colors are grayish black (N2) and very dark grayish brown (5Y 3/2); the light colors are gray (5Y 6/1) and gray (5Y 5/1). The ash beds are structureless except for a light-colored layer in Section 2, 60-66 cm, which contains burrows, 2-3 cm wide, that are filled with olive gray (5Y 4/2) silty clay.

Section 1 and the core catcher are moderately disturbed by drilling.

SMEAR SLIDE SUMMARY (%):

	1, 35 D	2, 10 M	2, 55 M	2, 64 M
TEXTURE:				
Sand	20	10	Tr	15
Silt	25	50	95	35
Clay	55	40	5	50
COMPOSITION:				
Accessory minerals	1	1	Tr	1
Clay	50	35	5	40
Diatoms	2	Tr	—	1
Feldspar	2	2	Tr	1
Foraminifers	1	1	Tr	1
Glass	15	50	95	35
Lithic fragments	10	Tr	—	—
Mica	—	1	Tr	3
Nannofossils	4	6	Tr	10
Opaques	1	2	Tr	1
Radiolarians	Tr	—	—	1
Silicoflagellates	10	—	—	2
Sponge spicules	1	1	—	1
Zeolite	—	2	—	—

792B-11X
1
2
CC

SITE 792 HOLE C CORE 1X CORED INTERVAL 136.8-146.4 mbsf

TIME-ROCK UNIT	FORAMINIFERS	NANNOFOSSILS	RADIOLARIANS	DIATOMS		PALEOMAGNETICS	PHYS. PROPERTIES	CHEMISTRY	SECTION	METERS	GRAPHIC LITHOLOGY	DRILLING DISTURB.	SED. STRUCTURES	SAMPLES
UPPER PLIOCENE		A/G CN12a	C/G			N		● [illegible]	CC					● ●

LITHOLOGIC DESCRIPTION

NANNOFOSSIL-RICH VITRIC SILTY CLAYSTONE

Major lithology: Except for the minor lithologies listed below, 90% of the core consists of olive gray (5Y 4/2) NANNOFOSSIL-RICH VITRIC SILTY CLAYSTONE. A burrow, 12 cm in diameter at 33 cm, is filled by olive gray (5Y 3/2) medium-grained sand.

Minor lithologies:
A VITRIC ASH layer at 13-18 cm is colored gray (5Y 6/1) in its upper and lower thirds, and gray (5Y 5/1) in the middle. Two 1-cm thick grayish black (N2) layers of coarse-grained scoriaceous sand occur at 26 and 27 cm.

The core is moderately disturbed by drilling from 0-40 cm, and very disturbed from 40-51 cm.

SMEAR SLIDE SUMMARY (%):

	CC, 8 D	CC, 10 M
TEXTURE:		
Sand	5	1
Silt	40	74
Clay	55	25
COMPOSITION:		
Accessory minerals	1	Tr
Clay	52	20
Diatoms	2	—
Feldspar	2	4
Foraminifers	1	Tr
Glass	25	68
Lithic fragments	Tr	Tr
Mica	2	1
Nannofossils	12	2
Opaques	—	5
Quartz	Tr	—
Radiolarians	Tr	—
Silicoflagellates	3	—

792C-1X, CC
0
10
20
30
40
50
60
70
80
90
100
110
120
130
140
150

SITE 792 HOLE D CORE 1X CORED INTERVAL 136.0-145.6 mbsf

TIME-ROCK UNIT	BIOSTRAT. ZONE/ FOSSIL CHARACTER: FORAMINIFERS	NANNOFOSSILS	RADIOLARIANS	DIATOMS	PALEOMAGNETICS	PHYS. PROPERTIES	CHEMISTRY	SECTION	METERS	GRAPHIC LITHOLOGY	DRILLING DISTURB.	SED. STRUCTURES	SAMPLES
UPPER PLIOCENE	N21 - N22 C/G	CN12a A/G	S. pentas C/G		N	[illegible]	[illegible]	1 CC		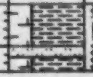			● ● ●

LITHOLOGIC DESCRIPTION

NANNOFOSSIL-RICH VITRIC SILTY CLAY

Major lithology: 90% of the core consists of structureless olive gray (5Y 4/2) NANNOFOSSIL-RICH VITRIC SILTY CLAYSTONE.

Minor lithologies:
A grayish black (N2), very fine-grained VITRIC SAND occurs at 31-33 cm, and a light gray (5Y 7/1) VITRIC SILT layer occurs at Section 1, 47-50 cm. Both of these layers are ash beds.

The core is very disturbed by drilling in Section 1, 0-15 cm and in the core catcher, and moderately disturbed in Section 1, 15-50 cm.

SMEAR SLIDE SUMMARY (%):

	1, 28 D	1, 47 M	CC, 16 D
TEXTURE:			
Sand	20	—	15
Silt	25	100	35
Clay	55	—	50
COMPOSITION:			
Clay	48	—	40
Diatoms	1	—	2
Feldspar	2	1	2
Foraminifers	4	—	2
Glass	25	98	30
Lithic fragments	7	Tr	8
Micrite	3	Tr	—
Nannofossils	15	Tr	12
Opaques	1	—	—
Pyroxene	—	—	2
Radiolarians	Tr	—	1
Silicoflagellates	3	—	3
Spicules	1	—	1

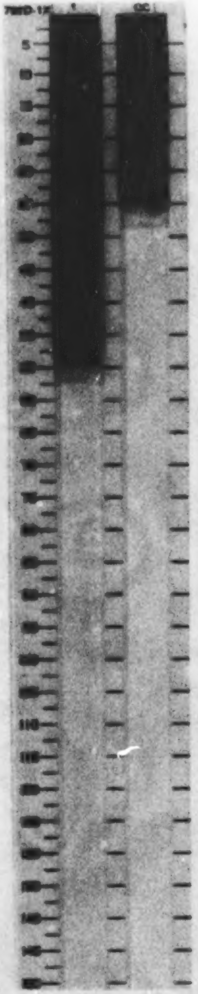

SITE 792 HOLE E CORE 1R CORED INTERVAL 135.6-145.2 mbsf

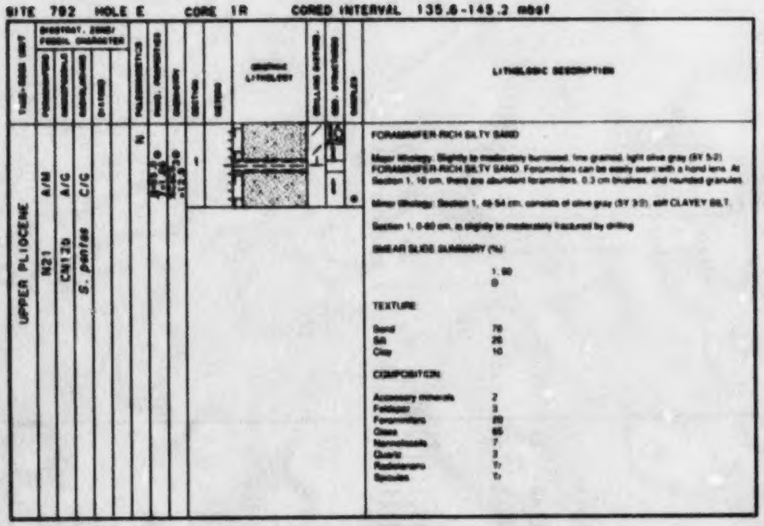
TIME-ROCK UNIT
BIOSTRAT. ZONE/FOSSIL CHARACTER
FORAMINIFERS
NANNOFOSSILS
RADIOLARIANS
DIATOMS
PALEOMAGNETICS
PHYS. PROPERTIES
CHEMISTRY
SECTION
METERS
GRAPHIC LITHOLOGY
DRILLING DISTURB.
SED. STRUCTURES
SAMPLES
UPPER PLIOCENE
N21 A/M
CN12b A/G
S. pentas C/G
N
1

LITHOLOGIC DESCRIPTION

FORAMINIFER-RICH SILTY SAND

Major lithology: Slightly to moderately burrowed, fine grained, light olive gray (5Y 5/2) FORAMINIFER-RICH SILTY SAND. Foraminifers can be easily seen with a hand lens. At Section 1, 10 cm, there are abundant foraminifers, 0.3 cm bivalves, and rounded granules.

Minor lithology: Section 1, 49-54 cm, consists of olive gray (5Y 3/2), stiff CLAYEY SILT.

Section 1, 0-60 cm, is slightly to moderately fractured by drilling.

SMEAR SLIDE SUMMARY (%):

	1, 50
	D
TEXTURE:	
Sand	70
Silt	20
Clay	10
COMPOSITION:	
Accessory minerals	2
Feldspar	3
Foraminifers	20
Glass	65
Nannofossils	7
Quartz	3
Radiolarians	Tr
Spicules	Tr

SITE 792 HOLE E CORE 2R CORED INTERVAL 145.2-154.8 mbsf

TIME-ROCK UNIT	FORAMINIFERS	NANNOFOSSILS	RADIOLARIANS	DIATOMS	PALEOMAGNETICS	PHYS. PROPERTIES	CHEMISTRY	SECTION	METERS	GRAPHIC LITHOLOGY	DRILLING DISTURB.	SED. STRUCTURES	SAMPLES
UPPER PLIOCENE	N21 A/M A/G	CN12a A/G	*S. pentas* C/G		N			1					●

LITHOLOGIC DESCRIPTION

NANNOFOSSIL-RICH VITRIC SILTY CLAY

Major lithology: Olive gray (5Y 4/2) NANNOFOSSIL-RICH VITRIC SILTY CLAY. The interval 11-17 cm is slightly burrowed, and the burrows are filled with medium- to coarse-grained volcaniclastic sand.

Minor lithology: At 17 cm there is a dark greenish gray (10Y5/1) pocket of silt-sized ash.

SMEAR SLIDE SUMMARY (%):

	1, 21
	D
TEXTURE:	
Sand	2
Silt	23
Clay	75
COMPOSITION:	
Accessory minerals	Tr
Biotite	Tr
Clay	62
Diatoms	3
Feldspar	1
Foraminifers	1
Glass	15
Lithic fragments	2
Micrite	1
Nannofossils	10
Radiolarians	Tr
Sponge spicules	5
[illegible]	Tr

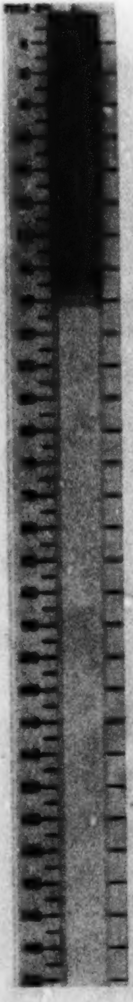

SITE 792 HOLE E CORE 3R CORED INTERVAL 154.8-164.5 mbsf

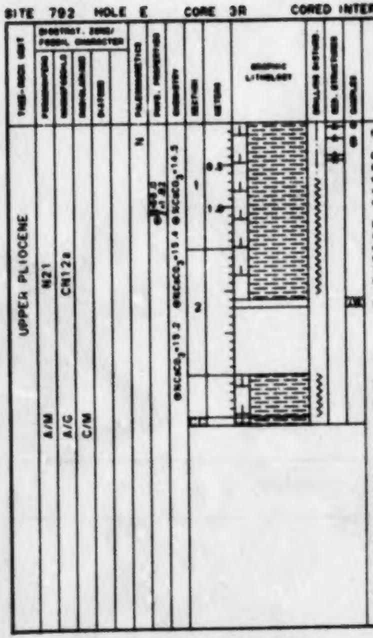
TIME-ROCK UNIT
BIOSTRAT. ZONE/ FOSSIL CHARACTER
FORAMINIFERS
NANNOFOSSILS
RADIOLARIANS
DIATOMS
PALEOMAGNETICS
PHYS. PROPERTIES
CHEMISTRY
SECTION
METERS
GRAPHIC LITHOLOGY
DRILLING DISTURB.
SED. STRUCTURES
SAMPLES
UPPER PLIOCENE
N21
A/M
CN12a
A/G
C/M
N
●%CaCO3=15.2 ●%CaCO3=15.4 ●%CaCO3=14.5
1
2
0.5
1.0

LITHOLOGIC DESCRIPTION

NANNOFOSSIL-RICH VITRIC SILTY CLAY

Major lithology: NANNOFOSSIL-RICH VITRIC SILTY CLAY comprises the entire core. It is light olive gray (5Y 5/2) in Section 1, 0-3 cm, and olive gray (5Y 4/2) in Section 1, 7-41 cm, where the core is only moderately disturbed by drilling. In the rest of the core, it has been very disturbed by drilling, and is mixed with the darker minor lithologies to homogenized olive gray (5Y 3/2).

Minor lithologies:
In the upper, less disturbed part of the core, there are three layers, 2-4 cm thick, of light olive gray (5Y 5/2), light gray (N7), and gray (5Y 6/1) VITRIC SILT, and four thin (1-3 cm thick) beds of grayish black (N2) and brownish black (5YR 2/1) ash layers that are CRYSTAL-VITRIC SANDY MUD except for the layer in Section 1, 44-46 cm, which is SCORIA PEBBLE-GRANULE GRAVEL.

SMEAR SLIDE SUMMARY (%):

	1, 5 M	1, 21 M	1, 26 D
TEXTURE:			
Sand	2	20	3
Silt	98	55	27
Clay	Tr	25	70
COMPOSITION:			
Accessory minerals	Tr	5	1
Clay	Tr	20	66
Diatoms	—	Tr	1
Feldspar	2	7	1
Foraminifers	—	—	1
Glass	97	58	12
Lithic fragments	1	Tr	1
Micrite	—	—	1
Nannofossils	Tr	2	12
Opaques	—	5	1
Oxide	—	2	—
Radiolarians	—	—	Tr
Silicoflagellates	—	—	2
Spicules	—	1	1

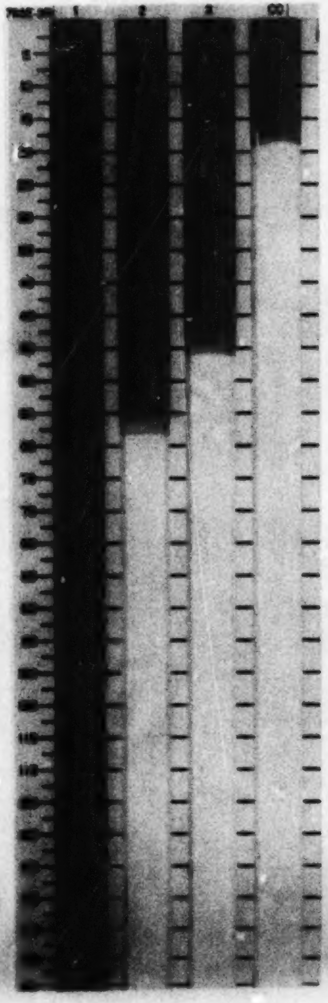
792E-3R
1
2
3
CC

SITE 792 HOLE E CORE 4R CORED INTERVAL 164.5-174.1 mbsf

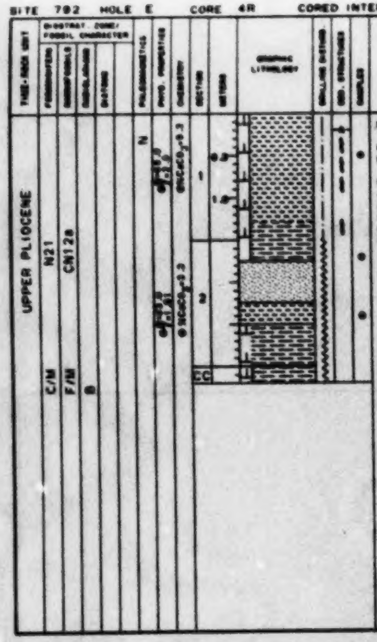
TIME-ROCK UNIT
BIOSTRAT. ZONE/ FOSSIL CHARACTER
FORAMINIFERS
NANNOFOSSILS
RADIOLARIANS
DIATOMS
PALEOMAGNETICS
PHYS. PROPERTIES
CHEMISTRY
SECTION
METERS
GRAPHIC LITHOLOGY
DRILLING DISTURB.
SED. STRUCTURES
SAMPLES
UPPER PLIOCENE
N21
C/M
CN12a
F/M
B
N
$CaCO_3$=0.3
$CaCO_3$=0.3
1
2
CC
0.5
1.0

LITHOLOGIC DESCRIPTION

NANNOFOSSIL-RICH CLAY

Major lithology: More than half (56%) of the core is composed of olive gray (5Y 4/2), slightly burrowed NANNOFOSSIL-RICH CLAY.

Minor lithologies:
A layer of structureless, silty, very coarse, grayish black (N2) VITRIC SAND in Section 2, 25-75 cm, comprises 16% of the core. It is underlain by a olive black (5Y 2/1), structureless CLAY (14% of the core). Variable contents of volcaniclastic and biogenic components give rise to two olive gray (5Y 3/2) variations from the major lithology: NANNOFOSSIL-RICH SILTY CLAY (9% of the core), and VITRIC SILTY CLAY (5%).

The core is moderately disturbed by drilling in Section 1 and is highly disturbed in the rest of the core.

SMEAR SLIDE SUMMARY (%):

	1, 50 D	2, 20 M	2, 81 M
TEXTURE:			
Sand	5	5	7
Silt	20	25	13
Clay	75	70	80
COMPOSITION:			
Accessory minerals	2	2	2
Biotite	Tr	—	—
Clay	60	60	60
Diatoms	Tr	1	Tr
Feldspar	5	2	2
Foraminifers	1	Tr	Tr
Glass	10	24	13
Lithic fragments	—	Tr	1
Micrite	2	1	1
Nannofossils	13	3	2
Opaques	1	—	1
Radiolarians	Tr	—	—
Silicoflagellates	Tr	Tr	—
Spicules	1	—	—
Zeolite	—	—	1

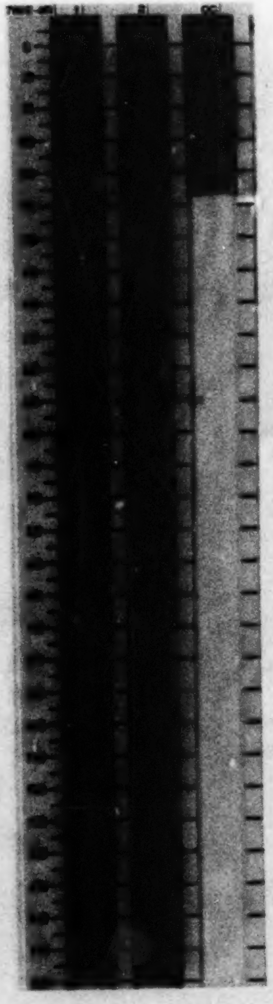
TIME-4R
1
2
CC
0
100

SITE 792 HOLE E CORE 5R CORED INTERVAL 174.1-183.7 mbsf

TIME-ROCK UNIT	BIOSTRAT. ZONE/ FOSSIL CHARACTER: FORAMINIFERS	NANNOFOSSILS	RADIOLARIANS	DIATOMS	PALEOMAGNETICS	PHYS. PROPERTIES	CHEMISTRY	SECTION	METERS	GRAPHIC LITHOLOGY	DRILLING DISTURB.	SED. STRUCTURES	SAMPLES
UPPER PLIOCENE	A/G N21 C/M	CN12a A/G	R/P		N			1 CC	0.5				

LITHOLOGIC DESCRIPTION

NANNOFOSSIL RICH VITRIC SILTY CLAY

Major lithology: Structureless, olive gray (5Y 4/2) NANNOFOSSIL RICH VITRIC SILTY CLAY constitutes 85% of the core.

Minor lithologies:
10% of the core is a dark gray (5Y 4/1) VITRIC SILTSTONE ash layer in Section 1, 25-32 cm, the first lithified interval in the hole. The remaining 5% of the core consists of olive (5Y 5/3) and gray (5Y 5/1) VITRIC SILT intervals at the bottom of Section 1 and in the core catcher.

The core is very disturbed in Section 1, 0-8 cm, moderately fractured in Section 1, 10-30 cm, moderately disturbed in Section 1, 32-75 cm, and very disturbed in the core catcher.

SMEAR SLIDE SUMMARY (%)

	1, 26 M	1, 63 D	1, 73 M
TEXTURE:			
Sand	20	10	30
Silt	70	30	60
Clay	10	60	10
COMPOSITION:			
Accessory minerals	—	Tr	Tr
Clay	10	50	10
Diatoms	1	1	Tr
Feldspar	2	1	1
Foraminifers	Tr	1	Tr
Glass	81	30	87
Lithic fragments	Tr	—	—
Micrite	Tr	2	—
Nannofossils	1	15	2
Opaques	5	—	Tr
Silicoflagellates	—	Tr	Tr
Spicules	—	Tr	—

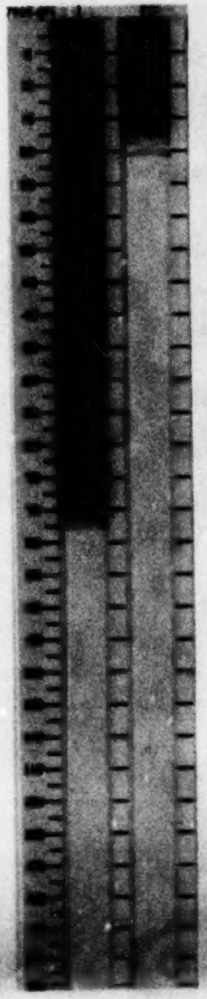

SITE 792 HOLE E CORE 8R CORED INTERVAL 183.7-193.4 mbsf

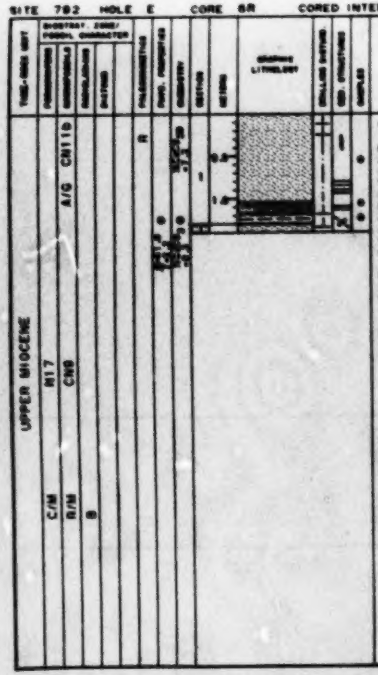
TIME-ROCK UNIT
BIOSTRAT. ZONE/ FOSSIL CHARACTER
FORAMINIFERS
NANNOFOSSILS
RADIOLARIANS
DIATOMS
PALEOMAGNETICS
PHYS. PROPERTIES
CHEMISTRY
SECTION
METERS
GRAPHIC LITHOLOGY
DRILLING DISTURB.
SED. STRUCTURES
SAMPLES
UPPER MIOCENE
N17
C/M
A/G CN11b
CN9
R/M
B
R
1
0.5
1.0
CC

LITHOLOGIC DESCRIPTION

VITRIC SAND AND VITRIC SANDSTONE

Major lithologies:
Approximately 30% of the core is olive gray (5Y 4/2, 3/2), dark gray (5Y 4/1), light olive gray (5Y 5/2), and olive black (5Y 2/1) semi-lithified VITRIC SAND and its lithified equivalent, VITRIC SANDSTONE. The ratio of semi-lithified to lithified material is about 30:70. Sorting is poor, and grain size varies from fine to coarse, with some granule-and pebble-bearing intervals. The lighter-colored intervals (Section 1, 50-63 cm and 92-102 cm) contain about 20% carbonate. Crude planar lamination occurs in Section 1, 80-92 cm and 105-110 cm, and slight burrowing occurs at Section 1, 35-50 cm. In Section 1, 104-118 cm, there is a microfault dipping approximately 40°, which juxtaposes finer-and coarser-grained sandstones.

Minor lithologies:
Section 1, 120-135 cm, contains thin (<10 cm thick) layers of grayish black (N2) VOLCANICLASTIC CONGLOMERATE with 3-6 mm-sized clasts, MUDSTONE, and CLAYSTONE.

The semi-lithified materials are moderately disturbed, and the rocks are moderately fractured by drilling.

SMEAR SLIDE SUMMARY (%):

	1, 54 D	1, 107 M	1, 122 M
TEXTURE:			
Sand	10	—	20
Silt	40	16	40
Clay	50	84	30
COMPOSITION:			
Accessory minerals	1	Tr	1
Biotite	Tr	—	—
Clay	50	84	30
Feldspar	2	1	2
Foraminifers	7	—	—
Glass	25	15	67
Glauconite	Tr	—	Tr
Lithic fragments	—	—	Tr
Micrite	5	—	—
Nannofossils	10	Tr	—
Spar Cement	Tr	—	—

SITE 792 HOLE E CORE 7R CORED INTERVAL 193.4-203.1 mbsf

TIME-ROCK UNIT	FORAMINIFERS	NANNOFOSSILS	RADIOLARIANS	DIATOMS	PALEOMAGNETICS	PHYS. PROPERTIES	CHEMISTRY	SECTION	METERS	GRAPHIC LITHOLOGY	DRILLING DISTURB.	SED. STRUCTURES	SAMPLES	LITHOLOGIC DESCRIPTION
UPPER MIOCENE	B	F/G CN9	B		R			1						VITRIC SANDY MUDSTONE AND VITRIC MUDDY SANDSTONE

Major lithologies:
60% of the core is olive gray (5Y 3/2) VITRIC SANDY MUDSTONE, and the remaining 40% is VITRIC MUDDY SANDSTONE. Slight burrowing occurs at 0-10 cm. Over the interval 30-35 cm, intense bioturbation by Chondrites has left burrows 3 mm in diameter filled with sand.

The intervals 0-10 cm and 22-35 cm are moderately fractured, and the interval 10-22 cm consists of drilling breccia.

SMEAR SLIDE SUMMARY & THIN SECTION (%):

	1, 1	1, 5	1, 20
	M	D	M
TEXTURE:			
Sand	55	20	30
Silt	20	30	30
Clay	25	50	40
COMPOSITION:			
Accessory minerals	3	10	10
Bioclast	Tr	—	—
Clay	25	50	40
Diatoms	1	—	—
Feldspar	8	2	3
Foraminifers	2	Tr	Tr
Glass	43	34	33
Lithic fragments	—	—	10
Micrite	—	—	1
Nannofossils	15	3	3
Pellets	Tr	—	—
Pore Space	Tr	—	—
Radiolarians	1	—	—
Rock fragment	2	—	—
Spicules	—	1	—

SITE 792 HOLE E CORE 8R CORED INTERVAL 203.1-212.6 mbsf

TIME-ROCK UNIT	BIOSTRAT. ZONE/ FOSSIL CHARACTER: FORAMINIFERS	NANNOFOSSILS	RADIOLARIANS	DIATOMS	PALEOMAGNETICS	PHYS. PROPERTIES	CHEMISTRY	SECTION	METERS	GRAPHIC LITHOLOGY	DRILLING DISTURB.	SED. STRUCTURES	SAMPLES	LITHOLOGIC DESCRIPTION
UPPER MIOCENE	B	F/G CN9	R/P		N/R	● [illegible]	● [illegible]	1						

VITRIC MUDDY SANDSTONE, VITRIC SANDSTONE AND VITRIC SANDY MUDSTONE

Major lithologies:
30% of the core is composed of olive black (5Y 2/1), slightly burrowed VITRIC MUDDY SANDSTONE, 27% of olive black (5Y 2/1) VITRIC SANDSTONE, and 23% of VITRIC SANDY MUDSTONE.

Minor lithology: The remaining 20% of the core (33-34 cm interval) is VITRIC SILT, which is lithified only in the dusky green (5G 3/2) middle part of the bed. The upper and lower parts of the ash bed are unlithified and dark gray (5Y 4/1) in color.

The core is moderately fractured throughout.

SMEAR SLIDE SUMMARY (%):

	1, 20 D	1, 32 M
TEXTURE:		
Sand	50	5
Silt	20	65
Clay	30	30
COMPOSITION:		
Accessory minerals	10	Tr
Clay	30	30
Feldspar	10	1
Foraminifers	Tr	—
Glass	40	68
Lithic fragments	10	—
Mica	—	Tr
Nannofossils	—	Tr
Opaques	—	1
Pyrite	—	Tr

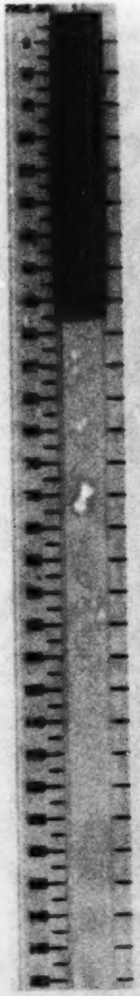

SITE 792

699

SITE 792 HOLE E CORE 9R CORED INTERVAL 212.6-222.2 mbsf

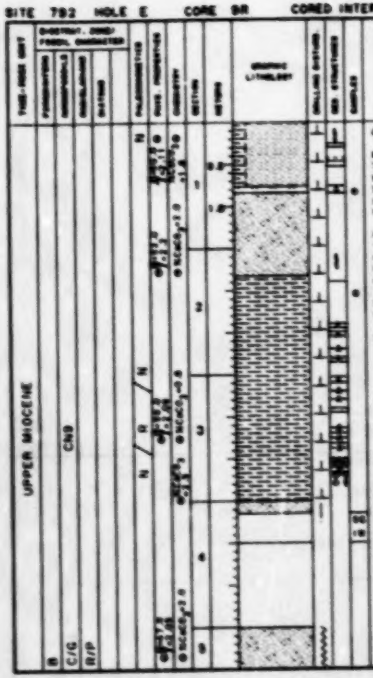
TIME-ROCK UNIT
BIOSTRAT. ZONE/FOSSIL CHARACTER
FORAMINIFERS
NANNOFOSSILS
RADIOLARIANS
DIATOMS
PALEOMAGNETICS
PHYS. PROPERTIES
CHEMISTRY
SECTION
METERS
GRAPHIC LITHOLOGY
DRILLING DISTURB.
SED. STRUCTURES
SAMPLES
UPPER MIOCENE
B
C/G
CN9
R/P
N
N
R
N
1
2
3
4
5
0.5
1.0
SS
TS

LITHOLOGIC DESCRIPTION

CLAYEY VITRIC SILTSTONE, VITRIC SILTY SANDSTONE AND VITRIC SANDSTONE

Major lithologies:
The core consists principally of the following completely interbedded lithologies, the intervals typically varying from 1 cm to 30 cm in thickness: 30% olive gray (5Y 3/2) CLAYEY VITRIC SILTSTONE, 20% olive black (5Y 2/1) VITRIC SILTY SANDSTONE, and 20% olive black (5Y 2/1) VITRIC SANDSTONE. The siltstones alternate between laminated and slightly to heavily bioturbated intervals in Section 3.

Minor lithologies:
15% of the core consists of olive gray (5Y 3/2) VITRIC SANDY SILTSTONE, a textural variation of the principal lithologies. Section 3, 103-105 cm, is a dark gray (5Y 4/1) PUMICEOUS PEBBLE GRANULE CONGLOMERATE (4% of the core) that displays inverse to normal grading.

Sections 1 through 3 are moderately fractured. Section 5 is moderately disturbed, and Section 5 is very disturbed.

SMEAR SLIDE SUMMARY (%):

	1, 80 M	2, 50 D
TEXTURE:		
Sand	80	60
Silt	10	20
Clay	10	20
COMPOSITION:		
Accessory minerals	1	10
Clay	15	20
Feldspar	5	10
Foraminifers	—	Tr
Glass	75	55
Lithic fragments	—	2
Mica	—	Tr
Nannofossils	—	3
Quartz	4	—
Spicules	—	Tr

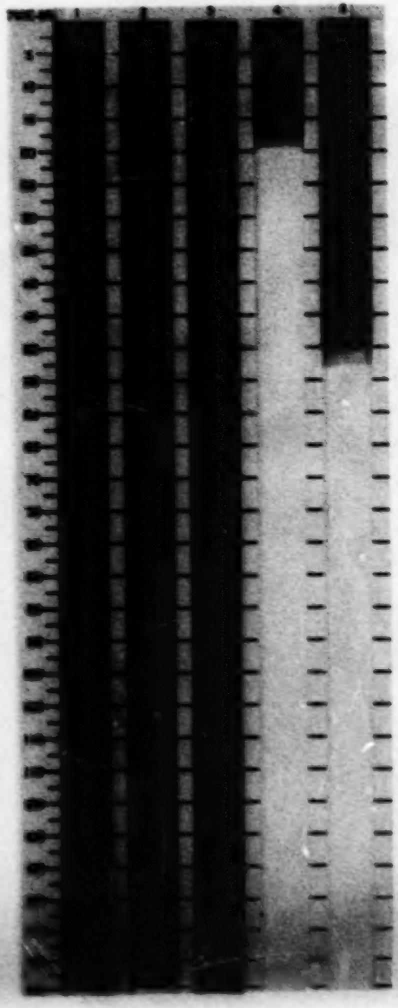

SITE 792 HOLE E CORE 10R CORED INTERVAL 222.2-231.9 mbsf

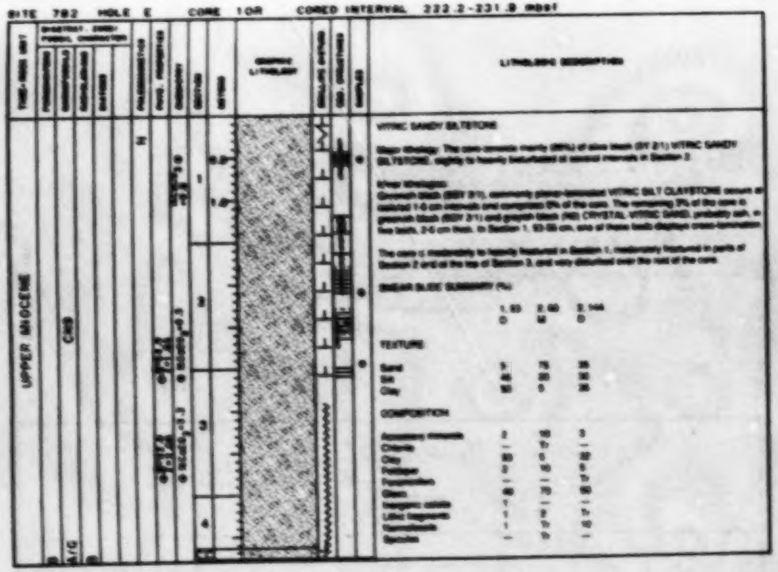
TIME-ROCK UNIT
BIOSTRAT. ZONE/FOSSIL CHARACTER
FORAMINIFERS
NANNOFOSSILS
RADIOLARIANS
DIATOMS
PALEOMAGNETICS
PHYS. PROPERTIES
CHEMISTRY
SECTION
METERS
GRAPHIC LITHOLOGY
DRILLING DISTURB.
SED. STRUCTURES
SAMPLES
UPPER MIOCENE
CN9
B
A/G
B
N
1
2
3
4

LITHOLOGIC DESCRIPTION

VITRIC SANDY SILTSTONE

Major lithology: The core consists mainly (95%) of olive black (5Y 2/1) VITRIC SANDY SILTSTONE, slightly to heavily bioturbated in several intervals in Section 2.

Minor lithologies:
Greenish black (5GY 2/1), commonly planar-laminated VITRIC SILTY CLAYSTONE occurs at selected 1-6 cm intervals and comprises 3% of the core. The remaining 2% of the core is greenish black (5GY 2/1) and grayish black (N2) CRYSTAL VITRIC SAND, probably ash, in five beds, 2-5 cm thick. In Section 1, 93-95 cm, one of these beds displays cross-lamination.

The core is moderately to heavily fractured in Section 1, moderately fractured in parts of Section 2 and at the top of Section 3, and very disturbed over the rest of the core.

SMEAR SLIDE SUMMARY (%):

	1, 93 D	2, 60 M	3, 146 D
TEXTURE:			
Sand	5	75	35
Silt	45	20	30
Clay	50	5	35
COMPOSITION:			
Accessory minerals	3	10	3
Opaques	—	Tr	—
Clay	50	5	37
Feldspar	3	10	5
Foraminifers	—	—	Tr
Glass	40	70	50
Inorganic calcite	1	—	—
Lithic fragments	1	2	Tr
Nannofossils	1	Tr	10
Spicules	—	Tr	—

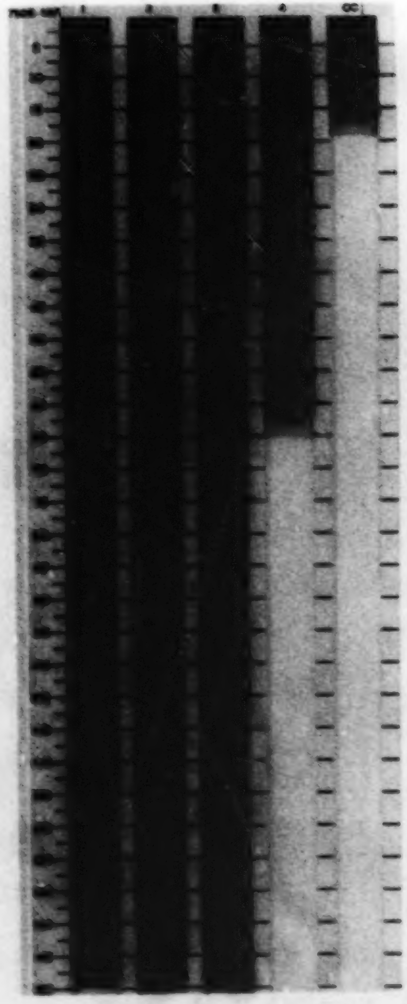

SITE 792 HOLE E CORE 11R CORED INTERVAL 231.9-241.5 mbsf

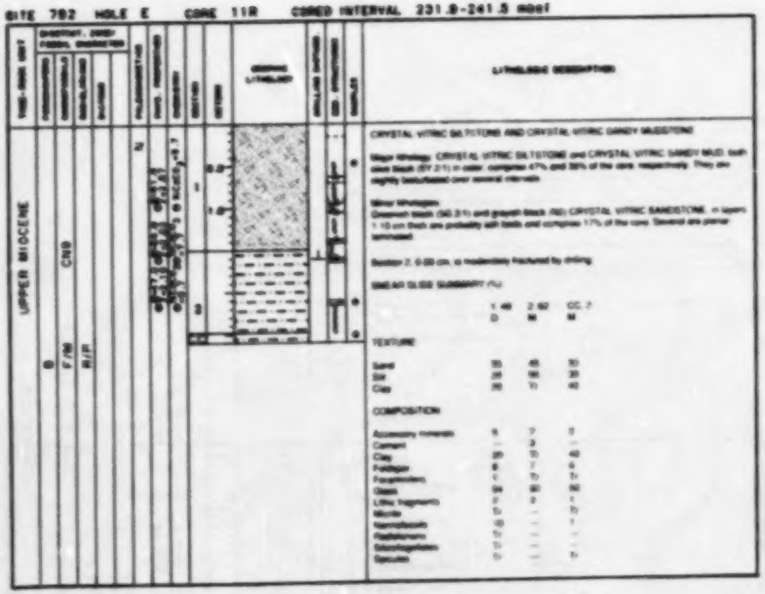
TIME-ROCK UNIT
BIOSTRAT. ZONE/FOSSIL CHARACTER
FORAMINIFERS
NANNOFOSSILS
RADIOLARIANS
DIATOMS
PALEOMAGNETICS
PHYS. PROPERTIES
CHEMISTRY
SECTION
METERS
GRAPHIC LITHOLOGY
DRILLING DISTURB.
SED. STRUCTURES
SAMPLES
UPPER MIOCENE
B
CN9
F/M
R/P
N
1
2
CC
0.5
1.0

LITHOLOGIC DESCRIPTION

CRYSTAL VITRIC SILTSTONE AND CRYSTAL VITRIC SANDY MUDSTONE

Major lithology: CRYSTAL VITRIC SILTSTONE and CRYSTAL VITRIC SANDY MUD, both olive black (5Y 2/1) in color, comprise 47% and 36% of the core, respectively. They are slightly bioturbated over several intervals.

Minor lithologies:
Greenish black (5G 2/1) and grayish black (N2) CRYSTAL VITRIC SANDSTONE, in layers 1-10 cm thick, are probably soft beds and comprise 17% of the core. Several are planar laminated.

Section 2, 0-20 cm, is moderately fractured by drilling.

SMEAR SLIDE SUMMARY (%):

	1, 40 D	2, 62 M	CC, 7 M
TEXTURE:			
Sand	35	45	30
Silt	35	55	30
Clay	30	Tr	40
COMPOSITION:			
Accessory minerals	6	7	3
Cement	—	3	—
Clay	30	Tr	40
Feldspar	8	7	6
Foraminifers	1	Tr	Tr
Glass	34	80	50
Lithic fragments	7	3	1
Mica	Tr	—	Tr
Nannofossils	10	—	1
Radiolarians	Tr	—	—
Silicoflagellates	Tr	—	—
Spicules	Tr	—	Tr

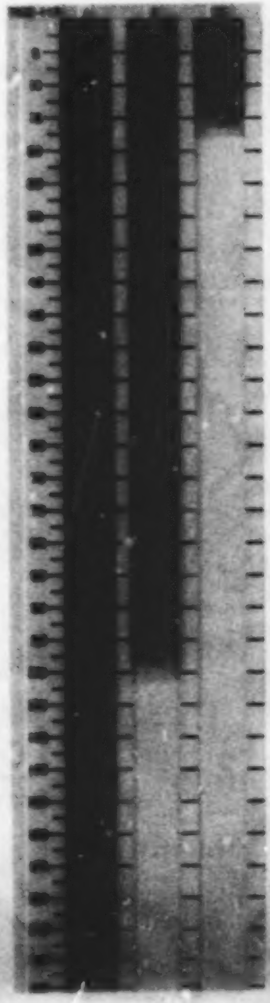

SITE 792 HOLE E CORE 12R CORED INTERVAL 241.0-251.2 mbsf

TIME-ROCK UNIT	FORAMINIFERS	NANNOFOSSILS	RADIOLARIANS	DIATOMS	PALEOMAGNETICS	PHYS. PROPERTIES	CHEMISTRY	SECTION	METERS	GRAPHIC LITHOLOGY	DRILLING DISTURB.	SED. STRUCTURES	SAMPLES	LITHOLOGIC DESCRIPTION
UPPER MIOCENE	N17 R/M	CN9 A/G	B		N	[illegible] [illegible]	● CaCO$_3$=11.6 ● CaCO$_3$=0.1	1 2 3 CC	0.5 1.0				●	see below

NANNOFOSSIL AND GRANULE RICH MUDDY SANDSTONE

Major lithology: Most of the core consists of dark gray (5Y 4/1), strongly burrowed NANNOFOSSIL AND GRANULE RICH MUDDY SANDSTONE. The granules are scattered throughout the core and consist of black basaltic scoria and light gray pumice. In Section 2, 80-85 cm, there is a concentration of scoria pebbles with diameters as large as 0.7 cm. Some of this sediment appears crudely laminated, but this could be a product of horizontal burrowing. Some of the muddy sandstone is pale olive (10Y 6/2) in color and is relatively rich in nannofossils (see smear slide data).

Minor lithology: Section 1, 63-65 cm, is a bed of dark gray (5GY 4/1) SILTY CLAYSTONE with faint parallel laminae. This is probably an ash layer.

Section 1, 0 cm, to Section 2, 59 cm, is slightly fractured by drilling. Section 3 is highly fractured.

SMEAR SLIDE SUMMARY (%):

	2, 112 M
TEXTURE:	
Sand	50
Silt	40
Clay	10
COMPOSITION:	
Accessory minerals	5
Clay	7
Feldspar	5
Glass	60
Mica	10
Nannofossils	20

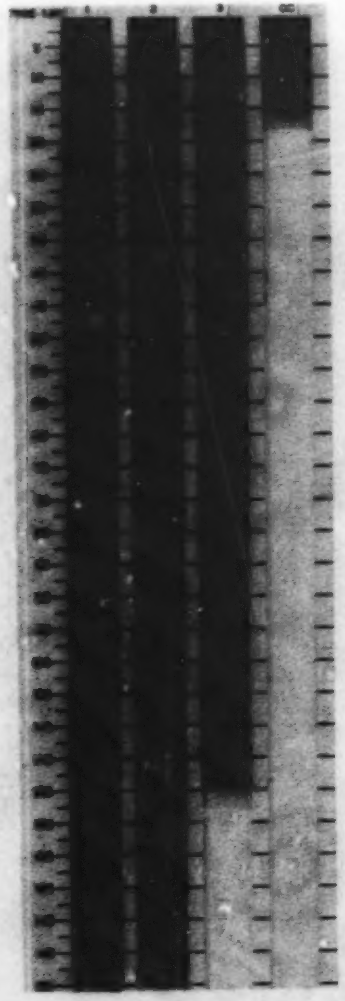

SITE 792 HOLE E CORE 13R CORED INTERVAL 251.2-260.9 mbsf

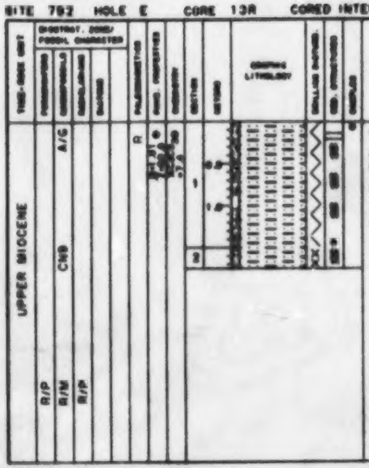
TIME-ROCK UNIT
BIOSTRAT. ZONE/ FOSSIL CHARACTER
FORAMINIFERS
NANNOFOSSILS
RADIOLARIANS
DIATOMS
PALEOMAGNETICS
PHYS. PROPERTIES
CHEMISTRY
SECTION
METERS
GRAPHIC LITHOLOGY
DRILLING DISTURB.
SED. STRUCTURES
SAMPLES
UPPER MIOCENE
R/P
CN9
A/G
R/M
R/P
R
1
2
0.5
1.0

LITHOLOGIC DESCRIPTION

GRANULE TO PEBBLE BEARING MUDDY SANDSTONE

Major lithology: Most of the core is dark gray (5GY 4/1), burrowed GRANULE- TO PEBBLE BEARING MUDDY SANDSTONE. Pumice and scoria pebbles are <1 cm in diameter.

Minor lithologies:
Section 1, 4-5 cm, is a remnant of the base of a bed of black fine SANDSTONE. Section 1, 18-25 cm, a greenish black (5GY 2/1) SILTY CLAYSTONE. Section 2, 21-28 cm, is a drilling breccia of greenish black (5GY 2/1) CLAYEY SILTSTONE.

In general, the core is highly fractured by drilling.

SMEAR SLIDE SUMMARY (%):

	1, 4 M
TEXTURE	
Sand	80
Silt	20
COMPOSITION	
Accessory minerals	10
Feldspar	15
Foraminifers	Tr
Glass	75
Spicules	Tr

SITE 792 HOLE E CORE 14R CORED INTERVAL 260.9-270.5 mbsf

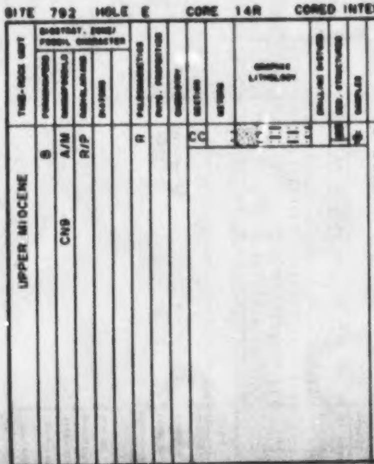
TIME-ROCK UNIT
BIOSTRAT. ZONE/ FOSSIL CHARACTER
FORAMINIFERS
NANNOFOSSILS
RADIOLARIANS
DIATOMS
PALEOMAGNETICS
PHYS. PROPERTIES
CHEMISTRY
SECTION
METERS
GRAPHIC LITHOLOGY
DRILLING DISTURB.
SED. STRUCTURES
SAMPLES
UPPER MIOCENE
B
CN9
A/M
R/P
R
CC

LITHOLOGIC DESCRIPTION

SILTY SANDSTONE AND MUDDY SANDSTONE

Major lithologies: Dark gray (5GY 4/1), burrowed, laminated SILTY SANDSTONE, grading upward into dark gray (5GY 4/1) MUDDY SANDSTONE with scattered granules of basaltic scoria.

THIN SECTION SUMMARY (%):

	CC, 19 M
TEXTURE	
Sand	30
Silt	30
Clay	40
COMPOSITION	
Accessory minerals	3
Clay	40
Feldspar	7
Foraminifers	2
Glass	40
Mica	Tr
Nannofossils	5
Radiolarians	3
Rock fragment	Tr
Spicules	Tr

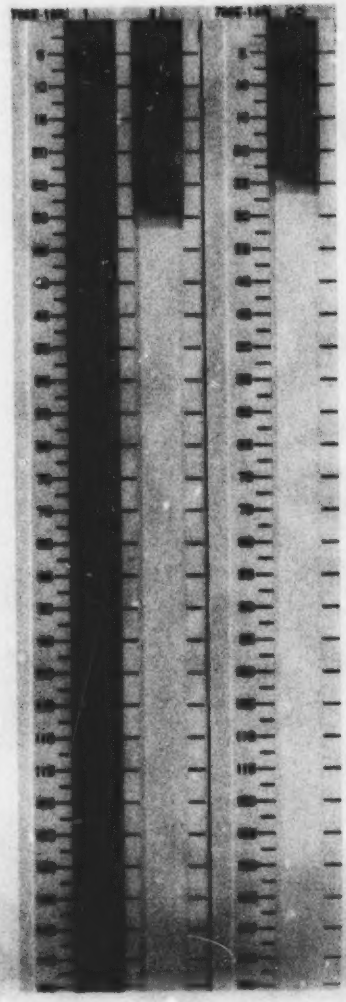
792E-13R 1
2
792E-14R CC

SITE 792 HOLE E CORE 15R CORED INTERVAL 270.5-280.2 mbsf

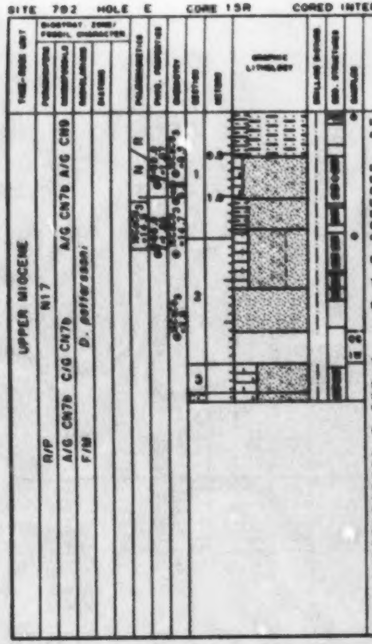
TIME-ROCK UNIT
BIOSTRAT. ZONE/ FOSSIL CHARACTER
FORAMINIFERS
NANNOFOSSILS
RADIOLARIANS
DIATOMS
PALEOMAGNETICS
PHYS. PROPERTIES
CHEMISTRY
SECTION
METERS
GRAPHIC LITHOLOGY
DRILLING DISTURB.
SED. STRUCTURES
SAMPLES
UPPER MIOCENE
R/P
N17
A/G CN7b
C/G CN7b
A/G CN7b
A/G CN9
F/M
D. petterssoni
N / R
1
2
3
0.5
1.0
CC
IW

LITHOLOGIC DESCRIPTION

NANNOFOSSIL-RICH SILTY SANDSTONE, MUDDY SANDSTONE, VITRIC SILTSTONE and VITRIC SANDSTONE

Major lithologies:
Most of the core consists of gray (5Y 5/1) to pale olive (10Y 6/2), burrowed NANNOFOSSIL-RICH SILTY SANDSTONE with scattered granules of pumice and scoria, and similarly burrowed MUDDY SANDSTONE. Maximum pebble size is 3.5 cm (pumice clasts). These lithologies are interbedded with thin to medium beds of greenish black (5GY 2/1) VITRIC SILTSTONE and VITRIC SANDSTONE containing basaltic glass. These beds contain local ripple and parallel laminations, and have sharp bases.

Minor lithology: Section 1, 141-146 cm, consists of pale olive (10Y 6/2) pumiceous gravel.

There is no drilling disturbance.

SMEAR SLIDE SUMMARY (%):

	1, 8	1, 149
	M	D
TEXTURE:		
Sand	—	30
Silt	80	50
Clay	20	20
COMPOSITION:		
Accessory minerals	1	—
Clay	14	10
Diatoms	—	1
Feldspar	2	1
Foraminifers	—	1
Glass	80	60
Inorganic calcite	—	2
Nannofossils	—	20
Opaques	1	1
Oxide	—	1
Quartz	2	2
Spicules	—	1

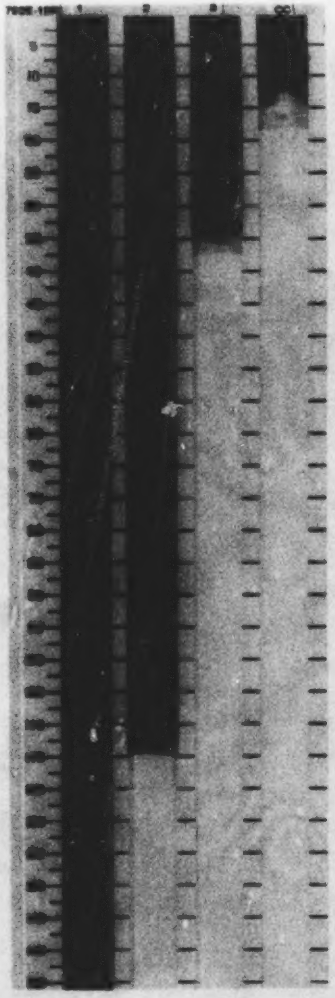
792E-15R
1
2
3
CC
5
10
15

SITE 792 HOLE E CORE 16R CORED INTERVAL 280.2-289.9 mbsf

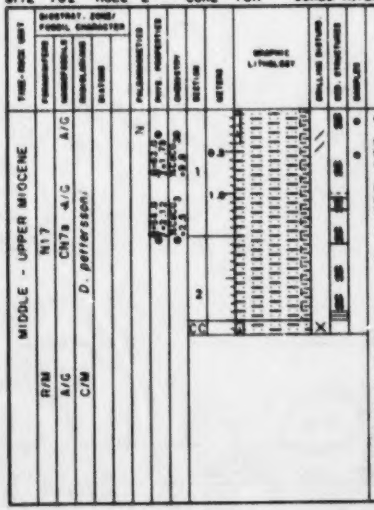
TIME-ROCK UNIT
BIOSTRAT. ZONE/ FOSSIL CHARACTER
FORAMINIFERS
NANNOFOSSILS
RADIOLARIANS
DIATOMS
PALEOMAGNETICS
PHYS. PROPERTIES
CHEMISTRY
SECTION
METERS
GRAPHIC LITHOLOGY
DRILLING DISTURB.
SED. STRUCTURES
SAMPLES
MIDDLE - UPPER MIOCENE
N17
R/M
CN7a A/G
A/G
A/G
D. pettersson
C/M
N
1
2
CC
0.5
1.0

LITHOLOGIC DESCRIPTION

GRANULE-BEARING MUDDY SANDSTONE

Major lithologies:
Most of the core consists of dark gray (5Y 4/1 and 5GY 4/1), burrowed GRANULE-BEARING MUDDY SANDSTONE. The granules consist of basaltic scoria.

Minor lithology: Section 1, 93-100 cm, 115-120 cm, and Section 2, 8-11 cm, 86-88 cm consist of thin beds of generally parallel laminated, olive black (5Y 2/1) VITRIC CLAYEY SILTSTONE.

Section 1, 30-50 cm, is slightly fractured by drilling.

SMEAR SLIDE SUMMARY (%):

	1, 15	1, 93
	D	D
TEXTURE		
Sand	20	—
Silt	70	60
Clay	10	40
COMPOSITION		
Clay	—	34
Feldspar	2	1
Glass	68	60
Inorganic calcite	5	—
Nannofossils	25	2
Opaques	—	1
Pyroxene	—	1
Quartz	—	1

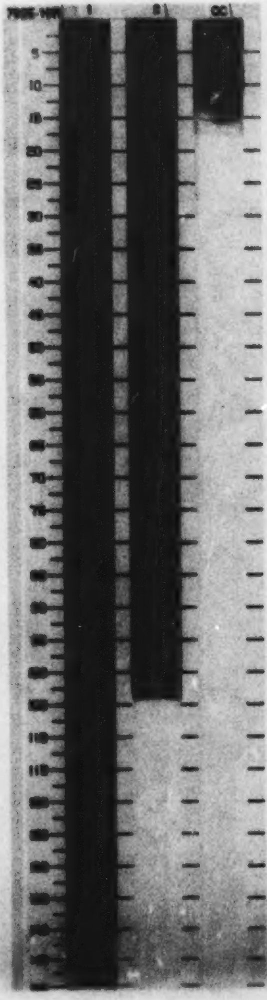
16R-1
1
2
CC
5
10
15

SITE 792 HOLE E CORE 17R CORED INTERVAL 289.8-299.5 mbsf

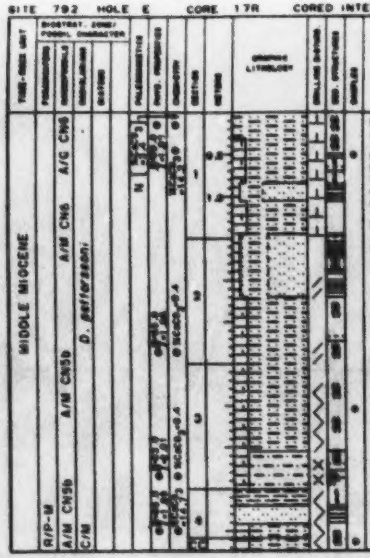
TIME-ROCK UNIT
BIOSTRAT. ZONE/FOSSIL CHARACTER
FORAMINIFERS
NANNOFOSSILS
RADIOLARIANS
DIATOMS
PALEOMAGNETICS
PHYS. PROPERTIES
CHEMISTRY
SECTION
METERS
GRAPHIC LITHOLOGY
DRILLING DISTURB.
SED. STRUCTURES
SAMPLES
MIDDLE MIOCENE
R/P-M
A/M CN5b
A/M CN5b
A/M CN6
A/G CN6
C/M
D. petterssoni
N
1
2
3
4
CC
0.5
1.0

LITHOLOGIC DESCRIPTION

NANNOFOSSIL-RICH MUDDY SANDSTONE, NANNOFOSSIL-RICH SANDY MUDSTONE AND VITRIC SILTSTONE

Major lithologies:
Most of the core consists of dark gray (5GY 4/1), burrowed NANNOFOSSIL-RICH MUDDY SANDSTONE and NANNOFOSSIL-RICH SANDY MUDSTONE, both with scattered scoria granules and sand grains. The remaining 20% of the core consists of sharp-based, locally graded and/or parallel laminated, thin beds of VITRIC SILTSTONE.

Minor lithology: Section 4, 0-18 cm, consists of dark gray (5GY 4/1) SILTY CLAYSTONE.

Section 1 is moderately fractured. Section 3, 30 cm, to CC is highly fractured by drilling.

SMEAR SLIDE SUMMARY (%):

	1, 51 M	3, 98 M	CC, 7 M
TEXTURE:			
Sand	80		80
Silt	20	80	10
Clay	—	20	10
COMPOSITION:			
Accessory minerals	5	—	Tr
Clay	—	14	—
Diatoms	—	1	—
Feldspar	10	1	5
Foraminifers	Tr	1	Tr
Glass	85	80	95
Lithic fragments	Tr	—	—
Nannofossils	—	1	Tr
Opaque	—	1	—
Quartz	—	1	—

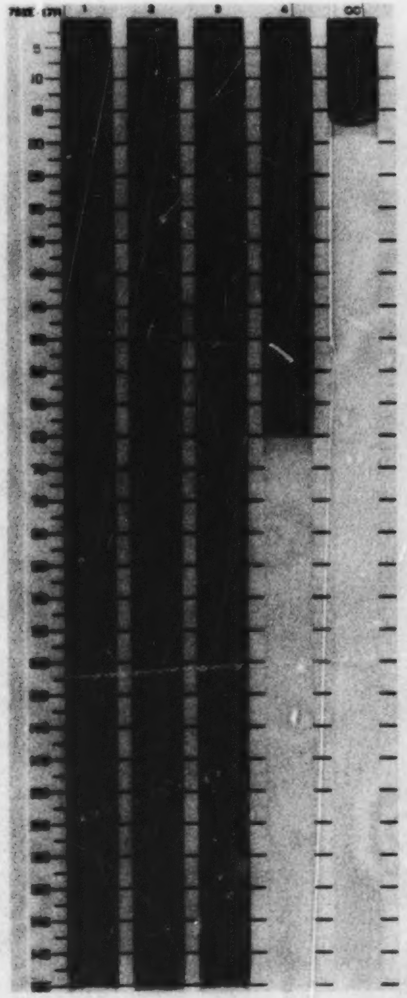
792E-17R
1
2
3
4
CC
0
10
20

SITE 792 HOLE E CORE 18R CORED INTERVAL 299.5-309.0 mbsf

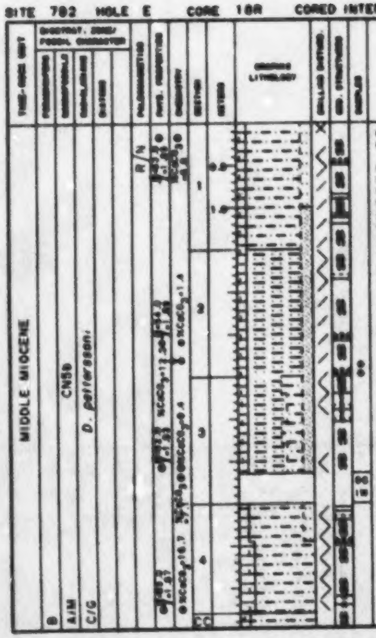
TIME-ROCK UNIT
BIOSTRAT. ZONE/FOSSIL CHARACTER
FORAMINIFERS
NANNOFOSSILS
RADIOLARIANS
DIATOMS
PALEOMAGNETICS
PHYS. PROPERTIES
CHEMISTRY
SECTION
METERS
GRAPHIC LITHOLOGY
DRILLING DISTURB.
SED. STRUCTURES
SAMPLES
MIDDLE MIOCENE
B
A/M
CN5b
C/G
D. petterssoni
R/N
1
2
3
4
CC
0.5
1.0
OG
IW

LITHOLOGIC DESCRIPTION

NANNOFOSSIL RICH MUDDY SANDSTONE, NANNOFOSSIL RICH SANDY MUDSTONE, VITRIC SILTSTONE AND VITRIC SANDSTONE

Major lithologies:
Most of the core consists of burrowed, dark gray (5GY 4/1) and grayish green (5GY 6/1) NANNOFOSSIL RICH MUDDY SANDSTONE and NANNOFOSSIL RICH SANDY MUDSTONE, with the lighter colors corresponding to intervals with higher carbonate contents. Sand- and granule-sized grains of basaltic scoria are scattered throughout the core. The remaining 20% of the core consists of sharp-based, locally graded and/or parallel laminated thin beds of grayish black (N2) or olive black (5Y 2/1) VITRIC SILTSTONE and VITRIC SANDSTONE (ash beds).

Minor lithology: Section 3, 86-87 cm, consists of olive black (5Y 2/1), fine SCORIACEOUS CONGLOMERATE.

Most of Sections 1 through 3 are slightly fractured by drilling. Section 4 is highly fractured.

SMEAR SLIDE SUMMARY (%):

	2, 136 D	2, 147 M
TEXTURE:		
Sand	—	70
Silt	15	30
Clay	85	—
COMPOSITION:		
Accessory minerals	—	2
Clay	56	—
Diatoms	2	—
Feldspar	1	5
Foraminifers	2	—
Glass	5	93
Nannofossils	30	—
Opaques	1	—
Quartz	1	—
Spicules	2	—

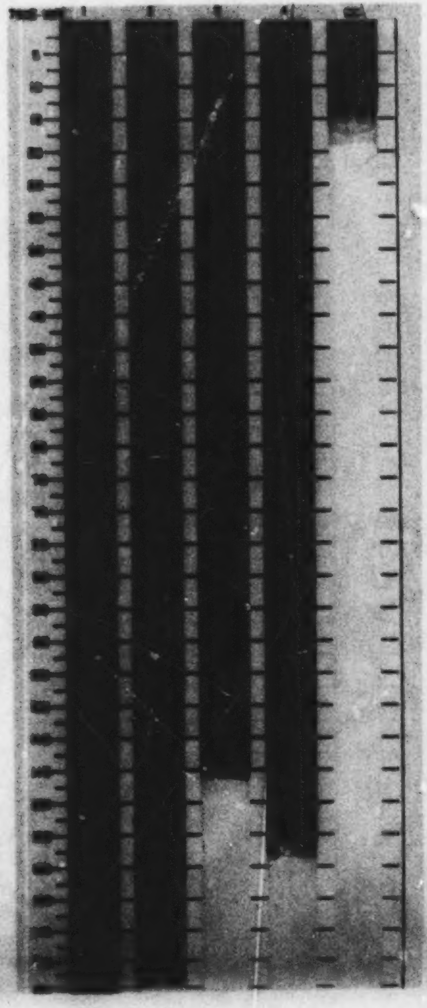

SITE 792 HOLE E CORE 19R CORED INTERVAL 309.0-318.6 mbsf

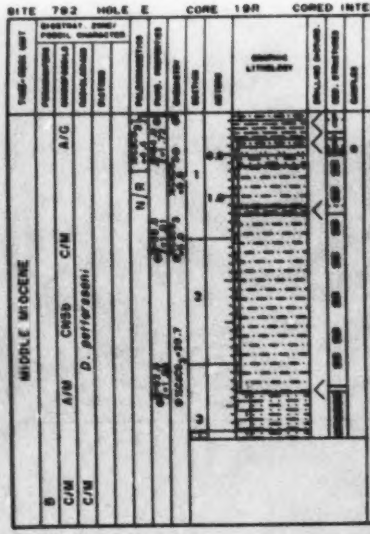
TIME-ROCK UNIT
BIOSTRAT. ZONE/ FOSSIL CHARACTER
FORAMINIFERS
NANNOFOSSILS
RADIOLARIANS
DIATOMS
PALEOMAGNETICS
PHYS. PROPERTIES
CHEMISTRY
SECTION
METERS
GRAPHIC LITHOLOGY
DRILLING DISTURB.
SED. STRUCTURES
SAMPLES
MIDDLE MIOCENE
B
C/M
A/M
CN5b
C/M
A/G
C/M
D. petterssoni
N/R
1
2
3
0.5
1.0

LITHOLOGIC DESCRIPTION

SANDY MUDSTONE AND NANNOFOSSIL-RICH MUDDY SANDSTONE

Major lithologies:
Most of the core consists of dark gray (5GY 4/1) and grayish green (5GY 5/1), strongly bioturbated, SANDY MUDSTONE and NANNOFOSSIL-RICH MUDDY SANDSTONE both with scattered granules and sand grains of [illegible].

Minor lithologies:
Section 1, 0-25 cm, is olive black (5Y 2/1) VITRIC SILTY CLAYSTONE. Section 1, 45-51 cm, is a graded bed of parallel laminated VITRIC SANDSTONE to VITRIC SILTSTONE. Section 1, 115-125 cm, is olive black (5Y 2/1) VITRIC CLAYEY SILTSTONE. Section 3, 20-30 cm, is a remnant of largely unrecovered grayish black (N2) VITRIC SANDSTONE. All these minor lithologies are basaltic ash beds.

Short intervals in this core are highly fractured. Otherwise, the core is essentially undisturbed by drilling.

SMEAR SLIDE SUMMARY (%):

	1, 47
	M
TEXTURE:	
Sand	20
Silt	60
Clay	20
COMPOSITION:	
Foraminifers	5
Glass	50
Micrite	15
Nannofossils	30
Spicules	Tr

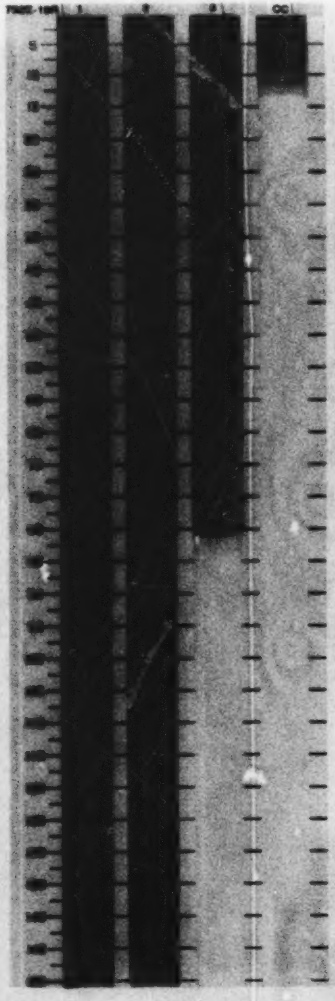
792E-19R
1
2
3
CC

SITE 792 HOLE E CORE 20R CORED INTERVAL 318.6-328.3 mbsf

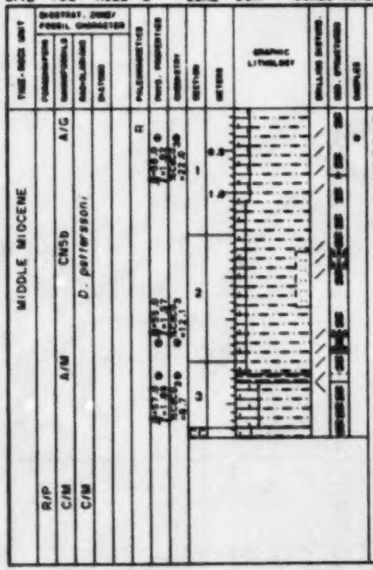
TIME-ROCK UNIT
BIOSTRAT. ZONE/ FOSSIL CHARACTER
FORAMINIFERS
NANNOFOSSILS
RADIOLARIANS
DIATOMS
PALEOMAGNETICS
PHYS. PROPERTIES
CHEMISTRY
SECTION
METERS
GRAPHIC LITHOLOGY
DRILLING DISTURB.
SED. STRUCTURES
SAMPLES
MIDDLE MIOCENE
R/P
CN5b
A/G
A/M
C/M
D. petterssoni
C/M
R
1
2
3
CC
0.5
1.0

LITHOLOGIC DESCRIPTION

NANNOFOSSIL RICH SANDY MUDSTONE

Major lithology: The core is almost entirely grayish green (5GY 6/1) strongly burrowed NANNOFOSSIL RICH SANDY MUDSTONE with scattered granule and sand-sized scoria grains. There are some pumice pebbles in the sediment. The most common trace fossil is Zoophycos, although Chondrites is also present.

Persistent dip of some burrows and scoria layers suggests a dip of 10°-20°.

Minor lithologies:
The core contains several ash layers of VITRIC SILTSTONE, VITRIC SANDSTONE and VITRIC SILTY CLAYSTONE. Some of these are graded. The ash beds are located in Section 1, 80-84 cm, Section 2, 14-19 cm, 31-36 cm, 76-83 cm, and Section 3, 17-27 cm. About half of the core is slightly fractured by drilling.

SMEAR SLIDE SUMMARY (%):

	1, 36
	D
TEXTURE:	
Silt	14
Clay	86
COMPOSITION:	
Accessory minerals	1
Clay	50
Diatoms	1
Feldspar	1
Foraminifers	1
Glass	8
Nannofossils	30
Opaques	1
Pyroxene	1
Quartz	1
Spicules	2

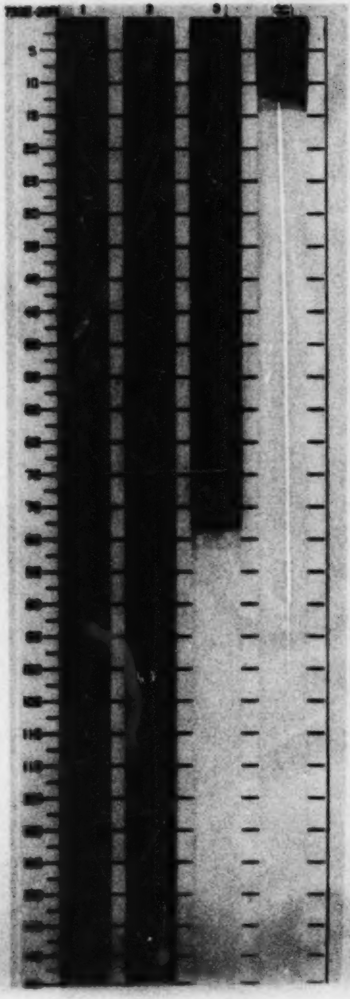

SITE 792 HOLE E CORE 21R CORED INTERVAL 328.3-337.9 mbsf

TIME-ROCK UNIT	FORAMINIFERS	NANNOFOSSILS	RADIOLARIANS	DIATOMS	PALEOMAGNETICS	PHYS. PROPERTIES	CHEMISTRY
MIDDLE MIOCENE	B	A/G CN5a A/G	F/P D. petterssoni		R	[illegible]	[illegible]

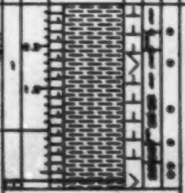

LITHOLOGIC DESCRIPTION

NANNOFOSSIL RICH VITRIC SILTY CLAYSTONE

Major lithology: 98% of the core consists of dark gray (5Y 4/1) NANNOFOSSIL RICH VITRIC SILTY CLAYSTONE. It is slightly burrowed in Section 1, 0-110 cm, and heavily bioturbated below that level to the base of Section 2. Zoophycos burrows occur in Section 2, 13-18 cm.

Minor lithology: Ash beds of dark gray (5GY 4/1) VITRIC CRYSTAL SILTY CLAYSTONE, and brownish black (5YR 2/1) VITRIC SILTSTONE and VITRIC SANDSTONE, in beds 0.5 to 5 cm thick, together comprise 2% of the core.

The entire core is moderately fractured except for the CC, which is highly fractured.

SMEAR SLIDE SUMMARY (%):

	1, 32 M	1, 76 M	1, 125 D	2, 15 M	2, 42 M	2, 52 D
TEXTURE:						
Sand	Tr	15	Tr	20	35	15
Silt	25	75	35	70	65	25
Clay	75	10	65	10	—	60
COMPOSITION:						
Accessory minerals	—	1	1	5	3	2
Clay	75	10	59	8	—	53
Feldspar	5	5	3	10	4	2
Foraminifers	—	—	—	—	—	1
Glass	12	76	15	75	86	25
Lithic fragments	1	3	2	Tr	7	Tr
Micrite	—	3	Tr	—	—	—
Nannofossils	5	1	15	2	Tr	15
Opaques	2	Tr	1	—	—	2
Pollen	—	1	—	—	—	—
Radiolarians	—	—	2	—	—	—
Sponge spicules	—	—	2	—	—	—

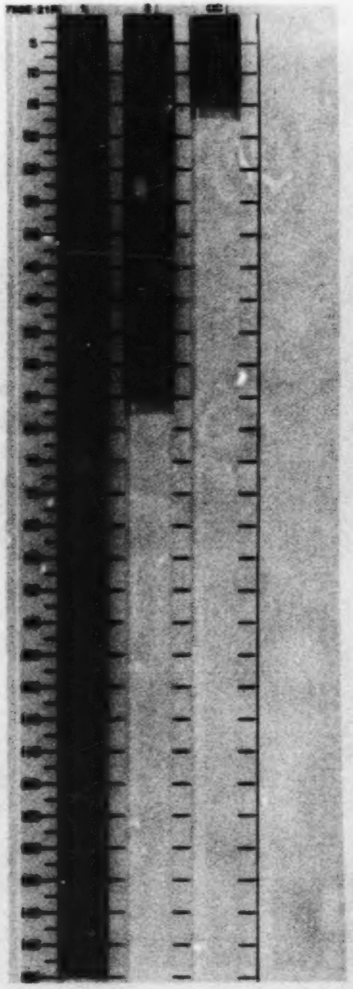

SITE 792 HOLE E CORE 22R CORED INTERVAL 337.9-347.6 mbsf

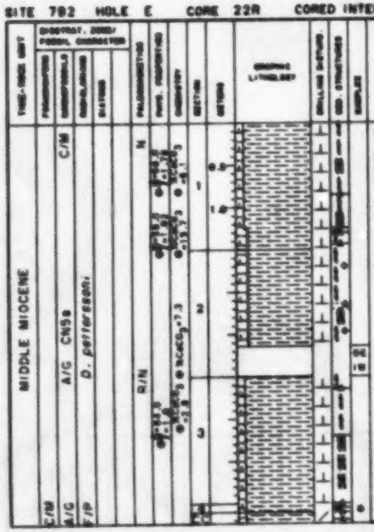
TIME-ROCK UNIT
BIOSTRAT. ZONE/ FOSSIL CHARACTER
FORAMINIFERS
NANNOFOSSILS
RADIOLARIANS
DIATOMS
PALEOMAGNETICS
PHYS. PROPERTIES
CHEMISTRY
SECTION
METERS
GRAPHIC LITHOLOGY
DRILLING DISTURB.
SED. STRUCTURES
SAMPLES
MIDDLE MIOCENE
C/M
A/G CN5a
D. petterssonii
C/M
A/G
F/P
N
R/N
1
2
3
0.5
1.0

LITHOLOGIC DESCRIPTION

NANNOFOSSIL RICH VITRIC SILTY CLAYSTONE AND VITRIC SILTY CLAYSTONE

Major lithology: Very dark gray (5Y 3/1) and dark gray (5Y 4/1), slightly to heavily bioturbated NANNOFOSSIL RICH VITRIC SILTY CLAYSTONE and VITRIC SILTY CLAYSTONE compose 96% of the core.

Minor lithology: The remaining 4% of the core is composed of seven brownish black (5YR 2/1) VITRIC SANDSTONE ash beds 1-5 cm thick.

The core is moderately fractured throughout.

SMEAR SLIDE SUMMARY (%):

	4, 8 M
TEXTURE:	
Sand	3
Silt	37
Clay	60
COMPOSITION:	
Accessory minerals	1
Clay	60
Feldspar	2
Glass	20
Micrite	1
Nannofossils	15
Radiolarians	1
Spicules	Tr

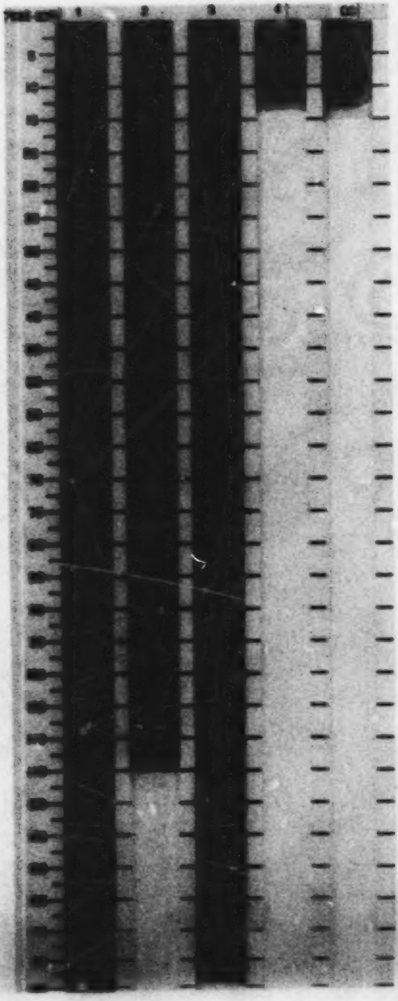

SITE 792 HOLE E CORE 23R CORED INTERVAL 347.6-357.3 mbsf

TIME-ROCK UNIT	FORAMINIFERS	NANNOFOSSILS	RADIOLARIANS	DIATOMS	PALEOMAGNETICS	PHYS. PROPERTIES	CHEMISTRY	SECTION	METERS	GRAPHIC LITHOLOGY	DRILLING DISTURB.	SED. STRUCTURES	SAMPLES
MIDDLE MIOCENE	N10 R/M	CN5a A/M	D. alata F/P		N	[illegible]	[illegible]	1 2 CC	0.5 1.0				●

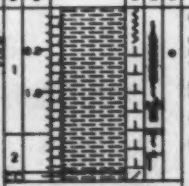

LITHOLOGIC DESCRIPTION

NANNOFOSSIL-RICH VITRIC SILTY CLAYSTONE

Major lithology: Dark gray (5Y 4/1), heavily to slightly bioturbated NANNOFOSSIL-RICH SILTY CLAYSTONE comprises 93% of the core. A Scolicia burrow is located in Section 1, 110 cm.

Minor lithology: The remaining 7% of the core is composed of five brownish black (5YR 2/1) VITRIC SANDSTONE ash beds 1-5 cm thick.

Section 1, 0-30 cm, is drilling breccia. The rest of the core is moderately fractured.

SMEAR SLIDE SUMMARY (%):

	1, 58 D
TEXTURE:	
Sand	20
Silt	20
Clay	60
COMPOSITION:	
Accessory minerals	1
Clay	60
Feldspar	2
Foraminifers	1
Glass	17
Glauconite	Tr
Lithic fragments	Tr
Nannofossils	10
Radiolarians	1
Silicoflagellates	Tr
Spicules	Tr

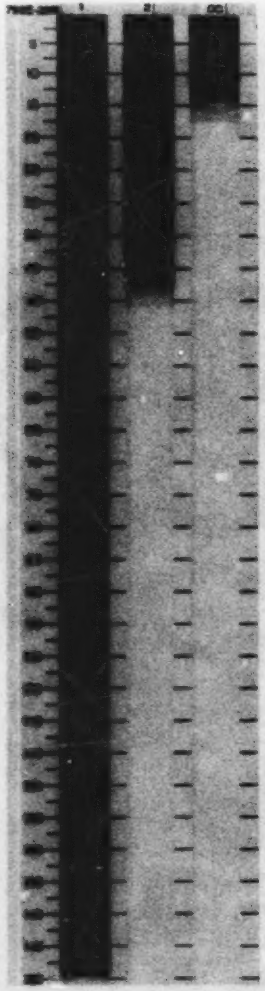

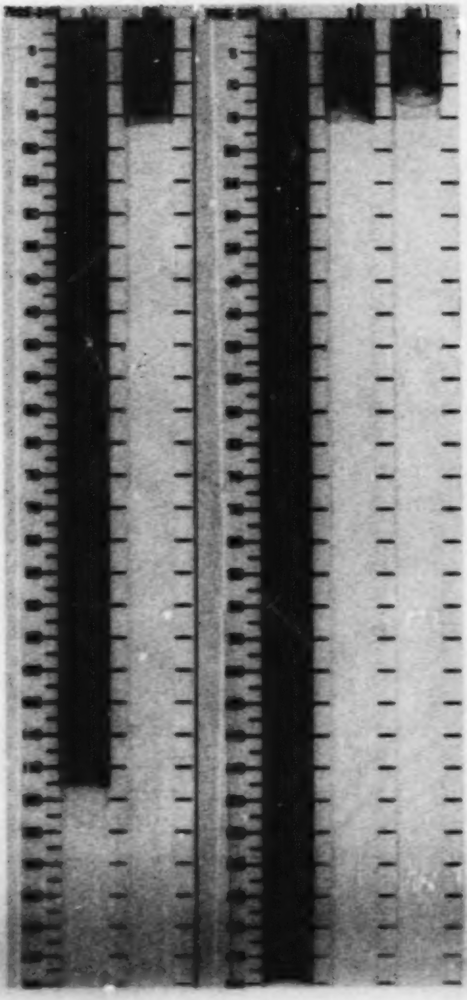

SITE 792 HOLE E CORE 24R CORED INTERVAL 357.3-367.0 mbsf

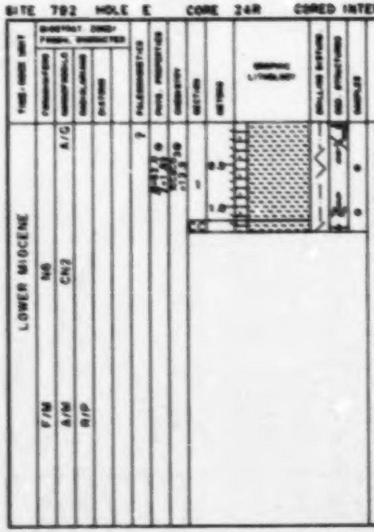

LITHOLOGIC DESCRIPTION

NANNOFOSSIL RICH CLAYSTONE

Major lithology: Gray (5Y 5/1) NANNOFOSSIL RICH CLAYSTONE, slightly burrowed in Section 1, 18-43 cm, 80-90 cm and 100-113 cm, and heavily burrowed from 90-110 cm. In Section 1 there are sub-vertical fractures at 26-28 cm, and a microfault at 113-117 cm.

Minor lithology: In Section 1, 5-10 cm, there is a brownish black (5YR 2/1) VITRIC SANDSTONE, overlain by a 5-cm thick NANNOFOSSIL RICH VITRIC SILTY CLAYSTONE that appears to have resulted from the mixing by burrowers of part of the sandstone with the overlying claystone.

The core is moderately to highly fractured.

SMEAR SLIDE SUMMARY (%):

	1, 95 D	1, 106 D
TEXTURE:		
Sand	—	5
Silt	25	10
Clay	75	85
COMPOSITION:		
Accessory minerals	1	2
Clay	65	80
Feldspar	1	2
Foraminifers	1	Tr
Glass	5	5
Mica	1	1
Nannofossils	25	10
Silicoflagellates	Tr	—

SITE 792 HOLE E CORE 25R CORED INTERVAL 367.0-376.6 mbsf

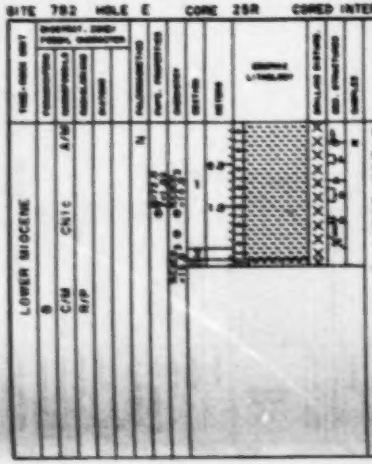

LITHOLOGIC DESCRIPTION

NANNOFOSSIL RICH CLAYSTONE

Major lithology: 90% of the core is dark gray (5GY 4/1), dark green (5GY 4/2), olive black (5Y 2/1) and light greenish gray (5GY 7/1) NANNOFOSSIL RICH CLAYSTONE. Subvertical fractures occur in a rotated drilling biscuit in Section 1, 143-150 cm.

Minor lithology: Five layers of olive black (5Y 2/1) CRYSTAL VITRIC SANDY SILTSTONE, 3-13 cm thick, constitute 10% of the core. One layer, in Section 1, 20-28 cm, is planar laminated.

The core consists of drilling biscuits.

SMEAR SLIDE SUMMARY (%):

	1, 26 M
TEXTURE:	
Sand	25
Silt	75
COMPOSITION:	
Accessory minerals	2
[illegible]	Tr
Feldspar	5
Glass	[illegible]
Lithic fragments	5

SITE 792 HOLE E CORE 28R CORED INTERVAL 378.6-388.3 mbsf

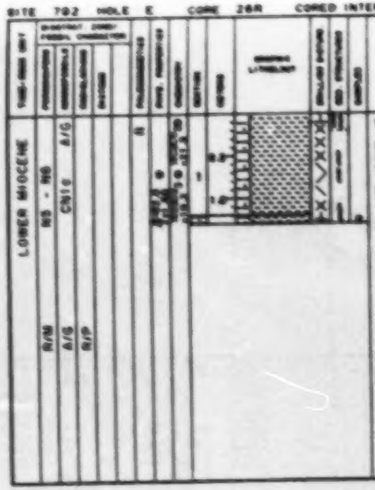
TIME-ROCK UNIT
BIOSTRAT. ZONE/FOSSIL CHARACTER
FORAMINIFERS
NANNOFOSSILS
RADIOLARIANS
DIATOMS
PALEOMAGNETICS
PHYS. PROPERTIES
CHEMISTRY
SECTION
METERS
GRAPHIC LITHOLOGY
DRILLING DISTURB.
SED. STRUCTURES
SAMPLES
LOWER MIOCENE
N5 - N6
R/M
CN1c
A/G
A/G
R/P
1
0.5
1.0
CC

LITHOLOGIC DESCRIPTION

NANNOFOSSIL-RICH CLAYSTONE

Major lithology: The uppermost 93% of the core is grayish green (5GY 5/1) and dark gray (5GY 4/1) NANNOFOSSIL-RICH CLAYSTONE. The only structure is a water escape feature in Section 1, 5 cm.

Minor lithology: The lowermost 7% of the core consists of a 4 cm thick layer of light gray (5Y 7/1) NANNOFOSSIL CLAYSTONE in the CC.

Portions of the core have been moderately or highly fractured; the rest is drilling breccia.

SMEAR SLIDE SUMMARY (%):

	CC, 5
	D
TEXTURE:	
Sand	7
Silt	20
Clay	73
COMPOSITION:	
Accessory minerals	1
Clay	52
Feldspar	1
Glass	5
Micrite	Tr
Nannofossils	40
Spicules	1

cm
1
CC
0
10
20
30
40
50
60
70
80
90
100
110
120
130
140
150

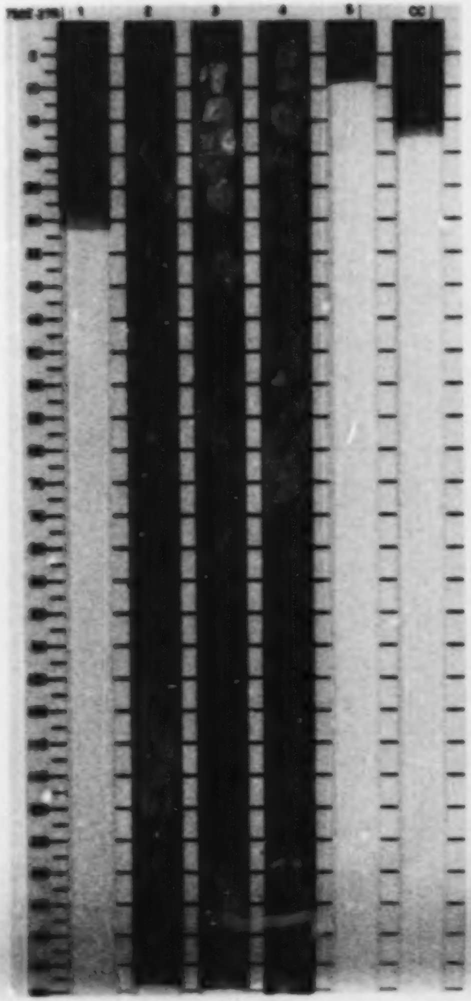

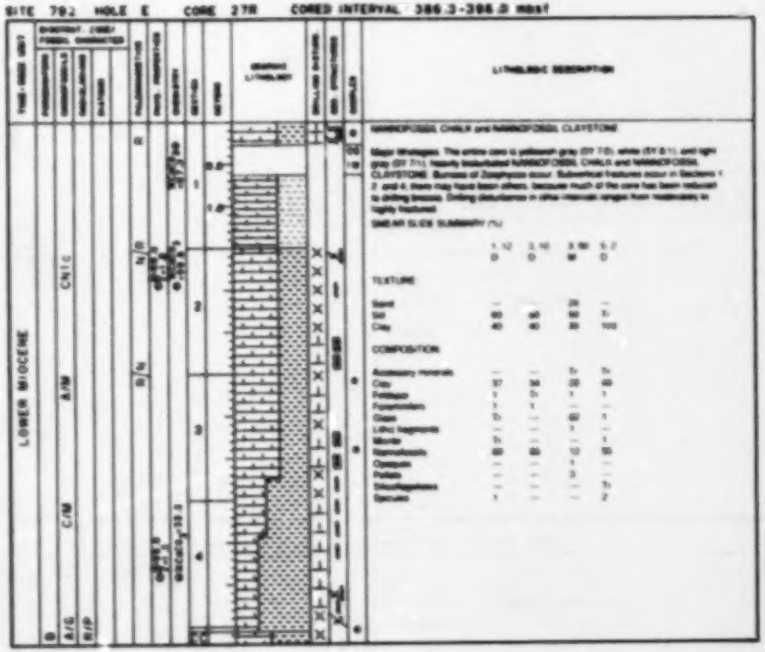
SITE 792 HOLE E CORE 27R CORED INTERVAL 386.2-396.0 mbsf
LOWER MIOCENE
CN1c
A/M
C/M
B
A/G
R/P
B
B/N
N/B
1
2
3
4
CC
0.5
1.0

LITHOLOGIC DESCRIPTION

NANNOFOSSIL CHALK and NANNOFOSSIL CLAYSTONE

Major lithologies: The entire core is yellowish gray (5Y 7/2), white (5Y 8/1), and light gray (5Y 7/1), heavily bioturbated NANNOFOSSIL CHALK and NANNOFOSSIL CLAYSTONE. Burrows of Zoophycos occur. Subvertical fractures occur in Sections 1, 2, and 4; there may have been others, because much of the core has been reduced to drilling breccia. Drilling disturbance in other intervals ranges from moderately to highly fractured.

SMEAR SLIDE SUMMARY (%):

	1, 12 D	2, 10 D	3, 90 M	5, 7 D
TEXTURE:				
Sand	—	—	20	—
Silt	60	60	60	Tr
Clay	40	40	20	100
COMPOSITION:				
Accessory minerals	—	—	Tr	Tr
Clay	37	38	20	48
Feldspar	1	Tr	1	1
Pyroclastics	1	1	—	—
Quartz	Tr	—	60	1
Lithic fragments	—	—	1	—
Micrite	Tr	—	—	1
Nannofossils	60	60	10	50
Opaques	—	—	1	—
Pellets	—	—	3	—
Silicoflagellates	—	—	—	Tr
Spicules	1	—	—	2

SITE 792 HOLE E CORE 28R CORED INTERVAL 396.0-405.6 mbsf

TIME-ROCK UNIT	FORAMINIFERS	NANNOFOSSILS	RADIOLARIANS	DIATOMS	PALEOMAGNETICS
UPPER OLIGOCENE - LOWER MIOCENE	P22/N3 R/M P22/N3 F/M-R N5 - N6	CN1c A/M A/G C/M	B		N/R

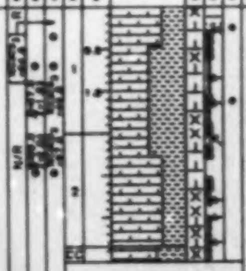

LITHOLOGIC DESCRIPTION

NANNOFOSSIL CLAYSTONE AND NANNOFOSSIL CHALK

Major lithologies:
Dark gray (5GY 4/1), heavily bioturbated NANNOFOSSIL CLAYSTONE comprises [illegible] of the core, in four layers 12-45 cm thick, and as 2-6 cm layers alternating with less burrowed grayish green (5GY 5/1) NANNOFOSSIL CHALK layers of similar thickness that constitute 20% of the core.

Minor lithologies:
The remaining 10% of the core is composed of about equal proportions of discrete, 2-7 cm thick beds, of dark gray (5GY 4/1) CRYSTAL VITRIC SILTSTONE and olive black (5Y 2/1) very fine-grained CRYSTAL VITRIC SANDSTONE.

A subvertical fracture occurs in Section 1, 25-35 cm; more may have been obliterated by drilling, which has moderately fractured to highly fragmented the core.

SMEAR SLIDE SUMMARY (%):

	1, 25 M	1, 111 D
TEXTURE:		
Sand	—	Tr
Silt	10	20
Clay	90	80
COMPOSITION:		
Accessory minerals	Tr	—
Clay	60	75
Glass	1	2
Micrite	Tr	—
Nannofossils	35	17
Radiolarians	1	—
Zeolite	—	5

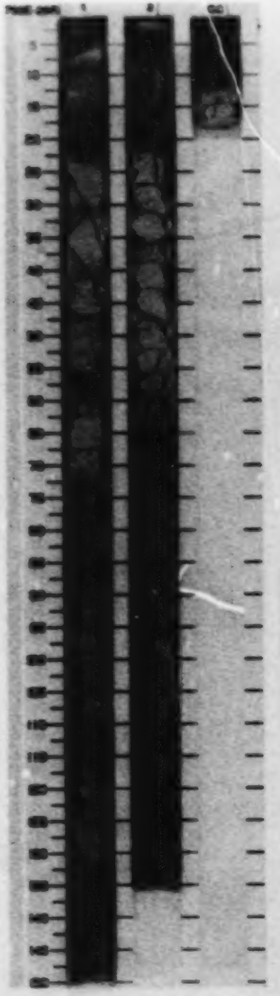

SITE 792 HOLE E CORE 29R CORED INTERVAL 405.6-415.2 mbsf

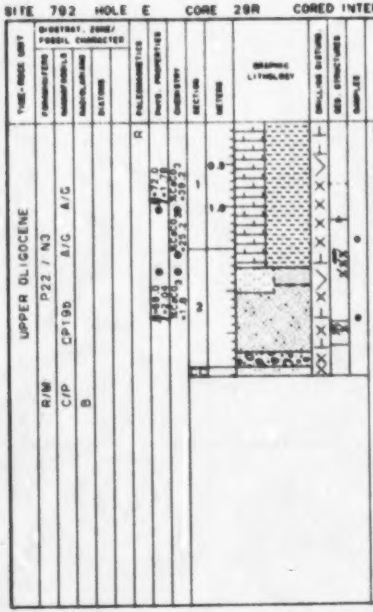
TIME-ROCK UNIT
BIOSTRAT. ZONE/ FOSSIL CHARACTER
FORAMINIFERS
NANNOFOSSILS
RADIOLARIANS
DIATOMS
PALEOMAGNETICS
PHYS. PROPERTIES
CHEMISTRY
SECTION
METERS
GRAPHIC LITHOLOGY
DRILLING DISTURB.
SED. STRUCTURES
SAMPLES
UPPER OLIGOCENE
P22 / N3
R/M
CP19b
A/G
A/G
C/P
B
R
0.5
1.0
1
2
CC

LITHOLOGIC DESCRIPTION

NANNOFOSSIL CLAYSTONE, NANNOFOSSIL RICH CLAYSTONE AND CRYSTAL VITRIC SILTY SANDSTONE

Major lithology: 50% of the core consists of olive black (5Y 2/1) NANNOFOSSIL RICH CLAYSTONE and NANNOFOSSIL CLAYSTONE, and 20% of horizontally bedded, olive black and greenish black (5GY 2/1) CRYSTAL VITRIC SILTY SANDSTONE that is fine grained, well sorted and laminated in Section 1, 78-84 cm. One isolated bed of this lithology in Section 1, 120-121 cm, may represent an ash bed.

Minor lithologies:
Olive black CRYSTAL VITRIC SILTSTONE, an interbedded textural variation of the major lithology sandstone, comprises 25% of the core, as well as an isolated thin bed in Section 1, 115-117 cm, that may be an ash layer. In Section 2, 125-135 cm, there is an indurated piece of breccia with angular pebble and granule sized clasts of sandstone and burrowed claystone in a siltstone matrix.

Fractures occur at four levels in Section 1.

Drilling has moderately and highly fractured some intervals, and reduced others to drilling breccia.

SMEA[illegible]IDE SUMMARY (%)

	1, 140 D	2, 82 D
TEXTURE:		
Sand	—	70
Silt	20	30
Clay	80	—
COMPOSITION:		
Accessory minerals	—	5
Cement	—	20
Clay	75	—
Feldspar	—	5
Foraminifers	Tr	—
Glass	—	70
Nannofossils	25	—

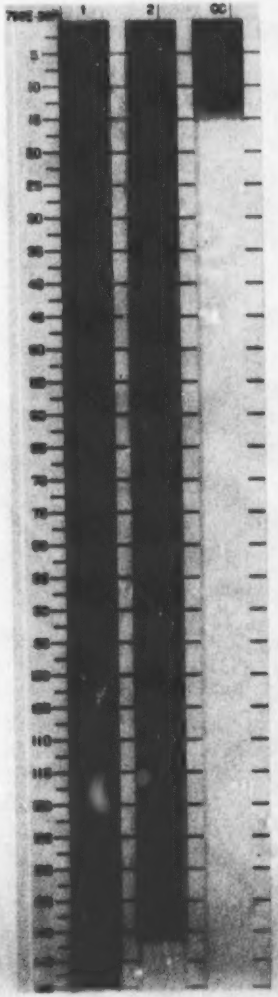

SITE 792 HOLE E CORE 30R CORED INTERVAL 415.2-424.9 mbsf

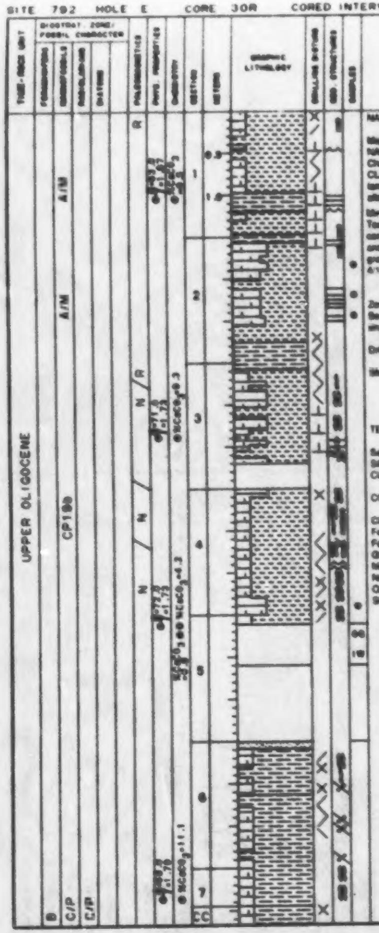

LITHOLOGIC DESCRIPTION

NANNOFOSSIL-RICH CLAYSTONE AND CLAYEY VITRIC SILTSTONE

Major lithologies: Dark greenish gray (10GY 4/1), slightly to heavily bioturbated NANNOFOSSIL-RICH CLAYSTONE comprises 42% of the core. Zoophycos and Chondrites burrows are present. Another 15% of the core is greenish black (5G 2/1) CLAYEY VITRIC SILTSTONE, commonly planar-laminated and, more rarely, wavy-laminated. In smear slide analyses, and indeterminate amount of its glass appears altered to zeolite.

Minor lithologies:
Textural and compositional variations of the major lithologies and their percentages of the core are: grayish green (5GY 5/1) NANNOFOSSIL CLAYSTONE, 14%, dark gray (5GY 4/1) and grayish green (5GY 6/1) NANNOFOSSIL-RICH SILTY CLAYSTONE, 15%, and dark grayish green (10GY 2.5/1) CLAYSTONE, 10%. Three 2-8 cm thick beds of dark gray (5GY 4/1) VITRIC SILTSTONE, which may be ash fall beds, together comprise 2% of the core.

Zones of wavy, subvertical fractures have deformed some of the more clayey intervals, as in Section 1, 50-65 cm, Section 4, 50-60 cm, and Section 6, 60-65 and 80-98 cm. Dewatering structures are also present.

Drilling deformation varies from absent to drilling breccia.

SMEAR SLIDE SUMMARY (%):

	2, 34 D	2, 90 D	2, 94 D	4, 140 M
TEXTURE:				
Sand	—	—	5	—
Silt	20	10	65	40
Clay	80	90	30	60
COMPOSITION:				
Clay	69	90	30	56
Feldspar	1	1	2	Tr
Foraminifers	—	—	Tr	—
Glass	—	—	68	—
Micrite	—	1	Tr	—
Nannofossils	30	2	Tr	45
Opaques	—	1	—	—
Silt	—	5	—	—

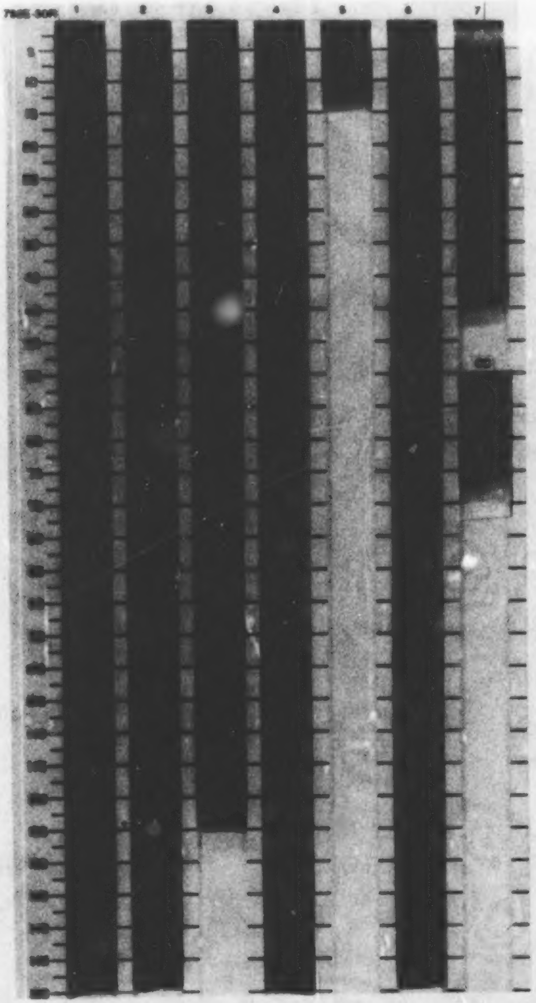

SITE 792 HOLE E CORE 31R CORED INTERVAL 424.9-434.6 mbsf

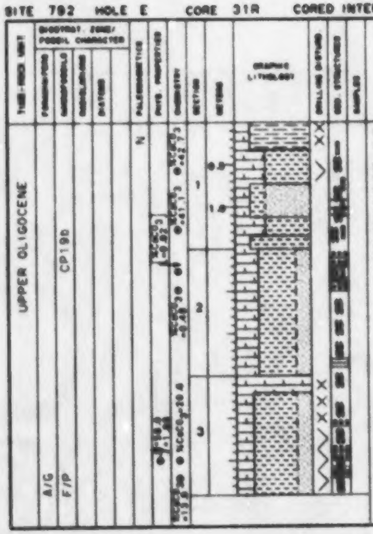
TIME-ROCK UNIT
BIOSTRAT. ZONE/ FOSSIL CHARACTER
FORAMINIFERS
NANNOFOSSILS
RADIOLARIANS
DIATOMS
PALEOMAGNETICS
PHYS. PROPERTIES
CHEMISTRY
SECTION
METERS
GRAPHIC LITHOLOGY
DRILLING DISTURB.
SED. STRUCTURES
SAMPLES
UPPER OLIGOCENE
CP19b
A/G
F/P
N
1
2
3
0.5
1.0

LITHOLOGIC DESCRIPTION

NANNOFOSSIL CLAYSTONE, NANNOFOSSIL RICH CLAYSTONE, VITRIC SILTSTONE AND VITRIC SANDSTONE

Major lithologies:
Most of the core consists of gray (5Y 6/1) and grayish green (5GY 6/1), strongly burrowed NANNOFOSSIL CLAYSTONE and NANNOFOSSIL RICH CLAYSTONE, with widespread dewatering veinlets. Interbedded with these lithologies are thin beds of medium dark gray (N4) VITRIC SILTSTONE and VITRIC SANDSTONE. Most of these beds are graded and some contain parallel and/or ripple lamination.

Minor lithologies:
Section 2, 133-142 cm, is a graded, parallel laminated bed of gray (5YR 6/1) VITRIC SILT (ash). Section 3, 0-22 cm, is burrowed, yellowish gray (5Y 8/1) NANNOFOSSIL CHALK.

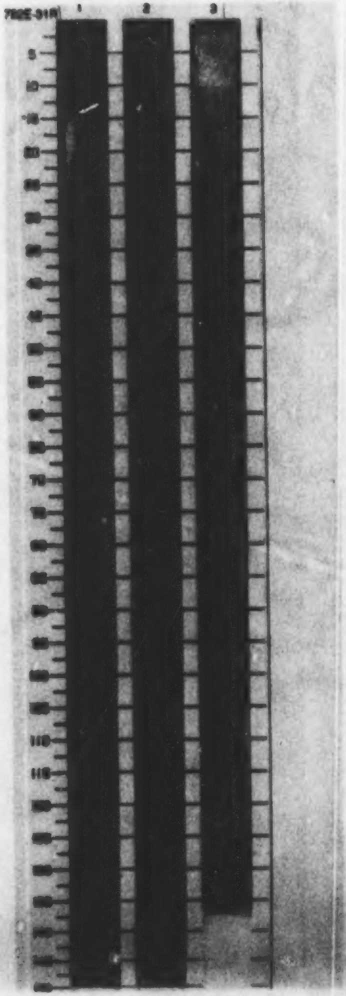
792E-31R
1
2
3
5
10
15
20
110
115

SITE 792 HOLE E CORE 32R CORED INTERVAL 434.6-444.2 mbsf

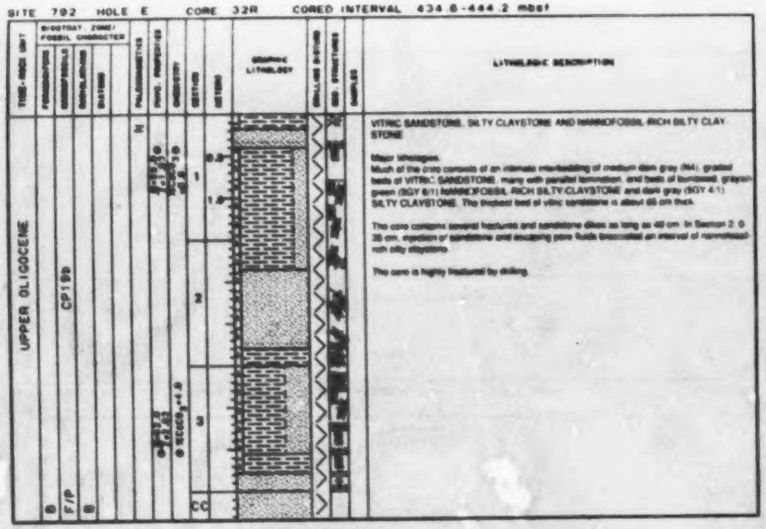
TIME-ROCK UNIT
BIOSTRAT. ZONE/ FOSSIL CHARACTER
FORAMINIFERS
NANNOFOSSILS
RADIOLARIANS
DIATOMS
PALEOMAGNETICS
PHYS. PROPERTIES
CHEMISTRY
SECTION
METERS
GRAPHIC LITHOLOGY
DRILLING DISTURB.
SED. STRUCTURES
SAMPLES
UPPER OLIGOCENE
B
F/P
CP19b
B
N
1
2
3
CC

LITHOLOGIC DESCRIPTION

VITRIC SANDSTONE, SILTY CLAYSTONE AND NANNOFOSSIL-RICH SILTY CLAYSTONE

Major lithologies:
Much of the core consists of an intimate interbedding of medium dark gray (N4), graded beds of VITRIC SANDSTONE, many with parallel lamination, and beds of burrowed, grayish green (5GY 6/1) NANNOFOSSIL-RICH SILTY CLAYSTONE and dark gray (5GY 4/1) SILTY CLAYSTONE. The thickest bed of vitric sandstone is about 65 cm thick.

The core contains several fractures and sandstone dikes as long as 40 cm. In Section 2, 0-35 cm, injection of sandstone and escaping pore fluids brecciated an interval of nannofossil-rich silty claystone.

The core is highly fractured by drilling.

SITE 792 HOLE E CORE 33R CORED INTERVAL 444.2-453.9 mbsf

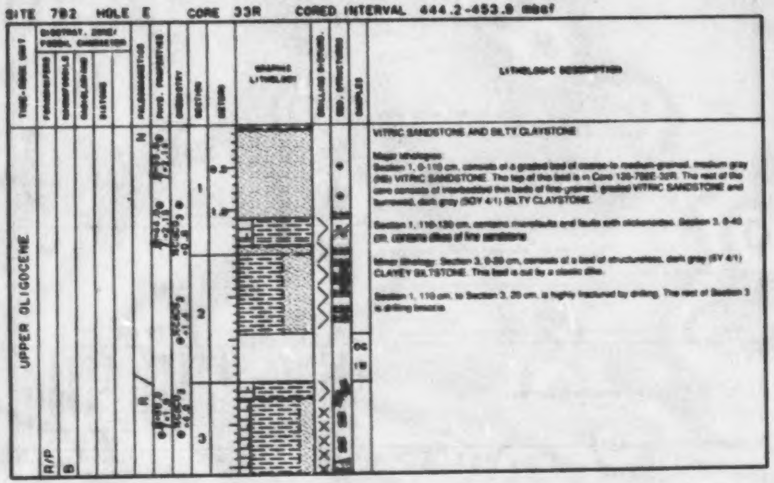
TIME-ROCK UNIT
BIOSTRAT. ZONE/ FOSSIL CHARACTER
FORAMINIFERS
NANNOFOSSILS
RADIOLARIANS
DIATOMS
PALEOMAGNETICS
PHYS. PROPERTIES
CHEMISTRY
SECTION
METERS
GRAPHIC LITHOLOGY
DRILLING DISTURB.
SED. STRUCTURES
SAMPLES
UPPER OLIGOCENE
R/P
B
N
R
1
2
3
CC

LITHOLOGIC DESCRIPTION

VITRIC SANDSTONE AND SILTY CLAYSTONE

Major lithologies:
Section 1, 0-110 cm, consists of a graded bed of coarse- to medium-grained, medium gray (N5) VITRIC SANDSTONE. The top of this bed is in Core 126-792E-32R. The rest of the core consists of interbedded thin beds of fine-grained, graded VITRIC SANDSTONE and burrowed, dark gray (5GY 4/1) SILTY CLAYSTONE.

Section 1, 110-130 cm, contains microfaults and faults with slickensides. Section 3, 0-40 cm, contains dikes of fine sandstone.

Minor lithology: Section 3, 0-20 cm, consists of a bed of structureless, dark gray (5Y 4/1) CLAYEY SILTSTONE. This bed is cut by a clastic dike.

Section 1, 110 cm, to Section 3, 20 cm, is highly fractured by drilling. The rest of Section 3 is drilling breccia.

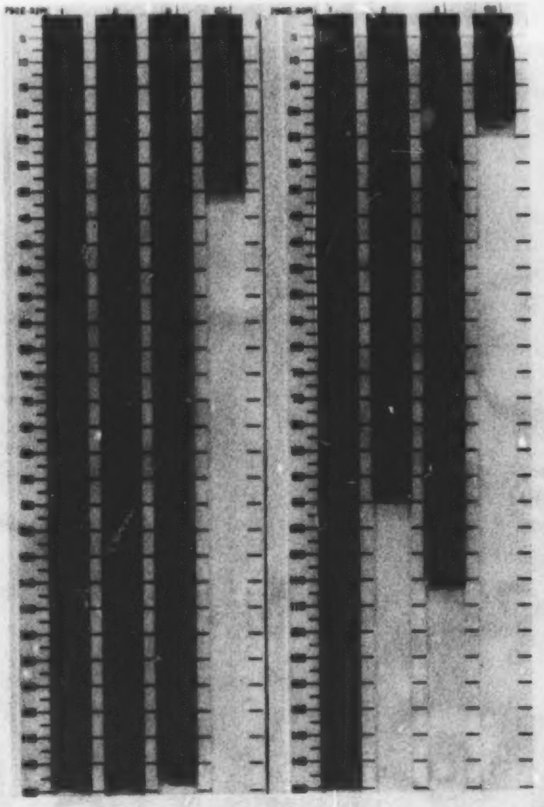
792E-32R
1
2
3
CC
792E-33R
1
2
3
CC

SITE 792 HOLE E CORE 34R CORED INTERVAL 453.9-463.5 mbsf

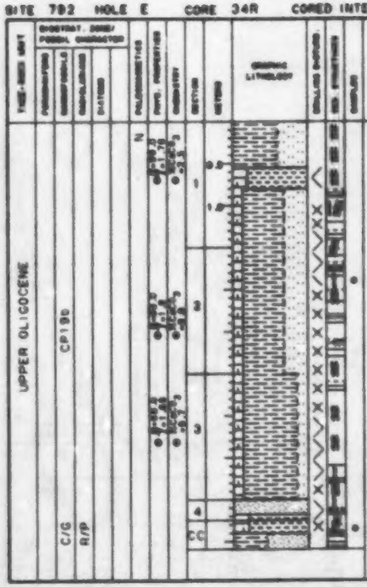
TIME-ROCK UNIT
BIOSTRAT. ZONE/FOSSIL CHARACTER
FORAMINIFERS
NANNOFOSSILS
RADIOLARIANS
DIATOMS
PALEOMAGNETICS
PHYS. PROPERTIES
CHEMISTRY
SECTION
METERS
GRAPHIC LITHOLOGY
DRILLING DISTURB.
SED. STRUCTURES
SAMPLES
UPPER OLIGOCENE
CP19b
C/G
R/P
N
1
2
3
4
CC
0.5
1.0

LITHOLOGIC DESCRIPTION

CLAYEY SILTSTONE, VITRIC SILTSTONE, VITRIC SANDSTONE AND NANNOFOSSIL RICH CLAYSTONE

Major lithologies:
Most of the core consists of interbedded thin beds of dark gray (5Y 4/1) CLAYEY SILTSTONE and greenish black (5GY 2/1) VITRIC SILTSTONE and VITRIC SANDSTONE. About 10% of the core consists of burrowed, dark gray (5GY 4/1), NANNOFOSSIL RICH CLAYSTONE. Zoophycos burrows are common.

In the core catcher, nannofossil-rich claystone is injected by sandstone dikes.

Bedding in Section 1 dips at about 5°.

Minor lithologies:
Section 1, 112-120 cm, a NANNOFOSSIL SILTY CLAYSTONE. Section 2, 37-50 cm, a NANNOFOSSIL SILTSTONE.

Most of the core is either highly fractured, or consists of drilling breccia.

SMEAR SLIDE SUMMARY (%):

	2, 40 M	CC, 16 D
TEXTURE:		
Sand	—	90
Silt	60	10
Clay	40	—
COMPOSITION:		
Accessory minerals	6	Tr
Feldspar	—	Tr
Foraminifers	5	—
Glass	44	95
Micrite	5	—
Nannofossils	40	—
Silicoflagellates	—	5

SITE 792 HOLE E CORE 35R CORED INTERVAL 463.5-473.2 mbsf

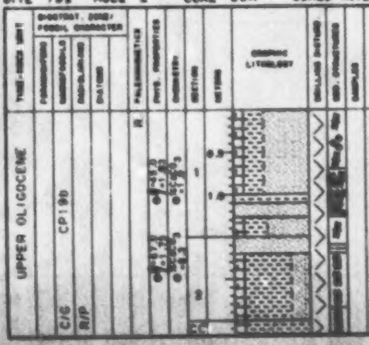
TIME-ROCK UNIT
BIOSTRAT. ZONE/FOSSIL CHARACTER
FORAMINIFERS
NANNOFOSSILS
RADIOLARIANS
DIATOMS
PALEOMAGNETICS
PHYS. PROPERTIES
CHEMISTRY
SECTION
METERS
GRAPHIC LITHOLOGY
DRILLING DISTURB.
SED. STRUCTURES
SAMPLES
UPPER OLIGOCENE
CP19b
C/G
R/P
R
1
2
CC
0.5
1.0

LITHOLOGIC DESCRIPTION

CLAYSTONE AND VITRIC SANDSTONE

Major lithologies:
Overall there are roughly equal amounts of burrowed, dark gray (5GY 4/1) CLAYSTONE and beds of graded, dark gray (N3) and medium dark gray (N4) VITRIC SANDSTONE, some with parallel lamination. The carbonate content of the claystone is well below the limit necessary for designation as a nannofossil-rich lithology.

All of Section 1, and Section 2, 0-30 cm, contain a zone of sandstone injection as a long vertical dike. Locally beds are offset on opposite sides of the dike due to bedding parallel injection.

The core is highly fractured by drilling.

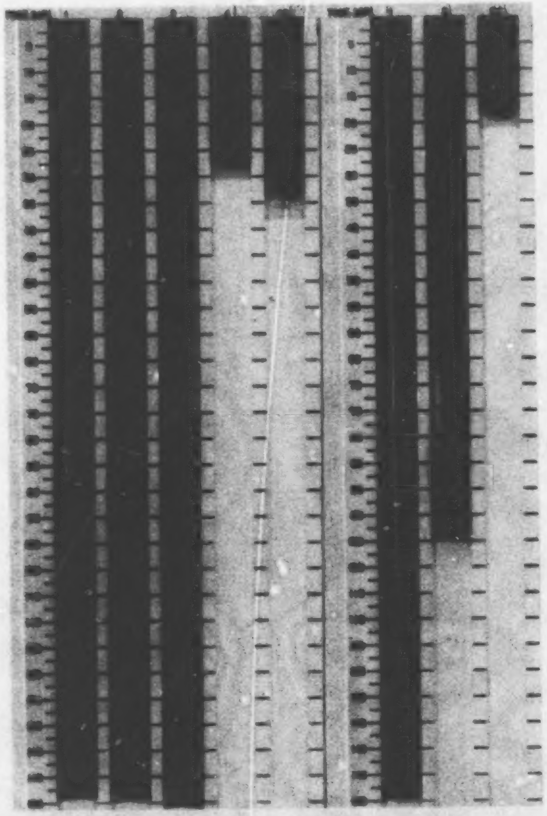

SITE 792 HOLE E CORE 38R CORED INTERVAL 473.2-482.8 mbsf

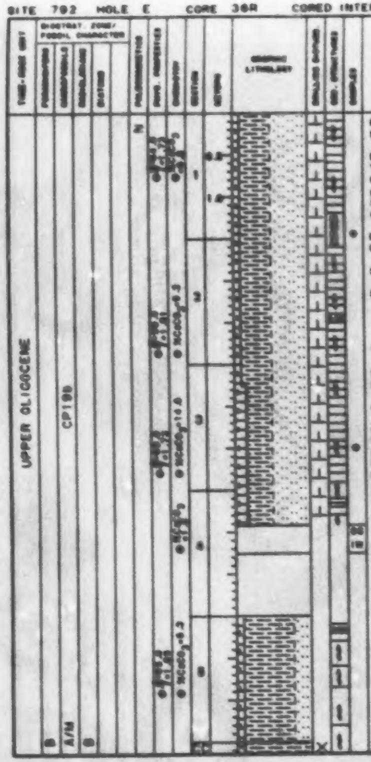

LITHOLOGIC DESCRIPTION

NANNOFOSSIL-RICH SILTY CLAYSTONE, VITRIC SILTSTONE AND VITRIC SANDSTONE

Major lithologies:
The core consists of a rhythmic interbedding of very thin to thin beds of moderately burrowed, dark gray (5GY 4/1) NANNOFOSSIL-RICH SILTY CLAYSTONE, and graded, parallel laminated, locally rippled, beds of dark gray (5GY 4/1) VITRIC SILTSTONE and vitric sandstone. The maximum grain size in all these beds is medium sand.

Minor lithology: Section 1, 117-150 cm, consists of burrowed NANNOFOSSIL-RICH SILTY CLAYSTONE.

Sections 1 through 4 are moderately fractured by drilling.

SMEAR SLIDE SUMMARY (%):

	1, 144 M	3, 100 D
TEXTURE:		
Silt	40	30
Clay	60	70
COMPOSITION:		
Clay	20	5
Feldspar	—	5
Glass	30	75
Micrite	10	—
Nannofossils	40	10

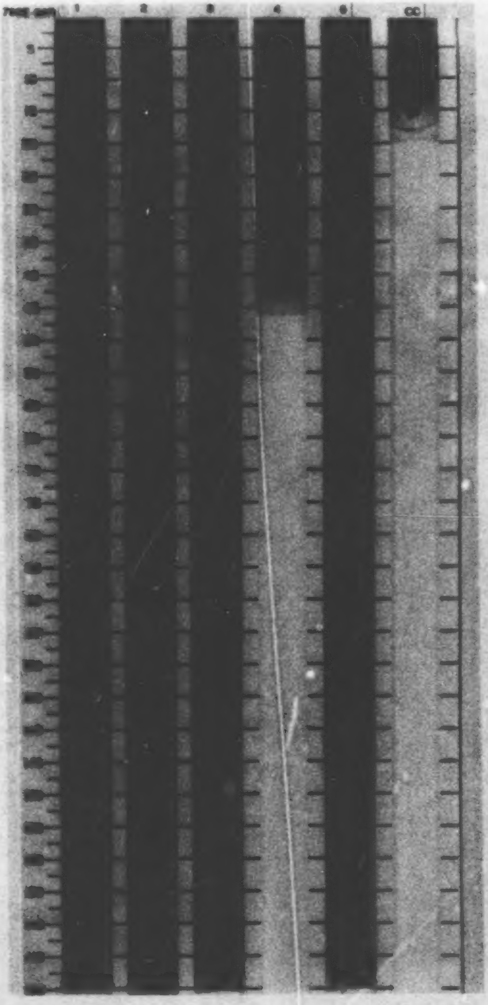

SITE 792 HOLE E CORE 37R CORED INTERVAL 482.8-492.3 mbsf

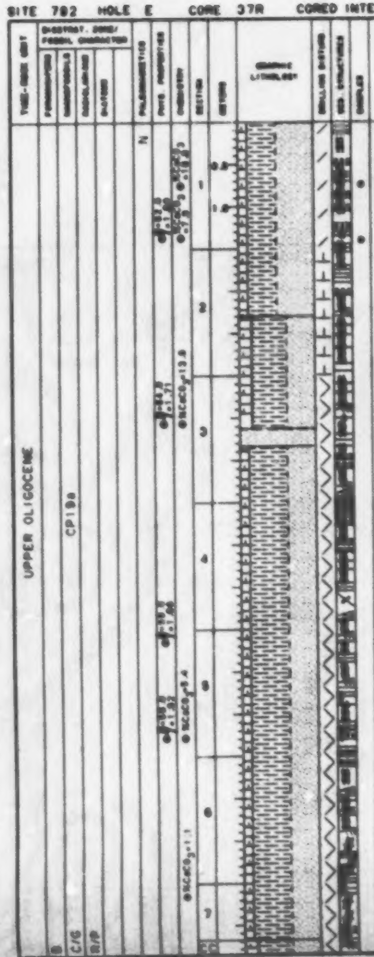
TIME-ROCK UNIT
BIOSTRAT. ZONE/FOSSIL CHARACTER
FORAMINIFERS
NANNOFOSSILS
RADIOLARIANS
DIATOMS
PALEOMAGNETICS
PHYS. PROPERTIES
CHEMISTRY
SECTION
METERS
GRAPHIC LITHOLOGY
DRILLING DISTURB.
SED. STRUCTURES
SAMPLES
UPPER OLIGOCENE
CP19a
B
C/G
R/P
N
●%CaCO3=13.8
●%CaCO3=9.4
●%CaCO3=1.1
0.5
1.0
1
2
3
4
5
6
7
CC

LITHOLOGIC DESCRIPTION

NANNOFOSSIL RICH SILTY CLAYSTONE AND VITRIC SANDSTONE

Major lithologies:
This core is characterized by an interbedding of burrowed, grayish green (5GY 6/1) NANNOFOSSIL RICH SILTY CLAYSTONE and thin to medium graded beds of greenish black (5GY 2/1) VITRIC SANDSTONE. Sandstone beds contain parallel and local ripple lamination. Bedding dips at 9°.

In Section 6, 110-120 cm, there is a sandstone dike. Section 7, 20-40 cm, contains a mineral-filled vein. The filling is gypsum.

Minor lithologies:
Section 1, 140-142 cm, is a bed of grayish black (N2) VITRIC SILTY CLAYSTONE (ash). Section 3, 50-51 cm, Section 5, 66-67 cm and 123-134 cm are olive black (5Y 2/1) VITRIC SILTSTONE (ash).

Section 1 is slightly fractured and Section 2 is moderately fractured by drilling. The rest of the core is highly fractured.

SMEAR SLIDE SUMMARY (%):

	1, 73 D	1, 140 M
TEXTURE:		
Silt	40	40
Clay	60	60
COMPOSITION:		
Clay	20	—
Feldspar	—	Tr
Glass	45	90
Micrite	10	—
Nannofossils	25	5
Quartz	—	5

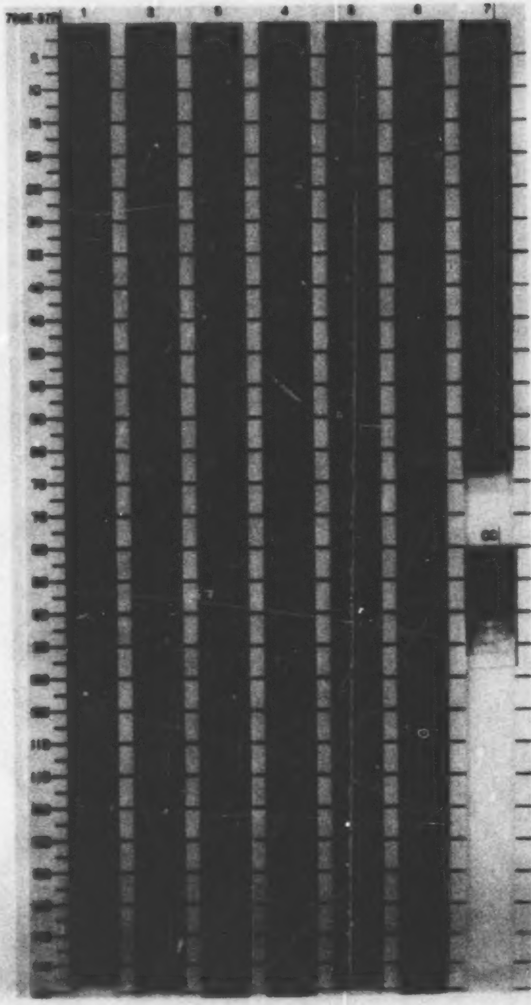
792E-37R
1
2
3
4
5
6
7
CC

SITE 792 HOLE E CORE 38R CORED INTERVAL 492.5-502.2 mbsf

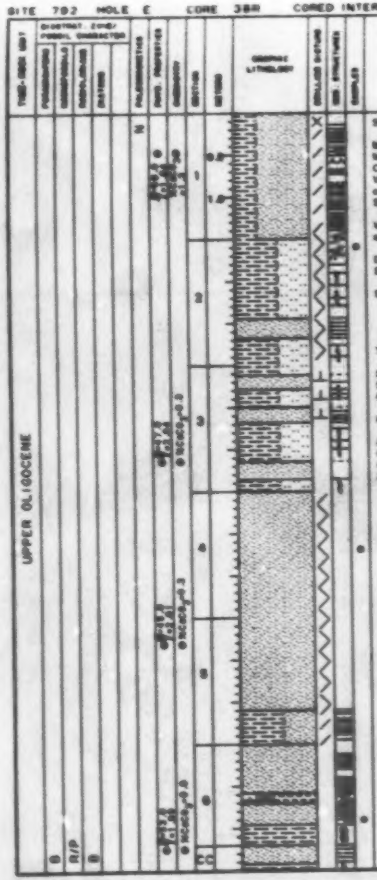
TIME-ROCK UNIT
BIOSTRAT. ZONE/FOSSIL CHARACTER
FORAMINIFERS
NANNOFOSSILS
RADIOLARIANS
DIATOMS
PALEOMAGNETICS
PHYS. PROPERTIES
CHEMISTRY
SECTION
METERS
GRAPHIC LITHOLOGY
DRILLING DISTURB.
SED. STRUCTURES
SAMPLES
UPPER OLIGOCENE
B
R/P
B
N
0.5
1
1.0
2
3
4
5
6
CC

LITHOLOGIC DESCRIPTION

SILTY CLAYSTONE, VITRIC SILTSTONE AND VITRIC SANDSTONE

Major lithologies:
Much of the core consists of thinly interbedded, burrowed, dark gray (5GY 4/1) SILTY CLAYSTONE and graded beds of parallel-laminated, locally rippled, dark gray (5Y 4/1) VITRIC SILTSTONE and VITRIC SANDSTONE. Section 4, 0 cm, to Section 5, 110 cm, consists of a 2.6-m-thick bed of medium-grained, structureless, dark gray (5Y 4/1) VITRIC SANDSTONE, containing about 10% olivine and zeolites.

Veins in Section 1 and Section 2 are filled with calcite. A vein in Section 6, 70-80 cm, appears to be filled with a zeolite mineral.

Drilling deformation is variable, with the greatest amount of deformation characterizing Sections 2, 4 and 5, all of which are highly fractured.

SMEAR SLIDE SUMMARY (%):

	2, 18 M	4, 70 D	6, 90 M
TEXTURE:			
Sand	—	80	100
Silt	—	20	—
Clay	—	—	—
COMPOSITION:			
Accessory minerals	—	10	—
Glass	—	90	—
Inorganic calcite	100	—	—
Zeolite	—	—	100

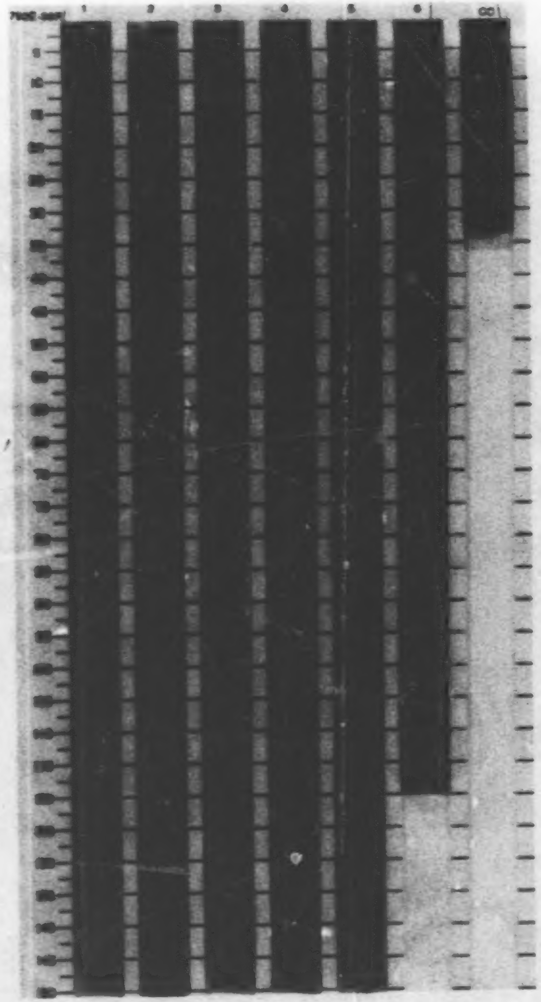
792E-38R
1
2
3
4
5
6
CC

SITE 792 HOLE E CORE 39R CORED INTERVAL 502.2-511.9 mbsf

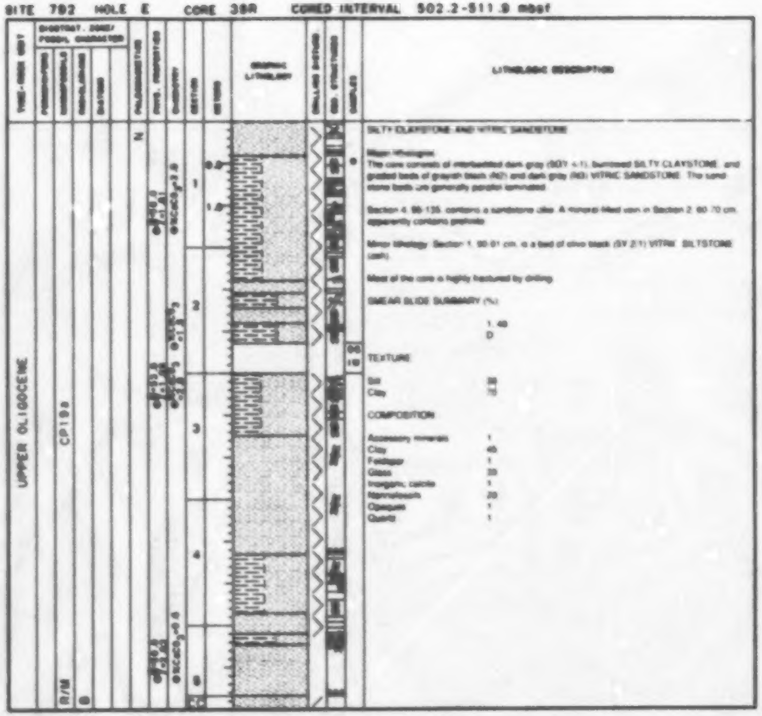
TIME-ROCK UNIT
BIOSTRAT. ZONE/ FOSSIL CHARACTER
FORAMINIFERS
NANNOFOSSILS
RADIOLARIANS
DIATOMS
PALEOMAGNETICS
PHYS. PROPERTIES
CHEMISTRY
SECTION
METERS
GRAPHIC LITHOLOGY
DRILLING DISTURB.
SED. STRUCTURES
SAMPLES
UPPER OLIGOCENE
CP19a
R/M
B
N
1
2
3
4
5
CC

LITHOLOGIC DESCRIPTION

SILTY CLAYSTONE AND VITRIC SANDSTONE

Major lithologies:

The core consists of interbedded dark gray (5GY 4/1), burrowed SILTY CLAYSTONE, and graded beds of grayish black (N2) and dark gray (N3) VITRIC SANDSTONE. The sandstone beds are generally parallel laminated.

Section 4, 99-135, contains a sandstone dike. A mineral-filled vein in Section 2, 60-70 cm, apparently contains prehnite.

Minor lithology: Section 1, 90-91 cm, is a bed of olive black (5Y 2/1) VITRIC SILTSTONE (ash).

Most of the core is highly fractured by drilling.

SMEAR SLIDE SUMMARY (%):

	1, 40
	D
TEXTURE	
Silt	30
Clay	70
COMPOSITION	
Accessory minerals	1
Clay	45
Feldspar	1
Glass	30
Inorganic calcite	1
Nannofossils	20
Opaques	1
Quartz	1

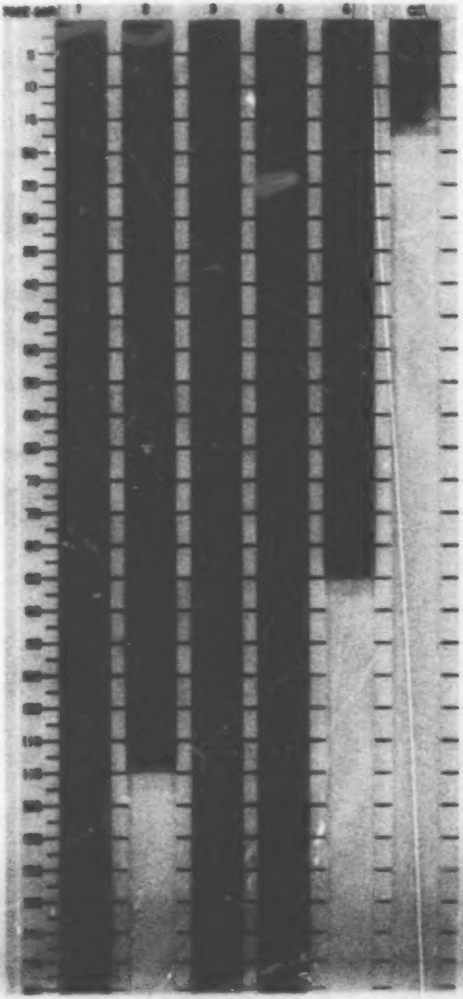

SITE 792 HOLE E CORE 40R CORED INTERVAL 511.8-521.8 mbsf

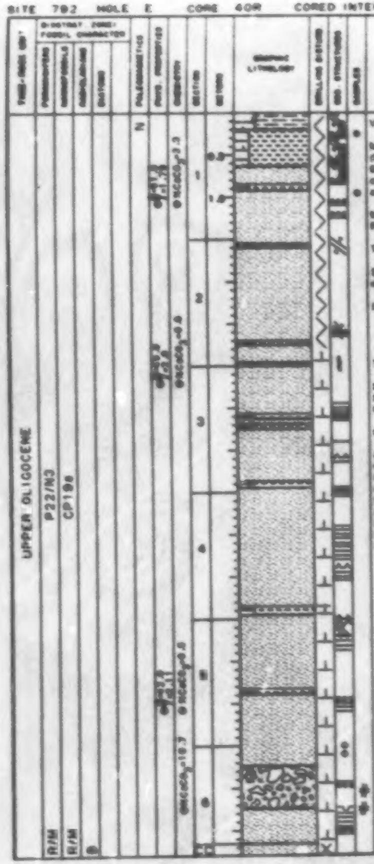
TIME-ROCK UNIT
BIOSTRAT. ZONE/FOSSIL CHARACTER
FORAMINIFERS
NANNOFOSSILS
RADIOLARIANS
DIATOMS
PALEOMAGNETICS
PHYS. PROPERTIES
CHEMISTRY
SECTION
METERS
GRAPHIC LITHOLOGY
DRILLING DISTURB.
SED. STRUCTURES
SAMPLES
UPPER OLIGOCENE
P22/N3
CP19b
R/M
R/M
B
N
●%CaCO3=3.3
●%CaCO3=0.0
●%CaCO3=0.9
●%CaCO3=10.7
1
2
3
4
5
6
CC
0.5
1.0

LITHOLOGIC DESCRIPTION

VITRIC SANDSTONE

Major lithology: Grayish black (N2), dark gray (N3), medium dark gray (N4), and dark gray (5GY 4/1) VITRIC SANDSTONE, fairly well sorted, medium- to very fine-grained, composes 90% of the core. Normally graded bedding is common in Section 1, and single graded units occur in Sections 2, 5 and 6. Planar laminations are common (especially in Sections 3, 4, 5 and 6); wavy laminations occur in Section 3, 110 cm and Section 4, 83 and 140 cm.

Minor lithology: The remaining 10% of the core is greenish black (5G 2/1) NANNOFOSSIL-RICH CLAYSTONE, in undisturbed to slightly bioturbated beds 3-37 cm thick.

Three fractures filled with a whitish mineral (most likely zeolite) occur in Sections 1, 2 and 5.

Sections 1 and 2 are highly fractured, and the rest of the core is moderately fractured by drilling.

SMEAR SLIDE & THIN SECTION SUMMARY (%):

	1, 28 D	1, 56 D	6, 56 D	6, 73 D
TEXTURE:				
Sand	—	80	100	100
Silt	70	20	—	—
Clay	30	—	—	—
COMPOSITION:				
Accessory minerals	5	15	3	10
Cement	—	—	35	20
Feldspar	5	—	3	5
Glass	50	75	30	60
Mica	—	10	—	—
Micrite	10	—	—	—
Nannofossils	30	—	—	—
Rock fragment	—	—	29	5
Silicoflagellates	—	2	—	—

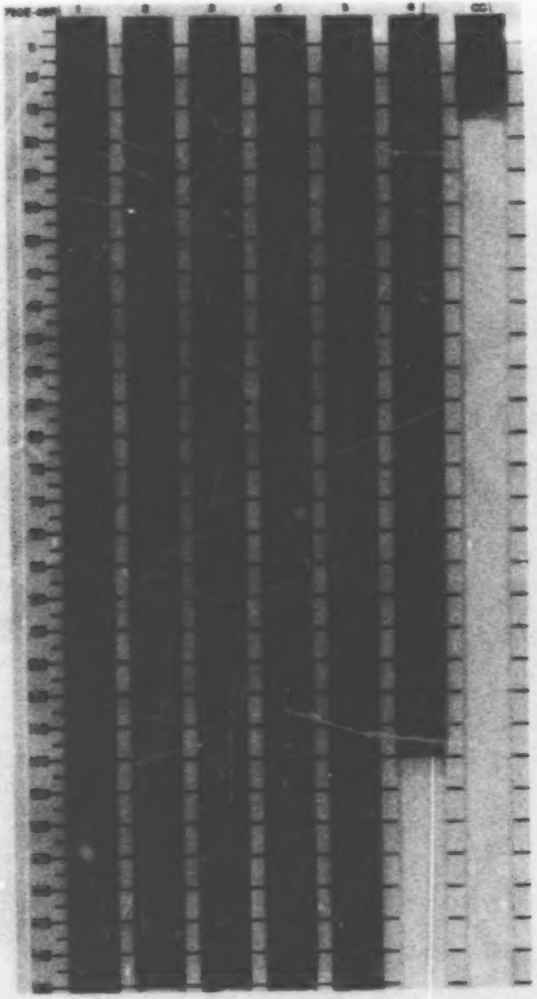
792E-40R
1
2
3
4
5
6
CC

SITE 792 HOLE E CORE 41R CORED INTERVAL 521.6-531.2 mbsf

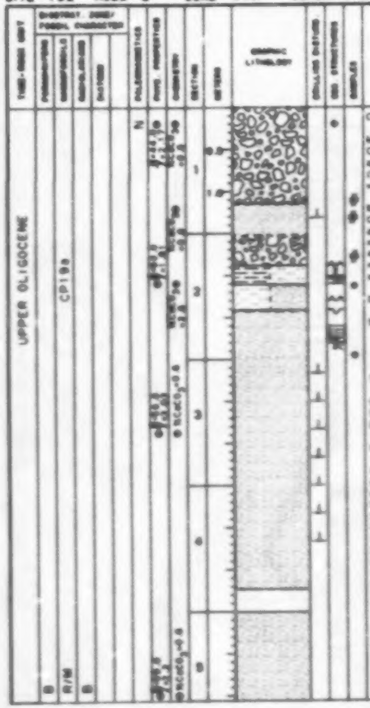
TIME-ROCK UNIT
BIOSTRAT. ZONE/FOSSIL CHARACTER
FORAMINIFERS
NANNOFOSSILS
RADIOLARIANS
DIATOMS
PALEOMAGNETICS
PHYS. PROPERTIES
CHEMISTRY
SECTION
METERS
GRAPHIC LITHOLOGY
DRILLING DISTURB.
SED. STRUCTURES
SAMPLES
UPPER OLIGOCENE
B
CP19a
R/M
B
N
1
2
3
4
5

LITHOLOGIC DESCRIPTION

CRYSTAL VITRIC SANDSTONE

Major lithology: Most of the core (87%) is black (N1), grayish black (N2), and dark gray (N CRYSTAL VITRIC SANDSTONE. Most of the sandstone is well sorted, but various interv are coarse grained and granule rich (Section 1, 0-4 cm and 117-150 cm) or granule bearin (Section 4), medium to coarse or very coarse grained (Sections 3 and 4, respectively), or very fine grained and silty to medium grained (Section 1, 61-150 cm).

Minor lithology: Most of the remaining material in the core is a grayish black (N2) VOLCANIC SANDY GRANULE PEBBLE CONGLOMERATE with rounded to angular, variably altered volcanic rock clasts. The clasts are colored light greenish gray (5G 8/1), black (N1), medium gray (N5), and light gray. In Section 1, 3-117 cm, the sand/granule/pebble ratio is 40:40:20, the maximum clast size is 18 mm, and the mean size of the 10 largest clasts is [illegible] mm. In Section 2, 4-30 cm, the sand/granule/pebble ratio is 30:40:30, and maximum clast size is 11 mm.

Drilling has moderately fractured the core in Section 3 and the top of Section 4.

SMEAR SLIDE & THIN SECTION SUMMARY (%):

	1, 100 M	1, 129 M	2, 24 M	2, 62 M	2, 147 D
TEXTURE:					
Sand	100	98	100	—	80
Silt	—	2	—	20	20
Clay	—	—	—	80	—
COMPOSITION:					
Accessory minerals	10	10	5	—	5
Cement	35	40	45	—	—
Clay	—	—	—	79	10
Feldspar	15	10	15	3	5
Foraminifers	—	—	—	Tr	—
Glass	35	30	20	—	73
Lithic fragments	—	—	—	1	1
Micrite	—	—	—	1	—
Nannofossils	—	—	—	1	—
Opaques	—	—	—	1	—
Rock fragment	5	10	15	—	—
Zeolite	—	—	—	15	1

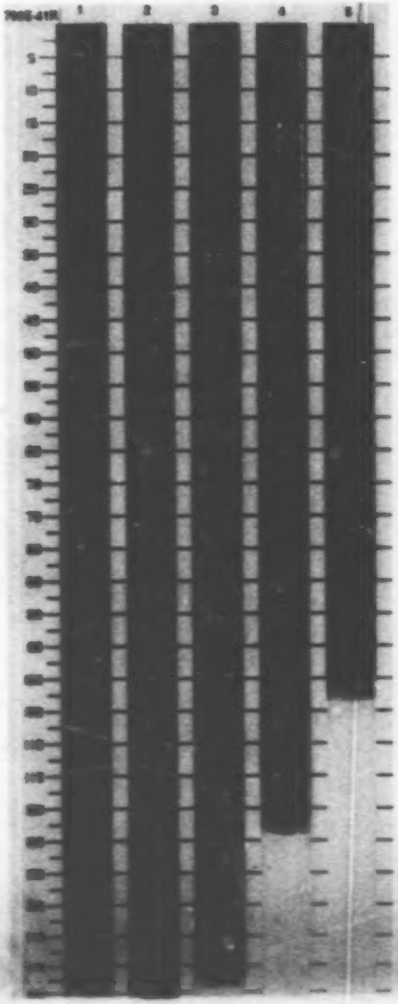
792E-41R
1
2
3
4
5

SITE 792 HOLE E CORE 42R CORED INTERVAL 531.2-540.8 mbsf

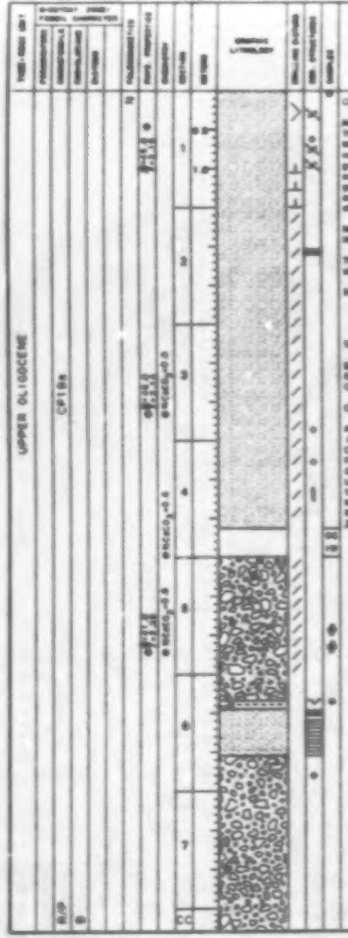

LITHOLOGIC DESCRIPTION

CRYSTAL VITRIC SANDSTONE AND VOLCANIC-LITHIC GRANULE CONGLOMERATE

Major lithologies:
The entire core is grayish black (N2) and greenish black (5G 2/1), except for the minor lithology. Section 1, 0 cm, to Section 6, 107 cm: a CRYSTAL VITRIC SANDSTONE comprising [illegible]% of the core. It is generally well sorted and ranges in grain size from [illegible] sand to very fine-grained, faintly laminated sand. Most of the rest of the core ([illegible]%) is a well-rounded VOLCANIC-LITHIC GRANULE CONGLOMERATE with sand/granule/pebble ratios varying from [illegible] to [illegible]. The maximum clast size is [illegible] mm and the mean size of the ten largest clasts is [illegible] mm. Most of the clasts are andesitic, but claystone rip-up clasts are located in Section 4, [illegible] cm, and Section 6, [illegible] cm.

Minor lithology: Section [illegible], [illegible] cm, a greenish black ([illegible]), slightly bioturbated NANNOFOSSIL-RICH CLAYSTONE.

There are three fractures in Section 1. Drilling disturbance varies from moderately and slightly fractured to undisturbed.

SMEAR SLIDE & THIN SECTION SUMMARY (%):

	1, 1 D	3, 60 D	5, 110 D	6, 37 M
TEXTURE:				
Sand	[illegible]	[illegible]	[illegible]	[illegible]
Silt	[illegible]	—	—	[illegible]
Clay	—	—	—	[illegible]
COMPOSITION:				
Accessory minerals	[illegible]	[illegible]	[illegible]	—
[illegible]	—	[illegible]	[illegible]	—
Clay	—	—	—	[illegible]
Feldspar	[illegible]	[illegible]	[illegible]	[illegible]
Glass	[illegible]	[illegible]	[illegible]	[illegible]
Lithic fragments	[illegible]	—	—	—
[illegible]	—	—	—	[illegible]
[illegible]	—	—	—	[illegible]
Rock fragments	—	[illegible]	[illegible]	—
[illegible]	[illegible]	—	—	[illegible]

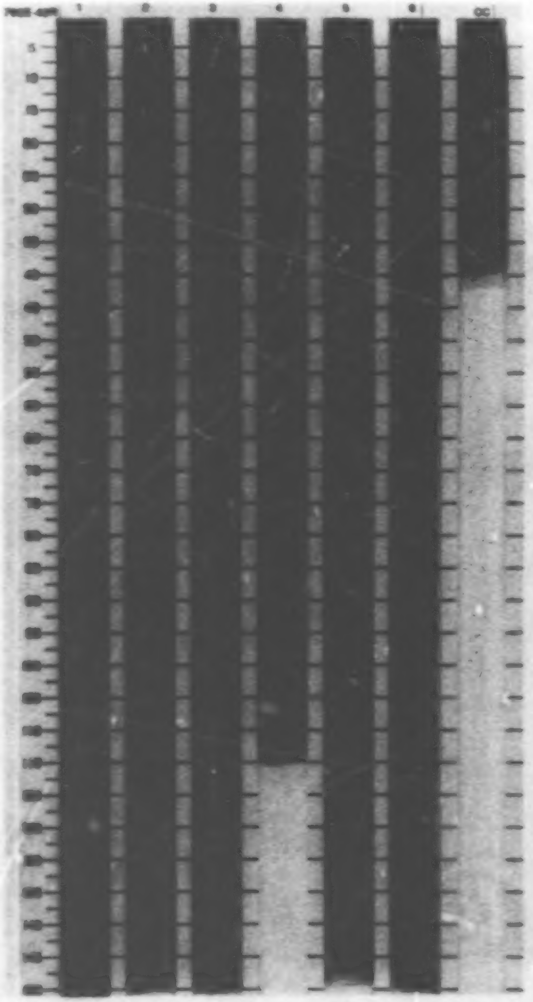

SITE 792 HOLE E CORE 43R CORED INTERVAL 540.6-550.3 mbsf

TIME-ROCK UNIT	BIOSTRAT. ZONE/ FOSSIL CHARACTER: FORAMINIFERS	NANNOFOSSILS	RADIOLARIANS	DIATOMS	PALEOMAGNETICS	PHYS. PROPERTIES	CHEMISTRY	SECTION	METERS	GRAPHIC LITHOLOGY	DRILLING DISTURB.	SED. STRUCTURES	SAMPLES
UPPER OLIGOCENE	C/M	CP19 B			N			1	0.5 1.0				
								2				X	
								3					●
								4					●
								5					●
								6					
								7					

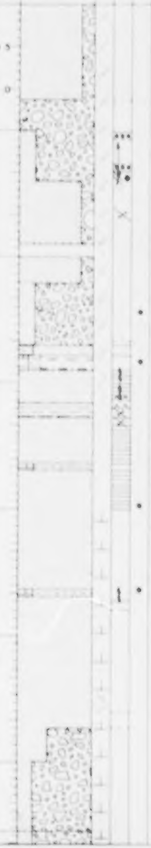

LITHOLOGIC DESCRIPTION

CRYSTAL-VITRIC SANDSTONE [illegible]

Major lithologies:

[illegible]

SMEAR SLIDE SUMMARY (%):

TEXTURE:

Sand

Silt

Clay

COMPOSITION:

[illegible]

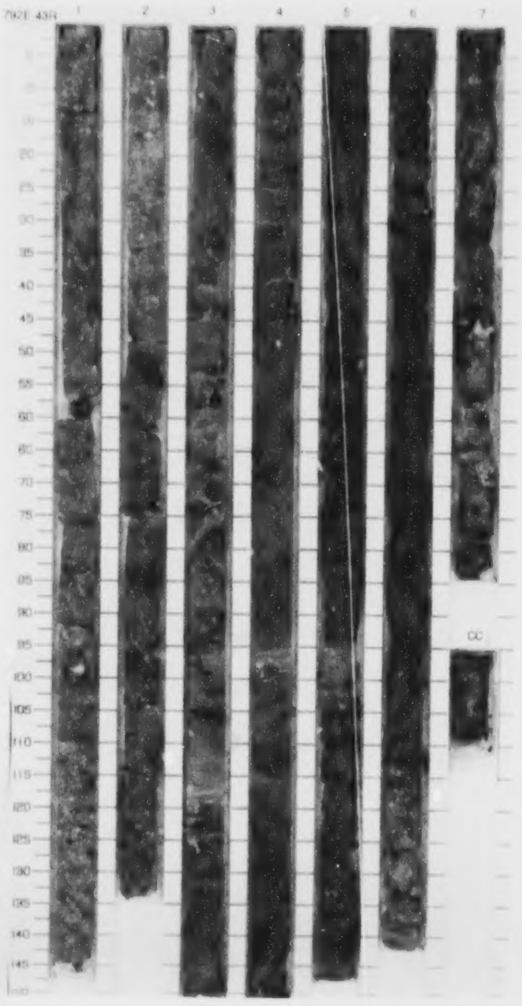

792E-43R
1
2
3
4
5
6
7
CC
5
10
15
20
25
30
35
40
45
50
55
60
65
70
75
80
85
90
95
100
105
110
115
120
125
130
135
140
145
150

SITE 792 HOLE E CORE 44R CORED INTERVAL [illegible]

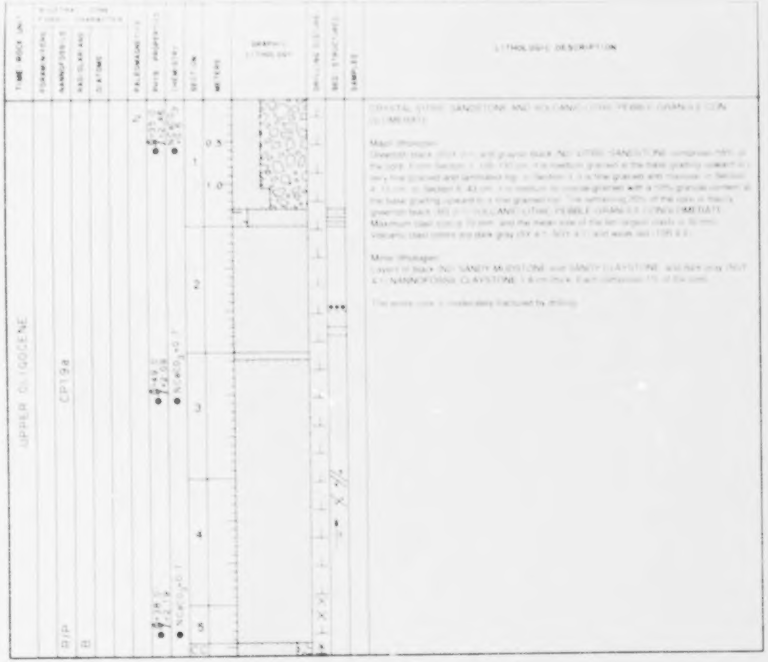
TIME-ROCK UNIT
BIOSTRAT. ZONE/FOSSIL CHARACTER
FORAMINIFERS
NANNOFOSSILS
RADIOLARIANS
DIATOMS
PALEOMAGNETICS
PHYS. PROPERTIES
CHEMISTRY
SECTION
METERS
GRAPHIC LITHOLOGY
DRILLING DISTURB.
SED. STRUCTURES
SAMPLES
LITHOLOGIC DESCRIPTION
UPPER OLIGOCENE
CP19a
B/P
B
N
0.5
1.0
1
2
3
4
5
CC

CRYSTAL-LITHIC SANDSTONE AND VOLCANIC-LITHIC PEBBLE GRANULE CONGLOMERATE

Major lithologies:
Greenish black (5GY 2/1) and grayish black (N2) LITHIC SANDSTONE comprises 74% of the core. From Section 1, 105-150 cm, it is medium grained at the base grading upward to a very fine grained and laminated top. In Section 2, it is fine grained and massive. In Section 4, 15 cm, to Section 5, 43 cm, it is medium to coarse grained with a 10% granule content at the base grading upward to a fine grained top. The remaining 25% of the core is mainly greenish black (5G 2/1) VOLCANIC-LITHIC PEBBLE GRANULE CONGLOMERATE. Maximum clast size is 70 mm, and the mean size of the ten largest clasts is 30 mm. Volcanic clast colors are dark gray (5Y 4/1, N3, 4/1) and weak red (10R 4/2).

Minor lithologies:
Layers of black (N2) SANDY MUDSTONE and SANDY CLAYSTONE, and dark gray (N3/ 4/1) NANNOFOSSIL CLAYSTONE 1-6 cm thick. Each comprises 1% of the core.

The entire core is moderately fractured by drilling.

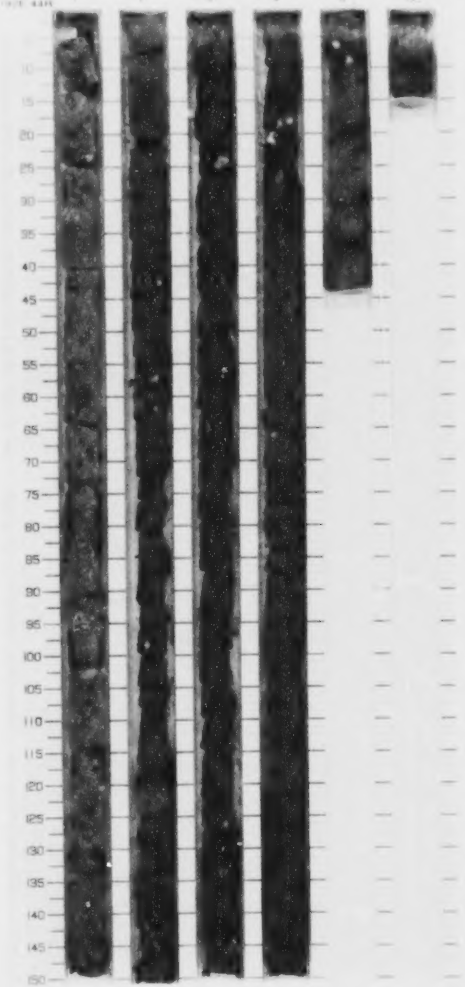
CORE 44R
1
2
3
4
5
CC
10
15
20
25
30
35
40
45
50
55
60
65
70
75
80
85
90
95
100
105
110
115
120
125
130
135
140
145
150

SITE 792 HOLE E CORE 45R CORED INTERVAL 560.0-569.7 mbsf

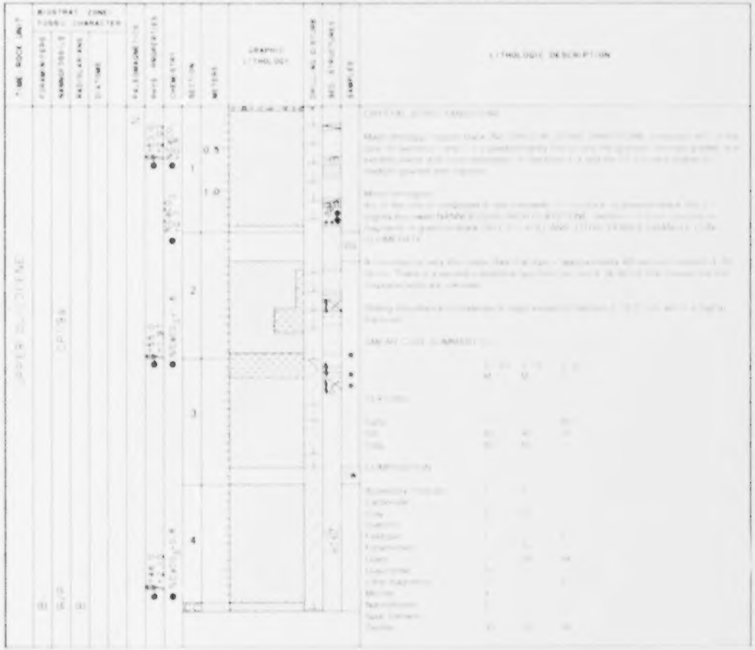
TIME-ROCK UNIT
BIOSTRAT. ZONE/ FOSSIL CHARACTER
FORAMINIFERS
NANNOFOSSILS
RADIOLARIANS
DIATOMS
PALEOMAGNETICS
PHYS. PROPERTIES
CHEMISTRY
SECTION
METERS
GRAPHIC LITHOLOGY
DRILLING DISTURB.
SED. STRUCTURES
SAMPLES
UPPER OLIGOCENE
CP19
0.5
1.0
1
2
3
4
CC

LITHOLOGIC DESCRIPTION

[illegible]

SMEAR SLIDE SUMMARY (%):

TEXTURE:

Sand
Silt
Clay

COMPOSITION:

Accessory minerals
Carbonate
Clay
Quartz
Feldspar
Ferromagnesian
Glass
Glauconite
Lithic fragments
Micrite
Nannofossils
Spar Cement
Zeolite

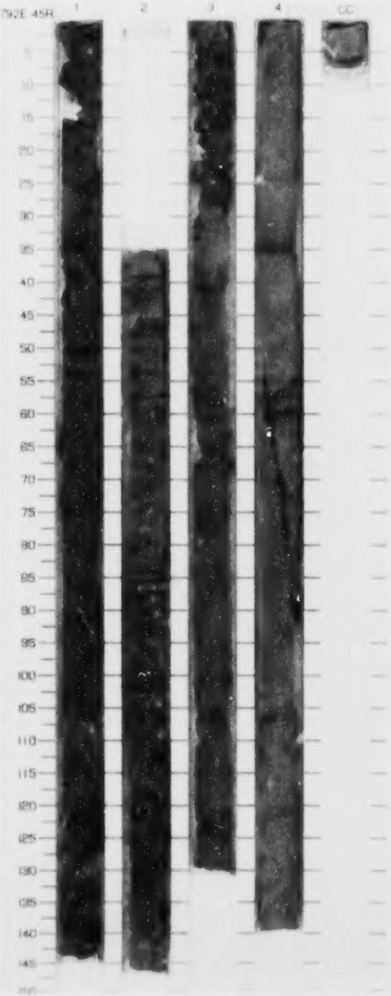
792E 45R
1
2
3
4
CC
5
10
15
20
25
30
35
40
45
50
55
60
65
70
75
80
85
90
95
100
105
110
115
120
125
130
135
140
145
150

SITE 792 HOLE E CORE [illegible] CORED INTERVAL [illegible]

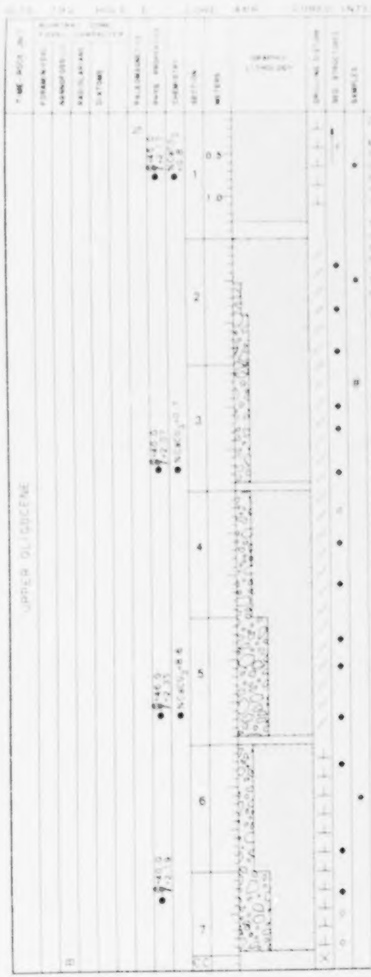
TIME-ROCK UNIT
BIOSTRAT. ZONE / FOSSIL CHARACTER
FORAMINIFERS
NANNOFOSSILS
RADIOLARIANS
DIATOMS
PALEOMAGNETICS
PHYS. PROPERTIES
CHEMISTRY
SECTION
METERS
GRAPHIC LITHOLOGY
DRILLING DISTURB.
SED. STRUCTURES
SAMPLES
UPPER OLIGOCENE
B
0.5
1
1.0
2
3
4
5
6
7
CC

LITHOLOGIC DESCRIPTION

ZEOLITE-RICH VITRIC SANDSTONE AND VITRIC PEBBLY SANDSTONE

Major lithologies:

[illegible] ZEOLITE-RICH VITRIC SAND-STONE [illegible] VITRIC PEBBLY SANDSTONE [illegible]

[illegible]

[illegible]

SMEAR SLIDE & THIN SECTION SUMMARY (%):

TEXTURE:

Sand

Silt

Clay

COMPOSITION:

Accessory minerals

Cement

Clay

Feldspar

Glass

Olivine

Opaques

Pore Space

Rock fragment

Zeolite

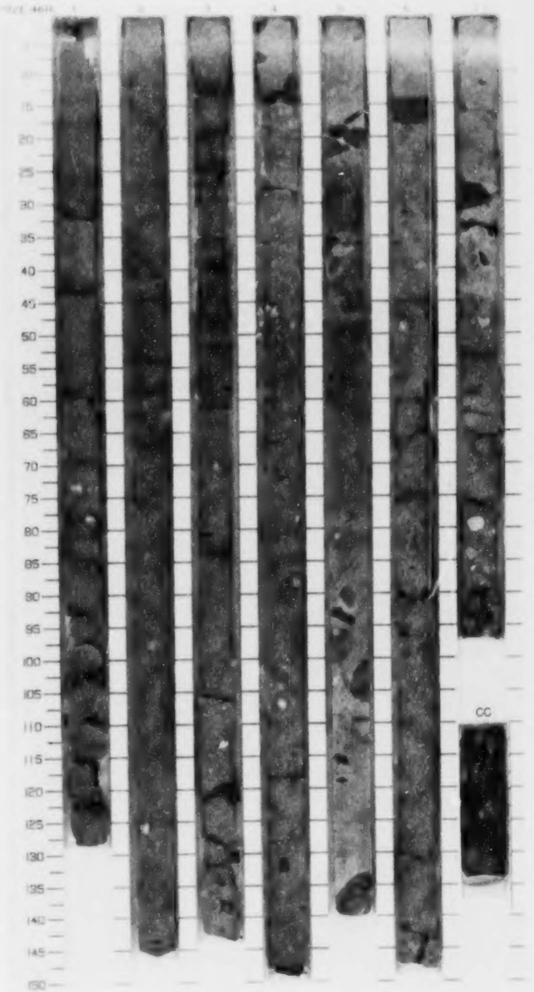
1
2
3
4
5
6
7
CC
0
10
15
20
25
30
35
40
45
50
55
60
65
70
75
80
85
90
95
100
105
110
115
120
125
130
135
140
145
150

SITE 792 HOLE E CORE 47R CORED INTERVAL 579.4-588.6 mbsf

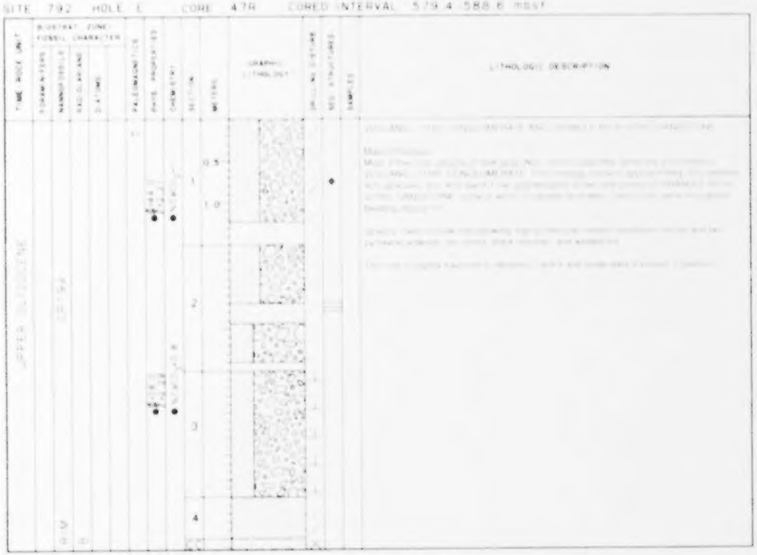
TIME-ROCK UNIT
BIOSTRAT. ZONE/ FOSSIL CHARACTER
FORAMINIFERS
NANNOFOSSILS
RADIOLARIANS
DIATOMS
PALEOMAGNETICS
PHYS. PROPERTIES
CHEMISTRY
SECTION
METERS
GRAPHIC LITHOLOGY
DRILLING DISTURB.
SED. STRUCTURES
SAMPLES
LITHOLOGIC DESCRIPTION
UPPER OLIGOCENE
0.5
1.0
1
2
3
4
CC

[illegible]

[illegible]

[illegible]

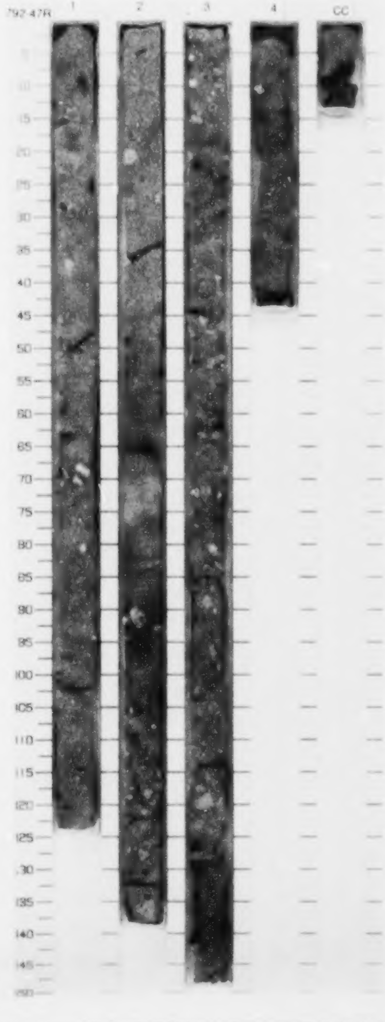
792-47R
1
2
3
4
CC
5
10
15
20
25
30
35
40
45
50
55
60
65
70
75
80
85
90
95
100
105
110
115
120
125
130
135
140
145
150

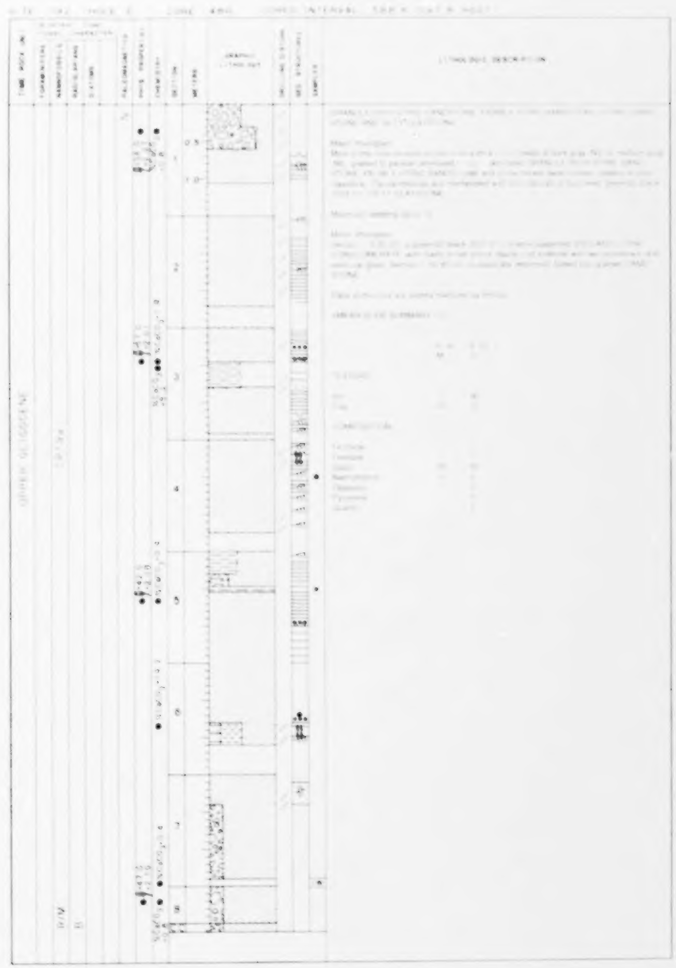
SITE 792 HOLE E CORE 48R CORED INTERVAL
LITHOLOGIC DESCRIPTION
GRAPHIC LITHOLOGY
UPPER OLIGOCENE

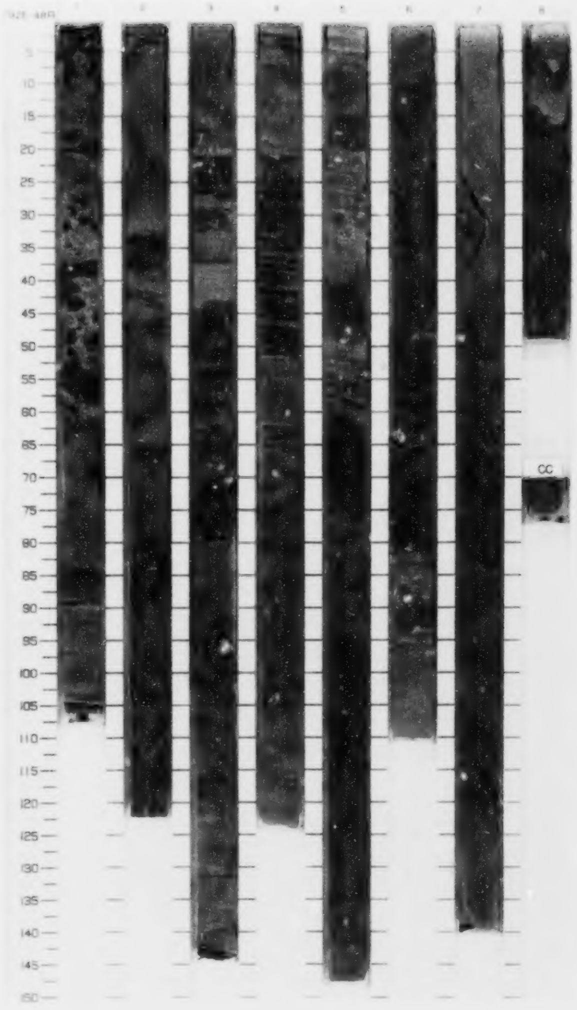
792E-48R
1
2
3
4
5
6
7
8
CC
5
10
15
20
25
30
35
40
45
50
55
60
65
70
75
80
85
90
95
100
105
110
115
120
125
130
135
140
145
150

SITE 792 HOLE E CORE 49R CORED INTERVAL 597.8-607.4 mbsf

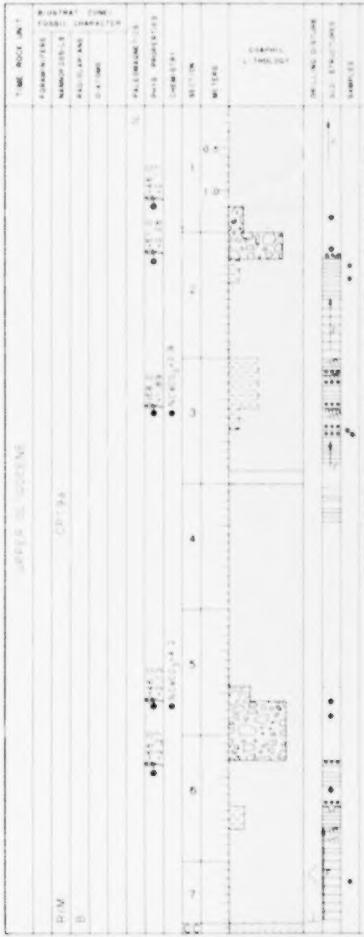
TIME-ROCK UNIT
BIOSTRAT. ZONE/ FOSSIL CHARACTER
FORAMINIFERS
NANNOFOSSILS
RADIOLARIANS
DIATOMS
PALEOMAGNETICS
PHYS. PROPERTIES
CHEMISTRY
SECTION
METERS
GRAPHIC LITHOLOGY
DRILLING DISTURB.
SED. STRUCTURES
SAMPLES
UPPER OLIGOCENE
CP19a
R/M
B
0.5
1.0
1
2
3
4
5
6
7
CC

LITHOLOGIC DESCRIPTION

[illegible]

Major lithologies:

[illegible]

Minor lithologies:

[illegible]

SMEAR SLIDE SUMMARY (%):

	[illegible]	[illegible]	[illegible]	[illegible]	[illegible]
	M	[illegible]	[illegible]	M	[illegible]
TEXTURE:					
Sand	[illegible]	[illegible]	[illegible]	[illegible]	[illegible]
Silt	[illegible]	[illegible]	[illegible]	[illegible]	[illegible]
Clay	[illegible]	[illegible]	[illegible]	[illegible]	[illegible]
COMPOSITION:					
Clay	[illegible]	[illegible]	[illegible]	[illegible]	[illegible]
Feldspar	[illegible]	[illegible]	[illegible]	[illegible]	[illegible]
Glass	[illegible]	[illegible]	[illegible]	[illegible]	[illegible]
[illegible]	[illegible]	[illegible]	[illegible]	[illegible]	[illegible]
Nannofossils	[illegible]	[illegible]	[illegible]	[illegible]	[illegible]
Opaques	[illegible]	[illegible]	[illegible]	[illegible]	[illegible]
Pyroxene	[illegible]	[illegible]	[illegible]	[illegible]	[illegible]
Quartz	[illegible]	[illegible]	[illegible]	[illegible]	[illegible]

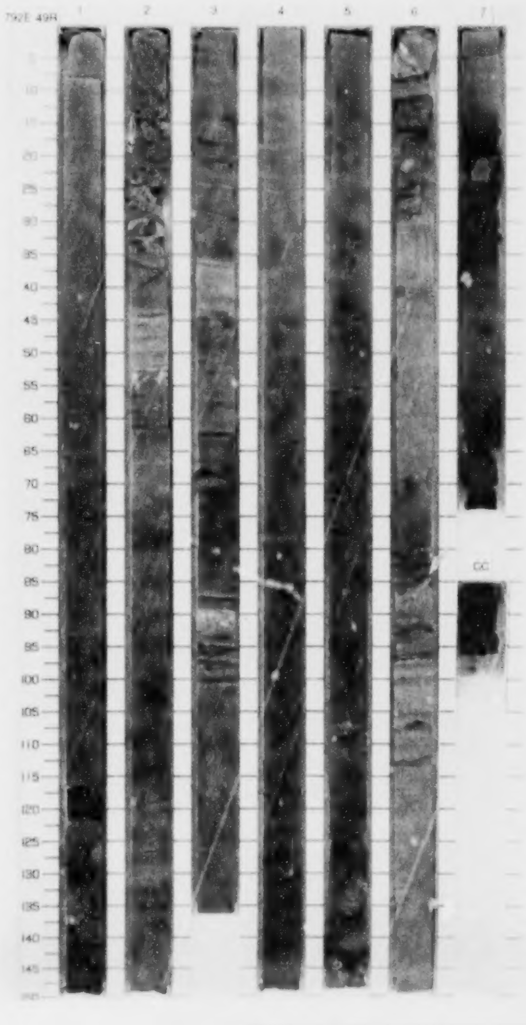
792E 49R
1
2
3
4
5
6
7
CC
0
5
10
15
20
25
30
35
40
45
50
55
60
65
70
75
80
85
90
95
100
105
110
115
120
125
130
135
140
145
150

SITE 792 HOLE E CORE 70R CORED INTERVAL 607.4-617.1 mbsf

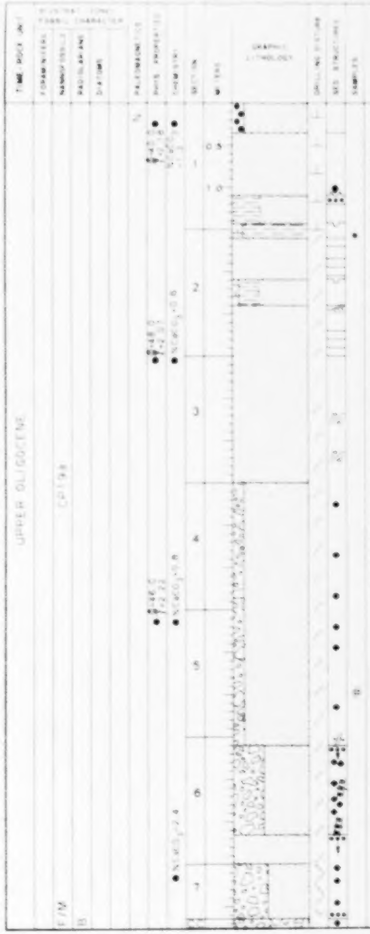

LITHOLOGIC DESCRIPTION

VITRIC SANDSTONE, VITRIC PEBBLY SANDSTONE, VOLCANIC LITHIC CONGLOMERATE, AND NANNOFOSSIL-RICH SILTY CLAYSTONE

Major lithologies:
Much of the core consists of dark gray (N3, N4) and dark greenish gray (5G 4/1), generally structureless, locally parallel-laminated VITRIC SANDSTONE and VITRIC PEBBLY SANDSTONE. In Sections 6 and 7, the sediment becomes matrix-supported, fine pebble VOLCANIC LITHIC CONGLOMERATE with clasts of nannofossil-rich silty claystone up to 1 cm in diameter. The volcanic clasts include red scoria, andesite and dacite. Thin-bedded intervals in the core consist of graded beds of fine-grained VITRIC SANDSTONE and burrowed NANNOFOSSIL-RICH SILTY CLAYSTONE.

There is a zone of soft-sediment deformation in a sandstone bed in Section 7, 50-90 cm. Small clastic dikes occur in Section 6. There are micro-faults in Section 3. Bedding dips at 8°.

Section 1 is moderately fractured by drilling. Section 7 is highly fractured. The rest of the core is only slightly fractured.

SMEAR SLIDE & THIN SECTION SUMMARY (%):

	2, 8	5, 90
	D	T
TEXTURE:		
Sand	—	100
Silt	30	—
Clay	70	—
COMPOSITION:		
Accessory minerals	—	5
Cement	—	11
Clay	49	—
Feldspar	2	10
Glass	30	40
Nannofossils	15	—
Opaques	1	—
Pore Space	—	4
Quartz	2	—
Rock fragment	—	30

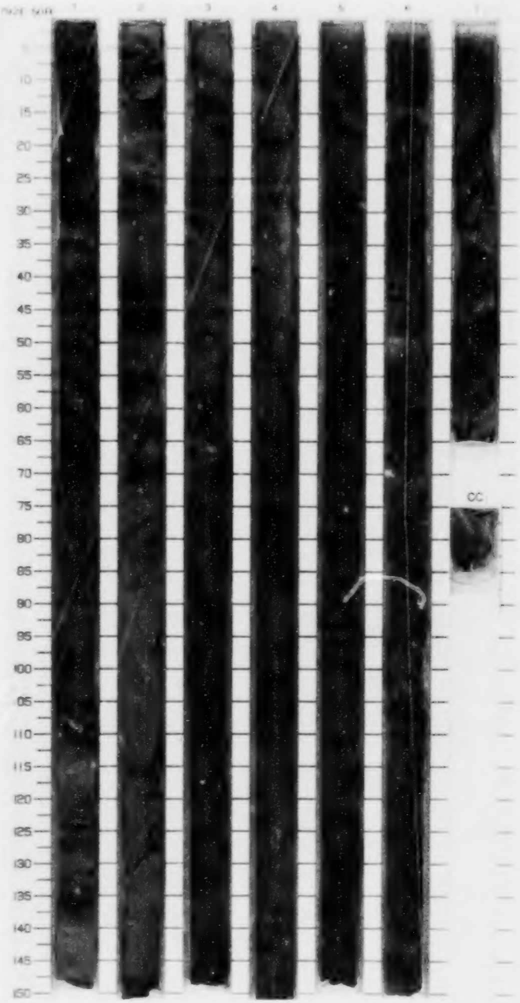

SITE 792 HOLE E CORE 51R CORED INTERVAL 617.1-626.8 mbsf

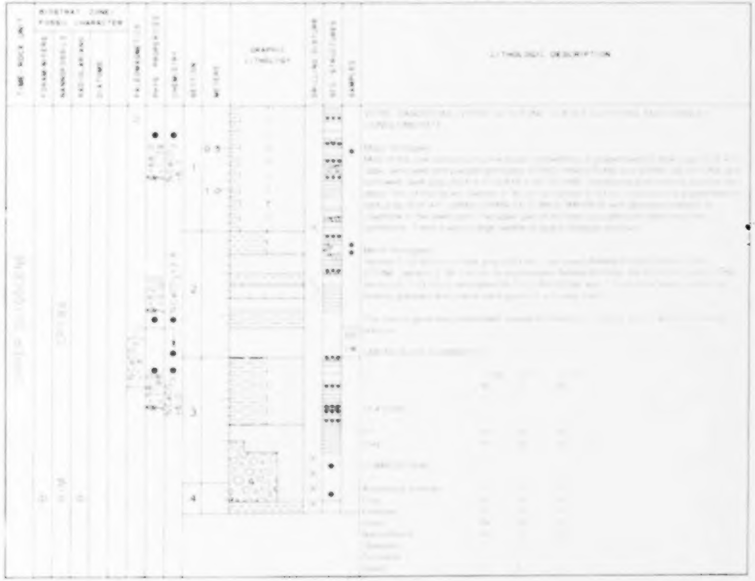
TIME-ROCK UNIT
BIOSTRAT. ZONE/FOSSIL CHARACTER
FORAMINIFERS
NANNOFOSSILS
RADIOLARIANS
DIATOMS
PALEOMAGNETICS
PHYS. PROPERTIES
CHEMISTRY
SECTION
METERS
GRAPHIC LITHOLOGY
DRILLING DISTURB.
SED. STRUCTURES
SAMPLES
LITHOLOGIC DESCRIPTION
0.5
1.0
1
2
3
4

[illegible]

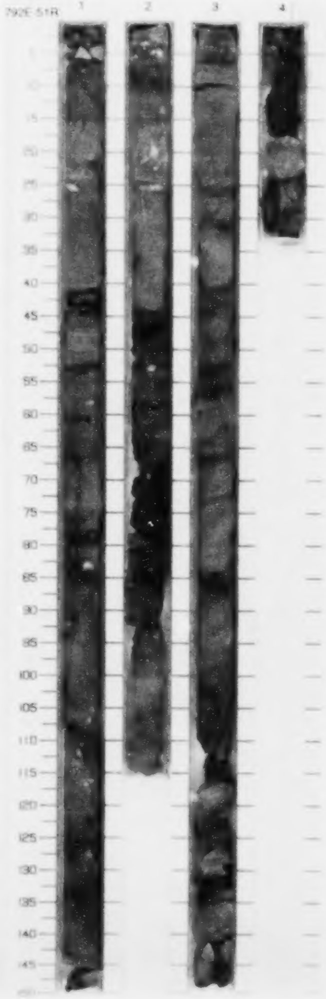
792E-51R
1
2
3
4
5
10
15
20
25
30
35
40
45
50
55
60
65
70
75
80
85
90
95
100
105
110
115
120
125
130
135
140
145
150

SITE 792 HOLE E CORE 52R CORED INTERVAL 626.8-636.4 mbsf

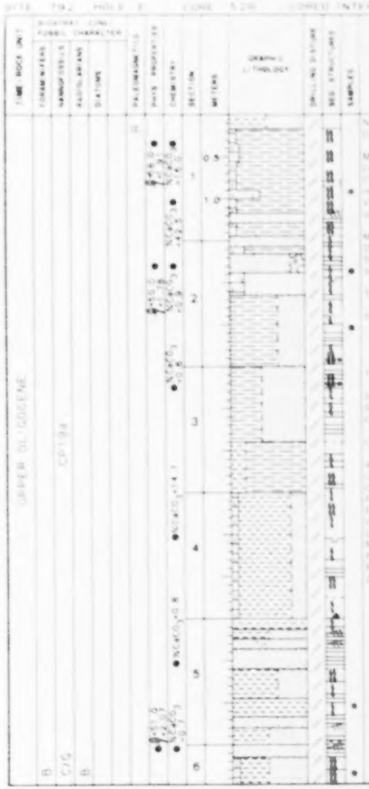
TIME-ROCK UNIT
BIOSTRAT. ZONE/ FOSSIL CHARACTER
FORAMINIFERS
NANNOFOSSILS
RADIOLARIANS
DIATOMS
PALEOMAGNETICS
PHYS. PROPERTIES
CHEMISTRY
SECTION
METERS
GRAPHIC LITHOLOGY
DRILLING DISTURB.
SED. STRUCTURES
SAMPLES
UPPER OLIGOCENE
CP19a
B
C/G
B
0.5
1.0
1
2
3
4
5
6

LITHOLOGIC DESCRIPTION

NANNOFOSSIL SILTY CLAYSTONE, NANNOFOSSIL CLAYSTONE AND VITRIC CRYSTAL SANDSTONE

Major lithologies:
Light greenish gray (5G 7/1) [illegible] slightly bioturbated NANNOFOSSIL SILTY CLAYSTONE and NANNOFOSSIL CLAYSTONE comprise 60% of the core. Most of the rest of the core (30%) is dark gray (5GY 4/1), dusky green (5G 3/2), and olive black (5Y 2/1) VITRIC CRYSTAL SANDSTONE, typically fine grained to very fine grained and planar laminated, with rare cross-laminations, normal grading, and [illegible].

Minor lithologies:
Dark greenish gray (5G 4/1) SILTY CLAYSTONE and olive black (5Y 2/1) SANDY SILTSTONE are [illegible] lithologies that comprise [illegible] of the core. [illegible] Section 5, [illegible] cm is a concentration of [illegible] plant matter.

The entire core is slightly fractured by drilling.

SMEAR SLIDE SUMMARY (%):

	1, 40	2, 103	5, 103	6, 33
	M	M	M	
TEXTURE:				
Sand	5	40	40	75
Silt	35	30	20	25
Clay	60	30	40	—
COMPOSITION:				
Accessory minerals	—	—	Tr	5
Cement	—	2	—	—
Clay	50	20	30	—
Feldspar	—	5	10	5
Foraminifers	Tr	—	—	—
Glass	5	25	20	35
Lithic fragments	—	5	—	—
Nannofossils	30	—	10	—
Plant	—	—	20	—
Radiolarians	Tr	—	—	—
Zeolite	10	10	5	30

126 792E 53R NO RECOVERY

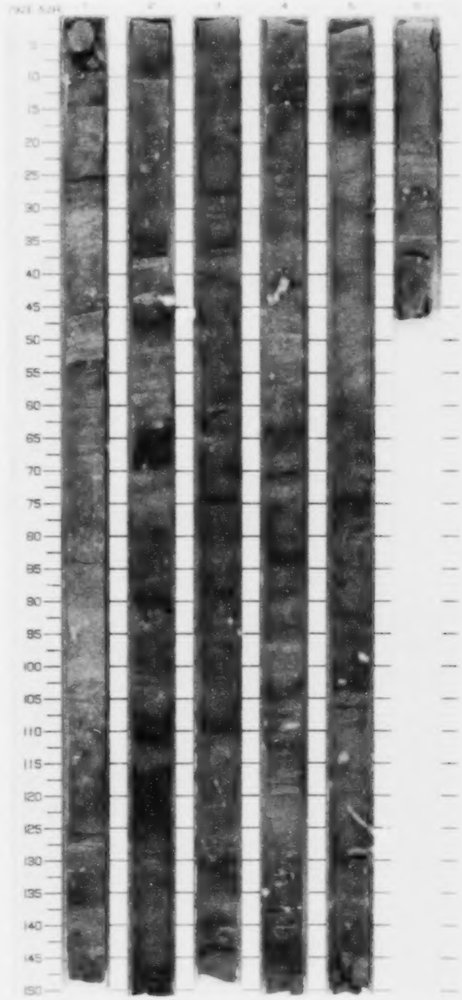
792E 52R
1
2
3
4
5
6
5
10
15
20
25
30
35
40
45
50
55
60
65
70
75
80
85
90
95
100
105
110
115
120
125
130
135
140
145
150

SITE 792 HOLE E CORE 54R CORED INTERVAL 646.1-655.7 mbsf

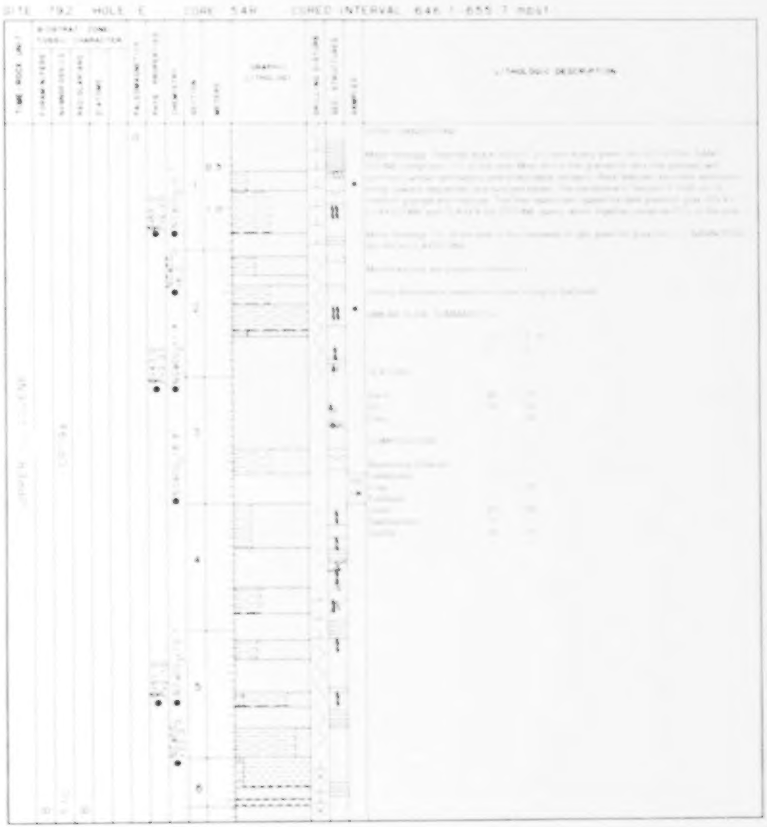

[illegible]

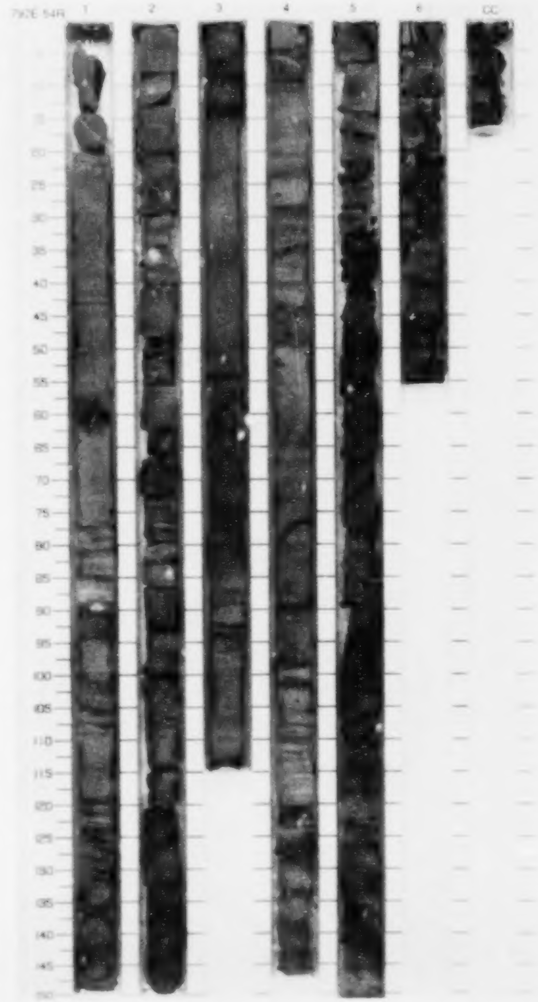
792E 54R
1
2
3
4
5
6
CC
10
15
20
25
30
35
40
45
50
55
60
65
70
75
80
85
90
95
100
105
110
115
120
125
130
135
140
145
150

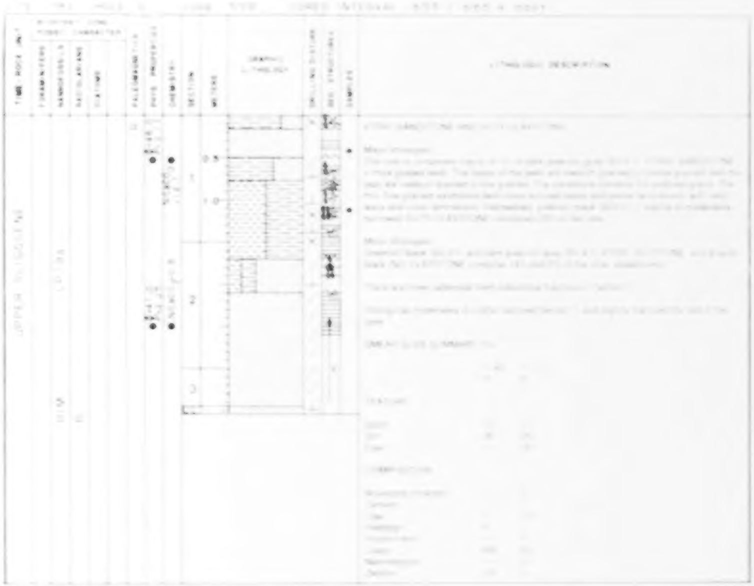
TIME-ROCK UNIT
BIOSTRAT. ZONE / FOSSIL CHARACTER
FORAMINIFERS
NANNOFOSSILS
RADIOLARIANS
DIATOMS
PALEOMAGNETICS
PHYS. PROPERTIES
CHEMISTRY
SECTION
METERS
GRAPHIC LITHOLOGY
DRILLING DISTURB.
SED. STRUCTURES
SAMPLES
LITHOLOGIC DESCRIPTION
UPPER OLIGOCENE
0.5
1.0
1
2
3
CC

Major lithologies:

Minor lithologies:

SMEAR SLIDE SUMMARY (%):

TEXTURE:

Sand
Silt
Clay

COMPOSITION:

[illegible]

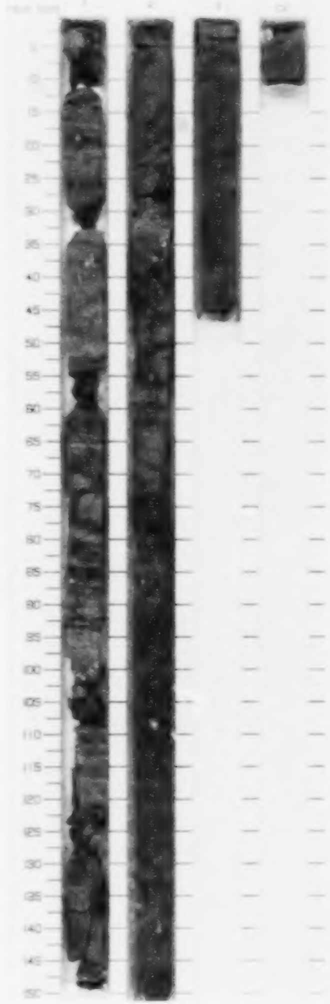
1
2
3
CC
0
10
15
20
25
30
35
40
45
50
55
60
65
70
75
80
85
90
95
100
105
110
115
120
125
130
135
140
145
150

SITE 792 HOLE E CORE 56R CORED INTERVAL 665.4-675.1 mbsf

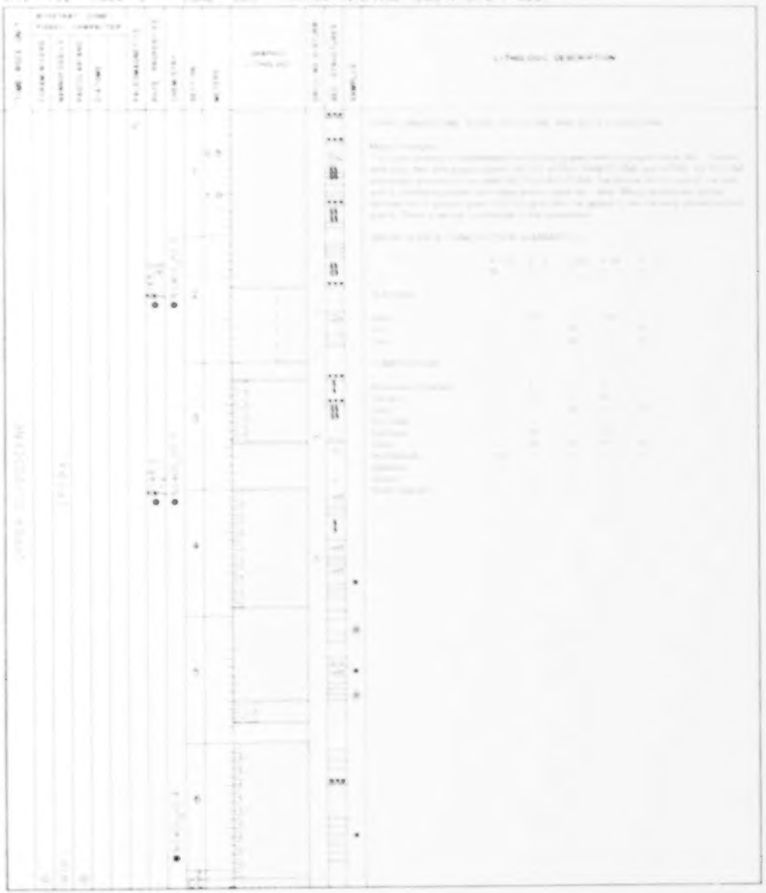
TIME-ROCK UNIT
BIOSTRAT. ZONE/FOSSIL CHARACTER
FORAMINIFERS
NANNOFOSSILS
RADIOLARIANS
DIATOMS
PALEOMAGNETICS
PHYS. PROPERTIES
CHEMISTRY
SECTION
METERS
GRAPHIC LITHOLOGY
DRILLING DISTURB.
SED. STRUCTURES
SAMPLES
LITHOLOGIC DESCRIPTION

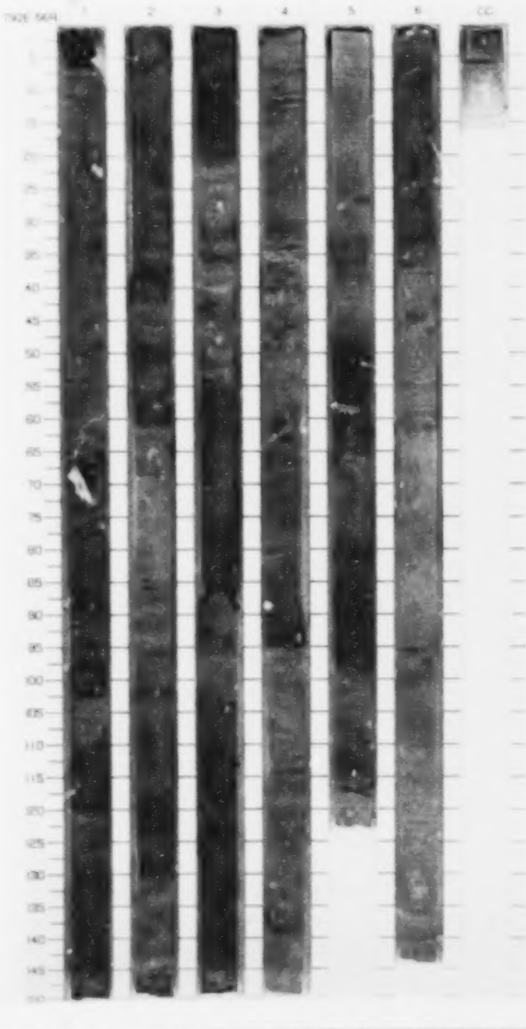
792E-56R
1
2
3
4
5
6
CC
0
5
10
15
20
25
30
35
40
45
50
55
60
65
70
75
80
85
90
95
100
105
110
115
120
125
130
135
140
145
150

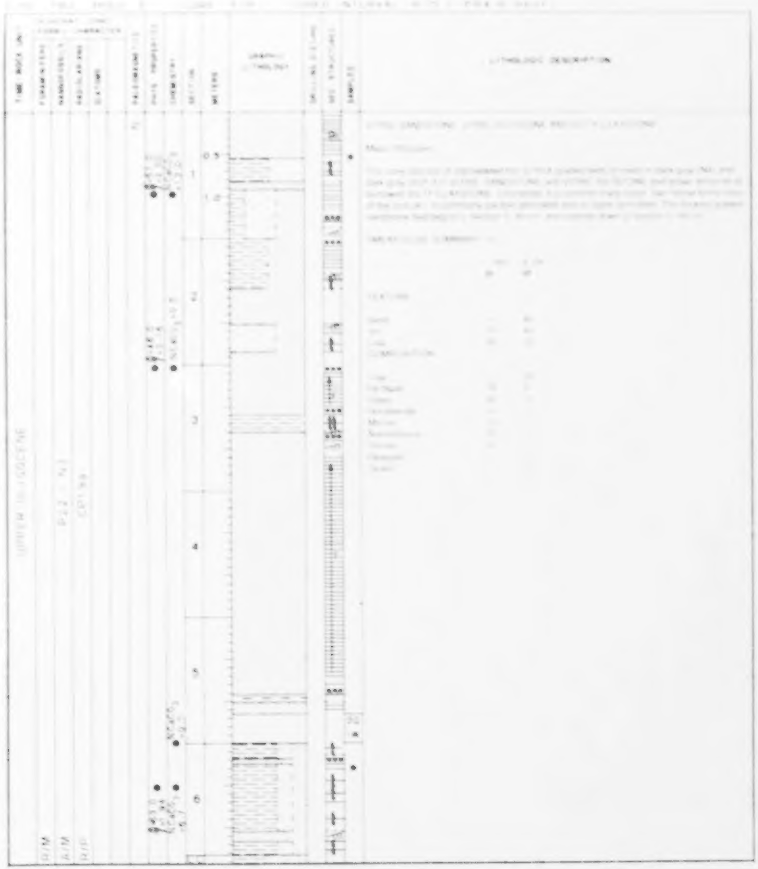
LITHOLOGIC DESCRIPTION
GRAPHIC LITHOLOGY
0.5
1
1.0
2
3
4
5
6

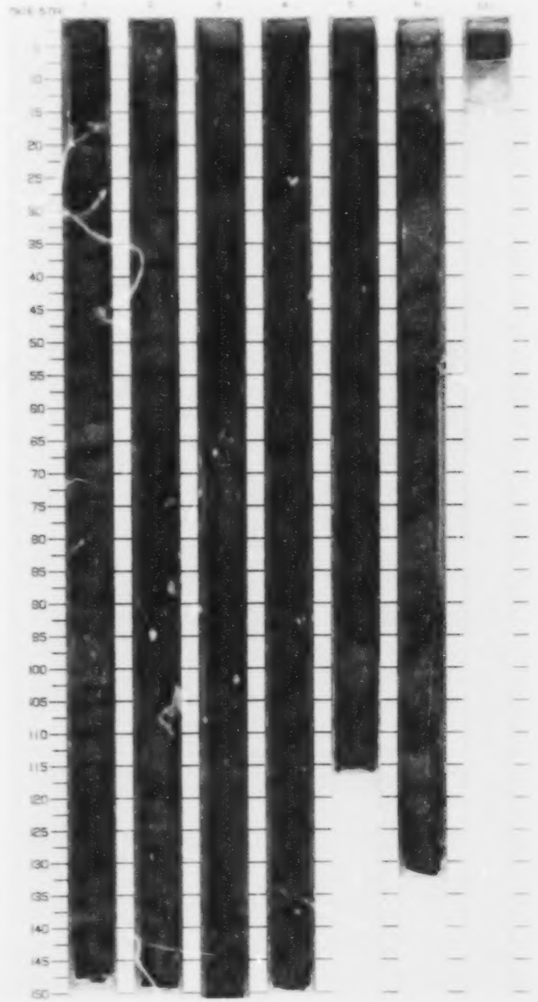
1
2
3
4
5
6
CC
0
5
10
15
20
25
30
35
40
45
50
55
60
65
70
75
80
85
90
95
100
105
110
115
120
125
130
135
140
145
150

SITE 792 HOLE E CORE 58R CORED INTERVAL 684.8-694.4 mbsf

TIME-ROCK UNIT
BIOSTRAT. ZONE/FOSSIL CHARACTER
FORAMINIFERS
NANNOFOSSILS
RADIOLARIANS
DIATOMS
PALEOMAGNETICS
PHYS. PROPERTIES
CHEMISTRY
SECTION
METERS
GRAPHIC LITHOLOGY
DRILLING DISTURB.
SED. STRUCTURES
SAMPLES
LITHOLOGIC DESCRIPTION
0.5
1.0
1
2
3
4
CC

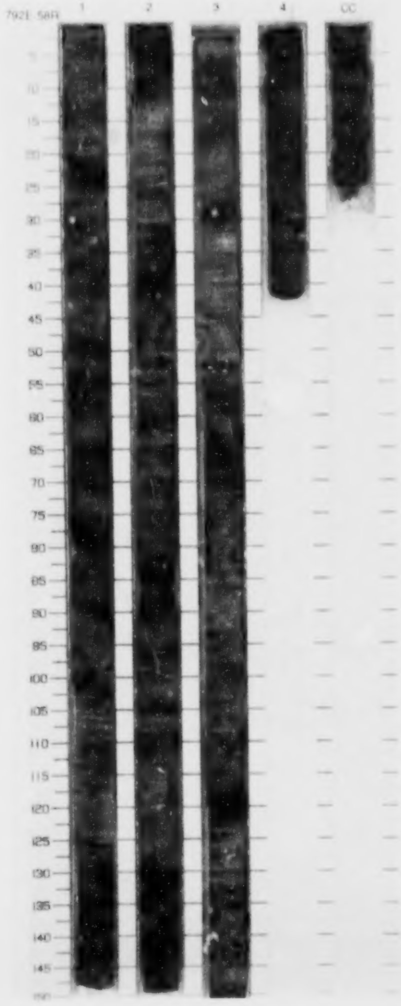
792E 58R
1
2
3
4
CC
5
10
15
20
25
30
35
40
45
50
55
60
65
70
75
80
85
90
95
100
105
110
115
120
125
130
135
140
145
150

SITE 792 HOLE E CORE 59R CORED INTERVAL [illegible] mbsf

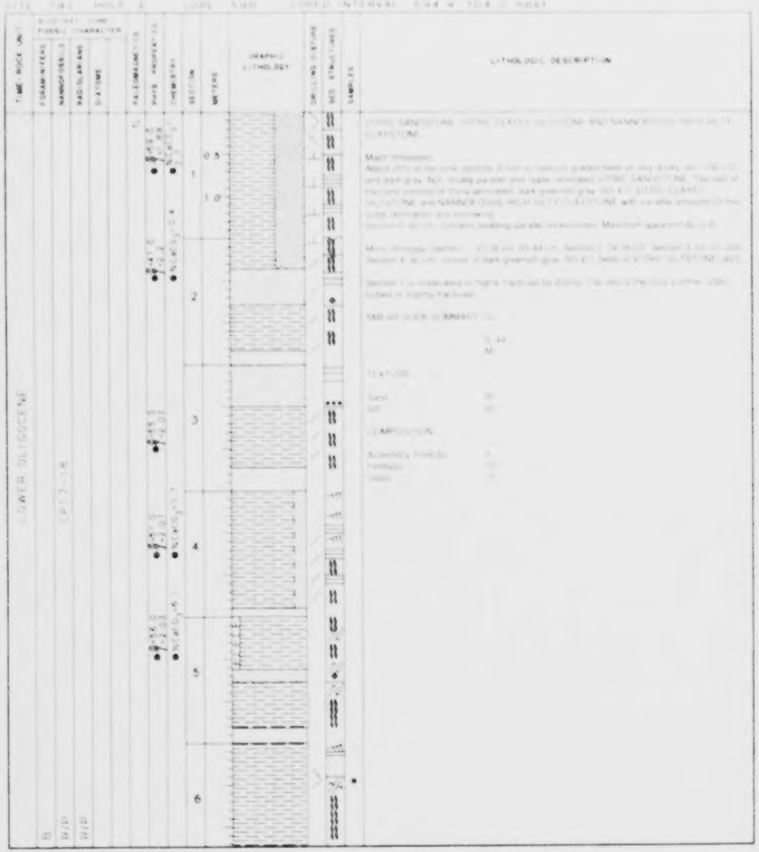
TIME-ROCK UNIT
BIOSTRAT. ZONE / FOSSIL CHARACTER
FORAMINIFERS
NANNOFOSSILS
RADIOLARIANS
DIATOMS
PALEOMAGNETICS
PHYS. PROPERTIES
CHEMISTRY
SECTION
METERS
GRAPHIC LITHOLOGY
DRILLING DISTURB.
SED. STRUCTURES
SAMPLES
LOWER OLIGOCENE
CP17-18
B
R/P
R/P
1
2
3
4
5
6
0.5
1.0

LITHOLOGIC DESCRIPTION

VITRIC SANDSTONE, VITRIC CLAYEY SILTSTONE, AND NANNOFOSSIL-RICH SILTY CLAYSTONE

Major lithologies:
About 20% of the core consists of [illegible] VITRIC SANDSTONE. The rest of the core consists of [illegible] dark greenish gray [illegible] VITRIC CLAYEY SILTSTONE and NANNOFOSSIL-RICH SILTY CLAYSTONE with variable amounts of [illegible]

[illegible]

Minor lithology: [illegible]

Section [illegible]

SMEAR SLIDE SUMMARY (%):

	[illegible]
	M
TEXTURE:	
Sand	[illegible]
Silt	[illegible]
COMPOSITION:	
Authigenic minerals	[illegible]
Feldspar	[illegible]
Glass	[illegible]

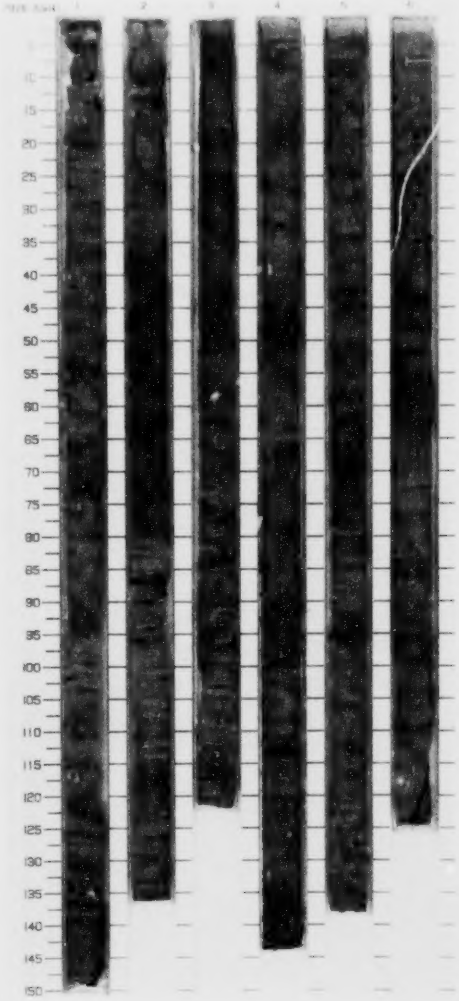
1
2
3
4
5
6
0
10
15
20
25
30
35
40
45
50
55
60
65
70
75
80
85
90
95
100
105
110
115
120
125
130
135
140
145
150

SITE 792 HOLE E CORE 60R CORED INTERVAL 704.0-713.6 mbsf

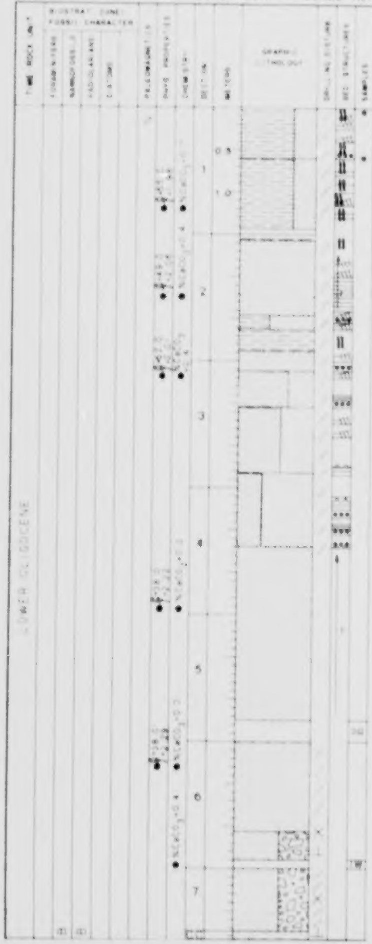
TIME-ROCK UNIT
BIOSTRAT. ZONE/FOSSIL CHARACTER
FORAMINIFERS
NANNOFOSSILS
RADIOLARIANS
DIATOMS
PALEOMAGNETICS
PHYS. PROPERTIES
CHEMISTRY
SECTION
METERS
GRAPHIC LITHOLOGY
DRILLING DISTURB.
SED. STRUCTURES
SAMPLES
LOWER OLIGOCENE
0.5
1.0
1
2
3
4
5
6
7
CC
IW
OG

LITHOLOGIC DESCRIPTION

VITRIC SANDSTONE

Major lithology: Brownish black (5YR 2/1) and greenish black (5GY 2/1) normally graded VITRIC SANDSTONE [illegible]

Minor lithologies: [illegible] SILTY CLAYSTONE [illegible] SILTSTONE [illegible] SILTY SANDSTONE [illegible] VITRIC SILTSTONE [illegible] and VOLCANIC [illegible] CONGLOMERATE [illegible]

[illegible]

Most of the core is slightly [illegible] by drilling.

SMEAR SLIDE SUMMARY (%):

	[illegible]	[illegible]
	[illegible]	M
TEXTURE:		
Sand	—	[illegible]
Silt	[illegible]	[illegible]
Clay	[illegible]	[illegible]
COMPOSITION:		
Accessory minerals	[illegible]	[illegible]
Clay	[illegible]	[illegible]
Feldspar	[illegible]	[illegible]
Glass	[illegible]	[illegible]
Lithic Fragments	—	[illegible]
Mica	[illegible]	—
Zeolite	[illegible]	[illegible]

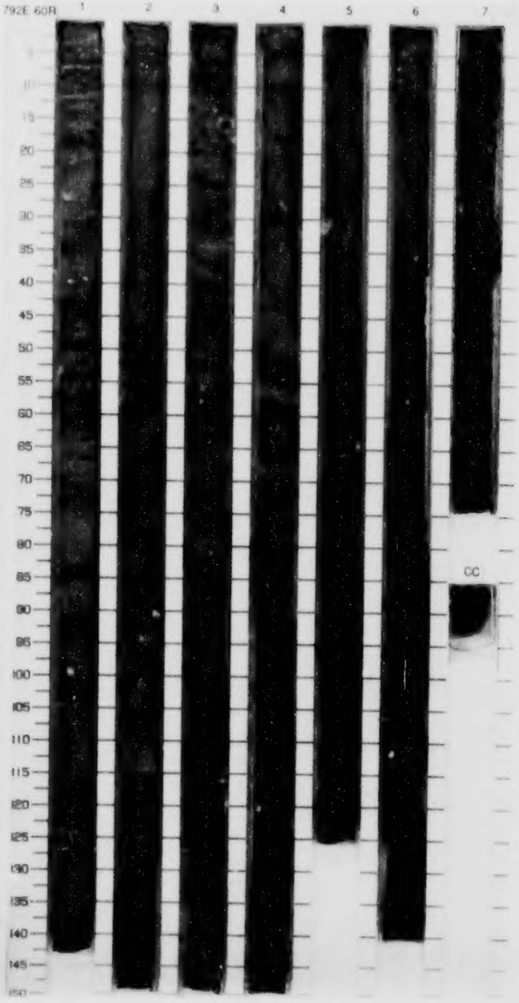
792E 60R
1
2
3
4
5
6
7
CC
5
10
15
20
25
30
35
40
45
50
55
60
65
70
75
80
85
90
95
100
105
110
115
120
125
130
135
140
145
150

SITE 792 HOLE E CORE 61R CORED INTERVAL [illegible] mbsf

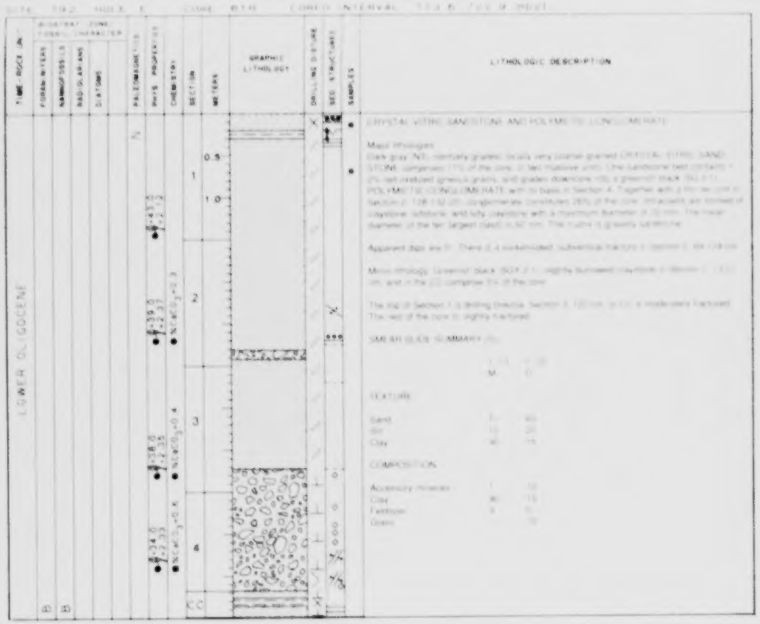
TIME-ROCK UNIT
BIOSTRAT. ZONE/ FOSSIL CHARACTER
FORAMINIFERS
NANNOFOSSILS
RADIOLARIANS
DIATOMS
PALEOMAGNETICS
PHYS. PROPERTIES
CHEMISTRY
SECTION
METERS
GRAPHIC LITHOLOGY
DRILLING DISTURB.
SED. STRUCTURES
SAMPLES
LOWER OLIGOCENE
B
B
N
φ=43.0 γ=2.12
φ=39.0 γ=2.37
φ=38.0 γ=2.35
φ=34.0 γ=2.33
%CaCO3=0.3
%CaCO3=0.4
%CaCO3=0.6
1
2
3
4
CC
0.5
1.0

LITHOLOGIC DESCRIPTION

CRYSTAL VITRIC SANDSTONE AND POLYMICTIC CONGLOMERATE

Major lithologies:
Dark gray (N3), normally graded, locally very coarse-grained CRYSTAL VITRIC SANDSTONE comprises 71% of the core in two massive units. One sandstone bed contains 2% red oxidized igneous grains, and grades downcore into a greenish black (5G 2/1) POLYMICTIC CONGLOMERATE with its base in Section 4. Together with a thinner unit in Section 2, 128-132 cm, conglomerate constitutes 26% of the core. Intraclasts are formed of claystone, siltstone, and silty claystone with a maximum diameter of 70 mm. The mean diameter of the ten largest clasts is 50 mm. The matrix is gravelly sandstone.

Apparent dips are 0°. There is a mineralized, subvertical fracture in Section 2, 44 cm.

Minor lithology: Greenish black (5GY 2/1), slightly burrowed claystone in Section 2, [illegible] cm, and in the CC comprise 3% of the core.

The top of Section 1 is drilling breccia. Section 3, 120 cm, to CC is moderately fractured. The rest of the core is slightly fractured.

SMEAR SLIDE SUMMARY (%):

	1, 03	2, 30
	M	D
TEXTURE:		
Sand	—	65
Silt	10	20
Clay	90	15
COMPOSITION:		
Accessory minerals	1	10
Clay	90	15
Feldspar	5	5
Glass	—	70

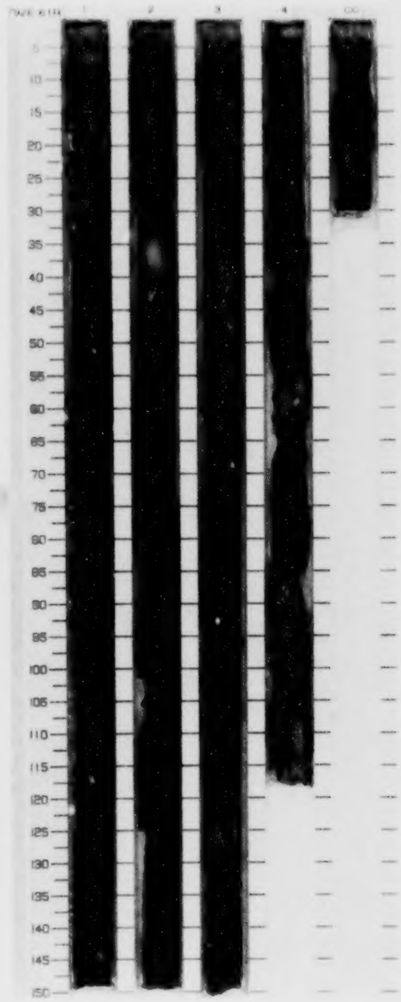
792E-61R
1
2
3
4
CC
5
10
15
20
25
30
35
40
45
50
55
60
65
70
75
80
85
90
95
100
105
110
115
120
125
130
135
140
145
150

SITE 792 HOLE E CORE 62R CORED INTERVAL 722.8-732.5 mbsf

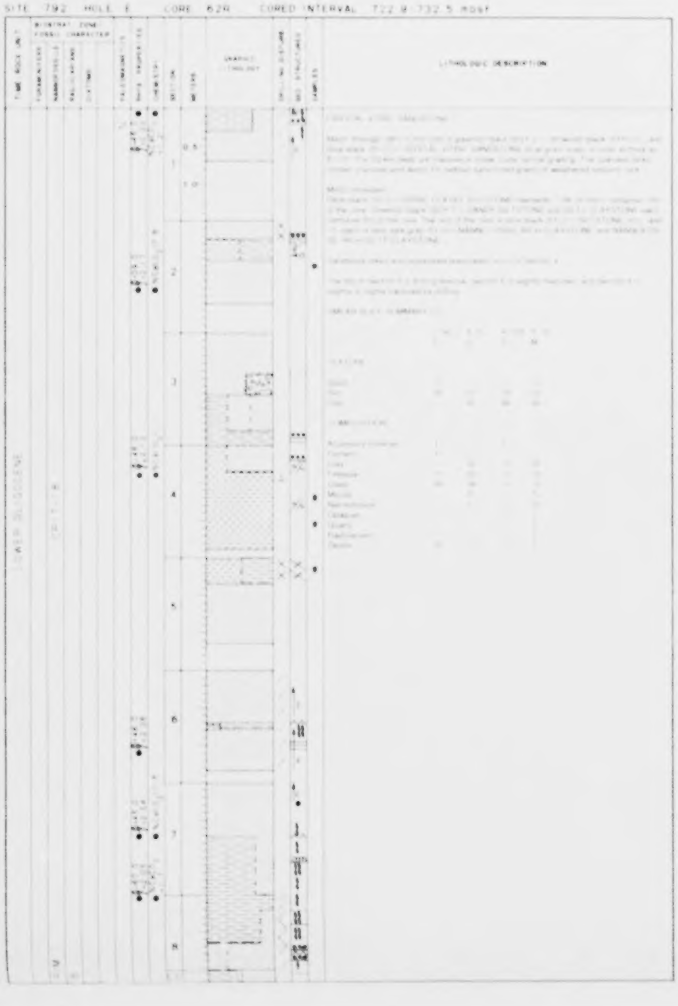
TIME-ROCK UNIT
BIOSTRAT. ZONE/FOSSIL CHARACTER
FORAMINIFERS
NANNOFOSSILS
RADIOLARIANS
DIATOMS
PALEOMAGNETICS
PHYS. PROPERTIES
CHEMISTRY
SECTION
METERS
GRAPHIC LITHOLOGY
DRILLING DISTURB.
SED. STRUCTURES
SAMPLES
LOWER OLIGOCENE
0.5
1.0
1
2
3
4
5
6
7
8
CC

LITHOLOGIC DESCRIPTION

[illegible]

[illegible]

[illegible]

[illegible]

SMEAR SLIDE SUMMARY (%):

TEXTURE:

Sand
Silt
Clay

COMPOSITION:

Accessory minerals
Carbonate
Clay
Feldspar
Glass
Micrite
Nannofossils
Opaques
Quartz
Radiolarians
Zeolite

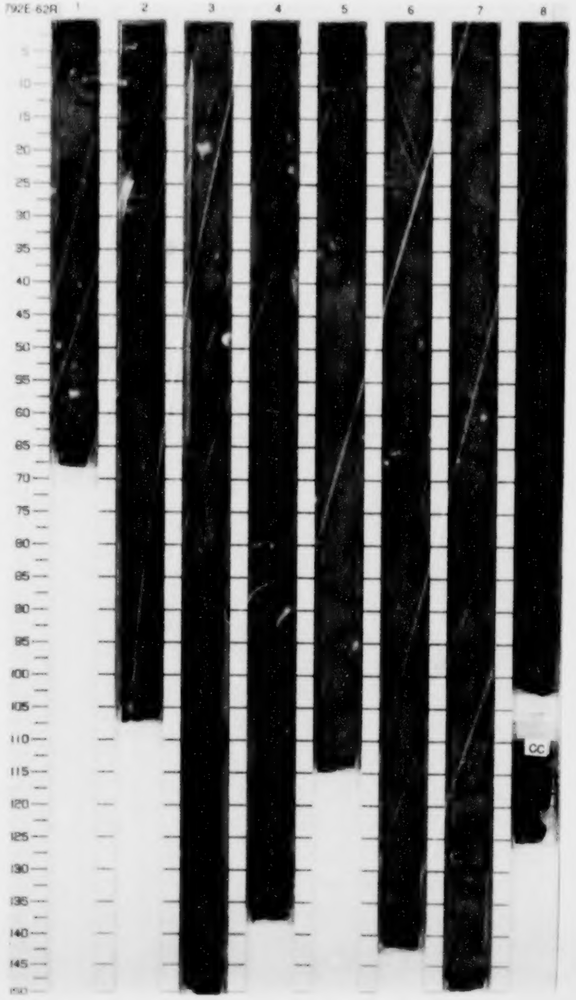
792E-62R
1
2
3
4
5
6
7
8
CC
5
10
15
20
25
30
35
40
45
50
55
60
65
70
75
80
85
90
95
100
105
110
115
120
125
130
135
140
145
150

SITE 792 HOLE E CORE 63R CORED INTERVAL 732.5-742.2 mbsf

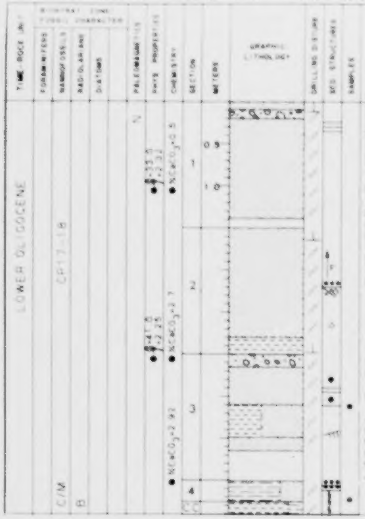
TIME-ROCK UNIT
BIOSTRAT. ZONE/ FOSSIL CHARACTER
FORAMINIFERS
NANNOFOSSILS
RADIOLARIANS
DIATOMS
PALEOMAGNETICS
PHYS. PROPERTIES
CHEMISTRY
SECTION
METERS
GRAPHIC LITHOLOGY
DRILLING DISTURB.
SED. STRUCTURES
SAMPLES
LOWER OLIGOCENE
CP17-18
C/M
B
N
φ=33.5
γ=2.32
%CaCO₃=0.5
φ=47.8
γ=2.25
%CaCO₃=2.7
%CaCO₃=2.92
1
2
3
4
CC
0.5
1.0
F

LITHOLOGIC DESCRIPTION

CRYSTAL VITRIC SANDSTONE

Major lithology: Dark gray (N3), massive, fine to medium grained CRYSTAL VITRIC SANDSTONE comprises 79% of the core. One bed in Section 2 and two beds in Section 3 are normally graded. Claystone intraclasts up to 22 mm in diameter are present in Section 1.

Bedding planes have an apparent dip of 2° on the split core surface and 10° true dip.

Minor lithologies: The remainder of the core is composed of greenish black (5GY 2/1) CLAYSTONE (9%), SILTY CLAYSTONE (6%), and tuff sedimentary BRECCIA (6%) that has claystone clasts up to 8 mm in diameter in a medium-grained sand to granule matrix.

Drilling has slightly fractured the entire core.

SMEAR SLIDE SUMMARY (%):

	3, 81	4, 30
	M	M
TEXTURE:		
Silt	25	30
Clay	75	70
COMPOSITION:		
Accessory minerals	—	—
Clay	64	65
Feldspar	5	—
Glass	25	—
Nannofossils	—	1
Zeolite	—	30

SITE 792 HOLE E CORE 64R CORED INTERVAL 742.2-751.8 mbsf

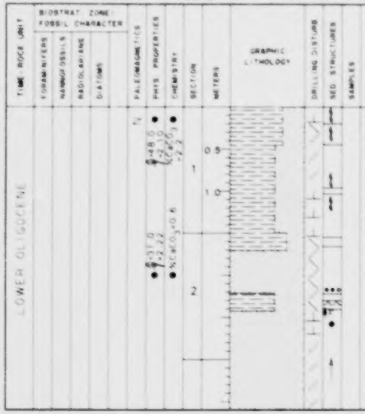
TIME-ROCK UNIT
BIOSTRAT. ZONE/ FOSSIL CHARACTER
FORAMINIFERS
NANNOFOSSILS
RADIOLARIANS
DIATOMS
PALEOMAGNETICS
PHYS. PROPERTIES
CHEMISTRY
SECTION
METERS
GRAPHIC LITHOLOGY
DRILLING DISTURB.
SED. STRUCTURES
SAMPLES
LOWER OLIGOCENE
N
φ=48.0
γ=2.10
%CaCO₃=2.2
φ=31.0
γ=2.22
%CaCO₃=0.6
1
2
0.5
1.0

LITHOLOGIC DESCRIPTION

CRYSTAL VITRIC SANDSTONE AND VITRIC SILTY CLAYSTONE

Major lithologies:
60% of the core consists of greenish black (5G 2/1) and brownish black (5YR 2/1) CRYSTAL VITRIC SANDSTONE in two massive beds (57 and 119 cm thick) that are granule rich and very coarse grained at their bases. Thinner sandstone beds (1–7 cm thick) are normally graded, fine grained and planar laminated. These are interbedded with brownish black (5YR 2/1) slightly burrowed VITRIC SILTY CLAYSTONE that comprises 39% of the core.

Minor lithology: 1% of the core is greenish black (5G 2/1) thinly laminated SANDY SILTSTONE.

The core is slightly to highly fractured by drilling.

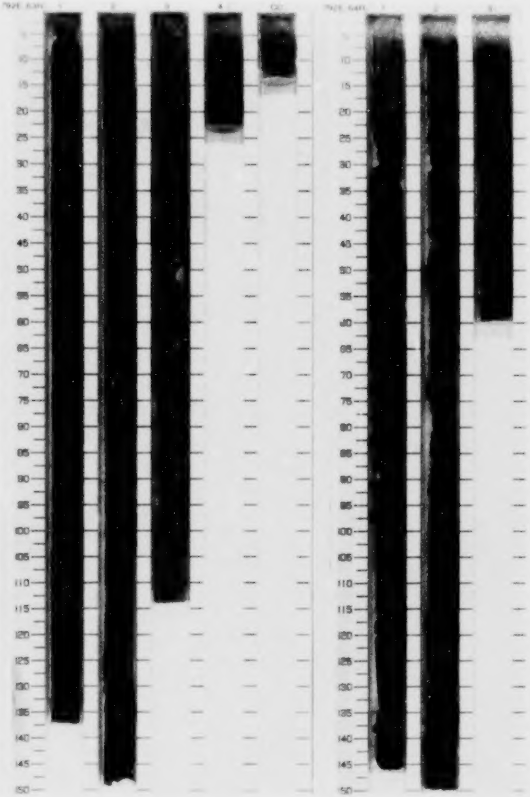
792E-63R
1
2
3
4
CC
792E-64R
1
2
3
0
5
10
15
20
25
30
35
40
45
50
55
60
65
70
75
80
85
90
95
100
105
110
115
120
125
130
135
140
145
150

SITE 792 HOLE E CORE 65R CORED INTERVAL 751.8-761.5 mbsf

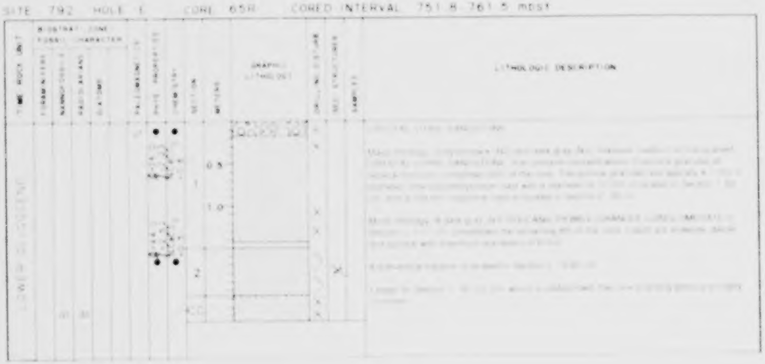
TIME-ROCK UNIT
BIOSTRAT. ZONE/FOSSIL CHARACTER
FORAMINIFERS
NANNOFOSSILS
RADIOLARIANS
DIATOMS
PALEOMAGNETICS
PHYS. PROPERTIES
CHEMISTRY
SECTION
METERS
GRAPHIC LITHOLOGY
DRILLING DISTURB.
SED. STRUCTURES
SAMPLES
LITHOLOGIC DESCRIPTION
LOWER OLIGOCENE
0.5
1.0
1
2
CC

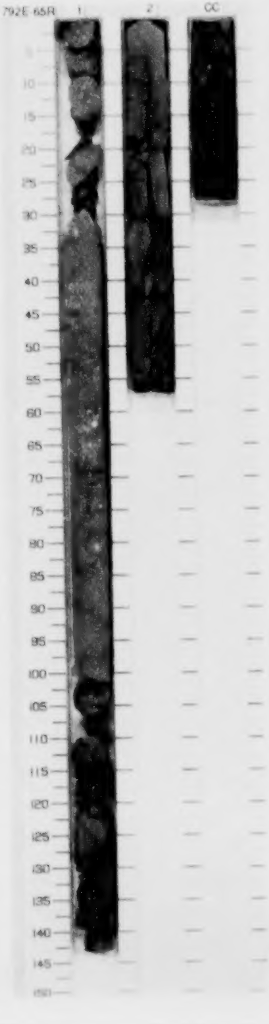
792E 65R
1
2
CC
5
10
15
20
25
30
35
40
45
50
55
60
65
70
75
80
85
90
95
100
105
110
115
120
125
130
135
140
145
150

SITE 792 HOLE E CORE [illegible] CORED INTERVAL [illegible] mbsf

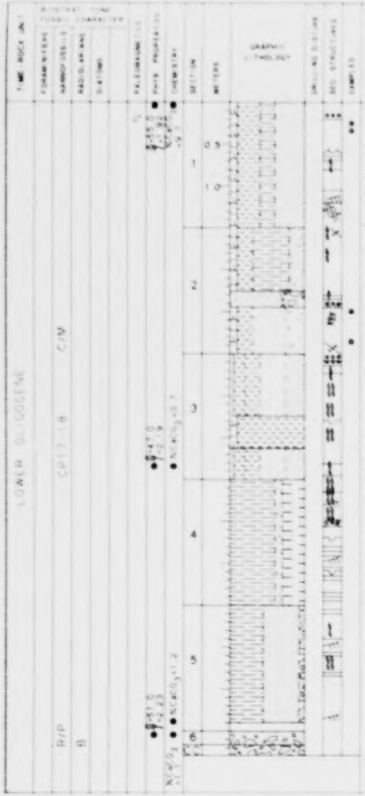
TIME-ROCK UNIT
BIOSTRAT. ZONE/FOSSIL CHARACTER
FORAMINIFERS
NANNOFOSSILS
RADIOLARIANS
DIATOMS
PALEOMAGNETICS
PHYS. PROPERTIES
CHEMISTRY
SECTION
METERS
GRAPHIC LITHOLOGY
DRILLING DISTURB.
SED. STRUCTURES
SAMPLES
LOWER OLIGOCENE
CP17-18
C/M
R/P
B
1
2
3
4
5
6
0.5
1.0
NCaCO3

LITHOLOGIC DESCRIPTION

VITRIC CLAYEY SILTSTONE, VITRIC SILTY CLAYSTONE, AND VOLCANIC [illegible] SANDSTONE

Major lithologies:
Dark greenish gray (5G 4/1) and dark gray (5Y 4/1) VITRIC CLAYEY SILTSTONE and VITRIC SILTY CLAYSTONE together comprise [illegible] of the core. Another [illegible] of the core consists of interbedded dark greenish gray (5G 4/1) and dark gray (5Y 4/1) fine- to very fine-grained sandstone beds [illegible] cm thick, which display planar lamination, normal grading, and scoured bases.

Minor lithologies:
The rest of the core is composed of [illegible] of greenish gray (5G [illegible]) NANNOFOSSIL-RICH CLAYSTONE ([illegible]), dark greenish gray (5G 4/1) SANDY CLAYSTONE ([illegible]), SILTY SANDSTONE ([illegible]), CLAYSTONE ([illegible]), and, in Section 6 and the CC, greenish gray (5G [illegible]) VOLCANIC PEBBLE-GRANULE CONGLOMERATE. The conglomerate has a maximum clast size of [illegible] mm and a mean size of [illegible] mm for the [illegible] largest pebbles.

Subvertical, sediment-filled fractures [illegible] mm thick, occur in Section [illegible]. A subvertical sandstone dike, [illegible] cm thick, is located in Section [illegible]. There is a small channel-filled clay immediately beneath the dike.

Drilling disturbance is slight.

SMEAR SLIDE SUMMARY (%):

	[illegible]	[illegible]	[illegible]	[illegible]
	M	D	M	M
TEXTURE:				
Sand	[illegible]			
Silt		[illegible]	[illegible]	[illegible]
Clay		[illegible]	[illegible]	[illegible]
COMPOSITION:				
Accessory minerals		[illegible]	[illegible]	
Amphibole	[illegible]			
Clay		[illegible]	[illegible]	[illegible]
Feldspar	[illegible]	[illegible]		
Glass	[illegible]			
Inorganic calcite				
Micrite			[illegible]	
Nannofossils			[illegible]	
Zeolite	[illegible]		[illegible]	

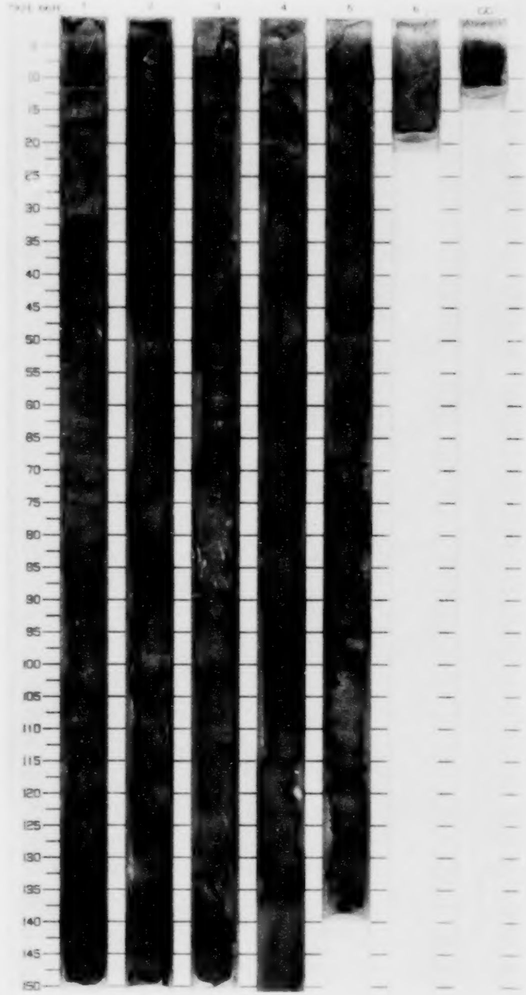
cm
1
2
3
4
5
6
CC
0
5
10
15
20
25
30
35
40
45
50
55
60
65
70
75
80
85
90
95
100
105
110
115
120
125
130
135
140
145
150

SITE 792 HOLE E CORE 67R CORED INTERVAL 771.2-780.9 mbsf

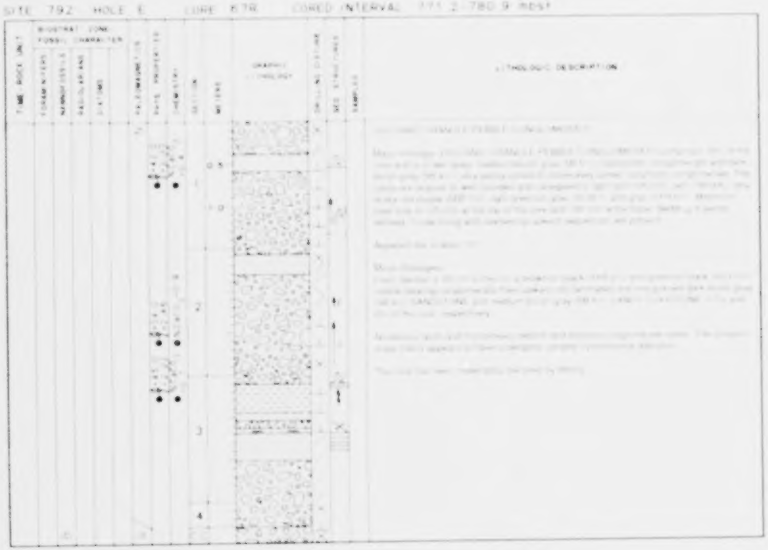
TIME-ROCK UNIT
BIOSTRAT. ZONE/ FOSSIL CHARACTER
FORAMINIFERS
NANNOFOSSILS
RADIOLARIANS
DIATOMS
PALEOMAGNETICS
PHYS. PROPERTIES
CHEMISTRY
SECTION
METERS
GRAPHIC LITHOLOGY
DRILLING DISTURB.
SED. STRUCTURES
SAMPLES
0.5
1
1.0
2
3
4

LITHOLOGIC DESCRIPTION

[illegible]

[illegible]

[illegible]

[illegible]

[illegible]

[illegible]

SITE 792 HOLE E CORE 68R CORED INTERVAL 780.9-790.6 mbsf

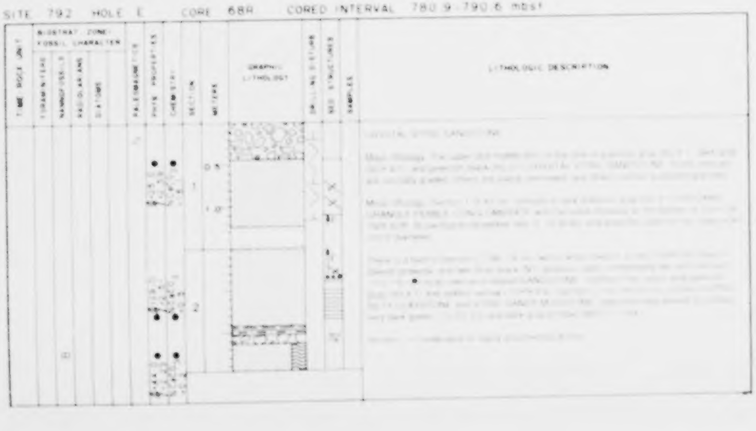
TIME-ROCK UNIT
BIOSTRAT. ZONE/ FOSSIL CHARACTER
FORAMINIFERS
NANNOFOSSILS
RADIOLARIANS
DIATOMS
PALEOMAGNETICS
PHYS. PROPERTIES
CHEMISTRY
SECTION
METERS
GRAPHIC LITHOLOGY
DRILLING DISTURB.
SED. STRUCTURES
SAMPLES
0.5
1
1.0
2

LITHOLOGIC DESCRIPTION

[illegible]

[illegible]

[illegible]

[illegible]

[illegible]

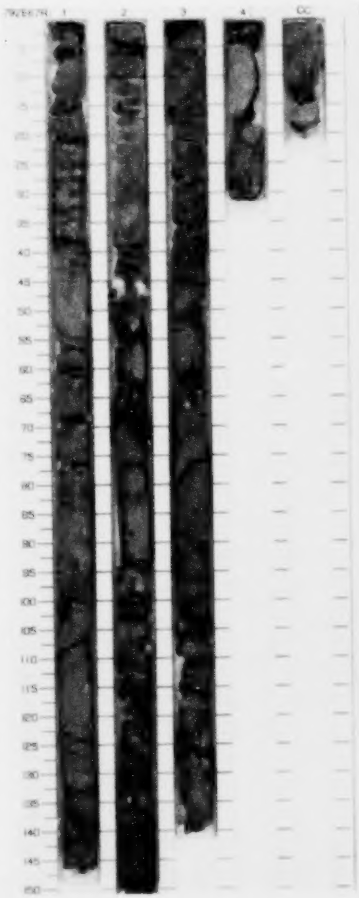
792E-67R
1
2
3
4
CC
5
10
15
20
25
30
35
40
45
50
55
60
65
70
75
80
85
90
95
100
105
110
115
120
125
130
135
140
145
150

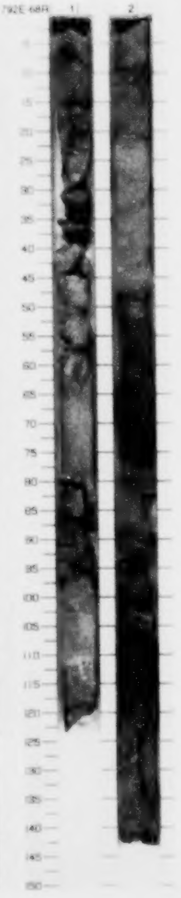
792E-68R
1
2
5
10
15
20
25
30
35
40
45
50
55
60
65
70
75
80
85
90
95
100
105
110
115
120
125
130
135
140
145
150

SITE 792 HOLE E CORE 69R CORED INTERVAL 790.6-800.2 mbsf

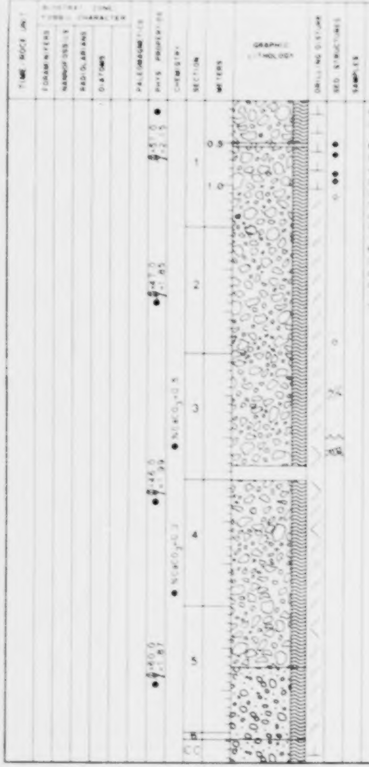
TIME-ROCK UNIT
BIOSTRAT. ZONE/FOSSIL CHARACTER
FORAMINIFERS
NANNOFOSSILS
RADIOLARIANS
DIATOMS
PALEOMAGNETICS
PHYS. PROPERTIES
CHEMISTRY
SECTION
METERS
GRAPHIC LITHOLOGY
DRILLING DISTURB.
SED. STRUCTURES
SAMPLES
φ=51.0 γ=2.15
φ=47.0 γ=1.85
φ=46.0 γ=1.99
φ=40.0 γ=1.87
NC: CaCO₃=0.5
NC: CaCO₃=0.3
1
2
3
4
5
6
CC
0.5
1.0

LITHOLOGIC DESCRIPTION

HYDROTHERMALLY ALTERED VOLCANIC PEBBLE GRANULE CONGLOMERATE AND OTHER VOLCANICLASTIC ROCKS OF UNCERTAIN GRAIN SIZE

Major lithology: The entire core consists of HYDROTHERMALLY ALTERED VOLCANIC PEBBLE GRANULE CONGLOMERATE and other volcaniclastic rocks of uncertain grain size. The principal colors in the upper part of the core are very dark green (7.5 GY 3/2) and dark grayish blue (5BG 3/2). From Section 4, 36 cm, to the CC, light grayish blue (5BG 6/1) colors predominate over medium greenish gray (5G 5/1) shades. Grain sizes are indeterminate because most of the rock is severely altered pumice; only fragments of dacite and andesite retain some freshness and maintain the appearance of conglomerate in some intervals.

Minor lithologies: In Section 1, 50 cm, is a layer of greenish black (5G 2/1) SILICIFIED CLAYSTONE or SILICIFIED SILTSTONE. Section 4, 76-86 cm, is a brecciated mixture of altered volcaniclastic rock and claystone clasts. Section 5, 75 cm, to the CC is also brecciated.

The core is slightly fractured by drilling.

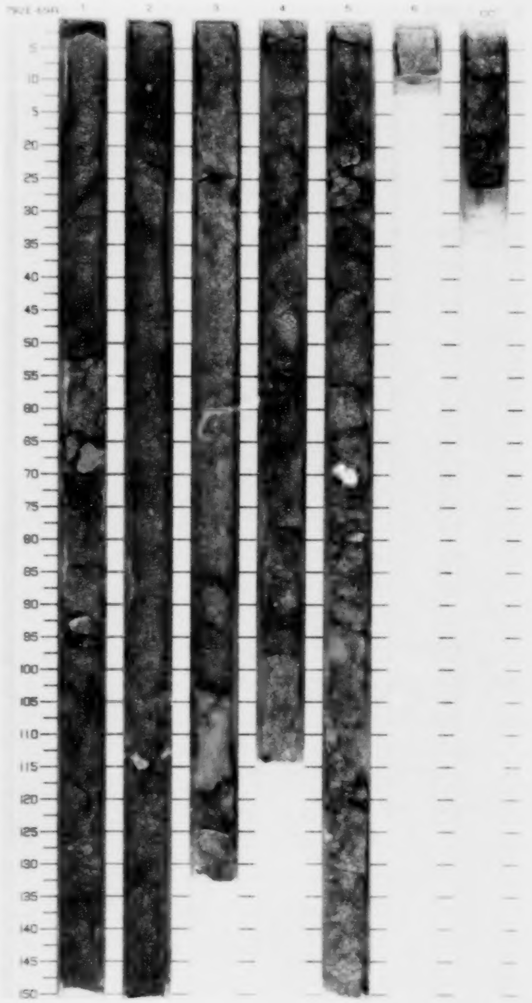
792E-69R
1
2
3
4
5
6
CC
5
10
15
20
25
30
35
40
45
50
55
60
65
70
75
80
85
90
95
100
105
110
115
120
125
130
135
140
145
150

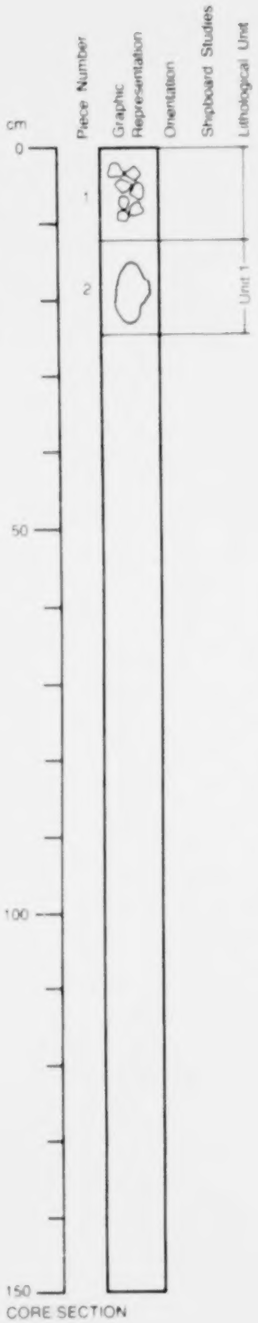
cm
Piece Number
Graphic Representation
Orientation
Shipboard Studies
Lithological Unit
0
1
2
Unit 1
50
100
150
CORE SECTION

126-792E-70R-CC

Piece 1 : Sediment Unit V

See sedimentary visual core description.

UNIT 1: PORPHYRITIC ANDESITE

Piece 2

CONTACTS: None
PHENOCRYSTS: Orthopyroxene pseudomorphs are sometimes mantled with clinopyroxene; some fresh orthopyroxene present.
Plagioclase - 35%, 0.2-5 mm, euhedral, zoned, glomeroporphyritic clots.
Clinopyroxene - 5%, 0.1-5 mm, euhedral, fresh.
Orthopyroxene - 10%, 0.1-5 mm, euhedral, 90% replaced by smectite, rimmed by clinopyroxene.
Magnetite - 1%, 0.1-0.5 mm, subhedral.
GROUNDMASS: Fine grained altered glass with microphenocrysts of plagioclase and pyroxenes.
VESICLES: None
COLOR: Medium light gray, N6.
STRUCTURE: Massive.
ALTERATION: Moderately altered, glass and partly altered orthopyroxene.
VEINS/FRACTURES: <1%, <1 mm, along fractures, celadonite and smectite veins.
ADDITIONAL COMMENTS: Xenoliths of plagioclase-orthopyroxene-clinopyroxene diabase and finer grained andesite.

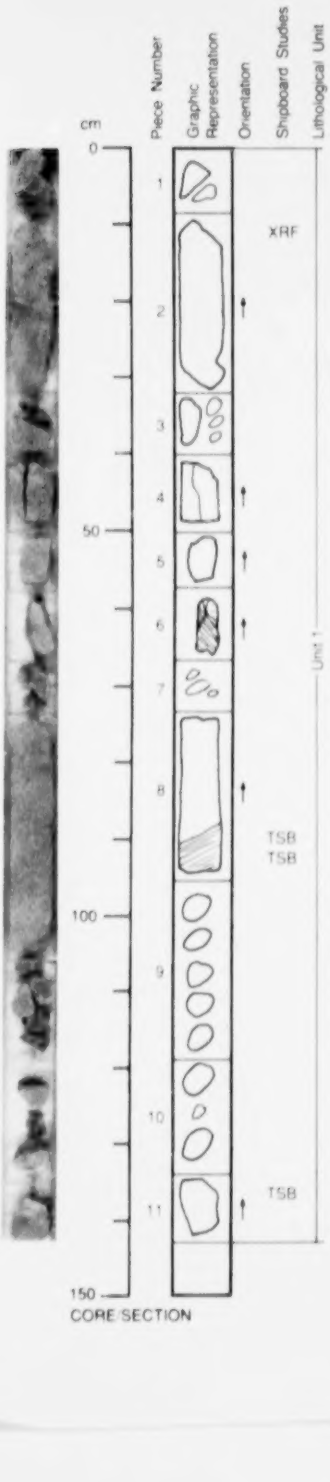
cm
Piece Number
Graphic Representation
Orientation
Shipboard Studies
Lithological Unit
0
50
100
150
1
2
3
4
5
6
7
8
9
10
11
XRF
TSB
TSB
TSB
Unit 1
CORE/SECTION

126-792E-71R-1

UNIT 1: PORPHYRITIC ANDESITE

Pieces 1-11

CONTACTS: None.
PHENOCRYSTS: Orthopyroxene pseudomorphs are sometimes mantled with clinopyroxene, some fresh orthopyroxene present.
Plagioclase - 35%, 0.2-5 mm, euhedral, zoned, glomeroporphyritic clots.
Clinopyroxene - 5%, 0.1-5 mm, euhedral, fresh.
Orthopyroxene - 10%, 0.1-5 mm, euhedral, 90% replaced by smectite, rimmed by clinopyroxene.
Magnetite - 1%, 0.1-0.5 mm, subhedral.
GROUNDMASS: Fine grained altered glass with microphenocrysts of plagioclase and pyroxenes.
VESICLES: None.
COLOR: Medium light gray, N6.
STRUCTURE: Massive.
ALTERATION: Moderately altered, glass and partly altered orthopyroxene.
VEINS/FRACTURES: <1%, <1 mm, along fractures, celadonite and smectite veins.
ADDITIONAL COMMENTS: Xenoliths of plagioclase-orthopyroxene-clinopyroxene diabase and finer-grained andesite. Hyaloclastite layers in Pieces 6 (3 cm thick) and 8 (4 cm thick).

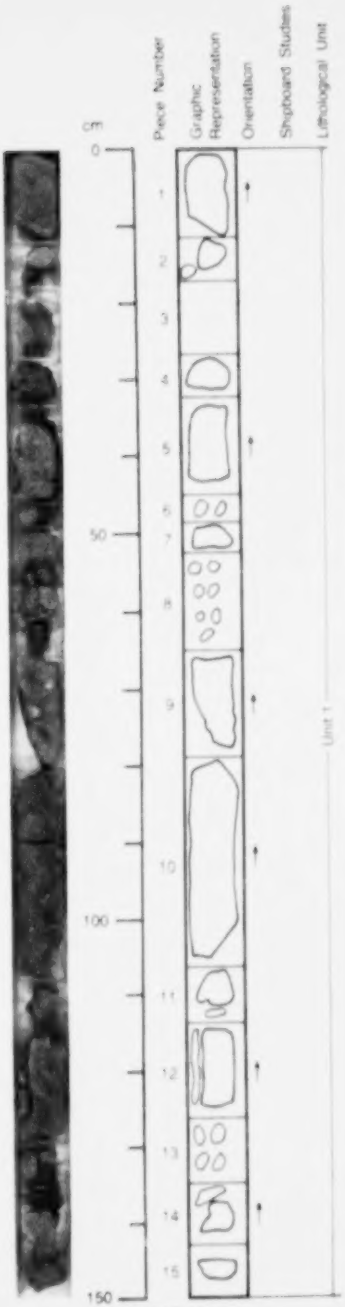
cm
Piece Number
Graphic Representation
Orientation
Shipboard Studies
Lithological Unit
0
50
100
150
1
2
3
4
5
6
7
8
9
10
11
12
13
14
15
Unit 1
CORE SECTION

126-792E-71R-2

UNIT 1: PORPHYRITIC ANDESITE

Pieces 1-15

CONTACTS: None.

PHENOCRYSTS: Orthopyroxene pseudomorphs are sometimes mantled with clinopyroxene; some fresh orthopyroxene present.

Plagioclase - 35%, 0.2-5 mm, euhedral, zoned, glomeroporphyritic clots.

Clinopyroxene - 5%, 0.1-5 mm, euhedral, fresh.

Orthopyroxene - 10%, 0.1-5 mm, euhedral, 90% replaced by smectite, rimmed by clinopyroxene.

Magnetite - 1%, 0.1-0.5 mm, subhedral.

GROUNDMASS: Fine-grained altered glass with microphenocrysts of plagioclase and pyroxenes.

VESICLES: None.

COLOR: Medium light gray, N6.

STRUCTURE: Massive.

ALTERATION: Moderately altered, glass and partly altered orthopyroxene.

VEINS/FRACTURES: <1%, <1 mm, along fractures, celadonite and smectite veins.

ADDITIONAL COMMENTS: Xenoliths of plagioclase-orthopyroxene-clinopyroxene diabase and finer grained andesite.

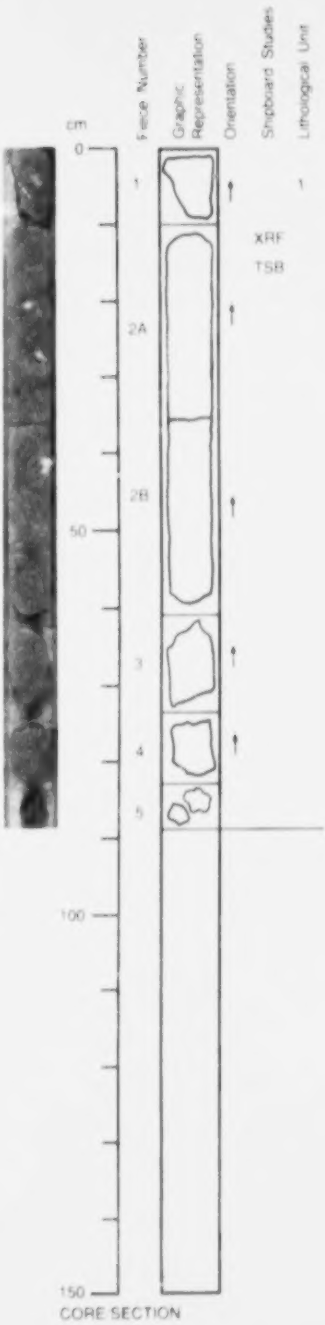
cm
Piece Number
Graphic Representation
Orientation
Shipboard Studies
Lithological Unit
0
50
100
150
1
2A
2B
3
4
5
XRF
TSB
1
CORE SECTION

126-792E-71R-3

UNIT 1: PORPHYRITIC ANDESITE

Pieces 1-5

CONTACTS: None

PHENOCRYSTS: Orthopyroxene pseudomorphs are sometimes mantled with clinopyroxene, some fresh orthopyroxene present.
Plagioclase - 35%, 0.2-5 mm, euhedral, zoned, glomeroporphyritic clots.
Clinopyroxene - 5%, 0.1-5 mm, euhedral, fresh.
Orthopyroxene - 10%, 0.1-5 mm, euhedral, 90% replaced by smectite, rimmed by clinopyroxene.
Magnetite - 1%, 0.1-0.5 mm, subhedral.

GROUNDMASS: Fine-grained altered glass with microphenocrysts of plagioclase and pyroxenes.

VESICLES: None

COLOR: Medium light gray, N6.

STRUCTURE: Massive.

ALTERATION: Moderately altered, glass and partly altered orthopyroxene.

VEINS/FRACTURES: <1%, <1 mm, along fractures, celadonite and smectite veins.

ADDITIONAL COMMENTS: Xenoliths of plagioclase-orthopyroxene-clinopyroxene diabase and finer-grained andesite.

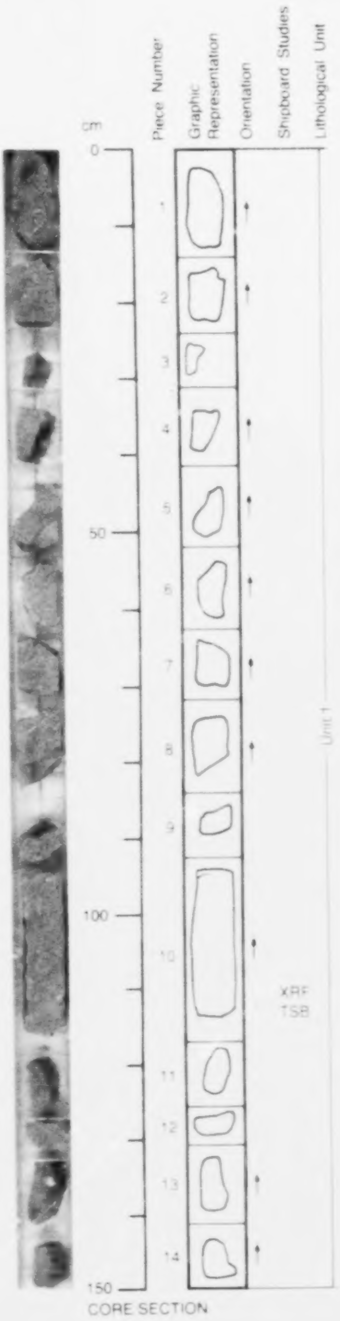
cm
Piece Number
Graphic Representation
Orientation
Shipboard Studies
Lithological Unit
0
50
100
150
1
2
3
4
5
6
7
8
9
10
11
12
13
14
XRF
TSB
Unit 1
CORE SECTION

126-792E-72R-1

UNIT 1: PORPHYRITIC ANDESITE

Pieces 1-14

CONTACTS: None.
PHENOCRYSTS: Orthopyroxene pseudomorphs are sometimes mantled with clinopyroxene; some fresh orthopyroxene present.
Plagioclase - 35%, 0.2-5 mm, euhedral, zoned, glomeroporphyritic clots.
Clinopyroxene - 5%, 0.1-5 mm, euhedral, fresh.
Orthopyroxene - 10%, 0.1-5 mm, euhedral, 90% replaced by smectite, rimmed by clinopyroxene.
Magnetite - 1%, 0.1-0.5 mm, subhedral.
GROUNDMASS: Fine-grained altered glass with microphenocrysts of plagioclase and pyroxenes.
VESICLES: None.
COLOR: Medium light gray, N6.
STRUCTURE: Massive.
ALTERATION: Moderately altered, glass and partly altered orthopyroxene.
VEINS/FRACTURES: <1%, <1 mm, along fractures; celadonite and smectite veins.
ADDITIONAL COMMENTS: Xenoliths of plagioclase-orthopyroxene-clinopyroxene diabase and finer grained andesite.

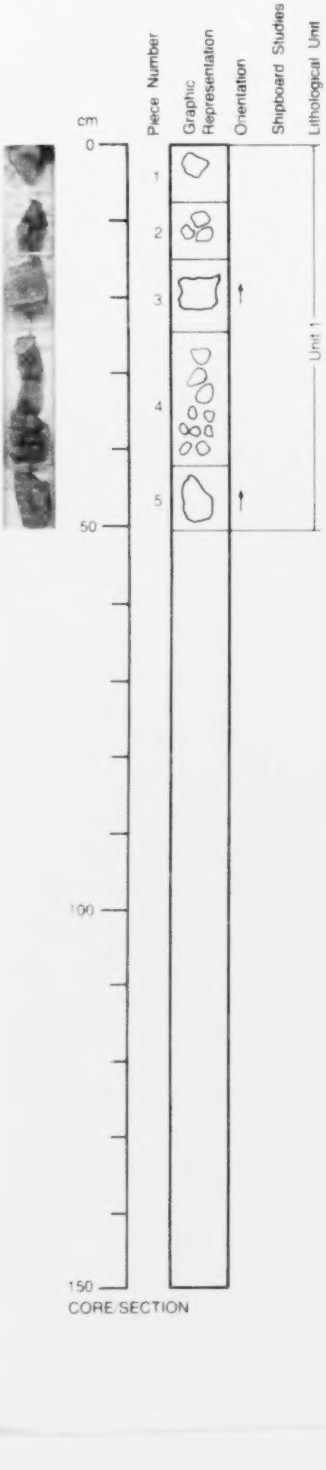
cm
Piece Number
Graphic Representation
Orientation
Shipboard Studies
Lithological Unit
0
50
100
150
1
2
3
4
5
Unit 1
CORE/SECTION

126-792E-72R-2

UNIT 1: PORPHYRITIC ANDESITE

Pieces 1-5

CONTACTS: None.
PHENOCRYSTS: Orthopyroxene pseudomorphs are sometimes mantled with clinopyroxene, some fresh orthopyroxene present.
Plagioclase - 35%, 0.2-5 mm, euhedral, zoned, glomeroporphyritic clots.
Clinopyroxene - 5%, 0.1-5 mm, euhedral, fresh.
Orthopyroxene - 10%, 0.1-5 mm, euhedral, 90% replaced by smectite, rimmed by clinopyroxene.
Magnetite - 1%, 0.1-0.5 mm, subhedral.
GROUNDMASS: Fine-grained altered glass with microphenocrysts of plagioclase and pyroxenes.
VESICLES: None.
COLOR: Medium light gray, N6.
STRUCTURE: Massive.
ALTERATION: Moderately altered, glass and partly altered orthopyroxene.
VEINS/FRACTURES: <1%, <1 mm, along fractures; celadonite and smectite veins.
ADDITIONAL COMMENTS: Xenoliths of plagioclase-orthopyroxene-clinopyroxene diabase and finer-grained andesite.

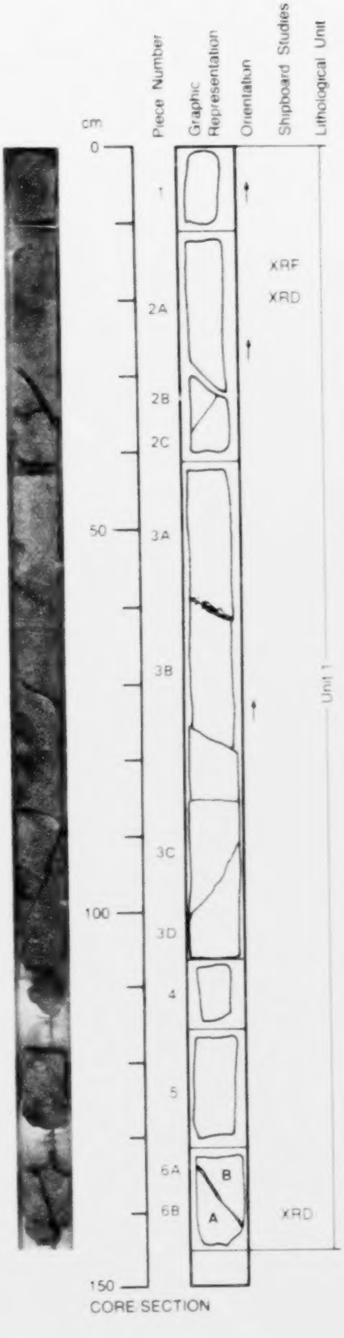
cm
Piece Number
Graphic Representation
Orientation
Shipboard Studies
Lithological Unit
0
50
100
150
1
2A
2B
2C
3A
3B
3C
3D
4
5
6A
6B
B
A
XRF
XRD
XRD
Unit 1
CORE SECTION

126-792E-73R-1

UNIT 1: PORPHYRITIC ANDESITE

Pieces 1-6

CONTACTS: None
PHENOCRYSTS:
- Plagioclase - 35%, 0.2-5 mm, euhedral, zoned
- Clinopyroxene - 5%, 0.2-5 mm, euhedral fresh
- Orthopyroxene - 5%, 0.2-5 mm, euhedral, replaced by smectite
- Magnetite - 1%, 0.1-0.5 mm, subhedral
- Quartz - 0.5%, 0.1-0.4 mm, anhedral rounded

GROUNDMASS: Fine grained altered glass with microphenocrysts of pyroxenes and plagioclase laths
VESICLES: None
COLOR: Light medium gray, N6
STRUCTURE: Massive
ALTERATION: Moderately altered glass and partly altered orthopyroxene.
VEINS/FRACTURES: <1%, 1 mm, along fractures, celadonite and smectite veins.
ADDITIONAL COMMENTS: 5 mm thick chlorite vein in Pieces 6A and B

126-792E-73R-2

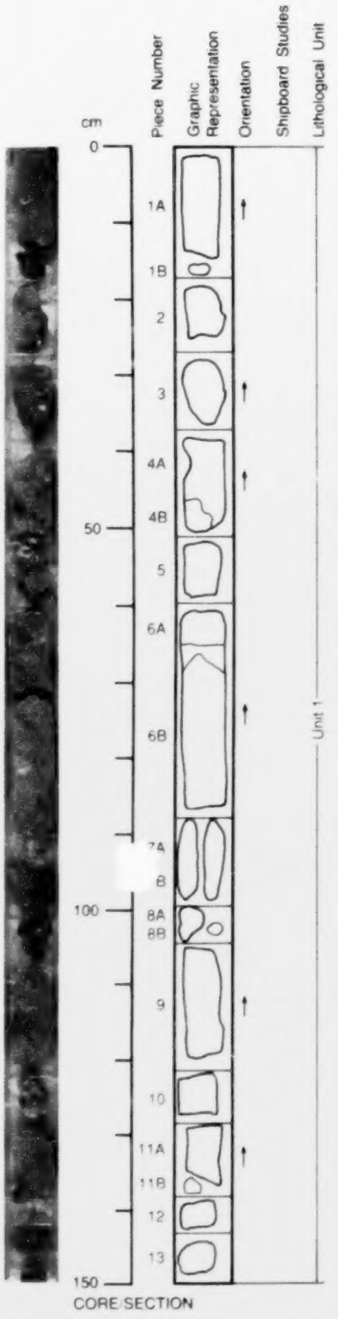
cm
Piece Number
Graphic Representation
Orientation
Shipboard Studies
Lithological Unit
0
50
100
150
1A
1B
2
3
4A
4B
5
6A
6B
7A
7B
8A
8B
9
10
11A
11B
12
13
Unit 1
CORE/SECTION

UNIT 1: PORPHYRITIC ANDESITE

Pieces 1-13

CONTACTS: None.
PHENOCRYSTS:
Plagioclase - 35%, 0.2-5 mm, euhedral, zoned.
Clinopyroxene - 5%, 0.2-5 mm, euhedral fresh.
Orthopyroxene - 5%, 0.2-5 mm, euhedral, replaced by smectite.
Magnetite - 1%, 0.1-0.5 mm, subhedral.
Quartz - 0.5%, 0.1-0.4 mm, anhedral rounded.
GROUNDMASS: Fine-grained altered glass with microphenocrysts of pyroxenes and plagioclase laths.
VESICLES: None.
COLOR: Light medium gray, N6.
STRUCTURE: Massive.
ALTERATION: Moderately altered glass and partly altered orthopyroxene.
VEINS/FRACTURES: <1%, 1 mm, along fractures, celadonite and smectite veins.
ADDITIONAL COMMENTS: 8 cm of breccia-hyaloclastite with contact to flow beneath (Piece 6A).

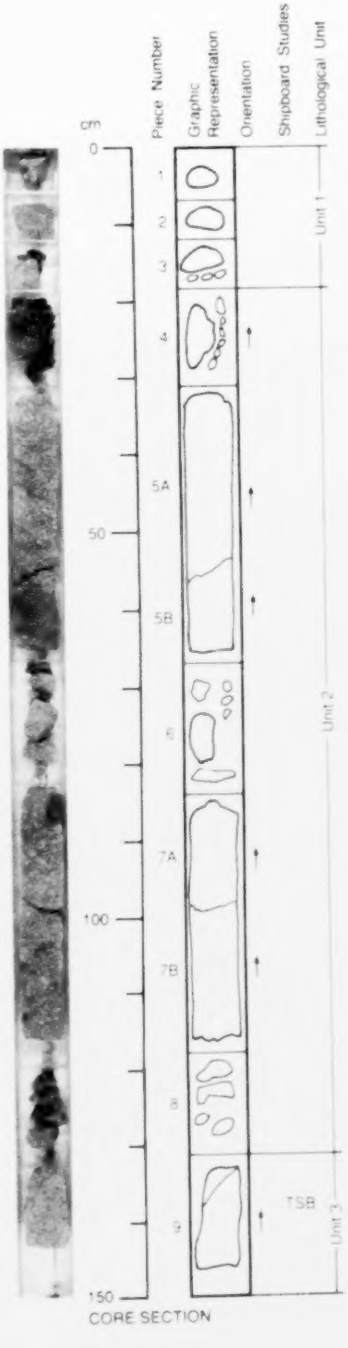

126-792E-74R-1

UNIT 1: PORPHYRITIC ANDESITE

Pieces 1-3

CONTACTS: None.
PHENOCRYSTS:
- Plagioclase - 35%, 0.2-5 mm, euhedral, zoned.
- Clinopyroxene - 5%, 0.2-5 mm, euhedral fresh.
- Orthopyroxene - 5%, 0.2-5 mm, euhedral, replaced by smectite.
- Magnetite - 1%, 0.1-0.5 mm, subhedral.
- Quartz - 0.5%, 0.1-0.4 mm, anhedral rounded.

GROUNDMASS: Fine-grained altered glass with microphenocrysts of pyroxenes and plagioclase laths.
VESICLES: None.
COLOR: Light medium gray, N6.
STRUCTURE: Massive.
ALTERATION: Moderately altered glass and partly altered orthopyroxene.
VEINS/FRACTURES: None.

UNIT 2: ANDESITIC HYALOCLASTITE BRECCIA

Pieces 4-9

CONTACTS: In Piece 9 at the base there is a clear contact to a massive andesite lava. In the basal 3 mm an accumulation of broken ilmenite grains is present.
PHENOCRYSTS: The rock contains plagioclase-orthopyroxene-clinopyroxene andesite and plagioclase-clinopyroxene-quartz dacite fragments in a hydrothermally altered glassy matrix.
- Plagioclase - 30%, 0.1-3 mm, euhedral, zoned, clustered.
- Clinopyroxene - 3%, 0.2-2 mm, subeuhedral.
- Opaques - 1%, 0.1-0.5 mm, subhedral, 8% in basal layer.
- Orthopyroxene - 1%, 0.1-3 mm, subhedral, altered to smectite.

GROUNDMASS: Fine grained, altered into smectite and chlorite.
VESICLES: None.
COLOR: Grayish green, 10GY 5/2.
STRUCTURE: Glassy fragmental rock with clast and matrix, fragmented and broken crystals.
ALTERATION: Glass and orthopyroxene are altered.
VEINS/FRACTURES: None.
ADDITIONAL COMMENTS: Quartz phenocrysts in xenoliths are rounded and partly resorbed.

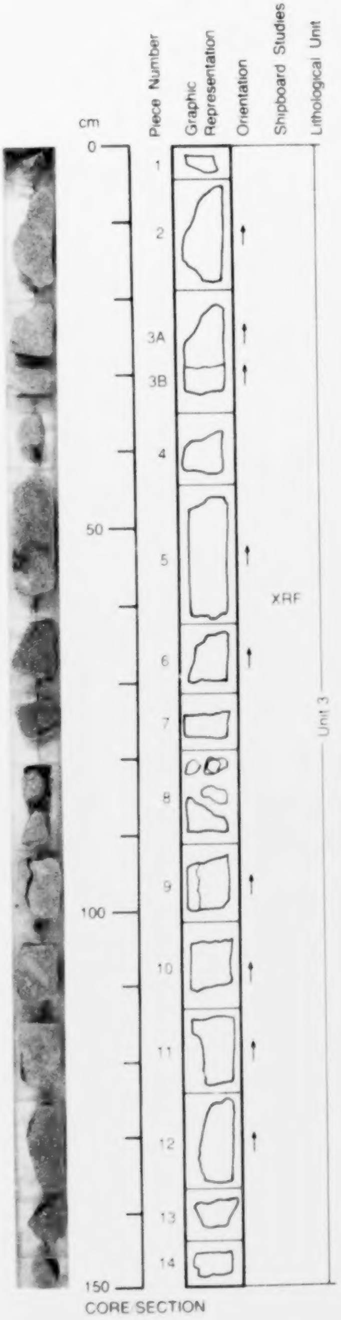
cm
Piece Number
Graphic Representation
Orientation
Shipboard Studies
Lithological Unit
0
50
100
150
1
2
3A
3B
4
5
6
7
8
9
10
11
12
13
14
XRF
Unit 3
CORE/SECTION

126-792E-74R-2

UNIT 3: PORPHYRITIC ANDESITE

Pieces 1-14

CONTACTS: None

PHENOCRYSTS:

- Plagioclase - 35%, 0.2-5 mm, euhedral, zoned
- Clinopyroxene - 5%, 0.2-5 mm, euhedral fresh
- Orthopyroxene - 5%, 0.2-5 mm, euhedral, replaced by smectite
- Magnetite - 1%, 0.1-0.5 mm, subhedral
- Quartz - 0.5%, 0.1-0.4 mm, anhedral rounded

GROUNDMASS: Fine grained altered glass with microphenocrysts of pyroxenes and plagioclase laths

VESICLES: None

COLOR: Light medium gray, N6

STRUCTURE: Massive

ALTERATION: Moderately altered glass and partly altered orthopyroxene

VEINS/FRACTURES: <1%, 1 mm, along fractures, celadonite and smectite veins

ADDITIONAL COMMENTS: 2-3 fragments of hyaloclastite material in Piece 8
Hydrothermal alteration along veins and fractures in Pieces 9 and 11

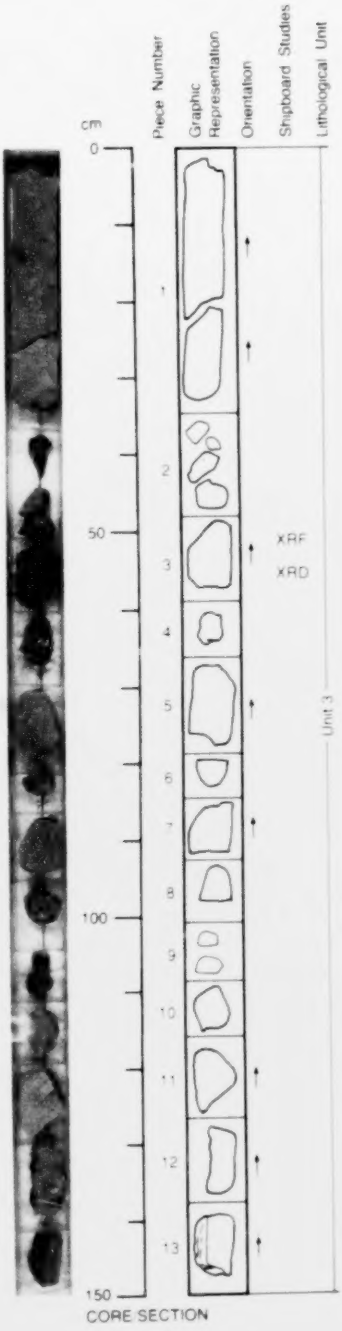
cm
Piece Number
Graphic Representation
Orientation
Shipboard Studies
Lithological Unit
0
50
100
150
1
2
3
4
5
6
7
8
9
10
11
12
13
XRF
XRD
Unit 3
CORE/SECTION

126-792E-75R-1

UNIT 3: PORPHYRITIC ANDESITE

Pieces 1-13

CONTACTS: None
PHENOCRYSTS:
- Plagioclase - 35%, 0.2-5 mm, euhedral, zoned
- Clinopyroxene - 5%, 0.2-5 mm, euhedral fresh
- Orthopyroxene - 5%, 0.2-5 mm, euhedral, replaced by smectite
- Magnetite - 1%, 0.1-0.5 mm, subhedral
- Quartz - 0.5%, 0.1-0.4 mm, anhedral rounded

GROUNDMASS: Fine-grained altered glass with microphenocrysts of pyroxenes and plagioclase laths
VESICLES: None
COLOR: Light medium gray, N6
STRUCTURE: Massive
ALTERATION: Moderately altered glass and partly altered orthopyroxene
VEINS/FRACTURES: <1%, 1 mm, along fractures, celadonite and smectite veins
ADDITIONAL COMMENTS: Interlayered green hyaloclastite in Piece 4

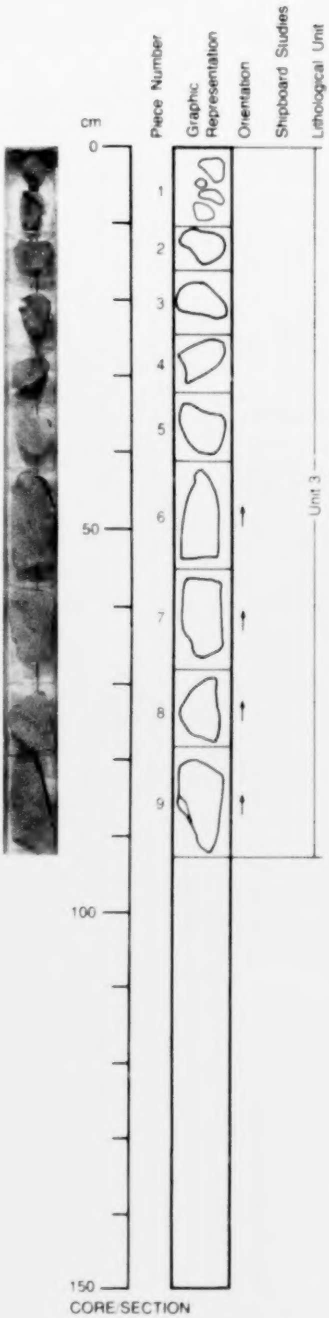
cm
Piece Number
Graphic Representation
Orientation
Shipboard Studies
Lithological Unit
0
50
100
150
1
2
3
4
5
6
7
8
9
Unit 3
CORE/SECTION

126-792E-75R-2

UNIT 3: PORPHYRITIC ANDESITE

Pieces 1-9

CONTACTS: None
PHENOCRYSTS:
- Plagioclase - 35%, 0.2-5 mm, euhedral, zoned
- Clinopyroxene - 5%; 0.2-5 mm, euhedral fresh
- Orthopyroxene - 5%, 0.2-5 mm, euhedral, replaced by smectite
- Magnetite - 1%, 0.1-0.5 mm, subhedral
- Quartz - 0.5%, 0.1-0.4 mm, anhedral rounded

GROUNDMASS: Fine-grained altered glass with microphenocrysts of pyroxenes and plagioclase laths
VESICLES: None
COLOR: Light medium gray, N6
STRUCTURE: Massive
ALTERATION: Moderately altered glass and partly altered orthopyroxene
VEINS/FRACTURES: <1%, 1 mm, along fractures, celadonite and smectite veins

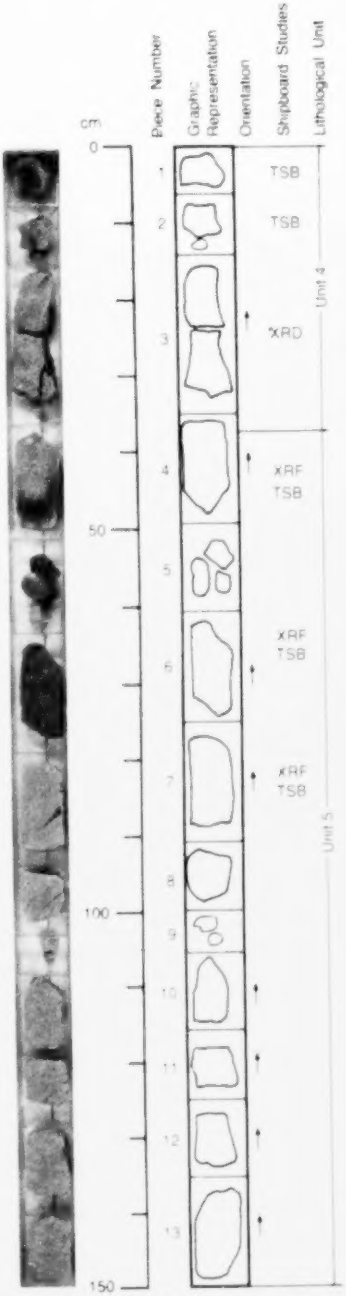
cm
Piece Number
Graphic Representation
Orientation
Shipboard Studies
Lithological Unit
0
50
100
150
1
2
3
4
5
6
7
8
9
10
11
12
13
TSB
TSB
XRD
XRF
TSB
XRF
TSB
XRF
TSB
Unit 4
Unit 5
CORE SECTION

126-792E-76R-1

UNIT 4: VOLCANIC BRECCIA

Pieces 1-4

CONTACTS: Good visible contact with massive andesite lava at top of Piece 4.
PHENOCRYSTS: All the phenocrysts are altered in the clasts but only orthopyroxene is altered in the matrix.
- Plagioclase - 35%, 0.2-4 mm, euhedral, glomeroporphyritic clots fresh in the clasts but altered to chlorite in the matrix.
- Clinopyroxene - 3%, 0.2-4 mm, euhedral fresh in clasts, replaced by prehnite and smectite in matrix.
- Orthopyroxene - 1%, 0.2-3 mm, euhedral, replaced by smectite.
- Magnetite - 1%, 0.1-0.2 mm.

GROUNDMASS: Fine-grained smectite and chlorite (with prehnite) in matrix.
VESICLES: 10%, 0.2 mm, round, even, vesicles only present in the clasts.
COLOR: Greenish gray matrix (5G 6/1) and dark gray clasts (N3).
STRUCTURE: Brecciated with angular to rounded gray clasts in a green matrix.
ALTERATION: Moderately altered glass and olivine, replaced by smectite and chlorite.
VEINS/FRACTURES: None.

UNIT 5: PORPHYRITIC ANDESITE

Pieces 4-13

CONTACTS: None.
PHENOCRYSTS:
- Plagioclase - 35%, 0.2-4 mm, sub-euhedral, zoned and clustered.
- Orthopyroxene - 7%, 0.1-2 mm, euhedral, altered to smectite.
- Clinopyroxene - 3%, 0.1-2 mm, euhedral fresh.
- Magnetite - 1%, 0.1-0.2 mm, sub-euhedral.
- Quartz - 1%, 0.1-0.2 mm, anhedral rounded.

GROUNDMASS: Fine-grained altered glass with microphenocrysts of plagioclase, pyroxenes and magnetite.
VESICLES: None.
COLOR: Light medium gray, N6.
STRUCTURE: Massive.
ALTERATION: Moderately altered glass and orthopyroxene.
VEINS/FRACTURES: <1%, 1 mm, along fractures, celadonite and smectite veins.

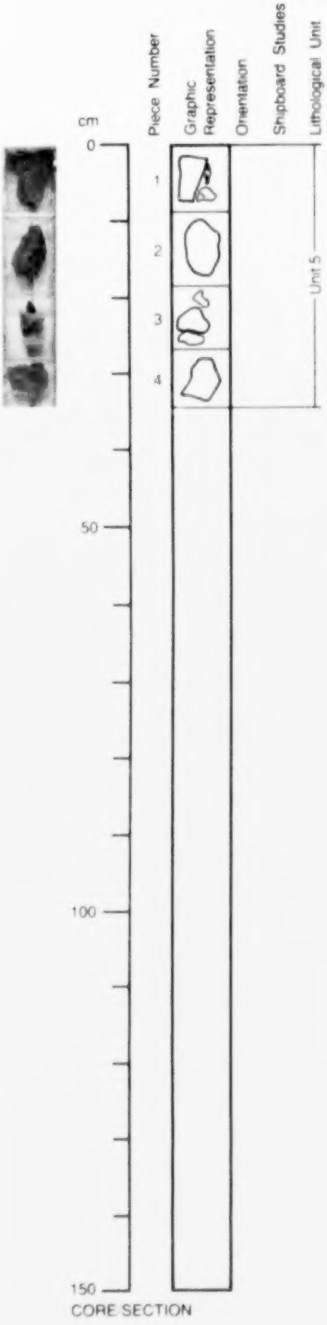
cm
Piece Number
Graphic Representation
Orientation
Shipboard Studies
Lithological Unit
0
1
2
3
4
Unit 5
50
100
150
CORE SECTION

126-792E-76R-2

UNIT 5: PORPHYRITIC ANDESITE

Pieces 1-4

CONTACTS: None

PHENOCRYSTS:

Plagioclase - 35%, 0.2-4 mm, sub-euhedral, zoned and clustered

Orthopyroxene - 7%, 0.1-2 mm, euhedral, altered to smectite

Clinopyroxene - 3%, 0.1-2 mm, euhedral fresh

Magnetite - 1%, 0.1-0.2 mm, sub-euhedral

Quartz - 1%, 0.1-0.2 mm, anhedral rounded

GROUNDMASS: Fine-grained altered glass with microphenocrysts of plagioclase, pyroxenes and magnetite.

VESICLES: None

COLOR: Light medium gray, N6

STRUCTURE: Massive

ALTERATION: Moderately altered glass and orthopyroxene.

VEINS/FRACTURES: <1%, 1 mm, along fractures, celadonite and smectite veins.

ADDITIONAL COMMENTS: Contact with hyaloclastite in Piece 4. Layer 0.5 cm thick.

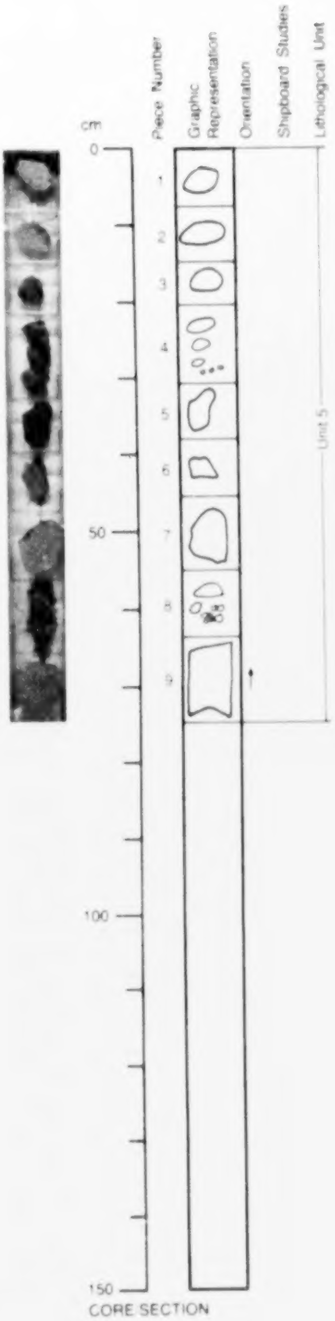
cm
Piece Number
Graphic Representation
Orientation
Shipboard Studies
Lithological Unit
0
1
2
3
4
5
6
50
7
8
9
Unit 5
100
150
CORE SECTION

126-792E-77R-1

UNIT 5: PORPHYRITIC ANDESITE

Pieces 1-9

CONTACTS: None
PHENOCRYSTS:
Plagioclase - 35%, 0.2-4 mm, sub-euhedral, zoned and clustered.
Orthopyroxene - 7%, 0.1-2 mm, euhedral, altered to smectite.
Clinopyroxene - 3%, 0.1-2 mm, euhedral fresh.
Magnetite - 1%, 0.1-0.2 mm, sub-euhedral.
Quartz - 1%, 0.1-0.2 mm, anhedral rounded.
GROUNDMASS: Fine-grained altered glass with microphenocrysts of plagioclase, pyroxenes and magnetite.
VESICLES: None
COLOR: Light medium gray, N6.
STRUCTURE: Massive.
ALTERATION: Moderately altered glass and orthopyroxene.
VEINS/FRACTURES: <1%, 1 mm, along fractures, celadonite and smectite veins.
ADDITIONAL COMMENTS: Hyaloclastite layers or hydrothermal alteration in Pieces 4 and 8.

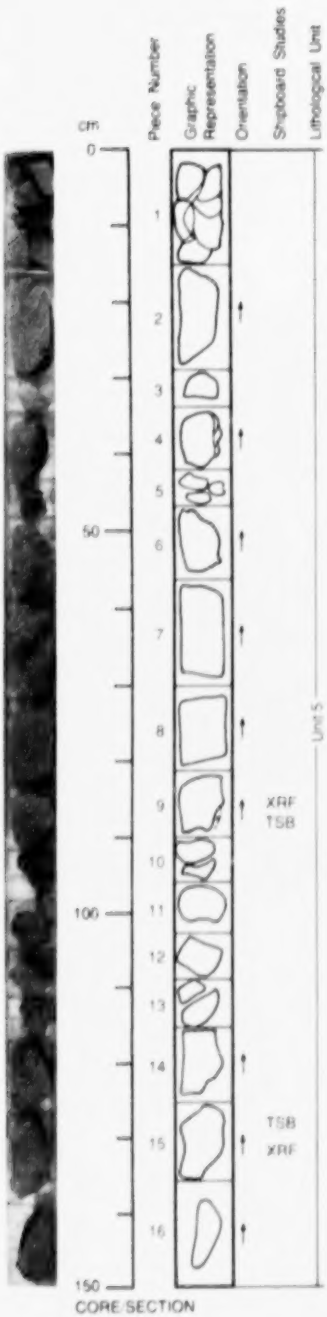
cm
0
50
100
150
Piece Number
Graphic Representation
Orientation
Shipboard Studies
Lithological Unit
1
2
3
4
5
6
7
8
9
10
11
12
13
14
15
16
XRF
TSB
TSB
XRF
Unit 5
CORE/SECTION

126-792E-78R-1

UNIT 5: PORPHYRITIC ANDESITE

Pieces 1-16

CONTACTS: None.
PHENOCRYSTS:
- Plagioclase - 35%, 0.2-4 mm, sub-euhedral, zoned and clustered.
- Orthopyroxene - 7%, 0.1-2 mm, euhedral, altered to smectite.
- Clinopyroxene - 3%, 0.1-2 mm, euhedral fresh.
- Magnetite - 1%, 0.1-0.2 mm, sub-euhedral.
- Quartz - 1%, 0.1-0.2 mm, anhedral rounded.

GROUNDMASS: Fine-grained altered glass with microphenocrysts of plagioclase, pyroxenes and magnetite.
VESICLES: None.
COLOR: Light medium gray, N6.
STRUCTURE: Massive.
ALTERATION: Moderately altered glass and orthopyroxene.
VEINS/FRACTURES: <1%, 1 mm, along fractures; celadonite and smectite veins.

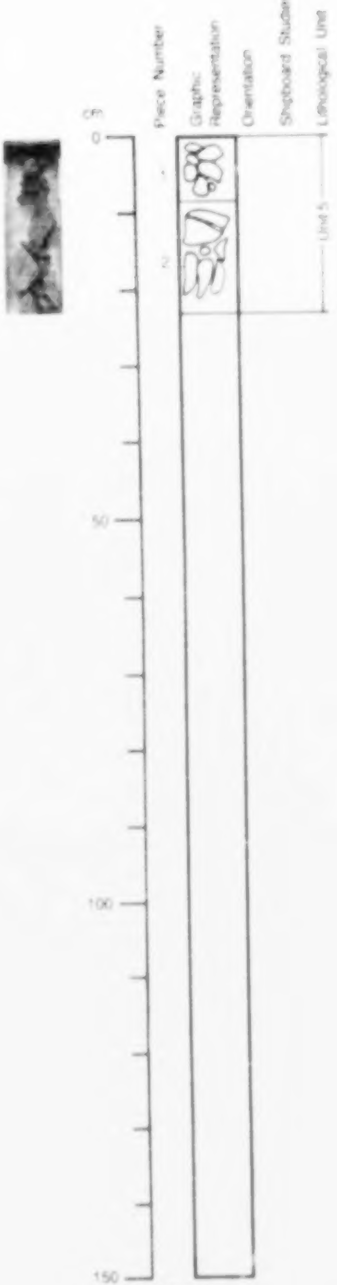
cm
Piece Number
Graphic Representation
Orientation
Shipboard Studies
Lithological Unit
0
1
2
Unit 5
50
100
150
CORE SECTION

126-792E-78R-2

UNIT 5: PORPHYRITIC ANDESITE

Pieces 1-2

CONTACTS: None.
PHENOCRYSTS:
Plagioclase : 35%, 0.2-4 mm, sub-euhedral, zoned and clustered.
Orthopyroxene : 7%, 0.1-2 mm, euhedral, altered to smectite.
Clinopyroxene : 3%, 0.1-2 mm, euhedral fresh.
Magnetite : 1%, 0.1-0.2 mm, sub-euhedral.
Quartz : 1%, 0.1-0.2 mm, anhedral rounded.
GROUNDMASS: Fine-grained altered glass with microphenocrysts of plagioclase, pyroxenes and magnetite.
VESICLES: None.
COLOR: Light medium gray, N6.
STRUCTURE: Massive.
ALTERATION: Moderately altered glass and orthopyroxene.
VEINS/FRACTURES: <1%, 1 mm, along fractures, celadonite and smectite veins.

[illegible]

N/A

COMMENTS

[illegible] filling [illegible]

FILLING

COMMENTS

[illegible] filled with smectite

COMMENTS: [illegible] No piece # given.

[illegible]

COMMENTS

N/A

[illegible] smectite

FILLING

COMMENTS: [illegible] No piece # given.

[illegible]

COMMENTS

N/A

FILLING

COMMENTS: [illegible] No piece # given.

[illegible] WHERE SAMPLED: Unit [illegible]

ROCK NAME: [illegible]

GRAIN SIZE: [illegible]

TEXTURE: [illegible]

PRIMARY MINERALOGY	PERCENT PRESENT	PERCENT ORIGINAL	SIZE (mm)	COMPOSITION	MORPHOLOGY	COMMENTS
PHENOCRYSTS						
Plagioclase	N.A.	15	[illegible]		[illegible]	[illegible]
Clinopyroxene	N.A.	1	[illegible]		[illegible]	[illegible]
Orthopyroxene	N.A.	Trace	N.A.		N.A.	[illegible]
Magnetite	N.A.	N.A.	N.A.		N.A.	[illegible] with small [illegible]
GROUNDMASS						
N.A.	N.A.	N.A.	N.A.		N.A.	[illegible]

VESICLES/ CAVITIES	PERCENT	LOCATION	SIZE (mm)	FILLING	SHAPE

COMMENTS: [illegible]

[illegible] WHERE SAMPLED: Unit [illegible]

ROCK NAME: [illegible]

GRAIN SIZE: [illegible]

TEXTURE: [illegible]

PRIMARY MINERALOGY	PERCENT PRESENT	PERCENT ORIGINAL	SIZE (mm)	COMPOSITION	MORPHOLOGY	COMMENTS
PHENOCRYSTS						
Plagioclase		[illegible]	[illegible]		[illegible]	[illegible]
Clinopyroxene		1	[illegible]		[illegible]	[illegible]
GROUNDMASS						
Plagioclase	N.A.	[illegible]	[illegible]		N.A.	[illegible]
Altered glass	N.A.	N.A.	[illegible]		N.A.	

SECONDARY MINERALOGY	PERCENT	REPLACING/ FILLING	COMMENTS

VESICLES/ CAVITIES	PERCENT	LOCATION	SIZE (mm)	FILLING	SHAPE
[illegible]	[illegible]			[illegible]	[illegible]

COMMENTS: [illegible]

[illegible]-478-31 (128-130 cm) OBSERVER: LTP WHERE SAMPLED: Unit 5

ROCK NAME: Clinopyroxene-basalt or andesite

GRAIN SIZE: Fine

TEXTURE: Porphyritic-vesicular

PRIMARY MINERALOGY	PERCENT PRESENT	PERCENT ORIGINAL	SIZE (mm)	COMPOSITION	MORPHOLOGY	COMMENTS
PHENOCRYSTS						
Clinopyroxene	N/A	1	</=2		Euhedral	Fresh exsolution along cleavages.
Plagioclase	N/A	N/A	N/A		Euhedral	Replaced by zeolites.
Orthopyroxene	N/A	[illegible]	[illegible]		N/A	Pseudomorphs of replaced smectites.
GROUNDMASS						
N/A	N/A	N/A	N/A		N/A	40% highly vesicular groundmass.

SECONDARY MINERALOGY	PERCENT	REPLACING/FILLING	COMMENTS
Clays			Smectites filling up small vesicles.
Zeolites			Filling big elongated vesicles.

VESICLES/CAVITIES	PERCENT	LOCATION	SIZE (mm)	FILLING	SHAPE
Vesicles	40		1-5	Smectites, zeolites	Rounded, elongated

COMMENTS: Clasts in a lapilli-tuff? are pebbly granule conglomerate. Broken and or complete crystals plagioclase, clinopyroxene, and quartz. Matrix is probably formed of zeolites. No piece # given.

[illegible]-41A-34 (11-17 cm) OBSERVER: LTP WHERE SAMPLED:

ROCK NAME: Clinopyroxene-olivine-plagioclase basalt

GRAIN SIZE: Fine

TEXTURE: Porphyritic

PRIMARY MINERALOGY	PERCENT PRESENT	PERCENT ORIGINAL	SIZE (mm)	COMPOSITION	MORPHOLOGY	COMMENTS
PHENOCRYSTS						
Olivine	8	N/A	[illegible]		Euhedral	Pseudomorphs of smectite, some crystals remain fresh.
Plagioclase	20	N/A	[illegible]		Euhedral	Fresh, including clinopyroxene.
Clinopyroxene	4	N/A	[illegible]		Euhedral	Partly altered.
GROUNDMASS						
Glass	N/A	N/A	<0.1		N/A	Glass is completely replaced by hydrated cryptocrystalline isotropic material.
Olivine	N/A	N/A	[illegible]		N/A	
Plagioclase	N/A	N/A	[illegible]		N/A	

SECONDARY MINERALOGY	PERCENT	REPLACING/FILLING	COMMENTS
Clays			Smectites from alteration of olivine and clinopyroxene fill vesicles.

VESICLES/CAVITIES	PERCENT	LOCATION	SIZE (mm)	FILLING	SHAPE
Vesicles	1		<0.5	Smectites	Irregular

COMMENTS: No piece # given. Groundmass is 60%.

```
[illegible]

PRIMARY          PERCENT PERCENT  SIZE      COMPO-
MINERALOGY       PRESENT ORIGINAL (mm)      SITION        MORPHOLOGY       COMMENTS

PHENOCRYSTS
[illegible]                                                [illegible]      Partly altered to smectites.
[illegible]                                                [illegible]      Fresh.
[illegible]                                                N/A
[illegible]                                                N/A              Altered to smectites (and celadonite).
                                                                            Includes plagioclase and magnetite.
[illegible]                                                N/A              Fresh "stubby twinning".

GROUNDMASS
[illegible]                                                N/A              Microcrystalline groundmass.
[illegible]                                                N/A              Microcrystalline groundmass.

[illegible]

[illegible]

PRIMARY          PERCENT PERCENT  SIZE      COMPO-
MINERALOGY       PRESENT ORIGINAL (mm)      SITION        MORPHOLOGY       COMMENTS

PHENOCRYSTS
[illegible]

GROUNDMASS
[illegible]

[illegible]
```

[illegible] ([illegible] cm) OBSERVER: LTP WHERE SAMPLED:

ROCK NAME: Amphibole-dacite

GRAIN SIZE: Fine

TEXTURE: Porphyritic

PRIMARY MINERALOGY	PERCENT PRESENT	PERCENT ORIGINAL	SIZE (mm)	COMPOSITION	MORPHOLOGY	COMMENTS
PHENOCRYSTS						
Plagioclase	N/A	[illegible]	0.5		Euhedral	Fresh
Orthopyroxene	N/A	Tr	[illegible]		Euhedral	Fresh
[illegible]	N/A	N/A	N/A		Euhedral	Included in amphibole
Amphibole	N/A	[illegible]	4		Euhedral	Fresh-zoned
Quartz	N/A	[illegible]	[illegible]		N/A	
GROUNDMASS						
[illegible]	N/A	N/A	N/A		N/A	Groundmass is cryptocrystalline

VESICLES/CAVITIES	PERCENT	LOCATION	SIZE (mm)	FILLING	SHAPE
Vesicles	0				

COMMENTS: Amphibole-dacite in volcaniclastic bed. No piece # given.

[illegible] ([illegible] cm) OBSERVER: LTP WHERE SAMPLED:

ROCK NAME: N/A

GRAIN SIZE: Fine grained

TEXTURE: Porphyritic

PRIMARY MINERALOGY	PERCENT PRESENT	PERCENT ORIGINAL	SIZE (mm)	COMPOSITION	MORPHOLOGY	COMMENTS
PHENOCRYSTS						
Plagioclase	N/A	[illegible]	[illegible]		Euhedral	Glomeroporphyritic; oscillatory zoned. Fresh.
Opaque	N/A	[illegible]	[illegible]		Euhedral	Often as inclusions in amphibole.
Quartz	N/A	N/A	[illegible]		Subeuhedral	Embayed
Amphibole	N/A	[illegible]	[illegible]		Euhedral	Fresh, zoned (green pleochroism).
GROUNDMASS						
Plagioclase	N/A	N/A	[illegible]		N/A	[illegible] apparently fresh, isotropic glass
Amphibole	N/A	N/A	[illegible]		N/A	Apparently fresh isotropic glass.

VESICLES/CAVITIES	PERCENT	LOCATION	SIZE (mm)	FILLING	SHAPE
Vesicles	0				

COMMENTS: Lots of amphibole, opaque and plagioclase. Glass is fractured and along cracks, there is development of smectites. No piece # given.

[illegible]

[illegible] 792E-71R-01 (Piece 11,134-142 cm)   OBSERVER: LTP   WHERE SAMPLED:

ROCK NAME: Orthopyroxene-clinopyroxene andesite

GRAIN SIZE: Fine

TEXTURE: Porphyritic

PRIMARY MINERALOGY	PERCENT PRESENT	PERCENT ORIGINAL	SIZE (mm)	COMPO-SITION	MORPHOLOGY	COMMENTS
PHENOCRYSTS						
Plagioclase	30	30	[illegible]		Subhedral	Zoned and clustered.
Clinopyroxene	15	15	[illegible]		Euhedral	Inclusions, lamellae, fresh.
Orthopyroxene	1	14	[illegible]		Euhedral	Altered to smectites (very few preserved).
Magnetite	1	1	[illegible]		Subhedral	In the groundmass.
Olivine	N/A	N/A	N/A		N/A	Perhaps a few crystals of olivine pseudomorphs.
GROUNDMASS						
Plagioclase	N/A	N/A	[illegible]		N/A	
Clinopyroxene	N/A	N/A	[illegible]		N/A	
Orthopyroxene	N/A	N/A	[illegible]		N/A	
Glass	N/A	N/A	N/A		N/A	Glass completely devitrified.

SECONDARY MINERALOGY	PERCENT	REPLACING/FILLING	COMMENTS
Clays	[illegible]	Orthopyroxene, glass	

VESICLES/CAVITIES	PERCENT	LOCATION	SIZE (mm)	FILLING	SHAPE
Vesicles	[illegible]				

COMMENTS: Individual quartz xenocrysts surrounded by clinopyroxene. Big inclusions with the same mineralogy as the andesite, coarser grained than the andesite - flow-aligned plagioclase microlites/laths. Original groundmass was [illegible], present is [illegible].

[illegible] 69R-01 (62-67 cm)   OBSERVER: LTP   WHERE SAMPLED:

ROCK NAME: Orthopyroxene-clinopyroxene-andesite

GRAIN SIZE: Fine

TEXTURE: Porphyritic

PRIMARY MINERALOGY	PERCENT PRESENT	PERCENT ORIGINAL	SIZE (mm)	COMPO-SITION	MORPHOLOGY	COMMENTS
PHENOCRYSTS						
Plagioclase	[illegible]	[illegible]	[illegible]		Euhedral	Zoned and clustered in glomeroporphyritic clots.
Clinopyroxene	[illegible]	[illegible]	[illegible]		Euhedral	Fresh.
Opaque	[illegible]	[illegible]	[illegible]		Euhedral	Fresh.
Orthopyroxene	[illegible]	[illegible]	[illegible]		Euhedral	Altered to smectites. Some crystals are preserved.
GROUNDMASS						
Feldspar	N/A	N/A	[illegible]		N/A	Microcrystalline groundmass: includes flow aligned feldspars.
Clinopyroxene	N/A	N/A	[illegible]		N/A	
Orthopyroxene	N/A	N/A	[illegible]		N/A	Microlites. Altered to smectites.
Glass	N/A	N/A	N/A		N/A	

SECONDARY MINERALOGY	PERCENT	REPLACING/FILLING	COMMENTS
Clays	[illegible]	Orthopyroxene, glass	Smectites replacing orthopyroxene and preserved in the groundmass.

VESICLES/CAVITIES	PERCENT	LOCATION	SIZE (mm)	FILLING	SHAPE
Vesicles	[illegible]				

COMMENTS: No piece # given. Present groundmass is [illegible] and original is [illegible]. Orthopyroxene altered with smectite and mantled by clinopyroxene.

[illegible] OBSERVER: [illegible] WHERE SAMPLED: [illegible]

ROCK NAME: [illegible]

GRAIN SIZE: [illegible]

TEXTURE: [illegible]

PRIMARY MINERALOGY	PERCENT PRESENT	PERCENT ORIGINAL	SIZE (mm)	COMPO-SITION	MORPHOLOGY	COMMENTS
PHENOCRYSTS						
Plagioclase	[illegible]	[illegible]	[illegible]		[illegible]	Fresh.
Clinopyroxene	[illegible]	[illegible]	[illegible]		[illegible]	[illegible]
Magnetite	[illegible]	[illegible]	[illegible]		[illegible]	[illegible]
Orthopyroxene	[illegible]	[illegible]	[illegible]		[illegible]	Almost all altered to smectite.
GROUNDMASS						
Glass	N/A	N/A	N/A		[illegible]	[illegible] partly altered to smectite.
Plagioclase	N/A	N/A	[illegible]		[illegible]	

SECONDARY MINERALOGY	PERCENT	REPLACING/FILLING	COMMENTS
[illegible]	[illegible]	[illegible]	

VESICLES	PERCENT	LOCATION	SIZE (mm)	FILLING	SHAPE
[illegible]	[illegible]				

COMMENTS: [illegible]

[illegible] OBSERVER: [illegible] WHERE SAMPLED: [illegible]

ROCK NAME: [illegible]

GRAIN SIZE: [illegible]

TEXTURE: [illegible]

PRIMARY MINERALOGY	PERCENT PRESENT	PERCENT ORIGINAL	SIZE (mm)	COMPO-SITION	MORPHOLOGY	COMMENTS
PHENOCRYSTS						
[illegible]	[illegible]	[illegible]	[illegible]		[illegible]	
[illegible]	[illegible]	[illegible]	[illegible]		[illegible]	[illegible]
[illegible]	[illegible]	[illegible]	[illegible]		[illegible]	
[illegible]	[illegible]	[illegible]	[illegible]		[illegible]	[illegible] altered to smectite; [illegible]
GROUNDMASS						
[illegible]	N/A	N/A	N/A		N/A	[illegible] altered to smectite.
[illegible]	N/A	N/A	N/A		N/A	

SECONDARY MINERALOGY	PERCENT	REPLACING/FILLING	COMMENTS
[illegible]	[illegible]	[illegible]	
[illegible]	[illegible]	[illegible]	

VESICLES	PERCENT	LOCATION	SIZE (mm)	FILLING	SHAPE
[illegible]					

COMMENTS: [illegible]

```
[illegible]-[illegible]R-[illegible] (Piece 10,17-18 cm)      OBSERVER: TOR      WHERE SAMPLED: Unit [illegible]

ROCK NAME: Plagioclase-two pyroxene-andesite

GRAIN SIZE: Fine

TEXTURE: Intersertal, porphyritic

PRIMARY          PERCENT PERCENT  SIZE        COMPO-
MINERALOGY       PRESENT ORIGINAL (mm)        SITION          MORPHOLOGY          COMMENTS

PHENOCRYSTS:
Plagioclase      [illegible]  [illegible]  [illegible]                  Subhedral           Highly zoned
Clinopyroxene    [illegible]  [illegible]  N/A                          Euhedral
[illegible]      [illegible]  [illegible]  N/A                          Euhedral
Orthopyroxene    [illegible]  [illegible]  [illegible]                  Euhedral            Altered to smectite
[illegible]      [illegible]  [illegible]  [illegible]                  Anhedral

GROUNDMASS:
Glass            N/A     N/A      N/A                         N/A                 [illegible]
Plagioclase      N/A     N/A      [illegible]                 Laths

SECONDARY                REPLACING/
MINERALOGY       PERCENT FILLING                                                  COMMENTS
Clay             [illegible]  Orthopyroxene, glass                    Smectite

VESICLES:                         SIZE
VESICLES         PERCENT LOCATION (mm)          FILLING                          SHAPE
Vesicles         [illegible]

COMMENT: [illegible]

[illegible]      (Piece [illegible])      OBSERVER: TOR      WHERE SAMPLED:

ROCK NAME: [illegible]

GRAIN SIZE: [illegible]

TEXTURE: Porphyritic

PRIMARY          PERCENT PERCENT  SIZE        COMPO-
MINERALOGY       PRESENT ORIGINAL (mm)        SITION          MORPHOLOGY          COMMENTS

PHENOCRYSTS:
Plagioclase      [illegible]  [illegible]  [illegible]                  [illegible]         [illegible]
Clinopyroxene    [illegible]  [illegible]  [illegible]                  [illegible]         [illegible]
[illegible]      [illegible]  [illegible]  [illegible]                  N/A
[illegible]      N/A     N/A      N/A                         N/A                 [illegible]
Orthopyroxene    [illegible]  [illegible]  [illegible]                  N/A                 [illegible]

GROUNDMASS:
[illegible]      [illegible]  [illegible]  N/A                          N/A                 [illegible]
                                                                                  [illegible]

SECONDARY                REPLACING/
MINERALOGY       PERCENT FILLING                                                  COMMENTS
[illegible]      [illegible]  Orthopyroxene, glass                    [illegible]

VESICLES:                         SIZE
VESICLES         PERCENT LOCATION (mm)          FILLING                          SHAPE
Vesicles         [illegible]

COMMENT: [illegible]
```

126-792E-[illegible] (Piece [illegible]) OBSERVER: [illegible] WHERE SAMPLED: At magnetite accumulation layer

ROCK NAME: Porphyritic 2 pyroxene andesite

GRAIN SIZE: [illegible] mm

TEXTURE: Porphyritic-intersertal accumulation

PRIMARY MINERALOGY	PERCENT PRESENT	PERCENT ORIGINAL	SIZE (mm)	COMPOSITION	MORPHOLOGY	COMMENTS
PHENOCRYSTS						
Plagioclase	[illegible]	[illegible]	[illegible]		Euhedral	
Clinopyroxene	[illegible]	[illegible]	[illegible]		Subhedral	
Opaque (magnetite)	[illegible]	[illegible]	[illegible]		Subhedral	Accumulation at contact between two flows
Orthopyroxene		[illegible]	[illegible]		Subhedral	
GROUNDMASS						
Glass	[illegible]	[illegible]	N/A		N/A	

SECONDARY MINERALOGY	PERCENT	REPLACING/FILLING	COMMENTS
Clays	[illegible]	[illegible]	[illegible]

VESICLES/CAVITIES	PERCENT	LOCATION	SIZE (mm)	FILLING	SHAPE
[illegible]	[illegible]				

COMMENTS: [illegible] accumulation of ore mineral [illegible] Matrix in this region [illegible] base of flow.

126-792E-[illegible] (Piece [illegible]) OBSERVER: [illegible] WHERE SAMPLED: [illegible]

ROCK NAME: [illegible]

GRAIN SIZE: [illegible]

TEXTURE: [illegible]

PRIMARY MINERALOGY	PERCENT PRESENT	PERCENT ORIGINAL	SIZE (mm)	COMPOSITION	MORPHOLOGY	COMMENTS
PHENOCRYSTS						
Plagioclase	[illegible]	[illegible]	[illegible]		[illegible]	
Clinopyroxene	[illegible]	[illegible]	[illegible]		[illegible]	
Magnetite	[illegible]	[illegible]	[illegible]		[illegible]	
Orthopyroxene	[illegible]	[illegible]	[illegible]		[illegible]	
[illegible]	[illegible]	[illegible]	[illegible]		[illegible]	
GROUNDMASS						
Glass	[illegible]	[illegible]	[illegible]		[illegible]	[illegible]
Plagioclase	[illegible]	[illegible]	[illegible]		[illegible]	

SECONDARY MINERALOGY	PERCENT	REPLACING/FILLING	COMMENTS
Clays	[illegible]	Orthopyroxene [illegible]	[illegible]

VESICLES/CAVITIES	PERCENT	LOCATION	SIZE (mm)	FILLING	SHAPE
[illegible]	[illegible]				

COMMENTS: [illegible]

[illegible] (Piece 1, 1-2 cm) OBSERVER: LTP WHERE SAMPLED: Altered zone (glassy part)

ROCK NAME: Pyroclastic breccia (andesitic)

GRAIN SIZE: Fine

TEXTURE: Porphyritic

PRIMARY MINERALOGY	PERCENT PRESENT	PERCENT ORIGINAL	SIZE (mm)	COMPOSITION	MORPHOLOGY	COMMENTS
PHENOCRYSTS						
Plagioclase	N/A	N/A	0.5		Euhedral	Chloritized.
Clinopyroxene	N/A	N/A	4		N/A	Replaced by smectites and prehnite.
Orthopyroxene	N/A	N/A	2		Euhedral	Replaced by smectites, iron oxides.
GROUNDMASS						
[illegible]	N/A	N/A	N/A		N/A	Orthopyroxene surrounded by clinopyroxene ~2 mm. Groundmass: 80%, both altered completely, transformed to chlorite and smectites.

SECONDARY MINERALOGY	PERCENT	REPLACING/FILLING	COMMENTS
Clay	[illegible]		Replacing minerals and groundmass.
Chlorite	30		Replacing minerals (mainly phenocrysts).
Prehnite	15		Replacing clinopyroxene.

VESICLES/CAVITIES	PERCENT	LOCATION	SIZE (mm)	FILLING	SHAPE
Vesicles	[illegible]				

COMMENTS: Clasts: altered clinopyroxene-orthopyroxene andesite, [illegible] cm up to [illegible] cm. Groundmass: glassy becoming partly replaced by smectites. Clots of clinopyroxene including small plagioclase laths, very fresh. Clinopyroxene and plagioclase crystals, whole or broken, very fresh. Orthopyroxene - generally replaced by smectites (some relicts).

[illegible] (Piece 1, 1-3 cm) OBSERVER: [illegible] WHERE SAMPLED:

ROCK NAME: Pyroclastic breccia

GRAIN SIZE: Fine

TEXTURE: Porphyritic

PRIMARY MINERALOGY	PERCENT PRESENT	PERCENT ORIGINAL	SIZE (mm)	COMPOSITION	MORPHOLOGY	COMMENTS
PHENOCRYSTS						
Plagioclase	17	[illegible]	[illegible]		Euhedral	
Clinopyroxene	[illegible]	5	N/A		Euhedral	Partly altered to smectite.
Magnetite	[illegible]	1	N/A		Subhedral	
Orthopyroxene	[illegible]	5	N/A		Euhedral	
GROUNDMASS						
Glass	N/A	N/A	N/A		N/A	Glass and plagioclase are presently [illegible], originally [illegible].
Plagioclase	N/A	N/A	N/A		N/A	Glass and plagioclase are presently [illegible], originally [illegible].

SECONDARY MINERALOGY	PERCENT	REPLACING/FILLING	COMMENTS
Clays	[illegible]	Orthopyroxene, clinopyroxene, plagioclase, groundmass	

VESICLES/CAVITIES	PERCENT	LOCATION	SIZE (mm)	FILLING	SHAPE
Vesicles	[illegible]				

[illegible]

[illegible]

[illegible]

[illegible]92E-78R-1 (Piece 15,133-136 cm)   OBSERVER: LEE   WHERE SAMPLED:

ROCK NAME: Quartz-bearing andesite (2 pyroxenes)

GRAIN SIZE: Fine

TEXTURE: Porphyritic

PRIMARY MINERALOGY	PERCENT PRESENT	PERCENT ORIGINAL	SIZE (mm)	COMPO-SITION	MORPHOLOGY	COMMENTS
PHENOCRYSTS						
Plagioclase	25	25	[illegible]		N/A	
Clinopyroxene	[illegible]	[illegible]	[illegible]		N/A	Fresh, sometimes clustered with plagioclase.
Orthopyroxene	1	1	[illegible]		N/A	Partly altered to smectites. Some crystals are still fresh.
Quartz	1	1	[illegible]		N/A	
GROUNDMASS						
Plagioclase	N/A	N/A	[illegible]		N/A	
Clinopyroxene	N/A	N/A	[illegible]		N/A	
Glass	N/A	N/A	N/A		N/A	Glass altered to brown microcrystalline material.

SECONDARY MINERALOGY	PERCENT	REPLACING/ FILLING	COMMENTS
Clays	10	Orthopyroxene, glass	

VESICLES/ CAVITIES	PERCENT	LOCATION	SIZE (mm)	FILLING	SHAPE
Vesicles	0				

COMMENTS: 1 crystal of fresh orthopyroxene. Present groundmass is [illegible]; original was [illegible]

SITE 793 HOLE A CORE 1H CORED INTERVAL 0.0-4.2 mbsf

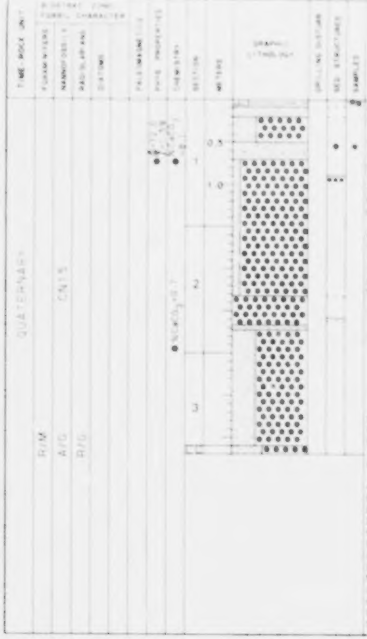
TIME-ROCK UNIT
BIOSTRAT. ZONE/ FOSSIL CHARACTER
FORAMINIFERS
NANNOFOSSILS
RADIOLARIANS
DIATOMS
PALEOMAGNETICS
PHYS. PROPERTIES
CHEMISTRY
SECTION
METERS
GRAPHIC LITHOLOGY
DRILLING DISTURB.
SED. STRUCTURES
SAMPLES
QUATERNARY
CN15
R/M
A/G
R/G
1
2
3
0.5
1.0

LITHOLOGIC DESCRIPTION

PUMICEOUS GRANULE PEBBLE GRAVEL AND PUMICEOUS PEBBLE GRANULE GRAVEL

Major lithologies:
Dark gray (5Y 4/1, N4) and brownish gray (2.5Y 5/2) PUMICEOUS GRANULE PEBBLE GRAVEL and PUMICEOUS PEBBLE GRANULE GRAVEL. Sand:granule:pebble ratios range from 30:60:10 to 10:20:70. Maximum pebble sizes range from 21 to 40 mm, and mean sizes of the ten largest clasts vary from 10 to 17 mm. Most pumice clast colors are gray (5Y 6/1) and light gray (N7), although two large clasts in Section 1, 96-104 cm, have greenish black (5GY 2/1) surface stains. Two intervals show crude inverse grading.

Minor lithologies:
Section 1, 0-8 cm (mudline layer) is grayish brown (10YR 5/2) NANNOFOSSIL-RICH VITRIC CLAYEY SILT grading upward into NANNOFOSSIL-RICH VITRIC SILTY CLAY. Section 2, 67-71 cm, is a soft intraclast of dark grayish brown (2.5Y 4/2) coarse to very fine grained LITHIC VITRIC SAND. Section 1, 117-121 cm, is dark gray (5Y 4/1) very coarse to fine grained VITRIC SAND.

The core is undisturbed by drilling.

SMEAR SLIDE SUMMARY (%):

	[illegible]	[illegible]	[illegible]
	M	M	M
TEXTURE:			
Sand	—	20	5
Silt	10	25	20
Clay	90	55	75
COMPOSITION:			
Accessory minerals	Tr	5	1
Biotite	Tr	—	—
Clay	38	43	60
Diatoms	1	1	1
Feldspar	—	1	1
Foraminifers	2	5	5
Glass	40	40	10
Lithic fragments	—	1	5
Nannofossils	15	1	15
Opaques	1	2	—
Radiolarians	3	1	5
Silicoflagellates	Tr	Tr	2
Spicules	—	2	2

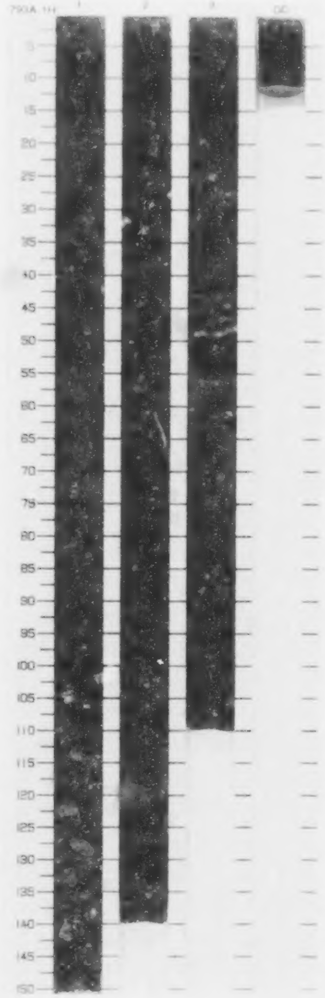
793A-1H
1
2
3
CC
0
5
10
15
20
25
30
35
40
45
50
55
60
65
70
75
80
85
90
95
100
105
110
115
120
125
130
135
140
145
150

SITE 793 HOLE A CORE 2H CORED INTERVAL 4.2-13.5 mbsf

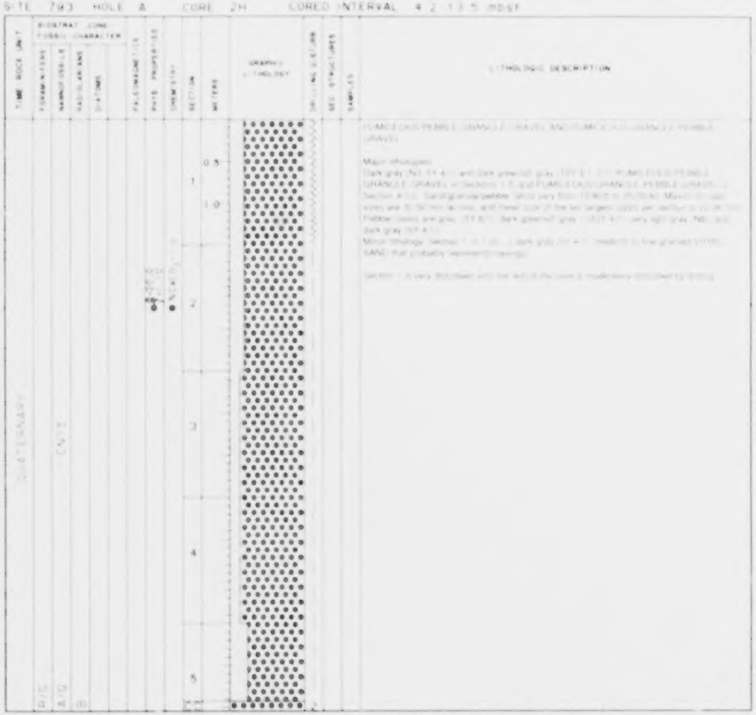
TIME-ROCK UNIT
BIOSTRAT. ZONE/FOSSIL CHARACTER
FORAMINIFERS
NANNOFOSSILS
RADIOLARIANS
DIATOMS
PALEOMAGNETICS
PHYS. PROPERTIES
CHEMISTRY
SECTION
METERS
GRAPHIC LITHOLOGY
DRILLING DISTURB.
SED. STRUCTURES
SAMPLES
QUATERNARY
CN15
B/G
A/G
B
0.5
1.0
1
2
3
4
5
CC

LITHOLOGIC DESCRIPTION

PUMICEOUS PEBBLE GRANULE GRAVEL AND PUMICEOUS GRANULE PEBBLE GRAVEL

Major lithologies:
Dark gray (N3; 5Y 4/1) and dark greenish gray ([illegible]) PUMICEOUS PEBBLE GRANULE GRAVEL in Sections 1-3, and PUMICEOUS GRANULE PEBBLE GRAVEL in Section 4 ([illegible]). Sand/granule/pebble ratios vary from [illegible] to [illegible]. Maximum clast sizes are [illegible] mm across, and mean size of the ten largest clasts per section is [illegible]. Pebble clasts are gray (5Y 6/1), dark greenish gray ([illegible]), very light gray (N8), and dark gray (5Y 4/1).
Minor lithology: Section 1, 0-7 cm(?), dark gray (5Y 4/1) medium- to fine-grained VITRIC SAND that probably represents cavings.

Section 1 is very disturbed and the rest of the core is moderately disturbed by drilling.

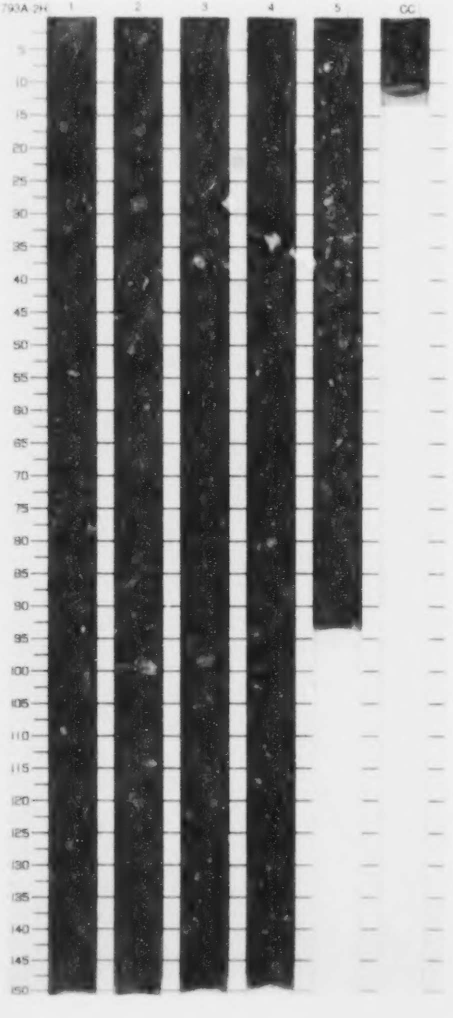
793A-2H
1
2
3
4
5
CC
5
10
15
20
25
30
35
40
45
50
55
60
65
70
75
80
85
90
95
100
105
110
115
120
125
130
135
140
145
150

SITE 793 HOLE A CORE 3H CORED INTERVAL 13.5-23.0 mbsf

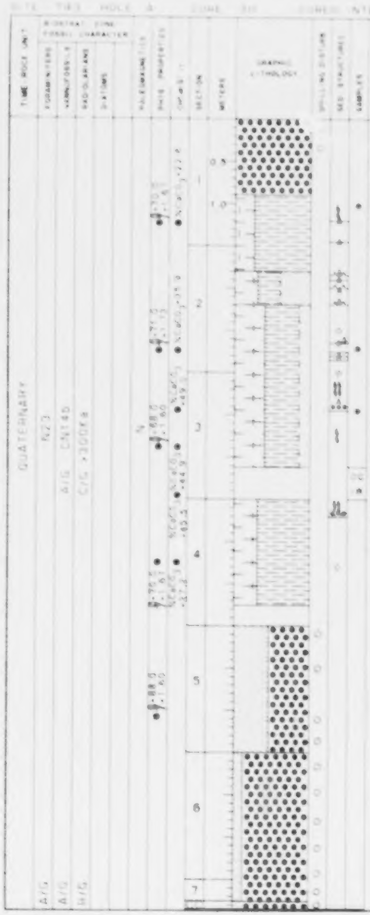
TIME-ROCK UNIT
BIOSTRAT. ZONE/FOSSIL CHARACTER
FORAMINIFERS
NANNOFOSSILS
RADIOLARIANS
DIATOMS
PALEOMAGNETICS
PHYS. PROPERTIES
CHEMISTRY
SECTION
METERS
GRAPHIC LITHOLOGY
DRILLING DISTURB.
SED. STRUCTURES
SAMPLES
QUATERNARY
N23
A/G CN14b
C/G >300Ka
A/G
A/G
R/G
N
1
2
3
4
5
6
7
0.5
1.0
CC

LITHOLOGIC DESCRIPTION

PUMICEOUS GRAVEL, PUMICEOUS PEBBLY SAND AND FORAMINIFER NANNOFOSSIL SILTY CLAY

Major lithologies:
Section 1, 0-85 cm, and Sections 5 through CC consist of gray (5Y 6/1) and dark gray (5Y 4/1), structureless PUMICEOUS GRAVEL and PUMICEOUS PEBBLY SAND. The soupy nature of much of this material contributes to its homogeneous appearance. Pebbles locally account for 80% of the sediment. The rest of the core is predominantly dark gray (5Y 4/1) and light gray (N7), burrowed FORAMINIFER NANNOFOSSIL SILTY CLAY with scattered clasts of pumice as large as 3 cm in diameter.

Minor lithologies: The foraminifer nannofossil silty clay contains graded interbeds, <10 cm thick, of olive black (5Y 2/1), grayish green (5G 5/2) and grayish black (N2) VITRIC SILT and fine-grained VITRIC SAND, particularly in VITRIC SILT, fine-grained VITRIC SAND, and GRANULE GRAVEL, all only a few centimeters thick.

Section 1, 0-40 cm, and Sections 5 through CC are soupy.

SMEAR SLIDE SUMMARY (%):

	1, 130 D	2, 121 M	3, 45 D
TEXTURE:			
Silt	20	20	20
Clay	80	80	80
COMPOSITION:			
Accessory minerals	Tr	Tr	—
Diatoms	3	—	3
Foraminifers	10	3	15
Glass	64	40	67
Micrite	—	40	—
Nannofossils	20	10	[illegible]
Spicules	3	—	—

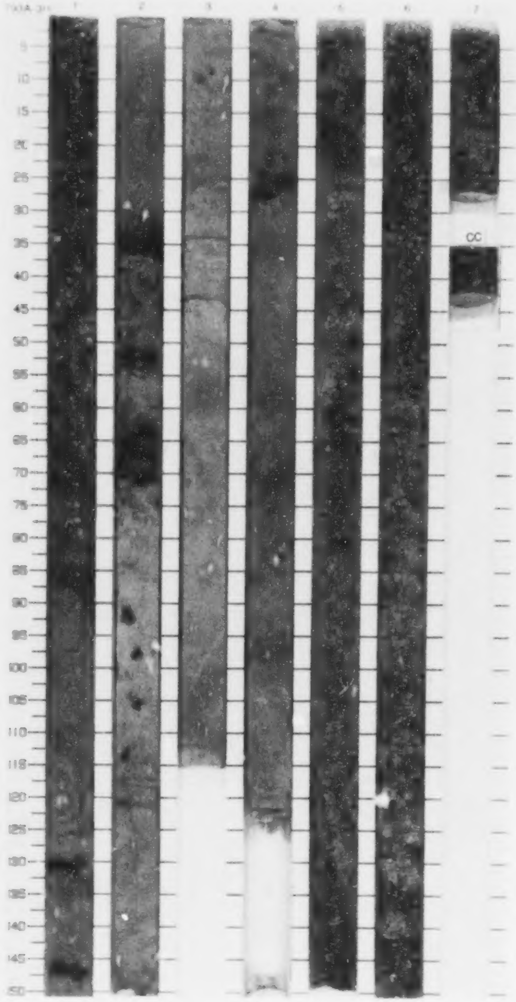
793A-3H
1
2
3
4
5
6
7
CC
5
10
15
20
25
30
35
40
45
50
55
60
65
70
75
80
85
90
95
100
105
110
115
120
125
130
135
140
145
150

SITE 793 HOLE A CORE 4H CORED INTERVAL 23.0-32.5 mbsf

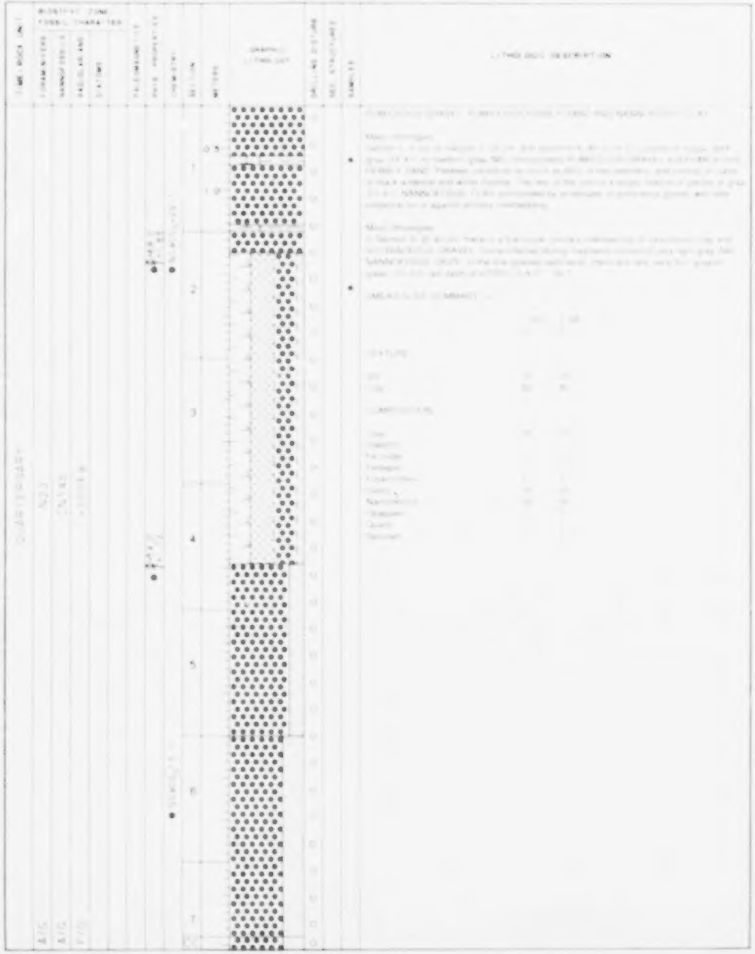
TIME-ROCK UNIT
BIOSTRAT. ZONE/FOSSIL CHARACTER
FORAMINIFERS
NANNOFOSSILS
RADIOLARIANS
DIATOMS
PALEOMAGNETICS
PHYS. PROPERTIES
CHEMISTRY
SECTION
METERS
GRAPHIC LITHOLOGY
DRILLING DISTURB.
SED. STRUCTURES
SAMPLES
QUATERNARY
N23
A/G
A/G
F/G
0.5
1.0
1
2
3
4
5
6
7
CC

LITHOLOGIC DESCRIPTION

[illegible]

Major lithologies:
[illegible] NANNOFOSSIL [illegible]

Minor lithologies:
[illegible] GRAVEL [illegible] NANNOFOSSIL OOZE [illegible]

SMEAR SLIDE SUMMARY (%):

TEXTURE:

Silt
Clay

COMPOSITION:

Clay
[illegible]

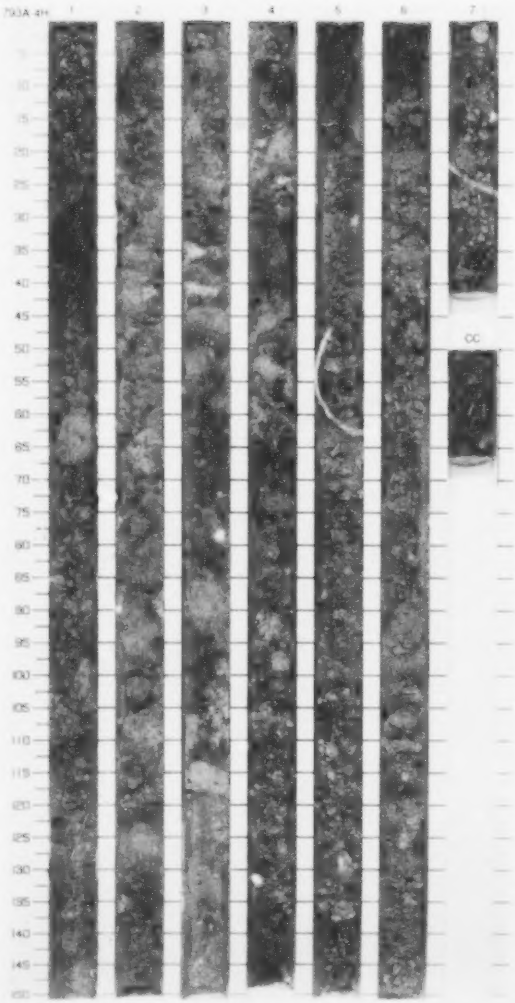
793A 4H
1
2
3
4
5
6
7
CC
5
10
15
20
25
30
35
40
45
50
55
60
65
70
75
80
85
90
95
100
105
110
115
120
125
130
135
140
145
150

SITE 793 HOLE A CORE 5H CORED INTERVAL [illegible]

TIME-ROCK UNIT	FORAMINIFERS	NANNOFOSSILS	RADIOLARIANS	DIATOMS	PALEOMAGNETICS	PHYS. PROPERTIES	CHEMISTRY	SECTION	METERS	GRAPHIC LITHOLOGY	DRILLING DISTURB.	SED. STRUCTURES	SAMPLES	LITHOLOGIC DESCRIPTION
QUATERNARY	A/G N22	A/G CN14a	F/G <0.005		N			1 2 3 4 5 6 7 8 CC	0.5 1.0					NANNOFOSSIL SILTY CLAY, NANNOFOSSIL [illegible] and PUMICEOUS GRAVEL

LITHOLOGIC DESCRIPTION

NANNOFOSSIL SILTY CLAY, NANNOFOSSIL [illegible] and PUMICEOUS GRAVEL

Major lithologies:

This core is a very [illegible] fragments [illegible] NANNOFOSSIL SILTY CLAY, dark gray [illegible] NANNOFOSSIL [illegible] PUMICEOUS GRAVEL [illegible]

Minor lithology: Section [illegible] and Section [illegible] medium gray (N6) and dark gray [illegible] [illegible]

SMEAR SLIDE SUMMARY (%):

TEXTURE:

Sand
Silt
Clay

COMPOSITION:

Accessory minerals
Clay
Chlorite
Feldspar
Foraminifers
Glass
Inorganic calcite
Nannofossils
Opaques
Quartz
Spicules

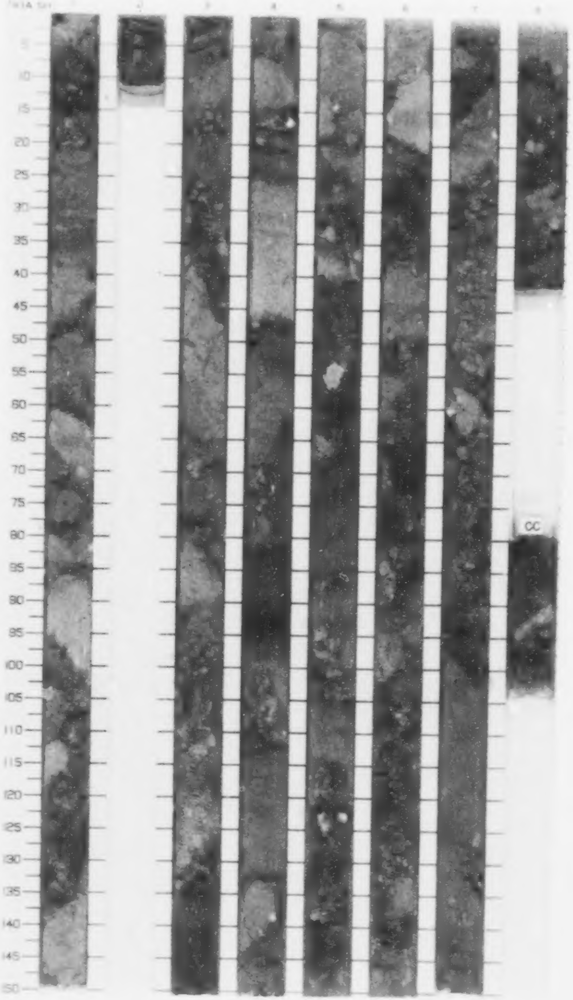
793A-5H 1
2
3
4
5
6
7
8
CC
5
10
15
20
25
30
35
40
45
50
55
60
65
70
75
80
85
90
95
100
105
110
115
120
125
130
135
140
145
150

SITE 793 HOLE A CORE 6H CORED INTERVAL 42.0-51.6 mbsf

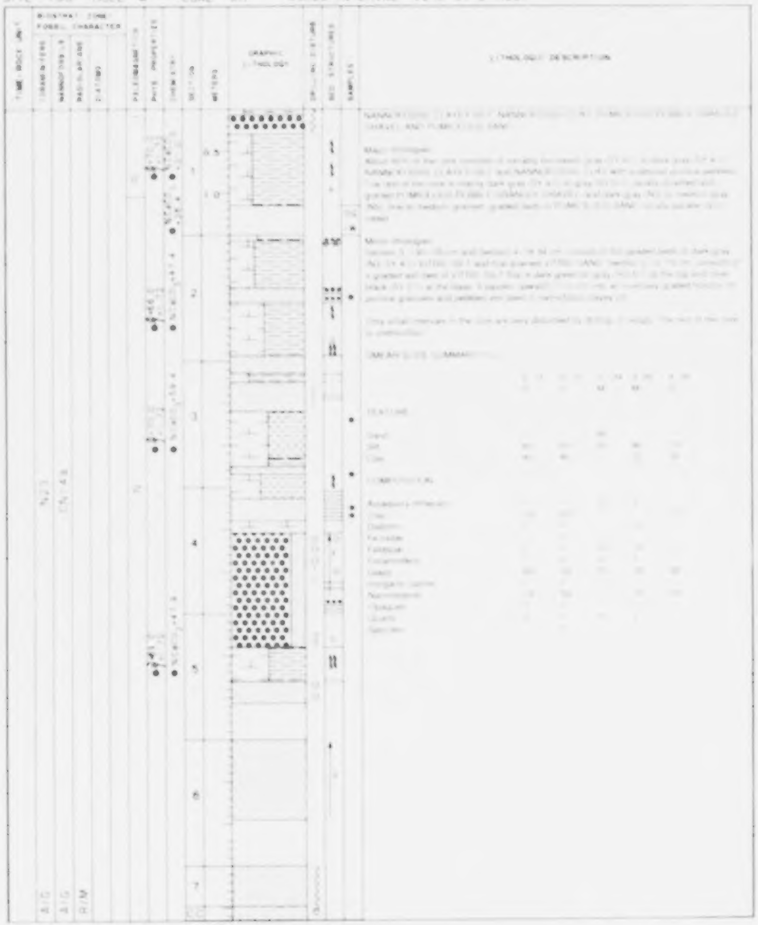
TIME-ROCK UNIT
BIOSTRAT. ZONE/FOSSIL CHARACTER
FORAMINIFERS
NANNOFOSSILS
RADIOLARIANS
DIATOMS
PALEOMAGNETICS
PHYS. PROPERTIES
CHEMISTRY
SECTION
METERS
GRAPHIC LITHOLOGY
DRILLING DISTURB.
SED. STRUCTURES
SAMPLES
LITHOLOGIC DESCRIPTION
N23
CN14a
A/G
A/G
R/M
N
1
2
3
4
5
6
7
CC
0.5
1.0
Major lithologies:
Minor lithologies:
SMEAR SLIDE SUMMARY (%):
TEXTURE:
Sand
Silt
Clay
COMPOSITION:
Accessory minerals
Clay
Diatoms
Foraminifers
Feldspar
Glass
Nannofossils
Quartz

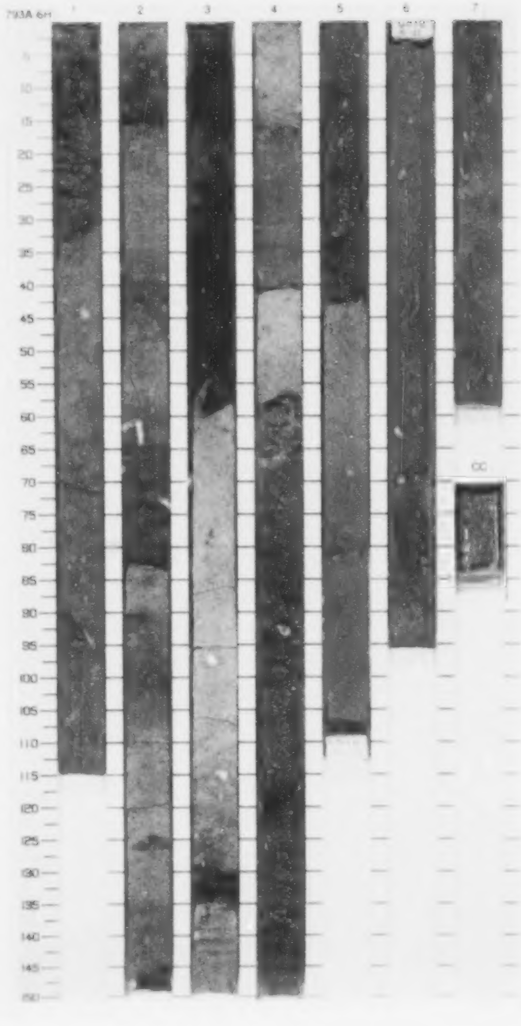
793A 6H
1
2
3
4
5
6
7
CC
0
5
10
15
20
25
30
35
40
45
50
55
60
65
70
75
80
85
90
95
100
105
110
115
120
125
130
135
140
145
150

SITE 793 HOLE B CORE 7H CORED INTERVAL 51.8-61.3 mbsf

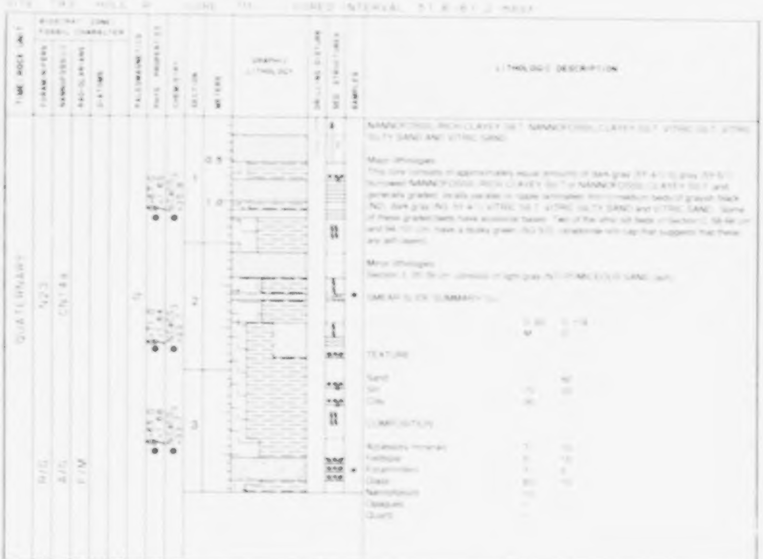
TIME-ROCK UNIT
BIOSTRAT. ZONE/FOSSIL CHARACTER
FORAMINIFERS
NANNOFOSSILS
RADIOLARIANS
DIATOMS
PALEOMAGNETICS
PHYS. PROPERTIES
CHEMISTRY
SECTION
METERS
GRAPHIC LITHOLOGY
DRILLING DISTURB.
SED. STRUCTURES
SAMPLES
QUATERNARY
N23
CN14b
R/G
A/G
F/M
0.5
1.0
1
2
3

LITHOLOGIC DESCRIPTION

NANNOFOSSIL-RICH CLAYEY SILT, NANNOFOSSIL CLAYEY SILT, VITRIC SILT, VITRIC SILTY SAND AND VITRIC SAND

Major lithologies:
This core consists of approximately equal amounts of dark gray (5Y 4/1) to gray (5Y 5/1) burrowed NANNOFOSSIL-RICH CLAYEY SILT or NANNOFOSSIL CLAYEY SILT and generally graded, locally parallel or ripple laminated, thin to medium beds of grayish black (N2), dark gray (N3, 5Y 4/1) VITRIC SILT, VITRIC SILTY SAND and VITRIC SAND. Some of these graded beds have erosional bases. Two of the vitric silt beds in Section 2, 58-64 cm and 94-101 cm, have a dusky green (5G 3/2) nannofossil-rich cap that suggests that these are [illegible].

Minor lithologies:
Section 3, 35-39 cm consists of light gray (N7) PUMICEOUS SAND (ash).

SMEAR SLIDE SUMMARY (%):

	2, 80 M	3, 118 D
TEXTURE:		
Sand	—	40
Silt	70	55
Clay	30	—
COMPOSITION:		
Accessory minerals	Tr	10
Feldspar	5	10
Foraminifers	Tr	5
Glass	60	75
Nannofossils	35	—
Opaques	Tr	—
Quartz	Tr	—

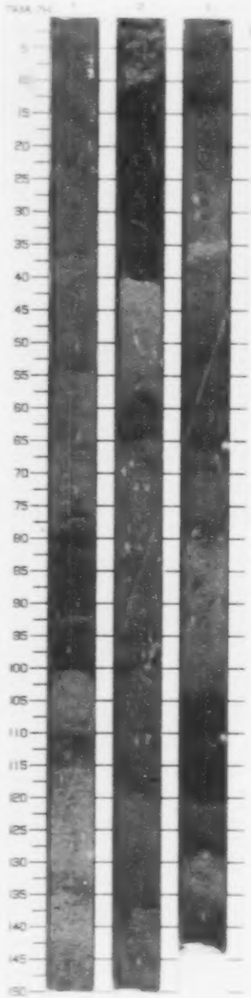
793B-7H
1
2
3
5
10
15
20
25
30
35
40
45
50
55
60
65
70
75
80
85
90
95
100
105
110
115
120
125
130
135
140
145
150

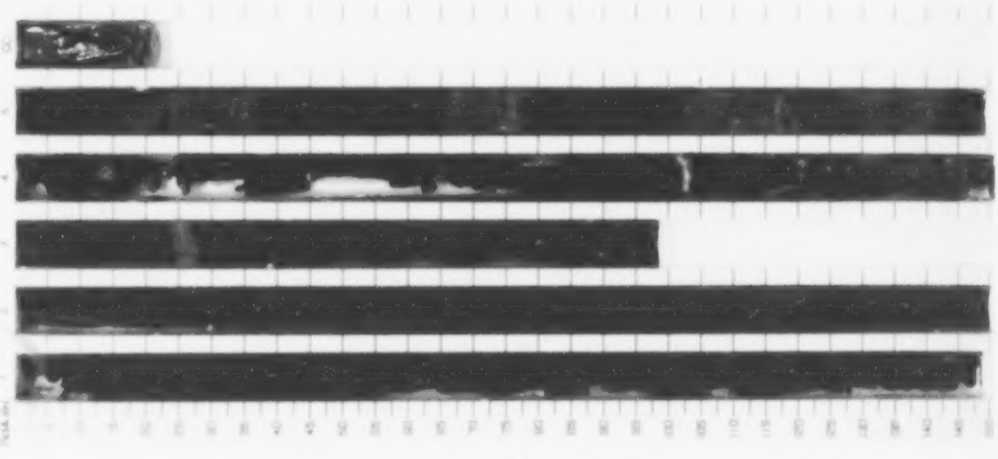
793A-8H
CC
1
2
3
4
5

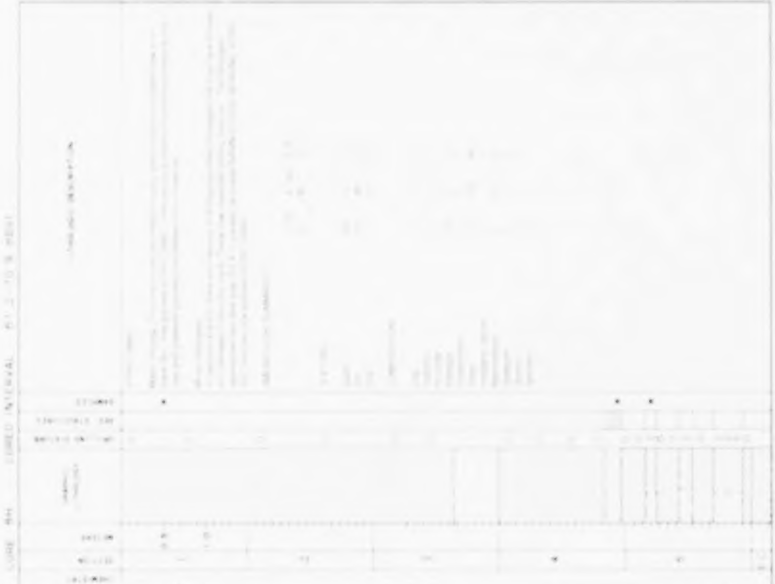
SITE 793 HOLE A CORE 8H CORED INTERVAL 61.2-70.8 mbsf
LITHOLOGIC DESCRIPTION

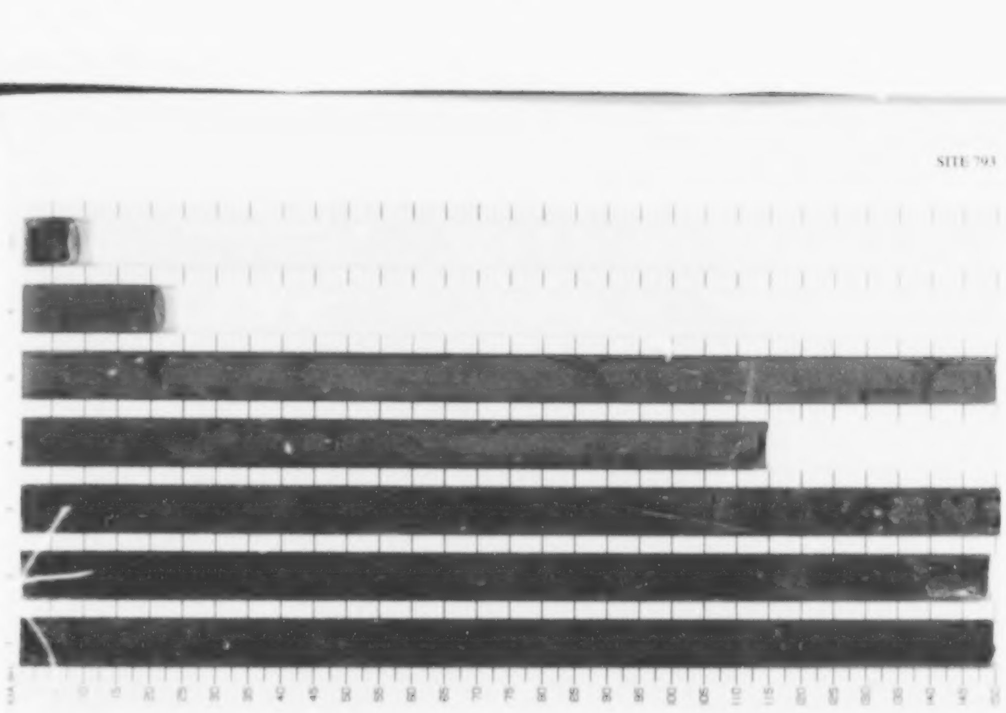

LITHOLOGIC DESCRIPTION
GRAPHIC LITHOLOGY
QUATERNARY

SITE 793 HOLE A CORE 10H CORED INTERVAL 80.5-90.1 mbsf

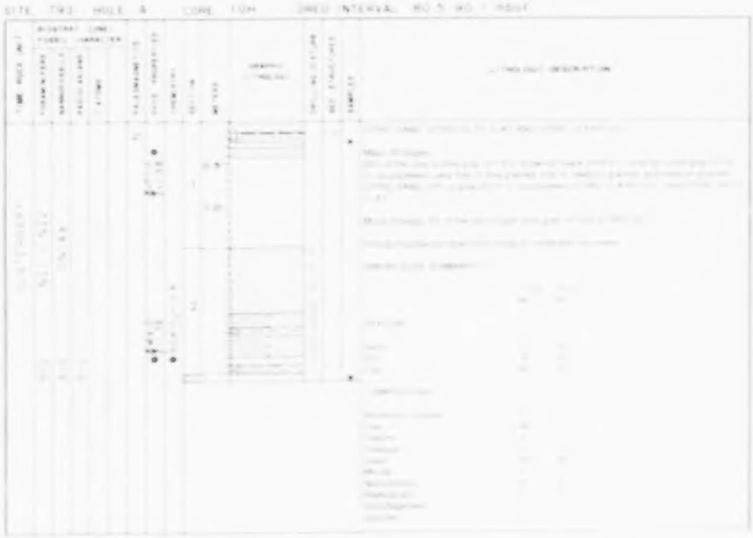

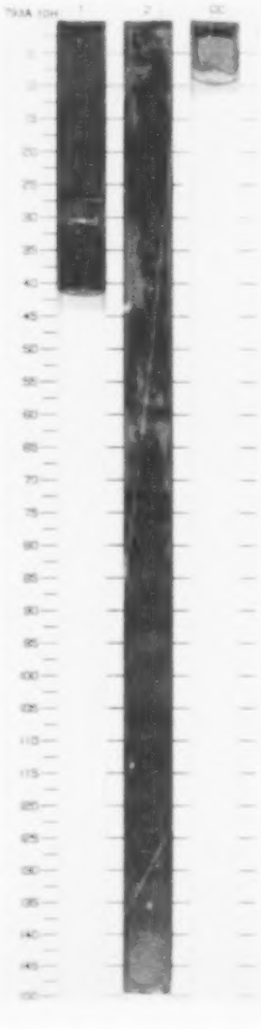
793A-10H
1
2
CC
5
10
15
20
25
30
35
40
45
50
55
60
65
70
75
80
85
90
95
100
105
110
115
120
125
130
135
140
145
150

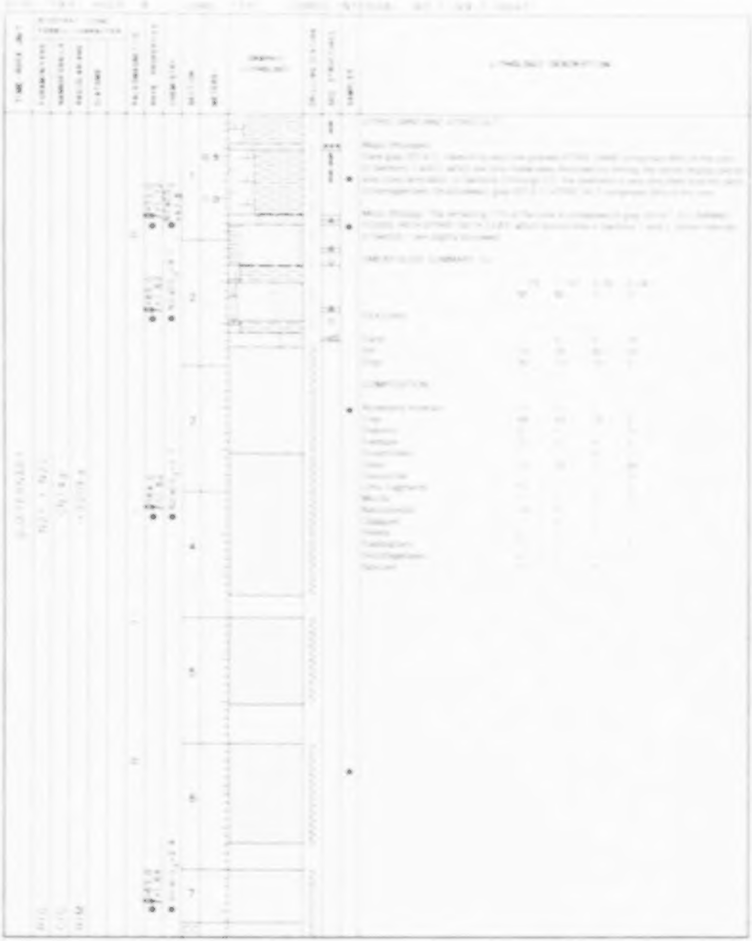

LITHOLOGIC DESCRIPTION

[illegible]

SMEAR SLIDE SUMMARY (%):

TEXTURE:

COMPOSITION:

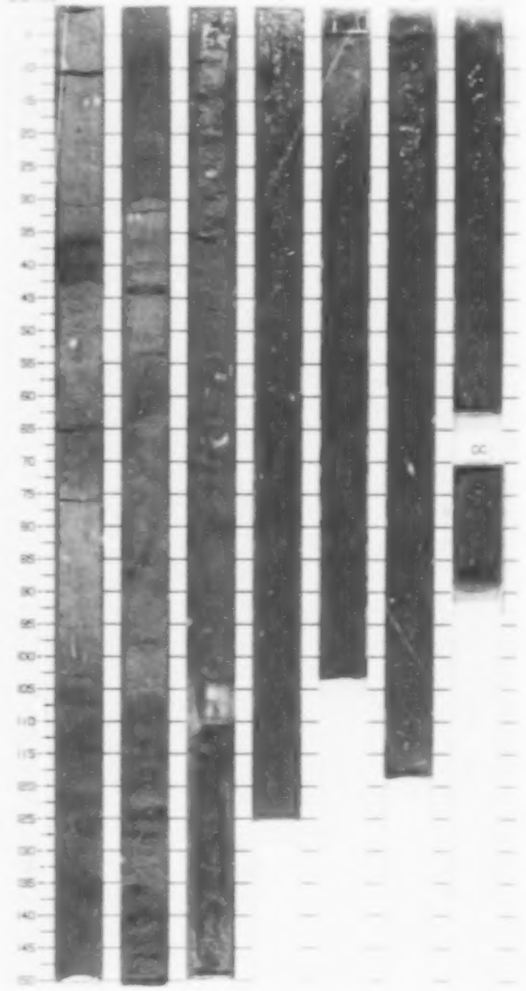

SITE 793 HOLE B CORE 1R CORED INTERVAL 586.5-594.7 mbsf

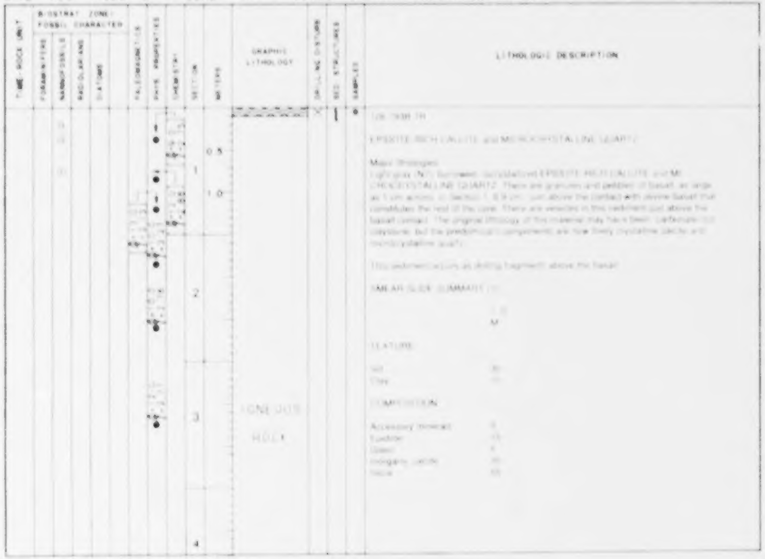
TIME-ROCK UNIT
BIOSTRAT. ZONE/ FOSSIL CHARACTER
FORAMINIFERS
NANNOFOSSILS
RADIOLARIANS
DIATOMS
PALEOMAGNETICS
PHYS. PROPERTIES
CHEMISTRY
SECTION
METERS
GRAPHIC LITHOLOGY
DRILLING DISTURB.
SED. STRUCTURES
SAMPLES
1
0.5
1.0
2
3
4
IGNEOUS ROCK

LITHOLOGIC DESCRIPTION

[illegible] 793B-1R

EPIDOTE-RICH CALCITE and MICROCRYSTALLINE QUARTZ

Major lithologies:
Light gray (N7) burrowed, [illegible] EPIDOTE-RICH CALCITE and MICROCRYSTALLINE QUARTZ. There are granules and pebbles of basalt, as large as 1 cm across, in Section 1, 8-9 cm, just above the contact with olivine basalt that constitutes the rest of the core. There are vesicles in this sediment just above the basalt contact. The original lithology of this material may have been carbonate-rich claystone, but the predominant components are now finely crystalline calcite and microcrystalline quartz.

This sediment occurs as drilling fragments above the basalt.

SMEAR SLIDE SUMMARY (%):

	1, 8 M
TEXTURE:	
Silt	[illegible]
Clay	[illegible]
COMPOSITION:	
Accessory minerals	[illegible]
Epidote	[illegible]
Glass	[illegible]
Inorganic calcite	[illegible]
Quartz	[illegible]

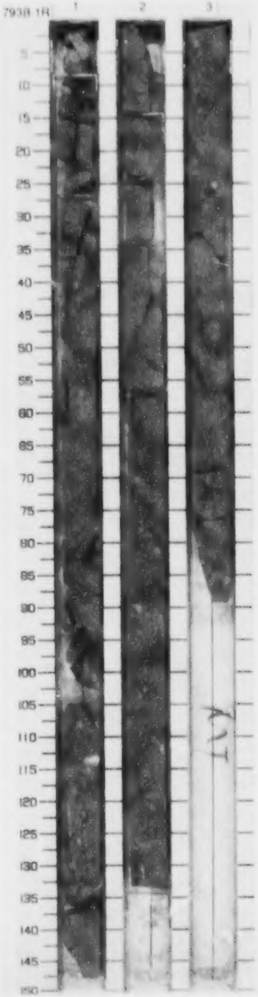
793B-1R
1
2
3
5
10
15
20
25
30
35
40
45
50
55
60
65
70
75
80
85
90
95
100
105
110
115
120
125
130
135
140
145
150

SITE 793 HOLE B CORE 2R CORED INTERVAL 594.70-604.30 mbsf

TIME-ROCK UNIT	BIOSTRAT. ZONE / FOSSIL CHARACTER: FORAMINIFERS	NANNOFOSSILS	RADIOLARIANS	DIATOMS	PALEOMAGNETICS	PHYS. PROPERTIES	CHEMISTRY	SECTION	METERS	GRAPHIC LITHOLOGY	DRILLING DISTURB.	SED. STRUCTURES	SAMPLES	LITHOLOGIC DESCRIPTION
MIDDLE MIOCENE	N10 A/P	CN4 C/G	D. alata - C. costata R/P			●	●	1 2 3	0.5 1.0				● ●	see below

NANNOFOSSIL CLAYSTONE

Major lithology: Grayish green (5GY 6/1) burrowed NANNOFOSSIL CLAYSTONE with very thin, patchy burrowed bands of mafic volcanic granules and pebbles as large as 5 mm across.

Minor lithology: Section 1, 8-13 cm: consists of a drilling fragment of burrowed NANNOFOSSIL-RICH VITRIC CLAYEY SILTSTONE.

The core is moderately to highly fractured by drilling.

SMEAR SLIDE SUMMARY (%):

	1, 10 M	1, 33 D
TEXTURE:		
Silt	60	15
Clay	40	85
COMPOSITION:		
Accessory minerals	—	Tr
Clay	30	47
Diatoms	—	Tr
Feldspar	Tr	1
Glass	60	1
Nannofossils	10	50
Opaques	—	Tr

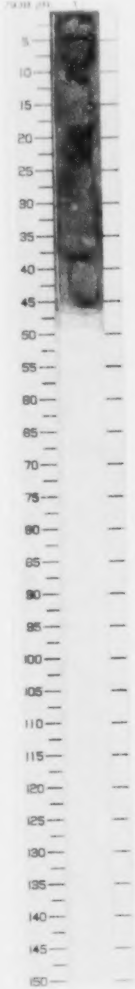

SITE 793 HOLE B CORE 3R CORED INTERVAL 604.3-614.0 mbsf

TIME-ROCK UNIT	FORAMINIFERS	NANNOFOSSILS	RADIOLARIANS	DIATOMS	SECTION	METERS	LITHOLOGIC DESCRIPTION
MIDDLE MIOCENE	N9-N10 B/P	CN4 C/G	B		1 2 3 4 CC	0.5 1.0	

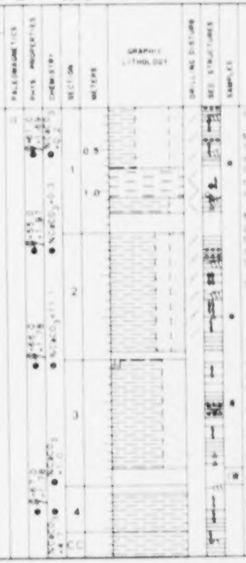
PALEOMAGNETICS
PHYS. PROPERTIES
CHEMISTRY
GRAPHIC LITHOLOGY
DRILLING DISTURB.
SED. STRUCTURES
SAMPLES

LITHOLOGIC DESCRIPTION

VITRIC SANDSTONE, VITRIC SILTSTONE and SILTY CLAYSTONE

Major lithologies:
The core is predominantly thin to medium graded beds, consisting of a lower, very thin to thin division of fine-grained, parallel- or ripple-laminated VITRIC SANDSTONE or VITRIC SILTSTONE, overlain by a thicker division of parallel-laminated SILTY CLAYSTONE that becomes strongly burrowed at the top. This uppermost sediment locally contains bands of scattered black volcanic sand that have been mixed into the sediment by burrowers.

Minor lithology: Section 1, 78-101 cm, consists of a bed of poorly sorted, very coarse-grained PEBBLY MUDDY SANDSTONE with a sharp top and base that contains a cobble of basalt 7 cm in diameter, and what are interpreted as large clasts of claystone(?) or clayey siltstone. These are believed to be much larger than the core diameter, and their interpretation as clasts is not unequivocal.

SMEAR SLIDE SUMMARY (%):

	1, 68 D	2, 100 M	3, 52 D
TEXTURE:			
Sand	80	60	—
Silt	20	10	15
Clay	—	30	85
COMPOSITION:			
Accessory minerals	5	—	—
Clay	—	20	—
Feldspar	5	2	1
Foraminifers	Tr	—	—
Glass	90	38	25
Inorganic calcite	—	30	—
Nannofossils	—	10	—

793B-3R

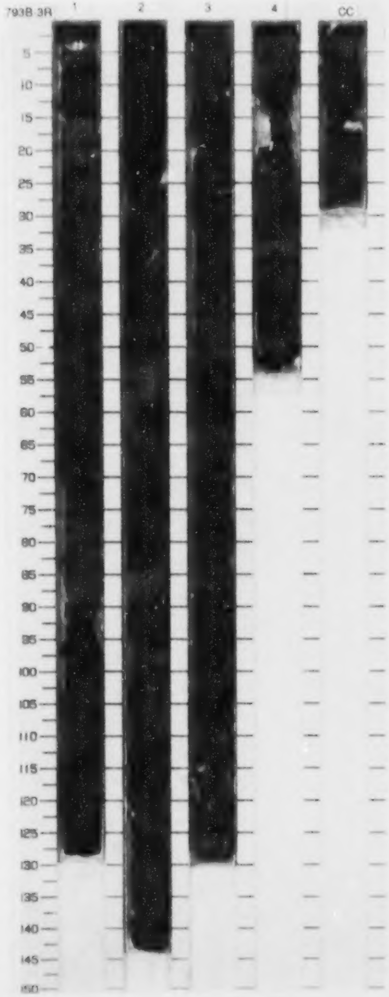
1
2
3
4
CC
5
10
15
20
25
30
35
40
45
50
55
60
65
70
75
80
85
90
95
100
105
110
115
120
125
130
135
140
145
150

SITE 793 HOLE B CORE 4R CORED INTERVAL 614.0-623.6 mbsf

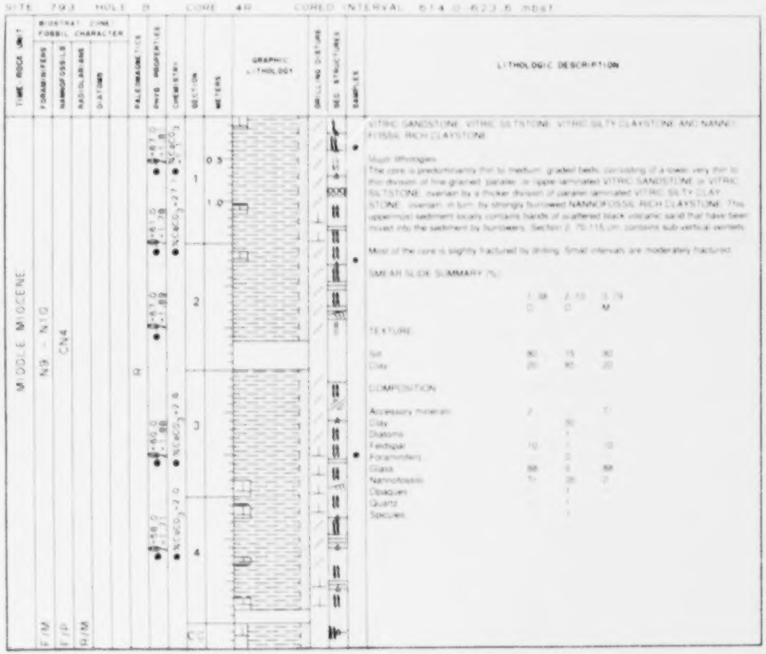
TIME-ROCK UNIT
BIOSTRAT. ZONE/ FOSSIL CHARACTER
FORAMINIFERS
NANNOFOSSILS
RADIOLARIANS
DIATOMS
PALEOMAGNETICS
PHYS. PROPERTIES
CHEMISTRY
SECTION
METERS
GRAPHIC LITHOLOGY
DRILLING DISTURB.
SED. STRUCTURES
SAMPLES
LITHOLOGIC DESCRIPTION
MIDDLE MIOCENE
N9 - N10
CN4
F/M
F/P
R/M
R
φ=67.0 γ=1.8
%CaCO3
φ=61.0 γ=1.78
%CaCO3=27
φ=67.0 γ=1.88
φ=60.0 γ=1.88
%CaCO3=2.6
φ=58.0 γ=1.71
%CaCO3=2.0
0.5
1.0
1
2
3
4
CC

VITRIC SANDSTONE, VITRIC SILTSTONE, VITRIC SILTY CLAYSTONE AND NANNOFOSSIL RICH CLAYSTONE

Major lithologies:

The core is predominantly thin to medium, graded beds, consisting of a lower very thin to thin division of fine grained, parallel- or ripple-laminated VITRIC SANDSTONE or VITRIC SILTSTONE, overlain by a thicker division of parallel laminated VITRIC SILTY CLAYSTONE, overlain in turn by strongly burrowed NANNOFOSSIL RICH CLAYSTONE. The uppermost sediment locally contains bands of scattered black volcanic sand that have been mixed into the sediment by burrowers. Section 2, 70-115 cm, contains sub-vertical veinlets.

Most of the core is slightly fractured by drilling. Small intervals are moderately fractured.

SMEAR SLIDE SUMMARY (%):

	1, 38 D	2, 10 D	3, 79 M
TEXTURE:			
Silt	80	15	80
Clay	20	85	20
COMPOSITION:			
Accessory minerals	2	—	Tr
Clay	—	80	—
Diatoms	—	1	—
Feldspar	10	1	10
Foraminifers	—	2	—
Glass	88	5	88
Nannofossils	Tr	20	2
Opaques	—	1	—
Quartz	—	1	—
Spicules	—	1	—

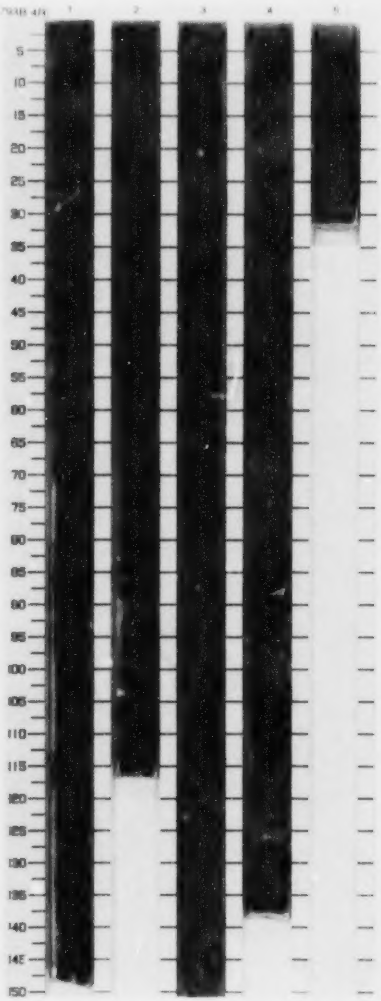
793B 4R
1
2
3
4
5
5
10
15
20
25
30
35
40
45
50
55
60
65
70
75
80
85
90
95
100
105
110
115
120
125
130
135
140
145
150

SITE 793 HOLE B CORE 5R CORED INTERVAL 623.6-633.3 mbsf

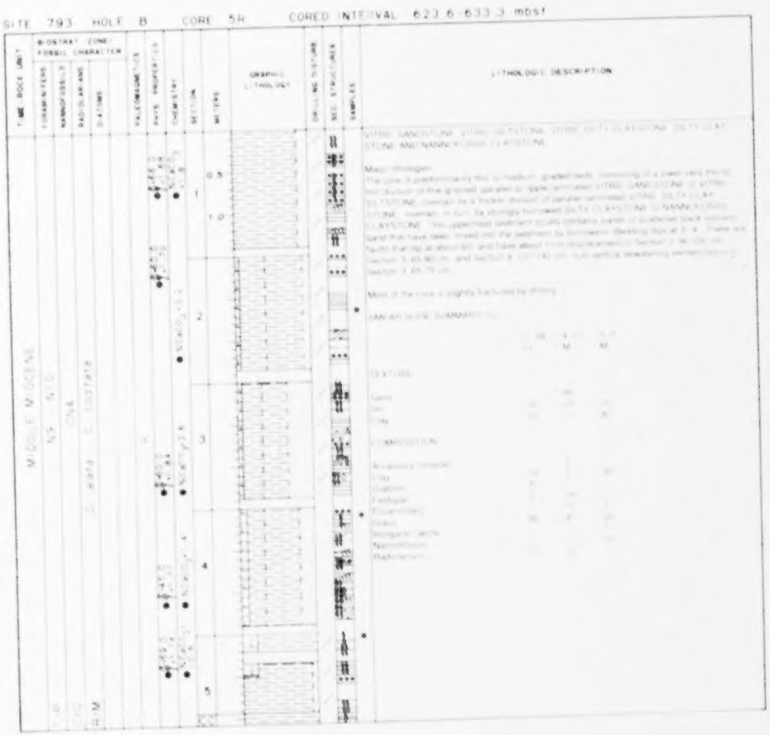
TIME-ROCK UNIT
BIOSTRAT. ZONE/ FOSSIL CHARACTER
FORAMINIFERS
NANNOFOSSILS
RADIOLARIANS
DIATOMS
PALEOMAGNETICS
PHYS. PROPERTIES
CHEMISTRY
SECTION
METERS
GRAPHIC LITHOLOGY
DRILLING DISTURB.
SED. STRUCTURES
SAMPLES
MIDDLE MIOCENE
N9 - N10
CN4
D. alata - C. costata
R/M
0.5
1.0
1
2
3
4
5

LITHOLOGIC DESCRIPTION

VITRIC SANDSTONE, VITRIC SILTSTONE, VITRIC SILTY CLAYSTONE, SILTY CLAYSTONE AND NANNOFOSSIL CLAYSTONE

Major lithologies:
The core is predominantly thin to medium, graded beds, consisting of a lower very thin [illegible] division of fine-grained, parallel or ripple-laminated VITRIC SANDSTONE or VITRIC SILTSTONE, overlain by a thicker division of parallel-laminated VITRIC SILTY CLAYSTONE, overlain in turn by strongly burrowed SILTY CLAYSTONE to NANNOFOSSIL CLAYSTONE. The uppermost sediment locally contains [illegible] of scattered black volcanic sand that have been mixed into the sediment by burrowers. Bedding dips at [illegible]. There are faults that dip at about 60° and have about 1 cm displacement in Section 2, [illegible] cm, Section 3, 65-80 cm, and Section 4, 137-142 cm. [illegible] vertical dewatering [illegible] in Section 3, 65-75 cm.

Most of the core is slightly fractured by drilling.

SMEAR SLIDE SUMMARY (%):

	1, 98	4, 20	5, 7
	D	M	M
TEXTURE:			
Sand	[illegible]	[illegible]	[illegible]
Silt	[illegible]	[illegible]	[illegible]
Clay	[illegible]	[illegible]	[illegible]
COMPOSITION:			
Accessory minerals	[illegible]	[illegible]	[illegible]
Clay	[illegible]	[illegible]	[illegible]
Quartz	[illegible]	[illegible]	[illegible]
Feldspar	[illegible]	[illegible]	[illegible]
[illegible]	[illegible]	[illegible]	[illegible]
Glass	[illegible]	[illegible]	[illegible]
Inorganic calcite	[illegible]	[illegible]	[illegible]
Nannofossils	[illegible]	[illegible]	[illegible]
Radiolarians	[illegible]	[illegible]	[illegible]

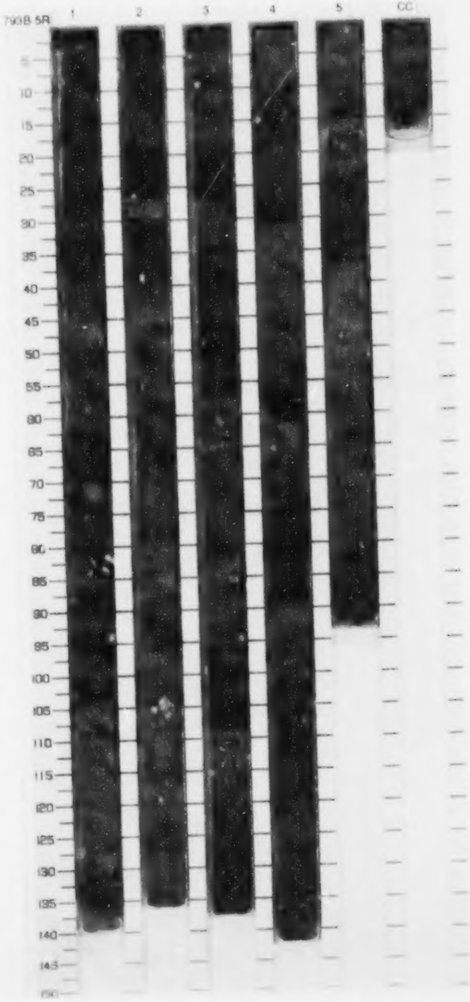
793B 5R
1
2
3
4
5
CC
5
10
15
20
25
30
35
40
45
50
55
60
65
70
75
80
85
90
95
100
105
110
115
120
125
130
135
140
143
150

SITE 793 HOLE B CORE 68R CORED INTERVAL 633.3-642.8 mbsf

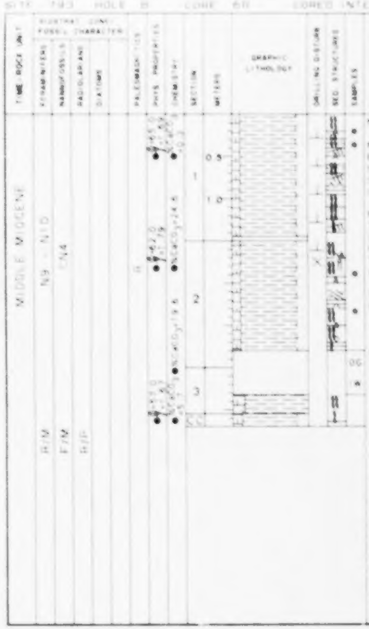
TIME-ROCK UNIT
BIOSTRAT. ZONE/FOSSIL CHARACTER
FORAMINIFERS
NANNOFOSSILS
RADIOLARIANS
DIATOMS
PALEOMAGNETICS
PHYS. PROPERTIES
CHEMISTRY
SECTION
METERS
GRAPHIC LITHOLOGY
DRILLING DISTURB.
SED. STRUCTURES
SAMPLES
MIDDLE MIOCENE
N9 - N10
CN4
R/M
F/M
R/P
R
%CaCO3=24.6
%CaCO3=19.6
1
2
3
CC
0.5
1.0
OG
IW

LITHOLOGIC DESCRIPTION

NANNOFOSSIL CLAYSTONE AND VITRIC SILTY CLAYSTONE

Major lithologies:
Beds of strongly burrowed, greenish gray (5G 5/1) NANNOFOSSIL CLAYSTONE, 2-29 cm thick, comprise 53% of the core. Another 29% of the core is dark gray (5Y 4/1) VITRIC SILTY CLAYSTONE, in beds 3-13 cm thick, commonly planar laminated with less common cross lamination.

Minor lithologies:
There are four beds of greenish gray (5G 5/1) and medium light gray (N6) VITRIC SILT, 4-22 cm thick, and two beds of light gray (N7), fine-grained VITRIC SANDSTONE, 6 and 9 cm thick, that respectively comprise 11% and 5% of the core. These beds are planar laminated. Two pumice clasts occur in the core, one 5 mm in diameter in Section 1, 97 cm, and one 17 x 35 mm in cross section in Section 2, 116 cm.

Section 2 contains a dewatering structure at 24 cm, a microfault at 75 cm, and a small slump structure at 83-86 cm.

The core is slightly fractured to undisturbed by drilling.

SMEAR SLIDE SUMMARY (%):

	1, 20 D	1, 37 M	2, 39 D	2, 81 M
TEXTURE:				
Sand	Tr	60	—	5
Silt	36	30	14	85
Clay	64	10	86	10
COMPOSITION:				
Accessory minerals	Tr	Tr	—	1
Clay	60	10	74	10
Feldspar	Tr	1	—	2
Foraminifers	—	—	—	Tr
Glass	30	88	10	80
Mica	1	1	1	Tr
Nannofossils	2	2	15	2
Pellets	—	—	—	1
Radiolarians	1	—	Tr	1
Spicules	1	—	Tr	1

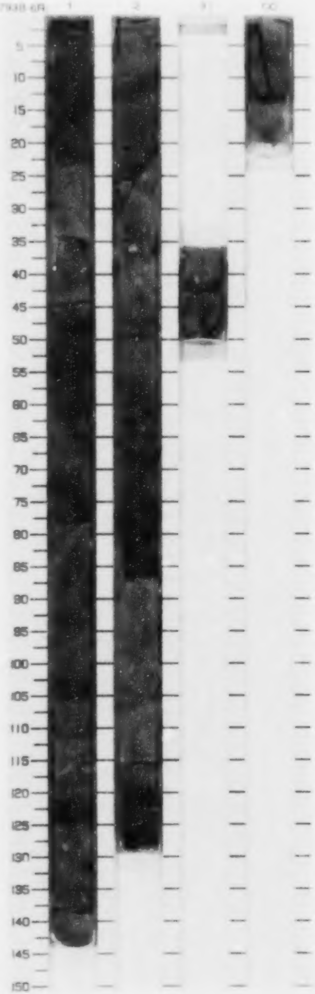
793B-68R
1
2
3
CC
5
10
15
20
25
30
35
40
45
50
55
60
65
70
75
80
85
90
95
100
105
110
115
120
125
130
135
140
145
150

SITE 793 HOLE B CORE 7R CORED INTERVAL 642.8-652.4 mbsf

TIME-ROCK UNIT	FORAMINIFERS	NANNOFOSSILS	RADIOLARIANS	DIATOMS	PALEOMAGNETICS	PHYS. PROPERTIES	CHEMISTRY	SECTION	METERS	GRAPHIC LITHOLOGY	DRILLING DISTURB.	SED. STRUCTURES	SAMPLES
MIDDLE MIOCENE	N9 - N10 C/G	CN4 A/G	D. alata - C. costata R/P		R	●	●	1 CC			×	≋	●●● ●●

LITHOLOGIC DESCRIPTION

NANNOFOSSIL CLAYSTONE

Major lithology: Strongly bioturbated, greenish gray ([illegible]) NANNOFOSSIL CLAYSTONE comprises 96% of the core.

Minor lithology: Two layers of very dark gray ([illegible]) SANDY SILTY CLAYSTONE, each 2 cm thick and probably representing ash falls, comprise the remaining 4% of the core.

Drilling has highly fractured the top 10 cm of the core, and moderately fractured the rest.

SMEAR SLIDE SUMMARY (%):

	1, 4 M	1, 30 D	1, 35 D	CC, 1 M	CC, 13 M
TEXTURE:					
Sand	5	5	Tr	50	15
Silt	60	35	20	40	35
Clay	35	60	80	10	50
COMPOSITION:					
Accessory minerals	Tr	—		10	2
Clay	60	50	53	10	40
Feldspar	2	5	Tr	20	1
Foraminifers			1	Tr	10
Quartz	35	35	12	58	30
Mica					1
Micrite	Tr	3	2		3
Nannofossils	1	15	30	1	5
Radiolarians	Tr		1		
Spicules			1		1

793B 7R
1
CC
5
10
15
20
25
30
35
40
45
50
55
60
65
70
75
80
85
90
95
100
105
110
115
120
125
130
135
140
145
150

SITE 793 HOLE B CORE 8R CORED INTERVAL 652.4-662.1 mbsf

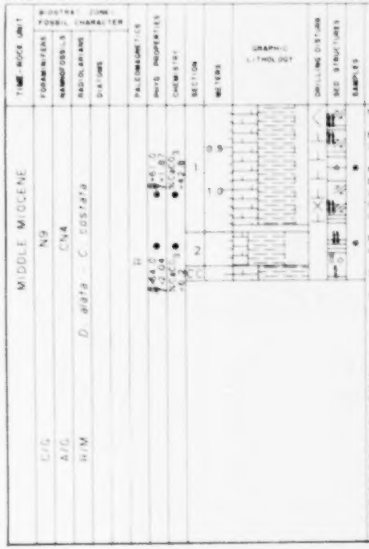
TIME-ROCK UNIT
BIOSTRAT. ZONE/ FOSSIL CHARACTER
FORAMINIFERS
NANNOFOSSILS
RADIOLARIANS
DIATOMS
PALEOMAGNETICS
PHYS. PROPERTIES
CHEMISTRY
SECTION
METERS
GRAPHIC LITHOLOGY
DRILLING DISTURB.
SED. STRUCTURES
SAMPLES
MIDDLE MIOCENE
N9
C/G
CN4
A/G
D. alata - C. costata
R/M
R
%CaCO₃
1
2
CC
0.5
1.0

LITHOLOGIC DESCRIPTION

NANNOFOSSIL CLAYSTONE

Major lithology: 75% of the core is composed of greenish gray (5G 6/1) NANNOFOSSIL CLAYSTONE, much of which is strongly bioturbated, in layers 5-40 cm thick.

Minor lithology: Intervals of very dark gray (5Y 3/1) VITRIC SILTSTONE (12%), greenish black (5GY 2/1) VITRIC SANDSTONE (8%), very dark gray (5Y 3/1) CLAYEY SILTSTONE (4%) and SILTY CLAYSTONE (3%), all 1-12 cm thick, comprise the rest of the core. These lithologies are typically planar laminated. Two intervals have basal cross lamination, and one has a scoured base.

Microfaults occur in Section 1, 10-15 cm, 43-49 cm, 96-100 cm and 117-122 cm, the latter with slickensided surfaces that dip 60°.

Section 1, 0-30 cm, is highly fractured, and the rest of the core is moderately fractured.

SMEAR SLIDE SUMMARY (%):

	1, 78 M	2, 13 M
TEXTURE:		
Sand	90	Tr
Silt	10	40
Clay	—	60
COMPOSITION:		
Accessory minerals	Tr	Tr
Clay	—	34
Feldspar	Tr	2
Glass	99	60
Mica	—	1
Nannofossils	1	2
Radiolarians	—	Tr
Spicules	—	1

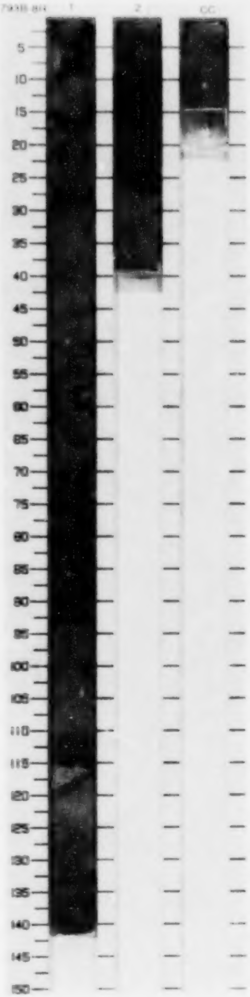
793B-8R
1
2
CC
5
10
15
20
25
30
35
40
45
50
55
60
65
70
75
80
85
90
95
100
105
110
115
120
125
130
135
140
145
150

SITE 793 HOLE B CORE 9R CORED INTERVAL 662.1-671.8 mbsf

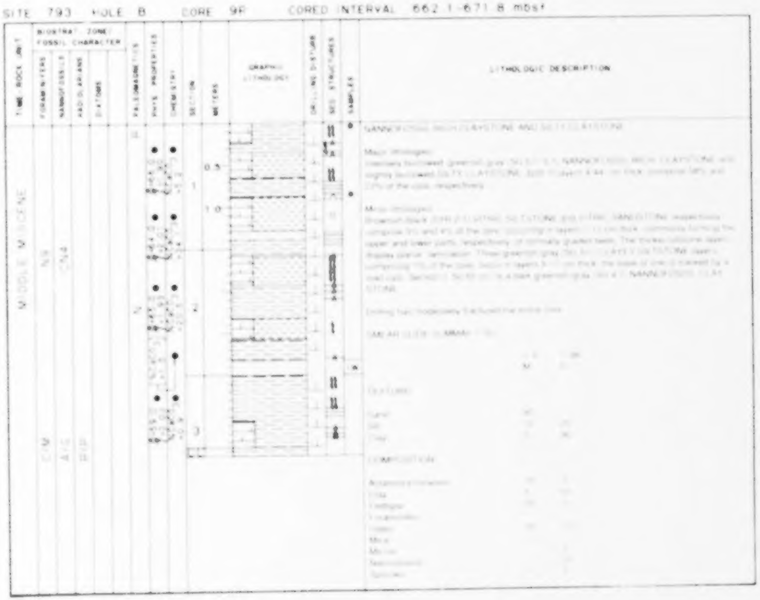
TIME-ROCK UNIT
BIOSTRAT. ZONE/ FOSSIL CHARACTER
FORAMINIFERS
NANNOFOSSILS
RADIOLARIANS
DIATOMS
PALEOMAGNETICS
PHYS. PROPERTIES
CHEMISTRY
SECTION
METERS
GRAPHIC LITHOLOGY
DRILLING DISTURB.
SED. STRUCTURES
SAMPLES
MIDDLE MIOCENE
N9
CN4
C/M
A/G
B/P
R
N
1
2
3
0.5
1.0

LITHOLOGIC DESCRIPTION

NANNOFOSSIL-RICH CLAYSTONE AND SILTY CLAYSTONE

Major lithologies:
Intensely bioturbated greenish gray [illegible] NANNOFOSSIL-RICH CLAYSTONE and slightly bioturbated SILTY CLAYSTONE [illegible] thick comprise [illegible] and [illegible] of the core, respectively.

Minor lithologies:
Brownish black [illegible] SILTSTONE and [illegible] SANDSTONE, respectively, comprise [illegible] and [illegible] of the core, occurring in layers [illegible] cm thick, commonly forming the upper and lower parts, respectively, of normally graded beds. The thicker siltstone layers display planar lamination. Three greenish gray [illegible] CLAYEY SILTSTONE layers comprising [illegible] of the core [illegible] layers [illegible] cm thick; the base of one is marked by a [illegible]. Section 2, [illegible] cm is a dark greenish gray [illegible] NANNOFOSSIL CLAYSTONE.

Drilling has moderately fractured the entire core.

SMEAR SLIDE SUMMARY (%):

	[illegible]	[illegible]
	M	D
TEXTURE:		
Sand	[illegible]	
Silt	[illegible]	[illegible]
Clay	[illegible]	[illegible]
COMPOSITION:		
Accessory minerals	[illegible]	[illegible]
Clay	[illegible]	[illegible]
Feldspar	[illegible]	[illegible]
[illegible]		
Quartz	[illegible]	[illegible]
Mica		
Micrite		[illegible]
Nannofossils		[illegible]
Spicules		[illegible]

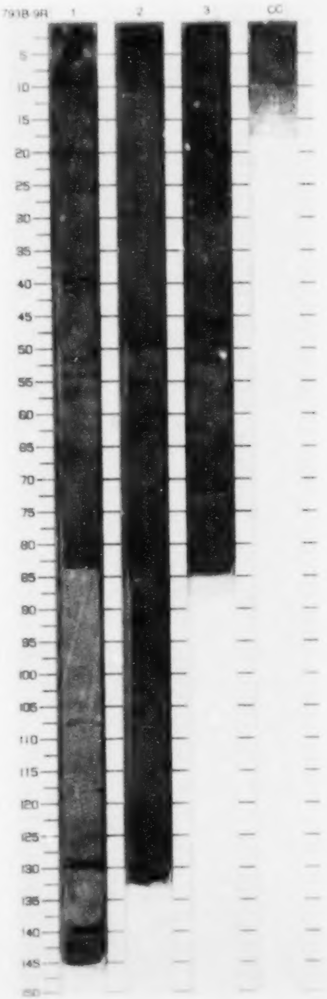
793B-9R
1
2
3
CC
5
10
15
20
25
30
35
40
45
50
55
60
65
70
75
80
85
90
95
100
105
110
115
120
125
130
135
140
145
150

SITE 793 HOLE B CORE 10R CORED INTERVAL 671.8-681.4 mbsf

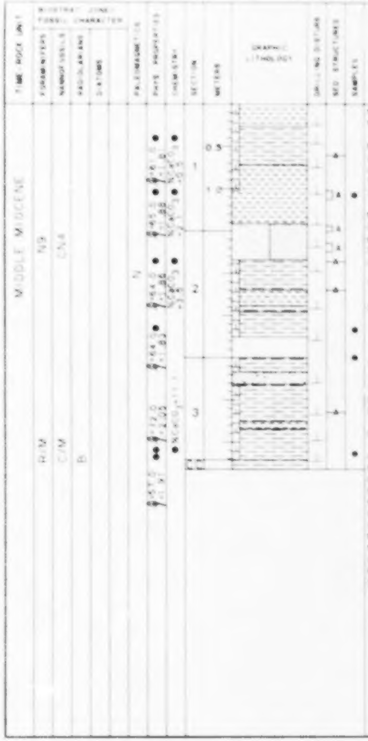
TIME-ROCK UNIT
BIOSTRAT. ZONE/ FOSSIL CHARACTER
FORAMINIFERS
NANNOFOSSILS
RADIOLARIANS
DIATOMS
PALEOMAGNETICS
PHYS. PROPERTIES
CHEMISTRY
SECTION
METERS
GRAPHIC LITHOLOGY
DRILLING DISTURB.
SED. STRUCTURES
SAMPLES
MIDDLE MIOCENE
N9
CN4
R/M
C/M
B
N
0.5
1.0
1
2
3
CC

LITHOLOGIC DESCRIPTION

NANNOFOSSIL-RICH CLAYSTONE, NANNOFOSSIL-RICH SILTY CLAYSTONE, AND NANNOFOSSIL-RICH CLAYEY SILTSTONE

Major lithologies:
Greenish gray (5G 6/1, 5/1), strongly bioturbated NANNOFOSSIL-RICH CLAYSTONE comprises 45% of the core. Slightly burrowed, greenish gray (5G 5/1) NANNOFOSSIL-RICH SILTY CLAYSTONE and NANNOFOSSIL-RICH CLAYEY SILTSTONE together comprise 37% of the core.

Minor lithologies:
Greenish gray (5G 5/1) VITRIC SILTSTONE and olive black (5Y 2/1) VITRIC SANDSTONE each comprise 7% of the core. The remaining material is dark gray (5Y 4/1) SILTY CLAYSTONE (4%) and greenish gray (5G 5/1) SANDY SILTSTONE (3%). These lithologies are commonly planar or wedge laminated.

The entire core is moderately disturbed by drilling.

SMEAR SLIDE SUMMARY (%):

	1, 101 D	2, 113 D	3, 7 M	3, 110 D
TEXTURE:				
Sand	100	10	—	5
Silt	Tr	35	60	65
Clay	—	55	40	30
COMPOSITION:				
Accessory minerals	2	1	—	—
Biotite	—	Tr	—	—
Clay	—	48	24	25
Feldspar	5	2	Tr	2
Foraminifers	Tr	Tr	Tr	—
Glass	91	40	55	58
Lithic fragments	Tr	—	—	—
Micrite	—	—	Tr	—
Nannofossils	Tr	7	20	15
Opaques	1	—	—	—
Radiolarians	1	—	1	—
Spicules	—	1	—	—

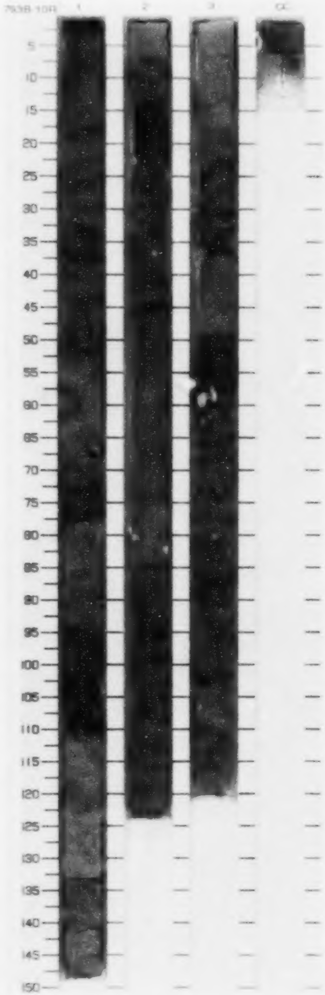
793B-10R
1
2
3
CC
5
10
15
20
25
30
35
40
45
50
55
60
65
70
75
80
85
90
95
100
105
110
115
120
125
130
135
140
145
150

SITE 793 HOLE B CORE 11R CORED INTERVAL 681.4-691.1 mbsf

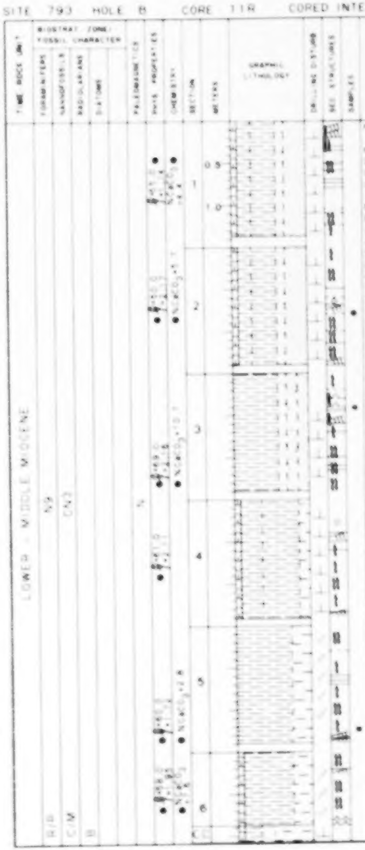
TIME-ROCK UNIT
BIOSTRAT. ZONE/ FOSSIL CHARACTER
FORAMINIFERS
NANNOFOSSILS
RADIOLARIANS
DIATOMS
PALEOMAGNETICS
PHYS. PROPERTIES
CHEMISTRY
SECTION
METERS
GRAPHIC LITHOLOGY
DRILLING DISTURB.
SED. STRUCTURES
SAMPLES
LOWER - MIDDLE MIOCENE
N9
CN3
R/P
C/M
B
N
1
2
3
4
5
6
CC
0.5
1.0

LITHOLOGIC DESCRIPTION

NANNOFOSSIL-RICH SILTY CLAYSTONE AND SILTY CLAYSTONE

Major lithologies:
Dark gray (5Y 4/1), moderately to intensely bioturbated NANNOFOSSIL-RICH SILTY CLAYSTONE (40%), and structureless SILTY CLAYSTONE (39%) occur as couplets 6-34 cm thick.

Minor lithologies:
Bioturbation has disseminated sandy silt layers into finer lithologies, producing dark gray (5Y 4/1) SANDY MUDSTONE beds 2-29 cm thick (9% of the core). Olive black (5Y 2/1) and very dark gray (5Y 3/1) VITRIC SANDSTONE layers 2-11 cm thick, and VITRIC SILTSTONE layers 1-8 cm thick comprise 7% and 6% of the core, respectively, and commonly display planar lamination and basal cross lamination. Section 3, 31-49 cm is an interval of syn-sedimentary slumping.

The core is moderately to slightly fractured by drilling.

SMEAR SLIDE SUMMARY (%):

	2, 77	3, 41	5, 103
	M	M	M
TEXTURE:			
Sand	—	70	5
Silt	28	10	55
Clay	72	20	40
COMPOSITION:			
Accessory minerals	1	10	Tr
Clay	11	15	33
Feldspar	Tr	2	1
Foraminifers	—	—	Tr
Glass	70	63	50
Lithic fragments	1	10	11
Mica	—	—	1
Nannofossils	8	[illegible]	10
Opaques	Tr	—	—
Radiolarians	—	Tr	10
Spicules	10	—	1
Unknown	1		

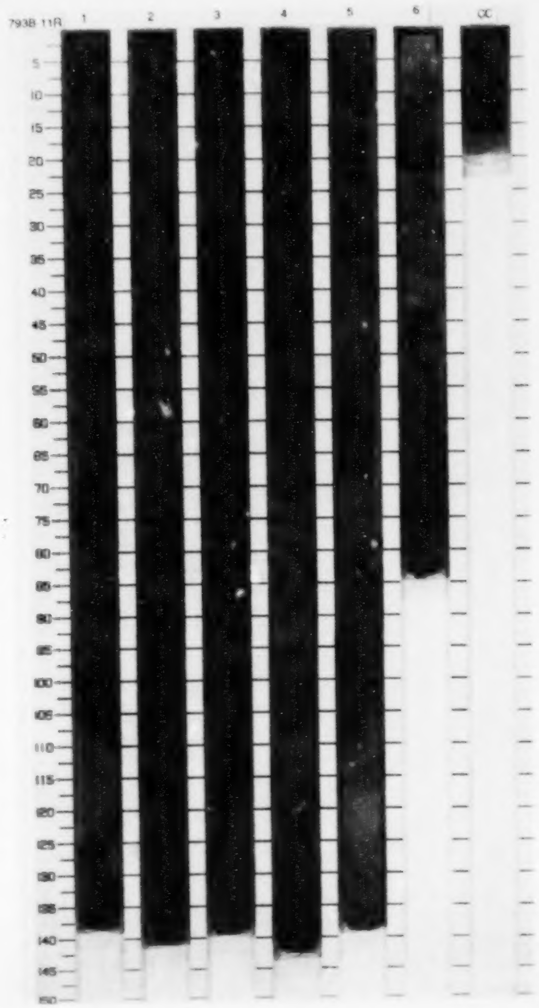
793B 11R
1
2
3
4
5
6
CC
5
10
15
20
25
30
35
40
45
50
55
60
65
70
75
80
85
90
95
100
105
110
115
120
125
130
135
140
145
150

SITE 793 HOLE B CORE 12R CORED INTERVAL 691.1-700.8 mbsf

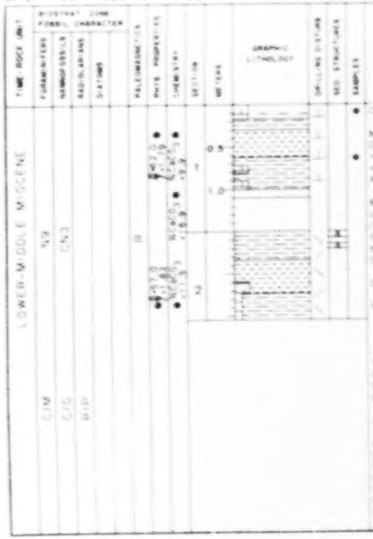
TIME-ROCK UNIT
BIOSTRAT. ZONE/ FOSSIL CHARACTER
FORAMINIFERS
NANNOFOSSILS
RADIOLARIANS
DIATOMS
PALEOMAGNETICS
PHYS. PROPERTIES
CHEMISTRY
SECTION
METERS
GRAPHIC LITHOLOGY
DRILLING DISTURB.
SED. STRUCTURES
SAMPLES
LOWER-MIDDLE MIOCENE
N9
CN3
C/M
C/G
R
1
2
0.5
1.0

LITHOLOGIC DESCRIPTION

CLAYSTONE AND SILTY CLAYSTONE

Major lithologies:
Dark greenish gray (10GY 4/1) heavily bioturbated CLAYSTONE and slightly bioturbated medium greenish gray (10GY 5/1) SILTY CLAYSTONE comprise 37% and 31% of the core, respectively. Some of the coarser intervals are planar laminated, with rare cross lamination. A dewatering structure occurs in Section 1, 20-24 cm.

Minor lithologies:
Locally, the principal lithologies are enriched in nannofossils, producing light greenish gray (10GY 6/1) NANNOFOSSIL-RICH CLAYSTONE and NANNOFOSSIL-RICH SILTY CLAYSTONE (17% and 6% of the core, respectively). Bioturbation of thin, sandy ash layers with the principal lithologies has produced dark greenish gray (10Y 5/1) NANNOFOSSIL-RICH SANDY MUDSTONE (8% of the core).

Drilling has moderately fractured Section 1, and moderately to slightly fractured Section 2.

SMEAR SLIDE SUMMARY (%):

	1, 9	1, 58
	M	D
TEXTURE:		
Sand	15	5
Silt	75	10
Clay	10	85
COMPOSITION:		
Accessory minerals	—	T
Clay	10	85
Fe oxide	Tr	—
Feldspar	T	T
Glass	88	10
Micrite	—	—
Nannofossils	2	5

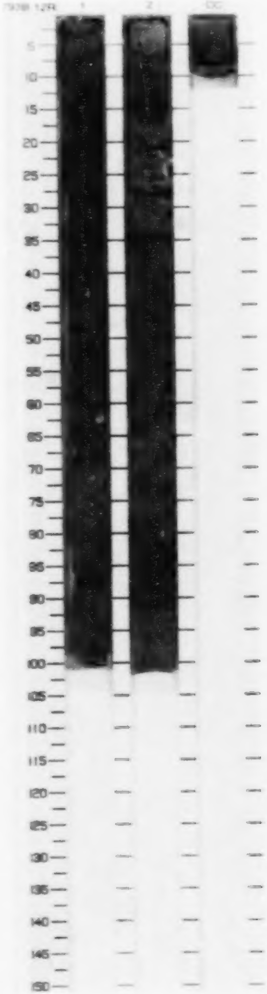
793B 12R
1
2
CC
5
10
15
20
25
30
35
40
45
50
55
60
65
70
75
80
85
90
95
100
105
110
115
120
125
130
135
140
145
150

SITE 793 HOLE B CORE 13R CORED INTERVAL 700.8-710.4 mbsf

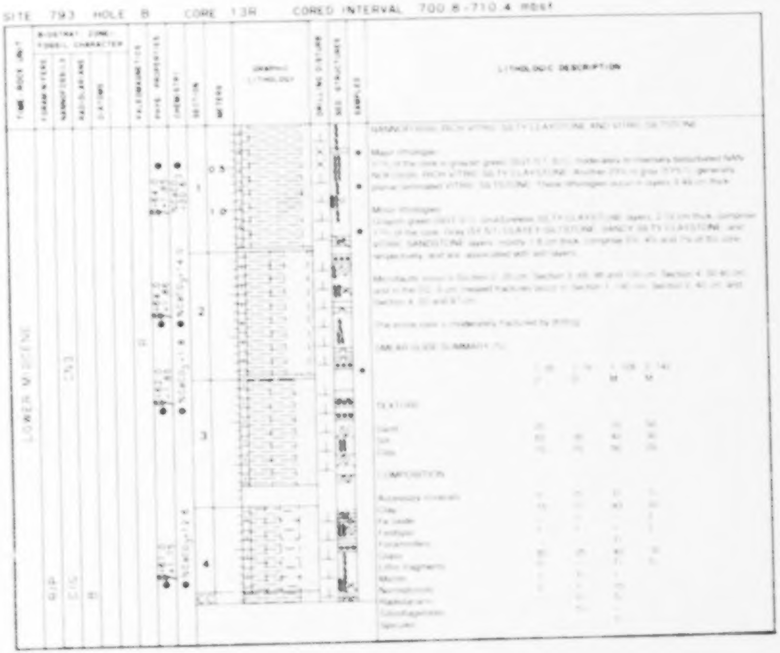
TIME-ROCK UNIT
BIOSTRAT. ZONE/FOSSIL CHARACTER
FORAMINIFERS
NANNOFOSSILS
RADIOLARIANS
DIATOMS
PALEOMAGNETICS
PHYS. PROPERTIES
CHEMISTRY
SECTION
METERS
GRAPHIC LITHOLOGY
DRILLING DISTURB.
SED. STRUCTURES
SAMPLES
LOWER MIOCENE
B/P
CN3
C/G
B
R
0.5
1.0
1
2
3
4
CC

LITHOLOGIC DESCRIPTION

NANNOFOSSIL-RICH VITRIC SILTY CLAYSTONE AND VITRIC SILTSTONE

Major lithologies:
[illegible]% of the core is grayish green (5GY 5/1, 6/1), moderately to intensely bioturbated NANNOFOSSIL-RICH VITRIC SILTY CLAYSTONE. Another [illegible]% is gray (5Y 5/1), generally planar-laminated VITRIC SILTSTONE. These lithologies occur in layers 3-40 cm thick.

Minor lithologies:
Grayish green (5GY 5/1) tuffaceous SILTY CLAYSTONE layers, 2-10 cm thick, comprise [illegible]% of the core. Gray (5Y 5/1) CLAYEY SILTSTONE, SANDY SILTY CLAYSTONE, and VITRIC SANDSTONE layers, mostly 1-8 cm thick, comprise [illegible]%, [illegible]% and [illegible]% of the core, respectively, and are associated with silt layers.

Microfaults occur in Section 2, 20 cm; Section 3, 45, 90 and 130 cm; Section 4, 30-40 cm; and in the CC. [illegible] healed fractures occur in Section 1, 140 cm; Section 2, 40 cm; and Section 4, 33 and 87 cm.

The entire core is moderately fractured by drilling.

SMEAR SLIDE SUMMARY (%):

	[illegible]	[illegible]	[illegible]	[illegible]
	D	D	M	M
TEXTURE:				
Sand	[illegible]		[illegible]	[illegible]
Silt	[illegible]	[illegible]	[illegible]	[illegible]
Clay	[illegible]	[illegible]	[illegible]	[illegible]
COMPOSITION:				
Accessory minerals	[illegible]	[illegible]	[illegible]	[illegible]
Clay	[illegible]	[illegible]	[illegible]	[illegible]
Fe-oxide	[illegible]	[illegible]	[illegible]	[illegible]
Feldspar	[illegible]	[illegible]	[illegible]	[illegible]
Foraminifers	[illegible]		[illegible]	
Glass	[illegible]	[illegible]	[illegible]	[illegible]
Lithic fragments	[illegible]		[illegible]	[illegible]
Micrite	[illegible]	[illegible]	[illegible]	
Nannofossils	[illegible]	[illegible]	[illegible]	
Radiolarians		[illegible]	[illegible]	
Silicoflagellates		[illegible]	[illegible]	
Spicules			[illegible]	

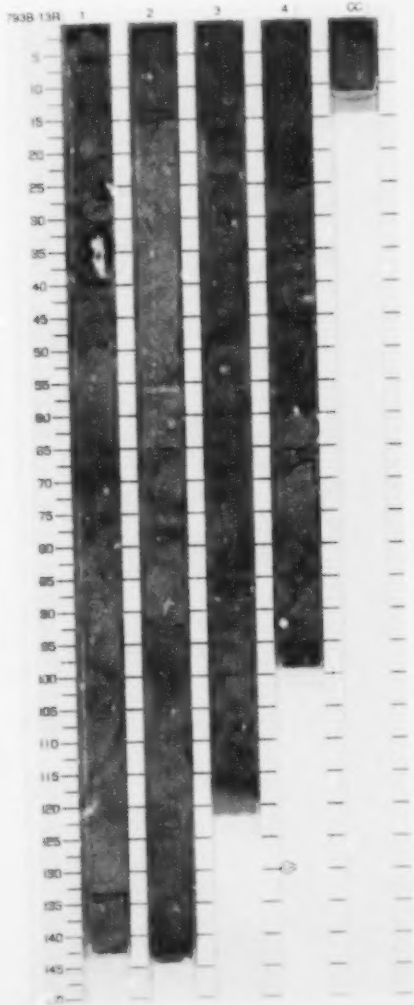
793B 13R
1
2
3
4
CC
5
10
15
20
25
30
35
40
45
50
55
60
65
70
75
80
85
90
95
100
105
110
115
120
125
130
135
140
145
150

SITE 793 HOLE B CORE 14R CORED INTERVAL 710.4-720.1 mbsf

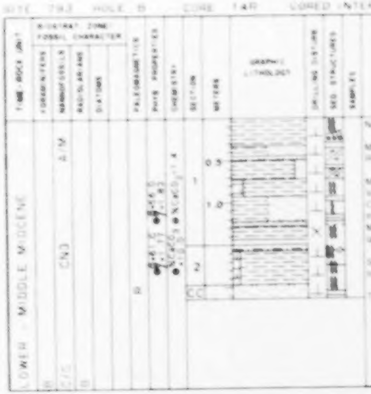
TIME-ROCK UNIT
BIOSTRAT. ZONE/ FOSSIL CHARACTER
FORAMINIFERS
NANNOFOSSILS
RADIOLARIANS
DIATOMS
PALEOMAGNETICS
PHYS. PROPERTIES
CHEMISTRY
SECTION
METERS
GRAPHIC LITHOLOGY
DRILLING DISTURB.
SED. STRUCTURES
SAMPLES
LOWER - MIDDLE MIOCENE
B
C/G
B
A/M
CN3
B
1
2
CC
0.5
1.0

LITHOLOGIC DESCRIPTION

NANNOFOSSIL-RICH SILTY CLAYSTONE

Major lithology: Slightly to intensely bioturbated, grayish green (10Y 5/1) NANNOFOSSIL-RICH SILTY CLAYSTONE, in layers 4-25 cm thick, comprises 62% of the core.

Minor lithologies:
Very dark gray (5Y 3/1) VITRIC SILTSTONE and dark gray (5GY 4/1) VITRIC SILTY CLAYSTONE comprise 16% and 13% of the core, respectively, and occur in layers 1-13 cm thick. The remaining 8% of the core consists of very dark gray (5Y 3/1) SANDY MUDSTONE, in part nannofossil-rich, and a grayish green (5GY 5/1) VITRIC SANDSTONE layer, 4 cm thick, that probably represents an ash bed.

Several of the coarser lithologies display planar lamination. One bed contains cross-lamination. Microfaults occur in Section 1, 45-53 cm, 56-60 cm, and 68-73 cm.

The core is moderately fractured by drilling.

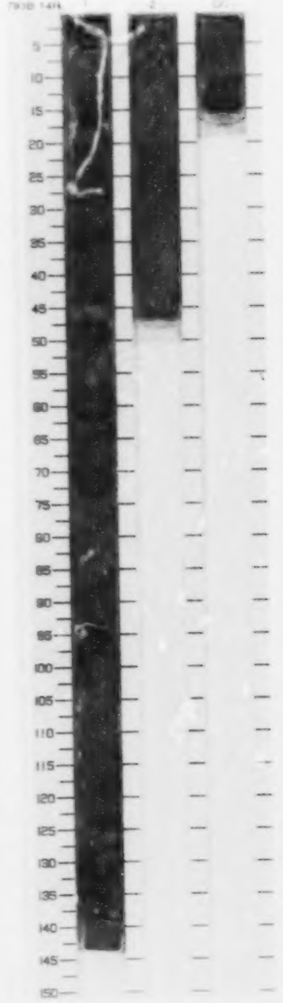
793B 14R
1
2
CC
5
10
15
20
25
30
35
40
45
50
55
60
65
70
75
80
85
90
95
100
105
110
115
120
125
130
135
140
145
150

SITE 793 HOLE B CORE 15R CORED INTERVAL 720.1-729.7 mbsf

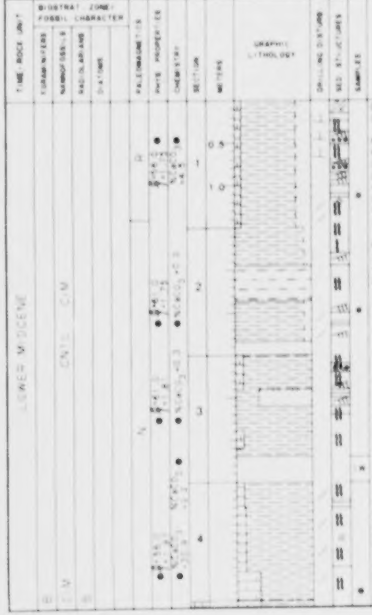
TIME-ROCK UNIT
BIOSTRAT. ZONE/ FOSSIL CHARACTER
FORAMINIFERS
NANNOFOSSILS
RADIOLARIANS
DIATOMS
PALEOMAGNETICS
PHYS. PROPERTIES
CHEMISTRY
SECTION
METERS
GRAPHIC LITHOLOGY
DRILLING DISTURB.
SED. STRUCTURES
SAMPLES
LOWER MIOCENE
CN1c C/M
B
R
N
1
2
3
4
0.5
1.0

LITHOLOGIC DESCRIPTION

CLAYEY SILTSTONE, VITRIC SILTSTONE AND NANNOFOSSIL-RICH CLAYEY SILTSTONE

Major lithologies:
Most of the core consists of dark gray (5GY 4/1) CLAYEY SILTSTONE, either parallel laminated or strongly burrowed. The parallel laminated variety generally forms the top of a graded bed that has a lower division, <5 cm thick, of dark gray (5Y 4/1) VITRIC SILTSTONE. In Sections 3 and 4, the burrowed facies is grayish green (5GY 5/1) NANNOFOSSIL-RICH CLAYEY SILTSTONE. All burrowed sediment contains scattered sand-sized grains of black vitric sand and local pebbles of pumice. The largest pumice pebble is 1.5 cm in diameter (Section 4, 55 cm).

Minor lithologies:
Section 2, 47-87 cm consists of SANDY MUDSTONE with a high content of sand-sized scoria and pumice. Color is dark gray (5GY 4/1). Section 4, 110 cm, through CC is grayish green (5GY 5/1) strongly burrowed NANNOFOSSIL SILTY CLAYSTONE.

Section 1 is slightly to moderately fractured by drilling. Section 4 is slightly fractured.

SMEAR SLIDE SUMMARY (%):

	1, 112	2, 90	4, 130
	M	D	D
TEXTURE:			
Silt	90	90	80
Clay	10	10	20
COMPOSITION:			
Clay	—	10	60
Feldspar	1	2	1
Glass	90	83	10
Inorganic calcite	2	—	3
Micrite	1	—	—
Nannofossils	2	1	25
Opaques	1	2	—
Quartz	2	2	—

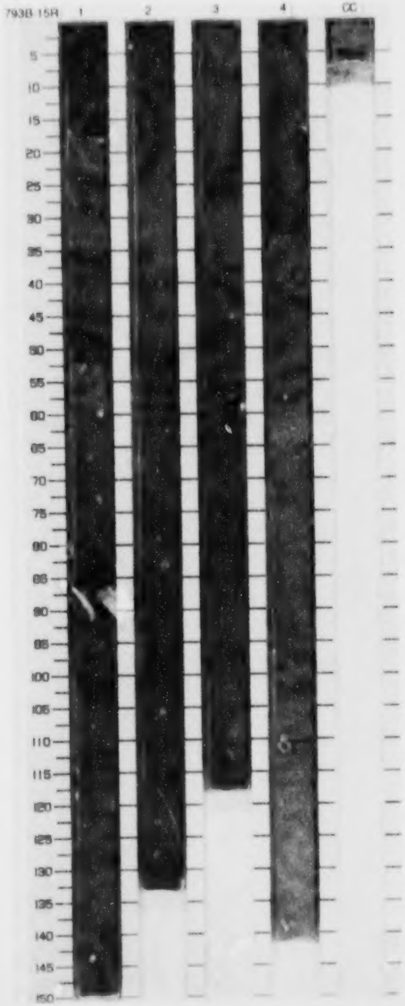
793B-15R
1
2
3
4
CC
5
10
15
20
25
30
35
40
45
50
55
60
65
70
75
80
85
90
95
100
105
110
115
120
125
130
135
140
145
150

SITE 793 HOLE B CORE 16R CORED INTERVAL 729.7-739.1 mbsf

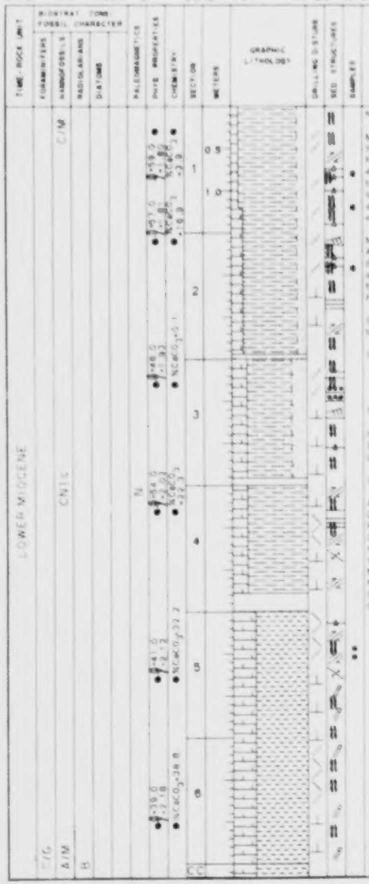

TIME-ROCK UNIT
BIOSTRAT. ZONE/FOSSIL CHARACTER
FORAMINIFERS
NANNOFOSSILS
RADIOLARIANS
DIATOMS
PALEOMAGNETICS
PHYS. PROPERTIES
CHEMISTRY
SECTION
METERS
GRAPHIC LITHOLOGY
DRILLING DISTURB.
SED. STRUCTURES
SAMPLES
LOWER MIOCENE
C/M
CN1c
C/G
A/M
B
N
%CaCO3=3.9
%CaCO3=16.9
%CaCO3=0.1
%CaCO3=22.3
%CaCO3=33.2
%CaCO3=38.8
0.5
1.0
1
2
3
4
5
6
CC

LITHOLOGIC DESCRIPTION

NANNOFOSSIL RICH VITRIC SILTY CLAYSTONE AND NANNOFOSSIL CLAYSTONE

Major lithologies:
Sections 1 through 4 consist of grayish green (5GY 6/1), strongly burrowed NANNOFOSSIL RICH VITRIC SILTY CLAYSTONE. There are extensional micro faults in Sections 1, 2 and 4. Below this lithology, there is a compositional and color change that is slightly gradational but that is most striking between Sections 4 and 5. From Section 5 to CC, the sediment is light reddish brown (5YR 6/4), strongly burrowed NANNOFOSSIL CLAYSTONE with abundant, sub-vertical, extensional veinlets. This part of the core also contains several extensional micro faults. Some of the fault surfaces have slickensides.

Minor lithologies:
About 10% of Sections 1 through 4 consists of graded beds <10 cm thick of gray (5YR 6/1), dark gray (5YR 4/1), greenish black (5G 2/1) and medium gray (N5) VITRIC SANDSTONE and VITRIC SILTSTONE. The thicker beds are parallel laminated or ripple laminated. The thinner examples are probably ash beds. Section 5, 13-15 cm, consists of medium-grained PUMICEOUS SANDSTONE.

Section 1 is slightly fractured by drilling. The rest of the core is moderately to highly fractured.

SMEAR SLIDE SUMMARY (%):

	1, 80 D	1, 109 D	2, 42 D	5, 44 M	5, 52 D
TEXTURE:					
Sand	—	—	10	—	—
Silt	20	30	90	10	10
Clay	80	70	—	90	90
COMPOSITION:					
Accessory minerals	Tr	—	5	5	—
Clay	25	36	—	50	37
Feldspar	2	1	50	10	1
Glass	48	30	40	—	8
Hornblende	—	1	—	—	—
Inorganic calcite	12	2	—	—	1
Micrite	—	—	—	30	1
Nannofossils	10	25	2	10	50
Opaques	—	1	—	—	1
Quartz	—	2	—	—	1

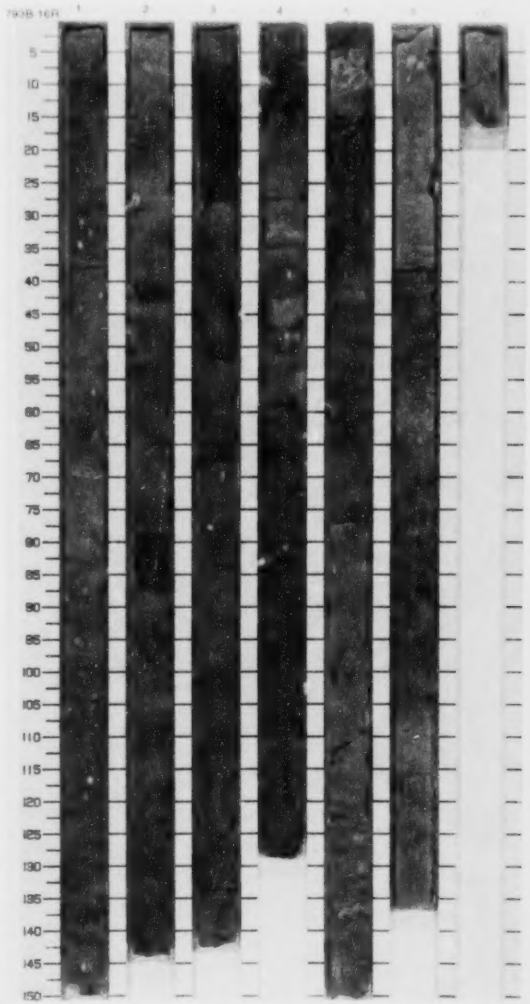

793B 16R
1
2
3
4
5
6
CC
5
10
15
20
25
30
35
40
45
50
55
60
65
70
75
80
85
90
95
100
105
110
115
120
125
130
135
140
145
150

SITE 793 HOLE B CORE 17R CORED INTERVAL 739.1-748.8 mbsf

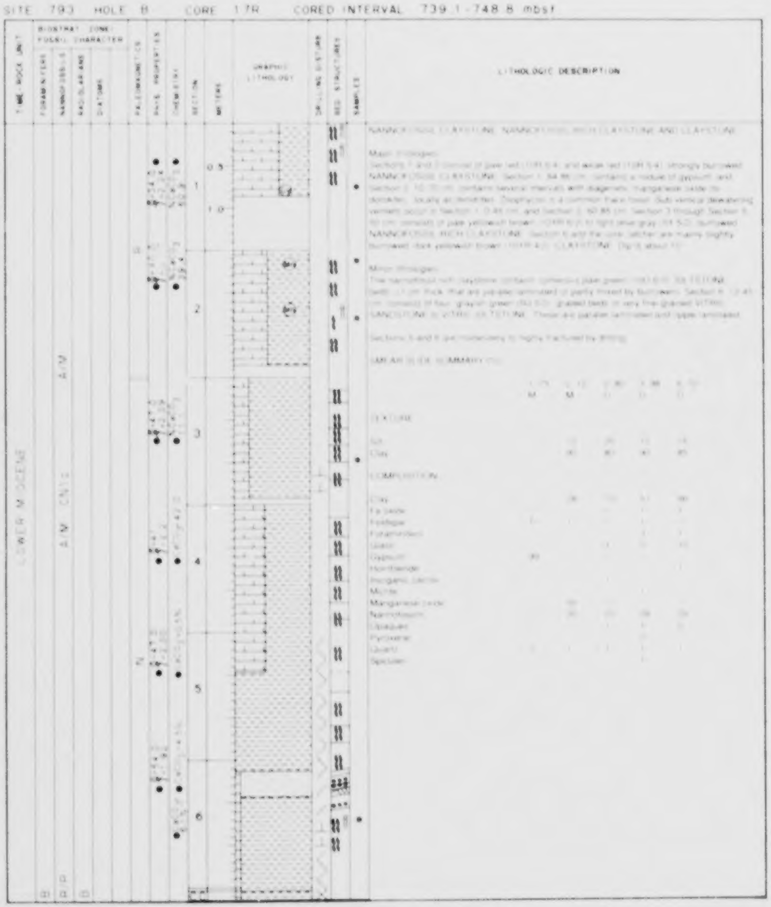
TIME-ROCK UNIT
BIOSTRAT. ZONE/FOSSIL CHARACTER
FORAMINIFERS
NANNOFOSSILS
RADIOLARIANS
DIATOMS
PALEOMAGNETICS
PHYS. PROPERTIES
CHEMISTRY
SECTION
METERS
GRAPHIC LITHOLOGY
DRILLING DISTURB.
SED. STRUCTURES
SAMPLES
LOWER MIOCENE
A/M CN1c
A/M
B
P/P
B
R
N
1
2
3
4
5
6
0.5
1.0

LITHOLOGIC DESCRIPTION

NANNOFOSSIL CLAYSTONE, NANNOFOSSIL-RICH CLAYSTONE AND CLAYSTONE

Major lithologies:
Sections 1 and 2 consist of pale red (10R 6/4) and weak red (10R 5/4) strongly burrowed NANNOFOSSIL CLAYSTONE. Section 1, 84-86 cm, contains a nodule of gypsum and Section 2, 10-70 cm, contains several intervals with diagenetic manganese oxide (?) dendrites, locally as dendrites. Zoophycos is a common trace fossil. Sub-vertical dewatering veinlets occur in Section 1, 0-44 cm, and Section 2, 60-85 cm. Section 3 through Section 6, 50 cm consists of pale yellowish brown (10YR 6/2) to light olive gray (5Y 5/2) burrowed NANNOFOSSIL-RICH CLAYSTONE. Section 6 and the core catcher are mainly slightly burrowed dark yellowish brown (10YR 4/2) CLAYSTONE. Dip is about 10°.

Minor lithologies:
The nannofossil-rich claystone contains numerous pale green (10G 6/2) SILTSTONE beds (<1 cm thick) that are parallel-laminated or partly mixed by burrowers. Section 6, 12-41 cm, consists of four grayish green (5G 5/2) graded beds of very fine-grained VITRIC SANDSTONE to VITRIC SILTSTONE. These are parallel-laminated and ripple-laminated.

Sections 5 and 6 are moderately to highly fractured by drilling.

SMEAR SLIDE SUMMARY (%):

	1, 75 M	2, 12 M	2, 80 D	3, 88 D	6, 70 D
TEXTURE:					
Silt	—	[illegible]	[illegible]	[illegible]	[illegible]
Clay	—	[illegible]	[illegible]	[illegible]	[illegible]
COMPOSITION:					
Clay	—	[illegible]	[illegible]	[illegible]	[illegible]
Fe oxide	—	—	[illegible]	[illegible]	[illegible]
Feldspar	[illegible]	[illegible]	[illegible]	[illegible]	[illegible]
Foraminifers	—	—	—	[illegible]	[illegible]
Glass	—	—	[illegible]	[illegible]	[illegible]
Gypsum	[illegible]	—	—	—	—
Hornblende	—	—	—	—	[illegible]
Inorganic calcite	—	—	[illegible]	—	—
Mica	—	—	—	[illegible]	—
Manganese oxide	—	[illegible]	[illegible]	—	[illegible]
Nannofossils	—	[illegible]	[illegible]	[illegible]	[illegible]
Opaques	—	—	[illegible]	[illegible]	[illegible]
Pyroxene	—	—	—	[illegible]	—
Quartz	[illegible]	[illegible]	[illegible]	[illegible]	[illegible]
Spicules	—	—	—	[illegible]	—

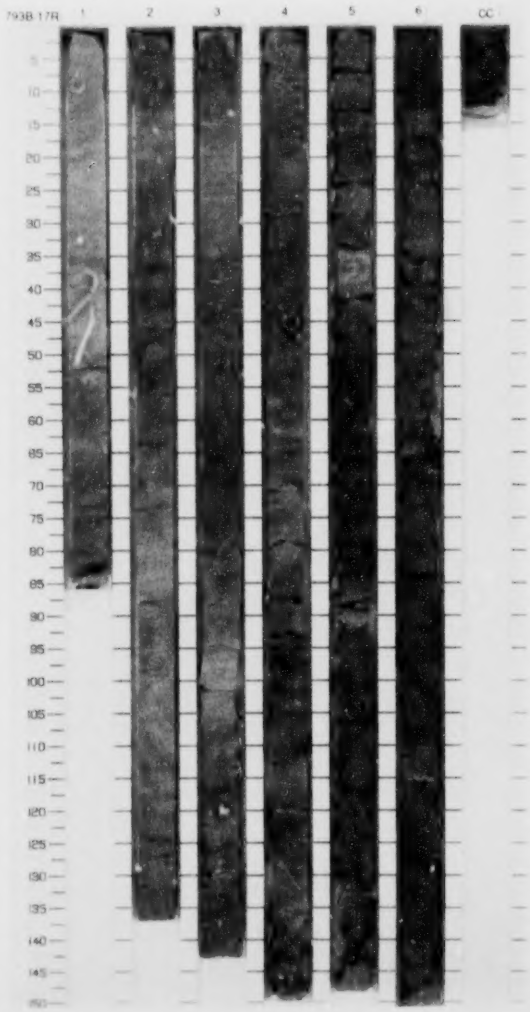
793B-17R
1
2
3
4
5
6
CC
5
10
15
20
25
30
35
40
45
50
55
60
65
70
75
80
85
90
95
100
105
110
115
120
125
130
135
140
145
150

SITE 793 HOLE B CORE 18R CORED INTERVAL 748.8-758.4 mbsf

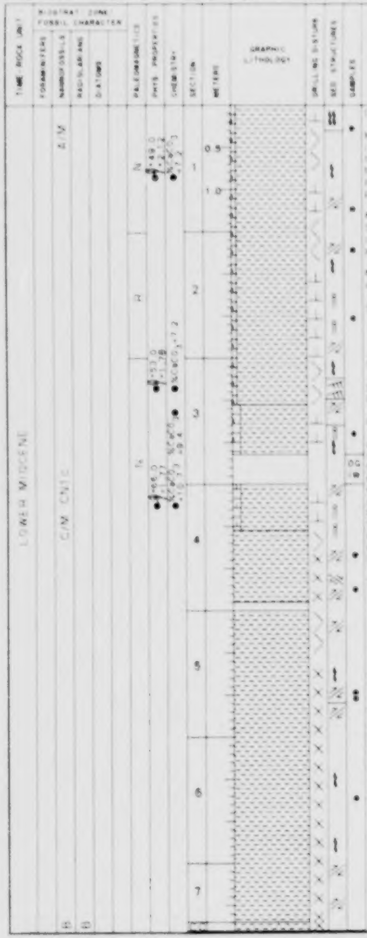
TIME-ROCK UNIT
BIOSTRAT. ZONE/FOSSIL CHARACTER
FORAMINIFERS
NANNOFOSSILS
RADIOLARIANS
DIATOMS
PALEOMAGNETICS
PHYS. PROPERTIES
CHEMISTRY
SECTION
METERS
GRAPHIC LITHOLOGY
DRILLING DISTURB.
SED. STRUCTURES
SAMPLES
LOWER MIOCENE
C/M CN1c
A/M
B
B
N
R
N
1
2
3
4
5
6
7
0.5
1.0
OG
IW

LITHOLOGIC DESCRIPTION

CLAYSTONE

Major lithology: Most of the core consists of light olive gray (5Y 5/2), pale yellowish brown (10YR 6/2), dark gray (5GY 4/1), grayish green (10GY 5/2), olive gray (5Y 3/2) and reddish brown (5YR 4/4) CLAYSTONE that is only slightly burrowed. Section 1 contains local large benthic foraminifers. This sediment contains numerous, extensional micro-faults, sub-vertical dewatering veinlets, and slickensided surfaces. In Section 6, the sediment has a bedding parallel fissility.

Minor lithologies:
Section 1, 30-31 cm, Section 2, 140-141 cm, and Section 5, 107-109 cm consist of variably colored beds of VITRIC SILTSTONE. Section 3, 25-80 cm, contains 3 sharp-based beds of parallel and ripple laminated VITRIC SILTSTONE.

Most of the core is moderately to highly fractured by drilling. Sections 3, 80 cm, through CC are drilling breccia.

SMEAR SLIDE SUMMARY (%):

	1, 28 D	1, 130 D	2, 25 M	2, 100 D	3, 90 D	4, 45 D	4, 137 D
TEXTURE:							
Silt	5	20	7	10	20	10	—
Clay	95	80	93	90	80	90	100
COMPOSITION:							
Accessory minerals	—	—	—	10	—	—	—
Clay	43	70	90	78	20	80	95
Fe oxide	1	—	—	—	—	—	—
Feldspar	Tr	—	—	2	—	—	—
Foraminifers	—	—	1	—	—	—	—
Glass	2	30	5	10	60	20	5
Micrite	—	—	—	—	10	—	—
Nannofossils	50	—	1	—	10	—	—
Opaques	1	—	—	—	—	—	—
Quartz	2	Tr	Tr	—	Tr	—	—
Unknown	1	—	—	—	—	—	—

SMEAR SLIDE SUMMARY (%):

	5, 38 M	5, 106 D	6, 72 D
TEXTURE:			
Silt	25	10	10
Clay	75	90	90
COMPOSITION:			
Accessory minerals	—	—	10
Clay	—	—	85
Fe oxide	—	Tr	—
Feldspar	1	2	5
Glass	98	94	—
Opaques	—	1	—
Quartz	—	2	—

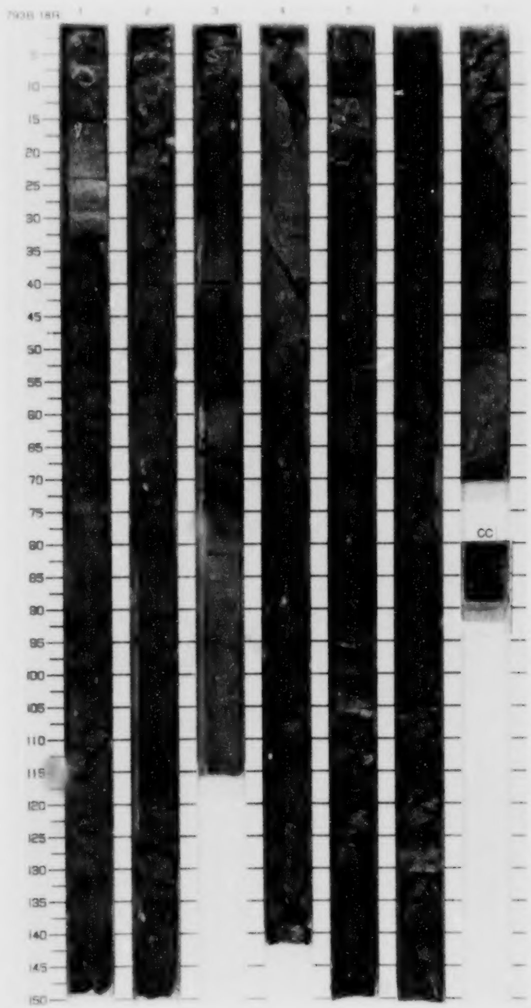
793B 18R
1
2
3
4
5
6
7
CC
5
10
15
20
25
30
35
40
45
50
55
60
65
70
75
80
85
90
95
100
105
110
115
120
125
130
135
140
145
150

SITE 793 HOLE B CORE 19R CORED INTERVAL 758.4-768.0 mbsf

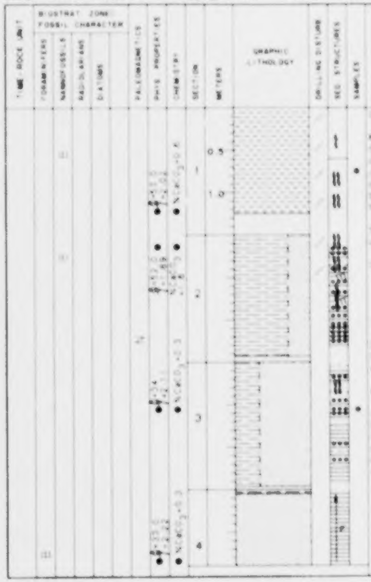
TIME-ROCK UNIT
BIOSTRAT. ZONE/FOSSIL CHARACTER
FORAMINIFERS
NANNOFOSSILS
RADIOLARIANS
DIATOMS
PALEOMAGNETICS
PHYS. PROPERTIES
CHEMISTRY
SECTION
METERS
GRAPHIC LITHOLOGY
DRILLING DISTURB.
SED. STRUCTURES
SAMPLES
B
B
B
N
$NCaCO_3=0.4$
$NCaCO_3=0.3$
$NCaCO_3=0.3$
1
2
3
4
0.5
1.0

LITHOLOGIC DESCRIPTION

CLAYSTONE, SILTY CLAYSTONE AND VITRIC SANDSTONE

Major lithologies:
Section 1, 0-80 cm: consists of pale yellowish brown (10YR 6/2), slightly burrowed, fissile CLAYSTONE. There is a sharp change below this level to slightly calcareous, grayish green (5GY 5/1), strongly burrowed CLAYSTONE. The rest of the core consists of equal amounts of grayish green (5GY 5/1) burrowed SILTY CLAYSTONE, and dark gray (N3), sharp based, graded, generally thin to medium beds of VITRIC SANDSTONE. An exceptionally thick sandstone, 80 cm thick, occurs in Section 4.

Section 1 and Section 2, 0-50 cm, are slightly fractured by drilling. The rest of the core is undisturbed.

SMEAR SLIDE SUMMARY (%):

	1, 75 D	4, 57 D
TEXTURE:		
Sand	—	20
Silt	30	60
Clay	70	20
COMPOSITION:		
Clay	10	20
Feldspar	1	6
Glass	86	72
Hornblende	—	1
Opaques	3	1
Quartz	—	—

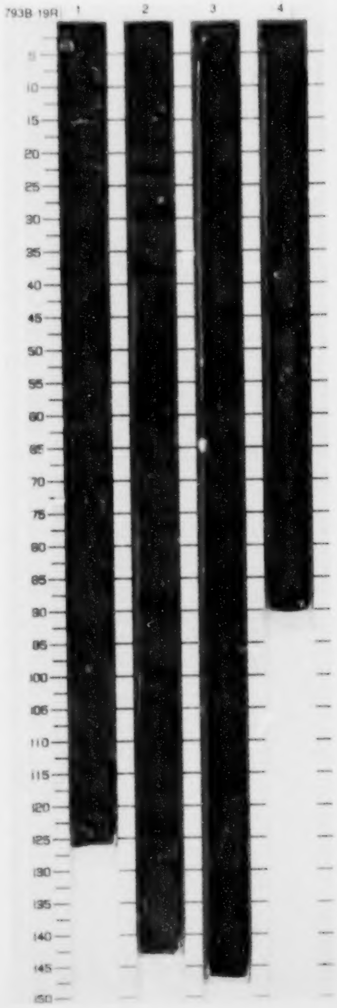
793B-19R
1
2
3
4
5
10
15
20
25
30
35
40
45
50
55
60
65
70
75
80
85
90
95
100
105
110
115
120
125
130
135
140
145
150

SITE 793 HOLE B CORE 20R CORED INTERVAL 768.0-777.7 mbsf

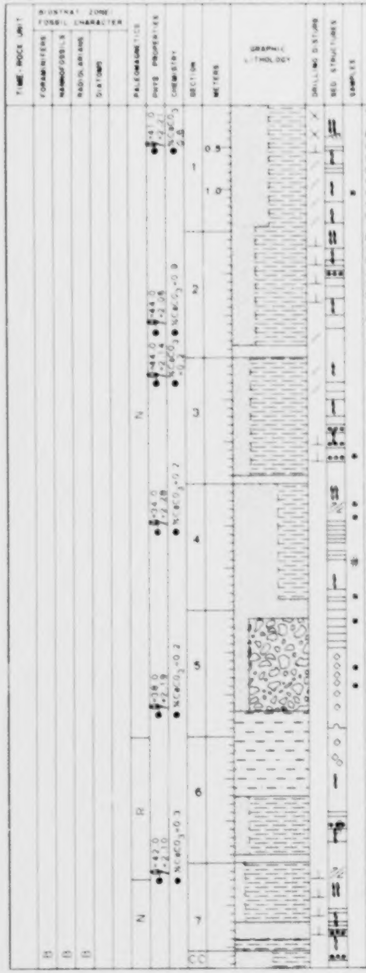
TIME-ROCK UNIT
BIOSTRAT. ZONE/ FOSSIL CHARACTER
FORAMINIFERS
NANNOFOSSILS
RADIOLARIANS
DIATOMS
PALEOMAGNETICS
PHYS. PROPERTIES
CHEMISTRY
SECTION
METERS
GRAPHIC LITHOLOGY
DRILLING DISTURB.
SED. STRUCTURES
SAMPLES
B
B
B
N
R
N
φ=41.0
γ=2.12
%CaCO₃=0.8
φ=44.0
γ=2.06
%CaCO₃=0.0
φ=44.0
γ=2.14
%CaCO₃=0.4
φ=34.0
γ=2.28
%CaCO₃=0.2
φ=38.0
γ=2.19
%CaCO₃=0.2
φ=42.0
γ=2.10
%CaCO₃=0.3
1
2
3
4
5
6
7
CC
0.5
1.0

LITHOLOGIC DESCRIPTION

VITRIC SANDSTONE AND CLAYEY SILTSTONE

Major lithologies:
Interbedded very thin to medium, graded beds of dark gray (5GY 4/1, N3) to greenish black (5G 2/1), parallel- to ripple-laminated VITRIC SANDSTONE and dark gray (5GY 4/1) to grayish green (5GY 6/1), burrowed CLAYEY SILTSTONE. A few sandstone beds have scoured bases. The clayey siltstone has local concentrations of sand-sized pumice and scoria grains. In Section 6, 71 cm, to CC, the color of the clayey siltstone includes dark yellowish brown (10YR 4/2), olive gray (5Y 3/2), dark greenish gray (5G 4/1), and light olive gray (5Y 5/2). Extensional microfaults occur in Sections 4 and 7.

Minor lithologies:
Section 5, 45-125 cm, consists of dark gray (5GY 4/1), poorly sorted PEBBLE CONGLOMERATE with pumice pebbles as large as 5x2 cm in cross section, and clayey siltstone clasts at least 10 cm across. This is the lower part of a graded conglomerate-sandstone bed. Section 5, 125 cm, to Section 6, 71 cm, is a clast-rich mud flow with a matrix of SANDY MUDSTONE and deformed clasts. Maximum mud clast diameter is at least 20 cm. Section 7, 56-64 cm and 70-90 cm, are graded beds of light bluish gray (5B 7/1), fine- to medium-grained PUMICEOUS SANDSTONE.

Some of the core is slightly fractured by drilling.

SMEAR SLIDE & THIN SECTION SUMMARY (%):

	1, 108 D	3, 118 D	4, 25 D	4, 40 D	3, 96 T	4, 135 D	5, 11 D
TEXTURE							
Sand	—	—	—	—	95	—	—
Silt	85	80	80	65	5	80	80
Clay	15	20	20	35	—	20	20
COMPOSITION							
Accessory minerals	—	—	—	—	10	—	—
Cement	—	—	—	—	30	—	—
Clay	10	20	5	30	—	20	20
Fe oxide	1	—	—	—	—	1	—
Feldspar	2	3	1	1	20	3	3
Foraminifers	—	—	—	—	Tr	—	—
Glass	82	75	88	64	30	69	74
Hornblende	—	—	1	1	—	—	—
Inorganic calcite	—	—	1	—	—	—	—
Micrite	—	—	—	—	—	—	—
Opaques	3	2	1	2	—	3	1
Quartz	1	1	—	—	5	3	1
Rock fragment	—	—	—	—	10	—	—

SMEAR SLIDE SUMMARY (%):

	5, 69 D	5, 90 D
TEXTURE		
Sand	30	—
Silt	60	75
Clay	10	25
COMPOSITION		
Accessory minerals	—	1
Clay	10	25
Feldspar	5	Tr
Glass	81	69
Hornblende	3	—
Opaques	1	1
Quartz	1	Tr

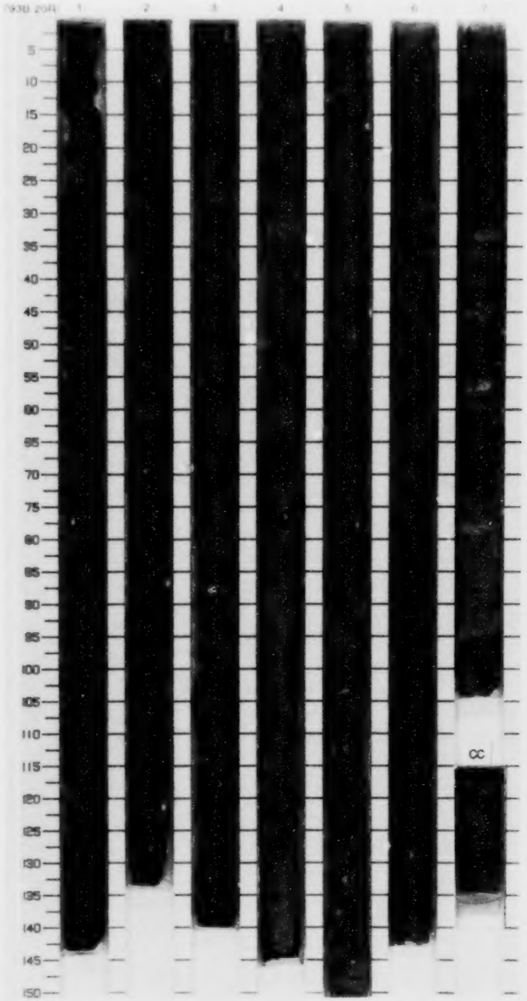
793B 20R
1
2
3
4
5
6
7
CC
5
10
15
20
25
30
35
40
45
50
55
60
65
70
75
80
85
90
95
100
105
110
115
120
125
130
135
140
145
150

SITE 793 HOLE B CORE 21R CORED INTERVAL 777.7-787.3 mbsf

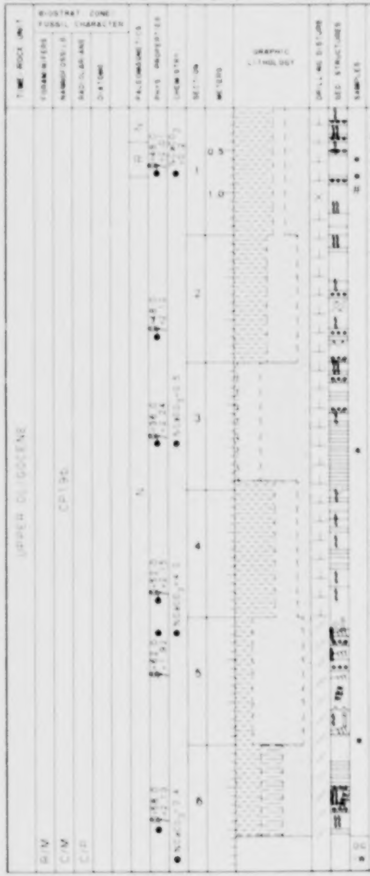
TIME-ROCK UNIT
BIOSTRAT. ZONE/ FOSSIL CHARACTER
FORAMINIFERS
NANNOFOSSILS
RADIOLARIANS
DIATOMS
PALEOMAGNETICS
PHYS. PROPERTIES
CHEMISTRY
SECTION
METERS
GRAPHIC LITHOLOGY
DRILLING DISTURB.
SED. STRUCTURES
SAMPLES
UPPER OLIGOCENE
CP19b
B/M
C/M
C/P
N
R
0.5
1.0
1
2
3
4
5
6
OG

LITHOLOGIC DESCRIPTION

VITRIC SILTSTONE, CLAYSTONE, AND CRYSTAL VITRIC SANDSTONE

Major lithologies:
Olive black (5Y 2/1) VITRIC SILTSTONE (38% of the core), CLAYSTONE (32%), and grayish green (5G 5/2) CRYSTAL VITRIC SANDSTONE (28%) occur as divisions of normally graded beds. The vitric component has been largely altered. The sandstone-siltstone basal portions of the graded beds are planar laminated and commonly have scoured bases. The claystone upper portions are slightly to heavily bioturbated. Trace fossils include Zoophycos. A healed fracture occurs in Section 2, 90 cm. A fine-grained sandstone dike and a dewatering structure occur in Section 5, at 88-92 cm and 106-110 cm, respectively.

Minor lithologies:
Dark gray (5Y 4/1) SILTY CLAYSTONE and CLAYEY SILTSTONE comprise 5% and 1% of the core, respectively.

The core is moderately to slightly fractured by drilling.

SMEAR SLIDE & THIN SECTION SUMMARY (%):

	1, 40	1, 90	[illegible], 93	[illegible], 101	[illegible], 141
	M	M	D	T	D
TEXTURE:					
Sand	—	100	95	100	—
Silt	5	—	5	—	15
Clay	95	—	—	—	85
COMPOSITION:					
Accessory minerals	Tr	5	4	5	Tr
Cement	—	—	5	15	—
Clay	94	—	—	—	80
Feldspar	1	10	10	5	1
Glass	5	82	80	75	—
Lithic fragments	—	3	—	—	5
Mica	Tr	—	—	—	Tr
Micrite	—	—	—	—	Tr
Nannofossils	—	—	—	—	4
Quartz	—	—	1	—	—
Radiolarians	—	—	—	—	1
Rock fragment	—	—	Tr	—	—
Zeolite	—	—	—	—	14

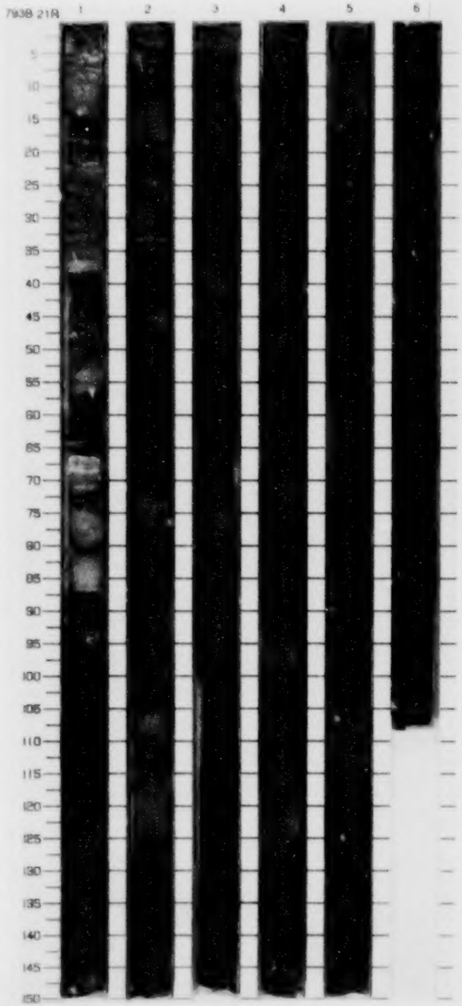
793B 21R
1
2
3
4
5
6
5
10
15
20
25
30
35
40
45
50
55
60
65
70
75
80
85
90
95
100
105
110
115
120
125
130
135
140
145
150

SITE 793 HOLE B CORE 22R CORED INTERVAL 787.3-797.0 mbsf

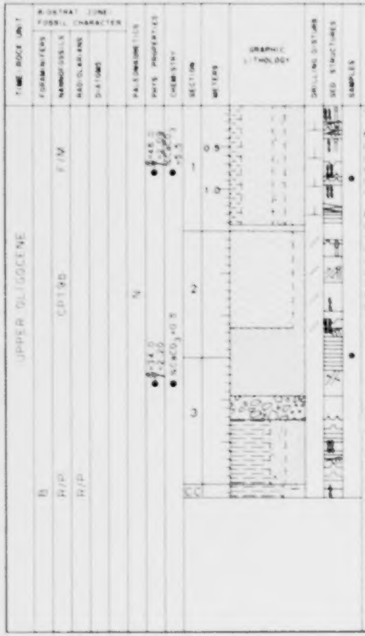
TIME-ROCK UNIT
BIOSTRAT. ZONE/ FOSSIL CHARACTER
FORAMINIFERS
NANNOFOSSILS
RADIOLARIANS
DIATOMS
PALEOMAGNETICS
PHYS. PROPERTIES
CHEMISTRY
SECTION
METERS
GRAPHIC LITHOLOGY
DRILLING DISTURB.
SED. STRUCTURES
SAMPLES
UPPER OLIGOCENE
B
F/M
CP19B
R/P
R/P
N
γ=48.0
ϕ=2.60
$\%CaCO_3$=3.5
γ=34.0
ϕ=2.20
$\%CaCO_3$=0.5
1
2
3
CC
0.5
1.0

LITHOLOGIC DESCRIPTION

VITRIC SILTSTONE AND VITRIC SANDSTONE

Major lithologies:
Greenish black (5GY 2/1) VITRIC SILTSTONE and VITRIC SANDSTONE, respectively, comprise 38% and 26% of the core. The vitric component has been largely altered. The sandstone and siltstone are typically in graded sequences with scoured bases and planar laminations. Load casts, dewatering structures, and fractures are present. There is a microfault in Section 2, 51-55 cm.

Minor lithologies:
Greenish black (5GY 2/1) VITRIC SANDY SILTSTONE comprises 11% of the core. Another 11% is represented by a single bed of olive black (5Y 2/1) GRANULE PEBBLE VOLCANIC CONGLOMERATE with a maximum pebble size of 8 mm. The mean size of the ten largest clasts is 7 mm. Most clasts are the same color as the matrix; 3% are colored red (10R 4/6) and very light gray (N8). The remaining 3% of the core consists of greenish black (5G 2/1) SILTY CLAYSTONE and SANDY MUDSTONE, and dark gray (5GY 4/1) NANNOFOSSIL-RICH SILTY CLAYSTONE. The siltstone and silty claystone are slightly to moderately bioturbated.

SMEAR SLIDE SUMMARY (%):

	1, 81	3, 7
	M	D
TEXTURE:		
Sand	—	100
Silt	10	—
Clay	90	—
COMPOSITION:		
Accessory minerals	1	3
Bioclast	—	1
Cement	—	5
Clay	80	—
Feldspar	Tr	10
Foraminifers	Tr	—
Glauconite	Tr	—
Lithic fragments	Tr	20
Nannofossils	10	—
Radiolarians	Tr	—
Unknown	—	58
Zeolite	9	—

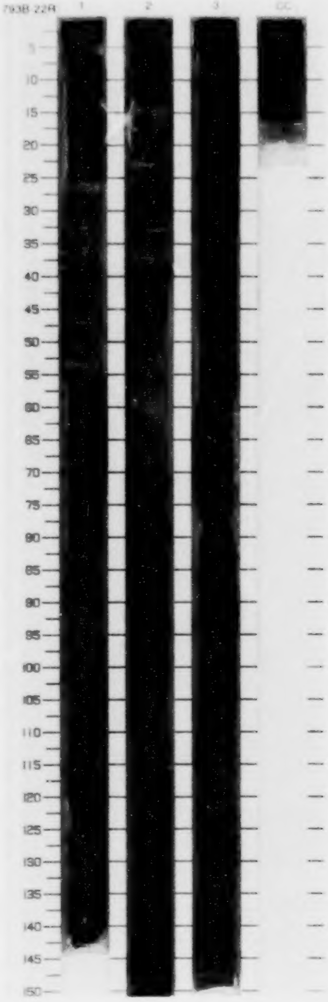
793B-22R
1
2
3
CC
5
10
15
20
25
30
35
40
45
50
55
60
65
70
75
80
85
90
95
100
105
110
115
120
125
130
135
140
145
150

SITE 793 HOLE B CORE 23R CORED INTERVAL 797.0-806.7 mbsf

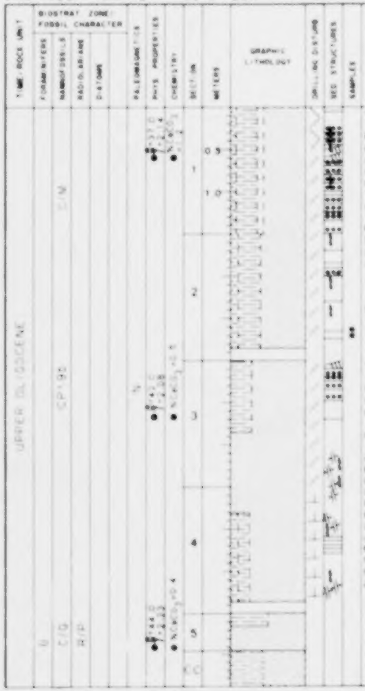
TIME-ROCK UNIT
BIOSTRAT. ZONE/ FOSSIL CHARACTER
FORAMINIFERS
NANNOFOSSILS
RADIOLARIANS
DIATOMS
PALEOMAGNETICS
PHYS. PROPERTIES
CHEMISTRY
SECTION
METERS
GRAPHIC LITHOLOGY
DRILLING DISTURB.
SED. STRUCTURES
SAMPLES
UPPER OLIGOCENE
B
C/M
CP19b
C/G
R/P
0.5
1.0
1
2
3
4
5
CC

LITHOLOGIC DESCRIPTION

VITRIC SANDSTONE AND VITRIC SILTY CLAYSTONE

Major lithologies:
69% of the core consists of dark reddish brown (5YR 3/2) VITRIC SANDSTONE, mostly interbedded with reddish brown (5YR 3/2) VITRIC SILTY CLAYSTONE in 3-6 cm thick normally graded beds with scoured bases and slightly bioturbated tops. There are two thicker beds of sandstone: 47 cm thick in Sections 3 and 4, and 30 cm thick in Section 5. The vitric component has been largely altered. There are several sub-vertical fractures: two in Section 3, one in Section 4, and one in Section 5 are filled with gypsum.

Minor lithologies:
Dark reddish brown (5YR 3/2) CLAYSTONE and VITRIC SILTSTONE comprise 1% of the core. An isolated lump of greenish gray (5G 6/1) GYPSUM, 7 cm long, occurs in the core catcher.

The core is undisturbed to slightly or moderately fractured by drilling.

SMEAR SLIDE SUMMARY (%):

	[illegible] D	[illegible] D
TEXTURE:		
Sand	—	100
Silt	10	—
Clay	90	—
COMPOSITION:		
Accessory minerals	[illegible]	[illegible]
Biosilica	[illegible]	[illegible]
Cement	—	20
Clay	75	—
Fe-oxide	[illegible]	—
Feldspar	[illegible]	—
Glass	[illegible]	56
Lithic fragments	[illegible]	20
Mica	[illegible]	—
Nannofossils	[illegible]	—
Radiolarians	—	[illegible]
Zeolite	[illegible]	—

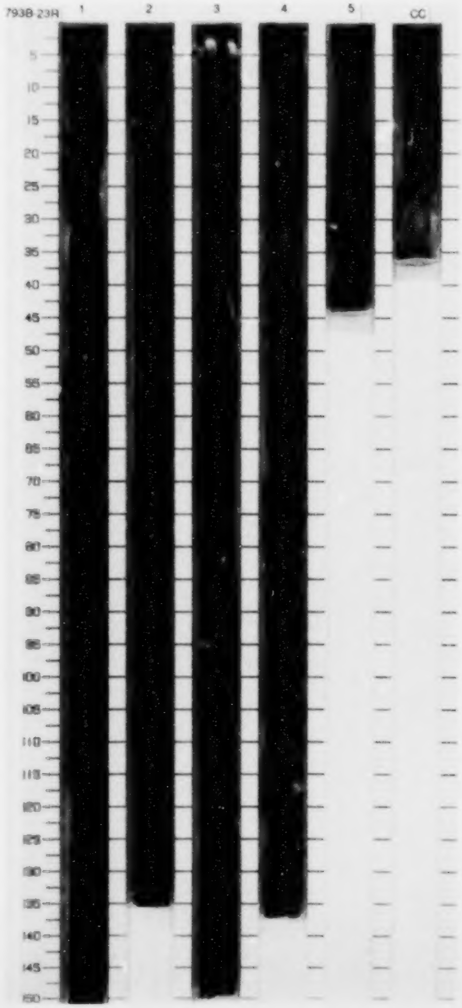
793B-23R
1
2
3
4
5
CC
5
10
15
20
25
30
35
40
45
50
55
60
65
70
75
80
85
90
95
100
105
110
115
120
125
130
135
140
145
150

SITE 793 HOLE B CORE 24R CORED INTERVAL 806.7-816.4 mbsf

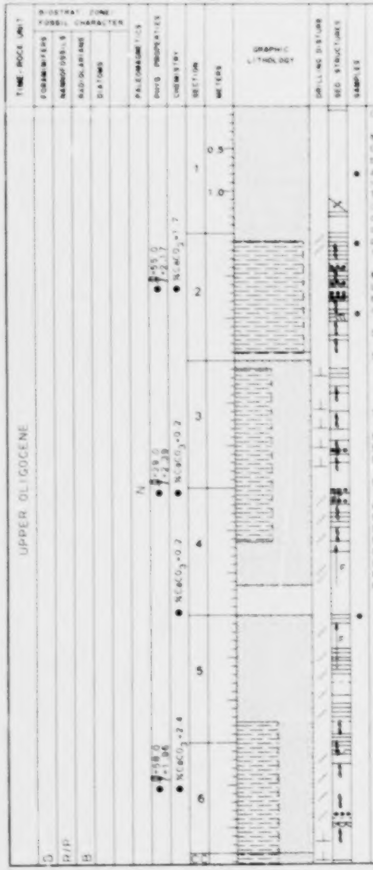
TIME-ROCK UNIT
BIOSTRAT. ZONE/ FOSSIL CHARACTER
FORAMINIFERS
NANNOFOSSILS
RADIOLARIANS
DIATOMS
PALEOMAGNETICS
PHYS. PROPERTIES
CHEMISTRY
SECTION
METERS
GRAPHIC LITHOLOGY
DRILLING DISTURB.
SED. STRUCTURES
SAMPLES
UPPER OLIGOCENE
C
R/P
B
N
φ=55.0
γ=2.17
%CaCO₃=1.7
φ=29.0
γ=2.38
%CaCO₃=0.2
%CaCO₃=0.2
φ=58.0
γ=1.96
%CaCO₃=2.4
1
2
3
4
5
6
CC
0.5
1.0

LITHOLOGIC DESCRIPTION

CRYSTAL VITRIC SANDSTONE AND VITRIC SILTY CLAYSTONE

Major lithologies:
CRYSTAL VITRIC SANDSTONE comprises 63% of the core. The vitric component has been largely altered. A grayish black (N2) layer in Sections 1 and 2, 159 cm thick, is massive and medium to fine grained. A brownish black (5YR 2/1) bed in Section 5, 0-87 cm, is normally graded from coarse to fine sandstone, and contains <1% red (2.5YR 4/6) grains. The rest of the sandstone occurs as grayish black (N2), black (N1), and brownish black (5YR 2/1), basal divisions, 2-11 cm thick, of beds that grade up into slightly bioturbated caps of greenish black (5GY 2/1) VITRIC SILTY CLAYSTONE, 1-22 cm thick. The latter lithology comprises 20% of the core. The graded beds commonly have scoured bases and basal planar laminations. Bedding dips at 4°. Sub vertical structures are a fracture in Section 1, 111-130 cm, and a vein, 0.5 mm across, filled with gypsum in Section 4, 12-16 cm.

Minor lithologies:
Lithologies transitional between the principal ones, either in the graded beds or as bioturbated mixtures, include SANDY SILTSTONE and SANDY CLAYSTONE, together with rare intervals of CLAYSTONE; they comprise 17% of the core.

Sections 3 to CC are slightly to moderately fractured by drilling.

SMEAR SLIDE SUMMARY (%):

	1, 80 D	2, 11 M	2, 95 D	5, 1 D
TEXTURE:				
Sand	100	—	—	90
Silt	—	65	35	10
Clay	—	35	65	—
COMPOSITION:				
Accessory minerals	10	5	1	15
Cement	15	—	—	20
Clay	—	20	65	—
Feldspar	10	5	1	10
Glass	50	60	25	50
Lithic fragments	15	1	5	5
Micrite	—	2	1	—
Nannofossils	—	10	2	—

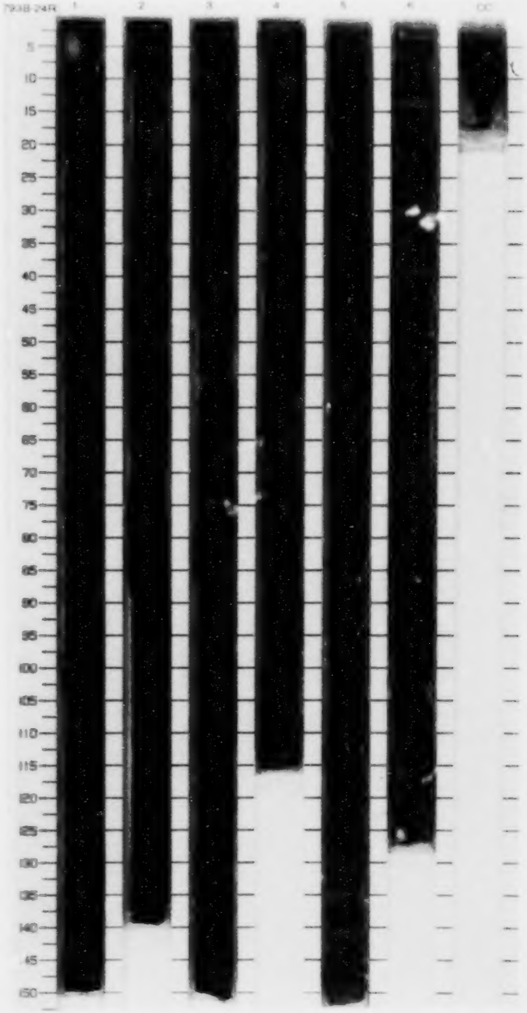
793B-24R
1
2
3
4
5
6
CC
5
10
15
20
25
30
35
40
45
50
55
60
65
70
75
80
85
90
95
100
105
110
115
120
125
130
135
140
145
150

SITE 793 HOLE B CORE 25R CORED INTERVAL 816.4-825.7 mbsf

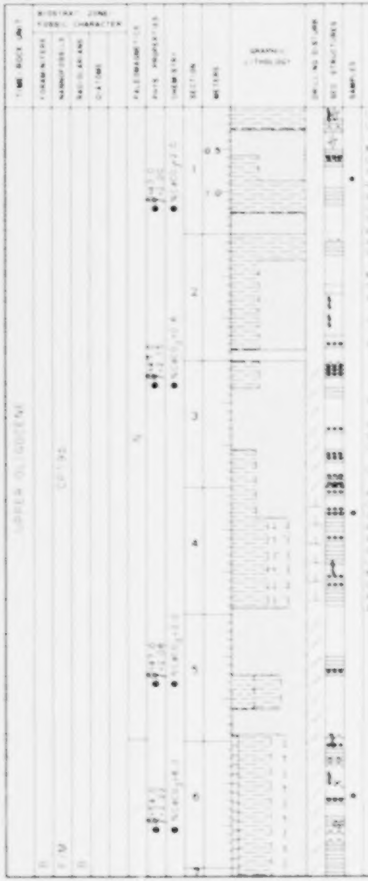
TIME-ROCK UNIT
BIOSTRAT. ZONE/ FOSSIL CHARACTER
FORAMINIFERS
NANNOFOSSILS
RADIOLARIANS
DIATOMS
PALEOMAGNETICS
PHYS. PROPERTIES
CHEMISTRY
SECTION
METERS
GRAPHIC LITHOLOGY
DRILLING DISTURB.
SED. STRUCTURES
SAMPLES
UPPER OLIGOCENE
CP19b
N
0.5
1.0
1
2
3
4
5
6
7
B
F/M
B

LITHOLOGIC DESCRIPTION

CRYSTAL VITRIC SANDSTONE, VITRIC CLAYEY SILTSTONE, AND VITRIC SILTY CLAYSTONE

Major lithologies:
[illegible]

Minor lithologies:
[illegible]

The core is undisturbed to slightly fractured by drilling.

SMEAR SLIDE SUMMARY (%):

	[illegible]	[illegible]	[illegible]
TEXTURE:			
Sand	[illegible]	[illegible]	[illegible]
Silt	[illegible]	[illegible]	[illegible]
Clay			[illegible]
COMPOSITION:			
Accessory minerals	[illegible]	[illegible]	[illegible]
Cement	[illegible]	[illegible]	[illegible]
Clay			[illegible]
Feldspar	[illegible]	[illegible]	[illegible]
Foraminifers	[illegible]		[illegible]
Glass	[illegible]	[illegible]	
Lithic fragments	[illegible]	[illegible]	[illegible]
Nannofossils		[illegible]	[illegible]
Opaques			[illegible]
Radiolarians			
Zeolite	[illegible]	[illegible]	[illegible]

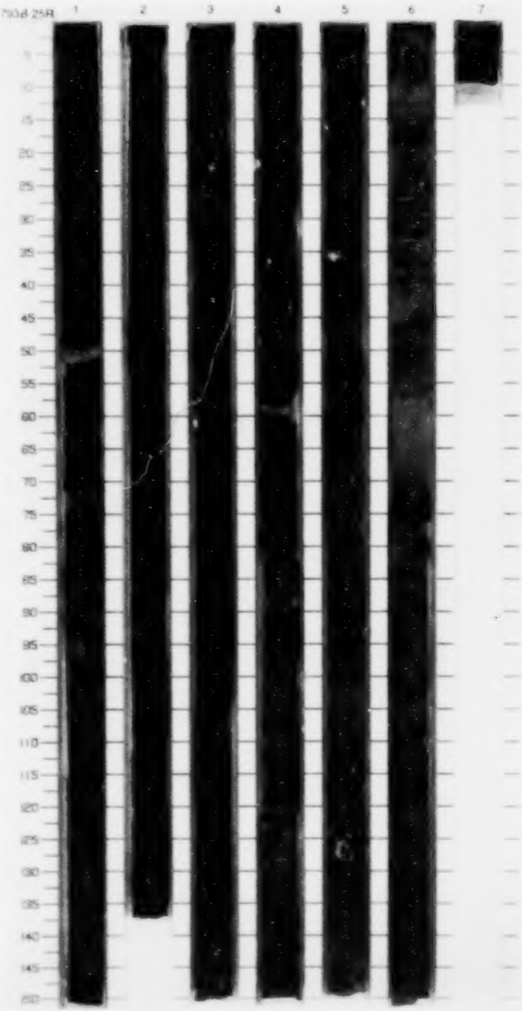
793B 25R
1
2
3
4
5
6
7
5
10
15
20
25
30
35
40
45
50
55
60
65
70
75
80
85
90
95
100
105
110
115
120
125
130
135
140
145
150

SITE 793 HOLE B CORE 26R CORED INTERVAL 825.7-835.4 mbsf

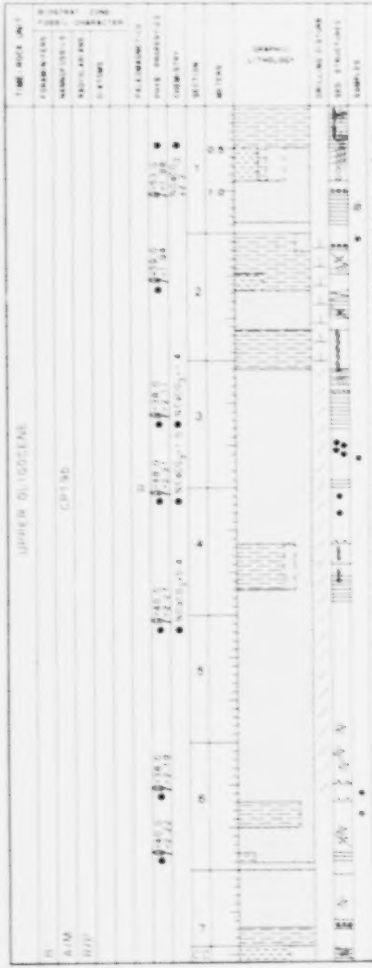
TIME-ROCK UNIT
BIOSTRAT. ZONE/ FOSSIL CHARACTER
FORAMINIFERS
NANNOFOSSILS
RADIOLARIANS
DIATOMS
PALEOMAGNETICS
PHYS. PROPERTIES
CHEMISTRY
SECTION
METERS
GRAPHIC LITHOLOGY
DRILLING DISTURB.
SED. STRUCTURES
SAMPLES
UPPER OLIGOCENE
CP19b
0.5
1.0
1
2
3
4
5
6
7
CC
R
A/M
B/M

LITHOLOGIC DESCRIPTION

CRYSTAL VITRIC SANDSTONE

Major lithology: Dark greenish gray (5G 4/1) and grayish black (N2) CRYSTAL VITRIC SANDSTONE comprises [illegible]% of the core, mostly in beds [illegible] cm thick. The vitric component has been largely altered. Most of the beds are fine grained and planar laminated. A massive, medium-grained bed in Section 3 contains volcanic lithic clasts up to 15 mm in diameter and claystone clasts as large as 15 mm. Some of the sandstone occurs as basal divisions [illegible] cm thick, of thin graded beds that pass upward into slightly bioturbated, dark greenish gray (5G 4/1) VITRIC SILTY CLAYSTONE and CLAYEY SILTSTONE, which together constitute [illegible]% of the core. Subvertical micro-fractures, some filled with gypsum, occur throughout the core.

Minor lithologies:
Dark greenish gray (5G 4/1) CLAYSTONE ([illegible]%), SANDY SILTSTONE ([illegible]%), and SILTSTONE comprise bioturbated [illegible] graded intervals in the upper parts of the sand-based graded beds.

The core is unfractured to slightly fractured by drilling.

SMEAR SLIDE & THIN SECTION SUMMARY (%):

	[illegible]	2, [illegible]	3, [illegible]	[illegible]	[illegible]
	D	M	M	D	D
TEXTURE:					
Sand	[illegible]			[illegible]	
Silt	[illegible]	[illegible]	[illegible]		[illegible]
Clay		[illegible]	[illegible]		[illegible]
COMPOSITION:					
Accessory minerals	[illegible]	[illegible]		[illegible]	[illegible]
Cement	[illegible]				
Clay		[illegible]	[illegible]	[illegible]	[illegible]
Fe-oxide		[illegible]			
Feldspar	[illegible]	[illegible]	[illegible]	[illegible]	[illegible]
Glass	[illegible]	[illegible]	[illegible]		[illegible]
Micrite			[illegible]		
Nannofossils		[illegible]	[illegible]		[illegible]
Opaques			[illegible]		[illegible]
Radiolarians					[illegible]
Rock fragment	[illegible]				
Zeolite				[illegible]	

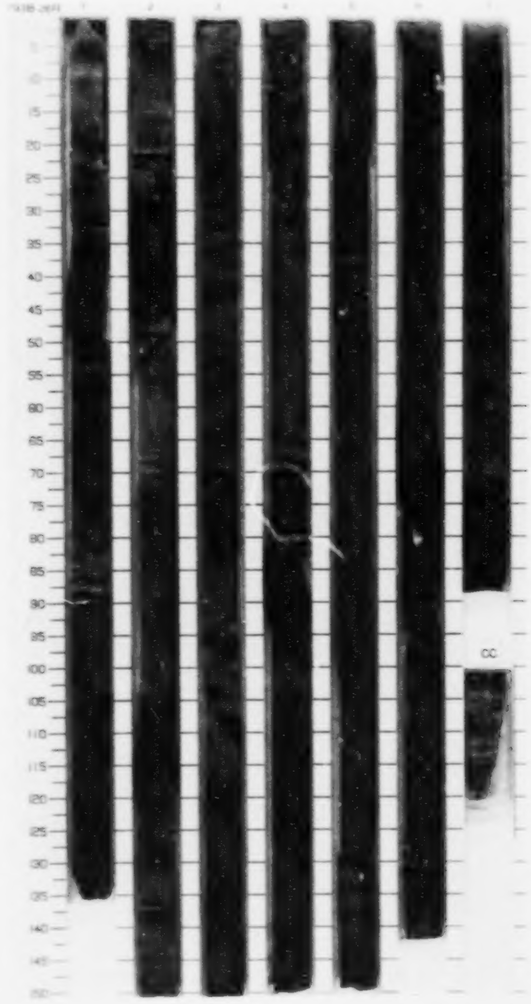
793B-26R
1
2
3
4
5
6
7
5
10
15
20
25
30
35
40
45
50
55
60
65
70
75
80
85
90
95
100
105
110
115
120
125
130
135
140
145
150
CC

SITE 793 HOLE B CORE 27R CORED INTERVAL 835.4-845.1 mbsf

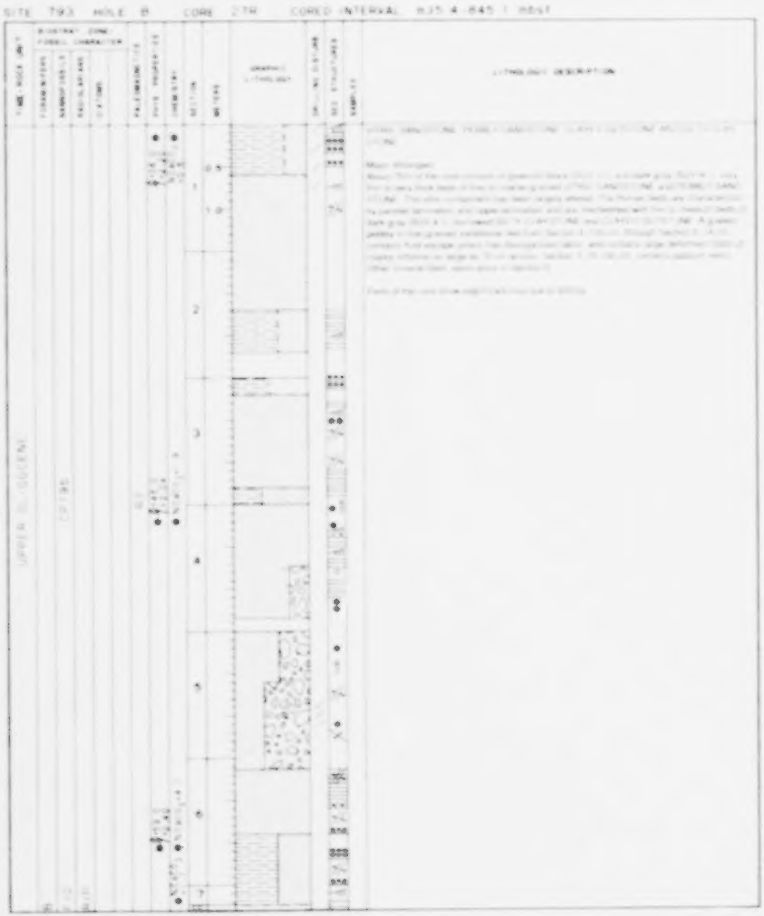
TIME-ROCK UNIT
BIOSTRAT. ZONE/FOSSIL CHARACTER
FORAMINIFERS
NANNOFOSSILS
RADIOLARIANS
DIATOMS
PALEOMAGNETICS
PHYS. PROPERTIES
CHEMISTRY
SECTION
METERS
GRAPHIC LITHOLOGY
DRILLING DISTURB.
SED. STRUCTURES
SAMPLES
LITHOLOGIC DESCRIPTION
UPPER OLIGOCENE
CP19b
0.5
1.0
1
2
3
4
5
6
7

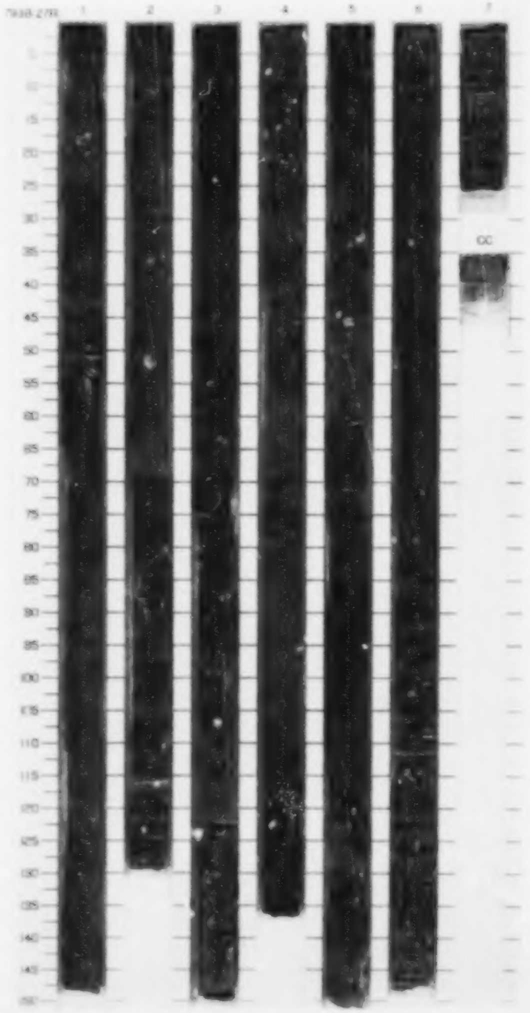
793B-27R
1
2
3
4
5
6
7
CC
0
5
10
15
20
25
30
35
40
45
50
55
60
65
70
75
80
85
90
95
100
105
110
115
120
125
130
135
140
145
150

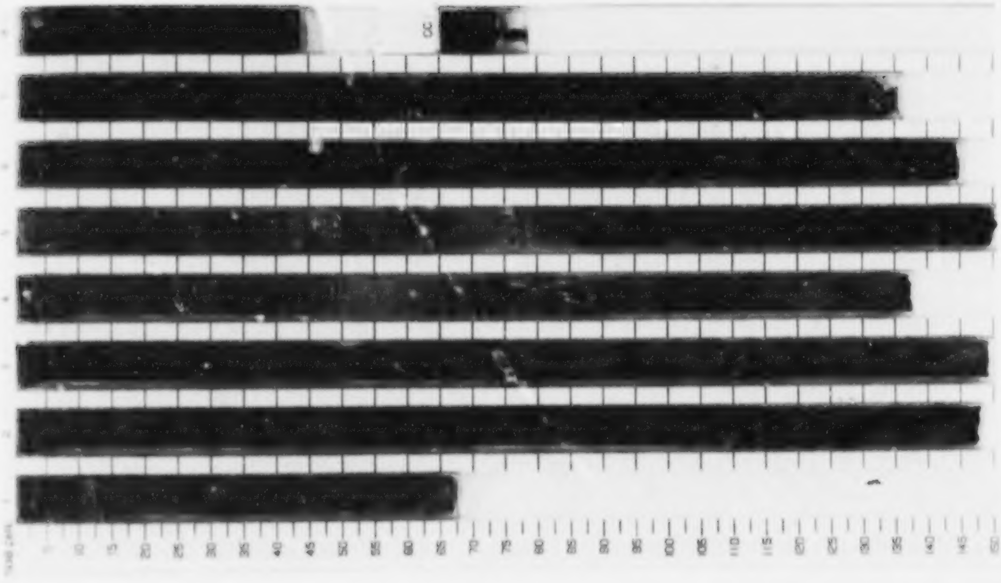
CC
1
2
3
4
5
6
7
8
5
10
15
20
25
30
35
40
45
50
55
60
65
70
75
80
85
90
95
100
105
110
115
120
125
130
135
140
145
150

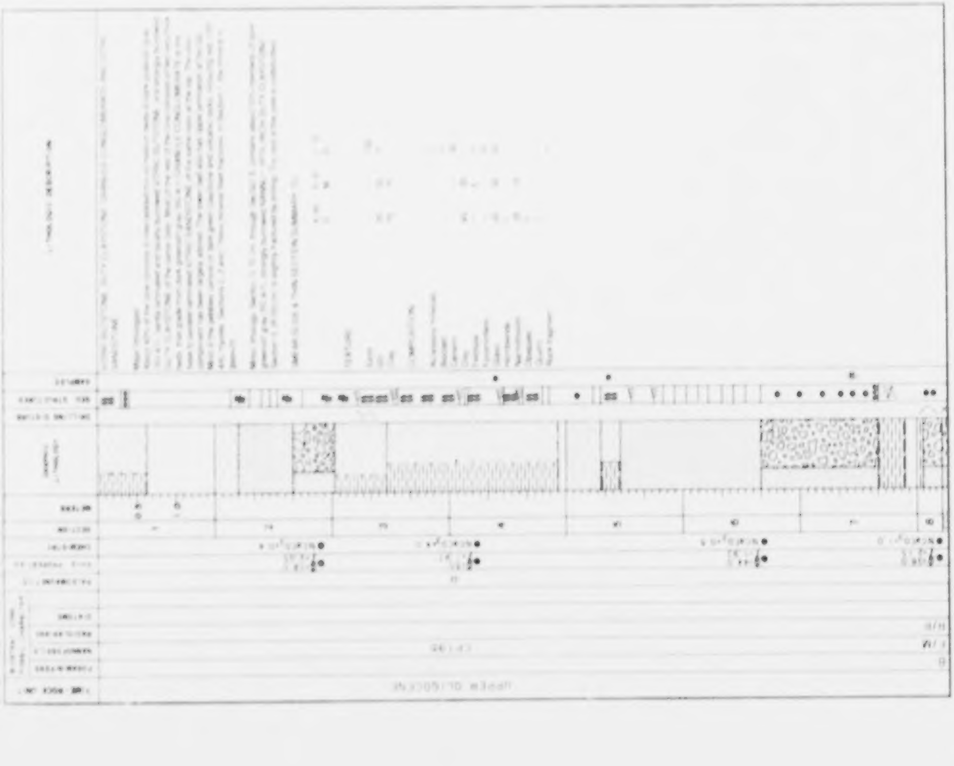

SITE 793 HOLE B CORE 29R CORED INTERVAL 854.7-864.4 mbsf

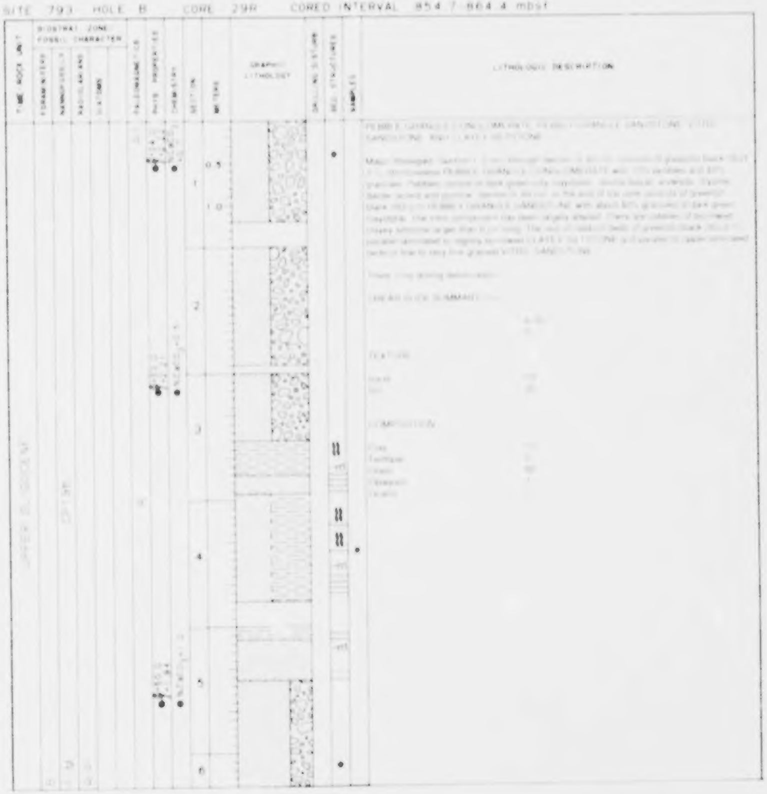
TIME-ROCK UNIT
BIOSTRAT. ZONE/FOSSIL CHARACTER
FORAMINIFERS
NANNOFOSSILS
RADIOLARIANS
DIATOMS
PALEOMAGNETICS
PHYS. PROPERTIES
CHEMISTRY
SECTION
METERS
GRAPHIC LITHOLOGY
DRILLING DISTURB.
SED. STRUCTURES
SAMPLES
LITHOLOGIC DESCRIPTION
0.5
1.0
1
2
3
4
5
6

PEBBLE-GRANULE CONGLOMERATE, PEBBLY-GRANULE SANDSTONE, VITRIC SANDSTONE, AND CLAYEY SILTSTONE

[illegible]

SMEAR SLIDE SUMMARY (%):

TEXTURE:

Sand

Silt

COMPOSITION:

Clay

Feldspar

Glass

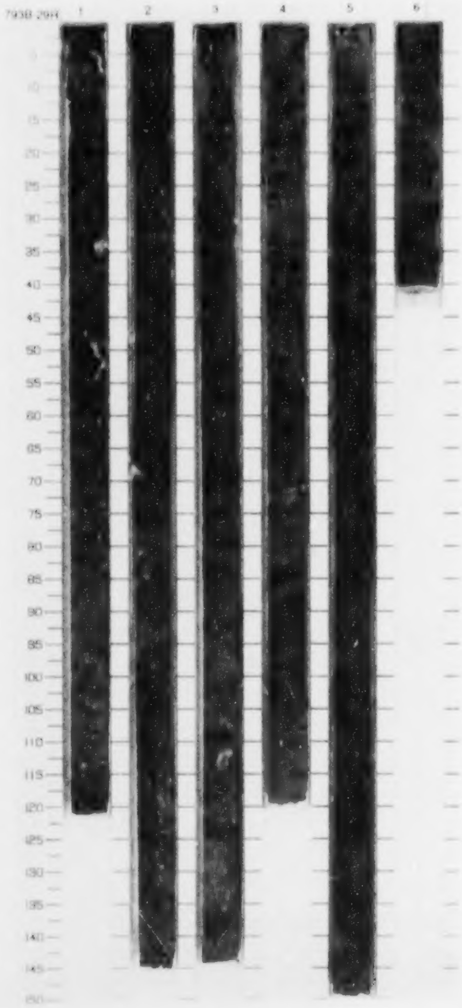
793B-29R
1
2
3
4
5
6
0
10
15
20
25
30
35
40
45
50
55
60
65
70
75
80
85
90
95
100
105
110
115
120
125
130
135
140
145
150

SITE 793 HOLE B CORE 30R CORED INTERVAL 864.4-874.0 mbsf

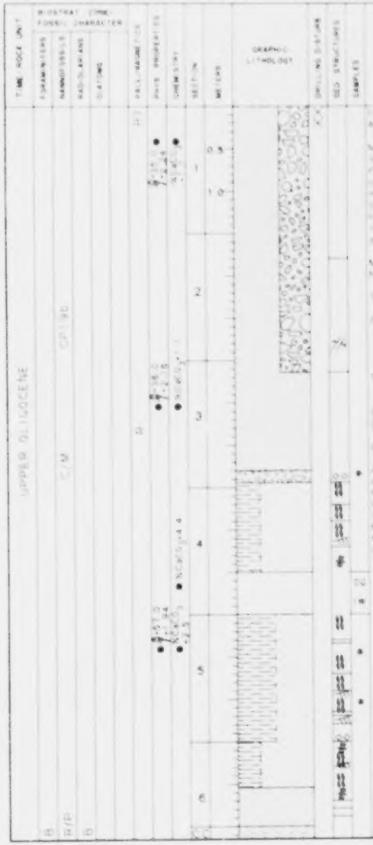
TIME ROCK UNIT
BIOSTRAT. ZONE/FOSSIL CHARACTER
FORAMINIFERS
NANNOFOSSILS
RADIOLARIANS
DIATOMS
PALEOMAGNETICS
PHYS. PROPERTIES
CHEMISTRY
SECTION
METERS
GRAPHIC LITHOLOGY
DRILLING DISTURB.
SED. STRUCTURES
SAMPLES
UPPER OLIGOCENE
CP19b
C/M
B
R/P
B
0.5
1.0
1
2
3
4
5
6
CC
IW
OG

LITHOLOGIC DESCRIPTION

PEBBLY SANDSTONE, VITRIC SANDSTONE, VITRIC SILTSTONE, CLAYEY SILTSTONE AND SILTY CLAYSTONE

Major lithologies:
Sections 1 through 3 consist of three beds of greenish black (5GY 2/1), structureless PEBBLY SANDSTONE and VITRIC SANDSTONE. Sand content is 60-70%. The vitric component has been largely altered. The rest of the core consists of interbedded thin to medium beds of dark gray (5GY 4/1) parallel laminated to slightly burrowed CLAYEY SILTSTONE or SILTY CLAYSTONE, and parallel- to ripple-laminated beds of fine- to very fine-grained VITRIC SILTSTONE or VITRIC SANDSTONE. Bedding dips at 8°. Section 3, 100-150 cm, and Section 4, 60-70 cm, have mineral-filled fractures. Section 4, 90-100 cm, and Section 5, 140-150 cm, have clastic dikes of silty claystone.

Minor lithology: Section 5, 90-97 cm and 102-105 cm, consists of greenish gray (5G 6/1) NANNOFOSSIL-RICH SILTY CLAYSTONE.

There is no drilling deformation.

SMEAR SLIDE SUMMARY (%):

	3, 137	5, 45	5, 104
	D	M	D
TEXTURE:			
Silt	10	10	20
Clay	90	90	80
COMPOSITION:			
Accessory minerals	1		[illegible]
Clay	90		41
Feldspar	2		[illegible]
Glass		90	30
Inorganic calcite	10	5	1
Micrite			1
Nannofossils	2	5	20
Opaques			1

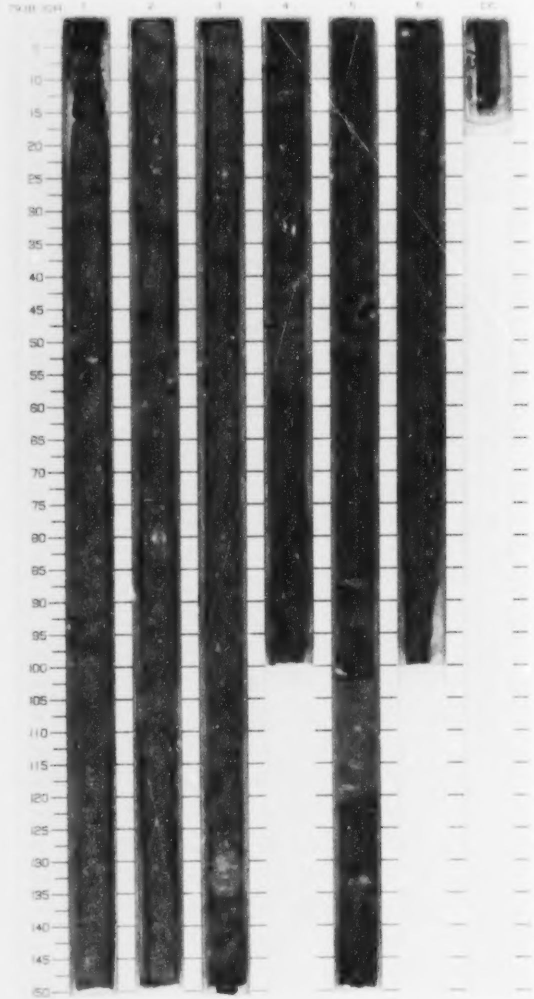
793B-30R
1
2
3
4
5
6
CC
5
10
15
20
25
30
35
40
45
50
55
60
65
70
75
80
85
90
95
100
105
110
115
120
125
130
135
140
145
150

SITE 793 HOLE B CORE 31R CORED INTERVAL 874.0-883.7 mbsf

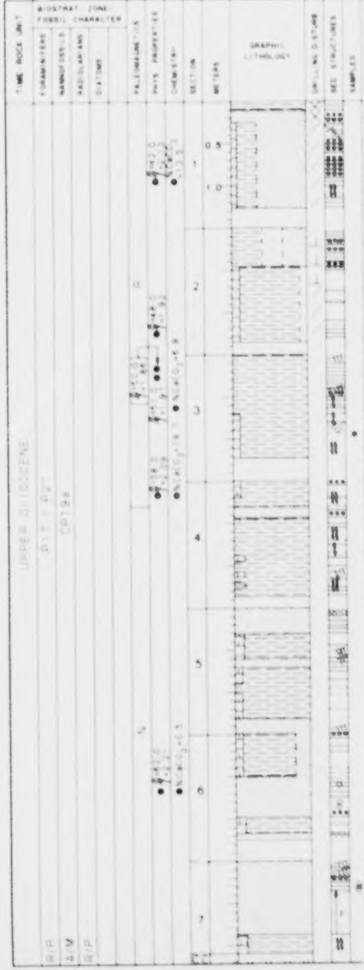
TIME-ROCK UNIT
BIOSTRAT. ZONE/ FOSSIL CHARACTER
FORAMINIFERS
NANNOFOSSILS
RADIOLARIANS
DIATOMS
PALEOMAGNETICS
PHYS. PROPERTIES
CHEMISTRY
SECTION
METERS
GRAPHIC LITHOLOGY
DRILLING DISTURB.
SED. STRUCTURES
SAMPLES
UPPER OLIGOCENE
P21 / P22
CP19b
R/P
A/M
R/P
N
1
2
3
4
5
6
7
0.5
1.0

LITHOLOGIC DESCRIPTION

VITRIC SANDSTONE, VITRIC SILTSTONE, CLAYEY SILTSTONE AND NANNOFOSSIL-RICH CLAYEY SILTSTONE

Major lithologies:
There is a fine scale interbedding of very thin to medium beds of dark gray (5GY 4/1) to greenish black (5GY 2/1), parallel to ripple laminated, fine grained VITRIC SANDSTONE or VITRIC SILTSTONE, parallel laminated to burrowed CLAYEY SILTSTONE of the same color, and gray (5Y 6/1) burrowed NANNOFOSSIL-RICH CLAYEY SILTSTONE. Sandstone plus siltstone form about 50% of the core. The vitric component has been largely altered. There are relatively steep normal faults that dip at 45° in Section 2, 30-50 cm, and Section 3, 80-90 cm.

Minor lithologies:
Section 4, 114-117 cm, consists of light bluish gray (5B 7/1) medium grained PUMICEOUS SANDSTONE (ash). Section 7, 50-87 cm, consists of olive black (5Y 2/1) coarse grained GRANULE-RICH SANDSTONE that grades upward into fine grained sandstone.

Sections 1, 2 and 4, and Section 6, 0-50 cm, are slightly to moderately fractured by drilling.

SMEAR SLIDE & THIN SECTION SUMMARY (%):

	3, 44 D	7, 38 D
TEXTURE:		
Sand	—	100
Silt	20	Tr
Clay	80	—
COMPOSITION:		
Accessory minerals	—	[illegible]
Carbonate	—	25
Clay	56	—
Fe-oxide	[illegible]	—
Feldspar	[illegible]	20
Glass	15	50
Hornblende	[illegible]	—
Mica	[illegible]	—
Nannofossils	15	—
Opaques	[illegible]	—
Quartz	[illegible]	—
Rock fragment	—	[illegible]

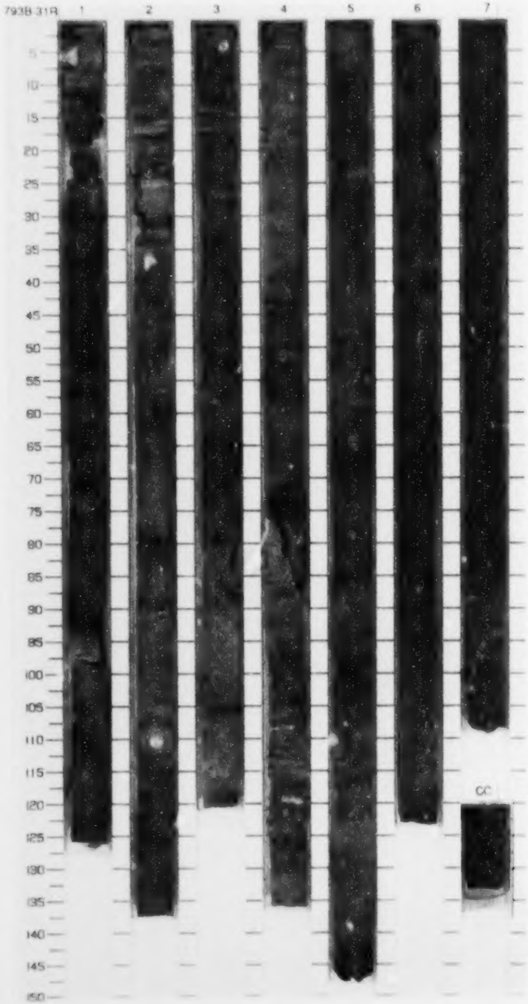
793B-31R
1
2
3
4
5
6
7
CC
5
10
15
20
25
30
35
40
45
50
55
60
65
70
75
80
85
90
95
100
105
110
115
120
125
130
135
140
145
150

SITE 793 HOLE B CORE 32R CORED INTERVAL 883.7-893.3 mbsf

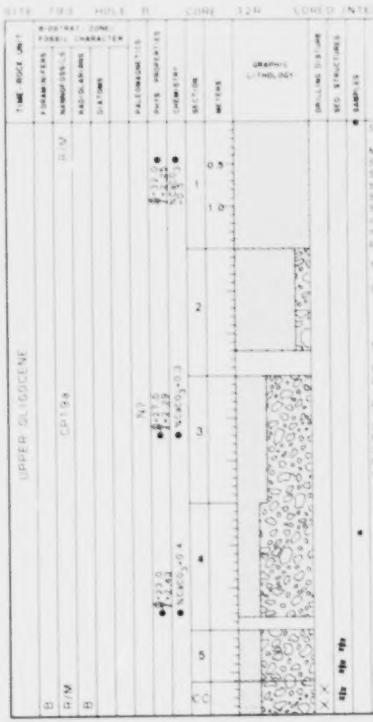
TIME-ROCK UNIT
BIOSTRAT. ZONE/FOSSIL CHARACTER
FORAMINIFERS
NANNOFOSSILS
RADIOLARIANS
DIATOMS
PALEOMAGNETICS
PHYS. PROPERTIES
CHEMISTRY
SECTION
METERS
GRAPHIC LITHOLOGY
DRILLING DISTURB.
SED. STRUCTURES
SAMPLES
UPPER OLIGOCENE
B
R/M
CP19a
R/M
B
N?
0.5
1.0
1
2
3
4
5
CC

LITHOLOGIC DESCRIPTION

SANDSTONE, PEBBLY SANDSTONE AND SANDY CONGLOMERATE

Major lithologies:
Sections 1 and 2 consist of greenish black (5G 2/1) structureless, very coarse-grained SANDSTONE to PEBBLY SANDSTONE as a single graded bed. The vitric component has been largely altered. Sections 3 through CC consist of greenish black (5G 2/1) structureless SANDY CONGLOMERATE, with about 40% sand matrix, 30% granules, and 30% pebbles. Section 5 contains three claystone clasts as large as ~5 cm long. Volcanic pebbles in the conglomerate include: brick red rhyolite with quartz phenocrysts, orthopyroxene and magnetite; olivine orthopyroxene plagioclase basalt; two-pyroxene andesite; white and red pumice; and basaltic scoria.

The core catcher is drilling breccia. Otherwise, the core is undisturbed by drilling.

SMEAR SLIDE SUMMARY (%):

	1, 3	4, 38
	M	M
TEXTURE:		
Silt	10	
Clay	90	
COMPOSITION:		
Clay	50	—
Feldspar	—	5
Glass	40	85
Nannofossils	10	—
Oxide	—	10

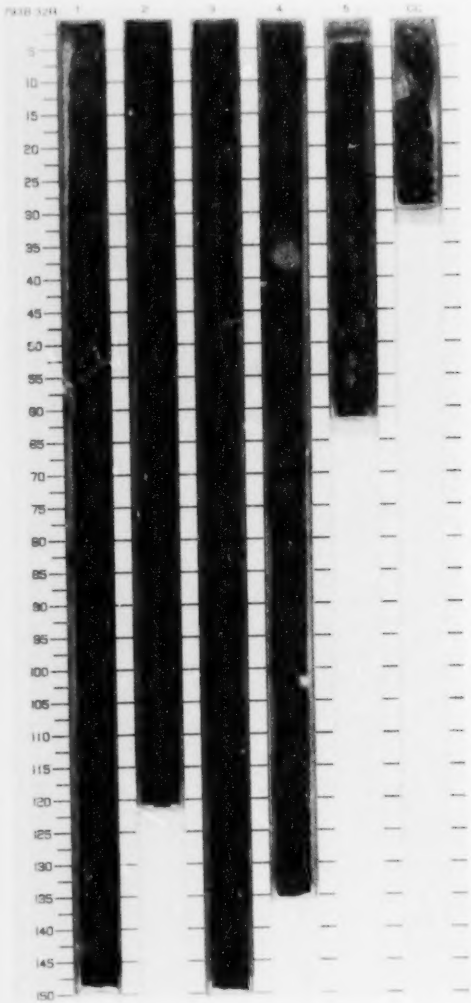
793B-32R
1
2
3
4
5
CC
5
10
15
20
25
30
35
40
45
50
55
60
65
70
75
80
85
90
95
100
105
110
115
120
125
130
135
140
145
150

SITE 793 HOLE B CORE 33R CORED INTERVAL 893.3-903.0 mbsf

TIME-ROCK UNIT	BIOSTRAT. ZONE/ FOSSIL CHARACTER: FORAMINIFERS	NANNOFOSSILS	RADIOLARIANS	DIATOMS	PALEOMAGNETICS	PHYS. PROPERTIES	CHEMISTRY	SECTION	METERS
UPPER OLIGOCENE	B	C/M CP19a	C/P [illegible]			● [illegible]	● [illegible]	1	0.5 1.0
								2	
						● [illegible]	● NCaCO₃=8.5	3	
								4	
						● [illegible]	● NCaCO₃=0.4 ● NCaCO₃=0.6	5	
								6	
						● [illegible]	● NCaCO₃=0.1	7	

GRAPHIC LITHOLOGY — DRILLING DISTURB. — SED. STRUCTURES — SAMPLES

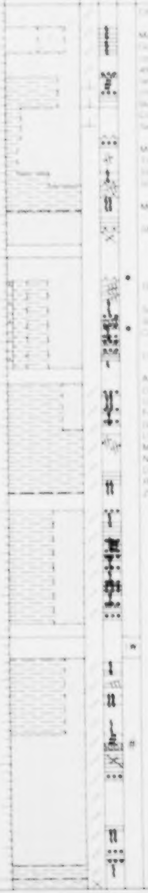

LITHOLOGIC DESCRIPTION

CRYSTAL VITRIC SANDSTONE AND VITRIC SILTY CLAYSTONE

Major lithologies:
Grayish black (N2) CRYSTAL VITRIC SANDSTONE and VITRIC SILTY CLAYSTONE comprise [illegible] and [illegible] of the core, respectively. The clay component has been largely altered. Much of the sandstone occurs in six fine- to medium-grained, graded beds with laminated tops, [illegible] cm thick. The rest of the sandstone forms the basal divisions, [illegible] cm thick, of thin, graded beds with slightly [illegible] tops of greenish black ([illegible]) [illegible] grayish black (N2) VITRIC SILTY CLAYSTONE. [illegible] in Sections [illegible] and [illegible] in Sections [illegible], and [illegible] in Sections [illegible].

Minor lithologies:
The remainder of the core consists of textural variants of the major lithologies: CLAYEY SILTSTONE ([illegible]), NANNOFOSSIL-RICH CLAYEY SILTSTONE ([illegible]), VITRIC SANDY SILTSTONE ([illegible]), and VITRIC SILTSTONE ([illegible]).

Most of the core is undisturbed to slightly fractured by drilling.

SMEAR SLIDE & THIN SECTION SUMMARY (%):

	1, 25 D	3, 94 M	5, 138 D
TEXTURE:			
Sand	80	[illegible]	100
Silt	20	[illegible]	
Clay		[illegible]	
COMPOSITION:			
Accessory minerals	[illegible]	[illegible]	[illegible]
Cement	20		[illegible]
Clay		[illegible]	
Feldspar	[illegible]	[illegible]	[illegible]
Glass	[illegible]		[illegible]
Lithic fragments	[illegible]	[illegible]	
Micrite		[illegible]	
Nannofossils		[illegible]	
Opaques		[illegible]	
Radiolarians		[illegible]	
Zeolite		[illegible]	

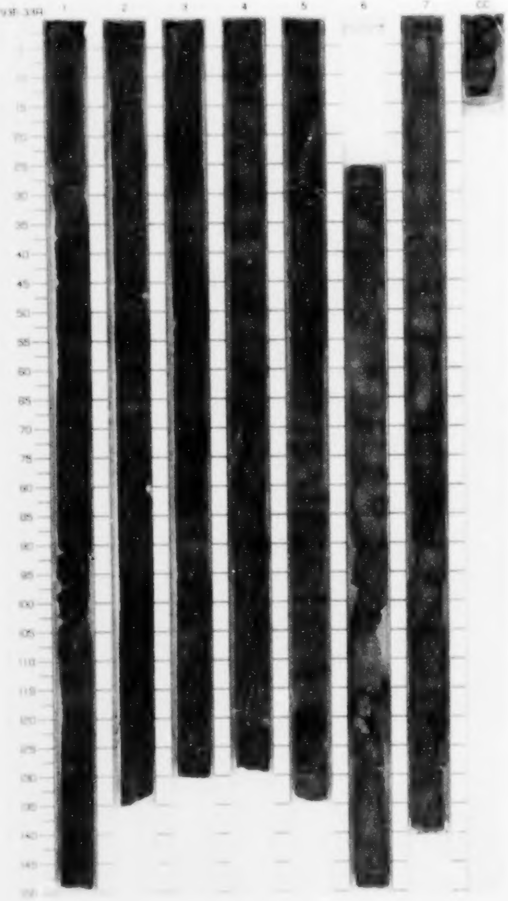

SITE 793 HOLE B CORE 34R CORED INTERVAL 903.0-912.6 mbsf

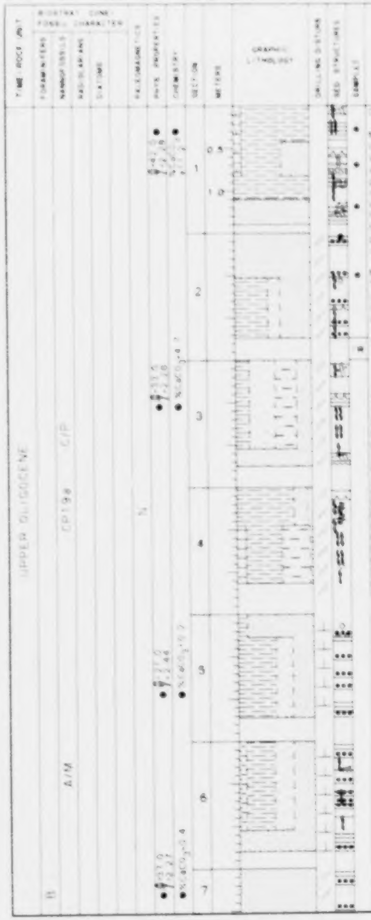
TIME-ROCK UNIT
BIOSTRAT. ZONE/FOSSIL CHARACTER
FORAMINIFERS
NANNOFOSSILS
RADIOLARIANS
DIATOMS
PALEOMAGNETICS
PHYS. PROPERTIES
CHEMISTRY
SECTION
METERS
GRAPHIC LITHOLOGY
DRILLING DISTURB.
SED. STRUCTURES
SAMPLES
UPPER OLIGOCENE
B
CP19a C/P
A/M
N
0.5
1.0
1
2
3
4
5
6
7

LITHOLOGIC DESCRIPTION

CRYSTAL VITRIC SANDSTONE AND VITRIC SILTY CLAYSTONE

Major lithologies:
Greenish black (5G 2/1), olive black (5Y 2/1), and brownish black (5YR 2/1) CRYSTAL VITRIC SANDSTONE comprises 45% of the core. The vitric component has been largely altered. The sandstone occurs in six beds, 23-51 cm thick, all but one of which are fine grained, parallel laminated, and grade upward into siltstone. One bed, in Section 2, is inverse graded from fine to medium sand and contains pumice granules. The rest of the sandstone occurs as the basal divisions of thin graded beds that are capped by slightly to heavily bioturbated, dark gray (5GY 4/1, 5Y 4/1) VITRIC SILTY CLAYSTONE. Two micro faults occur in Section 1. Two sub vertical sandstone dikes are located in Section 4. A gypsum filled fracture occurs in Section 2. An ash layer in Section 1, 70-72 cm, shows convolution due to wet sediment deformation.

Minor lithologies:
The remainder of the core consists of textural variants of the major lithologies: SILTSTONE (10%), SANDY MUDSTONE (9%), and CLAYEY SILTSTONE (3%), together with two intervals of NANNOFOSSIL RICH CLAYEY SILTSTONE (2%). The core is undisturbed to slightly or moderately fractured by drilling.

SMEAR SLIDE SUMMARY (%):

	1, 28 D	1, 54 M	1, 119 D	2, 50 D
TEXTURE:				
Sand	10	5	100	80
Silt	25	25	—	20
Clay	65	70	—	—
COMPOSITION:				
Accessory minerals	2	1	2	15
Cement	—	—	Tr	Tr
Clay	71	61	—	—
Feldspar	5	1	5	15
Glass	15	20	90	55
Lithic fragments	2	1	Tr	15
Micrite	—	—	1	—
Nannofossils	5	15	2	
Opaques	—	1		
Radiolarians	—	Tr		

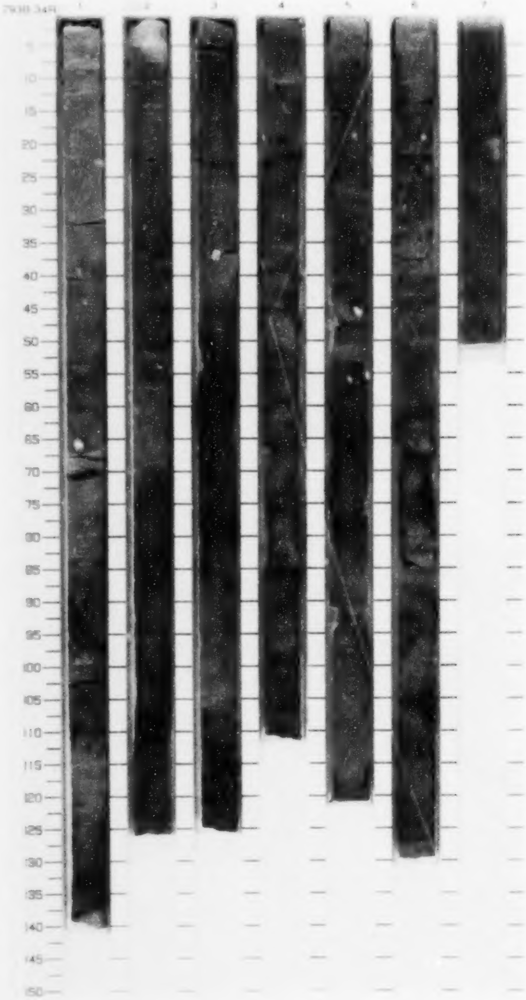
793B-34R
1
2
3
4
5
6
7
5
10
15
20
25
30
35
40
45
50
55
60
65
70
75
80
85
90
95
100
105
110
115
120
125
130
135
140
145
150

SITE 793 HOLE B CORE 35R CORED INTERVAL 912.6-922.3 mbsf

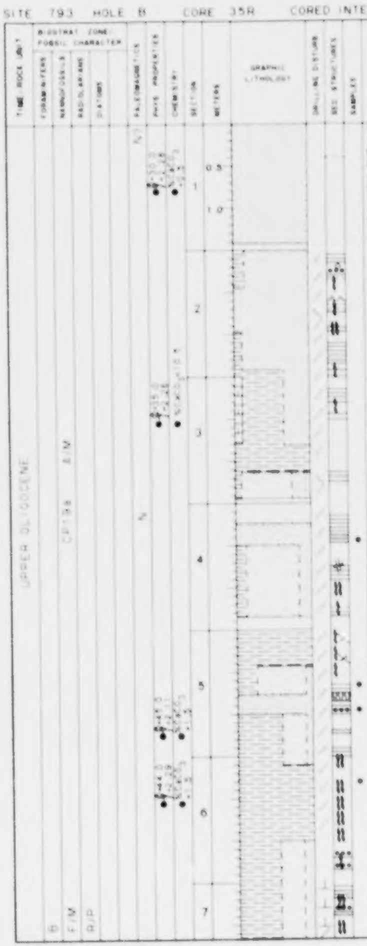
TIME-ROCK UNIT
BIOSTRAT. ZONE/ FOSSIL CHARACTER
FORAMINIFERS
NANNOFOSSILS
RADIOLARIANS
DIATOMS
PALEOMAGNETICS
PHYS. PROPERTIES
CHEMISTRY
SECTION
METERS
GRAPHIC LITHOLOGY
DRILLING DISTURB.
SED. STRUCTURES
SAMPLES
UPPER OLIGOCENE
CP19B
A/M
B
F/M
R/P
N?
N
0.5
1.0
1
2
3
4
5
6
7

LITHOLOGIC DESCRIPTION

VITRIC SILTY CLAYSTONE, CRYSTAL VITRIC SANDSTONE AND VITRIC SILTSTONE

Major lithologies:
Dark gray (5Y 4/1) slightly to intensely bioturbated VITRIC SILTY CLAYSTONE comprises 48% of the core. Trace fossils include *Chondrites* and *Zoophycos*. Grayish black (N2) greenish black (5G 2/1, 5GY 2/1) CRYSTAL VITRIC SANDSTONE and VITRIC SILTSTONE comprise 27% and 25% of the core, respectively. Section 1 is a crudely graded very coarse to medium grained sandstone bed; four other sandstone beds are 20-27 cm thick; four siltstone beds are 25-23 cm thick. The rest of the sandstone and siltstone occurs as thin (1-10 cm) divisions of graded beds that contain planar and wavy laminations. The vitric component has been largely altered.

Convolute bedding occurs in Section 5, 30-45 cm. A gypsum-lined microfracture occurs in Section 4, and two healed microfractures in Section 7.

Most of the core is slightly fractured by drilling.

SMEAR SLIDE SUMMARY (%):

	1, 44 M	[illegible] D	[illegible] M	[illegible] M
TEXTURE:				
Sand	100	—	100	5
Silt	—	20	—	15
Clay	—	80	—	80
COMPOSITION:				
Accessory minerals	1	1	10	—
Cement	5	—	5	—
Clay	—	30	—	75
Feldspar	1	2	20	1
Foraminifers	Tr	1	—	—
Glass	80	20	40	12
Inorganic calcite	Tr	—	—	—
Lithic fragments	—	5	20	5
Micrite	—	5	—	—
Nannofossils	1	25	—	8
Opaques	—	1	—	—

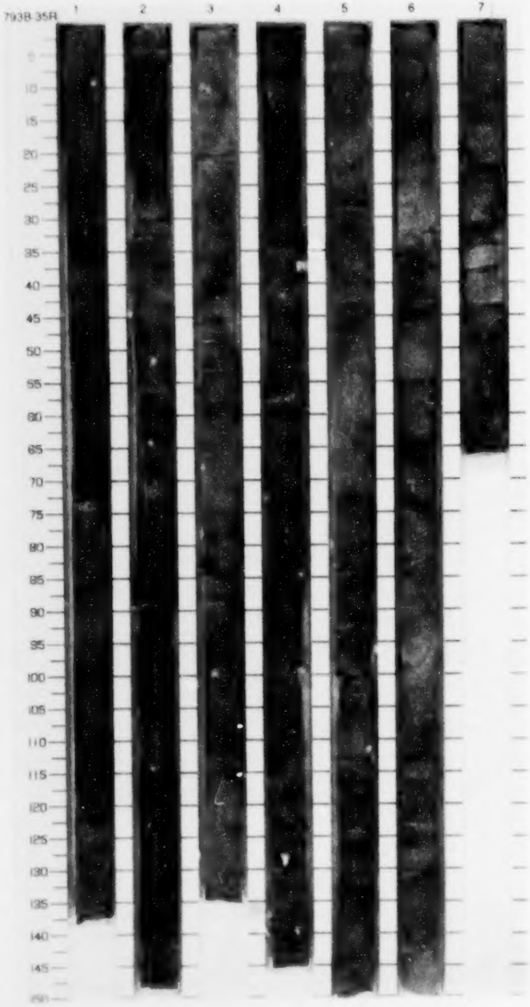
793B-35R
1
2
3
4
5
6
7
5
10
15
20
25
30
35
40
45
50
55
60
65
70
75
80
85
90
95
100
105
110
115
120
125
130
135
140
145
150

SITE 793 HOLE B CORE 36R CORED INTERVAL 922.3-932.0 mbsf

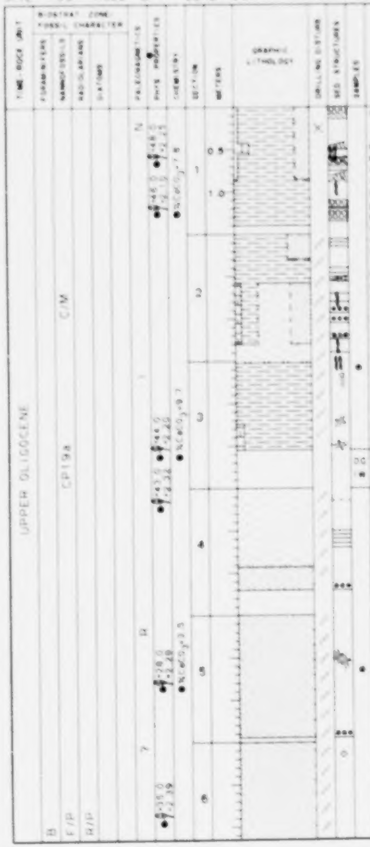
TIME-ROCK UNIT
BIOSTRAT. ZONE/ FOSSIL CHARACTER
FORAMINIFERS
NANNOFOSSILS
RADIOLARIANS
DIATOMS
PALEOMAGNETICS
PHYS. PROPERTIES
CHEMISTRY
SECTION
METERS
GRAPHIC LITHOLOGY
DRILLING DISTURB.
SED. STRUCTURES
SAMPLES
UPPER OLIGOCENE
B
F/P
R/P
C/M
CP19a
N
I
R
?
φ=48.0
γ=2.15
φ=48.0
γ=2.45
%CaCO3=7.8
φ=44.0
γ=2.26
φ=43.0
γ=2.32
%CaCO3=9.7
φ=28.0
γ=2.49
%CaCO3=3.5
φ=35.0
γ=2.39
1
2
3
4
5
6
0.5
1.0
X
OG
IW

LITHOLOGIC DESCRIPTION

CRYSTAL VITRIC SANDSTONE, VITRIC SILTSTONE AND VITRIC CLAYEY SILTSTONE

Major lithologies:
Most of the core consists of dark greenish gray (5G 4/1) and grayish black (N2) CRYSTAL VITRIC SANDSTONE (47%), VITRIC SILTSTONE (24%), and dark greenish gray (5G 4/1) VITRIC CLAYEY SILTSTONE (18%). The vitric component has been largely altered. In Sections 1 and 2, these lithologies comprise thin, normally graded beds with common parallel lamination and more rare, cross lamination. In the lower part of the core, individual beds tend to be 25-145 cm thick. The sandstone from Section 4, 92 cm to the bottom of the core is a single, inverse to normal graded unit 3.2 m thick. It contains lithic sedimentary and volcanic clasts 14 mm in diameter in Section 6, and siltstone and claystone intraclasts 20-30 mm in diameter in Section 5.

Post depositional structures include convolute bedding in Section 1, 11 and 148 cm; dewatering structures in Section 3, 9-42 cm; and two zeolite filled microfractures in Section 5, 50-58 cm.

Minor lithologies:
The rest of the core consists of dark gray (5GY 4/1) SILTY CLAYSTONE (5%) and NANNOFOSSIL RICH SILTY CLAYSTONE (4%), and greenish black (5GY 2/1) CLAYSTONE. The core is slightly fractured by drilling.

SMEAR SLIDE SUMMARY (%):

	3, 8	5, 96
	M	D
TEXTURE:		
Sand	—	40
Silt	10	35
Clay	90	25
COMPOSITION:		
Accessory minerals	Tr	5
Clay	85	20
Feldspar	Tr	10
Glass	5	51
Lithic fragments	Tr	10
Nannofossils	10	4

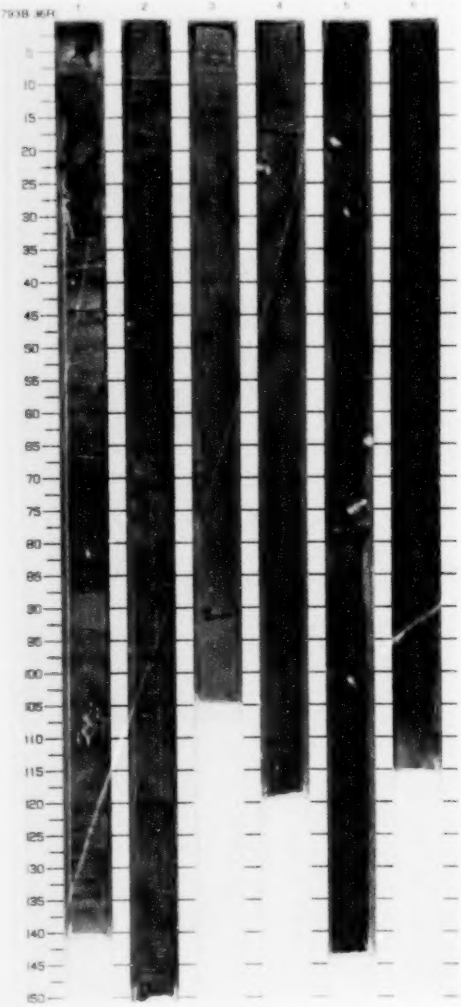
793B 36R
1
2
3
4
5
6
5
10
15
20
25
30
35
40
45
50
55
60
65
70
75
80
85
90
95
100
105
110
115
120
125
130
135
140
145
150

SITE 793 HOLE B CORE 37R CORED INTERVAL 932.0-941.6 mbsf

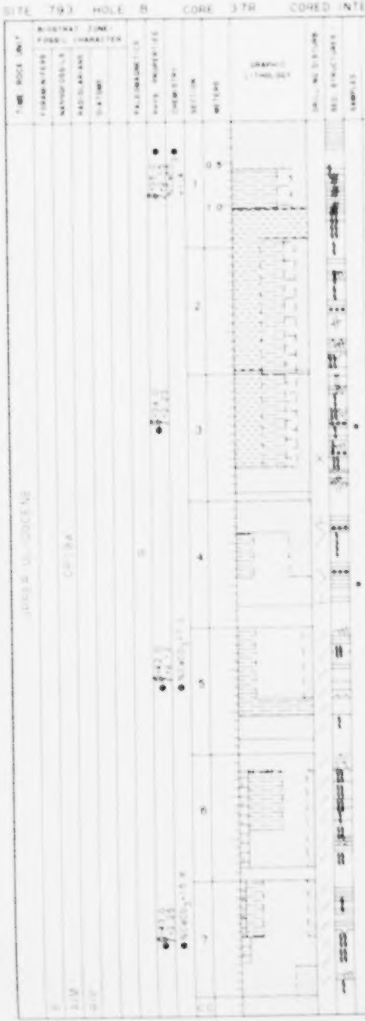
TIME ROCK UNIT
BIOSTRAT. ZONE/ FOSSIL CHARACTER
FORAMINIFERS
NANNOFOSSILS
RADIOLARIANS
DIATOMS
PALEOMAGNETICS
PHYS. PROPERTIES
CHEMISTRY
SECTION
METERS
GRAPHIC LITHOLOGY
DRILLING DISTURB.
SED. STRUCTURES
SAMPLES
UPPER OLIGOCENE
CP19A
B
R/M
R/M
0.5
1.0
1
2
3
4
5
6
7
CC

LITHOLOGIC DESCRIPTION

VITRIC SILTSTONE AND CRYSTAL VITRIC SANDSTONE

Major lithologies:
VITRIC SILTSTONE, slightly to heavily bioturbated, in various shades of gray, greenish black [illegible] and generally darker CRYSTAL VITRIC SANDSTONE [illegible] comprise [illegible] and [illegible] of the core, respectively. The vitric component has been largely altered. Each of these lithologies occurs as [illegible] thick, well [illegible] graded [illegible] with each other and with the minor lithologies. Planar lamination is common; cross lamination and wavy laminations are rare. [illegible] depositional structures include [illegible] in Section 1, [illegible] in Section 3, a [illegible] in Section 3 and two [illegible] in Section 5.

Minor lithologies:
The rest of the core consists of variously colored SILTY CLAYSTONE [illegible], CLAYSTONE [illegible], NANNOFOSSIL-RICH SILTY CLAYSTONE [illegible], SANDY MUDSTONE [illegible] and CLAYEY SILTSTONE [illegible].

Drilling deformation is severe in Sections 1-3; Sections 4-5 moderately to highly fractured and Sections 6-7 are slightly fractured.

SMEAR SLIDE SUMMARY (%):

	3, [illegible]	3, [illegible]
	D	M
TEXTURE:		
Sand	[illegible]	
Silt		[illegible]
Clay		[illegible]
COMPOSITION:		
Accessory minerals	[illegible]	[illegible]
Clay	[illegible]	[illegible]
Feldspar	[illegible]	[illegible]
Glass	[illegible]	[illegible]
Lithic fragments	[illegible]	[illegible]
Micrite		[illegible]
Nannofossils		[illegible]

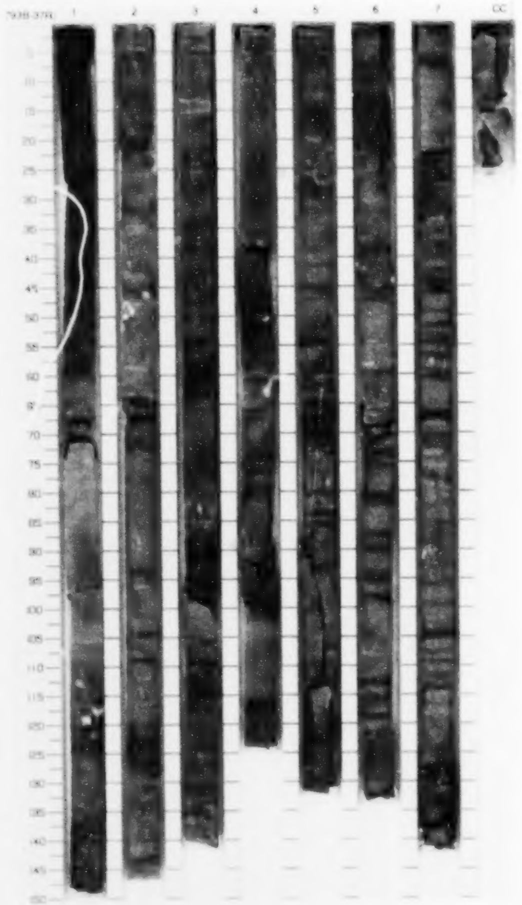
793B-37R
1
2
3
4
5
6
7
CC
5
10
15
20
25
30
35
40
45
50
55
60
65
70
75
80
85
90
95
100
105
110
115
120
125
130
135
140
145
150

SITE 793 HOLE B CORE 38R CORED INTERVAL 941.6-951.3 mbsf

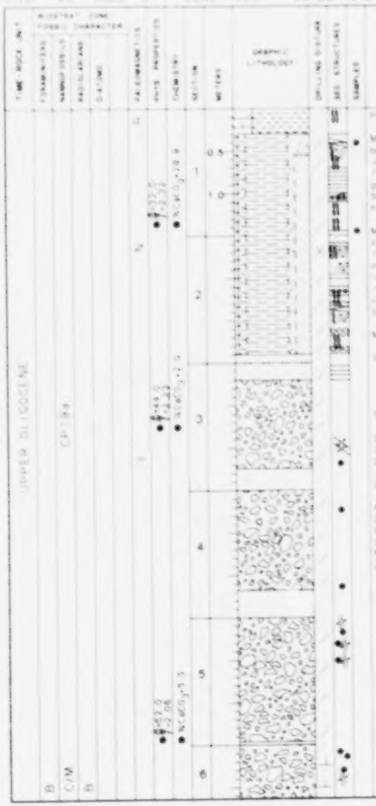
TIME-ROCK UNIT
BIOSTRAT. ZONE / FOSSIL CHARACTER
FORAMINIFERS
NANNOFOSSILS
RADIOLARIANS
DIATOMS
PALEOMAGNETICS
PHYS. PROPERTIES
CHEMISTRY
SECTION
METERS
GRAPHIC LITHOLOGY
DRILLING DISTURB.
SED. STRUCTURES
SAMPLES
UPPER OLIGOCENE
CP19a
B
C/M
B
R
N
?
φ=33.6
γ=2.32
%CaCO3=28.9
φ=44.6
γ=2.23
%CaCO3=12.5
φ=37.6
γ=2.06
%CaCO3=3.5
1
2
3
4
5
6
0.5
1.0

LITHOLOGIC DESCRIPTION

POLYMICTIC CONGLOMERATE

Major lithology: The lower 58% of the core consists of dark greenish gray (5G 4/1) and olive black (5Y 2/1) POLYMICTIC CONGLOMERATE with pumice and volcanic lithic clasts, and claystone and siltstone intraclasts larger than 10 cm. Maximum sizes of volcanic clasts are 7-13 mm. Mean sizes of the ten largest clasts in each section are 3-10 mm, and sand: granule:pebble ratios are 40:40:20, 25:40:35, and 45:30:25 in Sections 1 to 3, respectively. Structural features are microfaults in Section 1, microfractures in Section 3, and zeolite-filled fractures in Sections 5 and 6.

Minor lithologies:
In Sections 1 and 2, thin, graded beds of dark gray (5Y 4/1) VITRIC SILTY CLAYSTONE, 7-18 cm thick, with planar laminations and less common wedge and cross laminations are intercalated gradationally with dark greenish gray (5G 4/1), greenish gray (5G 5/1, 5BG 6/1) slightly to intensely bioturbated NANNOFOSSIL-RICH CLAYSTONE layers 3-30 cm thick. These lithologies respectively comprise only 15% and 12% of the core. Related lithologies comprise the rest of the core: VITRIC SANDSTONE (8%), VITRIC SANDY SILTSTONE (4%), VITRIC SILTSTONE (3%), and VITRIC CLAYEY SILTSTONE (1%).

Most of the core is slightly fractured by drilling.

SMEAR SLIDE SUMMARY (%):

	1, 45	1, 139
	D	M
TEXTURE:		
Sand	25	5
Silt	75	25
Clay	—	70
COMPOSITION:		
Accessory minerals	Tr	1
Clay	—	60
Feldspar	Tr	5
Glass	100	—
Nannofossils	Tr	8
Zeolite	—	25

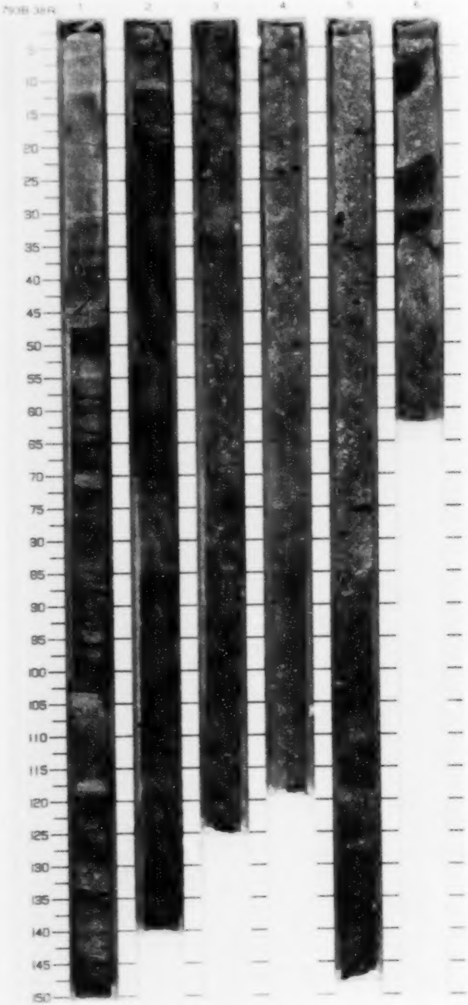
793B-38R
1
2
3
4
5
6
5
10
15
20
25
30
35
40
45
50
55
60
65
70
75
80
85
90
95
100
105
110
115
120
125
130
135
140
145
150

SITE 793 HOLE B CORE 39R CORED INTERVAL 951.3-961.0 mbsf

TIME-ROCK UNIT	BIOSTRAT. ZONE/ FOSSIL CHARACTER: FORAMINIFERS	NANNOFOSSILS	RADIOLARIANS	DIATOMS	PALEOMAGNETICS	PHYS. PROPERTIES	CHEMISTRY	SECTION	METERS	GRAPHIC LITHOLOGY	DRILLING DISTURB.	SED. STRUCTURES	SAMPLES	LITHOLOGIC DESCRIPTION
UPPER OLIGOCENE	B	F/M	B					1	0.5		× × ×			PEBBLY PUMICEOUS SANDSTONE, SANDSTONE AND SILTY CLAYSTONE Major lithologies: 45% of the core is greenish black (10Y 2/1), crudely laminated PEBBLY PUMICEOUS SANDSTONE and medium-grained SANDSTONE with shale intraclasts flattened parallel to bedding. The rest of the core is greenish black (5GY 2/1) SILTY CLAYSTONE. The silty claystone is cut by a fault that dips at 40°. This short core consists of drilling breccia.

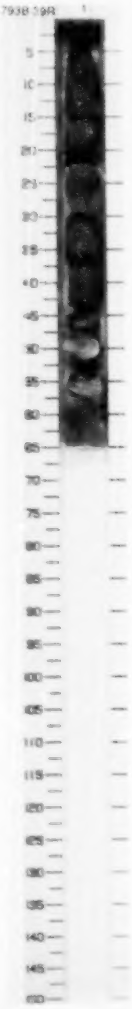
793B-39R
1
5
10
15
20
25
30
35
40
45
50
55
60
65
70
75
80
85
90
95
100
105
110
115
120
125
130
135
140
145
150

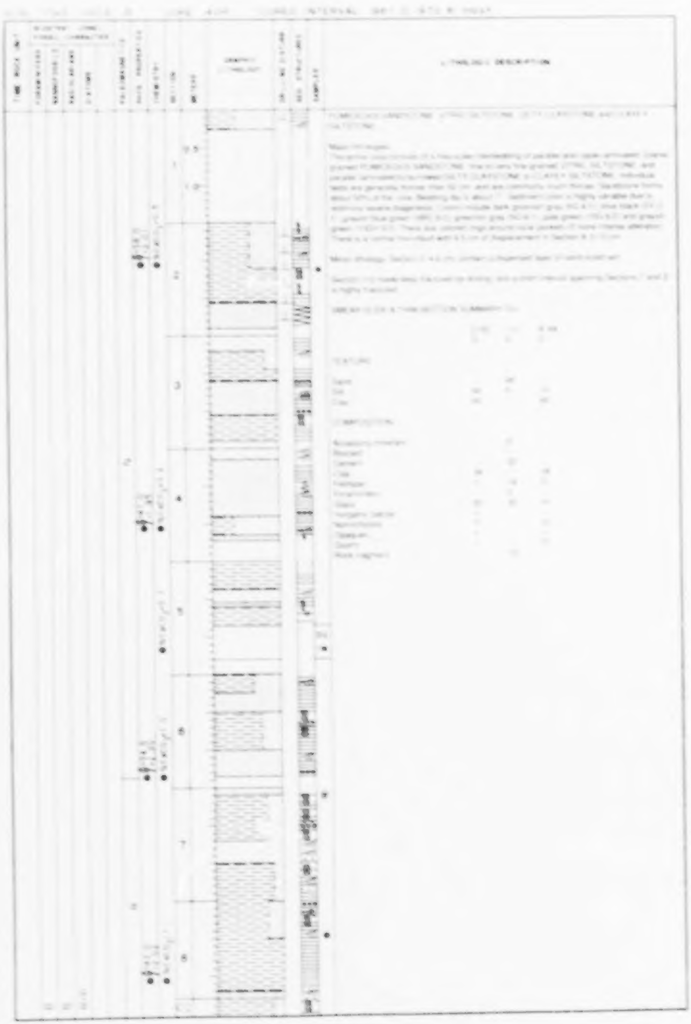

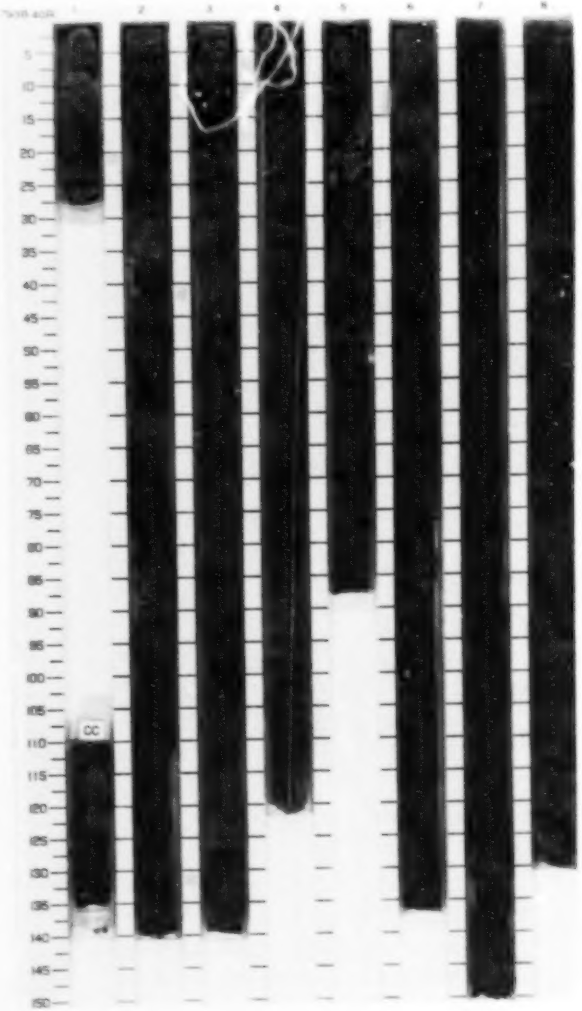

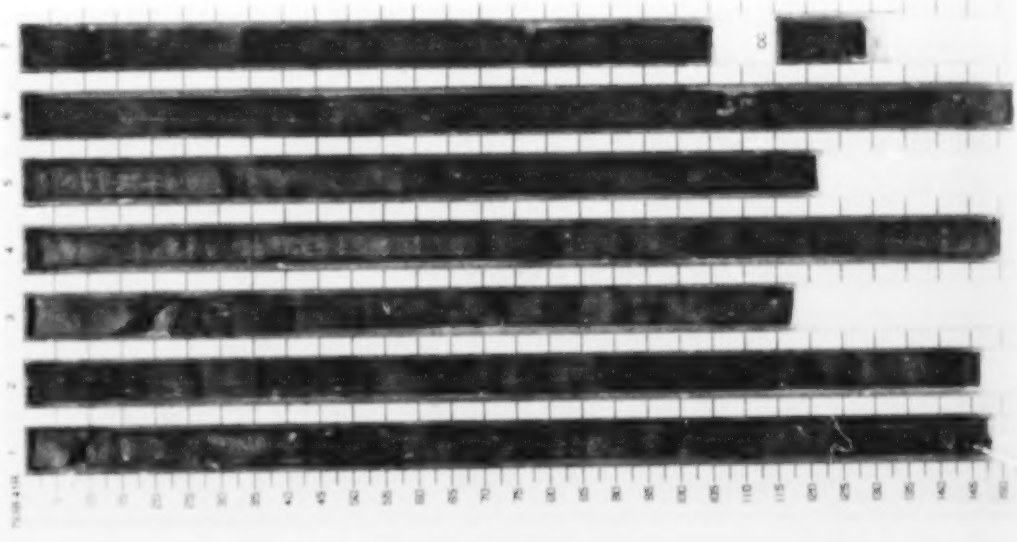
1
2
3
4
5
6
7
CC
793B-4R
0
5
10
15
20
25
30
35
40
45
50
55
60
65
70
75
80
85
90
95
100
105
110
115
120
125
130
135
140
145
150

SITE 793 HOLE B CORE 4 R CORED INTERVAL
LITHOLOGIC DESCRIPTION

SITE 793 HOLE B CORE 42R CORED INTERVAL 980.3-989.7 mbsf

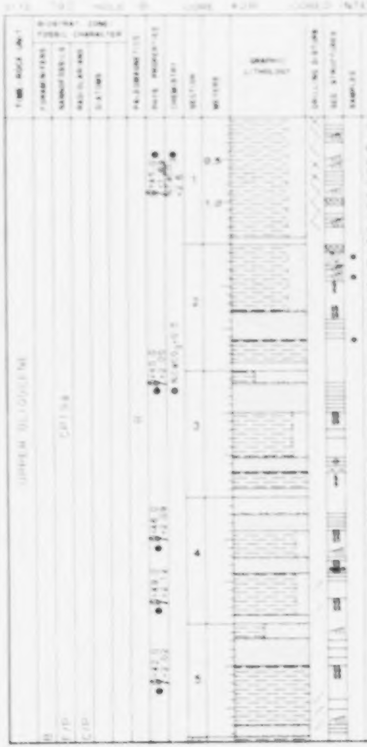
TIME-ROCK UNIT
BIOSTRAT. ZONE/ FOSSIL CHARACTER
FORAMINIFERS
NANNOFOSSILS
RADIOLARIANS
DIATOMS
PALEOMAGNETICS
PHYS. PROPERTIES
CHEMISTRY
SECTION
METERS
GRAPHIC LITHOLOGY
DRILLING DISTURB.
SED. STRUCTURES
SAMPLES
UPPER OLIGOCENE
CP19
B
F/P
C/P
0.5
1.0
1
2
3
4
5

LITHOLOGIC DESCRIPTION

SILTY CLAYSTONE, VITRIC SILTSTONE AND PUMICEOUS SANDSTONE

Major lithologies: About 75% of the core consists of very thinly and thinly interbedded dark greenish gray (5G 4/1) and greenish black (5G 2/1) parallel laminated to burrowed SILTY CLAYSTONE and parallel to ripple laminated VITRIC SILTSTONE. The vitric component has been largely altered. Most of the siltstones has the same color as the silty claystone, but some beds are medium bluish gray (5B 5/1). The rest of the core consists of medium to thick beds of greenish black (5G 2/1), dark greenish gray (5G 4/1) and medium bluish gray (5B 5/1) parallel to ripple laminated PUMICEOUS SANDSTONE. The basal part of these beds may be inversely graded due to the occurrence of relatively large, low density pumice clasts well above the base of the beds.

Bedding dips at 7° (Section 3, 3-15 cm), indicates a normal microfault.

Most of Section 1 is highly fractured by drilling, or is a drilling breccia. Parts of Sections 4 and 5 are slightly fractured.

SMEAR SLIDE SUMMARY (%):

	1, 75 D	2, 40 D	3, 100 D
TEXTURE:			
Silt	40	30	20
Clay	60	70	80
COMPOSITION:			
Clay	40	54	70
Fe-oxide	—	—	—
Feldspar	—	1	Tr
Glass	44	30	15
Inorganic calcite	—	—	—
Micrite	—	—	—
Nannofossils	5	5	—
Opaques	—	—	—
Quartz	—	—	Tr

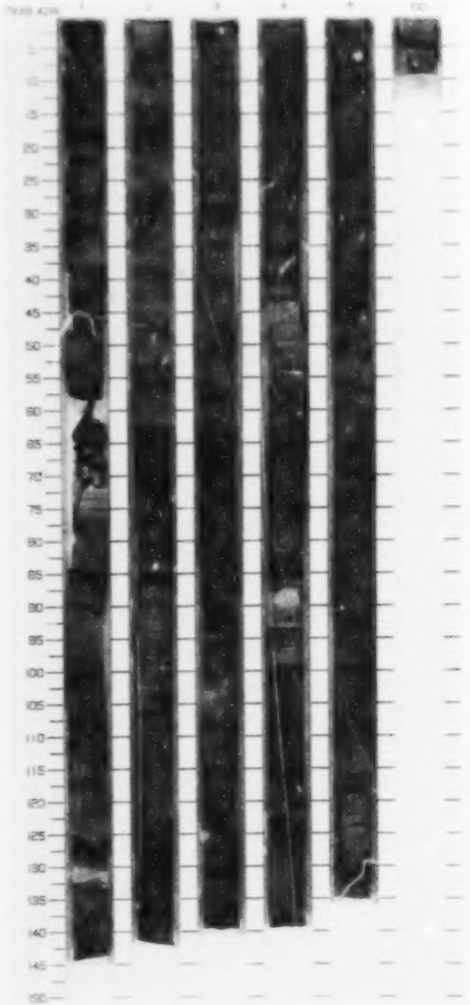
793B-42R
1
2
3
4
5
CC
5
10
15
20
25
30
35
40
45
50
55
60
65
70
75
80
85
90
95
100
105
110
115
120
125
130
135
140
145
150

SITE 793 HOLE B CORE 43R CORED INTERVAL 989.7-999.4 mbsf

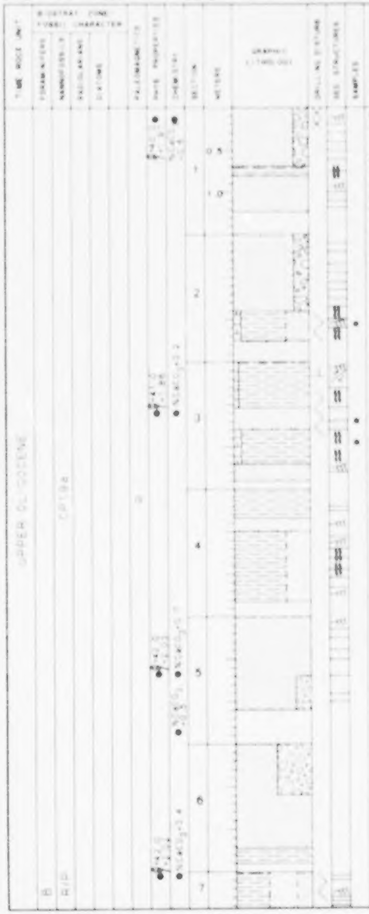
TIME-ROCK UNIT
BIOSTRAT. ZONE/FOSSIL CHARACTER
FORAMINIFERS
NANNOFOSSILS
RADIOLARIANS
DIATOMS
PALEOMAGNETICS
PHYS. PROPERTIES
CHEMISTRY
SECTION
METERS
GRAPHIC LITHOLOGY
DRILLING DISTURB.
SED. STRUCTURES
SAMPLES
UPPER OLIGOCENE
CP19B
B
R/P
0.5
1.0
1
2
3
4
5
6
7

LITHOLOGIC DESCRIPTION

PUMICEOUS SANDSTONE, PUMICEOUS AND SCORIACEOUS PEBBLY SANDSTONE, VITRIC SILTSTONE, SILTY CLAYSTONE AND NANNOFOSSIL-RICH SILTY CLAYSTONE

Major lithologies:
About 50% of the core consists of thick to very thick beds of dusky blue green (5BG 3/2) to greenish black (5GY 2/1) to grayish blue green (5BG 5/2) to pale green (10G 6/2) to dark greenish gray (5G 4/1), structureless or parallel- to ripple-laminated, very coarse to fine grained PUMICEOUS SANDSTONE and PUMICEOUS AND SCORIACEOUS PEBBLY SANDSTONE. Some levels in these beds are rich in pumice pebbles as large as 1.3 cm across; the upward transitions into these levels show inverse grading. The rest of the core consists of a very thin to medium scale interbedding of greenish black (5GY 2/1), parallel laminated to burrowed SILTY CLAYSTONE, graded beds of parallel- to ripple-laminated VITRIC SILTSTONE, and light olive gray (5Y 5/2), burrowed NANNOFOSSIL-RICH SILTY CLAYSTONE. The vitric component has been largely altered. Bedding dips at [illegible]

Short intervals in Sections 2, 3 and 7 are highly fractured by drilling.

SMEAR SLIDE SUMMARY (%):

	2, 107	3, 70	3, 90
	D	D	D
TEXTURE:			
Silt	80	80	80
Clay	20	20	20
COMPOSITION:			
Clay	[illegible]	[illegible]	[illegible]
Feldspar	[illegible]	[illegible]	[illegible]
Glass	[illegible]	[illegible]	[illegible]
Hornblende	[illegible]		
Nannofossils	[illegible]	[illegible]	[illegible]
Opaques	[illegible]	[illegible]	[illegible]
Quartz	[illegible]	[illegible]	[illegible]

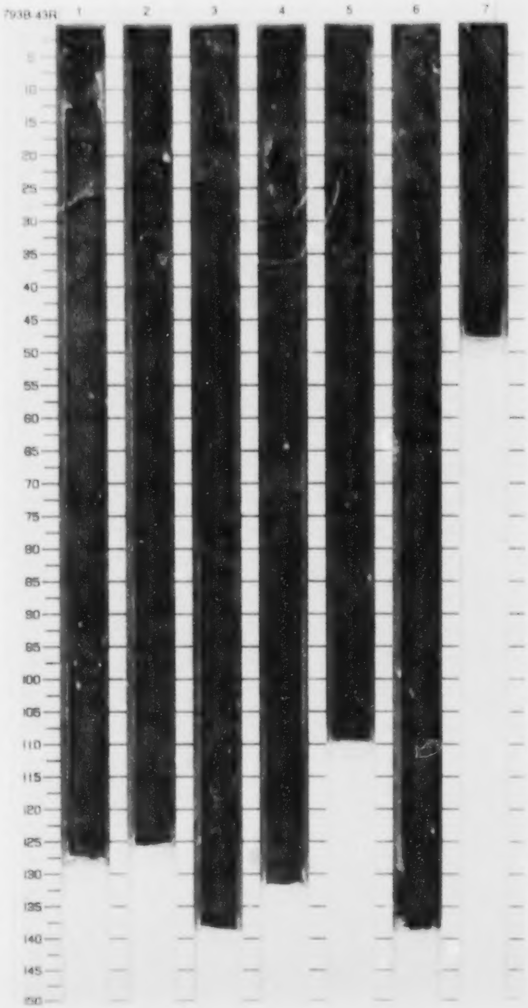
793B-43R
1
2
3
4
5
6
7
5
10
15
20
25
30
35
40
45
50
55
60
65
70
75
80
85
90
95
100
105
110
115
120
125
130
135
140
145
150

SITE 793 HOLE B CORE 44R CORED INTERVAL 999.4-1009.1 mbsf

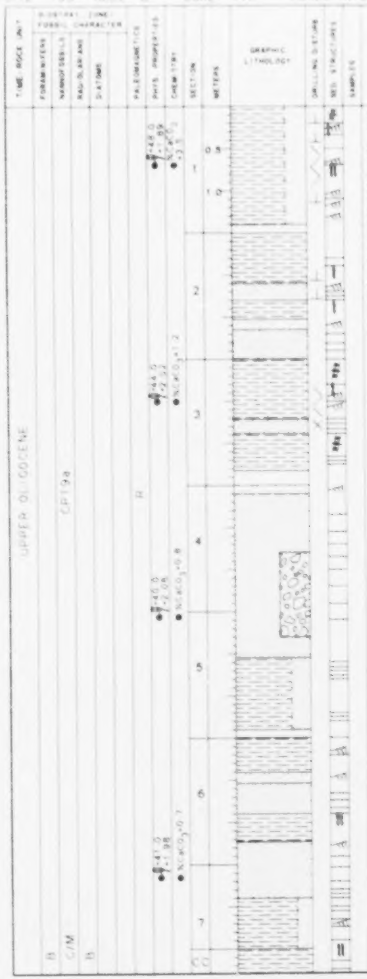
TIME-ROCK UNIT
BIOSTRAT. ZONE/FOSSIL CHARACTER
FORAMINIFERS
NANNOFOSSILS
RADIOLARIANS
DIATOMS
PALEOMAGNETICS
PHYS. PROPERTIES
CHEMISTRY
SECTION
METERS
GRAPHIC LITHOLOGY
DRILLING DISTURB.
SED. STRUCTURES
SAMPLES
UPPER OLIGOCENE
B
CP19a
C/M
B
R
φ=48.0
γ=1.89
%CaCO3=3.5
φ=44.0
γ=2.22
%CaCO3=1.2
φ=40.0
γ=2.06
%CaCO3=0.8
φ=41.0
γ=1.98
%CaCO3=0.7
1
0.5
1.0
2
3
4
5
6
7
CC

LITHOLOGIC DESCRIPTION

SILTY CLAYSTONE, VITRIC SILTSTONE, VITRIC SANDSTONE, PUMICEOUS SANDSTONE AND PUMICEOUS GRANULE CONGLOMERATE

Major lithologies:
About 60% of the core consists of greenish black (5GY 2/1), parallel laminated to lightly burrowed SILTY CLAYSTONE. This lithology contains thin interbeds of greenish black (5GY 2/1) to medium gray (N5), parallel to ripple laminated VITRIC SILTSTONE and VITRIC SANDSTONE. The rest of the core consists of medium to very thick, graded beds of coarse- to fine-grained greenish black (5GY 2/1) and grayish blue green (5BG 5/2) PUMICEOUS SANDSTONE, in one case with a basal division of PUMICEOUS GRANULE CONGLOMERATE. The conglomerate bed is inversely graded, with the greatest concentration of pumice clasts well above the base of the bed. This inverse grading is due to the low density of pumice clasts, and does not indicate significant grain interaction during transport. Clasts in the conglomerate consist of black scoria and white and red pumice.

Most of Section 1 is moderately to highly fractured by drilling. Short intervals in Sections 2 and 3 show similar fracturing.

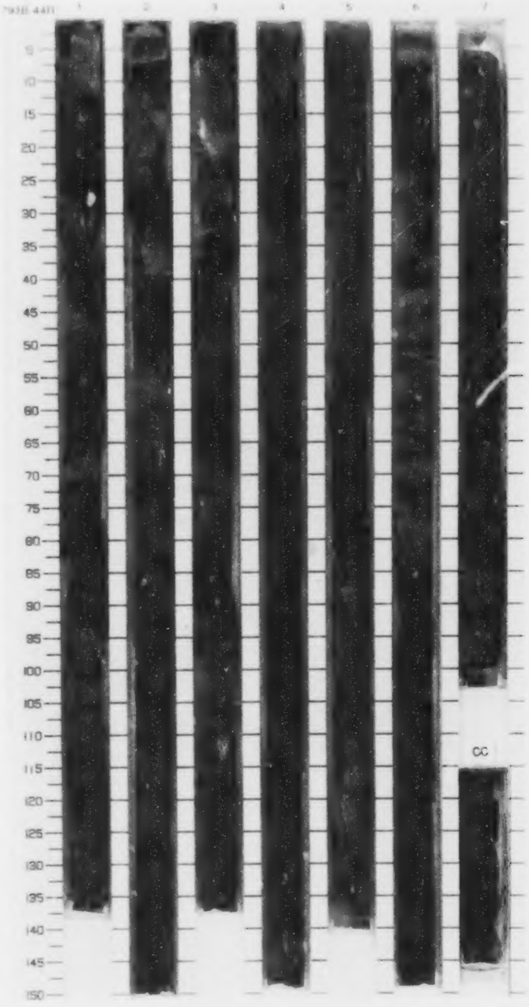
793B-44R
1
2
3
4
5
6
7
5
10
15
20
25
30
35
40
45
50
55
60
65
70
75
80
85
90
95
100
105
110
115
120
125
130
135
140
145
150
CC

SITE 793 HOLE B CORE 45R CORED INTERVAL 1009.1-1018.7 mbsf

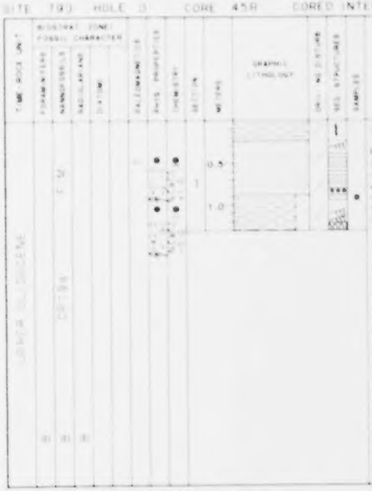
TIME-ROCK UNIT
BIOSTRAT. ZONE/ FOSSIL CHARACTER
FORAMINIFERS
NANNOFOSSILS
RADIOLARIANS
DIATOMS
PALEOMAGNETICS
PHYS. PROPERTIES
CHEMISTRY
SECTION
METERS
GRAPHIC LITHOLOGY
DRILLING DISTURB.
SED. STRUCTURES
SAMPLES
UPPER OLIGOCENE
CP19b
1
0.5
1.0
B
B
B

LITHOLOGIC DESCRIPTION

SILTY CLAYSTONE AND SANDSTONE

Major lithologies:

Section 1, 0–75 cm and 88–131 cm: consists of two different colors (greenish black (5GY 2/1) [illegible] medium bluish gray (5B 5/1)) of SILTY CLAYSTONE. The upper interval is bioturbated, whereas the lower one is locally laminated and contains very thin interbeds of more silty rippled sediment. This lower interval is rich in volcanic glass, which has been largely altered. The rest of the core consists of a graded bed of greenish black (5GY 2/1) coarse- to very fine-grained SANDSTONE, with some nodules of dark green [illegible] granules.

The entire core is slightly fractured by drilling.

SMEAR SLIDE SUMMARY (%):

	1, [illegible]
	D
TEXTURE:	
Silt	[illegible]
Clay	[illegible]
COMPOSITION:	
Clay	[illegible]
Feldspar	[illegible]
Quartz	[illegible]
Rock fragments	[illegible]
Nannofossils	[illegible]
Opaques	[illegible]

793B-45R

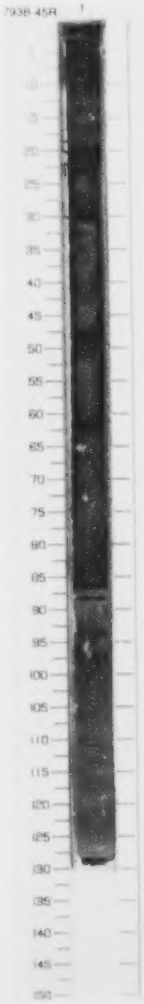
1
5
10
15
20
25
30
35
40
45
50
55
60
65
70
75
80
85
90
95
100
105
110
115
120
125
130
135
140
145
150

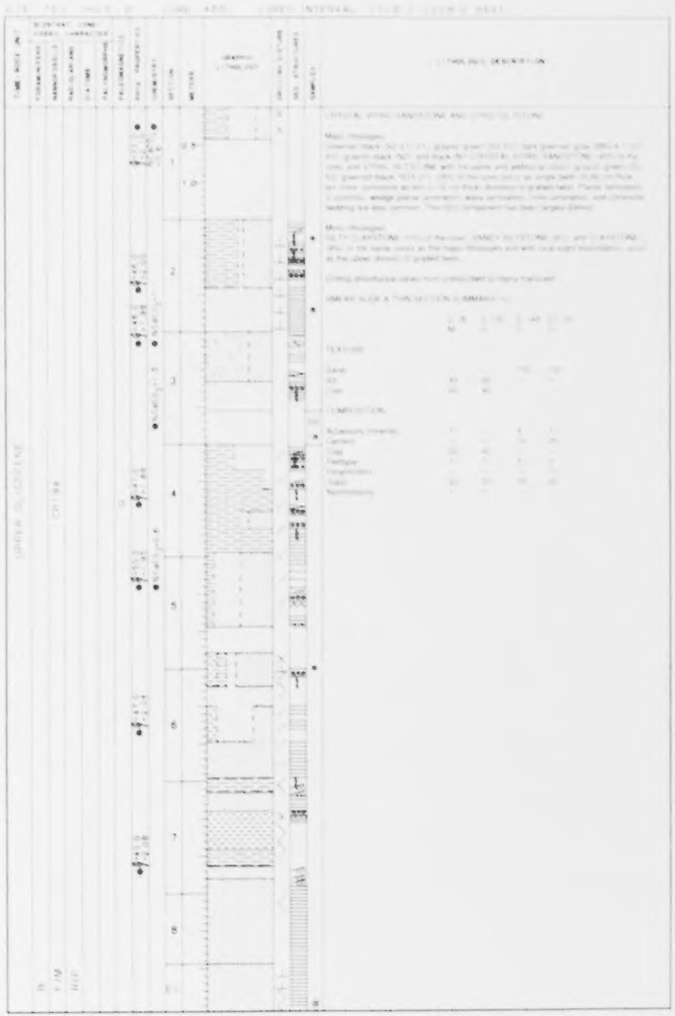

LITHOLOGIC DESCRIPTION

Major lithologies:

Minor lithologies:

SMEAR SLIDE & THIN SECTION SUMMARY (%):

TEXTURE:

Sand

Silt

Clay

COMPOSITION:

Accessory minerals

Cement

Clay

Feldspar

Glass

GRAPHIC LITHOLOGY
METERS
SECTION
SAMPLES
1
2
3
4
5
6
7
8
CC

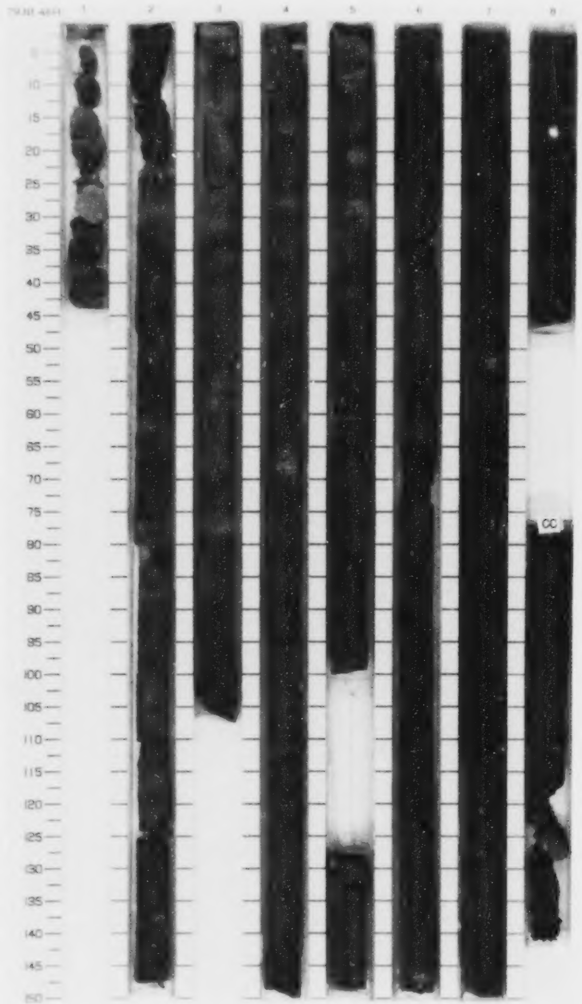

1
2
3
4
5
6
7
8
CC
0
10
15
20
25
30
35
40
45
50
55
60
65
70
75
80
85
90
95
100
105
110
115
120
125
130
135
140
145
150

SITE 793 HOLE B CORE 47R CORED INTERVAL 1028.0-1037.6 mbsf

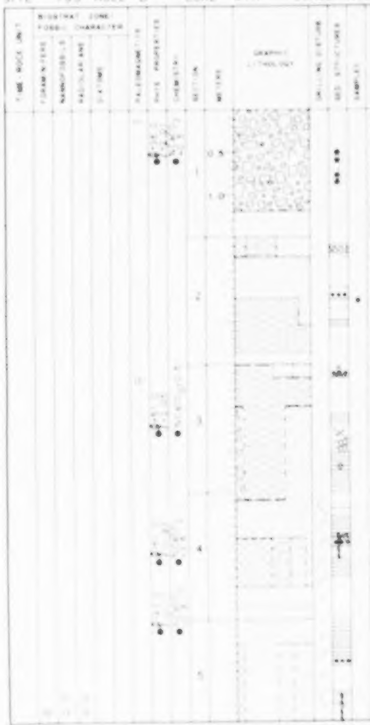
TIME-ROCK UNIT
BIOSTRAT. ZONE/ FOSSIL CHARACTER
FORAMINIFERS
NANNOFOSSILS
RADIOLARIANS
DIATOMS
PALEOMAGNETICS
PHYS. PROPERTIES
CHEMISTRY
SECTION
METERS
GRAPHIC LITHOLOGY
DRILLING DISTURB.
SED. STRUCTURES
SAMPLES
1
2
3
4
5
0.5
1.0

LITHOLOGIC DESCRIPTION

SANDY GRANULE PEBBLE VOLCANIC LITHIC CONGLOMERATE, CRYSTAL VITRIC SANDSTONE AND VITRIC SILTSTONE

Major lithologies:
The upper part ([illegible] cm) of Section 1 is a single bed of greenish black [illegible] SANDY GRANULE PEBBLE VOLCANIC LITHIC CONGLOMERATE [illegible] [illegible] [illegible] [illegible] CRYSTAL VITRIC SANDSTONE and dark greenish gray [illegible] VITRIC SILTSTONE [illegible] [illegible]

Minor lithologies:
[illegible] VITRIC SILTY CLAYSTONE [illegible] VITRIC CLAYEY SILTSTONE [illegible] and VITRIC SANDY SILTSTONE [illegible] Sections 4 and 5 are slightly disturbed by drilling.

SMEAR SLIDE SUMMARY (%):

	[illegible]	[illegible]
TEXTURE:		
Sand	[illegible]	[illegible]
Silt	[illegible]	[illegible]
Clay	[illegible]	[illegible]
COMPOSITION:		
Accessory minerals		
[illegible]	[illegible]	[illegible]
Clay	[illegible]	[illegible]
Feldspar	[illegible]	[illegible]
[illegible]	[illegible]	[illegible]
Lithic fragments	[illegible]	[illegible]
Mica	[illegible]	[illegible]
Nannofossils	[illegible]	[illegible]

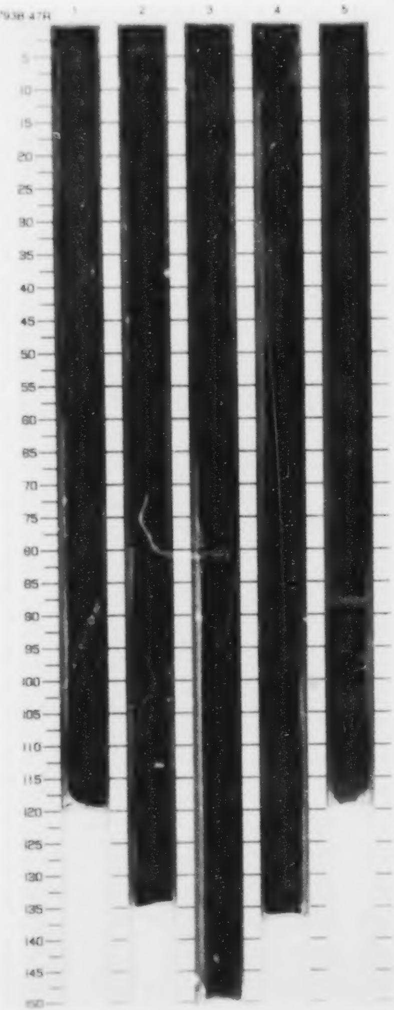
793B-47R
1
2
3
4
5
5
10
15
20
25
30
35
40
45
50
55
60
65
70
75
80
85
90
95
100
105
110
115
120
125
130
135
140
145
150

SITE 793 HOLE B CORE 48R CORED INTERVAL 1037.8-1047.5 mbsf

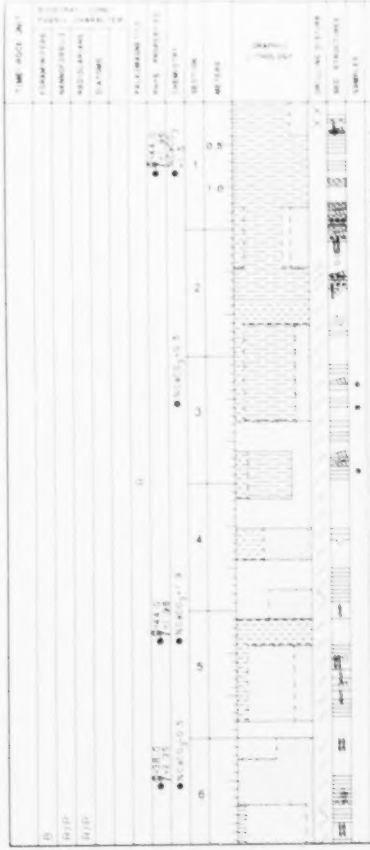
TIME-ROCK UNIT
BIOSTRAT. ZONE/ FOSSIL CHARACTER
FORAMINIFERS
NANNOFOSSILS
RADIOLARIANS
DIATOMS
PALEOMAGNETICS
PHYS. PROPERTIES
CHEMISTRY
SECTION
METERS
GRAPHIC LITHOLOGY
DRILLING DISTURB.
SED. STRUCTURES
SAMPLES
0.5
1.0
1
2
3
4
5
6
B
B/P
B/P
B

LITHOLOGIC DESCRIPTION

VITRIC SILTSTONE AND CRYSTAL VITRIC SANDSTONE

Major lithologies:
Dark greenish gray (5G 4/1), dark gray (5GY 4/1), and greenish black (5GY 2/1) VITRIC SILTSTONE, and greenish black (5G 2/1), brownish black (5YR 2/1), grayish green (5G 5/2), and grayish black (N2) CRYSTAL VITRIC SANDSTONE comprise 50% and 24% of the core respectively, as the coarser members of graded beds. The vitric component has been largely altered. Planar lamination is common; cross-lamination, wavy lamination, load casts, and convolute bedding are also present.

Minor lithologies:
The rest of the core is composed of the finer divisions of graded beds: greenish gray (5G 5/1), dark greenish gray (5BG 4/1), and dark gray (5Y 4/1) slightly to intensely bioturbated CLAYEY SILTSTONE (18%), SILTY CLAYSTONE (13%), and CLAYSTONE (15%). Slickensided microfaults with zeolite filling occur in Section 2, 120 cm and Section 6, 75 cm.

Most of the core is slightly fractured by drilling.

SMEAR SLIDE SUMMARY (%):

	2, 33	3, 47	3, 106
	D	D	D
TEXTURE:			
Sand	30	80	15
Silt	50	20	55
Clay	20	—	30
COMPOSITION:			
Accessory minerals	—	5	—
Cement	5	10	—
Clay	15	—	30
Feldspar	—	5	—
Glass	80	75	68
Lithic fragments	—	5	—
Nannofossils	—	—	2

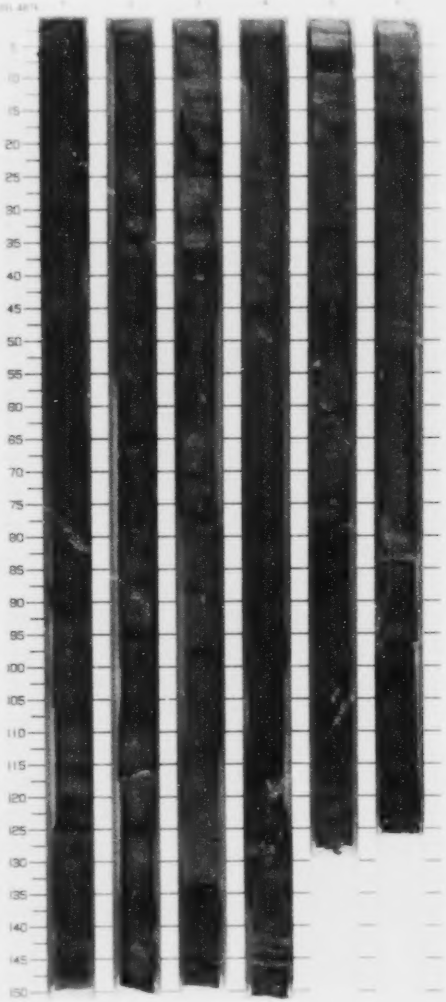
CM
1
2
3
4
5
6
5
10
15
20
25
30
35
40
45
50
55
60
65
70
75
80
85
90
95
100
105
110
115
120
125
130
135
140
145
150

SITE 793 HOLE B CORE 49R CORED INTERVAL 1047.3-1057.0 mbsf

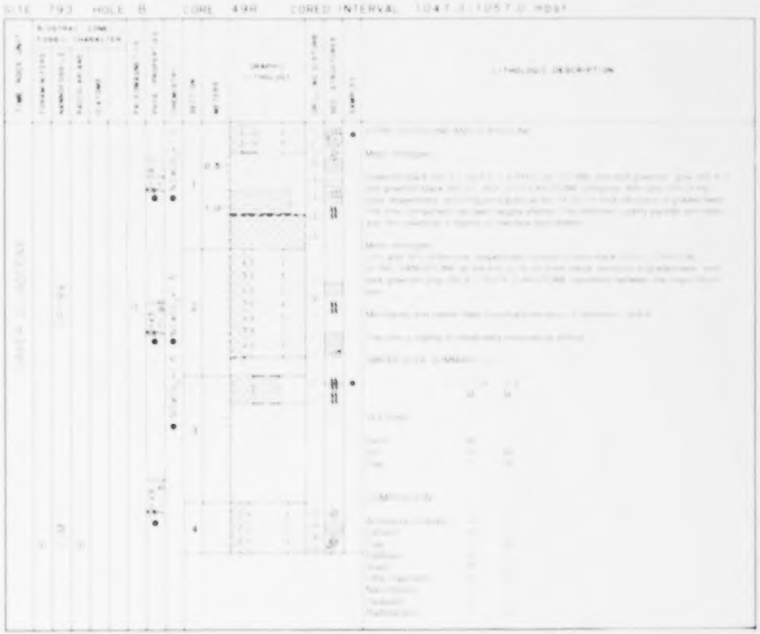
TIME-ROCK UNIT
BIOSTRAT. ZONE/FOSSIL CHARACTER
FORAMINIFERS
NANNOFOSSILS
RADIOLARIANS
DIATOMS
PALEOMAGNETICS
PHYS. PROPERTIES
CHEMISTRY
SECTION
METERS
GRAPHIC LITHOLOGY
DRILLING DISTURB.
SED. STRUCTURES
SAMPLES
LITHOLOGIC DESCRIPTION
SMEAR SLIDE SUMMARY (%):
TEXTURE:
COMPOSITION:

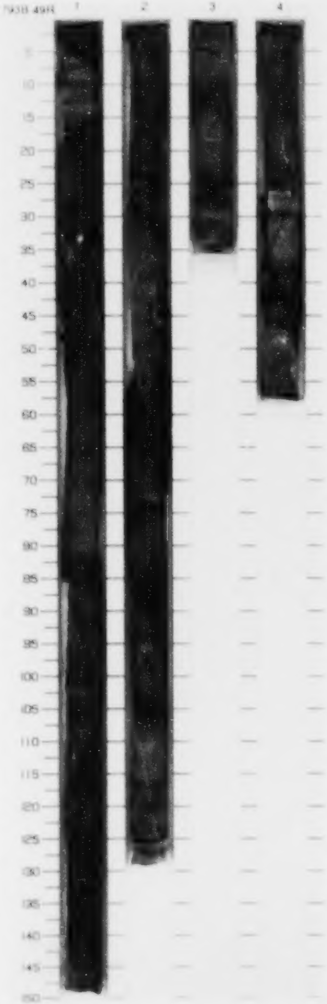
793B-49R
1
2
3
4
5
10
15
20
25
30
35
40
45
50
55
60
65
70
75
80
85
90
95
100
105
110
115
120
125
130
135
140
145
150

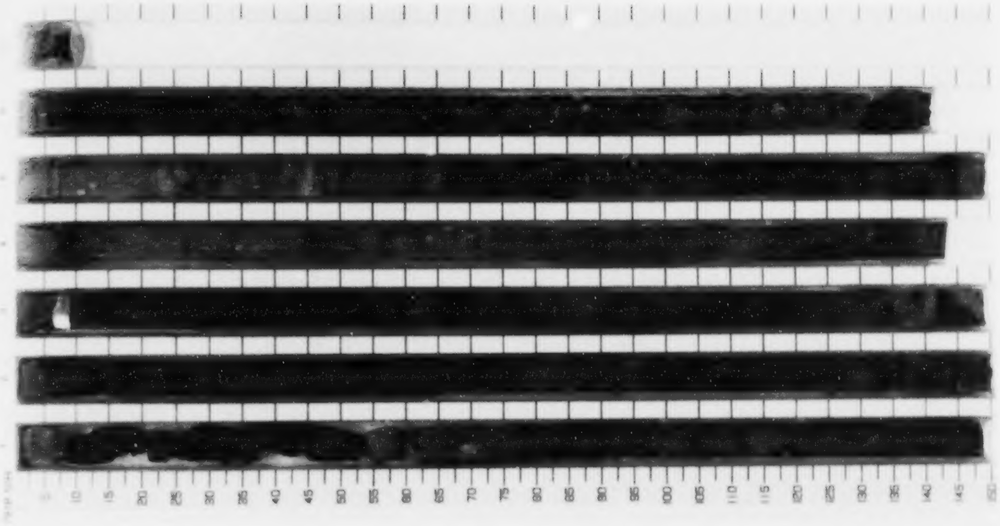

5
10
15
20
25
30
35
40
45
50
55
60
65
70
75
80
85
90
95
100
105
110
115
120
125
130
135
140
145
150

UPPER OLIGOCENE

SITE 793 HOLE B CORE 51R CORED INTERVAL 1066.7-1076.4 mbsf

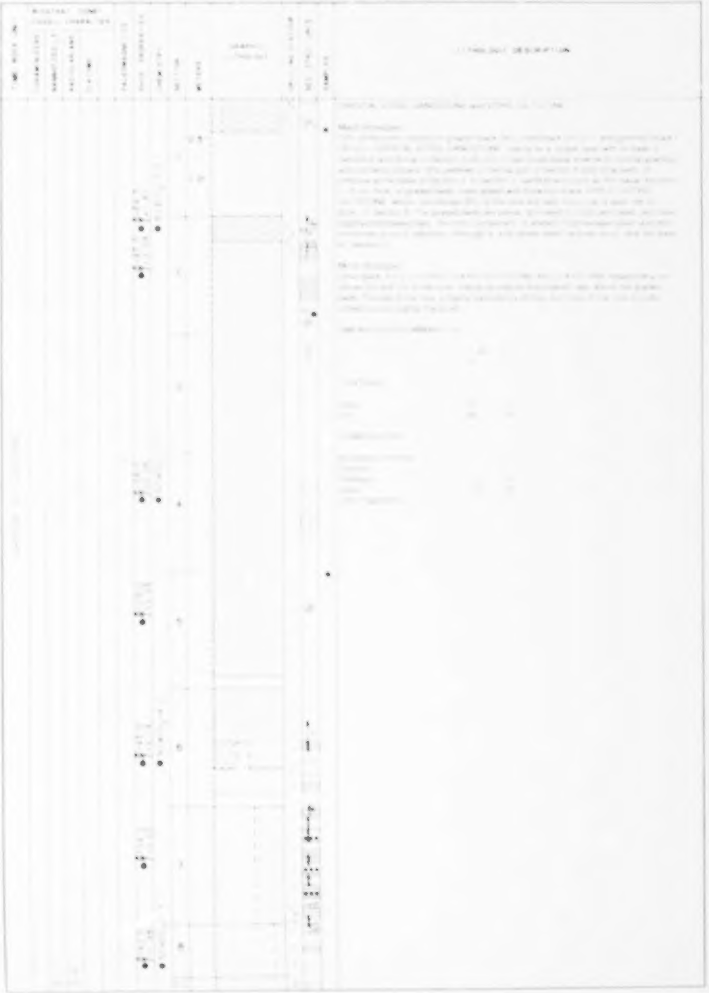
BIOSTRAT. ZONE/ FOSSIL CHARACTER
GRAPHIC LITHOLOGY
LITHOLOGIC DESCRIPTION

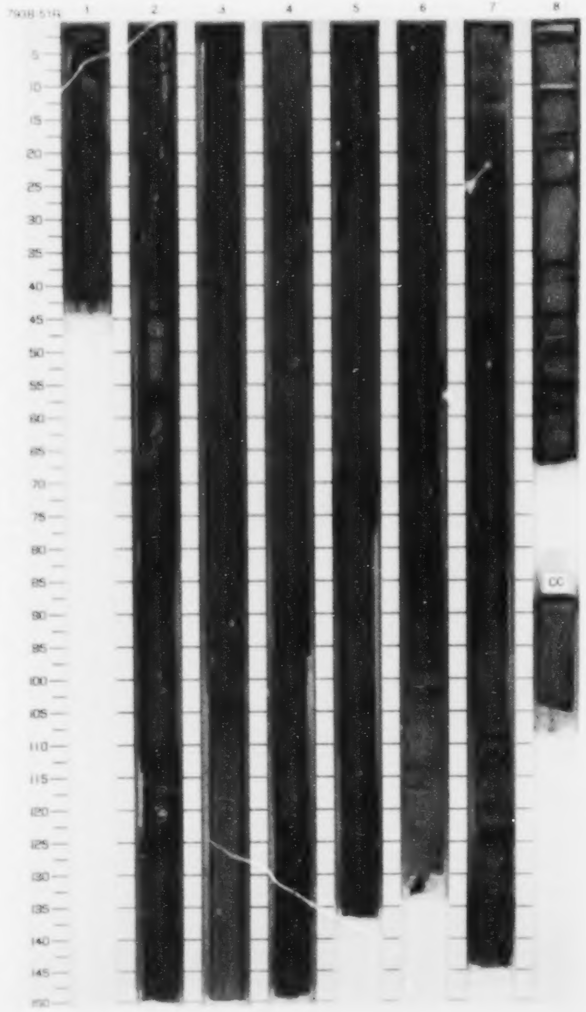
793B-51R
1
2
3
4
5
6
7
8
CC
5
10
15
20
25
30
35
40
45
50
55
60
65
70
75
80
85
90
95
100
105
110
115
120
125
130
135
140
145
150

SITE 793 HOLE B CORE [illegible] CORED INTERVAL [illegible]

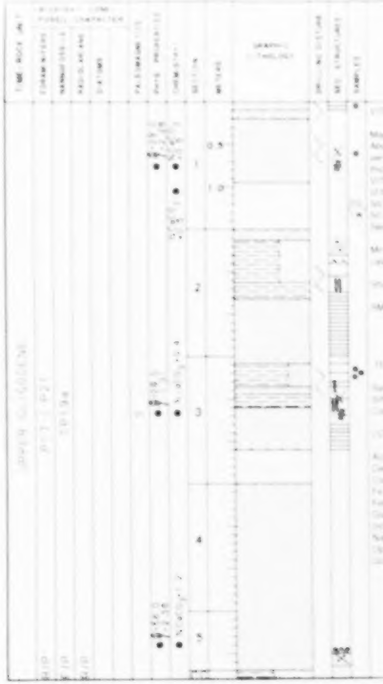
TIME-ROCK UNIT
BIOSTRAT. ZONE / FOSSIL CHARACTER
FORAMINIFERS
NANNOFOSSILS
RADIOLARIANS
DIATOMS
PALEOMAGNETICS
PHYS. PROPERTIES
CHEMISTRY
SECTION
METERS
GRAPHIC LITHOLOGY
DRILLING DISTURB.
SED. STRUCTURES
SAMPLES
UPPER OLIGOCENE
1
2
3
4
5
0.5
1.0

LITHOLOGIC DESCRIPTION

VITRIC SANDSTONE, VITRIC SILTSTONE AND SILTY CLAYSTONE

Major lithologies:
About 70% of the core consists of thin to very thick beds of grayish black (N2), fine to very coarse-grained, parallel-laminated to unstructured VITRIC SANDSTONE. The thickest bed is about 3 m thick. The uppermost part of some of these beds fines to VITRIC SILTSTONE. The rest of the core consists of interbedded very thin to thin beds of fine- to very fine-grained vitric sandstone and dark greenish gray (5G 4/1), burrowed SILTY CLAYSTONE. Bedding dips at 7°. Sub-vertical fractures occur in Section 1, [illegible] cm, Section [illegible], [illegible] cm, and Section 5, [illegible] cm. There is a normal microfault in Section [illegible], [illegible] cm.

Minor lithology: Section [illegible], [illegible] cm, consists of crystalline, granule-sized grains of calcite, apparently as an alteration of pumice grains.

Short intervals in Sections 1 through 5 are highly fractured by drilling.

SMEAR SLIDE SUMMARY (%):

	[illegible]	[illegible]	[illegible]	[illegible]	[illegible]	[illegible]
TEXTURE:						
Sand	[illegible]	[illegible]	[illegible]	[illegible]	[illegible]	[illegible]
Silt	[illegible]	[illegible]	[illegible]	[illegible]	[illegible]	[illegible]
Clay	[illegible]	[illegible]	[illegible]	[illegible]	[illegible]	[illegible]
COMPOSITION:						
Accessory minerals	[illegible]	[illegible]	[illegible]	[illegible]	[illegible]	[illegible]
Cement	[illegible]	[illegible]	[illegible]	[illegible]	[illegible]	[illegible]
Clay	[illegible]	[illegible]	[illegible]	[illegible]	[illegible]	[illegible]
Fe-oxide	[illegible]	[illegible]	[illegible]	[illegible]	[illegible]	[illegible]
Feldspar	[illegible]	[illegible]	[illegible]	[illegible]	[illegible]	[illegible]
Glass	[illegible]	[illegible]	[illegible]	[illegible]	[illegible]	[illegible]
Inorganic calcite	[illegible]	[illegible]	[illegible]	[illegible]	[illegible]	[illegible]
Nannofossils	[illegible]	[illegible]	[illegible]	[illegible]	[illegible]	[illegible]
Opaques	[illegible]	[illegible]	[illegible]	[illegible]	[illegible]	[illegible]
Quartz	[illegible]	[illegible]	[illegible]	[illegible]	[illegible]	[illegible]

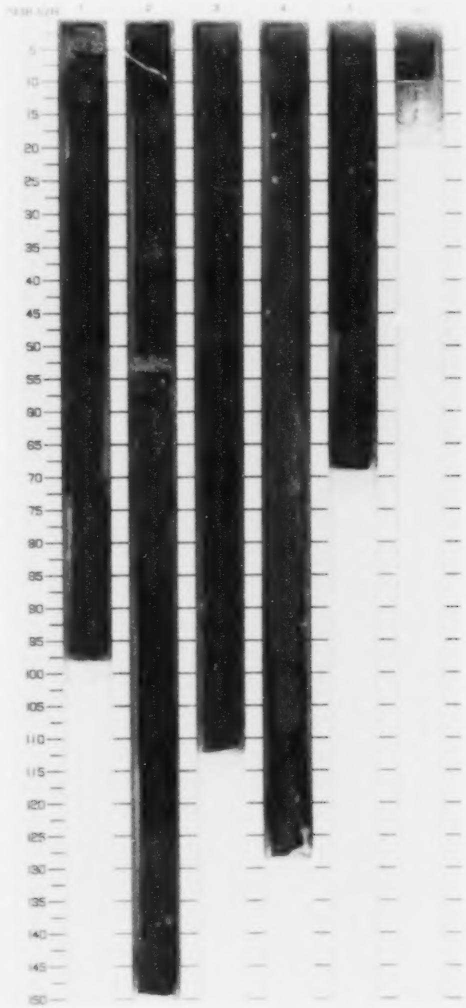
1
2
3
4
5
CC
0
5
10
15
20
25
30
35
40
45
50
55
60
65
70
75
80
85
90
95
100
105
110
115
120
125
130
135
140
145
150

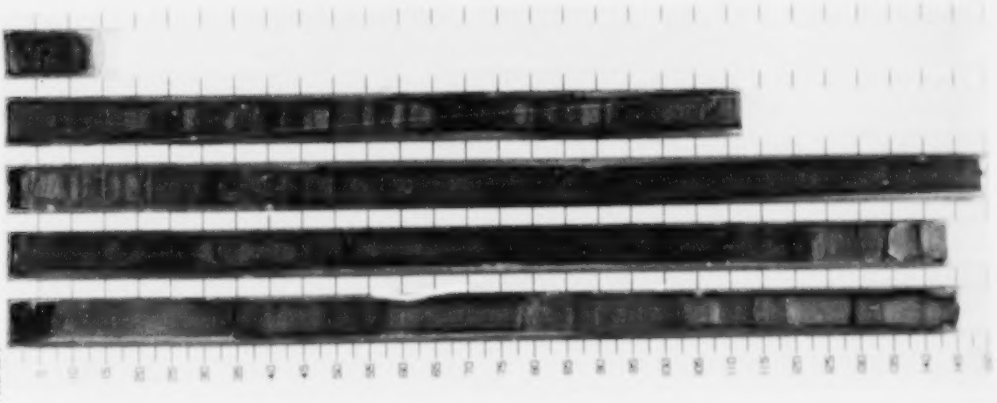
793B-53R
1
2
3
4
CC

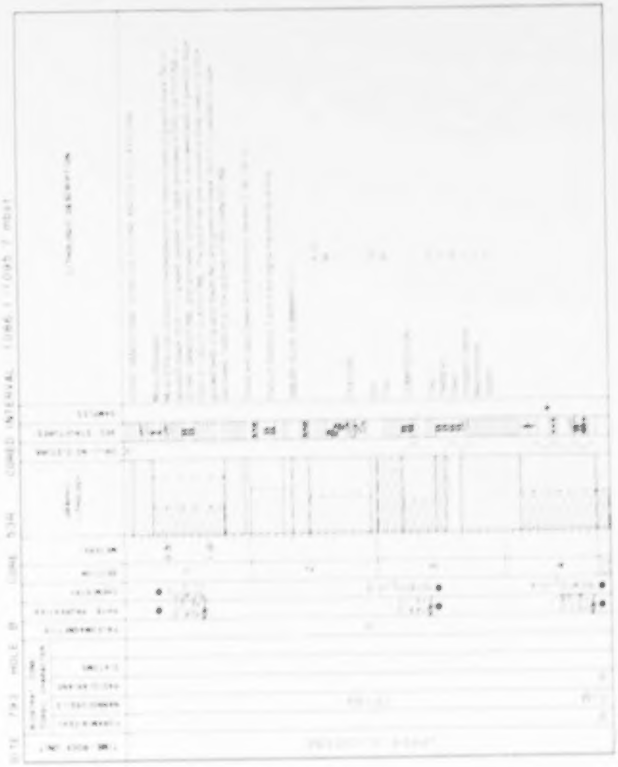
SITE 793 HOLE B CORE 53R CORED INTERVAL 1086.1-1095.7 mbsf
LITHOLOGIC DESCRIPTION

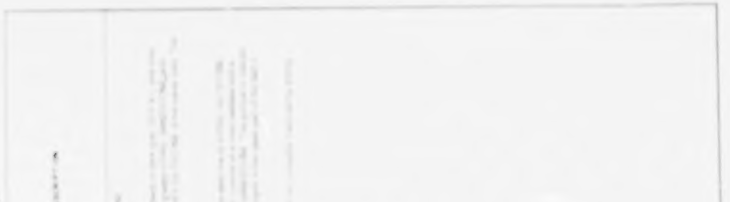

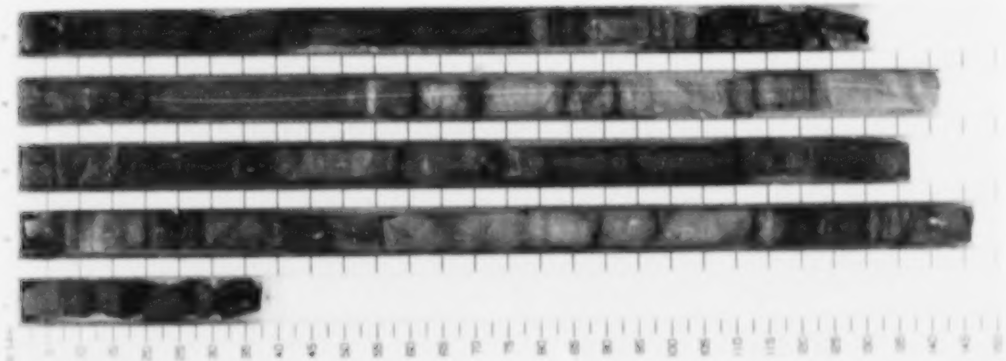

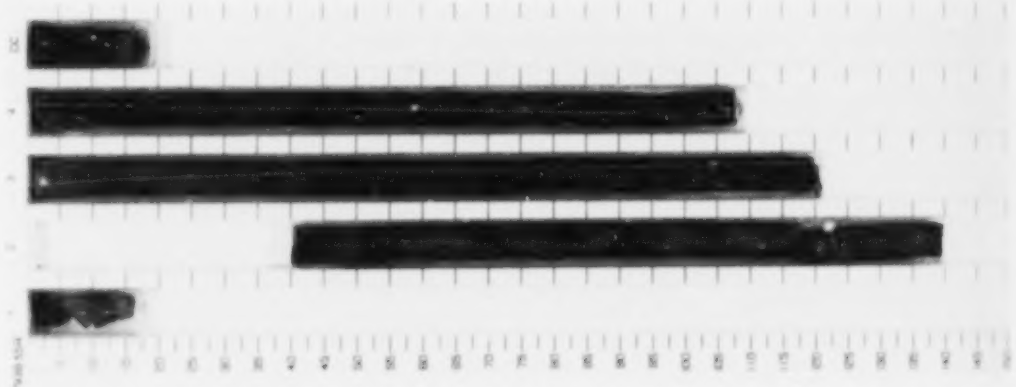

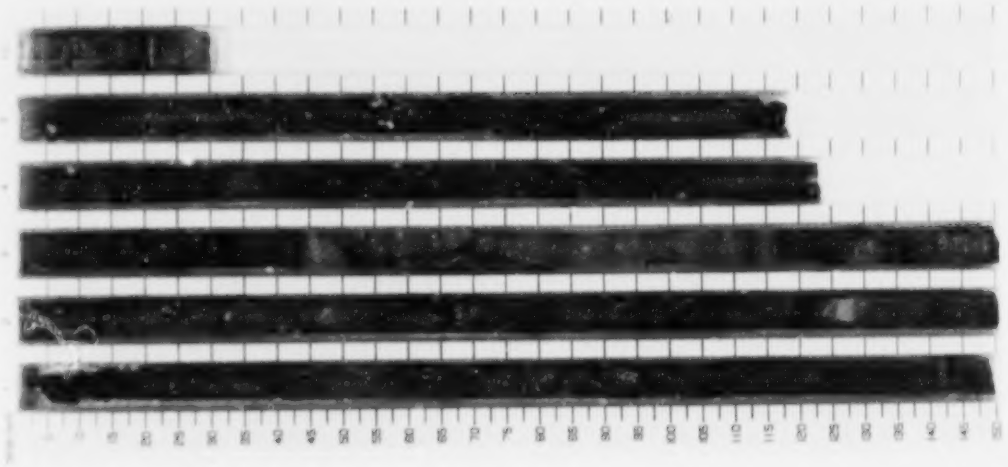

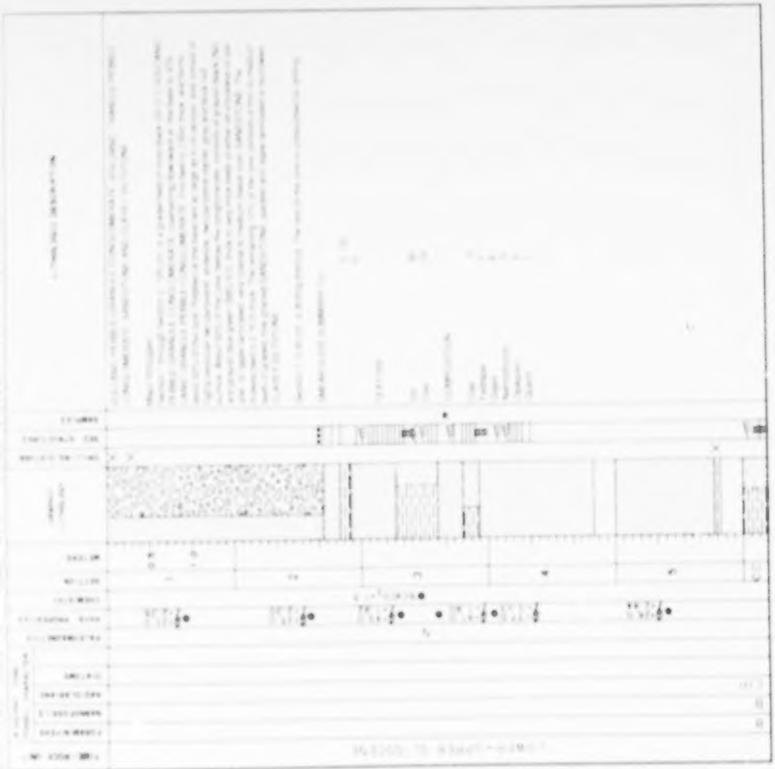

SITE 793 HOLE B CORE 57R CORED INTERVAL 1124.7-1134.0 mbsf

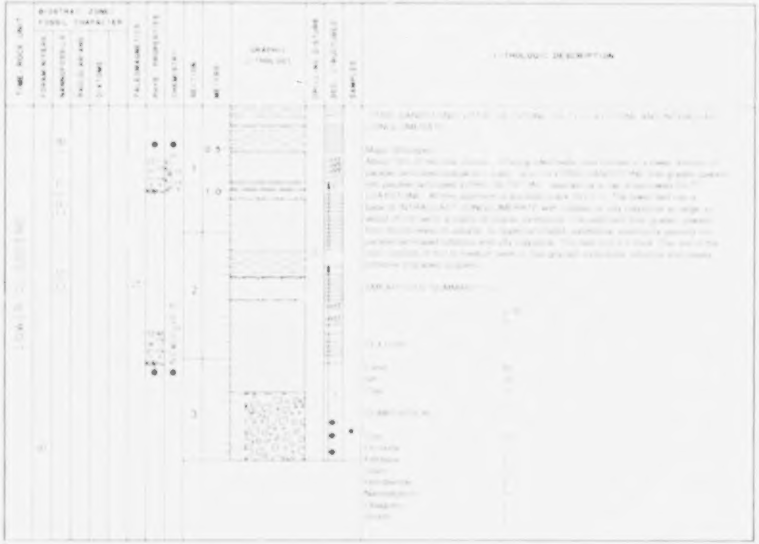
TIME-ROCK UNIT
BIOSTRAT. ZONE/FOSSIL CHARACTER
FORAMINIFERS
NANNOFOSSILS
RADIOLARIANS
DIATOMS
PALEOMAGNETICS
PHYS. PROPERTIES
CHEMISTRY
SECTION
METERS
GRAPHIC LITHOLOGY
DRILLING DISTURB.
SED. STRUCTURES
SAMPLES
LITHOLOGIC DESCRIPTION
0.5
1
1.0
2
3
Major lithologies:
SMEAR SLIDE SUMMARY
TEXTURE:
Sand
Silt
Clay
COMPOSITION:
Feldspar
Nannofossils

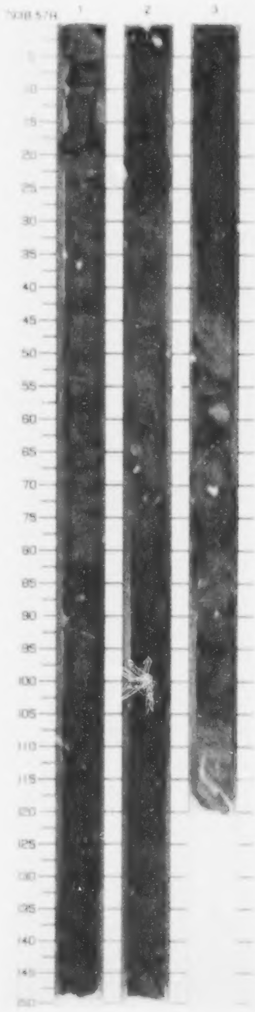
793B 57R
1
2
3
5
10
15
20
25
30
35
40
45
50
55
60
65
70
75
80
85
90
95
100
105
110
115
120
125
130
135
140
145
150

SITE 793 HOLE B CORE 58R CORED INTERVAL 1134.0-1143.6 mbsf

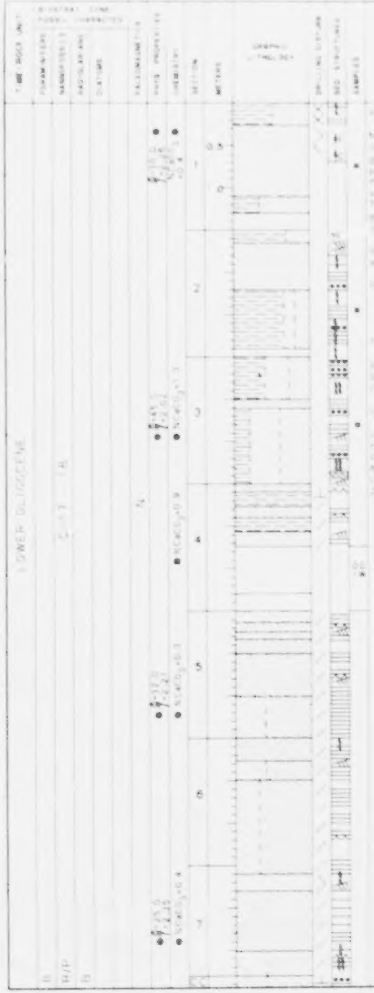
TIME-ROCK UNIT
BIOSTRAT. ZONE/FOSSIL CHARACTER
FORAMINIFERS
NANNOFOSSILS
RADIOLARIANS
DIATOMS
PALEOMAGNETICS
PHYS. PROPERTIES
CHEMISTRY
SECTION
METERS
GRAPHIC LITHOLOGY
DRILLING DISTURB.
SED. STRUCTURES
SAMPLES
LOWER OLIGOCENE
N
B
F/P
1
2
3
4
5
6
7
0.5
1.0
CC

LITHOLOGIC DESCRIPTION

VITRIC SANDSTONE, VITRIC SILTSTONE AND CLAYEY SILTSTONE

Major lithologies:

Sections 1, 2 and 3 contain thick graded beds of olive black (5Y 2/1), dark greenish gray (5G 4/1), greenish black (5GY 2/1) and brownish black (5YR 2/1), structureless or parallel to ripple-laminated, coarse to fine grained VITRIC SANDSTONE. The rest of the core is a fine scale interbedding of thin to very thin beds of similar vitric sandstone, VITRIC SILTSTONE, and parallel laminated to slightly burrowed CLAYEY SILTSTONE. The interbedded facies are color banded; colors include grayish blue green (5BG 5/2), greenish black (5G 2/1, 5GY 2/1), grayish black (N2), dark gray (N3), moderate blue green (5BG 4/6) and dark greenish gray (5BG 4/1).

Section 1, 0-30 cm, is drilling breccia or highly fractured by drilling. Sections 5 through [illegible] are all slightly fractured.

SMEAR SLIDE SUMMARY (%):

	1, 70	2, 46	3, 80
	D	M	D
TEXTURE:			
Sand	—	90	—
Silt	54	10	30
Clay	46	—	70
COMPOSITION:			
Clay	41	—	70
Feldspar	—	—	[illegible]
Glass	54	90	[illegible]
Nannofossils	5	—	[illegible]
Opaques	—	—	[illegible]
Zeolite	—	—	[illegible]

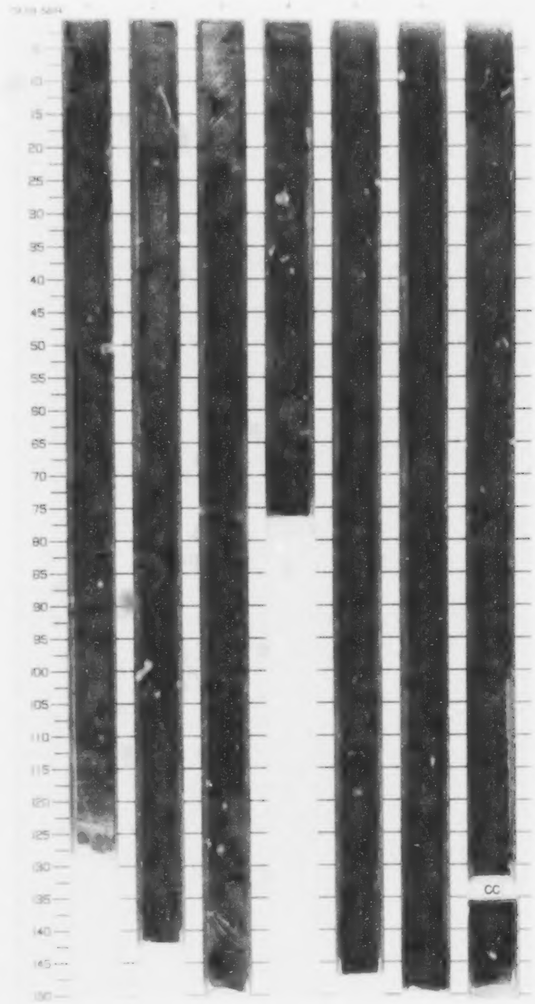
1
2
3
4
5
6
7
CC
5
10
15
20
25
30
35
40
45
50
55
60
65
70
75
80
85
90
95
100
105
110
115
120
125
130
135
140
145
150

SITE 793 HOLE B CORE 59R CORED INTERVAL 1143.6-1153.2 mbsf

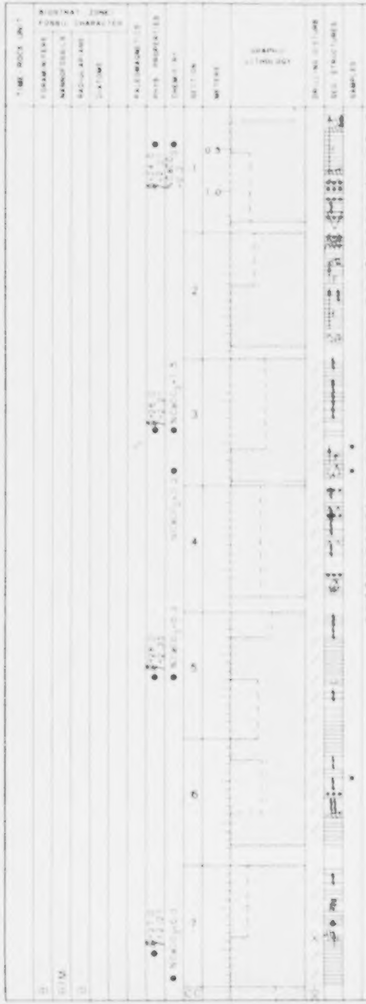

LITHOLOGIC DESCRIPTION

[illegible] SANDSTONE AND [illegible] SILTSTONE

Major lithologies:
[illegible]

Minor lithologies:
[illegible]

[illegible]

SMEAR SLIDE SUMMARY (%):

	[illegible]	[illegible]	[illegible]
TEXTURE:			
Sand	[illegible]	[illegible]	[illegible]
Silt	[illegible]	[illegible]	[illegible]
Clay	[illegible]	[illegible]	[illegible]
COMPOSITION:			
Accessory minerals	[illegible]	[illegible]	[illegible]
Cement	[illegible]	[illegible]	[illegible]
Clay	[illegible]	[illegible]	[illegible]
Feldspar	[illegible]	[illegible]	[illegible]
[illegible]	[illegible]	[illegible]	[illegible]
Glass	[illegible]	[illegible]	[illegible]
Lithic fragments	[illegible]	[illegible]	[illegible]
Mica	[illegible]	[illegible]	[illegible]
Nannofossils	[illegible]	[illegible]	[illegible]
Plant	[illegible]	[illegible]	[illegible]
Radiolarians	[illegible]	[illegible]	[illegible]

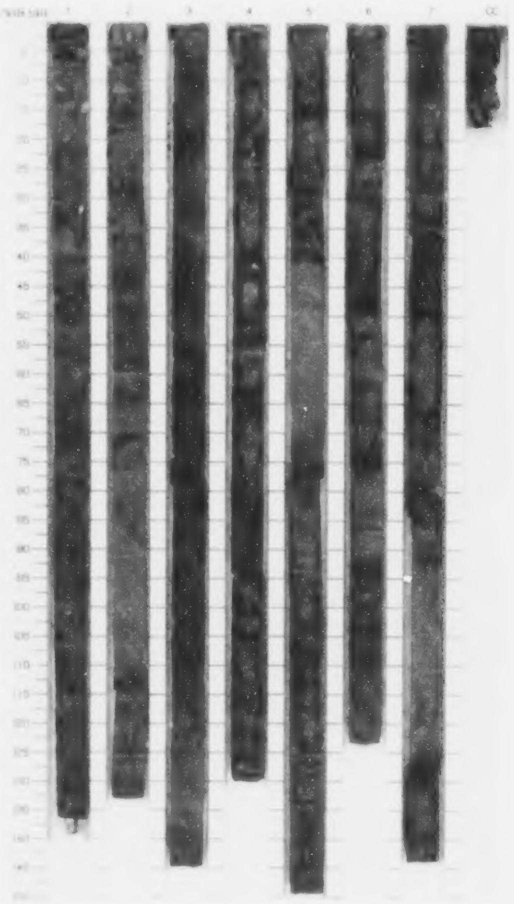
cm
1
2
3
4
5
6
7
CC
5
10
15
20
25
30
35
40
45
50
55
60
65
70
75
80
85
90
95
100
105
110
115
120
125
130
135
140
145
150

SITE 793 HOLE B CORE 60R CORED INTERVAL 1153.2-1162.9 mbsf

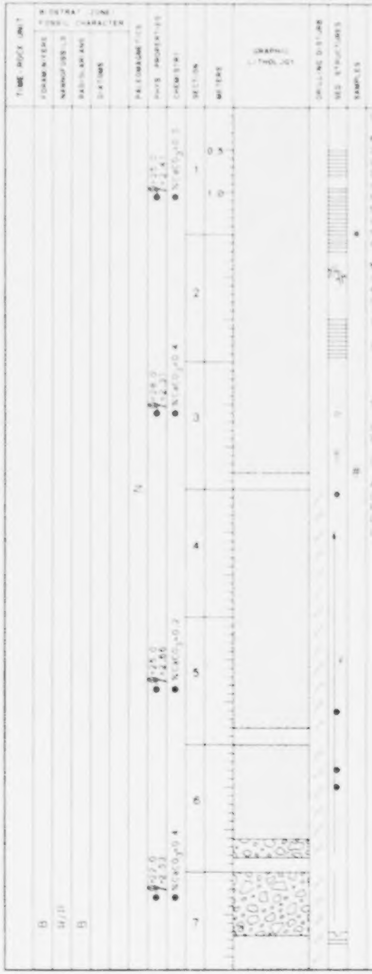
TIME-ROCK UNIT
BIOSTRAT. ZONE/ FOSSIL CHARACTER
FORAMINIFERS
NANNOFOSSILS
RADIOLARIANS
DIATOMS
PALEOMAGNETICS
PHYS. PROPERTIES
CHEMISTRY
SECTION
METERS
GRAPHIC LITHOLOGY
DRILLING DISTURB.
SED. STRUCTURES
SAMPLES
B
R/B
B
N
φ=25.0 γ=2.41
%CaCO3=0.3
φ=28.0 γ=2.31
%CaCO3=0.4
φ=25.0 γ=2.46
%CaCO3=0.2
φ=22.0 γ=2.52
%CaCO3=0.4
1
2
3
4
5
6
7
0.5
1.0

LITHOLOGIC DESCRIPTION

CRYSTAL-VITRIC SANDSTONE

Major lithology: 90% of the core consists of grayish black (N2) and greenish black (5GY 2/1) medium-grained CRYSTAL-VITRIC SANDSTONE. The vitric component has been largely altered. The sandstone has planar laminated divisions in Sections 1 and 2; in Section 3, it is medium to coarse grained with a well rounded claystone pebble 21 mm in diameter. In Section 4, it is normally graded from coarse to medium sand. Section 4, 60 cm, to Section 6, 110 cm, is the upper, main part of a normally graded bed that has a basal division of conglomerate (see Minor lithology). This upper part of the bed grades upward from very coarse-grained sandstone with volcanic granules to medium-grained sandstone. Post-depositional structures include two zeolite-filled subvertical fractures and a dewatering pipe.

Minor lithology: Grayish black (N2) VOLCANIC CONGLOMERATE in Sections 6 and 7 constitutes 10% of the core. Sand-granule-pebble ratios are 65:30:5 in Section 6 and 40:30:30 in Section 7. Maximum clast size is 5-7 mm; mean size of the ten largest clasts is 3-5 mm. Siltstone clasts 12-20 mm in size are present in Section 6.

The core is undisturbed to slightly fractured by drilling.

SMEAR SLIDE & THIN SECTION SUMMARY (%):

	1, 148	3, 128
	D	D
TEXTURE:		
Sand	80	100
Silt	20	—
COMPOSITION:		
Accessory minerals	3	10
Cement	30	45
Feldspar	5	10
Glass	58	40
Lithic fragments	5	—

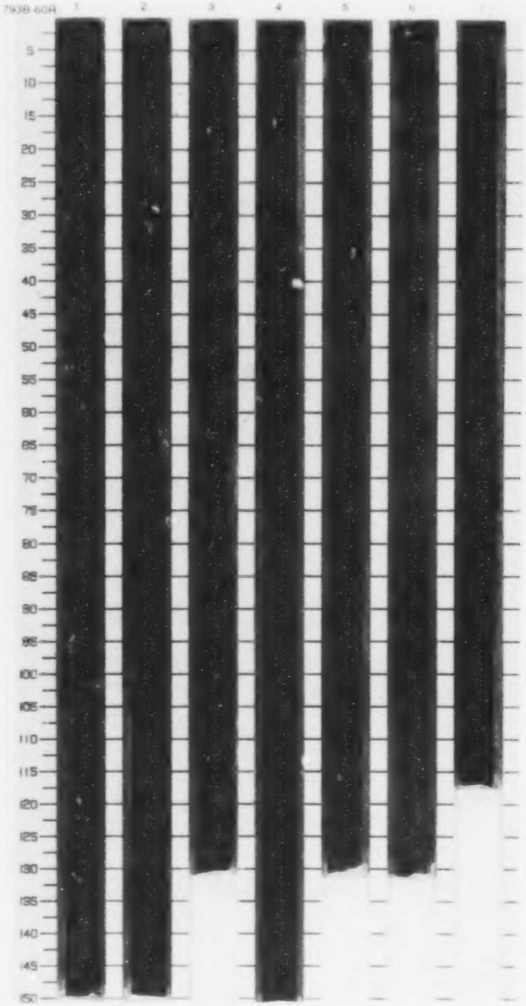
793B-60R
1
2
3
4
5
6
7
5
10
15
20
25
30
35
40
45
50
55
60
65
70
75
80
85
90
95
100
105
110
115
120
125
130
135
140
145
150

SITE 793 HOLE B CORE 61R CORED INTERVAL 1162.9-1172.6 mbsf

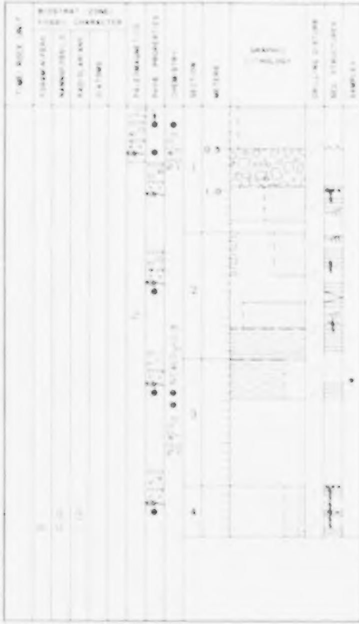

LITHOLOGIC DESCRIPTION

[illegible]

Major Lithologies:

[illegible]

Minor lithology: [illegible]

[illegible]

SMEAR SLIDE SUMMARY (%):

TEXTURE:

Sand

Silt

Clay

COMPOSITION:

Accessory minerals

Clay

Feldspar

Glass

Mica

Nannofossils

Opaques

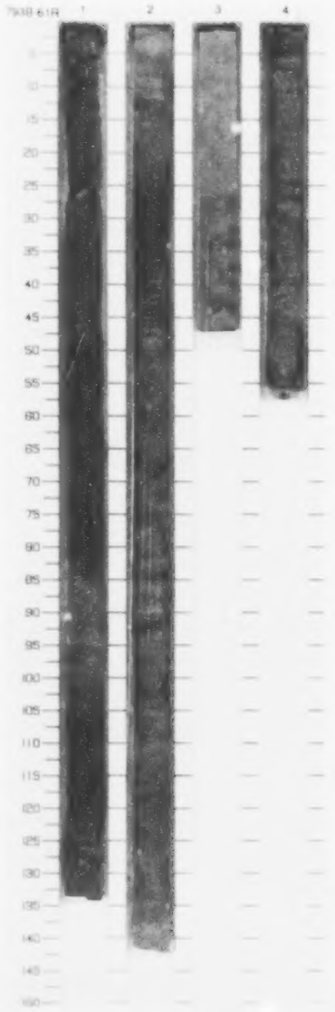
793B-61R
1
2
3
4
5
10
15
20
25
30
35
40
45
50
55
60
65
70
75
80
85
90
95
100
105
110
115
120
125
130
135
140
145
150

SITE 793 HOLE B CORE 62R CORED INTERVAL 1172.6-1182.2 mbsf

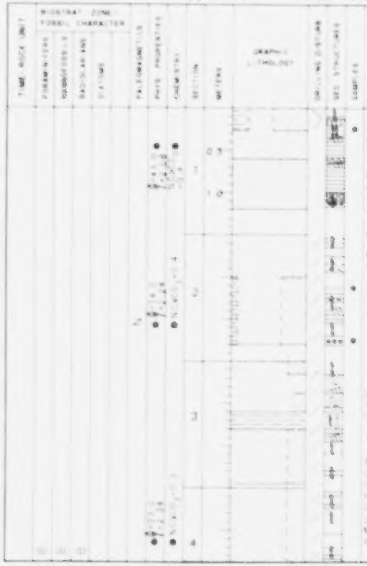
TIME-ROCK UNIT
BIOSTRAT. ZONE/FOSSIL CHARACTER
FORAMINIFERS
NANNOFOSSILS
RADIOLARIANS
DIATOMS
PALEOMAGNETICS
PHYS. PROPERTIES
CHEMISTRY
SECTION
METERS
GRAPHIC LITHOLOGY
DRILLING DISTURB.
SED. STRUCTURES
SAMPLES
0.5
1.0
1
2
3
4

LITHOLOGIC DESCRIPTION

VITRIC SILTSTONE AND CRYSTAL-VITRIC SANDSTONE

Major lithologies:

[illegible]

Minor lithology: Four brownish black (5YR 2/1) [illegible] LAYERS, [illegible] cm thick, [illegible] of the core.

The core is undisturbed to slightly fractured by drilling.

SMEAR SLIDE SUMMARY (%):

	[illegible] M	[illegible] D	[illegible] M
TEXTURE:			
Sand	[illegible]	[illegible]	[illegible]
Silt	[illegible]	[illegible]	[illegible]
Clay	[illegible]	[illegible]	[illegible]
COMPOSITION:			
Accessory minerals	[illegible]	[illegible]	[illegible]
Cement	[illegible]	[illegible]	[illegible]
Clay	[illegible]	[illegible]	[illegible]
Feldspar	[illegible]	[illegible]	[illegible]
Glass	[illegible]	[illegible]	[illegible]
Lithic fragments	[illegible]	[illegible]	[illegible]
Mica	[illegible]	[illegible]	[illegible]
Radiolarians	[illegible]	[illegible]	[illegible]

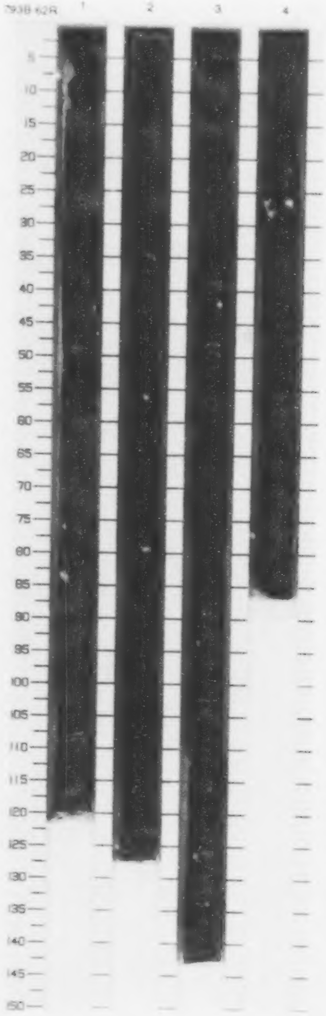
793B 62R
1
2
3
4
5
10
15
20
25
30
35
40
45
50
55
60
65
70
75
80
85
90
95
100
105
110
115
120
125
130
135
140
145
150

SITE 793 HOLE B CORE 63R CORED INTERVAL 1182.2-1191.9 mbsf

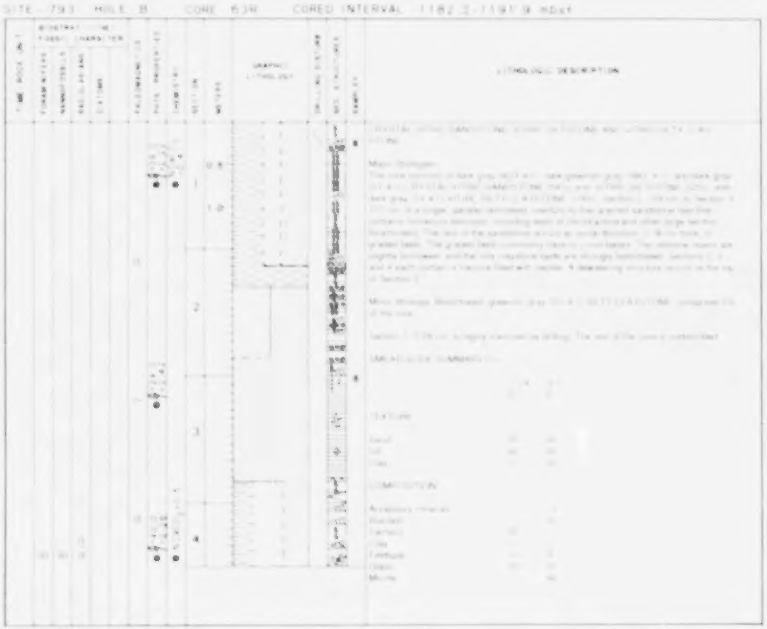
TIME-ROCK UNIT
BIOSTRAT. ZONE/ FOSSIL CHARACTER
FORAMINIFERS
NANNOFOSSILS
RADIOLARIANS
DIATOMS
PALEOMAGNETICS
PHYS. PROPERTIES
CHEMISTRY
SECTION
METERS
GRAPHIC LITHOLOGY
DRILLING DISTURB.
SED. STRUCTURES
SAMPLES
0.5
1.0
1
2
3
4

LITHOLOGIC DESCRIPTION

[illegible]

Major lithologies:

[illegible]

Minor lithology: [illegible]

[illegible]

SMEAR SLIDE SUMMARY (%):

TEXTURE:

Sand
Silt
Clay

COMPOSITION:

Accessory minerals
[illegible]
[illegible]
Clay
Feldspar
Glass
Micrite

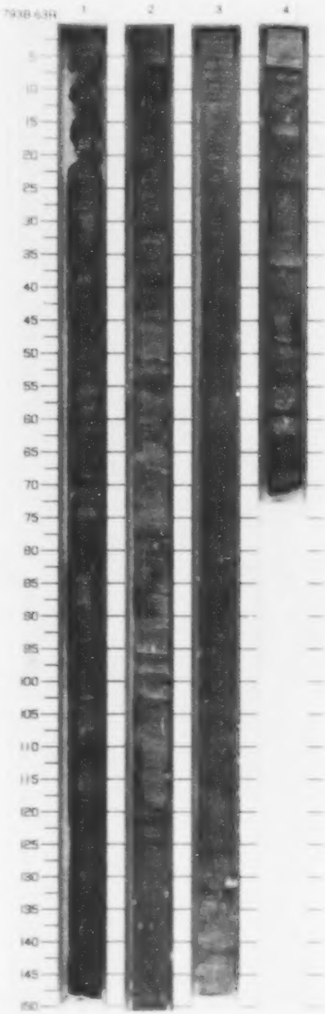
793B-63R
1
2
3
4
5
10
15
20
25
30
35
40
45
50
55
60
65
70
75
80
85
90
95
100
105
110
115
120
125
130
135
140
145
150

SITE 793 HOLE B CORE 64R CORED INTERVAL 1191.8-1201.5 mbsf

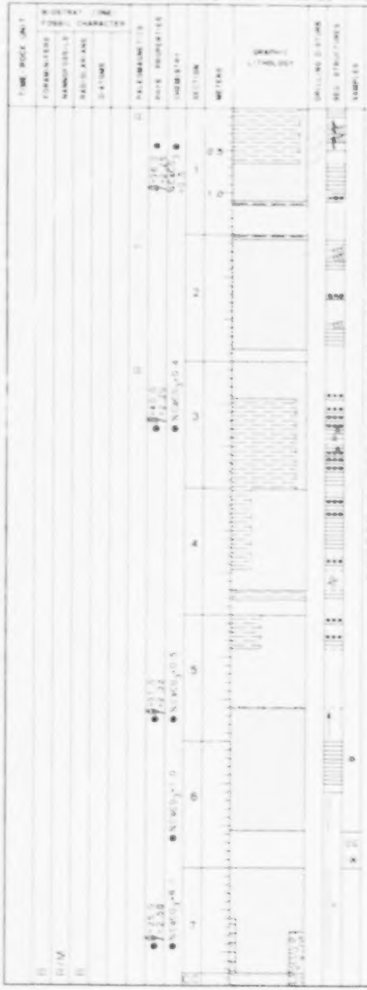
TIME-ROCK UNIT
BIOSTRAT. ZONE/FOSSIL CHARACTER
FORAMINIFERS
NANNOFOSSILS
RADIOLARIANS
DIATOMS
PALEOMAGNETICS
PHYS. PROPERTIES
CHEMISTRY
SECTION
METERS
GRAPHIC LITHOLOGY
DRILLING DISTURB.
SED. STRUCTURES
SAMPLES
B
R/M
B
0.5
1.0
1
2
3
4
5
6
7
CC

LITHOLOGIC DESCRIPTION

VITRIC SANDSTONE, FORAMINIFER-BEARING VITRIC SANDSTONE, VITRIC SILTSTONE AND SILTY CLAYSTONE

Major lithologies:
About 90% of the core consists of olive black (5Y 2/1) and greenish black (5GY 2/1) thick to very thick, graded beds of fine- to medium-grained VITRIC SANDSTONE. Some of the sandstone is [illegible], some parallel laminated, and some ripple laminated. Several of these sandstone beds have [illegible]. Large benthic foraminifers in sandstones of Sections 3 and 7 justify the name FORAMINIFER-BEARING VITRIC SANDSTONE. The rest of the core consists of a fine-scale interbedding of graded beds of olive black (5Y 2/1) and greenish black (5GY 2/1) very fine-grained VITRIC SANDSTONE, VITRIC SILTSTONE and parallel laminated to burrowed SILTY CLAYSTONE. There is a mineral-filled fracture in Section 4, [illegible] cm.

Minor lithologies:
Section 2, [illegible] cm: [illegible] beds, [illegible] thick, of sharp-topped fine-grained VITRIC SANDSTONE [illegible]. Section 7, [illegible] cm: [illegible] consist of greenish black (5GY 2/1) medium-coarse-grained GRANULE-RICH VITRIC SANDSTONE that forms the lower division of a 2 m thick graded bed.

Section 1, [illegible] cm, is slightly fractured by drilling.

SMEAR SLIDE SUMMARY (%):

TEXTURE:

Sand
Silt
Clay

COMPOSITION:

Clay
Feldspar
[illegible]
Glass
Opaques
Quartz

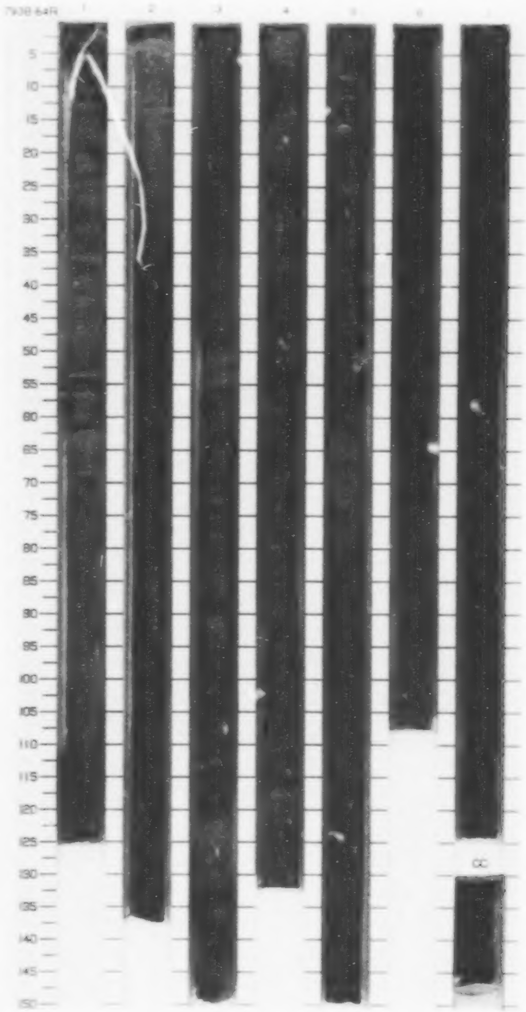
793B 64R
1
2
3
4
5
6
7
CC
5
10
15
20
25
30
35
40
45
50
55
60
65
70
75
80
85
90
95
100
105
110
115
120
125
130
135
140
145
150

SITE 793 HOLE B CORE 65R CORED INTERVAL 1201.5-1211.1 mbsf

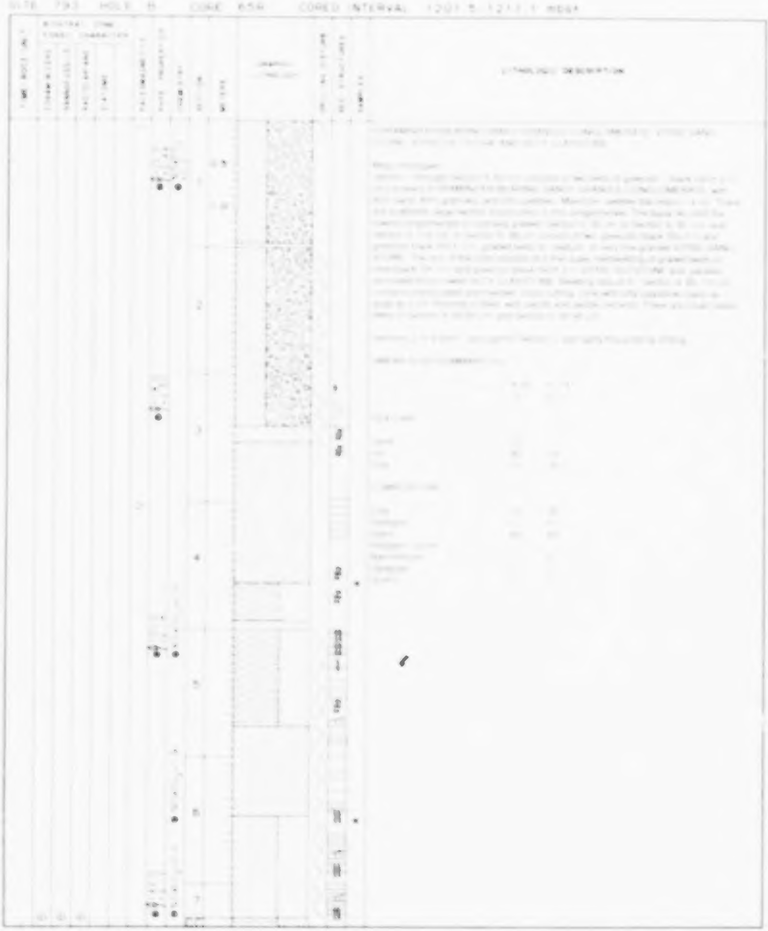

TIME-ROCK UNIT
BIOSTRAT. ZONE/FOSSIL CHARACTER
FORAMINIFERS
NANNOFOSSILS
RADIOLARIANS
DIATOMS
PALEOMAGNETICS
PHYS. PROPERTIES
CHEMISTRY
SECTION
METERS
GRAPHIC LITHOLOGY
DRILLING DISTURB.
SED. STRUCTURES
SAMPLES
1
2
3
4
5
6
7

LITHOLOGIC DESCRIPTION

[illegible]

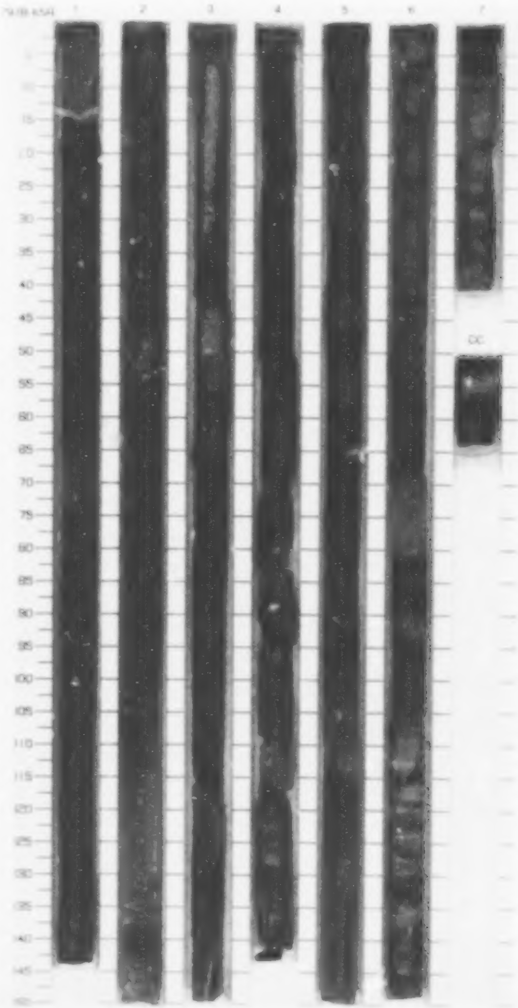

793B-65R
1
2
3
4
5
6
7
CC
0
5
10
15
20
25
30
35
40
45
50
55
60
65
70
75
80
85
90
95
100
105
110
115
120
125
130
135
140
145
150

SITE 793 HOLE B CORE 65R CORED INTERVAL 1211.1-1220.8 mbsf

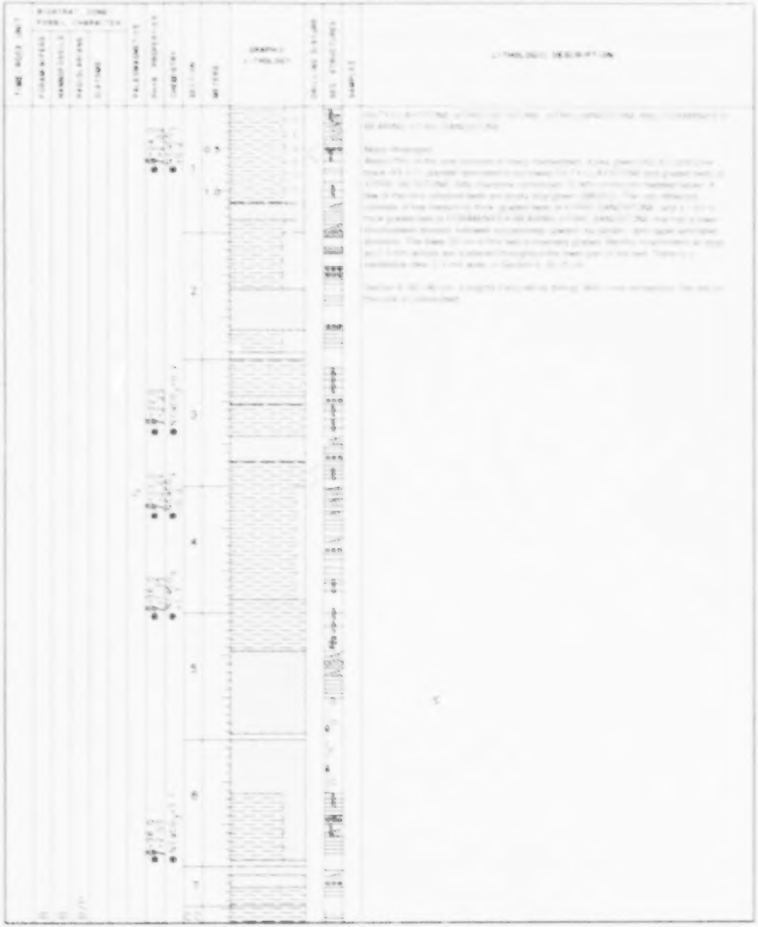
TIME-ROCK UNIT
BIOSTRAT. ZONE/FOSSIL CHARACTER
FORAMINIFERS
NANNOFOSSILS
RADIOLARIANS
DIATOMS
PALEOMAGNETICS
PHYS. PROPERTIES
CHEMISTRY
SECTION
METERS
0.5
1.0
1
2
3
4
5
6
7
CC
GRAPHIC LITHOLOGY
DRILLING DISTURB.
SED. STRUCTURES
SAMPLES
LITHOLOGIC DESCRIPTION

[illegible]

[illegible]

[illegible]

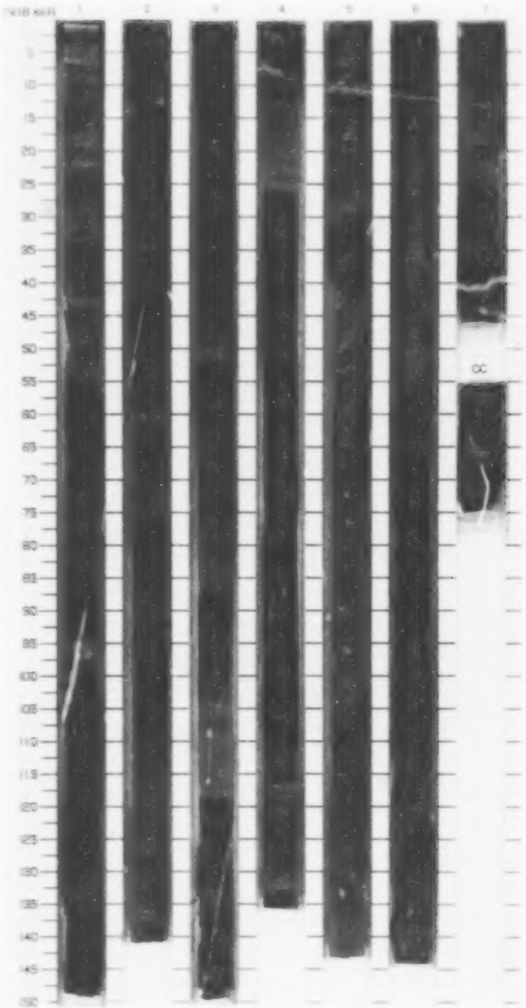
CM
1
2
3
4
5
6
7
5
10
15
20
25
30
35
40
45
50
55
60
65
70
75
80
85
90
95
100
105
110
115
120
125
130
135
140
145
150
CC

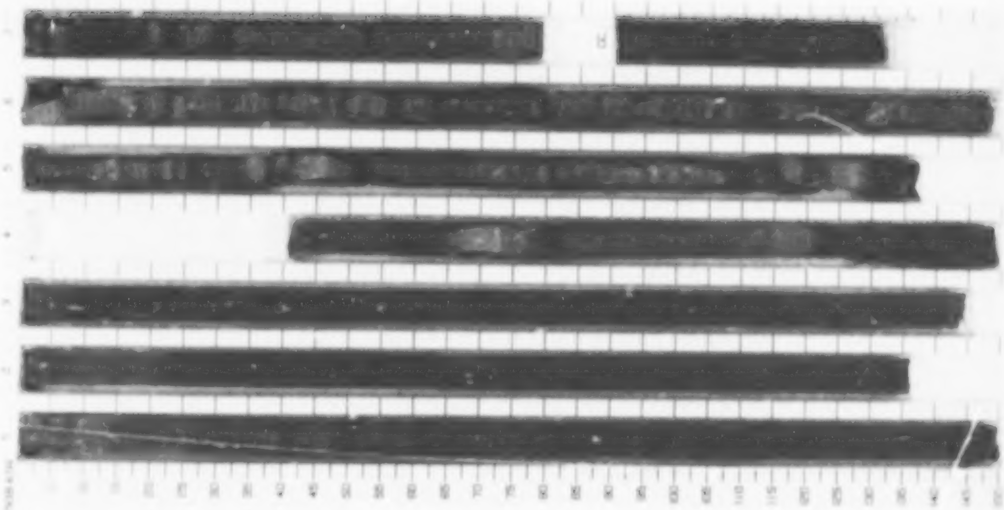

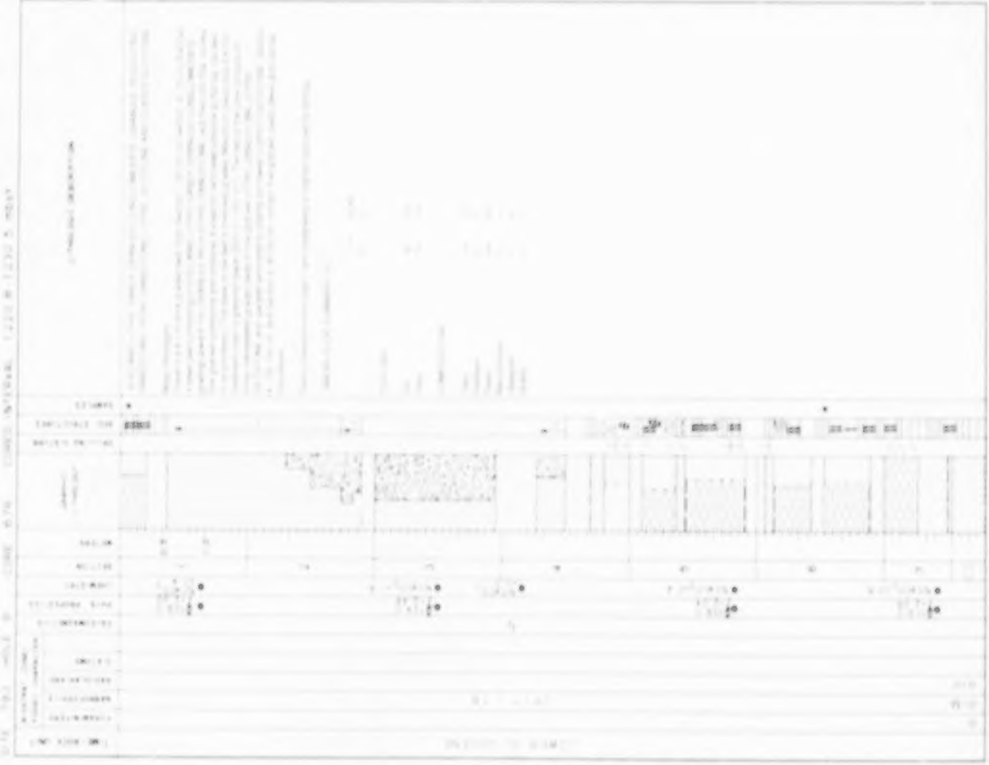

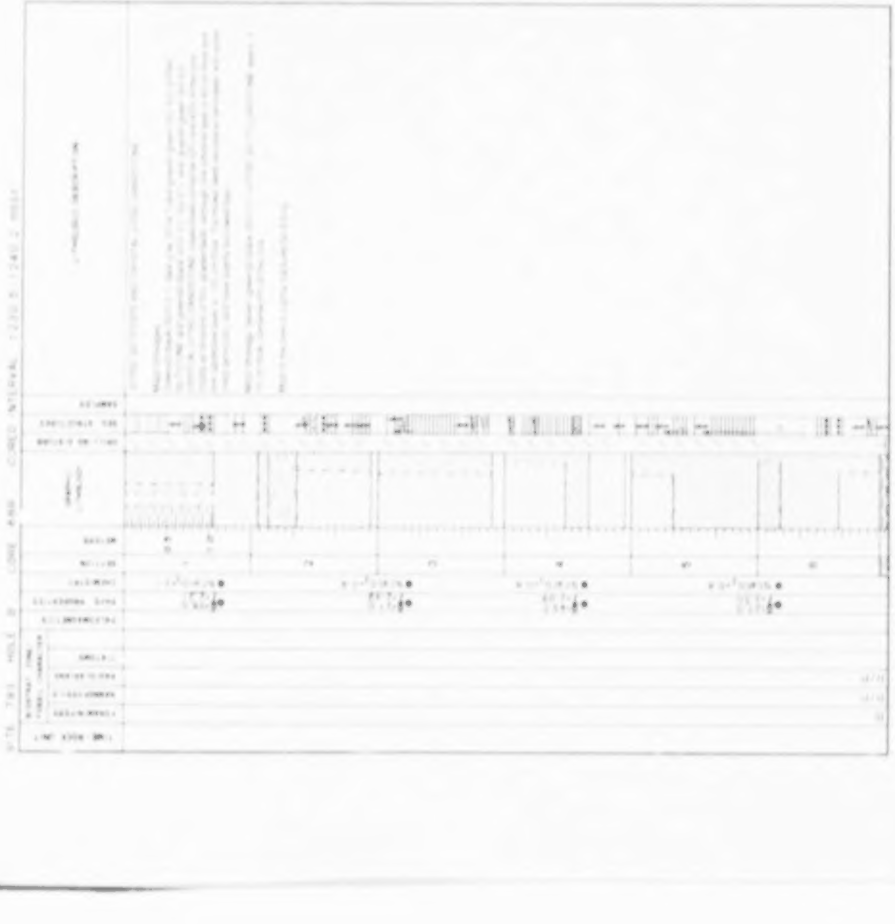

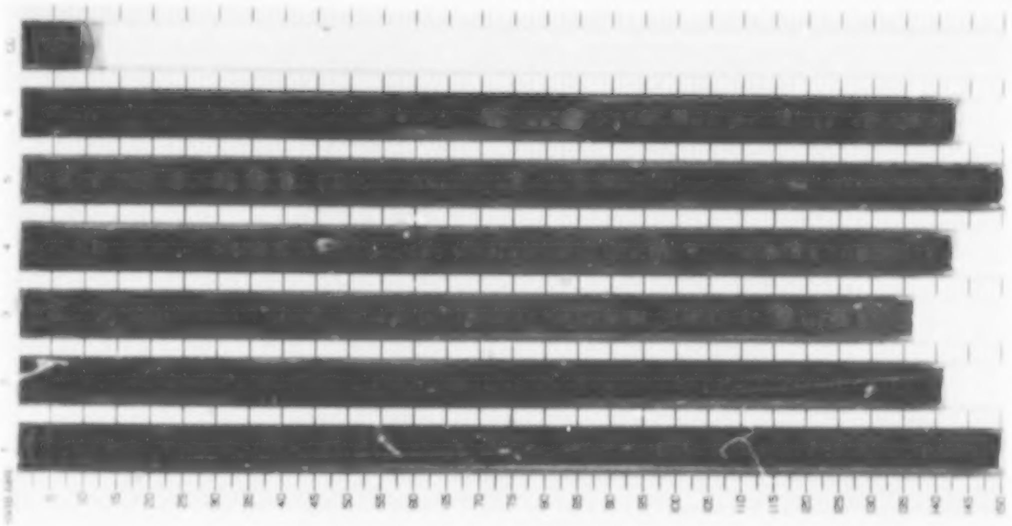

SITE 793 HOLE B CORE 69R CORED INTERVAL 1240.2-1249.8 mbsf

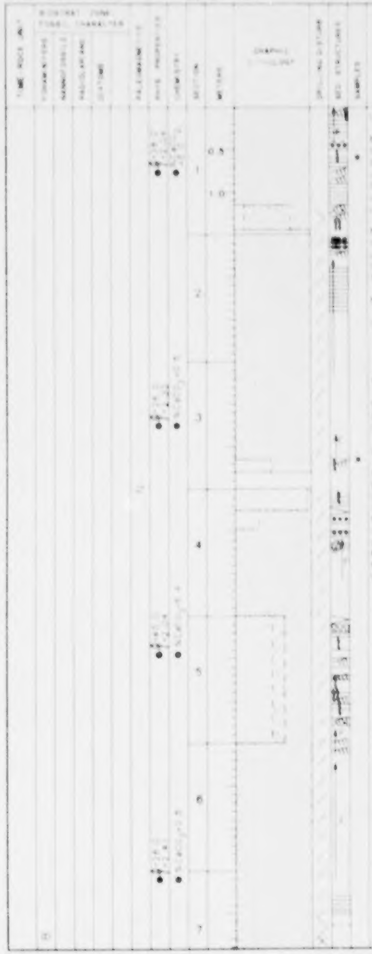
TIME-ROCK UNIT
BIOSTRAT. ZONE/ FOSSIL CHARACTER
FORAMINIFERS
NANNOFOSSILS
RADIOLARIANS
DIATOMS
PALEOMAGNETICS
PHYS. PROPERTIES
CHEMISTRY
SECTION
METERS
GRAPHIC LITHOLOGY
DRILLING DISTURB.
SED. STRUCTURES
SAMPLES
1
2
3
4
5
6
7
0.5
1.0

LITHOLOGIC DESCRIPTION

CRYSTAL VITRIC SANDSTONE

Major lithology: Dark gray (5Y 4/1), grayish black (N2), dark greenish gray (5BG 4/1, 5G 4/1), greenish black (5G 2/1, 5GY 2/1) CRYSTAL VITRIC SANDSTONE [illegible] of the core, most of it in four beds [illegible] cm thick, that vary from [illegible] coarse-grained sandstone to very fine grained and thinly laminated sandstone. The thickest bed in Sections 3 and 5 is normally graded, greenish black (5G 2/1), altered [illegible]. There are a few [illegible] about 1 mm in diameter.

Minor lithologies:
In Sections 1, 3 and 5, some of the sandstone [illegible] have [illegible] of graded beds capped by slightly to moderately bioturbated SILTSTONE and SANDY SILTSTONE [illegible] cm thick. These lithologies respectively comprise [illegible]% and [illegible]% of the core.

Most of the core is slightly fractured by drilling.

SMEAR SLIDE SUMMARY (%):

	1, 80	3, 72
	M	D
TEXTURE:		
Sand	—	[illegible]
Silt	[illegible]	[illegible]
Clay	[illegible]	—
COMPOSITION:		
Accessory minerals	—	[illegible]
Biotite	—	[illegible]
Calcite	—	[illegible]
Clay	[illegible]	—
Feldspar	—	[illegible]
Glass	[illegible]	[illegible]
Lithic fragments	—	[illegible]
Mica	—	—
Nannofossils	[illegible]	—
Opaques	—	[illegible]

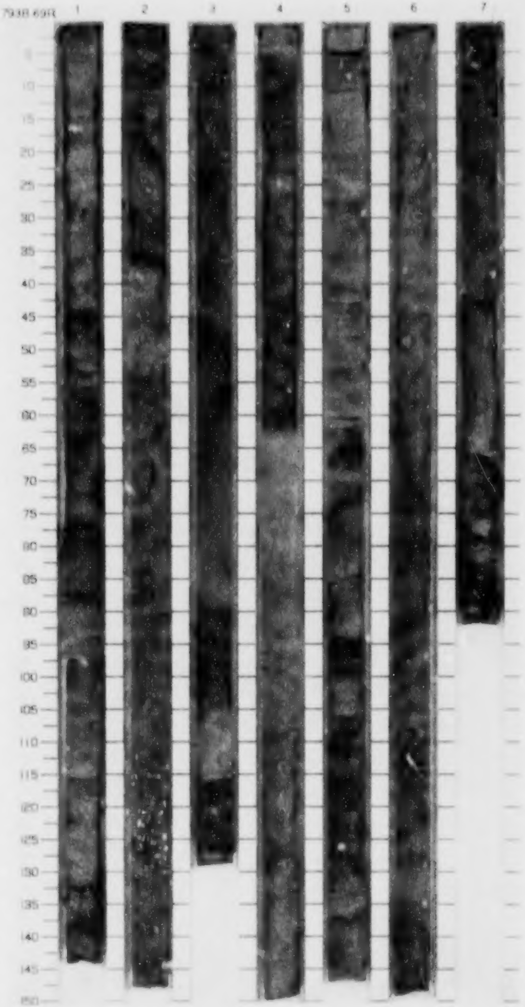
793B 69R
1
2
3
4
5
6
7
5
10
15
20
25
30
35
40
45
50
55
60
65
70
75
80
85
90
95
100
105
110
115
120
125
130
135
140
145
150

SITE 793 HOLE B CORE 70R CORED INTERVAL 1249.8-1259.4 mbsf

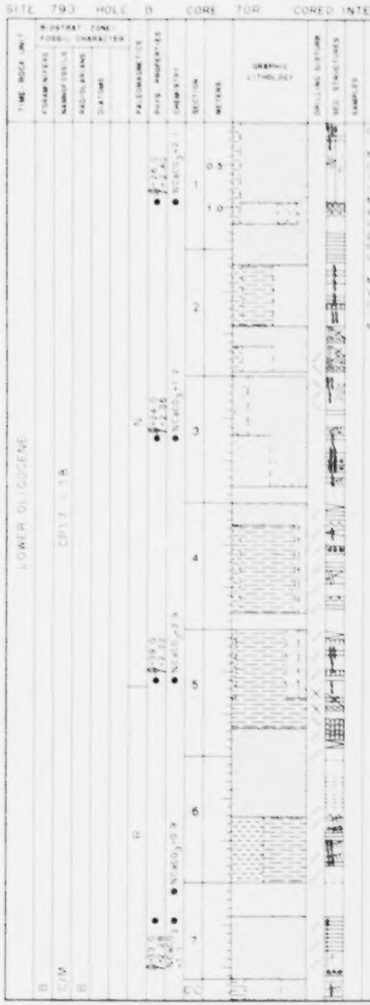
TIME-ROCK UNIT
BIOSTRAT. ZONE/FOSSIL CHARACTER
FORAMINIFERS
NANNOFOSSILS
RADIOLARIANS
DIATOMS
PALEOMAGNETICS
PHYS. PROPERTIES
CHEMISTRY
SECTION
METERS
GRAPHIC LITHOLOGY
DRILLING DISTURB.
SED. STRUCTURES
SAMPLES
LOWER OLIGOCENE
CP17 - 18
B
C/M
B
N
R
1
2
3
4
5
6
7
CC
0.5
1.0

LITHOLOGIC DESCRIPTION

CRYSTAL VITRIC SANDSTONE AND VITRIC SILTY CLAYSTONE

Major lithologies:

Greenish black (5GY 2/1), dark greenish gray (5BG 4/1, 5G 4/1), and dark gray (5GY 4/1) CRYSTAL VITRIC SANDSTONE and dark greenish gray (5BG 4/1) and dark gray (5Y 4/1) VITRIC SILTY CLAYSTONE comprise 58% and 20% of the core, respectively. Much of the sandstone is in seven layers, 23-104 cm thick. The thickest bed (Sections 5 and 6) is graded from structureless, medium-grained sandstone to fine-grained, parallel-laminated sandstone. Other layers are basal divisions, several centimeters thick, of graded beds. The siltstone, in layers 1-16 cm thick, consists of slightly to moderately bioturbated caps of graded beds. There are water escape features in Section 2, a micro-fault in Section 3, and fractures in Sections 1, 2, 4, and 5.

Minor lithologies:

VITRIC SILTSTONE (7%), CLAYSTONE (8%), and VITRIC SILTY SANDSTONE (7%) comprise the remainder of the core, as middle or upper divisions of the graded beds.

Most of the core is undisturbed to slightly fractured by drilling.

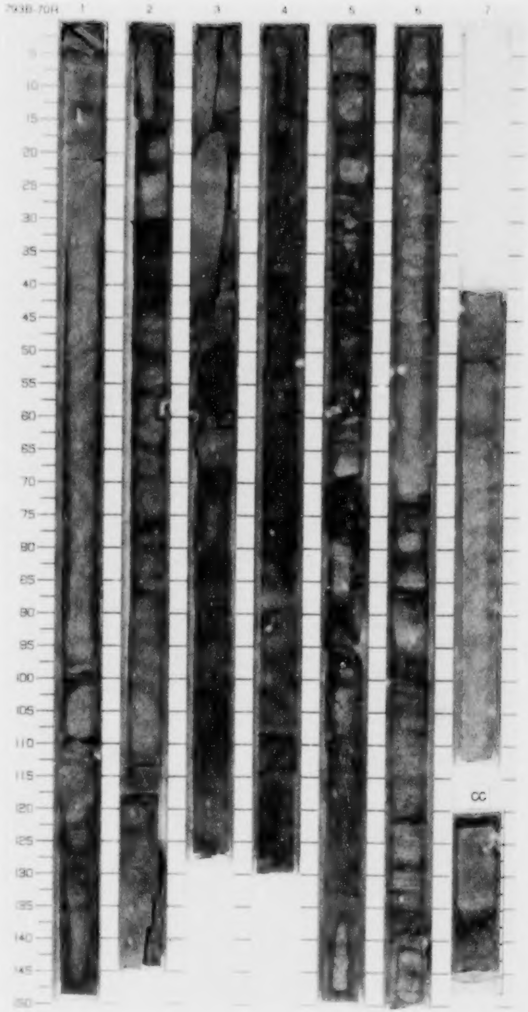
793B-70R
1
2
3
4
5
6
7
CC
0
10
15
20
25
30
35
40
45
50
55
60
65
70
75
80
85
90
95
100
105
110
115
120
125
130
135
140
145
150

SITE 793 HOLE B CORE 71R CORED INTERVAL 1259.4-1268.7 mbsf

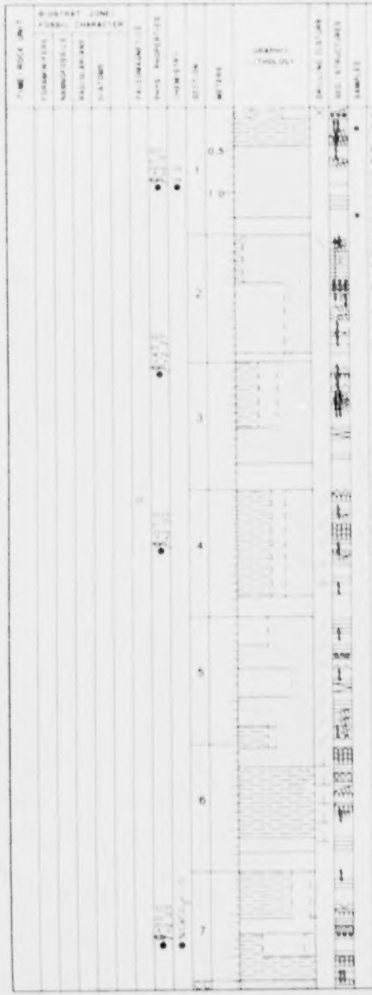
TIME-ROCK UNIT
BIOSTRAT. ZONE/ FOSSIL CHARACTER
FORAMINIFERS
NANNOFOSSILS
RADIOLARIANS
DIATOMS
PALEOMAGNETICS
PHYS. PROPERTIES
CHEMISTRY
SECTION
METERS
GRAPHIC LITHOLOGY
DRILLING DISTURB.
SED. STRUCTURES
SAMPLES
0.5
1.0
1
2
3
4
5
6
7

LITHOLOGIC DESCRIPTION

CRYSTAL-VITRIC SANDSTONE, VITRIC SILTSTONE AND VITRIC CLAYEY SILTSTONE

Major lithologies:
Most of the core is composed of dark greenish gray (5BG 4/1), dark gray (5Y 4/1, 5GY 4/1), grayish green (5G 5/2), and brownish black (5YR 2/1) CRYSTAL-VITRIC SANDSTONE (40%) in the lower; greenish black (5G 2/1), dark gray (5Y 4/1, 5GY 4/1), medium dark gray (N4), and dark greenish gray (5BG 4/1) VITRIC SILTSTONE (20%); and dark greenish gray (5G 4/1), dark gray (5Y 4/1), greenish gray (5G 5/1), grayish green (5G 5/2), and olive black (5Y 2/1) VITRIC CLAYEY SILTSTONE (25%). Five sandstone layers and one layer each of siltstone and clayey siltstone are thicker than 30 cm. These lithologies are generally divisions of graded beds, the finer tops being slightly to intensely bioturbated. The coarser sandstone divisions are planar, wavy, and cross laminated. A calcite filled fracture occurs at the base of Section 5.

Minor lithology: Eight layers of dark greenish gray (5G 4/1) and olive black (5Y 2/1) VITRIC SILTY CLAYSTONE, 1-30 cm thick, comprise 15% of the core as intensely bioturbated caps of graded beds.

The top 40% of the core is undisturbed, the middle 30% slightly fractured, and the bottom 30% moderately fractured by drilling.

SMEAR SLIDE SUMMARY (%):

	1, 20	1, 100
	M	D
TEXTURE:		
Sand	10	30
Silt	45	60
Clay	45	10
COMPOSITION:		
Accessory minerals	[illegible]	[illegible]
Biotite	—	10
Clay	41	15
Feldspar	5	10
Glass	42	37
Mica	—	10
Nannofossils	3	—
Opaques	5	3

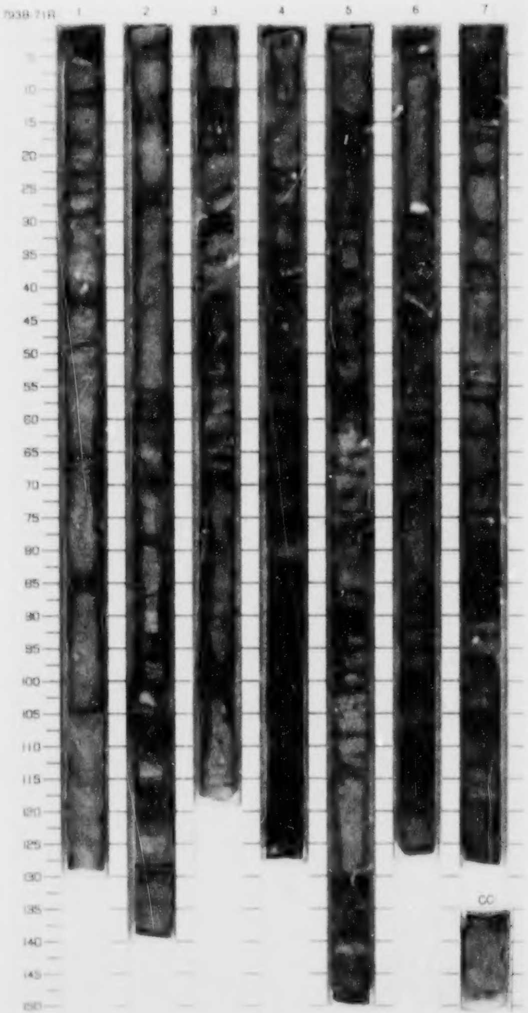
793B-71R
1
2
3
4
5
6
7
CC
5
10
15
20
25
30
35
40
45
50
55
60
65
70
75
80
85
90
95
100
105
110
115
120
125
130
135
140
145
150

SITE 793 HOLE B CORE 72R CORED INTERVAL 1268.7-1278.4 mbsf

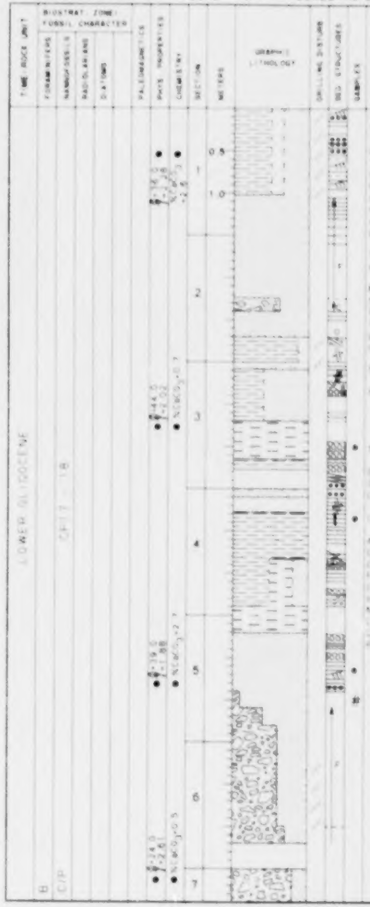
TIME-ROCK UNIT
BIOSTRAT. ZONE/ FOSSIL CHARACTER
FORAMINIFERS
NANNOFOSSILS
RADIOLARIANS
DIATOMS
PALEOMAGNETICS
PHYS. PROPERTIES
CHEMISTRY
SECTION
METERS
GRAPHIC LITHOLOGY
DRILLING DISTURB.
SED. STRUCTURES
SAMPLES
LOWER OLIGOCENE
B
C/P
CP17 - 18
φ=34.0
γ=2.38
%CaCO$_3$=2.6
φ=44.0
γ=2.02
%CaCO$_3$=0.7
φ=39.0
γ=1.88
%CaCO$_3$=2.7
φ=24.0
γ=2.61
%CaCO$_3$=0.5
1
2
3
4
5
6
7
0.5
1.0

LITHOLOGIC DESCRIPTION

VOLCANIC LITHIC GRANULE CONGLOMERATE, GRANULE-RICH VITRIC SANDSTONE, VITRIC SANDSTONE, VITRIC SILTSTONE AND CLAYEY SILTSTONE

Major lithologies:
Two very thick beds, spanning parts of Sections 1, 2, 5, 6 and 7 consist of olive black (5Y 2/1) VOLCANIC LITHIC GRANULE CONGLOMERATE, grading upward into GRANULE-RICH VITRIC SANDSTONE, and then into VITRIC SANDSTONE. This rock is structureless or parallel laminated. The upper bed has an inversely graded base. The rest of the core (about 40% of recovery) consists of very thin to thick beds of parallel and ripple laminated, olive black (5Y 2/1) and pale green (10G 6/2), fine to very fine grained VITRIC SANDSTONE, VITRIC SILTSTONE and CLAYEY SILTSTONE.

There are extensional microfaults, sub-vertical fractures and veinlets in Sections 2, 3 and 4.

Minor lithologies:
Section 5, 25-90 cm, consists of very fine grained grayish green (5G 5/2) CARBONATE VITRIC SANDSTONE, with calcite of unknown origin. Section 3, 70-115 cm, Section 4, 110-128 cm, and Section 4, 140 cm to Section 5, 25 cm, consist of beds of grayish green (5G 5/2), fine to very fine grained MUDDY SANDSTONE with a lower division of convolute laminae.

Some intervals are slightly fractured by drilling.

SMEAR SLIDE & THIN SECTION SUMMARY (%):

	3, 100 D	4, 34 D	5, 85 D	5, 90 D
TEXTURE:				
Sand	—	—	—	100
Silt	54	15	90	—
Clay	46	85	10	—
COMPOSITION:				
Accessory minerals	—	—	—	5
Cement	—	—	—	40
Clay	40	75	10	—
Feldspar	[illegible]	[illegible]	[illegible]	[illegible]
Glass	50	25	29	50
Inorganic calcite	1	—	60	—
Nannofossils	—	2	—	—
Opaques	[illegible]	3	[illegible]	—
Quartz	[illegible]	[illegible]	[illegible]	—
Rock fragments	—	—	—	5

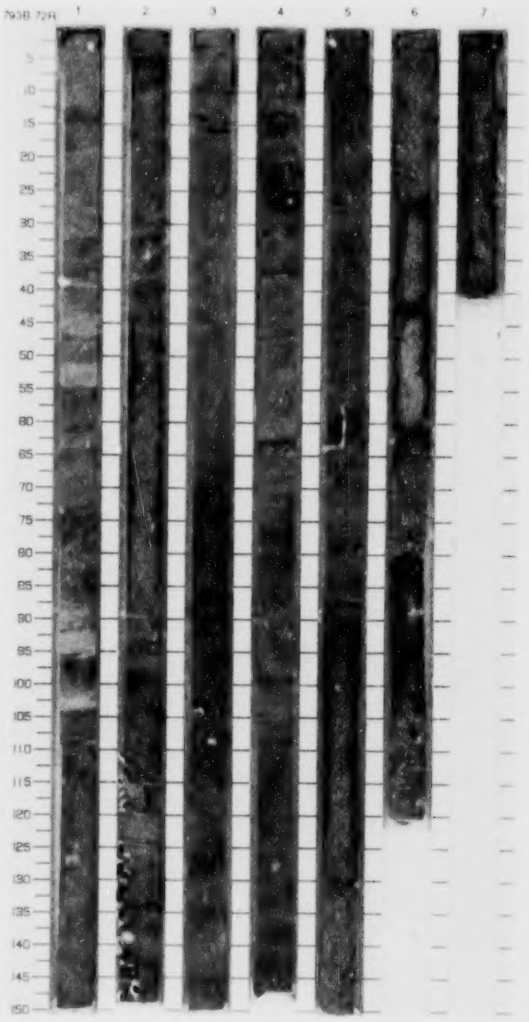
793B 72R
1
2
3
4
5
6
7
5
10
15
20
25
30
35
40
45
50
55
60
65
70
75
80
85
90
95
100
105
110
115
120
125
130
135
140
145
150

SITE 793 HOLE B CORE 73R CORED INTERVAL 1278.4-1288.0 mbsf

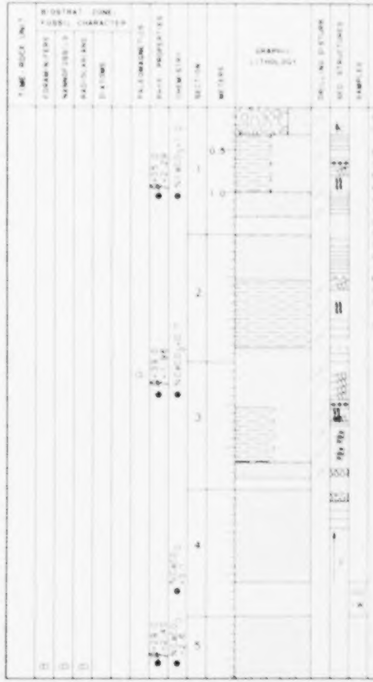
TIME-ROCK UNIT
BIOSTRAT. ZONE/ FOSSIL CHARACTER
FORAMINIFERS
NANNOFOSSILS
RADIOLARIANS
DIATOMS
PALEOMAGNETICS
PHYS. PROPERTIES
CHEMISTRY
SECTION
METERS
GRAPHIC LITHOLOGY
DRILLING DISTURB.
SED. STRUCTURES
SAMPLES
0.5
1.0
1
2
3
4
5
B
B
B

LITHOLOGIC DESCRIPTION

BIOCLAST-BEARING VITRIC SANDSTONE, VITRIC SANDSTONE, VITRIC SILTSTONE AND SILTY CLAYSTONE

Major lithologies:
Section 1, 18 cm, through Section 3 consists of a 2-m-thick graded bed of greenish black (5G 2/1) coarse to fine grained BIOCLAST-BEARING VITRIC SANDSTONE, with parallel and ripple lamination at the top. The bioclasts are as large as 1.4 cm across and appear to be calcareous red algae. About 20% of the core consists of medium to thick graded beds of VITRIC SANDSTONE and VITRIC SILTSTONE. The color of these is greenish black (5GY 2/1), dark greenish gray (5G 4/1) to blackish red (5R 2/2). The rest of the core is mainly thinly interbedded graded beds of VITRIC SILTSTONE and SILTY CLAYSTONE with similar colors. These facies are parallel laminated, ripple laminated or burrowed. Bedding dips at 8°.

Minor lithology: Section 1, 0-18 cm, consists of greenish black (5GY 2/1) to blackish red (5R 2/2) inversely graded SANDY GRANULE CONGLOMERATE with a maximum clast diameter of 1.8 cm.

Section 1, part of Section 2, and most of Section 3 are slightly fractured by drilling.

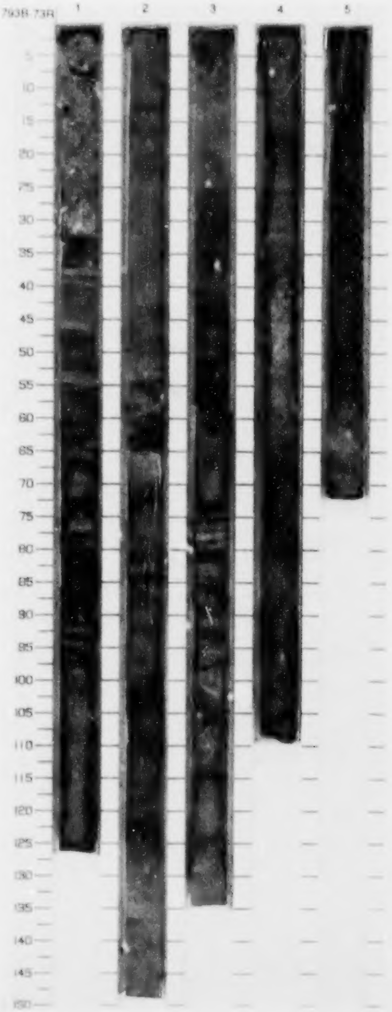
793B-73R
1
2
3
4
5
5
10
15
20
25
30
35
40
45
50
55
60
65
70
75
80
85
90
95
100
105
110
115
120
125
130
135
140
145
150

SITE 793 HOLE B CORE 74R CORED INTERVAL 1288.0-1297.7 mbsf

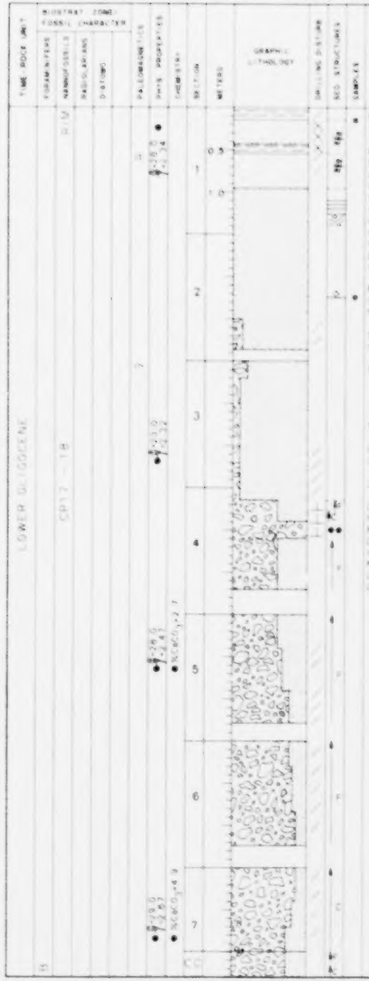
TIME-ROCK UNIT
BIOSTRAT. ZONE/ FOSSIL CHARACTER
FORAMINIFERS
NANNOFOSSILS
RADIOLARIANS
DIATOMS
PALEOMAGNETICS
PHYS. PROPERTIES
CHEMISTRY
SECTION
METERS
GRAPHIC LITHOLOGY
DRILLING DISTURB.
SED. STRUCTURES
SAMPLES
LOWER OLIGOCENE
R/M
CP17 – 18
B
R
?
1
2
3
4
5
6
7
CC
0.5
1.0

LITHOLOGIC DESCRIPTION

BIOCLAST-BEARING SANDY GRANULE CONGLOMERATE, GRANULE-RICH VITRIC SANDSTONE, AND VITRIC SANDSTONE

Major lithologies:
Sections 2, 75 cm, through CC consist of a 7.7-m-thick, inversely to normally graded unit of greenish black (5G 2/1, 5GY 2/1), structureless BIOCLAST-BEARING SANDY GRANULE CONGLOMERATE, GRANULE-RICH VITRIC SANDSTONE, and VITRIC SANDSTONE. Maximum clast size is about 2 cm. There are intraclasts of silty claystone as large as 8 cm across in Section 6, 40-45 cm. White clasts of calcareous red algae occur in Sections 4 through CC. Section 1, 53 cm, through Section 2, 75 cm, consists of a graded bed of greenish black (5G 2/1), medium-grained vitric sandstone near the base to VITRIC SILTSTONE at the top. The basal 2 cm contains pumice pebbles as large as 1.2 cm in diameter. There are clastic dikes and a normal microfault in Section 1.

Minor lithology: Section 1, 0-18 cm, consists of greenish black (5G 2/1) SILTY CLAYSTONE. Section 1, 18-53 cm, consists of greenish black (5G 2/1) SILTSTONE with floating clasts, as large as 5 cm across, of silty claystone.

Section 1, 20-50 cm, is drilling breccia. Large intervals of Sections 3 through 7 are moderately to slightly fractured.

SMEAR SLIDE SUMMARY (%):

	1, 15	2, 74
	D	M
TEXTURE:		
Silt	30	20
Clay	70	80
COMPOSITION:		
Clay	60	75
Fe-oxide	1	—
Feldspar	2	5
Glass	30	20
Inorganic calcite	1	—
Nannofossils	4	—
Opaques	1	—
Quartz	1	—

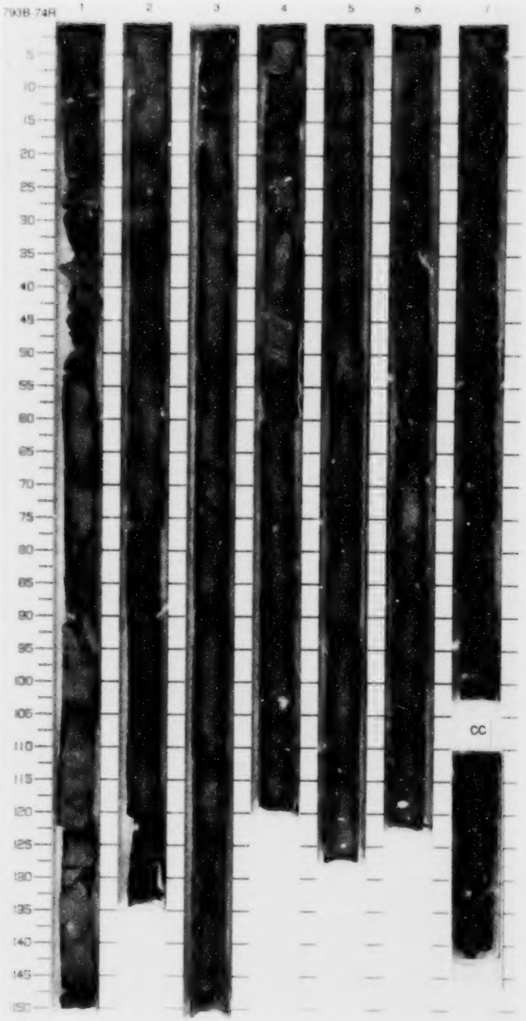
793B-74R
1
2
3
4
5
6
7
CC
5
10
15
20
25
30
35
40
45
50
55
60
65
70
75
80
85
90
95
100
105
110
115
120
125
130
135
140
145
150

SITE 793 HOLE B CORE 75R CORED INTERVAL 1297.7-1307.3 mbsf

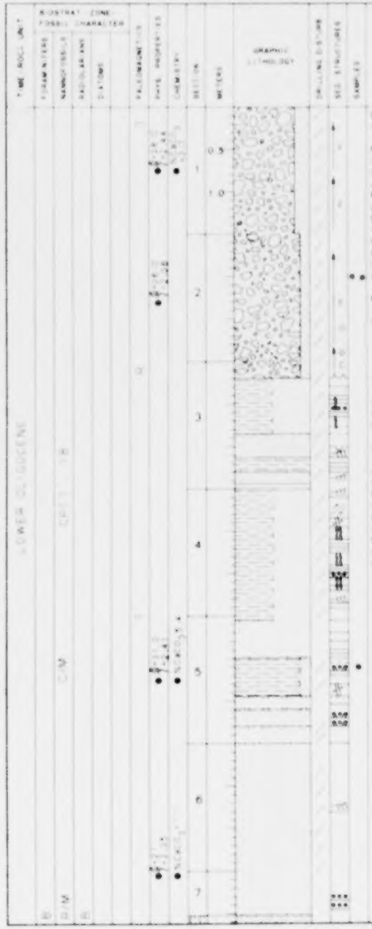
TIME-ROCK UNIT
BIOSTRAT. ZONE/FOSSIL CHARACTER
FORAMINIFERS
NANNOFOSSILS
RADIOLARIANS
DIATOMS
PALEOMAGNETICS
PHYS. PROPERTIES
CHEMISTRY
SECTION
METERS
GRAPHIC LITHOLOGY
DRILLING DISTURB.
SED. STRUCTURES
SAMPLES
LOWER OLIGOCENE
CP17-18
C/M
R/M
B
0.5
1.0
1
2
3
4
5
6
7

LITHOLOGIC DESCRIPTION

BIOCLAST-BEARING VITRIC CONGLOMERATE, VITRIC SANDSTONE, VITRIC SILTSTONE AND SILTY CLAYSTONE

Major lithologies:
Sections 1, 0 cm, through 2, 35 cm, consist of greenish black (5GY 2/1), structureless, inversely to normally graded BIOCLAST-BEARING VITRIC CONGLOMERATE. The upper part of this bed occurs in Core 74R. Volcanic clasts are aphyric andesites. Maximum pebble size is 1.5 cm. Sand:granule:pebble ratio is 20:40:40. The bioclastic grains are pebbles of calcareous red algae. Sections 5 through CC consist of one very thick bed and two medium beds of greenish black (5G 2/1), fine to very fine grained VITRIC SANDSTONE with "snowflake"-like alteration spots, and diffused dewatering fractures. The rest of the core consists of thin to medium interbeds of fine-grained vitric sandstone, VITRIC SILTSTONE, and parallel laminated to burrowed SILTY CLAYSTONE. Sections 3, 4 and 5 contain steep fractures, mineral-filled fractures and microfaults.

Most of the core is slightly fractured by drilling.

SMEAR SLIDE SUMMARY (%):

	[illegible]	[illegible]	[illegible]
	M	D	D
TEXTURE:			
Sand		[illegible]	
Silt		80	[illegible]
Clay		[illegible]	[illegible]
COMPOSITION:			
Accessory minerals		[illegible]	[illegible]
Clay		[illegible]	[illegible]
Feldspar		[illegible]	[illegible]
Glass		80	[illegible]
Hornblende		[illegible]	
Inorganic calcite	TR	[illegible]	[illegible]
Nannofossils			[illegible]
Opaques		[illegible]	[illegible]
Quartz		[illegible]	[illegible]

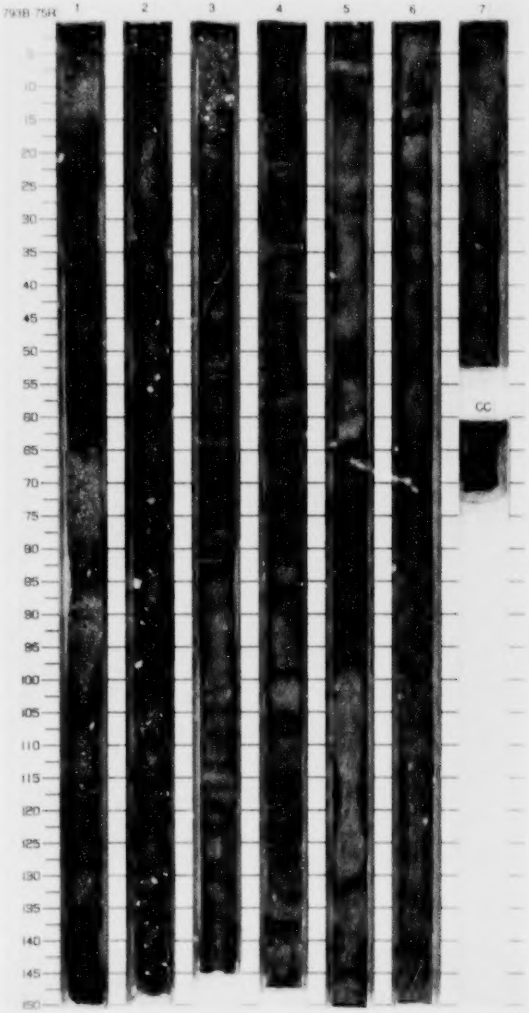
793B 75R
1
2
3
4
5
6
7
CC
0
10
15
20
25
30
35
40
45
50
55
60
65
70
75
80
85
90
95
100
105
110
115
120
125
130
135
140
145
150

SITE 793 HOLE B CORE 76R CORED INTERVAL 1307.2-1317.0 mbsf

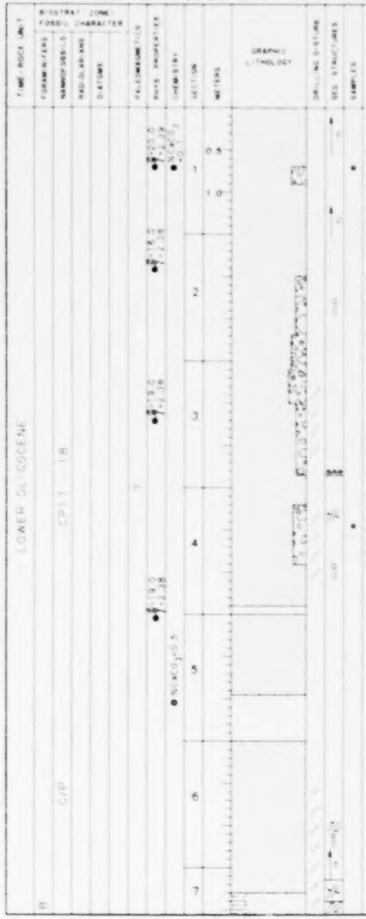
TIME-ROCK UNIT
BIOSTRAT. ZONE/FOSSIL CHARACTER
FORAMINIFERS
NANNOFOSSILS
RADIOLARIANS
DIATOMS
PALEOMAGNETICS
PHYS. PROPERTIES
CHEMISTRY
SECTION
METERS
GRAPHIC LITHOLOGY
DRILLING DISTURB.
SED. STRUCTURES
SAMPLES
LOWER OLIGOCENE
CP17-18
C/P
B
?
0.5
1.0
1
2
3
4
5
6
7
%CaCO3=0.5

LITHOLOGIC DESCRIPTION

VITRIC SANDSTONE AND BIOCLAST-BEARING VITRIC-LITHIC PEBBLY SANDSTONE

Major lithologies:
This core consists of parts of two very thick, graded beds of greenish black (5GY 2/1), structureless VITRIC SANDSTONE and BIOCLAST-BEARING VITRIC-LITHIC PEBBLY SANDSTONE. The uppermost bed continues into Core 75R. Grain size fluctuates as a result of variations in the content of volcanic and bioclastic granules and pebbles. The bioclastic grains consist of calcareous red algae. The vitric sandstone has "snowflake-like" alteration spots. Steeply dipping dewatering fractures occur in Section 2, 90-120 cm, Section 4, 90-110 cm, and Section 6, 110-120 cm. Mineral-filled fractures occur in Section 4, 30-40 cm, and Section 7, 30-40 cm. Microfaults occur in Section 6, 100-110 cm, and Section 7, 40-50 cm.

Minor lithologies:
Section 7, 17-55 cm, consists of interbedded, fine-grained VITRIC SANDSTONE, VITRIC SILTSTONE, SILTY CLAYSTONE, and BRECCIATED CLAYSTONE, that has been fractured in the fault in this interval. All this sediment is greenish black (5GY 2/1).

Parts of Sections 3, 4, 6 and 7 are slightly fractured by drilling.

SMEAR SLIDE SUMMARY (%):

	1, 20 D	4, 45 D
TEXTURE:		
Silt	90	35
Clay	10	65
COMPOSITION:		
Clay	10	68
Feldspar	5	—
Glass	74	30
Hornblende	2	—
Inorganic calcite	—	2
Opaques	5	1
Quartz	4	1

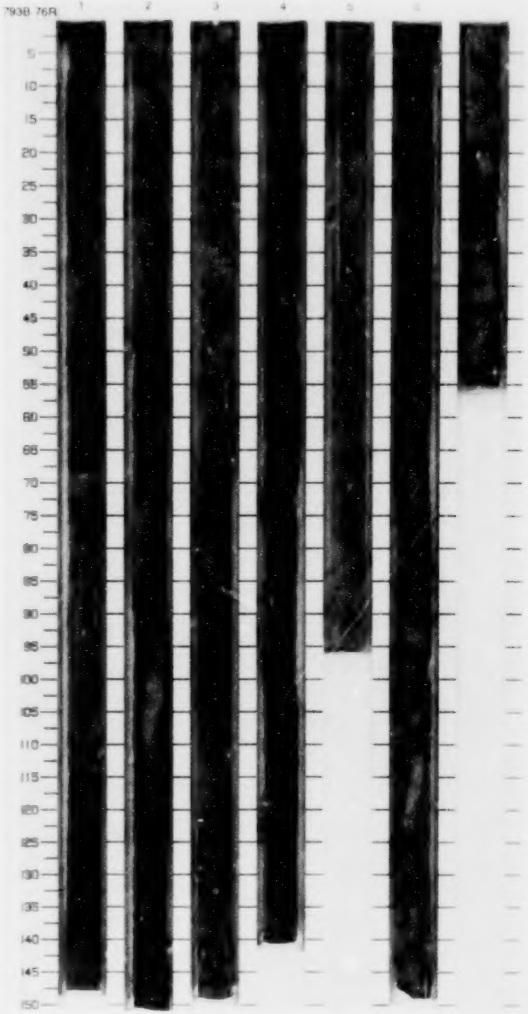
793B 76R
1
2
3
4
5
6
7
5
10
15
20
25
30
35
40
45
50
55
60
65
70
75
80
85
90
95
100
105
110
115
120
125
130
135
140
145
150

SITE 793 HOLE B CORE 77R CORED INTERVAL 1317.0-1326.7 mbsf

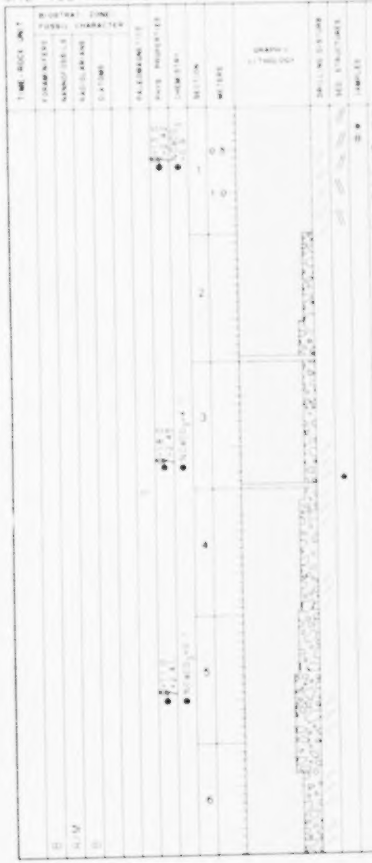
TIME-ROCK UNIT
BIOSTRAT. ZONE/ FOSSIL CHARACTER
FORAMINIFERS
NANNOFOSSILS
RADIOLARIANS
DIATOMS
PALEOMAGNETICS
PHYS. PROPERTIES
CHEMISTRY
SECTION
METERS
GRAPHIC LITHOLOGY
DRILLING DISTURB.
SED. STRUCTURES
SAMPLES
0.5
1.0
1
2
3
4
5
6
B
R/M
B

LITHOLOGIC DESCRIPTION

VITRIC SANDSTONE AND BIOCLAST-BEARING VITRIC-LITHIC PEBBLY SANDSTONE

Major lithologies:
The sediment consists of greenish black [illegible] VITRIC SANDSTONE and BIOCLAST-BEARING VITRIC-LITHIC PEBBLY SANDSTONE. Grain size [illegible] result of variations in the content of volcanic and bioclastic granules and pebbles. The bioclastic grains [illegible] calcareous red algae. The vitric sandstone has [illegible]. A mudstone [illegible] at the base of Section [illegible]. The maximum clast size of pebbles is [illegible]. Bioclastic grains are as large as 1 cm in diameter.

Parts of Sections 1 and 3 through 6 are slightly fractured by drilling.

SMEAR SLIDE & THIN SECTION SUMMARY (%):

	[illegible]	[illegible]
TEXTURE:		
Sand		[illegible]
Silt	[illegible]	[illegible]
Clay	[illegible]	
COMPOSITION:		
Accessory minerals	[illegible]	
Bioclast		[illegible]
Cement		[illegible]
Clay	[illegible]	
Feldspar	[illegible]	[illegible]
Glass	[illegible]	[illegible]
Inorganic calcite	[illegible]	
Micrite	[illegible]	
Opaques	[illegible]	
Quartz	[illegible]	

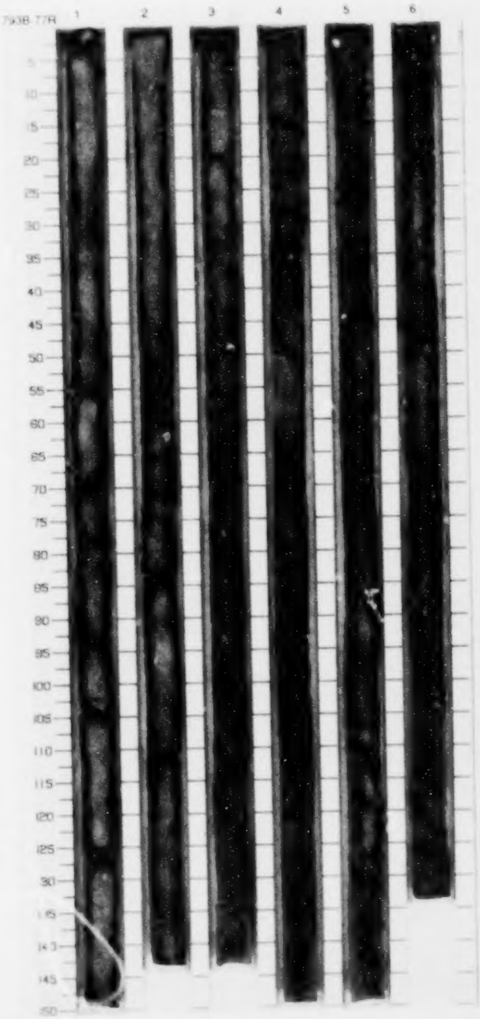
793B-77R
1
2
3
4
5
6
5
10
15
20
25
30
35
40
45
50
55
60
65
70
75
80
85
90
95
100
105
110
115
120
125
130
135
140
145
150

SITE 793 HOLE B CORE 78R CORED INTERVAL 1326.7-1336.4 mbsf

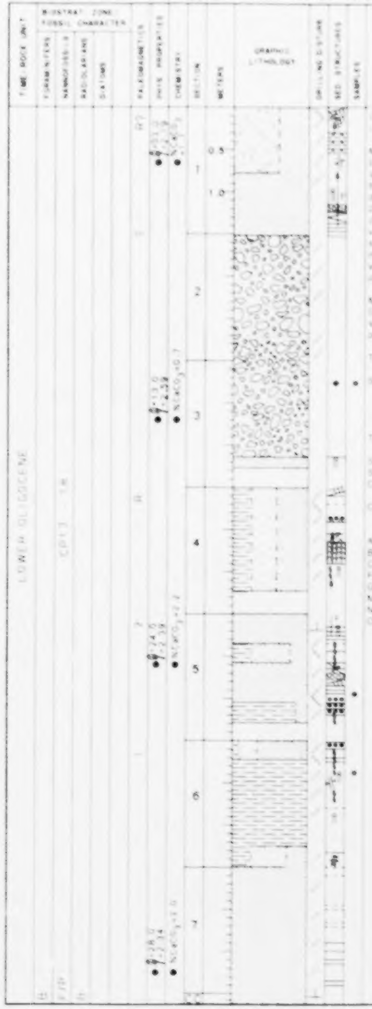
TIME-ROCK UNIT
BIOSTRAT. ZONE/ FOSSIL CHARACTER
FORAMINIFERS
NANNOFOSSILS
RADIOLARIANS
DIATOMS
PALEOMAGNETICS
PHYS. PROPERTIES
CHEMISTRY
SECTION
METERS
GRAPHIC LITHOLOGY
DRILLING DISTURB.
SED. STRUCTURES
SAMPLES
LOWER OLIGOCENE
CP13 - 16
0.5
1.0
1
2
3
4
5
6
7

LITHOLOGIC DESCRIPTION

CRYSTAL VITRIC SANDSTONE AND VOLCANICLITHIC SANDY PEBBLE GRANULE CONGLOMERATE

Major lithologies:
Dark gray (5Y 4/1, 5GY 4/1) and dark greenish gray (5G 4/1, 5BG 4/1) CRYSTAL VITRIC SANDSTONE comprises 42% of the core in five graded beds, 22-148 cm thick, that are planar laminated in their lower portions. Sandstone also occurs as basal divisions, 1-7 cm thick, of parallel laminated, graded beds. A bed of greenish black (5G 2/1) VOLCANICLITHIC SANDY PEBBLE GRANULE CONGLOMERATE from Section 2, 0 cm, to Section 3, 115 cm, comprises 28% of the core. Sand/granule/pebble ratios vary from 40/50/10 at the top to 40/40/20 at the bottom of this bed. Maximum clasts sizes vary from 20 mm near the top to 14 mm near the base, and the corresponding mean sizes of the ten largest pebbles are 8 mm and 7 mm. Pebbles consist of highly vesicular two pyroxene andesite, two pyroxene dacite, glass and brick red pumice. The core contains water escape structures and zeolite-filled fractures.

Minor lithologies:
Greenish black (5G 2/1) VITRIC SILTY CLAYSTONE, VITRIC SILTSTONE, and VITRIC SANDY SILTSTONE respectively comprise 16%, 12% and 2% of the core, occurring as slightly to intensely burrowed upper divisions of graded beds.

The core is slightly fractured by drilling.

SMEAR SLIDE SUMMARY (%):

	3, 27 M	5, 95 D	6, 44 M
TEXTURE:			
Sand	20	40	10
Silt	50	50	40
Clay	30	10	50
COMPOSITION:			
Accessory minerals	3	10	—
Bioclast	—	Tr	—
Clay	30	10	50
Feldspar	2	18	2
Glass	65	60	40
Micrite	—	—	3
Nannofossils	—	—	2
Opaques	—	2	3

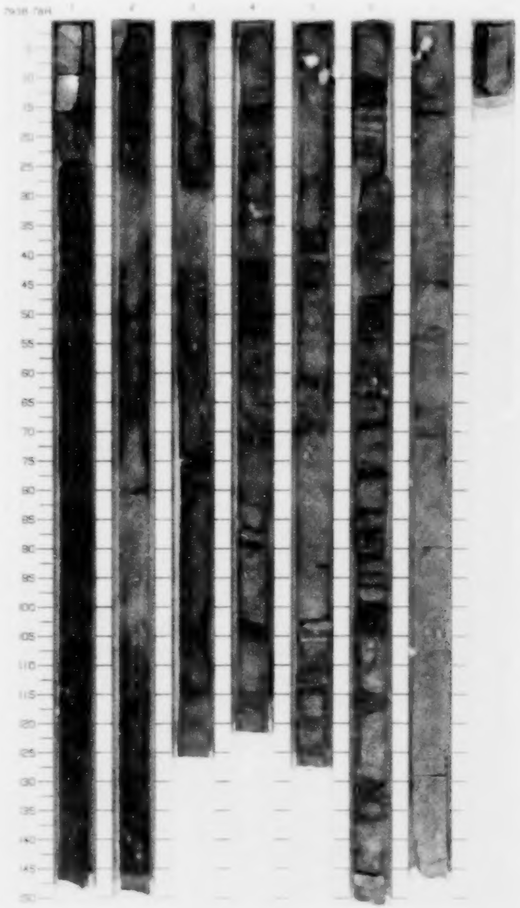
793B-78R 1 2 3 4 5 6 7 CC
0 5 10 15 20 25 30 35 40 45 50 55 60 65 70 75 80 85 90 95 100 105 110 115 120 125 130 135 140 145 150

SITE 793 HOLE B CORE 79R CORED INTERVAL 1336.4-1346.0 mbsf

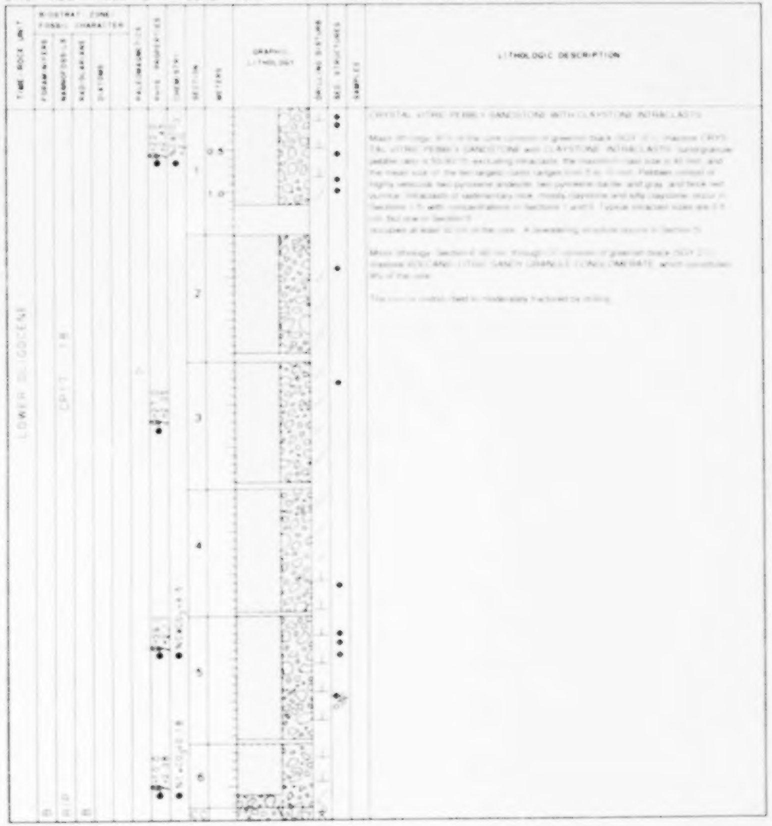
TIME-ROCK UNIT
BIOSTRAT. ZONE/FOSSIL CHARACTER
FORAMINIFERS
NANNOFOSSILS
RADIOLARIANS
DIATOMS
PALEOMAGNETICS
PHYS. PROPERTIES
CHEMISTRY
SECTION
METERS
GRAPHIC LITHOLOGY
DRILLING DISTURB.
SED. STRUCTURES
SAMPLES
LITHOLOGIC DESCRIPTION
LOWER OLIGOCENE
CP17-18
B
B/P
B
1
2
3
4
5
6
0.5
1.0

CRYSTAL VITRIC PEBBLY SANDSTONE WITH CLAYSTONE INTRACLASTS

Major lithology: 91% of the core consists of greenish black (5GY 2/1), massive CRYSTAL VITRIC PEBBLY SANDSTONE with CLAYSTONE INTRACLASTS. Sand:granule:pebble ratio is 50:30:20, excluding intraclasts; the maximum clast size is 40 mm, and the mean size of the ten largest clasts ranges from 5 to 10 mm. Pebbles consist of highly vesicular two-pyroxene andesite, two-pyroxene dacite, and gray and brick red pumice. Intraclasts of sedimentary rock, mostly claystone and silty claystone, occur in Sections 1-5, with concentrations in Sections 1 and 5. Typical intraclast sizes are 3-7 cm, but one in Section 5 occupies at least 10 cm of the core. A dewatering structure occurs in Section 5.

Minor lithology: Section 6, 60 cm, through CC consists of greenish black (5GY 2/1), massive VOLCANIC LITHIC SANDY GRANULE CONGLOMERATE, which constitutes 9% of the core.

The core is slightly to moderately fractured by drilling.

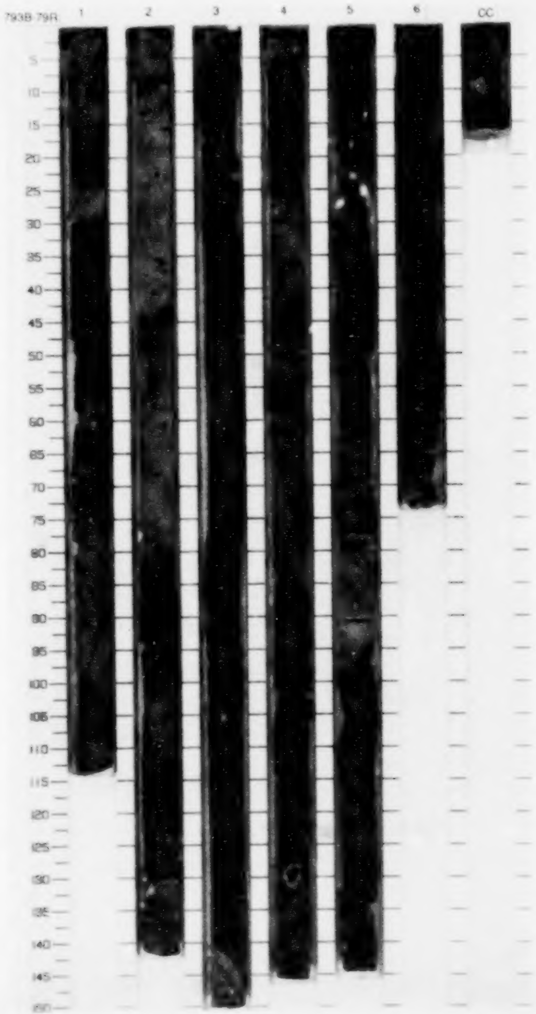
793B-79R
1
2
3
4
5
6
CC
5
10
15
20
25
30
35
40
45
50
55
60
65
70
75
80
85
90
95
100
105
110
115
120
125
130
135
140
145
150

SITE 793 HOLE B CORE 80R CORED INTERVAL 1346.0-1355.7 mbsf

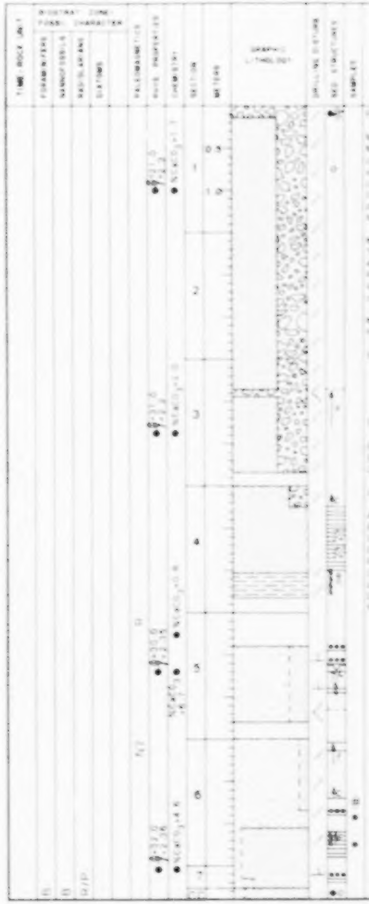
TIME-ROCK UNIT
BIOSTRAT. ZONE/ FOSSIL CHARACTER
FORAMINIFERS
NANNOFOSSILS
RADIOLARIANS
DIATOMS
PALEOMAGNETICS
PHYS. PROPERTIES
CHEMISTRY
SECTION
METERS
GRAPHIC LITHOLOGY
DRILLING DISTURB.
SED. STRUCTURES
SAMPLES
0.5
1.0
1
2
3
4
5
6
7
B
B
B/P

LITHOLOGIC DESCRIPTION

PEBBLY CRYSTAL VITRIC SANDSTONE

Major lithology: PEBBLY CRYSTAL VITRIC SANDSTONE comprises 81% of the core. Much of it occurs in a single, greenish black (5GY 2/1), massive, coarse graded and conglomeratic bed from Section 1, 0 cm, to Section 4, 27 cm, with a maximum clast size of 15 mm and a mean size of 11 mm for the ten largest clasts. The pebble-sized clasts consist of two-pyroxene andesite, two-pyroxene dacite, and gray and brick-red pumice. Other sandstone beds, colored brownish black (5YR 2/1), greenish black (5GY 2/1) and dark gray (N4) (1–11 cm thick), are generally planar laminated and normally graded. Microfaults occur in Section 4, and a dewatering structure in Section 5.

Minor lithologies:
Two intervals in the uppermost sandstone unit (Section 1, 0–13 cm, and Section 3, 0–43 cm) contain enough pebbles and granules to be termed VOLCANIC LITHIC SANDY PEBBLE-GRANULE CONGLOMERATE (2% of the core). Greenish black (5G 2/1) VITRIC SILTSTONE and VITRIC SILTY CLAYSTONE comprise 14% and 3% of the core, respectively, and occur as the upper divisions of graded beds.

Most of the core is only slightly fractured by drilling, but Section 5 is moderately to highly fractured.

SMEAR SLIDE & THIN SECTION SUMMARY (%):

	3, 13 D	4, 92 M	6, CA D
TEXTURE:			
Sand	100	5	80
Silt	—	75	20
Clay	—	20	—
COMPOSITION:			
Accessory minerals	5	1	—
Pumice	5	—	30
Cement	20	—	2
Clay	—	67	—
Feldspar	15	10	15
Glass	45	20	40
Lithic fragments	—	—	5
Opaques	—	2	—
Rock fragment	10	—	—

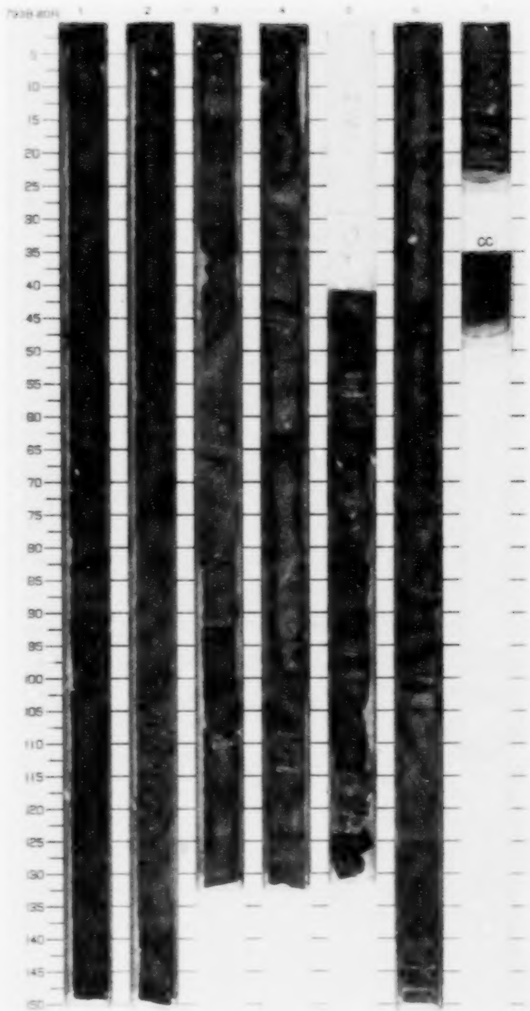
793B-80R
1
2
3
4
5
6
7
CC
5
10
15
20
25
30
35
40
45
50
55
60
65
70
75
80
85
90
95
100
105
110
115
120
125
130
135
140
145
150

SITE 793 HOLE B CORE 81R CORED INTERVAL 1355.7-1365.3 mbsf

LITHOLOGIC DESCRIPTION

CRYSTAL-VITRIC SANDSTONE AND VITRIC SILTSTONE

Major lithologies:

[illegible] CRYSTAL-VITRIC SANDSTONE and VITRIC SILTSTONE [illegible]

Minor lithologies:

[illegible] VITRIC SILTY CLAYSTONE [illegible] VITRIC SANDY SILTSTONE [illegible] and CLAYSTONE [illegible]

[illegible]

SMEAR SLIDE SUMMARY (%):

TEXTURE:

Sand
Silt
Clay

COMPOSITION:

Accessory minerals
Cement
Clay
Feldspar
Glass
Inorganic calcite
Lithic fragments
Mica
Nannofossils
Opaques
Radiolarians

LOWER OLIGOCENE

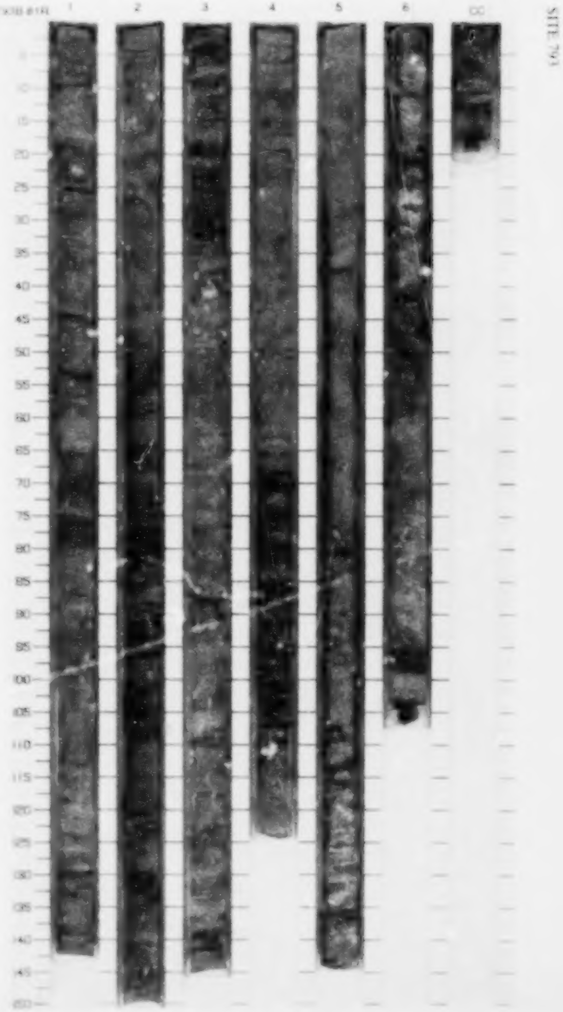
CM
1
2
3
4
5
6
CC
0
10
20
30
40
50
60
70
80
90
100
110
120
130
140
150

SITE 793 HOLE B CORE 82R CORED INTERVAL 1365.3-1374.9 mbsf

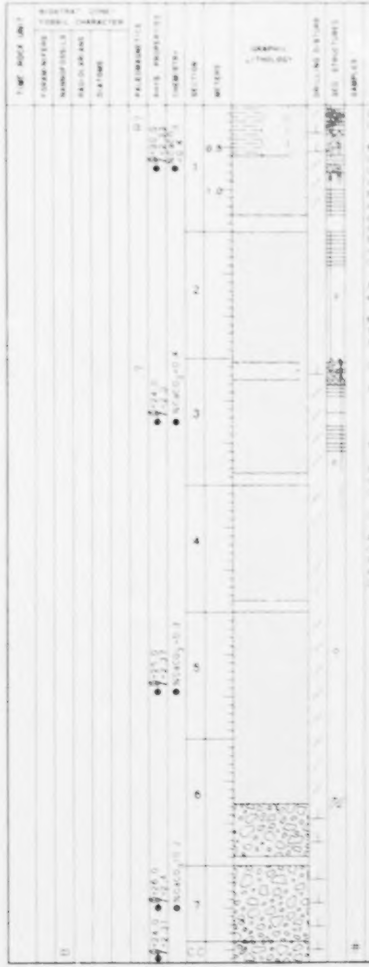
TIME-ROCK UNIT
BIOSTRAT. ZONE/FOSSIL CHARACTER
FORAMINIFERS
NANNOFOSSILS
RADIOLARIANS
DIATOMS
PALEOMAGNETICS
PHYS. PROPERTIES
CHEMISTRY
SECTION
METERS
GRAPHIC LITHOLOGY
DRILLING DISTURB.
SED. STRUCTURES
SAMPLES
0.5
1.0
1
2
3
4
5
6
7
CC

LITHOLOGIC DESCRIPTION

CRYSTAL-VITRIC SANDSTONE AND VOLCANIC LITHIC COBBLE-PEBBLE CONGLOMERATE

Major lithologies:
Dark greenish gray (5G 4/1), greenish black (5G 2/1), and greenish black (5GY 2/1) CRYSTAL-VITRIC SANDSTONE comprises 75% of the core. It is in beds 2-10 cm thick in the upper part of the core, as the planar laminated basal divisions of thin graded beds. Most of the sandstone, however, is in two beds, 244 cm and 527 cm thick, that are very coarse grained and granule-rich in their lower parts, and grade into very fine grained, planar laminated tops. The lower, thickest sandstone bed is underlain by a single bed of dark gray (N3/ 4/1) VOLCANIC LITHIC COBBLE-PEBBLE CONGLOMERATE, which comprises 19% of the core. Its angular to sub-rounded clasts have a maximum size larger than 100 mm, with mean size of 70 mm for the ten largest clasts. Clast lithologies are basaltic andesite and andesite.

All the beds are severely altered. Sections 1 and 3 contain zeolite-filled fractures, water escape structures, and microfaults.

Minor lithologies:
The rest of the core is composed of VITRIC SILTSTONE (4%), VITRIC SILTY CLAYSTONE (2%), and VITRIC CLAYEY SILTSTONE (2%), as the tops of graded beds.

Drilling has slightly to moderately fractured all but Section 3 of the core.

SMEAR SLIDE & THIN SECTION SUMMARY (%):

	CC, 17 D
TEXTURE:	
Sand	50
Silt	20
Clay	30
COMPOSITION:	
Accessory minerals	[illegible]
Clay	28
Feldspar	5
Foraminifers	[illegible]
Glass	61

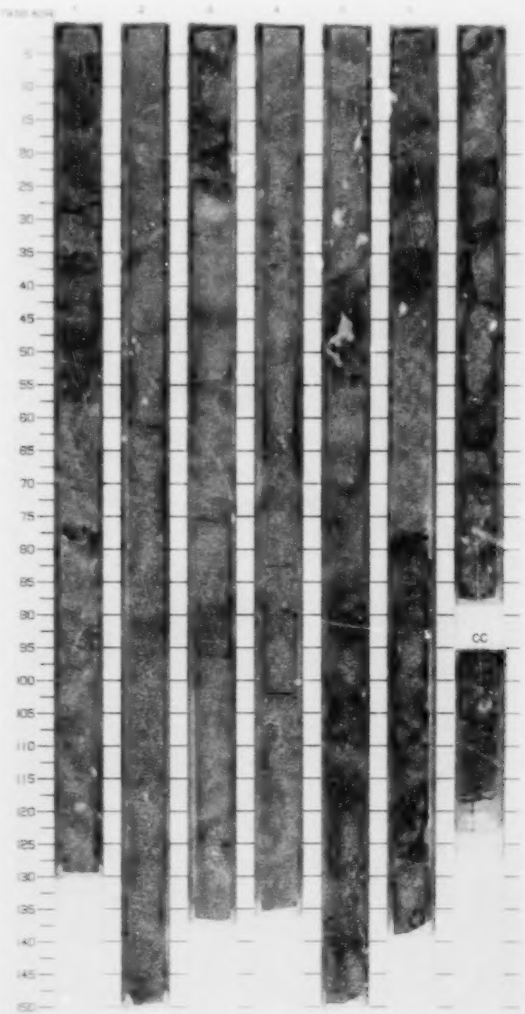

SITE 793 HOLE B CORE 83R CORED INTERVAL 1374.9-1384.5 mbsf

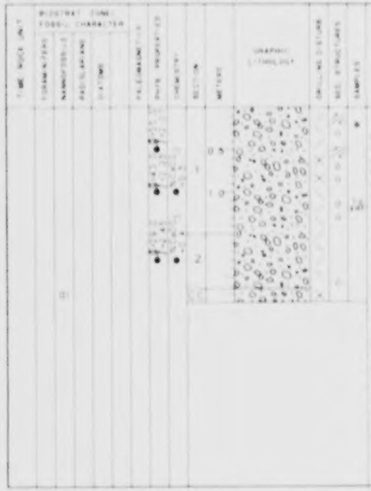
TIME-ROCK UNIT
BIOSTRAT. ZONE/FOSSIL CHARACTER
FORAMINIFERS
NANNOFOSSILS
RADIOLARIANS
DIATOMS
PALEOMAGNETICS
PHYS. PROPERTIES
CHEMISTRY
SECTION
METERS
GRAPHIC LITHOLOGY
DRILLING DISTURB.
SED. STRUCTURES
SAMPLES
0.5
1.0
1
2
CC

LITHOLOGIC DESCRIPTION

VOLCANIC BRECCIA AND VOLCANIC MICROBRECCIA

Major lithology: The core consists entirely of grayish green (5G 5/2), very poorly sorted VOLCANIC BRECCIA and VOLCANIC MICROBRECCIA with a matrix of zeolitic claystone. The matrix forms about 10% of the rock in Section 1, whereas in Section 2 there is little claystone matrix between sand- and granule-sized volcanic grains. All clasts are angular. Clasts in Section 1 are as large as 10 cm in diameter and consist of vesicular andesite with chilled margins. The larger clasts are olive black (5Y 2/1). There are fault surfaces with slickensides in Section 1, 15-25 cm and 50-60 cm.

The core is highly fractured by drilling.

SMEAR SLIDE SUMMARY (%):

	1, 20
	M
TEXTURE:	
Silt	10
Clay	90
COMPOSITION:	
Feldspar	Tr
Glass	96
[illegible]	Tr
Opaques	1
Quartz	Tr

SITE 793 HOLE B CORE 84R CORED INTERVAL 1384.5-1394.2 mbsf

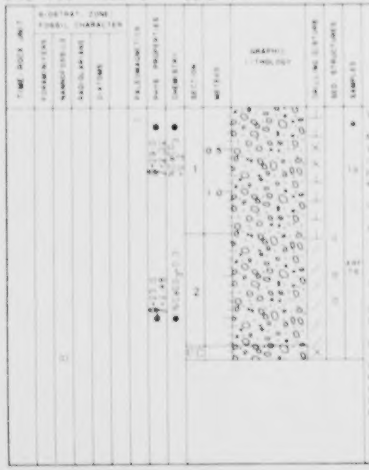
TIME-ROCK UNIT
BIOSTRAT. ZONE/FOSSIL CHARACTER
FORAMINIFERS
NANNOFOSSILS
RADIOLARIANS
DIATOMS
PALEOMAGNETICS
PHYS. PROPERTIES
CHEMISTRY
SECTION
METERS
GRAPHIC LITHOLOGY
DRILLING DISTURB.
SED. STRUCTURES
SAMPLES
0.5
1.0
1
2
CC

LITHOLOGIC DESCRIPTION

VOLCANIC BRECCIA AND VOLCANIC MICROBRECCIA

Major lithology: The core consists entirely of grayish green (5G 5/2), very poorly sorted VOLCANIC BRECCIA and VOLCANIC MICROBRECCIA. All clasts are angular. Clasts in Sections 1 and 2 are as large as 4 and 11 cm in diameter, respectively. Clasts are predominantly vesicular, plagioclase-rich andesites with smectite in the vesicles, and with zoned plagioclase. The larger clasts are olive black (5Y 2/1).

Section 1 is moderately fractured by drilling; Section 2 is slightly fractured.

SMEAR SLIDE SUMMARY (%):

	1, 20
	M
TEXTURE:	
Silt	10
Clay	90
COMPOSITION:	
Clay	85
Feldspar	1
Glass	10
Opaques	1
Quartz	Tr

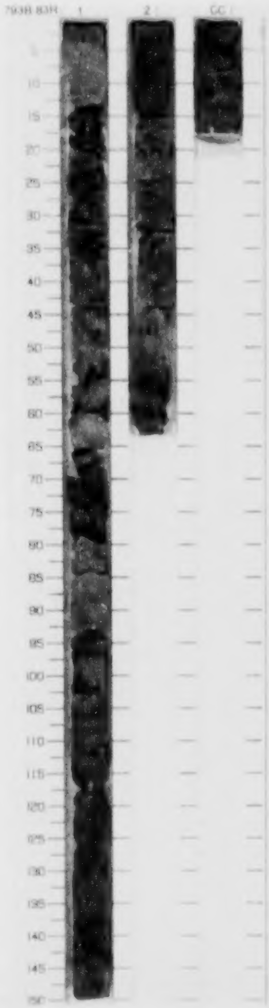
793B 83R
1
2
CC
5
10
15
20
25
30
35
40
45
50
55
60
65
70
75
80
85
90
95
100
105
110
115
120
125
130
135
140
145
150

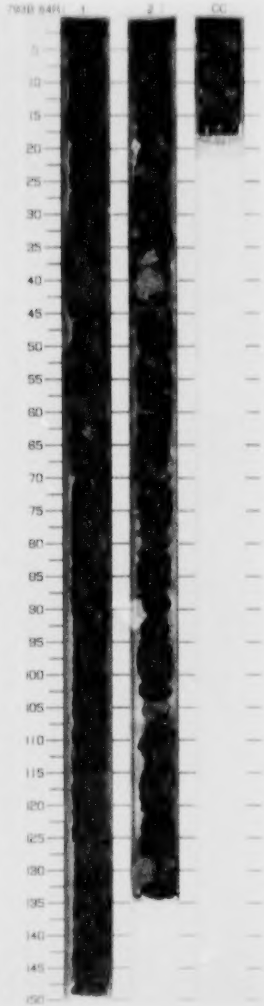
793B 84R
1
2
CC
5
10
15
20
25
30
35
40
45
50
55
60
65
70
75
80
85
90
95
100
105
110
115
120
125
130
135
140
145
150

SITE 793 HOLE B CORE 85R CORED INTERVAL 1394.2-1403.9 mbsf

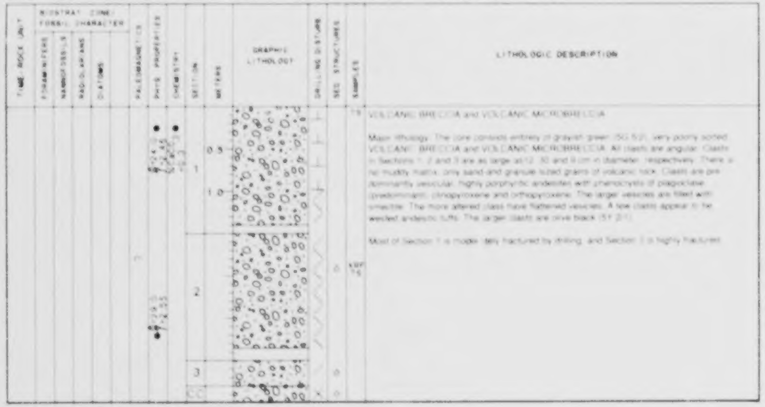
TIME-ROCK UNIT
BIOSTRAT. ZONE/ FOSSIL CHARACTER
FORAMINIFERS
NANNOFOSSILS
RADIOLARIANS
DIATOMS
PALEOMAGNETICS
PHYS. PROPERTIES
CHEMISTRY
SECTION
METERS
GRAPHIC LITHOLOGY
DRILLING DISTURB.
SED. STRUCTURES
SAMPLES
LITHOLOGIC DESCRIPTION
0.5
1.0
1
2
3
CC
TS
XRF TS

VOLCANIC BRECCIA and VOLCANIC MICROBRECCIA

Major lithology: The core consists entirely of grayish green (5G 5/2), very poorly sorted VOLCANIC BRECCIA and VOLCANIC MICROBRECCIA. All clasts are angular. Clasts in Sections 1, 2 and 3 are as large as 12, 30 and 9 cm in diameter, respectively. There is no muddy matrix, only sand- and granule-sized grains of volcanic rock. Clasts are predominantly vesicular, highly porphyritic andesites with phenocrysts of plagioclase (predominant), clinopyroxene and orthopyroxene. The larger vesicles are filled with smectite. The more altered clasts have flattened vesicles. A few clasts appear to be welded andesitic tuffs. The larger clasts are olive black (5Y 2/1).

Most of Section 1 is moderately fractured by drilling, and Section 2 is highly fractured.

126 793B 91R NO RECOVERY

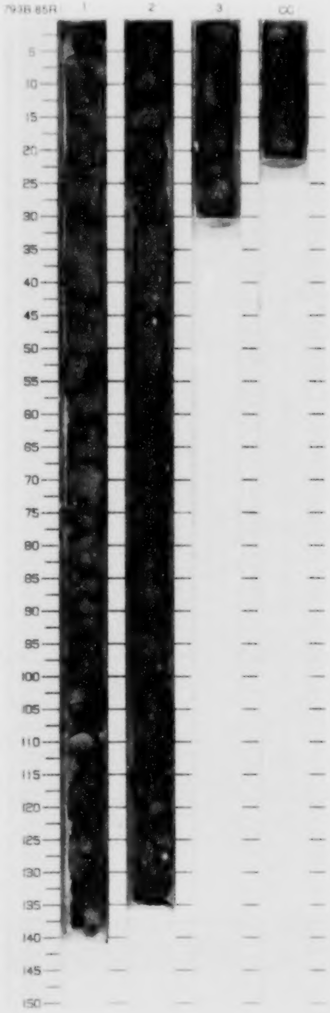
793B 85R
1
2
3
CC
5
10
15
20
25
30
35
40
45
50
55
60
65
70
75
80
85
90
95
100
105
110
115
120
125
130
135
140
145
150

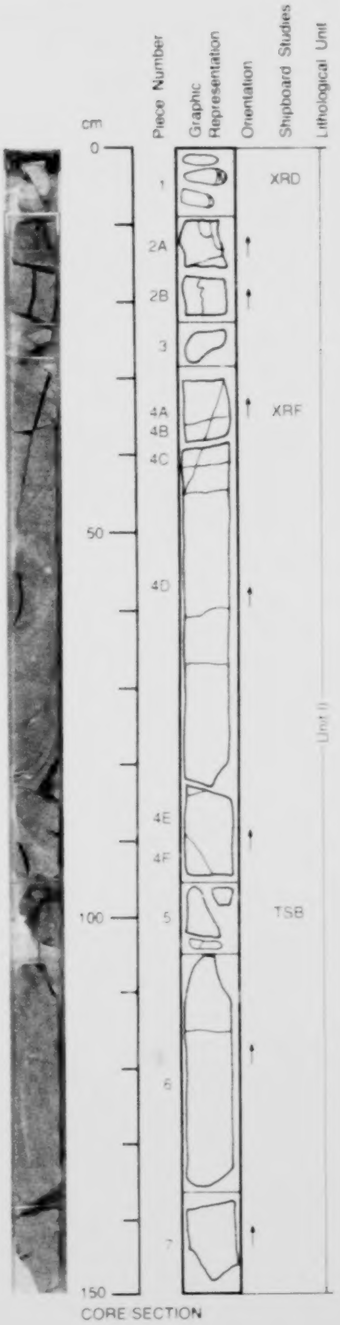
cm
Piece Number
Graphic Representation
Orientation
Shipboard Studies
Lithological Unit
0
50
100
150
1
2A
2B
3
4A
4B
4C
4D
4E
4F
5
6
7
XRD
XRF
TSB
Unit II
CORE SECTION

126-793B-1R-1

UNIT II: DIABASE

Pieces 1-7

CONTACTS: Upper baked, lower chilled.
PHENOCRYSTS: In glomeroporphyritic clots and at lower chilled margin.
Olivine - 5-7%, 1-3 mm, subhedral, altered to smectite.
Clinopyroxene - 2-15%, 2-6 mm, euhedral, twinned, with exsolution lamellae.
Orthopyroxene - 1%, 1-2 mm, sometimes rounded.
GROUNDMASS: Plagioclase (41%, 0.1-0.5 mm), clinopyroxene (18%, 0.1-0.5 mm), orthopyroxene (<1%, 0.1 mm), opaque (4%, 0.05-0.5 mm), glass (26%), vesicles (8%).
VESICLES: 8%, 0.1 mm, equant, random.
Miaroles: In bands and inclusions.
COLOR: Gray.
STRUCTURE: Sill.
ALTERATION: Smectite.
VEINS/FRACTURES: 1%, 5-10 mm, subhorizontal, roughly at 10 cm spacing.

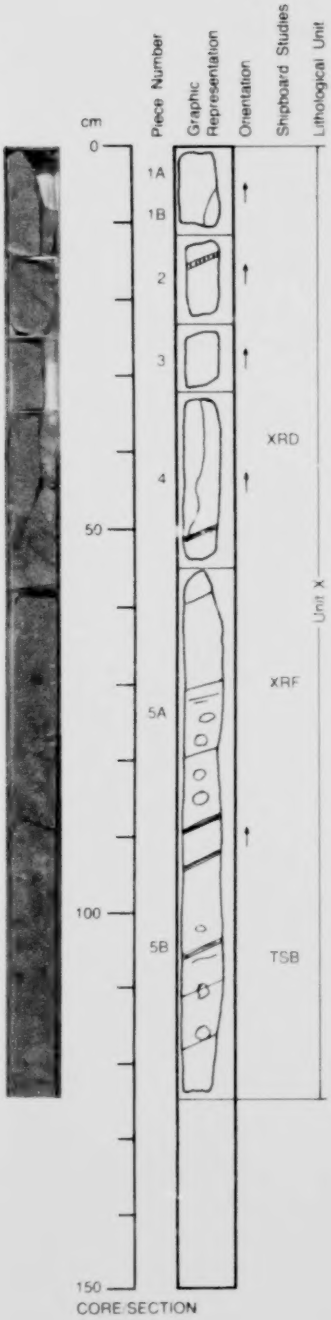
cm
Piece Number
Graphic Representation
Orientation
Shipboard Studies
Lithological Unit
0
50
100
150
1A
1B
2
3
4
5A
5B
XRD
XRF
TSB
Unit X
CORE/SECTION

126-793B-1R-2

UNIT II: DIABASE

Pieces 1-5

CONTACTS: Upper baked, lower chilled
PHENOCRYSTS: In glomeroporphyritic clots, and at lower chilled margin
  Olivine - 5-7%, 1-3 mm, subhedral; altered to smectite
  Clinopyroxene - 2-15%, 2-6 mm, euhedral, twinned, with exsolution lamellae
  Orthopyroxene - 1%, 1-2 mm, sometimes rounded
GROUNDMASS: Plagioclase (41%, 0.1-0.5 mm); clinopyroxene (18%, 0.1-0.5 mm), orthopyroxene (<1%, 0.1 mm); opaque (4%, 0.05-0.5 mm); glass (26%); vesicles (8%)
VESICLES: 8%, 0.1 mm, equant, random
  Miaroles: In bands and inclusions
COLOR: Gray
STRUCTURE: Sill
ALTERATION: Smectite
VEINS/FRACTURES: 1%, 5-10 mm, subhorizontal, roughly at 10 cm spacing

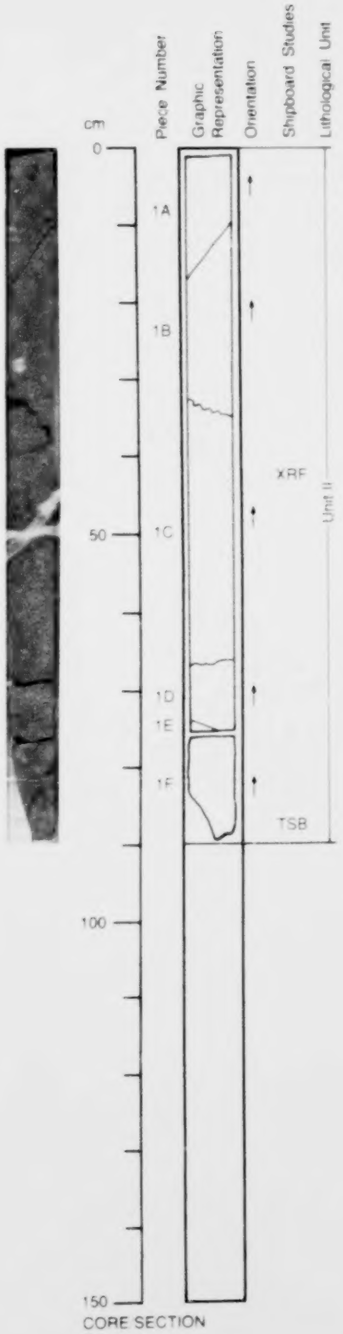
cm
Piece Number
Graphic Representation
Orientation
Shipboard Studies
Lithological Unit
0
50
100
150
1A
1B
1C
1D
1E
1F
XRF
TSB
Unit II
CORE SECTION

126-793B-1R-3

UNIT II: DIABASE

Pieces 1A-F

CONTACTS: Upper baked, lower chilled.
PHENOCRYSTS: In glomeroporphyritic clots, and at lower chilled margin.
Olivine - 5-7%, 1-3 mm, subhedral, altered to smectite.
Clinopyroxene - 2-15%, 2-6 mm, euhedral, twinned, with exsolution lamellae.
Orthopyroxene - 1%, 1-2 mm, sometimes rounded.
GROUNDMASS: Plagioclase (41%, 0.1-0.5 mm), clinopyroxene (18%, 0.1-0.5 mm), orthopyroxene (<1%, 0.1 mm), opaque (4%, 0.05-0.5 mm), glass (26%), vesicles (8%).
VESICLES: 8%, 0.1 mm, equant, random.
Miaroles: In bands and inclusions.
COLOR: Gray.
STRUCTURE: Sill.
ALTERATION: Smectite.
VEINS/FRACTURES: 1%, 5-10 mm, subhorizontal, roughly at 10 cm spacing.

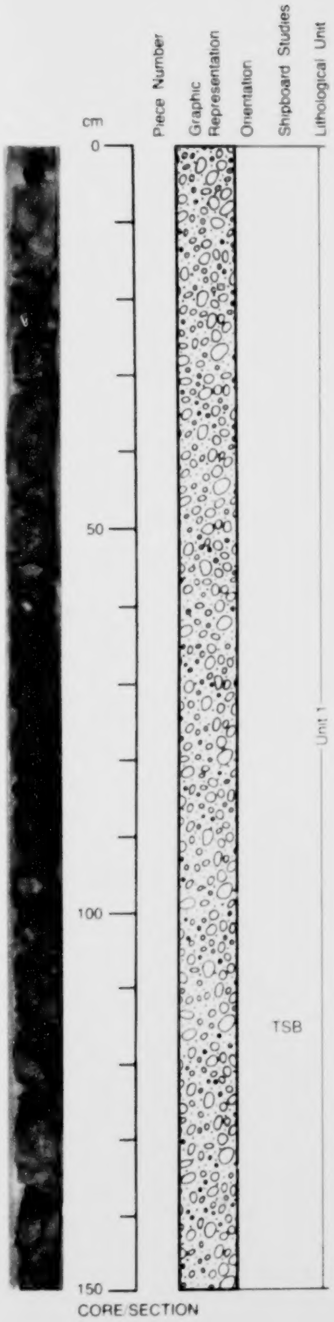
cm
Piece Number
Graphic Representation
Orientation
Shipboard Studies
Lithological Unit
0
50
100
150
TSB
Unit 1
CORE/SECTION

126-793B-86R-1

UNIT 1: VERY FRACTURED VOLCANIC BRECCIA

CONTACTS: Clasts of andesite lava.

PHENOCRYSTS: Clasts of volcanic breccia with angular fragments of altered glass-clinopyroxene crystals up to 5-6 mm. Vesicles filled with smectites, quartz and/or calcite.
Plagioclase - 5-10%, 0.5-1.0 mm, euhedral.
Clinopyroxene - 5-20%, 0.5-2.0 mm, euhedral.
Orthopyroxene - 1-5%, 0.5-2.0 mm, euhedral.

GROUNDMASS: Fine-grained with tiny (<0.1 mm) plagioclase laths.

VESICLES: 2-5%, rounded, mostly filled with clays or with smectite lining.

COLOR: Greenish gray.

ALTERATION: Groundmass altered to clay and orthopyroxene altered to hematite and iron oxides. Plagioclase and clinopyroxene are generally fresh.

ADDITIONAL COMMENTS: Very fractured volcanic breccia with clasts as large as 11 cm. Matrix appears deformed and there are some mineral filled fractures. Could be a fault zone. Rounded clasts of clinopyroxene-plagioclase-altered olivine or orthopyroxene vesicles filled with smectites, quartz and/or calcite. Perhaps chilled fragments of the same composition (pillow fragments). Some clasts look like hyaloclastites.

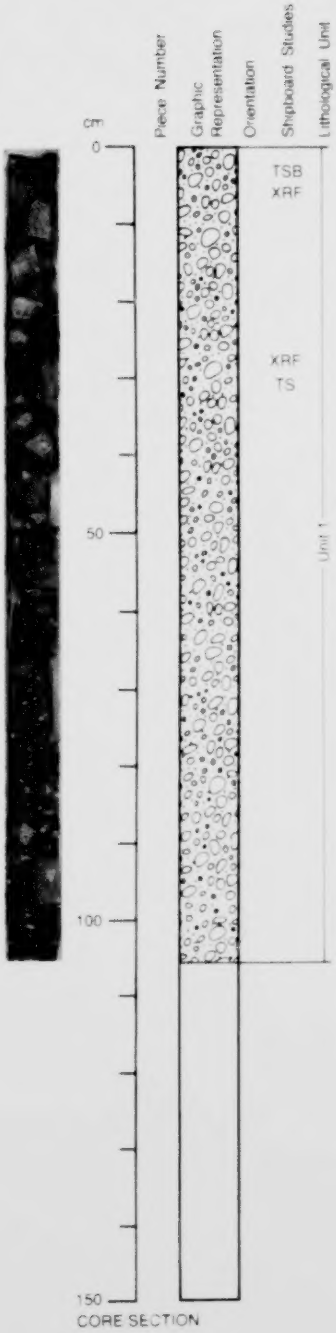
cm
Piece Number
Graphic Representation
Orientation
Shipboard Studies
Lithological Unit
0
50
100
150
TSB
XRF
XRF
TS
Unit 1
CORE SECTION

126-793B-86R-2

UNIT 1: VERY FRACTURED VOLCANIC BRECCIA

CONTACTS: Clasts of andesite lava.

PHENOCRYSTS: Clasts of volcanic breccia with angular fragments of altere glass, clinopyroxene crystals up to 5-6 mm. Vesicles filled with smectites, quartz and/or calcite.

Plagioclase - 5-10%, 0.5-1.0 mm, euhedral.
Clinopyroxene - 5-20%, 0.5-2.0 mm, euhedral.
Orthopyroxene - 1-5%, 0.5-2.0 mm, euhedral.

GROUNDMASS: Fine-grained with tiny (<0.1 mm) plagioclase laths.

VESICLES: 2-5%, rounded, mostly filled with clays or with smectite lining.

COLOR: Greenish gray.

ALTERATION: Groundmass altered to clay, and orthopyroxene altered to hematite and iron oxides. Plagioclase and clinopyroxene are generally fresh.

ADDITIONAL COMMENTS: Very fractured volcanic breccia with clasts as large as 6 cm. Matrix appears deformed and there are some mineral-filled fractures. Could be a fault zone. Rounded clasts of clinopyroxene, plagioclase-altered olivine or orthopyroxene vesicles filled with smectites, quartz and/or calcite. Perhaps chilled fragments of the same composition (pillow fragments). Some clasts look like hyaloclastites.

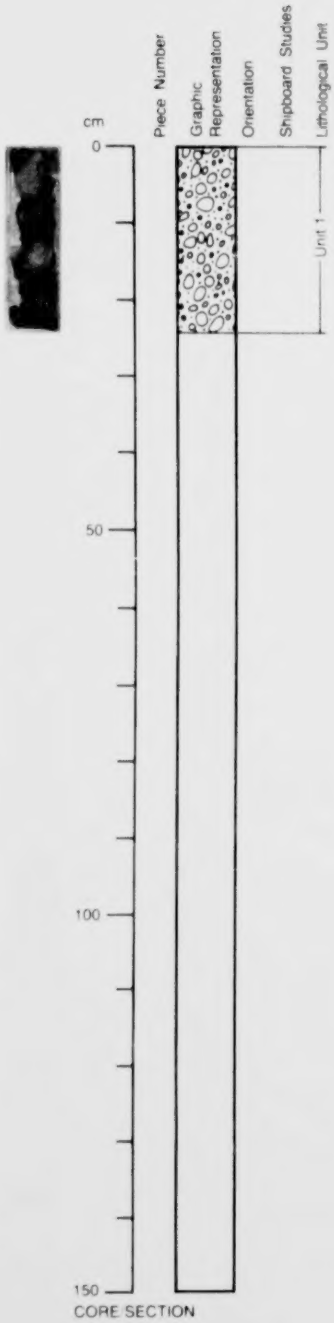
cm
0
50
100
150
Piece Number
Graphic Representation
Orientation
Shipboard Studies
Lithological Unit
Unit 1
CORE SECTION

126-793B-86R-CC

UNIT 1: VERY FRACTURED VOLCANIC BRECCIA

CONTACTS: Clasts of andesite lava.

PHENOCRYSTS: Clasts of volcanic breccia with angular fragments of altered glass clinopyroxene crystals up to 5-6 mm. Vesicles filled with smectites, quartz and/or calcite.

Plagioclase - 5-10%, 0.5-1.0 mm, euhedral.
Clinopyroxene - 5-20%, 0.5-2.0 mm, euhedral.
Orthopyroxene - 1-5%, 0.5-2.0 mm, euhedral.

GROUNDMASS: Fine-grained with tiny (<0.1 mm) plagioclase laths.

VESICLES: 2-5%, rounded, mostly filled with clays or with smectite lining.

COLOR: Greenish gray.

ALTERATION: Groundmass altered to clay, and orthopyroxene altered to hematite and iron oxides. Plagioclase and clinopyroxene are generally fresh.

ADDITIONAL COMMENTS: Very fractured volcanic breccia with clasts as large as 5 cm. Matrix appears deformed and there are some mineral-filled fractures. Could be a fault zone. Rounded clasts of clinopyroxene-plagioclase-altered olivine or orthopyroxene vesicles filled with smectites, quartz and/or calcite. Perhaps chilled fragments of the same composition (pillow fragments). Some clasts look like hyaloclastites.

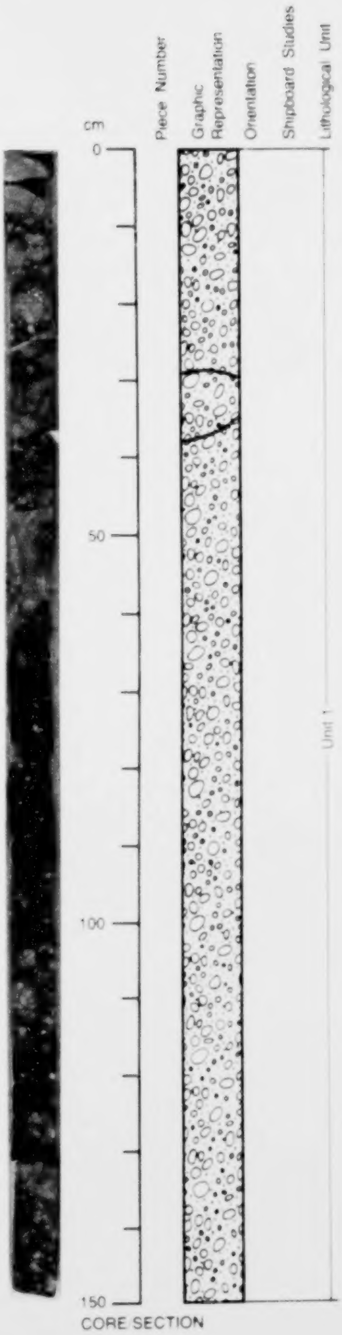
cm
0
50
100
150
Piece Number
Graphic Representation
Orientation
Shipboard Studies
Lithological Unit
Unit 1
CORE SECTION

126-793B-87R-1

UNIT 1: VOLCANIC BRECCIA

PHENOCRYSTS: Orthopyroxene clinopyroxene plagioclase andesite with vesicles filled with smectites.

GROUNDMASS: Angular clasts of the same rocks with opaque minerals looking like chalcopyrite. The groundmass of the smaller clasts is altered to blue smectites. Cement is a chemical percipitate (native?). Silicified. Native copper is in the cement or at the border of the clasts.

ADDITIONAL COMMENTS: Very poorly sorted, angular volcanic breccia with clasts from granule to 10 cm and 5% porosity filled in with pale green and clear mineral cements (heulandite-clinoptilolite). Clasts are oligomictic, 2 pyroxene andesite. The cement contains rare crystals of native copper. Some clasts include altered olivine or orthopyroxene with smectites-opaque minerals (magnetite or ilmenite). The main difference that exists between the clasts is the abundance of vesicles in the groundmass. These vesicles are filled with smectites, perhaps zeolites.

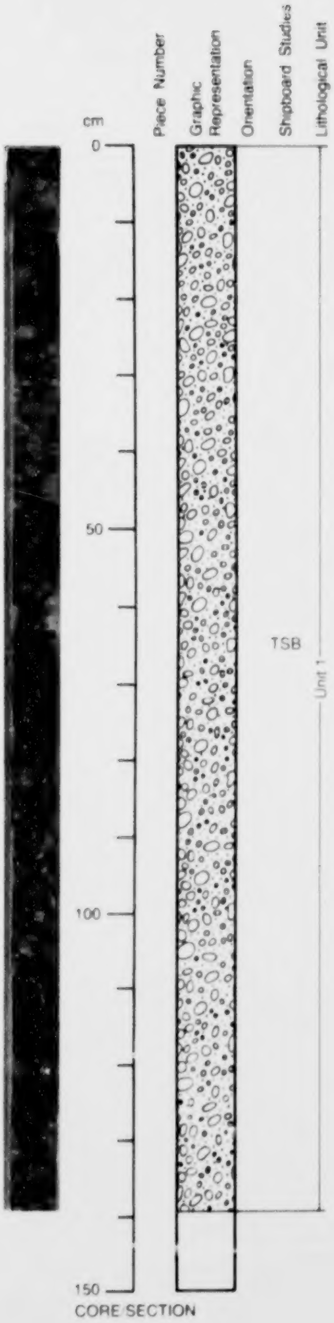
cm
0
50
100
150
Piece Number
Graphic Representation
Orientation
Shipboard Studies
Lithological Unit
TSB
Unit 1
CORE SECTION

126-793B-87R-2

UNIT 1: VOLCANIC BRECCIA

PHENOCRYSTS: Orthopyroxene-clinopyroxene-plagioclase andesite with vesicles filled with smectites.

GROUNDMASS: Angular clasts of the same rocks with opaque minerals looking like chalcopyrite. The groundmass of the smaller clasts is altered to blue smectites. Cement is a chemical percipitate (native?). Silicified. Native copper is in the cement or at the border of the clasts.

VESICLES: "Vug" filled with heulandite/clinoptilolite (mixture).

ADDITIONAL COMMENTS: Very poorly sorted, angular volcanic breccia with clasts from granule to 6 cm and 5% porosity filled in with pale green and clear mineral cements (heulandite-clinoptilolite). Clasts are oligomictic, 2 pyroxene andesite. The cement contains rare crystals of native copper. Some clasts include altered olivine or orthopyroxene with smectites-opaque minerals (magnetite or ilmenite). The main difference that exists between the clasts is the abundance of vesicles in the groundmass. These vesicles are filled with smectites, perhaps zeolites.

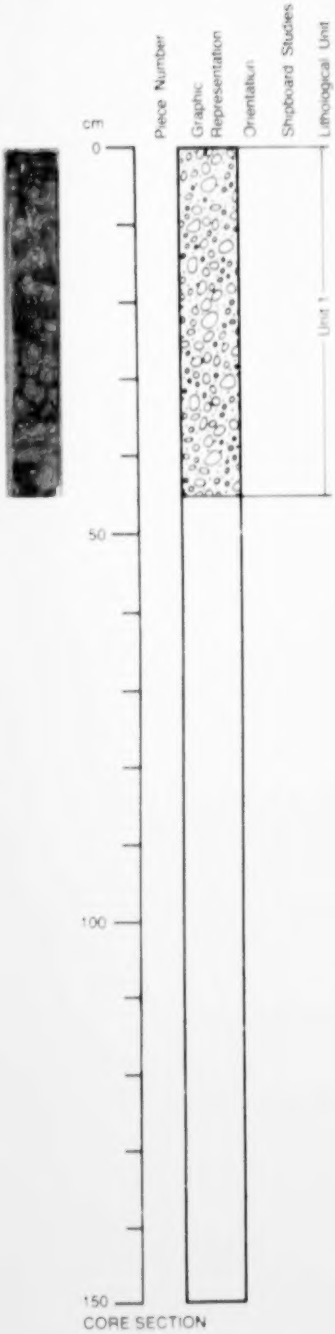
cm
Piece Number
Graphic Representation
Orientation
Shipboard Studies
Lithological Unit
0
50
100
150
Unit 1
CORE SECTION

126-793B-87R-3

UNIT 1: VOLCANIC BRECCIA

PHENOCRYSTS: Orthopyroxene-clinopyroxene-plagioclase andesite with vesicles filled with smectites.

GROUNDMASS: Angular clasts of the same rocks with opaque minerals looking like chalcopyrite. The groundmass of the smaller clasts is altered to blue smectites. Cement is a chemical percipitate (native?). Silicified. Native copper is in the cement or at the border of the clasts.

ADDITIONAL COMMENTS: Very poorly sorted, angular volcanic breccia with clasts from granule to 12 cm and 5% porosity filled in with pale green and clear mineral cements (heulandite-clinoptiolite). Clasts are oligomictic, 2 pyroxene andesite. The cement contains rare crystals of native copper. Some clasts include altered olivine or orthopyroxene with smectites-opaque minerals (magnetite or ilmenite). The main difference that exists between the clasts is the abundance of vesicles in the groundmass. These vesicles are filled with smectites, perhaps zeolites.

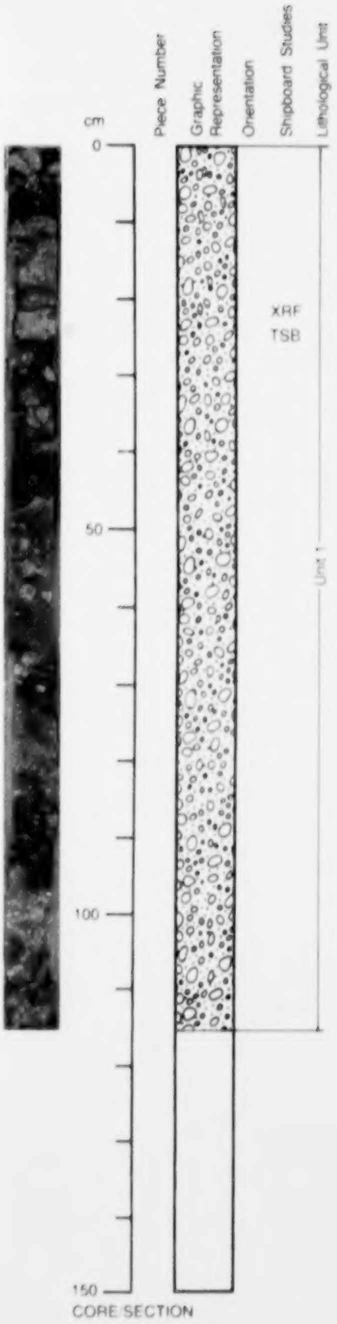
cm
Piece Number
Graphic Representation
Orientation
Shipboard Studies
Lithological Unit
0
50
100
150
XRF
TSB
Unit 1
CORE/SECTION

126-793B-87R-4

UNIT 1: VOLCANIC BRECCIA

PHENOCRYSTS: Orthopyroxene-clinopyroxene-plagioclase andesite with vesicles filled with smectites.

GROUNDMASS: Angular clasts of the same rocks with opaque minerals looking like chalcopyrite. The groundmass of the smaller clasts is altered to blue smectites. Cement is a chemical percipitate (native?). Silicified. Native copper is in the cement or at the border of the clasts.

ADDITIONAL COMMENTS: Very poorly sorted, angular volcanic breccia with clasts from granule to 10 cm and 5% porosity filled in with pale green and clear mineral cements (heulandite-clinoptilolite). Clasts are oligomictic, 2 pyroxene andesite. The cement contains rare crystals of native copper. Little pore-filling cement and more sandy matrix than 126-793B-87R-1. Some clasts include altered olivine or orthopyroxene with smectites-opaque minerals (magnetite or ilmenite). The main difference that exists between the clasts is the abundance of vesicles in the groundmass. These vesicles are filled with smectites, perhaps zeolites.

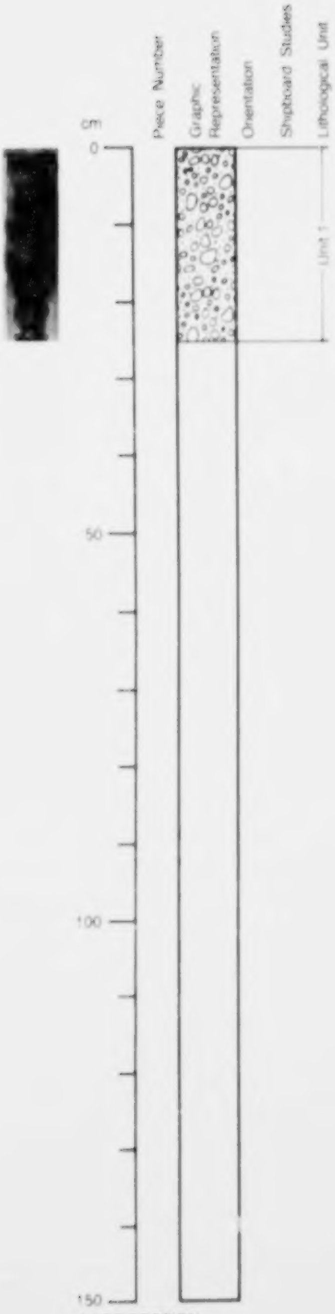
cm
Piece Number
Graphic Representation
Orientation
Shipboard Studies
Lithological Unit
0
50
100
150
Unit 1
CORE SECTION

126-793B-87R-CC

UNIT 1: VOLCANIC BRECCIA

PHENOCRYSTS: Orthopyroxene-clinopyroxene-plagioclase andesite with vesicles filled with smectites.

GROUNDMASS: Angular clasts of the same rocks with opaque minerals looking like chalcopyrite. The groundmass of the smaller clasts is altered to blue smectites. Cement is a chemical percipitate (native?). Silicified. Native copper is in the cement or at the border of the clasts.

ADDITIONAL COMMENTS: Drilling breccia. Very poorly sorted, angular volcanic breccia with clasts from granule to 10 cm and 5% porosity filled in with pale green and clear mineral cements (heulandite-clinoptilolite). Clasts are oligomictic: 2 pyroxene andesite. The cement contains rare crystals of native copper. Some clasts include altered olivine or orthopyroxene with smectites, opaque minerals (magnetite or ilmenite). The main difference that exists between the clasts is the abundance of vesicles in the groundmass. These vesicles are filled with smectites, perhaps zeolites.

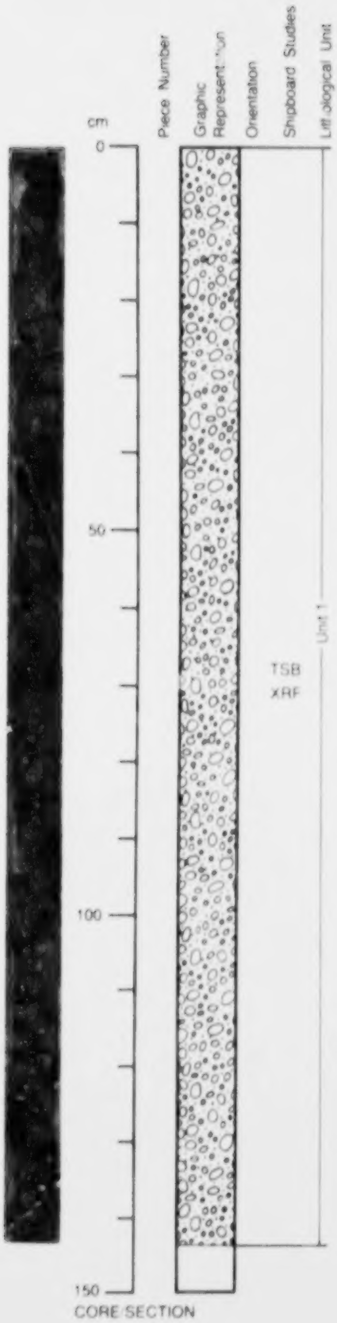
cm
Piece Number
Graphic Representation
Orientation
Shipboard Studies
Lithological Unit
0
50
100
150
TSB
XRF
Unit 1
CORE/SECTION

126-793B-88R-1

UNIT 1: VOLCANIC BRECCIA

PHENOCRYSTS: Intersertal porphyritic andesite with clinopyroxene and above all orthopyroxene and plagioclase.

VESICLES: Vesicular orthopyroxene-plagioclase andesite. The vesicles are filled with zeolites, smectites and copper. Some vesicles are flattened and filled with smectite. One clast contains a vesicle filled with zeolites and native copper. Some clasts contain altered orthopyroxene in smectites.

ADDITIONAL COMMENTS: 1-57 cm: Volcanic breccia with clasts as large as 6 cm. Matrix is a crystal-shard tuff. The shards are altered glass with smectite and chlorite; 57 to 143 cm: Volcanic Breccia with clasts up to ~8 cm. Average diameter of 10 largest clasts is ~6 cm. Matrix is composed of granules and fine pebbles of the same material and small amounts of mineral cement. Clasts are vesicular lava. Some vesicles are filled with white zeolite and flecks of native copper. Clasts have chilled margins.

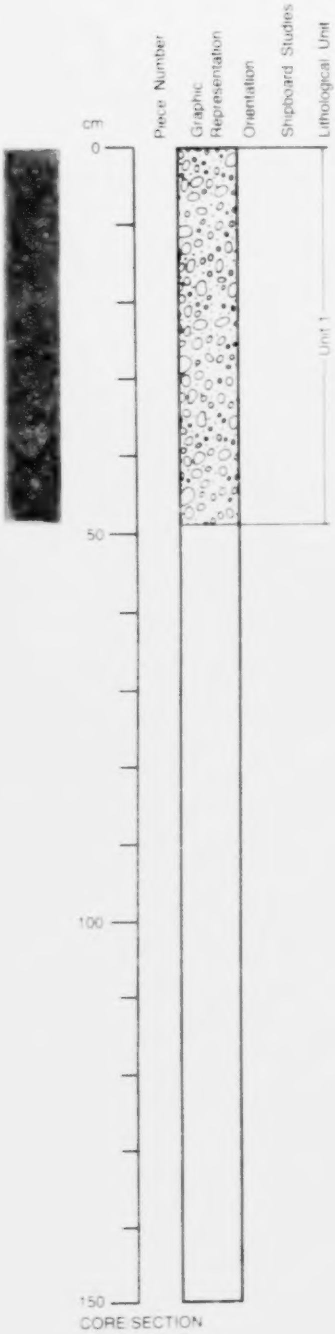
cm
Piece Number
Graphic Representation
Orientation
Shipboard Studies
Lithological Unit
0
50
100
150
Unit 1
CORE SECTION

126-793B-88R-2

UNIT 1: VOLCANIC BRECCIA

PHENOCRYSTS: Intersertal-porphyritic andesite with clinopyroxene and above all orthopyroxene and plagioclase.

VESICLES: Vesicular orthopyroxene-plagioclase andesite. The vesicles are filled with zeolites, smectites and copper. Some vesicles are flattened and filled with smectite. One clast contains a vesicle filled with zeolites and native copper. Some clasts contain altered orthopyroxene in smectites.

ADDITIONAL COMMENTS: Volcanic breccia with clasts to ~6 cm. Average diameter of 10 largest clasts is ~4 cm. Matrix is composed of granules and fine pebbles of the same material and small amounts of mineral cement. Clasts are vesicular lava. Some vesicles are filled with white zeolite and flecks of native copper. Clasts have chilled margins.

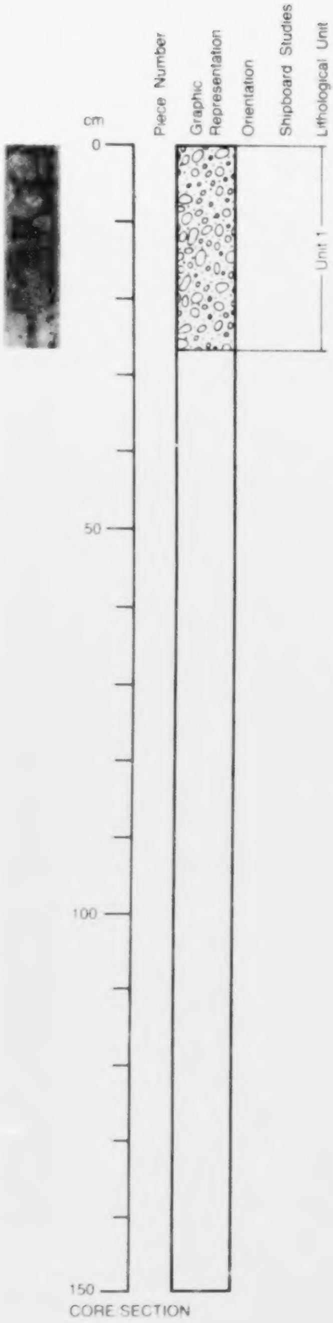
cm
Piece Number
Graphic Representation
Orientation
Shipboard Studies
Lithological Unit
0
50
100
150
Unit 1
CORE SECTION

126-793B-88R-CC

UNIT 1: VOLCANIC BRECCIA

PHENOCRYSTS: Intersertal-porphyritic andesite with clinopyroxene and above all orthopyroxene and plagioclase.

VESICLES: Vesicular orthopyroxene plagioclase andesite. The vesicles are filled with zeolites, smectites and copper. Some vesicles are flattened and filled with smectite. One clast contains a vesicle filled with zeolites and native copper. Some clasts contain altered orthopyroxene in smectites.

ADDITIONAL COMMENTS: Volcanic breccia with clasts up to ~8 cm. Average diameter of 10 largest clasts is ~6 cm. Matrix is composed of granules and fine pebbles of the same material and small amount of mineral cement. Clasts are vesicular lava. Some vesicles are filled with white zeolite and flecks of native copper. Clasts have chilled margins.

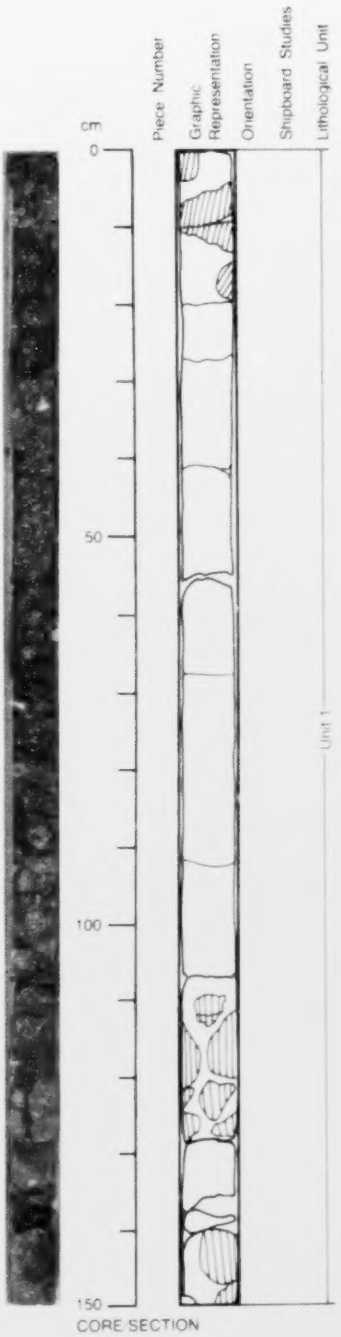
cm
0
50
100
150
Piece Number
Graphic Representation
Orientation
Shipboard Studies
Lithological Unit
Unit 1
CORE SECTION

126-793B-89R-1

UNIT 1: BASALTIC ANDESITE

Pieces clasts

CONTACTS: Chilled margins are common at the edge of clasts, often paler in color (
altered) with a finer-grained texture. Margins are truncated by matrix. Possible pi
talus breccia deposit.

PHENOCRYSTS: Virtually aphyric, with less than 2% phenocrysts.

GROUNDMASS: Commonly trachytic texture, flow aligned plagioclase micropheno
diverging around vesicles and crystal clots.

VESICLES: Vesiculation is around 5%. Vesicles range between 1-10 mm and betw
spherical/rounded and elongate/almond shaped. Vesicles filled (0-100%) with v
minerals. These are dominantly gypsum, some zeolites, and smectite.

ALTERATION: Phenocrysts are in varying states of alteration.
Clinopyroxene - 95% fresh, some celadonite + smectite.
Orthopyroxene - 60% fresh - celadonite + smectite + crystobalite(?).
Plagioclase - 70% fresh - smectite.

VEINS/FRACTURES: Gypsum veins are present, crossing the matrix.

ADDITIONAL COMMENTS: Breccia matrix: angular shards of altered glass, fresh c
and basalt fragments.

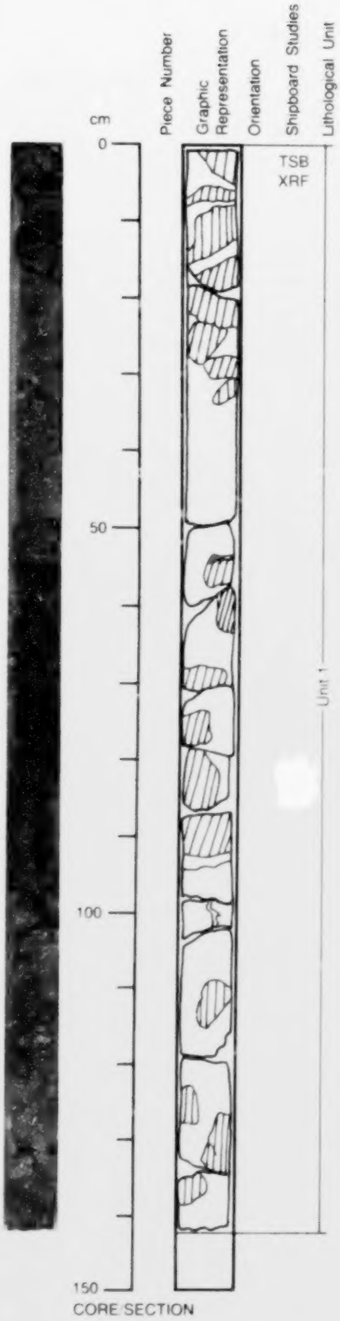
cm
Piece Number
Graphic Representation
Orientation
Shipboard Studies
Lithological Unit
0
50
100
150
TSB
XRF
Unit 1
CORE/SECTION

126-793B-89R-2

UNIT 1: BASALTIC ANDESITE

Pieces clasts

CONTACTS: Chilled margins are common at the edge of clasts, often paler in color (more altered) with a finer-grained texture. Margins are truncated by matrix. Possible pillow-talus breccia deposit.

PHENOCRYSTS: 20% clinopyroxene and orthopyroxene, clinopyroxene up to 7 mm in length.

GROUNDMASS: Commonly trachytic texture, flow aligned plagioclase microphenocrysts diverging around vesicles and crystal clots.

VESICLES: Vesiculation is around 5%. Vesicles range between 1-10 mm and between spherical/rounded and elongate/almond-shaped. Vesicles filled (0-100%) with various minerals. These are dominantly gypsum, some zeolites, and smectite.

ALTERATION: Phenocrysts are in varying states of alteration.
Clinopyroxene - 95% fresh, some celadonite - smectite.
Orthopyroxene - 60% fresh - celadonite - smectite - crystobalite(?)
Plagioclase - 70% fresh - smectite.

VEINS/FRACTURES: Gypsum veins are present, crossing the matrix.

ADDITIONAL COMMENTS: Breccia matrix. Angular shards of altered glass, fresh crystals, and basalt fragments.

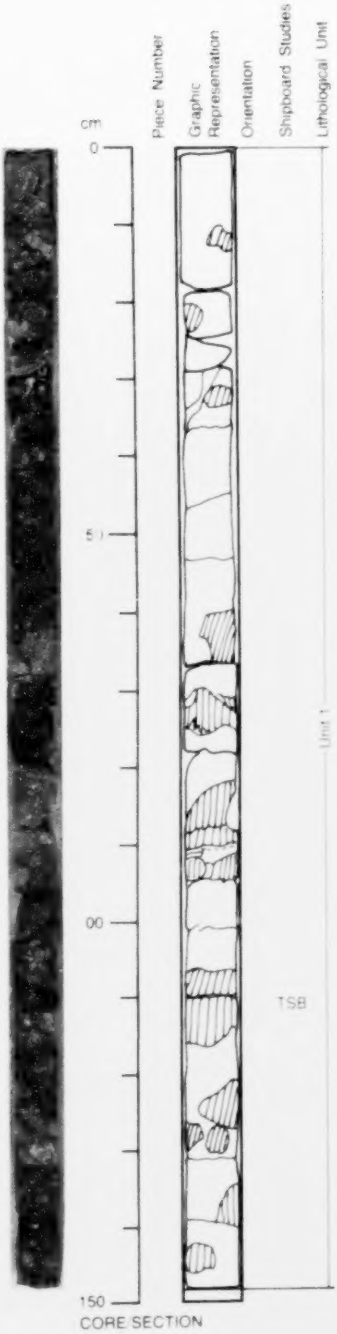
cm
Piece Number
Graphic Representation
Orientation
Shipboard Studies
Lithological Unit
0
50
100
150
TSB
Unit 1
CORE SECTION

126-793B-89R-3

UNIT 1: BASALTIC ANDESITE

Pieces clasts

CONTACTS: Chilled margins are common at the edge of clasts, often paler in color (more altered) with a finer grained texture. Margins are truncated by matrix. Possible pillow talus breccia deposit.

PHENOCRYSTS: 15-25% crystals. The proportions are orthopyroxene 55%, clinopyroxene 43%, and plagioclase 2%.

GROUNDMASS: Commonly trachytic texture, flow aligned plagioclase microphenocrysts diverging around vesicles and crystal clots.

VESICLES: Vesiculation is around 5%. Vesicles range between 1-10 mm and between spherical/rounded and elongate/almond-shaped. Vesicles filled (0-100%) with various minerals. These are dominantly gypsum, some zeolites, and smectite.

ALTERATION: Phenocrysts are in varying states of alteration.

Clinopyroxene: 95% fresh, some celadonite + smectite.

Orthopyroxene: 60% fresh: celadonite + smectite + crystobalite(?).

Plagioclase: 70% fresh: smectite.

VEINS FRACTURES: Gypsum veins are present, crossing the matrix.

ADDITIONAL COMMENTS: Breccia matrix: angular shards of altered glass, fresh crystals and basalt fragments.

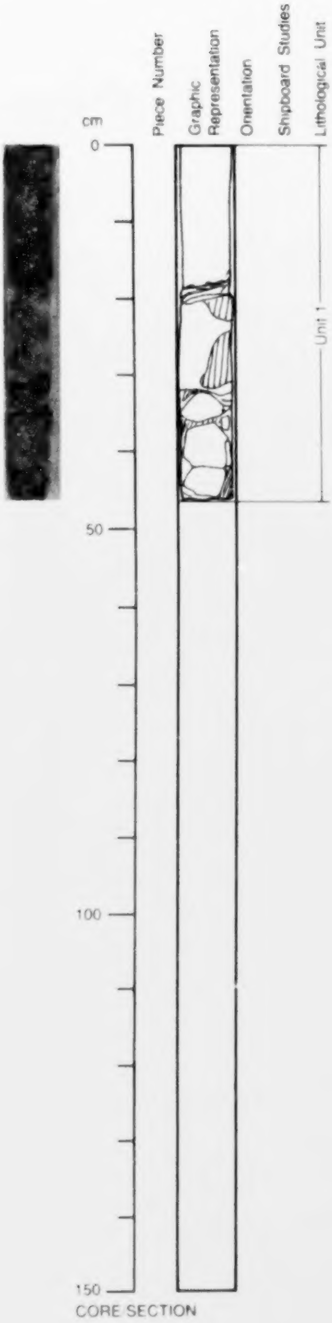
cm
Piece Number
Graphic Representation
Orientation
Shipboard Studies
Lithological Unit
0
50
100
150
Unit 1
CORE SECTION

126-793B-89R-4

UNIT 1: BASALTIC ANDESITE

Pieces clasts

CONTACTS: Chilled margins are common at the edge of clasts, often paler in color (more altered) with a finer-grained texture. Margins are truncated by matrix. Possible pillow-talus breccia deposit.

PHENOCRYSTS: 15-25% crystals. The proportions are orthopyroxene 55%, clinopyroxene 40%, plagioclase 5%.

GROUNDMASS: Commonly trachytic texture, flow aligned plagioclase microphenocrysts diverging around vesicles and crystal clots.

VESICLES: Vesiculation is around 5%. Vesicles range between 1-10 mm and between spherical/rounded and elongate/almond shaped. Vesicles filled (0-100%) with various minerals. These are dominantly gypsum, some zeolites, and smectite.

ALTERATION: Phenocrysts are in varying states of alteration.
Clinopyroxene - 95% fresh, some celadonite - smectite
Orthopyroxene - 60% fresh - celadonite - smectite - crystobalite(?)
Plagioclase - 70% fresh - smectite

VEINS/FRACTURES: Gypsum veins are present, crossing the matrix.

ADDITIONAL COMMENTS: Breccia matrix: angular shards of altered glass, fresh crystals, and basalt fragments.

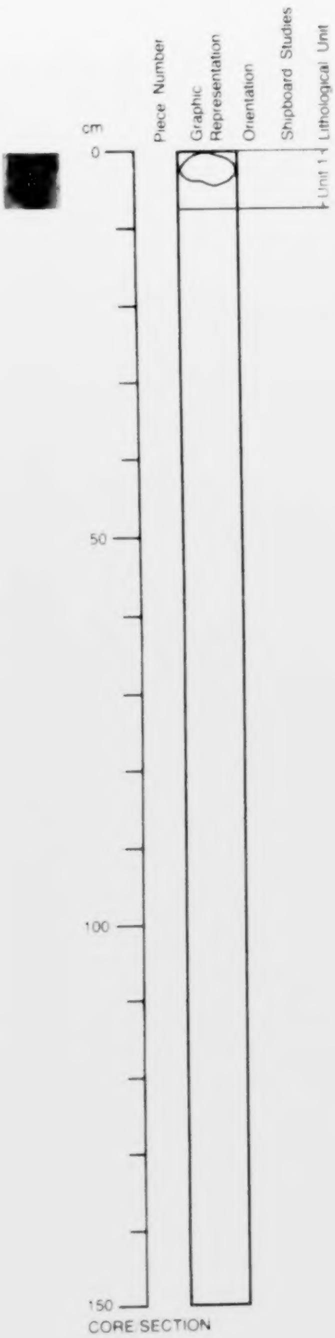
cm
0
50
100
150
CORE SECTION
Piece Number
Graphic Representation
Orientation
Shipboard Studies
Lithological Unit
Unit 1

126-793B-90R-CC

UNIT 1: IGNEOUS ROCKS

COLOR: 5YR 3/1, 2.5Y 5/2, 2.5Y 4/2. Matrix 10GY 3/2 to 5G 2/1.
ADDITIONAL COMMENTS: Very irregular shaped volcanic clast with some "attached" medium to coarse crystal-vitric matrix; clast is mottled.

126-793B-92R-1

UNIT 2: VOLCANIC BRECCIA (0-140 CM); PLAGIOCLASE-BASALTIC ANDESITE (140-150 CM)

Pieces N/A

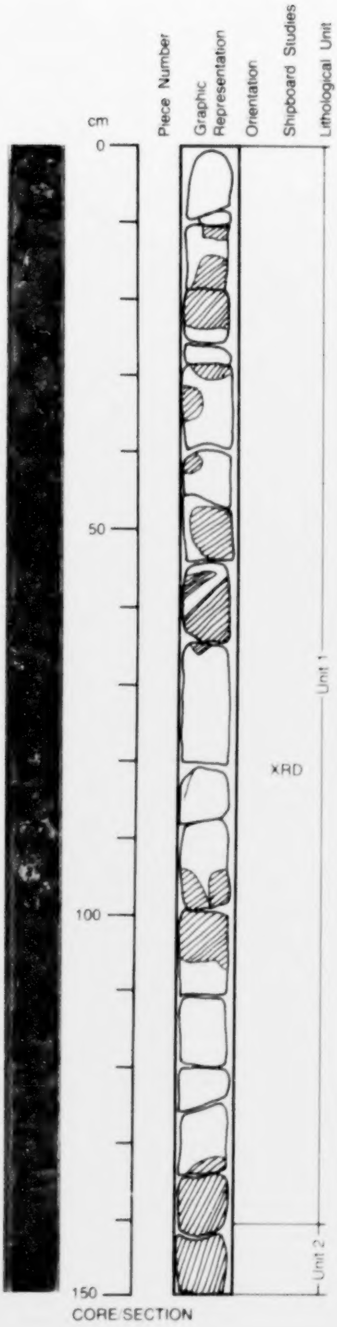
cm
0
50
100
150
Piece Number
Graphic Representation
Orientation
Shipboard Studies
Lithological Unit
XRD
Unit 1
Unit 2
CORE/SECTION

CONTACTS: Not observed.
PHENOCRYSTS: Clinopyroxene and orthopyroxene phenocrysts.
GROUNDMASS: Sand to cobble-size clasts.
VESICLES: Vesicles are filled with zeolites and smectites; vesicles are flattened.
COLOR: 5G 3/2 matrix with dark gray and gray/light gray clasts (0-140 cm).
STRUCTURE: Massive.
ALTERATION: No alteration.
VEINS/FRACTURES: No veins/fractures.
ADDITIONAL COMMENTS: Zeolite cements, some of the clasts have chilled margins; orthopyroxene crystals up to 5-6 mm, clinopyroxene crystals as large as 2-3 mm; native copper in the matrix with smectites and zeolites.

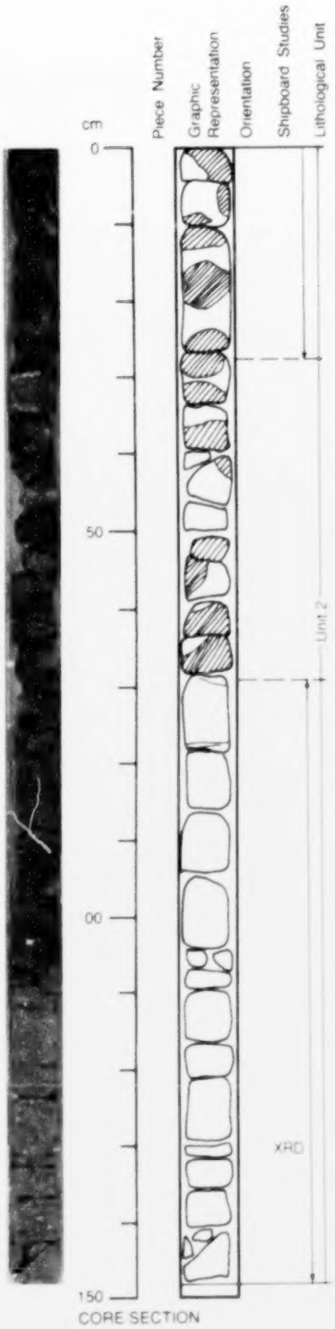
cm
Piece Number
Graphic Representation
Orientation
Shipboard Studies
Lithological Unit
0
50
100
150
CORE SECTION
Unit 2
XRD

126-793B-92R-2

UNIT 2: VOLCANIC BRECCIA (28-70 CM); VOLCANIC LAVA (0-28,70-150 CM)

Pieces N/A

CONTACTS: Not observed.
PHENOCRYSTS: Clinopyroxene and orthopyroxene phenocrysts.
GROUNDMASS: Clasts up to 4 cm diameter at 53-60 cm; clinopyroxene up to 5-15 mm at 7-150 cm.
VESICLES: Stretched at 70-90, 130-150 cm; equant vesicles at 90-130 cm; 1-3 mm in diameter.
COLOR: (5G 3/2) matrix with dark gray (5Y 4/1) clasts (28-70 cm); black? (5Y 2/1) at 0-28, 70-150 cm.
STRUCTURE: Laminated cement at base of flow at 28 cm.
ALTERATION: Orthopyroxene is more altered to smectite at 70-150 cm.
VEINS/FRACTURES: Not observed.
ADDITIONAL COMMENTS: Cavities are filled with zeolite cement (28-70 cm); no chilled margin (70-150 cm); orthopyroxene and clinopyroxene are fresh; large vug with zeolite and native copper at 101 cm.

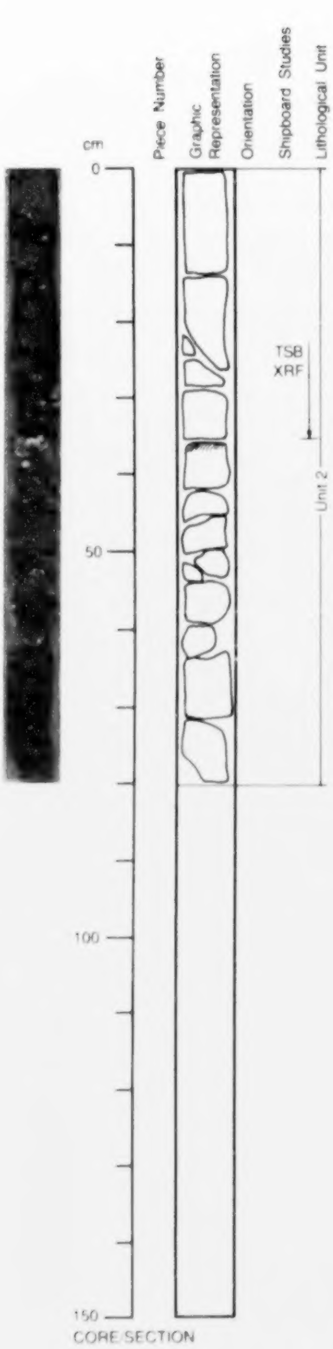
cm
0
50
100
150
Piece Number
Graphic Representation
Orientation
Shipboard Studies
Lithological Unit
TSB
XRF
Unit 2
CORE/SECTION

126-793B-92R-3

UNIT 2: VOLCANIC BRECCIA (35-80 CM); ANDESITE (0-35 CM)

Pieces N/A

CONTACTS: Not observed.
PHENOCRYSTS: Clinopyroxene and orthopyroxene phenocrysts.
GROUNDMASS: Clasts up to 6 cm size.
VESICLES: Flat to elongated vesicles filled with smectites and zeolites at 0-35 cm; 1-5 cm and ~0.02 mm diameter vesicles.
COLOR: Black? (5Y 2/1) at 0-35 cm; (5G 3/2) matrix with black? (5Y 2/1) clasts at 35-80 cm.
STRUCTURE: None observed.
ALTERATION: Not observed.
VEINS/FRACTURES: None observed.
ADDITIONAL COMMENTS: No evidence of chilled margin; zeolite cemented zone at 35-37 cm; clinopyroexe-orthopyroxene-plagioclase porphyritic basicandesite at 0-35 cm.

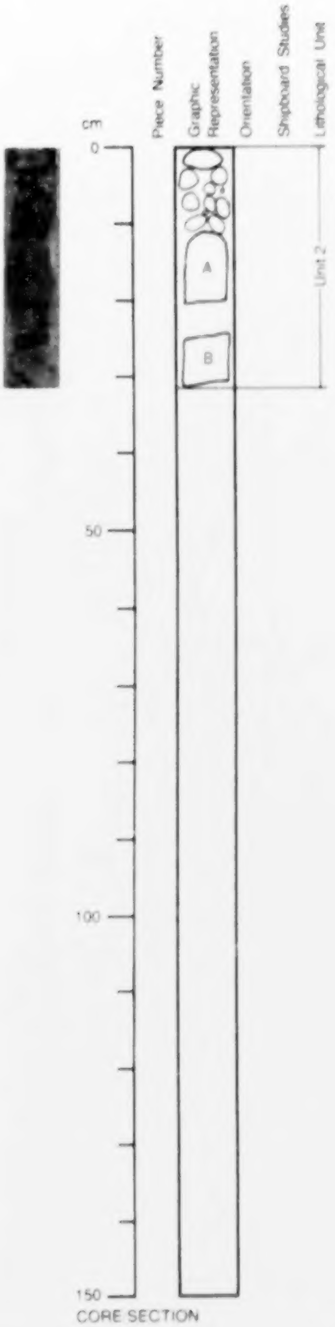
cm
Piece Number
Graphic Representation
Orientation
Shipboard Studies
Lithological Unit
0
50
100
150
A
B
Unit 2
CORE/SECTION

126-793B-92R-CC

UNIT 2: VOLCANIC BRECCIA/LAVA

Pieces N/A

CONTACTS: Not observed.
PHENOCRYSTS: Clinopyroxene and orthopyroxene phenocrysts.
GROUNDMASS: Clasts.
VESICLES: Not observed.
COLOR: Mainly black? (5Y 2/1).
STRUCTURE: None observed.
ALTERATION: Not observed.
VEINS/FRACTURES: None observed.
ADDITIONAL COMMENTS: Clinopyroxene>orthopyroxene>plagioclase; large piece (a) is solid lava; piece (b) is a lava clast in the matrix.

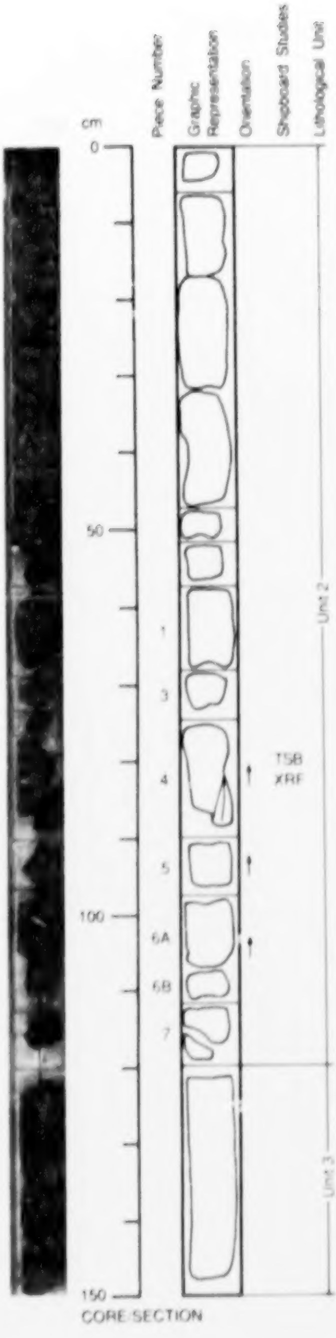
cm
Piece Number
Graphic Representation
Orientation
Shipboard Studies
Lithological Unit
0
50
100
150
1
3
4
5
6A
6B
7
TSB
XRF
Unit 2
Unit 3
CORE/SECTION

126-793B-93R-1

UNIT 2: VOLCANIC BRECCIA

Pieces N/A

CONTACTS: Not observed.
PHENOCRYSTS: Clinopyroxene and orthopyroxene phenocrysts; some Plagioclase microphenocrysts.
GROUNDMASS: Fine grained.
VESICLES: Open to completely filled with smectite; bands of flattened vesicles, rounded and elongated vesicles filled with smectites and zeolites in the altered groundmass.
COLOR: (5GY 3/2) matrix with gray (N5) clasts, pebbles and cobbles.
STRUCTURE: Not observed.
ALTERATION: Altered shards of glass, groundmass altered; hexagonal smectite pseudomorphs after orthopyroxene and olivine; orthopyroxene altered to smectites.
VEINS/FRACTURES: None observed.
ADDITIONAL COMMENTS: Angular clasts; matrix is composed of mm size angular shards of glass or rocks/crystals; cement is partly vesicular filled with zeolites and smectites.

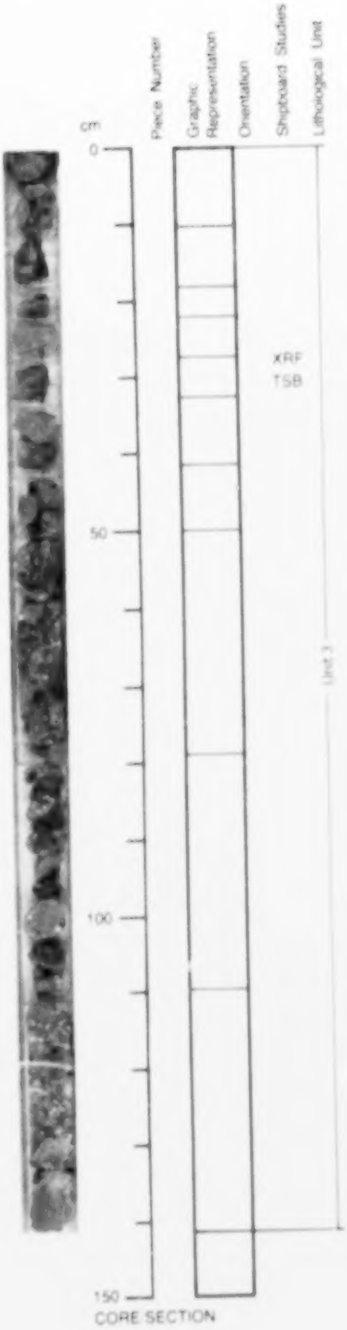
cm
Piece Number
Graphic Representation
Orientation
Shipboard Studies
Lithological Unit
0
50
100
150
XRF
TSB
Unit 3
CORE SECTION

126-793B-93R-2

UNIT 3: VOLCANIC BRECCIA/LAVA

Pieces N/A

CONTACTS: Not observed.
PHENOCRYSTS: Clinopyroxene and orthopyroxene phenocrysts.
GROUNDMASS: Felsicmicrolites.
VESICLES: 1-2 mm diameter, elongate vesicles at 0-42 cm.
COLOR: Dark gray (N4) clasts (0-42 cm), greenish gray (5GY 6/1) clasts (42-142 cm).
STRUCTURE: Not observed.
ALTERATION: Altered clasts, phenocrysts fresh.
VEINS/FRACTURES: Fractured clasts cemented by zeolite.
ADDITIONAL COMMENTS: Most clasts are sparsely phyric from 0-100 cm; color contrast in clasts probably cooling or alteration feature.

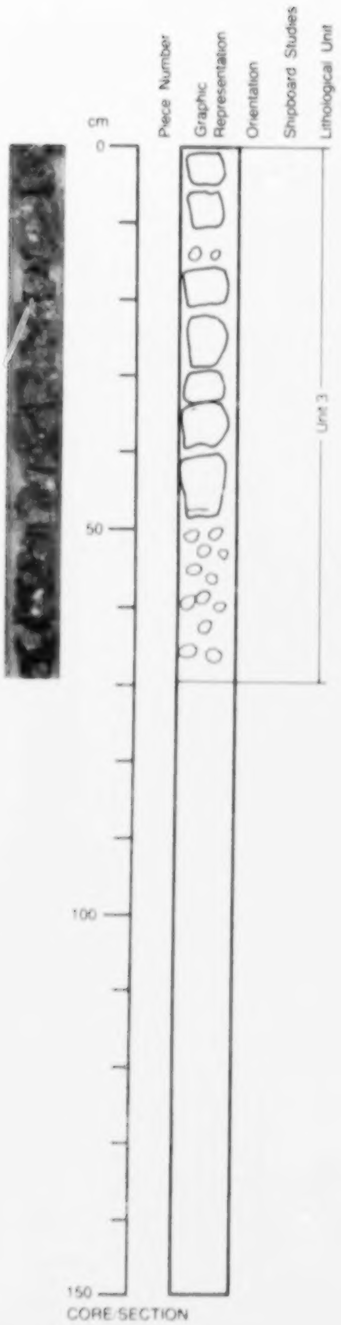
cm
Piece Number
Graphic Representation
Orientation
Shipboard Studies
Lithological Unit
0
50
100
150
Unit 3
CORE/SECTION

126-793B-93R-3

UNIT 3: VOLCANIC BRECCIA AND ANDESITE

Pieces N/A

CONTACTS: Not observed.
PHENOCRYSTS: Clinopyroxene and orthopyroxene phenocrysts.
GROUNDMASS: Clasts 0.5 to 3 mm in size.
VESICLES: Vesicles are flattened and filled with smectites.
COLOR: Dark greenish gray (5GY 4/1) and very dark gray (N3) clasts.
STRUCTURE: Not observed.
ALTERATION: Angular shards of altered glass, altered orthopyroxene.
VEINS/FRACTURES: Veins in the lower part of the section are filled with zeolites.
ADDITIONAL COMMENTS: Porphyritic. Clinopyroxene>Orthopyroxene-Plagioclase andesite. Clinopyroxene is fresh; clasts from 33-43 cm have lobate contours with lighter rims indicating chilled margins.

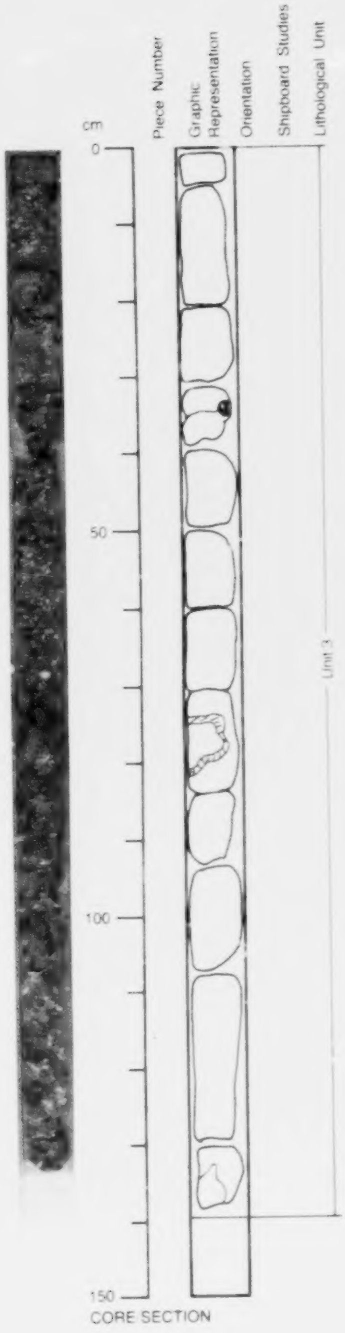
cm
Piece Number
Graphic Representation
Orientation
Shipboard Studies
Lithological Unit
0
50
100
150
Unit 3
CORE SECTION

126-793B-94R-1

UNIT 3: VOLCANIC BRECCIA AND LAVA

Pieces N/A

CONTACTS: Not observed
PHENOCRYSTS: Clinopyroxene and orthopyroxene phenocrysts
GROUNDMASS: Trachytic alignment of Plagioclase; chilled margins of glass (devitrified); many small feldspar laths partly siliceous
VESICLES: Spherical, elongate vesicles filled with zeolites, smectites and gypsum vesicles are elongated along the margins, rounded in the interior
COLOR: Gray (N5) to dark greenish gray (5G 4/1) to pale gray/green clasts
STRUCTURE: Broken pillows
ALTERATION: Some altered orthopyroxene and glass
VEINS/FRACTURES: Radial pillow-style fractures within clasts; some gypsum and zeolite veins
ADDITIONAL COMMENTS: Clasts are all with chilled margins; native copper; zeolite cement; Clinopyroxene>Plagioclase; sparsely phyric (less than 5%)

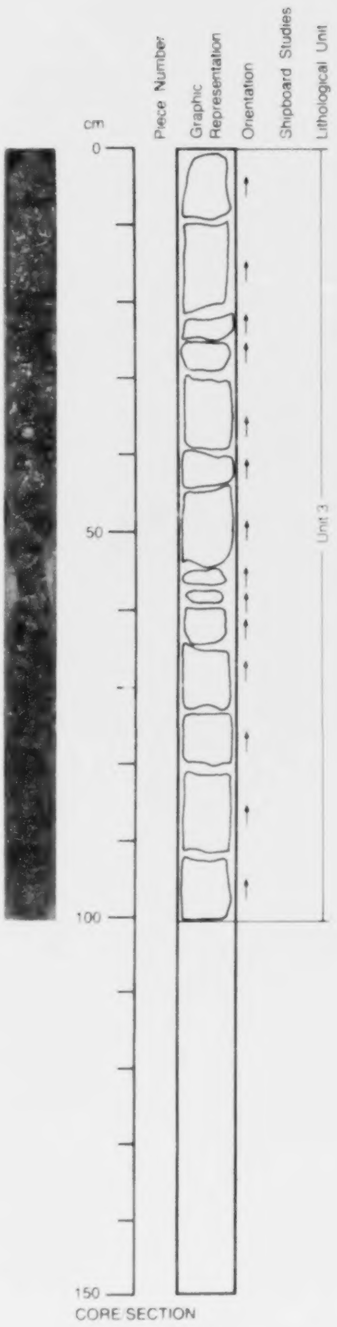
cm
Piece Number
Graphic Representation
Orientation
Shipboard Studies
Lithological Unit
0
50
100
150
Unit 3
CORE SECTION

126-793B-94R-2

UNIT 3: PILLOW-BRECCIA WITH HYALOCLASTIC MATRIX

CONTACTS: None.

PHENOCRYSTS: All fresh, some orthopyroxene alteration.

Plagioclase - < 1%, 0.5 - 1.0 mm.
Clinopyroxene - 1%, 0.5 - 1.0 mm.
Orthopyroxene - 1%, 1.0 mm.

GROUNDMASS: Trachytic alignment of plagioclase in groundmass. Original vitrophyric texture? Devitrified glass.

VESICLES: Spherical, rounded at chilled margins; filled with smectite.

COLOR: Pale gray - green.

STRUCTURE: Broken pillows in a shard glass and lava fragment matrix. Very poorly sorted, clasts 0.5 - 10.0 cm.

ALTERATION: Smectite replaces orthopyroxene. Glass devitrified.

ADDITIONAL COMMENTS: Clast lava type: sparse phyric basaltic andesite to andesite.

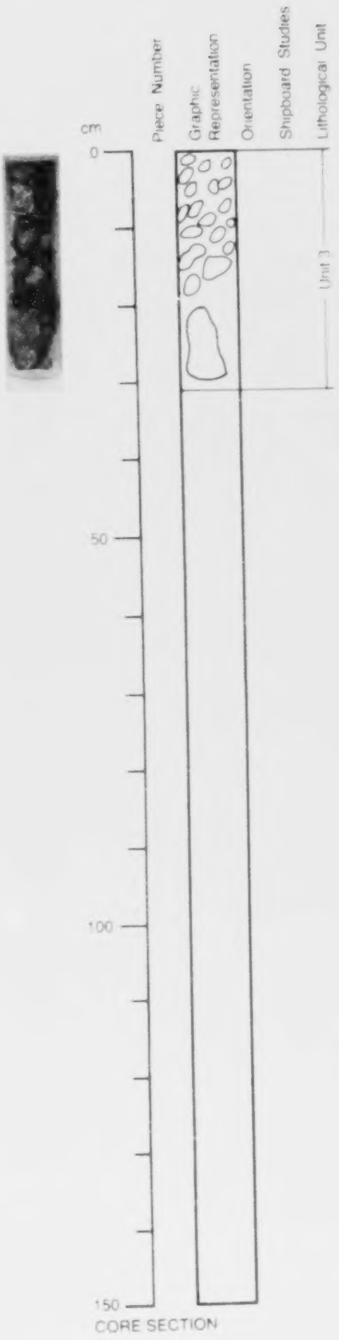
cm
0
50
100
150
Piece Number
Graphic Representation
Orientation
Shipboard Studies
Lithological Unit
Unit 3
CORE SECTION

126-793B-94R-CC

UNIT 3: PILLOW-BRECCIA WITH HYALOCLASTIC MATRIX

CONTACTS: None
PHENOCRYSTS: All fresh, some orthopyroxene alteration.
Plagioclase - <1%, 0.5-1.0 mm
Clinopyroxene - 1%, 0.5-1.0 mm
Orthopyroxene - 1%, 1.0 mm
GROUNDMASS: Trachytic alignment of plagioclase in groundmass. Original vitrophyric texture? Devitrified glass.
VESICLES: Spherical, rounded at chilled margins, filled with smectite.
COLOR: Pale gray - green.
STRUCTURE: Broken pillows in a shard glass and lava fragment matrix. Very poorly sorted clasts 0.5-10.0 cm.
ALTERATION: Smectite replaces orthopyroxene. Glass devitrified.
ADDITIONAL COMMENTS: Clast lava type: sparse phyric basaltic andesite to andesite.

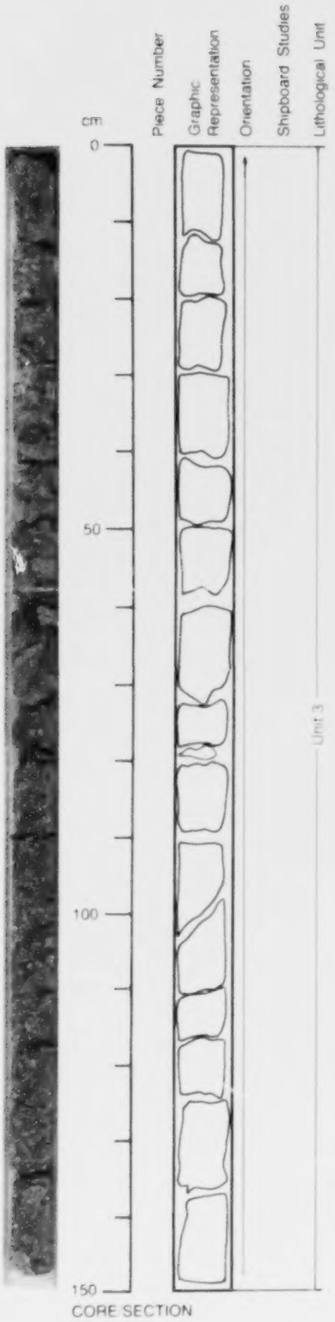
cm
0
50
100
150
Piece Number
Graphic Representation
Orientation
Shipboard Studies
Lithological Unit
Unit 3
CORE SECTION

126-793B-95R-1

UNIT 3: PILLOW-BRECCIA WITH HYALOCLASTIC MATRIX

CONTACTS: None

PHENOCRYSTS: All fresh, some orthopyroxene alteration.

Plagioclase - < 1%, 0.5 - 1.0 mm.
Clinopyroxene - 1%, 0.5 - 1.0 mm.
Orthopyroxene - 1%, 1.0 mm.

GROUNDMASS: Trachytic alignment of plagioclase in groundmass. Original vitrophyric texture? Devitrified glass.

VESICLES: Spherical, rounded at chilled margins, filled with smectite.

COLOR: Pale gray - green.

STRUCTURE: Broken pillows in a shard glass and lava fragment matrix. Very poorly sorted clasts 0.5 - 10.0 cm.

ALTERATION: Smectite replaces orthopyroxene. Glass devitrified.

ADDITIONAL COMMENTS: Clast lava type: sparse phyric basaltic andesite to andesite.

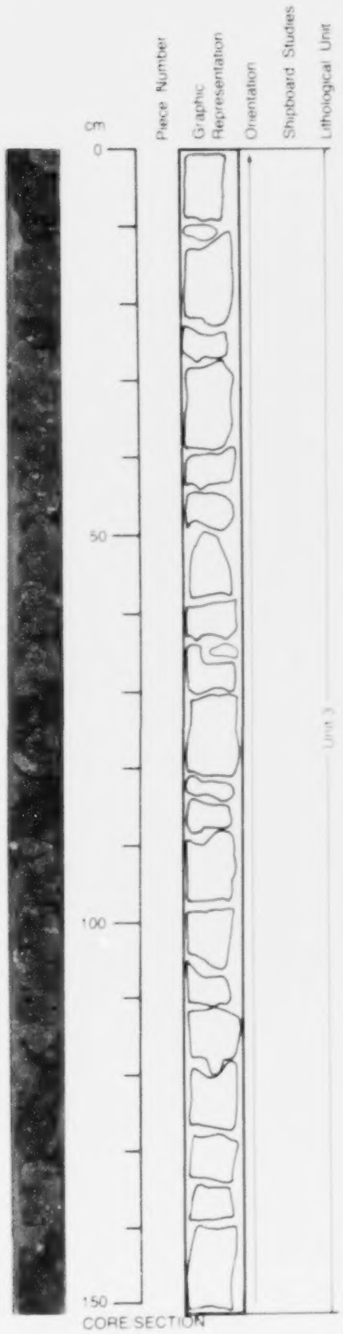
cm
Piece Number
Graphic Representation
Orientation
Shipboard Studies
Lithological Unit
0
50
100
150
Unit 3
CORE SECTION

126-793B-95R-2

UNIT 3: PILLOW-BRECCIA WITH HYALOCLASTIC MATRIX

CONTACTS: None.
PHENOCRYSTS: All fresh, some orthopyroxene alteration.
Plagioclase - < 1%, 0.5 - 1.0 mm.
Clinopyroxene - 1%, 0.5 - 1.0 mm.
Orthopyroxene - 1%, 1.0 mm.
GROUNDMASS: Trachytic alignment of plagioclase in groundmass. Original vitrophyric texture? Devitrified glass.
VESICLES: Spherical, rounded at chilled margins, filled with smectite.
COLOR: Pale gray - green.
STRUCTURE: Broken pillows in a shard-glass and lava fragment matrix. Very poorly sorted clasts 0.5 - 10.0 cm.
ALTERATION: Smectite replaces orthopyroxene. Glass devitrified.
ADDITIONAL COMMENTS: Clast lava type: sparse-phyric basaltic andesite to andesite in interval 30 - 50 cm; 25% of the clasts are very porphyritic basaltic andesite.

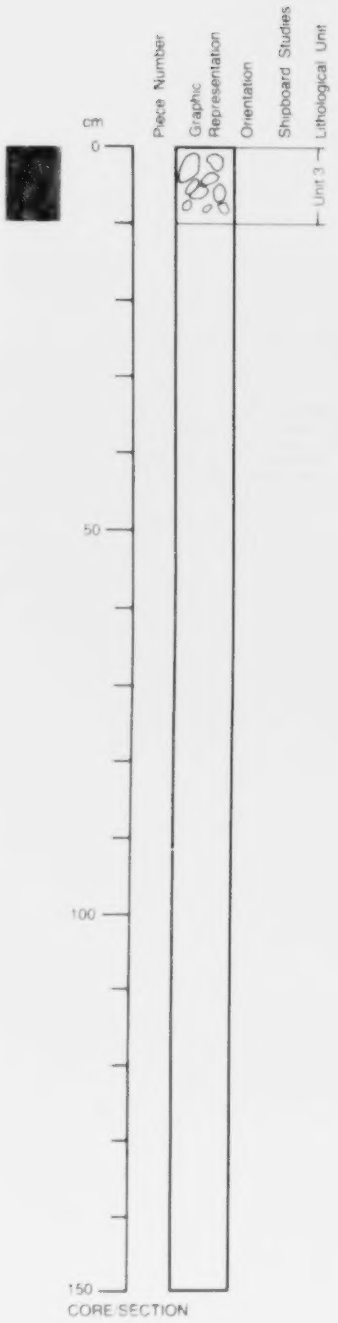
cm
Piece Number
Graphic Representation
Orientation
Shipboard Studies
Lithological Unit
0
Unit 3
50
100
150
CORE/SECTION

126-793B-95R-CC

UNIT 3: PILLOW-BRECCIA WITH HYALOCLASTIC MATRIX

CONTACTS: None.

PHENOCRYSTS: All fresh, some orthopyroxene alteration.

- Plagioclase - < 1%, 0.5 - 1.0 mm.
- Clinopyroxene - 1%, 0.5 - 1.0 mm.
- Orthopyroxene - 1%, 1.0 mm.

GROUNDMASS: Trachytic alignment of plagioclase in groundmass. Original vitrophyric texture? Devitrified glass.

VESICLES: Spherical, rounded at chilled margins, filled with smectite.

COLOR: Pale gray - green.

STRUCTURE: Broken pillows in a shard glass and lava fragment matrix. Very poorly sorted clasts 0.5 - 10.0 cm.

ALTERATION: Smectite replaces orthopyroxene. Glass devitrified.

ADDITIONAL COMMENTS: Clast lava type: sparse phyric basaltic andesite to andesite.

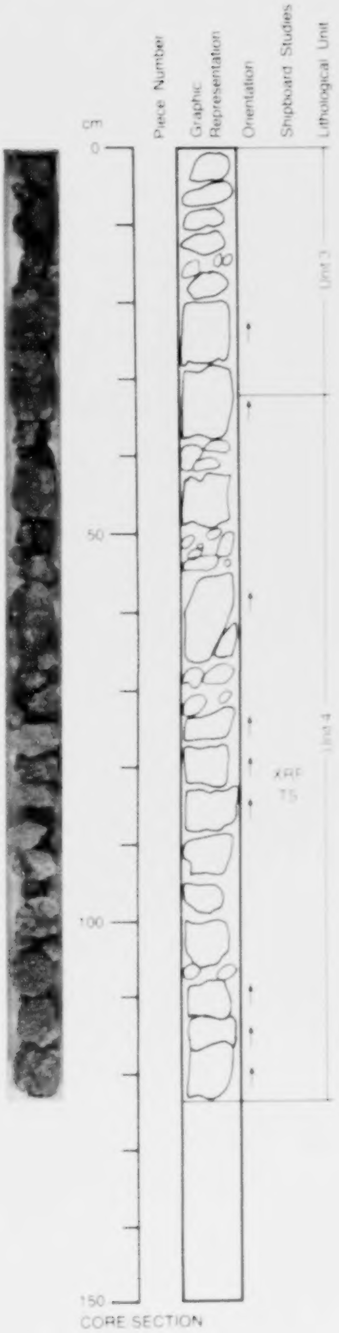

126-793B-96R-1

UNIT 3: PILLOW-BRECCIA WITH HYALOCLASTIC MATRIX

CONTACTS: None.
PHENOCRYSTS: All fresh, some orthopyroxene alteration.
Plagioclase - < 1%, 0.5 - 1.0 mm.
Clinopyroxene - 1%, 0.5 - 1.0 mm.
Orthopyroxene - 1%, 1.0 mm.
GROUNDMASS: Trachytic alignment of plagioclase in groundmass. Original vitrophyric texture? Devitrified glass.
VESICLES: Spherical, rounded at chilled margins, filled with smectite.
COLOR: Pale gray - green.
STRUCTURE: Broken pillows in a shard glass and lava fragment matrix. Very poorly sorted clasts 0.5 - 10.0 cm.
ALTERATION: Smectite replaces orthopyroxene. Glass devitrified.
ADDITIONAL COMMENTS: Clast lava type: sparse phyric basaltic-andesite to andesite.

UNIT 4: PORPHYRITIC BASALTIC ANDESITE

CONTACTS: None.
PHENOCRYSTS:
Plagioclase - < 1%, 0.5 - 2.0 mm, euhedral.
Clinopyroxene - 5%, 1.0 - 5.0 mm, euhedral.
Orthopyroxene - 5%, 1.0 - 5.0 mm, euhedral.
GROUNDMASS: Aligned plagioclase microphenocrysts. Trachytic texture.
VESICLES: Elongate, almond shaped, vesicles are empty, 1-4 mm.
COLOR: Medium bluish gray, 5B 5/1.
STRUCTURE: None.
ALTERATION: Orthopyroxene altered at margins and along cleavages to smectite and celadonite - filled fractures.
ADDITIONAL COMMENTS: Above description applies to interval from 33 cm to 95 cm.

UNIT 4: APHYRIC BASALTIC-ANDESITE

CONTACTS: None.
PHENOCRYSTS: No phenocrysts present.
GROUNDMASS: Aligned plagioclase microphenocrysts, trachytic texture.
VESICLES: 3%. Up to 1.0 cm, elongate, vesicles are empty.
COLOR: Medium bluish gray.
STRUCTURE: None.
ALTERATION: Orthopyroxene altered at margins and along cleavages to smectite and celadonite - filled fractures.
ADDITIONAL COMMENTS: Above description applies to clast at 106 cm.

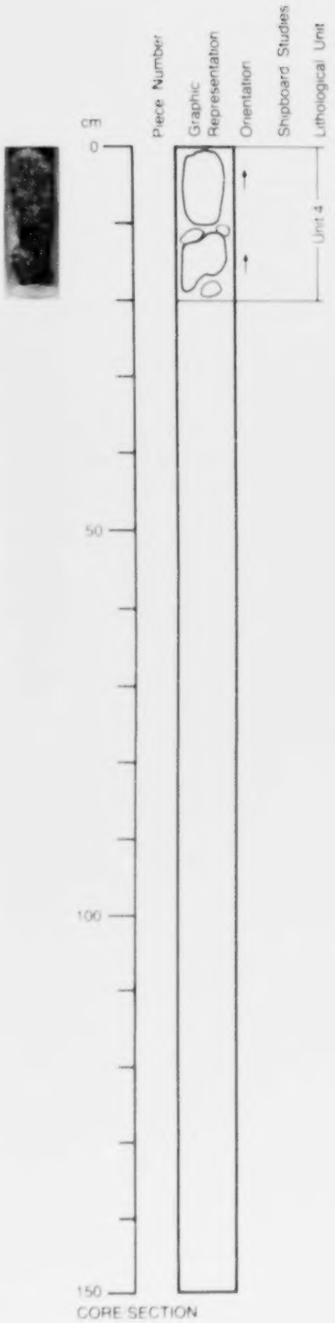
cm
Piece Number
Graphic Representation
Orientation
Shipboard Studies
Lithological Unit
0
50
100
150
Unit 4
CORE SECTION

126-793B-96R-CC

UNIT 4: PILLOW BRECCIA WITH HYALOCLASTIC MATRIX

CONTACTS: None.

PHENOCRYSTS: All fresh, some orthopyroxene alteration.

Plagioclase - < 1%, 0.5 - 1.0 mm.
Orthopyroxene - 1%, 1.0 mm.
Clinopyroxene - 1%, 0.5 - 1.0 mm.

GROUNDMASS: Trachytic alignment of plagioclase in groundmass. Original vitrophyric texture? Devitrified glass.

VESICLES: Spherical, rounded at chilled margins, vesicles filled with smectite.

COLOR: Pale gray green.

STRUCTURE: Broken pillows in a shard glass and lava fragment matrix, very poorly sorted.

ALTERATION: Smectite replacing orthopyroxene. Glass devitrified.

ADDITIONAL COMMENTS: Clast lava type: sparse-phyric basaltic andesite to andesite. Clasts 2-3 cm.

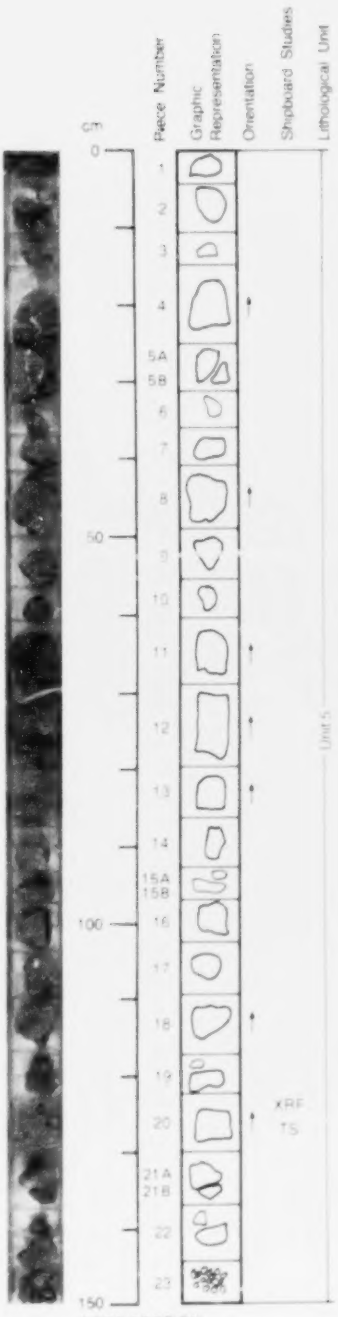
cm
Piece Number
Graphic Representation
Orientation
Shipboard Studies
Lithological Unit
0
50
100
150
1
2
3
4
5A
5B
6
7
8
9
10
11
12
13
14
15A
15B
16
17
18
19
20
21A
21B
22
23
XRF
TS
Unit 5

CORE SECTION

126-793B-97R-1

UNIT 5: BASALTIC ANDESITE MASSIVE LAVA

Pieces 1-23

CONTACTS: None
PHENOCRYSTS:
Clinopyroxene - 5%, 0.5 - 5.0 mm, euhedral.
Orthopyroxene - 5%, 0.5 - 5.0 mm, euhedral.
GROUNDMASS: Fine-grained with plagioclase laths.
VESICLES: 0.5-5.0 mm; elongated; random; vesicles empty, but walls are coated with celadonite and/or zeolites.
COLOR: Medium light gray, N6.
STRUCTURE: Massive.
ALTERATION: Both orthopyroxene and clinopyroxene altered at margins and along cleavages to celadonite and smectite. Some orthopyroxene crystals completely altered.

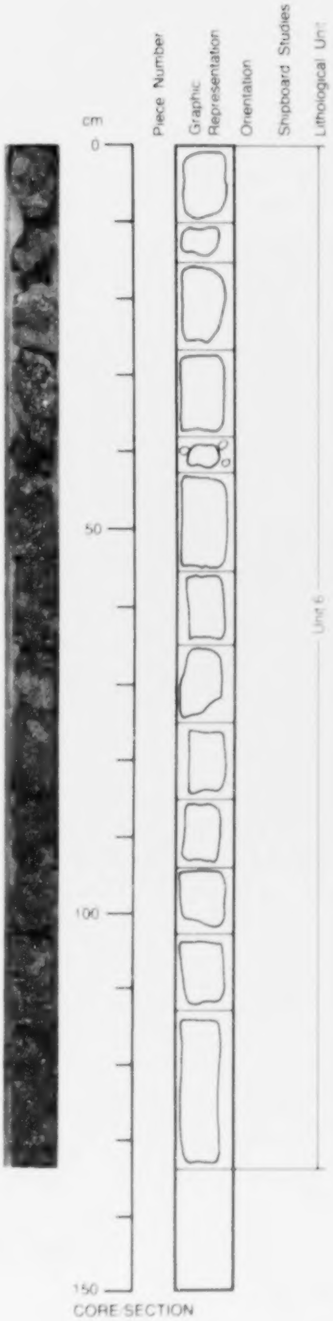
cm
Piece Number
Graphic Representation
Orientation
Shipboard Studies
Lithological Unit
0
50
100
150
Unit 6
CORE-SECTION

126-793B-98R-1

UNIT 6: HYALOCLASTIC - MONOMICTIC CLASTS

PHENOCRYSTS: Sparsely phyric clinopyroxene andesite.
Clinopyroxene - 1%, 4.0 mm, fresh.
Plagioclase - 0.1 mm, fresh.
GROUNDMASS: Fine grained.
VESICLES: Rounded to elongated, vesicles filled with smectite.
STRUCTURE: Chilled rim with no phenocrysts, very flattened vesicles. Groundmass invaded by smectites.
ADDITIONAL COMMENTS: Matrix: zeolites and copper. Clasts: 0.2-6.0 cm.

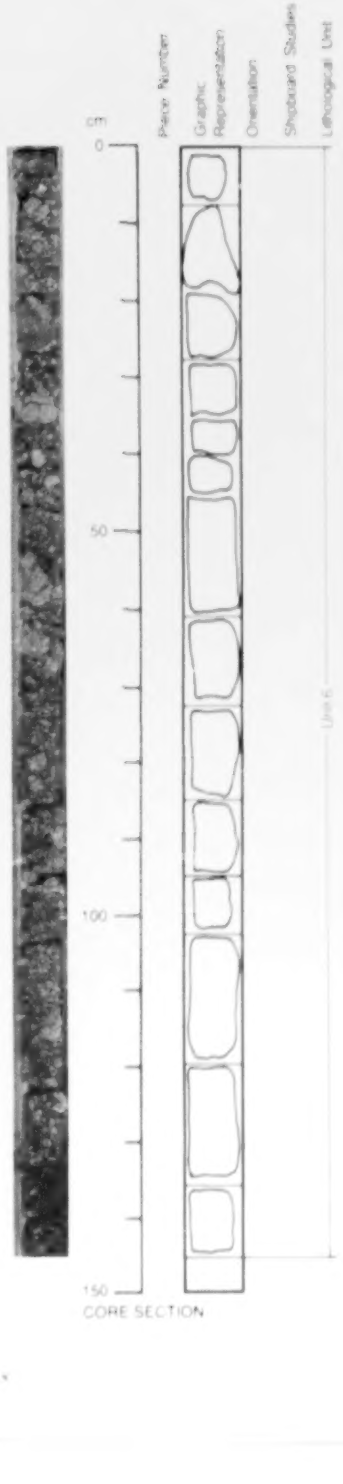
cm
Piece Number
Graphic Representation
Orientation
Shipboard Studies
Lithological Unit
0
50
100
150
Unit 6
CORE SECTION

126-793B-98R-2

UNIT 6: MONOMICTIC HYALOCLASTITE

CONTACTS: None.
PHENOCRYSTS: Almost aphyric.
Clinopyroxene - < 1%.
Feldspar - 1%, 2 mm.
GROUNDMASS: Light colored groundmass. Smectite veins in groundmass.
VESICLES: Flattened; vesicles are flattened and filled with smectites. On the chilled rims the vesicles are filled with zeolites and/or calcite.
COLOR: Light colored groundmass.
VEINS/FRACTURES: Smectite veins in the groundmass.
ADDITIONAL COMMENTS: Matrix: zeolites and copper. Clasts: size ranges from 0.2-10 cm. All the clasts are rimmed with a chilled margin. Elongated shaped vesicles also occur in the core of the bigger clasts. Only the smaller (0.1 mm) clasts are rounded.

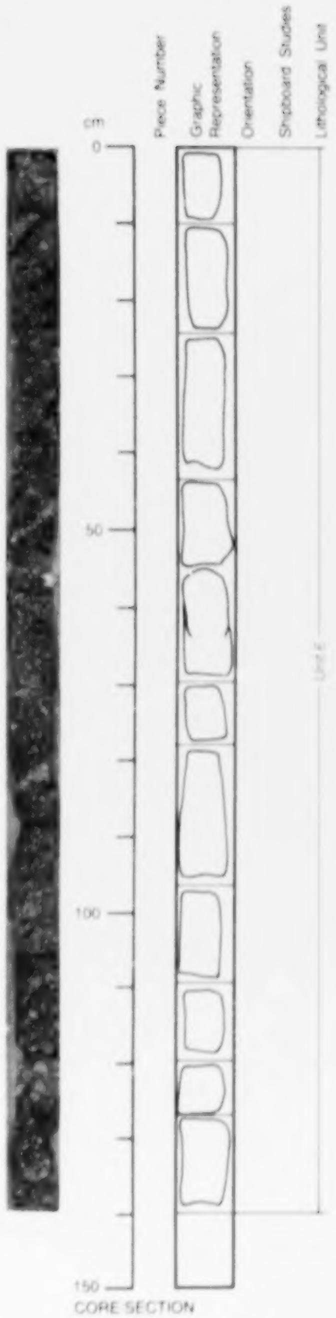
cm
Piece Number
Graphic Representation
Orientation
Shipboard Studies
Lithological Unit
0
50
100
150
Unit 6
CORE SECTION

126-793B-98R-3

UNIT 6: MONOMICTIC HYALOCLASTITE

CONTACTS: None
PHENOCRYSTS: Almost aphyric
  Clinopyroxene - < 1%
  Feldspar - 1%, 2 mm
GROUNDMASS: Light colored groundmass. Smectite veins in groundmass.
VESICLES: Flattened - vesicles are flattened and filled with smectites. On the chilled rims the vesicles are filled with zeolites and/or calcite.
VEINS/FRACTURES: Smectite veins in the groundmass.
ADDITIONAL COMMENTS: Matrix: zeolites and copper. Some matrix looks more ferrous and the intervals are filled with zeolites. Clasts: size ranges from 0.2-10 cm. All the clasts are rimmed with a chilled margin. Elongated shaped vesicles also occur in the core of the biggest clasts. Only the smaller (0.1 mm) clasts are rounded. Open cracks cutting through the clasts and the matrix is filled with zeolites.

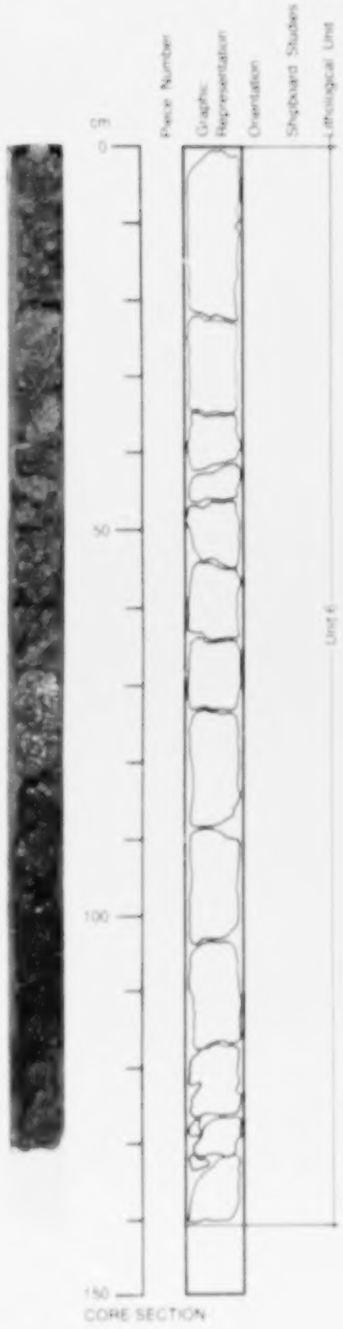
cm
0
50
100
150
CORE SECTION
Piece Number
Graphic Representation
Orientation
Shipboard Studies
Lithological Unit
Unit 6

126-793B-98R-4

UNIT 6: MONOMICTIC HYALOCLASTITE

Continued from 98R Section 3.

126-793B-98R-CC

UNIT 6: HYALOCLASTITE

CONTACTS: None

ADDITIONAL COMMENTS: Clasts: andesite with sparse phenocrysts of clinopyroxene and plagioclase. Small, rounded vesicles filled with smectites and zeolites.

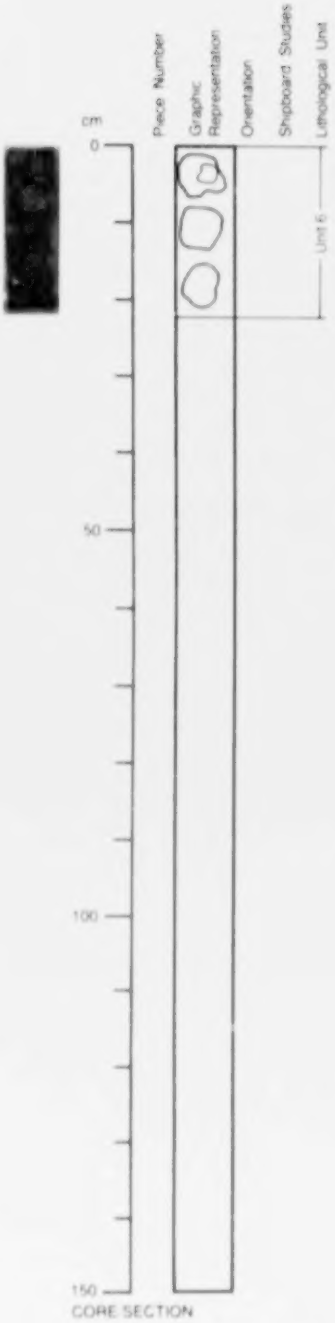
cm
0
50
100
150
Piece Number
Graphic Representation
Orientation
Shipboard Studies
Lithological Unit
Unit 6
CORE SECTION

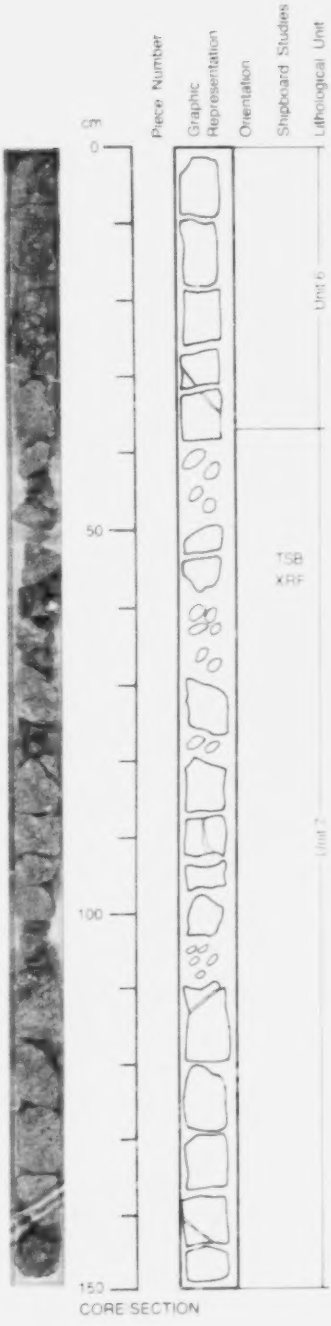

126-793B-99R-1

UNIT 6: BRECCIA

PHENOCRYSTS: Both porphyritic and aphyric clasts in zeolite and smectite cement.
Clinopyroxene : 5-10%, 1-4 mm, partially fresh.
Orthopyroxene : 3-5%, 1-2 mm, very altered.
Plagioclase : < 1%, 0.5 mm.
Olivine? : Now smectite pseudomorphs.
GROUNDMASS: Fine-grained laths.
VESICLES: Elongated; lineations of smectite filled, elongated vesicles cross the pillows; also smectite and zeolite filled fractures.
COLOR: Gray.
ADDITIONAL COMMENTS: Hyaloclastite texture. Isolated pyroxene crystals plus mostly nonvesicular aphyric shards.

UNIT 7: BRECCIA

CONTACTS: Lower pillow contact missing.
PHENOCRYSTS: Both porphyritic and aphyric clasts in zeolite and smectite cement.
Clinopyroxene : 5-10%, 1-4 mm, partially fresh.
Orthopyroxene : 3-5%, 1-2 mm, very altered.
Plagioclase : < 1%, 0.5 mm.
Olivine? : Now smectite pseudomorphs.
GROUNDMASS: Fine-grained laths.
VESICLES: Elongated; lineations of smectite filled, elongated vesicles cross the pillows; also smectite and zeolite filled fractures (especially at 90 cm).
COLOR: Gray.
ADDITIONAL COMMENTS: Hyaloclastite texture. Isolated pyroxene crystals plus mostly nonvesicular aphyric shards. Possibly glassy rims of pillows in lower portion of section despite relative absence of phenocrysts.

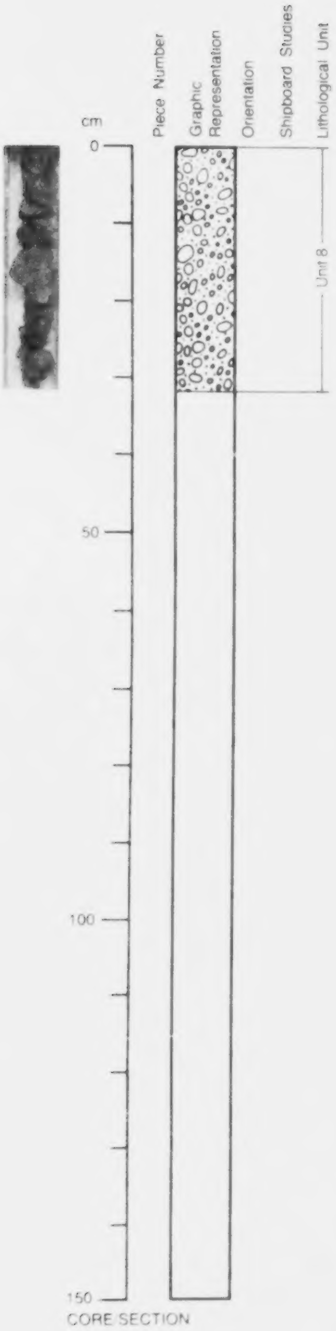
cm
Piece Number
Graphic Representation
Orientation
Shipboard Studies
Lithological Unit
0
50
100
150
Unit 8
CORE/SECTION

126-793B-99R-2

UNIT 8: BRECCIA

ADDITIONAL COMMENTS: Breccia: 0.5-5.0 cm clasts of clinopyroxene, orthopyroxene and plagioclase lava.

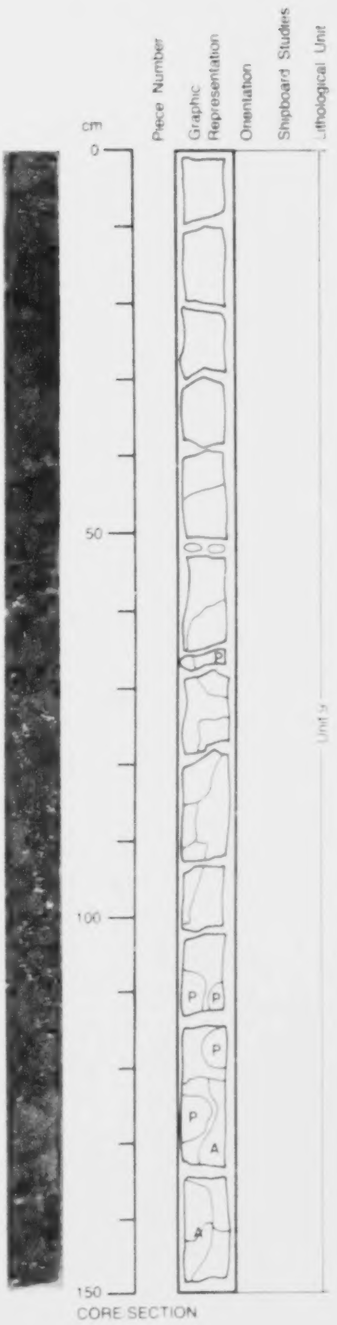
cm
Piece Number
Graphic Representation
Orientation
Shipboard Studies
Lithological Unit
0
50
100
150
P
P
P
P
A
A
Unit 9
CORE SECTION

126-793B-100R-1

UNIT 9: HETEROLITHIC BRECCIA

CONTACTS: Glassy rims are noticeable on the aphyric clasts.

PHENOCRYSTS: Porphyritic clasts contain plagioclase, trace; orthopyroxene, 3-8%, 0.5-2 mm, smectite pseudomorphs; clinopyroxene, 5-10%, 2-6 mm. Aphyric clasts contain plagioclase, <1%, 0.5 mm, fresh; clinopyroxene, <1%, <=4 mm, fresh; orthopyroxene, <1%, <=1 mm, smectite pseudomorphs.

GROUNDMASS: Felty feldspar laths, gray.

VESICLES: Porphyritic clasts: <5% vesicles, 0.1-0.2 mm in diameter, usually stretched. Aphyric clasts: ~5% vesicles, 1.2 mm in diameter, usually stretched, and 0.2 mm in diameter, circular, both open with smectite lining and filled with zeolite.

COLOR: See groundmass.

ALTERATION: See main comments.

ADDITIONAL COMMENTS: Clasts: 0.5-10 cm in diameter. Matrix: Altered glass shards plus clinopyroxene plus orthopyroxene crystals. Cement: zeolite, not calcite.

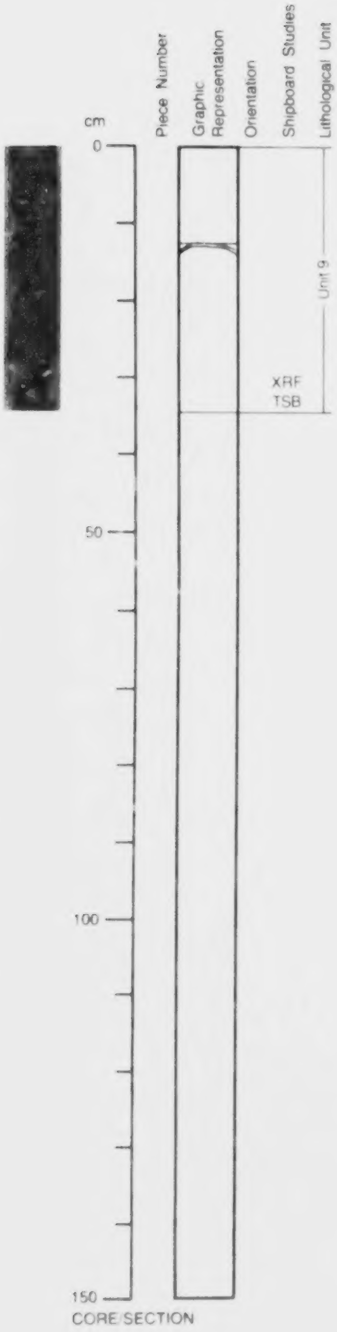
cm
0
50
100
150
Piece Number
Graphic Representation
Orientation
Shipboard Studies
Lithological Unit
Unit 9
XRF
TSB
CORE/SECTION

126-793B-100R-2

UNIT 9: HYALOCLASTITE

CONTACTS: Chilled lobate highly vesicular contact at about 12 cm.
PHENOCRYSTS:
  Plagioclase - 1-2%; 1 mm.
  Clinopyroxene - 1-2%; <4 mm, sparsely phyric.
  Orthopyroxene - 1-2%.
GROUNDMASS: The contact with the groundmass is marked by a white border.
VESICLES: 10%, up to 16 mm, elongated to rounded - rounded vesicles up to 1 mm are filled with zeolites. Elongated partially filled vesicles up to 16 mm.
COLOR: Light green, with a dark green-gray groundmass.
STRUCTURE: Matrix is like the previous section, only difference is more abundant crystallized zeolites.
ADDITIONAL COMMENTS: Clasts are sometimes more porphyritic (30% of phenocrysts opx=cpx, altered olivine?).

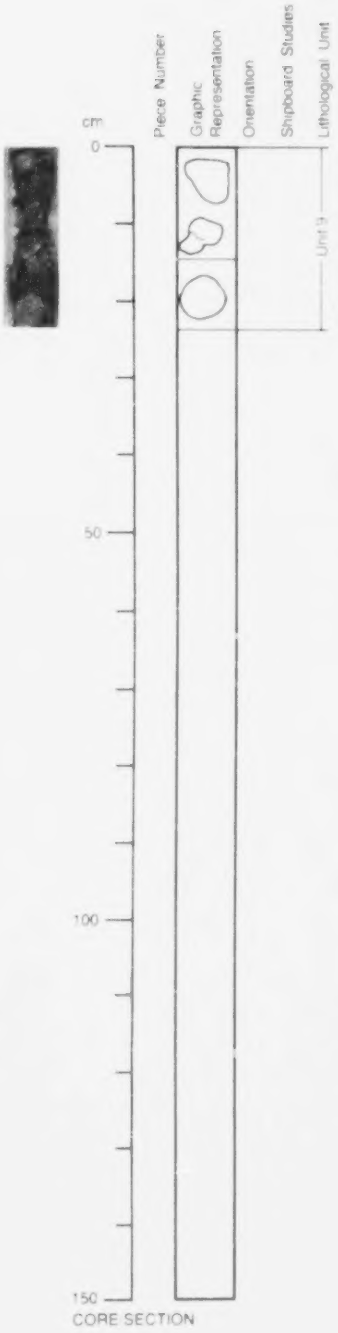
cm
Piece Number
Graphic Representation
Orientation
Shipboard Studies
Lithological Unit
0
50
100
150
Unit 9
CORE SECTION

126-793B-100R-CC

UNIT 9: HYALOCLASTITE

STRUCTURE: Matrix is like the previous section (126-793B-100R-2).
ADDITIONAL COMMENTS: Clasts in top part of the pillow.

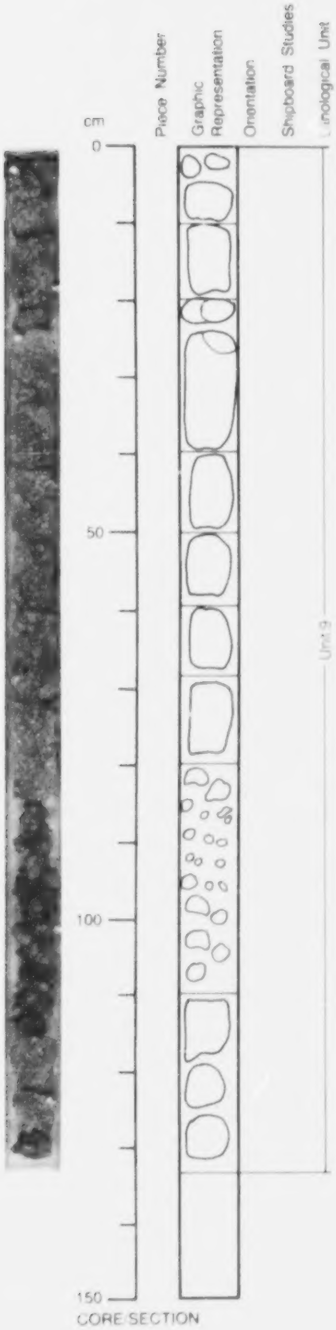
cm
Piece Number
Graphic Representation
Orientation
Shipboard Studies
Lithological Unit
0
50
100
150
Unit 9
CORE/SECTION

126-793B-101R-1

UNIT 9: HYALOCLASTIC-PORPHYRITIC

CLINOPYROXENE-ORTHOPYROXENE-PLAGIOCLASE BASIC ANDESITE

PHENOCRYSTS:
Clinopyroxene : 10-30%, up to 5 mm.
Orthopyroxene : 10-30%, altered to smectites.
Plagioclase : A few plagioclase phenocrysts.

GROUNDMASS: Crystal and shards of altered glass. Crystals in the mature clinopyroxene (fresh, up to 5 mm). Shards of altered glass. Cement is composed of zeolites and smectites.

VESICLES: 1-3 mm, flattened; chilled rim with flattened vesicles filled with smectites.

COLOR: N3 to 5GY 4/1.

STRUCTURE: In some clasts the chilled margin is perfectly visible. Very fine cooling fractures filled with zeolites are perpendicular to the chilled rims. Color is greenish white. The core of the chilled clasts are richer in small plagioclase laths (0.1-0.3 mm).

ADDITIONAL COMMENTS: Clasts are 0.1 - 6.0 cm.

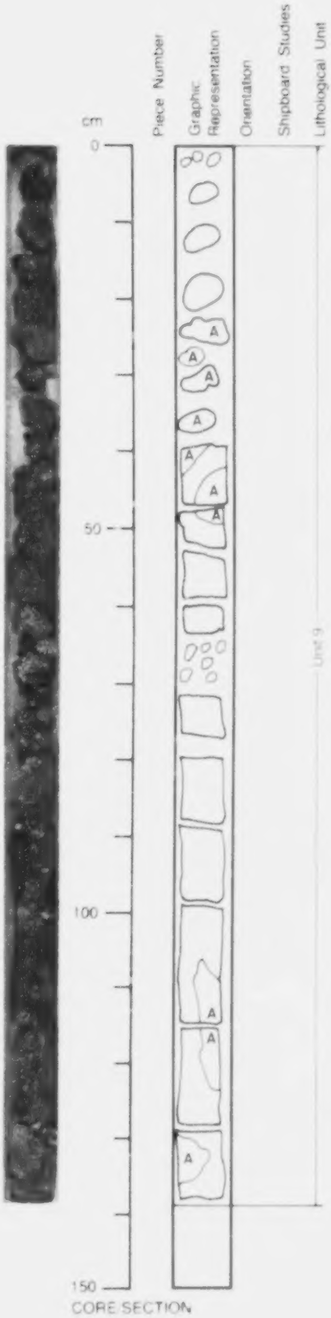
cm
0
50
100
150
Piece Number
Graphic Representation
Orientation
Shipboard Studies
Lithological Unit
A
Unit 9
CORE SECTION

126-793B-102R-1

UNIT 9: HYALOCLASTITE BRECCIA/APHYRIC LAVA

PHENOCRYSTS:
- Clinopyroxene - 2-4%; 1-3 mm.
- Orthopyroxene - 2-4%; 1-3 mm.

GROUNDMASS: Consists of glass shards and pyroxene crystals cemented by zeolites (heulandite-clinoptilolite); thoroughly green (smectite not chlorite). More matrix than clasts.

VESICLES: < 5%.

COLOR: Green.

ADDITIONAL COMMENTS: Breccia: 0-20 cm: 1-2 cm clasts with mostly aphyric hyaloclastic textures. 40-140 cm: mostly (entirely?) aphyric clasts. Here the aphyric lava pieces are clearly clasts with chilled margins; clasts 0.5-7.0 cm diameter. Aphyric lava pieces: 20-40 cm. Clinopyroxene and orthopyroxene together comprise 2-4%.

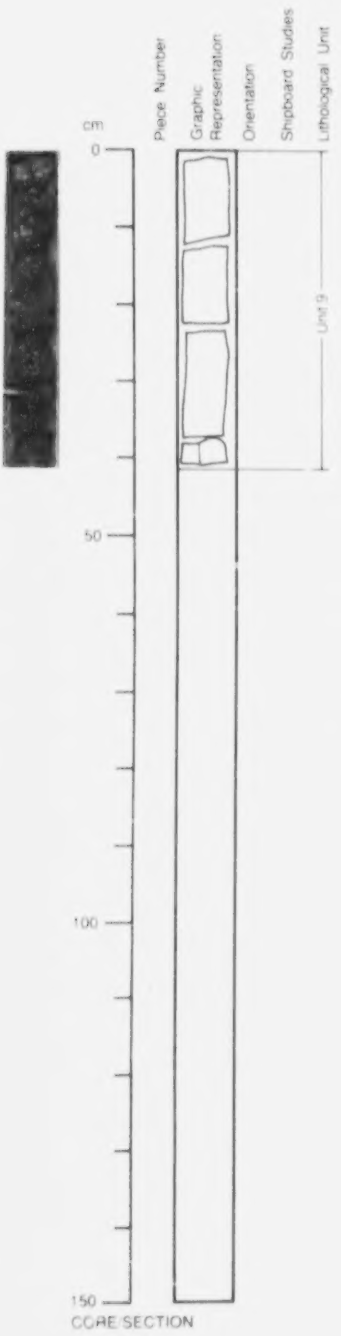
cm
Piece Number
Graphic Representation
Orientation
Shipboard Studies
Lithological Unit
0
50
100
150
Unit 9
CORE/SECTION

126-793B-102R-2

UNIT 9: HYALOCLASTITE BRECCIA

GROUNDMASS: More matrix than clasts
ADDITIONAL COMMENTS:Mostly (entirely?) aphyric clasts, clasts 1.0-4.0 cm diameter

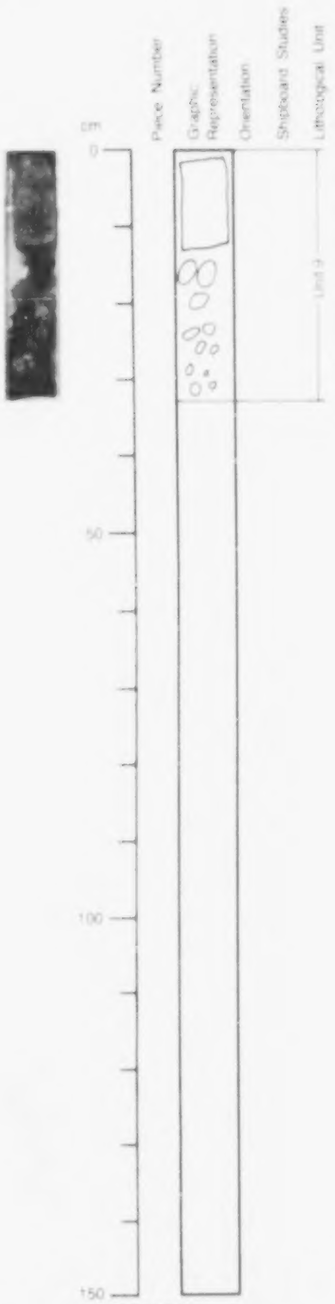
cm
0
50
100
150
Piece Number
Graphic Representation
Orientation
Shipboard Studies
Lithological Unit
Unit 9
CORE SECTION

126-793B-102R-CC

UNIT 9: HYALOCLASTITE BRECCIA

GROUNDMASS: Matrix consists of glass shards and pyroxene crystals cemented by zeolites (heulandite-clinoptilolite); thoroughly green (smectite not chlorite). More matrix than clasts.

COLOR: Green.

ADDITIONAL COMMENTS: Mostly (entirely?) aphyric clasts; clasts 0.5-7.0 cm diameter.

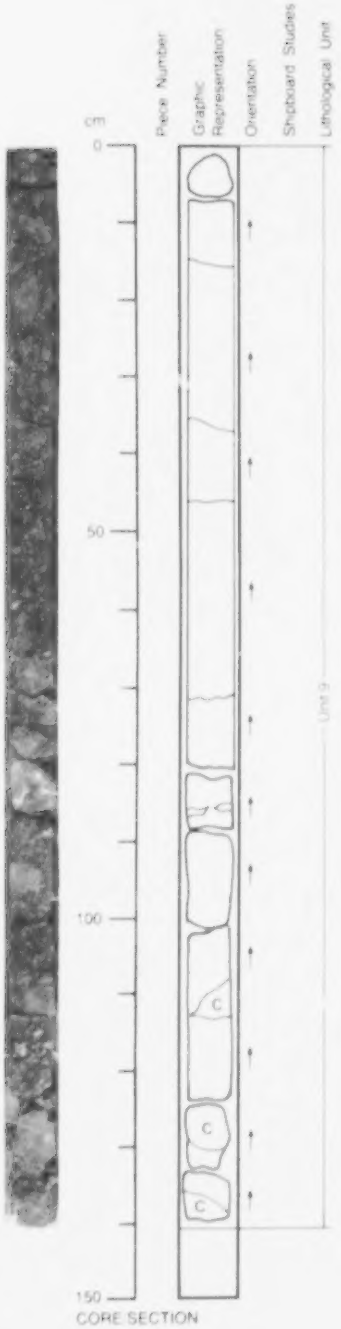
Piece Number
Graphic Representation
Orientation
Shipboard Studies
Lithological Unit
cm
0
50
100
150
C
C
C
Unit 9
CORE SECTION

126-793B-103R-1

UNIT 9: HYALOCLASTITE

PHENOCRYSTS:
Plagioclase : 2%; 0.2-1.0 mm; euhedral; partially altered.
Clinopyroxene : 2%; 0.2-2.0 mm; euhedral; partially altered.
Orthopyroxene : 2%; 0.2-2.0 mm; euhedral; partially altered.

GROUNDMASS: Fined grained. Altered glass with clinopyroxene-orthopyroxene-plagioclase crystals in zeolite cement. Glass is altered to smectite. Zeolite vein at 84 cm, 2 mm thick. Greenish black. Matrix is more abundant than clasts, but clasts increase in size and abundanse downward through core 126-793B-103R.

VESICLES: 5%; round; random; filled with smectite or zeolite coating on walls.

COLOR: Medium light gray.

ALTERATION: All phenocrysts are partially altered to smectite (orthopyroxene, clinopyroxene) or sericite (plagioclase).

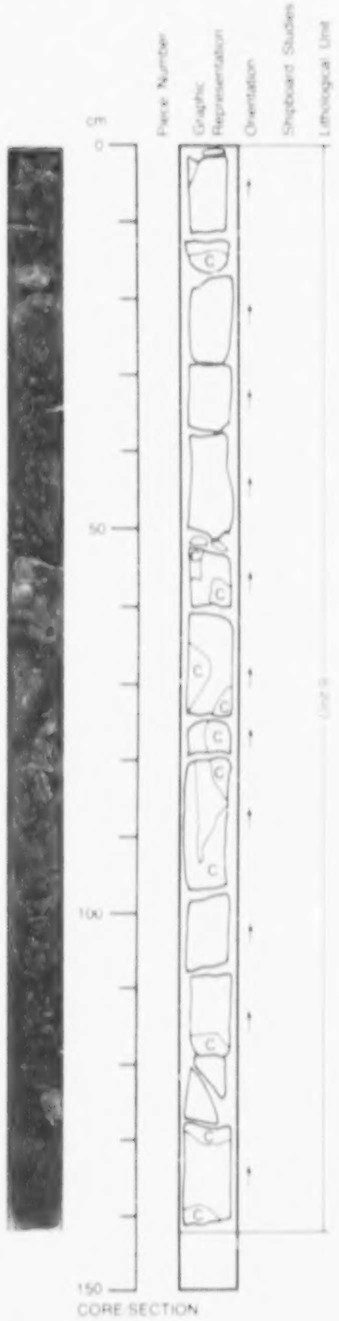
cm
0
50
100
150
CORE SECTION
Piece Number
Graphic Representation
Orientation
Shipboard Studies
Lithological Unit
C
Unit 9

126-793B-103R-2

UNIT 9: HYALOCLASTITE

PHENOCRYSTS:
Plagioclase - 2%, 0.2-1.0 mm, euhedral, partially altered.
Clinopyroxene - 2%, 0.2-2.0 mm, euhedral, partially altered.
Orthopyroxene - 2%, 0.2-2.0 mm, euhedral, partially altered.

GROUNDMASS: Fined grained. Altered glass with clinopyroxene-orthopyroxene-plagioclase crystals in zeolite cement. Glass is altered to smectite. Greenish black. Matrix is more abundant than clasts, but clasts increase in size and abundance downward through core 126-793B-103R.

VESICLES: 5%, round, random, filled with smectite or zeolite coating on walls.

COLOR: Medium light gray.

ALTERATION: All phenocrysts are partially altered to smectite (orthopyroxene, clinopyroxene) or sericite (plagioclase).

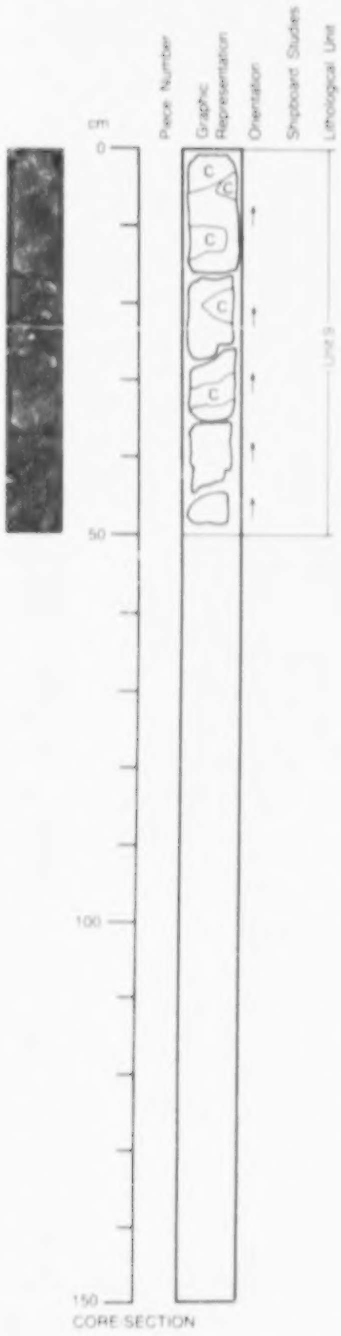
cm
0
50
100
150
Piece Number
Graphic Representation
Orientation
Shipboard Studies
Lithological Unit
C
C
C
C
C
Unit 9
CORE SECTION

126-793B-103R-3

UNIT 9: HYALOCLASTITE

PHENOCRYSTS:
Plagioclase - 2%; 0.2-1.0 mm; euhedral; partially altered.
Clinopyroxene - 2%; 0.2-2.0 mm; euhedral; partially altered.
Orthopyroxene - 2%; 0.2-2.0 mm; euhedral; partially altered.
GROUNDMASS: Fined grained. Altered glass withclinopyroxene orthopyroxene plagioclase crystals in zeolite cement. Glass is altered to smectite. Greenish black. Matrix is more abundant than clasts, but clasts increase in size and abundance downward through core 126-793B-103R.
VESICLES: 5%; round; random; filled with smectite or zeolite coating on walls.
COLOR: Medium light gray.
ALTERATION: All phenocrysts are partially altered to smectite (orthopyroxene, clinopyroxene) or sericite (plagioclase).

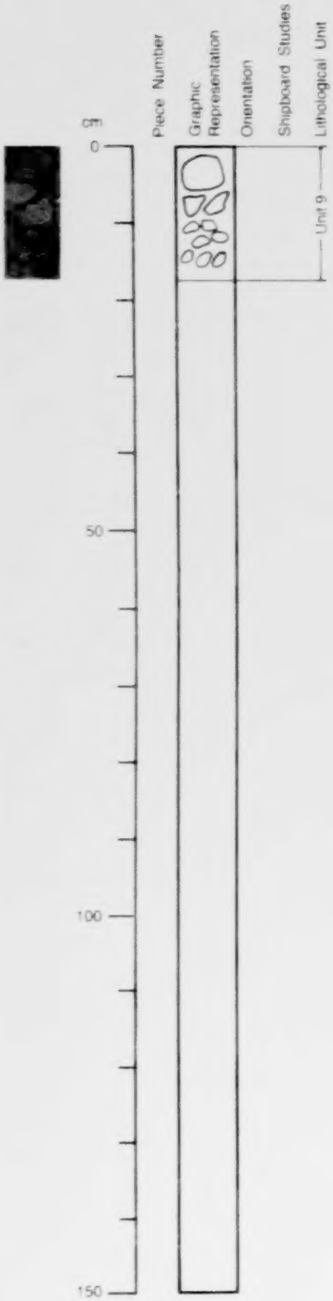
cm
Piece Number
Graphic Representation
Orientation
Shipboard Studies
Lithological Unit
0
50
100
150
Unit 9
CORE SECTION

126-793B-103R-CC

UNIT 9: HYALOCLASTITE

PHENOCRYSTS:

Plagioclase - 2%, 0.2-1.0 mm, euhedral, partially altered.
Clinopyroxene - 2%, 0.2-2.0 mm, euhedral, partially altered.
Orthopyroxene - 2%, 0.2-2.0 mm, euhedral, partially altered.

GROUNDMASS: Fine-grained. Altered glass with clinopyroxene + orthopyroxene + plagioclase crystals in zeolite cement. Glass is altered to smectite. Greenish black. Matrix is more abundant than clasts, but clasts increase in size and abundance downward through core 126-793B-103R.

VESICLES: 5%, round, random, filled with smectite or zeolite coating on walls.

COLOR: Medium light gray.

ALTERATION: All phenocrysts are partially altered to smectite (orthopyroxene, clinopyroxene) or sericite (plagioclase).

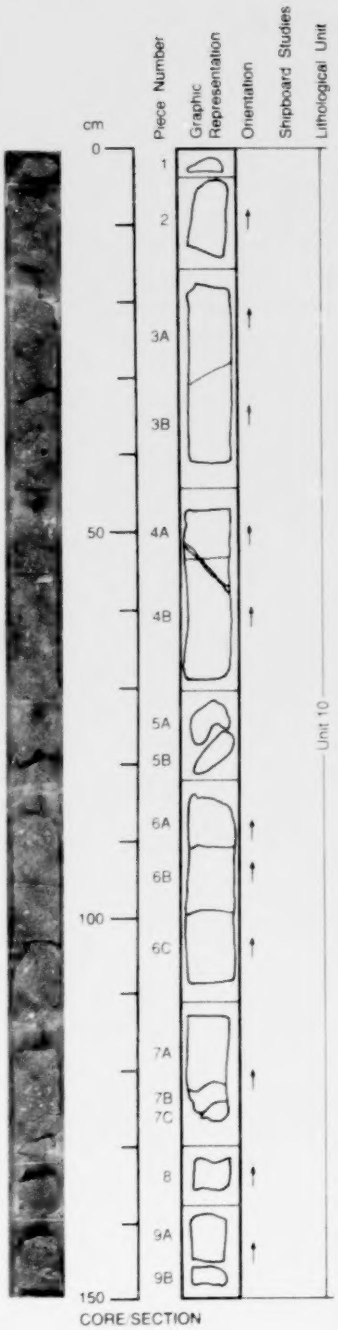
cm
Piece Number
Graphic Representation
Orientation
Shipboard Studies
Lithological Unit
0
50
100
150
1
2
3A
3B
4A
4B
5A
5B
6A
6B
6C
7A
7B
7C
8
9A
9B
Unit 10
CORE/SECTION

126-793B-104R-1

UNIT 10: BASALTIC ANDESITE

Pieces 1-9

CONTACTS: Clear contact between altered glass (green) and gray chilled margin of lava in Piece 4A and 4B.

PHENOCRYSTS:
Plagioclase - 5%, 0.3-2.0 mm, euhedral.
Clinopyroxene - 10%, 0.5-8.0 mm, euhedral.
Orthopyroxene - 3%, 0.3-5.0 mm, euhedral.

GROUNDMASS: Fine-grained with plagioclase laths < 0.3 mm.

VESICLES: 5%, 0.2 - 100 mm; elongated; random; filled with clays or zeolites. Some vesicles open with secondary minerals on vesicle walls. Native copper found in a few.

COLOR: Medium bluish gray.

STRUCTURE: Massive lava with alteration along fissures.

ALTERATION: Phenocrysts are generally fresh throughout core, but within the green bands, the clinopyroxene and orthopyroxene phenocrysts are altered along margins and cleavages.

VEINS/FRACTURES: Thin (0.1-1.0 mm) white zeolite veins throughout section. Thick, 1-5 cm vein in altered zone in Pieces 2, 3, 4, and 6B.

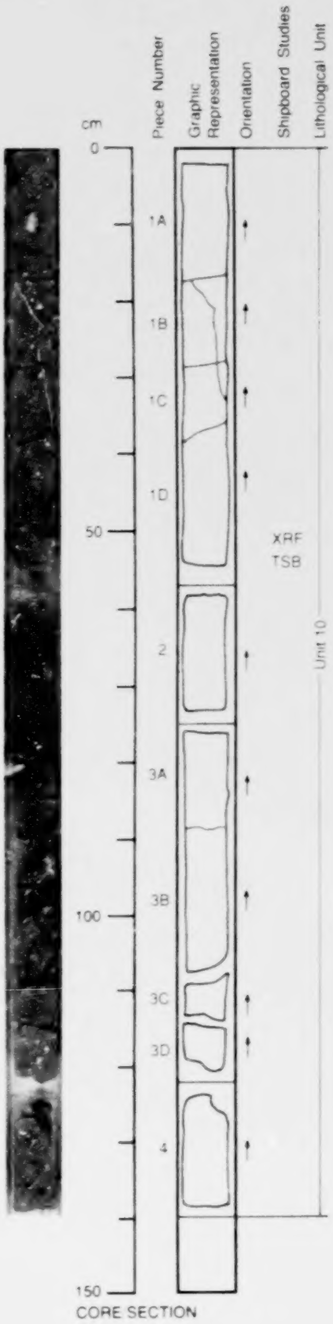
cm
Piece Number
Graphic Representation
Orientation
Shipboard Studies
Lithological Unit
0
1A
1B
1C
1D
50
XRF
TSB
2
3A
3B
100
3C
3D
4
Unit 10
150
CORE SECTION

126-793B-104R-2

UNIT 10: BASALTIC ANDESITE

Pieces 1-4

PHENOCRYSTS:
Plagioclase - 5%, 0.3-2.0 mm, euhedral
Clinopyroxene - 10%, 0.5-8.0 mm, euhedral
Orthopyroxene - 3%, 0.3-5.0 mm, euhedral

GROUNDMASS: Fine-grained with plagioclase laths < 0.3 mm.

VESICLES: 5%, 0.2 - 100 mm, elongated, random, filled with clays or zeolites. Some vesicles open with secondary minerals on vesicle walls. Native copper found in a few.

COLOR: Medium bluish gray.

STRUCTURE: Massive lava with alteration along fissures.

ALTERATION: Phenocrysts are generally fresh throughout core, but within the green bands, the clinopyroxene and orthopyroxene phenocrysts are altered along margins and cleavages.

VEINS/FRACTURES: Zeolite vein through Pieces 1B and 1C.

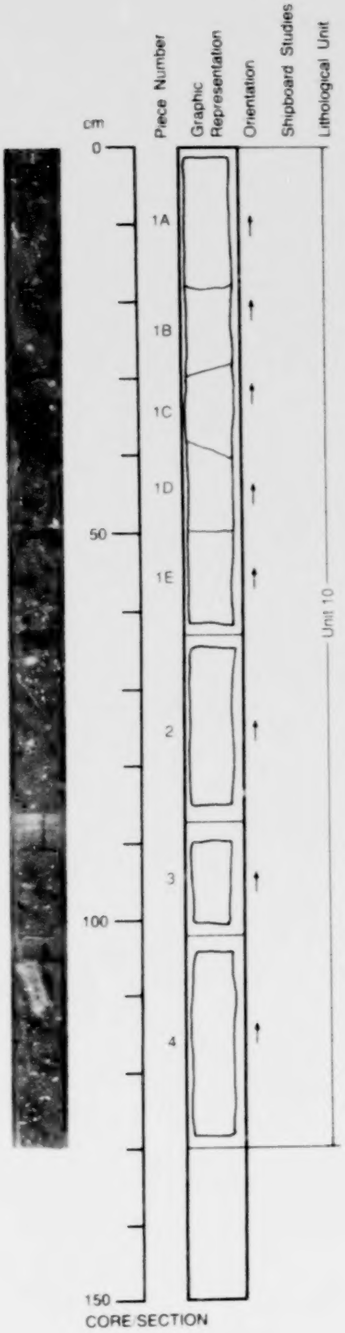
cm
Piece Number
Graphic Representation
Orientation
Shipboard Studies
Lithological Unit
0
1A
1B
1C
1D
50
1E
Unit 10
2
3
100
4
150
CORE/SECTION

126-793B-104R-3

UNIT 10: BASALTIC ANDESITE

Pieces 1-4

PHENOCRYSTS:
Plagioclase - 5%, 0.3-2.0 mm, euhedral.
Clinopyroxene - 10%, 0.5-8.0 mm, euhedral.
Orthopyroxene - 3%, 0.3-5.0 mm, euhedral.
GROUNDMASS: Fine-grained with plagioclase laths < 0.3 mm.
VESICLES: 5%, 0.2 - 100 mm, elongated, random, filled with clays or zeolites. Some vesicles open with secondary minerals on vesicle walls. Native copper found in a few.
COLOR: Medium bluish gray.
STRUCTURE: Massive lava with alteration along fissures.
ALTERATION: Phenocrysts are generally fresh throughout core, but within the green bands, the clinopyroxene and orthopyroxene phenocrysts are altered along margins and cleavages.

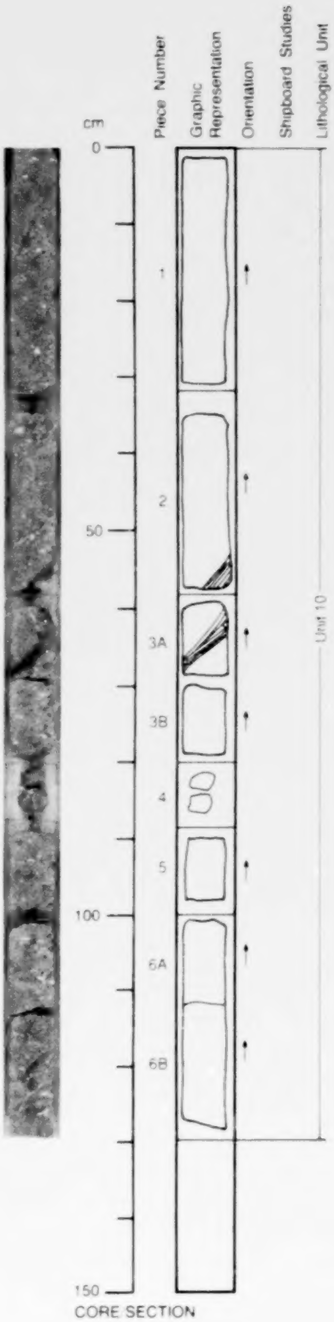
cm
Piece Number
Graphic Representation
Orientation
Shipboard Studies
Lithological Unit
0
50
100
150
1
2
3A
3B
4
5
6A
6B
Unit 10
CORE SECTION

126-793B-104R-4

UNIT 10: BASALTIC ANDESITE

Pieces 1-6

PHENOCRYSTS:
Plagioclase - 5%, 0.3-2.0 mm, euhedral.
Clinopyroxene - 10%, 0.5-8.0 mm, euhedral.
Orthopyroxene - 3%, 0.3-5.0 mm, euhedral.

GROUNDMASS: Fine-grained with plagioclase laths < 0.3 mm.

VESICLES: 5%, 0.2 - 100 mm, elongated, random, filled with clays or zeolites. Some vesicles open with secondary minerals on vesicle walls. Native copper found in a few.

COLOR: Medium bluish gray.

STRUCTURE: Massive lava with alteration along fissures.

ALTERATION: Phenocrysts are generally fresh throughout core, but within the green bands, the clinopyroxene and orthopyroxene phenocrysts are altered along margins and cleavages.

ADDITIONAL COMMENTS: Green hyaloclastite band in Pieces 2 and 3A.

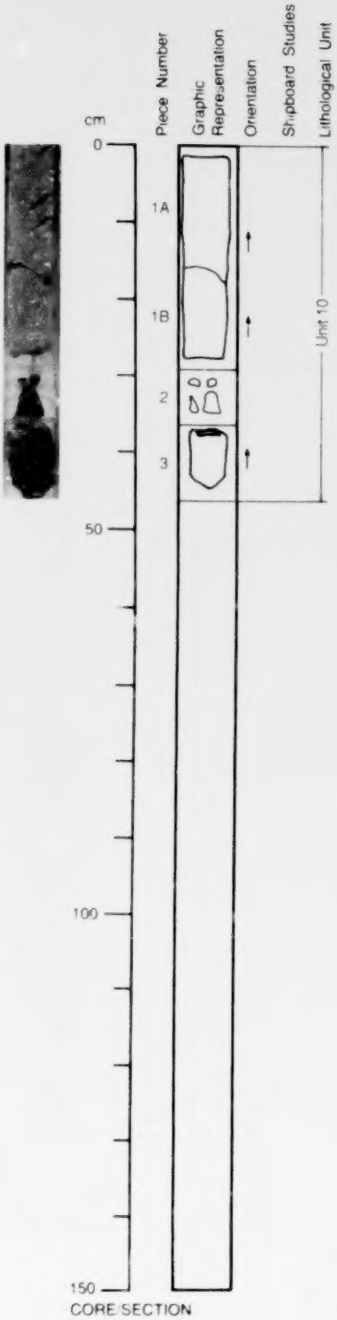
cm
Piece Number
Graphic Representation
Orientation
Shipboard Studies
Lithological Unit
0
50
100
150
1A
1B
2
3
Unit 10
CORE/SECTION

126-793B-104R-CC

UNIT 10: BASALTIC ANDESITE

Pieces 1-2

PHENOCRYSTS:
Plagioclase - 5%, 0.3-2.0 mm, euhedral
Clinopyroxene - 10%, 0.5-8.0 mm, euhedral
Orthopyroxene - 3%, 0.3-5.0 mm, euhedral
GROUNDMASS: Fine-grained with plagioclase laths < 0.3 mm.
VESICLES: 5%, 0.2 - 100 mm, elongated, random, filled with clays or zeolites. Some vesicles open with secondary minerals on vesicle walls. Native copper found in a few.
COLOR: Medium bluish gray.
STRUCTURE: Massive lava with alteration along fissures.
ALTERATION: Phenocrysts are generally fresh throughout core, but within the green bands, the clinopyroxene and orthopyroxene phenocrysts are altered along margins and cleavages.
ADDITIONAL COMMENTS: Glassy margin at bottom of Piece 2.

UNIT 10: MONOMICTITE HYALOCLASTITE BRECCIA

Piece 3

CONTACTS: Glassy margin at top of Piece 3 which is the contact to the basaltic andesite.
PHENOCRYSTS: Plagioclase phyric basic andesite.
GROUNDMASS: Chilled glassy shards, clinopyroxene, altered orthopyroxene crystals. Zeolite and smectite cement.
ADDITIONAL COMMENTS: Volcanic clastics 35%, chilled glassy shards 50%, cement 20%.

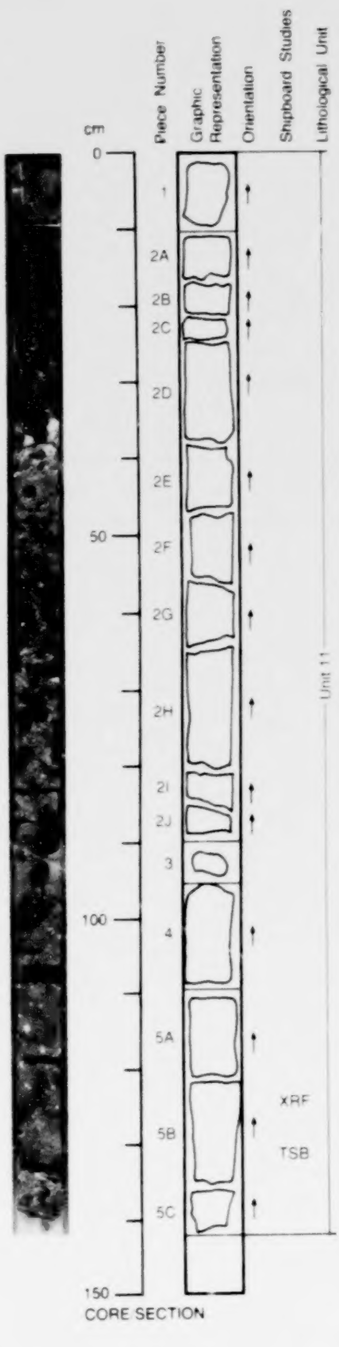
cm
Piece Number
Graphic Representation
Orientation
Shipboard Studies
Lithological Unit
0
50
100
150
1
2A
2B
2C
2D
2E
2F
2G
2H
2I
2J
3
4
5A
5B
5C
XRF
TSB
Unit 11
CORE SECTION

126-793B-105R-1

UNIT 11: BASALTIC ANDESITE PILLOW LAVAS

Pieces 1, 4-5B

CONTACTS: Chilled, darker glassy margins mark pillow rims.
PHENOCRYSTS:
Plagioclase - 5%, 1-3 mm, euhedral.
Clinopyroxene - 8%, 2-10 mm, euhedral.
Orthopyroxene - 5%, 1-3 mm, euhedral.
GROUNDMASS: Fine-grained, non-aligned laths of plagioclase.
VESICLES: < 1%, spherical to tabular, sporadic, filled with radiating, white zeolite (heulandite-clinoptilolite). Some vesicles remain open.
COLOR:Medium bluish gray.
ALTERATION: Orthopyroxene rims are altered to smectite.
ADDITIONAL COMMENTS: Stellate spherulitic arrangement of clinopyroxene, often nucleated around orthopyroxene pseudomorphs.

UNIT 11: HYALOCLASTITE BRECCIA

Pieces 2, 5C

PHENOCRYSTS:
Orthopyroxene - 5%, 1-2 mm.
Clinopyroxene - 10%, 2-5 mm.
GROUNDMASS: Altered glass shards, 1-10 mm pyroxene crystals.
VESICLES: 2-4 cm, sparse, zeolite and native copper in vesicles.
COLOR: Greenish black.
ADDITIONAL COMMENTS: Highly altered clasts of porphyritic andesite.

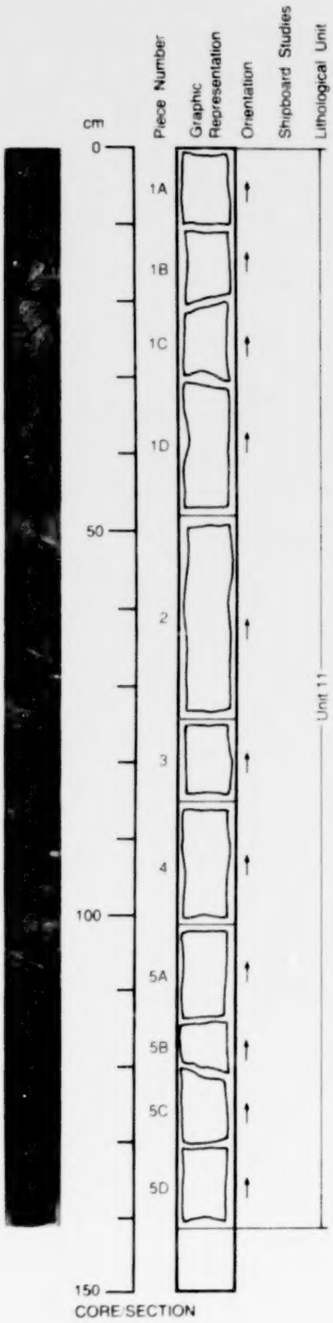
cm
Piece Number
Graphic Representation
Orientation
Shipboard Studies
Lithological Unit
0
50
100
150
1A
1B
1C
1D
2
3
4
5A
5B
5C
5D
Unit 11
CORE/SECTION

126-793B-105R-2

UNIT 11: HYALOCLASTITE BRECCIA

Pieces 1-5

PHENOCRYSTS: Clasts: porphyritic basaltic andesite, 5-20 cm diameter.
Orthopyroxene - 5%, 0.5 - 3.0 mm, euhedral.
Clinopyroxene - 10-15%, 2-6 mm, euhedral, stellate clusters.
Plagioclase - 2%, 0.5-1.0 mm, euhedral.
GROUNDMASS: Felty feldspar.
VESICLES: < 5%, elongate, filled with white and orange zeolite and native copper.
COLOR: Medium bluish gray.
ADDITIONAL COMMENTS: Matrix: hyaloclastite mixture of altered glass shards (1-10mm), pyroxene crystals, and zeolite+smectite cement.

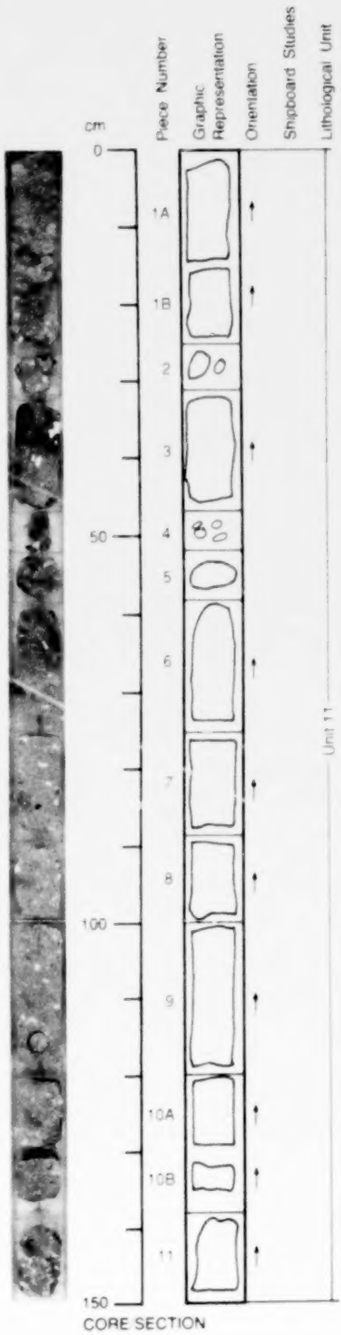
cm
Piece Number
Graphic Representation
Orientation
Shipboard Studies
Lithological Unit
0
50
100
150
1A
1B
2
3
4
5
6
7
8
9
10A
10B
11
Unit 11
CORE SECTION

126-793B-105R-3

UNIT 11: HYALOCLASTITE BRECCIA

Piece 1A

PHENOCRYSTS: Clasts: porphyritic basaltic andesite.
Orthopyroxene - 5%, 0.5 - 3.0 mm, euhedral.
Clinopyroxene - 10-15%, 2-6 mm, euhedral, stellate clusters.
Plagioclase - 2%, 0.5-1.0 mm, euhedral.
GROUNDMASS: Felty feldspar.
VESICLES: < 5%, elongate, filled with white and orange zeolite and native copper.
COLOR: Medium bluish gray.
ADDITIONAL COMMENTS: Matrix: hyaloclastite mixture of altered glass shards (1-10 mm), pyroxene crystals, and zeolite+smectite cement.

UNIT 11: PILLOW LAVA

Pieces 1B-10A

CONTACTS: Chilled margins at both pillows (see comments).
PHENOCRYSTS: Amygdules 2-20 mm diameter, filled with zeolite and native copper.
Stellate clinopyroxene clusters.
Orthopyroxene - 5%, 0.5 - 3.0 mm euhedral.
Clinopyroxene - 10-15%, 2-6 mm, euhedral, stellate clusters.
Plagioclase - 2%, 0.5-1.0 mm, euhedral.
ADDITIONAL COMMENTS: Piece 1 to 3 and Piece 6 to 10G are separate pillows with chilled margins.

UNIT 11: HYALOCLASTITE BRECCIA

Pieces 10B and 11

PHENOCRYSTS:
Orthopyroxene - 5%, 0.5 mm, altered.
Clinopyroxene - 10%, 1.5 mm, serrate occasionally.
Plagioclase - 10%, 0.5 mm, euhedral, fresh.
GROUNDMASS: Trachytic feldspar. Matrix: glass shards, 1-4 mm, plus pyroxene and feldspar crystals with orange zeolite cement.
VESICLES: < 2%, filled with smectite.
COLOR: Greenish black.
ADDITIONAL COMMENTS: Clasts about 4 cm in diameter.

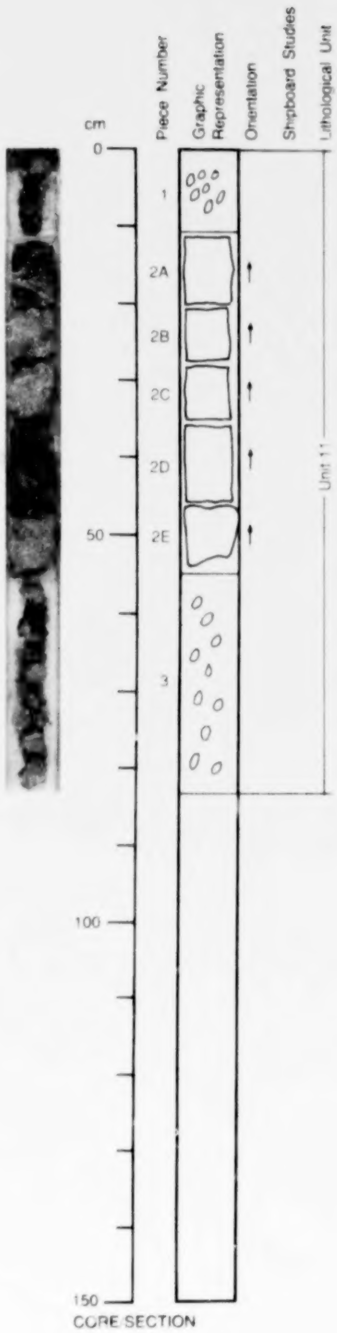
cm
Piece Number
Graphic Representation
Orientation
Shipboard Studies
Lithological Unit
0
50
100
150
1
2A
2B
2C
2D
2E
3
Unit 11
CORE/SECTION

126-793B-105R-4

UNIT 11: HYALOCLASTITE BRECCIA

Pieces 1-3

PHENOCRYSTS:
Plagioclase - 10%, 0.5 mm, euhedral, fresh
Clinopyroxene - 10%, 1.5 mm, serrate occasionally
Orthopyroxene - 5%, 0.5 mm, altered
GROUNDMASS: Trachytic feldspar. Matrix: glass shards, 1-4 mm, plus pyroxene and feldspar crystals with orange zeolite cement
VESICLES: < 2%, filled with smectite
COLOR: Greenish black
ADDITIONAL COMMENTS: Clasts about 4 cm in diameter

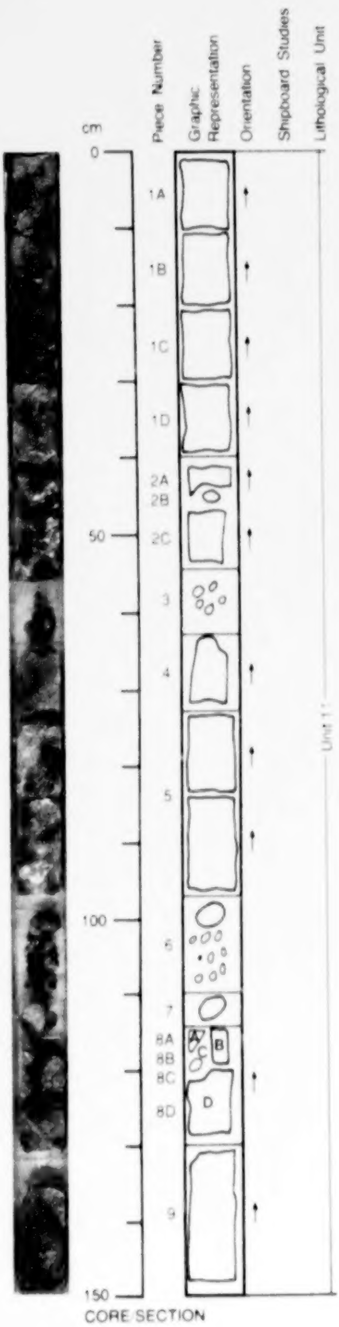
cm
Piece Number
Graphic Representation
Orientation
Shipboard Studies
Lithological Unit
0
50
100
150
1A
1B
1C
1D
2A
2B
2C
3
4
5
6
7
8A
8B
8C
8D
9
A
B
C
D
Unit 11
CORE SECTION

126-793B-106R-1

UNIT 11: HYALOCLASTITE BRECCIA

Pieces 1-9

PHENOCRYSTS:
Plagioclase - 10%, 0.5-1.0 mm, euhedral, fresh.
Clinopyroxene - 10%, 1.0 mm, euhedral, fresh.
Orthopyroxene - 2%, 0.5 mm, altered, fresh.
GROUNDMASS: Intersertal? Matrix: hyaloclastite, altered glass shards, 1-3 mm. Cement is zeolite. Smectite in interstices up to 1 cm in diameter.
VESICLES: 1-2 mm diameter, elongate, filled with smectite, zeolite, and native copper.
COLOR: Greenish gray.
ADDITIONAL COMMENTS: Clasts 1 - 10 cm in diameter.

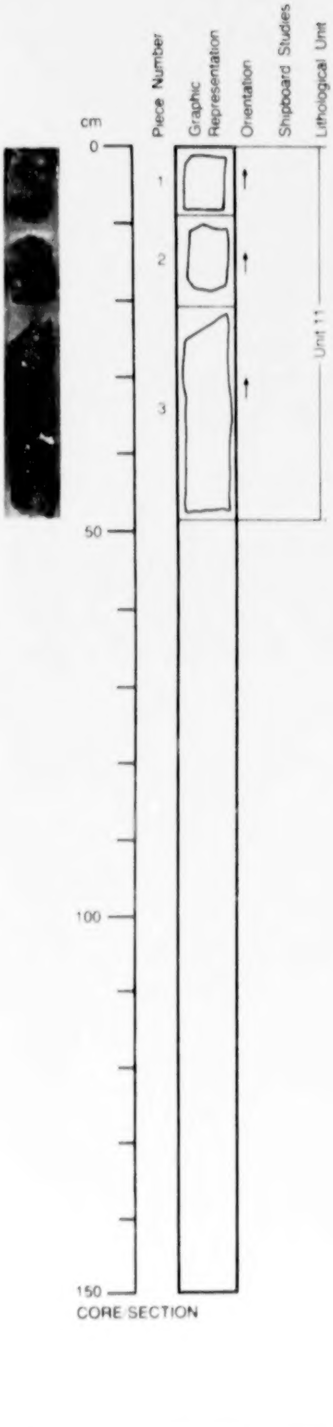
cm
0
50
100
150
Piece Number
Graphic Representation
Orientation
Shipboard Studies
Lithological Unit
1
2
3
Unit 11
CORE SECTION

126-793B-106R-2

UNIT 11: HYALOCLASTITE BRECCIA

Pieces 1-2

PHENOCRYSTS
- Plagioclase - 10%, 0.5-1.0 mm, euhedral, fresh
- Clinopyroxene - 10%, 1.0 mm, euhedral, fresh
- Orthopyroxene - 2%, 0.5 mm, altered, fresh

GROUNDMASS: Intersertal? Matrix: hyaloclastite, altered glass shards, 1-3 mm. Cement is zeolite. Smectite in interstices up to 1 cm in diameter.

VESICLES: 1-2 mm diameter; elongate, filled with smectite, zeolite, and native copper.

COLOR: Greenish gray.

ADDITIONAL COMMENTS: Clasts 1 - 10 cm in diameter.

UNIT 11: PORPHYRITIC ANDESITE LAVA

Piece 3

CONTACTS: No contacts observed.

PHENOCRYSTS:
- Plagioclase - 8%, 0.5-2.0 mm, euhedral, fresh
- Clinopyroxene - 12%, 1.0-5.0 mm, euhedral, fresh
- Orthopyroxene - 10%, 1.0-3.0 mm, euhedral, fresh

GROUNDMASS: Intersertal plagioclase and clinopyroxene.

VESICLES: < 5%, 0.2 - 0.3 mm, vesicles are open, lined with smectite, or filled with zeolite (no native copper).

ADDITIONAL COMMENTS: Very fresh.

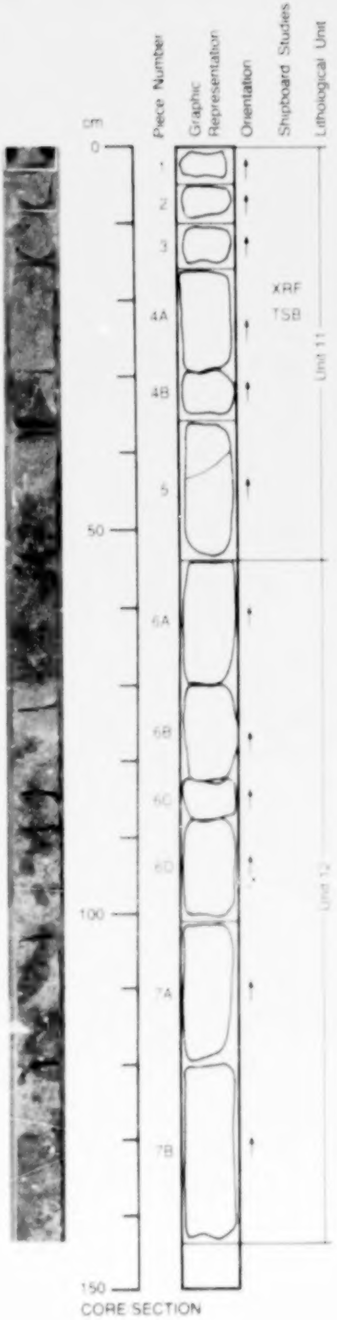
cm
Piece Number
Graphic Representation
Orientation
Shipboard Studies
Lithological Unit
0
50
100
150
1
2
3
4A
4B
5
6A
6B
6C
6D
7A
7B
XRF
TSB
Unit 11
Unit 12
CORE SECTION

126-793B-107R-1

UNIT 11: CLINOPYROXENE-ORTHOPYROXENE-PLAGIOCLASE PHYRIC ANDESITE

Pieces 1-4

PHENOCRYSTS:
Plagioclase - 20%, 3.0 mm, euhedral, fresh.
Clinopyroxene - 10%, ~4.0 mm, euhedral, fresh.
Orthopyroxene - 5%, ~4.0 mm, euhedral. Partially altered to smectite, clustered with clinopyroxene.
GROUNDMASS: Fine grained.
VESICLES: ~10%, circular, sometime elongate, partly filled with smectites.

UNIT 11: HYALOCLASTITE BRECCIA

Piece 5

CONTACTS: Chilled contact at top of Piece 5 with andesite lava above. This contact is marked by a chilled rim, rich in flattened vesicles and filled with zeolites and smectites.
VESICLES: 30%, flattened vesicles filled with zeolites and smectites.
VEINS/FRACTURES: Vertical fractures filled with zeolites.

UNIT 12: ANDESITIC BRECCIA

Pieces 6-7

PHENOCRYSTS: Clasts from 0.5-7.0 cm. These clasts are formed of clinopyroxene, orthopyroxene, plagioclase andesite similar to Pieces 1-4. Chilled rims very rich in vesicles that are filled with zeolites and smectites.
Plagioclase - 20%, 3.0 mm, euhedral, fresh.
Clinopyroxene - 10%, ~4.0 mm, euhedral, fresh.
Orthopyroxene - 5%, ~4.0 mm, euhedral, fresh.
GROUNDMASS: Chilled glass shards with clinopyroxene crystals from 0.1 up to 6.0 mm. Cement is zeolite and smectite.
VESICLES: Filled with zeolites and smectites.

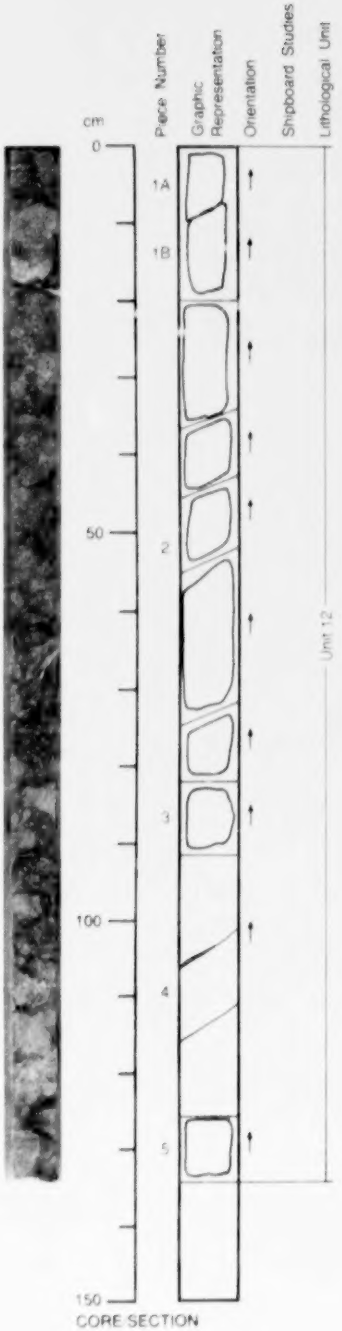
cm
Piece Number
Graphic Representation
Orientation
Shipboard Studies
Lithological Unit
0
50
100
150
1A
1B
2
3
4
5
Unit 12
CORE SECTION

126-793B-107R-2

UNIT 12: ANDESITIC BRECCIA WITH HYALOCLASTITE MATRIX

Pieces 1-5

PHENOCRYSTS: Clasts 0.5 - 6.0 cm. Chilled rims of andesite.
  Plagioclase - 5%. Up to 1.0 mm, euhedral, fresh.
  Clinopyroxene - 10%, 4.0 mm, euhedral, fresh.
  Orthopyroxene - 5%, 4.0 mm, euhedral, altered to smectites.
GROUNDMASS: Matrix. Dark green glassy shards, 0.2-1.0 mm. Zeolite and smectite cement. Plagioclase present.
VESICLES: < 10%, 3.0 mm, flattened or rounded, filled with zeolites and smectites.
COLOR: Dark green.
VEINS/FRACTURES: 70%, cracks and veins filled with smectites.

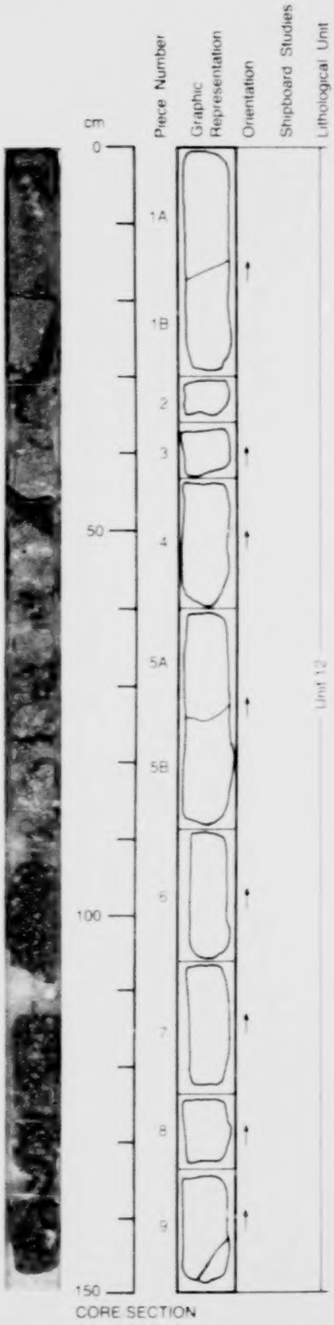
cm
Piece Number
Graphic Representation
Orientation
Shipboard Studies
Lithological Unit
0
50
100
150
1A
1B
2
3
4
5A
5B
6
7
8
9
Unit 12
CORE SECTION

126-793B-107R-3

UNIT 12: BRECCIA WITH CRYSTAL TUFF MATRIX

Pieces 1-9

PHENOCRYSTS: Clasts increase in size (2-20 cm) down section in Pieces 1-5 ("minipillow"). In Pieces 6-9, clasts are smaller (0.5-2.0 cm). In Pieces 6-9 the clasts have inclusions rich in smectites.
Plagioclase - 5%, ~2.0 mm, euhedral.
Clinopyroxene - ~10%, 3.00 mm, euhedral, fresh.
Orthopyroxene - 5%, ~10.0 mm, euhedral, altered in smectites.
GROUNDMASS: Gray, with small plagioclase laths. Matrix: Crystal tuff, glassy shards and clinopyroxene-plagioclase crystals. Cement is smectite.
VESICLES: ~12%, flattened or rounded, filled with zeolites and smectites.
COLOR: Gray.
ADDITIONAL COMMENTS: Inclusions composed of smectite mantled by clinopyroxene.

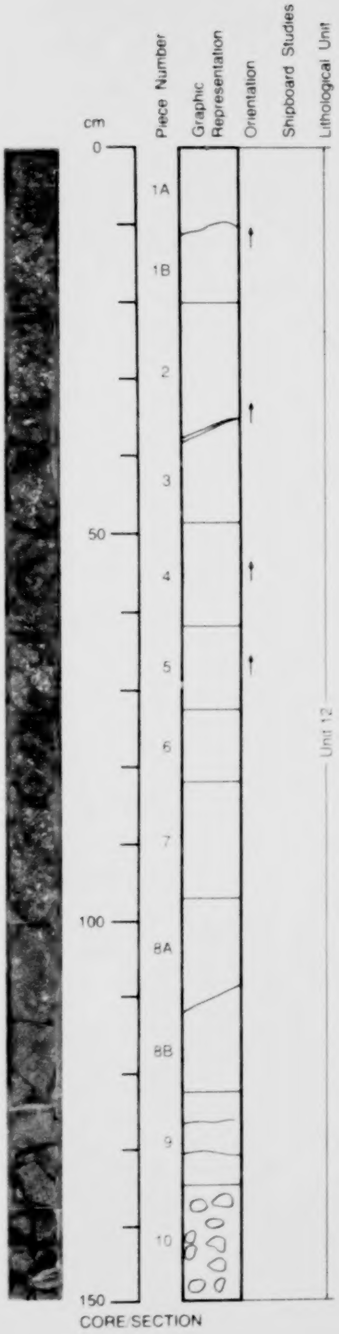
cm
Piece Number
Graphic Representation
Orientation
Shipboard Studies
Lithological Unit
0
50
100
150
1A
1B
2
3
4
5
6
7
8A
8B
9
10
Unit 12
CORE SECTION

126-793B-107R-4

UNIT 12: CLINOPYROXENE-ORTHOPYROXENE ANDESITE

Pieces 1-3, 5-7

PHENOCRYSTS: Clasts size ranges from 0.5-7.0 cm. These clasts are chilled.
Plagioclase - 5%, ~ 1.0 mm, euhedral.
Clinopyroxene - 10%, Up to 5.0 mm, euhedral.
Orthopyroxene - 8%, Up to 7.0 mm, euhedral, altered to smectites, often clustered with clinopyroxene.

GROUNDMASS: Cement is composed of zeolites and smectites. Matrix is composed of glass shards altered to smectites.

UNIT 12: CLINOPYROXENE-ORTHOPYROXENE ANDESITE

Pieces 4, 8 - 10

PHENOCRYSTS: "Big clasts" of clinopyroxene orthopyroxene andesite.
Plagioclase - 5%, ~ 1.0 mm, euhedral.
Clinopyroxene - 10%, Up to 5.0 mm, euhedral.
Orthopyroxene - 8%, Up to 7.0 mm, euhedral, altered to smectites, often clustered with clinopyroxene.

GROUNDMASS: Microcrystalline with tiny feldspar microlites. Cement is composed of zeolites and smectites.

VESICLES: 15%, Up to 4.0 mm, rounded or slightly flattened, filled with zeolites and/or smectites. Copper is present in the vesicles.

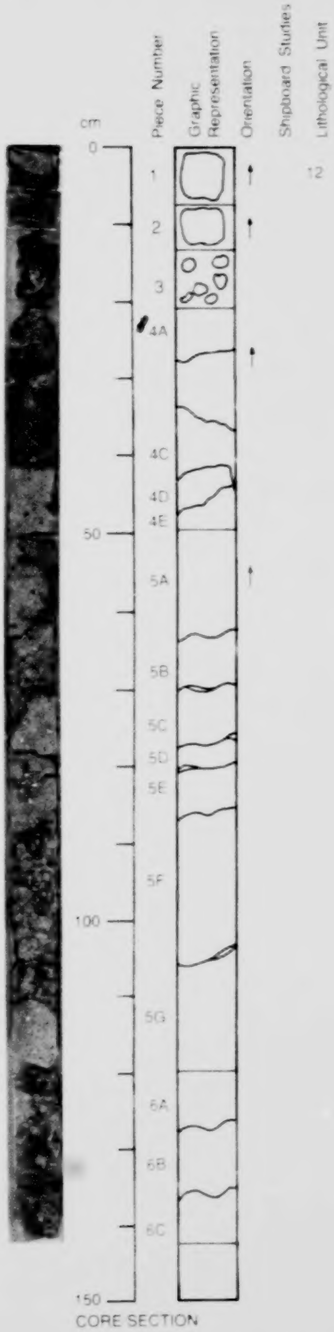
cm
Piece Number
Graphic Representation
Orientation
Shipboard Studies
Lithological Unit
0
50
100
150
1
2
3
4A
4C
4D
4E
5A
5B
5C
5D
5E
5F
5G
6A
6B
6C
12
CORE SECTION

126-793B-108R-1

UNIT 12: BRECCIA

Pieces 1-4, 5(A, D, E)

PHENOCRYSTS: "Pillows" chilled against the matrix.
Plagioclase - 3%. Up to 1.0 mm, euhedral.
Clinopyroxene - 10%. Up to 5.0 mm, euhedral, fresh.
Orthopyroxene - 5%. Up to 3.0 mm, euhedral, altered to smectites.

GROUNDMASS: Groundmass with small feldspars (feldspars seem more abundant in the groundmass of these pieces). The matrix that is present in Pieces 4A and 4B is a tuff very similar to core 126-793B-107R-3, formed of small shards of glass. Piece 4B contains a reworked "clast" formed of a pillow-clast with its rims surrounded by fine-grained tuffs.

VESICLES: 10%, circular, slightly elongated, filled with smectites.

VEINS/FRACTURES: Veins or cracks filled with smectites.

UNIT 12: BRECCIA

Pieces 5 (B,C,F,G) - 6

PHENOCRYSTS: "Clasts" 0.5-10.0 cm, andesite, similar to Pieces 1-4.
Plagioclase - 3%. Up to 1.0 mm, euhedral.
Clinopyroxene - 10%. Up to 5.0 mm, euhedral, fresh.
Orthopyroxene - 5%. Up to 3.0 mm, euhedral, altered in smectites.

GROUNDMASS: Matrix is crystal tuff with glassy shards. The crystals are mainly clinopyroxene, similar to core 126-793B-107R.

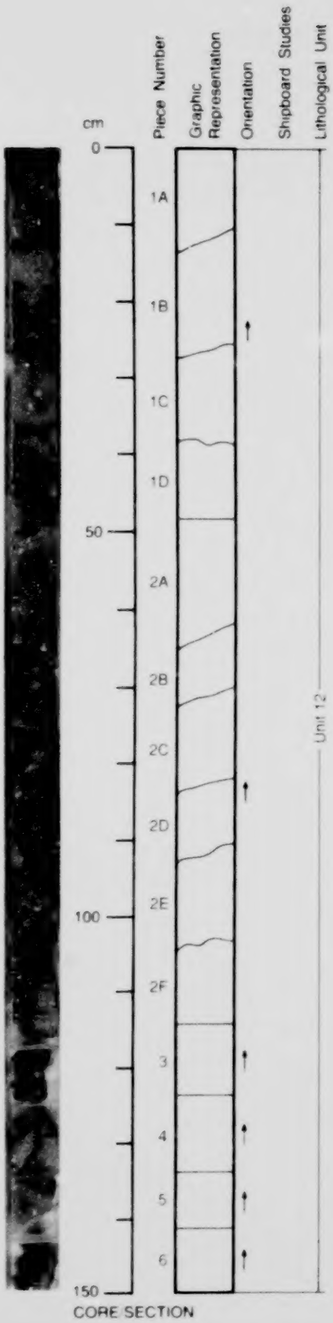
cm
Piece Number
Graphic Representation
Orientation
Shipboard Studies
Lithological Unit
0
50
100
150
1A
1B
1C
1D
2A
2B
2C
2D
2E
2F
3
4
5
6
Unit 12
CORE/SECTION

126-793B-108R-2

UNIT 12: ANDESITIC CLASTS IN A CRYSTAL TUFF MATRIX

Pieces 1-6

PHENOCRYSTS: Andesitic clasts are chilled. Similar to section 793B-108R-1.
Plagioclase - 3%. Up to 1.0 mm, euhedral.
Clinopyroxene - 10%; Up to 5.0 mm, euhedral, fresh.
Orthopyroxene - 5%. Up to 3.0 mm, euhedral, altered to smectites.

GROUNDMASS: Matrix is crystal tuff with glassy shards. The crystals are mainly clinopyroxene, similar to core 126-793B-108R.

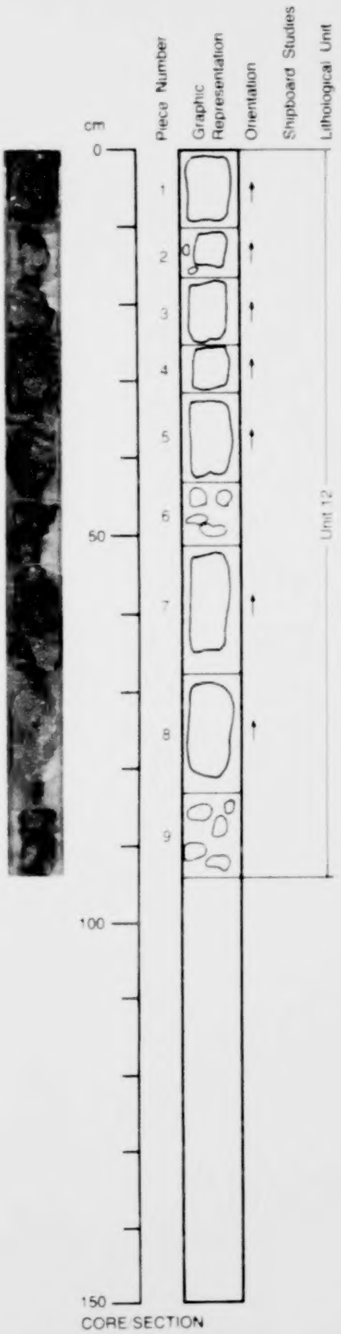
cm
Piece Number
Graphic Representation
Orientation
Shipboard Studies
Lithological Unit
0
50
100
150
1
2
3
4
5
6
7
8
9
Unit 12
CORE SECTION

126-793B-108R-3

UNIT 12: ANDESITIC BRECCIA

Pieces 1-9

PHENOCRYSTS: Clinopyroxene>orthopyroxene>plagioclase with very big clinopyroxene crystals up to 1 cm in diameter.

GROUNDMASS: "Matrix" contains crystals, glassy shards, and gray lithic fragments.

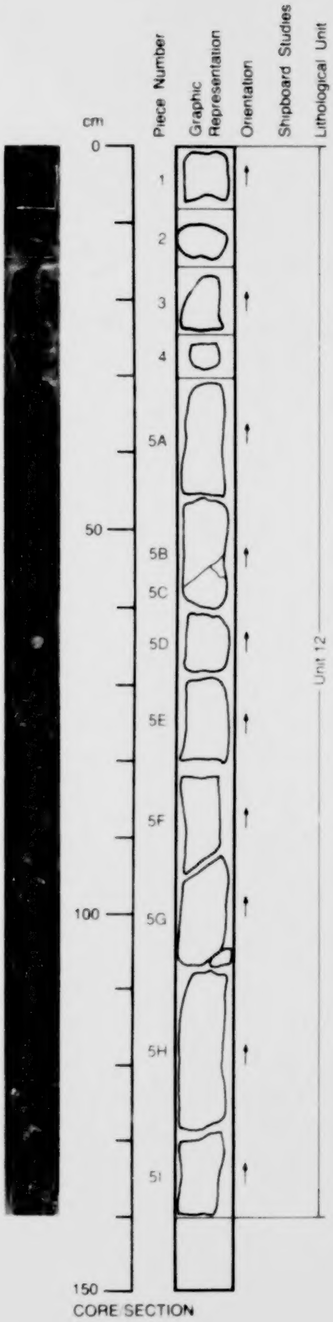
cm
0
50
100
150
CORE SECTION
Piece Number
Graphic Representation
Orientation
Shipboard Studies
Lithological Unit
1
2
3
4
5A
5B
5C
5D
5E
5F
5G
5H
5I
Unit 12

126-793B-109R-1

UNIT 12: ANDESITE BRECCIA IN HYALOCLASTITIC MATRIX

Pieces 1-5

CONTACTS: None internally visible within clasts.
PHENOCRYSTS: Clasts of 1 - 8 cm in size in a greenish gray to dark greenish gray matrix.
Plagioclase - - 5%, 0.5 mm, euhedral, fresh.
Clinopyroxene - 5%, 0.5-3.0 mm, euhedral, fresh.
Orthopyroxene - 2%, 0.5-1.0 mm; euhedral, altered.
GROUNDMASS: Altered, with plagioclase microlites, smectites, and celadonite. Matrix contains clasts of lava, altered glass shards and crystal fragments/phenocrysts.
VESICLES: 0.2%, filled with zeolites.
COLOR: Dark greenish gray.
ALTERATION: Groundmass altered to smectite and celadonite. Orthopyroxene altered to celadonite and smectite plus an iron oxide mineral (brown).
ADDITIONAL COMMENTS: About 20% of the clasts have broken chilled margins.

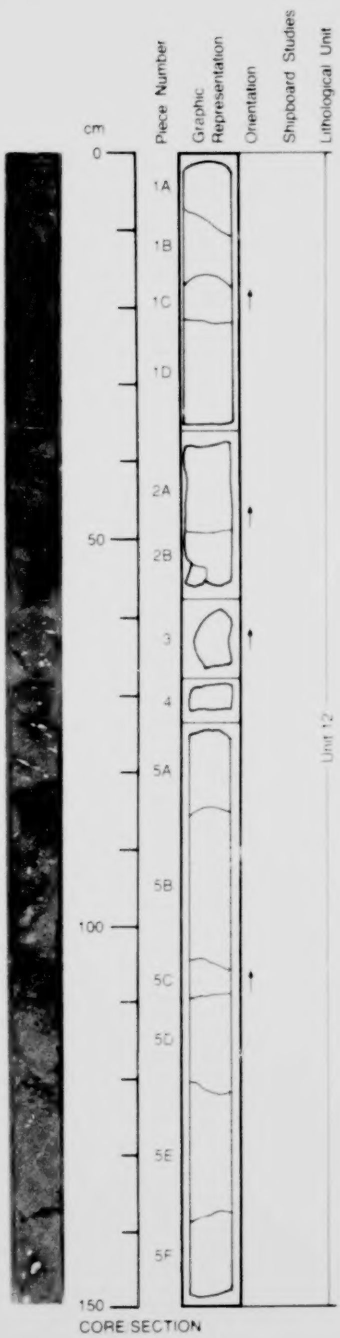
cm
Piece Number
Graphic Representation
Orientation
Shipboard Studies
Lithological Unit
0
50
100
150
1A
1B
1C
1D
2A
2B
3
4
5A
5B
5C
5D
5E
5F
Unit 12
CORE SECTION

126-793B-109R-2

UNIT 12: ANDESITE BRECCIA IN HYALOCLASTITIC MATRIX

Pieces 1-5

CONTACTS: None internally visible within clasts.
PHENOCRYSTS: Clasts of 1 - 8 cm in size in a greenish gray to dark greenish gray matrix.
Plagioclase: ~5%, 0.5 mm, euhedral, fresh.
Clinopyroxene: 5%, 0.5-3.0 mm, euhedral, fresh.
Orthopyroxene: 2%, 0.5-1.0 mm, euhedral, altered.
GROUNDMASS: Altered, with plagioclase microlites, smectites, and celadonite. Matrix contains clasts of lava, altered glass shards and crystal fragments phenocrysts.
VESICLES: 0.2%, filled with zeolites.
COLOR: Dark greenish gray.
ALTERATION: Groundmass altered to smectite and celadonite. Orthopyroxene altered to celadonite and smectite plus an iron oxide mineral (brown).
ADDITIONAL COMMENTS: About 20% of the clasts have broken chilled margins.

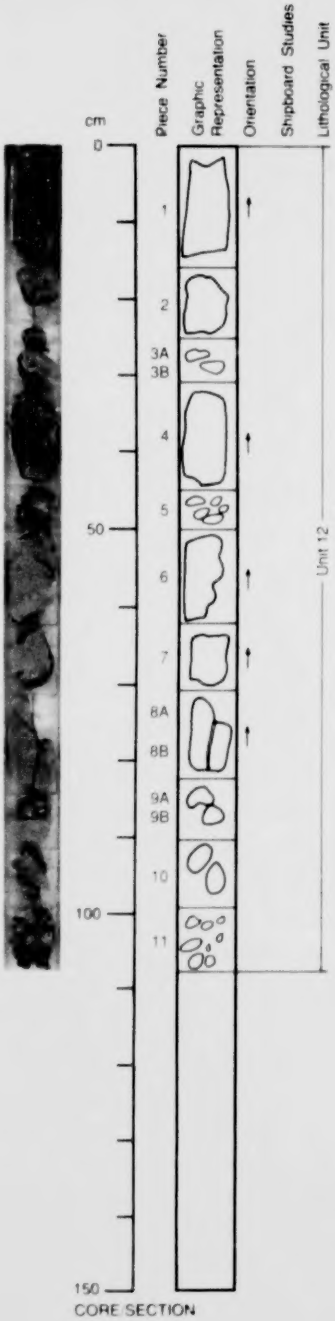
cm
Piece Number
Graphic Representation
Orientation
Shipboard Studies
Lithological Unit
0
50
100
150
1
2
3A
3B
4
5
6
7
8A
8B
9A
9B
10
11
Unit 12
CORE SECTION

126-793B-109R-3

UNIT 12: ANDESITE BRECCIA IN HYALOCLASTITIC MATRIX

Pieces 1-7, 9-11

CONTACTS: None internally visible within clasts.
PHENOCRYSTS: Clasts of 1 - 8 cm in size in a greenish gray to dark greenish gray matrix.
Plagioclase - ~5%, 0.5 mm, euhedral, fresh.
Clinopyroxene - 5%, 0.5-3.0 mm, euhedral, fresh.
Orthopyroxene - 2%, 0.5-1.0 mm, euhedral, altered.
GROUNDMASS: Altered, with plagioclase microlites, smectites, and celadonite. Matrix contains clasts of lava, altered glass shards and crystal fragments/phenocrysts.
VESICLES: 0-2%, filled with zeolites.
COLOR: Dark greenish gray.
ALTERATION: Groundmass altered to smectite and celadonite. Orthopyroxene altered to celadonite and smectite plus an iron oxide mineral (brown).
ADDITIONAL COMMENTS: About 20% of the clasts have broken chilled margins.

UNIT 12: BASALTIC ANDESITE CLAST

Pieces 8 (A & B)

CONTACTS: None.
PHENOCRYSTS:
Plagioclase - 1%, < 1.0 mm, lath.
Clinopyroxene - 1%, 1.0 mm, fresh, green.
Orthopyroxene - 3%, 1.0-3.0 mm, altered to Fe oxide and clay.
GROUNDMASS: Fine grained, < 0.2 mm plagioclase laths, microlites.
VESICLES: 3%, 4 mm, elongate, aligned, empty.
COLOR: Dusky yellow green.
STRUCTURE: None.
ALTERATION: Groundmass altered mostly to clays.
ADDITIONAL COMMENTS: Similar alteration to Core 126-793B-110R and lower in the section.

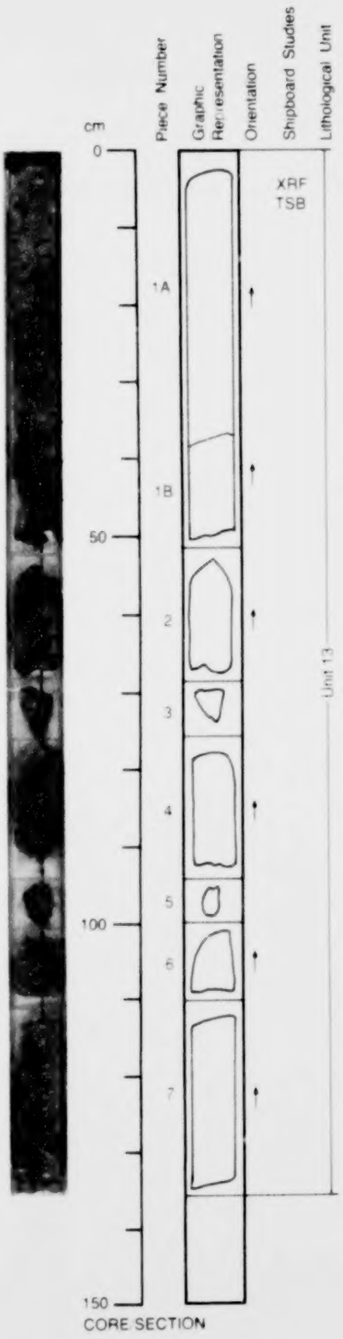
cm
Piece Number
Graphic Representation
Orientation
Shipboard Studies
Lithological Unit
0
50
100
150
1A
1B
2
3
4
5
6
7
XRF
TSB
Unit 13
CORE SECTION

126-793B-110R-1

UNIT 13: MASSIVE BASALTIC ANDESITE LAVA

Pieces 1-7

CONTACTS: None
PHENOCRYSTS:
Clinopyroxene - 10%, 0.3-10.0 mm, euhedral, generally fresh.
Orthopyroxene - 10%, 0.3-10.0 mm, euhedral, 80% altered.
GROUNDMASS: Fine-grained altered glass with plagioclase laths.
VESICLES: 1-5%, 0.2-5.0 mm, elongated, concentrated in certain zones. Mostly empty with smectite and celadonite lining on vesicle walls. Some zeolite filled.
COLOR: Medium bluish gray.
STRUCTURE: Massive lava flow.
ALTERATION: Orthopyroxene altered to a brown clay mineral. Native copper present in orthopyroxene pseudomorphs. Clinopyroxene 40% altered to smectite. Plagioclase laths are fresh. Alteration along cleavages and margins, but alteration from interior and out to surface is not uncommon.
VEINS/FRACTURES: Zeolite and smectite-filled veins (< 1 mm in size) are common.

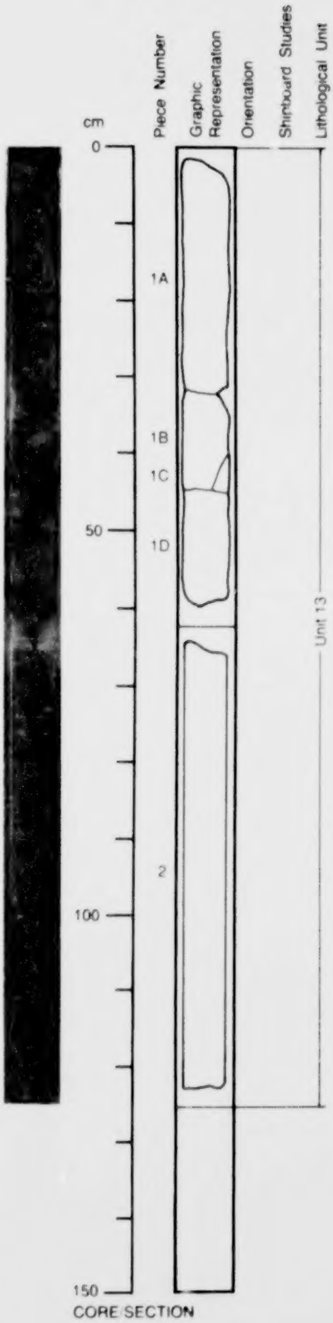
cm
Piece Number
Graphic Representation
Orientation
Shipboard Studies
Lithological Unit
0
50
100
150
1A
1B
1C
1D
2
Unit 13
CORE/SECTION

126-793B-110R-2

UNIT 13: MASSIVE BASALTIC ANDESITE LAVA

Pieces 1-2

CONTACTS: None
PHENOCRYSTS:
Clinopyroxene - 10%, 0.3-10.0 mm, euhedral, generally fresh.
Orthopyroxene - 10%, 0.3-10.0 mm, euhedral, 80% altered.
GROUNDMASS: Fine-grained altered glass with plagioclase laths.
VESICLES: 1-5%, 0.2-5.0 mm, elongated, concentrated in certain zones. Mostly empty with smectite and celadonite lining on vesicle walls. Some zeolite filled.
COLOR: Medium bluish gray.
STRUCTURE: Massive lava flow.
ALTERATION: Orthopyroxene altered to a brown clay mineral. Native copper present in orthopyroxene pseudomorphs. Clinopyroxene 40% altered to smectite. Plagioclase laths are fresh. Alteration along cleavages and margins, but alteration from interior and out to surfaces is not uncommon.
VEINS/FRACTURES: Zeolite and smectite-filled veins (< 1 mm in size) are common.

126-793B-110R-3

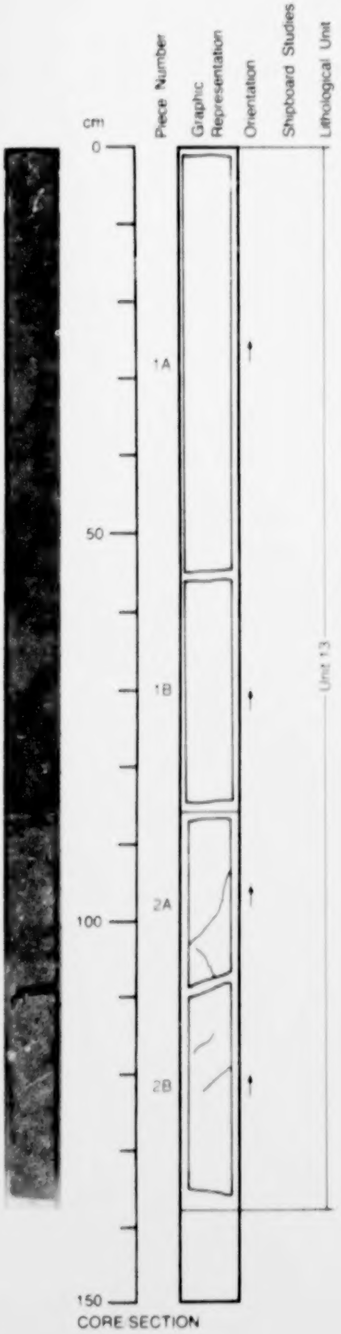
cm
0
50
100
150
Piece Number
Graphic Representation
Orientation
Shipboard Studies
Lithological Unit
1A
1B
2A
2B
Unit 13
CORE SECTION

UNIT 13: MASSIVE BASALTIC ANDESITE LAVA

Pieces 1-2

CONTACTS: None
PHENOCRYSTS:
Clinopyroxene - 10%; 0.3-10.0 mm; euhedral; generally fresh.
Orthopyroxene - 10%; 0.3-10.0 mm; euhedral; 80% altered.
GROUNDMASS: Fine-grained altered glass with plagioclase laths.
VESICLES: 1-5%; 0.2-5.0 mm; elongated; concentrated in certain zones. Mostly empty with smectite and celadonite lining on vesicle walls. Some zeolite filled.
COLOR: Medium bluish gray.
STRUCTURE: Massive lava flow.
ALTERATION: Othopyroxene altered to a brown clay mineral. Native copper present in orthopyroxene pseudomorphs. Clinopyroxene 40% altered to smectite. Plagioclase laths are fresh. Alteration along cleavages and margins, but alteration from interior and out to surfaces is not uncommon.
VEINS/FRACTURES: Zeolite and smectite filled veins (< 1 mm in size) are common. Zeolite veins in Piece 2 are less than 1 mm thick.

126-793B-110R-4

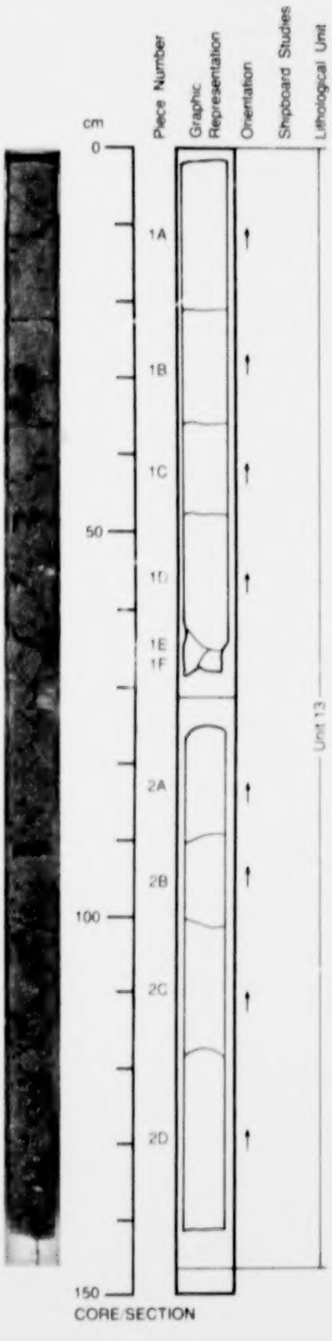
cm
Piece Number
Graphic Representation
Orientation
Shipboard Studies
Lithological Unit
0
50
100
150
1A
1B
1C
1D
1E
1F
2A
2B
2C
2D
Unit 13
CORE/SECTION

UNIT 13: MASSIVE BASALTIC ANDESITE LAVA

Pieces 1-2

CONTACTS: None.

PHENOCRYSTS: Phenocryst more altered towards the bottom of section through 126-793B-110R-05 Piece 6B.
Clinopyroxene - 10%, 0.3-10.0 mm, euhedral, generally fresh.
Orthopyroxene - 10%, 0.3-10.0 mm, euhedral, 80% altered.

GROUNDMASS: Fine-grained altered glass with plagioclase laths.

VESICLES: 1-5%, 0.2-5.0 mm, elongated, concentrated in certain zones. Mostly empty with smectite and celadonite lining on vesicle walls. Some zeolite filled.

COLOR: Brown, olive gray.

STRUCTURE: Massive lava flow.

ALTERATION: Orthopyroxene altered to brown clay mineral. Native copper present in orthopyroxene pseudomorphs. Clinopyroxene 40% altered to smectite. Plagioclase laths are fresh. Alteration along cleavages and margins, but alteration from interior and out to surfaces is uncommon.

VEINS/FRACTURES: Zeolite and smectite filled veins (< 1 mm in size) are common.

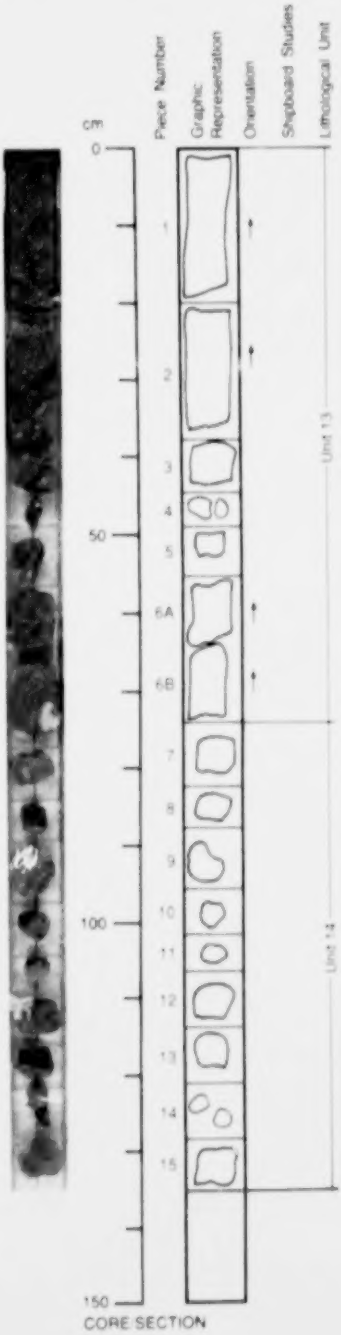

126-793B-110R-5

UNIT 13: MASSIVE BASALTIC ANDESITE LAVA

Pieces 1-3

CONTACTS: None
PHENOCRYSTS: Phenocrysts more altered towards the bottom of section
Clinopyroxene - 10%, 0.3-10.0 mm, euhedral, generally fresh
Orthopyroxene - 10%, 0.3-10.0 mm, euhedral, 80% altered
GROUNDMASS: Fine-grained altered glass with plagioclase laths
VESICLES: 1-5%, 0.2-5.0 mm, elongated, concentrated in certain zones. Mostly empty with smectite and celadonite lining on vesicle walls. Some zeolite filled.
COLOR: Brown, olive gray
STRUCTURE: Massive lava flow
ALTERATION: Orthopyroxene altered to brown clay mineral. Native copper present in orthopyroxene pseudomorphs. Clinopyroxene 40% altered to smectite. Plagioclase laths are fresh. Alteration along cleavages and margins, but alteration from interior and out to surfaces is not uncommon.
VEINS/FRACTURES: Zeolite and smectite filled veins (< 1 mm in size) are common.

UNIT 13: MASSIVE BASALTIC ANDESITE LAVA

Pieces 4-6B

CONTACTS: None
PHENOCRYSTS: Down section decrease in phenocryst abundance to Piece 6B.
Clinopyroxene - 3%, 0.3-10.0 mm, euhedral, generally fresh
Orthopyruxene - 3%, 0.3-10.0 mm, euhedral, 80% altered
GROUNDMASS: Fine-grained altered glass with plagioclase laths
VESICLES: 1-5%, 0.2-5.0 mm, elongated, concentrated in certain zones. Mostly empty with smectite and celadonite lining on vesicle walls. Some zeolite filled.
COLOR: Brown, olive gray
STRUCTURE: Massive lava flow
ALTERATION: Orthopyroxene altered to brown clay mineral. Native copper present in orthopyroxene pseudomorphs. Clinopyroxene 40% altered to smectite. Plagioclase laths are fresh. Alteration along cleavages and margins, but alteration from interior and out to surfaces is not uncommon.
VEINS/FRACTURES: Zeolite and smectite filled veins (< 1 mm common in size) are common.

UNIT 14: APHYRIC-SPARSELY PHYRIC BASALTIC ANDESITE

Pieces 7-15

CONTACTS: None, not present with overlying flow
PHENOCRYSTS: Phenocrysts are < 1% of total.
Plagioclase - < 0.5 mm, fresh
Clinopyroxene - 0.5 mm, fresh
Orthopyroxene - 0.3 mm, semi-fresh
GROUNDMASS: Trachytic alignment of feldspars, also some dark laths - quenched pyroxene?
VESICLES: 1-7%, elongate, sub-parallel alignment, in bands, open
COLOR: Light olivine gray
STRUCTURE: Bands of vesiculation
ALTERATION: Semi-alteration of rare orthopyroxene at margins.

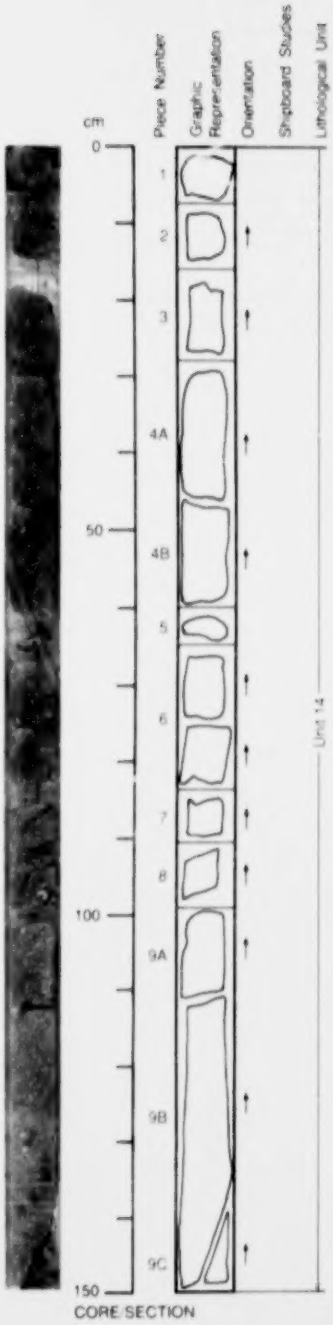
cm
Piece Number
Graphic Representation
Orientation
Shipboard Studies
Lithological Unit
0
50
100
150
1
2
3
4A
4B
5
6
7
8
9A
9B
9C
Unit 14
CORE/SECTION

126-793B-111R-1

UNIT 14: BASALTIC ANDESITE, SETTLED FLOW

Pieces 1-9

CONTACTS: None
PHENOCRYSTS: There is an increase in crystal density towards the base of the flow.
Pieces 1-3 contain 7-10% phenocrysts (upper section). Pieces 4-9 contain 15% phenocrysts. Settling of crystals within the flow.
Plagioclase - 2%, 0.5-1.0 mm, fresh, euhedral.
Clinopyroxene - 10%, 1.0-10.0 mm, fresh, some alteration, euhedral.
Orthopyroxene - 5%, 1.0-3.0 mm, fresh, euhedral.
GROUNDMASS: Fine-grained, plagioclase laths, not orientated, intersertal texture(?).
VESICLES: 0.5-2%, 1.0-3.0 mm, spherical to slightly elongate ; vesicles are open.
COLOR: Dusky yellowish green.
STRUCTURE: None.
ALTERATION: Some hydrothermal veining recognized by smectite-celadonite rich zones.
Orthopyroxene altered to smectite-celadonite-Fe oxides etc.
ADDITIONAL COMMENTS: Native copper present as small grains in oxidized crystals.

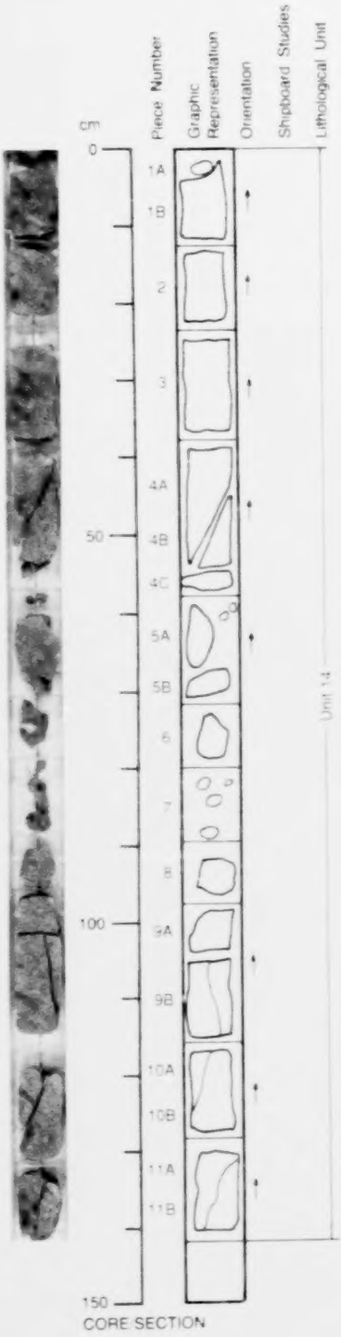
cm
Piece Number
Graphic Representation
Orientation
Shipboard Studies
Lithological Unit
0
50
100
150
1A
1B
2
3
4A
4B
4C
5A
5B
6
7
8
9A
9B
10A
10B
11A
11B
Unit 14
CORE SECTION

126-793B-111R-2

UNIT 14: BASALTIC ANDESITE, SETTLED FLOW

Pieces 1-11

CONTACTS: None
PHENOCRYSTS:
Plagioclase - 2%, 0.5-1.0 mm, fresh, euhedral
Clinopyroxene - 10%, 1.0-10.0 mm, fresh, some alteration, euhedral
Orthopyroxene - 5%, 1.0-3.0 mm, fresh, euhedral
GROUNDMASS: Fine-grained, plagioclase laths, not orientated, intersertal texture(?)
VESICLES: 0.5-2%, 1.0-3.0 mm, spherical to slightly elongate, vesicles are open
COLOR: Dusky yellowish green
STRUCTURE: None
ALTERATION: Some hydrothermal veining recognized by smectite-celadonite rich zones.
Orthopyroxene altered to smectite-celadonite-Fe oxides etc.
ADDITIONAL COMMENTS: Native copper present as small grains in oxidized crystals

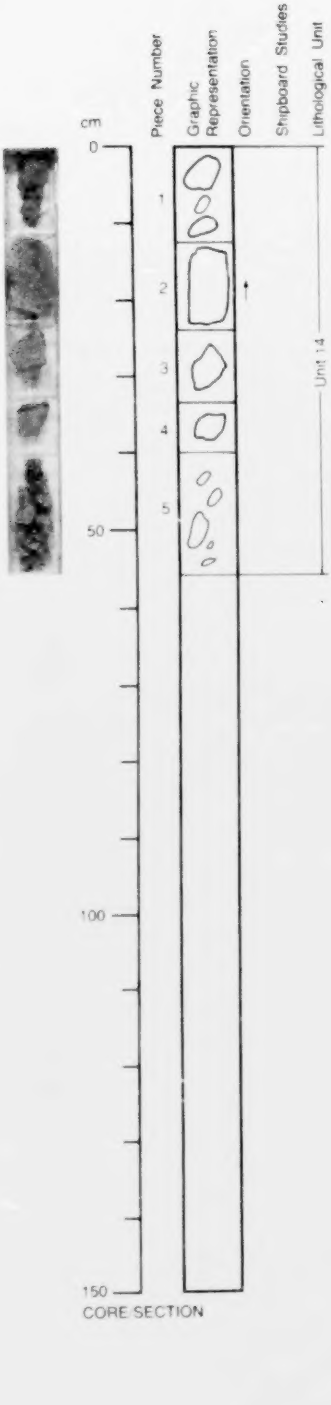
cm
Piece Number
Graphic Representation
Orientation
Shipboard Studies
Lithological Unit
0
50
100
150
1
2
3
4
5
Unit 14
CORE SECTION

126-793B-111R-3

UNIT 14: BASALTIC ANDESITE, SETTLED FLOW

Pieces 1-5

CONTACTS: None
PHENOCRYSTS:
Plagioclase - 2%, 0.5-1.0 mm, fresh, euhedral
Clinopyroxene - 10%, 1.0-10.0 mm, fresh, some alteration, euhedral
Orthopyroxene - 5%, 1.0-3.0 mm, fresh, euhedral
GROUNDMASS: Fine grained, plagioclase laths, not orientated, intersertal texture(?)
VESICLES: 0.5-2%, 1.0-3.0 mm, spherical to slightly elongate; vesicles are open
COLOR: Dusky yellowish green
STRUCTURE: None
ALTERATION: Some hydrothermal veining recognized by smectite-celadonite rich zones
Orthopyroxene altered to smectite-celadonite-Fe oxides etc
ADDITIONAL COMMENTS: Native copper present as small grains in oxidized crystals

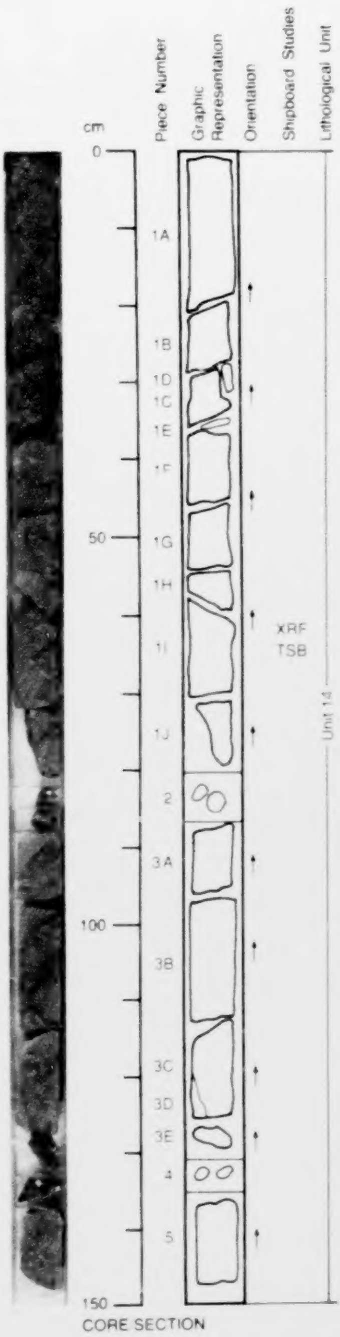
cm
Piece Number
Graphic Representation
Orientation
Shipboard Studies
Lithological Unit
0
50
100
150
1A
1B
1D
1C
1E
1F
1G
1H
1I
1J
2
3A
3B
3C
3D
3E
4
5
XRF
TSB
Unit 14
CORE SECTION

126-793B-112R-1

UNIT 14: PORPHYRITIC LAVA

Piece 1

CONTACTS: None.
PHENOCRYSTS: Phenocryst content decreases from about 20% in Piece 1A to 8% in Piece 1J.
- Plagioclase - 1-2%, 0.5 mm.
- Clinopyroxene - 5%, 1.0 mm.
- Orthopyroxene - 1-2%, 1.0 mm, rusty.

GROUNDMASS: Fine-grained, plagioclase laths, not orientated, intersertal texture(?).
VESICLES: ~2%, 1.0-3.0 mm; spherical to slightly elongate; vesicles are open.
COLOR: Dusky yellowish green.
STRUCTURE: None.
ALTERATION: Some hydrothermal veining recognized by smectite-celadonite rich zones. Orthopyroxene altered to smectite-celadonite-Fe oxides etc.
ADDITIONAL COMMENTS: Native copper present as small grains in oxidized crystals.

UNIT 14: SPARSELY-PHYRIC, NON-VESICULAR LAVA

Pieces 2-3A

PHENOCRYSTS:
- Plagioclase - 2%, 0.5 mm, fresh, euhedral.
- Clinopyroxene - 1%, 1.0-2.0 mm, fresh, euhedral.
- Orthopyroxene - 1%, Up to 1.0 mm, highly altered.

VESICLES: Non-vesicular.
ADDITIONAL COMMENTS: Piece 3A changes from sparsely phyric to 10% crystals (with 2-3 mm diameters) at 94 cm. Sharp contact with broken crystals.

UNIT 14: PORPHYRITIC LAVA

Pieces 3B-5

PHENOCRYSTS:
- Plagioclase - 1%, < 1.0 mm, euhedral, fresh.
- Clinopyroxene - 10%, 3.0-15.0 mm, euhedral, fresh.
- Orthopyroxene - 5%, 2.0-3.0 mm, euhedral, altered to smectite.

GROUNDMASS: Fairly holocrystalline.
VESICLES: 5%, 1 mm, elongate.
ADDITIONAL COMMENTS: Similar to Core 126-793B-111R.

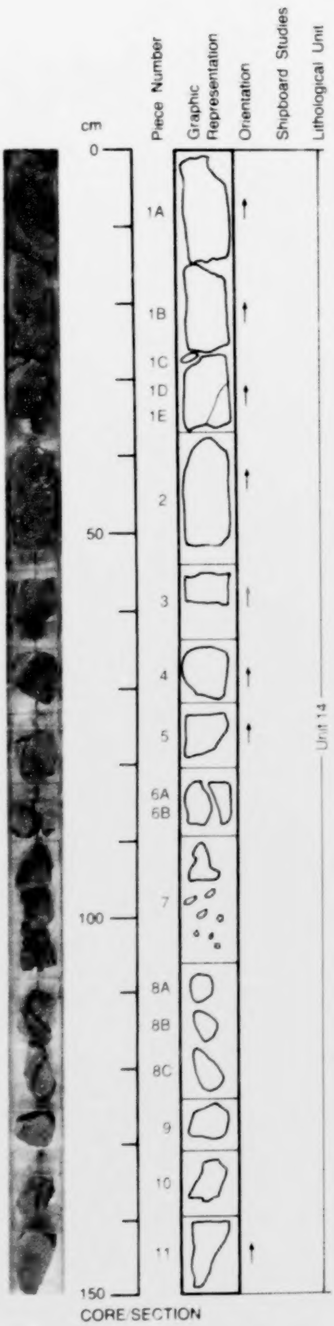
cm
Piece Number
Graphic Representation
Orientation
Shipboard Studies
Lithological Unit
0
50
100
150
1A
1B
1C
1D
1E
2
3
4
5
6A
6B
7
8A
8B
8C
9
10
11
Unit 14
CORE/SECTION

126-793B-112R-2

UNIT 14: PORPHYRITIC LAVA

Pieces 1-7

PHENOCRYSTS:
Plagioclase - 1%, < 1.0 mm, euhedral, fresh
Clinopyroxene - 10%, 3.0-15.0 mm, euhedral, fresh
Orthopyroxene - 5%, 2.0-3.0 mm, euhedral, altered to smectite
GROUNDMASS: Fairly holocrystalline
VESICLES: 5%, 1 mm, elongate
ADDITIONAL COMMENTS: Similar to Core 126-793B-111R

UNIT 14: SPARSELY-PHYRIC LAVA

Pieces 8-11

PHENOCRYSTS:
Plagioclase - 5%, 0.5 mm, long, fresh, euhedral
Clinopyroxene - 1%, 1.0-2.0 mm, fresh, euhedral
Orthopyroxene - < 1%, 1.0 mm, altered
GROUNDMASS: Looks fresh, intersertal
VESICLES: ~5%, up to 10 mm long and 1 mm wide, elongate

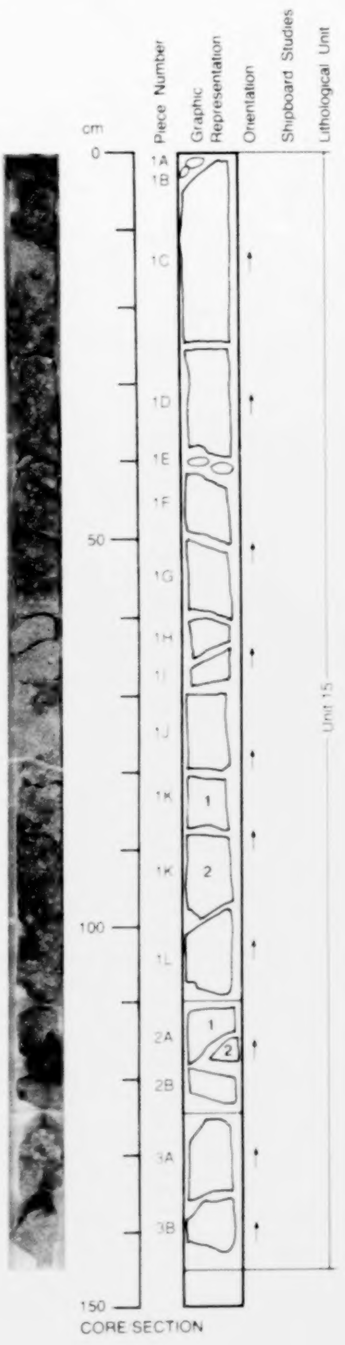
cm
Piece Number
Graphic Representation
Orientation
Shipboard Studies
Lithological Unit
0
50
100
150
1A
1B
1C
1D
1E
1F
1G
1H
1I
1J
1K
1
1K
2
1L
2A
1
2
2B
3A
3B
Unit 15
CORE SECTION

126-793B-113R-1

UNIT 15: HYALOCLASTITE BRECCIA

Pieces 1-3

PHENOCRYSTS:
Plagioclase - 1%, 0.5-1.0 mm, euhedral, fresh.
Clinopyroxene - 5%, 1.0-3.0 mm, euhedral, fresh.
Orthopyroxene - 1%, 0.5-1.5 mm, euhedral, altered.
GROUNDMASS: Trachytic feldspar laths. Matrix is altered glass shards, (1-10 mm in size), and crystals of pyroxene in smectite > zeolite cement. Medium bluish gray in color.
VESICLES: < 2%, smectite filled.
COLOR: Medium gray.
ADDITIONAL COMMENTS: Clasts 1-10 cm with chilled margins (good example at 58 cm).

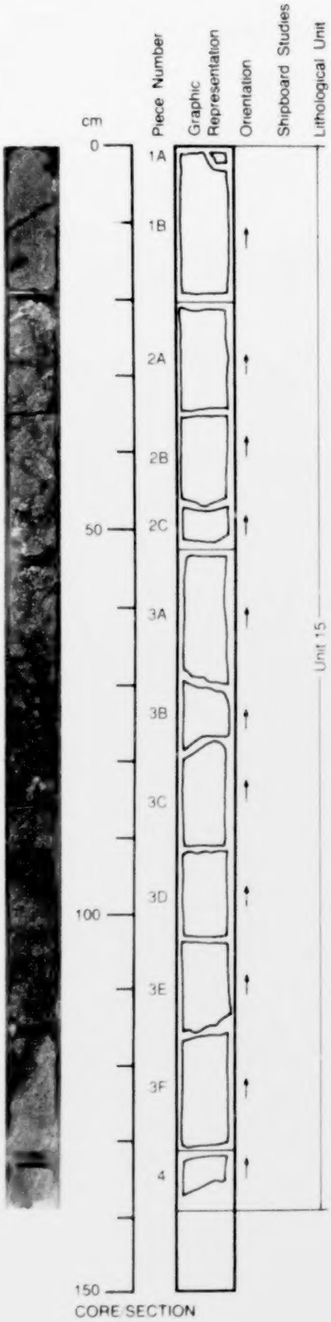
cm
Piece Number
Graphic Representation
Orientation
Shipboard Studies
Lithological Unit
0
50
100
150
1A
1B
2A
2B
2C
3A
3B
3C
3D
3E
3F
4
Unit 15
CORE/SECTION

126-793B-113R-2

UNIT 15: MASSIVE LAVA

Piece 1

CONTACTS: No contacts
PHENOCRYSTS:
Plagioclase - 5%; 0.5-1.0 mm; euhedral, fresh
Clinopyroxene - 8%; 2.5-5.0 mm; euhedral, fresh
Orthopyroxene - 5%; 0.5-1.0 mm; euhedral, fresh
GROUNDMASS: Intersertal, fresh
VESICLES: 3%; 0.5-1.0 mm; filled with smectite > zeolite > native copper

UNIT 15: HYALOCLASTITE BRECCIA

Pieces 2-3E

CONTACTS: No contacts
PHENOCRYSTS: Highly altered
Plagioclase - 5%; 0.5-1.0 mm
Clinopyroxene - 8%; 2.5-5.0 mm
Orthopyroxene - 5%; 0.5-1.0 mm
GROUNDMASS: Intersertal, highly altered. Matrix is zeolite dominated in Piece 2 and smectite dominated in Piece 3.
VESICLES: 3%; 0.5-1.0 mm; filled with smectite > zeolite > native copper
ADDITIONAL COMMENTS: Clasts are 1-6 cm in size. Highly altered version of Piece 1.

UNIT 15: HYALOCLASTITE BRECCIA

Pieces 3F-4

CONTACTS: No contacts
PHENOCRYSTS:
Plagioclase - 5%; 0.5-1.0 mm
Clinopyroxene - 8%; 2.5-5.0 mm
Orthopyroxene - 5%; 0.5-1.0 mm
GROUNDMASS: Intersertal
VESICLES: 3%; 0.5-1.0 mm; filled with smectite > zeolite > native copper
ADDITIONAL COMMENTS: Pieces 3F and 4 contain a 20 cm pillow Piece of same lava type but intermediate in freshness between Piece 1 and 2-3E.

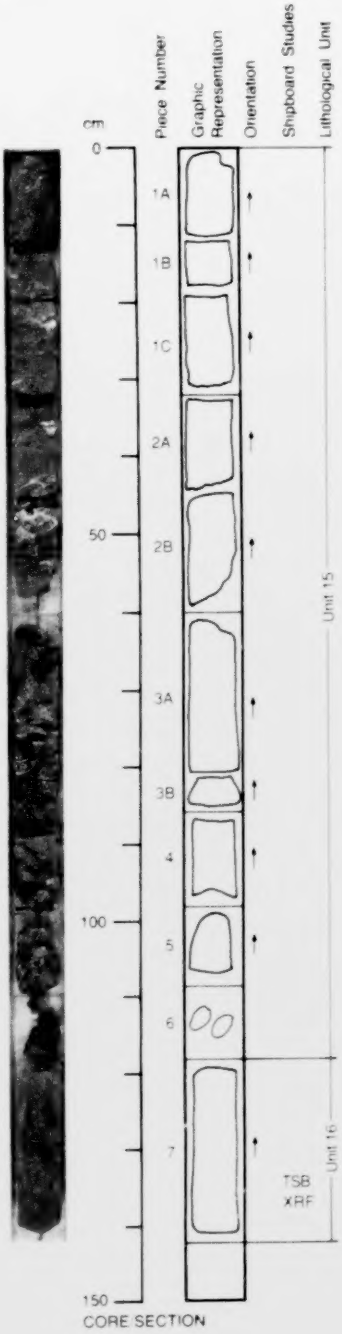
cm
Piece Number
Graphic Representation
Orientation
Shipboard Studies
Lithological Unit
0
50
100
150
1A
1B
1C
2A
2B
3A
3B
4
5
6
7
Unit 15
Unit 16
TSB
XRF
CORE SECTION

126-793B-113R-3

UNIT 15: HYALOCLASTITE BRECCIA

Pieces 1-6

CONTACTS: No contacts.
PHENOCRYSTS:
Plagioclase - 5%; 0.5-1.0 mm.
Clinopyroxene - 8%; 2.5-5.0 mm.
Orthopyroxene - 5%; 0.5-1.0 mm.
GROUNDMASS: Intersertal. Zeolite cement at 45-50 cm, but mostly smectite cement.
VESICLES: 3%; 0.5-1.0 mm; filled with smectite > zeolite > native copper.
ADDITIONAL COMMENTS: Mostly 10 cm-sized clasts (also at base of section 2) of porphyritic lava.

UNIT 16: APHYRIC LAVA

Piece 7

CONTACTS: No contacts.
PHENOCRYSTS:
Clinopyroxene - < 1%; 1.0 mm; partly altered to smectite.
GROUNDMASS: Groundmass is composed of felty feldspar laths and pyroxene.
VESICLES: 2%; 1-2 mm diameter; elongate; partly filled with smectite and native copper; glassy rims on vesicles.

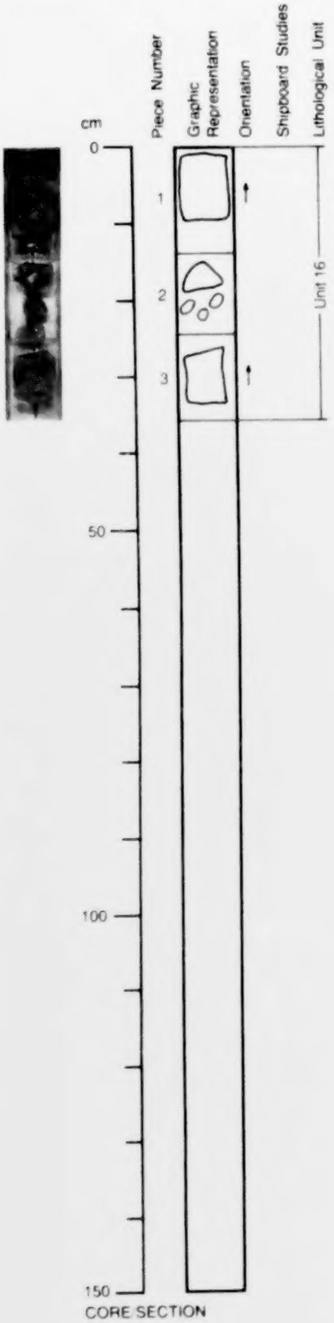
cm
Piece Number
Graphic Representation
Orientation
Shipboard Studies
Lithological Unit
0
1
2
3
Unit 16
50
100
150
CORE SECTION

126-793B-113R-4

UNIT 16: APHYRIC LAVA

CONTACTS: No contacts.
PHENOCRYSTS:
Clinopyroxene - < 1%; 1.0 mm; partly altered to smectite.
GROUNDMASS: Groundmass is composed of felty feldspar laths and pyroxene.
VESICLES: 2%; up to 10 mm; elongate; partly filled with smectite and native copper; glassy rims on vesicles.

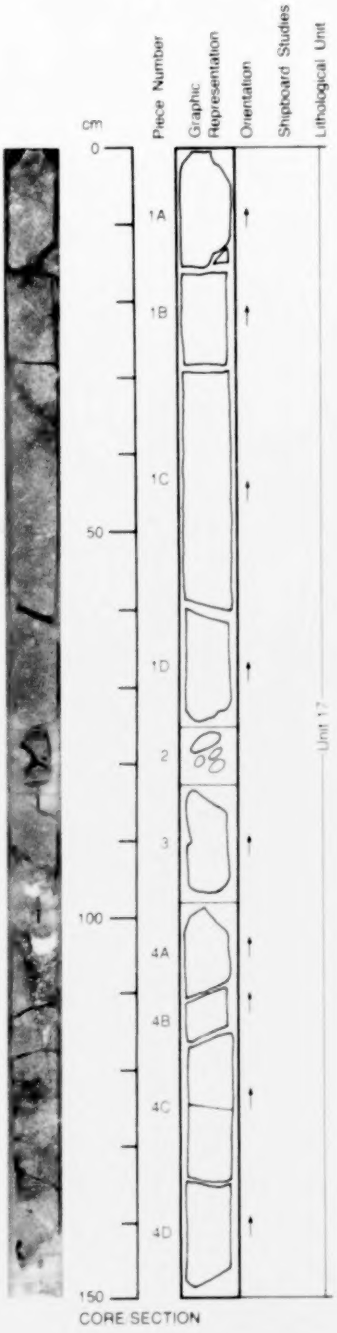
cm
Piece Number
Graphic Representation
Orientation
Shipboard Studies
Lithological Unit
0
50
100
150
1A
1B
1C
1D
2
3
4A
4B
4C
4D
Unit 17
CORE SECTION

126-793B-114R-1

UNIT 17: HYALOCLASTITE BRECCIA

Pieces 1-4

CONTACTS: Clasts are 1-10 cm in diameter. Pieces 1C and 1D contain one pillow Piece greater than 40 cm in diameter. Next lower contact is in Piece 3. Pieces 4A-4C contain one pillow Piece 20 cm in diameter.

PHENOCRYSTS: Most clasts are from 0-130 cm in size. Clast at bottom of Piece 4D is more typical of clasts in Unit 15 (Core 126-793B-113) with clinopyroxene >/= orthopyroxene > plagioclase.

Plagioclase - 5%, 1-2 mm, fresh, euhedral.

Clinopyroxene - 2-5%, 1-6 mm, altered, euhedral.

Orthopyroxene - 1-2%, < 0.5 mm, very altered.

GROUNDMASS: Quite fresh. Matrix is composed of glass shards, pyroxene and plagioclase crystals with smectite and zeolite cement. Color is darkgreenish gray.

VESICLES: 1%, 1 mm, zeolite and smectite filling.

COLOR: Medium gray.

ADDITIONAL COMMENTS: Coarse, heterolithic.

126-793B-114R-2

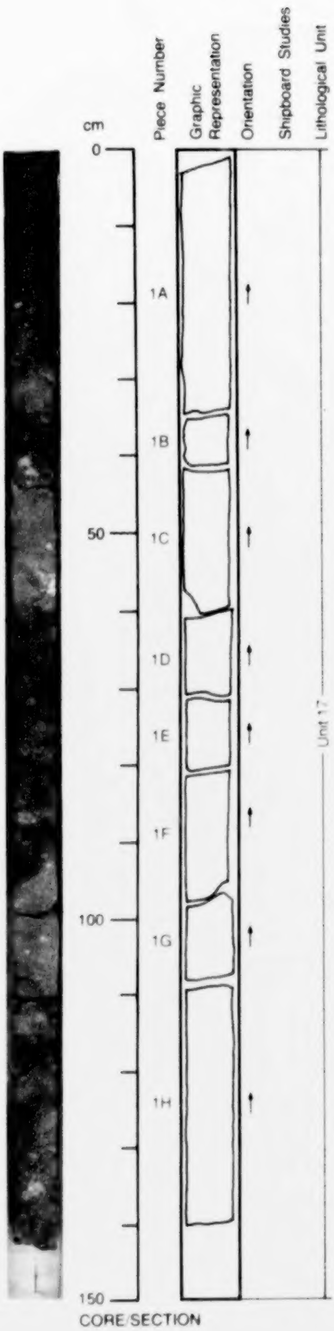
cm
Piece Number
Graphic Representation
Orientation
Shipboard Studies
Lithological Unit
0
50
100
150
1A
1B
1C
1D
1E
1F
1G
1H
Unit 17
CORE/SECTION

UNIT 17: HYALOCLASTITE BRECCIA

Piece 1

CONTACTS: Clasts are 1-4 cm, with two ~20 cm in diameter at 40-60 and 88-108 cm.
PHENOCRYSTS: All clasts are clinopyroxene > orthopyroxene >/= plagioclase, similar to those at the base of Section 126-793B-114R-1.
Plagioclase - 2%; 0.5 mm; fresh, euhedral.
Clinopyroxene - 5%; 1-6 mm; euhedral, fresh.
Orthopyroxene - 2%; 1.0 mm; fresh and altered.
GROUNDMASS: Quite fresh. Matrix is a hyaloclastite.
VESICLES: 2%; 1 mm; filled with smectite greater than zeolite.
COLOR: Medium gray.

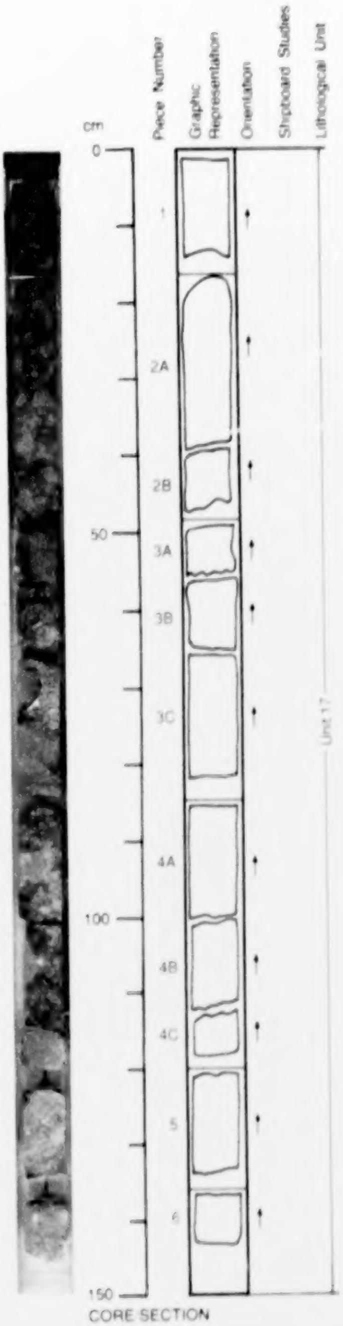
cm
Piece Number
Graphic Representation
Orientation
Shipboard Studies
Lithological Unit
0
50
100
150
1
2A
2B
3A
3B
3C
4A
4B
4C
5
6
Unit 17
CORE SECTION

126-793B-114R-3

UNIT 17: HYALOCLASTITE BRECCIA

Pieces 1-6

PHENOCRYSTS: All clasts are clinopyroxene >> orthopyroxene >> plagioclase, similar to those at the base of Section 126-793B-114R-1. Clasts are 1-8 cm in diameter, and largest in Pieces 3C and 4C-5.

Plagioclase - 2%, 0.5 mm, fresh, euhedral.

Clinopyroxene - 5%, 1-6 mm, euhedral, fresh.

Orthopyroxene - 2%, 1.0 mm, fresh and altered.

GROUNDMASS: Quite fresh. Matrix of glass, pillow shards and crystals in smectite, zeolite and native copper cement.

VESICLES: 2%, 1 mm, filled with smectite greater than zeolite.

COLOR: Medium gray.

ADDITIONAL COMMENTS: Similar to Sections 126-793B-114R-1 and 2.

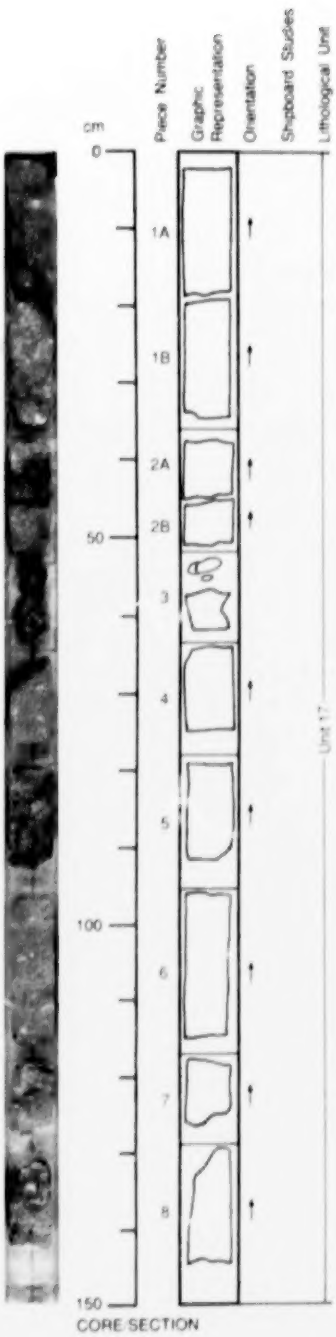
cm
Piece Number
Graphic Representation
Orientation
Shipboard Studies
Lithological Unit
0
50
100
150
1A
1B
2A
2B
3
4
5
6
7
8
Unit 17
CORE SECTION

126-793B-114R-4

UNIT 17: HYALOCLASTITE BRECCIA

Pieces 1-7

PHENOCRYSTS: All clasts are clinopyroxene >> orthopyroxene >= plagioclase, similar to those at the base of section 1. Clasts are typically 1-5 cm in size, but 15 cm in Piece 1, and 18 cm in Piece 6.

Plagioclase - 2%, 0.5 mm, fresh, euhedral.
Clinopyroxene - 5%, 1-6 mm, euhedral, fresh.
Orthopyroxene - 2%, 1.0 mm, fresh and altered.

GROUNDMASS: Quite fresh. Matrix of glass, pillow shards and crystals in smectite, zeolite, and native copper cement.

VESICLES:2%, 1 mm, filled with smectite greater than zeolite.

COLOR: Medium gray.

ADDITIONAL COMMENTS: Similar to Sections 126-793B-114R-1 and 2.

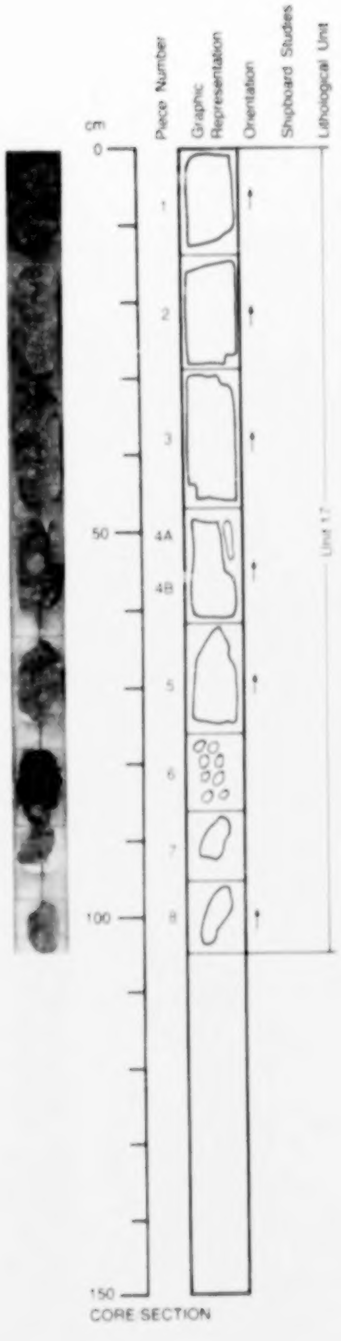
cm
Piece Number
Graphic Representation
Orientation
Shipboard Studies
Lithological Unit
0
50
100
150
1
2
3
4A
4B
5
6
7
8
Unit 17
CORE SECTION

126-793B-114R-5

UNIT 17: HYALOCLASTITE BRECCIA

Pieces 1-8

PHENOCRYSTS: All clasts are clinopyroxene >> orthopyroxene >> plagioclase, similar to those at the base of Section 126-793B-114R-1. Clasts are typically 1-8 cm in diameter.
Plagioclase - 2%, 0.5 mm, fresh, euhedral.
Clinopyroxene - 5%, 1-6 mm, euhedral, fresh.
Orthopyroxene - 2%, 1.0 mm, fresh and altered.
GROUNDMASS: Quite fresh. Matrix of glass, pillow shards and crystals in smectite, zeolite and native copper cement.
VESICLES: 2%, 1 mm, filled with smectite greater than zeolite.
COLOR: Medium gray.
ADDITIONAL COMMENTS: Similar to Sections 126-793B-114R-1 and 2. Piece 6 is drilling hash. Pieces 7 and 8 are isolated clasts of the same lava type.

126-793B-[illegible] (Piece 5,102-104 cm) OBSERVER: TOR WHERE SAMPLED: Unit 7

ROCK NAME: Plagioclase-clinopyroxene-olivine diabase

GRAIN SIZE: Medium

TEXTURE: Subophitic-intersertal

PRIMARY MINERALOGY	PERCENT PRESENT	PERCENT ORIGINAL	SIZE (mm)	COMPO-SITION	MORPHOLOGY	COMMENTS
PHENOCRYSTS						
Olivine	[illegible]	2.9	N/A		N/A	
Plagioclase	41	41	N/A		N/A	
Clinopyroxene	18.3	18.3	N/A		N/A	
Oxes	4.2	4.2	N/A		N/A	
GROUNDMASS						
Glass	[illegible]	33.6	N/A		N/A	

SECONDARY MINERALOGY	PERCENT	REPLACING/ FILLING	COMMENTS
Clays	36.5	Olivine and glass	

VESICLES/ CAVITIES	PERCENT	LOCATION	SIZE (mm)	FILLING	SHAPE
Vesicles	5				

COMMENTS: Point counting of described thin section.

126-793B-[illegible] (Piece 5,102-104 cm) OBSERVER: LTP WHERE SAMPLED:

ROCK NAME: Olivine-clinopyroxene diabase

GRAIN SIZE: Medium

TEXTURE: Intersertal-intergranular

PRIMARY MINERALOGY	PERCENT PRESENT	PERCENT ORIGINAL	SIZE (mm)	COMPO-SITION	MORPHOLOGY	COMMENTS
PHENOCRYSTS						
Olivine	2	1	2		Subeuhedral	Altered to smectites.
Plagioclase	40	40	0.1-1		Subhedral	Fresh; intersertal texture.
Clinopyroxene	20	20	0.1-0.5		Subeuhedral	Fresh; intersertal texture.
Opaques	5	5	0.05-0.1		Subhedral	
Orthopyroxene	<0.5	<0.5	0.2		Subhedral	Fresh, minor groundmass phase.
GROUNDMASS						
Glass	30	N/A	N/A		10%	Smectites replacing probably glass. Plagioclase and clinopyroxene in dark band.

SECONDARY MINERALOGY	PERCENT	REPLACING/ FILLING	COMMENTS
Clays			Smectites filling up vesicles or replacing glass.
Smectites			Intersertal, in between the plagioclase laths.

VESICLES/ CAVITIES	PERCENT	LOCATION	SIZE (mm)	FILLING	SHAPE
Vesicles	15	Random	1-4	Smectites	Rounded or polygonal

COMMENTS: Darker bands or inclusions are formed of the same rocks but finer grained and the groundmass was more rich in glass, now transformed to smectites. Minerals like feldspars and clinopyroxene are quenched. Vesicles are more abundant, bigger and lined by smectites. Around the vesicles, the groundmass is formed of glass now recrystallized to brown opaque material with few small feldspars microlites formed during devitrification. The darker color is due to smectites replacing the glass.

126-793B-[illegible] (Piece [illegible]) OBSERVER: [illegible] WHERE SAMPLED: Unit [illegible], middle

ROCK NAME: Plagioclase-clinopyroxene-olivine-diabase

GRAIN SIZE: Fine

TEXTURE: Porphyritic-intersertal

PRIMARY MINERALOGY	PERCENT PRESENT	PERCENT ORIGINAL	SIZE (mm)	COMPO-SITION	MORPHOLOGY	COMMENTS
PHENOCRYSTS						
Olivine	[illegible]	[illegible]	[illegible]		Euhedral	Altered to smectite.
Plagioclase	[illegible]	[illegible]	[illegible]		Subhedral	
Clinopyroxene	20	20	[illegible]		Subhedral	Glomeroporphyritic clots with orthopyroxene.
Opaques	[illegible]	[illegible]	[illegible]		N/A	
Orthopyroxene	[illegible]	[illegible]	[illegible]		Subhedral	
GROUNDMASS						
Glass	[illegible]	[illegible]	N/A		N/A	Altered to smectite.

SECONDARY MINERALOGY	PERCENT	REPLACING/FILLING	COMMENTS
Clays	[illegible]	Olivine, orthopyroxene, glass	
Carbonate	Tr	Olivine	

VESICLES/CAVITIES	PERCENT	LOCATION	SIZE (mm)	FILLING	SHAPE
Vesicles	0				

COMMENTS: Clinopyroxene has simple twinning.

126-793B-[illegible] (Piece [illegible]) OBSERVER: [illegible] WHERE SAMPLED: Chilled margin of the sill.

ROCK NAME: Olivine-clinopyroxene-orthopyroxene basalt

GRAIN SIZE: Fine

TEXTURE: Porphyritic

PRIMARY MINERALOGY	PERCENT PRESENT	PERCENT ORIGINAL	SIZE (mm)	COMPO-SITION	MORPHOLOGY	COMMENTS
PHENOCRYSTS						
Olivine	N/A	[illegible]	[illegible]		Sub-euhedral	Altered to calcite and smectites.
Plagioclase	N/A	[illegible]	[illegible]		Euhedral	[illegible]
Clinopyroxene	N/A	[illegible]	[illegible]		Euhedral	Zoned, twinned + [illegible] lamellae. Often clustered with olivine.
Orthopyroxene	N/A	[illegible]	[illegible]		Sub-euhedral	Clustered with clinopyroxene and olivine.
GROUNDMASS						
Plagioclase	N/A	N/A	[illegible]		N/A	Quenched mineral crystallites
Clinopyroxene	N/A	N/A	[illegible]		N/A	Microcrystalline

SECONDARY MINERALOGY	PERCENT	REPLACING/FILLING	COMMENTS
Clays			Replaced olivine
Carbonate			Calcite, replaced olivine

VESICLES/CAVITIES	PERCENT	LOCATION	SIZE (mm)	FILLING	SHAPE
Vesicles	[illegible]		[illegible]	Smectite	Rounded

COMMENTS: Glomeroporphyritic aggregates suggesting [illegible] with olivine + clinopyroxene + orthopyroxene. Plagioclase may be an inclusion or small laths in orthopyroxene. Glass is [illegible] in between the phenocrysts [illegible].

126-793B-28R-1 OBSERVER: TOR WHERE SAMPLED:

ROCK NAME: Plagioclase-clinopyroxene-basalt

GRAIN SIZE: Fine

TEXTURE: Vesicular-porphyritic-intersertal

PRIMARY MINERALOGY	PERCENT PRESENT	PERCENT ORIGINAL	SIZE (mm)	COMPO-SITION	MORPHOLOGY	COMMENTS
PHENOCRYSTS						
Plagioclase	5	5	0.5-2		Euhedral	Glomeroporphyritic clots, fresh.
Clinopyroxene	1	1	0.2-1		Euhedral	Fresh.
GROUNDMASS						
Glass	N/A	N/A	N/A		N/A	Devitrified.
Plagioclase	N/A	N/A	<0.2		Laths	
Clinopyroxene	N/A	N/A	<0.1		N/A	

VESICLES/ CAVITIES	PERCENT	LOCATION	SIZE (mm)	FILLING	SHAPE
Vesicles	25	Random	0.2-4	None	Rounded-elongated

COMMENTS: The plagioclase phenocrysts do not contain any fluid inclusions. The plagioclase laths show alignment around vesicles and phenocrysts ([illegible] texture). Groundmass is 95%. No top or bottom interval on piece # 3 cm.

126-793B-108R-[illegible] (129-131 cm) OBSERVER: LTP WHERE SAMPLED:

ROCK NAME: Clinopyroxene-orthopyroxene-plagioclase andesite

GRAIN SIZE: Fine

TEXTURE: Porphyritic

PRIMARY MINERALOGY	PERCENT PRESENT	PERCENT ORIGINAL	SIZE (mm)	COMPO-SITION	MORPHOLOGY	COMMENTS
PHENOCRYSTS						
Plagioclase	N/A	[illegible]	[illegible]		Euhedral	Clustered in glomeroporphyritic aggregates, zoned.
Clinopyroxene	N/A	10	[illegible]		Subhedral	Fresh, zoned, partly corroded.
Orthopyroxene	[illegible]	N/A	[illegible]		Euhedral	Altered in smectites and or zeolites.
GROUNDMASS						
Plagioclase	N/A	N/A	0.1		[illegible]	Groundmass altered in a brown-opaque material.

SECONDARY MINERALOGY	PERCENT	REPLACING/ FILLING	COMMENTS
Clays			Replacing orthopyroxene.
Zeolites			Replacing orthopyroxene-partly plagioclase-filling up vesicles.

VESICLES/ CAVITIES	PERCENT	LOCATION	SIZE (mm)	FILLING	SHAPE
Vesicles	2		[illegible]	Zeolites	Lobate

COMMENTS: Clast in a conglomerate. Isolated clinopyroxene crystals sometimes clustered with orthopyroxene, never with plagioclase. Orthopyroxene altered in smectite and/or zeolites. Plagioclase beginning to be replaced by zeolites. No piece # given.

126-793B-[illegible] (125-128 cm)   OBSERVER: LTP   WHERE SAMPLED:

ROCK NAME: Clinopyroxene-orthopyroxene-plagioclase andesite

GRAIN SIZE:

TEXTURE: Porphyritic

PRIMARY MINERALOGY	PERCENT PRESENT	PERCENT ORIGINAL	SIZE (mm)	COMPO-SITION	MORPHOLOGY	COMMENTS
PHENOCRYSTS						
Plagioclase	~15	N/A	<1		Euhedral	Altered to smectites and zeolite.
Clinopyroxene	2	N/A	<0.5		N/A	Fresh. Includes opaques.
Orthopyroxene	<1	N/A	0.5		N/A	Replaced by smectite/zeolite.
GROUNDMASS						
N/A	N/A	N/A	N/A		N/A	Groundmass: Replaced by opaque, reddish material.

VESICLES/CAVITIES	PERCENT	LOCATION	SIZE (mm)	FILLING	SHAPE
Vesicles	0				

COMMENTS: Clasts of clinopyroxene-orthopyroxene plagioclase. Andesitic clasts are clinopyroxene-orthopyroxene-plagioclase. Zeolite cement. No piece # given. Groundmass is N/A.

126-793B-[illegible] cm)   OBSERVER: LTP   WHERE SAMPLED:

ROCK NAME: Hornblende-dacitic crystal tuff

GRAIN SIZE:

TEXTURE:

PRIMARY MINERALOGY	PERCENT PRESENT	PERCENT ORIGINAL	SIZE (mm)	COMPO-SITION	MORPHOLOGY	COMMENTS
PHENOCRYSTS						
Plagioclase	N/A	N/A	N/A		N/A	Fresh. Oscillatory zoned.
Clinopyroxene	N/A	N/A	N/A		N/A	Fresh.
Opaques	N/A	N/A	N/A		N/A	Included in clinopyroxene and hornblende.
Hornblende	N/A	N/A	N/A		N/A	Fresh.
Quartz	N/A	N/A	N/A		Subhedral	Embayed.
GROUNDMASS						
N/A	N/A	N/A	N/A		N/A	

VESICLES/CAVITIES	PERCENT	LOCATION	SIZE (mm)	FILLING	SHAPE
Vesicles	0				

COMMENTS: Crystal tuff of hornblende-quartz dacite. No piece # given.

126-793B-56R-02 (Piece 1,75-76 cm) OBSERVER: LTF WHERE SAMPLED:

ROCK NAME: Clinopyroxene-plagioclase andesite

GRAIN SIZE: Fine

TEXTURE: Porphyritic/flow aligned

PRIMARY MINERALOGY	PERCENT PRESENT	PERCENT ORIGINAL	SIZE (mm)	COMPO-SITION	MORPHOLOGY	COMMENTS
PHENOCRYSTS						
Plagioclase	5	N/A	0.5		Euhedral	Altered to smectite and zeolite.
Clinopyroxene	5	N/A	</=1		Euhedral	Fresh.
GROUNDMASS						
N/A	N/A	N/A	N/A		N/A	Groundmass altered to brown opaque iron stained material.

SECONDARY MINERALOGY	PERCENT	REPLACING/ FILLING	COMMENTS
Clays			Smectite/filling up vesicles.
Zeolites			Replacing plagioclase/filling vesicles.

VESICLES/ CAVITIES	PERCENT	LOCATION	SIZE (mm)	FILLING	SHAPE
Vesicles	20		</=0.2	Smectite, zeolite	Lobate, flattened

COMMENTS: Clasts in a sandstone/conglomerate. Some andesitic clasts look fresher with glass still present, more porphyritic and with a fluidal texture. Clinopyroxene-plagioclase clots. Zeolite cement. Groundmass is 70%.

126-793B-56R-02 (85-86 cm) OBSERVER: LTF WHERE SAMPLED:

ROCK NAME: Clinopyroxene-orthopyroxene-plagioclase andesite

GRAIN SIZE: Fine

TEXTURE: Porphyritic/flow aligned

PRIMARY MINERALOGY	PERCENT PRESENT	PERCENT ORIGINAL	SIZE (mm)	COMPO-SITION	MORPHOLOGY	COMMENTS
PHENOCRYSTS						
Plagioclase	N/A	15	0.7		Euhedral	Fresh-zoned/flow aligned.
Clinopyroxene	N/A	3	0.7		Euhedral	Fresh/clustered with orthopyroxene.
Orthopyroxene	N/A	2	0.5		Euhedral	Sometimes fresh/replaced.
GROUNDMASS						
N/A	N/A	N/A	N/A		N/A	Groundmass replaced by an opaque/brown material (iron stained).

VESICLES/ CAVITIES	PERCENT	LOCATION	SIZE (mm)	FILLING	SHAPE
Vesicles	2		0.2	Smectite	Rounded

COMMENTS: Other clasts altered intersertal quenched basalt (uncommon). The other clasts are clinopyroxene-orthopyroxene-plagioclase andesite. Clinopyroxene-plagioclase crystals or clots. Zeolite cement. Very similar to sample 126-793B-83R-02, 39-40cm. No piece # given.

[illegible] OBSERVER: [illegible] WHERE SAMPLED:

ROCK NAME: Clinopyroxene-orthopyroxene-plagioclase andesite

GRAIN SIZE: Fine

TEXTURE: Porphyritic

PRIMARY MINERALOGY	PERCENT PRESENT	PERCENT ORIGINAL	SIZE (mm)	COMPO-SITION	MORPHOLOGY	COMMENTS
PHENOCRYSTS						
Plagioclase	[illegible]	N/A	[illegible]		Euhedral-subhedral	Isolated to clustered with clinopyroxene and orthopyroxene beginning to alter
Clinopyroxene	[illegible]	N/A	[illegible]		Euhedral	Zoned-isolated or clustered with orthopyroxene
Oxides	N/A	[illegible]	N/A		N/A	
Orthopyroxene	N/A	[illegible]	[illegible]		Euhedral	Altered to Fe-oxides and smectites. Clustered with clinopyroxene and plagioclase
GROUNDMASS						
Plagioclase	N/A	[illegible]	N/A		N/A	Microphenocrysts
Clinopyroxene	N/A	[illegible]	N/A		N/A	Microphenocrysts

SECONDARY MINERALOGY	PERCENT	REPLACING-FILLING	COMMENTS
Clays			Replacing orthopyroxene and glass

VESICLES/CAVITIES	PERCENT	LOCATION	SIZE (mm)	FILLING	SHAPE
Vesicles	[illegible]				

COMMENTS: Clast in a volcaniclastic sediment. [illegible] clinopyroxene crystals. Cement is smectite. The order of appearance in the glomeroporphyritic clots are orthopyroxene, plagioclase, clinopyroxene, oxides. No piece # given. [illegible] of groundmass altered to smectites.

[illegible] OBSERVER: [illegible] WHERE SAMPLED: In a sedimentary unit

ROCK NAME: Clinopyroxene-orthopyroxene-plagioclase andesite

GRAIN SIZE:

TEXTURE:

PRIMARY MINERALOGY	PERCENT PRESENT	PERCENT ORIGINAL	SIZE (mm)	COMPO-SITION	MORPHOLOGY	COMMENTS
PHENOCRYSTS						
Plagioclase	[illegible]	N/A	[illegible]		N/A	Partly altered-zoned (zeolites?)
Clinopyroxene	N/A	[illegible]	[illegible]		Euhedral	Zoned-very fresh
Oxides	N/A	[illegible]	[illegible]		Euhedral	
Orthopyroxene	[illegible]	N/A	[illegible]		Euhedral	Mantled by clinopyroxene-altered to smectite (some are preserved)
GROUNDMASS						
N/A	N/A	N/A	N/A		N/A	Altered groundmass rather rich in glass; now replaced by smectites.

VESICLES/CAVITIES	PERCENT	LOCATION	SIZE (mm)	FILLING	SHAPE
Vesicles	[illegible]				

COMMENTS: Very similar to sample [illegible], but main differences: (1) less porphyritic, (2) clinopyroxene + orthopyroxene clustered but no plagioclase present. Seems less differentiated than sample [illegible]. No piece # given. Groundmass is [illegible].

126-793B-84R-01 (75-78 cm) OBSERVER: REX WHERE SAMPLED: As clast in breccia

ROCK NAME: Clinopyroxene-phyric basalt-andesite

GRAIN SIZE: Fine (1 mm phenocrysts)

TEXTURE: Porphyritic

PRIMARY MINERALOGY	PERCENT PRESENT	PERCENT ORIGINAL	SIZE (mm)	COMPO-SITION	MORPHOLOGY	COMMENTS
PHENOCRYSTS						
Plagioclase	0	0	N/A		N/A	May not be any-possibly clinopyroxene phyric.
Clinopyroxene	7	7	0.2-1		Subhedral-euhedral	Fresh.
Oxide	<1	<1	0.2		Anhedral	
GROUNDMASS						
Glass	0	93	N/A		N/A	Completely replaced by clays and cristobalite.

SECONDARY MINERALOGY	PERCENT	REPLACING/ FILLING	COMMENTS
Clays	47	Replacing	Groundmass glass.
Cristobalite	45	Replacing	Groundmass glass (+ feldspar?).

VESICLES/ CAVITIES	PERCENT	LOCATION	SIZE (mm)	FILLING	SHAPE
Vesicles	0				

COMMENTS: Clast is dominantly clinopyroxene phyric. Matrix to whole breccia contains clinopyroxene, altered orthopyroxene, and replaced plagioclase. Clinopyroxene looks pale green in PPL. Na or Cr? in clinopyroxene? Plagioclase replaced by isotropic mineral, (zeolite of some kind?). No piece # given.

126-793B-84R-02 (39-40 cm) OBSERVER: LTY WHERE SAMPLED:

ROCK NAME: Clinopyroxene-orthopyroxene-plagioclase andesite

GRAIN SIZE: Fine

TEXTURE: Porphyritic/flow aligned

PRIMARY MINERALOGY	PERCENT PRESENT	PERCENT ORIGINAL	SIZE (mm)	COMPO-SITION	MORPHOLOGY	COMMENTS
PHENOCRYSTS						
Plagioclase	35	N/A	<2		Euhedral	Altered to smectites/zeolites/calcite.
Clinopyroxene	N/A	10	1		Euhedral	Fresh, includes opaques.
Opaques	N/A	1	0.1		Subhedral	Early crystallizing phase present in inclusions and also in the groundmass.
Quartz	N/A	Tr	0.1		Subhedral	Rounded.
Orthopyroxene	5	N/A	0.5		N/A	Altered to smectite.
GROUNDMASS						
N/A	N/A	N/A	N/A		N/A	49% groundmass is altered to smectites.

SECONDARY MINERALOGY	PERCENT	REPLACING/ FILLING	COMMENTS
Clays			Groundmass/replacing plagioclase and orthopyroxene.
Zeolites			Filling vesicles/replacing plagioclase.

VESICLES/ CAVITIES	PERCENT	LOCATION	SIZE (mm)	FILLING	SHAPE	COMMENTS
Vesicles	3		<<0.1		Lobate or flattened	Filled with zeolites/smectites.

COMMENTS: Very similar to 126-793B-85R-03, 19-25 cm but much more altered. Looks like basement at Hole 792E. No piece # given.

[illegible] OBSERVER: [illegible] WHERE SAMPLED:

ROCK NAME: Orthopyroxene-clinopyroxene-plagioclase andesite

GRAIN SIZE: Fine

TEXTURE: Porphyritic "fluidal"

PRIMARY MINERALOGY	PERCENT PRESENT	PERCENT ORIGINAL	SIZE (mm)	COMPO-SITION	MORPHOLOGY	COMMENTS
PHENOCRYSTS						
Plagioclase	N/A	[illegible]	[illegible]		Euhedral	Fresh-zoned, sometimes altered in zeolites
Clinopyroxene	N/A	[illegible]	[illegible]		Euhedral	Fresh-zoned; clustered with orthopyroxene, some crystals are corroded
Orthopyroxene	N/A	[illegible]	[illegible]		Euhedral	Partly altered to smectites
GROUNDMASS						
N/A	N/A	N/A	N/A		N/A	"Pseudo-welded" trachytic textured with flattened vesicles. Altered to smectites. Groundmass + vesicles = [illegible]

SECONDARY MINERALOGY	PERCENT	REPLACING/FILLING	COMMENTS
Clays			Replacing the groundmass; filling vesicles

VESICLES/CAVITIES	PERCENT	LOCATION	SIZE (mm)	FILLING	SHAPE
Vesicles	[illegible]		[illegible]	Smectites, zeolites	Elongated

COMMENTS: "Fluidal" is a descriptive type of texture [illegible] [illegible]

[illegible] OBSERVER: [illegible] WHERE SAMPLED:

ROCK NAME: [illegible] andesite

GRAIN SIZE:

TEXTURE: [illegible]

PRIMARY MINERALOGY	PERCENT PRESENT	PERCENT ORIGINAL	SIZE (mm)	COMPO-SITION	MORPHOLOGY	COMMENTS
PHENOCRYSTS						
Plagioclase	N/A	[illegible]	[illegible]		Euhedral	Zoned, rather fresh, clustered, sometimes altered to smectites
Clinopyroxene	N/A	[illegible]	[illegible]		Subhedral	Fresh, corroded, embayed, sometimes clustered with orthopyroxene
Opaque	N/A	[illegible]	[illegible]		Euhedral	
Orthopyroxene	N/A	[illegible]			Euhedral	Partly altered to smectites, some crystals are fresh.
GROUNDMASS						
Plagioclase	N/A	N/A	[illegible]		N/A	[illegible] groundmass, microcrystalline

VESICLES/CAVITIES	PERCENT	LOCATION	SIZE (mm)	FILLING	SHAPE
Vesicles	[illegible]		[illegible]	[illegible]	[illegible]

COMMENTS: Vesicles are [illegible] [illegible]

126-793B-88R-1 (117-119 cm) OBSERVER: REX WHERE SAMPLED: In breccia-conglomerate horizon (clast)

ROCK NAME: Porphyritic basalt

GRAIN SIZE: Phenocrysts 0.5-4 mm

TEXTURE: Porphyritic to glomeroporphyritic

PRIMARY MINERALOGY	PERCENT PRESENT	PERCENT ORIGINAL	SIZE (mm)	COMPO-SITION	MORPHOLOGY	COMMENTS
PHENOCRYSTS						
Olivine	0	4	1-4		Sub-euhedral	Totally pseudomorphed-probably olivine.
Plagioclase	13	13	0.5-1		Subhedral	Zoned, many fluid inclusions.
Clinopyroxene	5	6	0.5-3		Euhedral	Zoned, twinned.
Orthopyroxene	1-2	2	0.5-1		Euhedral	Some alteration, [illegible], could be two generations of orthopyroxene growth?
GROUNDMASS						
Microlitic glass	74	74	N/A		N/A	Microlites of plagioclase (<0.01 mm) in a glassy matrix-some patches of less microlitic glass.

SECONDARY MINERALOGY	PERCENT	REPLACING/ FILLING		COMMENTS
Hematite-clay	4	Replacing	Olivine?	

VESICLES/ CAVITIES	PERCENT	LOCATION	SIZE (mm)	FILLING	SHAPE	COMMENTS
Vesicles	2	Random	0.3-1	None	Rounded-moderately elongate	Walls lined with clays.

COMMENTS: No piece # given.

126-793B-89R-CC (29-31 cm) OBSERVER: LIT WHERE SAMPLED:

ROCK NAME: Clinopyroxene-orthopyroxene-plagioclase andesite

GRAIN SIZE:

TEXTURE: Porphyritic

PRIMARY MINERALOGY	PERCENT PRESENT	PERCENT ORIGINAL	SIZE (mm)	COMPO-SITION	MORPHOLOGY	COMMENTS
PHENOCRYSTS						
Plagioclase	N/A	1	[illegible]		Euhedral	Oscillatory zoned-fresh.
Clinopyroxene	N/A	10	[illegible]		Euhedral	Fresh/zoned, clustered with orthopyroxene.
Orthopyroxene	1	1	[illegible]		Euhedral	Partly altered to smectites, sometimes fresh.
GROUNDMASS						
Feldspar	N/A	[illegible]	[illegible]		N/A	Groundmass: microcrystalline.

VESICLES/ CAVITIES	PERCENT	LOCATION	SIZE (mm)	FILLING	SHAPE
Vesicles	5	Groundmass	1-4	Smectites	Rounded

COMMENTS: Orthopyroxene mantled by clinopyroxene. Clots of orthopyroxene + clinopyroxene or clinopyroxene + plagioclase. Two types of orthopyroxene: bigger phenocrysts altered to smectites. Smaller phenocrysts fresh and mantled by clinopyroxene. No piece # given.

126-793B-[illegible] ([illegible] cm) OBSERVER: [illegible] WHERE SAMPLED: [illegible]

ROCK NAME: Clinopyroxene-orthopyroxene-plagioclase andesite

GRAIN SIZE: Fine

TEXTURE: Porphyritic

PRIMARY MINERALOGY	PERCENT PRESENT	PERCENT ORIGINAL	SIZE (mm)	COMPOSITION	MORPHOLOGY	COMMENTS
PHENOCRYSTS						
Plagioclase	N.R.	[illegible]	[illegible]		Subhedral	Fresh-oscillatory zoned.
Clinopyroxene	N.R.	[illegible]	[illegible]		Euhedral	Fresh.
Orthopyroxene	N.R.	[illegible]	[illegible]		Euhedral	Fresh to slightly altered to smectites. Clustered with orthopyroxene and clinopyroxene.
GROUNDMASS						
Feldspar	N.R.	N.R.	[illegible]		N.R.	[illegible] microcrystalline.

VESICLES/CAVITIES	PERCENT	LOCATION	SIZE (mm)	FILLING	SHAPE	COMMENTS
Vesicles	[illegible]		[illegible]		Rounded	Filled with zeolites and smectites.

COMMENTS: Orthopyroxene-clinopyroxene [illegible] on piece # given.

126-793B-[illegible] ([illegible] cm) OBSERVER: [illegible] WHERE SAMPLED: [illegible]

ROCK NAME: Clinopyroxene-orthopyroxene-plagioclase andesite

GRAIN SIZE: Fine

TEXTURE: Porphyritic

PRIMARY MINERALOGY	PERCENT PRESENT	PERCENT ORIGINAL	SIZE (mm)	COMPOSITION	MORPHOLOGY	COMMENTS
PHENOCRYSTS						
Plagioclase	N.R.	[illegible]	[illegible]		Subhedral	Fresh-oscillatory zoned.
Clinopyroxene	N.R.	[illegible]	[illegible]		Euhedral	Fresh.
Orthopyroxene	N.R.	[illegible]	[illegible]		Euhedral	Fresh to slightly altered to smectites. Clustered with orthopyroxene and clinopyroxene.
GROUNDMASS						
Feldspar	N.R.	N.R.	[illegible]		N.R.	[illegible] microcrystalline.

VESICLES/CAVITIES	PERCENT	LOCATION	SIZE (mm)	FILLING	SHAPE	COMMENTS
Vesicles	[illegible]		[illegible]		Rounded	Filled with zeolites and smectites.

COMMENTS: Orthopyroxene-clinopyroxene [illegible] on piece # given.

126-793B-[illegible]R-1 (Piece 1,69-75 cm) OBSERVER: [illegible] WHERE SAMPLED:

ROCK NAME: Plagioclase-clinopyroxene andesite

GRAIN SIZE: Fine

TEXTURE: Porphyritic, intersertal

PRIMARY MINERALOGY	PERCENT PRESENT	PERCENT ORIGINAL	SIZE (mm)	COMPO-SITION	MORPHOLOGY	COMMENTS
PHENOCRYSTS						
Plagioclase	6	6	0.8-2		Euhedral	Fresh, relatively simple growth history.
Clinopyroxene	3	4	0.5-2		Euhedral	Both fresh and smectite alteration; twinned.
Orthopyroxene	2	2	N/A		N/A	None fresh.
GROUNDMASS						
Plagioclase + magnetite + clinopyroxene	88	N/A	N/A		N/A	Trachytic alignment.

VESICLES/ CAVITIES	PERCENT	LOCATION	SIZE (mm)	FILLING	SHAPE
Vesicles	5	Zeolite + smectites		Round	

COMMENTS: Groundmass quite fresh, with some smectite glass between plagioclase +/- clinopyroxene; partly devitrified. Sample is a clast; the zeolite, smectite, clinopyroxene and plagioclase matrix is seen in one corner, as well as part of an adjacent clast.

126-793B-[illegible]R-[illegible] (3-6 cm) OBSERVER: [illegible] WHERE SAMPLED:

ROCK NAME: Clinopyroxene-orthopyroxene andesite

GRAIN SIZE:

TEXTURE: Porphyritic, intersertal

PRIMARY MINERALOGY	PERCENT PRESENT	PERCENT ORIGINAL	SIZE (mm)	COMPO-SITION	MORPHOLOGY	COMMENTS
PHENOCRYSTS						
Plagioclase	N/A	[illegible]	[illegible]		Euhedral	
Clinopyroxene	[illegible]	[illegible]	[illegible]		Euhedral	Twinned, zoned.
Orthopyroxene	[illegible]	[illegible]	N/A		N/A	Little smectite-altered pyroxene shapes, no [illegible] figures.
GROUNDMASS						
Plagioclase + pyroxene + magnetite	84	N/A	N/A		N/A	Flow aligned (trachytic) alteration is patchy.

VESICLES/ CAVITIES	PERCENT	LOCATION	SIZE (mm)	FILLING	SHAPE
Vesicles	[illegible]	Smectite, zeolites	0.2-1	Round	

COMMENTS: No glass [illegible]

[illegible] OBSERVER: [illegible] WHOLE SAMPLED

ROCK NAME: [illegible] andesite

GRAIN SIZE: Fine

TEXTURE: Porphyritic, [illegible]

PRIMARY MINERALOGY	PERCENT PRESENT	PERCENT ORIGINAL	SIZE (mm)	COMPOSITION	MORPHOLOGY	COMMENTS
PHENOCRYSTS						
Plagioclase	N/A	[illegible]	[illegible]		Euhedral	Fresh.
Clinopyroxene	N/A	[illegible]	[illegible]		Euhedral	Fresh, twinned.
Orthopyroxene	N/A	[illegible]	[illegible]		Euhedral	[illegible]
GROUNDMASS						
Plagioclase + [illegible]	[illegible]	[illegible]	[illegible]		[illegible]	[illegible]

SECONDARY MINERALOGY	PERCENT	LOCATION	SIZE (mm)	FILLING	SHAPE	COMMENTS
VESICLES	[illegible]		[illegible]			[illegible]

COMMENTS: [illegible]

[illegible] OBSERVER: [illegible] WHOLE SAMPLED

ROCK NAME: [illegible]

GRAIN SIZE: Fine

TEXTURE: [illegible]

PRIMARY MINERALOGY	PERCENT PRESENT	PERCENT ORIGINAL	SIZE (mm)	COMPOSITION	MORPHOLOGY	COMMENTS
PHENOCRYSTS						
[illegible]					[illegible]	[illegible]
[illegible]	[illegible]	[illegible]	[illegible]		[illegible]	[illegible]
GROUNDMASS						
[illegible]	N/A	N/A	N/A		[illegible]	[illegible]
[illegible]	N/A	N/A			[illegible]	[illegible]
[illegible]	N/A	N/A			[illegible]	
[illegible]	N/A	N/A			[illegible]	

SECONDARY MINERALOGY	PERCENT	REPLACING / FILLING	COMMENTS
[illegible]	[illegible]	[illegible]	

VESICLES	PERCENT	LOCATION	SIZE (mm)	FILLING	SHAPE	COMMENTS
[illegible]	[illegible]	[illegible]	[illegible]		[illegible]	[illegible]

COMMENTS: [illegible]

[illegible] (Piece 4A, 44-45 cm) OBSERVER: [illegible] WHERE SAMPLED:

ROCK NAME: Clinopyroxene-orthopyroxene andesite

GRAIN SIZE: Fine

TEXTURE: Porphyritic; intersertal

PRIMARY MINERALOGY	PERCENT PRESENT	PERCENT ORIGINAL	SIZE (mm)	COMPOSITION	MORPHOLOGY	COMMENTS
PHENOCRYSTS						
Plagioclase	N/A	1	1-2		Euhedral	Fresh.
Clinopyroxene	N/A	11	1-3		Euhedral	Fresh, twinned, zoned.
Orthopyroxene	N/A	17	1-4		Euhedral	Generally fresh, some smectite to calcite alteration.
GROUNDMASS						
Plagioclase + pyroxene + magnetite	71	N/A	N/A		N/A	Flow aligned, intersertal.

FRACTURES/CAVITIES	PERCENT	LOCATION	SIZE (mm)	FILLING	SHAPE
Vesicles	1		0.7	Smectite lined	

[illegible] (27-29 cm) OBSERVER: [illegible] WHERE SAMPLED: Flow top

ROCK NAME: Andesite

GRAIN SIZE: Fine grained with 1 mm phenocrysts

TEXTURE: Porphyritic; fluidal groundmass

PRIMARY MINERALOGY	PERCENT PRESENT	PERCENT ORIGINAL	SIZE (mm)	COMPOSITION	MORPHOLOGY	COMMENTS
PHENOCRYSTS						
Plagioclase	1	1	1-1.5		Euhedral	Fresh.
Clinopyroxene	1	1	0.5-1		Euhedral	Fresh, zoned.
Orthopyroxene	0.5	1	0.5-1		Euhedral	Some fresh, replaced by smectite.
GROUNDMASS						
Plagioclase	50	50	N/A		Euhedral	Laths are 0.05 by 0.2 mm.
Glass	40	40	N/A		N/A	
Pyroxene/clinopyroxene	7	7	N/A		Subhedral	

SECONDARY MINERALOGY	PERCENT	REPLACING/FILLING	COMMENTS
Clays	0.5	Replacing	Smectite; orthopyroxene.
Clays	40	Replacing	Smectite; glass in interstitial.

FRACTURES/CAVITIES	PERCENT	LOCATION	SIZE (mm)	FILLING	SHAPE	COMMENTS
Vesicles	1	Random	0.2	Smectite	Spherical	Walls coated with smectite.

COMMENTS: Some vesicles filled with zeolite (chabazite); some glomeroporphyritic clots of plagioclase-clinopyroxene; groundmass plagioclase is aligned in trachytic texture (flow). No plate # given.

```
125-793B-[illegible] [illegible] cm                  OBSERVER: [illegible]        WHERE SAMPLED: [illegible]

ROCK NAME: Orthopyroxene-clinopyroxene-plagioclase andesite

GRAIN SIZE: Fine

TEXTURE: Porphyritic, intersertal

PRIMARY          PERCENT PERCENT  SIZE         COMPO-
MINERALOGY       PRESENT ORIGINAL (mm)         SITION              MORPHOLOGY            COMMENTS

 PHENOCRYSTS
Plagioclase      [illegible]  [illegible]  [illegible]             Euhedral
Clinopyroxene    5       5        [illegible]                      Euhedral         Fresh, with fluid inclusions, zoned.
Orthopyroxene    12      12       [illegible]                      Euhedral         Partly altered to smectite along margins
                                                                                    and cleavages.

 GROUNDMASS
Glass            N/A     N/A      N/A                              N/A              Devitrified.
Plagioclase      N/A     N/A      [illegible]                      Laths

SECONDARY                   REPLACING/
MINERALOGY       PERCENT    FILLING                                                 COMMENTS
Clay             [illegible]  Orthopyroxene, glass                  And fractures in the thin section.
Zeolite          [illegible]  Orthopyroxene

VESICLES/                           SIZE
CAVITIES         PERCENT  LOCATION  (mm)             FILLING                        SHAPE        COMMENTS
Vesicles         [illegible]  Random  [illegible]    Empty                          Elongated    Smectite lining in
                                                                                                 vesicle walls.

COMMENTS: [illegible] Present groundmass is [illegible], original was [illegible].

125-793B-[illegible] (Piece [illegible], [illegible] cm)    OBSERVER: [illegible]      WHERE SAMPLED: [illegible]

ROCK NAME: Orthopyroxene-clinopyroxene andesite

GRAIN SIZE: Fine

TEXTURE: Porphyritic, intersertal

PRIMARY          PERCENT PERCENT  SIZE         COMPO-
MINERALOGY       PRESENT ORIGINAL (mm)         SITION              MORPHOLOGY            COMMENTS

 PHENOCRYSTS
Clinopyroxene    [illegible]  1   [illegible]                      Euhedral         Fresh.
Orthopyroxene    [illegible]  [illegible]  [illegible]             Euhedral         Partly altered to smectite.

 GROUNDMASS
Glass            N/A     N/A      N/A                              N/A              Devitrified
Plagioclase      N/A     N/A      [illegible]                      Laths            Alignment of laths around crystals.
Clinopyroxene    N/A     N/A      [illegible]                      N/A
Orthopyroxene    N/A     N/A      [illegible]                      N/A

SECONDARY                   REPLACING/
MINERALOGY       PERCENT    FILLING                                                 COMMENTS
Clays            [illegible]  Orthopyroxene and glass
Zeolites         [illegible]  Trace

VESICLES/                           SIZE
CAVITIES         PERCENT  LOCATION  (mm)             FILLING                        SHAPE        COMMENTS
Vesicles         N/A                                                                Round        [illegible] in thin
                                                                                                 section, smectite lined
                                                                                                 walls.

COMMENTS: Alteration of orthopyroxene along margins and cleavages. Present groundmass is [illegible], original was [illegible].
```

126-793B-98R-01 (54-55 cm)   OBSERVER: REX   WHERE SAMPLED:

ROCK NAME: Basaltic andesite

GRAIN SIZE: Fine groundmass 1-3 mm phenocrysts

TEXTURE: Porphyritic

PRIMARY MINERALOGY	PERCENT PRESENT	PERCENT ORIGINAL	SIZE (mm)	COMPOSITION	MORPHOLOGY	COMMENTS
PHENOCRYSTS						
Olivine	0	1	1		Rounded-subhedral	Possible reabsorbed.
Clinopyroxene	5	5	1-4		Euhedral-subhedral	Zoned, fluid inclusion.
Orthopyroxene	2	4	1-2		N/A	
GROUNDMASS						
Plagioclase	50	50	0.2		Laths	
Clinopyroxene	2	2	0.1		Laths	
Glass	10	38	N/A		N/A	Some interstitial glass may be fresh.

SECONDARY MINERALOGY	PERCENT	REPLACING/ FILLING	COMMENTS
Clays	2	Replacing	Orthopyroxene.
Clays	28	Replacing	Glass.
Zeolites			Filling vesicles.
Fe hydroxide/oxide	0.5	Replacing	Olivine.
Iddingsite	0.5	Replacing	Olivine.

VESICLES/ CAVITIES	PERCENT	LOCATION	SIZE (mm)	FILLING	SHAPE	COMMENTS
Vesicles	5	Random	1-4	50	Elongate to spherical	Aligned and 1/2 filled by zeolites and clays in some cases.

COMMENTS: No piece # given.

126-793B-100R-01 (28-29 cm)   OBSERVER: REX   WHERE SAMPLED:

ROCK NAME: Andesite

GRAIN SIZE: Fine grained <0.5 mm

TEXTURE: Aphyric, trachytic groundmass

PRIMARY MINERALOGY	PERCENT PRESENT	PERCENT ORIGINAL	SIZE (mm)	COMPOSITION	MORPHOLOGY	COMMENTS
PHENOCRYSTS						
Plagioclase	0.2	0.2	0.7		Euhedral-subhedral	
Clinopyroxene	0.5	0.5	0.2-0.5		Euhedral	
Orthopyroxene	0.1	0.5	0.5		Euhedral	
GROUNDMASS						
Glass	10	10	N/A		Interstitial	
Plagioclase	88	88	N/A		Laths	Aligned in trachytic texture.
Clinopyroxene	1	1	N/A		Laths	
Oxide	<0.1	<0.1	N/A		Cubes	Red brown in ppl.

SECONDARY MINERALOGY	PERCENT	REPLACING/ FILLING	COMMENTS
Clays	10	Replacing	Glass in groundmass.

VESICLES/ CAVITIES	PERCENT	LOCATION	SIZE (mm)	FILLING	SHAPE	COMMENTS
Vesicles	5	Random	0.1-1	Zeolites	Spherical	Zeolites on walls, smectite in center.

COMMENTS: Generally aphyric vesicular andesite. No piece # given.

```
[illegible]                              OBSERVER: [illegible]      WHERE SAMPLED: [illegible]

ROCK NAME: Andesite

GRAIN SIZE: Fine grained

TEXTURE: [illegible]

PRIMARY         PERCENT PERCENT  SIZE       COMPO-
MINERALOGY      PRESENT ORIGINAL (mm)       SITION          MORPHOLOGY            COMMENTS

PHENOCRYSTS
Plagioclase     [illegible]                                 Subhedral             Zoned, with glass inclusions.
Clinopyroxene   [illegible]                                 Subhedral/anhedral    Zoned, glass inclusions and [illegible]
                                                                                  lamellae.
Orthopyroxene   [illegible]                                 Euhedral

GROUNDMASS
Glass           [illegible]                                 n/a                   Completely altered to [illegible].
Plagioclase     [illegible]                                 Subhedral
Clinopyroxene   [illegible]                                 Subhedral
Oxide           [illegible]                                 n/a

SECONDARY                 REPLACING/
MINERALOGY      PERCENT   FILLING                                    COMMENTS
Clays           [illegible]                                 Glass within the groundmass
[illegible]     [illegible]                                 Orthopyroxene sites

VESICLES/                          SIZE
CAVITIES        PERCENT LOCATION   (mm)       FILLING                     SHAPE          COMMENTS
Vesicles        [illegible] Random            [illegible]                 Spherical      Thin coating of smectite
                                                                                         on walls.

COMMENTS: [illegible]

[illegible]                              OBSERVER: [illegible]      WHERE SAMPLED: [illegible]

ROCK NAME: [illegible] andesite

GRAIN SIZE: [illegible]

TEXTURE: [illegible]

PRIMARY         PERCENT PERCENT  SIZE       COMPO-
MINERALOGY      PRESENT ORIGINAL (mm)       SITION          MORPHOLOGY            COMMENTS

PHENOCRYSTS
Plagioclase     [illegible]                                 Subhedral             [illegible]
Clinopyroxene   [illegible]                                 Subhedral
Orthopyroxene   [illegible]                                 Subhedral

GROUNDMASS
Plagioclase     [illegible]                                 [illegible]
Clinopyroxene   [illegible]                                 [illegible]           [illegible]
Glass           [illegible]                                 n/a
Orthopyroxene   [illegible]                                 [illegible]

SECONDARY                 REPLACING/
MINERALOGY      PERCENT   FILLING                                    COMMENTS
Clays           [illegible] [illegible]                     [illegible]

VESICLES/                          SIZE
CAVITIES        PERCENT LOCATION   (mm)       FILLING                     SHAPE          COMMENTS
Vesicles        [illegible] Random            [illegible]                 [illegible]    [illegible]

COMMENTS: [illegible]
```

126-793B-127R-1 (Piece 2A,17-18 cm) OBSERVER: REX WHERE SAMPLED:

ROCK NAME: Andesite

GRAIN SIZE: Fine groundmass

TEXTURE: Porphyritic

PRIMARY MINERALOGY	PERCENT PRESENT	PERCENT ORIGINAL	SIZE (mm)	COMPO-SITION	MORPHOLOGY	COMMENTS
PHENOCRYSTS						
Plagioclase	[illegible]	[illegible]	0.5-4	Anorthite 70	Euhedral	Zoned, with fluid inclusions.
Clinopyroxene	5	5	0.5-3		Euhedral-subhedral	
Orthopyroxene	0.2	1	0.5-1		Euhedral	Dominantly altered to smectite.
GROUNDMASS						
Plagioclase	55	55	0.2		Euhedral	Laths in glass.
Glass	10	22	N/A		N/A	
Oxide	7	N/A	N/A		N/A	

SECONDARY MINERALOGY	PERCENT	REPLACING/ FILLING	COMMENTS
Clays	0.8	Replacing	Smectite replacing orthopyroxene.
Clays	5	Replacing	Celadonite replacing groundmass and orthopyroxene.
Zeolites	5	Filling	Vesicles.
Smectite	10	Replacing	Glass in groundmass.

VESICLES/ CAVITIES	PERCENT	LOCATION	SIZE (mm)	FILLING	SHAPE	COMMENTS
Vesicles	5	Random	1-5	Vesicle	Sub-spherical	Filled with zeolites and smectite.

COMMENTS: Groundmass texture intersertal to microphyric. Some veins of celadonite (1 mm) crossing section. Some orthopyroxene phenocrysts rimmed by clinopyroxene laths.

126-793B-112R-01 (Piece 1A,0-5 cm)   OBSERVER: REX   WHERE SAMPLED: Orange spot lava flow

ROCK NAME: Boninitic basaltic andesite

GRAIN SIZE: Fine groundmass, 5 mm phenocrysts

TEXTURE: Porphyritic

PRIMARY MINERALOGY	PERCENT PRESENT	PERCENT ORIGINAL	SIZE (mm)	COMPO-SITION	MORPHOLOGY	COMMENTS
PHENOCRYSTS						
Olivine	0	6	<5		Euhedral and subrounded	Altered to clays, calcite, Fe-oxide.
Clinopyroxene	4	4	0.2-1		Euhedral	Rare chromium-spinel inclusions.
Spinel	0.1	0.1	.005-.1		Euhedral cubes	Reddish tint in ppl.
Orthopyroxene	1	[illegible]	0.2-1		Euhedral	Altered along fractures, rimmed by clinopyroxene.
GROUNDMASS						
Plagioclase	41	33	0.1		Subhedral	
Clinopyroxene	25	25	0.1-0.2		Subhedral-quench acicular	
Orthopyroxene	8	8	0.1		Subhedral-quench acicular	
Spinel	1	1	0.02		Subhedral	Some cubes.
Glass	~20	20	N/A		N/A	Interstitial, possibly zeolite replaced.

SECONDARY MINERALOGY	PERCENT	REPLACING/ FILLING	COMMENTS
Clays	0.5	Replacing	Olivine.
Clays	1	Replacing	Orthopyroxene.
Carbonate	0.5	Replacing	Olivine (calcite).
Zeolites	1	Replacing	Glass.
Fe-oxide	1	Replacing	Olivine, Fe-oxide + hydroxide.
Celadonite	1	Replacing	Olivine.
Native copper	Trace	Replacing	Olivine.

VESICLES/ CAVITIES	PERCENT	LOCATION	SIZE (mm)	FILLING	SHAPE
Vesicles	0.5	Random	1	No	Sub-spherical/spherical

COMMENTS: "Orange spots" may represent complete mineral cluster; in this region rounded euhedral pseudomorphs after olivine cluster in alignment, and are "cemented" by orthopyroxene and clinopyroxene. Chromium-spinel inclusions present in pseudomorphs and "cement" native copper present within the orange spot region.

126-793B-112R-01 (Piece 11,83-84 cm)   OBSERVER: TOP   WHERE SAMPLED:

ROCK NAME: Basaltic andesite

GRAIN SIZE: Fine grained groundmass

TEXTURE: Porphyritic, intersertal, [illegible]

PRIMARY MINERALOGY	PERCENT PRESENT	PERCENT ORIGINAL	SIZE (mm)	COMPO-SITION	MORPHOLOGY	COMMENTS
PHENOCRYSTS						
Clinopyroxene	1	1	0.1-1		Euhedral	
Orthopyroxene	8	12	0.5-2		Euhedral	Partly altered to smectite along margins and fractures.
GROUNDMASS						
Plagioclase	40	40	N/A		Laths	
Glass	20	40	N/A		N/A	Devitrified.

SECONDARY MINERALOGY	PERCENT	REPLACING/ FILLING	COMMENTS
Clays	4	Replacing	Orthopyroxene.
Clays	15	Replacing glass and filling fractures	
Zeolites	10	Filling	Vesicles and replacing glass.

VESICLES/ CAVITIES	PERCENT	LOCATION	SIZE (mm)	FILLING	SHAPE
Vesicles	2	Random	0.1-1	Zeolites	

```
126-793B-113R-03 (Piece 7,136-137 cm)      OBSERVER: TOR         WHERE SAMPLED:

ROCK NAME: Andesite

GRAIN SIZE: Fine

TEXTURE: Aphyric with trachytic groundmass
--------------------------------------------------------------------------------------------------------------

PRIMARY          PERCENT PERCENT  SIZE        COMPO-
MINERALOGY       PRESENT ORIGINAL (mm)        SITION              MORPHOLOGY            COMMENTS

PHENOCRYSTS
Clinopyroxene     1        1      0.1-0.3                         Euhedral              Altered along cleavages.

GROUNDMASS
Glass             N/A     N/A    N/A                              N/A                   Devitrified.
Plagioclase       N/A     N/A    <0.1                             N/A                   Aligned around crystals.
Clinopyroxene     N/A     N/A    N/A                              N/A
Magnetite         N/A     N/A    <0.05                            N/A

SECONDARY                     REPLACING/
MINERALOGY       PERCENT       FILLING                                                  COMMENTS
Clays             8          Filling                                Fractures.
Clays             35         Replacing glass
Zeolites          10
--------------------------------------------------------------------------------------------------------------
VESICLES/                              SIZE
CAVITIES         PERCENT  LOCATION   (mm)            FILLING                        SHAPE        COMMENTS
Vesicles          5       Random     0.3-2           Empty                          Elongated   Zeolites on vesicle
                                                                                                walls.
--------------------------------------------------------------------------------------------------------------
COMMENTS: Present groundmass is 51%, original was 99%.
```

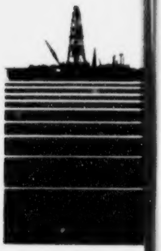

SECTION 5: POLICY

JOIDES ADVISORY GROUPS*

Executive Committee (EXCOM)

Charles E. Helsley
University of Hawaii

Roger N. Anderson (Wireline Logging Services liaison)
Columbia University

D. James Baker, Jr. (JOI liaison)
Joint Oceanographic Institutions, Inc.

Christopher R. Barnes
Geological Survey of Canada

Bernard Biju-Duval
IFREMER (France)

James C. Briden
Natural Environment Research Council (U.K.)

Douglas R. Caldwell
Oregon State University

Craig E. Dorman
Woods Hole Oceanographic Institution

Robert A. Duce
University of Rhode Island

Hans J. Dürbaum
Bundesanstalt für Geowissenschaften und Rohstoffe

Edward A. Frieman
University of California, San Diego

C.G.A. Harrison
University of Miami

G. Ross Heath
University of Washington

Donald F. Heinrichs (NSF liaison)
National Science Foundation (U.S.)

Arthur E. Maxwell
University of Texas at Austin

William J. Merrell
Texas A&M University at Galveston

Ralph Moberly (PCOM liaison)
University of Hawaii

Takahisa Nemoto
University of Tokyo

Philip D. Rabinowitz (Science Operator liaison)
Texas A&M University

C. Barry Raleigh
Columbia University

Jan H. Stel
Netherlands Council of Oceanic Research

Planning Committee (PCOM)

Ralph Moberly
University of Hawaii

Garrett W. Brass
University of Miami

Darrel S. Cowan
University of Washington

Olav Eldholm
University of Oslo

Louis E. Garrison (Science Operator liaison)
Texas A&M University

Richard D. Jarrard (Wireline Logging Services liaison)
Columbia University

Hugh C. Jenkyns
Oxford University

Miriam Kastner
University of California, San Diego

Yves P. Lancelot
Université Pierre et Marie Curie

Marcus G. Langseth
Columbia University

Margaret Leinen
University of Rhode Island

Bruce Malfait (NSF liaison)
National Science Foundation (U.S.)

John Malpas
Memorial University

Nicklas G. Pisias
Oregon State University

Thomas E. Pyle (JOI liaison)
Joint Oceanographic Institutions, Inc.

Thomas H. Shipley
University of Texas at Austin

Asahiko Taira
University of Tokyo

Brian E. Tucholke
Woods Hole Oceanographic Institution

Ulrich von Rad
Bundesanstalt für Geowissenschaften und Rohstoffe

Joel Watkins
Texas A&M University

Central and Eastern Pacific Detailed Planning Group (CEPDPG)

David K. Rea
University of Michigan

Helmut Beiersdorf
Bundesanstalt für Geowissenschaften und Rohstoffe

Earl E. Davis
Geological Survey of Canada

Martin F.J. Flower
University of Illinois, Chicago

Peter A. Floyd
University of Keele

Jean Francheteau
Université Pierre et Marie Curie

Loren W. Kroenke
University of Hawaii

Hakuyu Okada
Kyushu University

Constance A. Sancetta
Columbia University

Seymour O. Schlanger
Northwestern University

Hans Joachim Schrader
University of Bergen

William V. Sliter
U.S. Geological Survey

Downhole Measurements Panel (DMP)

Paul F. Worthington
British Petroleum Company, Ltd.

Keir Becker (LITHP liaison)
University of Miami

Sebastian Bell
Geological Survey of Canada

Bobb Carson
Lehigh University

Darrel S. Cowan (PCOM liaison)
University of Washington

Joris M. Gieskes
University of California, San Diego

Xenia Golovchenko (Wireline Logging Services liaison)
Columbia University

Eddie P. Howell
Arco Oil and Gas Company

---

*Membership at time of cruise

Daniel E. Karig
Cornell University

Hajimu Kinoshita
Chiba University

Marcus G. Langseth (PCOM liaison)
Columbia University

Peter Lysne
Sandia National Laboratories

Roger H. Morin
U.S. Geological Survey

Suzanne O'Connell (Science Operator liaison)
Texas A&M University

J. P. Pozzi
Ecole Normale Supérieure

Carl Sondergeld
Amoco Production Company

Ove Stephansson
University of Lulea

Heinrich Villinger
Alfred Wegener Institute for Polar and Marine Research

Roy H. Wilkens
University of Hawaii

Fluid Processes in Accretionary Prisms Working Group (FPAPWG)

Graham K. Westbrook
University of Birmingham

Keir Becker
University of Miami

Joris M. Gieskes
University of California, San Diego

Roy D. Hyndman
Pacific Geoscience Centre (Canada)

Daniel E. Karig
Cornell University

Xavier Le Pichon
Ecole Normale Supérieure

J. Casey Moore
University of California, Santa Cruz

E. Nuti
Istituto Internazionale de Geotermia

Thomas H. Shipley
University of Texas at Austin

Erwin Suess
GEOMAR (F.R.G.)

Roland von Huene
GEOMAR (F.R.G.)

Information Handling Panel (IHP)

Ted C. Moore, Jr.
Exxon Production Research Company

Cristina Broglia (Wireline Logging Services liaison)
Columbia University

Raymond V. Ingersoll
University of California, Los Angeles

Meirion T. Jones
Institute of Oceanographic Sciences (U.K.)

Yves P. Lancelot (PCOM liaison)
Université Pierre et Marie Curie

Alfred R. Loeblich, Jr.
University of California, Los Angeles

Michael S. Loughridge
National Geophysical Data Center (U.S.)

Russell B. Merrill (Science Operator liaison)
Texas A&M University

Judit Nowak
Bundesanstalt für Geowissenschaften und Rohstoffe

Niklas G. Pisias (PCOM liaison)
Oregon State University

John B. Saunders
Naturhistorisches Museum (Switzerland)

André Schaaf
Université Claude Bernard

Henry Spall
U.S. Geological Survey

Kensaku Tamaki
University of Tokyo

Lithospheric Panel (LITHP)

Rodey Batiza
University of Hawaii

Keir Becker
University of Miami

Garrett W. Brass (PCOM liaison)
University of Miami

Lawrence M. Cathles
Cornell University

Sierd Cloetingh
Vrije Universiteit

Henry Elderfield
Cambridge University

Jörg Erzinger
Universitat Giessen

James M. Franklin
Geological Survey of Canada

Toshitsugu Fujii
University of Tokyo

Susan E. Humphris
Woods Hole Oceanographic Institution

John Malpas (PCOM liaison)
Memorial University

Catherine Mevel
Université Pierre et Marie Curie

Jason Phipps Morgan
Massachusetts Institute of Technology

John C. Mutter
Columbia University

John A. Orcutt
University of California, San Diego

Julian A. Pearce
University of Newcastle upon Tyne

Michael R. Perfit
University of Florida

Guy M. Smith
St. Louis University

Ocean History Panel (OHP)

Nicholas J. Shackleton
Cambridge University

Eric J. Barron
Pennsylvania State University

Wolfgang H. Berger
University of California, San Diego

William A. Berggren
Woods Hole Oceanographic Institution

Margaret L. Delaney
University of Southern California, Santa Cruz

André W. Droxler
Rice University

Robert E. Garrison
University of California, Santa Cruz

Eystein Jansen
Columbia University

Hugh C. Jenkyns (PCOM liaison)
Oxford University

Dennis V. Kent
Columbia University

Alan C. Mix
Oregon State University

Nicklas G. Pisias (PCOM liaison)
Oregon State University

Tsunemasa Saito
Yamagata University

Ruediger Stein
Universität Giessen

Edith Vincent
Université Pierre et Marie Curie

Pollution Prevention and Safety Panel (PPSP)

Mahlon M. Ball
U.S. Geological Survey

Yutaka Aoki
Japex Geoscience Institute, Inc.

Carl Brenner (Databank liaison)
Columbia University

E. Cassani
AGIP S.p.A. (Italy)

George E. Claypool
Mobil Oil Company

Claude Delas
Total Compagnie Française des Pétroles

Mimi Fortier
Canadian Oil and Gas Lands Administration

Louis E. Garrison (Science Operator liaison)
Texas A&M University

Arthur R. Green
Exxon Production Research Company

Paul Haseldonckx
Deminex (F.R.G.)

Stephen Lewis (SSP liaison)
U.S. Geological Survey

David B. MacKenzie
Littleton, Colorado

Ralph Moberly (PCOM liaison)
University of Hawaii

David G. Roberts
British Petroleum Company, Ltd.

Sedimentary and Geochemical Processes Panel (SGPP)

Erwin Suess
GEOMAR (F.R.G.)

Jacques Boulegue
Paris, France

Nicholas Christie-Blick
Columbia University

Shirley Dreiss
University of California, Santa Cruz

Henry Elderfield
Cambridge University

Philip N. Froelich
Columbia University

Martin B. Goldhaber
U.S. Geological Survey

Makoto Ito
Chiba University

Noel P. James
Memorial University of Newfoundland

Miriam Kastner (PCOM liaison)
University of California, San Diego

Judith A. McKenzie
Eidgenossische Technische Hochschule

Larry Mayer
Université Pierre et Marie Curie

Jürgen Mienert
Woods Hole Oceanographic Institution

William R. Normark
U.S. Geological Survey

Frederick Prahl
Oregon State University

Dorrik Stow
University of Nottingham

Ulrich von Rad (PCOM liaison)
Bundesanstalt für Geowissenschaften und Rohstoffe

Sedimented Ridges Detailed Planning Group (SRDPG)

Robert S. Detrick
University of Rhode Island

Harald Backer
GEOMAR (F.R.G.)

Keir Becker
University of Miami

Wilfred B. Bryan
Woods Hole Oceanographic Institution

David Chapman
University of Utah

Earl E. Davis
Geological Survey of Canada

Craig B. Forster
Utah State University

James M. Franklin
Geological Survey of Canada

Hiromi Fujimoto
University of Tokyo

Steven P. Howard
Texas A&M University

Mitchell W. Lyle
Oregon State University

Catherine Mevel
Université Pierre et Marie Curie

Michael J. Mottl
University of Hawaii

Bernd Simoneit
Oregon State University

Robert Zierenberg
U.S. Geological Survey

Shipboard Measurements Panel (SMP)

Kate Moran
Bedford Institute of Oceanography

Ian L. Gibson
University of Waterloo

Joris M. Gieskes (DMP liaison)
University of California, San Diego

John W. King
University of Rhode Island

Margaret Leinen (PCOM liaison)
University of Rhode Island

Michael Mottl
University of Hawaii

J. Mike Rhodes
University of Massachusetts

Adrian Richards
Technische Hogeschool te Delft (Netherlands)

Asahiko Taira (PCOM liaison)
University of Tokyo

Ellen Thomas
Wesleyan University

Hidekazu Tokuyama
University of Tokyo

Site Survey Panel (SSP)

Gregory S. Mountain
Columbia University

Mahlon M. Ball (PPSP liaison)
U.S. Geological Survey

Carl Brenner (Databank liaison)
Columbia University

Frederick K. Duennebier
University of Hawaii

Robert B. Kidd
University College of Swansea

Yves P. Lancelot (PCOM liaison)
Université Pierre et Marie Curie

Birger Larsen
Technical University of Denmark

Stephen Lewis
U.S. Geological Survey

Alain Mauffret
Université Pierre et Marie Curie

Audrey W. Meyer (Science Operator liaison)
Texas A&M University

Heinrich Meyer
Bundesanstalt für Geowissenschaften and Rohstoffe

John W. Peirce
Petro Canada

Thomas E. Pyle (JOI liaison)
Joint Oceanographic Institutions, Inc.

Kiyoshi Suyehiro
University of Tokyo

Joel Watkins (PCOM liaison)
Texas A&M University

Technology and Engineering Development Committee (TEDCOM)

Charles Sparks
Institut Français du Pétrole

Jean Bonnasse Gahot
Elf Aquitaine

Garrett W. Brass (PCOM liaison)
University of Miami

Martin E. Chenevert
University of Texas at Austin

William R. Cotten
Chevron Services Company

Bert R. Dennis
Los Alamos National Laboratories

David D. Grassick
Enterprise Oil plc

Barry W. Harding (Science Operator liaison)
Texas A&M University

Junzo Kasahara
University of Tokyo

Keith Manchester
Bedford Institute of Oceanography

Archie R. McLerran
Solana Beach, California

Keith Millheim
Amoco Production Company

Heinrich Rischmuller
Bundesanstalt für Geowissenschaften and Rohstoffe

Frank J. Schuh
Intertech Operations Technology, Inc.

Paul N. Stanton
Exxon Production Research Company

Harald Strand
Norsk Hydro

Walter W. Svendsen
Longyear Company

Paul F. Worthington (DMP liaison)
British Petroleum Company, Ltd.

Tectonics Panel (TECP)

Ian W. D. Dalziel
University of Texas at Austin

Sebastian Bell (DMP liaison)
Geological Survey of Canada

Roger Buck
Columbia University

Dan M. Davis
State University of New York, Stony Brook

Olav Eldholm (PCOM liaison)
University of Oslo

David C. Engebretson
Western Washington University

Karl Hinz
Bundesanstalt für Geowissenschaften and Rohstoffe

David G. Howell
U.S. Geological Survey

Hans Christian Larsen
Greenland Geological Survey

Gregory F. Moore (WPAC liaison)
University of Hawaii

Yujiro Ogawa
Kyushu University

Robin P. Riddihough
Geological Survey of Canada

François Roure
Institut Français du Pétrole

Thomas H. Shipley (PCOM liaison)
University of Texas at Austin

Brian E. Tucholke (PCOM liaison)
Woods Hole Oceanographic Institution

Peter R. Vogt
U.S. Naval Research Laboratory

Anthony B. Watts
Columbia University

Graham K. Westbrook
University of Birmingham

Western Pacific Detailed Planning Group (WPDPG)

James B. Gill
University of California, Santa Cruz

Kent Brooks
University of Copenhagen

David S. Cronan
Imperial College

James V. Eade
CCOP/SOPAC (Fiji)

Roy D. Hyndman
Pacific Geoscience Centre (Canada)

H. R. Kudrass
Bundesanstalt für Geowissenschaften and Rohstoffe

Gregory F. Moore
University of Hawaii

James Natland
University of California, San Diego

Claude Rangin
Université Pierre et Marie Curie

Steven D. Scott
University of Toronto

Kensaku Tamaki
University of Tokyo

Brian Taylor
University of Hawaii

SAMPLE-DISTRIBUTION POLICY[1]

Distribution of Ocean Drilling Program (ODP) and Deep Sea Drilling Project (DSDP) samples is undertaken in order to (1) provide support to shipboard scientists in achieving the scientific objectives of their cruise and to support shore-based investigators who are preparing contributions to ODP reports, (2) provide individual investigators with materials to conduct detailed studies beyond the scope of ODP reports, (3) provide micropaleontological reference centers with samples for reference and comparison purposes, and (4) provide educators with samples for teaching purposes.

Funding for sample-related activities must be secured by the investigator independently of requesting the samples.

The Ocean Drilling Program Curator is responsible for distributing samples and for preserving and conserving core material. The Curator, who may accept advice from chairmen of the appropriate JOIDES advisory panels, is responsible for enforcing the provisions of this Sample Distribution Policy. He is responsible for maintaining a record of all samples that have been distributed, both on board ship and subsequently from the repositories, indicating the recipients and the nature of investigations proposed. This information is available to interested investigators on request.

Every sample distributed from the ship or from a repository is labeled with a standard identifier, which includes leg number, hole number, core and section numbers, and interval within the section from which the sample was removed. It is imperative that this standard identifier be associated with all data reported in the literature, and that residues of the sample remain labeled throughout their lives, so that later workers can relate the data to the cores.

Distribution of sample materials is made directly from the repositories (Lamont-Doherty Geological Observatory, Scripps Institution of Oceanography, and Texas A&M University) by the Curator or his designated representative.

1. *Distribution of Samples for Research Leading to Contributions to ODP Reports*

Any investigator who wishes to contribute to the reports of a scheduled cruise may write to the Curator, Ocean Drilling Program, 1000 Discovery Drive, College Station, Texas 77845-9547, U.S.A., in order to request samples from that cruise. Requests for a specific cruise must be received by the Curator at least TWO MONTHS in advance of the departure of that cruise, in order to allow time for review of the request in conjunction with other requests, so that a suitable shipboard sampling program can be assembled. The request should include a statement of the nature of the proposed research, the size and approximate number of samples required to complete the study, and any particular sampling technique or equipment which may be required. Requests will be reviewed by the Staff Representative and co-chief scientists of the cruise and by the Curator. Approval/disapproval will be based on the scientific requirements of the cruise as determined by the appropriate JOIDES advisory panel(s). The scope of a request must be such that samples can be processed, that proposed research can be completed, and that the paper can be written in time for submission to the relevant ODP cruise report.

Except for rare, specific instances involving ephemeral properties, the total volume of samples removed during a cruise-related sampling program will not exceed one-quarter of the volume of core recovered, and no interval will be depleted. One-half of all recovered materials will be retained in the archives in as pristine a condition as is practicable. Investigators requesting shipboard samples of igneous materials may receive a maximum of 100 igneous samples per cruise.

Because many sample requests are received for shipboard work and because the time of the shipboard party is at a premium, co-chief scientists are strongly urged to limit shipboard sampling to the minimum necessary to accomplish the cruise objectives. Shore-based investigators whose requests for cruise-related samples are approved should expect that they will receive the samples after the cores are returned to the repository, and should schedule research activities accordingly.

Co-chief scientists may invite investigators who are not cruise participants to perform special studies of selected core samples in direct support of shipboard activities. If this occurs, the names and addresses of these investigators and details of all samples loaned or distributed to them must be forwarded to the Curator, via the ODP Staff Representative to that cruise, immediately after the cruise. These investigators are expected to contribute to the cruise reports as though they had been cruise participants. All requirements of the Sample-Distribution Policy apply.

Any publication of results other than in ODP reports within twelve (12) months of completion of the cruise must be approved and authored by the whole shipboard party and, where appropriate, shore-based investigators. After twelve (12) months, individual investigators may submit related papers for open publication, provided they have already submitted their contributions to ODP reports and had them accepted. Investigations which are not completed in time for inclusion in the ODP reports for a specific cruise may be published in a later edition of the ODP reports; however, they may not appear in another journal until the report for which they were intended has been published.

2. *Distribution of Samples for Research Leading to Publication Outside of the ODP Reports*

   A. Researchers who wish to use samples for studies beyond the scope of the ODP reports should obtain sample request forms from the Curator, Ocean Drilling Program, 1000 Discovery Drive, College Station, Texas 77845-9547, U.S.A. Requestors are required to specify the quantities and intervals of core required, to make a clear statement of the nature of the proposed research, to state the time which will be required to complete the work and to submit results for publication, and to specify funding status and the availability of equipment and space for the research.

   Additionally, if the requestor has received samples from ODP or from DSDP previously, he/she will be required to account for the disposition of those samples by citing published works, four (4) copies of which must be sent to the Curator. If no report has been published, this requirement can be fulfilled by sending a brief (two- or three-page) report of the status of the research.

   If the requestor has never before received samples from ODP or DSDP, he/she will be required to show that the samples will be used for responsible research. This requirement can be met by providing the Curator with a copy of the requestor's résumé and bibliography. If the requestor is a student working on a higher degree, he/she can meet this requirement by sending a copy of his/her dissertation or research proposal endorsed by the student's advisor.

   Unused and residual samples should be returned and data should be sent to the Curator if the project has terminated. Paleontological materials may be returned either to the Curator at ODP or to one of the designated micropaleontological reference centers. If material is returned to a reference center, notify the Curator when it is sent.

   Requests for samples from researchers in industrial laboratories will be honored in the same manner as those from academic organizations. Industrial investigators have the same obligations as other investigators to publish all results promptly in the open literature and to provide the Curator with copies of all reports published and of all data acquired in their research.

   In order to ensure that all requests for highly desirable but limited samples can be considered together, approval of requests and distribution of samples will be delayed until twelve (12) months after completion of the cruise or two (2) months after official publication of the core descriptions, whichever occurs earlier. The only exceptions to this policy will be made for specific requests involving ephemeral properties. Requests for samples may be based on core descriptions published in ODP reports produced by the shipboard party, copies of which are on file at various institutions throughout the world. Copies of original core logs and data are kept on open file at ODP, and at the repositories at Lamont-Doherty Geological Observatory and Scripps Institution of Oceanography.

---

[1] Revised October 1988.

B. Most investigations can be accomplished handily with sample volumes of 10 mL or less. Investigators must provide explicit justification of requests for larger sample sizes or for frequent intervals within a core. Requests which exceed reasonable size or frequency limits will require more time to process and are unlikely to be granted in their entirety.

Requests for samples from thin layers, from stratigraphically important boundaries, or from sections which are badly depleted or in unusually high demand may be delayed in order to coordinate requests from several investigators or while the Curator seeks advice from the community. Investigators who submit such requests may expect to receive suggestions for alternative sampling programs or for joining with a research consortium which will share the samples. In any event, such exceptional requests will require more time for processing than will more routine requests.

Investigators who wish to study ephemeral properties may request a waiver of the twelve-month waiting period; however, such requests will be referred automatically to the relevant co-chiefs. If such a request is approved, the investigator will join the shore-based contributors to the shipboard science effort, and will incur the obligations thereof (see section 1).

C. Samples will not be provided until the requestor assures the Curator that funding for the proposed research is available or unnecessary. If a sample request is dependent in any way on proposed funding, the Curator is prepared to provide the proposed funding organization with information on the availability (or potential availability) of suitable samples.

D. Investigators who receive samples incur the following obligations:

(1) To publish significant results promptly; however, no contribution may be submitted for publication prior to twelve (12) months following the termination of the relevant leg unless it is approved and authored by the entire shipboard party.

(2) To acknowledge in all publications that the samples were supplied through the assistance of the international Ocean Drilling Program and others as appropriate.

(3) To submit four (4) copies of reprints of all published works to the Curator, Ocean Drilling Program, 1000 Discovery Drive, College Station, Texas 77845-9547, U.S.A. These reprints will be distributed to the repositories and to the ship. All reprints received will be logged in an on-line bibliographic data base.

(4) To submit all final analytical data obtained from the samples to the Data Librarian, Ocean Drilling Program, 1000 Discovery Drive, College Station, Texas 77845-9547, U.S.A. Please consult announcements in the *JOIDES Journal* or call (409–845-2673) for information on acceptable data formats. Investigators should be aware that they may have other data obligations under the National Science Foundation's Ocean Science Data Policy or under relevant policies of other funding agencies which require submission of data to national data centers.

(5) To return all unused or residual samples, in good condition and with a detailed explanation of any processing they may have undergone, upon termination of the proposed research. In particular, all thin sections and smear slides manufactured on board the vessel or in the repositories are to be returned to the Curator. Paleontological materials may be returned either to the Curator at ODP or to one of the designated micropaleontological reference centers.

Failure to honor these obligations will prejudice future applications for samples.

E. Cores are available for examination by interested parties at the repositories. Investigators are welcome to visit the repositories in order to inspect cores and to specify sample locations when that is required for their research; however, time and space in the workrooms are limited, so advance appointments are required. Occasionally, the space may be fully booked several weeks in advance, so investigators are urged to call for appointments well ahead in order to avoid disappointment. Only the Curator or his delegate may actually remove samples from the cores.

F. A reference library of thin sections, smear slides, and archive photographs is maintained in the repositories for the use of visiting investigators. All thin sections and smear slides produced on board the ship or in repositories belong to this library.

3. *Distribution of Samples to Micropaleontological Reference Centers*

As a separate and special category of repository activity, selected samples are distributed to micropaleontological reference centers, where the prepared material may be studied by visitors. Foraminifers, calcareous nannofossils, and diatoms can be viewed; radiolarians will be prepared in the future. The present centers are (1) U.S. East Coast: Lamont-Doherty Geological Observatory, Palisades, NY 10964 (Ms. Rusty Lotti; telephone, 914–359-2900; telex, 7105762653 LAMONTGEO); (2) U.S. National Museum: Smithsonian Institution, Washington, D.C. 20560 (Dr. Martin Buzas; telephone, 202–357-1390; telex, 264729); (3) U.S. Gulf Coast: Texas A&M University, Department of Oceanography, College Station, TX 77843 (Dr. Stefan Gartner; telephone, 409–845-8479; telex, 792779/ODP TAMU); (4) U.S. West Coast: Scripps Institution of Oceanography, La Jolla, CA 92093 (Dr. William Riedel; telephone, 619–534-4386); telex, 910337127 IUC WWD SIOSDG); (5) Western Europe: Natural History Museum, CH-4001 Basel, Switzerland (Mr. J. B. Saunders; telephone, 061-29-55-64); (6) U.S.S.R.: Institute of the Lithosphere, Staromonet 22, Moscow 109180, U.S.S.R. (Dr. Ivan Basov; telephone, 231-48-36); (7) Japan: National Science Museum, Department of Geology, 3-23-1 Hyakunin-cho, Shinjuku-ku, Tokyo 160, Japan (Dr. Y. Tanimura; telephone, 03-364-2311; telemail, 03-364-2316); (8) New Zealand: New Zealand Geological Survey, P.O Box 30368, Lower Hutt, New Zealand (Dr. Tony Edwards; telephone, (04) 699059).

Further details concerning the micropaleontological reference centers are reported periodically in the *JOIDES Journal*.

4. *Distribution of Samples for Educational Purposes*

Samples may be available in limited quantities to college-level educators for teaching purposes. Interested educators should request application forms from the Curator, Ocean Drilling Program, 1000 Discovery Drive, College Station, Texas 77845-9547, U.S.A. Requestors are required to specify preferred sample size and location, to make a very clear statement of the nature of the course work in which the samples will be used, to explain how the samples will be prepared and how they will be used in the classroom, to explain in detail why similar materials derived from outcrops or dredge hauls cannot be used (it is NOT acceptable to argue that it requires less effort for the requestor to obtain samples from ODP than to assemble them from other sources), and to certify that funds are available to prepare the materials for classroom use. In general, only samples of materials which are abundant in the collection and which are in little demand for research purposes should be requested for educational purposes. The Curator will not approve requests for materials which are limited in supply or for which demand (real or potential) is great, including most paleontological materials.

5. *Distribution of Data*

The Deep Sea Drilling Project and the Ocean Drilling Program have routinely captured much of the data generated on board ship and published in Program reports. Additionally, data supplied by investigators who have received samples are incorporated into the data bases, so data sets which are larger than can be published are available to investigators. Magnetic, downhole-logging, seismic-reflection, bathymetric, and other data collected by the drilling vessel become available for distribution to investigators at the same time as core samples.

Requests for ODP and DSDP data should be addressed to the Data Librarian, Ocean Drilling Program, 1000 Discovery Drive, College Station, Texas 77845-9547, U.S.A. Many varieties of DSDP data are included in ODP data bases. Information on sources of DSDP data is available from the ODP Data Librarian.

A charge will be made to recover material expenses greater than $25.00 incurred in filling individual requests. If required, estimates of charges can be furnished before the work is performed.

Chart Transposed to

End of Volume.

Drilling locations

Leg	Location	Sites
Phase 1 1968–1970		
1	North Atlantic	1–7
2	North Atlantic	8–12
3	South Atlantic	13–22
4	Central Atlantic	23–31
5	North Pacific	32–43
6	North Pacific	44–60
7	Central Pacific	61–67
8	Central Pacific	68–75
9	Central Pacific	76–84
Phase 2 1970–1972		
10	Gulf of Mexico	85–97
11	North Atlantic	98–108
Re-entry trials		109–110
12	North Atlantic	111–119
13	Mediterranean	120–134
14	Central Atlantic	135–144
15	Caribbean	146–154
16	Central Pacific	155–163
17	Central Pacific	164–171
18	North Pacific	172–182
19	North Pacific	183–193
20	North Pacific	194–202
21	Coral Sea	203–210
22	Indian Ocean	211–218
23	Arabian Sea	219–230
24	Indian Ocean	231–238
25	Indian Ocean	239–249
Phase 3 1972–1975		
26	Indian Ocean	250–258
27	Indian Ocean	259–263
28	Antarctic	264–274
29	Tasman Sea	275–284
30	South Pacific	285–289
31	North Pacific	290–302
32	North Pacific	303–313
33	North Pacific	314–318
34	South Pacific	319–321
35	South Pacific	322–325
36	South Atlantic	326–331
37	North Atlantic	332–335
38	Arctic	336–352
39	Atlantic	353–359
40	South Atlantic	360–365
41	South Atlantic	366–370
42A	Mediterranean	371–378
42B	Black Sea	379–381
43	North Atlantic	382–387
44	North Atlantic	388–392
44A	North Atlantic	393–394
IPOD 1 1975–1983		
45	North Atlantic	395–396
46	North Atlantic	396A–396B
47	North Atlantic	397–398
48	North Atlantic	399–406
49	North Atlantic	407–414
50	North Atlantic	415–416
51A	North Atlantic	417–417A
51B	North Atlantic	417B–417D
52	North Atlantic	417D–418A
53	North Atlantic	418A–418B
54	Central Pacific	419–429
55	North Pacific	430–433
56	North Pacific	434–437
57	North Pacific	438–441
58	North Pacific	442–446
59	North Pacific	447–451
60	North Pacific	452–461
61	Central Pacific	462
62	North Pacific	463–466
63	North Pacific	467–473
64	Gulf of California	474–481
65	Gulf of California	482–485
66	Central Pacific	486–493
67	Central Pacific	494–500
68	Central Pacific	502–503
69	Central Pacific	504–505, 501
70	Central Pacific	506–510, 504B
71	South Atlantic	511–514
72	South Atlantic	515–518
73	South Atlantic	519–524
74	South Atlantic	525–529
75	South Atlantic	530–532
76	North Atlantic	533–534
77	Caribbean	535–540
78	North Atlantic	541–543, 395A, B
79	North Atlantic	544–547
80	North Atlantic	548–551
81	North Atlantic	552–555
82	North Atlantic	556–564
83	Central Pacific	504B
84	Central Pacific	565–570
85	Central Pacific	571–575
86	North Pacific	576–581
87	North Pacific	582–584
88	North Pacific	581
89	Central Pacific	585–586, 462A
90	South Pacific	587–594
91	Central Pacific	595–596
92	Central Pacific	597–602, 504B
93	North Atlantic	603–605
94	North Atlantic	606–611
95	North Atlantic	612–613, 603
96	Gulf of Mexico	614–624

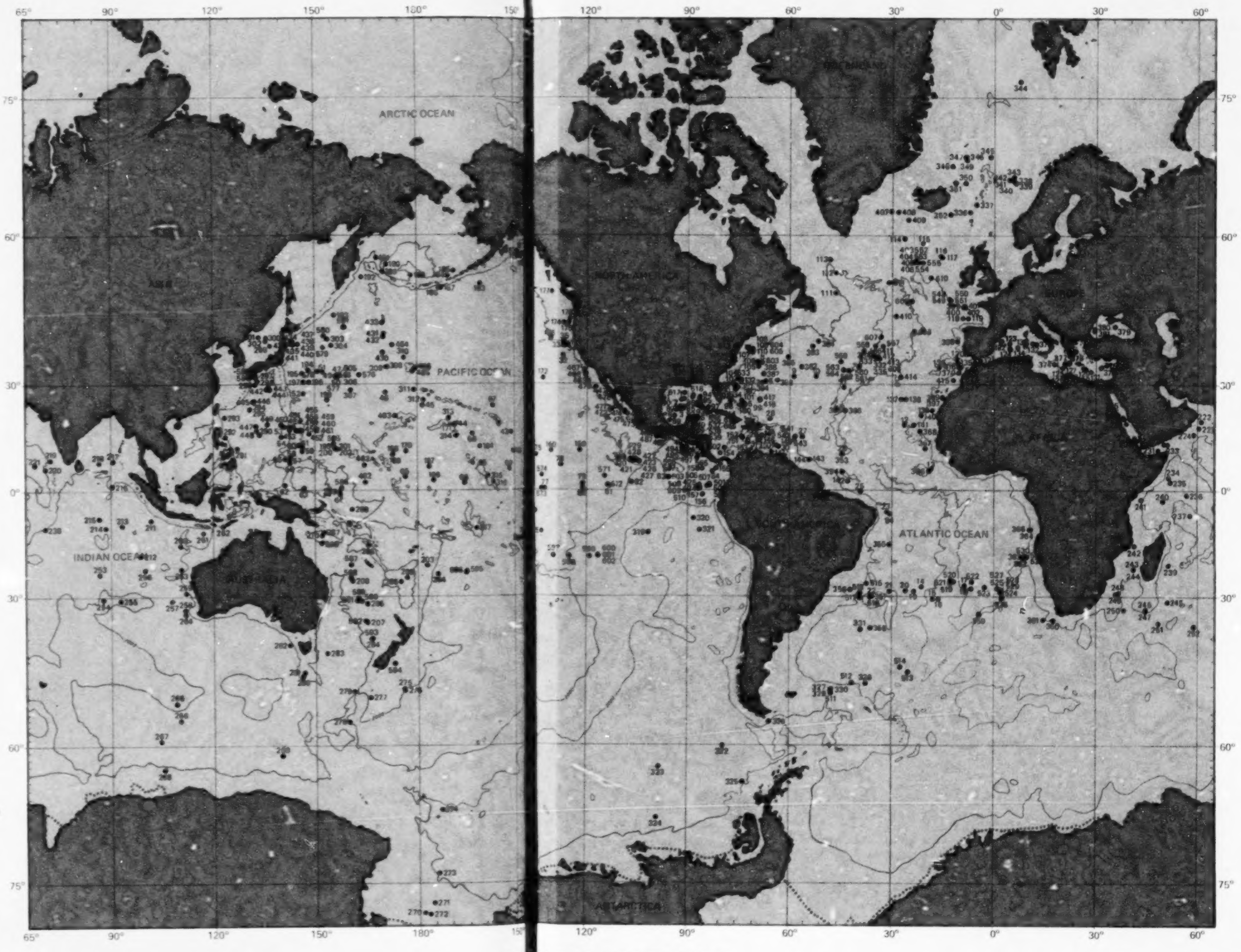

DE EA DRILLING PROJECT

Texas A&M University, Science Operator

ISSN 0884-5883

126

Volume 126A: Chapter 4: Figure 3. Forearc basin multichannel seismic (MCS) data. VE = 6.7.

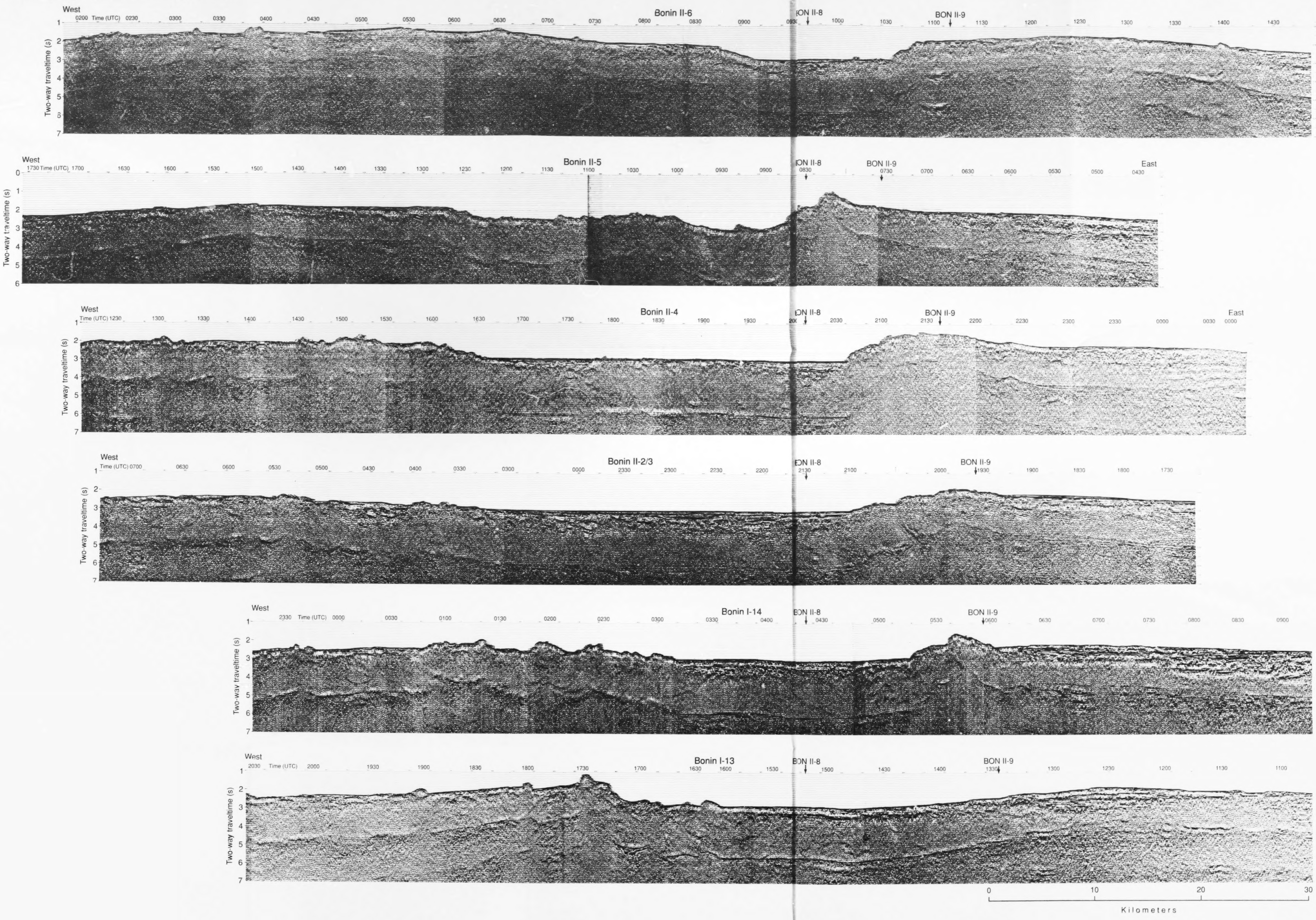

NS1-38/2:

Volume 126A: Chapter 4: Figure 10. Sumisu Rift MCS data.

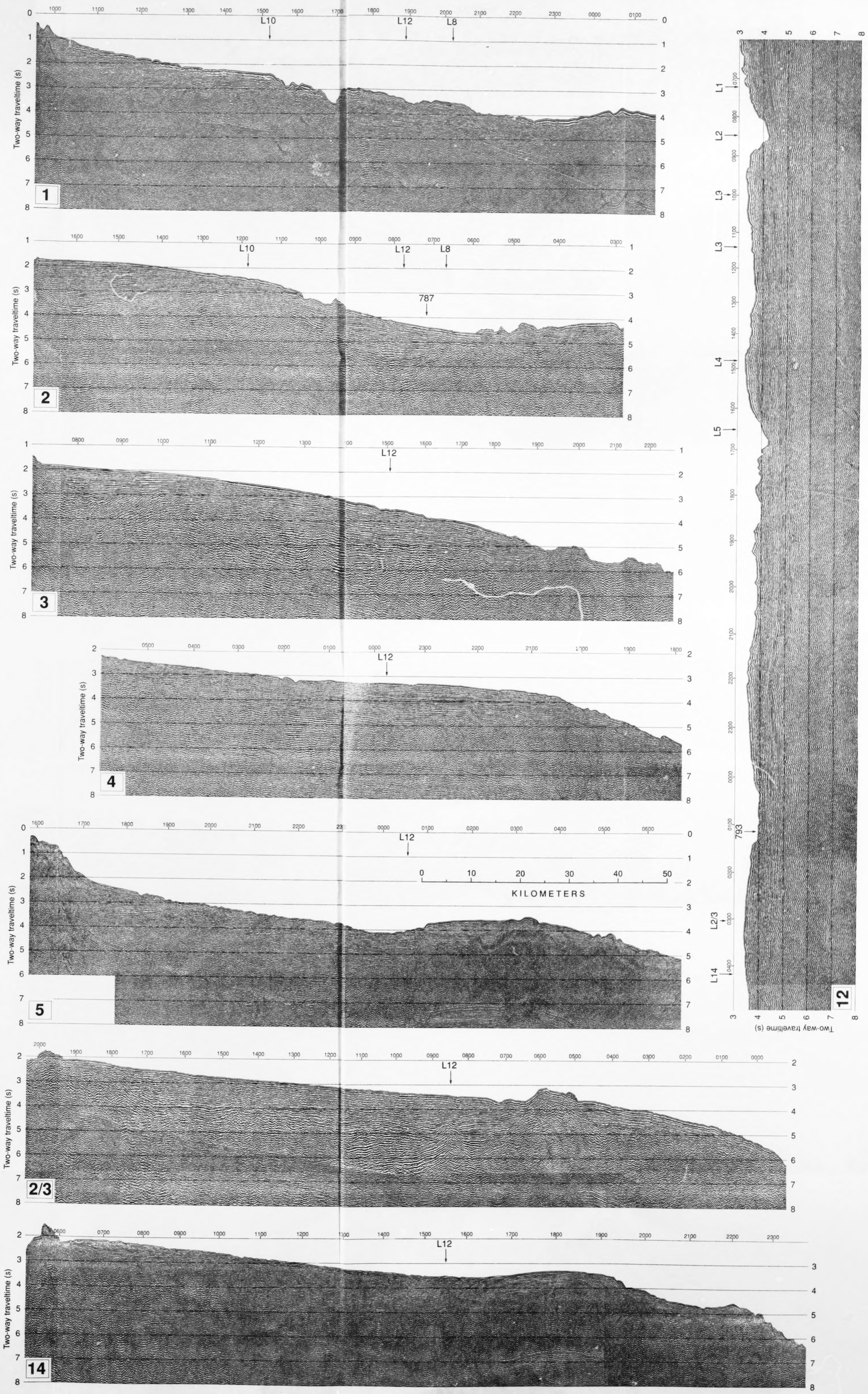

best copy available

Schlumberger

DIPMETER
COMPUTED
RESULT

FORMATION
MICRO-SCANNER

A Borehole Imaging System

* A Mark of Schlumberger

Using the following logs: 4 PAD FMS

Company:	OCEAN DRILLING PROJECT		
Well:	HOLE 792-E		
Field:	BONIN ARC		
County	OFFSHORE		
State			
Reference No:	14765	Run no.	1
Date Logged:	24-JUN-1989	Date Processed:	8-FEB-1990

Elevations: KB: 35.40 DF: 34.4 GL: 0.00

Permanent Datum: 0.00 Depth Units: METRES

FOLD HERE

The well name, location and borehole reference data were furnished by the customer.

All interpretations are opinions based on inferences from electrical or other measurements and we cannot, and do not guarantee the accuracy or correctness of any interpretations, and we shall not, except in the case of gross or willful negligence on our part, be liable or responsible for any loss, costs, damages or expenses incurred or sustained by anyone resulting from any interpretations made by any of our officers, agents or employees. These interpretations are also subject to Clause 4 of our General Terms and Conditions as set out in our current

FIELD RECORDING	Engineer:	DIANA	Location:	HOOS	Cyberpack Version:	31.360
COMPUTATION	Analyst	D LEE	Center	HDC	Baseline:	16.3

Remarks

STATIC IMAGES

STATIC IMAGES

ZONE FROM 2104.0 M TO 2090.0 M

DEPTH SCALE = 1/ 5

IMAGE SCALE = 1/ 5

BITSIZE = 9.88

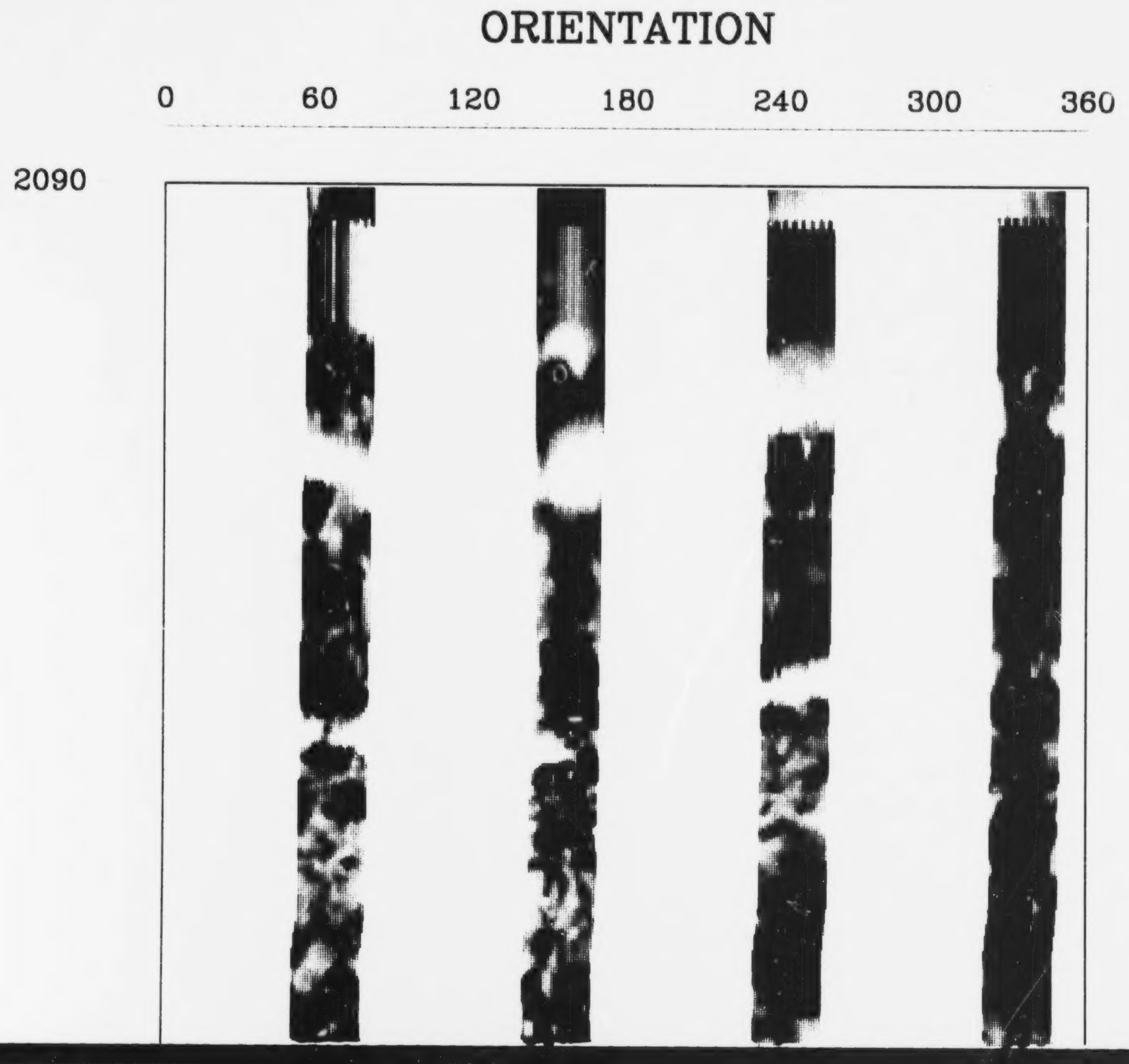

2091

2092

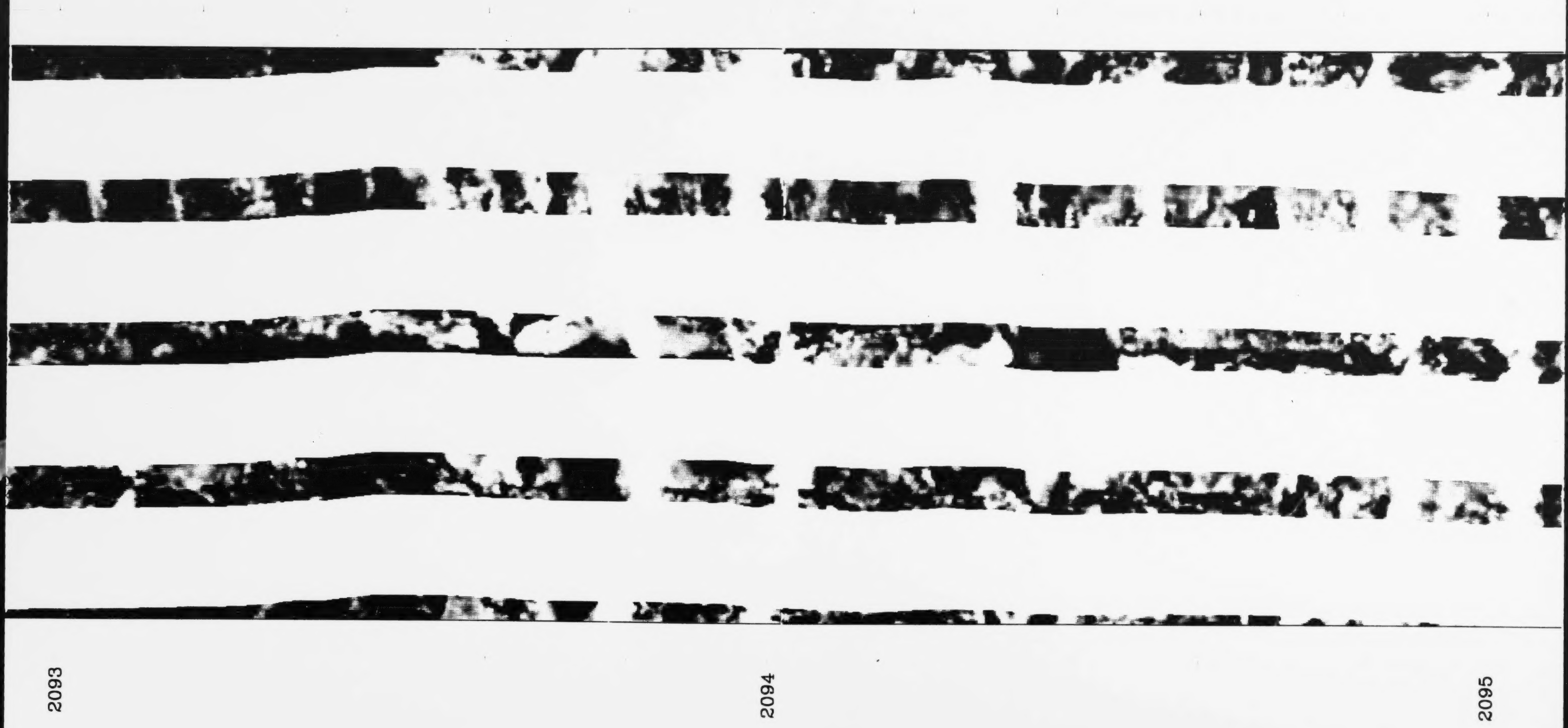
2093
2094
2095

2096

2097

2098

2099

2100
2101

2102
2103

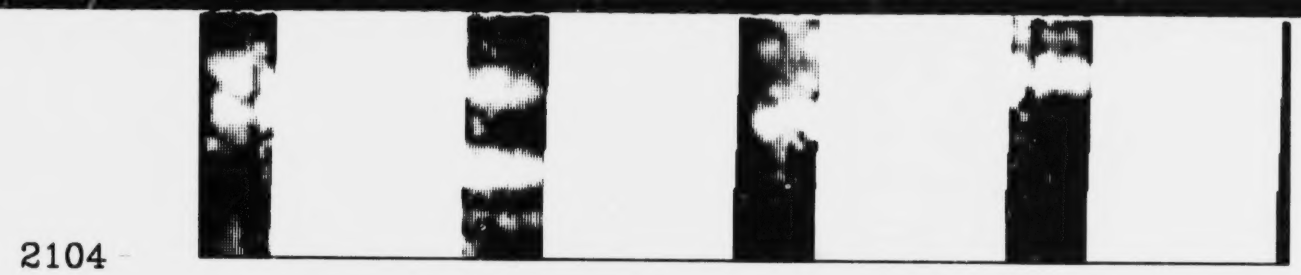

STATIC IMAGES

ZONE FROM 2144.0 M TO 2104.0 M

DEPTH SCALE = 1/ 5

IMAGE SCALE = 1/ 5

BITSIZE = 9.88

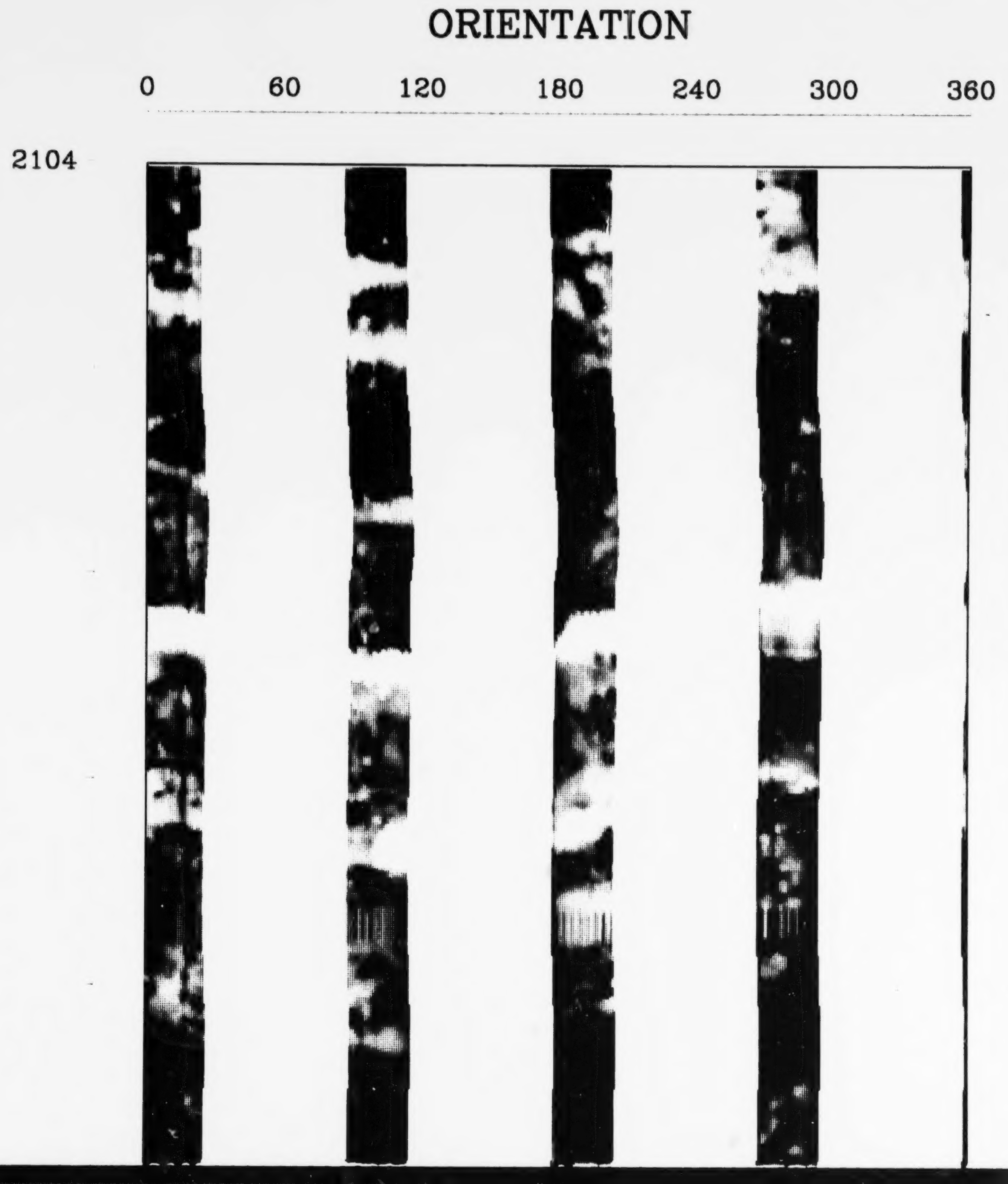

2105
2106
2107

2108
2109

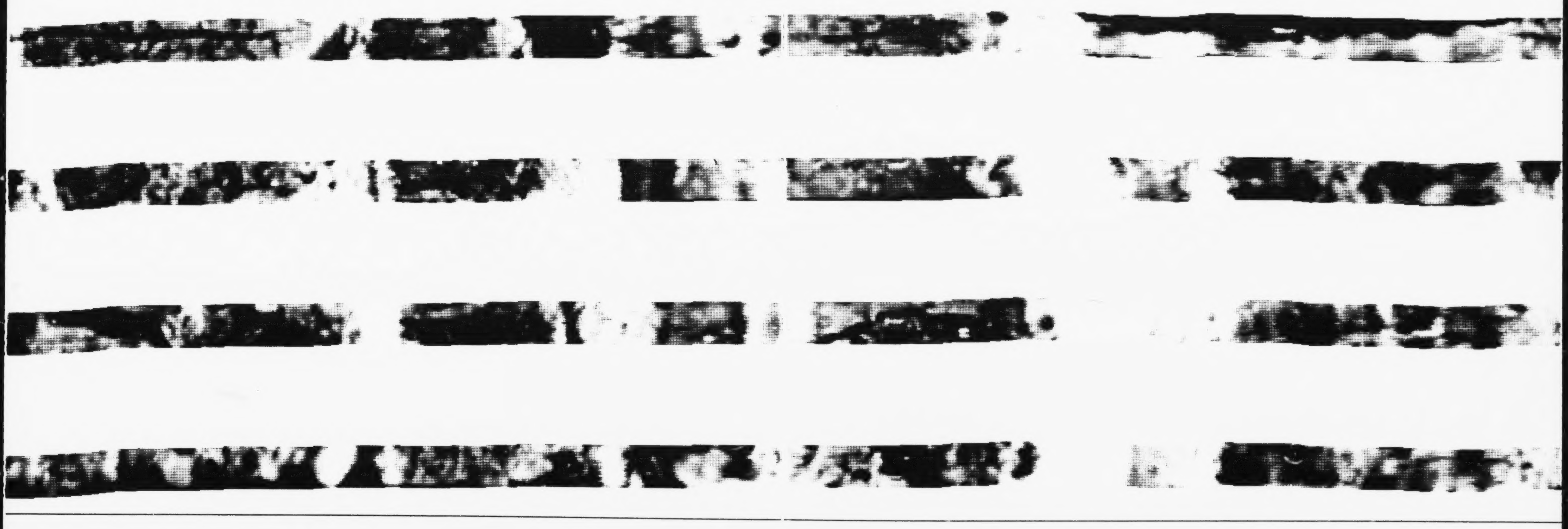

2110
2111

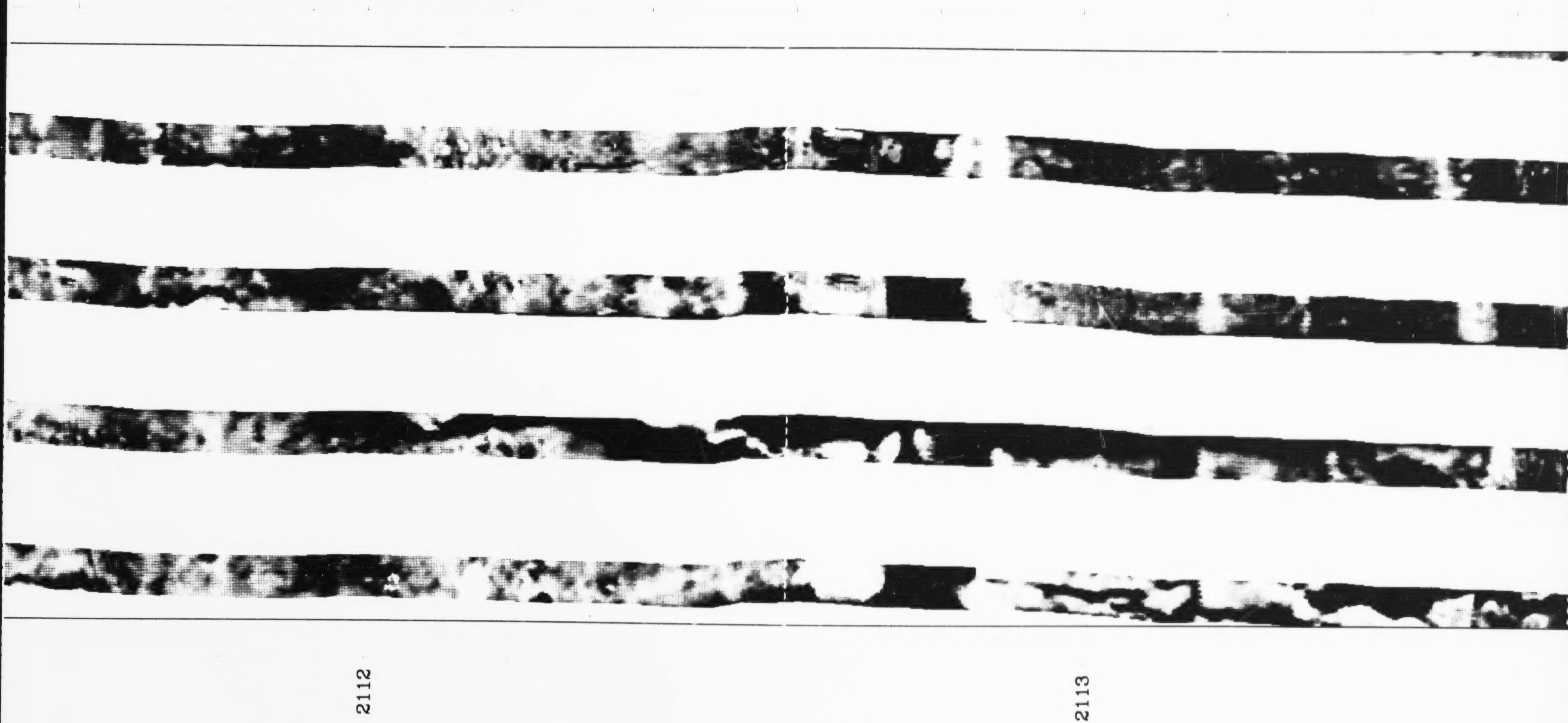

2112
2113

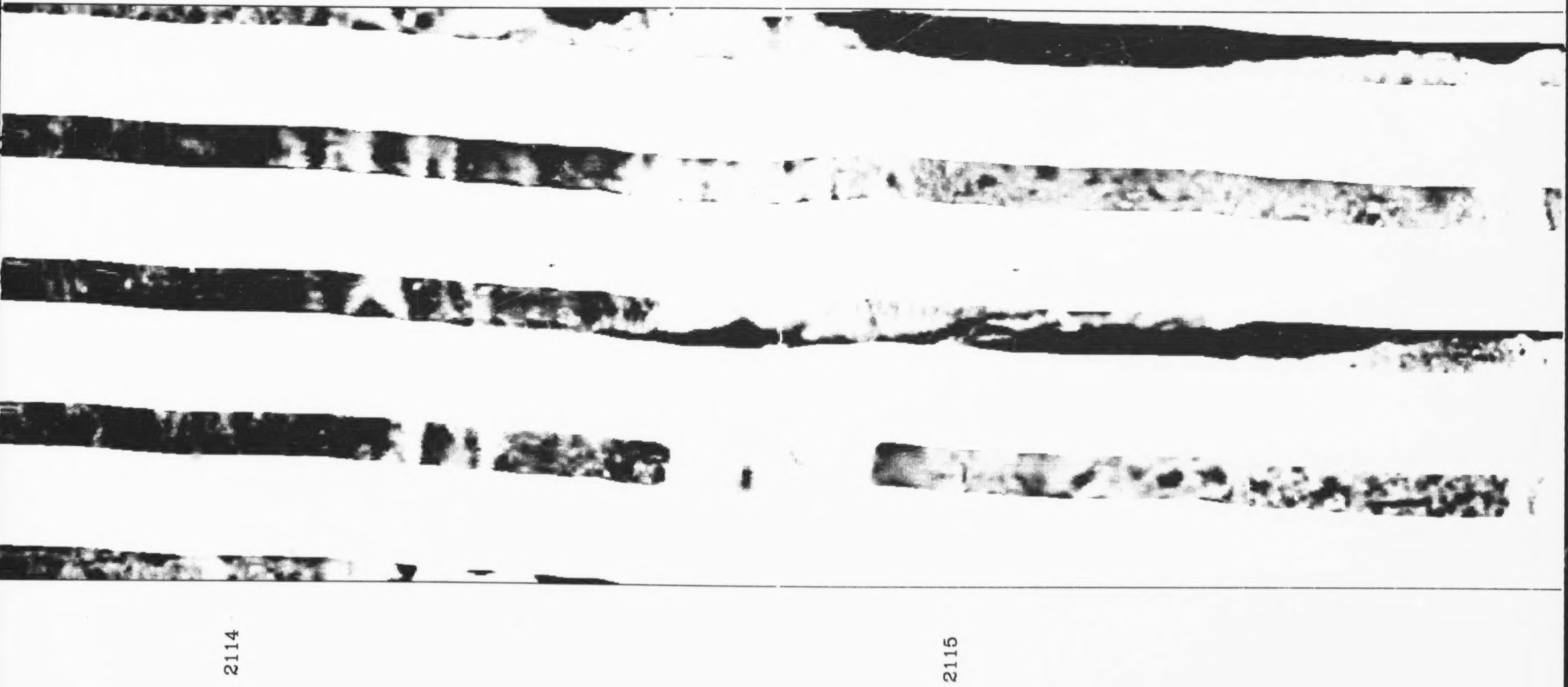
2114
2115

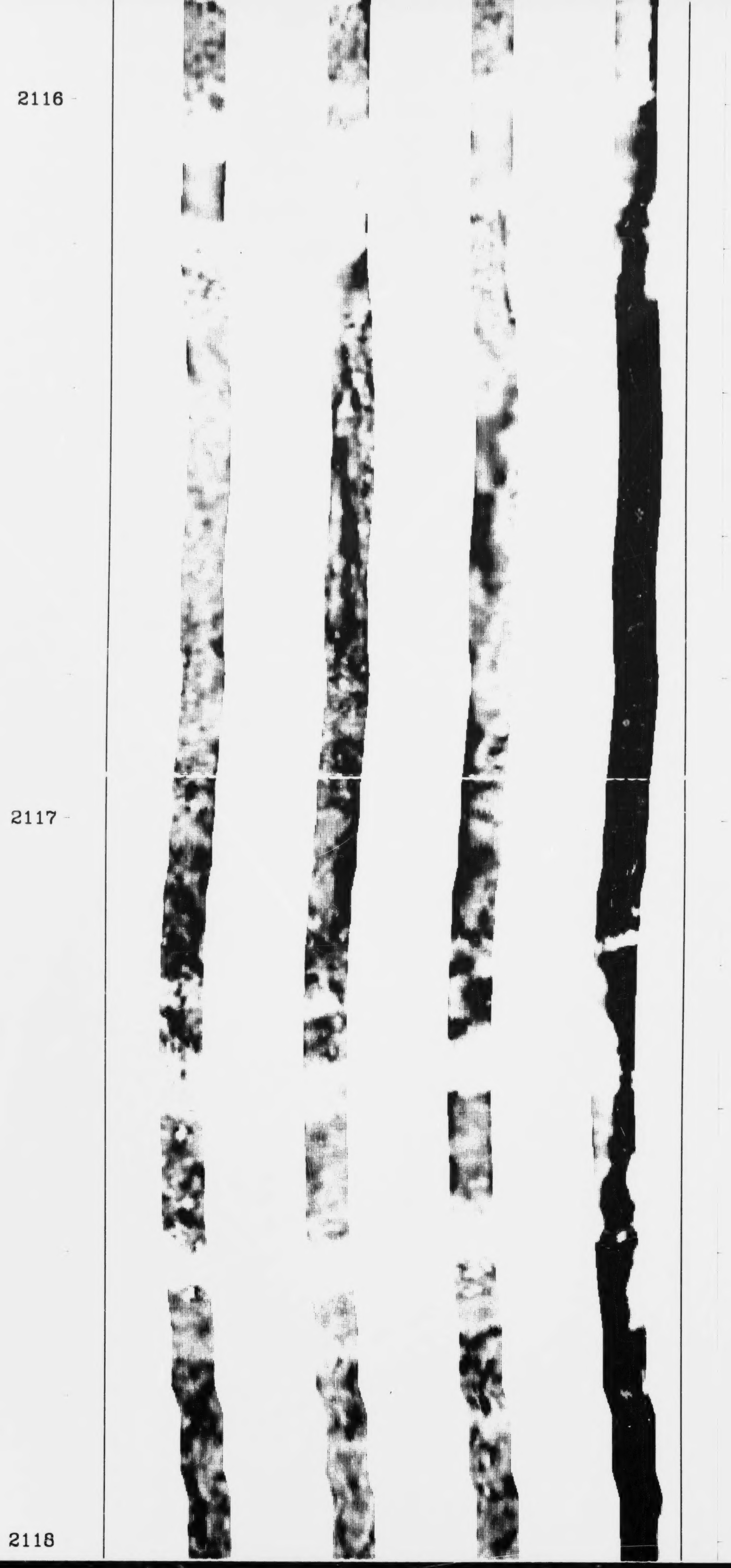

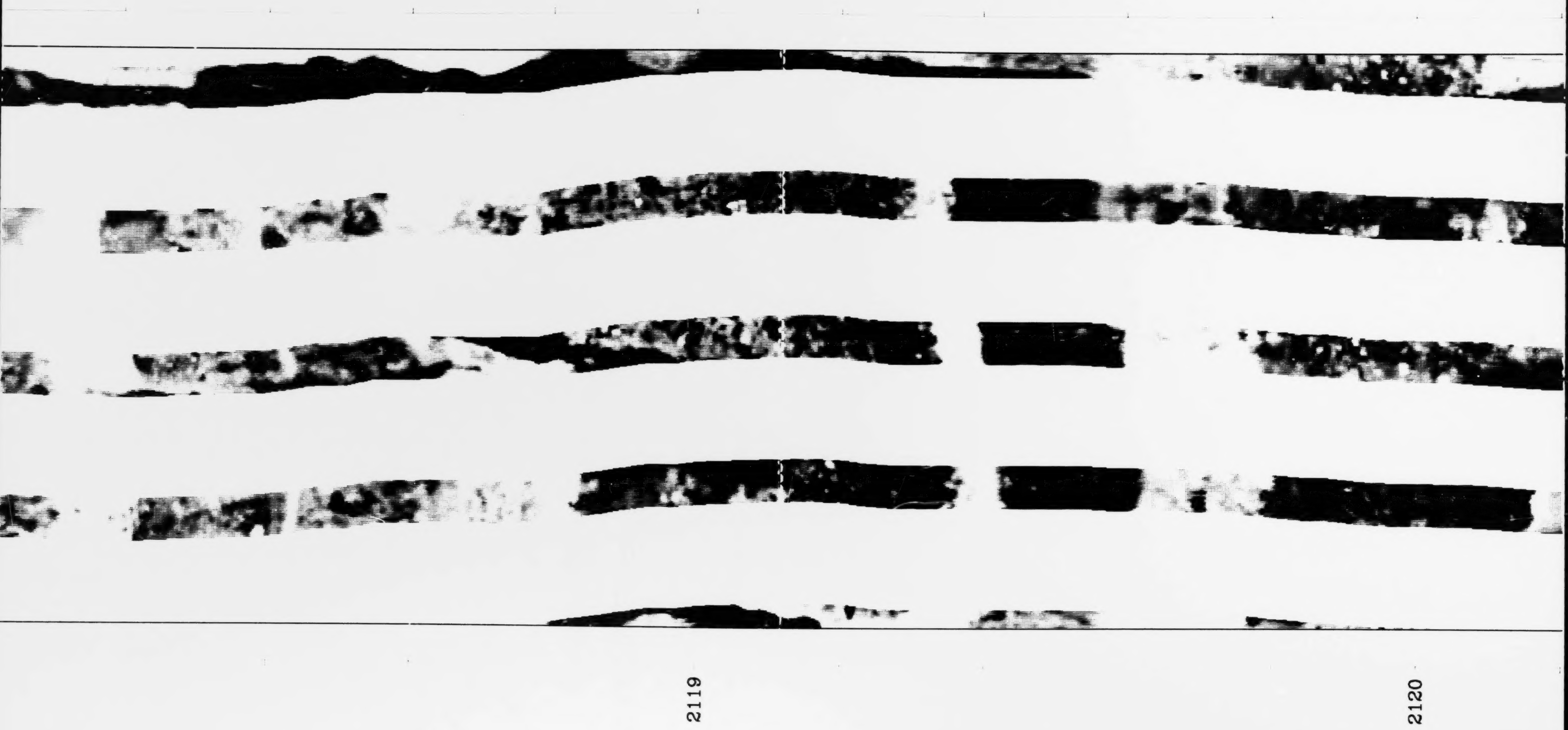
2119
2120

2121
2122

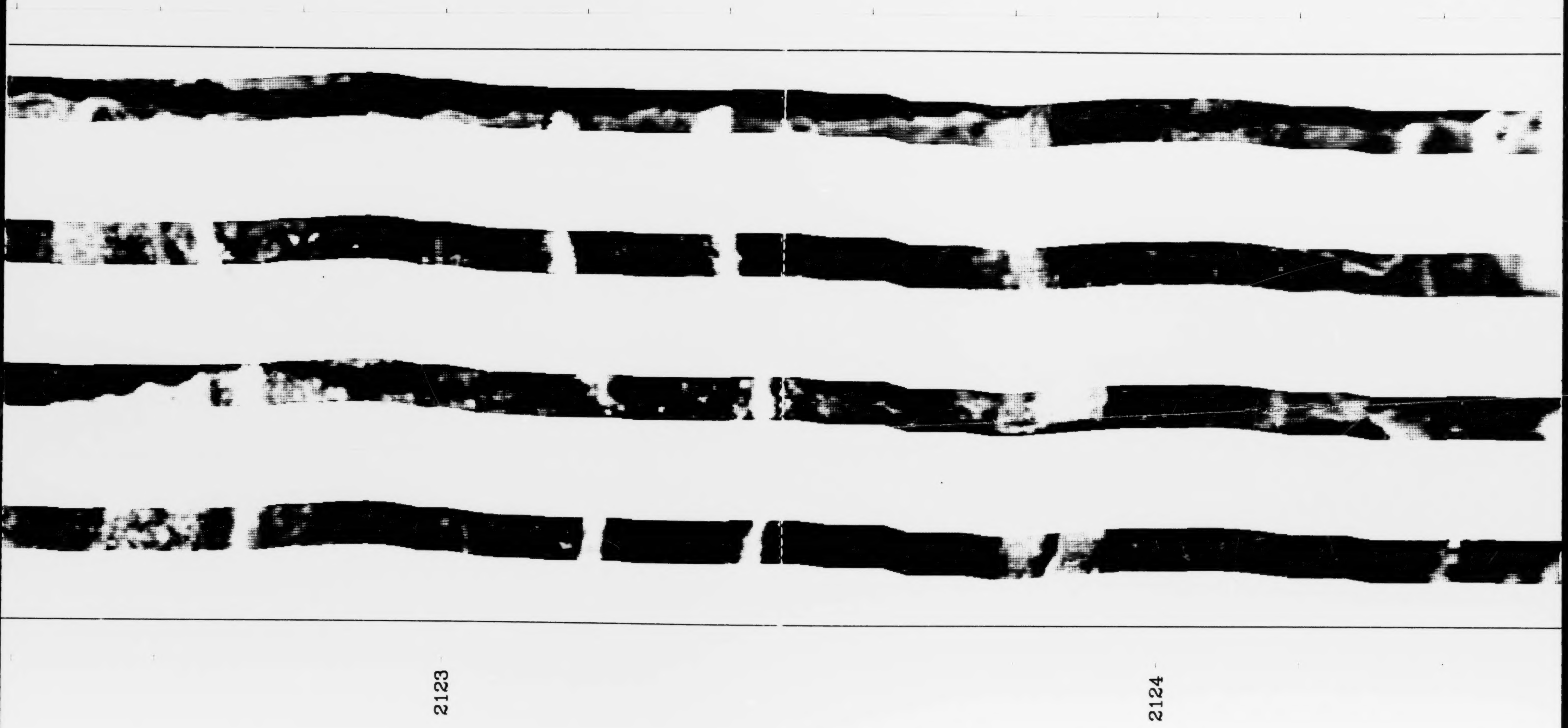
2123
2124

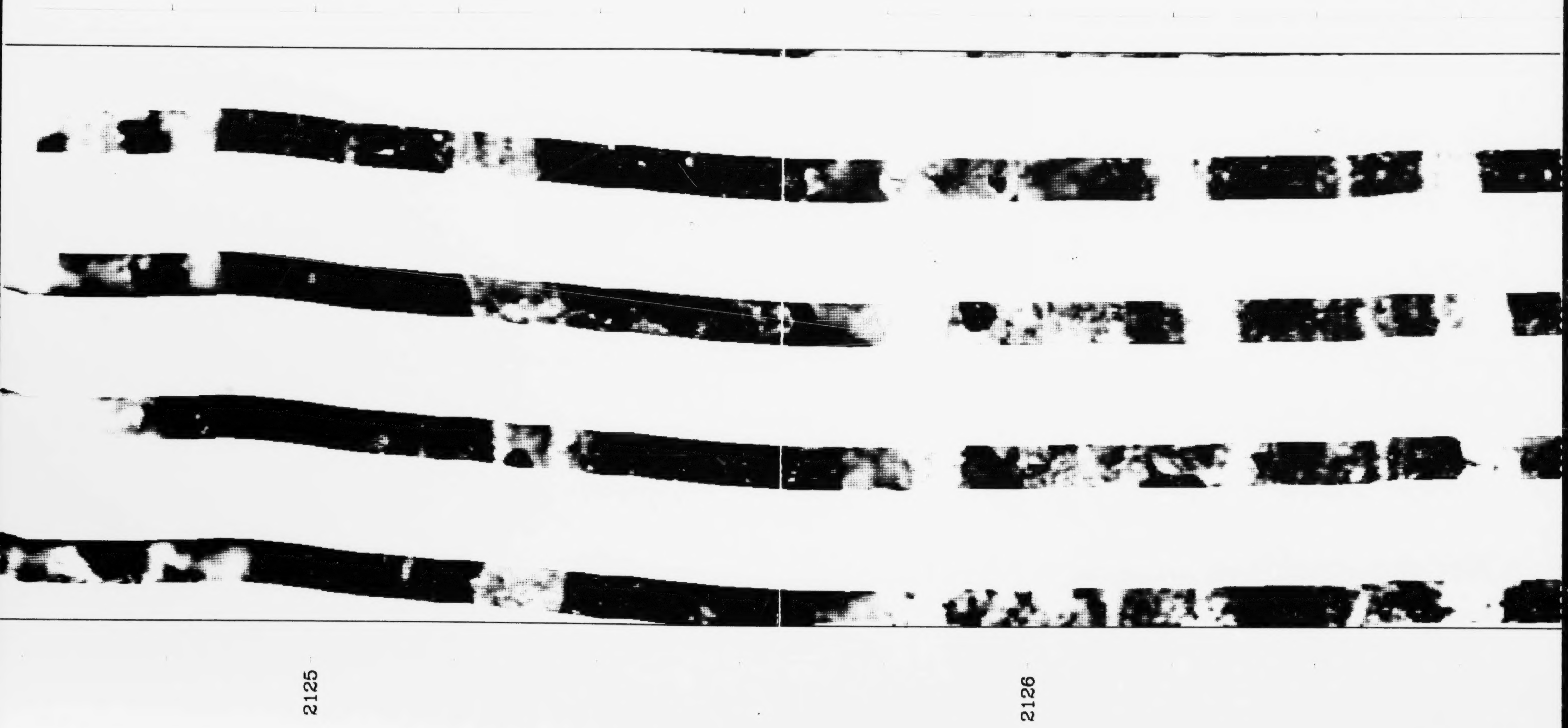
2125
2126

2127
2128

2129
2130
2131

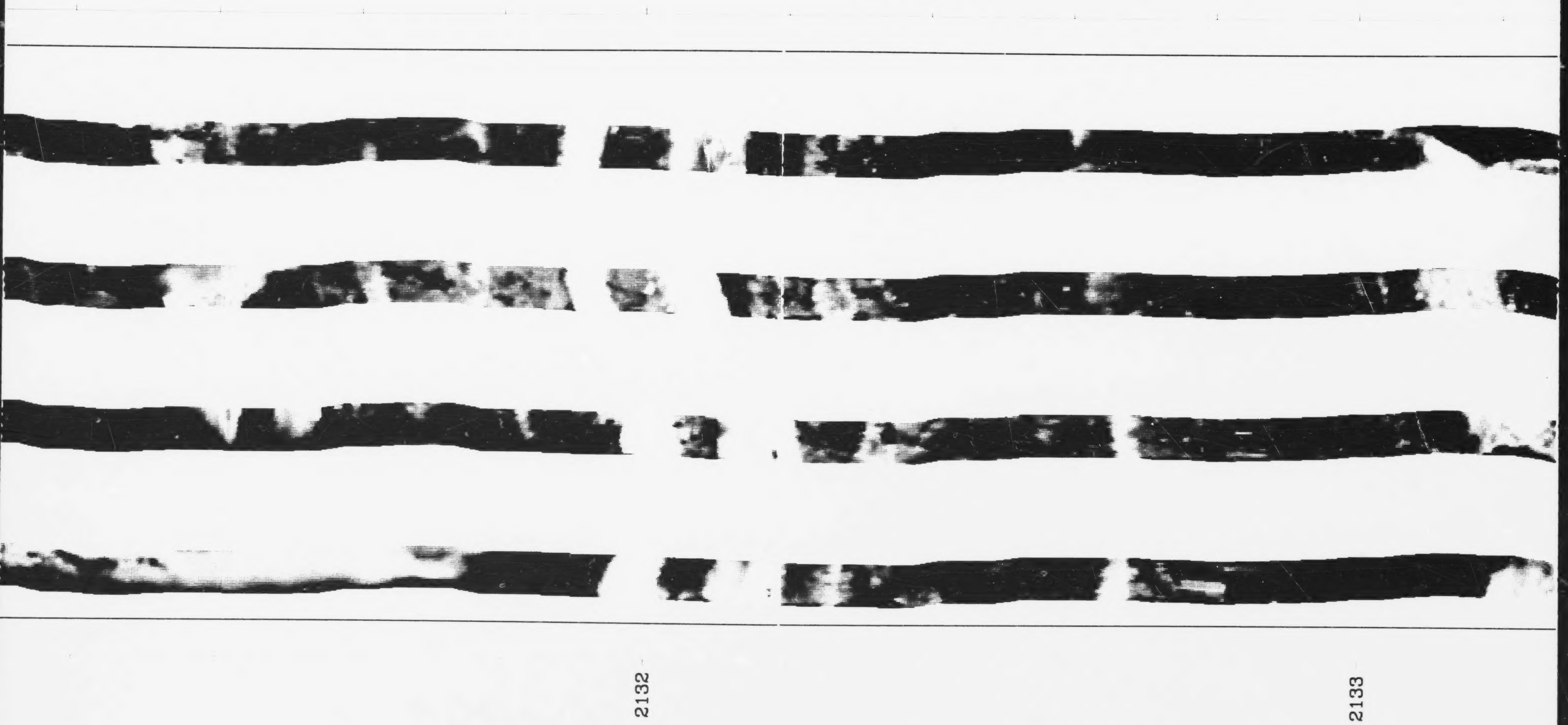
2132
2133

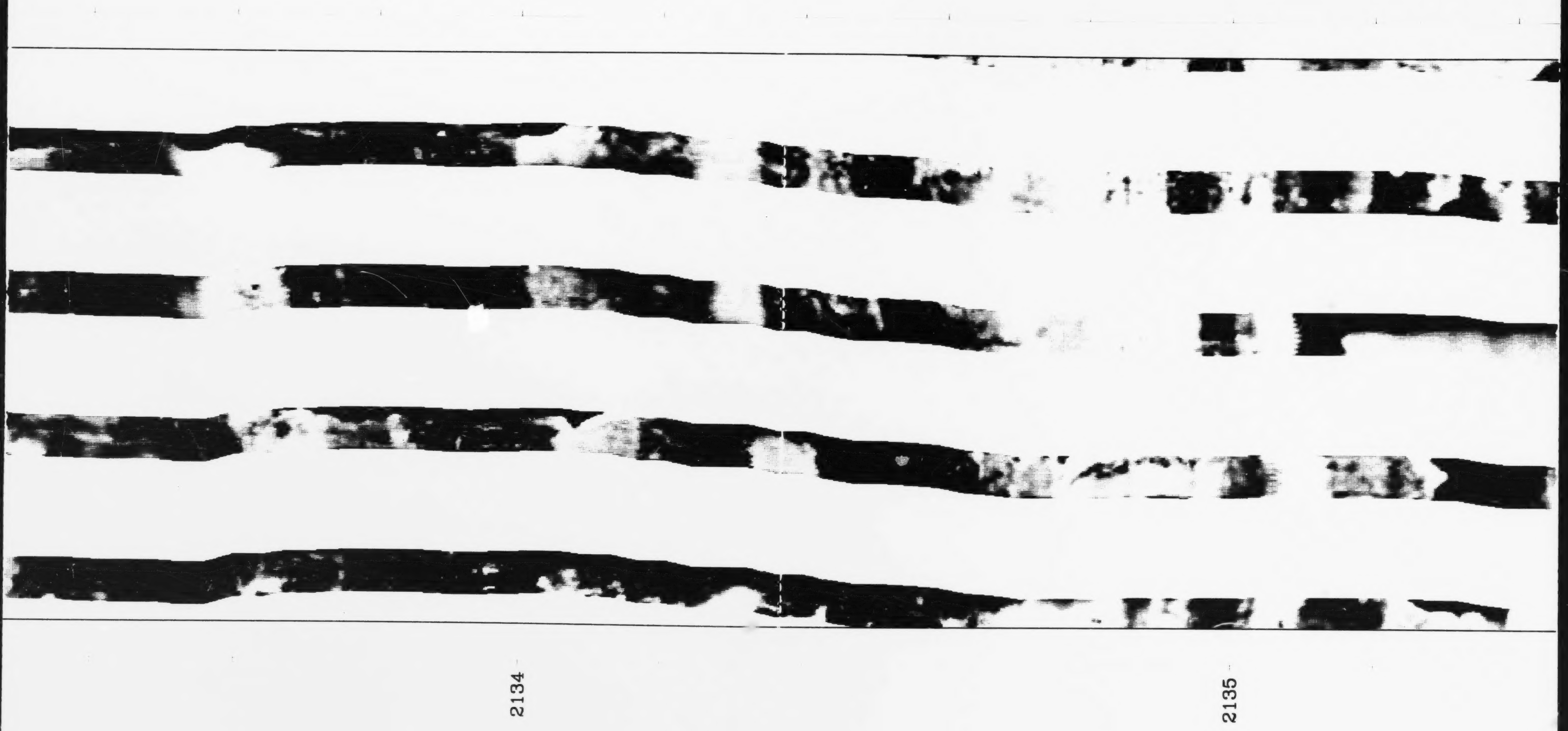
2134
2135

2136
2137

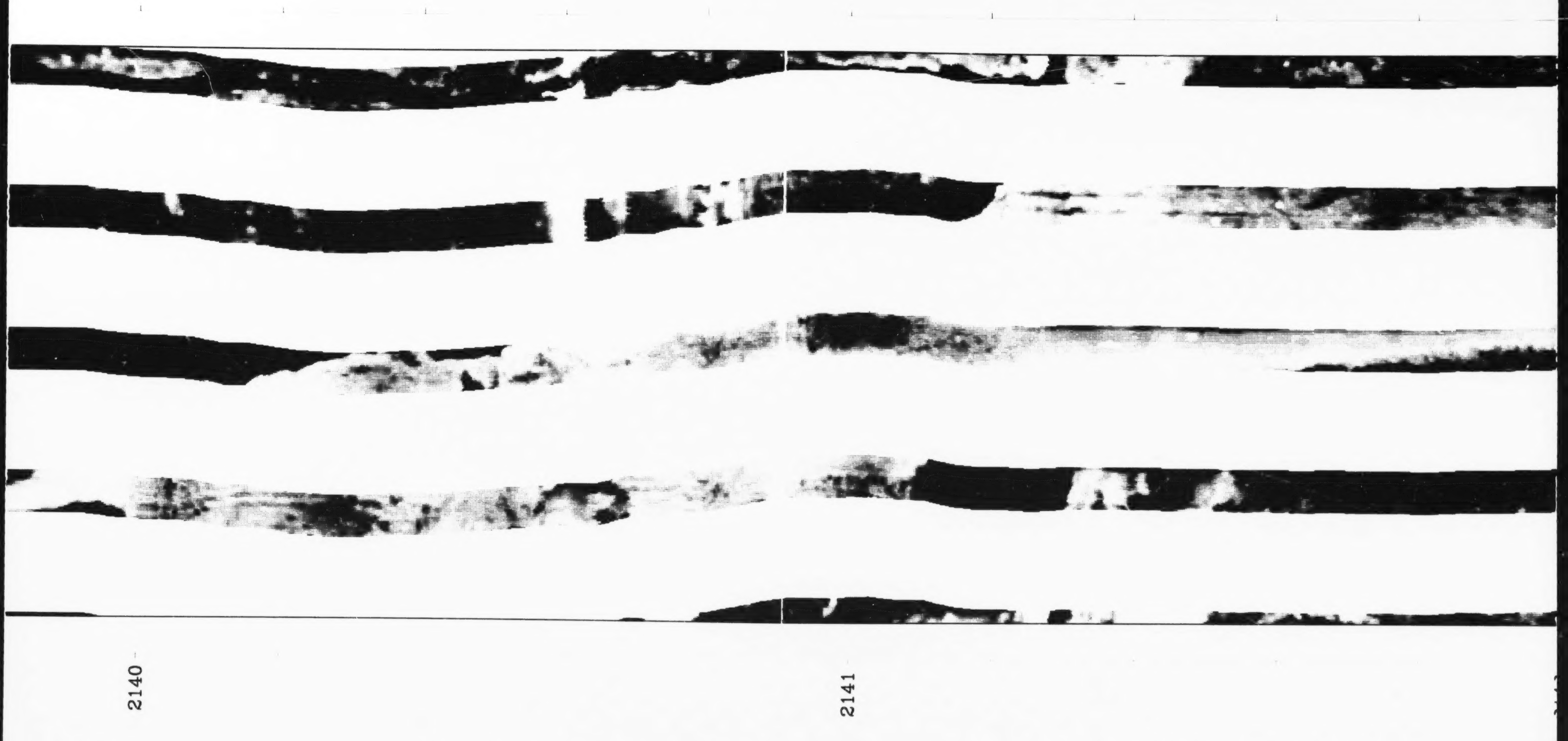
2140
2141

2142
2143
2144

STATIC IMAGES

ZONE FROM 2184.0 M TO 2144.0 M

DEPTH SCALE = 1/ 5

IMAGE SCALE = 1/ 5

BITSIZE = 9.88

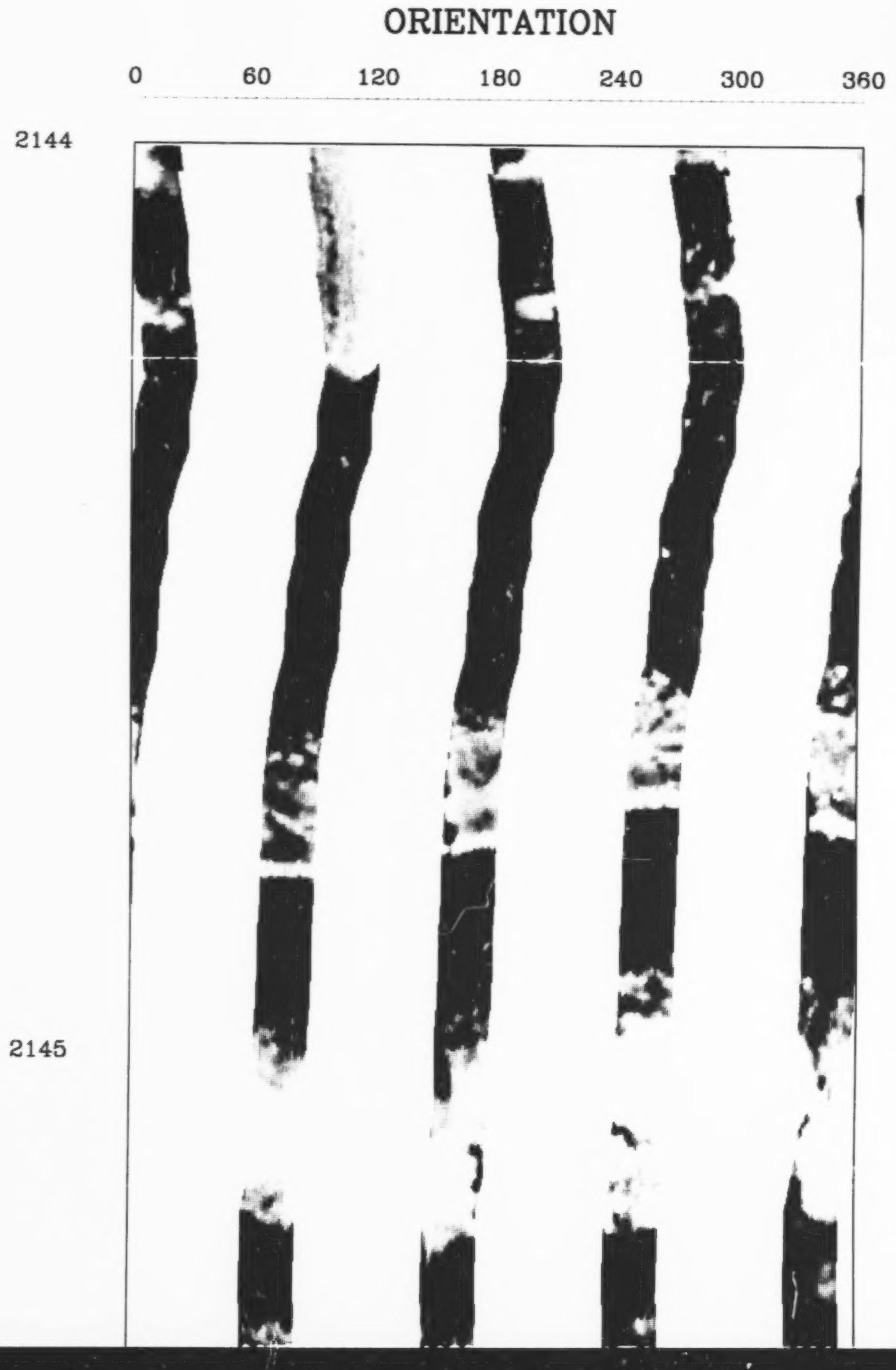

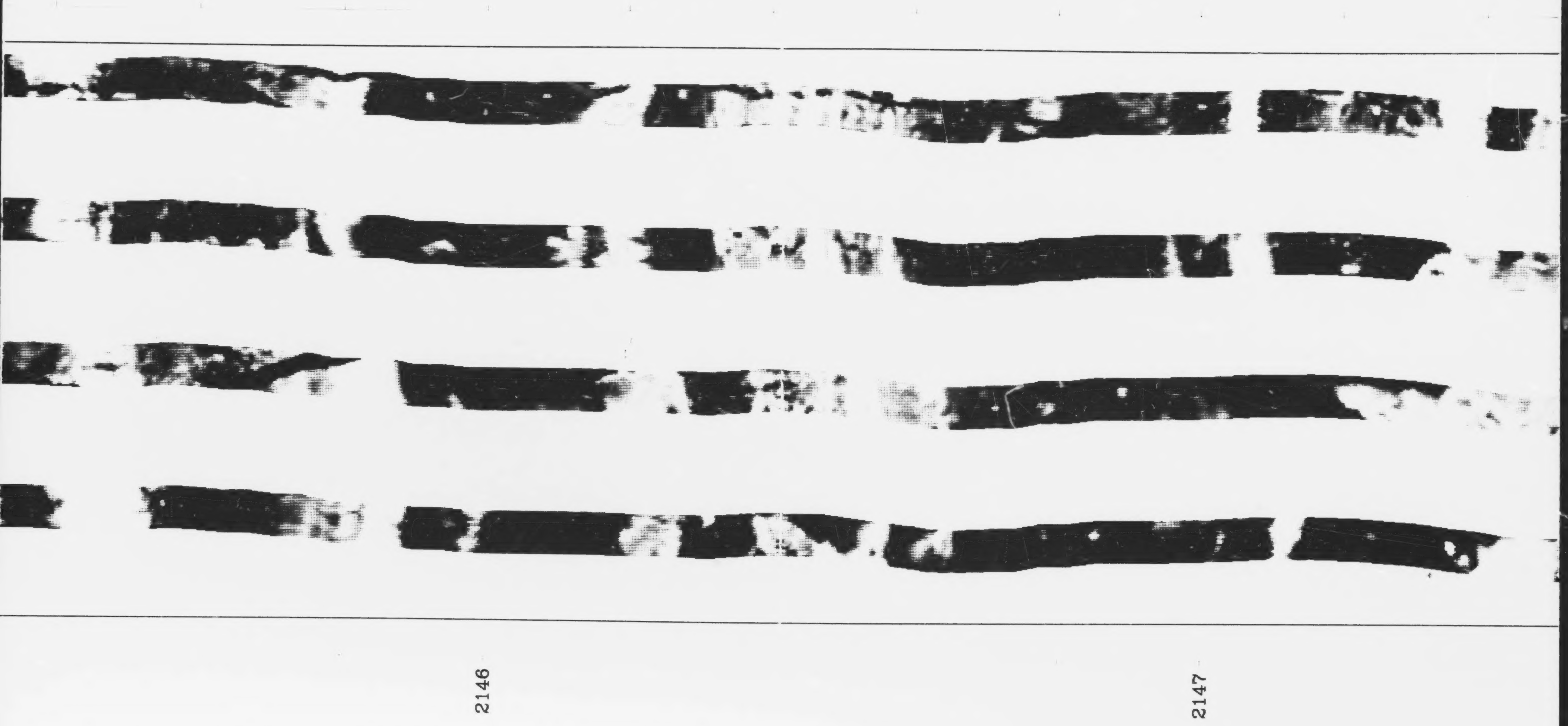
2146
2147

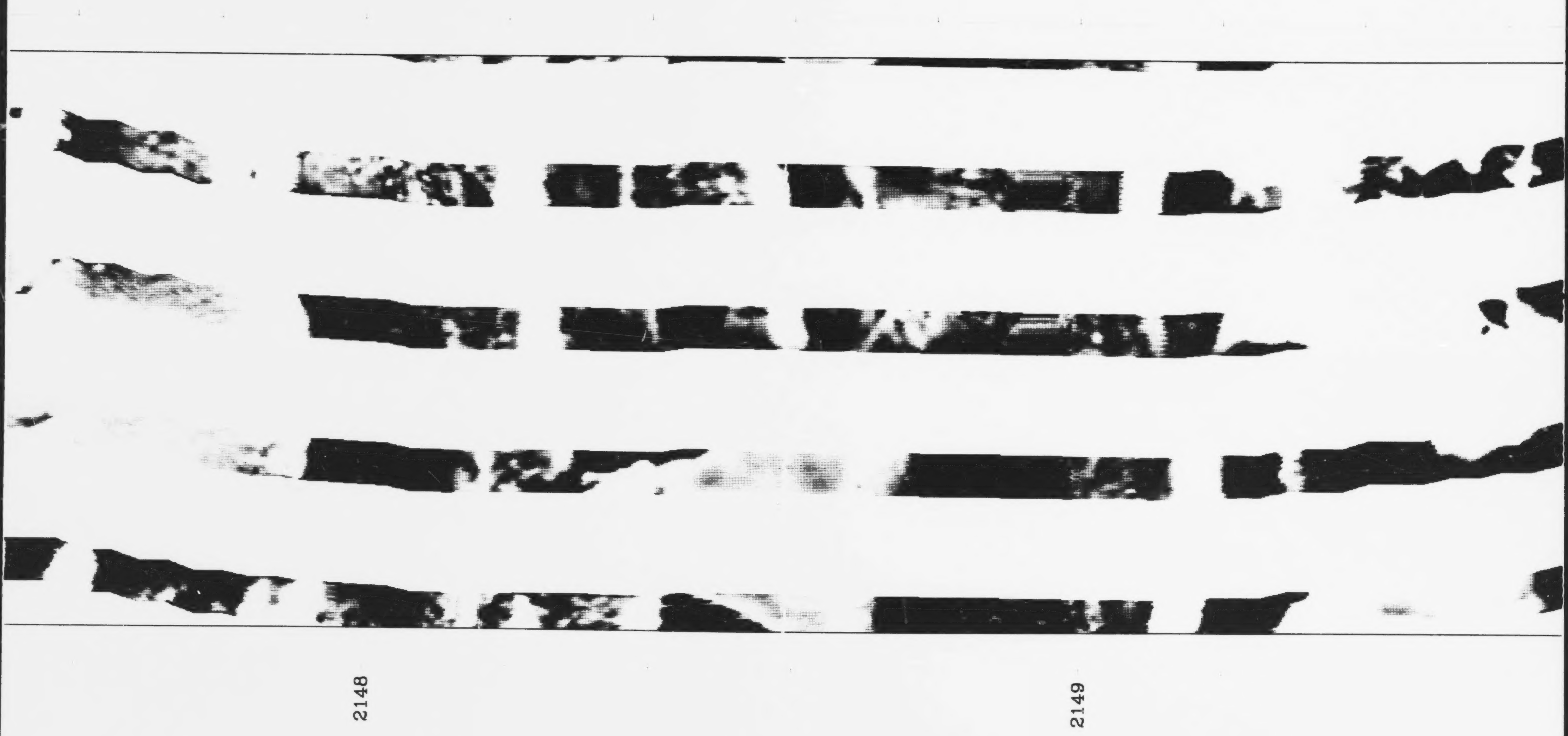
2148
2149

2150
2151

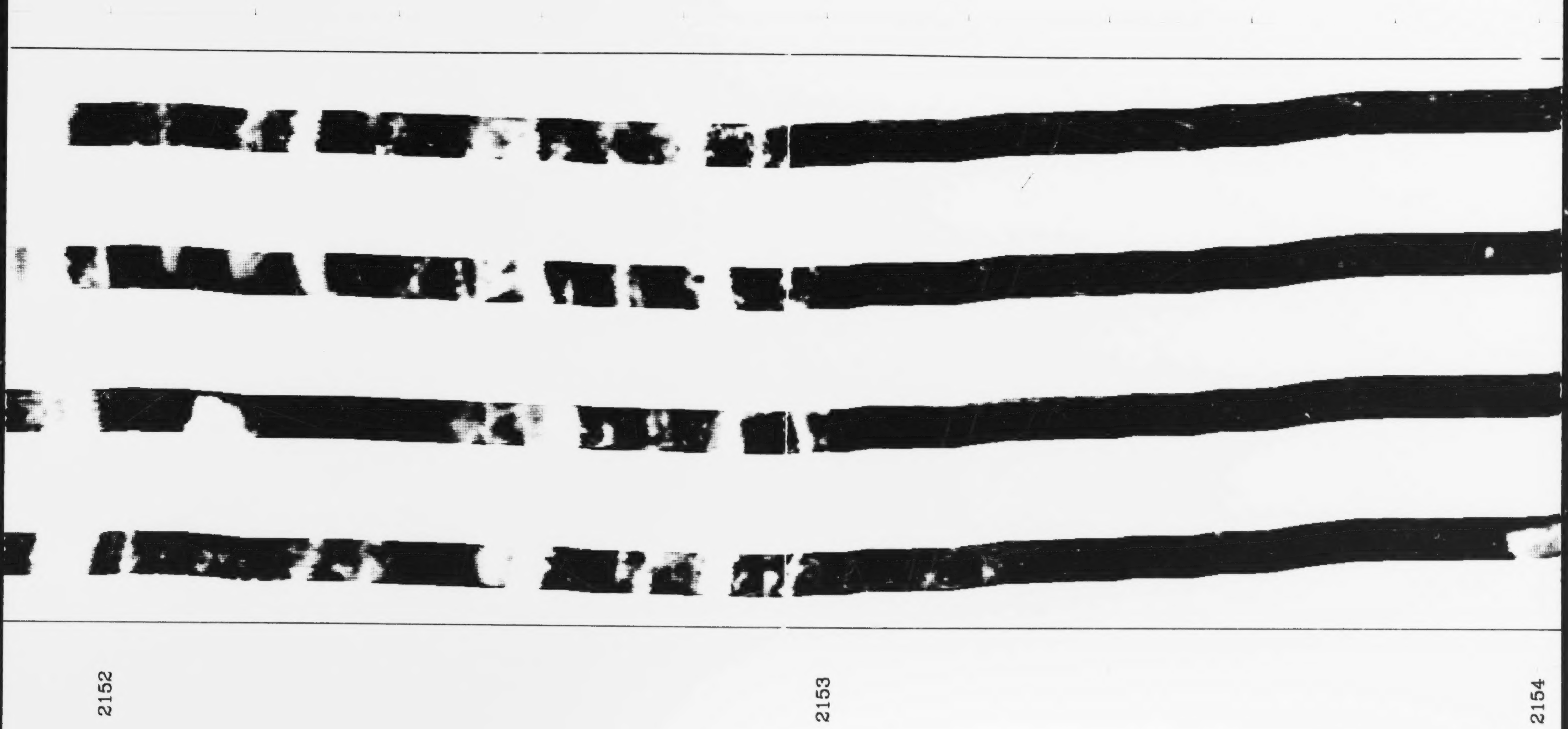
2152
2153
2154

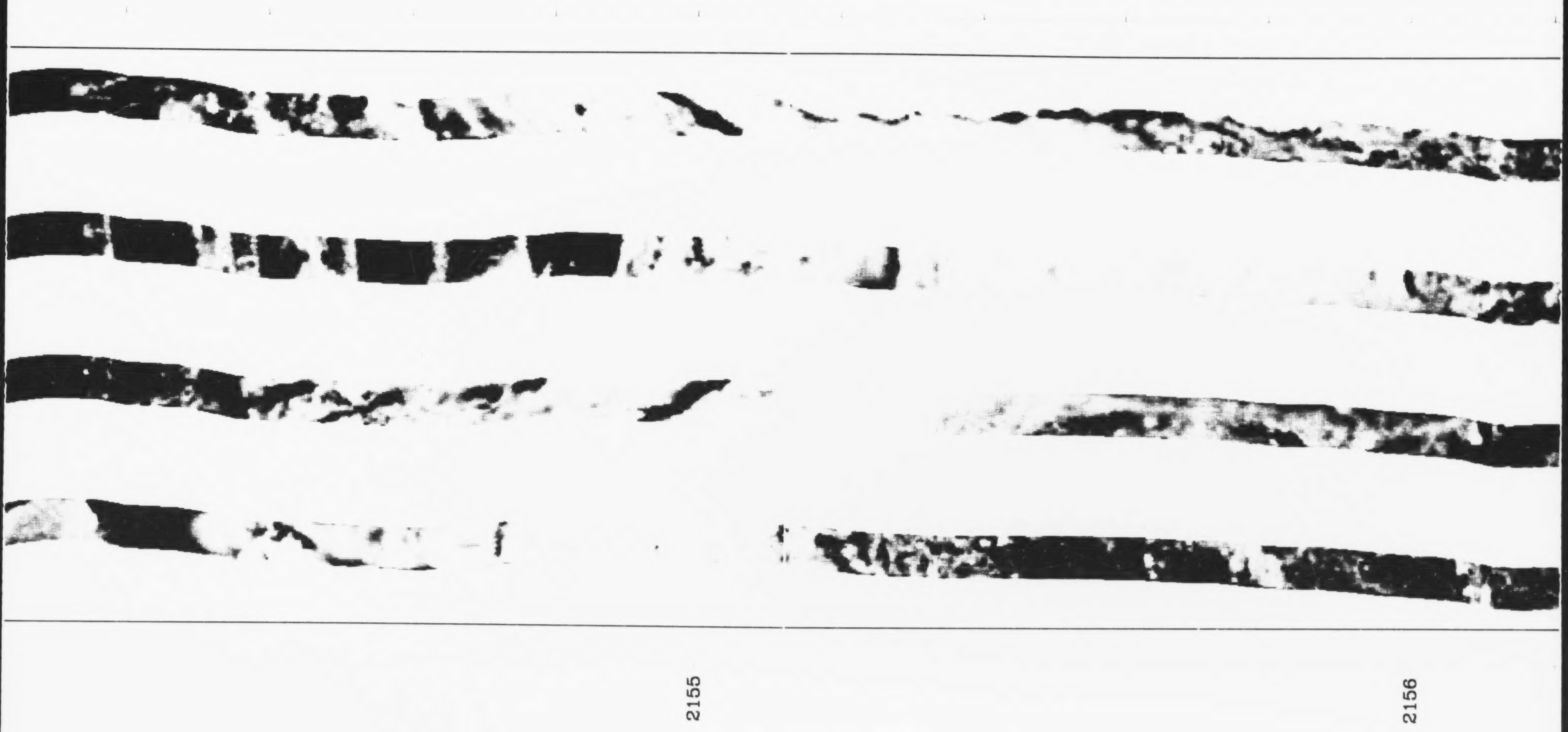

2155
2156

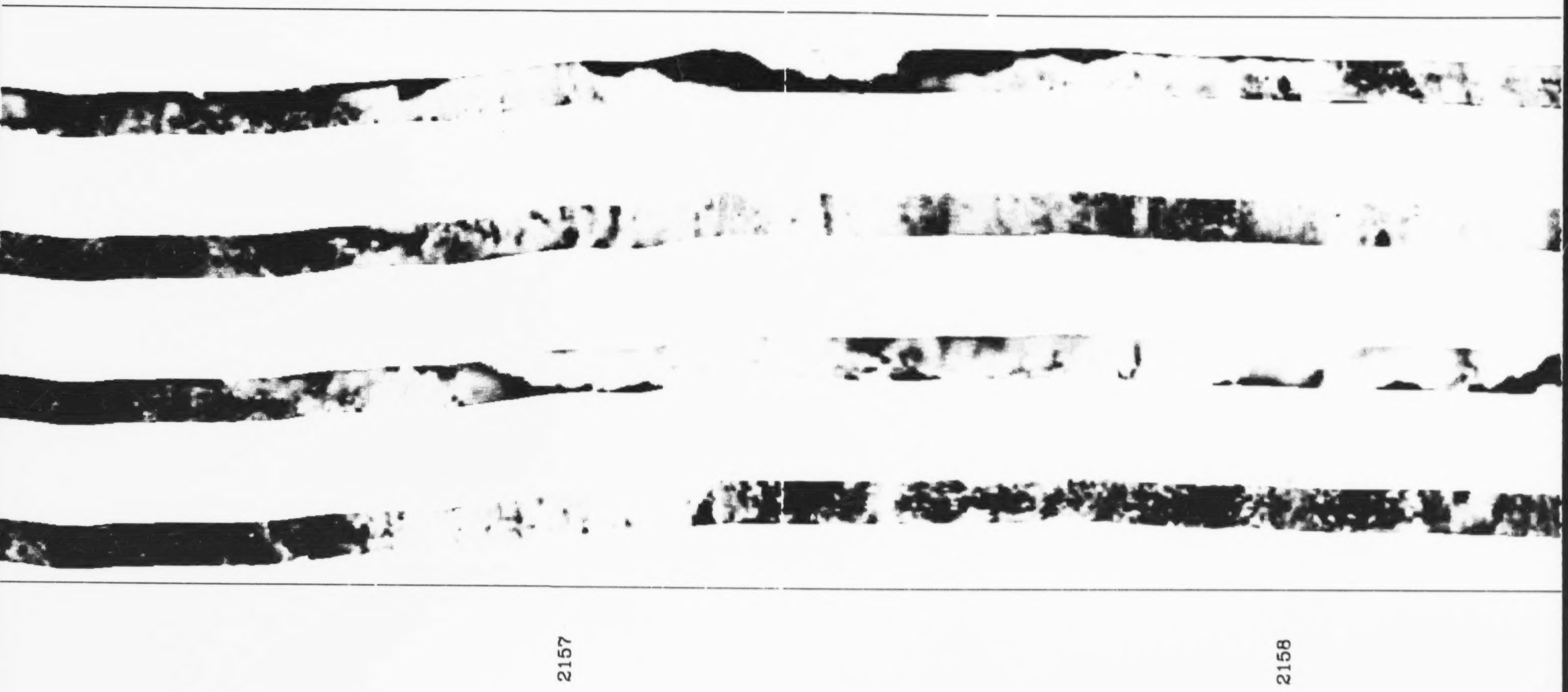
2157
2158

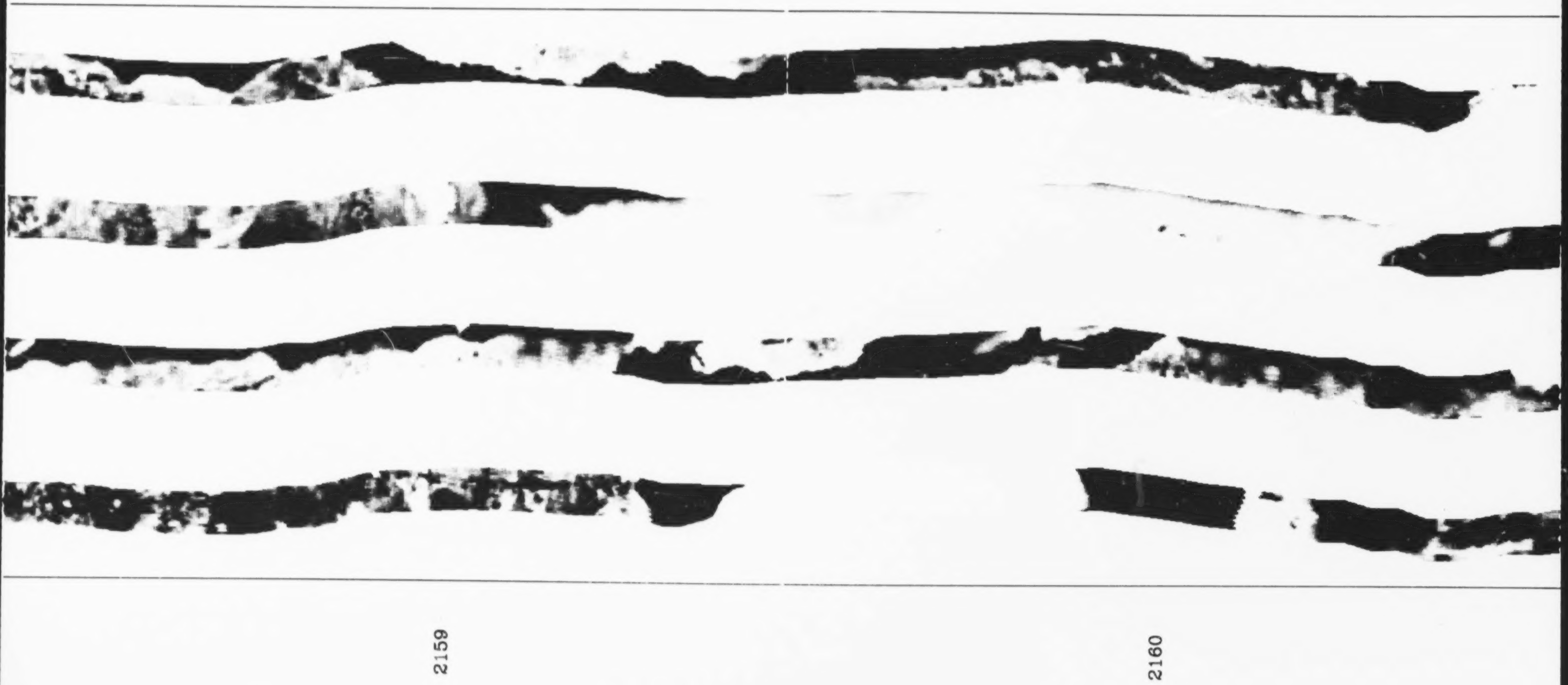
2159
2160

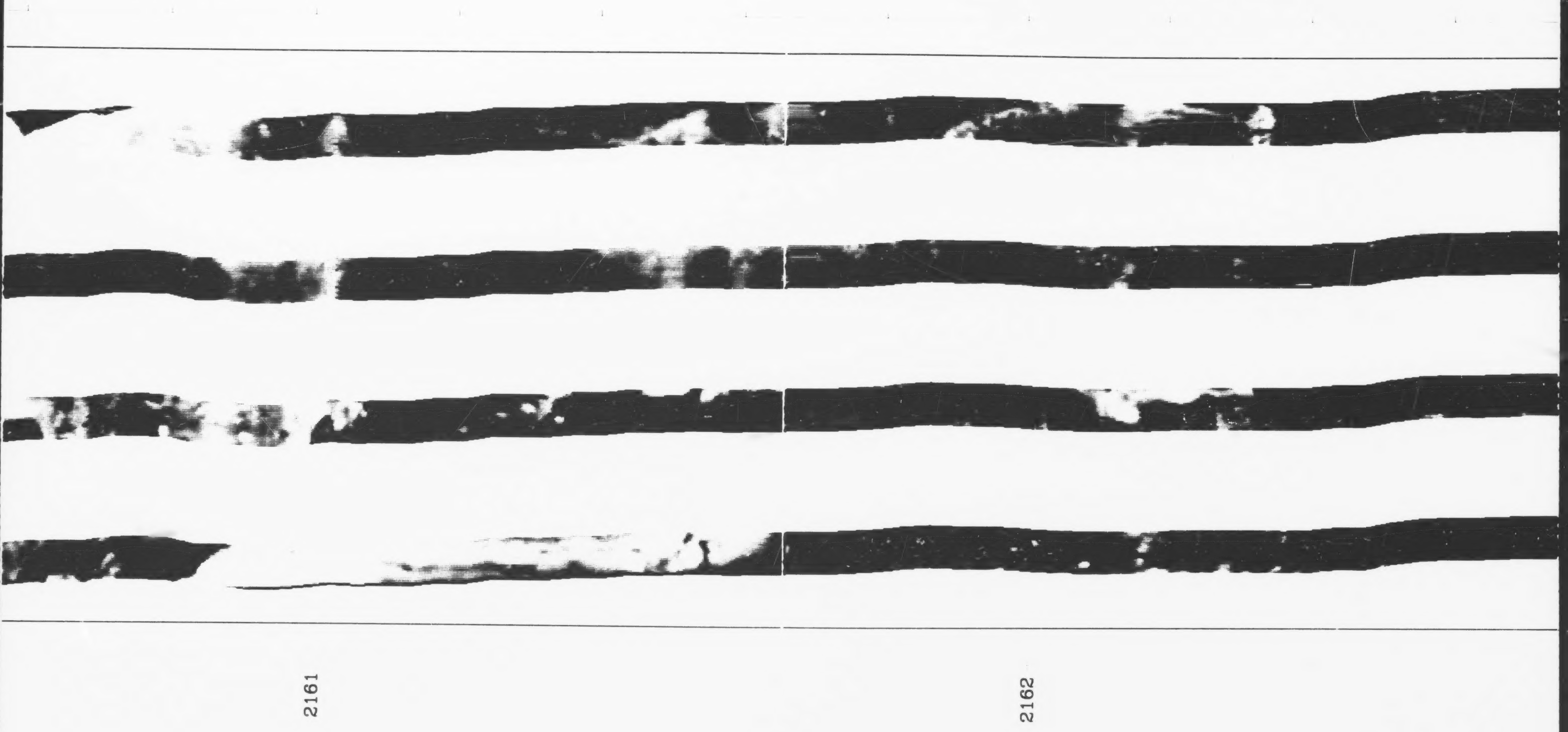
2161
2162

2163
2164

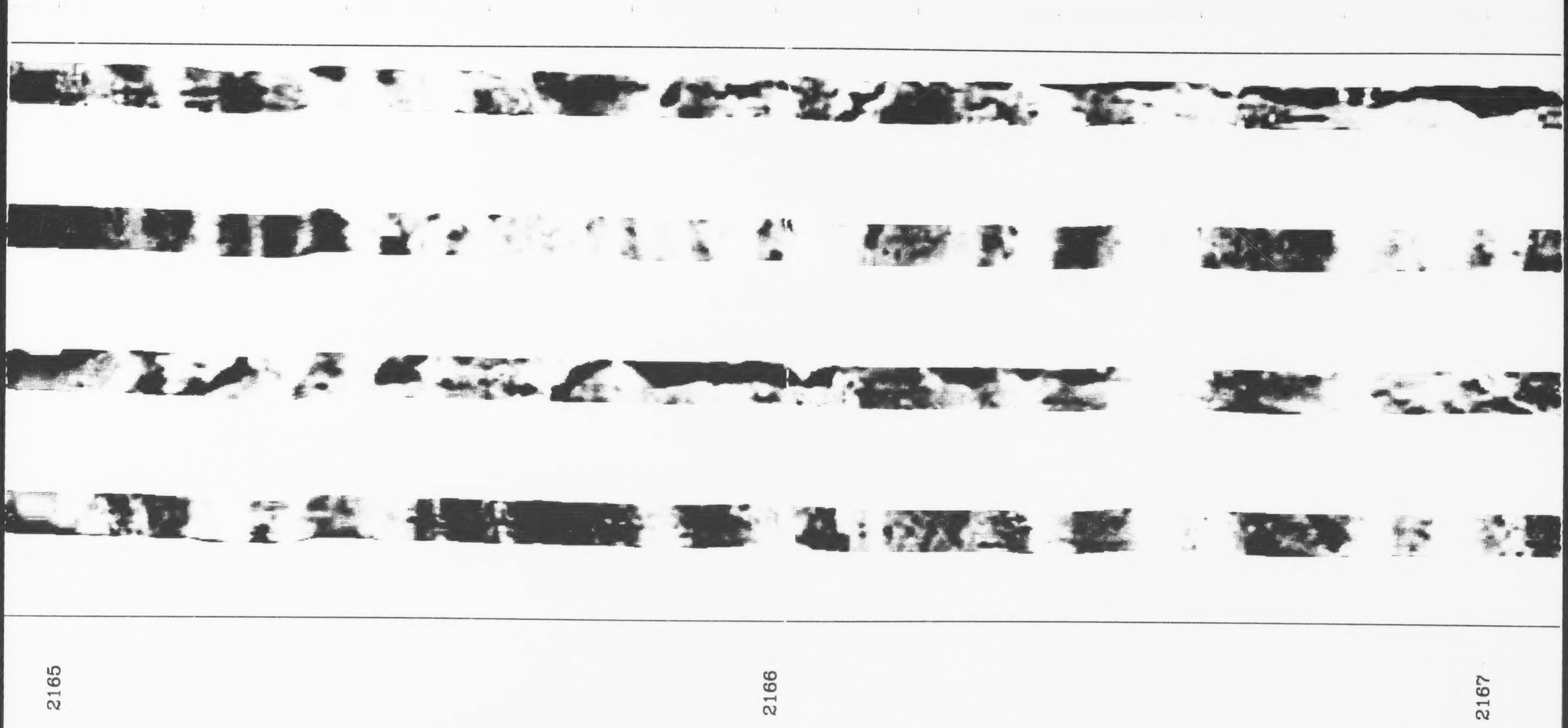
2165
2166
2167

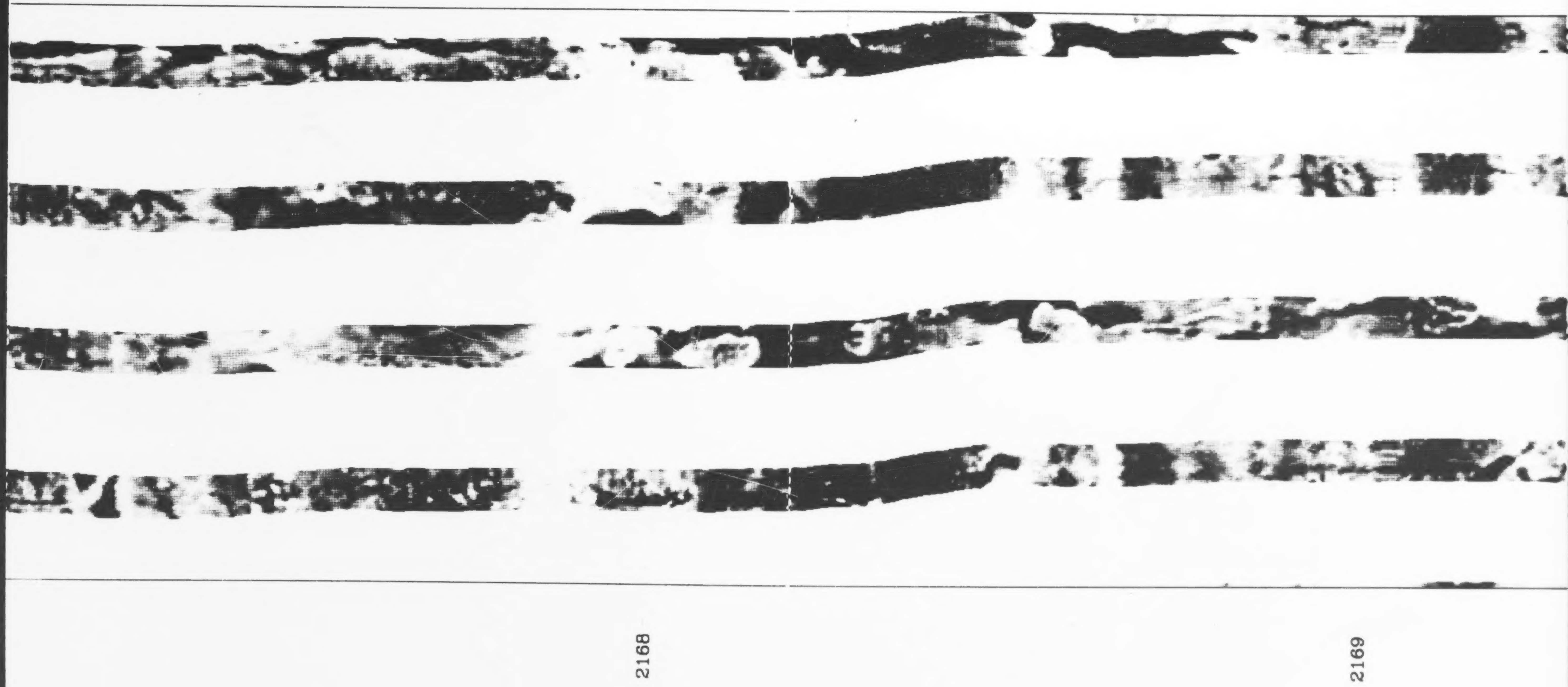
2168
2169

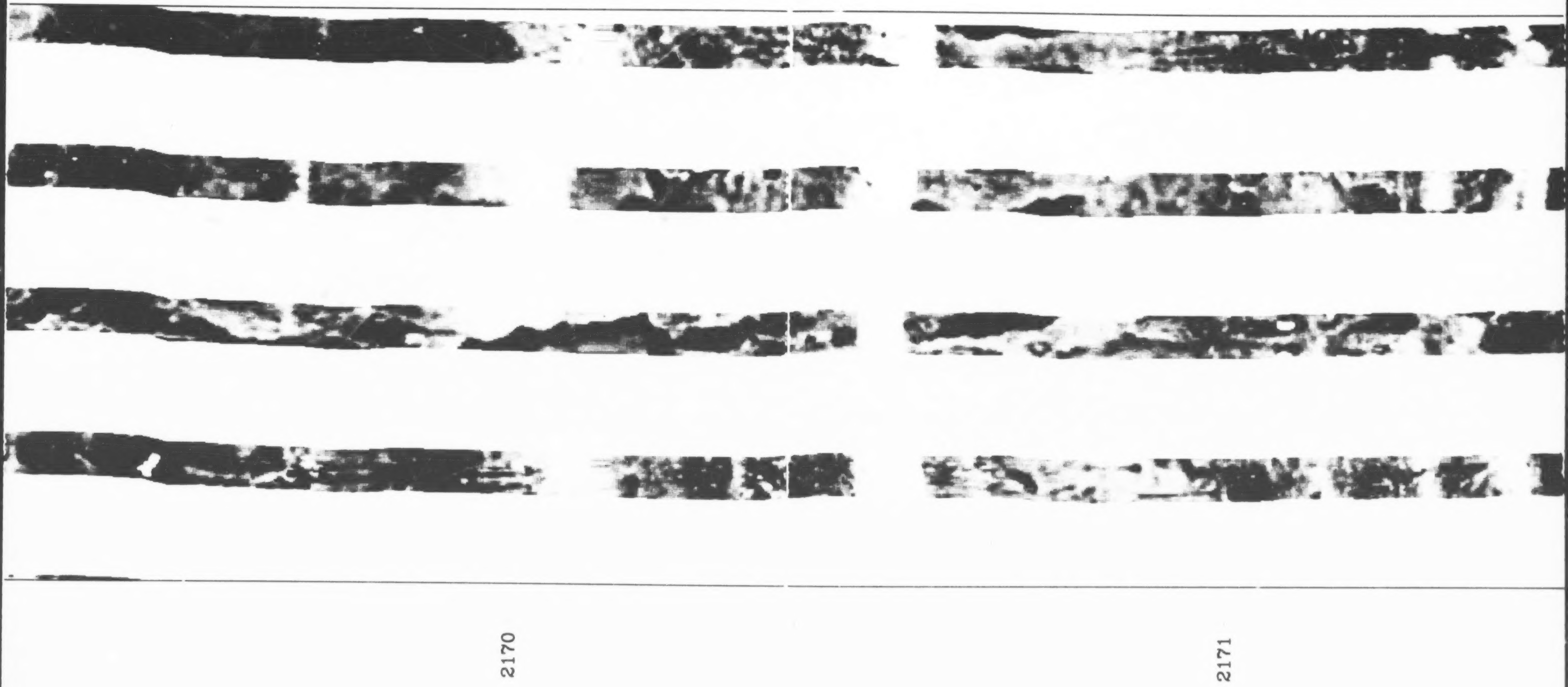
2170
2171

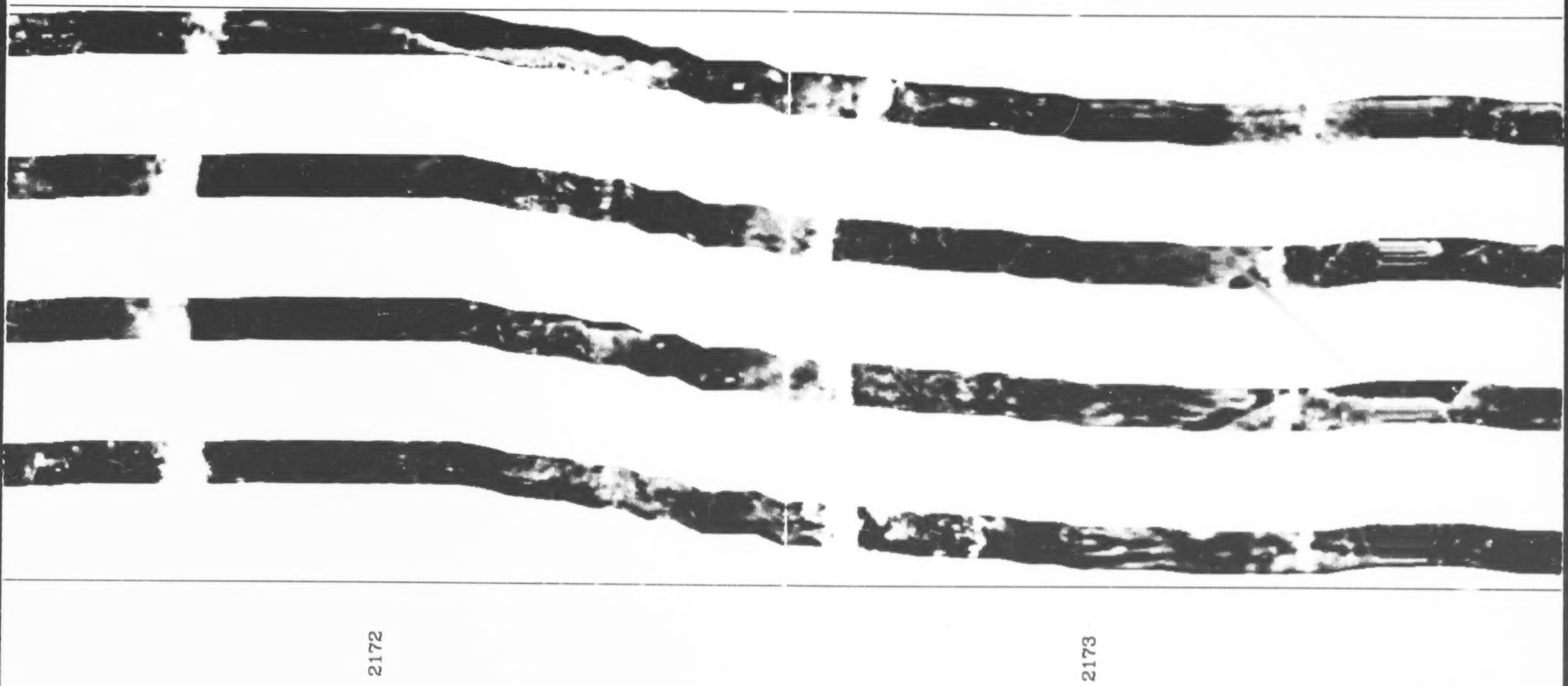
2172
2173

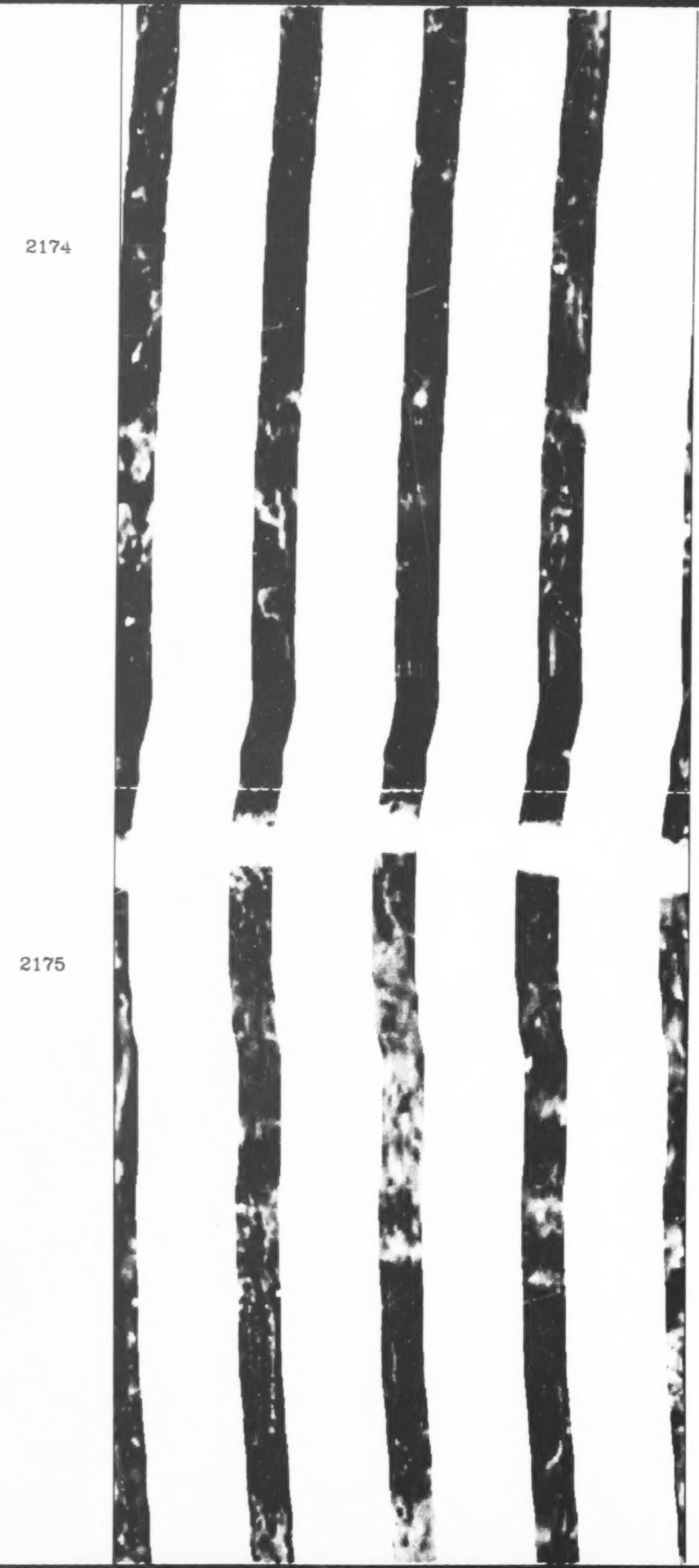
2174
2175

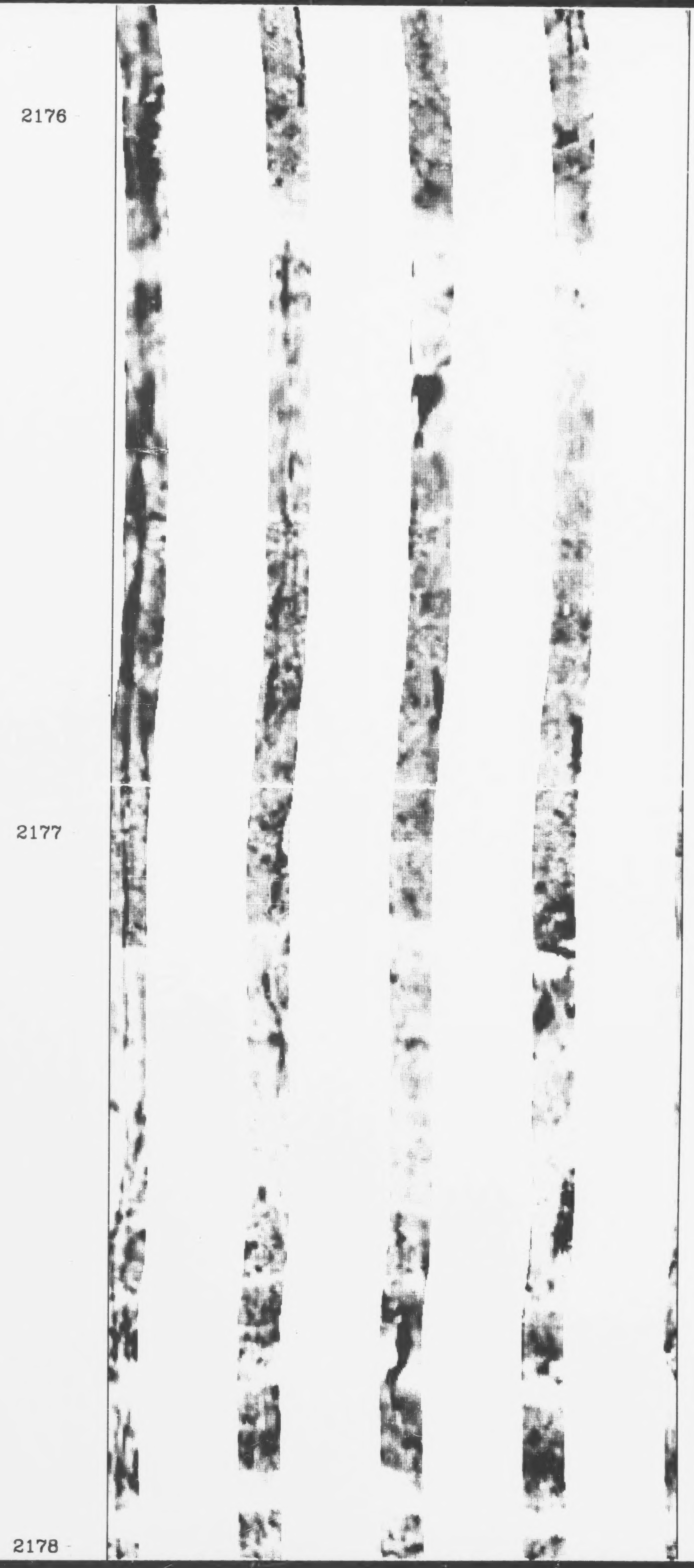
2176
2177
2178

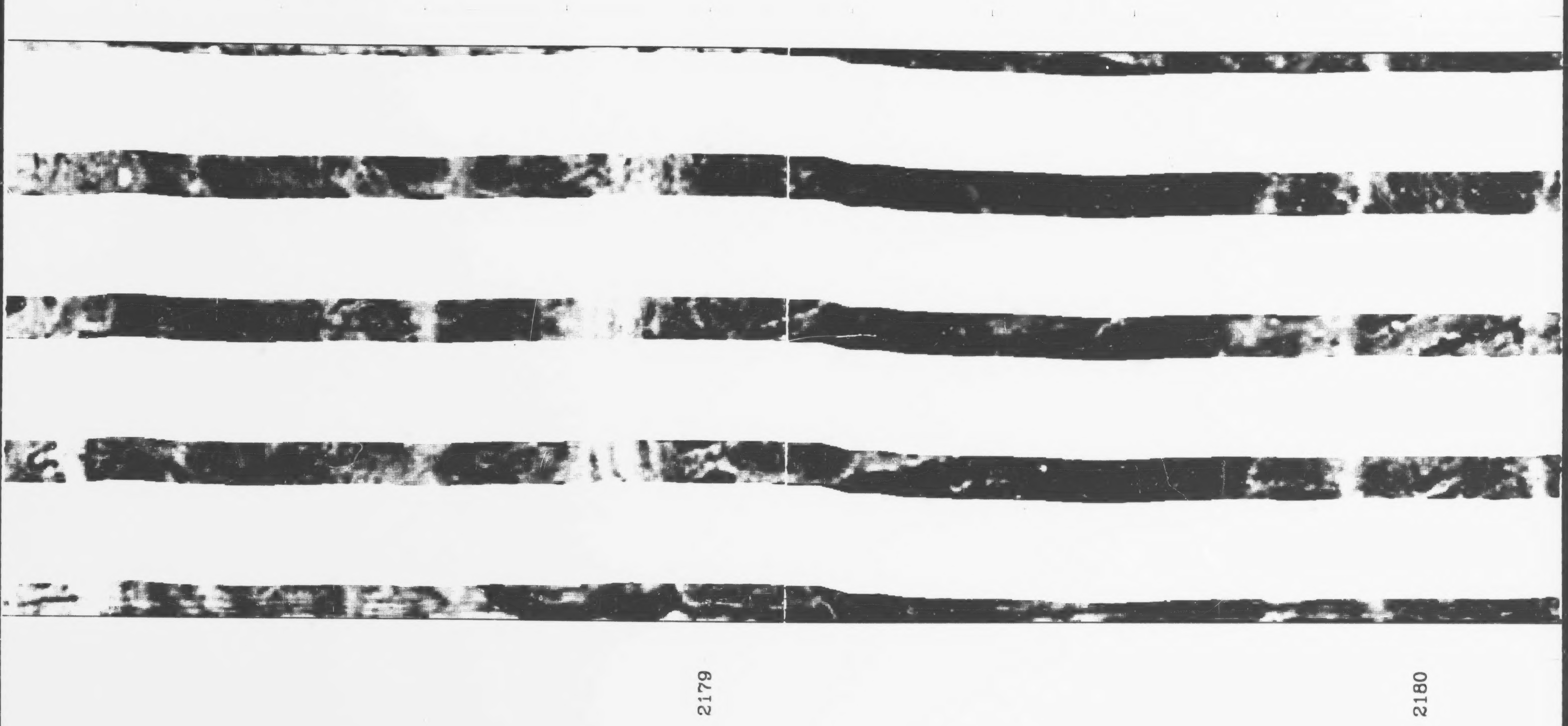

2179
2180

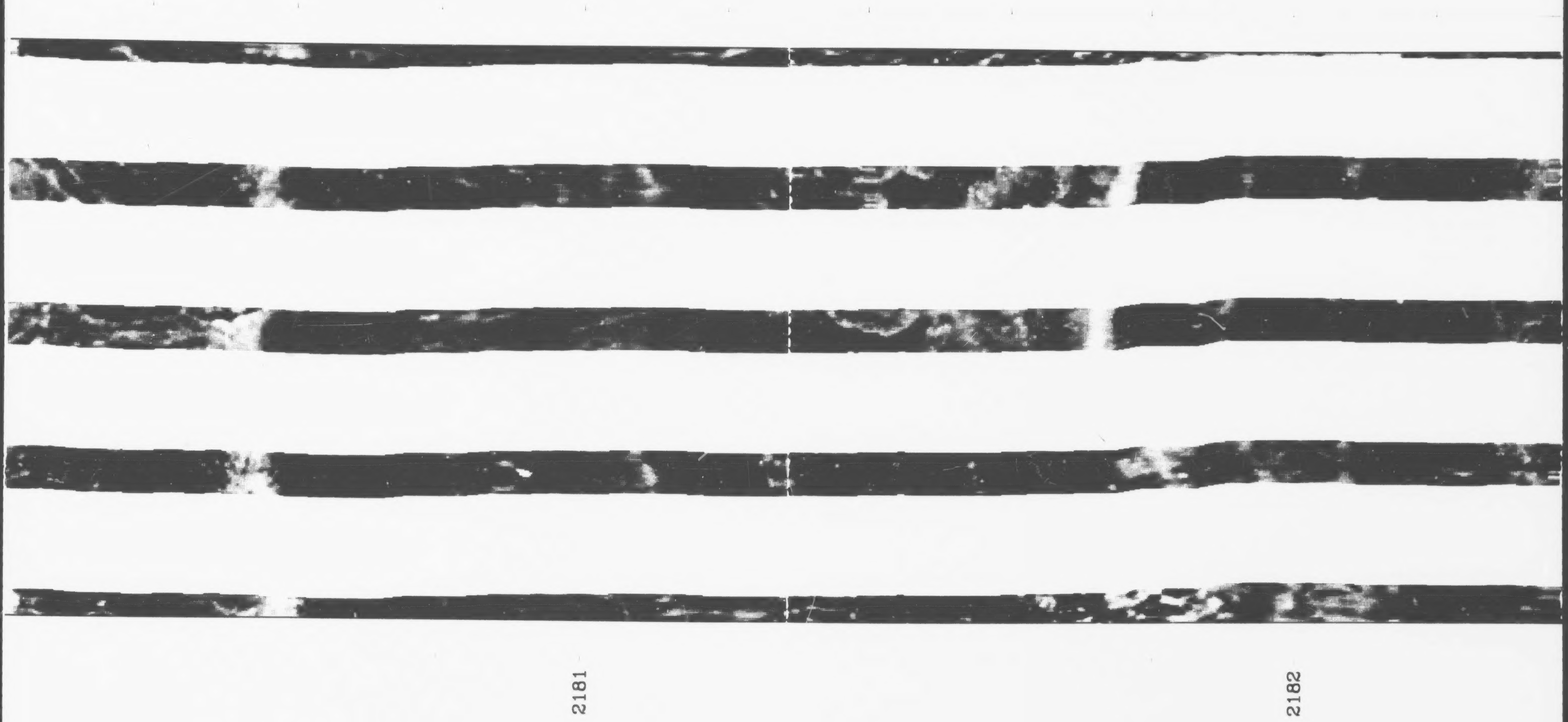
2181
2182

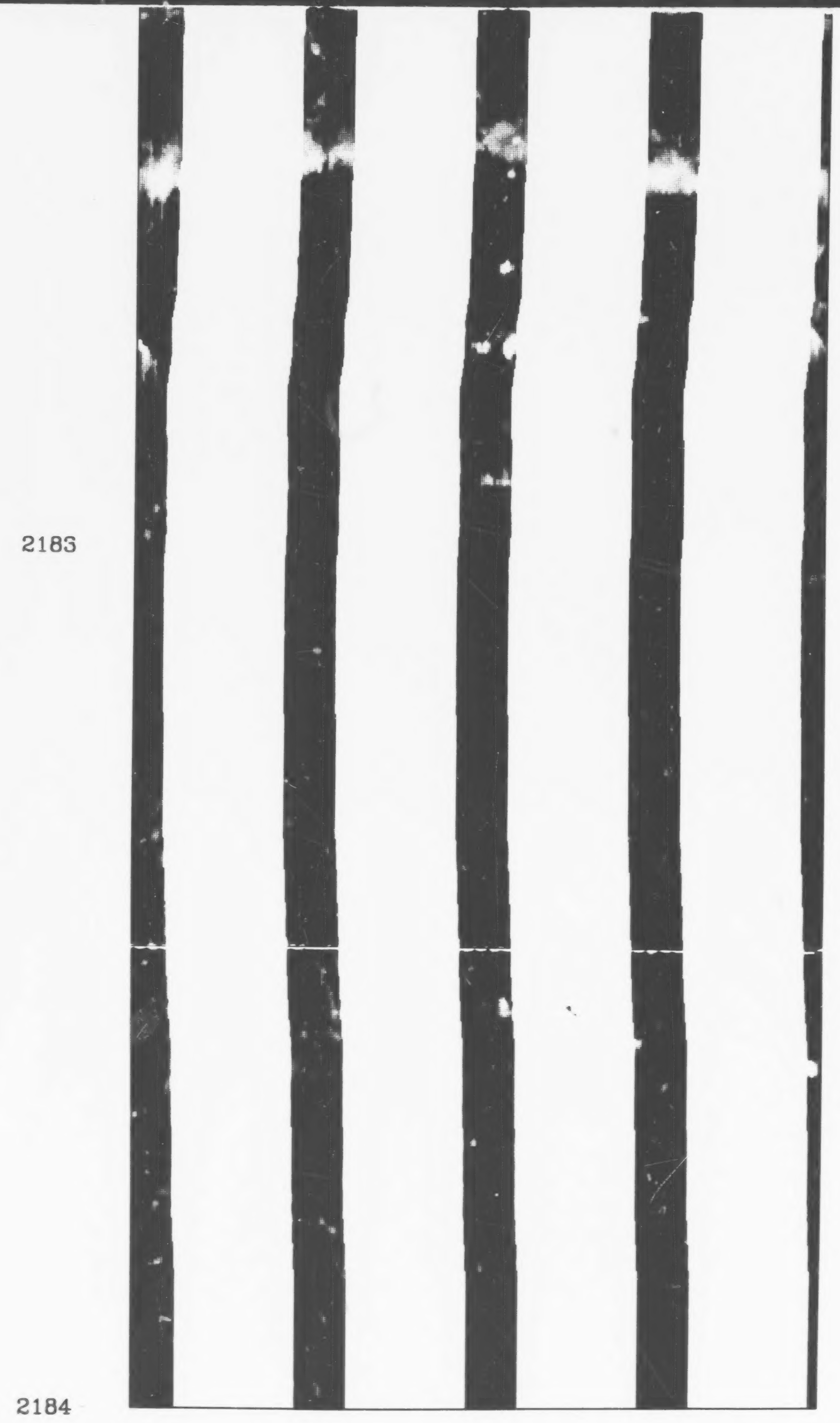

STATIC IMAGES

ZONE FROM 2204.0 M TO 2184.0 M

DEPTH SCALE = 1/ 5

IMAGE SCALE = 1/ 5

BITSIZE = 9.88

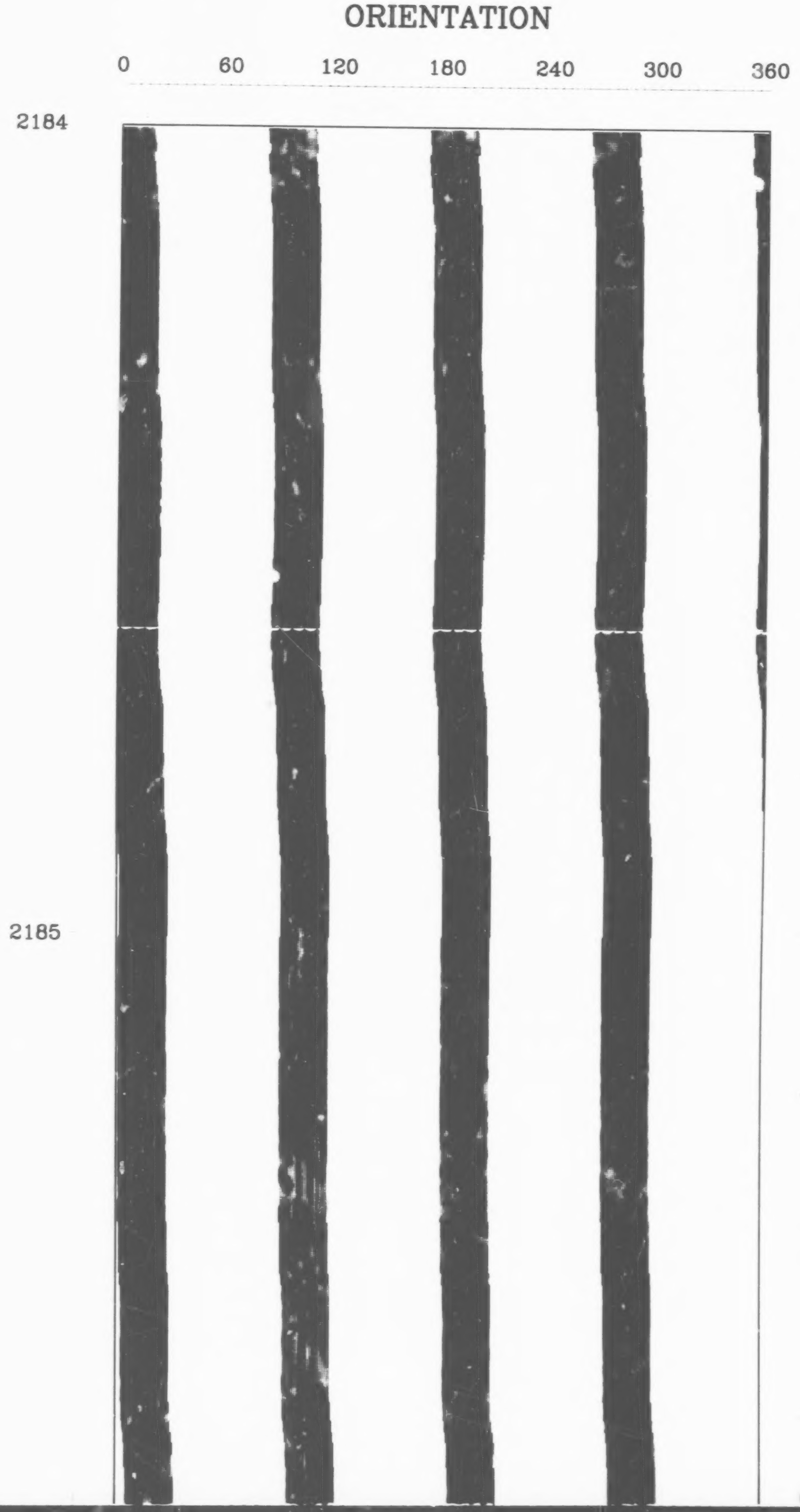

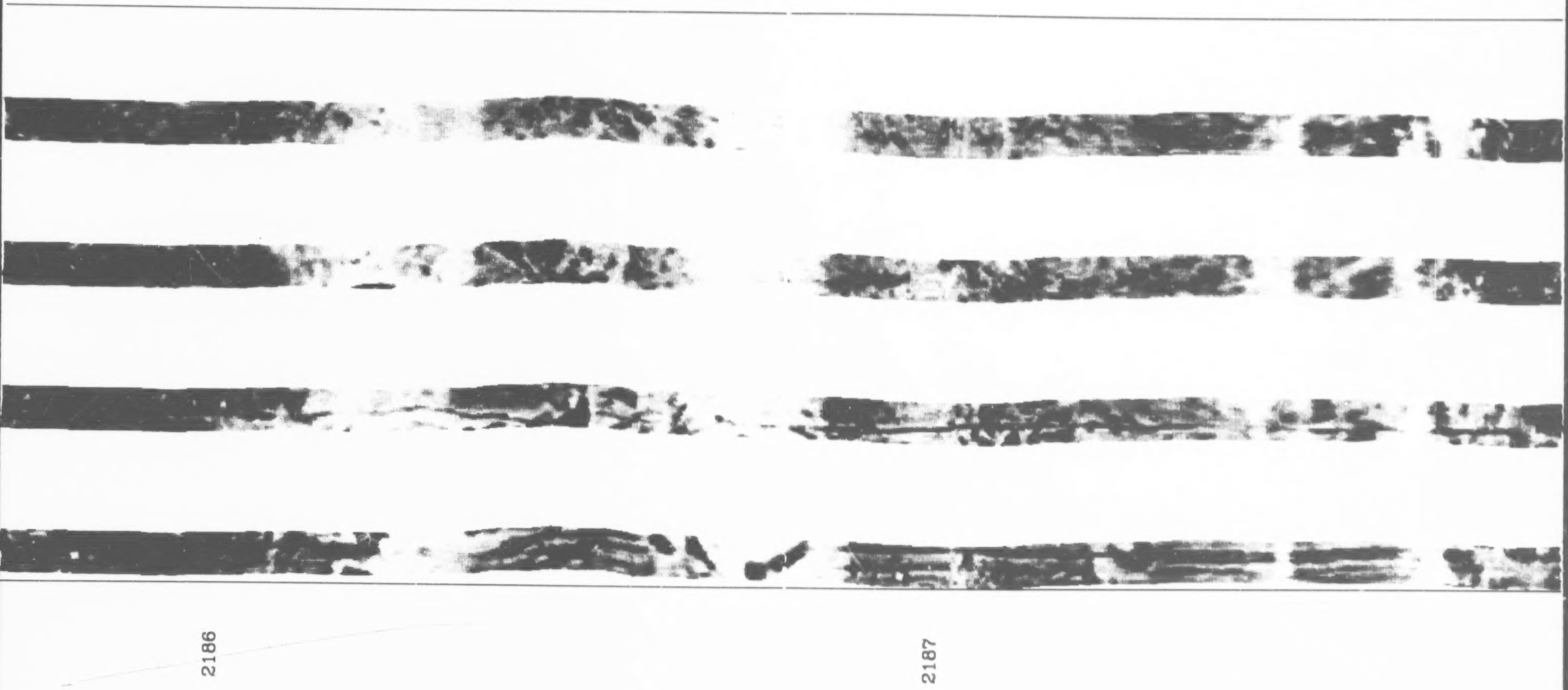
2186
2187

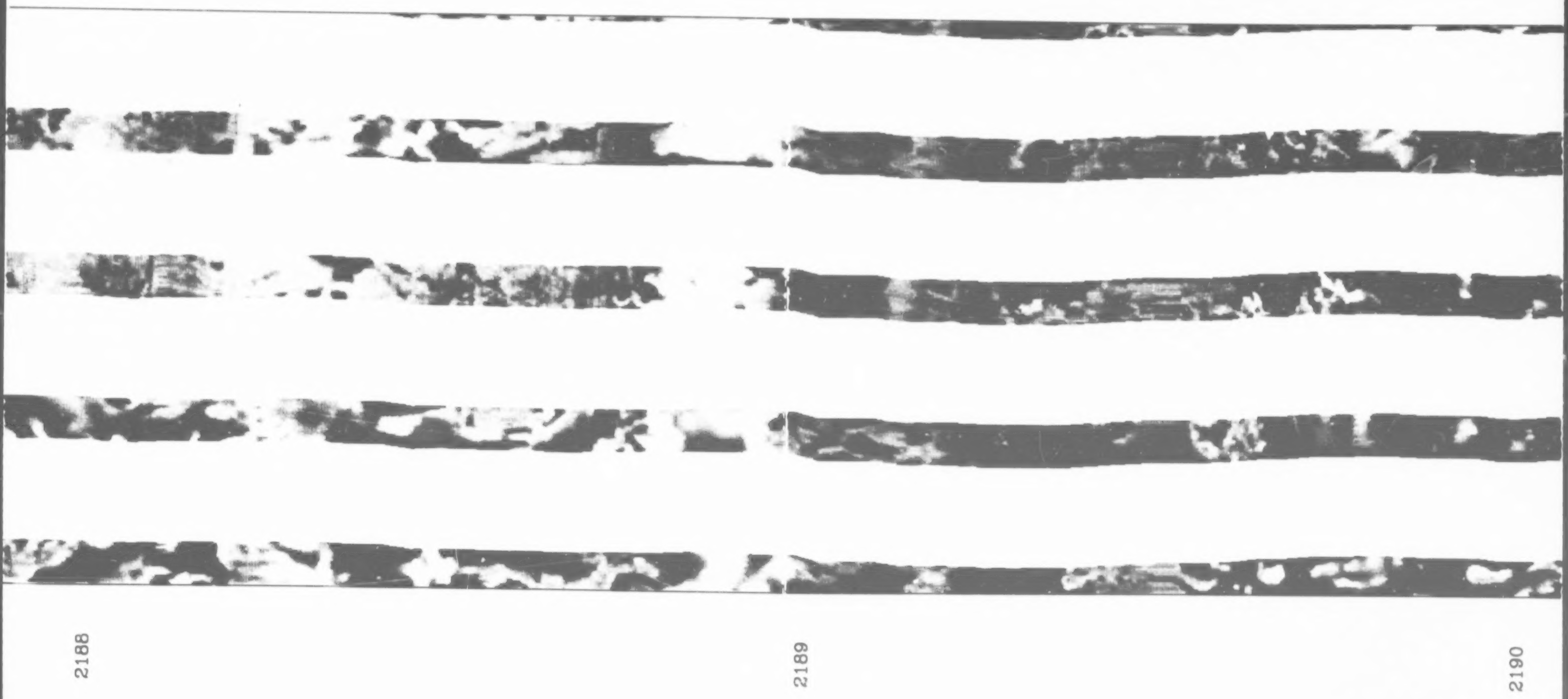
2188
2189
2190

2191
2192

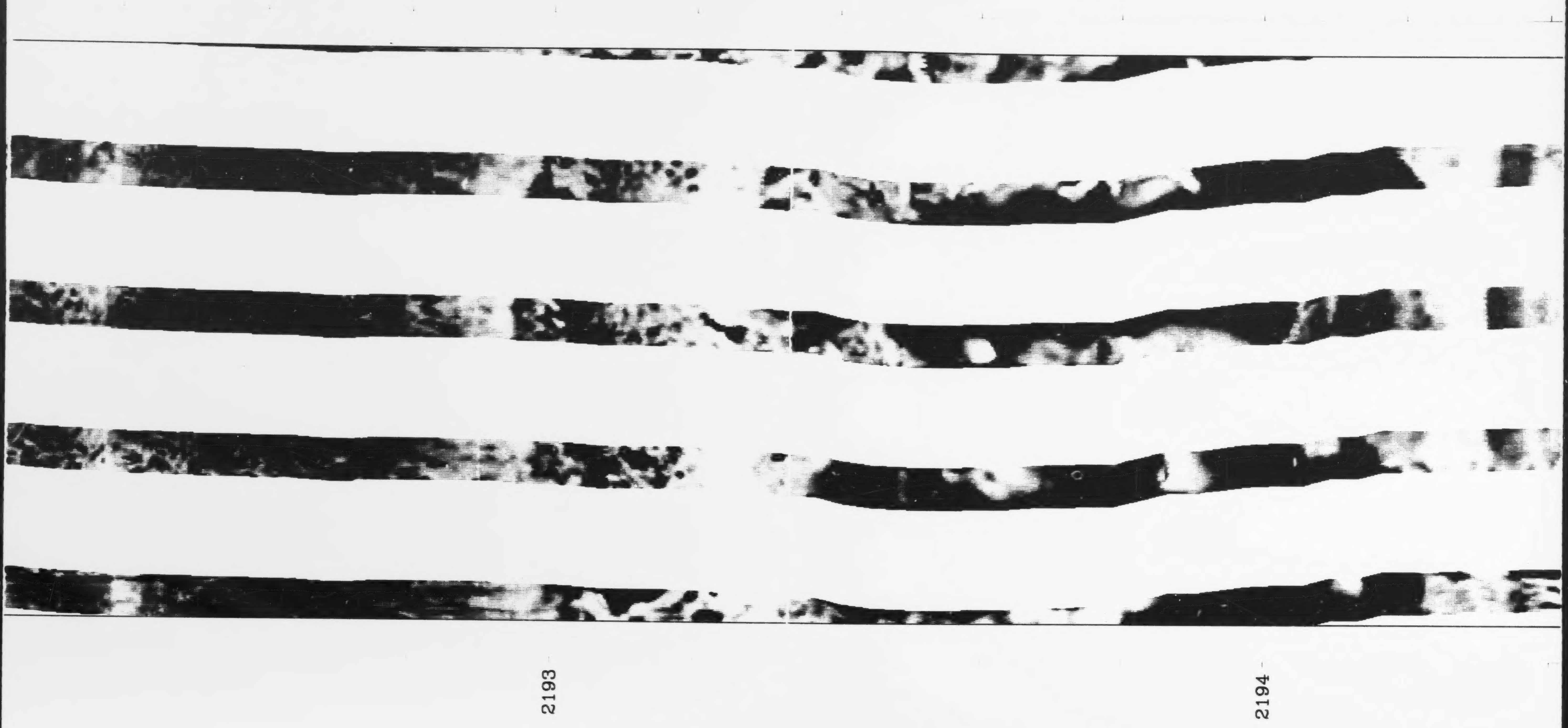
2193
2194

[redacted]

2195

2196

2197

2198

2199
2200

2201
2202
2203

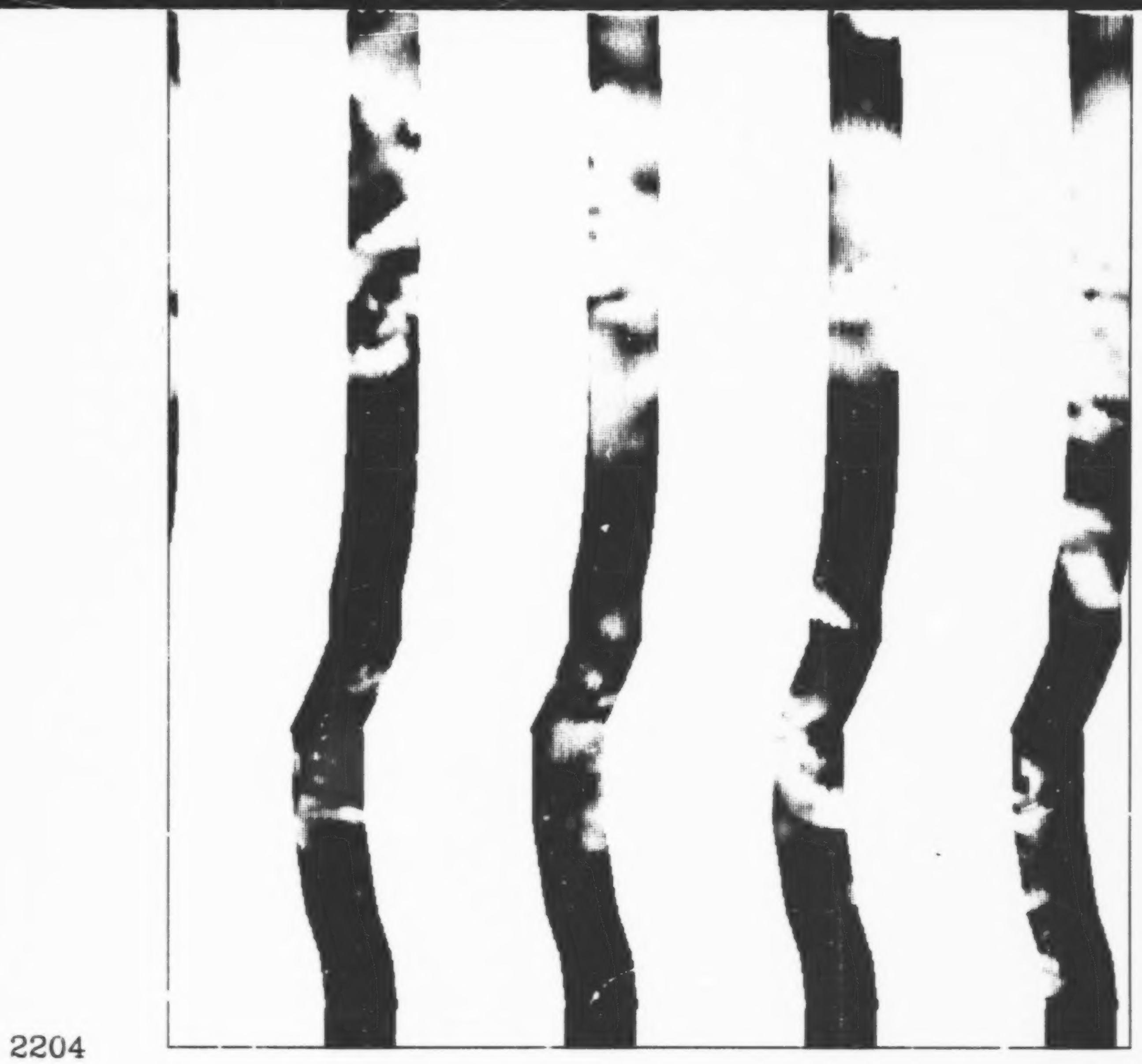

STATIC IMAGES

ZONE FROM 2244.0 M TO 2204.0 M

DEPTH SCALE = 1/ 5

IMAGE SCALE = 1/ 5

BITSIZE = 9.88

CRIENTATION

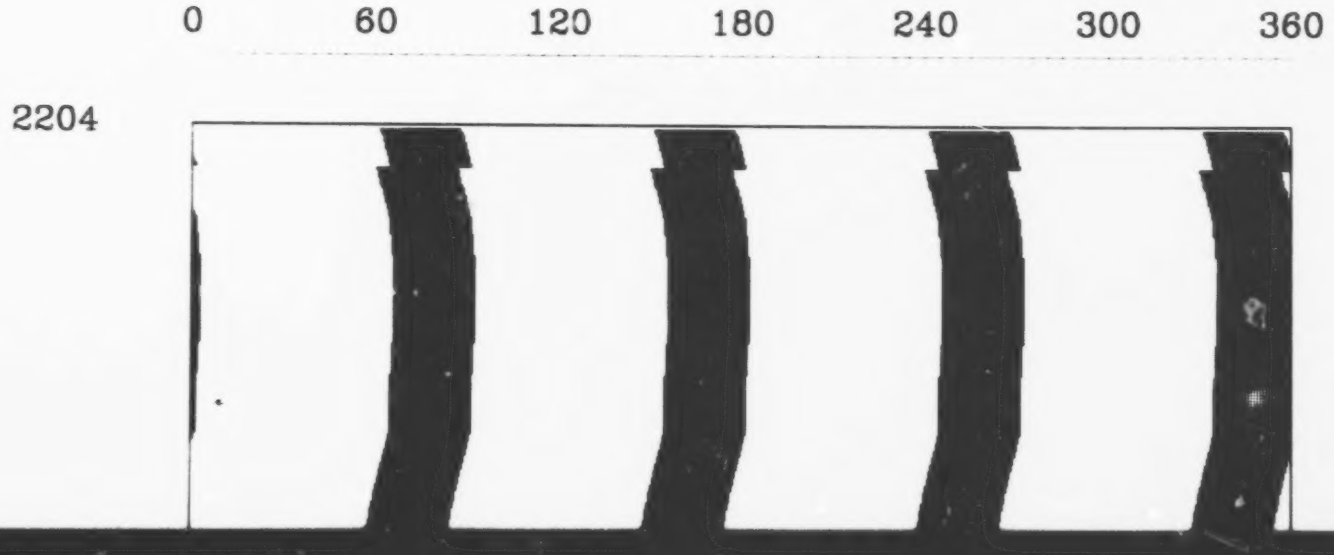

2205
2206

2207
2208

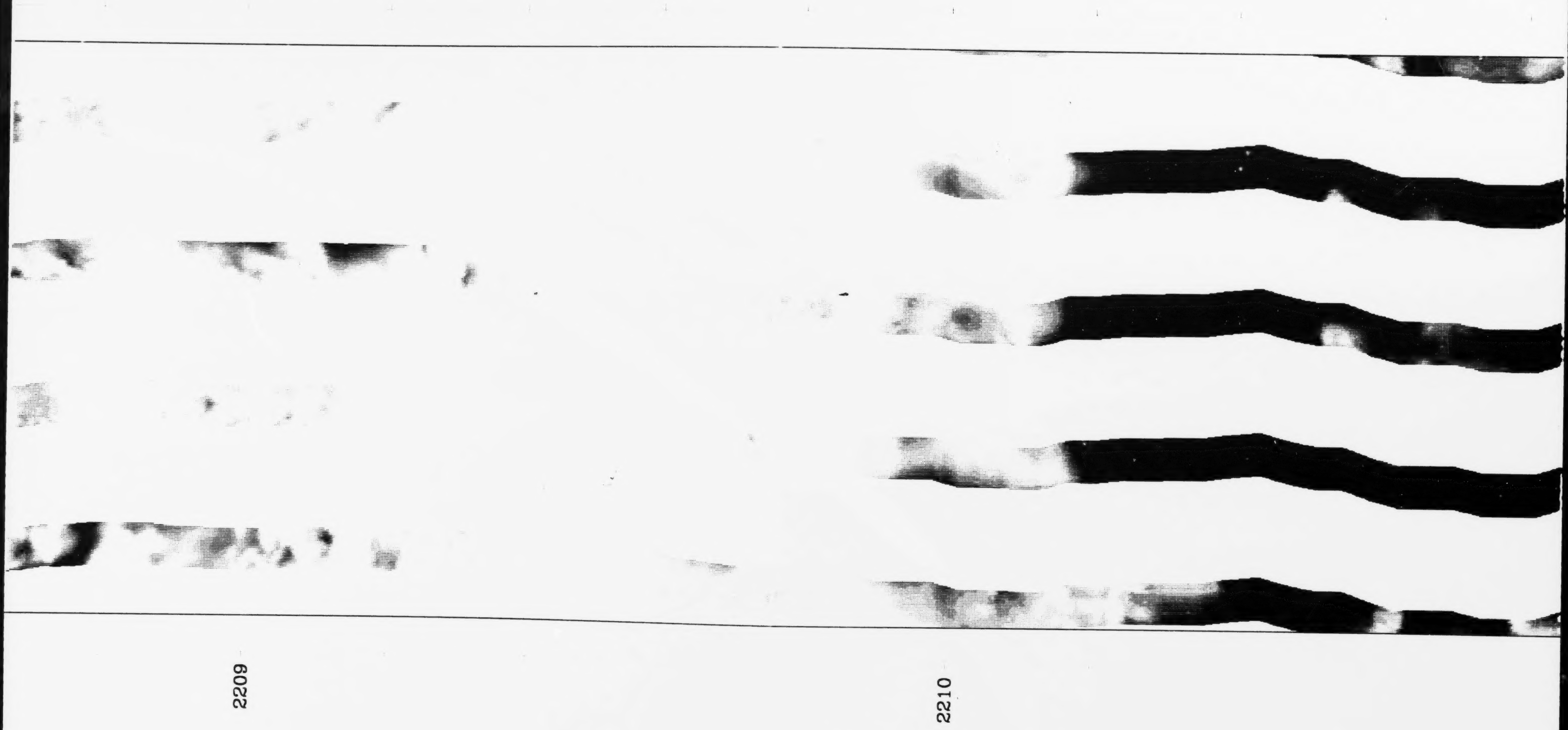
2209
2210

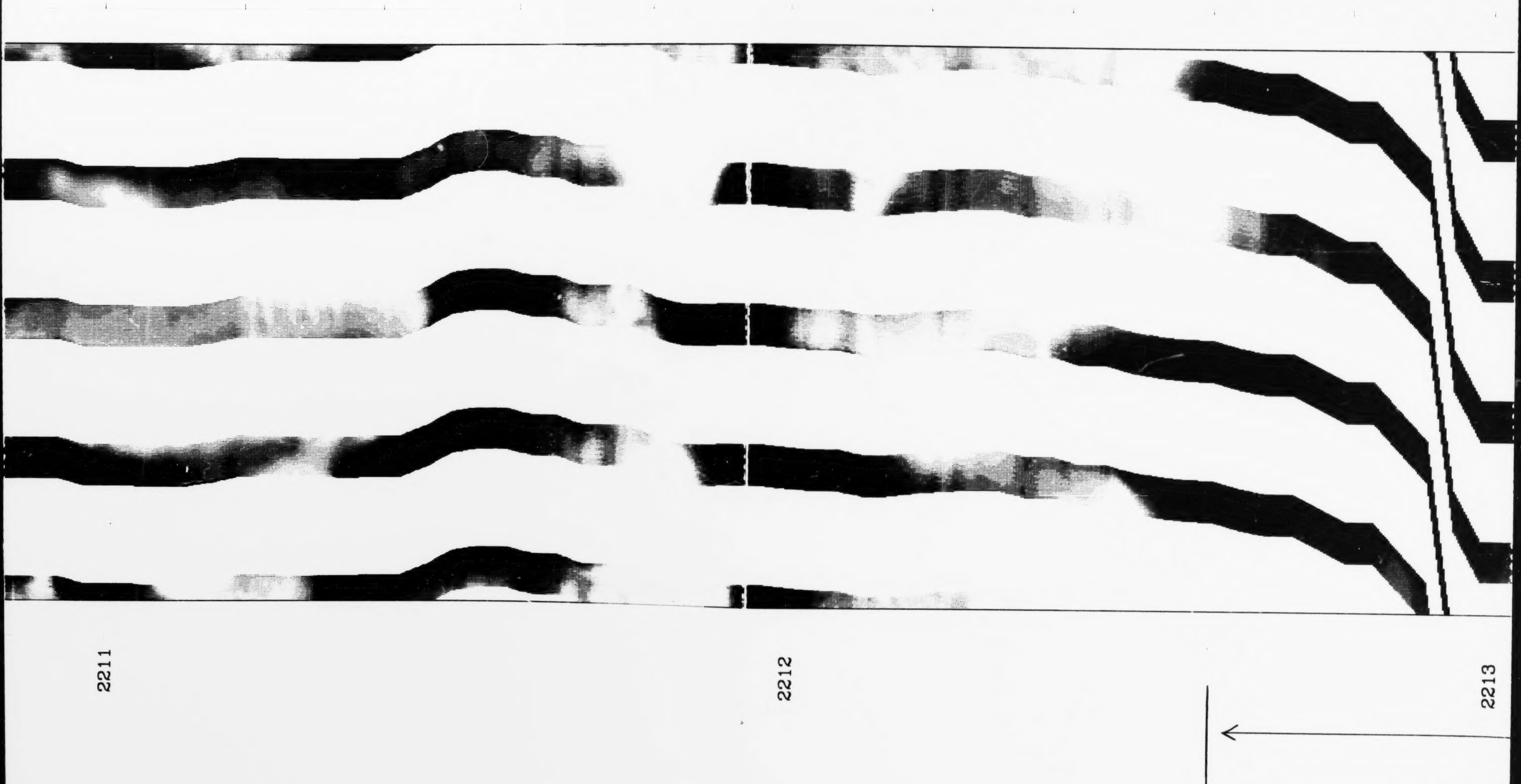
2211
2212
2213

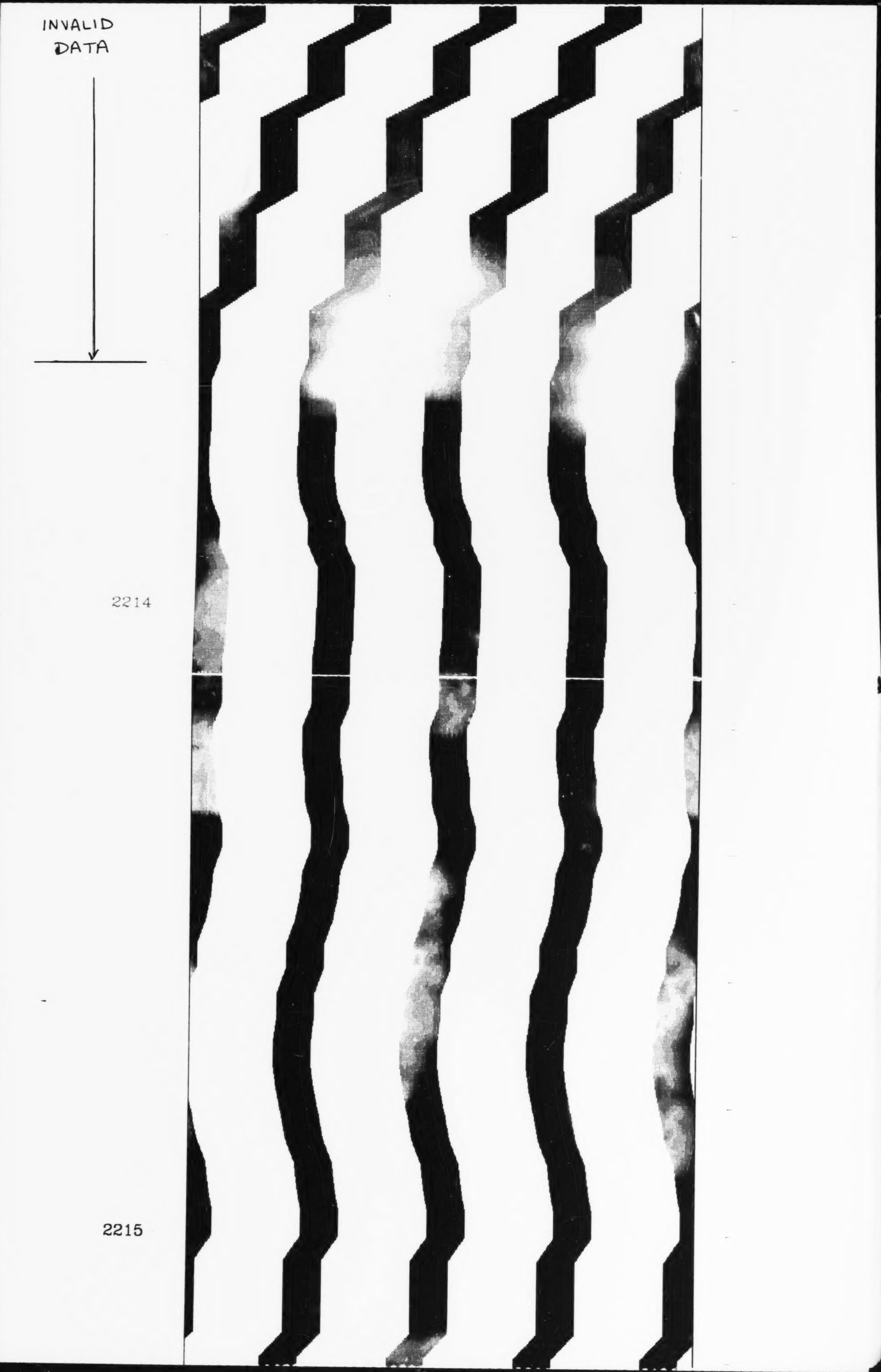
INVALID
DATA
2214
2215

2216
2217

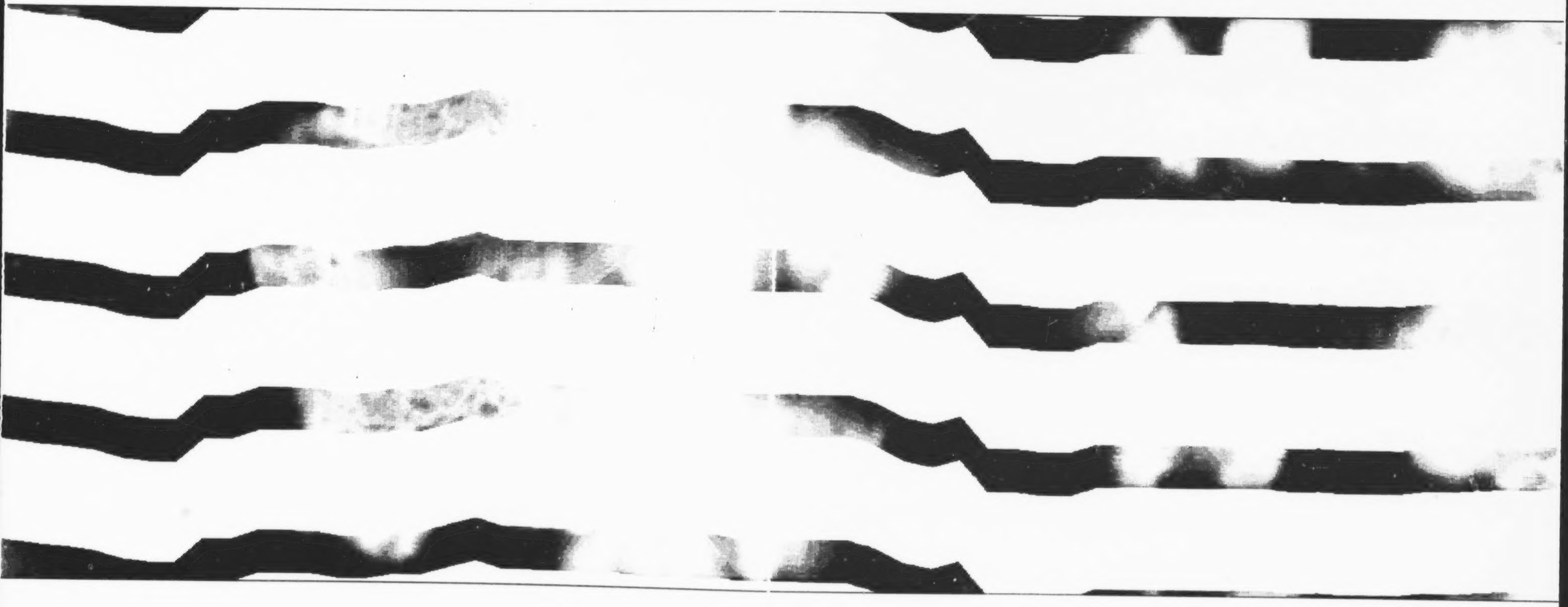
2218
2219

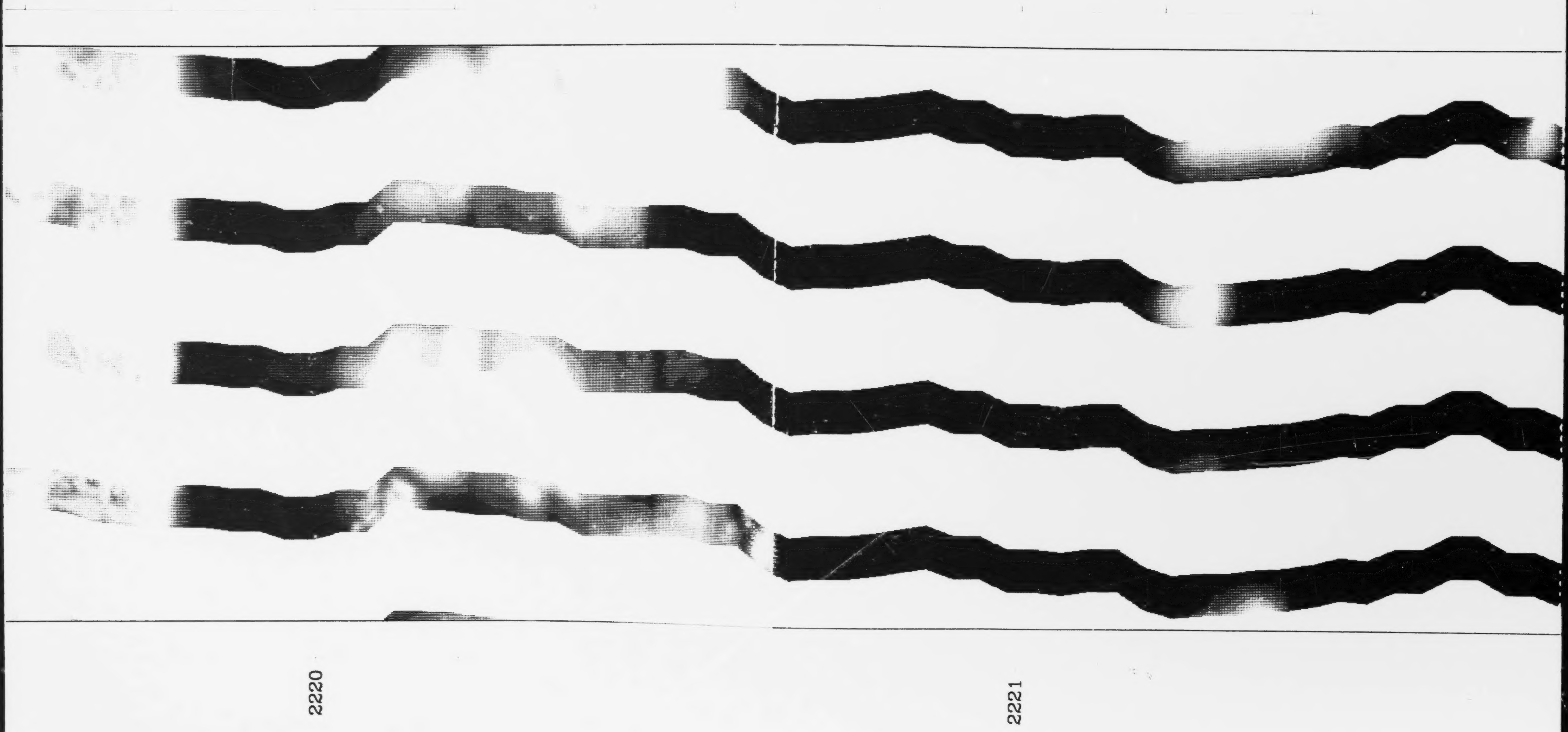
2220
2221

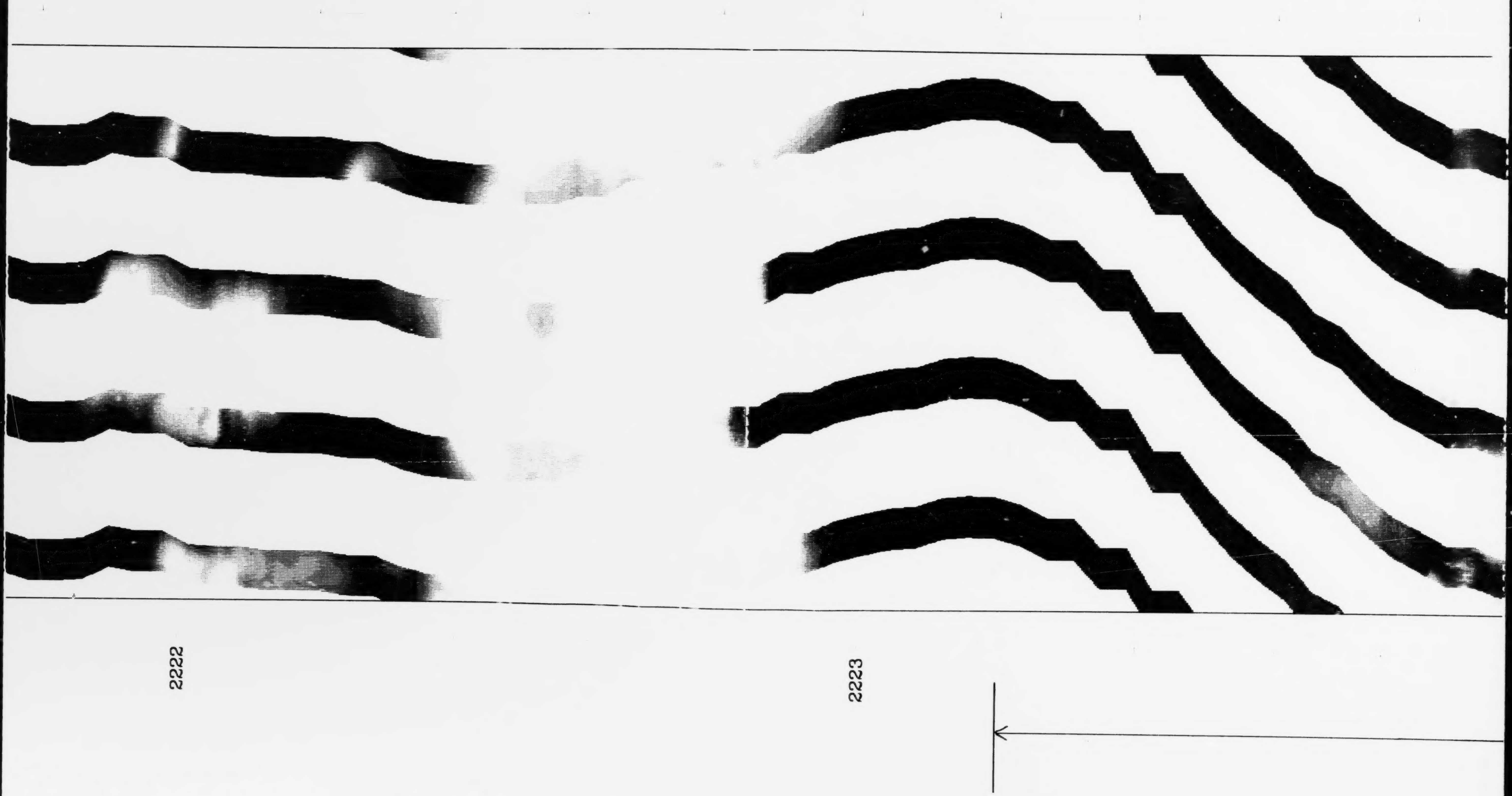
2222
2223

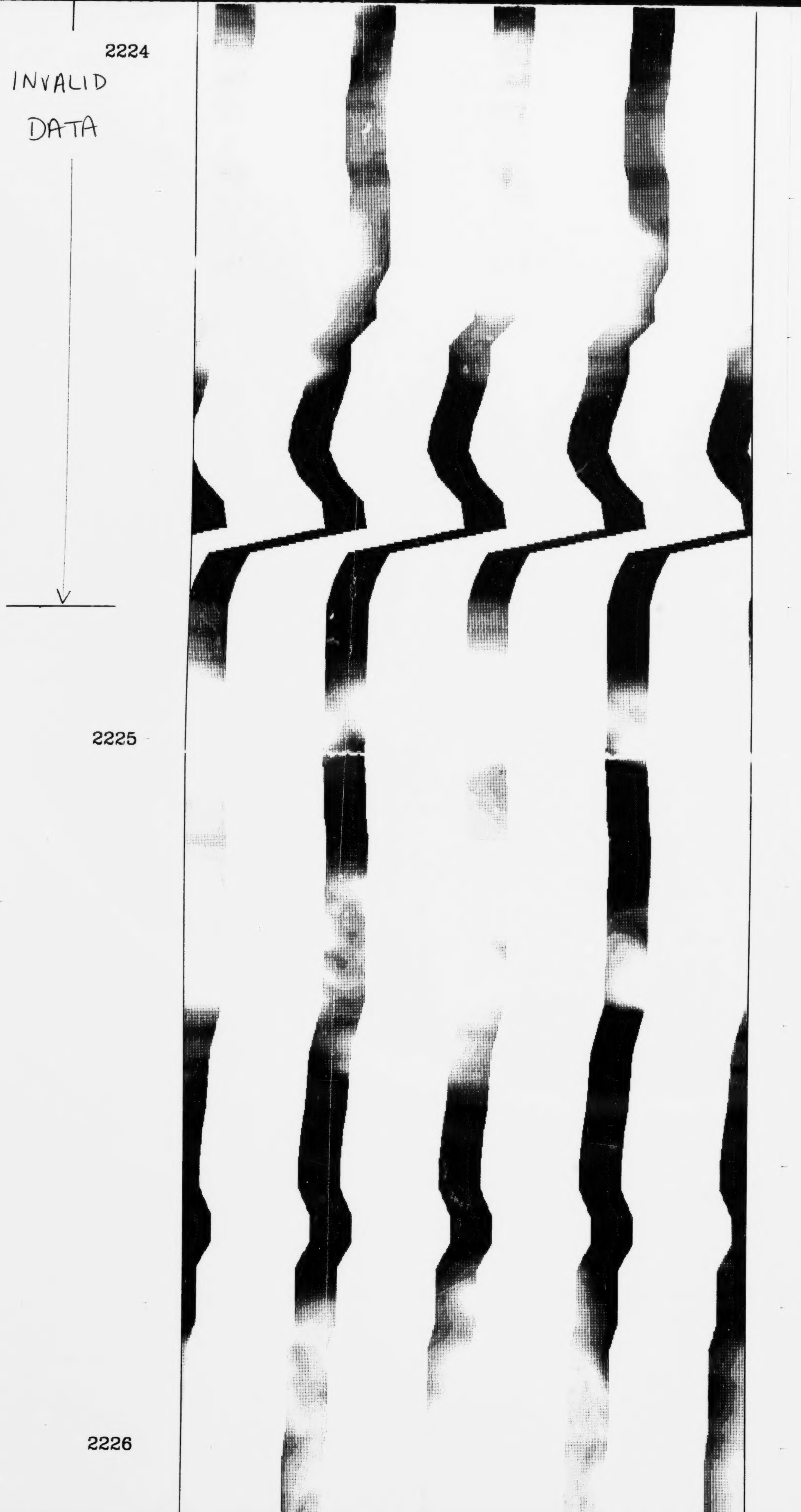

INVALID
DATA

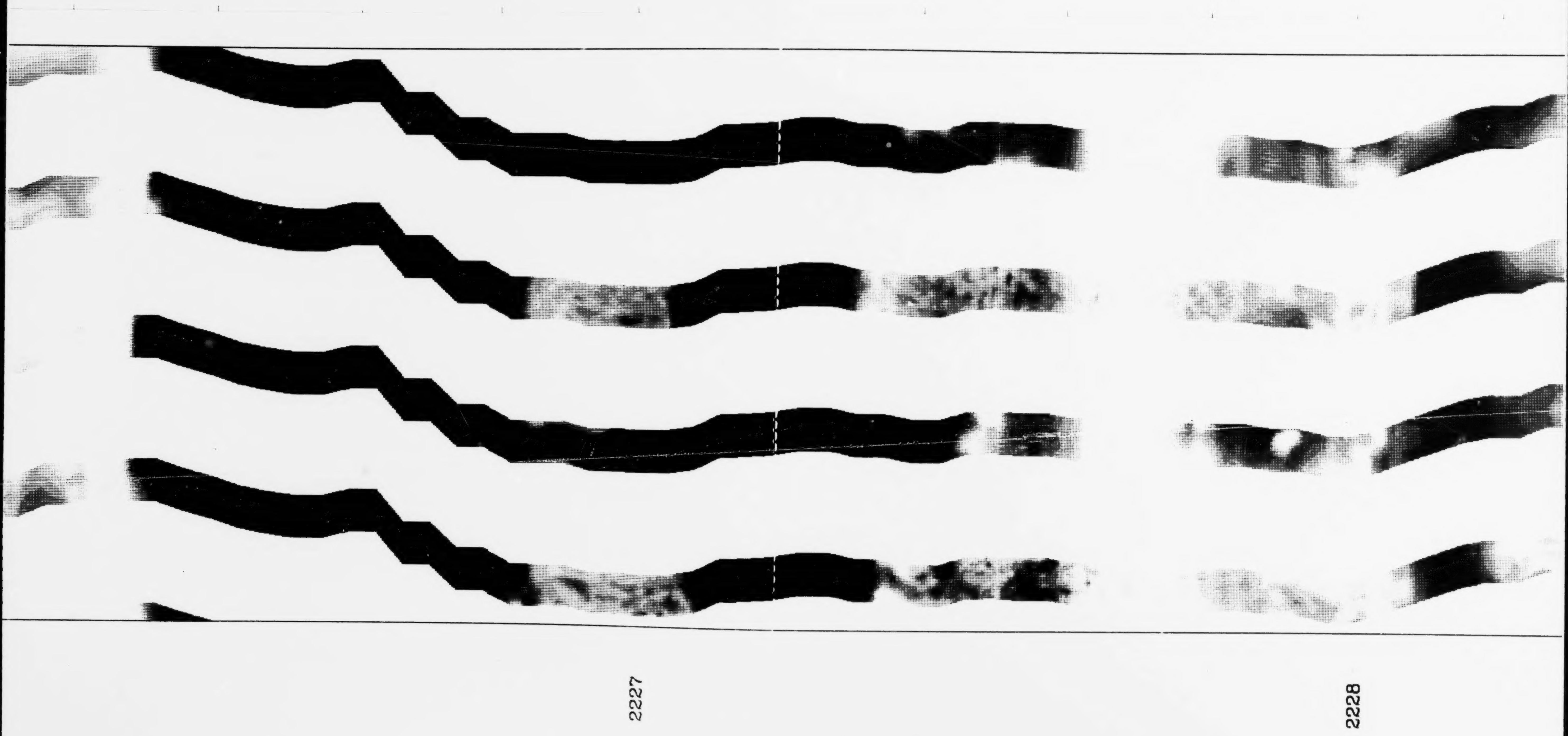
2227
2228

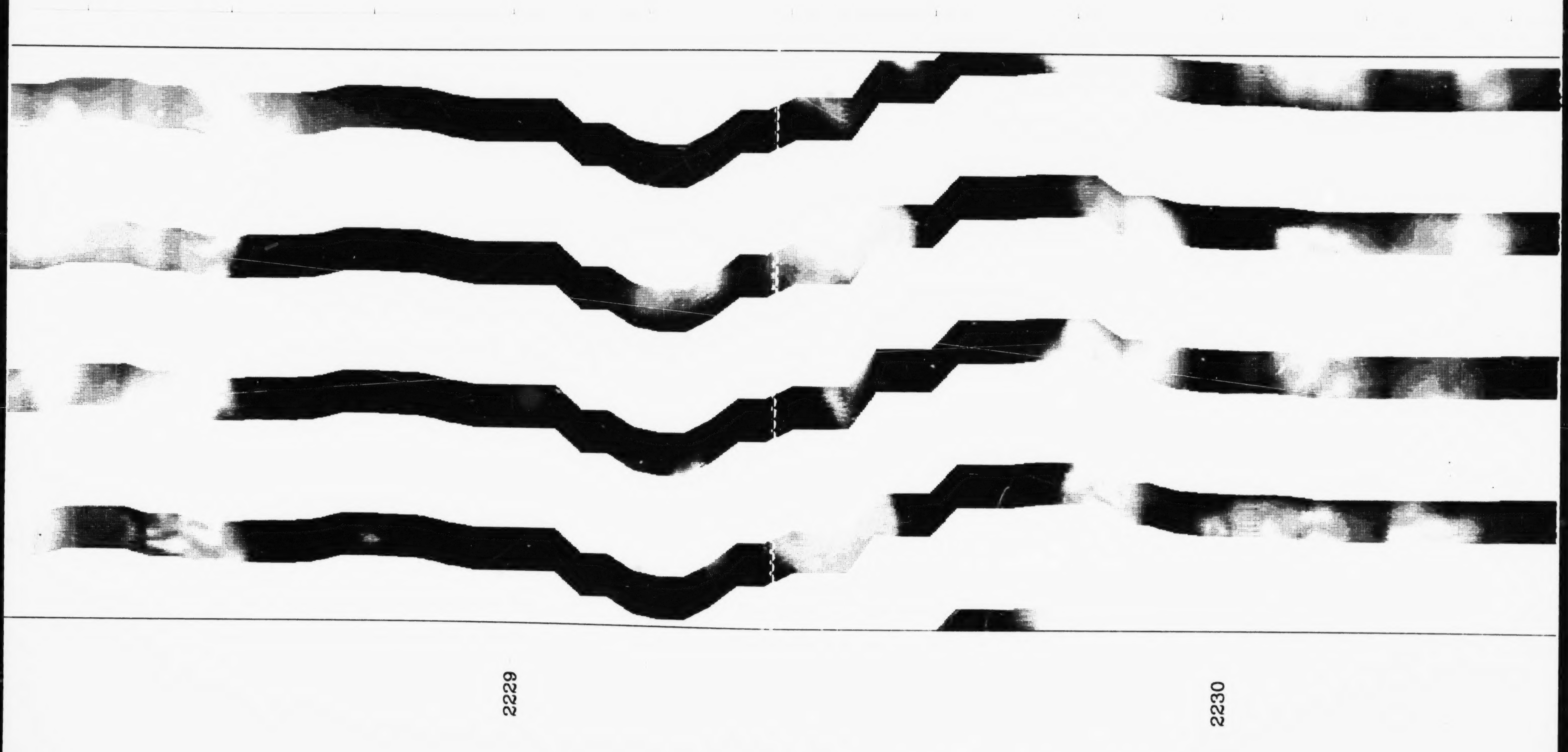
2229
2230

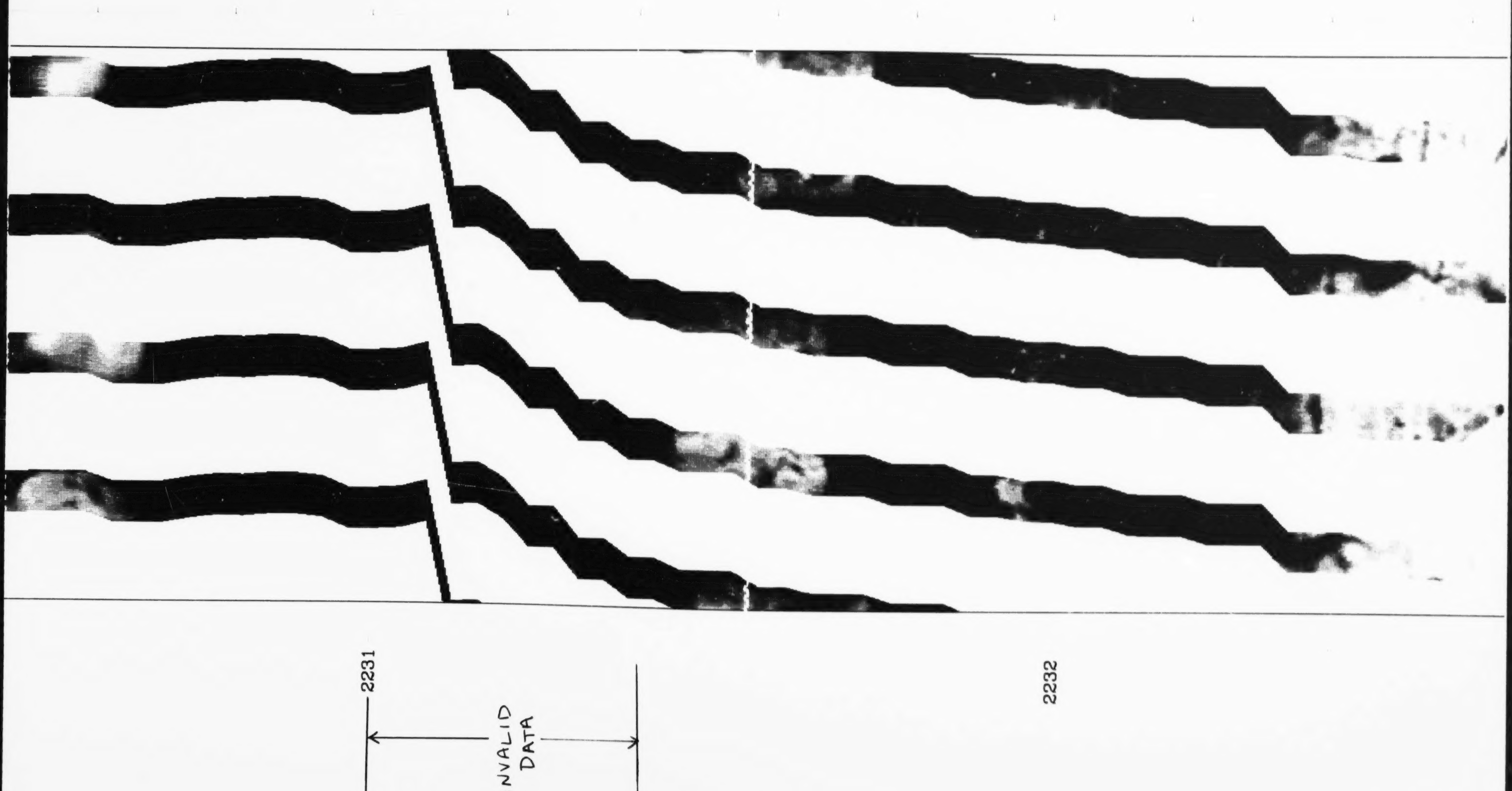

2231
INVALID DATA
2232

2233
2234

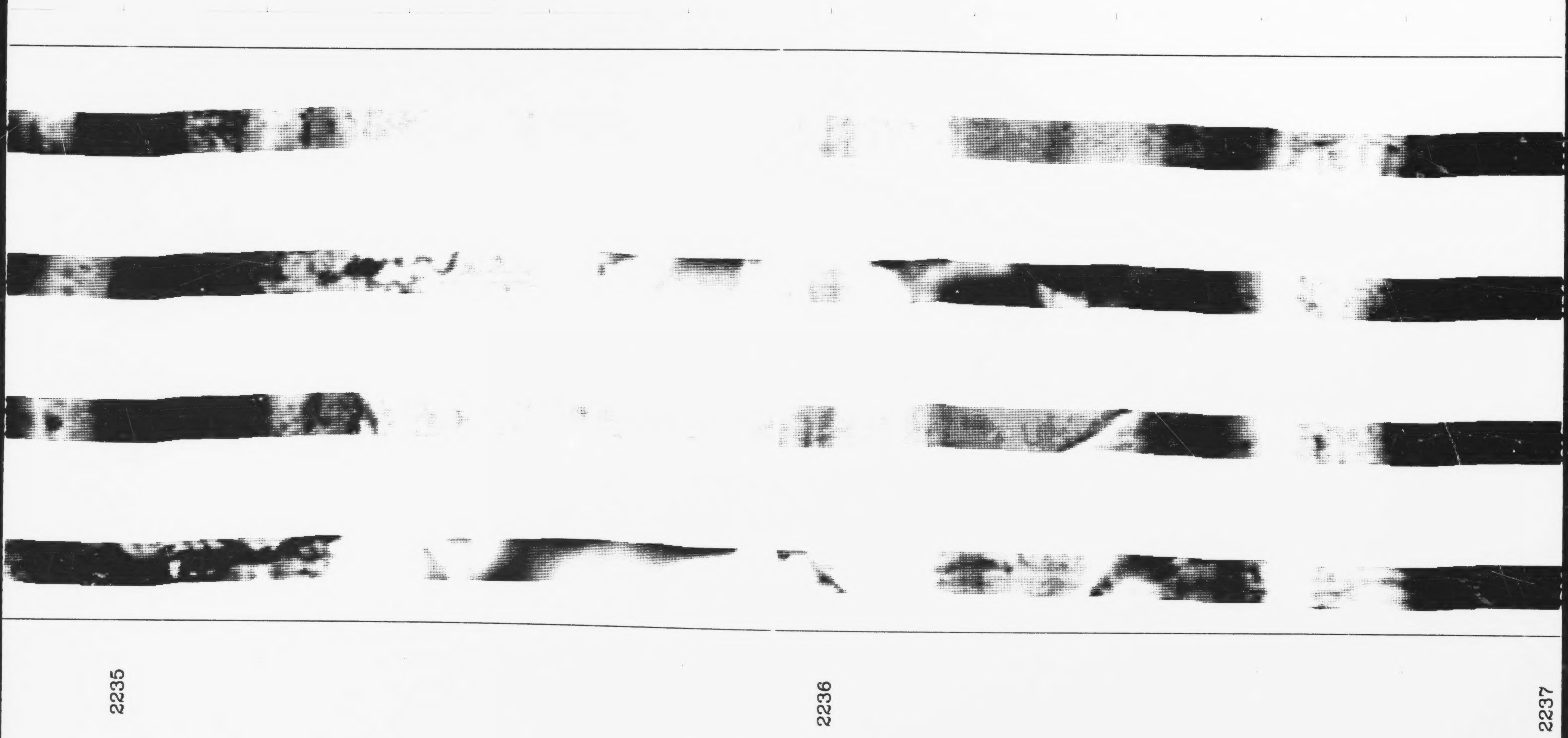
2235
2236
2237

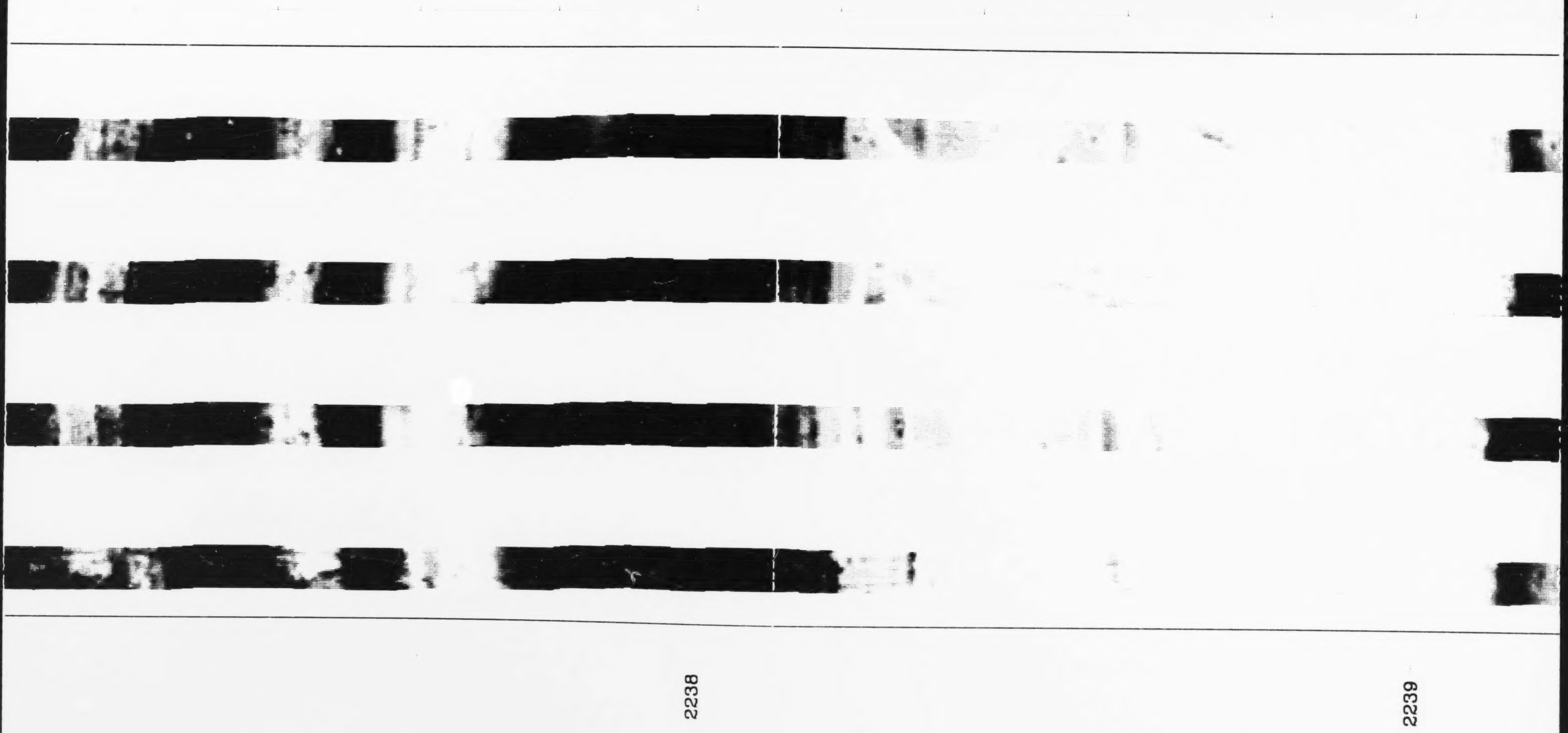
2238
2239

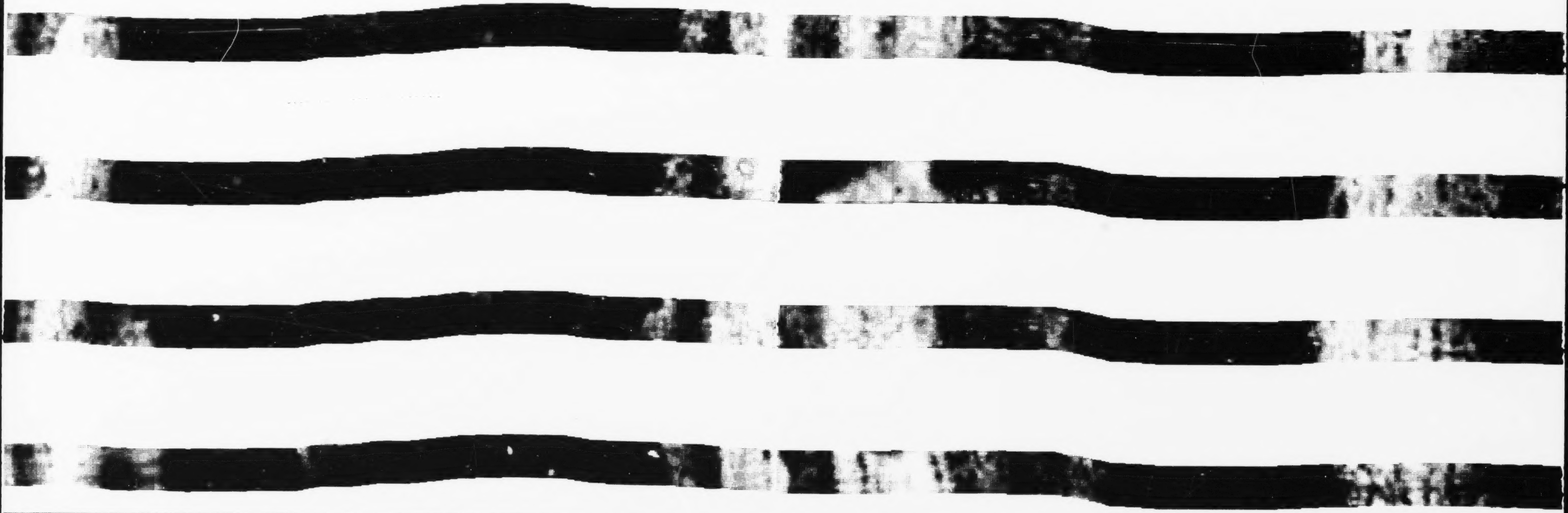

2240
2241

2242
2243

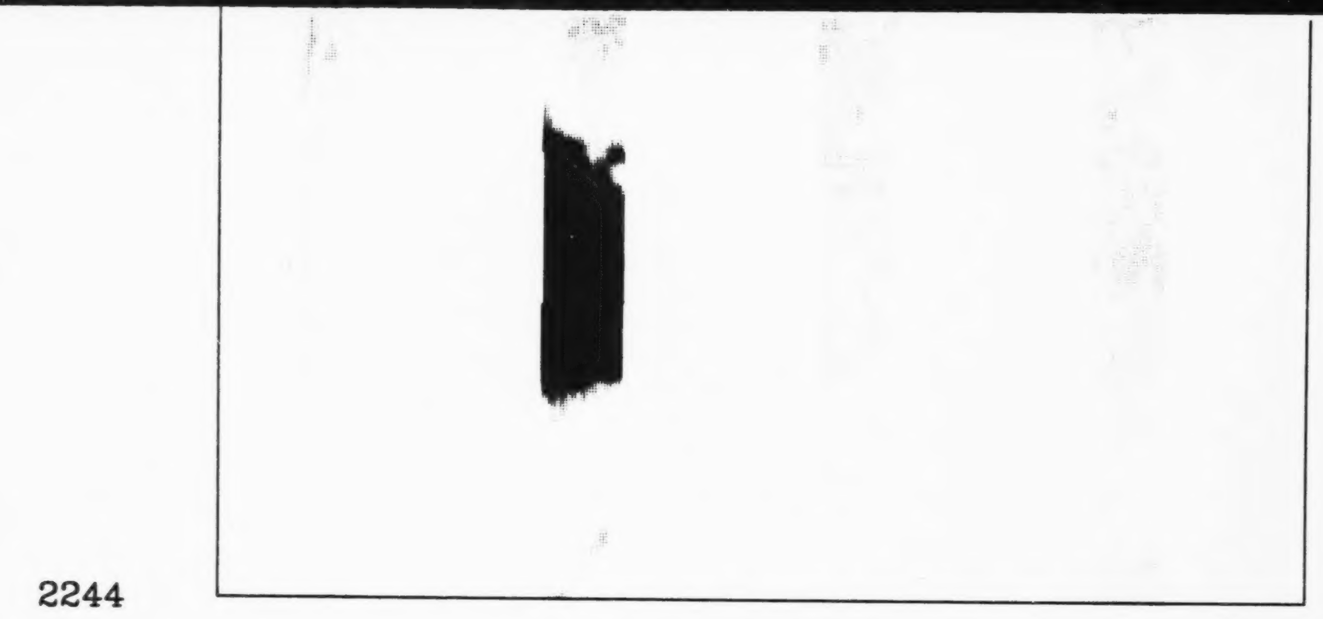

STATIC IMAGES

ZONE FROM 2284.0 M TO 2244.0 M

DEPTH SCALE = 1/ 5

IMAGE SCALE = 1/ 5

BITSIZE = 9.88

ORIENTATION

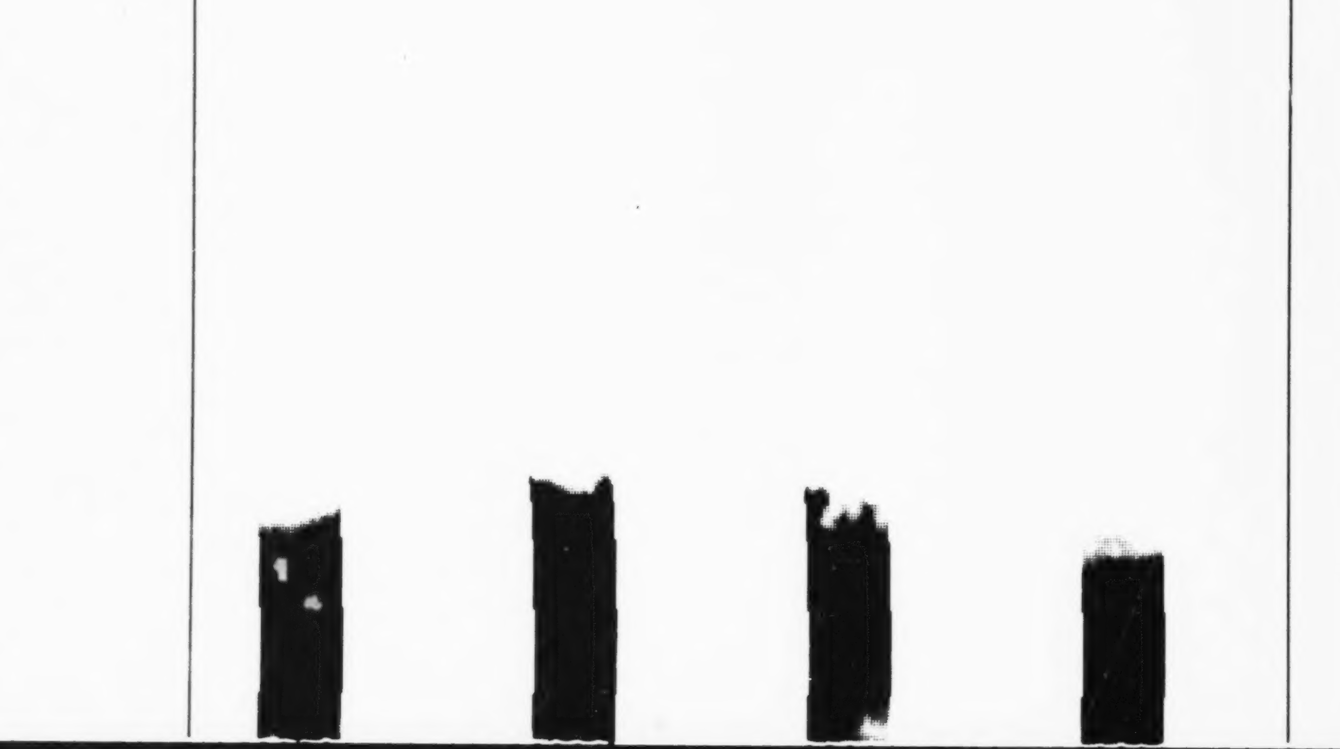

2245
2246

[redacted]

2250
2251

[illegible] [redacted]

[illegible] [redacted]

[illegible] [redacted]

[illegible] [redacted]

2252

2253

[redacted]

2254

2255

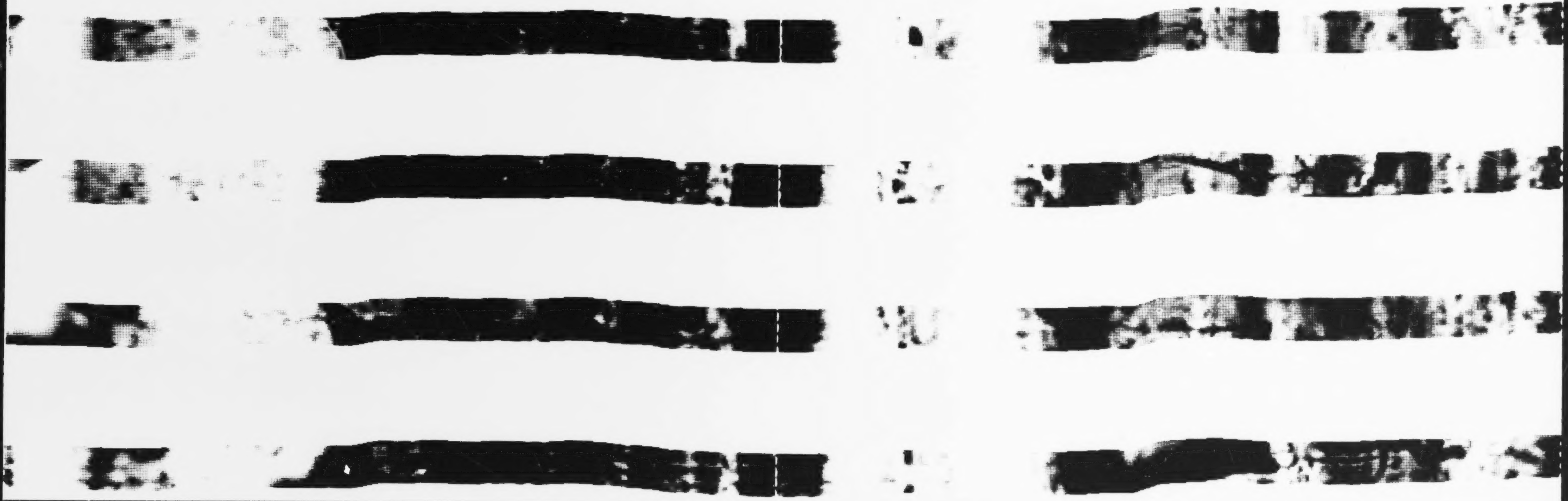
2256
2257

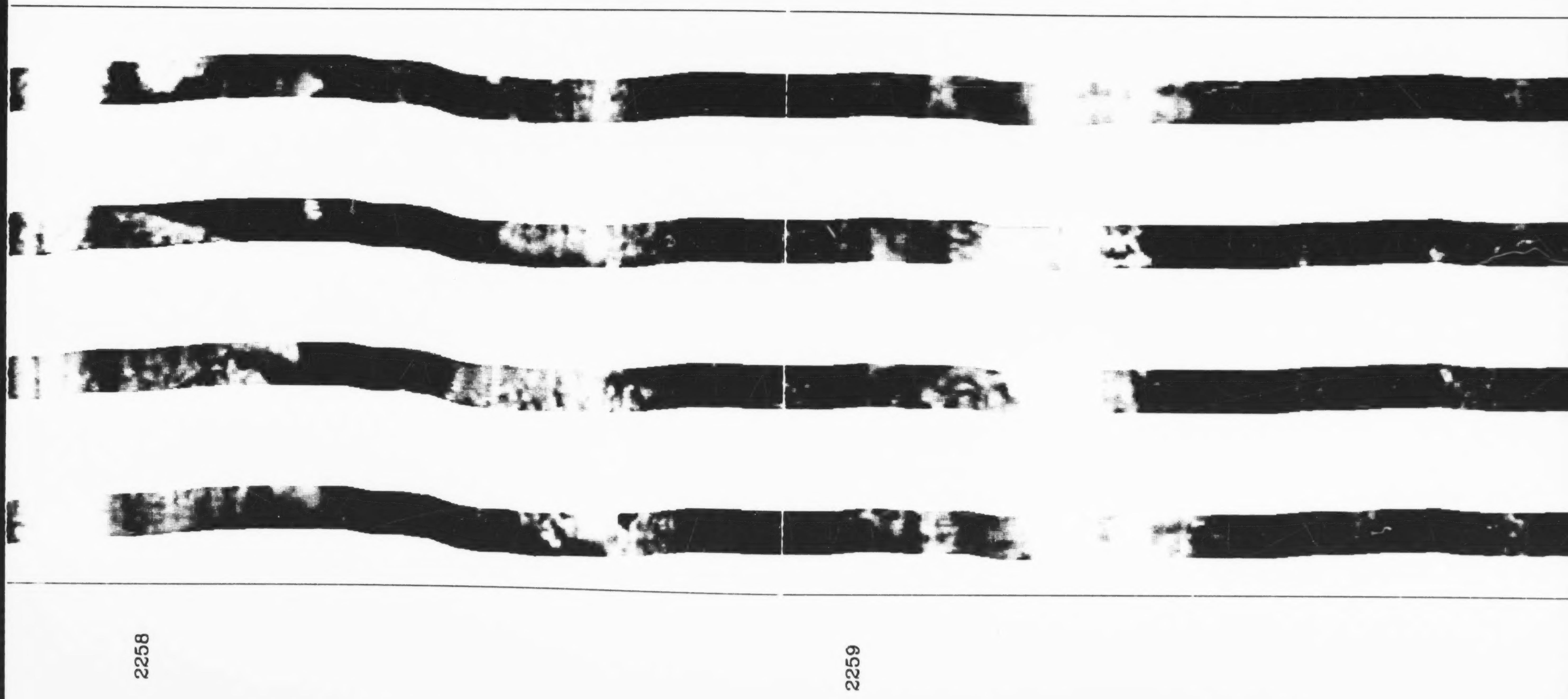
2258
2259

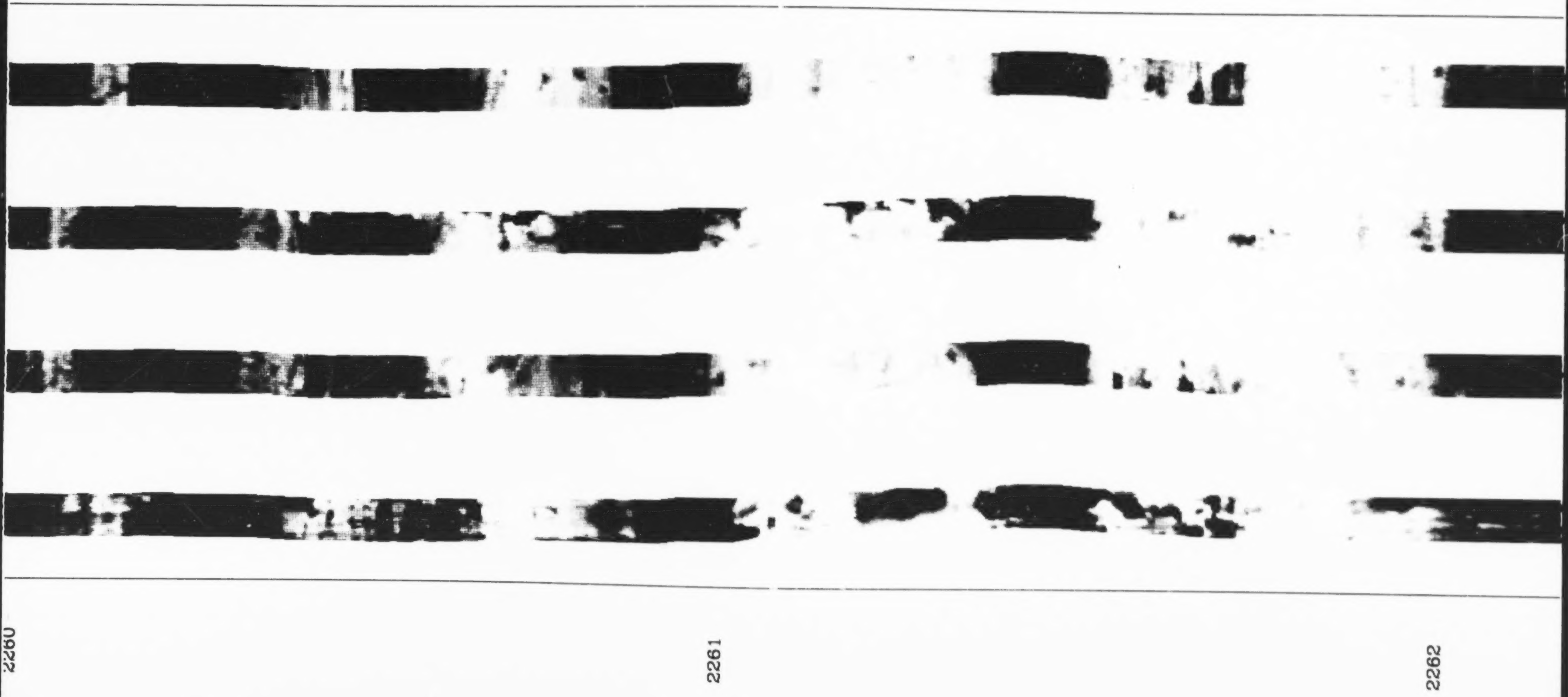
2260
2261
2262

[redacted]

2265

2266

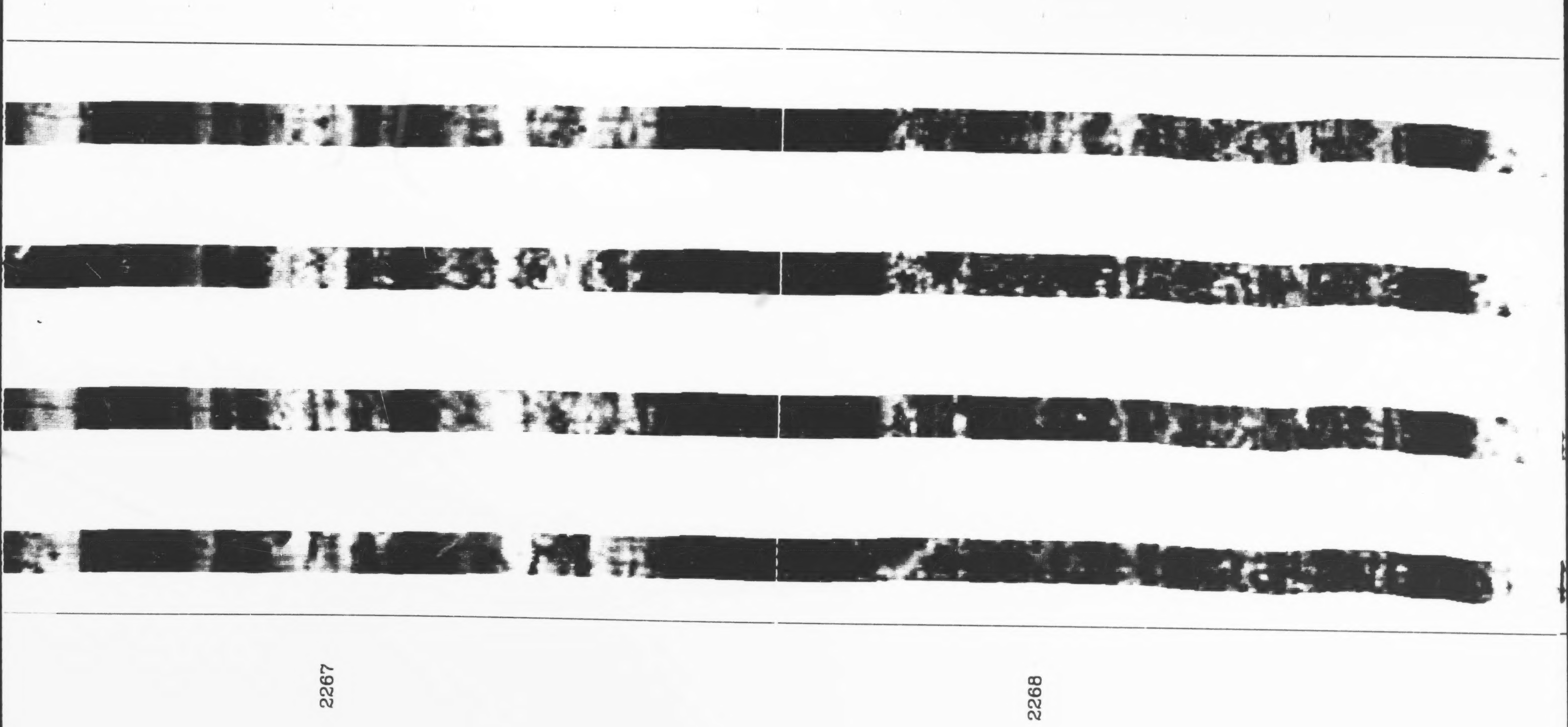
2267
2268

2269

2270

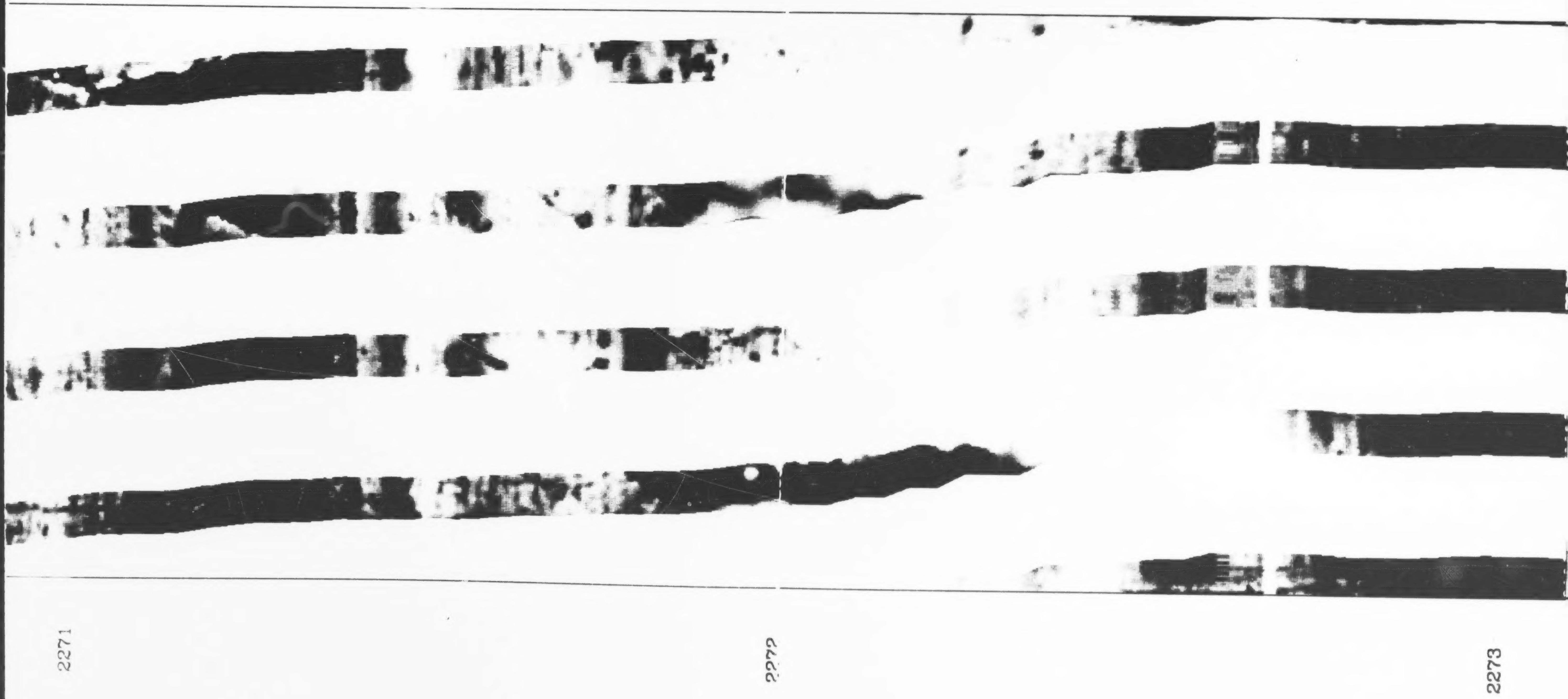
2271
2272
2273

2274

2275

[redacted]

[redacted]

[redacted]

[redacted]

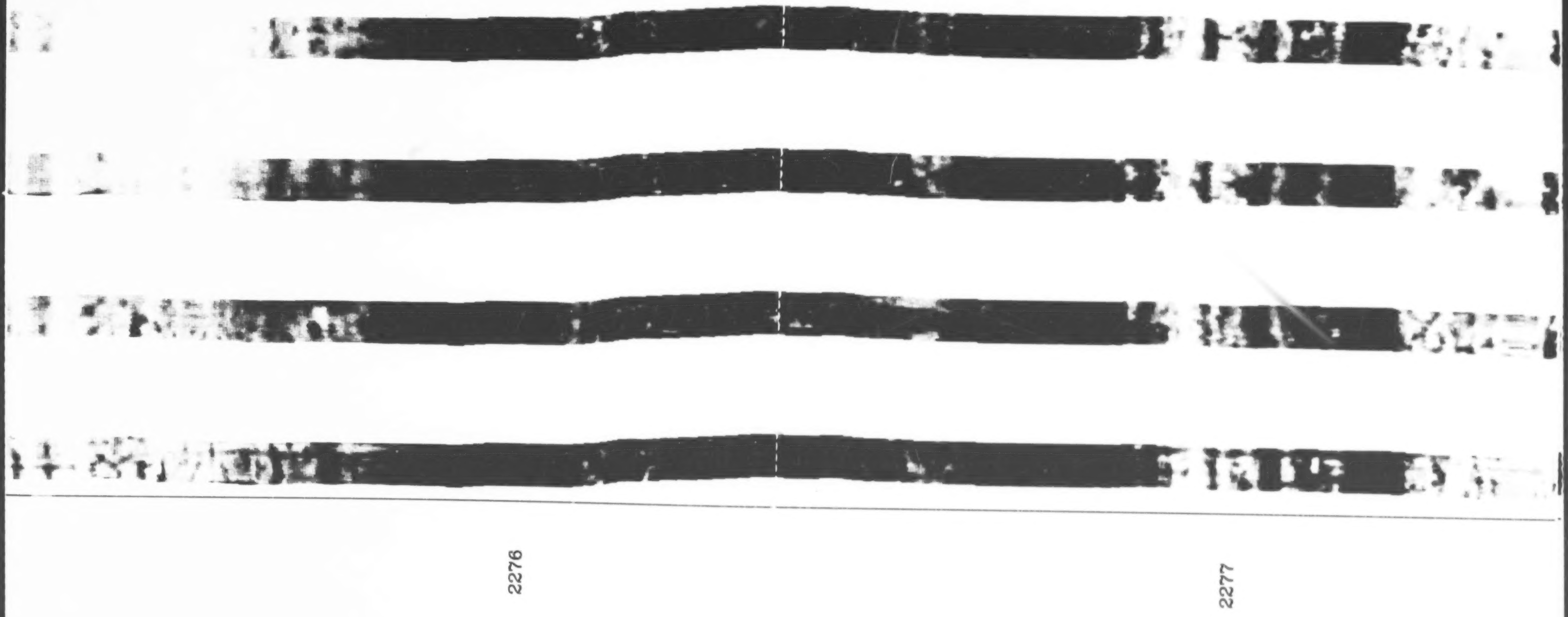
2276
2277

2278

2279

[redacted]

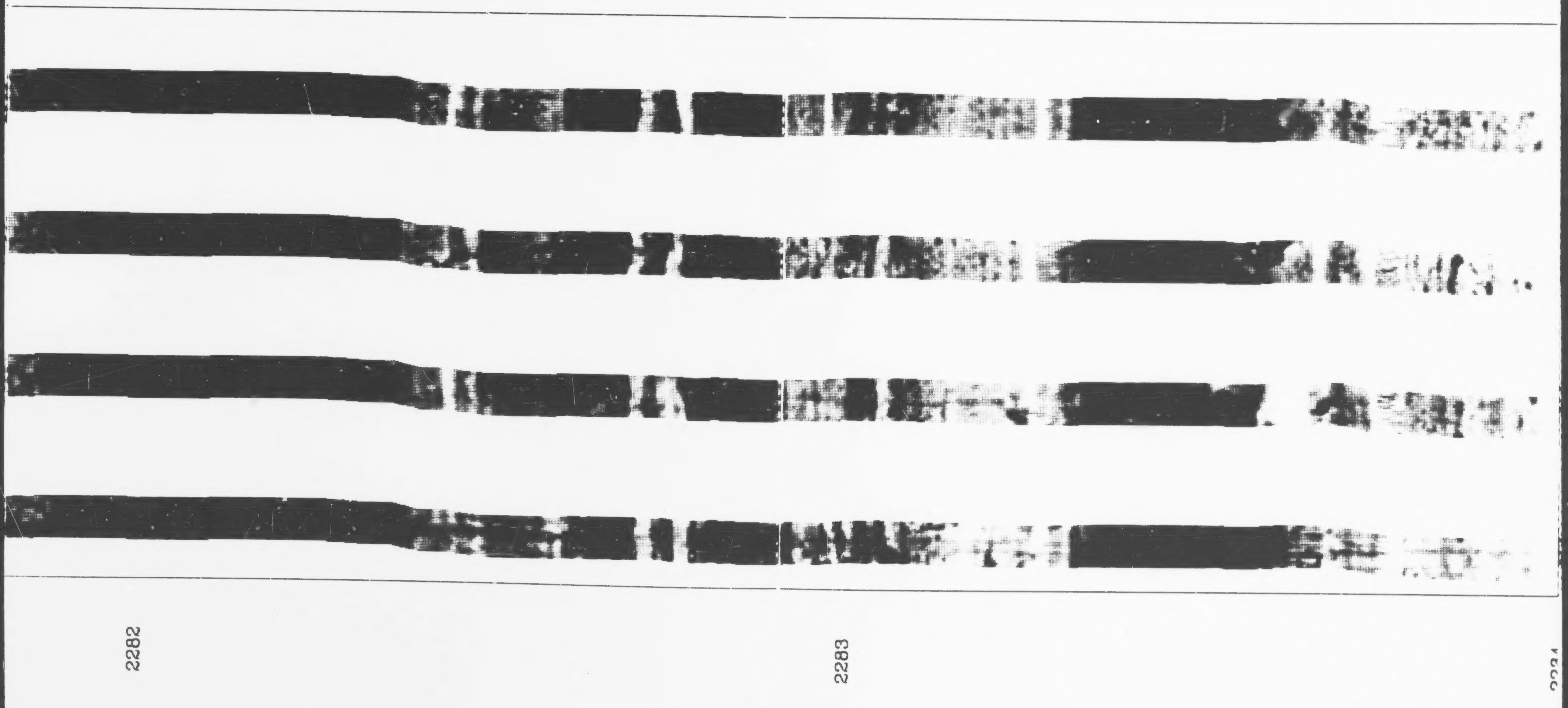
2282
2283

STATIC IMAGES

ZONE FROM 2324.0 M TO 2284.0 M

DEPTH SCALE = 1/ 5

IMAGE SCALE = 1/ 5

BITSIZE = 9.88

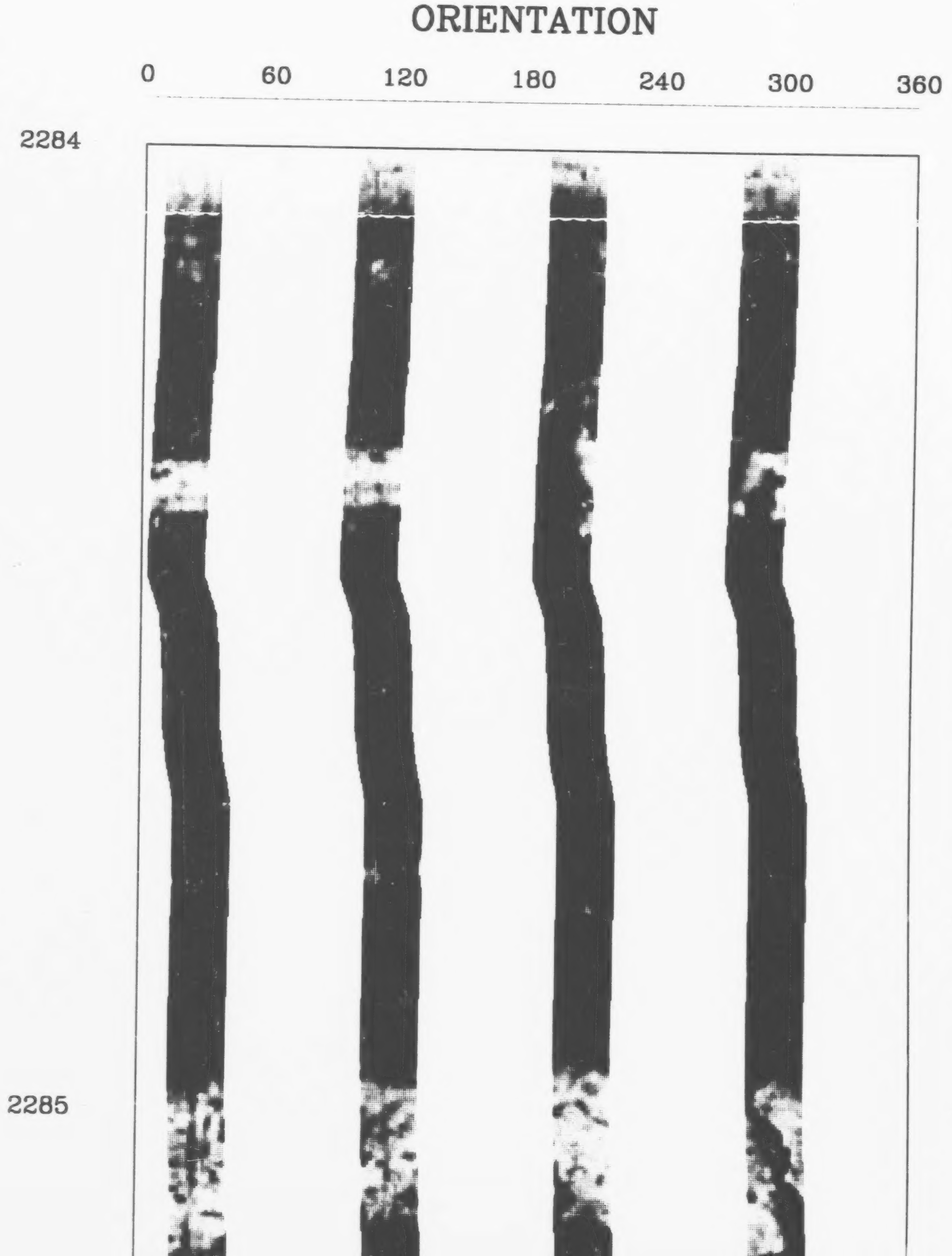

2288

2289

[redacted]

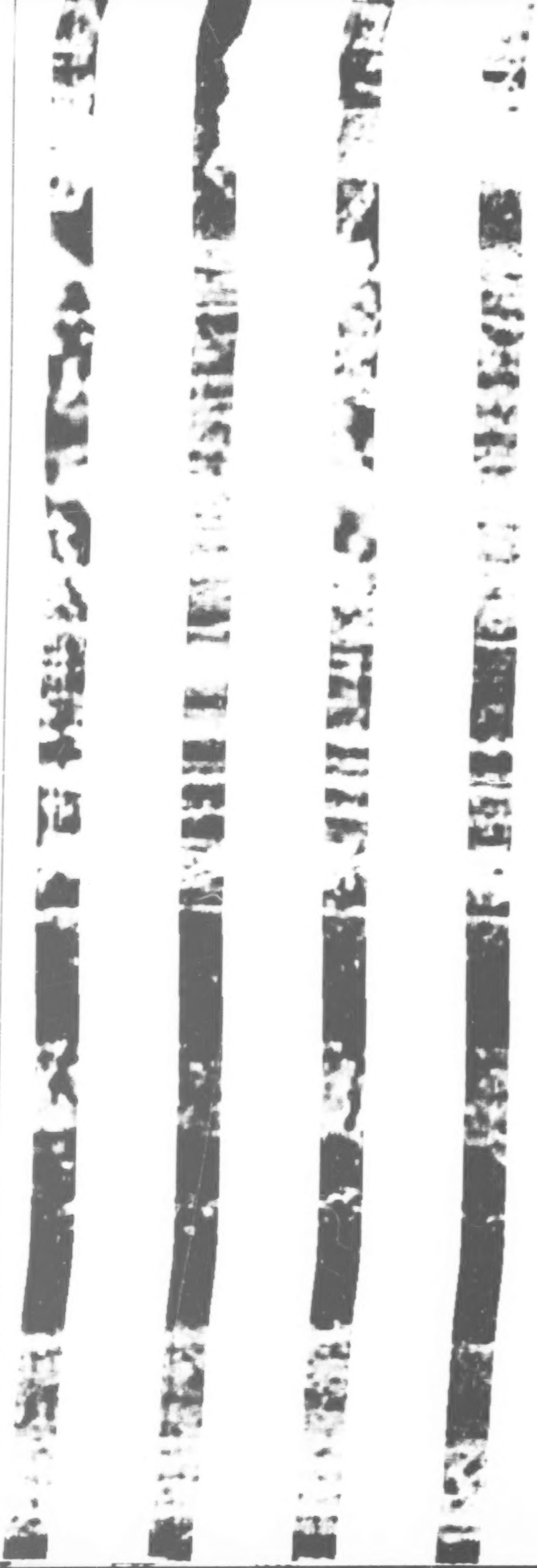

2292

2293

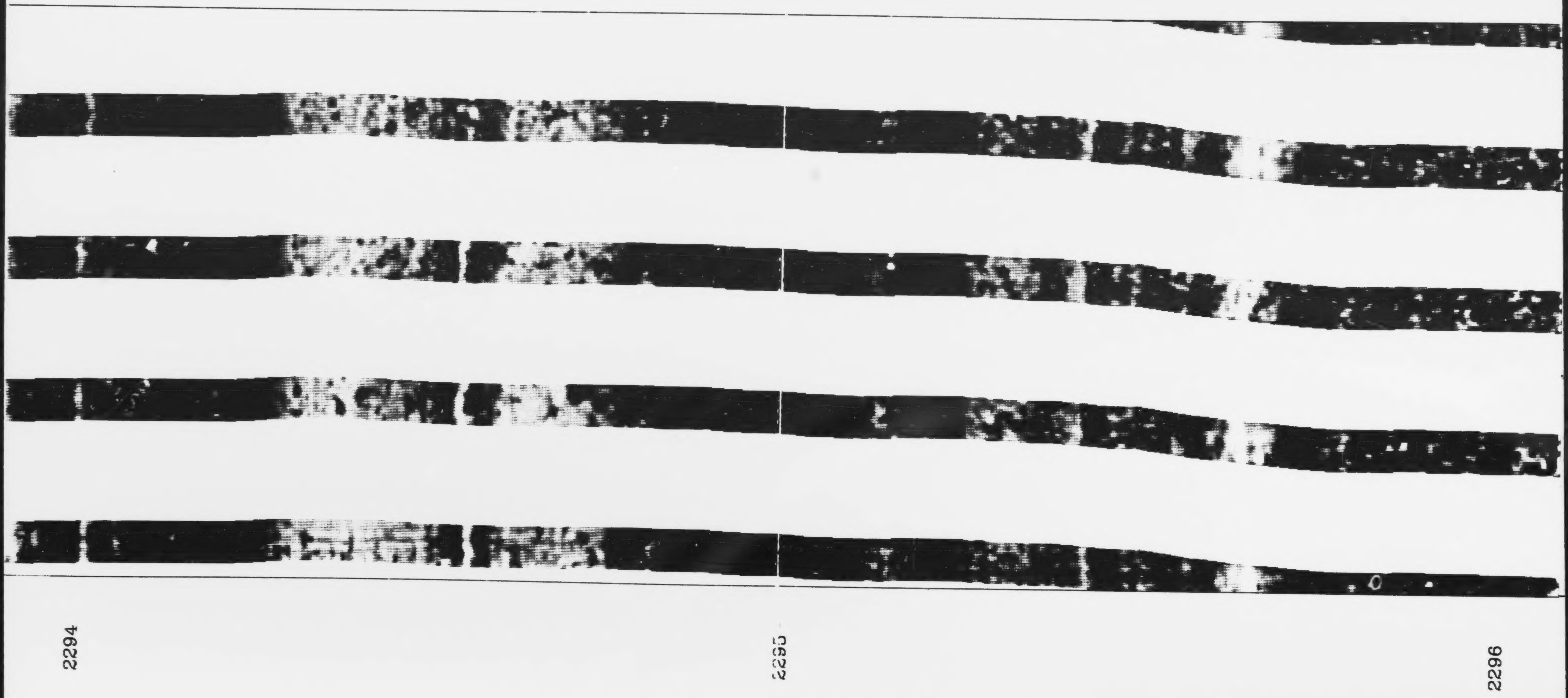
2294
2295
2296

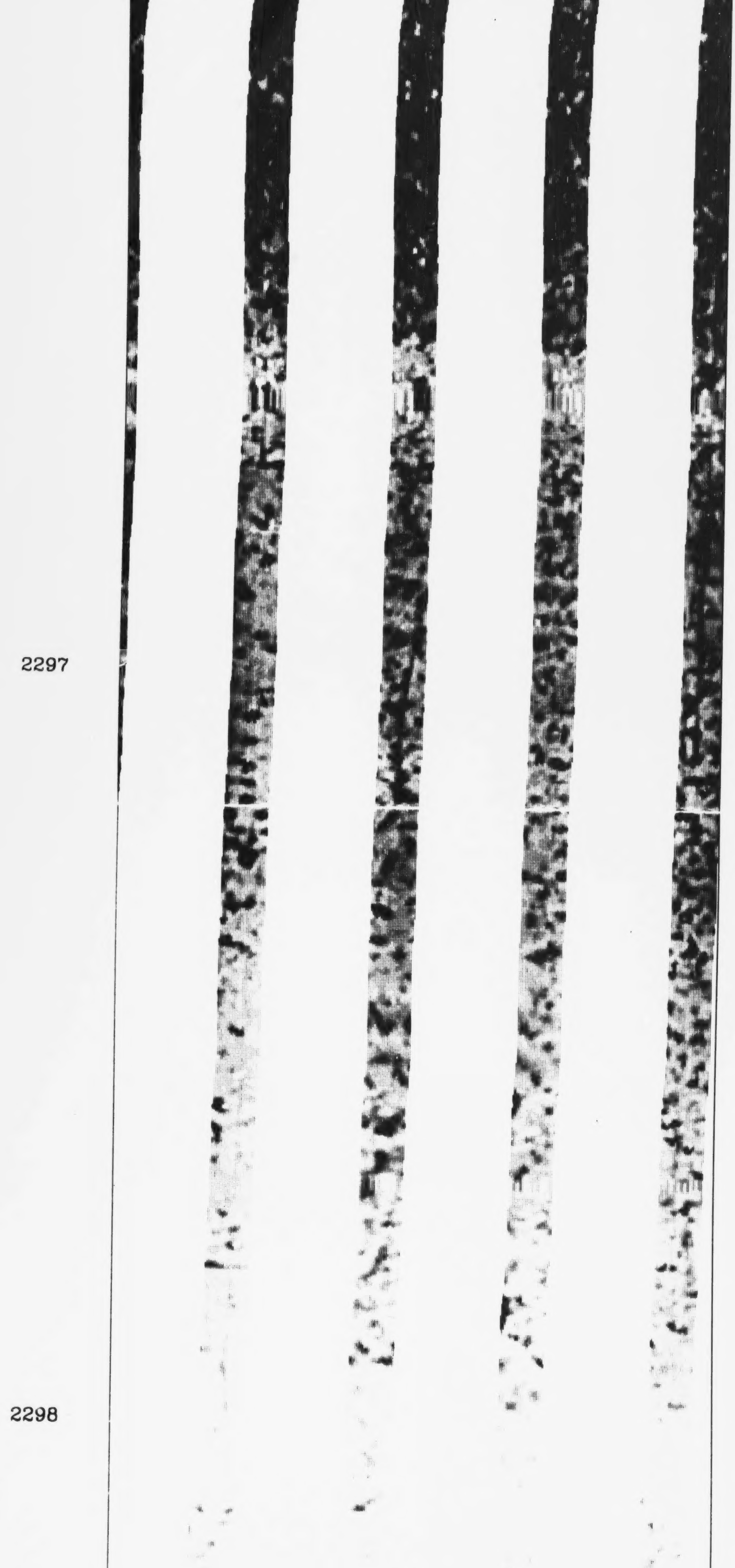
2297
2298

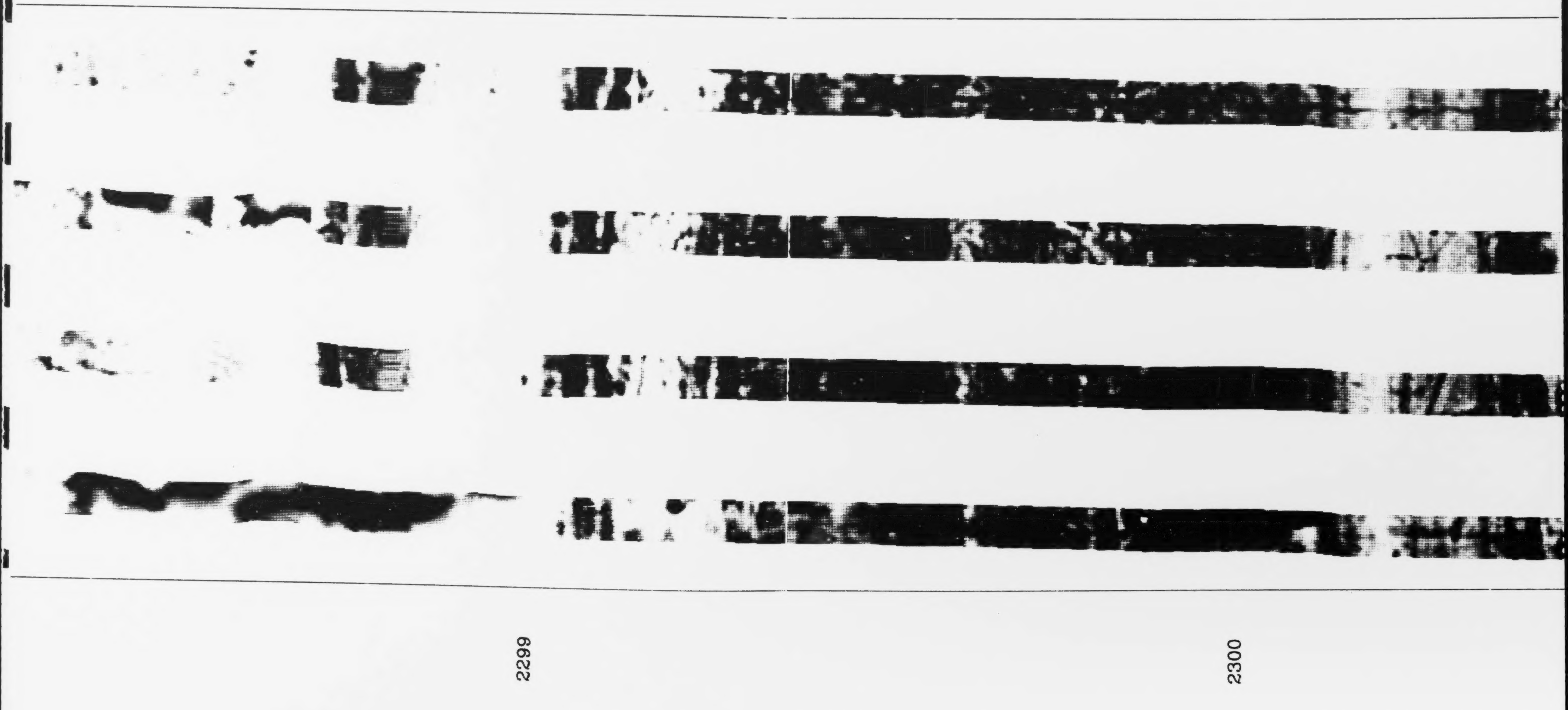
2299
2300

2301

2302

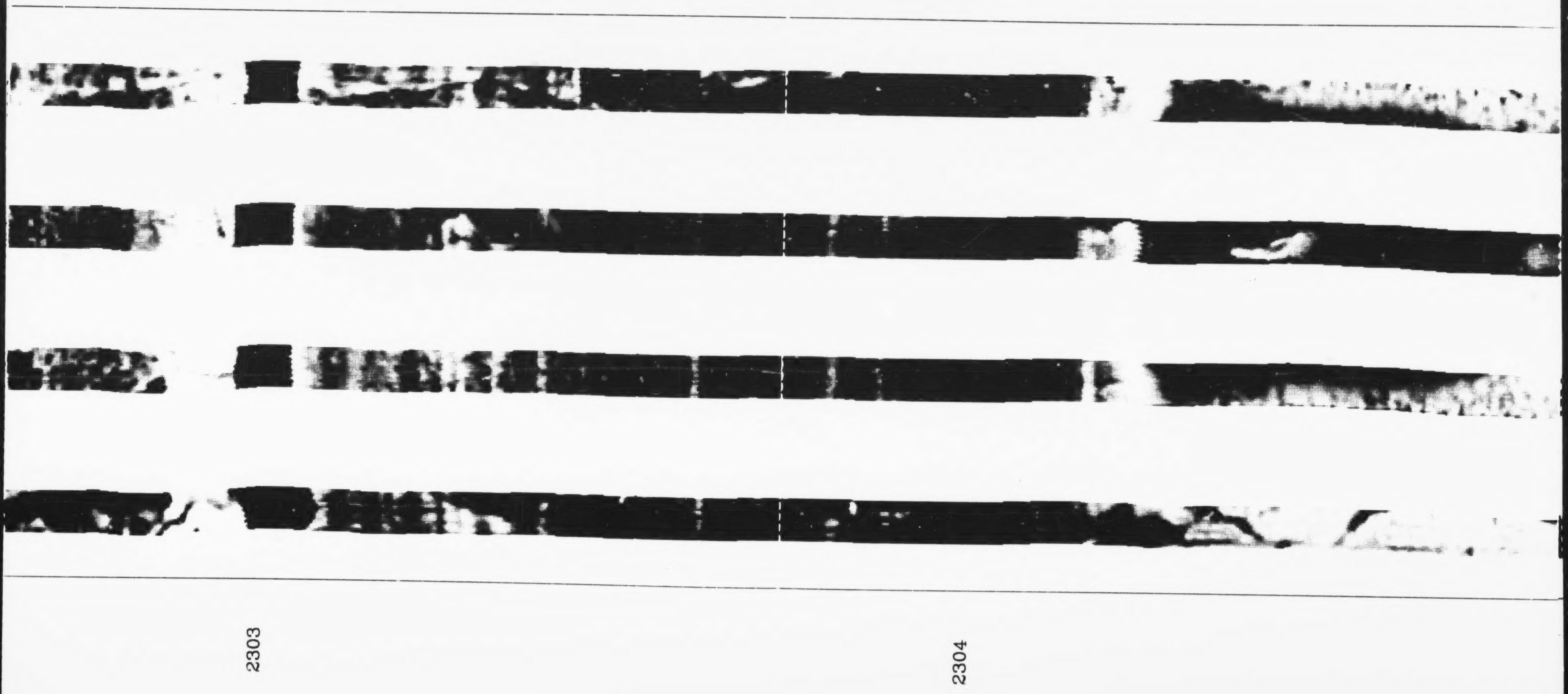
2303
2304

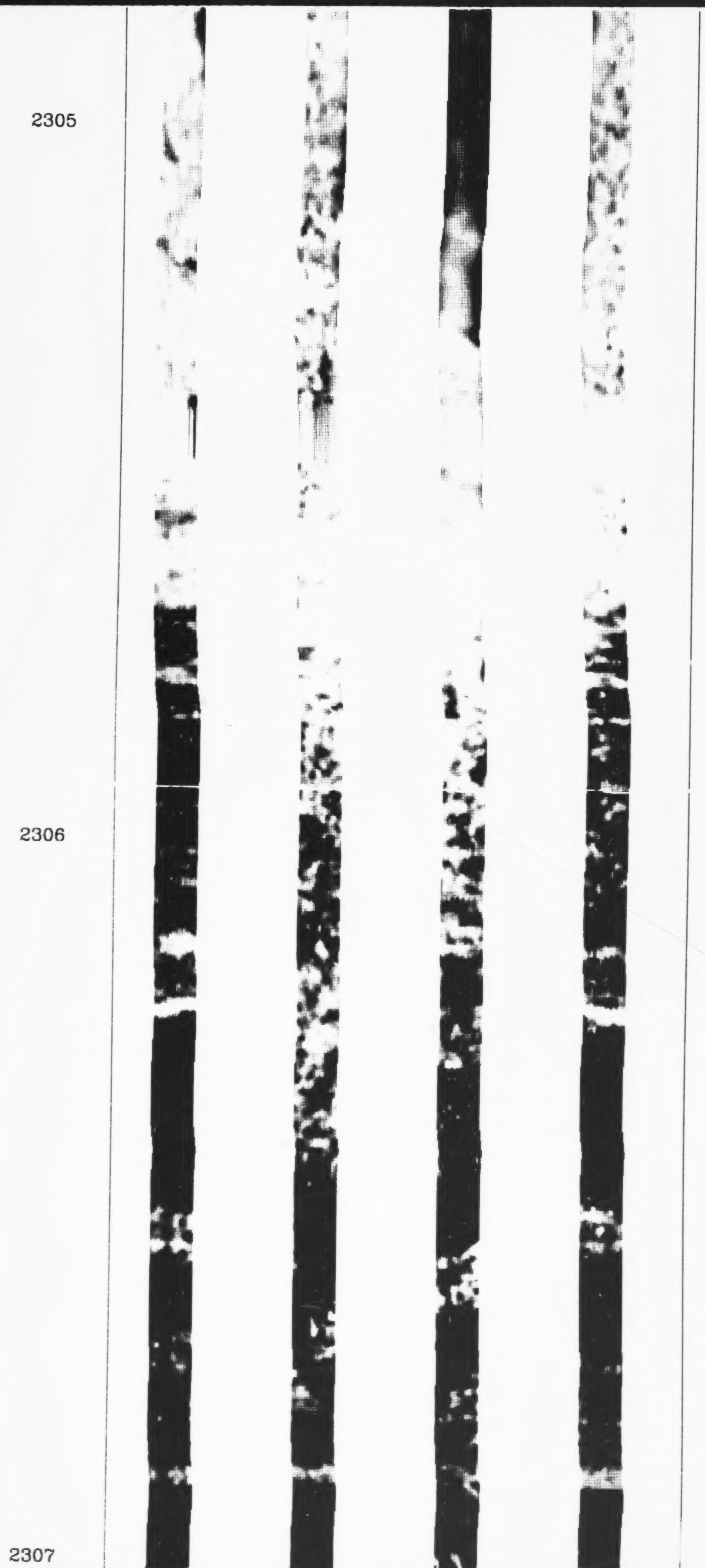
2305
2306
2307

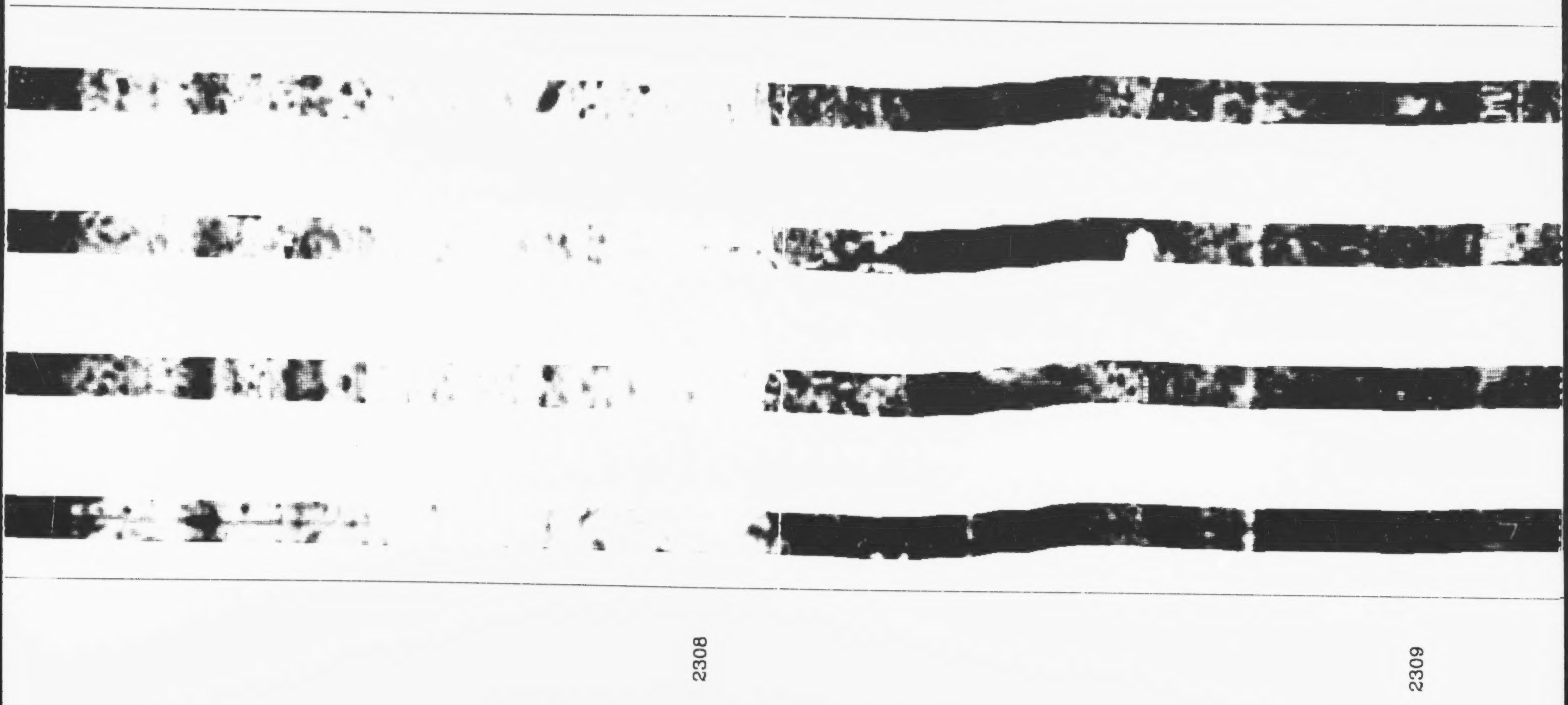
2308
2309

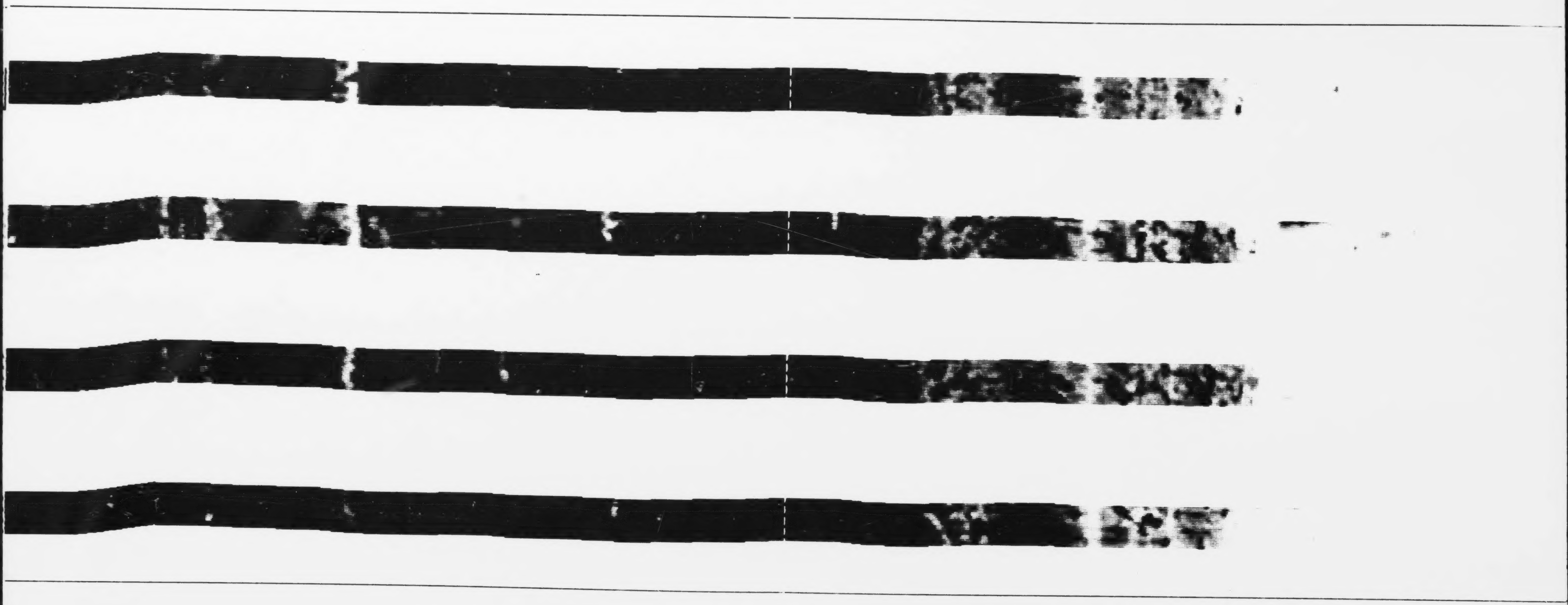
2310
2311

2312

[redacted]

2313

2316

[illegible]

2317

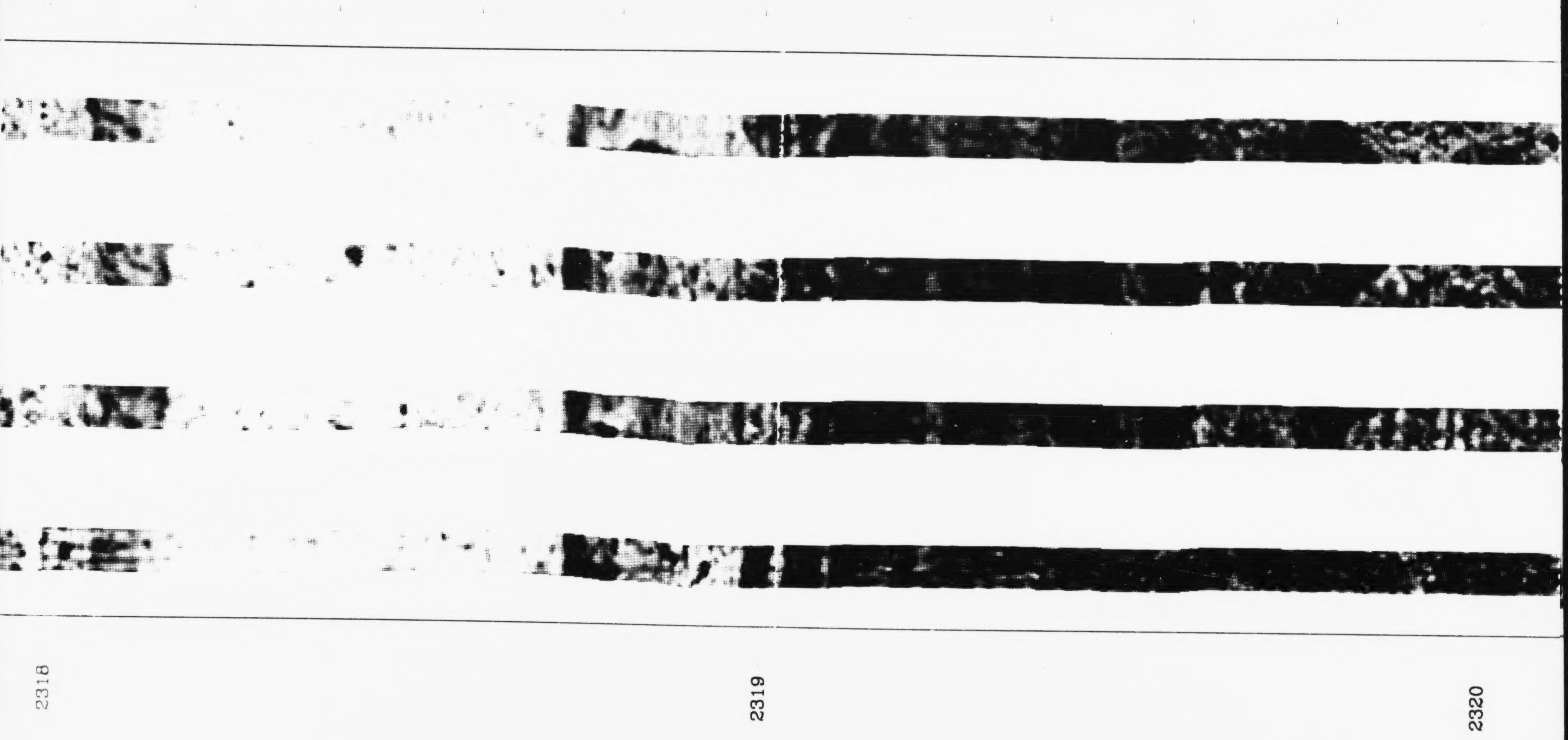
2318
2319
2320

2321
2322

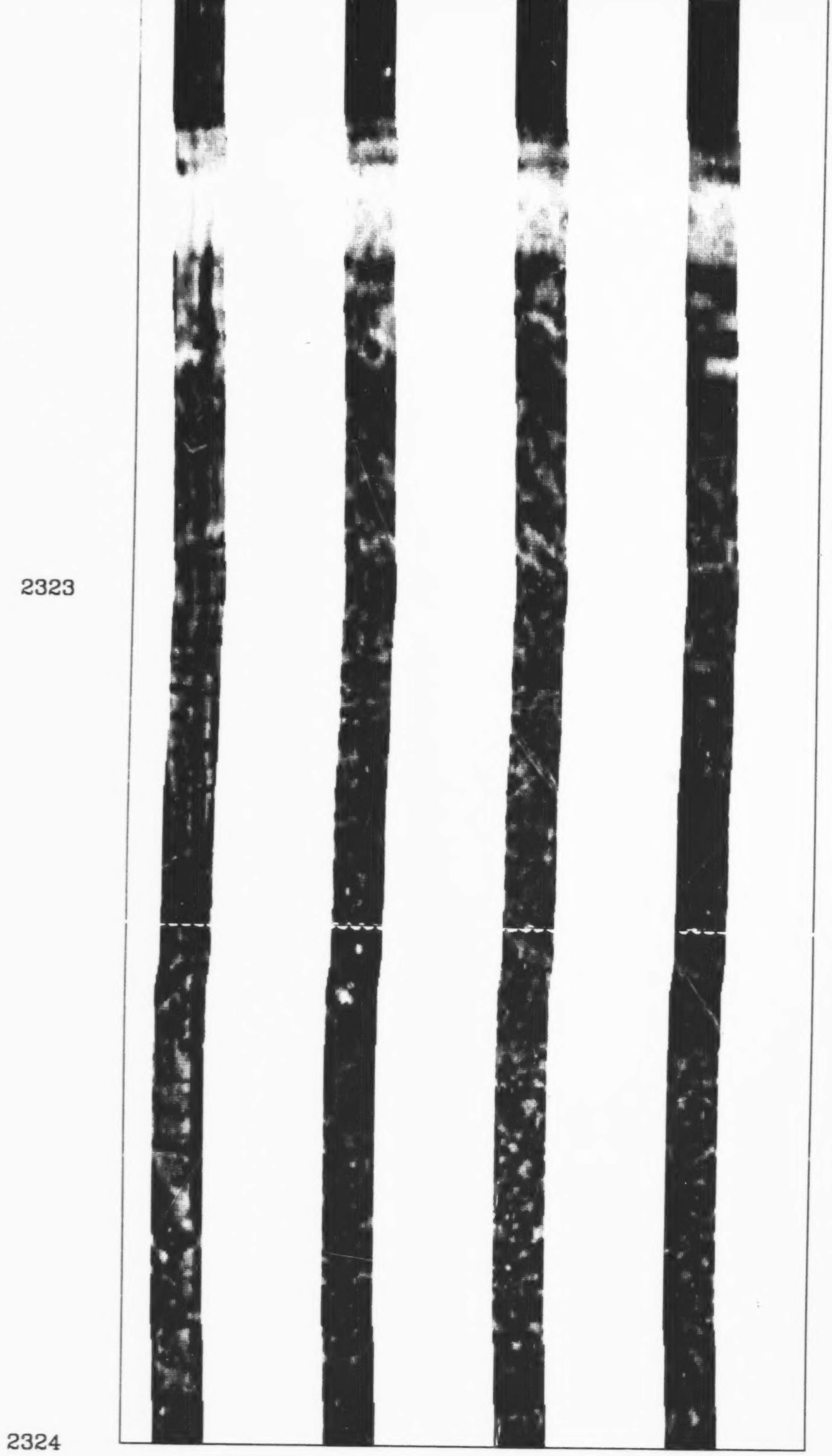

STATIC IMAGES

ZONE FROM 2364.0 M TO 2324.0 M

DEPTH SCALE = 1/ 5

IMAGE SCALE = 1/ 5

BITSIZE = 9.88

ORIENTATION

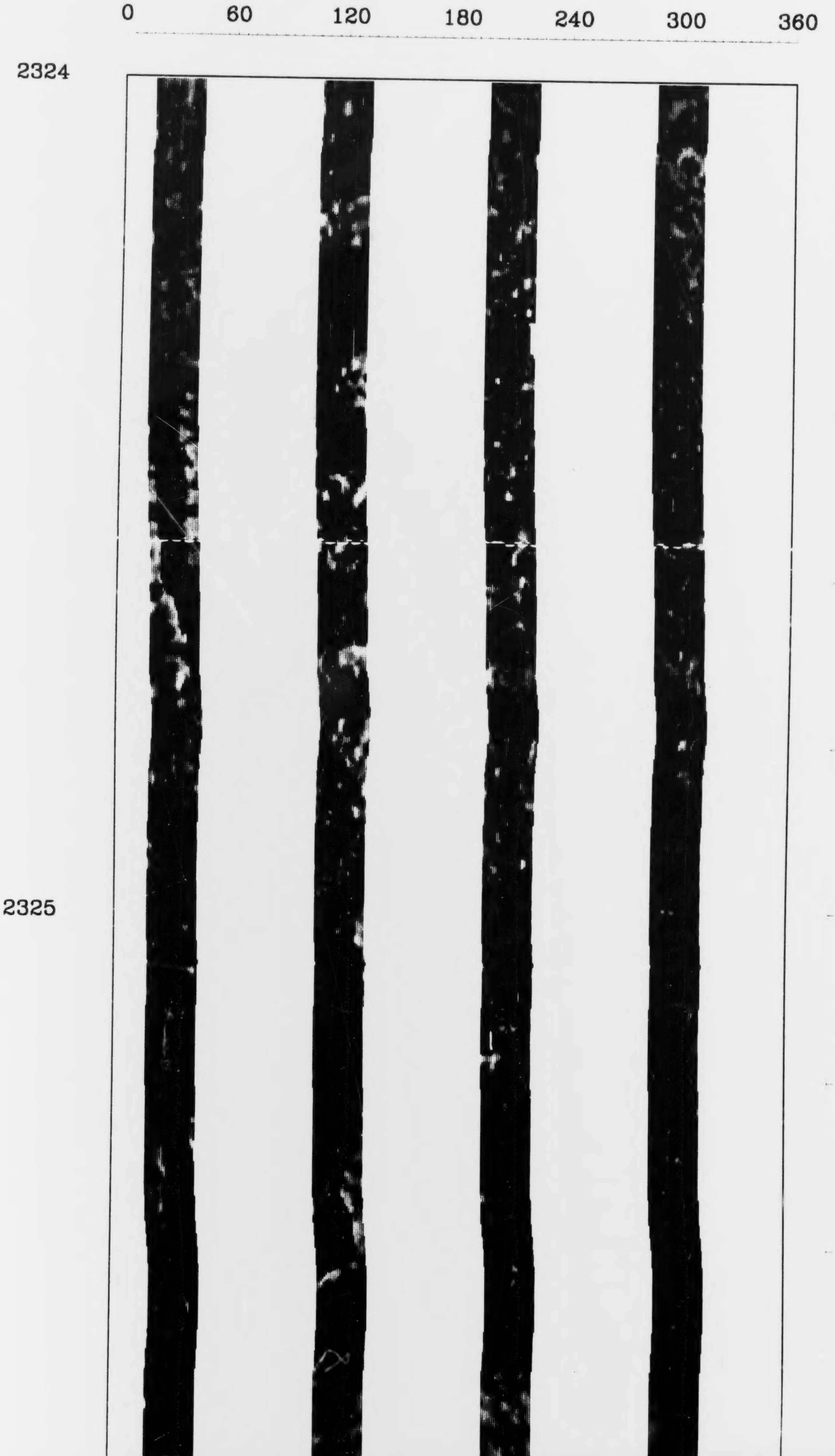

2326
2327

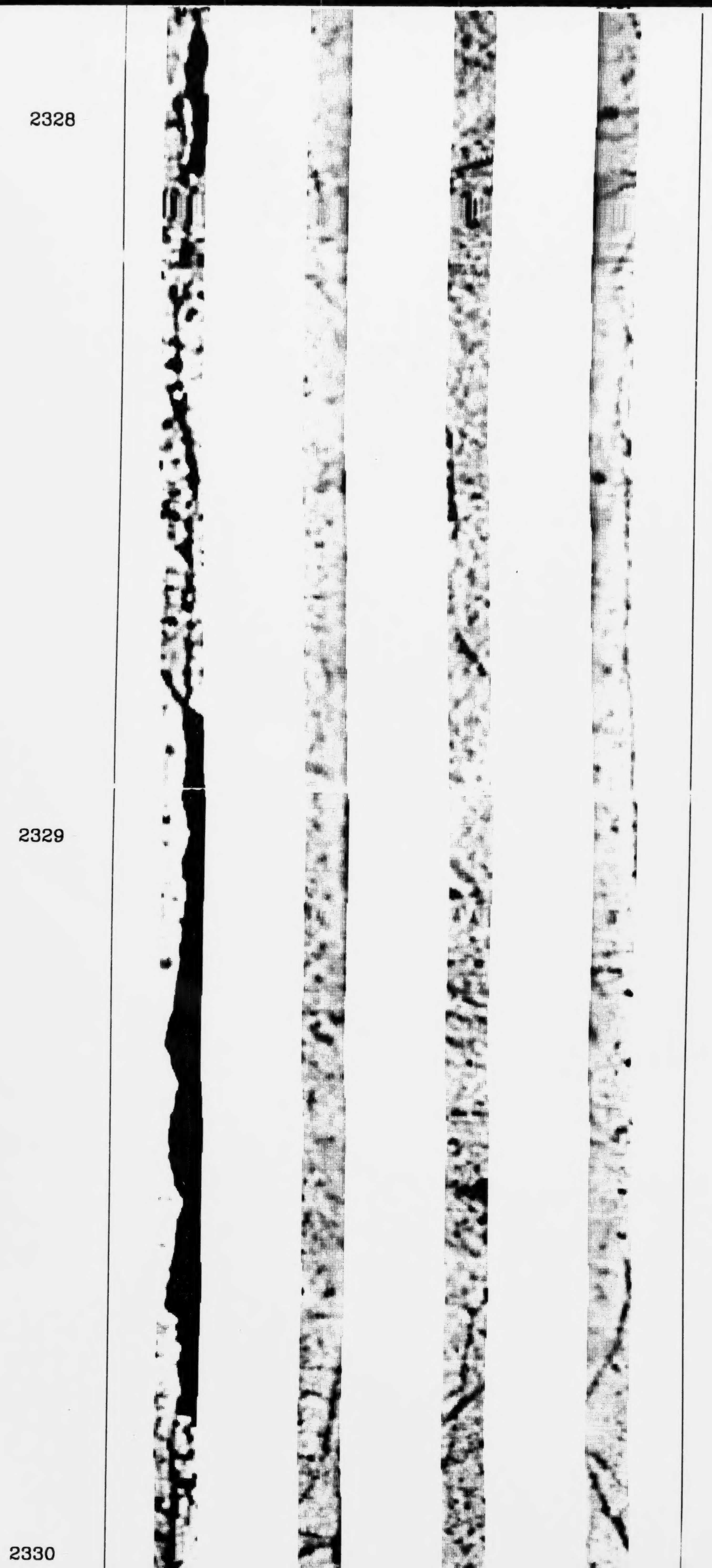
2328
2329
2330

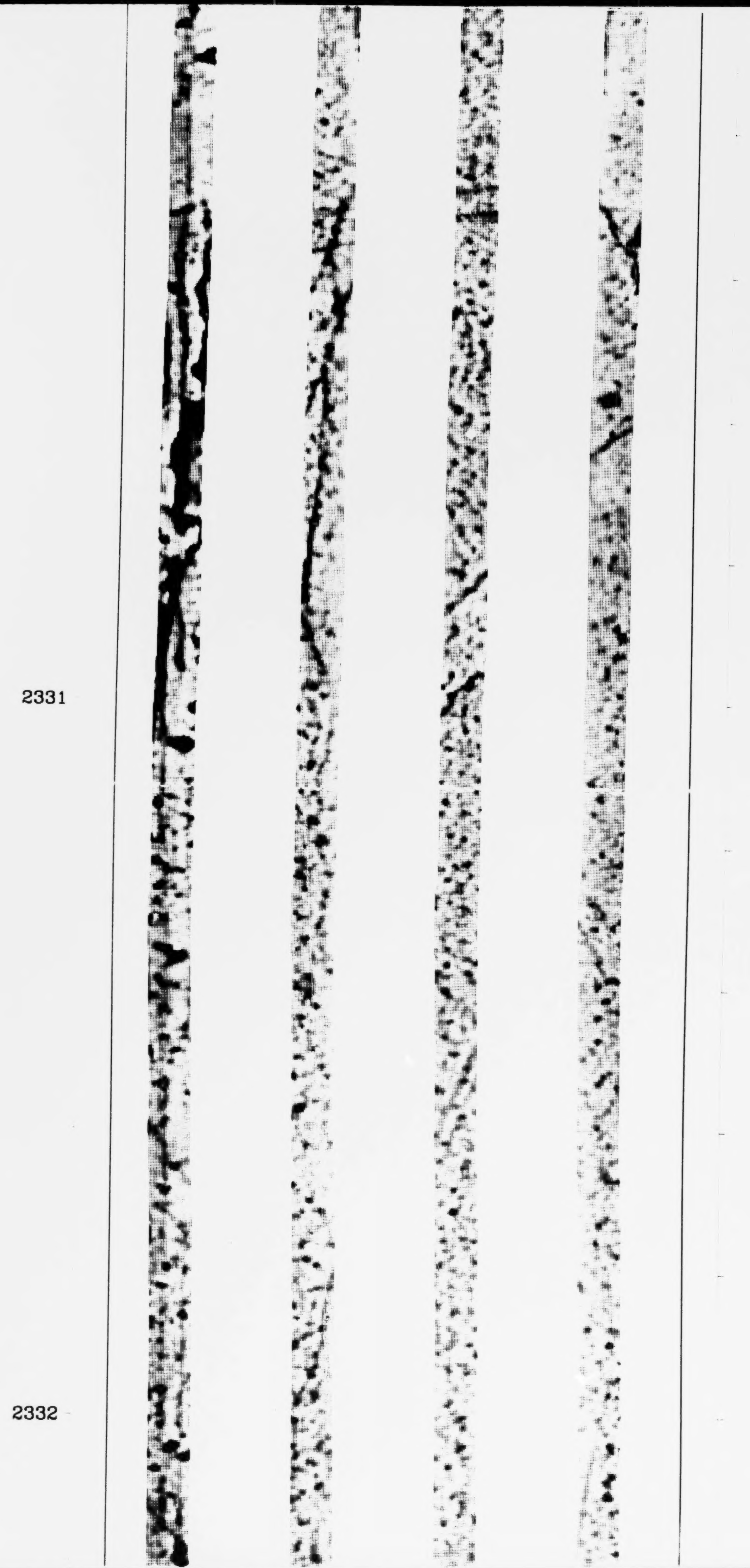
2331
2332

2333
2334

2335
2336

2337
2338

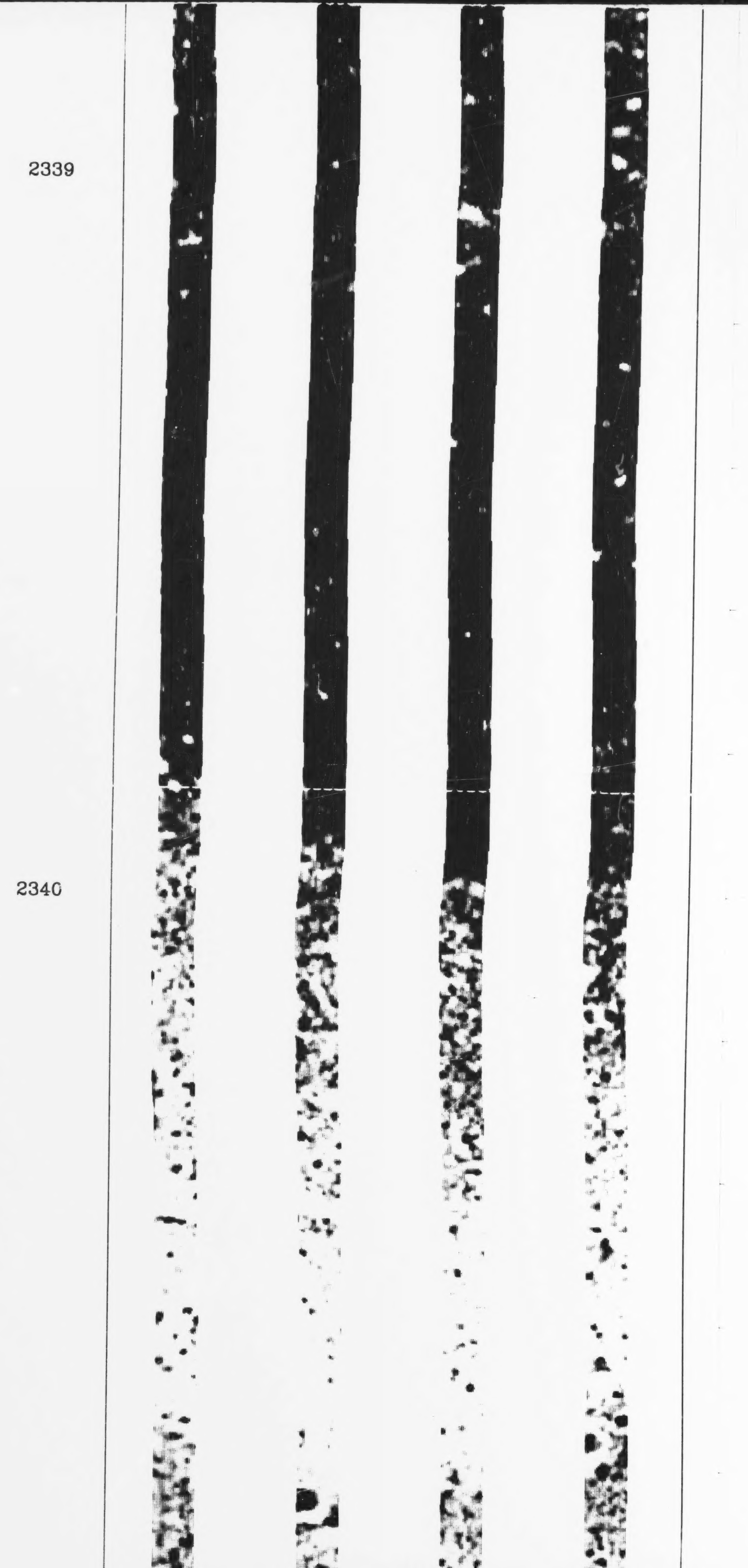
2339
2340

2341

2342

2343

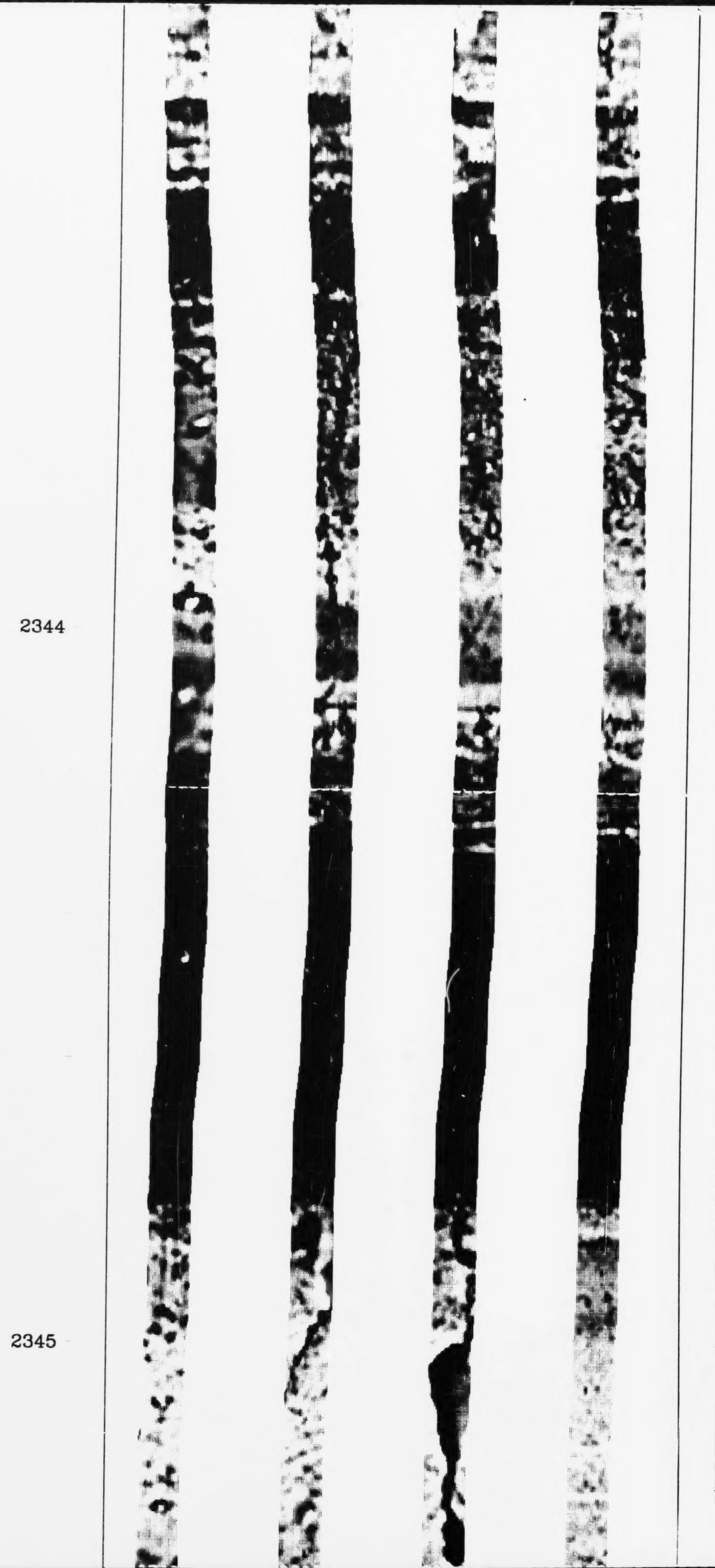
2344
2345

2346

2347

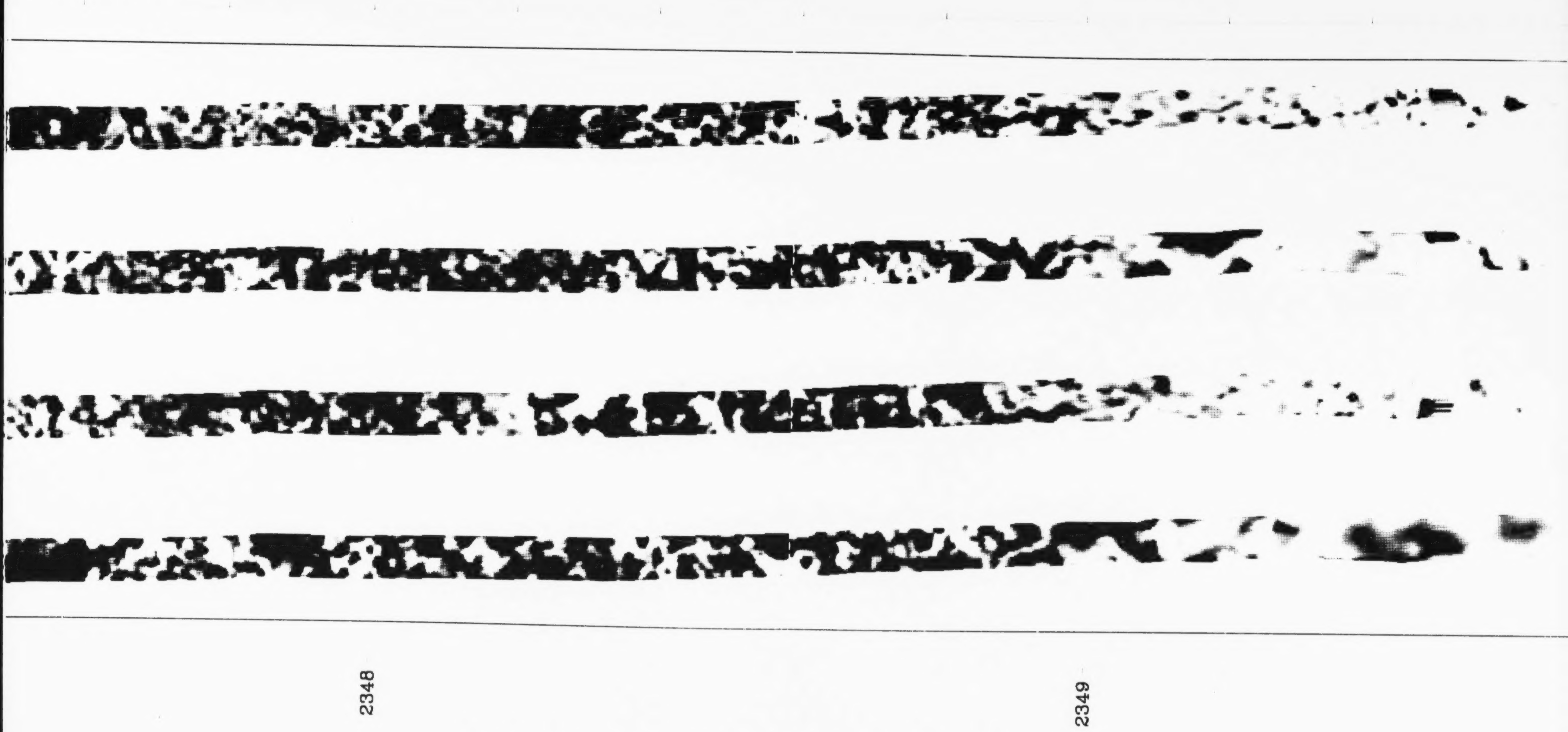
2348
2349

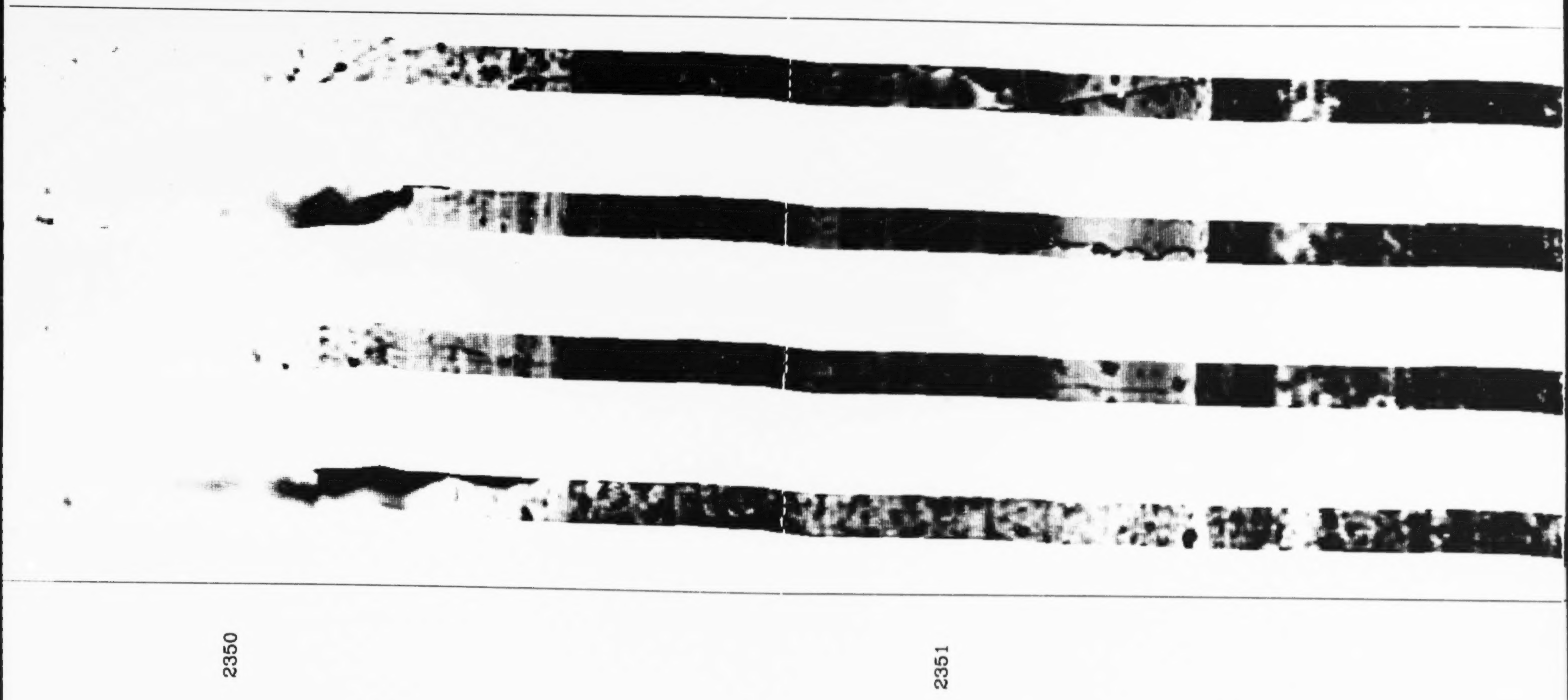

2350
2351

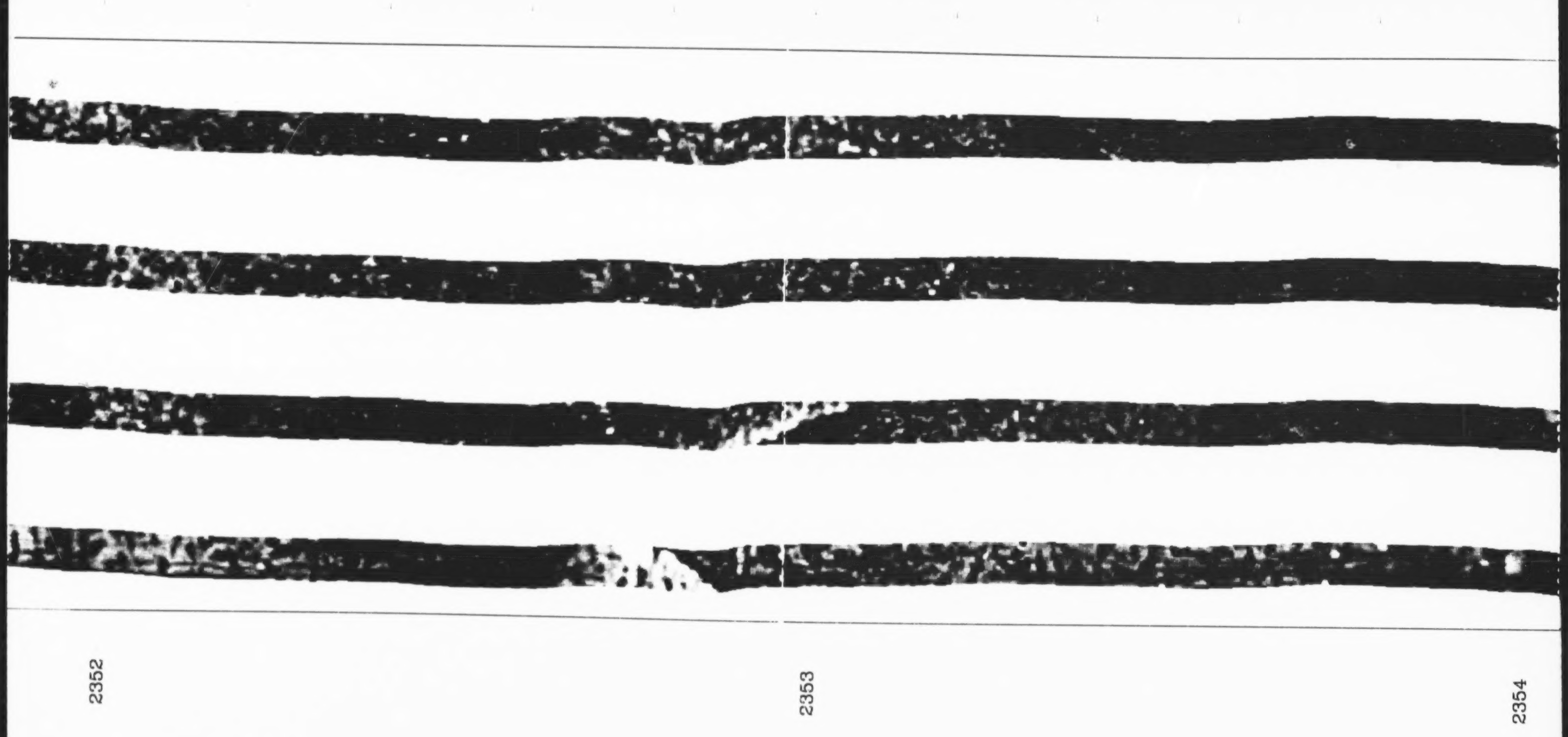

2352
2353
2354

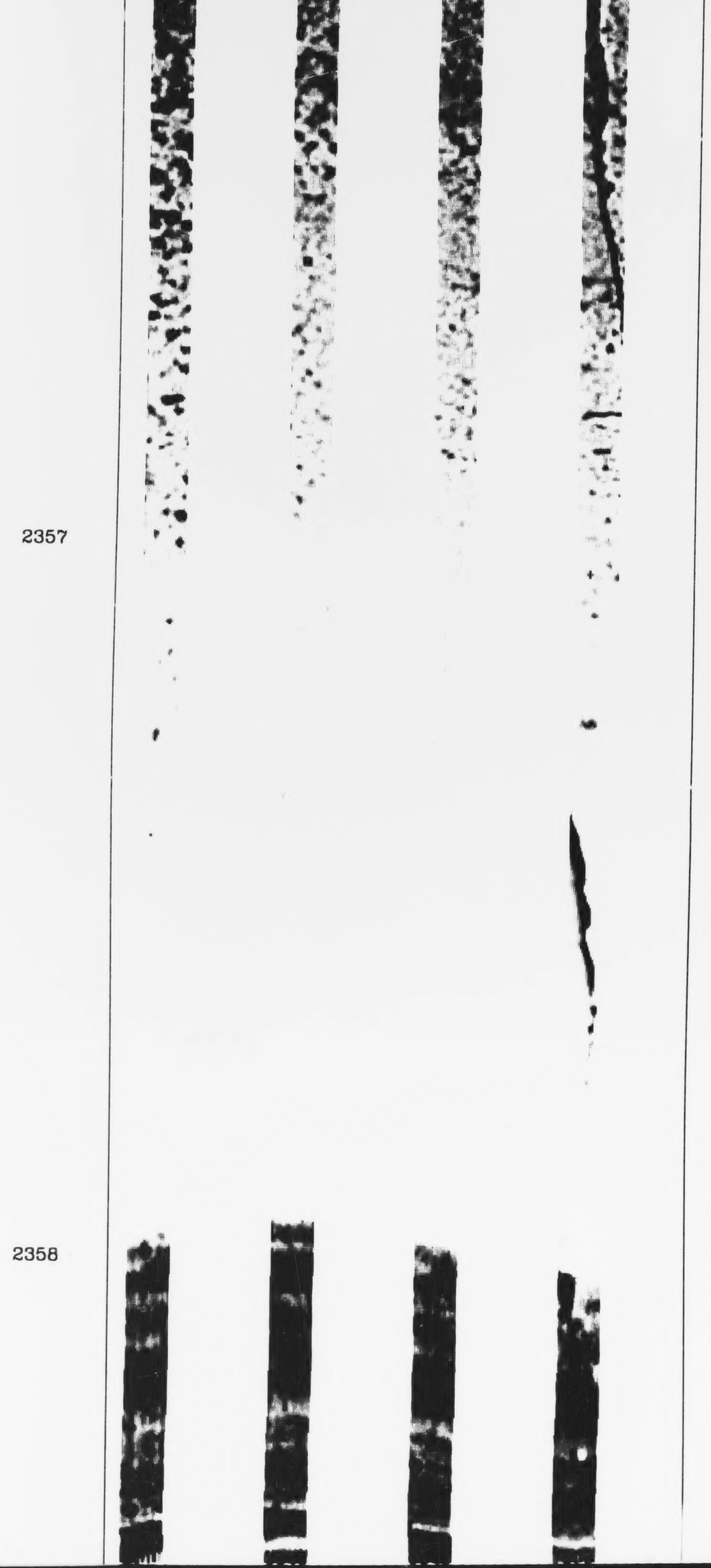
2357
2358

2359
2360

2361

2362

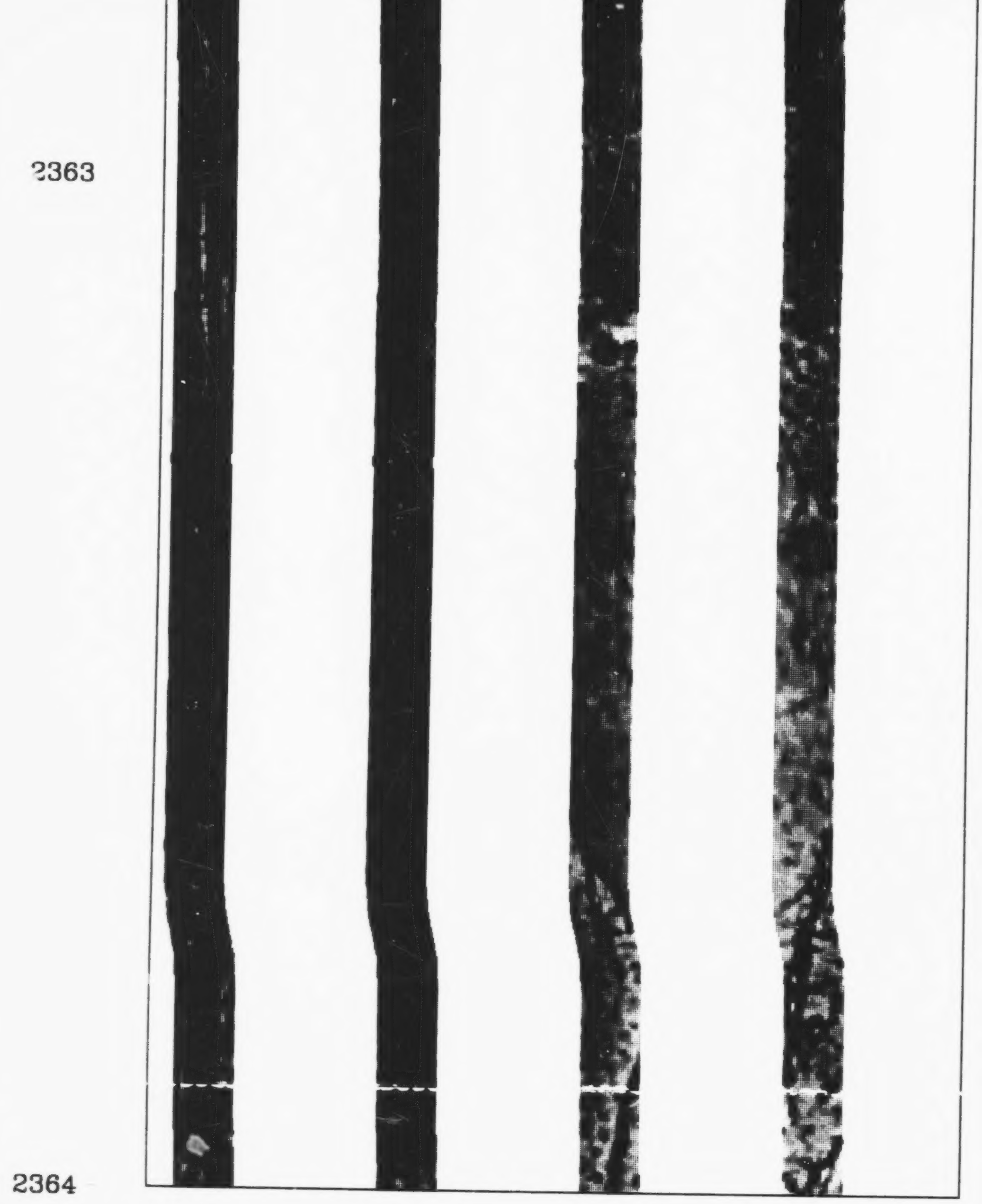

STATIC IMAGES

ZONE FROM 2404.0 M TO 2364.0 M

DEPTH SCALE = 1/ 5

IMAGE SCALE = 1/ 5

BITSIZE = 9.88

ORIENTATION

0 60 120 180 240 300 360

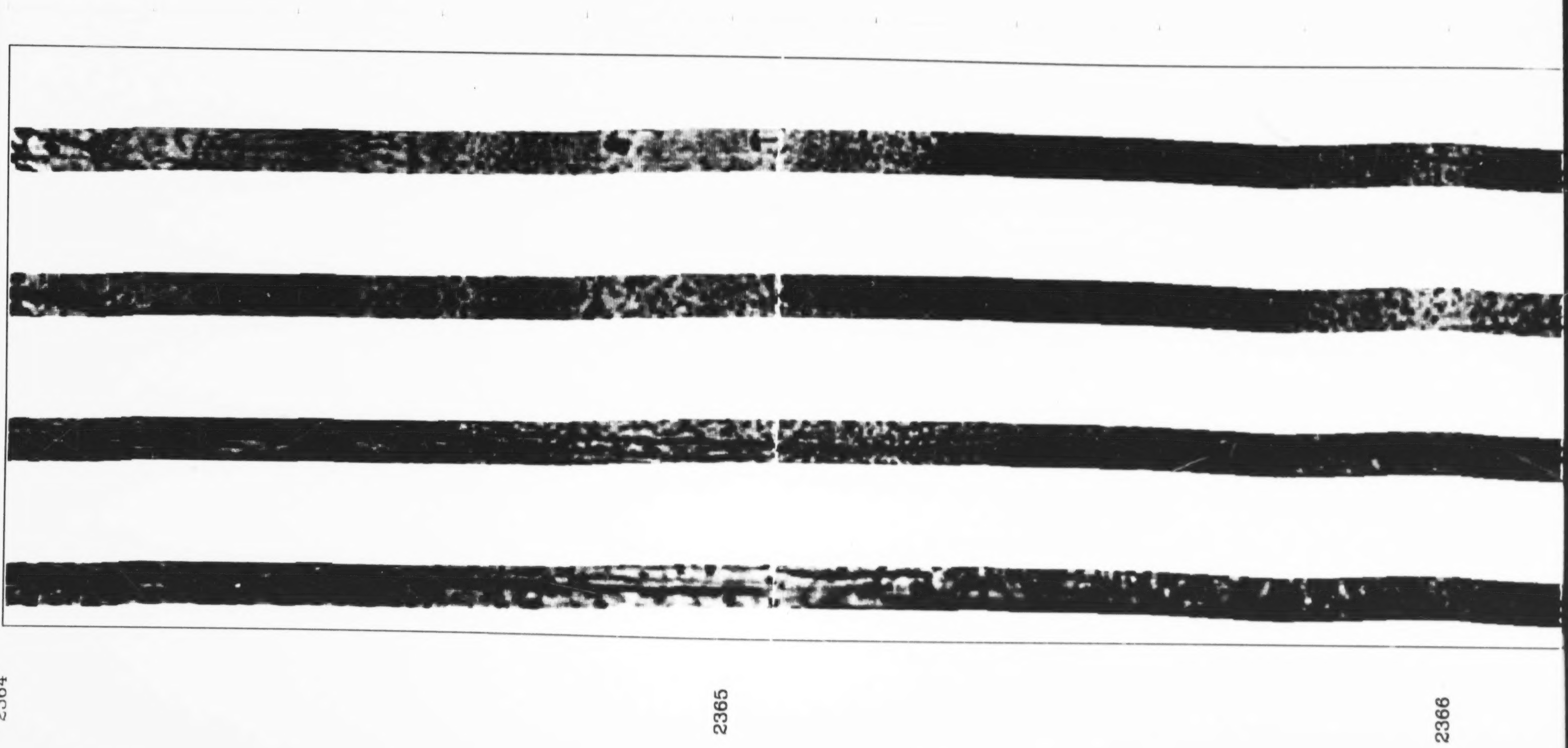
2365
2366

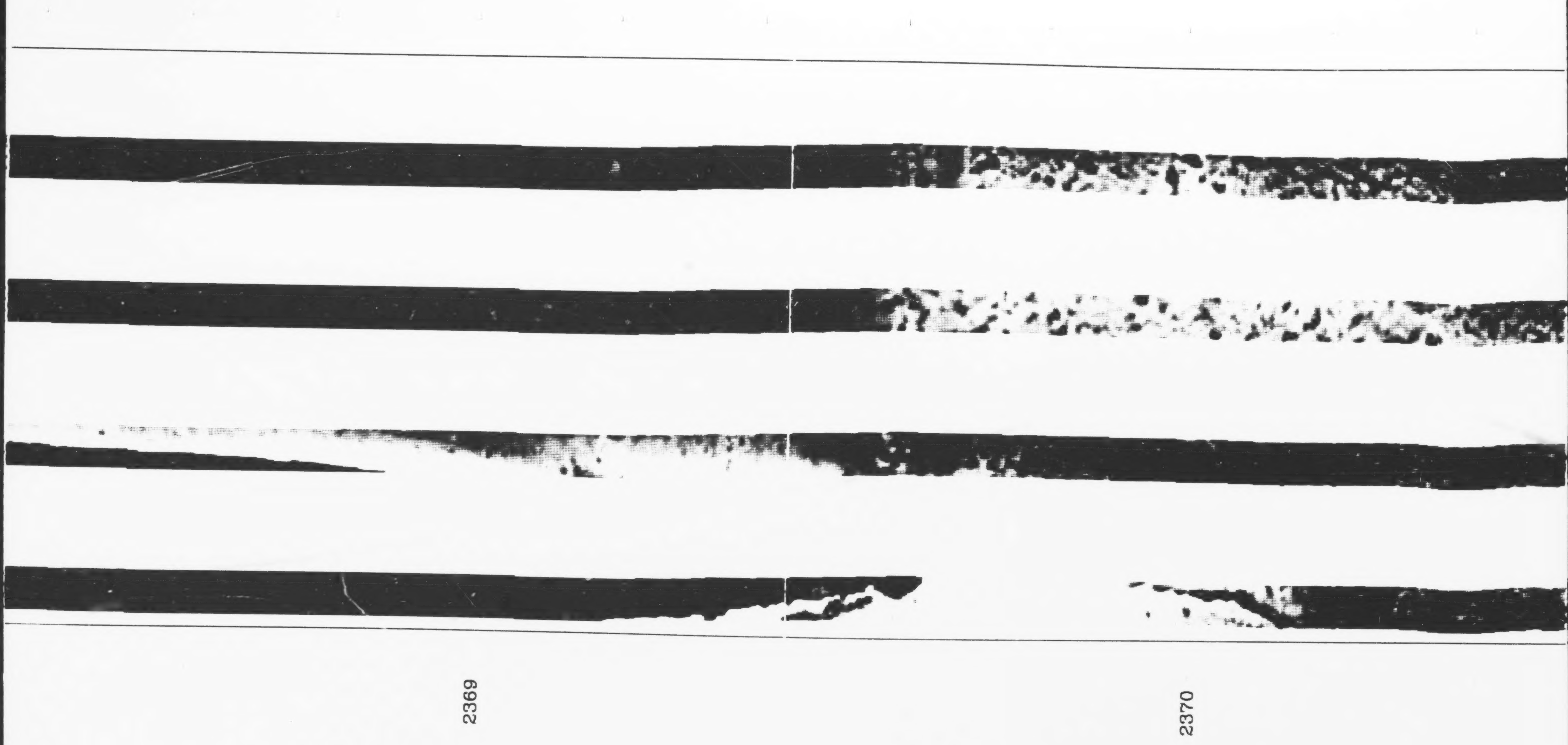
2369
2370

2371
2372

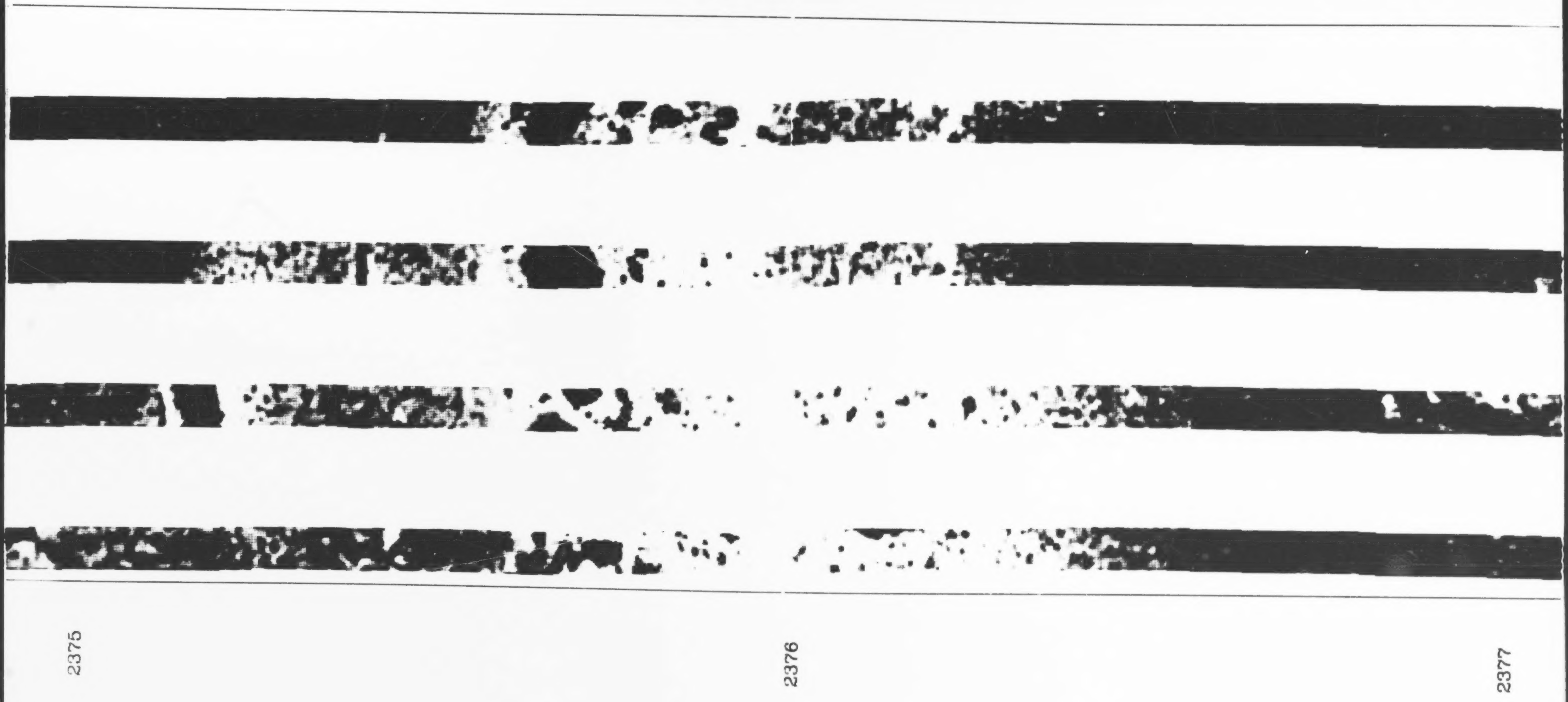
2375
2376
2377

[redacted]

[redacted]

[redacted]

[redacted]

2382
2383

[redacted]

[redacted]

[redacted]

[redacted]

[redacted]

[redacted]

[redacted]

[redacted]

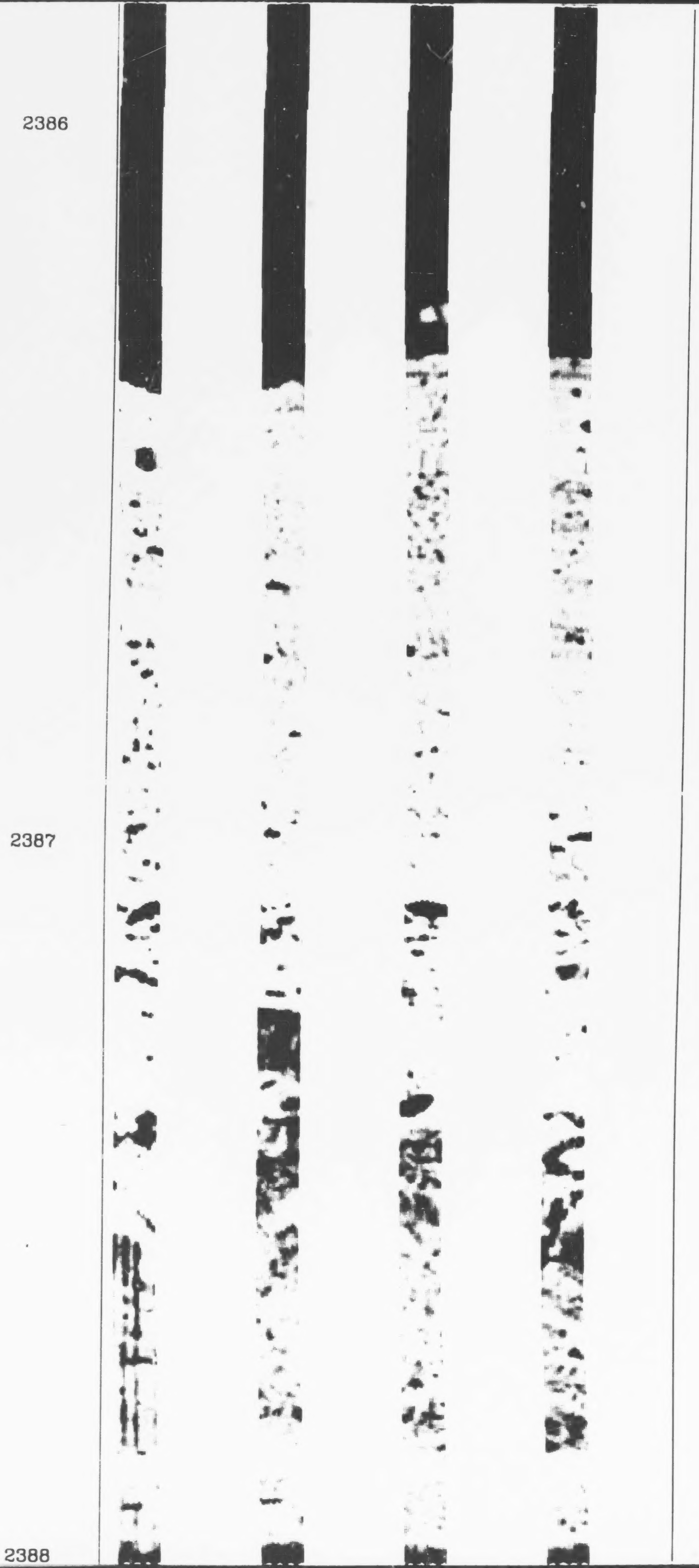
2386
2387
2388

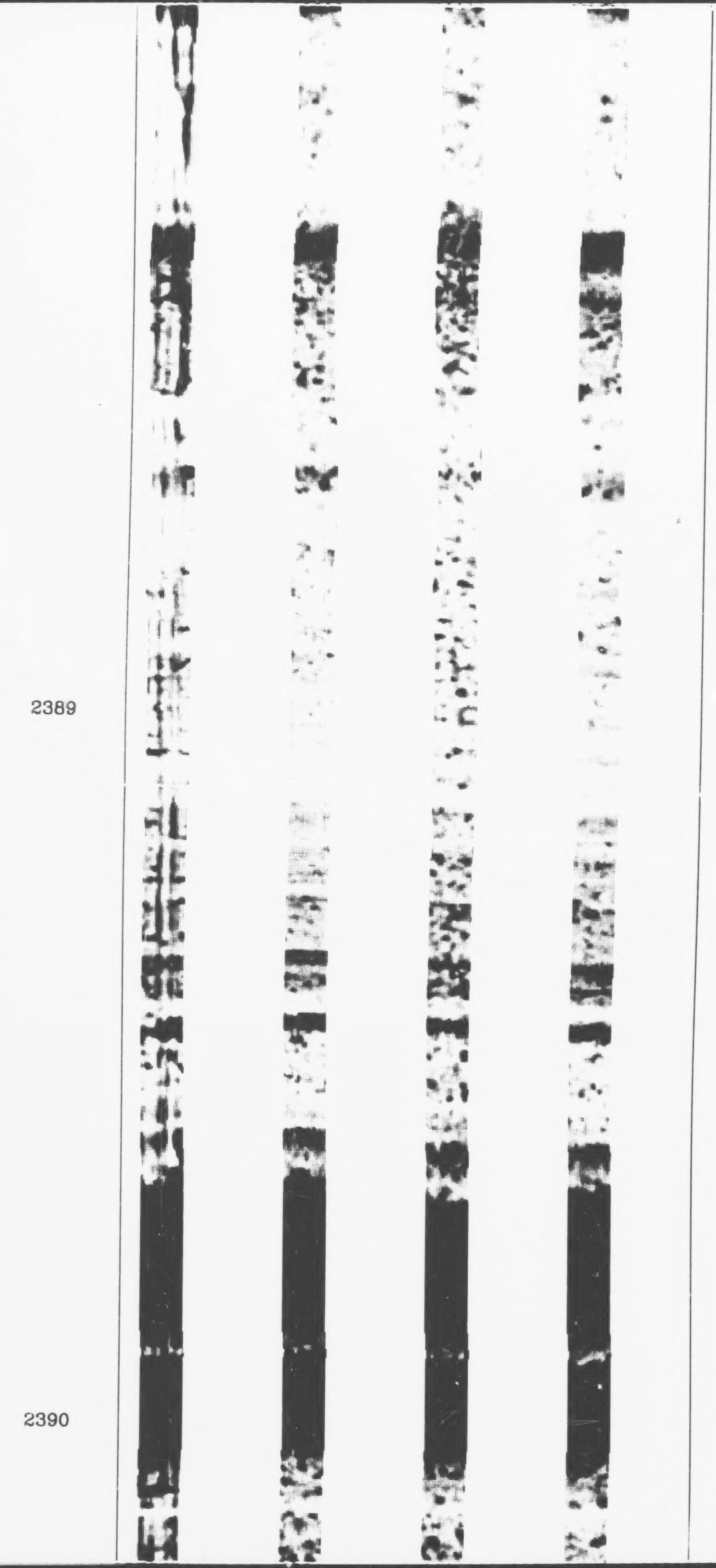
2389
2390

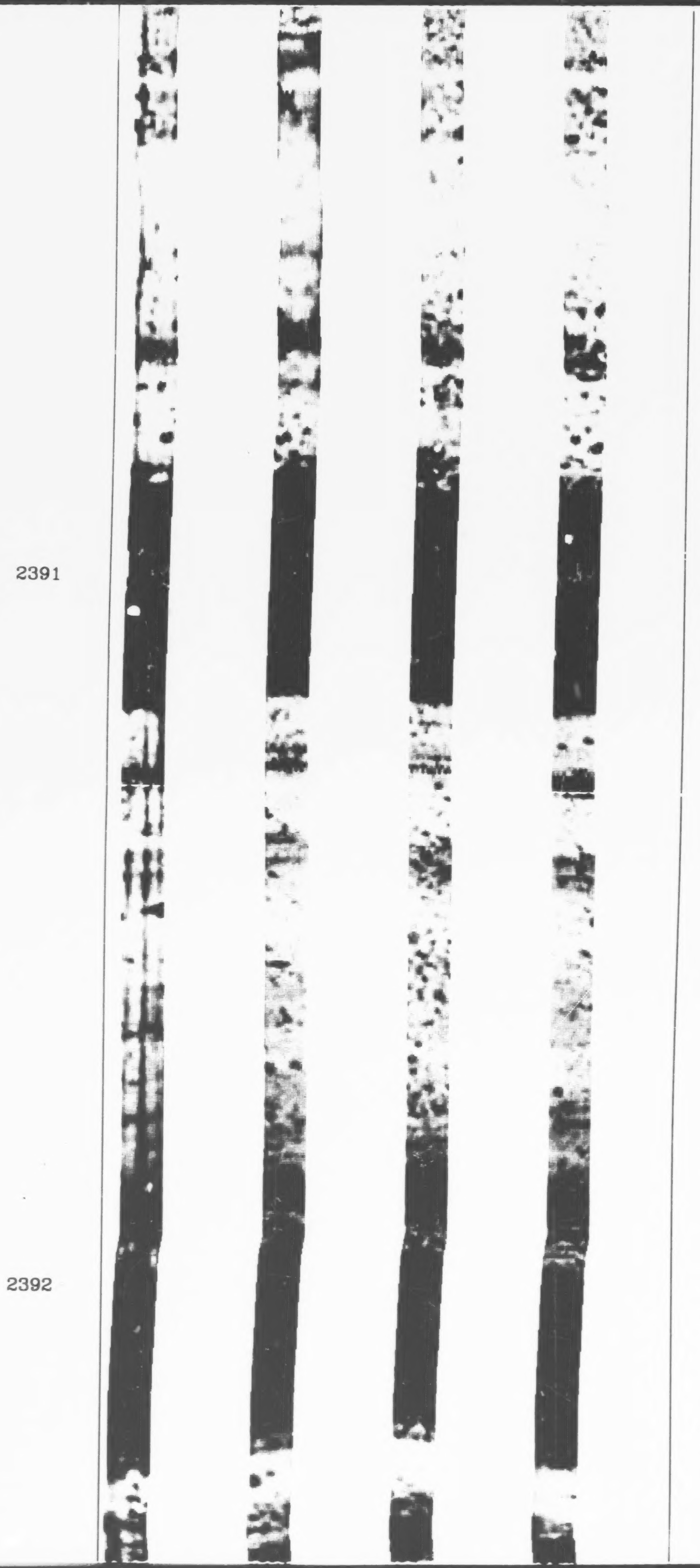
2391
2392

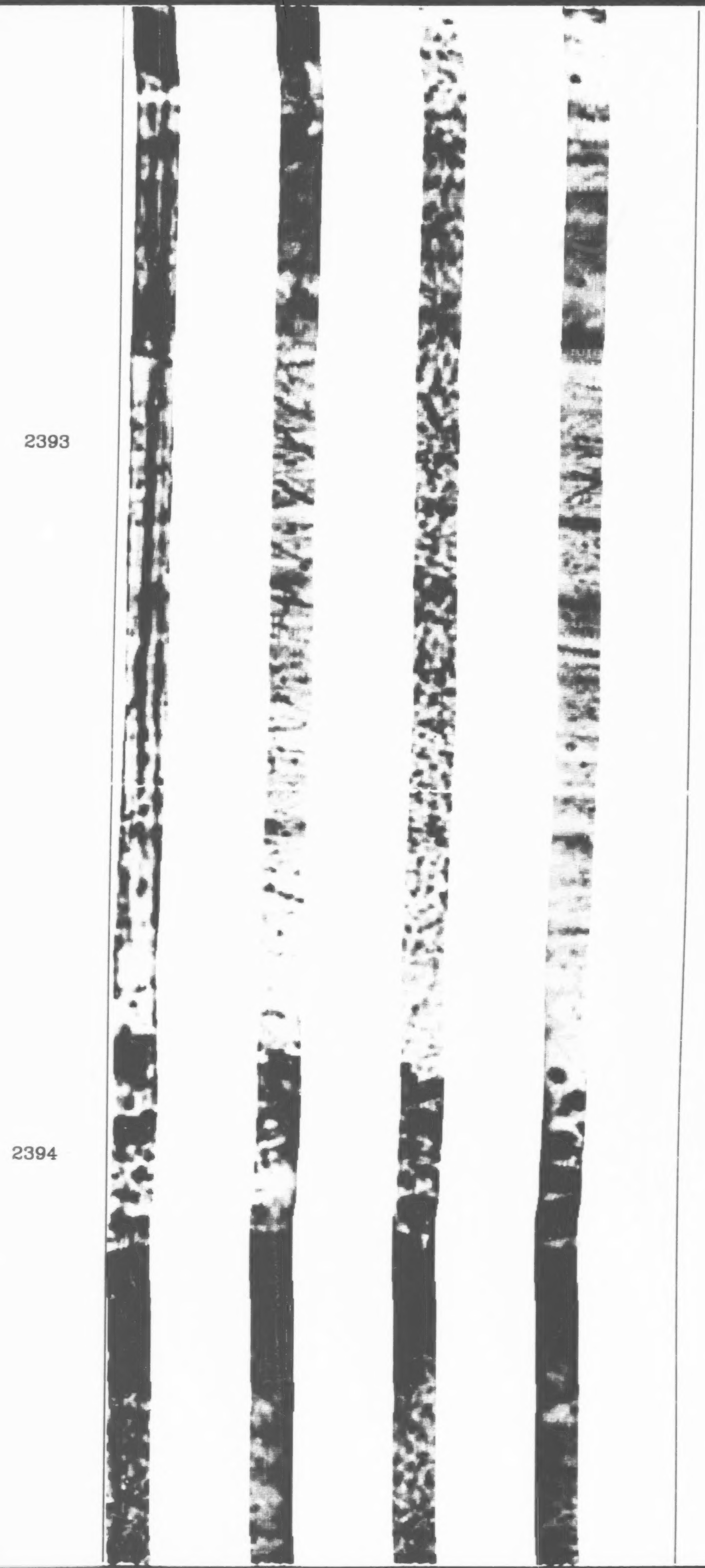
2393
2394

2397

2398

[redacted]

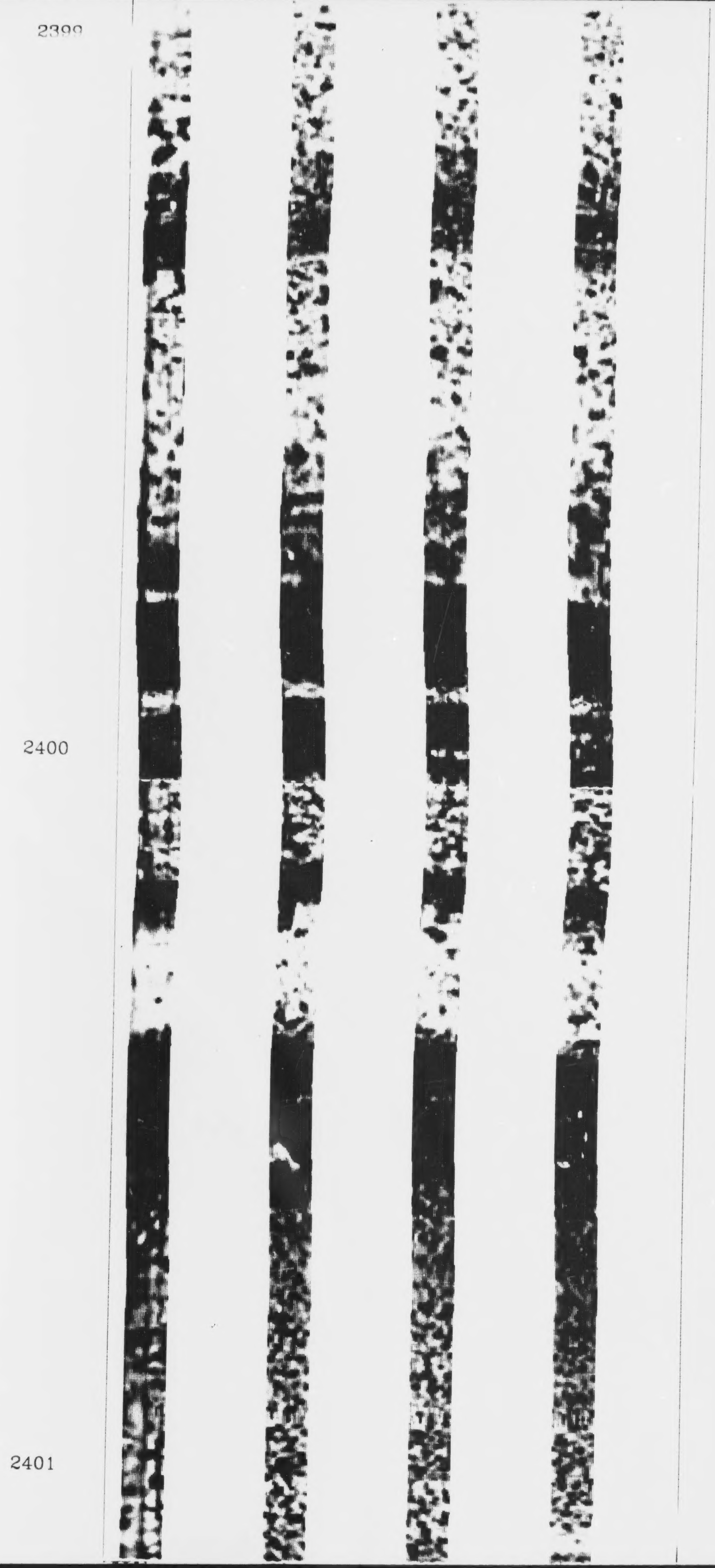
2399
2400
2401

2402 [illegible]

2403 [illegible]

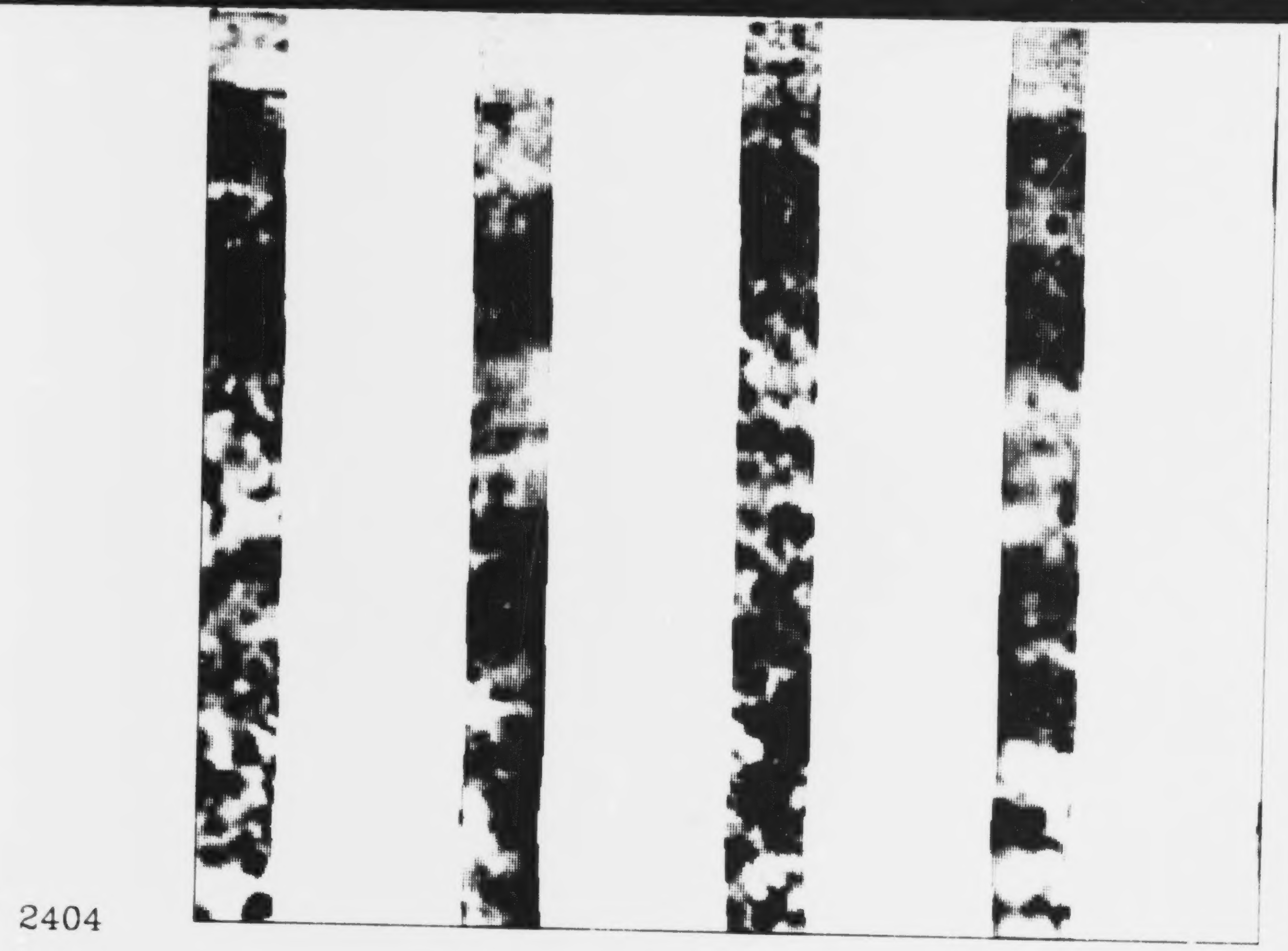

BITSIZE = 9.88

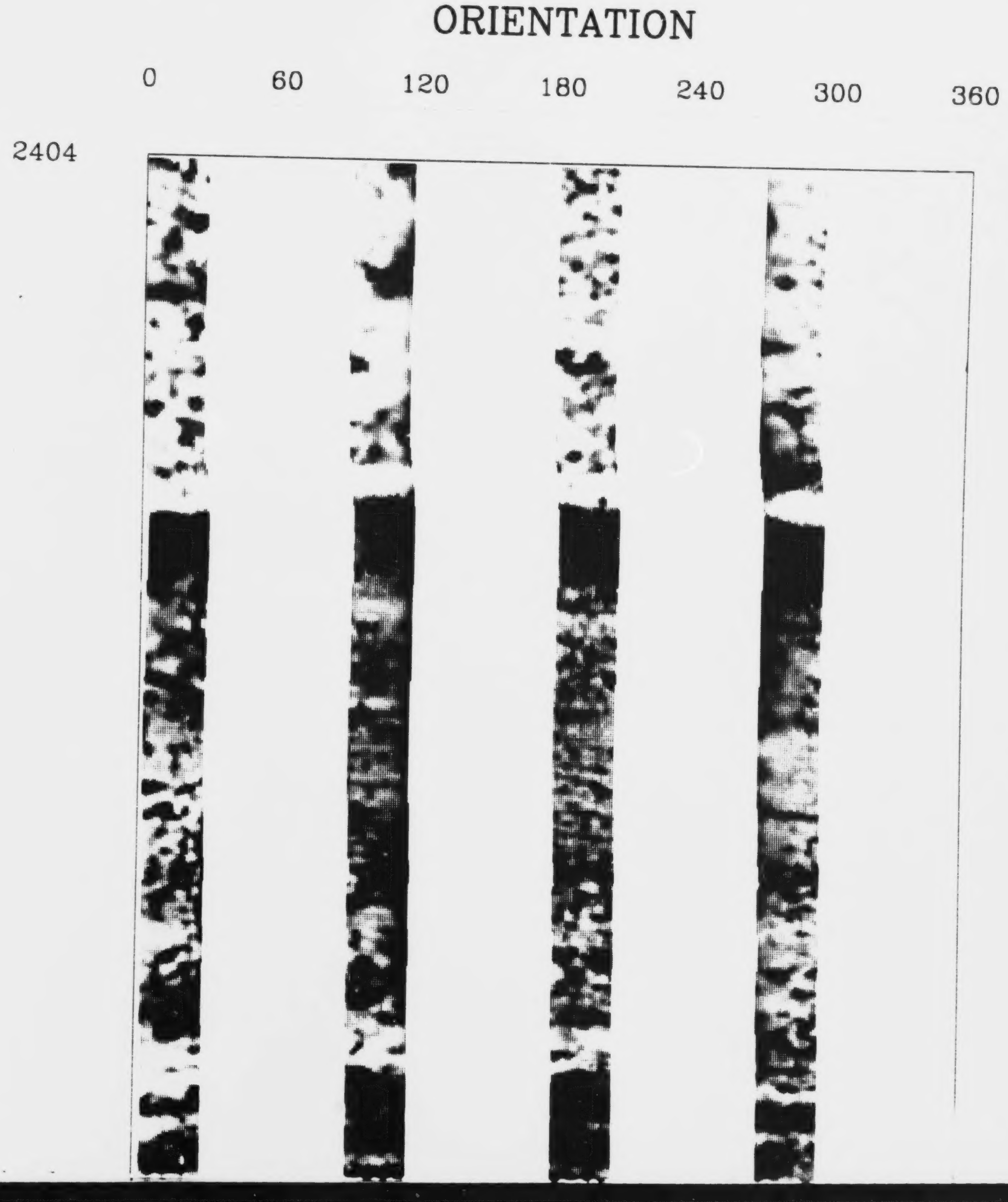

[redacted]

2410

2411

2412

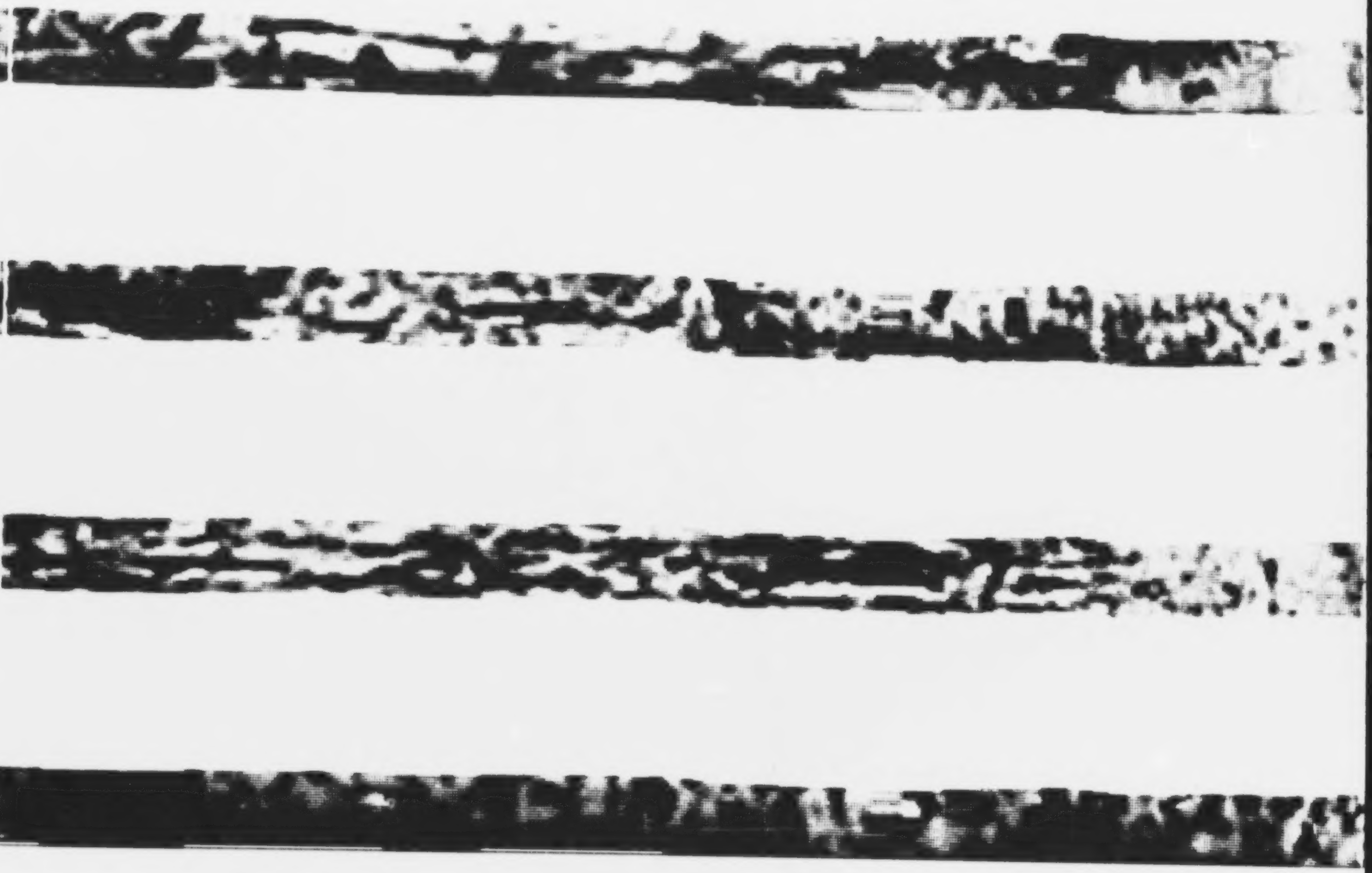

2413

2414
2415

2417
2418

2419

2420

2421
2422

2423

2424

[redacted]

2430

[illegible]

2431

2432

2433

2434

[redacted]

2435

2436

2437

2438
2439

2440

2441

2442

2443

2444

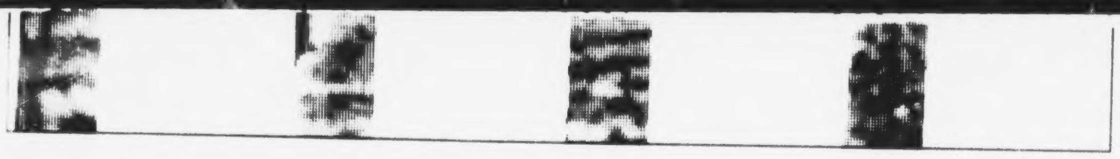

STATIC IMAGES

ZONE FROM 2484.3 M TO 2444.4 M

DEPTH SCALE = 1/ 5

IMAGE SCALE = 1/ 5

BITSIZE = 9.88

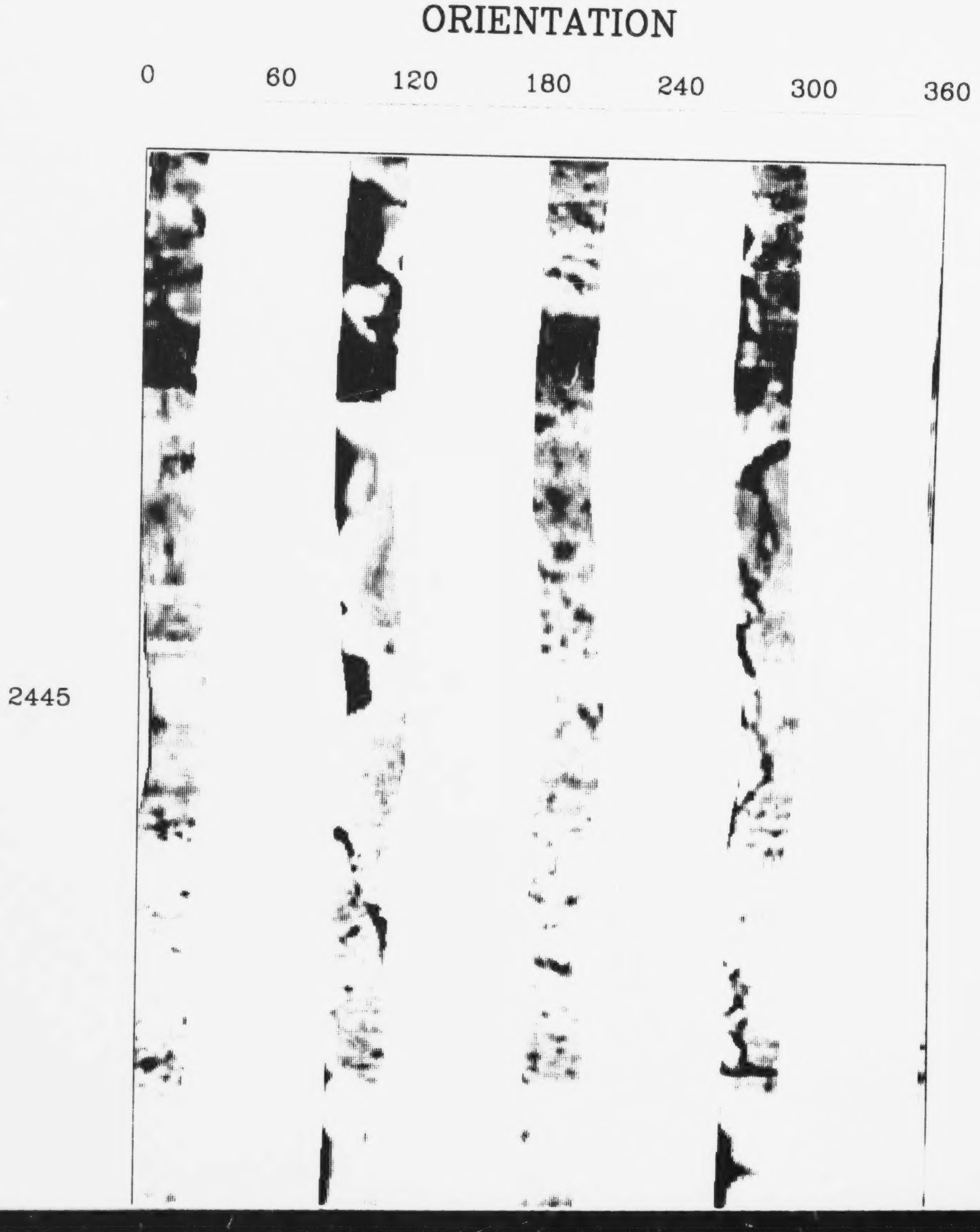

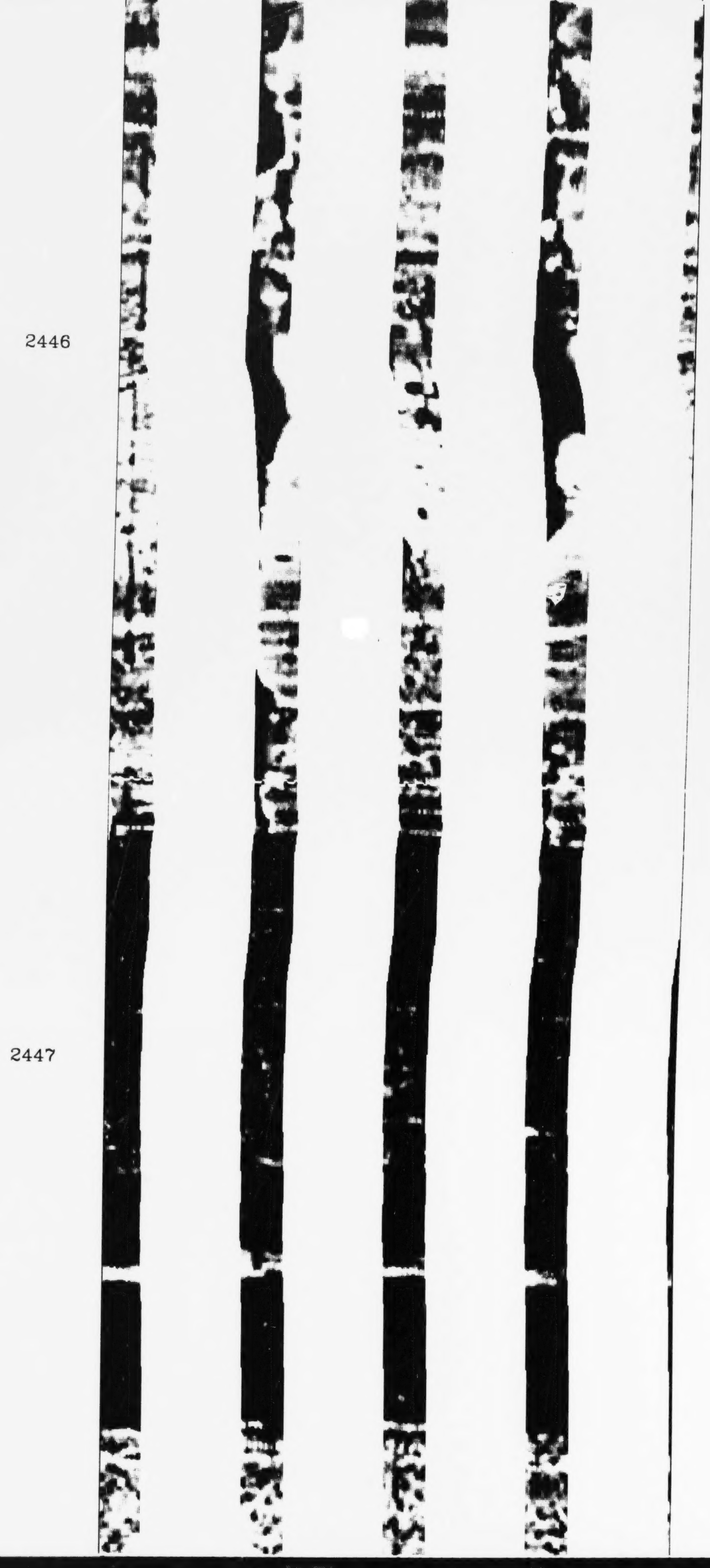
2446
2447

2450
2451
2452

2453
2454

2455 [illegible]

2456 [illegible]

2457

2458

2459

2460

2461
2462
2463

[illegible]

2464

2465

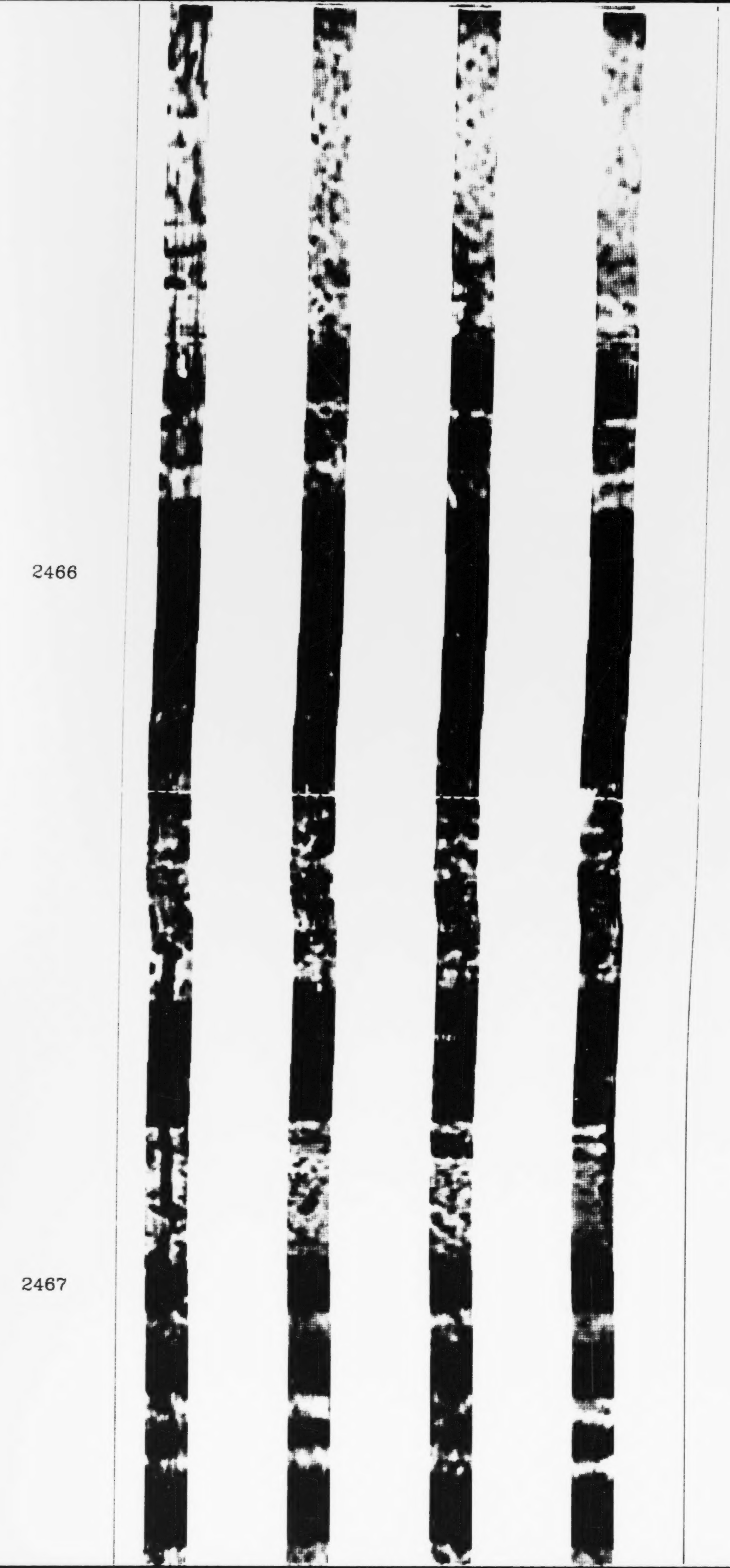
2466
2467

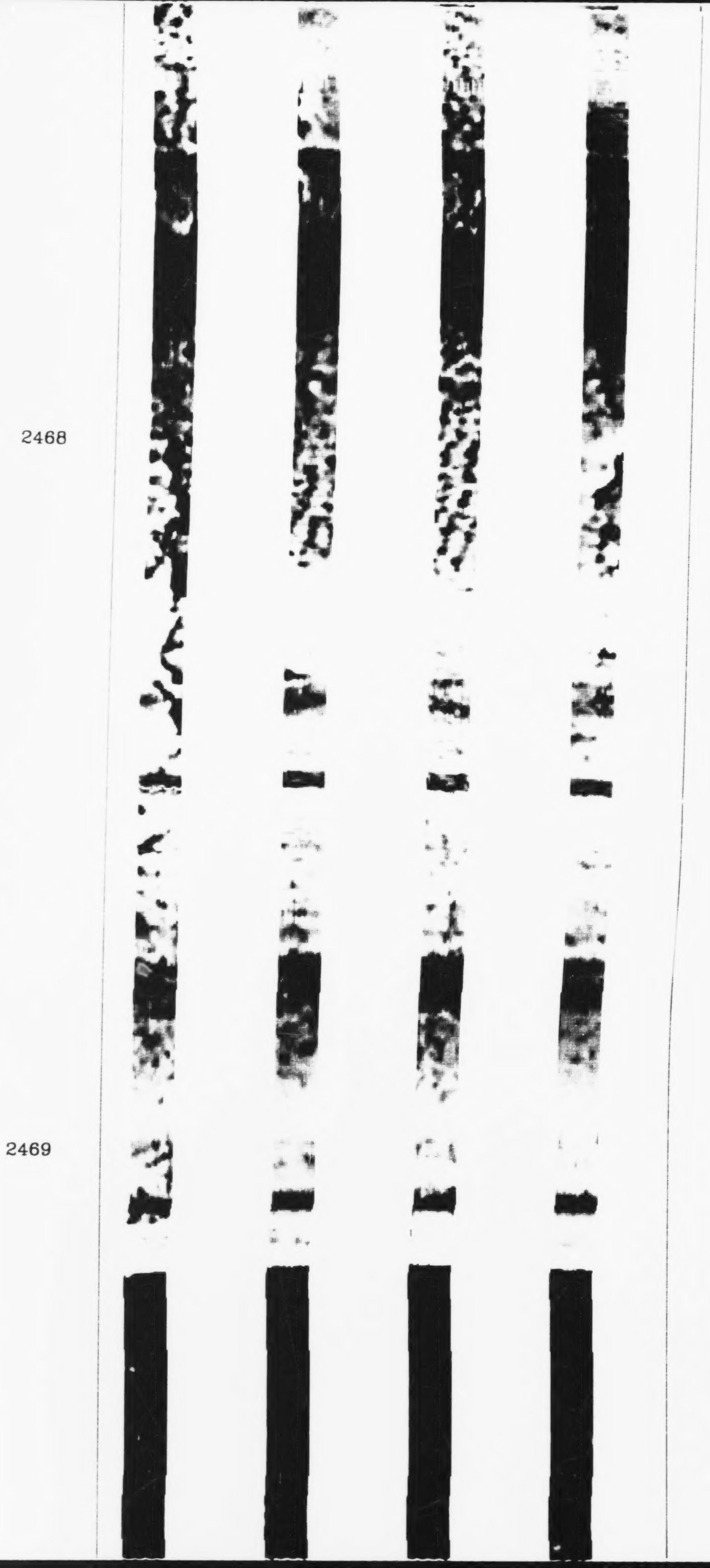
2468
2469

2470

2471

2472
2473

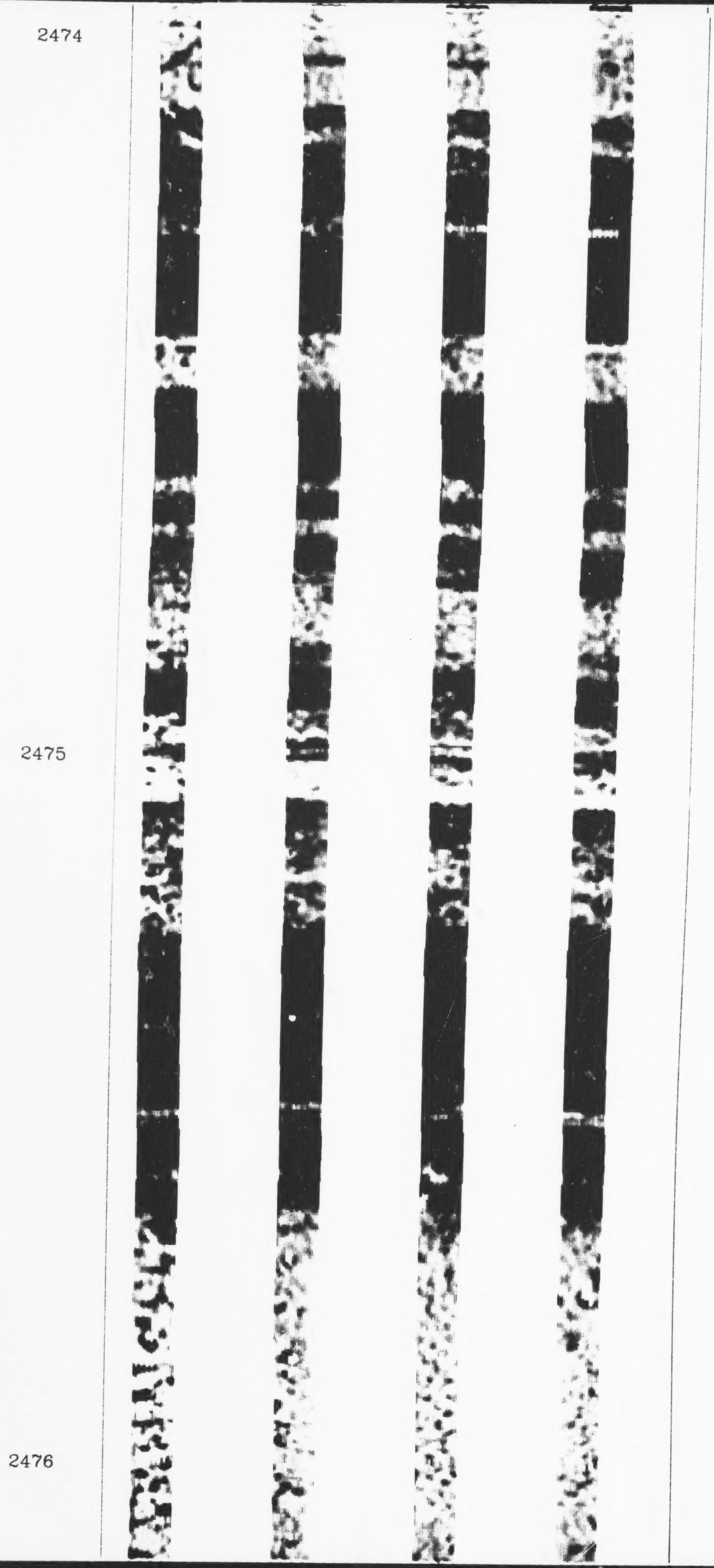
2474
2475
2476

2477
2478

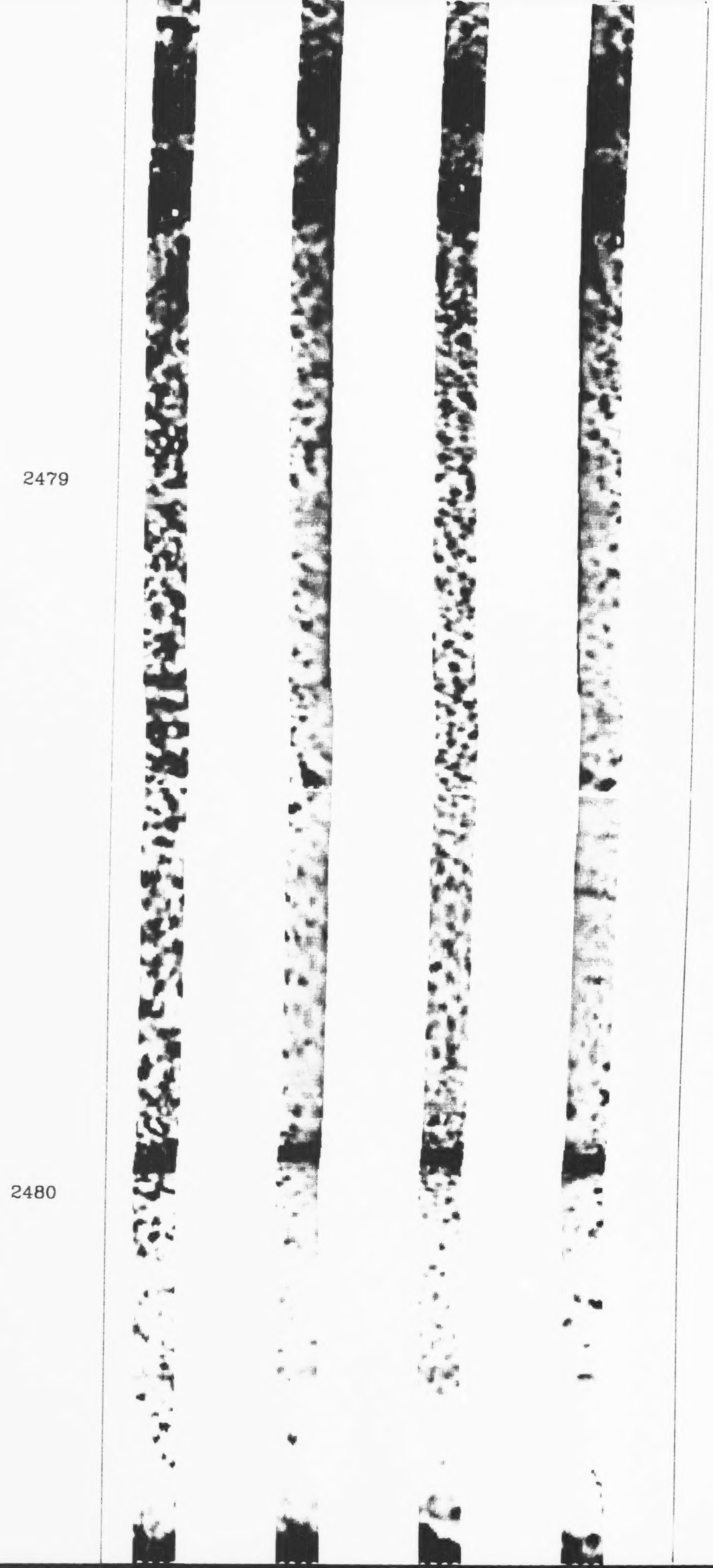
2479
2480

2481

[redacted] [redacted] [redacted] [redacted]

2482

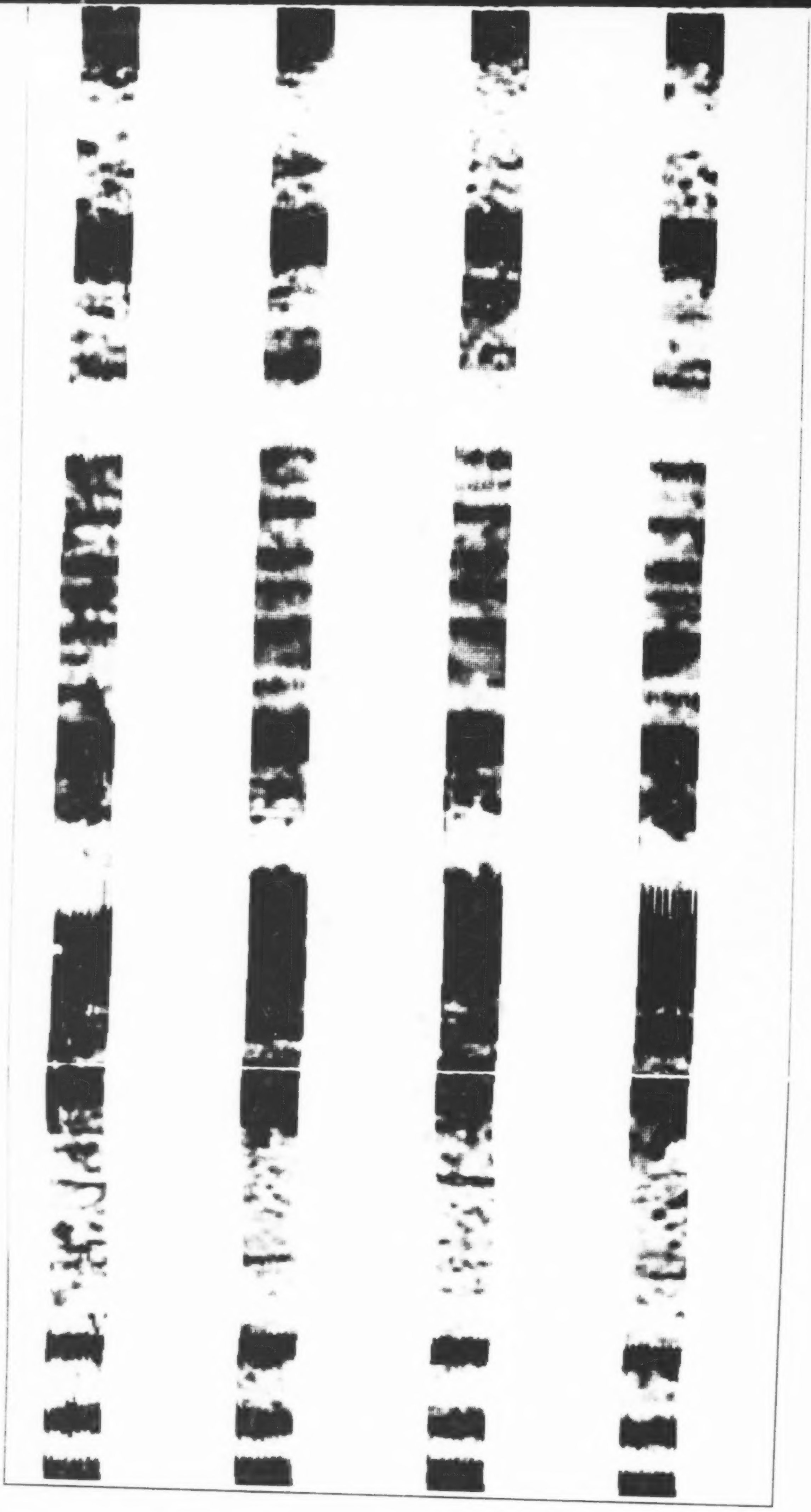

2483
2484

SCHLUMBERGER

FMS
BOREHOLE
IMAGING

COMPANY	LAMONT–DOHERTY GEOLOGICAL
WELL	ODP HOLE–793B
FIELD	IZU–BONIN FOREARC BASIN
COUNTRY	OCEAN
RUN	1
DATE LOGGED	16 – JUN – 89
REFERENCE	STATIC PS-1 3536-3565

STATIC NORMALIZATION

PASS 1 (23577)

FILE : MEST.003

ZONE FROM 3565.0 M TO 3543.0 M

DEPTH SCALE = 1/ 5

IMAGE SCALE = 1/ 5

BITSIZE = 9.88

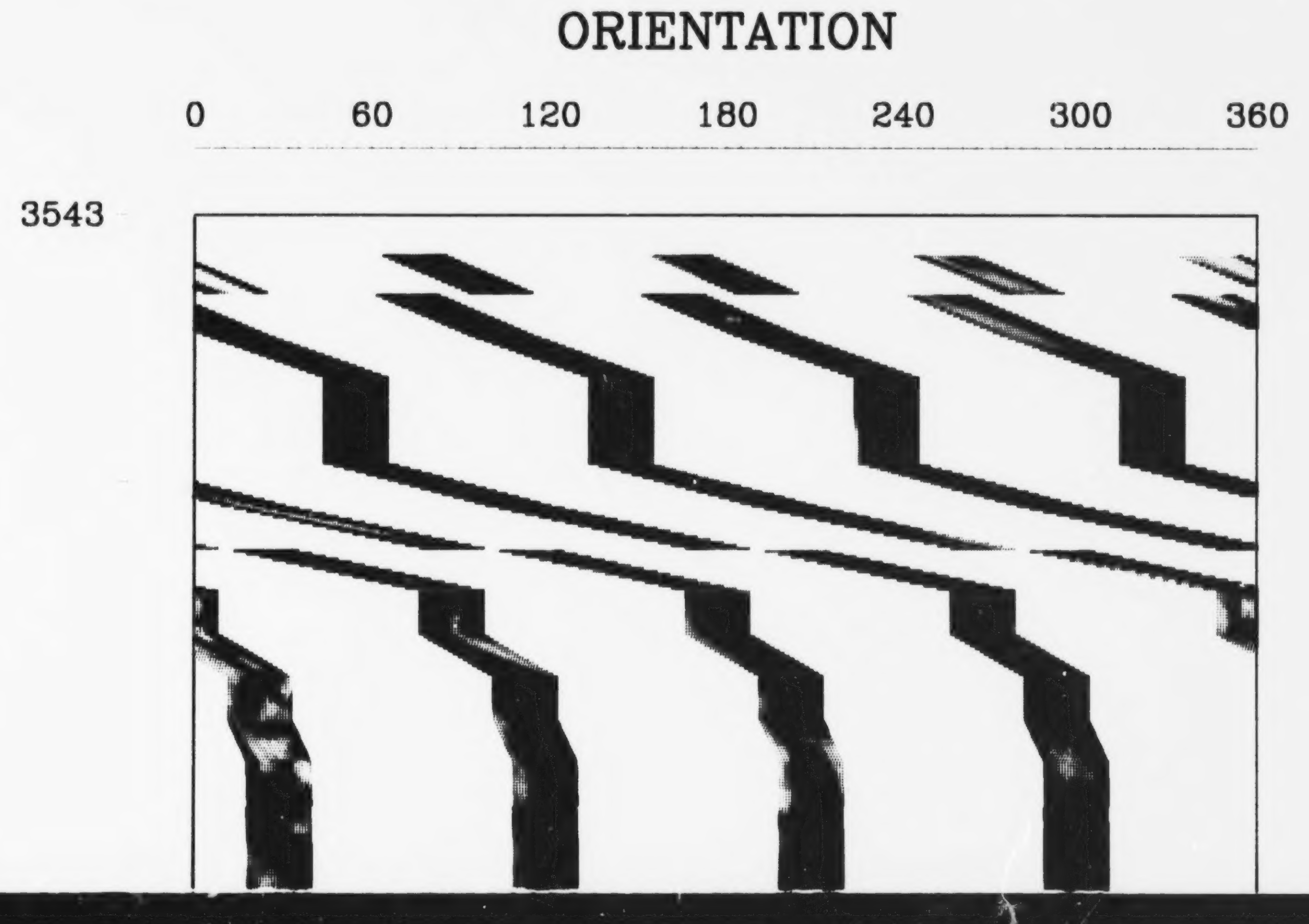

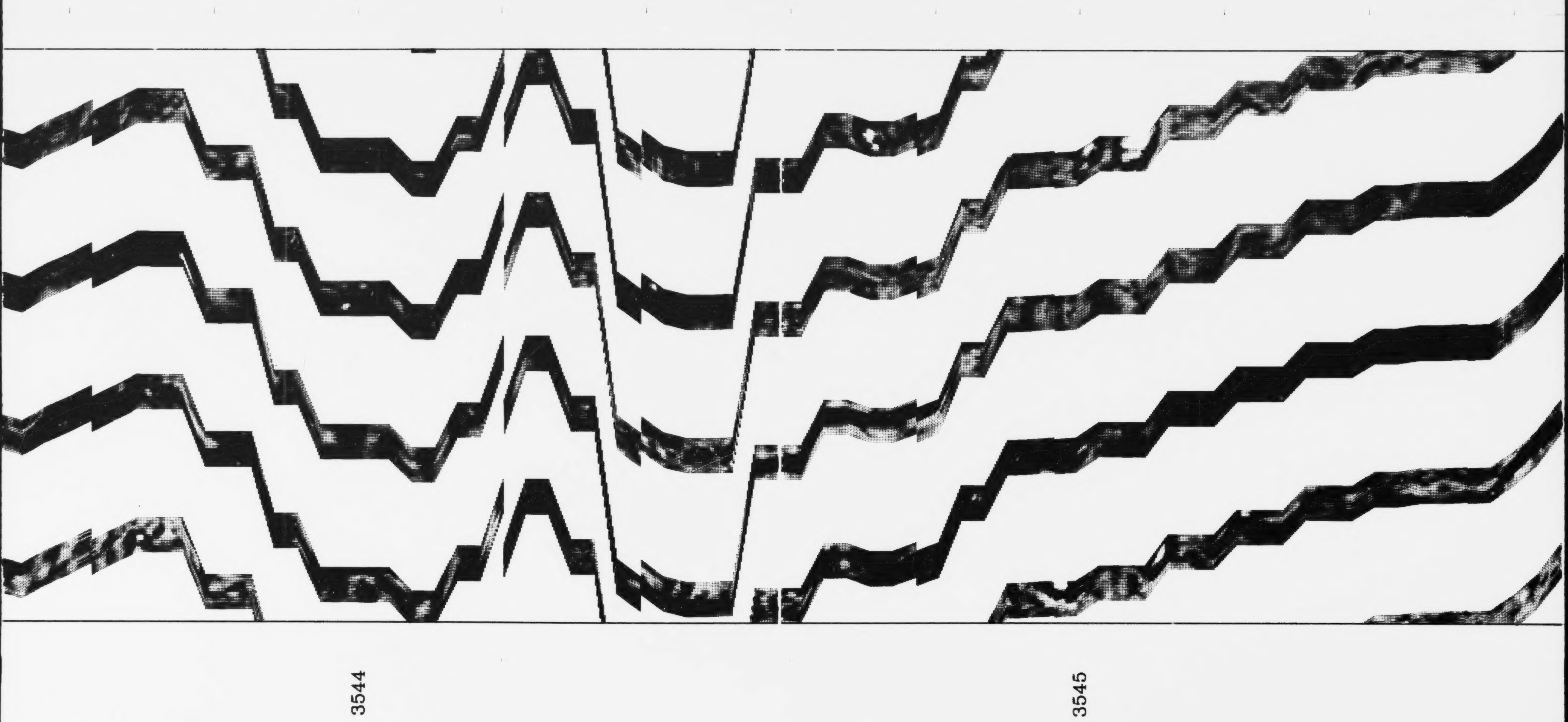
3544
3545

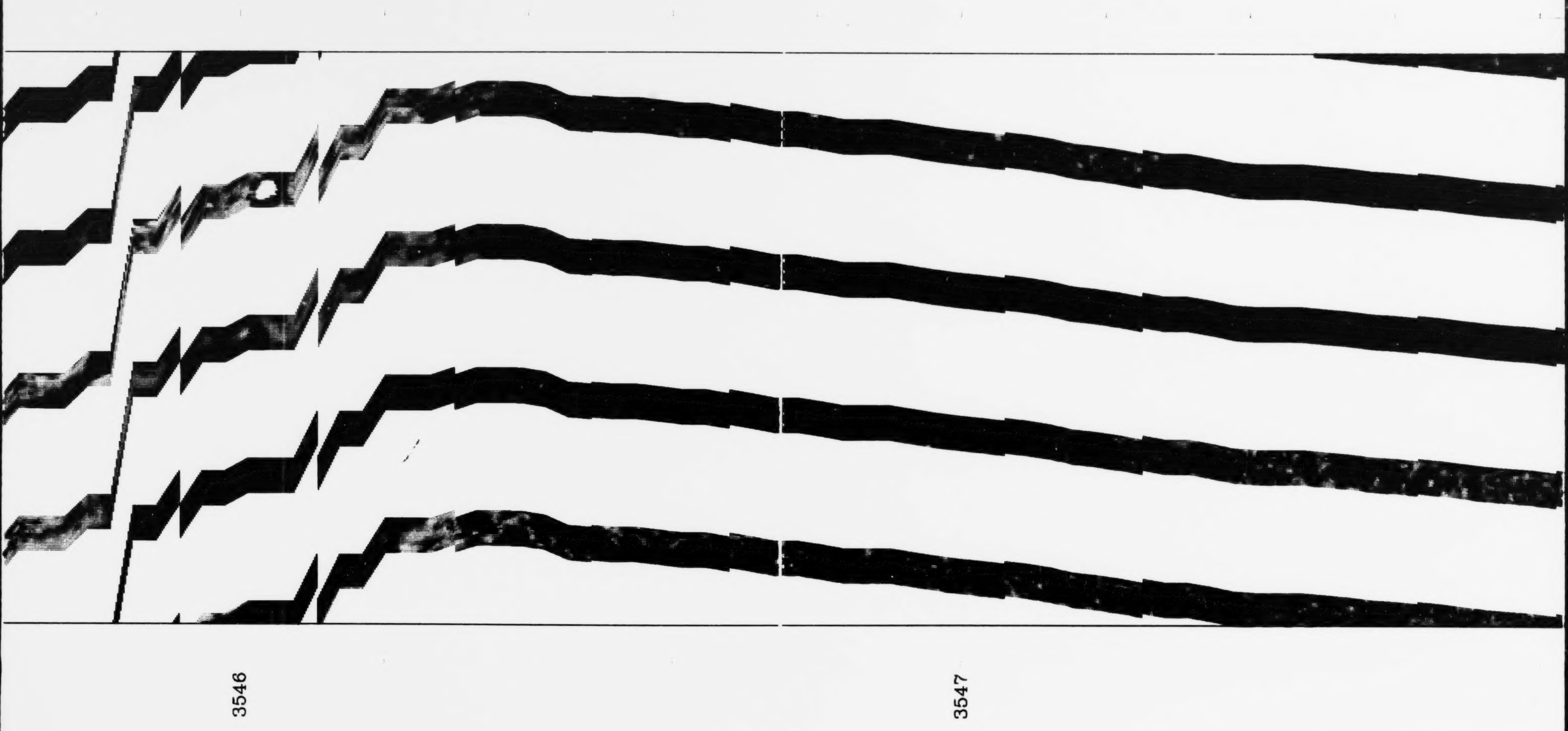
3546
3547

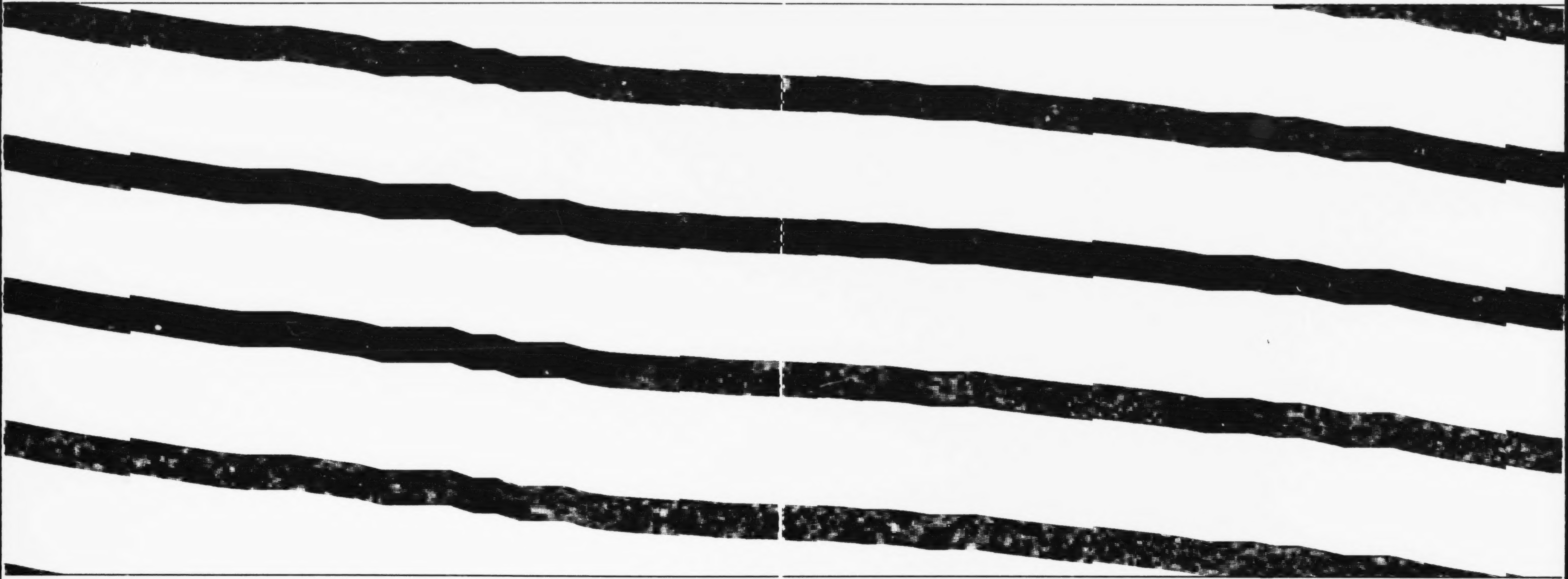

3548

3549

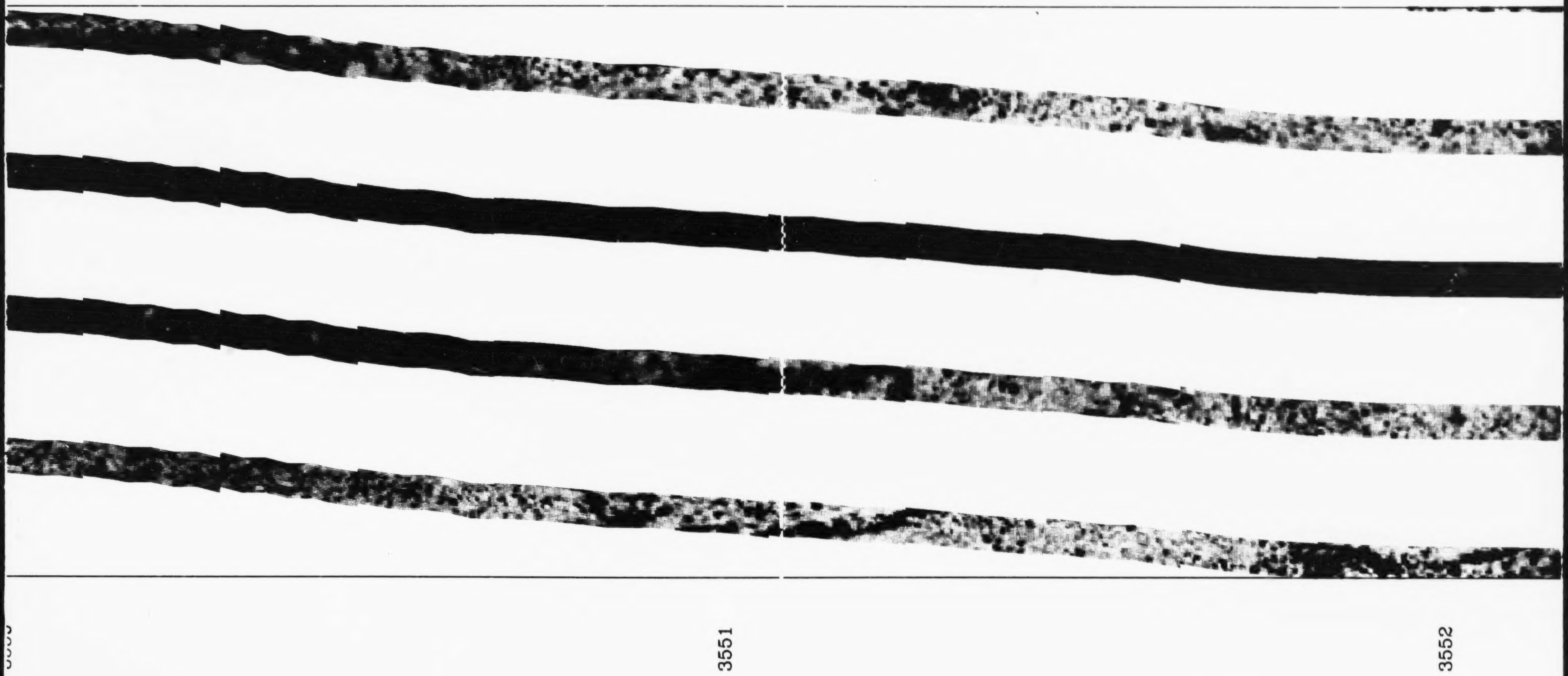
3551
3552

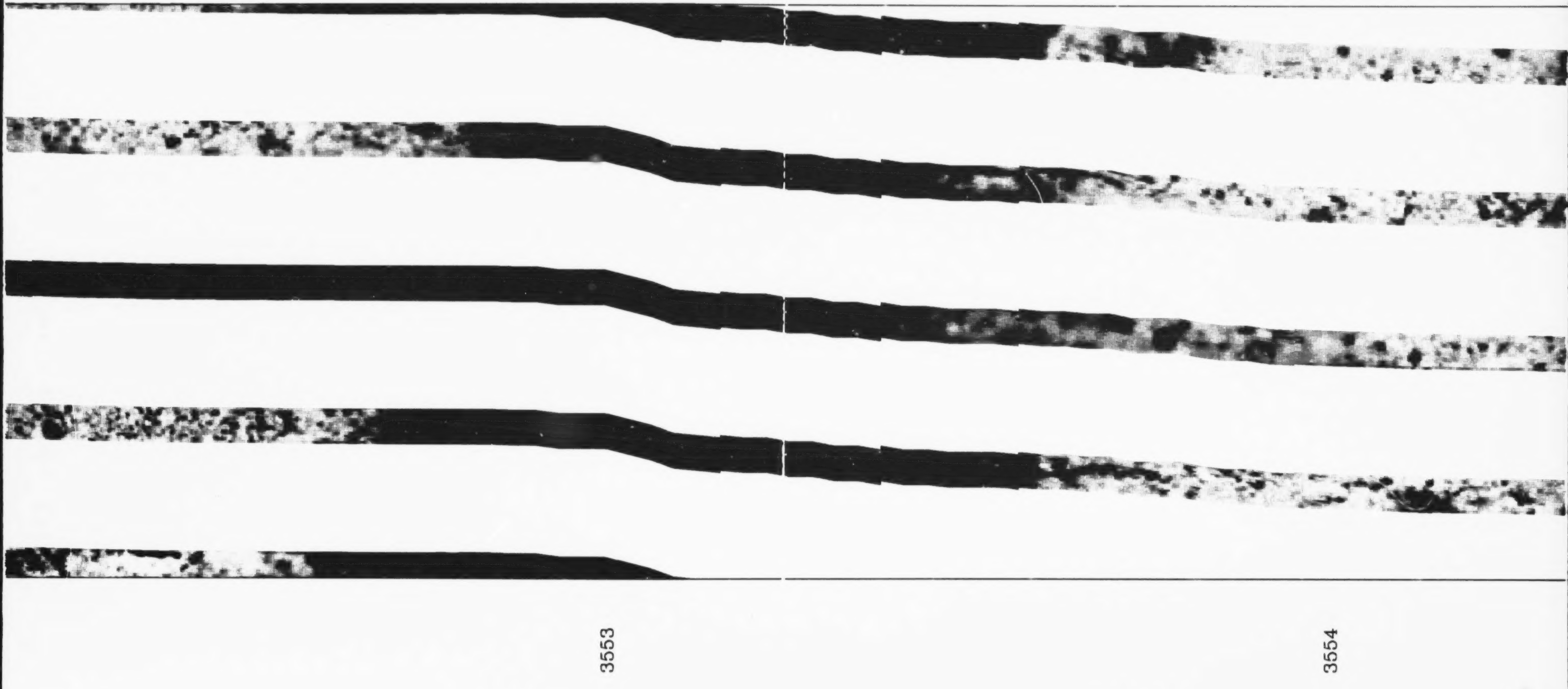
3553
3554

3555
3556

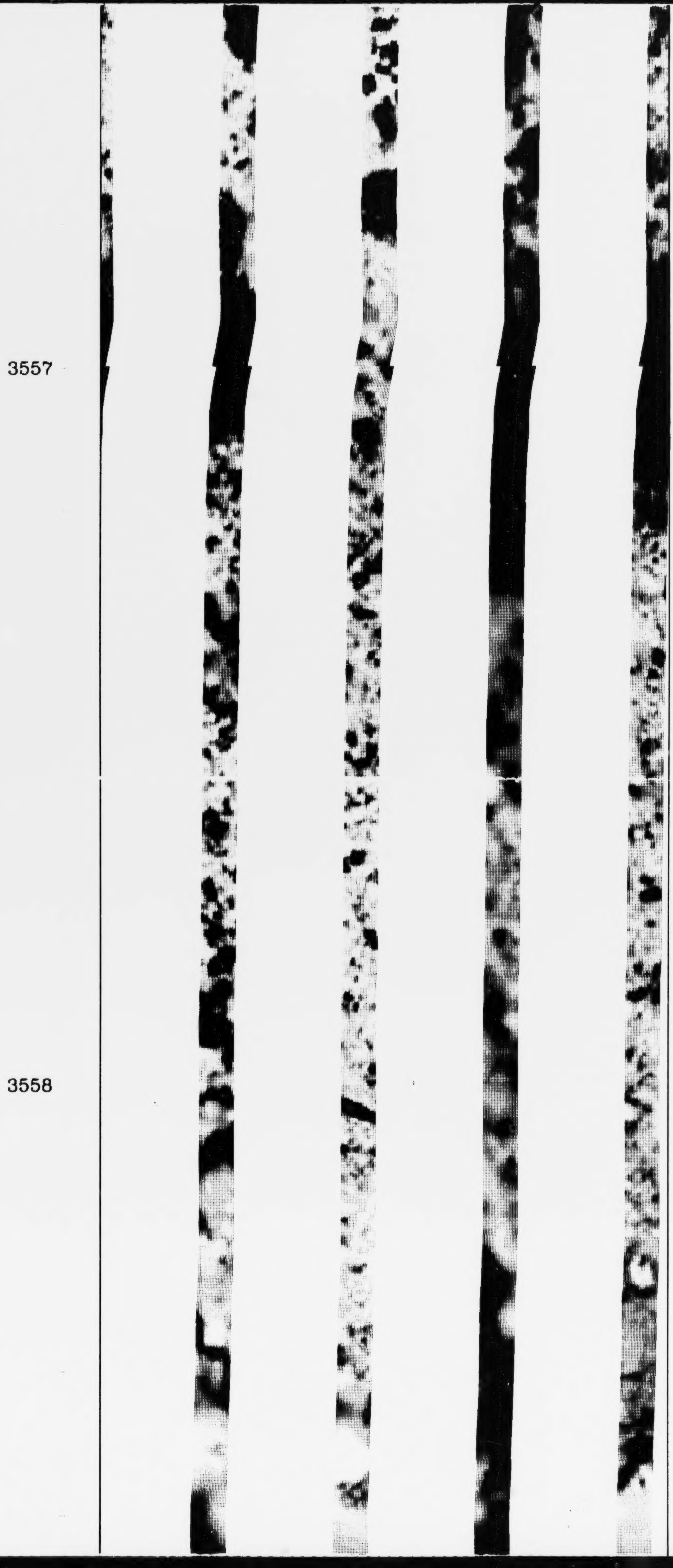
3557
3558

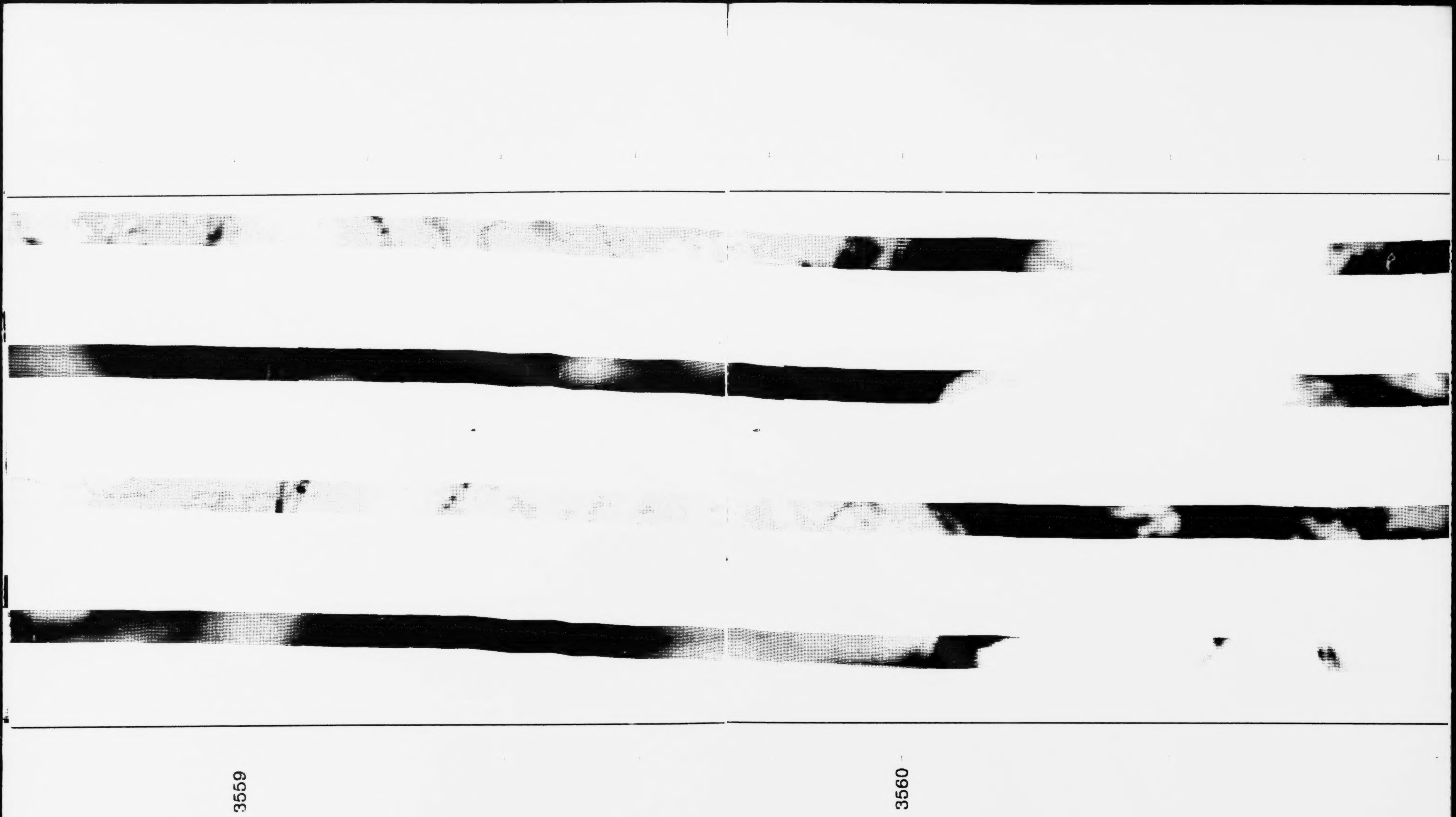
3559
3560

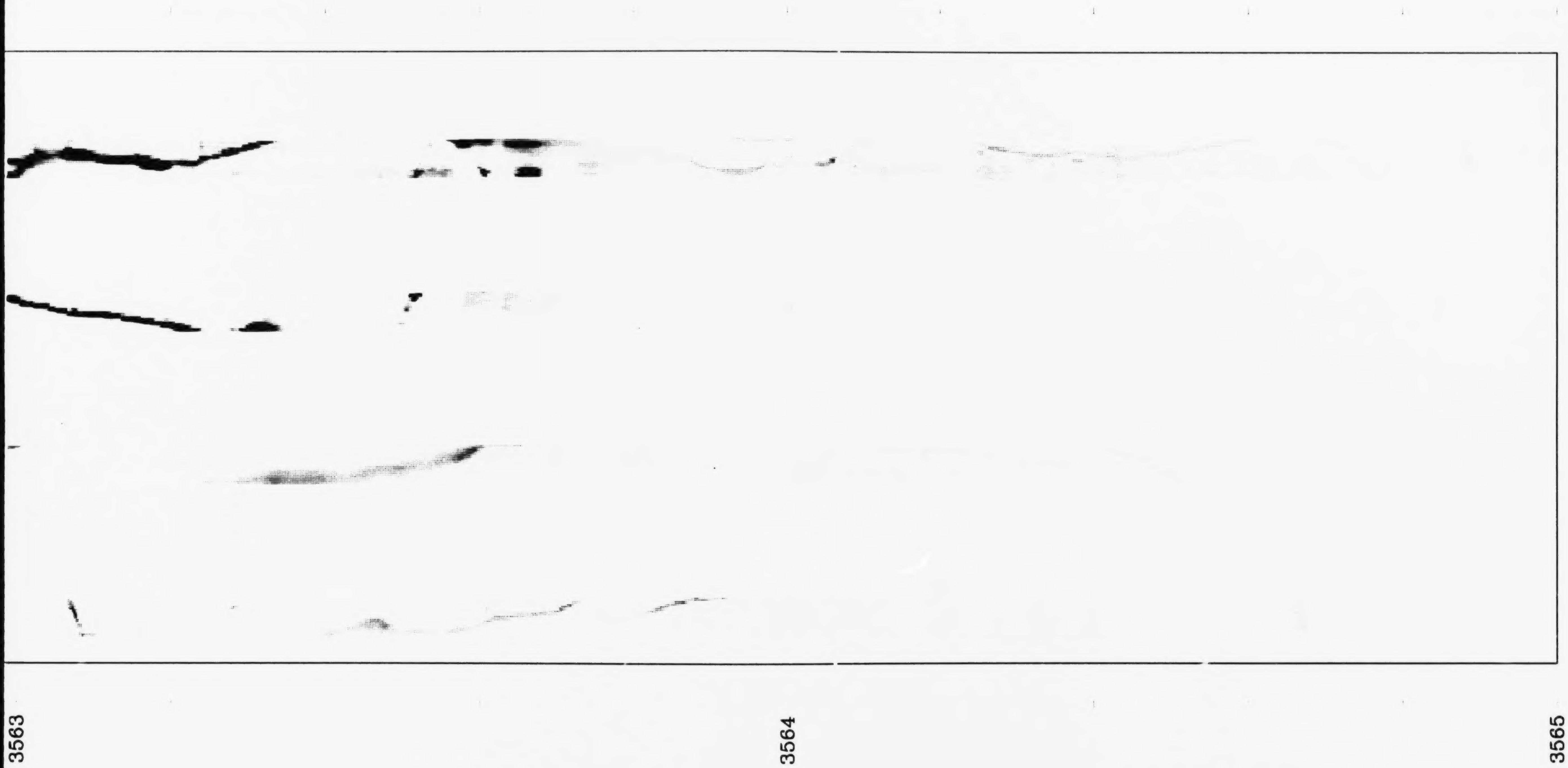
3563
3564
3565

SCHLUMBERGER

FMS
BOREHOLE
IMAGING

COMPANY	LAMONT–DOHERTY GEOLOGICAL
WELL	ODP HOLE–793B
FIELD	IZU–BONIN FOREARC BASIN
COUNTRY	OCEAN
RUN	1
DATE LOGGED	16 – JUN – 89
REFERENCE	STATIC PS–1 3565–3600

STATIC NORMALIZATION

PASS 1 (23577)

FILE : MEST.003

ZONE FROM 3600.0 M TO 3565.0 M

DEPTH SCALE = 1/ 5

IMAGE SCALE = 1/ 5

BITSIZE = 9.88

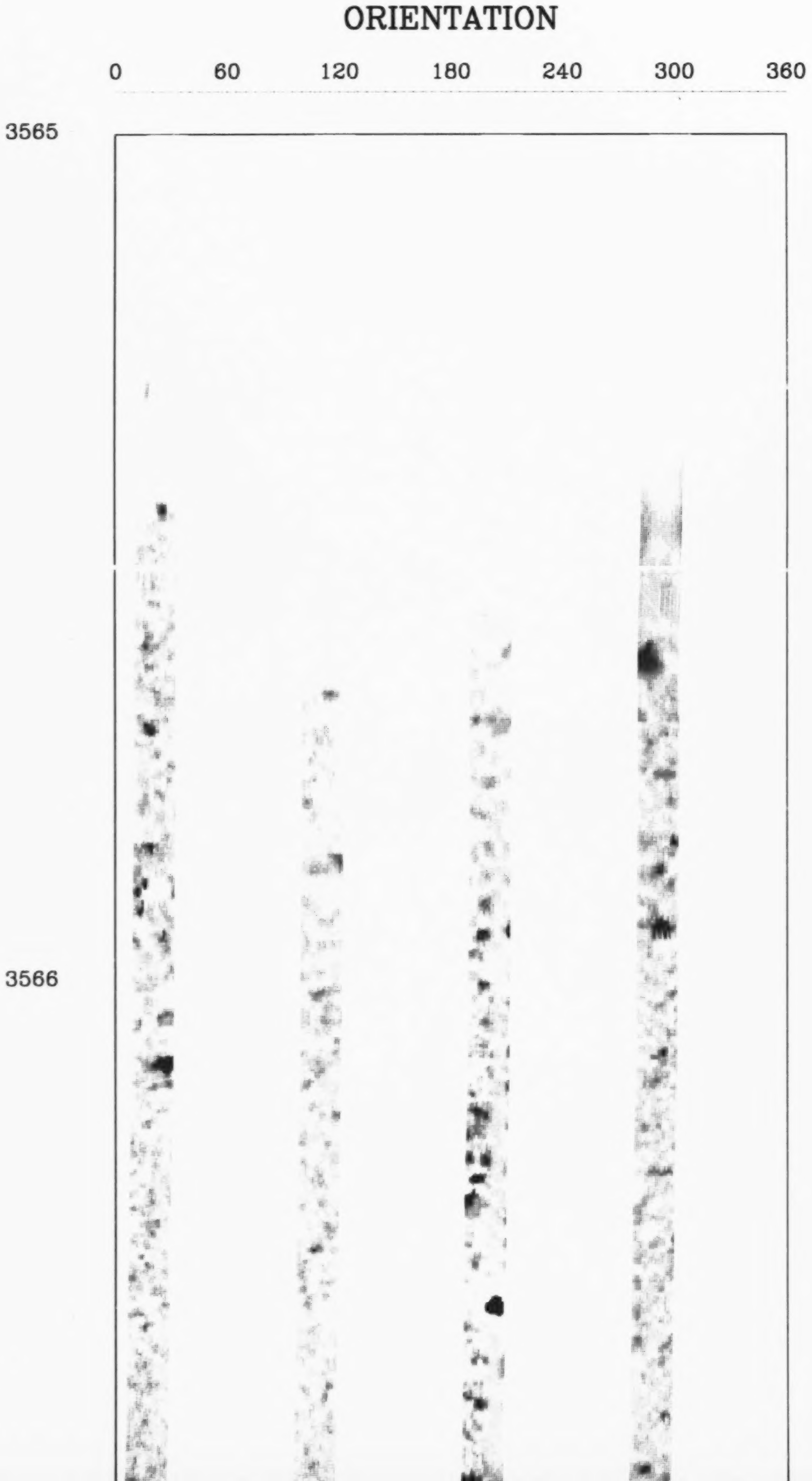

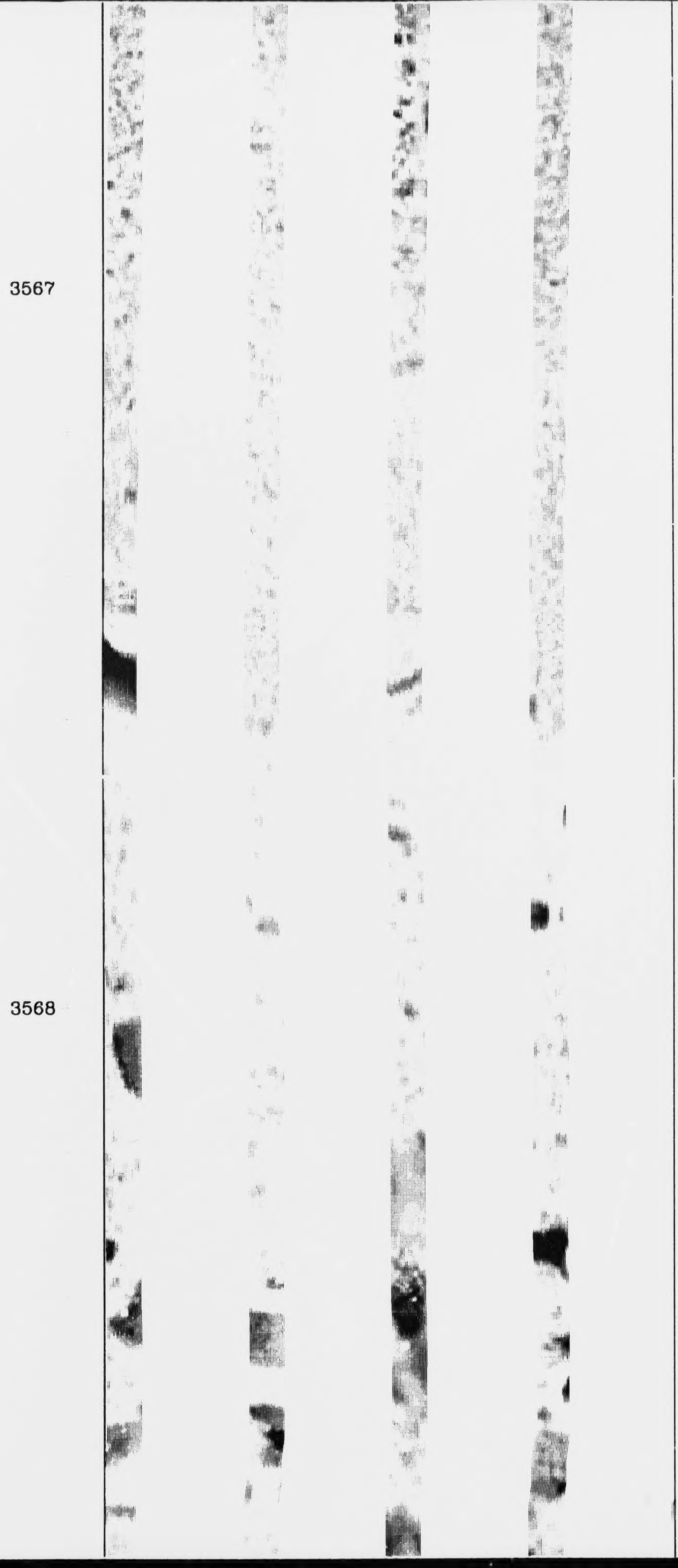
3567
3568

3571

3572

3573

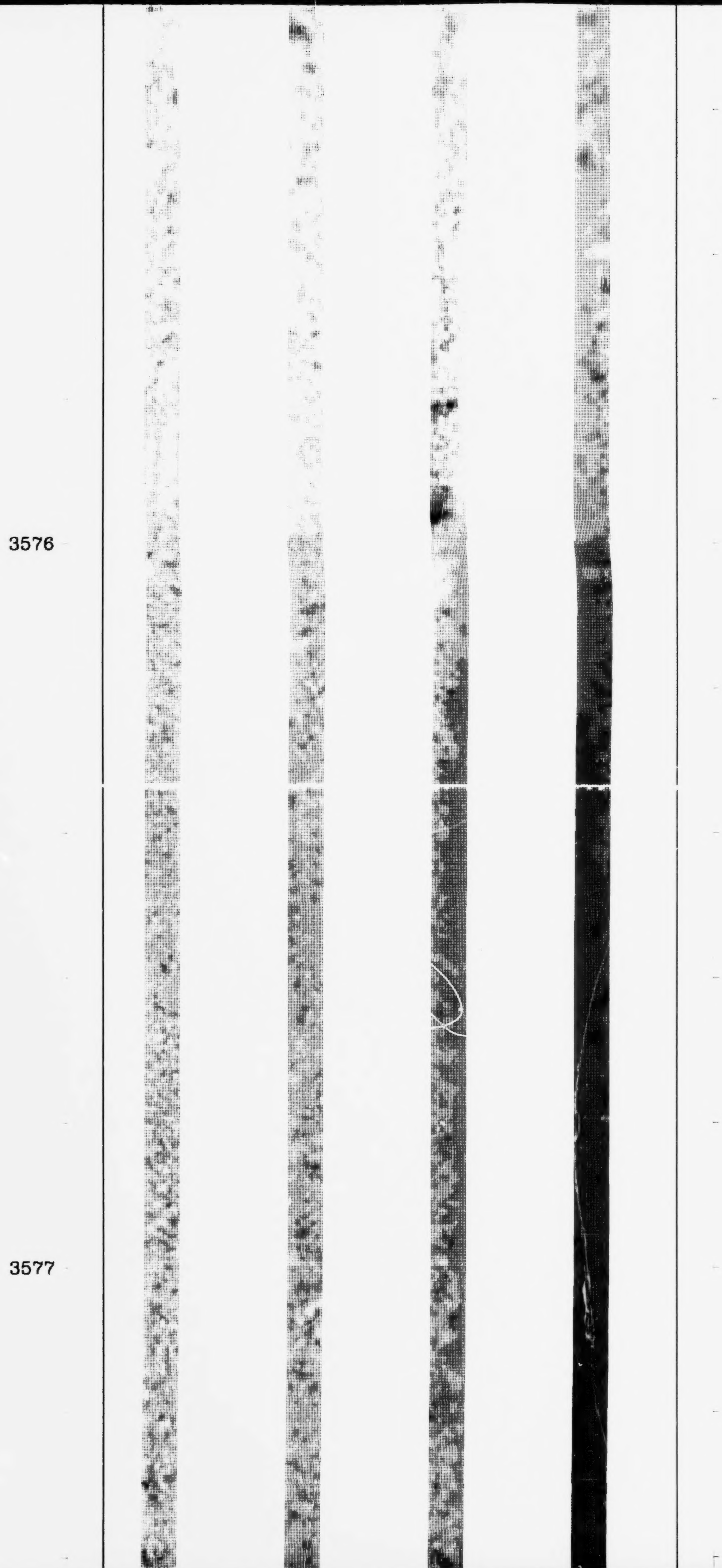
3576
3577

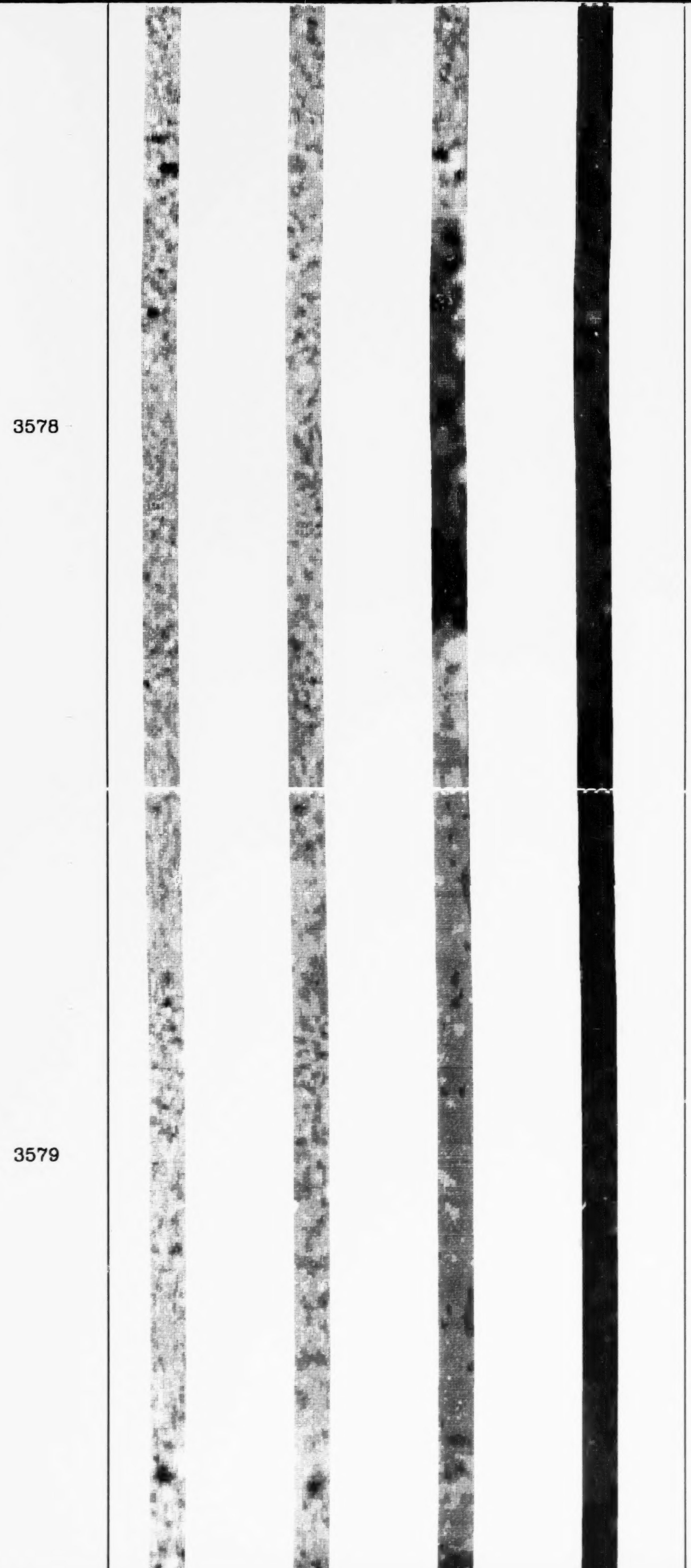
3578
3579

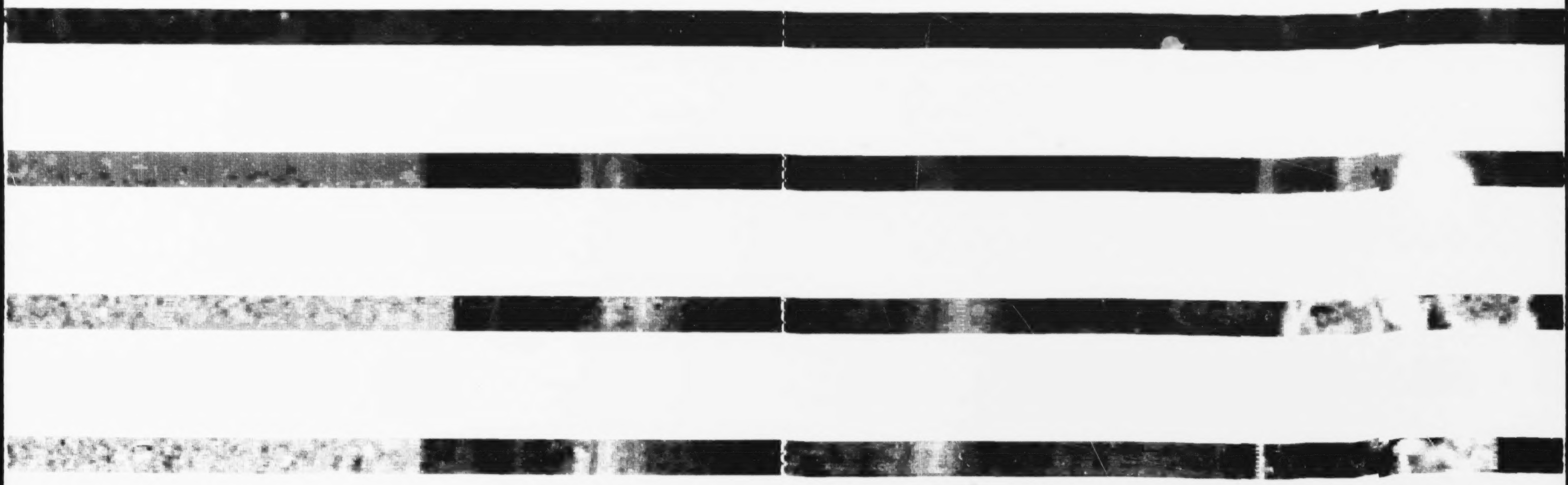

3580

3581

3582

3583

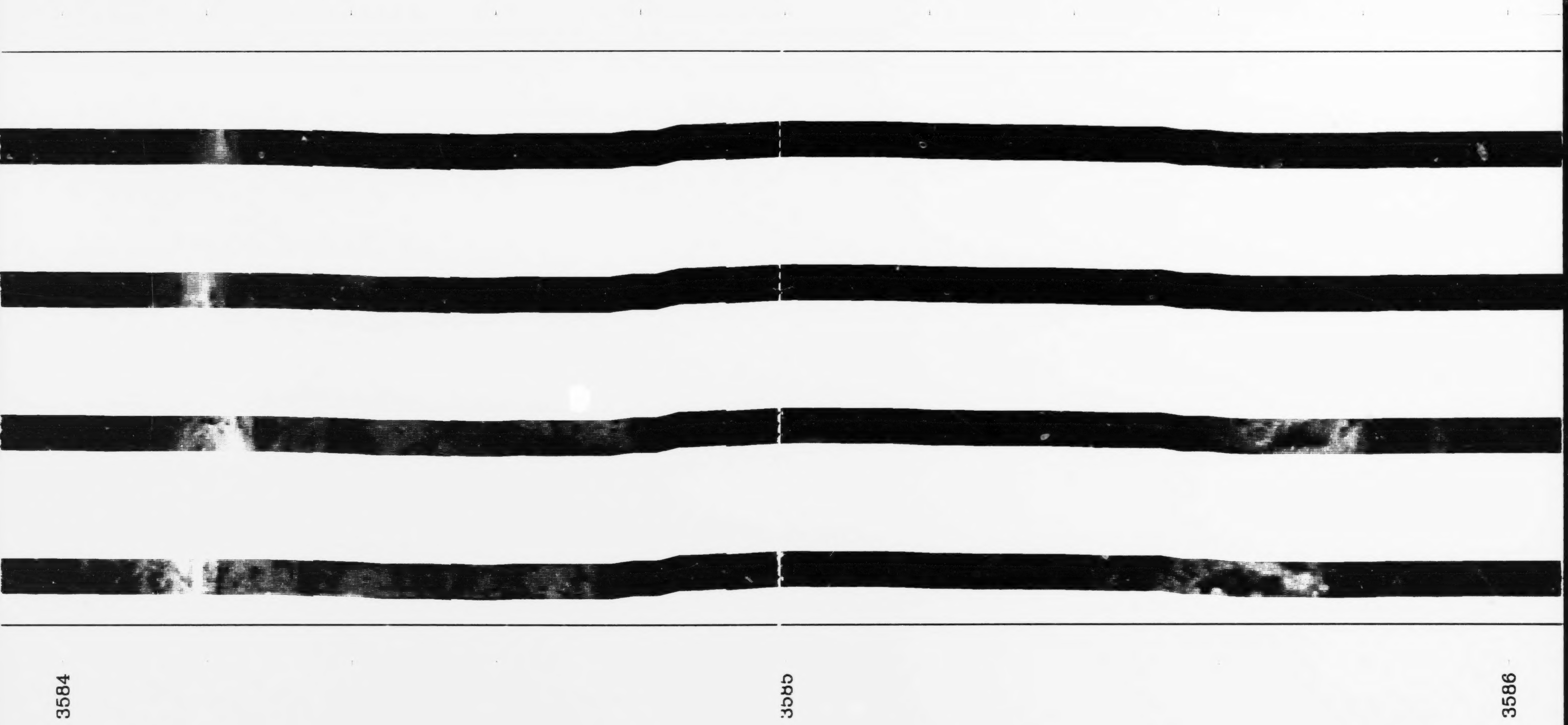
3584
3585
3586

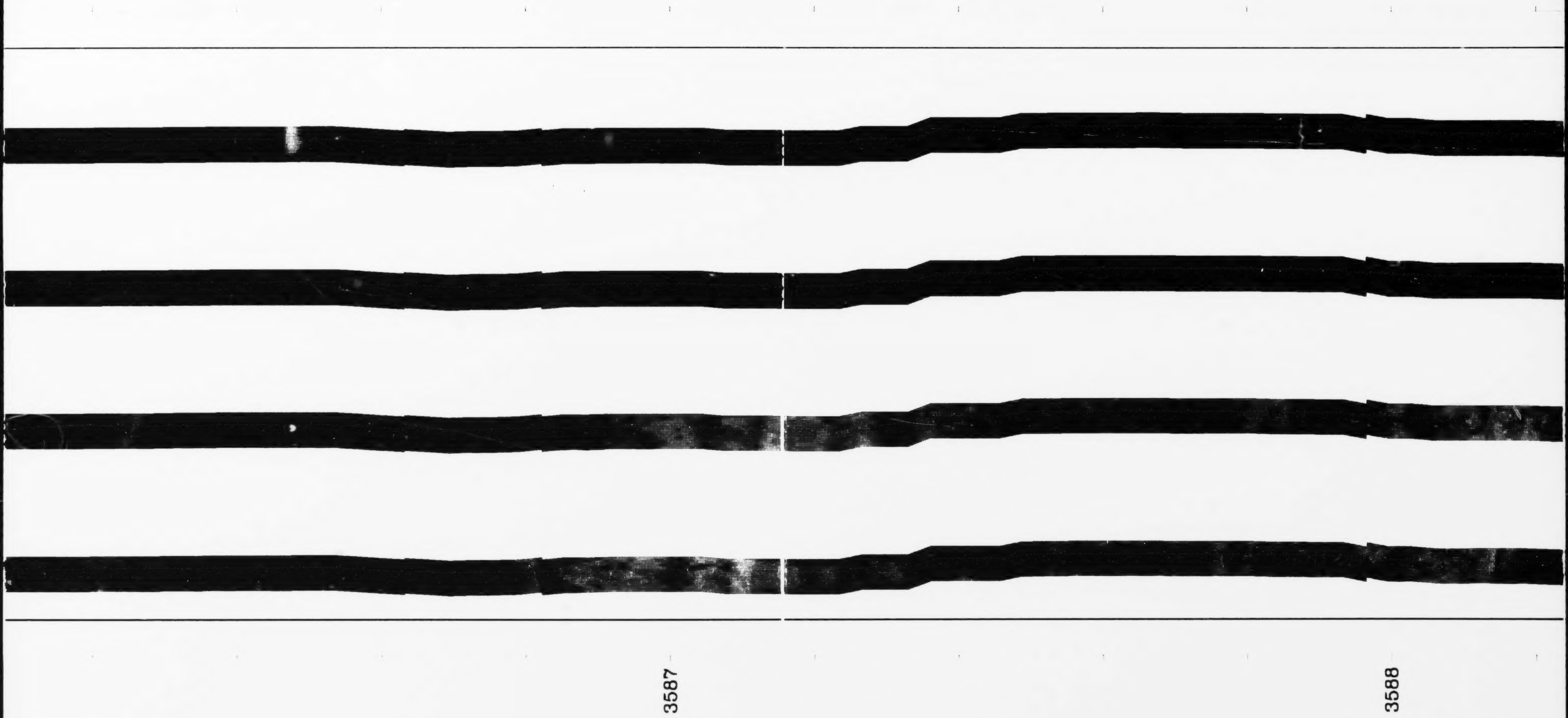
3587
3588

3589

3590

3591

3592

3597

3598

3599

SCHLUMBERGER

FMS
BOREHOLE
IMAGING

COMPANY	LAMONT–DOHERTY GEOLOGICAL
WELL	ODP HOLE–793B
FIELD	IZU–BONIN FOREARC BASIN
COUNTRY	OCEAN
RUN	1
DATE LOGGED	16 – JUN – 89
REFERENCE	STATIC PS-1 3600-3630

STATIC NORMALIZATION

PASS 1 (23577)

FILE : MEST.003

ZONE FROM 3630.0 M TO 3600.0 M

DEPTH SCALE = 1/ 5

IMAGE SCALE = 1/ 5

BITSIZE = 9.88

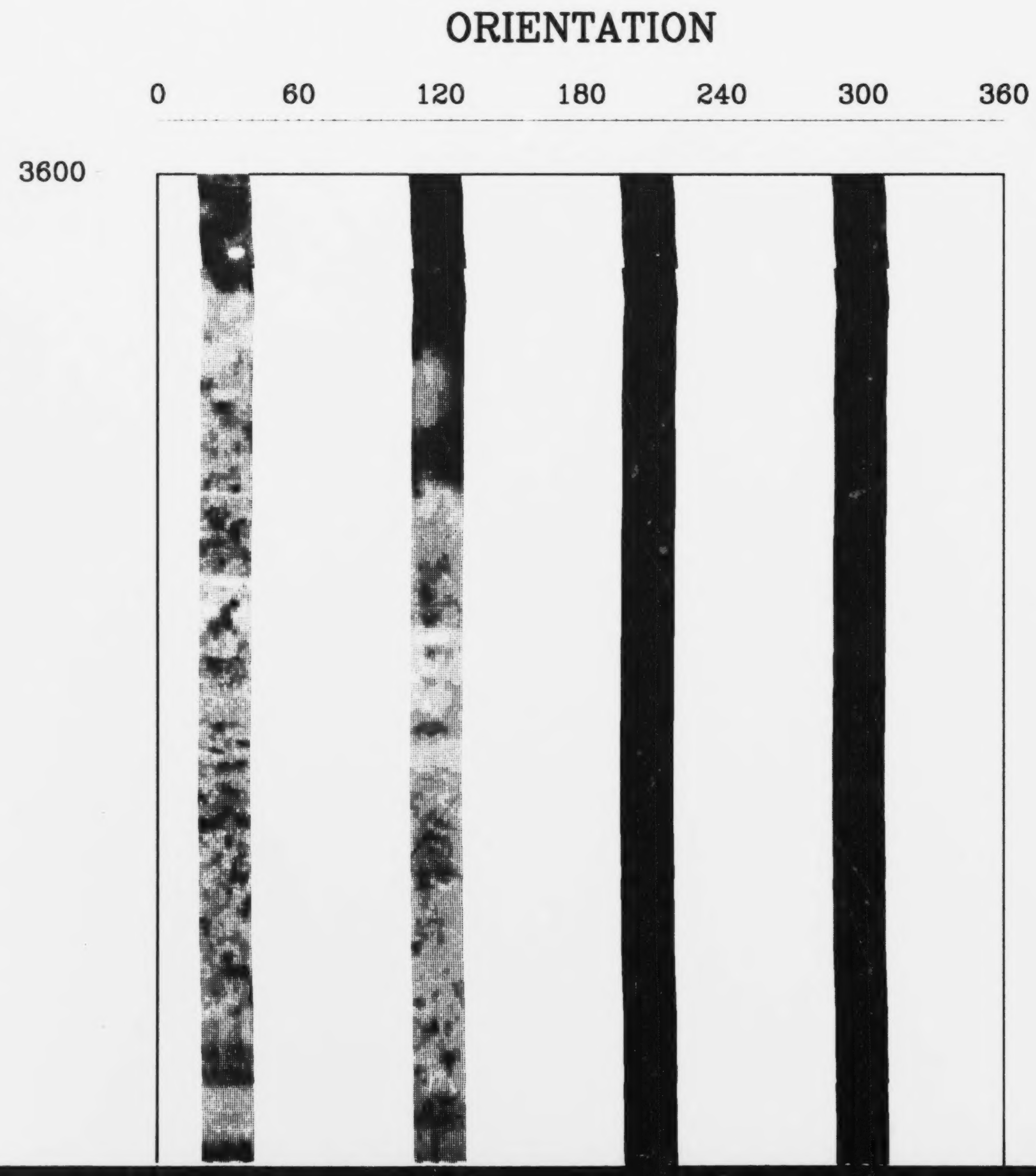

3601
3602
3603

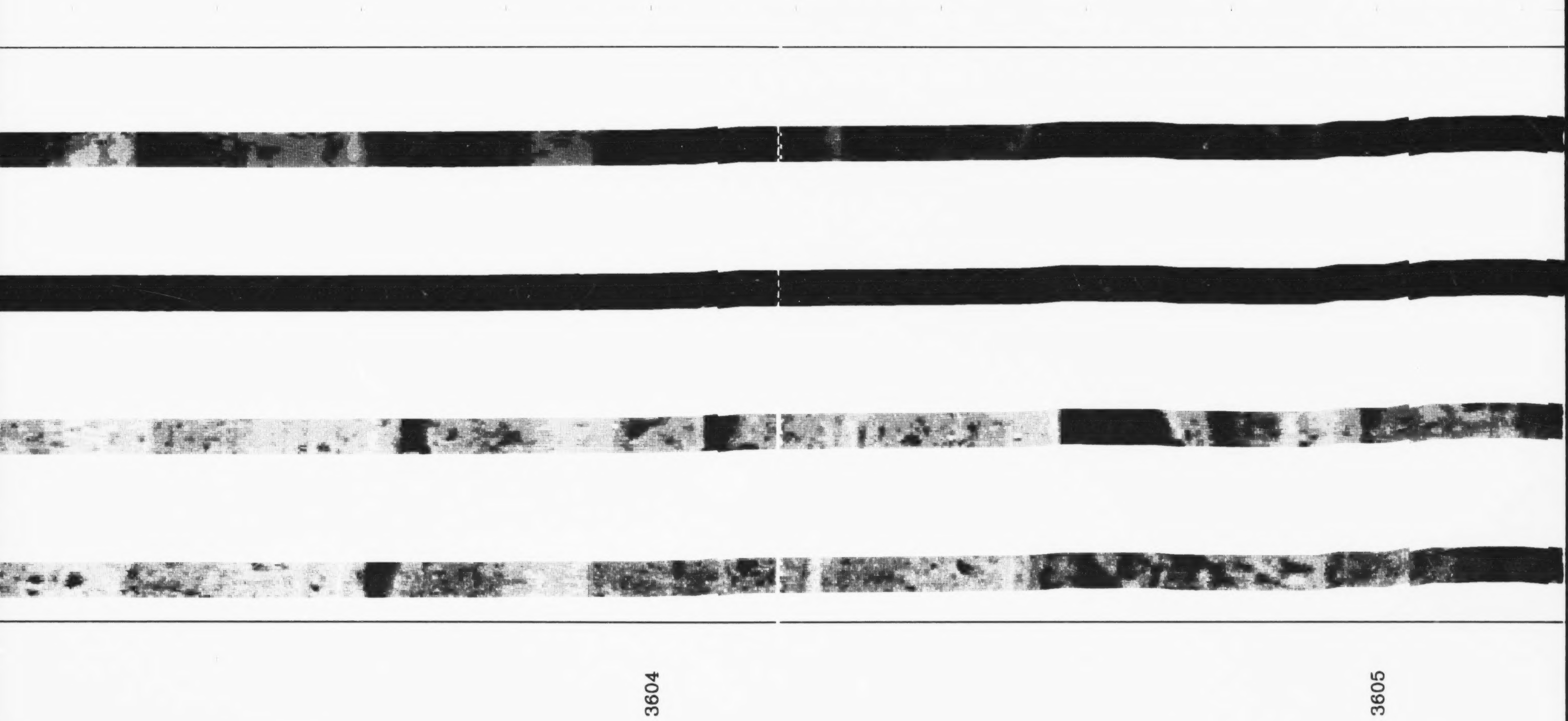
3604
3605

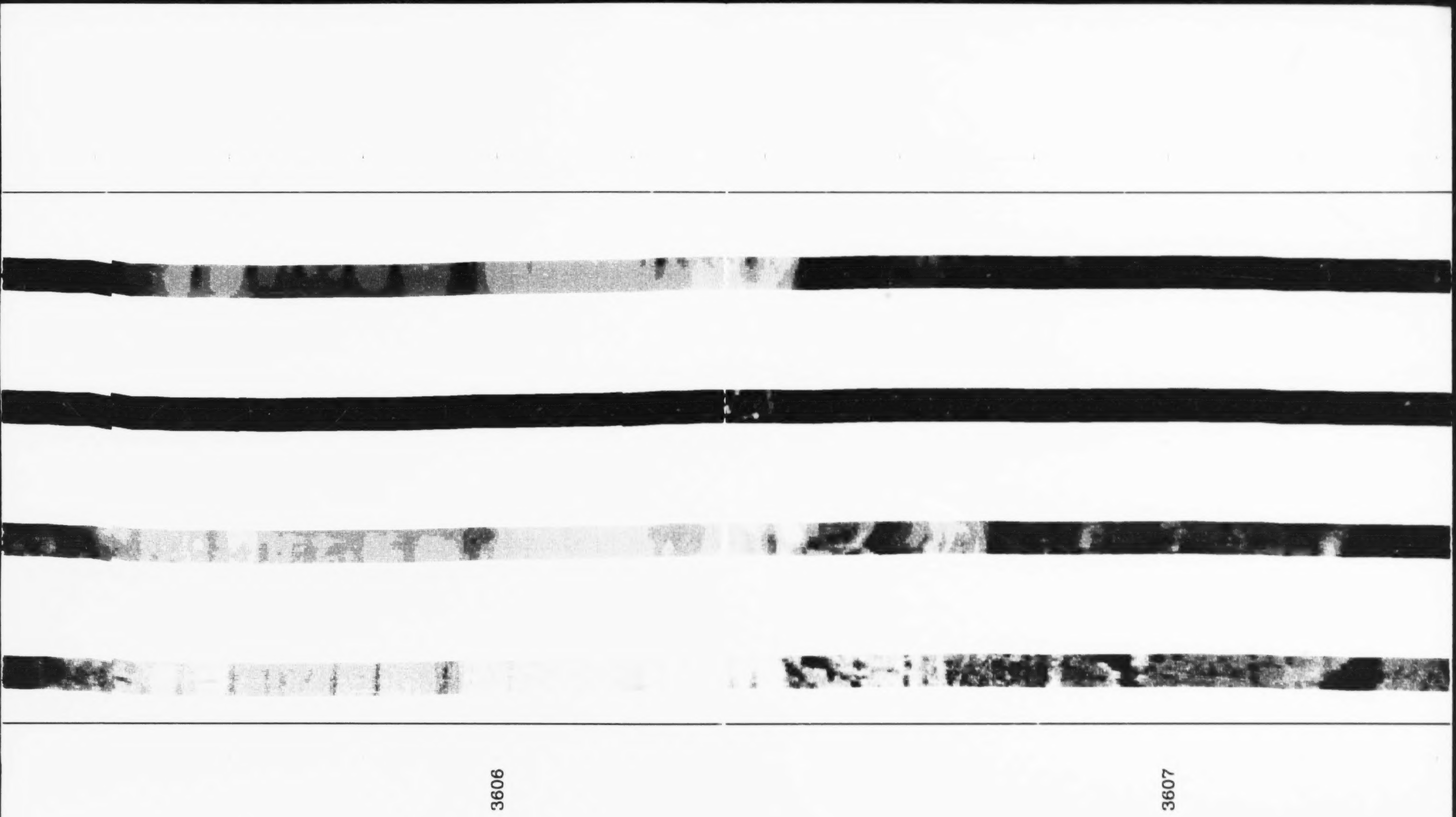
3606
3607

3608

3609

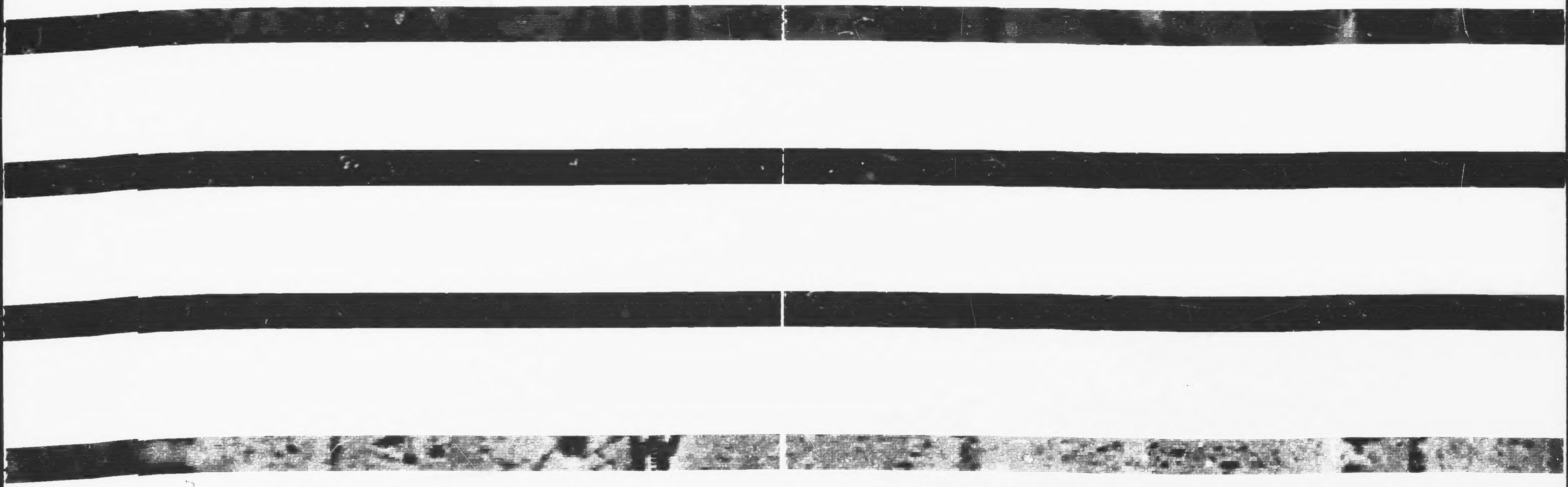
3610
3611

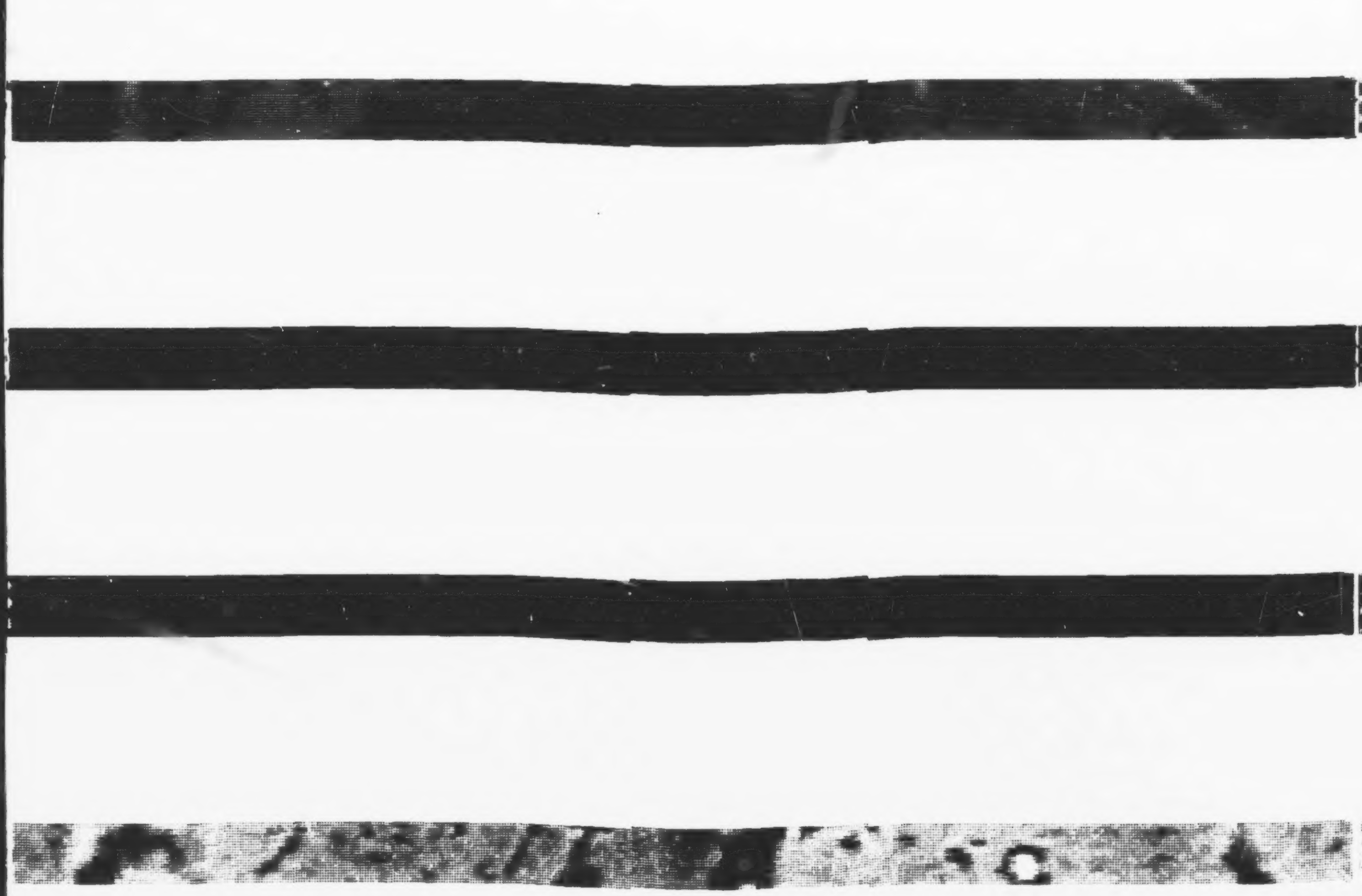

3612

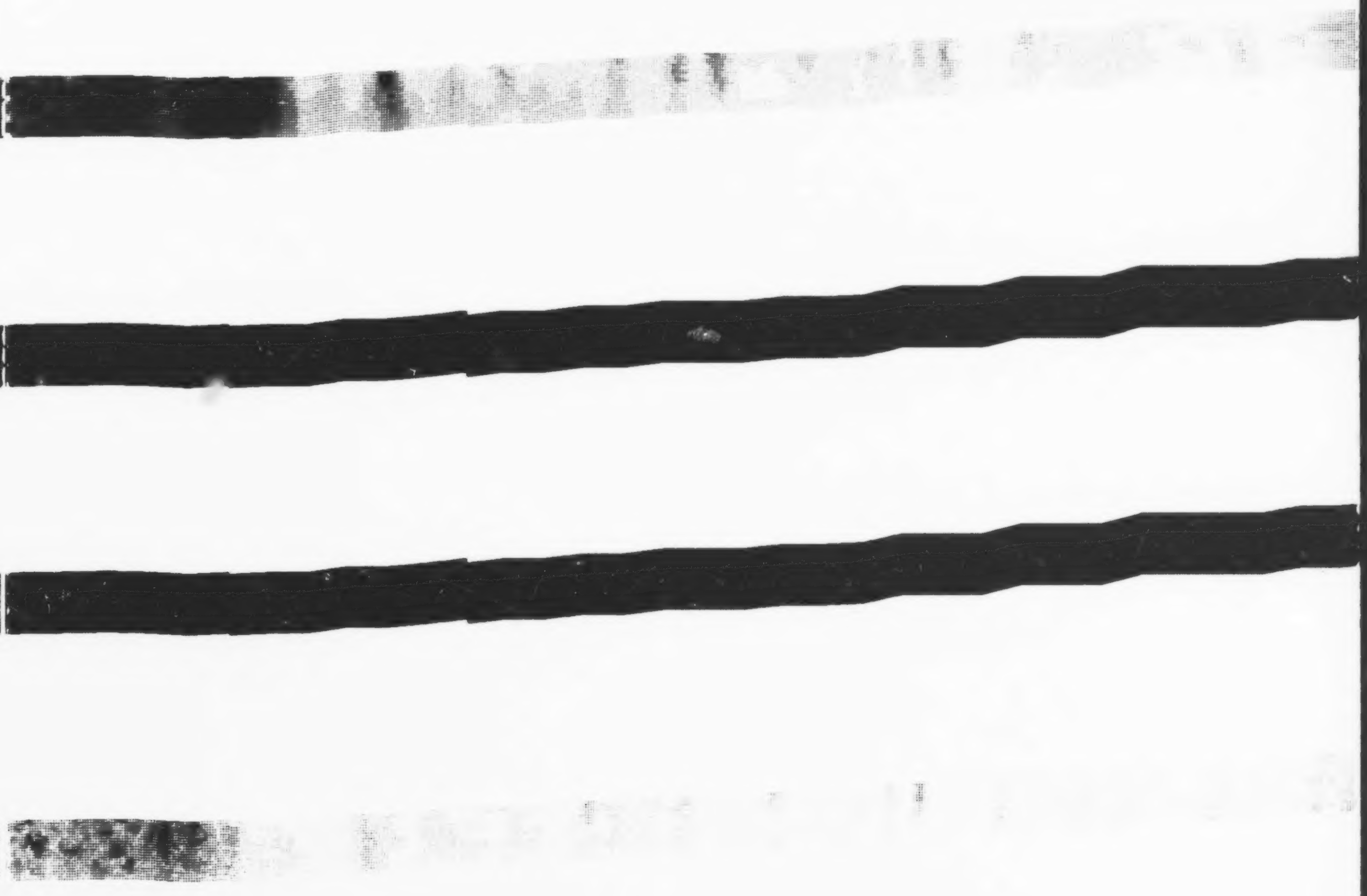

3613

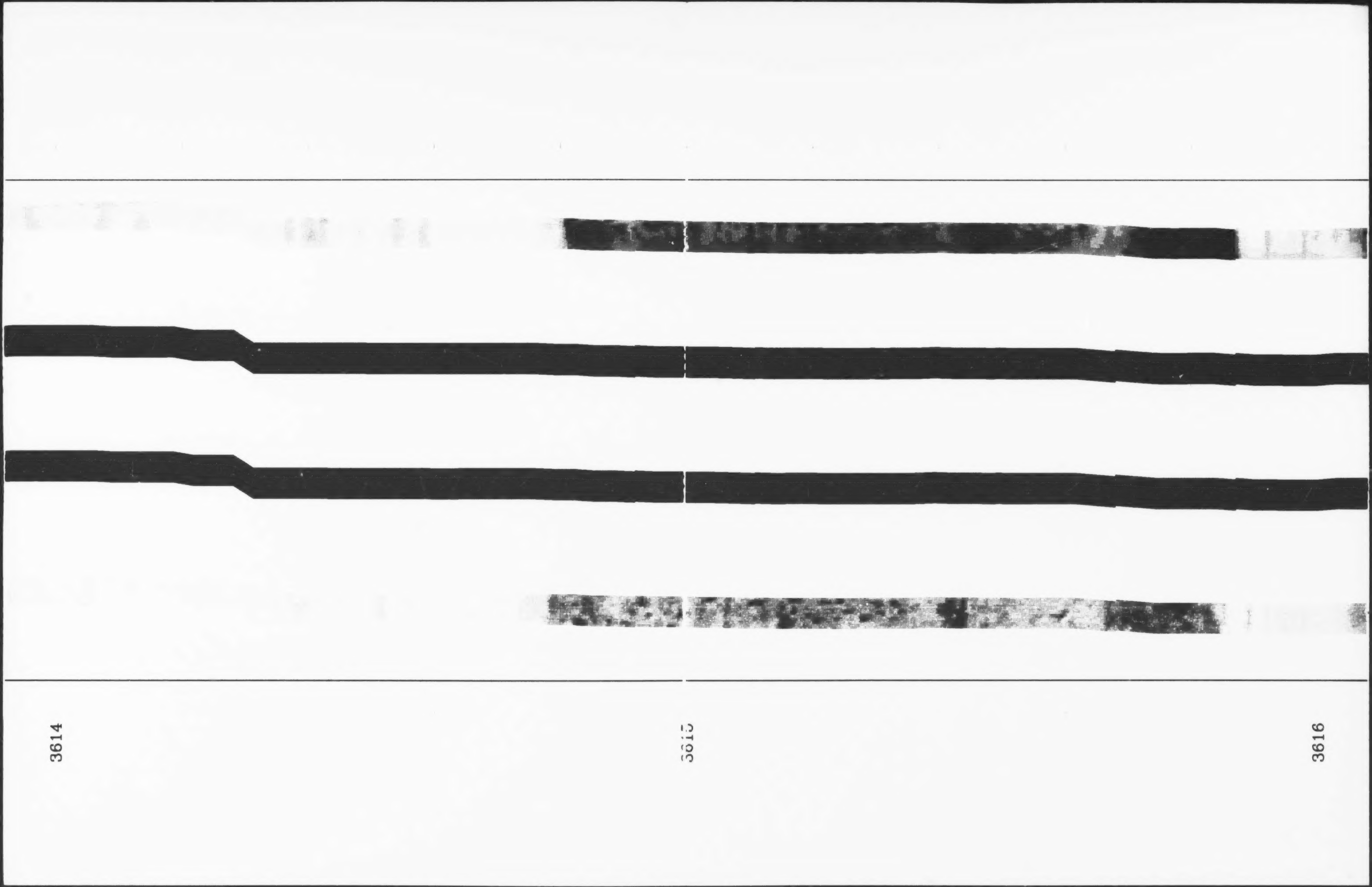
3614
3615
3616

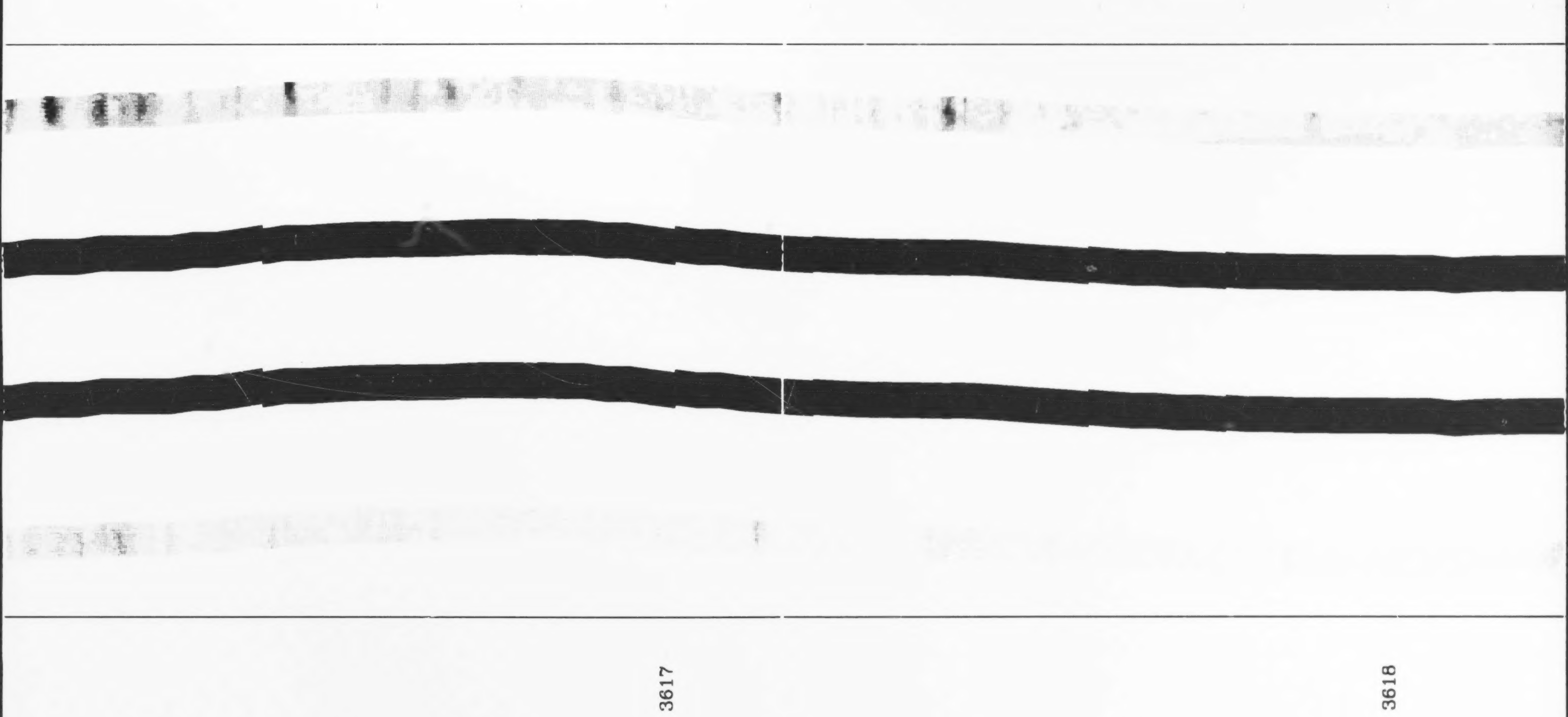
3617
3618

3619
3620

3621

3622

[redacted]

[redacted]

3623

[redacted]

[redacted]

3624

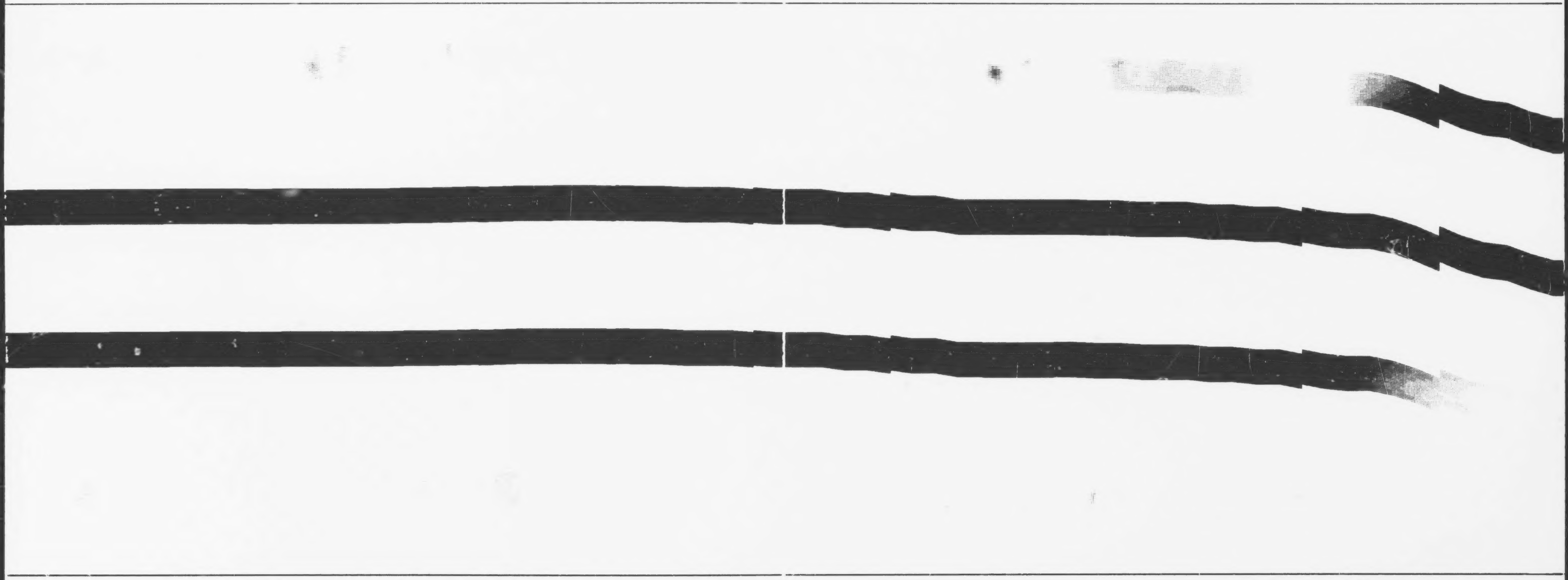
3625
3626

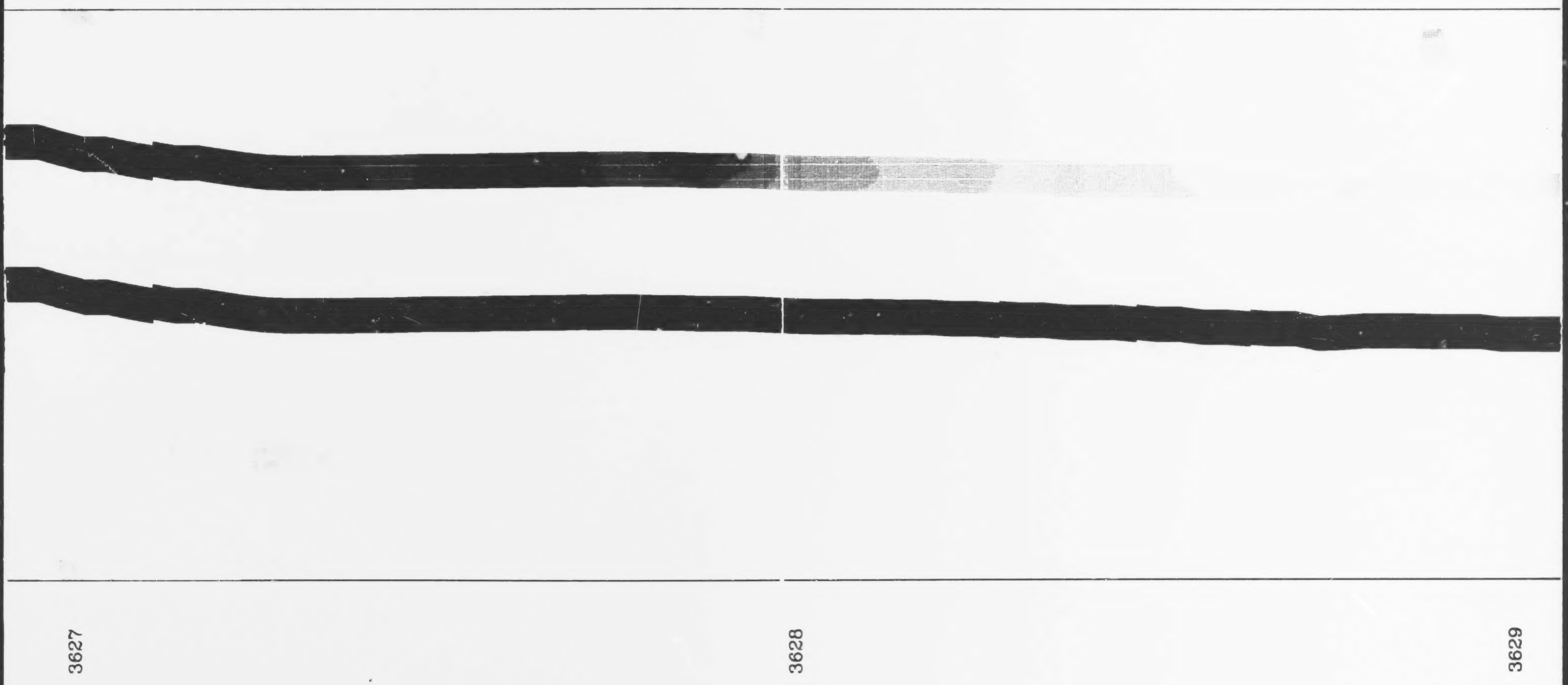
3627
3628
3629

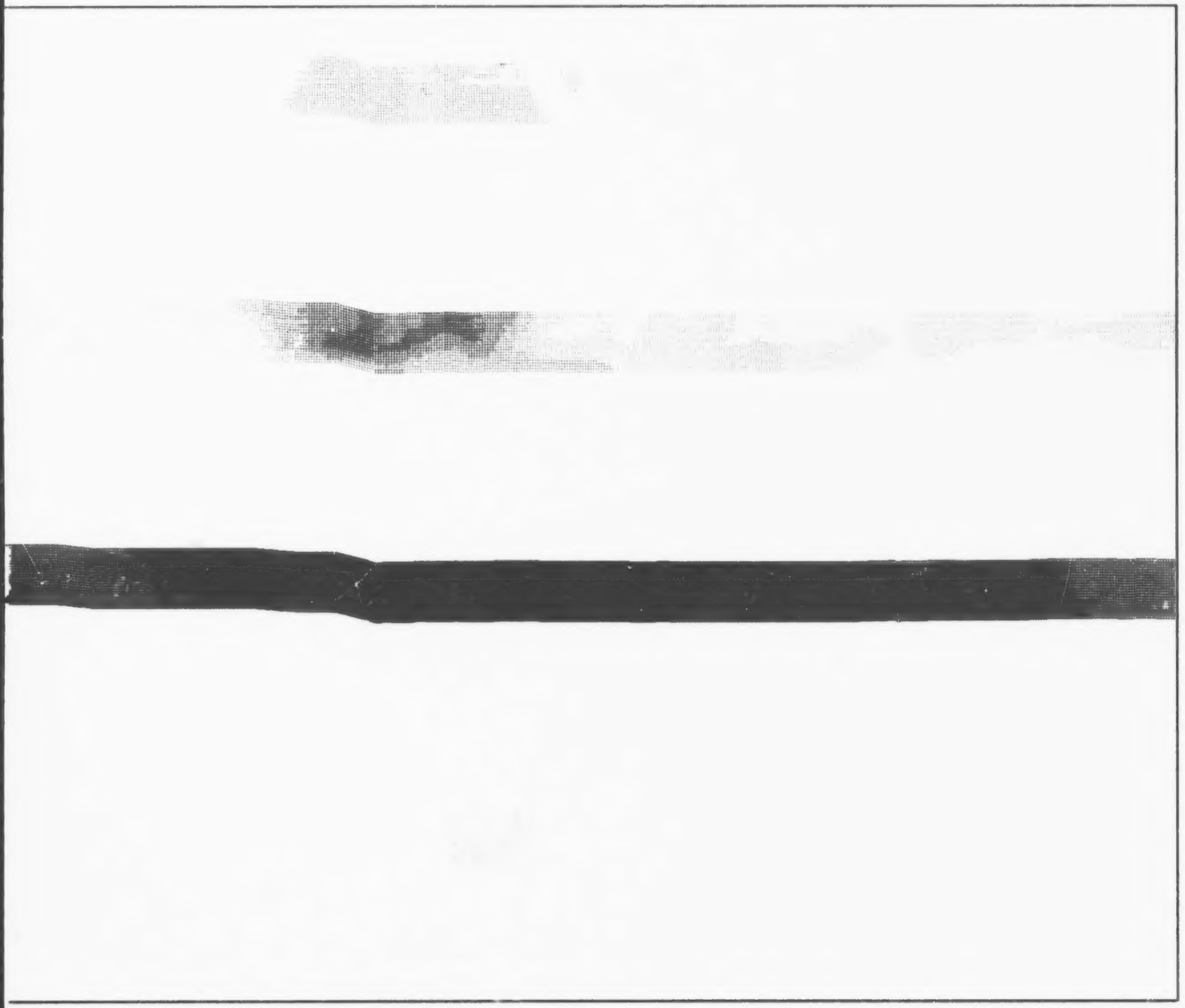

SCHLUMBERGER

FMS
BOREHOLE
IMAGING

COMPANY	LAMONT-DOHERTY GEOLOGICAL
WELL	ODP HOLE-793B
FIELD	IZU-BONIN FOREARC BASIN
COUNTRY	OCEAN
RUN	1
DATE LOGGED	16 - JUN - 89
REFERENCE	STATIC PS-1 3630 3665

STATIC NORMALIZATION

PASS 1 (23577)

FILE : MEST.003

ZONE FROM 3665.0 M TO 3630.0 M

DEPTH SCALE = 1/ 5

IMAGE SCALE = 1/ 5

BITSIZE = 9.88

ORIENTATION

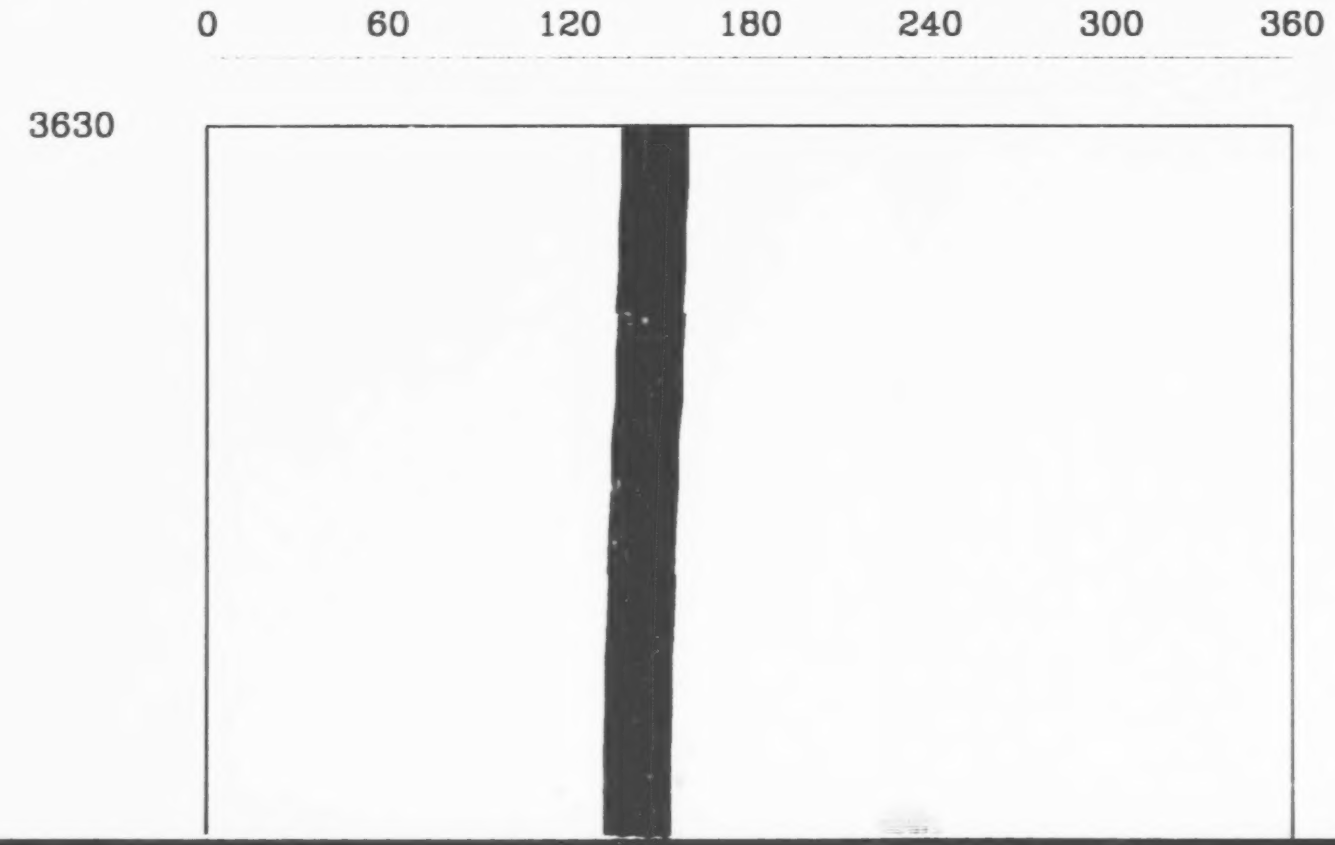

3631

3632

3633

3634

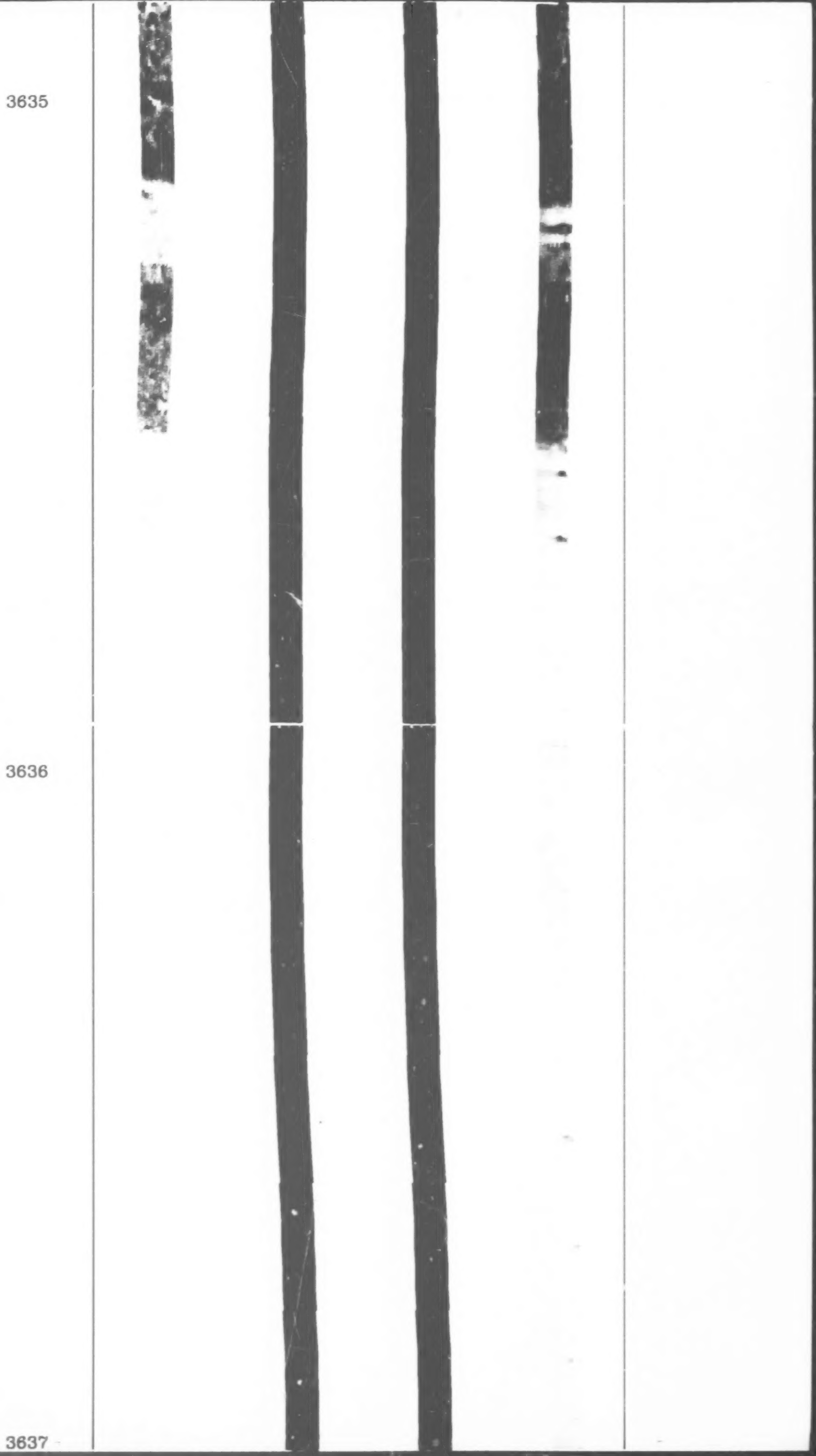

3635
3636
3637

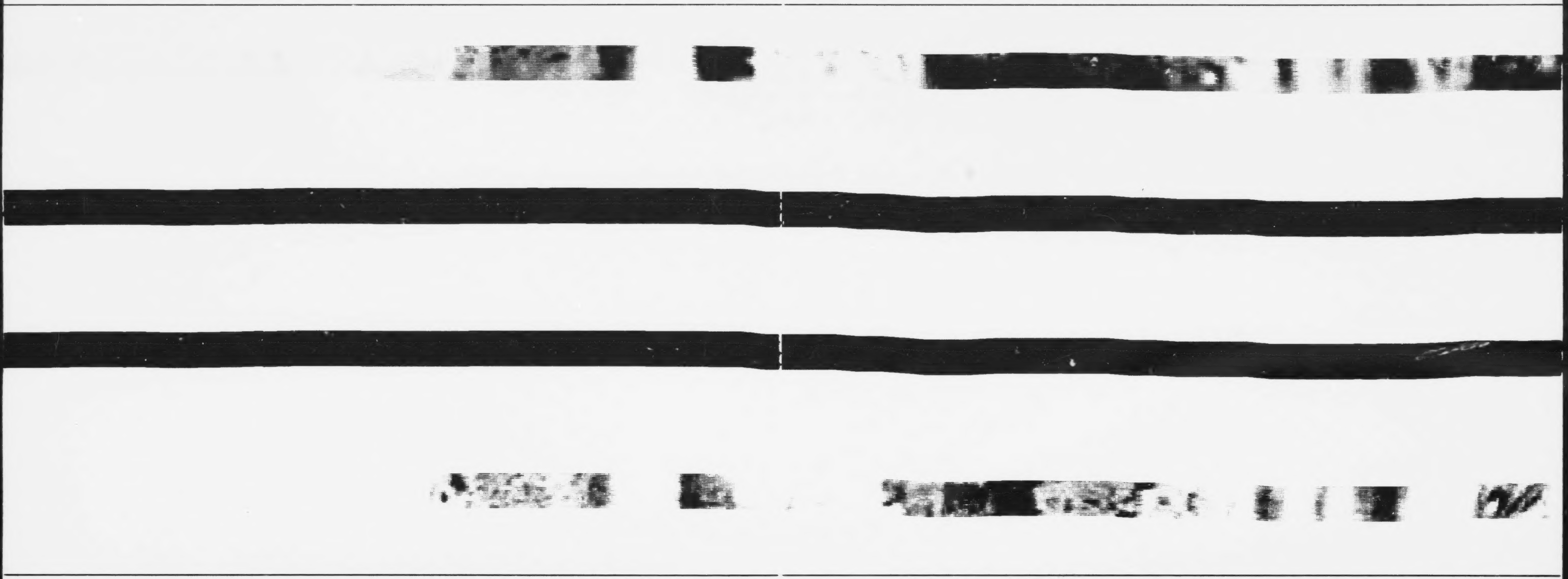

3638

3639

3640
3641

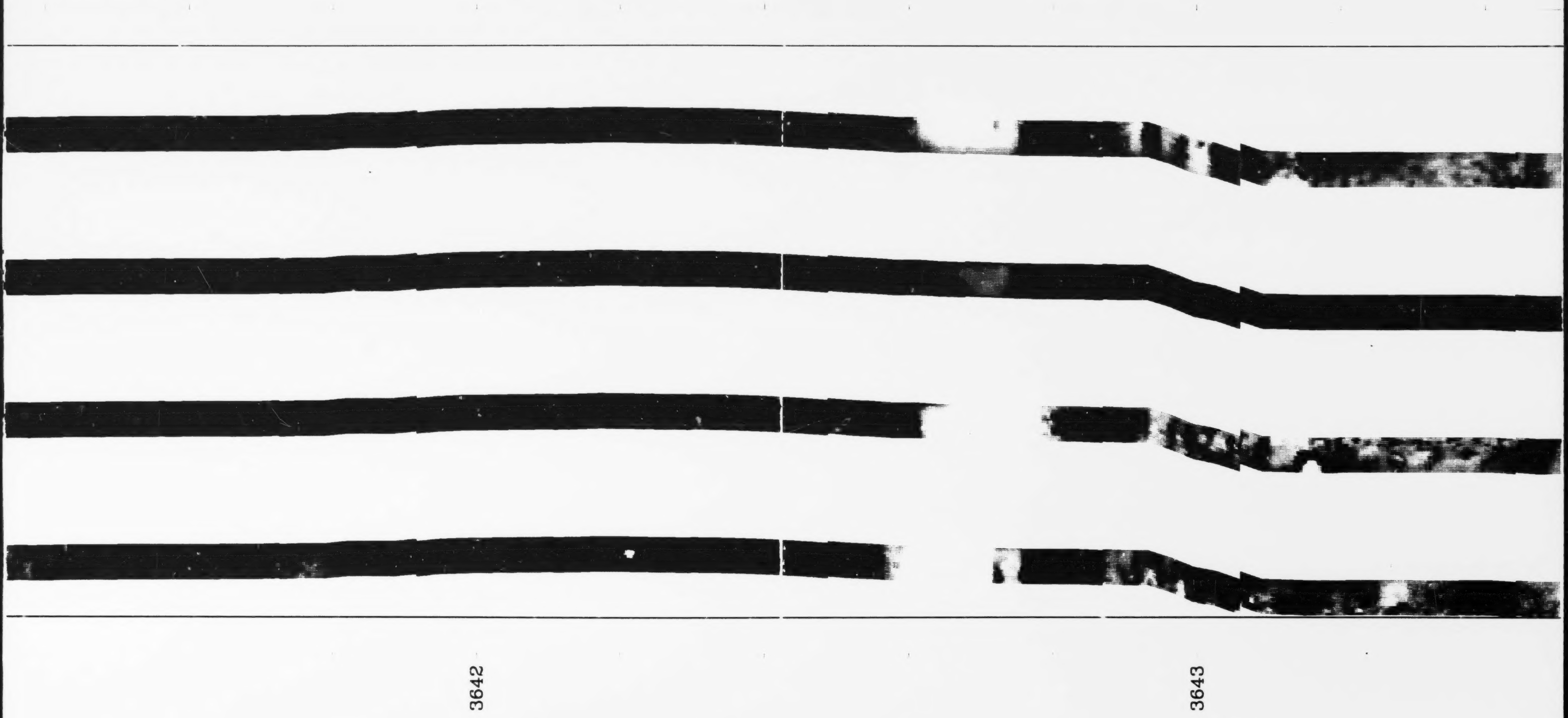
3642
3643

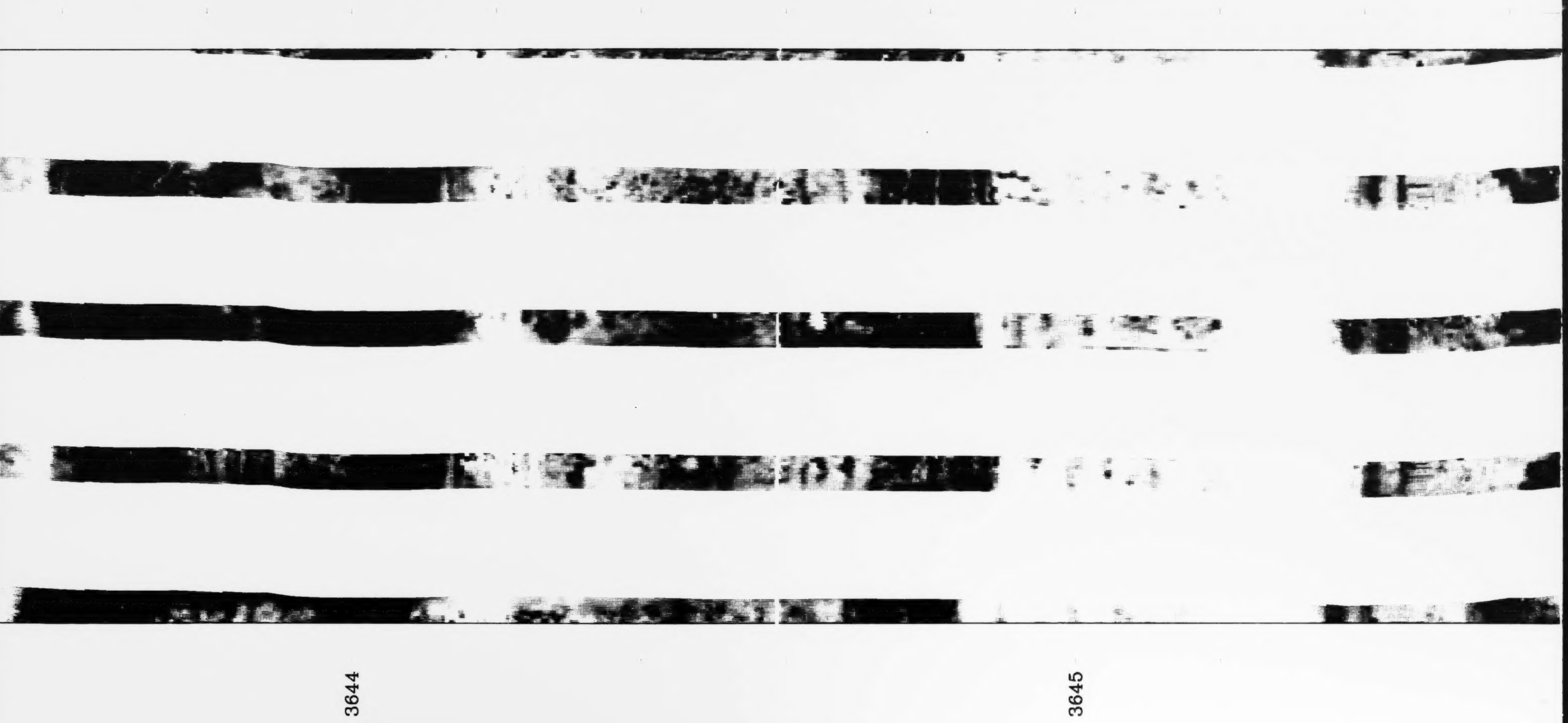
3644
3645

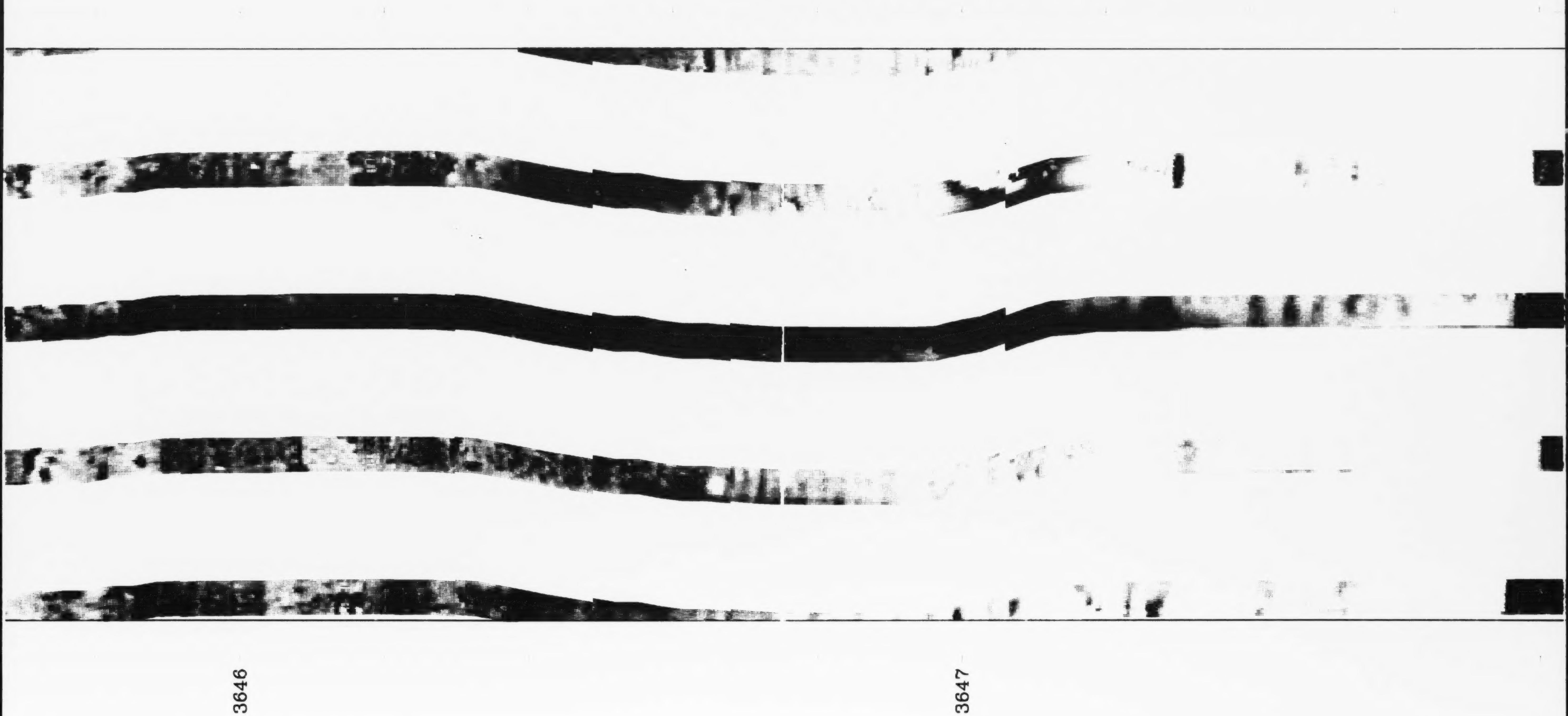
3646
3647

3648
3649

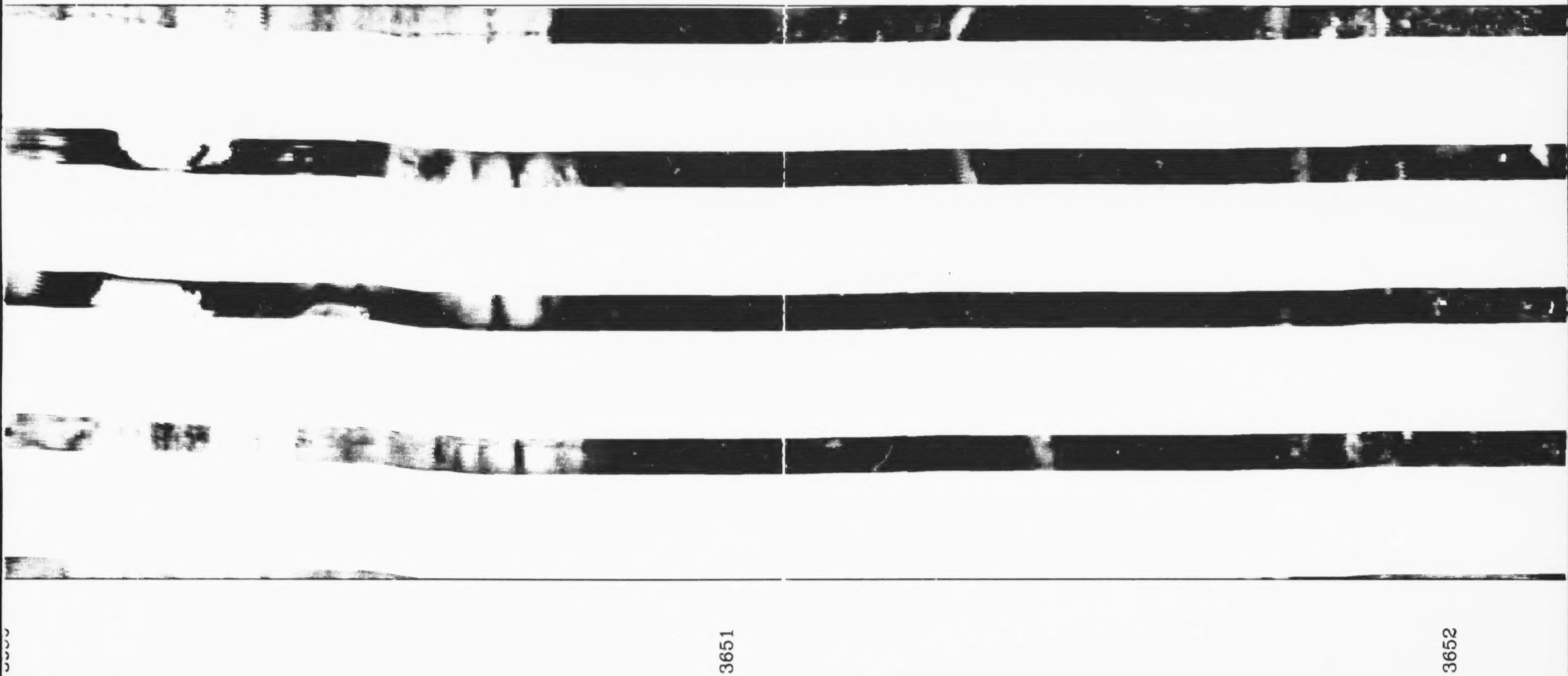
3651
3652

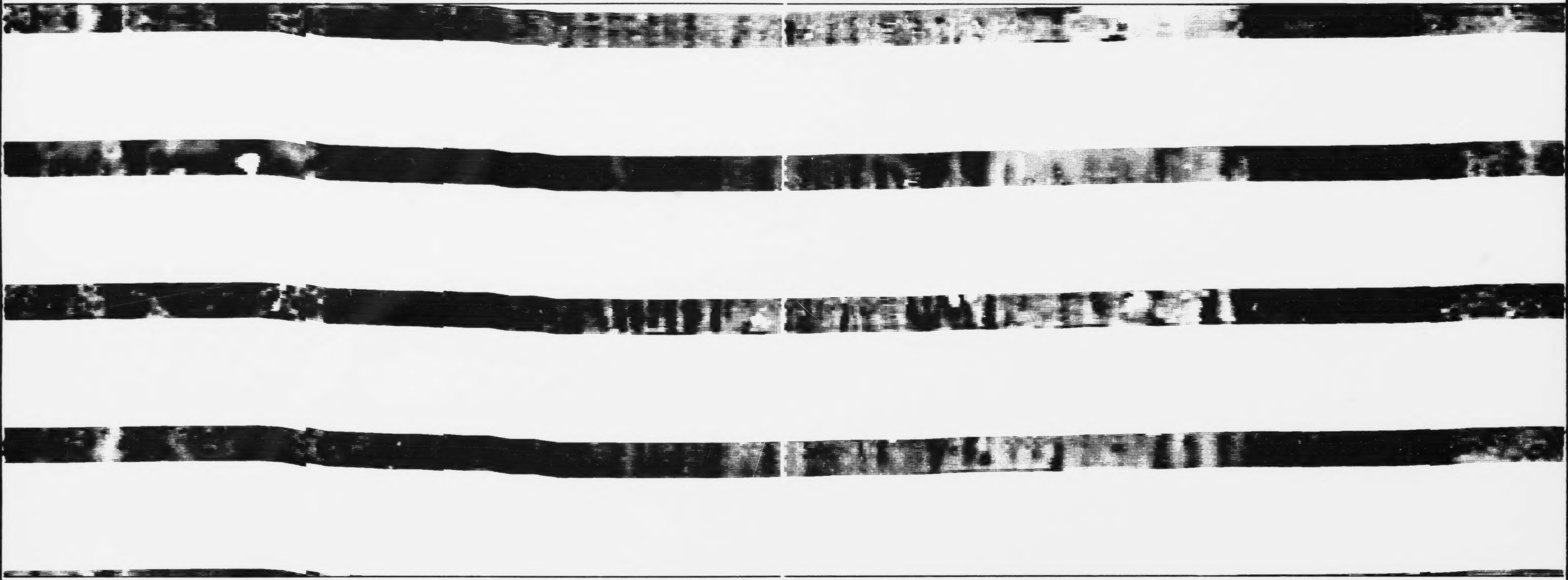

3653

3654

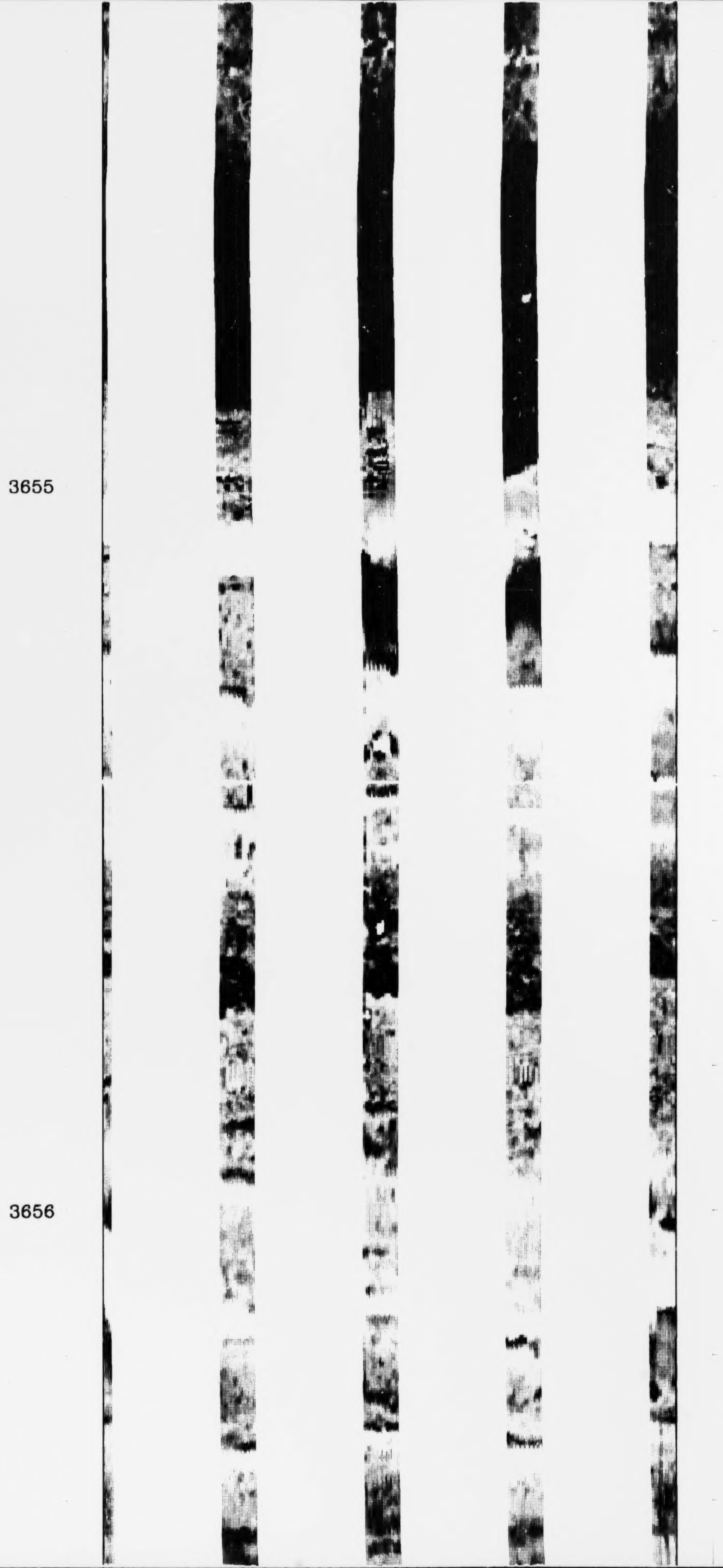
3655
3656

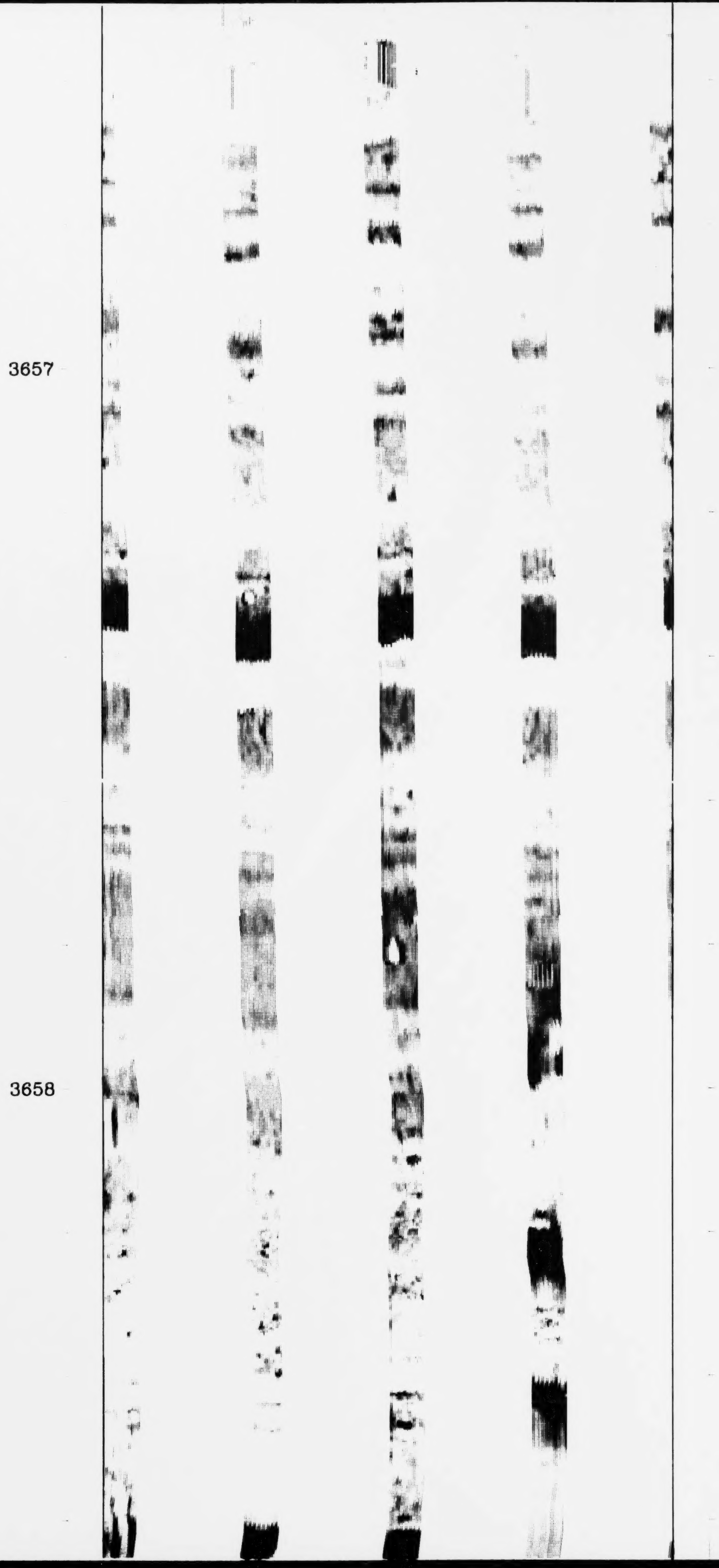
3657
3658

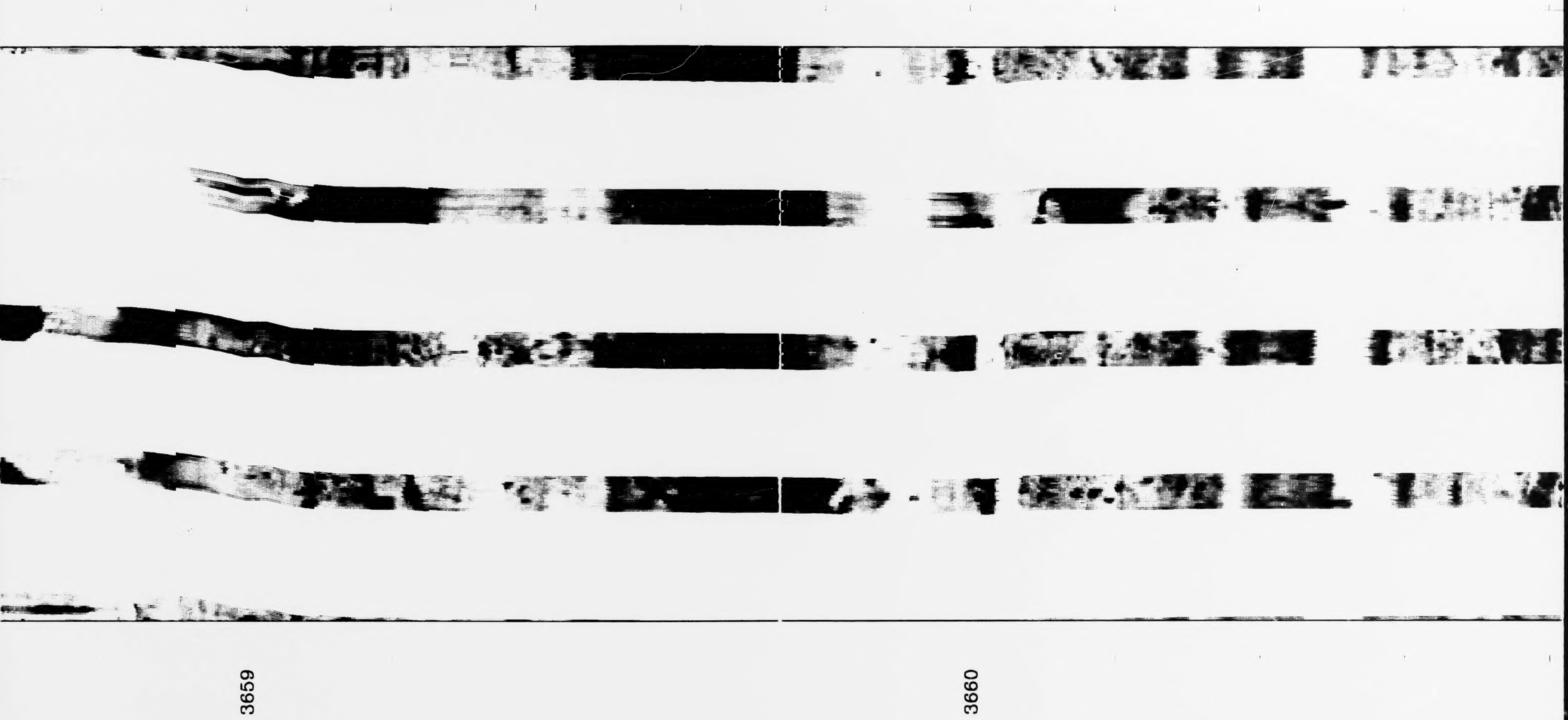
3659
3660

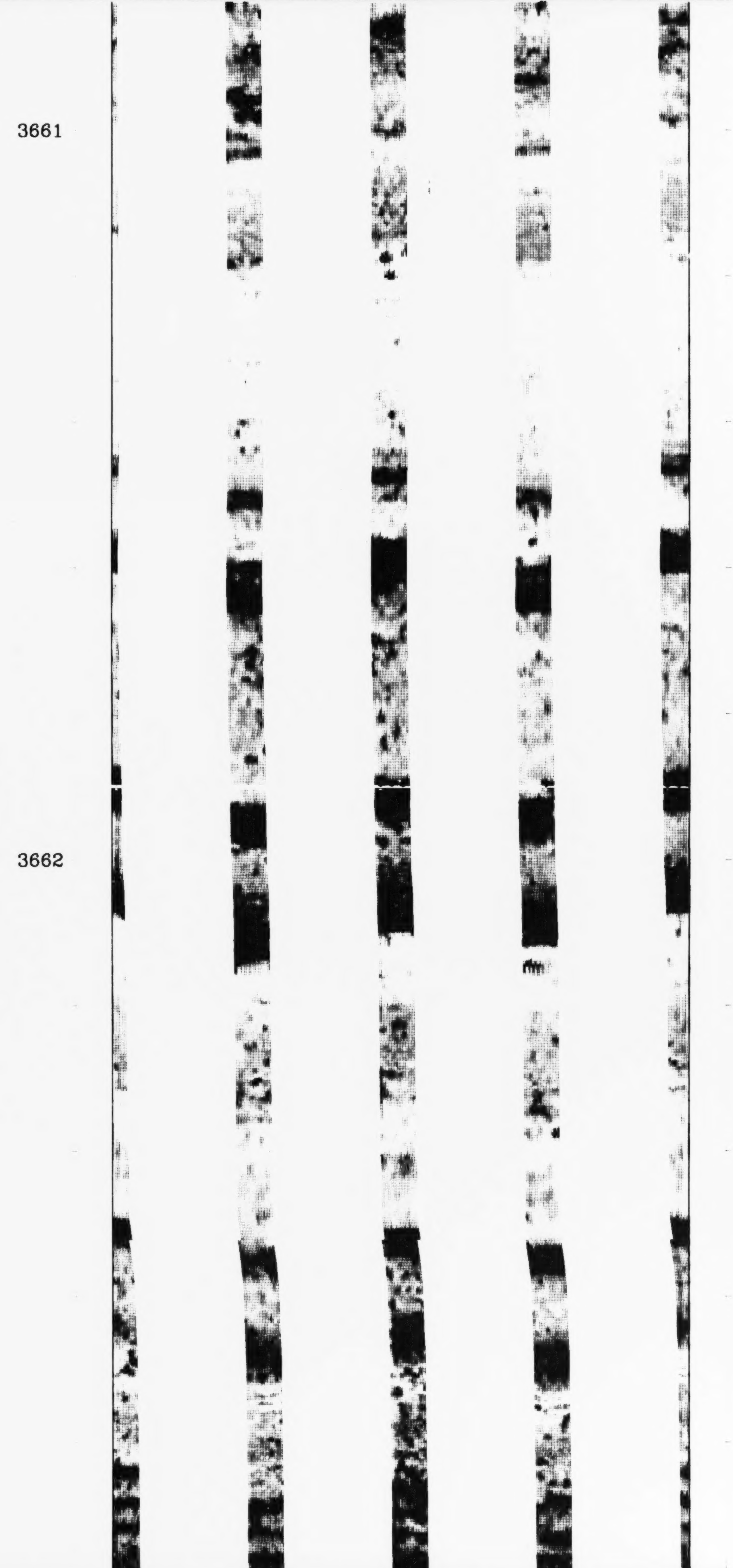
3661
3662

3663
3664
3665

SCHLUMBERGER

FMS
BOREHOLE
IMAGING

COMPANY	LAMONT-DOHERTY GEOLOGICAL
WELL	ODP HOLE-793B
FIELD	IZU-BONIN FOREARC BASIN
COUNTRY	OCEAN
RUN	1
DATE LOGGED	16 – JUN – 89
REFERENCE	STATIC PS-1 3665 3700

STATIC NORMALIZATION

PASS 1 (23577)

FILE : MEST.003

ZONE FROM 3700.0 M TO 3665.0 M

DEPTH SCALE = 1/ 5

IMAGE SCALE = 1/ 5

BITSIZE = 9.88

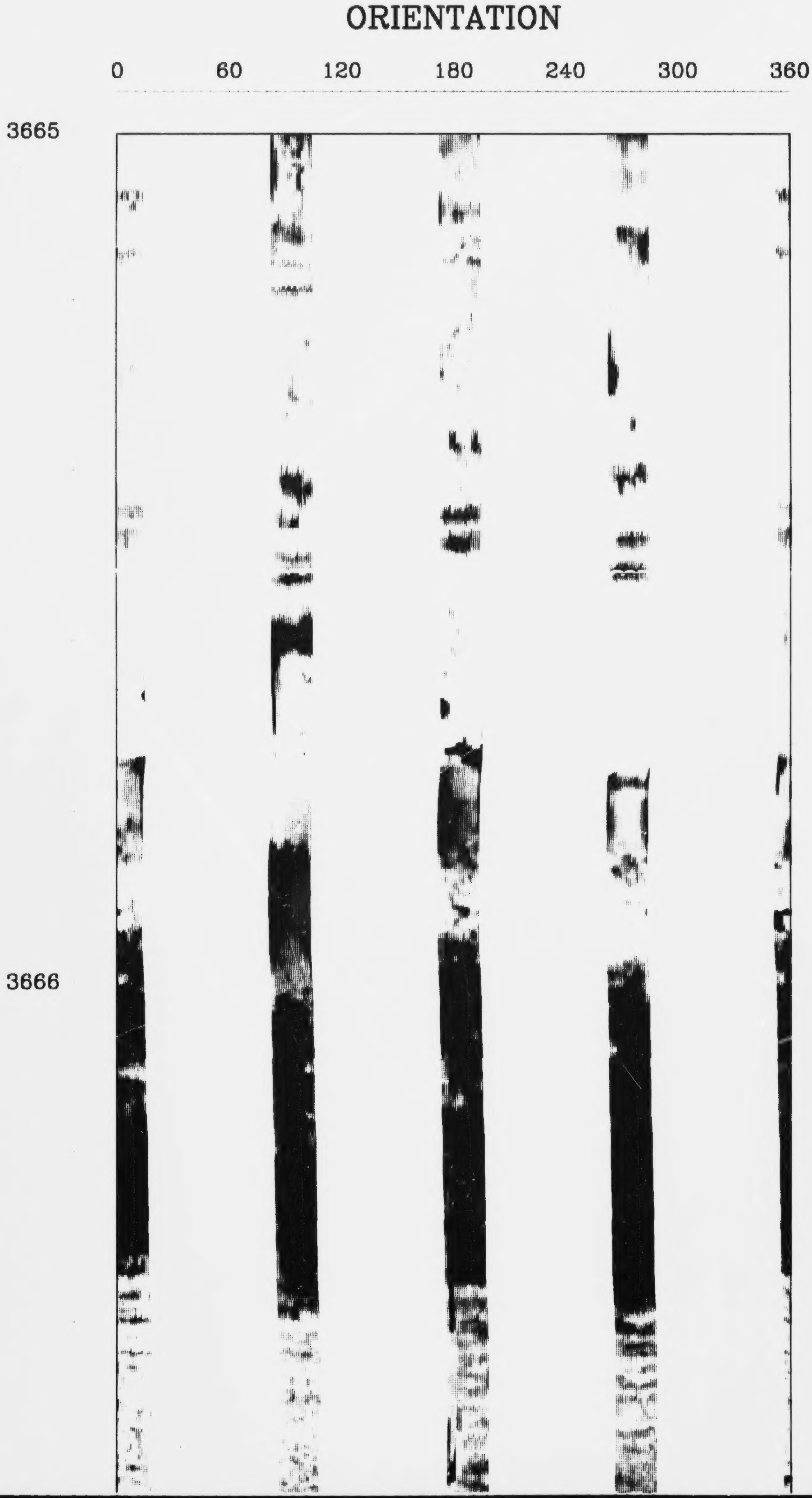

3667
3668

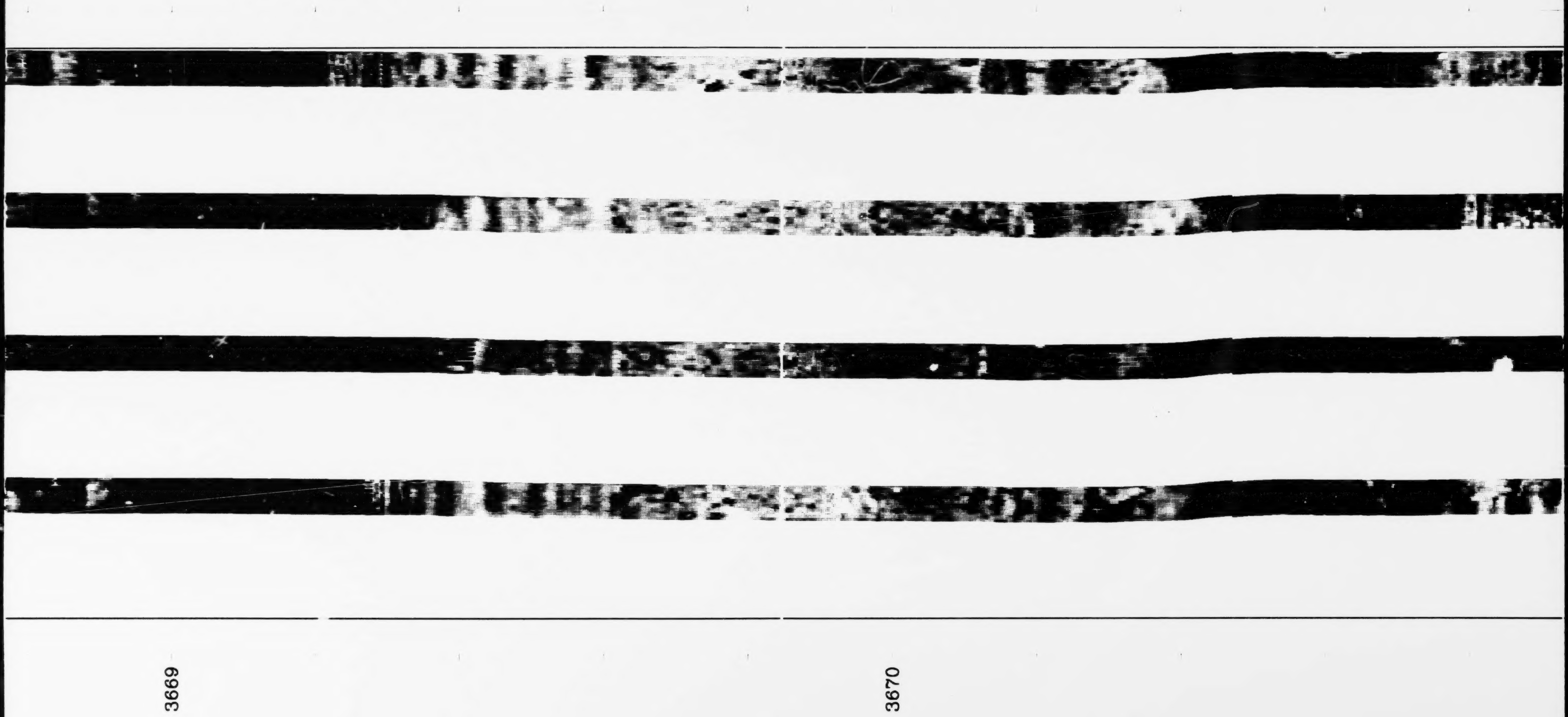
3669
3670

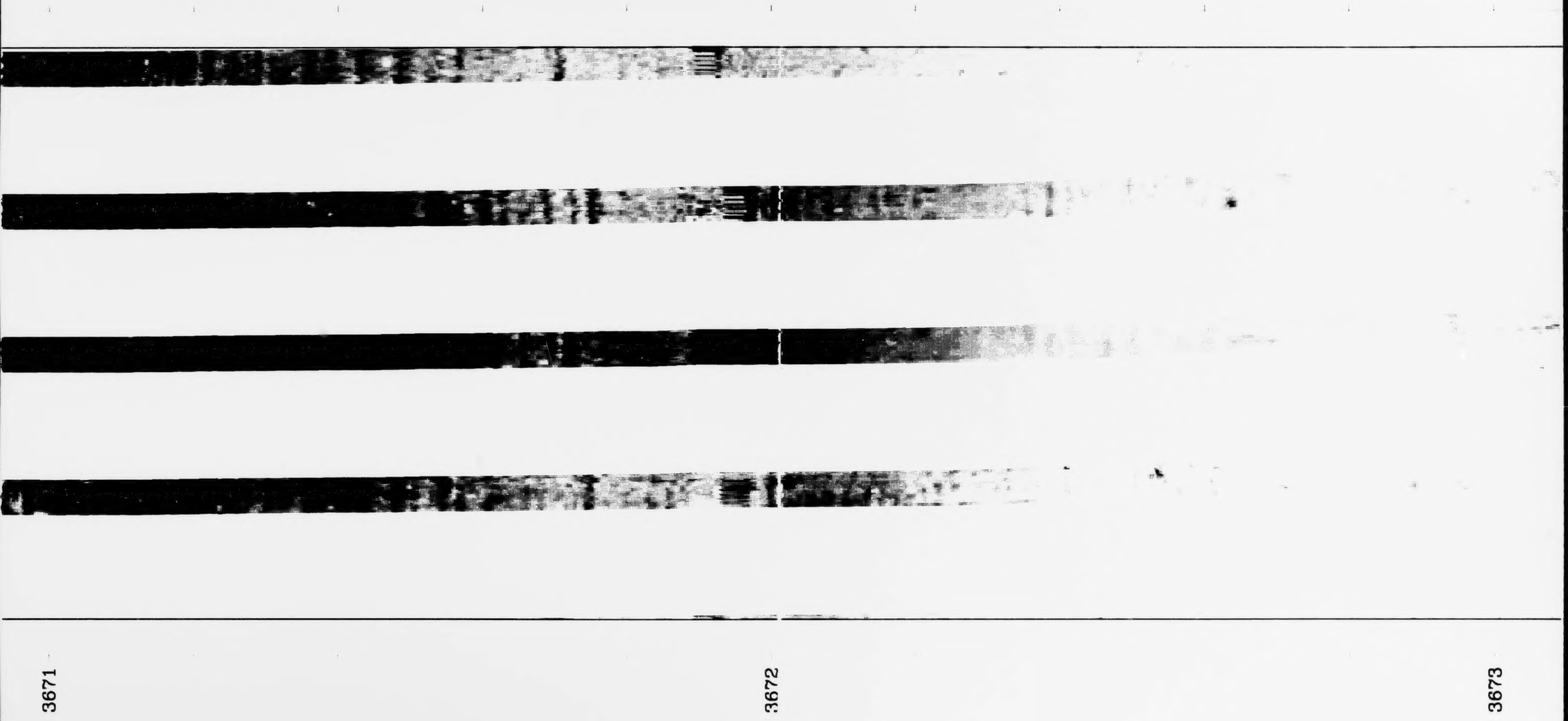
3671
3672
3673

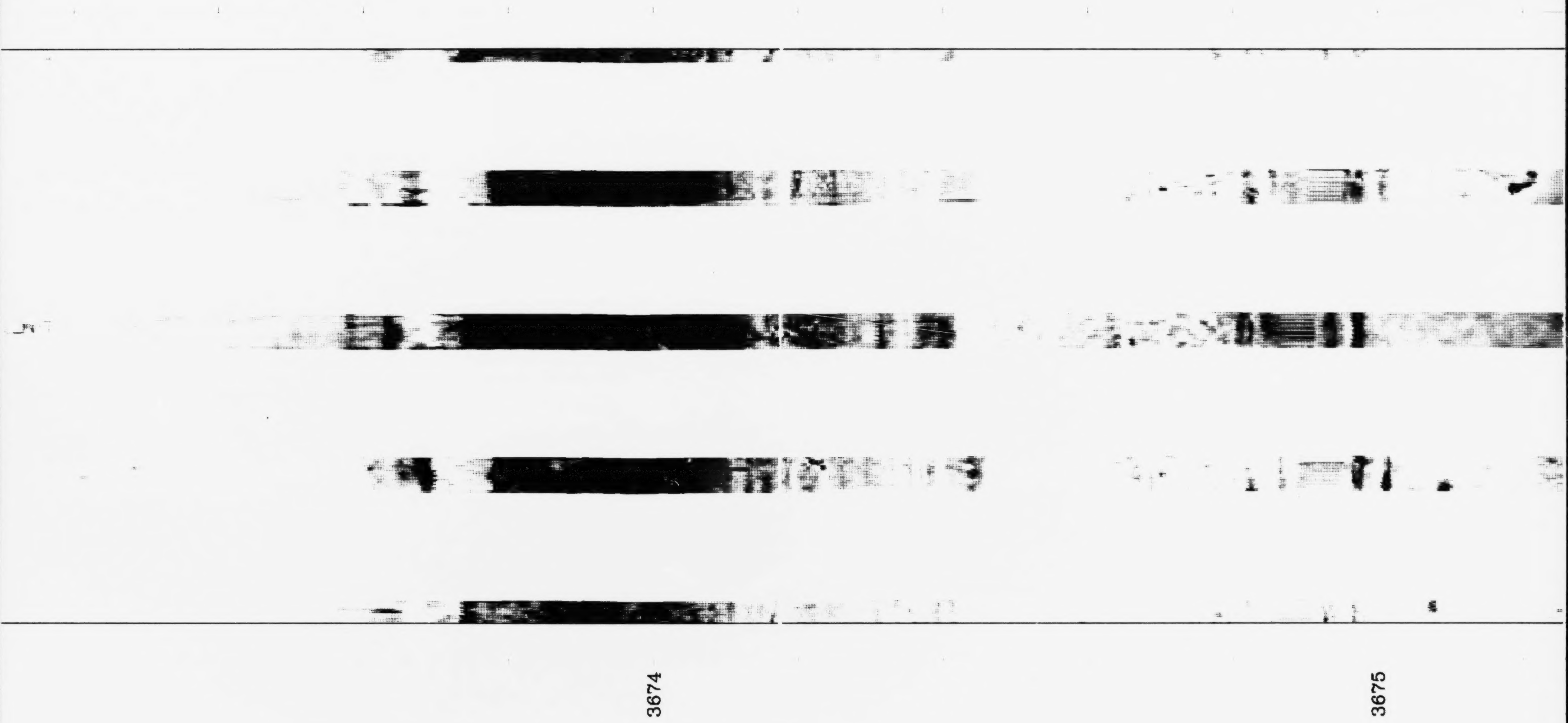
3674
3675

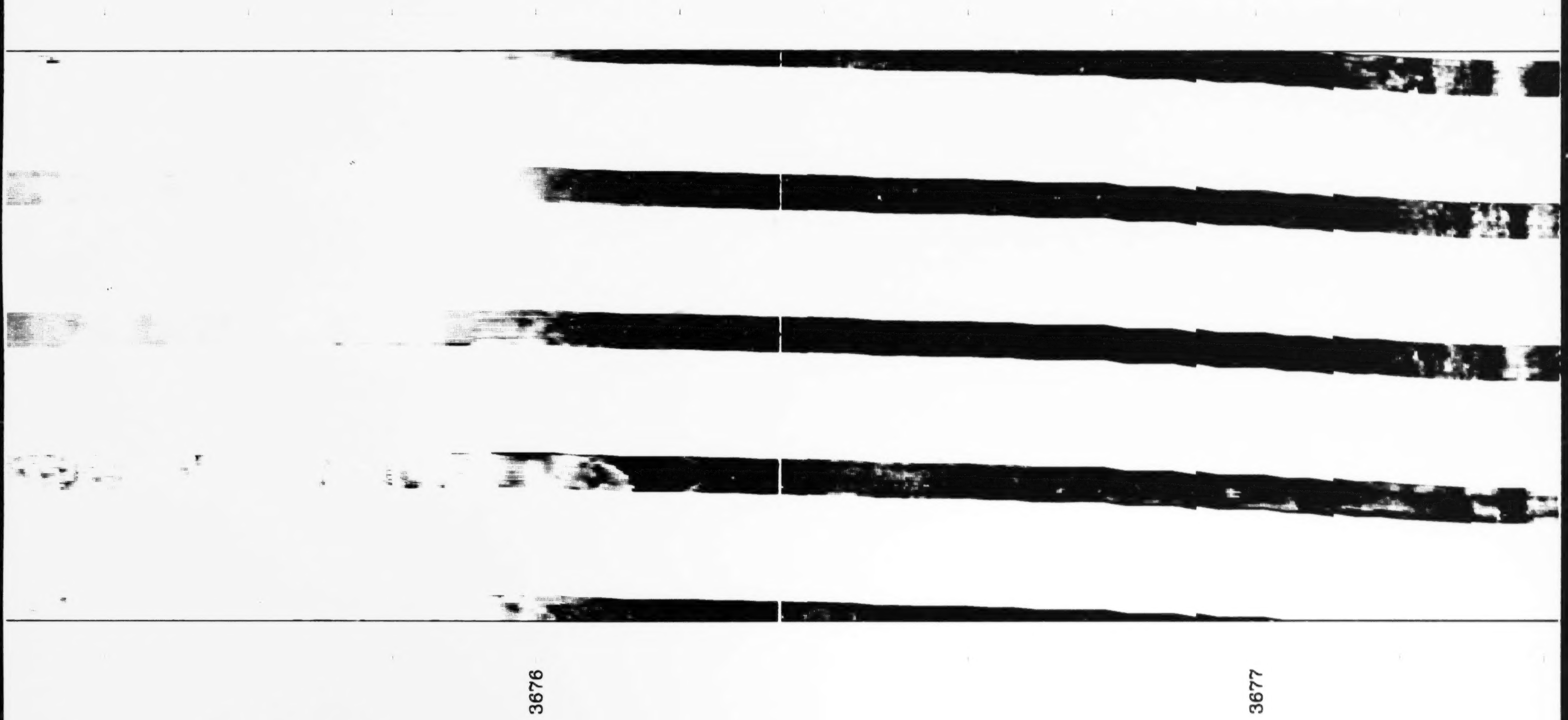
3676
3677

3678
3679

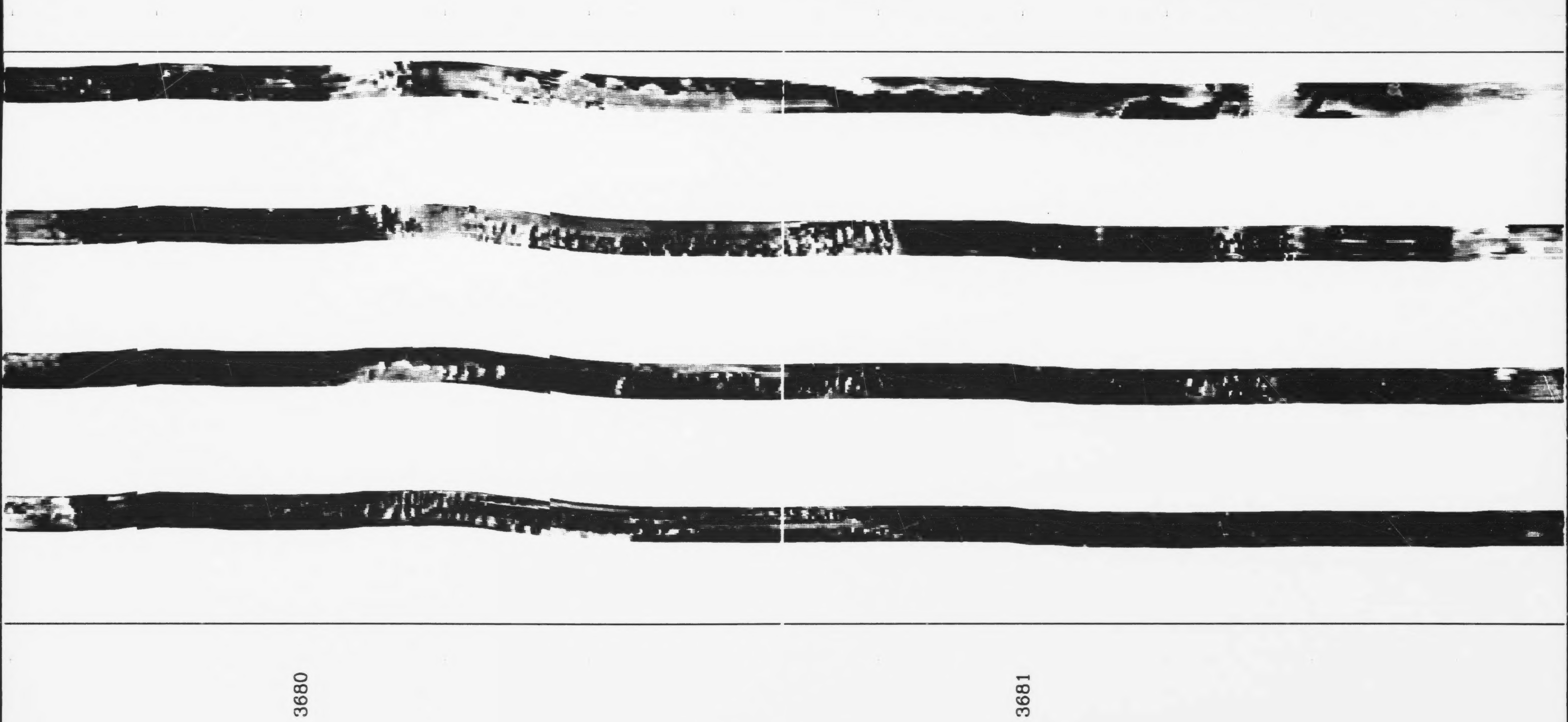
3680
3681

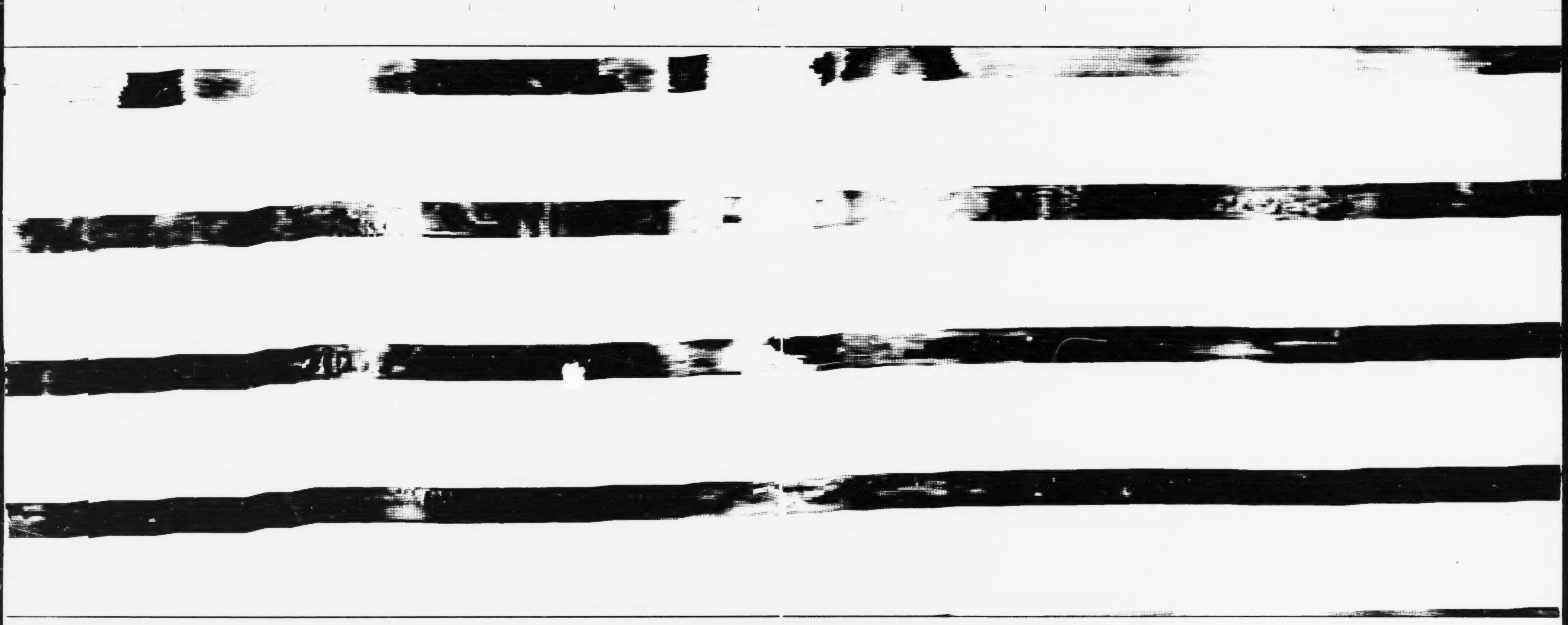

3682
3683

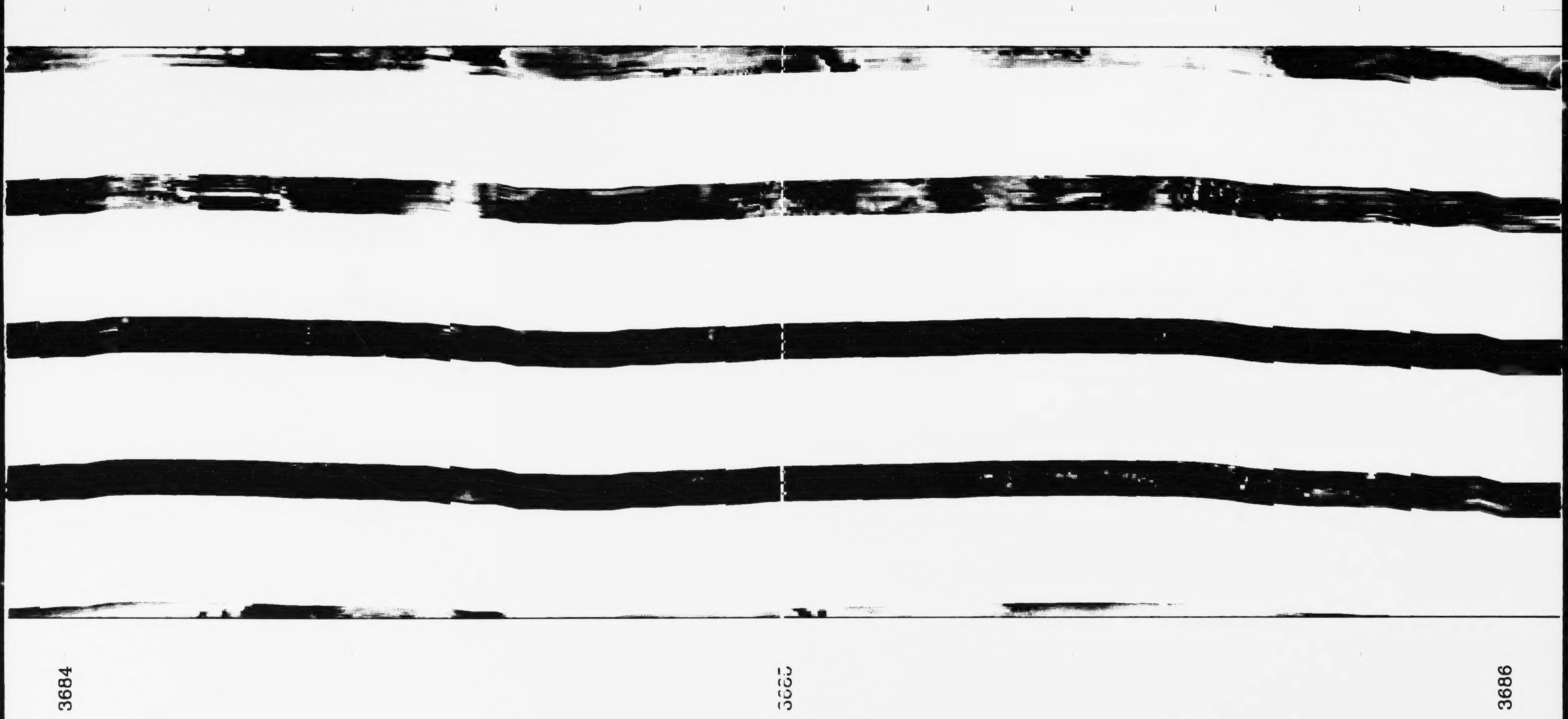
3684
3685
3686

3687
3688

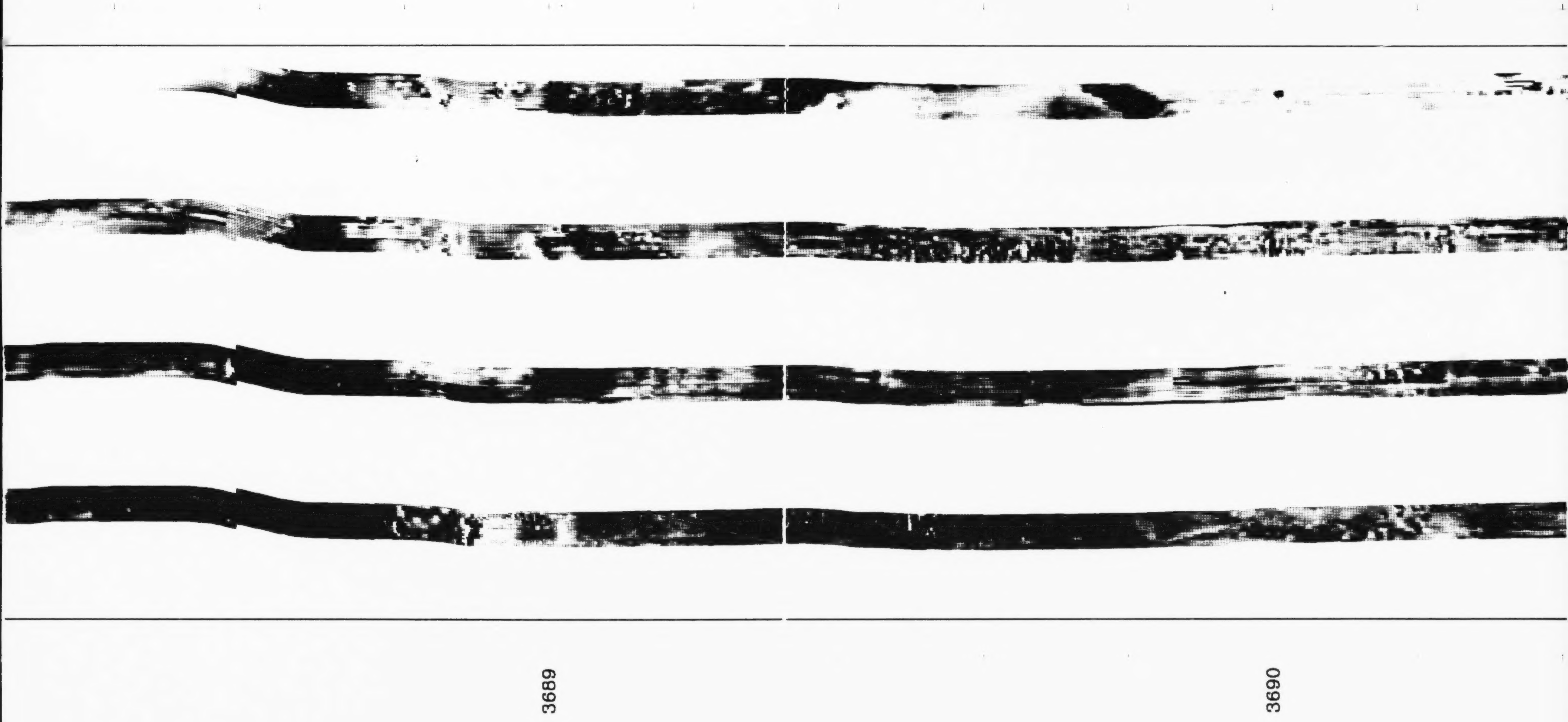
3689
3690

3691

3692

3693
3694

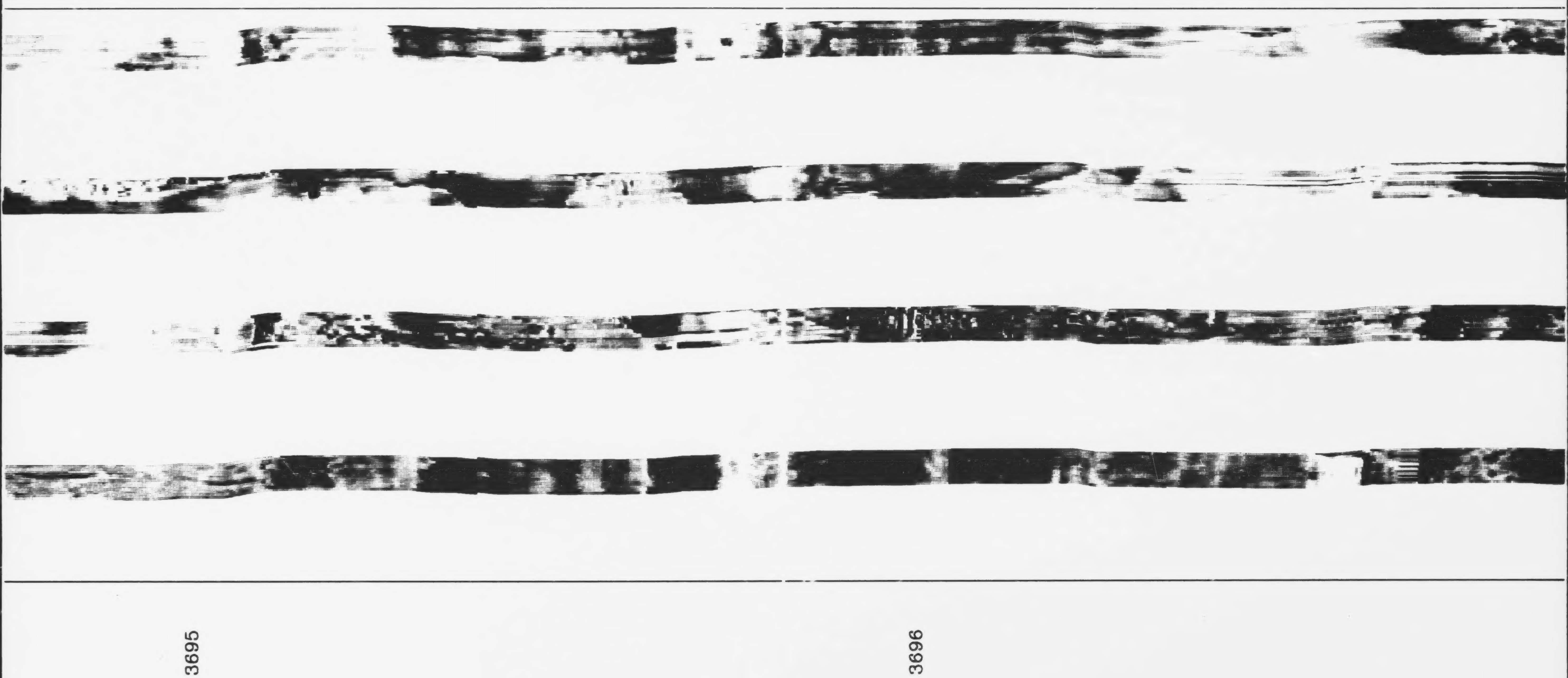

3695
3696

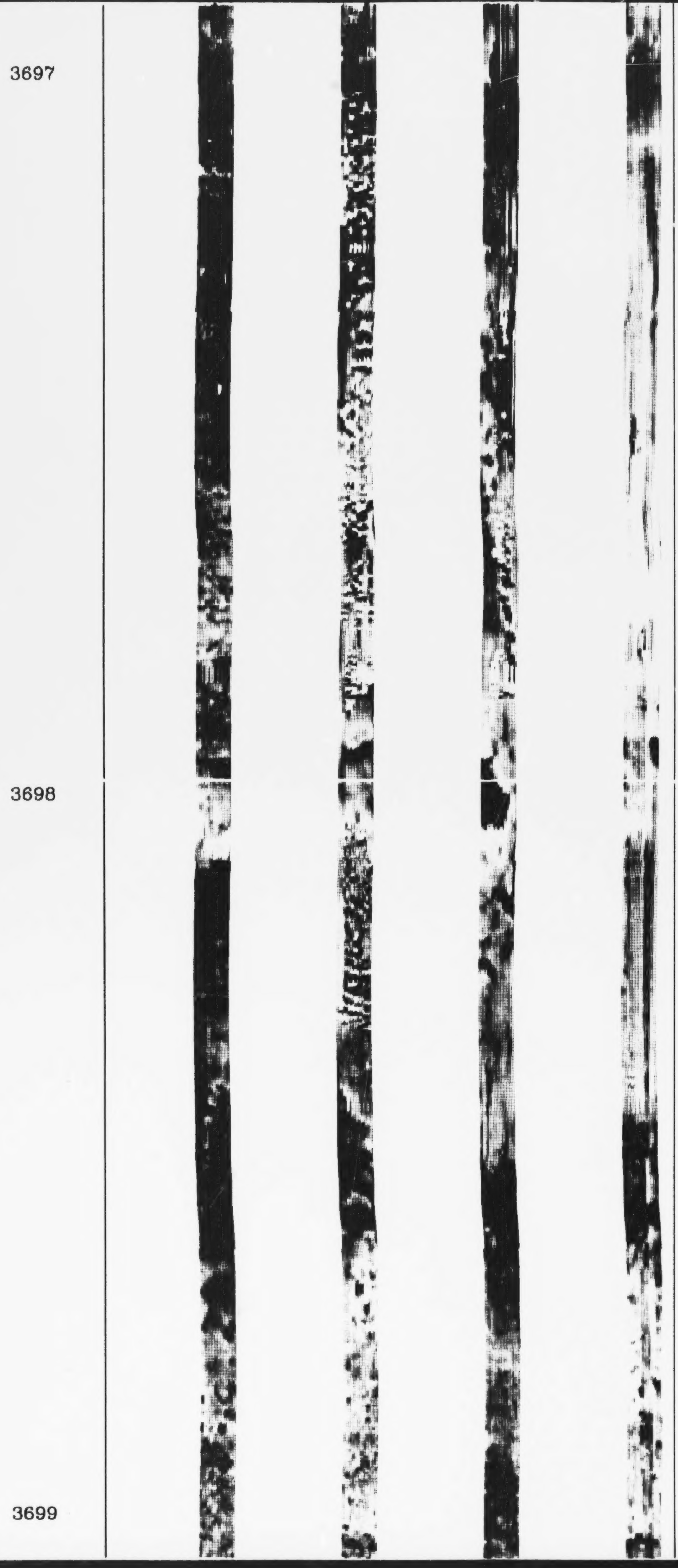
3697
3698
3699

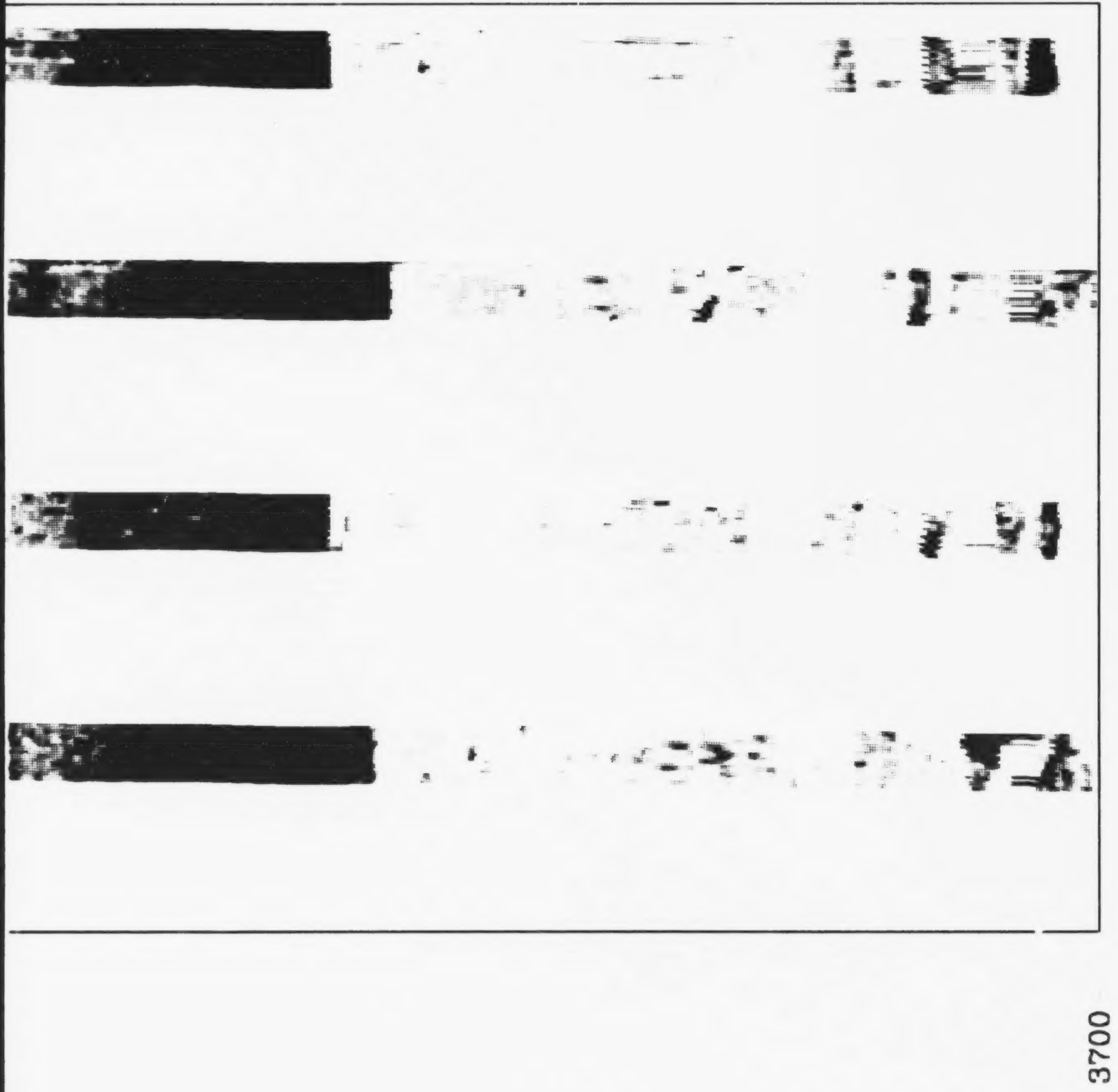

SCHLUMBERGER

FMS
BOREHOLE
IMAGING

COMPANY	LAMONT–DOHERTY GEOLOGICAL
WELL	ODP HOLE–793B
FIELD	IZU–BONIN FOREARC BASIN
COUNTRY	OCEAN
RUN	1
DATE LOGGED	16 – JUN – 89
REFERENCE	STATIC PS-1 3700-3724

STATIC NORMALIZATION

PASS 1 (23577)

FILE : MEST.003

ZONE FROM 3723.9 M TO 3700.0 M

DEPTH SCALE = 1/ 5

IMAGE SCALE = 1/ 5

BITSIZE = 9.88

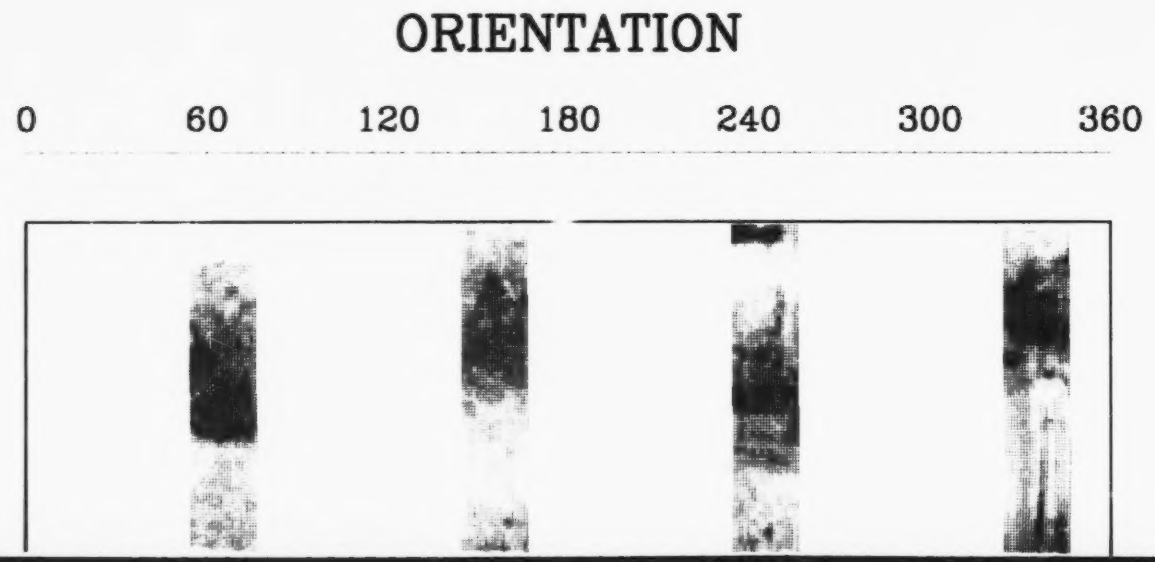

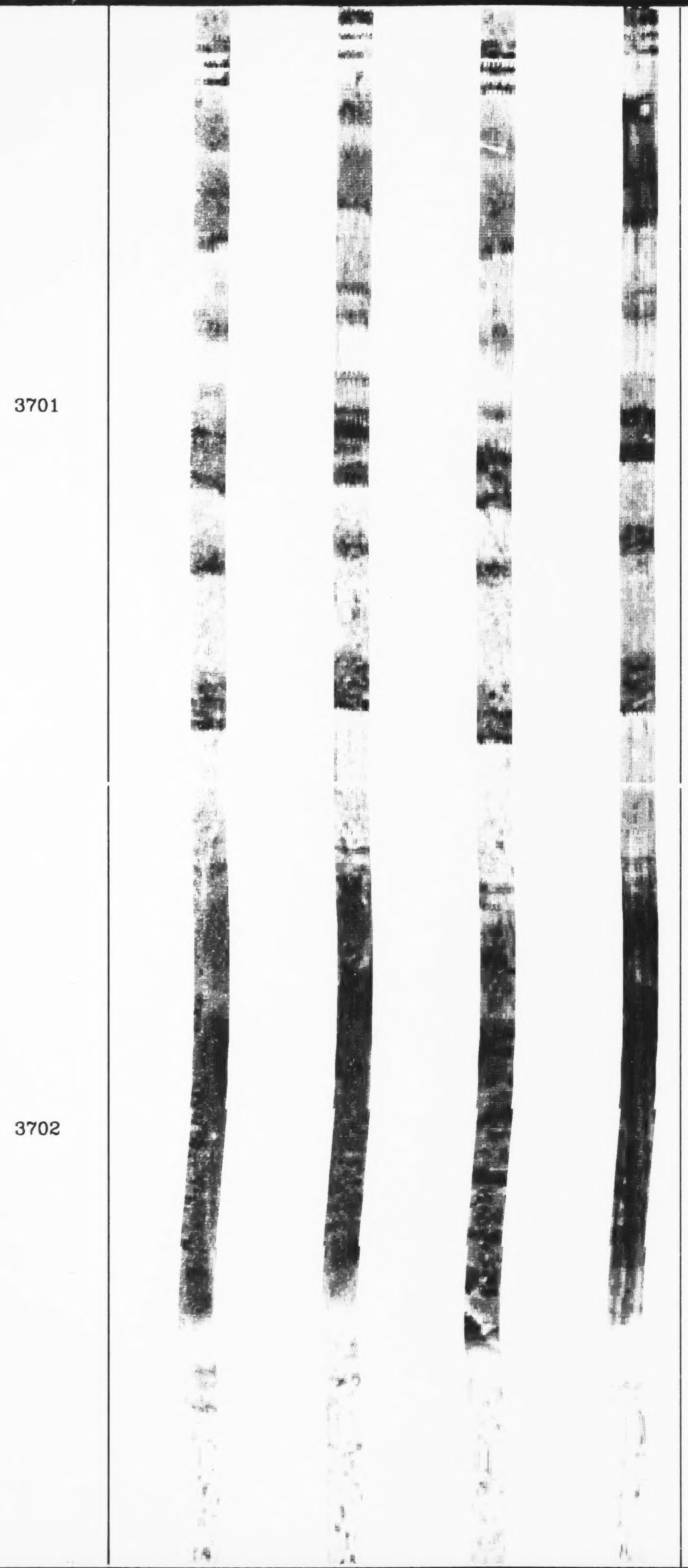

3701
3702

3703

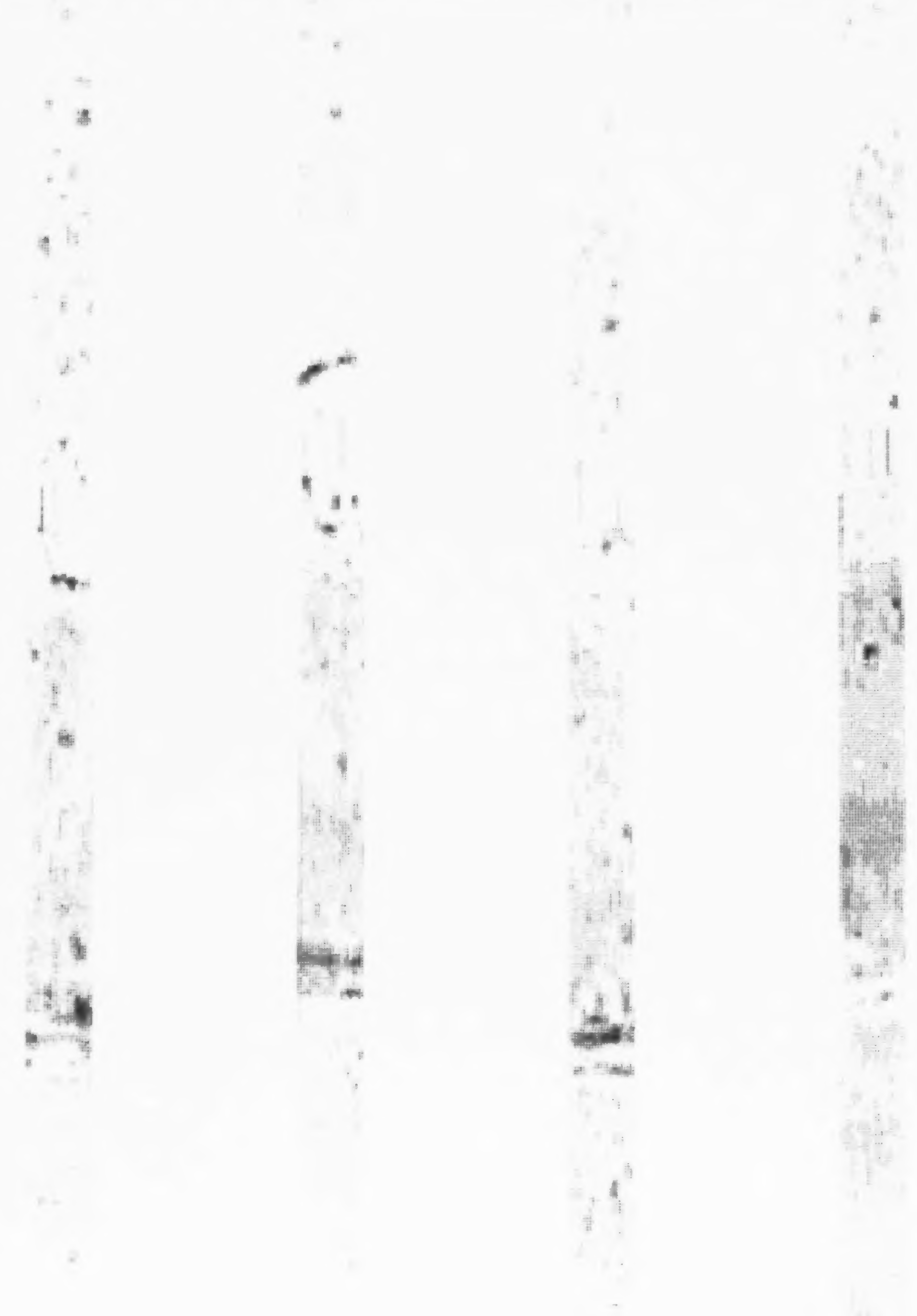

3704

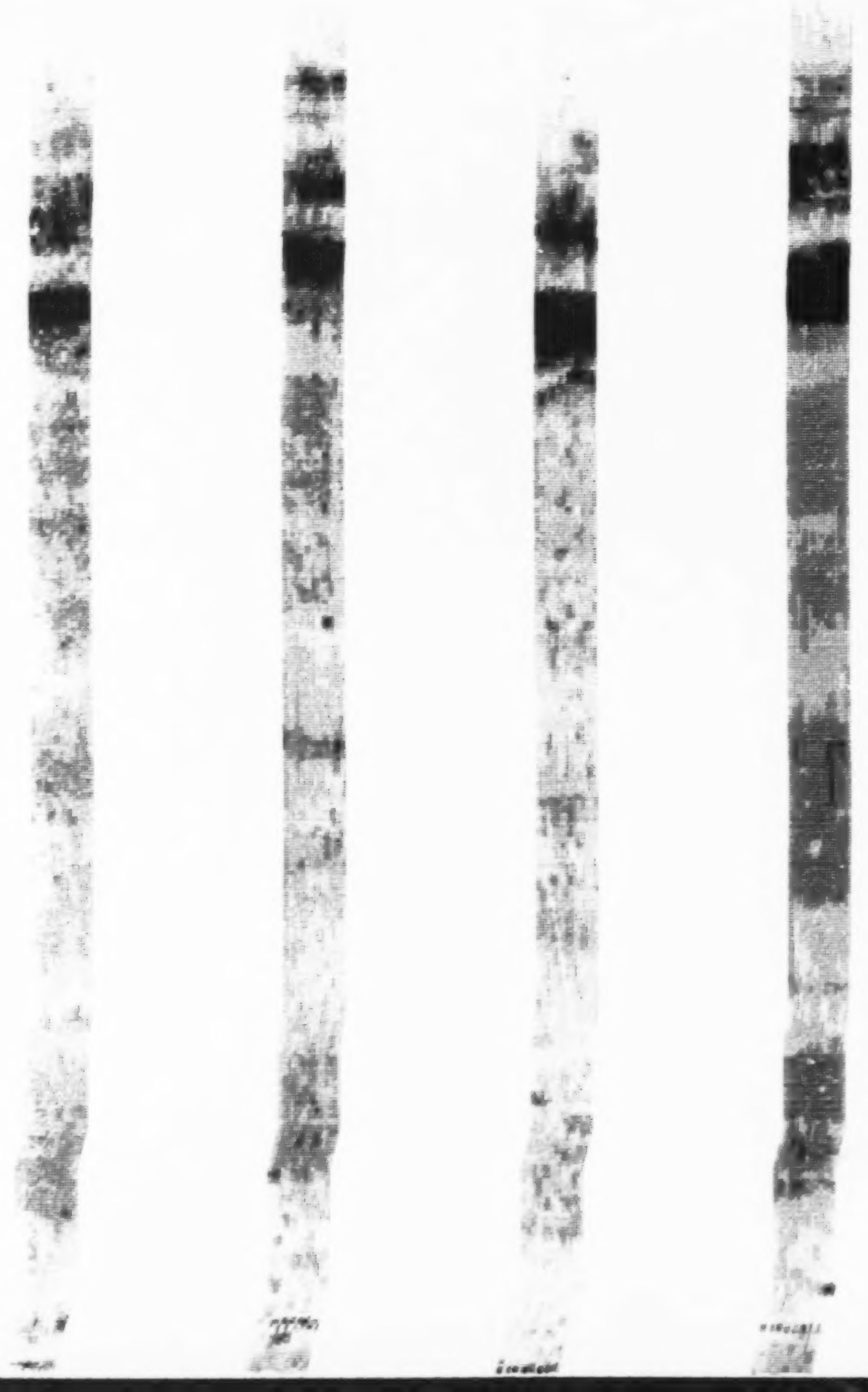

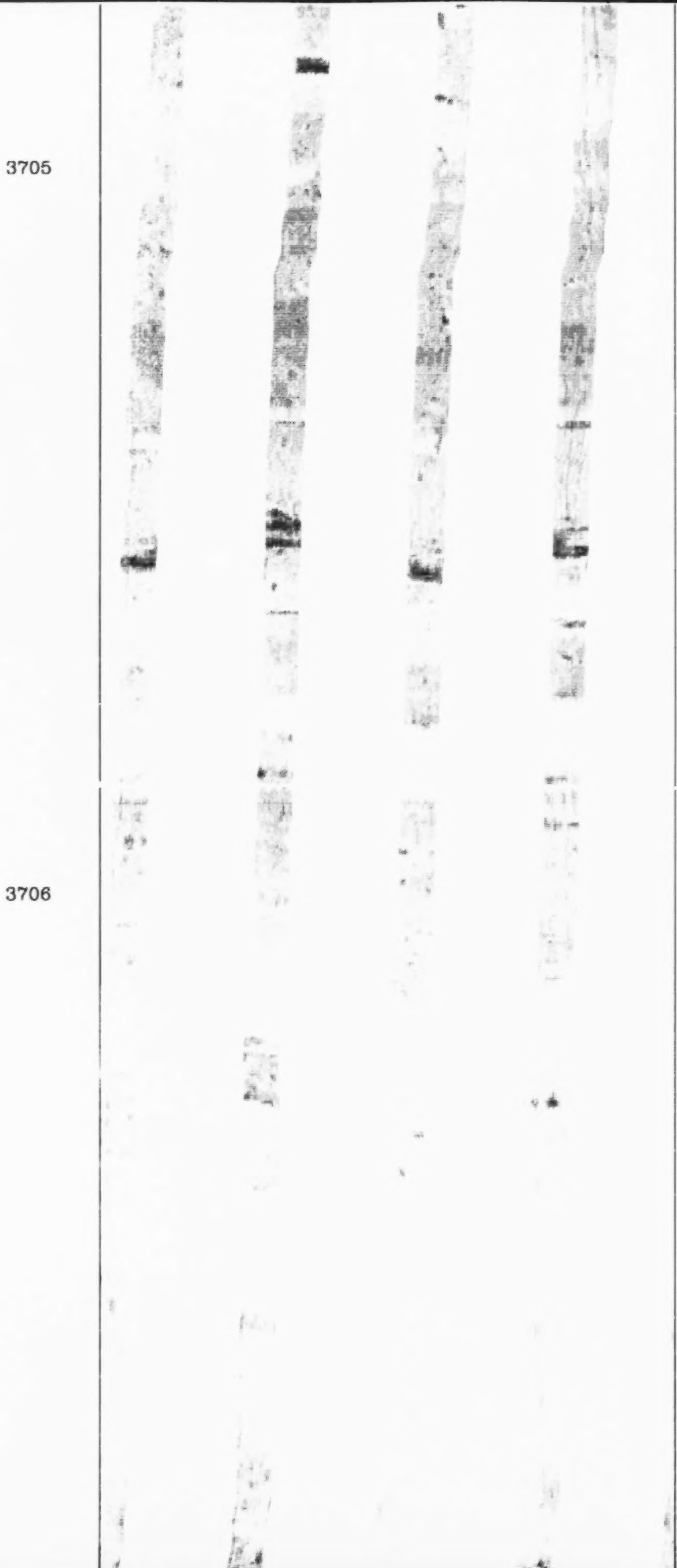

3705
3706

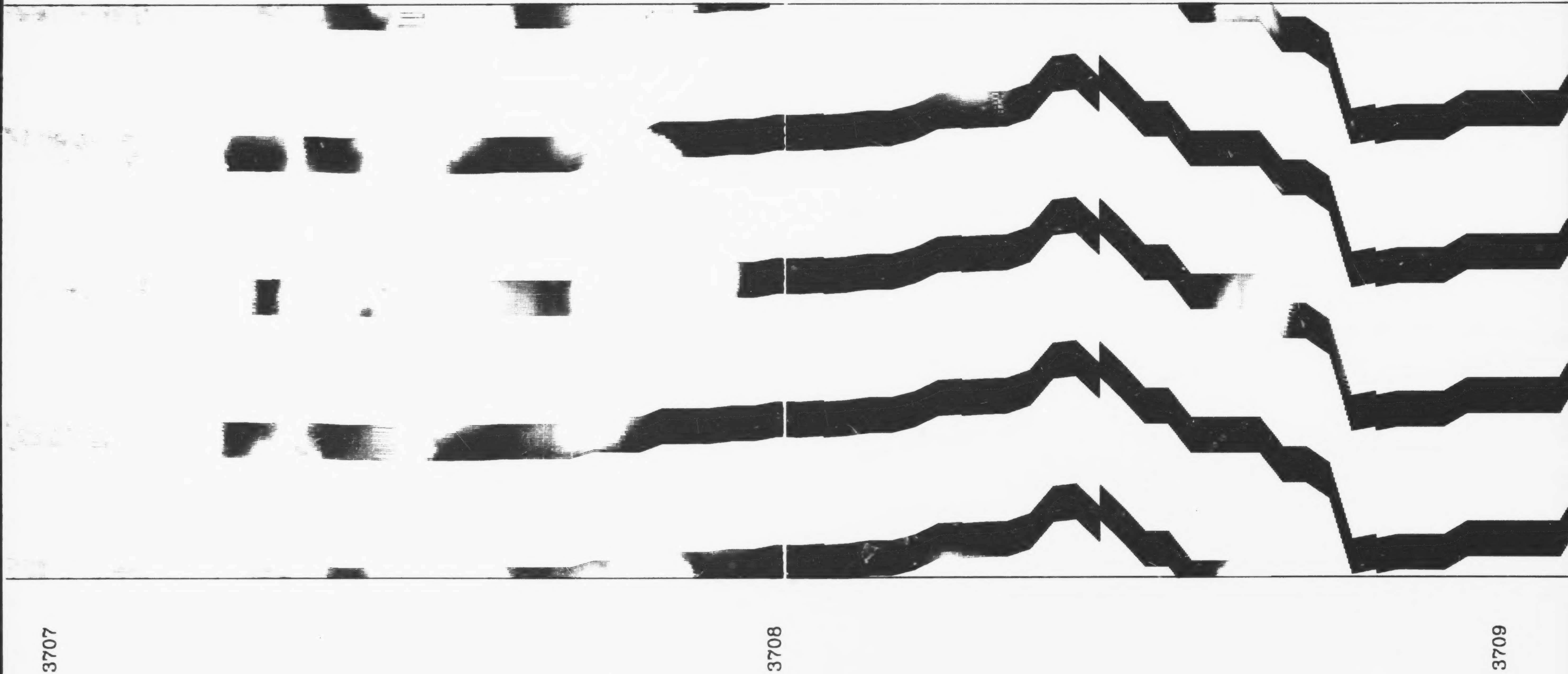
3707
3708
3709

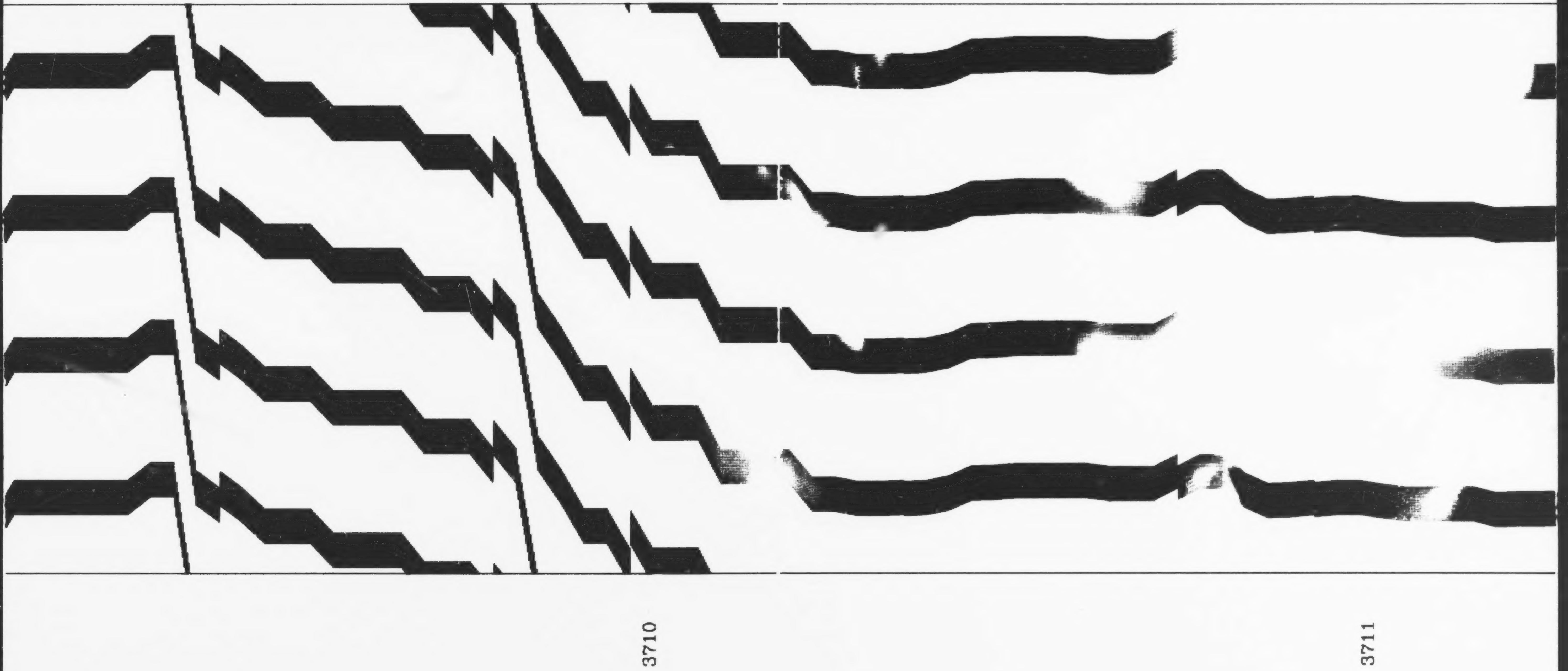
3710
3711

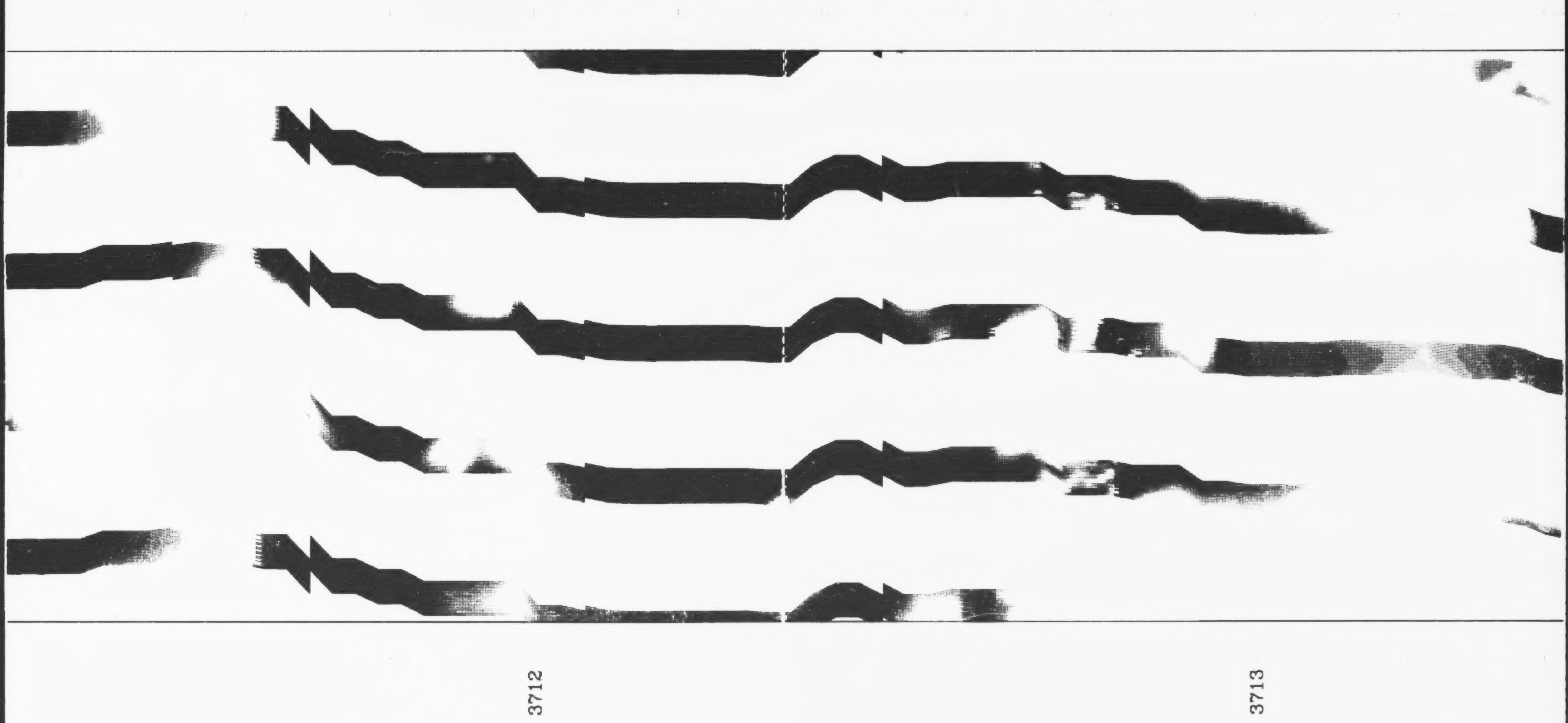
3712
3713

3714
3715

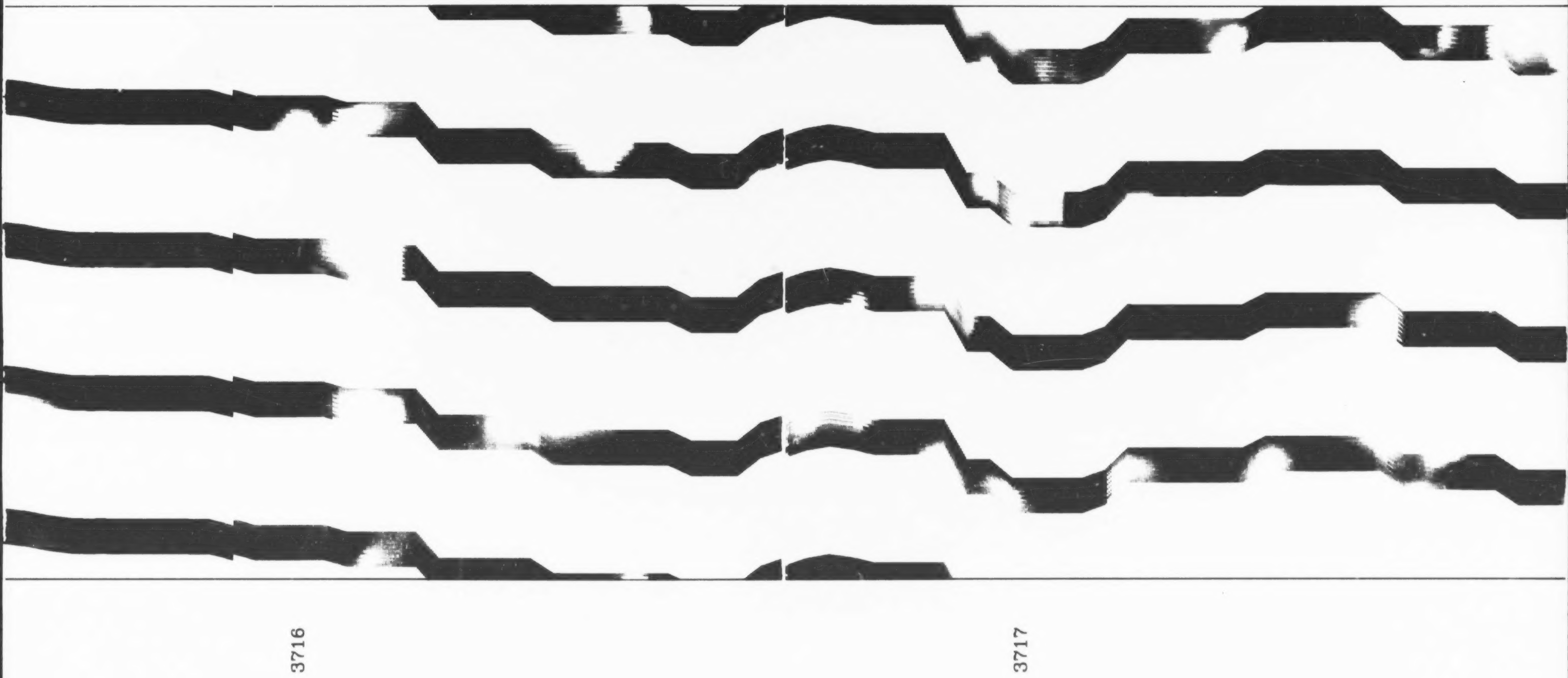
3716
3717

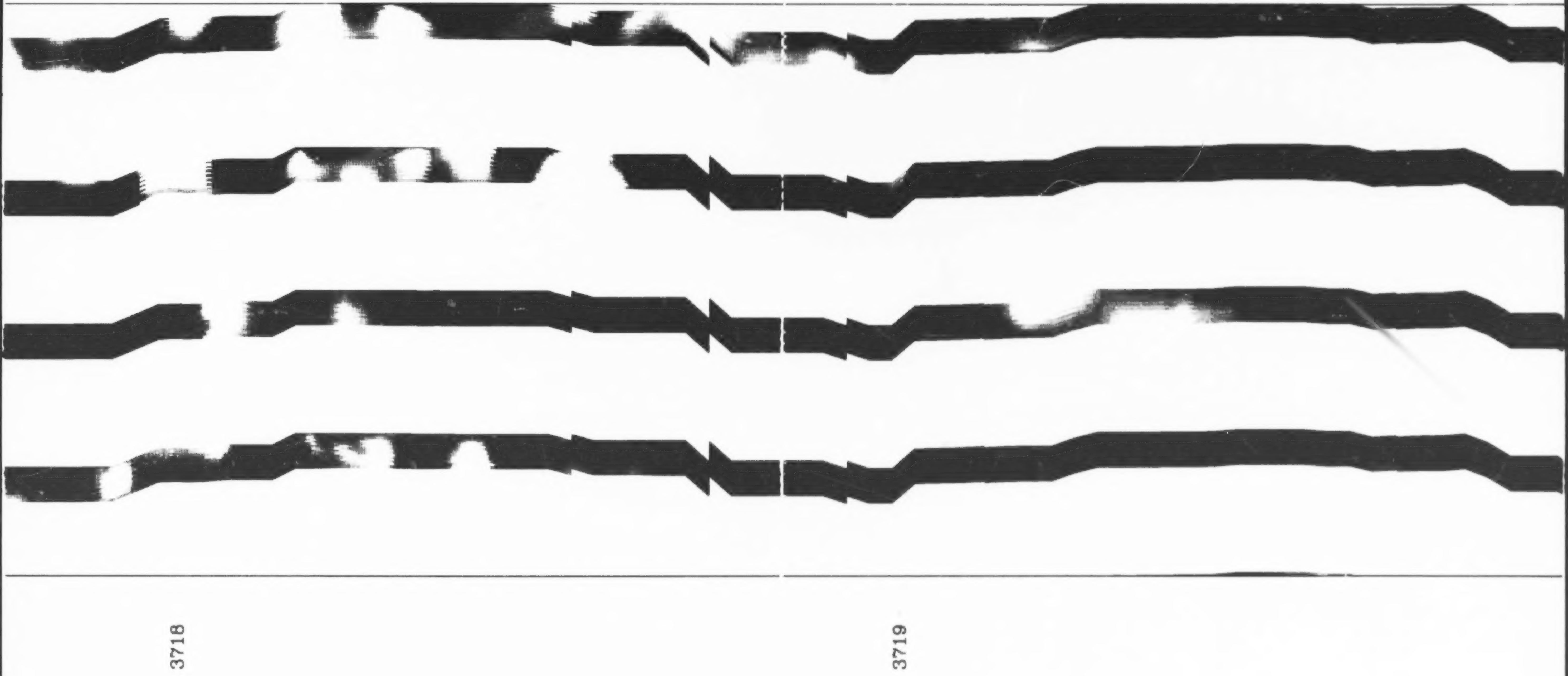
3718
3719

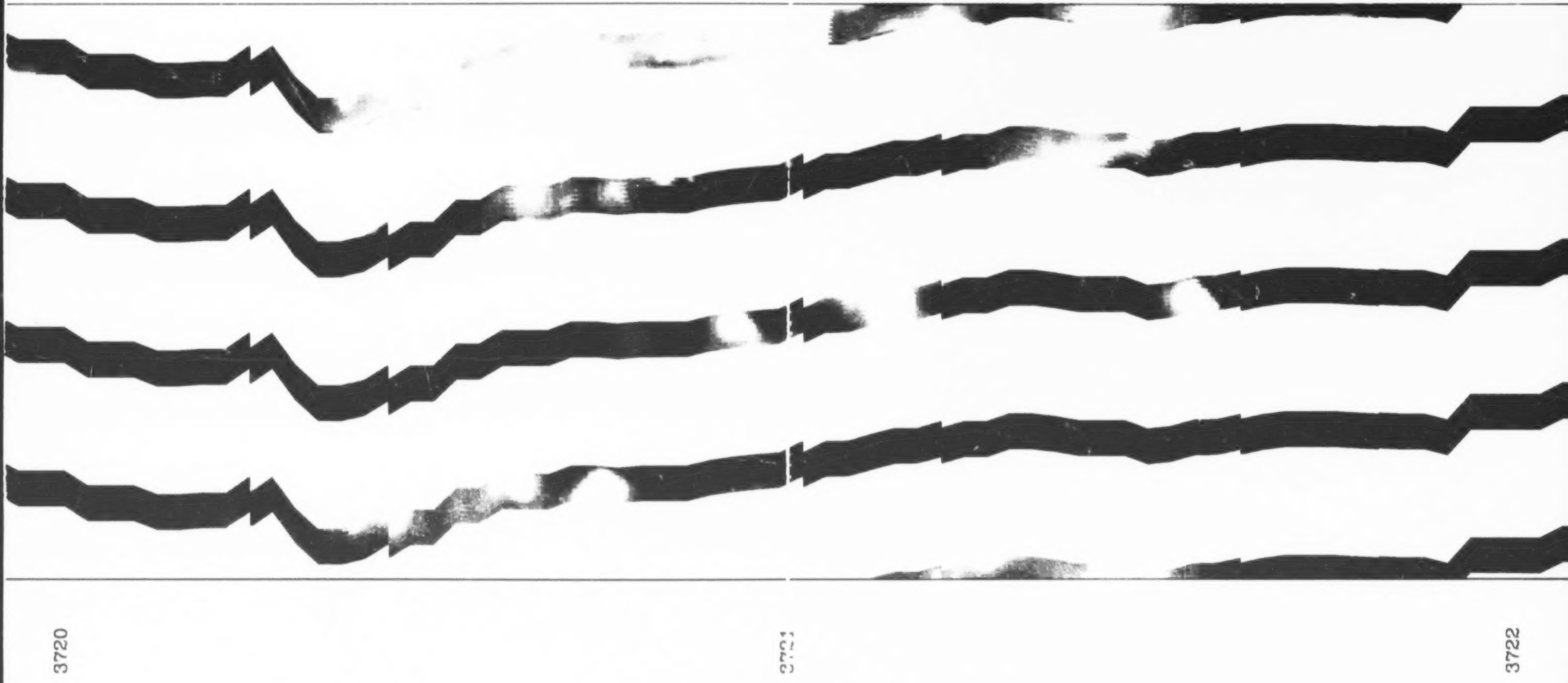
3720
3721
3722

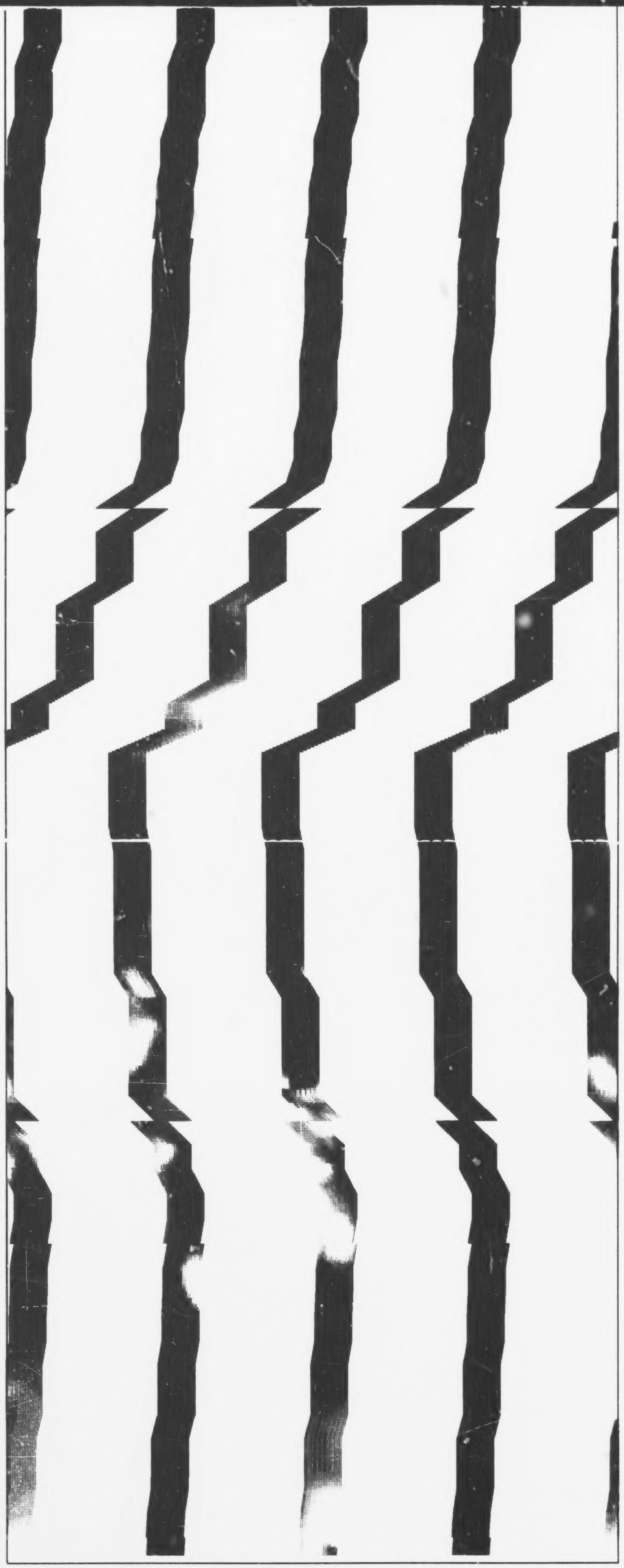

SCHLUMBERGER

FMS
BOREHOLE
IMAGING

COMPANY	LAMONT-DOHERTY GEOLOGICAL
WELL	ODP HOLE-793B
FIELD	IZU-BONIN FOREARC BASIN
COUNTRY	OCEAN
RUN	1
DATE LOGGED	16 - JUN - 89
REFERENCE	STATIC PS-1 4023-4062

STATIC NORMALIZATION

PASS 1 (23577)

FILE : MEST.001

ZONE FROM 4062.0 M TO 4023.0 M

DEPTH SCALE = 1/ 5

IMAGE SCALE = 1/ 5

BITSIZE = 9.88

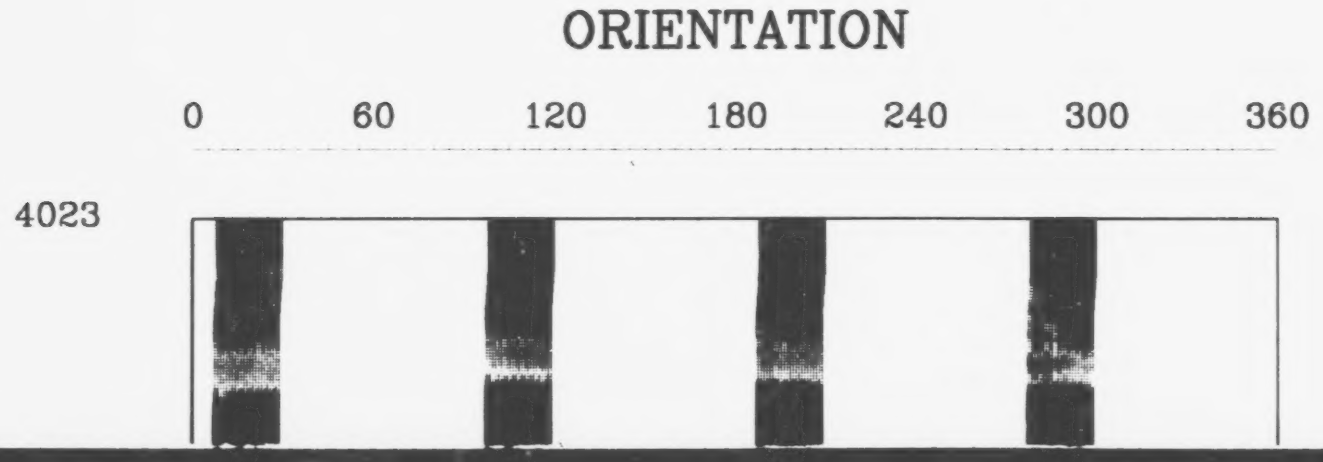

4024

4025

4026

4027

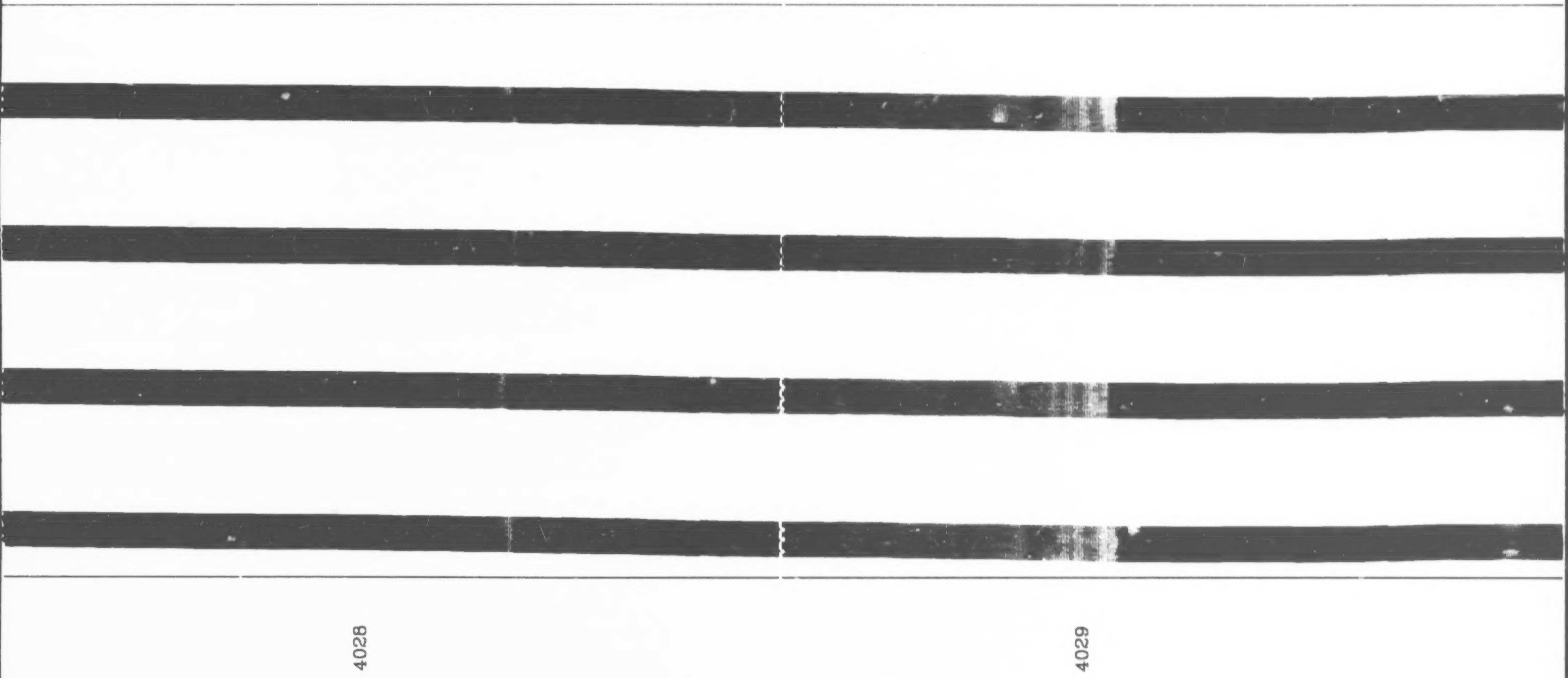
4028
4029

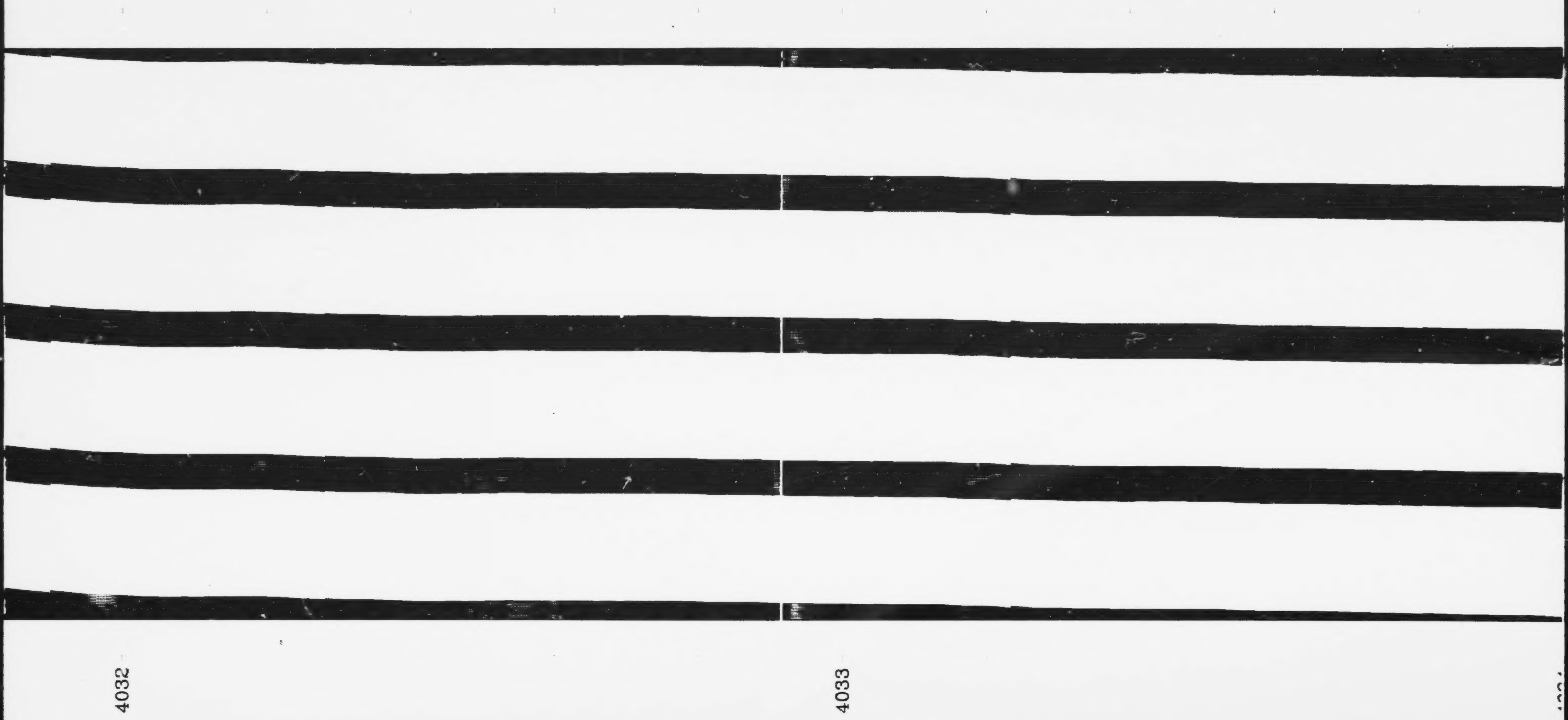
4032
4033

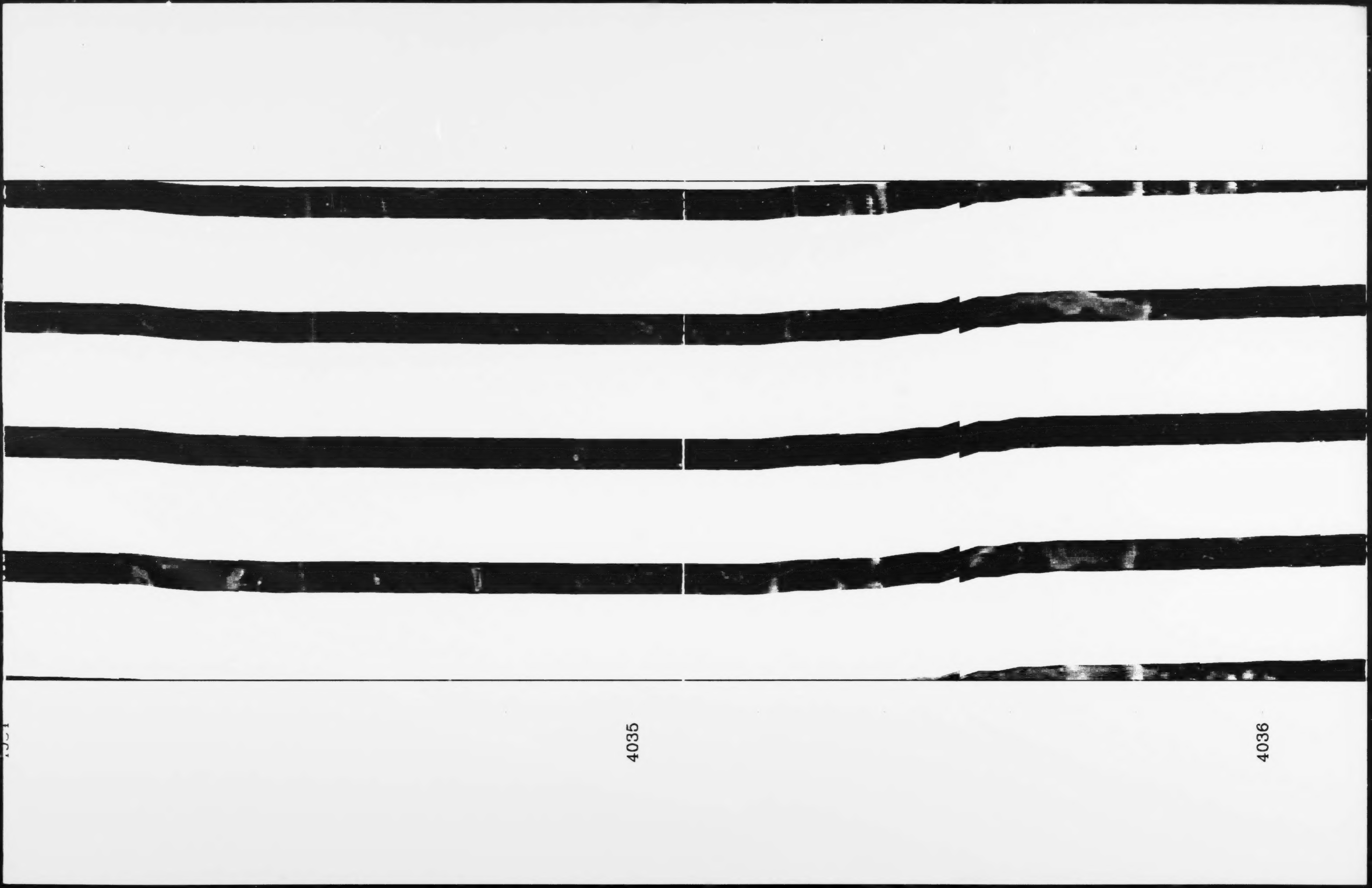
4035
4036

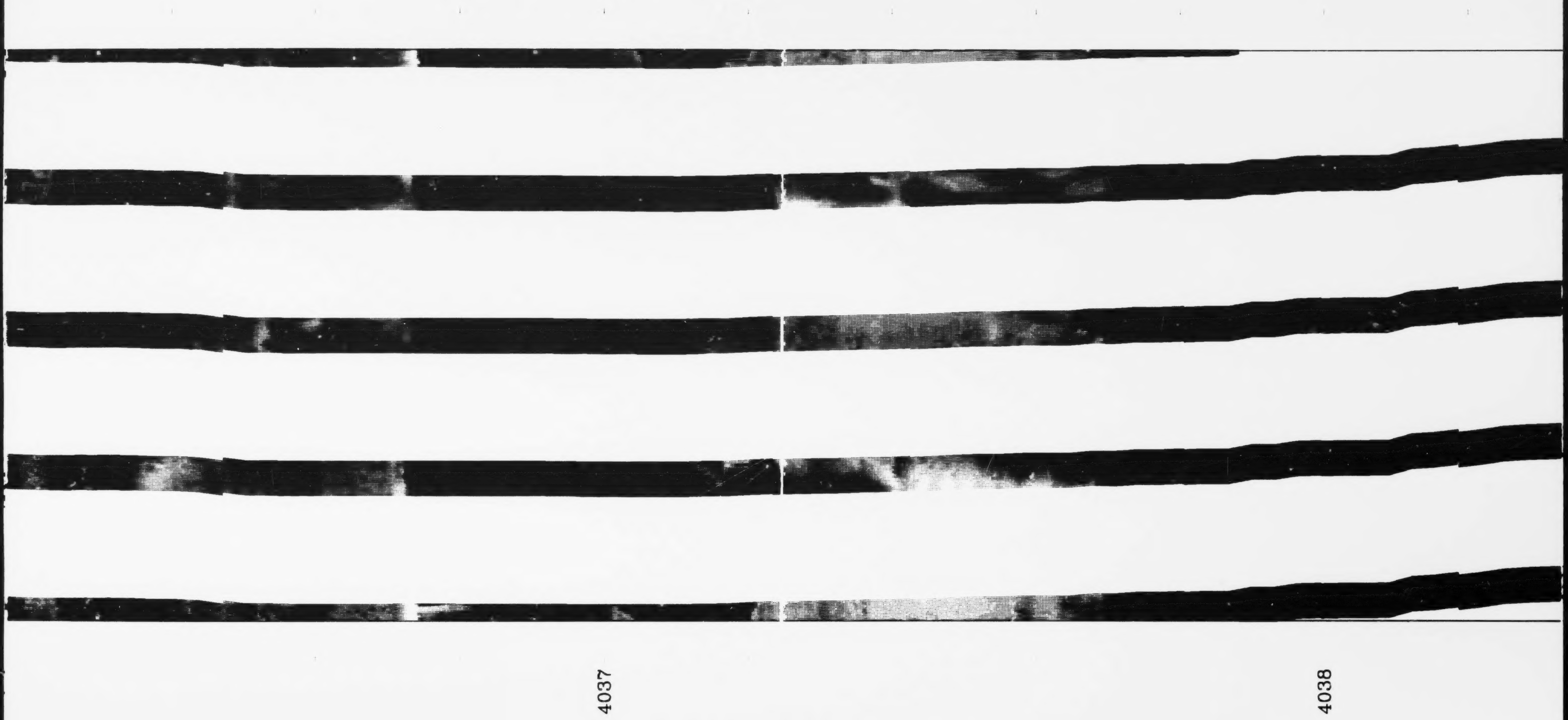
4037
4038

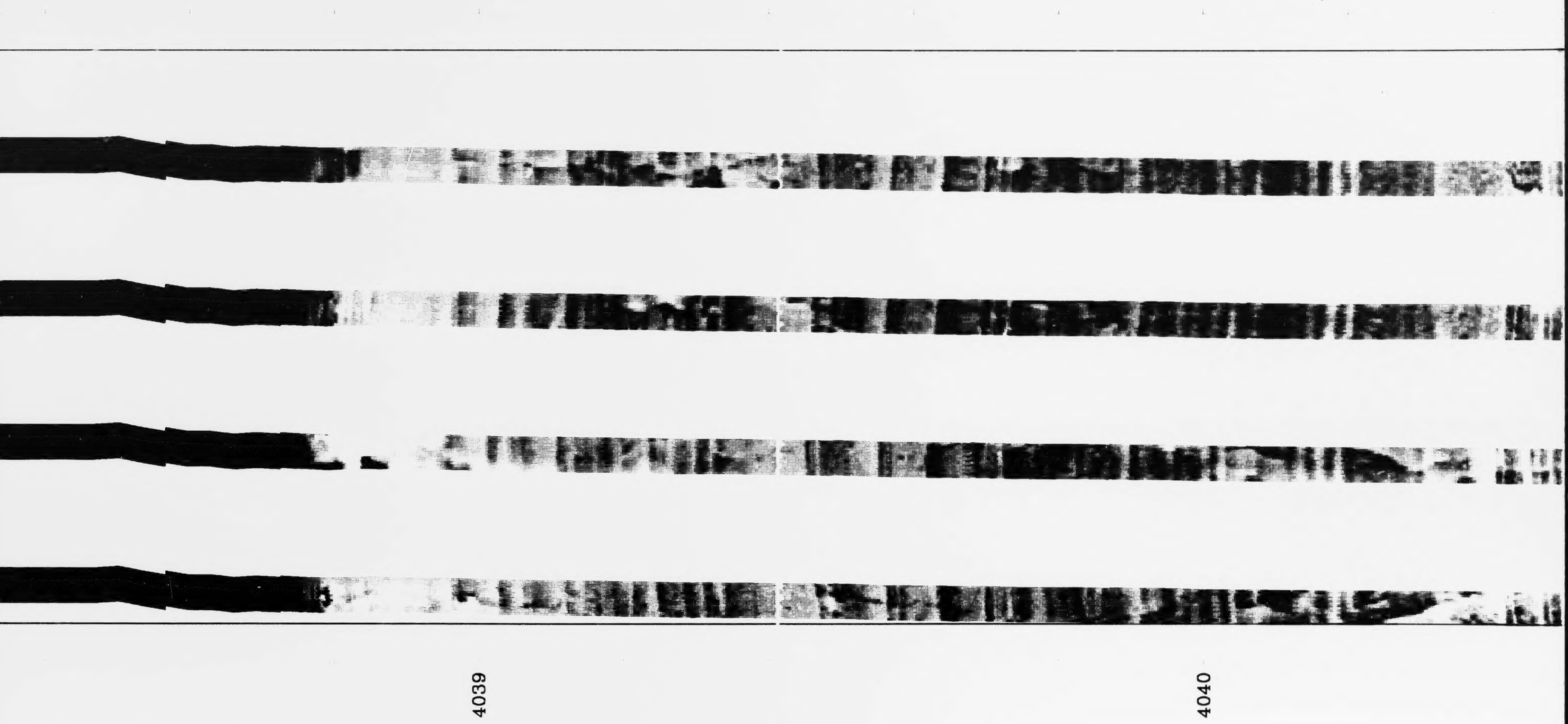
4039
4040

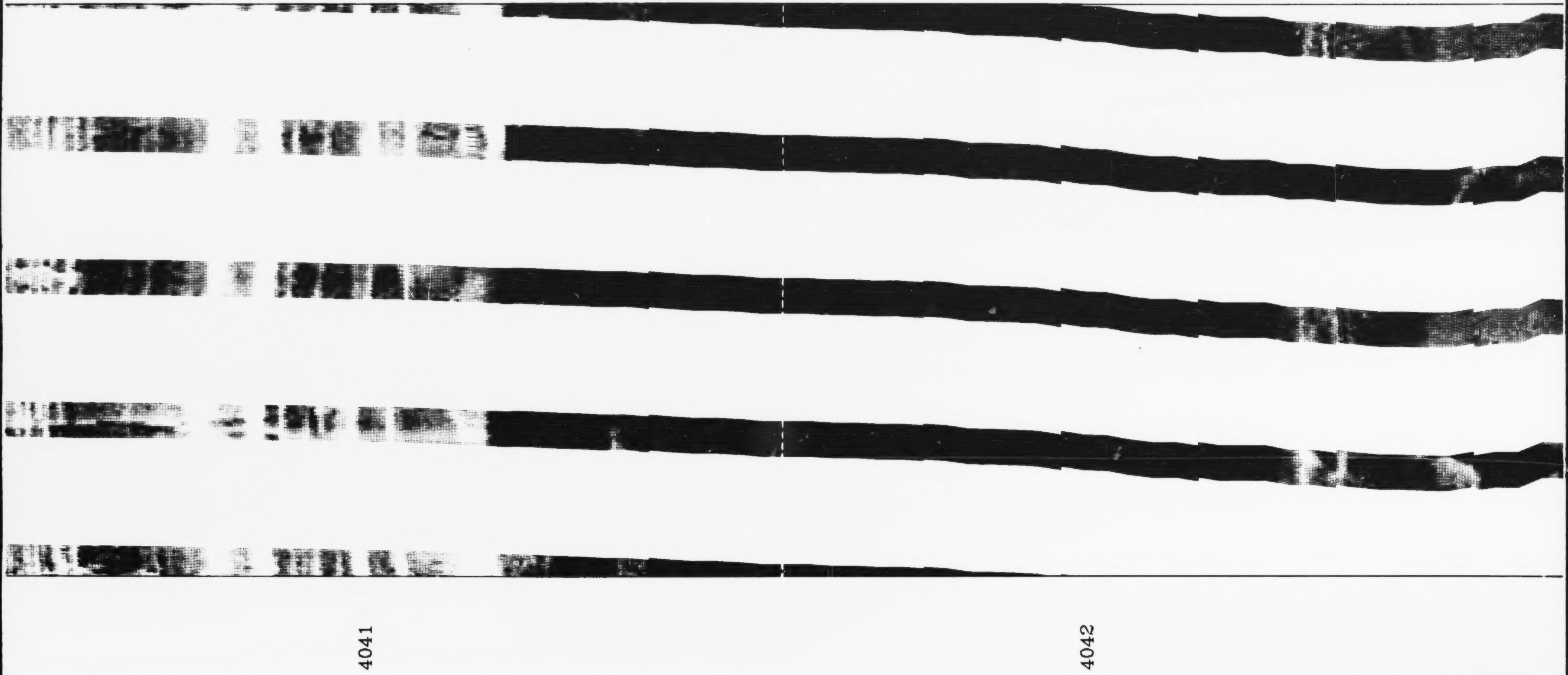
4041
4042

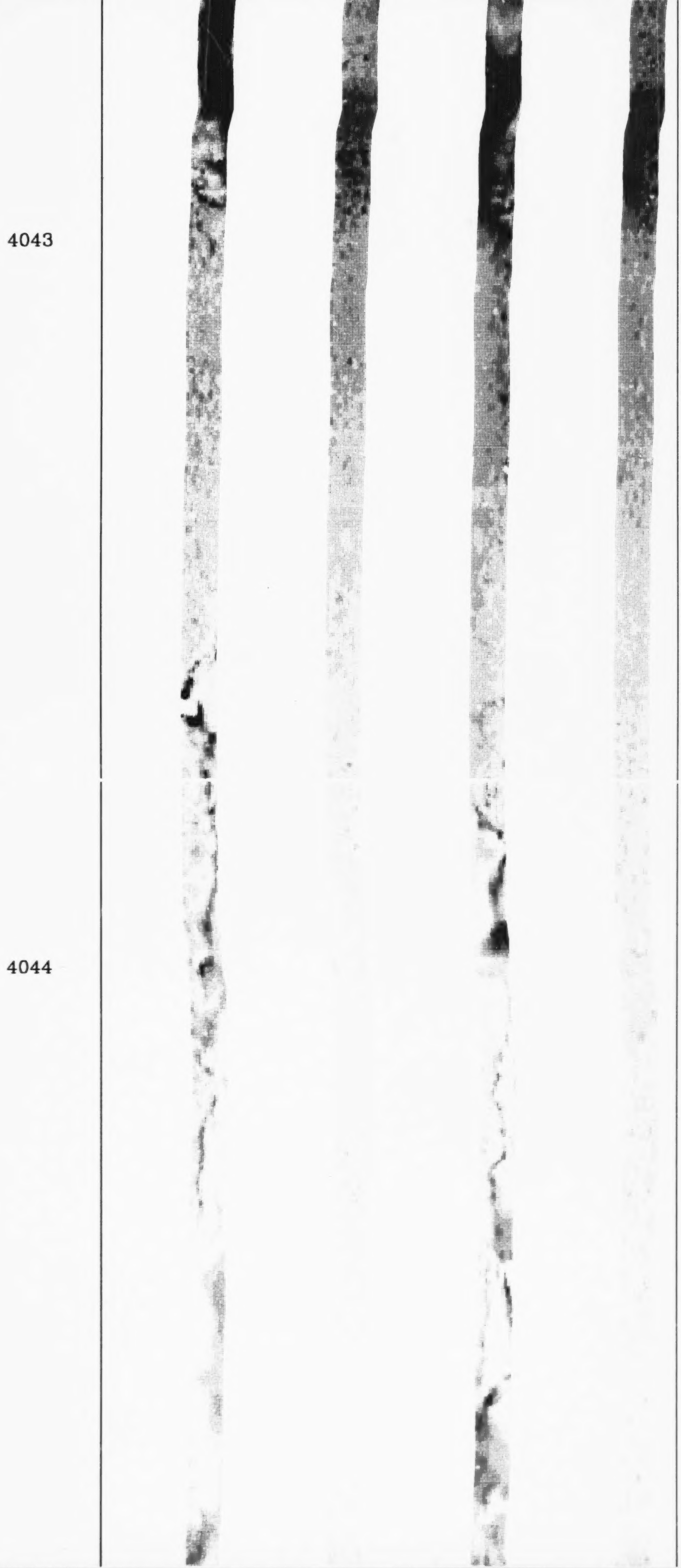
4043
4044

4045

4046

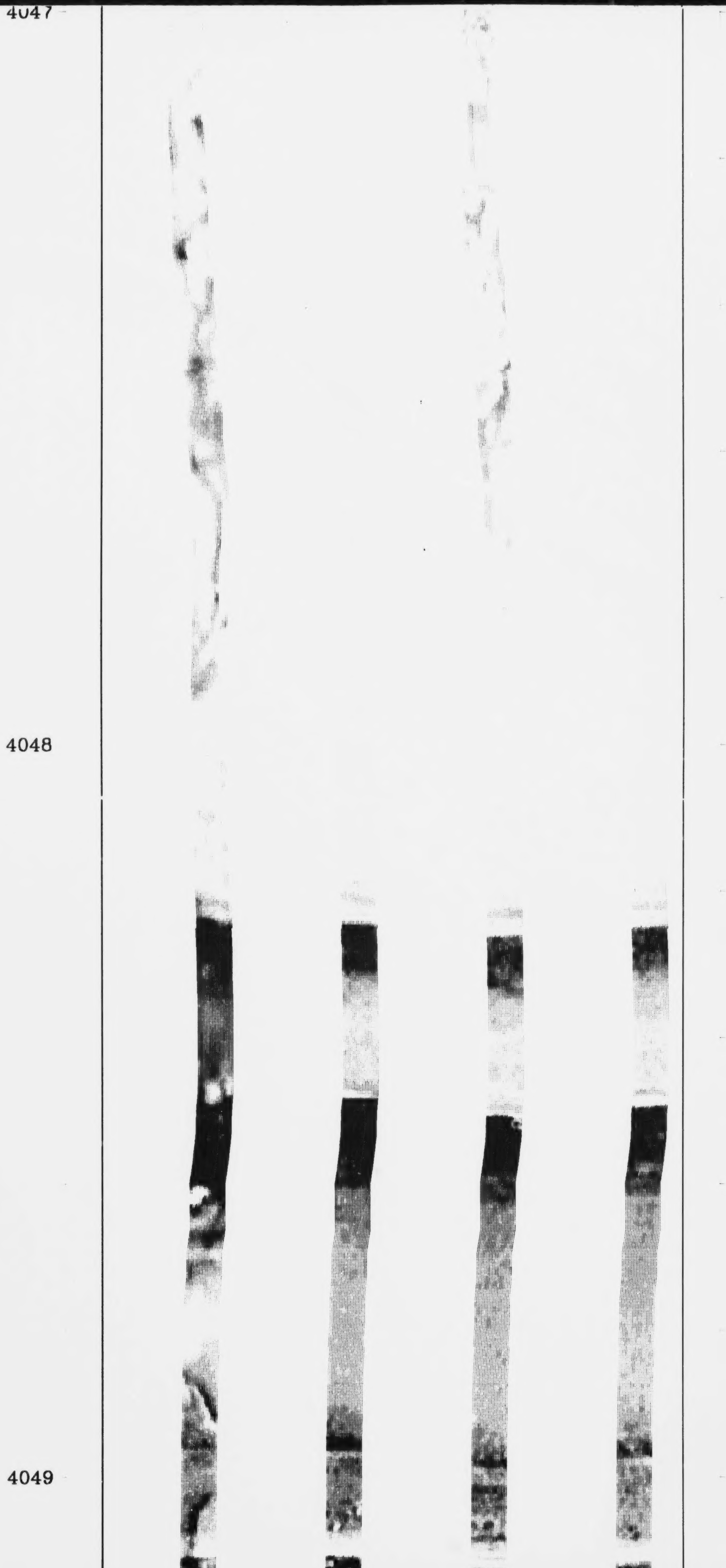
4047
4048
4049

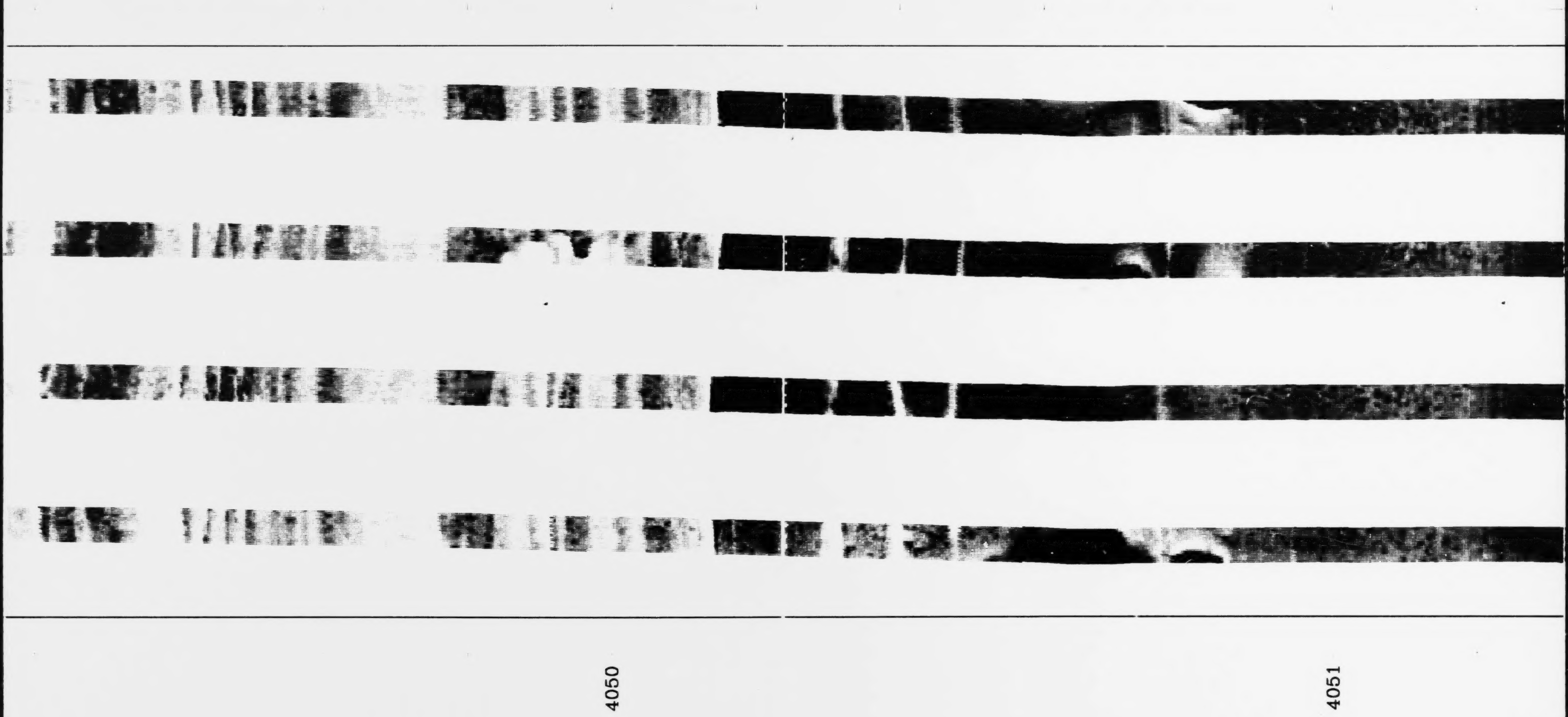
4050
4051

4052

4053

4054

4055

4056

4057

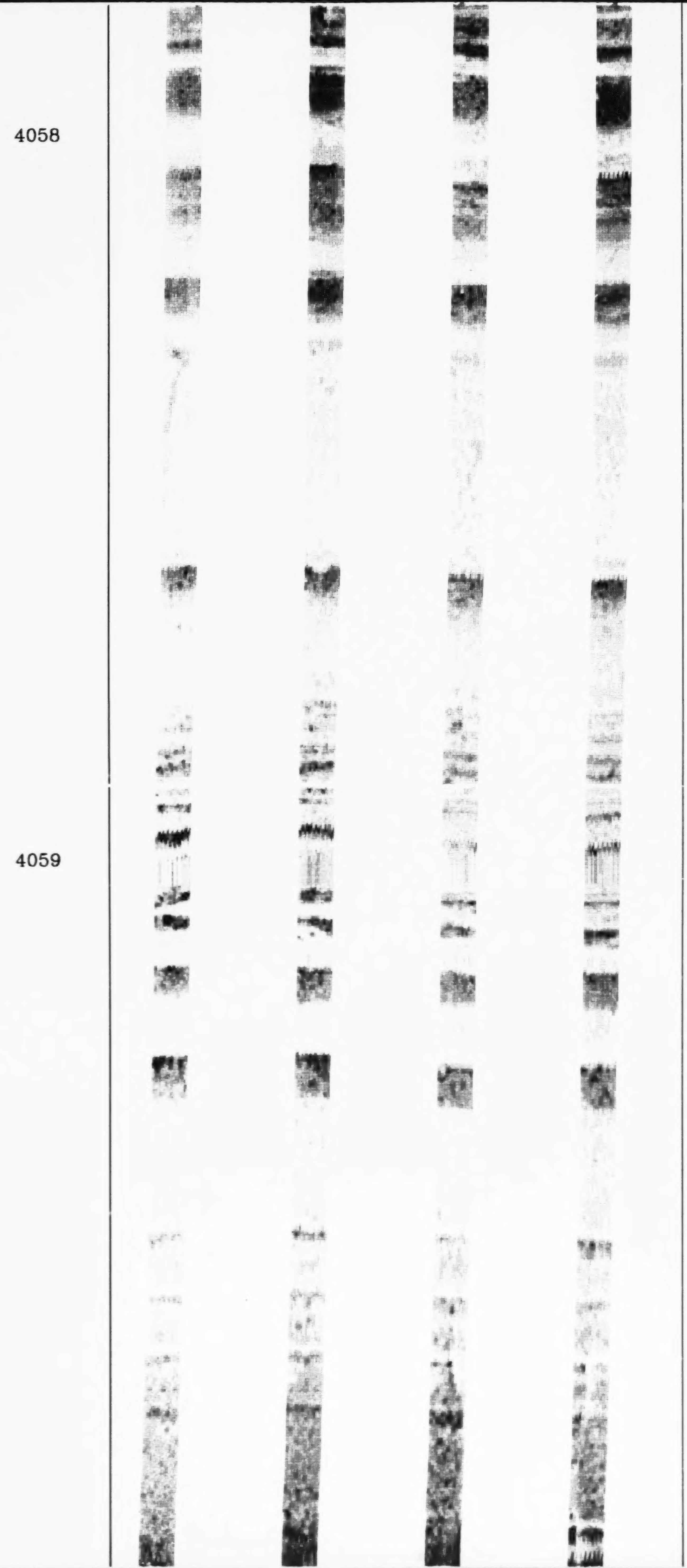
4058
4059

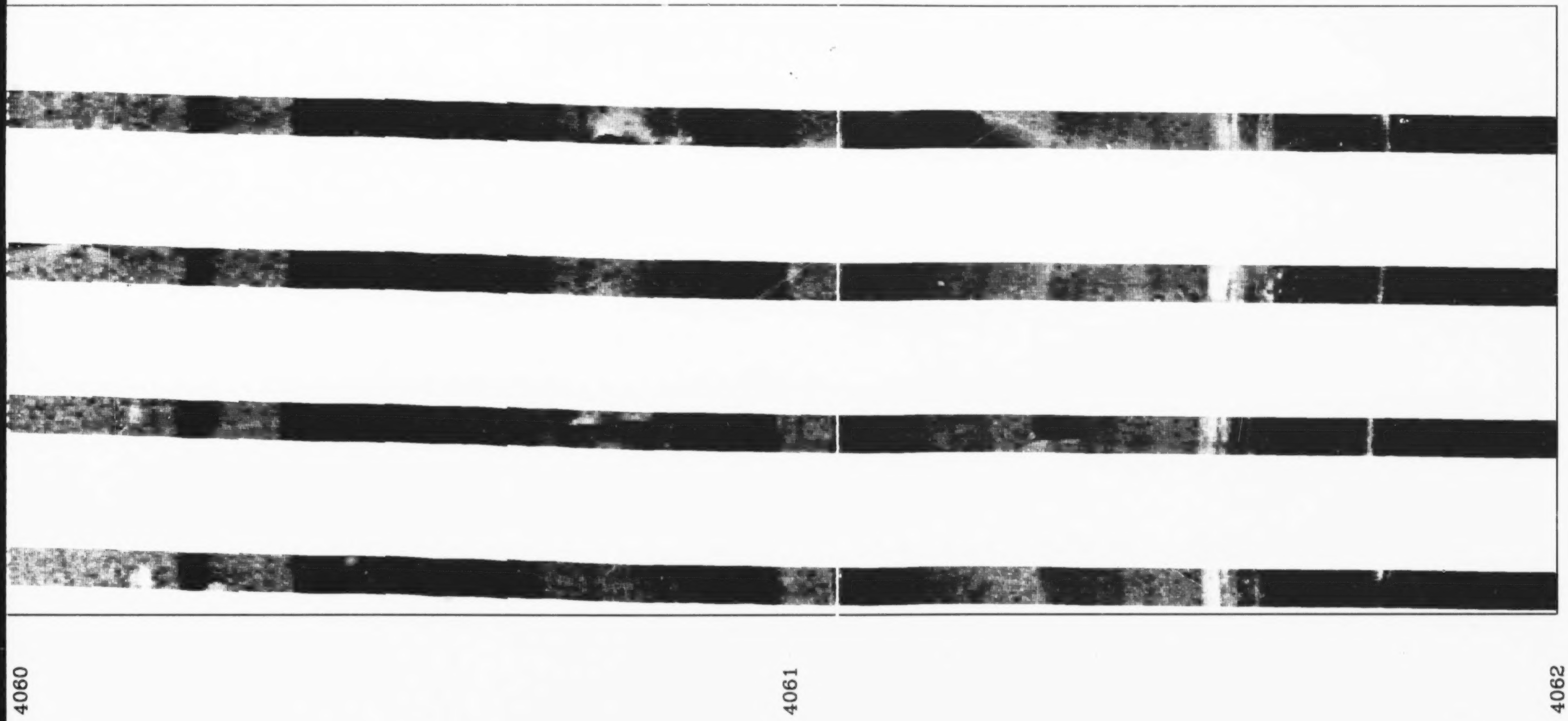
4060
4061
4062

SCHLUMBERGER

FMS
BOREHOLE
IMAGING

COMPANY	LAMONT–DOHERTY GEOLOGICAL
WELL	ODP HOLE–793B
FIELD	IZU–BONIN FOREARC BASIN
COUNTRY	OCEAN
RUN	1
DATE LOGGED	16 – JUN – 89
REFERENCE	STATIC PS–1 4062–4100

STATIC NORMALIZATION

PASS 1 (23577)

FILE : MEST.001

ZONE FROM 4100.0 M TO 4062.0 M

DEPTH SCALE = 1/ 5

IMAGE SCALE = 1/ 5

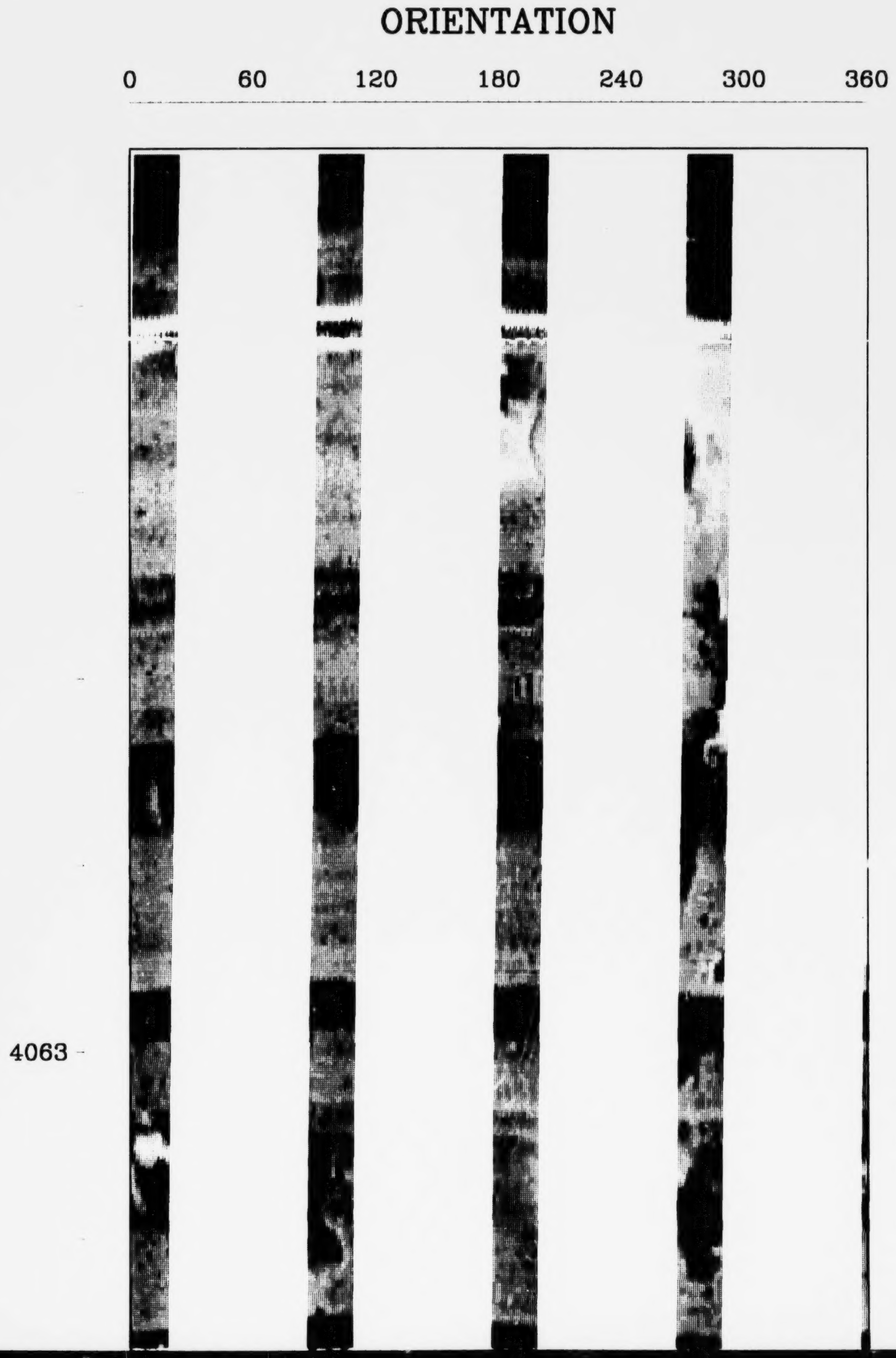

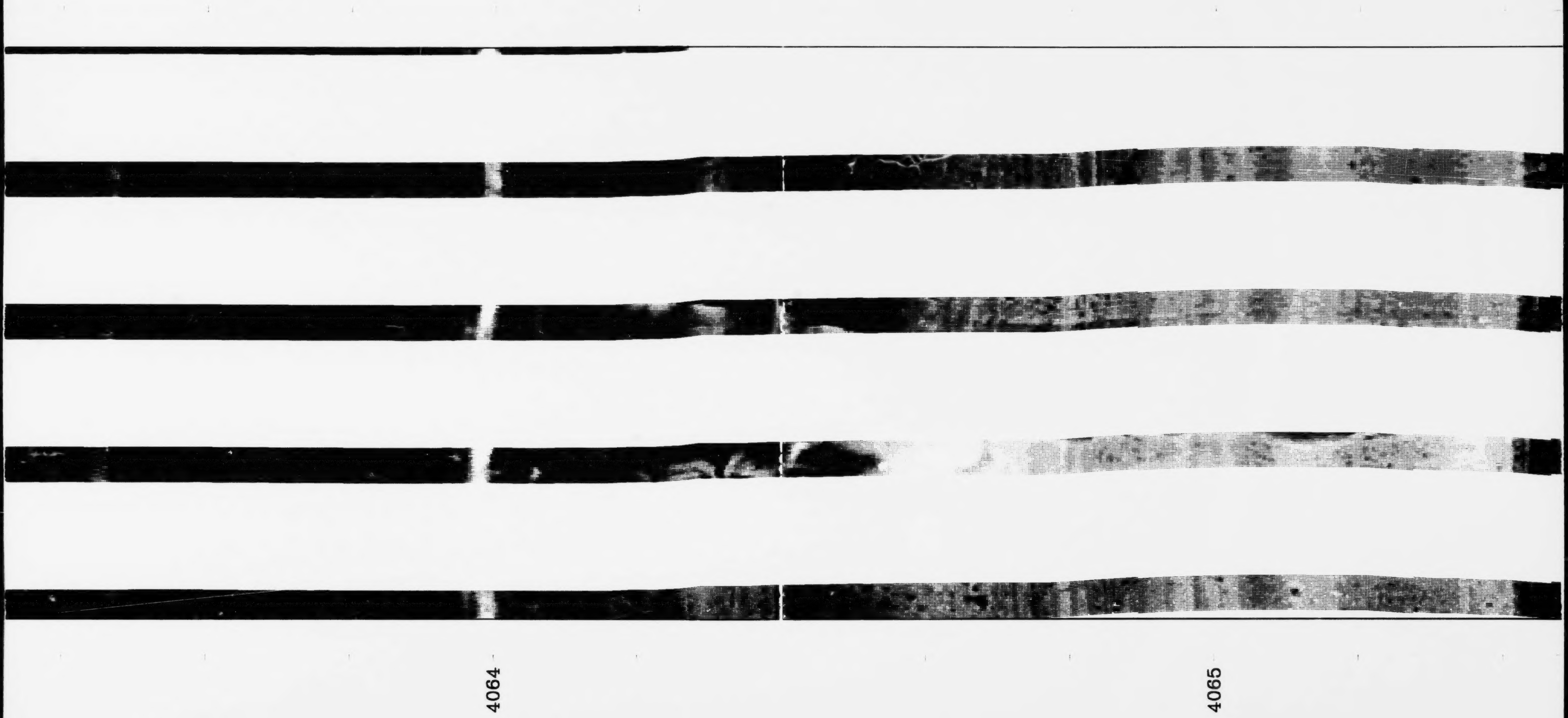
4064
4065

4066
4067

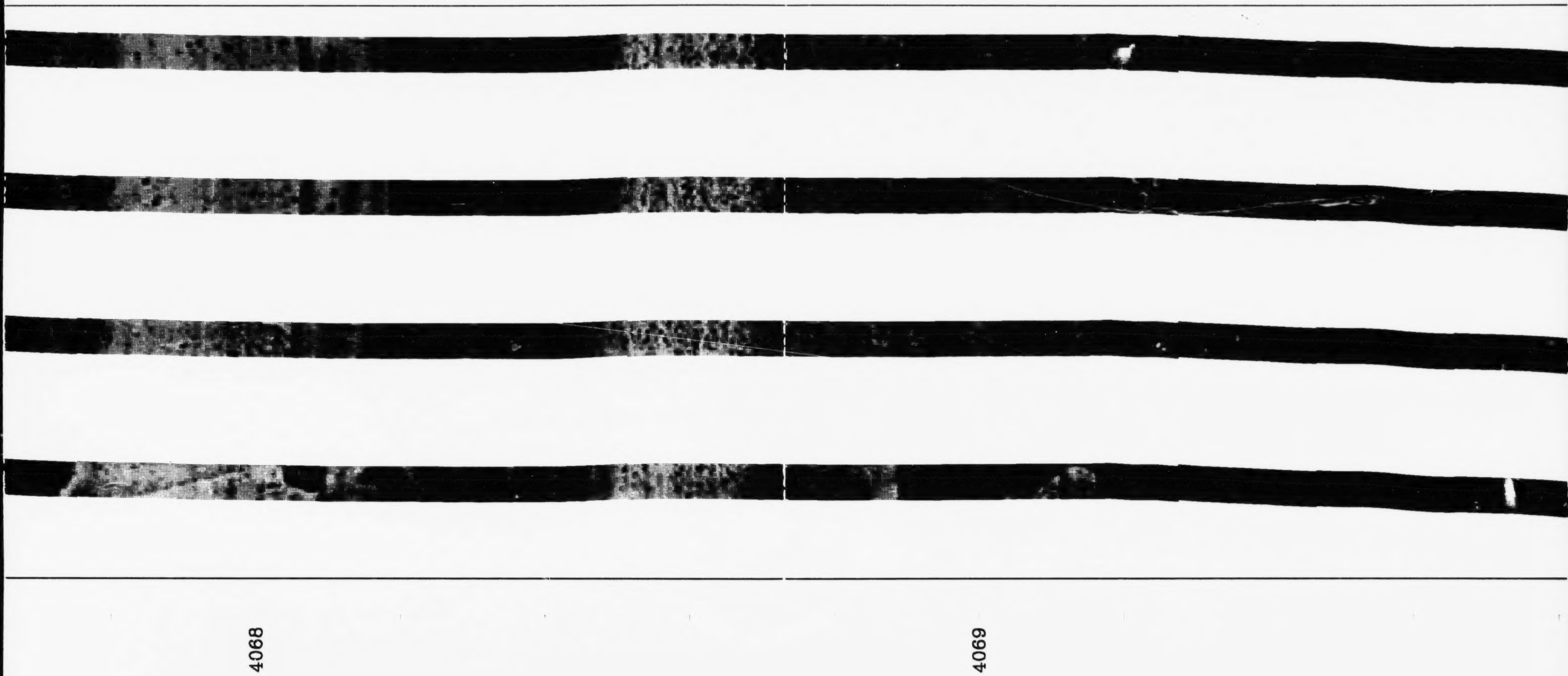
4068
4069

4070

4071

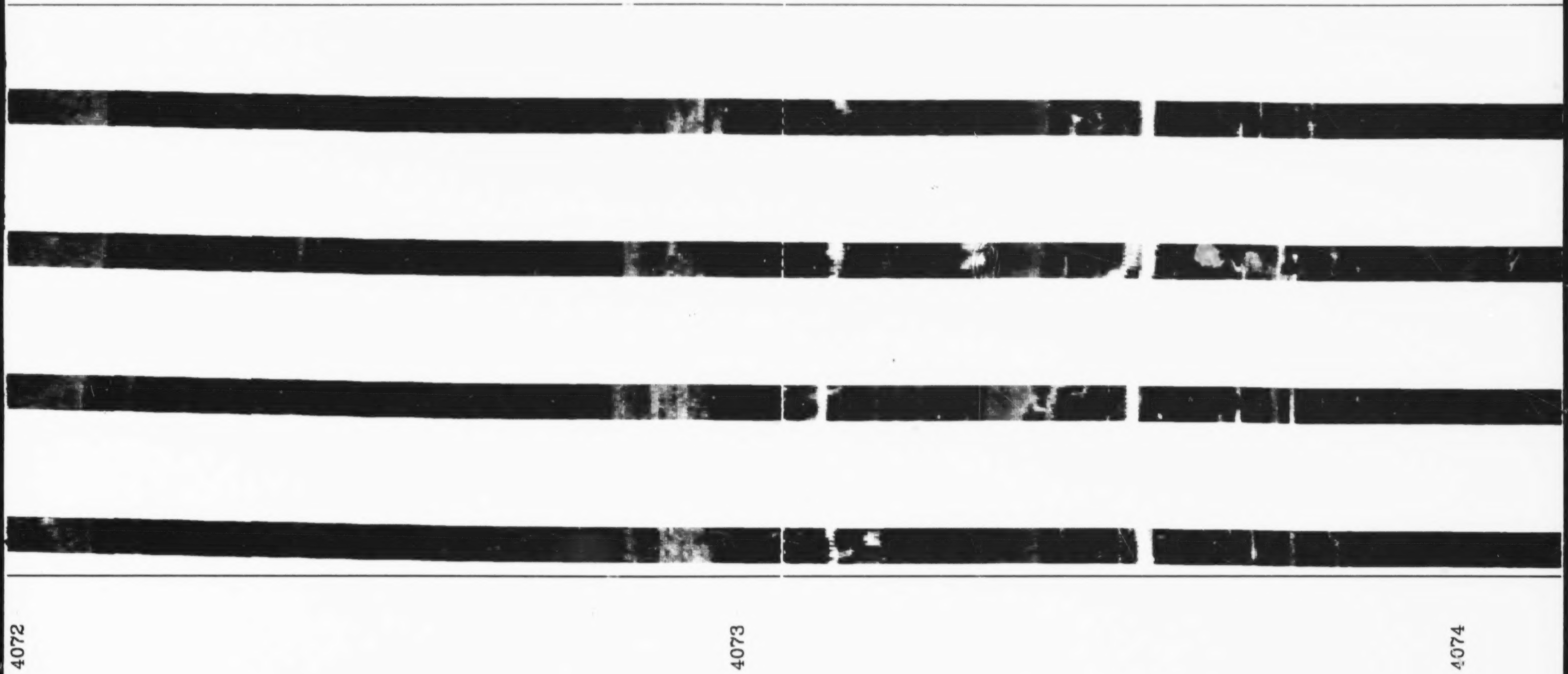
4072
4073
4074

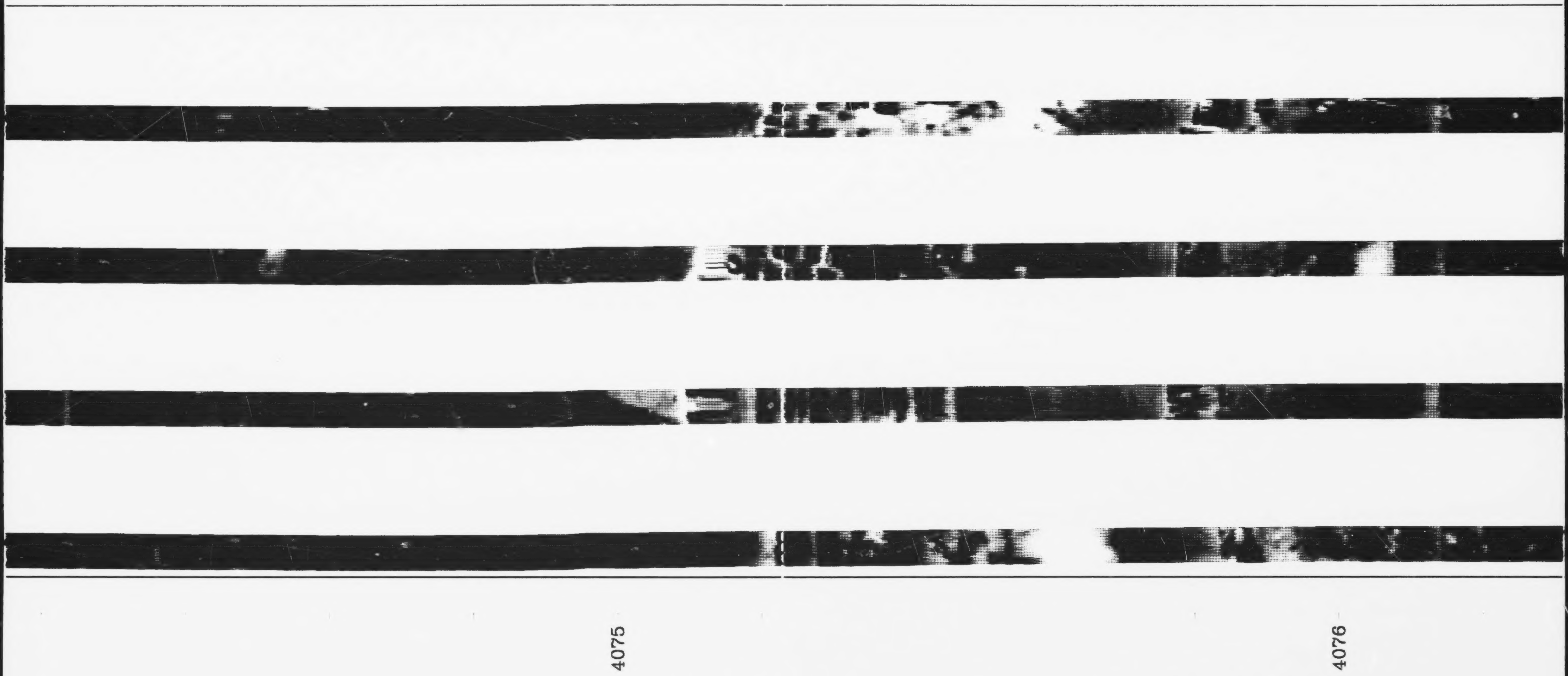
4075
4076

4077

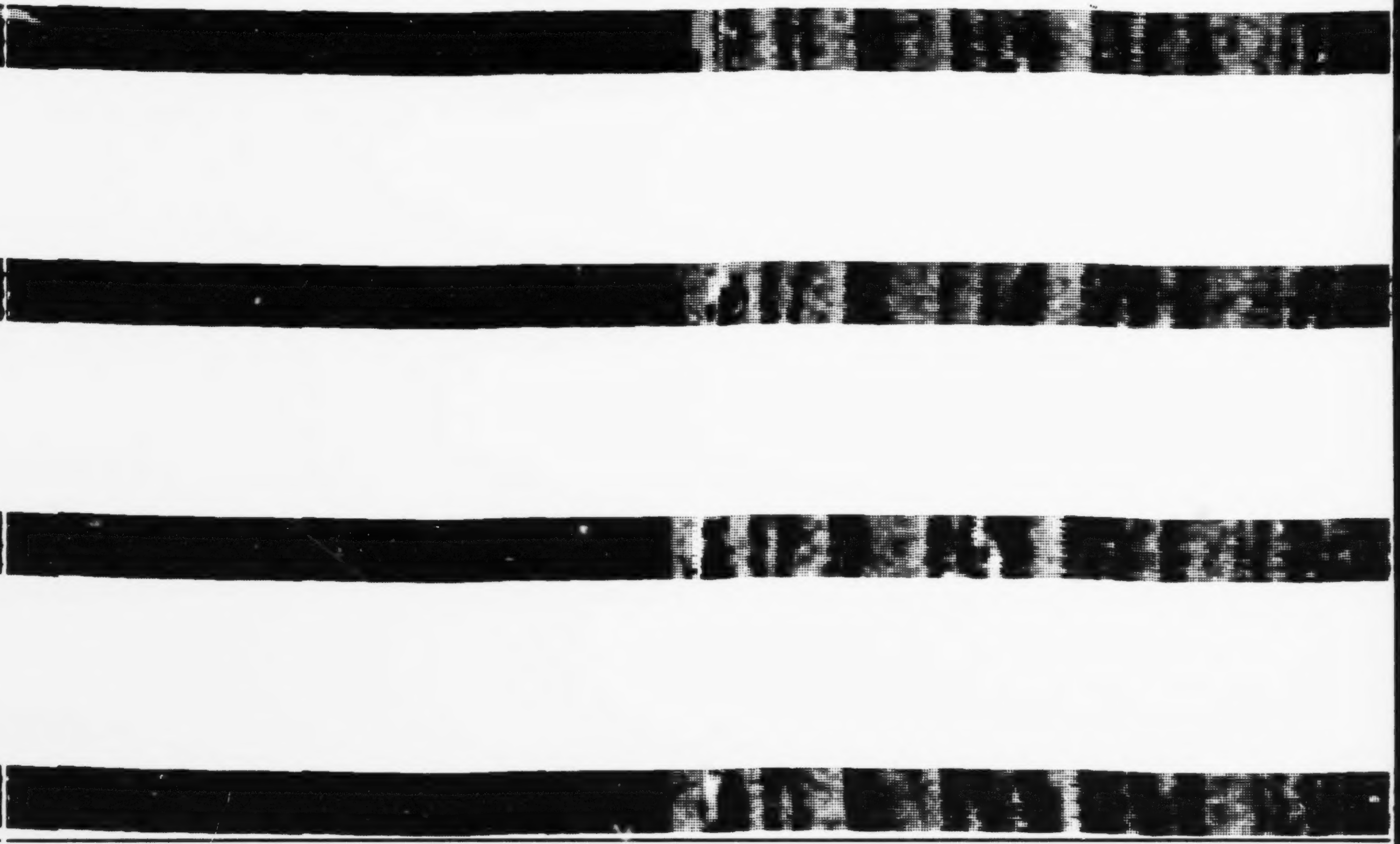

4078

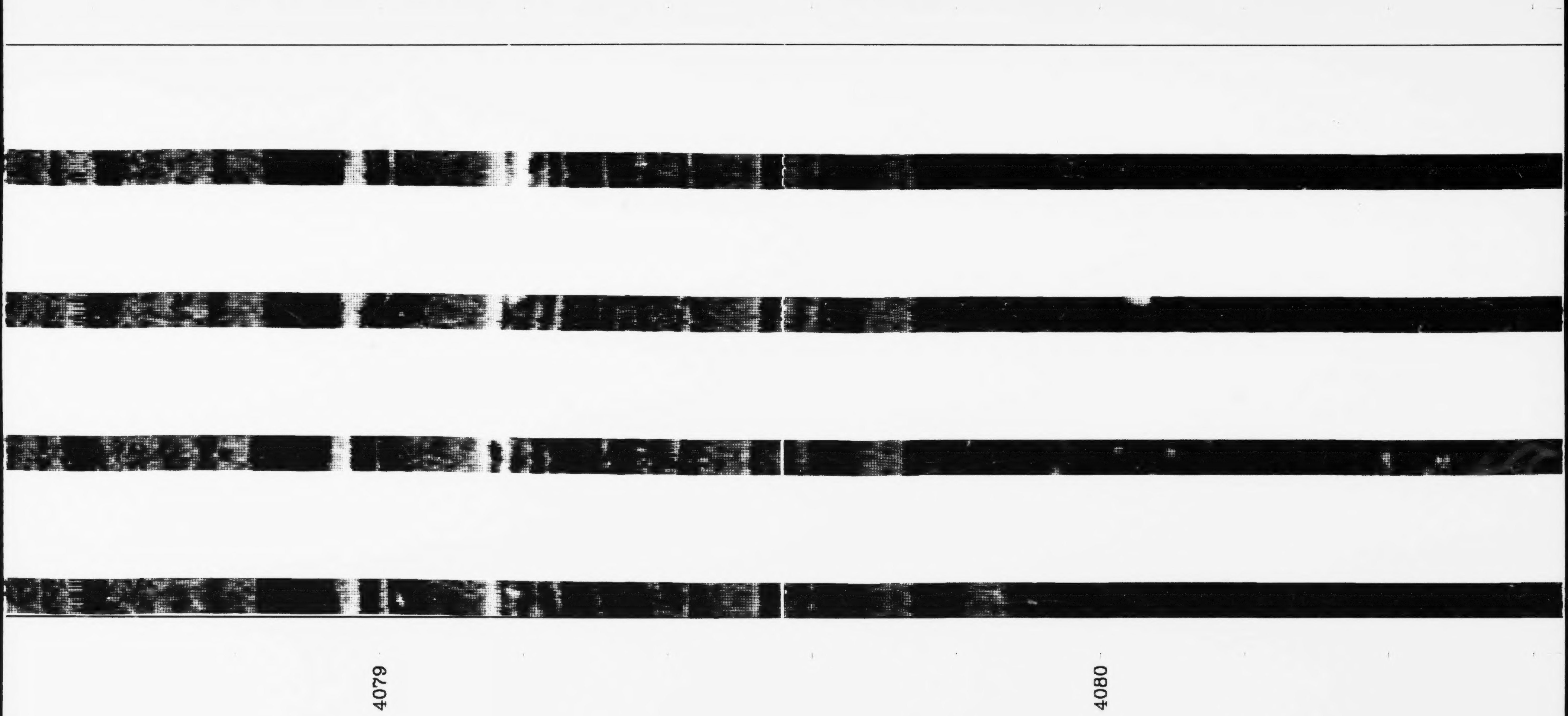
4079
4080

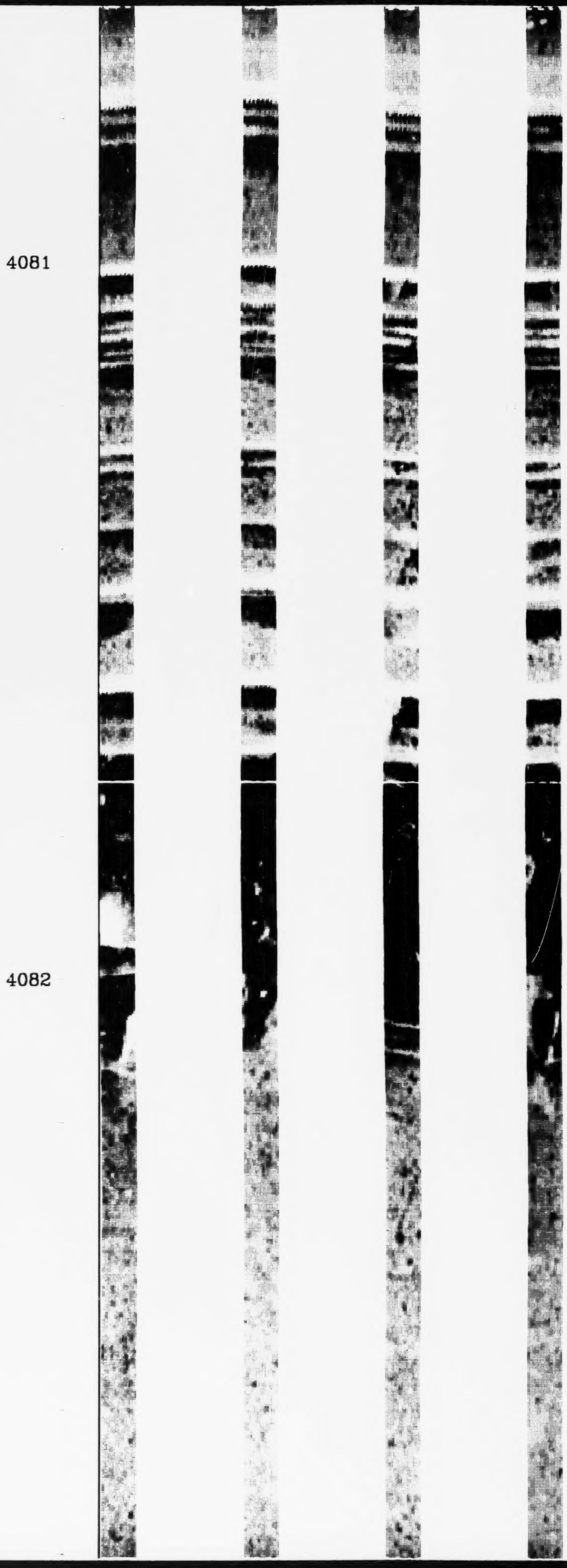
4081
4082

4083

4084

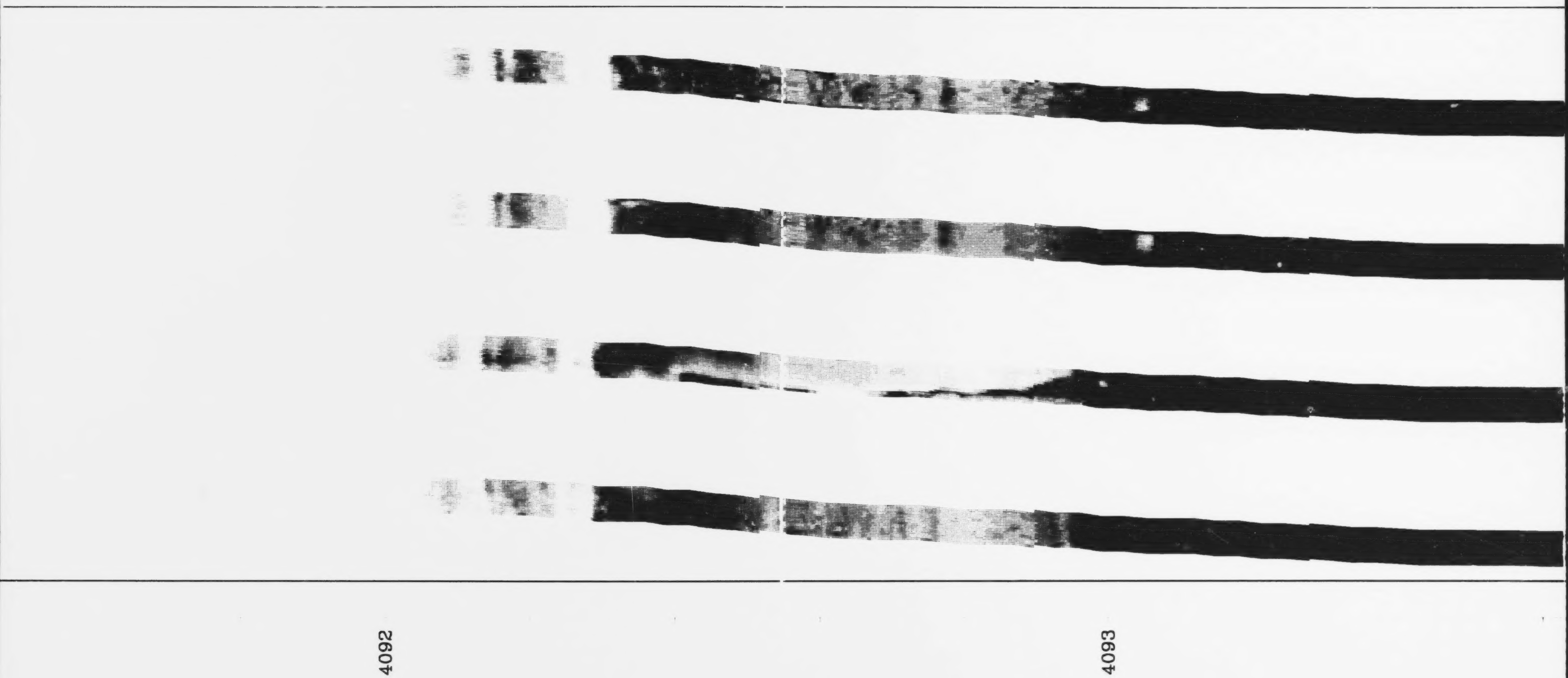
4092
4093

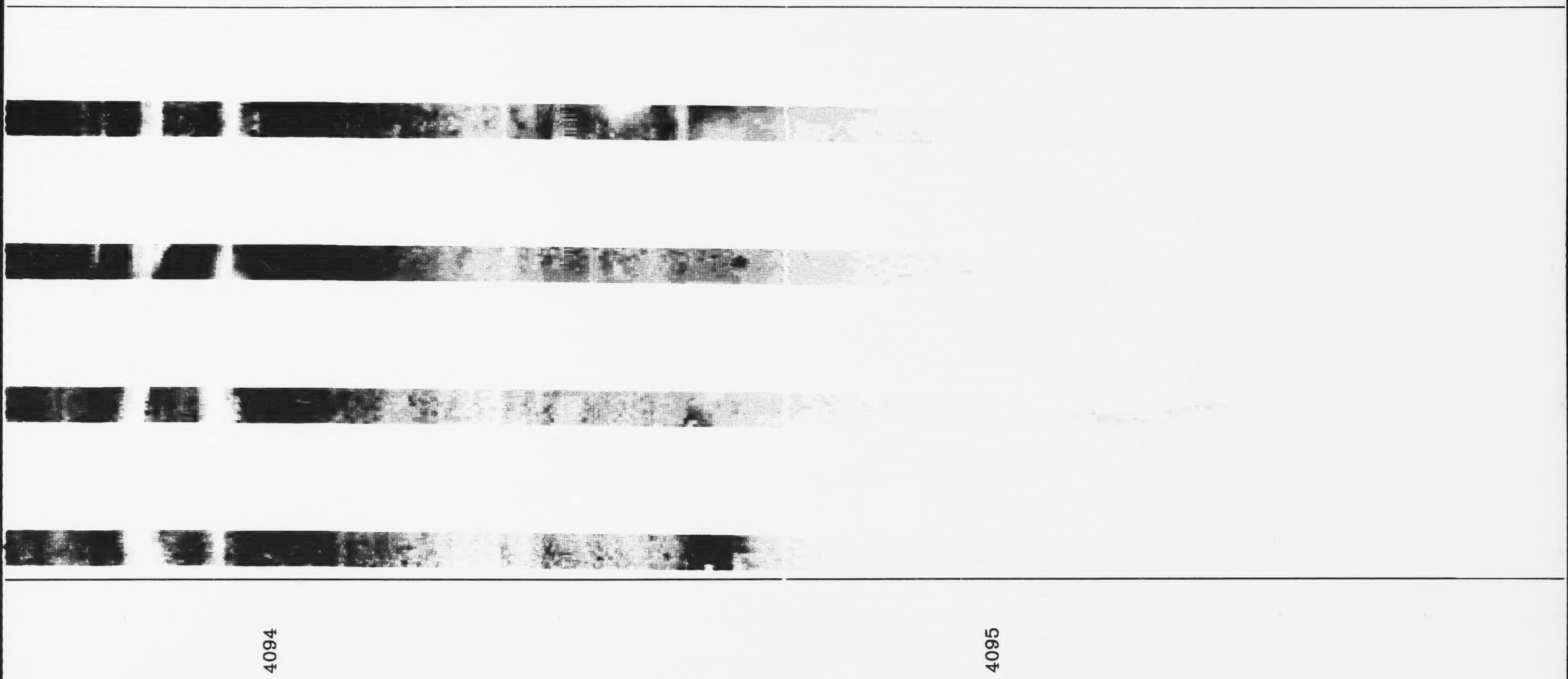
4094
4095

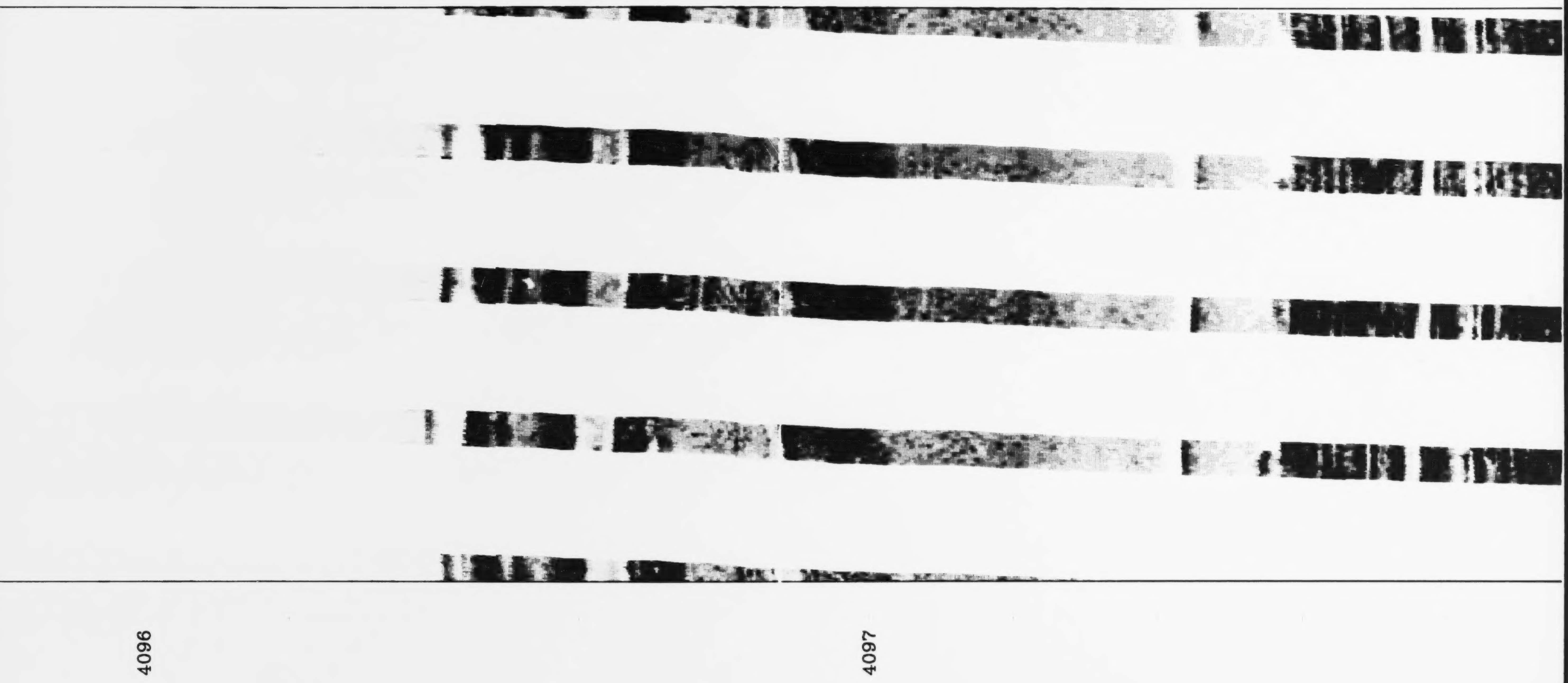
4096
4097

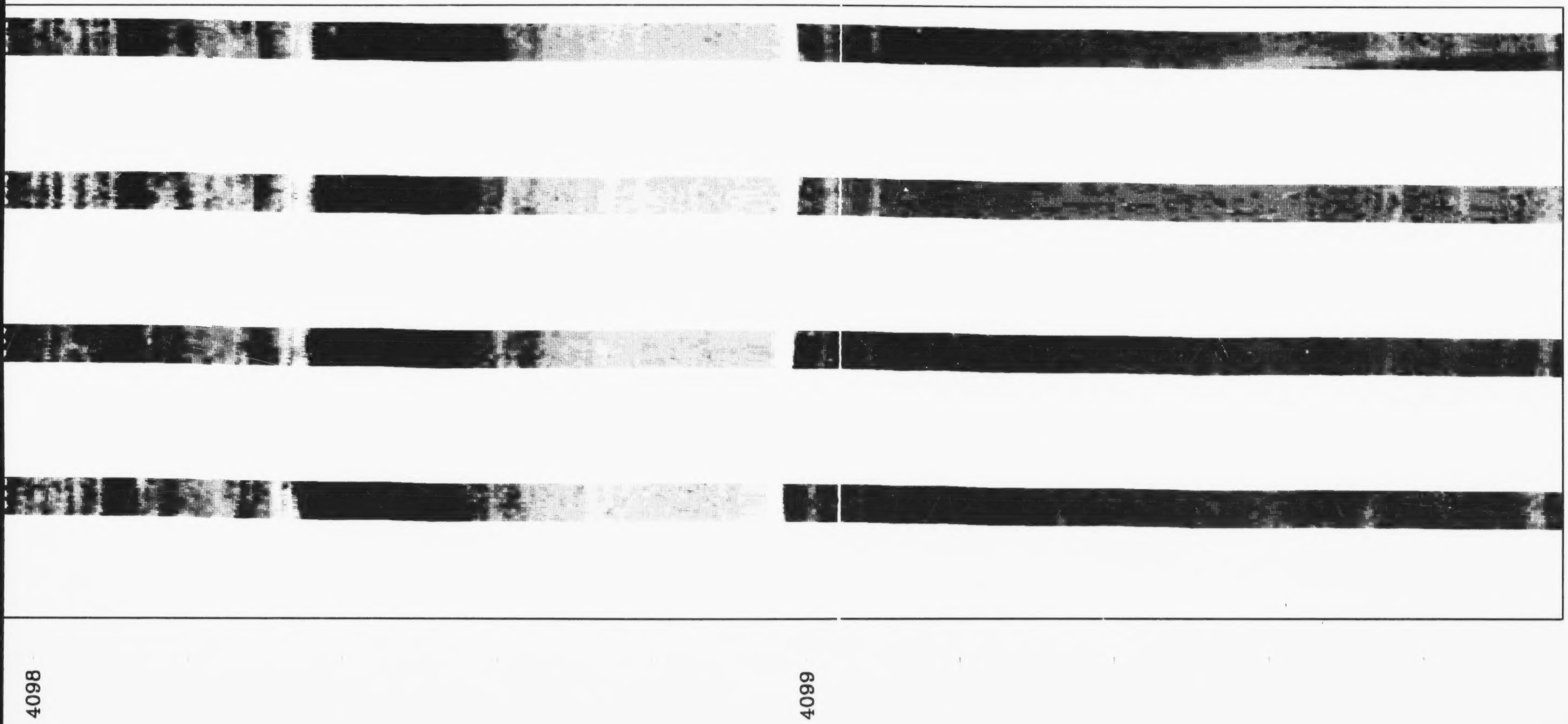
4098
4099

SCHLUMBERGER

FMS
BOREHOLE
IMAGING

COMPANY	LAMONT-DOHERTY GEOLOGICAL
WELL	ODP HOLE-793B
FIELD	IZU-BONIN FOREARC BASIN
COUNTRY	OCEAN
RUN	1
DATE LOGGED	16 - JUN - 89
REFERENCE	STATIC PS-1 4100-4130

STATIC NORMALIZATION

PASS 1 (23577)

FILE : MEST.001

ZONE FROM 4130.0 M TO 4100.0 M

DEPTH SCALE = 1/ 5

IMAGE SCALE = 1/ 5

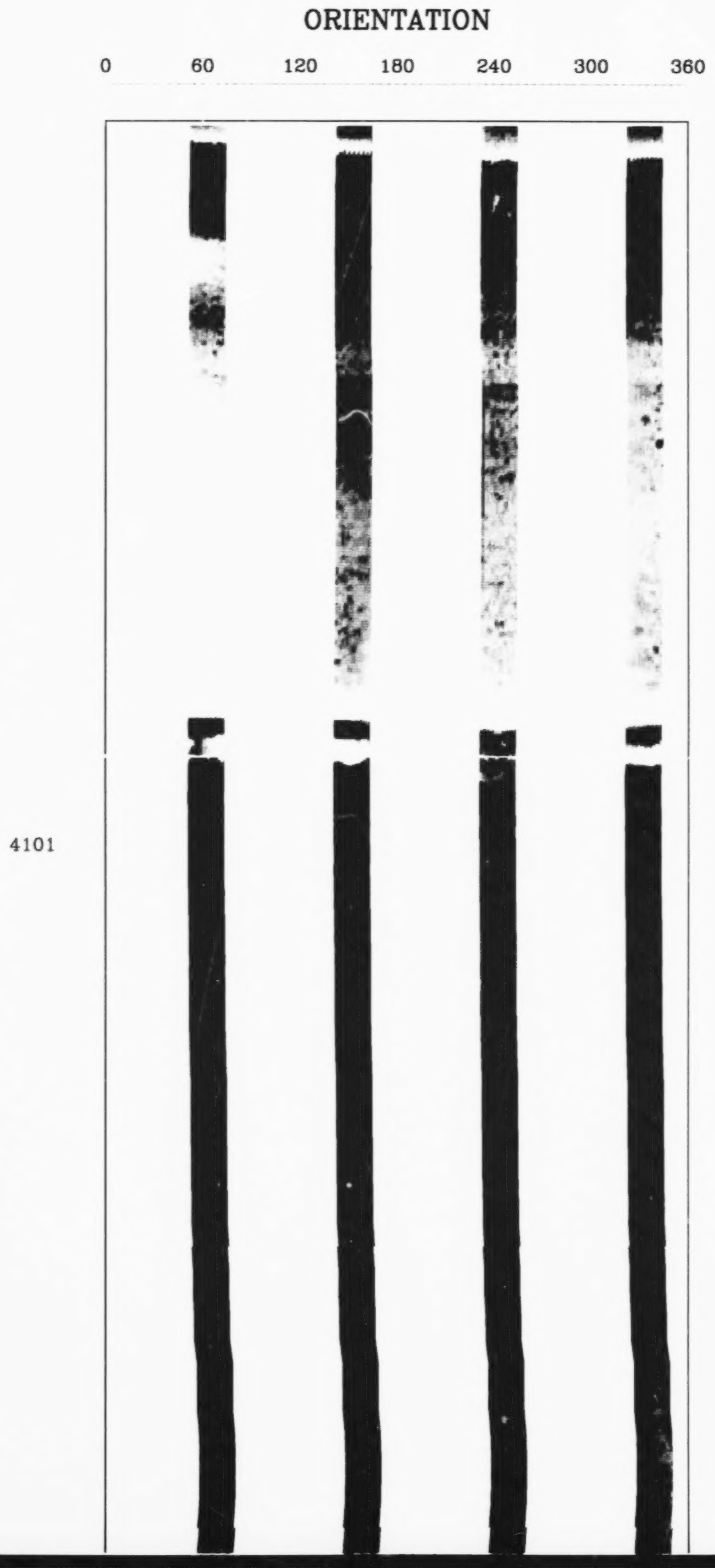
ORIENTATION
0
60
120
180
240
300
360
4101

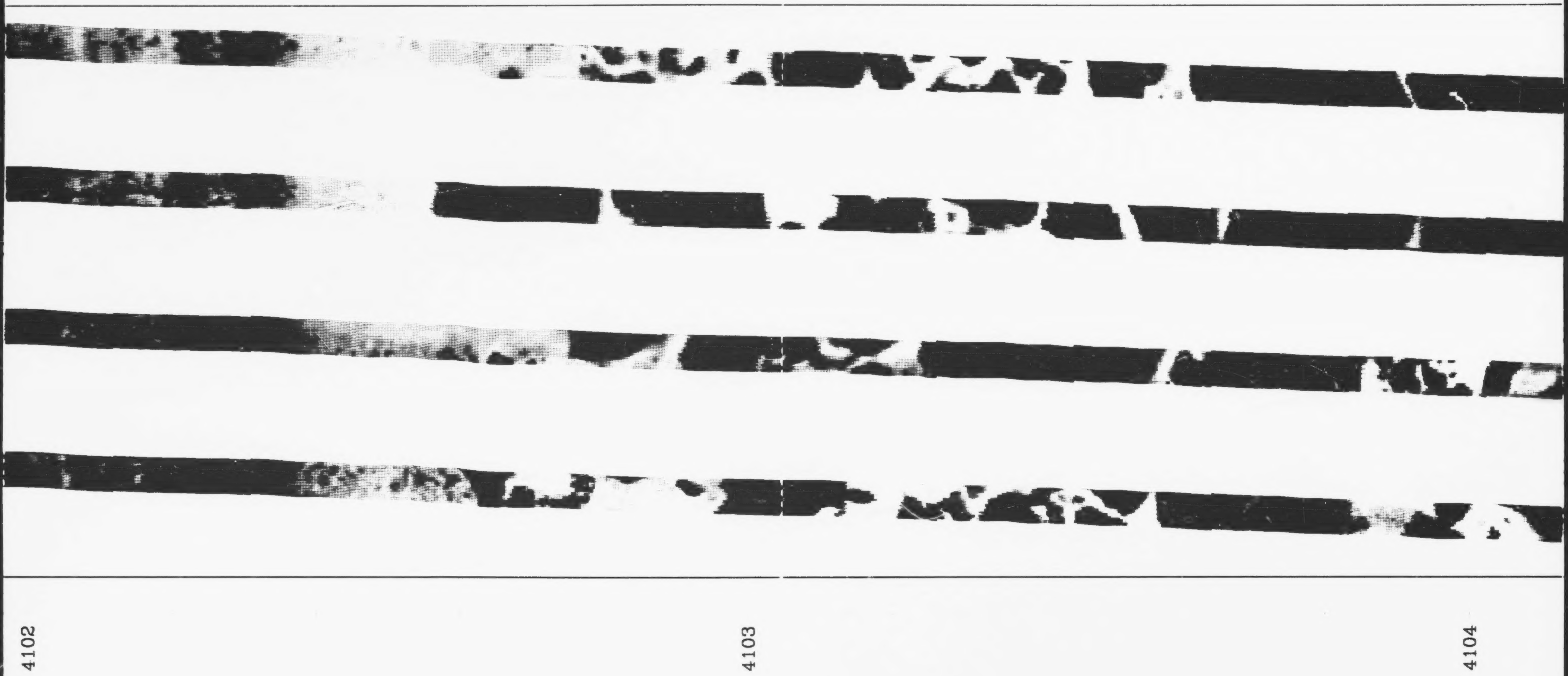
4102
4103
4104

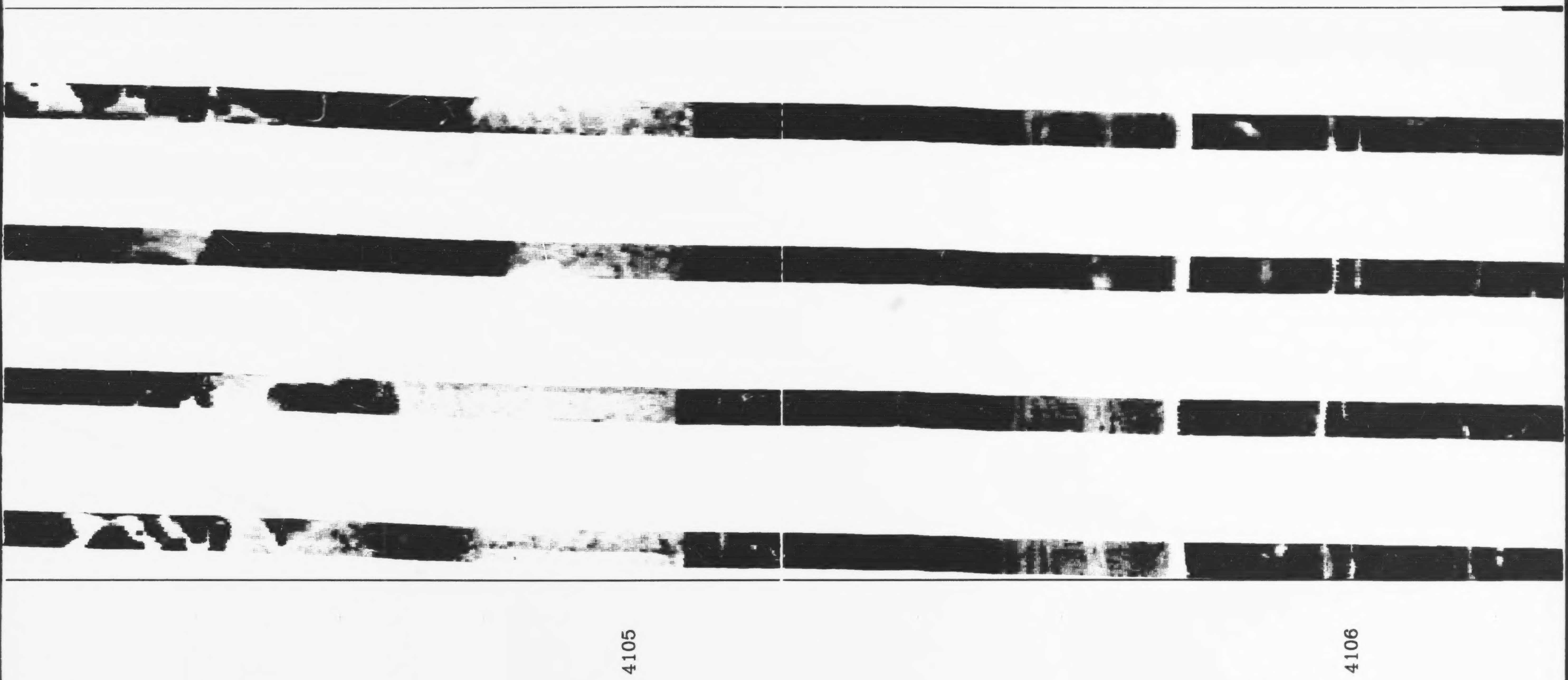

4105
4106

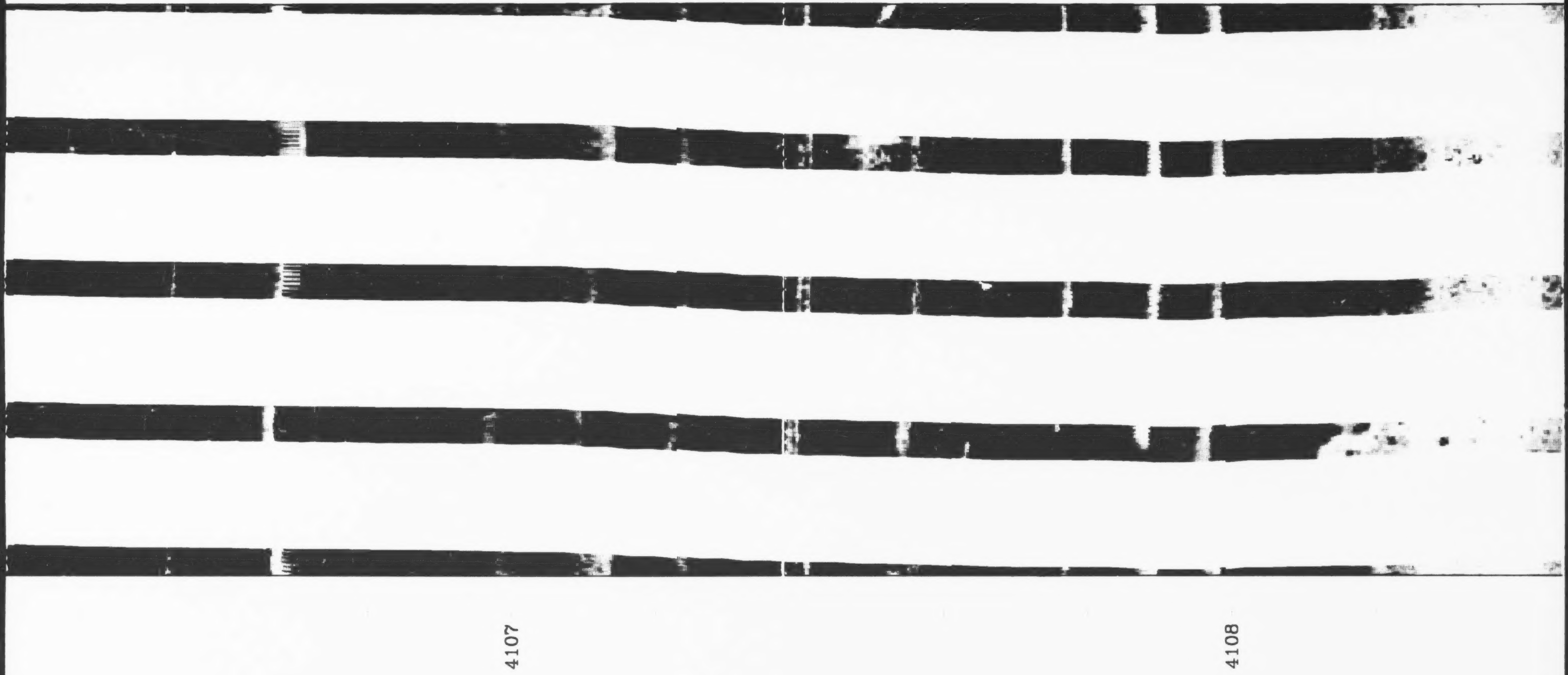
4107
4108

4109
4110

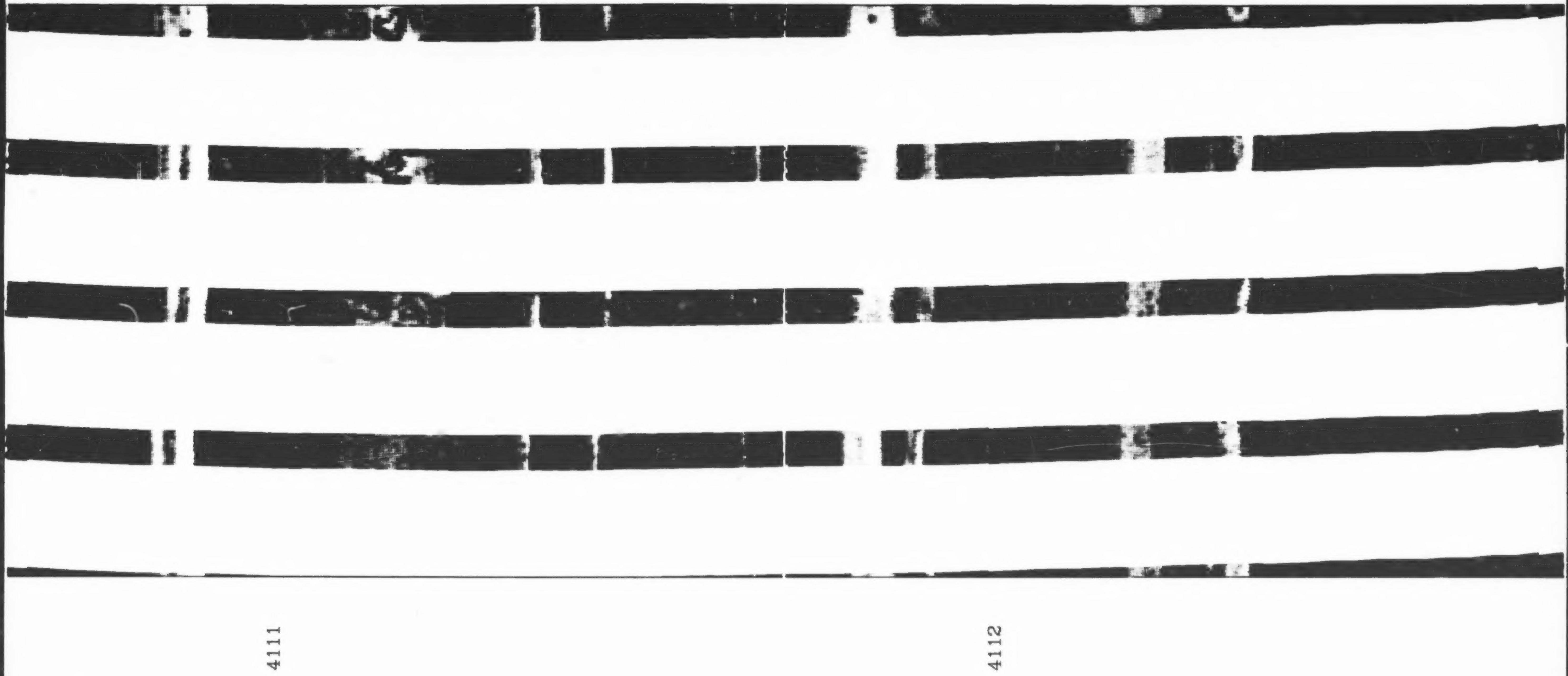
4111
4112

4113
4114

[redacted]

4115

4116

4117

4118

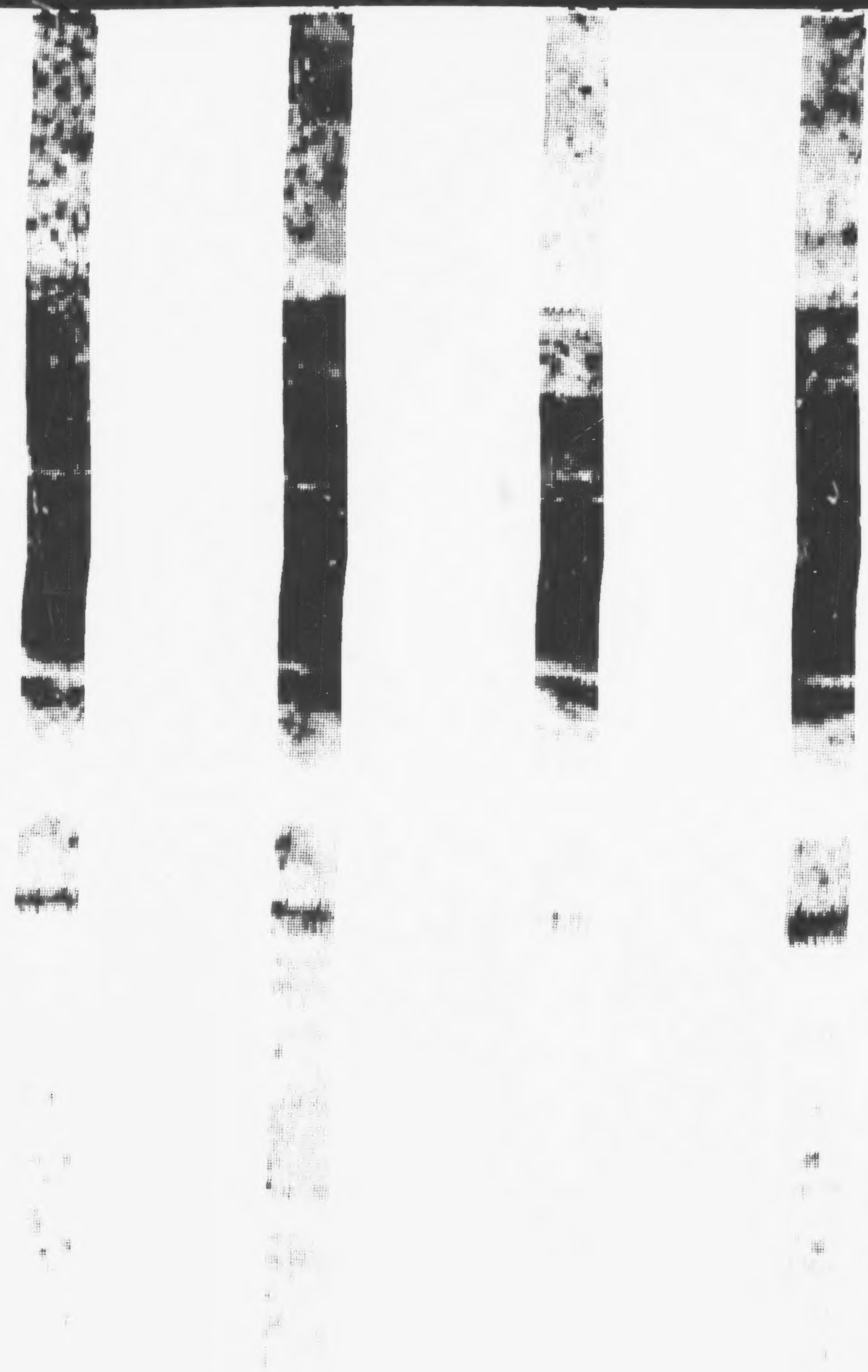

4119

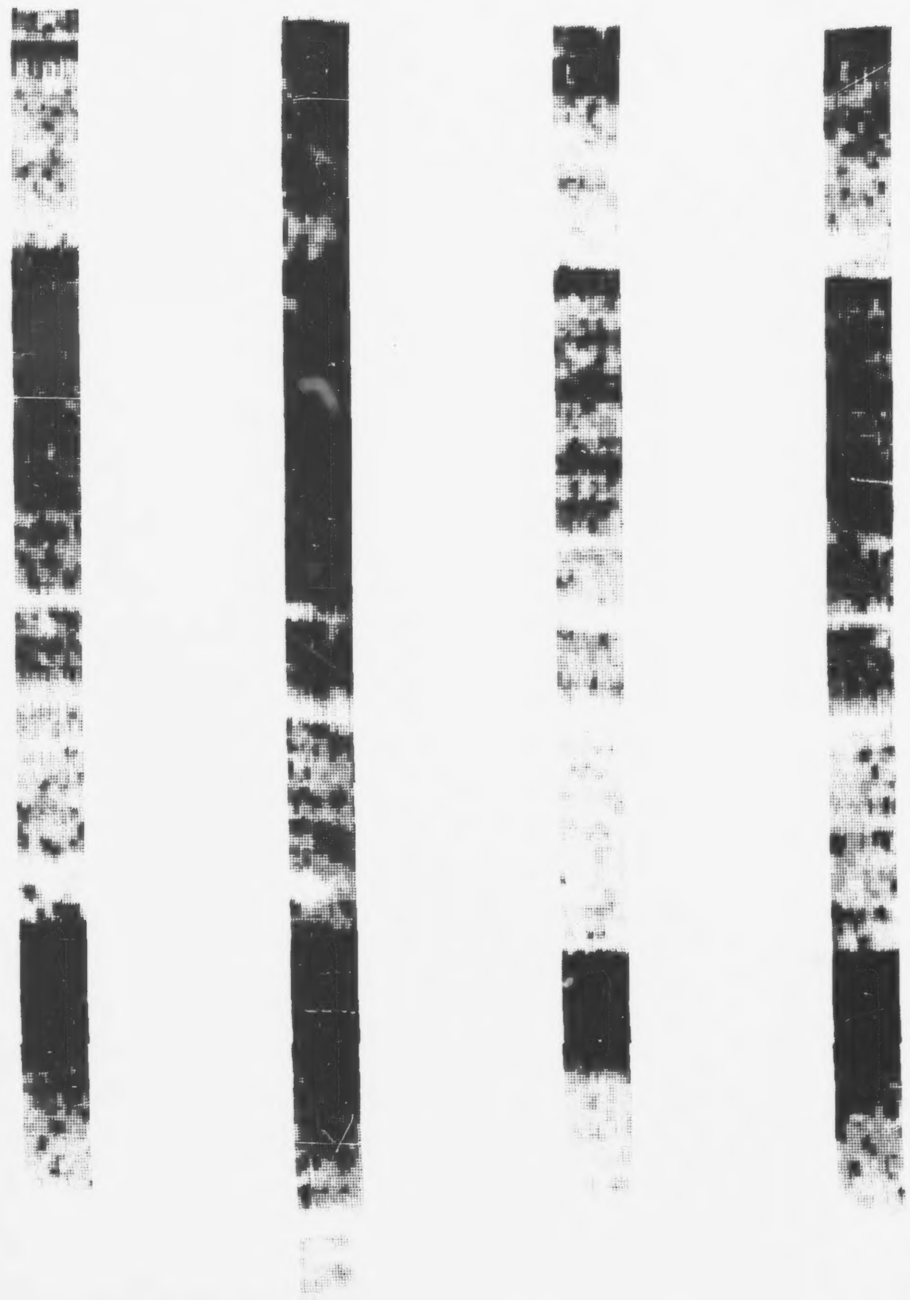

[redacted]

4122

4123

4124 [illegible]

4125 [illegible]

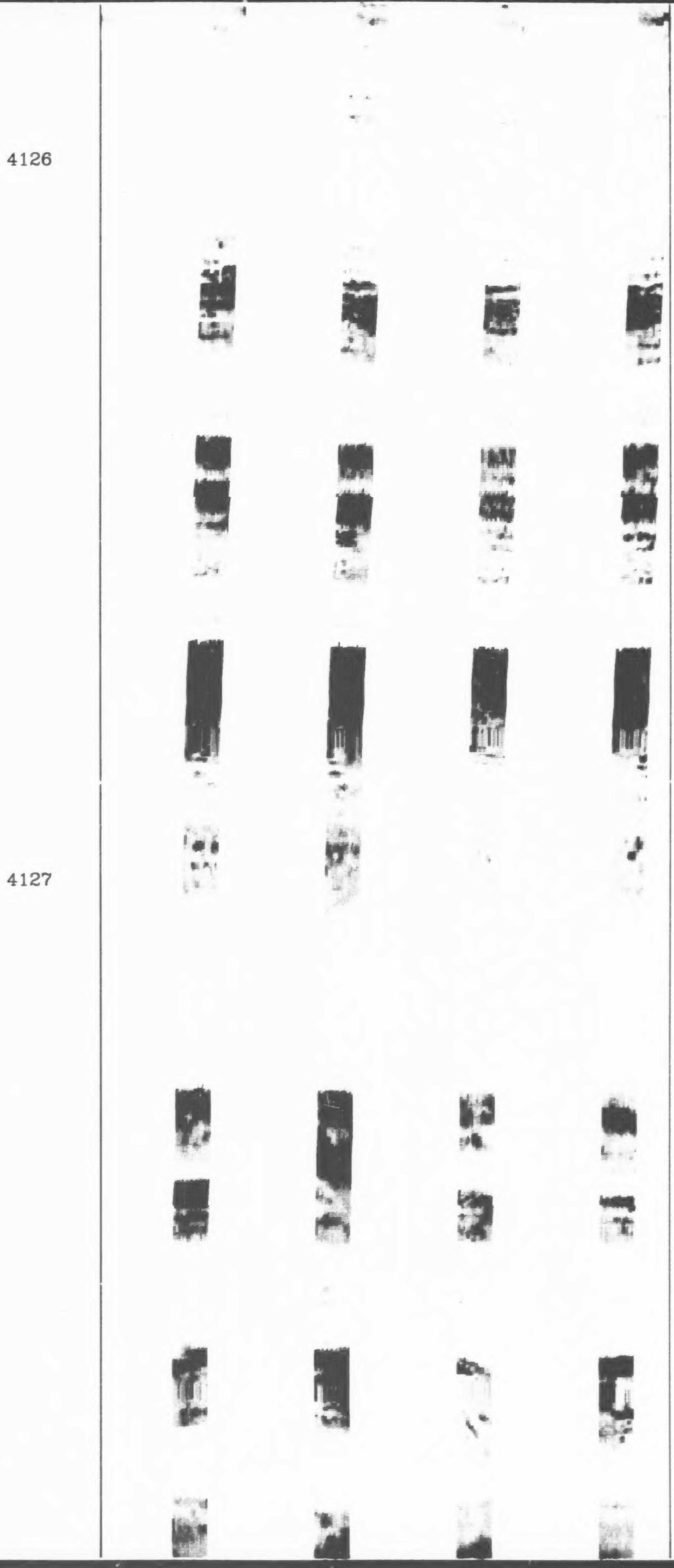
4126
4127

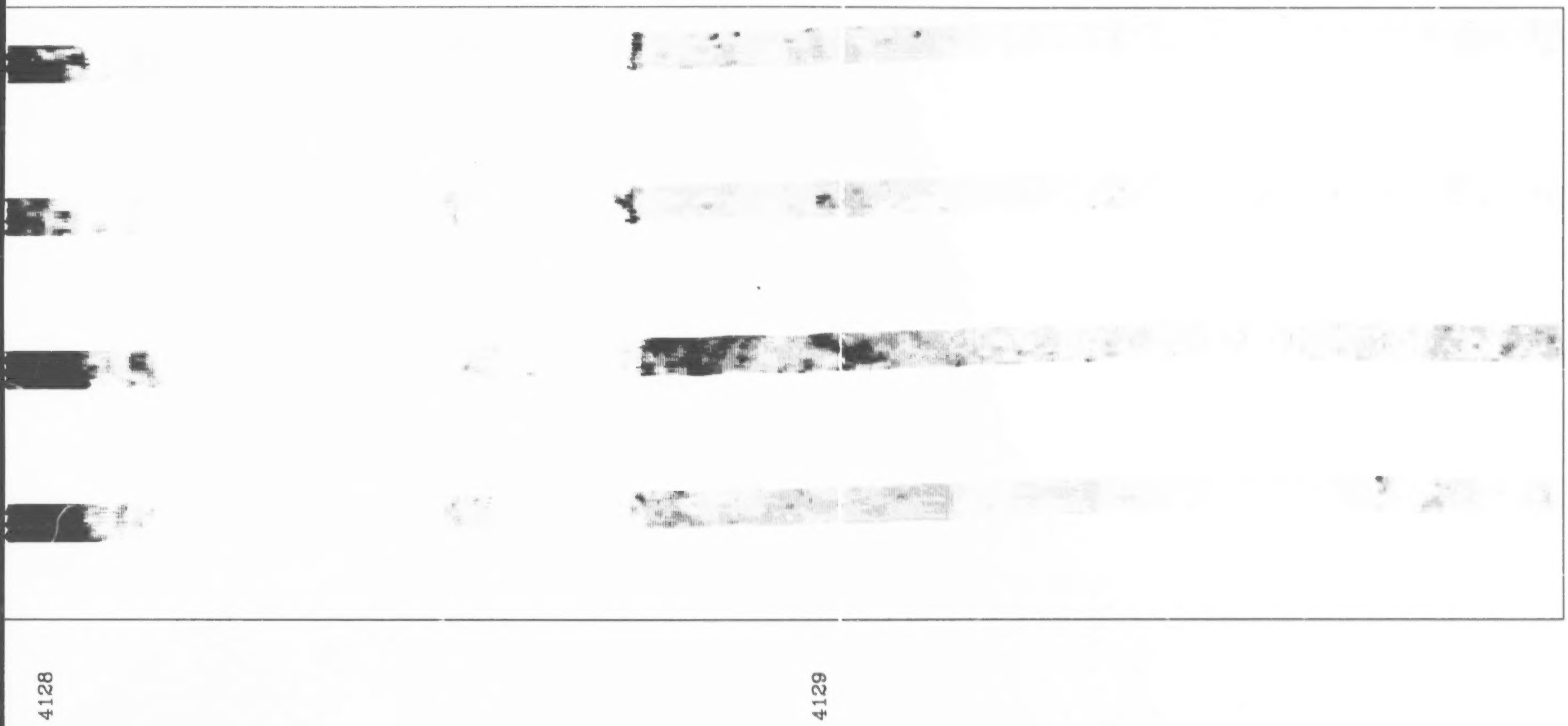
4128
4129

SCHLUMBERGER

FMS
BOREHOLE
IMAGING

COMPANY	LAMONT–DOHERTY GEOLOGICAL
WELL	ODP HOLE–793B
FIELD	IZU–BONIN FOREARC BASIN
COUNTRY	OCEAN
RUN	1
DATE LOGGED	16 – JUN – 89
REFERENCE	STATIC PS-1 4130-4165

STATIC NORMALIZATION
PASS 1 (23577)
FILE : MEST.001

ZONE FROM 4165.0 M TO 4130.0 M

DEPTH SCALE = 1/ 5

IMAGE SCALE = 1/ 5

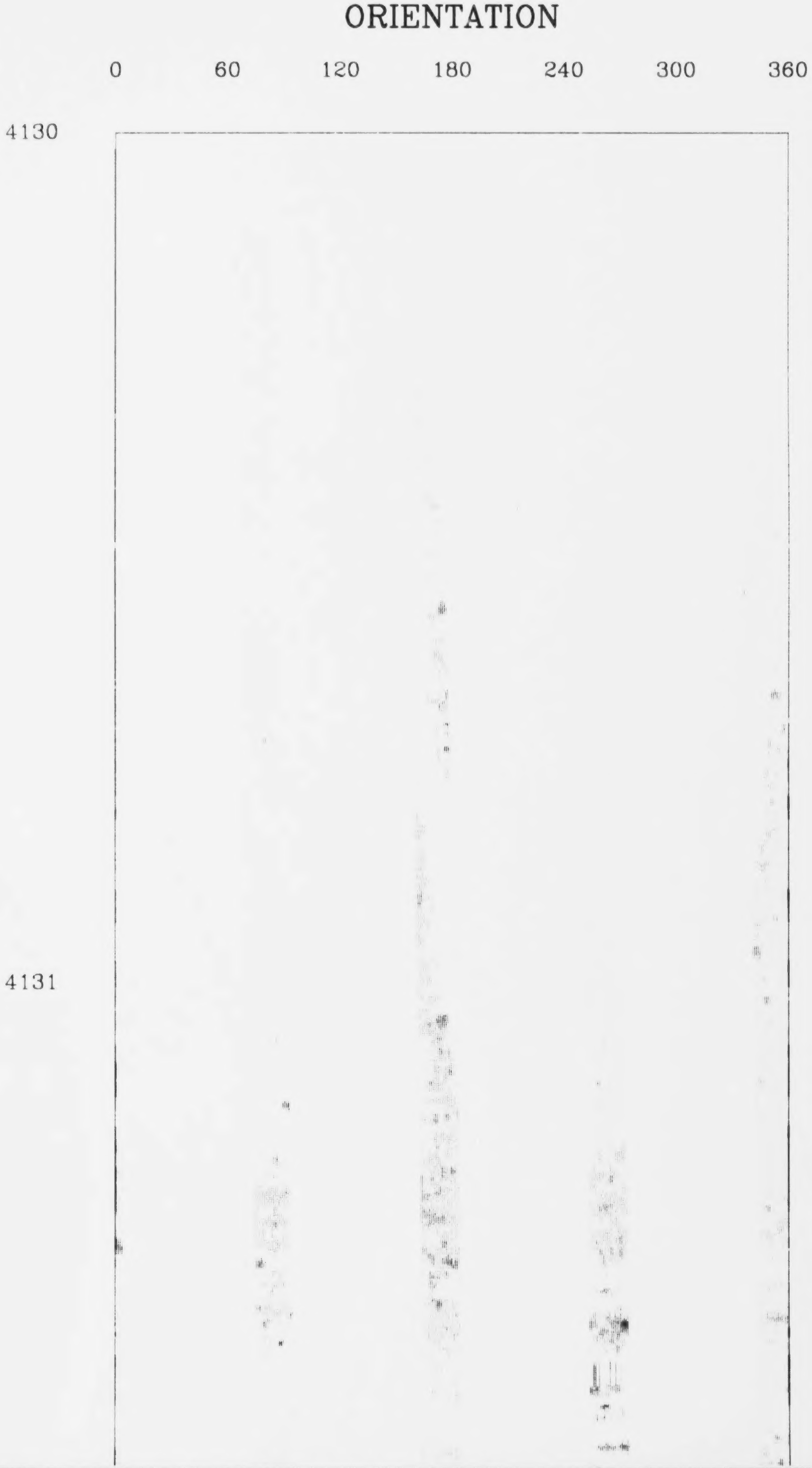

4132

4133

4139

[redacted]

[redacted]

4140

4141

4142

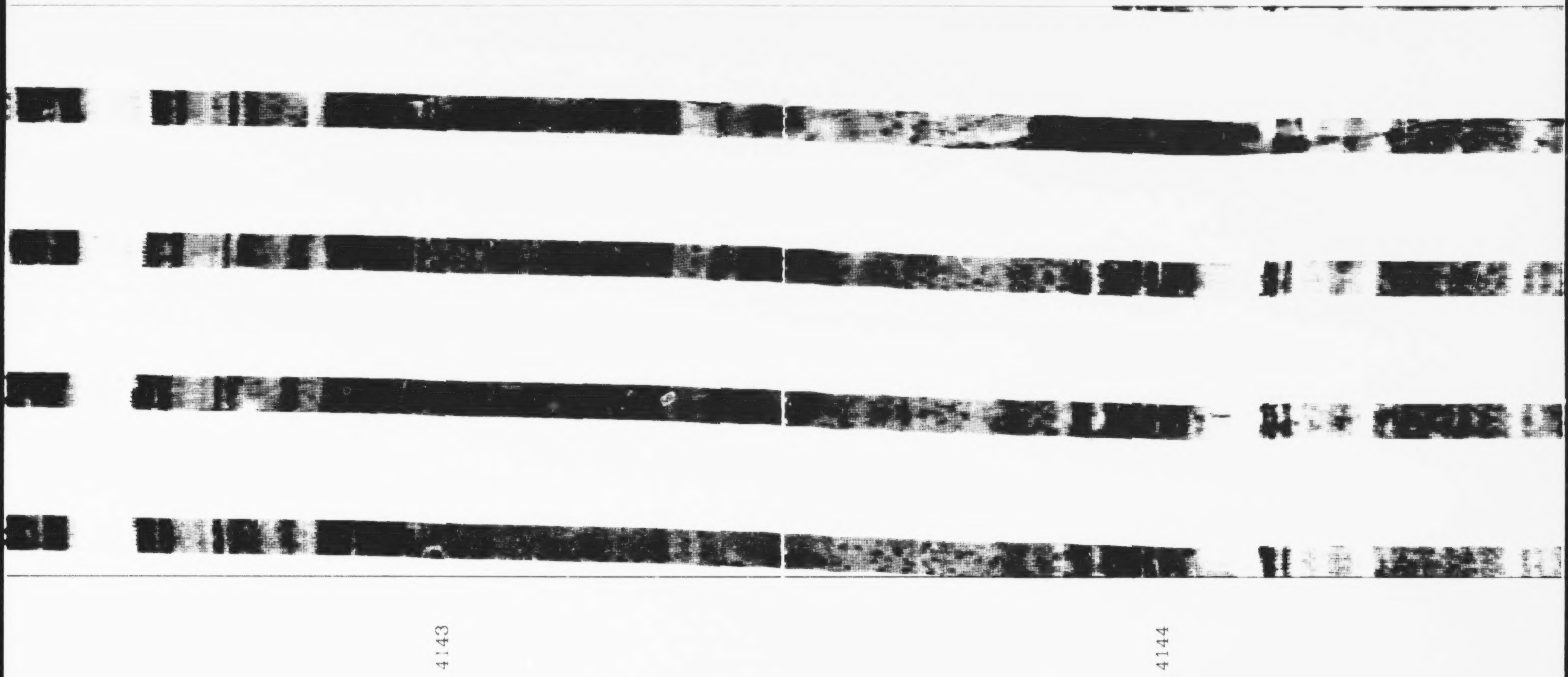
4143
4144

[illegible]

[illegible]

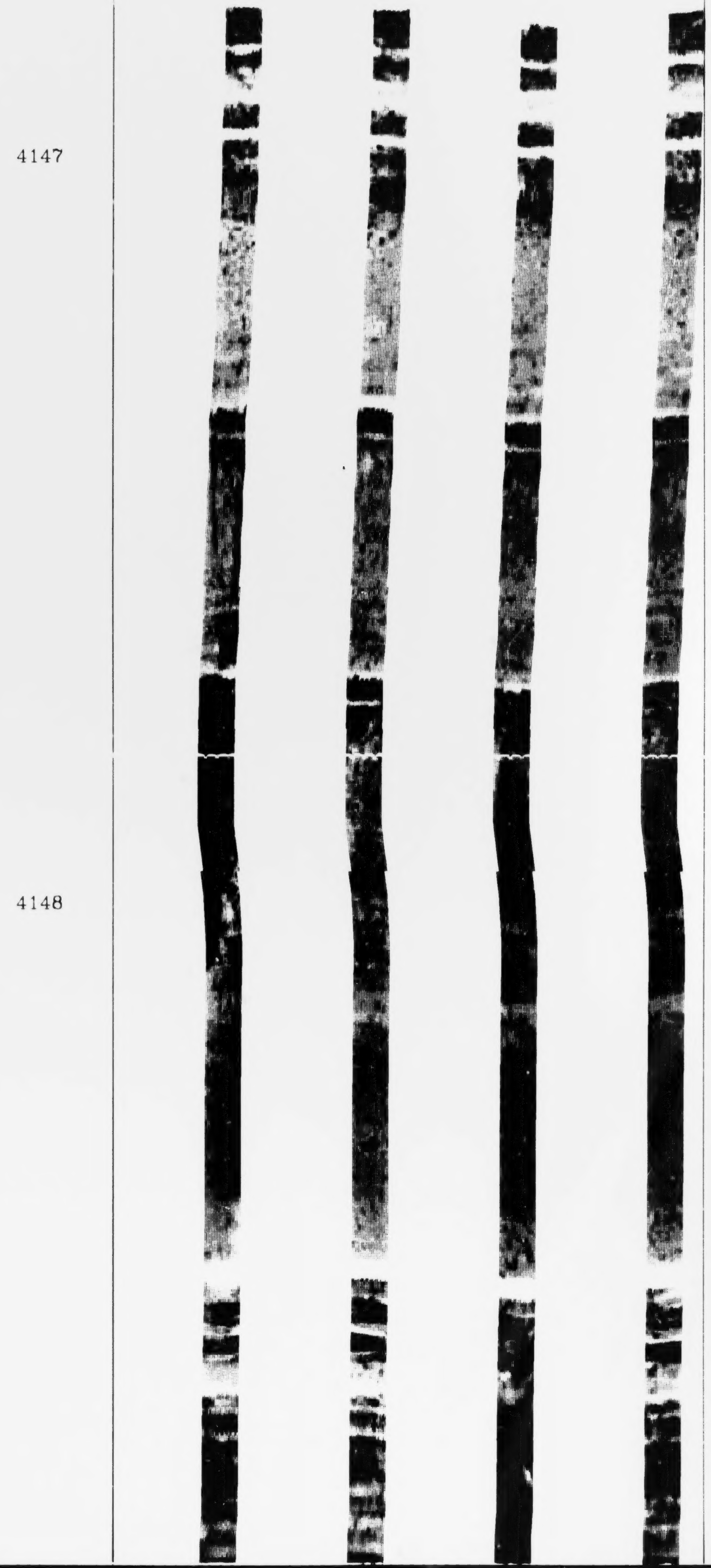
4147
4148

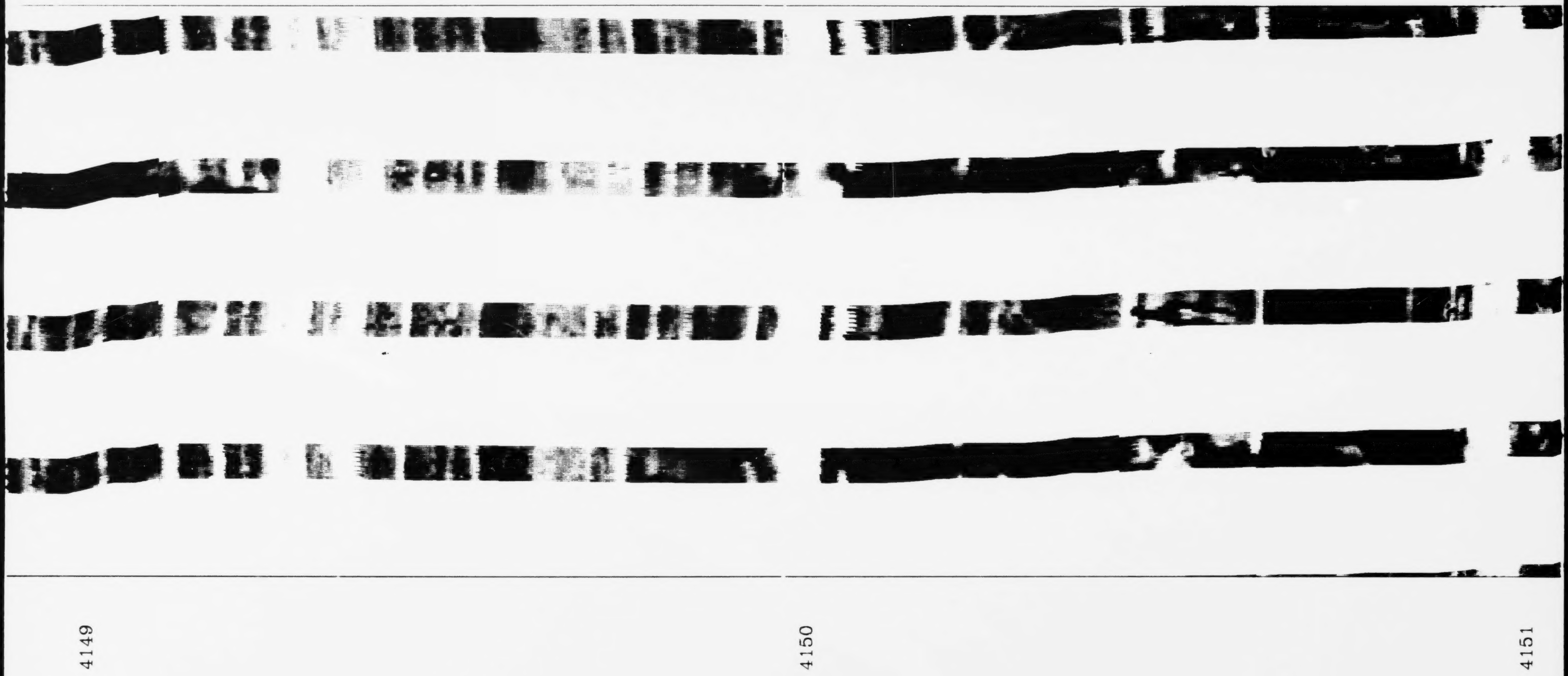
4149
4150
4151

4152

4153

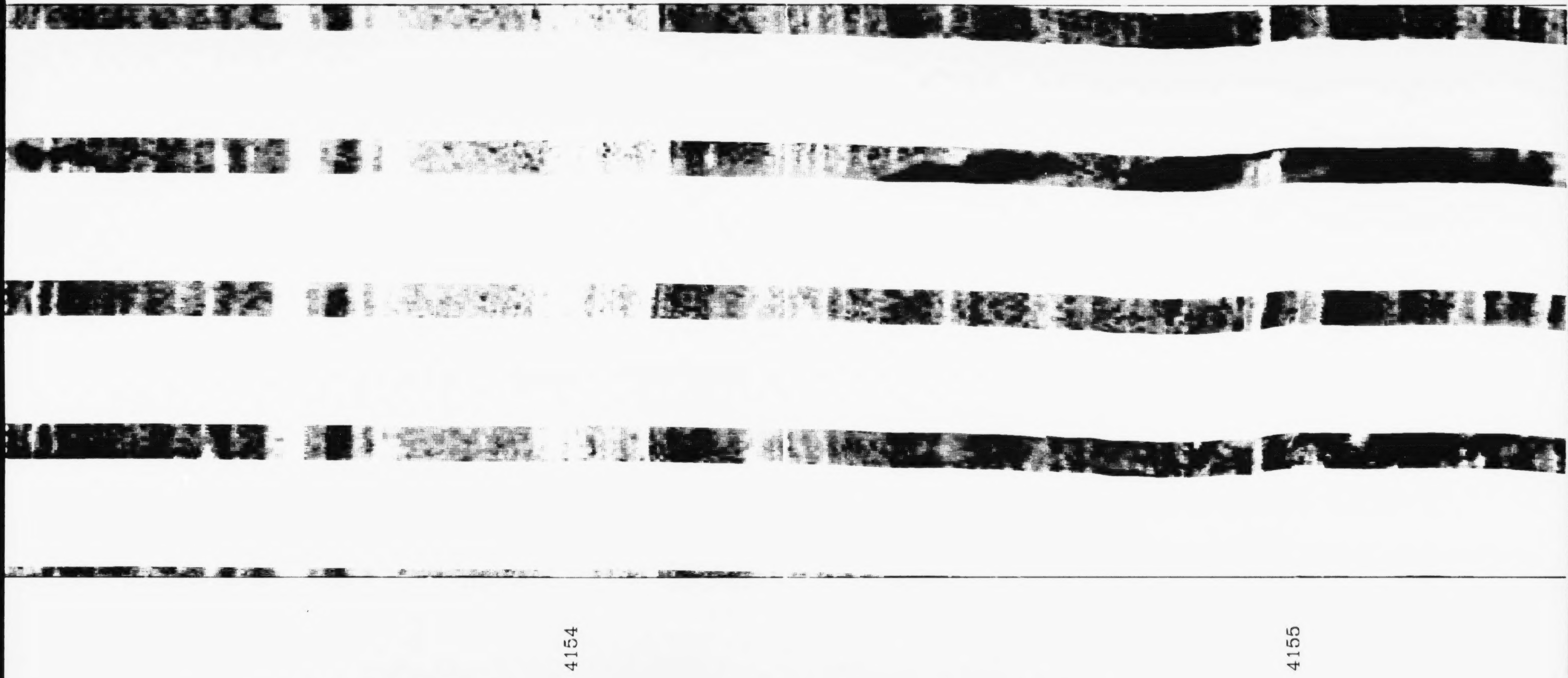
4154
4155

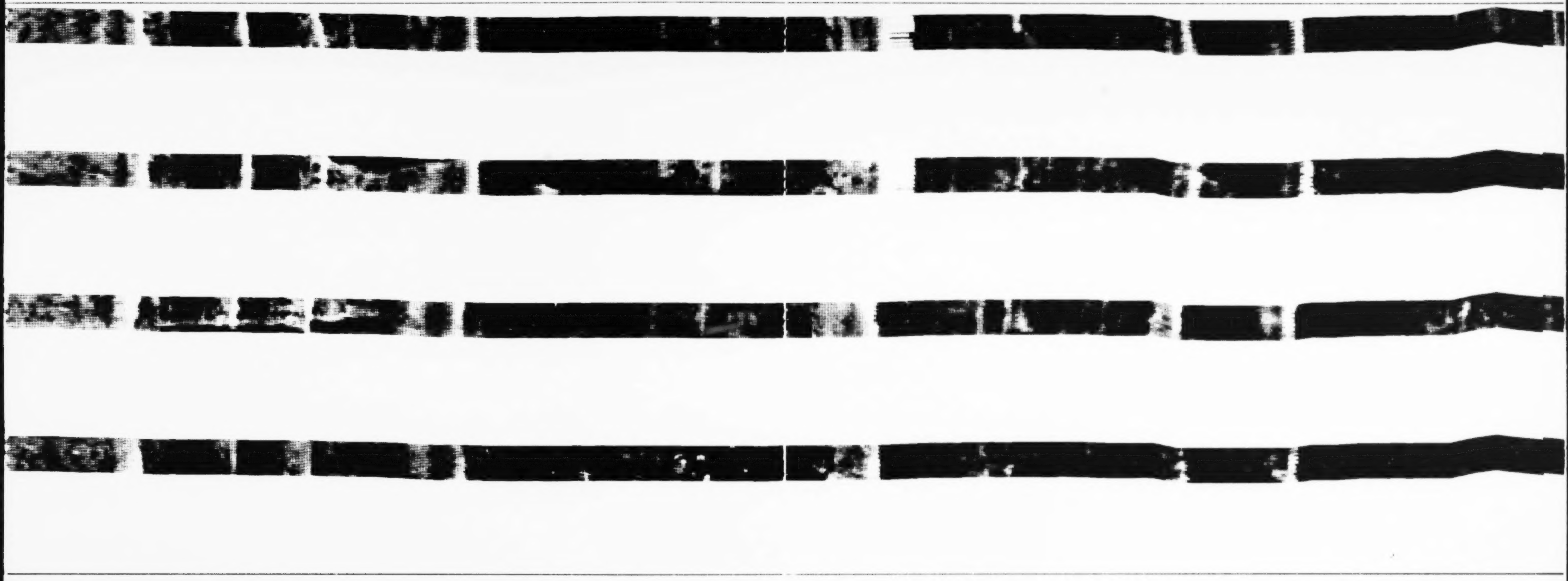

4156
4157

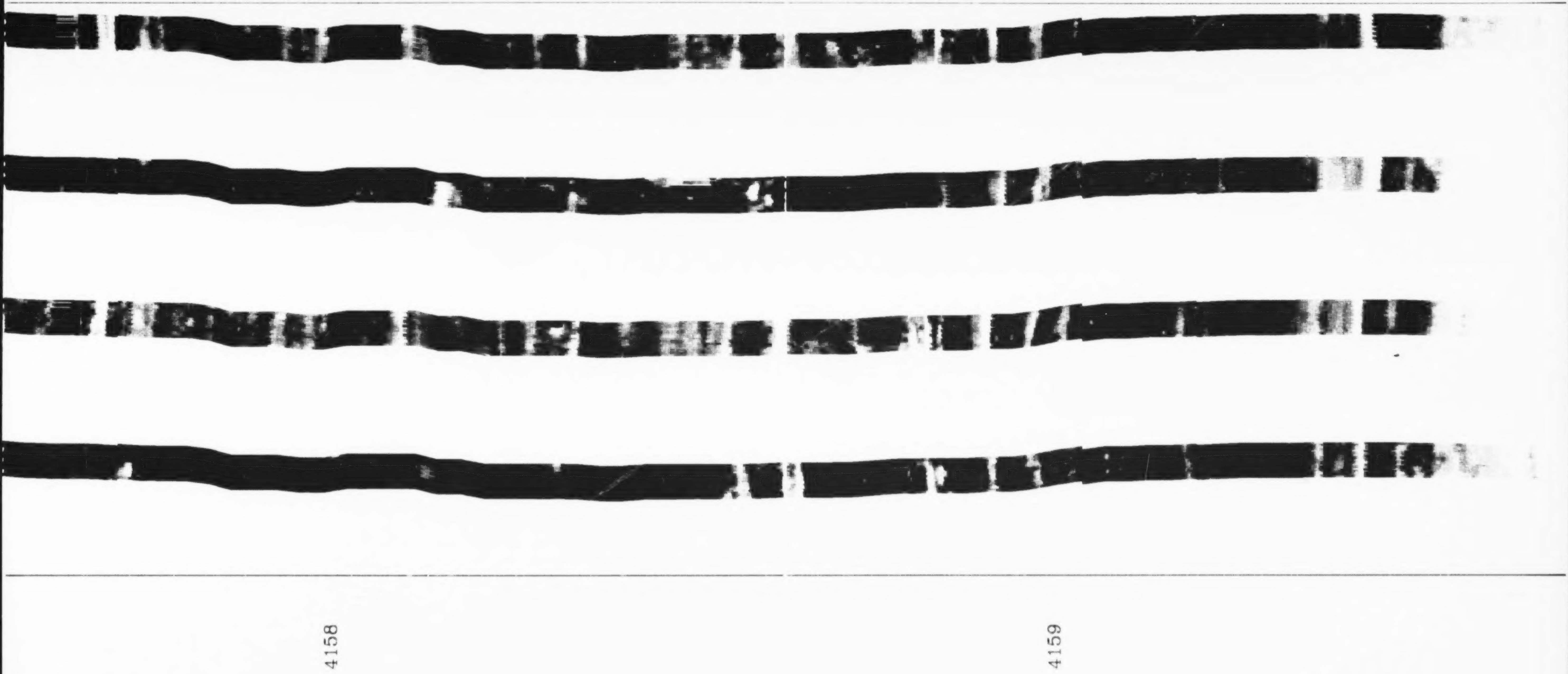
4158
4159

4160

[illegible]

4161

[redacted]

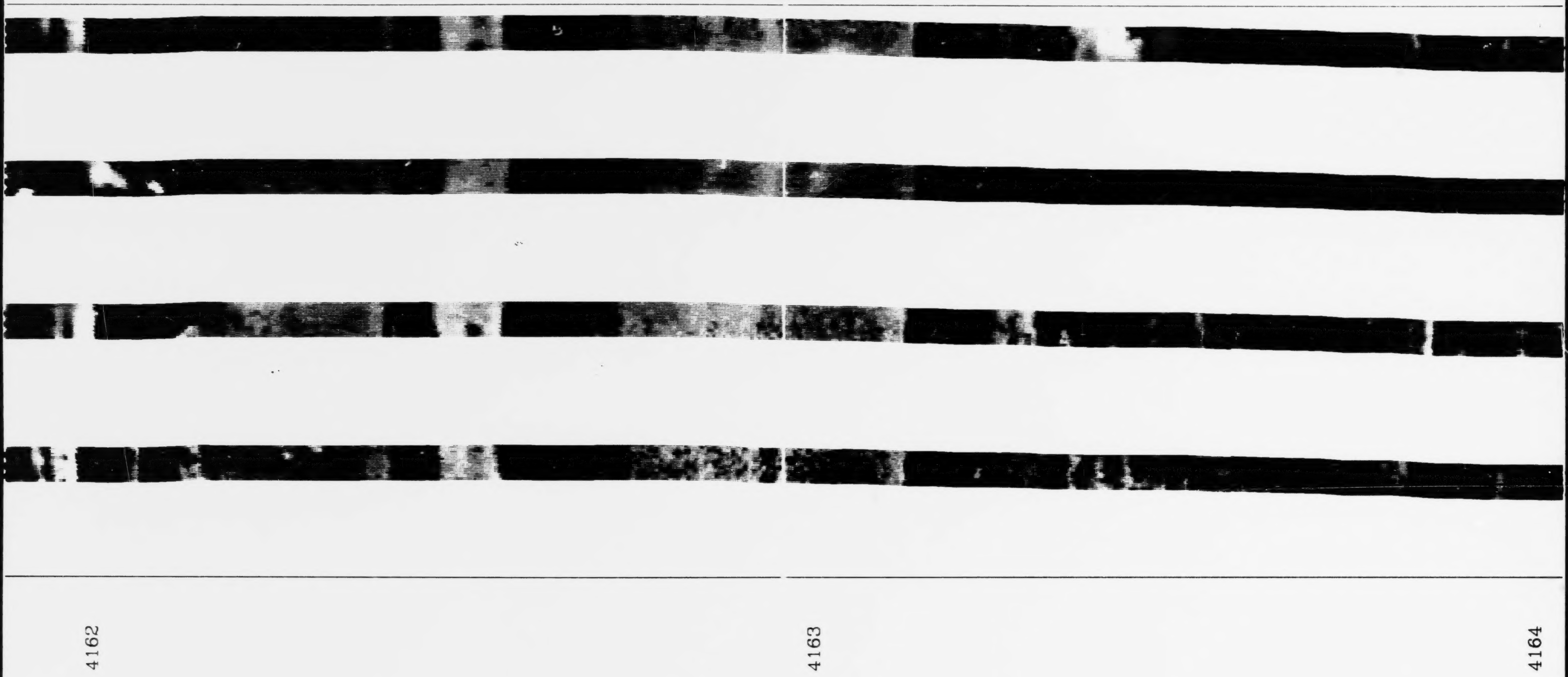
4162
4163
4164

SCHLUMBERGER

FMS
BOREHOLE
IMAGING

COMPANY	LAMONT-DOHERTY GEOLOGICAL
WELL	ODP HOLE-793B
FIELD	IZU-BONIN FOREARC BASIN
COUNTRY	OCEAN
RUN	1
DATE LOGGED	16 - JUN - 89
REFERENCE	STATIC PS 1 4165 4200

STATIC NORMALIZATION

PASS 1 (23577)

FILE : MEST.001

ZONE FROM 4200.0 M TO 4165.0 M

DEPTH SCALE = 1/ 5

IMAGE SCALE = 1/ 5

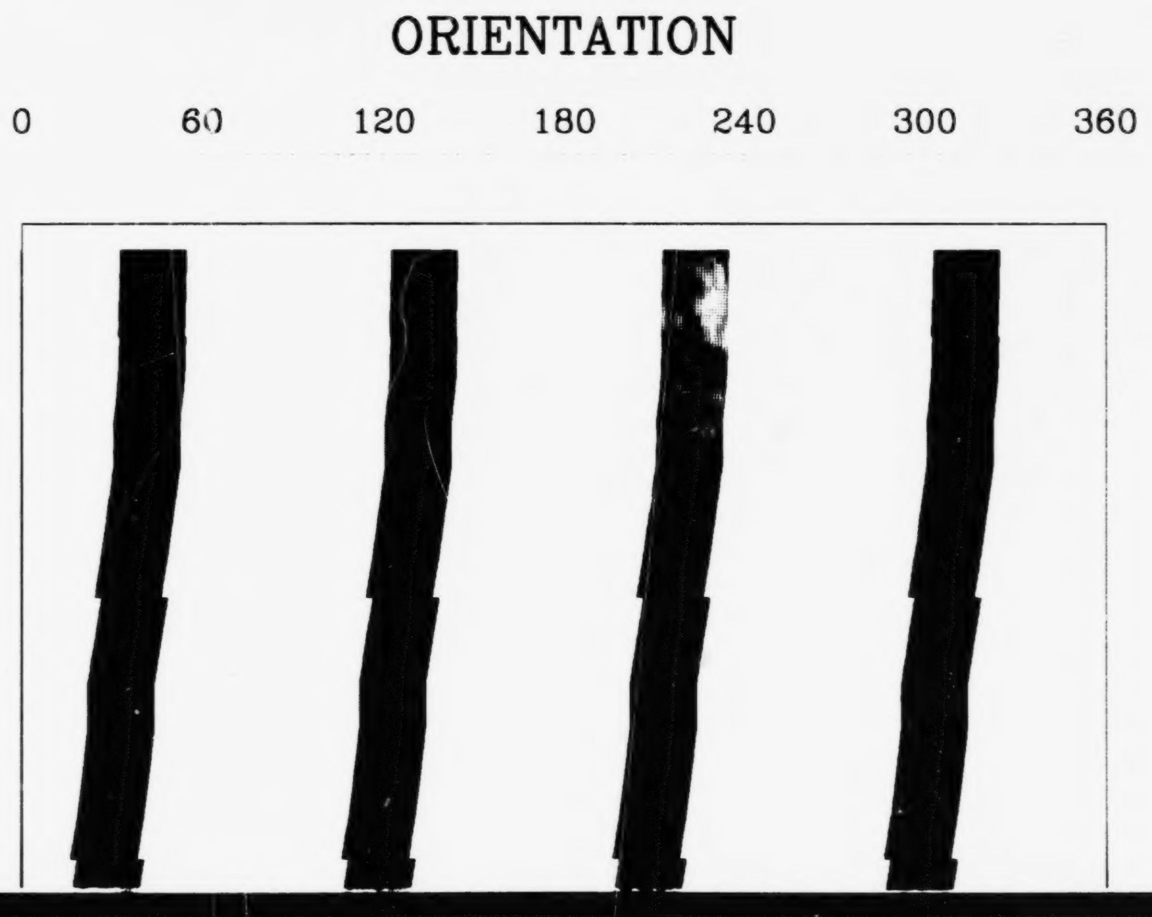

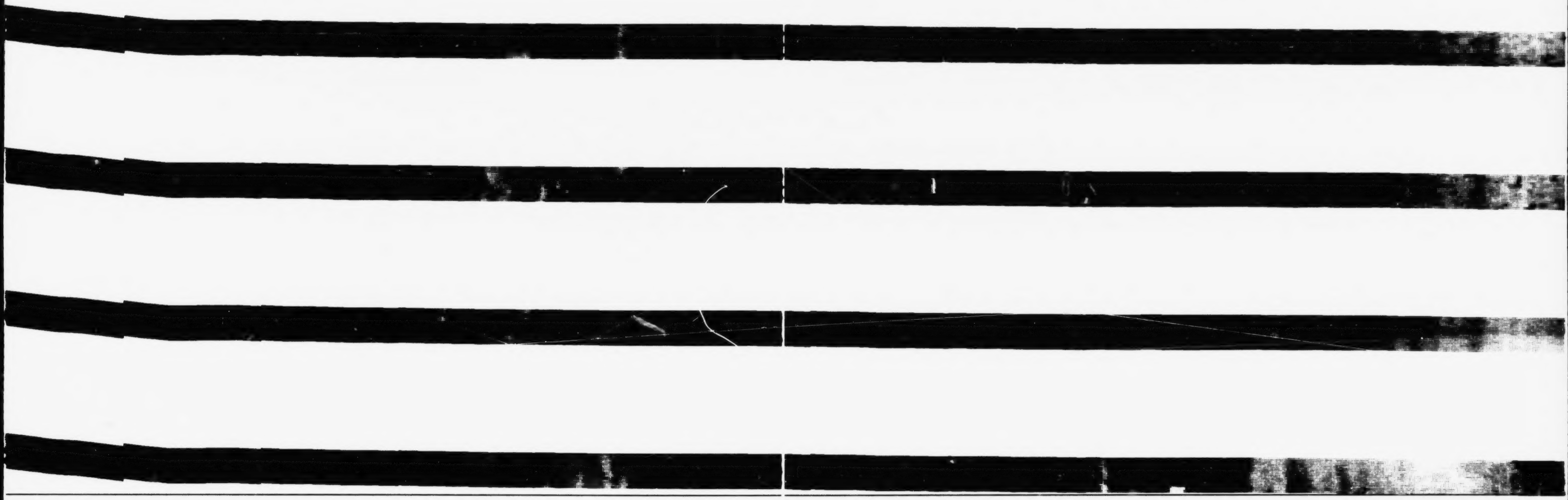

4166
4167

4168

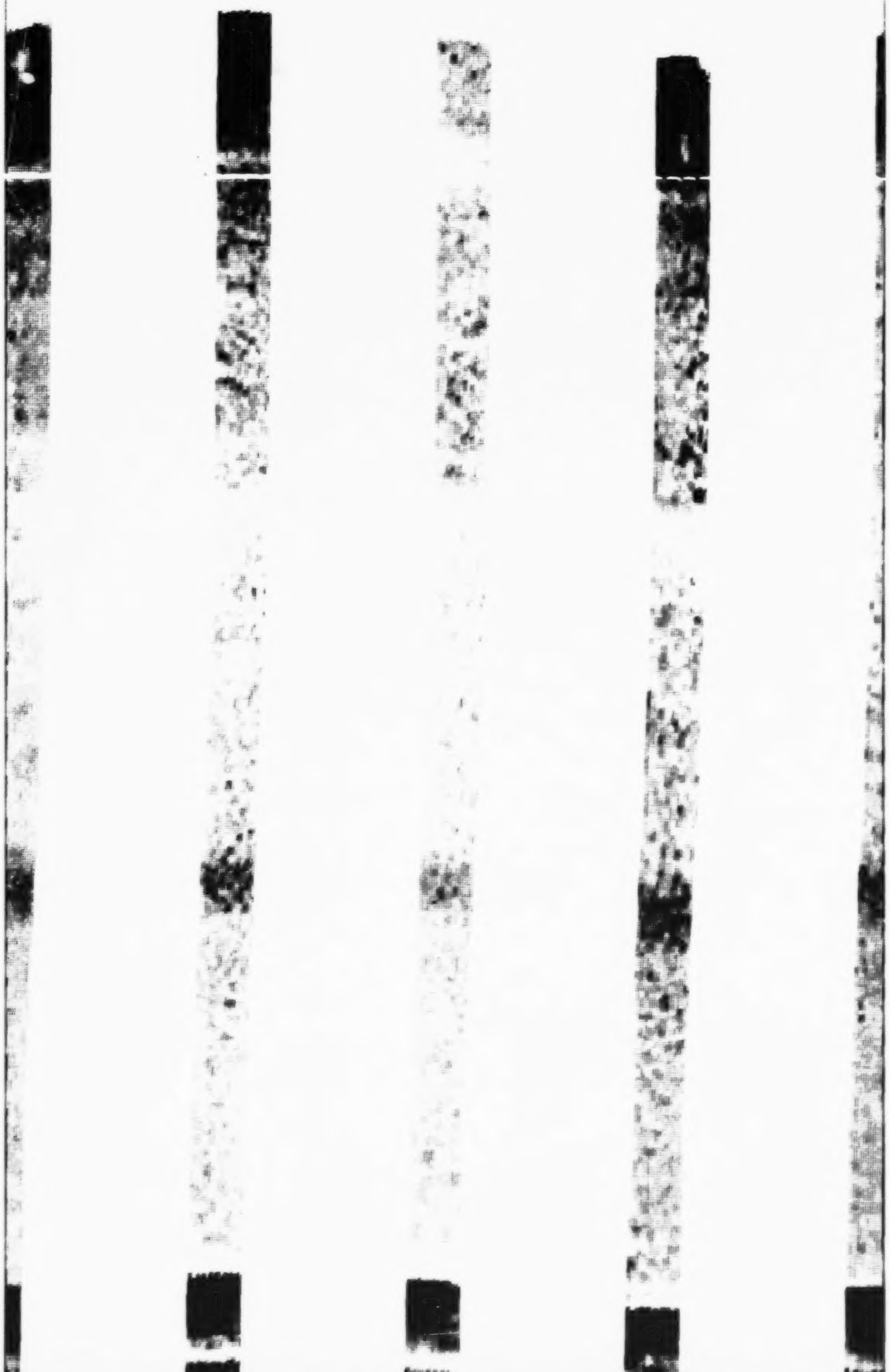

4169

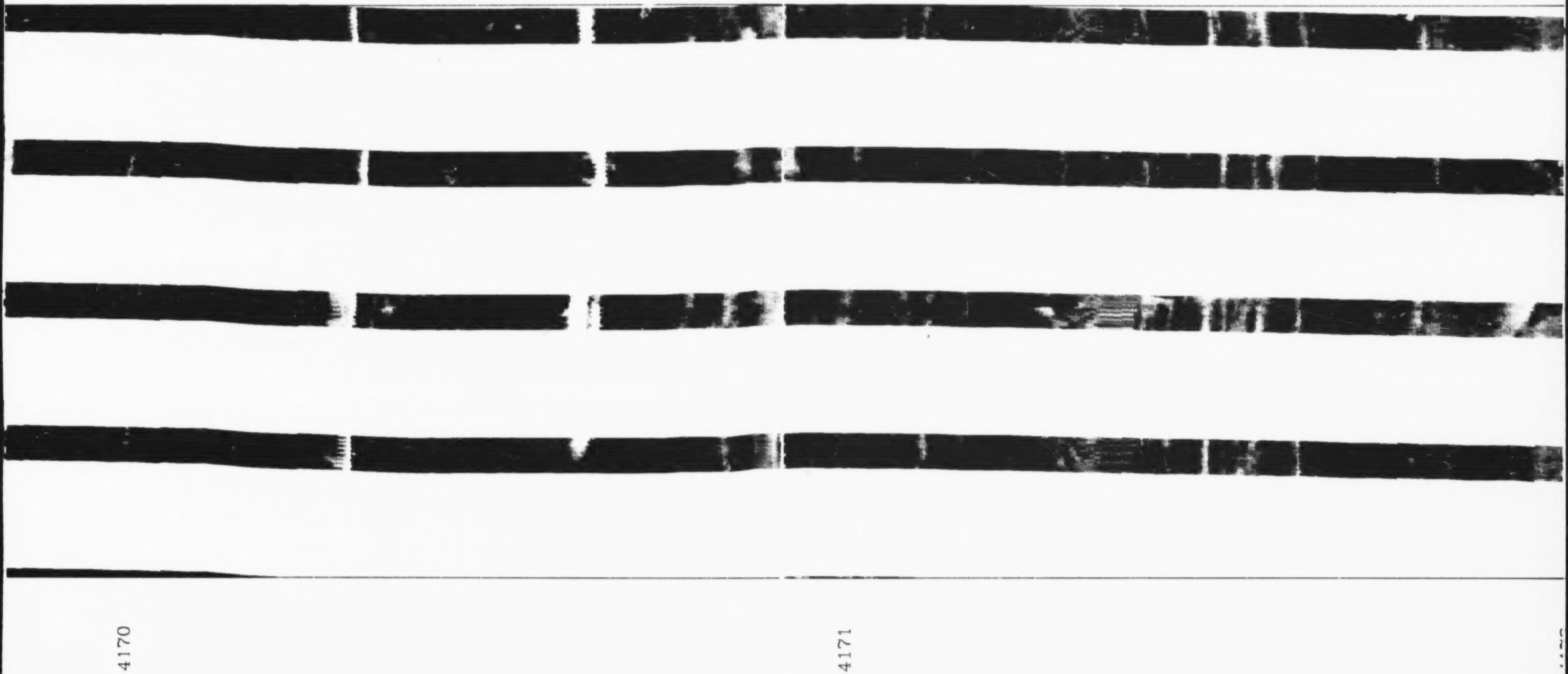
4170
4171

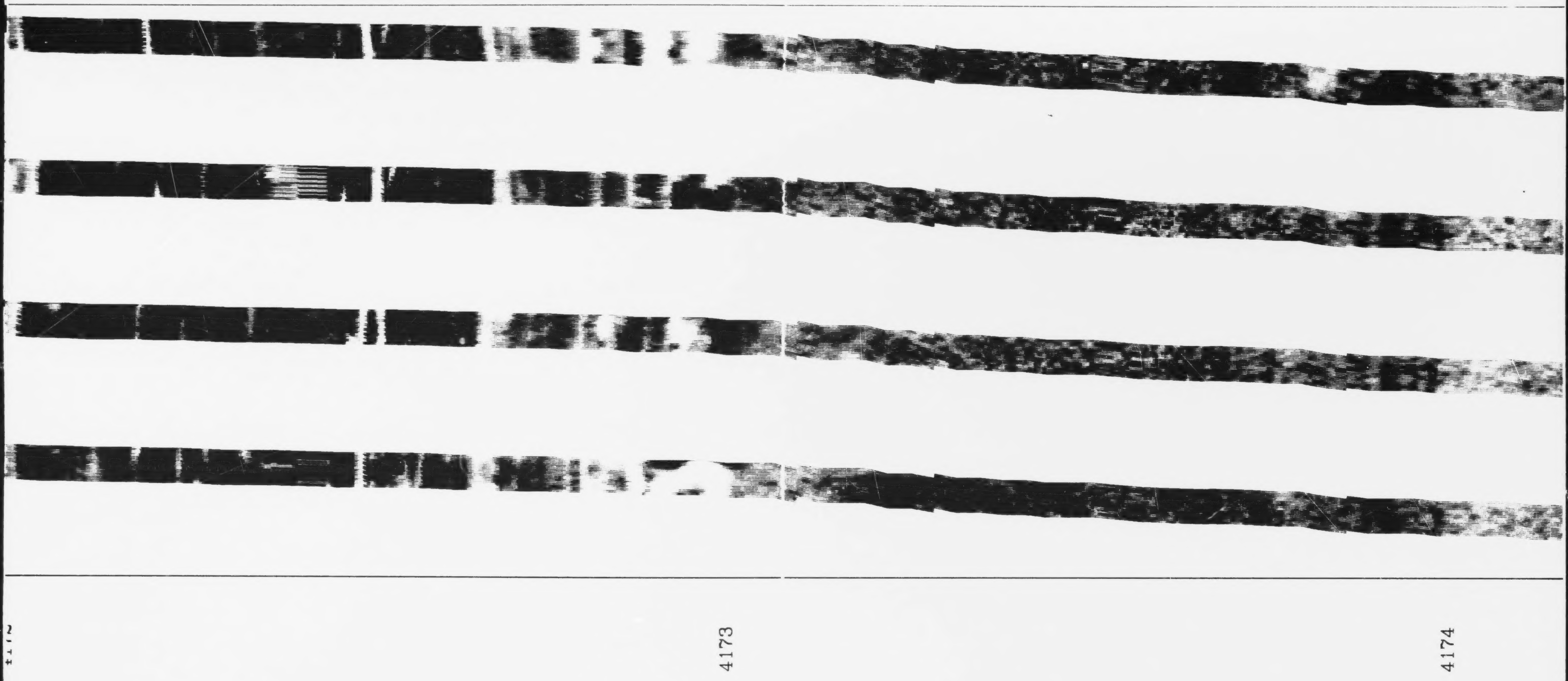
4173
4174

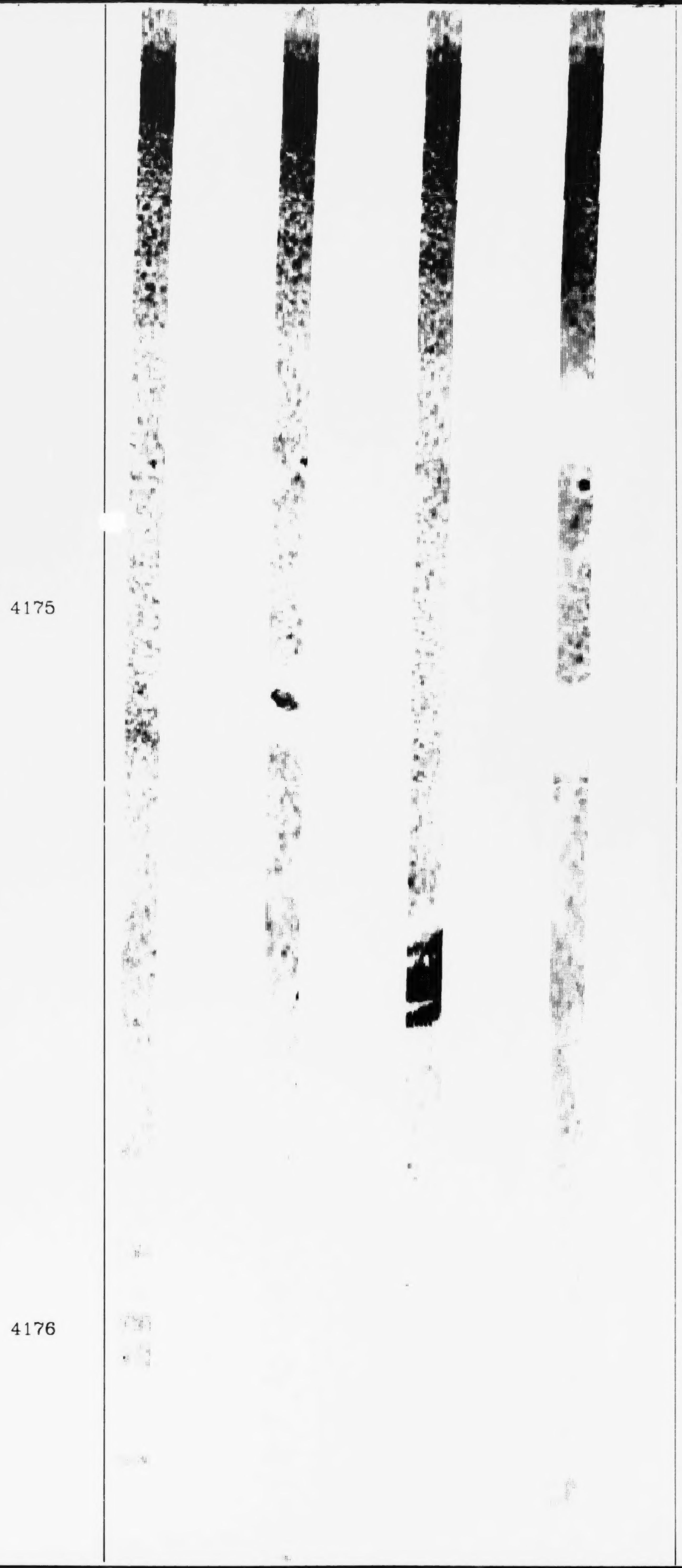
4175
4176

4177

4178

4179

4180

[redacted]

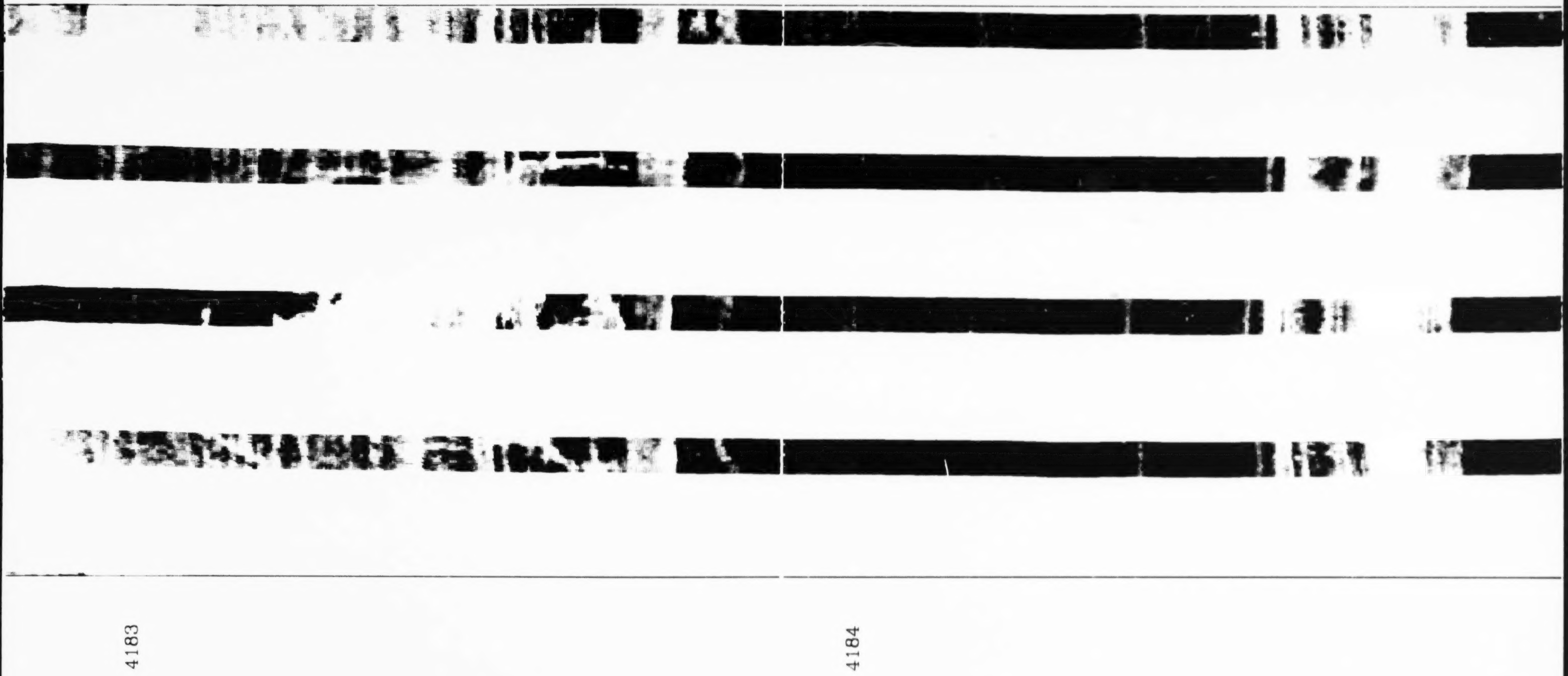
4183
4184

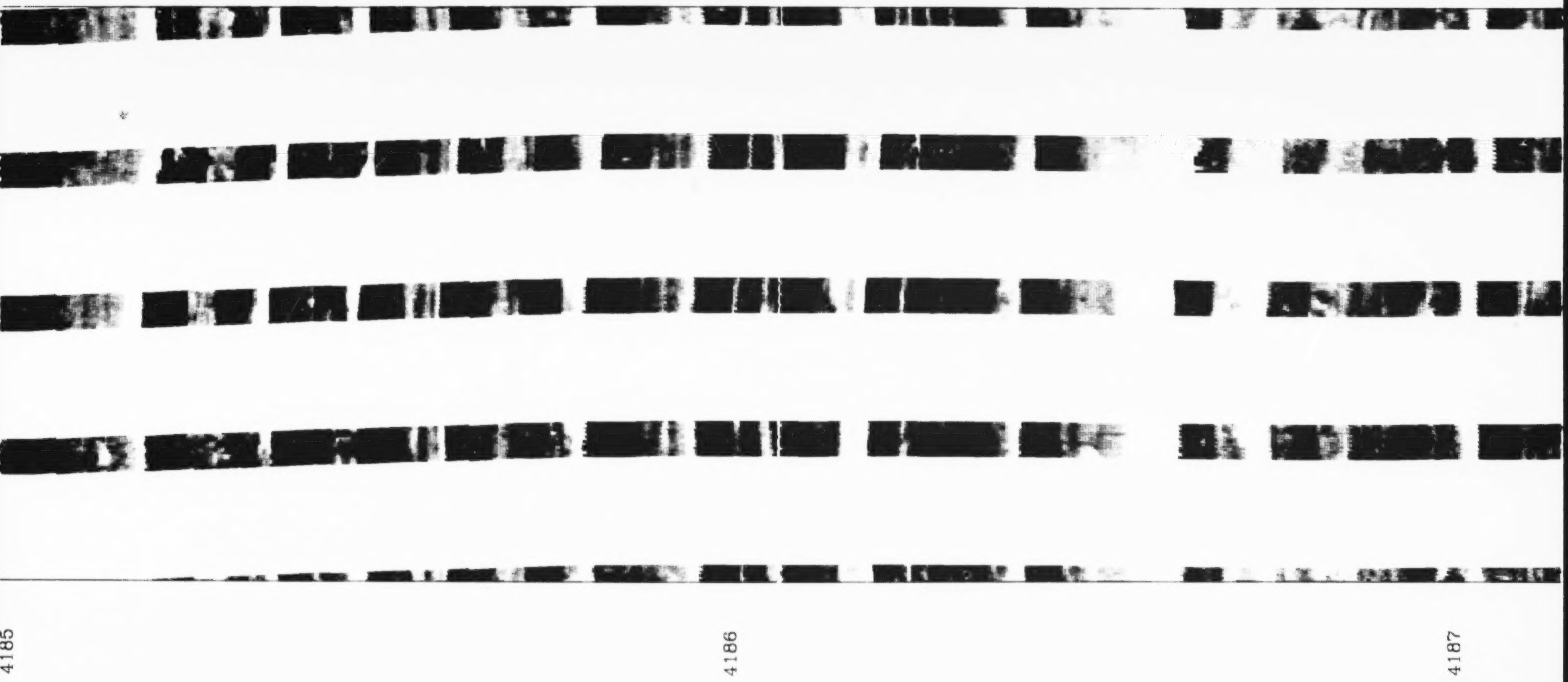
4185
4186
4187

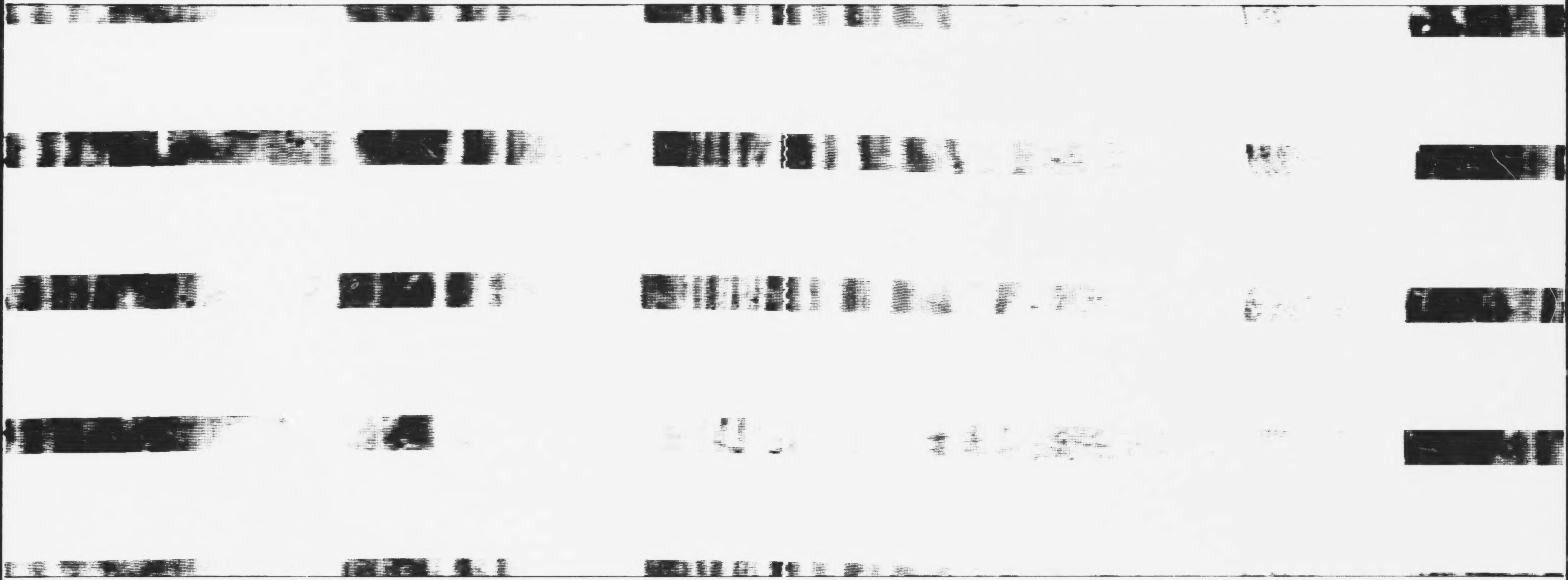
4188
4189

4190

[redacted]

4191

[redacted]

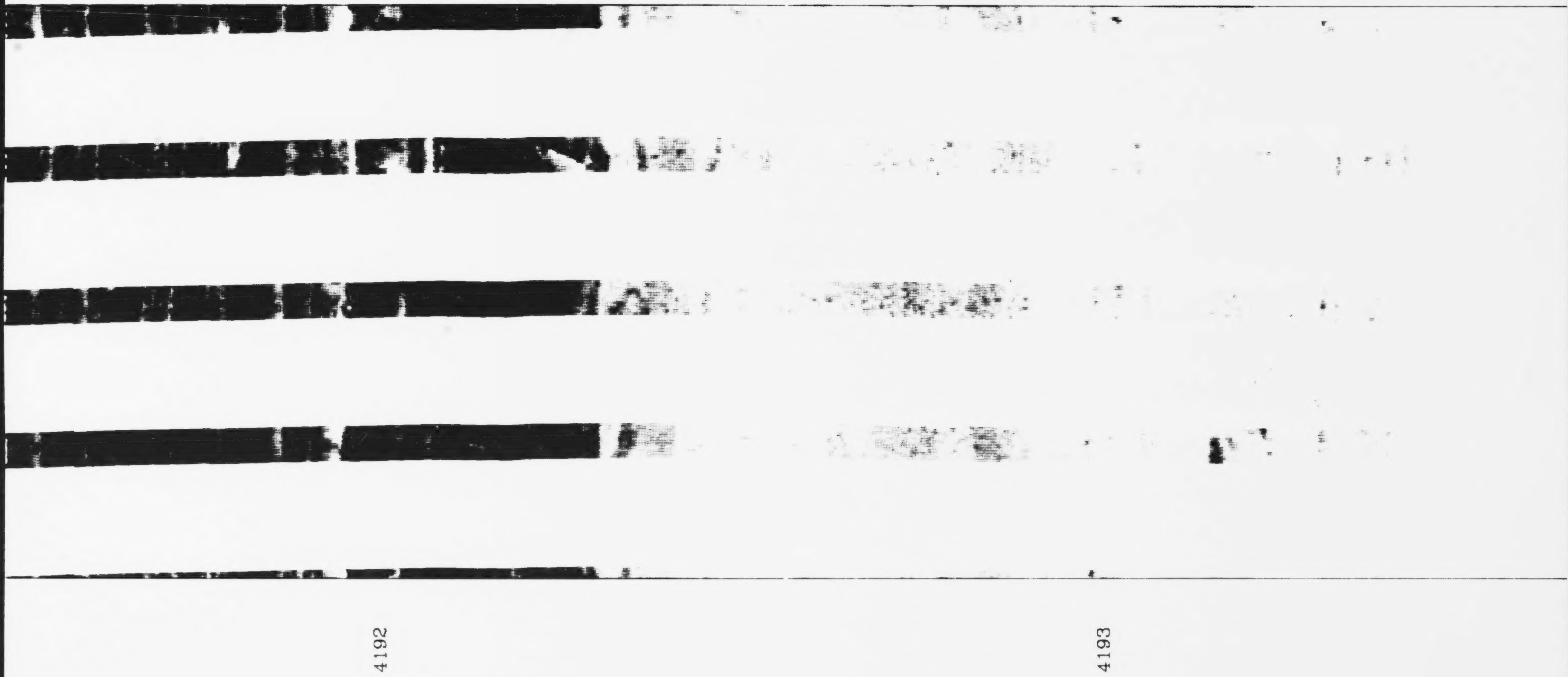
4192
4193

[redacted]

4194

4195

4196

4197

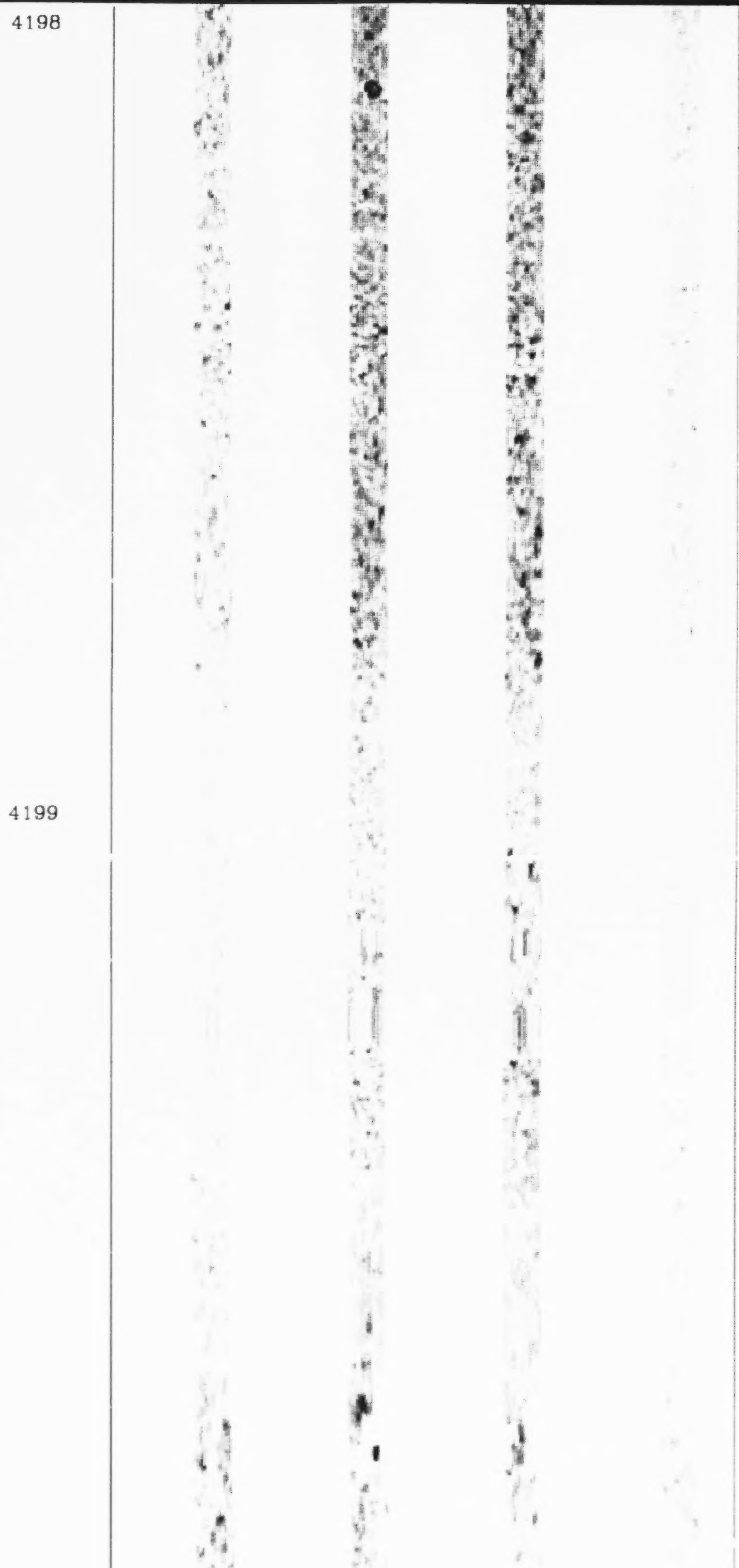
4198
4199

SCHLUMBERGER

FMS
BOREHOLE
IMAGING

COMPANY	LAMONT-DOHERTY GEOLOGICAL
WELL	ODP HOLE-793B
FIELD	IZU-BONIN FOREARC BASIN
COUNTRY	OCEAN
RUN	1
DATE LOGGED	16 - JUN - 89
REFERENCE	STATIC PS 1 4200 4230

ZONE FROM 4230.0 M TO 4200.0 M
DEPTH SCALE = 1/ 5
IMAGE SCALE = 1/ 5

STATIC NORMALIZATION
PASS 1 (23577)
FILE : MEST.001

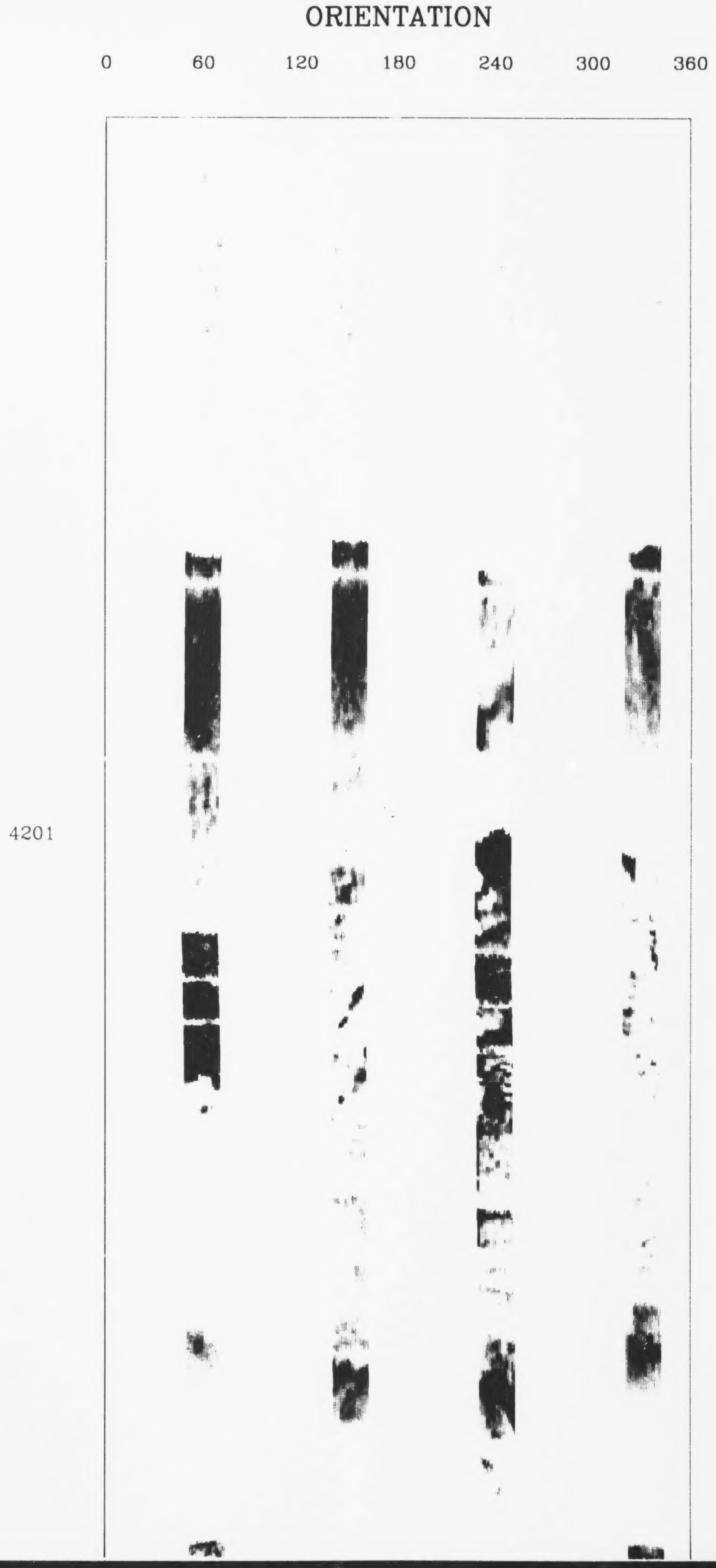
ORIENTATION
0
60
120
180
240
300
360
4201

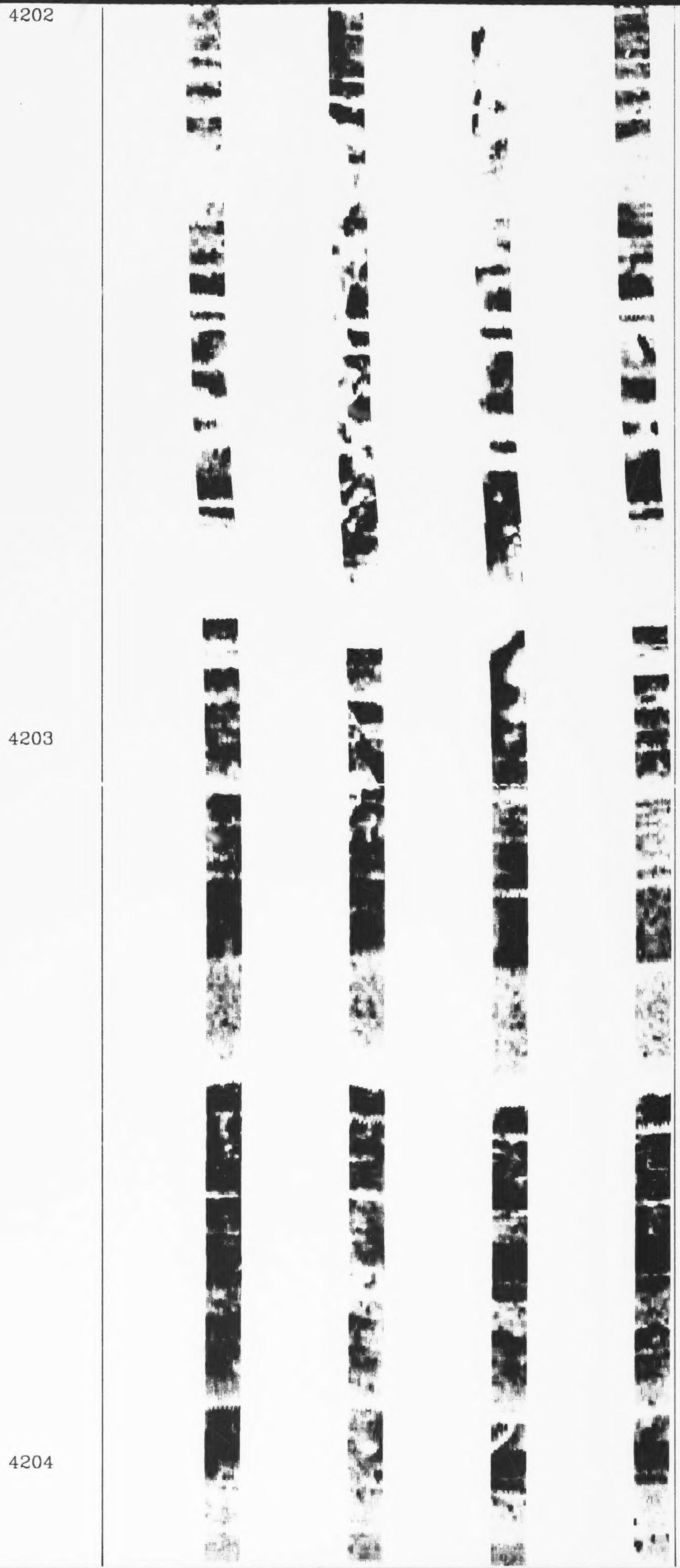
4202
4203
4204

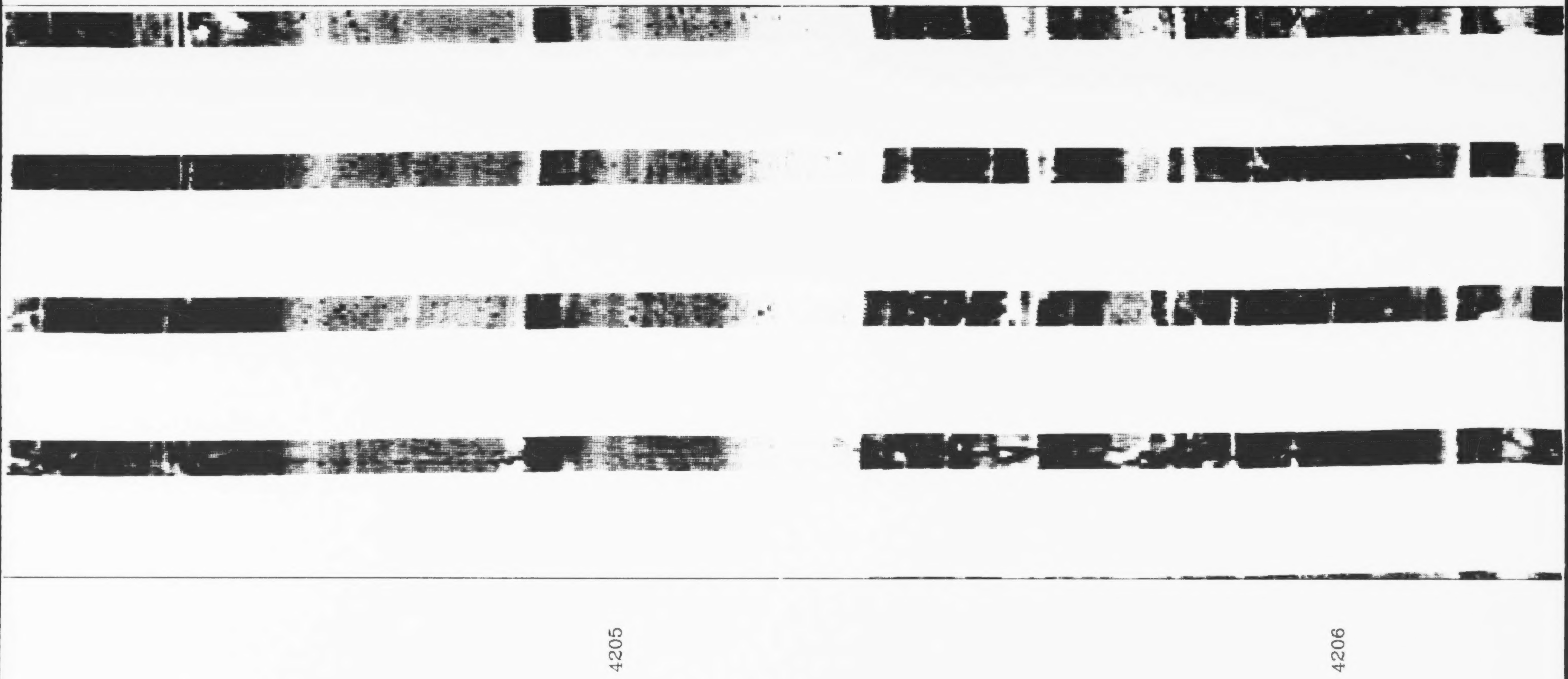
4205
4206

[redacted]

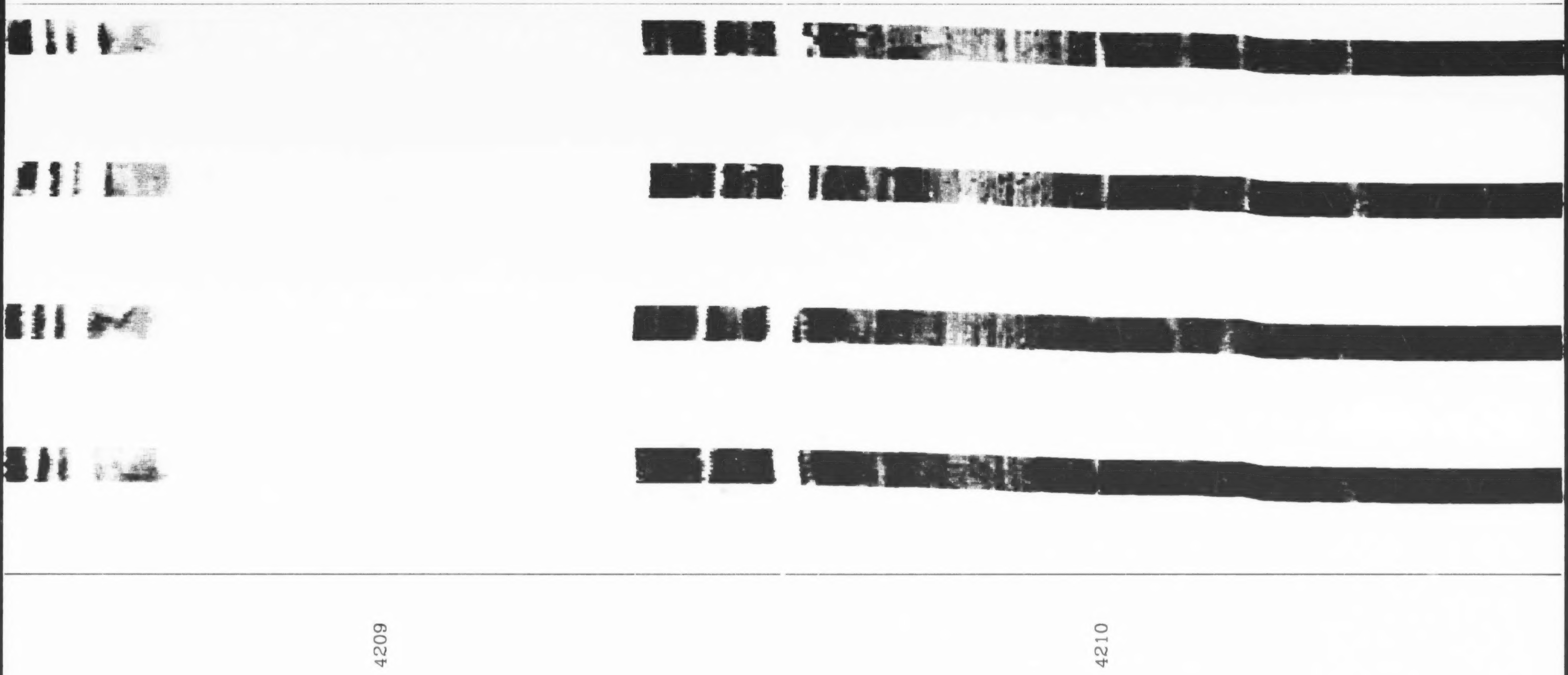
4209
4210

4211

[illegible]

4212

4213

[illegible]

4214

[illegible]

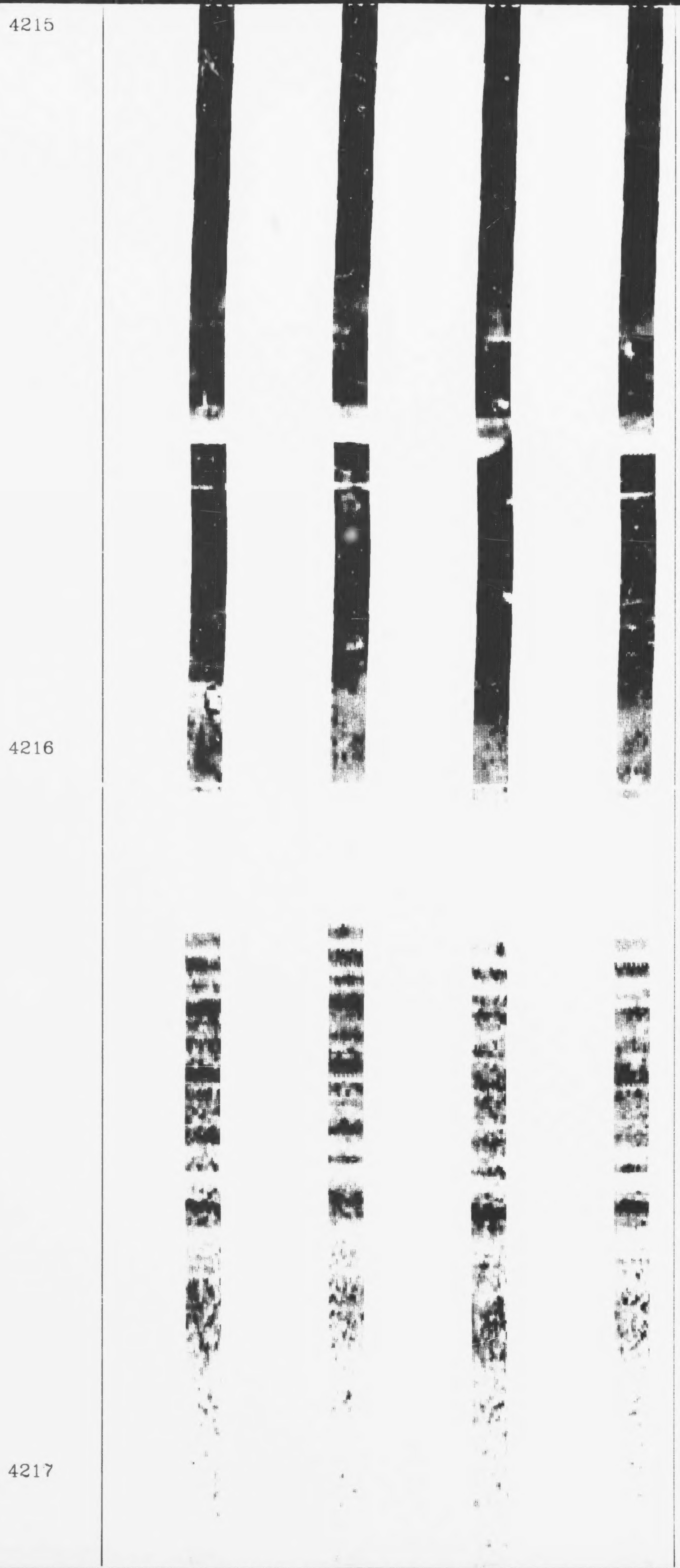
4215
4216
4217

4218

4219

[redacted]

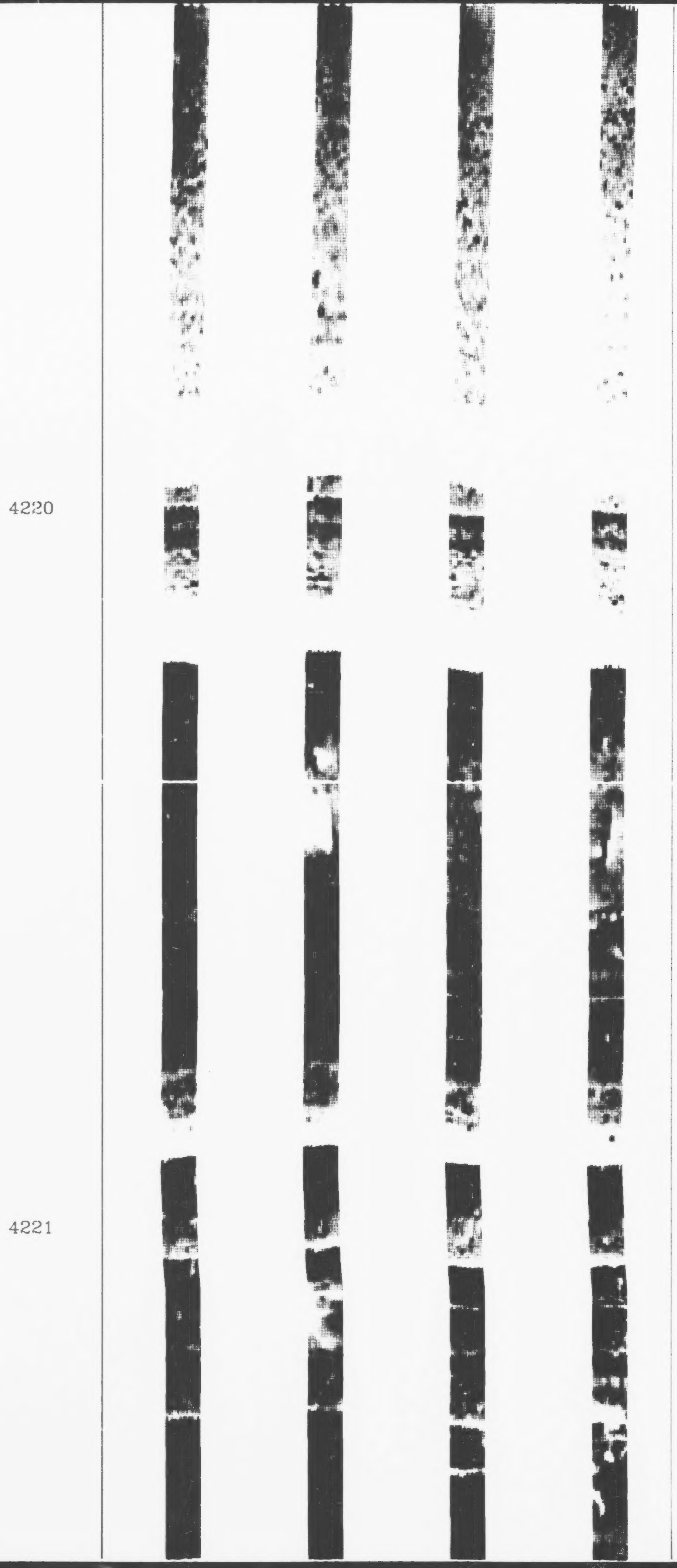
4220
4221

4224 [redacted]

4225 [redacted]

[redacted]

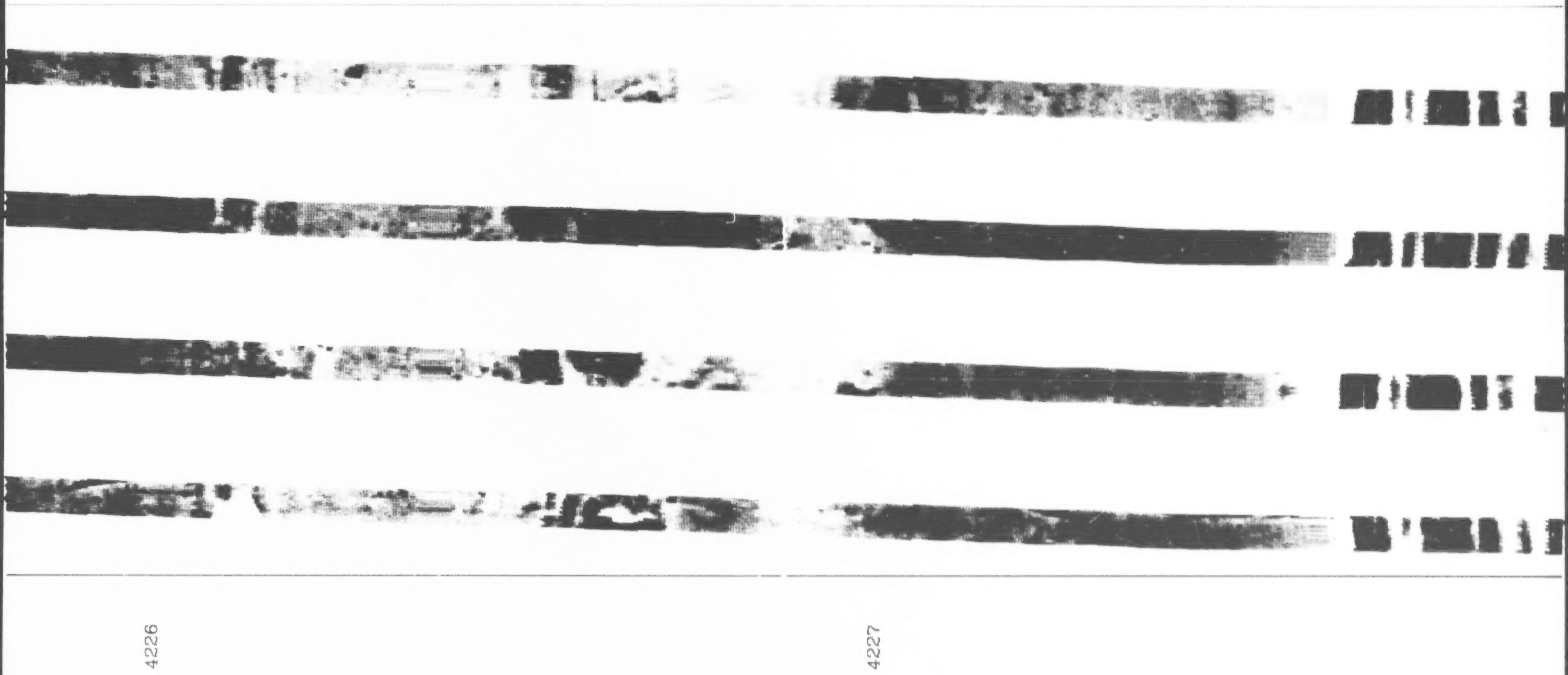
4226
4227

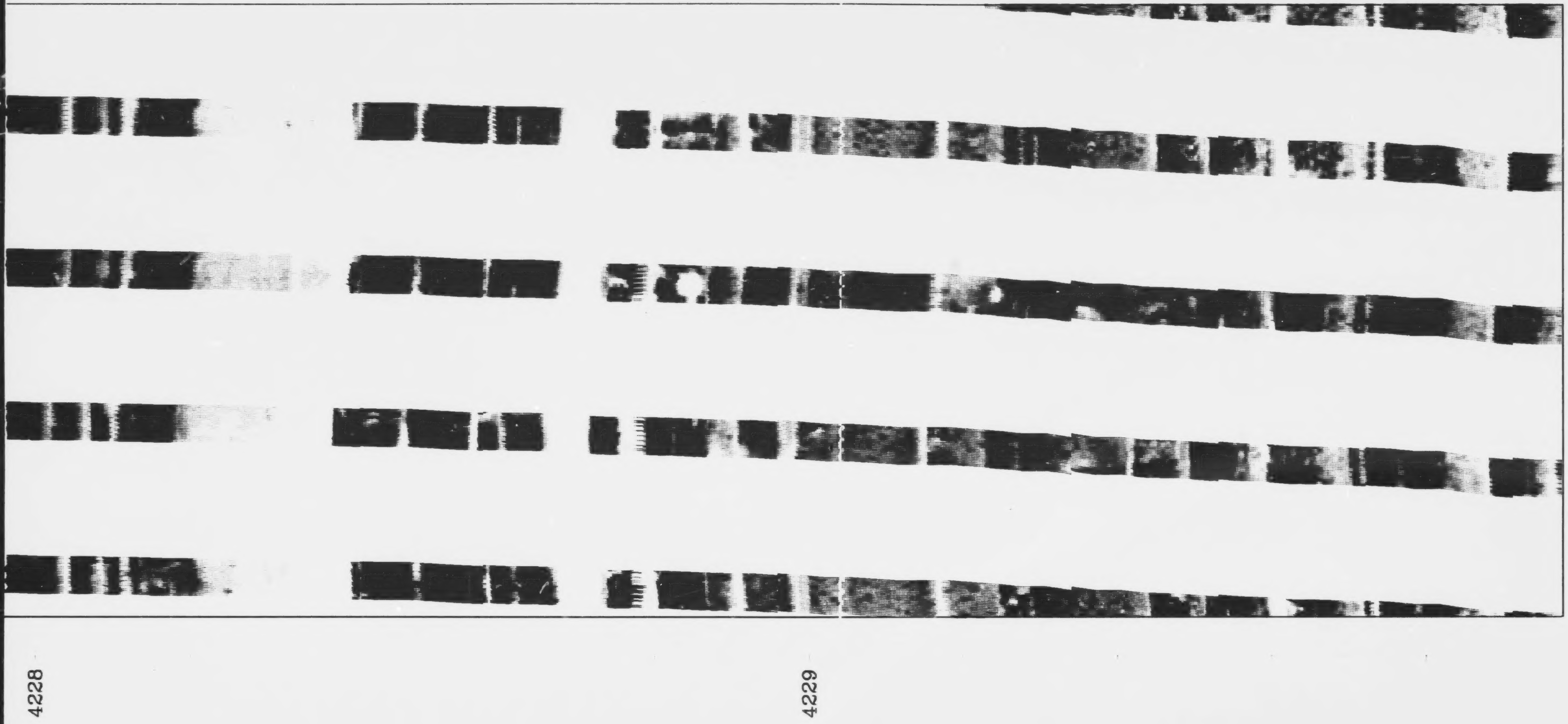
4228
4229

SCHLUMBERGER

FMS
BOREHOLE
IMAGING

COMPANY	LAMONT–DOHERTY GEOLOGICAL
WELL	ODP HOLE–793B
FIELD	IZU–BONIN FOREARC BASIN
COUNTRY	OCEAN
RUN	1
DATE LOGGED	16 – JUN – 89
REFERENCE	STATIC PS-1 4230–4265

STATIC NORMALIZATION

PASS 1 (23577)

FILE : MEST.001

ZONE FROM 4265.0 M TO 4230.0 M

DEPTH SCALE = 1/ 5

IMAGE SCALE = 1/ 5

BITSIZE = 9.88

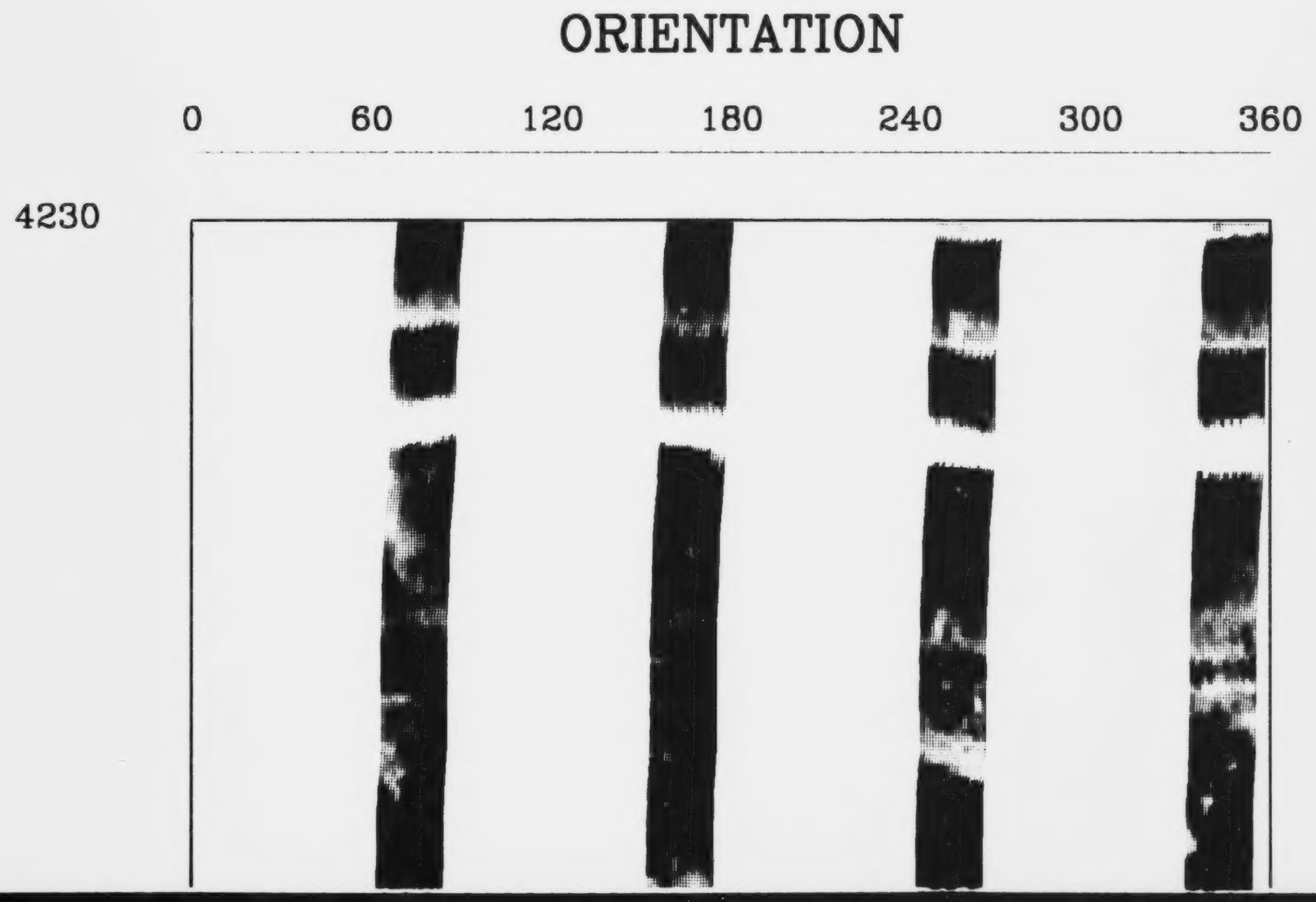

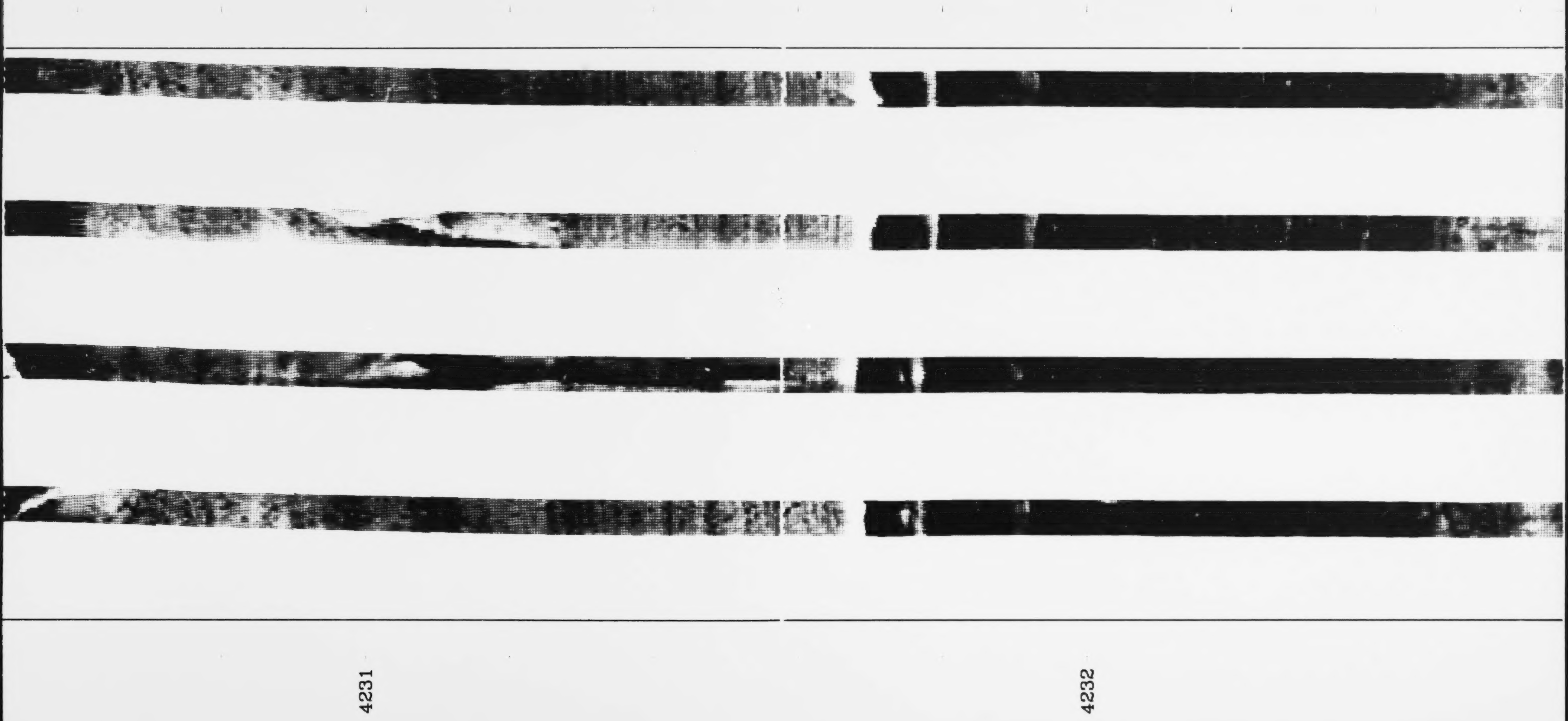
4231
4232

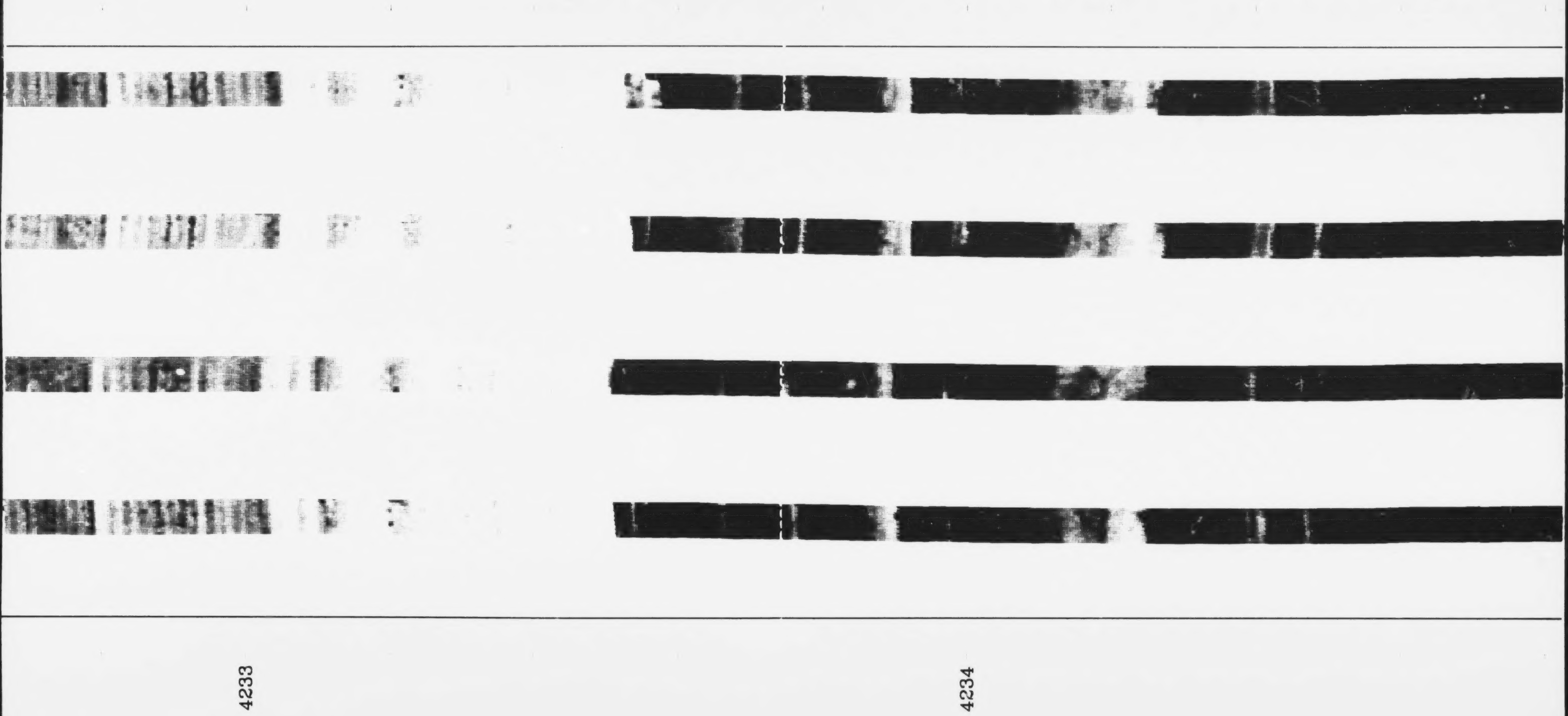
4233
4234

4235
4236

4237

4238

4239

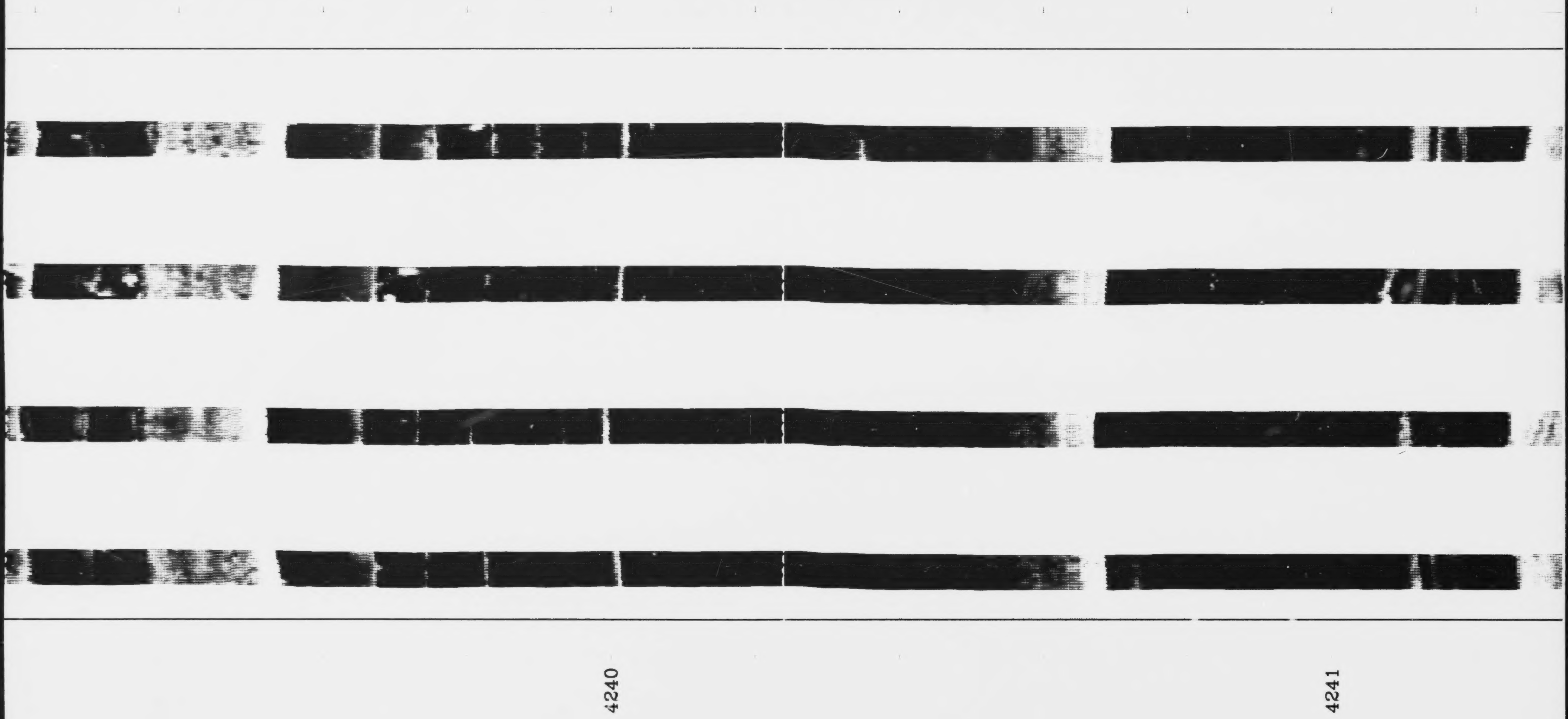
4240
4241

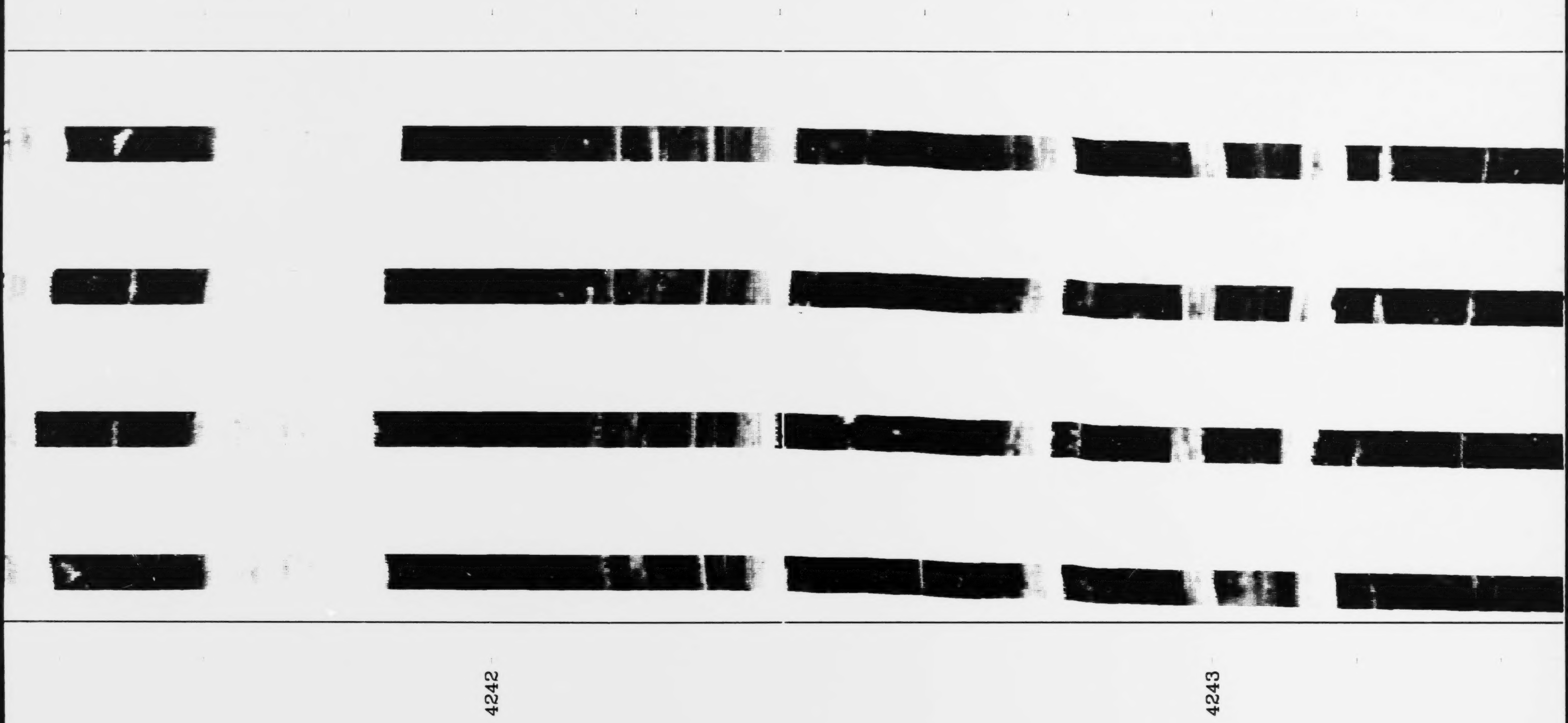
4242
4243

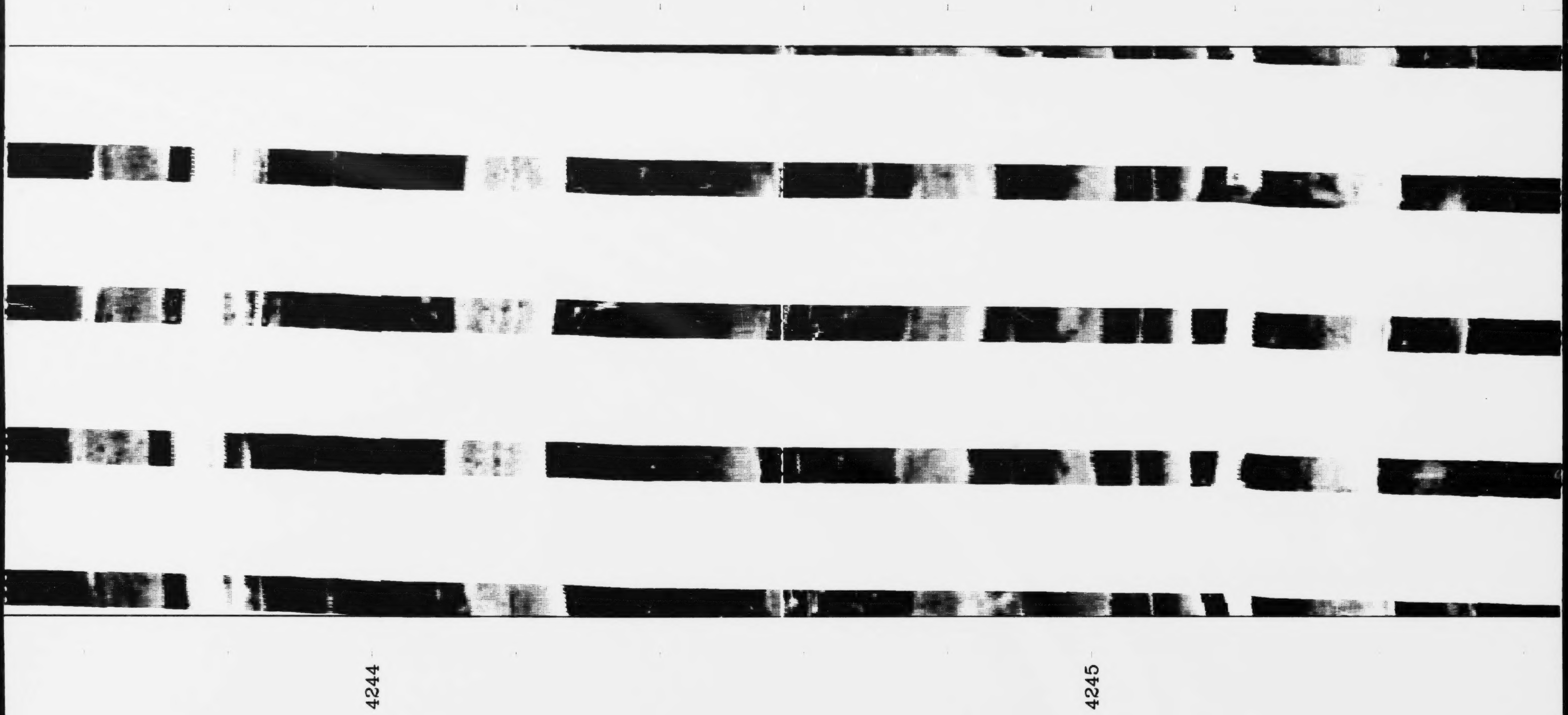
4244
4245

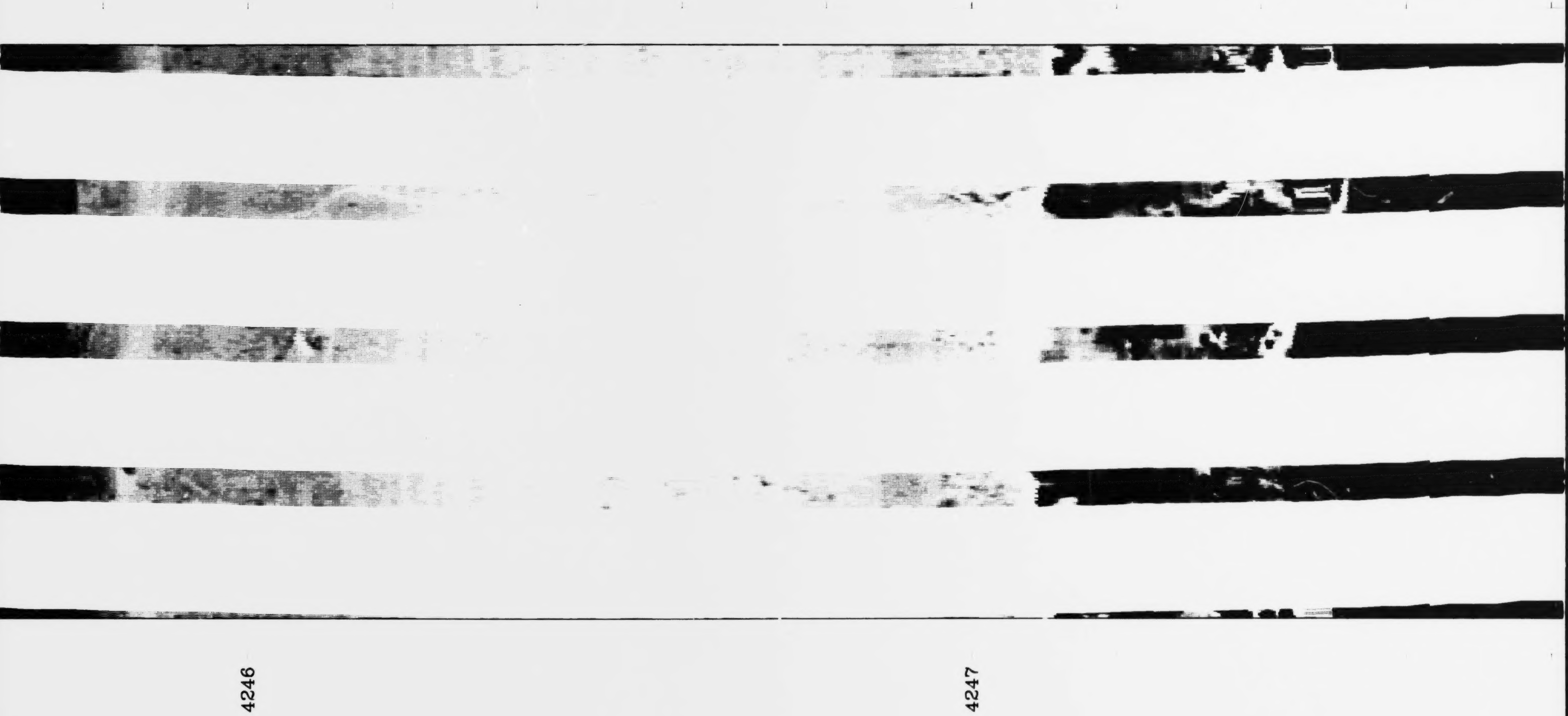

4246
4247

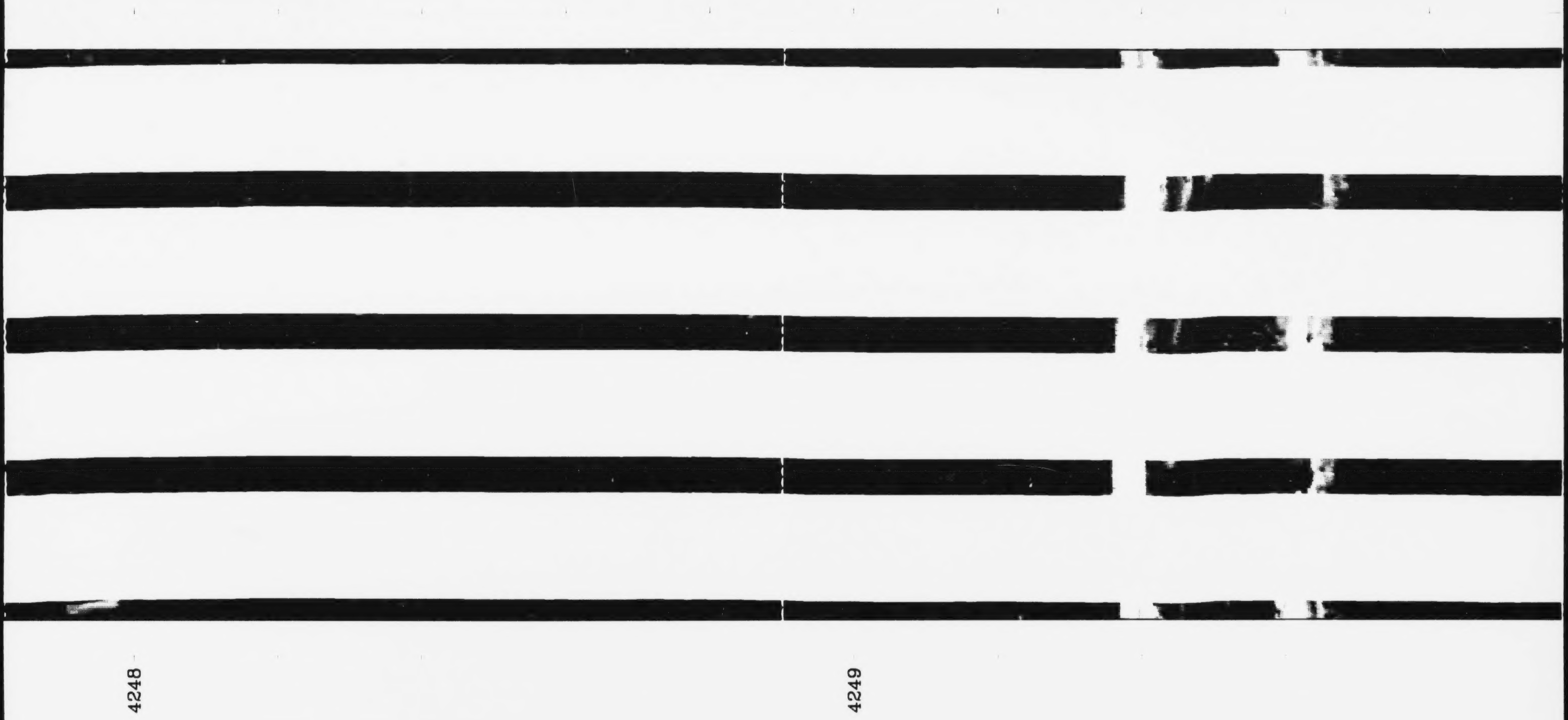
4248
4249

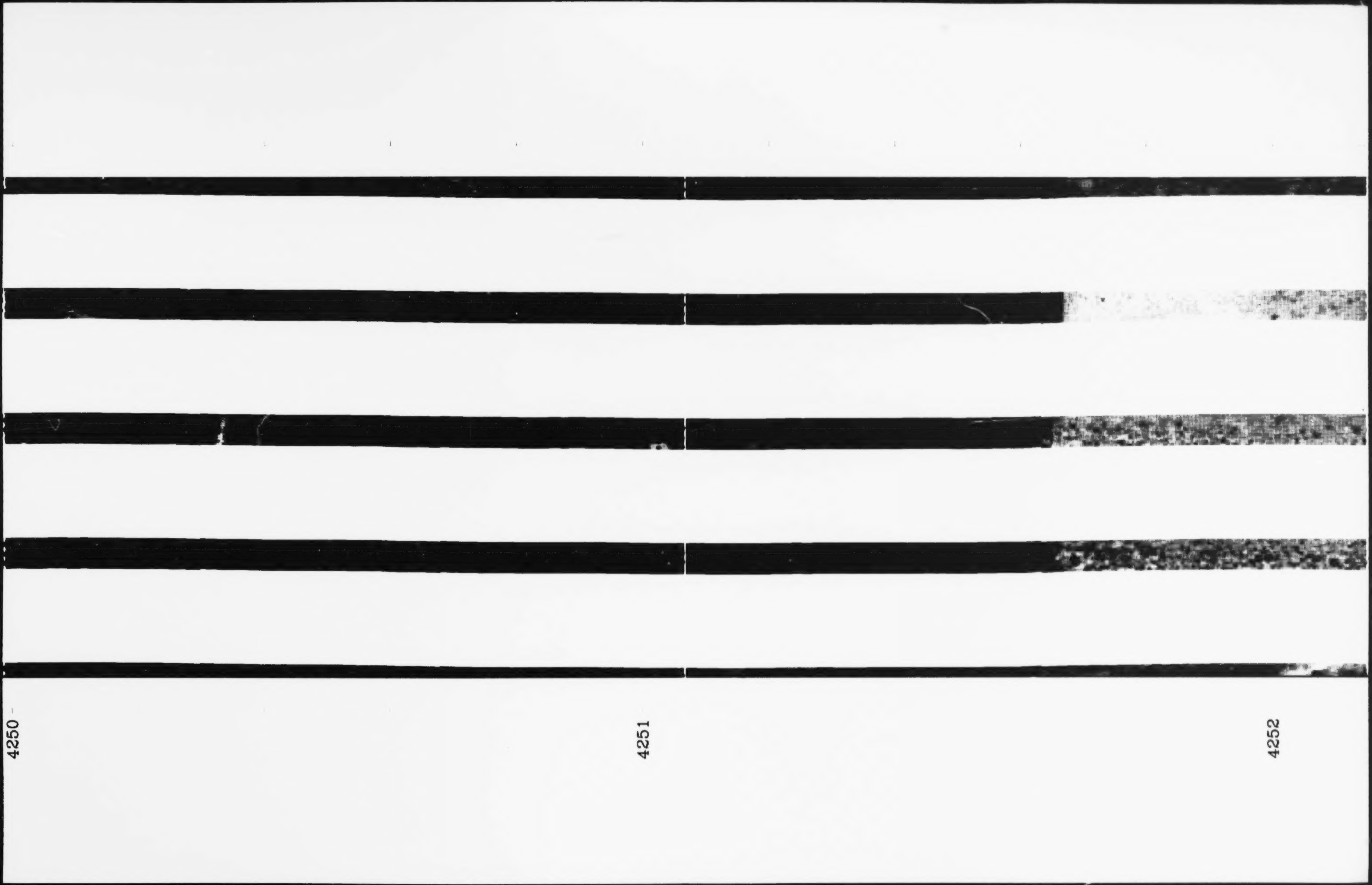
4250
4251
4252

4253

4254

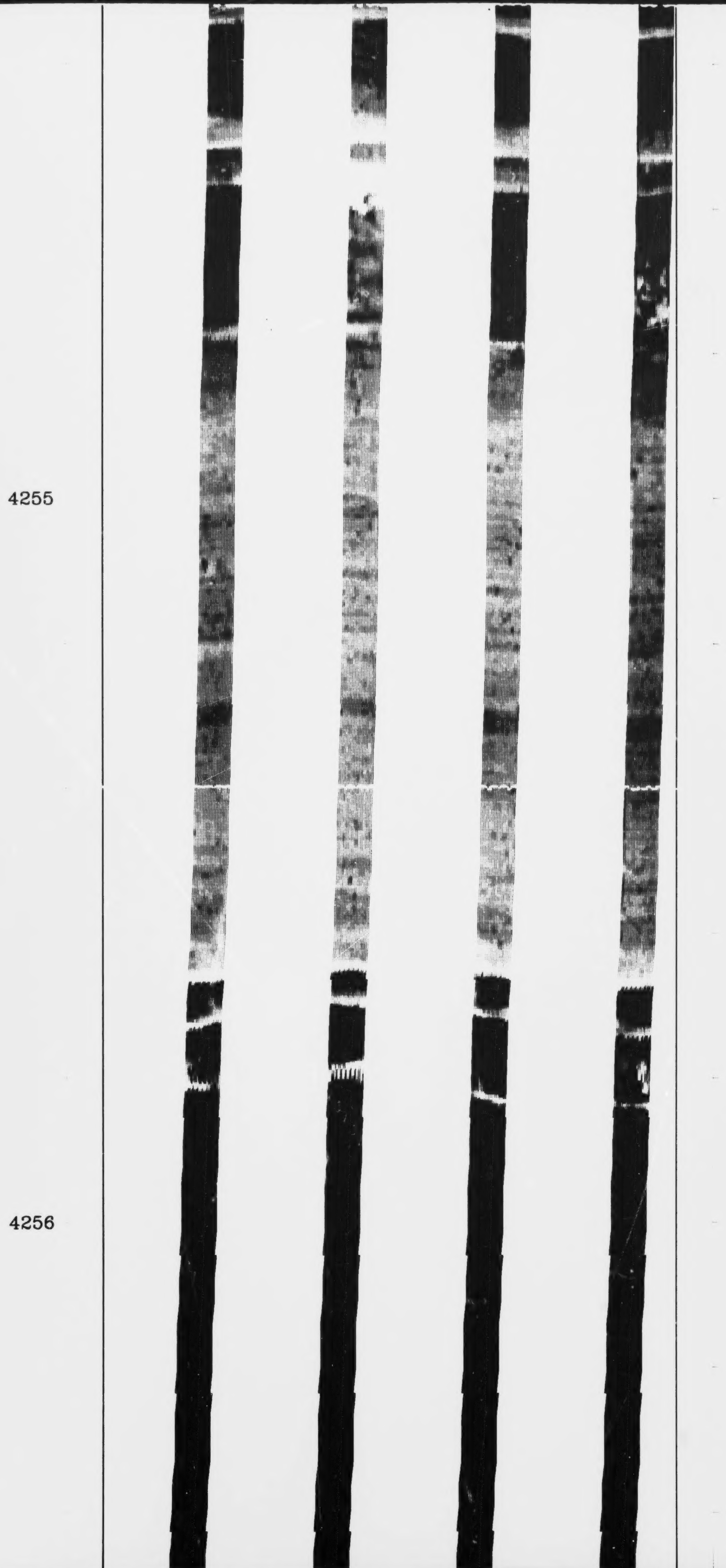
4255
4256

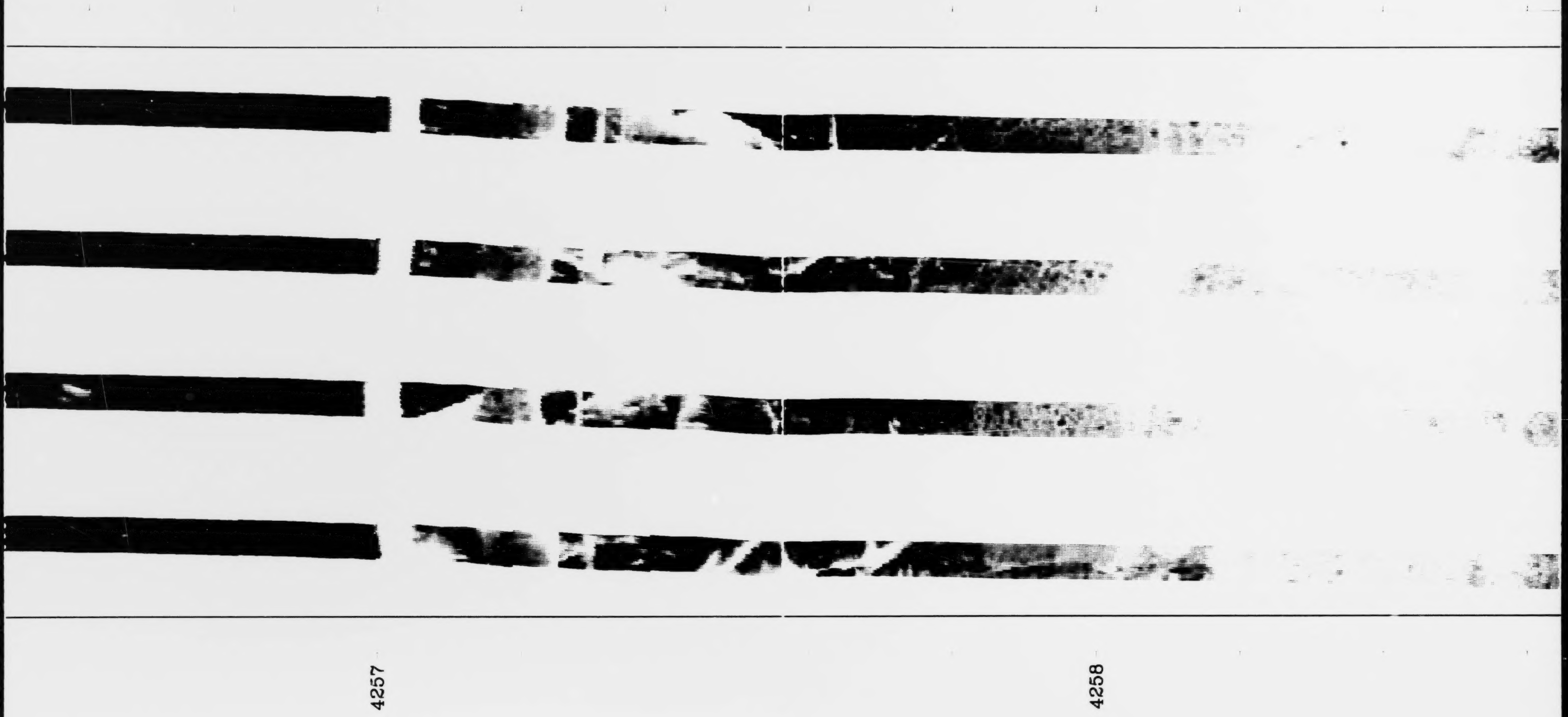
4257
4258

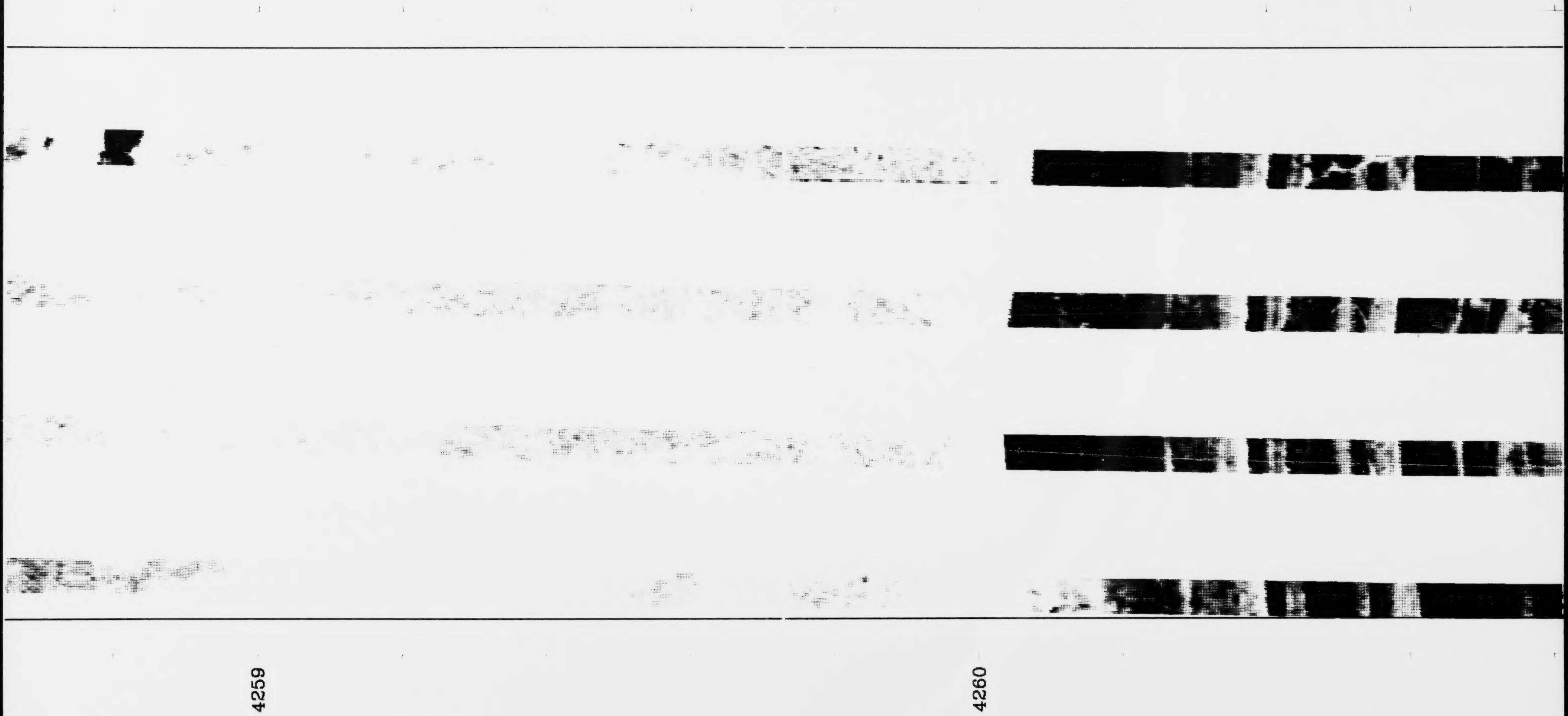
4259
4260

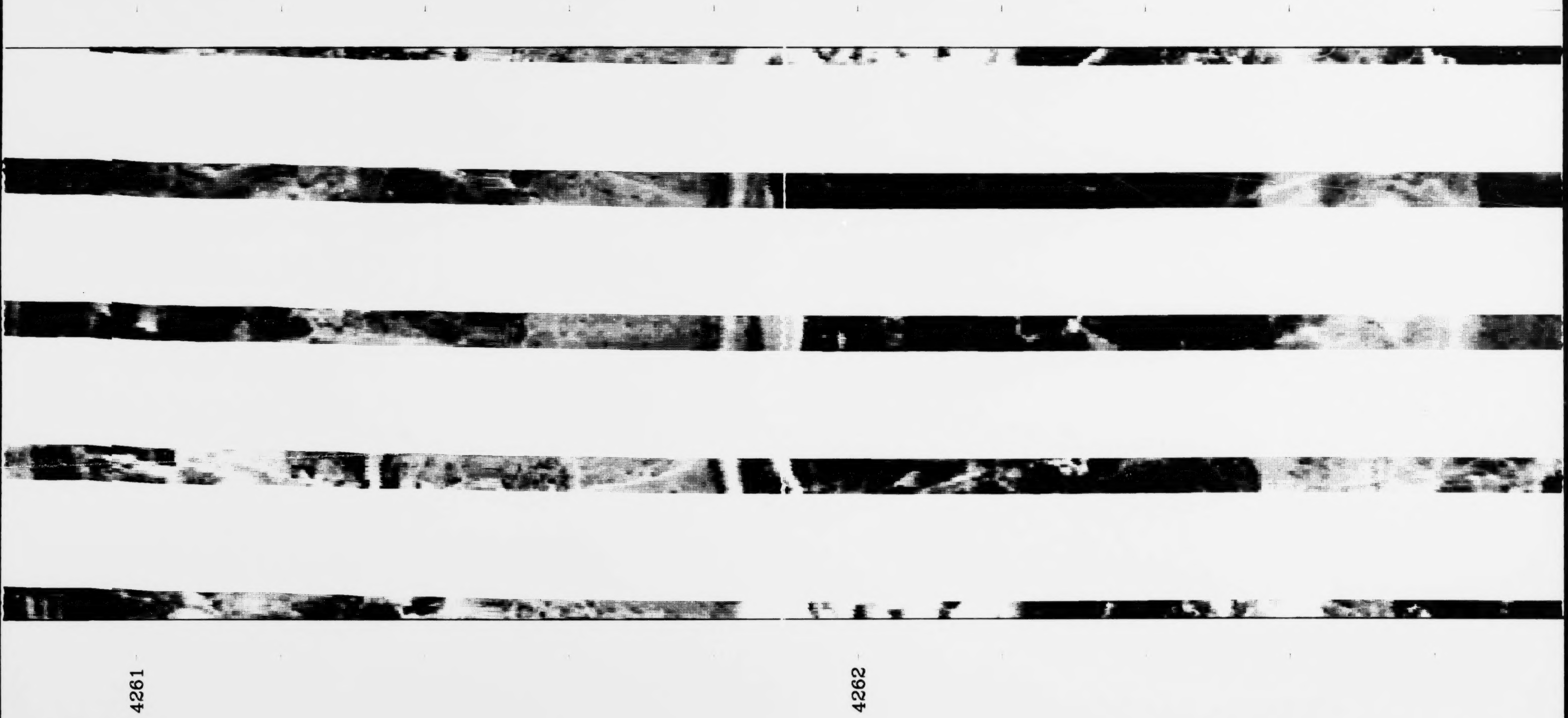
4261
4262

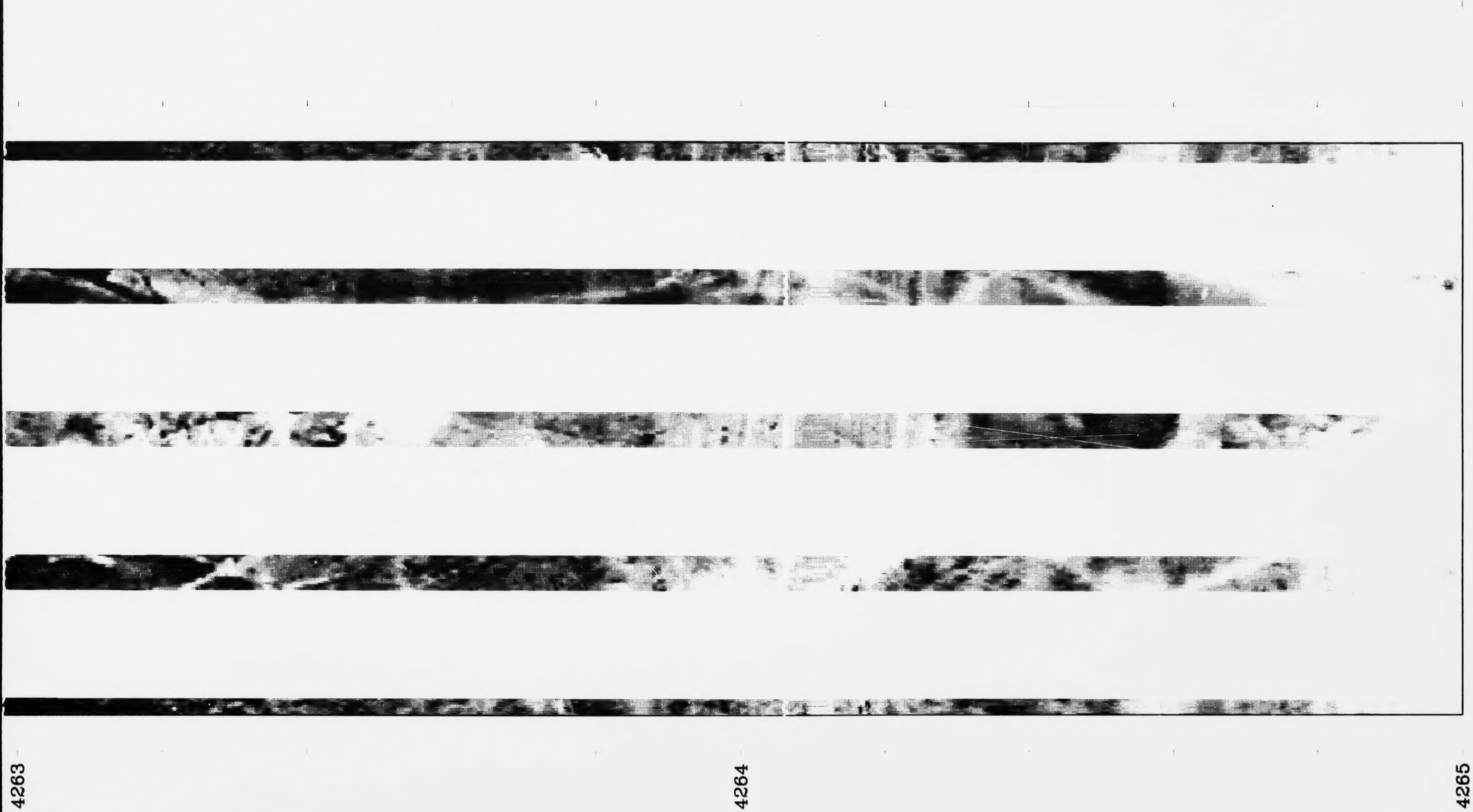
4263
4264
4265

SCHLUMBERGER

FMS
BOREHOLE
IMAGING

COMPANY	LAMONT-DOHERTY GEOLOGICAL
WELL	ODP HOLE-793B
FIELD	IZU-BONIN FOREARC BASIN
COUNTRY	OCEAN
RUN	1
DATE LOGGED	16 - JUN - 89
REFERENCE	STATIC PS 1 4265-4300

STATIC NORMALIZATION

PASS 1 (23577)

FILE : MEST.001

ZONE FROM 4300.0 M TO 4265.0 M

DEPTH SCALE = 1/ 5

IMAGE SCALE = 1/ 5

BITSIZE = 9.88

ORIENTATION

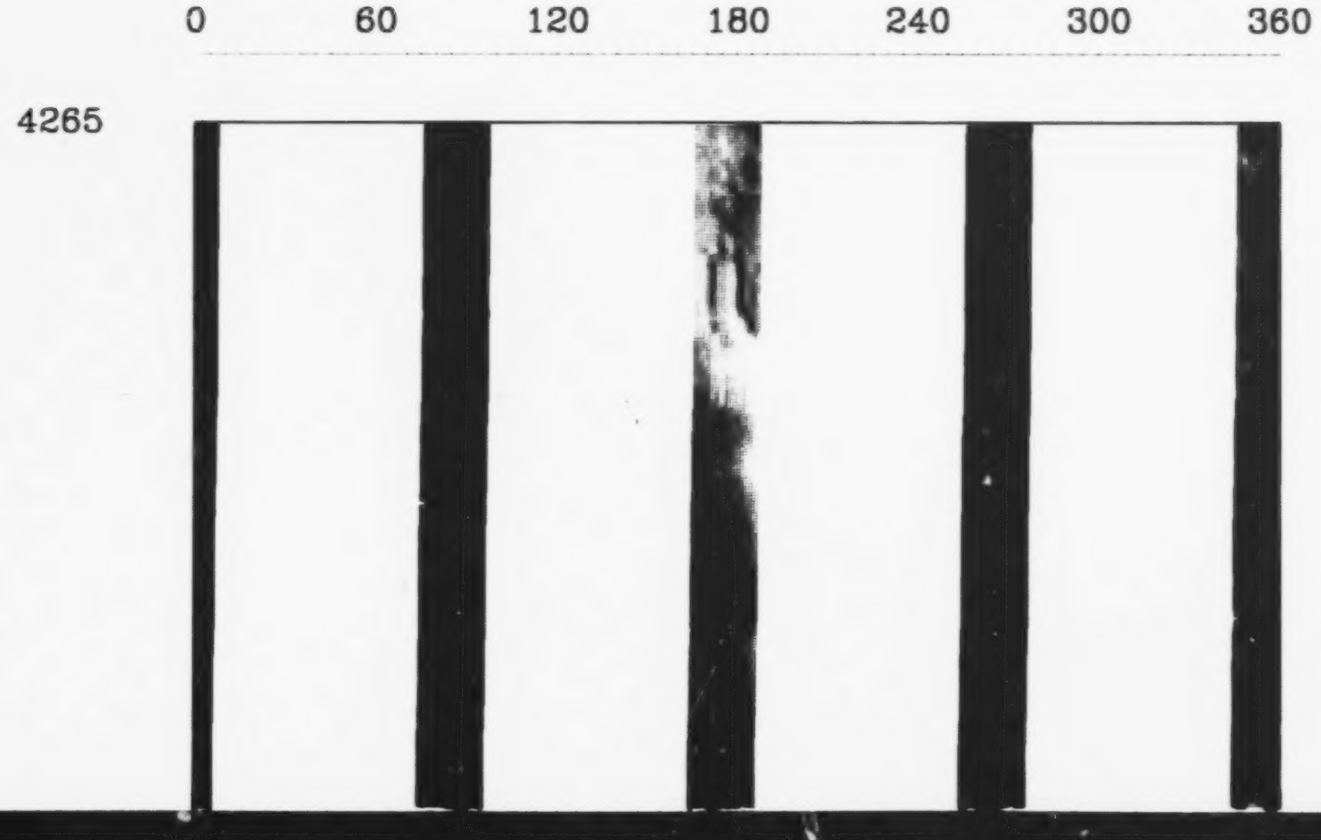

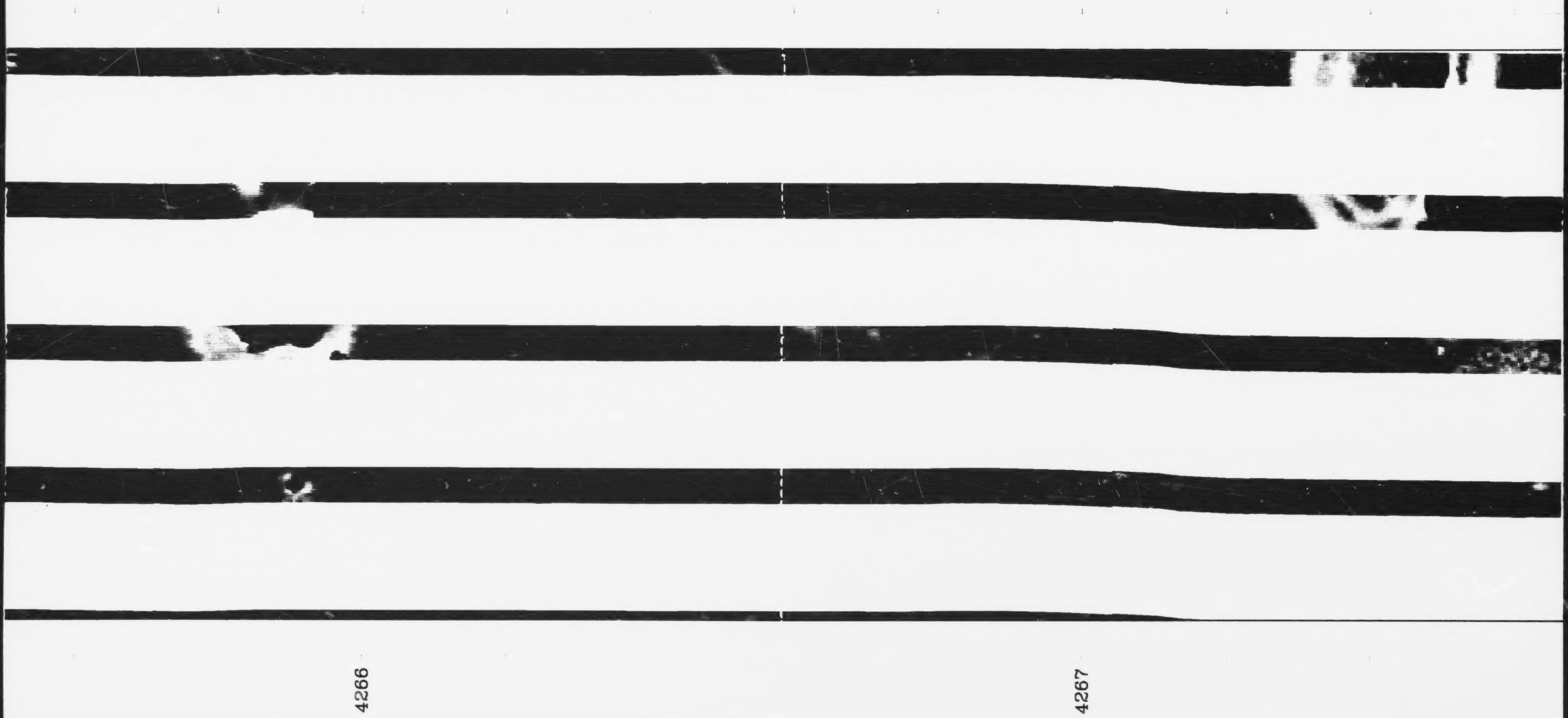
4266
4267

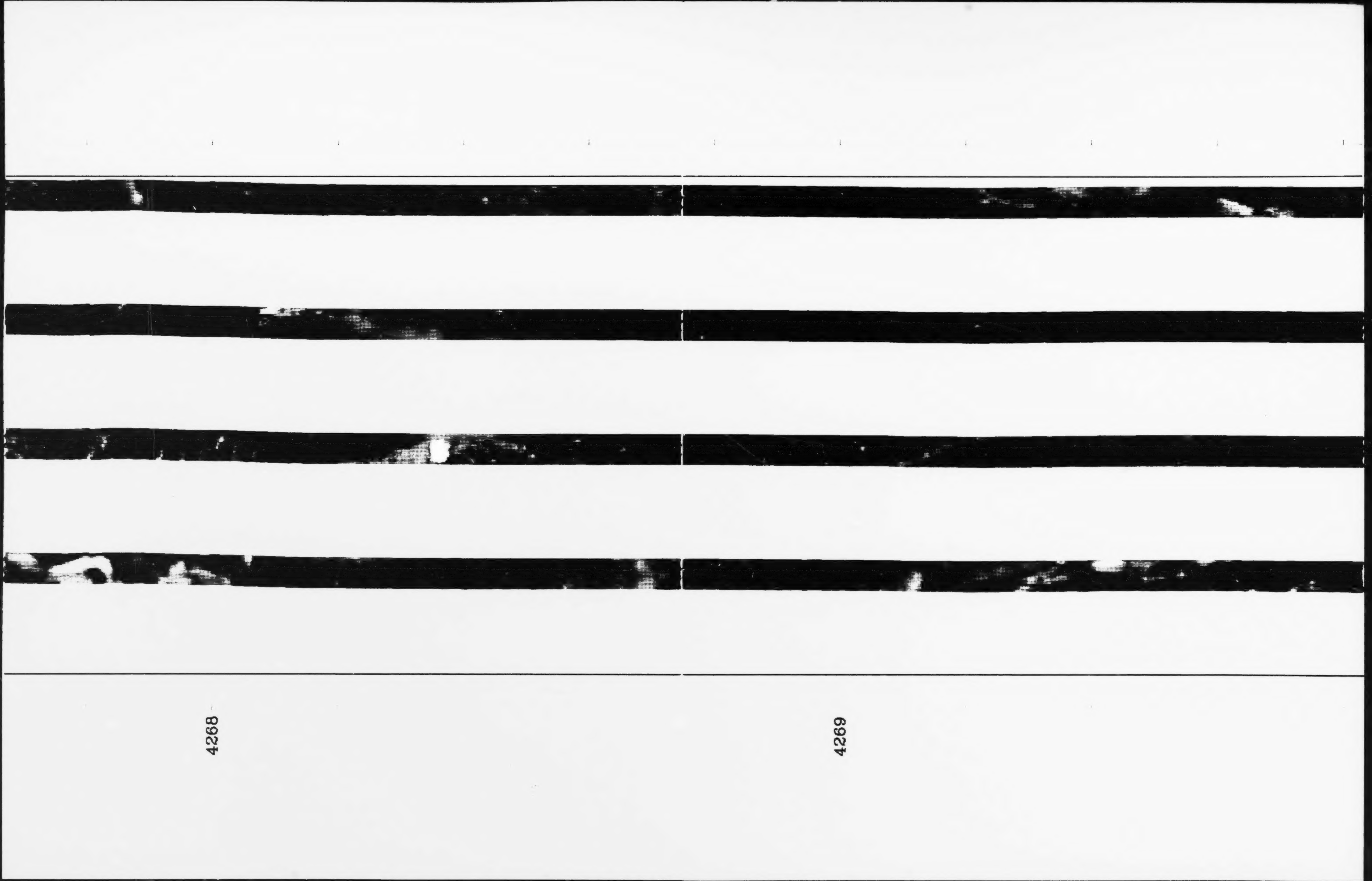
4268
4269

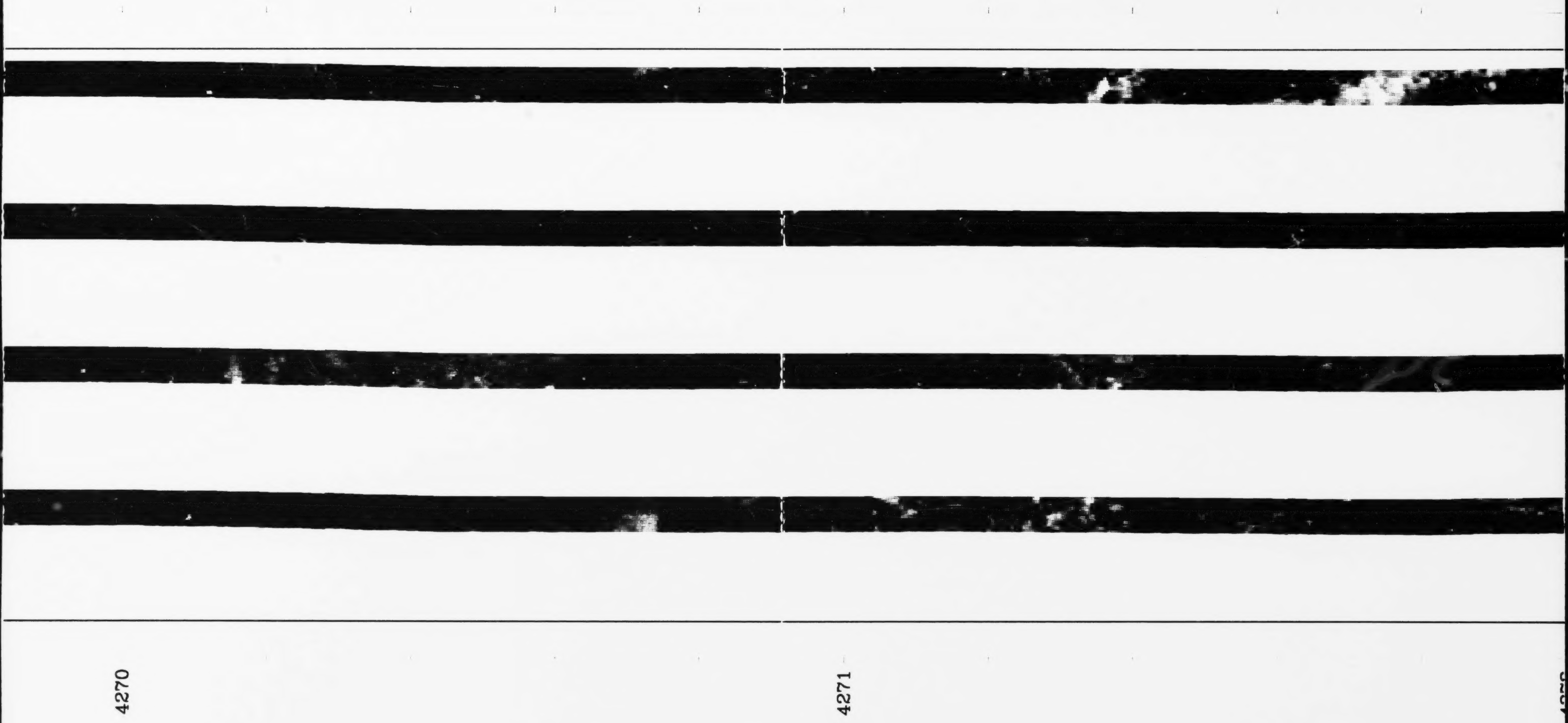
4270
4271

4273

4274

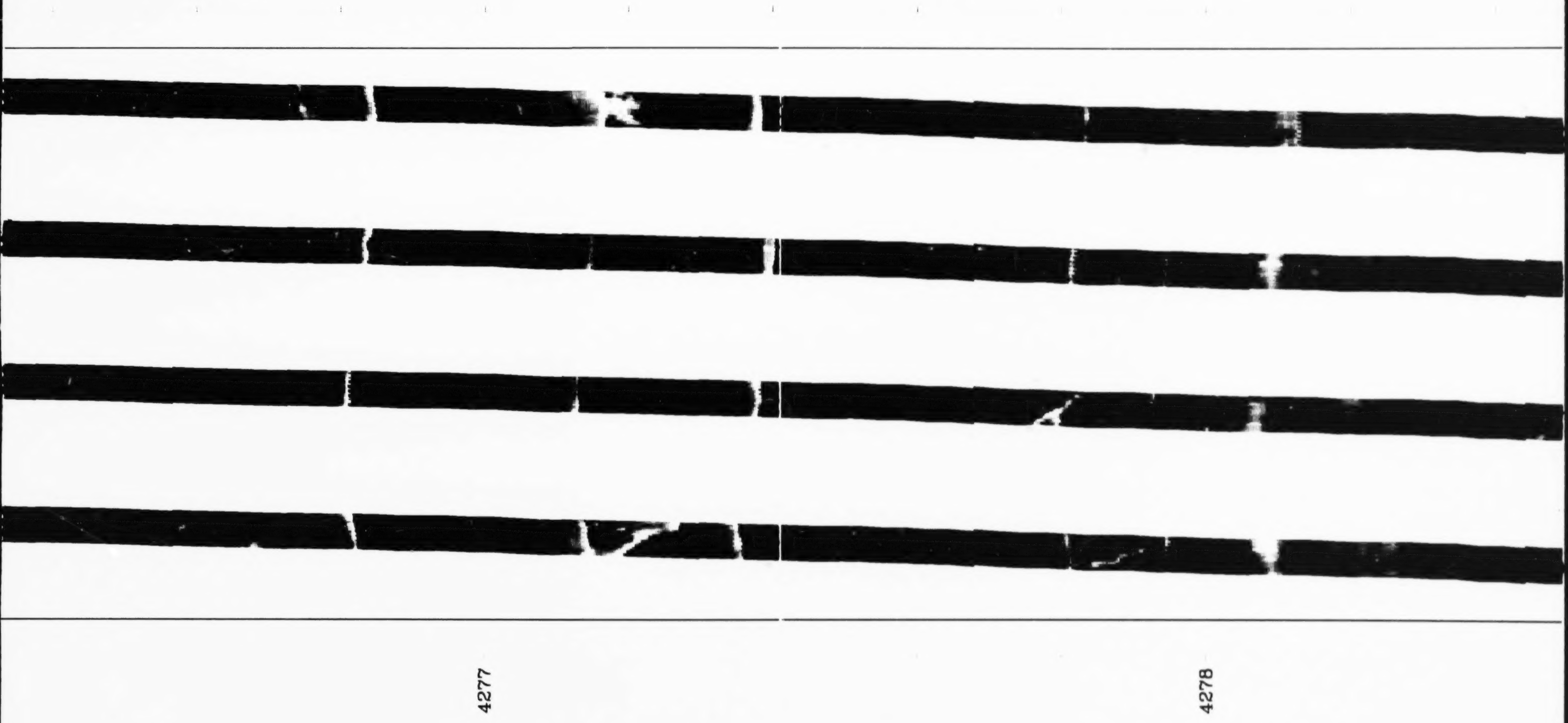
4277
4278

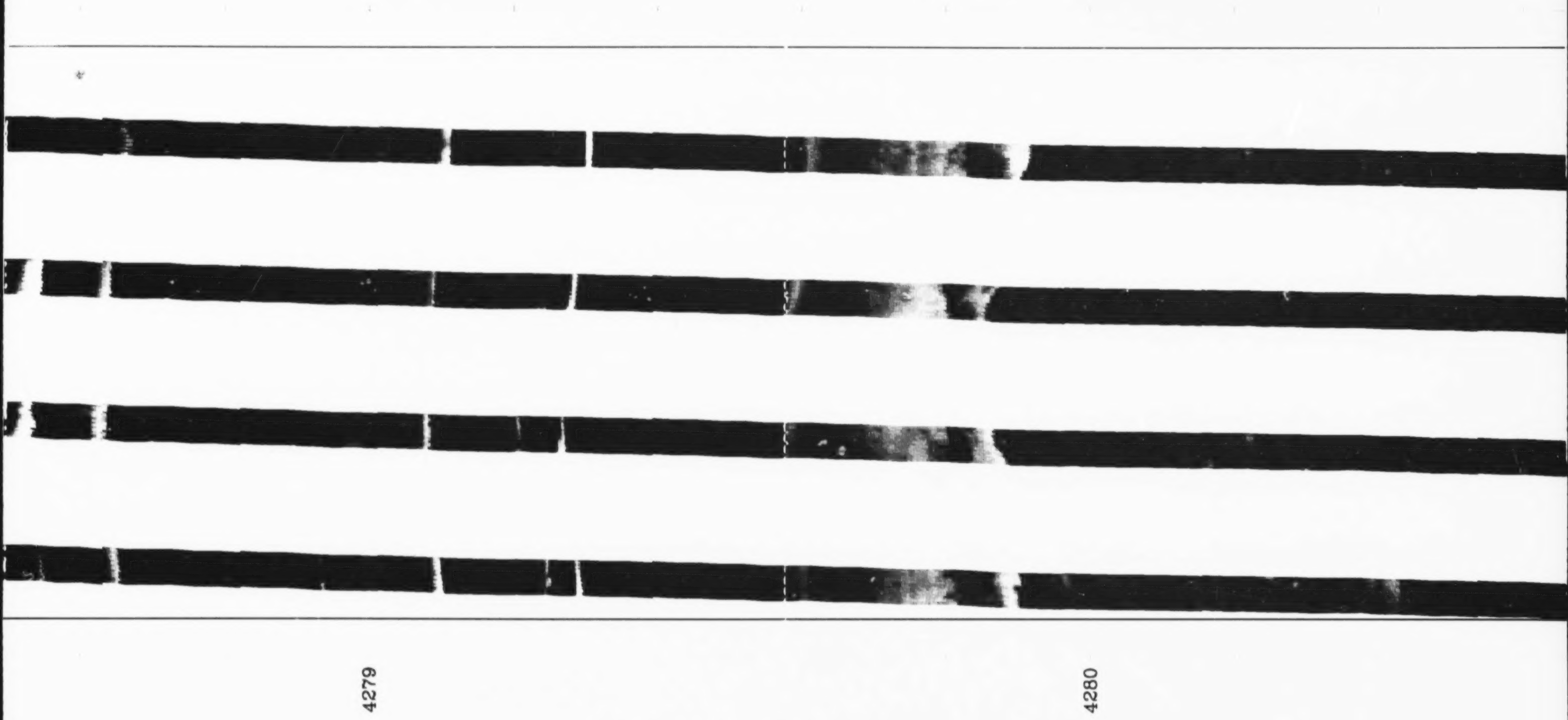
4279
4280

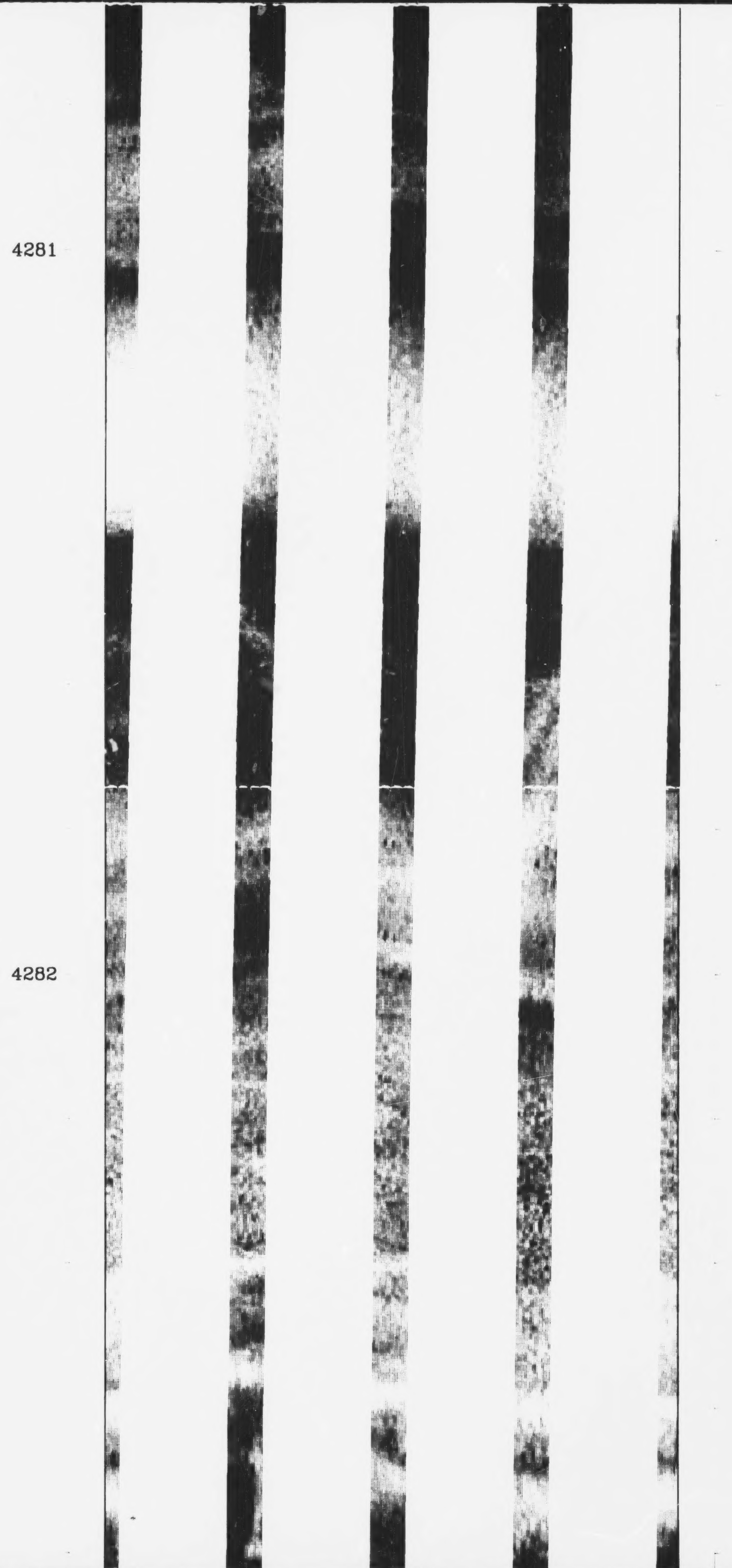
4281
4282

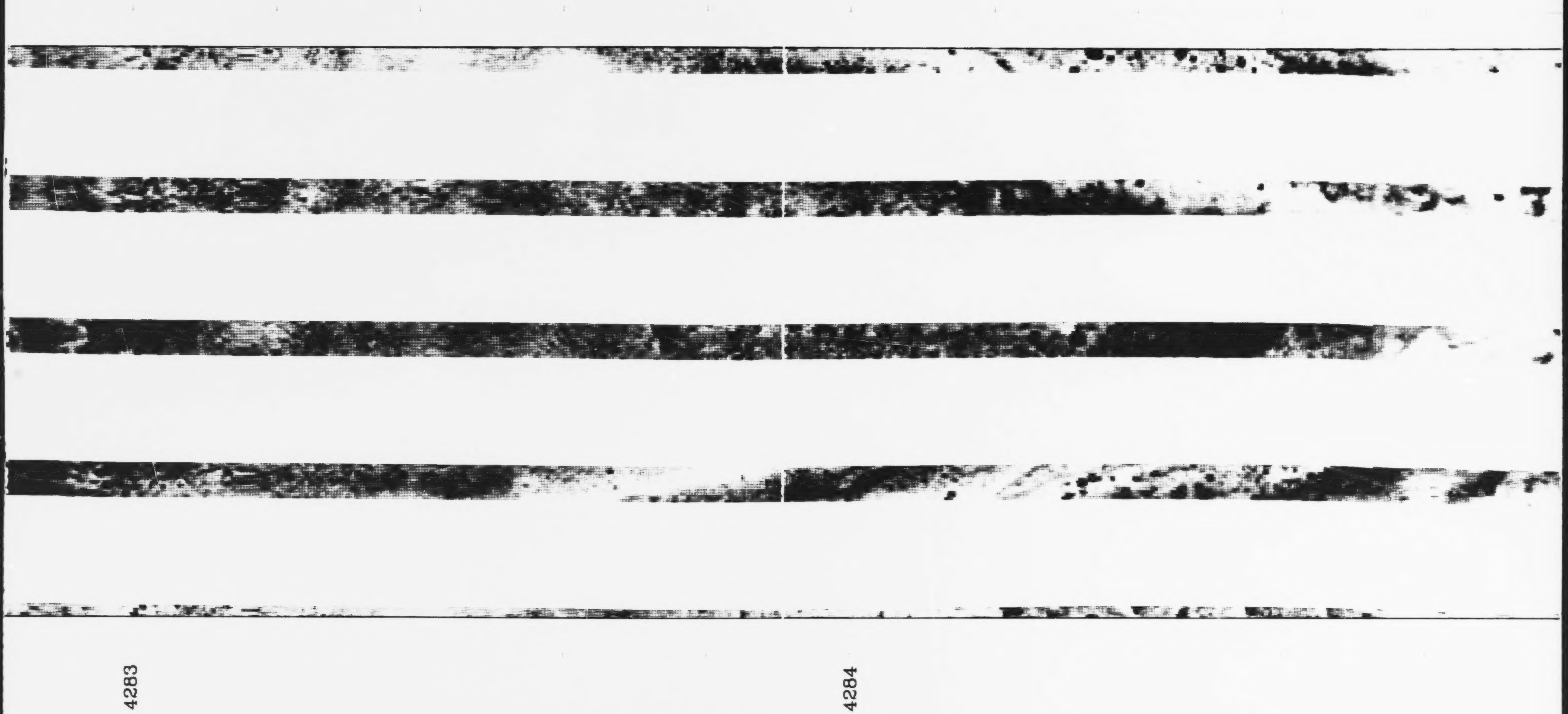
4283
4284

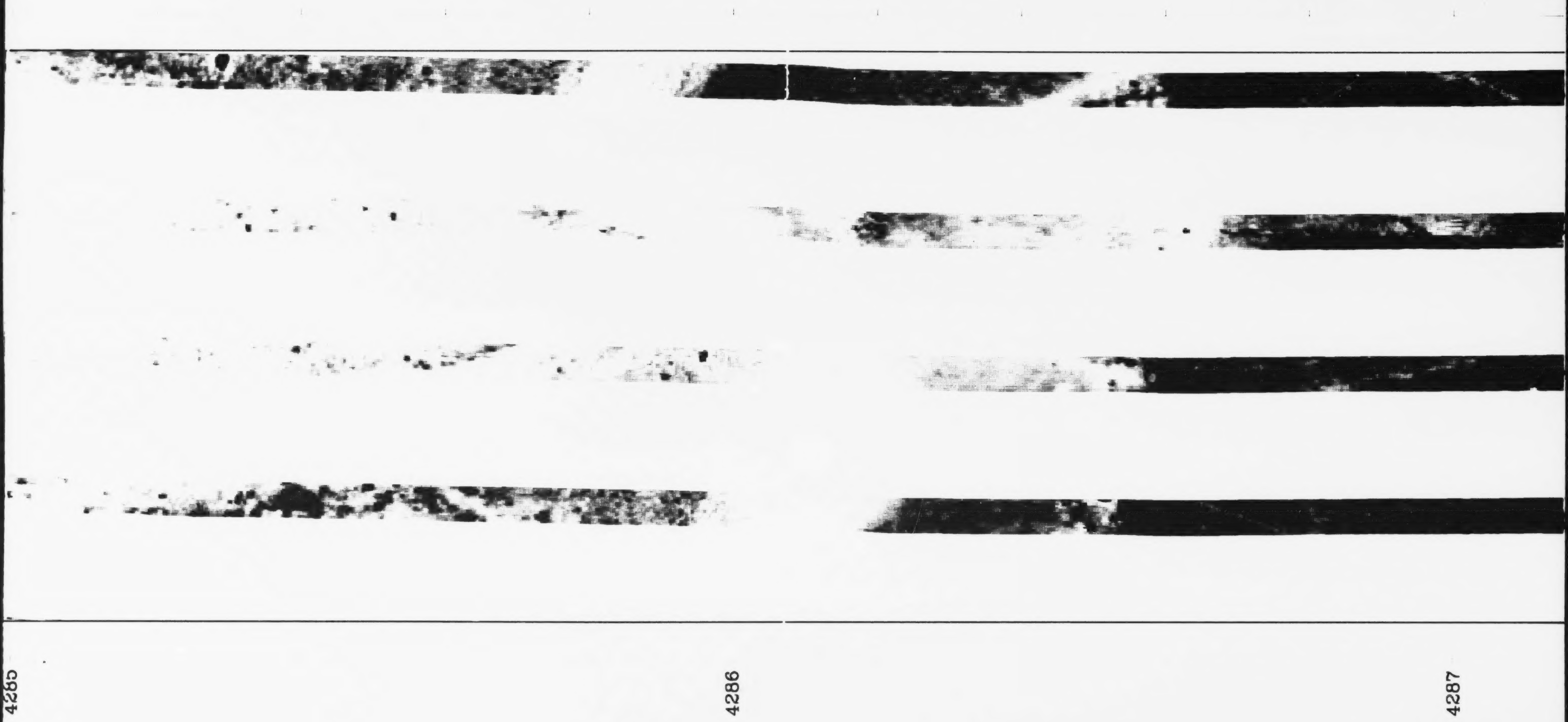
4285
4286
4287

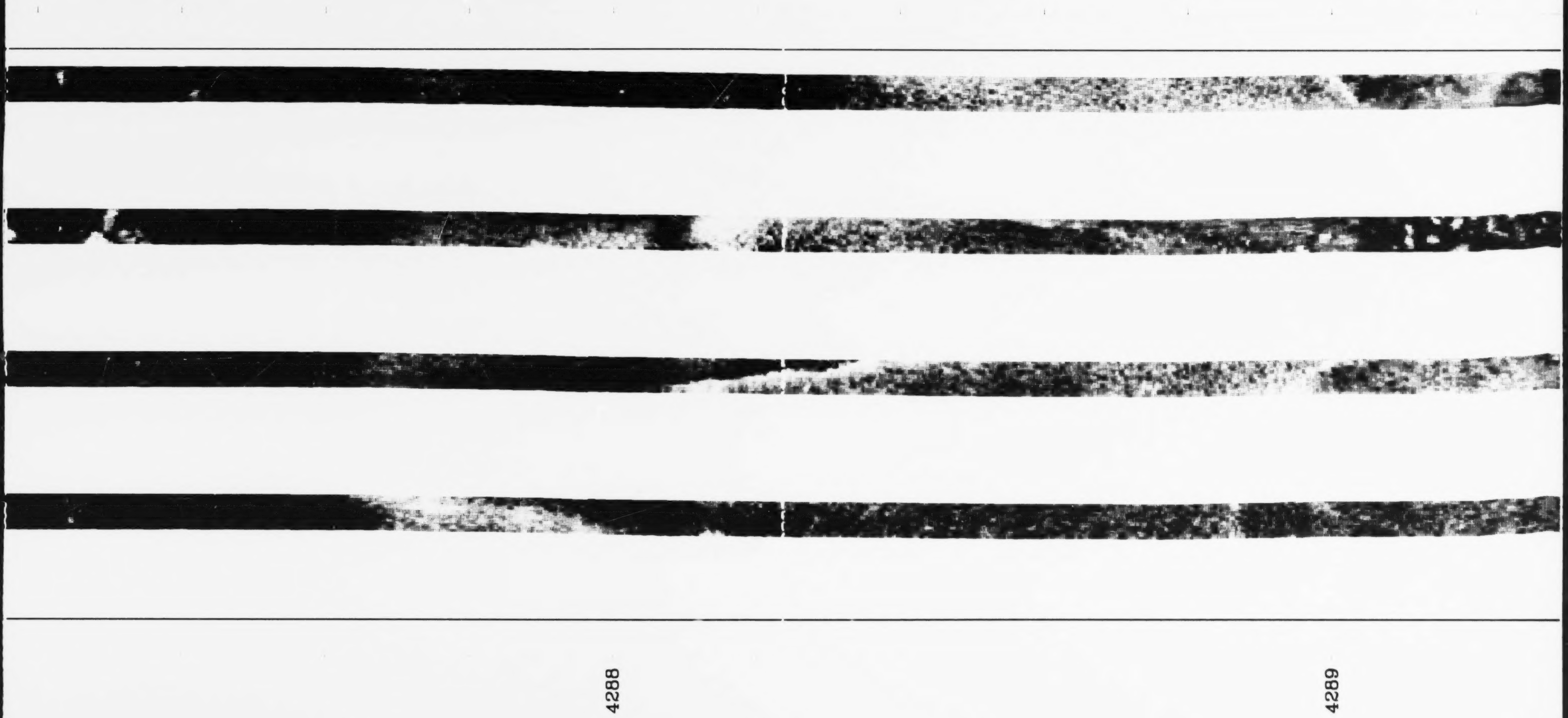
4288
4289

4290

4291

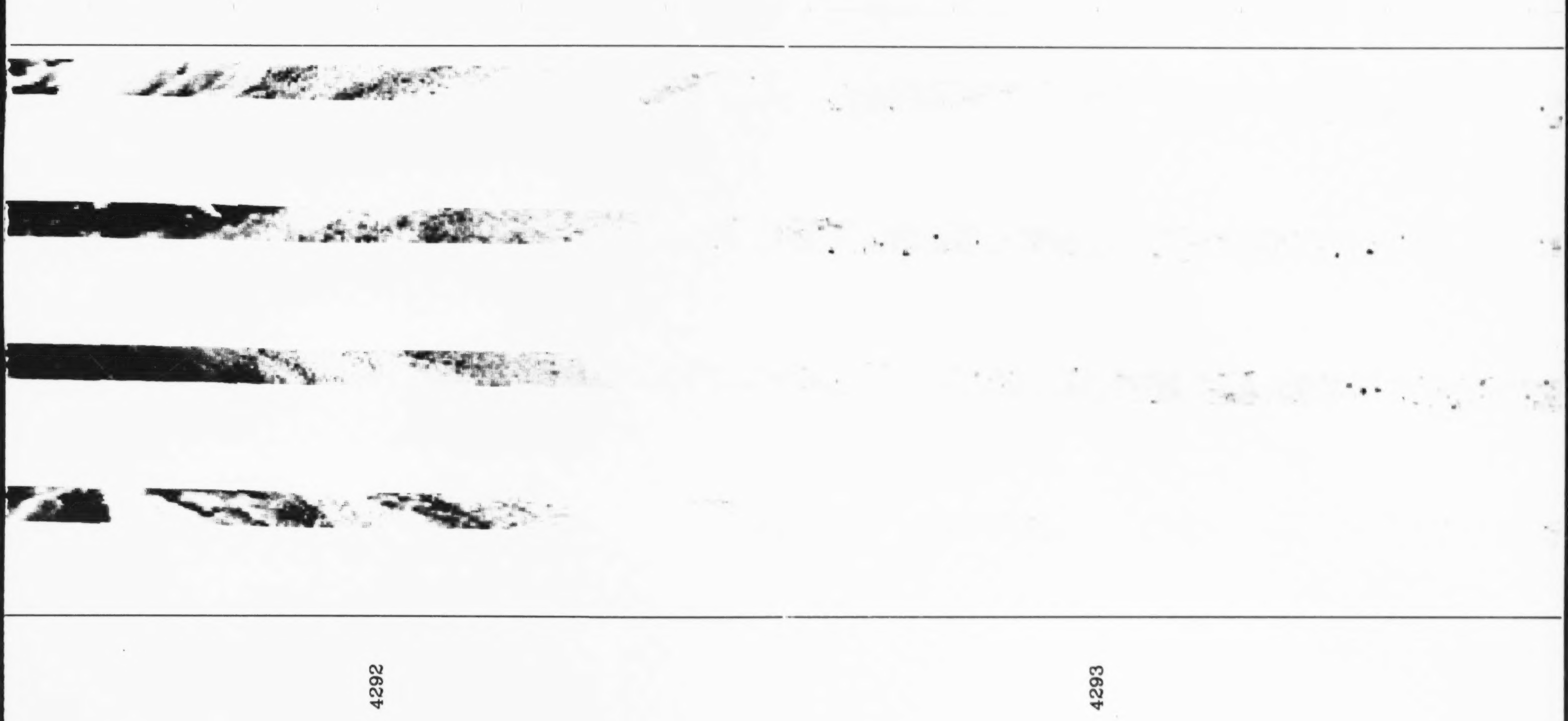
4292
4293

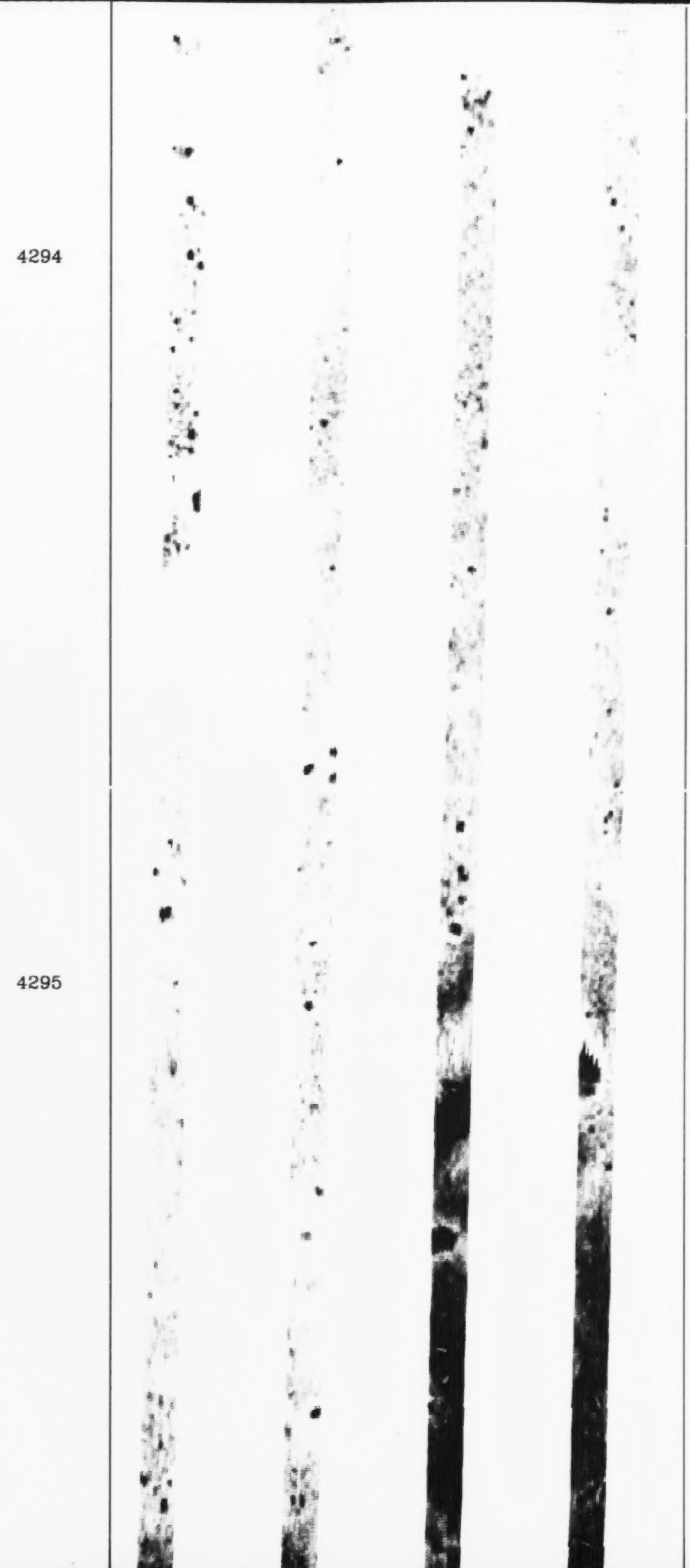
4294
4295

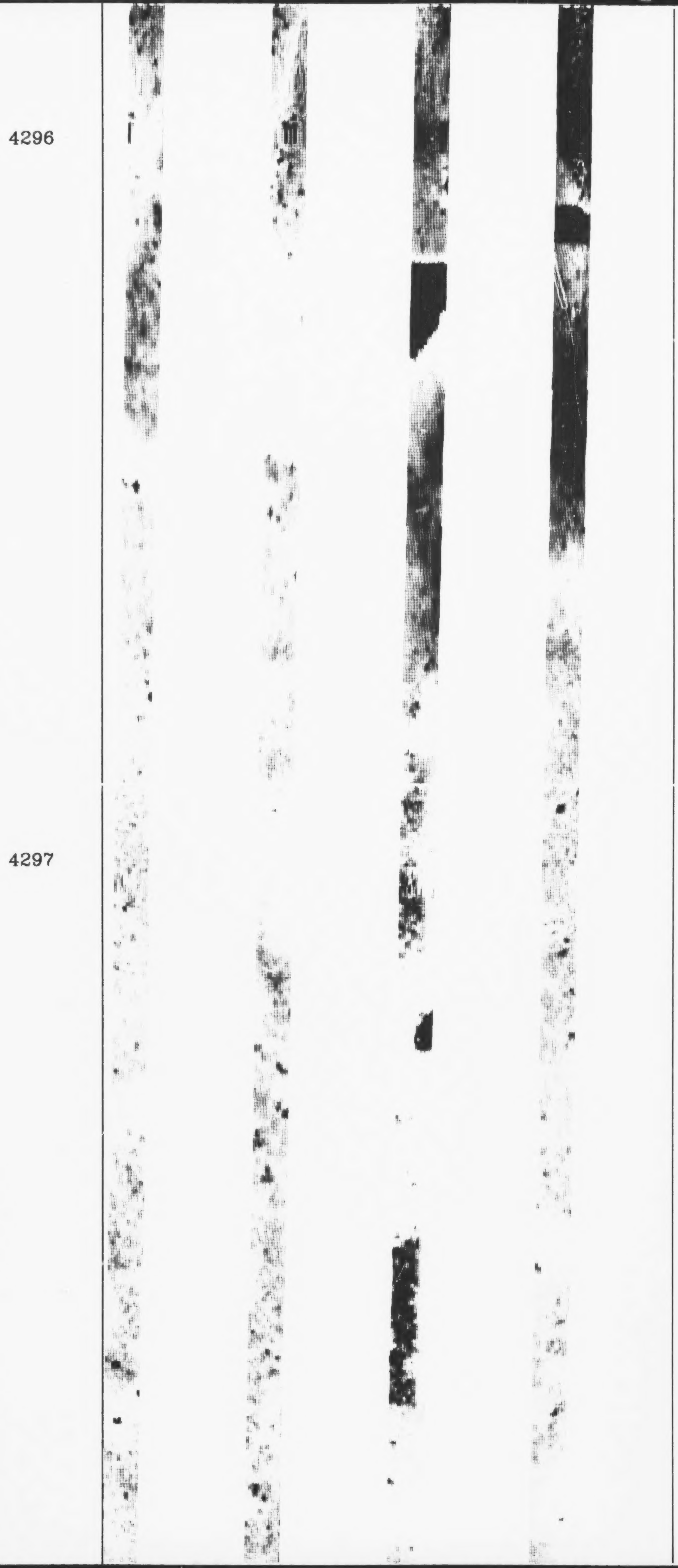
4296
4297

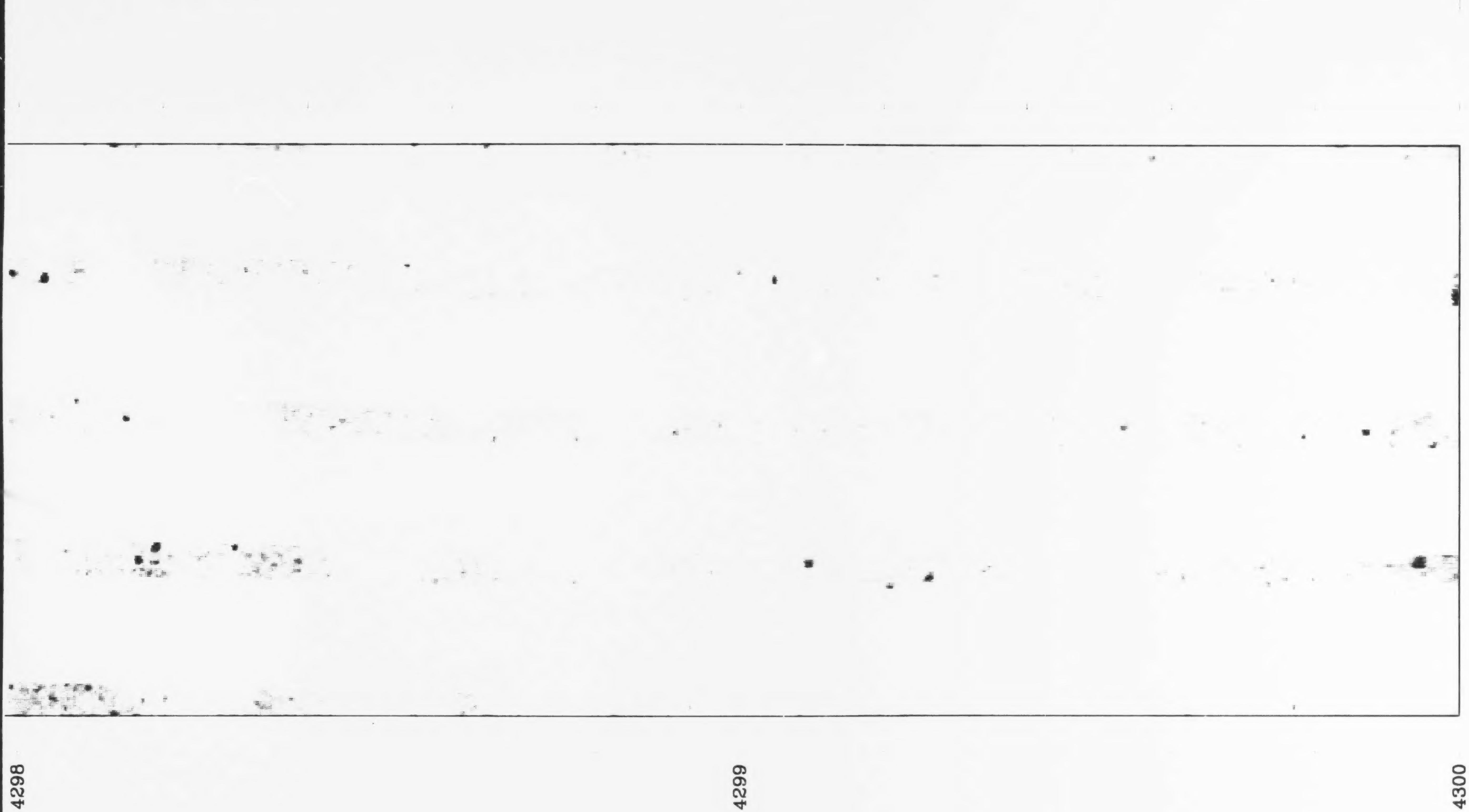
4298
4299
4300

SCHLUMBERGER

FMS
BOREHOLE
IMAGING

COMPANY	LAMONT-DOHERTY GEOLOGICAL
WELL	ODP HOLE-793B
FIELD	IZU-BONIN FOREARC BASIN
COUNTRY	OCEAN
RUN	1
DATE LOGGED	16 - JUN - 89
REFERENCE	STATIC PS-1 4300-4330

BORMAP 004E02 - ENGINEER LISTING : BORENG.006

STATIC NORMALIZATION

PASS 1 (23577)

FILE : MEST.001

ZONE FROM 4330.0 M TO 4300.0 M

DEPTH SCALE = 1/ 5

IMAGE SCALE = 1/ 5

BITSIZE = 9.88

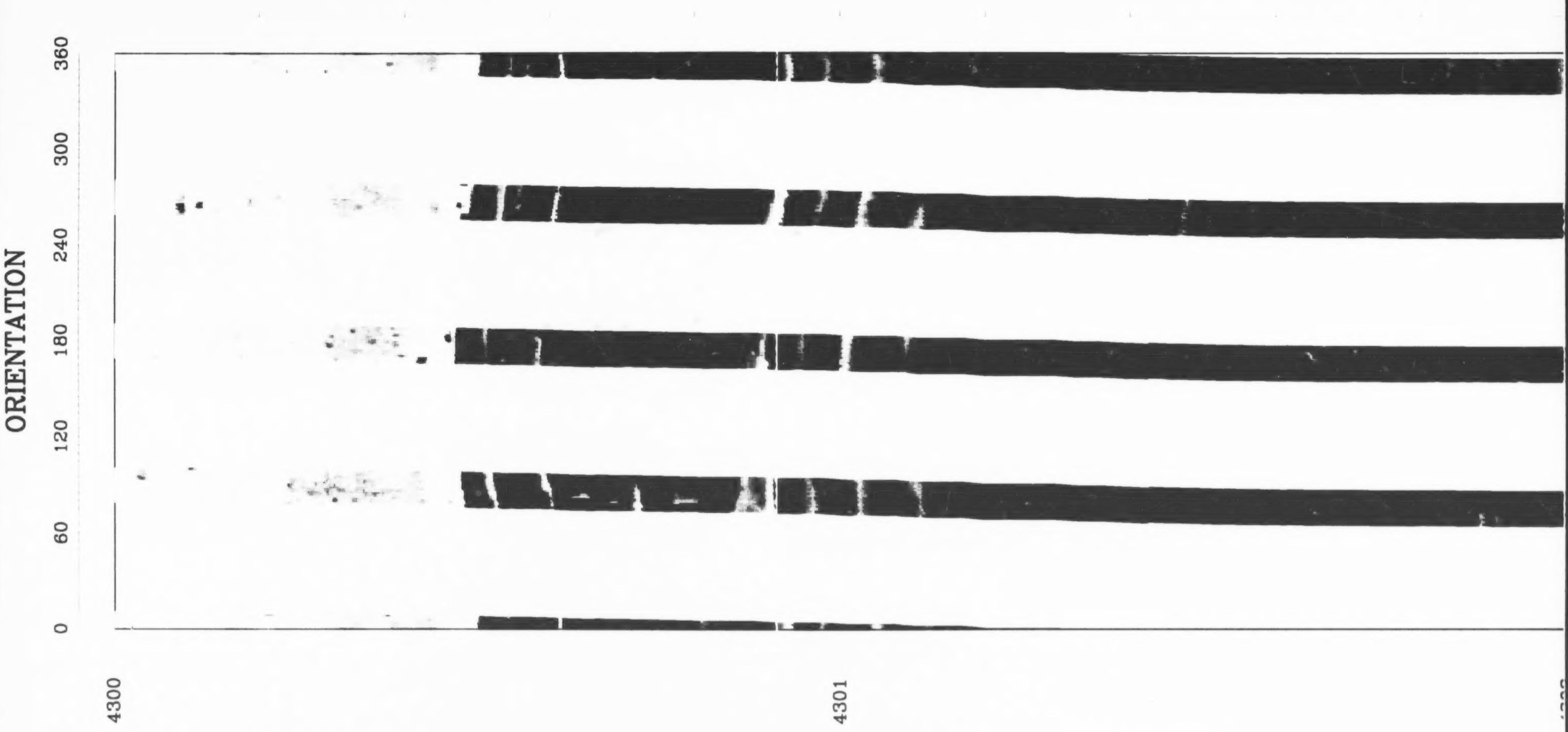
ORIENTATION
0
60
120
180
240
300
360
4300
4301

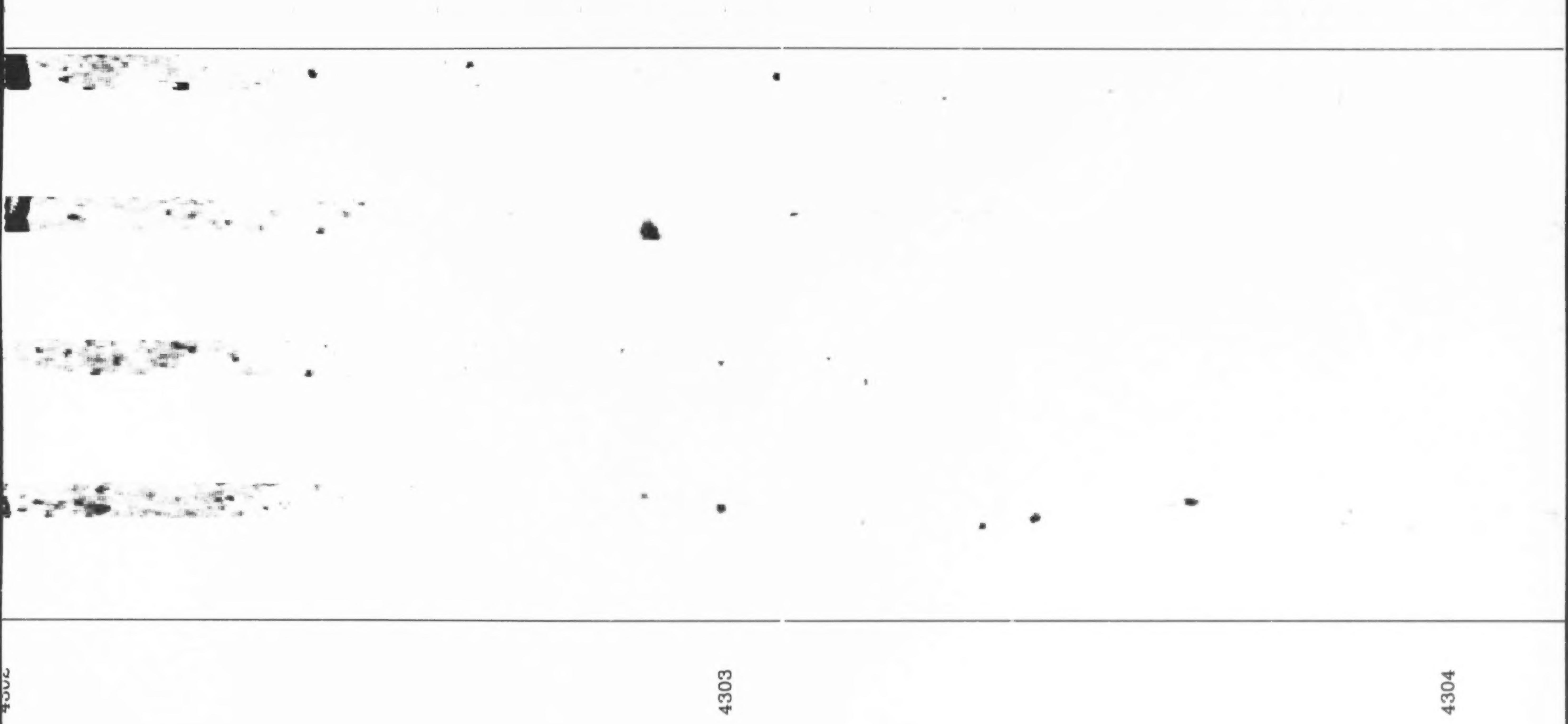
4302
4303
4304

[redacted]

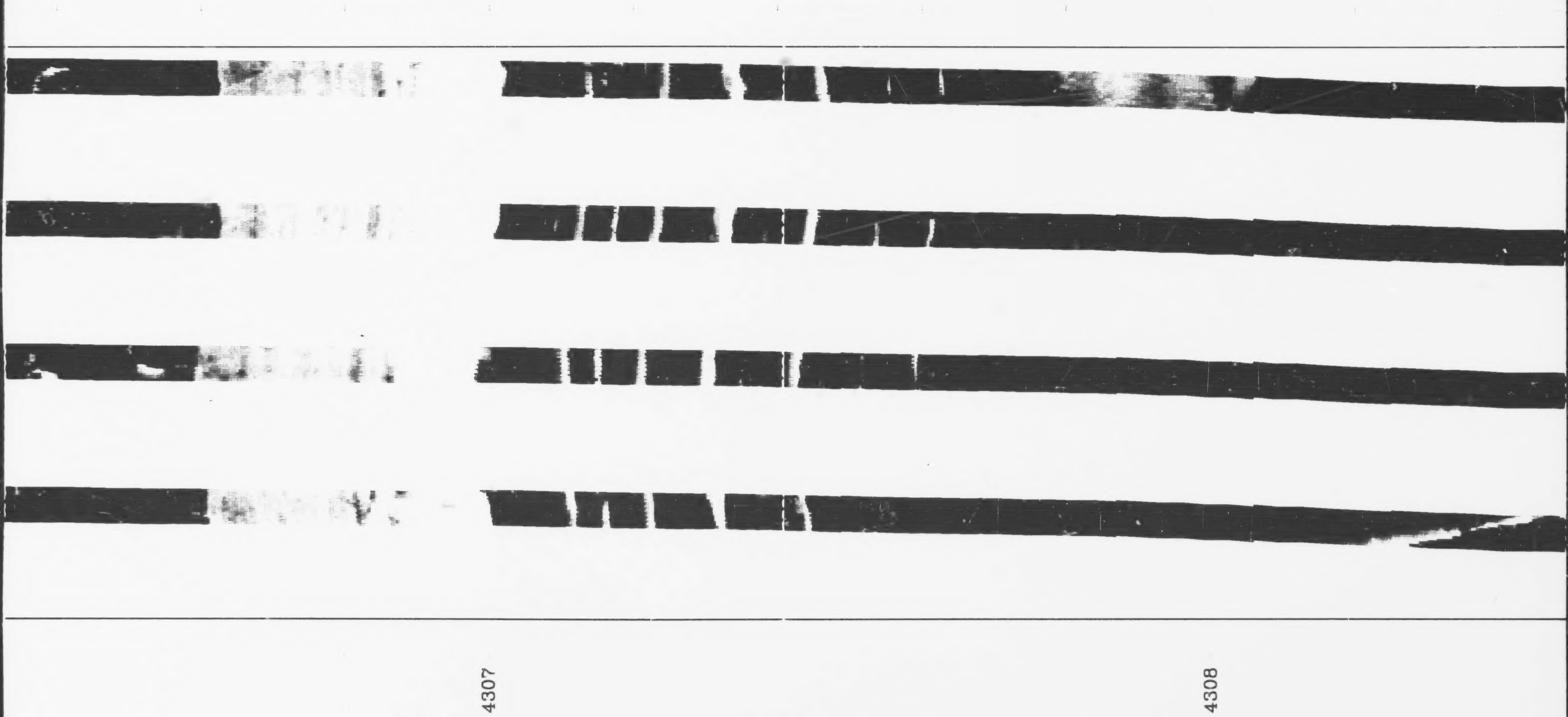
4307
4308

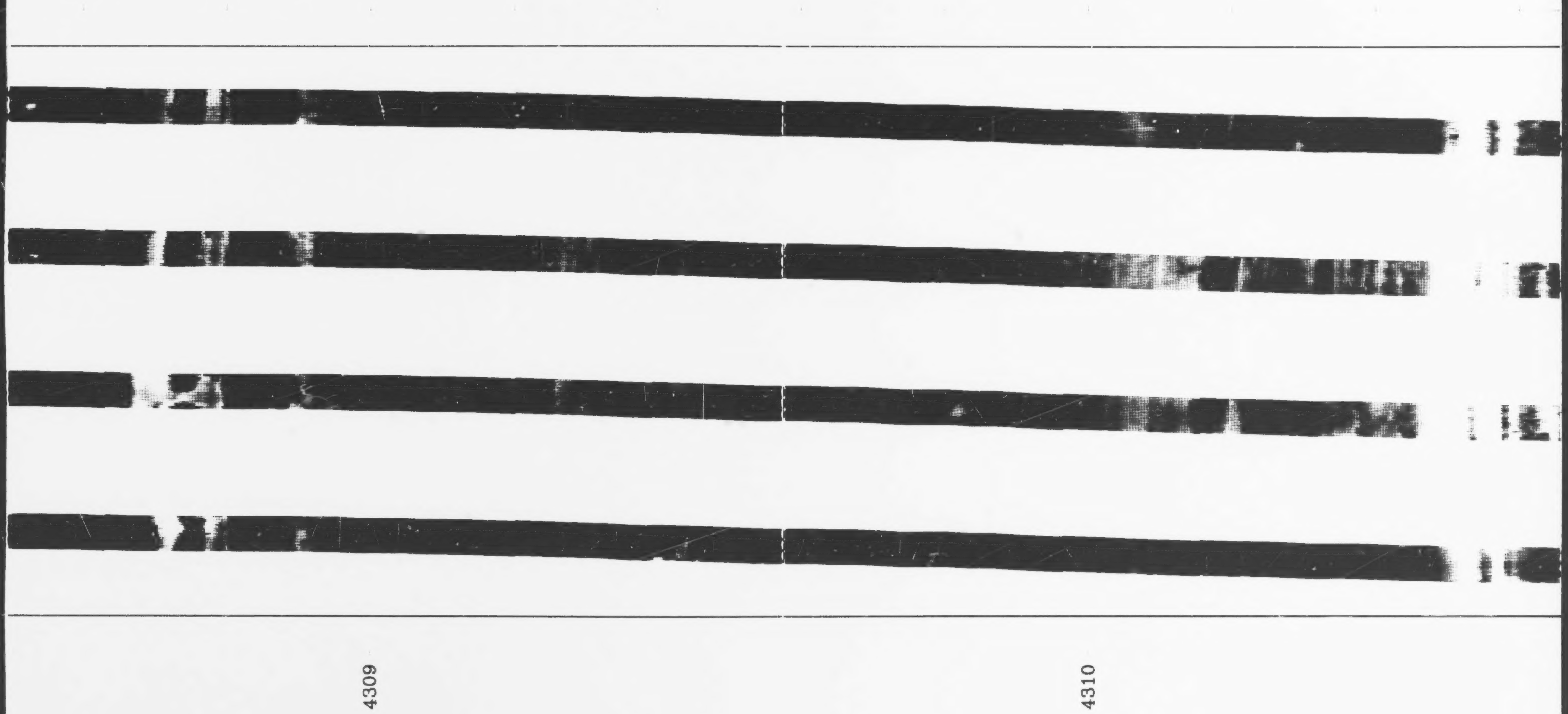
4309
4310

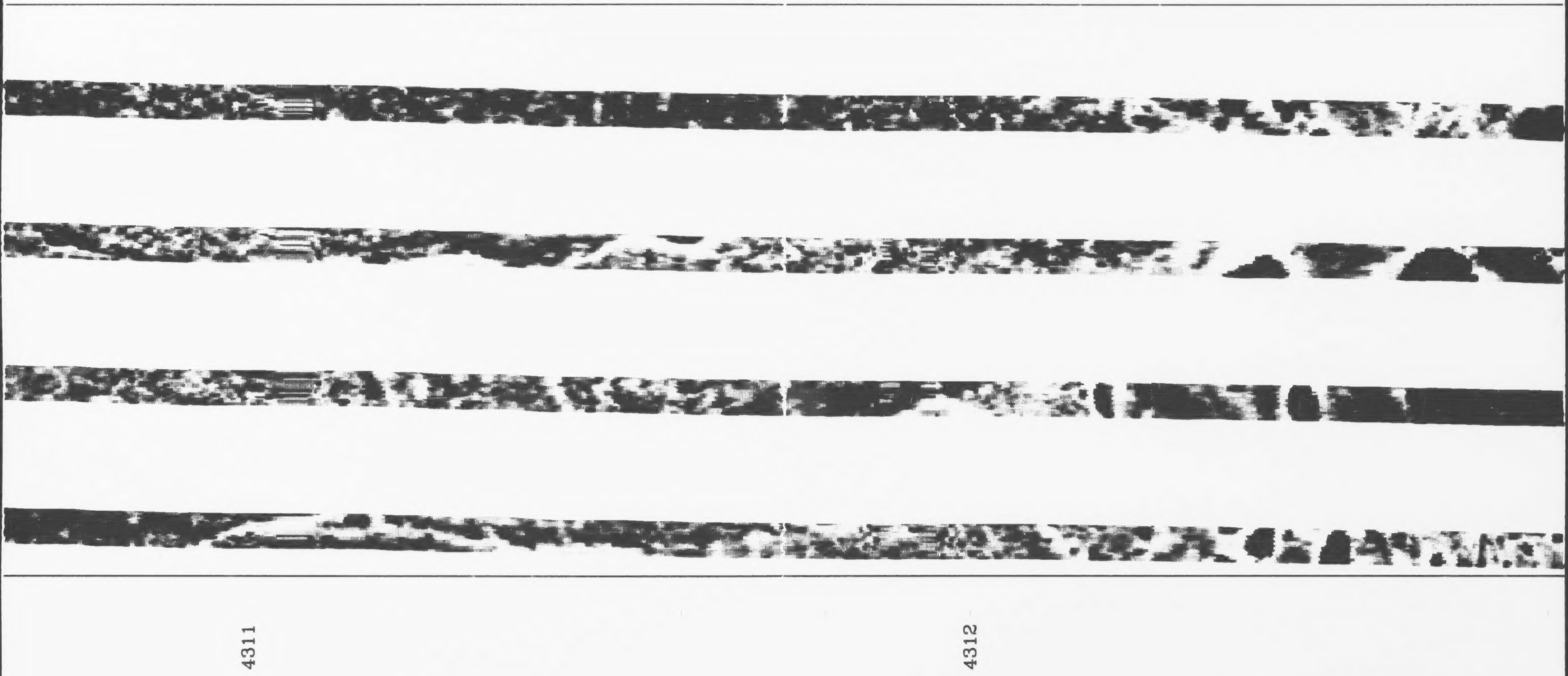
4311
4312

4313
4314

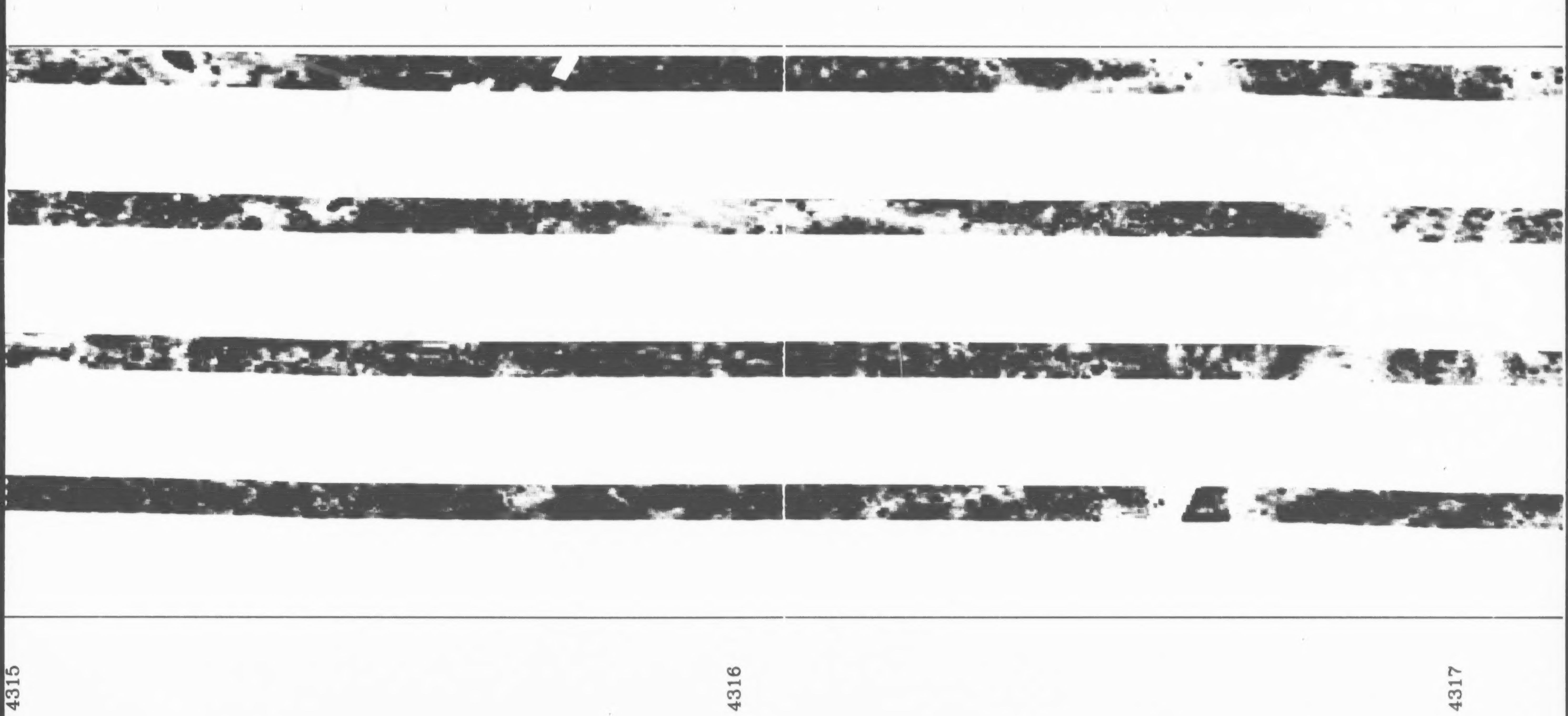
4315
4316
4317

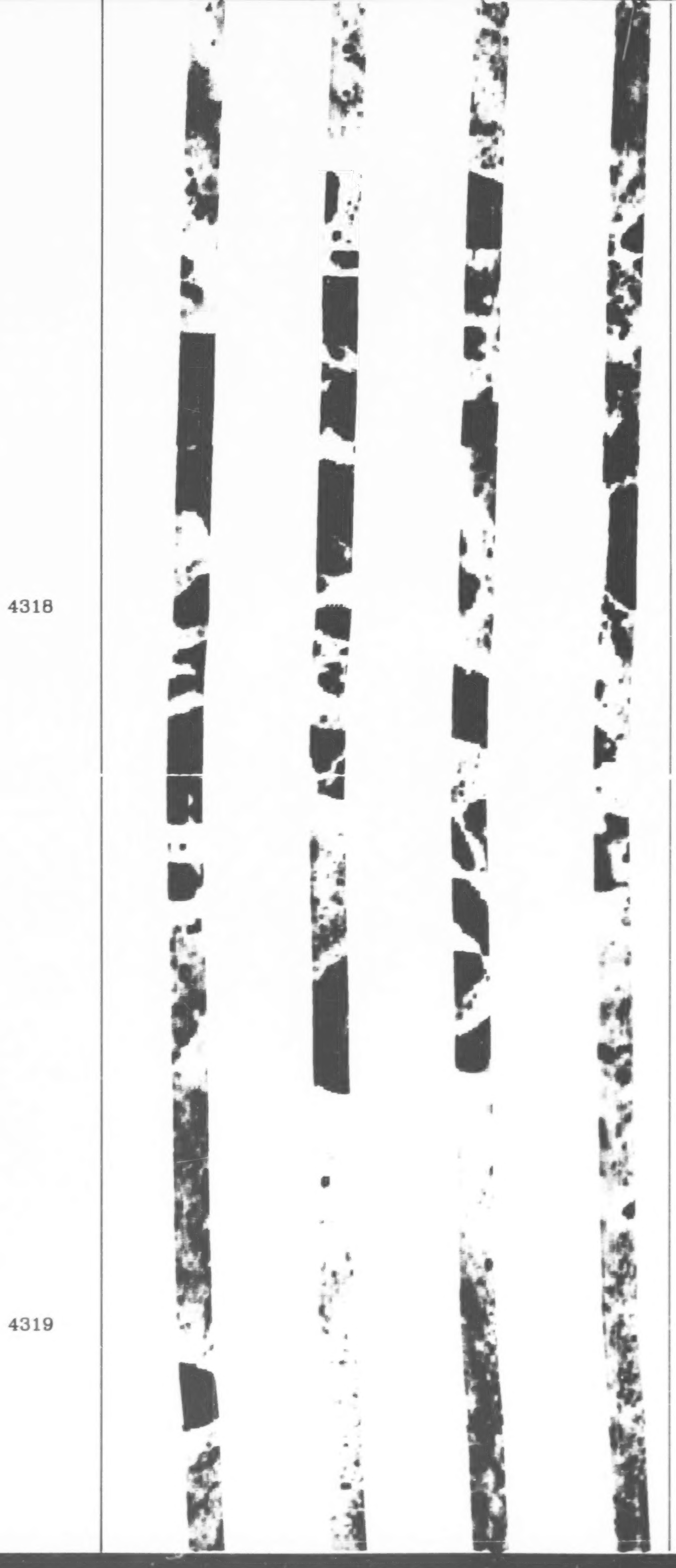
4318
4319

4320
4321

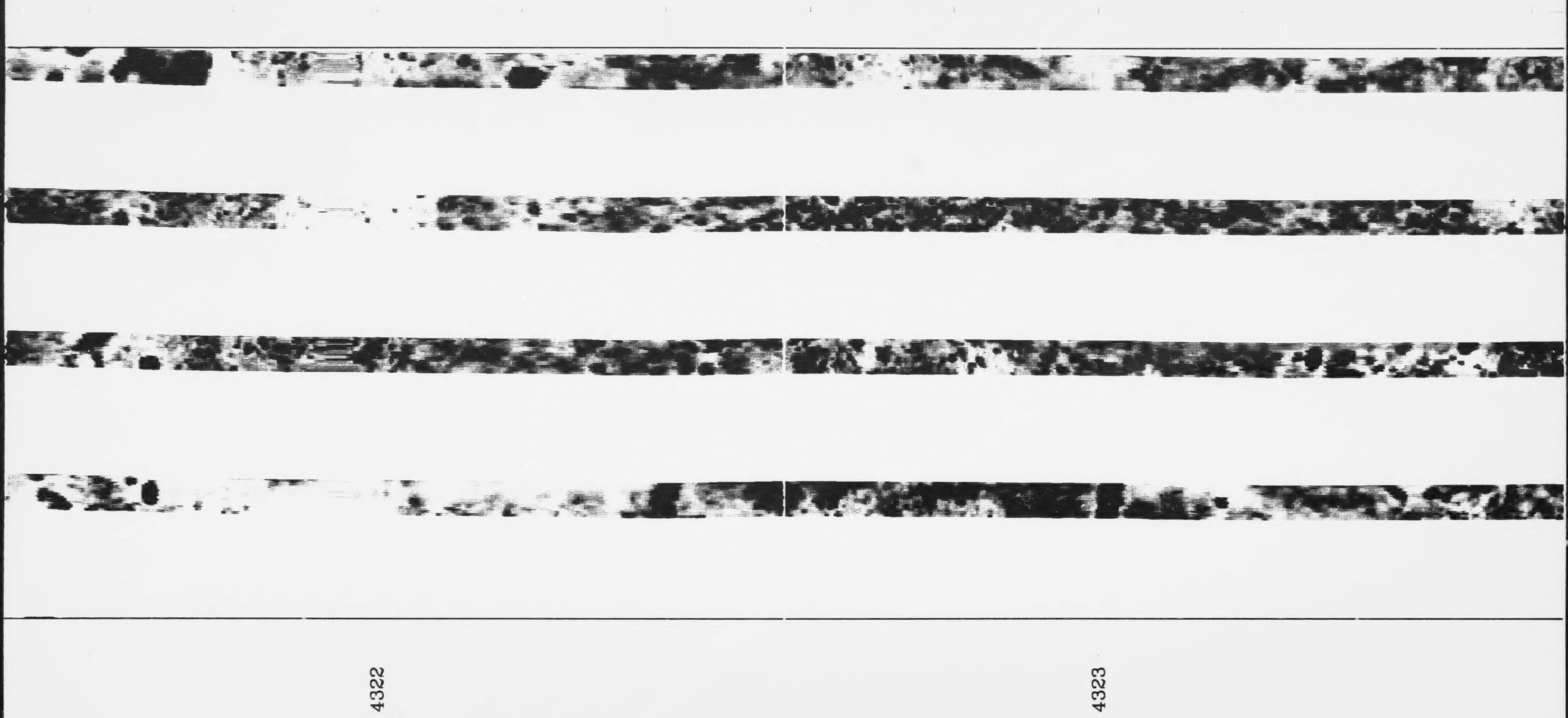
4322
4323

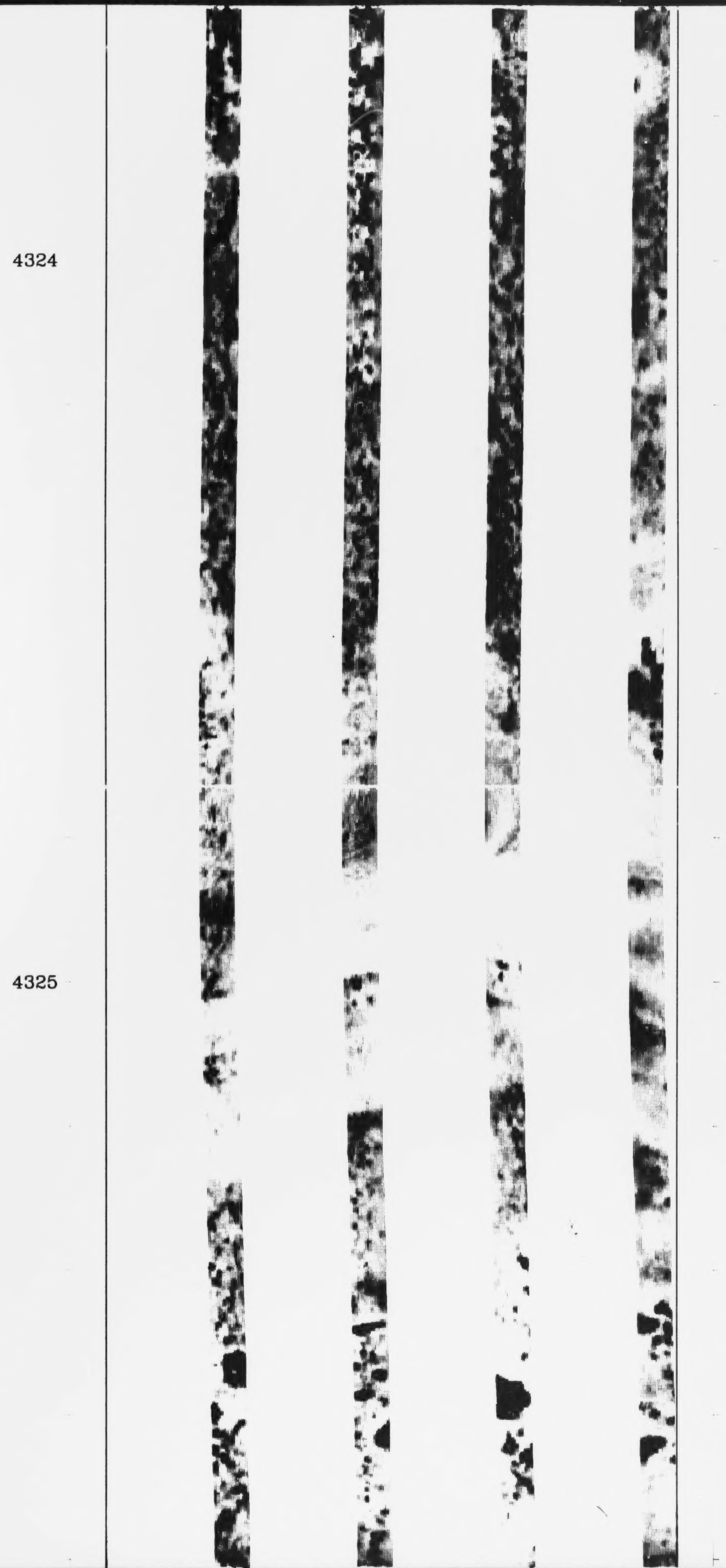
4324
4325

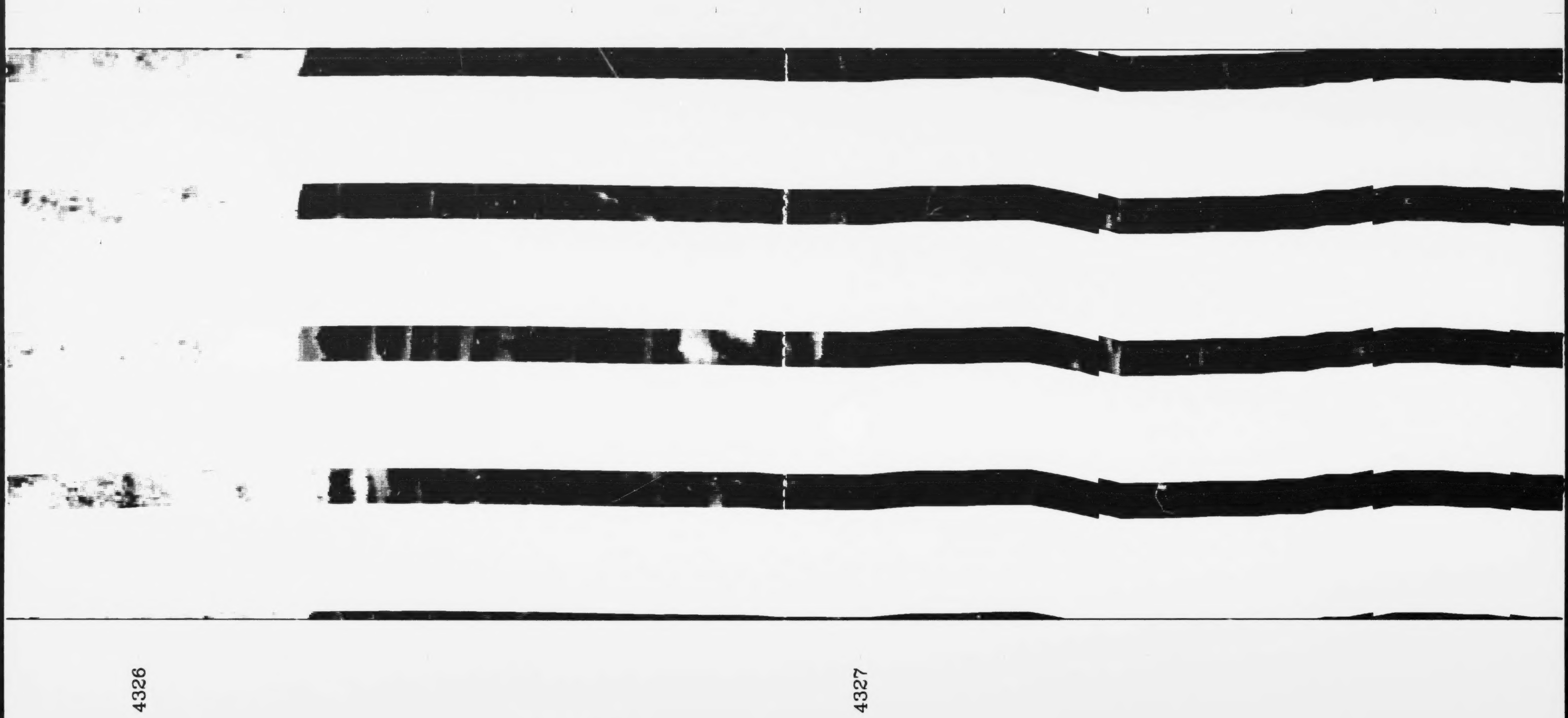
4326
4327

4328
4329
4330

SCHLUMBERGER

FMS
BOREHOLE
IMAGING

COMPANY	LAMONT-DOHERTY GEOLOGICAL
WELL	ODP HOLE-793B
FIELD	IZU-BONIN FOREARC BASIN
COUNTRY	OCEAN
RUN	1
DATE LOGGED	16 - JUN - 89
REFERENCE	STATIC PS-1 4330-4365

STATIC NORMALIZATION

PASS 1 (23577)

FILE : MEST.001

ZONE FROM 4365.0 M TO 4330.0 M

DEPTH SCALE = 1/ 5

IMAGE SCALE = 1/ 5

BITSIZE = 9.88

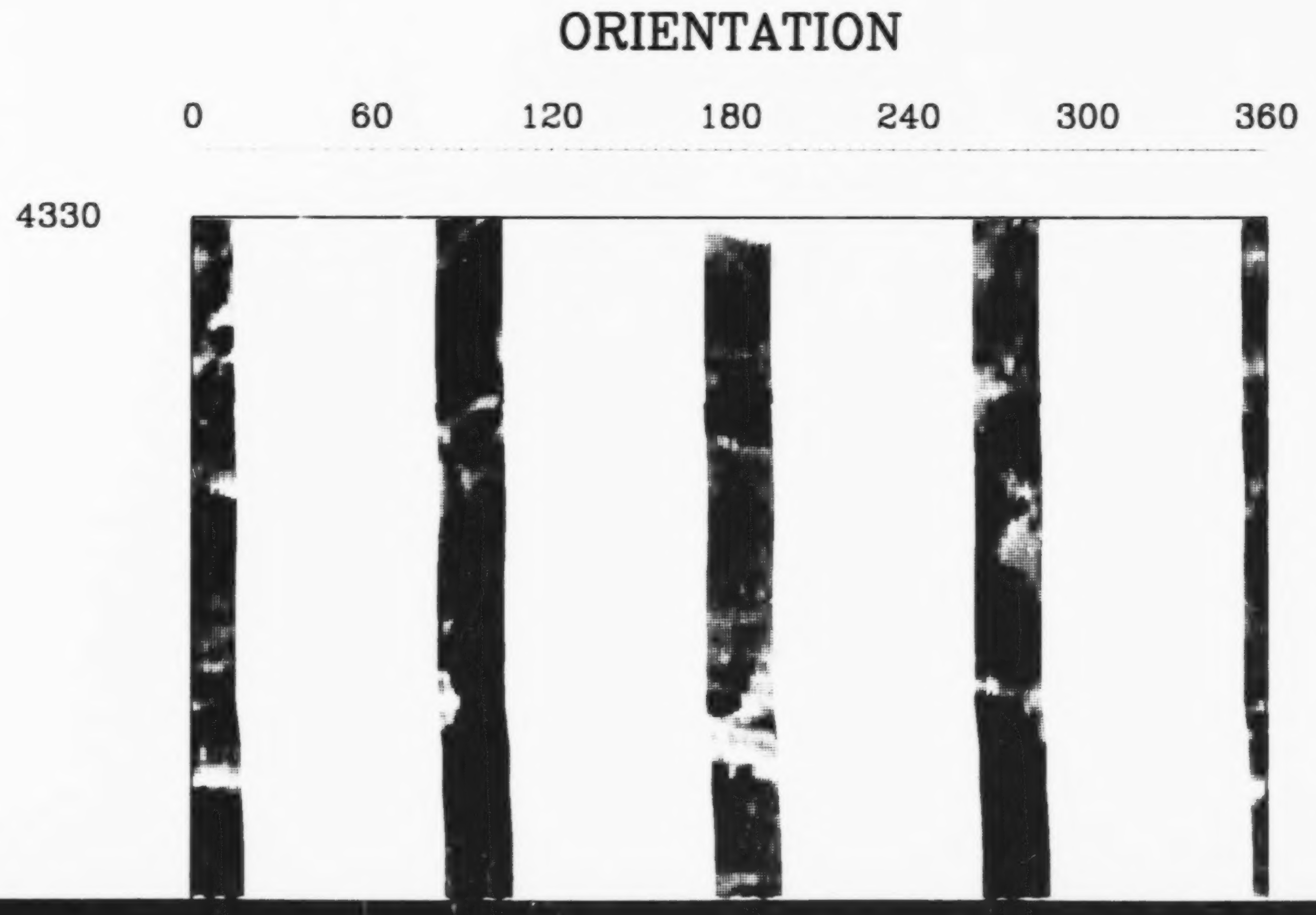

4331
4332

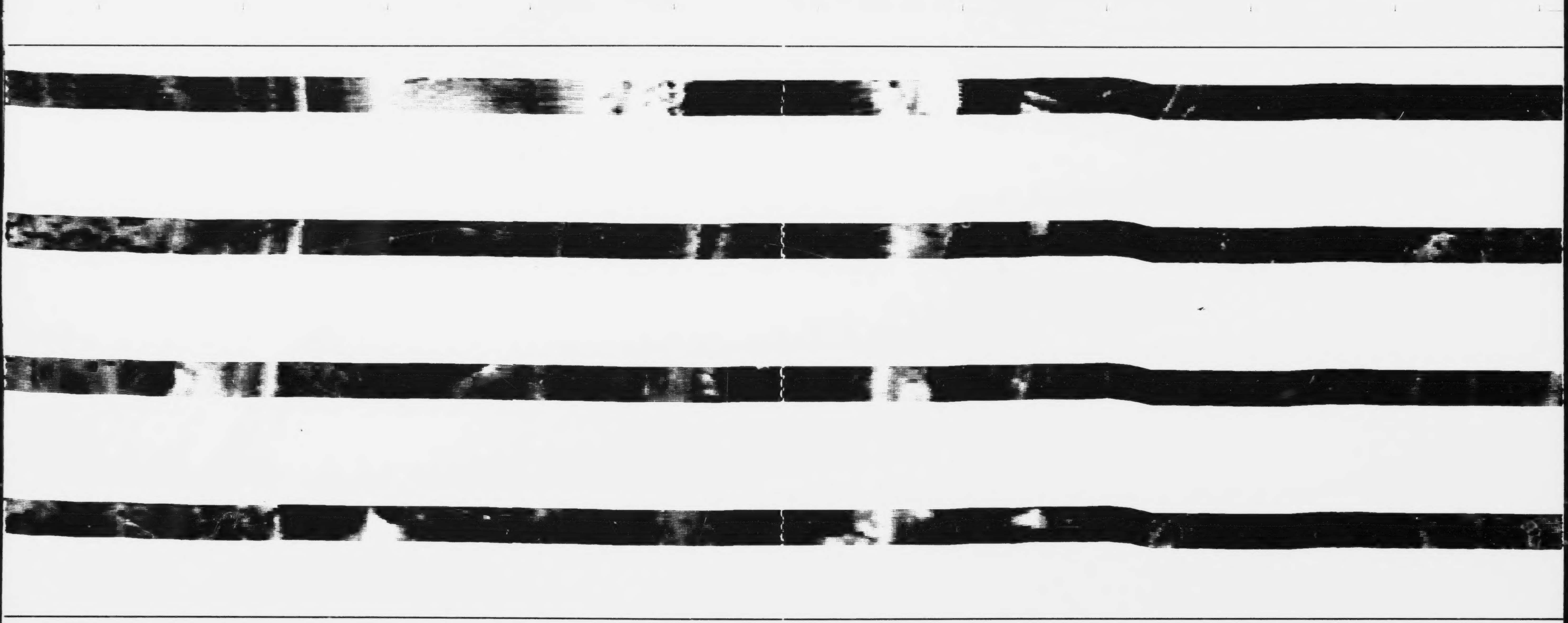

4333

4334

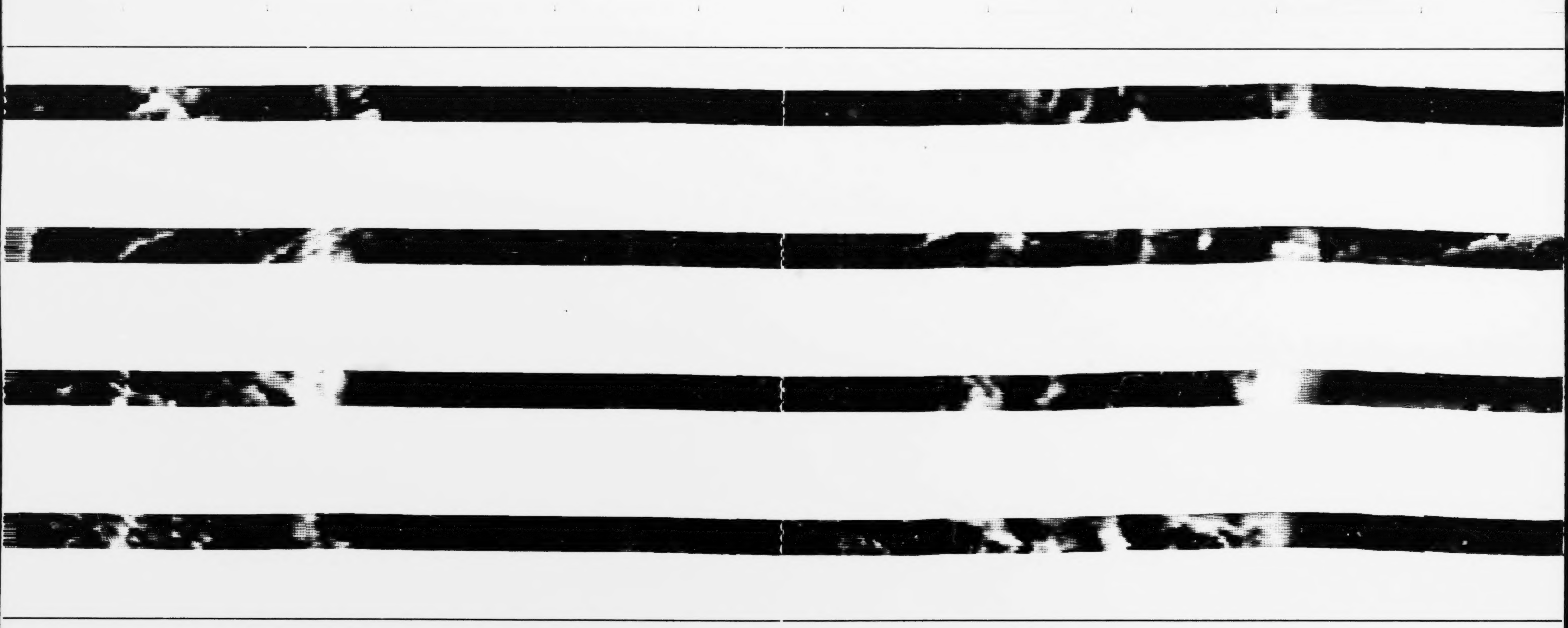

4335
4336

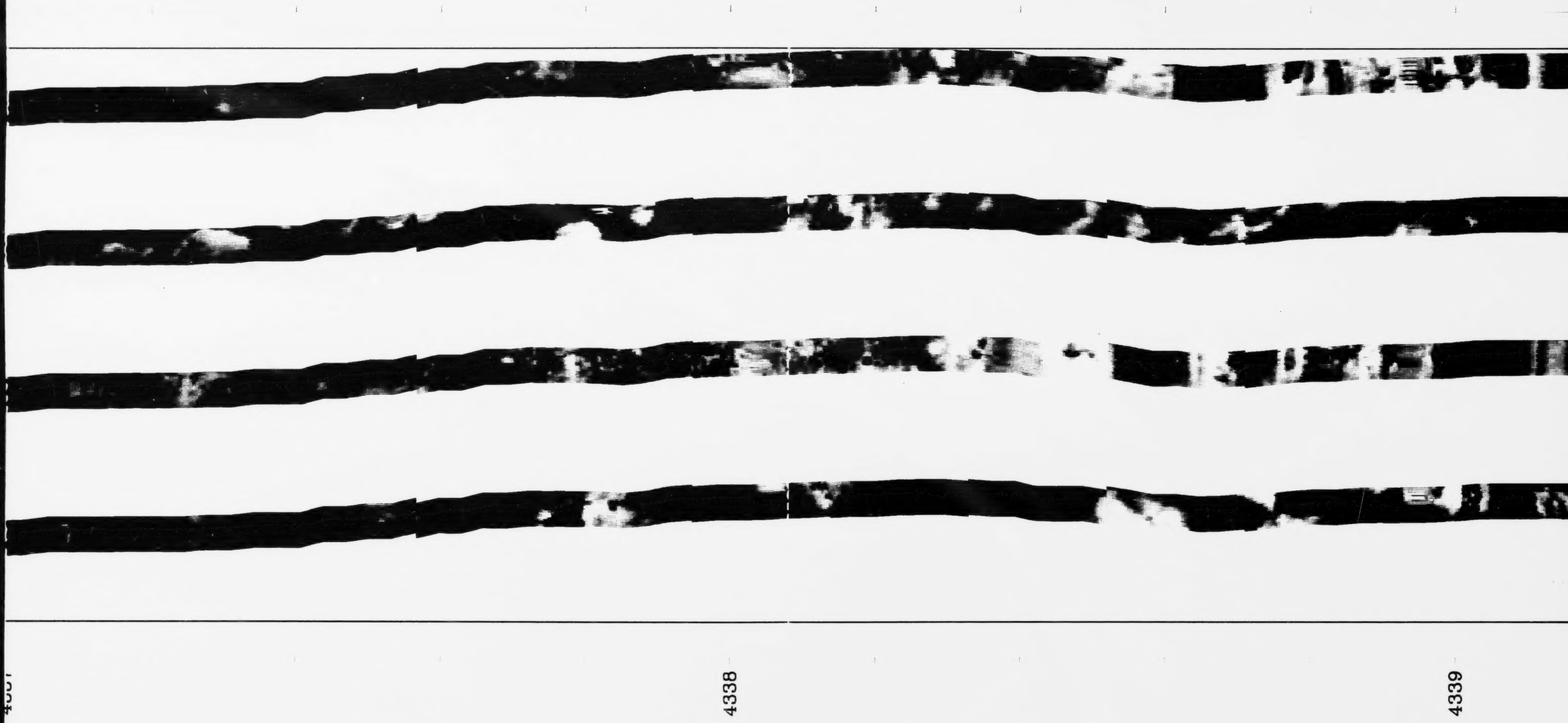
4338
4339

4340
4341

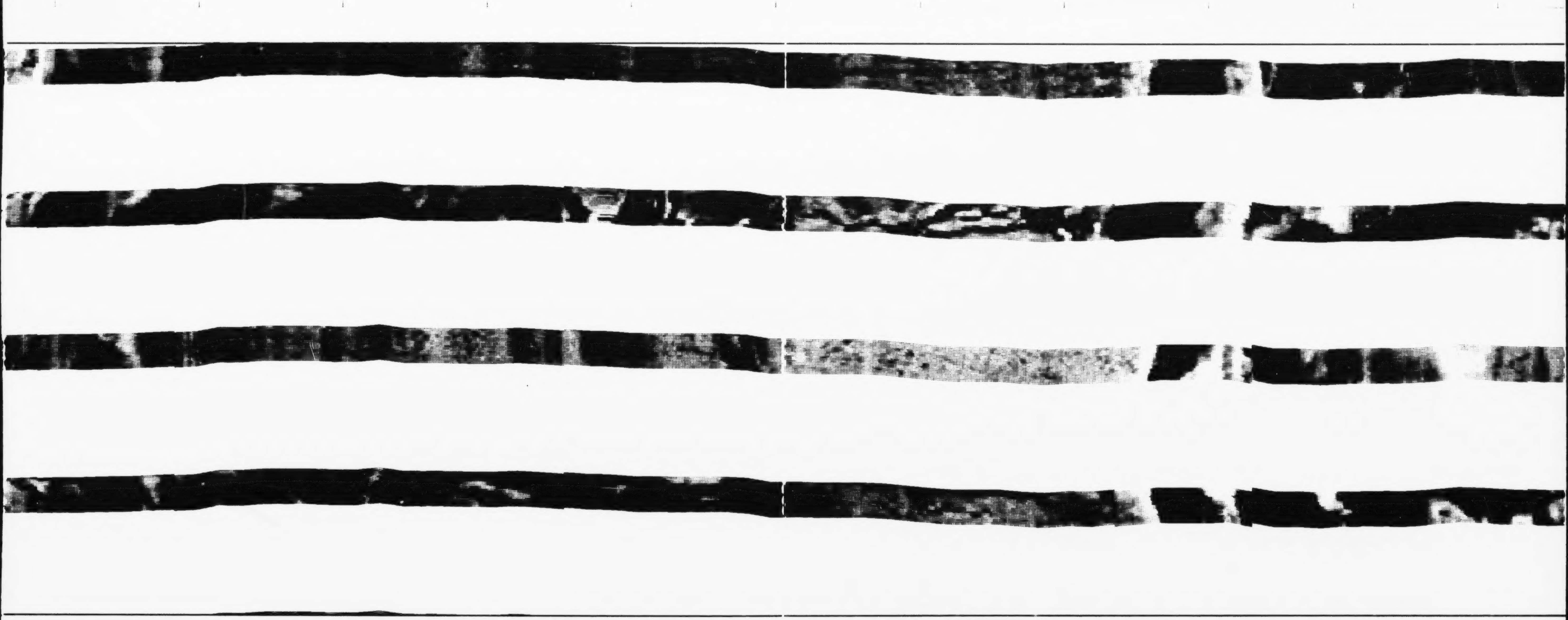
4342
4343

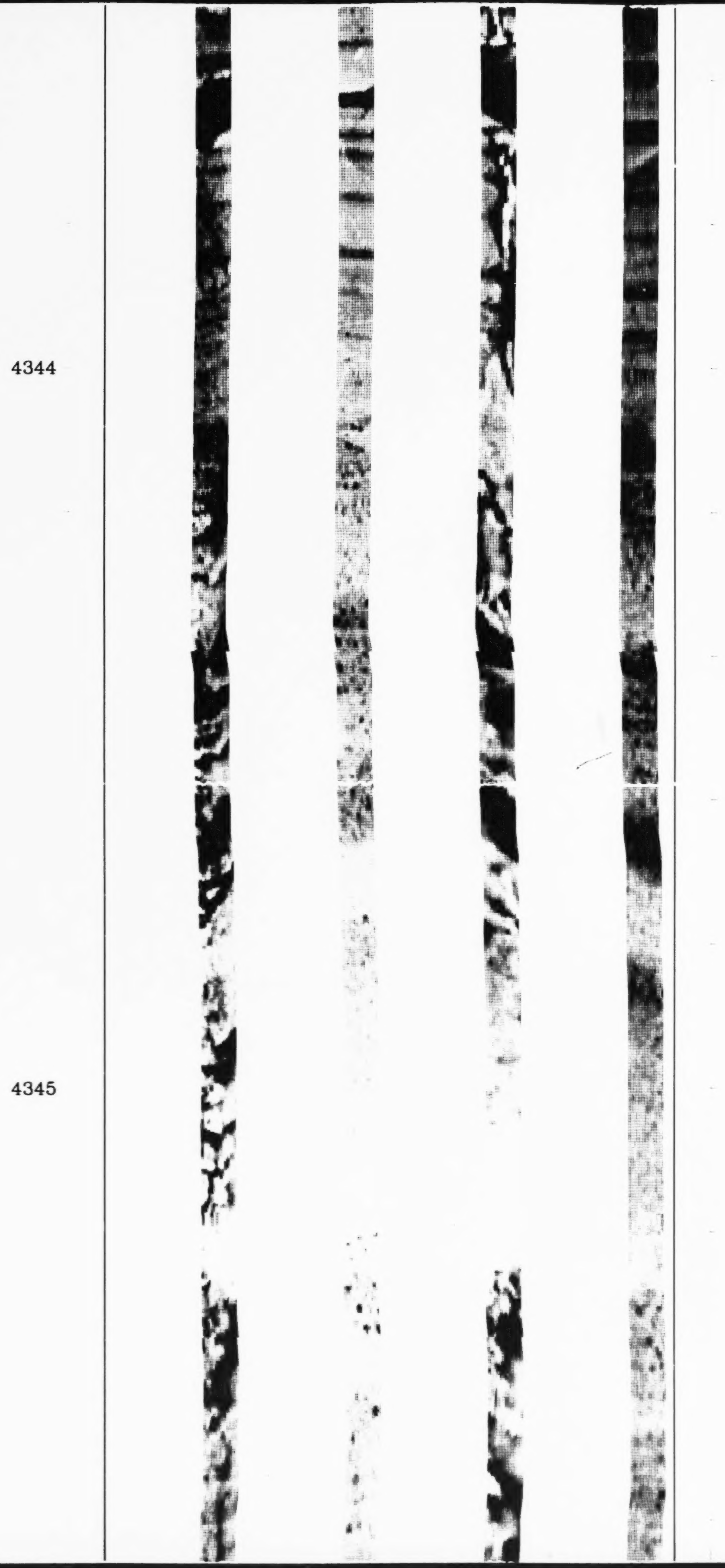
4344
4345

4346

4347

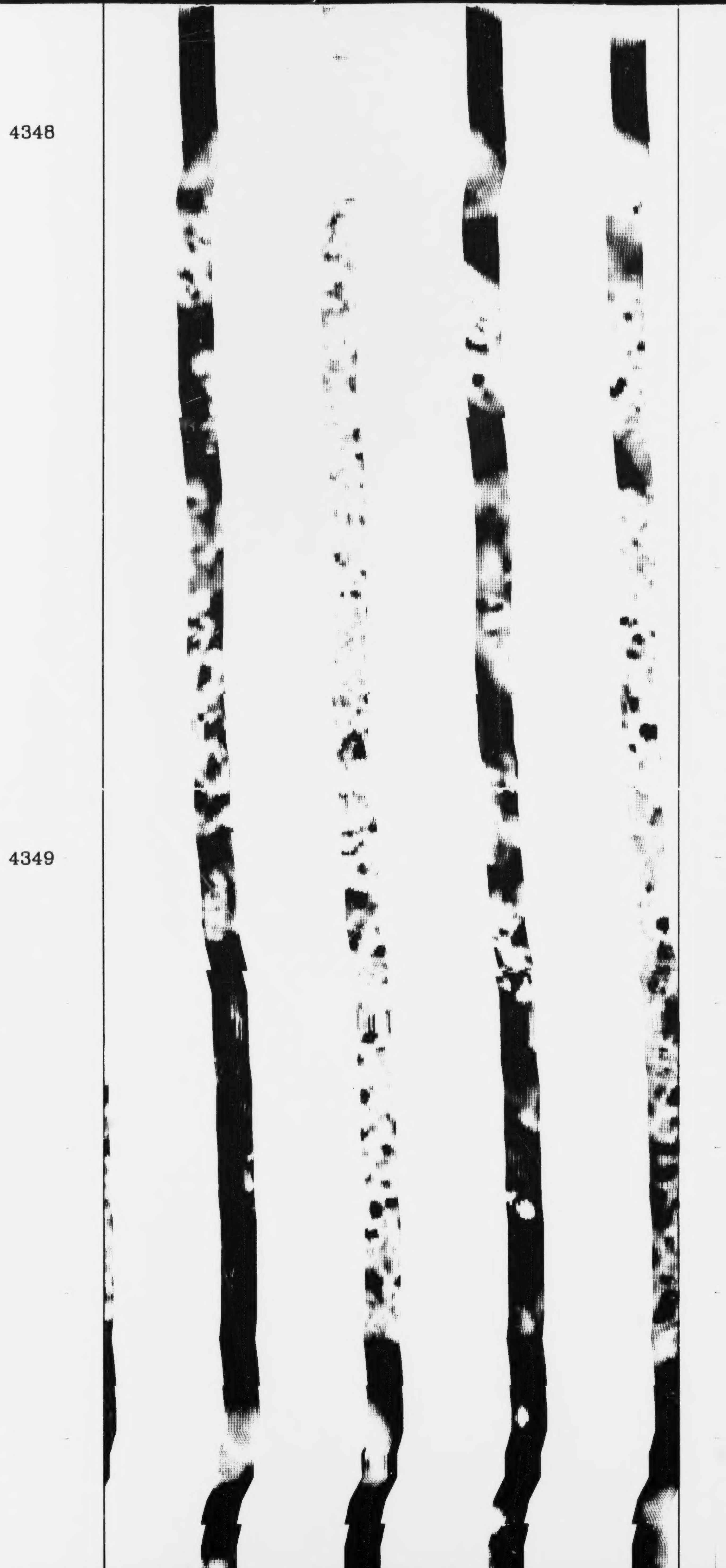
4348
4349

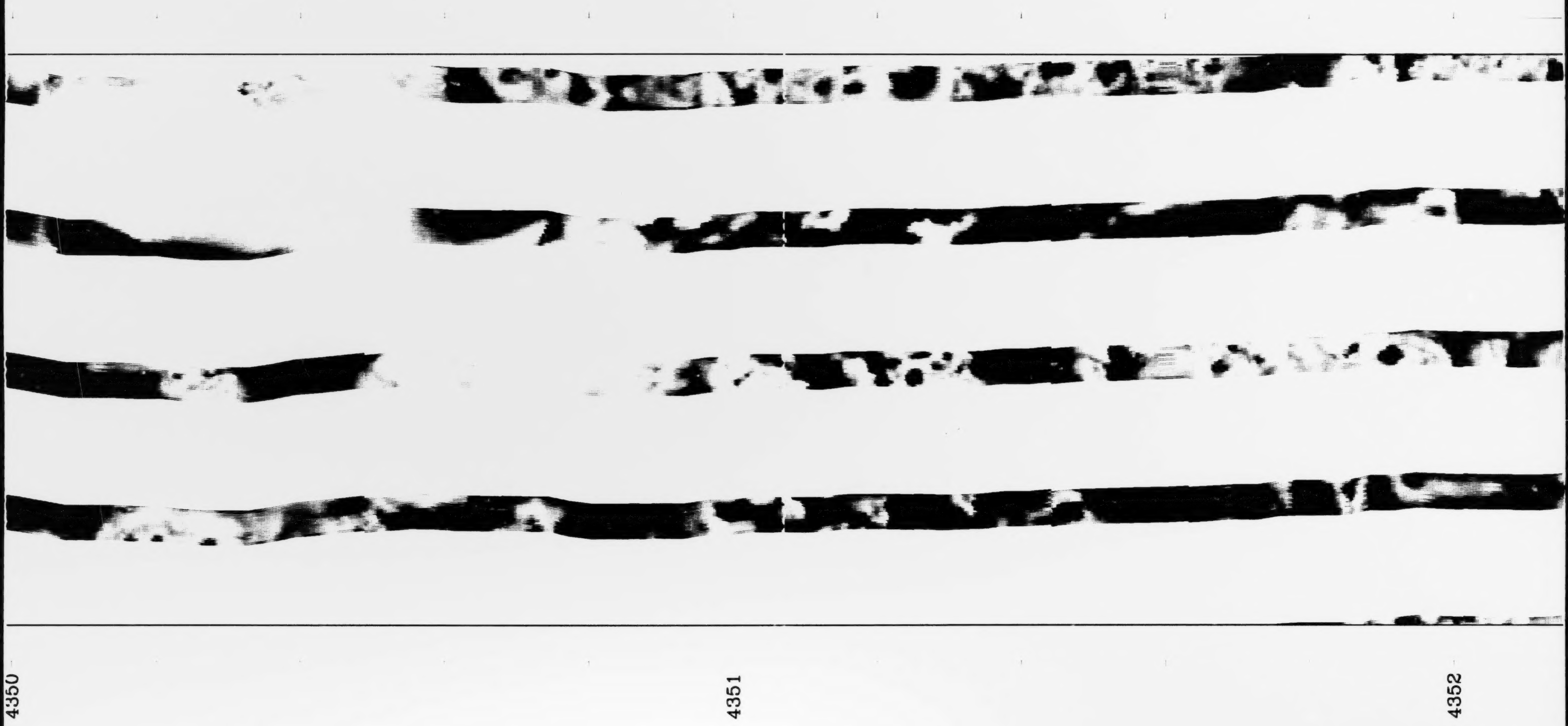
4350
4351
4352

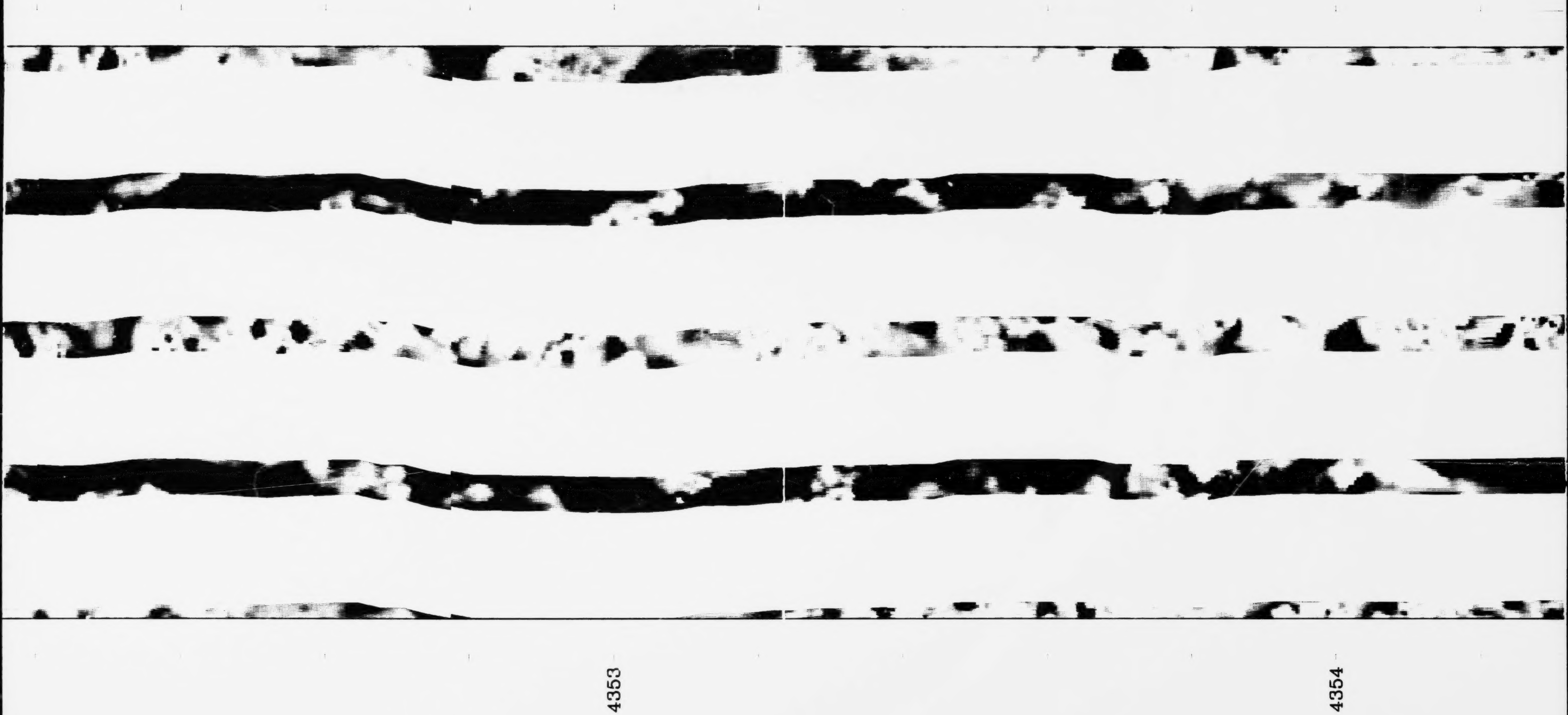
4353
4354

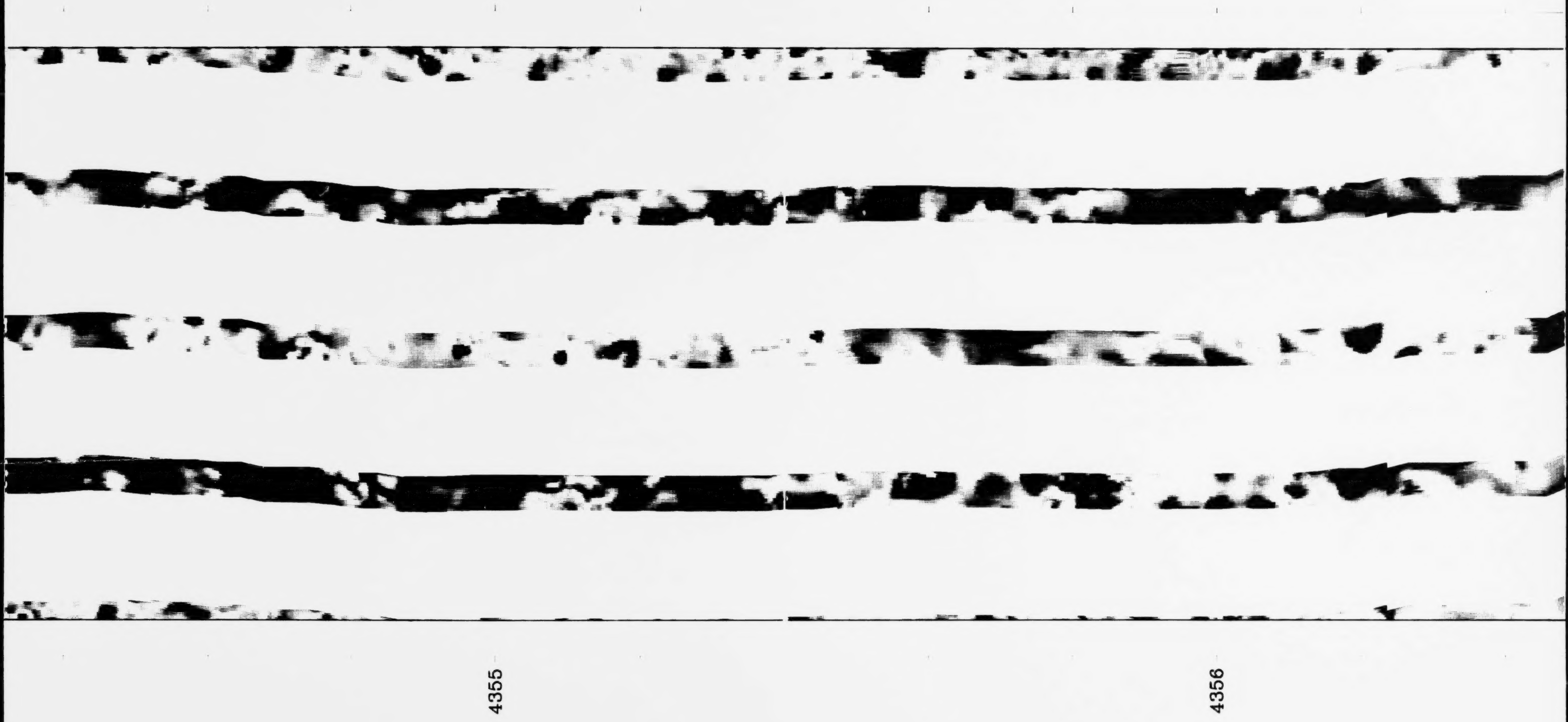
4355
4356

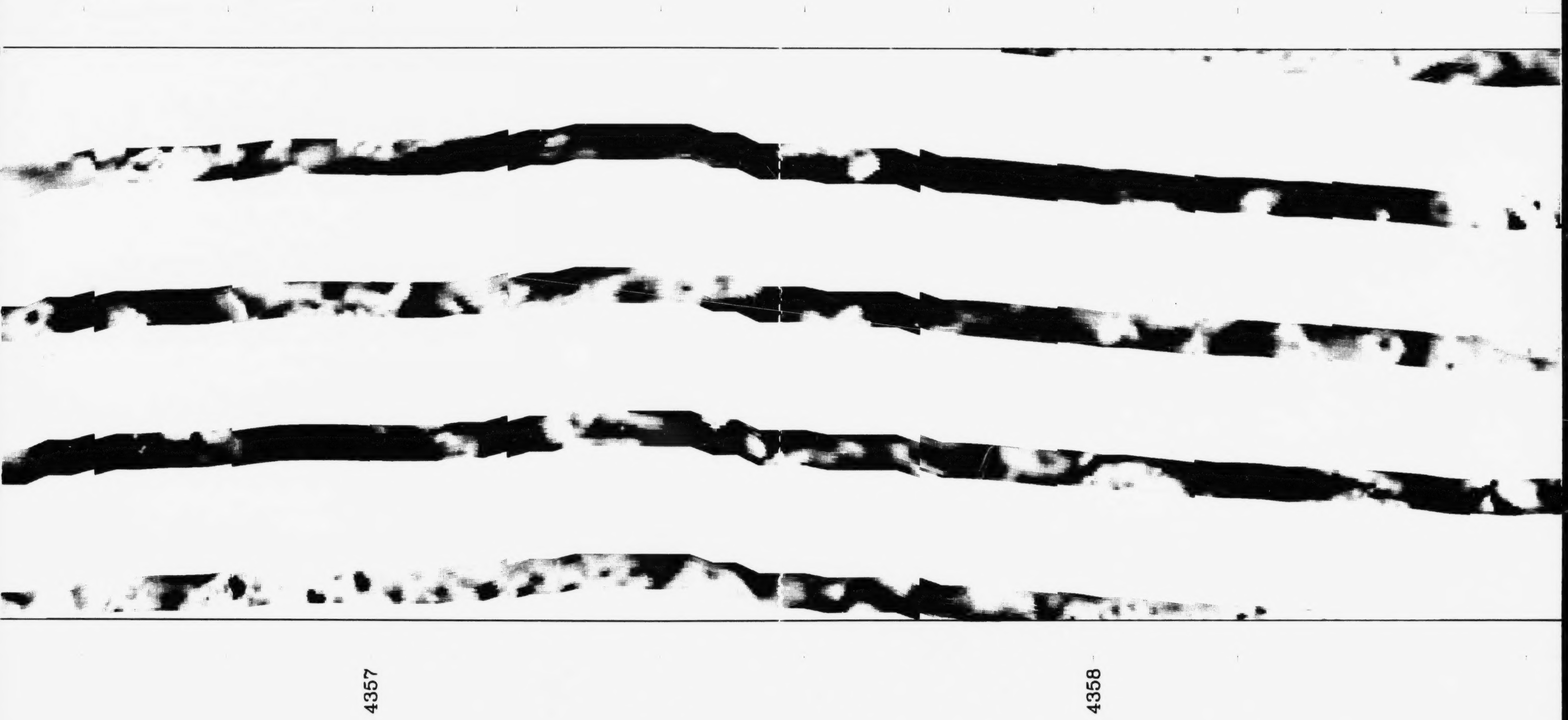
4357
4358

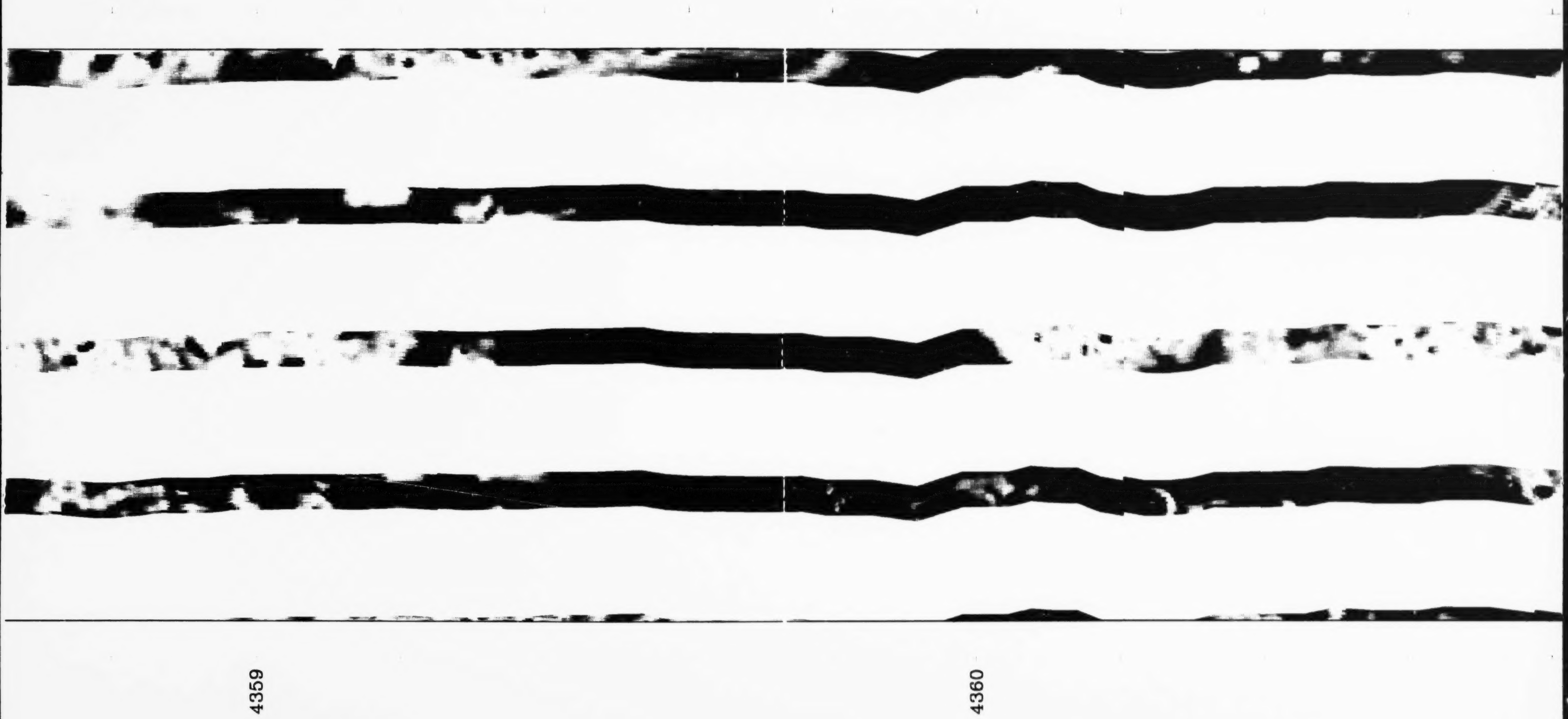
4359
4360

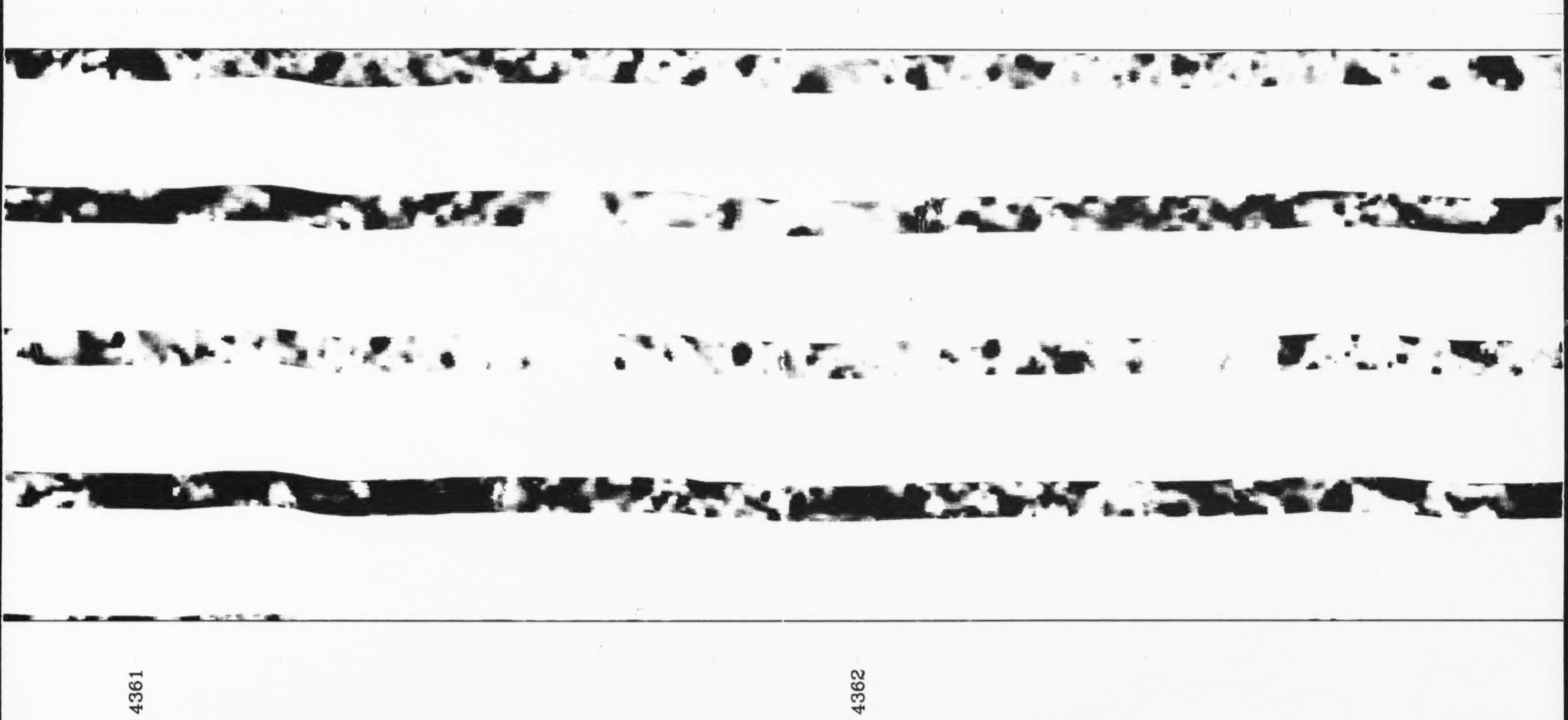
4361
4362

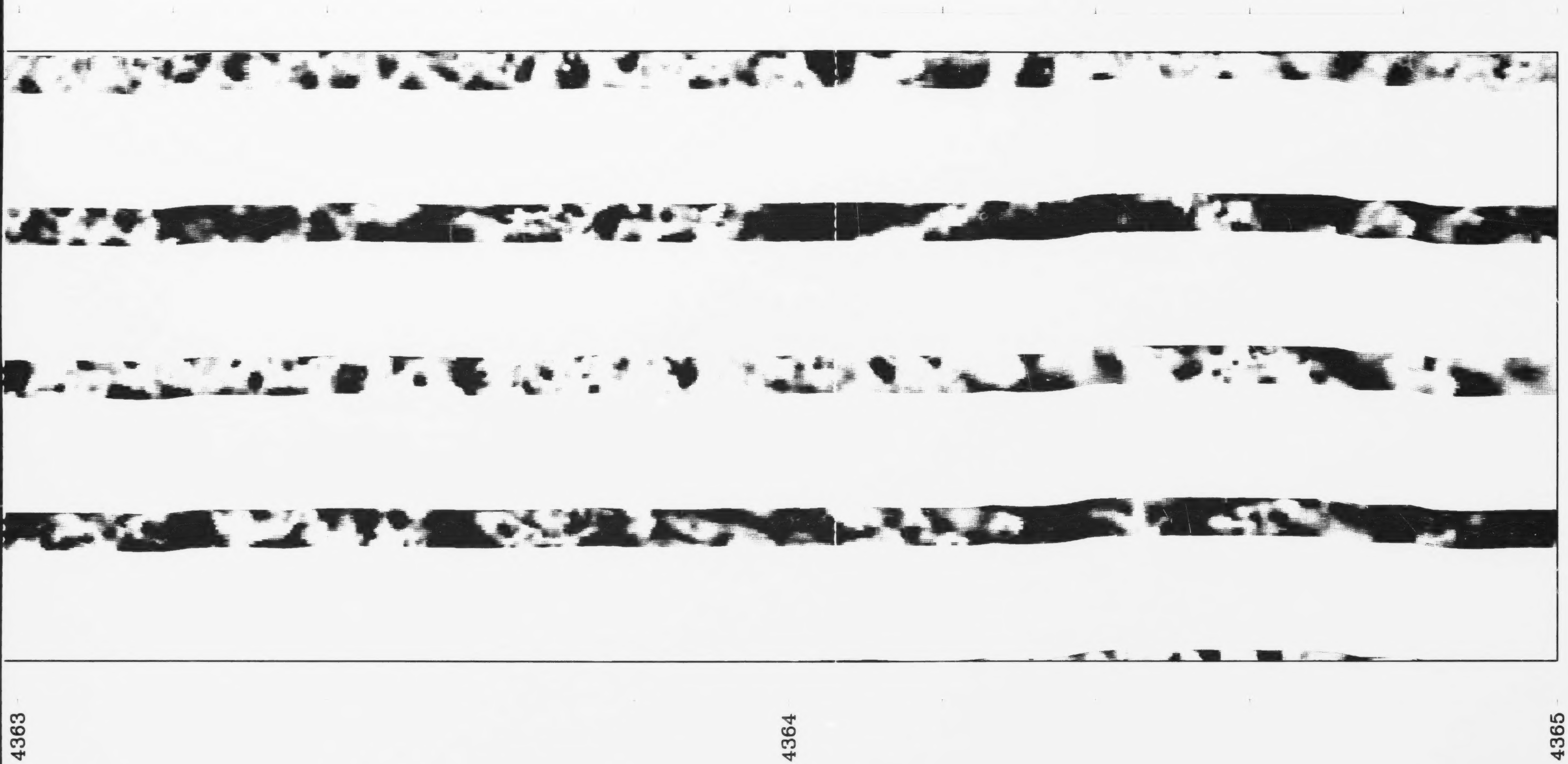
4363
4364
4365

SCHLUMBERGER

FMS
BOREHOLE
IMAGING

COMPANY	LAMONT–DOHERTY GEOLOGICAL
WELL	ODP HOLE–793B
FIELD	IZU–BONIN FOREARC BASIN
COUNTRY	OCEAN
RUN	1
DATE LOGGED	16 – JUN – 89
REFERENCE	STATIC PS–1 4365–4400

STATIC NORMALIZATION

PASS 1 (23577)

FILE : MEST.001

ZONE FROM 4400.0 M TO 4365.0 M

DEPTH SCALE = 1/ 5

IMAGE SCALE = 1/ 5

BITSIZE = 9.88

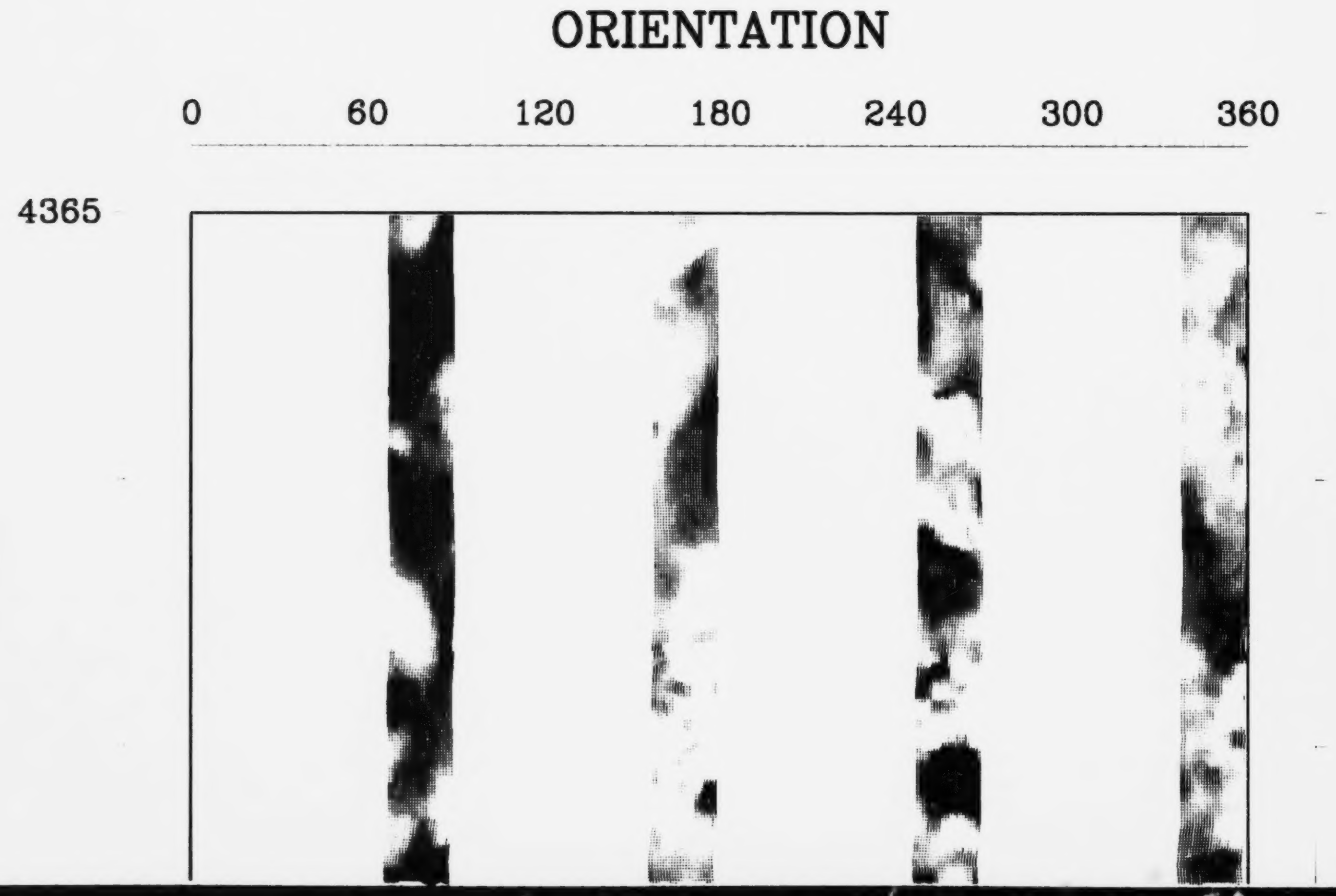

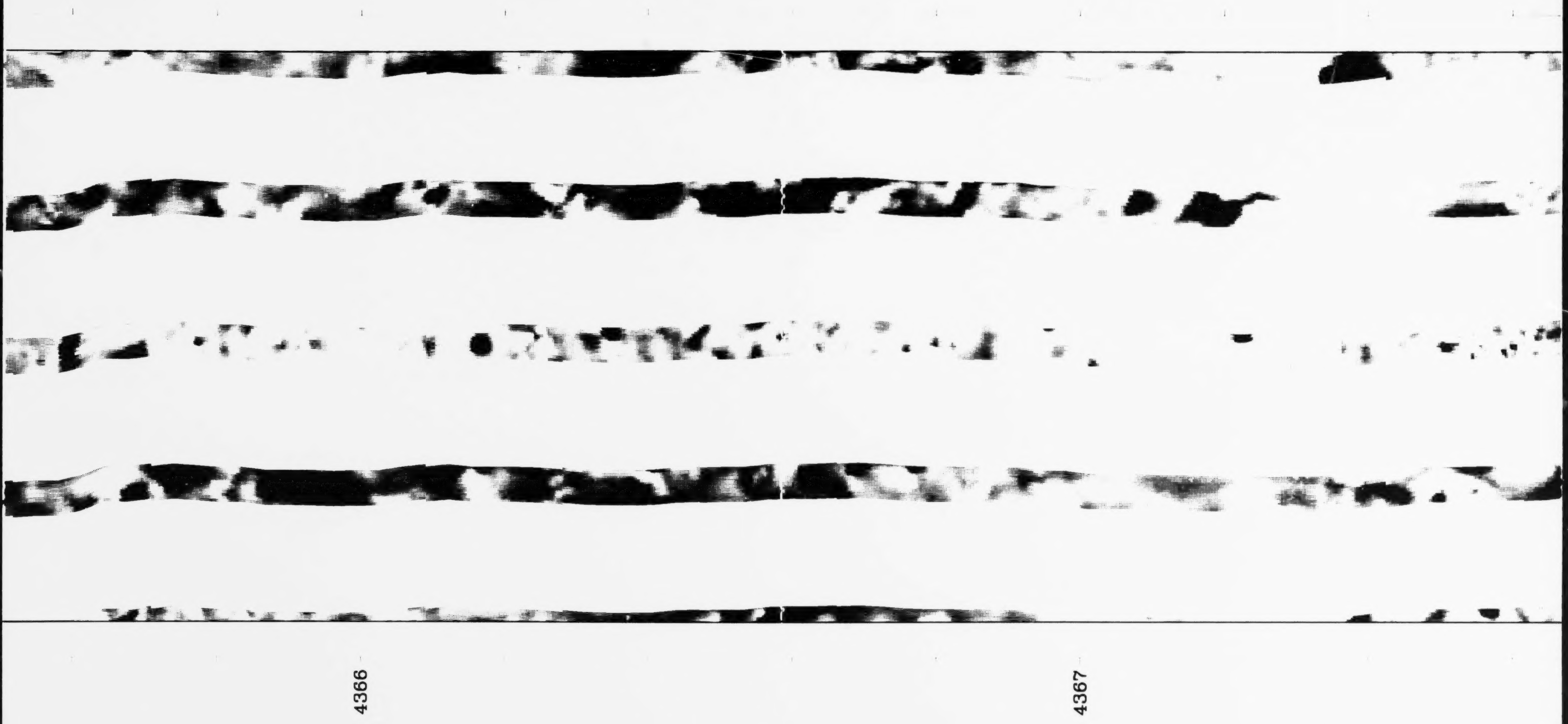
4366
4367

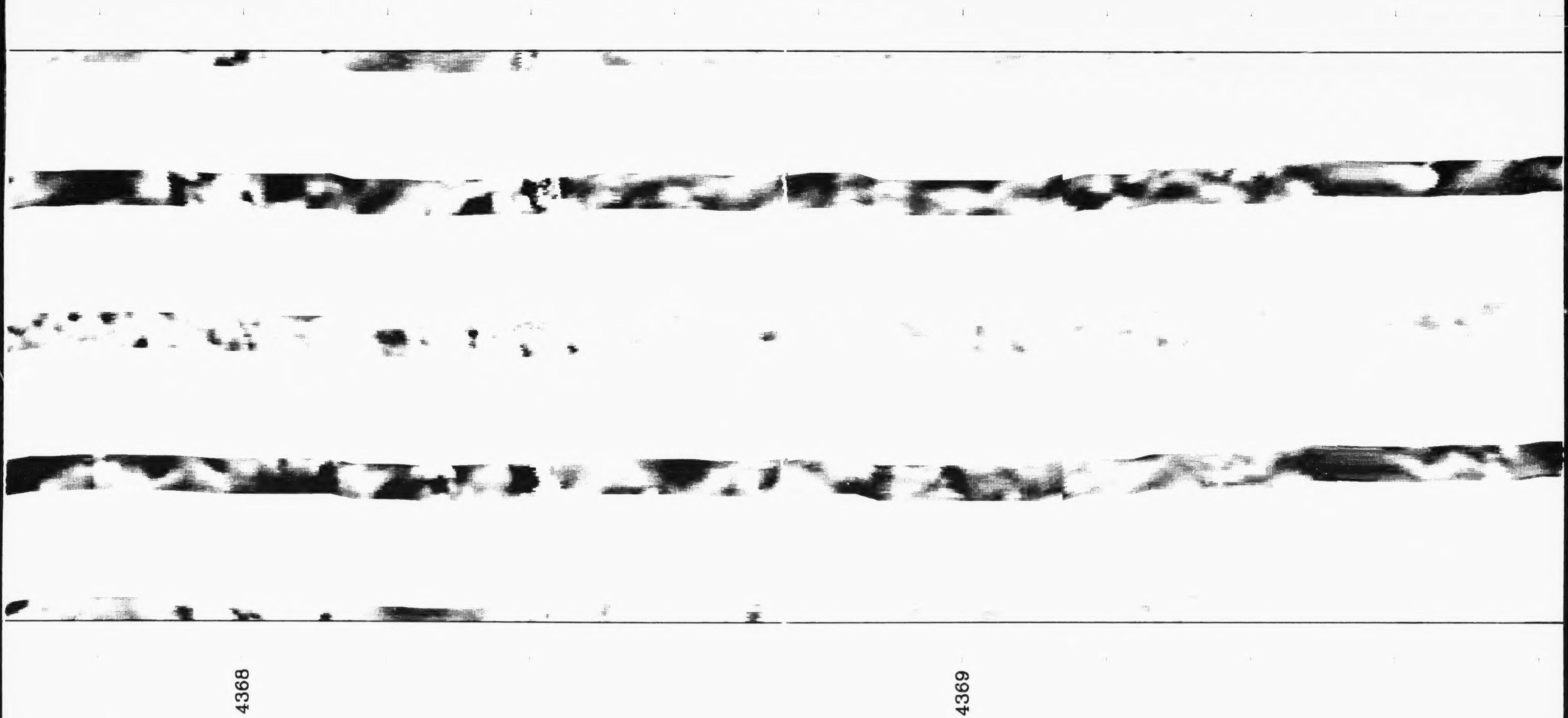
4368
4369

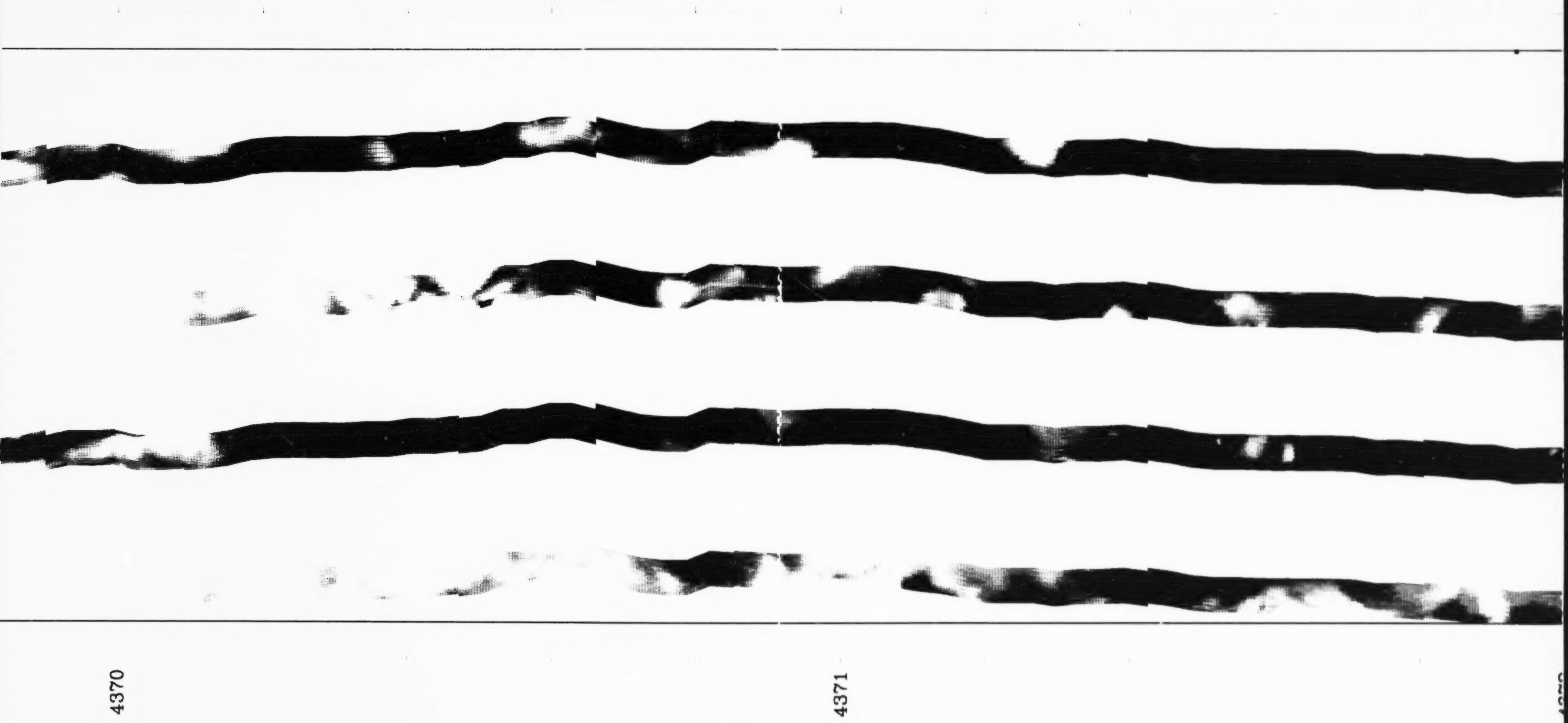
4370
4371

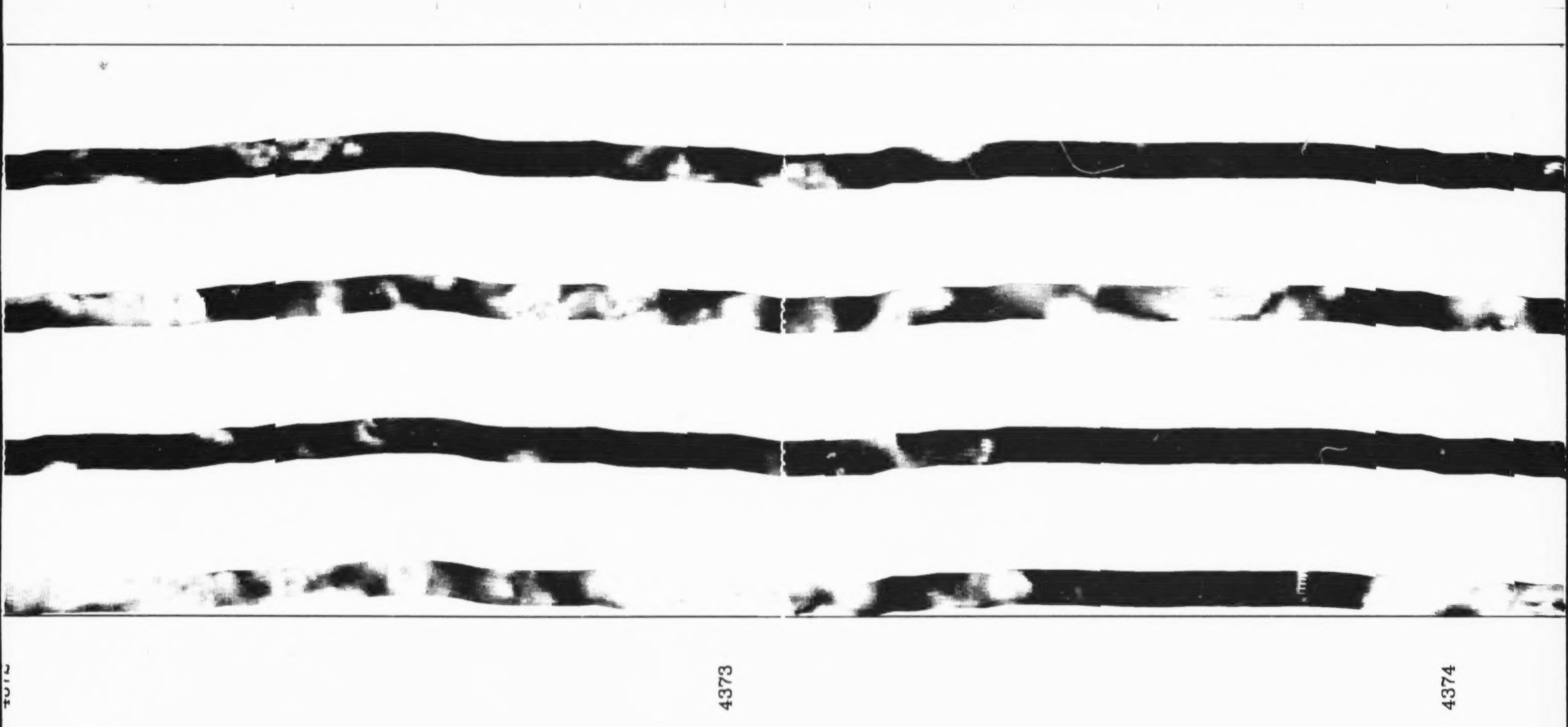
4373
4374

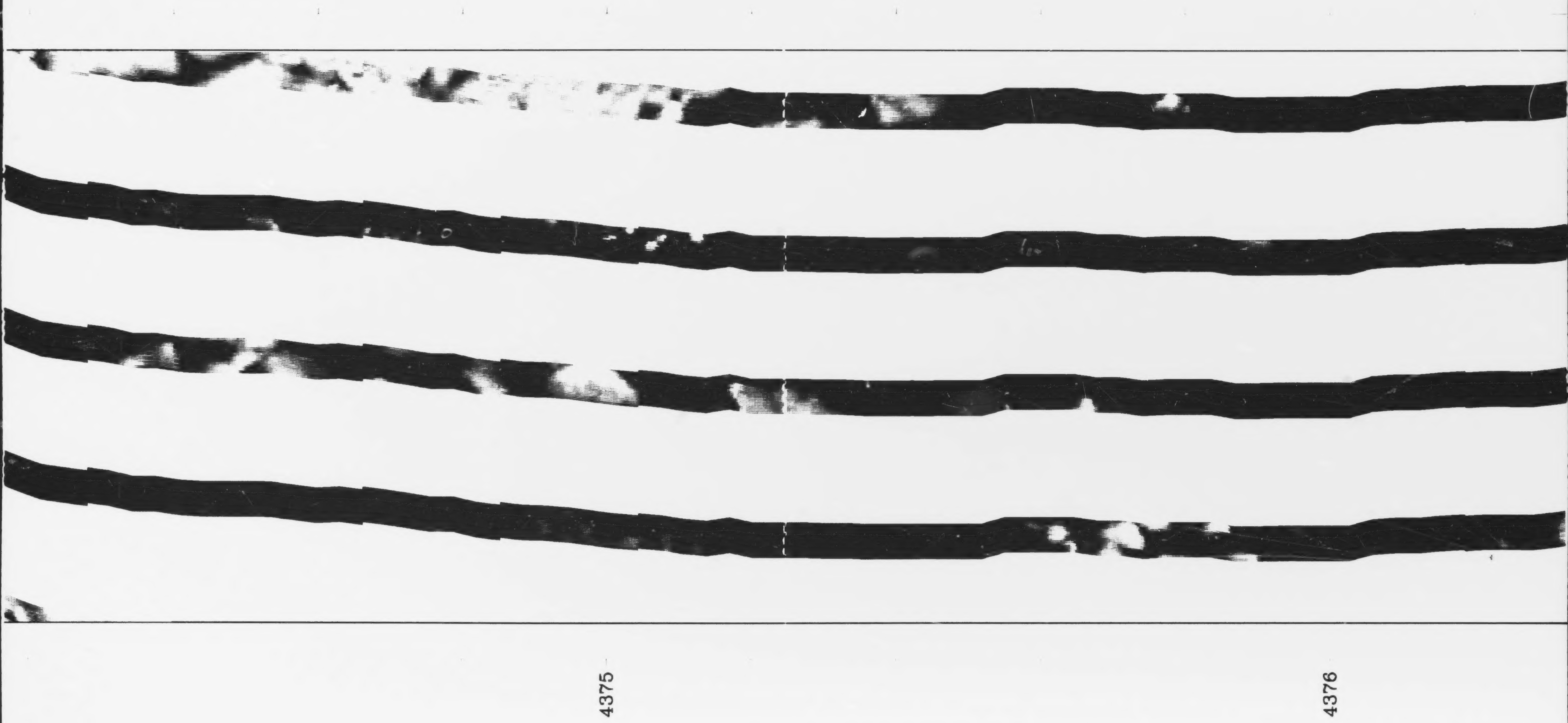
4375
4376

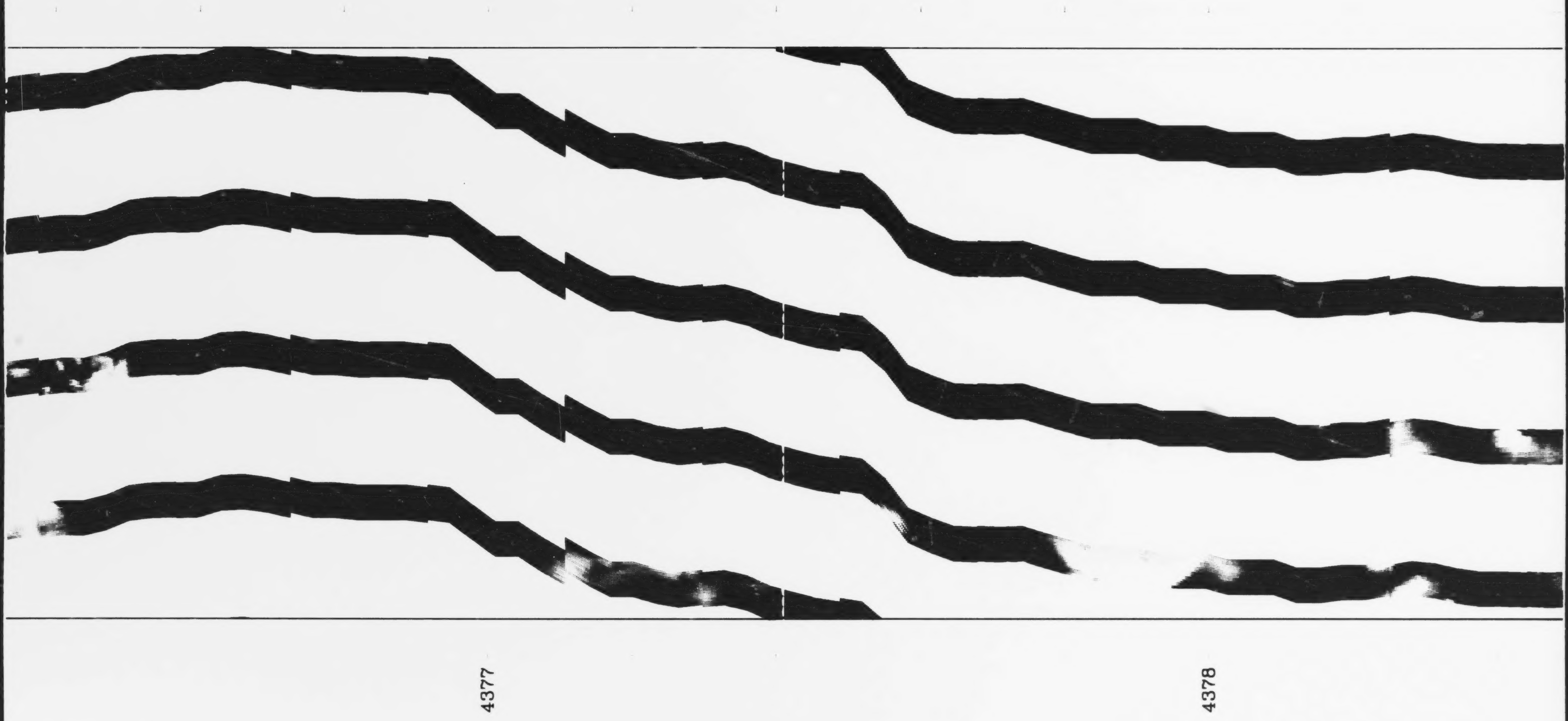
4377
4378

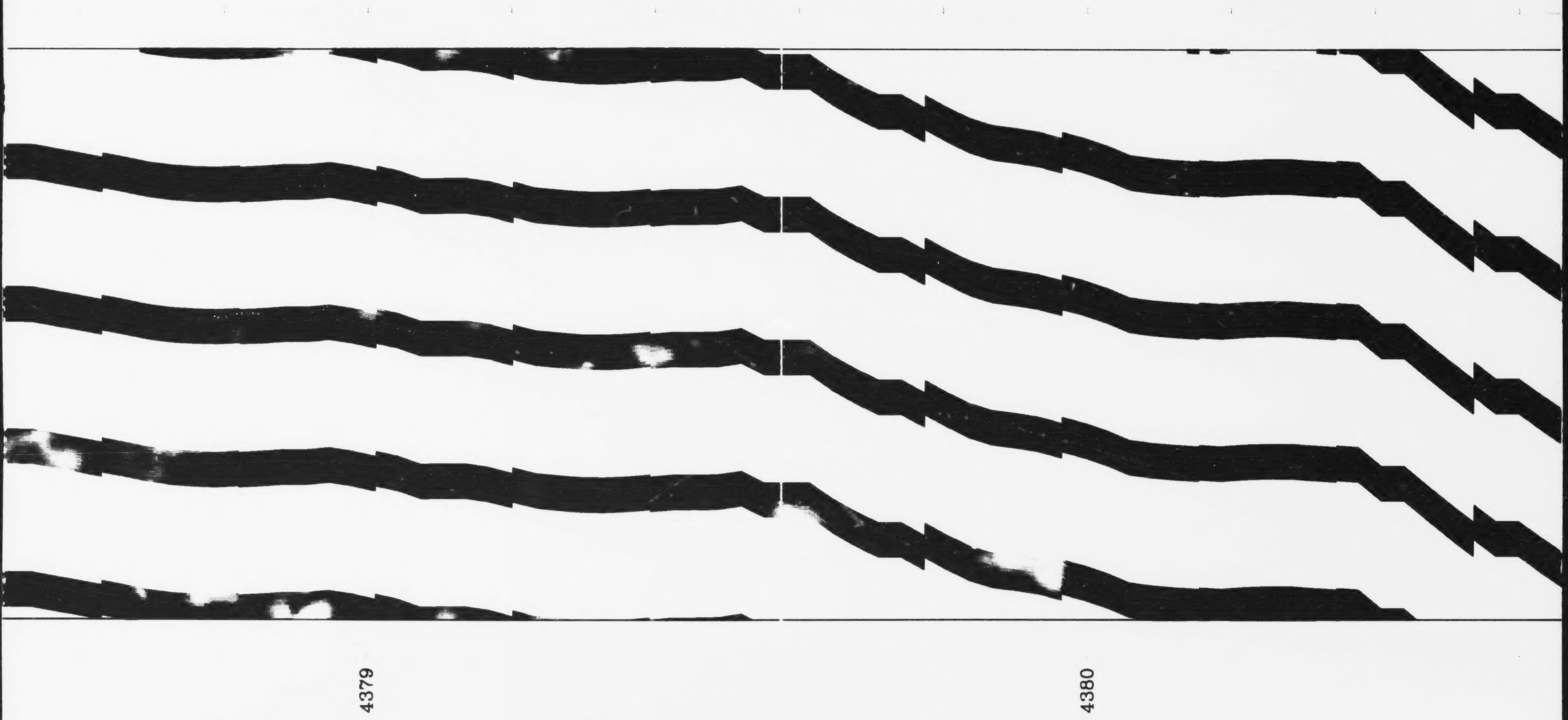
4379
4380

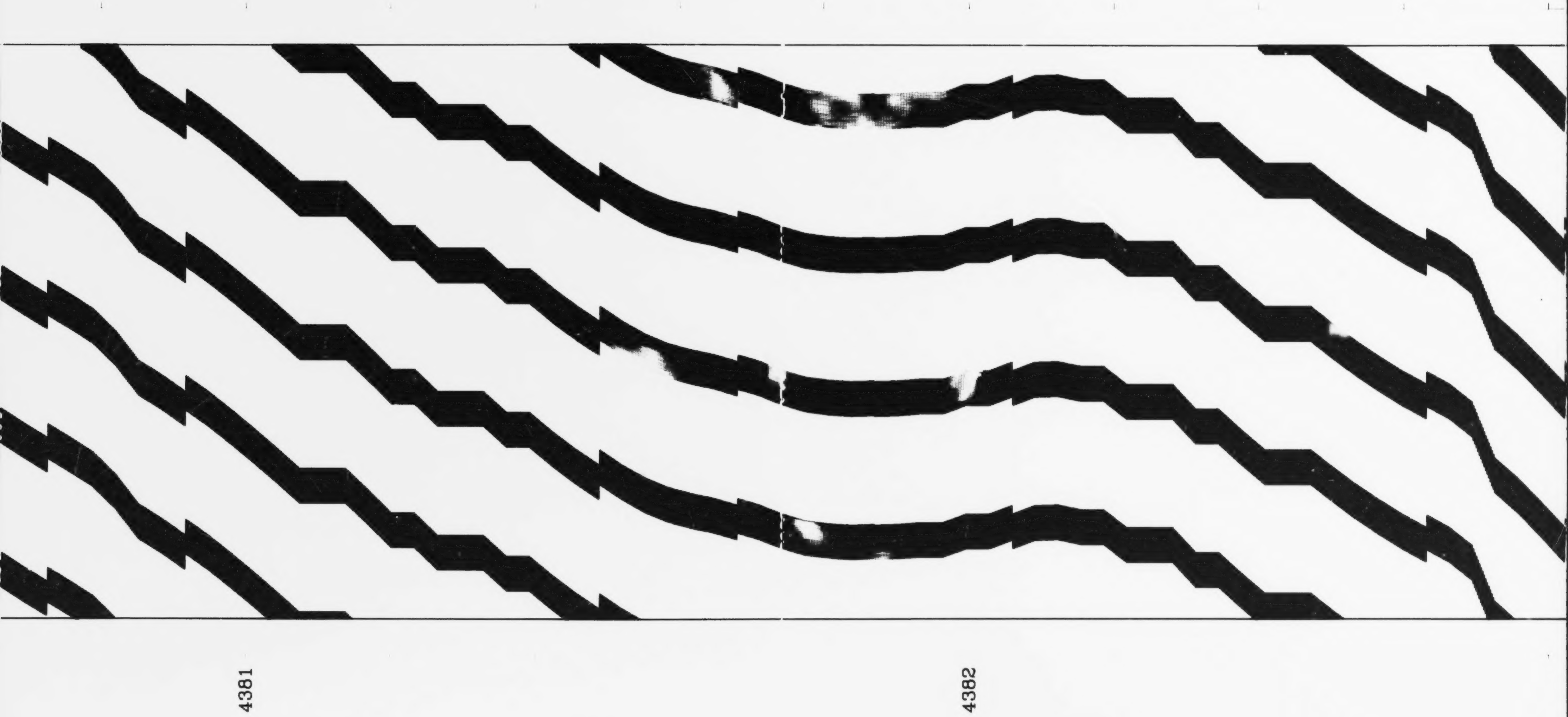
4381
4382

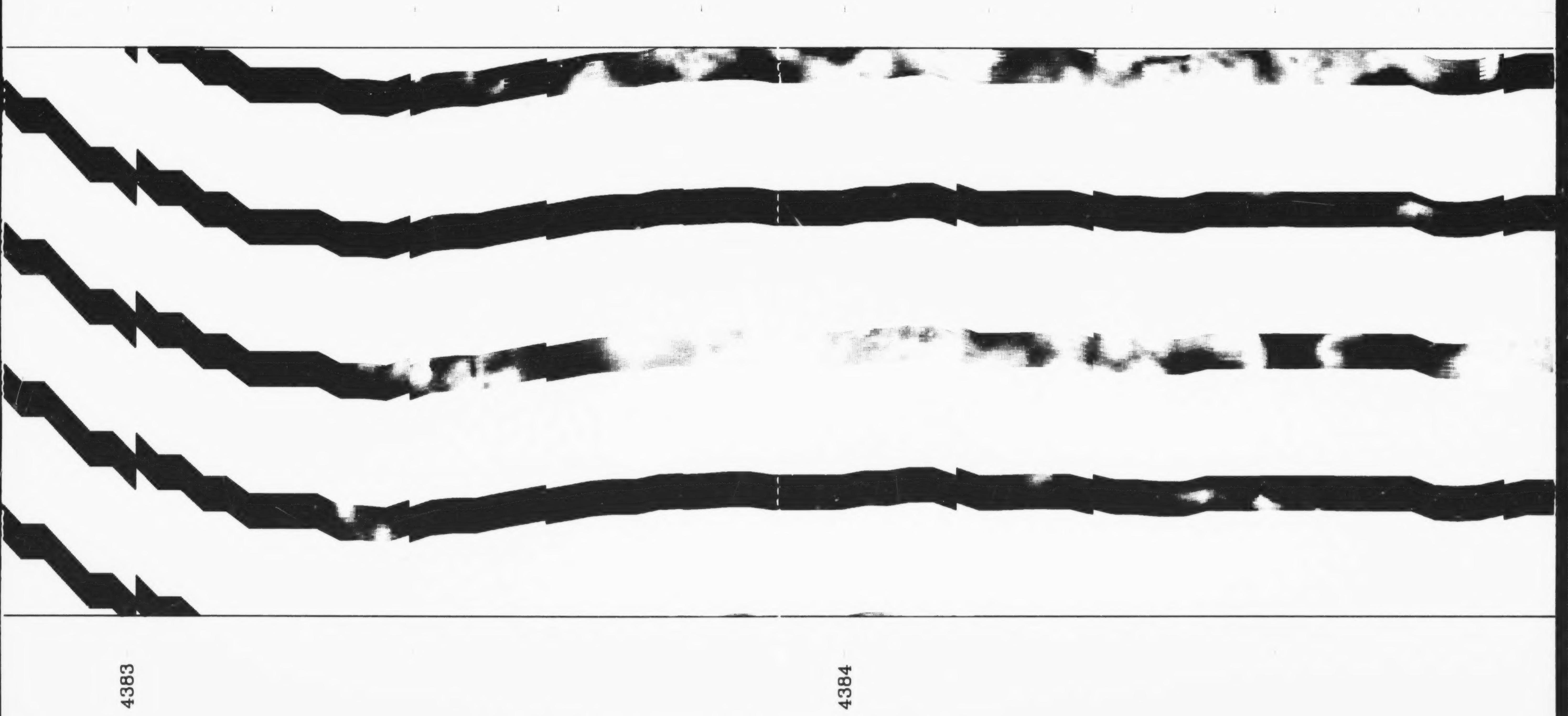
4383
4384

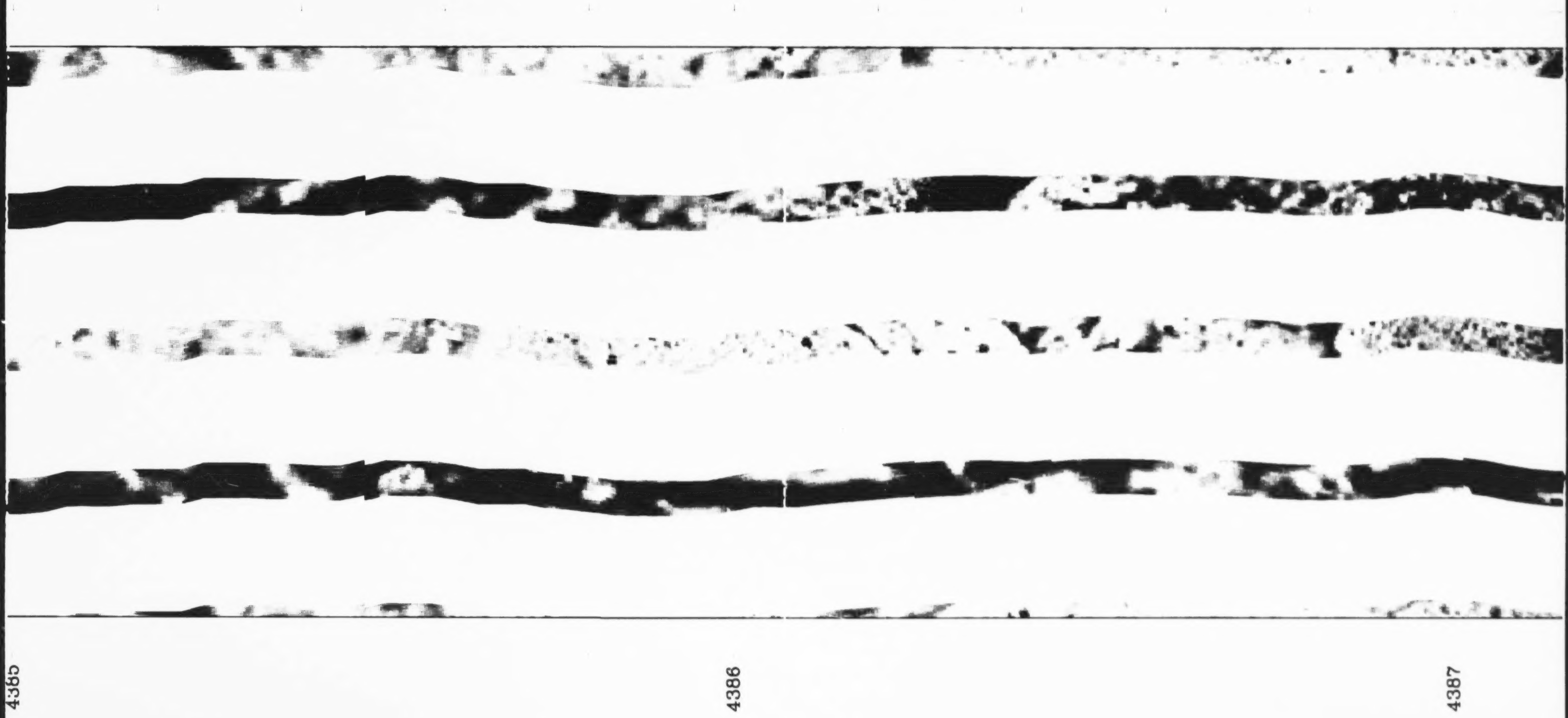
4385
4386
4387

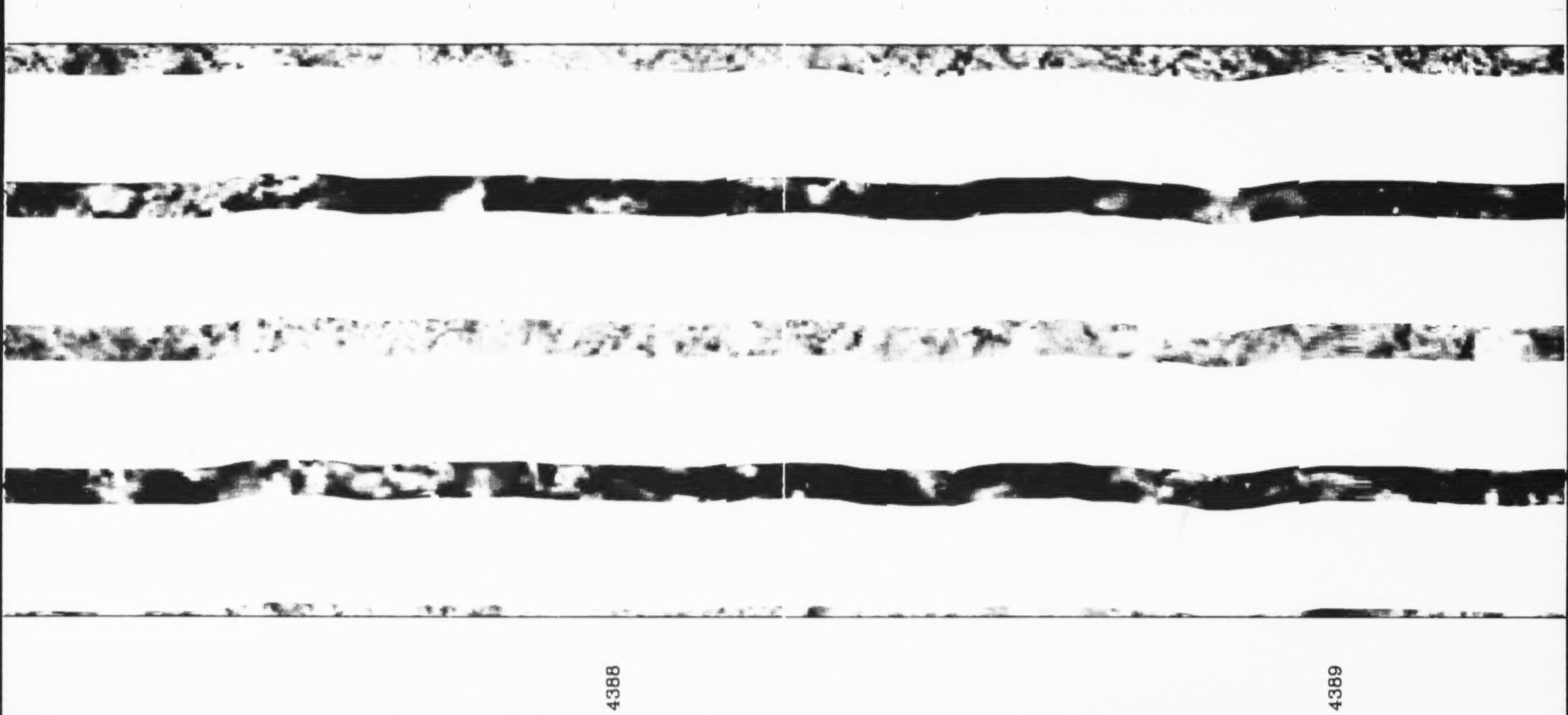
4388
4389

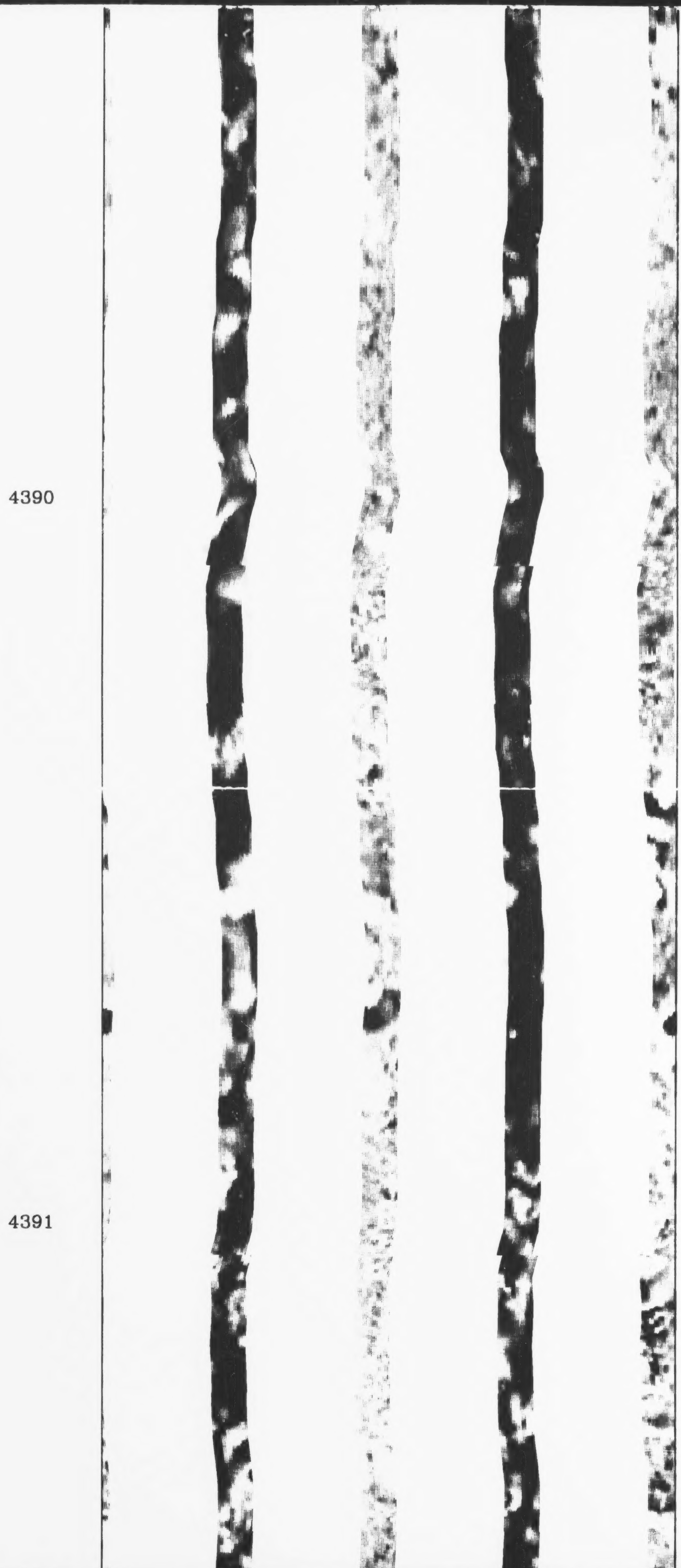
4390
4391

4392
4393

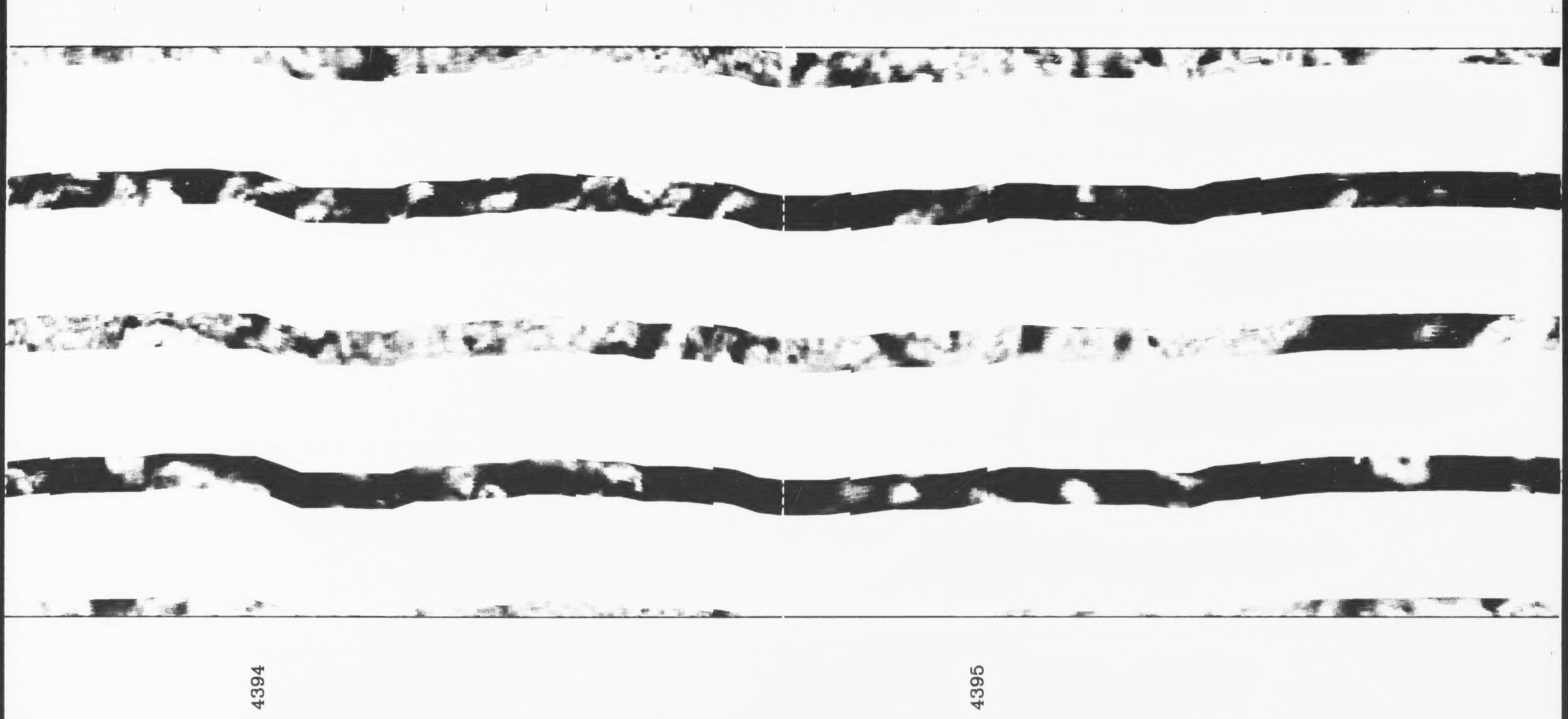

4394
4395

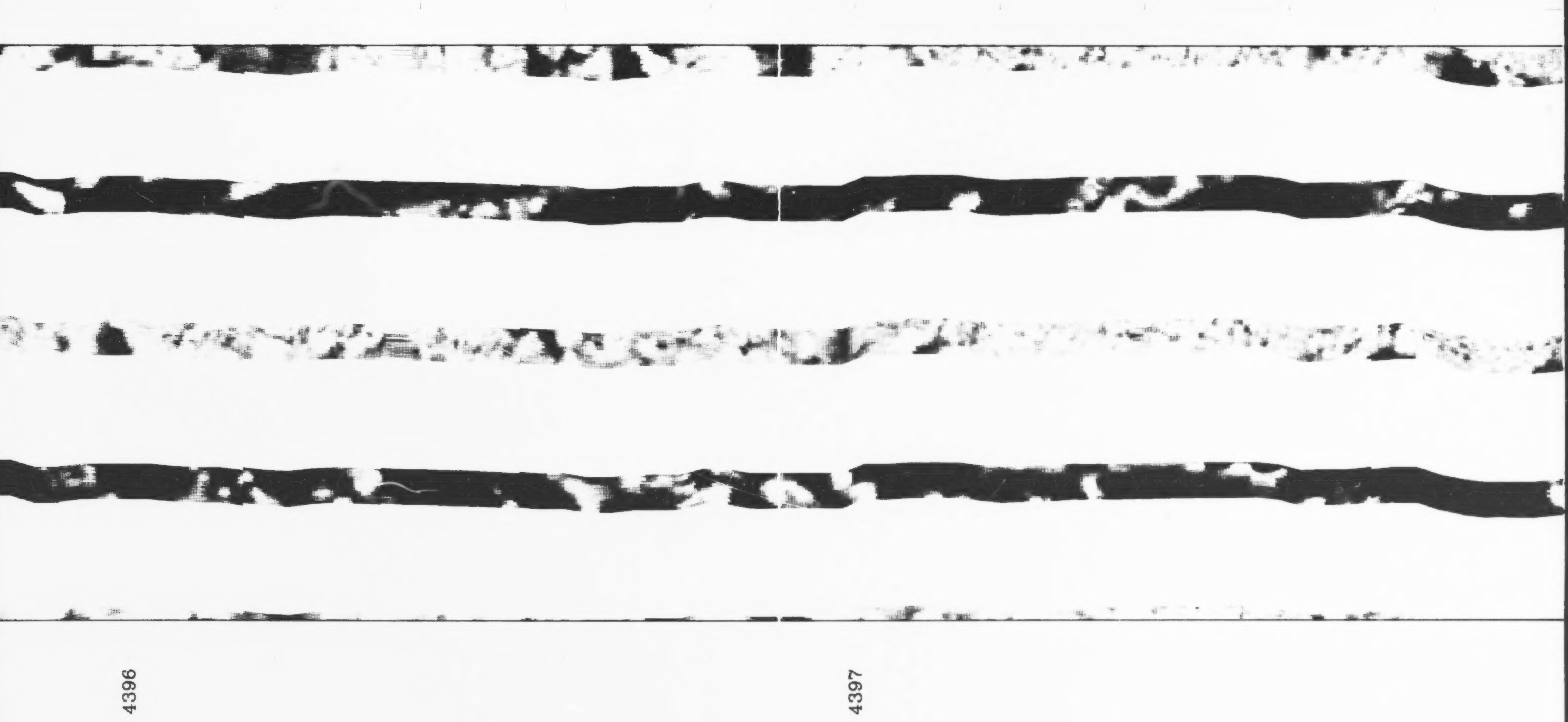
4396
4397

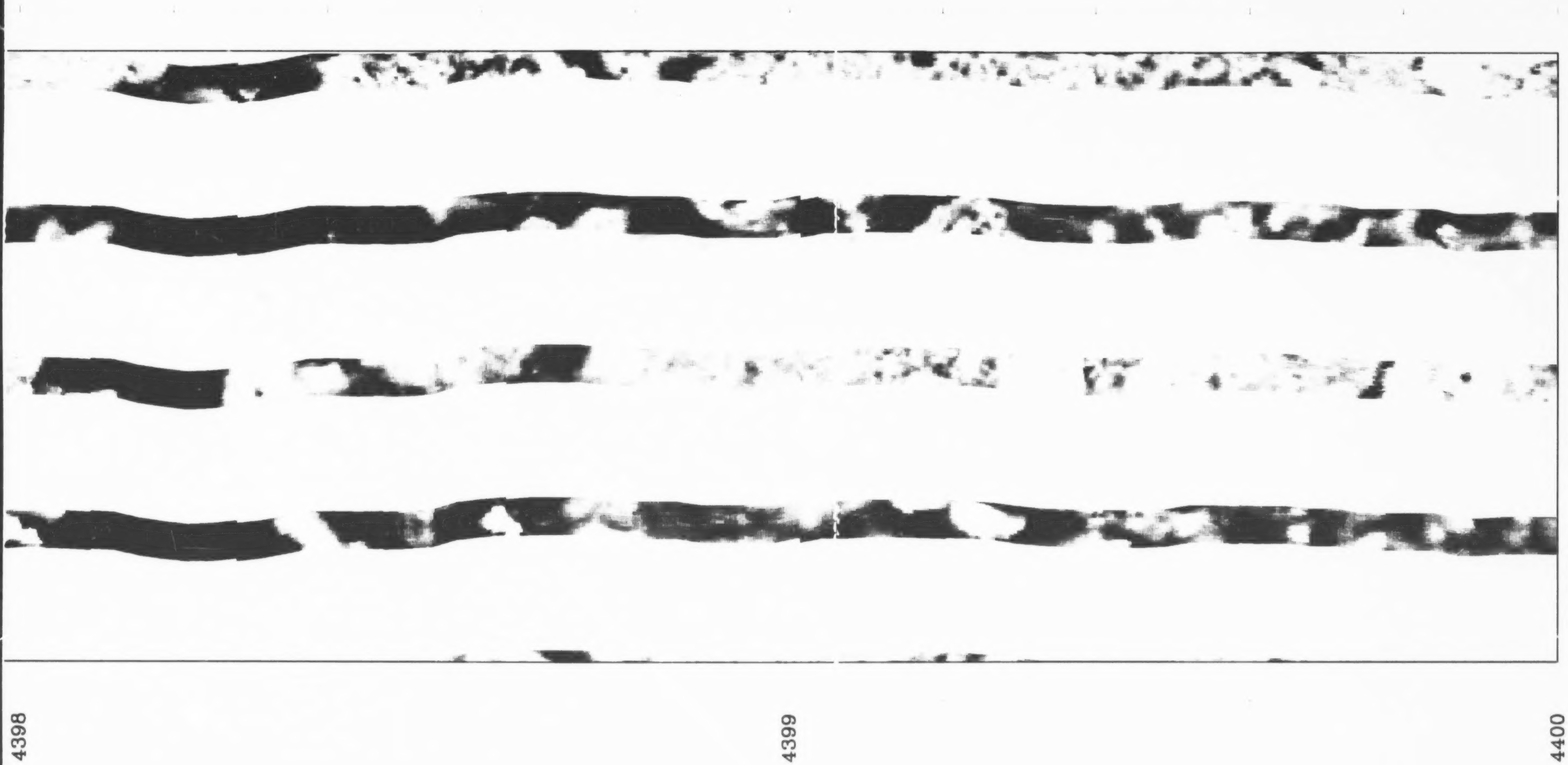
4398
4399
4400

BORMAP 004E02 - ENGINEER LISTING : BORENG.003

SCHLUMBERGER

FMS
BOREHOLE
IMAGING

COMPANY	LAMONT-DOHERTY GEOLOGICAL
WELL	ODP HOLE-793B
FIELD	IZU-BONIN FOREARC BASIN
COUNTRY	OCEAN
RUN	1
DATE LOGGED	16 - JUN - 89
REFERENCE	STATIC PS 1 4400 4430

STATIC NORMALIZATION

PASS 1 (23577)

FILE : MEST.001

ZONE FROM 4430.0 M TO 4400.0 M

DEPTH SCALE = 1/ 5

IMAGE SCALE = 1/ 5

BITSIZE = 9.88

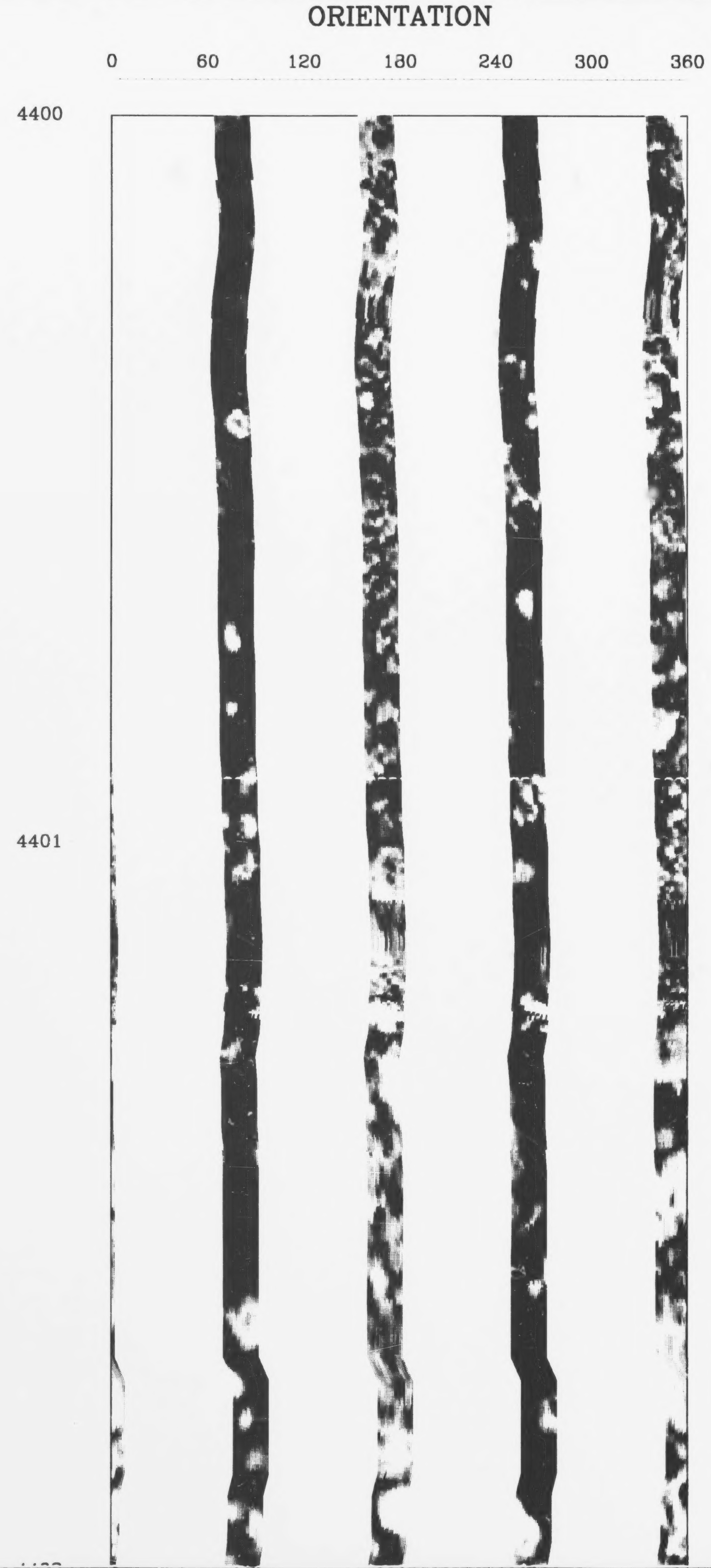
ORIENTATION
0
60
120
180
240
300
360
4400
4401

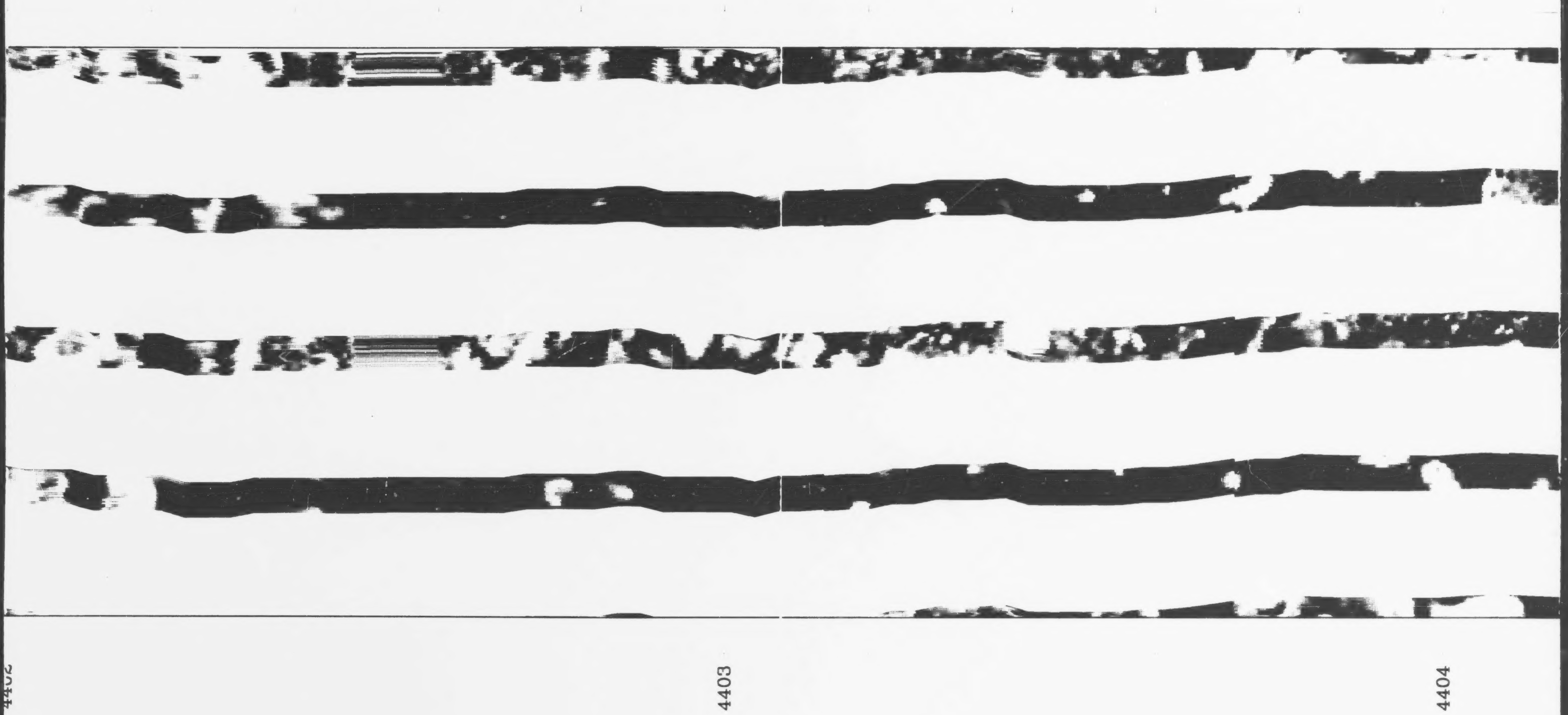
4402
4403
4404

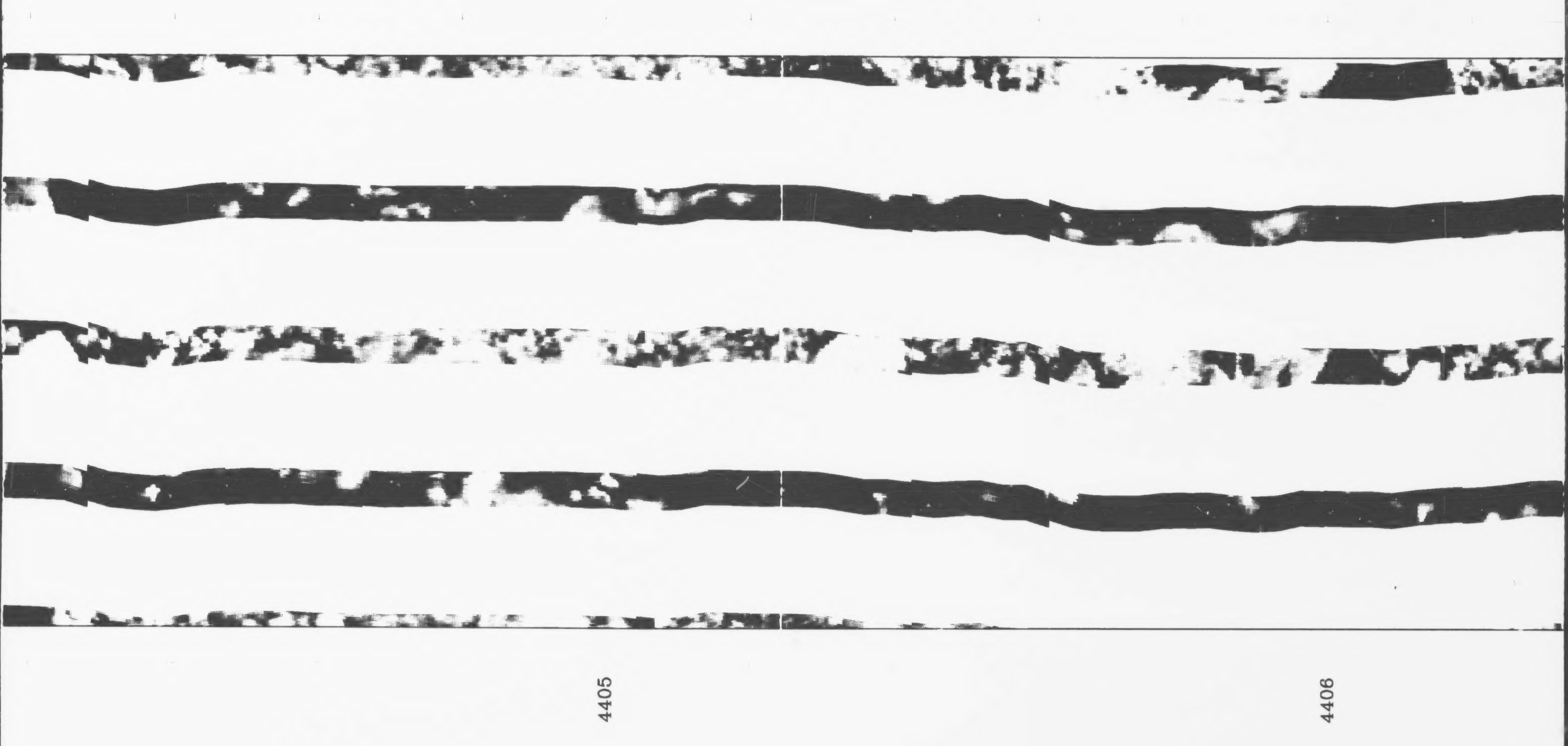
4405
4406

4407
4408

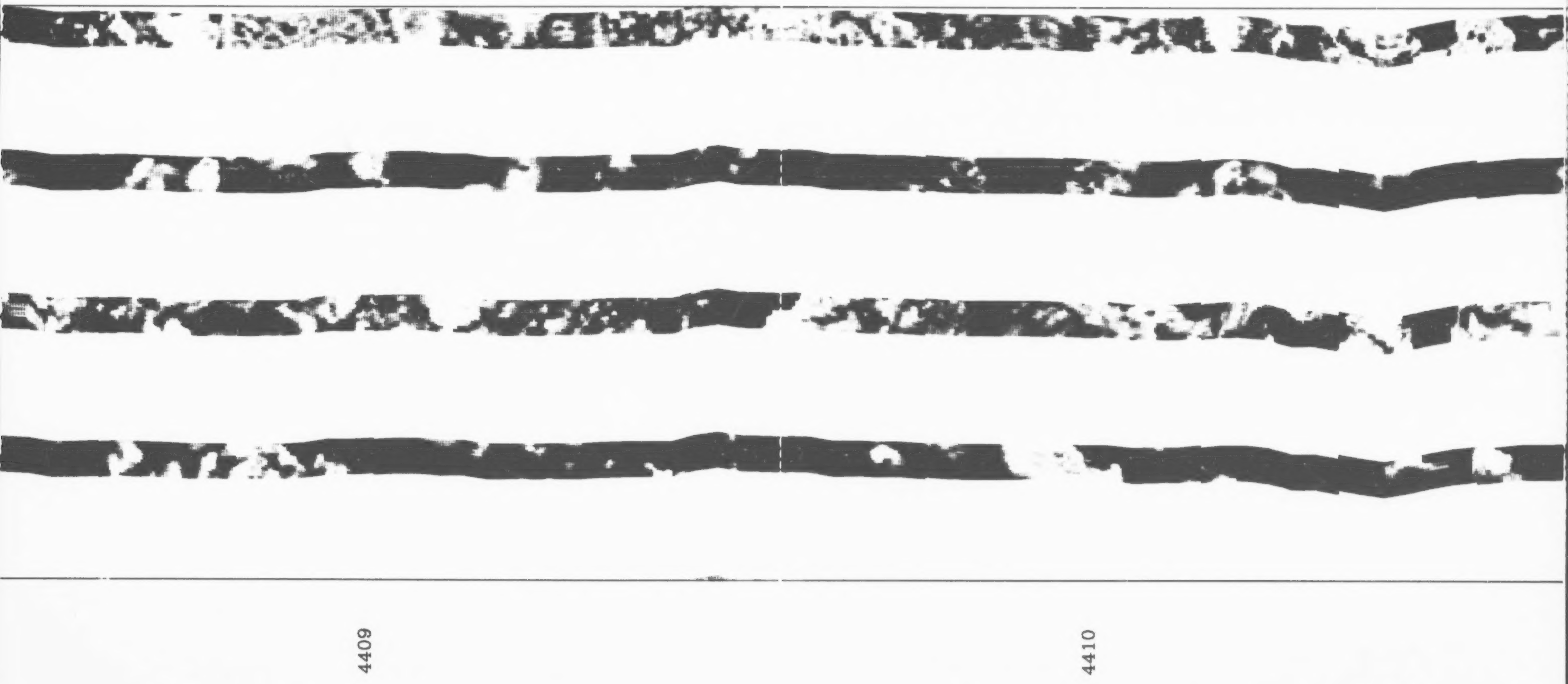

4409
4410

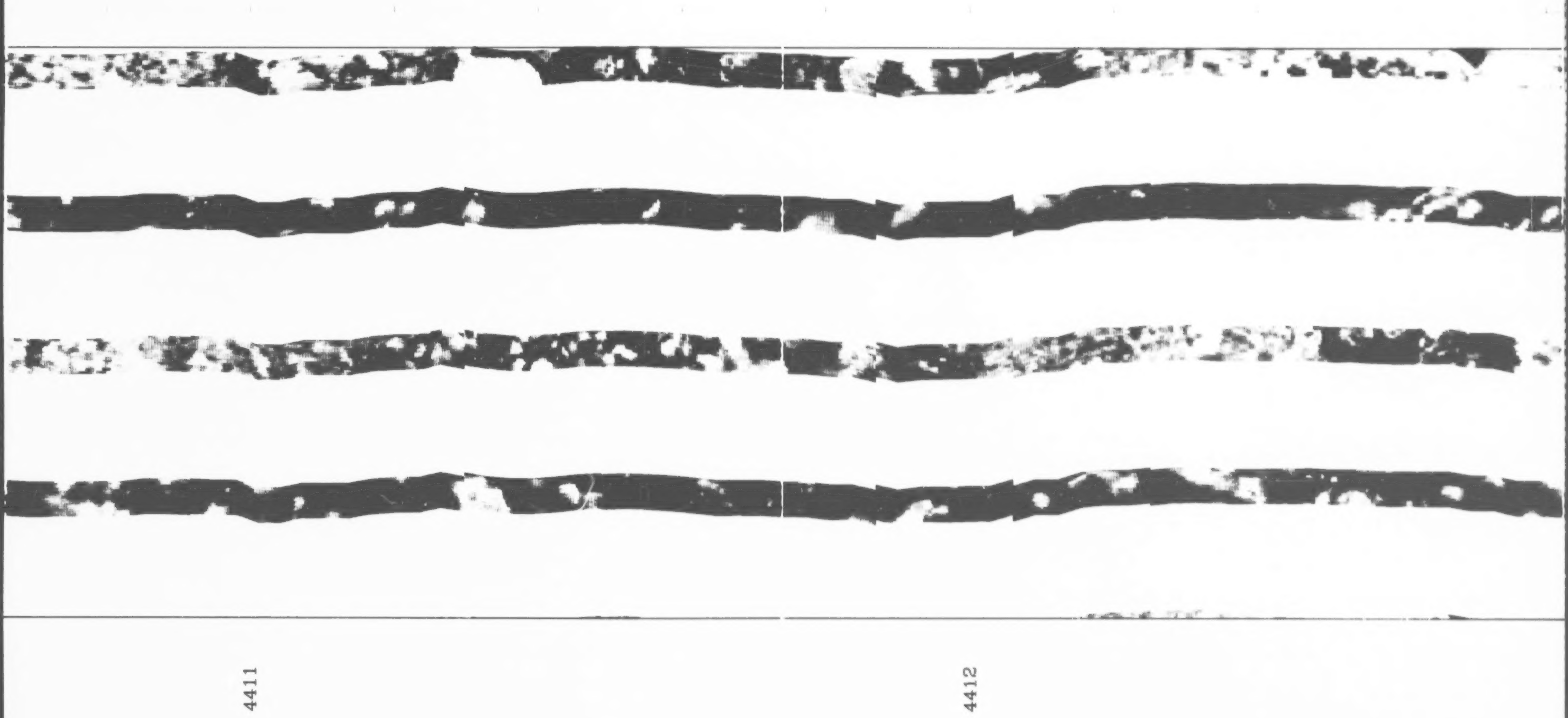
4411
4412

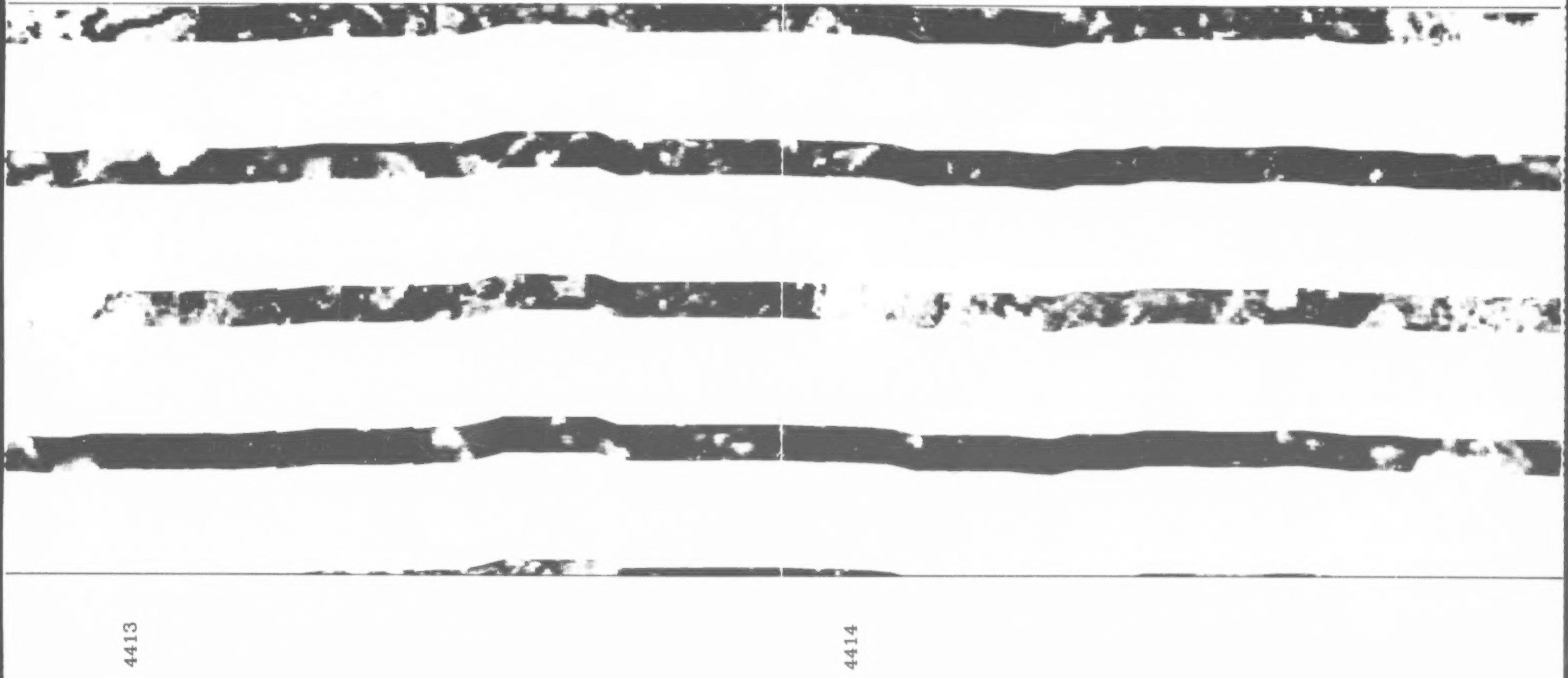
4413
4414

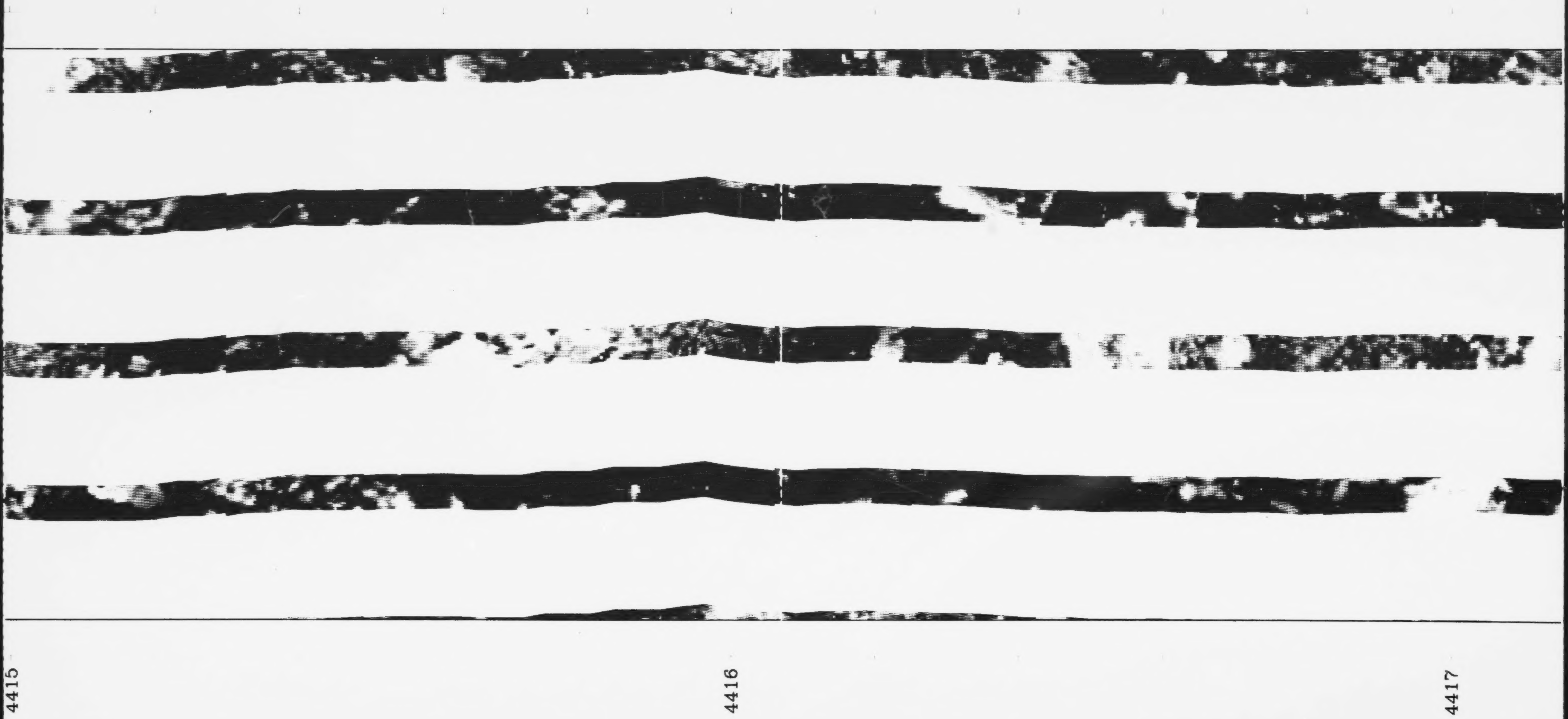
4415
4416
4417

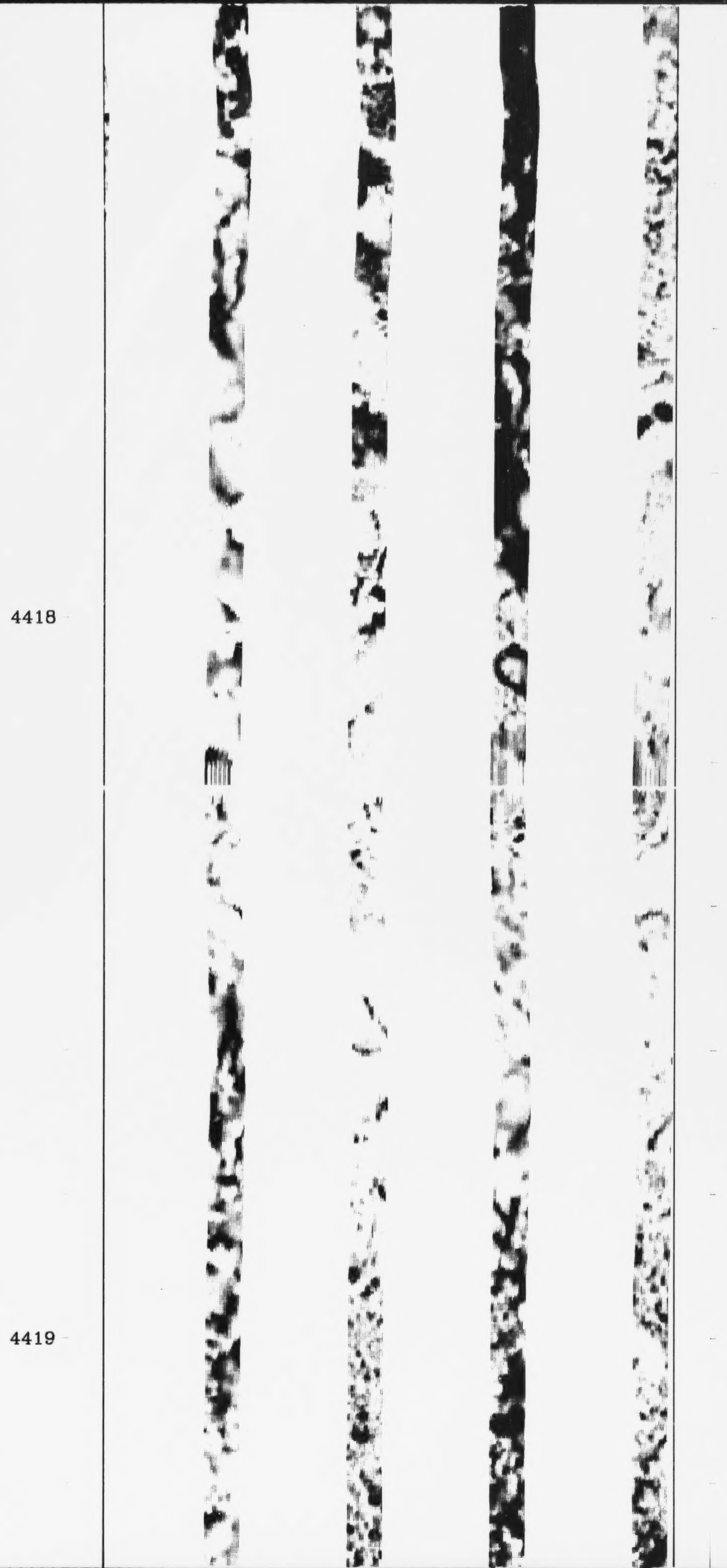
4418
4419

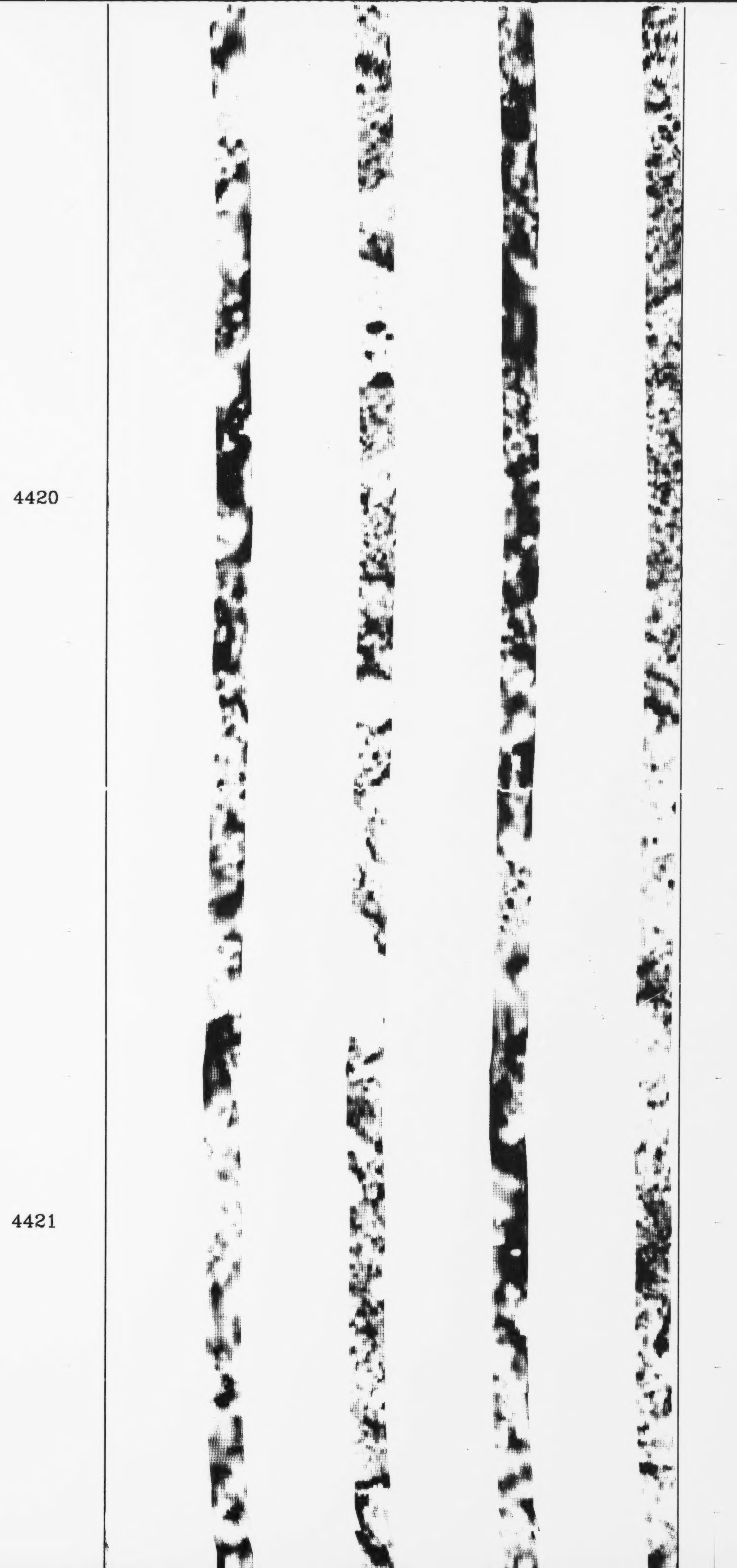
4420
4421

4422
4423

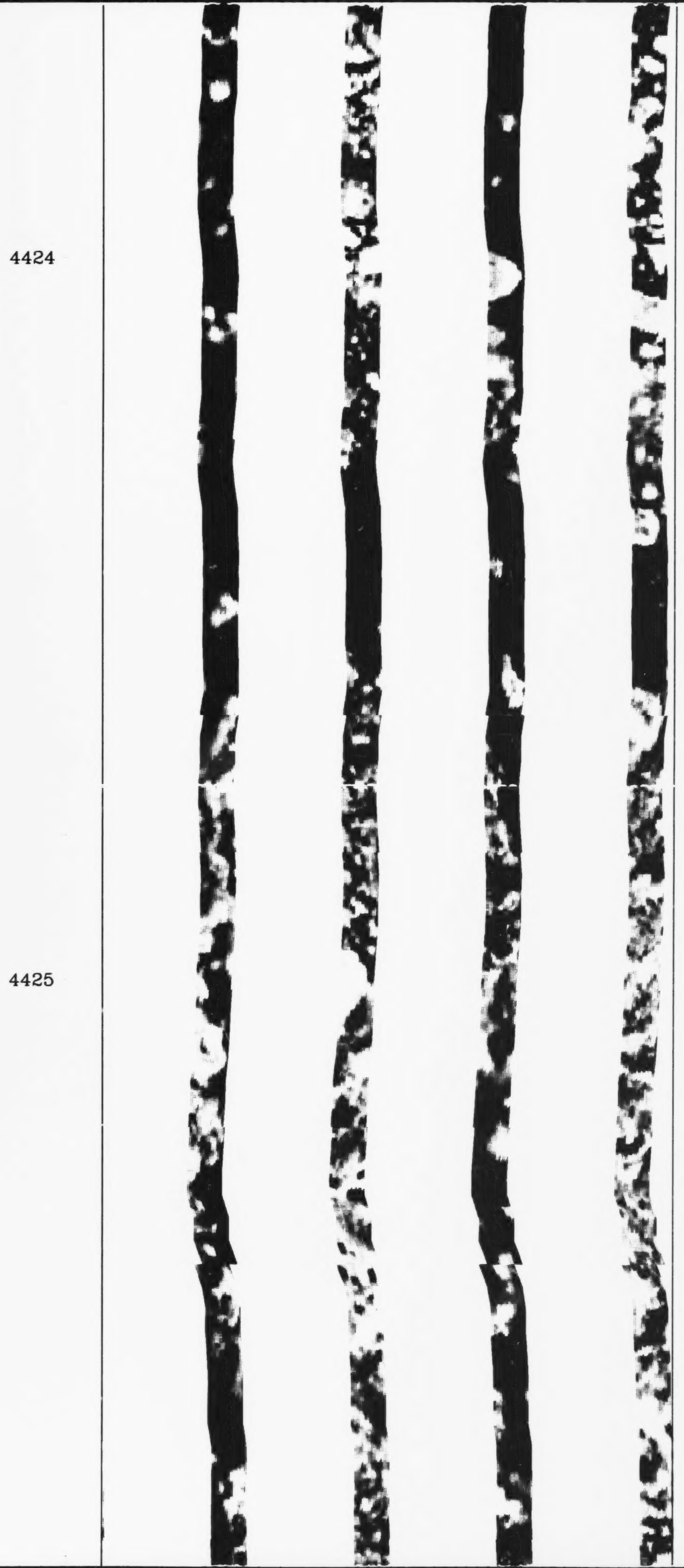
4424
4425

4426

4427

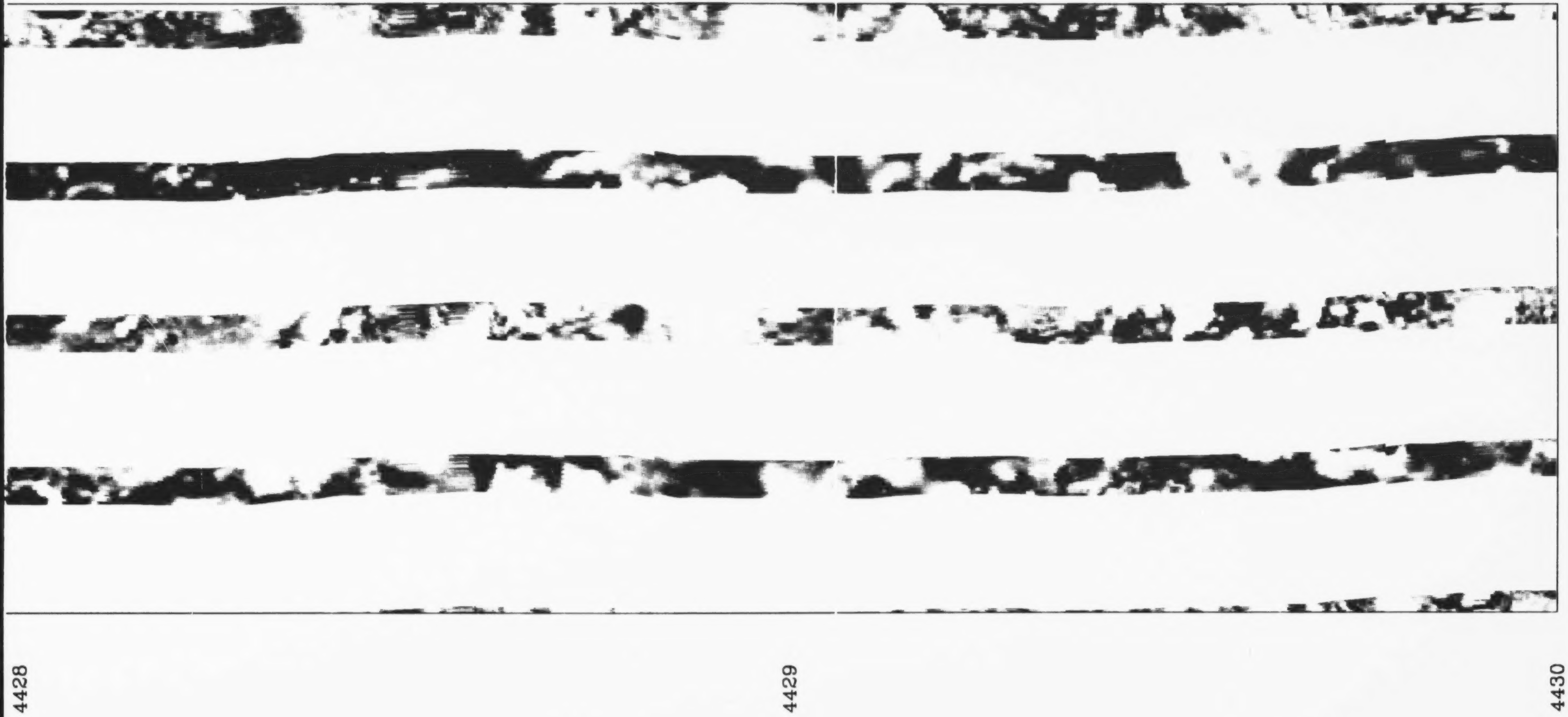
4428
4429
4430

SCHLUMBERGER

FMS
BOREHOLE
IMAGING

COMPANY	LAMONT-DOHERTY GEOLOGICAL
WELL	ODP HOLE-793B
FIELD	IZU-BONIN FOREARC BASIN
COUNTRY	OCEAN
RUN	1
DATE LOGGED	16 - JUN - 89
REFERENCE	STATIC PS-1 4430-4465

STATIC NORMALIZATION

PASS 1 (23577)

FILE : MEST.001

ZONE FROM 4465.0 M TO 4430.0 M

DEPTH SCALE = 1/ 5

IMAGE SCALE = 1/ 5

BITSIZE = 9.88

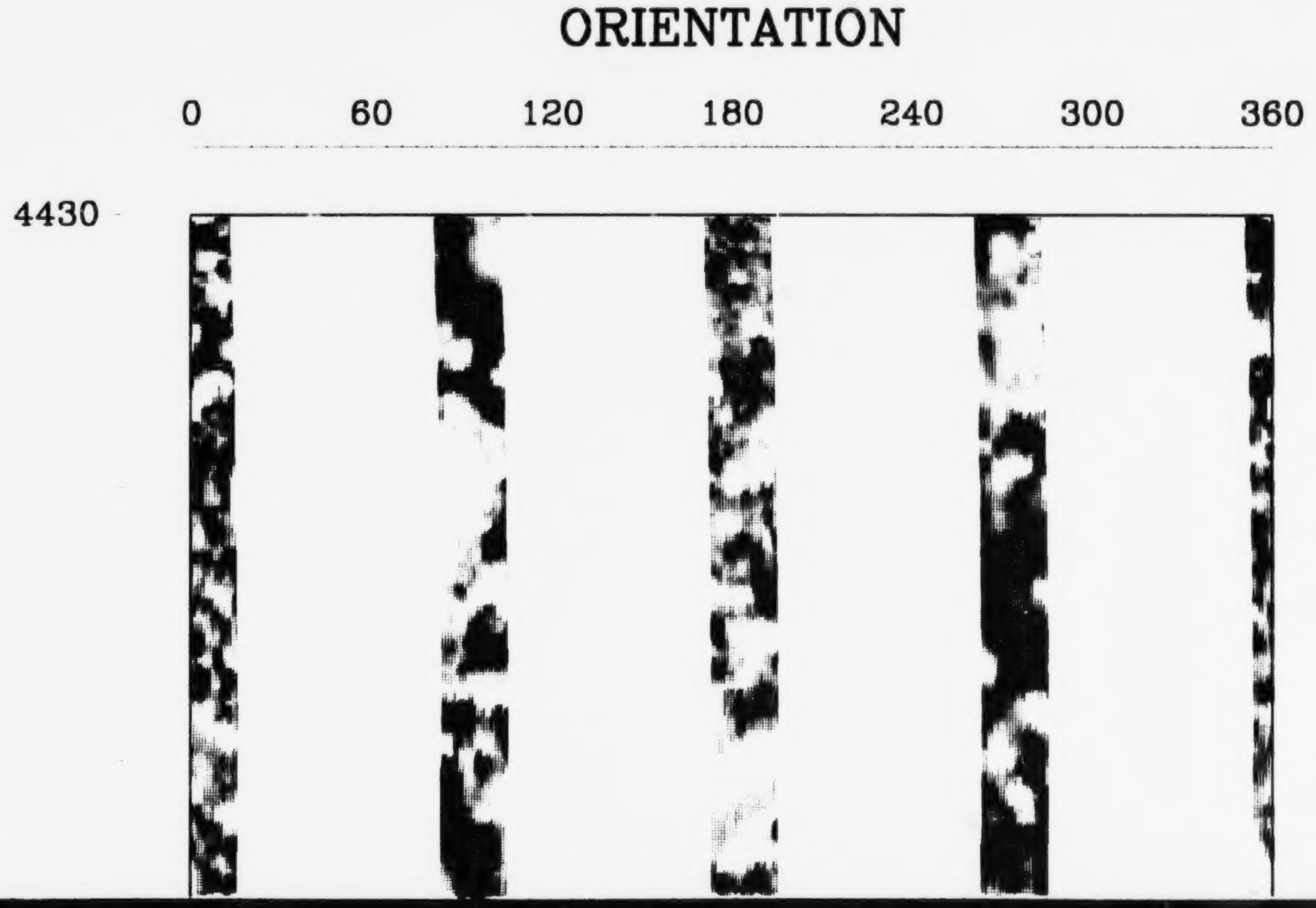

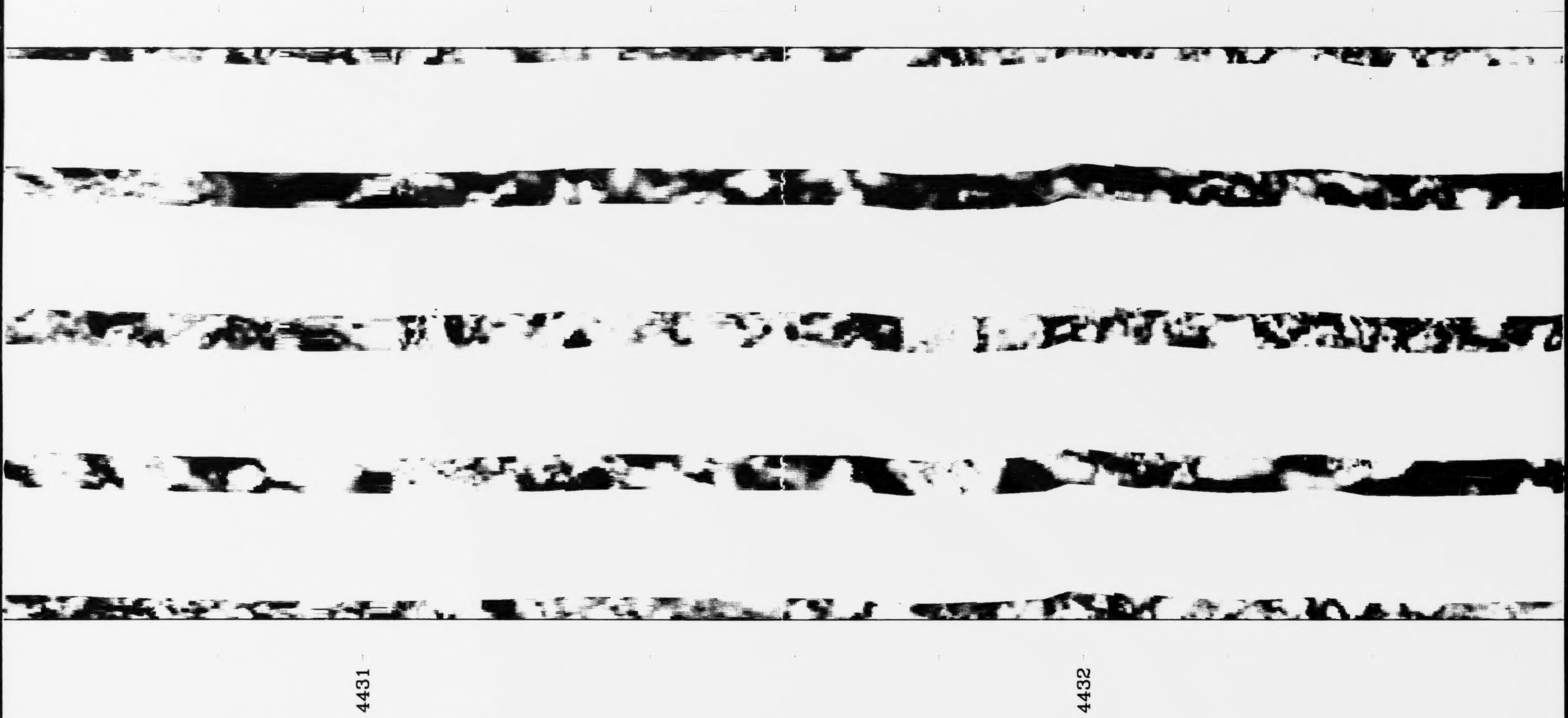
4431
4432

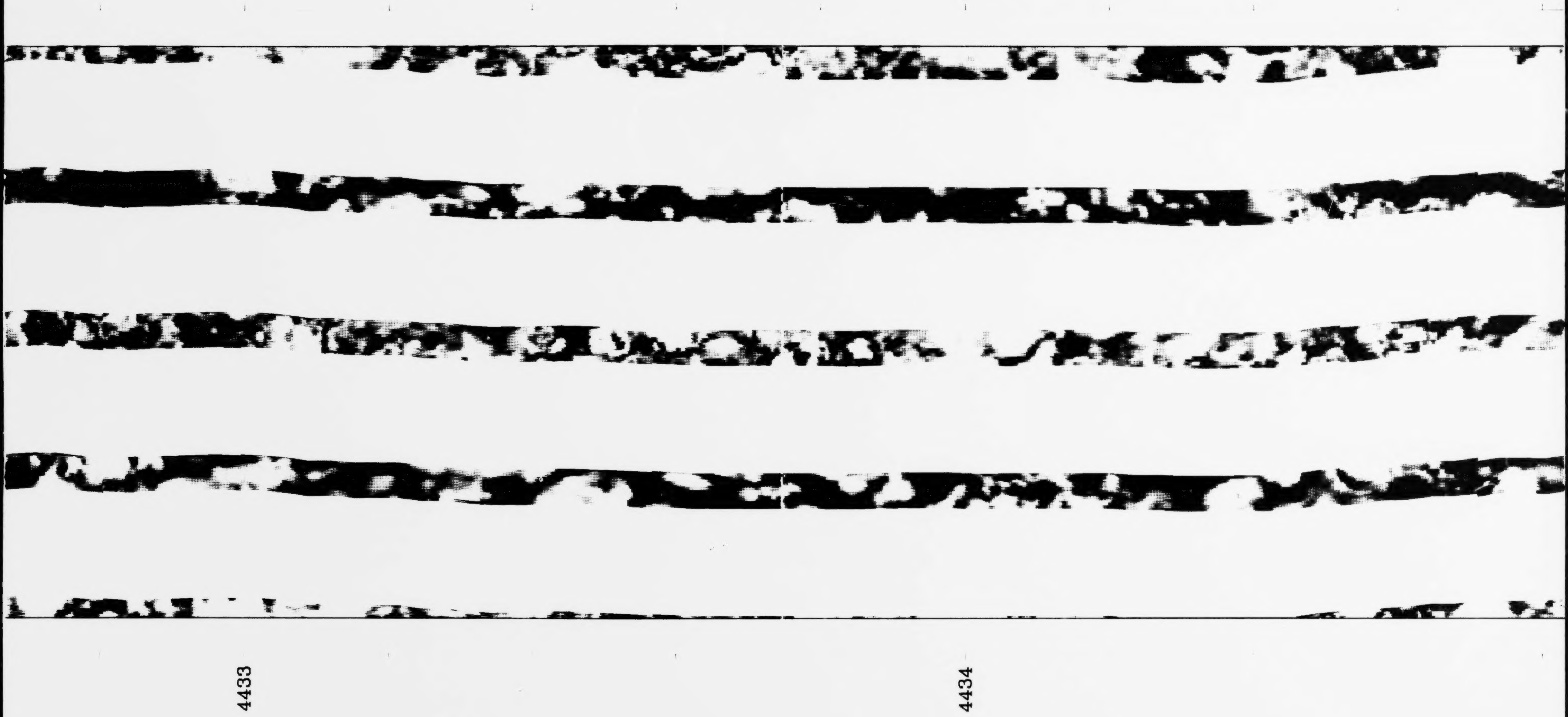
4433
4434

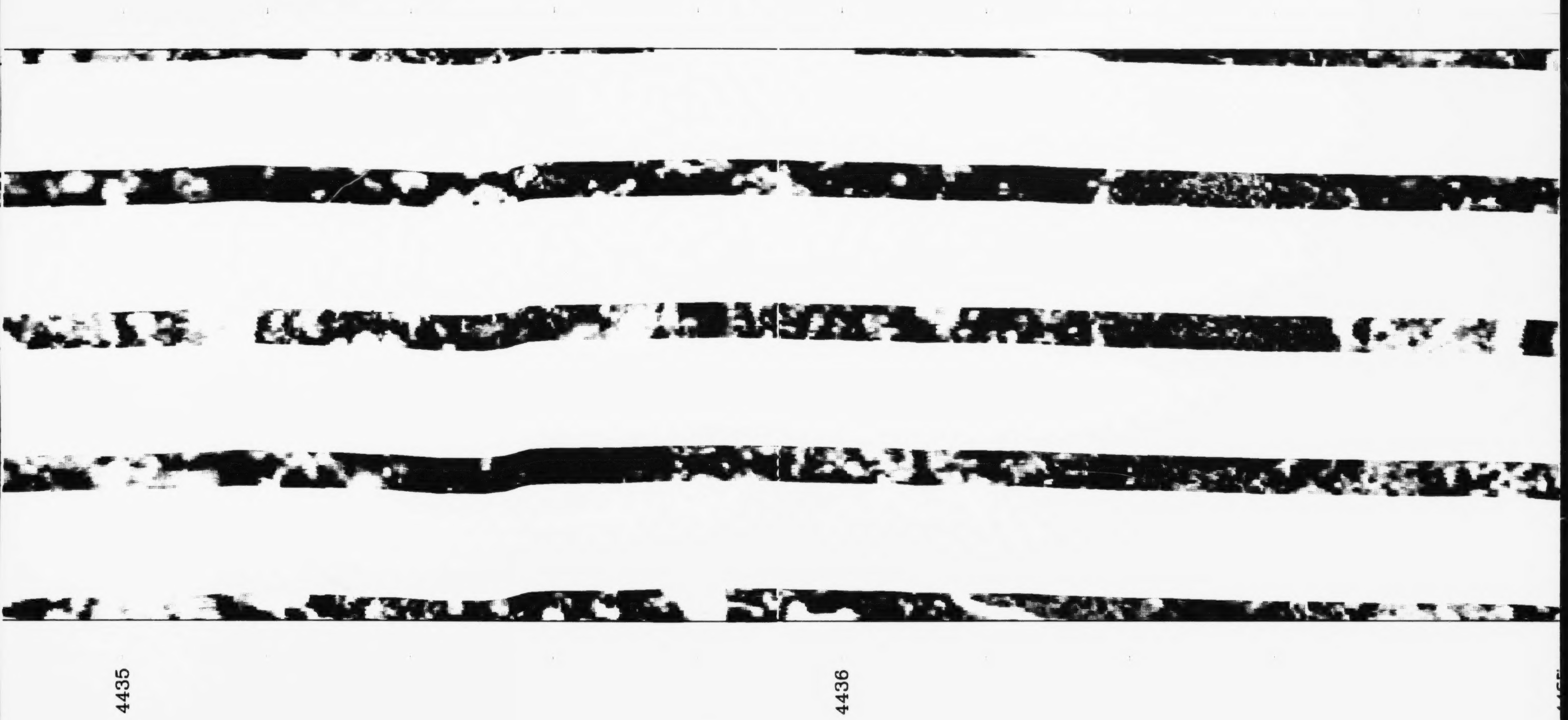
4435
4436

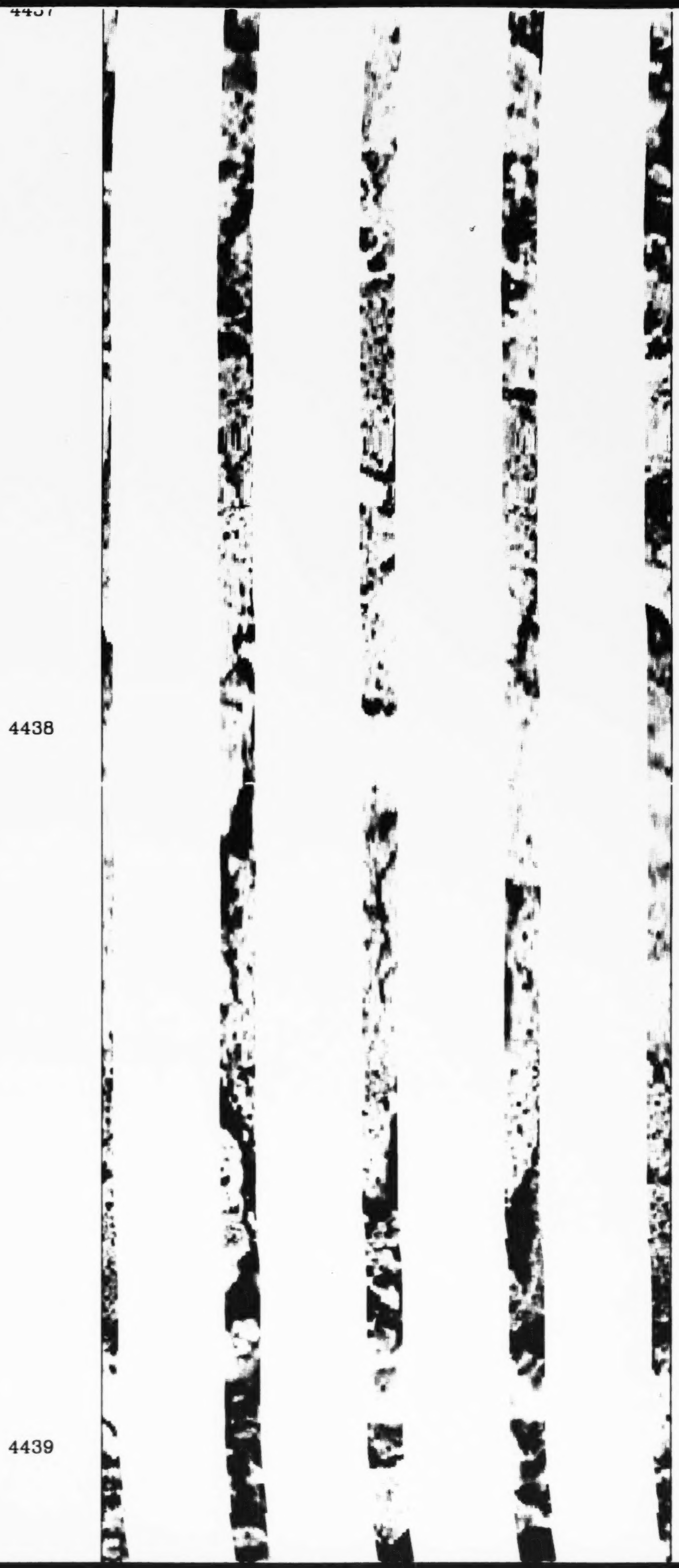
4437
4438
4439

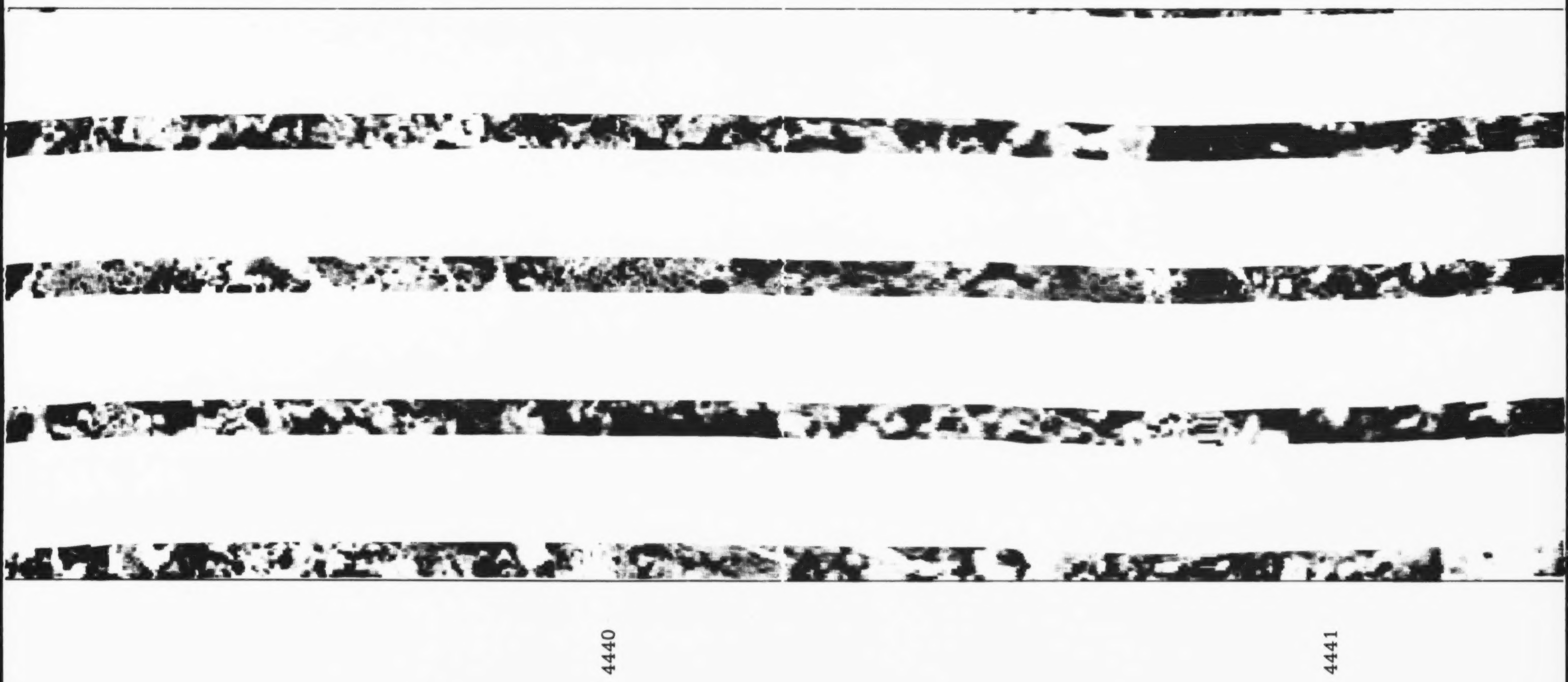
4440
4441

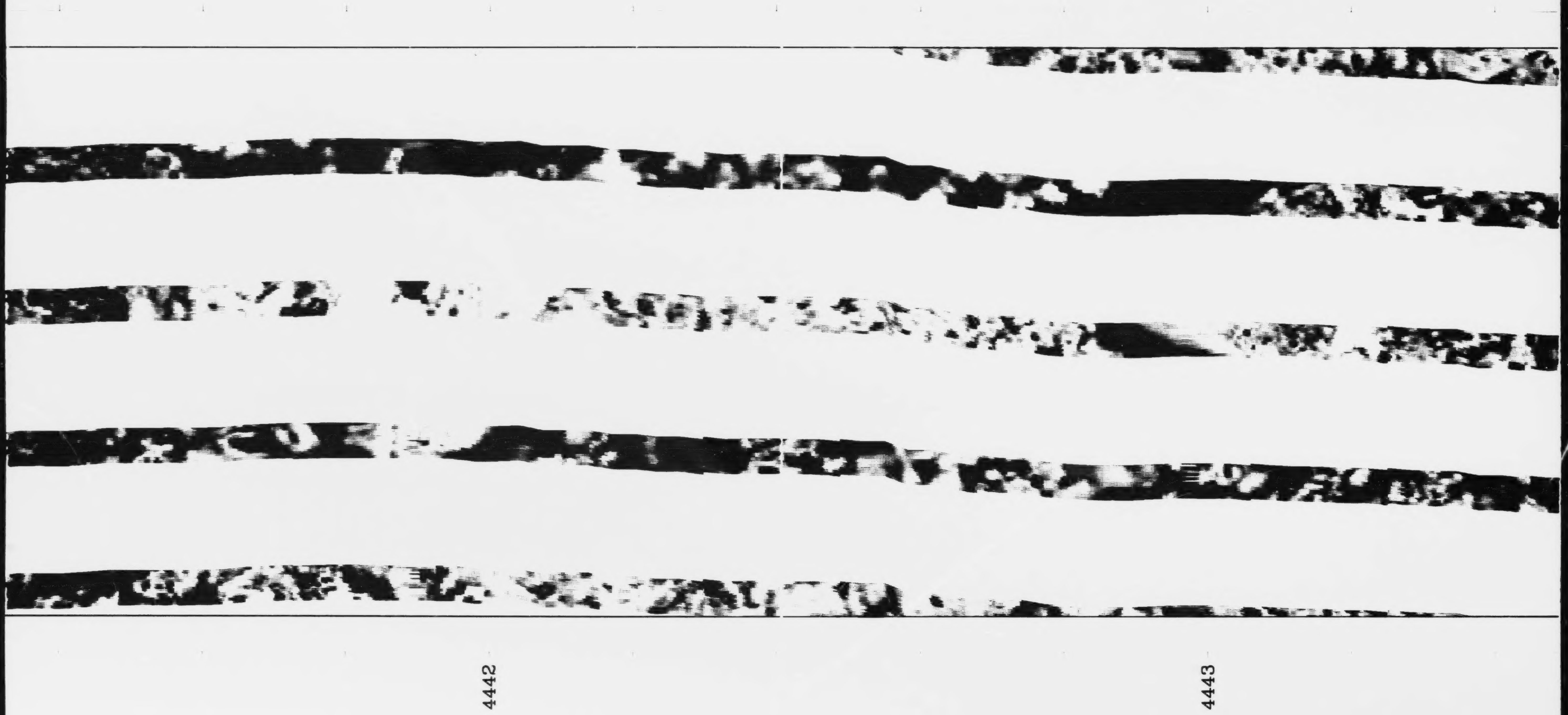
4442
4443

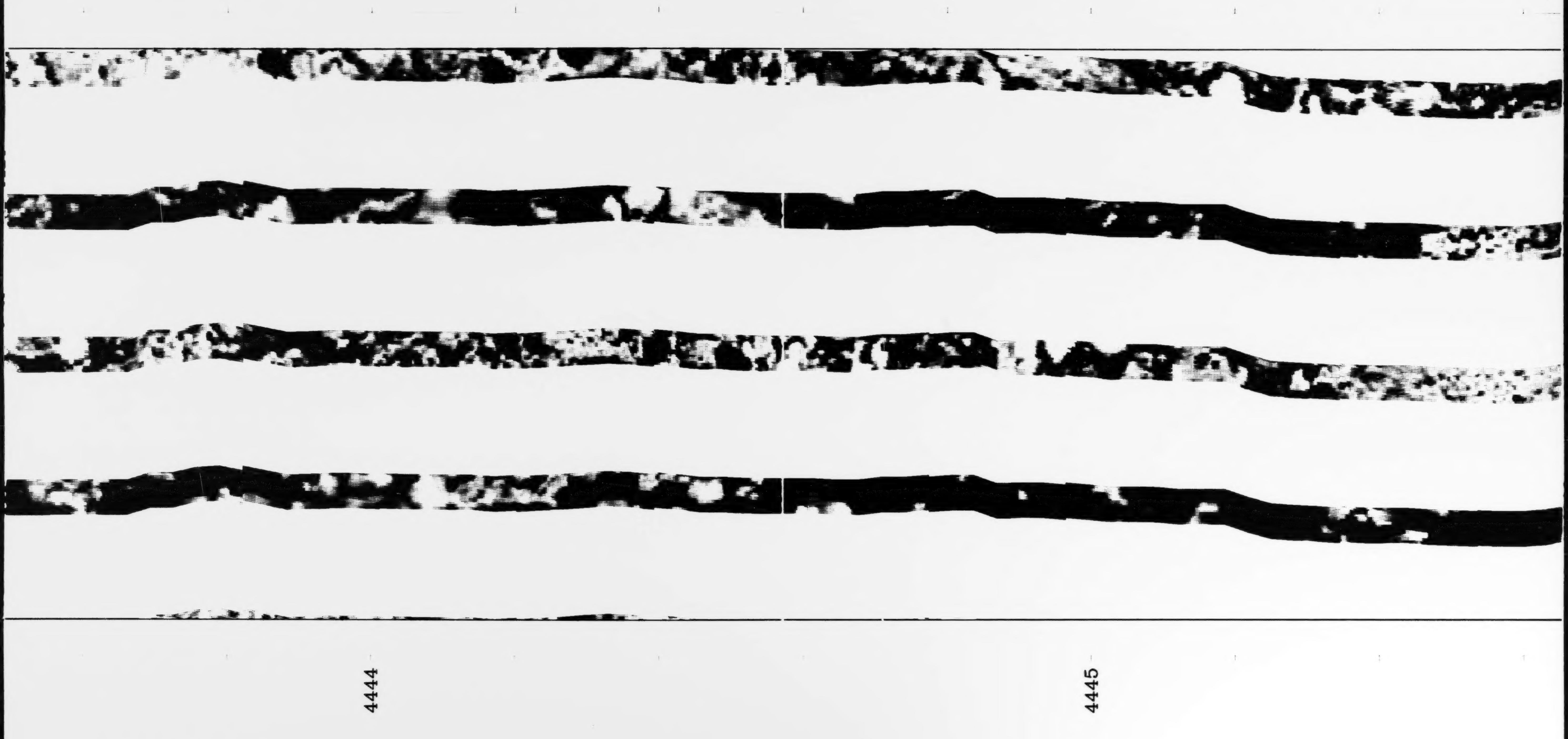

4444
4445

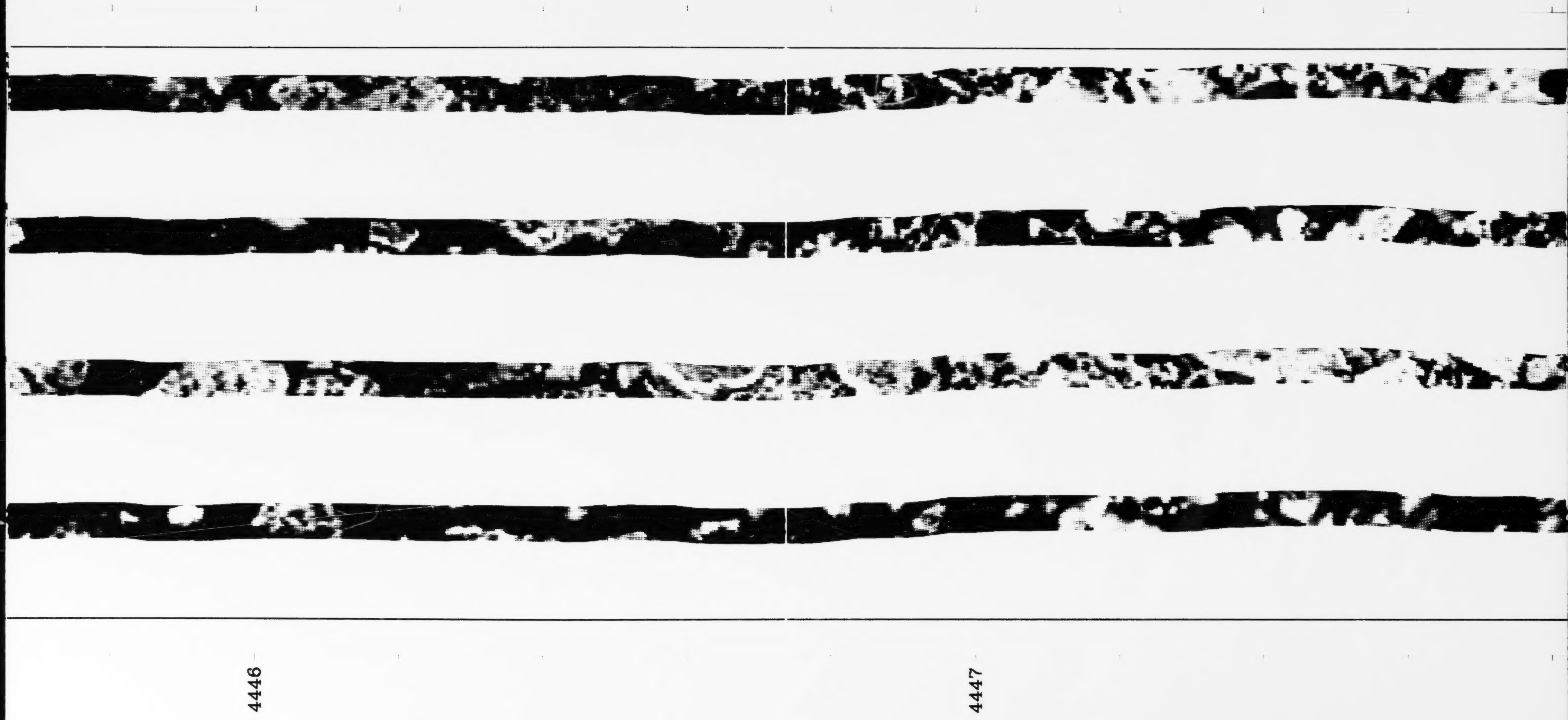
4446
4447

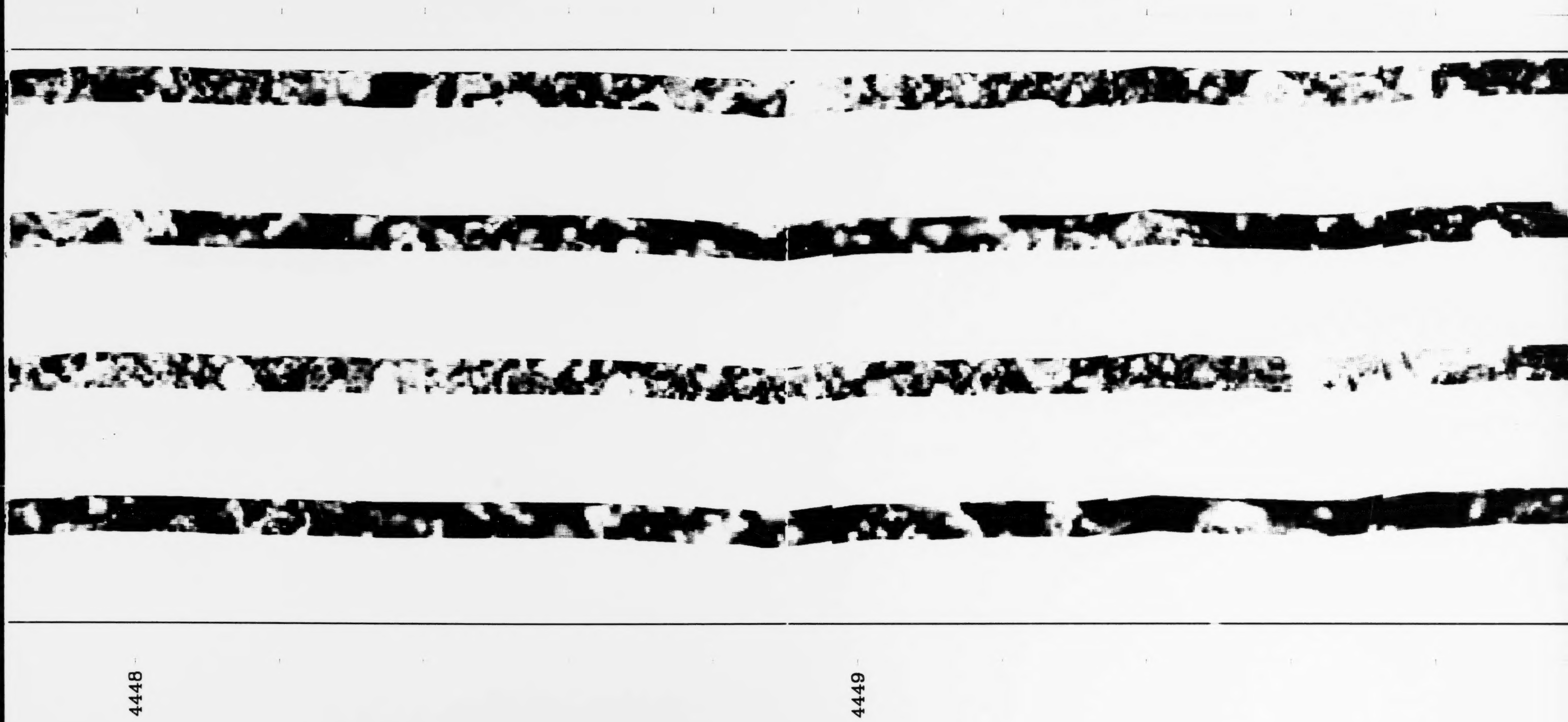
4448
4449

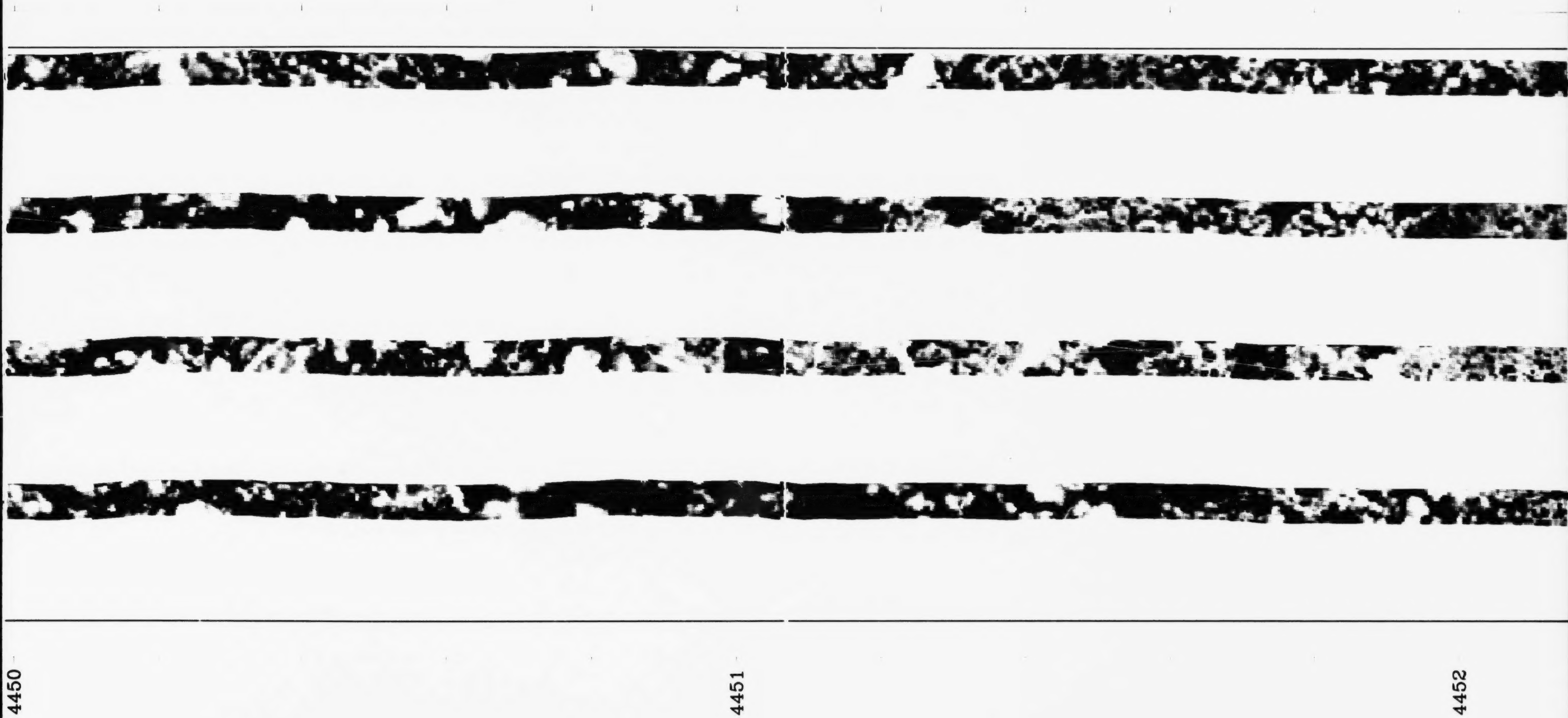

4450
4451
4452

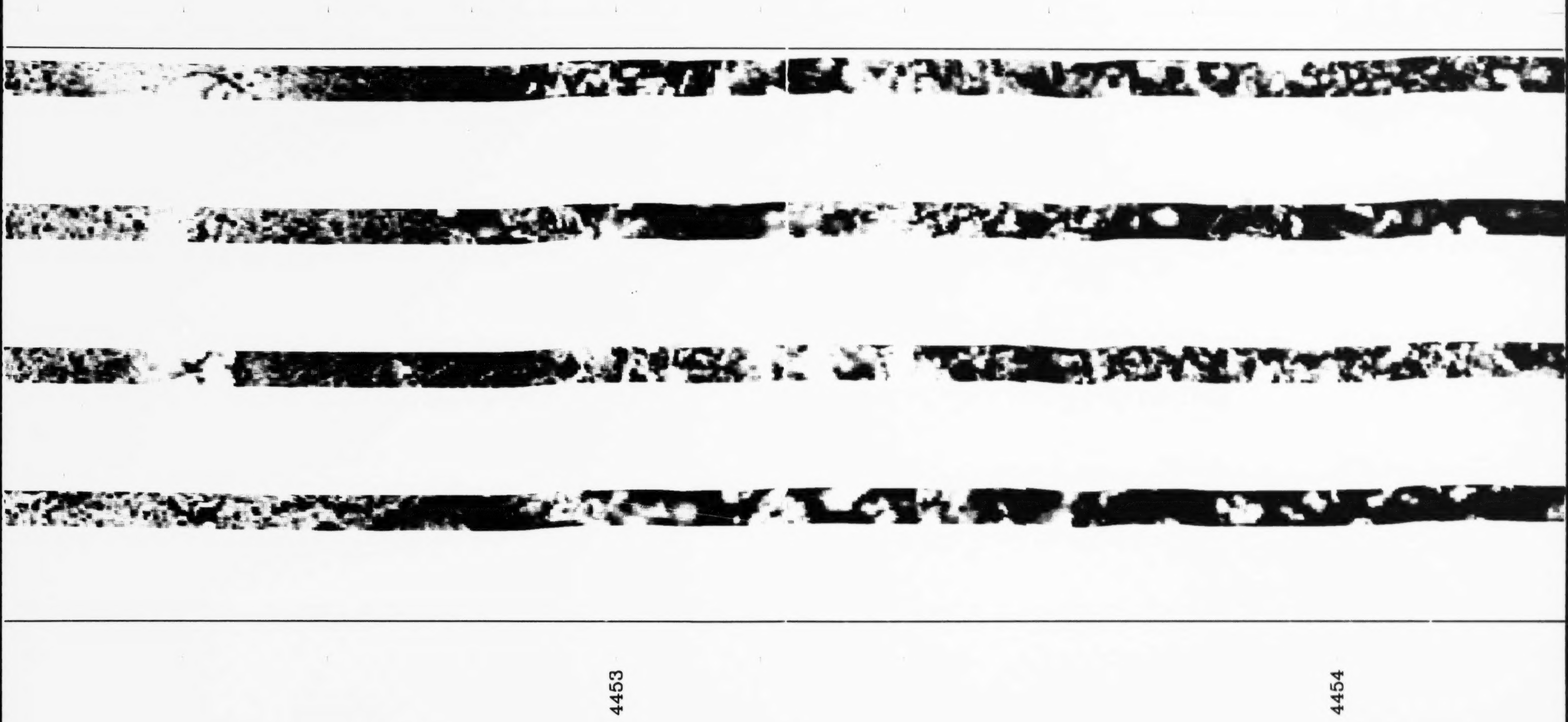
4453
4454

4457
4458

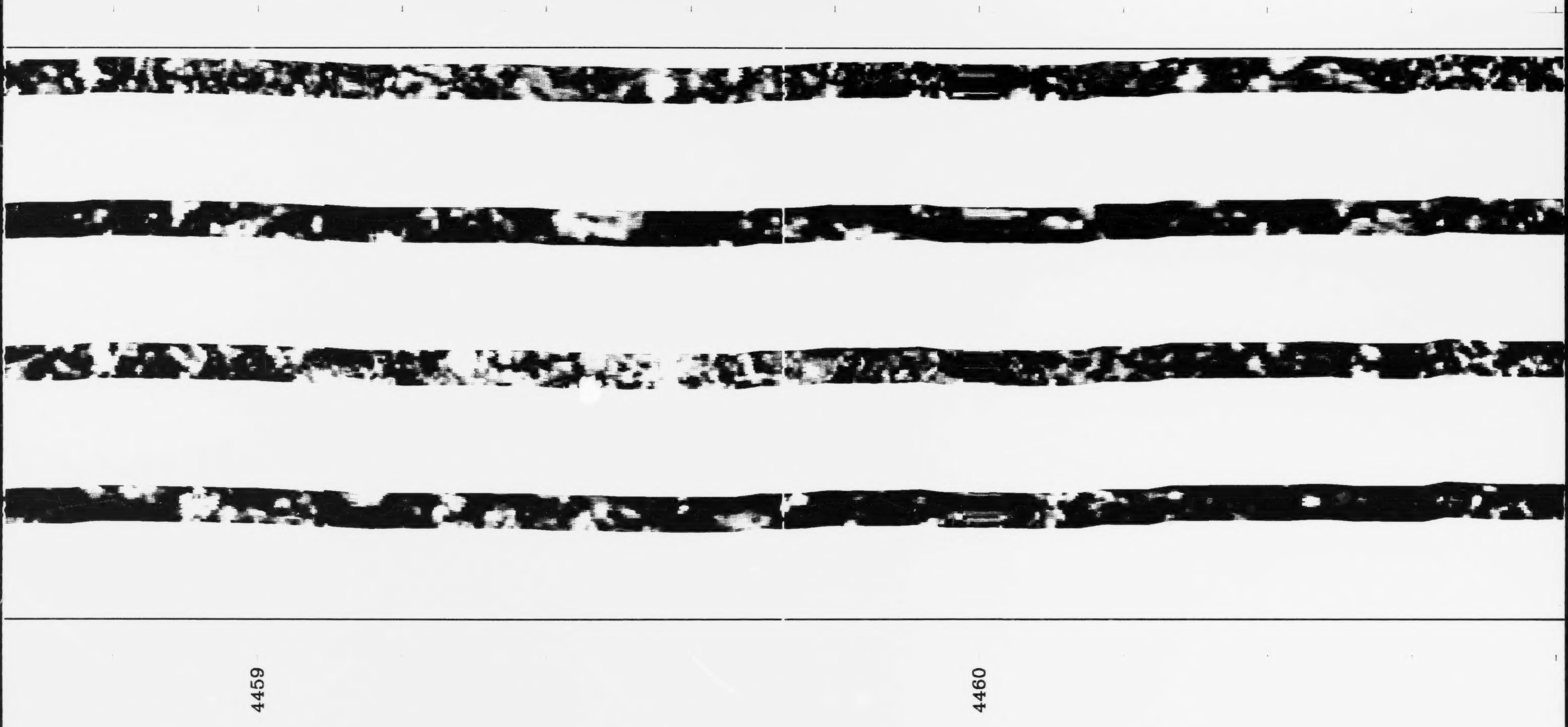
4459
4460

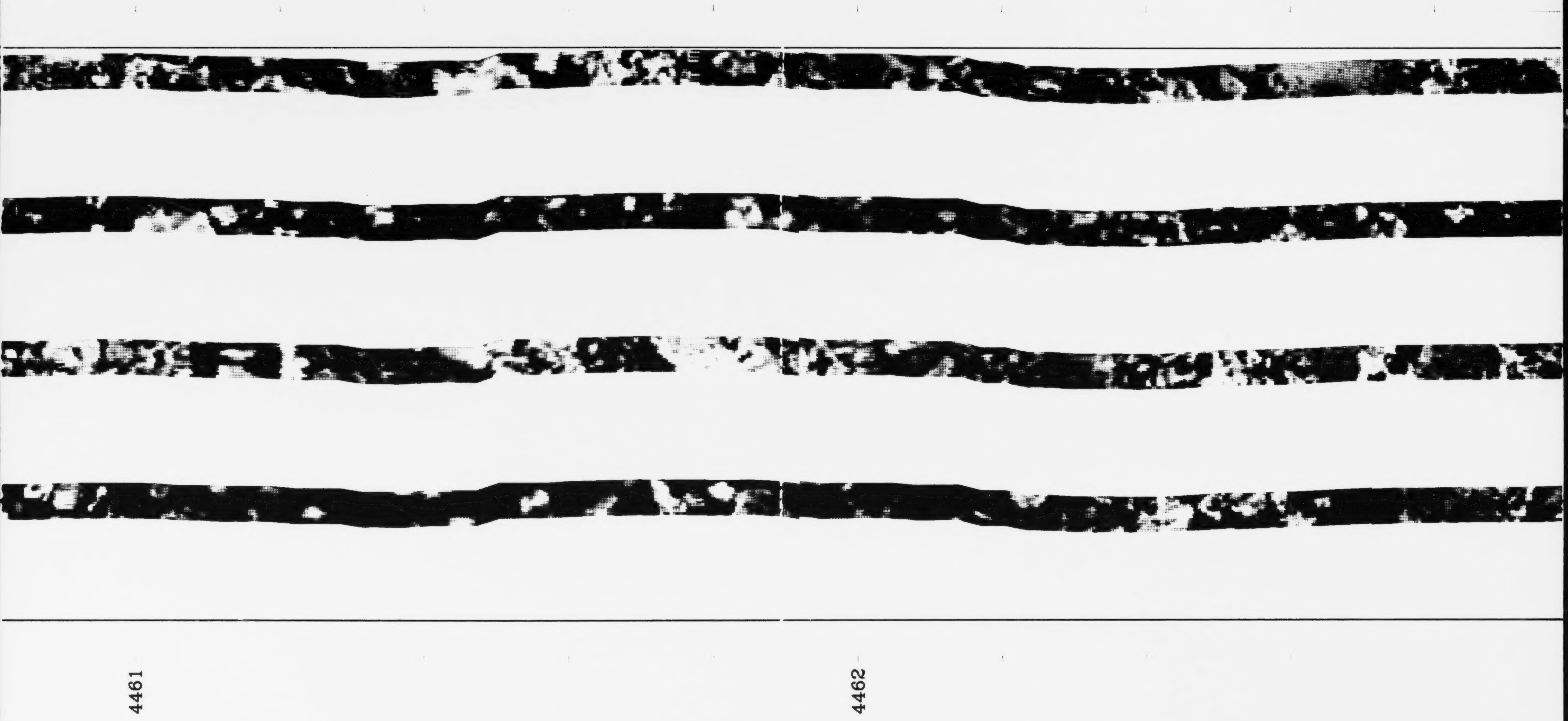

4461
4462

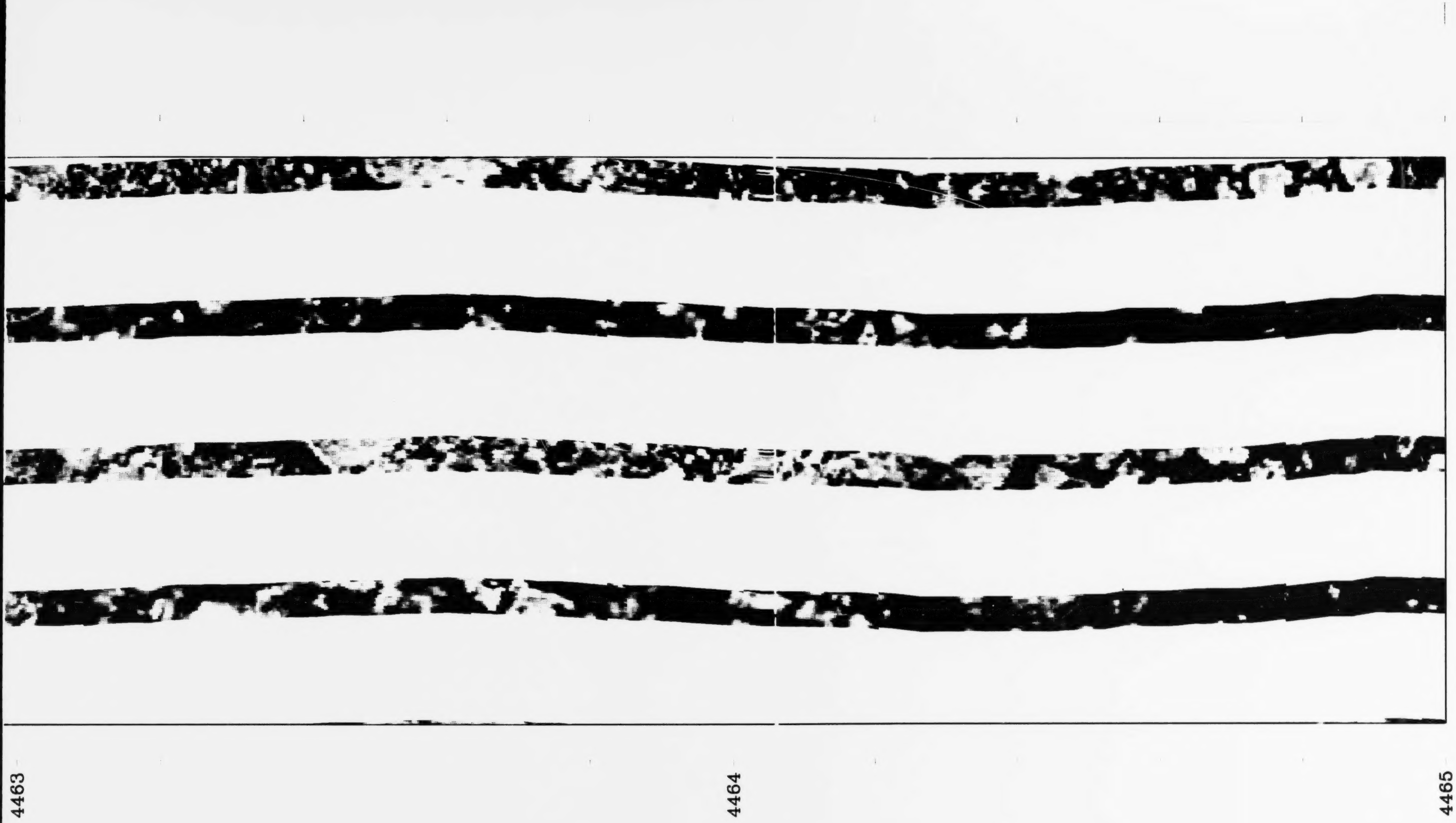
4463
4464
4465

SCHLUMBERGER

FMS
BOREHOLE
IMAGING

COMPANY	LAMONT-DOHERTY GEOLOGICAL
WELL	ODP HOLE-793B
FIELD	IZU-BONIN FOREARC BASIN
COUNTRY	OCEAN
RUN	1
DATE LOGGED	16 -- JUN - 89
REFERENCE	STATIC PS-1 4465-4500

STATIC NORMALIZATION

PASS 1 (23577)

FILE : MEST.001

ZONE FROM 4500.0 M TO 4465.0 M

DEPTH SCALE = 1/ 5

IMAGE SCALE = 1/ 5

BITSIZE = 9.88

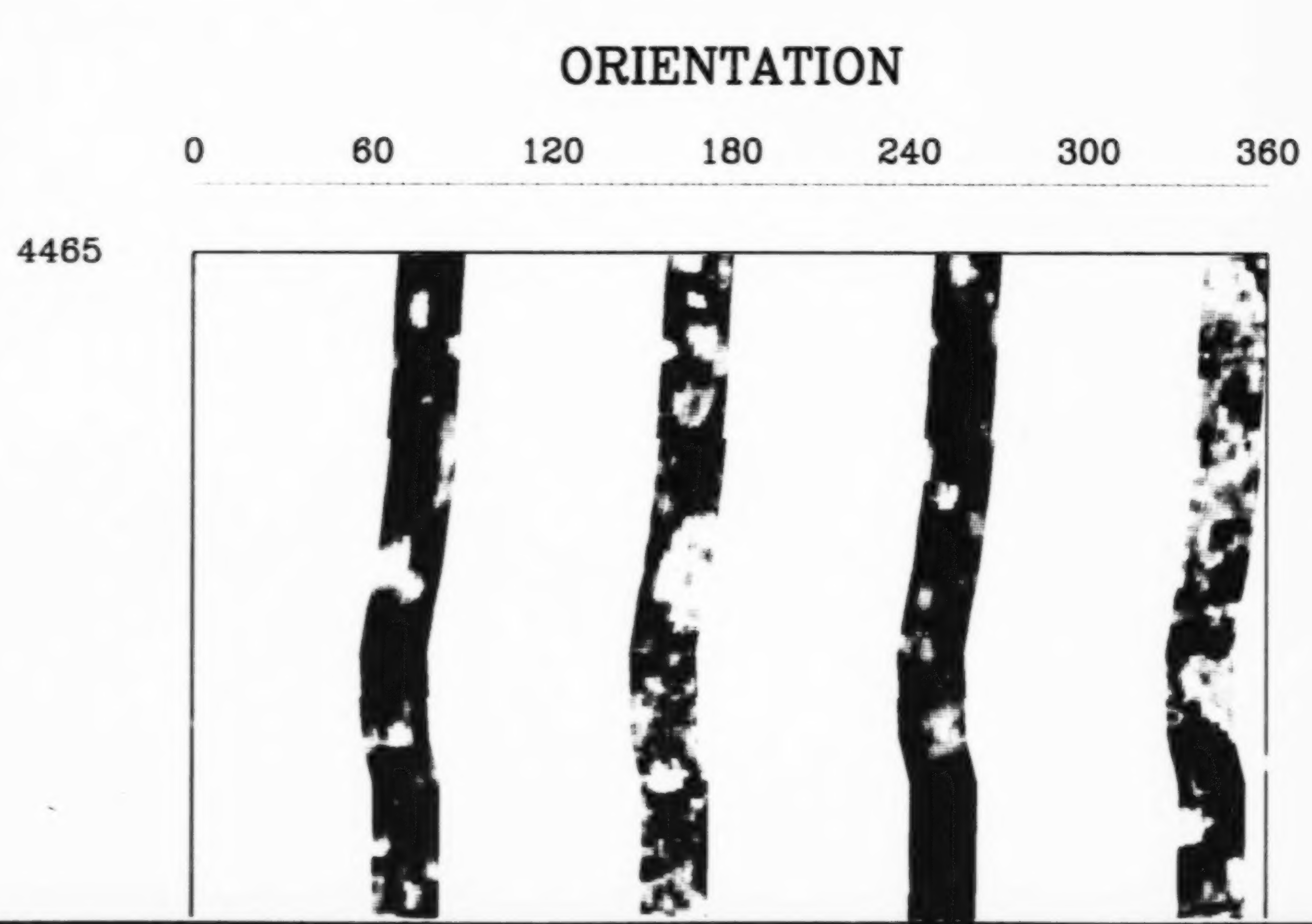

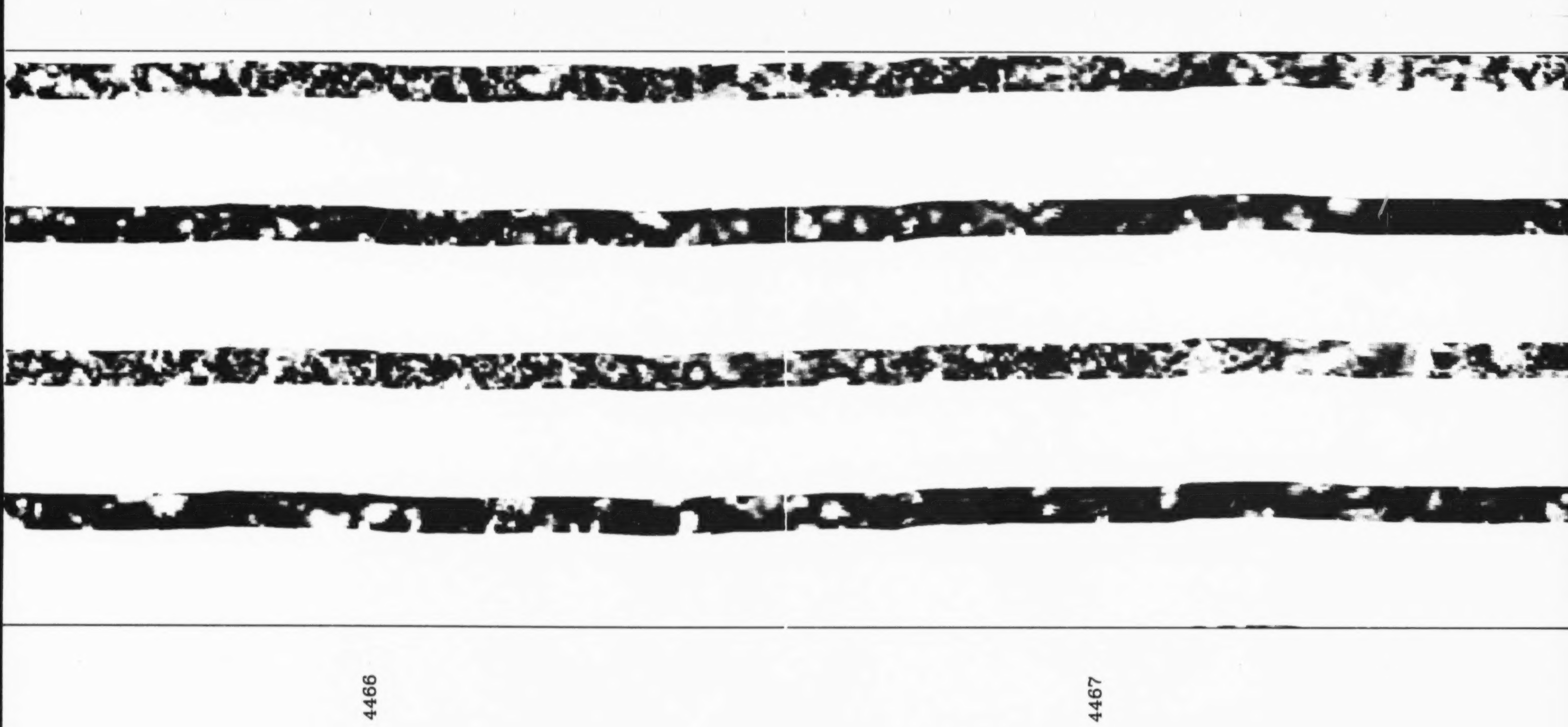
4466
4467

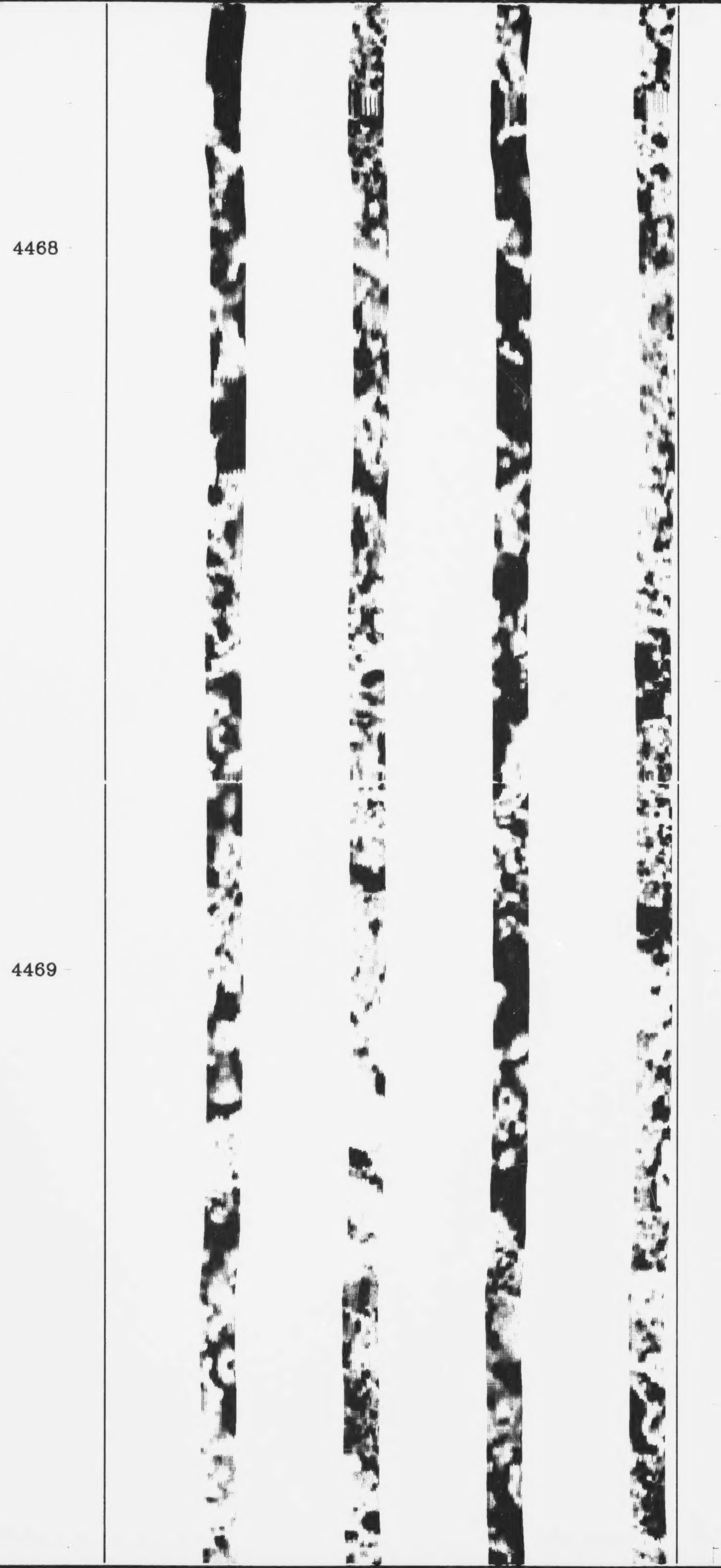
4468
4469

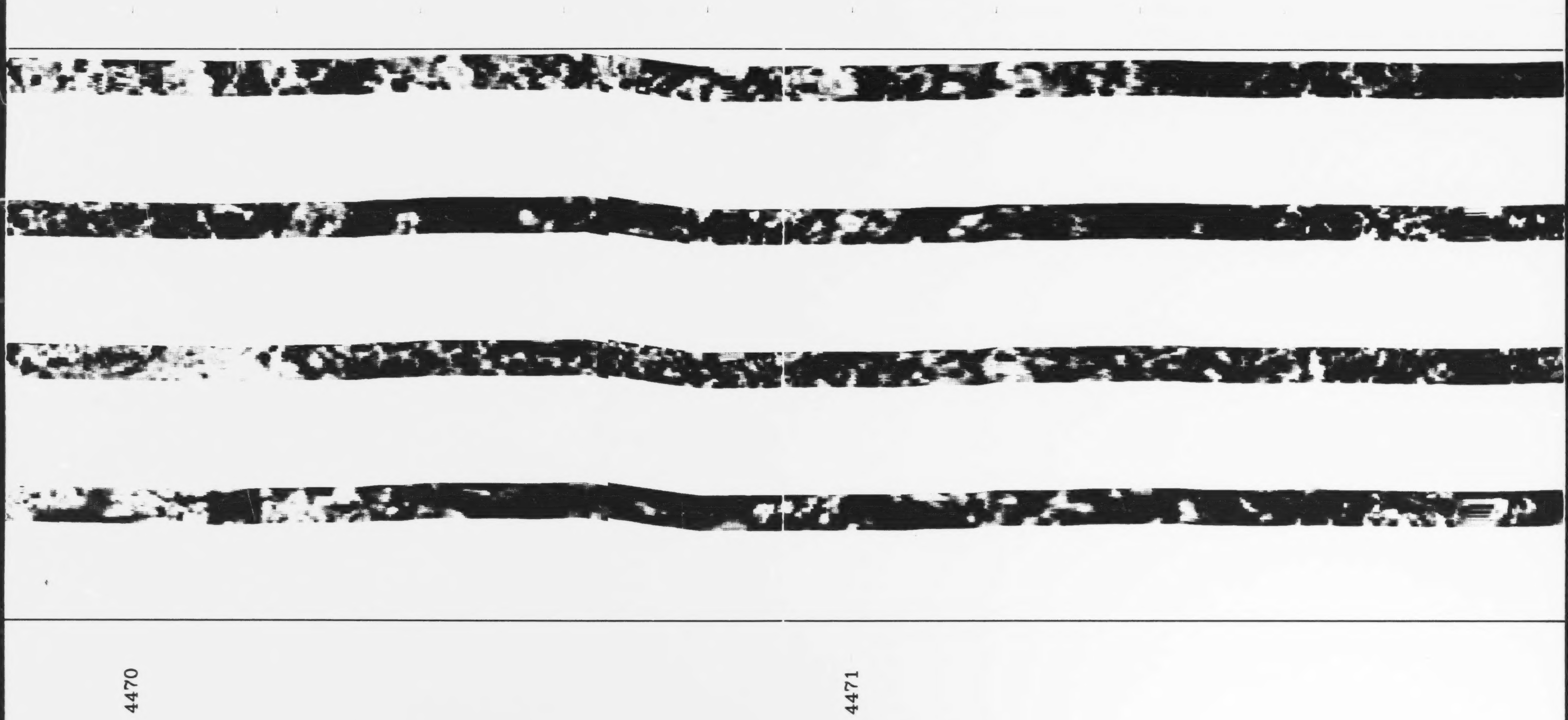
4470
4471

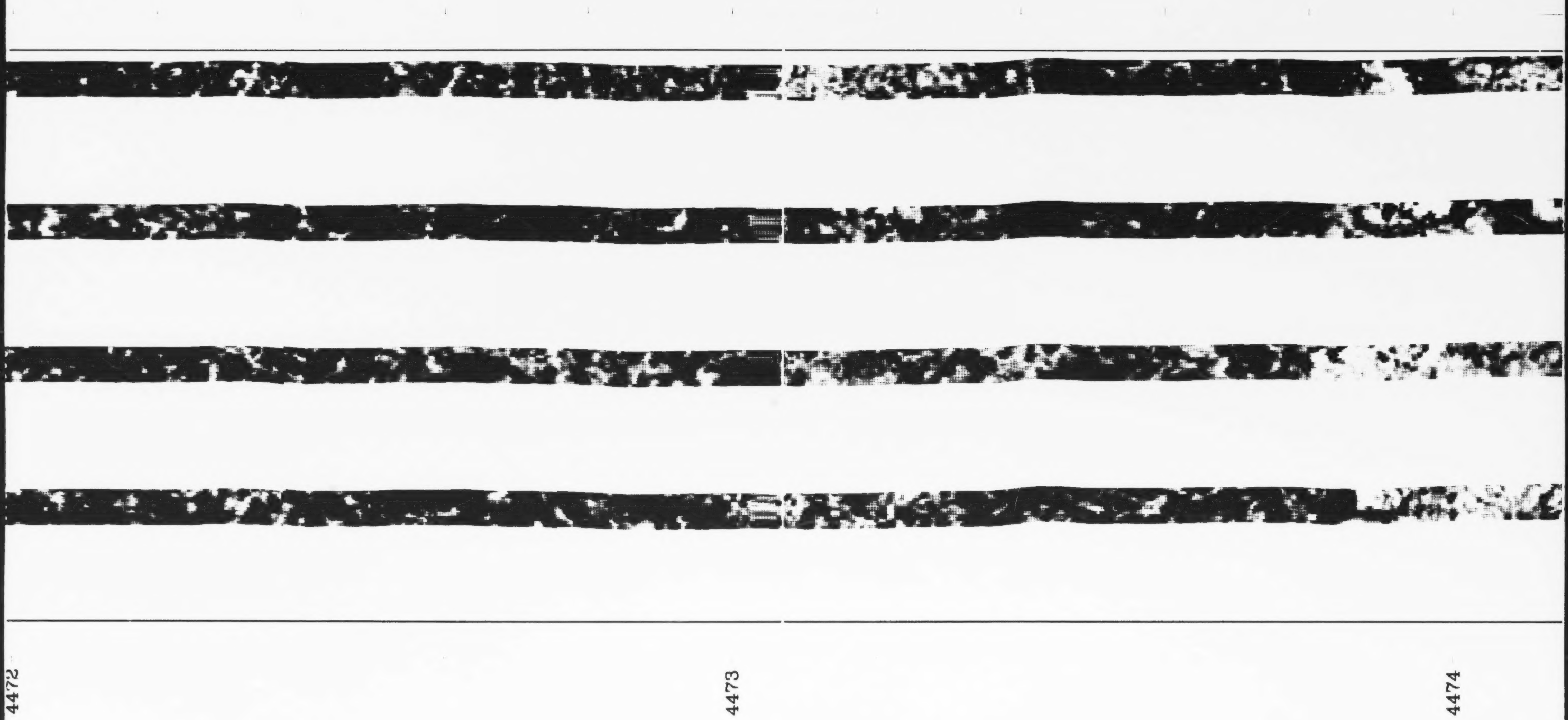

4472
4473
4474

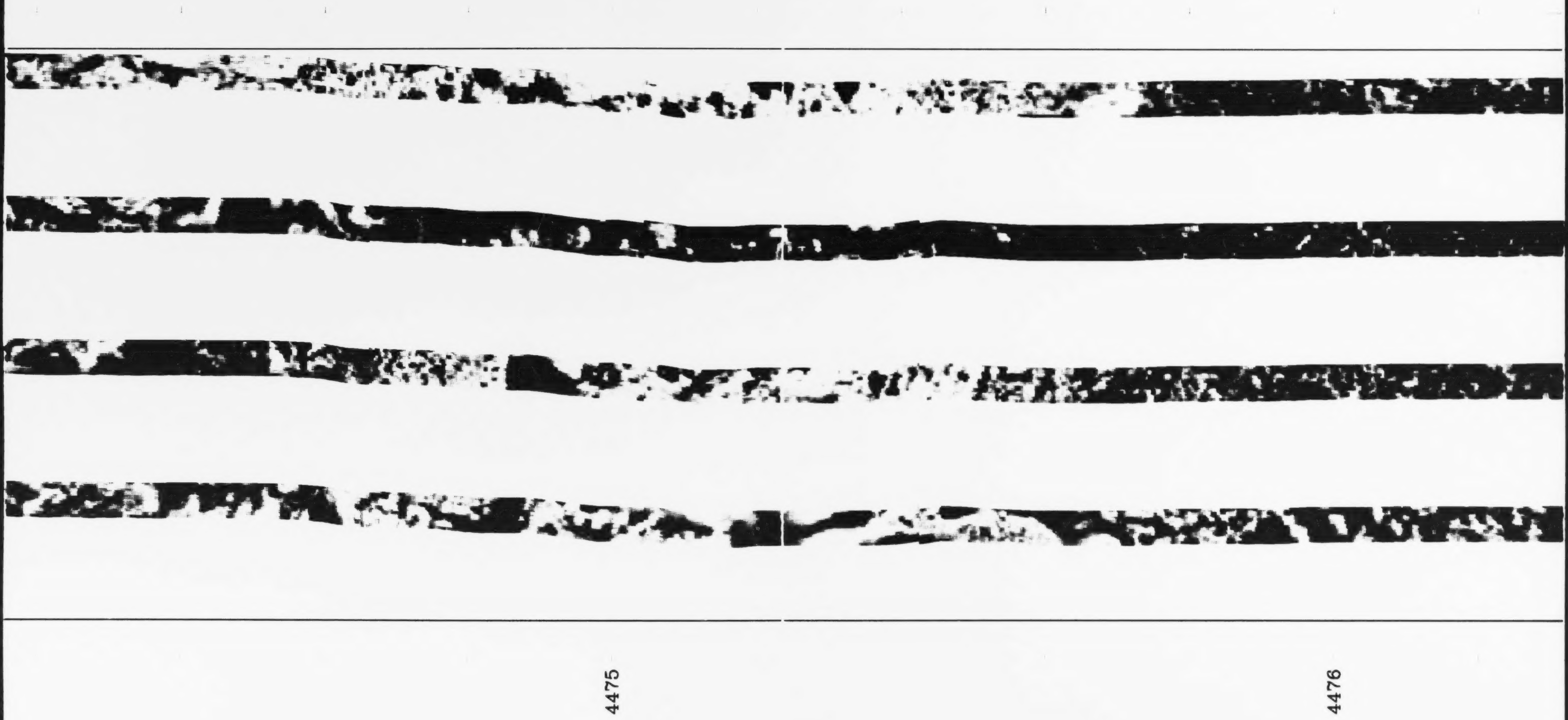
4475
4476

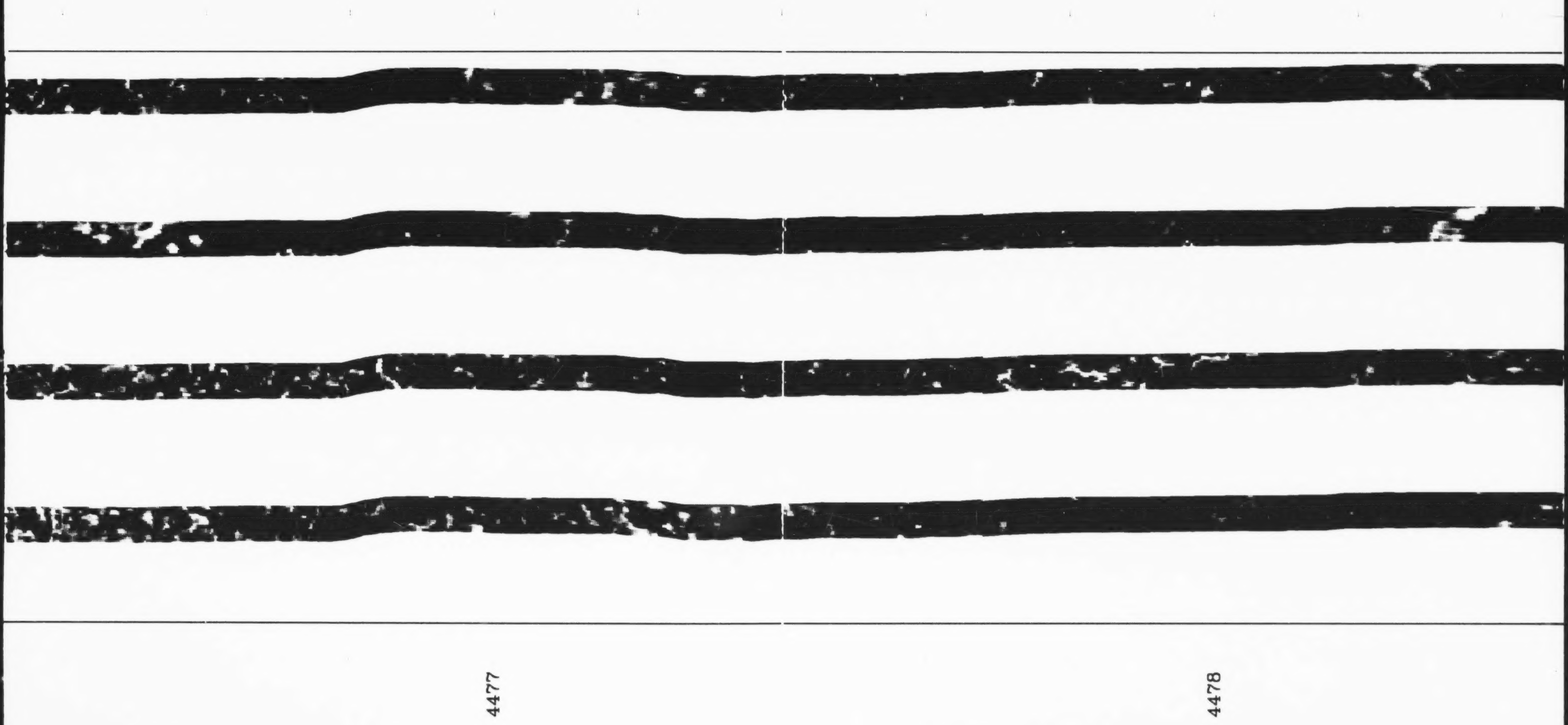
4477
4478

4479

4480

4481

4482

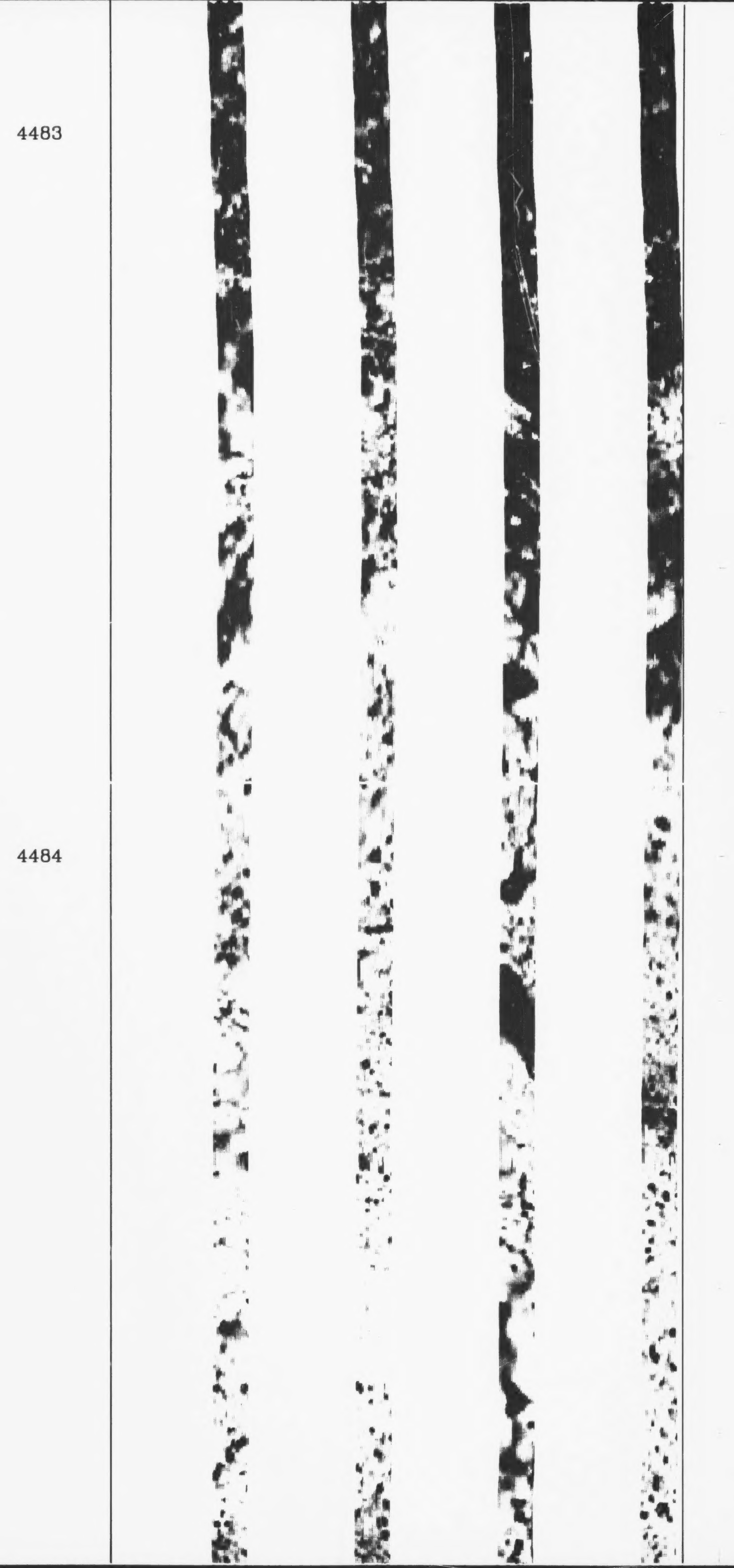
4483
4484

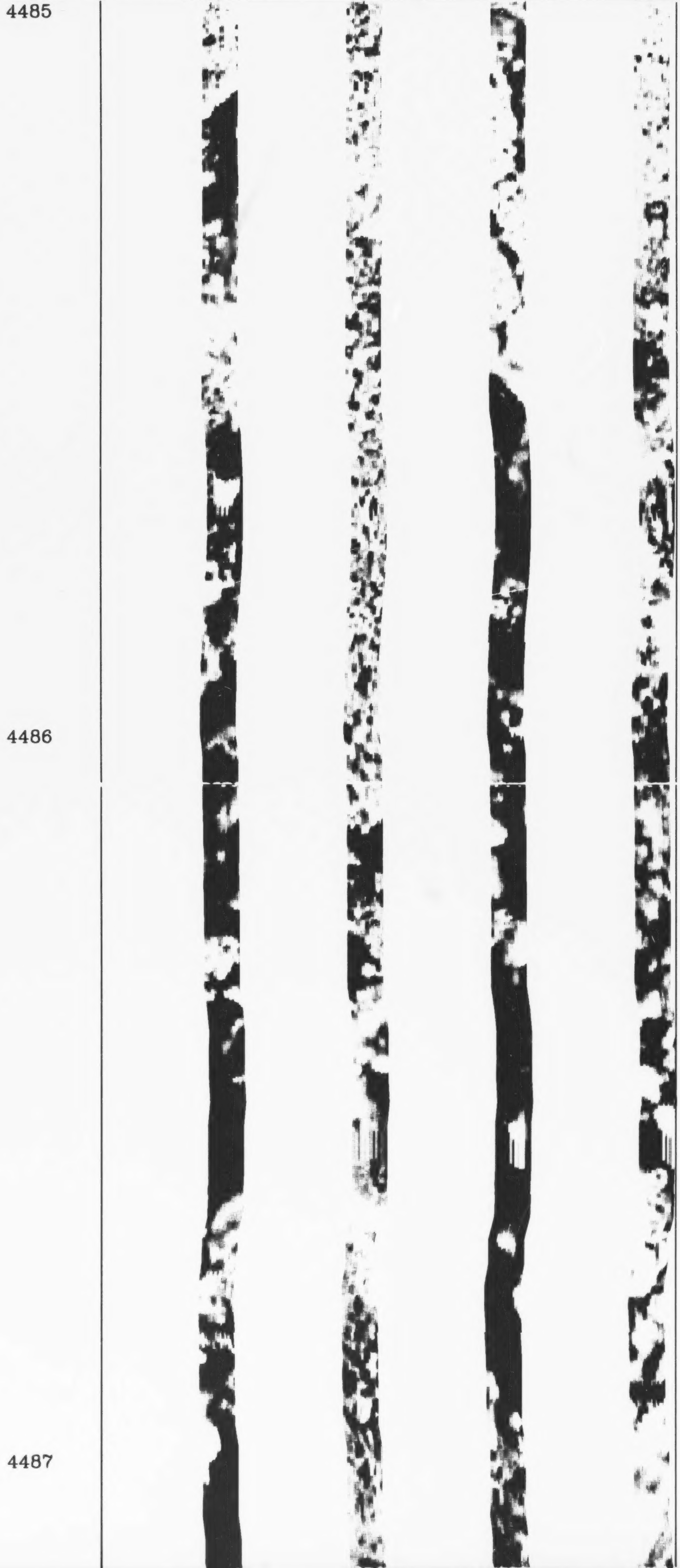

4485
4486
4487

4488
4489

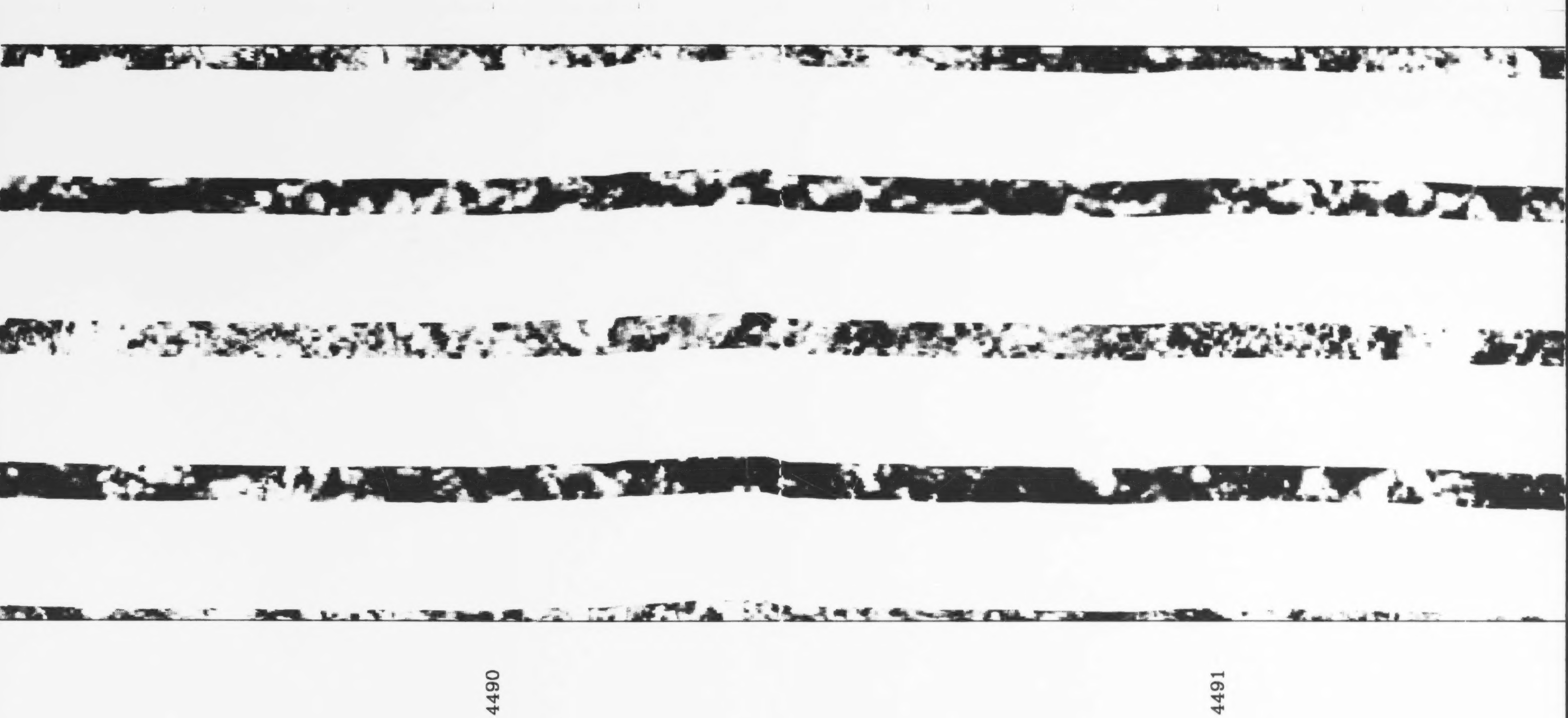
4490
4491

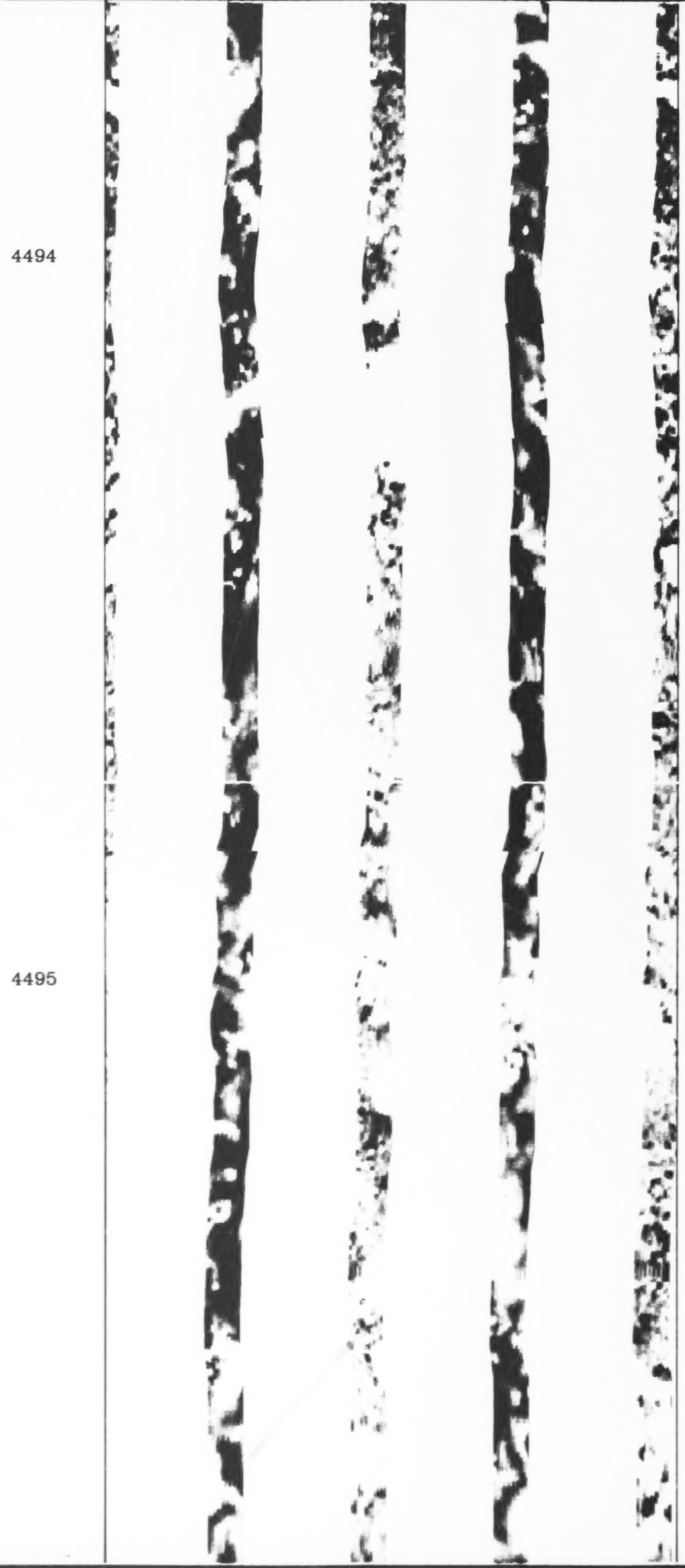
4494
4495

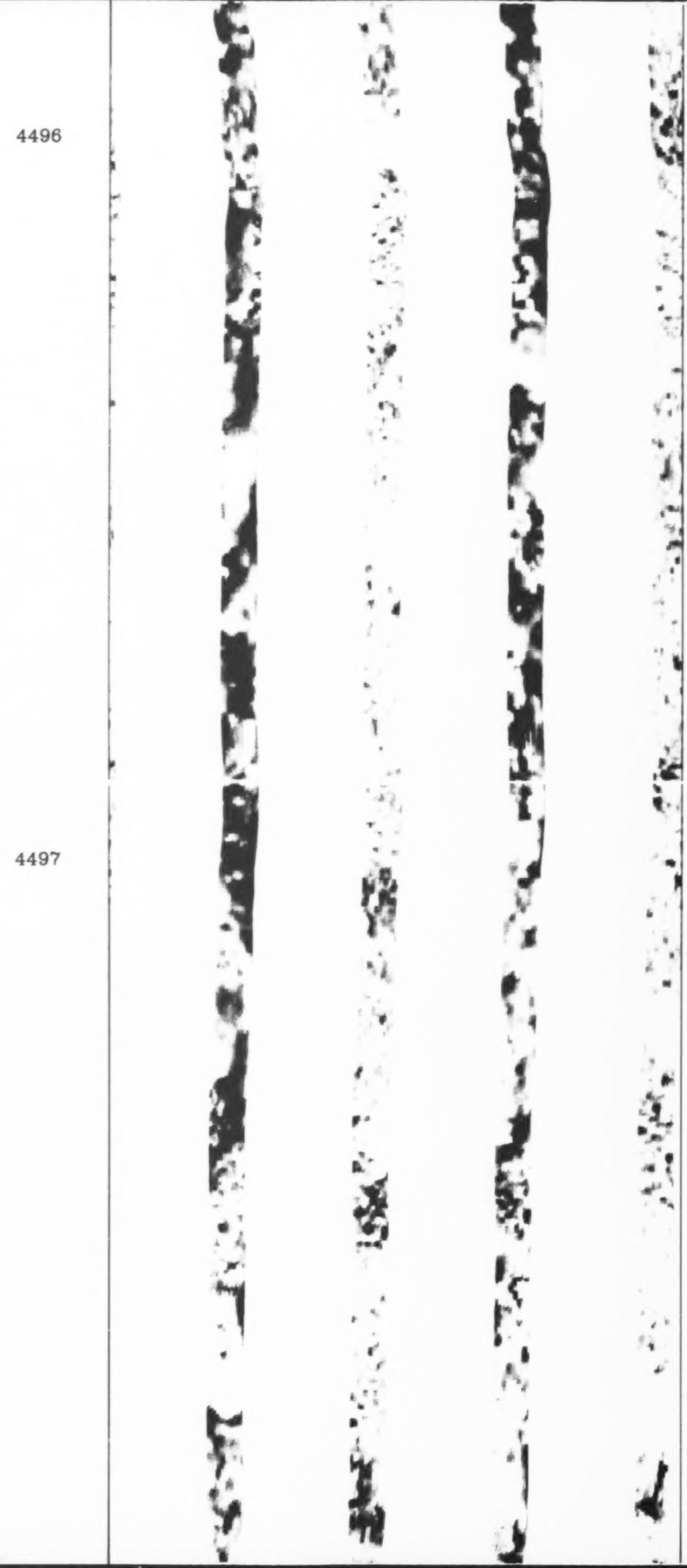
4496
4497

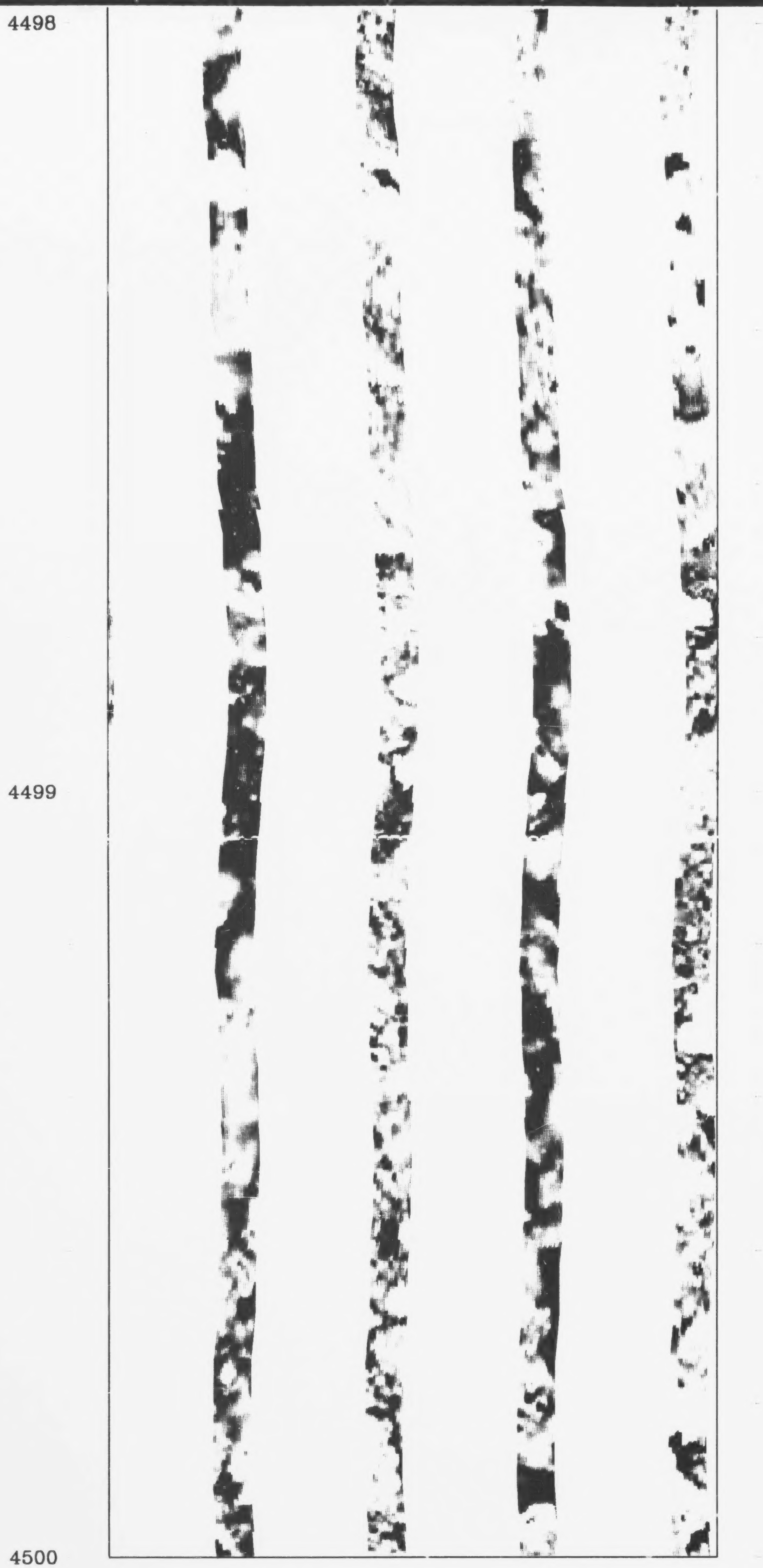
4498
4499
4500

SCHLUMBERGER

FMS
BOREHOLE
IMAGING

COMPANY	LAMONT-DOHERTY GEOLOGICAL
WELL	ODP HOLE-793B
FIELD	IZU-BONIN FOREARC BASIN
COUNTRY	OCEAN
RUN	1
DATE LOGGED	16 - JUN - 89
REFERENCE	STATIC PS 1 4500 4523

STATIC NORMALIZATION

STATIC - NORMALIZATION

PASS 1 (23577)

FILE : MEST.001

ZONE FROM 4522.8 M TO 4500.0 M

DEPTH SCALE = 1/ 5

IMAGE SCALE = 1/ 5

BITSIZE = 9.88

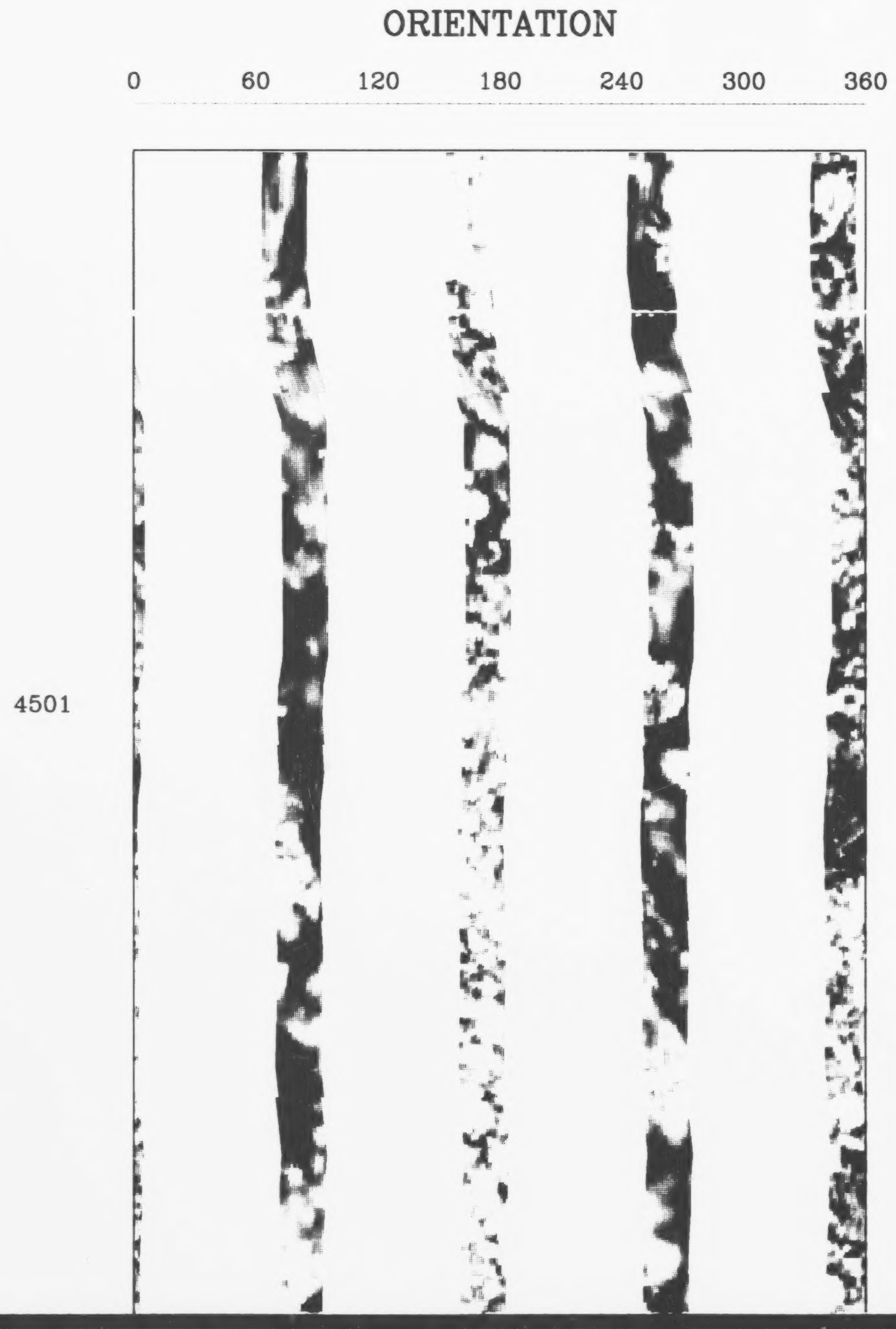

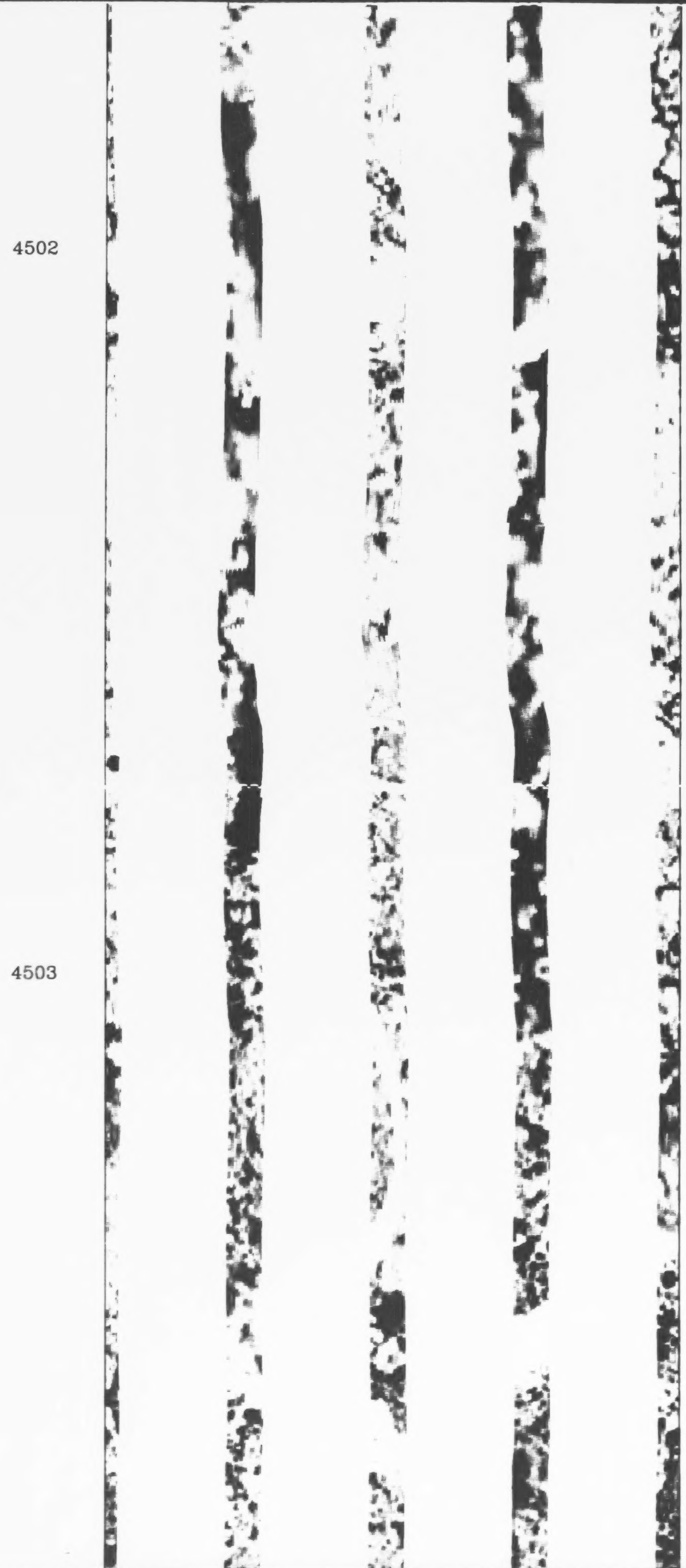
4502
4503

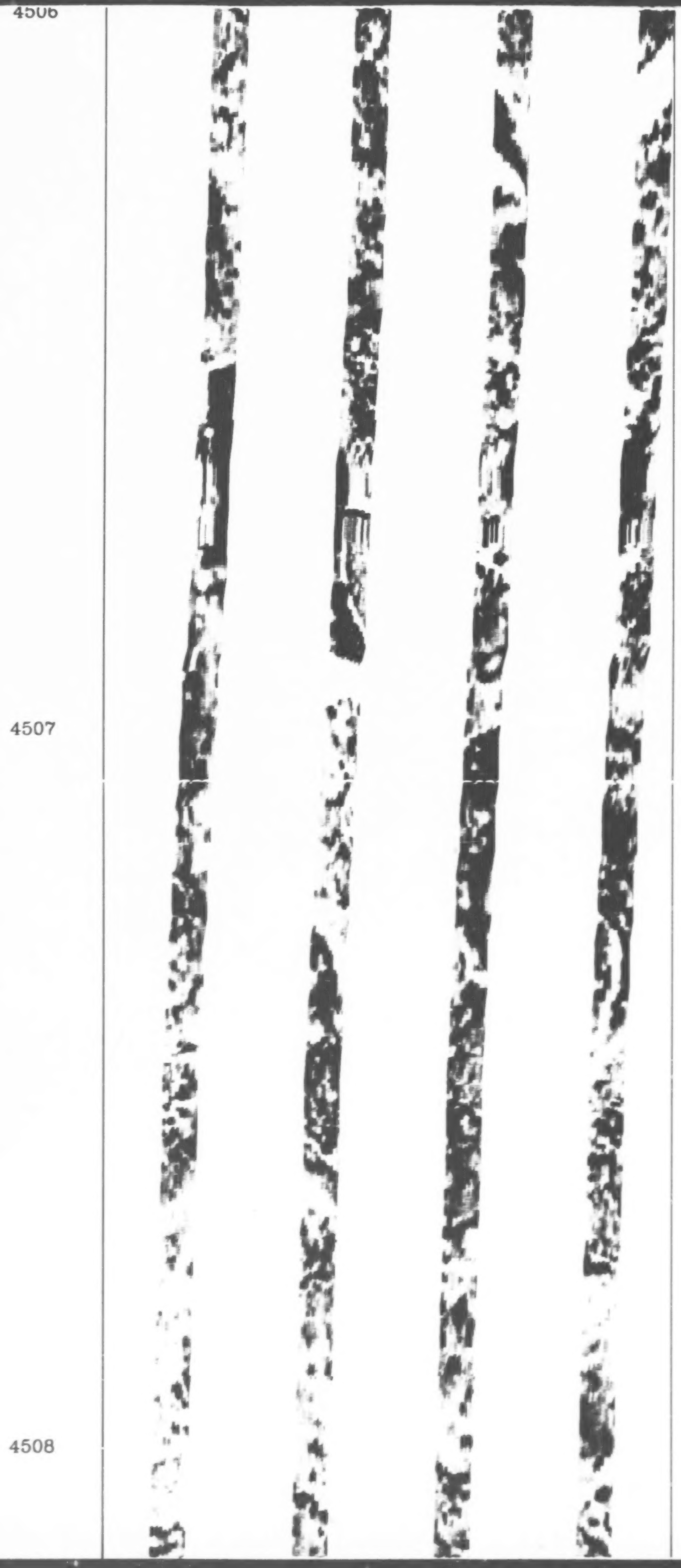
4506
4507
4508

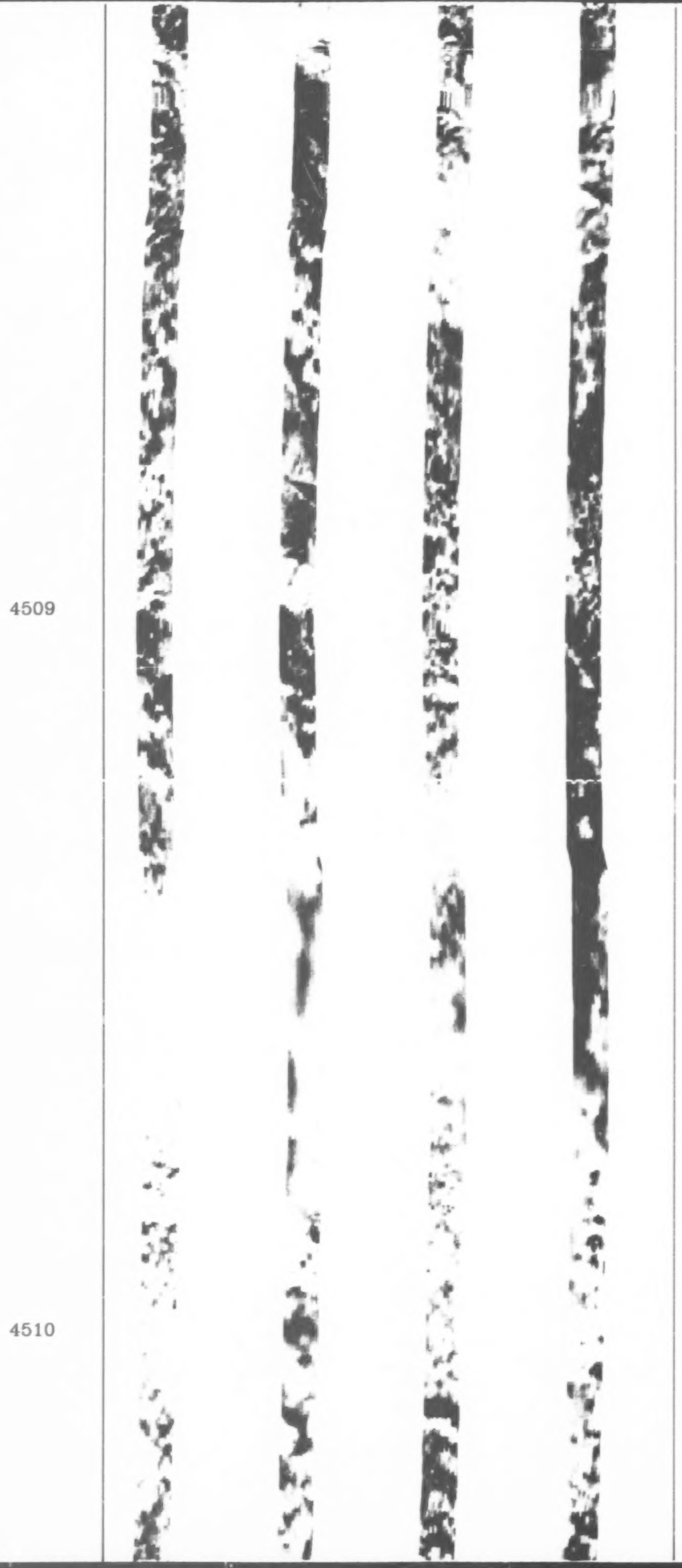
4509
4510

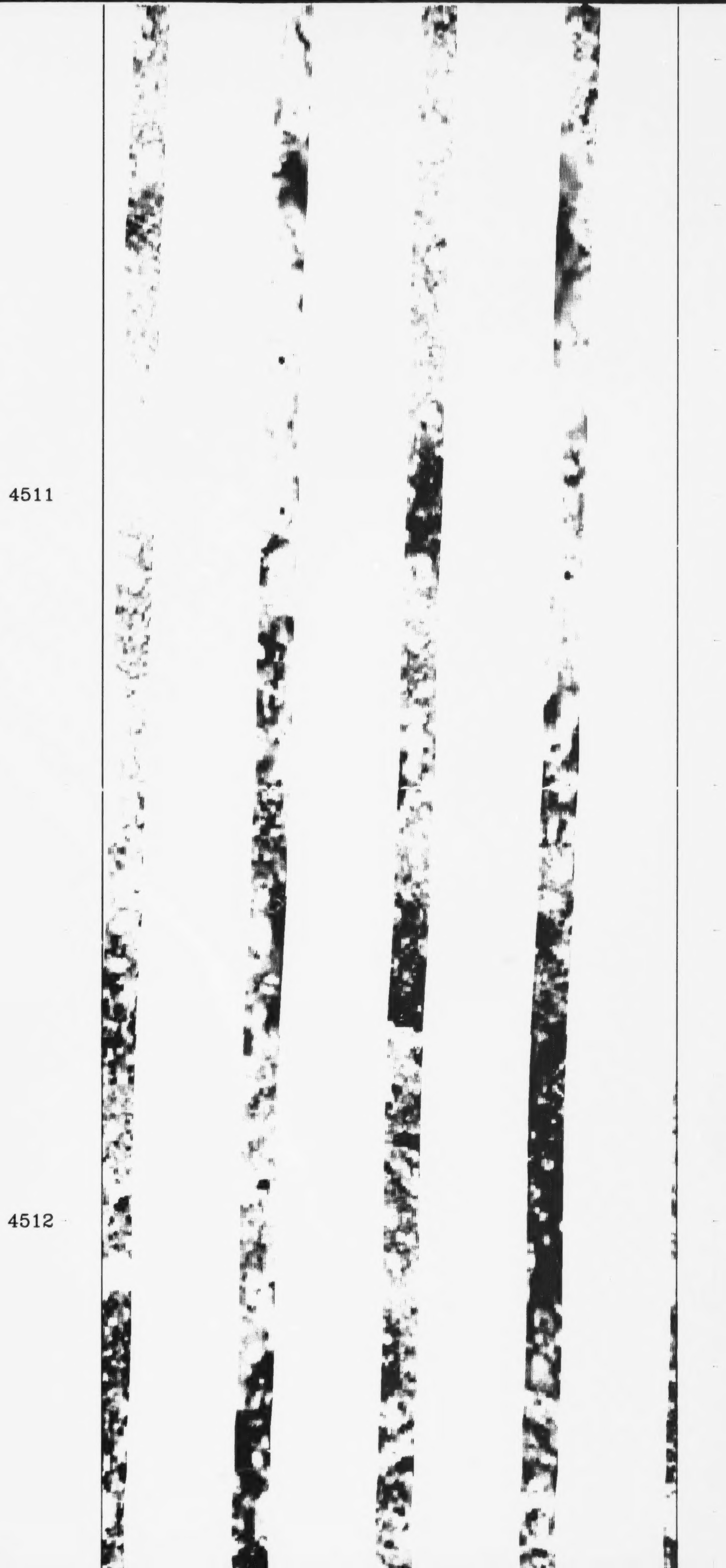
4511
4512

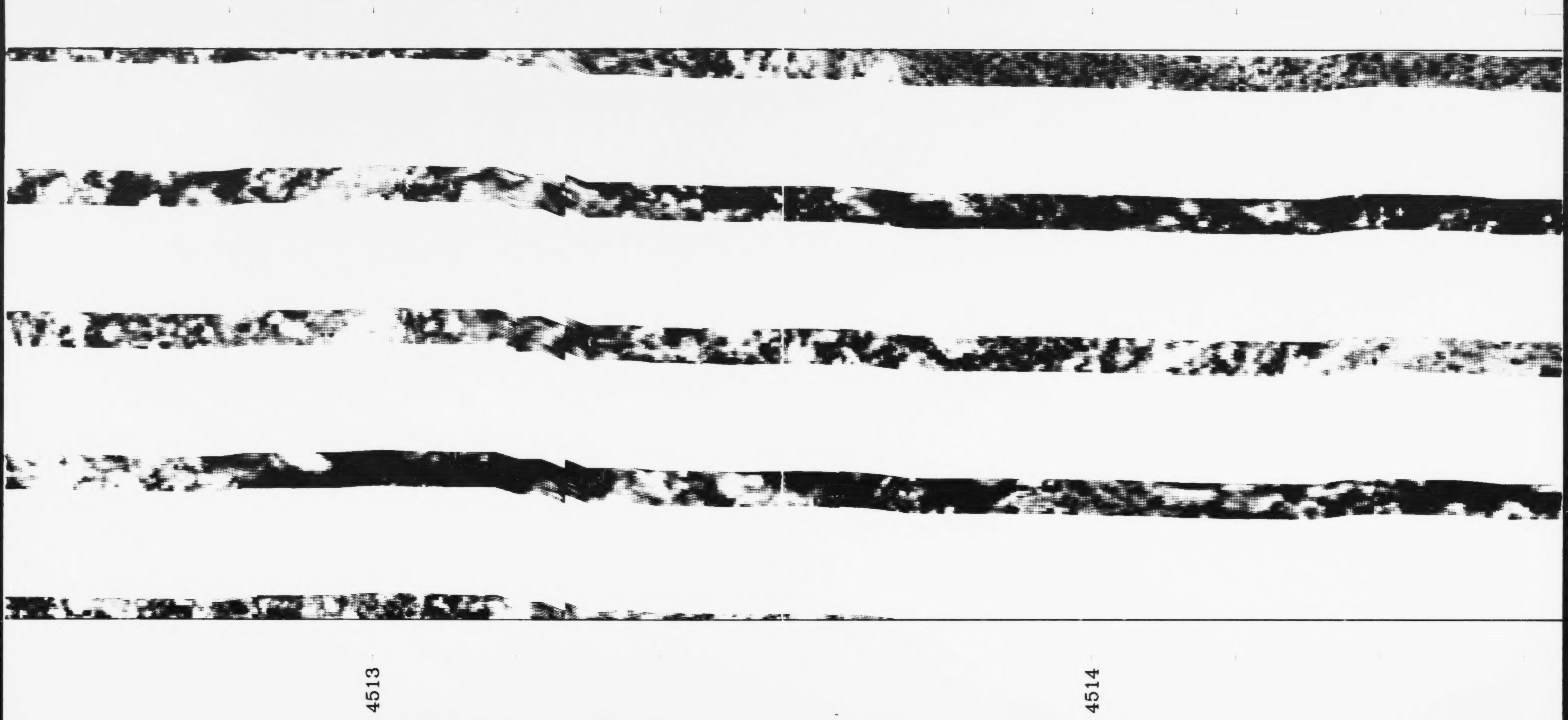
4513
4514

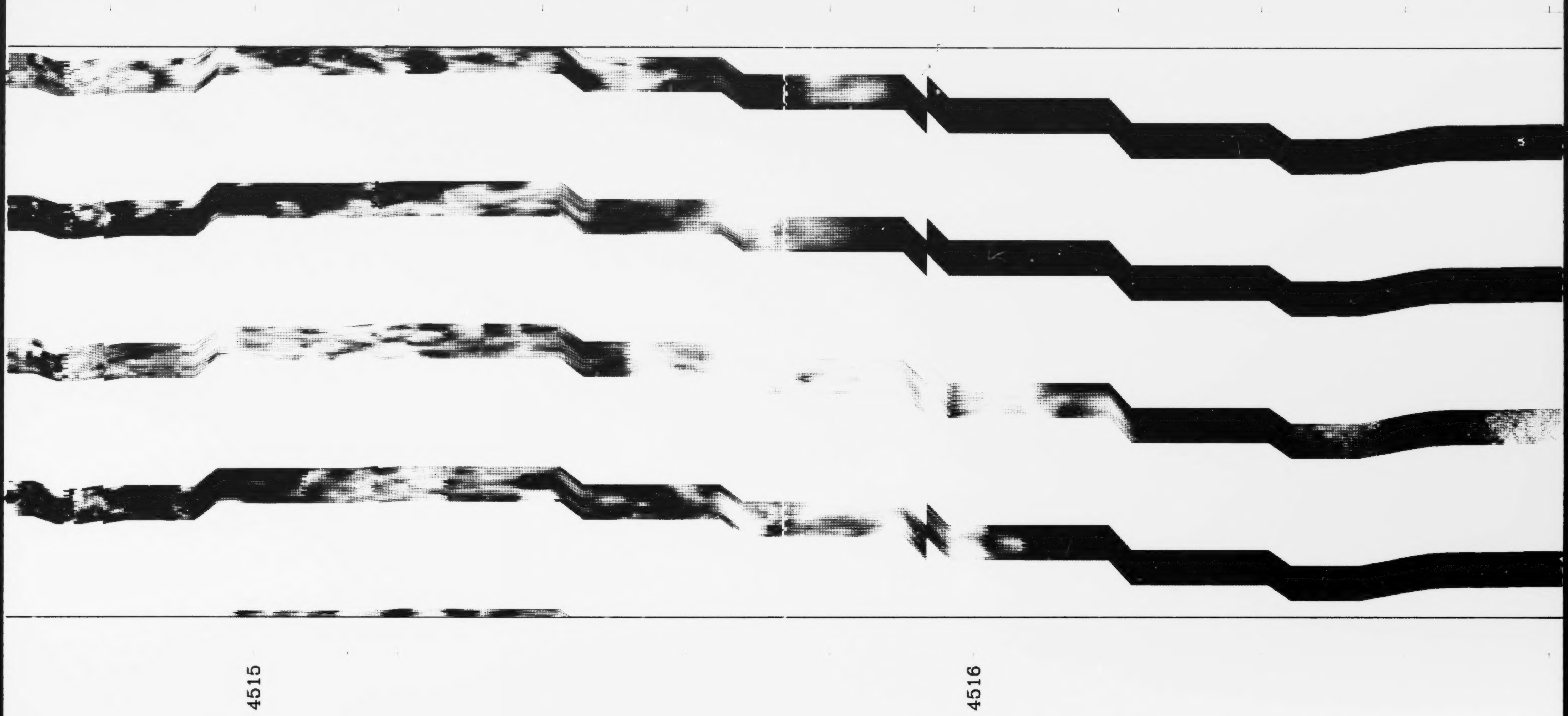
4515
4516

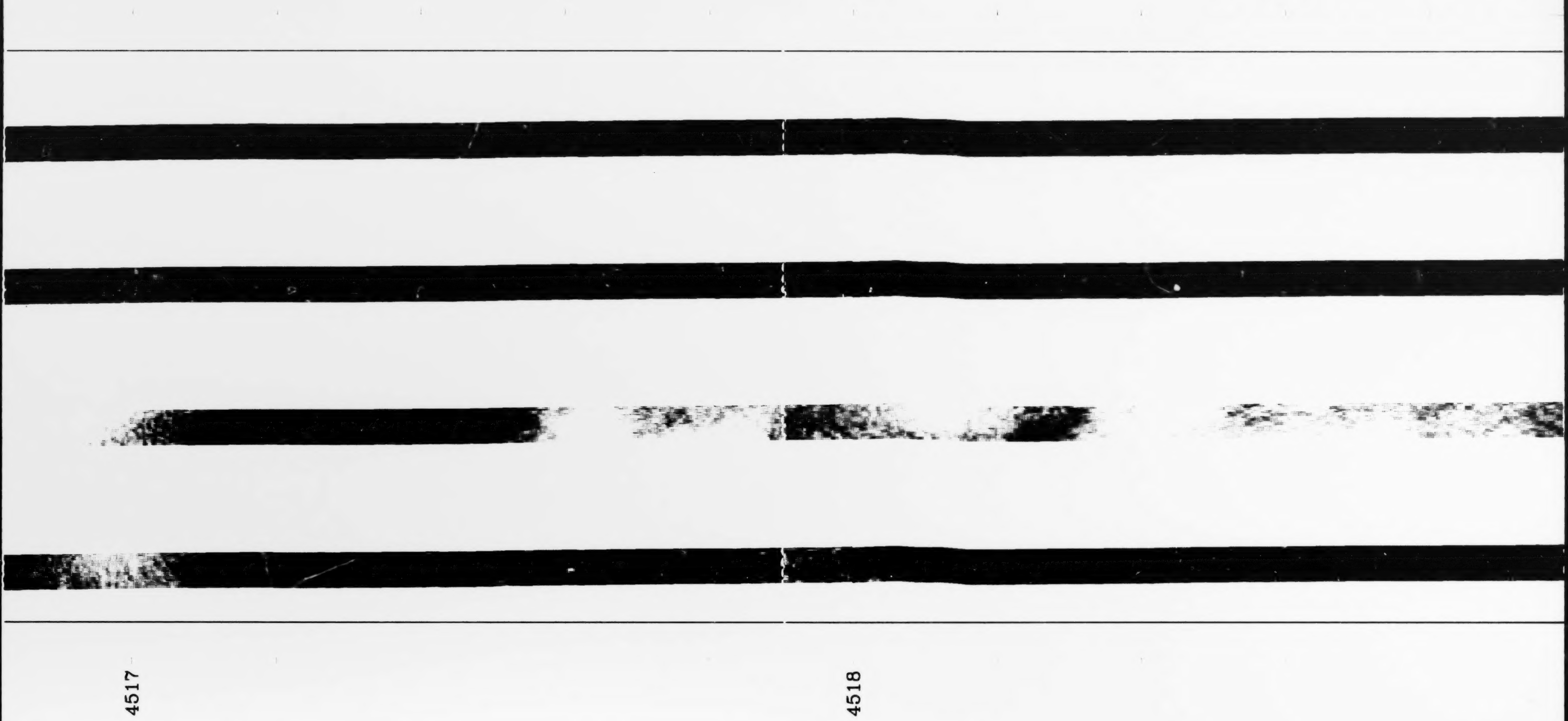
4517
4518

4519

4520

4521

4522